PET and SPECT in Neurology

Rudi A. J. O. Dierckx
Andreas Otte
Erik F. J. de Vries
Aren van Waarde
Editors

Klaus L. Leenders
Guest Editor

Second Edition

Springer

PET and SPECT in Neurology

Rudi A. J. O. Dierckx • Andreas Otte
Erik F. J. de Vries • Aren van Waarde
Editors

Klaus L. Leenders
Guest Editor

PET and SPECT in Neurology

Second Edition

Springer

Editors
Rudi A. J. O. Dierckx
Nuclear Medicine and Molecular Imaging
University Medical Center Groningen
Groningen
The Netherlands

Erik F. J. de Vries
Nuclear Medicine and Molecular Imaging
University Medical Center Groningen
Groningen
The Netherlands

Andreas Otte
Faculty of Electrical Engineering,
Medical Engineering and Computer Science
Offenburg University
Offenburg
Germany

Aren van Waarde
Nuclear Medicine and Molecular Imaging
University Medical Center Groningen
Groningen
The Netherlands

Guest Editor
Klaus L. Leenders
Neurology
University Medical Center Groningen
Groningen
The Netherlands

ISBN 978-3-030-53167-6 ISBN 978-3-030-53168-3 (eBook)
https://doi.org/10.1007/978-3-030-53168-3

This Springer imprint is published by the registered company Springer Nature Switzerland AG
The registered company address is: Gewerbestrasse 11, 6330 Cham, Switzerland

Foreword

When in 2014 the editors published the first edition of this 3-volume series, dedicated to the use of PET and SPECT in the CNS, a major undertaking saw the light in print. These were significant multi-authored books, providing the most comprehensive review of this challenging field at the time.

Now, in 2020, a second edition is launched, demonstrating the success of this initial endeavour. With a further major effort, over 50% of the numerous chapters are either entirely novel or rewritten anew, by an impressive list of international contributors. The team deserves warm congratulations for this achievement.

In 2014, PET-MR had just emerged as a novel imaging modality, and the medical applications of machine learning, or artificial intelligence, had hardly surfaced. PET imaging of Tau had just made it.

Now, in 2020, amazing progress in the understanding of the brain is being made, and even dedicated brain PET and PET-MR imaging instruments are in development (Catana 2019). Yet, with its hundred billion neurons, the brain keeps its mystery and continues to engage and stimulate our enquiry.

Little by little progress is being made, from decoding consciousness (Sohn 2019) to growing neurons from reprogrammed skin fibroblasts (Kofler 2019). We now understand that protein deposits in the brain may precede clinical manifestations by years, great advances have been made in extracting quantitative data from such studies (as shown with PET-CT and amyloid and tau numerical data) and that we can intervene effectively, inter alia, in receptor deficiencies and in deep brain stimulation. The brain connectome is unravelling, with it, a greater understanding of, amongst others, pain and drug-induced addictions, the dementias and movement disorders. All of this and much more is being critically reviewed by 119 chapters spread into these 3 major volumes.

It is hence perfect timing that the Second Edition shines a new light at the significant progress made in PET and SPECT, describing and analysing latest information from novel biological radionuclide probes, neuroreceptors and the clinical progress achieved.

University College London
London, UK

Peter Josef Ell,

References

1. Catana C (2019) Development of Dedicated Brain PET Imaging Devices: Recent Advances and Future Perspectives. J Nucl Med 60:1044–1052.
2. Kofler N (2019) Brain in a Dish, Babies by Design: What It Means to Be Human. Nature 569:333–334.
3. Sohn E (2019) Decoding the Neuroscience of Consciousness. Nature 571:S2–S5.

Preface

Neuroscientists of today dispose of a powerful armament for functional, physiological and molecular imaging that has never made more impressive advances than before, helping to better understand the mechanisms of diseases and to develop and design drug treatment options with a superior efficacy and safety profile. Among these instruments, positron emission tomography (PET) and single-photon emission computed tomography (SPECT) have become forerunners in the *in vivo* imaging arena, and for this reason, the present trilogy, now in its second, completely revised and supplemented edition, is dedicated to PET and SPECT. The volumes of this trilogy are *PET and SPECT in Psychiatry, PET and SPECT in Neurology* and *PET and SPECT in Neurobiological Systems*. In all volumes, we have again assembled the combined expertise of the renowned authors of the first edition and expanded this by some new authors for the second edition, whose dedication to the investigation of psychiatric and neurological disorders or of neurobiological systems through nuclear medicine technology has achieved international recognition.

The editors, who are nuclear medicine specialists, radiochemists and biologists with a strong exposure to neurosciences, have again invited experts from the psychiatry, neurology, and medical physics fields to enhance the editorial board as guest editors for each volume of the trilogy. For *PET and SPECT in Psychiatry* this was Iris Sommer, professor of cognitive aspects of neurological and psychiatric disorders; for *PET and SPECT in Neurology* it remained Klaus (Nico) L. Leenders, emeritus professor of neurology; and for *SPECT in Neurobiological Systems* it was Adriaan A. Lammertsma, professor of medical physics and PET.

We are very happy that our trilogy has become a state-of-the-art compendium with top downloads already for the first edition. This is certainly also due to the production and distribution by one of the premier publishers in the field, guaranteeing a high quality of reproduction and allowing for the inclusion of many colour figures, which is essential in the field of neuroimaging. We are intrigued by the enthusiastic response from contributors from all over the world who made this endeavour successful and are confident that the second edition continues to live up to this onus. Finally, we would like to thank Mrs. Gesa Frese from *Springer-Verlag* for her continuous help and support during the development of the second edition of this book series.

We sincerely hope that the new trilogy will still serve as a key tool not only for all physicians in nuclear medicine, psychiatry, neurology, or geriatrics but also for

all professionals working to understand or treat brain disorders. With today's ageing population, PET and SPECT imaging can provide new insights into the processes that may lead to unhealthy ageing of the brain. May this book series serve as a guide towards the present use of PET and SPECT in brain disorders and as a catalyst for future research. The progress achieved by PET and SPECT in the diagnosis of the many facets of diseases disposed in the neurosciences has been astounding. Nevertheless, in line with the Socratic paradox "*I know that I know nothing*", it seems that we are still at the beginning of understanding the brain. This book hopes to provide a renewed platform to further contribute to this quest, at the benefit of patients suffering from neurologic and psychiatric disorders.

Groningen, The Netherlands — Rudi A. J. O. Dierckx
Offenburg, Germany — Andreas Otte
Groningen, The Netherlands — Erik F. J. de Vries
Groningen, The Netherlands — Aren van Waarde

Contents

Part I Basics

1 Nuclear Medicine Imaging Tracers for Neurology 3
Philip H. Elsinga

2 Tracer Kinetic Modelling 37
Adriaan A. Lammertsma

3 Quantification in Brain SPECT: Noninvasive Cerebral Blood Flow Measurements Using ^{99m}Tc-Labeled Tracers 53
Hiroshi Matsuda

4 From Positron to Pattern: A Conceptual and Practical Overview of ^{18}F-FDG PET Imaging and Spatial Covariance Analysis 73
Sanne K. Meles, Jelmer G. Kok, Remco J. Renken, and Klaus L. Leenders

5 Artificial Intelligence in the Analysis of PET Scans of the Human Brain 105
Kim Mouridsen and Ronald Borra

6 MRI/PET Brain Imaging 119
Georg Schramm, Koen Van Laere, Peter Jan Van Laar, and Michel Koole

7 The Default Network of the Brain 165
Koene R. A. Van Dijk and Alexander Drzezga

8 Use of Nuclear Medicine Molecular Neuroimaging to Model Brain Molecular Connectivity 181
Carlos A. Sanchez-Catasus, Martijn L. T. M. Müller, Peter Paul De Deyn, Rudi A. J. O. Dierckx, Nicolaas I. Bohnen, and Lester Melie-Garcia

Part II Dementia

9 PET Neuroimaging in Dementia Conditions 211
Daniela Perani, Silvia Paola Caminiti, Giulia Carli, and Giacomo Tondo

10 Aβ Imaging in Aging, Alzheimer's Disease, and Other Neurodegenerative Conditions 283
Victor L. Villemagne, Vincent Doré, Samantha Burnham, and Christopher C. Rowe

11 PET Imaging of the α4β2* Nicotinic Acetylcholine Receptors in Alzheimer's Disease 345
Osama Sabri, Philipp M. Meyer, Hermann-Josef Gertz, Solveig Tiepolt, Peter Brust, Henryk Barthel, and Swen Hesse

12 Neuroimaging Findings in Mild Cognitive Impairment 367
Federico Massa, Matteo Bauckneht, Enrico Peira, Caterina Lapucci, Agnese Picco, Selene Capitanio, Dario Arnaldi, Luca Roccatagliata, Andrea Chincarini, and Flavio Nobili

13 Impact of the New Conceptual Framework of Alzheimer's Disease in Imaging Studies 427
Bruno Dubois, Nicolas Villain, Claudia Jacova, and Olga Uspenskaya

14 Perfusion SPECT: Its Role in the Diagnosis and Differential Diagnosis of Alzheimer's Disease, with Particular Emphasis on Guidelines 453
Ronald W. J. van Rheenen, Gilles N. Stormezand, Jacoba P. van Amerongen, Andreas Otte, Peter Paul De Deyn, and Rudi A. J. O. Dierckx

15 Nuclear Imaging in Frontotemporal Dementia 469
Fransje E. Reesink, Gilles N. Stormezand, Rudi A. J. O. Dierckx, and Peter Paul De Deyn

16 Parkinsonian Dementias: PET Findings 491
Prabesh Kanel, Martijn L. T. M. Müller, and Nicolaas I. Bohnen

17 SPECT/PET Findings in Dementia with Lewy Bodies 515
Sedigheh Zabihi, Tim Whitfield, and Zuzana Walker

18 SPECT and PET in Vascular Dementia 563
Yumin Zheng and Zhi Zhou

19 Value of MIBG in the Differential Diagnosis of Neurodegenerative Disorders 577
Mitsuhiro Yoshita

Part III Cerebrovascular Disorders

20 Perfusion Imaging in Healthy Human Aging 593
Sabine L. Collette, Auke P. Appelman, and Reinoud P. H. Bokkers

21 Carotid Plaque Imaging with SPECT/CT and PET/CT 607
Riemer H. J. A. Slart, Hendrikus H. Boersma, and Clark J. Zeebregts

22 PET in Brain Arteriovenous Malformations and Cerebral Proliferative Angiopathy 629
J. Marc C. van Dijk, Timo Krings, Janine Doorduin, and Riemer H. J. A. Slart

23 PET Reveals Pathophysiology in Ischemic Stroke 651
Wolf-Dieter Heiss and Olivier Zaro-Weber

Part IV Movement Disorders

24 Parkinson's Disease 675
Michele Matarazzo, Andre C. Felicio, and A. Jon Stoessl

25 Computer-Aided Diagnosis of Parkinson's Disease, Based on SPECT Scans of the Dopamine Transporter 709
Francisco P. M. Oliveira and Durval C. Costa

26 PET and SPECT Imaging in Atypical Parkinsonian Syndromes 729
Martin Niethammer, Yoon Young Choi, Chris C. Tang, and David Eidelberg

27 Amyotrophic Lateral Sclerosis 759
Martin R. Turner and Marco Pagani

28 PET in Huntington's Disease 783
H. P. H. (Berry) Kremer

29 PET and SPECT Imaging in Dystonia 799
Evelien Zoons, Jan Booij, Bauke de Jong, and Marina A. J. Tijssen

30 PET and SPECT Imaging in Hyperkinetic Movement Disorders . . . 821
Evelien Zoons, Sarvi Sharifi, Jan Booij, Bauke de Jong, and Marina A. J. Tijssen

31 Clinical Applications of [^{123}I]FP-CIT SPECT Imaging 849
Jan Booij, Marina A. J. Tijssen, and Henk W. Berendse

Part V Inflammatory Disorders

32 PET Imaging of Microglia Activation and Infection in Neuropsychiatric Disorders with Potential Infectious Origin 873
Hans Christiaan Klein, Lot de Witte, Robert Bransfield, and Peter Paul De Deyn

33 PET Imaging in Multiple Sclerosis 893
Chris W. J. van der Weijden, Jan F. Meilof, and Erik F. J. de Vries

34 PET and SPECT Imaging of Neurotoxicity 917
Erik F. J. de Vries, Rudi A. J. O. Dierckx, and Didima M. G. de Groot

35 PET and SPECT in Hepatic and Uraemic Encephalopathy 947
Georg Berding, Frank Bengel, and Karin Weissenborn

Part VI Epilepsy

36 PET in Epilepsy 969
Matthias Koepp, Marian Galovic, and Maria Ilyas-Feldmann

37 Imaging Evaluation of Epilepsy: Functional and Structural Approaches 983
Sara K. Inati and William H. Theodore

38 SISCOM (Subtraction Ictal SPECT with Coregistration to MRI) . . 1007
Hwareung Lee, Jung Sik Kim, Ji Hyun Kim, and Seung Bong Hong

Part VII Tumors of the Nervous System

39 Gliomas 1027
Karl Herholz

40 Single-Photon Emission Computed Tomography [Neuro-SPECT] Imaging of Brain Tumors 1051
George A. Alexiou, Spyridon Tsiouris, and Andreas D. Fotopoulos

41 The Value of Positron Emission Tomography for Differentiating Brain Tumor Progression and Treatment-Induced Changes 1067
Bart R. J. van Dijken, Roelien H. Enting, Hanne-Rinck Jeltema, Miranda C. A. Kramer, Rudi A. J. O. Dierckx, and Anouk van der Hoorn

42 Imaging Brain Metastases of Neuroendocrine Tumors 1083
Klaas Pieter Koopmans and A. H. Brouwers

43 Traumatic Brain Injury: Nuclear Medicine Neuroimaging 1095
Carlos A. Sanchez-Catasus, Gilles N. Stormezand, David Vállez García, Eloísa Le Riverend Morales, Reinaldo Galvizu Sánchez, and Rudi A. J. O. Dierckx

Part VIII Other Subjects

44 Anaesthesia and PET of the Brain 1123
Anthony Absalom and Ram Adapa

45 PET Imaging in Altered States of Consciousness: Coma, Sleep, and Hypnosis 1149
Estelle A. C. Bonin, Géraldine Martens, Helena Cassol, Camille Chatelle, Steven Laureys, and Aurore Thibaut

46 Modulation of CNS Functions by Deep Brain Stimulation: Insights Provided by Molecular Imaging 1177
Alexandre Boutet, Mehr Jain, Dave Gwun, Pablo Rusjan, Clemens Neudorfer, Gavin J. B. Elias, Jürgen Germann, Alexander Bilbily, Walter Kucharczyk, Alfonso Fasano, Gwenn S. Smith, and Andres M. Lozano

47 Radionuclide Imaging Studies in Pediatric Neurology 1245
Ajay Kumar, Csaba Juhasz, and Harry T. Chugani

Part I

Basics

Nuclear Medicine Imaging Tracers for Neurology

1

Philip H. Elsinga

Contents

1.1 Introduction 4
1.2 Glucose Consumption 7
1.3 Translocator Protein TSPO 7
1.4 GABA Receptor 8
1.5 Dopaminergic System 8
1.5.1 Dopamine Transporter (DAT) 9
1.5.2 D_1 Receptor 11
1.5.3 D_2 Receptor 12
1.5.4 D_2/D_3 Agonists 12
1.6 Beta-Amyloid Deposition 13
1.7 NMDA Receptor, Glycine Transport 14
1.8 P-Glycoprotein 14
1.9 Cholinergic System 16
1.10 Metabotropic Glutamate-5 Receptor 17
1.11 Vesicular Monoamine Transporter 18
1.12 Adenosine Receptors 19
1.13 Serotonergic System 20
1.13.1 Serotonin Transporter 20
1.13.2 5-HT Receptor Ligands 21
1.14 Nonadrenergic System 22
1.15 Opioid Receptors 22
1.16 Monoamine Oxidase 23
1.17 SV2A Receptors 24
1.18 Sigma Receptors 24
1.19 Tau Protein Deposition 25

P. H. Elsinga (✉)
Department of Nuclear Medicine and Molecular Imaging, University of Groningen, University Medical Center Groningen, Groningen, The Netherlands
e-mail: p.h.elsinga@umcg.nl

R. A. J. O. Dierckx et al. (eds.), *PET and SPECT in Neurology*,
https://doi.org/10.1007/978-3-030-53168-3_1

1.20 Phosphodiesterase..... 25
1.21 P2X7 Receptor..... 26
1.22 (Re)Myelination..... 27
1.23 Cannabinoid Receptors..... 27
1.24 Conclusions..... 27
References..... 28

Abstract

Tracers to investigate neurological disorders with positron emission tomography (PET) or single-photon emission computed tomography (SPECT) have found many applications. Several molecular targets can be studied in the human brain in vivo, both in health and disease. Initially, most attention was given to tracers for translocator protein (TSPO), deposition of beta-amyloid, and the dopaminergic system. Many clinical studies have been published with application of a variety of tracers for these targets. During the past few years, more tracers have reached the stage of human studies such as imaging agents for tau protein, P2X7 receptor, SV2A receptor, and the cholinergic system. Other targets of interest that have been studied in man to a lesser extent are *N*-methyl-D-aspartic acid (NMDA), serotonergic, adenosine, gamma-aminobutyric acid (GABA), sigma, opioid, and metabotropic glutamate subtype 5 (mGlu5) receptors. In addition, several transporter systems have received a great deal of attention. Many tracers for new molecular targets are under development and may open new horizons in the future. Most PET tracers for the brain were initially labeled with ^{11}C but were later replaced by ^{18}F-labeled analogs, since this radionuclide enables longer scanning protocols, dissemination to other hospitals, and commercialization. This initial chapter will highlight PET tracers that have already reached the state of human application.

1.1 Introduction

This chapter describes positron emission tomography (PET) and single-photon emission computed tomography (SPECT) tracers that have been validated in humans and are applied in clinical studies. Many other tracers with potentially improved properties are currently under preclinical evaluation. In Table 1.1, an overview is given of molecular targets and processes associated with neurological diseases and available tracers for nuclear medicine imaging in humans.

An ideal nuclear medicine imaging tracer for brain imaging should satisfy the following requirements:

- Simple automated synthesis procedure suitable for reliable and robust production and low radiation burden for personnel. For clinical studies, GMP compliance is a prerequisite.
- Appropriate molar activity which should be sufficiently high, so that tracer binding is minimally affected by nonradioactive counterparts. Especially for

Table 1.1 Overview of nuclear medicine tracers and their application in clinical studies

Target	Related disease	Tracers (human application)	Binding mechanism
TSPO	MS, AD, stroke, PD, HD, schizophrenia	[^{11}C]PK11195, DAA and PBR derivatives, [^{18}F]GE180	Antagonist
GABA	Stroke	[^{11}C]/[^{18}F]Flumazenil	Antagonist
Dopaminergic system	PD, HD, tardive dyskinesia, schizophrenia, autism, ADHD, drug abuse, depression	[^{18}F]FDOPA, [^{11}C] SCH23390	Vesicular storage D_1 antagonist
		[^{11}C]Raclopride, [^{123}I] IBZM	D_2 antagonist
		[^{11}C]PHNO	D_2 agonist
		[^{18}F]FP-CIT, [^{18}F] FE-PE2I [^{99m}Tc]TRODAT-1, [^{123}I]PE2I, [^{123}I]-β-CIT	Dopamine transporter
ß-Amyloid	AD, MCI	[^{11}C]PIB	Staining agent
		[^{18}F]Florbetaben/ florbetapir	
NMDA	Schizophrenia	[^{11}C]GSK-931145 [^{18}F]GE179	Antagonist
P-Glycoprotein	Neurodegeneration	[^{11}C]Verapamil, [^{11}C] dLop, [^{11}C]metoclopramide	Substrate
Cholinergic system	AD, PD, HD, schizophrenia	[^{11}C]MP4A [^{18}F]FEOBV	Acetylcholinesterase inhibitor VAChT ligand
		[^{18}F]FP-TZTP [^{18}F]ASEM, [^{11}C] CHIBA-1001 [^{18}F]A-85360, [^{18}F] flubatine	M_2 antagonist α_7-nAChR ligands $\alpha_4\beta_2$-nAChR ligands
mGlu-5	Depression, anxiety, schizophrenia, PD	[^{11}C]ABP688, [^{18}F] PSS232 [^{18}F]FPEB	Antagonist
VMAT2	PD, AD, HD	[^{11}C]DTPZ, [^{18}F] AV-133 [^{18}F]FP-DTBZ	
Adenosine receptor	PD, AD, epilepsy, sleep, neuroinflammation	[^{11}C]MPDX, [^{11}C] preladenant	A_1 antagonist A_{2a} antagonist
		[^{11}C]TSMX	A_{2a} antagonist
P2X7 Serotonergic system	Neuroinflammation Depression, anxiety, OCD, schizophrenia	[^{18}F]JNJ-64413739 [^{11}C]JNJ54173717 [^{11}C]DASB	Antagonist Serotonin transporter ligand
		[^{11}C]WAY100635, [^{18}F]MPPF	5-HT_{1A} antagonist
		[^{11}C]Cimbi-36	5-HT_{2A} agonist

(continued)

Table 1.1 (continued)

Target	Related disease	Tracers (human application)	Binding mechanism
Norephedrine	Depression	[^{11}C] Methylreboxetine	NE transporter ligand
Opioid receptors	Analgesia, shock, appetite, thermoregulation	[^{11}C]Carfentanil	Mu opioid receptor antagonist
Monoamine oxidase	Neurodegenerative and inflammatory processes	[^{11}C]Deprenyl	MAO inhibitor
Energy	Neurodegenerative and inflammatory processes	[^{18}F]FDG	Glucose consumption
Neuronal activity SV2A Sigma	Neurodegenerative and inflammatory processes AD AD	[^{15}O]Water [^{11}C]/[^{18}F]UCB-J [^{11}C]SA4503, [^{18}F] fluspidine	Blood flow Synaptic density Ligands
Tau protein	AD	[^{18}F]THK523, [^{18}F] AV1541	Staining agent
Phosphodies-terase-PDE-4 Phosphodies-terase-PDE-10	Depression Neurodegeneration	[^{11}C]Rolipram [^{11}C]IMA107, [^{11}C] Lu AE92680, [^{18}F] MNI589	Breakdown of cAMP
Demyelinization	Multiple sclerosis	[^{11}C]MeDAS	Staining agent
Cannabinoid R2	Neuroinflammation	[^{11}C]NE40	Antagonist

targets with low densities, high specific radioactivity is an important issue. In addition some compounds (e.g., opioid ligands) are pharmacologically active at very small concentrations, resulting in a need for ultra-high molar activities.

- Log*P* between 1.5 and 4 in order to passively cross the blood–brain barrier, enabling high accumulation of target bound radioactivity.
- High affinity (i.e., a low value for K_D, resulting in a high binding potential B_{max}/K_D) to achieve sufficient target-bound radioactivity and high specificity so that the measured radioactive signal represents binding to the target of interest.
- Metabolic stability to ensure that measured radioactivity represents binding of the administered tracer and not binding of a metabolite. Metabolites should not enter the brain.
- Low affinity for *P*-glycoprotein since *P*-glycoprotein can transport tracers out of the brain resulting in low brain uptake.
- Appropriate radionuclide: the radioactive half-life should match the rate of the physiological process of interest.

So to summarize: Radioactivity accumulation should represent target density or functionality, enabling the acquisition of quantitative data (Elsinga 2002). Since the ideal tracer does not exist, PET data should be interpreted with care. The following text discusses tracers for the human brain, arranged by molecular target.

1.2 Glucose Consumption

The most generally applied tracer in PET is 2-[^{18}F]fluoro-2-desoxyglucose (FDG). In neurology, FDG is used for quantifying the regional cerebral glucose consumption rate. In several neurological diseases (dementia, PD, AD, stroke), glucose consumption is reduced in specific brain regions, indicating impaired functionality of these areas. Many recent studies with FDG focus on quantification, differential diagnosis, pattern recognition (Nobili et al. 2018; Kogan et al. 2019), and on dual modality imaging (PET and MRI) aiming to increase its clinical utility. Numerous articles including review papers on the use of FDG have appeared in the literature. In many cases, FDG is applied in combination with tracers for other targets, as described in Chap. 1 (Demetriades 2002; Mielke and Heis 1998). In addition, several chapters in this volume will address the use of FDG-PET imaging.

1.3 Translocator Protein TSPO

Microglia act as resident macrophages in the brain governing the immune response. Activated microglia cells are associated with neuroinflammation, which plays an important role in the onset of neurodegenerative disease. TSPO, formerly known as the peripheral benzodiazepine receptor (PBR), is overexpressed by activated microglia (Politis et al. 2012). Several PET tracers for TSPO have been developed. (*R*)-[^{11}C]PK11195 [1-(2-chlorophenyl)-*N*-methyl-*N*-(1-methylpropyl)-3-isoquinoline carboxamide] was the first non-benzodiazepine and selective TSPO ligand (Hashimoto et al. 1989). The compound has nanomolar affinity for TSPO (Chauveau et al. 2008). This PET tracer is widely applied in TSPO PET imaging. (*R*)-[^{11}C]PK11195 has been used in many studies of the human CNS, including studies in multiple sclerosis, Alzheimer's disease (AD), Parkinson's disease (PD), amyotrophic lateral sclerosis, Huntington's disease, HIV, herpes encephalitis, and schizophrenia. Although (*R*)-[^{11}C]PK11195 shows increased brain uptake in several neurodegenerative disorders, the ligand has several disadvantages. The sensitivity is low, and it is difficult to quantify small changes in TSPO expression. (*R*)-[^{11}C]PK11195 displays a low brain penetration, high plasma protein binding, and high nonspecific binding because of its high lipophilicity. This results in a low signal-to-noise ratio. The lack of sensitivity and specificity of (*R*)-[^{11}C]PK11195 has hampered development of a standard method for quantitative data analysis. (*R*)-[^{11}C]PK11195 PET has been used mainly for assessing microglia/macrophage activation in various neurodegenerative disorders, as an indication of neuronal and tissue damage. A (metabolite-corrected) plasma input with a reversible two-tissue compartment model was shown to be the best approach for analyzing (*R*)-[^{11}C]PK11195 kinetics in brain. Because of the disadvantages of (*R*)-[^{11}C]PK11195, second- and third-generation TSPO tracers have been developed that should additionally distinguish TSPO polymorphism. Most of these new TSPO tracers are still in the early stage of investigation. Preclinical research efforts are aimed to resolve the following issues: (1) metabolic stability of the tracer, (2) adequate binding

potential (BP), (3) appropriate kinetics of the ligand receptor interaction, and (4) suitable quantification methods (Narayanaswami et al. 2018; Best et al. 2019).

Radioligands such as [^{11}C]PBR28, [^{11}C]DAA1106, [^{18}F]FEDAA1106, and [^{18}F]PBR111 have been developed to image TSPO in vivo (Dollé et al. 2009; de Vries et al. 2006). Published data using the second-generation tracers [^{11}C]DAA1106 and [^{18}F]FEDAA1106 in humans are promising, as they showed significantly higher brain uptake than [^{11}C]PK11195. Furthermore, increased [^{11}C]DAA1106 binding was reported in AD patients (Yasuno et al. 2008). A study using [^{11}C]PBR28 found focal increases of radiotracer binding in the brain of multiple sclerosis patients. In addition, third-generation TSPO-tracers such as [^{18}F]GE180 have been developed. [^{18}F]GE180 was studied in a head-to-head comparison with [^{11}C]PBR28 (Zanotti-Fregonara et al. 2018). It was concluded that kinetic modeling for [^{18}F]GE180 was more challenging than that for [^{11}C]PBR28 because of poor brain penetration.

1.4 GABA Receptor

The development of epilepsy has been associated with the impairment of gamma-aminobutyric acid (GABA) neurotransmission in the brain. The high-affinity ligand [^{11}C]flumazenil has been used widely for the investigation of GABA receptors (Hammers 2004) and was labeled in various positions (Halldin et al. 1988). [^{11}C]Flumazenil is available commercially in the United States and has been approved by the Food and Drug Administration (FDA) for use in various clinical trials. Using [^{11}C]flumazenil with PET in patients with acute hemispheric ischemic stroke, it was shown that this tracer can distinguish between irreversibly damaged and viable neuronal tissue during early onset of the disease. With [^{11}C]flumazenil, a reduction in the number of GABA/central benzodiazepine receptors was observed in the hippocampus of patients with mesial temporal lobe epilepsy, caused by unilateral hippocampal sclerosis. [^{11}C]Flumazenil has also been used to estimate the synaptic density of benzodiazepine receptors in persons who became blind. Compared with sighted controls, a significantly lower benzodiazepine receptor density was reported in the cerebellum of the blind subjects. In recent years, the ^{18}F-analog [^{18}F]flumazenil has become available (Hodolic et al. 2016). As flumazenil contains already a fluorine atom, [^{11}C]flumazenil and [^{18}F]flumazenil are chemically and pharmacologically identical, but with ^{18}F prolonged scanning protocols are possible. However, the synthesis of [^{18}F]flumazenil proceeds with low radiochemical yields, which has hampered widespread acceptance of [^{18}F]flumazenil (Zhang et al. 2019).

1.5 Dopaminergic System

The dopaminergic system plays a major role in neurological and psychiatric disorders such as PD, Huntington's disease, tardive dyskinesia, and schizophrenia. The neurotransmitter dopamine plays an important role in the control of movement, cognition, and emotion. Changed levels of dopamine also play a role in various

neuropsychiatric disorders, such as autism, attention deficit hyperactivity disorder, and drug abuse. Knowledge on altered dopamine synthesis and dopamine receptor densities is important for understanding the mechanisms underlying the pathogenesis and therapy of these diseases (Elsinga et al. 2006).

PET and SPECT tracers have been developed to measure presynaptic dopamine synthesis and transport. For measuring dopamine synthesis, the most commonly used tracer is 6-[^{18}F]FDOPA, whereas for dopamine transport, several radiolabeled tropane analogs are used in the clinic. Postsynaptically, dopamine exerts actions through several dopamine receptor subtypes. The dopamine receptor family consists of five subtypes D_1–D_5. In order to investigate the role of each receptor subtype, selective and high-affinity PET radioligands are required. To a lesser extent, work has been published related to radioiodinated tracers for SPECT. For the dopamine D_1 and D_2/D_3 subtypes, the most commonly used ligands are [^{11}C]SCH23390 (Kosaka et al. 2010) and [^{11}C]raclopride. [^{18}F]Fallypride is suitable for the investigation of extrapyramidal D_2 receptors. For SPECT studies of D_2/D_3 receptors, [^{123}I]IBZM is commercially available. For the other subtypes, no suitable radioligands have been developed (Tissingh et al. 1997).

6-[^{18}F]Fluoro-L-DOPA (FDOPA) is used to evaluate the central dopaminergic function of presynaptic neurons (Eidelberg et al. 1990; Sioka et al. 2010). Uptake of FDOPA is an indicator of DOPA transport into the neurons, its decarboxylation by amino acid decarboxylase (AADC) to 6-[^{18}F]fluorodopamine, and the capacity for dopamine storage, mainly in the striatum. 6-[^{18}F]Fluorodopamine can be converted by catechol-*O*-methyltransferase (COMT) to 3-*O*-methyl-6-[^{18}F]fluoro-L-DOPA, which is uniformly distributed throughout the brain. 6-[^{18}F]Fluorodopamine is also metabolized via monoamine oxidase to 6-[^{18}F]fluoro-3,4-dihydroxyphenylacetic acid and subsequently by COMT to yield 6-[^{18}F]fluorochomovanillic acid. In clinical studies, AADC is commonly inhibited with carbidopa. As a result of this inhibition of peripheral AADC, the delivery of FDOPA to the brain is increased.

The first FDOPA PET study of human brain was reported in 1983, showing increased accumulation of radioactivity in the striatum. In patients with established bilateral PD, FDOPA PET showed influx constant reductions in the caudate, putamen, striatal nigra, and midbrain. The decline with age in FDOPA uptake was more rapid in PD than in normal subjects. FDOPA PET is a good tool to monitor the progression of PD and the impact of therapies. The availability of FDOPA has improved since several robust nucleophilic [^{18}F]fluorination methods have become available (Zarrad et al. 2017; Tredwell et al. 2014).

1.5.1 Dopamine Transporter (DAT)

DAT is another important target for investigation of presynaptic dopaminergic function (Brooks 2010). The function of DAT is critical for the effects of antidepressant drugs. The use of DAT ligands has a practical benefit. In 6-[^{18}F]FDOPA PET, for example, medication with L-DOPA or other drugs is usually stopped before the PET scan, and patients sometimes receive inhibitors for AADC and COMT to reduce the

peripheral metabolism of the tracer. Usually, these pretreatments are not needed for PET scans with DAT tracers. Of course, effects of other medication on DAT images should be taken into account.

Several PET ligands of different chemical classes have been investigated to study DAT. The first reported tracers were [^{11}C]nomifensine and [^{18}F]GBR13119 followed by [^{11}C]*d-threo*-methylphenidate. Later, tropane analogs have been developed. [^{11}C]-β-CFT and [^{11}C]-β-CIT showed high affinity and were metabolically stable. The major drawback of [^{11}C]-β-CIT was its low selectivity toward DAT, although [^{123}I]-β-CIT (DaTSCAN, developed in the early 1990s, Innis et al. 1991) is clinically being used as a SPECT tracer (Nocker et al. 2012). [^{123}I]-β-CIT is commercially available. A significant correlation of the striatal uptake of [^{123}I]-ß-CIT with the severity and duration of PD has been reported. [^{123}I]-β-CIT scan is a useful tool in daily clinical practice to confirm diagnosis of PD and to differentiate PD from other diseases. [^{123}I]-β-CIT SPECT can contribute to treatment selection and can be used to monitor the effectiveness of therapies. In later years, an [^{18}F]analog of β-CIT has been developed. [^{18}F]FP-CIT PET images of striatal uptake were superior to those of [^{123}I]-β-CIT obtained with SPECT. Plasma analysis using [^{18}F]FP-CIT indicated the presence of only one minor metabolite. [^{18}F]FP-CIT (Hong et al. 2018; Yoo et al. 2018) has become an equally useful tracer in clinical practice as [^{123}I]-β-CIT (Sihver et al. 2007, see also Chap. 32 in this volume).

In order to circumvent the disadvantages, i.e., the limited availability, of cyclotron-produced radionuclides, ^{99m}Tc-labeled DAT tracers were developed (Kung et al. 1996). These tracers contain neutral lipophilic complexes that contain *N*-(alkylthiolate)tropane, aminobis(ethylthiolate), and a complex of ^{99m}Tc. [^{99m}Tc]TRODAT-1 belongs to this group (Chen et al. 2013). Using [^{99m}Tc]TRODAT-1 scintigraphy, the loss of DAT in PD patients could be measured very accurately. [^{99m}Tc]TRODAT-1 has been successfully applied to correlate striatal DAT expression with therapeutic results in patients with attention deficit hyperactivity disorder (ADHD). Patients with elevated striatal DAT responded better to methylphenidate therapy than those with lower DAT levels. On the basis of these results, the possible use of DAT measurements to predict a response to methylphenidate therapy was suggested. As a follow-up result, the decrease of DAT levels in ADHD patients who underwent methylphenidate therapy (measured with SPECT and [^{99m}Tc]TRODAT-1) correlated with an improvement in clinical symptoms. Caution has to be exercised in the interpretation of [^{99m}Tc]TRODAT-1 scans, since the uptake of this tracer is affected by age and sex (Mozley et al. 2001). [^{99m}Tc]TRODAT-1 is still used on regular basis, and several publications on PD in combination with this SPECT-tracer have appeared.

Other tropane tracers have been used as a biomarker for the integrity of presynaptic dopaminergic nerve cells in patients with movement disorders. ^{123}I-labeled *N*-(3-iodoprop-2*E*-enyl)-2-β-carbomethoxy-3β-(4-methylphenyl) nortropane, or PE2I, has about tenfold higher in vitro selectivity for the DAT over the serotonin transporter (SERT) compared to DaTSCAN (Ziebell 2011). Furthermore, [^{123}I]PE2I has faster kinetics than [^{123}I]-β-CIT. Because of its rapid kinetics, [^{123}I]PE2I binding to the DAT can be quantified with kinetic or graphical analysis. Since [^{123}I]PE2I is a

selective radioligand with optimal kinetic properties for accurate quantification of DAT availability in the striatum, it is currently considered the best radioligand for DAT imaging in the human brain with SPECT. More recently, ^{11}C-methyl and ^{18}F-fluoroethyl analogs of PE2I have been developed for human use. Studies in nonhuman primates concluded that the kinetics and metabolic behavior of [^{18}F]FE-PE2I were more favorable than those of [^{11}C]PE2I. All studies indicated highest tracer uptake in the striatum. [^{11}C]PE2I has been used in several human PET studies comparing controls with myoclonic epilepsy or with addicted counterparts. Application of various kinetic modeling procedures demonstrated a higher DAT activity in controls. The radioactive half-life of ^{11}C-PE2I may be too short for proper estimation of the striatal distribution volume, and [^{18}F]FE-PE2I may be better in this respect (Seki et al. 2010). Thus, [^{18}F]FE-PE2I is now more frequently used in human PET studies (Jakobson Mo et al. 2018).

1.5.2 D_1 Receptor

Two PET ligands, [^{11}C]NNC112 and [^{11}C]SCH23390, have been applied for human studies of the dopamine D_1 receptor (Catafau et al. 2010; Farde et al. 1987). In a PET study of D_1 receptor distribution in human brain, [^{11}C]NNC112 showed major localization of radioactivity in the striatum and neocortex. The striatum/cerebellum and neocortex/cerebellum ratios were 3.8 and 1.8, respectively. In a study in patients with schizophrenia in comparison with normal subjects, it was shown that the binding potential of [^{11}C]NNC112 was significantly elevated in the dorsolateral prefrontal cortex of patients with schizophrenia compared with healthy controls (Abi-Dargham et al. 2002). In recent years no new studies have been published with this radiotracer.

Other PET studies of D_1 receptor distribution in human brain employed [^{11}C]SCH23390, which accumulated mainly in striatum. [^{11}C]SCH23390 is currently the most common PET-tracer for D_1 receptors. Striatum-to-cerebellum ratios and kinetic constants are commonly used as parameters for quantitative imaging. PET scans of schizophrenic patients were similar to those obtained in healthy control subjects (Karlsson et al. 2002). With [^{11}C]SCH23390, it was possible to assess dopamine receptor occupancies in the striatum of patients treated with antipsychotics. Binding potential of the D_1 receptors in the striatum and frontal cortex decreased with age. There was no gender difference in D_1 binding potentials. In a study in patients with Huntington's disease, significant reductions of both the D_1 ([^{11}C]SCH23390) and D_2 ([^{11}C]raclopride) binding potentials in the striatum were shown. A comparative study using [^{11}C]NNC112 and [^{11}C]SCH23390 was performed in patients with schizophrenia and age-matched controls. The D_1 binding potential of both tracers in the frontal cortex, anterior cingulate, temporal cortex, and striatum of the schizophrenia patients was significantly lower than those of controls (Kosaka et al. 2010). Recent publications with [^{11}C]SCH23390 are relating D_1R availability to pathology (Plavén-Sigray et al. 2018; Stenkrona et al. 2019). Inconsistent results between groups have been discussed in literature and might by due to demographic factors.

1.5.3 D_2 Receptor

The D_2 receptor in the striatum has been one of the major targets of PET imaging. [^{11}C]*N*-methylspiperone, an analog of butyrophenone neuroleptics, was one of the first radioligands. Compared to [^{11}C]*N*-methylspiperone which also has affinity for the 5-HT_2 receptor, [^{11}C]raclopride has a higher selectivity for D_2 receptors. [^{11}C]Raclopride binds reversibly to D_2 receptors, which is an ideal property for estimation of B_{max} (Sioka et al. 2010; Elsinga et al. 2006). For this reason, [^{11}C]raclopride has been widely used as a D_2 receptor ligand. Several lines of evidence have indicated that [^{11}C]raclopride binding is reduced when the synaptic concentration of endogenous dopamine is increased. For the measurement of extrastriatal D_2 receptors that are expressed in much lower densities than D_2R in the striatum, ligands with very high affinity are required, in order to achieve sufficient binding to D_2 receptor. For this purpose, [^{11}C]FLB457 was developed (Narendran et al. 2011a). Another high-affinity benzamide, [^{18}F]fallypride, was also developed for this purpose. The longer half-life of this ^{18}F-labeled ligand enabled quantification of D_2 receptors in the caudate and putamen, using a prolonged scan protocol lasting 2 or 3 h (Millet et al. 2012). Both high-affinity tracers have also been used to measure dopamine release after administration of amphetamine. It should be noted that compounds within the benzamide class, such as raclopride and FLB457, do not only bind to D_2 receptors but also bind to D_3 receptors. The development of a D2-selective PET tracer has remained a challenge.

[^{123}I]IBZM (Kung et al. 1990) is a commercially available SPECT tracer for D_2/D_3 receptors. Comparative studies have reported a good correlation of the regional cerebral distribution of [^{123}I]IBZM and [^{11}C]raclopride. Calculated values for receptor density or receptor occupancy of the two tracers show systematic differences, which can be attributed to either the analysis method or the imaging modality (Catafau et al. 2009). In recent years, [^{123}I]IBZM has not been reported anymore in research articles.

1.5.4 D_2/D_3 Agonists

The use of agonists as imaging tracers may offer several advantages because they are supposed to bind only to the high-affinity state of the receptor, whereas antagonist tracers bind to both the high- and low-affinity binding sites. (−)-[^{11}C]-*N*-propylnorapomorphine (Narendran et al. 2011b) and (+)-[^{11}C]PHNO (4-propyl-9-hydroxynaphthoxazine) (Willeit et al. 2006) are successful D_2 receptor ligands. After exerting effects on second messenger systems, agonists will dissociate because of a conformational change of the receptor protein, back to the low-affinity state. In comparison to antagonists, receptor binding of radiolabeled agonists is expected to be more sensitive to changes in endogenous dopamine levels that compete with injected radioligands for binding to the receptor. As has been discussed in the section on dopamine synthesis and transport, the level of extracellular dopamine is an important parameter in neurological and psychiatric diseases.

It was shown that the binding of (−)[^{11}C]-*N*-propylnorapomorphine was indeed more sensitive to alterations in endogenous dopamine levels than [^{11}C]raclopride. This agonist tracer has not been used anymore in recent years and has been replaced by (+)-[^{11}C]PHNO. Its structure is based on naphtoxazine. (+)-[^{11}C]PHNO has been evaluated in several animal species and in humans. PHNO displayed higher binding potential values compared to [^{11}C]-*N*-propylnorapomorphine. The affinity of (+)-[^{11}C]PHNO for D_3 receptors is higher than for D_2 receptors. (+)-[^{11}C]PHNO has shown to be useful for evaluation of new drugs, estimation of receptor occupancy, and assessment of levels of extracellular dopamine under pathological conditions (Graff-Guerrero et al. 2008).

1.6 Beta-Amyloid Deposition

Many advances have been made to understand the neuropathological processes in AD. The accumulation of beta-amyloid is a primary event leading to the formation of neurofibrillary tangles and loss of synapses and neurons (Huang and Mucke 2012). The first clinically useful tracer for beta-amyloid imaging was ^{11}C-labeled Pittsburgh compound B (PIB) (Klunk et al. 2004). PIB is an analog of thioflavin T that binds to fibrillar beta-amyloid deposits with high sensitivity and specificity. PIB binds to both extracellular amyloid plaques and vascular amyloid deposits. At tracer dosages, PIB does not bind to neurofibrillary tangles or Lewy bodies (Zhang et al. 2012).

To improve the accessibility of beta-amyloid imaging, a second generation of ^{18}F-amyloid tracers was developed. Four ^{18}F-amyloid imaging agents are in advanced stages of development: flutemetamol, a 3′-fluoro analog of PIB (Thurfjell et al. 2012); florbetapir, a styrylpyridine derivative (Doraiswamy et al. 2012); FDDNP, a naphthol analog (Ossenkoppele et al. 2012); and florbetaben, a derivative of stilbene (Barthel and Sabri 2011). With the exception of FDDNP, these tracers show comparable results to PIB in clinical populations, although their nonspecific binding in white matter appears to be higher.

2-(1-(6-[(2-[^{18}F]Fluoroethyl)(methyl)amino]-2-naphthyl)ethylidene)malononitrile ([^{18}F]FDDNP) showed higher binding in AD than in the healthy brain. Despite its slow clearance kinetics, [^{18}F]FDDNP is used for the detection of neurofibrillary tangles and beta-amyloid plaques in patients with AD. In a comparative study between [^{11}C]PIB and [^{18}F]FDDNP, [^{11}C]PIB showed higher binding in patients with AD than in controls and patients with mild cognitive impairment (MCI). [^{18}F]FDDNP uptake was higher in brains of AD patients than in healthy controls, but MCI could not be distinguished from AD or from controls. Differences in binding potentials between patients with AD, or MCI, and healthy controls were more pronounced for PIB.

[^{18}F]florbetaben, [^{18}F]florbetapir, and [^{18}F]flutemetamol are clinically approved. They show very high sensitivity and specificity to detect beta-amyloid plaques. All three PET tracers are licensed to pharmaceutical industry. The clinical value of these tracers and the role of beta-amyloid in AD in particular are still under debate (Sala-Llonch et al. 2019; Palermo et al. 2019; Paghera et al. 2019).

With newly developed technology to get antibodies in the brain using transferrin as a vector, specific bifunctional transferrin beta-amyloid ^{124}I-labeled constructs were developed that specifically target the soluble neurotoxic beta-amyloid aggregates rather than insoluble fibrils. The expression of these soluble oligomers correlates better with disease severity than the insoluble plaques. The method has not yet been tested in humans (Sehlin and Syvänen 2019).

1.7 NMDA Receptor, Glycine Transport

Glycine acts as a neurotransmitter and is a modulator of the neuroexcitatory activity of the *N*-methyl-D-aspartate (NMDA) receptor. Impaired function of the NMDA receptor is responsible for cognitive dysfunction in patients suffering from neuropsychiatric diseases, like schizophrenia (Zorumski and Izumi 2012). Specific transporters are responsible for the uptake of glycine into the brain. The high-affinity transporters, GlyT-1 and GlyT-2, terminate the activity of glycine on the NMDA receptor in the synapse. GlyT-1 has been shown to maintain low levels of glycine at the synapse. Inhibition of GlyT-1 would increase glycine concentrations around the synapse, resulting in enhanced activity of the NMDA receptor. Several imaging agents for GlyT-1, such as [^{18}F]-2,4-dichloro-*N*-((1-(propylsulphonyl)-4-(6-fluoropyridine-2-yl)piperidine-4-yl)methyl)benzamide ([^{18}F]MK-6577 and [^{11}C]GSK931145, have been developed. Although the tracer is slowly metabolized, [^{11}C]GSK931145 has been successfully evaluated for the visualization of GlyT-1a in the human brain (Gunn et al. 2011). [^{18}F]GE-179 was developed as a next-generation NMDA antagonist and displayed a low nanomolar affinity of 2.4 nM. The tracer showed favorable kinetic properties. First human studies showed reproducible brain uptake (McGinnity et al. 2014). With [^{18}F]GE-179 it was possible to measure increased uptake around epileptic foci as a result of enhanced NMDA activation (McGinnity et al. 2015). A fully automated GMP-compliant synthesis method has been published (Yue et al. 2019).

1.8 P-Glycoprotein

Permeability of the blood–brain barrier (BBB) is an important factor in the maintenance of cerebral homeostasis (Bartels 2011). The BBB only allows entry of lipophilic compounds with low molecular weights by passive diffusion. In addition, the barrier contains transporters such as P-glycoprotein (P-gp), multidrug resistance-associated protein (MRP), and organic anion-transporting polypeptides (OATPs). The action of these carrier systems results in rapid efflux of harmful compounds from the central nervous system (CNS). P-gp is the most studied efflux transporter. PET studies related to P-gp were aimed at (1) direct evaluation of the effect of P-gp modulators on the cerebral uptake of therapeutic drugs, (2) assessment of mechanisms underlying drug resistance in epilepsy, (3) examination of the role of the BBB

in the pathophysiology of neurodegenerative and affective disorders, and (4) exploration of the relationship between polymorphisms of transporter genes and the pharmacokinetics of test compounds within the CNS (Colabufo et al. 2010; Elsinga et al. 2005).

Several radiotracers have been prepared to study P-glycoprotein function in vivo with PET, whereas some other PET tracers unintendedly proved to be P-gp substrates. These include alkaloids ([^{11}C]colchicine), anticancer drugs ([^{11}C]daunorubicin, [^{18}F]paclitaxel, [^{11}C]tariquidar, [^{11}C]elacridar), calcium antagonists ([^{11}C]-*R*-(+)-verapamil), ß-adrenoceptor antagonists ((*S*)-[^{11}C]carazolol, [^{18}F]-(*S*)-1′-fluorocarazolol, [^{11}C]carvedilol), serotonin 5-HT$_{1A}$ receptor antagonists ([^{18}F]MPPF), opioid receptor antagonists ([^{11}C]loperamide, [^{11}C]carfentanil), and various ^{64}Cu-labeled copper complexes. (*R*)-[^{11}C]verapamil is by far the most investigated PET tracer for P-gp. The tracer has been administered to healthy volunteers, and blocking studies with the immunosuppressant agent cyclosporin A were carried out. The results indicated that P-gp activity at the human BBB can be measured despite the high lipophilicity of (*R*)-[^{11}C]verapamil. Using tracer distribution volume as parameter, (*R*)-[^{11}C]verapamil uptake in the midbrain was significantly increased (18%) in Parkinson's disease patients compared with healthy controls. This suggests a decrease in P-gp activity at the BBB of PD patients (Bartels et al. 2010). (*R*)-[^{11}C]Verapamil has been further investigated in epileptic patients (Shin et al. 2016), and the effect of age on P-gp function/expression was investigated (Bauer et al. 2009). A drawback of [^{11}C]verapamil is its metabolic instability. Therefore deuterated [^{18}F]fluoroverapamil derivatives have been synthesized and preclinically evaluated. [^{18}F]d7-verapamil was shown to be the most stable verapamil derivative, maintaining its affinity for P-gp (Raaphorst et al. 2018).

Loperamide is an opiate agonist and a substrate for P-gp at the BBB. [^{11}C]Loperamide ([^{11}C]Lop) has been applied for studying P-gp function and multidrug resistance in tumors and normal tissues noninvasively. However, demethylation of [^{11}C]Lop to [*N*-methyl-^{11}C]-*N*-desmethyl-loperamide ([^{11}C]dLop) hampers its use as PET tracer for P-gp function since [^{11}C]dLop is also a good substrate for P-gp. Therefore, [^{11}C]dLop has been studied as a PET tracer for studying P-gp function (Seneca et al. 2009). In a study with healthy volunteers, there was minimal brain uptake of [^{11}C]dLop. There were five hydrophilic radiometabolites. Because of much lower nonspecific binding, [^{11}C]dLop is preferred over [^{11}C]verapamil. Surprisingly, the usability of [^{11}C]dLop has not been further investigated in recent years.

During a search for ^{18}F-labeled Pgp-substrates, [^{18}F]MC225 was identified as a promising tracer with improved metabolic stability compared to [^{11}C]verapamil and an increased basal uptake, as it is a weak P-gp substrate. This may enable not only assessment of decreased but also increased function/expression of P-glycoprotein (Savolainen et al. 2017). Another weak P-gp substrate, [^{11}C]metoclopramide, has already been evaluated in primates and humans. The relative importance of both the influx hindrance and the efflux enhancement components of P-glycoprotein was reported (Tournier et al. 2019).

1.9 Cholinergic System

Acetylcholine is an endogenous neurotransmitter at cholinergic synapses and acts on nicotinic and muscarinic receptors to mediate functions, such as attention, memory, cognition, and consciousness. Degeneration of cholinergic neurons has been observed in several neurodegenerative diseases, such as AD and PD (van Waarde et al. 2011). Acetylcholinesterase (AChE) is the enzyme that terminates cholinergic actions by the rapid hydrolysis of acetylcholine to choline and acetate. AChE has been a target for radioligand development as well as drug development because its levels decrease in AD. Radiolabeled AChE inhibitors and substrates have been developed for mapping AChE in vivo in brain. For measurements of AChE activity, various labeled esters of 1-methyl-4-hydroxypiperidine have been developed (Irie et al. 1996). *N*-[^{11}C]methylpiperidin-4-yl acetate ([^{11}C]MP4A) has a tertiary amine structure that makes it lipophilic, and therefore, the tracer can passively cross the BBB. [^{11}C]MP4A is specifically hydrolyzed by AChE. The hydrophilic metabolite, *N*-[^{11}C]methylpiperidinol ([^{11}C]MP4OH), is trapped in the brain. [^{11}C]MP4A has been tested as PET tracer for the AChE activity in patients with AD and PD (Shinotoh et al. 2004). For kinetic analysis, usually a three-compartment model is used to measure AChE. The parameter k_3 reflecting hydrolysis of the tracer is altered in disease. In a study of patients with AD, cortical regions displayed a reduced k_3 value compared with controls. The reduction in k_3 was both regionally and individually heterogeneous. In another study with patients with PD and ten Parkinson's patients with associated dementia (PDD) compared with age-matched controls, the cortical k_3 values for [^{11}C]MP4A were strongly reduced in PDD and slightly decreased in PD compared with controls. The PDD group had lower parietal k_3 values for [^{11}C]MP4A than patients with Parkinson's disease.

In contrast to AChE which acts both pre- and post-synaptically, the vesicular acetylcholine transporter (VAChT) is a glycoprotein regulating the accumulation of acetylcholine only into the presynaptic vesicles of cholinergic neurons. The cholinergic innervation is decreased at early stages of AD and PD. Therefore, VAChT is considered as a significant diagnostic target and an indicator for cholinergic neuronal integrity and function. A large number of vesamicol derivatives have been tested for their affinity to VAChT. [^{18}F]fluoroethyl benzovesamicol (FEOBV) emerged as a promising PET tracer for VAChT imaging. The compound has high affinity for VAChT and negligible affinity to sigma receptors. Most vesamicol derivatives have affinity for both VAChT and sigma receptors. FEOBV has been successfully used in human PET studies. These can involve short static scans made 3 h post-injection, with white matter as a reference region to estimate regional gray matter VAChT binding (Petrou et al. 2014). Binding data with respect to AD and PD have been published, showing a decreased uptake of [^{18}F]FEOBV in gray matter in patients compared to healthy control subjects (Aghourian et al. 2017).

Neuronal $\alpha_4\beta_2$ nicotinic cholinergic receptors (nAChRs) are part of a heterogeneous family of ligand-gated ion channels expressed in the central nervous system. Their activation by acetylcholine and nicotine causes a rapid increase in cellular permeability to ions, such as Na^+ and Ca^{2+}. nAChR dysfunction is implicated in

diseases such as schizophrenia, Huntington's disease, AD, and PD. nAChRs also play a significant role in nicotine addiction (Palma et al. 2012). 3-[2(*S*)-2-Azetidinylmethoxy]pyridine (A-85380) is a highly potent and selective $\alpha_4\beta_2$ nAChR agonist with subnanomolar affinity. 6-[^{18}F]Fluoro-A-85380 and 2-[^{18}F]fluoro-A-85380 have been studied for $\alpha_4\beta_2$ nAChR imaging in the brain. A-85380 has also been labeled as 5-[^{123}I]iodo-A-85380 for SPECT. These compounds displayed slow kinetics. Next-generation PET tracers based on the (homo)epibatidine scaffold, [^{18}F]flubatine, [^{18}F]AZAN, and [^{18}F]XTRA, were reported to have faster kinetics enabling scanning times of 90 min, or less. Most effort was put in the further development of [^{18}F]flutabine as a clinical tool to study the human brain (Sabri et al. 2015; Sabri et al. 2018). Recently, [^{18}F]XTRA and [^{18}F]nifene have shown to be also promising for human studies (Coughlin et al. 2018; Mukherjee et al. 2018). Kinetic modeling and dosimetry studies have been published.

The α_7 subtype of nAChR also plays a role in neurodegeneration. It has been suggested that this subtype mediates the phosphorylation of tau protein and also modulates immunological processes. The agonist 4-[^{11}C]Methylphenyl-1,4-diazabicyclo[3.2.2]nonane-4-carboxylate ([^{11}C]CHIBA-1001), a 4-methyl-substituted derivative of SSR180711, has been developed as a PET agent for the study of α_7-nAChR (Sakata et al. 2011) and was successfully evaluated to determine receptor occupancy by tropisetron (Ishikawa et al. 2011). [^{18}F]ASEM has been investigated in patients with schizophrenia (Wong et al. 2018). The data suggest decreased distribution volume in cingulate cortex, frontal cortex, and hippocampus in schizophrenic patients compared to healthy controls.

Muscarinic cholinergic M_2 subtype-selective tracers have been developed since this subtype is lost in the cerebral cortex in AD. M_2-selective PET tracers would offer the possibility to quantify such losses. Most tracers for cholinergic receptors have not demonstrated subtype selectivity. Tracers that are subtype selective in vitro typically do not cross the BBB. 3-((3-(3-Fluoropropyl)thio)-1,2,5-thiadiazol-4-yl)-1,2,5,6-tetrahydro-1-methylpyridine (FP-TZTP), a muscarinic agonist based on a series of non-fluorinated analogs, has been radiolabeled with ^{18}F ([^{18}F]FP-TZTP). [^{18}F]FP-TZTP was found to be a promising imaging agent for the M_2 receptor (Podruchny et al. 2003). In human studies, an age-related increase in M_2 receptor binding potential was found in healthy control subjects, using [^{18}F]FP-TZTP and PET. No recent studies on M_2 receptors have been reported.

1.10 Metabotropic Glutamate-5 Receptor

Glutamate is an important excitatory neurotransmitter at neuronal synapses in the brain. Glutamate produces its excitatory effects by acting on cell-surface ionotropic or metabotropic glutamate receptors (mGluRs). Of the eight subtypes, mGluR5 is usually found with moderate to high density in postsynaptic neurons of the frontal cortex, caudate, putamen, nucleus accumbens, olfactory tubercle, and hippocampus, whereas the density in the cerebellum is low (Homayoun and Moghaddam 2010). Dysfunction of mGluR5 is implicated in a variety of diseases of the CNS,

including anxiety, depression, schizophrenia, PD, drug addiction, and withdrawal. Radiolabeled analogs of 2-methyl-6-(phenylethynyl)-pyridine (MPEP) have been developed as potent, highly selective PET tracers for mGluR5. A drawback is their high lipophilicity, lack of mGluR subtype selectivity, and unfavorable brain accumulation kinetics. As a second-generation tracer for mGluR5, 3-(6-methyl-pyridin-2-ylethynyl)-cyclohex-2-enone-*O*-[^{11}C]-methyl-oxime ([^{11}C]ABP688) was evaluated. This tracer showed high and specific radioactivity uptake in rodent and human brain (DeLorenzo et al. 2011). [^{11}C]ABP688 has been used in several studies to investigate changes of mGlu-5 binding in depression, alcohol abuse, schizophrenia, and epilepsy. Except from alcohol abuse, the distribution volume was reduced in all cases. As a follow-up, 3-(pyridin-2-ylethynyl)-cyclohex-2-enone-*O*-(3-(2-[^{18}F]fluoroethoxy)propyl-oxime ([^{18}F]PSS232) was developed to enable prolonged study protocols. First-in-man studies showed that its brain uptake corresponds to known mGlu-5 distribution and can be quantified using a two-tissue compartment model. Because reference tissue models are available, no arterial sampling is needed, making this PET tracer very promising for clinical application (Warnock et al. 2018).

[^{18}F]FPEB was published at the same time and was synthesized by direct [^{18}F]fluorination and removal of the ylide functionality (Stephenson et al. 2015). [^{18}F]FPEB proved to be a weak P-glycoprotein substrate (Jung et al. 2019). Using this tracer, mGlu5 receptors were shown to be upregulated in PD patients compared to controls. An upregulation of mGlu5 receptors was also detected in postcentral gyrus and cerebellum of male subjects with autism. Other human studies with this tracer were related to alcohol abuse and reward (Leurquin-Sterk et al. 2018).

1.11 Vesicular Monoamine Transporter

The vesicular monoamine transporter (VMAT2) is present in monoaminergic neurons of the brain and is responsible for transporting neurotransmitters (dopamine, norepinephrine, and serotonin) into the neuron and storing them in vesicles for synaptic release. Decreases in the VMAT2 level are implicated in movement disorders, such as PD, AD, and Huntington's disease (Brooks et al. 2003). VMAT2 has been studied with PET using [^{11}C]dihydrotetrabenazine (2-hydroxy-3-isobutyl-9-[^{11}C]methoxy-10-methoxy-1,2,3,4,6,7,-hexahydro-11b*H*-benzo[α]-quinolizine) ([^{11}C]DTBZ) (Koeppe et al. 1996). Binding of DTBZ to the vesicular monoamine transporter is stereospecific. The (+)-enantiomer showed a high-affinity in vitro binding to the VMAT2 in rat striatum, whereas the (−)-enantiomer was inactive. [^{11}C]DTBZ has been applied for investigation of VMAT2 in the human brain with PET (Koeppe et al. 2008). In normal subjects and PD patients, a decrease of the distribution volume of [^{11}C]DTBZ was found in the putamen with increasing age. Parkinson patients displayed a significant reduction in distribution volume in the putamen and in the caudate nucleus. Later studies revealed a significant correlation of [^{11}C]DTBZ binding reduction with severity of the loss of motor functions. In addition, it was shown that PET with (+)[^{11}C]DTBZ can differentiate Lewy body

dementia from AD. The trend that is observed for several targets in this chapter also holds true for DTBZ, namely, that a promising ^{18}F-analog has become available: the [^{18}F]fluoropropyl derivative [^{18}F]FP-DTBZ, also called [^{18}F]AV-133 (florbenazine). Its synthesis was already published in 2010. Also for this PET tracer the (+)-enantiomer proved to be active (Naganawa et al. 2018). A human study concerning VMAT2 in LBD and AD has been published, showing lowered VMAT2 densities (Villemagne et al. 2012). In recent years several studies were conducted in PD patients, which also examined the link of PD with obstipation.

1.12 Adenosine Receptors

Adenosine is an endogenous modulator of a variety of physiological functions in the CNS. During the last two decades, the receptor subtypes A_1R and $A_{2A}R$ have been extensively studied. There is growing evidence that these adenosine receptor subtypes could be promising therapeutic targets for neurodegenerative diseases such as AD and PD and for other neurological pathologies such as epilepsy, ischemic brain disorders, or sleep disorders.

Several PET tracers for the adenosine receptor have been reported (Ishiwata et al. 2007). A_1 receptors have been studied using [1-methyl-^{11}C]-8-dicyclopropylmethyl-1-methyl-3-propylxanthine (MPDX). [^{11}C]MPDX PET studies in healthy volunteers showed the highest binding potential in striatum followed by the thalamus. Also, Logan plot analysis with arterial input was applied. The distribution pattern of [^{11}C]MPDX in the brain was different from that of blood flow as measured by [^{15}O]water (Fukumitsu et al. 2008).

For A_{2a} receptors, PET tracers for human use have also been developed. The distribution in brain of [^{11}C]KF18446 is in agreement with the distribution of $A_{2A}R$ known from postmortem studies in humans as well as in rodents and monkeys. A two-tissue, three-compartment model was used to measure the distribution of $A_{2A}R$ in the brain using metabolite-corrected arterial input function.

Furthermore, Mishina reported differences of $A_{2A}R$ and D_2R expression in the striata of drug-naive PD patients and those with dyskinesia and alterations of these receptor systems after antiparkinsonian therapy. The binding potential of striatal $A_{2A}R$ was measured using PET and [7-methyl-^{11}C]-(*E*)-8-(3,4,5-trimethoxystyryl)-1,3,7-trimethylxanthine ([^{11}C]TMSX) in drug-naive patients with PD, seven PD patients with mild dyskinesia, and six elderly control subjects (Mishina et al. 2011). The binding potential of [^{11}C]TMSX was increased in the putamen of PD patients with dyskinesia. $A_{2A}R$ were asymmetrically downregulated in the putamen in drug-naive patients with PD, and this asymmetric regulation of $A_{2A}Rs$ seems to compensate for the decrease in dopamine. Their study also showed that $A_{2A}Rs$ were increased in human putamen after antiparkinsonian therapy. [^{11}C]Preladenant was developed as a PET tracer based on the non-xanthine SCH442416 scaffold (Zhou et al. 2014). After successful evaluation in rats and primates, human studies were conducted in healthy subjects (for initial validation) and in PD patients for investigation of A_{2a} receptor occupancy by the drug

istradefylline (Ishibashi et al. 2018). Binding potentials were calculated from computed *k*-values, derived from a SRTM2 fit.

A few ^{18}F-tracers for $A_{2A}R$ have been developed, based on the non-xanthine scaffold SCH442416 (Khanapur et al. 2017). Also, [^{18}F]CPFPX was developed as a radiofluorinated xanthine for the A_1 receptor (Nabbi-Schroeter et al. 2018). All these ^{18}F-fluorinated analogs look promising. [^{18}F]CPFPX has reached the stage of human studies and was successfully employed to measure A_1 receptor occupancies in the human brain (Elmenhorst et al. 2012).

1.13 Serotonergic System

Serotonin (5-hydroxytryptamine, 5-HT) has diverse physiological roles as a neurotransmitter in the central nervous system. It is also a regulator of smooth muscle function and platelet aggregation. The brain 5-HT system has been implicated in several neuropsychiatric disorders, including major depression, anxiety, obsessive–compulsive disorder, and schizophrenia.

1.13.1 Serotonin Transporter

The transmission of serotonin is controlled in part by the serotonin transporter (SERT), which regulates the concentration of free and active 5-HT in the synaptic cleft (Jayanthi and Ramamoorthy 2005). Trans-1,2,3,5,6,10-β-Hexahydro-6-[4-([^{11}C]methylthio)phenyl[pyrrolo-[2,1-a]isoquinoline ([^{11}C]McN5652) binds selectively to the SERT, and the regional distribution of its binding in humans correlates well with the known distribution of the SERT. The drawback of [^{11}C]McN5652 is its high nonspecific binding and slow release from specific binding sites. [^{11}C]-*N*,*N*-Dimethyl-2-(2-amino-4-cyanophenylthio)benzylamine ([^{11}C]DASB) was found to be a promising tracer for SERT imaging (Houle et al. 2000). It displays nanomolar affinity for SERT and has 1000-fold greater affinity for SERT over dopamine transporter and norepinephrine transporter. Several human PET studies with [^{11}C]DASB have been performed (Turkheimer et al. 2012). The highest uptake was in the midbrain, thalamus, hypothalamus, and striatum, reaching a maximum at 30–40 min. After blocking with citalopram, an 80% reduction in specific binding of [^{11}C]DASB in SERT-rich regions was measured. The metabolism of [^{11}C]DASB was rapid, with about 50% of the intact compound remaining in plasma at 20 min after injection. No difference in regional SERT binding potential was found between depressed patients and normal subjects. However, in patients with major depression and with even more negativistic dysfunctional attitudes, a higher SERT binding potential was measured, which led to low extracellular 5-HT. It is concluded that [^{11}C]DASB is a useful tool for antidepressant development, PET studies in obsessive–compulsive disorder (Lee et al. 2018), and alcoholism.

4-[^{18}F]F-ADAM (*N*-((*E*)-4-[^{18}F]Fluorobut-2-*en*-1-yl)-2β-carbomethoxy-3β-(4′-fluoro phenyl)nortropane) turned out to be the most suitable SERT tracer out of a

series of ^{18}F-analogs. The tracer has been used in human studies. Most optimal scanning time was 120–140 min after injection. Subjects with depression had lower SERT availability than controls (Yeh et al. 2015).

1.13.2 5-HT Receptor Ligands

Effects of 5-HT are also mediated by receptors (5-HT$_1$ to 5-HT$_7$). 5-HT$_{1A}$ receptors function both as presynaptic autoreceptors in the raphe nuclei and as postsynaptic receptors in the terminal fields. The 5-HT$_{1A}$ receptor is involved in modulation of emotion and is implicated in the pathogenesis of anxiety, depression, hallucinogenic behavior, motion sickness, dementia, schizophrenia, and eating disorders. Many psychiatric drugs modulate serotonergic transmission or specifically target the 5-HT$_{1A}$ receptors. Various compounds have been developed for quantification of these receptors (Passchier and van Waarde 2001). [^{11}C]WAY100635 was developed as a highly selective, silent antagonist at both pre- and postsynaptic sites (Pike et al. 1995; Takano et al. 2011). Analogs of WAY100635 bearing bulkier cycloalkylcarbonyl groups appear to be more resistant to amide hydrolysis. However, the increased lipophilicity also reduces receptor affinity. Major problem of the WAY family is the often troublesome radiochemical synthesis. In parallel to evaluation of the WAY100635 compound, a series of arylpiperazine benzamido derivatives was synthesized that selectively bind to 5-HT$_{1A}$ receptors. Studies showed that benzoyl substituents affected the inhibition constant (K_i) of the compound. A fluoro analog, *p*-[^{18}F]MPPF, displayed a high binding affinity to 5-HT$_{1A}$ receptors (Shiue et al. 1997; Aznavour and Zimmer 2007). A large number of human studies have been performed both with [^{11}C]WAY100635 and [^{18}F]MPPF under various pathophysiological conditions. The number of PET studies with these tracers is continuously growing, and no important improvements regarding tracer development have been made.

The 5-HT$_{2A}$ receptor modulates cortical GABAergic, glutamatergic, and dopaminergic neurotransmission. An adequate balance of 5-HT$_{2A}$ receptor activity at inhibitory and excitatory neurons is needed for normal neuronal functioning. The 5-HT$_{2A}$ receptor has been implicated in various physiological functions and pathological conditions, including schizophrenia, major depression, anxiety, and sleep disorders. Various 5-HT$_{2A}$ receptor tracers have been proposed as PET radiopharmaceutical for 5-HT$_{2A}$ receptor quantification, most notably [^{11}C]*N*-methylspiperone, [^{18}F]altanserin, [^{18}F]setoperone, and [^{11}C]MDL 100,907). [^{11}C]MDL 100,907 appeared to be the most promising 5-HT$_{2A}$ tracer (Lundkvist et al. 1996) because of its high brain uptake with high target-to-nontarget contrast, prototypical 5-HT$_{2A}$ receptor selectivity, and absence of blood–brain barrier penetrating radiolabeled metabolites interfering with 5-HT$_{2A}$ receptor quantification (Talbot et al. 2012). Despite these results, [^{11}C]MDL 100,907 has become obsolete. [^{11}C]Cimbi-36, the first agonist PET tracer for 5-HT$_{2A}$ receptors, proved to be more useful for in vivo measurements of serotonin release as its binding is more sensitive to endogenous serotonin levels compared to antagonists. It should be noted that [^{11}C]Cimbi-36 is

metabolized by ^{11}C-demethylation. The small molecule radiolabeled metabolites display non-displaceable binding. [^{11}C]Cimbi-36 has been applied in human PET studies (da Cunha-Bang et al. 2019).

1.14 Nonadrenergic System

Many diseases affect the sympathetic nervous system, and imaging of pathological changes of noradrenergic neurotransmission has been an important area of PET research. Most postganglionic sympathetic neurons in the autonomic nervous system release the neurotransmitter norepinephrine (NE), which stimulates adrenergic receptors in various organs. The NET is a transmembrane protein located in the adrenergic nerve terminals that is responsible for active reuptake (uptake 1) of NE released from neurons. NE is stored in neuronal vesicles and is released upon stimulation. Brain norepinephrine transporters (NETs) are involved in various neurological and psychiatric disorders, including depression, attention deficit hyperactivity disorder, drug addiction, and eating disorders. NETs are also the site of action of many antidepressant drugs in the brain. Several radiolabeled NET inhibitors, for example, [^{11}C]desipramine, have been tested as radiopharmaceuticals for PET imaging, but they showed high nonspecific binding. Reboxetine ((*RS*)-2-[(*RS*)-2-ethoxyphenoxy)benzyl]morpholine) is a specific NET inhibitor with a high affinity and selectivity. It has been developed for the treatment of depressive illness. Among the different reboxetine derivatives that have been tested, (*S*,*S*)-methylreboxetine is considered a promising PET ligand. [^{11}C]Methylreboxetine ([^{11}C]MRB, [^{11}C]MeNER) has been tested in man for the investigation of cocaine addiction (Ding et al. 2010). The results suggest that (a) brain NET concentration declines with age in healthy controls and (b) there is a significant upregulation of NET in thalamus and dorsomedial thalamic nucleus in cocaine-addicted individuals. No new PET tracers for NETs have been developed during the last few years.

1.15 Opioid Receptors

Opioids such as morphine are commonly used analgesics in clinical practice (Waldhoer et al. 2004). Three opioid receptors that mediate opioid effects have been identified: δ (enkephalin preferring), κ (dynorphin preferring), and μ (morphine and ß-endorphin preferring). The opioid receptors play an important role in the regulation of analgesia, shock, appetite, thermoregulation, and cardiovascular, mental, and endocrine function. The μ opioid receptors are the major receptors to mediate the analgesic effects of opioids, although δ and κ receptors are also important in antinociception. Opioids have been found to protect cells in the heart and brain from ischemic injury via the δ receptors. On the other hand, κ antagonists prevent neurodegeneration. The κ opioid receptors have been implicated in several brain disorders, including drug abuse, epilepsy, Tourette's syndrome, and AD. Diprenorphine is a highly potent and non-subtype-selective opioid receptor antagonist with

subnanomolar affinity (Koepp and Duncan 2000). Diprenorphine has been labeled as [6-*O-methyl-11C*]diprenorphine ([^{11}C]DPN). PET studies have been reported in human brain using high and low specific activity [^{11}C]DPN. After pretreatment with 1 mg/kg naloxone, the uptake of [^{11}C]DPN was reduced to background levels throughout the brain. [^{11}C]DPN PET has been applied to study endogenous opiate response to pain in patients with rheumatoid arthritis. There were significant increases in [^{11}C]DPN binding in association with a reduction in pain in most areas of the brain. Also, decreases in [^{11}C]DPN binding in various cortical areas and the thalamus in patients with poststroke pain were found. These findings suggest that there are substantial increases in opioid receptor occupancy by endogenous opioid peptides during pain.

Research on κ opioid receptors has shifted to the use of agonist tracers and ^{18}F-analogs of antagonists (Li et al. 2018). [^{11}C]LY2795050 has been applied as a promising tracer for κ opioid receptor imaging and has been tested in human studies (test-retest reproducibility, blocking with LY2456302, receptor occupancy studies) (Naganawa et al. 2016).

[^{11}C]carfentanil is the tracer of choice for μ opioid receptors at this moment. Its first application goes back to the 1980s. The tracer is mainly taken up in cortical regions and thalamus. Bound [^{11}C]carfentanil can be displaced by other antagonists; thus the tracer can be used to determine μ opioid receptor occupancy and availability. Also studies related to addiction and reward were successful (Nummenmaa et al. 2018). As carfentanil is a very potent drug, the administered dose should be kept very low (<1 μg), in order to avoid any pharmacological effect. For human PET studies, [^{11}C]carfentanil should be prepared with ultrahigh specific radioactivity.

1.16 Monoamine Oxidase

Monoamine oxidase (MAO) is a mitochondrial enzyme which inactivates dopamine, noradrenaline, and serotonin in the brain. Two isoforms (A and B) of the enzyme have been identified. MAO-A preferentially oxidizes serotonin and noradrenaline, whereas MAO-B preferentially oxidizes phenethylamine. MAO-B is highly abundant in astrocytes. Astrocyte activity and thus the activity of MAO-B are upregulated in neuroinflammatory and neurodegenerative processes including PD and AD. Dopamine is a substrate for both enzymes. MAO-A is mainly involved in depression and anxiety, whereas MAO-B is involved in neurodegenerative diseases.

To measure MAO-A activity, the MAO-A inhibitor [^{11}C]harmine was developed for PET studies of MAO-A distribution and concentration in the brain of patients with psychiatric and neurological disorders or with neuroendocrine tumors. It was shown that tumors in patients with midgut carcinoids and endocrine pancreatic tumors could be visualized with [^{11}C]harmine (Sacher et al. 2012). [^{11}C]-L-deprenyl, an irreversible inhibitor, has been developed for measurement of MAO-B activity (Fowler et al. 1987). It was found that [^{11}C]-L-deprenyl uptake was increased in hippocampus, temporal lobes, and white matter of AD patients. The same has been found in patients with amyotrophic lateral sclerosis (ALS). This increased uptake

has been ascribed to an increased presence of activated astrocytes. Astrocytosis measured with deuterated [^{11}C]-L-deprenyl in MCI patients can be considered as an early phenomenon of AD (Carter et al. 2012). A carbamate-based reversible MAO-B inhibitor, [^{11}C]SL251188, was synthesized by ^{11}C-carbonylation and showed favorable results in nonhuman primates. First-in-man studies have been performed in controls and patients with depression. Preclinical studies on ^{18}F-fluorinated deprenyl analogs are also underway, but these compounds are degraded to brain-penetrating radioactive metabolites, as is [^{11}C]-L-deprenyl (Nag et al. 2016).

1.17 SV2A Receptors

In recent years, the synaptic vesicle glycoprotein 2A (SV2A) has been proposed as indicator for the disruption and alteration of synapses, which is associated with several brain diseases. The SV2A protein plays an important role in proper functioning of the nervous system. A few PET tracers developed by UCB S.A. were used in human studies: [^{11}C]UCB-J and [^{18}F]UCB-H. Both compounds are very similar but have either a [^{18}F]fluoro or a [^{11}C]methyl substituent on the pyridine ring. These compounds bind with nanomolar affinity to the SV2A protein. The biodistribution of the UCB-based PET tracers is uniform throughout the healthy brain. In 2015, a first-in-man study with [^{18}F]UCB-H was published, and its biodistribution and radiation dosimetry were determined (Bretin et al. 2015). Slightly later, also [^{11}C]UCB-J was tested in humans. A comparative study showed that [^{11}C]UCB-J has a higher binding potential than [^{18}F]UCB-H (Mercier et al. 2017). Finally [^{18}F]UCB-J, having the same methyl group but a ^{18}F substitution on the trifluorophenyl ring, showed the same excellent imaging properties than [^{11}C]UCB-J and could benefit from the longer half-life and lower positron energy of ^{18}F. For both [^{11}C] and [^{18}F]UCB-J, there are still some radiochemical challenges: the reliability and yield of the synthesis should be increased. One study was published in which 10 AD patients and 11 healthy controls were compared. Hippocampal SV2A binding was significantly reduced in the AD brain (Chen et al. 2018).

1.18 Sigma Receptors

Sigma receptors are categorized in the sigma-1 and sigma-2 subtypes. Sigma-1 receptors are abundantly expressed in the brain. These receptors are located in the cell membrane and the mitochondria-associated membrane of the endoplasmic reticulum of neurons, where they are playing a role in regulation of ion channels and neurotransmitter receptors. Therefore sigma-1 receptors are recognized as potentially interesting targets for imaging and therapy in brain disorders. One of the first sigma-1 PET tracers was [^{11}C]SA4503, which could be easily prepared by ^{11}C-methylation. [^{11}C]SA4503 showed a decreased uptake in frontal, temporal, and occipital lobes, cerebellum, and thalamus of patients with early AD (Mishina et al. 2008). The tracer has also been applied in PET studies to determine the receptor

occupancy of atypical antipsychotics. More recently, (*S*)-[^{18}F]fluspidine has been investigated for imaging of sigma-1 receptors in humans (Ludwig et al. 2019). Its radiosynthesis proceeds through a one-step ^{18}F-fluorination, in high radiochemical yields. This PET tracer displayed <5% plasma metabolites in healthy volunteers. Application of (*S*)-[^{18}F]fluspidine in patients with CNS disorders is still pending.

1.19 Tau Protein Deposition

Tau proteins stabilize microtubuli which play a fundamental role in neuronal activity. Similar to deposition of beta-amyloid, deposition of tau protein in the form of neurofibrillary tangles is also associated with neurodegeneration and cognitive impairment. These tangles already form before disease becomes manifest. Tau protein can aggregate in different ways, which affects the selectivity of PET tracers. Six isoforms of tau occur, with either three (3*R*) or four repeats (4*R*) of the microtubules. Different isoforms can cause the same tauopathy. Besides accumulation of tau protein in AD brain and dementia variants, this accumulation is also observed in other tauopathies including Pick's disease, PSP, and chronic traumatic encephalopathy. Several PET tracers have been developed for tau imaging. As both tau aggregates and beta-amyloid contain beta sheets, it has been challenging to develop selective PET tracers. Furthermore densities for tau aggregates are up to ten times lower than for beta-amyloid. The so-called first-generation tau tracer [^{18}F]AV-1451 (T807; flortaucipir) shows about 25-fold affinity for tau over beta-amyloid and is very specific and sensitive for the AD type of tau protein (Saint-Aubert et al. 2017). This tracer is currently in use at many PET sites because of its favorable kinetics and uptake pattern, which has been confirmed by Braak staining. [^{18}F]AV-1451 mainly binds to paired helical filaments (PHF)-tau which are characteristic lesions in AD brain. The ultimate value in clinical decision-making using [^{18}F]AV-1451 is still not clear, more research is needed to validate [^{18}F]AV-1451 (Wang and Edison 2019).

Second-generation PET tau tracers have been developed aiming at a more accurate staging of AD, less non-specific binding, and improvement of binding selectivity. The chemical structures are based on the same scaffolds as the first-generation tracers, therefore their binding sites are similar, but they display less non-specific binding. This generation includes [^{18}F]MK-6240, APN-1607([^{18}F]PM-PBB3), [^{18}F]GTP1, and [^{18}F]PI-2620. These tracers have been used in human PET studies comparing healthy subjects with AD patients. Different PET tracers have affinity for specific types of tau proteins. Binding differences between tau tracers could thus be used for the differential diagnosis of tauopathies.

1.20 Phosphodiesterase

Phosphodiesterase 10A is an enzyme responsible for the breakdown of cAMP and cGMP, which are important second messengers involved in the regulation of cellular functions through effectors. PDE10A affects the signaling of G-coupled

receptors, such as dopamine receptors, besides many other physiological processes. Within the brain, PDE10A is mainly localized in striatum. PDE10A inhibitors were developed as potential therapeutic agents in neurodegenerative diseases. Based on these inhibitors, several tracers were prepared to study PDE10A with PET. Some of these have reached the stage of human PET studies and were used to quantify PDE10A in healthy subjects and in different patient populations. Data acquired in healthy volunteers suggest that [^{11}C]IMA107, [^{11}C]Lu AE92686, and [^{18}F]MNI589 are the most promising tracers for PDE10A, with the lowest nonspecific binding. Based on the application and logistics of the scan, one might either prefer an ^{11}C- or a ^{18}F-tracer. The tracers showed a loss of PDE10A activity in the caudate and putamen of patients with PD or schizophrenia (Boscutti et al. 2019).

PDE4 is another isozyme involved in the breakdown of cAMP and implied in similar pathology as PDE10A. However, PDE4 is expressed in other parts of the brain, such as cortical regions related to working memory. For imaging of PDE4 with PET, (*R*)-[^{11}C]rolipram is the only radiotracer that has been used in human studies. Originally the tracer was developed for cardiac studies, but more recently it has also been applied for the brain. In a study where subjects received SSRI medication and were scanned with [^{11}C]rolipram, it was found that PDE4 inhibitors have antidepressant effects (Fujita et al. 2017). In another PET study, loss of PDE4 in cortical areas was found in PD patients (Niccolini et al. 2017).

1.21 P2X7 Receptor

The purinergic P2X7 receptor is an ion channel which is mainly present on activated microglia and therefore an important target in neurodegeneration and neuroinflammation, like TSPO. Stimulation of these receptors results in release of proinflammatory cytokines. Several preclinical experiments have demonstrated the role of P2X7 receptors in amyloid plaque formation, cognition, neuron loss, and motor coordination. Antagonism of P2X7 is in many cases neuroprotective. PET imaging of P2X7 receptors can be of great value to obtain more knowledge on neurodegeneration and to monitor treatment.

[^{11}C]JNJ54173717 is a tracer showing nanomolar affinity for human P2X7 (K_d 1.6 nM), good brain penetration, and low nonspecific binding in rats and primates. The tracer has recently been applied to quantify P2X7 receptors in humans (Van Weehaeghe et al. 2019). Distribution volumes show little variation in most cortical regions and are higher in brainstem and striatum. No differences were found between uptake in healthy controls and patients with PD. [^{18}F]JNJ64413739 has a structure related to [^{11}C]JNJ54173717 but has a longer radioactive half-life and has been investigated in healthy subjects (Koole et al. 2019). Future work should prove the value of this tracer in PET studies on P2X7 receptors.

1.22 (Re)Myelination

Demyelination is a major hallmark of multiple sclerosis (MS). Neuroinflammation results in the formation of demyelinated lesions. In the pathogenesis of MS, failure of compensatory mechanisms such as remyelination results in disability. Remyelination seems to be a dynamic phenomenon in MS, which is not well understood and is evident in white matter lesions. Some drugs have a positive impact on remyelination. The development of remyelination strategies may be boosted by PET with appropriate tracers to quantitatively assess remyelination. Beta amyloid tracers have been tried for this purpose but are not sufficiently selective. [^{11}C]MeDAS, a stilbene derivative, showed favorable binding characteristics for PET imaging of myelin. Its binding was limited to white matter regions, and [^{11}C]MeDAS showed high sensitivity and specificity for myelin in animal models (de Paula Faria et al. 2014). The clinical value of [^{11}C]MeDAS needs to be determined.

1.23 Cannabinoid Receptors

Cannabinoid (CB) receptors are G-protein-coupled receptor proteins. There are two subtypes CB1 and CB2. CB2 has mostly been studied with PET as this subtype is involved in neuroinflammatory processes and activated microglia. It has been demonstrated that CB2 is strongly overexpressed during neuroinflammation. The most promising tracer for CB receptors that has been developed thus far is [^{11}C]NE40. This tracer has been applied in humans, and its biodistribution in AD patients and healthy control subjects was compared (Ahmad et al. 2016). Full kinetic modeling was performed. Surprisingly, the binding of [^{11}C]NE40 was significantly lower in AD patients than in controls. The authors suggest that [^{11}C]NE40 may have a higher affinity/selectivity for CB1 than for CB2 receptors.

1.24 Conclusions

For a variety of neurotransmitter systems and transporters, useful PET and SPECT tracers are currently available that can be applied to study neurologic and psychiatric diseases in man. These tracers have proven to be able to image the molecular target of interest. Some of them are labeled with ^{18}F and commercially available. Increased availability of PET tracers will stimulate multicenter studies that may demonstrate their value for clinical diagnosis and treatment evaluation. Since most physiological processes interact, studies combining two or more CNS tracers will become more common. Several examples of such studies have already been published in the literature. Clinical applications of PET will be highlighted in more detail in other chapters of this book.

Recent review papers have summarized the current status of tracers for neurodegenerative diseases (Tiepolt et al. 2019; Narayanaswami et al. 2018; Bauckneht

Table 1.2 Overview of targets that are under investigation with respect to the development of nuclear medicine tracers

Target	Related disease	Tracers (preclinical application)	Binding mechanism
Alpha-synuclein	AD, PD	No suitable tracers	Staining agent
D_3 receptor	Psychosis, neurodegeneration	Mixed D_2/D_3 tracers	Antagonists
ROS	Neuroinflammation	[^{11}C]hydromethidine	Trapping by oxidation
Sphingosine 1-phophate receptor	MS	[^{11}C]TZ3321	CNS homeostasis
Toll-like receptor	Neuroinflammation	No tracers available	Antagonists
Receptor for advanced glycation end products (RAGE)	AD	[^{18}F]RAGER	Beta-amyloid transport
NLRP3	AD	No tracers available	Antagonist
COX-1 COX-2	Neuroinflammation Neuroinflammation	[^{18}F]PS2 [^{11}C]MC1	Enzyme inhibitor Enzyme inhibitor

et al. 2019). Besides the processes mentioned in Sects. 1.2–1.23, several other targets in the brain may need to be investigated to gain understanding of the pathophysiology of neurologic and psychiatric diseases. Table 1.2 summarizes some of these targets. Several new tracers are in the preclinical stage of development. For the sake of clarity, only a few tracers are listed in the table.

In conclusion, several tracers have been validated and can be applied in patient studies in order to measure physiological processes quantitatively. Several new targets have also been discovered, and tracers for these targets are under development. This demonstrates the huge interest in clinically validated tracers for PET imaging.

References

Abi-Dargham A, Mawlawi O, Lombardo I et al (2002) Prefrontal dopamine D_1 receptors and working memory in schizophrenia. J Neurosci 22:3708–3719

Aghourian M, Legault-Denis C, Soucy JP et al (2017) Quantification of brain cholinergic denervation in Alzheimer's disease using PET imaging with [^{18}F]FEOBV. Mol Psychiatry 22:1531–1538

Ahmad R, Postnov A, Bormans G et al (2016) Decreased in vivo availability of the cannabinoid type 2 receptor in Alzheimer's disease. Eur J Nucl Med Mol Imaging 43:2219–2227

Aznavour N, Zimmer L (2007) [^{18}F]MPPF as a tool for the in vivo imaging of 5-HT_{1A} receptors in animal and human brain. Neuropharmacology 52:695–707

Bartels AL (2011) Blood-brain barrier P-glycoprotein function in neurodegenerative disease. Curr Pharm Des 17:2771–2777

Bartels AL, de Klerk OL, Kortekaas R et al (2010) [^{11}C]verapamil to assess P-gp function in human brain during aging, depression and neurodegenerative disease. Curr Top Med Chem 10:1775–1784

Barthel H, Sabri O (2011) Florbetaben to trace amyloid-β in the Alzheimer brain by means of PET. J Alzheimers Dis 26(Suppl 3):117–121

Bauckneht M, Capitanio S, Raffa S (2019) Molecular imaging of multiple sclerosis: from the clinical demand to novel radiotracers. EJNMMI Radiopharm Chem 4:6

Bauer M, Karch R, Neumann F et al (2009) Age dependency of cerebral P-gp function measured with (R)-[^{11}C]verapamil and PET. Eur J Clin Pharmacol 65:941–946

Best L, Ghadery C, Pavese N et al (2019) New and old TSPO PET Radioligands for imaging brain microglial activation in neurodegenerative disease. Curr Neurol Neurosci Rep 19:24

Bretin F, Bahri MA, Bernard C et al (2015) Biodistribution and radiation dosimetry for the novel SV2A radiotracer [^{18}F]UCB-H: first-in-human study. Mol Imaging Biol 17:557–564

Brooks DJ (2010) Imaging dopamine transporters in Parkinson's disease. Biomark Med 4:651–660

Brooks DJ, Frey KA, Marek KL (2003) Assessment of neuroimaging techniques as biomarkers of the progression of Parkinson's disease. Exp Neurol 184(Suppl 1):S68–S79

Boscutti G, Rabiner EA, Plisson C (2019) PET Radioligands for imaging of the PDE10A in human: current status. Neurosci Lett 691:11–17

Carter SF, Scholl M, Almkvist O et al (2012) Evidence for astrocytosis in prodromal Alzheimer disease provided by ^{11}C-deuterium-L-deprenyl: a multitracer PET paradigm combining [^{11}C]-Pittsburgh compound B and [^{18}F]FDG. J Nucl Med 53:37–46

Catafau AM, Suarez M, Bullich S, Barcelona Clinical Imaging in Psychiatry Group (2009) Within-subject comparison of striatal D2 receptor occupancy measurements using [^{123}I]IBZM SPECT and [^{11}C]Raclopride PET. NeuroImage 46:447–458

Catafau AM, Searle GE, Bullich S et al (2010) Imaging cortical dopamine D_1 receptors using [^{11}C]NNC112 and ketanserin blockade of the 5-HT_{2A} receptors. J Cereb Blood Flow Metab 30:985–993

Chauveau F, Boutin H, Van Camp N et al (2008) Nuclear imaging of neuroinflammation: a comprehensive review of [^{11}C]PK11195 challengers. Eur J Nucl Med Mol Imaging 35:2304–2319

Chen KC, Yang YK, Howes O et al (2013) Striatal dopamine transporter availability in drug-naive patients with schizophrenia: a case-control SPECT study with [^{99m}Tc]-TRODAT-1 and a meta-analysis. Schizophr Bull 39:378–386

Chen MK, Mecca AP, Naganawa M et al (2018) Assessing synaptic density in Alzheimer disease with synaptic vesicle glycoprotein 2A positron emission tomographic imaging. JAMA Neurol 75:1215–1224

Colabufo NA, Berardi F, Perrone MG et al (2010) Substrates, inhibitors and activators of P-glycoprotein: candidates for radiolabeling and imaging perspectives. Curr Top Med Chem 10:1703–1714

Coughlin JM, Slania S, Du Y et al (2018) [^{18}F]XTRA PET for enhanced imaging of the Extrathalamic α4β2 nicotinic acetylcholine receptor. J Nucl Med 59:1603–1608

da Cunha-Bang S, Ettrup A, Mc Mahon B et al (2019) Measuring endogenous changes in serotonergic neurotransmission with [^{11}C]Cimbi-36 positron emission tomography in humans. Transl. Psychiatry 9:134

de Vries EF, Dierckx RA, Klein HC (2006) Nuclear imaging of inflammation in neurologic and psychiatric disorders. Curr Clin Pharmacol 1:229–242

DeLorenzo C, Kumar JS, Mann JJ (2011) In vivo variation in metabotropic glutamate receptor subtype 5 binding using positron emission tomography and [^{11}C]ABP688. J Cereb Blood Flow Metab 31:2169–2180

Demetriades AK (2002) Functional neuroimaging in Alzheimer's type dementia. J Neurol Sci 15:247–251

Ding YS, Singhal T, Planeta-Wilson B et al (2010) PET imaging of the effects of age and cocaine on the norepinephrine transporter in the human brain using (S,S)-[^{11}C]-O-methylreboxetine and HRRT. Synapse 64:30–38

Dollé F, Luus C, Reynolds A et al (2009) Radiolabelled molecules for imaging the translocator protein (18 kDa) using positron emission tomography. Curr Med Chem 16:2899–2923

Doraiswamy PM, Sperling RA, Coleman RE et al (2012) Amyloid-β assessed by [^{18}F]florbetapir-PET and 18-month cognitive decline: a multicenter study. Neurology 79:1636–1644

Eidelberg D, Moeller JR, Dhawan V et al (1990) The metabolic anatomy of Parkinson's disease: complementary [^{18}F]FDG and [^{18}F]FDOPA positron emission tomography studies. Mov Disord 5:203–213

Elmenhorst D, Meyer PT, Matusch A et al (2012) Caffeine occupancy of human cerebral A1 adenosine receptors: in vivo quantification with [^{18}F]CPFPX and PET. J Nucl Med 53:1723–1729

Elsinga PH (2002) Radiopharmaceutical chemistry for positron emission tomography. Methods 27:208–217

Elsinga PH, Hendrikse NH, Bart J et al (2005) Positron emission tomography studies on binding of central nervous system drugs and P-glycoprotein function in the rodent brain. Mol Imaging Biol 7:37–44

Elsinga PH, Hatano K, Ishiwata K (2006) PET tracers for imaging of the dopaminergic system. Curr Med Chem 13:2139–2153

Farde L, Halldin C, Stone-Elander S et al (1987) PET analysis of human dopamine receptor subtypes using [^{11}C]SCH23390 and [^{11}C]raclopride. Psychopharmacology 92:278–284

de Paula Faria D, Copray S, Sijbesma JW et al (2014) PET imaging of focal demyelination and remyelination in a rat model of multiple sclerosis: comparison of [^{11}C]MeDAS, [^{11}C]CIC and [^{11}C]PIB. Eur J Nucl Med Mol Imaging 41:995–1003

Fowler JS, MacGregor RR, Wolf AP et al (1987) Mapping human brain monoamine oxidase a and B with ^{11}C-labelled suicide inactivators and PET. Science 235:481–485

Fujita M, Richards EM, Niciu MJ et al (2017) cAMP signaling in brain is decreased in unmedicated depressed patients and increased by treatment with a selective serotonin reuptake inhibitor. Mol Psychiatry 22:754–759

Fukumitsu N, Ishii K, Kimura Y et al (2008) Adenosine A1 receptors using 8-dicyclopropylmethyl-1-[^{11}C]methyl-3-propylxanthine PET in Alzheimer's disease. Ann Nucl Med 22:841–847

Graff-Guerrero A, Willeit M, Ginovart N et al (2008) Brain region binding of the D2/3 agonist [^{11}C]-(+)-PHNO and the D2/3 antagonist [^{11}C]raclopride in healthy humans. Hum Brain Mapp 29:400–410

Gunn RN, Murthy V, Catafau AM et al (2011) Translational characterization of [^{11}C]GSK931145, a PET ligand for the glycine transporter type 1. Synapse 65:1319–1332

Halldin C, Stone-Elander S, Thorell JO et al (1988) ^{11}C-labelling of Ro 15-1788 in two different positions and also ^{11}C-labelling of its main metabolite R0 15-3890 for PET-studies of benzodiazepine receptors. Int J Rad Appl Instrum A 39:993–997

Hammers A (2004) Flumazenil positron emission tomography and other ligands for functional imaging. Neuroimaging Clin N Am 14:537–551

Hashimoto K, Inoue O, Suzuki K et al (1989) Synthesis and evaluation of [^{11}C]PK 11195 for in vivo study of peripheral-type benzodiazepine receptors using positron emission tomography. Ann Nucl Med 3:63–71

Hodolic M, Topakian R, Pichler R (2016) [^{18}F]fluorodeoxyglucose and [^{18}F]flumazenil positron emission tomography in patients with refractory epilepsy. Radiol Oncol 50:247–253

Homayoun H, Moghaddam B (2010) Group 5 metabotropic glutamate receptors: role in modulating cortical activity and relevance to cognition. Eur J Pharmacol 639:33–39

Hong CM, Ryu HS, Ahn BC (2018) Early perfusion and dopamine transporter imaging using [^{18}F]FP-CIT PET/CT in patients with parkinsonism. Am J Nucl Med Mol Imaging 8:360–372

Houle S, Ginovart N, Hussey D et al (2000) Imaging the serotonin transporter with positron emission tomography: initial human studies with [^{11}C]DAPP and [^{11}C]DASB. Eur J Nucl Med 27:1719–1722

Huang Y, Mucke L (2012) Alzheimer mechanisms and therapeutic strategies. Cell 148:1204–1222

Innis R, Baldwin R, Sybirska E et al (1991) Single photon emission computed tomography imaging of monoamine reuptake sites in primate brain with [^{123}I]CIT. Eur J Pharmacol 200:369–370

Irie T, Fukushi K, Namba H et al (1996) Brain acetylcholinesterase activity: validation of a PET-tracer in a rat model of Alzheimer's disease. J Nucl Med 37:649–655

Ishibashi K, Miura Y, Wagatsuma K et al (2018) Occupancy of adenosine A_{2A} receptors by istradefylline in patients with Parkinson's disease using [^{11}C]preladenant PET. Neuropharmacology 143:106–112

Ishikawa M, Sakata M, Toyohara J et al (2011) Occupancy of α7 nicotinic acetylcholine receptors in the brain by Tropisetron: a positron emission tomography study using [^{11}C]CHIBA-1001 in healthy human subjects. Clin Psychopharmacol Neurosci 9:111–116

Ishiwata K, Kimura Y, de Vries EFJ et al (2007) PET tracers for mapping adenosine receptors as probes for diagnosis of CNS disorders. Cent Nerv Syst Agents Med Chem 7:57–77

Jakobson Mo S, Axelsson J, Jonasson L et al (2018) Dopamine transporter imaging with [^{18}F]FE-PE2I PET and [^{123}I]FP-CIT SPECT-a clinical comparison. EJNMMI Res 8:100

Jayanthi LD, Ramamoorthy S (2005) Regulation of monoamine transporters: influence of psychostimulants and therapeutic antidepressants. AAPS J 7:E728–E738

Jung KH, Oh SJ, Kang KJ et al (2019) Effects of P-gp and Bcrp as brain efflux transporters on the uptake of [^{18}F]FPEB in the murine brain. Synapse 73(11):e22123

Karlsson P, Farde L, Halldin C et al (2002) PET study of D_1 dopamine receptor binding in neuroleptic-naive patients with schizophrenia. Am J Psychiatry 159:761–767

Khanapur S, van Waarde A, Dierckx RA et al (2017) Preclinical evaluation and quantification of [^{18}F]Fluoroethyl and [^{18}F]Fluoropropyl analogs of SCH442416 as Radioligands for PET imaging of the adenosine A2A receptor in rat brain. J Nucl Med 58:466–472

Klunk WE, Engler H, Norgberg A et al (2004) Imaging brain amyloid in Alzheimer's disease with Pittsburgh compound-B. Ann Neurol 55:306–319

Koepp MJ, Duncan JS (2000) PET: opiate neuroreceptor mapping. Adv Neurol 83:145–156

Koeppe RA, Frey KA, Vander Borght TM et al (1996) Kinetic evaluation of [^{11}C]dihydrotetrabenazine by dynamic PET measurement of vesicular monoamine transporter. J Cereb Blood Flow Metab 16:1288–1299

Koeppe RA, Gilman S, Junck L et al (2008) Differentiating Alzheimer's disease from dementia with Lewy bodies and Parkinson's disease with (+)-[^{11}C]dihydrotetrabenazine positron emission tomography. Alzheimers Dement 4(1 Suppl 1):S67–S76

Kogan RV, de Jong BA, Renken RJ, JPND-PETMETPAT Working Group et al (2019) Factors affecting the harmonization of disease-related metabolic brain pattern expression quantification in [^{18}F]FDG-PET (PETMETPAT). Alzheimers Dement (Amst) 11:472–482

Koole M, Schmidt ME, Hijzen A et al (2019) [^{18}F]JNJ-64413739, a novel PET ligand for the P2X7 Ion Channel: radiation dosimetry, kinetic modeling, test-retest variability, and occupancy of the P2X7 antagonist JNJ-54175446. J Nucl Med 60:683–690

Kosaka J, Takahashi H, Ito H (2010) Decreased binding of [^{11}C]NNC112 and [^{11}C]SCH23390 in patients with chronic schizophrenia. Life Sci 86:814–818

Kung HF, Alavi A, Chang W et al (1990) In vivo SPECT imaging of CNS D_2 dopamine receptors: initial studies with [^{123}I] IBZM in humans. J Nucl Med 31:573–579

Kung HF, Kim HJ, Kung MP et al (1996) Imaging of dopamine transporters in human with [^{99m}Tc] TRODAT-1. Eur J Nucl Med 23:1527–1530

Lee J, Kim BH, Kim E et al (2018) Higher serotonin transporter availability in early-onset obsessive-compulsive disorder patients undergoing escitalopram treatment: a [^{11}C]DASB PET study. Hum Psychopharmacol 33(1)

Leurquin-Sterk G, Ceccarini J, Crunelle CL et al (2018) Cerebral dopaminergic and glutamatergic transmission relate to different subjective responses of acute alcohol intake: an in vivo multimodal imaging study. Addict Biol 23:931–944

Li S, Cai Z, Zheng MQ, Holden D et al (2018) Novel ^{18}F-labeled κ-opioid receptor antagonist as PET radiotracer: synthesis and in vivo evaluation of [^{18}F]LY2459989 in nonhuman primates. J Nucl Med 59:140–146

Ludwig FA, Fischer S, Houska R et al (2019) In vitro and in vivo human metabolism of (S)-[^{18}F]Fluspidine - a Radioligand for imaging σ1 receptors with positron emission tomography (PET). Front Pharmacol 10:534

Lundkvist C, Halldin C, Ginovart N et al (1996) [^{11}C]MDL 100907, a radioligand for selective imaging of 5-HT_{2A} receptors with positron emission tomography. Life Sci 58:187–192

McGinnity CJ, Hammers A, Riaño Barros DA et al (2014) Initial evaluation of [^{18}F]GE-179, a putative PET tracer for activated N-methyl D-aspartate receptors. J Nucl Med 55:423–430
McGinnity CJ, Koepp MJ, Hammers A et al (2015) NMDA receptor binding in focal epilepsies. J Neurol Neurosurg Psychiatry 86:1150–1157
Mercier J, Provins L, Valade A (2017) Discovery and development of SV2A PET tracers: potential for imaging synaptic density and clinical applications. Drug Discov Today Technol 25:45–52
Mielke R, Heis WD (1998) Positron emission tomography for diagnosis of Alzheimer's disease and vascular dementia. J Neural Transm Suppl 53:237–250
Millet P, Moulin-Sallanon M, Tournier BB (2012) Quantification of dopamine D2/3 receptors in rat brain using factor analysis corrected [^{18}F]Fallypride images. NeuroImage 62:1455–1468
Mishina M, Ohyama M, Ishii K et al (2008) Low density of sigma1 receptors in early Alzheimer's disease. Ann Nucl Med 22:151–156
Mishina M, Ishiwata K, Naganawa M et al (2011) Adenosine A_{2A} receptors measured with [^{11}C]TMSX PET in the striata of Parkinson's disease patients. PLoS One 6:e17338
Mozley LH, Gur RC, Mozley PD, Gur RE (2001) Striatal dopamine transporters and cognitive functioning in healthy men and women. Am J Psychiatry 158:1492–1499
Mukherjee J, Lao PJ, Betthauser TJ et al (2018) Human brain imaging of nicotinic acetylcholine α4β2 receptors using [^{18}F]Nifene: selectivity, functional activity, toxicity, aging effects, gender effects, and extrathalamic pathways. J Comp Neurol 526:80–95
Nabbi-Schroeter D, Elmenhorst D, Oskamp A et al (2018) Effects of long-term caffeine consumption on the adenosine A1 receptor in the rat brain: an in vivo PET study with [^{18}F]CPFPX. Mol Imaging Biol 20:284–291
Nag S, Fazio P, Lehmann L et al (2016) In vivo and in vitro characterization of a novel MAO-B inhibitor Radioligand, ^{18}F-labeled deuterated Fluorodeprenyl. J Nucl Med 57:315–320
Naganawa M, Dickinson GL, Zheng MQ et al (2016) Receptor occupancy of the κ-opioid antagonist LY2456302 measured with positron emission tomography and the novel radiotracer [^{11}C]LY2795050. J Pharmacol Exp Ther 356:260–266
Naganawa M, Lim K, Nabulsi NB et al (2018) Evaluation of pancreatic VMAT2 binding with active and inactive enantiomers of [^{18}F]FP-DTBZ in healthy subjects and patients with type 1 diabetes. Mol Imaging Biol 20:835–845
Narayanaswami V, Dahl K, Bernard-Gauthier V et al (2018) Emerging PET radiotracers and targets for imaging of neuroinflammation in neurodegenerative diseases: outlook beyond TSPO. Mol Imaging 17:1–25
Narendran R, Mason NS, May MA (2011a) Positron emission tomography imaging of dopamine $D_{2/3}$ receptors in the human cortex with [^{11}C]FLB 457: reproducibility studies. Synapse 65:35–40
Narendran R, Martinez D, Mason NS et al (2011b) Imaging of dopamine $D_{2/3}$ agonist binding in cocaine dependence: a [^{11}C]NPA positron emission tomography study. Synapse 65:1344–1349
Niccolini F, Wilson H, Pagano G et al (2017) Loss of phosphodiesterase-4 in Parkinson disease: relevance to cognitive deficits. Neurology 89:586–593
Nobili F, Festari C, Altomare D et al (2018) Automated assessment of FDG-PET for differential diagnosis in patients with neurodegenerative disorders. EANM-EAN task force for the prescription of FDG-PET for dementing neurodegenerative disorders. Eur J Nucl Med Mol Imaging 45:1557–1566
Nocker M, Seppi K, Donnemiller E (2012) Progression of dopamine transporter decline in patients with the Parkinson variant of multiple system atrophy: a voxel-based analysis of [^{123}I]β-CIT SPECT. Eur J Nucl Med Mol Imaging 39:1012–1020
Nummenmaa L, Saanijoki T, Tuominen L et al (2018) μ-Opioid receptor system mediates reward processing in humans. Nat Commun 9:1500
Ossenkoppele R, Tolboom N, Foster-Dingley JC (2012) Longitudinal imaging of Alzheimer pathology using [^{11}C]PIB, [^{18}F]FDDNP and [^{18}F]FDG PET. Eur J Nucl Med Mol Imaging 39:990–1000

Paghera B, Altomare D, Peli A et al (2019) Comparison of visual criteria for amyloid-PET reading: could their merging reduce the inter-raters variability? Q J Nucl Med Mol Imaging. [Epub ahead of print]

Palermo G, Tommasini L, Aghakhanyan G et al (2019) Clinical correlates of cerebral amyloid deposition in Parkinson's disease dementia: evidence from a PET study. J Alzheimers Dis 70:595–607

Palma E, Conti L, Roseti C et al (2012) Novel approaches to study the involvement of α7-nAChR in human diseases. Curr Drug Targets 13:579–586

Passchier J, van Waarde A (2001) Visualisation of serotonin-1A (5-HT_{1A}) receptors in the central nervous system. Eur J Nucl Med 28:113–129

Petrou M, Frey KA, Kilbourn MR et al (2014) In vivo imaging of human cholinergic nerve terminals with (−)-5-[^{18}F]fluoroethoxybenzovesamicol: biodistribution, dosimetry, and tracer kinetic analyses. J Nucl Med 55:396–404

Pike VW, McCarron JA, Lammertsma AA et al (1995) First delineation of 5-HT_{1A} receptors in human brain with PET and [^{11}C]WAY-100635. Eur J Pharmacol 283:R1–R3

Plavén-Sigray P, Matheson GJ, Gustavsson P et al (2018) Is dopamine D_1 receptor availability related to social behavior? A positron emission tomography replication study. PLoS One 13(3):e0193770

Podruchny TA, Connolly C, Bokde A (2003) In vivo muscarinic-2 receptor imaging in cognitively normal young and older volunteers. Synapse 48:39–44

Politis M, Su P, Piccini P (2012) Imaging of microglia in patients with neurodegenerative disorders. Front Pharmacol 3:96

Raaphorst RM, Luurtsema G, Schokker CJ et al (2018) Improving metabolic stability of fluorine-18 labeled verapamil analogs. Nucl Med Biol 64-65:47–56

Sabri O, Becker GA, Meyer PM et al (2015) First-in-human PET quantification study of cerebral α4β2 nicotinic acetylcholine receptors using the novel specific radioligand (−)-[^{18}F]Flubatine. NeuroImage 118:199–208

Sabri O, Meyer PM, Gräf S et al (2018) Cognitive correlates of α4β2 nicotinic acetylcholine receptors in mild Alzheimer's dementia. Brain 141:1840–1854

Sacher J, Rabiner EA, Clark M et al (2012) Dynamic, adaptive changes in MAO-A binding after alterations in substrate availability: an in vivo [^{11}C]-harmine positron emission tomography study. J Cereb Blood Flow Metab 32:443–446

Saint-Aubert L, Lemoine L, Chiotis K et al (2017) Tau PET imaging: present and future directions. Mol Neurodegener 12:19

Sakata M, Wu J, Toyohara J (2011) Biodistribution and radiation dosimetry of the α7 nicotinic acetylcholine receptor ligand [^{11}C]CHIBA-1001 in humans. Nucl Med Biol 38:443–448

Sala-Llonch R, Falgàs N, Bosch B et al (2019) Regional patterns of [^{18}F]florbetaben uptake in presenilin 1 mutation carriers. Neurobiol Aging 81:1–8

Savolainen H, Windhorst AD, Elsinga PH et al (2017) Evaluation of [^{18}F]MC225 as a PET radiotracer for measuring P-glycoprotein function at the blood-brain barrier in rats: kinetics, metabolism, and selectivity. J Cereb Blood Flow Metab 37:1286–1298

Sehlin D, Syvänen S (2019) Engineered antibodies: new possibilities for brain PET? Eur J Nucl Med Mol Imaging 46(13):2848–2858

Seki C, Ito H, Ichimiya T et al (2010) Quantitative analysis of dopamine transporters in human brain using [^{11}C]PE2I and positron emission tomography: evaluation of reference tissue models. Ann Nucl Med 24:249–260

Seneca N, Zoghbi SS, Liow JS (2009) Human brain imaging and radiation dosimetry of [^{11}C]-N-desmethyl-loperamide, a PET radiotracer to measure the function of P-glycoprotein. J Nucl Med 50:807–813

Shin JW, Chu K, Shin SA et al (2016) Clinical applications of simultaneous PET/MR imaging using (R)-[^{11}C]verapamil with cyclosporine a: preliminary results on a surrogate marker of drug-resistant epilepsy. Am J Neuroradiol 37:600–606

Shinotoh H, Fukushi K, Nagatsuka S et al (2004) Acetylcholinesterase imaging: its use in therapy evaluation and drug design. Curr Pharm Des 10:1505–1517

Shiue CY, Shiue GG, Mozley PD et al (1997) P-[^{18}F]MPPF: a potential radioligand for PET-studies of 5-HT1A receptors in humans. Synapse 25:147–154

Sihver W, Drewes B, Schulze A (2007) Evaluation of novel tropane analogues in comparison with the binding characteristics of [^{18}F]FP-CIT and [^{131}I]beta-CIT. Nucl Med Biol 34:211–219

Sioka C, Fotopoulos A, Kyritsis AP (2010) Recent advances in PET imaging for evaluation of Parkinson's disease. Eur J Nucl Med Mol Imaging 37:1594–1603

Stenkrona P, Matheson GJ, Halldin C et al (2019) D_1-dopamine receptor availability in first-episode neuroleptic naive psychosis patients. Int J Neuropsychopharmacol 22:415–425

Stephenson NA, Holland JP, Kassenbrock A et al (2015) Iodonium ylide-mediated radiofluorination of [^{18}F]FPEB and validation for human use. J Nucl Med 56:489–492

Takano H, Ito H, Takahashi H et al (2011) Serotonergic neurotransmission in the living human brain: a positron emission tomography study using [^{11}C]DASB and [^{11}C]WAY100635 in young healthy men. Synapse 65:624–633

Talbot PS, Slifstein M, Hwang DR et al (2012) Extended characterisation of the serotonin 2A ($5\text{-}HT_{2A}$) receptor-selective PET radiotracer [^{11}C]MDL100907 in humans: quantitative analysis, test-retest reproducibility, and vulnerability to endogenous 5-HT tone. NeuroImage 59:271–285

Thurfjell L, Lötjönen J, Lundqvist R et al (2012) Combination of biomarkers: PET [^{18}F]flutemetamol imaging and structural MRI in dementia and mild cognitive impairment. Neurodegener Dis 10:246–249

Tiepolt S, Patt M, Aghakhanyan G (2019) Current status/need for tracers to diagnose neurodegenerative diseases. EJNMMI Radiopharm Chem 4:17

Tissingh G, Booij J, Winogrodzka A et al (1997) IBZM- and CIT-SPECT of the dopaminergic system in parkinsonism. J Neural Transm Suppl 50:31–37

Tournier N, Bauer M, Pichler V et al (2019) Impact of P-glycoprotein function on the brain kinetics of the weak substrate [^{11}C]metoclopramide assessed with PET imaging in humans. J Nucl Med 60:985–991

Tredwell M, Preshlock SM, Taylor NJ et al (2014) A general copper-mediated nucleophilic ^{18}F-fluorination of arenes. Angew Chem Int Ed Engl 53:7751–7755

Turkheimer FE, Selvaraj S, Hinz R et al (2012) Quantification of ligand PET studies using a reference region with a displaceable fraction: application to occupancy studies with [^{11}C]DASB as an example. J Cereb Blood Flow Metab 32:70–80

Villemagne VL, Okamura N, Pejoska S et al (2012) Differential diagnosis in Alzheimer's disease and dementia with Lewy bodies via VMAT2 and amyloid imaging. Neurodegener Dis 10:161–165

van Waarde A, Ramakrishnan NK, Rybczynska AA (2011) The cholinergic system, sigma-1 receptors and cognition. Behav Brain Res 221:543–554

Waldhoer M, Bartlett SE, Whistler JL (2004) Opioid receptors. Annu Rev Biochem 73:953–990

Wang YT, Edison P (2019) Tau imaging in neurodegenerative diseases using positron emission tomography. Curr Neurol Neurosci Rep 19:45

Warnock G, Sommerauer M, Mu L et al (2018) A first-in-man PET study of [^{18}F]PSS232, a fluorinated ABP688 derivative for imaging metabotropic glutamate receptor subtype 5. Eur J Nucl Med Mol Imaging 45:1041–1051

Van Weehaeghe D, Koole M, Schmidt ME et al (2019) [^{11}C]JNJ54173717, a novel P2X7 receptor radioligand as marker for neuroinflammation: human biodistribution, dosimetry, brain kinetic modelling and quantification of brain P2X7 receptors in patients with Parkinson's disease and healthy volunteers. Eur J Nucl Med Mol Imaging 46(10):2051–2064

Willeit M, Ginovart N, Kapur S et al (2006) High-affinity states of human brain dopamine $D_{2/3}$ receptors imaged by the agonist [^{11}C]-(+)-PHNO. Biol Psychiatry 59:389–394

Wong DF, Kuwabara H, Horti AG et al (2018) Brain PET imaging of α7-nAChR with [^{18}F]ASEM: reproducibility, occupancy, receptor density, and changes in schizophrenia. Int J Neuropsychopharmacol 21:656–667

Yasuno F, Ota M, Ito H et al (2008) Increased binding of peripheral benzodiazepine receptor in Alzheimer‘s disease measured by positron emission tomography with [^{11}C]DAA1106. Biol Psychiatry 64:835–841

Yeh YW, Ho PS, Chen CY et al (2015) Suicidal ideation modulates the reduction in serotonin transporter availability in male military conscripts with major depression: a 4-[^{18}F]-ADAM PET study. World J Biol Psychiatry 16:502–512

Yoo HS, Chung SJ, Kim SJ et al (2018) The role of [^{18}F]FP-CIT PET in differentiation of progressive supranuclear palsy and frontotemporal dementia in the early stage. Eur J Nucl Med Mol Imaging 45:1585–1595

Yue X, Xin Y, Chugani HT et al (2019) Automated production of a N-methyl-D-aspartate receptor radioligand [^{18}F]GE179 for clinical use. Appl Radiat Isot 148:246–252

Zanotti-Fregonara P, Pascual B, Rizzo G et al (2018) Head-to-head comparison of [^{11}C]PBR28 and [^{18}F]GE180 for quantification of the translocator protein in the human brain. J Nucl Med 59:1260–1266

Zarrad F, Zlatopolskiy BD, Krapf P et al (2017) A practical method for the preparation of ^{18}F-labeled aromatic amino acids from nucleophilic [^{18}F]fluoride and Stannyl precursors for electrophilic Radiohalogenation. Molecules 15:22

Zhang S, Han D, Tan X (2012) Diagnostic accuracy of [^{18}F]FDG and [^{11}C]PIB-PET for prediction of short-term conversion to Alzheimer’s disease in subjects with mild cognitive impairment. Int J Clin Pract 66:185–198

Zhang X, Basuli F, Swenson RE (2019) An azeotropic drying-free approach for copper-mediated radiofluorination without addition of base. J Labelled Comp Radiopharm 62:139–145

Zhou X, Khanapur S, Huizing AP et al (2014) Synthesis and preclinical evaluation of 2-(2-furanyl)-7-[2-[4-[4-(2-[^{11}C]methoxyethoxy)phenyl]-1-piperazinyl]ethyl]7H-pyrazolo[4,3-e][1,2,4]triazolo[1,5-c]pyrimidine-5-amine ([^{11}C]Preladenant) as a PET tracer for the imaging of cerebral adenosine A2A receptors. J Med Chem 57:9204–9210

Ziebell M (2011) Evaluation of the superselective radioligand [^{123}I]PE2I for imaging of the dopamine transporter in SPECT. Dan Med Bull 58:B4279

Zorumski CF, Izumi Y (2012) NMDA receptors and metaplasticity: mechanisms and possible roles in neuropsychiatric disorders. Neurosci Biobehav Rev 36:989–1000

Tracer Kinetic Modelling

2

Adriaan A. Lammertsma

Contents

2.1 Introduction 38
2.2 Principles of Modelling 38
2.3 Single-Tissue Compartment Model 40
2.4 Principles and Practice of Quantification 42
2.5 An Example: Measurement of CBF Using [^{15}O]H_2O 43
2.6 Two-Tissue Compartment Model 43
2.7 Reference Tissue Models 47
2.8 Parametric Methods 49
2.9 Conclusions 50
References 51

Abstract

This chapter provides an overview of the basic principles of quantification of cerebral PET studies using compartmental modelling. Both single- and two-tissue compartment models are presented with emphasis on volume of distribution and non-displaceable binding potential as outcome measures. Next, both full and simplified reference tissue models are introduced, obviating the need for arterial cannulation. Finally, a brief overview is given of various parametric methods enabling calculations at a voxel level.

A. A. Lammertsma (✉)
Department of Radiology and Nuclear Medicine, Amsterdam University Medical Centers, Amsterdam, The Netherlands
e-mail: aa.lammertsma@amsterdamumc.nl

R. A. J. O. Dierckx et al. (eds.), *PET and SPECT in Neurology*,
https://doi.org/10.1007/978-3-030-53168-3_2

2.1 Introduction

Positron emission tomography (PET) is a tomographic imaging technique that is characterized by its quantitative nature and high sensitivity. It allows for accurate measurements of regional tissue radioactivity concentrations. In general, uptake of radioactivity in tissue follows intravenous injection of minute (tracer) amounts of molecules labelled with a positron emitter such as carbon-11 or fluorine-18. As tissue uptake depends on physiological or molecular processes, PET images provide in vivo information on these biological processes (Phelps 2004) rather than on anatomy. By using different tracers, different processes such as perfusion, metabolism, pre- and postsynaptic receptor density and affinity, neurotransmitter release, enzyme activity and drug delivery and uptake can be measured.

PET radioactivity measurements are based on coincidence detection, i.e. the simultaneous detection of the two annihilation photons (travelling in opposite directions) resulting from a single positron emission. This so-called coincidence detection of the two annihilation photons means that the line of response along which the original annihilation took place is known and therefore it is possible to perform accurate correction for tissue attenuation along this line of response, e.g. by measuring attenuation using an external positron source or by using density information from an accompanying CT scan. In addition, PET has unrivalled sensitivity allowing for measurements of tracer concentrations at a picomolar level. At present, PET is the most selective and sensitive method for measuring molecular pathways and interactions in vivo (Jones 1996).

In routine clinical (nuclear medicine) practice, such as in staging using [^{18}F]FDG, it is customary to inject the tracer, wait (in case of [^{18}F]FDG for 1 h) and acquire a static scan of tracer uptake. In general, increased uptake is then associated with an increase in the physiological or molecular process being monitored. Net uptake at a certain time after injection, however, is a complex interplay between delivery, uptake, retention and clearance. Therefore, increased uptake can also be due to increased availability, i.e. either increased plasma concentration or increased flow, or decreased clearance. From a single static scan, it is not possible to separate the various components that contribute to the total signal, such as specific binding, nonspecific binding and free tracer in tissue. This clearly is illustrated in Fig. 2.1, where an image of total uptake (left) is compared with that of specific binding (right). Interpreting a change in uptake as being due to a change in specific signal rests on the assumption that the other components contributing to the total signal do not change. Although this may seem quite obvious, it is often forgotten in clinical practice.

2.2 Principles of Modelling

As mentioned above, PET allows for accurate measurements of regional tissue radioactivity concentrations. The purpose of a PET study, however, is to obtain quantitative values of parameters that characterize a physiological, biochemical or

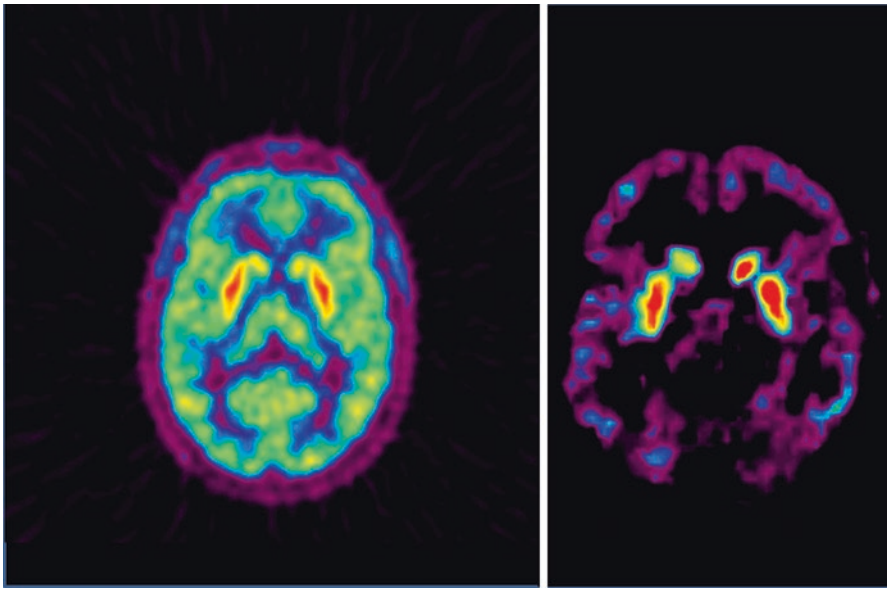

Fig. 2.1 Uptake of the NK1 receptor ligand [^{11}C]R116301 in a normal volunteer with (*left*) a total uptake image (60–90 min after injection) and (*right*) a parametric image on non-displaceable binding potential (BP_{ND}) representing specific signal only

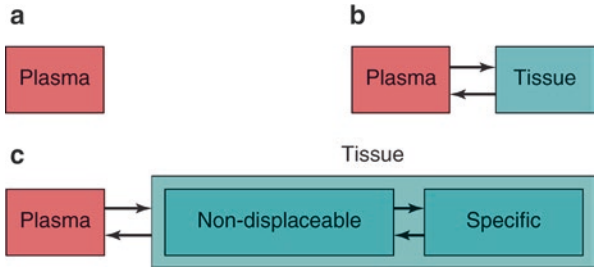

Fig. 2.2 Structure of compartment models with (**a**) no-, (**b**) one- and (**c**) two-tissue compartments

pharmacokinetic process. In other words, a tracer kinetic model, describing the process under study, is required to translate the measurements of radioactivity into quantitative values of these biological parameters. Although other models are available, in practice, all PET studies are analysed using compartment models (Gunn et al. 2001). These compartments not necessarily are distinct anatomical compartments but a convenient way to describe different kinetic "states" of the tracer. The most common models are single- and two-tissue compartment models (Fig. 2.2).

The simplest model, a zero-tissue compartment model (Fig. 2.2a), can be used for a blood volume tracer, such as [^{15}O]CO or [^{11}C]CO (Phelps et al. 1979a). CO binds to red cells and remains in the vascular space (no tissue compartment). As CO binds to red cells, a correction for the small- to large-vessel haematocrit ratio is needed to obtain values of blood volume (Lammertsma et al. 1984). This clearly illustrates that

one should always be aware of underlying assumptions in the model, as differences between capillary and large-vessel haematocrit could easily be overlooked.

A more common model is the single-tissue compartment model (Fig. 2.2b). In this case, the tracer is taken up by tissue, but it has either no further interactions within tissue (e.g. [^{15}O]H_2O; Frackowiak et al. 1980) or its kinetics are such that no additional tissue compartments can be identified (e.g. [^{11}C]flumazenil; Koeppe et al. 1991). In a two-tissue compartment model, a second tissue compartment is introduced with additional rate constants to describe exchange of tracer between the two tissue compartments (Huang et al. 1980). In general, the first compartment represents free and non-specifically bound tracer and the second compartment metabolized (e.g. [^{18}F]FDG; Phelps et al. 1979b) or bound (e.g. [^{11}C]raclopride; Farde et al. 1989) tracer.

Since the introduction of quantitative PET, there has been confusion about the nomenclature of both the models themselves and the parameters associated with them. Initially, single-tissue compartment models were referred to as either single (tissue) or two (blood and tissue) compartment models, and a similar problem existed for two-tissue compartment models. Fortunately, in recent years, there is consensus to classify models according to the number of tissue compartments involved. More importantly, a multitude of symbols has been used to indicate parameters associated with these models, in particular volume of distribution and binding potential. To provide clarity, in 2007, consensus was reached about the nomenclature related to reversibly bound ligands (Innis et al. 2007), and, wherever possible, this nomenclature will be used here.

2.3 Single-Tissue Compartment Model

As mentioned above, the single-tissue compartment model (Fig. 2.3) can be used for tracers where no second-tissue compartment is present or identifiable. The differential equation describing this model is given by:

$$dC_T(t)/dt = K_1 \cdot C_P(t) - k_2 \cdot C_T(t) \tag{2.1}$$

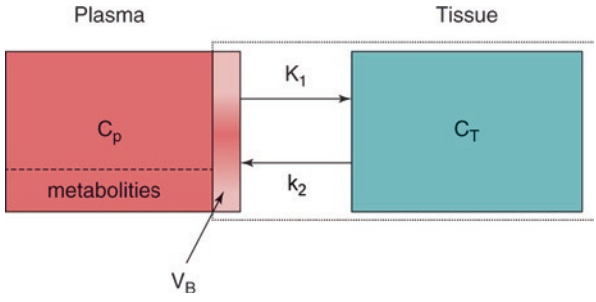

Fig. 2.3 Schematic diagram of the general single-tissue compartment model. C_P and C_T represent arterial plasma and tissue concentrations, K_1 and k_2 influx and efflux rate constants, and V_B blood volume within the PET region

where C_T and C_P are tissue and arterial plasma concentrations as function of time t and K_1 and k_2 rate constants for influx into and efflux out of tissue, respectively. This differential equation provides a mathematical description of the fact that the rate of change of the concentration in tissue depends on the balance between total rate of influx and total rate of efflux. The rate constant K_1 depends on two components according to:

$$K_1 = E \cdot F \tag{2.2}$$

where E is the first-pass extraction fraction and F blood flow (perfusion). It has been well documented that E itself depends on F according to (Renkin 1959; Crone 1963):

$$E = 1 - \exp\left(-\mathrm{PS} / F\right) \tag{2.3}$$

where PS represents the permeability surface area product. This equation illustrates that E is constant for flow values that are small compared with PS. For higher flow values, however, E starts to decrease, reflecting the phenomenon that the chance of a molecule to cross the capillary wall reduces if flow increases.

An important parameter, independent of the actual model, is the volume of distribution V_T, which is the ratio of tissue and plasma concentrations under steady-state conditions, i.e. at equilibrium when both concentrations are time independent:

$$V_T = C_T / C_P \tag{2.4}$$

At equilibrium, the single-tissue compartment model reduces to:

$$0 = K_1 \cdot C_P - k_2 \cdot C_T \tag{2.5}$$

Rearranging results in:

$$C_T / C_P = K_1 / k_2 \tag{2.6}$$

In other words, for the single-tissue compartment model, it follows that:

$$V_T = K_1 / k_2 \tag{2.7}$$

The general solution of Eq. (2.1), with or without Eq. (2.7), is:

$$C_T(t) = K_1 \cdot C_P(t) \otimes \exp\left(-k_2 \cdot t\right) = K_1 \cdot C_P(t) \otimes \exp\left\{-\left(K_1 / V_T\right) \cdot t\right\} \tag{2.8}$$

where $\otimes$ represents the convolution operation.

In practice, a PET scanner does not only measure uptake in tissue but rather total uptake in a region of interest (ROI) or voxel. In other words, intravascular activity should also be taken into account. Consequently, the concentration measured by the PET scanner is given by:

$$C_{\mathrm{PET}}(t) = (1 - V_{\mathrm{B}}) \cdot C_{\mathrm{T}}(t) + V_{\mathrm{B}} \cdot C_{\mathrm{A}}(t) \tag{2.9}$$

where V_B represents (fractional) blood volume, $C_A(t)$ represents arterial whole blood concentration as function of time and $C_T(t)$ is given by Eq. (2.8).

2.4 Principles and Practice of Quantification

Equation (2.9) illustrates a couple of basic principles of quantification of PET studies. Firstly, it clearly illustrates that activity is delivered to tissue through the circulation, and therefore, for full quantification, the arterial plasma concentration $C_P(t)$ needs to be measured as function of time. If the tracer is metabolized and (ideally) its radioactive metabolites do not cross the blood-brain barrier, $C_P(t)$ represents the time-activity curve of parent tracer only. In other words, in general, the metabolite-corrected arterial plasma curve is needed. Secondly, although $C_P(t)$ provides input to tissue, intravascular activity is a mixture of parent tracer, its radiolabelled metabolites and indeed tracer (or metabolites) bound to blood cells. Consequently, as a second input function, the non-metabolite-corrected arterial whole blood curve $C_A(t)$ is needed. Thirdly, the convolution in Eq. (2.9) indicates that the tissue concentration $C_T(t)$ does not depend on the instantaneous $C_P(t)$ value but rather on its history. This is just a mathematical representation of the fact that tissue clearance is not instantaneous. Finally, apart from the measured variables $C_P(t)$, $C_A(t)$ and $C_{PET}(t)$, Eq. (2.9) contains two tissue related unknown parameters K_1 and V_T. With two unknown parameters, it will be clear that it is not possible to solve Eq. (2.9) using a single (static) scan (i.e. Figure 2.1b cannot be derived from Fig. 2.1a without additional information).

To derive quantitative values of both K_1 and V_T, dynamic scanning is required. In contrast to most diagnostic procedures where a static scan is acquired sometime after tracer injection, in a dynamic scanning protocol, the patient is first positioned within the scanner. With the patient in the scanner, the tracer is injected, and, at the same time, a (dynamic) scan is started with an overall length that is dictated primarily by the kinetics of the process/tracer under study. To date, most scanners acquire data in list mode (each event has a time stamp), but during data processing, counts are binned into successive time frames. Reconstruction of these frames provides a series of images as function of time. From these frames, time-activity curves (i.e. $C_T(t)$) can be generated at either a voxel or a region of interest (ROI) level.

$C_A(t)$ can be obtained by continuous arterial blood sampling (Boellaard et al. 2001) during scanning. Additional manual arterial blood samples are needed to obtain $C_P(t)$. These samples are needed to obtain plasma to whole blood ratios and

parent fractions, both as function of time. Curves are fitted to both manual data sets, and $C_A(t)$ is multiplied with both curves, resulting in $C_P(t)$. When all data are available, a voxel or ROI time-activity curve $C_T(t)$ can be fitted for K_1 and V_T (or k_2) using the operational equation (Eq. 2.9), together with input functions $C_P(t)$ and $C_A(t)$ and standard non-linear regression techniques (Cunningham 1985).

2.5 An Example: Measurement of CBF Using [^{15}O]H_2O

As mentioned earlier, the single-tissue compartment model can be used for tracers that enter tissue but have no further interaction within that tissue. Such a tracer is ideal for measuring tissue perfusion, and the best example is [^{15}O]H_2O (Lammertsma et al. 1989). Water is freely diffusible in the brain, at least at normal and reduced flow values. In addition, it is metabolically inert (no interaction in tissue). Being freely diffusible means that the first-pass extraction fraction is 100%, i.e. $E = 1$. From Eq. (2.2), it follows that $K_1 = F$ and, from Eq. (2.7), $k_2 = F/V_T$ where, in the brain, F represents cerebral blood flow (CBF).

For perfusion, not the arterial plasma concentration is relevant but rather the whole blood concentration. For water, this makes little difference, as concentrations are nearly the same. In this case, $V_T = C_T/C_A$ (at equilibrium), and it can be seen that the volume of distribution is identical to the partition coefficient of water.

As the partition coefficient of water is close to 1 (Herscovitch and Raichle 1985; Lammertsma et al. 1992), the venous concentration of [^{15}O]H_2O will be similar to the tissue concentration, and it will not be possible to separate these from each other. In other words, the fractional blood volume in Eq. (2.9) is essentially the fractional arterial blood volume V_A, which in the brain is in the order of about 1% (except in the vicinity of large arteries). In practice, V_A is left out of the equation, as it reduces precision (one more parameter to fit) and it has been shown that fitted F values are essentially the same when V_A is included or excluded. Therefore, for [^{15}O]H_2O, Eq. (2.9) reduces to:

$$C_{PET}(t) = C_T(t) = F \cdot C_A(t) \otimes \exp\left\{-\left(F / V_T\right) \cdot t\right\} \tag{2.10}$$

A schematic diagram showing the principles of obtaining F and V_T from measured tissue and arterial blood time-activity curves is shown in Fig. 2.4.

2.6 Two-Tissue Compartment Model

The most widely used tracer kinetic model is the two-tissue compartment model (Fig. 2.5), as it is used for both metabolism and neuroreceptor studies. The standard (reversible) two-tissue compartment model contains four rate constants (K_1 to k_4), but for tracers that are trapped in the final compartment, it reduces to an irreversible two-tissue compartment model in which $k_4 = 0$.

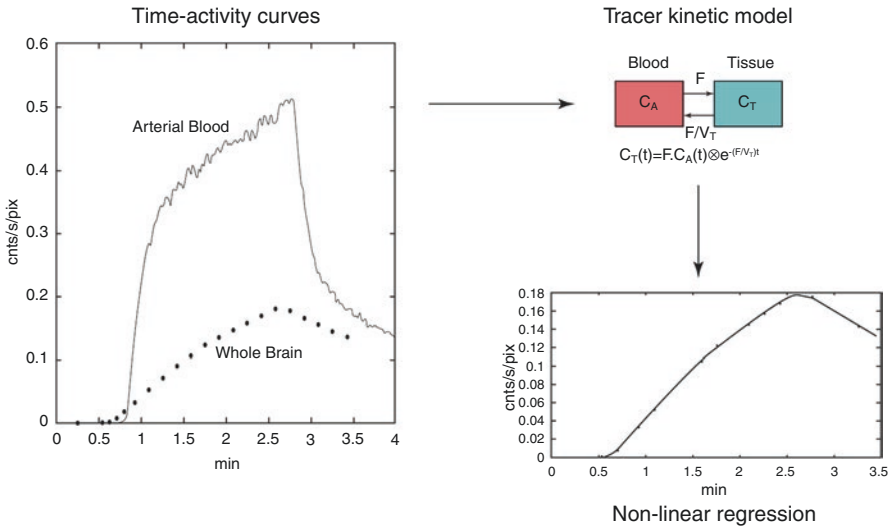

Fig. 2.4 Schematic diagram showing the fitting process, in this case, for flow F and volume of distribution V_T using $[^{15}O]H_2O$ as tracer. The *left panel* shows arterial blood and whole brain $[^{15}O]H_2O$ time-activity curves. The tissue curve is then fitted using the arterial whole blood curve as input function together with the model shown in the *right upper panel*. The best fit is shown in the *lower right panel*. Note that additional parameters are needed to account for delay and dispersion of the arterial input function

It should be noted that, for receptor studies, the reversible two-tissue compartment model is already based on an important assumption. In reality, the total tissue signal obtained with a receptor ligand is the sum of three components: free ligand, non-specifically bound ligand (e.g. protein binding) and specifically bound ligand. The corresponding compartment model would require six rate constants, but deriving six parameter values from a single tissue time-activity curve essentially is impossible. In addition, in nearly all cases, a third compartment is not identifiable. Therefore, the assumption is made that kinetics of non-specific binding are fast enough, so that free and non-specific compartments can be lumped together into a single non-displaceable compartment, resulting in a model with four rate constants (Fig. 2.5). Equation (2.9) also applies to this model, except that in this case C_T is given by:

$$C_T(t) = C_{ND}(t) + C_S(t) \tag{2.11}$$

where C_{ND} and C_S represent concentrations in non-displaceable and specific compartments, respectively.

From Fig. 2.5, it can be seen that the underlying differential equations are given by

$$dC_{ND}(t)/dt = K_1 C_P(t) - k_2 C_{ND}(t) - k_3 C_{ND}(t) + k_4 C_S(t) \tag{2.12}$$

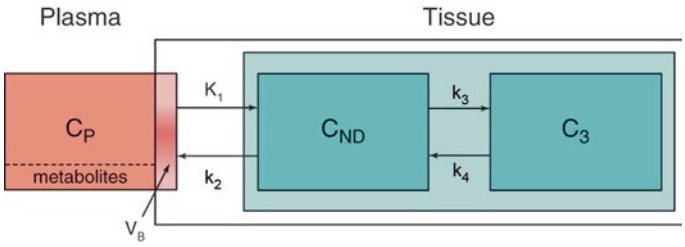

Fig. 2.5 Schematic diagram of the two-tissue compartment model. C_P, C_{ND} and C_S represent arterial plasma, non-displaceable tissue and specific tissue concentrations, K_1 to k_4 rate constants characterizing transport between compartments, and V_B blood volume within the PET region

$$\mathrm{d}C_S(t)/\mathrm{d}t = k_3 C_{ND}(t) - k_4 C_S(t) \tag{2.13}$$

Solving these differential equations results in a non-linear equation which, in contrast to the single-tissue compartment model, contains two convolutions (Phelps et al. 1979b). Again, as for the single-tissue compartment model, a voxel or ROI time-activity curve $C_T(t)$ can then be fitted for the four rate constants and V_B using Eq. (2.9), combined with the operational equation derived from Eqs. (2.12) and (2.13). Fitting five parameters from a single time-activity curve, however, can be quite challenging, especially in the presence of noise. As a result, precision of the fitted rate constants (also called micro-parameters) can be quite poor. Fortunately, from a biological point of view, macro-parameters (i.e. a combination of various micro-parameters) are still of great interest. Especially for receptor studies, the most interesting macro-parameter is the non-displaceable binding potential BP_{ND}, which is given by:

$$BP_{ND} = k_3 / k_4 \tag{2.14}$$

For a receptor, ligand, the rate constants k_3 and k_4 are related to pharmacological parameters (Innis et al. 2007):

$$k_3 = f_{ND} \cdot k_{on} \cdot B_{avail} \tag{2.15}$$

$$k_4 = k_{off} \tag{2.16}$$

where f_{ND} represents the free fraction in the non-displaceable compartment and B_{avail} the number of available receptors and k_{on} and k_{off} represent the rate constants for association and dissociation of the ligand-receptor complex, respectively.

The free fraction f_{ND} is needed in Eq. (2.15), as free and non-specific compartments had been lumped together. In addition, Eq. (2.15) contains B_{avail}, as occupancy by endogenous neurotransmitters cannot be excluded in an in vivo study. Only if this level of occupancy is low, B_{avail} will approach the pharmacological parameter

B_{max}, the maximum number of receptors. Another pharmacological parameter is the equilibrium dissociation constant K_d (Innis et al. 2007):

$$K_d = k_{off} / k_{on} \tag{2.17}$$

From Eqs. (2.14–2.17), it follows that (Mintun et al. 1984):

$$BP_{ND} = f_{ND} \cdot B_{avail} / K_d \tag{2.18}$$

Equation (2.18) illustrates that, if f_{ND} is constant, BP_{ND} depends on both number of available receptors (B_{avail}) and affinity of the ligand for the receptor (K_d). Often it is assumed that a change in BP_{ND} reflects a change in receptor density. This assumption, however, is only valid when there is independent evidence that affinity is unchanged. B_{avail} and K_d can be measured separately, but this requires multiple scans in the same subject using tracer injections with different specific activities.

For many tracers fitted BP_{ND} cannot be used because of lack of precision. In that case, data can be analysed using the volume of distribution V_T (Eq. 2.4). Clearly, the relationship given in Eq. (2.7) does not hold for a two-tissue compartment model. Again, however, it is possible to derive a relationship between V_T and the various rate constants by considering equilibrium conditions. In this case, both $dC_{ND}(t)/dt$ and $dC_S(t)/dt$ can be set to 0. From Eq. (2.13), it follows that:

$$C_S = \left(k_3 / k_4\right) \cdot C_{ND} \tag{2.19}$$

where C_S and C_{ND} are independent of time.

From Eqs. (2.4), (2.11) and (2.19), it follows that:

$$V_T = \left(C_{ND} + C_S\right) / C_P = \left(1 + k_3 / k_4\right) \cdot C_{ND} / C_P \tag{2.20}$$

Next, from Eqs. (2.12) and (2.13), it follows that under equilibrium conditions:

$$C_{ND} = \left(K_1 / K_2\right) \cdot C_P \tag{2.21}$$

Finally, combining Eqs. (2.14), (2.20) and (2.21) results in:

$$V_T = K_1 / k_2 \cdot \left(1 + k_3 / k_4\right) = K_1 / k_2 \cdot \left(1 + BP_{ND}\right) \tag{2.22}$$

Although in practice it is never used, it is of interest to consider non-specific binding as a separate kinetic process with rate constants k_5 and k_6. Analogues to the derivation of Eq. (2.22), it can be shown that the volume of distribution V_T is then given by:

$$V_T = K_1 / k_2 \cdot \left(1 + BP_{ND} + k_5 / k_6\right) \tag{2.23}$$

Equation (2.23) clearly shows that V_T represents the total tissue signal, i.e. the sum of specific and non-specific signals. The large discrepancy between summed and parametric BP_{ND} images in Fig. 2.1 can be explained by a relatively large non-specific signal. Note, however, that a V_T image is only "contaminated" by non-specific binding, whilst a summed image also suffers from flow and plasma clearance effects.

V_T can be used as outcome measure of receptors studies, provided the signal is dominated by specific binding. A classical example is [^{11}C]flumazenil, where the non-specific binding is approximately 10% (Koeppe et al. 1991).

If a direct measurement of BP_{ND} cannot be used due to lack of precision, it is still possible to extract it indirectly from V_T provided there is a region in the brain that is devoid of the receptor under study, a so-called reference region. In that case, V_T for the target region is given by Eq. (2.22) and the volume of distribution V_T' of the reference region by Eq. (2.7):

$$V_T^{'} = K_1^{'} / k_2^{'} \tag{2.24}$$

If the level of non-specific binding is constant across the brain, the following equality holds:

$$K_1 / k_2 = K_1^{'} / k_2^{'} \tag{2.25}$$

By combining Eqs. (2.22), (2.24) and (2.25), it follows that (Lammertsma et al. 1996):

$$BP_{ND} = V_T / \left(K_1 / k_2\right) - 1 = V_T / V_T^{'} - 1 \tag{2.26}$$

2.7 Reference Tissue Models

Using Eq. (2.26), BP_{ND} can still be obtained even if direct fitting results in unstable estimates. The main disadvantage of the method represented by this equation is the fact that it still requires a metabolite-corrected arterial plasma input function to estimate V_T and V_T'. To overcome this problem, the so-called reference tissue models have been developed that use the time-activity curve of the reference region (i.e. a region devoid of receptors) as an indirect input function, obviating the need for arterial cannulation. If such a reference tissue exists, it is also possible to derive BP_{ND} directly without arterial sampling. Figure 2.6 shows the (full) reference tissue model. The corresponding differential equations are:

$$\mathrm{d}C_{ND}\left(t\right) / \mathrm{d}t = K_1 C_P\left(t\right) - k_2 C_{ND}\left(t\right) - k_3 C_{ND}\left(t\right) + k_4 C_S\left(t\right) \tag{2.27}$$

$$\mathrm{d}C_S\left(t\right) / \mathrm{d}t = k_3 C_{ND}\left(t\right) - k_4 C_S\left(t\right) \tag{2.28}$$

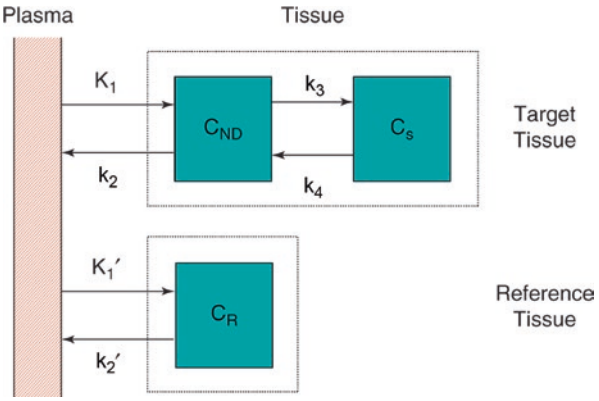

Fig. 2.6 Schematic diagram of the full-reference tissue model. C_{ND} and C_S represent non-displaceable and specific concentrations in the target tissue, and C_R represents the concentration in the reference tissue

$$dC_R(t)/dt = K_1' C_p(t) - k_2' C_R(t) \tag{2.29}$$

where $C_R(t)$ represents the tissue concentration as function of time in the reference tissue.

Solving Eqs. (2.27)–(2.29) results in an equation in which $C_T(t)$ is expressed as function of $C_R(t)$ and the parameters R_1 (=K_1/K_1'), k_2, k_3 and BP_{ND} (Lammertsma et al. 1996). As the target tissue curve is now expressed as a function of the reference tissue curve rather than the plasma input function, K_1 cannot be estimated but only the ratio R_1, i.e. K_1 target tissue relative to K_1' reference tissue. These K_1 values do not have to be the same, and so the model does take into account differences in delivery between target and reference tissues.

The full-reference tissue model essentially combines a two-tissue compartment model for the target region with a single-tissue compartment model (no receptors) for the reference tissue. Although this gives full account of all kinetic parameters, in practice fits converge slowly mainly because of high correlation between k_2 and k_3. To obtain more stable fits, the model was further simplified by reducing the number of parameters from four to three (Lammertsma and Hume 1996). This was achieved by assuming that the exchange between non-displaceable and specific compartments is relatively fast, i.e. by treating the target tissue also as a single-tissue compartment with an apparent rate of clearance that is reduced by a factor $1 + BP_{ND}$. The resulting simplified reference tissue model (SRTM) is shown in Fig. 2.7, and its kinetics can be described by the following differential equations:

$$dC_T(t)/dt = K_1 C_P(t) - k_2 C_T(t)/(1 + BP_{ND}) \tag{2.30}$$

$$dC_R(t)/dt = K_1' C_p(t) - k_2' C_R(t) \tag{2.31}$$

Solving Eqs. (2.30) and (2.31) again results in an equation in which $C_T(t)$ is expressed as function of $C_R(t)$, in this case, with three parameters R_1, k_2 and BP_{ND} (Lammertsma and Hume 1996):

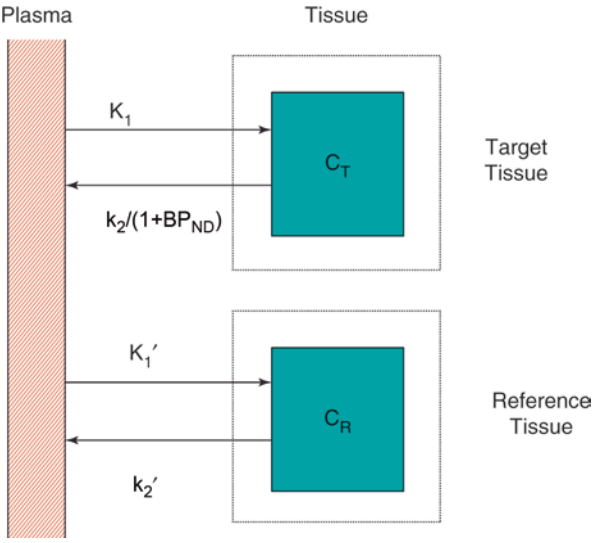

Fig. 2.7 Schematic diagram of the simplified reference tissue model. C_T and C_R represent total concentrations in target and reference tissues, respectively

$$C_T(t) = R_1 \cdot C_R(t) + \left\{k_2 - R_1 \cdot k_2 / \left(1 + \mathrm{BP_{ND}}\right)\right\} \cdot C_R(t) \otimes \exp\left\{-k_2 \cdot t / \left(1 + \mathrm{BP_{ND}}\right)\right\} \quad (2.32)$$

The main differences with the full-reference tissue model are (1) reduction of the number of parameters from four to three and (2) reduction of the number of convolutions from two to one. Although SRTM assumes fast exchange between non-displaceable and specific compartments, this assumption does not seem to be too critical (Buchert and Thiele 2008). Indeed, originally SRTM was developed and validated for analysing [^{11}C] raclopride kinetics, which are best described by two-tissue compartments. Nevertheless, BP_{ND} values obtained using SRTM and full-reference tissue models were identical (Lammertsma and Hume 1996).

Although reference tissue models are convenient, as they do not require arterial cannulation and labour-intensive measurements of radiolabelled plasma metabolites, it is important to stress that, for new tracers and applications, use of any reference tissue model should be validated against the most appropriate plasma input model for that tracer.

2.8 Parametric Methods

In general, the model equations presented so far are used to fit ROI data, i.e. time-activity curves generated for specific (predefined) ROIs. Ideally, fits should be performed at the voxel level, thereby generating images of the parameters of interest (the so-called parametric images). Although, in theory, it is possible to fit individual

voxel data, in practice, this is not feasible. Firstly, non-linear regression is too slow to generate parametric images within a reasonable amount of time. Secondly, non-linear regression is sensitive to noise, resulting in noisy images with outliers.

To generate parametric images, some form of linearization of the model equations is required. Several methods have been developed using either a graphical approach or multilinear regression analysis (Patlak et al. 1983; Blomqvist 1984; Logan et al. 1990, 1996; Ichise et al. 2002, 2003). These methods involve some sort of transformation of variables or direct integration of differential equations. As such, they are "approximations" of the full compartmental equations, and a given linearized model should be validated against the full non-linear model.

An interesting, more general, approach is the basis function method, which in theory can be used for all compartment models. The method is best known for its implementation of SRTM, also known as RPM (Gunn et al. 1997). Equation (2.32) contains both a linear and a convolution term. The basic idea of the basis function method is to pre-calculate the convolution for a set of "basis" functions that cover the entire range of physiological values. For a pre-calculated convolution, Eq. (2.32) becomes linear, and the coefficients can be obtained by linear regression. This process is repeated for each basis function, and the linear fit with the lowest residual sum of squares is kept. From the coefficients of this fit, the actual model parameters are calculated.

Using SRTM at a voxel level (i.e. RPM) provides the opportunity to reduce the number of parameters even further (Wu and Carson 2002), as R_1 and k_2 are obtained for all voxels. Given R_1 and k_2, k_2' can be calculated using Eq. (2.25). However, k_2' should be a constant as it refers to the same reference region. This can be utilized by running RPM twice. After the first run, k_2' is calculated for each voxel (from R_1 and k_2), and in the second run, k_2' is fixed to the median value (not mean, as this would be sensitive to outliers) from the first run, effectively reducing the number of parameters to two.

Parametric methods should be validated against their full compartmental counterparts. For each tracer, several parametric methods should be investigated, as no single method is ideal for all applications. In other words, for each new ligand, the optimal parametric method should be determined separately.

2.9 Conclusions

Quantitative analysis of PET data requires dynamic scanning and measurements of both arterial whole blood and metabolite-corrected plasma input functions. In case of neuroreceptor studies, reference tissue models can be used provided a region devoid of these receptors is available. To fully utilize the spatial resolution of the scanner, parametric methods should be used. The optimal model should, however, be determined for each new ligand, and simplifications such as reference tissue models and parametric methods should always be validated.

References

Blomqvist G (1984) On the construction of functional maps in positron emission tomography. J Cereb Blood Flow Metab 4:629–632

Boellaard R, Van Lingen A, Van Balen SCM et al (2001) Characteristics of a new fully programmable blood sampling device for monitoring blood radioactivity during PET. Eur J Nucl Med 28:81–89

Buchert R, Thiele F (2008) The simplified reference tissue model for SPECT/PET brain receptor studies. Interpretation of its parameters. Nuklearmedizin 47:167–174

Crone C (1963) The permeability of capillaries in various organs as determined by use of the 'indicator diffusion' method. Acta Physiol Scand 58:292–305

Cunningham VJ (1985) Non-linear regression techniques in data analysis. Med Inf 10:137–142

Farde L, Eriksson L, Blomquist G et al (1989) Kinetic analysis of central [^{11}C]raclopride binding to D2-dopamine receptors studied by PET—a comparison to the equilibrium analysis. J Cereb Blood Flow Metab 9:696–708

Frackowiak RSJ, Lenzi GL, Jones T et al (1980) Quantitative measurement of regional cerebral blood flow and oxygen metabolism in man, using ^{15}O and positron emission tomography: theory, procedure, and normal values. J Comput Assist Tomogr 4:727–736

Gunn RN, Lammertsma AA, Hume SP et al (1997) Parametric imaging of ligand-receptor binding in PET using a simplified reference region model. NeuroImage 6:279–287

Gunn RN, Gunn SR, Cunningham VJ (2001) Positron emission tomography compartmental models. J Cereb Blood Flow Metab 21:635–652

Herscovitch P, Raichle ME (1985) What is the correct value for the brain-blood partition coefficient for water? J Cereb Blood Flow Metab 5:65–69

Huang SC, Phelps ME, Hoffman EJ et al (1980) Noninvasive determination of local cerebral metabolic rate of glucose in man. Am J Phys 238:E69–E82

Ichise M, Toyama H, Innis RB et al (2002) Strategies to improve neuroreceptor parameter estimation by linear regression analysis. J Cereb Blood Flow Metab 22:1271–1281

Ichise M, Liow JS, Lu JQ et al (2003) Linearized reference tissue parametric imaging methods: application to [11C]DASB positron emission tomography studies of the serotonin transporter in human brain. J Cereb Blood Flow Metab 23:1096–1112

Innis RB, Cunningham VJ, Delforge J et al (2007) Consensus nomenclature for in vivo imaging of reversibly binding radioligands. J Cereb Blood Flow Metab 27:1533–1539

Jones T (1996) The role of positron emission tomography within the spectrum of medical imaging. Eur J Nucl Med 23:207–211

Koeppe RA, Holthoff VA, Frey KA et al (1991) Compartmental analysis of [^{11}C] flumazenil kinetics for the estimation of ligand transport rate and receptor distribution using positron emission tomography. J Cereb Blood Flow Metab 11:735–744

Lammertsma AA, Hume SP (1996) Simplified reference tissue model for PET receptor studies. NeuroImage 4:153–158

Lammertsma AA, Brooks DJ, Beaney RP et al (1984) In vivo measurement of regional cerebral haematocrit using positron emission tomography. J Cereb Blood Flow Metab 4:317–322

Lammertsma AA, Frackowiak RSJ, Hoffman JM et al (1989) The $C^{15}O_2$ build-up technique to measure regional cerebral blood flow and volume of distribution of water. J Cereb Blood Flow Metab 9:461–4707

Lammertsma AA, Martin AJ, Friston KJ et al (1992) In vivo measurement of the volume of distribution of water in cerebral grey matter: effects on the calculation of regional cerebral blood flow. J Cereb Blood Flow Metab 12:291–295

Lammertsma AA, Bench CJ, Hume SP et al (1996) Comparison of methods for analysis of clinical [^{11}C]raclopride studies. J Cereb Blood Flow Metab 16:42–52

Logan J, Fowler JS, Volkow ND et al (1990) Graphical analysis of reversible radio-ligand binding from time-activity measurements applied to [*N*-^{11}C-methyl]-(−)-cocaine PET studies in human subjects. J Cereb Blood Flow Metab 10:740–747

Logan J, Fowler JS, Volkow ND et al (1996) Distribution volume ratios without blood sampling from graphical analysis of PET data. J Cereb Blood Flow Metab 16:834–840
Mintun MA, Raichle ME, Kilbourn MR et al (1984) A quantitative model for the in vivo assessment of drug binding sites with positron emission tomography. Ann Neurol 15:217–227
Patlak CS, Blasberg RG, Fenstermacher JD (1983) Graphical evaluation of blood-to-brain transfer constants from multiple-time uptake data. J Cereb Blood Flow Metab 3:1–7
Phelps ML (2004) PET: molecular imaging and its biological applications. Springer, New York
Phelps ME, Huang SC, Hoffman EJ et al (1979a) Validation of tomographic measurement of cerebral blood volume with C-11 labeled carboxyhaemoglobin. J Nucl Med 20:328–334
Phelps ME, Huang SC, Hoffman EJ et al (1979b) Tomographic measurement of local cerebral glucose metabolic rate in humans with (F-18)2-fluoro-2-deoxy-D-glucose: validation of method. Ann Neurol 6:371–388
Renkin EM (1959) Transport of potassium-42 from blood to tissue in isolated mammalian skeletal muscles. Am J Phys 197:1205–1210
Wu Y, Carson RE (2002) Noise reduction in the simplified reference tissue model for neuroreceptor functional imaging. J Cereb Blood Flow Metab 22:1440–1452

3 Quantification in Brain SPECT: Noninvasive Cerebral Blood Flow Measurements Using ^{99m}Tc-Labeled Tracers

Hiroshi Matsuda

Contents

3.1 Introduction 54
3.2 Method 55
3.2.1 Theory of Graphical Analysis 55
3.2.2 Brain Perfusion Index (BPI) 55
3.2.3 Comparison of BPI and CBF Values Measured by Other Invasive Methods 58
3.2.4 Alternative Approach to Estimation of BPI 58
3.2.5 Calculation of Regional CBF from BPI 59
3.2.6 Consecutive rCBF Measurements at Baseline and Acetazolamide Challenge 61
3.3 Clinical Application 63
3.3.1 Cerebrovascular Diseases 63
3.3.2 Heart Failure 66
3.3.3 Idiopathic Normal Pressure Hydrocephalus 66
3.3.4 Neurodegenerative Disorders 67
3.3.5 Mood Disorders 68
3.3.6 Other Neuropsychiatric Diseases 68
3.4 Conclusion 68
References 69

Abstract

An absolute cerebral blood flow (CBF) measurement is necessary for detection of diffuse cerebral involvement and helpful for management of patients. Of the various measurement methods that have been employed in single photon emission computed tomography (SPECT), a noninvasive method using radionuclide angiography of ^{99m}Tc-labeled tracers has been widely used because of its simplicity without the need for any blood sampling. Brain perfusion index (BPI) is

H. Matsuda (✉)
Integrative Brain Imaging Center, National Center of Neurology and Psychiatry, Kodaira, Tokyo, Japan
e-mail: matsudah@ncnp.go.jp

R. A. J. O. Dierckx et al. (eds.), *PET and SPECT in Neurology*,
https://doi.org/10.1007/978-3-030-53168-3_3

determined by graphical analysis of time activity curves for aortic arch and brain within 30 s immediately after bolus injection of the tracer. This BPI is converted to global CBF using a regression line equation between BPI and global CBF measured using ^{133}Xe-SPECT. Then, regional CBF is calculated from global CBF, a linearization correction factor, and global mean SPECT counts. Obtained CBF values show good correlations with those obtained by other invasive methods with arterial blood sampling. This noninvasive technique has been applied to various neuropsychiatric diseases including cerebrovascular diseases, neurodegenerative disorders, and mood disorders for the early and differential diagnosis and objective evaluation of therapeutic effects.

3.1 Introduction

Quantitative evaluation of cerebral blood flow (CBF) allows assessment of diffuse cerebral involvement and enables longitudinal studies. Absolute CBF measurements hold promise for optimal patient selection and management, especially in cerebrovascular disease. They may also provide added value in larger patient populations with various neuropsychiatric disorders.

Various approaches have been described for the absolute CBF quantification by means of single photon emission computed tomography (SPECT). The earliest method applied ^{133}Xe, which was either inhaled or injected intravenously. Following equilibrium, the regional CBF (rCBF) is calculated from regional clearance of the inert ^{133}Xe gas washout by means of a pixel-based exponential fit derived from dynamic SPECT data sets. The blood time-activity curve is noninvasively estimated from an end-tidal air activity curve. Despite high precision this method suffers from several disadvantages mainly due to low spatial resolution related to the low gamma energy of ^{133}Xe and instrumentation applied. In addition, there is a need for dedicated, sensitive instrumentation with fast dynamic SPECT capabilities. Instrumentation, in addition involves a xenon trap and room ventilation, and a cooperative patient willing and able to breathe through a tightly fitting breathing mask for the duration of the study. ^{133}Xe SPECT studies have markedly decreased in number due to these disadvantages and have been replaced by methods employing either *N*-isopropyl-(iodine-123)-*p*-iodoamphetamine (^{123}I-IMP) or the technetium-99 m labeled products ethyl cysteinate dimer (^{99m}Tc-ECD) and hexamethylpropylene amine oxime (^{99m}Tc-HMPAO). However, most of these approaches require some form of arterial blood sampling. Although several investigators have proposed one-point sampling of arterial blood instead of invasive continuous or interval arterial sampling to estimate the integral of the input function for quantification of CBF (Iida et al. 1994), even single-point sampling is difficult in daily clinical practice. For clinical applications, noninvasive SPECT techniques without any blood sampling are desirable.

Two decades ago the author developed a noninvasive method for CBF quantification using radionuclide angiography of ^{99m}Tc-labeled tracers (Matsuda et al.

1992, 1993, 1995). This simple method without the need for any blood sampling has been used worldwide and was listed as a method for absolute CBF quantification in the guidelines and recommendations for perfusion imaging in cerebral ischemia from the council on cerebrovascular radiology of the American Heart Association (Latchaw et al. 2003). This article reviews the methodology and clinical applications of this noninvasive method.

3.2 Method

3.2.1 Theory of Graphical Analysis

The theoretical model of blood-brain exchange was employed to measure CBF using ^{99m}Tc-labeled tracers. In the unidirectional transfer process across the blood-brain barrier, brain radioactivity as a function of time, $B(t)$, is expressed as follows:

$$B(t) = k_u \int_0^t A(\tau)\,d\tau + V_n \cdot A(t) \tag{3.1}$$

where $A(t)$ is the arterial activity as a function of measurement time (t), τ is time, k_u is the unidirectional influx rate constant, and V_n is the initial distribution volume for the tracer which is the space of the exchangeable region plus the plasma space. Dividing Eq. (3.1) by $A(t)$ yields

$$\frac{B(t)}{A(t)} = k_u \frac{\int_0^t A(\tau)\,d\tau}{A(t)} + V_n \tag{3.2}$$

The graphical approach by plotting $B(t)/A(t)$ versus $\int_0^t A(\tau)/A(t)$ from each group of data gives an unidirectional influx rate of ku as a slope of a straight line and Vn as the ordinate intercept of this line. This graphical Patlak-Gjedde analysis (Patlak et al. 1983; Patlak and Blasberg 1985) does not require the determination of a specific compartment model.

3.2.2 Brain Perfusion Index (BPI)

In this method, the passage through the thoracic aorta to the brain is monitored after bolus injection of a ^{99m}Tc-labled tracer into the right brachial vein using a large-field gamma-camera. Following the injection, a sequence of 100 frames at 1-s intervals is started in a 128 × 128 format, with the patient lying in the supine position, facing the detector (Fig. 3.1).

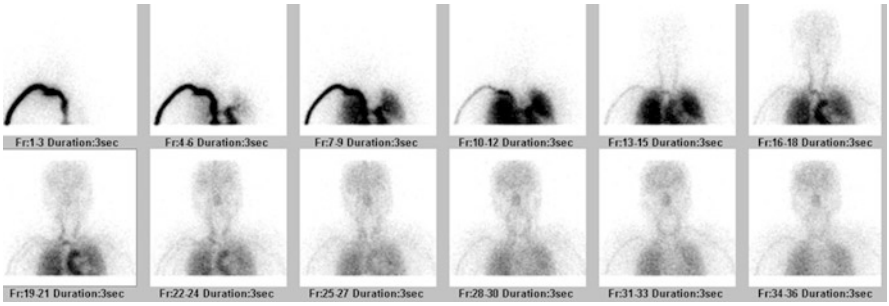

Fig. 3.1 Radionuclide angiography of ^{99m}Tc-ECD. The passage through the thoracic aorta to the brain is monitored using a large-field gamma camera. A sequence of 100 frames at 1 s intervals is acquired. Each sequential image of three merged frames is shown

Regions of interest (ROI) are hand-drawn over the aortic arch (ROI_{aorta}) and bilateral brain hemispheres (ROI_{brain}). The size of the ROIs is approximately 55 pixels and 300 pixels for ROI_{aorta} and ROI_{brain}, respectively. The activity of the aortic arch is monitored instead of the arterial activity to minimize the invasiveness of the procedure without the need for arterial blood sampling. Time-activity curves for these ROIs are processed with a five-point smoothing technique. Then, the time delay of the brain activity to the aortic arch activity is corrected by shifting the brain activity curve to the left to match the peak times or ascending parts of both curves. A fully automatic setting program for an ascending aorta ROI was proposed to improve the throughput, repeatability, and reproducibility (Masunaga et al. 2014).

In this graphical approach, a linear phase is discernible during an 8–12 s period within the first 30 s after tracer injection, indicating the presence of unidirectional tracer uptake (Fig. 3.2). Thereafter the tracer transfer into brain is less than expected if transport into the brain tissue continues to be unidirectional. The divergence of expected and measured activities reflects both the loss of radioactivity from the brain to blood and the rapid decrease of the lipophilic content of the tracer in the blood.

Graphically obtained slope (k_u) according to Eq. (3.2) depends on the size ratio of ROI_{brain} to ROI_{aorta}. To eliminate this dependence, a brain perfusion index (BPI) is developed as follows, where the size ratio of ROI_{brain} to ROI_{aorta} is set to 10 for standardization. This standardization makes it possible to compare BPI among subjects.

$$\mathrm{BPI} = 100 * k_u * \frac{10 * (\text{size of } \mathrm{ROI}_{aorta})}{(\text{size of } \mathrm{ROI}_{brain})} \tag{3.3}$$

Direct comparison of BPI for ^{99m}Tc-HMPAO with that for ^{99m}Tc-ECD in the same individuals demonstrated a highly significant correlation between these two tracers but approximately 7% lower BPI values for ^{99m}Tc-ECD than those for ^{99m}Tc-HMPAO (Matsuda et al. 1995). This lower BPI might be due to low first-pass brain extraction for ^{99m}Tc-ECD as compared with that for ^{99m}Tc-HMPAO. Friberg et al. (1994) reported an average first-pass extraction ratio of 0.60 for ^{99m}Tc-ECD

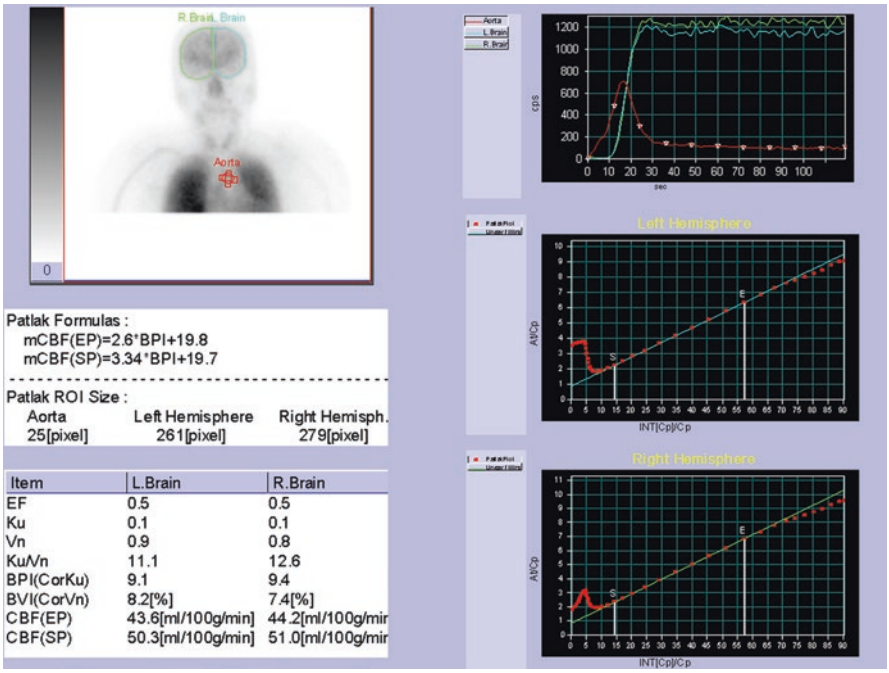

Fig. 3.2 Determination of brain perfusion index. Regions of interest (ROI) are hand-drawn over the aortic arch and bilateral brain hemispheres. Patlak-Gjedde graphical analysis of time activity curves for aorta and brain provides a linear phase during an 8–12 s period within the first 30 s after tracer injection. Brain perfusion index is calculated from graphically obtained slope (k_u) after correction of size of ROIs for brain hemisphere and aortic arch

when CBF was 46 ml/100 g/min, while Andersen et al. (1988) reported a higher average first-pass brain extraction ratio of 0.72 for ^{99m}Tc-HMPAO when CBF was 59 ml/100 g/min. BPI represents the unidirectional influx rate from blood to brain, which is proportional to a product of CBF and the first-pass extraction ratio. Thus BPI depends on the first-pass extraction ratio for the used tracer under constant CBF. However, differences between ^{99m}Tc-ECD BPI and ^{99m}Tc-HMPAO BPI were smaller than were expected from the difference in the first-pass extraction ratios, possibly attributable to a difference in radiochemical purity between the two tracers. The radiochemical purity of ^{99m}Tc-HMPAO is somewhat lower than that of ^{99m}Tc-ECD. The lower the radiochemical purity, the smaller BPI becomes.

Reproducibility for calculation of BPI was evaluated. To determine the influence of ROI selection and curve shift for correction of time delay of brain and aortic arch curves independent observers conducted a repeat analysis of the same radionuclide angiograms. Intra-observer coefficients of variation ranged from 4.0% (Matsuda et al. 1992) to 5.3, 5.6, and 7.9% (Van Laere et al. 1999). Interobserver coefficient of variation was reported to be 4.8% (Zaknun et al. 2008). Automated setting of ROI_{aorta} can improve both intra- and interobserver reproducibility particularly for naive observers (Groiselle et al. 2000).

Attention must be paid to dead-time count loss by gamma camera during radionuclide angiography. The brain activity curve is inevitably delayed in relation to the aortic arch activity curve. The total count rate is higher during estimation of activity in the aortic arch than during estimation of cerebral activity. Most of the injected tracer is present in the field soon after the injection, and thus counting efficiency is lower during the estimation of aortic arch activity. Arterial input appears to be underestimated due to excessive count loss, resulting in overestimation of BPI by over 3% when injecting 370 MBq of ^{99m}Tc-labeled tracers (Inoue et al. 1997).

3.2.3 Comparison of BPI and CBF Values Measured by Other Invasive Methods

Hemispheric BPI values for ^{99m}Tc-HMPAO and CBF values obtained from dynamic SPECT measurements by the ^{133}Xe inhalation method were compared in 38 hemispheres of 19 same individuals (Matsuda et al. 1992). BPI values showed a highly significant positive correlation (correlation coefficient = 0.926) with global CBF (gCBF) obtained from the early picture method in a ^{133}Xe-SPECT study. The regression line equation is global CBF = 2.75 × BPI + 17.7.

In comparison with CBF values measured using ^{123}I-IMP SPECT with continuous arterial blood sampling (Murase et al. 1999), BPI showed significant correlation coefficients of 0.629 and 0.856 for ^{99m}Tc-HMPAO and ^{99m}Tc-ECD, respectively.

In comparison with CBF values measured using $H_2{}^{15}O$ PET with continuous arterial blood sampling (Takasawa et al. 2004), BPI for ^{99m}Tc-HMPAO showed a significant correlation coefficient of 0.831.

3.2.4 Alternative Approach to Estimation of BPI

Murase et al. (1999, 2001) proposed spectral analysis for the estimation of BPI using radionuclide angiography for ^{99m}Tc-labeled tracers. This analysis has been mostly applied to dynamic positron emission tomography measurements. This analysis has been introduced as a non-compartmental tracer kinetic modeling technique, which can be used to characterize the reversible and irreversible components of acyclic, connected systems and to estimate the minimum number of compartments. This technique is applicable to systems in which the measured data can be expressed as a positively weighted sum of convolution integrals of the input function with an exponential function that has real-valued non-positive decay constants. BPI measured using graphical analysis and spectral analysis showed highly significant correlations (Murase et al. 1999; Van Laere et al. 2001) with equal interobserver reproducibility (Takasawa et al. 2003). Since BPI measured using spectral analysis appears to be proportional to CBF because of independence from the first-pass brain extraction ratio, it is larger by over 20% and more highly correlated to CBF values obtained from ^{123}I-IMP SPECT with continuous arterial blood sampling than BPI measured using graphical analysis (Murase et al. 1999). These results suggest that spectral

analysis provides a more reliable BPI than graphical analysis particularly in acetazolamide challenge (Takasawa et al. 2002). However this spectral analysis has not prevailed among users because of unavailability of an automated program.

3.2.5 Calculation of Regional CBF from BPI

To calculate regional CBF (rCBF) and to correct for incomplete retention of ^{99m}Tc-labeled tracers in the brain, Lassen et al. (1988) proposed the following linearization algorithm of a curve-linear relationship between the brain activity and CBF. This algorithm is based on kinetic models for ^{99m}Tc-HMPAO (Fig. 3.3) and ^{99m}Tc-ECD (Fig. 3.4):

$$F_i = F_r \cdot \frac{\alpha \cdot \left(C_i / C_r\right)}{\left[1 + \alpha - \left(C_i / C_r\right)\right]} \tag{3.4}$$

where F_i and F_r represent rCBF values for a region i and α reference region, respectively, and C_i and C_r are the SPECT counts for the region i and the reference region respectively. Acquisition of SPECT data usually starts at 10 min after tracer injection. Global brain is used as the reference region in this method. α is a correction factor for the linearization. The optimum value of the correction factor α is estimated from the following equations:

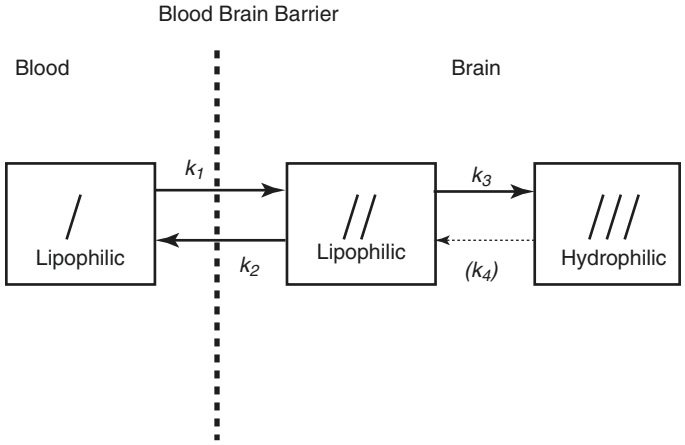

Fig. 3.3 Three-compartment unit-membrane model of solute exchange of lipophilic ^{99m}Tc-HMPAO. The first compartment is the freely diffusible lipophilic tracer in the blood pool outside the brain. The second compartment is the freely diffusible lipophilic tracer inside the brain. The third compartment is the hydrophilic form retained in the brain. K_1 is the influx constant, k_2 is the back diffusion rate constant, k_3 is the lipophilic to hydrophilic conversion constant, and k_4 is the hypothetical reverse conversion constant. Experimentally, it has been shown that no such reverse conversion takes place; therefore $k_4 \fallingdotseq 0$

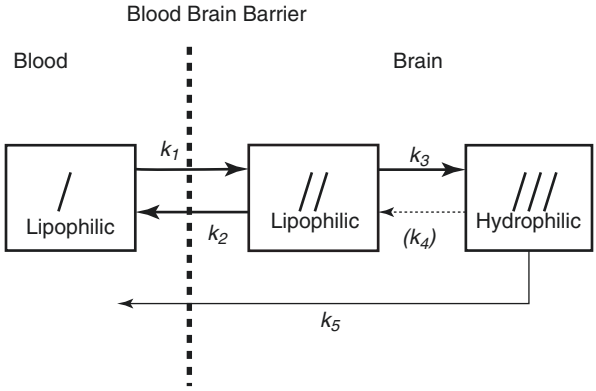

Fig. 3.4 Three-compartment unit-membrane model of solute exchange of lipophilic ^{99m}Tc-ECD. A slow loss of hydrophilic tracer or metabolites is present and not subject to detectable reuptake in tissue. k_5 represents a pathway from compartment III to blood

Table 3.1 Average values of transfer constants, brain-to-blood partition coefficient (λ) and α ratios for ^{99m}Tc-HMPAO and ^{99m}Tc-ECD

	^{99m}Tc-HMPAO	^{99m}Tc-ECD
k_2 (min^{-1})	0.69	0.22
k_3 (min^{-1})	0.8	0.57
k_4 (min^{-1})	0	0
k_5 (min^{-1})	0	0.0038
λ (ml/g)	0.67	1.33
α	1.18	2.59

$$\alpha = \frac{k_3}{k_{2r}} \tag{3.5}$$

$$k_{2r} = \frac{K_{1r}}{\lambda} = \frac{E \cdot F_r}{\lambda} \tag{3.6}$$

where k_3 is the conversion rate constant from lipophilic to hydrophilic tracer in the brain, k_{2r} is the rate of the back-diffusion from a reference region in the brain to the blood, and K_{1r} is the influx rate constant from the blood to a reference region in the brain. λ is the brain-blood partition coefficient of the lipophilic tracer and E describes the first-pass brain extraction of the lipophilic tracer across the blood-brain barrier. Average values for these rate constants and λ have been reported (Table 3.1). Lassen's correction algorithm assumes that k_3 and λ are the same in all regions. k_3 and λ were set to the reported mean values of 0.80 and 0.67 for ^{99m}Tc-HMPAO and 0.57 and 1.33 for ^{99m}Tc-ECD, respectively. An almost threefold smaller k_{2r} value for ^{99m}Tc-ECD than that for ^{99m}Tc-HMPAO results in the higher default α value of 2.6 in the linearization algorithm for ^{99m}Tc-ECD than the default α value of 1.5 in that for ^{99m}Tc-HMPAO. When CBF in the reference region ranged from 20 to 60 ml/100 g/min, optimum α values estimated using Eqs. (3.5) and (3.6) ranged from 3.2 to 1.2 for ^{99m}Tc-HMPAO and from 6.3 to 2.1 for ^{99m}Tc-ECD. The use of the fixed α value in the linearization algorithm gives rise to deviation of the obtained rCBF values

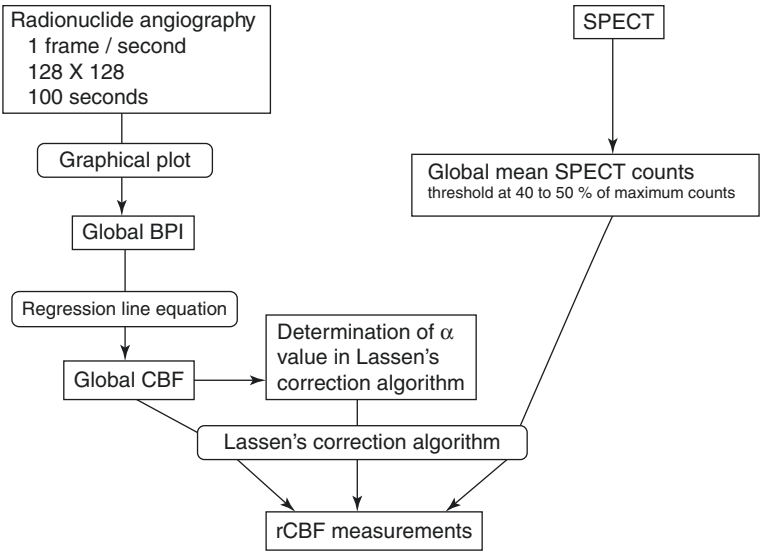

Fig. 3.5 Flowchart of the rCBF measurement procedure comprising radionuclide angiography and SPECT using ^{99m}Tc-labeled tracers. The gCBF converted from BPI using a regression line equation between BPI and gCBF measured using ^{133}Xe-SPECT, the linearization correction factor α, and the global mean SPECT counts obtained from the threshold at 40–50% of maximum counts are substituted into Lassen's algorithm for the linearization correction (Eq. 3.4) to estimate rCBF. The default value of α is 1.5 for ^{99m}Tc-HMPAO and 2.6 for ^{99m}Tc-ECD

from true rCBF values when using optimized α values that vary with CBF in a reference region. However, less deviation of obtained rCBF values from true values may be expected in the presence of a higher α value.

A flowchart of the rCBF measurement procedure comprising radionuclide angiography to estimate gCBF and SPECT to estimate rCBF using ^{99m}Tc-labeled tracers is demonstrated in Fig. 3.5. Global mean SPECT counts are calculated from threshold at 40–50% of maximum SPECT counts. Thus original SPECT images (Fig. 3.6a) are converted to rCBF SPECT images without any blood sampling (Fig. 3.6b).

3.2.6 Consecutive rCBF Measurements at Baseline and Acetazolamide Challenge

Takeuchi et al. (1997) applied these noninvasive rCBF measurements using ^{99m}Tc-ECD to a split dose protocol (Fig. 3.7) for the consecutive evaluation of baseline rCBF and cerebral perfusion reserve with acetazolamide challenge. Radionuclide angiography after bolus injection of ^{99m}Tc-ECD is performed for 100 s to obtain gCBF at baseline using graphical analysis. Ten minutes after the first injection of ^{99m}Tc-ECD, first SPECT at baseline is started. Then 10 min before the second

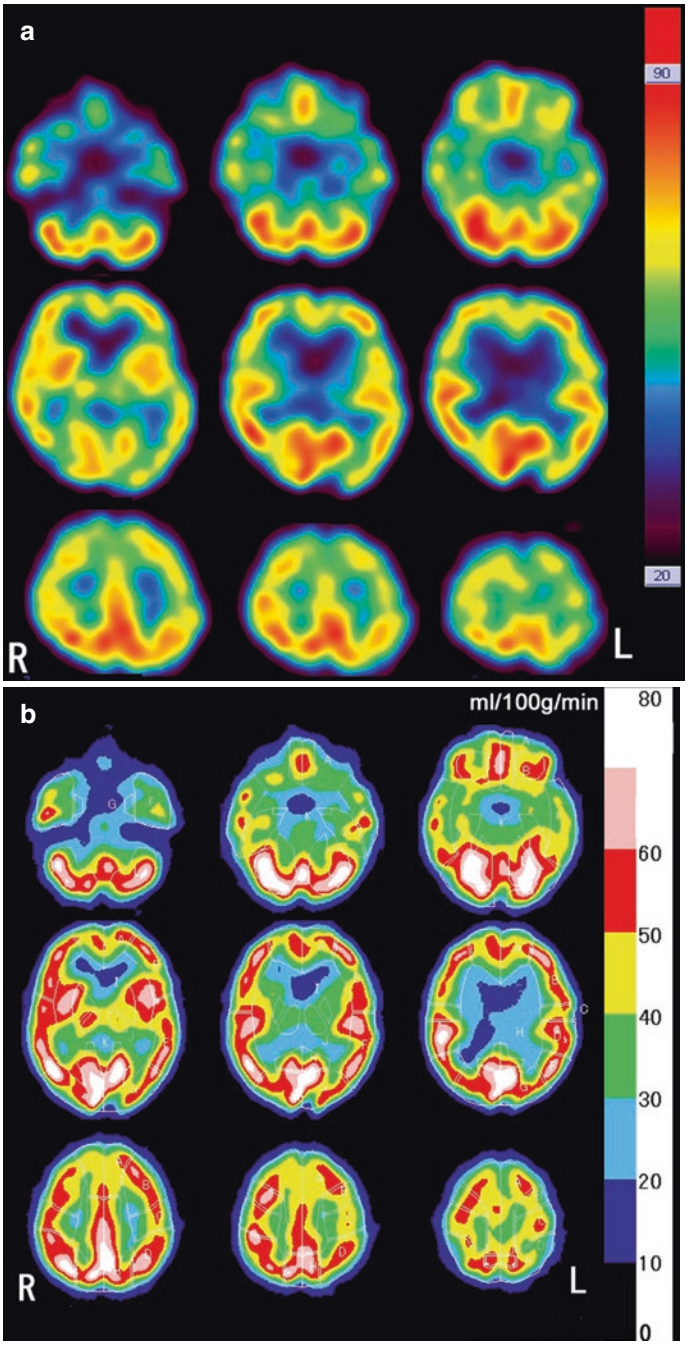

Fig. 3.6 Conversion of original ^{99m}Tc-ECD SPECT to rCBF SPECT images. (**a**) Original SPECT images. (**b**) rCBF SPECT images

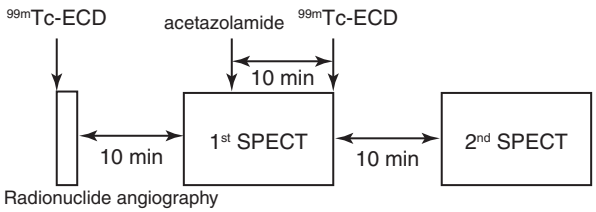

Fig. 3.7 Study protocol for the consecutive evaluation of baseline rCBF and cerebral perfusion reserve with acetazolamide challenge. Radionuclide angiography after bolus injection of ^{99m}Tc-ECD is performed for 100 s to obtain gCBF at baseline using graphical analysis. Ten minutes after the first injection of ^{99m}Tc-ECD, first SPECT at baseline is started. Then 10 min before the second injection of ^{99m}Tc-ECD, acetazolamide is intravenously injected during acquisition of projection data for the first SPECT. Immediately after the completion of the first SPECT an additional dose of ^{99m}Tc-ECD is injected and 10 min later the second SPECT is started

injection of ^{99m}Tc-ECD, 1000 mg acetazolamide is intravenously injected during acquisition of projection data for the first SPECT. Acetazolamide does not modify the tracer distribution of the brain during this acquisition of the first SPECT since tracer distribution has been already determined during radionuclide angiography. Immediately after the completion of the first SPECT an additional dose of ^{99m}Tc-ECD is injected and 10 min later the second SPECT is started. Total time span required for this procedure is less than 50 min.

To extract SPECT data for the acetazolamide challenge, the first SPECT data were subtracted from the second SPECT data after decay correction of ^{99m}Tc. Post-acetazolamide gCBF is estimated from the baseline gCBF, baseline global mean SPECT count, and post-acetazolamide global mean SPECT count as follows:

$$\text{post-acetazolamide gCBF} = \text{baseline gCBF} \cdot \frac{\alpha \cdot \chi}{(1+\alpha-\chi)} \tag{3.7}$$

where χ is post-acetazolamide global mean SPECT count/baseline global mean SPECT count. Using these baseline gCBF and post-acetazolamide gCBF, rCBF values at baseline and acetazolamide challenge are measured using SPECT data according to Eq. (3.4). Acetazolamide induced a 40% gCBF increase in subjects without apparent vascular lesions, in contrast to only a 13–16% increase in subjects with bilateral vascular lesions (Takeuchi et al. 1997). This noninvasive method without any blood sampling is easy to use and is helpful to detect regional abnormalities of hemodynamic reserve in cerebrovascular diseases.

3.3 Clinical Application

3.3.1 Cerebrovascular Diseases

Many investigators have used quantitative assessment of gCBF and rCBF using ^{99m}Tc-labeled tracers to aid therapy planning in patients with cerebrovascular

diseases. Automatic estimation of rCBF has been often performed by a three-dimensional stereotaxic ROI template on anatomically standardized SPECT mages (Takeuchi et al. 2002).

In acute cerebral ischemia, affected tissue inevitably develops infarction unless early recovery of cerebral blood flow is achieved. Shimosegawa et al. (1994) reported predictability of complete infarction within 6 h of onset using semi-quantitative analysis of brain perfusion SPECT. Intravenous thrombolysis with recombinant tissue plasminogen activator or endovascular recanalization has been attempted for acute hemispheric ischemic stroke, but the problem of symptomatic intracerebral hemorrhage has been recognized. When thrombolytic therapy is considered, it is important to identify patients who are at increased risk of hemorrhagic transformation. Umemura et al. (2000) demonstrated that the regions where residual rCBF ranged from 25 to 35 ml/100 g/min could be recovered by early recanalization within 7 h after onset. However, the regions where residual rCBF was severely decreased to less than 20 ml/100 g/min were at risk of hemorrhagic transformation, and the use of thrombolytic or anticoagulation agents would be likely to promote the development of serious hemorrhage. On the other hand, the presence of hyperperfusion on brain perfusion SPECT 1 hour after thrombolysis using tissue plasminogen activator was predictive of symptom improvement in the first 24-h period (Abumiya et al. 2014).

Garai et al. (2002) observed no effect of acetazolamide provocation on gCBF in patients awaiting carotid endarterectomy with severe stenosis of the internal carotid artery on at least one side, indicating a lack of cerebrovascular reserve capacity. On the other hand, migraine patients showed a significant increase of over 20% in gCBF after acetazolamide provocation.

Hyperperfusion syndrome is a critical complication after carotid endarterectomy and carotid artery stenting. Once an intracerebral hemorrhage occurs, serious morbidity or mortality may ensue. It is important, therefore, to estimate in advance whether candidates for elective carotid artery stenting are at higher risk of hyperperfusion syndrome following stenting. Fujimoto et al. (2004) and Iwata et al. (2011) identified decreased cerebral vasoreactivity in the affected middle cerebral artery territory measured using pre- and post-acetazolamide challenge SPECT as a good predictor of hyperperfusion syndrome after surgery. Moreover pre- and post-acetazolamide challenge SPECT was also effective for narrowing down patients at high risk of hemodynamic ischemic stroke during cardiac surgery (Imasaka et al. 2015).

The balloon occlusion test of the unilateral internal carotid artery has been used to predict whether the patient can tolerate either temporary or permanent occlusion of the internal carotid artery. Ratio of rCBF during balloon occlusion over that at baseline well correlated with mean stump pressure of the internal carotid artery (Torigai et al. 2013). In contrast asymmetry index of rCBF during balloon occlusion did not correlate with mean stump pressure. These results suggest that dual rCBF measurements during balloon occlusion and at baseline are able to detect cerebral collateral-flow redistribution more accurately than asymmetry index alone during balloon occlusion.

For secondary prevention of stroke, blood pressure should be carefully controlled in hypertensive stroke patients with carotid artery occlusive diseases. Some conventional antihypertensive medications lower CBF and worsen outcome after acute ischemic stroke, probably as a result of reduced cerebral perfusion within and adjacent to the affected area. Walters et al. (2001) and Nazir et al. (2004, 2005) investigated the effect of the angiotensin-converting enzyme inhibitor, perindopril, or angiotensin II receptor antagonist, losartan, on gCBF using ^{99m}Tc-HMPAO. They found that both perindopril and losartan lowered blood pressure without lowering gCBF. rCBF measurements were also elucidative of preventive mechanism of calcium channel blocker, lomerizine, for migraine (Ikeda et al. 2018). Lomerizine treatment increased rCBF in an elderly migraineur by approximately 20%.

Ischemic stroke is a common cause of morbidity and mortality in cocaine addicts. Johnson et al. (1998b) demonstrated dose-dependent cocaine-induced reductions of gCBF and rCBF in dopamine-rich areas. This cocaine-induced ischemia was prevented by the L-type calcium channel antagonist, isradipine pretreatment (Johnson et al. 1998a).

Diabetes mellitus considerably increases the risk of stroke due to cerebral artery damage. Macrovascular complications are typically seen in type 2 diabetes mellitus, while cerebral microvascular injury can be detected in both types 1 and 2. Hyperglycemia leads to structural damage of capillaries and endothelial dysfunction, and the permeability of the blood-brain barrier is also altered in diabetics. Káplár et al. (2009) investigated whether there was any difference of gCBF in the effects of these two types of diabetes mellitus. They found that both baseline and acetazolamide challenged gCBF were significantly lower in type 2 than in type 1 patients. Regionally the circulation of the frontal lobe is particularly damaged in type 2 patients. These findings call attention to the necessity of a "holistic view" of treatment, including lifestyle modifications to preserve CBF and reduce disease progression.

There has been striking improvement in the survival of patients with acute cerebrovascular disease in recent years. There has therefore been increased interest in the social rehabilitation of these patients and in their functional outcome. Accordingly, attempts have been made to predict in advance the social rehabilitation, functional outcome, and independence of cerebrovascular disease patients who have survived the acute phase of the disease. Tamamoto et al. (2000) focused on the relationship between rehabilitative efficacy evaluated by the Barthel index score and CBF. They found that global CBF before the start of rehabilitation tended to be more correlated with the Barthel Index scores after rehabilitation than those before rehabilitation. Regionally the strongest correlation was found between the rCBF of the frontal lobe and the Barthel index score after rehabilitation. rCBF measures of the frontal lobe may be helpful for prediction of the efficacy of rehabilitation and drawing up the rehabilitation protocol for each individual patient.

3.3.2 Heart Failure

Identifying predictors of survival in patients with systolic heart failure is an area of intense investigation. Kim et al. (2012) proposed measures of gCBF using radionuclide angiography of ^{99m}Tc-ECD as a good predictor. They reported that patients with global CBF less than 35.4 ml/100 g/min were at increased risk of death or urgent heart transplantation. Brain circulation is characterized by the autoregulation of blood flow over a wide range of perfusion pressures. Compensatory mechanisms exist that maintain perfusion to vital organs, such as the brain in response to the progressive reduction of cardiac output. However brain perfusion is reversibly decreased, and cognitive dysfunction develops in the advanced stages of systolic heart failure despite these compensatory mechanisms. This CBF decrease may result from a neurohormonal response to maintain cardiac output and systemic hemodynamics. In patients with heart failure, the activity of the sympathetic and renin-angiotensin systems becomes exaggerated. This heightened neurohormonal system activity in patients with advanced heart failure may increase vascular resistance and contribute to the reduction of CBF (Choi et al. 2006). Angiotensin-converting enzyme inhibitors and angiotensin II receptor agonists have been shown to increase gCBF measured using ^{99m}Tc-HMPAO (Kamishirado et al. 1997) and prevent cognitive impairment in patients with heart failure.

3.3.3 Idiopathic Normal Pressure Hydrocephalus

The diagnosis of idiopathic normal pressure hydrocephalus as a contributing cause of dementia is difficult in patients with dementia of mixed origins, for example, normal pressure hydrocephalus associated with multi-infarct dementia or Alzheimer's disease. Correction of the hydrocephalic process should improve morbidity and achieve the best outcome for such patients. However, the usefulness of cerebrospinal fluid shunting is unclear because the resultant ventricular dilatation is difficult to relate to a true hydrocephalic process, and the degree to which hydrocephalus contributes to the neurological deficits is uncertain. Chang et al. (2009) investigated gCBF and cerebrovascular reactivity to acetazolamide in 162 patients with a proposed diagnosis of idiopathic normal pressure hydrocephalus. Preoperative gCBF did not differ between responders and non-responders to shunt placement. On the other hand responders showed lower preoperative cerebrovascular reactivity than non-responders. Responders with the complete triad of normal pressure hydrocephalus had significantly lower preoperative gCBF and cerebrovascular reactivity than those with the incomplete triad. Postoperative gCBF and cerebrovascular reactivity increased significantly in responders. Impairment of cerebrovascular reactivity in responders is probably due to compression of small-caliber vessels by increased water content and high tissue pressure in the periventricular white matter resulting from increased bulk diffusion of cerebrospinal fluid flow through the brain interstitium.

3.3.4 Neurodegenerative Disorders

Global CBF in patients with Parkinson's disease has been reported to be lower than that in normal controls by several investigators. Imon et al. (1999) reported gCBF decreases of 11% and 20% in patients with Hoehn and Yahr stage I and II disease and stage III and IV disease respectively as compared with healthy controls. This decrease may result from vasoconstriction due to loss of dopaminergic innervation of blood vessels more prominently in advanced Parkinson's disease. Medication-induced hallucination in Parkinson's disease has been reported to be associated with rCBF reduction particularly in left temporal areas (Okada et al. 1999). Dementia with Lewy bodies showed decreased rCBF in occipital lobes in 76% of patients, possibly related to visual hallucination (Tateno et al. 2008). In the recent diagnostic criteria for dementia with Lewy bodies (McKeith et al. 2017), "generalized low uptake on SPECT/PET perfusion/metabolism scan with reduced occipital activity +/− the cingulate island sign on FDG-PET imaging" was listed as one of three supportive biomarkers. Imabayashi et al. (2016) reported a 7% decrease of gCBF in patients with dementia with Lewy bodies as compared with those with Alzheimer's disease.

The clinical differential diagnosis between Parkinson's disease, Parkinson variant of multiple system atrophy, and progressive supranuclear palsy is often difficult in the early stages of the disease because of the similarity of symptoms and the lack of diagnostic markers. Kimura et al. (2011) demonstrated rCBF reduction in the anterior cingulate gyrus and thalamus in progressive supranuclear palsy and rCBF reduction in the cerebellum in multiple system atrophy. These rCBF changes may be helpful for the differential diagnosis of Parkinsonian syndrome. Quantification of rCBF in patients with corticobasal degeneration has revealed widespread rCBF decrease in the frontal, parietal, and temporal cortices, basal ganglia, thalamus, pons, and cerebellum (Hossain et al. 2003).

Spinocerebellar ataxia type 6 is an autosomal dominant cerebellar ataxia caused by CAG trinucleotide expansion. This disease causes rCBF decrease only in the cerebellum. This rCBF decrease is associated with both the duration of illness and severity of dysarthria (Honjo et al. 2004). The efficacy of transcranial magnetic stimulation on rCBF has been investigated in patients with inherited spinocerebellar degeneration. Shiga et al. (2002) found a significant alleviation of truncal ataxia in patients after 3 weeks of active transcranial magnetic stimulation. rCBF showed 11% and 15% increases selectively in cerebellum and pons, respectively. In patients with autoimmune cerebellar ataxia, intravenous immunoglobulin therapy has been reported to alleviate the ataxia with rCBF increase in cerebellum (Nanri et al. 2009).

Kogure et al. (2000) reported a 9% decrease of gCBF in patients with early Alzheimer's disease as compared with healthy controls. Longitudinal rCBF reductions in Alzheimer's disease were more prominent in parieto-temporal areas than in other areas (Kimura et al. 2012). Parietal rCBF along with posterior volume of white matter hyperintensity on MRI negatively correlated with cognitive function (Tabei et al. 2017).

White matter lesions were associated with decreased rCBF in frontal, parietal, and medial temporal lobes in patients with mild cognitive impairment (Ishibashi et al. 2018).

3.3.5 Mood Disorders

A circuit that connects the limbic system, thalamus, and prefrontal cortex is proposed as a neuroanatomical model that plays an important role for the regulation of mood. Depression may cause frontal dysfunction that can be evaluated using SPECT as frontal hypoperfusion (Narita et al. 2004). Iidaka et al. (1997) demonstrated significant negative correlations between the Hamilton scale for depression and rCBF in the bilateral lower frontal cortex in patients with mood disorder. Ohgami et al. (2005) reported an increase of gCBF in remission from that in depressive state in patients with major depression. Significant negative correlations were seen between gCBF and duration of previous episode of depression.

3.3.6 Other Neuropsychiatric Diseases

Noninvasive gCBF and rCBF quantification using ^{99m}Tc-labeled tracers has been applied to various other neuropsychiatric diseases. Patients with chronic pain showed rCBF decrease in bilateral thalami (Nakabeppu et al. 2001). rCBF reduction is frequently observed in patients with traumatic brain injury, which is related to symptoms in the absence of other objective findings, such as post-traumatic amnesia, vertigo or personality changes (Kinuya et al. 2004: Hofman et al. 2001). Patients with neuropsychiatric systemic lupus erythematosus showed lower gCBF than non-neuropsychiatric patients (Tatsukawa et al. 2005). This result supports the contention that the pathophysiology underlying neuropsychiatric systemic lupus erythematosus is related to microvascular damage, small vessel vasculopathy, and autoantibody-mediated neuronal cell injury. Suzuki et al. (2010) reported rCBF decrease in the limbic system in chronic alcoholic patients. This decrease may be related to the occurrence of memory impairment, emotional disorders, and blackouts attributable to alcohol consumption. Right-side dominant rCBF asymmetry was reported in patients with oral cenesthopathy (Umezaki et al. 2013). This asymmetry in oral cenesthopathy disappeared after modified electroconvulsive therapy (Uezato et al. 2012).

3.4 Conclusion

Routine quantification of gCBF measured using a short period of radionuclide angiography of ^{99m}Tc-labeled tracers is a simple and reproducible method, which can be easily added to the standard brain perfusion SPECT without additional cost or increase in the patient's radiation burden. Combined with rCBF quantification

it provides an additional tool for the management of acute and chronic cerebrovascular diseases and for the early and differential diagnosis of various neuropsychiatric diseases and serves as a tool for the objective evaluation of therapeutic effects.

References

Abumiya T, Katoh M, Moriwaki T et al (2014) Utility of early post-treatment single-photon emission computed tomography imaging to predict outcome in stroke patients treated with intravenous tissue plasminogen activator. J Stroke Cerebrovasc Dis 23:896–901

Andersen AR, Friberg HH, Schmidt JF et al (1988) Quantitative measurements of cerebral blood flow using SPECT and [^{99m}Tc]-d,l-HM-PAO compared to xenon-133. J Cereb Blood Flow Metab 8:S69–S81

Chang C-C, Asada H, Mimura T et al (2009) A prospective study of cerebral blood flow and cerebrovascular reactivity to acetazolamide in 162 patients with idiopathic normal-pressure hydrocephalus: clinical article. J Neurosurg 111:610–617

Choi BR, Kim JS, Yang YJ et al (2006) Factors associated with decreased cerebral blood flow in congestive heart failure secondary to idiopathic dilated cardiomyopathy. Am J Cardiol 97:1365–1369

Friberg L, Andersen AR, Lassen NA et al (1994) Retention of ^{99m}Tc-bicisate in the human brain after intracarotid injection. J Cereb Blood Flow Metab 14(Suppl 1):S19–S27

Fujimoto S, Toyoda K, Inoue T et al (2004) Diagnostic impact of transcranial color-coded real-time sonography with echo contrast agents for hyperperfusion syndrome after carotid endarterectomy. Stroke 35:1852–1856

Garai I, Varga J, Szomj E et al (2002) Quantitative assessment of blood flow reserve using ^{99m}Tc-HMPAO in carotid stenosis. Eur J Nucl Med 29:216–220

Groiselle C, Rocchisani J-M, Moretti J-L (2000) Improving the measurement of the ^{99}Tc^{m}-ECD brain perfusion index by temporal analysis. Nucl Med Commun 21:811–816

Hofman PAM, Stapert SZ, Van Kroonenburgh MJ et al (2001) MR imaging, single-photon emission CT, and neurocognitive performance after mild traumatic brain injury. AJNR Am J Neuroradiol 22:441–449

Honjo K, Ohshita T, Kawakami H et al (2004) Quantitative assessment of cerebral blood flow in genetically confirmed spinocerebellar ataxia type 6. Arch Neurol 61:933–937

Hossain AKMM, Murata Y, Zhang L et al (2003) Brain perfusion SPECT in patients with corticobasal degeneration: analysis using statistical parametric mapping. Mov Disord 18:697–703

Iida H, Itoh H, Nakazawa M et al (1994) Quantitative mapping of regional cerebral blood flow using iodine-123-IMP and SPECT. J Nucl Med 35:2019–2030

Iidaka T, Nakajima T, Suzuki Y et al (1997) Quantitative regional cerebral blood flow measured by Tc-99m HMPAO SPECT in mood disorder. Psychiatry Res 68:143–154

Ikeda K, Aoyagi J, Hanashiro S et al (2018) Preventive treatment with lomerizine increases cerebral blood flows during the interictal phase of migraine. J Stroke Cerebrovasc Dis 27:998–1002

Imabayashi E, Yokoyama K, Tsukamoto T et al (2016) The cingulate island sign within early Alzheimer's disease-specific hypoperfusion volumes of interest is useful for differentiating Alzheimer's disease from dementia with Lewy bodies. EJNMMI Res 6:67

Imasaka K, Yasaka M, Tayama E et al (2015) Obstructive carotid and/or intracranial artery disease rarely affects the incidence of haemodynamic ischaemic stroke during cardiac surgery: a study on brain perfusion single-photon emission computed tomography with acetazolamide. Eur J Cardiothorac Surg 48:739–746

Imon Y, Matsuda H, Ogawa M et al (1999) SPECT image analysis using statistical parametric mapping in patients with Parkinson's disease. J Nucl Med 40:1583–1589

Inoue Y, Momose T, Ohtake T et al (1997) Effect of deadtime loss on quantitative measurement of cerebral blood flow with technetium-99m hexamethylpropylene amine oxime. Eur J Nucl Med 24:1418–1421

Ishibashi M, Kimura N, Aso Y et al (2018) Effects of white matter lesions on brain perfusion in patients with mild cognitive impairment. Clin Neurol Neurosurg 168:7–11

Iwata T, Mori T, Tajiri H et al (2011) Predictors of hyperperfusion syndrome before and immediately after carotid artery stenting in single-photon emission computed tomography and transcranial color-coded real-time sonography studies. Neurosurgery 68:649–655

Johnson B, Barron B, Fang B et al (1998a) Isradipine prevents global and regional cocaine-induced changes in brain blood flow: a preliminary study. Psychopharmacology 136:335–341

Johnson B, Lamki L, Fang B et al (1998b) Demonstration of dose-dependent global and regional cocaine-induced reductions in brain blood flow using a novel approach to quantitative single photon emission computerized tomography. Neuropsychopharmacology 18:377–384

Kamishirado H, Inoue T, Fujito T et al (1997) Effect of enalapril maleate on cerebral blood flow in patients with chronic heart failure. Angiology 48:707–713

Káplár M, Paragh G, Erdei A et al (2009) Changes in cerebral blood flow detected by SPECT in type 1 and type 2 diabetic patients. J Nucl Med 50:1993–1998

Kim M-S, Kim J-S, Yun S-C et al (2012) Association of cerebral blood flow with the development of cardiac death or urgent heart transplantation in patients with systolic heart failure. Eur Heart J 33:354–362

Kimura N, Hanaki S, Masuda T et al (2011) Brain perfusion differences in parkinsonian disorders. Mov Disord 26:2530–2537

Kimura N, Kumamoto T, Masuda T et al (2012) Evaluation of the regional cerebral blood flow changes during long-term donepezil therapy in patients with Alzheimer's disease using 3DSRT. J Neuroimaging 22:299–304

Kinuya K, Kakuda K, Nobata K et al (2004) Role of brain perfusion single-photon emission tomography in traumatic head injury. Nucl Med Commun 25:333–337

Kogure D, Matsuda H, Ohnishi T et al (2000) Longitudinal evaluation of early Alzheimer's disease using brain perfusion SPECT. J Nucl Med 41:1155–1162

Lassen NA, Andersen AR, Friberg L et al (1988) The retention of [^{99m}Tc]-d,l-HM-PAO in the human brain after intracarotid bolus injection: a kinetic analysis. J Cereb Blood Flow Metab 8:S13–S22

Latchaw RE, Yonas H, Hunter GJ et al (2003) Guidelines and recommendations for perfusion imaging in cerebral ischemia: a scientific statement for healthcare professionals by the Writing Group on Perfusion Imaging, from the Council on Cardiovascular Radiology of the American Heart Association. Stroke 34:1084–1104

Masunaga Y, Uchiyama Y, Ofuji A et al (2014) Development of an automatic ROI setting program for input function determination in ^{99m}Tc-ECD non-invasive cerebral blood flow quantification. Phys Med 30:513–520

Matsuda H, Tsuji S, Shuke N et al (1992) A quantitative approach to technetium-99m hexamethylpropylene amine oxime. Eur J Nucl Med 19:195–200

Matsuda H, Tsuji S, Shuke N et al (1993) Noninvasive measurements of regional cerebral blood flow using technetium-99m hexamethylpropylene amine oxime. Eur J Nucl Med 20:391–401

Matsuda H, Yagishita A, Tsuji S et al (1995) A quantitative approach to technetium-99m ethyl cysteinate dimer: a comparison with technetium-99m hexamethylpropylene amine oxime. Eur J Nucl Med 22:633–637

McKeith IG, Boeve BF, Dickson DW et al (2017) Diagnosis and management of dementia with Lewy bodies: fourth consensus report of the DLBConsortium. Neurology 89:88–100

Murase K, Inoue T, Fujioka H et al (1999) An alternative approach to estimation of the brain perfusion index for measurement of cerebral blood flow using technetium-99m compounds. Eur J Nucl Med 26:1333–1339

Murase K, Fujioka H, Inoue T et al (2001) Reproducibility of the brain perfusion index for measuring cerebral blood flow using technetium-99m compounds. Eur J Nucl Med 28:1640–1646

Nakabeppu Y, Nakajo M, Gushiken T et al (2001) Decreased perfusion of the bilateral thalami in patients with chronic pain detected by Tc-99m-ECD SPECT with statistical parametric mapping. Ann Nucl Med 15:459–463

Nanri K, Okita M, Takeguchi M et al (2009) Intravenous immunoglobulin therapy for autoantibody-positive cerebellar ataxia. Intern Med 48:783–790

Narita H, Odawara T, Iseki E et al (2004) Psychomotor retardation correlates with frontal hypoperfusion and the modified Stroop test in patients with major depression under 60-years-old. Psychiatry Clin Neurosci 58:389–395

Nazir FS, Overell JR, Bolster A et al (2004) The effect of losartan on global and focal cerebral perfusion and on renal function in hypertensives in mild early ischaemic stroke. J Hypertens 22:989–995

Nazir FS, Overell JR, Bolster A et al (2005) Effect of perindopril on cerebral and renal perfusion on normotensives in mild early ischaemic stroke: a randomized controlled trial. Cerebrovasc Dis 19:77–83

Ohgami H, Nagayama H, Akiyoshi J et al (2005) Contributing factors to changes of cerebral blood flow in major depressive disorder. J Affect Disord 87:57–63

Okada K, Suyama N, Oguro H et al (1999) Medication-induced hallucination and cerebral blood flow in Pfarkinson's disease. J Neurol 246:365–368

Patlak CS, Blasberg RG, Fenstermacher JD (1983) Graphical evaluation of blood-to-brain transfer constants from multiple-time uptake data. J Cereb Blood Flow Metab 3:1–7

Patlak CS, Blasberg RG (1985) Graphical evaluation of blood-to-brain transfer constants from multiple-time uptake data. Generalizations. J Cereb Blood Flow Metab 5:584–590

Shiga Y, Tsuda T, Itoyama Y et al (2002) Transcranial magnetic stimulation alleviates truncal ataxia in spinocerebellar degeneration. J Neurol Neurosurg Psychiatry 72:124–126

Shimosegawa E, Hatazawa J, Inugami A et al (1994) Cerebral infarction within six hours of onset: prediction of completed infarction with technetium-99m-HMPAO SPECT. J Nucl Med 35:1097–1103

Suzuki Y, Oishi M, Ogawa K et al (2010) Atrophy of the parahippocampal gyrus and regional cerebral blood flow in the limbic system in chronic alcoholic patients. Alcohol 44:439–445

Tabei KI, Kida H, Hosoya T et al (2017) Prediction of cognitive decline from white matter hyperintensity and single-photon emission computed tomography in Alzheimer's disease. Front Neurol 8:408

Takasawa M, Murase K, Oku N et al (2002) Assessment of acetazolamide reactivity in cerebral blood flow using spectral analysis and technetium-99m hexamethylpropylene amine oxime. J Cereb Blood Flow Metab 22:1004–1009

Takasawa M, Murase K, Oku N et al (2003) Interobserver variability of cerebral blood flow measurements obtained using spectral analysis and technetium-99m labeled compounds. Ann Nucl Med 17:255–259

Takasawa M, Murase K, Oku N et al (2004) Spectral analysis of ^{99m}Tc-HMPAO, for estimating cerebral blood flow: a comparison with H_2 ^{15}O PET. Ann Nucl Med 18:243–249

Takeuchi R, Matsuda H, Yonekura Y et al (1997) Noninvasive quantitative measurements of regional cerebral blood flow using technetium-99m-L,L-ECD SPECT activated with acetazolamide: quantification analysis by equal-volume-split ^{99m}Tc-ECD consecutive SPECT method. J Cereb Blood Flow Metab 17:1020–1032

Takeuchi R, Yonekura Y, Matsuda H et al (2002) Usefulness of a three-dimensional stereotaxic ROI template on anatomically standardised ^{99m}Tc-ECD SPET. Eur J Nucl Med Mol Imaging 29:331–341

Tamamoto F, Sumi Y, Nakanishi A et al (2000) Usefulness of cerebral blood flow (CBF) measurements to predict the functional outcome for rehabilitation in patients with cerebrovascular disease (CVD). Ann Nucl Med 14:47–52

Tateno M, Kobayashi S, Shirasaka T et al (2008) Comparison of the usefulness of brain perfusion SPECT and MIBG myocardial scintigraphy for the diagnosis of dementia with Lewy bodies. Dement Geriatr Cogn Disord 26:453–457

Tatsukawa H, Ishii K, Haranaka M et al (2005) Evaluation of average amount of cerebral blood flow measured by brain perfusion index in patients with neuropsychiatric systemic lupus erythematosus. Lupus 14:445–449

Torigai T, Mase M, Ohno T et al (2013) Usefulness of dual and fully automated measurements of cerebral blood flow during balloon occlusion test of the internal carotid artery. J Stroke Cerebrovasc Dis 22:197–204

Uezato A, Yamamoto N, Kurumaji A et al (2012) Improvement of asymmetrical temporal blood flow in refractory oral somatic delusion after successful electroconvulsive therapy. J ECT 28:50–51

Umemura A, Suzuka T, Yamada K (2000) Quantitative measurement of cerebral blood flow by ^{99m}Tc-HMPAO SPECT in acute ischaemic stroke: usefulness in determining therapeutic options. J Neurol Neurosurg Psychiatry 69:472–478

Umezaki Y, Katagiri A, Watanabe M et al (2013) Brain perfusion asymmetry in patients with oral somatic delusions. Eur Arch Psychiatry Clin Neurosci 263:315–323

Van Laere K, Van de Wiele C, Van Belle Y, et al (1999) Variability study of a non-invasive approach to the absolute quantification of cerebral blood flow with ^{99m}Tc-ECD using aortic activity as the arterial input estimate. Nucl Med Commun 20:33–40

Van Laere K, Dumont F, Koole M et al (2001) Non-invasive methods for absolute cerebral blood flow measurement using ^{99m}Tc-ECD: a study in healthy volunteers. Eur J Nucl Med 28:862–872

Walters MR, Bolster A, Dyker AG et al (2001) Effect of perindopril on cerebral and renal perfusion in stroke patients with carotid disease. Stroke 32:473–478

Zaknun JJ, Leblhuber F, Schktanz H (2008) Value of cerebral blood flow quantification in the diagnosis of dementia. Nucl Med Commun 29:260–269

From Positron to Pattern: A Conceptual and Practical Overview of ^{18}F-FDG PET Imaging and Spatial Covariance Analysis

4

Sanne K. Meles, Jelmer G. Kok, Remco J. Renken, and Klaus L. Leenders

Contents

4.1 ^{18}F-FDG PET Imaging 74
4.1.1 Basic Concepts in PET 74
4.1.2 ^{18}F-FDG PET Imaging 77
4.1.3 Studying Brain Function with ^{18}F-FDG PET 79
4.2 Analysis of Resting-State ^{18}F-FDG PET Images 80
4.2.1 Image Registration 80
4.2.2 Normalization 81
4.2.3 Analysis of Variance and Covariance 83
4.2.4 Principal Component Analysis 84
4.3 SSM PCA 87
4.3.1 Defining the Data 87
4.3.2 Normalization with the Scaled Subprofile Model (SSM) 87
4.3.3 Calculating Eigenvectors from a Covariance Matrix 88
4.3.4 Calculating Subject Scores and Selecting Disease-Related Components 89
4.3.5 Prospective Application of the Pattern 91
4.3.6 Validation 91
4.3.7 Visualization and Interpretation of PC Maps 92
4.3.8 Advantages of SSM PCA Over Univariate SPM Models 94

S. K. Meles (✉)
Department of Neurology, University of Groningen, University Medical Center Groningen, Groningen, The Netherlands
e-mail: s.k.meles@umcg.nl

J. G. Kok · R. J. Renken
Neuroimaging Center, Department of Neuroscience, University of Groningen, University Medical Center Groningen, Groningen, The Netherlands
e-mail: j.g.kok02@umcg.nl; r.j.renken@umcg.nl

K. L. Leenders
Department of Nuclear Medicine and Molecular Imaging, University of Groningen, University Medical Center Groningen, Groningen, The Netherlands
e-mail: k.l.leenders@umcg.nl

R. A. J. O. Dierckx et al. (eds.), *PET and SPECT in Neurology*,
https://doi.org/10.1007/978-3-030-53168-3_4

Appendix: Effects of Normalization..... 95
Global Mean Normalization..... 96
Log Transformation and Demean in the SSM..... 97
Practical Examples..... 97
References..... 101

Abstract

Imaging of brain glucose metabolism with ^{18}F-2-fluoro-2-deoxy-D-glucose positron emission tomography (^{18}F-FDG PET) can give important information regarding disease-related changes in underlying neuronal systems, when combined with appropriate analytical methods. One such method is the scaled subprofile model combined with principal component analysis (SSM PCA). This model takes into account the relationships (covariance) between voxels to identify disease-related patterns. By quantifying disease-related pattern expression on a scan-by-scan basis, this technique allows objective assessment of disease activity in individual subjects. This chapter provides an overview of steps involved in pattern identification in ^{18}F-FDG PET data and is divided into three sections. Section 1 introduces basic concepts in nuclear imaging and explores the cellular underpinnings of signals measured with ^{18}F-FDG PET. Section 2 describes relevant basic concepts in ^{18}F-FDG PET image analysis including anatomical registration, normalization, and analysis of variance and covariance. Section 3 is dedicated to SSM PCA specifically. The goal of this chapter is to make the technique more accessible to readers without a mathematics or neuroimaging background. Although many excellent texts on this topic exist, the current chapter aims to provide a more conceptual overview, including some discussion points that are not always formally described in literature.

4.1 ^{18}F-FDG PET Imaging

4.1.1 Basic Concepts in PET

Positron emission tomography (PET) allows measurement of the local tissue accumulations of injected radioactive tracers. The type of tracer that is used depends on the focus of the PET study. For instance, tracers can bind to specific receptor sites, allowing quantification of the distribution of a receptor in a tissue. Tracers can also be metabolically active compounds and allow measurement of the activity of a particular enzyme or biochemical pathway. Tracers are "tagged" with a radioactive atom. Radioactive decay of this atom is central to PET technology. A simplified explanation of radioactive decay necessary to understand PET technology is provided in the next paragraphs.

Atoms consist of protons, neutrons, and electrons. Protons and neutrons can be found in the nucleus, whereas electrons orbit around the nucleus. Protons have a

positive charge, and electrons are negatively charged. The number of protons determines to what chemical element the atom belongs. Elements can have multiple isotopes. Isotopes of an element have the same number of protons in their nucleus, but a variable number of neutrons. In order for a nucleus to be stable, a certain balance is needed between protons and neutrons in the nucleus. Most naturally occurring isotopes have stable nuclei. Isotopes of an element with an unstable nucleus are referred to as radioisotopes. These isotopes will spontaneously emit particles or photons (or both) from its nucleus in order to regain stability. In this process, mass is converted into energy. This is called radioactive decay.

Different modes of radioactive decay exist. PET is designed to measure positron emission. In radioactive decay by positron emission, a proton in the nucleus is transformed into a neutron and a positron. A positron is the antiparticle of an electron (i.e., a positively charged electron, also called a β+ particle). When a positron is emitted, it travels a distance before it annihilates with an electron (a β− particle) from the surrounding matter. The annihilation of the masses of the two β particles results in the conversion and emission of two gamma (γ) rays. Gamma rays consist of high-energy photons. In the case of positron emission and annihilation, each γ-ray contains 511 keV in energy. These two γ-rays always originate simultaneously and are emitted in opposite directions. They form a so-called back-to-back pair (Fig. 4.1a).

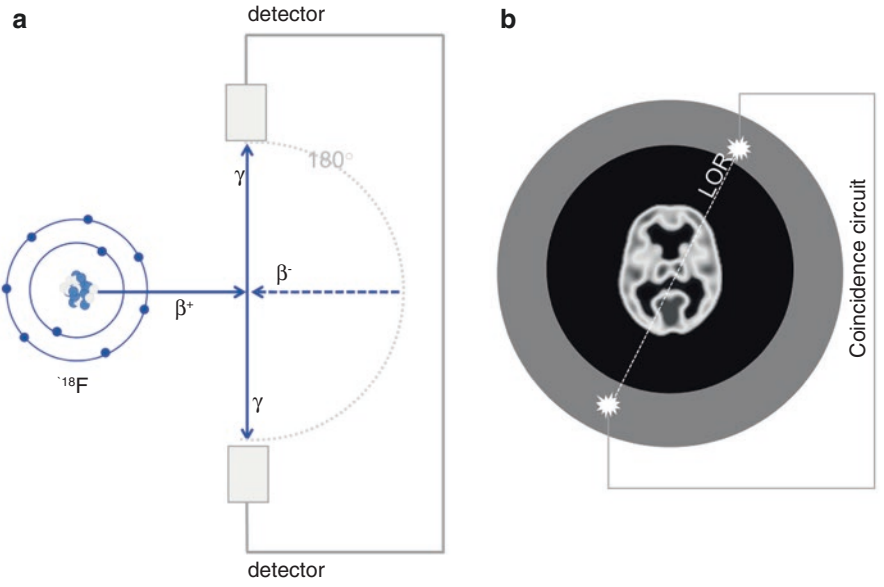

Fig. 4.1 Schematic of an annihilation event in positron emission (**a**) and its detection (**b**). (**a**)The positron travels a short distance before it loses its kinetic energy and then annihilates with an electron (β^-) from the surrounding matter. The mass of the two particles is converted into two opposing photon beams (γ-rays), traveling at approximately 180° from each other with an energy of 511 keV each. (**b**) In a PET camera, a ring of detectors is placed around the patient. Opposing detectors, connected via a coincidence circuit, record annihilation photons only when they arrive simultaneously. The origin of the annihilation event is inferred along the line of response (LOR)

A PET camera consists of a large number of small scintillation detectors positioned on a ring around the patient. Scintillation detectors use inorganic crystals that absorb γ-rays and then fluoresce. The γ-rays are converted into visible light by the crystal. The light signal is multiplied and transformed into an electric current. The strength of this current is proportional to the intensity of the light from the crystal and thus to the energy of the γ-ray that was detected.

A PET camera can determine the origin of the detected γ-ray in the tissue of the patient, by using the principle of γ-ray pairs. If one γ-ray is detected by a crystal, then its twin must be detected by the opposite crystal within a certain time window (a few nanoseconds). Such an event is called a coincidence event. Opposing crystals are linked via coincidence circuits. From a coincidence event, the origin of the annihilation can be inferred along a "line of response" (LOR) running between the two detectors (Fig. 4.1b). Modern electronics permit measurement of the time interval between detection of the first and the second photon of the same photon pair. This means that the origin of the photon pairs (the point of annihilation) can be pinpointed to a part of the LOR, close to the true event (Karp et al. 2008; Surti and Karp 2016). PET data thus consists of many back-to-back photon pairs, connected with LORs through the patient, from which the locations of the multiple annihilations are estimated. Because the detector system is a stationary ring that completely surrounds the patients, it is possible to acquire data from many different angular views (projections) simultaneously. From these multiple projections of the detected emissions, images can be reconstructed using mathematical algorithms (Cherry et al. 2012). In the final 3D PET image, each pixel (or voxel) has a value which reflects the number of coincidence events ("counts") that belong to that particular coordinate. Thus, the more radioactive decay in a certain part of the tissue, the higher the counts for the corresponding pixel in the image.

The spatial resolution of PET depends on its accuracy and precision in pinpointing the exact location of annihilation events. Even with sophisticated computerized techniques, the reconstructed location of the annihilation event is not exact. Current state-of-the-art PET systems have a maximum resolution of just under 3 mm. This limitation is inherent to physical properties of PET. First, the PET system assumes γ-rays pairs to be emitted at a 180° angle, but this is not always the case. Second, after emission, the positron travels a short distance (a few millimeters (Phelps et al. 1975)) before it annihilates with an electron.

Some commonly used PET tracers in neurology and their half-lives are listed in Table 4.1. Fluorine-18 (^{18}F) is the most commonly used radioisotope in clinical

Table 4.1 Commonly used isotopes in PET

Isotope	Half-life (min)	Product	Examples of tracers
^{11}C	20.38	^{11}B	^{11}C-methionine: amino-acid transport ^{11}C-raclopride: dopamine receptors
^{15}O	2.03	^{15}N	^{15}O-water: perfusion ^{15}O-oxygen: oxygen utilization
^{18}F	109.8	^{18}O	^{18}F-FDG: glucose utilization ^{18}F-Fdopa: activity of aromatic amino-acid decarboxylase

practice. It is produced in a particle accelerator (cyclotron). An important advantage of ^{18}F is its relatively long half-life, which facilitates regional production of ^{18}F tracers and distribution to other hospitals. The main application of ^{18}F is labeling of fluorodeoxyglucose (FDG), which provides a measure of glucose utilization in the cells of the body. ^{18}F-FDG is the most widely used positron-emitting radiopharmaceutical with a wide range of clinical applications.

4.1.2 ^{18}F-FDG PET Imaging

The tracer ^{18}F-2-fluoro-2-deoxy-D-glucose (^{18}F-FDG) is an analogue of glucose. In normal conditions, glucose is the predominant metabolic substrate for brain tissue, and the brain's oxygen consumption is almost entirely for the oxidative metabolism of glucose (Fox et al. 1988). The brain holds minimal glycogen stores, and therefore, a permanent supply of glucose via the blood is necessary. Glucose is transported through the blood-brain barrier via GLUT transporters. Once in the cell, glucose undergoes numerous transformations to end up in three main metabolic pathways. The goal of each of these pathways is to create energy (in the form of ATP) for cells to function. The first step for any of these pathways is the phosphorylation of glucose into glucose-6-phosphate, a reaction catalyzed by the enzyme hexokinase. Hexokinase is the rate-controlling enzyme for all of the subsequent pathways. The enzymatic rate of this first step is equivalent to measuring the glucose utilization rate (Fig. 4.2a).

It has been attempted to quantify regional glucose metabolism with ^{14}C-glucose, but the many transformations and pathways for radioactively labeled glucose to enter are complex, leading to many different metabolites. Moreover, ^{14}C-glucose is very rapidly converted to CO_2 and H_2O, and CO_2 is too rapidly cleared from the cerebral tissue to allow measurement (Raichle et al. 1975; Sacks 1957). In the 1970s, this problem was solved by Sokoloff and colleagues, who applied a deoxyglucose analogue, 2-deoxy-D-glucose (2-DG), labeled with ^{14}C (Sokoloff et al. 1977). The deoxy variant of glucose is phosphorylated by hexokinase, at a definable rate relative to that of glucose. However, unlike glucose-6-phosphate, ^{14}C-2-DG-6-phosphate is not metabolized further and is essentially trapped in the tissue, allowing quantification of hexokinase. Therefore, regional deoxyglucose uptake measured with PET reflects the first step of the glucose metabolic pathway. Reivich et al. were the first to measure cerebral glucose metabolism with the deoxyglucose method in humans (Reivich et al. 1979). Instead of ^{14}C, ^{18}F was used as the radioisotope. ^{18}F-FDG behaves similarly as ^{14}C-DG and glucose (because fluorine behaves biochemically like hydrogen) and can measure glucose utilization accurately and reliably.

The kinetics of accumulation of ^{18}F-FDG-6-PO_4 can be described with a three-compartment model (Reivich et al. 1979). A description of tracer kinetic modeling is beyond the scope of this chapter and can be found elsewhere (Heiss 2014). In brief, after intravenous administration of ^{18}F-FDG, the regional cerebral metabolic rate of glucose (CMRglc) can be determined using the ^{18}F concentration in the tissue (measured with PET), the concentration of ^{18}F-FDG in the arterial plasma

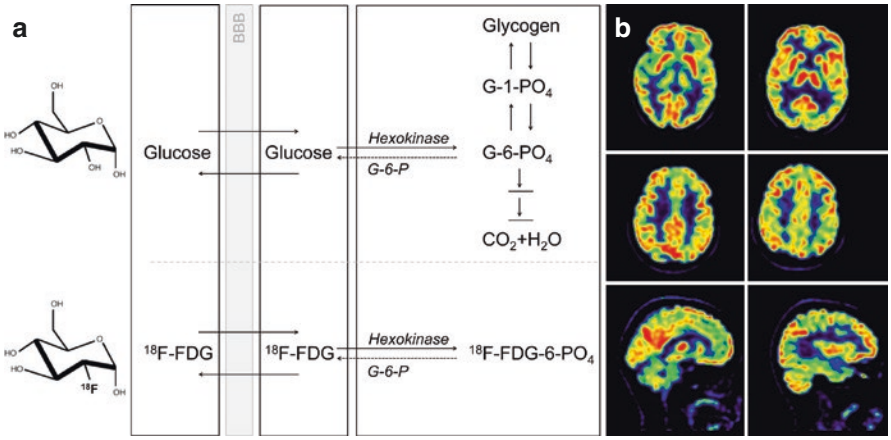

Fig. 4.2 (**a**) Schematic of the behavior of glucose and ^{18}F-FDG in brain tissue. Glucose and ^{18}F-FDG are similarly transported over the blood-brain barrier (BBB) and are both metabolites for the enzyme hexokinase. FDG-6-phosphate (^{18}F-FDG-6-PO_4) is trapped in the brain tissue, whereas glucose-6-phosphate (G-6-PO_4) can be metabolized further and has many metabolites. The dashed arrow represents the activity of glucose-6-phosphatase (G-6-P), which catalyzes the hydrolysis of G-6-PO_4 and ^{18}F-FDG-6-PO_4 back to glucose, and ^{18}F-FDG, respectively. This is a slow process (Sokoloff et al. 1977). (Adapted from (Heiss 2014) with permission from Springer Verlag Heidelberg). (**b**) Visual representation of an ^{18}F-FDG PET study of a 65-year-old healthy individual. The participant fasted for at least 6 h before the investigation. ^{18}F-FDG PET imaging was performed in a 3D mode using a Siemens Biograph mCT-64 PET/CT system. A 6 min static frame was acquired starting 30 min after the injection of 205 MBq ^{18}F-FDG in 4 mL saline. ^{18}F-FDG uptake and image acquisition were performed in the resting state with eyes closed in a dimly lit room with minimal auditory stimulation. The image was iteratively reconstructed with OSEM 3D, including point spread function and time-of-flight modeling (3 iterations/21 subsets, matrix 400), and smoothed with a Gaussian 2 mm full-width at half-maximum filter. Voxel size is 2 mm. Scatter and attenuation corrections were applied based on the acquired low-dose CT

(time-activity curve of blood tracer concentration), and the concentration of glucose in the plasma. In this situation, multiple sequential PET images are obtained (i.e., a dynamic protocol). When performed in this manner, PET provides absolute measures of regional CMRglc (i.e., in physiological units).

Thus, for a fully quantitative determination of *absolute* regional glucose utilization, arterial blood sampling is required, which is an invasive and time-consuming procedure. Already early on it was recognized that "raw counts" data could be analyzed instead of physiological units, obviating the need for arterial blood sampling (Fox et al. 1984). In current clinical practice and most experimental designs, arterial blood sampling is not strictly necessary, because the *relative* regional distribution of ^{18}F-FDG (raw counts) can be visually assessed and/or statistically analyzed.

In a clinical setting, ^{18}F-FDG is injected intravenously, and patients subsequently rest in a quiet, dimly lit room for 30–45 min, at which time metabolic equilibrium is reached. Next, a single static image with a frame duration of 5–15 min is acquired, and a low-dose CT scan is performed for attenuation correction. The corrected, reconstructed ^{18}F-FDG PET images are visually assessed by an expert reader in the context of the available clinical information. When performed according to the

guidelines, ^{18}F-FDG PET imaging in a clinical setting is easy, reliable, and accurate (Varrone et al. 2009). ^{18}F-FDG PET has an established role for a number of diagnostic indications in neurology, one of which is the differential diagnosis of neurodegenerative brain diseases.

An example of an ^{18}F-FDG PET image of a healthy control participant is given in Fig. 4.2b. Resting-state ^{18}F-FDG uptake is much higher in gray matter compared with white matter. In healthy controls, ^{18}F-FDG uptake is typically highest in the basal ganglia, primary visual cortex, cingulate cortex, and frontal cortex, with lower values in other cortical and subcortical areas, brain stem, and cerebellum (Heiss 2014).

4.1.3 Studying Brain Function with ^{18}F-FDG PET

The goal of neuroimaging is to understand how the brain functions under different circumstances and conditions, including disease. In the past decade, the focus of neuroimaging studies has converged on the study of brain networks (Friston 2011). Networks encompass connections between neurons and can be described in terms of structure and function. Structure dictates which neurons are connected. Function is dynamic, and this term is used to describe neuronal activity that assembles on the backbone of a relatively fixed anatomical structure (Buzsaki et al. 2013). A synapse may be present between two neurons, but the connection may be used to different degrees depending on the situation (Fornito et al. 2016). The main principle of functional neuroimaging techniques is that localized changes in neuronal activity can be mapped by measuring changes in energy metabolism or hemodynamics, which are thought to reflect the underlying cellular events.

Brain activity is determined by signaling between neurons. Neural signaling is achieved with the generation and propagation of action potentials across synapses. Energy metabolism (glucose metabolism) increases almost linearly with the frequency of action potentials (Kadekaro et al. 1985). Action potentials themselves do not require energy, as they are passive electrical consequences of K^+ and Na^+ fluxes across the cell membrane upon depolarization. Restoring ionic gradients and resting membrane potentials in the cell after an action potential does require energy. In primates, the major energetic burden is located at the nerve terminals from the postsynaptic neuron (the neuropil) (Sokoloff 1993). This is because there are a large number of synapses per neuron, and during signaling, postsynaptic passive Na^+ influx acts as an amplifier of the initial signal. Reversing ion fluxes after postsynaptic currents has been estimated to cost 74% of the energy used in signaling (Attwell and Laughlin 2001). Of note, energy metabolism in the postsynaptic neuron increases with both excitatory (glutamatergic) and inhibitory (GABA-ergic) signaling (Buzsaki et al. 2007; Jueptner and Weiller 1995). The only way to determine which has occurred is to look downstream at the next synapses in the projection zones of those neurons (Sokoloff 1993).

To sustain brain activity, neurons continuously require energy in the form of adenosine triphosphate (ATP). Under normal physiological conditions, generation of ATP is supported almost exclusively by the oxidative (i.e., aerobic) metabolism

of glucose. Only around 10% of ATP is generated by anaerobic metabolism through glycolysis (Vaishnavi et al. 2010). The products of glycolysis, such as lactate, can subsequently be metabolized further using oxygen. Astroglia are thought to play an important role in the latter process, in which lactate is also exchanged between neurons and glia cells (Magistretti and Allaman 2015).

Glucose and oxygen supplies are maintained by an adequate regulation of cerebral blood flow (CBF). The relationship of the cerebral metabolic rate of glucose (CMRglc), the cerebral metabolic rate of oxygen ($CMRO_2$), and cerebral blood flow (CBF) to the underlying cellular events is complex and still not completely understood. Counter-intuitively, CBF increases do not simply serve to adjust glucose and oxygen delivery to the variable energy demands of neuronal tissue. Activation studies have shown that in response to a task (i.e., an increase in neuronal activity), CBF and CMRglc increase together, but far exceed $CMRO_2$ (Fox and Raichle 1986; Fox et al. 1988). Several models have been used to explain the cellular underpinnings of neurovascular coupling and uncoupling (Lin et al. 2008; Lin et al. 2009; Lin et al. 2010).

An important advantage of measuring CMRglc is that it provides a direct, physiologically specific signal that can be quantified. This was elegantly demonstrated by several early autoradiography studies with ^{14}C-deoxyglucose (Sokoloff 1993). For example, in rats, retinal stimulation with flashes of light of a known, calibrated intensity resulted in proportional increases in local CMRglc in the primary projection areas from the retina, whereas local CMRglc remained unchanged in structures that did not receive direct projections from the retina (Batipps et al. 1981).^{18}F-FDG PET measurements are indicative of a steady state of neuronal activity during the uptake and scanning interval.

Relative to other tissues, the brain's energy demand is high in the resting state and during sleep and increases with only a fraction of its baseline metabolism with activity. In the resting state, most of this energy is also devoted to neuronal signaling (i.e., synaptic function) (Sibson et al. 1998). In activation (or task-based) studies, local changes in ^{18}F-FDG uptake in response to a task are studied to localize brain functions. Studies in which subjects are in a resting state, which means there is no specific sensory stimulation and patients are not engaged in any behavioral or physical task, can give information about time-invariant aspects of brain function. Several neuroimaging and electroencephalography (EEG) studies have shown that spontaneous neuronal activity is highly organized at rest and that several conditions (including disease) can alter resting-state neuronal activity.

4.2 Analysis of Resting-State ^{18}F-FDG PET Images

4.2.1 Image Registration

Voxel-wise image analyses usually start with the registration of each image to standard space. This is because this type of analysis of brain images is hampered by the differences in brain morphology between subjects. In image registration, the brain

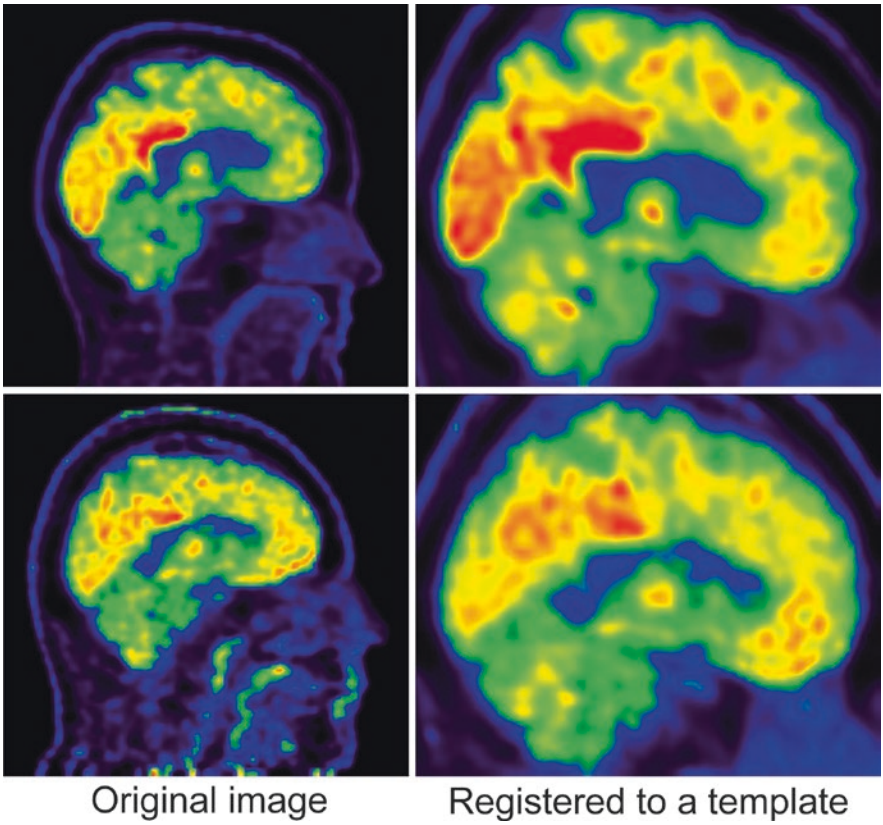

Fig. 4.3 Example of two healthy controls showing the reconstructed ^{18}F-FDG PET image, and the images after registration to an ^{18}F-FDG PET specific template in standard space (Della Rosa et al. 2014)

images of subjects are translated to another image (usually a template), such that voxels/regions can be compared between subjects. Image registration entails the estimation of the optimal spatial transformation between two images. ^{18}F-FDG PET images are often directly registered to a template such that all the images are in the same space. An example of ^{18}F-FDG PET image registration is given in Fig. 4.3. A more detailed explanation of image registration can be found elsewhere (Herholz et al. 2004).

4.2.2 Normalization

By adhering to strict scanning protocols, it is attempted to minimize the differences between each scanning session (Varrone et al. 2009). By image registration, morphological differences are accounted for. However, considerable inter-individual

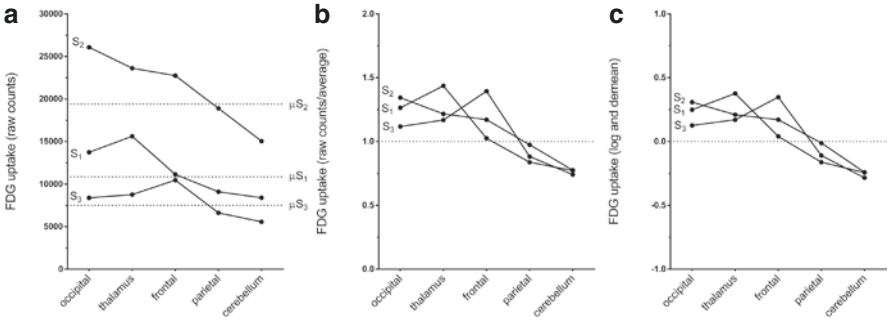

Fig. 4.4 Two types of normalization. Raw voxel values (i.e., raw count data) (**a**); ratio-normalized voxel values (**b**); and voxel values normalized according to the SSM (**c**) are depicted for five different coordinates in three healthy controls (S_1, S_2, and S_3). The average voxel value was calculated for each subject, by taking all voxels in the image within a gray matter mask. This average voxel value is indicated for each subject in (**a**) with the dashed line (μS_1, μS_2, and μS_3). In (**b**) each voxel value was divided by the corresponding subject average. This results in voxel values centered around 1 for each subject. In (**c**) voxel values within the same mask were log-transformed, and subsequently the log mean was subtracted from the data. This results in voxel values centered around zero for each coordinate and each subject. In (**a** and **b**), data is non-negative. In (**c**), negative values are present

differences in ^{18}F-FDG uptake remain present. This is because there may be slight differences in the dose of ^{18}F-FDG injected, or due to baseline metabolic differences between people (even after fasting). This is apparent in Fig. 4.4a, which shows the average brain FDG uptake for three healthy controls, scanned with identical protocols. These large inter-individual differences will obscure underlying task-evoked or disease-dependent patterns of altered metabolism.

This can be solved with tracer kinetic modeling, which transforms count data into physiological units using information from arterial blood sampling. However, as stated previously, this entails an invasive, time-consuming procedure. A solution is normalizing the raw count data to a reference value. It should be noted that any ^{18}F-FDG PET study that does not apply arterial blood sampling cannot study absolute differences of ^{18}F-FDG uptake, but can only make inferences on relative differences.

Several approaches are used to normalize raw count data. Some researchers choose a reference region which is thought to be unaffected by the disease process. The average ^{18}F-FDG uptake in that region is measured, and all voxel values in each image are subsequently divided by this value (Borghammer et al. 2008). An important limitation of this approach is that it requires a priori assumptions. For example, in the study of Parkinson's disease, some authors have chosen the cerebellum as a reference region, whereas it is now known that the cerebellum plays an important part in parkinsonism (Bostan et al. 2013; Rodriguez-Oroz et al. 2009). For ^{18}F-FDG studies which study brain-wide metabolism, choosing a reference region may therefore be problematic. Still, in other radiotracer studies, a reference region can be very useful.

A frequently used alternative is to ratio-normalize each voxel value to the subject's average whole-brain uptake (usually within a gray matter mask), which is

referred to as global mean normalization (Fig. 4.4b). An equivalent approach is the scaled subprofile model (SSM), in which the data is first log-transformed, and subsequently the log mean is subtracted (Fig. 4.4c). The appendix provides additional details on these two methods and the associated issues.

4.2.3 Analysis of Variance and Covariance

After applying some type of normalization, a straightforward approach to investigating differences in cerebral glucose metabolism between patients and controls is by comparing the mean ^{18}F-FDG uptake in each region (or each voxel) between the groups with multiple *t* tests. This is an example of analysis of *variance*. Variance is a measure of spread of the data. It is equal to the square of the standard deviation of the data:

$$\mathrm{var}\left(X\right) = s^2 = \frac{\sum_{i=1}^{n}\left(X_i - \bar{X}\right)^2}{\left(n-1\right)}$$

where $\bar{X}$ indicates the average of variable *X*. This formula can be rewritten as:

$$\mathrm{var}\left(X\right) = \frac{\sum_{i=1}^{n}\left(X_i - \bar{X}\right)\left(X_i - \bar{X}\right)}{\left(n-1\right)}$$

Multiple *t* tests between voxel values in two or more groups can be easily performed. If a cluster of voxels holds significantly lower values in patients compared to controls, then this brain region shows decreased ^{18}F-FDG uptake in the disease state, which reflects a loss of synaptic integrity. The interpretation of such statistical parametric mapping (SPM)-based group contrasts is thus very straightforward. Several studies have used a voxel-based SPM analysis to identify group differences between patients with a neurodegenerative disease and healthy age-matched controls (Eckert et al. 2005; Juh et al. 2004; Teune et al. 2010; Yong et al. 2007). These univariate patterns give a good impression of the brain regions involved in disease.

Covariance is a measure of how much two variables change together. The formula for covariance is very similar to the formula for variance, but includes an additional variable (variable *Y*):

$$\mathrm{cov}\left(X,Y\right) = \frac{\sum_{i=1}^{n}\left(X_i - \bar{X}\right)\left(Y_i - \bar{Y}\right)}{\left(n-1\right)}$$

A positive covariance indicates that as *X* increases, so does *Y*; and a negative covariance indicates that as *X* increases, *Y* decreases (or vice versa). If the covariance is zero, *X* and *Y* are unrelated. The concepts variance and covariance are explained in a schematic in Fig. 4.5.

If there are more than two variables (i.e., more than two dimensions), covariance (C) can be stored in a matrix. If we have three variables (*x*, *y*, and *z*), the diagonal

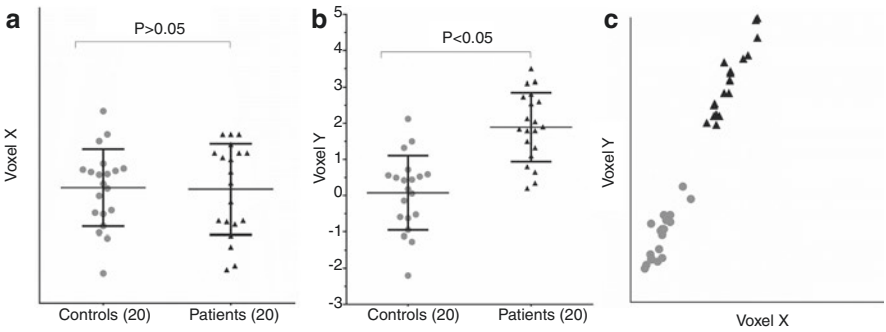

Fig. 4.5 A schematic, easy representation of variance and covariance (mock data). Two voxels are considered in a patient group and a control group. The mean in ^{18}F-FDG uptake (normalized counts) in voxel *X* is compared between patients and controls with a *t* test (**a**), which does not show a significant difference. The mean value for voxel *Y* does show a significant difference (patients higher than controls) (**b**). Voxel *X* and voxel *Y* are correlated; a higher value in voxel *X* predicts a higher value in voxel *Y*. These two variables thus show positive covariance (C)

entries in this matrix reflect the variance. The off-diagonal entries reflect the covariance between *x* and *y*, *x* and *z*, and *y* and *z*. The matrix is symmetric around the diagonal.

$$C = \begin{pmatrix} \mathbf{cov}(\boldsymbol{x},\boldsymbol{x}) & \mathrm{cov}(x,y) & \mathrm{cov}(x,z) \\ \mathrm{cov}(y,x) & \mathbf{cov}(\boldsymbol{y},\boldsymbol{y}) & \mathrm{cov}(y,z) \\ \mathrm{cov}(z,x) & \mathrm{cov}(z,y) & \mathbf{cov}(\boldsymbol{z},\boldsymbol{z}) \end{pmatrix}$$

4.2.4 Principal Component Analysis

In data with only a few dimensions, it is easy to appreciate the "patterns" in the data (i.e., the relationship between variables). However, when the dimensionality of the data increases, as is the case in typical neuroimaging data (>100,000 voxels and dozens of subjects), relationships between variables can no longer be presented graphically. Principal component analysis (PCA) reduces the number of dimensions and can hereby aid in identifying patterns in complex datasets. In this section, we will explore what PCA does in a simple, two-dimensional example.

Imagine we have studied the values of two voxels (*X* and *Y*) in ten controls and ten patients. PCA requires a dataset with a mean of zero. Therefore, we first subtract $\bar{X}$ from each observation of *X* and $\bar{Y}$ from each observation of *Y*. A plot of the data is shown in Fig. 4.6 (this is mock data, so the values do not represent true voxel values).

From Fig. 4.6b, it is clear that the two voxels are related. We can infer that these two variables have a positive covariance. The variance-covariance matrix for these variables is:

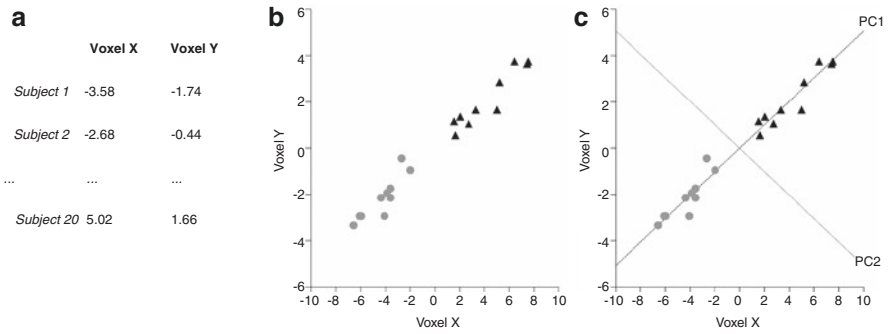

Fig. 4.6 Two voxels were studied in 20 subjects (mock data). The data points were demeaned (**a**). (**b**) shows these values for voxel *X* and voxel *Y* in ten controls (grey circles) and ten patients (black triangles). In (**c**), the first eigenvector (PC1) and the second eigenvector (PC2) are drawn. PC2 is perpendicular (orthogonal) to PC1. PC = principal component

$$\mathrm{cov}(X,Y) = \begin{matrix} 22.97 & 11.57 \\ 11.57 & 6.01 \end{matrix}$$

The variance of voxel *X* is 22.97 and the variance of voxel *Y* is 6.01. The covariance of the two voxels is 11.57. From the covariance matrix, we can calculate the **eigenvectors** and the **eigenvalues** of this dataset (how this is done is beyond the scope of this chapter):

$$eigenvectors = \begin{matrix} 0.45 & -0.89 \\ -0.89 & -0.45 \end{matrix} \qquad eigenvalues = \begin{matrix} 0.14 \\ 28.84 \end{matrix}$$

The eigenvectors describe the lines that are plotted in Fig. 4.6c. The first eigenvector, called principal component (PC) 1, almost perfectly fits the data points. The second eigenvector, PC2, describes how much the data points deviate from PC1. Thus, this process of taking the eigenvectors from the covariance matrix has enabled the extraction of lines that characterize the data.

The first eigenvector explains most of the variability in the data. This eigenvector therefore has the highest eigenvalue. In PCA, eigenvectors (or components) are always ordered in terms of how much of the variability in the data they describe. The component with the highest eigenvalue is principal component 1, the one with the second highest eigenvalue is principal component 2, and so on. The number of principal components depends on the dimensionality of the data. A PC is always perpendicular (also called *orthogonal*) to all other PCs.

The rest of the steps involve transforming the data such that they are expressed in terms of PC1 and PC2. This means that each data point will obtain a new value in terms of PC1 and PC2. This is essentially a rotation by which PC1 and PC2 describe the new axes. Note that in Fig. 4.7a, this rotation effectively removes the

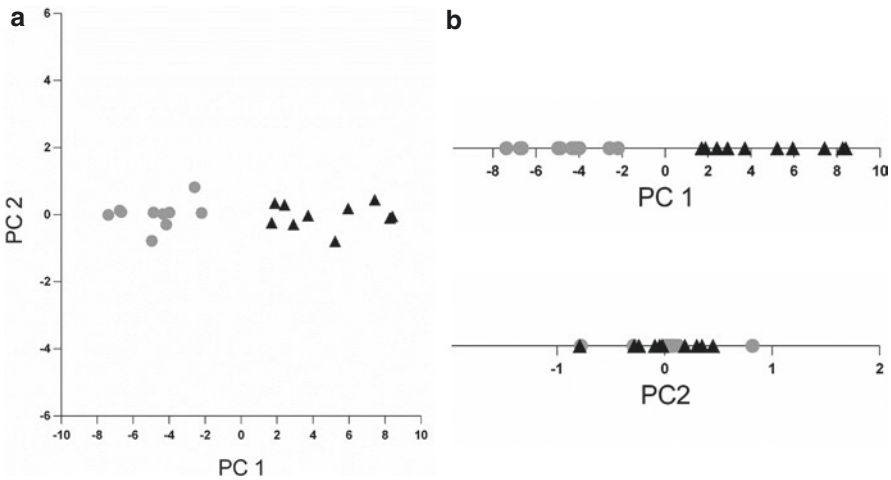

Fig. 4.7 Rotation of the data such that PC1 values are plotted along the *x*-axis, and PC2 values are plotted along the *y*-axis (**a**). The data can be reduced in dimensionality (from two-dimensional to one-dimensional) when only one PC is considered (**b**). PC1 contains the information of interest (it separates the two groups), and PC2 can be discarded

covariance from the data. The new values can be calculated by multiplying the original, demeaned voxel values with each eigenvector. We could also decide to only keep PC1, since this eigenvector describes the most important effects in the data, and we can discard PC2. This is a way of reducing the dimensionality of the data (Fig. 4.7b). We have discarded some of the information (the PC with the lowest eigenvalue), but kept the most important effects in one dimension (the PC with the largest eigenvalue).

In the example above, we have explained PCA with 20 subjects but just 2 voxels. In that mock data, there were only two eigenvectors. In neuroimaging studies, there are many more voxels than there are subjects. In such studies, the number of possible eigenvectors is limited to the number of subjects minus 1. This can be intuitively understood when we imagine a situation where we have just two subjects with three voxels each (voxels *x*, *y*, and *z*). The voxels determine the axes: a three-dimensional grid with axes *x*, *y*, and *z*. The subjects are plotted in this three-dimensional grid: each subject has a value for each voxel. With only two subjects, just one eigenvector (running exactly between the two points) can be calculated. Now imagine we have three subjects in the same space. In this situation, two eigenvectors can be calculated. Since these three subjects are in one plane, a third eigenvector cannot be determined. This same principle works for multi-dimensional space. In other words, the possible number of eigenvectors depends on the length of the shortest dimension. As noted above, in neuroimaging, the shortest dimension is usually the number of subjects. For example, in the typical situation where we have 40 subjects (20 controls and 20 patients) and > 100,000 voxels, 39 eigenvectors can be determined.

4.3 SSM PCA

Now that the concepts variance, covariance, and PCA have been explained, we will give an overview of the steps involved in scaled subprofile model (SSM) and principal component analysis (PCA). SSM PCA was first introduced by Moeller and colleagues for region-of-interest (ROI) data (Eidelberg et al. 1994; Moeller et al. 1987; Moeller and Strother 1991) and was later extended to whole-brain voxel-wise analyses (Eidelberg 2009; Habeck et al. 2008; Ma et al. 2007; Spetsieris and Eidelberg 2011). This approach combines a type of normalization (SSM) with principal component analysis (PCA) to find patterns (components) that can potentially discriminate between neuroimaging data of two groups. Here, we explain the method in a conceptual manner, such that an audience with a limited mathematics background can follow the steps involved.

4.3.1 Defining the Data

Usually, SSM PCA is applied to ^{18}F-FDG PET data that are acquired in a static imaging protocol and registered to a template in Montreal Neurological Institute (MNI) brain space. The data are typically smoothed (8–10 mm full width at half maximum) to improve the signal to noise ratio. A threshold of the whole-brain maximum is applied to remove out-of-brain voxels. The threshold value is usually chosen as the value that is 35% of the whole-brain maximum. This results in a mask of mainly gray matter (see Spetsieris and Eidelberg (2011) for details and alternatives). This mask is created for each subject, and the masks for all subjects are combined to include only those voxels that are shared between all participants. The remaining data can be stored in a matrix where subjects are in rows and voxels are in columns (Fig. 4.8).

4.3.2 Normalization with the Scaled Subprofile Model (SSM)

First, the SSM is applied, which refers to the normalization of the raw count data. This preprocessing starts with the log transformation of each voxel value for each

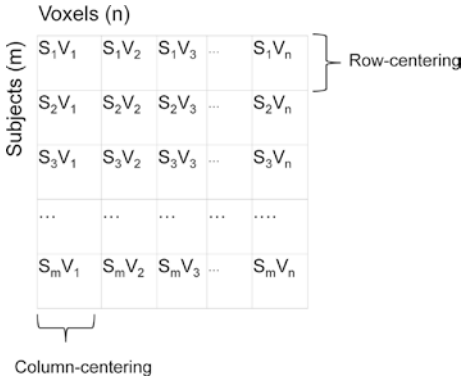

Fig. 4.8 Data matrix (D) with *m* subjects (S_m) and *n* voxels (v_n). Removal of the subject mean (row-centering) and group mean (column-centering) is indicated

subject. Subsequently, the mean for each subject is removed (row-centering). These two steps combined serve to remove subject-specific scaling effects (also see the appendix and Fig. 4.4c). Next, the mean per voxel is removed (column-centering). This mean per voxel is referred to as the group mean profile (GMP). The remaining data matrix consists of residual voxel values for each subject. For each subject, this is termed the "subject residual profile" (SRP). Because all SRPs are in the same scale, the SRPs can now be compared between subjects (and thus between groups).

4.3.3 Calculating Eigenvectors from a Covariance Matrix

After normalization, a PCA is performed on the SRP data matrix. First, a covariance matrix is determined. The formula for covariance was introduced previously:

$$\operatorname{cov}(X,Y) = \frac{\sum_{i=1}^{n}(X_i - \bar{X})(Y_i - \bar{Y})}{(n-1)}$$

Remember that the SRP matrix has a mean of zero, because the data was log-transformed and the mean was subtracted. Therefore, we can ignore the terms $\bar{X}$ and $\bar{Y}$. In other words:

$$\operatorname{cov}(X,Y) = \frac{\sum_{i=1}^{n}(X_i)(Y_i)}{(n-1)}$$

The covariance between all voxels across all subjects can be determined from the voxel * voxel covariance matrix. We arrive at the voxel * voxel covariance matrix by multiplying the transpose of D with D itself (D′ * D). This can be visualized as follows (Fig. 4.9):

Since we usually have thousands of voxels, the voxel * voxel data matrix (S_{vox}) will be quite large, and calculating the eigenvectors from S_{vox} will require a lot of computational power. This can be solved by determining the eigenvectors from the subject * subject covariance matrix (S_{sub}) instead and left-multiplying these with the transposed SRP (Spetsieris and Eidelberg 2011).

The eigenvectors from S_{vox} are referred to as group invariant subprofiles (GIS) in literature (Eidelberg 2009; Spetsieris and Eidelberg 2011). The terms eigenvector, GIS, and PC are often used interchangeably. As described in Sect. 2, the components in PCA are always ordered in terms of variance accounted for. Thus, PC1 explains most of the variance in the data, PC2 less, and so on. The last component accounts for only a small percentage of the total variance.

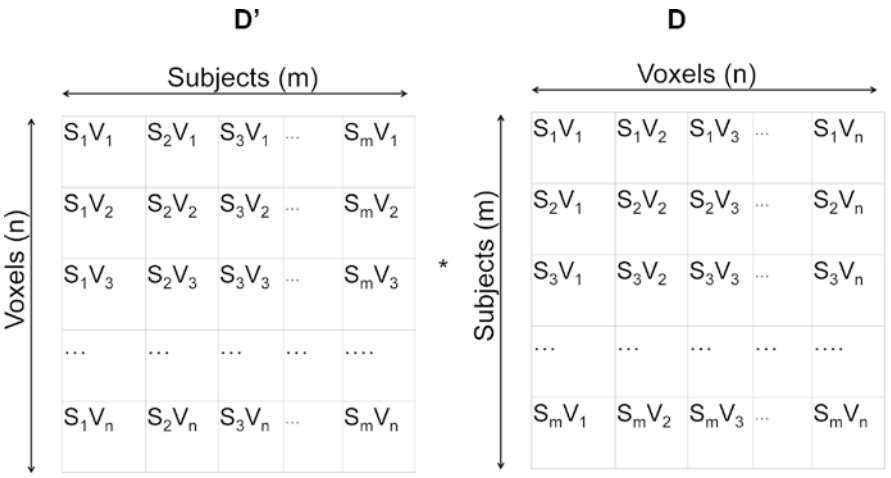

Fig. 4.9 The product (not shown here) will show the variance across the diagonal of the matrix, and the off-diagonal entries will show the covariance between the voxels. Thus, the entire matrix describes the spatial variance and covariance relationships between voxels across subjects

4.3.4 Calculating Subject Scores and Selecting Disease-Related Components

In order to reduce the dimensionality of the data, we need to project each data point (each SRP) onto each PC. Each subject will receive a score on each PC. These so-called subject scores (SS) are easily computed by the inner product of the two vectors:

$$\mathrm{SS} = \mathrm{SRP} * \mathrm{PC}$$

In the case of n subjects, this will result in a matrix of subject scores on each PC, with a maximum of $n - 1$ PCs (Fig. 4.10):

The subject scores will determine which PC is of interest to the study. On some PCs, the subject scores will be significantly different between patients and controls. These components may thus contain the disease-related changes that are of interest and may be selected for further analysis. Of note, the subject scores on each PC are inspected, to ensure that the mean subject score in patients is higher than the mean subject score in controls. This convention aids in the interpretation of the PC maps, as will be discussed later. In case the calculated mean scores are higher in controls than in patients, both the subject scores and the associated PC are multiplied by -1.

There are several ways to decide which PC (or combination of PCs) constitute(s) the final disease-related pattern (Spetsieris and Eidelberg 2011). In some studies, a

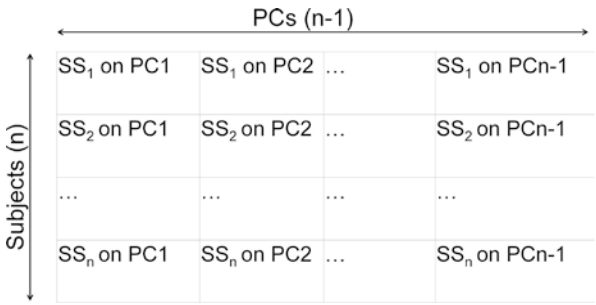

Fig. 4.10 Matrix of subject scores on each PC

single PC is chosen (usually PC1) if it discriminates significantly between controls and patients. Consecutive, smaller PCs are not included (even if these also discriminate between patients and controls) (Niethammer and Eidelberg 2012; Wu et al. 2013; Wu et al. 2014). A disadvantage of that approach is that it assumes that the relevant disease-related information is captured in a single component, which may not be the case. On the other hand, an important consideration is the risk of overfitting. Including more components may yield a pattern that gives a better fit of the initial sample, but may be limited in its relevance or generality across new datasets from the same population.

In previous studies by our group (Meles et al. 2018a; Meles et al. 2018b; Teune et al. 2013; Teune et al. 2014a; Teune et al. 2014b), combinations of principal components were selected using a forward stepwise logistic regression model. First, the components that explain the top 50% of the total variance in the data are selected. This is an arbitrary threshold that assumes that the lower 50% includes only noisy components that explain very small sources of variance in the data (a few percent) and are probably not disease-related. The combination of components that together give the lowest Akaike information criterion (AIC) of the model is selected (Akaike 1974). In other words, we combine the least possible number of components that together give the optimum discrimination between groups (trade-off between discriminative power and parsimony of the model). The selected components are subsequently combined linearly into a single PC vector using the coefficients determined by the logistic regression model.

We have re-evaluated the data in previously published disease-related patterns (Teune et al. 2013; Teune et al. 2014a; Teune et al. 2014b) and found that a combination of components as selected by the logistic model gave better discrimination of groups compared to the selection of PC1 alone. This does not imply that this model can be applied blindly to any dataset. In every analysis, each separate component should be inspected carefully, for instance, by visually checking if the component could potentially reflect disease activity or noise.

An important consideration is that PCA is susceptible to outliers. One outlier may contribute overwhelmingly to the variance, resulting in a first PC that accounts for most of the variance (i.e., >90%). The rest of the components are always orthogonal to this first, "faulty" PC, and thus even the remaining PCs are influenced by this issue, even though they reflect the effects of interest in the data (Habeck et al.

2010). It is thus advisable to always check each PC visually and in terms of variance accounted for. It may be necessary to re-run the analysis, excluding a problematic case.

Of note, when PCA is performed without this double-centering procedure, the chance that the first few components will reflect group-dependent differences in brain function is reduced (Moeller and Strother 1991; Spetsieris and Eidelberg 2011). In such a scenario, the first PC will reflect major sources of variance stemming from global mean values. This PC does not discriminate patients from controls. The disease-related pattern (i.e., the component that can discriminate between groups) shifts in order of importance, to a lower eigenvalue.

4.3.5 Prospective Application of the Pattern

Once a pattern has been identified, it can be applied to new scans. Scans of new subjects are registered to the same template and masked using the same parameters as in the original dataset. Next, the data are log-transformed, the mean per subject is subtracted, and the SRP for each subject is calculated by subtracting the group mean profile (GMP) that was determined from the original pattern identification dataset. Finally, the pattern is projected onto the new data to calculate the subject score:

$$\mathrm{SS} = \mathrm{SRP} * \mathrm{PC}$$

Subject scores are usually z-transformed with reference to the control group:

$$Z_{\mathrm{SS}} = \frac{\mathrm{SS} - \mu_{\mathrm{SS\,HC}}}{\sigma_{\mathrm{SS\,HC}}}$$

SS refers to the ("raw") subject score, $\mu_{\mathrm{SS\,HC}}$ refers to the mean raw subject score of the control group, $\sigma_{\mathrm{SS\,HC}}$ refers to the standard deviation of the raw subject scores in the control group, and Z_{SS} refers to the z-transformed subject score of the new subject. This implies that the mean z-score of controls will be set to zero, with a standard deviation of 1. If the new dataset was acquired in a different manner than the original pattern identification dataset (for instance, the subjects were scanned on a different PET system), it may be necessary to z-transform the new data to a control cohort that was acquired under the same circumstances (Kogan et al. 2019).

4.3.6 Validation

One cannot assume that components that result from PCA are intrinsically meaningful. PCA is a mathematical operation, and aspects such as variance ordering and orthogonality are true by design (Habeck and Moeller 2011). Even if the signals only consist of noise, PCA will achieve a data reduction. Disease-related patterns

may be found by coincidence, and therefore, it is important to check empirically if the findings that were determined on the derivation set hold in a completely new dataset. If the pattern successfully discriminates between patients and controls in a new dataset, it is likely that this pattern can be interpreted as disease-related. This can be substantiated if subject scores correlate to other markers of disease such as disease duration or severity (measured with a validated scale) in new subjects. If significant correlations are found, this would mean that the identified component has some meaning other than a purely mathematical dimension.

In some cases, a testing set may not be available. This can be (partly) solved using a leave-one-out cross validation (LOOCV). In LOOCV, the analysis described above is repeated several times, each time leaving out one subject. Imagine patient *x* is part of our identification sample. We have included 20 controls and 20 patients. We leave out patient *x* and re-determine the pattern on the remaining 20 controls and 19 patients. We subsequently calculate the subject score of this pattern in patient *x*. We now have the LOOCV subject score for patient *x*. This procedure can be repeated for each subject (patients and controls). It results in subject scores for each subject, which are independent from the pattern identification step. The difference between LOOCV subject scores in controls and patients can be determined with a *t* test. If significant, the original pattern is considered a predictor for the disease in new cases.

4.3.7 Visualization and Interpretation of PC Maps

PCs can be visualized as 3D brain images, in which each voxel has a weight (the voxel value). Positive and negative weights indicate the direction of the principal component vector with respect to the mean. Voxels with a greater absolute weight in the pattern will be dominant in determining the subject score on that PC. This does not mean that weaker voxel weights should be discarded. "Although highly weighted regions may have a greater influence on the pattern score, regional values alone are not as predictive as whole pattern expression in performance measures" (Spetsieris et al. 2015). PCs are vectors, which do not have a direction. If controls have higher subject scores on a PC compared to patients, then the PC map is multiplied with −1 by convention. Subsequently, positive voxel weights are color-coded red in PC maps, and negative voxel weights are color-coded blue.

In order to interpret the pattern topography itself, it is useful to apply a threshold to the PC image, which somehow indicates which regions are most important. Several approaches have been applied in literature. For instance, all voxel values in the PC map can be transformed to *Z*-values. Next, only the highest and lowest voxel values in this "*Z*-map" are displayed (at a certain threshold, for instance, $Z > 1.96$ corresponding to $P < 0.05$). Regions that survive this threshold are interpreted as the most important regions of the pattern; these regions are likely most involved in the disease process.

An important issue arises when small sample sizes (20/20) are used, as is usually the case in neuroimaging studies. Pattern maps will likely be variable depending on

the specific sample of patients and controls. Thus, voxel weights in the pattern may fluctuate (this is also the case for univariate approaches). Identification of the areas most affected by the disease process becomes less reliable. This could be solved by collecting many different datasets of controls and patients and determining the disease-related pattern for each dataset. Imagine we have 1000 datasets of 20 controls and 20 patients. Then we can derive 1000 patterns. We can study the distribution of voxel weights across the different patterns. For each voxel, we can determine the mean voxel weight and its standard deviation. If a particular voxel has a similar weight in each pattern and does not fluctuate much across populations (i.e., it has a small standard deviation), then this voxel gives a reliable contribution to the pattern and is interpreted as being important in the disease. In contrast, if a voxel has a negative weight in some populations, but a positive voxel weight in others (i.e., the distribution straddles 0), then this voxel is probably unreliable. In summary, if we have such a distribution of voxel weights for each voxel, we can test which voxels in the pattern are reliable.

In reality, such a study is hampered by small numbers of subjects in most datasets and varying imaging protocols across centers which impedes pooling of datasets. To approximate this distribution per voxel, we apply a bootstrap estimation procedure. A bootstrap estimation procedure entails repeating the PCA several (~1000) times on randomly sampled data (with replacement) from the pool of patients and controls. In each iteration, the control and patient group contain the same number of images. This means that some subjects are represented more than once in some iterations, whereas others are completely omitted. We are thus creating multiple datasets from just one derivation set, which is similar to the LOOCV procedure. In contrast to the LOOCV, a bootstrap allows us to reuse subjects. For each iteration, each voxel will get a voxel weight. With multiple iterations, it is possible to analyze the distribution of weights of a voxel with a point estimate (average) of w and a standard deviation of s_w. Using this distribution, we can determine thresholds, which can subsequently be used to display only those voxels that we consider stable enough to be interpreted as part of the disease topography.

Again, one approach to this threshold is to make a Z-map using the bootstrap distribution. Each voxel will receive a z-value: $z = w/s_w$. "Sufficiently small variability of a voxel weight around its point estimate results in a Z-value of large magnitude, and indicates a reliable contribution to the covariance pattern" (Habeck et al. 2008). One can chose a certain z-threshold to show only stable voxels (e.g., $|z| > 1.96$ corresponding to a P-value of <0.05).

In previous studies, we chose to apply the confidence interval (CI) as a threshold. For each average voxel weight (w), we can determine a CI interval based on the distribution of the voxel weights from the bootstrap. This confidence interval (e.g., 90%) has an upper and a lower bound. For positive regions, we display only those voxels for which the lower bound of the confidence interval is larger than zero. For the negative regions, we display only those voxels for which the upper bound of the confidence interval is smaller than zero. Voxels for which the confidence interval straddles zero are not visualized.

The maps that follow from the bootstrap estimation procedure are only used for visualization. It is likely that those voxels that survive the chosen threshold after a bootstrap estimation procedure are truly related to the disease process and not coincidentally found in a given sample. Thus, if a pattern were to be identified in a completely new set of controls and patients, it is likely that those regions would be identified again.

In summary, several validation procedures are necessary when identifying a disease-related pattern with SSM PCA. First, it is important to calculate its expression in a new dataset to ascertain that the pattern can be generalized to new subjects. If a validation set is not available, a leave-one-out cross validation can be applied. This approach tests whether the pattern is a good predictor of the disease in a new subject. Ideally, subject scores are also correlated to some aspects of the disease, such as disease duration or severity of symptoms. Finally, the stability of the pattern is assessed with a bootstrap estimation procedure. Stable regions will probably be found again if the pattern was to be re-derived in a completely new population and may thus be interpreted as important regions in the pathophysiology of the disease.

4.3.8 Advantages of SSM PCA Over Univariate SPM Models

In reality, neither mass-univariate nor SSM PCA can provide an exact description of the pathophysiological mechanisms that underlie the disease and give rise to alterations in neuroimaging signals (Moeller and Habeck 2006). That said, SSM PCA has a few advantages over univariate approaches. The core issue in univariate approaches is that they assume that voxels are independent, which is not the case. The signal in neuroimaging data stems from the communication between neurons over synapses. The strength of neuroimaging lies in the detection of these interactions, to ultimately understand the network-level changes in certain conditions. Disregarding interactions between voxels means that most of the data of interest is in fact discarded (O'Toole et al. 2007). Multivariate approaches such as SSM PCA take into account the interactions (covariance) between voxels, and patterns that result from these analyses are more easily interpreted in the context of network-level changes.

The assumption of independent voxels in mass-univariate analyses also leads to a technical issue. In voxel-by-voxel comparisons, 10^4 to 10^5 voxels are compared between two groups, with an equal number of *t* tests. Performing multiple *t* tests leads to an inflation of the error rate. In such cases the α-level has to be corrected for multiple comparisons. This correction can be either too liberal (leading to type I errors) or too conservative (leading to type II errors), potentially "correcting away" true effects of interest in the data. Some solutions have been proposed (Genovese et al. 2002), but investigators are often willing to tolerate higher ($p > 0.05$) false-positive rates. For example, voxel clusters at uncorrected levels of $P < 0.001$ are often reported for standard F- or T-statistics (Moeller and Habeck 2006). In contrast, multivariate analyses such as SSM PCA have enhanced statistical power, as correction for multiple comparisons is not necessary.

In addition, it is generally accepted that PCA-based multivariate approaches have better sensitivity and replicability compared to univariate approaches (Habeck et al. 2008; Habeck et al. 2010). SSM PCA is especially relevant when making predictions in new cases. Habeck et al. compared SSM PCA pattern analysis to univariate approaches in the study of Alzheimer's disease (AD). In the univariate approach, AD patients and controls were compared using SPM with a *t* test. The area that gave the best group separation in the derivation sample was chosen as the region of interest (ROI). The ROI in this study was the right parietotemporal area. Signal values in this ROI were inspected in new AD subjects, which were subsequently classified as AD if the signal in that ROI surpassed a fixed threshold level obtained from the derivation sample. The multivariate approach entailed the identification of the AD-related pattern (ADRP) with SSM PCA. ADRP subject scores were calculated in scans of new AD patients, and these subjects were classified as AD if the subject score surpassed a fixed threshold level obtained from the derivation sample. Although both methods were able to distinguish between patients and controls in the derivation sample, the classification of new subjects was significantly better when the ADRP was used. Even when the most important area was omitted from the scans (i.e., the voxel values in the right parietotemporal area were set to zero in each subject), ADRP subject scores remained stable. According to the authors, "this demonstrates how multivariate analysis takes into account the interregional correlation structure in the data, and is thus not critically dependent on the inclusion of any particular brain region and can withstand dropping out even the most salient areas" (Habeck et al. 2008). This also supports the concept that pathological processes have a widely distributed effect on brain function in neurodegeneration.

Appendix: Effects of Normalization

In this example we demonstrate effects of ratio normalization versus log transformation and subtraction of the mean, as applied in the scaled subprofile model (SSM). In this example, we consider ^{18}F-FDG uptake in two regions, *A* and *B*, in healthy controls and patients. Region *B* is affected by the disease. Metabolism in this region has changed compared to the control population with ΔB. In our example, region *A* is unaffected in both groups. For each subject, there is a scaling factor q which accounts for effects due to, for instance, the amount of radioactive label administered. The term q is a subject-specific scaling factor which we need to eliminate from the data.

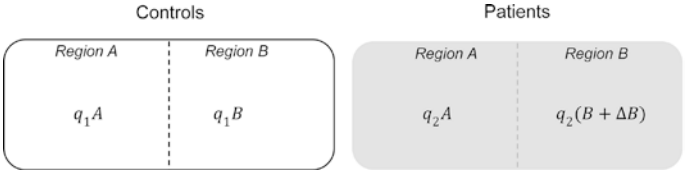

We introduce another term n, which indicates the relative size of region A.

$$\text{Mean brain uptake}: \; nA + (1-n)B \qquad 0 < n < 1$$

Often, ^{18}F-FDG uptake is altered in a few areas due to the disease. In such a case, A will contribute much more to the whole-brain average than B. Situations where B contributes only a small proportion to the whole-brain average include, for instance, early Parkinson's disease, or even its prodromal phases.

One can imagine situations where large parts of the brain are affected by the disease. For instance, in advanced Alzheimer's disease, we would expect hypometabolism in large parts of the cerebral cortex. In that case, B contributes overwhelmingly to the whole-brain average. As a result, whole-brain and average ^{18}F-FDG uptake will be lower in patients compared to controls.

As discussed in the main text, a normalization is needed. Two options are discussed. The first method is global mean normalization by proportional scaling, which is commonly applied and entails dividing each voxel value by the subject mean. The second method is the normalization procedure as applied in SSM PCA. In the SSM, data is first log-transformed and subsequently the subject mean is subtracted. In this example we will show that:

1. Scaling effects (q) are eliminated in both methods.
2. Both normalization techniques can introduce artifacts in (the unaffected) region A.

Global Mean Normalization

In global mean normalization, ^{18}F-FDG uptake in each voxel is divided by the mean uptake of the whole brain. For our example, the corrected values are shown in below figure

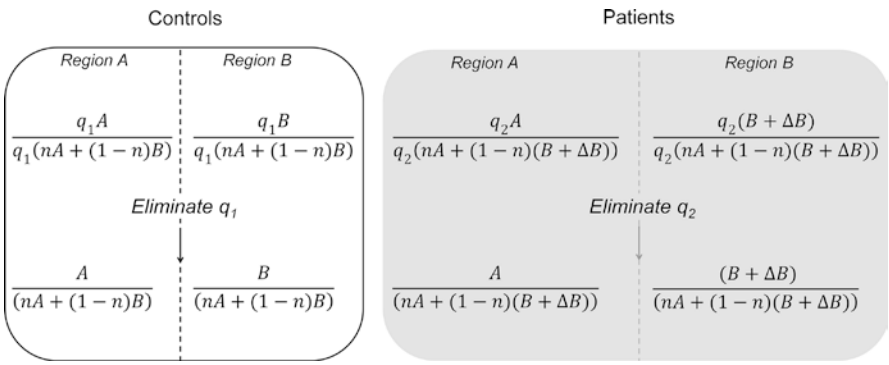

Although ^{18}F-FDG uptake in region A is the same in the control and patient population, the values in this area are different after global mean normalization.

Thus, the change in signal in region *B* due to pathology resulted in an altered signal in region *A* after global mean normalization (i.e., it produced an artifact).

Log Transformation and Demean in the SSM

In the SSM, the data are first log-transformed, and next we subtract the mean (see below figure). The fact that factor *q* can be eliminated in the SSM indicates that any multiplicative effect in the data can be removed, just like it can be eliminated in the global mean normalization. Thus, both methods are invariant to scaling effects (also see Spetsieris and Eidelberg (2011)).

Practical Examples

We modeled the formulas above in MATLAB, with two values for *n* (0.9 and 0.1) and variable values for ΔB. For *A* and *B*, we chose the same (realistic) fixed values.

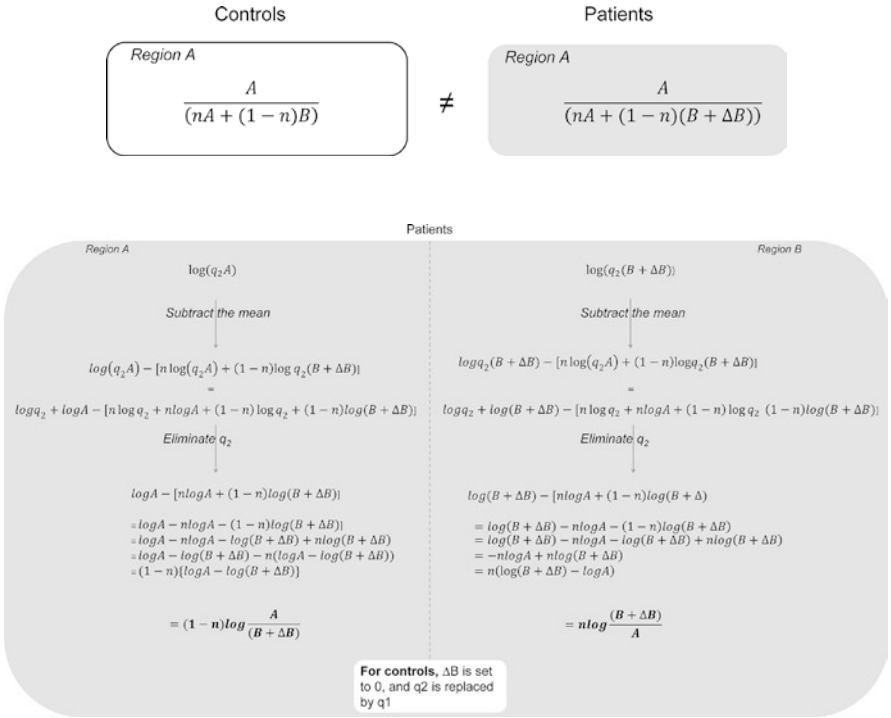

Example 1: Changes in a few regions.

In this situation, ^{18}F-FDG changes are present in a few brain regions. In patients, most of the brain is unchanged, and thus A contributes most to the average (n is close to 1).

We plotted the values for A and B after global mean normalization ("A_{mean}" and "B_{mean}") and after SSM normalization ("A_{log}" and "B_{log}"). On the x-axis, we show the values for ΔB, ranging from −1000 (i.e., a decrease in B) to +1000 (i.e., an increase in B). Furthermore, we chose: $A = 1001$, $n = 0.9$ and $B = 1001$. The result is shown in Fig. 4.11a.

It is clear that there is an offset difference between the two methods. This is inherent to subtracting the mean versus dividing by the mean. When region B becomes hypometabolic, there is a slight (artificial) increase in region A. However, the changes in region A as a function of ΔB, even for extreme values of ΔB, are relatively small. The slope for the new values in A and B after each normalization procedure are almost equal.

Example 2: Changes in most of the brain.

In this situation, most of the cortex of the brain shows altered ^{18}F-FDG uptake in patients. Only a few brain regions have intact ^{18}F-FDG uptake (A), and these brain regions only contribute marginally to the whole-brain average. The altered brain areas (B) dominate the whole-brain metabolism, and ΔB is large. To simulate this situation, we repeated the example ($A = 1001$, $B = 1001$), but this time we chose $n = 0.1$. The result is shown in Fig. 4.11b. This example illustrates that both methods can cause an artifactual increase in A, when there is extreme hypometabolism in B.

To summarize, the grand mean normalization and the normalization in the SSM are equivalent methods. We illustrated that normalization to any mean is useful to eliminate subject-specific scaling factors in ^{18}F-FDG-PET data, but inherently can induce artificial increases and decreases. This is a known issue in any imaging study where absolute values are not available, be it univariate or multivariate. It is therefore important that patients and controls have similar values of average ^{18}F-FDG brain uptake (i.e., global metabolic rate (GMR)).

This issue has been addressed in several publications concerning the spatial covariance pattern that was identified in Parkinson's disease (Parkinson's disease-related pattern, PDRP). This pattern is characterized by relatively increased metabolism in subcortical structures (globus pallidus, putamen, thalamus, cerebellum, and pons), relatively increased metabolism in the sensorimotor cortex, and relatively decreased metabolism in the lateral frontal and parieto-occipital areas (Fig. 4.12). It has been posited that the PDRP reflects normalization artifacts due to GMR differences between controls and patients (Borghammer et al. 2008; Borghammer et al. 2009). Specifically, widespread cortical decreases, rather than subcortical increases,

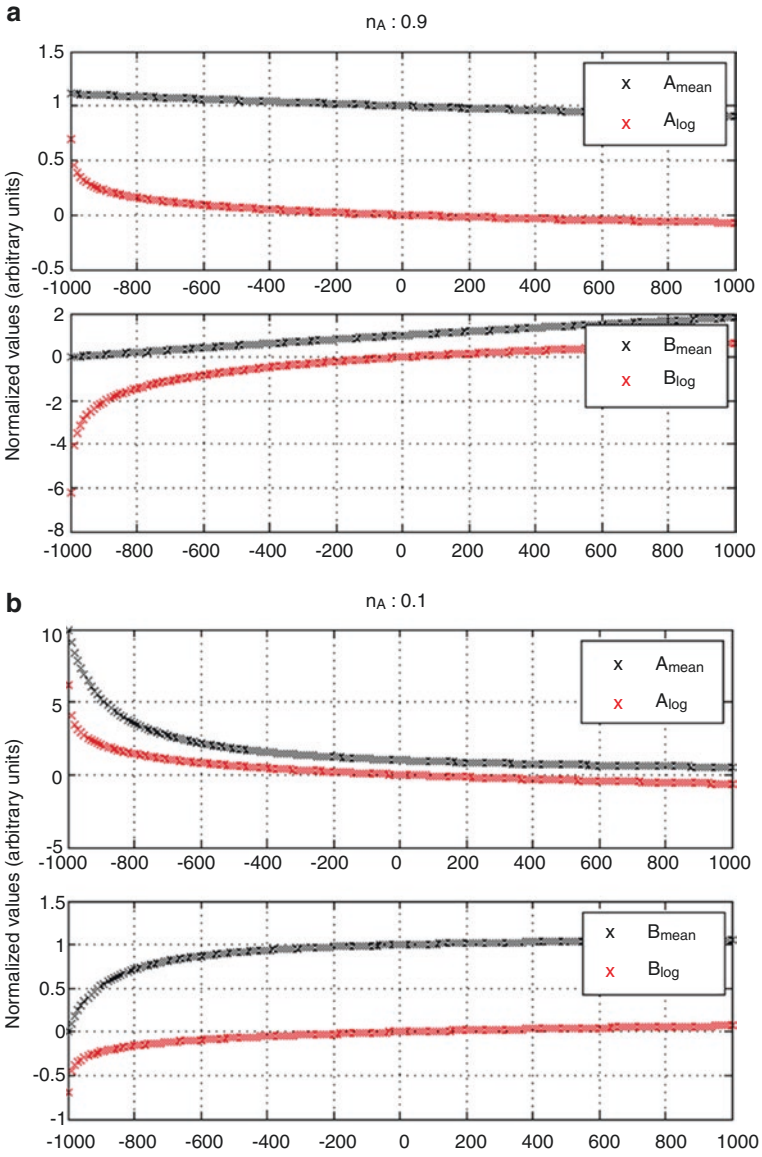

Fig. 4.11 The normalized values for region A are plotted for the global mean normalization method (A_{mean}: black) and for the SSM (A_{log}: red). The normalized values for region B are also plotted for both regions (B_{mean} and B_{log}). In *a*, the results of example 1 are shown ($n = 0.9$; $A = 1001$ and ΔB ranges from −1000 to 1000). In b, the results of example 2 are shown ($n = 0.1$; $A = 1001$ and ΔB ranges from −1000 to +1000)

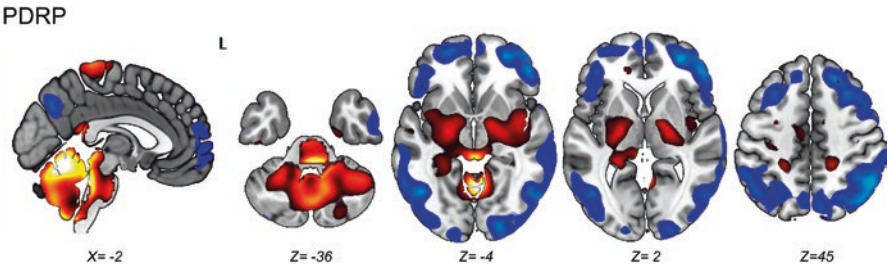

Fig. 4.12 The Parkinson's disease-related pattern (PDRP) identified in 17 controls and 19 PD subjects. Stable voxels are displayed, determined after a bootstrap resampling (90% confidence interval not straddling zero). Overlay on a T_1 MRI template. Positive voxel weights are color-coded red (relative hypermetabolism), and negative voxel weights are color-coded blue (relative hypometabolism). L = Left. Coordinates in the axial (*Z*) and sagittal (*X*) planes are in Montreal Neurological Institute (MNI) space

were suggested to be characteristic of the PD disease process (Borghammer et al. 2010). However, both theoretical and empirical evidence is available to support the contention that the PDRP topography holds true pathophysiological meaning and that the "red PDRP nodes" are central to PD pathophysiology.

Spetsieris et al. showed that GMR reductions in PD patients were not significant relative to healthy controls after 15 years of illness. GMR reductions also did not correlate with symptom duration (in contrast to PDRP scores) (Spetsieris and Eidelberg 2011). Ma et al. analyzed absolute ^{18}F-FDG uptake (with arterial blood sampling) in 24 patients with early-stage PD (Hoehn and Yahr I–II) and 24 controls. Both absolute (physiological units) and relative (after global mean ratio normalization) scan data was analyzed with a univariate model (SPM). A group contrast of relative count data revealed increased metabolism in the globus pallidus, ventral thalamus, dorsal pons/midbrain, and sensorimotor cortex, but cortical metabolic decreases were not found. There was no significant difference in mean whole-brain CMRglc between patients and controls. When absolute measures (physiological units without global mean normalization) were compared between groups in a similar univariate SPM analysis, no differences were found between controls and patients. This was attributed to the marked reduction in between-subject variability achieved with the normalization step. A similar analysis was also performed in repeat scans of PD patients. Globally normalized values for the "hypermetabolic regions" showed greater reproducibility than the corresponding absolute values (in physiological units). Thus, instead of introducing bias, the authors concluded that, when the global metabolic rate is carefully matched across groups, global normalization enhances the sensitivity of PET to detect meaningful regional differences. The SSM PCA disease-related pattern that was identified in the same data was similar to the SPM pattern but also included some additional regions (Ma et al. 2009).

A PDRP has also been identified by first normalizing the data to the cerebellum (non-log; every voxel divided by average cerebellar uptake), which was very similar to the original PDRP. In addition, the "red" and "blue" parts of the PDRP have also been used as separate vectors to calculate subject scores. Interestingly, both were

able to discriminate between controls and PD patients of a new dataset, in which the red pattern performed the best (Spetsieris and Eidelberg 2011). In addition, when the "red" and "blue" vectors were calculated separately in longitudinal FDG PET scans of de novo PD patients and controls (three scans per subject over a 48-month period), the rate of progression of the red regions was the greatest and significantly higher compared to controls. By contrast, the expression of the blue pattern did not differ from controls at any of the three time points (Ma et al. 2009). Moreover, if the "blue" areas in the PDRP define or cause the "red" areas in the PDRP, then the "red" areas should disappear when the PDRP is re-derived in a subspace that excludes the "blue" areas. This was not the case; a PDRP derived in the red voxel subspace was very similar to the "red" vector of the original PDRP, and subject scores for these two patterns were significantly correlated (Spetsieris and Eidelberg 2011). Finally, Dhawan et al. studied a group of healthy participants in whom global metabolic activity was experimentally decreased by sleep induction (with secobarbital). Participants were scanned with ^{18}F-FDG PET while awake and during stage II sleep (monitored with EEG recordings). Sleep-induced reductions in global metabolic activity did not increase PDRP expression in these controls. In addition, an SSM PCA pattern comparing sleep and wake scans did not disclose any PDRP-like subcortical increases (Dhawan et al. 2012).

References

Akaike H (1974) A new look at the statistical model identification. IEEE Trans Automat Contr 19:716–723

Attwell D, Laughlin SB (2001) An energy budget for signaling in the grey matter of the brain. J Cereb Blood Flow Metab 21:1133–1145

Batipps M, Miyaoka M, Shinohara M, Sokoloff L, Kennedy C (1981) Comparative rates of local cerebral glucose utilization in the visual system of conscious albino and pigmented rats. Neurology 31:58–62

Borghammer P, Jonsdottir KY, Cumming P, Ostergaard K, Vang K, Ashkanian M, Vafaee M, Iversen P, Gjedde A (2008) Normalization in PET group comparison studies--the importance of a valid reference region. NeuroImage 40:529–540

Borghammer P, Cumming P, Aanerud J, Gjedde A (2009) Artefactual subcortical hyperperfusion in PET studies normalized to global mean: lessons from Parkinson's disease. NeuroImage 45:249–257

Borghammer P, Chakravarty M, Jonsdottir KY, Sato N, Matsuda H, Ito K, Arahata Y, Kato T, Gjedde A (2010) Cortical hypometabolism and hypoperfusion in Parkinson's disease is extensive: probably even at early disease stages. Brain Struct Funct 214:303–317

Bostan AC, Dum RP, Strick PL (2013) Cerebellar networks with the cerebral cortex and basal ganglia. Trends Cogn Sci 17:241–254

Buzsaki G, Kaila K, Raichle M (2007) Inhibition and brain work. Neuron 56:771–783

Buzsaki G, Logothetis N, Singer W (2013) Scaling brain size, keeping timing: evolutionary preservation of brain rhythms. Neuron 80:751–764

Cherry SR, Sorenson JA, Phelps MA (2012) Physics in nuclear medicine. Elsevier Saunders, Philadelphia

Della Rosa PA, Cerami C, Gallivanone F, Prestia A, Caroli A, Castiglioni I, Gilardi MC, Frisoni G, Friston K, Ashburner J, Perani D, EADC-PET Consortium (2014) A standardized [18F]-FDG-PET template for spatial normalization in statistical parametric mapping of dementia. Neuroinformatics 12:575–593

Dhawan V, Tang CC, Ma Y, Spetsieris P, Eidelberg D (2012) Abnormal network topographies and changes in global activity: absence of a causal relationship. NeuroImage 63:1827–1832
Eckert T, Barnes A, Dhawan V, Frucht S, Gordon MF, Feigin AS, Eidelberg D (2005) FDG PET in the differential diagnosis of parkinsonian disorders. NeuroImage 26:912–921
Eidelberg D (2009) Metabolic brain networks in neurodegenerative disorders: a functional imaging approach. Trends Neurosci 32:548–557
Eidelberg D, Moeller JR, Dhawan V, Spetsieris P, Takikawa S, Ishikawa T, Chaly T, Robeson W, Margouleff D, Przedborski S (1994) The metabolic topography of parkinsonism. J Cereb Blood Flow Metab 14:783–801
Fornito A, Zalesky A, Bullmore E (2016) Fundamentals of brain network analysis. Elsevier, Amsterdam
Fox PT, Raichle ME (1986) Focal physiological uncoupling of cerebral blood flow and oxidative metabolism during somatosensory stimulation in human subjects. Proc Natl Acad Sci U S A 83:1140–1144
Fox PT, Mintun MA, Raichle ME, Herscovitch P (1984) A noninvasive approach to quantitative functional brain mapping with H2 (15)O and positron emission tomography. J Cereb Blood Flow Metab 4:329–333
Fox PT, Raichle ME, Mintun MA, Dence C (1988) Nonoxidative glucose consumption during focal physiologic neural activity. Science 241:462–464
Friston KJ (2011) Functional and effective connectivity: a review. Brain Connect 1:13–36
Genovese CR, Lazar NA, Nichols T (2002) Thresholding of statistical maps in functional neuroimaging using the false discovery rate. NeuroImage 15:870–878
Habeck C, Moeller JR (2011) Intrinsic functional-connectivity networks for diagnosis: just beautiful pictures? Brain Connect 1:99–103
Habeck C, Foster NL, Perneczky R, Kurz A, Alexopoulos P, Koeppe RA, Drzezga A, Stern Y (2008) Multivariate and univariate neuroimaging biomarkers of Alzheimer's disease. NeuroImage 40:1503–1515
Habeck C, Stern Y, Alzheimer's Disease Neuroimaging Initiative (2010) Multivariate data analysis for neuroimaging data: overview and application to Alzheimer's disease. Cell Biochem Biophys 58:53–67
Heiss WD (2014) Cerebral Glucose Metabolism. In: Dierckx RAJO, Otte A, de Vries EFJ, van Waarde A, Luiten PGM (eds) PET and SPECT of neurobiological systems. Springer-Verlag, Berlin Heidelberg, p 85
Herholz K, Herscovitch P, Heiss W (2004) NeuroPET; PET in neuroscience and clinical neurology. Springer-Verlag, Berlin Heidelberg
Jueptner M, Weiller C (1995) Review: does measurement of regional cerebral blood flow reflect synaptic activity? Implications for PET and fMRI. NeuroImage 2:148–156
Juh R, Kim J, Moon D, Choe B, Suh T (2004) Different metabolic patterns analysis of parkinsonism on the 18F-FDG PET. Eur J Radiol 51:223–233
Kadekaro M, Crane AM, Sokoloff L (1985) Differential effects of electrical stimulation of sciatic nerve on metabolic activity in spinal cord and dorsal root ganglion in the rat. Proc Natl Acad Sci U S A 82:6010–6013
Karp JS, Surti S, Daube-Witherspoon ME, Muehllehner G (2008) Benefit of time-of-flight in PET: experimental and clinical results. J Nucl Med 49:462–470
Kogan RV, de Jong BA, Renken RJ, Meles SK, van Snick PJH, Golla S, Rijnsdorp S, Perani D, Leenders KL, Boellaard R, JPND-PETMETPAT Working Group (2019) Factors affecting the harmonization of disease-related metabolic brain pattern expression quantification in [(18) F]FDG-PET (PETMETPAT). Alzheimers Dement (Amst) 11:472–482
Lin AL, Fox PT, Yang Y, Lu H, Tan LH, Gao JH (2008) Evaluation of MRI models in the measurement of CMRO2 and its relationship with CBF. Magn Reson Med 60:380–389
Lin AL, Fox PT, Yang Y, Lu H, Tan LH, Gao JH (2009) Time-dependent correlation of cerebral blood flow with oxygen metabolism in activated human visual cortex as measured by fMRI. NeuroImage 44:16–22

Lin AL, Fox PT, Hardies J, Duong TQ, Gao JH (2010) Nonlinear coupling between cerebral blood flow, oxygen consumption, and ATP production in human visual cortex. Proc Natl Acad Sci U S A 107:8446–8451

Ma Y, Tang C, Spetsieris PG, Dhawan V, Eidelberg D (2007) Abnormal metabolic network activity in Parkinson's disease: test-retest reproducibility. J Cereb Blood Flow Metab 27:597–605

Ma Y, Tang C, Moeller JR, Eidelberg D (2009) Abnormal regional brain function in Parkinson's disease: truth or fiction? NeuroImage 45:260–266

Magistretti PJ, Allaman I (2015) A cellular perspective on brain energy metabolism and functional imaging. Neuron 86:883–901

Meles SK, Kok JG, De Jong BM, Renken RJ, de Vries JJ, Spikman JM, Ziengs AL, Willemsen ATM, van der Horn HJ, Leenders KL, Kremer HPH (2018a) The cerebral metabolic topography of spinocerebellar ataxia type 3. Neuroimage Clin 19:90–97

Meles SK, Renken RJ, Janzen A, Vadasz D, Pagani M, Arnaldi D, Morbelli S, Nobili F, Mayer G, Leenders KL, Oertel WHO (2018b) The metabolic pattern of idiopathic REM sleep behavior disorder reflects early-stage Parkinson's disease. J Nucl Med 59(9):1437–1444

Moeller JR, Habeck CG (2006) Reciprocal benefits of mass-univariate and multivariate modeling in brain mapping: applications to event-related functional MRI, H(2) (15)O-, and FDG-PET. Int J Biomed Imaging 2006:79862

Moeller JR, Strother SC (1991) A regional covariance approach to the analysis of functional patterns in positron emission tomographic data. J Cereb Blood Flow Metab 11:A121–A135

Moeller JR, Strother SC, Sidtis JJ, Rottenberg DA (1987) Scaled subprofile model: a statistical approach to the analysis of functional patterns in positron emission tomographic data. J Cereb Blood Flow Metab 7:649–658

Niethammer M, Eidelberg D (2012) Metabolic brain networks in translational neurology: concepts and applications. Ann Neurol 72:635–647

O'Toole AJ, Jiang F, Abdi H, Penard N, Dunlop JP, Parent MA (2007) Theoretical, statistical, and practical perspectives on pattern-based classification approaches to the analysis of functional neuroimaging data. J Cogn Neurosci 19:1735–1752

Phelps ME, Hoffman EJ, Huang SC, Ter-Pogossian MM (1975) Effect of positron range on spatial resolution. J Nucl Med 16:649–652

Raichle ME, Larson KB, Phelps ME, Grubb RL Jr, Welch MJ, Ter-Pogossian MM (1975) In vivo measurement of brain glucose transport and metabolism employing glucose- -11C. Am J Phys 228:1936–1948

Reivich M, Kuhl D, Wolf A, Greenberg J, Phelps M, Ido T, Casella V, Fowler J, Hoffman E, Alavi A, Som P, Sokoloff L (1979) The [18F]fluorodeoxyglucose method for the measurement of local cerebral glucose utilization in man. Circ Res 44:127–137

Rodriguez-Oroz MC, Jahanshahi M, Krack P, Litvan I, Macias R, Bezard E, Obeso JA (2009) Initial clinical manifestations of Parkinson's disease: features and pathophysiological mechanisms. Lancet Neurol 8:1128–1139

Sacks W (1957) Cerebral metabolism of isotopic glucose in normal human subjects. J Appl Physiol 10:37–44

Sibson NR, Dhankhar A, Mason GF, Rothman DL, Behar KL, Shulman RG (1998) Stoichiometric coupling of brain glucose metabolism and glutamatergic neuronal activity. Proc Natl Acad Sci U S A 95:316–321

Sokoloff L (1993) Sites and mechanisms of function-related changes in energy metabolism in the nervous system. Dev Neurosci 15:194–206

Sokoloff L, Reivich M, Kennedy C, Des Rosiers MH, Patlak CS, Pettigrew KD, Sakurada O, Shinohara M (1977) The [^{14}C]deoxyglucose method for the measurement of local cerebral glucose utilization: theory, procedure, and normal values in the conscious and anesthetized albino rat. J Neurochem 28:897–916

Spetsieris PG, Eidelberg D (2011) Scaled subprofile modeling of resting state imaging data in Parkinson's disease: methodological issues. NeuroImage 54:2899–2914

Spetsieris PG, Ko JH, Tang CC, Nazem A, Sako W, Peng S, Ma Y, Dhawan V, Eidelberg D (2015) Metabolic resting-state brain networks in health and disease. Proc Natl Acad Sci U S A 112:2563–2568

Surti S, Karp JS (2016) Advances in time-of-flight PET. Phys Med 32:12–22

Teune LK, Bartels AL, de Jong BM, Willemsen AT, Eshuis SA, de Vries JJ, van Oostrom JC, Leenders KL (2010) Typical cerebral metabolic patterns in neurodegenerative brain diseases. Mov Disord 25:2395–2404

Teune LK, Renken RJ, Mudali D, De Jong BM, Dierckx RA, Roerdink JB, Leenders KL (2013) Validation of parkinsonian disease-related metabolic brain patterns. Mov Disord 28:547–551

Teune LK, Renken RJ, de Jong BM, Willemsen AT, van Osch MJ, Roerdink JB, Dierckx RA, Leenders KL (2014a) Parkinson's disease-related perfusion and glucose metabolic brain patterns identified with PCASL-MRI and FDG-PET imaging. Neuroimage Clin 5:240–244

Teune LK, Strijkert F, Renken RJ, Izaks GJ, de Vries JJ, Segbers M, Roerdink JB, Dierckx RA, Leenders KL (2014b) The Alzheimer's disease-related glucose metabolic brain pattern. Curr Alzheimer Res 11:725–732

Vaishnavi SN, Vlassenko AG, Rundle MM, Snyder AZ, Mintun MA, Raichle ME (2010) Regional aerobic glycolysis in the human brain. Proc Natl Acad Sci U S A 107:17757–17762

Varrone A, Asenbaum S, Vander Borght T, Booij J, Nobili F, Nagren K, Darcourt J, Kapucu OL, Tatsch K, Bartenstein P, Van Laere K, European Association of Nuclear Medicine Neuroimaging Committee (2009) EANM procedure guidelines for PET brain imaging using [18F]FDG, version 2. Eur J Nucl Med Mol Imaging 36:2103–2110

Wu P, Wang J, Peng S, Ma Y, Zhang H, Guan Y, Zuo C (2013) Metabolic brain network in the Chinese patients with Parkinson's disease based on 18F-FDG PET imaging. Parkinsonism Relat Disord 19:622–627

Wu P, Yu H, Peng S, Dauvilliers Y, Wang J, Ge J, Zhang H, Eidelberg D, Ma Y, Zuo C (2014) Consistent abnormalities in metabolic network activity in idiopathic rapid eye movement sleep behaviour disorder. Brain 137:3122–3128

Yong SW, Yoon JK, An YS, Lee PH (2007) A comparison of cerebral glucose metabolism in Parkinson’s disease, Parkinson's disease dementia and dementia with Lewy bodies. Eur J Neurol 14:1357–1362

Artificial Intelligence in the Analysis of PET Scans of the Human Brain

5

Kim Mouridsen and Ronald Borra

Contents

5.1 Introduction 106
5.2 Artificial Intelligence 107
5.3 Scope of Classical Statistics Versus Deep Learning 109
5.4 Inferring CT and MR Information 110
5.5 Image Reconstruction 111
5.6 Dose Reduction 112
5.7 Automated Detection of Pathology 112
5.8 Considerations for the Future 114
References 115

Abstract

Artificial intelligence (AI) is being intensely studied, evaluated, and applied in healthcare and especially in medical imaging. Having shown performance equaling that of experienced radiologists in tasks such as detecting pneumonia on chest X-rays and identifying cancerous long nodules on X-ray, AI is poised to radically optimize many areas of medical practice from early detection of disease to prediction of progression and personalization of therapeutic strategy. Artificial intelligence extends classical statistical techniques and machine learning, both of which characteristically involve manually establishing imaging features hypothesized to modulate a certain outcome. With AI, predictive features are automatically established in a data-driven fashion, which in turn implies that raw

K. Mouridsen (✉)
Center of Functionally Integrative Neuroscience and MINDLab, Inst. of Clinical Medicine, Aarhus University, Aarhus C, Denmark
e-mail: kim@cfin.au.dk

R. Borra
University Medical Center Groningen, Groningen, The Netherlands

R. A. J. O. Dierckx et al. (eds.), *PET and SPECT in Neurology*,
https://doi.org/10.1007/978-3-030-53168-3_5

unprocessed data can be fully utilized, human bias can be avoided, and previously unrealized disease mechanisms potentially can be discovered. Here we discuss applications of AI in PET imaging for image reconstruction, attenuation correction without CT, dose reduction, automatic identification of pathology, and differentiation of disease progression. One of the costs of more automated analyses and better accuracy with AI compared to classical machine learning is larger volumes of training data; however, the field is rapidly evolving, and we discuss possible mitigations as well as other directions for valuable future applications of AI in PET imaging.

5.1 Introduction

Deep learning may be considered the big bang moment for artificial intelligence (AI). The idea of mimicking human brain architecture to build "intelligent" machines dates back at least to the period 1930–1950 where research in neurology showed that the brain consists of networks of neurons exchanging electrical signals and concurrently researchers showed that any form of computation can be performed digitally. Over the years, however, mathematical models based on idealized neurons organized in a hierarchical structure were realized to be unstable, brittle, in the sense that training the same network more than once led to different solutions and networks could yield surprising results given previously unseen input.

The pursuit for electronic brains gave way for less ambitious or "flat" models such as support vector machines and even classical logistic regression for tasks where a set of input variables should be combined to form a classification or prediction. In general interest in neural networks was replaced by developments in what is often referred to as classical machine learning. Despite a much simpler structure, classical machine learning techniques often demonstrate good classification or predictive accuracy, have been extensively applied in medical imaging, and lie at the heart of the relatively new field of radiomics, where tissue imaging features are manually crafted, for instance, with texture analysis, and combined into estimates of tissue type or presence of disease, for instance.

The idea that superior performance could be obtained by replicating neuronal architecture was not entirely abandoned, but it was not until the period 2006–2012 that neural networks accomplished the breakthroughs leading to today's enthusiasm. In this period Geoffrey Hinton, among others, discovered robust methods to train neural networks and laid the foundation for the field now known as deep learning. It centers on artificial neural networks with "neurons" or nodes, as they are called, organized in hierarchically connected layers, of which there can be hundreds and the total number of free parameters on the scale of millions; see Figure 5.1b for a schematic illustration.

As an indicator of progress, the annual ImageNet challenge considers a database of one million images from one thousand categories. By 2011 only classical machine learning had been attempted with the best algorithms reaching an accuracy around 75%. In 2012 deep learning yielded a remarkable 84.3% accuracy (Krizhevsky et al.

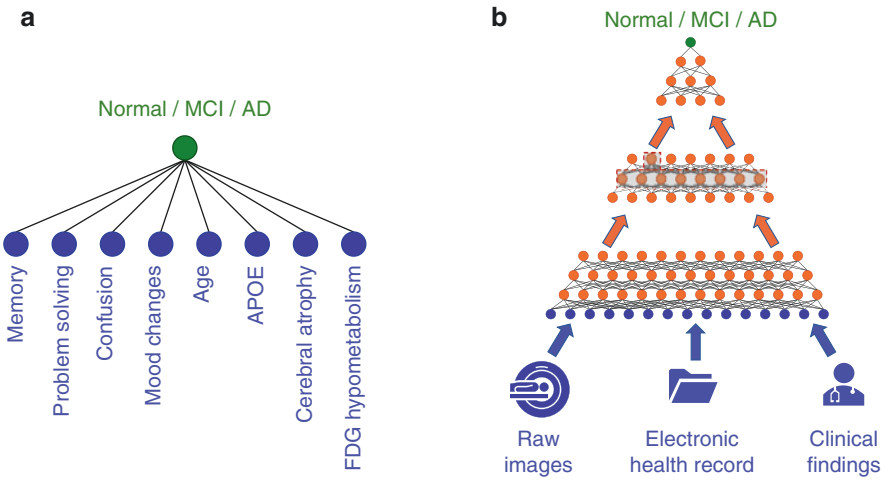

Fig. 5.1 (**a**) Graphic representation of the idea of combining a number of input variables into a single value. (**b**) Schematic illustration of an artificial neural network

2012). Perhaps the most surprising development was in 2015 where a deep neural network was reported to exceed human performance in image classification (He et al. 2015).

Clearly a natural domain for application of deep learning is medical imaging, and the technology has already demonstrated notable success. One study showed that a deep neural network (DNN) outperformed four radiologists in detecting pneumonia on chest X-rays (Rajpurkar et al. 2017). Another study found that a DNN outperformed 17 out of 18 radiologists in a task of identifying cancerous long nodules on X-rays (Hwang et al. 2019). With increasing demand for value and efficiency in healthcare, and not least medical imaging, AI is poised—inter alia—to improve early disease detection, accelerate image reading, and guide therapeutic decision-making.

As a crucial component in routine diagnostics as well as clinical trials, nuclear medicine stands to make important advances in combination with AI methodology. So far the field appears less explored than other advanced imaging modalities. A search on PubMed (October 18, 2019) for deep learning revealed only 65 publications with positron emission tomography against 271 with computed tomography and 420 with magnetic resonance imaging. In the following, we discuss current research directions, results, and future opportunities.

5.2 Artificial Intelligence

To better understand the potential and opportunities for AI in PET imaging, we offer a brief introduction and overview of methods from a "user's" perspective. Although the terminology is ambiguous, artificial intelligence is often used as an overarching term for methods aimed at identifying and parameterizing patterns in data. This can

be as simple as a classical regression model, where a number of observed quantities are combined to form an estimate or prediction of a target quantity. In a linear regression, this target is a value such as the volume of a tissue type or the level of metabolism. If the target is a category, such as presence or absence of disease, the same linear combination can be formed but is then transformed to represent the probability for each of the two, or more, classes. This is called logistic regression. Figure 5.1a displays graphically the idea of combining a number of input variables into a single value.

As we will see below, the state-of-the-art deep learning models, which can be said to be at the other end of the spectrum of mathematical complexity compared to regression, consist fundamentally of exactly the same simple building blocks, namely, linear combinations of predictors. This is illustrated in Figure 5.1b, where the small highlighted part of the larger network has exactly the structure of a regression model shown in Figure 5.1a. The difference is that deep neural networks comprise hierarchies of non-linear transformations of the basic linear combinations.

One advantage is that throughout the layers the model itself is able to construct combinations of input variables which are predictive for the target outcome. This allows tremendous flexibility in transforming—or encoding—the connection between predictors and response, where these hierarchical models also have the capacity to naturally uncover complex interactions across predictors. Interactions are also possible in classical regression models, but they must be specified manually a priori, and typically only subsets of pairs of variables are considered practically feasible.

Another advantage is that since it is possible to have even very high numbers of nodes in the input layer, it is feasible to input raw data such as image volumes (PET, MRI, CT), text (electronic health records, clinical findings), and signals (EEG, MEG). In contrast, with classical regression, raw data is typically filtered, aggregated, and subjected to manual feature extraction until rather few representative quantities are left. Broadly speaking, a regression model can in this case be seen as the result of human feature engineering followed by statistical fitting, whereas a neural network automates the entire process. The manual steps in classical data analyses prompt risk of bias, missing critical information and even overfitting, compromising generalizability. The latter is an often overlooked problem in classical scientific data analyses. Whereas the regression model itself is thoroughly treated by statistical software and estimates are properly corrected for level of data noise and number of parameters, the many choices of which parameters to include and how they are transformed and combined are not factored into the final results, although substantially influencing the degrees of freedom and potentially limiting reproducibility (Simmons et al. 2011; Ioannidis 2005).

A third advantage is that deep learning models have the capability to continue improving in performance as the volume of input data increases. Simple models such as regressions are naturally limited in their ability to model complex relations between inputs and outputs, whereas deep neural networks, with up to millions of parameters, are able to encode much more complex relations, such as the

differences in disease progression across diverse populations. The volume of parameters is at the same time the major limitation of deep neural networks when data is scarce, where classical models may be more robustly applied.

5.3 Scope of Classical Statistics Versus Deep Learning

As we have seen, modern deep neural networks extend in terms of architecture the classical regression model. However, the purpose and the methods for fitting the two approaches differ considerably. From a traditional statistical point of view, linear combinations are used in an inferential way to quantify the degree (and type) of influence a predictor seemingly exerts on an outcome measure. This has been qualified, for instance, by the amount of change in response that would be expected by a one-unit change in the value of the predictor. Formally, significance tests have been used as an indicator for whether such an effect should be considered manifest or could have occurred by chance.

Considering regression as a (very) simple machine learning model means changing one's perspective. Instead of focusing on quantification of individual predictor's effect on the response, we focus on making the most accurate predictions. For this purpose, the inferential question of whether a predictor is statistically significant is less relevant, and instead the focus is on the collective predictive ability. This could be conceived as a loss, but if, for instance, the input for a prediction, e.g., prediction of progression of dementia, is an entire image, it can be argued that it is not the individual voxels but rather their combined effects and interactions which are of interest. In this case the notion of effect of a single element may be less meaningful in that the voxel may have negligible influence in itself but may contribute via complex interactions with other tissue regions. The matter of whether an element provides actual information, however, persists but manifests in a different way. Namely, if a predictor does not consistently contribute to prediction of the response, its coefficient parameter will typically be low or zero. This is ensured by a mechanism during model development referred to as cross-validation, which may be seen as an even stricter control than traditional statistical inference based on *p*-values. During model development data used for fitting is typically split in a training partition and a validation partition. This systematically simulates the real-world setting where the model must make predictions for new and previously unseen cases. Hence if a predictor has an apparently strong effect on the outcome in the training data, but performance on the validation data is low, then the estimated strength of each predictor is adjusted accordingly. As a result, the final model will have "proven" that it performs well on the data on which it was trained but is also expected to perform well on unseen cases. This is a very important and valuable criteria especially for methods intended to be used in actual clinical settings. It is important to note that in traditional statistics, all data points are typically used for model fitting and *p*-values used for inference are based on in-sample estimates. Hence it can be argued that artificial intelligence algorithms undergo a stricter scrutiny than traditional

statistical models and foster greater requirements for predictors than traditional inference.

As an additional note, *p*-values are influenced not only by the size of the effect they are associated with but also by the number of observations in the study. Accordingly, as studies increase in volume of samples, assuming that the effect of a predictor remains constant, the *p*-value will in any case become smaller. Therefore even the most scientifically negligible effects will eventually become statistically significant. In contrast, the actual influence and therefore predictive ability of the variable remain the same, and therefore the performance of the model will not change (Mouridsen 2015). Measurement of model performance can therefore be argued to give a more robust picture of the face value of predictors.

5.4 Inferring CT and MR Information

A challenge for quantitative PET imaging is the spatially accurate source of photon emission. The tissue-dependent attenuation, such as Compton scatter, of the gamma-rays compromises precise volumetric reconstruction. A common resolution to this problem is to acquire an additional CT, typically in combined PET/CT systems, which yield clear identification of bone structures which can be used as a basis to establish a photon attenuation correction map. However this may not always be a practical solution wherefore deep learning has been considered to alleviate this problem in different settings.

For instance, with combined PET/MR scanners, a CT scan for attenuation correction is unavailable. At the same time, while standard MRI sequences are excellent at displaying soft-tissue contrast, MRI poorly displays bone and can therefore not be used per se as a basis for attenuation correction. This can be mediated to some extent using very short echo times, but errors remain in the attenuation correction. As an alternative it has been suggested to generate a pseudo-CT image from MRI (Liu et al. 2018a). With 40 subjects for whom T1 MRI as well as plain CT was acquired, an encoder-decoder type neural network was constructed aiming to input an MR image and output a segmented CT image. The pseudo-CT images were shown to match actual segmented CT with a Dice coefficient of 0.803 ± 0.021 for bone. In a prospective study with five patients, a significantly lower PET reconstruction error was demonstrated with deep learning-based attenuation correction than with standard Dixon-based soft-tissue and air segmentation and anatomic CT-based template registration.

An alternative idea is to directly estimate a pseudo-CT image with tissue segmentation from the uncorrected PET image, thereby avoiding the extra step involved in acquiring a second image modality. One procedure for this was recently proposed (Liu et al. 2018b). This study uses a similar encoder-decoder structure network as in Liu et al. (2018a) except for the addition of short-cut connections making the architecture appear comparable to the U-net (Ronneberger et al. 2015). The network was trained based on 100 subjects and validated on an additional 28. The authors report a Dice coefficient for bone segmentation of 0.75 ± 0.03 compared to actual non-contrast CT and ^{18}F-FDG-PET errors less than 2% compared to CT.

Looking beyond attenuation correction, the possibility for image-to-image translation may also be useful, for instance, in diagnostic workup where two modalities are necessary. For instance, amyloid deposition is a useful biomarker in patients suspected of cognitive decline, where absence of amyloid depositions in the cortex can rule out Alzheimer's disease. Being established as SUV relative to a reference region, PET imaging should therefore ideally be supplemented by a structural MR acquisition. However, this may not be feasible in the clinic. As an alternative (Choi and Lee 2018) suggests producing a pseudo-T1 MRI from ^{18}F-florbetapir PET. The model was trained using 163 patients from the ADNI study. The authors used a so-called generative adversarial neural network which is an approach in which two competing networks are trained in parallel (Goodfellow et al. 2014). One is trained with the aim to generate realistic MR images from PET, while the other is trained to determine whether an MR image is artificially generated or actually acquired**.** Performance test in 98 subjects from 8 independent sites showed an absolute error in standardized SUV significantly smaller than for other MR-less approaches such as template matching and segmentation.

5.5 Image Reconstruction

PET images are created via a complex process where scintillation in the inorganic crystals in the PET scanner is converted to spatially resolved maps of metabolic activity. This process holds a number of possible applications for artificial intelligence. Raw data produced in a PET acquisition are in the form of a sinogram representing the number of photon coincidence detections in pairs of detectors. Conversion from sinogram data to tissue maps is known as image reconstruction. This can be accomplished with so-called filtered backprojection (FBP) which is computationally efficient but has a range of limitations including tendency to produce streaks across images from high-uptake areas and sensitivity to shot noise. Statistical methods acknowledge the randomness in the underlying physical processes and avoid the artifacts of FBP but are slow because they require iterative maximization of a likelihood function, for instance, using expectation maximization (MLEM).

In Cui et al. (2017), the authors suggest improving the MLEM by using stacked autoencoders to automatically extract important image features. However it has also been suggested to entirely bypass traditional image reconstruction and simply construct metabolic maps from raw sinogram data (Häggström et al. 2019). By presenting a neural network on the input side with sinogram data and on the output side spatial maps established with traditional, but time-consuming, image reconstruction, the authors demonstrate that the network becomes capable of prospectively producing spatial maps from sinogram data with similar quality but more than 100 times faster.

PET image quality depends on the features of the scintillating crystals. More coarsely pixelated crystals are less sensitive to noise but produce blurred images, whereas thin-pixelated crystals yield higher spatial accuracy but at the cost of noise sensitivity. Hong et al. (2018) suggest that comparable image resolution and better

noise properties can be obtained with large crystals of bin sizes a factor 4 larger than thin crystals using a deep residual convolutional neural network. For an application of denoising with combined PET/CT data, see, for instance, Cui et al. (2019).

5.6 Dose Reduction

One of the main limitations for wider use of PET in the clinic is the necessity of a radioactive tracer. Due to radiation exposure, PET imaging is often limited to terminally ill or elderly patients. If the radiation dose could be reduced without substantially compromising image quality, the more general clinical value of PET could increase tremendously.

With image quality depending on the balance of bed duration and radiation dose, early work (Xiang et al. 2017) used a reduction in acquisition time from 12 min to 3 min following a standard dose of ^{18}F-2-deoxyglucose to simulate the effect of administering a dose 75% below the standard. Using a concatenation of convolutional neural networks with the pseudo-low-dose (i.e., short scan duration) images as input and standard-dose (long scan duration) images as output to predict, the study shows in 16 patients that in particular when the low-dose PET is complemented by T1 MR competitive image quality is seen relative to a state-of-the-art technique however 500 times faster.

Later, Xu et al. (2017) administered standard-dose ^{18}F-fluorodeoxyglucose (370 MBq) in nine patients with glioblastoma with a PET/MR scanner. Low-dose PET was simulated by randomly selecting only 0.5% of the count events based on raw listmode data corresponding to a 200× reduction in dose. The authors used so-called residual learning where a neural network is trained to learn the difference between low-dose PET as input and standard-dose PET as output. This is found to be a more robust training strategy for deep networks. The resulting network demonstrated to produce superior performance in estimating standard-dose PET from low-dose PET compared to state-of-the-art techniques.

Clearly synthetic images reconstructed from lower resolution will not match standard acquisitions numerically exact, but for clinical purposes, a more relevant question is whether similar diagnostic conclusions are reached with the synthetic images. To study this, Chen et al. (2019) considered amyloid (fluorine 18 [^{18}F]-florbetaben) PET/MR acquisitions in 39 subjects and a neural network architecture similar to Xu et al. (2017). Expert human assessment of amyloid status with synthetic images yielded good accuracy compared to full-dose images with an accuracy of 89% corresponding to 71 out of 80 readings and was found to be similar to intrareader reproducibility of full-dose images (73 of 80 [91%]).

5.7 Automated Detection of Pathology

Combined PET and CT imaging plays a major role in managing oncological patients and in particular for radiation therapy planning. Outlining the gross tumor as well as pathological lymph nodes is a time-consuming manual task. In addition to the

time requirement, the manual intervention also limits reproducibility and standardization. Automation of this task is therefore potentially a clinically valuable application of artificial intelligence. This task has previously been approached with traditional machine learning methods such as k-nearest neighbors, Markov random fields, adaptive random walk with k-means, and decision trees (Yu et al. 2009; Comelli et al. 2018; Yang et al. 2015; Stefano et al. 2017; Berthon et al. 2017).

Using a deep learning approach, Moe et al. (2019) describe a method for automatic delineation of gross tumor volume as well as pathological lymph nodes. This is based on the often used U-Net convolutional architecture (Ronneberger et al. 2015)**.** Imaging regimen included FDG-PET and CT. The best correspondence with manual outlining was seen when using PET and CT images in combination, followed by PET only. The Dice coefficient for PET/CT was 0.75 ± 0.12, whereas for CT only this dropped to 0.65 ± 0.17. This was based on a training set of 142, validation set of 15, and test set of 42 patients stratified on tumor T-stage.

In a smaller study (Huang et al. 2018), however with combined PET and CT data from two sites, a convolutional architecture also based on the U-net was proposed to segment gross tumor volume. To mitigate the challenge of a lower number of patients, this study explicitly used simulated data augmentation in the form of rotating the images, horizontal mirroring, changing the contrast, and image scaling. The resulting median Dice score as calculated with leave-one-out cross-validation was 0.785 with a range of 0.482 to 0.868.

Correct delineation of tumor volume in clinical practice also depends on the ability to differentiate between lesions due to tumor progression and tissue damage due to radiotherapy. For instance, radiosurgery treatment of patients with brain metastases may result in radiation necrosis rates between 25% and 50% (Minniti et al. 2011). Mis-interpretation of treatment-induced change as tumor progression may lead to unwarranted treatment approaches or cessation of effective therapy as well as biased estimation of therapeutic success in clinical trials.

Whereas reports (Chao et al. 2001) on the use of FDG-PET for differentiating metastasis relapse from radiation damage are ambiguous on the clinical value, with sensitivities and specificities ranging from 40% to 100%, the MET and FDOPA PET have more consistently demonstrated clinical feasibility with sensitivities and specificities around 80%. Similarly for the differentiation of treatment-related damage and progression of glioma, PET imaging with FET and FDOPA has shown clinically relevant performance. While artificial intelligence may be hypothesized to improve these performances by a more detailed analysis of lesion extent and texture notably the implementation of dynamic PET (Galldiks et al. 2012), where subtle patterns in the uptake curves may hold further clues, which can be exploited by computationally intensive methods.

Detection of disease can also have a more global aim than regional gross tumor or metastasis identification and delineation. For instance, detection of Alzheimer's disease (AD) is important for diagnostic purposes and is expected to become even more critical with the advent of therapies to potentially delay onset, slow progression, or even cure the disease. At the heart of this task is separation of prodromal AD cases from patients with mild cognitive impairment (MCI) who will not progress to AD. It is speculated that a deeper understanding of the progression from MCI to AD

is necessary also at the time of development of pharmacological interventions—since only a fraction of patients with symptoms of MCI develop AD, the patients who would not progress to AD will seemingly dilute actual therapeutic effects for those who will progress. Being able to design studies such that only patients predicted to progress to AD from MCI are included will increase the statistical power for detection of actual effects.

FDG-PET plays an important role in the diagnosis of AD due to its ability to show metabolic activity which is recognized to preceed anatomical changes, as observed with MRI, and account for the cognitive and functional decline observed with the disease. However, success in developing automated methods for predicting which MCI cases will progress to AD has been limited with accuracies typically not exceeding 80% (Lu et al. 2018).

One larger study (Lu et al. 2018) considers 1.051 patients from the publicly available ADNI dataset with structural MRI as well as FDG-PET. Subjects were divided in normal controls, stable mild cognitive impairment (sMCI) class, progressive mild cognitive impairment (pMCI) class, and those clinically diagnosed with Alzheimer's disease. A deep learning approach was suggested which simultaneously analyzes images across different spatial resolutions. This produces a number of classifiers, which are then combined into a single result via so-called ensemble learning. An accuracy of 82.51(5.35) was demonstrated for automatically differentiating between stable and progressive MCI. For the classification of NC versus AD, the accuracy reported was 93.58 (5.20). The principle of combining multiple classifications into one has also previously been explored in a subset of the ADNI data (Ortiz et al. 2016).

This study employed a strategy of pre-training the neural network using a so-called autoencoder approach. Autoencoders have previously shown efficiency in detection of AD in a smaller subset of 311 subjects from the ADNI data (Liu et al. 2014). One of the challenges in deep learning models, which contain a large number of unknown parameters, is finding suitable starting values (known as initialization). An autoencoder can be used to mitigate this problem by effectively reducing the complex information in raw data to more compact distillation. This is accomplished by channeling the high-dimensional raw data through a lower-dimensional layer of hidden units in neural network and then optimizing this layer such that it can at the same time reproduce the input data. This is similar to traditional principal component analysis, where raw data is reduced to principal components which are linear combinations of data input. Autoencoders generalize this approach by using non-linear transformations. The many layers in a deep neural network can now be initialized in a bottom-up approach where each layer is initialized by the hidden layer of an appropriate autoencoder.

5.8 Considerations for the Future

Across medical imaging and healthcare in general, there are a seemingly endless stream of new ideas for application of AI and a corresponding multitude of proof-of-concept-level studies. However the uptake in clinical practice is still minimal. In 2017 and 2018, only around 14 algorithms were approved by the Food and Drug Administration (FDA) in the USA. It is a concern that few of the companies behind

these products have published peer-reviewed papers let alone conducted prospective clinical trials. This shows a trend where validation of technology as well as actual clinical value is lacking.

One reason for the lack of validation studies is that datasets in medical imaging are typically small. While some of the largest medical imaging datasets used for deep learning contains in the order of 100.000 patients, run-of-the-mill research studies are much smaller with cohort sizes from around 30 to a few thousands. This may be due to limited funding, but privacy concerns also make compilation of large data volumes from different sites across the world let alone commercial participation difficult. Research publications, such as those reviewed here, do offer validations, but only the so-called cross-validations which are essentially made by randomly splitting the dataset into training and testing. The testing dataset therefore, statistically, has the same properties as the training data which may not be the case if new data is acquired with another machine or at another hospital. Also inclusion and exclusion criteria must be exactly identical. For clinical uptake not only larger datasets with representative samples are critical to show consistent high accuracy, but the technologies must be tested prospectively in the clinic to show actual value. With smaller datasets the risk of bias also increases, and bias in AI is a concern. However in fairness this should be compared to human bias which has also been reported to be significant (Topol 2019). In the case of AI, the bias is in principle avoidable by having representative data samples. Finally although cross-validation is the typical performance metric used in AI studies, the field lacks a standard for how this is performed. Without such standardization, it is difficult to compare performance across studies. In classical statistics, *p*-values have the role of a standardized measure of significance. Although such single measures may be misused or overinterpreted, as has been the case with *p*-values (Ioannidis 2005), efforts toward developing standardized reporting practices will be beneficial.

For the first wave of AI enthusiasm algorithm performance has been the center of attention. To move the field forward, increase trust in AI technology, and increase clinical acceptance, the pursuit to develop explainable AI will likely have a substantial role. A common criticism of deep neural networks is that they are black boxes unable to account for their otherwise high accuracy. In Europe, the General Data Protection Regulation (GDPR) stipulates that decisions relating to a patient may not fully rely on automated processing, often taken to mean that patients have a right to an explanation for decisions. As the field moves forward, the ability of algorithms to account for their decisions may not only benefit patients but also be the source of many new insights and discoveries based on combinations of imaging and health record data made possible by modern versions of artificial intelligence.

References

Berthon B et al (2017) Head and neck target delineation using a novel PET automatic segmentation algorithm. Radiother Oncol 122:242–247

Chao ST, Suh JH, Raja S, Lee SY, Barnett G (2001) The sensitivity and specificity of FDG PET in distinguishing recurrent brain tumor from radionecrosis in patients treated with stereotactic radiosurgery. Int J Cancer 96:191–197

Chen KT et al (2019) Ultra-low-dose (18)F-Florbetaben amyloid PET imaging using deep learning with multi-contrast MRI inputs. Radiology 290:649–656
Choi H, Lee DS (2018) Generation of structural MR images from amyloid PET: application to MR-less quantification. J Nucl Med 59:1111–1117
Comelli A, Stefano A, Benfante V, Russo G (2018) Normal and abnormal tissue classification in positron emission tomography oncological studies. Pattern Recogn Image Anal 28:106–113
Cui J, Liu X, Wang Y, Liu H (2017) Deep reconstruction model for dynamic PET images. PLoS One 12:e0184667
Cui J et al (2019) PET image denoising using unsupervised deep learning. Eur J Nucl Med Mol Imaging 46(13):2780–2789
Galldiks N et al (2012) Role of O-(2-(18)F-fluoroethyl)-L-tyrosine PET for differentiation of local recurrent brain metastasis from radiation necrosis. J Nucl Med 53:1367–1374
Goodfellow IJ et al (2014) Generative adversarial nets. In: Proceedings of the 27th International Conference on Neural Information Processing Systems, vol 2. MIT Press, Montreal, pp 2672–2680
Häggström I, Schmidtlein CR, Campanella G, Fuchs TJ (2019) DeepPET: a deep encoder–decoder network for directly solving the PET image reconstruction inverse problem. Med Image Anal 54:253–262
He K, Zhang X, Ren S, Sun J (2015) Delving deep into rectifiers: surpassing human-level performance on ImageNet classification. In: Proceedings of the 2015 IEEE International Conference on Computer Vision (ICCV). IEEE Computer Society, Washington, D.C., pp 1026–1034
Hong X et al (2018) Enhancing the image quality via transferred deep residual learning of coarse PET Sinograms. IEEE Trans Med Imaging 37:2322
Huang B et al (2018) Fully automated delineation of gross tumor volume for head and neck cancer on PET-CT using deep learning: a dual-center study. Contrast Media Mol Imaging 2018:8923028
Hwang EJ et al (2019) Development and validation of a deep learning-based automatic detection algorithm for active pulmonary tuberculosis on chest radiographs. Clin Infect Dis 69:739–747
Ioannidis JP (2005) Why most published research findings are false. PLoS Med 2:e124
Krizhevsky A, Sutskever I, Hinton GE (2012) ImageNet classification with deep convolutional neural networks. In: Proceedings of the 25th International Conference on Neural Information Processing Systems, vol 1. Curran Associates Inc., Lake Tahoe, Nevada, pp 1097–1105
Liu S et al (2014) 2014 IEEE 11th International Symposium on Biomedical Imaging (ISBI). IEEE, Piscataway, pp 1015–1018
Liu F, Jang H, Kijowski R, Bradshaw T, McMillan AB (2018a) Deep learning MR imaging-based attenuation correction for PET/MR imaging. Radiology 286:676–684
Liu F et al (2018b) A deep learning approach for (18)F-FDG PET attenuation correction. EJNMMI Phys 5:24
Lu D, Popuri K, Ding GW, Balachandar R, Beg MF (2018) Multiscale deep neural network based analysis of FDG-PET images for the early diagnosis of Alzheimer's disease. Med Image Anal 46:26–34
Minniti G et al (2011) Stereotactic radiosurgery for brain metastases: analysis of outcome and risk of brain radionecrosis. Radiat Oncol 6:48
Moe Y et al. (2019) Deep learning for automatic tumour segmentation in PET/CT images of patients with head and neck cancers
Mouridsen K (2015) Behavioral methods in consciousness research. Oxford University Press, Oxford
Ortiz A, Munilla J, Gorriz JM, Ramirez J (2016) Ensembles of deep learning architectures for the early diagnosis of the Alzheimer's disease. Int J Neural Syst 26:1650025
Rajpurkar P et al. (2017), CheXNet: radiologist-level pneumonia detection on chest X-rays with deep learning
Ronneberger O, Fischer P, Brox T (2015) In: Navab N, Hornegger J, Wells WM, Frangi AF (eds) Medical Image Computing and Computer-Assisted Intervention—MICCAI 2015. Springer International Publishing, Cham, pp 234–241

Simmons JP, Nelson LD, Simonsohn U (2011) False-positive psychology: undisclosed flexibility in data collection and analysis allows presenting anything as significant. Psychol Sci 22:1359–1366

Stefano A et al (2017) An enhanced random walk algorithm for delineation of head and neck cancers in PET studies. Med Biol Eng Comput 55:897–908

Topol E (2019) Deep medicine: how artificial intelligence can make healthcare human again. Basic Books Inc., New York

Xiang L et al (2017) Deep auto-context convolutional neural networks for standard-dose PET image estimation from low-dose PET/MRI. Neurocomputing 267:406–416

Xu J, Gong E, Pauly J, Zaharchuk G (2017) 200x Low-dose PET Reconstruction using Deep Learning

Yang J, Beadle BM, Garden AS, Schwartz DL, Aristophanous M (2015) A multimodality segmentation framework for automatic target delineation in head and neck radiotherapy. Med Phys 42:5310–5320

Yu H, Caldwell C, Mah K, Mozeg D (2009) Coregistered FDG PET/CT-based textural characterization of head and neck cancer for radiation treatment planning. IEEE Trans Med Imaging 28:374–383

MRI/PET Brain Imaging

6

Georg Schramm, Koen Van Laere, Peter Jan Van Laar, and Michel Koole

Contents

6.1 MRI Basics 120
6.1.1 Nuclear Magnetic Resonance (NMR) 120
6.1.2 Magnetic Resonance Imaging (MRI) 122
6.2 MR Imaging Sequences 123
6.2.1 Spin Echo (SE) Sequence 123
6.2.2 Gradient Echo (GE) Sequence 124
6.2.3 Echo-Planar Imaging (EPI) Sequence 125
6.3 MR Imaging Contrasts 127
6.3.1 T_1, T_2, and PD-Weighted Image Contrasts 127
6.3.2 Inversion Recovery (IR) 128
6.3.3 Susceptibility-Weighted Imaging (SWI) 129
6.3.4 Diffusion-Weighted Imaging (DWI) 129
6.3.5 Perfusion-Weighted Imaging (PWI) 131
6.3.6 MR Angiography (MRA) 136
6.3.7 Advanced Functional MRI Techniques 137
6.3.8 High-Field MRI 139
6.4 PET Basics 141
6.5 [^{15}O]H_2O Brain PET 142
6.6 [^{18}F]FDG Brain PET 143
6.7 Simultaneous [^{15}O]H_2O and [^{18}F]FDG Brain PET 146
6.8 Integrated PET/MRI Quantification 149
6.9 Future Perspectives of Hybrid PET/MRI 153
References 154

G. Schramm · K. Van Laere · M. Koole (✉)
Division of Nuclear Medicine, UZ/KU Leuven, Leuven, Belgium
e-mail: michel.koole@kuleuven.be

P. J. Van Laar
Division of Radiology, University Groningen, University Medical Center Groningen, Groningen, The Netherlands

R. A. J. O. Dierckx et al. (eds.), *PET and SPECT in Neurology*,
https://doi.org/10.1007/978-3-030-53168-3_6

Abstract

Multimodal brain imaging has become an established clinical and research tool for diagnosis and disease progression of brain disorders. Among available imaging modalities, magnetic resonance imaging (MRI) and positron-emission tomography (PET) can provide a wide spectrum of data for the in vivo mapping of neurobiological functions and brain morphology while demonstrating to relationships between behavioral and neurobiological factors. Since MRI mostly uses endogenous contrast mechanisms to visualize and quantify tissue characteristics, optimal sequence design is essential for the diagnostic information of MRI. On the other hand, PET imaging is always based on the exogenous contrast of an injected PET tracer. Therefore, characteristics of the PET tracer determine the quantitative and diagnostic potential of PET. This chapter will focus on both of these modalities and shortly discuss the potential of multimodal or hybrid MR/PET imaging. We will not cover MR spectroscopy nor specific applications of $H_2{}^{15}O$ PET since this will be discussed in other chapters of this book.

6.1 MRI Basics

6.1.1 Nuclear Magnetic Resonance (NMR) (Gibby 2005; Pooley 2005.; McRobbie 2003; NessAiver 1997; Elster and Burdette 2001)

Nuclei with an odd mass or odd atomic number have an intrinsic spin angular moment with an associated magnetic moment. In the presence of an external magnetic field B_0, the magnetic moment of nuclei with a one half spin will line up in parallel with the applied magnetic field with an either spin-aligned or spin-opposed orientation. The energy difference between the two orientations is very small at room temperature with a small majority of nuclei populating the lower energy spin-aligned orientation. This will cause a net macroscopic magnetization M_0 which will be directed parallel to B_0 and which strength will depend on the spatial spin density and the magnetic field strength. Next to this magnetization, nuclei will tend to precess in phase around the magnetic field with a frequency depending on the nucleus, the molecular structure, and the strength of the magnetic field. This frequency is traditionally called the Larmor frequency. Generating a MR signal is a two-phase process. During the transmission phase, a radio frequency (RF) signal induces a "spin flip" resulting in a rotating transversal magnetization in the plane perpendicular to the longitudinal external magnetic field B_0 and in a residual longitudinal component if the flip angle (FA) is not 90°. During the receiving phase, the transversal magnetization is picked up to generate the MR signal. During transmission, the RF excitation frequency must fit the Larmor frequency to have optimal resonance

conditions, hence the term magnetic resonance. The Larmor frequency for the ^{1}H nucleus amounts to 42.58 MHz/Tesla (Fig. 6.1).

After excitation and during the receiving phase, relaxation occurs when magnetization returns to the state prior to RF excitation. One can differentiate two types of relaxation. Longitudinal relaxation describes the relaxation where the longitudinal magnetization component is exponentially restored to initial net longitudinal magnetization M_0. This relaxation is referred to as spin-lattice relaxation and is quantified by the longitudinal relaxation time constant T_1. Transverse relaxation corresponds to the so-called spin-spin relaxation and describes the exponential decrease of the transverse magnetization component perpendicular to the longitudinal external magnetic field. The representative parameter is the transverse relaxation time constant T_2. Both relaxation processes take place simultaneously with relaxation times T_1 and T_2 being characteristic for a specific tissue type. While the T_1-relaxation time is within the range of 300 ms (fat) to 3000 ms (fluids), T_2-relaxation times are always much shorter ranging from 30 ms (muscle) to 2000 ms

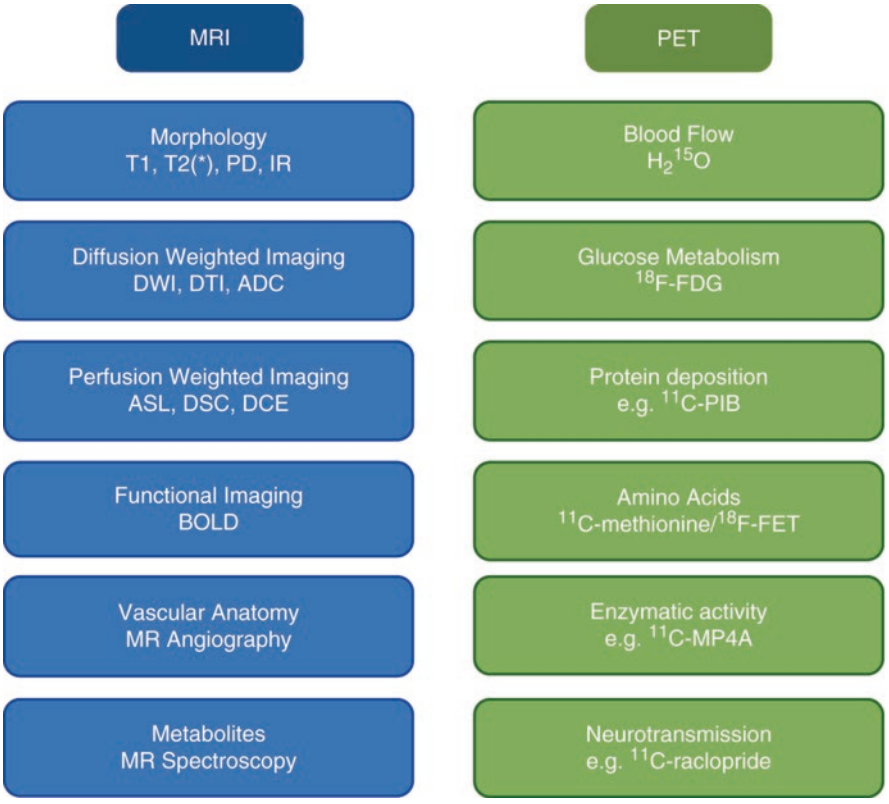

Fig. 6.1 Schematic overview of MRI and PET imaging potential

(fluids) (De Bazelaire et al. 2004). Specifically for brain imaging and for a 3 T magnetic field, T_1-relaxation times are 832 ms for white matter and 1331 ms for gray matter, while T_2-relaxation times are 79.6 and 110 ms, respectively (Wansapura et al. 1999).

6.1.2 Magnetic Resonance Imaging (MRI) (Paschal and Morris 2004; Hennig 1999; Elster and Burdette 2001; NessAiver 1997; McRobbie 2003)

MRI consists of applying the NMR principle to construct an image representing the proton density of different tissue voxels. Many of those protons are water protons such that MRI is particularly well suited for imaging soft tissue structures. The frequency of the proton MR signal is proportional to the magnetic field to which they are subjected during relaxation. An image can be made by producing a set of well-calibrated magnetic field gradients in all directions so that a certain magnetic field strength can be associated with a given location. In the longitudinal direction, a slice selective excitation is induced by applying a magnetic field gradient, a so-called slice selection gradient. This way, Larmor frequency and RF excitation fulfill the resonance condition in a specific axial slice such that only the magnetization of that slice is excited and contributes to the signal. In one of the transversal directions, phase encoding is applied with different phase-encoding gradients between RF excitation and readout. This is achieved by briefly switching on a magnetic field gradient in that direction when neither excitation nor readout is performed. This additional magnetic field gradient will induce differences in spinning rate such that when the gradient is switched back off again, proton spinning is dephased along this direction, and the signal is phase encoded. Finally, frequency encoding is applied along the other transversal direction by applying a readout gradient. This way, the frequency of the signal during readout is dependent on the spatial location in that direction. The signal of all voxels from the selected slice is recorded simultaneously in the so-called *k*-space by performing sequentially different phase-encoding steps. This *k*-space represents the Fourier transform of the MR image. The central part of *k*-space covers the lower spatial frequency range of the image representing the contrast and signal-to-noise content, while the outer part of *k*-space contains the high frequencies or resolution content. In case of contrast-enhanced MRI, the central part of *k*-space could be sampled first using a more centric approach, while for very fast scan techniques, spiral-like trajectories could be considered instead of the line at a time strategy. Multi-slice imaging and exploiting *k*-space symmetry can further reduce the acquisition time substantially.

During the phase encoding, phase is also encoded outside of the field of view (FOV), such that structures or body parts that are positioned outside of the FOV but within the encoded image slice contribute to the image and can cause aliasing artifacts in the phase-encoding direction. Other artifacts that mainly propagate in the phase-encoding direction are motion artifacts due to the movement of spins between the phase encoding and signal reading. During movement through the magnetic

gradient field, spins change frequency and thus acquire an additional phase shift causing a spatial mismapping of the signal of these protons. In the frequency-encoding direction, the pace of spatial encoding and sampling is such that physiological motion only causes limited spatial blurring in that direction.

In contrast, chemical shift artifacts can arise in the frequency-encoding direction. The chemical bounding of protons causes a shift in their precession frequency due to magnetic shielding provided by the electron shell. For the same field strength, protons bound to water have higher resonance frequencies than protons bound to lipids. Therefore, spatial encoding by the frequency-encoding gradient will shift fat relative to water in the frequency-encoding direction resulting in dark and/or white band at the interfaces between water and fat. This chemical shift artifact can be reduced by suppressing the signal from fat using saturation or inversion recovery techniques. Another method to minimize chemical shift artifacts is to use a wider receiver bandwidth, such that the bandwidth for each pixel is wider and thus a given chemical shift corresponds to fewer pixels. Drawback of wider receiver bandwidth is however a lower signal-to-noise ratio.

6.2 MR Imaging Sequences (Bitar et al. 2006; Boyle et al. 2006; Poustchi-Amin et al. 2001)

In standard clinical setting, parameters of MR sequences are chosen such that images are generated with a contrast depending on the proton density, and thus tissue composition, or on the differences between T_1- and/or T_2-relaxation times between different tissue types. To understand how contrast is generated, one needs to be aware that after RF excitation, signal intensity of the transversal magnetization decays very fast due to T_2 relaxation. This is called the free induction decay (FID) of the signal. Due to local microscopic magnetic field inhomogeneities and chemical shift effects, the signal actually decays much faster with a shorter effective time constant T_2*. Therefore, an echo of the original signal is generated and measured. The time between initial excitation RF pulse and the echo signal is the echo time TE and one of the key sequence parameters together with the repetition time TR which represents the time between two consecutive RF excitation pulses. In general, standard MRI sequences can be subdivided in three classes depending on how the echo of the original signal is generated and how the readout of the signal is performed.

6.2.1 Spin Echo (SE) Sequence

Following the excitation pulse, the net magnetization in the transverse plane will start to dephase due to T_2 relaxation, and signal intensity will drop very fast. A short time after the excitation pulse, a 180° pulse is transmitted causing the spins to rephase and the signal to rise again. This signal is sampled and called an echo of the initial net transversal magnetization. Echo time is twice the time between the initial excitation RF pulse and 180° RF pulse. The initial excitation pulse used to induce a

flip angle (FA) of 90°; however, smaller or larger flip angles are used as well. Advantage of a SE sequence is the strong signal which is compensated for local field inhomogeneities and different chemical shifts and is therefore less susceptible to artifacts. Rephasing however requires longer minimal echo times due to the additional 180° pulse and longer repetition times for an acceptable signal. This will increase total scan time and therefore the risk for motion, while a larger amount of RF energy will be deposited in the body. In order to reduce acquisition time, multiple echoes are generated after a single excitation pulse using an echo train (Harms et al. 1986). The sequences are called turbo spin echo (TSE) or fast spin echo (FSE) sequences. The number of echoes is called the turbo factor, and measurement time is reduced by this factor compared to standard SE imaging. However, contrast in fast spin echo needs to be described differently compared to standard spin echo sequences since multiple echoes are generated at different echo times. From these echoes, the ones corresponding to the central part of the *k*-space will determine image contrast, and the time between these echoes and the excitation pulse is called the effective TE.

Since a 180° rephasing pulse is used for the echo, SE and FSE sequences are insensitive to microscopic magnetic field inhomogeneities caused by iron deposition or specific tissue composition. Therefore, real T_2 weighting is only possible by this kind of sequences, excluding T_2* contrast and opposed-phase imaging. On the other hand, SE and FSE sequences generate a strong signal compensated for local field inhomogeneities and therefore less sensitive to artifacts. Examples of T_2 weighting can be found in Figs. 6.2 and 6.3.

6.2.2 Gradient Echo (GE) Sequence

GE sequences differ from SE sequences in the way the echo is formed. GE sequences create an echo by reversing the polarity of the readout or frequency-encoding gradient. A gradient pulse directly after the RF pulse enhances dephasing of spin frequencies such that the FID occurs considerably faster than under normal conditions. By reversing the polarity of the gradient, dephasing of the spins is reversed and spins start rephasing till at a certain moments all spins are in phase again and the echo is generated and measured. This gradient polarity reversal technique can work much faster than a 180° pulse for rephasing spins. This technique can be combined with a partial FA, which means smaller than 90°, making this approach very suitable for fast imaging sequences. Since a partial FA decreases the amount of magnetization flipped into the transverse plane, longitudinal magnetization is recovered faster, allowing a shorter TE and TR and thus decreased scan times while preserving image quality and limiting RF deposits. On the other hand, GE sequences are susceptible to microscopic magnetic field inhomogeneities and chemical shift effects. GE imaging sequences therefore produce T_2*-weighted images reflecting faster spin dephasing and signal loss due to both spin-spin interactions and magnetic field inhomogeneities and allowing opposed-phase imaging. Due to different resonance frequencies of water and fat, the signal intensity from a voxel containing both water

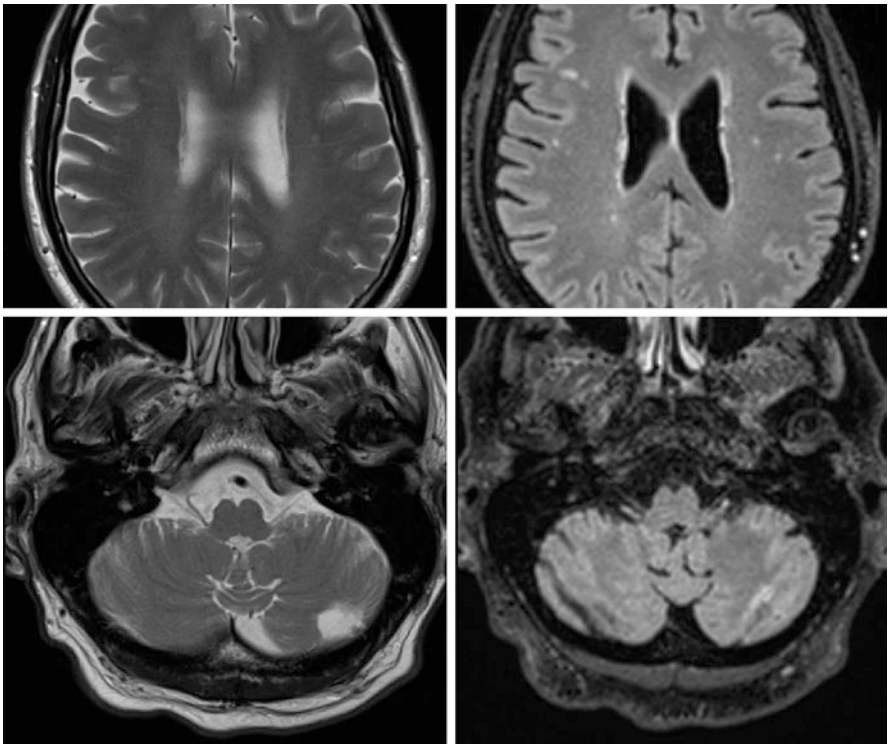

Fig. 6.2 T_2-weighted TSE (*left column*) and FLAIR (*right column*) brain imaging. *First row*: subcortical white matter hyperintensities better visible on FLAIR compared to T_2. *Second row*: cerebellar infarct visible on T_2 TSE which can be missed on FLAIR

and fat will oscillate, reaching a minimum when fat and water are out of phase and a maximum when they are in phase. If the echo is created with fat and water in phase, their signals will add up. When the echo is performed when they are out of phase, their signals will be subtracted. This way, water and fat can be separated. For spin echo sequences, these effects are not feasible since phase shifts due to chemical shift are canceled by the 180° refocusing pulse.

6.2.3 Echo-Planar Imaging (EPI) Sequence

EPI sequences are a very fast way of acquiring MRI data and form the basis for many advanced MRI applications such as diffusion, perfusion, and functional imaging. The excitation pulse is followed by a gradient echo train to continuously measure the MR signal and fill the *k*-space completely (single shot) or partially (segmented acquisition) within a single TR interval. The gradient echo train consists of fast oscillating gradients for frequency encoding in the readout direction and short gradient pulses for phase encoding. Therefore, a high-performance gradient

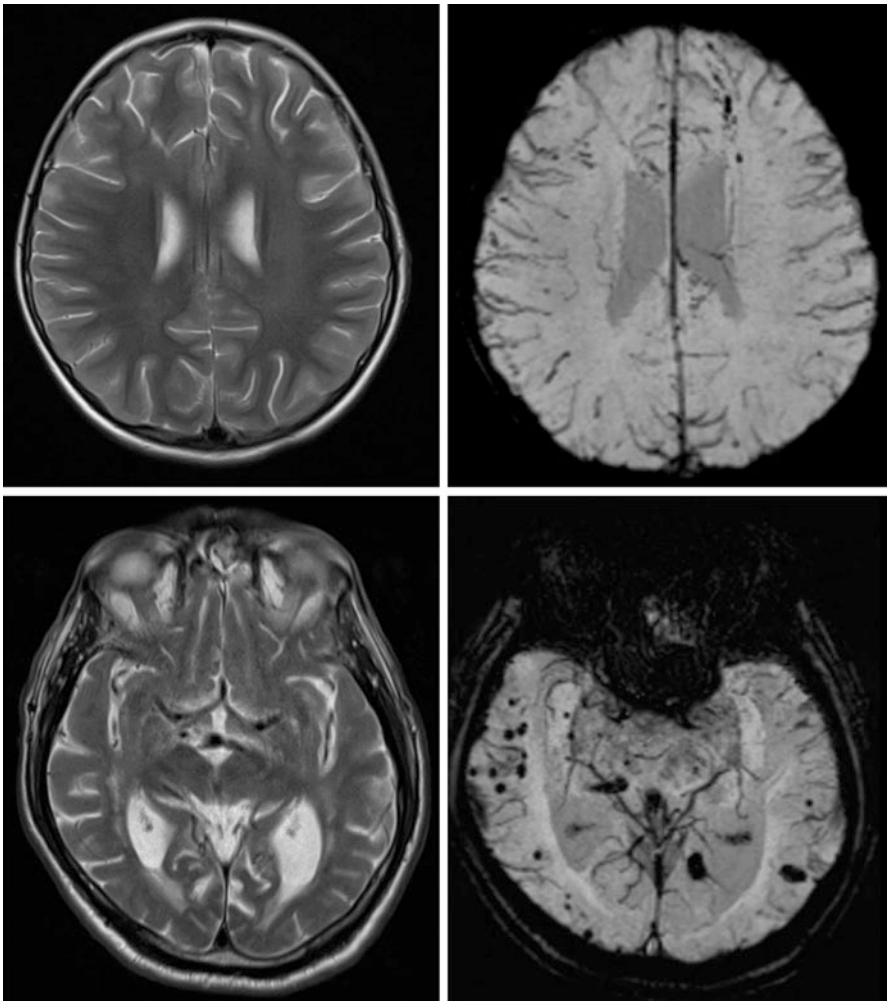

Fig. 6.3 T_2-weighted TSE (*left column*) and SWI (*right column*) brain imaging. *First row*: diffuse axonal injury in an 8-year-old girl—multiple hypointense focal lesions on SWI not visible on T_2 TSE, secondary to susceptibility from blood products after trauma. *Second row*: normotensive demented patient with cerebral amyloid angiopathy—multiple *black dots* on SWI in subcortical white matter in parietal and occipital lobes

system is required with short rise times to allow frequent gradient switching. Specific compositions of readout and phase-encoding gradients define the spatial encoding and the trajectory to fill up *k*-space. Several types of trajectories such as spiral trajectories can be compiled to optimize sampling of *k*-space and reduce scanning time. However, this often results in poorer spatial resolution. Spatial encoding of EPI sequences is sensitive to magnetic susceptibility and can be disturbed by gradient imperfections. Increasing the scan time and using segmented rather than

single-shot sequences can reduce artifacts. Due to the narrow readout bandwidth in the phase-encoding direction, chemical shift artifacts are possible in this direction requiring fat signal suppression.

The contrast generated with an EPI sequence is determined by the echo sequence and additional contrast-related gradient pulses. Both SE-EPI and GE-EPI are available.

6.3 MR Imaging Contrasts

The possibility of performing MRI with different image contrasts often results in considering MRI as a multimodal imaging technique or at least as multispectral imaging. Different contrast mechanisms are available such as proton density contrast and contrast based on relaxation along and perpendicular to the static magnetic field; chemical shift contrast of particular use for molecular imaging; motion-weighted contrast for imaging blood flow, tissue perfusion, and diffusion; susceptibility-weighted contrast used for functional MRI; and other advanced contrast mechanisms such as magnetization transfer.

6.3.1 T_1, T_2, and PD-Weighted Image Contrasts (Gibby 2005; Pooley 2005; McRobbie 2003; NessAiver 1997)

In case of SE sequences, the effect of T_2 relaxation on the image is controlled by TE, while the impact of T_1 relaxation is dependent on TR. For a sequence with a short TR and very short TE, spins will undergo very limited dephasing due to T_2 relaxation, and without T_1 relaxation, all tissue types would generate a similar MR signal. However, the short TR will not allow the net magnetization in the longitudinal direction to recover fully between two RF excitation pulses. The recovered longitudinal magnetization will depend on the T_1-relaxation time of the underlying tissue type. Fat, for instance, with a shorter T_1-relaxation time will have a larger net longitudinal magnetization restored than water with a longer T_1-relaxation time. Consequently, the transversal magnetization generated during the next RF excitation pulse will be higher for fat than for water, and therefore, the contribution of fluids to the overall signal will be lower. In this case the MR signal is T_1 weighted, meaning that contrast is dependent on T_1 relaxation differences between tissues where tissues with longer T_1-relaxation times contribute less to the signal and therefore appear darker in the MR image.

If the TE of a SE sequence is prolonged, dephasing of spins due to T_2 relaxation will be more pronounced and will depend on the differences in T_2-relaxation times between tissue types. If a longer TE is combined with a relatively long TR, full recovery of the net longitudinal magnetization is obtained for all tissues, and tissue differences in T_1 relaxation are canceled out. Consequently, the transversal magnetization generated during the next RF excitation pulse is the same for all tissues such that the MR signal will be dependent only on differences in T_2 relaxation and the

MR image contrast will be T_2 weighted. Water, for instance, has a long T_2-relaxation time and will still show some phase coherence in case of a long TE, while most other tissues will have dephased much more and will contribute less to the MR signal. Hence, water will appear bright in a T_2-weighted image, while other tissue types will have lower intensities (see Figs. 6.2 and 6.3).

If a sequence combines a short TE with a long TR, T_2 relaxation will have a very limited impact on the image contrast, while the net longitudinal magnetization will have recovered for most tissue types. Thus, the MR contrast will be dominated neither by T_1 relaxation nor by T_2 relaxation but will depend only on the proton density (PD) of the different underlying tissue types. A tissue type with a high proton density such as water will produce a high MR signal and appear bright, while tissues containing few protons will generate a low signal and appear dark.

SE sequences are especially suited for acquiring images of the same slice with different contrast. Generating a second echo with a longer TE within the same TR interval and with the same phase encoding will generate a PD-weighted image for the echo with the short TE and a more T_2-weighted image for the echo with longer TE. This way, a T_2- and PD-weighted image of the same slice position can be acquired without increasing overall acquisition time. Specifically for FSE sequences, a short TR for T_1-weighted sequences limits the echo train length. Therefore, FSE sequences are preferably used for T_2-weighted imaging.

Contrary to SE sequences where the FA is mostly fixed to 90°, GE sequences use a range of flip angles, and contrast is determined mainly by FA and TE. If FA decreases, T_2* weighting is favored since the residual longitudinal magnetization will be higher and the recovery of longitudinal magnetization for a given T_1 and TR will be more pronounced. A high FA and short TE will generate T_1 weighting, while a medium FA and short TE corresponds to PD-weighted contrast.

Given these types of contrast, it is not easy to decide on the best image contrast for a given pathology. In general, T_1-weighted contrast allows a clear delineation of anatomical brain structures, while for brain pathologies involving edema, T_2- or PD-weighted contrast could be preferred (Fullerton 1984).

6.3.2 Inversion Recovery (IR)

Inversion recovery (IR) sequences are frequently used to generate T_1-contrast-weighted images. IR sequences can be considered a standard sequence preceded by a 180° excitation pulse in the longitudinal direction. This 180° excitation pulse will induce T_1 relaxation that takes twice as long as for a standard sequence. No T_2 relaxation will occur since no transversal magnetization component is generated. After a specific time interval of T_1 relaxation, called the inversion time TI, a standard sequence is applied to generate an image. Because of this preceding 180° excitation pulse, one can make better use of differences in T_1 relaxation between various tissues to create higher T_1-weighted image contrast. This is however at the expense of longer acquisition times compared to standard T_1-weighted sequences. TR time is now defined as the time interval between two 180° excitation pulses in the

longitudinal direction. Since TE is relatively short compared to TI, image contrast of IR sequences is mainly determined by TI. Choosing this TI appropriately will suppress the signal from specific tissue types. If, for instance, the standard sequence part of an IR sequence is started at the time the longitudinal magnetization vector of fat or cerebrospinal fluid (CSF) crosses the zero line, no magnetization can be flipped into the transversal plane, and therefore no signal can be generated for this tissue type. In case of fat, this type of IR sequence is called short TI inversion recovery (STIR) (de Kerviler et al. 1998) and is very effective in those cases where fat signal interferes with the given pathology such as the detection of water in fatty tissue in case of inflammation in the joints or infiltrating tumors in bone marrow. The IR sequence for suppressing the signal of CSF is called fluid-attenuated inversion recovery (Eastwood and Hudgins 1998; Simonson et al. 1996) (FLAIR) (see Fig. 6.2). This sequence is very useful for visualizing demyelinating diseases and to assess vascular white matter hyperintensities and infarctions.

6.3.3 Susceptibility-Weighted Imaging (SWI)

The uniformity of the static magnetic field B_0 is slightly distorted by the magnetic susceptibility or magnetizability of substances that are present in the FOV. This magnetic susceptibility exhibited by a tissue or substance will result in signal loss (Wendt et al. 1988). In particular the magnetic susceptibility of oxygenated and deoxygenated blood differ, with oxygenated blood being diamagnetic and decreasing local field strength, while deoxygenated blood is paramagnetic and increasing local field strength. Protons in the tissue surrounding the blood vessels are affected by this microscopic field variation, resulting in a loss of phase coherence. This induces signal cancelation and a decrease in total signal intensity. Next to phase changes at blood/tissue interfaces, the difference in magnetic susceptibility between oxygenated and deoxygenated blood, although small, also induces T_2* changes between the arterial and venous bed of the vascular system. Using 3D GE sequences, susceptibility-weighted imaging (SWI) picks up these subtle differences in magnetic susceptibility in order to detect bleedings and small iron depositions (Chavhan et al. 2009) (see Fig. 6.3) or as part of a multimodal imaging approach for neurodegenerative diseases (Haller et al. 2010) such as Alzheimer's (Ramani et al. 2006) and multiple sclerosis (MS) (Langkammer et al. 2013; Tavazzi et al. 2007; Walsh et al. 2014).

6.3.4 Diffusion-Weighted Imaging (DWI) (Luypaert et al. 2001; Bammer 2003; Le Bihan et al. 2006; Huisman 2003; Hagmann et al. 2006)

Diffusion reflects the Brownian, a random movement of water molecules at microlevel. This random motion is hindered by cell membranes, fibers, or large molecules such as proteins, while concentration of these obstacles depends on tissue type or

pathology (tumor tissue, abscess, and edema). Measuring the mobility of water molecules therefore gives indirect information about the tissue structures in terms of cell density and granularity such that tissue types can be better characterized and differentiated.

The contrast of diffusion-weighted imaging (DWI) is based on the mobility of the extracellular water by adding diffusion gradients to the imaging sequence. The spins of immobile water molecules will dephase by the first gradient pulse but will rephase by the second gradient pulse such that no impact on the signal is observed. Contrary, the spins of water molecules moving along the direction of the diffusion gradients during the time interval between the gradients will not be rephased by the second gradient and will stay dephased compared to the spins of the immobile water molecules, and thus the signal will decrease. The more water molecules diffuse during the time interval between the two diffusion gradients, the more they will remain dephased after the second gradient, and the more the recorded signal will be weakened. Weakening of the signal is limited to diffusion along the direction of the gradients, so diffusion gradients are applied in three perpendicular spatial directions. The diffusion magnitudes calculated along these three directions are averaged to provide a measure for a global diffusion-weighted image called a trace image.

DWI sequences are usually T_2-weighted ultrafast 3D SE-EPI sequences sensitized for diffusion by adding diffusion gradients symmetrically before and after the 180° rephasing pulse. Therefore, contrast of DWI images is both diffusion and T_2 weighted such that a strong signal could correspond to diffusion restriction as well as T_2 shine through of a T_2-sensitive lesion. The diffusion gradient pulses are characterized by the b value which is essentially dependent on the gradient amplitude, gradient duration, and time interval between the two gradients. In clinical practice a T_2-weighted image with a b value of zero is combined with a diffusion-weighted image with a high b value (see Fig. 6.4).

If DWI images are acquired for different b values, the amount and speed of movement can be quantified by the apparent diffusion coefficient (ADC)

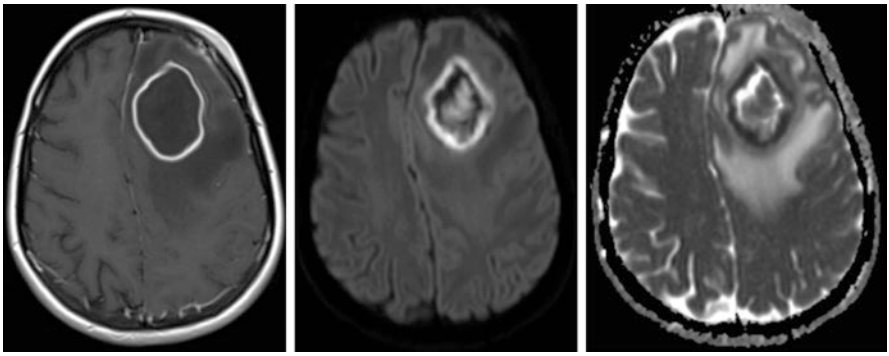

Fig. 6.4 Left frontal abscess after complicated sinusitis with ring enhancement on T_1-weighted DCE-MRI with Ga-DTPA and restricted diffusion (high DWI and low ADC) in the border and central in the lesion

(Vandecaveye et al. 2008; Thoeny et al. 2012) (see Fig. 6.4). The ADC is calculated by fitting an exponential diffusion model to the signal intensities from images acquired with different *b* values. This way, only information on diffusion is retained, and T_2 shines through of T_2-sensitive lesions is avoided. Whereas fast-moving molecules will quickly lose all of their phase coherence and signal intensity, even at low *b* values, slow-moving molecules will retain high signal intensities far into the higher ranges of *b* values. A solid tumor will show high signal intensity on a high *b* value image and low signal intensity on the corresponding ADC map, whereas apoptosis or necrosis will commonly appear as areas of low signal intensity on high *b* value images with high signal intensity on the corresponding ADC map.

This way, post-therapeutic changes induced by radiation therapy or chemotherapy generate a high signal intensity (edema) or low signal intensity (necrosis) on high *b* value images but generally show high signal intensity on corresponding ADC map. ADC information proves clinically relevant for other brain pathologies (Schaefer et al. 2000) such as degenerative (Vitali et al. 2011; Kim et al. 2011; Horsfield and Jones 2002) (Creutzfeldt-Jakob's disease) or inflammatory pathologies (MS) (Tavazzi et al. 2007).

6.3.5 Perfusion-Weighted Imaging (PWI)

Generally, two approaches can be applied for perfusion-weighted MRI. The first approach uses endogenously generated contrast, while the second approach relies on the intravenous administration of MR-sensitive contrast agents. PWI information can be used to quantify brain blood volume and extract temporal information about brain blood flow on the level of microcirculation.

6.3.5.1 Arterial Spin Labeling (ASL)

Arterial spin labeling (Detre et al. 1992; Williams et al. 1992; Ferré et al. 2013; Van Laar 2008) is a PWI technique that does not require exogenous contrast agents. It uses the intravascular water in the arterial blood compartment as endogenous tracer. Water molecules are magnetically labeled by applying locally a 180° RF pulse to invert the longitudinal magnetization of arterial blood upstream just below the region of interest. With a time delay called the transit time TI, this arterial blood, tagged with an inverted net magnetization, will flow into the region of interest and act as a freely diffusible paramagnetic tracer. The inflowing inverted spins of the arterial water molecules will start to exchange with water molecules in brain tissue, reducing tissue magnetization and consequently weakening MR signal and image intensity. Next to this tag image, a reference image is acquired by repeating the sequence without tagging the hydrogen nuclei of the intravascular water. Reference and tag image are subtracted to provide a perfusion image, reflecting the amount of arterial blood entering the region of interest during the TI interval.

Major drawback of ASL is the rapid T_1 relaxation and therefore limited life span of the tracer. Since a TI interval is required for blood to flow from the labeling location to the region of interest, labeled water within the arterial blood is decaying, and

labeling efficiency is decreased depending on the spatial position of the labeling region, blood flow, and vessel geometry. This can make ASL particularly challenging for studying cerebral vascular pathologies with limited blood flow.

Because ASL techniques require image subtraction and the flow-related signal is only a few percent of the tag and reference signal, motion can significantly degrade image quality and lead to large errors of the cerebral blood flow estimation. Ultrafast imaging sequences, such as EPI and FSE, or interleaved acquisitions of reference and tag data, provide higher SNR data and can significantly attenuate the effects of motion.

Techniques for ASL perfusion imaging can be sorted into two categories. The first category, continuous ASL (CASL) (Detre and Alsop 1999), uses a flow-driven continuous inversion technique where a constant RF pulse is applied off-resonance in the presence of a constant labeling gradient along the flow direction of the arterial blood. The frequency offset of the RF pulse is determined by the gradient strength and the desired distance from the inversion plane (called the labeling plane) to the region of interest. As arterial blood flows along the direction of the labeling gradient, the spins of arterial water experience a frequency sweep and are being inverted as they pass through the labeling plane. Once inverted, these water molecules will flow into the region of interest and influence the magnetic properties of the vascular bed of the target tissue.

The CASL approach requires arteries in a fairly straight segment along the labeling gradient and a sufficiently high blood flow such that frequency sweep is large compared to the relaxation time of arterial blood and small with respect to the amplitude of the RF pulse. Therefore, larger gradient strengths are required for smaller arteries with lower blood flow. Applying off-resonance RF pulses continuously during CASL causes saturation of protons bound to macromolecules (proteins, membranes, etc.) as their T_2 is very short, giving a very wide frequency band. The permanent exchanges between the unbound protons in water close to the macromolecules and protons bound to these molecules result in a magnetization transfer (MT) from the bound to unbound protons, reducing the observed MRI signal from the unbound protons in tissue and affecting quantification. To overcome this effect, a distal labeling is performed in the control experiment to produce identical MT effects. A small separate labeling coil, placed on the neck to label the common carotid arteries, can also avoid this effect since the FOV of the labeling coil is confined to the neck region and does not reach the brain, thus eliminating off-resonance effects, with the added benefit that it also greatly reduces the RF power deposition compared to a volume coil. Substantial RF power deposition in the body during CASL may be of concern for the routine use at high magnetic field strengths.

Next to CASL, pulsed arterial spin labeling (PASL) (Edelman et al. 1994; Kim 1995; Wong et al. 1997) can also be used as a technique for tagging water in arterial blood. Unlike CASL, where arterial blood is continuously inverted in a thin labeling plane, PASL techniques rely on a short RF pulse for inverting magnetization of all the water molecules contained in a thick region or slab proximal to the brain. Following this inversion, blood from this slab flows into the region of interest during an inflow time TI and interacts with the non-inverted water of brain tissue, after

which the image is acquired. The control image is acquired in the absence of the slab-selective inversion.

Advantages of PASL over CASL (Wong et al. 1998) are the small MT effects and the lower RF power deposition due to the use of short RF labeling pulses, compared to the long continuous pulses used in CASL. The latter may become an important issue at high magnetic field strengths, such as 7 T and above. The major advantage of CASL techniques is the higher SNR compared to PASL, combined with a higher labeling efficiency because the labeling plane can, on average, be placed closer to the region of interest compared to the thick labeling slabs required in PASL. A post-labeling delay between end of the labeling interval and start of image acquisition can be included in the sequence. If this delay is longer than expected TI, all labeled water will have entered the region of interest prior to image acquisition, and concentration of labeled water in the arterial vessels will be minimized to avoid overestimation of blood flow and vascular volume artifacts. For PASL, determining the temporal width of the volume of labeled water is not straightforward since it depends on the spatial extent of the inversion slab, the arterial blood flow, and the geometry of the proximal vessels, while for CASL, estimating the TI is more evident.

A hybrid approach that simulates CASL using many short pulses termed "pseudo continuous" or "pulsed continuous" ASL (pCASL) (Dai et al. 2008; Wu et al. 2007) combines these two approaches to provide better sensitivity and ease of implementation for body coil transmitters. Several methods also exist for spatially selective labeling, uniquely allowing the perfusion distribution of single arterial territories to be measured. Velocity-selective labeling (VS-ASL) (Wong et al. 2006) has also been explored as a means of eliminating arterial transit time dependence. With this technique, the tagging scheme selectively saturates flowing spins with no spatial selectivity. This is accomplished with an RF and gradient pulse train that effectively dephases the MR signal from protons that are flowing faster than a specified cutoff velocity while rephasing the signal from slower flowing protons. The advantage of this approach is a small and uniform transit delay for the delivery of the tagged blood to the tissues of interest.

Clinical applications of ASL have demonstrated the challenge of optimizing labeling timing, in particular the post-labeling delay or TI time, to allow all labeled blood to enter the microvasculature while not losing too much signal to T_1 decay because of delay times. Several studies of ASL in acute stroke have been reported revealing that ASL underestimates flow in many of the cases (Chalela et al. 2000; Siewert et al. 1997), and imaging performed with a longer wait before acquisition, either post-labeling delay or TI, was more consistent with other findings (Yoneda et al. 2003; Wolf et al. 2003).

ASL can provide either baseline measurements for between group comparison or serial measurements in individual subjects. As a serial measure, it can be used for fMRI with shorter timescale changes within a single scanning session or for changes on longer timescales to image the changes in the brain with normal aging (Wang et al. 2008).

On the other hand, the repeatability and noninvasiveness of ASL makes this technique suitable for monitoring neurological effects of pharmacologic agents and

drug administration (Wang et al. 2011; Chen et al. 2011; Detre et al. 2009; Nordin et al. 2013), although vascular and neuronal effects of ASL cannot be separated. The temporal stability of ASL makes it also valuable for the study of brain activation changes over longer timescales (Wang et al. 2005). Activation studies with ASL may improve understanding of a number of important neural functions, such as memory consolidation or emotional state (Brown et al. 2007; O'Gorman et al. 2008).

In terms of clinical applications for ASL, stroke and cerebrovascular diseases are logical indications, but ASL also offers several important advantages for tumor blood flow assessment (Warmuth et al. 2003). Because of its insensitivity to vascular permeability, blood flow measurements are not confounded by permeability factors as in dynamic susceptibility contrast. Therefore, absolute blood flow quantification is feasible such that tumor blood flow can be used as an indicator of tumor grade (Järnum et al. 2010; Schlemmer et al. 2009; Wolf et al. 2005) and tumor blood flow values can be compared throughout the duration of therapy. Since ASL is insensitive to susceptibility variations that can result from surgical interventions or hemorrhage and high-resolution anatomical information can be acquired in the same scanning session, it can be a useful pre- and postoperative tool.

In the context of dementia, ASL may be useful in the early detection of AD-related changes in subjects with mild cognitive impairment (Alsop et al. 2000, 2008, 2010; Wolk and Detre 2012; Johnson et al. 2005). Loss of tissue and metabolic function are important hallmarks of dementia. In Alzheimer's disease, loss of tissue is detected in the medial temporal lobes including the hippocampus. Metabolic imaging has demonstrated functional decreases in the posterior-inferior temporal cortex, the superior temporal-parietal association cortex, the posterior cingulated cortex, and in advanced cases also the frontal association cortex. ASL perfusion MRI to patients diagnosed with AD has found similar regions of decreased function, while blood flow was relatively preserved in the medial temporal, superior temporal, and inferior frontal regions.

6.3.5.2 Dynamic Susceptibility-Weighted Contrast-Enhanced MRI (DSC-MRI)

DCS-MRI (Sourbron 2010; Ostergaard et al. 1996a, 1996b; Verma et al. 2013) uses an intravenous bolus injection of a paramagnetic tracer such as a gadolinium-DTPA chelate (diethylenetriaminepentaacetic acid) combined with dynamic imaging technique which measures the signal changes induced by the tracer in the tissue as a function of time. Using T_2*-weighted ultrafast EPI sequences, data sampling is performed on a timescale smaller than typical tracer transit times through the capillary bed. This way the tracer is essentially intravascular during the first pass of the bolus, and pure perfusion weighting is achieved. With these sequences, T_2* signal loss due susceptibility effects of the contrast agent during first pass is picked up, and this signal decrease is used to compute the relative perfusion of that region (see Fig. 6.5). The DSC-MRI hemodynamic parameters are typically obtained from the time susceptibility curve while eliminating tracer recirculation effects. Typical quantitative parameters are time to peak (TTP), mean transit time (MTT), cerebral blood volume (CBV), and cerebral blood flow (CBF = CBV/MTT).

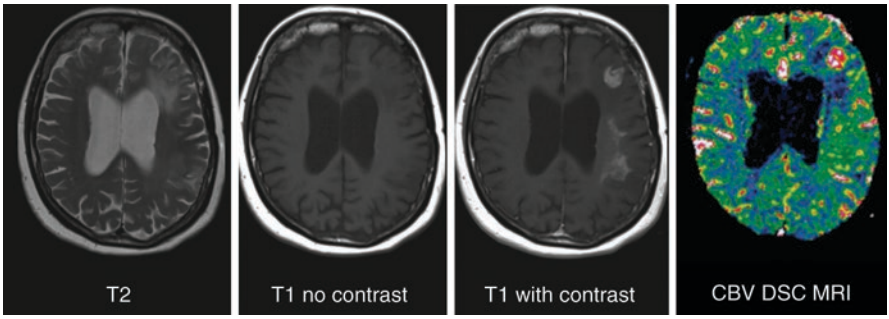

Fig. 6.5 T_2 hyperintense lesion in left frontal lobe and left frontoparietal white matter in a patient after resection and radiotherapy of low-grade astrocytoma. Enhancement and elevated CBV indicating degeneration to high-grade astrocytoma

In comparison to other MR perfusion techniques (Weber et al. 2003), DSC-MRI has several advantages, such as better SNR, shorter scan times, ease of use, and greater availability for commercial scanners. These advantages make DSC-MRI the most widely used perfusion technique for the brain, although it is increasingly being challenged in recent years because of quantification issues (Calamante 2009). Since the technique remains highly sensitive to susceptibility artifacts, its application in patients with hemorrhages, calcifications, or surgical clips is limited. The administration of a contrast agent also makes DSC-MRI more invasive compared to ASL and difficult to conduct in patients with renal impairment. On the other hand, T_1 shortening of the blood due to the administration of a contrast agent, such as gadolinium-DTPA, prohibits further ASL acquisitions. Contrast media in larger vessels in the field of view can interfere with the blood flow measurements, whereas this effect is small for ASL. In case of blood-brain barrier breakdown, the tracer extravasates into the interstitial space causing an accelerated T_1 relaxation of the surrounding brain tissue, loss of T_2* weighting, and potential errors in the calculation of the hemodynamic parameters.

6.3.5.3 Dynamic Contrast-Enhanced (DCE) MR

While T_2* effects are significantly stronger for intravascular paramagnetic contrast media such as gadolinium-DTPA, T_1 relaxation of water molecules of surrounding brain tissue is strongly accelerated as well. This signal can be picked by T_1-weighted DCE-MRI sequences using EPI or rapid gradient echo techniques (Cha 2003). Although in the brain, DCE-MRI signal changes remain weaker than DSC-MRI, technological advances leading to shorter echo times, and higher field strengths have improved the DCE-MRI data quality. While DCE-MRI has less temporal resolution than DSC-MRI, it has some advantages compared to DSC-MRI such as better spatial resolution that allows a better characterization of the vascular microenvironment of the lesion and robustness to the presence of susceptibility artifacts.

Specific indications are vessel wall imaging and imaging of inflammation where an increased vascular permeability is expected, imaging of neovascularization

corresponding to an increased vascularity, and fibrous tissue characterization which induces an increased distribution volume (Bley et al. 2005; Kerwin et al. 2003; Desai et al. 2005; Yuan et al. 2002; Wasserman et al. 2002; Kramer et al. 2004).

6.3.6 MR Angiography (MRA)

MRI sensitivity to movement in terms of spatial encoding perturbations and artifacts can be used to develop vascular imaging approaches based on signal changes that are linked to flow. Techniques such as time-of-flight MRA (TOF MRA) or phase-contrast MRA (PC MRA) apply endogenous vascular contrast, while contrast-enhanced MRA exploits the relaxation properties of exogenous contrast agents to visualize vascular structures (van Laar et al. 2006; Ozsarlak et al. 2004).

MR angiography techniques are generally T_1-weighted echo-gradient-based sequences. When endogenous vascular contrast is used, strategies are implemented to suppress the background signal represented by the stationary tissue such that vascular signal is favored over that of the surrounding tissues (Foo et al. 2005).

TOF MRA generates contrast between blood flow and stationary tissue by changing the magnitude of magnetization such that moving spins generated a high signal, while the signal of stationary tissue spins will be diminished. Using repetition times much shorter than the relaxation times of brain tissue, spins in a predefined slice do not fully recover after each repetition, and the MR signal decreases with the number of excitation pulses until equilibrium is reached. Moving spins that flow into this slice are not saturated and therefore have a greater signal, creating contrast between saturated stationary tissue and blood. Drawbacks are the long acquisition time and saturation of in-plane blood vessels, while the signal of stationary tissues with short T_1-relaxation time such as fat, hematoma, or thrombus can be poorly suppressed.

PC MRA on the other hand generates contrast between blood flow and stationary tissue by changing the phase of magnetization such that the phase of moving spins is shifted relative to the phase of stationary spins. This technique uses a bipolar flow encoding gradient of given intensity to dephase spins in the transversal direction in proportion to their velocity in the direction of the gradient. This generated phase difference between stationary and moving spins can be picked up to derive contrast between flowing blood and brain tissue.

Next to TOF MRA and PC MRA, time-resolved ASL (Robson et al. 2010) has been developed as a noninvasive alternative to angiography.

In the case of CE MRA (Zhang et al. 2007a), signal differences are achieved not only by employing the appropriate sequence parameters but also by intravenously injecting a contrast agent into the vascular system to selectively shorten the T_1 relaxation of the blood. Using a T_1-weighted imaging sequence during the first pass of the contrast agent, the shortened T_1 relaxation of blood causes the blood to give rise to a very large signal producing a very high contrast between arteries and surrounding tissues and veins.

While MRA using endogenous contrast can be disturbed by complex or turbulent flows, the blood signal of CE MRA is minimally affected by dephasing caused by

complex flows and susceptibility variations. The key factor for CE MRA signal is to acquire data at the right moment, during the passage of the contrast agent bolus. Because the CE MRA techniques are relatively insensitive to this signal loss, they provide high-quality images with fewer artifacts than the non-CE methods. Because effects of saturation are minimal, large fields of view can be imaged with high SNR to demonstrate large vascular areas in a short acquisition time. The short imaging time permits acquisition in a single breath-hold interval, providing high-quality images even in areas affected by respiratory motion.

6.3.7 Advanced Functional MRI Techniques

Next to the MRI techniques which were mentioned above and which are used extensively in a clinical setting, other MRI techniques will be discussed in brief. These methods are mainly used for addressing scientific questions rather than for clinical diagnosis or therapy evaluation. However, for specific brain pathologies, they could move from a research setting into clinical tools in the near future.

6.3.7.1 BOLD fMRI

Neuronal activity not only increases local oxygen consumption but also induces an even higher increase in local blood supply, due to neurovascular coupling. Therefore, neuronal activity is reflected by a higher oxygenated over deoxygenated blood ratio, which causes a local paramagnetic effect. This blood-oxygenation-level-dependent (BOLD) effect can be picked up by MRI as a weak, transient T_2*-weighted signal rise, very similar to SWI. Since the BOLD contrast is poor, fast T_2*-sensitive sequences with high SNR and sufficient temporal resolution are required for functional MRI (fMRI) studies. Disadvantages of using BOLD contrast for fMRI studies are related to motion artifacts caused by head motion, breathing, and cardiac pulsation and susceptibility artifacts causing signal distortion or signal loss at tissue interfaces with bone structures and air cavities. BOLD fMRI also maps neuronal activity using an indirect effect which can lead to imprecise localization of the activated zone due to spatial discrepancies between activated neurons and corresponding vascular variations in the oxy- over deoxy-hemoglobin ratio.

As an alternative to BOLD fMRI, ASL can be used to detect variations in perfusion after neuronal activation. Like BOLD, ASL only indirectly reflects neuronal activity by detecting vascular changes. However, it provides an absolute quantitative measure of cerebral blood flow (CBF) compared to BOLD, which is a complex function of a number of physiological variables, especially oxygen utilization, cerebral blood flow, and cerebral blood volume. Moreover ASL fMRI is less sensitive to baseline signal drift and low-frequency noise and may provide higher spatial specificity for neuronal activity. Several studies have shown that ASL measurements have decreased intersubject and intersession variability as compared to BOLD (Aguirre et al. 2002, 2005; Tjandra et al. 2005), possibly due to a more direct link between CBF and neural activity. On the other hand, SNR of ASL is lower, while in general less imaging coverage and lower temporal resolution is provided than with

BOLD fMRI. This is because of the acquisition of a tag and control dataset, the need to wait for tagged blood to flow into the imaging region and the need to acquire data before the tagged blood signal, has fully relaxed. Therefore, ASL fMRI is particularly suitable for experimental paradigms with task repetitions at low frequency or with long stimulus durations (Wang et al. 2003). However, further development of single-shot ASL acquisition protocols (Wong et al. 2000; Günther et al. 2005) with whole-brain coverage will keep on challenging BOLD fMRI, as these sequences provide similar temporal resolution and spatial coverage with improved temporal stability and without susceptibility artifacts. It has also been suggested to combine ASL with BOLD imaging, as ASL perfusion measurements can aid in the interpretation of the BOLD signal change and, when combined with BOLD, provide an indicator of oxygen utilization (Hoge et al. 1999).

In a research setting, fMRI is widely used for neuropsychological and cognitive studies. In task-based fMRI, specific tasks are performed during fMRI data acquisitions; such that the neuronal activity changes during task performance can be monitored. Acquisitions are repeated in time during a succession of different tasks following an activation paradigm. This activation paradigm comprises the task sequence and mode of repetition. It consists of at least a baseline task and other tasks, which only differ from the baseline task by a specific activity. Analysis is based on a statistical comparison of the signal variations measured in each pixel between different states of activation and thus relate to the differences between the two tasks.

Next to task-based fMRI, fMRI can also be used to study brain functioning, while subjects are not engaged in any specific task. These resting-state fMRI or RS-fMRI studies monitor the functional brain activity during resting state as spontaneous low-frequency BOLD signal fluctuations (Van Dijk et al. 2010; Buckner et al. 2008). Interregional temporal correlations of these BOLD signal fluctuations provide estimates for the temporal correlation between neurophysiological measurements obtained in different brain areas and thus for resting-state functional connectivity (RSFC). This coherent activity of functionally related brain areas is an important feature of healthy brain functioning (Fox and Raichle 2007; van den Heuvel et al. 2009).

Since RS-fMRI is noninvasive and does not require cognitive task performance during image acquisition, its setup is substantially simpler than other functional neuroimaging methods. RS-fMRI detects multiple brain networks presenting consistent intercorrelations of low-frequency activity, including the primary sensorimotor network, the primary visual and extrastriate visual networks, the frontoparietal attention networks, and the default-mode network (DMN), which is directly associated with episodic memory retrieval, self-referential processes, social cognition, and mind wandering (van den Heuvel and Hulshoff Pol 2010; De Luca et al. 2006). Functional connectivity abnormalities in one or more of those networks may be found in psychiatric and neurological disorders while showing significant correlations with behavioral changes and cognitive deficits (Broyd et al. 2009; Greicius 2008; Damoiseaux et al. 2012; Galvin et al. 2011; Kwak et al. 2010; Sheline et al. 2010; Cole et al. 2011; Anticevic et al. 2012). Given its feasibility and reliable and

replicable results (Chou et al. 2012; Koch et al. 2010), RSFC abnormalities associated with the above disorders could have future potential as a disease biomarker in a clinical setting, both for diagnosis and treatment monitoring (Koch et al. 2012; Van Dijk and Sperling 2011).

6.3.7.2 Diffusion Tensor Imaging (DTI) MRI

While DW-MRI measures differences in water mobility without taking into account the direction of the displacements, DTI MRI detects motion of water molecules in different directions and can characterize the mobility in terms of anisotropic diffusion (fractional anisotropy), main diffusion direction, and preferred directions or restrictions (Hagmann et al. 2006). This is particularly of interest for nerve fibers since it can be applied indirectly to reconstruct nerve fiber trajectories. Since nerve fibers consist of axon bundles running in parallel with concentric layers of myelin-restricting transversal diffusion, water diffusion will preferably follow the direction of the fibers while being restricted in the direction perpendicular to the fibers. This causes anisotropic diffusion in white matter tissue of the brain. By performing diffusion-weighted acquisitions in different directions, a tensor can be determined characterizing the diffusion. This diffusion tensor can give information about nerve fiber lesions in white matter or spinal cord and allows tracking of the nerve fiber trajectories in the brain. The latter can provide valuable preoperative information for brain tumor resection or can be of diagnostic use (Stahl et al. 2007; Agosta et al. 2011; Horsfield and Jones 2002). Fiber tractography (Nucifora et al. 2007) can also be combined with fMRI to study the connectivity between functionally different brain regions and to analyze brain maturation and development in terms of myelinization.

The accuracy of fiber tractography is limited by possible fiber crossings in the same voxel leading to errors in fiber trajectories. Diffusion measurements in more different directions can increase the accuracy, albeit at the expense of longer acquisition times.

6.3.8 High-Field MRI

Increasing the magnetic field strength yields images with a better signal-to-noise ratio (SNR), a higher spatial resolution, shorter acquisition times, and a better contrast for tissue characterization (Schick 2005; Stafford and Challenges 2003; Panebianco et al. 2013; Mri and Quick 2011). In terms of relaxation times, T_1-relaxation time increases, while T_2-relaxation time decreases. Therefore, MRI sequences require appropriate adjustment for the slower longitudinal relaxation, while a shorter TE is needed to comply with the reduced T_2-relaxation time.

Both TOF MRA (Nguyen and Yang n.d.) and ASL benefit from the intrinsically higher SNR and the lengthening of blood T_1 relaxation providing better contrast between tissue and the circulating blood. Increased contrast between tissue and paramagnetic contrast agents will allow a reduced injection dose of these agents. Higher sensitivity to magnetic susceptibility has a positive impact on the detection

of hemorrhages, first-pass perfusion imaging, and BOLD fMRI signal. In terms of chemical shift, the larger gap between the resonance frequencies of fat and water makes saturation of the fat signal much easier and more homogeneous.

Besides these advantages, high-field MRI has some limitations as well (Schick 2005; Stafford and Challenges 2003). Due to the shortened wavelength of the RF pulse, now being much shorter than the FOV, RF excitation occurs much more inhomogeneous. On the other hand, the increased magnetic susceptibility can be diminished by reducing the TE and making the sequence less T_2* sensitive or by choosing segmented rather than single-shot sequences and increasing the bandwidth. Finally, during high-field MRI, the amount of RF energy deposited in tissue is increased significantly and needs to be addressed by increasing TR, limiting the number of slices, reducing the flip angle, or shortening the length of echo train.

In this context, it is also worthwhile to briefly mention parallel imaging (Glockner et al. 2005; Deshmane et al. 2012; Setsompop et al. 2008). Multiple small diameter coil elements can be combined in a phased array to record signals simultaneously and independently. Each coil element has a limited receiving range and a sensitivity profile that depends on the distance from the coil element. Therefore, the signal received by each coil element contains spatial data such as position coil position, reception level, and sensitivity level. This information can be combined with the gradient-induced spatial encoding to reconstruct the image. Since small diameter coils have higher signal-to-noise ratios than coils with larger diameters and noise between the different elements in the phased array is not correlated, the signal will have a better SNR than that one large coil.

Techniques combining the signals of several coil elements in a phased array to reconstruct an image are called parallel acquisition techniques. These techniques can be used to increase SNR, improve image quality for the same acquisition time, or reduce the acquisition time. The latter is particularly suitable for breath-hold sequences or for improving the temporal resolution of perfusion imaging (Olivertaylor 2012), functional imaging, and dynamic imaging of movements while reducing flow and motion artifacts. Especially cardiac and abdominal MRI or MRA (Wilson et al. 2004) can benefit from this approach.

In terms of reconstruction, two approaches have been presented (Blaimer et al. 2004). The first approach combines the images from each coil to reconstruct the global image in the spatial domain (i.e. SENSE or sensitivity encoding) (Zhang et al. 2007b) and is the most widely spread in present commercially available parallel MR sequences, while the second approach combines the frequency signals of each coil in the Fourier domain (GRAPPA or generalized autocalibrating partially parallel acquisition) (Hoge and Brooks 2008).

In the context of ultrahigh-field MRI (Wiesinger et al. 2006), parallel transmission techniques, where the independent RF pulses from an array of small coils can be combined to a more complex and adaptive RF pulse, offer multiple potential improvements in radio frequency transmission (Katscher et al. 2003; Katscher and Börnert 2006). More advanced RF transmission can lead to shorter pulse duration and reduce energy disposition in the patient, while patient-specific inhomogeneities can be corrected for, especially in ultrahigh-field MRI. Therefore, advanced parallel

acquisition techniques allow sequences of the echo-planar type and ultrafast gradient echo type, even at a very high field (Webb and Collins 2010; Harvey and Hoogeveen n.d.).

6.4 PET Basics

PET has extensively been used to explore a variety of physiological, biochemical, and pharmacological processes and to study aspects of the complex interaction of several neurotransmitter systems in the brain (Kenneth et al. 2002; Savitz and Drevets 2013; Smith and Jakobsen 2009). Because of the extremely low amounts of PET radiotracers (a compound labeled with a radionuclide) needed for imaging, its administration causes no pharmacological or functional changes in the physiology of the organism. Therefore, PET can measure nanomolar molecular concentrations and is highly sensitive and quantitative compared to MR-based techniques. The most challenging aspect is the development of suitable PET tracers for brain imaging which need to match a relatively small window of appropriate lipophilicity and molecular weight and affinity while demonstrating high target specificity and appropriate behavior in terms of metabolization.

A typical PET study involves the injection of a radiotracer into the venous blood stream of a subject. This radiotracer is delivered to the brain by the arterial flow. After crossing the blood-brain barrier, it might bind reversibly or irreversibly to its targets, which may either be neuroreceptors, transporter vesicles, or be metabolized by endogenous enzymes. If the tracer is inert, it will diffuse across the blood-brain barrier and will not be bound or trapped. In parallel to these biochemical processes, the radioactive label will decay, emitting a positron that annihilates through the simultaneous emission of two 511 keV photons in opposite directions. These photon pairs will be detected by the PET scanner within a predefined timing window (usually 6–10 ns) as a pair of coinciding detections. Therefore, PET is also being referred to as coincidence imaging. Over the total duration of the emission scan, data are acquired and corrected for physical effects such as attenuation, scatter, dead time, and detector response. These corrected data are binned into different time frames, and each time frame is reconstructed using an analytical or iterative reconstruction algorithm. This way a three-dimensional image of the radiotracer distribution in the brain is generated at various time points after tracer injection. These PET data are denoted dynamic and represent the temporal and spatial distribution of radiotracer concentration in brain tissue. The temporal evolution of radiotracer concentration in individual brain voxels or regions can be visualized by a time-activity curve (TAC). These TACs form the basis for quantifying the physiological (e.g., blood flow) and/or pharmacological aspect (e.g., receptor-binding site density, enzyme activity) of the system of interest.

Appropriate in vivo quantification of molecular targets with PET imaging is relatively complex due to the fact that tracers are administered intravenously and not directly applied to the target tissue. Therefore, delivery of the tracer to the brain can be influenced by the local blood flow, free tracer concentration in the plasma, and

peripheral tracer clearance due to metabolization and excretion. Moreover, total brain activity is measured with PET brain imaging, while often specifically bound, nonspecifically bound, and free tracer need to be separated to estimate the specific tracer kinetics.

In terms of mathematical analysis, brain uptake of a radioactive tracer is often described within the theoretical framework of compartments. Compartment modeling allows the description of systems that vary in time, but not in space. One of the assumptions for compartmental modeling is that there are no spatial concentration gradients within each department but only gradients in time. In fact, a compartment represents a unique state of the tracer and is defined as a space with separate uptake and clearance rate constants where the radioactive tracer concentration is assumed homogeneous. Rate constants of each compartment are assumed time invariant at least over the duration of the study and considered to be representative for the steady state of the system and the properties of the ligand. A compartment may have a physical analog such as the interstitial fluid compartment but can also be considered as a tracer being in bound or unbound state. Once the exchange paths between compartments have been specified, the mass balance for each compartment can be described as a set of ordinary differential equations where the tracer concentration in the vascular arterial compartment drives the model.

In the next paragraphs, brain PET perfusion imaging will be discussed, introducing elementary compartmental modeling. The basic kinetic blood flow model will be linked to a more general one-tissue compartment model and extended to a two tissue compartment model. The latter will be considered for the quantification of [^{18}F]FDG brain PET imaging. Finally, the potential to acquire PET information from multiple tracers simultaneously will be discussed.

6.5 [^{15}O]H_2O Brain PET

PET can be used to study neuronal activation by measuring the changes in regional cerebral perfusion and local large vessel blood flow since changes in neuronal activity are very closely related to perfusion. These PET studies use blood flow tracers like radiolabeled water or butanol which enter brain tissue via diffusion. Kety and Schmidt first described this basic exchange model for nonradioactive substances using the Fick principle (Kety and Schmidt 1948). The Fick principle states that, when a fluid with known flow F runs through a compartment which is in steady state, the rate at which a substance is extracted from the fluid by the compartment is equal to the difference in concentration of this substance when entering and leaving the compartment. Applying this principle to the passage of tracer within capillaries and considering the smallest scale such that the blood compartment represents a single capillary and the compartment is the tissue in the immediate vicinity, the change in tracer concentration in tissue over time $C_{\text{tissue}}(t)$ can be described as difference between the tracer concentration in arterial blood $C_{\text{arterial}}(t)$ and in venous blood $C_{\text{venous}}(t)$:

$$\frac{dC_{tissue}(t)}{dt} = F\left(C_{arterial}(t) - C_{venous}(t)\right). \tag{6.1}$$

The partition coefficient ρ is defined as the ratio of the tissue to venous blood concentration of the tracer. For tracers with high extraction, one can assume that the tracer concentration in the venous blood will be in equilibrium with the tissue concentration. Therefore, the tracer concentration in tissue over time $C_{tissue}(t)$ is described by:

$$\frac{dC_{tissue}(t)}{dt} = FC_{arterial}(t) - \frac{F}{\rho}C_{tissue}(t). \tag{6.2}$$

Since the tracer concentration can be measured in arterial blood and in tissue and one typically assumes that the same input function is valid for all brain tissue, Eq. 6.2 can be solved for blood flow F and partition coefficient ρ as a function of $C_{tissue}(t)$ and $C_{arterial}(t)$. Note that this model is only valid when blood flow remains constant during PET imaging and the PET tracer is inert and rapidly and freely diffusible in brain tissue.

Since the radioisotope [^{15}O] has a very short half-life of only 2 min, blood flow measurements with PET require a cyclotron in the proximity of the PET scanner in order to produce [^{15}O] on demand and immediately before tracer injection and data acquisition. Moreover, quantification involves the invasive procedure of arterial blood sampling. These prerequisites limit the number of imaging centers capable of performing these PET blood flow measurements.

6.6 [^{18}F]FDG Brain PET

The approach for modeling blood flow tracers is closely related to a one-tissue compartment model which describes the bidirectional flux of tracer between blood and tissue. This model is characterized by the time-varying tracer concentration in tissue $C_{tissue}(t)$ and in the arterial blood $C_{arterial}(t)$ and two first-order kinetic rate constants K_1 and k_2. In this way the tracer flux from arterial plasma to tissue is $K_1C_{plasma}(t)$, while the tracer flux from tissue to blood is $k_2C_{tissue}(t)$. Therefore, the net tracer flux into tissue is describes as:

$$\frac{dC_{tissue}(t)}{dt} = K_1C_{plasma}(t) - k_2C_{tissue}(t). \tag{6.3}$$

To solve Eq. 6.3 for K_1 and k_2, both $C_{plasma}(t)$ and $C_{tissue}(t)$ need to be determined. $C_{plasma}(t)$ can be measured by drawing blood samples from an arterial line at regular time points during the PET scan. On the other hand, $C_{tissue}(t)$ can be determined from the PET measurement. Since PET measures however all activity present in the brain, both intra- and extravascular, the activity concentration in brain tissue $C_{tissue}(t)$ relates to the total activity concentration measured by PET $C_{PET}(t)$ as:

$$C_{\mathrm{PET}}(t) = (1 - V_{\mathrm{blood}})C_{\mathrm{tissue}}(t) + V_{\mathrm{blood}}C_{\mathrm{blood}}(t). \tag{6.4}$$

V_{blood} represents the blood fraction present in the brain ($0 \leq V_{\mathrm{blood}} \leq 1$), while $C_{\mathrm{blood}}(t)$ denotes the activity concentration in the blood compartment of the brain. For the human brain, the blood is assumed to occupy about 5% of the brain volume (Phelps et al. 1979); hence, V_{blood} typically has a value of about 0.05.

The partition coefficient in the context of high extraction tracers can be defined more generally as the ratio of the steady-state concentrations between two compartments and is numerically identical to the tissue distribution volume V_{T}. If we consider tracer concentrations in blood and tissue in equilibrium, i.e., no net tracer transfer between the two compartments, the gradient $\frac{\mathrm{d}C_{\mathrm{tissue}}(t)}{\mathrm{d}t}$ in Eq. 6.3 can be set to zero, and the following equation for the distribution volume V_T is valid:

$$V_{\mathrm{T}} = \frac{C_{\mathrm{tissue}}(t)}{C_{\mathrm{plasma}}(t)} = \frac{K_1}{k_2} \tag{6.5}$$

If the tracer is inert and does not interact with any receptor system or does not undergo any chemical changes, but simply diffuses into and back out of the cells, a one-tissue compartment model would be an appropriate model.

This assumption is not valid for measuring energy metabolism with 2-fluoro-2-deoxy-D-glucose labeled with the fluorine radioisotope ^{18}F ([^{18}F]FDG). The substance is a glucose analog that is trapped in brain tissue since it is being metabolized in the mitochondria to its 6-phosphate form FDG-6-PO_4 through the enzyme hexokinase. Therefore, a one-tissue compartment model needs to be extended with an extra compartment to accurately describe the trapping behavior of the tracer (see Fig. 6.6). In this case the activity concentration in brain tissue $C_{\mathrm{tissue}}(t)$ can be written as:

$$C_{\mathrm{tissue}}(t) = C_{\mathrm{free}}(t) + C_{\mathrm{trapped}}(t), \tag{6.6}$$

The concentration of free radioligand in tissue is denoted by $C_{\mathrm{free}}(t)$, while $C_{\mathrm{trapped}}(t)$ represents the concentration of tracer trapped in tissue. Since no dephosphorylation of FDG-6-PO_4 is observed (Lucignani et al. 1993) for a PET measurement of less than 1 h post injection, no tracer clearance from this trapping compartment is expected ($k_4 \cong 0$) (see Fig. 6.6). Therefore, only the uptake rate constant needs to be taken into account for this compartment, and the tracer concentration in the two compartments can be described by the following partial differential equations:

$$\frac{\mathrm{d}C_{\mathrm{free}}(t)}{\mathrm{d}t} = K_1 C_{\mathrm{plasma}}(t) - k_2 C_{\mathrm{free}}(t) - k_3 C_{\mathrm{free}}(t), \tag{6.7}$$

$$\frac{\mathrm{d}C_{\mathrm{trapped}}(t)}{\mathrm{d}t} = k_3 C_{\mathrm{free}}(t). \tag{6.8}$$

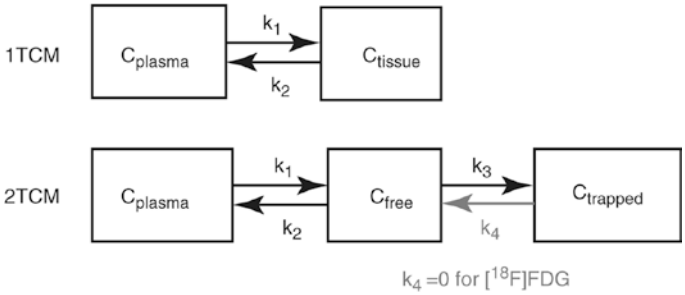

Fig. 6.6 Schematic overview of a one-tissue (*1TCM*) and two-tissue compartment model (*2TCM*) with corresponding rate constants. For [18F]FDG, the clearance rate constant for the second compartment k_4 can be assumed zero

If we assume steady-state conditions for the free tracer in tissue, the gradient in Eq. 6.7 can be set to zero, and the trapping rate can be expressed as:

$$\frac{\mathrm{d}C_{\text{trapped}}(t)}{\mathrm{d}t} = K_1 \frac{k_3}{k_2 + k_3} C_{\text{plasma}}(t) \tag{6.9}$$

Instead of V_T, the influx rate constant K_i, also named metabolic rate, trapping rate, or accumulation rate constant, can be considered as an endpoint, defined as:

$$K_i = K_1 \frac{k_3}{k_2 + k_3} \tag{6.10}$$

Since [18F]FDG is a glucose analog, trapping rate has proven to be proportional to the glucose metabolic rate. The value of the ratio between [18F]FDG and glucose metabolic rate is called the lumped constant (LC), which is determined by a combination of several factors. For human brain tissue, LC values are assumed to be around 0.8.

For radioligands with irreversible kinetic behavior, late static scanning can be considered as is common for [18F]FDG-PET. These radioligands often provide high-specific to nonspecific binding ratios such that tracer uptake at a later time point postinjection reflects the amount of specific tracer binding and therefore represents valid quantitative endpoint for the underlying physiological process.

For regional analysis, [18F]FDG brain PET scans are typically spatially normalized to a predefined stereotactic template space using an average [18F]FDG brain PET template. In this way anatomical structures can more easily be identified in a spatially standardized fashion and predefined volumes of interest can be projected onto the brain PET data to allow a VOI-based quantification of [18F]FDG uptake. In addition, this spatial standardization allows cortical tracer uptake to be projected onto the cortical surface of a standard brain. These so-called stereotactic surface projections (3D-SSP) provide a convenient 3D visualization for visual inspection and further quantitative analysis. In a next step, [18F]FDG brain PET datasets can be compared individually on a voxel-by-voxel basis with an age- and gender-matched

database of normal values. *Z*-scores on a voxel level, determining the deviation from normal mean uptake values in terms of number of standard deviations, can be calculated and displayed as overlay in 3D-SSP views. These *Z*-score maps allow straightforward identification of brain regions with abnormal uptake values and of hypometabolic patterns that can be specific for neurodegenerative diseases (see Fig. 6.7).

Static, normalized [^{18}F]FDG brain PET scans are a valuable early and differential diagnostic tool for neurodegenerative diseases (Grimmer et al. 2004) and can be used for differentiation of movement disorders, for localization of the functional deficit zone in epilepsy, and to assess brain tumor burden and staging. Combined with [^{11}C]PIB brain PET reflecting the amyloid burden in brain tissue (Villemagne et al. 2011, 2012) (see Fig. 6.8), FDG-PET can be part of a multimodal and multitracer approach to differentiate different types of dementias such as Alzheimer's disease, dementia with Lewy bodies, frontotemporal lobar degeneration, semantic dementia, primary progressive nonfluent aphasia, and multiple system atrophy (Drzezga 2010).

6.7 Simultaneous [^{15}O]H_2O and [^{18}F]FDG Brain PET

In contrast to MRI, where different types of tissue contrast can be generated during one scanning session, information provided by a PET imaging session is typically limited to a single tracer. Multiple tracer protocols for PET imaging generally require that the signal of one tracer has decayed to sufficiently low levels due to both physical and biological decay before the signal of subsequent tracers can be measured. In this context, consecutive brain PET imaging with [^{11}C]PIB and [^{18}F]FDG takes up to a little more than 2 h, where first a 1-h dynamic [^{11}C]PIB brain PET scan is acquired starting at the time of injection, followed by the injection of [^{18}F]FDG and an additional time interval of 1 h between the end of the [^{11}C]PIB brain PET scan and the start of the static [^{18}F]FDG brain PET scan (Meyer et al. 2011). This way, cross talk between the [^{11}C]PIB and [^{18}F]FDG signal is avoided as the [^{18}F]FDG brain PET scan is started 2 h after the injection of [^{11}C]PIB, corresponding to a delay of six times the half-life of [^{11}C].

However, in some cases it is possible to acquire the PET signal of two different PET tracers simultaneously and separate the signal afterward based on the different kinetic behavior of the two tracers (Kadrmas et al. 2013; Kadrmas and Hoffman 2013; El Fakhri et al. 2013; Joshi et al. 2009; Black et al. 2009). As an example, kinetics of [^{15}O]H_2O and [^{18}F]FDG brain PET, for instance, generate highly distinct TACs, enabling the use of temporal information to separate the tracer signals. For this purpose, two sets of temporal basis functions are defined, which model either the slowly decaying [^{18}F]FDG or the fast-decaying water dynamics (Verhaeghe and Reader 2013). These basis functions are formed by convolution of a generating function, estimated from the measured head curve, with a set of predetermined decaying exponential functions. Moreover, this temporal basis function approach effectively permits fully 4D image reconstruction such that every time point in the

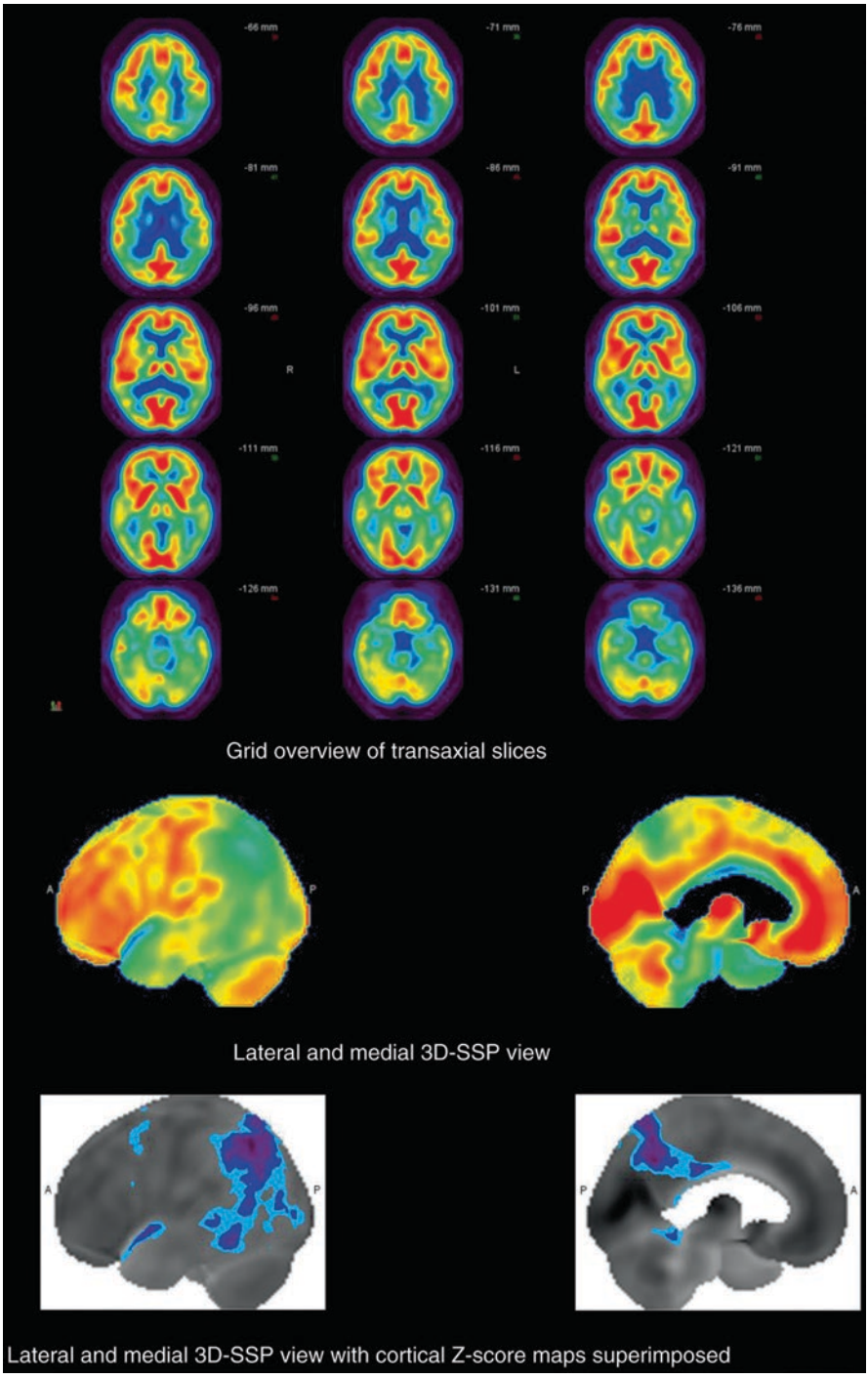

Fig. 6.7 [^{18}F]FDG brain PET data of a patient suffering from Alzheimer's disease (AD)

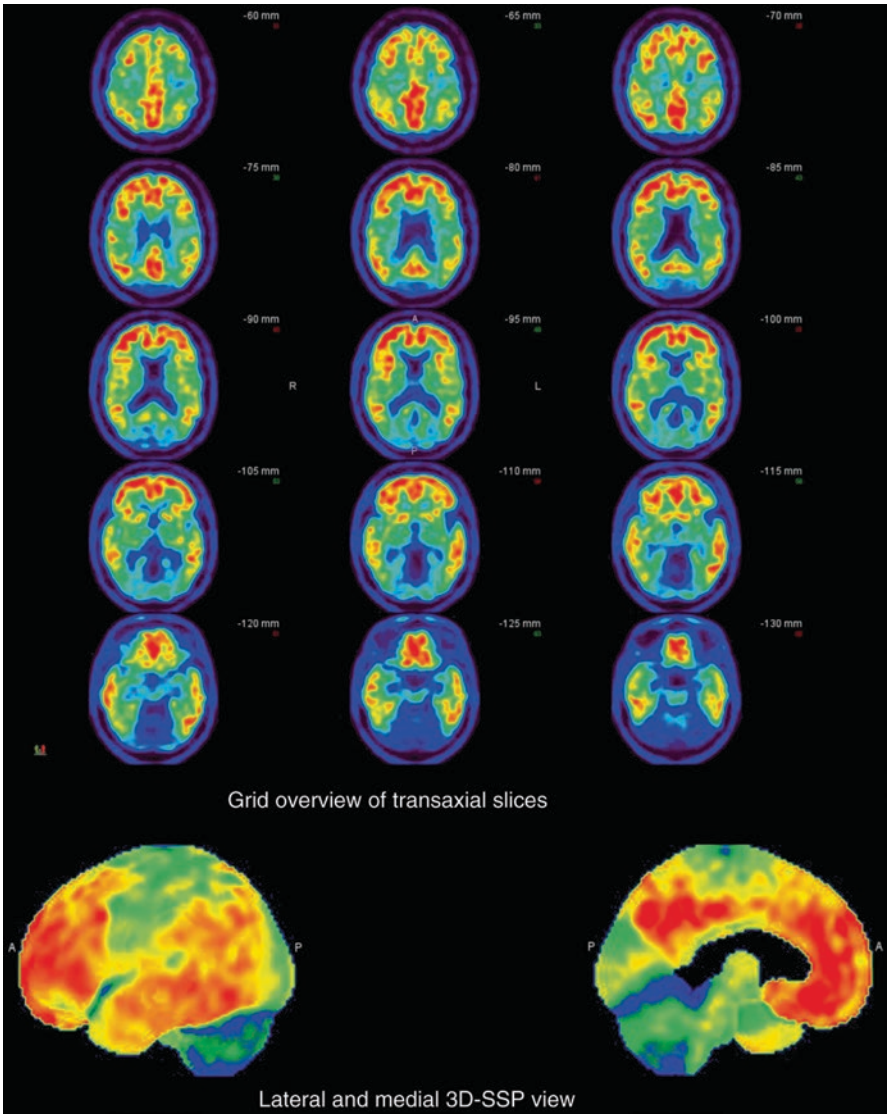

Fig. 6.8 [^{11}C]PIB brain PET data of the same AD patient as in Fig. 6.7

reconstructed image benefits from far more acquired data than a conventional frame-by-frame approach. Based on simulation studies, simultaneous imaging using the basis function method reduces noise to below that of conventional individual imaging, while [^{15}O]H_2O activation maps created using the basis functions method showed increased t-values in the activated region, indicating increased confidence that the difference between activated and baseline conditions is genuine rather than noise related. These simulation studies showed that dual-tracer imaging

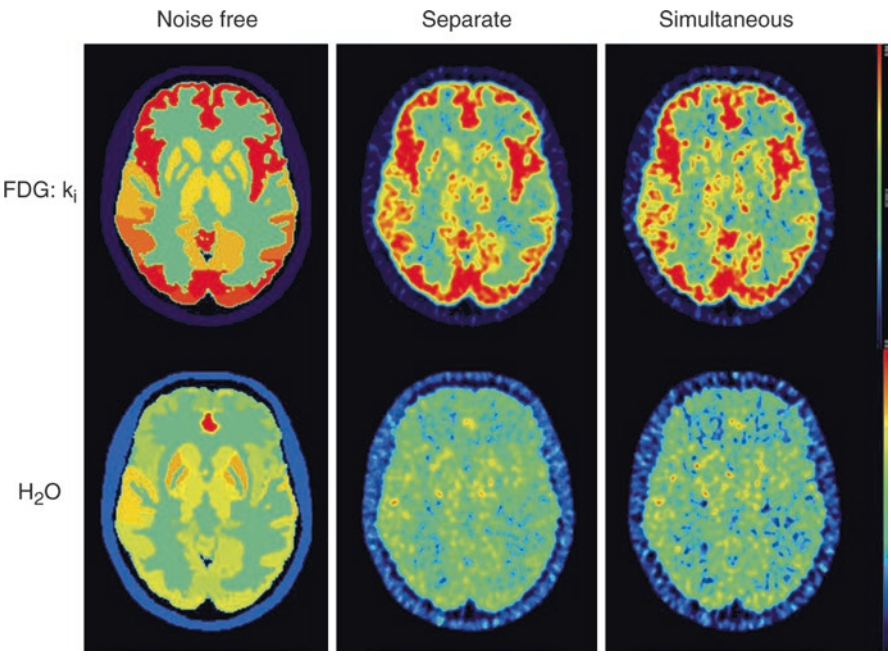

Fig. 6.9 Example of reconstructed images from simulated PET data for simultaneous imaging of [^{18}F]FDG and [^{15}O]H_2O. Simultaneous imaging (*right*) compared to separate imaging (*middle*) and the noise-free "ground truth" image (*left*)

using basis functions to separate [^{18}F]FDG and [^{15}O]H_2O components is feasible, and resulting image data are comparable to those obtained from individual PET scans (see Fig. 6.9).

Another approach to separate the information of two different PET isotopes is to use the different decays schemes of the radioisotopes. If one of the two radioactive isotopes is a pure positron emitter and the second isotope emits an additional high-energy gamma in a cascade simultaneously with positron emission, detection of this auxiliary prompt gamma in coincidence with the annihilation event allows us to identify the corresponding 511 keV photon pair as originating from the second isotope (Andreyev and Celler 2011).

6.8 Integrated PET/MRI Quantification

Currently available hybrid PET/MRI systems allow a straightforward integration of MRI and PET information (Catana et al. 2012). Figure 6.11 gives some examples of the imaging potential of a hybrid PET/MRI system for brain imaging where different types of image information can be acquired in a "one-stop shop" setting (Drzezga et al. 2012; Martinez-Möller et al. 2012). At the moment, fully integrated PET/MRI

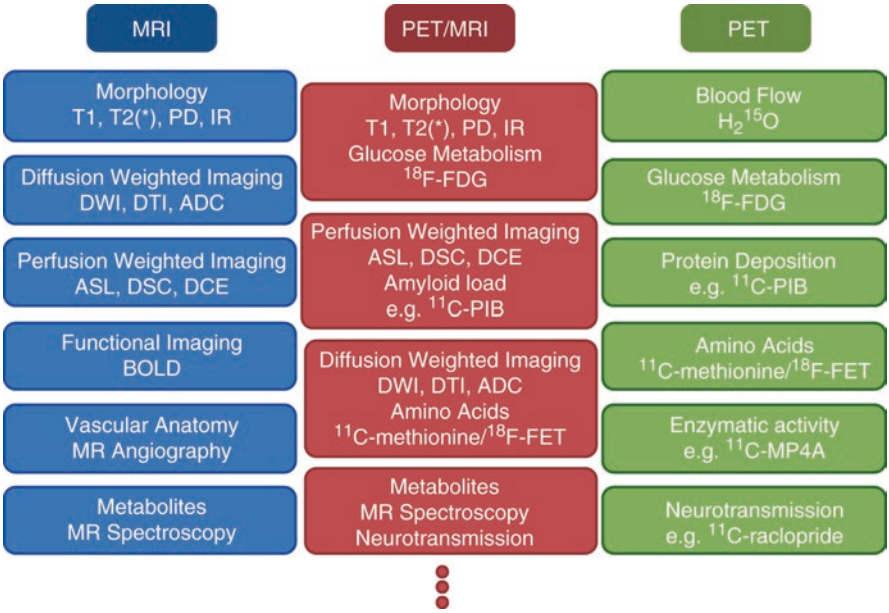

Fig. 6.10 Some examples of the imaging potential of hybrid PET/MRI

systems are also being commercialized which allow simultaneous acquisition of MRI and PET information (Delso et al. 2011; Grant et al. 2016) (Fig. 6.10).

In terms of reconstruction, the most challenging of fully integrated PET/MR brain imaging is the attenuation correction and the creation of a reliable attenuation map (Torigian et al. 2013). While an attenuation map relies on the information about tissue electron density, MRI only gives information about tissue proton density. Different methodologies are suggested to generate an attenuation map based on MRI information (Hofmann et al. 2009; Bezrukov et al. 2013). One of these approaches is to use a dedicated DIXON MRI sequence such that segmentation of MRI data into four tissue classes, i.e., background, lungs, fat, and soft tissue, is rather straightforward (Martinez-Möller et al. 2009). Actually a DIXON MRI sequence acquires MRI datasets with fat and water in phase and fat and water out of phase, such that datasets with only fat tissue and only water can be generated very easily. Based on these MRI data, an attenuation map is generated by assigning appropriate narrow beam attenuation values to these four tissue classes, while other tissue classes such as cortical bone are discarded. This approach proved to be a good approximation for quantitative [^{18}F]FDG whole-body PET imaging except for bone lesions (Drzezga et al. 2012; Kim et al. 2012). However, in case of [^{18}F]FDG brain PET imaging, 3.7–17.7% reduced activity is observed in cortical regions compared to the center of the brain with the underestimation increasing in image planes with relative higher skull contribution. Therefore, hybrid methods combining DIXON and UTE MRI sequences are presented (Berker et al. 2012). While DIXON

sequences perform well for separating, air, water, and fat, ultrashort echo time (Keereman et al. 2010) or UTE sequences allow the visualization of cortical bone since the very short echo times of these sequences are adapted to the very fast T_2 relaxation of cortical bone due to the very limited water content of these tissues types. This way, attenuation of the skull can be included in the attenuation map leading to improved quantification of [^{18}F]FDG uptake in the brain (Ladefoged et al. 2017; Sekine et al. 2016).

In terms of quantification, high-resolution anatomical MR information can be used to facilitate manual or semiautomatic delineation of the appropriate volume of interest (VOI) especially when the PET data itself provide limited anatomical landmarks. While manual delineation can be time-consuming and observer dependent, methodologies have been developed that allow automatic VOI generation (Svarer et al. 2005; Hammers et al. 2003) with freesurfer (https://surfer.nmr.mgh.harvard.edu/) currently being considered as the state of the art for brain parcellation. These methods create an individualized VOI probability map on the basis of a database of several MRI datasets, where a template VOI set has been defined manually on each MRI dataset. Nonlinear image registration between these MRI datasets and the MRI dataset of interest allows transfer of these individually defined templates VOI sets to the MRI dataset of interest. Based on the degree of overlap of the transferred VOI sets, a VOI probability map is created specifically for that particular PET dataset. When the generated VOI map is based on more than one template VOI set, VOI delineation proved to be better reproducible and showed less variation as compared to manual delineation or transfer of only a single template VOI set. This methodology allows a fast, objective, and reproducible assessment of regional brain PET values.

In addition, a high-resolution anatomical MRI image spatially aligned to the PET image offers the possibility to migitate partial volume effects in brain PET imaging. Due to the limited resolution of PET imaging, the reconstructed activity distribution will be a blurred version of the true activity distribution. Furthermore, the typical brain PET reconstruction voxel size (2 × 2 × 2 mm or bigger) is relatively large compared to the cortical thickness. Hence, many of the studied PET voxels are only partly composed of the target brain tissue, which, in most cases, is a specific gray matter brain structure. Indeed, the PET estimate actually reflects the blurred activity concentration of different underlying adjacent tissue types, like gray matter, white matter, and cerebrospinal fluid, with different activity concentrations. Therefore, the estimated PET signal of the target tissue is confounded. One can correct for this partial volume effect by using aligned spatial distribution maps for gray matter, white matter, and cerebrospinal fluid, generated by segmenting the structural MRI image (Rousset et al. 2007). This correction is often performed after PET reconstruction. In that case, the actual tracer concentration in the target tissue is estimated based on the segmentation information and on an estimate of the resolution in the reconstructed image (see Fig. 6.11). Many different partial volume correction (PVC) techniques have been proposed in the past (Erlandsson et al. 2012). These approaches recover the true activity concentration very well in most cortical regions, but their accuracy typically depends heavily on the accuracy of the MRI

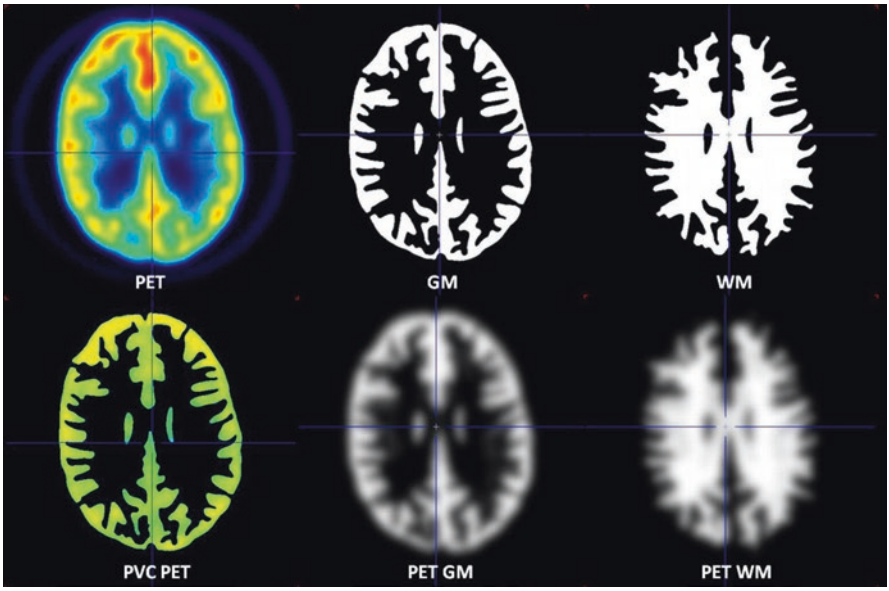

Fig. 6.11 Brain phantom experiment to illustrate partial volume correction methodology to correct for PVE between gray matter (*GM*) and white matter (*WM*) in [^{18}F]FDG brain PET imaging

segmentation. As an alternative, the resolution of the PET images can be improved by modeling the system resolution during PET reconstruction. Unfortunately, these images suffer from Gibbs artifacts. These can be suppressed, e.g., by applying a smoothing prior during reconstruction, which penalizes fast intensity changes. To avoid that the tissue edges get blurred too, the smoothing prior should only be applied between voxels of the same tissue class, by exploiting the segmentation maps from the aligned MRI (Baete et al. 2004). This method is referred to as PET reconstruction using a segmentation-based anatomical prior. While this approach still requires accurate segmentation of the MRI data, new anatomical priors have been proposed that improve the PET reconstruction by incorporating the aligned high-resolution anatomical MRI image without the need for segmentation (Vunckx et al. 2012; Somayajula et al. 2011; Bowsher et al. 2004) (see Fig. 6.12). Post-reconstruction PVC methods provide an estimate for the actual tracer uptake per unit gray matter tissue, whereas PET reconstruction with an anatomical prior yields an accurate estimate for the uptake in each voxel, which can be converted to an estimate for the gray matter tracer uptake through the use of tissue distribution maps (Baete et al. 2004). Correction of the PVE is particularly important when comparing healthy volunteers with elderly subjects or with patients suffering from neurodegenerative disorders where the presence of regional cerebral atrophy is suspected.

Finally, MR angiography of large vessel structures can be used to facilitate the segmentation and extraction of the arterial PET signal such that an image-derived arterial input function can be determined and integrated into the pharmacokinetic modeling of PET data. This approach will potentially result in a noninvasive and more accurate quantification of the biological and physiological parameters of the target tissue.

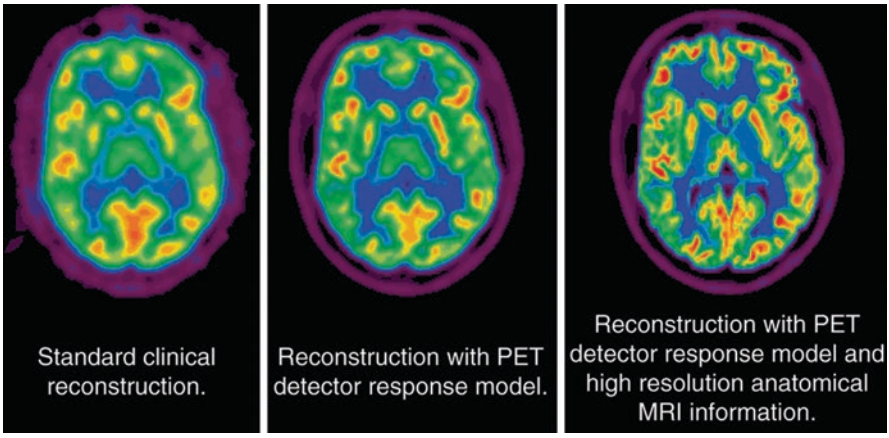

Fig. 6.12 Comparison of different types of brain PET reconstruction in terms of resolution properties

6.9 Future Perspectives of Hybrid PET/MRI

In terms of patient care, integrated PET/MRI offers several potential advantages. Since two modalities are combined in a "one-stop shop," scanning can be done in a more time-effective way, while sedation, if needed, can be limited to one scanning session. Therefore, overall patient comfort can be improved. Meanwhile, the tracer dose for PET imaging could be reduced since the MRI protocols now determine total scan time compared to the PET imaging protocols in the case of PET/CT.

In terms of radiation exposure, hybrid PET/MRI limits radiation exposure to the PET component and as such substantially reduces the total radiation dose, especially compared to whole-body PET/CT when a diagnostic CT is acquired. While this is desirable for all patients, this especially concerns pediatric patients and adult cancer patients with good prognosis but needing frequent follow-up imaging. More personalized treatments could also result in multiple molecular imaging sessions with labeled antibodies. Since kinetics of antibodies are such that labeling with long-lived positron emitters such as ^{89}zirconium and ^{124}iodine is required for quantification, radiation exposure of the patient can become a critical aspect of the treatment.

Whether simultaneous acquisition of PET and MRI data has really clinical added value in brain imaging may be questioned, since information from different modalities can be integrated by software registration. While this approach could be sufficient to answer most clinical questions, the conceptual advantage of simultaneous data acquisition becomes imperative when addressing questions which require synchronous recordings of region-bound functional parameters that change rapidly over time. This specifically applies for brain connectivity analysis where functionally or effectively connected brain networks will be investigated by component and correlation analyses of simultaneous acquired functional MRI data and [^{18}F]FDG-PET data. On the other hand, simultaneous PET/MRI can measure BOLD or ASL fMRI, MR spectroscopy, and PET receptor-binding kinetics in nonsteady-state

conditions of a fast functional brain response. This way high-resolution structural MRI, fMRI responses, and changes in neurotransmission obtained from PET can be correlated spatially and temporally such that temporal relatedness and physiological equivalence of the separately observed regional phenomena can be demonstrated.

On the other hand, an integrated PET/MRI approach will facilitate cross-validation and multimodal interpretation of the integrated image data provided by both modalities. This way, MRI and PET information can be evaluated as complementary, confirmatory, or redundant such that MRI/PET imaging protocols can be developed to maximize the potential of combining both modalities. Meanwhile, clinical applications can be identified where PET and MRI information are likely to be complementary. This can contribute to more effective and rational use of MRI/PET imaging. As an example, cerebral blood flow can be measured simultaneously with the PET data using MRI techniques (Wintermark et al. 2005). Using the MRI instead of the PET component for brain blood flow measurements may not only make the measurement more time efficient but also more accessible for centers which do not have a cyclotron for onsite tracer production. As the MRI is used for brain blood flow measurements, other more specific PET tracers can be used with regard to the brain pathology being studied. This could also apply for ASL MRI which uses blood as an endogenous, freely diffusible tracer for cerebral blood flow. Since [^{18}F]FDG-PET and ASL MRI identify similar regional abnormalities and could have comparable diagnostic accuracy as proven in a small population of AD patients (Musiek et al. 2012), other PET tracers could be considered instead of [^{18}F]FDG-PET targeting other pathways of the AD pathology and therefore providing better insight in the relationship between structural, functional, and metabolic changes in Alzheimer's disease in specific or neurodegenerative disorders in general.

To conclude, hybrid PET/MRI could prove beneficial for many clinical applications. For brain tumors, a combined PET/MRI approach could improve diagnostic accuracy, therapy planning, and therapy monitoring of medication and/or radiotherapy. For cerebrovascular disorders, simultaneously PET/MRI might help in understanding the relationship and penumbra mismatch between MR PWI/DWI and PET. This could lead to new PWI imaging thresholds for a better selection of patients beyond 4.5-h time window who could benefit from thrombolytic therapy. In case of epilepsy, hybrid PET/MRI can provide the accurate spatial co-registration of PET and MRI data which is crucial for surgery planning. In the context of dementia, a hybrid PET/MRI approach could improve early diagnosis and monitoring of disease progression. Future studies will determine the potential of hybrid PET/MRI in terms of clinical value and cost-effectiveness.

References

Agosta F et al (2011) White matter damage in Alzheimer disease and its relationship to gray matter atrophy. Radiology 258(3):853–863. http://www.ncbi.nlm.nih.gov/pubmed/21177393. Accessed 8 Dec 2013

Aguirre GK et al (2002) Experimental design and the relative sensitivity of BOLD and perfusion fMRI. Neuroimage 15(3):488–500. http://www.ncbi.nlm.nih.gov/pubmed/11848692. Accessed 9 Dec 2013

Aguirre GK, Detre JA, Wang J (2005) Perfusion fMRI for functional neuroimaging. Int Rev Neurobiol 66:213–236. http://www.ncbi.nlm.nih.gov/pubmed/16387205. Accessed 9 Dec 2013

Alsop DC, Detre JA, Grossman M (2000) Assessment of cerebral blood flow in Alzheimer's disease by spin-labeled magnetic resonance imaging. Ann Neurol 47(1):93–100. http://www.ncbi.nlm.nih.gov/pubmed/10632106. Accessed 9 Dec 2013

Alsop DC et al (2008) Hippocampal hyperperfusion in Alzheimer's disease. NeuroImage 42(4):1267–1274. http://www.pubmedcentral.nih.gov/articlerender.fcgi?artid=2675915&tool=pmcentrez&rendertype=abstract. Accessed 9 Dec 2013

Alsop DC et al (2010) Arterial spin labeling blood flow MRI: its role in the early characterization of Alzheimer's disease. J Alzheimers Dis 20(3):871–880. http://www.pubmedcentral.nih.gov/articlerender.fcgi?artid=3643892&tool=pmcentrez&rendertype=abstract. Accessed 11 Aug 2013

Andreyev A, Celler A (2011) Dual-isotope PET using positron-gamma emitters. Phys Med Biol 56(14):4539–4556

Anticevic A et al (2012) The role of default network deactivation in cognition and disease. Trends Cogn Sci 16(12):584–592. http://www.ncbi.nlm.nih.gov/pubmed/23142417. Accessed 22 Sept 2013

Baete K et al (2004) Anatomical-based FDG-PET reconstruction for the detection of hypometabolic regions in epilepsy. IEEE Trans Med Imaging 23(4):510–519. http://www.ncbi.nlm.nih.gov/pubmed/15084076. Accessed 9 Dec 2013

Bammer R (2003) Basic principles of diffusion-weighted imaging. Eur J Radiol 45:169–184

Berker Y et al (2012) MRI-based attenuation correction for hybrid PET/MRI systems: a 4-class tissue segmentation technique using a combined ultrashort-echo-time/Dixon MRI sequence. J Nucl Med 53(5):796–804. http://www.ncbi.nlm.nih.gov/pubmed/22505568. Accessed 30 May 2013

Bezrukov I et al (2013) MR-based PET attenuation correction for PET/MR imaging. Semin Nucl Med 43(1):45–59. http://www.ncbi.nlm.nih.gov/pubmed/23178088. Accessed 24 May 2013

Bitar R et al (2006) MR pulse sequences: what every radiologist wants to know but is afraid to ask. Radiographics 26(2):513–537. http://www.ncbi.nlm.nih.gov/pubmed/16549614. Accessed 11 Nov 2013

Black NF, McJames S, Kadrmas DJ (2009) Rapid multi-tracer PET tumor imaging with F-FDG and secondary shorter-lived tracers. IEEE Trans Nucl Sci 56(5):2750–2758. http://www.pubmedcentral.nih.gov/articlerender.fcgi?artid=2799294&tool=pmcentrez&rendertype=abstract. Accessed 9 Dec 2013

Blaimer M et al (2004) SMASH, SENSE, PILS, GRAPPA: how to choose the optimal method. Top Magn Reson Imaging 15(4):223–236. http://www.ncbi.nlm.nih.gov/pubmed/15548953. Accessed 9 Dec 2013

Bley TA et al (2005) High-resolution MRI in giant cell arteritis: imaging of the wall of the superficial temporal artery. AJR Am J Roentgenol 184(1):283–287. http://www.ncbi.nlm.nih.gov/pubmed/15615989. Accessed 9 Dec 2013

Bowsher JE et al (2004) Utilizing MRI information to estimate F18-FDG distributions in rat flank tumors. In: IEEE symposium conference record nuclear science 2004. IEEE, Piscataway, pp 2488–2492, http://ieeexplore.ieee.org/lpdocs/epic03/wrapper.htm?arnumber=1462760. Accessed 9 Dec 2013

Boyle GE et al (2006) An interactive taxonomy of MR imaging sequences. Radiographics 26(6):e24; quiz e24. http://www.ncbi.nlm.nih.gov/pubmed/16971691. Accessed 8 Dec 2013

Brown GG, Clark C, Liu TT (2007) Measurement of cerebral perfusion with arterial spin labeling: part 2. Applications. J Int Neuropsychol Soc 13(3):526–538. http://www.pubmedcentral.nih.gov/articlerender.fcgi?artid=2408863&tool=pmcentrez&rendertype=abstract. Accessed 24 Sept 2013

Broyd SJ et al (2009) Default-mode brain dysfunction in mental disorders: a systematic review. Neurosci Biobehav Rev 33(3):279–296. http://www.ncbi.nlm.nih.gov/pubmed/18824195. Accessed 9 Dec 2013

Buckner RL, Andrews-Hanna JR, Schacter DL (2008) The brain's default network: anatomy, function, and relevance to disease. Ann N Y Acad Sci 1124:1–38. http://www.ncbi.nlm.nih.gov/pubmed/18400922. Accessed 15 Nov 2013

Calamante F (2009) Artifacts and pitfalls in perfusion MR imaging. In: Clinical MR neuroimaging. Cambridge University Press, Cambridge, pp 137–155

Catana C et al (2012) PET/MRI for neurologic applications. J Nucl Med 53(12):1916–1925. http://www.ncbi.nlm.nih.gov/pubmed/23143086. Accessed 6 June 2013

Cha S (2003) Perfusion MR imaging: basic principles and clinical applications. Magn Reson Imaging Clin N Am 11(3):403–413. http://www.ncbi.nlm.nih.gov/pubmed/14768726. Accessed 9 Dec 2013

Chalela JA et al (2000) Magnetic resonance perfusion imaging in acute ischemic stroke using continuous arterial spin labeling. Stroke 31(3):680–687. http://www.ncbi.nlm.nih.gov/pubmed/10700504. Accessed 9 Dec 2013

Chavhan GB et al (2009) Principles, techniques, and applications of T2*-based MR imaging and its special applications. Radiographics 29(5):1433–1449. http://www.pubmedcentral.nih.gov/articlerender.fcgi?artid=2799958&tool=pmcentrez&rendertype=abstract. Accessed 8 Dec 2013

Chen Y et al (2011) Quantification of cerebral blood flow as biomarker of drug effect: arterial spin labeling phMRI after a single dose of oral citalopram. Clin Pharmacol Ther 89(2):251–258. http://www.ncbi.nlm.nih.gov/pubmed/21191380. Accessed 8 Aug 2013

Chou Y et al (2012) Investigation of long-term reproducibility of intrinsic connectivity network mapping: a resting-state fMRI study. AJNR Am J Neuroradiol 33(5):833–838. http://www.pubmedcentral.nih.gov/articlerender.fcgi?artid=3584561&tool=pmcentrez&rendertype=abstract. Accessed 9 Dec 2013

Cole MW et al (2011) Variable global dysconnectivity and individual differences in schizophrenia. Biol Psychiatry 70(1):43–50. http://www.pubmedcentral.nih.gov/articlerender.fcgi?artid=3204885&tool=pmcentrez&rendertype=abstract. Accessed 9 Dec 2013

Dai W et al (2008) Continuous flow-driven inversion for arterial spin labeling using pulsed radio frequency and gradient fields. Magn Reson Med 60(6):1488–1497. http://www.pubmedcentral.nih.gov/articlerender.fcgi?artid=2750002&tool=pmcentrez&rendertype=abstract. Accessed 7 Nov 2013

Damoiseaux JS et al (2012) Functional connectivity tracks clinical deterioration in Alzheimer's disease. Neurobiol Aging 33(4):828.e19–828.e30. http://www.pubmedcentral.nih.gov/articlerender.fcgi?artid=3218226&tool=pmcentrez&rendertype=abstract. Accessed 9 Dec 2013

De Bazelaire CMJ et al (2004) Radiology of abdominal and pelvic tissues measured in vivo at 3.0 T: preliminary results. Radiology 230(3):652–659

De Kerviler E et al (1998) Fat suppression techniques in MRI: an update. Biomed Pharmacother 52(2):69–75. http://www.ncbi.nlm.nih.gov/pubmed/9755798. Accessed 8 Dec 2013

De Luca M et al (2006) fMRI resting state networks define distinct modes of long-distance interactions in the human brain. Neuroimage 29(4):1359–1367. http://www.ncbi.nlm.nih.gov/pubmed/16260155. Accessed 9 Dec 2013

Delso G et al (2011) Performance measurements of the Siemens mMR integrated whole-body PET/MR scanner. J Nucl Med 52(12):1914–1922. http://www.ncbi.nlm.nih.gov/pubmed/22080447. Accessed 23 May 2013

Desai MY et al (2005) Delayed contrast-enhanced MRI of the aortic wall in Takayasu's arteritis: initial experience. AJR Am J Roentgenol 184(5):1427–1431. http://www.ncbi.nlm.nih.gov/pubmed/15855090. Accessed 3 Dec 2013

Deshmane A et al (2012) Parallel MR imaging. J Magn Reson Imaging 72:55–72

Detre JA, Alsop DC (1999) Perfusion magnetic resonance imaging with continuous arterial spin labeling: methods and clinical applications in the central nervous system. Eur J Radiol 30(2):115–124. http://www.ncbi.nlm.nih.gov/pubmed/10401592

Detre JA et al (1992) Perfusion imaging. Magn Reson Med 23(1):37–45. http://www.ncbi.nlm.nih.gov/pubmed/1734182. Accessed 8 Dec 2013

Detre JA et al (2009) Arterial spin-labeled perfusion MRI in basic and clinical neuroscience. Curr Opin Neurol 22(4):348–355

Drzezga A (2010) Amyloid-plaque imaging in early and differential diagnosis of dementia. Ann Nucl Med 24(2):55–66. http://www.ncbi.nlm.nih.gov/pubmed/20082230. Accessed 10 June 2013

Drzezga A et al (2012) First clinical experience with integrated whole-body PET/MR: comparison to PET/CT in patients with oncologic diagnoses. J Nucl Med 53(6):845–855. http://www.ncbi.nlm.nih.gov/pubmed/22534830. Accessed 23 May 2013

Eastwood JD, Hudgins PA (1998) New techniques in magnetic resonance imaging. Curr Opin Ophthalmol 9(6):54–60. http://www.ncbi.nlm.nih.gov/pubmed/10387337. Accessed 8 Dec 2013

Edelman RR et al (1994) Qualitative mapping of cerebral blood flow and functional localization with echo-planar MR imaging and signal targeting with alternating radio frequency. Radiology 192(2):513–520. http://www.ncbi.nlm.nih.gov/pubmed/8029425. Accessed 8 Dec 2013

El Fakhri G et al (2013) Dual-tracer PET using generalized factor analysis of dynamic sequences. Mol Imaging Biol 15(6):666–674. http://www.pubmedcentral.nih.gov/articlerender.fcgi?artid=3812387&tool=pmcentrez&rendertype=abstract. Accessed 9 Dec 2013

Elster AD, Burdette JH (2001) Questions & answers in magnetic resonance imaging, 2nd edn. Mosby, St. Louis

Erlandsson K et al (2012) A review of partial volume correction techniques for emission tomography and their applications in neurology, cardiology and oncology. Phys Med Biol 57(21):R119–R159. http://www.ncbi.nlm.nih.gov/pubmed/23073343. Accessed 1 Mar 2013

Ferré J-C et al (2013) Arterial spin labeling (ASL) perfusion: techniques and clinical use. Diagn Interv Imaging 94(12):1211–1223. http://www.ncbi.nlm.nih.gov/pubmed/23850321. Accessed 8 Aug 2013

Foo TKF, Polzin JA, Thomasson DM (2005) MR angiography physics: an update. Magn Reson Imaging Clin N Am 13(1):1–22. http://www.ncbi.nlm.nih.gov/pubmed/15760754. Accessed 9 Dec 2013

Fox MD, Raichle ME (2007) Spontaneous fluctuations in brain activity observed with functional magnetic resonance imaging. Nat Rev Neurosci 8(9):700–711. http://www.ncbi.nlm.nih.gov/pubmed/17704812. Accessed 22 Nov 2013

Fullerton GD (1984) Characterization of proton NMR relaxation times in normal and pathological tissues by correlation with other tissue parameters. Magn Reson Imaging 2:97–106

Galvin JE et al (2011) Resting bold fMRI differentiates dementia with Lewy bodies versus Alzheimer disease. Neurology 76:1797–1803. http://www.pubmedcentral.nih.gov/articlerender.fcgi?artid=3100121&tool=pmcentrez&rendertype=abstract. Accessed 25 Nov 2013

Gibby WA (2005) Basic principles of magnetic resonance imaging. Neurosurg Clin N Am 16(1):1–64. http://www.ncbi.nlm.nih.gov/pubmed/15561528. Accessed 8 Dec 2013

Glockner JF et al (2005) Parallel MR imaging: a user's guide. Radiographics 25(5):1279–1297

Greicius M (2008) Resting-state functional connectivity in neuropsychiatric disorders. Curr Opin Neurol 21(4):424–430. http://www.ncbi.nlm.nih.gov/pubmed/18607202. Accessed 5 Mar 2013

Grant AM et al (2016) NEMA NU 2-2012 performance studies for the SiPM-based ToF-PET component of the GE SIGNA PET/MR system. Med Phys 43(5):2334. https://www.ncbi.nlm.nih.gov/pubmed/27147345

Grimmer T et al (2004) Region-specific decline of cerebral glucose metabolism in patients with frontotemporal dementia: a prospective 18F-FDG-PET study. Dement Geriatr Cogn Disord 18(1):32–36. http://www.ncbi.nlm.nih.gov/pubmed/15084791. Accessed 12 June 2013

Günther M, Oshio K, Feinberg DA (2005) Single-shot 3D imaging techniques improve arterial spin labeling perfusion measurements. Magn Reson Med 54(2):491–498. http://www.ncbi.nlm.nih.gov/pubmed/16032686. Accessed 9 Dec 2013

Hagmann P et al (2006) Understanding diffusion MR imaging techniques: from scalar diffusion-weighted imaging to diffusion tensor imaging and beyond. Radiographics 26(Suppl 1):S205–S223. http://www.ncbi.nlm.nih.gov/pubmed/17050517

Haller S et al (2010) Cerebral microhemorrhage and iron deposition in mild cognitive impairment: susceptibility-weighted MR imaging assessment. Radiology 257(3):764–773. http://www.ncbi.nlm.nih.gov/pubmed/20923870. Accessed 8 Dec 2013

Hammers A et al (2003) Three-dimensional maximum probability atlas of the human brain, with particular reference to the temporal lobe. Hum Brain Mapp 19(4):224–247. http://www.ncbi.nlm.nih.gov/pubmed/12874777. Accessed 13 Aug 2013

Harms SE et al (1986) Multiple spin echo magnetic resonance imaging of the brain. Radiographics 6(1):117–134. http://www.ncbi.nlm.nih.gov/pubmed/3592525

Harvey PR, Hoogeveen RM (n.d.) MultiTransmit parallel RF transmission technology setting the benchmark in clinical high-field imaging

Hennig J (1999) K-space sampling strategies. Eur Radiol 9(6):1020–1031. http://www.ncbi.nlm.nih.gov/pubmed/10415232. Accessed 8 Dec 2013

Hofmann M et al (2009) Towards quantitative PET/MRI: a review of MR-based attenuation correction techniques. Eur J Nucl med Mol imaging 36(Suppl 1):S93–S104. http://www.ncbi.nlm.nih.gov/pubmed/19104810. Accessed 3 Mar 2013

Hoge WS, Brooks DH (2008) Using GRAPPA to improve autocalibrated coil sensitivity estimation for the SENSE family of parallel imaging reconstruction algorithms. Magn Reson Med 60(2):462–467. http://www.ncbi.nlm.nih.gov/pubmed/18666113. Accessed 9 Dec 2013

Hoge RD et al (1999) Investigation of BOLD signal dependence on cerebral blood flow and oxygen consumption: the deoxyhemoglobin dilution model. Magn Reson Med 42(5):849–863. http://www.ncbi.nlm.nih.gov/pubmed/10542343

Horsfield MA, Jones DK (2002) Applications of diffusion-weighted and diffusion tensor MRI to white matter diseases—a review. NMR Biomed 15(7-8):570–577. http://www.ncbi.nlm.nih.gov/pubmed/12489103. Accessed 10 Aug 2013

Huisman TAGM (2003) Diffusion-weighted imaging: basic concepts and application in cerebral stroke and head trauma. Eur Radiol 13(10):2283–2297. http://www.ncbi.nlm.nih.gov/pubmed/14534804. Accessed 8 Dec 2013

Järnum H et al (2010) Perfusion MRI of brain tumours: a comparative study of pseudo-continuous arterial spin labelling and dynamic susceptibility contrast imaging. Neuroradiology 52(4):307–317. http://www.pubmedcentral.nih.gov/articlerender.fcgi?artid=2836404&tool=pmcentrez&rendertype=abstract. Accessed 9 Dec 2013

Johnson NA et al (2005) Pattern of cerebral hypoperfusion in Alzheimer disease and mild cognitive impairment measured with arterial spin-labeling MR imaging: initial experience. Radiology 234(3):851–859. http://www.pubmedcentral.nih.gov/articlerender.fcgi?artid=1851934&tool=pmcentrez&rendertype=abstract. Accessed 9 Dec 2013

Joshi AD et al (2009) Signal separation and parameter estimation in noninvasive dual-tracer PET scans using reference-region approaches. J Cereb Blood Flow Metab 29(7):1346–1357. http://www.ncbi.nlm.nih.gov/pubmed/19401708. Accessed 9 Dec 2013

Kadrmas DJ, Hoffman JM (2013) Methodology for quantitative rapid multi-tracer PET tumor characterizations. Theranostics 3(10):757–773. http://www.ncbi.nlm.nih.gov/pubmed/24312149. Accessed 9 Dec 2013

Kadrmas DJ, Rust TC, Hoffman JM (2013) Single-scan dual-tracer FLT+FDG PET tumor characterization. Phys Med Biol 58(3):429–449. http://www.pubmedcentral.nih.gov/articlerender.fcgi?artid=3553659&tool=pmcentrez&rendertype=abstract. Accessed 9 Dec 2013

Katscher U, Börnert P (2006) Parallel RF transmission in MRI. NMR Biomed 19(3):393–400. http://www.ncbi.nlm.nih.gov/pubmed/16705630. Accessed 9 Dec 2013

Katscher U et al (2003) Transmit SENSE. Magn Reson Med 49(1):144–150. http://www.ncbi.nlm.nih.gov/pubmed/12509830. Accessed 9 Dec 2013

Keereman V et al (2010) MRI-based attenuation correction for PET/MRI using ultrashort echo time sequences. J Nucl Med 51(5):812–818. http://www.ncbi.nlm.nih.gov/pubmed/20439508. Accessed 9 Dec 2013

Kenneth LD et al (eds) (2002) Neuropsychopharmacology – the fifth generation of progress first edit. Lippincott, Williams and Wilkins, Philadelphia. http://www.acnp.org/publications/neuro5thgeneration.aspx

Kerwin W et al (2003) Quantitative magnetic resonance imaging analysis of neovasculature volume in carotid atherosclerotic plaque. Circulation 107(6):851–856. http://www.ncbi.nlm.nih.gov/pubmed/12591755. Accessed 3 Dec 2013

Kety SS, Schmidt CF (1948) The nitrous oxide method for the quantitative determination of cerebral blood flow in man: theory, procedure and normal values. J Clin Invest 27(4):476–483. http://www.pubmedcentral.nih.gov/articlerender.fcgi?artid=439518&tool=pmcentrez&rendertype=abstract. Accessed 7 Mar 2013

Kim SG (1995) Quantification of relative cerebral blood flow change by flow-sensitive alternating inversion recovery (FAIR) technique: application to functional mapping. Magn Reson Med 34(3):293–301. http://www.ncbi.nlm.nih.gov/pubmed/7500865. Accessed 8 Dec 2013

Kim JH et al (2011) Diffusion-weighted imaging and magnetic resonance spectroscopy of sporadic Creutzfeldt-Jakob disease: correlation with clinical course. Neuroradiology 53(12):939–945. http://www.ncbi.nlm.nih.gov/pubmed/21221559. Accessed 8 Dec 2013

Kim JH et al (2012) Comparison of segmentation-based attenuation correction methods for PET/MRI: evaluation of bone and liver standardized uptake value with oncologic PET/CT data. J Nucl Med 53(12):1878–1882. http://www.ncbi.nlm.nih.gov/pubmed/23081993. Accessed 3 Sept 2013

Koch W et al (2010) Effects of aging on default mode network activity in resting state fMRI: does the method of analysis matter? Neuroimage 51(1):280–287. http://www.ncbi.nlm.nih.gov/pubmed/20004726. Accessed 9 Dec 2013

Koch W et al (2012) Diagnostic power of default mode network resting state fMRI in the detection of Alzheimer's disease. Neurobiol Aging 33(3):466–478. http://www.ncbi.nlm.nih.gov/pubmed/20541837. Accessed 9 Dec 2013

Kramer CM et al (2004) Magnetic resonance imaging identifies the fibrous cap in atherosclerotic abdominal aortic aneurysm. Circulation 109(8):1016–1021. http://www.pubmedcentral.nih.gov/articlerender.fcgi?artid=2957882&tool=pmcentrez&rendertype=abstract. Accessed 9 Dec 2013

Kwak Y et al (2010) Altered resting state cortico-striatal connectivity in mild to moderate stage Parkinson's disease. Front Syst Neurosci 4:143. http://www.pubmedcentral.nih.gov/articlerender.fcgi?artid=3009475&tool=pmcentrez&rendertype=abstract. Accessed 9 Dec 2013

Langkammer C et al (2013) Quantitative susceptibility mapping in multiple sclerosis. Radiology 267(2):551. http://www.ncbi.nlm.nih.gov/pubmed/23315661. Accessed 17 Nov 2013

Ladefoged CN et al (2017) A multi-Centre evaluation of eleven clinically feasible brain PET/MRI attenuation correction techniques using a large cohort of patients. NeuroImage 147:346–359. https://www.ncbi.nlm.nih.gov/pubmed/27988322

Le Bihan D et al (2006) Artifacts and pitfalls in diffusion MRI. J Magn Reson Imaging 24(3):478–488. http://www.ncbi.nlm.nih.gov/pubmed/16897692. Accessed 8 Dec 2013

Lucignani G et al (1993) Measurement of regional cerebral glucose utilization with fluorine-18-FDG and PET in heterogeneous tissues: theoretical considerations and practical procedure. J Nucl Med 34(3):360–369. http://www.ncbi.nlm.nih.gov/pubmed/8441024. Accessed 12 Mar 2013

Luypaert R et al (2001) Diffusion and perfusion MRI: basic physics. Eur J Radiol 38:19–27

Martinez-Möller A et al (2009) Tissue classification as a potential approach for attenuation correction in whole-body PET/MRI: evaluation with PET/CT data. J Nucl Med 50(4):520–526. http://www.ncbi.nlm.nih.gov/pubmed/19289430. Accessed 3 June 2013

Martinez-Möller A et al (2012) Workflow and scan protocol considerations for integrated whole-body PET/MRI in oncology. J Nucl Med 53(9):1415–1426. http://www.ncbi.nlm.nih.gov/pubmed/22879079. Accessed 13 May 2013

McRobbie DW (2003) MRI from picture to proton. Cambridge University Press, Cambridge/New York

Meyer PT et al (2011) Dual-biomarker imaging of regional cerebral amyloid load and neuronal activity in dementia with PET and 11C-labeled Pittsburgh compound B. J Nucl Med 52(3):393–400. http://www.ncbi.nlm.nih.gov/pubmed/21321269. Accessed 30 Nov 2013

Mri HF, Quick BHH (2011) Seven Tesla MRI: from technical developments to imaging applications. 10–12 Apr

Musiek ES et al (2012) Direct comparison of fluorodeoxyglucose positron emission tomography and arterial spin labeling magnetic resonance imaging in Alzheimer's disease. Alzheimers

Dement 8(1):51–59. http://www.pubmedcentral.nih.gov/articlerender.fcgi?artid=3264701&tool=pmcentrez&rendertype=abstract. Accessed 8 Aug 2013
NessAiver M (1997) All you really need to know about MRI physics. Simply Physics, Baltimore
Nguyen P, Yang P (n.d.) Great vessels
Nordin LE et al (2013) Cortical responses to amphetamine exposure studied by pCASL MRI and pharmacokinetic/pharmacodynamic dose modeling. Neuroimage 68:75–82. http://www.ncbi.nlm.nih.gov/pubmed/23246855. Accessed 8 Aug 2013
Nucifora PGP et al (2007) Diffusion-tensor MR imaging and tractography: exploring brain microstructure and connectivity. Radiology 245(2):367–384. http://www.ncbi.nlm.nih.gov/pubmed/17940300. Accessed 8 Dec 2013
O'Gorman RL et al (2008) Increased cerebral perfusion in adult attention deficit hyperactivity disorder is normalised by stimulant treatment: a non-invasive MRI pilot study. Neuroimage 42(1):36–41. http://www.ncbi.nlm.nih.gov/pubmed/18511306. Accessed 9 Dec 2013
Oliver-taylor A (2012) Parallel transmission methods for arterial spin labelling magnetic resonance imaging
Ostergaard L, Weisskoff RM et al (1996a) High resolution measurement of cerebral blood flow using intravascular tracer bolus passages. Part I: mathematical approach and statistical analysis. Magn Reson Med 36(5):715–725. http://www.ncbi.nlm.nih.gov/pubmed/8916022. Accessed 9 Dec 2013
Ostergaard L, Sorensen AG et al (1996b) High resolution measurement of cerebral blood flow using intravascular tracer bolus passages. Part II: experimental comparison and preliminary results. Magn Reson Med 36(5):726–736. http://www.ncbi.nlm.nih.gov/pubmed/8916023. Accessed 9 Dec 2013
Ozsarlak O et al (2004) MR angiography of the intracranial vessels: technical aspects and clinical applications. Neuroradiology 46(12):955–972. http://www.ncbi.nlm.nih.gov/pubmed/15580489. Accessed 9 Dec 2013
Panebianco V et al (2013) High-field PET/MRI and MRS: potential clinical and research applications. Clin Transl Imaging 1(1):17–29. http://link.springer.com/10.1007/s40336-013-0004-4. Accessed 26 Mar 2013
Paschal CB, Morris HD (2004) K-space in the clinic. J Magn Reson Imaging 19(2):145–159. http://www.ncbi.nlm.nih.gov/pubmed/14745747. Accessed 8 Dec 2013
Phelps ME et al (1979) Tomographic measurement of local cerebral glucose metabolic rate in humans with (F-18)2-fluoro-2-deoxy-D-glucose: validation of method. Ann Neurol 6(5):371–388. http://www.ncbi.nlm.nih.gov/pubmed/117743. Accessed 8 Mar 2013
Pooley RA (2005) AAPM/RSNA physics tutorial for residents: fundamental physics of MR imaging. Radiographics 25(4):1087–1099. http://www.ncbi.nlm.nih.gov/pubmed/16009826. Accessed 19 Nov 2013
Poustchi-Amin M et al (2001) Principles and applications of echo-planar imaging: a review for the general radiologist. Radiographics 21(3):767–779. http://www.ncbi.nlm.nih.gov/pubmed/11353123. Accessed 8 Dec 2013
Ramani A, Jensen JH, Helpern JA (2006) Quantitative MR imaging in Alzheimer disease. Radiology 241(1):26–44. http://www.ncbi.nlm.nih.gov/pubmed/16990669. Accessed 8 Dec 2013
Robson PM et al (2010) Time-resolved vessel-selective digital subtraction MR angiography of the cerebral vasculature with arterial spin labeling. Radiology 257(2):507–515. http://www.pubmedcentral.nih.gov/articlerender.fcgi?artid=2957593&tool=pmcentrez&rendertype=abstract. Accessed 9 Dec 2013
Rousset O et al (2007) Partial volume correction strategies in PET. PET Clinics 2(2):235–249. http://linkinghub.elsevier.com/retrieve/pii/S1556859807000338. Accessed 10 Feb 2013
Savitz JB, Drevets WC (2013) Neuroreceptor imaging in depression. Neurobiol Dis 52:49–65. http://www.ncbi.nlm.nih.gov/pubmed/22691454. Accessed 18 Mar 2013
Schaefer PW, Grant PE, Gonzalez RG (2000) Diffusion-weighted MR imaging of the brain. Radiology 217(2):331–345. http://www.ncbi.nlm.nih.gov/pubmed/11058626. Accessed 18 Dec 2013

Schick F (2005) Whole-body MRI at high field: technical limits and clinical potential. Eur Radiol 15(5):946–959. http://www.ncbi.nlm.nih.gov/pubmed/15856252. Accessed 10 Aug 2013

Schlemmer H-P et al (2009) An integrated MR/PET system: prospective applications. Abdom Imaging 34(6):668–674. http://www.pubmedcentral.nih.gov/articlerender.fcgi?artid=2774419&tool=pmcentrez&rendertype=abstract. Accessed 30 Aug 2013

Setsompop K et al (2008) Design algorithms for parallel transmission in magnetic resonance imaging. 1–158

Sekine T et al (2016) Clinical evaluation of zero-Echo-time attenuation correction for brain 18F-FDG PET/MRI: comparison with atlas attenuation correction. J Nucl Med 57(12):1927–1932. https://www.ncbi.nlm.nih.gov/pubmed/27339875

Sheline YI et al (2010) Resting-state functional MRI in depression unmasks increased connectivity between networks via the dorsal nexus. Proc Natl Acad Sci U S A 107(24):11020–11025. http://www.pubmedcentral.nih.gov/articlerender.fcgi?artid=2890754&tool=pmcentrez&rendertype=abstract. Accessed 9 Dec 2013

Siewert B et al (1997) Comparison of EPISTAR and T2*-weighted gadolinium-enhanced perfusion imaging in patients with acute cerebral ischemia. Neurology 48(3):673–679. http://www.ncbi.nlm.nih.gov/pubmed/9065546. Accessed 9 Dec 2013

Simonson TM et al (1996) Echo-planar FLAIR imaging in evaluation of intracranial lesions. Radiographics 16(3):575–584. http://www.ncbi.nlm.nih.gov/pubmed/8897625. Accessed 8 Dec 2013

Smith DF, Jakobsen S (2009) Molecular tools for assessing human depression by positron emission tomography. Eur Neuropsychopharmacol 19(9):611–628. http://www.ncbi.nlm.nih.gov/pubmed/19502013. Accessed 18 Mar 2013

Somayajula S et al (2011) PET image reconstruction using information theoretic anatomical priors. IEEE Trans Med Imaging 30(3):537–549. http://www.pubmedcentral.nih.gov/articlerender.fcgi?artid=3331595&tool=pmcentrez&rendertype=abstract. Accessed 9 Dec 2013

Sourbron S (2010) Technical aspects of MR perfusion. Eur J Radiol 76(3):304–313. https://doi.org/10.1016/j.ejrad.2010.02.017

Stafford RJ, Challenges T (2003) High field limitations MRI: technology, applications, safety, and Limitations. Med Phys 32

Stahl R et al (2007) White matter damage in Alzheimer disease and mild cognitive impairment: assessment with diffusion-tensor MR imaging and parallel imaging techniques. Radiology 243(2):483–492. http://www.ncbi.nlm.nih.gov/pubmed/17456872. Accessed 8 Dec 2013

Svarer C et al (2005) MR-based automatic delineation of volumes of interest in human brain PET images using probability maps. Neuroimage 24(4):969–979. http://www.ncbi.nlm.nih.gov/pubmed/15670674. Accessed 5 Mar 2013

Tavazzi E et al (2007) Quantitative diffusion weighted imaging measures in patients with multiple sclerosis. Neuroimage 36(3):746–754. http://www.ncbi.nlm.nih.gov/pubmed/17498974. Accessed 8 Dec 2013

Thoeny HC, De Keyzer F, King AD (2012) Diffusion-weighted MR imaging in the head and neck. Radiology 263(1):19–32. http://www.ncbi.nlm.nih.gov/pubmed/23151830

Tjandra T et al (2005) Quantitative assessment of the reproducibility of functional activation measured with BOLD and MR perfusion imaging: implications for clinical trial design. Neuroimage 27(2):393–401. http://www.ncbi.nlm.nih.gov/pubmed/15921936. Accessed 9 Dec 2013

Torigian DA et al (2013) PET/MR imaging: technical. Radiology 267(1):26–44

Van den Heuvel MP, Hulshoff Pol HE (2010) Exploring the brain network: a review on resting-state fMRI functional connectivity. Eur Neuropsychopharmacol 20(8):519–534. http://www.ncbi.nlm.nih.gov/pubmed/20471808. Accessed 30 Nov 2013

Van den Heuvel MP et al (2009) Functionally linked resting-state networks reflect the underlying structural connectivity architecture of the human brain. Hum Brain Mapp 30(10):3127–3141. http://www.ncbi.nlm.nih.gov/pubmed/19235882. Accessed 7 Nov 2013

Van Dijk KRA, Sperling RA (2011) Defaulting on the default network: increased risk for dementia. Neurology 76(6):498–500. http://www.ncbi.nlm.nih.gov/pubmed/21228298. Accessed 9 Dec 2013

Van Dijk KRA et al (2010) Intrinsic functional connectivity as a tool for human connectomics: theory, properties, and optimization. J Neurophysiol 02138:297–321

Van Laar PJ (2008) Brain perfusion territory imaging: methods and clinical applications of selective arterial. Radiology 246(2):354–364

Van Laar PJ et al (2006) Magnetic resonance evaluation of the cerebral circulation in obstructive arterial disease. Cerebrovasc Dis 21(5-6):297–306. http://www.ncbi.nlm.nih.gov/pubmed/16490938. Accessed 30 Nov 2013

Vandecaveye V, De Keyzer F, Hermans R (2008) Diffusion-weighted magnetic resonance imaging in neck lymph adenopathy. Cancer Imaging 8:173–180. http://www.pubmedcentral.nih.gov/articlerender.fcgi?artid=2556503&tool=pmcentrez&rendertype=abstract. Accessed 23 Sept 2013

Verhaeghe J, Reader AJ (2013) Simultaneous water activation and glucose metabolic rate imaging with PET. Phys Med Biol 58(3):393–411. http://www.ncbi.nlm.nih.gov/pubmed/23296197. Accessed 28 Mar 2013

Verma N et al (2013) Differentiating tumor recurrence from treatment necrosis: a review of neuro-oncologic imaging strategies. Neuro Oncol 15(5):515–534. http://www.ncbi.nlm.nih.gov/pubmed/23325863

Villemagne VL et al (2011) Longitudinal assessment of Aβ and cognition in aging and Alzheimer disease. Ann Neurol 69(1):181–192. http://www.pubmedcentral.nih.gov/articlerender.fcgi?artid=3045039&tool=pmcentrez&rendertype=abstract. Accessed 10 June 2013

Villemagne VL et al (2012) Aβ imaging: feasible, pertinent, and vital to progress in Alzheimer's disease. Eur J Nucl Med Mol Imaging 39(2):209–219. http://www.pubmedcentral.nih.gov/articlerender.fcgi?artid=3261395&tool=pmcentrez&rendertype=abstract. Accessed 13 June 2013

Vitali P et al (2011) Diffusion-weighted MRI hyperintensity patterns differentiate CJD from other rapid dementias. Neurology 76(20):1711–1719. http://www.pubmedcentral.nih.gov/articlerender.fcgi?artid=3100134&tool=pmcentrez&rendertype=abstract. Accessed 10 Nov 2013

Vunckx K et al (2012) Evaluation of three MRI-based anatomical priors for quantitative PET brain imaging. IEEE Trans Med Imaging 31(3):599–612. http://www.ncbi.nlm.nih.gov/pubmed/22049363

Walsh AJ et al (2014) Longitudinal MR imaging of iron in multiple sclerosis: an imaging marker of disease. Radiology 270(1):186–196. http://pubs.rsna.org/doi/abs/10.1148/radiology.13130474. Accessed 8 Dec 2013

Wang J, Wang J et al (2003) Arterial spin labeling perfusion fMRI with very low task frequency. Magn Reson Med 49(5):796–802. http://www.ncbi.nlm.nih.gov/pubmed/12704760. Accessed 8 Aug 2013

Wang J et al (2005) Perfusion functional MRI reveals cerebral blood flow pattern under psychological stress. Proc Natl Acad Sci U S A 102(49):17804–17809. http://www.pubmedcentral.nih.gov/articlerender.fcgi?artid=1292988&tool=pmcentrez&rendertype=abstract. Accessed 9 Dec 2013

Wang Z et al (2008) Assessment of functional development in normal infant brain using arterial spin labeled perfusion MRI. NeuroImage 39(3):973–978. http://www.pubmedcentral.nih.gov/articlerender.fcgi?artid=2268607&tool=pmcentrez&rendertype=abstract. Accessed 9 Dec 2013

Wang DJJ et al (2011) Potentials and challenges for arterial spin labeling in pharmacological. Magn Reson Imaging 337(2):359–366

Wansapura JP et al (1999) NMR relaxation times in the human brain at 3.0 tesla. J Magn Reson Imaging 9(4):531–538. http://www.ncbi.nlm.nih.gov/pubmed/10232510

Warmuth C, Gunther M, Zimmer C (2003) Quantification of blood flow in brain tumors: comparison of arterial spin labeling and dynamic susceptibility-weighted contrast-enhanced MR imaging. Radiology 228(2):523–532. http://www.ncbi.nlm.nih.gov/pubmed/12819338. Accessed 9 Dec 2013

Wasserman BA et al (2002) Carotid artery atherosclerosis: in vivo morphologic characterization with gadolinium-enhanced double-oblique MR imaging initial results. Radiology 223(2):566–573. http://www.ncbi.nlm.nih.gov/pubmed/11997569. Accessed 9 Dec 2013

Webb AG, Collins CM (2010) Parallel transmit and receive technology in high-field magnetic resonance neuroimaging. Int J Imaging Syst Technol 23:2–13

Weber M-A et al (2003) Comparison of arterial spin-labeling techniques and dynamic susceptibility-weighted contrast-enhanced MRI in perfusion imaging of normal brain tissue. Invest Radiol 38(11):712–718. http://www.ncbi.nlm.nih.gov/pubmed/14566181. Accessed 9 Dec 2013

Wendt RE et al (1988) MR imaging of susceptibility-induced magnetic field inhomogeneities. Radiology 168(3):837–841. http://www.ncbi.nlm.nih.gov/pubmed/3406413. Accessed 8 Dec 2013

Wiesinger F et al (2006) Potential and feasibility of parallel MRI at high field. NMR Biomed 19(3):368–378. http://www.ncbi.nlm.nih.gov/pubmed/16705638. Accessed 9 Dec 2013

Williams DS et al (1992) Magnetic resonance imaging of perfusion using spin inversion of arterial water. Proc Natl Acad Sci U S A 89(1):212–216. http://www.ncbi.nlm.nih.gov/pubmed/8412609

Wilson GJ et al (2004) Parallel imaging in MR angiography. Top Magn Reson Imaging 15(3):169–185. http://www.ncbi.nlm.nih.gov/pubmed/15479999. Accessed 9 Dec 2013

Wintermark M et al (2005) Comparative overview of brain perfusion imaging techniques. J Neuroradiol 32(5):294–314. http://www.ncbi.nlm.nih.gov/pubmed/16424829. Accessed 9 Dec 2013

Wolf RL et al (2003) Susceptibility contrast and arterial spin labeled perfusion MRI in cerebrovascular disease. J Neuroimaging 13(1):17–27. http://www.ncbi.nlm.nih.gov/pubmed/12593127. Accessed 9 Dec 2013

Wolf RL et al (2005) Grading of CNS neoplasms using continuous arterial spin labeled perfusion MR imaging at 3 Tesla. J Magn Reson Imaging 22(4):475–482. http://www.ncbi.nlm.nih.gov/pubmed/16161080. Accessed 9 Dec 2013

Wolk DA, Detre JA (2012) Arterial spin labeling MRI: an emerging biomarker for Alzheimer's disease and other neurodegenerative conditions. Curr Opin Neurol 25(4):421–428. http://www.pubmedcentral.nih.gov/articlerender.fcgi?artid=3642866&tool=pmcentrez&rendertype=abstract. Accessed 30 Aug 2013

Wong EC, Buxton RB, Frank LR (1997) Implementation of quantitative perfusion imaging techniques for functional brain mapping using pulsed arterial spin labeling. NMR Biomed 10(4–5):237–249. http://www.ncbi.nlm.nih.gov/pubmed/9430354. Accessed 8 Dec 2013

Wong EC, Buxton RB, Frank LR (1998) A theoretical and experimental comparison of continuous and pulsed arterial spin labeling techniques for quantitative perfusion imaging. Magn Reson Med 40(3):348–355. http://www.ncbi.nlm.nih.gov/pubmed/9727936. Accessed 8 Dec 2013

Wong EC, Luh WM, Liu TT (2000) Turbo ASL: arterial spin labeling with higher SNR and temporal resolution. Magn Reson Med 44(4):511–515. http://www.ncbi.nlm.nih.gov/pubmed/11025504. Accessed 8 Dec 2013

Wong EC et al (2006) Velocity-selective arterial spin labeling. Magn Reson Med 55(6):1334–1341. http://www.ncbi.nlm.nih.gov/pubmed/16700025. Accessed 8 Dec 2013

Wu W-C et al (2007) A theoretical and experimental investigation of the tagging efficiency of pseudocontinuous arterial spin labeling. Magn Reson med 58(5):1020–1027. http://www.ncbi.nlm.nih.gov/pubmed/17969096. Accessed 7 Nov 2013

Yoneda K et al (2003) Comparison of FAIR technique with different inversion times and post contrast dynamic perfusion MRI in chronic occlusive cerebrovascular disease. Magn Reson Imaging 21(7):701–705. http://www.ncbi.nlm.nih.gov/pubmed/14559333. Accessed 9 Dec 2013

Yuan C et al (2002) Contrast-enhanced high resolution MRI for atherosclerotic carotid artery tissue characterization. J Magn Reson Imaging 15(1):62–67. http://www.ncbi.nlm.nih.gov/pubmed/11793458. Accessed 2 Dec 2013

Zhang H, Maki JH, Prince MR (2007a) 3D contrast-enhanced MR angiography. J Magn Reson Imaging 25(1):13–25. http://www.ncbi.nlm.nih.gov/pubmed/17154188. Accessed 9 Dec 2013

Zhang Z et al (2007b) Reduction of transmitter B1 inhomogeneity with transmit SENSE slice-select pulses. Magn Reson Med 57(5):842–847. http://www.pubmedcentral.nih.gov/articlerender.fcgi?artid=3041897&tool=pmcentrez&rendertype=abstract. Accessed 9 Dec 2013

The Default Network of the Brain

7

Koene R. A. Van Dijk and Alexander Drzezga

Contents

7.1 Discovery of the Default Network 166
7.2 Measuring Default Network Function 168
7.2.1 Deactivation During Attention-Demanding Cognitive Tasks 168
7.2.2 Tasks That Rely on Default Network Activation 169
7.2.3 Assessment of Functional Connectivity 169
7.2.4 Molecular Function and Metabolic Connectivity 172
7.2.5 Clinical Relevance of Measuring Default Network Integrity 173
References 175

Abstract

Continued advancement of sophisticated imaging procedures over the last decades has allowed the assessment of large-scale functional-anatomic brain networks. Among the identified networks, a frequently investigated system is the so-called default network. This network was originally identified as a set of brain regions consistently deactivated during tasks that require externally oriented attention. Later imaging studies showed that this network is active during inter-

K. R. A. Van Dijk (✉)
Digital Medicine and Translational Imaging, Early Clinical Development, Pfizer Inc, Cambridge, MA, USA
e-mail: koene.vandijk@pfizer.com

A. Drzezga
Department of Nuclear Medicine, Medical Faculty and University Hospital Cologne, University of Cologne, Cologne, Germany

German Center for Neurodegenerative Diseases (DZNE), Bonn/Köln, Germany

Institute of Neuroscience and Medicine, Molecular Organization of the Brain (INM-2), Forschungzentrum Jülich, Jülich, Germany
e-mail: alexander.drzezga@uk-koeln.de

R. A. J. O. Dierckx et al. (eds.), *PET and SPECT in Neurology*,
https://doi.org/10.1007/978-3-030-53168-3_7

nally focused cognitive processes such as moral decision-making and planning of future behavior, and also that it can reliably be identified during resting conditions. A growing number of studies indicate that various brain disorders are associated with dysfunction of brain networks, leading to the notion that measures of functional network integrity may serve as marker of neurologic and psychiatric disease states. For instance, disconnection of default network regions seems evident in very early stages of Alzheimer's disease, and a striking topographical overlap has been shown between default network regions and the spatial distribution of different diagnostic markers of Alzheimer's disease such as amyloid deposition, hypometabolism, and brain atrophy. In this chapter, we cover milestones that led to the discovery of the default network, methodological advancements that allow more precise measurements of neuronal networks, pitfalls of functional network measures, and a number of potential clinical applications.

7.1 Discovery of the Default Network

The set of brain regions we refer to as the *default network*, or *default mode network*, was first noted as a by-product of experiments aimed at mapping human brain function. In experiments that were common in the 1990s, positron emission tomography (PET) with suitable tracers (e.g., $H_2{}^{15}O$) or functional magnetic resonance imaging (fMRI) making use of the blood oxygenation level-dependent (BOLD) contrast was used to measure changes in regional cerebral blood flow. Before these neuroimaging techniques were available, basic research into brain function would consist of animal experiments with more or less successful translation to humans. Clinical research in those days was aimed at determining cognitive deficits in patients with known focal brain damage. The use of PET and fMRI for mapping cognitive functions turned out immensely successful because using these imaging techniques, scientists were able to determine fairly precisely the location of neuronal correlates of cognition in healthy study subjects. In a typical task-based experiment, or activation study, healthy young adults would perform a cognitive task in the scanner. Brain images acquired during, for instance, a language task would then be compared with brain images acquired during a reference condition that often consisted of simply resting in the scanner. Based on the theory of neurovascular coupling, brain regions with *higher* blood flow during the task would then be considered *activated* by the task. Thus, in the example of a language task, areas of the brain showing statistically higher signal during the language task would be attributed to language function.

Using neuroimaging techniques such as PET and fMRI, most researchers were initially focused on brain regions that showed higher levels of blood flow or oxygenation during specific tasks. However, Shulman et al. (1997) reported that during a number of different tasks (object discrimination, visual search, spatial attention, language, memory, and imagery), one particular set of brain regions would consistently show *lower* levels of blood flow during the tasks (see Fig. 7.1a). Blood flow

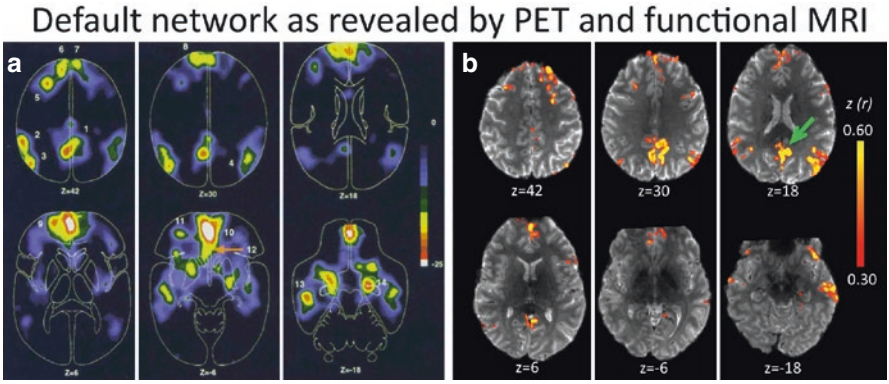

Fig. 7.1 (**a**) The default network of the human brain as it was originally identified in a meta-analysis of nine positron emission tomography (*PET*) studies (132 healthy young adults) from Shulman et al. (1997) (Reprinted with permission). The colored brain regions were more active in passive task states as compared to active tasks states. (**b**) The default network identified using functional connectivity MRI (fcMRI) while a single subject was resting in the scanner. The color scale indicates functional connectivity (Pearson correlation coefficient after Fishers *r*-to-*z* transformation) with the signal from a seed region placed in the posterior cingulate cortex as indicated by the *green arrow* (Adapted from Van Dijk et al. (2012b))

decreases during attention-demanding tasks were interpreted as decreases in brain activation, also referred to as deactivation. These consistent decreases during tasks suggested the existence of an organized functional-anatomic network that is more active during passive task conditions. Since humans are most of the time not engaged in attention-demanding goal-directed behavior, Raichle and colleagues referred to this network as representing a "default mode of brain function" (Raichle et al. 2001). After the publication by Raichle et al., the field started to refer to this set of brain regions as the "default network" or "default mode network." Greicius et al. (2003) showed that regions of the default network not only appear as deactivated regions during most attention-demanding cognitive tasks but in addition show high functional coherence while people are simply resting in the scanner (see Fig. 7.1b).

Brain regions associated with the default network are the posterior cingulate cortex, medial prefrontal cortex, inferior parietal lobule, lateral temporal cortex, and regions of the parahippocampal and entorhinal cortex (Buckner et al. 2008; Greicius et al. 2003; Raichle et al. 2001; Shulman et al. 1997; Ward et al. 2014). The relative ease of measuring this network during rest using standard neuroimaging techniques, in combination with initial findings of vulnerability of the default network to neurologic and psychiatric disease states, caused the default network to be a popular brain network to study which, in turn, led to an explosion of the number of papers on this topic published each year (see Fig. 7.2).

There is a growing interest in measuring structural connectivity of the default network and of other neuronal systems. While measures of brain structure, such as structural brain connectivity using diffusion magnetic resonance imaging, are beyond the scope of the present chapter, we would like to mention that several large

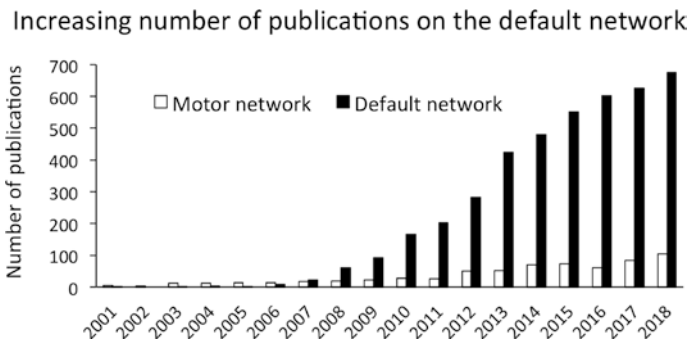

Fig. 7.2 There has been a steady increase in the number of papers published on the default network since the publication by Raichle et al. (2001) in which the term default mode was associated with the network described by Shulman et al. (1997). The graph shows the number of publications per year from 2001 until 2018 for the search terms ["motor network" OR "somatomotor network"](open bars) and ["default network" OR "default mode network" (closed bars)] (source https://www.ncbi.nlm.nih.gov/pubmed/, December 1, 2019)

multisite collaborative projects, such as the "Human Connectome Project" in the United States and the "Developing Human Connectome Project," "Human Brain Project," and the "UK Biobank" in Europe, are expected to shed more light on the complex relationship between brain structure and function during health and disease states.

7.2 Measuring Default Network Function

The main methods to assess default network function are (1) observing regions of deactivation during attention-demanding cognitive tasks, (2) probing the network with tasks that specifically rely on default network activation, (3) assessment of functional connectivity in terms of coherent BOLD fMRI signals either during task states or during the resting state, and finally (4) using FDG-PET to determine the molecular function and metabolic connectivity.

7.2.1 Deactivation During Attention-Demanding Cognitive Tasks

While the most commonly used clinical radiotracer for the assessment of brain function is ^{18}F-FDG (18-fluorodeoxyglucose for measuring glucose consumption), scientific activation studies performed in healthy young adults in the late 1980s and into the 1990s primarily used $H_2{}^{15}O$ (oxygen-15-water for measuring cerebral blood flow). Those studies were aimed at mapping cognitive functions such as language and decision-making under attention-demanding experimental conditions. The half-life of $H_2{}^{15}O$ is only 122 s (as opposed to 110 min for ^{18}F-FDG), which made it

suitable for repeated assessment of blood flow during different experimental conditions within one scanning session. Using $H_2{}^{15}O$-PET, many brain regions were identified that were implicated in a range of cognitive abilities. As mentioned in the previous section, an analysis by Shulman et al. (1997) of data of several PET experiments indicated that a common set of brain regions—which was only later termed the default network—showed consistent deactivation during various attention-demanding cognitive tasks. This means that those regions are more active in passive task conditions relative to many active task states. When it turned out that changes in blood oxygenation, as indirect measure of neuronal function, could be determined using BOLD fMRI without the use of radiotracers (Kwong et al. 1992; Ogawa et al. 1992), fMRI became the method of choice for studying brain function in healthy young adults. Parametric manipulation of task difficulty during BOLD fMRI experiments confirmed that the more a person is focused on an attention-demanding task, the more deactivation of the default network occurs (McKiernan et al. 2003).

7.2.2 Tasks That Rely on Default Network Activation

In addition to attention-demanding tasks that deactivate the default network, one can also ask people to perform tasks in the scanner that specifically *activate* the default network. Tasks relying on conceptual knowledge, moral decision-making, the ability to think what other people are thinking (i.e., theory of mind), remembering the past, and imagining the future are all associated with activation of default network regions and are therefore considered core functions of the network (e.g., Addis et al. 2007; Binder et al. 1999; Buckner et al. 2008; Mitchell et al. 2006; Shenhav and Greene 2012). Another suggested role of the default network is the exploratory monitoring of the external environment, a function that is suspended when a person is engaged in a task that requires focused attention (Gusnard et al. 2001; Shulman et al. 1997). In situations when people are left to think to themselves, the default network seems to integrate information from past experiences, replay events from memory, and construct mental simulations about possible future events (Buckner et al. 2008; Schacter et al. 2007).

7.2.3 Assessment of Functional Connectivity

Functional connectivity, defined as temporally correlated remote neurophysiological events (Friston 1994), can be estimated within individual subjects using functional neuroimaging measures such as EEG, MEG, and fMRI. The most commonly used method for assessing brain functional connectivity is fMRI and is often referred to as functional connectivity MRI (fcMRI). Using fcMRI, patterns of synchronous fluctuations in the blood oxygenation level-dependent (BOLD) signal are measured (Biswal et al. 1995). These analyses involve data processing, including steps to remove unwanted signals such as physiological noise caused by heart rate,

breathing, and head motion. If, after data preprocessing, two or more brain regions show a similar pattern in fluctuations over time, we designate these regions as being functionally connected. While functional connectivity does not equate to structural connectivity, fcMRI can be used as noninvasive probe of integrity of neuronal systems (for review, see Van Dijk et al. 2010).

Biswal and colleagues in 1995 used BOLD fMRI to show that a region in the left somatomotor cortex exhibits signal fluctuations that are highly correlated with signal fluctuations in the whole somatomotor system including contralateral somatomotor cortex (Biswal et al. 1995). It is important to realize that the somatomotor system exhibits these coherent signal fluctuations when a person is simply resting in the scanner, that is, when a person is not engaged in active behavior that relies on the somatomotor system. This technique of mapping functional systems by analyzing coherent fluctuations in remote brain areas increased in popularity when Greicius et al. (2003) decided to place a region of interest—also called a "seed region"—in a core node of the default network. When they extracted the signal from that seed region and computed the correlation strength between the seed and every other voxel in the brain, the results robustly revealed the default network (Greicius et al. 2003). During those years, data-driven techniques that do not rely on choosing a specific seed region also revealed coherent activity patterns in large-scale brain systems such as the somatomotor and default network (Beckmann et al. 2005; De Luca et al. 2006). While it is relatively easy to measure these networks while people are resting in the scanner, it is important to note that most networks, including the default network, also show functional connectivity during many tasks (Fransson 2006; Smith et al. 2009; Van Dijk et al. 2010). This means that functional connectivity methods can be applied to data acquired during rest but also during active task conditions (for applications and discussion, see Fair et al. (2007). When one is interested in how functional connectivity changes during different conditions of a task, other methods, such as psychophysiological interaction analysis, are suitable (Friston et al. 1997; McLaren et al. 2012).

Over the last years, different authors have focused on different networks as measured during rest. Besides the default network, often-mentioned systems are those involved in keeping attention focused on a task (dorsal attention network or salience network; see, e.g., Fox et al. 2005 and Seeley et al. 2007, respectively) or networks performing executive control functions such as allocating attention to one stimulus and then actively switching attention to another stimulus when cued to do so (Seeley et al. 2007; Vincent et al. 2008). Efforts of determining an exact number of meaningful neuronal networks will offer different results based on the methods employed and the behavior of the subject during the scan. Moreover, while these fcMRI metrics show fairly stable measurements from one session to the next (e.g., Shehzad et al. 2009; Van Dijk et al. 2010), the correlational measures do not capture moment-to-moment changes in coherence (Chang and Glover 2010; Hutchison et al. 2013; Lurie et al. 2020).

Potential pitfalls when using fcMRI to determine functional network integrity are contamination of the BOLD signal by the before-mentioned sources of

physiological noise such as heart rate, respiration (Birn et al. 2006; Chang and Glover 2009), and head motion (Power et al. 2012; Satterthwaite et al. 2012; Van Dijk et al. 2012a). It is crucial that investigators that apply fcMRI are aware of these confounding factors since they often bias results in studies where patients are compared to healthy controls in the direction of hypothesized effects. For instance, one might find lower coherence in the default network in the patient group which may not be due to a specific brain disorder but rather to more head movement in the patient group during the scan. Discussion of additional caveats when working with measures of functional network integrity and interpretation of functional network changes when structural brain changes are also present are beyond the scope of this chapter but are topics of active research.

With the increasing availability of high-quality neuroimaging datasets and advances in computational approaches to complex biological systems, a field has emerged in which the brain is treated as graph with brain regions as nodes and functional or structural connections as edges or links between the nodes (Bullmore and Sporns 2009; Drzezga et al. 2011; Rubinov and Sporns 2010; Sepulcre et al. 2010; Stam and Reijneveld 2007; van den Heuvel et al. 2008). Graph theory applied to structural and functional brain images has shown that the human brain is shaped by an economic trade-off between minimizing costs and maximizing efficiency of information processing whereby the brain exhibits properties of a *complex network* that sits in between a regular low-cost/low-efficiency lattice network and a high-cost/high-efficiency random network (see Fig. 7.3).

While complex brain network analysis techniques often take the whole brain into account and are not necessarily aimed at identifying (just) the default network, it turns out that the brain's main cortical hubs largely—but not fully—overlap with

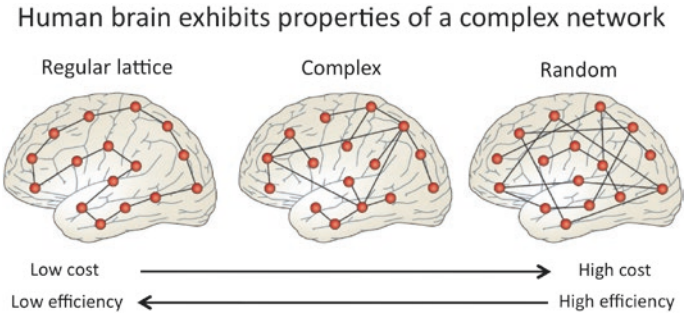

Fig. 7.3 The human brain exhibits properties of a complex network that sits in between an orderly regular lattice structure and an unorderly random network. The healthy human brain shows a balance between minimizing costs and maximizing processing efficiency. While the default network is known to include many key relay stations that are important for this cost/efficiency trade-off, graph theoretical measures of the human brain go beyond the default network and are starting to show promise to identify changes in brain network structure in neurologic and psychiatric disease states (Adapted with permission from Macmillan Publishers Ltd.: Nature Reviews Neuroscience, Bullmore and Sporns, copyright 2012)

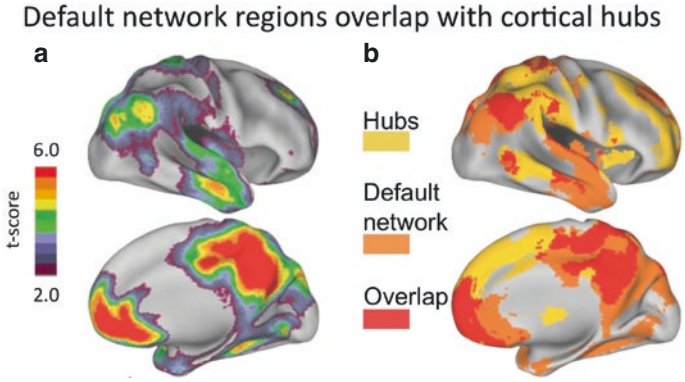

Fig. 7.4 (**a**) Map of the default network as voxels exhibiting greater activity during blocks of passive fixation than during externally directed tasks. Six independent fMRI blocked-design studies were included, each comprising 30 participants matched on age and gender for a total of 180 healthy young adults. The scale is average *t*-score. The map of the default network is consistent with prior meta-analyses (e.g., Shulman et al. (1997) as shown in Fig. 7.1a). (**b**) Overlap of the default network with a map of degree connectivity representing cortical hubs (Adapted with permission from Buckner et al. (2009))

default network regions (see Fig. 7.4). One potential role of these hub regions is that they act as relay stations for information processing serving as connector regions between different (sub)networks. Other complex brain network analyses suggest that default network regions display extensive local connectivity between and within certain bordering brain areas (see Buckner et al. 2009; Sepulcre et al. 2010; Tomasi and Volkow 2010 for discussion). Complex brain network analysis relies first on time-series analyses within an individual subject, but the next step requires analyses of patters across large groups of subjects. This may have utility in detecting abnormal connectomics due to neurologic and psychiatric disease states (Bullmore and Sporns 2012; Rubinov and Sporns 2010; Dichter et al. 2015; Derks et al. 2017), but the practical utility of network measures for diagnostic and/or treatment decisions within an individual patient remains to be determined.

7.2.4 Molecular Function and Metabolic Connectivity

The abovementioned fcMRI methods rely on functional connectivity between brain regions to be estimated within individual subjects. ^{18}F-FDG-PET traditionally does not provide information regarding change in neuronal function over time but rather offers a snapshot reflecting synaptic glutamatergic activity which then serves as summary measure of neuronal function over the duration of the scan. This means that within one subject, connectivity between two given regions (region A and B) cannot be computed using traditional FDG-PET as in both regions only a single value will be obtained. However, a correlation between the values in region A can be computed with the values in region B across subjects. This approach using PET

was used before the availability of fMRI BOLD methods (e.g., Horwitz et al. 1984; McIntosh 1999), and the same concept has successfully been applied to structural MRI data of older adults with and without dementia (e.g., He et al. 2008; Seeley et al. 2009). Across-subject analysis of FDG-PET data has been termed "metabolic connectivity" in a study by Morbelli et al. (2012), in which they demonstrated reduced resting metabolic connectivity in prodromal Alzheimer's disease both in hypometabolic and non-hypometabolic areas and they suggested that metabolic disconnection (reflecting early diaschisis) may antedate remote hypometabolism (early sign of synaptic degeneration) (Morbelli et al. 2012).

Thanks to increasing temporal resolution of modern PET imaging systems, metabolic connectivity can now also be studied within a single subject or patient using functional PET (fPET; Villien et al. 2014). This method employs a constant infusion of radiotracer and enables assessment of changes in brain metabolism over the course of a task paradigm or during resting-state conditions.

7.2.5 Clinical Relevance of Measuring Default Network Integrity

There are several lines of evidence indicating that default network integrity may serve as marker of brain function with relevance for several neurologic and psychiatric disease states (for review, see Fox and Greicius 2010; Teipel et al. 2016). One example where loss of deactivation during task conditions and disconnection measured during resting-state conditions across the spectrum of prodromal and clinical disease phases is Alzheimer's disease. Loss of task-related deactivation in Alzheimer's disease was shown for the default network using fMRI (Lustig et al. 2003) and for other association regions using $H_2{}^{15}O$ PET (Drzezga et al. 2005). With the development of PET tracers such as ^{11}C-Pittsburgh compound B (11C-PiB; Klunk et al. 2004; Mathis et al. 2004), in vivo measurement of fibrillar amyloid beta, one of the major neuropathological hallmarks of Alzheimer's disease, became possible. It turned out that older adults who presented with elevated ^{11}C-PiB uptake, but who were otherwise still cognitively normal, showed loss of deactivation of the default network during fMRI task performance (Sperling et al. 2009).

In situations where patients may have difficulty performing a cognitive task in the scanner, or in multisite collaborative studies where it is difficult to implement a behavioral task protocol and monitor task compliance, a resting-state fMRI scan has been shown to be useful. Disconnection of regions of the default network during rest has been reported in Alzheimer's disease (Greicius et al. 2004) and also in patients who are at high risk of developing the disease (Filippini et al. 2009; Sorg et al. 2007). In addition, even older adults who show no clinical signs of Alzheimer's disease but who have elevated amyloid values as measured using ^{11}C-PiB-PET showed decreases in fcMRI measures of the default network (Hedden et al. 2009; Mormino et al. 2011; Sheline et al. 2010). Finally, regional overlap of default network disconnection, amyloid burden, and neuronal dysfunction was shown using resting-state fcMRI, ^{11}C-PiB-PET, and ^{18}F-FDG-PET, respectively (Drzezga et al. 2011), lending support to the hypothesis that

Alzheimer's disease-associated amyloid deposition tends to concentrate in default network areas (Buckner et al. 2005) or more generally in functional hubs of the brain that overlap with typical default network areas and other critical nodes of large-scale functional networks (Buckner et al. 2009). These findings indicate that assessment of the default mode network and other major neuronal networks may serve as marker of functional brain integrity, prior to occurrence of symptoms of memory loss due to Alzheimer's disease-related pathology and also prior to anatomical changes that will only later become visible with structural brain imaging techniques (Sperling et al. 2011).

Availability of in vivo assessment of tau aggregates using tracers such as ^{18}F-AV-1451 (T807; Chien et al. 2013; Xia et al. 2013) as well as adaptation of PET tau imaging in large longitudinal cohort studies such as the Alzheimer's Disease Neuroimaging Initiative (ADNI) has offered a view that multiple networks may be differentially affected by pathologies that may show its effects at different (pre) clinical disease stages (see, e.g., Jones et al. 2017; Hoenig et al. 2018; Sepulcre et al. 2018).

Applying PET tracers for imaging amyloid and tau deposition in the brain, recent studies were able to identify characteristic networks of amyloid deposition in the brain as well as specific "tau networks" of tau distribution in patients with Alzheimer's disease (Pereira et al. 2018; Kim et al. 2019; Hoenig et al. 2018). Substantial overlap between amyloid deposition, tau aggregation, and functional-anatomic networks was demonstrated, particularly for the default network. These findings indicate that Alzheimer pathology shows a preference for development within the default network, potentially due to high susceptibility of this network and potential spreading of the molecular pathologies along its connectivity pathways. These findings have further fueled the so-called network degeneration hypothesis, postulating that neurodegenerative disorders are possibly characterized by the way molecular pathologies are spreading along functional networks of the brain (see, for review, Drzezga 2018).

It is unlikely that default network dysfunction is exclusively indicative of (preclinical) Alzheimer's disease because this network has been implicated in a range of different conditions (for an early review, see Fox and Greicius 2010). In addition, most studies referenced in this chapter showed functional network characteristics based on group averages of normal control subjects or group differences between patients and controls, but it has become clear that these large-scale functional networks, when measured at high spatial resolution in individual subjects, show consistent fractionation within individuals (Braga et al. 2019) of which clinical utility remains to be determined. In the coming years, we will likely learn more about sensitivity and specificity of measures of neuronal network dysfunction and its clinical utility in a range of different conditions.

Besides investigating which neurologic and psychiatric disease affects which brain system, there are a number of other clinical applications for measuring the connectional architecture of the brain. One such example is presurgical mapping of functional brain areas in patients that might otherwise be scanned while performing a task but who have difficulty with task comprehension and/or task compliance (Liu

et al. 2009; Lee et al. 2016) with recent publications confirming utility but also calling for further investigations into subject-level variability before widespread clinical implementation (Sair et al. 2017). Another potential clinical application is determining brain function in individual patients with disorders of consciousness where a minimal conscious state might be differentiated from vegetative state using default network measures (Fernandez-Espejo et al. 2012). And finally, resting-state functional network measures have been used for image-guided manipulation using transcranial magnetic stimulation (TMS) of brain networks in psychiatric diseases (Fox et al. 2012). With continued efforts of improved data acquisition and analysis techniques, including higher spatial and temporal resolution MRI (Smith et al. 2011; Triantafyllou et al. 2005; Setsompop et al. 2012; Van Dijk et al. 2012b), and simultaneous PET/MR data acquisition (Heiss 2009; Marsden et al. 2002), additional translational research for clinical applications is likely to follow.

References

Addis DR, Wong AT, Schacter DL (2007) Remembering the past and imagining the future: common and distinct neural substrates during event construction and elaboration. Neuropsychologia 45:1363–1377

Beckmann CF, DeLuca M, Devlin JT, Smith SM (2005) Investigations into resting-state connectivity using independent component analysis. Philos Trans R Soc Lond Ser B Biol Sci 360:1001–1013

Binder JR, Frost JA, Hammeke TA, Bellgowan PS, Rao SM, Cox RW (1999) Conceptual processing during the conscious resting state. A functional MRI study. J Cogn Neurosci 11:80–95

Birn RM, Diamond JB, Smith MA, Bandettini PA (2006) Separating respiratory-variation-related fluctuations from neuronal-activity-related fluctuations in fMRI. NeuroImage 31:1536–1548

Biswal B, Yetkin FZ, Haughton VM, Hyde JS (1995) Functional connectivity in the motor cortex of resting human brain using echo-planar MRI. Magn Reson Med 34:537–541

Braga RM, Van Dijk KRA, Polimeni JR, Eldaief MC, Buckner RL (2019) Parallel distributed networks resolved at high resolution reveal close juxtaposition of distinct regions. J Neurophysiol 121(4):1513–1534

Buckner RL, Snyder AZ, Shannon BJ, LaRossa G, Sachs R, Fotenos AF, Sheline YI, Klunk WE, Mathis CA, Morris JC et al (2005) Molecular, structural, and functional characterization of Alzheimer's disease: evidence for a relationship between default activity, amyloid, and memory. J Neurosci 25:7709–7717

Buckner RL, Andrews-Hanna JR, Schacter DL (2008) The brain's default network: anatomy, function, and relevance to disease. Ann N Y Acad Sci 1124:1–38

Buckner RL, Sepulcre J, Talukdar T, Krienen FM, Liu H, Hedden T, Andrews-Hanna JR, Sperling RA, Johnson KA (2009) Cortical hubs revealed by intrinsic functional connectivity: mapping, assessment of stability, and relation to Alzheimer's disease. J Neurosci 29:1860–1873

Bullmore E, Sporns O (2009) Complex brain networks: graph theoretical analysis of structural and functional systems. Nat Rev Neurosci 10:186–198

Bullmore E, Sporns O (2012) The economy of brain network organization. Nat Rev Neurosci 13:336–349

Chang C, Glover GH (2009) Relationship between respiration, end-tidal CO(2), and BOLD signals in resting-state fMRI. NeuroImage 47(4):1381–1393

Chang C, Glover GH (2010) Time-frequency dynamics of resting-state brain connectivity measured with fMRI. NeuroImage 50:81–98

Chien DT, Bahri S, Szardenings AK, Walsh JC, Mu F, Su MY, Shankle WR, Elizarov A, Kolb HC (2013) Early clinical PET imaging results with the novel PHF-tau radioligand [F-18]-T807. J Alzheimers Dis 34:457–468

De Luca M, Beckmann CF, De Stefano N, Matthews PM, Smith SM (2006) fMRI resting state networks define distinct modes of long-distance interactions in the human brain. NeuroImage 29:1359–1367

Derks J, Dirkson AR, de Witt Hamer PC, van Geest Q, Hulst HE, Barkhof F, Pouwels PJ, Geurts JJ, Reijneveld JC, Douw L (2017) Connectomic profile and clinical phenotype in newly diagnosed glioma patients. Neuroimage Clin 14:87–96

Dichter GS, Gibbs D, Smoski MJ (2015) A systematic review of relations between resting-state functional-MRI and treatment response in major depressive disorder. J Affect Disord 172:8–17

Drzezga A (2018) The network degeneration hypothesis: spread of neurodegenerative patterns along neuronal brain networks. J Nucl Med 59:1645–1648

Drzezga A, Grimmer T, Peller M, Wermke M, Siebner H, Rauschecker JP, Schwaiger M, Kurz A (2005) Impaired cross-modal inhibition in Alzheimer disease. PLoS Med 2:e288

Drzezga A, Becker JA, Van Dijk KRA, Sreenivasan A, Talukdar T, Sullivan C, Schultz AP, Sepulcre J, Putcha D, Greve D et al (2011) Neuronal dysfunction and disconnection of cortical hubs in non-demented subjects with elevated amyloid burden. Brain 134:1635–1646

Fair DA, Schlaggar BL, Cohen AL, Miezin FM, Dosenbach NU, Wenger KK, Fox MD, Snyder AZ, Raichle ME, Petersen SE (2007) A method for using blocked and event-related fMRI data to study "resting state" functional connectivity. NeuroImage 35:396–405

Fernandez-Espejo D, Soddu A, Cruse D, Palacios EM, Junque C, Vanhaudenhuyse A, Rivas E, Newcombe V, Menon DK, Pickard JD et al (2012) A role for the default mode network in the bases of disorders of consciousness. Ann Neurol 72:335–343

Filippini N, MacIntosh BJ, Hough MG, Goodwin GM, Frisoni GB, Smith SM, Matthews PM, Beckmann CF, Mackay CE (2009) Distinct patterns of brain activity in young carriers of the APOE-epsilon4 allele. Proc Natl Acad Sci U S A 106:7209–7214

Fox MD, Buckner RL, White MP, Greicius MD, Pascual-Leone A (2012) Efficacy of transcranial magnetic stimulation targets for depression is related to intrinsic functional connectivity with the subgenual cingulate. Biol Psychiatry 72(7):595–603

Fox MD, Greicius M (2010) Clinical applications of resting state functional connectivity. Front Syst Neurosci 4:19. https://doi.org/10.3389/fnsys.2010.00019

Fox MD, Snyder AZ, Vincent JL, Corbetta M, Van Essen DC, Raichle ME (2005) The human brain is intrinsically organized into dynamic, anticorrelated functional networks. Proc Natl Acad Sci U S A 102:9673–9678

Fransson P (2006) How default is the default mode of brain function? Further evidence from intrinsic BOLD signal fluctuations. Neuropsychologia 44:2836–2845

Friston KJ (1994) Functional and effective connectivity in neuroimaging: a synthesis. Hum Brain Mapp 2:56–87

Friston KJ, Buechel C, Fink GR, Morris J, Rolls E, Dolan RJ (1997) Psychophysiological and modulatory interactions in neuroimaging. NeuroImage 6:218–229

Greicius MD, Krasnow B, Reiss AL, Menon V (2003) Functional connectivity in the resting brain: a network analysis of the default mode hypothesis. Proc Natl Acad Sci U S A 100:253–258

Greicius MD, Srivastava G, Reiss AL, Menon V (2004) Default-mode network activity distinguishes Alzheimer's disease from healthy aging: evidence from functional MRI. Proc Natl Acad Sci U S A 101:4637–4642

Gusnard DA, Raichle ME, Raichle ME (2001) Searching for a baseline: functional imaging and the resting human brain. Nat Rev Neurosci 2:685–694

He Y, Chen Z, Evans A (2008) Structural insights into aberrant topological patterns of large-scale cortical networks in Alzheimer's disease. J Neurosci 28:4756–4766

Hedden T, Van Dijk KRA, Becker JA, Mehta A, Sperling RA, Johnson KA, Buckner RL (2009) Disruption of functional connectivity in clinically normal older adults harboring amyloid burden. J Neurosci 29:12686–12694

Heiss WD (2009) The potential of PET/MR for brain imaging. Eur J Nucl Med Mol Imaging 36(Suppl 1):S105–S112

Hoenig MC, Bischof GN, Seemiller J, Hammes J, Kukolja J, Onur ÖA, Jessen F, Fliessbach K, Neumaier B, Fink GR, van Eimeren T, Drzezga A (2018) Networks of tau distribution in Alzheimer's disease. Brain 141(2):568–581

Horwitz B, Duara R, Rapoport SI (1984) Intercorrelations of glucose metabolic rates between brain regions: application to healthy males in a state of reduced sensory input. J Cereb Blood Flow Metab 4:484–499

Hutchison RM, Womelsdorf T, Allen EA, Bandettini PA, Calhoun VD, Corbetta M, Della Penna S, Duyn JH, Glover GH, Gonzalez-Castillo J, Handwerker DA, Keilholz S, Kiviniemi V, Leopold DA, de Pasquale F, Sporns O, Walter M, Chang C (2013) Dynamic functional connectivity: promise, issues, and interpretations. NeuroImage 80:360–378

Jones DT, Graff-Radford J, Lowe VJ, Wiste HJ, Gunter JL, Senjem ML, Botha H, Kantarci K, Boeve BF, Knopman DS, Petersen RC, Jack CR Jr (2017) Tau, amyloid, and cascading network failure across the Alzheimer's disease spectrum. Cortex 97:143–159

Kim J, Ghadery C, Cho SS, Mihaescu A, Christopher L, Valli M, Houle S, Strafella AP (2019) Network patterns of Beta-amyloid deposition in Parkinson's disease. Mol Neurobiol 56:7731–7740

Klunk WE, Engler H, Nordberg A, Wang Y, Blomqvist G, Holt DP, Bergström M, Savitcheva I, Huang GF, Estrada S, Ausén B, Debnath ML, Barletta J, Price JC, Sandell J, Wall A, Koivisto P, Antoni G, Mathis CA, Långström B (2004) Imaging brain amyloid in Alzheimer's disease with Pittsburgh compound-B. Ann Neurol 55:306–319

Kwong KK, Belliveau JW, Chesler DA, Goldberg IE, Weisskoff RM, Poncelet BP, Kennedy DN, Hoppel BE, Cohen MS, Turner R et al (1992) Dynamic magnetic resonance imaging of human brain activity during primary sensory stimulation. Proc Natl Acad Sci U S A 89:5675–5679

Lee MH, Miller-Thomas MM, Benzinger TL, Marcus DS, Hacker CD, Leuthardt EC, Shimony JS (2016) Clinical resting-state fMRI in the preoperative setting: are we ready for prime time? Top Magn Reson Imaging 25(1):11–18

Liu H, Buckner RL, Talukdar T, Tanaka N, Madsen JR, Stufflebeam SM (2009) Task-free presurgical mapping using functional magnetic resonance imaging intrinsic activity. J Neurosurg 111(4):746–754

Lurie DJ, Kessler D, Bassett DS, Betzel RF, Breakspear M, Keilholz S et al (2020) Questions and controversies in the study of time-varying functional connectivity in resting fMRI. Netw Neurosci 4(1):30–69. https://doi.org/10.1162/netn_a_00116

Lustig C, Snyder AZ, Bhakta M, O'Brien KC, McAvoy M, Raichle ME, Morris JC, Buckner RL (2003) Functional deactivations: change with age and dementia of the Alzheimer type. Proc Natl Acad Sci U S A 100:14504–14509

Marsden PK, Strul D, Keevil SF, Williams SC, Cash D (2002) Simultaneous PET and NMR. Br J Radiol 75:S53–S59

Mathis CA, Wang Y, Klunk WE (2004) Imaging beta-amyloid plaques and neurofibrillary tangles in the aging human brain. Curr Pharm Des 10:1469–1492

McIntosh AR (1999) Mapping cognition to the brain through neural interactions. Memory 7:523–548

McKiernan KA, Kaufman JN, Kucera-Thompson J, Binder JR (2003) A parametric manipulation of factors affecting task-induced deactivation in functional neuroimaging. J Cogn Neurosci 15:394–408

McLaren DG, Ries ML, Xu G, Johnson SC (2012) A generalized form of context-dependent psychophysiological interactions (gPPI): a comparison to standard approaches. NeuroImage 61:1277–1286

Mitchell JP, Macrae CN, Banaji MR (2006) Dissociable medial prefrontal contributions to judgments of similar and dissimilar others. Neuron 50:655–663

Morbelli S, Drzezga A, Perneczky R, Frisoni GB, Caroli A, van Berckel BN, Ossenkoppele R, Guedj E, Didic M, Brugnolo A et al (2012) Resting metabolic connectivity in prodromal Alzheimer's disease. A European Alzheimer Disease Consortium (EADC) project. Neurobiol Aging 33:2533–2550

Mormino EC, Smiljic A, Hayenga AO, Onami SH, Greicius MD, Rabinovici GD, Janabi M, Baker SL, Yen IV, Madison CM et al (2011) Relationships between beta-amyloid and functional connectivity in different components of the default mode network in aging. Cereb Cortex 21(10):2399–2407

Ogawa S, Tank DW, Menon RS, Ellermann JM, Kim SG, Merkle H, Ugurbil K (1992) Intrinsic signal changes accompanying sensory stimulation: functional brain mapping with magnetic resonance imaging. Proc Natl Acad Sci U S A 89:5951–5955

Pereira JB, Strandberg TO, Palmqvist S, Volpe G, van Westen D, Westman E, Hansson O, Alzheimer's Disease Neuroimaging Initiative (2018) Amyloid network topology characterizes the progression of Alzheimer's disease during the predementia stages. Cereb Cortex 28:340–349

Power JD, Barnes KA, Snyder AZ, Schlaggar BL, Petersen SE (2012) Spurious but systematic correlations in functional connectivity MRI networks arise from subject motion. NeuroImage 59:2142–2154

Raichle ME, MacLeod AM, Snyder AZ, Powers WJ, Gusnard DA, Shulman GL (2001) A default mode of brain function. Proc Natl Acad Sci U S A 98:676–682

Rubinov M, Sporns O (2010) Complex network measures of brain connectivity: uses and interpretations. NeuroImage 52:1059–1069

Satterthwaite TD, Wolf DH, Loughead J, Ruparel K, Elliott MA, Hakonarson H, Gur RC, Gur RE (2012) Impact of in-scanner head motion on multiple measures of functional connectivity: relevance for studies of neurodevelopment in youth. NeuroImage 60:623–632

Schacter DL, Addis DR, Buckner RL (2007) Remembering the past to imagine the future: the prospective brain. Nat Rev Neurosci 8:657–661

Sair HI, Agarwal S, Pillai JJ (2017) Application of resting state functional MR imaging to presurgical mapping: language mapping. Neuroimaging Clin N Am 27(4):635–644

Seeley WW, Menon V, Schatzberg AF, Keller J, Glover GH, Kenna H, Reiss AL, Greicius MD (2007) Dissociable intrinsic connectivity networks for salience processing and executive control. J Neurosci 27:2349–2356

Seeley WW, Crawford RK, Zhou J, Miller BL, Greicius MD (2009) Neurodegenerative diseases target large-scale human brain networks. Neuron 62:42–52

Sepulcre J, Grothe MJ, d'Oleire Uquillas F, Ortiz-Terán L, Diez I, Yang HS, Jacobs HIL, Hanseeuw BJ, Li Q, El-Fakhri G, Sperling RA, Johnson KA (2018) Neurogenetic contributions to amyloid beta and tau spreading in the human cortex. Nat Med 24(12):1910–1918

Sepulcre J, Liu H, Talukdar T, Martincorena I, Yeo BT, Buckner RL (2010) The organization of local and distant functional connectivity in the human brain. PLoS Comput Biol 6:e1000808

Setsompop K, Gagoski BA, Polimeni JR, Witzel T, Wedeen VJ, Wald LL (2012) Blipped-controlled aliasing in parallel imaging for simultaneous multislice echo planar imaging with reduced g-factor penalty. Magn Reson Med 67(5):1210–1224

Shehzad Z, Kelly AM, Reiss PT, Gee DG, Gotimer K, Uddin LQ, Lee SH, Margulies DS, Roy AK, Biswal BB et al (2009) The resting brain: unconstrained yet reliable. Cereb Cortex 19:2209–2229

Sheline YI, Raichle ME, Snyder AZ, Morris JC, Head D, Wang S, Mintun MA (2010) Amyloid plaques disrupt resting state default mode network connectivity in cognitively normal elderly. Biol Psychiatry 67:584–587

Shenhav A, Greene JD (2012) Moral judgments recruit domain-general valuation mechanisms to integrate representations of probability and magnitude. Neuron 67:667–677

Shulman GL, Fiez JA, Corbetta M, Buckner RL, Miezin FM, Raichle ME, Petersen SE (1997) Common blood flow changes across visual tasks: II.: decreases in cerebral cortex. J Cogn Neurosci 9:648–663

Smith SM, Fox PT, Miller KL, Glahn DC, Fox PM, Mackay CE, Filippini N, Watkins KE, Toro R, Laird AR et al (2009) Correspondence of the brain's functional architecture during activation and rest. Proc Natl Acad Sci U S A 106:13040–13045

Smith SM, Miller KL, Moeller S, Xu J, Auerbach EJ, Woolrich MW, Beckmann CF, Jenkinson M, Andersson J, Glasser MF et al (2011) Temporally-independent functional modes of spontaneous brain activity. Proc Natl Acad Sci U S A 109:3131–3136

Sorg C, Riedl V, Muhlau M, Calhoun VD, Eichele T, Laer L, Drzezga A, Forstl H, Kurz A, Zimmer C et al (2007) Selective changes of resting-state networks in individuals at risk for Alzheimer's disease. Proc Natl Acad Sci U S A 104:18760–18765

Sperling RA, Laviolette PS, O'Keefe K, O'Brien J, Rentz DM, Pihlajamaki M, Marshall G, Hyman BT, Selkoe DJ, Hedden T et al (2009) Amyloid deposition is associated with impaired default network function in older persons without dementia. Neuron 63:178–188

Sperling RA, Aisen PS, Beckett LA, Bennett DA, Craft S, Fagan AM, Iwatsubo T, Jack CR Jr, Kaye J, Montine TJ et al (2011) Toward defining the preclinical stages of Alzheimer's disease: recommendations from the National Institute on Aging-Alzheimer's association workgroups on diagnostic guidelines for Alzheimer's disease. Alzheimers Dement 7:280–292

Stam CJ, Reijneveld JC (2007) Graph theoretical analysis of complex networks in the brain. Nonlinear Biomed Phys 1:3

Teipel S, Grothe MJ, Zhou J, Sepulcre J, Dyrba M, Sorg C, Babiloni C (2016) Measuring cortical connectivity in Alzheimer's disease as a brain neural network pathology: toward clinical applications. J Int Neuropsychol Soc 22(2):138–163

Tomasi D, Volkow ND (2010) Functional connectivity density mapping. Proc Natl Acad Sci U S A 107:9885–9890

Triantafyllou C, Hoge RD, Krueger G, Wiggins CJ, Potthast A, Wiggins GC, Wald LL (2005) Comparison of physiological noise at 1.5 T, 3 T and 7 T and optimization of fMRI acquisition parameters. NeuroImage 26:243–250

van den Heuvel MP, Stam CJ, Boersma M, Hulshoff Pol HE (2008) Small-world and scale-free organization of voxel-based resting-state functional connectivity in the human brain. NeuroImage 43:528–539

Van Dijk KRA, Hedden T, Venkataraman A, Evans KC, Lazar SW, Buckner RL (2010) Intrinsic functional connectivity as a tool for human connectomics: theory, properties, and optimization. J Neurophysiol 103:297–321

Van Dijk KRA, Sabuncu MR, Buckner RL (2012a) The influence of head motion on intrinsic functional connectivity MRI. NeuroImage 59:431–438

Van Dijk KRA, Triantafyllou C, Keil B, Hedden T, Wald LL , Buckner RL (2012b) Detailed anatomical localization of intrinsic connectivity networks using high spatial resolution fMRI at 7 tesla. In: Neuroscience meeting planner. Program no. 79.13. 2012, New Orleans

Villien M, Wey HY, Mandeville JB, Catana C, Polimeni JR, Sander CY, Zürcher NR, Chonde DB, Fowler JS, Rosen BR, Hooker JM (2014) Dynamic functional imaging of brain glucose utilization using fPET-FDG. NeuroImage 100:192–199

Vincent JL, Kahn I, Snyder AZ, Raichle ME, Buckner RL (2008) Evidence for a frontoparietal control system revealed by intrinsic functional connectivity. J Neurophysiol 100:3328–3342

Ward A, Schultz AP, Huijbers W, Van Dijk KRA, Hedden T, Sperling RA (2014) The parahippocampal gyrus links the default mode cortical network with the medial temporal lobe memory system. Hum Brain Mapp 35(3):1061–1073

Xia CF, Arteaga J, Chen G, Gangadharmath U, Gomez LF, Kasi D, Lam C, Liang Q, Liu C, Mocharla VP, Mu F, Sinha A, Su H, Szardenings AK, Walsh JC, Wang E, Yu C, Zhang W, Zhao T, Kolb HC (2013) [(^{18})F]T807, a novel tau positron emission tomography imaging agent for Alzheimer's disease. Alzheimers Dement 9(6):666–676

8 Use of Nuclear Medicine Molecular Neuroimaging to Model Brain Molecular Connectivity

Carlos A. Sanchez-Catasus, Martijn L. T. M. Müller, Peter Paul De Deyn, Rudi A. J. O. Dierckx, Nicolaas I. Bohnen, and Lester Melie-Garcia

C. A. Sanchez-Catasus (✉)
Division of Nuclear Medicine, Department of Radiology, University of Michigan, Ann Arbor, MI, USA

Department of Nuclear Medicine and Molecular Imaging, University of Groningen, University Medical Center Groningen, Groningen, The Netherlands
e-mail: carlosas@umich.edu

M. L. T. M. Müller
Division of Nuclear Medicine, Department of Radiology, University of Michigan, Ann Arbor, MI, USA

Morris K. Udall Center of Excellence for Parkinson's Disease Research, University of Michigan, Ann Arbor, MI, USA
e-mail: mtmuller@umich.edu

P. P. De Deyn
Department of Neurology and Alzheimer Center, University of Groningen, University Medical Center Groningen, Groningen, The Netherlands

R. A. J. O. Dierckx
Department of Nuclear Medicine and Molecular Imaging, University of Groningen, University Medical Center Groningen, Groningen, The Netherlands
e-mail: r.a.dierckx@umcg.nl

N. I. Bohnen
Division of Nuclear Medicine, Department of Radiology, University of Michigan, Ann Arbor, MI, USA

Morris K. Udall Center of Excellence for Parkinson's Disease Research, University of Michigan, Ann Arbor, MI, USA

Department of Neurology, University of Michigan, Ann Arbor, MI, USA

Neurology Service and GRECC, Veterans Administration Ann Arbor Healthcare System, Ann Arbor, MI, USA
e-mail: nbohnen@umich.edu

R. A. J. O. Dierckx et al. (eds.), *PET and SPECT in Neurology*,
https://doi.org/10.1007/978-3-030-53168-3_8

L. Melie-Garcia
Laboratoire de Recherche en Neuroimagerie (LREN), Centre Hospitalier Universitaire Vaudois (CHUV), Lausanne, Switzerland

Applied Signal Processing Group, Swiss Federal Institute of Technology Lausanne (EPFL), Lausanne, Switzerland

Contents

8.1 Introduction 182
8.2 From Topography to Topology: The Graph Theoretical Analysis 184
8.3 Brain Molecular Networks: The Connectivity Matrix 186
8.3.1 Brain Molecular Connectivity in the Context of Structural and Functional Connectivity 190
8.4 Network Metrics 191
8.4.1 Integration 192
8.4.2 Segregation 192
8.4.3 Centrality 193
8.5 Brain Connectivity Analysis 195
8.6 Sparse Inverse Covariance Estimation (SICE) 196
8.7 Example Studies 197
8.7.1 Age-Associated Metabolic Network Changes 197
8.7.2 Modularity of Amyloid Networks 199
8.7.3 Cerebrovascular Reactivity in MCI 200
8.7.4 SICE Application to Multimodal Neuroimaging 202
8.8 Final Remarks 202
A Lexicon of the Most Commonly Used Network Metrics 204
References 205

Abstract

We introduce basic concepts of brain networks and discuss methods to model and analyze brain molecular connectivity using positron emission tomography (PET) and single-photon emission computed tomography (SPECT). Basic elements of network analytic methods, including graph theory, and the connectivity matrix as a basis for network analysis will be discussed in more detail. Statistical methods to compare networks will be reviewed. A specific brain network analysis method called sparse inverse covariance estimation (SICE) is presented as an alternative to Pearson correlation to estimate the brain molecular connectivity matrix. Finally, we will discuss examples from published research to illustrate the practical application of brain molecular connectivity analysis concepts.

8.1 Introduction

This chapter will focus on the construction and analysis of brain molecular networks using nuclear medicine molecular neuroimaging. The advance of multimodal neuroimaging techniques and mathematical analysis methods has provided a great

opportunity to more comprehensively capture brain network functioning. Traditional methods of nuclear medicine molecular neuroimaging analysis have emphasized analysis based on a single or small number of brain regions. This reductionist approach of using a "process of elimination" has led to a better understanding of brain functioning. Although this method is fruitful to understand the relationship between a specific brain region and behavioral or clinical function, it generally will fail to more fully capture the wide spectrum of behavioral functions or clinical symptomatology. That is because dysfunction of one specific brain region will propagate through the larger network and will affect regions that are both directly structurally connected or indirectly functionally connected. A classic example of this is diaschisis where local dysfunction in a single brain region may cause remote deafferentation effects (Monakow 1914).

In recent years there has been a growing interest in multivariate methods to analyze nuclear medicine molecular images. The first attempts to model brain networks using multivariate analysis methods were made in the last two decades of the last century by analyzing covariations of FDG-PET data (Horwitz et al. 1984; Horwitz et al. 1987; Metter et al. 1984; Clark and Stoessl 1986; Moeller et al. 1987; Eidelberg et al. 1994). For example, studies by Eidelberg et al. (1994) demonstrated the existence of specific brain metabolic covariance profiles in Parkinson disease (PD) that were associated with some of the motor and cognitive symptoms of PD (Eidelberg et al. 1994).

The dawn of the so-called connectomic era spurred mainly MR-based brain connectivity analysis (Sporns et al. 2005). Brain networks were modeled by analyzing structural connectivity using diffusion tensor images (DTI) and functional connectivity through functional magnetic resonance imaging (fMRI) as well as electroencephalography (EEG) and magnetoencephalography (MEG) (Fornito and Bullmore 2015). More recently, there is a renewed interest in brain molecular connectivity, based on molecular PET and SPECT, to define networks using radiotracers that can capture network of brain metabolism, neurotransmission, and proteinopathies among others. Many of the ideas and methods developed for the analysis of brain networks for MRI/EEG/MEG neuroimaging modalities have been gradually adapted for the analysis of brain networks based on PET and SPECT. Prevailing methods include seed-based correlation analysis (Lee et al. 2008), principal component analysis (PCA) (Manzanera et al. 2019), independent component analysis (ICA) (Gu et al. 2019), and methods based on pairwise covariance of brain regions (Yakushev et al. 2017; Sala and Perani 2019; Huang et al. 2010). The feasibility of the latter has also been shown in the analysis of cerebral blood flow (CBF) networks using SPECT (Melie-Garcia et al. 2013; Sanchez-Catasus et al. 2017; Sanchez-Catasus et al. 2018).

Perhaps due to its relative simplicity and practical feasibility, one of the most widespread methods is based on a pairwise covariance analysis of brain regions in conjunction with graph theory. This methodology allows for using metrics that capture the strength or "health" of the brain network. A specific type of the pairwise covariance approach is the sparse inverse covariance estimation (SICE) methodology that has gained recent interest (Huang et al. 2010). In this chapter, we aim to

introduce and discuss the basic elements of these methods targeting readers working in the field of neuro-nuclear medicine who may not be familiar with the underlying principles of these approaches.

Section 2 presents basic concepts of network and graph theoretical analysis. Section 3 defines the concept of the connectivity matrix which may have especially application for networks based on nuclear medicine molecular neuroimaging. In Sect. 4, frequently used network metrics are discussed in more detail. Section 5 presents the analysis of brain molecular connectivity based on the statistical comparison of metrics from at least two networks. Section 6 addresses the SICE methodology as an alternative to more standard Pearson correlation coefficient-based method. Finally, Sect. 7 will briefly discuss some recently published studies to illustrate the major concepts explained in this chapter.

8.2 From Topography to Topology: The Graph Theoretical Analysis

A key concept of graph theory is the notion of topology. Topology can be illustrated with a common network concept that one can encounter when traveling by subway in a large city. In Fig. 8.1, the left map of the London subway shows a precise spatial description of the railway (or lines) layout, i.e., the subway topography, the right map represents the relative locations of subway stations and connecting lines, i.e., the subway topology. These two maps do not coincide with regard to the relative

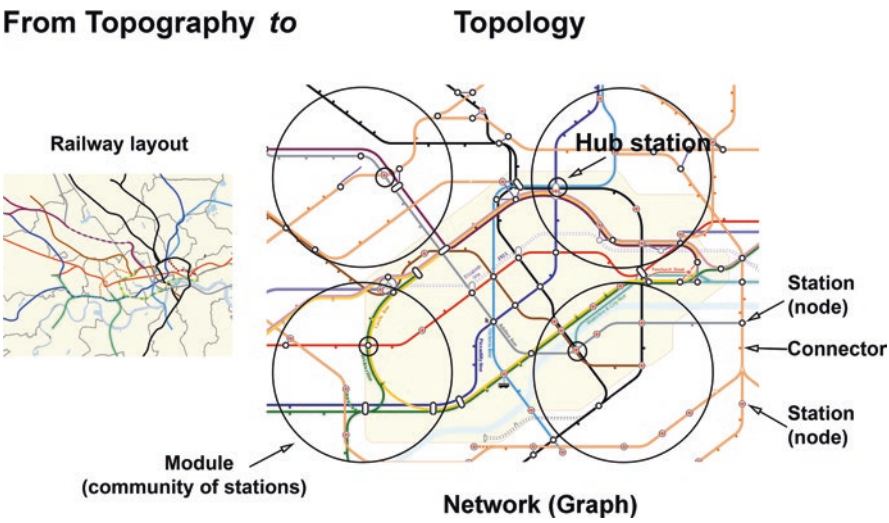

Fig. 8.1 The topographical (left) and the topological maps (right) of the London subway. Both maps are partially shown and modules (large circles) and hubs (small circles) are for illustrative purposes only. Topographical map source: https://en.wikipedia.org/wiki/File:London_Underground_with_Greater_London_map.svg. Topological map source: https://en.wikipedia.org/wiki/List_of_London_Underground_stations

position of the stations, neither in distance nor in location of lines. For example, two stations may be topographically (physically) distant but with a direct connection they can be topologically close and vice versa. The direct connection cannot be easily derived from the topographical map but is readily recognized from the topological map. The topological map is a "graph" and represents a network.

A graph is composed of two main topological elements (see also Fig. 8.1), the nodes (the stations in the subway example), and the connectors or edges (the connecting lines). While the topological map makes it easier to extract relevant information for travel on the subway, this would not be sufficient to compare the London subway with the subway of another large city, for example, to compare which subway system is more efficient. This is why quantitative measures of the network (graph) are needed. Graph theory, founded by Swiss mathematician Leonhard Euler as early as the eighteenth century (Biggs et al. 1986), is the mathematical framework for calculating these network metrics. In general, network metrics can be grouped into measures of integration, segregation, and centrality. In this section we will provide an intuitive concept of these measures. Section 4 will address these measures in more detail.

In network analysis, the concept of integration is related to communication between all the nodes of the network, i.e., how well-connected are any pair of nodes. A measure of integration in the example of the London subway would be the average number of stations that must be crossed to go from any part of the city to another; the lower the number of stations, the higher the efficiency of the subway integration.

In contrast to network integration, network segregation is related to the partition of the network into smaller graphs or a cluster of connected nodes (subgraphs). In case of the London subway graph, a natural partition is defined by taking different subgraphs formed by the stations and its direct topological neighbors. In some stations, neighboring stations are better connected than in others. For example, suppose that a particular station is out of service due to an electrical failure, if its neighboring stations are well connected to each other, it will be more easy to reroute (reconnect) the passengers to the final destination.

A more complex metric of segregation is related to what extent the whole subway can be divided into modules (i.e., groups of stations within the large circles in Fig. 8.1) in such a way that the number of connections between the stations within the module is the maximum possible while the number of connections between modules is the minimal necessary to maintain the whole subway optimally interconnected. For example, when a group of stations (module) is out of service, the remaining subway still can continue to operate due to the relative independence among modules. Therefore, a modular structure increases flexibility, stability, and robustness.

Centrality refers to the level of influence of a node on other nodes. The nodes with the highest centrality (or influence) are called hubs and are key elements in network functioning. Some nodes have a high influence on communications between modules (connector hubs), for example, the subway stations within the small circles in Fig. 8.1. Other nodes facilitate communication between the nodes that make up each module (provincial hubs). Connector hubs are crucial for network integration while provincial hubs are critical for network segregation. In Sect. 4 centrality measures are described to differentiate these two types of hubs.

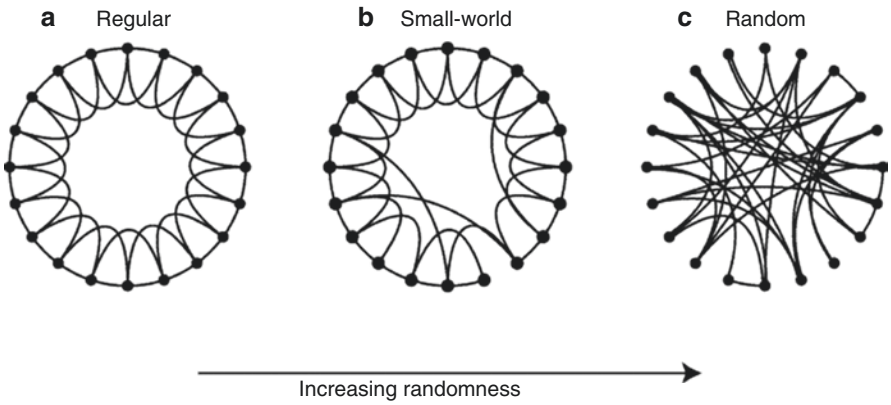

Fig. 8.2 Representation of a computational model of small-world (complex) networks which positions between regular and random networks. (Adapted from Watts and Strogatz (1998) with permission)

If networks were to be ranked, at one end of the spectrum would be a regular (ordered) network. In a regular network each node is directly connected to its neighboring nodes (short direct connection), but without direct connections to distant nodes; i.e., a network with low integration but high segregation (Fig. 8.2a). At the other end of the spectrum would be a random network. In a random network, direct connections between any two nodes are random (Fig. 8.2c); i.e., in a random network, the integration is high and the segregation is low. In the middle of these two extremes is a complex network (Fig. 8.2b), in which there is a balance between integration and segregation. A complex network has a "small-world" topology (Watts and Strogatz 1998). The concept of "small-world" comes from the social sciences and reflects the fact that two persons (nodes) who do not know each other are nevertheless connected by a relatively short chain of persons known to each other (a.k.a., the "six degrees of separation" theory).

Unlike ordered and random networks, a complex network has a modular structure and the presence of hubs (see also London subway example). These London subway concepts can be applied also to brain network analysis. Brain networks follow a "small-world" topology, with an efficient modular structure and the presence of hubs (Bullmore and Sporns 2009; Rubinov and Sporns 2010; Fornito et al. 2013). Notably, these properties remain across different spatial scales: from micro (networks of neurons) to macro (networks of brain regions).

8.3 Brain Molecular Networks: The Connectivity Matrix

We will use an example with FDG-PET to illustrate the application of network analysis to molecular imaging. Network analysis is not limited to FDG PET; the methodology described here can also be applied to PET (or SPECT) of other molecular tracers (see study examples in Sects. 8.7.2 and 8.7.3).

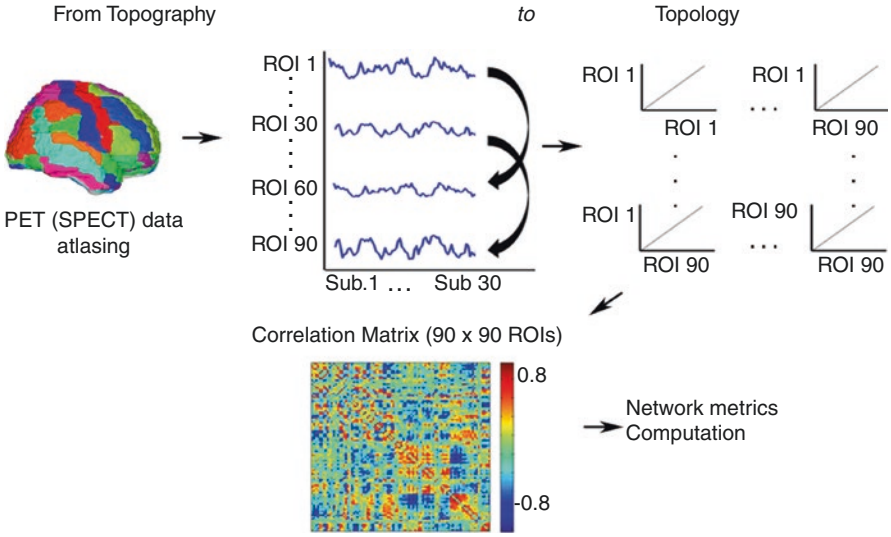

Fig. 8.3 Construction of a brain glucose metabolic network using FDG-PET data. The color bar indicates the value of the correlation coefficient coming from the brain metabolic co-variations among 90 anatomical brain regions (AAL atlas). The diagonal elements of the constructed matrix (self-correlations) are set to zero

In this example, we assume that there is a group of FDG-PET images corresponding to 30 healthy control subjects (or 30 patients with the same CNS disorder). The images of each subject can be segmented into different regions of interest (ROIs) using a brain atlas, for instance, the automated anatomical labeling (AAL) atlas (Tzourio-Mazoyer et al. 2002). If we plot the mean voxel value of each ROI for the 30 subjects, we have a measure of how each ROI varies across subjects (Fig. 8.3). Figure 8.3 shows that ROI 1 and ROI 60 (although with different amplitudes) change similarly. The same for ROIs 30 and 90. A simple way to measure how similar the variations are between any pair of ROIs across subjects is by calculating the Pearson's correlation coefficient between two different ROIs. If this process is performed for every pair of ROIs, a matrix of Pearson's correlation coefficients is obtained (Fig. 8.3).

The correlation matrix defines "the connectivity matrix," also known as the adjacency matrix, and can be seen as a network (or a graph) of interactions between all pairs of brain regions. In this example, the network nodes are the ROIs (equivalent to the subway stations) and the connectors are the Pearson correlation coefficients between any two ROIs; the FDG-PET data of a group 30 individuals have been transformed from a topographic space to a topological one (the brain glucose metabolic network). This connectivity model assumes that covariations in brain metabolism between different regions form a network.

The connectivity matrix is a basic concept of brain network analysis common to other neuroimaging modalities. For example, for DTI MRI the connectivity matrix is based on the number of tracts or streamlines connecting the ROIs, and for fMRI

the connectivity matrix is based on temporal correlations of the BOLD signal. A fundamental difference is that the connectivity matrix using PET (or SPECT) is group-based due to the "static" nature of the data while DTI and fMRI based networks can be constructed on an individual base. In recent years, however, several methods have been developed that allow the extraction of individual information from a group-based connectivity matrix (Batalle et al. 2013; Raj et al. 2010; Saggar et al. 2015; Tijms et al. 2012; Zhou et al. 2011). Other alternatives have also been proposed for single-subject level analysis (Titov et al. 2017; Tomasi et al. 2017). The development and validation of optimal methods for single-subject analysis is perhaps one of the most important research directions in the near future, since it opens the door to the use of molecular network analysis in clinical practice.

In the above FDG-PET example, the Pearson's correlation was used. One of the problems with this statistical measure is that it estimates the association between two brain regions without considering the influence that other brain regions may have on that relationship. One way to solve the problem is to use the partial correlation measure. This requires, however, more subjects than the number of ROIs, which could be cost-prohibitive for PET or SPECT imaging studies. One possible solution is to reduce the number of ROIs, using only those that are relevant in the context of an a priori hypothesis. However, this approach has the risk that ROIs that could potentially be important may be ignored. In addition, by reducing the number of ROIs, the resulting network may not be a complex network (i.e., small-world, modularity, and the presence of hubs). Although the use of partial correlation is the optimal method to build the connectivity matrix, a recent study showed that the Pearson's correlation is also valid to study brain molecular connectivity using radiotracer probes, albeit with certain limitations (Veronese et al. 2019).

Another important point relates to the connectivity weights between brain regions. Connections between different neuronal units are not the same in terms of the number of synapses, axonal density, or the degree of fiber myelination. These differences can be represented by different connectivity weights between brain regions, for example, using the value of Pearson's correlation coefficient between ROIs as shown in Fig. 8.3. Weights based on the Pearson's correlation range from +1 (perfect positive correlation) to −1 (perfect negative correlation or anti-correlation). Many brain connectivity studies, however, rule out or ignore negative correlations, since its meaning is not entirely clear. Some network metrics also cannot be defined if negative correlations are considered. Several researchers attribute the negative correlations to statistical artifacts (Saad et al. 2012; Murphy et al. 2009; Murphy and Fox 2017), while other authors believe that negative correlations may reflect inhibition or deactivation (Anticevic et al. 2012). A possible alternative is to consider the absolute value of the resulting correlation coefficient when calculating network metrics, assuming that the relevant biological information is the presence of a statistical interaction, regardless of the correlation sign. However, the role of negative correlations will need further clarification for a better understanding in the case of brain molecular connectivity analysis.

Another important consideration is related to the extent that a given weight represents a biological connection or may be only due to noise or a spurious link.

Networks based on correlation matrices have a nonzero value in every off-diagonal element of the matrix, that is, every node is connected to every other. However, brain networks tend to be sparse by following a principle of economics, which means that the total cost of wiring in the network is less than if the same nodes were randomly connected, but at the same time maximizing the efficiency of information processing (economically connected) (Bullmore and Sporns 2012).

To address this problem, thresholds are usually applied to the correlation matrix to eliminate weights that may be due to false connections. In brain molecular imaging connectivity studies, the most used threshold method applies a global threshold to all elements of the connectivity matrix. Weights that survive the threshold are set to one (connection) and zero (no connection) otherwise, which results in a binary graph. This has the advantage that it is easier to not only characterize the network but also to make statistical comparisons (Sect. 5). The most commonly used method to define a threshold uses the concept of network density (also termed "cost" or "sparsity" in the literature). Network density represents the proportion of suprathreshold connections of all possible connections. Since threshold selection is arbitrary, the connectivity matrix is thresholded in a range of network densities instead. The area under the curve (AUC) across the threshold range is often used as the descriptor of a given network metric (Fornito et al. 2013).

A widely used criterion to choose the threshold range (both lower and upper thresholds) is based on avoiding a fragmented or fully connected network. In this case, the lower threshold is selected as the minimum network density, below which the network would be fragmented. The network is not fragmented when all its nodes are connected by an edge path, forming a single connected component. Also, as the network density decreases, it tends to be a regular network. On the other hand, to select the upper threshold, a threshold in which the network is fully connected should be avoided, as this occurs at higher densities.

Furthermore, selection of the lower and upper threshold is often dependent on the specific brain disorder and type of data used. This often will require an exploratory analysis of the data set, which will limit the use of an a priori selection. Nonetheless, the range between the upper and lower threshold moves typically from 0.1 (10% of all possible connections) to 0.5 (50%). The example in the Sect. 8.7.1 illustrates the concept of network metrics evaluation across a range of network densities.

In summary, the most common analysis of brain molecular connectivity is accomplished by using unweighted (binary) undirected graphs, that are based on Pearson's correlation, discarding negative weights, and are only based on group-level analysis. Even with these simplifications, this method can provide important information about the molecular organization of the brain in various brain disorders. Moreover, in recent years there have been advances in the weighted graph approach and increasing calls for use across all neuroimaging modalities (Bassett and Bullmore 2017). There are also alternative methods for connectivity matrix thresholding. However, each of these thresholding methods has its own advantages and limitations. Detailed discussion of these methods is beyond the scope of this chapter but have been reviewed by Fornito et al. (Fornito et al. 2013).

8.3.1 Brain Molecular Connectivity in the Context of Structural and Functional Connectivity

Different neuroimaging modalities are proxies of different brain characteristics, e.g., DTI can be used for estimation of brain structure (principally white matter), fMRI can be used for function, and molecular imaging (PET and SPECT) for molecular activity. The information provided by these techniques allows modeling of different aspects of large-scale brain networks.

Brain structural connectivity based on DTI refers to anatomical connections between brain areas through fiber bundles. Structural connectivity is relatively stable on a short time scale (e.g., minutes) although it is subject to change on a larger time scale. In contrast, brain functional connectivity based on fMRI is related to the temporal statistical dependence between brain regions, regardless of whether these regions are connected by nerve fibers (direct structural links), with changes that can be in short periods of time (e.g., seconds). Previous studies support the notion that structural and functional connectivity are correlated (Skudlarski et al. 2008; Honey et al. 2010). If there is a strong structural connection between two brain regions, it is likely that the corresponding functional connection is also strong, although the opposite is not always true (Koch et al. 2002; Mišić et al. 2016). This is because the structural connectivity infers a direct physical or anatomical connection between any two regions, while functional connectivity incorporates direct and indirect statistical associations. In this sense, molecular-imaging based brain metabolic connectivity is more analogous to fMRI-based functional connectivity, since there could be indirect metabolic covariations ("connections") without a specific anatomical substrate. Indeed, recent studies have shown an association between functional connectivity by fMRI and glucose metabolism derived from FDG-PET (Passow et al. 2015; Riedl et al. 2016), suggesting that the analysis of both could be complementary.

Brain molecular connectivity can also be modeled for radiotracers targeting neurotransmission systems, e.g., dopamine. In this case, the connectivity model reflects covariations of neurotransmitter binding in a given region with neurotransmitter binding in other regions (Hahn et al. 2019). Likewise, network analysis of radiotracers that visualize brain pathology (e.g., β-amyloid plaques) assumes that the pathology spreads in a network-like manner (Sepulcre et al. 2013; Pereira et al. 2018).

It is important to note that brain connectivity inferred by either DTI, fMRI, or based on molecular radiotracers does not make any explicit reference to a specific directionality, so it is not possible to estimate the causal directionality of the connectivity. This is reflected in the symmetry of the connectivity matrix (in which the upper half above the main diagonal is a mirror of the lower half) (Fig. 8.3). In these cases, the graph corresponding to the connectivity matrix is "undirected." The so-called "effective connectivity" analysis aims to overcome this limitation through methods designed to capture the direct causal influences between brain regions (Friston 2011; David et al. 2008). More recently, a novel approach to infer effective connectivity has been suggested using the simultaneous acquisition of fMRI and FDG-PET (Riedl et al. 2016).

8.4 Network Metrics

The earlier introduced concepts of integration, segregation, and centrality metrics can be defined at a local (nodal level) and network-wide level. Figure 8.4 provides a simplification of networks to visually guide the explanation of these network metrics. Appendix A provides a lexicon of the most commonly used network metrics. Figure 8.4a shows a connectivity matrix of a hypothetical network of only 24 nodes. These nodes could be 24 London subway stations or 24 brain ROIs based on FDG-PET imaging as explained in Sects. 2 and 3, respectively. Figure 8.4b–d shows the representation of the connectivity matrix in the form of graphs displaying some simple but fundamental topological measures (shortest path, B; triad, C; and modules, D). The graph is undirected and binary, and direct connections (edges) between many pairs of nodes do not exist, although there may be indirect connections through other intermediate nodes. This is a real-life representation. For example, many stations in the London subway do not have direct connections, but are interconnected through others. Similarly, many direct edges in an FDG-PET based connectivity matrix (e.g.,

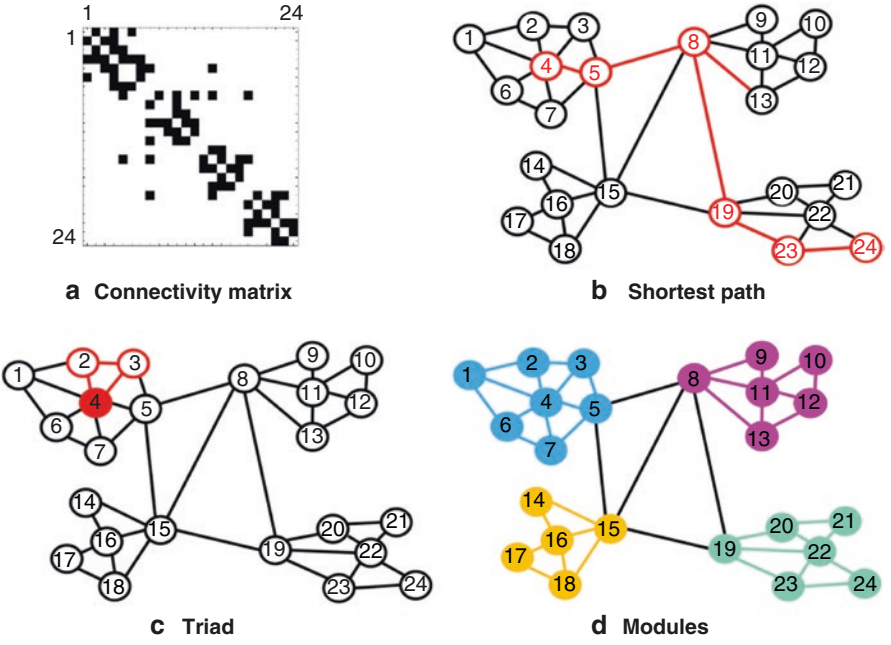

Fig. 8.4 Basics of network metrics. (**a**) Shows a connectivity matrix of a hypothetical network of 24 nodes. The nodes appear in order from 1 to 24 (rows or columns). Each small black square represents a binary connection between two nodes. (**b–d**) Display the graphic representation of the connectivity matrix, showing some fundamental topological measures (shortest path, triad and modules)

derived from Pearson's correlation coefficient) could be weak not surviving a predefined threshold. This also illustrates the idea that the formation of complex networks follows a principle of economy as stated in Sect. 3.

8.4.1 Integration

Integration metrics highlight how well-connected any pair of nodes is within the network. The topological concept of *shortest path* (Fig. 8.4b) is relevant for this concept. The shortest path is the topological distance between two nodes, for example, between nodes 4 and 24 in Fig. 8.4b. The length is the minimum number of edges between these nodes. The *path length* of a particular node (e.g., node 4) represents the shortest path of that particular node to each of the other nodes in the graph (i.e., average of *shortest path* from node 4 to node 5, node 4 to node 6, node 4 to node 7, etc.). As each node is characterized by a *path length*, the average *path length* across all nodes represents the *characteristic path length* of the network *(*average of path length node 4, path length node 5, path length node 6, etc.). *Path length* is a measure of nodal integration, and *characteristic path length* is a measure of network integration. A large *path length* of a node reflects a weakly connected node to the network as a whole. The opposite holds if path length is small. In this context, the definition of "large" or "small" is based on comparison with the node's path length in a reference control network (*see* Sect. 5 for metrics statistical comparison).

The *global efficiency* at the nodal level (also known as *nodal efficiency*) is another metric of integration. It is defined as the average of the inverse shortest path from a given node to all other nodes. Similarly, the global efficiency of the network is the *average of the global efficiency* of all nodes. The *global efficiency* (network-wide) and the *characteristic path length* are inversely related.

8.4.2 Segregation

Unlike integration measures, segregation metrics are related to how well the neighbors of a node are connected. A triad is the main concept involved with this measure (Fig. 8.4c). A triad is formed when a node is connected to any two connected neighbors. A classic measure of segregation is the nodal *clustering coefficient*, defined as the ratio between the number of triads present and the maximum number of triads that could be formed around a node. For example, the clustering coefficient of node 4 in Fig. 8.4 is 0.6 since there are 6 triads around node 4 and the maximum number of possible triads is 10 (e.g., a possible triad would be formed by the node 4 with nodes 5 and 2 if they were directly connected). The clustering coefficient can be interpreted as the probability of connection between any two neighbors of a given node. So, the *average clustering coefficient* of the network is the mean nodal clustering index across all nodes.

Another metric of segregation is the *local efficiency*. At the nodal level, it is defined as the *global efficiency* calculated on the subgraph created by the node's neighbors. Note that the concept of *global efficiency* (network-wide) defined above as a metric of integration (based on the shortest path) is used here as a metric of segregation. The difference is that the network, in this case, is only formed by the neighbors of the specific node (subnetwork or subgraph around the node) after removing it. Likewise, the *average of the local efficiency* of all nodes is the whole network level version of this metric. The *local efficiency* (network-wide) and the *average clustering coefficient* are directly related.

Modularity is a more complex segregation measure (as discussed in Sect. 2). This metric reflects the extent to which a network can be subdivided into modules (communities of nodes) with a maximal within-module and minimal between-module connectivity (Bullmore and Sporns 2009; Rubinov and Sporns 2010; Fornito et al. 2013; Garcia et al. 2018). Figure 8.4d shows in different colors the four modules that make up our hypothetical network. The modularity index Q is a network property that allows quantifying the degree of modularity of a network (Rubinov and Sporns 2010). The Q index varies from 1 to −1. If Q index >0 and is also higher than the Q index for random networks, the network has a modular structure. To calculate the Q index, the community structure needs to be determined first. In real life, community structure detection methods are based on heuristic algorithms that result in a different partition from run to run. Therefore, to have a robust estimate of the community, the analysis requires to find a consensus partition representative of the modular structure of the network (Garcia et al. 2018).

Characteristic path length and the *average clustering coefficient* (or equivalent metrics) are usually considered the two main properties of small-world topology (introduced in Sect. 2). A metric that summarizes this is the small-worldness (also termed σ). This metric reflects to what extent a network shows an optimal balance between *characteristic path length* (integration) and *average clustering coefficient* (segregation). To assess σ, both c*haracteristic path length* and *average clustering coefficient* must be relative (ratio) to these identical average measures of a reference random graph. This results in *lambda* (λ) for the *characteristic path length* and *gamma* (γ) for the *average clustering coefficient*. σ is the ratio between γ and λ. In a complex network, σ is greater than unity because the *characteristic path length* of a complex network and a random network is expected to be similar, unlike the *average clustering coefficient* that must be greater in the complex network.

8.4.3 Centrality

The metrics of centrality measure the level of influence of a given node on other nodes in the network. The simplest measure of centrality is the *nodal degree*, defined as the number of direct connections that a node has with other nodes. For example, the nodal degree of node 4 is six because it has six direct connections to nodes 1–3 and 5–7 (Fig. 8.4b). For binary and undirected graphs, this metric is calculated as

the sum of the number of connections (black squares) across the rows or columns of the connectivity matrix (Fig. 8.4a). The *mean degree* is the average of the degrees of all nodes (network-wide degree).

The *nodal degree* version of a weighted (no binary) network is the *nodal strength*, defined as the sum of the weights of all edges connected to a node. The mean strength is the average of the strength of all nodes (network-wide strength). The *strength* (both nodal and network-wide) is useful even when using binary matrices for network metrics calculation. Before binarization, this metric serves as an exploratory step of the analysis of the dataset as it is a relatively simple measure of connectivity and less abstract than other high-order metrics. It still may be useful to normalize the *nodal strength* by the average across nodes (also known as the *strength of association*), as it is a more intuitive summary of nodal connectivity.

Another important property related to the *nodal degree* (*strength*) is the distribution of degree (strength) values across all nodes. The degree (strength) distribution allows to determine whether the network of interest contains hubs and to understand possible influences that they may have on the network.

Two other widely used metrics are the closeness and betweenness centralities. The first is the same metric defined above as nodal efficiency as a measure of integration, while the second is the ratio between all shortest paths that pass through the node and all shortest paths in the graph.

Two other, more complex, metrics of centrality are the *participation coefficient* and *within-module degree z-score*. Both these metrics reflect the connectivity of each node in relation to the modular organization of the brain. The participation coefficient is defined as the ratio between the number of connections that the node has outside its module (intermodular) and the total number of connections in the whole network. For example, nodes 5, 8, 15 and 19 in Fig. 8.4 have a high participation coefficient compared to other nodes, since they have intermodular connections. The within-module degree *z*-score for a given node is the nodal degree (as defined above), but restricted to only connections inside the module to which that node belongs. For example, nodes 4, 11, 16 and 22 in Fig. 8.4 have a high within-module degree *z*-score compared to other nodes.

These two last metrics provide a more appropriate way to identify the presence of hubs in correlation-based network analyses (Power et al. 2013). For instance, connector hubs have a high participation coefficient and relative high within-module degree *z*-score (nodes 5, 8, 15 and 19 in Fig. 8.4). Connector hubs have a fundamental role in network integration, and they are important in network resilience. So-called "provincial" hubs have low participation coefficient but high within-module degree *z*-score (nodes 4, 11, 16 and 22 in Fig. 8.4). Provincial hubs are fundamental in network segregation.

To identify connector hubs and provincial hubs, the modular structure of the network must first be determined. Thus, modularity is not just a segregation metric, it interrelates segregation, integration, and centrality metrics. Modularity is a key integrative concept in complex network metrics.

Detailed mathematical definitions of network metrics can be found elsewhere (Rubinov and Sporns 2010). Open-source software is readily available on

multiple websites to calculate graph metrics and perform brain connectivity analysis (e.g., (Melie-García et al. 2010; Hosseini et al. 2012; Mijalkov et al. 2017).).

8.5 Brain Connectivity Analysis

Connectivity analysis is generally performed by a statistical comparison of metrics of at least two networks. For example, comparison of network integrity of patients with a specific CNS disorder to a group of control subjects, or longitudinal assessment of network changes within a single group.

Data resampling allows for statistical comparison of network metrics (based on the connectivity matrix) between groups (or time points). One form of resampling uses a non-parametric permutation test. In this procedure: (1) ROI data of each subject are randomly reassigned (a "permutation") to one of the two groups such that each randomized group has the same number of participants as the original ones (typically 1000 permutations or more); (2) the connectivity matrix is calculated for each randomized group; (3) binary connectivity matrices at different network densities (range of densities) are obtained by applying thresholds (as described in Sect. 3); (4) network metrics are estimated for all networks (from randomized groups) in each density; (5) differences in network metrics between randomized groups, in each density, are obtained resulting in a permutation distribution of the difference under the null hypothesis; (6) the real difference between groups in network metrics (for each density) is placed in the corresponding permutation distribution and a p-value of two tails is calculated based on its percentile position. As a critical value, the 95% confidence interval of each network metric distribution is usually considered (two-tailed test of the null hypothesis at $p < 0.05$).

Another form of resampling is by generating bootstrap samples from both networks. Normally statistical inference is based on sampling distributions of sample statistics. The bootstrap method is a way to find the sampling distribution, at least approximately, of a single sample. Therefore, the sample must represent the population from which it was extracted. In our particular case, for each of the two groups (networks), new samples (1000 or more), called bootstrap samples or resamples, are created by sampling with replacement from the original random sample (each resample is the same size as the original sample). Replacement means that after randomly drawing one observation from the original sample, we replace it before drawing the next observation, that results in two randomized groups. From here, the method follows the **steps 2–6** as described above for the permutation test. The main difference between the two procedures is in how the randomized groups are created. It is important to emphasize that in the case of the bootstrap method, the original sample should represent the population at large.

It is also important to control for multiple comparisons when comparing network metrics at the nodal level. Typically, the false discovery rate correction (FDR) procedure is used for this purpose (Benjamini and Hochberg 1995).

8.6 Sparse Inverse Covariance Estimation (SICE)

As discussed earlier, using partial correlation is the preferred method to build the connectivity matrix. The estimation of partial correlations is usually achieved by the maximum likelihood estimation (MLE) of the inverse covariance matrix, but for that estimate to be reliable, the number of subjects must be greater than the number of ROIs. Huang et al. (2010) introduced the idea of analyzing brain metabolic connectivity based on FDG-PET using so-called graphical lasso, in which a constraint imposed on MLE allows for estimation of the inverse covariance matrix even when the number of subjects is less than the number of ROIs (Huang et al. 2010). The connectivity matrix estimated by this approach is binary (1 = connection, 0 = no connection). Instead of the exact value of the nonzero entries in the inverse covariance matrix, this methodology discovers the zero entries (i.e., no connection) by using a regularization parameter (known as λ; not related to the small worldness metric) that controls the zero entries number in the connectivity matrix. The λ parameter controls a trade-off between the likelihood fit of the inverse covariance estimation and matrix sparsity. A small λ will result in a higher likelihood fit of the inverse covariance estimation, while a large λ will result in a sparser estimation (low network density or sparsity). Since whole brain networks tend to be sparse, λ should be relatively high. Hence the name sparse inverse covariance estimation (SICE). λ, however, cannot be too high since it reduces the likelihood fit of the inverse covariance estimation. The determination of λ is a key step when using SICE although there is no gold standard for the selection of this parameter. One proposed λ selection method is Stability Approach to Regularization Selection (StARS) (Liu et al. 2010). This method selects the minimum λ necessary to capture the correct structure of the connectivity matrix and at the same time guarantees a relatively low matrix sparsity (low network density) and replicability under random sampling. An important assumption of SICE analysis is multivariate normality distribution of the data.

Since SICE matrices are also graphs, all previously described network metrics and statistical inference methods are applicable. Nevertheless, the original idea of the analysis of SICE matrices was based on submatrices and their interactions (also applicable to any other type of connectivity matrix). The submatrix based approach involves subdividing the connectivity matrix into smaller submatrices. For example, Huang et al. (Huang et al. 2010) made this subdivision based on 42 ROIs of cerebral regions to be the most affected by Alzheimer disease (AD), as revealed by FDG-PET (Horwitz et al. 1984). These ROIs were then distributed in four submatrices representing ROIs of the frontal, parietal, occipital, and temporal lobes successively (Fig. 8.5). The submatrix based analysis consists of calculating the total number of connections within a submatrix (number of black dots within red squares in Fig. 8.5) and the total number of connections between two submatrices. The total number of connections within a submatrix represents the "short distance" connections, while between two submatrices they represent the "long distance" connections (i.e., the interaction between two submatrices). For instance, in Fig. 8.5, the connections within the temporal lobe are decreased in the matrix representing the AD group

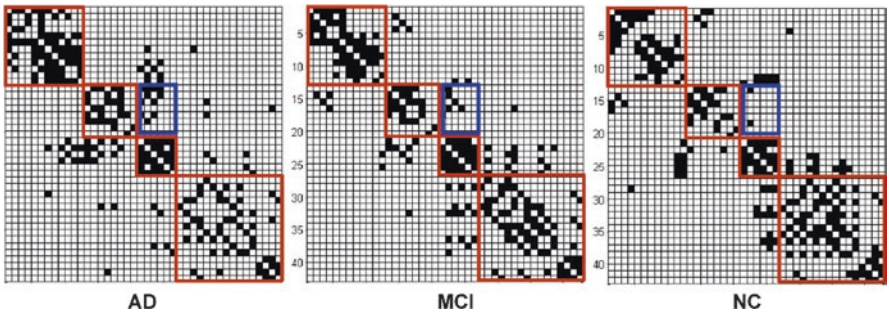

Fig. 8.5 Brain connectivity models using SICE. The figure shows the model for AD dementia, MCI and normal control (NC) subjects. The red squares, from top left to bottom right, represent the ROIs of the frontal, parietal, occipital, and temporal lobes. The blue square represents the interaction between the parietal and occipital lobes. (*Image adapted from Huang et al. (*2010*)*)

compared to the control group, while they are increased between the parietal and occipital lobes (blue squares).

In addition, Huang et al. (2010) showed a monotonous property of SICE, which allowed them to develop a quasi-measure for the strength of functional connections. The monotonous property of SICE states that if two regions of the brain are not connected at a certain λ, they will never be connected as λ becomes larger. Recent articles used this concept (e.g., see (Caminiti et al. 2017; Sala et al. 2017)).

8.7 Example Studies

In this section, findings of selected articles are briefly described to illustrate the concepts explained in previous sections.

8.7.1 Age-Associated Metabolic Network Changes

This example highlights the utility of *characteristic path length* and *average clustering coefficient* (main properties of small-world topology) as well as the *betweenness* centrality. Liu et al. (2014) investigated whether small-world topology of the brain metabolic network changes with aging (Liu et al. 2014). The authors built two brain networks based on FDG-PET using partial correlation: one from healthy young adults (mean age = 36.5 years, 113 individuals) and the other from healthy older adults (mean age = 56.3 years, 110 individuals). The connectivity matrices associated with each group were binarized and the statistical differences were assessed using a non-parametric permutation test in a range of network density (sparsity) between 10% and 50%. They found that networks from both young and old adults showed small-world topologies. However, the *characteristic path length* and the *average clustering coefficient* were increased in the older group compared to the younger group (Figs. 8.6 and 8.7, respectively).

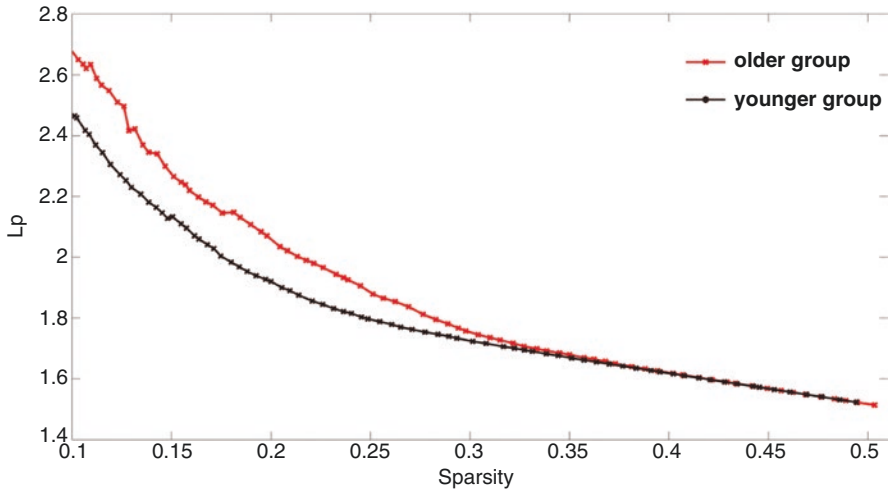

Fig. 8.6 The *characteristic path* length (Lp) as a function of sparsity (S). The graph shows that two groups have same Lp value when sparsity ranges from 33% to 50% and the older group (red line) has larger Lp at 10% < S < 33%. (*Image reproduced from Liu et al. (*2014*)*)

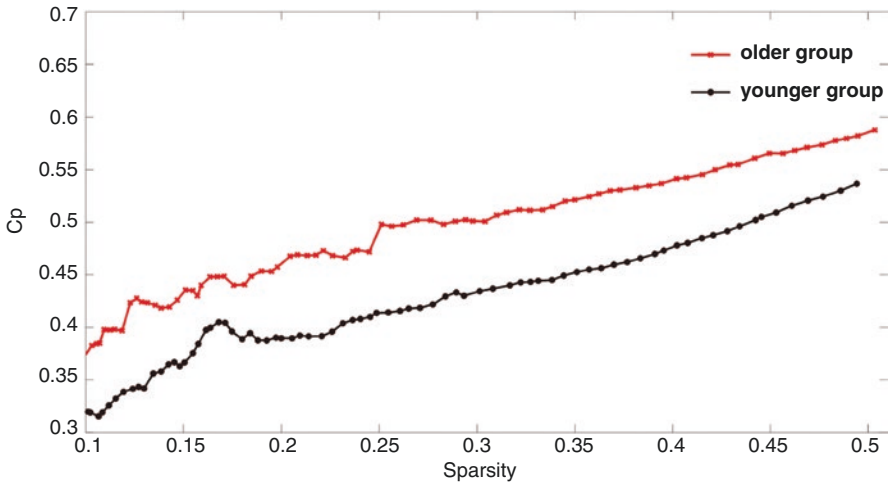

Fig. 8.7 The *average clustering coefficient* (Cp) as a function of sparsity (S). The graph shows that, at a wide range of sparsity (10% < S < 50%), the older subjects (red line) have larger Cp values than the younger subjects (black line). (*Image reproduced from Liu et al. (*2014*)*)

Liu et al. (2014) also analyzed *nodal centrality* using the *betweenness*. They found that the younger group showed higher *betweenness* in the hippocampus and auditory cortex on the left side, and the amygdala and superior frontal gyrus on the right side. In contrast, the older group showed higher *betweenness* in the orbital frontal cortex bilaterally and the right insula (Fig. 8.8).

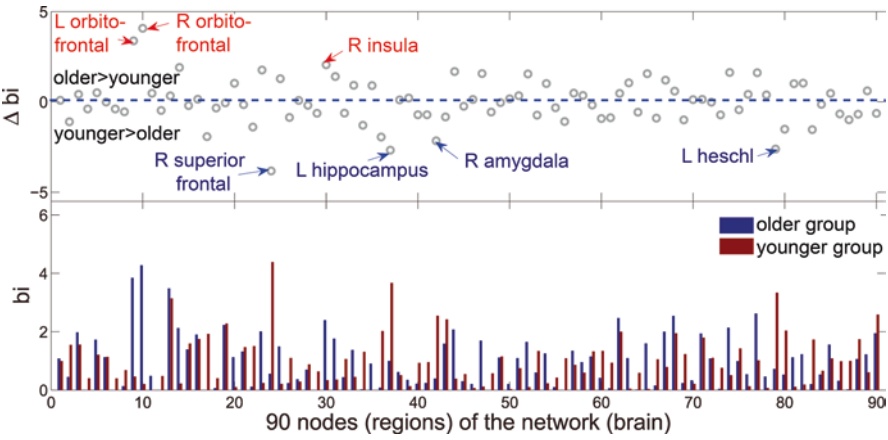

Fig. 8.8 The betweenness centrality (bi) of the two groups. The upper graph shows the regional changes (Δbi, *Δbi = bi_older -bi_younger*) between the two groups. The regions labeled in the upper graph indicate significant bi changes. These results were obtained from a network density of 16%. (*Images adapted from* Liu et al. (2014))

Similar results with respect to the *characteristic path length* have also been found when comparing age-matched controls with patients with mild cognitive impairment (MCI) and AD in network analyses based on FDG-PET (Sanabria-Diaz et al. 2013) and perfusion SPECT (Sanchez-Catasus et al. 2018), in both cases using simple correlation matrices. The increase of the *characteristic path length* was interpreted as a result of loss of brain connectivity due to AD pathology. Findings of these studies suggest that brain changes, whether age-associated or associated with cognitive change, can be adequately captured by network metrics based on FDG-PET and perfusion SPECT. Both age- and cognition-associated brain changes have a perceptible effect on the topology of the brain metabolic network.

8.7.2 Modularity of Amyloid Networks

In this example, we will focus on the utility of modularity analysis. Pereira et al. (2018) analyzed the topology of the amyloid network in non-demented individuals in different stages of Aβ accumulation (Pereira et al. 2018). The authors analyzed three groups of subjects according to Aβ42 levels in the cerebro-spinal fluid (CFS) and Florbetapir β-amyloid PET biomarkers (CSF−/PET−, n = 291; CSF+/PET−, n = 81; and CSF+/PET+, n = 272). PET-based β-amyloid networks were created using partial correlation (Figs. 8.9a, b).

Similar to the previously described study by Liu et al. (2014), they use binary matrices and non-parametric permutation test in a range of network densities between 5% and 15%. They performed a modularity analysis and used several network metrics at the nodal level. Two modules were identified that were present in the three groups (Fig. 8.10). One of these modules comprised several regions that

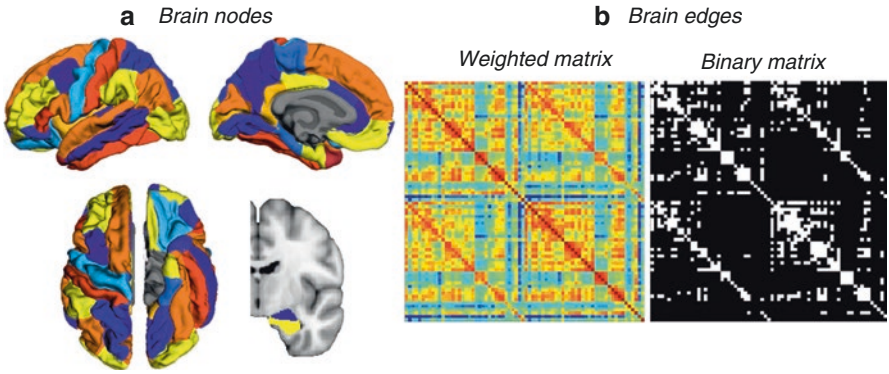

Fig. 8.9 (**a**) Brain parcellation (72 ROIs). (**b**) Weighted and binary matrices (*Image reproduced from Pereira et al. (*2018*)*)

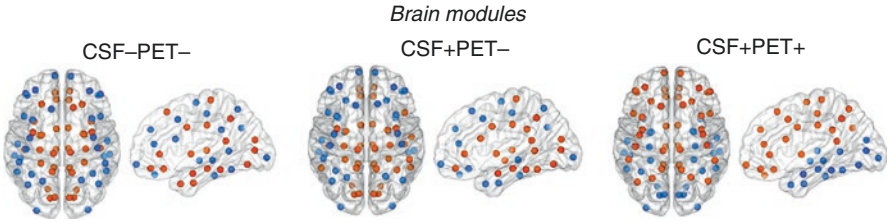

Fig. 8.10 The two modules identified in the three groups studied. The spheres represent the nodes belonging to each module (orange and blue colors). (*Image reproduced from Pereira et al. (*2018*)*)

are part of the default mode network (anterior cingulate, posterior cingulate and precuneus) but also included additional lateral temporal and parietal areas in the CSF + PET− group and lateral frontal in the CSF + PET+ group. These findings are in line with the current pathological knowledge of spread of β-amyloid pathology with progression to AD dementia (Braak and Braak 1991). This suggests that analysis of the topology of the amyloid network could potentially be used to assess disease progression in stages prior to dementia.

8.7.3 Cerebrovascular Reactivity in MCI

This example will highlight the complementary role of network analysis in interpreting univariate analysis results. Sanchez-Catasus et al. (2017) examined cerebrovascular reactivity (CVR) in MCI and healthy conditions by analyzing vasodilator-induced changes in the topology of the CBF network (Sanchez-Catasus et al. 2017). For this purpose, four networks were constructed (based on simple correlation): two using CBF SPECT data at baseline and under the vasodilatory challenge of acetazolamide (ACZ) corresponding to 26 MCI patients and two equivalent networks from 26 matching cognitively normal controls. The strength of association

and the clustering coefficient were used as network metrics (network-wide and nodal). The data were analyzed by a 2 (group: Control and MCI) × 2 (condition: basal and ACZ) design. Simple main effects and their interactions were statistically determined using the bootstrap resampling approach. A 2 × 2 design was also used for voxel-based univariate analysis. In addition, voxel-based univariate analysis of MRI data was carried out. Results showed no significant differences between groups in response to the ACZ challenge by the univariate approach. In contrast, the network analysis showed different patterns of changes in the strength of association and clustering coefficient (network-wise and nodal). However, the most striking finding was the crossover interaction between group and condition found in the network analysis, particularly for the nodal clustering coefficient (Fig. 8.11a). This interaction effect showed a pattern of decrease of the *clustering coefficient* in the MCI group that partially overlapped with the default mode network, which is a target of AD-like neurodegenerative process. Surprisingly, this pattern also partially corresponded with the regional CBF reduction found in the MCI group in the baseline condition (Fig. 8.11b). The overlap increases if the atrophy found by MRI analysis is considered (Fig. 8.11c), suggesting that the functional and structural abnormalities found by the univariate approach in the baseline condition could explain the ACZ-induced changes found by the graph theoretical analysis. In this example, both multivariate and univariate analysis approaches provided complimentary information that led to a more comprehensive understanding of CVR in MCI.

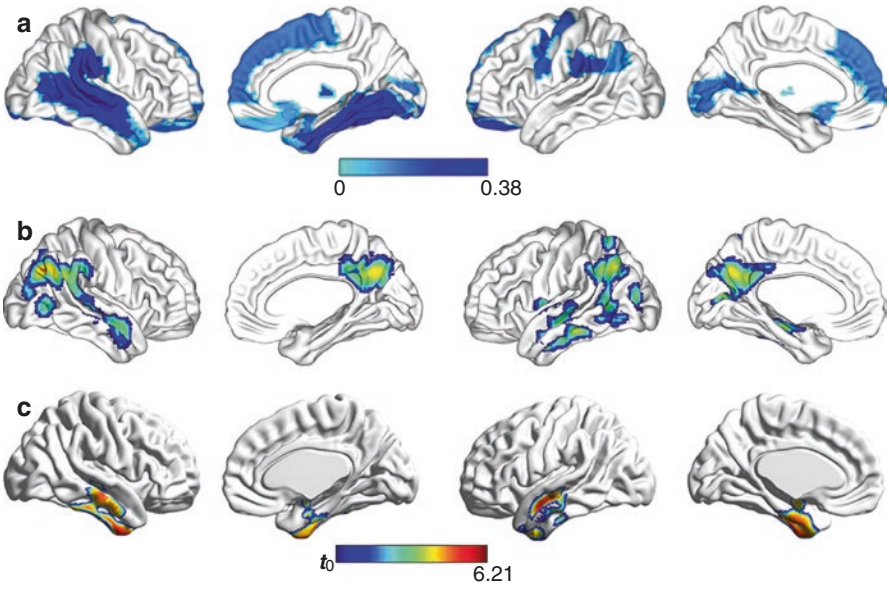

Fig. 8.11 (**a**) Decrease of the clustering coefficient in the MCI group network induced by the vasodilatory challenge (crossover interaction between group and condition); (**b**) hypoperfusion in the MCI group in the baseline condition; and (**c**) atrophy in the MCI group. (*Images adapted from Sanchez-Catasus et al. (2017)*)

8.7.4 SICE Application to Multimodal Neuroimaging

This example will highlight the versatility of SICE analysis. Li et al. (2018) compared networks of patients with AD (n = 116; 64 m/52f) and MCI (n = 116; 64 m/52 f) to networks constructed with normal subjects (n = 116; 62 m/54 f), based on structural MRI, FDG-PET and Florbetapir β-amyloid PET (Li et al. 2018). The authors used the SICE methodology to create connectivity matrices for each group that included the three image modalities. The authors used the same ROIs as Huang et al. (2010), excluding frontal ROIs (see Sect. 6). For illustrative purposes results are only discussed for one of the multimodal connectivity models. The models presented in Fig. 8.12 demonstrate how network connectivity can be applied to a single modality but also the interaction between modalities (e.g., interactions of the β-amyloid network with the metabolic or with a network based on structural brain volumes). The figure shows a gradient of decreasing number of connections (black dots) within modalities from control to MCI and then to AD dementia, while the interaction between modalities gradually increased between these groups. This analysis would be impossible using simple correlation connectivity matrices and the partial correlation option would have required a very large sample of data, with a prohibitive cost in PET studies.

8.8 Final Remarks

The network analysis methods described in this chapter provide a powerful tool for a better understanding of metabolic, perfusion, neurotransmitter, and neuropathological brain changes, particularly in the context of aging and neurodegenerative diseases. These multivariate methods allow for analysis of the neuroimaging data and subsequent results that could be missed when a univariate brain region or even voxel-based whole brain analysis is used. Both approaches, however, are complementary, and simultaneous analysis and interpretation provide a higher level of understanding of brain function than either one alone.

The abundance of metrics that graph analysis of network properties provides allows for a detailed description of network properties. For example, nuclear medicine neuroimaging-based connectivity studies commonly use the main properties of small-world topology, i.e., the characteristic path length and average clustering coefficient (or equivalent network-wide or local metrics). This level of analysis characterizes networks within the spectrum from random to regular (ordered) topologies. Other commonly used graph analysis metrics involve centrality metrics, which allow the identification of hubs, but without distinction between connectors and provincial hubs. We emphasize that modularity analysis is important to take into account, as it offers an integrative analysis of complex network metrics, properly defining, for example, connectors and provincial hubs.

The plethora of graph analysis metrics to choose from poses also a challenge in selecting the appropriate measures. A first consideration to be made in the selection

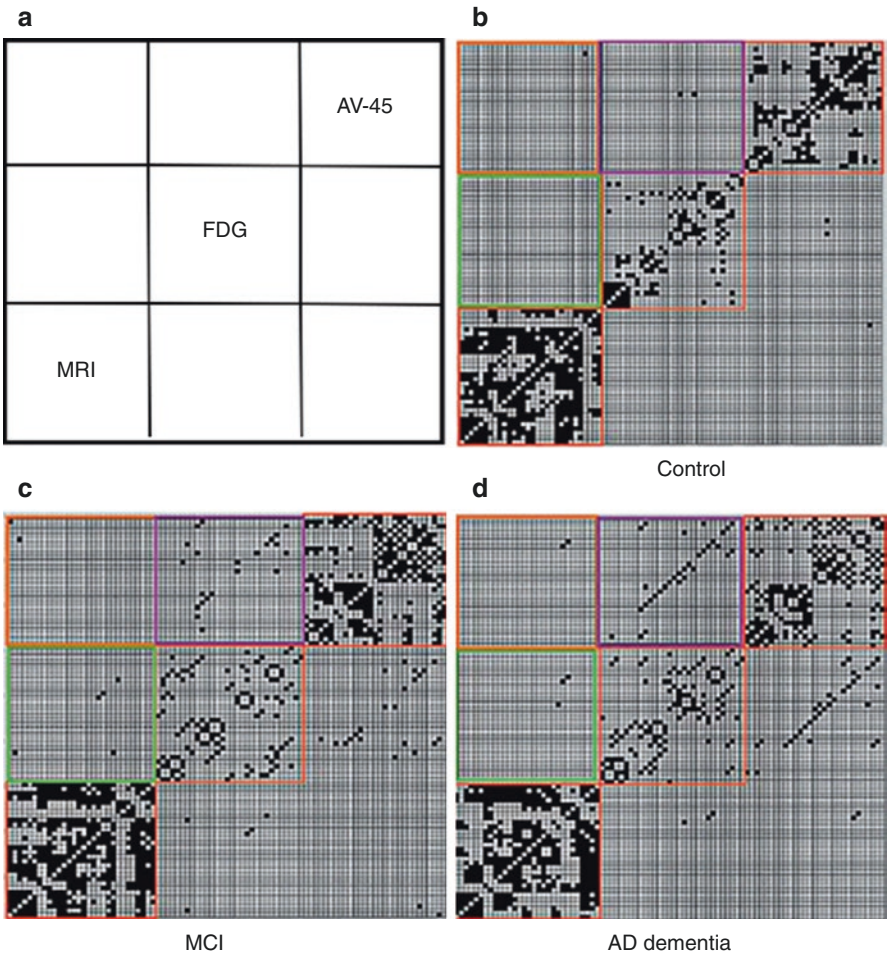

Fig. 8.12 Brain connectivity models using SICE based on multimodal data. (**a**) Matrix indicative of the subdivision into submatrices (30 × 30 ROIs) of the data corresponding to AV-45 (Florbetapir-PET), FDG-PET, and MRI (brain volumes). The figure shows the model for normal control (**b**), MCI (**c**), and AD dementia (**d**). (*Images adapted from Li et al. (*2018*)*)

of one of these two methods is whether complex multivariate approaches are justified or if the specific scientific question can be solved with univariate methodology. A second consideration is to properly select those metrics that will address the a priori scientific hypothesis. A final consideration, which is especially important for nuclear molecular neuroimaging studies, is whether network analysis adequately reflects the underlying biology, for example, known neurotransmitter distribution and/or neuropathology. Network analysis of radiotracers with limited specificity will inherently be noisier. However, this problem exists also in univariate analysis approaches.

The study of brain molecular connectivity using nuclear medicine neuroimaging has gradually matured, but there are many remaining challenges. Solving such challenges will offer new opportunities to expand our knowledge of molecular brain networks. A multimodal approach using complementary network information from both MRI and nuclear molecular imaging will ultimately provide a more comprehensive insight into brain network functioning. PET and SPECT brain network analysis tools are now able to overcome limitations of standard univariate approach in neuro-nuclear medicine. We anticipate that molecular brain network analysis may become part of clinical nuclear medicine practice in the near future.

A Lexicon of the Most Commonly Used Network Metrics

- ***Shortest path:*** Topological distance between two nodes, also called *Length,* as the minimum number of edges between two nodes.
- ***Path length:*** Shortest path of a given node to each of the other nodes.
- ***Characteristic path length:*** Average path length node across all nodes.
- ***Global efficiency:*** Average of the inverse shortest path from a given node to all other nodes. At the network level, it is the average of the global efficiency of all nodes.
- ***Triad:*** Formed when a node is connected to any two connected neighbors.
- ***Clustering coefficient:*** The ratio between the number of triads present around a node and the maximum number of triads that could be formed around that node. At the network level, it is the average of the clustering coefficient of all nodes.
- ***Local efficiency (nodal level):*** The global efficiency calculated on the subgraph created by the node's neighbors. At the network level, it is the average of the local efficiency of all nodes.
- ***Modularity***: The extent to which a network can be subdivided into modules (communities of nodes) with a maximal within-module and minimal between-module connectivity.
- ***The small-worldness (σ):*** The extent to which a network shows an optimal balance between *characteristic path length* (integration) and *average clustering coefficient* (segregation).
- ***Degree*****:** The number of direct connections that a node has with other nodes. At the network level, it is the average of the degrees of all nodes.
- ***Strength:*** The sum of the weights of all edges connected to a node. At the network level, it is the average of the strength of all nodes.
- ***Closeness centrality:*** The same as the global efficiency at the nodal level.
- ***Betweenness centrality:*** The ratio between all shortest paths that pass through the node and all shortest paths in the graph.
- ***Participation coefficient:*** The ratio between the number of connections that the node has outside its module (intermodular) and the total number of connections in the whole network.
- ***Within-module degree z-score:*** The nodal degree but restricted to only connections inside the module to which that node belongs.

References

Anticevic A, Cole MW, Murray JD, Corlett PR, Wang XJ, Krystal JH (2012) The role of default network deactivation in cognition and disease. Trends Cogn Sci 16(12):584–592

Bassett DS, Bullmore ET (2017) Small-world brain networks revisited. Neuroscientist 23(5):499–516

Batalle D, Munoz-Moreno E, Figueras F, Bargallo N, Eixarch E, Gratacos E (2013) Normalization of similarity-based individual brain networks from gray matter MRI and its association with neurodevelopment in infants with intrauterine growth restriction. NeuroImage 83:901–911

Benjamini Y, Hochberg Y (1995) Controlling the false discovery rate: a practical and powerful approach to multiple testing. J R Stat Soc Series B 1:289–300

Biggs N, Lloyd E, Wilson R (1986) Graph theory. Oxford University Press, Oxford, pp 1736–1936

Braak H, Braak E (1991) Neuropathological stageing of Alzheimer-related changes. Acta Neuropathol 82(4):239–259

Bullmore E, Sporns O (2009) Complex brain networks: graph theoretical analysis of structural and functional systems. Nat Rev Neurosci 10(3):186–198

Bullmore E, Sporns O (2012) The economy of brain network organization. Nat Rev Neurosci 13(5):336–349

Caminiti SP, Tettamanti M, Sala A, Presotto L, Iannaccone S, Cappa SF et al (2017) Metabolic connectomics targeting brain pathology in dementia with Lewy bodies. J Cereb Blood Flow Metab 37(4):1311–1325

Clark CM, Stoessl AJ (1986) Glucose use correlations: a matter of inference. J Cereb Blood Flow Metab 6(4):511–512

David O, Guillemain I, Saillet S, Reyt S, Deransart C, Segebarth C et al (2008) Identifying neural drivers with functional MRI: an electrophysiological validation. PLoS Biol 6(12):2683–2697

Eidelberg D, Moeller JR, Dhawan V, Spetsieris P, Takikawa S, Ishikawa T et al (1994) The metabolic topography of parkinsonism. J Cereb Blood Flow Metab 14(5):783–801

Fornito A, Bullmore ET (2015) Connectomics: a new paradigm for understanding brain disease. Eur Neuropsychopharmacol 25(5):733–748

Fornito A, Zalesky A, Breakspear M (2013) Graph analysis of the human connectome: promise, progress, and pitfalls. NeuroImage 80:426–444

Friston KJ (2011) Functional and effective connectivity: a review. Brain Connect 1(1):13–36

Garcia JO, Ashourvan A, Muldoon SF, Vettel JM, Bassett DS (2018) Applications of community detection techniques to brain graphs: algorithmic considerations and implications for neural function. Proc IEEE Inst Electr Electron Eng 106(5):846–867

Gu SC, Ye Q, Yuan CX (2019) Metabolic pattern analysis of 18F-FDG PET as a marker for Parkinson's disease: a systematic review and meta-analysis. Rev Neurosci

Hahn A, Lanzenberger R, Kasper S (2019) Making sense of connectivity. Int J Neuropsychopharmacol 22(3):194–207

Honey CJ, Thivierge JP, Sporns O (2010) Can structure predict function in the human brain? NeuroImage 52(3):766–776

Horwitz B, Duara R, Rapoport SI (1984) Intercorrelations of glucose metabolic rates between brain regions: application to healthy males in a state of reduced sensory input. J Cereb Blood Flow Metab 4(4):484–499

Horwitz B, Grady CL, Schlageter NL, Duara R, Rapoport SI (1987) Intercorrelations of regional cerebral glucose metabolic rates in Alzheimer's disease. Brain Res 407(2):294–306

Hosseini SM, Hoeft F, Kesler SR (2012) GAT: a graph-theoretical analysis toolbox for analyzing between-group differences in large-scale structural and functional brain networks. PLoS One 7(7):e40709

Huang S, Li J, Sun L, Ye J, Fleisher A, Wu T et al (2010) Learning brain connectivity of Alzheimer's disease by sparse inverse covariance estimation. NeuroImage 50(3):935–949

Koch MA, Norris DG, Hund-Georgiadis M (2002) An investigation of functional and anatomical connectivity using magnetic resonance imaging. NeuroImage 16(1):241–250

Lee DS, Kang H, Kim H, Park H, Oh JS, Lee JS et al (2008) Metabolic connectivity by interregional correlation analysis using statistical parametric mapping (SPM) and FDG brain PET; methodological development and patterns of metabolic connectivity in adults. Eur J Nucl Med Mol Imaging 35(9):1681–1691

Li Q, Wu X, Xie F, Chen K, Yao L, Zhang J et al (2018) Aberrant connectivity in mild cognitive impairment and Alzheimer disease revealed by multimodal neuroimaging data. Neurodegener Dis 18(1):5–18

Liu H, Roeder K, Wasserman L (2010) Stability approach to regularization selection (StARS) for high dimensional graphical models. Adv Neural Inf Process Syst 24:1432–1440

Liu Z, Ke L, Liu H, Huang W, Hu Z (2014) Changes in topological organization of functional PET brain network with normal aging. PLoS One 9(2):e88690

Manzanera OM, Meles SK, Leenders KL, Renken RJ, Pagani M, Arnaldi D et al (2019) Scaled subprofile modeling and convolutional neural networks for the identification of Parkinson's disease in 3D nuclear imaging data. Int J Neural Syst 1950010

Melie-García L, Sanabria-Diaz G, Iturria-Medina Y, Alemán-Gómez Y (2010) MorphoConnect: toolbox for studying structural brain networks using morphometric descriptors. In: 16th annual meeting of the Organization for Human Brain Mapping. Human Brain Mapping (HBM), Barcelona

Melie-Garcia L, Sanabria-Diaz G, Sanchez-Catasus C (2013) Studying the topological organization of the cerebral blood flow fluctuations in resting state. NeuroImage 64:173–184

Metter EJ, Riege WH, Kuhl DE, Phelps ME (1984) Cerebral metabolic relationships for selected brain regions in healthy adults. J Cereb Blood Flow Metab 4(1):1–7

Mijalkov M, Kakaei E, Pereira JB, Westman E, Volpe G (2017) BRAPH: a graph theory software for the analysis of brain connectivity. PLoS One 12(8):e0178798

Mišić B, Betzel RF, de Reus MA, van den Heuvel MP, Berman MG, McIntosh AR et al (2016) Network-level structure-function relationships in human neocortex. Cereb Cortex 26(7):3285–3296

Moeller JR, Strother SC, Sidtis JJ, Rottenberg DA (1987) Scaled subprofile model: a statistical approach to the analysis of functional patterns in positron emission tomographic data. J Cereb Blood Flow Metab 7(5):649–658

Monakow C (1914) Die Lokalisation im Grosshirn und der Abbau der Funktion durch Kortikale Herde. J. F. Bergman, Wiesbaden, pp 26–34

Murphy K, Fox MD (2017) Towards a consensus regarding global signal regression for resting state functional connectivity MRI. NeuroImage 154:169–173

Murphy K, Birn RM, Handwerker DA, Jones TB, Bandettini PA (2009) The impact of global signal regression on resting state correlations: are anti-correlated networks introduced? NeuroImage 44(3):893–905

Passow S, Specht K, Adamsen TC, Biermann M, Brekke N, Craven AR et al (2015) Default-mode network functional connectivity is closely related to metabolic activity. Hum Brain Mapp 36(6):2027–2038

Pereira JB, Strandberg TO, Palmqvist S, Volpe G, van Westen D, Westman E et al (2018) Amyloid network topology characterizes the progression of Alzheimer's disease during the Predementia stages. Cereb Cortex 28(1):340–349

Power JD, Schlaggar BL, Lessov-Schlaggar CN, Petersen SE (2013) Evidence for hubs in human functional brain networks. Neuron 79(4):798–813

Raj A, Mueller SG, Young K, Laxer KD, Weiner M (2010) Network-level analysis of cortical thickness of the epileptic brain. NeuroImage 52(4):1302–1313

Riedl V, Utz L, Castrillón G, Grimmer T, Rauschecker JP, Ploner M et al (2016) Metabolic connectivity mapping reveals effective connectivity in the resting human brain. Proc Natl Acad Sci U S A 113(2):428–433

Rubinov M, Sporns O (2010) Complex network measures of brain connectivity: uses and interpretations. NeuroImage 52(3):1059–1069

Saad ZS, Gotts SJ, Murphy K, Chen G, Jo HJ, Martin A et al (2012) Trouble at rest: how correlation patterns and group differences become distorted after global signal regression. Brain Connect 2(1):25–32

Saggar M, Hosseini SM, Bruno JL, Quintin EM, Raman MM, Kesler SR et al (2015) Estimating individual contribution from group-based structural correlation networks. NeuroImage 120:274–284

Sala A, Perani D (2019) Brain molecular connectivity in neurodegenerative diseases: recent advances and new perspectives using positron emission tomography. Front Neurosci 13:617

Sala A, Caminiti SP, Presotto L, Premi E, Pilotto A, Turrone R et al (2017) Altered brain metabolic connectivity at multiscale level in early Parkinson's disease. Sci Rep 7(1):4256

Sanabria-Diaz G, Martinez-Montes E, Melie-Garcia L (2013) Glucose metabolism during resting state reveals abnormal brain networks organization in the Alzheimer's disease and mild cognitive impairment. PLoS One 8(7):e68860

Sanchez-Catasus CA, Sanabria-Diaz G, Willemsen A, Martinez-Montes E, Samper-Noa J, Aguila-Ruiz A et al (2017) Subtle alterations in cerebrovascular reactivity in mild cognitive impairment detected by graph theoretical analysis and not by the standard approach. Neuroimage Clin 15:151–160

Sanchez-Catasus CA, Willemsen A, Boellaard R, Juarez-Orozco LE, Samper-Noa J, Aguila-Ruiz A et al (2018) Episodic memory in mild cognitive impairment inversely correlates with the global modularity of the cerebral blood flow network. Psychiatry Res Neuroimaging 282:73–81

Sepulcre J, Sabuncu MR, Becker A, Sperling R, Johnson KA (2013) In vivo characterization of the early states of the amyloid-beta network. Brain 136(Pt 7):2239–2252

Skudlarski P, Jagannathan K, Calhoun VD, Hampson M, Skudlarska BA, Pearlson G (2008) Measuring brain connectivity: diffusion tensor imaging validates resting state temporal correlations. NeuroImage 43(3):554–561

Sporns O, Tononi G, Kötter R (2005) The human connectome: a structural description of the human brain. PLoS Comput Biol 1(4):e42

Tijms BM, Series P, Willshaw DJ, Lawrie SM (2012) Similarity-based extraction of individual networks from gray matter MRI scans. Cereb Cortex 22(7):1530–1541

Titov D, Diehl-Schmid J, Shi K, Perneczky R, Zou N, Grimmer T et al (2017) Metabolic connectivity for differential diagnosis of dementing disorders. J Cereb Blood Flow Metab 37(1):252–262

Tomasi DG, Shokri-Kojori E, Wiers CE, Kim SW, Demiral SB, Cabrera EA et al (2017) Dynamic brain glucose metabolism identifies anti-correlated cortical-cerebellar networks at rest. J Cereb Blood Flow Metab 37(12):3659–3670

Tzourio-Mazoyer N, Landeau B, Papathanassiou D, Crivello F, Etard O, Delcroix N et al (2002) Automated anatomical labeling of activations in SPM using a macroscopic anatomical parcellation of the MNI MRI single-subject brain. NeuroImage 15(1):273–289

Veronese M, Moro L, Arcolin M, Dipasquale O, Rizzo G, Expert P et al (2019) Covariance statistics and network analysis of brain PET imaging studies. Sci Rep 9(1):2496

Watts DJ, Strogatz SH (1998) Collective dynamics of 'small-world' networks. Nature 393(6684):440–442

Yakushev I, Drzezga A, Habeck C (2017) Metabolic connectivity: methods and applications. Curr Opin Neurol 30(6):677–685

Zhou L, Wang Y, Li Y, Yap PT, Shen D (2011) Hierarchical anatomical brain networks for MCI prediction: revisiting volumetric measures. PLoS One 6(7):e21935

Part II

Dementia

PET Neuroimaging in Dementia Conditions

9

Daniela Perani, Silvia Paola Caminiti, Giulia Carli, and Giacomo Tondo

Contents

9.1 Introduction 213
9.2 [18F]FDG-PET: A Marker of Neurodegeneration 218
9.2.1 Evidence in AD Spectrum 219
9.2.2 Evidence in FTLD Spectrum 222
9.2.3 Evidence in α-Synuclein Spectrum 226
9.2.4 Evidence in Prion Diseases Spectrum 227
9.2.5 Strengths 229
9.2.6 Weaknesses 231
9.3 PET Markers of Amyloidosis 231
9.3.1 Evidence in AD Spectrum 232
9.3.2 Evidence in FTLD Spectrum 233
9.3.3 Evidence in α-Synuclein Spectrum 235
9.3.4 Strengths 236
9.3.5 Weaknesses 236
9.4 PET Markers of Tauopathy 238
9.4.1 Evidence in AD Spectrum 239
9.4.2 Evidence in FTLD Spectrum 241
9.4.3 Evidence in α-Synuclein Spectrum 243
9.4.4 Strengths 243

D. Perani (✉)
Vita-Salute San Raffaele University, Milan, Italy

In vivo human molecular and structural neuroimaging Unit, Division of Neuroscience, IRCCS San Raffaele Scientific Institute, Milan, Italy

Nuclear Medicine Unit, San Raffaele Hospital, Milan, Italy
e-mail: perani.daniela@hsr.it

S. P. Caminiti · G. Carli · G. Tondo
Vita-Salute San Raffaele University, Milan, Italy

In vivo human molecular and structural neuroimaging Unit, Division of Neuroscience, IRCCS San Raffaele Scientific Institute, Milan, Italy
e-mail: caminiti.silviapaola@hsr.it; carli.giulia@hsr.it; tondo.giacomo@hsr.it

R. A. J. O. Dierckx et al. (eds.), *PET and SPECT in Neurology*,
https://doi.org/10.1007/978-3-030-53168-3_9

9.4.5 Weaknesses..... 244
9.5 PET Markers of Neuroinflammation..... 244
9.5.1 Evidence in AD Spectrum..... 247
9.5.2 Evidence in FTLD Spectrum..... 249
9.5.3 Evidence in α-Synuclein Spectrum..... 250
9.5.4 Evidence in Prion Diseases Spectrum..... 251
9.5.5 Strengths..... 252
9.5.6 Weaknesses..... 252
9.6 Relationships Amongst Amyloid, Tau, Neurodegeneration and Neuroinflammation Biomarkers..... 254
9.7 PET Imaging: New Frontiers in Dementia..... 256
9.8 Conclusion..... 257
References..... 258

Abstract

In neurodegenerative diseases, several studies have increasingly highlighted that the same neuropathology can trigger different clinical phenotypes or, vice versa, that similar clinical phenotypes can be triggered by different underlying neuropathologies. This evidence called for the adoption of a pathology spectrum-based approach. Conditions belonging to the same or different spectrum of diseases share brain deposition of abnormal protein aggregates, which lead to aberrant biochemical, metabolic, functional and structural changes. Positron emission tomography (PET) is a well-recognized and unique tool for the *in vivo* assessment of brain metabolism, molecular changes and protein load, and novel PET techniques are emerging for the study of specific protein alterations. The availability of PET neuroimaging tools for the assessment of brain function, molecular biology and neuropathology has opened new venues in research, in diagnostic design and in the conduction of new clinical trials. Appropriate use of PET tools is crucial in supporting a prompt diagnosis and in evaluating drug targets aiming to slow down or prevent dementia. This chapter critically reviews the role of distinct PET molecular tracers (i.e. neurodegeneration, amyloid, tau and neuroinflammation) in different neurodegenerative spectrum of diseases, highlighting their strengths and weaknesses, with special emphasis on methodological challenges and future applications.

Abbreviations

[^{11}C]PiB	Carbon-11-labelled Pittsburgh Compound B
[^{18}F]FDG	Fluorine-18-fluorodeoxyglucose
AD	Alzheimer's disease
ALS	Amyotrophic lateral sclerosis
Aβ	Amyloid beta
bvFTD	Behavioural variant of frontotemporal dementia
CBD	Corticobasal degeneration
CBS	Corticobasal syndrome

CJD	Creutzfeldt–Jakob disease
CSF	Cerebral spinal fluid
DAT	Dopamine transporter
DED	Deuterium-L-deprenyl
DLB	Dementia with Lewy bodies
EOAD	Early-onset AD
fAD	Frontal variant of AD
FFI	Fatal familial insomnia
FTD	Frontotemporal dementia
FTLD	Frontotemporal lobar degeneration
FUS	Fused in sarcoma protein
GSS	Gerstmann–Sträussler syndrome
LOAD	Late-onset AD
lvAD	Logopenic variant of AD
lvPPA	Logopenic variant of primary progressive aphasia
MAO	Monoamine oxidase
MAPT	Microtubule-associated protein tau
MCI	Mild cognitive impairment
MRI	Magnetic resonance imaging
MSA	Multiple system atrophy
MSA-c	MSA-cerebellar
MSA-p	MSA-parkinsonian
PCA	Posterior cortical atrophy
PD	Parkinson's disease
PDD	Parkinson's disease with dementia
PET	Positron emission tomography
PGRN	Progranulin
PNFA	Progressive non-fluent aphasia variant
PPA	Primary progressive aphasia
PSP	Progressive supranuclear palsy
SD	Semantic dementia
SPECT	Single-photon emission tomography
SPM	Statistical parametric mapping
SUVrs	Standardized uptake value ratios
SV2A	Synaptic vesicle glycoprotein 2A
tAD	Typical AD
TDP-43	TAR DNA binding protein 43
TPSO	Translocator specific protein

9.1 Introduction

Dementia encompasses a wide range of disorders which are often difficult to diagnose with high accuracy. Dementia disorders can be classified by *in vivo* biomarkers, according to their underlying pathology, including amyloid beta peptide (Aβ), tau and α-synuclein, which can support clinical diagnosis. Alzheimer's disease

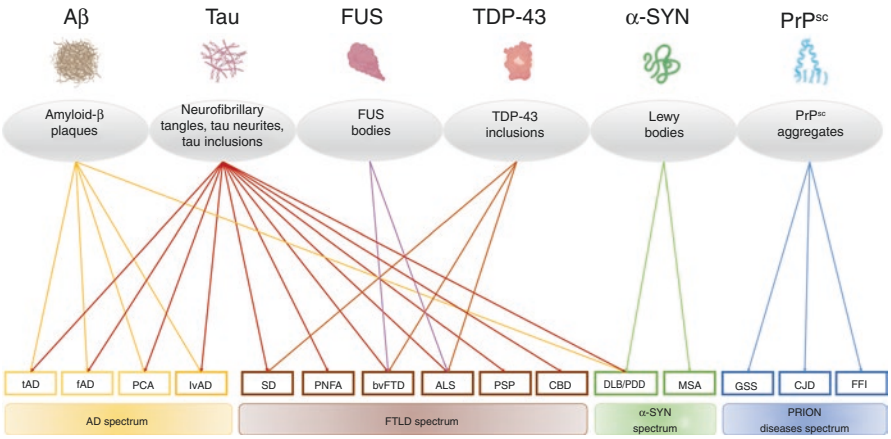

Fig. 9.1 Clinical and pathological spectrum associated with misfolded proteins in dementia conditions. The figure shows a scheme of the different spectra presented in this chapter. Several neurodegenerative diseases are associated with a misfolded and aggregated protein; hence, the term "proteinopathies" has been coined to emphasize the biological characterization of these disorders. Each spectrum includes diseases characterized by common features but also clinical variabilities. The same misfolded protein can be associated with different clinical phenotypes and the same clinical phenotype may be the result of deposition of different misfolded proteins. *Aβ* amyloid beta, *FUS* fused in sarcoma, *TDP-43* TAR DNA binding protein 43, *PrP*^{sc} scrapie prion protein, *AD* Alzheimer's disease, *tAD* typical AD, *fAD* frontal variant AD, *PCA* posterior cortical atrophy, *lvAD* logopenic variant AD, *FTLD* frontotemporal lobar degeneration, *SD* semantic dementia, *PNFA* primary progressive non-fluent aphasia, *bvFTD* behavioural variant of frontotemporal dementia, *ALS* amyotrophic lateral sclerosis, *PSP* progressive supranuclear palsy, *CBD* corticobasal degeneration, *α-SYN* α-synucleinopathy, *DLB* dementia with Lewy bodies, *PDD* Parkinson's disease dementia, *MSA* multiple system atrophy, *GSS* Gerstmann–Sträussler–Scheinker disease, *CJD* Creutzfeldt–Jakob disease, *FFI* fatal familial insomnia

(AD) is the leading cause of neurodegenerative dementia (Nichols et al. 2019), and it is pathologically characterized by extracellular amyloid plaques composed of Aβ and intracellular neurofibrillary tangles composed of hyperphosphorylated tau protein (Fig. 9.1) (Hardy 2006). The commonest clinical presentation of AD is an insidious cognitive decline which involves primarily episodic memory, progressively manifesting with visuospatial difficulties and executive and behavioural disturbances, interfering with activities of daily living (McKhann et al. 2011). Three atypical (non-memory) clinical syndromes are also recognized, especially in young-onset patients: posterior cortical atrophy (PCA), characterized by prominent visuospatial and visuo-perceptual difficulties and dyspraxia; logopenic variant (lvAD), clinically characterized by difficulties in word finding, anomia and impairments in working memory; and the frontal variant of AD (fAD), with severe behavioural disturbances (Dubois et al. 2014). In addition, a 65 years age cut-off has been proposed to distinguish the most common late-onset AD (LOAD) from the early-onset AD (EOAD), which is characterized by a fast disease progression and frequent atypical onset (Balasa et al. 2011).

Frontotemporal lobe degeneration (FTLD) encompasses variable neuropathology, including different neuronal inclusions composed by both 3R and 4R tau isoforms, TAR DNA binding protein 43 (TDP-43) and fused in sarcoma protein (FUS) (Fig. 9.1) (Mackenzie and Neumann 2016; Hu et al. 2007). Clinically, FTLD is an umbrella term which indicates a group of syndromes characterized by a progressive deterioration in behaviour, executive function, motor performances or language abilities and constituting the most frequent cause of dementia in the population younger than 65 years (Bang et al. 2015). Clinically, different major subtypes are recognized: the behavioural variant of frontotemporal dementia (bvFTD), a dysexecutive syndrome associated with behavioural disturbances and mood disorders; the progressive non-fluent aphasia variant (PNFA), usually progressing to bvFTD, progressive supranuclear palsy (PSP) or corticobasal degeneration (CBD) and presenting with a language disorder with non-fluent spontaneous speech, agrammatism and phonemic errors; and the semantic dementia (SD), characterized by problems in recognizing and understanding words, often associated with changes in personality and behaviour (Neary et al. 1998). As neurodegenerative disorders primarily involving language, PNFA and semantic aphasia are gathered together into the clinical group termed primary progressive aphasia (PPA), which includes also the logopenic variant (lv)PPA (Gorno-Tempini et al. 2011). The clinical progression of PPA may vary from a stable cognitive profile to a progressive deterioration leading to dementia, which can involve executive functions, memory, motor abilities and reasoning, while the designation of PPA-plus has been suggested to indicate a disease started as PPA and then progressed into a complex neurodegenerative disorder (Mesulam et al. 2014).

FTLD spectrum comprises also the so-called frontotemporal dementia (FTD)-related disorders, PSP and CBD (Olney et al. 2017), which are associated with intraneuronal and astrocytic aggregates of tau. The typical PSP clinical presentation includes progressive loss of balance with falls, vertical gaze palsy and problems with speech and swallowing (Ling 2016). CBD commonly manifests with asymmetric parkinsonism, dystonia, myoclonus and cognitive decline (Armstrong et al. 2013). PSP and CBD, however, share common pathology and clinical features, and overlap may exist (Ling 2016). Up to 15% of FTD patients develop amyotrophic lateral sclerosis (ALS), falling into the clinical syndrome termed FTD/ALS, in which behavioural and executive disturbance are associated with muscle weakness, fasciculations, spastic tone, hyperreflexia, dysarthria, dysphagia and respiratory failure (Olney et al. 2017).

Abnormal accumulation of α-synuclein is the pathological key feature of the group of neurodegenerative disorders within the α-synuclein spectrum, including Parkinson's disease (PD), PD with dementia (PDD), dementia with Lewy bodies (DLB) and multiple system atrophy (MSA). In PD, α-synuclein deposition generates the intracellular Lewy bodies, which mainly affect dopaminergic pathways (neurons and axons), while in PDD and in DLB, Lewy bodies are also widely distributed into the cortical areas (Goedert 2001). In MSA pathology, α-synuclein aggregates affect primarily oligodendrocytes, and the distribution involves several subcortical and cortical regions (McCann et al. 2014). In

addition, histopathological evidence suggests that α-synuclein often coexists with Aβ plaques and tau neurofibrillary tangles (Fig. 9.1) (Compta et al. 2014; Horvath et al. 2013). Within α-synuclein spectrum, the different diseases are clinically well characterized; common clinical features include motor impairments and several non-motor manifestations, namely, neuropsychiatric symptoms, visuospatial and executive deficits and dysautonomia (Barker and Williams-Gray 2016).

Prion diseases are a rare group of neurodegenerative conditions characterized by the abnormal accumulation of misfolded prion protein that includes syndromes, such as Gerstmann–Sträussler syndrome (GSS), Creutzfeldt–Jakob disease (CJD) and fatal familial insomnia (FFI) (Takada and Geschwind 2013) (Fig. 9.1). While prion diseases share with the proteinopathies a detrimental accumulation of misfolded proteins, they are commonly considered as different brain neurodegenerations since they are characterized by the tumultuous development of dementia with a rapid and inexorable course (Colby and Prusiner 2011).

In clinical practice, patients with different dementias may show substantial overlap, which hinders clinical decision-making. The last decades have progressively witnessed a shift from a purely clinical diagnosis to a biomarker-supported diagnosis, and molecular neuroimaging techniques such as positron emission tomography (PET) have played a leading role in the dementia research diagnostic workup (McKhann et al. 2011; Gorno-Tempini et al. 2011; Armstrong et al. 2013; Albert et al. 2011; Rascovsky et al. 2011; Sperling et al. 2011). In the past, the limited availability and high cost of PET scanning made it possible to defend the use of single-photon emission tomography (SPECT) imaging in the differential diagnosis of neurodegenerative disorders (Laforce Jr et al. 2018). The diagnostic performance of PET is higher than SPECT, and, nowadays, PET applications are significantly more widely available and affordable (Laforce Jr et al. 2018). For these reasons, PET has become the instrument of choice in nuclear medicine practice for the assessment of brain functional and molecular changes in cognitive disorders (O'Brien et al. 2014; Morinaga et al. 2010). Within this framework, PET-based neuroimaging by using adequate radiotracers plays a leading role in *in vivo* assessment of neurodegeneration, brain deposition of abnormal protein species and presence of neuroinflammatory responses, as well as many other biochemical and molecular changes (Perani et al. 2019). PET techniques are also crucial to disentangle the relationship between underlying neuropathology, brain dysfunction and clinical phenotypes. In this regard much is expected from combining brain metabolism, Aβ and tau imaging studies (Villemagne et al. 2018). Such endeavours should help in confirming whether the presence or concentration of Aβ triggers and/or accelerates the spread of tau deposition (Villemagne et al. 2017). These pathophysiological processes indeed can further be correlated with neurodegeneration, as measured with flourine-18-fluorodeoxyglucose ([^{18}F]FDG)-PET, and cognitive impairments. Given the complexity of neuropathological processes, it is very likely that future therapeutic approaches will necessitate a combined brain neuroimaging assessment.

PET techniques have provided major advances, promoting novel approaches to support an early and differential dementia diagnosis. Accurate ad hoc measures of PET images are mandatory, allowing the detection of also very subtle, but significant brain functional and pathological changes, even before the onset of clinical symptoms. Of note, several studies demonstrated that PET techniques fully show their diagnostic and prognostic value especially when appropriate quantitative or parametric methods are applied (Frisoni et al. 2013; Sokoloff 1981; Caroli et al. 2012; Perani et al. 2014). This is crucial for early interventions, personalized care planning and subject inclusion in clinical trials (Perani 2014; Iaccarino et al. 2019). These cardinal issues include timing and protocol of acquisition, parametric modelling and estimation, large normal database for statistical comparison and, in some cases, the critical definition of the reference region to be used for semi-quantification.

Here, we review the most recent evidence, advances, strengths and weaknesses of the four leading PET tools in the dementia research field, namely, the assessment of brain metabolism, amyloid and tau burden and neuroinflammation (for a schematic summary, see Fig. 9.2). The progressive implementation of these techniques, together with the standardization of appropriate analysis methodologies, will allow

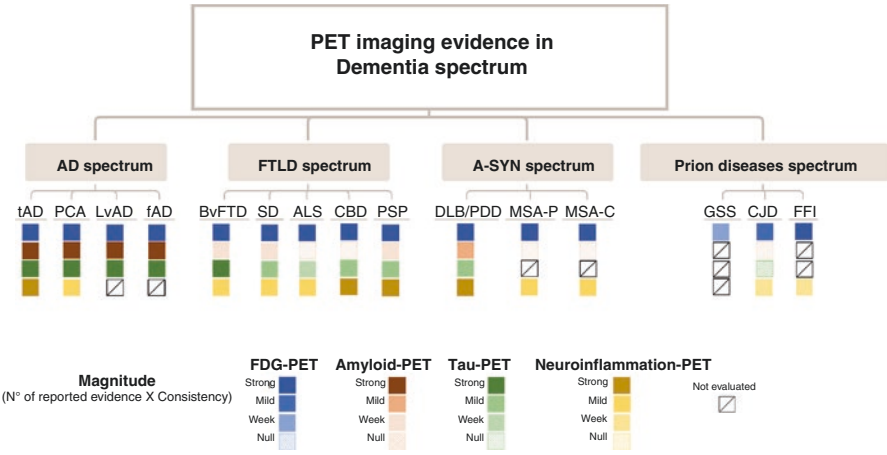

Fig. 9.2 PET neuroimaging evidence in dementia spectra. Graphical representation of the reviewed literature on neurodegeneration-, amyloid-, tau- and neuroinflammation-PET findings in dementia spectra. Colour gradients index magnitude of alteration, namely, the combination of number of reported evidence and consistency. *AD* Alzheimer's disease, *tAD* typical AD, *fAD* frontal AD, *PCA* posterior cortical atrophy, *lvAD* logopenic variant of AD, *FTLD* frontotemporal lobar degeneration, *bvFTD* behavioural variant of frontotemporal dementia, *SD* semantic dementia, *ALS* amyotrophic lateral sclerosis, *PSP* progressive supranuclear palsy, *CBD* corticobasal degeneration, *α-SYN* α-synucleinopathy, *DLB* dementia with Lewy bodies, *PDD* Parkinson's disease dementia, *MSA-P* parkinsonian type of multiple system atrophy, *MSA-c* cerebellar type MSA, *GSS* Gerstmann–Sträussler–Scheinker disease, *CJD* Creutzfeldt–Jakob disease, *FFI* fatal familial insomnia

unique breakthroughs in the study of neurodegenerative conditions and will have remarkable implications for diagnostic and prognostic algorithms and therapy monitoring.

9.2 [18F]FDG-PET: A Marker of Neurodegeneration

The large amount of data concerning the exploration of metabolic mechanism underlying [18F]FDG-PET lead to well determine its fundamentals (Perani 2014). The [18F]FDG-PET signal reflects astrocyte/neuron coupled energy consumption (Sokoloff 1981; Kadekaro et al. 1987; Pellerin and Magistretti 1994; Lundgaard et al. 2015). [^{18}F]FDG-PET signal reflects resting potentials (15% of [^{18}F]FDG-PET signal), action potentials (16% of [^{18}F]FDG-PET signal) and synaptic processes (44% of [^{18}F]FDG-PET signal) (Howarth et al. 2012).

Pioneering studies conducted by Kety and Sokoloff 60 years ago clearly showed that glucose is the obligatory energy substrate for the brain. Pellerin and Magistretti proposed that lactate is produced glycolytically by astrocytes and is transported to neurons to be used as a significant source of energy (Pellerin and Magistretti 1994). Recently, Zimmer et al. provided evidence that astrocytes account for a substantial proportion of glucose consumption, thus better defining their coupling (Zimmer et al. 2017).

[^{18}F]FDG-PET is a marker of synaptic integrity (Attwell and Laughlin 2001; Rocher et al. 2003). Decrease of brain metabolism, assessed by [^{18}F]FDG-PET, is considered a surrogate of synaptic dysfunction, which might be related to a variety of neuropathological events, including altered intracellular signalling cascades and mitochondria bioenergetics, impaired neurotransmitter release and accumulation of neurotoxic protein species (Perani 2014; Kato et al. 2016). Of note, tiny perturbations of glucose metabolism can be effectively detected by means of [^{18}F]FDG-PET. The high sensitivity of this tool leads to capture neurodegeneration not only due to local pathological and biochemical alterations but also due to long-distance functional deafferentations (Kato et al. 2016). At the molecular level, this implies that [^{18}F]FDG-PET reveals significant brain hypometabolism when neuronal death has not occurred yet, detecting the ongoing molecular changes that are perturbing the physiological synaptic functioning. Consistent evidence for highly specific patterns of [^{18}F]FDG-PET hypometabolism in distinct dementia conditions has been provided by several studies (Teune et al. 2010; Cerami et al. 2016; Perani et al. 2016; Teipel et al. 2015; Caminiti et al. 2017; Cerami et al. 2017a; Iaccarino et al. 2015) and before manifest brain atrophy occurs (Chételat et al. 2007; Bateman et al. 2012). Disease-specific hypometabolism, obtained with [^{18}F]FDG-PET imaging, can provide support to differential diagnosis of neurodegenerative conditions (Perani et al. 2014; Teune et al. 2010; Cerami et al. 2016; Caminiti et al. 2017; 2019). [^{18}F]FDG-PET hypometabolism has therefore been included in the clinical/research diagnostic criteria of several dementia conditions, as a supportive feature (McKhann et al. 2011; Gorno-Tempini et al. 2011; Armstrong et al. 2013; Rascovsky et al. 2011; Sperling et al. 2011; McKeith et al. 2017). To date, the relevance of

[^{18}F]FDG-PET has been supported by a number of international workgroups and consortia in the diagnostic workup of neurodegenerative diseases (Garibotto et al. 2017). The modality used to measure [^{18}F]FDG-PET patterns, however, critically influences diagnostic accuracy (Perani 2014; Iaccarino et al. 2017a). In this regard, the selection of appropriate and validated procedures represents a cardinal issue in [^{18}F]FDG-PET data analysis. In order to obtain an objective cut-off between normal and pathological findings, ad hoc methods need to be used, where the relative quantification or semi-quantification represents largely diffuse approaches worldwide. Different advanced parametric tools have been introduced to obtain statistical comparisons between the subject of interest and a cohort of healthy controls, including Neurostat, 3D-SSP and statistical parametric mapping (SPM). Overall, these tools run analysis at the voxel level and provide statistical maps of difference between the patients and normative data. The implementation of standardized [^{18}F]FDG-PET readouts and operator-independent maps is currently being called for by both US Society of Nuclear Medicine and Molecular Imaging and the European Association of Nuclear Medicine (Waxman et al. 2009; Morbelli et al. 2015). Brain hypometabolism patterns at single-subject level can be identified by means of a recently developed optimized SPM procedure, based on comparison with a large dataset of healthy controls (Perani et al. 2014; Della Rosa et al. 2014). The use of large healthy subjects datasets of PET scans (>50) is indeed recommended for single-subject SPM analysis (Gallivanone 2014). SPM single-subject method takes advantage of an optimized spatial normalization, based on a [^{18}F]FDG-PET dementia-specific template (http://inlab.ibfm.cnr.it/inlab/PET_template.php) (Della Rosa et al. 2014), and it has been also validated for utilization with different scanners (Presotto et al. 2017). The [^{18}F]FDG-PET SPM procedure allows the identification of disease-specific brain hypometabolism patterns in single individuals and performs better than visual qualitative assessment of [^{18}F]FDG-PET uptake images, as shown in cross-validation studies for diagnostic accuracy and also in cross-validation studies with other biomarkers (Perani et al. 2014; Perani et al. 2016; Iaccarino et al. 2017b; Caminiti et al. 2018). This method has been largely validated for differential dementia diagnosis (Perani et al. 2016; Caminiti et al. 2017; Cerami et al. 2017a) including also atypical parkinsonisms (Caminiti et al. 2017) and crucially for prognosis in prodromal cases (Perani et al. 2014; Perani et al. 2016; Iaccarino et al. 2017b; Caminiti et al. 2018; Cerami et al. 2015a).

9.2.1 Evidence in AD Spectrum

[^{18}F]FDG-PET represents an accurate tool able to distinguish AD patients from healthy subjects and other dementia conditions. The disease-specific hypometabolism pattern supports AD diagnosis since the earliest clinical phases, such as in subjects with mild cognitive impairment (MCI), as well as in preclinical cases (asymptomatic subjects at risk or asymptomatic carriers of pathogenetic mutations) (Perani et al. 2016; Iaccarino et al. 2017b; Caminiti et al. 2018; Cerami et al. 2015a).

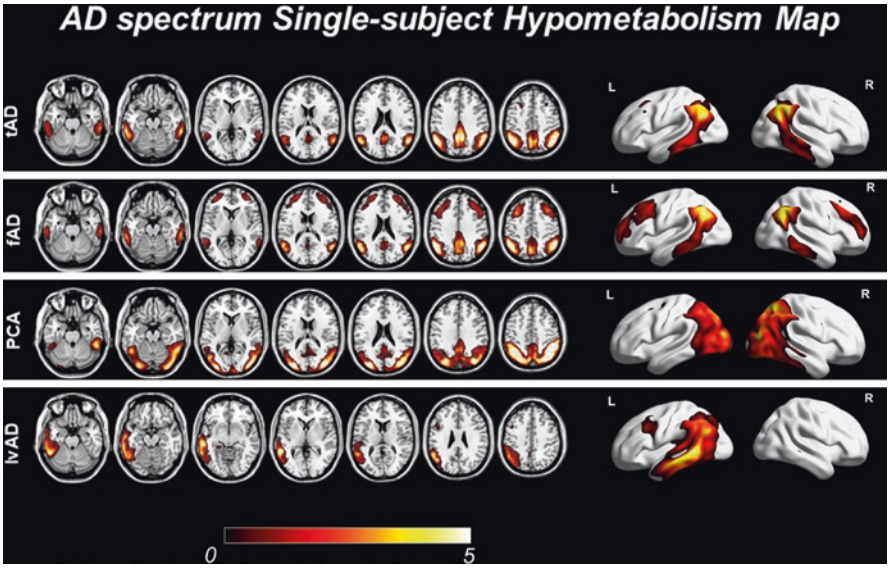

Fig. 9.3 Representative SPM-t-map at the single-subject level in AD spectrum. Figure shows prototypical examples of hypometabolism patterns in different variants of AD, from top to the bottom: typical AD-like hypometabolism pattern; frontal variant of AD-like hypometabolism pattern; posterior variant of AD-like hypometabolism pattern; logopenic variant of AD-like hypometabolism pattern. *AD* Alzheimer's disease, *tAD* typical AD, *fAD* frontal AD, *PCA* posterior cortical atrophy, *lvAD* logopenic variant of AD

In typical AD, the [^{18}F]FDG-PET metabolic pattern typically involves temporo-parietal association cortices, the precuneus and posterior cingulate cortex (Fig. 9.3). The AD-like bilateral temporo-parietal hypometabolism was described also in cohorts of patients with pathologically confirmed AD (Hoffman et al. 2000). The hypometabolism can start even two decades before symptom onset (Gordon et al. 2018; Benzinger et al. 2013). Frontal hypometabolism can be present, although more variably and in later stages (Mosconi et al. 2008; Ossenkoppele et al., 2012). Of note, the characteristic topographic distribution of cerebral hypometabolism represents the most proximal biomarker associated with clinical expression of AD, thus the major correlate of memory and cognitive impairments (Perani 2008) and also highly correlated with tau deposition (Ossenkoppele et al. 2016). Specific [^{18}F]FDG-PET regional brain metabolic dysfunctions are also associated with distinct neuropsychiatric subtypes of frontal AD patients, classified according to neuropsychiatric inventory scores (Ballarini et al. 2016). Specifically, a more severe hypometabolism in frontal and limbic structures was related to high hyperactivity scores implicated in behavioural control. A comparable positive correlation with these same regions was found for the affective neuropsychiatric scores. On the other hand, the apathetic scores were negatively correlated with metabolism in the bilateral orbitofrontal and dorsolateral frontal cortex known to be involved in motivation and decision-making processes.

A more severe bilateral hypometabolism in parietal and posterior cingulate cortices and precuneus is reported in patients with EOAD (onset <65 years) in comparison to patients with LOAD (onset >65 years) (Kim et al. 2005; Sakamoto et al. 2002). In addition, there is also evidence of different subtypes of AD (Whitwell et al. 2012) which have been far less investigated by means of [^{18}F]FDG-PET (Nestor et al. 2018). Notably, [^{18}F]FDG-PET reveals variant-specific hypometabolism patterns suggestive of the atypical form of AD, namely, PCA, lvAD and fAD, and already in prodromal phase (Sala et al. 2020).

In patients with PCA, [^{18}F]FDG-PET both at group and single-subject level reveals hypometabolism patterns involving lateral occipital cortex, lingual gyrus, cuneus, precuneus, posterior cingulate, the parietal lobe, the lateral posterior temporal cortex and the thalamus (see Fig. 9.3) (Sala et al. 2020; Whitwell et al. 2017a). Associative visual areas are usually the most affected regions; however, in few cases also the primary visual cortex can be involved (Cerami et al. 2015b). [^{18}F]FDG-PET revealed also specific hypometabolism of the frontal eye fields, which can occur secondary to the loss of input from the occipitoparietal regions, representing the possible neural dysfunctional substrate underlying oculomotor apraxia in PCA (Cerami et al. 2015b; Nestor et al. 2003). The hypometabolism in the right lateral temporo-occipital cortex represents a syndrome-specific signature that emerges from the comparison between PCA, DLB and typical AD cases (Rosenbloom et al. 2011; Spehl et al. 2015). Consistently, PCA can be distinguished from DLB when [^{18}F]FDG uptake is mostly asymmetric, with reductions in the right lateral temporo-occipital cortex and a relatively spared left occipital cortex, with 83% sensitivity, 85% specificity and 83% accuracy (Spehl et al. 2015).

In the fAD, [^{18}F]FDG-PET studies demonstrated a marked frontal hypometabolism, in addition to the typical AD hypometabolic pattern, namely, affecting the temporo-parietal regions and posterior cingulate cortex, reflecting perhaps a great pathology load (e.g. neurofibrillary tangles) in frontal regions (see Fig. 9.3) (Sala et al. 2020; Woodward et al. 2015). Moreover, fAD shows a severe hypometabolism in the characteristic AD regions when compared to bvFTD (Rabinovici et al. 2011), thus supporting differential diagnosis (Foster et al. 2007).

In lvAD, reduction of metabolism encompasses the left parietal and posterolateral temporal lobes, with a relative sparing of right temporo-parietal cortex (see Fig. 9.3) (Cerami et al. 2017a). The inferior and middle temporal gyrus, inferior parietal gyrus and angular gyrus, only in the left hemisphere, represent variant-specific hypometabolic core regions for lvAD (Sala et al. 2020). Hypometabolism in left inferior, middle and superior temporal gyri and left supramarginal gyrus is able to distinguish lvAD patients from typical AD ones, with area under the receiver operating characteristic curve of 0.89 (Madhavan et al. 2013).

In addition to the shared typical hypometabolism in common core regions, namely, precuneus and temporo-parietal cortex, bilaterally, the AD variants show specific hypometabolic hallmarks that are uniquely associated with the different clinical phenotypes, i.e. occipital regions for the PCA, left temporal regions for the lvAD and the superior and middle frontal regions for the fAD (Sala et al. 2020). These disease-specific hypometabolism patterns performed extremely well in

discriminating the AD variants (typical and atypical) from each other within the AD spectrum (Sala et al. 2020).

[^{18}F]FDG-PET is an effective tool also able to differentiate AD from other forms of dementia (Perani et al. 2014; Perani et al. 2016; Caminiti et al. 2019). AD and DLB patients may present partially overlapping profile of brain hypometabolism, except for a marked hypometabolism in the occipital cortex and seldom with relative preservation of metabolism in the posterior cingulate cortex in DLB (Perani et al. 2016; Caminiti et al. 2019; Nestor et al. 2018). Consistently, [^{18}F]FDG-PET hypometabolism maps show high discriminative power distinguishing DLB from AD conditions with an accuracy of >90% (Caminiti et al. 2019). As for the differential diagnosis between AD and FTLD, semi-quantitative assessment of [^{18}F]FDG-PET allows a high accuracy in the classification of patients (Perani et al. 2014; Perani et al. 2016). The level of currently available evidence was rated as good for differentiating AD from DLB and fair for distinguishing between AD and FTLD (Nestor et al. 2018).

This evidence suggests that AD variant-specific patterns of brain hypometabolism, highly consistent at single-subject level and already evident in the prodromal stages, represent relevant markers of neurodegeneration, with highly supportive diagnostic and prognostic role.

9.2.2 Evidence in FTLD Spectrum

FTLD spectrum is characterized by variable neuropathology which may induce synaptic dysfunction resulting in a decrease of [^{18}F]FDG uptake. [^{18}F]FDG-PET has been largely used to evaluate regional metabolic changes in FTLD spectrum, revealing a crucial role of this biomarker in differential diagnosis and early detection of brain functional abnormalities. Specifically, [^{18}F]FDG-PET can be regarded as a reliable imaging tool in the differentiation amongst FTLD subtypes (Matias-Guiu et al. 2014).

Patterns of hypometabolism in bvFTD have been largely investigated, reporting a significant hypometabolism in frontal lobe, limbic system and insular and temporal regions that were also associated with the dysfunction of connected subcortical structures (see Fig. 9.4) (Cerami et al. 2016; Franceschi et al. 2005; Diehl et al. 2004; Jeong et al. 2005; Salmon et al. 2003; Schroeter et al. 2008). Two bvFTD variants have been recently described, according to the hypometabolism features, namely, the frontal and temporo-limbic bvFTD variants (Cerami et al. 2016). Widespread hypometabolism in the dorsolateral and ventromedial frontal cortex characterizes frontal bvFTD variant, while predominant hypometabolism in the temporal lobes, including the poles, the hippocampal structures and amygdala, with a selective sparing of the dorsolateral prefrontal cortex was associated with the temporo-limbic variant (Cerami et al. 2016).

Several studies including those with *post-mortem* pathological confirmation assessed the role of [^{18}F]FDG-PET in differential diagnosis of bvFTD and AD, showing high sensitivity and specificity of this tool (Rabinovici et al. 2011; Foster

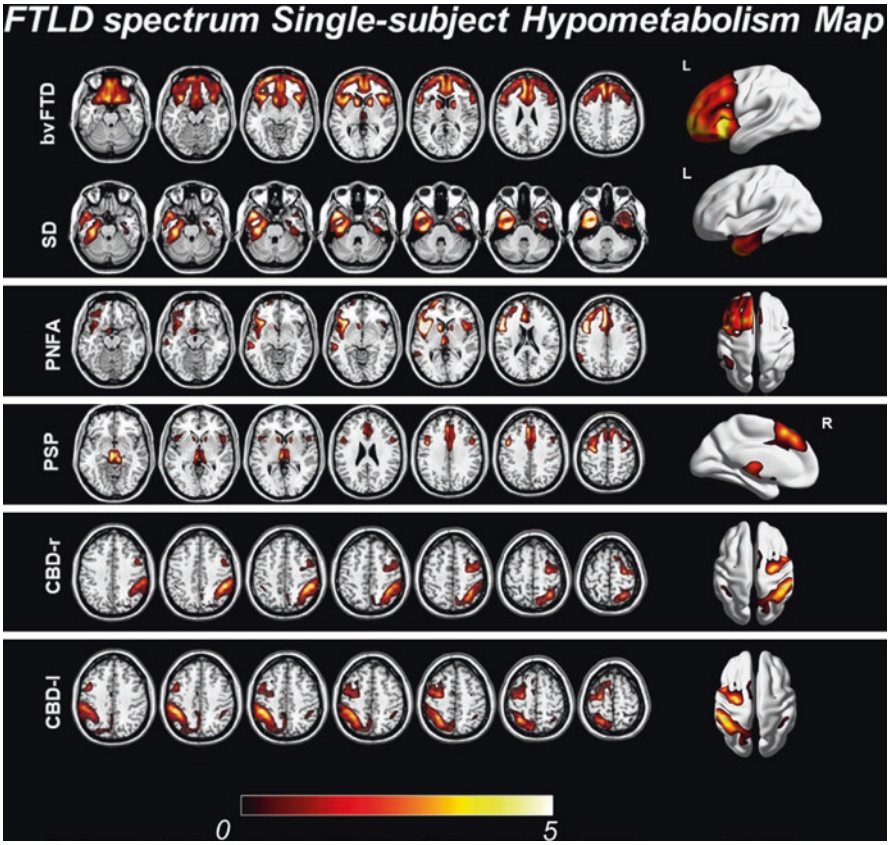

Fig. 9.4 Representative SPM-t-map at the single-subject level in FTLD spectrum. Figure shows prototypical examples of hypometabolism patterns in different variants of FTLD, from top to the bottom: behavioural variant of FTD-like hypometabolism pattern; semantic dementia-like hypometabolism pattern; PNFA-like hypometabolism pattern; PSP-like hypometabolism pattern; CBD left-like hypometabolism pattern; CBD right-like hypometabolism pattern. *FTLD* frontotemporal lobar degeneration, *bvFTD* behavioural variant of frontotemporal dementia, *SD* semantic dementia, *PNFA* primary non-fluent aphasia, *PSP* progressive supranuclear palsy, *CBD-l* corticobasal degeneration left, *CBD-r* corticobasal degeneration right

et al. 2007; Panegyres et al. 2009; Davison and O'Brien 2014). In this framework, anterior cingulate and anterior temporal cortices showed the higher specificity for the differential diagnosis with AD (Rabinovici et al. 2011). Although [^{18}F]FDG and carbon-11-labelled Pittsburgh Compound B ([^{11}C]PiB)-PET show similar accuracy in discriminating AD and bvFTD patients, hypometabolism pattern demonstrates higher specificity when the [^{18}F]FDG scans were classified quantitatively (Rabinovici et al. 2011).

PPA syndromes, which include selective language disorders with specific features, may be sometimes complicated by the presence of non-language cognitive symptoms (Mesulam et al. 2014), representing a prodromal stage to more complex

clinical pictures belonging to AD or the FTLD spectrum. Predominately anterior temporal lobe pattern of hypometabolism with left dominant asymmetry is consistently reported as the main metabolic signature of SD (see Fig. 9.4) (Iaccarino et al. 2015; Diehl et al. 2004; Nestor et al. 2006; Acosta-Cabronero et al. 2011). However, [^{18}F]FDG-PET hypometabolism pattern, at single-subject level, highlights some heterogeneity regarding the lateralization of hemispheric involvement (Cerami et al. 2017a; Iaccarino et al. 2015). Furthermore, in SD [^{18}F]FDG-PET reveals an involvement of limbic structures (Diehl et al. 2004; Kim et al. 2012a; Desgranges et al. 2007), the fusiform gyrus (Diehl et al. 2004; Nestor et al. 2006; Acosta-Cabronero et al. 2011; Drzezga et al. 2008; Mion et al. 2010) and the caudate and thalamus (Diehl et al. 2004; Desgranges et al. 2007). The topography of hypometabolism is highly associated with the clinical features of SD (Matias-Guiu et al. 2014). A longitudinal study showed that early pathological changes in metabolism are enough to produce specific neurocognitive profile in SD patients (Diehl-Schmid et al. 2006).

In PNFA patients the asymmetric hypometabolism is more evident in the left anterior perisylvian cortical area as well as in the fronto-insular cortex and supplementary motor area (see Fig. 9.4) (Nestor 2003). Thus, PNFA are characterized by asymmetric left frontal hypometabolism, which is subtle in some cases (Feher et al. 1991; Rabinovici et al. 2008). Hippocampal structures and amygdala result selectively spared (Cerami et al. 2017a). Of note, a recent follow-up study showed that specific metabolic signatures in PNFA patients are able to predict the clinical progression toward different form of dementia (Cerami et al. 2017a).The hypometabolism in the superior and inferior parietal cortex predicted the conversion to CBD, and an involvement of the basal ganglia, midbrain and cerebellum was present in those PNFA patients fulfilling PSP diagnostic criteria at the follow-up.

Asymmetric hypometabolism in the basal ganglia, thalamus and frontoparietal cortical regions, contralateral to the clinically affected side, was consistently reported in CBD patients (see Fig. 9.4) (Caminiti et al. 2017; Zhao et al. 2012; Niethammer et al. 2014). A recent study assessed the utility of [^{18}F]FDG-PET in differentiating amongst different neuropathologic substrata in a cohort of patients with corticobasal syndrome (CBS) (Pardini et al. 2019). In this study, *post-mortem* pathologic diagnosis identified three subgroups: CBS-CBD, CBS-AD and CBS-PSP. The whole group of CBS patients showed significant hypometabolism in frontoparietal regions, including the perirolandic area, basal ganglia and thalamus of the clinically more affected hemisphere, in comparison to healthy controls. A more evident, bilateral involvement of the basal ganglia characterized CBS-CBD subgroup. On the other hand, patients with CBS-AD and CBS-PSP presented with posterior, asymmetric hypometabolism and a more anterior hypometabolic pattern, including the medial frontal regions and the anterior cingulate, respectively. All the evidence suggests that [^{18}F]FDG-PET scans can help in the aetiologic diagnosis of CBS (Pardini et al. 2019).

Hypometabolism pattern in PSP patients involves basal ganglia, midbrain, anterior cingulate cortex, frontal operculi and primary motor cortex (see Fig. 9.4) (Caminiti et al. 2017; Zhao et al. 2012; Eckert et al. 2005; Hosaka et al. 2002). Thalamic hypometabolism was also variably reported in PSP (Akdemir et al. 2014).

Significant reductions of metabolism in the caudate nucleus, thalamus, midbrain and cingulate gyrus emerges from the comparison of PSP patients with controls but also with PD and MSA (Juh et al. 2004). Specifically, "pimple sign"—an oval/round-shaped region representing midbrain hypometabolism—has been proposed as a hypometabolic feature able to distinguish PSP from MSA and CBS (Botha et al. 2014). This sign showed high specificity (100%) to identify PSP patients, but low sensitivity (29%) since it is not present in all cases (Botha et al. 2014). A recent study reveals that visual rating of t-maps of brain hypometabolism in single subjects, obtained by optimized SPM voxel-wise procedure, allows an accurate differential diagnosis amongst PSP, CBD, DLB and MSA-cerebellar (MSA-c) patients with 98% sensitivity, 99% specificity and 99% accuracy (Caminiti et al. 2017). Histopathological changes in regions affected by brain hypometabolism were reported by *post-mortem* examination in PSP patients. Specifically, argyrophilic globosum neuronal tangles were found in the pons, while neuronal tangles with cytoplasmic inclusions and neuropil threads were found in the frontal lobe. In addition, tufted astrocytes were found in the frontal lobe, amygdala and both thalami (Tang et al. 2010).

PSP clinical subtypes, namely, the PSP-Richardson and the PSP-parkinsonism (Williams et al. 2005), present distinct patterns of glucose hypometabolism (Eckert et al. 2005). PSP-Richardson patients are characterized by severe thalamic and frontal cortex hypometabolism, whereas more significant putaminal hypometabolism can be found in PSP-parkinsonism patients. In this regard, Srulijes and colleagues identify the putamen/thalamus [^{18}F]FDG uptake ratio as an index able to discriminate between PSP-parkinsonism and PSP-Richardson patients (Srulijes et al. 2012).

Dalakas and colleagues in 1987 reported frontal and basal ganglia reduction of [^{18}F]FDG uptake, with a relative sparing of the cerebellum, in ALS patients (Dalakas et al. 1987). About 15% of ALS patients develop FTD (FTD/ALS) over the disease course; in addition 35% of ALS patients can manifest cognitive impairments with variable severity, generally involving executive functions (Phukan et al. 2012; Ringholz et al. 2005). [^{18}F]FDG-PET group-level studies in FTD/ALS patients reported hypometabolism in motor and non-motor cortices, encompassing frontal temporal and parietal regions (Canosa et al. 2016; Renard et al. 2011; Rajagopalan and Pioro 2015; Matías-Guiu et al. 2016). A large cohort study assessed brain hypometabolism in 170 ALS cases, including cognitively unimpaired ALS, ALS with cognitive impairments and FTD/ALS. The study revealed an increasing hypometabolism gradient in frontal brain regions going from cognitively unimpaired ALS to FTD/ALS patients, where ALS with cognitive impairments showed intermediate levels of frontal hypometabolism. Based on this background, although [^{18}F]FDG-PET is currently not supported in the clinical diagnosis of ALS (Nestor et al. 2018; Sala et al. 2019), it can be helpful in the diagnostic and prognostic evaluation of cognitive impairment in FTD/ALS spectrum.

The pattern of neurodegeneration as shown by [^{18}F]FDG-PET in clinically diagnosed sporadic and genetic FTLD cases was characterized in many cross-sectional and also some longitudinal studies, reviewed by (Meeter et al. 2017). A recent study assessed maps of brain relative hypometabolism and hypermetabolism at

single-subject level in six FTD/ALS patients carrying the C9orf72 mutation (Castelnovo et al. 2019). C9bvFTD cases were characterized by a prevalent frontal hypometabolism and C9SD by right temporal polar and lateral involvement, in accordance with the clinical diagnosis. Variable patterns of hypo- and hypermetabolism, instead, were found in C9ALS bulbar variant patients. The consistency between brain hypometabolism and different clinical phenotypes supports the diagnostic importance to capture specific brain dysfunction at single-subject level.

Unfortunately, the number of studies examining the relation of functional imaging markers with the underlying pathology is limited, and hitherto there is not reliable evidence in TDP-43 pathology or FUS by metabolic imaging (Steinacker et al. 2019; Gordon et al. 2016a; Diehl-Schmid et al. 2014).

9.2.3 Evidence in α-Synuclein Spectrum

α-Synuclein oligomers accumulate in synaptic terminals and spread in a prion-like manner through vulnerable synaptic circuits. Synaptic pathology plays, therefore, a central role in the pathogenesis of a-synucleinopathies (Calo et al. 2016). Specifically, the alterations in synaptic structure and function caused by the accumulation of abnormal α-synuclein are reported as a primary event in the pathogenesis of α-synuclein-related diseases (Calo et al. 2016). This synaptic dysfunction can be measured by [^{18}F]FDG-PET, which allows the detection of patterns of brain hypometabolism with disease-specific topography within the α-synuclein spectrum. [^{18}F]FDG-PET is able to distinguish DLB from MSA patients, identifying also different disease phenotypes such as cerebellar and parkinsonian subtypes of MSA (Caminiti et al. 2017).

DLB condition is characterized by a selective reduction of [^{18}F]FDG uptake in occipital cortex, specifically in associative occipital cortex and primary visual cortex (see Fig. 9.5) (McKeith et al. 2017). DLB shares with AD similar hypometabolic pattern in the temporo-parietal cortices (Perani et al. 2014; Teune et al. 2010; Caminiti et al. 2019; Presotto et al. 2017). In terms of differential diagnosis, pathological reduction of metabolism in lateral occipital cortex showed the highest sensitivity (88%), whereas the relative preservation of posterior cingulate metabolism (the "cingulate island sign") achieved the highest specificity (100%) (Lim et al. 2009). A recent study showed that occipital lobe hypometabolism has the highest discriminative power distinguishing DLB from AD and PD conditions with an accuracy of >90% (Caminiti et al. 2019). It has been also demonstrated that a posterior hypometabolism pattern represents an early marker able to distinguish patients with PD at higher risk of progression to dementia (i.e. PDD/DLB) after 4-year follow-up from those who will remain with normal cognition (Pilotto et al. 2018).

MSA patients exhibit altered glucose metabolism in the basal ganglia, putamen, pons and cerebellum, compared to PD and controls (Brajkovic et al. 2017). Consistently, decreased [^{18}F]FDG uptake in putamen, brainstem or cerebellum is part of the diagnostic criteria for possible MSA (see Fig. 9.5) (Gilman et al. 2008). Decreases in cerebellar glucose metabolism occur early in the course of the disease

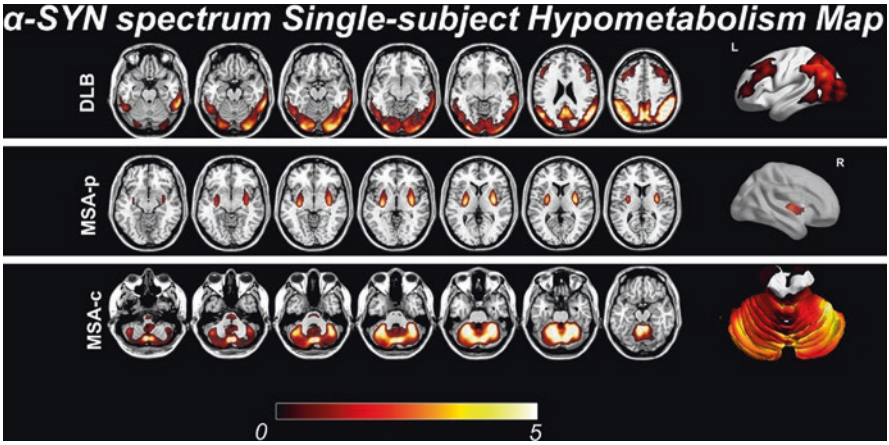

Fig. 9.5 Representative SPM-t-map at the single-subject level in α-synuclein spectrum. Figure shows prototypical examples of hypometabolism patterns in α-synuclein spectrum, from top to the bottom (bottom panel): DLB-like hypometabolism pattern; MSA-p-like hypometabolism pattern; MSA-c-like hypometabolism pattern. Colour scales indicate values of T-scores, corrected for age, obtained from comparison with a large group of healthy subjects, rendered on a high-resolution anatomical template. *α-SYN* α-synucleinopathy, *DLB* dementia with Lewy bodies, *PDD* Parkinson's disease dementia, *MSA-P* parkinsonian type of multiple system atrophy, *MSA-c* cerebellar type MSA

and contribute to cerebellar symptoms, whereas motor symptoms seem to precede putaminal hypometabolism (Lyoo et al. 2008). Patients with a diagnosis of probable MSA showed greater brain hypometabolism than patients with MSA and severe autonomic dysfunction (Kwon et al. 2009). These findings suggest that the pattern of glucose metabolism in MSA with predominant involvement of the autonomic nervous system may differ from that of MSA with involvement of the striatonigral or olivopontocerebellar systems.

According to the prevalent motor characteristics, MSA can be distinguished into a parkinsonian (MSA-p, where the predominant motor symptom is parkinsonism) and a cerebellar (MSA-c, where the predominant motor feature is cerebellar ataxia) subtype (Fanciulli and Wenning 2015). [^{18}F]FDG-PET reveals specific hypometabolic features characterizing the two clinical phenotypes. Specifically, hypometabolism mainly occurs in the putamen bilaterally in MSA-p and in the whole cerebellum in MSA-c (Fig. 9.5) (Caminiti et al. 2017; Zhao et al. 2012) in line with the neuropathology feature of these MSA subtypes (Ozawa et al. 2004).

9.2.4 Evidence in Prion Diseases Spectrum

Human prion diseases are uniformly fatal, progressive neurodegenerative disorders. The prion diseases are caused by accumulation of misfolded prion protein in the human brain. The histopathological features of prion diseases include characteristic

spongiform changes, neuronal cell loss and gliosis in various regions of the brain (Takada and Geschwind 2013; Puoti et al. 2012).

An *in vivo* PET imaging study evaluated [^{18}F]FDG-PET in six symptomatic and asymptomatic carriers of prion protein gene mutations associated with the GSS disease. Reduction of glucose metabolism was observed extensively in the neocortex, especially in parietal regions, but also in the basal ganglia and/or thalamus (Kepe et al. 2010).

The role of [^{18}F]FDG-PET in patients with CJD has been investigated only in few studies. [^{18}F]FDG-PET shows widespread hypometabolism in CJD, as opposed to other dementias such as AD or FTD which show specific patterns of reduced metabolism (Henkel et al. 2002; Goldman et al. 1993). Hypometabolism in parietal, temporal, frontal and occipital regions is consistently reported (Henkel et al. 2002; Goldman et al. 1993; Engler et al. 2003; Renard et al. 2013). In most CJD patients, alterations were asymmetric. Notably, histopathological astrocytosis (Engler et al. 2003), neuronal death (Goldman et al. 1993) and spongiform change show an association with reduction of [^{18}F]FDG uptake (Goldman et al. 1993; Matías-Guiu et al. 2017). A SPM semi-quantitative study of [^{18}F]FDG uptake in patients with CJD revealed hypometabolism in many cortical areas with an asymmetric pattern and sparing of the basal ganglia and thalamus (Kim et al. 2012b). Since the vacuolation and prion deposition did not always correlate with hypometabolism in subcortical structures (Mente et al. 2017), it can be hypothesized that cortical involvement occurs earlier in the progression of the disease; therefore, subcortical involvement can be detected by [^{18}F]FDG imaging in later stages. Two other studies, however, found an early involvement of the basal ganglia and thalamus, with [^{18}F]FDG-PET, in probable or pathologically confirmed sporadic CJD patients (Xing et al. 2012; Hamaguchi et al. 2005). A recent study with [^{18}F]FDG-PET identified also hypermetabolism in the limbic and mesolimbic structures, including medial temporal lobe in autopsy-confirmed cases of CJD, suggesting a possible relationship with microglial activation (Mente et al. 2017). [^{18}F]FDG-PET is not routinely used in the diagnostic evaluation of prion disease patients; however, increasing evidence supports the use in the clinical assessment of CJD (Matías-Guiu et al. 2017).

In FFI patients, a thalamic reduction of [^{18}F]FDG uptake was consistently found, proposing this feature as a hypometabolic hallmark of the disease, in agreement with the neuropathologic findings (Perani et al. 1993; Cortelli et al. 1997; Parchi et al. 1995; Mastrianni et al. 1999; Montagna et al. 2003). Thalamic hypometabolism is detectable since the early phase of the disease, while the involvement of other brain regions depends on disease duration (Perani et al. 1993; Cortelli et al. 1997; Parchi et al. 1995). Cortelli and colleagues (Cortelli et al. 1997) tested also the association between neuropathological and [^{18}F]FDG-PET findings in six FFI patients. They found that the hypometabolism was more widespread than neuronal loss and significantly correlated with the presence of protease-resistant prion protein (Cortelli et al. 1997). A recent study showed that FFI patients present a high variability in [^{18}F]FDG-PET hypometabolism at single-subject level and a less marked and extensive cortical involvement in comparison to CJD patients, with a selective involvement of the thalamus as the most characteristic finding (Prieto et al. 2015).

Thus, prion diseases exhibit characteristic patterns of brain hypometabolism, suggesting that the detection of these patterns by [^{18}F]FDG-PET imaging could orient the diagnosis (Prieto et al. 2015).

9.2.5 Strengths

In the research and clinical field of dementia, [^{18}F]FDG-PET is an established and well-validated marker of neurodegeneration. Results are a direct reflection of neural tissue state, efficiently depicting regional dysfunctions at the synaptic level, implying dysfunction without actual loss of neurons. The ability of [^{18}F]FDG-PET to detect disease-specific patterns of neurodegeneration led to the inclusion of brain hypometabolism as a supportive feature in the clinical/research diagnostic criteria of multiple dementia conditions (McKhann et al. 2011; Gorno-Tempini et al. 2011; Armstrong et al. 2013; Albert et al. 2011; Rascovsky et al. 2011; McKeith et al. 2017; Sperling et al. 2014). [^{18}F]FDG-PET represents an effective tool to provide essential information to improve early differential diagnoses amongst neurodegenerative diseases belonging to different spectrum and amongst clinical subtypes belonging to the same disease spectrum (Nestor et al. 2018) (Fig. 9.6).

The supportive role of [^{18}F]FDG-PET has also been demonstrated in differentiating DLB and atypical parkinsonian syndromes, with respect to neuroimaging of the presynaptic dopaminergic system. Due to the widespread availability of SPECT scans and approval from Europe (since 2000) and the United States (since 2011), dopamine transporter (DAT) radiotracers are often used in routine clinical practice, allowing the assessment *in vivo* of presynaptic nerve terminals integrity (Booij et al. 2001; Catafau and Tolosa 2004). However, dopamine presynaptic tracers are not a trustworthy tool to distinguish amongst parkinsonian disorders (Burn et al. 1994; Vlaar et al. 2007). In this regard, [^{18}F]FDG-PET provided a high diagnostic accuracy for differentiation between Lewy body diseases and atypical parkinsonism identifying disease-specific pattern topography (Caminiti et al. 2017; 2019), which is significantly better than presynaptic dopaminergic system radiotracers (Hellwig et al. 2012).

A growing body of evidence supports the value of [^{18}F]FDG-PET in the diagnosis of patients with atypical/unclear conditions (Mosconi et al. 2008; Silverman et al. 2001; Mosconi 2005; Bohnen et al. 2012; Elias et al. 2014; Herholz et al. 2007; Laforce Jr et al. 2010; Pakrasi and O'Brien 2005; Jagust et al. 2007). Importantly, [^{18}F]FDG-PET improving diagnostic accuracy can lead in the future to better and earlier treatment and better inclusion in clinical trials.

[^{18}F]FDG-PET shows also a crucial predictive and prognostic value. Indeed, [^{18}F]FDG-PET patterns of hypometabolism seem to be particularly accurate in predicting conversion from MCI to dementia, when compared to other biomarkers (e.g. amyloid-PET, magnetic resonance imaging, cerebrospinal fluid) (Perani et al. 2016; Anchisi et al. 2005; Bloudek et al. 2011; Dukart et al. 2016; Fellgiebel et al. 2007; Landau et al. 2010; Prestia et al. 2013; Robb et al. 2017; Shaffer et al. 2013; Yuan et al. 2009). In particular, [^{18}F]FDG-PET, analysed with appropriate semi-quantitative

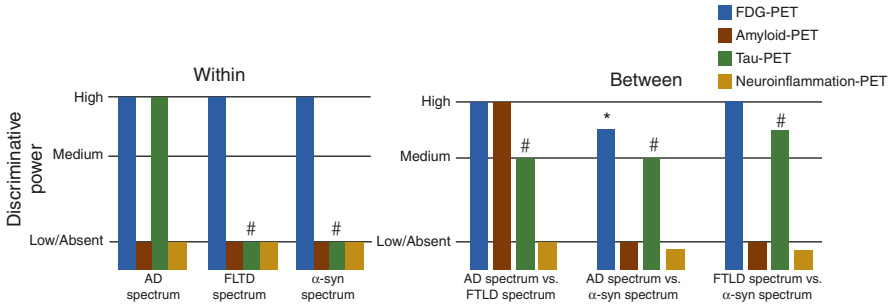

Fig. 9.6 Qualitative overview of the discriminative power of molecular PET neuroimaging measures presented in this chapter. Neurodegeneration-, amyloid-, tau- and neuroinflammation-PET role in differential diagnoses amongst clinical subtypes belonging to the same disease spectrum (**within—left panel**) and amongst neurodegenerative diseases belonging to different spectra (**between—right panel**). **Within:** [^{18}F]FDG-PET shows high discriminative power in within spectrum differential diagnoses for all dementia conditions. Although amyloid-PET is a good biomarker to capture AD pathology, it is not able to differentiate clinical phenotypes within the AD spectrum (Lehmann et al. 2013). Tau-PET has shown to be useful in within spectrum differential diagnosis for AD (Whitwell et al. 2018b; Nasrallah et al. 2018); however, it presents low specificity for non-AD-related tauopathies (Marquié et al. 2015). Most studies report evident but non-specific inflammatory responses in many neurodegenerative diseases. Neuroinflammation-PET imaging studies show sparse and questionable results in differential diagnosis within the same spectrum, due to small sample sizes, methodological differences amongst studies and intrinsic limitations of TSPO tracers (Best et al. 2019). **Between**: [^{18}F]FDG-PET shows high discriminative power for differentiating AD from FTLD spectra, and between FTLD and α-syn spectra. Diagnostic challenges may rise in differentiating PCA from DLB, due to topographical overlap in the hypometabolic pattern between the two conditions (Whitwell et al. 2017a). Amyloid-PET value is high in differentiating AD spectrum from the FTLD spectrum (Rabinovici et al. 2011), while the co-occurrence of amyloid and α-syn deposition in DLB/PDD hinders a clear, amyloid-PET-based, pathological differentiation between the AD and the α-syn spectrum (Ossenkoppele et al. 2015). However, in the α-syn spectrum, it may help in distinguishing DLB/PDD patients from MSA patients (Jellinger 2007). The selectivity of the current tau-PET radioligands for non-AD tauopathies is not well understood and affects their role in differential diagnosis amongst spectra (Marquié et al. 2015; Sander et al. 2016; Ishiki et al. 2017; Kikuchi et al. 2016; Lowe et al. 2016; Josephs et al. 2016). Low or "NA" discriminative power for neuroinflammation-PET imaging is due to paucity of studies comparing the different spectra. Abbreviations: *[^{18}F]FDG-PET* fluorine-18-fluorodeoxyglucose positron emission tomography, *AD* Alzheimer's disease, *FTLD* frontotemporal lobar degeneration, *α-syn* α-synucleinopathy, *NA* not available

parametric approaches, is able to correctly differentiate MCI subjects who converted to AD dementia or to other dementias (FTD and DLB) from those who remained stable or reverted to normal cognition (Perani et al. 2016; Caminiti et al. 2018; Cerami et al. 2015a). Thus, heterogeneous hypometabolism patterns in MCI can be identified, allowing clinicians to predict conversion not only to AD but also to non-AD dementia, avoiding multiple additional examinations and unnecessary delay in proper clinical management (Perani et al. 2016; Cerami et al. 2015a). Given its high predictive value, [^{18}F]FDG-PET will likely play a relevant role for candidate inclusion in future clinical trials as an accurate tool to select subjects at higher risk for short-term conversion to dementia (Garibotto et al. 2017). An accurate screening of

participants is crucial for optimizing trial effectiveness. In this regard, the sole use of amyloid positivity, as eligibility criterion, might lead to inclusion of amyloid-positive clinically stable subjects, especially in the older individuals (Iaccarino et al. 2019; Brookmeyer and Abdalla 2018). Of note, it has been recently showed that negative [^{18}F]FDG-PET scans are able to identify those MCI and healthy subjects who remain clinically stable with high negative predictive values (>0.80) (Iaccarino et al. 2019). This evidence further highlights the role of [^{18}F]FDG-PET, coupled to amyloid-PET, in the patient selection for future clinical trials.

9.2.6 Weaknesses

[^{18}F]FDG-PET results evaluating metabolic changes in neurodegenerative conditions have been and are largely based on qualitative methods (i.e. visual inspection). These approaches greatly depend on the observers' experience and may greatly reduce sensitivity and specificity, due to the lack of an objective cut-off between normal and pathological findings (Perani et al. 2014). A recent Cochrane review concluded that the current evidence is not enough to support the use of [^{18}F]FDG-PET in clinical diagnostic routine of prodromal dementia phase (Smailagic et al. 2015). These results are likely due to methodological heterogeneity across [^{18}F]FDG-PET literature, including data analysis procedures. In order to overcome these problems, two broad families of quantifications can be considered: either absolute or relative. Absolute [^{18}F]FDG-PET quantification requires advanced research settings since an arterial blood sampling has to be performed during the scan (Mosconi 2013). On the other hand, relative quantification requires the utilization of a reference value, such as the global mean or the mean value of an a priori defined reference region. Relative quantification, or semi-quantification, is definitely more diffuse worldwide, also because of the invasive nature of the absolute quantification and the resulting patient discomfort (Varrone et al. 2009). Despite the increasingly recognized need for objective measurements, few studies have focused on head-to-head comparisons between visual and quantitative assessments (Perani et al. 2014). Still, few studies have shown higher diagnostic (Foster et al. 2007) and prognostic (Patterson et al. 2011) performances when using semi-quantification methods, as well as more accurate differential diagnosis (Rabinovici et al. 2011).

9.3 PET Markers of Amyloidosis

To date, several tracers are available to assess amyloid plaque burden *in vivo*, with [^{11}C]PiB being the pioneering and most frequently used one for research purposes. [^{11}C]PiB binds to both extracellular amyloid plaques and vascular amyloid deposits (Bacskai et al. 2003). This tracer has a very high specificity for amyloid plaques, and it does not bind to non-Aβ inclusions such as neurofibrillary tangles or Lewy bodies (Fodero-Tavoletti et al. 2012; Lockhart et al. 2007). Three other [^{18}F]-labelled

Aβ tracers, [^{18}F]florbetapir, [^{18}F]florbetaben and [^{18}F]flutemetamol, have then received Food and Drug Administration and European Medicines Agency approval for clinical use (Villemagne et al. 2018).

9.3.1 Evidence in AD Spectrum

Neuropathologically, AD is typically characterized by the presence of Aβ plaques (Braak and Braak 1991). Accumulation of Aβ neuritic plaques is considered one of the hallmark pathologic changes associated with the AD clinical manifestations, from typical amnesic disease or LOAD to atypical variants (Galton et al. 2000; Hardy and Allsop 1991).

Aβ burden, as measured by PET, has been associated with both age and APOE*e4 carrier status (Morris et al. 2010; Rowe et al. 2010). *APOE* is a major susceptibility gene for AD (Roses and Saunders 1994). APOE*e4 carriers present with substantially higher Aβ deposition than non-carriers that are at the same clinical stage (Morris et al. 2010; Rowe et al. 2010).

The typical AD-like pattern of amyloid ligand accumulation is diffuse and symmetric, with a typical strong load in the posterior cingulate cortex and precuneus, plus orbitofrontal cortex and temporal lobe, followed by prefrontal and parietal cortices (Villemagne et al. 2018). This pattern of Aβ PET tracer retention is highly correlated with regional Aβ plaque density in *post-mortem* brain or biopsy samples (Ikonomovic et al. 2008; Sabbagh et al. 2011; Clark et al. 2011). Pioneering studies with PET and [^{11}C]PiB consistently demonstrated the ability to capture amyloid pathology in typical and atypical AD, and these findings have been correlated with ex vivo histologic measurements of Aβ plaque burden (Ikonomovic et al. 2008; Roe et al. 2013; Wolk et al. 2009). The uptake of [^{11}C]PiB tracer, however, did not show distinct topographic patterns associated with each AD variant (Xia et al. 2017) (Fig. 9.6).

Increased [^{11}C]PiB uptake in occipital regions relative to that found in typical AD has been reported in PCA series (Ng et al. 2007; Tenovuo et al. 2008; Formaglio et al. 2011; Rabinovici et al. 2010; Lehmann et al. 2013; Ossenkoppele et al. 2015; Santos-Santos et al. 2018). Wolk et al. (Wolk et al. 2012) described a lower ratio of anterior-to-posterior [^{11}C]PiB uptake relative to that in typical AD, with the opposite pattern for [^{18}F]FDG-PET, the latter consistent with the lower posterior hypometabolism in PCA. Lehmann et al. also reported some evidence of increased [^{11}C]PiB uptake in visual association cortex in PCA (Lehmann et al. 2013).

Of note, previous studies consistently reported no significant difference in the [^{11}C]PiB uptake between patients with EOAD and LOAD (Lehmann et al. 2013; Cho et al. 2013).

[^{11}C]PiB deposition was recently found in more than 95% of the patients with sporadic lvPPA (Santos-Santos et al. 2018). The pattern of amyloid uptake in lvPPA, often progressing to AD, is not clearly different from that in typical AD (Rabinovici et al. 2008; Lehmann et al. 2013; Wolk et al. 2012; Leyton et al. 2011). Other individual studies using *in vivo* biomarkers or neuropathological examination in patients

with lvPPA variably detected Aβ pathology in 57–100% of patients, thus supporting AD diagnosis (Santos-Santos et al. 2018; Spinelli et al. 2017; Giannini et al. 2017). Despite the prominence of language symptoms and evidence of more focal left hemisphere neurodegenerative change, these patients did not display any asymmetry in amyloid plaque distribution as measured by [^{11}C]PiB.

Since 2012, [^{18}F]-labelled amyloid radiotracers (i.e. [^{18}F]florbetaben, [^{18}F]florbetapir, [^{18}F]flutemetamol), with longer half-life than [^{11}C]PiB, entered clinical and research evaluation to support AD diagnosis (Masdeu 2017). All these amyloid-PET tracers bind with high affinity to fibrillar amyloid in neuritic plaques and have been validated against autopsy evidence (Wolk et al. 2011; Choi et al. 2011; Sabri et al. 2015; Klunk et al. 2004). Higher cortical retention of [^{18}F]florbetaben was found in AD as compared to age-matched controls or patients with frontotemporal dementia (Fodero-Tavoletti et al. 2012). [^{18}F]flutemetamol-PET showed good performance in differentiating between patients with AD and age-matched healthy controls (Vandenberghe et al. 2010). It is not fully understood whether or not the three [^{18}F]-labelled amyloid radiopharmaceuticals are equally specific and sensitive in the differential diagnosis between AD and healthy controls (Johnson et al. 2013a). All tracers were validated through a comparison with [^{11}C]PIB, showing high correlation with the latter (Johnson et al. 2013a). In this direction, the Centiloid Project provided methods to standardize amyloid-PET measures across the different tracers, making results obtained with [^{18}F]-labelled and [^{11}C]PiB Aβ tracers comparable (Klunk et al. 2015).

Amyloid-PET imaging has the potential clinical utility of aiding in differential diagnosis in EOAD and to support the clinical diagnosis of subjects with probable AD with improved diagnostic accuracy (Suppiah et al. 2019). There are, however, several problems to be addressed, particularly the presence of amyloid load of comparable pattern and amount in cognitively normal elderly individuals (Iaccarino et al. 2019; Brookmeyer and Abdalla 2018).

9.3.2 Evidence in FTLD Spectrum

Aβ deposition is not a pathological feature of FTLD, and these patients usually have no cortical amyloid-PET retention (Drzezga et al. 2008; Rowe et al. 2007; Rabinovici et al. 2007; Engler et al. 2008). Thus, this imaging tool has a crucial role in the differential diagnosis of FTLD and AD (Drzezga et al. 2008; Rowe et al. 2007; Rabinovici et al. 2007). FTLD and AD are the leading causes of early age-of-onset dementia, occurring with similar frequency in population younger than the age of 65 (Ratnavalli et al. 2002). Specifically, EOAD and FTLD are characterized by misdiagnosis rates ranging from 10% to 40%, reported even in expert centres (Alladi et al. 2007). In 62 EOAD patients and 45 FTLD patients matched for age and disease severity, [^{11}C]PiB visual reads had 89.5% sensitivity and 83% specificity to distinguish AD from FTLD patients (Rowe et al. 2007; Rabinovici et al. 2007; Villemagne et al. 2011a). Quantitative analysis of [^{11}C]PiB provided 89% sensitivity and 83% specificity (Rabinovici et al. 2011). However, a proportion of them may

have been clinically misdiagnosed, with AD as the pathological substrate for their dementia (Beach et al. 2012). It is possible that amyloid is present as secondary pathology also in FTLD, or as incidental amyloid deposition due to ageing processes, whereas the clinical syndrome is driven by non-AD pathologies (Jellinger and Attems 2010).

In CBS, a clinically and pathologically heterogeneous entity, mostly associated with underlying tauopathy, 25–50% present AD as the causative pathology *post-mortem* (Alladi et al. 2007; Lee et al. 2011; Ling et al. 2010; Dickson et al. 2002). Niccolini et al. reported no differences in cortical and subcortical amyloid uptake between patients with CBS and healthy controls, also confirmed at autopsy (Niccolini et al. 2018). A recent meta-analysis reported that the prevalence of Aβ positivity decreased with age in CBS. This study suggests that AD may be the causative pathology in young CBS patients, whereas a primary tauopathy becomes more likely with increasing age (Ossenkoppele et al. 2015). Amyloid-PET would theoretically be useful in identifying CBS patients with underlying AD pathology.

In PSP, two different autopsy studies have highlighted the presence of concomitant Aβ proteins in the brains (Tsuboi et al. 2003; Dugger et al. 2014). In a series of clinically PSP patients, evidence of Aβ deposition was seen by PET imaging in a relatively high proportion of PSP subjects (40%). However, Aβ deposition was not found to be correlated with clinical severity, magnetic resonance patterns of atrophy or tau deposition, suggesting to be mostly related to an age-dependent phenomenon (Whitwell et al. 2018a).

Aβ imaging also has been used to ascertain the absence of AD pathology in patients with PPA (Drzezga et al. 2008; Rabinovici et al. 2008; Leyton et al. 2011). A multicentre study involving 1251 patients diagnosed with PPA and a measure of Aβ pathology (Cerebral spinal fluid (CSF), PET or autopsy) indicated that Aβ positivity is more prevalent in lvPPA (86%) than in PNFA (20%) or SD (16%). The prevalence of Aβ positivity increased with advancing age in PNFA and SD, and those patients carrying APOE ε4 allele were more often Aβ positive than non-carriers (Bergeron et al. 2018).

The 90% of patients with SD is characterized by TDP-43 pathology, and it is only rarely due to a primary tauopathy or AD (Mackenzie et al. 2008; Josephs et al. 2004). Consistently, a recent study using [^{11}C]PiB found that five out of six TDP-43 SD patients were amyloid negative (Makaretz et al. 2018). Serrano and colleagues reported a positive amyloid scan in a patient with clinical FTLD. *Post-mortem* histopathologic examination confirmed the coexistence of amyloid plaques with TDP-43-positive histopathology (Serrano et al. 2014).

TDP-43 is the major component of aggregates composing the neuropathological hallmark of about 50% of FTLD cases and of 97% of ALS cases (Steinacker et al. 2019). Visualization of Aβ deposits in ALS has been investigated suggesting a link between ALS and AD (Hamilton and Bowser 2004). The relationship between FTD/ALS and amyloid precursor protein was observed in rodent models, and recent *post-mortem* immunohistochemical analysis has also shown Aβ deposition in 35–50% of all ALS patients, even without co-morbid dementia (Hamilton and Bowser 2004;

Bryson et al. 2012). Currently, there are three published case reports of ALS patients with co-morbid dementia scanned with [^{11}C]PiB. These reports suggest a potential role for [^{11}C]PIB-PET in the discrimination of various neurodegenerative proteinopathies such as AD and ALS with co-morbid FTD (Farid et al. 2015; Yamakawa et al. 2012). Very recently, Matías-Guiu et al., studying amyloid deposition with [^{18}F]florbetaben PET in a cohort of ALS patients, showed only a small number of patients with increased tracer uptake in several brain regions comparable to amyloid load observed in age-matched controls (Matías-Guiu et al. 2016). Therefore, cautious interpretation of these data and further investigations are required.

9.3.3 Evidence in α-Synuclein Spectrum

Aβ and α-synuclein may interact synergistically to enhance each other's aggregation and accelerate cognitive decline. The mechanisms by which these two aggregation-prone proteins interact remain unclear. However, growing evidence suggests that Aβ may influence α-synuclein pathology by modulating protein clearance, driving inflammation, activating kinases or directly altering α-synuclein aggregation (Marsh and Blurton-Jones 2012).

In DLB, which often presents also in co-morbidity with AD pathology, positivity to amyloid-PET was reported frequently (Ossenkoppele et al. 2015). Pure DLB cases are relatively rare (~20%), and Aβ deposition is often present (McKeith et al. 2017; Marsh and Blurton-Jones 2012). Four studies have compared amyloid brain imaging in DLB and AD; one found low global [^{11}C]PiB retention ratio in DLB (Kantarci et al. 2012); two other studies have also found lower cortical [^{11}C]PiB uptake in DLB compared with AD (Rowe et al. 2007; Villemagne et al. 2011a); and one study found no difference between DLB and AD, with very similar results in both groups in all cortical areas (Gomperts et al. 2008). Amyloid burden is higher in patients with DLB compared to PDD, but not as high as [^{11}C]PiB levels observed in AD (Gomperts et al. 2008; Fujishiro et al. 2010). [^{11}C]PiB binding has been linked to cognitive impairment in DLB (Gomperts et al. 2012). In PDD, [^{11}C]PIB binding was reported not to differ from PD patients or healthy individuals (Gomperts et al. 2008). However, cortical [^{11}C]PIB retention has been shown to predict cognitive decline in PD (Gomperts et al. 2012). Neuropathology studies confirm these findings by demonstrating greater amyloid pathology in DLB versus PDD/PD (Harding and Halliday 2001) and in PDD versus PD (Irwin et al. 2012). The presence of Aβ pathology in DLB may be the trigger of dementia onset and may influence the severity of cognitive impairment as well as dementia progression (Gomperts et al. 2012; Foster et al. 2010; Pletnikova et al. 2005).

While amyloid pathology is frequent in DLB, it is very rare in MSA (Jellinger 2007). Claassen et al. (Claassen et al. 2011) found no [^{11}C]PiB uptake in any of the three MSA patients included in their study, but in all the three DLB patients included. Kim et al. (Kim et al. 2013) reported no statistically significant differences in global [^{11}C]PIB binding between normal controls and MSA patients, neither when comparing the subgroups of MSA patients without and with dementia with normal

controls. These findings suggest that amyloid-PET imaging could be helpful in the differential diagnosis in cases where DLB and MSA may present with similar clinical symptoms (Fig. 9.6).

9.3.4 Strengths

In patients with dementia, amyloid-PET is recognized as a powerful tool to measure amyloid deposition (Fig. 9.6). Amyloid-PET imaging has the highest accuracy in ruling out AD (Chetelat et al. 2016), thus differentiating AD dementia from FTLD (Rabinovici et al. 2011), and in supporting AD diagnosis in subjects with MCI; in patients with suspected AD, but atypical presentation or aetiologically mixed presentation; and in patients with EOAD (Johnson et al. 2013b; Guerra et al. 2015).

9.3.5 Weaknesses

Major weakness is the presence of amyloid deposition in the elderly population as measured with PET (Rowe et al. 2010), consistently with Aβ depositions found in the brain of cognitively normal people at autopsy (Knopman et al. 2003). Approximately 25–35% of healthy elderly individuals have significant levels of Aβ deposition, predominantly in the posterior cingulate, precuneus and prefrontal regions, without overt clinical symptoms (Rowe et al. 2010; Mintun et al. 2006; Villemagne et al. 2008). The view that amyloid positivity equals AD dementia diagnosis has been challenged by the high prevalence of amyloid positivity in the elderly (about 44% in nonagenarians) despite normal cognitive function (Jansen et al. 2015). Moreover, brain amyloidosis across subjects appears more as a continuum rather than a clustered, binomial distribution (Fig. 9.7). In addition, the amyloid-PET visual reading classically refers to a binary lecture, i.e. negative or positive for amyloidosis; however, the current clinical experience provides evidence of borderline pathological values (Payoux et al. 2015). Although the interpretation of amyloid-PET in clinical practice is predominantly dichotomous through visual assessment, there is a growing body of evidence on the added value of standardized uptake value ratios (SUVrs) in the clinic (see Fig. 9.7 for an example) (Chen and Nasrallah 2017). The classification of amyloid positivity or negativity is dependent on the selected cut-off (Chételat et al. 2013), which varies according to the quantification method adopted for tracer binding estimation. To this regard, different quantification methods for amyloid-PET have been proposed, including either compartmental model binding tools or reference tissue model-based tools, with various regions of interests being suggested for the latter (see, for instance, (van Berckel et al. 2013)). Currently, no gold standard for amyloid-PET quantification has been yet established (van Berckel et al. 2013). Thus, the use of fully quantitative pipelines is highly recommended in intervention studies given the possible dependence of semi-quantified parameters on influencing factors such as cerebral blood flow (van Berckel et al. 2013).

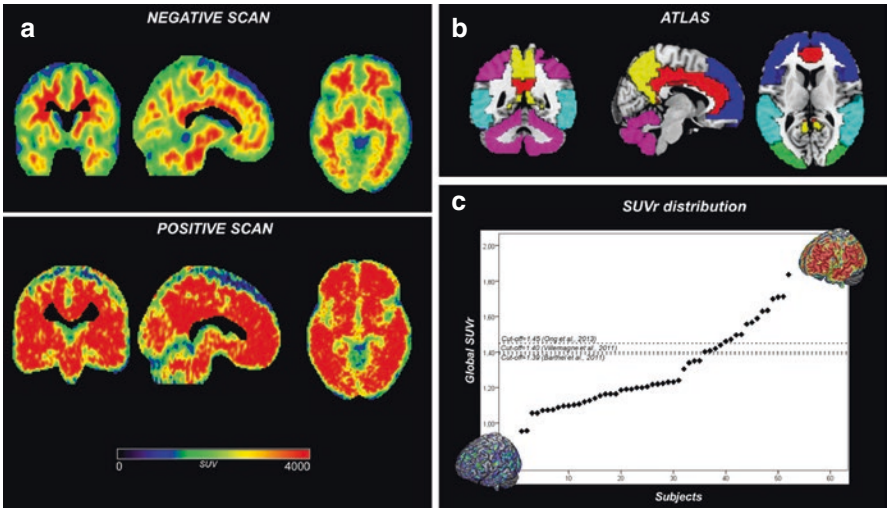

Fig. 9.7 Amyloid-PET quantification steps. (**a**) Example of [^{18}F]florbetaben-negative and [^{18}F] florbetaben-positive scans. (**b**) Regions of interest overlaid on a standardized template used to calculate and estimate regional standardized uptake value ratios (SUVrs), according to Presotto and colleagues (Presotto et al. 2018). Distribution of SUVr in a heterogeneous sample of subjects and patients ordered from lowest to highest amyloid-PET uptake, underlying the concept of amyloid continuum

As emerged by previous paragraphs, amyloid-PET cannot distinguish specific AD syndromes (Lehmann et al. 2013; Dronse et al. 2017) and amyloid-based pathologies, with most studies showing a non-specific pattern of amyloid burden diffusely distributed throughout the entire cortex across diseases (Maetzler et al. 2009; Kantarci et al. 2017; Baron et al. 2014). In addition, amyloid rate might not be the best predictor of speed of conversion from MCI to AD, as compared to [^{18}F]FDG-PET (Teipel et al. 2015; Iaccarino et al. 2017b). Amyloid-PET studies showed MCI patients presenting with wide variations in amyloid burden load (Villemagne et al. 2011b; Landau et al. 2016; Petersen et al. 2013), sometimes showing an intermediate "grey area" burden, challenging to classify as either positive or negative (Chételat et al. 2013). For these reasons a continuum in the amyloid load from negative to low or high deposition should be considered. This is allowed only by proper measurements.

An open question remains as to which amyloid-PET tracers are the most adequate to evaluate the efficacy of clinical trials. To date, the majority of clinical trials in AD have focused on amyloid therapies (e.g. (Sevigny et al. 2016; Salloway et al. 2014; Doody et al. 2014)), also including serial amyloid-PET scans to evaluate decreases in cerebral amyloid burden (Sevigny et al. 2016; Salloway et al. 2014). However, the adoption of amyloid-PET imaging for clinical trials has been criticized, since currently available amyloid-PET tracers measure fibrillary insoluble amyloid burden and are insensitive to toxic soluble amyloid oligomers (Kayed and Lasagna-Reeves 2013), which are much more clinically relevant and present in

the early phase of a disease (Haass and Selkoe 2007). Moreover, multi-tracer PET studies have revealed no clear association between amyloid accumulation and neurodegeneration (Lehmann et al. 2013; Dronse et al. 2017; Jagust et al. 2012; Jack et al. 2013) and only modest associations with cognitive status (Hedden et al. 2013; Ossenkoppele et al. 2014). The lack of a strong association between fibrillary amyloid burden and measures of cognition and neurodegeneration (Villemagne et al. 2017) suggests that clinical trials should be supported by other more sensitive and specific biomarkers. Accordingly, a recent study showed that the presence of ongoing downstream neurodegeneration both in healthy controls and amyloid-positive MCI subjects predicts a worse clinical outcome regardless of the upstream primary pathology. Adding the [^{18}F]FDG-PET status, the authors found a more rapid clinical progression rate in neurodegeneration-positive MCI subjects and healthy controls characterized by an AD-like hypometabolic pattern compared to those with non-AD patterns (Iaccarino et al. 2019). Thus, the inclusion of biomarkers of neurodegeneration can reduce the number of recruited subjects who are not on a trajectory to dementia, also avoiding exposure to possible side effects of the tested treatment.

9.4 PET Markers of Tauopathy

One of the most recent advances for *in vivo* PET imaging is the evaluation of cerebral tau burden (Okamura et al. 2016; Okamura et al. 2014a; Villemagne and Okamura 2014; Villemagne and Okamura 2015).

Tau protein is physiologically associated with the stabilization, assembly and functional integrity of microtubules, critical structures for cytoskeletal support and intracellular molecular transport (Wang and Mandelkow 2016; Villemagne et al. 2015). Abnormal tau aggregation is not exclusively present in the brains of AD patients, as it can also be detected in several other neurodegenerative diseases. Its hyperphosphorylation and accumulation is a key pathogenic event in a number of neurodegenerative conditions, i.e. *tauopathies*, and can potentially trigger remarkably different clinical phenotypes and disease courses (Villemagne et al. 2015; Dickson et al. 2011). In a normal brain, the ratio of 3R/4R tau is 1:1, but it can change across the different pathologies (Okamura et al. 2016; Villemagne et al. 2015). When agglomerating, hyperphosphorylated tau can additionally assume different conformations, such as paired helical filaments, straight filaments and irregular filaments (Villemagne et al. 2015). This biological complexity implies a considerably heterogeneous pathological picture which historically hampered the development of selective tau radioligands suitable for *in vivo* PET imaging (Villemagne and Okamura 2014).

Notwithstanding tau biological complexity, the synthesis of some radioligands is now available and is rapidly entering into research use and possibly for a potential validation in clinical practice (Okamura et al. 2016). To date, three broad groups of radioligands are under extensive evaluation, i.e. [^{18}F]THK5351, [^{18}F]THK5117 or

[^{18}F]THK5105 (Okamura et al. 2014b; Harada et al. 2015; Harada et al. 2016), [^{18}F]T807 (also known as [^{18}F]AV1451 or [^{18}F]flortaucipir) (Chien et al. 2013) and [^{11}C]PBB3 (Maruyama et al. 2013). Furthermore, novel second-generation tau-PET tracers, including [^{18}F]MK-6240 and [^{18}F]PI-2620, are coming in the research field with the aim of solving the shortcomings of first-generation tau tracers (no off-target binding). [^{18}F]MK-6240 has high affinity for neurofibrillary tangles with negligible off-target binding to monoamine oxidases (MAO)-A/B, as well as high brain uptake, homogenous distribution and rapid clearance (Hostetler et al. 2016; Pascoal et al. 2018). [^{18}F]PI-2620 has high signal-to-noise ratio and high affinity for neurofibrillary tangles with no MAO-A/B off-target binding and low-affinity binding to Aβ (Mueller et al. 2017).

9.4.1 Evidence in AD Spectrum

In the AD spectrum, tau-PET imaging has provided compelling evidence for a tight relationship between tau burden and synaptic dysfunction, grey matter atrophy and cognitive deficits (Ossenkoppele et al. 2016; Johnson et al. 2016; Schöll et al. 2016; Cho et al. 2016). Early reports additionally suggested that tau-PET was able to recapitulate the neuropathological Braak staging (Braak and Braak 1997), suggesting that it could be a valuable tool for the *in vivo* staging of AD pathology progression (Schöll et al. 2016; Schwarz et al. 2016) and confirming previous *post-mortem* evidence (Nelson et al. 2012; Murray et al. 2015). AD patients in the initial phases of the disease show high tracer retention in the medial temporal lobe (Wang and Mandelkow 2016), followed by involvement of other sentinel cortical regions, namely, the temporo-parietal cortices as the disease progresses, according to Braak and Braak stages I–VI (Schwarz et al. 2016).

Multiple reports showed a cross-sectional association between worsening of cognitive impairment and increasing cortical tau-PET binding, from normal cognition to MCI and AD dementia stages (Johnson et al. 2016; Schöll et al. 2016; Cho et al. 2016). Furthermore, PET studies using [^{18}F]THK5351 showed that higher temporal tau-PET uptake in AD patients was associated with an increased temporal atrophy and with the severity of cognitive impairment (Lockhart et al. 2016; Saint-Aubert et al. 2016; Sone et al. 2017). Temporal lobe involvement was associated with the degree of cognitive decline, regional grey matter atrophy and CSF tau levels (Cho et al. 2016; Brier et al. 2016; Gordon et al. 2016b; La Joie et al. 2018; Maass et al. 2017; Mattsson et al. 2017). Of note, the correspondence between tau accumulation, neurodegeneration and clinical manifestations stands in stark contrast with amyloid-PET evidence, which is not associated with specific patterns of neurodegeneration or cognitive impairment. Okamura and colleagues demonstrated that the degree of [^{18}F]THK5105 hippocampal retention correlated with cognitive performances in AD patients, differently from [^{11}C]PiB (Okamura et al. 2014a). Moreover, [^{18}F]AV-1451 retention in inferior temporal regions had a stronger correlation with the degree of cognitive impairment when compared to [^{11}C]PiB

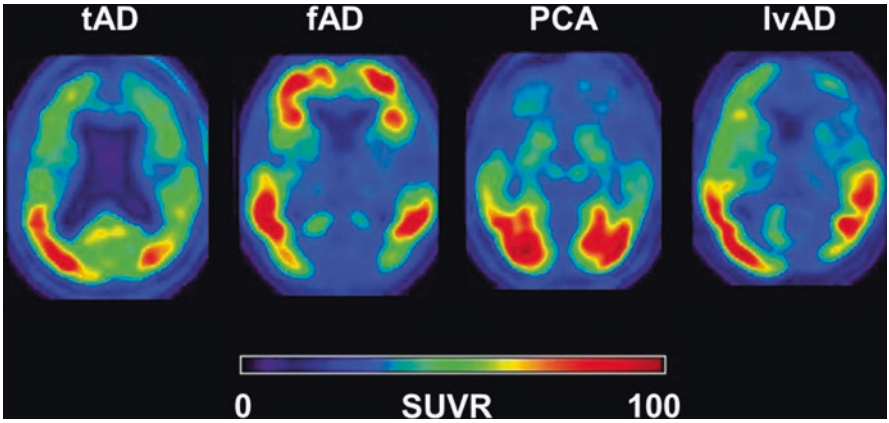

Fig. 9.8 Tau distribution in AD spectrum. [^{18}F]AV-1451 uptake topography in patients with typical and atypical AD. SUVr image intensities were normalized to each individual's global maximum. From left to right: typical AD; frontal AD; PCA and lvAD. *tAD* typical Alzheimer's disease, *fAD* frontal AD, *PCA* posterior cortical atrophy, *lvAD* logopenic variant of AD, *SUVR* standardized uptake value ratio. (Reprinted from Journal of Alzheimer's disease, 55, Dronse, Juliana, Fliessbach, Klausc; Bischof, Gérard…..Drzezga, Alexanderd, *In vivo* Patterns of Tau Pathology, Amyloid-β Burden, and Neuronal Dysfunction in Clinical Variants of Alzheimer's Disease, 465–471, Copyright (2017), with permission from IOS Press)

(Johnson et al. 2016). Similar results have been shown using other tau-PET tracers including [^{11}C]PBB3 (Maruyama et al. 2013; Shimada et al. 2017), [^{18}F]THK5317 (Chiotis et al. 2016) and [^{18}F]THR5117 (Harada et al. 2015; Ishiki et al. 2015).

The topographical specificity of tau-PET uptake distribution especially emerged for the AD variants (Fig. 9.8), which are known to present phenotype-specific patterns of neurodegeneration, as assessed with [^{18}F]FDG-PET. Patients with typical AD show a similar extent of [^{18}F]AV-1451 uptake in the entorhinal and cortical associative regions, whereas patients with atypical AD show higher levels of tracer uptake in the cortex than entorhinal regions (Whitwell et al. 2018b). EOAD patients show a greater involvement of neocortical regions than AD patients developing the disease at a later age (Scholl et al. 2017). A younger age at onset was associated with predominant tau deposition in wide regions of the neocortex, while an older age at onset was associated with increased [^{18}F]AV-1451 uptake, specifically in the medial temporal lobe (Ossenkoppele et al. 2016). Both EOAD and PCA showed symmetric and broadly distributed [^{18}F]AV-1451 uptake. EOAD had highest effect sizes in medial temporal and right temporo-parietal regions, while PCA had largest effect sizes in posterior cortical structures (Nasrallah et al. 2018). High [^{18}F]AV-1451 uptake in the right hippocampus, amygdala, fusiform gyrus and cuneus was shown to be associated with memory impairment in five typical AD patients, while high uptake in the right lingual gyrus was associated with visuospatial deficits in five PCA patients, and high uptake in the left anterior superior gyrus was associated with language deficits in four lvAD patients (Phillips et al. 2018).

9.4.2 Evidence in FTLD Spectrum

PET imaging has contributed significantly in the characterization of the neuronal deposition of tau throughout the disease course of FTLD. In the FTLD spectrum, FTLD-tau is present in ~50% of bvFTD patients and in ~70% of PNFA (Mackenzie et al. 2008; Kertesz et al. 2005; Rascovsky et al. 2013). FTLD-tau has three repeats (3R) or four repeats (4R). Accumulation of the 4R tau isoforms is predominant in PSP, CBD, PNFA and up to one third of patients presenting with bvFTD (Mackenzie and Neumann 2016; Spinelli et al. 2017; Lee et al. 2011; Perry et al. 2017; Hughes et al. 2002), whereas the 3R tau isoforms are predominantly accumulated in TDP-43 pathology, in the majority of patients with SD (~80% of cases) and FTD/ALS (Spinelli et al. 2017; Neumann et al. 2006). A *post-mortem* autoradiographic analysis demonstrated that [^{18}F]AV-1451 strongly binds to tau lesions in AD brains, but not to non-AD tauopathy or to Aβ-, α-synuclein- or TDP-43-containing lesions (Marquié et al. 2015). Consistently, Sander et al. (Sander et al. 2016) found high specific binding of [^{18}F]AV-1451 in AD *post-mortem* brain tissue, but moderate binding in FTLD with parkinsonism and low but displaceable binding in CBD. Yet, *in vivo* [^{18}F]AV-1451-PET studies appear to be more encouraging regarding tau pathology identification in FTLD spectrum (Laforce Jr et al. 2018). A study investigating 20 patients with bvFTD, 20 AD patients and 20 healthy controls revealed high [^{18}F]AV-1451 binding in the basal ganglia and in frontal, anterior cingulate and insula white matter of patients with bvFTD, which was helpful in distinguishing these patients from AD and healthy controls (Cho et al. 2018). In bvFTD, an autopsy series of 117 patients demonstrated 34 and 55 cases of FTLD-tau and FTLD-TDP-43, respectively (Perry et al. 2017). Consistently, a recent study showed a bimodal separation where five of ten patients with bvFTD showed frontotemporal tracer [^{18}F]AV-1451 uptake, possibly reflecting the differentiation between tau and TDP (Tsai et al. 2019).

In another study, using [^{18}F]AV-1451 in a sample composed of 40 PPA patients, SD showed elevated uptake (left>right) in anteromedial temporal lobes, compared to controls and PNFA; PNFA showed elevated uptake (left>right) in prefrontal white matter and in subcortical grey matter, compared to healthy controls and SD (Josephs et al. 2018). Another study reported increased [^{18}F]AV-1451 uptake in left greater than right frontal operculum, middle/inferior frontal gyri and left superior frontal gyri in PNFA compared to controls (Tsai et al. 2019). The reported notable tracer uptake in syndromes associated with TDP-43 pathology, such as SD, raises concerns about the specificity of [^{18}F]AV-1451 binding for FTLD tau pathology. In two patients with PET to autopsy correlation, mild [^{18}F]AV-1451 binding was seen in some areas with tau pathology (neurofibrillary tangles or argyrophilic grain disease), but binding patterns did not correspond with the distribution of FTLD TDP-43 type B inclusions (Tsai et al. 2019).

Recently, [^{18}F]THK5351 showed greater cortical uptake in FTLD than [^{18}F]AV-1451 (Jang et al. 2018), which overlaps with brain atrophy on magnetic resonance imaging (MRI) and shows good correlation with clinical phenotypes (Jang et al. 2018). Lee and colleagues showed higher binding (left>right) of the

tracer [^{18}F]THK5351 in the antero-inferior and lateral temporal cortices in five SD patients compared to controls, with a direct correlation with clinical severity and an inverse correlation with local glucose metabolism as measured with [^{18}F]FDG-PET (Lee et al. 2018a). High [^{18}F]THK-5351 retention in bilateral temporal lobes, predominantly on the left side, was confirmed by a subsequent study (Kobayashi et al. 2018). Schaeverbeke and colleagues reported increased [^{18}F]THK5351 binding in the supplementary motor area, left premotor cortex, thalamus, basal ganglia and midbrain in PNFA compared with controls and SD and an increased binding in the temporal lobes bilaterally in SD compared with controls and PNFA (Schaeverbeke et al. 2018).

The presence of MAO-B may confound the [^{18}F]THK5351-PET retention, as indicated by a previous study in which the administration of MAO-B inhibitors reduced the uptake of [^{18}F]THK5351 throughout the entire brain (Ng et al. 2017).

The *in vivo* PET study of tau burden in patients with PSP is challenging because of the high levels of off-target binding to neuromelanin and MAO-B in regions typically involved in this condition (Vermeiren et al. 2018). The tracers mostly found affected in PSP are [^{18}F]AV-1451 (Vermeiren et al. 2018; Marquie et al. 2017; Coakeley and Strafella 2017), [^{18}F]THK5351 (Ishiki et al. 2018) and [^{11}C]PBB3 (Perez-Soriano et al. 2017), and off-target binding may explain why some studies failed to detect differences between PSP patients and controls (Coakeley and Strafella 2017). Most studies, using [^{11}C]PBB3, [^{18}F]FDDNP and [^{18}F]THK5351 tracers, showed a typical distribution involving subcortical areas such as the striatum, thalamus, midbrain and cerebellum (Perez-Soriano et al. 2017; Kepe et al. 2013; Ishiki et al. 2017; Brendel et al. 2017), reflecting the tau distribution that has been observed in neuropathological studies (Dickson 1999). [^{18}F]AV-1451-PET studies commonly found highly increased radiotracer binding in the globus pallidus and midbrain relative to controls (Cho et al. 2017a; Passamonti et al. 2017; Smith et al. 2017a; Whitwell et al. 2017b; Schonhaut et al. 2017). However, this tracer seems to be not ideal to assess tau pathology in PSP, since no correlation was found with motor severity in patient groups; there was no increased tracer binding cortically in PSP patients, and variable degrees of subcortical binding were even detected in controls. One of these studies showed that elevated [^{18}F]AV-1451 uptake in the globus pallidus was the most useful feature in distinguishing PSP from healthy controls and PD (Schonhaut et al. 2017). However, another study using the same tracer found no significant tracer retention in PSP patients compared to PD and controls (Coakeley et al. 2017).

In CBD, tau-PET studies using different tau radioligands showed increased uptake in the globus pallidus and in the frontal and parietal cortices contralaterally to the most affected clinical side (Kikuchi et al. 2016). Tau deposition involving the basal ganglia, the thalamus and neocortical areas, which clearly distinguished CBD from AD patients, was found in a longitudinal PET study using [^{18}F]THK5317 (Chiotis et al. 2018). Higher [^{18}F]AV-1451 uptake has been found in the basal ganglia and in the precentral grey and white matter, mainly contralateral to the clinically most affected side, in 6 Aβ-negative CBD patients compared to 20 age-matched controls (Cho et al. 2017b). In this series, elevated precentral white matter

[^{18}F]AV-1451 binding correlated with motor severity (Cho et al. 2017b), while another series reported six of eight patients with CBD with asymmetric [^{18}F]AV-1451 binding in motor cortex and white matter (Smith et al. 2017b).

9.4.3 Evidence in α-Synuclein Spectrum

Using [^{18}F]AV-1451 PET, increased neocortical [^{18}F]AV-1451 retention was reported in DLB and also correlated to cognitive performances (Kantarci et al. 2017; Gomperts et al. 2016; Smith et al. 2018). The pattern of tau distribution mainly involved temporo-parietal cortices (Kantarci et al. 2017; Gomperts et al. 2016; Smith et al. 2018) but also the precuneus (Gomperts et al. 2016) and occipital cortex (Kantarci et al. 2017). However, tau binding in DLB patients was relatively lower than that of AD patients (Kantarci et al. 2017). Notably, 4 out of 17 of the DLB patients presenting with low amyloid burden had elevated [^{18}F]AV-1451 uptake in the inferior temporal cortex, suggesting an independent effect of tau pathology with respect to amyloid burden (Gomperts et al. 2016). A pattern similar to that of DLB, but with lower magnitude and extension, was observed in PD in the presence of cognitive decline ranging from mild to severe impairment (Gomperts et al. 2016). Lee and colleagues studied 12 idiopathic PD patients, 22 PD with cognitive impairment and 18 DLB patients using [^{18}F]AV-1451, for tau, and [^{18}F]florbetaben, for detection of β-amyloid deposits; the cohort also included 25 AD and 25 healthy controls (Lee et al. 2018b). DLB showed slightly increased [^{18}F]AV-1451 binding in the sensorimotor, parieto-temporal and visual cortices, compared with normal controls, and lower binding in temporal cortices when compared with AD. DLB with Aβ-positive scans also showed an increase of tau deposition in the same cortical regions (Lee et al. 2018b).

High[^{18}F]AV-1451 binding in the posterior putamen was found in 4 MSA-p. Tau tracer uptake was more prominent in the side ipsilateral to the greater putaminal atrophy, together with lower uptake of DAT PET contralateral to the clinically more affected side (Cho et al. 2017c). Considering the low probability for tau pathology to be present in these cases, as tau pathology was found to be very rare in MSA histopathology (Nagaishi et al. 2011), the elevated PET signal was most likely caused by off-target binding to overexpressed MAO in the neuroinflammatory process.

9.4.4 Strengths

There is tremendous potential for tau imaging to provide novel information on the earliest events in the pathophysiological cascade of AD and other dementias. Tau imaging studies show not only that tau tracer retention reflects the known distribution of aggregated tau in the brain seen in *post-mortem* studies (Braak and Braak 1997; Delacourte et al. 2002) but also that tau deposition is closely related to neurodegeneration, grey matter atrophy and tau CSF levels (Xia et al. 2017; Brier et al.

2016; Gordon et al. 2016b; Chiotis et al. 2018; van Eimeren et al. 2017). In contrast to Aβ imaging, for which the total amount in the brain is more relevant than the regional Aβ distribution as a possible driver of cognitive decline, tau-PET imaging provides crucial information about the topographical distribution of pathology in the brain (Villemagne et al. 2018). Moreover, several groups found robust differences in tracer retention between cognitively unimpaired elderly individuals, patients with AD (Johnson et al. 2016; Schöll et al. 2016; Cho et al. 2016; Okamura et al. 2017; Sarazin et al. 2016; Wang et al. 2016) and patients with atypical AD presentations (Ossenkoppele et al. 2016). Tau-PET imaging could be considered a good candidate biomarker useful to predict progression of AD and/or for disease staging.

9.4.5 Weaknesses

While providing a wealth of evidence with critical implications for disease tracking and possibly future monitoring of AD interventions, the above-mentioned studies have also highlighted several areas of criticisms which need further consideration. Of note, the selectivity of the current tau-PET radioligands for non-AD tauopathies is not well established. Previous autoradiographical studies on the most commonly adopted tau-PET compounds, such as the [^{18}F]AV-1451, have shown high affinity for the AD tauopathy (Marquié et al. 2015; Lowe et al. 2016), but not for the 4R tau aggregates typical of primary tauopathies, such as PSP or CBD, where *post-mortem* results are more heterogeneous and, overall, present less robust staining (Marquié et al. 2015; Sander et al. 2016; Ishiki et al. 2017; Kikuchi et al. 2016; Lowe et al. 2016; Josephs et al. 2016). Another area of concern regards consistent non-specific tau-PET binding in subcortical structures, especially in the striatum and in the choroid plexus, in healthy controls, suggesting that the currently available tau tracers could present off-target binding, such as to neuromelanin (Marquié et al. 2015; Lowe et al. 2016). Moreover, as tau pathology is predominantly located intraneuronally, tracers have the challenging task not only to cross the blood–brain barrier but also to enter the intra-neuronal compartment. The tracer specificity is further challenged by the lower concentration of tau aggregates with respect to Aβ levels in AD brain (Bischof et al. 2017). Finally, suitable quantification approaches remain to be established. Building on these premises, tau-PET diagnostic value, especially in non-AD tauopathies, needs further validation.

9.5 PET Markers of Neuroinflammation

Increasing evidence suggests that neuroinflammation plays a crucial role in the neurodegeneration processes (Ransohoff 2016). Many neurodegenerative diseases share the same pathological deposition of specific proteins, hence the term “proteinopathies” that introduced to focus on the biological characterization of these disorders (Perani et al. 2019). The pathological deposition of these specific proteins

is involved in a cascade of deleterious events which in turn lead to synaptic dysfunction and neuronal loss (Golde et al. 2013). Another common feature in neurodegenerative diseases is the chronic activation of innate immune cells within the central nervous system (Stephenson et al. 2018). Several preclinical studies have shown that specific protein species, including amyloid, tau and synuclein, can stimulate the activation of the neuroimmune cells, i.e. microglia and astrocytes (Zhang et al. 2005; Lee et al. 2013; Lian et al. 2016; Brelstaff et al. 2018). Starting from these evidences, a large part of research in neuroscience focused on the understanding of physiopathological mechanisms which link neuroinflammation and neurodegeneration (Subhramanyam et al. 2019; Pasqualetti et al. 2015). Elucidating the role of neuroinflammatory cells and mechanisms in neurodegenerative diseases may provide evidence for new reliable markers of disease severity and progression, as well as help in identifying targets for novel therapeutic strategies (Heneka et al. 2014; Du et al. 2017; Valera et al. 2016).

Microglia and astrocytes are the main constituent of the neuroimmune system, acting in relation to the cross-talk with other immune system players and depending on environmental physiological and pathological stimuli (Gentleman 2013). Microglial function *in vivo* is heterogeneous, and it is related to the expression of pro-inflammatory and protective activation phenotypes (Comi and Tondo 2017). Microglia neuroprotective activities include phagocytosis of apoptotic cells and cellular debris clearance, synaptic remodelling and neuronal circuits maintenance and release of steroids and neurotrophic factors (Ji et al. 2013; Kettenmann et al. 2011). Together with astrocytes, microglia represent the first line of response to any insult to the nervous system. Typically, microglia are activated at first, promoting inflammatory response through the release of signalling molecules, which activate astrocytes and influence the excitability of neurons (Russo and McGavern 2015). This homeostatic response can be beneficial, promoting recovery from the original insult, but can be also detrimental and may damage healthy neurons by producing reactive oxygen species and pro-inflammatory cytokines (Pekny and Pekna 2014).

Clinical studies confirmed that activation of both microglia and astrocytes is an early phenomenon in neurodegenerative disorders. However, the precise role of the different players of neuroinflammatory responses, as well as the complicate interactions during neurodegenerative processes, is still far to be completely clarified (Schain and Kreisl 2017; Chen et al. 2016; Rodriguez-Vieitez et al. 2016).

A precious tool for *in vivo* quantification of neuroinflammation is PET imaging, used for detecting both microglia activation and reactive astrocytosis in different neurodegenerative conditions (Cerami et al. 2017b; Narayanaswami et al. 2018). Given its unique ability to detect the dynamic changes characterizing inflammatory responses in the central nervous system, PET imaging of neuroinflammation can represent a marker for early disease identification and progression monitoring (Schain and Kreisl 2017; Best et al. 2019). Furthermore, shedding light on the pathogenesis of neurodegeneration, PET imaging of neuroinflammation may be fundamental in exploring the effectiveness of novel treatment targets and monitoring the therapeutic efficacy (Piel et al. 2014).

Microglia express the 18 kDa translocator protein (TSPO), an intracellular protein formerly known as peripheral benzodiazepine receptor (Papadopoulos et al. 2006). TSPO is a five-transmembrane domain protein mainly situated to the outer mitochondrial membrane which is involved in the transport of cholesterol into mitochondria, a fundamental step in steroid synthesis. TSPO has been also associated with other mitochondrial functions, such as mitochondrial membrane permeability, calcium-mediated signalling, generation of reactive species, cell proliferation and apoptosis (Gatliff and Campanella 2012). Although its roles are not completely defined yet, TSPO has been shown to be overexpressed by activated microglia, reactive astrocytes and vascular endothelium and, to a much lesser extent, in neurons, in case of neuroinflammatory response to insults of various aetiologies (Gatliff and Campanella 2012). Thus, TSPO density has been used as a biomarker for neuroinflammation in various neurological disorders (Chen and Guilarte 2008).

[^{11}C]PK11195 is the progenitor and the most widely used of a series of PET radiotracers which allow to *in vivo* measure TSPO levels (Turkheimer et al. 2015). Although [^{11}C]PK11195 provides a great deal of visual information on glial activation, its use can be problematic. [^{11}C]PK11195 has a low brain permeability and high non-specific plasma protein binding: this results in a low signal-to-noise ratio in PET imaging and in low specificity (Banati et al. 2000). In addition, it has a moderate intraindividual reproducibility (Jučaite et al. 2012). Since the introduction of [^{11}C]PK11195, many second-generation tracers have been developed, generally with greater specific binding than the prototype and with different sensitivity, signal-to-noise ratio, accumulation and binding stability (Fujita et al. 2017). They encompass [^{11}C]PBR28, [^{18}F]DPA-714, [^{18}F]FEPPA, [^{18}F]PBR06, [^{18}F]PBR11 and [^{11}C]DAA1106 which have been used to image glial activation in brain disorders (Vivash and O'Brien 2016). However, the first studies using second-generation TSPO tracers already evidenced large interindividual differences in tracer binding amongst healthy controls. This variation in binding affinity is a shared characteristic of all tested second-generation TSPO tracers, and it is due to the existence of a single nucleotide polymorphism in the TSPO gene, the rs6971, which results in three different genotypes with different binding affinity (Owen et al. 2012). Given the presence of individuals with low-affinity binding, and consequent negligible TSPO PET signal, as well as the notable difference in binding between individuals with mixed and high-affinity binding capacity (Collste et al. 2016), genotype evaluation is mandatory in clinical and research studies to avoid inaccurate interpretation of results. Of note, the quantification of TSPO overexpression in PET imaging studies may be particularly challenging, mainly due to the heterogeneous distribution of TSPO across the brain which hampers the identification of a clear reference region. Several clustering methods have been proposed to overcome this limitation (Turkheimer et al. 2007). Differences in analysis method together with the use of different tracers with different kinetic properties may explain some contrasting results in TSPO PET imaging studies (Turkheimer et al. 2015).

A third generation of tracers is currently under evaluation. Flutriciclamide [^{18}F]GE180 and [^{11}C]ER176 are third-generation TSPO tracers insensitive to the rs6971 polymorphism, but their clinical relevance needs to be totally determined

(Dupont et al. 2017). To date, [^{11}C]PK11195 remains the most validated TSPO radiotracer and is most widely used in human studies.

Astrocytes are the most numerous brain cell type and are involved in many physiological functions, including growth factors production, neuronal microenvironment and homeostasis maintenance and synaptic plasticity support (Vasile et al. 2017). Astrocytes may be activated in response to a plethora of pathogenic stimuli and participate in the neuroinflammatory response involved in the progression of neurodegenerative diseases (Li et al. 2019). Astrocyte activation generates different cellular phenotypes (Anderson et al. 2014) and leads to the production of several molecules which serve as markers for astrocytosis detection in preclinical and clinical studies (Sriram et al. 2004; Ekblom et al. 1993; Rodriguez-Vieitez and Nordberg 2018). Despite growing literature focusing on the role of astrocytosis in neurodegenerative processes, a high level of controversy remains about its role, given the complexity of responses and the heterogeneity of possible phenotypes (Li et al. 2019).

[^{11}C]deuterium-L-deprenyl (DED) is a PET tracer with high affinity and specificity for the MAO-B (Fowler et al. 1987), an enzyme expressed on the outer mitochondrial membrane and occurring predominantly in astrocytes (Saura et al. 1996). Thus the [^{11}C]DED has been used in several central nervous system diseases, such as AD, CJD and ALS, as well as in healthy older individuals, to track reactive astrocytosis (Engler et al. 2003; Rodriguez-Vieitez et al. 2016; Johansson et al. 2007; Carter et al. 2012; Santillo et al. 2011).

9.5.1 Evidence in AD Spectrum

Several studies have shown that neuroinflammatory responses are a crucial event in AD pathophysiology (Calsolaro and Edison 2016). Both Aβ plaques and tau neurofibrillary tangles have shown to activate microglia and induce neurotoxicity in preclinical studies (Asai et al. 2014; Maezawa et al. 2011; Marlatt et al. 2014; Morales et al. 2013). In AD brain, activated microglia and reactive astrocytes have been found to surround Aβ plaques (Cosenza-Nashat et al. 2009; McGeer et al. 1988). Consequently, neuroinflammatory responses are now considered to actively contribute to and drive AD pathogenesis (Heppner et al. 2015).

Most of the PET imaging studies in the neuroinflammation field focused on the study of microglia activation in AD (Best et al. 2019). The large majority of [^{11}C]PK11195 PET *in vivo* studies reported increased microglia activation, specifically involving temporo-parietal regions (consistently across different studies) and frontal, occipital and cingulate cortices (Cerami et al. 2017b). Increased cortical [^{11}C]PK11195 binding has been found also in MCI condition (Cagnin et al. 2001), especially in subjects with high cortical amyloid load (Okello et al. 2009; Parbo et al. 2017). The presence of an early and a late peak of microglia activation with a protective function in MCI and with a chronic deleterious role in late AD has been suggested (Fan et al. 2017). The detection of increased TSPO expression in the prodromal AD stage has obvious repercussions in elaborating and monitoring novel

disease-modifying therapies. Although some studies reported a relationship between neuroinflammation and amyloid deposition, as measured by [^{11}C]PIB-PET (Parbo et al. 2017; Fan et al. 2015a; Edison et al. 2013; Fan et al. 2015b; Edison et al. 2008), the co-localization of microglia activation and amyloid load is debated, due to the detection of microglia activation in absence of amyloid plaques (Okello et al. 2009; Yokokura et al. 2011), suggesting that these pathological processes may occur independently (Wiley et al. 2009). When assessed longitudinally, AD patients showed increased [^{11}C]PK11195 binding over time, associated with both progressively decreased brain metabolism as assessed by [^{18}F]FDG-PET and increased cortical amyloid deposition, as assessed by [^{11}C]PIB-PET (Fan et al. 2015b). The evidence of an inverse correlation between neuroinflammation and brain glucose hypometabolism suggests that chronic microglia activation may have a detrimental effect on neuronal function (Fan et al. 2015a), and, as a confirmation, it has been recently shown that neuroinflammation may impair large-scale network connectivity in AD (Passamonti et al. 2019). Notably, several studies showed a negative correlation between high levels of microglia activation and cognitive status, indicating the active role of cortical neuroinflammation in driving neuronal dysfunction (Fan et al. 2015a; Edison et al. 2008; Yokokura et al. 2011).

A few studies reported no differences in [^{11}C]PK11195 binding between AD and controls and between MCI and controls (Wiley et al. 2009; Schuitemaker et al. 2013). These negative results are most likely related to the small sample size and to differences in [^{11}C]PK11195 binding quantification (Schain and Kreisl 2017; Turkheimer et al. 2015).

Studies using second-generation TSPO radioligands in AD and MCI have shown contradictory results (Cerami et al. 2017b; Best et al. 2019). A study using [^{11}C]PBR28-PET reported that TSPO expression, especially in temporo-parietal regions, correlated with severity of dementia in AD, but failed to detect any difference between MCI and healthy controls, proposing [^{11}C]PBR28-PET as a marker of disease progression (Kreisl et al. 2013). The same group suggested the use of [^{11}C]PBR28-PET in differentiating AD clinical phenotypes, showing an increased uptake of [^{11}C]PBR28 in visual cortices in patients with PCA (Kreisl et al. 2017) and in limbic regions in patients with the amnestic variant of AD (Kreisl et al. 2013). In addition, these authors reported greater [^{11}C]PBR28-PET binding in early-onset AD than late-onset AD patients (Kreisl et al. 2013). Comparing AD patients with different rate of progression, a large study using [^{18}F]DPA714 revealed a higher TSPO expression in patients with slower clinical progression, suggesting a protective role of neuroinflammation in the early stages of AD (Hamelin et al. 2016). Overall, these results along with other findings from studies using second-generation TSPO tracers (Yasuno et al. 2012; Yasuno et al. 2008; Suridjan et al. 2015; Varrone et al. 2013; Golla et al. 2015) are not clear-cut, given the small sample size and the differences in methodological approach for TSPO quantification which may result in inconsistent data.

Activated astrocytes are key players in neuropathological changes which lead to neurodegeneration in AD. Astrocytes co-localize with Aβ plaques in *post-mortem* AD brain (Nagele et al. 2003), but their *in vivo* roles and functions are still not fully

elucidated. [^{11}C]DED-PET imaging has been used to investigate reactive astrocytosis in both AD patients and MCI subjects. Higher tracer binding has been detected in frontal, parietal and temporal cortices of AD patients and amyloid-positive MCI subjects compared to healthy controls (Carter et al. 2012; Santillo et al. 2011). The correlation between tracer uptake and hippocampal grey matter loss suggests that early atrocytosis may influence neuronal loss (Choo et al. 2014). Early reactive astrocytosis has been confirmed in the pre-symptomatic stage of genetic AD, where [^{11}C]DED binding has been found to correlate with higher amyloid deposition, indicating astrocytosis as an early driving force in AD pathology (Schöll et al. 2015). In a large longitudinal multi-tracer PET imaging study of subjects with autosomal dominant or sporadic AD, regional astrocytosis, brain glucose metabolism and cortical amyloid burden were assessed in pre-symptomatic stage and in symptomatic stage. Amyloid deposition in pre-symptomatic autosomal dominant AD started 17 years before expected symptom onset; at the same time, increased astrocytosis was found, which was then progressively declining, while amyloid burden increased with disease progression. As expected, brain glucose metabolism was found to reduce with disease progression (Rodriguez-Vieitez et al. 2016). These findings confirmed a prominent astrocyte activation in the early, pre-symptomatic dementia stage, when promising therapeutic potential is possible.

9.5.2 Evidence in FTLD Spectrum

Microglia activation is thought to play a role also in FTLD and in related tauopathies, and it has been investigated with *in vivo* PET imaging studies in both symptomatic patients and pre-symptomatic carriers of MAPT mutations (Cagnin et al. 2004; Miyoshi et al. 2010; Bevan-Jones et al. 2019). The first study investigating neuroinflammation in the FTLD spectrum involved five patients with a clinical diagnosis of FTD (four patients affected by SD and one patient affected by bvFTD) and showed increased [^{11}C]PK11195 binding in frontotemporal regions and in the putamen bilaterally, reflecting the distribution pattern of synaptic dysfunction and neuronal degeneration characterizing FTLD (Cagnin et al. 2004). These results have been recently replicated using the second-generation TSPO tracer [^{11}C]PBR28, whose binding was reported higher in frontal, temporal but also parietal and occipital regions in four FTLD patients (Kim et al. 2019).

In vivo characterization of neuroinflammation may serve as a precious tool in disease monitoring as shown in studies of genetic forms of FTLD (Miyoshi et al. 2010; Bevan-Jones et al. 2019). FTD with parkinsonism linked to chromosome 17 is a FTLD disorder due to mutations in the chromosome 17 involving the microtubule-associated protein tau (MAPT) or the progranulin (PGRN) gene, usually characterized by a dysexecutive syndrome associated with behavioural disturbances, parkinsonism and aphasia (Boeve and Hutton 2008). A study using a second-generation tracer, [^{11}C]DAA1106, investigated microglia activation in three pre-symptomatic MAPT gene mutation carriers, showing increased microglia activation in the frontal, occipital and posterior cingulate cortices in carriers compared

to controls (Miyoshi et al. 2010). In addition, the early presence of microglia activation has been reported in an asymptomatic MAPT mutation carrier, despite the lack of atrophy, as measured by MRI, or tau deposition, as measured by [^{18}F]AV-1451-PET (Bevan-Jones et al. 2019). These findings suggest the presence of neuroinflammation in genetic tauopathies even in an early, pre-symptomatic stage, representing a potential marker for monitoring of novel therapeutic approaches.

Microglia activation showing spatial correspondence with the topographical distribution of tau pathology has been revealed in other tauopathies, i.e. CBD and PSP. PSP and CBD are neurodegenerative parkinsonism with considerable clinical, pathological and genetic overlap (Ling and Macerollo 2018). Both diseases are pathologically characterized by neuronal and glial tau deposition, but with a different distribution, which affects primarily subcortical regions in PSP while involving white matter and cortical regions in CBD (Dickson 1999). Microglia activation has been reported in *post-mortem* examination of brains affected by tauopathies, including PSP and CBD (Sasaki et al. 2008). *In vivo* PET studies of neuroinflammation confirmed that microglia activation in these diseases follows the distribution of the corresponding pathology. In PSP, significant levels of activated microglia as measured by [^{11}C]PK11195 have been detected in the basal ganglia, midbrain, frontal lobe and cerebellum (Gerhard et al. 2006a; Passamonti et al. 2018), showing a pattern of distribution which clearly distinguished PSP patients from AD patients. [^{11}C]PK11195 binding in pallidus, midbrain and pons was found to correlate with disease severity (Passamonti et al. 2018). In CBD, increased [^{11}C]PK11195 binding was detected in basal ganglia, pons, precentral gyrus and post-central gyrus (Gerhard et al. 2004; Henkel et al. 2004), showing a lateralization according to the clinically more affected side. This suggested the involvement of microglia activation in CBD pathogenesis (Henkel et al. 2004).

9.5.3 Evidence in α-Synuclein Spectrum

Synuclein can directly generate a neuroinflammatory response (Reynolds et al. 2008), and activated microglia and reactive astrogliosis are common findings in *post-mortem* PD, DLB and MSA patients' brain (McGeer et al. 1988; Radford et al. 2015; Imamura et al. 2003), indicating a close relationship between neuroinflammation and neurodegeneration in synucleinopathies.

Coherently with neuropathological findings, *in vivo* [^{11}C]PK11195 PET studies in PD patients reported increased tracer bindings in the striatum, substantia nigra, putamen, brainstem, frontal and temporal cortices (Gerhard et al. 2006b; Ouchi et al. 2005; Kang et al. 2018; Bartels et al. 2010), positively correlating with motor impairment (Ouchi et al. 2005; Bartels et al. 2010). In a study comparing PD and DLB patients, increased microglia activation was detected in the basal ganglia and substantia nigra in both groups, while the cerebellum and association cortex were involved only in DLB group, in line with the neuropathology (Iannaccone et al. 2013). In addition, selecting patients within 1 year since the disease onset, the authors showed that microglia activation is an early phenomenon in

synucleinopathies (Iannaccone et al. 2013). In DLB a strong correlation between [^{11}C]PK11195 binding and cognitive decline has been reported, again suggesting a role of microglia activation in supporting neurodegeneration changes (Surendranathan et al. 2018). When comparing [^{11}C]PK11195 uptake in PD and PDD patients, an increased binding was found in cingulate, frontal, temporal and occipital cortices in both groups, confirming that cortical microglia activation may be present also in non-demented patients (Edison et al. 2013). However, PDD had a more widespread tracer cortical distribution, with a correlation with global cognition impairment, as measured by Mini Mental State Evaluation, and a large overlap with brain hypometabolism, as measured by [^{18}F]FDG-PET (Edison et al. 2013). As a confirmation, a co-localization between microglia activation and hypometabolism in frontal, temporal, parietal and occipital lobes was found in another study on PDD, with increased [^{11}C]PK11195 negatively correlating with MMSE score, thus implying that microglia activation may drive neuronal dysfunction in PDD (Fan et al. 2015a).

The presence of activated microglia has also been reported in MSA. *In vivo* studies on neuroinflammation in MSA, using [^{11}C]PK11195-PET imaging, showed increased tracer uptake in patients compared to controls in caudate nucleus, putamen, pallidum, substantia nigra, pons and cortical regions (Gerhard et al. 2003; Kübler et al. 2019), but without correlation with clinical parameters (Kübler et al. 2019).

[^{11}C]PK11195-PET imaging was also adopted to monitor MSA patients involved in a prospective clinical trial using minocycline, an anti-inflammatory drug (Dodel et al. 2010). After 24 weeks of treatment, there was a reduction in [^{11}C]PK11195 binding in some patients, showing the effectiveness of minocycline in reducing microglia activation but, again, without any clinical benefit during the overall study (Dodel et al. 2010). These findings suggest that microglia activation involves brain areas typically affected in MSA pathology, but the clinical relevance of these data still needs further investigation.

9.5.4 Evidence in Prion Diseases Spectrum

Prion diseases are rare, rapidly progressive devastating conditions caused by the accumulation of abnormally shaped proteins called prions and include sporadic, genetic and acquired forms (Geschwind and Wong 2014).

CJD is the most common form of human prion disease, and it is pathologically characterized by the typical spongiform degeneration of neurons which is accompanied by reactive astrocytosis and microglia activation (Geschwind and Wong 2014; Muhleisen et al. 1995; Obst et al. 2017; Liberski and Brown 2006). A recent study investigating *in vivo* microglia activation in symptomatic CJD showed a significantly higher [^{11}C]PK11195 binding in patients than in controls in the thalamus, basal ganglia, cerebellum, midbrain and parieto-occipital cortex, with a different pattern of distribution in case of sporadic or genetic transmission (Iaccarino et al. 2018a). Microglia activation was confirmed, along with neuronal loss and

astrogliosis, at the *post-mortem* evaluation (Iaccarino et al. 2018a). [^{11}C]DED-PET studies in CJD have provided an *in vivo* proof of the presence of reactive astrocytosis co-localized with spongiform neurodegeneration and neuronal loss, correlating also with brain glucose hypometabolism (Engler et al. 2003; Engler et al. 2012).

FFI is today considered one of the most common inherited prion diseases worldwide (Schmitz et al. 2017). *Post-mortem* studies reported microglia activation associated in FFI brains with neuronal apoptosis (Dorandeu et al. 1998). These findings were confirmed *in vivo* in a [^{11}C]PK11195-PET study involving one FFI symptomatic patient and eight carriers of the pathogenic mutation D178N-129met/val that showed higher and widespread TSPO expression in the patient and increased microglia activation, limited to the limbic structures, in half of the pre-symptomatic carriers (Iaccarino et al. 2018b). The involvement of key regions in the development of the disease, as the limbic regions in FFI, indicates again a primary role of microglia activation in driving neuronal alterations (Iaccarino et al. 2018b).

9.5.5 Strengths

Research on neuroinflammation has provided precious insights into the pathological processes underlying progressive neurodegeneration. *In vivo* PET imaging of neuroinflammatory responses, especially studies using the validated and widely used [^{11}C]PK11195 TSPO tracer, can serve as a unique tool in investigating dynamic changes in microglia activation over the disease course. TSPO expression has been proposed as a marker of disease progression, correlating with dementia severity (Fan et al. 2015b; Kreisl et al. 2013), and also as topographical marker of disease, helping to distinguish between atypical AD phenotypes (Kreisl et al. 2017) and different forms of dementia (Fig. 9.9) (Passamonti et al. 2018). Clarifying the role of microglia activation in the early phase of neurodegenerative diseases might provide reliable markers for monitoring novel disease-modifying therapies. TSPO radiotracers have been already used to monitor responses to anti-inflammatory therapy in parkinsonism (Dodel et al. 2010; Jucaite et al. 2015), but the lack of clinical repercussion in those studies imposes further investigations.

9.5.6 Weaknesses

Despite the development of second- and third-generation tracers, neuroinflammatory responses quantification is still a challenge. [^{11}C]PK11195 is the most validated TSPO radiotracer, but it has some clear limitations, such as the wide distribution across different tissues and the low brain permeability which result in a low signal-to-noise ratio, low specificity and moderate intraindividual reproducibility (Jučaite et al. 2012). The main limitation in the use of second-generation tracers is the presence of the rs6971 polymorphism which obliges to conduct the genotyping during

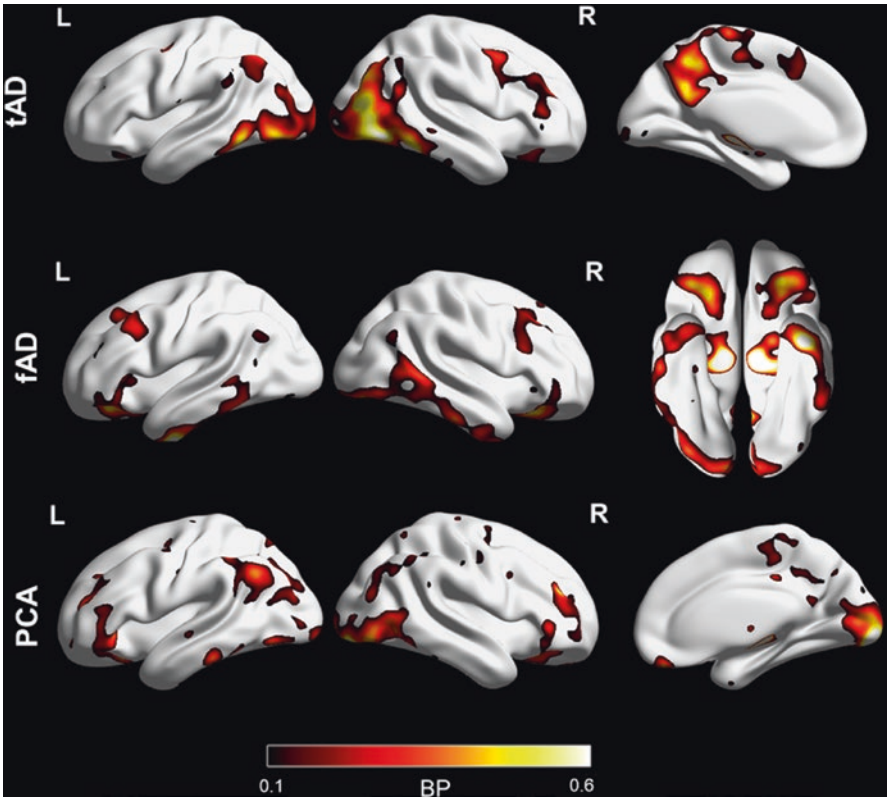

Fig. 9.9 Patterns of [^{11}C]-PK 11195 PET binding potential in three different AD variants. Patterns of [^{11}C]-PK 11195 PET binding potential obtained in three different single individuals with diagnosis of AD. The first subject had a diagnosis of typical AD: [^{11}C]-(R)-PK11195 PET revealed microglia activation involving the temporal regions, mainly on the right, and the parietal and the occipital regions bilaterally. The second subject had a diagnosis of frontal AD. [^{11}C]-(R)-PK11195 PET reveals a widespread bilateral microglia activation in frontal, temporal, parietal and occipital regions. The third subject had a diagnosis of a PCA. [^{11}C]-(R)-PK11195 PET analysis shows an increased BP in occipital and temporal cortex. *L* left, *R* right, *tAD* typical Alzheimer's disease, *fAD* frontal AD, *PCA* posterior cortical atrophy. *BP* binding potential. (Perani Daniela personal data)

the sample selection and to exclude low-affinity binders (Owen et al. 2012). The high signal of TSPO in the blood–brain barrier masks brain tissue signals, thus requiring kinetic correction and invasive arterial blood sampling, and, in addition, second-generation tracer binding still lacks a universally accepted and validated quantification method (Turkheimer et al. 2015; Rizzo et al. 2019). Lastly, TSPO is overexpressed by activated microglia, independently on the pro-inflammatory or anti-inflammatory phenotype, and reactive astrocytes, and to date there is no PET radiotracer able to distinguish between the different microglia expressions and populations that can play different functions.

9.6 Relationships Amongst Amyloid, Tau, Neurodegeneration and Neuroinflammation Biomarkers

The independent and/or synergistic effects of underlying pathology on neurodegeneration and cognition in neurodegenerative dementia have been elucidated by the *in vivo* molecular imaging. Whether such effects are sequential or parallel and whether (and if so at what stage of the disease) Aβ and/or tau either become or stop being the driver of cognitive decline are key issues in research (Villemagne et al. 2018). The different molecular paths that PET *in vivo* biomarkers can reveal in the timeframe of AD progression reflect the events leading to deposition of Aβ and phosphorylated tau, neuronal injury and neurodegeneration, which can run in parallel instead of in a sequential manner (Kato et al. 2016). Specifically, it could be possible to examine the potential interactive relationship between protein aggregation and neurodegeneration *in vivo*, in order to understand the contribution of tau and Aβ pathology to neurodegeneration. In AD patients, tau pathology was primarily observed in brain regions related to clinical symptoms and overlapped with synaptic dysfunction (Dronse et al. 2017). In contrast, amyloid deposition presents a diffuse distribution over the entire cortex (Dronse et al. 2017). These results suggest differences in the pathophysiology, with amyloid pathology deposited extracellularly in a more generalized fashion and tau pathology aggregating inside neurons, more directly linked to regional neuronal dysfunction. Consistently, multimodal imaging studies combining amyloid-PET with [^{18}F]FDG-PET reported a striking dissociation between the patterns of amyloid deposition and synaptic dysfunction; neurodegeneration prevailed in regions related to the clinical symptoms, while Aβ deposition was observed diffusely throughout the neocortex (Lehmann et al. 2013) showing that regional hypometabolism is unrelated to regional Aβ burden (Altmann et al. 2015). On the contrary, the considerable overlap between tau tracer uptake and glucose hypometabolism suggests that both biomarkers may represent complementary and interrelated aspects of AD pathology. A recent study examined the independent and interactive influences of neuroimaging biomarkers (i.e. Tau and amyloid-PET) on cognitive decline in participants ranging from cognitively normal to very mild symptomatic AD (Aschenbrenner et al. 2018). The authors found that amyloidosis may not be enough to cause observable cognitive declines and that tau-PET was the most consistent and significant predictor of cognitive decline. However, a strong interaction between tau-PET and amyloid-PET was related to cognition, indicating that declines in cognition are accelerated when both tau and amyloid are elevated.

Another multimodal PET imaging study assessed the differential contribution of neurofibrillary tangles (measured with [^{18}F]AV-1451) and Aβ burden (measured with [^{11}C]PiB) on degree of neurodegeneration (i.e. glucose metabolism measured with [^{18}F]FDG-PET) in patients with AD (Bischof et al. 2016). Most regions showed a direct relationship of tau pathology and hypometabolism, irrespective of Aβ. However, in the parietal region, an early site of amyloid deposition and decreased hypometabolism in AD, an interactive effect of Aβ and tau was observed, also

associated with the most pronounced reduction of glucose metabolism. This result may be indicative of the joint downstream effect of both protein pathologies in regions affected early in the course of the disease. From a spreading perspective (Brettschneider et al. 2015), it could be argued that tau burden starts in temporal regions and then spreads to adjacent parietal regions, where elevated levels of Aβ accelerate the propagation of tau to other regions. Consistently, two recent studies showed that cortical [^{18}F]AV-1451 binding, measured from AD cortical signature regions, was elevated in presence of high Aβ load (Johnson et al. 2016; Wang et al. 2016).

Tau radiotracers potentially offer additional value over [^{18}F]FDG, since they represent core elements of AD pathology serving as both neurodegenerative and pathophysiological biomarkers. Tau is more closely linked to hypometabolism and symptomatology than amyloid along with current conceptual models of the AD pathophysiological cascade (Jack Jr et al. 2013), even if the presence of Aβ may accelerate the propagation of tau during the neurodegenerative process. In addition, there may also be differences in metabolic susceptibility to the neurotoxicity of tau across brain regions and individuals.

In this context instead, the role of neuroinflammation still needs to be completely clarified. Microglia, the main player in neuroinflammatory responses to several kinds of insults, can be activated by both Aβ and tau (Lian et al. 2016; Brelstaff et al. 2018). A protective effect, related to pathologic protein clearance and neurotrophic factors production, has been hypothesized in the very early stage of neurodegeneration, while chronic microglia activation leads to neuronal dysfunction and loss via the production of cytokines and reactive oxygen species (Comi and Tondo 2017). Coherently, a double peak of activation has been suggested in AD, where in the initial phase microglia would try to repair the damage, while later on the same inflammatory players chronically activated could be ineffective and deleterious, conducing to progressive neuronal damage (Fan et al. 2017). Several reports confirmed the co-localization between activated microglia, overexpressing TSPO, and brain glucose hypometabolism, indicating their interplay in synaptic dysfunction and neuronal loss (Fan et al. 2015a; Edison et al. 2013). In addition, a topographical distribution of activated microglia in dysfunctional brain areas, clinically corresponding to a specific phenotype, has been reported in different neurodegenerative diseases (Kreisl et al. 2017; Henkel et al. 2004), reflecting the specific hypometabolic pattern (Nestor et al. 2003; Niccolini et al. 2018). Conversely, the correspondence between microglia activation and Aβ distribution appears less convincing (Cerami et al. 2017b), given the possibility to have microglia activation independently of amyloid load (Okello et al. 2009; Yokokura et al. 2011). Whether microglia activation in amyloidopathies is a cause (i.e. failing in the amyloid clearance) or the consequence of amyloid deposition is still debated, and the possibility of two parallel paths needs to be considered. To date, only one study assessed the relationships between levels of cortical microglial activation and the aggregated Aβ and tau load in MCI and AD (Parbo et al. 2018). The authors reported high levels of microglia activation in prodromal AD in the absence of detectable tau deposition, again suggesting that microglia activation is an early phenomenon in AD pathology, and

it may be an initial protective mechanism that fails in the later stage of the disease (Parbo et al. 2018).

Future studies with larger samples and longitudinal follow-up should explore the relationships between brain metabolism, amyloid binding, tau aggregation and microglia activation from prodromal phases to full-blown dementia.

9.7 PET Imaging: New Frontiers in Dementia

Pathological substrates causing neurodegenerative diseases are multiple and heterogeneous. Future *in vivo* imaging techniques will possibly account for this and track progression of various neuropathology events across networks in time. Some available PET tracers reveal some disadvantages including, but not limited to, binding affinity, presence of off-target binding, poor signal-to-noise ratio and clinical suitability issues. Amyloid-, tau- and neuroinflammation-PET techniques have seen a constant development of new-generation PET tracers in an attempt to overcome such limitations. In particular, the efforts regarding the development of fluorinated alternative of [^{11}C]-labelled tracers promoted and facilitated the implementation of PET techniques in clinical practice.

Notwithstanding the broad efforts, the greatest challenge in PET imaging is still represented by the lack of standardized methodology, which hampers both reproducibility and biological interpretation of findings. Thus, validation of methodology of analysis should be encouraged in order to obtain reliable and robust statistics, as well as identifying new suitable targets or developing new techniques (e.g. 4R tau-PET or a-synuclein PET). The validation of data analytical procedures for currently existing PET tracers should be one focus of future research.

Regarding the development of radiotracers for additional molecular applications, the implementation of PET tracers specific for α-synuclein aggregates is a crucial challenge. The Michael J. Fox Foundation launched a $2-million-prize competition (https://www.michaeljfox.org/research/imaging-prize.html) for the identification of an accurate α-synuclein tracer. The implementation of a compound able to target α-synuclein aggregates by *in vivo* PET imaging would have remarkable implications for clinical practice with respect to the α-synuclein spectrum, such as for disease monitoring, and clinical trials, thereby facilitating and accelerating drug development (Kotzbauer et al. 2017). The *in vivo* investigation of synaptic density using newly developed ad hoc *tracers* represents another exciting and breakthrough molecular imaging frontier, which is currently under validation (Finnema et al. 2016). [^{18}F]FDG-PET is a reliable measure of brain metabolism, considered to be a proxy for neuronal/synaptic activity and density (Rocher et al. 2003; Magistretti and Pellerin 1999; Stoessl 2017). At present, a large amount of evidence demonstrates the absolute value of [^{18}F]FDG-PET in detecting brain dysfunction and region-specific disorder in neurodegenerative dementias (Kato et al. 2016). *In vivo* quantification of synapses, however, may be possible using PET by means of a synapse-specific radioligand able to bind a protein ubiquitously present on neuronal synapses. In this regard, recently

synaptic density PET measurements, targeting the synaptic vesicle glycoprotein 2A (SV2A), began to be investigated, providing promising results (Finnema et al. 2016; Chen et al. 2018). SV2A is homogenously located in presynaptic terminals across brain regions (Finnema et al. 2016; Bajjalieh et al. 1994). A preliminary human imaging study showed that the [^{11}C]UCB-J tracer, targeting SV2A, has excellent properties, such as test-retest reproducibility, high brain uptake, rapid kinetics and displacement by levetiracetam, an antiepileptic drug targeting SV2A (Finnema et al. 2016; Finnema et al. 2018). Furthermore, in AD and epilepsy patients, [^{11}C]UCB-J reliably detected focal medial temporal synaptic loss (Finnema et al. 2016; Chen et al. 2018).

Recently, the PET radioligand [^{11}C]BU9908 has been developed for *in vivo* quantification of I2BS showing high specificity and selectivity (Kealey et al. 2013; Parker et al. 2014; Tyacke et al. 2012). PET studies evaluating [^{11}C]BU99008 expression could highlight the role of astroglial activation in disease progression and associations with symptomatology.

9.8 Conclusion

Recent studies have progressively highlighted how the same pathology can trigger different functional phenotypes. Given the recent advances in neuroimaging techniques, it is likely that the multimodal integration of pathological and functional biomarkers will be the key proxy to the most accurate identification of both underlying pathology and phenotypic syndromes. The increasing availability of PET *in vivo* biomarkers will likely favour the implementation of a spectrum-based research framework. PET molecular studies can give us the unique opportunity to understand *in vivo* specific pathologic contributions along the time course of neurodegenerative conditions, also providing crucial information on possible co-morbidities. The accuracy of a biomarker does not necessarily depend on binding specificity to a certain protein pathology, but mostly on its ability to discriminate patients in clinically unclear situations and secondly on its usefulness in the quantification of disease progression, e.g. brain glucose metabolism imaging that represents a valuable diagnostic biomarker for various conditions and is certainly not pathology-specific.

Although the clinical usefulness of amyloid-PET is recognized, it is particularly recommended for specific clinical subpopulations, such as early and atypical clinical presentations. The novel tau tracers are promising, given their tight relationship with neurodegeneration, but the lack of affinity for different tau isoforms and the evidence for non-specific bindings shown by several of these radioligands call for the development of novel compounds overcoming these limitations. In this context, [^{18}F]FDG-PET provides a well-validated key value to dementia diagnosis and prognosis and should be considered as one of the most demonstrated valuable tools for monitoring neurodegenerative disease status and progression and also for selecting candidates for clinical trials and evaluating treatment response in both AD and non-AD pathologies.

Nevertheless, in the context of molecular therapy strategies, pathology specificity of a biomarker is indispensable. The tracers' affinity to their targets strictly influences the specificity of a PET measure for detecting neuropathology *in vivo* in the different neurodegenerative conditions.

The progressive worldwide implementation and adoption of PET imaging techniques paves the way to improved understanding of the pathophysiology of neurodegenerative diseases also enabling a more precise approach to interventional trials, both for screening of participants and for outcome evaluation.

References

Acosta-Cabronero J, Patterson K, Fryer TD, Hodges JR, Pengas G, Williams GB et al (2011) Atrophy, hypometabolism and white matter abnormalities in semantic dementia tell a coherent story. Brain 134(7):2025–2035

Akdemir ÜÖ, Tokçaer AB, Karakus A, Kapucu LÖ (2014) Brain 18F-FDG PET imaging in the differential diagnosis of parkinsonism. Clin Nucl Med 39(3):e220–e226

Albert MS, DeKosky ST, Dickson D, Dubois B, Feldman HH, Fox NC et al (2011) The diagnosis of mild cognitive impairment due to Alzheimer's disease: recommendations from the National Institute on Aging-Alzheimer's association workgroups on diagnostic guidelines for Alzheimer's disease. Alzheimers Dement 7(3):270–279

Alladi S, Xuereb J, Bak T, Nestor P, Knibb J, Patterson K et al (2007) Focal cortical presentations of Alzheimer's disease. Brain 130(10):2636–2645

Altmann A, Ng B, Landau SM, Jagust WJ, Greicius MD (2015) Regional brain hypometabolism is unrelated to regional amyloid plaque burden. Brain 138(12):3734–3746

Anchisi D, Borroni B, Franceschi M, Kerrouche N, Kalbe E, Beuthien-Beumann B et al (2005) Heterogeneity of brain glucose metabolism in mild cognitive impairment and clinical progression to Alzheimer disease. Arch Neurol 62(11):1728–1733

Anderson MA, Ao Y, Sofroniew MV (2014) Heterogeneity of reactive astrocytes. Neurosci Lett 565:23–29

Armstrong MJ, Litvan I, Lang AE, Bak TH, Bhatia KP, Borroni B et al (2013) Criteria for the diagnosis of corticobasal degeneration. Neurology 80(5):496–503

Asai H, Ikezu S, Woodbury ME, Yonemoto GMS, Cui L, Ikezu T (2014) Accelerated neurodegeneration and neuroinflammation in transgenic mice expressing P301L tau mutant and tau-tubulin kinase 1. Am J Pathol 184(3):808–818

Aschenbrenner AJ, Gordon BA, Benzinger TLS, Morris JC, Hassenstab JJ (2018) Influence of tau PET, amyloid PET, and hippocampal volume on cognition in Alzheimer disease. Neurology 91(9):e859–e866

Attwell D, Laughlin SB (2001) An energy budget for signaling in the grey matter of the brain. J Cereb Blood Flow Metab 21(10):1133–1145

Bacskai BJ, Hickey GA, Skoch J, Kajdasz ST, Wang Y, Huang G et al (2003) Four-dimensional multiphoton imaging of brain entry, amyloid binding, and clearance of an amyloid-β ligand in transgenic mice. Proc Natl Acad Sci 100(21):12462–12467

Bajjalieh SM, Frantz GD, Weimann JM, McConnell SK, Scheller RH (1994) Differential expression of synaptic vesicle protein 2 (SV2) isoforms. J Neurosci 14(9):5223–5235

Balasa M, Gelpi E, Antonell A, Rey MJ, Sanchez-Valle R, Molinuevo JL et al (2011) Clinical features and APOE genotype of pathologically proven early-onset Alzheimer disease. Neurology 76(20):1720–1725

Ballarini T, Iaccarino L, Magnani G, Ayakta N, Miller BL, Jagust WJ et al (2016) Neuropsychiatric subsyndromes and brain metabolic network dysfunctions in early onset Alzheimer's disease. Hum Brain Mapp 37(12):4234–4247. https://doi.org/10.1002/hbm.23305

Banati RB, Newcombe J, Gunn RN, Cagnin A, Turkheimer F, Heppner F et al (2000) The peripheral benzodiazepine binding site in the brain in multiple sclerosis: quantitative in vivo imaging of microglia as a measure of disease activity. Brain 123(11):2321–2337

Bang J, Spina S, Miller BL (2015) Frontotemporal dementia. Lancet 386(10004):1672–1682

Barker RA, Williams-Gray CH (2016) The spectrum of clinical features seen with alpha synuclein pathology. Neuropathol Appl Neurobiol 42(1):6–19

Baron J-C, Farid K, Dolan E, Turc G, Marrapu ST, O'brien E et al (2014) Diagnostic utility of amyloid PET in cerebral amyloid angiopathy-related symptomatic intracerebral hemorrhage. J Cereb Blood Flow Metab 34(5):753–758

Bartels AL, Willemsen ATM, Doorduin J, De Vries EFJ, Dierckx RA, Leenders KL (2010) [11C]-PK11195 PET: quantification of neuroinflammation and a monitor of anti-inflammatory treatment in Parkinson's disease? Parkinsonism Relat Disord 16(1):57–59

Bateman RJ, Xiong C, Benzinger TLS, Fagan AM, Goate A, Fox NC et al (2012) Clinical and biomarker changes in dominantly inherited Alzheimer's disease. N Engl J Med 367(9):795–804

Beach TG, Monsell SE, Phillips LE, Kukull W (2012) Accuracy of the clinical diagnosis of Alzheimer disease at National Institute on Aging Alzheimer disease centers, 2005–2010. J Neuropathol Exp Neurol 71(4):266–273

Benzinger TLS, Blazey T, Jack CR, Koeppe RA, Su Y, Xiong C et al (2013) Regional variability of imaging biomarkers in autosomal dominant Alzheimer's disease. Proc Natl Acad Sci U S A 110(47):E4502–E4509

Bergeron D, Gorno-Tempini ML, Rabinovici GD, Santos-Santos MA, Seeley W, Miller BL et al (2018) Prevalence of amyloid-β pathology in distinct variants of primary progressive aphasia. Ann Neurol 84(5):729–740

Best L, Ghadery C, Pavese N, Tai YF, Strafella AP (2019) New and old TSPO PET radioligands for imaging brain microglial activation in neurodegenerative disease. Curr Neurol Neurosci Rep 19(5):24

Bevan-Jones WR, Cope TE, Jones PS, Passamonti L, Hong YT, Fryer T et al (2019) In vivo evidence for pre-symptomatic neuroinflammation in a MAPT mutation carrier. Ann Clin Transl Neurol 6(2):373–378

Bischof GN, Jessen F, Fliessbach K, Dronse J, Hammes J, Neumaier B et al (2016) Impact of tau and amyloid burden on glucose metabolism in Alzheimer's disease. Ann Clin Transl Neurol 3(12):934–939

Bischof GN, Endepols H, van Eimeren T, Drzezga A (2017) Tau-imaging in neurodegeneration. Methods 130:114–123

Bloudek LM, Spackman DE, Blankenburg M, Sullivan SD (2011) Review and meta-analysis of biomarkers and diagnostic imaging in Alzheimer's disease. J Alzheimers Dis 26(4):627–645

Boeve BF, Hutton M (2008) Refining frontotemporal dementia with parkinsonism linked to chromosome 17: introducing FTDP-17 (MAPT) and FTDP-17 (PGRN). Arch Neurol 65(4):460–464

Bohnen NI, Djang DSW, Herholz K, Anzai Y, Minoshima S (2012) Effectiveness and safety of 18F-FDG PET in the evaluation of dementia: a review of the recent literature. J Nucl Med 53(1):59–71

Booij J, Speelman JD, Horstink MWIM, Wolters EC (2001) The clinical benefit of imaging striatal dopamine transporters with [123 I] FP-CIT SPET in differentiating patients with presynaptic parkinsonism from those with other forms of parkinsonism. Eur J Nucl Med 28(3):266–272

Botha H, Whitwell JL, Madhaven A, Senjem ML, Lowe V, Josephs KA (2014) The pimple sign of progressive supranuclear palsy syndrome. Parkinsonism Relat Disord 20(2):180–185

Braak H, Braak E (1991) Neuropathological stageing of Alzheimer-related changes. Acta Neuropathol 82(4):239–259

Braak H, Braak E (1997) Frequency of stages of Alzheimer-related lesions in different age categories. Neurobiol Aging 18(4):351–357

Brajkovic L, Kostic V, Sobic-Saranovic D, Stefanova E, Jecmenica-Lukic M, Jesic A et al (2017) The utility of FDG-PET in the differential diagnosis of parkinsonism. Neurol Res 39(8):675–684

Brelstaff J, Tolkovsky AM, Ghetti B, Goedert M, Spillantini MG (2018) Living neurons with tau filaments aberrantly expose phosphatidylserine and are phagocytosed by microglia. Cell Rep 24(8):1939–1948

Brendel M, Schonecker S, Hoglinger G, Lindner S, Havla J, Blautzik J et al (2017) [(18) F]-THK5351 PET correlates with topology and symptom severity in progressive supranuclear palsy. Front Aging Neurosci 9:440

Brettschneider J, Del Tredici K, Lee VM-Y, Trojanowski JQ (2015) Spreading of pathology in neurodegenerative diseases: a focus on human studies. Nat Rev Neurosci 16(2):109

Brier MR, Gordon B, Friedrichsen K, McCarthy J, Stern A, Christensen J et al (2016) Tau and Aβ imaging, CSF measures, and cognition in Alzheimer's disease. Sci Transl Med 8(338):338ra66

Brookmeyer R, Abdalla N (2018) Estimation of lifetime risks of Alzheimer's disease dementia using biomarkers for preclinical disease. Alzheimers Dement 14(8):981–988

Bryson JB, Hobbs C, Parsons MJ, Bosch KD, Pandraud A, Walsh FS et al (2012) Amyloid precursor protein (APP) contributes to pathology in the SOD1G93A mouse model of amyotrophic lateral sclerosis. Hum Mol Genet 21(17):3871–3882

Burn DJ, Sawle GV, Brooks DJ (1994) Differential diagnosis of Parkinson's disease, multiple system atrophy, and Steele-Richardson-Olszewski syndrome: discriminant analysis of striatal 18F-dopa PET data. J Neurol Neurosurg Psychiatry 57(3):278–284

Cagnin A, Brooks DJ, Kennedy AM, Gunn RN, Myers R, Turkheimer FE et al (2001) In-vivo measurement of activated microglia in dementia. Lancet 358(9280):461–467

Cagnin A, Rossor M, Sampson EL, MacKinnon T, Banati RB (2004) In vivo detection of microglial activation in frontotemporal dementia. Ann Neurol 56(6):894–897

Calo L, Wegrzynowicz M, Santivañez-Perez J, Grazia SM (2016) Synaptic failure and α-synuclein. Mov Disord 31(2):169–177

Calsolaro V, Edison P (2016) Neuroinflammation in Alzheimer's disease: current evidence and future directions. Alzheimers Dement 12(6):719–732

Caminiti SP, Alongi P, Majno L, Volontè MA, Cerami C, Gianolli L et al (2017) Evaluation of an optimized [18F] fluoro-deoxy-glucose positron emission tomography voxel-wise method to early support differential diagnosis in atypical parkinsonian disorders. Eur J Neurol 24(5):687–e26

Caminiti SP, Ballarini T, Sala A, Cerami C, Presotto L, Santangelo R et al (2018) FDG-PET and CSF biomarker accuracy in prediction of conversion to different dementias in a large multicentre MCI cohort. NeuroImage Clin 18:167–177. https://doi.org/10.1016/j.nicl.2018.01.019

Caminiti SP, Sala A, Iaccarino L, Beretta L, Pilotto A, Gianolli L et al (2019) Brain glucose metabolism in Lewy body dementia: implications for diagnostic criteria. Alzheimers Res Ther 11(1):20

Canosa A, Pagani M, Cistaro A, Montuschi A, Iazzolino B, Fania P et al (2016) 18F-FDG-PET correlates of cognitive impairment in ALS. Neurology 86(1):44–49

Caroli A, Prestia A, Chen K, Ayutyanont N, Landau SM, Madison CM et al (2012) Summary metrics to assess Alzheimer disease–related hypometabolic pattern with ^{18}F-FDG PET: head-to-head comparison. J Nucl Med 53(4):592–600

Carter SF, Schöll M, Almkvist O, Wall A, Engler H, Långström B et al (2012) Evidence for astrocytosis in prodromal Alzheimer disease provided by 11C-deuterium-L-deprenyl: a multitracer PET paradigm combining 11C-Pittsburgh compound B and 18F-FDG. J Nucl Med 53(1):37–46

Castelnovo V, Caminiti SP, Riva N, Magnani G, Silani V, Perani D (2019) Heterogeneous brain FDG-PET metabolic patterns in patients with C9orf72 mutation. Neurol Sci 40(3):515–521

Catafau AM, Tolosa E (2004) Impact of dopamine transporter SPECT using 123I-Ioflupane on diagnosis and management of patients with clinically uncertain parkinsonian syndromes. Mov Disord 19(10):1175–1182

Cerami C, Della Rosa PA, Magnani G, Santangelo R, Marcone A, Cappa SF et al (2015a) Brain metabolic maps in mild cognitive impairment predict heterogeneity of progression to dementia. NeuroImage Clin 7:187–194

Cerami C, Crespi C, Della Rosa PA, Dodich A, Marcone A, Magnani G et al (2015b) Brain changes within the visuo-spatial attentional network in posterior cortical atrophy. J Alzheimers Dis 43(2):385–395

Cerami C, Dodich A, Lettieri G, Iannaccone S, Magnani G, Marcone A et al (2016) Different FDG-PET metabolic patterns at single-subject level in the behavioral variant of fronto-temporal dementia. Cortex 83:101–112

Cerami C, Dodich A, Greco L, Iannaccone S, Magnani G, Marcone A et al (2017a) The role of single-subject brain metabolic patterns in the early differential diagnosis of primary progressive aphasias and in prediction of progression to dementia. J Alzheimers Dis 55(1):183–197

Cerami C, Iaccarino L, Perani D (2017b) Molecular imaging of neuroinflammation in neurodegenerative dementias: the role of in vivo PET imaging. Int J Mol Sci 18(5):993

Chen M-K, Guilarte TR (2008) Translocator protein 18 kDa (TSPO): molecular sensor of brain injury and repair. Pharmacol Ther 118(1):1–17

Chen YJ, Nasrallah IM (2017) Brain amyloid PET interpretation approaches: from visual assessment in the clinic to quantitative pharmacokinetic modeling. Clin Trans Imaging 5(6):561–573

Chen W, Zhang XIA, Huang W (2016) Role of neuroinflammation in neurodegenerative diseases. Mol Med Rep 13(4):3391–3396

Chen M-K, Mecca AP, Naganawa M, Finnema SJ, Toyonaga T, Lin S et al (2018) Assessing synaptic density in Alzheimer disease with synaptic vesicle glycoprotein 2A positron emission tomographic imaging. JAMA Neurol 75(10):1215–1224

Chételat G, Desgranges B, Landeau B, Mézenge F, Poline JB, de La Sayette V et al (2007) Direct voxel-based comparison between grey matter hypometabolism and atrophy in Alzheimer's disease. Brain 131(1):60–71

Chételat G, La Joie R, Villain N, Perrotin A, de La Sayette V, Eustache F et al (2013) Amyloid imaging in cognitively normal individuals, at-risk populations and preclinical Alzheimer's disease. NeuroImage Clin 2:356–365

Chetelat G, Ossenkoppele R, Villemagne VL, Perrotin A, Landeau B, Mézenge F et al (2016) Atrophy, hypometabolism and clinical trajectories in patients with amyloid-negative Alzheimer's disease. Brain 139(9):2528–2539

Chien DT, Bahri S, Szardenings AK, Walsh JC, Mu F, Su M-Y et al (2013) Early clinical PET imaging results with the novel PHF-tau radioligand [F-18]-T807. J Alzheimers Dis 34(2):457–468

Chiotis K, Saint-Aubert L, Savitcheva I, Jelic V, Andersen P, Eriksson J et al (2016) Imaging in-vivo tau pathology in Alzheimer's disease with THK5317 PET in a multimodal paradigm. Eur J Nucl Med Mol Imaging 43(9):1686–1699

Chiotis K, Saint-Aubert L, Rodriguez-Vieitez E, Leuzy A, Almkvist O, Savitcheva I et al (2018) Longitudinal changes of tau PET imaging in relation to hypometabolism in prodromal and Alzheimer's disease dementia. Mol Psychiatry 23(7):1666–1673

Cho H, Seo SW, Kim J-H, Suh MK, Lee J-H, Choe YS et al (2013) Amyloid deposition in early onset versus late onset Alzheimer's disease. J Alzheimers Dis 35(4):813–821

Cho H, Choi JY, Hwang MS, Lee JH, Kim YJ, Lee HM et al (2016) Tau PET in Alzheimer disease and mild cognitive impairment. Neurology 87(4):375–383

Cho H, Choi JY, Hwang MS, Lee SH, Ryu YH, Lee MS et al (2017a) Subcortical 18F-AV-1451 binding patterns in progressive supranuclear palsy. Mov Disord 32(1):134–140

Cho H, Baek MS, Choi JY, Lee SH, Kim JS, Ryu YH et al (2017b) (18)F-AV-1451 binds to motor-related subcortical gray and white matter in corticobasal syndrome. Neurology 89(11):1170–1178

Cho H, Choi JY, Lee SH, Ryu YH, Lee MS, Lyoo CH (2017c) 18F-AV-1451 binds to putamen in multiple system atrophy. Mov Disord 32(1):171–173

Cho H, Seo SW, Choi JY, Lee HS, Ryu YH, Lee MS et al (2018) Predominant subcortical accumulation of (18)F-flortaucipir binding in behavioral variant frontotemporal dementia. Neurobiol Aging 66:112–121

Choi SR, Schneider JA, Bennett DA, Beach TG, Bedell BJ, Zehntner SP et al (2011) Correlation of amyloid PET ligand florbetapir $^{F}18$ binding with Aβ aggregation and neuritic plaque deposition in postmortem brain tissue. Alzheimer Dis Assoc Disord 26(1):8–16

Choo ILH, Carter SF, Schöll ML, Nordberg A (2014) Astrocytosis measured by 11 C-deprenyl PET correlates with decrease in gray matter density in the parahippocampus of prodromal Alzheimer's patients. Eur J Nucl Med Mol Imaging 41(11):2120–2126

Claassen DO, Lowe VJ, Peller PJ, Petersen RC, Josephs KA (2011) Amyloid and glucose imaging in dementia with Lewy bodies and multiple systems atrophy. Parkinsonism Relat Disord 17(3):160–165

Clark CM, Schneider JA, Bedell BJ, Beach TG, Bilker WB, Mintun MA et al (2011) Use of florbetapir-PET for imaging β-amyloid pathology. JAMA 305(3):275–283

Coakeley S, Strafella AP (2017) Imaging tau pathology in Parkinsonisms. NPJ Parkinsons Dis 3(1):22

Coakeley S, Cho SS, Koshimori Y, Rusjan P, Harris M, Ghadery C et al (2017) Positron emission tomography imaging of tau pathology in progressive supranuclear palsy. J Cereb Blood Flow Metab 37(9):3150–3160

Colby DW, Prusiner SB (2011) Prions. Cold Spring Harb Perspect Biol 3(1):a006833

Collste K, Forsberg A, Varrone A, Amini N, Aeinehband S, Yakushev I et al (2016) Test–retest reproducibility of [11 C] PBR28 binding to TSPO in healthy control subjects. Eur J Nucl Med Mol Imaging 43(1):173–183

Comi C, Tondo G (2017) Insights into the protective role of immunity in neurodegenerative disease. Neural Regen Res 12(1):64

Compta Y, Parkkinen L, Kempster P, Selikhova M, Lashley T, Holton JL et al (2014) The significance of α-synuclein, amyloid-β and tau pathologies in Parkinson's disease progression and related dementia. Neurodegener Dis 13(2–3):154–156

Cortelli P, Perani D, Parchi P, Grassi F, Montagna P, De Martin M et al (1997) Cerebral metabolism in fatal familial insomnia: relation to duration, neuropathology, and distribution of protease-resistent prion protein. Neurology 49(1):126–133

Cosenza-Nashat M, Zhao M, Suh H, Morgan J, Natividad R, Morgello S et al (2009) Expression of the translocator protein of 18 kDa by microglia, macrophages and astrocytes based on immunohistochemical localization in abnormal human brain. Neuropathol Appl Neurobiol 35(3):306–328

Dalakas MC, Hatazawa J, Brooks RA, Di Chiro G (1987) Lowered cerebral glucose utilization in amyotrophic lateral sclerosis. Ann Neurol 22(5):580–586

Davison CM, O'Brien JT (2014) A comparison of FDG-PET and blood flow SPECT in the diagnosis of neurodegenerative dementias: a systematic review. Int J Geriatr Psychiatry 29(6):551–561

Delacourte A, Sergeant N, Wattez A, Maurage C-A, Lebert F, Pasquier F et al (2002) Tau aggregation in the hippocampal formation: an ageing or a pathological process? Exp Gerontol 37(10–11):1291–1296

Della Rosa PA, Cerami C, Gallivanone F, Prestia A, Caroli A, Castiglioni I et al (2014) A standardized [18F]-FDG-PET template for spatial normalization in statistical parametric mapping of dementia. Neuroinformatics 12(4):575–593

Desgranges B, Matuszewski V, Piolino P, Chételat G, Mézenge F, Landeau B et al (2007) Anatomical and functional alterations in semantic dementia: a voxel-based MRI and PET study. Neurobiol Aging 28(12):1904–1913

Dickson DW (1999) Neuropathologic differentiation of progressive supranuclear palsy and corticobasal degeneration. J Neurol 246(2):II6–I15

Dickson DW, Bergeron C, Chin SS, Duyckaerts C, Horoupian D, Ikeda K et al (2002) Office of Rare Diseases neuropathologic criteria for corticobasal degeneration. J Neuropathol Exp Neurol 61(11):935–946

Dickson DW, Kouri N, Murray ME, Josephs KA (2011) Neuropathology of frontotemporal lobar degeneration-tau (FTLD-tau). J Mol Neurosci 45(3):384–389

Diehl J, Grimmer T, Drzezga A, Riemenschneider M, Förstl H, Kurz A (2004) Cerebral metabolic patterns at early stages of frontotemporal dementia and semantic dementia. A PET study. Neurobiol Aging 25(8):1051–1056

Diehl-Schmid J, Grimmer T, Drzezga A, Bornschein S, Perneczky R, Förstl H et al (2006) Longitudinal changes of cerebral glucose metabolism in semantic dementia. Dement Geriatr Cogn Disord 22(4):346–351

Diehl-Schmid J, Onur OA, Kuhn J, Gruppe T, Drzezga A (2014) Imaging frontotemporal lobar degeneration. Curr Neurol Neurosci Rep 14(10):489

Dodel R, Spottke A, Gerhard A, Reuss A, Reinecker S, Schimke N et al (2010) Minocycline 1-year therapy in multiple-system-atrophy: effect on clinical symptoms and [11C](R)-PK11195 PET (MEMSA-trial). Mov Disord 25(1):97–107

Doody RS, Thomas RG, Farlow M, Iwatsubo T, Vellas B, Joffe S et al (2014) Phase 3 trials of solanezumab for mild-to-moderate Alzheimer's disease. N Engl J Med 370(4):311–321

Dorandeu A, Wingertsmann L, Chrétien F, Delisle M, Vital C, Parchi P et al (1998) Neuronal apoptosis in fatal familial insomnia. Brain Pathol 8(3):531–537

Dronse J, Fliessbach K, Bischof GN, von Reutern B, Faber J, Hammes J et al (2017) In vivo patterns of tau pathology, amyloid-β burden, and neuronal dysfunction in clinical variants of Alzheimer's disease. J Alzheimers Dis 55(2):465–471

Drzezga A, Grimmer T, Henriksen G, Stangier I, Perneczky R, Diehl-Schmid J et al (2008) Imaging of amyloid plaques and cerebral glucose metabolism in semantic dementia and Alzheimer's disease. NeuroImage 39(2):619–633

Du L, Zhang Y, Chen Y, Zhu J, Yang Y, Zhang H-L (2017) Role of microglia in neurological disorders and their potentials as a therapeutic target. Mol Neurobiol 54(10):7567–7584

Dubois B, Feldman HH, Jacova C, Hampel H, Molinuevo JL, Blennow K et al (2014) Advancing research diagnostic criteria for Alzheimer's disease: the IWG-2 criteria. Lancet Neurol 13(6):614–629

Dugger BN, Adler CH, Shill HA, Caviness J, Jacobson S, Driver-Dunckley E et al (2014) Concomitant pathologies among a spectrum of parkinsonian disorders. Parkinsonism Relat Disord 20(5):525–529

Dukart J, Sambataro F, Bertolino A (2016) Accurate prediction of conversion to Alzheimer's disease using imaging, genetic, and neuropsychological biomarkers. J Alzheimers Dis 49(4):1143–1159

Dupont A-C, Largeau B, Santiago Ribeiro M, Guilloteau D, Tronel C, Arlicot N (2017) Translocator protein-18 kDa (TSPO) positron emission tomography (PET) imaging and its clinical impact in neurodegenerative diseases. Int J Mol Sci 18(4):785

Eckert T, Barnes A, Dhawan V, Frucht S, Gordon MF, Feigin AS et al (2005) FDG PET in the differential diagnosis of parkinsonian disorders. NeuroImage 26(3):912–921

Edison P, Archer HA, Gerhard A, Hinz R, Pavese N, Turkheimer FE et al (2008) Microglia, amyloid, and cognition in Alzheimer's disease: an [11C](R) PK11195-PET and [11C] PIB-PET study. Neurobiol Dis 32(3):412–419

Edison P, Ahmed I, Fan Z, Hinz R, Gelosa G, Chaudhuri KR et al (2013) Microglia, amyloid, and glucose metabolism in Parkinson's disease with and without dementia. Neuropsychopharmacology 38(6):938

Ekblom J, Jossan SS, Bergström M, Oreland L, Walum E, Aquilonius S (1993) Monoamine oxidase-B in astrocytes. Glia 8(2):122–132

Elias A, Woodward M, Rowe CC (2014) Management impact of FDG-PET in dementia: results from a tertiary center memory clinic. J Alzheimers Dis 42(3):885–892

Engler H, Lundberg P, Ekbom K, Nennesmo I, Nilsson A, Bergström M et al (2003) Multitracer study with positron emission tomography in Creutzfeldt-Jakob disease. Eur J Nucl Med Mol Imaging 30(1):85–95

Engler H, Santillo AF, Wang SX, Lindau M, Savitcheva I, Nordberg A et al (2008) In vivo amyloid imaging with PET in frontotemporal dementia. Eur J Nucl Med Mol Imaging 35(1):100–106

Engler H, Nennesmo I, Kumlien E, Gambini JP, Lundberg PO, Savitcheva I et al (2012) Imaging astrocytosis with PET in Creutzfeldt-Jakob disease: case report with histopathological findings. Int J Clin Exp Med 5(2):201

Fan Z, Aman Y, Ahmed I, Chetelat G, Landeau B, Chaudhuri KR et al (2015a) Influence of microglial activation on neuronal function in Alzheimer's and Parkinson's disease dementia. Alzheimers Dement 11(6):608–621

Fan Z, Okello AA, Brooks DJ, Edison P (2015b) Longitudinal influence of microglial activation and amyloid on neuronal function in Alzheimer's disease. Brain 138(12):3685–3698

Fan Z, Brooks DJ, Okello A, Edison P (2017) An early and late peak in microglial activation in Alzheimer's disease trajectory. Brain 140(3):792–803

Fanciulli A, Wenning GK (2015) Multiple-system atrophy. N Engl J Med 372(3):249–263

Farid K, Carter SF, Rodriguez-Vieitez E, Almkvist O, Andersen P, Wall A et al (2015) Case report of complex amyotrophic lateral sclerosis with cognitive impairment and cortical amyloid deposition. J Alzheimers Dis 47(3):661–667

Feher EP, Doody RS, Whitehead J, Pirozzolo FJ (1991) Progressive nonfluent aphasia with dementia: a case report. Top Geriatr 4(4):236–240

Fellgiebel A, Scheurich A, Bartenstein P, Müller MJ (2007) FDG-PET and CSF phospho-tau for prediction of cognitive decline in mild cognitive impairment. Psychiatry Res Neuroimaging 155(2):167–171

Finnema SJ, Nabulsi NB, Eid T, Detyniecki K, Lin S, Chen M-K et al (2016) Imaging synaptic density in the living human brain. Sci Transl Med 8(348):348ra96

Finnema SJ, Nabulsi NB, Mercier J, Lin S, Chen M-K, Matuskey D et al (2018) Kinetic evaluation and test–retest reproducibility of [11C] UCB-J, a novel radioligand for positron emission tomography imaging of synaptic vesicle glycoprotein 2A in humans. J Cereb Blood Flow Metab 38(11):2041–2052

Fodero-Tavoletti MT, Brockschnieder D, Villemagne VL, Martin L, Connor AR, Thiele A et al (2012) In vitro characterization of [18F]-florbetaben, an Aβ imaging radiotracer. Nucl Med Biol 39(7):1042–1048

Formaglio M, Costes N, Seguin J, Tholance Y, Le Bars D, Roullet-Solignac I et al (2011) In vivo demonstration of amyloid burden in posterior cortical atrophy: a case series with PET and CSF findings. J Neurol 258(10):1841–1851

Foster NL, Heidebrink JL, Clark CM, Jagust WJ, Arnold SE, Barbas NR et al (2007) FDG-PET improves accuracy in distinguishing frontotemporal dementia and Alzheimer's disease. Brain 130(10):2616–2635

Foster ER, Campbell MC, Burack MA, Hartlein J, Flores HP, Cairns NJ et al (2010) Amyloid imaging of Lewy body-associated disorders. Mov Disord 25(15):2516–2523

Fowler JS, MacGregor RR, Wolf AP, Arnett CD, Dewey SL, Schlyer D et al (1987) Mapping human brain monoamine oxidase A and B with 11C-labeled suicide inactivators and PET. Science 235(4787):481–485

Franceschi M, Pelati O, Raffaele S, Raffaele S, Franceschi M, Anchisi D et al (2005) Glucose metabolism and serotonin receptors in the frontotemporal lobe degeneration glucose metabolism and serotonin receptors in the frontotemporal lobe degeneration. Ann Neurol 57(2):216–225

Frisoni GB, Bocchetta M, Chételat G, Rabinovici GD, De Leon MJ, Kaye J et al (2013) Imaging markers for Alzheimer disease Which vs how. Neurology 81(5):487–500

Fujishiro H, Iseki E, Higashi S, Kasanuki K, Murayama N, Togo T et al (2010) Distribution of cerebral amyloid deposition and its relevance to clinical phenotype in Lewy body dementia. Neurosci Lett 486(1):19–23

Fujita M, Kobayashi M, Ikawa M, Gunn RN, Rabiner EA, Owen DR et al (2017) Comparison of four 11 C-labeled PET ligands to quantify translocator protein 18 kDa (TSPO) in human brain:(R)-PK11195, PBR28, DPA-713, and ER176—based on recent publications that measured specific-to-non-displaceable ratios. EJNMMI Res 7(1):84

Gallivanone F (2014) The impact of different 18FDG PET healthy subject scans for comparison with single patient in SPM analysis. Q J Nucl Med Mol Imaging 61(1):115–132

Galton CJ, Patterson K, Xuereb JH, Hodges JR (2000) Atypical and typical presentations of Alzheimer ' s disease: a clinical, neuropsychological , neuroimaging and pathological study of 13 cases. Brain:484–498

Garibotto V, Herholz K, Boccardi M, Picco A, Varrone A, Nordberg A et al (2017) Clinical validity of brain fluorodeoxyglucose positron emission tomography as a biomarker for Alzheimer's disease in the context of a structured 5-phase development framework. Neurobiol Aging 52:183–195

Gatliff J, Campanella M (2012) The 18 kDa translocator protein (TSPO): a new perspective in mitochondrial biology. Curr Mol Med 12(4):356–368

Gentleman SM (2013) Microglia in protein aggregation disorders: friend or foe? Neuropathol Appl Neurobiol 39(1):45–50
Gerhard A, Banati RB, Goerres GB, Cagnin A, Myers R, Gunn RN et al (2003) [11C](R)-PK11195 PET imaging of microglial activation in multiple system atrophy. Neurology 61(5):686–689
Gerhard A, Watts J, Trender-Gerhard I, Turkheimer F, Banati RB, Bhatia K et al (2004) In vivo imaging of microglial activation with [11C](R)-PK11195 PET in corticobasal degeneration. Mov Disord 19(10):1221–1226
Gerhard A, Trender-Gerhard I, Turkheimer F, Quinn NP, Bhatia KP, Brooks DJ (2006a) In vivo imaging of microglial activation with [11C](R)-PK11195 PET in progressive supranuclear palsy. Mov Disord 21(1):89–93
Gerhard A, Pavese N, Hotton G, Turkheimer F, Es M, Hammers A et al (2006b) In vivo imaging of microglial activation with [11C](R)-PK11195 PET in idiopathic Parkinson's disease. Neurobiol Dis 21(2):404–412
Geschwind MD, Wong K (2014) Prion diseases. Continuum (Minneap Minn):267–280
Giannini LAA, Irwin DJ, McMillan CT, Ash S, Rascovsky K, Wolk DA et al (2017) Clinical marker for Alzheimer disease pathology in logopenic primary progressive aphasia. Neurology 88(24):2276–2284
Gilman S, Wenning GK, Low PA, Brooks DJ, Mathias CJ, Trojanowski JQ et al (2008) Second consensus statement on the diagnosis of multiple system atrophy. Neurology 71(9):670–676
Goedert M (2001) Alpha-synuclein and neurodegenerative diseases. Nat Rev Neurosci 2(7):492
Golde TE, Borchelt DR, Giasson BI, Lewis J (2013) Thinking laterally about neurodegenerative proteinopathies. J Clin Invest 123(5):1847–1855
Goldman S, Liard A, Flament-Durand J, Luxen A, Bidaut LM, Stanus E et al (1993) Positron emission tomography and histopathology in Creutzfeldt-Jakob disease. Neurology 43(9):1828
Golla SSV, Boellaard R, Oikonen V, Hoffmann A, Van Berckel BNM, Windhorst AD et al (2015) Quantification of [18F] DPA-714 binding in the human brain: initial studies in healthy controls and Alzheimer's disease patients. J Cereb Blood Flow Metab 35(5):766–772
Gomperts SN, Rentz DM, Moran E, Becker JA, Locascio JJ, Klunk WE et al (2008) Imaging amyloid deposition in Lewy body diseases. Neurology 71(12):903–910
Gomperts SN, Locascio JJ, Marquie M, Santarlasci AL, Rentz DM, Maye J et al (2012) Brain amyloid and cognition in Lewy body diseases. Mov Disord 27(8):965–973
Gomperts SN, Locascio JJ, Makaretz SJ, Schultz A, Caso C, Vasdev N et al (2016) Tau positron emission tomographic imaging in the Lewy body diseases. JAMA Neurol 73(11):1334–1341
Gordon E, Rohrer JD, Fox NC (2016a) Advances in neuroimaging in frontotemporal dementia. J Neurochem 138:193–210
Gordon BA, Friedrichsen K, Brier M, Blazey T, Su Y, Christensen J et al (2016b) The relationship between cerebrospinal fluid markers of Alzheimer pathology and positron emission tomography tau imaging. Brain 139(Pt 8):2249–2260
Gordon BA, Blazey TM, Su Y, Hari-Raj A, Dincer A, Flores S et al (2018) Spatial patterns of neuroimaging biomarker change in individuals from families with autosomal dominant Alzheimer's disease: a longitudinal study. Lancet Neurol 17(3):241–250
Gorno-Tempini M, Hillis AE, Weintraub S, Kertesz A, Mendez M, Cappa SF et al (2011) Classification of primary progressive aphasia and its variants. Neurology 76(11):1006–1014
Guerra UP, Nobili FM, Padovani A, Perani D, Pupi A, Sorbi S et al (2015) Recommendations from the Italian Interdisciplinary Working Group (AIMN, AIP, SINDEM) for the utilization of amyloid imaging in clinical practice. Neurol Sci 36(6):1075–1081
Haass C, Selkoe DJ (2007) Soluble protein oligomers in neurodegeneration: lessons from the Alzheimer's amyloid β-peptide. Nat Rev Mol Cell Biol 8(2):101–112
Hamaguchi T, Kitamoto T, Sato T, Mizusawa H, Nakamura Y, Noguchi M et al (2005) Clinical diagnosis of MM2-type sporadic Creutzfeldt-Jakob disease. Neurology 64(4):643–648
Hamelin L, Lagarde J, Dorothée G, Leroy C, Labit M, Comley RA et al (2016) Early and protective microglial activation in Alzheimer's disease: a prospective study using 18 F-DPA-714 PET imaging. Brain 139(4):1252–1264

Hamilton RL, Bowser R (2004) Alzheimer disease pathology in amyotrophic lateral sclerosis. Acta Neuropathol 107(6):515–522
Harada R, Okamura N, Furumoto S, Furukawa K, Ishiki A, Tomita N et al (2015) [18F] THK-5117 PET for assessing neurofibrillary pathology in Alzheimer's disease. Eur J Nucl Med Mol Imaging 42(7):1052–1061
Harada R, Okamura N, Furumoto S, Furukawa K, Ishiki A, Tomita N et al (2016) 18F-THK5351: a novel PET radiotracer for imaging neurofibrillary pathology in Alzheimer disease. J Nucl Med 57(2):208–214
Harding AJ, Halliday GM (2001) Cortical Lewy body pathology in the diagnosis of dementia. Acta Neuropathol 102(4):355–363
Hardy J (2006) Alzheimer's disease: the amyloid cascade hypothesis: an update and reappraisal. J Alzheimers Dis 9(s3):151–153
Hardy J, Allsop D (1991) Amyloid deposition as the central event in the aetiology of Alzheimer's disease. Trends Pharmacol Sci 12:383–388
Hedden T, Oh H, Younger AP, Patel T (2013) a. Meta-analysis of amyloid-cognition relations in cognitively normal older adults. Neurology 80(14):1341–1348
Hellwig S, Amtage F, Kreft A, Buchert R, Winz OH, Vach W et al (2012) [18F] FDG-PET is superior to [123I] IBZM-SPECT for the differential diagnosis of parkinsonism. Neurology 79(13):1314–1322
Heneka MT, Kummer MP, Latz E (2014) Innate immune activation in neurodegenerative disease. Nat Rev Immunol 14(7):463
Henkel K, Zerr I, Hertel A, Gratz K-F, Schröter A, Tschampa HJ et al (2002) Positron emission tomography with [18 F] FDG in the diagnosis of Creutzfeldt-Jakob disease (CJD). J Neurol 249(6):699–705
Henkel K, Karitzky J, Schmid M, Mader I, Glatting G, Unger JW et al (2004) Imaging of activated microglia with PET and [11C] PK 11195 in corticobasal degeneration. Mov Disord 19(7):817–821
Heppner FL, Ransohoff RM, Becher B (2015) Immune attack: the role of inflammation in Alzheimer disease. Nat Rev Neurosci 16(6):358
Herholz K, Carter SF, Jones M (2007) Positron emission tomography imaging in dementia. Br J Radiol 80(special_issue_2):S160–S167
Hoffman JM, Welsh-Bohmer KA, Hanson M, Crain B, Hulette C, Earl N et al (2000) FDG PET imaging in patients with pathologically verified dementia. J Nucl Med 41(11):1920–1928
Horvath J, Herrmann FR, Burkhard PR, Bouras C, Kövari E (2013) Neuropathology of dementia in a large cohort of patients with Parkinson's disease. Parkinsonism Relat Disord 19(10):864–868
Hosaka K, Ishii K, Sakamoto S, Mori T, Sasaki M, Hirono N et al (2002) Voxel-based comparison of regional cerebral glucose metabolism between PSP and corticobasal degeneration. J Neurol Sci 199(1–2):67–71
Hostetler ED, Walji AM, Zeng Z, Miller P, Bennacef I, Salinas C et al (2016) Preclinical characterization of 18F-MK-6240, a promising PET tracer for in vivo quantification of human neurofibrillary tangles. J Nucl Med 57(10):1599–1606
Howarth C, Gleeson P, Attwell D (2012) Updated energy budgets for neural computation in the neocortex and cerebellum. J Cereb Blood Flow Metab 32(7):1222–1232
Hu WT, Parisi JE, Knopman DS, Boeve BF, Dickson DW, Ahlskog JE et al (2007) Clinical features and survival of 3R and 4R tauopathies presenting as behavioral variant frontotemporal dementia. Alzheimer Dis Assoc Disord 21(4):S39–S43
Hughes AJ, Daniel SE, Ben-Shlomo Y, Lees AJ (2002) The accuracy of diagnosis of parkinsonian syndromes in a specialist movement disorder service. Brain 125(Pt 4):861–870
Iaccarino L, Crespi C, Della Rosa PA, Catricalà E, Guidi L, Marcone A et al (2015) The semantic variant of primary progressive aphasia: clinical and neuroimaging evidence in single subjects. PLoS One 10(3):e0120197
Iaccarino L, Sala A, Caminiti SP, Perani D (2017a) The emerging role of PET imaging in dementia. F1000Res 6:1830

Iaccarino L, Chiotis K, Alongi P, Almkvist O, Wall A, Cerami C et al (2017b) A cross-validation of FDG-and Amyloid-PET biomarkers in mild cognitive impairment for the risk prediction to dementia due to Alzheimer's disease in a clinical setting. J Alzheimers Dis 59(2):603–614

Iaccarino L, Moresco RM, Presotto L, Bugiani O, Iannaccone S, Giaccone G et al (2018a) An in vivo 11 C-(R)-PK11195 PET and in vitro pathology study of microglia activation in Creutzfeldt-Jakob disease. Mol Neurobiol 55(4):2856–2868

Iaccarino L, Presotto L, Bettinardi V, Gianolli L, Roiter I, Capellari S et al (2018b) An in vivo 11C-PK PET study of microglia activation in fatal familial insomnia. Ann Clin Transl Neurol 5(1):11–18

Iaccarino L, Sala A, Perani D, ADN I (2019) Predicting long-term clinical stability in amyloid-positive subjects by FDG-PET. Ann Clin Transl Neurol 6(6):1113–1120

Iannaccone S, Cerami C, Alessio M, Garibotto V, Panzacchi A, Olivieri S et al (2013) In vivo microglia activation in very early dementia with Lewy bodies, comparison with Parkinson's disease. Parkinsonism Relat Disord 19(1):47–52

Ikonomovic MD, Klunk WE, Abrahamson EE, Mathis CA, Price JC, Tsopelas ND et al (2008) Post-mortem correlates of in vivo PiB-PET amyloid imaging in a typical case of Alzheimer's disease. Brain 131(6):1630–1645

Imamura K, Hishikawa N, Sawada M, Nagatsu T, Yoshida M, Hashizume Y (2003) Distribution of major histocompatibility complex class II-positive microglia and cytokine profile of Parkinson's disease brains. Acta Neuropathol 106(6):518–526

Irwin DJ, White MT, Toledo JB, Xie SX, Robinson JL, Van Deerlin V et al (2012) Neuropathologic substrates of Parkinson disease dementia. Ann Neurol 72(4):587–598

Ishiki A, Okamura N, Furukawa K, Furumoto S, Harada R, Tomita N et al (2015) Longitudinal assessment of tau pathology in patients with Alzheimer's disease using [18F]THK-5117 positron emission tomography. PLoS One 10(10):e0140311

Ishiki A, Harada R, Okamura N, Tomita N, Rowe CC, Villemagne VL et al (2017) Tau imaging with [18F] THK-5351 in progressive supranuclear palsy. Eur J Neurol 24(1):130–136

Ishiki A, Harada R, Kai H, Sato N, Totsune T, Tomita N et al (2018) Neuroimaging-pathological correlations of [(18)F]THK5351 PET in progressive supranuclear palsy. Acta Neuropathol Commun 6(1):53

Jack CR Jr, Knopman DS, Jagust WJ, Petersen RC, Weiner MW, Aisen PS et al (2013) Tracking pathophysiological processes in Alzheimer's disease: an updated hypothetical model of dynamic biomarkers. Lancet Neurol 12(2):207–216

Jack CR, Wiste HJ, Weigand SD, Knopman DS, Lowe V, Vemuri P et al (2013) Amyloid-first and neurodegeneration-first profiles characterize incident amyloid PET positivity. Neurology 81(20):1732–1740

Jagust W, Reed B, Mungas D, Ellis W, DeCarli C (2007) What does fluorodeoxyglucose PET imaging add to a clinical diagnosis of dementia? Neurology 69(9):871–877

Jagust WJ, Landau SM, Initiative ADN (2012) Apolipoprotein E, not fibrillar β-amyloid, reduces cerebral glucose metabolism in normal aging. J Neurosci 32(50):18227–18233

Jang YK, Lyoo CH, Park S, Oh SJ, Cho H, Oh M et al (2018) Head to head comparison of [(18) F] AV-1451 and [(18)F] THK5351 for tau imaging in Alzheimer's disease and frontotemporal dementia. Eur J Nucl Med Mol Imaging 45(3):432–442

Jansen WJ, Ossenkoppele R, Knol DL, Tijms BM, Scheltens P, Verhey FRJ et al (2015) Prevalence of cerebral amyloid pathology in persons without dementia: a meta-analysis. JAMA 313(19):1924–1938

Jellinger KA (2007) More frequent Lewy bodies but less frequent Alzheimer-type lesions in multiple system atrophy as compared to age-matched control brains. Acta Neuropathol 114(3):299–303

Jellinger KA, Attems J (2010) Prevalence of dementia disorders in the oldest-old: an autopsy study. Acta Neuropathol 119(4):421–433

Jeong Y, Cho SS, Park JM, Kang SJ, Lee JS (2005) 18F-FDG PET findings in frontotemporal dementia: an SPM analysis of 29 patients. J Nucl Med 46(2):233–240

Ji K, Akgul G, Wollmuth LP, Tsirka SE (2013) Microglia actively regulate the number of functional synapses. PLoS One 8(2):e56293
Johansson A, Engler H, Blomquist G, Scott B, Wall A, Aquilonius S-M et al (2007) Evidence for astrocytosis in ALS demonstrated by [11C](L)-deprenyl-D2 PET. J Neurol Sci 255(1–2):17–22
Johnson KA, Minoshima S, Bohnen NI, Donohoe KJ, Foster NL, Herscovitch P et al (2013a) Appropriate use criteria for amyloid PET: a report of the Amyloid imaging task force, the Society of Nuclear Medicine and Molecular Imaging, and the Alzheimer's Association. J Nucl Med 54(3):476–490
Johnson KA, Minoshima S, Bohnen NI, Donohoe KJ, Foster NL, Herscovitch P et al (2013b) Update on appropriate use criteria for amyloid PET imaging: Dementia experts , mild cognitive impairment, and education. Alzheimers Dement 9(4):e106–e109
Johnson KA, Schultz A, Betensky RA, Becker JA, Sepulcre J, Rentz D et al (2016) Tau positron emission tomographic imaging in aging and early Alzheimer disease. Ann Neurol 79(1):110–119
Josephs KA, Holton JL, Rossor MN, Godbolt AK, Ozawa T, Strand K et al (2004) Frontotemporal lobar degeneration and ubiquitin immunohistochemistry. Neuropathol Appl Neurobiol 30(4):369–373
Josephs KA, Whitwell JL, Tacik P, Duffy JR, Senjem ML, Tosakulwong N et al (2016) [18F] AV-1451 tau-PET uptake does correlate with quantitatively measured 4R-tau burden in autopsy-confirmed corticobasal degeneration. Acta Neuropathol 132(6):931–933
Josephs KA, Martin PR, Botha H, Schwarz CG, Duffy JR, Clark HM et al (2018) [(18) F]AV-1451 tau-PET and primary progressive aphasia. Ann Neurol 83(3):599–611
Jučaite A, Cselényi Z, Arvidsson A, Åhlberg G, Julin P, Varnäs K et al (2012) Kinetic analysis and test-retest variability of the radioligand [11 C](R)-PK11195 binding to TSPO in the human brain-a PET study in control subjects. EJNMMI Res 2(1):15
Jucaite A, Svenningsson P, Rinne JO, Cselenyi Z, Varnäs K, Johnström P et al (2015) Effect of the myeloperoxidase inhibitor AZD3241 on microglia: a PET study in Parkinson's disease. Brain 138(9):2687–2700
Juh R, Kim J, Moon D, Choe B, Suh T (2004) Different metabolic patterns analysis of parkinsonism on the 18F-FDG PET. Eur J Radiol 51(3):223–233
Kadekaro M, Vance WH, Terrell ML, Gary H, Eisenberg HM, Sokoloff L (1987) Effects of antidromic stimulation of the ventral root on glucose utilization in the ventral horn of the spinal cord in the rat. Proc Natl Acad Sci U S A 84(15):5492–5495
Kang Y, Mozley PD, Verma A, Schlyer D, Henchcliffe C, Gauthier SA et al (2018) Noninvasive PK11195-PET image analysis techniques can detect abnormal cerebral microglial activation in Parkinson's disease. J Neuroimaging 28(5):496–505
Kantarci K, Lowe VJ, Boeve BF, Weigand SD, Senjem ML, Przybelski SA et al (2012) Multimodality imaging characteristics of dementia with Lewy bodies. Neurobiol Aging 33(9):2091–2105
Kantarci K, Lowe VJ, Boeve BF, Senjem ML, Tosakulwong N, Lesnick TG et al (2017) AV-1451 tau and beta-amyloid positron emission tomography imaging in dementia with Lewy bodies. Ann Neurol 81(1):58–67
Kato T, Inui Y, Nakamura A, Ito K (2016) Brain fluorodeoxyglucose (FDG) PET in dementia. Ageing Res Rev 30:73–84. https://doi.org/10.1016/j.arr.2016.02.003
Kayed R, Lasagna-Reeves CA (2013) Molecular mechanisms of amyloid oligomers toxicity. J Alzheimers Dis 33(s1):S67–S78
Kealey S, Turner EM, Husbands SM, Salinas CA, Jakobsen S, Tyacke RJ et al (2013) Imaging imidazoline-I2 binding sites in porcine brain using 11C-BU99008. J Nucl Med 54(1):139–144
Kepe V, Ghetti B, Farlow MR, Bresjanac M, Miller K, Huang S et al (2010) PET of brain prion protein amyloid in Gerstmann–Sträussler–Scheinker disease. Brain Pathol 20(2):419–430
Kepe V, Bordelon Y, Boxer A, Huang S-C, Liu J, Thiede FC et al (2013) PET imaging of neuropathology in tauopathies: progressive supranuclear palsy. J Alzheimers Dis 36(1):145–153
Kertesz A, McMonagle P, Blair M, Davidson W, Munoz DG (2005) The evolution and pathology of frontotemporal dementia. Brain 128(9):1996–2005

Kettenmann H, Hanisch U-K, Noda M, Verkhratsky A (2011) Physiology of microglia. Physiol Rev 91(2):461–553

Kikuchi A, Okamura N, Hasegawa T, Harada R, Watanuki S, Funaki Y et al (2016) In vivo visualization of tau deposits in corticobasal syndrome by 18F-THK5351 PET. Neurology 87(22):2309–2316

Kim EJ, Cho SS, Jeong Y, Park KC, Kang SJ, Kang E et al (2005) Glucose metabolism in early onset versus late onset Alzheimer's disease: an SPM analysis of 120 patients. Brain 128(8):1790–1801

Kim E-J, Kim BC, Kim S-J, Jung DS, Sin J-S, Yoon Y-J et al (2012a) Clinical staging of semantic dementia in an FDG-PET study using FTLD-CDR. Dement Geriatr Cogn Disord 34(5–6):300–306

Kim E, Cho S, Jeong B, Kim Y, Seo SW, Na DL et al (2012b) Glucose metabolism in sporadic Creutzfeldt–Jakob disease: a statistical parametric mapping analysis of 18F-FDG PET. Eur J Neurol 19(3):488–493

Kim H-J, Jeon BS, Kim YE, Kim J-Y, Kim YK, Sohn C-H et al (2013) Clinical and imaging characteristics of dementia in multiple system atrophy. Parkinsonism Relat Disord 19(6):617–621

Kim M-J, McGwier M, Jenko KJ, Snow J, Morse C, Zoghbi SS et al (2019) Neuroinflammation in frontotemporal lobar degeneration revealed by ^{11}C-PBR28 PET. Ann Clin Transl Neurol

Klunk WE, Engler H, Nordberg A, Wang Y, Blomqvist G, Holt DP et al (2004) Imaging brain amyloid in Alzheimer's disease with Pittsburgh compound-B. Ann Neurol 55(3):306–319

Klunk WE, Koeppe RA, Price JC, Benzinger TL, Devous MD, Jagust WJ et al (2015) The Centiloid project: standardizing quantitative amyloid plaque estimation by PET. Alzheimers Dement 11(1):1–15

Knopman DS, Parisi JE, Salviati A, Floriach-Robert M, Boeve BF, Ivnik RJ et al (2003) Neuropathology of cognitively normal elderly. J Neuropathol Exp Neurol 62(11):1087–1095

Kobayashi R, Hayashi H, Kawakatsu S, Ishiki A, Okamura N, Arai H et al (2018) [(18)F]THK-5351 PET imaging in early-stage semantic variant primary progressive aphasia: a report of two cases and a literature review. BMC Neurol 18(1):109

Kotzbauer PT, Tu Z, Mach RH (2017) Current status of the development of PET radiotracers for imaging alpha synuclein aggregates in Lewy bodies and Lewy neurites. Clin Trans Imaging 5(1):3–14

Kreisl WC, Lyoo CH, McGwier M, Snow J, Jenko KJ, Kimura N et al (2013) In vivo radioligand binding to translocator protein correlates with severity of Alzheimer's disease. Brain 136(7):2228–2238

Kreisl WC, Lyoo CH, Liow J-S, Snow J, Page E, Jenko KJ et al (2017) Distinct patterns of increased translocator protein in posterior cortical atrophy and amnestic Alzheimer's disease. Neurobiol Aging 51:132–140

Kübler D, Wächter T, Cabanel N, Su Z, Turkheimer FE, Dodel R et al (2019) Widespread microglial activation in multiple system atrophy. Mov Disord 34(4):564–568

Kwon K-Y, Kim JS, Im KC, Lee MC, Chung SJ (2009) Comparison of cerebral glucose metabolism between possible and probable multiple system atrophy. J Mov Disord 2(1):22

La Joie R, Bejanin A, Fagan AM, Ayakta N, Baker SL, Bourakova V et al (2018) Associations between [(18)F]AV1451 tau PET and CSF measures of tau pathology in a clinical sample. Neurology 90(4):e282–e290

Laforce R Jr, Buteau JP, Paquet N, Verret L, Houde M, Bouchard RW (2010) The value of PET in mild cognitive impairment, typical and atypical/unclear dementias: a retrospective memory clinic study. Am J Alzheimers Dis Other Demen 25(4):324–332

Laforce R Jr, Soucy J-P, Sellami L, Dallaire-Théroux C, Brunet F, Bergeron D et al (2018) Molecular imaging in dementia: past, present, and future. Alzheimers Dement 14(11):1522–1552

Landau SM, Harvey D, Madison CM, Reiman EM, Foster NL, Aisen PS et al (2010) Comparing predictors of conversion and decline in mild cognitive impairment. Neurology 75(3):230–238

Landau SM, Horng A, Fero A, Jagust WJ, Weiner M, Aisen P et al (2016) Amyloid negativity in patients with clinically diagnosed Alzheimer disease and MCI. Neurology 86(15):1377–1385

Lee SE, Rabinovici GD, Mayo MC, Wilson SM, Seeley WW, DeArmond SJ et al (2011) Clinicopathological correlations in corticobasal degeneration. Ann Neurol 70(2):327–340

Lee DC, Rizer J, Hunt JB, Selenica M, Gordon MN, Morgan D (2013) Experimental manipulations of microglia in mouse models of Alzheimer's pathology: activation reduces amyloid but hastens tau pathology. Neuropathol Appl Neurobiol 39(1):69–85

Lee H, Seo S, Lee SY, Jeong HJ, Woo SH, Lee KM et al (2018a) [18F]-THK5351 PET imaging in patients with semantic variant primary progressive aphasia. Alzheimer Dis Assoc Disord 32(1):62–69

Lee SH, Cho H, Choi JY, Lee JH, Ryu YH, Lee MS et al (2018b) Distinct patterns of amyloid-dependent tau accumulation in Lewy body diseases. Mov Disord 33(2):262–272

Lehmann M, Ghosh PM, Madison C, Laforce R Jr, Corbetta-rastelli C, Weiner MW et al (2013) Diverging patterns of amyloid deposition and hypometabolism in clinical variants of probable Alzheimer's disease. Brain 136(Pt 3):844–858

Leyton CE, Villemagne VL, Savage S, Pike KE, Ballard KJ, Piguet O et al (2011) Subtypes of progressive aphasia: application of the international consensus criteria and validation using β-amyloid imaging. Brain 134(10):3030–3043

Li K, Li J, Zheng J, Qin S (2019) Reactive astrocytes in neurodegenerative diseases. Aging Dis 10(3):664

Lian H, Litvinchuk A, Chiang AC-A, Aithmitti N, Jankowsky JL, Zheng H (2016) Astrocyte-microglia cross talk through complement activation modulates amyloid pathology in mouse models of Alzheimer's disease. J Neurosci 36(2):577–589

Liberski PP, Brown P (2006) Astrocytes in transmissible spongiform encephalopathies (prion diseases). Folia Neuropathol 42:71

Lim SM, Katsifis A, Villemagne VL, Best R, Jones G, Saling M et al (2009) The 18F-FDG PET cingulate island sign and comparison to 123I-β-CIT SPECT for diagnosis of dementia with Lewy bodies. J Nucl Med 50(10):1638–1645

Ling H (2016) Clinical approach to progressive supranuclear palsy. J Mov Disord 9(1):3

Ling H, Macerollo A (2018) Is it useful to classify PSP and CBD as different disorders? Yes. Mov Disord Clin Pract 5(2):145–148

Ling H, O'Sullivan SS, Holton JL, Revesz T, Massey LA, Williams DR et al (2010) Does corticobasal degeneration exist? A clinicopathological re-evaluation. Brain 133(7):2045–2057

Lockhart A, Lamb JR, Osredkar T, Sue LI, Joyce JN, Ye L et al (2007) PIB is a non-specific imaging marker of amyloid-beta (Aβ) peptide-related cerebral amyloidosis. Brain 130(10):2607–2615

Lockhart SN, Baker SL, Okamura N, Furukawa K, Ishiki A, Furumoto S et al (2016) Dynamic PET measures of tau accumulation in cognitively normal older adults and Alzheimer's Disease Patients Measured Using [^{18}F] THK-5351. PLoS One 11(6):e0158460

Lowe VJ, Curran G, Fang P, Liesinger AM, Josephs KA, Parisi JE et al (2016) An autoradiographic evaluation of AV-1451 tau PET in dementia. Acta Neuropathol Commun 4(1):58

Lundgaard I, Li B, Xie L, Kang H, Sanggaard S, Haswell JDR et al (2015) Direct neuronal glucose uptake heralds activity-dependent increases in cerebral metabolism. Nat Commun 6:6807

Lyoo CH, Jeong Y, Ryu YH, Lee SY, Song TJ, Lee JH et al (2008) Effects of disease duration on the clinical features and brain glucose metabolism in patients with mixed type multiple system atrophy. Brain 131(2):438–446

Maass A, Landau S, Baker SL, Horng A, Lockhart SN, La Joie R et al (2017) Comparison of multiple tau-PET measures as biomarkers in aging and Alzheimer's disease. Neuroimage 157:448–463

Mackenzie IRA, Neumann M (2016) Molecular neuropathology of frontotemporal dementia: insights into disease mechanisms from postmortem studies. J Neurochem 138:54–70

Mackenzie IRA, Foti D, Woulfe J, Hurwitz TA (2008) Atypical frontotemporal lobar degeneration with ubiquitin-positive, TDP-43-negative neuronal inclusions. Brain 131(5):1282–1293

Madhavan A, Whitwell JL, Weigand SD, Duffy JR, Strand EA, Machulda MM et al (2013) FDG PET and MRI in logopenic primary progressive aphasia versus dementia of the Alzheimer's type. PLoS One 8(4):e62471

Maetzler W, Liepelt I, Reimold M, Reischl G, Solbach C, Becker C et al (2009) Cortical PIB binding in Lewy body disease is associated with Alzheimer-like characteristics. Neurobiol Dis 34(1):107–112

Maezawa I, Zimin PI, Wulff H, Jin L-W (2011) Amyloid-β protein oligomer at low nanomolar concentrations activates microglia and induces microglial neurotoxicity. J Biol Chem 286(5):3693–3706

Magistretti PJ, Pellerin L (1999) Cellular mechanisms of brain energy metabolism and their relevance to functional brain imaging. Philos Trans R Soc London Ser B Biol Sci 354(1387):1155–1163

Makaretz SJ, Quimby M, Collins J, Makris N, McGinnis S, Schultz A et al (2018) Flortaucipir tau PET imaging in semantic variant primary progressive aphasia. J Neurol Neurosurg Psychiatry 89(10):1024–1031

Marlatt MW, Bauer J, Aronica E, van Haastert ES, Hoozemans JJM, Joels M et al (2014) Proliferation in the Alzheimer hippocampus is due to microglia, not astroglia, and occurs at sites of amyloid deposition. Neural Plast 2014

Marquié M, Normandin MD, Vanderburg CR, Costantino IM, Bien EA, Rycyna LG et al (2015) Validating novel tau positron emission tomography tracer [F-18]-AV-1451 (T807) on postmortem brain tissue. Ann Neurol 78(5):787–800

Marquie M, Normandin MD, Meltzer AC, Siao Tick Chong M, Andrea NV, Anton-Fernandez A et al (2017) Pathological correlations of [F-18]-AV-1451 imaging in non-alzheimer tauopathies. Ann Neurol 81(1):117–128

Marsh SE, Blurton-Jones M (2012) Examining the mechanisms that link β-amyloid and α-synuclein pathologies. Alzheimers Res Ther 4(2):11

Maruyama M, Shimada H, Suhara T, Shinotoh H, Ji B, Maeda J et al (2013) Imaging of tau pathology in a tauopathy mouse model and in Alzheimer patients compared to normal controls. Neuron 79(6):1094–1108

Masdeu JC (2017) Future directions in imaging neurodegeneration. Curr Neurol Neurosci Rep 17(1):9

Mastrianni JA, Nixon R, Layzer R, Telling GC, Han D, DeArmond SJ et al (1999) Prion protein conformation in a patient with sporadic fatal insomnia. N Engl J Med 340(21):1630–1638

Matias-Guiu JA, Cabrera-Martín MN, García-Ramos R, Moreno-Ramos T, Valles-Salgado M, Carreras JL et al (2014) Evaluation of the new consensus criteria for the diagnosis of primary progressive aphasia using fluorodeoxyglucose positron emission tomography. Dement Geriatr Cogn Disord 38(3–4):147–152

Matías-Guiu JA, Pytel V, Cabrera-Martín MN, Galán L, Valles-Salgado M, Guerrero A et al (2016) Amyloid-and FDG-PET imaging in amyotrophic lateral sclerosis. Eur J Nucl Med Mol Imaging 43(11):2050–2060

Matías-Guiu JA, Guerrero-Márquez C, Cabrera-Martín MN, Gómez-Pinedo U, Romeral M, Mayo D et al (2017) Amyloid- and FDG-PET in sporadic Creutzfeldt-Jakob disease: Correlation with pathological prion protein in neuropathology. Prion 11(3):205–213. https://doi.org/10.1080/19336896.2017.1314427

Mattsson N, Scholl M, Strandberg O, Smith R, Palmqvist S, Insel PS et al (2017) (^{18})F-AV-1451 and CSF T-tau and P-tau as biomarkers in Alzheimer's disease. EMBO Mol Med 9(9):1212–1223

McCann H, Stevens CH, Cartwright H, Halliday GM (2014) α-Synucleinopathy phenotypes. Parkinsonism Relat Disord 20:S62–S67

McGeer PL, Itagaki S, Boyes BE, McGeer EG (1988) Reactive microglia are positive for HLA-DR in the substantia nigra of Parkinson's and Alzheimer's disease brains. Neurology 38(8):1285

McKeith IG, Boeve BF, Dickson DW, Halliday G, Taylor J-P, Weintraub D et al (2017) Diagnosis and management of dementia with Lewy bodies: fourth consensus report of the DLB consortium. Neurology 89(1):88–100

McKhann GM, Knopman DS, Chertkow H, Hyman BT, Jack CR, Kawas CH et al (2011) The diagnosis of dementia due to Alzheimer's disease: recommendations from the National Institute on Aging-Alzheimer's association workgroups on diagnostic guidelines for Alzheimer's disease. Alzheimers Dement 7(3):263–269

Meeter LH, Kaat LD, Rohrer JD, Van Swieten JC (2017) Imaging and fluid biomarkers in frontotemporal dementia. Nat Rev Neurol 13(7):406

Mente KP, O'Donnell JK, Jones SE, Cohen ML, Thompson NR, Bizzi A et al (2017) Fluorodeoxyglucose positron emission tomography (FDG-PET) Correlation of histopathology and MRI in Prion disease. Alzheimer Dis Assoc Disord 31(1):1–7. https://www.ncbi.nlm.nih.gov/pubmed/28121634

Mesulam M-M, Rogalski EJ, Wieneke C, Hurley RS, Geula C, Bigio EH et al (2014) Primary progressive aphasia and the evolving neurology of the language network. Nat Rev Neurol 10(10):554

Mintun MA, Larossa GN, Sheline YI, Dence CS, Lee SY, Mach RH et al (2006) [11C] PIB in a nondemented population: potential antecedent marker of Alzheimer disease. Neurology 67(3):446–452

Mion M, Patterson K, Acosta-Cabronero J, Pengas G, Izquierdo-Garcia D, Hong YT et al (2010) What the left and right anterior fusiform gyri tell us about semantic memory. Brain 133(11):3256–3268

Miyoshi M, Shinotoh H, Wszolek ZK, Strongosky AJ, Shimada H, Arakawa R et al (2010) In vivo detection of neuropathologic changes in presymptomatic MAPT mutation carriers: a PET and MRI study. Parkinsonism Relat Disord 16(6):404–408

Montagna P, Gambetti P, Cortelli P, Lugaresi E (2003) Familial and sporadic fatal insomnia. Lancet Neurol 2(3):167–176

Morales I, Jiménez JM, Mancilla M, Maccioni RB (2013) Tau oligomers and fibrils induce activation of microglial cells. J Alzheimers Dis 37(4):849–856

Morbelli S, Garibotto V, Van De Giessen E, Arbizu J, Chételat G, Drezgza A et al (2015) A Cochrane review on brain [18 F] FDG PET in dementia: limitations and future perspectives. Eur J Nucl Med Mol Imaging 42(10):1487–1491

Morinaga A, Ono K, Ikeda T, Ikeda Y, Shima K, Noguchi-Shinohara M et al (2010) A comparison of the diagnostic sensitivity of MRI, CBF-SPECT, FDG-PET and cerebrospinal fluid biomarkers for detecting Alzheimer's disease in a memory clinic. Dement Geriatr Cogn Disord 30(4):285–292

Morris JC, Roe CM, Xiong C, Fagan AM, Goate AM, Holtzman DM et al (2010) APOE predicts amyloid-beta but not tau Alzheimer pathology in cognitively normal aging. Ann Neurol 67(1):122–131

Mosconi L (2005) Brain glucose metabolism in the early and specific diagnosis of Alzheimer's disease: FDG-PET studies in MCI and AD. Eur J Nucl Med Mol Imaging 32(4):486–510

Mosconi L (2013) Glucose metabolism in normal aging and Alzheimer's disease: methodological and physiological considerations for PET studies. Clin Transl Imaging 1(4):217–233

Mosconi L, Tsui WH, Herholz K, Pupi A, Drzezga A, Lucignani G et al (2008) Multicenter standardized 18F-FDG PET diagnosis of mild cognitive impairment, Alzheimer's disease, and other dementias. Eur J Nucl Med Mol Imaging 49(3):390–398

Mueller et al (2017) Characterization of the novel PET Tracer PI-2620 for the assessment of Tau pathology in Alzheimer's disease and other tauopathies. J Nucl Med 58

Muhleisen H, Gehrmann J, Meyermann R (1995) Reactive microglia in Creutzfeldt-Jakob disease. Neuropathol Appl Neurobiol 21(6):505–517

Murray ME, Lowe VJ, Graff-Radford NR, Liesinger AM, Cannon A, Przybelski SA et al (2015) Clinicopathologic and 11C-Pittsburgh compound B implications of Thal amyloid phase across the Alzheimer's disease spectrum. Brain a J Neurol 138(5):1370–1381

Nagaishi M, Yokoo H, Nakazato Y (2011) Tau-positive glial cytoplasmic granules in multiple system atrophy. Neuropathology 31(3):299–305

Nagele RG, D'Andrea MR, Lee H, Venkataraman V, Wang H-Y (2003) Astrocytes accumulate Aβ42 and give rise to astrocytic amyloid plaques in Alzheimer disease brains. Brain Res 971(2):197–209

Narayanaswami V, Dahl K, Bernard-Gauthier V, Josephson L, Cumming P, Vasdev N (2018) Emerging PET radiotracers and targets for imaging of neuroinflammation in neurodegenerative diseases: outlook beyond TSPO. Mol Imaging 17:1536012118792317

Nasrallah IM, Chen YJ, Hsieh M-K, Phillips JS, Ternes K, Stockbower GE et al (2018) 18F-Flortaucipir PET/MRI correlations in nonamnestic and amnestic variants of Alzheimer disease. J Nucl Med 59(2):299–306

Neary D, Snowden JS, Gustafson L, Passant U, Stuss D, Black S et al (1998) Frontotemporal lobar degeneration: a consensus on clinical diagnostic criteria. Neurology 51(6):1546–1554

Nelson PT, Alafuzoff I, Bigio EH, Bouras C, Braak H, Cairns NJ et al (2012) Correlation of Alzheimer disease neuropathologic changes with cognitive status: a review of the literature. J Neuropathol Exp Neurol 71(5):362–381

Nestor PJ (2003) Progressive non-fluent aphasia is associated with hypometabolism centred on the left anterior insula. Brain 126(11):2406–2418

Nestor PJ, Caine D, Fryer TD, Clarke J, Hodges JR (2003) The topography of metabolic deficits in posterior cortical atrophy (the visual variant of Alzheimer's disease) with FDG-PET. J Neurol Neurosurg Psychiatry 74(11):1521–1529

Nestor PJ, Fryer TD, Hodges JR (2006) Declarative memory impairments in Alzheimer's disease and semantic dementia. NeuroImage 30(3):1010–1020

Nestor PJ, Altomare D, Festari C, Drzezga A, Rivolta J, Walker Z et al (2018) Clinical utility of FDG-PET for the differential diagnosis among the main forms of dementia. Eur J Nucl Med Mol Imaging 45(9):1509–1525

Neumann M, Sampathu DM, Kwong LK, Truax AC, Micsenyi MC, Chou TT et al (2006) Ubiquitinated TDP-43 in frontotemporal lobar degeneration and amyotrophic lateral sclerosis. Science 314(5796):130–133

Ng SY, Villemagne VL, Masters CL, Rowe CC (2007) Evaluating atypical dementia syndromes using positron emission tomography with carbon 11–labeled Pittsburgh compound B. Arch Neurol 64(8):1140–1144

Ng KP, Pascoal TA, Mathotaarachchi S, Therriault J, Kang MS, Shin M et al (2017) Monoamine oxidase B inhibitor, selegiline, reduces 18 F-THK5351 uptake in the human brain. Alzheimers Res Ther 9(1):25

Niccolini F, Wilson H, Hirschbichler S, Yousaf T, Pagano G, Whittington A et al (2018) Disease-related patterns of in vivo pathology in Corticobasal syndrome. Eur J Nucl Med Mol Imaging:1–13

Nichols E, Szoeke CEI, Vollset SE, Abbasi N, Abd-Allah F, Abdela J et al (2019) Global, regional, and national burden of Alzheimer's disease and other dementias, 1990–2016: a systematic analysis for the global burden of disease study. Lancet Neurol 18(1):88–106

Niethammer M, Tang CC, Feigin A, Allen PJ, Heinen L, Hellwig S et al (2014) A disease-specific metabolic brain network associated with corticobasal degeneration. Brain 137(11):3036–3046

O'Brien JT, Firbank MJ, Davison C, Barnett N, Bamford C, Donaldson C et al (2014) 18F-FDG PET and perfusion SPECT in the diagnosis of Alzheimer and Lewy body dementias. J Nucl Med 55(12):1959–1965

Obst J, Simon E, Mancuso R, Gomez-Nicola D (2017) The role of microglia in prion diseases: a paradigm of functional diversity. Front Aging Neurosci 9:207

Okamura N, Harada R, Furumoto S, Arai H, Yanai K, Kudo Y (2014a) Tau PET imaging in Alzheimer's disease. Curr Neurol Neurosci Rep 14(11):1–7

Okamura N, Furumoto S, Fodero-Tavoletti MT, Mulligan RS, Harada R, Yates P et al (2014b) Non-invasive assessment of Alzheimer's disease neurofibrillary pathology using 18F-THK5105 PET. Brain 137(6):1762–1771

Okamura N, Harada R, Furukawa K, Furumoto S, Tago T, Yanai K et al (2016) Advances in the development of tau PET radiotracers and their clinical applications. Ageing Res Rev:1–7

Okamura N, Furumoto S, Harada R, Tago T, Iwata R, Tashiro M et al (2017) Characterization of [18F] THK-5351, a novel PET tracer for imaging tau pathology in Alzheimer's disease. Eur J Neurol 24(1):130–136

Okello A, Edison P, Archer HA, Turkheimer FE, Kennedy J, Bullock R et al (2009) Microglial activation and amyloid deposition in mild cognitive impairment: a PET study. Neurology 72(1):56–62

Olney NT, Spina S, Miller BL (2017) Frontotemporal dementia. Neurol Clin 35(2):339–374

Ossenkoppele R, Tolboom N, Foster-Dingley JC, Adriaanse SF, Boellaard R, Yaqub M et al (2012) Longitudinal imaging of Alzheimer pathology using [^{11}C] PIB,[^{18}F] FDDNP and [^{18}F] FDG PET. Eur J Nucl Med Mol Imaging 39(6):990–1000

Ossenkoppele R, van der Flier WM, Verfaillie SCJ, Vrenken H, Versteeg A, van Schijndel RA et al (2014) Long-term effects of amyloid, hypometabolism, and atrophy on neuropsychological functions. Neurology 82(20):1768–1775

Ossenkoppele R, Jansen WJ, Rabinovici GD, Knol DL, van der Flier WM, van Berckel BNM et al (2015) Prevalence of amyloid PET positivity in dementia syndromes: a meta-analysis. JAMA 313(19):1939–1949. http://www.pubmedcentral.nih.gov/articlerender.fcgi?artid=4517678&tool=pmcentrez&rendertype=abstract

Ossenkoppele R, Schonhaut DR, Schöll M, Lockhart SN, Ayakta N, Baker SL et al (2016) Tau PET patterns mirror clinical and neuroanatomical variability in Alzheimer's disease. Brain 139(5):1551–1567

Ouchi Y, Yoshikawa E, Sekine Y, Futatsubashi M, Kanno T, Ogusu T et al (2005) Microglial activation and dopamine terminal loss in early Parkinson's disease. Ann Neurol 57(2):168–175

Owen DR, Yeo AJ, Gunn RN, Song K, Wadsworth G, Lewis A et al (2012) An 18-kDa translocator protein (TSPO) polymorphism explains differences in binding affinity of the PET radioligand PBR28. J Cereb Blood Flow Metab 32(1):1–5

Ozawa T, Paviour D, Quinn NP, Josephs KA, Sangha H, Kilford L et al (2004) The spectrum of pathological involvement of the striatonigral and olivopontocerebellar systems in multiple system atrophy: clinicopathological correlations. Brain 127(12):2657–2671

Pakrasi S, O'Brien JT (2005) Emission tomography in dementia. Nucl Med Commun 26(3):189–196

Panegyres PK, Rogers JM, McCarthy M, Campbell A, Wu JS (2009) Fluorodeoxyglucose-positron emission tomography in the differential diagnosis of early-onset dementia: a prospective, community-based study. BMC Neurol 9(1):41. https://doi.org/10.1186/1471-2377-9-41

Papadopoulos V, Baraldi M, Guilarte TR, Knudsen TB, Lacapère J-J, Lindemann P et al (2006) Translocator protein (18 kDa): new nomenclature for the peripheral-type benzodiazepine receptor based on its structure and molecular function. Trends Pharmacol Sci 27(8):402–409

Parbo P, Ismail R, Hansen KV, Amidi A, Mårup FH, Gottrup H et al (2017) Brain inflammation accompanies amyloid in the majority of mild cognitive impairment cases due to Alzheimer's disease. Brain 140(7):2002–2011

Parbo P, Ismail R, Sommerauer M, Stokholm MG, Hansen AK, Hansen KV et al (2018) Does inflammation precede tau aggregation in early Alzheimer's disease? A PET study. Neurobiol Dis 117:211–216

Parchi P, Castellani R, Cortelli P, Montagna P, Chen SG, Petersen RB et al (1995) Regional distribution of protease-resistant prion protein in fatal familial insomnia. Ann Neurol 38(1):21–29

Pardini M, Huey ED, Spina S, Kreisl WC, Morbelli S, Wassermann EM et al (2019) FDG-PET patterns associated with underlying pathology in corticobasal syndrome. Neurology 92(10):e1121–e1135

Parker CA, Nabulsi N, Holden D, Lin S, Cass T, Labaree D et al (2014) Evaluation of 11C-BU99008, a PET ligand for the imidazoline2 binding sites in rhesus brain. J Nucl Med 55(5):838–844

Pascoal TA, Shin M, Kang MS, Chamoun M, Chartrand D, Mathotaarachchi S et al (2018) In vivo quantification of neurofibrillary tangles with [(18)F]MK-6240. Alzheimers Res Ther 10(1):74

Pasqualetti G, Brooks DJ, Edison P (2015) The role of neuroinflammation in dementias. Curr Neurol Neurosci Rep 15(4):17

Passamonti L, Vázquez Rodríguez P, Hong YT, Allinson KSJ, Williamson D, Borchert RJ et al (2017) 18F-AV-1451 positron emission tomography in Alzheimer's disease and progressive supranuclear palsy. Brain 140(3):781–791

Passamonti L, Rodríguez PV, Hong YT, Allinson KSJ, Bevan-Jones WR, Williamson D et al (2018) [11C] PK11195 binding in Alzheimer disease and progressive supranuclear palsy. Neurology 90(22):e1989–e1996

Passamonti L, Tsvetanov K, Jones PS, Bevan-Jones WR, Arnold R, Borchert RJ, et al. Neuroinflammation and functional connectivity in Alzheimer's disease: interactive influences on cognitive performance. bioRxiv. 2019;532291

Patterson JC, Lilien DL, Takalkar A, Pinkston JB (2011) Early detection of brain pathology suggestive of early AD using objective evaluation of FDG-PET scans. Int J Alzheimers Dis 2011:946590

Payoux P, Delrieu J, Gallini A, Adel D, Salabert AS, Hitzel A et al (2015) Cognitive and functional patterns of nondemented subjects with equivocal visual amyloid PET findings. Eur J Nucl Med Mol Imaging 42(9):1459–1468

Pekny M, Pekna M (2014) Astrocyte reactivity and reactive astrogliosis: costs and benefits. Physiol Rev 94(4):1077–1098

Pellerin L, Magistretti PJ (1994) Glutamate uptake into astrocytes stimulates aerobic glycolysis: a mechanism coupling neuronal activity to glucose utilization. Proc Natl Acad Sci U S A 91(22):10625–10629

Perani D (2008) Functional neuroimaging of cognition. Handb Clin Neurol 88:61–111

Perani D (2014) FDG-PET and amyloid-PET imaging: the diverging paths. Curr Opin Neurol 27(4):405–413

Perani D, Cortelli P, Lucignani G, Montagna P, Tinuper P, Gallassi R et al (1993) [^{18}F] FDG PET in fatal familial insomnia: the functional effects of thalamic lesions. Neurology 43(12):2565

Perani D, Anthony P, Rosa D, Cerami C, Gallivanone F, Fallanca F et al (2014) Validation of an optimized SPM procedure for FDG-PET in dementia diagnosis in a clinical setting. NeuroImage Clin 6:445–454

Perani D, Cerami C, Caminiti SP, Santangelo R, Coppi E, Ferrari L et al (2016) Cross-validation of biomarkers for the early differential diagnosis and prognosis of dementia in a clinical setting. J Nucl Med Mol Imaging 43(3):499–508

Perani D, Iaccarino L, Lammertsma AA, Windhorst AD, Edison P, Boellaard R et al (2019) A new perspective for advanced positron emission tomography–based molecular imaging in neurodegenerative proteinopathies. Alzheimer's Dement 15(8):1081–1103

Perez-Soriano A, Arena JE, Dinelle K, Miao Q, McKenzie J, Neilson N et al (2017) PBB3 imaging in Parkinsonian disorders: Evidence for binding to tau and other proteins. Mov Disord 32(7):1016–1024

Perry DC, Brown JA, Possin KL, Datta S, Trujillo A, Radke A et al (2017) Clinicopathological correlations in behavioural variant frontotemporal dementia. Brain 140(12):3329–3345

Petersen RC, Aisen P, Boeve BF, Geda YE, Ivnik RJ, Knopman DS et al (2013) Mild cognitive impairment due to Alzheimer disease in the community. Ann Neurol 74(2):199–208

Phillips JS, Das SR, McMillan CT, Irwin DJ, Roll EE, Da Re F et al (2018) Tau PET imaging predicts cognition in atypical variants of Alzheimer's disease. Hum Brain Mapp 39(2):691–708

Phukan J, Elamin M, Bede P, Jordan N, Gallagher L, Byrne S et al (2012) The syndrome of cognitive impairment in amyotrophic lateral sclerosis: a population-based study. J Neurol Neurosurg Psychiatry 83(1):102–108

Piel M, Vernaleken I, Rösch F (2014) Positron emission tomography in CNS drug discovery and drug monitoring. J Med Chem 57(22):9232–9258

Pilotto A, Premi E, Caminiti SP, Presotto L, Turrone R, Alberici A et al (2018) Single-subject SPM FDG-PET patterns predict risk of dementia progression in Parkinson disease. Neurology 90(12):e1029–e1037

Pletnikova O, West N, Lee MK, Rudow GL, Skolasky RL, Dawson TM et al (2005) Aβ deposition is associated with enhanced cortical α-synuclein lesions in Lewy body diseases. Neurobiol Aging 26(8):1183–1192

Presotto L, Ballarini T, Caminiti SP, Bettinardi V, Gianolli L, Perani D (2017) Validation of 18 F–FDG-PET single-subject optimized SPM procedure with different PET scanners. Neuroinformatics 15(2):151–163

Presotto L, Iaccarino L, Sala A, Vanoli EG, Muscio C, Nigri A et al (2018) Low-dose CT for the spatial normalization of PET images: a validation procedure for amyloid-PET semi-quantification. NeuroImage Clin 20:153–160

Prestia A, Caroli A, Van Der Flier WM, Ossenkoppele R, Van Berckel B, Barkhof F et al (2013) Prediction of dementia in MCI patients based on core diagnostic markers for Alzheimer disease. Neurology 80(11):1048–1056

Prieto E, Domínguez-Prado I, Riverol M, Ortega-Cubero S, Ribelles MJ, Luquin MR et al (2015) Metabolic patterns in prion diseases: an FDG PET voxel-based analysis. Eur J Nucl Med Mol Imaging 42(10):1522–1529

Puoti G, Bizzi A, Forloni G, Safar JG, Tagliavini F, Gambetti P (2012) Sporadic human prion diseases: molecular insights and diagnosis. Lancet Neurol 11(7):618–628

Rabinovici GD, Furst AJ, O'neil JP, Racine CA, Mormino EC, Baker SL et al (2007) ^{11}C-PIB PET imaging in Alzheimer disease and frontotemporal lobar degeneration. Neurology 68(15):1205–1212

Rabinovici GD, Jagust WJ, Furst AJ, Ogar JM, Racine CA, Mormino EC et al (2008) Aβ amyloid and glucose metabolism in three variants of primary progressive aphasia. Ann Neurol 64(4):388–401

Rabinovici GD, Furst AJ, Alkalay A, Racine CA, O'neil JP, Janabi M et al (2010) Increased metabolic vulnerability in early-onset Alzheimer's disease is not related to amyloid burden. Brain 133(2):512–528

Rabinovici GD, Rosen HJ, Alkalay A, Kornak J, Furst AJ, Agarwal N et al (2011) Amyloid vs FDG-PET in the differential diagnosis of AD and FTLD. Neurology 77(23):2034–2042

Radford R, Rcom-H'cheo-Gauthier A, Wong MB, Eaton ED, Quilty M, Blizzard C et al (2015) The degree of astrocyte activation in multiple system atrophy is inversely proportional to the distance to α-synuclein inclusions. Mol Cell Neurosci 65:68–81

Rajagopalan V, Pioro EP (2015) Comparing brain structural MRI and metabolic FDG-PET changes in patients with ALS-FTD: 'the chicken or the egg?' question. J Neurol Neurosurg Psychiatry 86(9):952–958

Ransohoff RM (2016) How neuroinflammation contributes to neurodegeneration. Science 353(6301):777–783

Rascovsky K, Hodges JR, Knopman D, Mendez MF, Kramer JH, Neuhaus J et al (2011) Sensitivity of revised diagnostic criteria for the behavioural variant of frontotemporal dementia. Brain 134(9):2456–2477

Rascovsky K, Hodges J, Knopman D, Mendez M, Kramer J, Neuhaus J et al (2013) Can clinical features predict tau pathology in patients with behavioral variant frontotemporal dementia (bvFTD)?(P05. 101). AAN Enterprises 80

Ratnavalli E, Brayne C, Dawson K, Hodges JR (2002) The prevalence of frontotemporal. Neurology 58(11):1615–1621

Renard D, Collombier L, Castelnovo G, Fourcade G, Kotzki P-O, Labauge P (2011) Brain FDG-PET changes in ALS and ALS-FTD. Acta Neurol Belg 111(4):306

Renard D, Vandenberghe R, Collombier L, Kotzki P-O, Pouget J-P, Boudousq V (2013) Glucose metabolism in nine patients with probable sporadic Creutzfeldt–Jakob disease: FDG-PET study using SPM and individual patient analysis. J Neurol 260(12):3055–3064

Reynolds AD, Kadiu I, Garg SK, Glanzer JG, Nordgren T, Ciborowski P et al (2008) Nitrated alpha-synuclein and microglial neuroregulatory activities. J Neuroimmune Pharmacol 3(2):59–74

Ringholz GM, Appel SH, Bradshaw M, Cooke NA, Mosnik DM, Schulz PE (2005) Prevalence and patterns of cognitive impairment in sporadic ALS. Neurology 65(4):586–590

Rizzo G, Veronese M, Tonietto M, Bodini B, Stankoff B, Wimberley C et al (2019) Generalization of endothelial modelling of TSPO PET imaging: considerations on tracer affinities. J Cereb Blood Flow Metab 39(5):874–885

Robb C, Udeh-Momoh C, Wagenpfeil S, Schöpe J, Alexopoulos P, Perneczky R (2017) Biomarkers and functional decline in prodromal Alzheimer's disease. J Alzheimers Dis 58(1):69–78

Rocher AB, Chapon F, Blaizot X, Baron J-C, Chavoix C (2003) Resting-state brain glucose utilization as measured by PET is directly related to regional synaptophysin levels: a study in baboons. NeuroImage 20(3):1894–1898

Rodriguez-Vieitez E, Nordberg A (2018) Imaging neuroinflammation: quantification of astrocytosis in a multitracer PET approach. In: Biomarkers for Alzheimer's disease drug development. Springer, New York, pp 231–251

Rodriguez-Vieitez E, Saint-Aubert L, Carter SF, Almkvist O, Farid K, Schöll M et al (2016) Diverging longitudinal changes in astrocytosis and amyloid PET in autosomal dominant Alzheimer's disease. Brain 139(3):922–936

Roe CM, Fagan AM, Grant EA, Hassenstab J, Moulder KL, Dreyfus DM et al (2013) Amyloid imaging and CSF biomarkers in predicting cognitive impairment up to 7.5 years later. Neurology 80(19):1784–1791

Rosenbloom MH, Alkalay A, Agarwal N, Baker SL, O'Neil JP, Janabi M et al (2011) Distinct clinical and metabolic deficits in PCA and AD are not related to amyloid distribution. Neurology 76(21):1789–1796

Roses AD, Saunders AM (1994) APOE is a major susceptibility gene for Alzheimer's disease. Curr Opin Biotechnol 5(6):663–667

Rowe CC, Ng S, Ackermann U, Gong SJ, Pike K, Savage G et al (2007) Imaging β-amyloid burden in aging and dementia. Neurology 68(20):1718–1725

Rowe CC, Ellis KA, Rimajova M, Bourgeat P, Pike KE, Jones G et al (2010) Amyloid imaging results from the Australian imaging, biomarkers and lifestyle (AIBL) study of aging. Neurobiol Aging 31(8):1275–1283

Russo MV, McGavern DB (2015) Immune surveillance of the CNS following infection and injury. Trends Immunol 36(10):637–650

Sabbagh MN, Fleisher A, Chen K, Rogers J, Berk C, Reiman E et al (2011) Positron emission tomography and neuropathologic estimates of fibrillar amyloid-β in a patient with down syndrome and Alzheimer disease. Arch Neurol 68(11):1461–1466

Sabri O, Sabbagh MN, Seibyl J, Barthel H, Akatsu H, Ouchi Y et al (2015) Florbetaben PET imaging to detect amyloid beta plaques in Alzheimer's disease: phase 3 study. Alzheimers Dement 11(8):964–974

Saint-Aubert L, Almkvist O, Chiotis K, Almeida R, Wall A, Nordberg A (2016) Regional tau deposition measured by [(18)F]THK5317 positron emission tomography is associated to cognition via glucose metabolism in Alzheimer's disease. Alzheimers Res Ther 8(1):38

Sakamoto S, Ishii K, Sasaki M, Hosaka K, Mori T, Matsui M et al (2002) Differences in cerebral metabolic impairment between early and late onset types of Alzheimer's disease. J Neurol Sci 200(1–2):27–32

Sala A, Iaccarino L, Fania P, Vanoli EG, Fallanca F, Pagnini C et al (2019) Testing the diagnostic accuracy of [18F] FDG-PET in discriminating spinal-and bulbar-onset amyotrophic lateral sclerosis. Eur J Nucl Med Mol Imaging 46(5):1117–1131

Sala A, Caprioglio C, Santangelo R, Vanoli EG, Iannaccone S, Magnani G, Perani D (2020) Brain metabolic signatures across the Alzheimer's disease spectrum. Eur J Nucl Med Mol Imaging 47(2):256–269

Salloway S, Sperling R, Fox NC, Blennow K, Klunk W, Raskind M et al (2014) Two phase 3 trials of bapineuzumab in mild-to-moderate Alzheimer's disease. N Engl J Med 370(4):322–333

Salmon E, Garraux G, Delbeuck X, Collette F, Kalbe E, Zuendorf G et al (2003) Predominant ventromedial frontopolar metabolic impairment in frontotemporal dementia. NeuroImage 20(1):435–440

Sander K, Lashley T, Gami P, Gendron T, Lythgoe MF, Rohrer JD et al (2016) Characterization of tau positron emission tomography tracer [18 F] AV-1451 binding to postmortem tissue in Alzheimer's disease, primary tauopathies, and other dementias. Alzheimers Dement 12(11):1116–1124

Santillo AF, Gambini JP, Lannfelt L, Långström B, Ulla-Marja L, Kilander L et al (2011) In vivo imaging of astrocytosis in Alzheimer's disease: an 11 C-l-deuteriodeprenyl and PIB PET study. Eur J Nucl Med Mol Imaging 38(12):2202–2208

Santos-Santos MA, Rabinovici GD, Iaccarino L, Ayakta N, Tammewar G, Lobach I et al (2018) Rates of amyloid imaging positivity in patients with primary progressive aphasia. JAMA Neurol 75(3):342–352

Sarazin M, Lagarde J, Bottlaender M (2016) Distinct tau PET imaging patterns in typical and atypical Alzheimer's disease. Brain 139(5):1321–1324

Sasaki A, Kawarabayashi T, Murakami T, Matsubara E, Ikeda M, Hagiwara H et al (2008) Microglial activation in brain lesions with tau deposits: comparison of human tauopathies and tau transgenic mice TgTauP301L. Brain Res 1214:159–168

Saura J, Bleuel Z, Ulrich J, Mendelowitsch A, Chen K, Shih JC et al (1996) Molecular neuroanatomy of human monoamine oxidases a and B revealed by quantitative enzyme radioautography and in situ hybridization histochemistry. Neuroscience 70(3):755–774

Schaeverbeke J, Evenepoel C, Declercq L, Gabel S, Meersmans K, Bruffaerts R et al (2018) Distinct [(18)F]THK5351 binding patterns in primary progressive aphasia variants. Eur J Nucl Med Mol Imaging 45(13):2342–2357

Schain M, Kreisl WC (2017) Neuroinflammation in neurodegenerative disorders—a review. Curr Neurol Neurosci Rep 17(3):25

Schmitz M, Dittmar K, Llorens F, Gelpi E, Ferrer I, Schulz-Schaeffer WJ et al (2017) Hereditary human prion diseases: an update. Mol Neurobiol 54(6):4138–4149

Schöll M, Carter SF, Westman E, Rodriguez-Vieitez E, Almkvist O, Thordardottir S et al (2015) Early astrocytosis in autosomal dominant Alzheimer's disease measured in vivo by multi-tracer positron emission tomography. Sci Rep 5:16404

Schöll M, Lockhart SN, Schonhaut DR, O'Neil JP, Janabi M, Ossenkoppele R et al (2016) PET imaging of tau deposition in the aging human brain. Neuron 89(5):971–982

Scholl M, Ossenkoppele R, Strandberg O, Palmqvist S, Jogi J, , Swedish Bio F study et al. Distinct 18F-AV-1451 tau PET retention patterns in early- and late-onset Alzheimer's disease. Brain. 2017;140(9):2286–2294

Schonhaut DR, McMillan CT, Spina S, Dickerson BC, Siderowf A, Devous MD Sr et al (2017) 18F-flortaucipir tau positron emission tomography distinguishes established progressive supranuclear palsy from controls and Parkinson disease: a multicenter study. Ann Neurol 82(4):622–634

Schroeter ML, Raczka K, Neumann J, von Cramon DY (2008) Neural networks in frontotemporal dementia—a meta-analysis. Neurobiol Aging 29(3):418–426

Schuitemaker A, Kropholler MA, Boellaard R, van der Flier WM, Kloet RW, van der Doef TF et al (2013) Microglial activation in Alzheimer's disease: an (R)-[11C] PK11195 positron emission tomography study. Neurobiol Aging 34(1):128–136

Schwarz AJ, Yu P, Miller BB, Shcherbinin S, Dickson J, Navitsky M et al (2016) Regional profiles of the candidate tau PET ligand 18F-AV-1451 recapitulate key features of Braak histopathological stages. Brain 139(5):1539–1550

Serrano GE, Sabbagh MN, Sue LI, Hidalgo JA, Schneider JA, Bedell BJ et al (2014) Positive florbetapir PET amyloid imaging in a subject with frequent cortical neuritic plaques and frontotemporal lobar degeneration with TDP43-positive inclusions. J Alzheimers Dis 42(3):813–821

Sevigny J, Chiao P, Bussière T, Weinreb PH, Williams L, Maier M et al (2016) The antibody aducanumab reduces Aβ plaques in Alzheimer's disease. Nature 537(7618):50–56. https://doi.org/10.1038/nature19323

Shaffer JL, Petrella JR, Sheldon FC, Choudhury KR, Calhoun VD, Coleman RE et al (2013) Predicting cognitive decline in subjects at risk for Alzheimer disease by using combined cerebrospinal fluid, MR imaging, and PET biomarkers. Radiology 266(2):583–591

Shimada H, Kitamura S, Shinotoh H, Endo H, Niwa F, Hirano S et al (2017) Association between Abeta and tau accumulations and their influence on clinical features in aging and Alzheimer's disease spectrum brains: A [(11)C]PBB3-PET study. Alzheimers Dement (Amst) 6:11–20

Silverman DHS, Small GW, Chang CY, Lu CS, de Aburto MAK, Chen W et al (2001) Positron emission tomography in evaluation of dementia: regional brain metabolism and long-term outcome. JAMA 286(17):2120–2127

Smailagic N, Vacante M, Hyde C, Martin S, Ukoumunne O, Sachpekidis C (2015) ^{18}F-FDG PET for the early diagnosis of Alzheimer's disease dementia and other dementias in people with mild cognitive impairment (MCI). Cochrane Database Syst Rev 1:CD010632

Smith R, Schain M, Nilsson C, Strandberg O, Olsson T, Hägerström D et al (2017a) Increased basal ganglia binding of 18 F-AV-1451 in patients with progressive supranuclear palsy. Mov Disord 32(1):108–114

Smith R, Schöll M, Widner H, van Westen D, Svenningsson P, Hägerström D et al (2017b) In vivo retention of 18F-AV-1451 in corticobasal syndrome. Neurology 89(8):845–853
Smith R, Scholl M, Londos E, Ohlsson T, Hansson O (2018) (18)F-AV-1451 in Parkinson's Disease with and without dementia and in Dementia with Lewy Bodies. Sci Rep 8(1):4717
Sokoloff L (1981) Localization of functional activity in the central nervous system by measurement of glucose utilization with radioactive deoxyglucose. J Cereb Blood Flow Metab 1(1):7–36
Sone D, Imabayashi E, Maikusa N, Okamura N, Furumoto S, Kudo Y et al (2017) Regional tau deposition and subregion atrophy of medial temporal structures in early Alzheimer's disease: A combined positron emission tomography/magnetic resonance imaging study. Alzheimers Dement (Amst) 9:35–40
Spehl TS, Hellwig S, Amtage F, Weiller C, Bormann T, Weber WA et al (2015) Syndrome-specific patterns of regional cerebral glucose metabolism in posterior cortical atrophy in comparison to dementia with Lewy bodies and Alzheimer's disease—a [F-18]-Fdg pet study. J Neuroimaging 25(2):281–288
Sperling RA, Aisen PS, Beckett LA, Bennett DA, Craft S, Fagan AM et al (2011) Toward defining the preclinical stages of Alzheimer's disease: recommendations from the National Institute on Aging-Alzheimer's association workgroups on diagnostic guidelines for Alzheimer's disease. Alzheimers Dement 7(3):280–292
Sperling R, Mormino E, Johnson K (2014) The evolution of preclinical Alzheimer's disease: implications for prevention trials. Neuron 84(3):608–622. https://doi.org/10.1016/j.neuron.2014.10.038
Spinelli EG, Mandelli ML, Miller ZA, Santos-Santos MA, Wilson SM, Agosta F et al (2017) Typical and atypical pathology in primary progressive aphasia variants. Ann Neurol 81(3):430–443
Sriram K, Benkovic SA, Hebert MA, Miller DB, O'Callaghan JP (2004) Induction of gp130-related cytokines and activation of JAK2/STAT3 Pathway in astrocytes precedes up-regulation of glial fibrillary acidic protein in the 1-Methyl-4-phenyl-1, 2, 3, 6-tetrahydropyridine model of neurodegeneration KEY SIGNALING PATHWAY FOR ASTROGLIOSIS IN VIVO? J Biol Chem 279(19):19936–19947
Srulijes K, Reimold M, Liscic RM, Bauer S, Dietzel E, Liepelt-Scarfone I et al (2012) Fluorodeoxyglucose positron emission tomography in Richardson's syndrome and progressive supranuclear palsy-parkinsonism. Mov Disord 27(1):151–155
Steinacker P, Barschke P, Otto M (2019) Biomarkers for diseases with TDP-43 pathology. Mol Cell Neurosci 97:43–59
Stephenson J, Nutma E, van der Valk P, Amor S (2018) Inflammation in CNS neurodegenerative diseases. Immunology 154(2):204–219
Stoessl AJ (2017) Glucose utilization: still in the synapse. Nat Neurosci 20(3):382
Subhramanyam CS, Wang C, Hu Q, Dheen ST (2019) Microglia-mediated neuroinflammation in neurodegenerative diseases. In: Seminars in Cell & Developmental Biology. Elsevier, Amsterdam
Suppiah S, Didier M-A, Vinjamuri S (2019) The who, when, why, and how of PET Amyloid imaging in Management of Alzheimer's disease—review of literature and interesting images. Diagnostics 9(2):65
Surendranathan A, Su L, Mak E, Passamonti L, Hong YT, Arnold R et al (2018) Early microglial activation and peripheral inflammation in dementia with Lewy bodies. Brain 141(12):3415–3427
Suridjan I, Pollock BG, Verhoeff N, Voineskos AN, Chow T, Rusjan PM et al (2015) In-vivo imaging of grey and white matter neuroinflammation in Alzheimer's disease: a positron emission tomography study with a novel radioligand,[18 F]-FEPPA. Mol Psychiatry 20(12):1579
Takada LT, Geschwind MD (2013) Prion diseases. In: Seminars in neurology. Thieme Medical Publishers, New York, pp 348–356
Tang CC, Poston KL, Eckert T, Feigin A, Frucht S, Gudesblatt M et al (2010) Differential diagnosis of parkinsonism: a metabolic imaging study using pattern analysis. Lancet Neurol 9(2):149–158
Teipel S, Drzezga A, Grothe MJ, Barthel H, Chételat G, Schuff N et al (2015) Multimodal imaging in Alzheimer's disease: validity and usefulness for early detection. Lancet Neurol 14(10):1037–1053

Tenovuo O, Kemppainen N, Aalto S, Någren K, Rinne JO (2008) Posterior cortical atrophy: a rare form of dementia with in vivo evidence of amyloid-β accumulation. J Alzheimers Dis 15(3):351–355

Teune LK, Bartels AL, de Jong BM, Willemsen ATM, Eshuis SA, de Vries JJ et al (2010) Typical cerebral metabolic patterns in neurodegenerative brain diseases. Mov Disord 25(14):2395–2404

Tsai RM, Bejanin A, Lesman-Segev O, LaJoie R, Visani A, Bourakova V et al (2019) 18 F-flortaucipir (AV-1451) tau PET in frontotemporal dementia syndromes. Alzheimers Res Ther 11(1):13

Tsuboi Y, Josephs KA, Cookson N, Dickson DW (2003) APOE E4 is a determinant for Alzheimer type pathology in progressive supranuclear palsy. Neurology 60(2):240–245

Turkheimer FE, Edison P, Pavese N, Roncaroli F, Anderson AN, Hammers A et al (2007) Reference and target region modeling of [11C]-(R)-PK11195 brain studies. J Nucl Med 48(1):158–167

Turkheimer FE, Rizzo G, Bloomfield PS, Howes O, Zanotti-Fregonara P, Bertoldo A et al (2015) The methodology of TSPO imaging with positron emission tomography. Biochem Soc Trans 43(4):586–592

Tyacke RJ, Fisher A, Robinson ESJ, Grundt P, Turner EM, Husbands SM et al (2012) Evaluation and initial in vitro and ex vivo characterization of the potential positron emission tomography ligand, BU99008 (2-(4, 5-Dihydro-1H-imidazol-2-yl)-1-methyl-1H-indole), for the imidazoline2 binding site. Synapse 66(6):542–551

Valera E, Spencer B, Masliah E (2016) Immunotherapeutic approaches targeting amyloid-β, α-synuclein, and tau for the treatment of neurodegenerative disorders. Neurotherapeutics 13(1):179–189

van Berckel BNM, Ossenkoppele R, Tolboom N, Yaqub M, Foster-Dingley JC, Windhorst AD et al (2013) Longitudinal amyloid imaging using 11C-PiB: methodologic considerations. J Nucl Med 54(9):1570–1576

van Eimeren T, Bischof GN, Drzezga A (2017) Is tau imaging more than just upside-down ^{18}F-FDG imaging? J Nucl Med 58(9):1357–1359

Vandenberghe R, Van Laere K, Ivanoiu A, Salmon E, Bastin C, Triau E et al (2010) 18F-flutemetamol amyloid imaging in Alzheimer disease and mild cognitive impairment: a phase 2 trial. Ann Neurol 68(3):319–329

Varrone A, Asenbaum S, Vander Borght T, Booij J, Nobili F, Någren K et al (2009) EANM procedure guidelines for PET brain imaging using [18F]FDG, version 2. Eur J Nucl Med Mol Imaging 36(12):2103–2110

Varrone A, Mattsson P, Forsberg A, Takano A, Nag S, Gulyás B et al (2013) In vivo imaging of the 18-kDa translocator protein (TSPO) with [18 F] FEDAA1106 and PET does not show increased binding in Alzheimer's disease patients. Eur J Nucl Med Mol Imaging 40(6):921–931

Vasile F, Dossi E, Rouach N (2017) Human astrocytes: structure and functions in the healthy brain. Brain Struct Funct 222:5

Vermeiren C, Motte P, Viot D, Mairet-Coello G, Courade JP, Citron M et al (2018) The tau positron-emission tomography tracer AV-1451 binds with similar affinities to tau fibrils and monoamine oxidases. Mov Disord 33(2):273–281

Villemagne VL, Okamura N (2014) In vivo tau imaging: obstacles and progress. Alzheimers Dement 10(3):S254–S264

Villemagne VL, Okamura N (2015) ScienceDirect Tau imaging in the study of ageing, Alzheimer's disease, and other neurodegenerative conditions. Curr Opin Neurobiol 36:43–51

Villemagne VL, Pike KE, Darby D, Maruff P, Savage G, Ng S et al (2008) Aβ deposits in older non-demented individuals with cognitive decline are indicative of preclinical Alzheimer's disease. Neuropsychologia 46(6):1688–1697

Villemagne VL, Ong K, Mulligan RS, Holl G, Pejoska S, Jones G et al (2011a) Amyloid imaging with ^{18}F-florbetaben in Alzheimer disease and other dementias. J Nucl Med 52(8):1210–1217

Villemagne VL, Pike KE, Chételat G, Ellis KA, Mulligan RS, Bourgeat P et al (2011b) Longitudinal assessment of Aβ and cognition in aging and Alzheimer disease. Ann Neurol 69(1):181–192

Villemagne VL, Fodero-tavoletti MT, Masters CL, Rowe CC, Health A (2015) Tau imaging: early progress and future directions. Lancet Neurol 14(1):114–124

Villemagne VL, Dore V, Bourgeat P, Burnham SC, Laws S, Salvado O et al (2017) Aβ-amyloid and tau imaging in dementia. In: Seminars in nuclear medicine. Elsevier, Amsterdam, pp 75–88
Villemagne VL, Doré V, Burnham SC, Masters CL, Rowe CC (2018) Imaging tau and amyloid-β proteinopathies in Alzheimer disease and other conditions. Nat Rev Neurol 14(4):225
Vivash L, O'Brien TJ (2016) Imaging microglial activation with TSPO PET: lighting up neurologic diseases? J Nucl Med 57(2):165–168
Vlaar AMM, van Kroonenburgh MJPG, Kessels AGH, Weber WEJ (2007) Meta-analysis of the literature on diagnostic accuracy of SPECT in parkinsonian syndromes. BMC Neurol 7(1):27
Wang Y, Mandelkow E (2016) Tau in physiology and pathology. Nat Rev Neurosci 17(1):5–21
Wang L, Benzinger TL, Su Y, Christensen J, Friedrichsen K, Aldea P et al (2016) Evaluation of Tau imaging in staging Alzheimer disease and revealing interactions between beta-amyloid and tauopathy. JAMA Neurol 73(9):1070–1077
Waxman AD, Herholz K, Lewis DH, Herscovitch P, Minoshima S, Mountz JM et al (2009) Society of Nuclear Medicine procedure guideline for FDG PET brain imaging. J Nucl Med:1–12
Whitwell JL, Dickson DW, Murray ME, Weigand SD, Tosakulwong N, Senjem ML et al (2012) Neuroimaging correlates of pathologically defined subtypes of Alzheimer's disease: a case-control study. Lancet Neurol 11(10):868–877
Whitwell JL, Graff-Radford J, Singh TD, Drubach DA, Senjem ML, Spychalla AJ et al (2017a) 18F-FDG PET in posterior cortical atrophy and dementia with lewy bodies. J Nucl Med 58(4):632–638
Whitwell JL, Lowe VJ, Tosakulwong N, Weigand SD, Senjem ML, Schwarz CG et al (2017b) [18F] AV-1451 tau positron emission tomography in progressive supranuclear palsy. Mov Disord 32(1):124–133
Whitwell JL, Ahlskog JE, Tosakulwong N, Senjem ML, Spychalla AJ, Petersen RC et al (2018a) Pittsburgh compound B and AV-1451 positron emission tomography assessment of molecular pathologies of Alzheimer's disease in progressive supranuclear palsy. Parkinsonism Relat Disord 48:3–9
Whitwell JL, Graff-Radford J, Tosakulwong N, Weigand SD, Machulda M, Senjem ML et al (2018b) [(18) F]AV-1451 clustering of entorhinal and cortical uptake in Alzheimer's disease. Ann Neurol 83(2):248–257
Wiley CA, Lopresti BJ, Venneti S, Price J, Klunk WE, DeKosky ST et al (2009) Carbon 11–labeled Pittsburgh compound b and carbon 11–labeled (R)-PK11195 positron emission tomographic imaging in Alzheimer disease. Arch Neurol 66(1):60–67
Williams DR, de Silva R, Paviour DC, Pittman A, Watt HC, Kilford L et al (2005) Characteristics of two distinct clinical phenotypes in pathologically proven progressive supranuclear palsy: Richardson's syndrome and PSP-parkinsonism. Brain 128(6):1247–1258
Wolk DA, Price JC, Saxton JA, Snitz BE, James JA, Lopez OL et al (2009) Amyloid imaging in mild cognitive impairment subtypes. Ann Neurol 65(5):557–568
Wolk DA, Grachev ID, Buckley C, Kazi H, Grady MS, Trojanowski JQ et al (2011) Association between in vivo fluorine 18–labeled flutemetamol amyloid positron emission tomography imaging and in vivo cerebral cortical histopathology. Arch Neurol 68(11):1398–1403
Wolk DA, Price JC, Madeira C, Saxton JA, Snitz BE, Lopez OL et al (2012) Amyloid imaging in dementias with atypical presentation. Alzheimers Dement 8(5):389–398
Woodward MC, Rowe CC, Jones G, Villemagne VL, Varos TA (2015) Differentiating the frontal presentation of Alzheimer's disease with FDG-PET. J Alzheimers Dis 44(1):233–242
Xia C, Makaretz SJ, Caso C, McGinnis S, Gomperts SN, Sepulcre J et al (2017) Association of in vivo [18F] AV-1451 tau PET imaging results with cortical atrophy and symptoms in typical and atypical Alzheimer disease. JAMA Neurol 74(4):427–436
Xing X, Zhang J, Zhu F, Ma L, Yin D, Jia W et al (2012) Comparison of diffusion-weighted MRI with 18F-fluorodeoxyglucose-positron emission tomography/CT and electroencephalography in sporadic Creutzfeldt–Jakob disease. J Clin Neurosci 19(10):1354–1357
Yamakawa Y, Shimada H, Ataka S, Tamura A, Masaki H, Naka H et al (2012) Two cases of dementias with motor neuron disease evaluated by Pittsburgh compound B-positron emission tomography. Neurol Sci 33(1):87–92

Yasuno F, Ota M, Kosaka J, Ito H, Higuchi M, Doronbekov TK et al (2008) Increased binding of peripheral benzodiazepine receptor in Alzheimer's disease measured by positron emission tomography with [11C] DAA1106. Biol Psychiatry 64(10):835–841

Yasuno F, Kosaka J, Ota M, Higuchi M, Ito H, Fujimura Y et al (2012) Increased binding of peripheral benzodiazepine receptor in mild cognitive impairment–dementia converters measured by positron emission tomography with [11C] DAA1106. Psychiatry Res Neuroimaging 203(1):67–74

Yokokura M, Mori N, Yagi S, Yoshikawa E, Kikuchi M, Yoshihara Y et al (2011) In vivo changes in microglial activation and amyloid deposits in brain regions with hypometabolism in Alzheimer's disease. Eur J Nucl Med Mol Imaging 38(2):343–351

Yuan Y, Gu Z-X, Wei W-S (2009) Fluorodeoxyglucose–positron-emission tomography, single-photon emission tomography, and structural MR imaging for prediction of rapid conversion to Alzheimer disease in patients with mild cognitive impairment: a meta-analysis. Am J Neuroradiol 30(2):404–410

Zhang W, Wang T, Pei Z, Miller DS, Wu X, Block ML et al (2005) Aggregated α-synuclein activates microglia: a process leading to disease progression in Parkinson's disease. FASEB J 19(6):533–542

Zhao P, Zhang B, Gao S (2012) 18 [F]-FDG PET study on the idiopathic Parkinson's disease from several parkinsonian-plus syndromes. Parkinsonism Relat Disord 18:S60–S62

Zimmer ER, Parent MJ, Souza DG, Leuzy A, Lecrux C, Kim H-I et al (2017) [^{18}F]FDG PET signal is driven by astroglial glutamate transport. Nat Neurosci 1(3):393–395

Aβ Imaging in Aging, Alzheimer's Disease, and Other Neurodegenerative Conditions

10

Victor L. Villemagne, Vincent Doré, Samantha Burnham, and Christopher C. Rowe

Contents

10.1 Introduction 284
10.2 Aβ Imaging Radiotracers 285
10.2.1 ^{11}C-Labeled Radiotracers 287
10.2.2 ^{18}F-Labeled Radiotracers 288
10.3 Aβ Imaging in Alzheimer's Disease 292
10.4 Ante-mortem Post-mortem Correlations 294
10.5 Aβ Deposition in Non-demented Individuals and Its Relation with Cognition 295
10.6 Relation of Aβ Imaging with Other Biomarkers 298
10.6.1 FDG 299
10.6.2 CSF 299
10.6.3 Plasma Aβ 300

V. L. Villemagne (✉)
Department of Molecular Imaging and Therapy, Austin Health, Melbourne, VIC, Australia

Department of Medicine, University of Melbourne, Austin Health, Melbourne, VIC, Australia
e-mail: victorlv@unimelb.edu.au

V. Doré
Department of Molecular Imaging and Therapy, Austin Health, Melbourne, VIC, Australia

Health and Biosecurity Flagship, The Australian eHealth Research Centre, CSIRO, Melbourne, VIC, Australia
e-mail: Vincent.Dore@csiro.au

S. Burnham
Health and Biosecurity Flagship, The Australian eHealth Research Centre, CSIRO, Melbourne, VIC, Australia
e-mail: Samantha.Burnham@csiro.au

C. C. Rowe
Department of Molecular Imaging and Therapy, Austin Health, Melbourne, VIC, Australia

Department of Medicine, University of Melbourne, Austin Health, Melbourne, VIC, Australia

The Australian Dementia Network (ADNeT), Melbourne, VIC, Australia
e-mail: Christopher.ROWE@austin.org.au

R. A. J. O. Dierckx et al. (eds.), *PET and SPECT in Neurology*,
https://doi.org/10.1007/978-3-030-53168-3_10

10.6.4 MRI Volumetrics..... 300
10.6.5 Neuroinflammation..... 301
10.7 Relation of Aβ Deposition with Genetic Risks and Predisposing Factors..... 302
10.8 Aβ Imaging in Other Neurodegenerative Conditions..... 303
10.8.1 Cerebral Amyloid Angiopathy..... 303
10.8.2 Lewy Body Diseases..... 304
10.8.3 Frontotemporal Lobar Degeneration..... 305
10.8.4 Prion Diseases..... 306
10.8.5 Traumatic Brain Injury and Chronic Traumatic Encephalopathy..... 306
10.9 Clinical and Research Applications of Amyloid Imaging..... 307
10.9.1 Aβ Imaging in Large Observational Cohorts..... 307
10.9.2 Aβ Imaging in Disease-Specific Therapeutic Trials..... 308
10.9.3 The Centiloid Scale..... 308
10.9.4 Appropriate Use Criteria and Clinical Impact of Aβ Imaging..... 309
10.10 CODA..... 310
References..... 313

Abstract

In vivo imaging of β-amyloid (Aβ) has transformed the assessment of Aβ pathology and its changes over time, extending our insight into Aβ deposition in the brain by providing highly accurate, reliable, and reproducible quantitative statements of regional or global Aβ burden in the brain, proving essential in anti-Aβ therapeutic trials. Although cross-sectional evaluation of Aβ burden does not strongly correlate with cognitive impairment in AD, it does correlate with memory impairment and a higher risk for cognitive decline in the aging population and MCI subjects. This correlation with memory impairment, one of the earliest symptoms of AD, suggests that Aβ deposition is not part of normal aging. Longitudinal observations, coupled with different disease-specific biomarkers to assess potential downstream effects of Aβ, have confirmed that Aβ deposition in the brain starts decades before the onset of symptoms. Aβ imaging studies continue to refine our understanding of the role of Aβ deposition in Alzheimer's disease.

10.1 Introduction

Alzheimer's disease (AD) is a progressive and irreversible neurodegenerative disorder clinically characterized by memory loss and cognitive decline that severely affect the activities of daily living (Masters et al. 2006). AD is the leading cause of dementia in the elderly, leading invariably to death, usually within 7–10 years after diagnosis (Khachaturian 1985). The progressive nature of the neurodegeneration suggests an age-dependent process that ultimately leads to synaptic failure and neuronal damage in cortical areas of the brain essential for memory and other cognitive domains (Isacson et al. 2002). AD not only has devastating effects on the sufferers

and their caregivers, but it also has a tremendous socioeconomic impact on families and the health system, a burden which will only increase in the upcoming years as the population of most countries ages (Johnson et al. 2000). In the absence of reliable biomarkers, direct pathologic examination of brain tissue derived from either biopsy or autopsy remains the only definitive method for establishing a diagnosis of AD (O'Brien et al. 2000). The typical macroscopic picture is gross cortical atrophy, while, microscopically, there are widespread cellular degeneration and diffuse synaptic and neuronal loss, accompanied by reactive gliosis and the presence of the pathological hallmarks of the disease: intracellular neurofibrillary tangles (NFT) and extracellular amyloid plaques (Jellinger 1990; Masters 2005; Masters and Beyreuther 2006). While NFT are intraneuronal bundles of paired helical filaments mainly composed of the aggregates of an abnormally phosphorylated form of tau protein (Jellinger and Bancher 1998; Michaelis et al. 2002), neuritic plaques consist of dense extracellular aggregates of β-amyloid (Aβ) (Masters et al. 1985), surrounded by reactive gliosis and dystrophic neurites. Aβ is a 4 kDa 39–43 amino acid metalloprotein derived from the proteolytic cleavage of the amyloid precursor protein (APP), by β- and γ-secretases (Cappai and White 1999). To date, all available genetic, pathological, biochemical, and cellular evidence strongly supports the notion that an imbalance between the production and removal of Aβ leading to its progressive accumulation is central to the pathogenesis of AD (Villemagne et al. 2006). The "Aβcentric theory" (Masters et al. 2006) postulates that Aβ plaque deposition is the primary event in a cascade of effects that lead to neurofibrillary degeneration and dementia (Hardy 1997).

Despite new diagnostic criteria (McKhann et al. 2011), clinical diagnosis of AD is still largely based on progressive impairment of memory and decline in at least one other cognitive domain and by excluding other diseases that might also present with dementia such as frontotemporal lobar degeneration (FTLD), dementia with Lewy bodies (DLB), stroke, brain tumor, normal pressure hydrocephalus, or depression (Larson et al. 1996; Cummings et al. 1998). A variable period of up to 5 years of prodromal decline in cognition characterized by a relatively isolated impairment in short-term memory that may also be accompanied by impairments of working memory, known as amnestic mild cognitive impairment (MCI), usually precedes the formal diagnosis of AD (Petersen et al. 1999; Petersen 2000). At this point, there is no cure for AD nor proven way to slow the rate of disease progression. Symptomatic treatment with acetylcholinesterase inhibitors or a glutamatergic moderator provides modest benefit in some patients usually by temporary stabilization rather than a noticeable improvement in memory function (Masters et al. 2006).

10.2 Aβ Imaging Radiotracers

Aβ plaques and NFTs are the pathological hallmark brain lesions of AD. These microscopic aggregates are still well beyond the resolution of conventional neuroimaging techniques used for the clinical evaluation of patients with AD. Positron emission tomography (PET) is a sensitive molecular imaging technique that allows

Table 10.1 Applications of Aβ imaging

• Accurate and early diagnosis of AD pathology
• Assessment of the spatial and temporal pattern of Aβ deposition and its relation to age, cognitive performance, disease progression, genotype, and other disease biomarkers (tau imaging, neuroinflammation, MRI, CSF, etc.)
• Validation of new imaging, cognitive and fluid biomarkers
• Early detection allowing staging, prognosis, and early disease-specific interventions
• Disease-specific trials:
– Proof of target engagement
– Patient selection
– Establish target floor (and ceiling) values for trial inclusion
– Predict rate of cognitive decline,
– Predict risk of disease progression, staging
– Monitor effectiveness/Outcome measure
– Establish optimal window for intervention

in vivo quantification of radiotracer concentrations in the picomolar range, allowing the non-invasive assessment of molecular processes at their sites of action, detecting disease processes at asymptomatic stages when there is no evidence of anatomic changes on computed tomography (CT) and magnetic resonance imaging (MRI) (Phelps 2000). Since Aβ is at the center of AD pathogenesis, and given that several pharmacological agents aimed at reducing Aβ levels in the brain are being developed and tested, many efforts have been focused on generating radiotracers for imaging Aβ in vivo (Sair et al. 2004; Mathis et al. 2005; Villemagne et al. 2005). Several applications of Aβ imaging have been proposed (Table 10.1).

As a quantitative neuroimaging probe, the Aβ radiotracer must possess a number of key general properties: it should be a lipophilic, non-toxic small molecule with a high specificity and selectivity for Aβ, amenable for high specific activity labeling with ^{18}F or other long-lived radioisotope, with no radiolabeled metabolites that enter the brain, while reversibly binding to Aβ in a specific and selective fashion (Laruelle et al. 2003; Nordberg 2004; Pike 2009). Overall, binding affinity and lipophilicity are the most crucial properties for in vivo neuroimaging tracers. While high affinity for Aβ is desirable to provide an adequate signal-to-noise ratio, this high affinity might also delay reaching binding equilibrium requiring an extended scanning time. And while lipophilicity is necessary for the tracer to cross the blood-brain barrier (BBB), if the radiotracer is too lipophilic, its non-specific binding might be too high (Laruelle et al. 2003; Pike 2009).

Through the years, several compounds have been evaluated with different fortune as potential Aβ probes: monoclonal and anti-Aβ antibodies fragments, serum amyloid P, basic fibroblast growth factor, Aβ fragments, and derivatives of histopathological dyes such as Congo red, Chrysamine-G, and Thioflavin S and T (*for review*, *see* (Villemagne & Rowe 2010)). While selective tau imaging for in vivo NFT quantification is still in the early stages of development (Okamura et al. 2005; Maruyama et al. 2009; Ojida et al. 2009; Fodero-Tavoletti et al. 2011), several Aβ radiotracers found their way into human clinical trials.

Almost a decade after unsuccessful trials with anti-Aβ antibodies (Majocha et al. 1992), Aβ imaging came to fruition with the first report of successful imaging in an AD patient with ^{18}F-FDDNP, a tracer claimed to bind both plaques and NFT (Shoghi-Jadid et al. 2002). Since then, human Aβ imaging studies have been conducted in AD patients, normal controls, and patients with other dementias using ^{11}C-PiB (Klunk et al. 2004), ^{11}C-SB13 (Verhoeff et al. 2004), ^{11}C-ST1859 (Bauer et al. 2006), ^{11}C-BF227 (Kudo et al. 2007), ^{11}C-AZD2138 (Nyberg et al. 2009), ^{18}F-florbetaben (Rowe et al. 2008), ^{18}F-flutemetamol (Serdons et al. 2009a; b), ^{18}F-florbetapir (Wong et al. 2010), and ^{18}F-NAV4694—a.k.a. AZD4694 (Cselenyi et al. 2012; Rowe et al. 2013a; b)—with PET.

In order to test compounds that could have more widespread application, preliminary studies with SPECT Aβ radiotracers ^{123}I-CQ (Opazo et al. 2006) and ^{123}I-IMPY (Newberg et al. 2006) showed limited utility for the evaluation of Aβ burden in AD, although ^{123}I-IMPY might be useful in the evaluation of transmissible spongiform encephalopathies (Song et al. 2008). New SPECT radiotracers labeled with ^{123}I or those that could be potentially labeled with ^{99m}Tc are being evaluated (Qu et al. 2007a; b; Serdons et al. 2007; Lin et al. 2009).

While all of the aforementioned tracers bind with varying degrees of success to Aβ fibrils and brain homogenates of AD patients, Congo Red and Thioflavin T—and some of their derivatives—have recently been shown to also bind to soluble oligomeric forms of Aβ (Maezawa et al. 2008). On the other hand, Aβ-soluble species represent less than 1% of the total brain Aβ (McLean et al. 1999; Roberts et al. 2017), and the reported affinity of PiB for these soluble oligomers seems to be significantly lower than for Aβ fibrils (Maezawa et al. 2008). Until highly selective radiotracers are developed to bind the Aβ-soluble species, the contribution of these oligomers to the PET signal in sporadic AD from tracers such as ^{11}C-PiB is considered to be negligible (Mathis et al. 2007).

10.2.1 ^{11}C-Labeled Radiotracers

10.2.1.1 ^{11}C-PiB

^{11}C-PiB (PiB) was the most successful and, early on, the most widely used of available Aβ tracers. PiB has been shown to possess high affinity and high selectivity for fibrillar Aβ in plaques and in other Aβ-containing lesions (Klunk et al. 2001; Mathis et al. 2002; Mathis et al. 2005; Price et al. 2005; Ye et al. 2005; Cohen et al. 2012). In vitro studies with high specific activity ^{3}H-PiB demonstrated two binding sites for PiB (Klunk et al. 2005), and in in vitro studies, it has been used to establish the different binding sites in frontal cortex and hippocampus (Ni et al. 2013). Recent studies have shown that ^{11}C-PiB binds with high affinity to the N-terminally truncated and modified Aβ and AβN3-pyroglutamate species in senile plaques (Maeda et al. 2007). In vitro assessment of ^{3}H-PiB binding to white matter homogenates failed to show any specific binding (Fodero-Tavoletti et al. 2009a; b). PiB is a derivative of Thioflavin T, a fluorescent dye commonly used to assess fibrillization into β-sheet conformation (LeVine 3rd 1999), and as such PiB has been shown to bind

to a range of additional Aβ-containing lesions, including diffuse plaques and cerebral amyloid angiopathy (CAA) (Lockhart et al. 2007), as well as to Aβ oligomers—albeit with lower affinity (Maezawa et al. 2008). PiB also displayed lower affinity toward other misfolded proteins with a similar β-sheet secondary structure such as α-synuclein (Fodero-Tavoletti et al. 2007; Ye et al. 2008) and tau (Lockhart et al. 2007; Ikonomovic et al. 2008). This is relevant particularly since AD has been described as a "triple brain amyloidosis" (Trojanowski 2002). Most importantly, these studies have shown that, at the concentrations achieved during a PET scan, ^{11}C-PiB cortical retention in AD or DLB primarily reflects Aβ-related cerebral amyloidosis and not binding to Lewy bodies (LB) or NFT (Klunk et al. 2003; Fodero-Tavoletti et al. 2007; Lockhart et al. 2007; Ikonomovic et al. 2008). ^{11}C-PiB has consistently provided quantitative information on Aβ burden in vivo, contributing new insights into Aβ deposition in the brain, allowing earlier detection of AD pathology (Klunk et al. 2004; Mintun et al. 2006; Rowe et al. 2007; Cohen et al. 2012) and accurate differential diagnosis of the dementias (Ng et al. 2007a; b; Rabinovici et al. 2007; Rowe et al. 2007).

10.2.1.2 ^{11}C-BF227

^{11}C-BF-227 (BF227), a benzoxazole derivative, is also a promising tool as an Aβ imaging tracer (Okamura et al. 2004). In vitro binding studies with BF-227 demonstrated a K_i value of 4.3 nM for the compound to $A\beta_{1–42}$ fibrils (Kudo 2006). A PET study using BF-227 showed AD patients were clearly distinguishable from age-matched controls with AD patients displaying significantly higher tracer retention in the cerebral cortex than controls (Kudo et al. 2007). Regional parametric analysis of the images further demonstrated a higher BF-227 retention in the posterior association cortex in AD patients. Unlike PiB, BF-227 presents with similar binding affinities for Aβ and α-synuclein (Fodero-Tavoletti et al. 2009a; b).

A few other C-11 Aβ radiotracers have been tested in humans. The evaluation of the stilbene derivative, ^{11}C-SB13, showed that it could differentiate between five AD and six controls but had a lower effect size values when compared with ^{11}C-PiB (Verhoeff et al. 2004). A preliminary study with the anti-Aβ agent ^{11}C-ST1859 revealed small differences in radiotracer retention between nine AD patients and three healthy controls, but showed that the biodistribution and specificity of therapeutic agents can be assessed with PET (Bauer et al. 2006). Another Aβ radiotracer, ^{11}C-AZD2138, not only showed reversible binding but also displayed very low non-specific binding to white matter (Johnson et al. 2009; Nyberg et al. 2009).

10.2.2 ^{18}F-Labeled Radiotracers

Unfortunately, the 20-min radioactive decay half-life of carbon-11 (^{11}C) limits the use of ^{11}C-PiB to centers with an on-site cyclotron and ^{11}C radiochemistry expertise, making the cost of studies prohibitive for routine clinical use. To overcome these limitations, several Aβ tracers labeled with fluorine-18 (^{18}F; half-life of 110 min) that permits centralized production and regional distribution have been developed

and tested. Recent studies with the newly introduced ^{8}F-labeled Aβ-specific radiotracers, ^{18}F-florbetapir (Wong et al. 2010; Clark et al. 2011), ^{18}F-florbetaben (Rowe et al. 2008; Barthel et al. 2011; Villemagne et al. 2011a; b), ^{18}F-flutemetamol (Nelissen et al. 2009; Vandenberghe et al. 2010), and ^{18}F-NAV4694 (Rowe et al. 2013a; b), have been successfully replicating the results obtained with ^{11}C-PiB. The latest entry into the list of fluorinated Aβ radiotracers is ^{18}F-MK-3328, developed by Merck, that has the disadvantage that >17% of its cortical signal was attributed to binding to monoamine oxidase-B (MAO-B) (Sur et al. 2010).

10.2.2.1 ^{18}F-FDDNP

A marked progression in the development of Aβ imaging tracers was the synthesis and characterization by Barrio and colleagues of a very lipophilic radiofluorinated 6-dialkylamino-2-naphthyethylidene derivative that presents nanomolar affinity to Aβ fibrils (Barrio et al. 1999; Agdeppa et al. 2001a; b). ^{18}F-FDDNP is reported to bind both the extracellular Aβ plaques and the intracellular NFT in AD (Shoghi-Jadid et al. 2002) while also binding to prion plaques in Creutzfeldt-Jakob disease (CJD) brain tissue (Bresjanac et al. 2003). However, in vitro evaluation of FDDNP in concentrations similar to those achieved during a PET scan showed limited binding to both NFT and Aβ plaques (Thompson et al. 2009). ^{18}F-FDDNP was used to obtain the first human PET images of Aβ in an 82-year-old woman with AD. AD patients present with higher accumulation and slower clearance of ^{18}F-FDDNP than controls in brain areas such as the hippocampus (Shoghi-Jadid et al. 2002). Retention time of ^{18}F-FDDNP in these brain regions was correlated with lower memory performance scores, regional glucose hypometabolism, and brain atrophy (Small et al. 2002; Small et al. 2006). However, the dynamic range of ^{18}F-FDDNP cortical uptake values between HC and AD patients is small (9%). Direct comparison of ^{18}F-FDDNP with ^{11}C-PIB in monkeys (Noda et al. 2008) and in human subjects showed very limited dynamic range of ^{18}F-FDDNP (Shih et al. 1987; Tolboom et al. 2009a; b) and in a longitudinal study was found to be less useful than ^{11}C-PiB and ^{18}F-fluorodeoxyglucose (FDG) for examining disease progression (Ossenkoppele et al. 2012). ^{18}F-FDDNP has also been shown to bind to pure tauopathies, such as patients with progressive supranuclear palsy (Kepe et al. 2013) and in individuals suspected of chronic traumatic encephalopathy (Barrio et al. 2015; Chen et al. 2018; Omalu et al. 2018). Interestingly, ^{18}F-FDDNP still remains the only Aβ tracer showing retention in the medial temporal cortex of AD patients (Shih et al. 1987) and correlation with cerebrospinal fluid (CSF) tau (Tolboom et al. 2009a; b).

10.2.2.2 ^{18}F-NAV4694

Developed by AstraZeneca, the most salient features of ^{18}F-NAV4694 are, as with ^{11}C-AZD2138, fast tracer kinetics and low non-specific binding to white matter, similar to that one observed with ^{11}C-PiB, which is helpful for the detection of small Aβ cortical deposits at very early stages of the disease process (Sundgren-Andersson et al. 2009; Jureus et al. 2010). Head-to-head comparison with PIB suggests ^{18}F-NAV4694 has a better binding profile than PiB (Rowe et al. 2013a; b; Rowe et al. 2016). Clinical studies with ^{18}F-NAV4694 showed a clear distinction in tracer

retention between healthy controls and AD patients (Rowe et al. 2013a; b; Rowe et al. 2016). To this date, ^{18}F-NAV4694 remains the only main F-18 Aβ radiotracer that has not yet been presented to the Food and Drug Administration (FDA) for approval.

10.2.2.3 ^{18}F-Florbetaben

^{18}F-florbetaben (a.k.a. Neuraceq™; AV1; BAY94–9172), synthesized by Kung and colleagues (Zhang et al. 2005a; b), developed by Bayer Healthcare, and nowadays commercialized by Life Molecular Imaging Inc., has been shown to bind with high affinity to Aβ in brain homogenates and selectively labeled Aβ plaques and CAA in AD tissue sections (Zhang et al. 2005a; b). After injection into Tg2576 transgenic mice, ex vivo brain sections showed localization of ^{18}F-florbetaben in regions with Aβ plaques as confirmed by thioflavin binding (Zhang et al. 2005a, b). At tracer concentrations achieved during human PET studies, florbetaben did not show binding to LB or NFT-tau in post-mortem cortices from DLB or FTLD patients (Fodero-Tavoletti et al. 2012). In human studies, cortical retention of ^{18}F-florbetaben was higher at 90 min post-injection in all AD subjects compared to age-matched controls and FTLD patients, with binding matching the reported post-mortem distribution of Aβ plaques (Rowe et al. 2008). Recently completed phase II clinical studies further confirmed these results (Barthel et al. 2011). A longitudinal study in MCI subjects established the usefulness of FBB PET in predicting progression to AD (Ong et al. 2013; Ong et al. 2015). ^{18}F-Florbetaben is highly correlated with ^{11}C-PiB (Villemagne et al. 2012a; b; c; d; Rowe et al. 2017) and was used to detect the presence or absence of AD pathology in the brain in subjects from a wide spectrum of neurodegenerative diseases (Villemagne et al. 2011a; b) aiding in the differential diagnosis of dementia (Ceccaldi et al. 2018) and clarifying diagnosis in patients with ambiguous CSF results (Manca et al. 2019). It has been shown that ^{18}F-florbetaben can make accurate ante-mortem differential diagnosis of brain amyloidosis (Sabbagh et al. 2017), and phase III confirmed ^{18}F-florbetaben is highly associated with Aβ plaque pathology (Sabri et al. 2015), leading to its approval for clinical use by the FDA. ^{18}F-Florbetaben has been recently incorporated as an Aβ radiotracer to ADNI-3.

10.2.2.4 ^{18}F-Florbetapir

As ^{18}F-florbetaben, ^{18}F-florbetapir is a stilbene derivative that was also synthesized by Kung and colleagues at the University of Pennsylvania (Zhang et al. 2005a, b) and has been developed by Avid Radiopharmaceuticals. Initial in vitro evaluation showed binding to Aβ plaques in AD brain sections (Choi et al. 2009; Lin et al. 2009). The most salient feature of this tracer is its rapid reversible binding characteristics allowing scanning only at 45–50 min after injection, similar to ^{11}C-PiB (Wong et al. 2010). ^{18}F-Florbetapir (Lister-James et al. 2011) has become the most widely used Aβ radiotracer after ^{11}C-PiB and has been adopted as the Aβ radiotracer for ADNI 2 and also used in patient selection and to evaluate treatment response in a large number of multicenter therapeutic trials around the world. Several multicenter phase I and II studies in AD, MCI, and HC showed the ability of ^{18}F-florbetapir

to discriminate between AD and age-matched controls, with ~50% of the MCI subjects presenting with high ^{18}F-florbetapir retention (Fleisher et al. 2011). Multicenter studies using ^{18}F-florbetapir to assess the relationship between Aβ burden and cognition showed that in clinically normal older individuals, Aβ burden in the brain is associated with poorer memory performance (Sperling et al. 2012), while MCI subjects with high Aβ burden in the brain are at a significantly higher risk of cognitive decline over 18 months (Doraiswamy et al. 2012). An initial phase III study in 35 volunteers demonstrated a 96% agreement between ^{18}F-florbetapir and neuropathology for the detection of brain Aβ in vivo and no retention in young controls (Clark et al. 2011). An extension phase III in 59 volunteers established that ^{18}F-florbetapir has a sensitivity of 92% and a specificity of 100% for the detection of Aβ pathology (Clark et al. 2012). The use of ^{18}F-florbetapir changes patient management (Pontecorvo et al. 2017a; b), and using a combination of visual inspection with a semiquantitative approach improves diagnostic accuracy (Pontecorvo et al. 2017a; b). No significant difference in the rates of Aβ accumulation was observed when compared against PiB in longitudinal studies (Su et al. 2019), where a slow but steady increase in florbetapir signal was observed in young controls (Gonneaud et al. 2017), which was associated with incipient cognitive decline (Bischof et al. 2016) even at low Aβ levels (Landau et al. 2018). ^{18}F-Florbetapir (as Amyvid™) was the first radiotracer approved by the FDA for detection of Aβ in vivo and the first ^{18}F-labeled radiotracer approved by the FDA since FDG.

10.2.2.5 ^{18}F-Flutemetamol

Another fluorinated tracer, developed by GE Healthcare, that also completed a phase III study (Curtis et al. 2015) is ^{18}F-flutemetamol (a.k.a. GE067; Vizamyl™) (Serdons et al. 2009a; b). Phase I and II studies demonstrated that ^{18}F-flutemetamol can clearly differentiate between AD and HC (Nelissen et al. 2009; Vandenberghe et al. 2010) and that when combined with brain atrophy, it could be predictive of disease progression in MCI subjects (Thurfjell et al. 2012). ^{18}F-Flutemetamol brain retention is highly correlated with ^{11}C-PIB (Vandenberghe et al. 2010; Mountz et al. 2015; Lowe et al. 2017) and with neuropathology (Wolk et al. 2011; Wong et al. 2012; Thal et al. 2015; Thal et al. 2018) where no difference was found in the ^{18}F-flutemetamol regional brain distribution between MCI subjects and end-stage AD patients (Farrar et al. 2019). ^{18}F-Flutemetamol has been shown to aid in the clinical diagnosis and management of individuals presenting with memory decline (Zwan et al. 2017; Leuzy et al. 2019). ^{18}F-Flutemetamol has been approved for clinical use by the FDA.

All Aβ imaging radiotracers present a similar pattern of tracer retention in AD, with the highest retention in frontal, temporal, and posterior cingulate cortices, reflecting Aβ plaque burden (Fig. 10.1). While the cortical retention of ^{18}F-florbetapir, ^{18}F-florbetaben, and ^{18}F-flutemetamol provides a clear separation of AD patients from HC subjects, the degree of cortical retention with ^{18}F-florbetapir and ^{18}F-florbetaben is lower than with ^{11}C-PiB (Villemagne et al. 2012a; b; c; d; Wolk et al. 2012a; b), showing a narrower dynamic range of SUVR values that visually appears as a relatively higher degree of non-specific binding to white

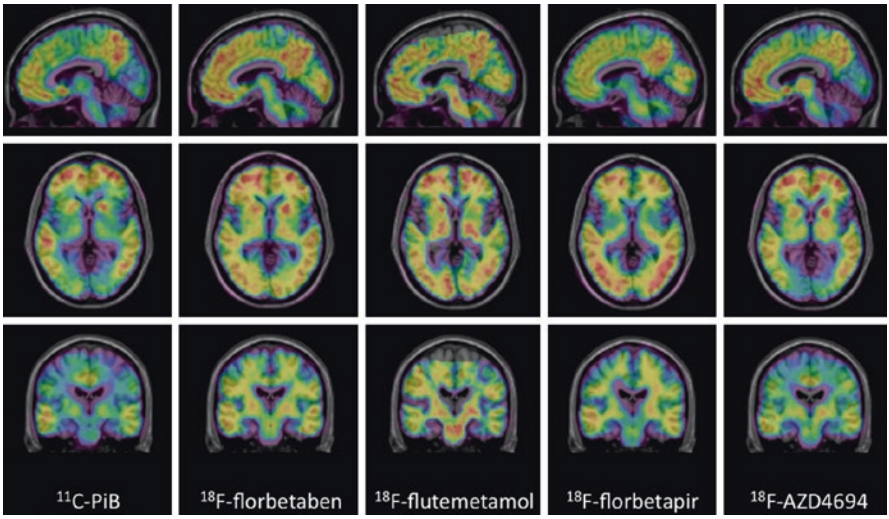

Fig. 10.1 Representative sagittal (top row), transaxial (middle row), and coronal (bottom row) PET images overlaid on MRI from Alzheimer's disease patients obtained with different Aβ imaging radiotracers. From left to right, ^{11}C-PiB, ^{18}F-florbetaben, ^{18}F-flutemetamol, ^{18}F-florbetapir, and ^{18}F-NAV4694. The images show the typical pattern of tracer retention in AD, with the highest retention in frontal, temporal, and posterior cingulate cortices, reflecting Aβ plaque burden

matter. While the cortical retention of ^{18}F-flutemetamol is similar to that of ^{11}C-PiB, the non-specific retention in white matter is much higher (Vandenberghe et al. 2010). Due to this lower signal-to-noise ratio, visual read-outs of the images are more challenging than with ^{11}C-PiB (Rowe and Villemagne 2011). These issues are not observed when using ^{18}F-NAV4694, which is an Aβ tracer that yields high contrast images with relatively low tracer retention in white matter and has proven to perform slightly better than ^{11}C-PiB (Rowe et al. 2016). While ^{11}C-PiB PET and ^{18}F-NAV4694 images in subjects with AD pathology usually clearly show high radiotracer retention in the gray matter in excess of that in subjacent white matter, these FDA-approved ^{18}F tracers frequently show loss of the normal gray-white matter demarcation as the predominant evidence of cortical Aβ deposition (Rowe and Villemagne 2011).

10.3 Aβ Imaging in Alzheimer's Disease

On visual inspection, cortical retention of Aβ tracers is higher in AD, with a regional brain distribution that is highest in frontal, cingulate, precuneus, striatum, parietal, and lateral temporal cortices, while occipital, sensorimotor, and mesial temporal cortices are much less affected (Villemagne et al. 2018). Both quantitative and visual assessment of PET images present a pattern of radiotracer retention that seems to replicate the sequence of Aβ deposition found at autopsy (Braak and Braak

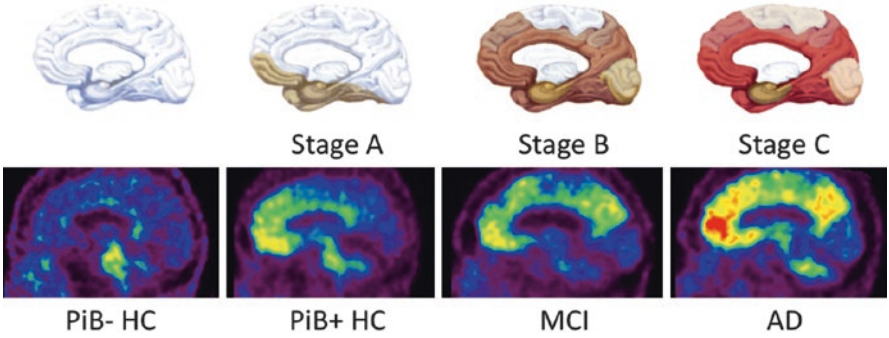

Fig. 10.2 *Top row*. Schematics showing the stages of Aβ deposition in the human brain as proposed by Braak and Braak (Braak and Braak 1997). *Bottom row*. Representative sagittal PET images showing the regional brain distribution of ^{11}C-PIB in two asymptomatic healthy age-matched controls, one with low (PiB- HC) and one with high Aβ burden (PiB+ HC), a subject classified as mild cognitive impairment (MCI) with significant Aβ deposition in the brain, and an Alzheimer's disease (AD) patient with even a higher Aβ burden in the brain. The pattern of PiB retention replicates the sequence of Aβ deposition described from post-mortem studies (Braak and Braak 1997)

1997), with initial deposition in the orbitofrontal cortex, inferior temporal, cingulate gyrus, and precuneus, followed by the remaining prefrontal cortex, lateral temporal, and parietal cortices (Fig. 10.2). Multimodality studies in early AD have shown that the regional pattern of Aβ deposition is similar to the anatomy of the "default network" (Buckner et al. 2005; Sperling et al. 2009), a specific, anatomically defined brain system responsible for internal modes of cognition, such as self-reflection processes, conscious resting state, or episodic memory retrieval (Buckner et al. 2008; Wermke et al. 2008), an association that is present even in non-demented subjects (Drzezga et al. 2011). The regional distribution of Aβ tracers in the brain sometimes varies with the specific Aβ distribution characteristic of the underlying pathology, for example, carriers of mutations associated with familial AD (Klunk et al. 2007; Koivunen et al. 2008a; b; Villemagne et al. 2009a; b) and subjects with posterior cortical atrophy (Ng et al. 2007a; b; Tenovuo et al. 2008; Kambe et al. 2010; Formaglio et al. 2011) or CAA (Johnson et al. 2007; Dierksen et al. 2010) each presenting a different regional ^{11}C-PiB distribution of retention to the one usually observed in sporadic AD (Klunk et al. 2004; Rowe et al. 2007).

Cross-sectional semiquantitative PET studies using diverse Aβ radiotracers have shown a robust difference in retention between AD patients and age-matched controls (Klunk et al. 2004; Price et al. 2005; Mintun et al. 2006; Kudo et al. 2007; Pike et al. 2007; Rabinovici et al. 2007; Rowe et al. 2007; Jack Jr. et al. 2008a; b; Morris et al. 2009; Furst et al. 2010; Rowe et al. 2010; Barthel et al. 2011; Fleisher et al. 2011; Villemagne et al. 2011a; b; Camus et al. 2012; Cselenyi et al. 2012). It should be noted that about 20–30% of clinically diagnosed probable AD patients have been shown to have a low Aβ imaging scan, which effectively rules out AD pathology as the etiology of the dementia.

Longitudinal studies have shown that significant, albeit small, increases in Aβ deposition can be measured but also that these increases in Aβ deposition are present across the whole spectrum of cognitive stages, from cognitively unimpaired individuals to AD dementia patients (Engler et al. 2006; Jack Jr. et al. 2009; Okello et al. 2009a; b; Resnick et al. 2010; Rinne et al. 2010; Sojkova et al. 2011a; b; Villemagne et al. 2011a; b; Villain et al. 2012; Jack Jr. et al. 2013; Villemagne et al. 2013; Landau et al. 2015). Aβ accumulation is observed in individuals considered to have low Aβ loads with about 7% of them progressing above the threshold in about 2.5 years (Vlassenko et al. 2011), and subtle cognitive decline is observed in those subthreshold individuals that accumulate Aβ over time (Landau et al. 2018). Aβ accumulation is a slow and protracted process that precedes by about two decades the onset of the typical phenotype of AD dementia (Jack Jr. et al. 2013; Villemagne et al. 2013; Landau et al. 2015). In individuals with the highest Aβ burdens independent of clinical classification and also as Alzheimer's dementia progresses, the rates of Aβ deposition start to slow down (Villain et al. 2012; Jack Jr. et al. 2013; Villemagne et al. 2013; Landau et al. 2015). This slower rate of Aβ deposition observed at the late stages of the disease might be attributed to a saturation of the process or, much more likely, extensive neuronal death that precludes production of Aβ.

10.4 Ante-mortem Post-mortem Correlations

While clinicopathological studies have shown that the accuracy of clinical assessments for the diagnosis of AD ranges between 70 and 90%, depending on the specialization of the center, the regional retention of radiotracers is highly correlated with regional Aβ plaques as reported at autopsy or biopsy (Bacskai et al. 2007; Ikonomovic et al. 2008; Leinonen et al. 2008a; b; Villemagne et al. 2009a; b; Burack et al. 2010; Clark et al. 2011; Kadir et al. 2011; Sabbagh et al. 2011; Sojkova et al. 2011a; b; Wolk et al. 2011; Clark et al. 2012; Wong et al. 2012; Curtis et al. 2015; Sabri et al. 2015), with a higher Aβ concentration in the frontal cortex than in the hippocampus, consistent with previous reports (Arnold et al. 2000; Naslund et al. 2000). As mentioned before, and in contrast with CSF studies, Aβ imaging studies can assess both the quantity and regional brain distribution of Aβ, as observed in the different patterns of regional distribution of Aβ observed in sporadic AD (Klunk et al. 2004; Nordberg 2007), familial AD (Klunk et al. 2007; Koivunen et al. 2008a; b; Villemagne et al. 2009a; b), familial British dementia (Villemagne et al. 2010), and CAA subjects (Johnson et al. 2007; Dierksen et al. 2010). The results from Aβ imaging might be considered for the brain regions to be sampled and stained for the neuropathological diagnosis of AD (Montine et al. 2012).

There have been a handful of cases reported with a discrepancy between a positive neuropathological finding or a strong biomarker profile of AD and a low PET signal (Leinonen et al. 2008a; b; Tomiyama et al. 2008; Cairns et al. 2009; Schöll et al. 2011; Sojkova et al. 2011a; b; Ikonomovic et al. 2012). For example, Tomiyama and colleagues reported a case of a novel APP mutation (E693Delta) where the

mutant Aβ does not fibrillize in the same way as wild-type Aβ (Inayathullah and Teplow 2011) in which the ^{11}C-PiB study showed low cortical retention (Tomiyama et al. 2008). Schöll and colleagues report on two subject carriers of the Artic APP mutation (Schöll et al. 2011). These two mutation carriers, while presenting with low ^{11}C-PiB retention, had a clear "AD pattern" of brain hypometabolism as measured by FDG, low $A\beta_{1-42}$, and elevated t-tau and p-tau in CSF (Schöll et al. 2011). On the one hand, these cases illustrate the possibility that different conformations of Aβ deposits (Levine 3rd and Walker 2010) may affect the binding of tracers and that Aβ imaging may not recognize all types of Aβ pathologies with equal sensitivity (Walker et al. 2008; Rosen et al. 2010). On the other, it raises issues not only in regard to the sensitivity of Aβ imaging (e.g., what is the minimal amount of Aβ detected by PET?) but also in regard to the evaluation of brain tissue (e.g., type of tissue dye, type of antibodies used for immunohistochemistry and ELISA, diagnostic criteria, etc.).

Second-generation radiofluorinated Aβ imaging radiotracers underwent phase III studies comparing ante-mortem PET with post-mortem findings. All these tracers showed a very high accuracy against neuropathology, with a sensitivity of 92% and a specificity of 100% for florbetapir (Clark et al. 2012), a sensitivity of 86% and a specificity of 92% for flutemetamol (Curtis et al. 2015), and a sensitivity of 98% and a specificity of 89% for florbetaben (Sabri et al. 2015). Based on the results of these phase III studies, all three tracers received Food and Drug Administration (FDA) and European Medicines Agency (EMA) approval for clinical use, specifically to *rule out* the presence of Aβ-amyloid in the brain.

10.5 Aβ Deposition in Non-demented Individuals and Its Relation with Cognition

About 25–35% of elderly subjects performing within normal limits on cognitive tests present with high cortical ^{11}C-PiB retention, predominantly in the prefrontal and posterior cingulate/precuneus regions (Mintun et al. 2006; Rowe et al. 2007; Aizenstein et al. 2008; Villemagne et al. 2008a; b; Mormino et al. 2009; Reiman et al. 2009a; b; Rowe et al. 2010). These findings are in perfect agreement with post-mortem reports that ~25% of non-demented older individuals over the age of 75 have Aβ plaques in the brain (Davies et al. 1988; Morris and Price 2001; Forman et al. 2007). Aβ deposition in these non-demented individuals (Mintun et al. 2006; Rowe et al. 2007; Aizenstein et al. 2008; Villemagne et al. 2008a; b) might reflect preclinical AD (Price and Morris 1999). Furthermore, the prevalence of subjects with high ^{11}C-PiB retention increases each decade at the same rate as the reported prevalence of plaques in non-demented subjects in autopsy studies (Rowe et al. 2010). While cross-sectional examination of these controls essentially show no significant differences in cognition (Mintun et al. 2006; Aizenstein et al. 2008; Jack Jr. et al. 2008a; b; Villemagne et al. 2008a; b; Rowe et al. 2010), significant cognitive differences in females were reported (Pike et al. 2011). More recently, Sperling and colleagues reported that high Aβ deposition in the brain was correlated with lower

immediate and delayed memory scores in otherwise healthy controls (Sperling et al. 2012). Interestingly, 23% of healthy elderly controls showed signs of neurodegeneration but no signs of Aβ pathology: This group of healthy elderly controls was defined by the presence of neurodegeneration in the absence of Aβ pathology and was proposed to have suspected non-Alzheimer's pathophysiology (SNAP) (Jack Jr. et al. 2012). While Aβ is a strong predictor of cognitive decline, neurodegeneration alone did not differ from those controls without neurodegeneration or Aβ in the brain (Burnham et al. 2016). When this basic approach was applied to the general population, it was found that almost all 50-year-old cases had no signs of either Aβ or neurodegeneration, while by 80 years old ~75% of the cohort presented signs of one or both markers (Jack Jr. et al. 2014). The detection of Aβ pathology at the presymptomatic stage is also of crucial importance because if this group truly represents preclinical AD (Price and Morris 1999; Thal et al. 2004; Backman et al. 2005; Small et al. 2007), it is precisely the group that may benefit the most from therapies aimed at reducing or eliminating Aβ from the brain before irreversible neuronal or synaptic loss occurs (Sperling et al. 2011a; b; c). Moreover, some individuals remain cognitively intact, while others develop cognitive impairment, despite carrying the same pathological burden, so factors that convey resilience or susceptibility to Aβ should also be considered.

Individuals fulfilling criteria for MCI are a heterogeneous group with a wide spectrum of underlying pathologies (Petersen 2000; Winblad et al. 2004). About 40–60% of carefully characterized subjects with MCI will subsequently progress to meet criteria for AD over a 3–4-year period (Petersen et al. 1995; Petersen et al. 1999; Petersen 2000). Aβ imaging has proven useful in identifying MCI individuals with and without AD pathology. Approximately 50–70% of the subjects classified as MCI present with high cortical ^{11}C-PiB retention (Price et al. 2005; Kemppainen et al. 2007; Pike et al. 2007; Forsberg et al. 2008; Lowe et al. 2009; Mormino et al. 2009). While most studies found that subjects classified as non-amnestic MCI show low Aβ levels in the brain (Pike et al. 2007; Lowe et al. 2009), other reports did not (Wolk et al. 2009). More specifically, subjects classified as non-amnestic single domain MCI usually do not show Aβ deposition, consistent with a non-AD underlying pathological process (Pike et al. 2007; Villemagne et al. 2011a; b).

Subjective cognitive impairment (SCI) or subjective cognitive decline (SCD) is believed to be an early behavioral manifestation along the AD spectrum that may precede objective MCI and is associated with up to a sixfold increased risk of developing AD (Jessen et al. 2010). In order to better characterize those SCI/SCD individuals that might have confounding personality or affective factors unrelated to AD, several studies evaluated the relationship between SCI/SCD and specific markers of AD pathology. While only a few individuals with SCI/SCD develop AD within a few years (Slot et al. 2019), these individuals are likely to already harbor Aβ in the brain (Buckley et al. 2016; Perrotin et al. 2017; Hu et al. 2019), but Aβ burden has a stronger association to worries than to the severity of the cognitive complaints (Verfaillie et al. 2019).

To date, the relationship between Aβ deposition and the development of clinical symptoms is not fully understood. Although Aβ burden as assessed by PET does not

correlate with measures of memory impairment in established clinical AD, it does correlate with memory impairment in MCI and healthy older subjects (Pike et al. 2007; Villemagne et al. 2008a; b). In subjects with MCI, this Aβ-related impairment is thought to be mediated through tau and hippocampal atrophy (Mormino et al. 2009; Sperling et al. 2019) while modulated by cognitive reserve (Roe et al. 2008; Rentz et al. 2010) and glucose metabolism (Cohen et al. 2009; Hanseeuw et al. 2017), although at the AD stage there is no longer correlation between glucose metabolism, cognition, and Aβ burden (Furst et al. 2010).

Longitudinal studies are helping clarify the relationship between Aβ burden and cognitive decline in healthy individuals and SCI/SCD and MCI subjects. High ^{11}C-PiB cortical retention in non-demented elderly subjects is associated with a greater risk of cognitive decline (Villemagne et al. 2008a; b; Resnick et al. 2010; Villemagne et al. 2011a; b). For example, the evaluation of either the cognitive trajectories (Villemagne et al. 2008a; b; Resnick et al. 2010) or changes in cognition prospectively (Morris et al. 2009; Villemagne et al. 2011a; b; Doraiswamy et al. 2012) shows that individuals with substantial Aβ deposition are more likely to present with cognitive decline. Aggregating the results from recently reported longitudinal studies reveals that 65% of MCI subjects with marked ^{11}C-PiB retention progressed to AD over 2–3 years, showing that MCI subjects with high Aβ deposition in the brain are >10 times more likely to progress to AD than those with low Aβ deposition, highlighting the clinical relevance and potential impact in patient management of Aβ imaging (Forsberg et al. 2008; Okello et al. 2009a; b; Wolk et al. 2009; Villemagne et al. 2011a; b; Rowe et al. 2013a; b). The observations that ^{11}C-PiB retention in non-demented individuals relates to episodic memory impairment, one of the earliest clinical symptoms of AD, and that extensive Aβ deposition is associated with a significant higher risk of cognitive decline in HC and with progression from MCI to AD emphasize the non-benign nature of Aβ deposition and support the hypothesis that Aβ deposition occurs well before the onset of symptoms, further suggesting that early disease-specific therapeutic intervention at the presymptomatic stage might be the most promising approach to either delay onset or halt disease progression (Sperling et al. 2011a; b; c).

The high prevalence of Aβ deposition in non-demented individuals raises questions in regard to Aβ toxicity and deposition. The evidence points to the fact that Aβ toxicity in the form of oligomers and Aβ deposition in the form of aggregates precede by many years the appearance of clinical symptoms (Price and Morris 1999). These neurotoxic processes eventually lead to synaptic and neuronal dysfunction, manifested as cognitive impairment, gray matter atrophy, and glucose hypometabolism (Eckert et al. 2003; Suo et al. 2004; Leuner et al. 2007). Therefore, it is highly likely that ^{11}C-PiB retention in non-demented individuals reflects preclinical AD (Mintun et al. 2006; Rowe et al. 2007; Aizenstein et al. 2008; Villemagne et al. 2008a; b). This may be associated or attributed to a different susceptibility/vulnerability to Aβ, at either a cellular (frontal neurons seem to be more resistant to Aβ than hippocampal neurons) (Roder et al. 2003; Resende et al. 2007), a regional (compensatory upregulation of choline acetyltransferase (ChAT) activity in the frontal cortex and hippocampi of MCI and

early AD subjects) (DeKosky et al. 2002), or an individual or personal level, either due to a particular cognitive reserve (Mortimer 1997; Stern 2002; Kemppainen et al. 2008; Roe et al. 2008), due to differences in Aβ conformation affecting toxicity and/or aggregation (Lockhart et al. 2005; Deshpande et al. 2006; Levine 3rd and Walker 2008; Walker et al. 2008), or because an idiosyncratic threshold must be exceeded for synaptic failure and neuronal death to ensue (Suo et al. 2004). These factors would help explain why some older individuals with a significant Aβ burden are cognitively unimpaired, while others with lower Aβ burden and no genetic predisposing factors have already developed the full clinical AD phenotype. Ongoing longitudinal studies will help identify those subjects that despite substantial Aβ deposition do not develop the AD phenotype, thus allowing to isolate genetic or environmental factors that may convey resistance to Aβ (Sojkova et al. 2011a; b).

The lack of a strong association between Aβ deposition and measures of cognition, synaptic activity, and neurodegeneration in AD, in addition to the evidence of Aβ deposition in a high percentage of MCI and asymptomatic HC, suggests that Aβ is an early and necessary, though not sufficient, cause for cognitive decline in AD (Villemagne et al. 2008a; b; Rabinovici et al. 2010; Sojkova et al. 2011a; b), indicating the involvement of other downstream mechanisms, likely triggered by Aβ such as NFT formation, synaptic failure, and eventually neuronal loss. Also at play are factors as age, years of education, occupational level, and brain volume among others that, under the umbrella of "cognitive reserve," appear to have a modulatory role between cognition and Aβ deposition (Roe et al. 2008; Chetelat et al. 2010a; b; Tucker and Stern 2011). Selective tau imaging studies are helping elucidate the bridge between Aβ deposition and the persistent decline in cognitive function observed in AD (Fodero-Tavoletti et al. 2011, Villemagne et al. 2015, Villemagne et al. 2018).

10.6 Relation of Aβ Imaging with Other Biomarkers

Another rapidly growing area is the exploration of the potential association between biomarkers of Aβ deposition or neurodegeneration (Wahlund and Blennow 2003; Morris et al. 2005; Sunderland et al. 2005; de Leon et al. 2006; Thal et al. 2006; Blennow et al. 2007; Shaw et al. 2007; Clark et al. 2008; Jack Jr. et al. 2010; Albert et al. 2011; McKhann et al. 2011; Storandt et al. 2012) and Aβ burden as measured by PET (Jack Jr. et al. 2008a; b; Jack Jr. et al. 2010). The new National Institute on Aging and Alzheimer's Association (NIA-AA) Research Framework—AT(N) (Jack Jr. et al. 2016; Jack et al. 2018)—is based on a biological definition of Alzheimer's disease and uses three kinds of biomarkers, markers of Aβ (A) and tau (T) pathology and markers of neuronal injury/neurodegeneration (N), for characterizing the physiopathology of AD. The implementation of the AT(N) classification is helping to refine prognosis in clinical practice and identify those at-risk individuals more likely to clinically progress, for their inclusion in therapeutic trials (Cummings 2019).

10.6.1 FDG

While the typical pattern of Aβ deposition in sporadic AD is highest in frontal, cingulate, precuneus, striatum, parietal, and lateral temporal cortices (Klunk et al. 2004), in FDG studies, the typical "AD pattern" is of temporoparietal and posterior cingulate hypometabolism with sparing of the basal ganglia, thalamus, cerebellum, and primary sensorimotor cortex (Salmon et al. 1994; Devanand et al. 1997; Coleman 2005; Jagust et al. 2007). Due to its high sensitivity (>90%) for detecting temporoparietal and posterior cingulate hypometabolism, FDG-PET has improved diagnostic and prognostic accuracy in patients with probable AD (Salmon et al. 1994; Kennedy et al. 1995; Small et al. 1995; Silverman et al. 2001; Silverman et al. 2002). A similar pattern of hypometabolism has been reported in normal elderly ApoE ε4 carriers (Reiman et al. 1996), MCI subjects (Chetelat et al. 2003, Chetelat et al. 2005, Mosconi et al. 2006), asymptomatic subjects with mutations associated with familial AD (Kennedy et al. 1995; Rossor et al. 1996), and subjects with a strong family history of AD (Mosconi et al. 2006a; b). FDG hypometabolism is correlated with cognition (Landau et al. 2009; Furst et al. 2010) and is predictive of future cognitive decline (Drzezga et al. 2003; Mosconi et al. 2004; Drzezga et al. 2005).

Visual assessment of PET images by clinicians blinded to the clinical status has demonstrated that ^{11}C-PiB was more accurate than FDG to distinguish AD from HC (Ng et al. 2007a; b) and slightly better than FDG in differentiating AD from FTLD (Rabinovici et al. 2011). Similarly, Aβ imaging outperforms FDG at identifying MCI subtypes (Lowe et al. 2009).

While some reports found no association between FDG and ^{11}C-PiB in AD (Furst et al. 2010), others found an inverse correlation between them in temporal and parietal cortices (Cohen et al. 2009), but no correlation has been shown in the frontal lobe (Klunk et al. 2004; Edison et al. 2007). A possible explanation for this dissociation is that there are compensatory mechanisms such as upregulation of ChAT in the frontal lobe of MCI individuals and mild AD patients (DeKosky et al. 2002; Ikonomovic et al. 2007) that might delay the manifestation of synaptic dysfunction; therefore, no hypometabolism is observed on FDG in the frontal lobe. Glucose metabolism in the frontal lobe eventually decreases as the disease progresses, and the characteristic temporoparietal pattern of AD becomes less apparent (Mielke et al. 1992; Herholz 1995). Conversely to what is observed in the frontal area, in AD patients ChAT is significantly decreased in the posterior cingulated gyrus (Ikonomovic et al. 2011), which is characterized by being one of the regions where marked and early Aβ deposition is associated with substantial hypometabolism (Drzezga et al. 2011; Yokokura et al. 2011).

10.6.2 CSF

Analysis of CSF allows simultaneous measurement of the concentration of the two main hallmarks of AD, Aβ and tau. It has been reported to be highly accurate in the diagnosis of AD as well of predicting cognitive decline (Blennow et al. 2007; de

Leon et al. 2007; Hansson et al. 2007; Mattsson et al. 2009; Mattsson et al. 2011). The typical CSF profile in AD is low $A\beta_{1–42}$ and high total (t-tau) and phosphorylated tau (p-tau) (Strozyk et al. 2003; Hampel et al. 2010). Slower Aβ clearance from the brain (Bateman et al. 2006; Mawuenyega et al. 2010) is likely to lead to Aβ deposition in the brain and lower CSF $A\beta_{1–42}$ concentrations. While there is no correlation between ^{11}C-PiB retention and CSF t-tau or p-tau (Tolboom et al. 2009a; b; Forsberg et al. 2010), several studies have reported a strong inverse correlation between Aβ deposition in the brain and CSF $A\beta_{1–42}$ (Fagan et al. 2006; Fagan et al. 2007; Forsberg et al. 2008; Koivunen et al. 2008a; b; Fagan et al. 2009; Grimmer et al. 2009; Landau et al. 2013; Mattsson et al. 2017). Both high Aβ burden and low CSF $A\beta_{1–42}$ have been observed in cognitively unimpaired individuals probably reflecting Aβ deposition years before the manifestation of the AD phenotype (Mintun et al. 2006; Fagan et al. 2007; Rowe et al. 2007; Aizenstein et al. 2008; Fagan et al. 2009). Large population studies, such as ADNI, AIBL, and DIAN (Shaw et al. 2007; Apostolova et al. 2010; Li et al. 2015; McDade et al. 2018), have been crucial for the validation of Aβ imaging and CSF assessments as antecedent biomarkers of AD as well as determining the longitudinal trajectories of these fluid biomarkers (Toledo et al. 2013; Fagan et al. 2014; Wang et al. 2018), while the introduction of automated immunoassay platforms has allowed reproducibility of results across time and across centers (Rozga et al. 2017; Schindler et al. 2018; Shaw et al. 2019). Given that CSF and Aβ imaging measure different biochemical pools of Aβ (Roberts et al. 2017), the inverse relationship between them is not linear (Toledo et al. 2015). This is also reflected in how these biomarkers change over time. In contrast to the sigmoid shape curve observed for longitudinal Aβ imaging studies in the brain (Jack Jr. et al. 2013; Villemagne et al. 2013), CSF $A\beta_{1–42}$ decreases over time tend to adopt a logarithmical shape (Toledo et al. 2013).

10.6.3 Plasma Aβ

In recent years, there has been a revolution in the ability to measure Aβ peptides and APP fragments in plasma. Several reports demonstrate that plasma Aβ levels can predict both CSF Aβ and brain Aβ with an accuracy ~90% (Fandos et al. 2017; Ovod et al. 2017; Nakamura et al. 2018; Palmqvist et al. 2019). The introduction of these tests will have immediate effects as an inexpensive way to identify individuals at risk of developing AD, lowering the costs of screening for therapeutic AD trials by reducing number of lumbar punctures and Aβ PET scans.

10.6.4 MRI Volumetrics

While Aβ imaging or CSF Aβ provides information in regard to Aβ pathology, CSF tau quantification, FDG, and structural MRI provide information related to the neurodegenerative process (Jack Jr. et al. 2010). Hippocampal and cortical gray matter atrophy and ventricular enlargement are typical, albeit not specific, MRI findings in

AD and MCI (Frisoni et al. 2010; Drago et al. 2011). Furthermore, it has been shown that the rates of hippocampal atrophy might be predictive of conversion from MCI to AD (Jack Jr. et al. 2008a; b).

Aβ deposition is associated with regional cerebral atrophy as measured by MRI (Archer et al. 2006; Bourgeat et al. 2010; Chetelat et al. 2010a; b; Becker et al. 2011) and correlates with the rates of cerebral atrophy (Becker et al. 2011; Tosun et al. 2011). Moreover, the data suggest that the relationship between Aβ deposition and cortical atrophy is sequential, where Aβ deposition precedes synaptic dysfunction and neuronal loss (Chetelat et al. 2010a, b, Drzezga et al. 2011, Forster et al. 2012), and then manifested as structural changes (Becker et al. 2011). While some reports did not find a correlation between atrophy trajectories and Aβ deposition (Josephs et al. 2008; Driscoll et al. 2010), most reported that those with high Aβ deposition showed a significantly higher rate of cortical atrophy compared to those with low Aβ burden (Chetelat et al. 2012; Sarro et al. 2016; Fletcher et al. 2018; Dang et al. 2019). These discrepancies might be due to degree of tau deposition in the brain, which is believed to mediate the effects of Aβ on brain volumetrics (Ossenkoppele et al. 2019; La Joie et al. 2020).

10.6.5 Neuroinflammation

Microglia are the primary resident immune surveillance cells in the brain and are thought to play a significant role in the pathogenesis of several neurodegenerative disorders including AD (Venneti et al. 2006). Activated microglia can be measured using radioligands for the translocator protein (TSPO), formerly known as the peripheral benzodiazepine receptor. The TSPO is upregulated on activated macrophages and microglia and has been established as a biomarker of neuroinflammation in the central nervous system. Most reports found that in AD there is no association between Aβ deposition and microglial activation measured by [^{11}C]PK11195 (Edison et al. 2008a; b; Okello et al. 2009a; b; Wiley et al. 2009) despite being an association between [^{11}C]PK11195 binding and both glucose hypometabolism and severity of dementia (Edison et al. 2008a; b; Yokokura et al. 2011). Higher TSPO tracer binding is observed in AD patients compared to elderly controls (Kreisl et al. 2018), but TSPO polymorphism affects the binding of these tracers in the brain (Kreisl et al. 2013). New developed radiotracers for activated microglia are focusing on cell membrane markers like P2X7 receptors (Berdyyeva et al. 2019; Hagens et al. 2020), as well as renewed interest on tracers binding to COX-1 and COX-2 (Kim et al. 2018). Also, PET studies assessing the relationship between Aβ deposition and neuroinflammation have been conducted using the MAO-B inhibitor ^{11}C-L-*d*-deprenyl as a marker for reactive astrocytosis (Carter et al. 2012; Rodriguez-Vieitez and Nordberg 2018). The most interesting issue in regard to imaging reactive astrocytosis is that, in contrast with activated microglia, it is an early phenomenon, suggesting it might be a better neuroinflammatory target at the preclinical and prodromal stages of AD (Scholl et al. 2015; Rodriguez-Vieitez et al. 2016).

10.7 Relation of Aβ Deposition with Genetic Risks and Predisposing Factors

Age is the strongest risk factor in sporadic AD, with the prevalence of the disease increasing exponentially with age. These risks are increased in the presence of the APOE ε4 allele (Farrer et al. 1997). Both risk factors have been directly associated with Aβ burden as measured by PET (Reiman et al. 2009a; b; Morris et al. 2010; Rowe et al. 2010).

To date, APOE ε4 is the most consistent genetic risk factor associated with sporadic AD, and its presence has been associated with an earlier age of onset and a dose-dependent—either one or two APOE ε4 alleles—higher risk of developing AD (Farrer et al. 1997). Examination of APOE ε4 allele status revealed that, independent of clinical classification, ε4 carriers present with significantly higher ^{11}C-PiB retention than non-ε4 carriers, further emphasizing the crucial role that APOE plays in the metabolism of Aβ (Reiman et al. 2009a; b; Morris et al. 2010; Rowe et al. 2010). When specific clinical groups are examined, the results— from either autopsy or Aβ imaging studies— are not that clear-cut. While some studies found significant differences in Aβ burden between AD ε4 carriers and non-ε4 carriers (Gomez-Isla et al. 1996; Drzezga et al. 2008; Grimmer et al. 2010), others did not (Berg et al. 1998; Klunk et al. 2004; Rowe et al. 2007; Rabinovici et al. 2010).

Both symptomatic and asymptomatic individual carriers of autosomal mutations within the APP or presenilin 1 or 2 genes associated with familial AD present with very high and early ^{11}C-PiB retention in the caudate nuclei, retention that seems to be independent of mutation type or disease severity (Klunk et al. 2007; Koivunen et al. 2008a; b; Remes et al. 2008; Villemagne et al. 2009a; b). Larger multicenter studies are helping elucidate the value of several biomarkers in these autosomal mutation carriers, assessment that might lead to better targeted disease-specific therapeutic strategies (Bateman et al. 2012; Benzinger et al. 2013).

While a similar pattern of Aβ deposition as seen in familial AD has been reported in adults with Down syndrome (Cohen et al. 2018), a completely different pattern of ^{11}C-PiB retention was observed in a mutation carrier of familial British dementia (Villemagne et al. 2010).

There are several other factors that have been associated with AD. Among these, the most relevant are vascular risk factors (VRF), such as diabetes, hypercholesterolemia, hypertension, hyperhomocysteinemia, etc. The influence of these VRF on AD pathology is an area that, despite the long and intense scientific debate, has not been clearly established (Viswanathan et al. 2009). Studies using MRI white matter hyperintense lesions as surrogate markers of vascular disease in association with assessment of Aβ deposition and cognition (Kuczynski et al. 2008; Marchant et al. 2011) suggest that cerebrovascular lesions may accelerate the clinical presentation of AD (Riekse et al. 2004) by having an independent effect on cognition (Vemuri et al. 2017; DeCarli et al. 2019).

As with AD, VRF are strongly age-dependent factors that share similar pathogenic pathways, such as oxidative stress or inflammation, so it is not easy to extricate one from the other in order to ascertain a causal, casual, or comorbid association

between them (Rosendorff et al. 2007). On the other hand, in light of the absence of disease-modifying therapies for AD, the relevance of these risk factors rests in the fact that early intervention, especially at middle age, might have an impact on delaying either the onset or progression of AD, as suggested by recent reports of a lowering incidence of AD (Satizabal et al. 2016; Pase et al. 2017).

10.8 Aβ Imaging in Other Neurodegenerative Conditions

Aβ imaging in a wide spectrum of neurodegenerative conditions has yielded diverse results. Although lower than in AD, similar patterns of ^{11}C-PiB retention are usually observed in DLB (Rowe et al. 2007; Gomperts et al. 2008; Maetzler et al. 2009). Cortical ^{11}C-PiB retention is also higher in subjects diagnosed with CAA (Johnson et al. 2007), while there is usually no cortical ^{11}C-PiB retention in patients with FTLD (Rabinovici et al. 2007; Rowe et al. 2007; Drzezga et al. 2008; Engler et al. 2008). Aβ imaging has also facilitated differential diagnosis in cases of patients with atypical presentations of dementia (Ng et al. 2007a; b; Wolk et al. 2012a; b).

10.8.1 Cerebral Amyloid Angiopathy

CAA, characterized by Aβ deposits in and around the media of small arteries and arterioles of the cerebral cortex and leptomeninges, has been found to be present in most patients with AD (Jellinger and Attems 2005). To this date, neuropathologic examination of the brain remains the only definitive method for diagnostic confirmation of CAA. However, the combination of Aβ imaging with ^{11}C-PiB PET and T2* susceptibility-weighted (SWI) MR imaging (Knudsen et al. 2001) allows for the concomitant assessment of molecular and structural changes in vivo. The combination of cerebral microhemorrhages (MH) and superficial siderosis (SS) has been suggested as a radiological marker for CAA (Feldman et al. 2008). Aβ imaging studies have shown both processes may be intimately associated with Aβ deposition (Dierksen et al. 2010; Dhollander et al. 2011), preferentially in posterior areas of the brain, showing a distinct pattern of ^{11}C-PiB retention than the one observed in sporadic AD (Johnson et al. 2007). Furthermore, focal Aβ deposition might be useful in predicting new MH in CAA patients (Gurol et al. 2012; Raniga et al. 2017). While deep subcortical MH are generally associated with VRF, lobar MH (particularly posterior) (Pettersen et al. 2008) are usually attributed to CAA (Knudsen et al. 2001; Vernooij et al. 2008). Lobar MH are a frequent finding in AD patients or even in cognitively normal older individuals, and they are strongly associated with increasing age and Aβ deposition (Yates et al. 2011). This association between Aβ and vascular lesions has crucial implications not only for the selection and risk stratification of individuals undergoing anticoagulant therapies but also in those enrolled in anti-Aβ therapeutic trials (Weller et al. 2009).

10.8.2 Lewy Body Diseases

While AD is the most common cause of dementia in the elderly, DLB accounts for 20% of the cases (McKeith et al. 2005). The pathological hallmark of DLB is the presence of α-synuclein-containing LB within the neocortical and limbic regions (McKeith et al. 2005; Kantarci et al. 2020), as well as substantial loss of pigmented dopaminergic neurons in the substantia nigra, reflected in a marked dopaminergic terminal denervation in the striatum (McKeith and Mosimann 2004). More refined neuropathological techniques have revealed extensive synaptic deposits of α-synuclein, more concordant with the DLB clinical phenotype than the usually sparse cortical LB (Schulz-Schaeffer 2010). Overlap of cognitive symptoms early in the disease course offers a challenge for clinicians making it difficult to distinguish between patients that will develop AD and those that will ultimately develop DLB. Post-mortem histopathological studies have identified that 50–80% of DLB cases often have cortical Aβ deposits with characteristics and a distribution similar to AD patients (McKeith et al. 2005; Rowe et al. 2007; Edison et al. 2008a; b; Kantarci et al. 2020). This has also been described as "mixed" DLB/AD or "Lewy body variant of AD." So-called "pure" DLB is much less common, and it is not clear if the clinical characteristics and prognosis differ from the mixed-pathology cases. On visual inspection, cortical Aβ tracer retention in DLB is generally lower and more variable than in AD, probably reflecting a larger spectrum of Aβ deposition (Rowe et al. 2007; Gomperts et al. 2008; Maetzler et al. 2009). Therefore Aβ imaging is not a useful tool in differentiating between AD and DLB, but might assist in the differential diagnosis of those cases ("pure" DLB) without Aβ deposition in the brain (Armstrong et al. 2000; Landau and Villemagne 2020).

Taking advantage of its high affinity for α-synuclein (Fodero-Tavoletti et al. 2009a; b), ^{11}C-BF227 has been used for the assessment of multiple system atrophy (MSA), a disease characterized by the glial accumulation of α-synuclein in the absence of Aβ plaques, showing a higher retention in MSA patients compared to age-matched controls (Kikuchi et al. 2010). Interestingly, while ^{11}C-BF227 retention in DLB patients was lower compared to AD in most cortical regions, DLB presented with significantly higher ^{11}C-BF227 retention in the amygdala (Furukawa et al. 2011).

In contrast to Aβ imaging, assessing the integrity of dopaminergic terminals via dopamine transporter (DAT) or vesicular monoamine transporter type 2 (VMAT2) imaging can robustly detect reductions of dopaminergic nigrostriatal afferents in DLB patients, assisting in the differential diagnosis from AD (O'Brien et al. 2004; Koeppe et al. 2008; Villemagne et al. 2012a; b; c; d; Gomperts et al. 2016).

Cortical Aβ is not usually present in cognitively intact Parkinson's disease (PD) patients, and no significant ^{11}C-PiB cortical retention is usually observed in these patients (Johansson et al. 2008; Mashima et al. 2017). Aβ deposits, both vascular and parenchymal, are frequent, however, in PD patients who develop dementia (PDD) (Edison et al. 2008a; b; Gomperts et al. 2008; Maetzler et al. 2008; Maetzler et al. 2009; Burack et al. 2010; Foster et al. 2010; Kalaitzakis et al. 2011; Gomperts et al. 2016).

The contribution of Aβ to the development of Lewy body diseases remains unclear, but cortical Aβ deposits are associated with extensive α-synuclein lesions and higher levels of insoluble α-synuclein lesions (Pletnikova et al. 2005), as well as exacerbation of neuronal injury (Masliah et al. 2001). Furthermore, it has been shown that in PD, CSF Aβ is predictive of cognitive decline (Siderowf et al. 2010). Along these lines, while Aβ imaging cannot contribute to the differential diagnosis between AD and DLB, it may have prognostic relevance in these Lewy body diseases. For example, similar to what has been reported for PDD, where higher Aβ burden was associated with a shorter prodromal phase before dementia (Halliday et al. 2008), Aβ burden in DLB patients was inversely correlated with the interval from onset of cognitive impairment to the full development of the DLB phenotype, faster rates of cortical atrophy, and faster rates of clinical progression (Rowe et al. 2007; Sarro et al. 2016; Donaghy et al. 2019).

10.8.3 Frontotemporal Lobar Degeneration

FTLD is a syndrome that can also be clinically difficult to distinguish from early-onset AD, especially at the initial stages of the disease. Based on clinical phenotype, FTLD has been categorized mainly into two classes: behavioral variant of FTLD (bvFTLD) with distinct changes in behavior and personality with little effect on language functions and progressive aphasias (comprised by semantic dementia (svFTLD), progressive non-fluent aphasia (nfvFTLD), and logopenic aphasia (lvFTLD)) showing progressive language deficits, with less obvious personality and behavioral changes (Rabinovici & Miller 2010).

Aβ deposition is not a pathological trait of FTLD, and definitive differential diagnosis can only be established after post-mortem examination of the human brain. Neuropathological examination of the brain in FTLD shows variable frontal and temporal atrophy (Cairns et al. 2007; Hodges and Patterson 2007; Snowden et al. 2007), microvacuolation, and neuronal loss, with white matter myelin loss, astrocytic gliosis, as well as neuronal and glial inclusions (Cairns et al. 2007). Three intraneuronal inclusion types have been identified in FTLD: (1) hyperphosphorylated tau (FTLD-tau), (2) ubiquitin-hyperphosphorylated and proteolysed TAR-DNA binding protein 43 (FTLD-TDP-43), and (3) fused sarcoma positive (FUS) (Taniguchi et al. 2004; Mott et al. 2005; Neumann et al. 2006; Neumann et al. 2009). Tau-positive inclusions account for approximately 40% of all FTLD cases, the remainder being tau negative and TDP-43/ubiquitin positive (Josephs et al. 2004). In bvFTLD, both tau and TDP-43 are equally prevalent; and while 90% of the SD cases show TDP-43 pathology, PNFA presents predominantly (70%) tau pathology (Josephs et al. 2004; Mackenzie et al. 2008). In contrast, logopenic progressive aphasia (LPA) is thought to be a language presentation of AD, with typical Aβ and NFT (Leyton et al. 2011). Absence of Aβ and tau deposition is considered one of the features of limbic-predominant age-related TDP-43 encephalopathy (LATE) (Nelson et al. 2019), a neurodegenerative condition that presents with an amnestic dementia similar to AD, which also presents a typical signature on FDG studies (Botha et al. 2018).

Aβ imaging has been helpful in the differential diagnosis between FTLD and AD (Rabinovici et al. 2007; Rowe et al. 2007; Drzezga et al. 2008; Engler et al. 2008). Furthermore, Aβ imaging has been used to ascertain the absence of AD pathology in the different FTLD aphasias (Drzezga et al. 2008; Rabinovici et al. 2008; Leyton et al. 2011). Despite displaying similar specificities, the diagnostic performance of Aβ imaging proved to be more sensitive for the diagnosis of FTLD than FDG (Rabinovici et al. 2011).

10.8.4 Prion Diseases

No cortical Aβ deposition is usually observed in sporadic Creutzfeldt-Jakob disease (CJD) cases (Villemagne et al. 2009a; b; Dulamea and Solomon 2016; Matias-Guiu et al. 2017). Due to the rapid progression and relatively short duration of symptomatic illness, sporadic CJD patients do not demonstrate appreciable PrP-plaque deposition at autopsy (Liberski 2004). Although some sporadic CJD molecular subtypes can manifest larger PrP plaques (Hill et al. 2003), the most common subtype usually demonstrates only very fine "synaptic" and small perivacuolar deposits (Hill et al. 2003; Liberski 2004). A study in transmissible spongiform encephalopathies showed that Aβ imaging with ^{11}C-BF227 might be able to distinguish between Gerstmann-Straussler-Scheinker disease (GSS) and sporadic CJD disease with clear tracer retention in brain regions of PrP deposition (Okamura et al. 2010).

10.8.5 Traumatic Brain Injury and Chronic Traumatic Encephalopathy

Traumatic brain injury (TBI) has been associated with a number of long-term sequelae, including an increased risk for dementia (Plassman et al. 2000; Barnes et al. 2014); however, the long-term effects of a single TBI event in regard to triggering AD-related proteinopathies remain controversial (Furst and Bigler 2016; LoBue et al. 2019). While some studies have reported higher cortical Aβ deposition in TBI (Malkki 2014; Gatson et al. 2016), others have found no evidence of it (Weiner et al. 2017). These discrepancies might be in part explained by slightly different definitions of TBI, as well as in the cause or severity of the event. A more careful selection of and better clinical and neuropsychological characterization of participants is needed to elucidate this issue.

Chronic traumatic encephalopathy (CTE) is a neurodegenerative 3R/4R tauopathy associated with a history of repetitive head trauma (McKee et al. 2018). However, in about 50% of CTE cases, other pathological protein deposits such as Aβ, α-synuclein, and TDP-43 are also present (McKee et al. 2013), which, added to a variable degree of cortical gray matter atrophy, make the interpretation of molecular imaging studies complicated.

10.9 Clinical and Research Applications of Amyloid Imaging

Aβ imaging has been widely used in research settings as well as in a host of disease-specific therapeutic trails while ascertaining its place as a diagnostic and prognostic tool in the clinical evaluation and management of dementia patients.

The application of Aβ imaging in research and clinical settings raises issues referring to the quantitative or semiquantitative approaches used to determine Aβ burden. Given that the studies are performed in individuals or populations who might not tolerate long scanning sessions, the majority of studies use a short 20- or 30-min PET scan when Aβ tracers reach, at different periods after injection, apparent steady state (Lopresti et al. 2005; Rowe et al. 2007; Yee et al. 2007; Edison et al. 2008a; b). While these image acquisition intervals are more than enough to obtain clinically useful images, it is unlikely they adequately or reliably establish Aβ burden in therapeutic trials (Rinne et al. 2010; Ostrowitzki et al. 2011; Ossenkoppele et al. 2012), where drug-induced changes in tracer metabolism, blood-brain barrier permeability, cerebral blood flow, gray matter atrophy, target conformation, etc. might affect Aβ tracer binding (Lopresti et al. 2005; Price et al. 2005). Finally, the issue of partial volume correction (PVC) raises several other questions: How much of the intrinsic noise of the PET signal is augmented by PVC? Should longitudinal studies be evaluated without PVC (Jack Jr. et al. 2013; Villemagne et al. 2013; Landau et al. 2015)? How to correct for spillover radioactivity from white matter? All these issues remain contentious.

10.9.1 Aβ Imaging in Large Observational Cohorts

Since the launch of the Alzheimer's Disease Neuroimaging Initiative (ADNI https://adni.loni.usc.edu) in the USA in 2003 ever-growing, similarly oriented consortia such as the Australian Imaging, Biomarker and Lifestyle (AIBL, https://aibl.csiro.au) Study of Ageing (Ellis et al. 2009) and Europe's Amyloid Imaging to Prevent Alzheimer's Disease (AMYPAD, http://amypad.eu) (Frisoni et al. 2019) have been organized and assembled around the world, setting the groundwork for biomarker discovery and the establishing of standards for early diagnosis of sporadic AD (Villemagne et al. 2014). A similar worldwide consortium, the Dominantly Inherited Alzheimer's Network (DIAN, https://dian.wustl.edu) (Morris et al. 2012), focuses on autosomal mutations leading to AD. The various accomplishments of these large cohort observational studies, especially in regard to Aβ imaging, have contributed substantially to a better understanding of the underlying physiopathology of aging and AD. These accomplishments are basically predicated in the trinity of multimodality, standardization, and sharing. This multimodality approach can now better identify those subjects with AD-specific traits that are more likely to present cognitive decline in the near future and that might represent the best candidates for smaller but more efficient therapeutic trials, trials that, by the gained and shared knowledge of some of the pathophysiological mechanisms underpinning aging and AD pathology, can be more focused on a specific target or a specific stage of the disease process.

10.9.2 Aβ Imaging in Disease-Specific Therapeutic Trials

Aβ imaging with PET is also contributing to the development of more effective therapies by allowing better selection of patients for multicenter anti-Aβ therapy trials around the world (Long and Holtzman 2019) and providing a means to ascertain target engagement and measure their impact on Aβ burden (Rinne et al. 2010; Ostrowitzki et al. 2011; Liu et al. 2015) as well as outcome measure of their effectiveness (Doody et al. 2014; Salloway et al. 2014; Sevigny et al. 2016).

While these studies represent one of the principal applications of Aβ imaging today, a key challenge for these trials is that reductions in Aβ burden, as measured by either CSF or PET, have not been accompanied with cognitive stabilization or improvement (Doody et al. 2014; Salloway et al. 2014; Sevigny et al. 2016). Furthermore, some of these therapies were associated with side effects such as edema and microhemorrhages. Other Aβ-centered therapeutic mechanisms have been attempted, such as inhibition or modulation of β- and γ-secretases, but most have been discontinued as well (Egan et al. 2019, Long and Holtzman 2019). Since study participants were, while mild, symptomatic AD patients, these setbacks have been attributed to treatment occurring too late in the course of disease, so trials like A4 have enrolled cognitively normal elderly individuals with high Aβ, aiming at preventing the cognitive decline expected in this cohort (Sperling et al. 2014). Others have argued that these failures are clear evidence that Aβ reduction will not be an effective strategy for treating AD and that Aβ as a target for treatment or preventing AD should be abandoned.

The contribution of Aβ imaging to the selection of patients for therapeutic trials needs to be complemented with adequate MRI sequences such as SWI or GRE for the detection of vascular pathology to rule out the possibility of vascular complications such as Aβ imaging-related abnormalities (ARIA), either as "vasogenic edema" and/or sulcal effusion (ARIA-E) or as hemosiderin deposits including MH and SS (ARIA-H) (Cordonnier 2010; Sperling et al. 2011a; b; c). The presence of MH is impacting on patient selection in therapeutic trials, and some anti-Aβ immunotherapy trials are already excluding individuals with MH. To make matters worse, about one third of non-demented individuals with high Aβ burden and no prior history of cerebrovascular disease show MH (Yates et al. 2011). While focal Aβ deposition might be a better predictor of a vascular event (Gurol et al. 2012), only longitudinal follow-up of large cohorts of patients will allow elucidation of the relevant risk factors for lobar MH.

10.9.3 The Centiloid Scale

One of the obstacles for the widespread implementation of Aβ imaging in therapeutic trials or comparison of results in different cohorts across different centers is that Aβ tracers present with differing pharmacological and pharmacokinetic properties, yielding results in different dynamic ranges. These issues, summed to the use of a diverse arsenal of quantitative approaches and contrasting criteria for the selection

of internal scaling region and different thresholds to separate high from low Aβ burden in the brain, pose a challenge when trying to compare results from different cohorts or different therapeutic trials that use different Aβ tracers as Aβ quantitative tools. Therefore, a method was developed to standardized all Aβ imaging results under a single common semiquantitative scale—called the Centiloid (Klunk et al. 2015)—to improve the clinical and research application of these Aβ tracers. Since then, all F-18-labeled radiotracers Aβ tracers currently in use have been cross-calibrated against PiB (Rowe et al. 2016; Rowe et al. 2017; Battle et al. 2018; Navitsky et al. 2018) to enable translation into Centiloids.

The other obstacle is to define a threshold. One of the issues is in regard to the utility of a cut-off given the continuous nature of Aβ deposition (Jagust 2011; Mormino et al. 2012). While thresholds are arbitrary, in order to adopt one, it needs to be shown that it is relevant and accurate from a diagnostic and/or prognostic point of view. From a clinical point of view, a visual binary read will help separate those with a significant Aβ burden in the brain from those with a null or low Aβ burden. Similar dilemmas arise in research settings. In order to avoid being trapped in this dichotomy, some researchers use tertiles (Resnick et al. 2010; Rowe et al. 2013a; b), while others are proposing to distinguish two thresholds for "positivity," one more sensitive, to detect the early stages of Aβ deposition usually in still cognitively unimpaired elderly individuals, and another, a higher one, that can more specifically ascribe the clinical phenotype of dementia to Aβ pathology (Klunk et al. 2012).

The introduction of the Centiloid scale has tried to solve this problem, and while it transforms all Aβ tracers' semiquantitative results into a single universal scale, the idiosyncratic properties of these Aβ tracers remain so they might be more or less sensitive or accurate to provide a similar statement to a similar Aβ burden in the brain. Most of the studies have used neuropathology to establish Centiloid thresholds. For example, a large multicenter study using neuropathology from pre-mortem ^{11}C-PiB studies found that below a threshold of 12.2 Centiloids can distinguish between plaques and no plaques, while a threshold of 24.4 Centiloids identified intermediate-to-high AD neuropathological changes (La Joie et al. 2018). Similar neuropathology-based thresholds were determined with other Aβ tracers such as ^{18}F-florbetaben yielding 21 Centiloids (Dore et al. 2019) or ^{18}F-florbetapir yielding 24 Centiloids (Navitsky et al. 2018).

10.9.4 Appropriate Use Criteria and Clinical Impact of Aβ Imaging

Also, clinical criteria for the appropriate use of Aβ imaging has been established highlighting the need to integrate Aβ imaging with a comprehensive clinical and cognitive evaluation performed by a clinician experienced in the evaluation of dementia, ensuring a positive impact on patient management (Johnson et al. 2013). These criteria clearly stipulate the specific cases Aβ imaging should be used, such as patients with persistent or progressive unexplained cognitive impairment, progressive atypical or unclear clinical presentation of dementia, or dementia onset in

individuals 65 years or younger (Johnson et al. 2013; Apostolova et al. 2016). It also outlines the inappropriate use of Aβ imaging, such as cases of probable AD with typical age of onset or to determine dementia severity, asymptomatic individuals or unconfirmed cognitive complaint, a family history of dementia or presence of the APOE ε4 allele, as well as non-medical use such as litigation for insurance purposes (Johnson et al. 2013; Apostolova et al. 2016).

These criteria are being tested in multicentre trials such as the Imaging Dementia—Evidence for Amyloid Scanning (IDEAS, https://www.ideas-study.org), assessing the clinical utility of Aβ imaging in the workup of patients with MCI or dementia of uncertain origin. The initial report from this trial showed that results from Aβ imaging were associated with *more than a 60%* change in the clinical management of these patients within 90 days, usually reflected in a change in acetylcholine esterase inhibitor medication (Rabinovici et al. 2019). Overall, Aβ imaging leads to change in diagnostic confidence and patient management in up to 60% of cases attending memory clinics (de Wilde et al. 2018; Rabinovici et al. 2019).

10.10 CODA

The clinical diagnosis of AD is typically based on progressive cognitive impairments while excluding other diseases. Clinical diagnosis of sporadic disease is challenging, however, often presenting mild and non-specific symptoms attributable to diverse and overlapping pathology presenting similar phenotypes. Overall, the accuracy of clinical diagnosis of AD compared to neuropathological examination ranges between 70% and 90% (Beach et al. 2012). While clinical criteria, together with current structural neuroimaging techniques (CT or MRI), are sufficiently sensitive and specific for the diagnosis of AD at the mid to late stages of the disease, they are focused on relatively non-specific features such as memory and functional activity decline or brain atrophy that are late features in the course of the disease. Confirmation of diagnosis of AD still relies on autopsy. But how reliable is pathology? How much of a "gold standard" is autopsy (Jellinger 2010; Scheltens and Rockwood 2011)? A more sensible paradigm, adopting a more fluid model that integrates all cognitive, biochemical, and imaging biomarkers that can provide a better predictive framework, has been proposed in the new diagnostic criteria for AD (Dubois et al. 2010; Sperling and Johnson 2010; McKhann et al. 2011), MCI (Albert et al. 2011), and preclinical AD (Sperling et al. 2011a; b; c). Along the same lines, Scheltens and Rockwood suggest that "a shift in focus from why people with AD have plaques and tangles to why not all people with plaques and tangles have AD would be welcome" (Scheltens and Rockwood 2011). While most people with AD pathology develop AD dementia, there are some that while having the pathology do not. What makes them different? What conveys resistance to some or, conversely, what makes others more vulnerable to the same pathological burden? Identifying these factors will allow a more discerning selection of individuals that will benefit from early intervention with anti-Aβ medication while also providing insights into potential preventive strategies or even new therapeutic approaches

(Sojkova and Resnick 2011; Sperling et al. 2011a; b; c). While the new diagnostic criteria has blurred once again the boundaries between MCI and AD (Morris 2012), it also allows for earlier diagnosis and therapeutic intervention, arguing that when there is a clear history of progressive cognitive decline, objective evidence from psychometric tests of episodic memory impairment and characteristic abnormalities in the CSF, and/or neuroimaging studies such as Aβ imaging, dementia is no more required for the diagnosis of probable AD (Dubois et al. 2010; Sperling and Johnson 2010; McKhann et al. 2011; Jack Jr. et al. 2016; Jack et al. 2018). Thus, as the criteria for the diagnosis of AD changes, Aβ imaging is likely, given its impact on patient management (Rabinovici et al. 2019), to play an increasingly important role in clinical practice provided it is accessible and affordable (Villemagne et al. 2010).

At this stage Aβ imaging, in combination with other modalities, is probably the best diagnostic tool to rule out Aβ pathology in individuals being evaluated for cognitive decline. The data to date clearly show that Aβ production and deposition is not a benign process with a more prominent role at the early, mostly asymptomatic, stages of the disease (Hyman 2011; Karran et al. 2011); therefore, anti-Aβ therapy at these stages seems a logical approach (Sperling et al. 2011a, b, c). On the other hand, we still do not have the full grasp of the long-term cognitive consequences of Aβ deposition. Longitudinal Aβ imaging, especially of cognitively unimpaired elderly individuals, is allowing the assessment of pathology almost simultaneously with tau, cognition, and other biomarkers of neurodegeneration. This will provide not only a better picture of how these different factors interact but also the weight or relevance this complementary and/or supplementary information plays at different stages of the disease.

The pathological process usually begins decades before symptoms are evident, making early identification difficult. This in turn precludes early intervention with disease-modifying medications during the presymptomatic period, which by arresting neuronal loss would presumably achieve the maximum benefits of such therapies (Villemagne et al. 2008a; b; Sperling et al. 2011a; b; c). Therefore, a change in the diagnostic paradigm is warranted, where diagnosis moves away from identification of signs and symptoms of neuronal failure—indicating that central compensatory mechanisms have been exhausted and extensive synaptic and neuronal damage is present—to the non-invasive detection of specific biomarkers for particular traits underlying the pathological process (Clark et al. 2008). Given the complexity and sometimes overlapping characteristics of these disorders, and despite recent advances in molecular neurosciences, it is unlikely that a single biomarker will be able to provide the diagnostic certainty required for the early detection of neurodegenerative diseases like AD, especially for the identification of at-risk individuals before the development of the typical phenotype. Therefore, a multimodality approach combining biochemical and neuroimaging methods is warranted (Shaw et al. 2007).

Biomarkers are important as they can be used to identify the risk of developing a disease (antecedent biomarkers), aid in identifying disease (diagnostic biomarkers), assess disease evolution (progression biomarkers), predict future disease course (prognostic biomarkers), or evaluate and/or customize therapy (theranostic

biomarkers). While CSF Aβ and tau, structural, and molecular neuroimaging (both FDG and Aβ imaging) are all good—specially if combined—diagnostic biomarkers for AD, evaluation of the data available to date suggests that Aβ imaging and CSF assessments of Aβ are good antecedent biomarkers at the preclinical and prodromal stages of the disease (Jack Jr. et al. 2010; Ossenkoppele et al. 2011; Villemagne et al. 2011a; b). Conversely, CSF assessments of tau and p-tau, structural neuroimaging, and FDG seem to be excellent biomarkers of disease progression (Jack Jr. et al. 2010). Despite the fact that Aβ accumulation is still ongoing at the AD stage (Villemagne et al. 2011a; b; Villain et al. 2012), and in contrast to what is observed at the preclinical and prodromal phases (Pike et al. 2007; Villemagne et al. 2008a; b; Cohen et al. 2012), Aβ burden at this stage is not correlated with markers of neurodegeneration, disease severity, or cognitive impairment (Hyman 2011; Karran et al. 2011). A review of the literature shows that quantification of $A\beta_{1-42}$, total tau, and p-tau in CSF and FDG and a long list of assessments of global or regional brain atrophy as well as white matter hyperintensities with MRI have all been proposed as predictors of conversion to AD (Chang and Silverman 2004; Smith et al. 2008; Jack Jr. et al. 2010). While larger longitudinal studies will further clarify the role of Aβ imaging in predicting conversion from MCI to AD, one of the most important conclusions to be drawn from these studies is that the likelihood of developing AD in a cognitively unimpaired individual with a low Aβ burden scan is extremely small (Villemagne et al. 2011a; b).

Another aspect to be considered is prediction of therapeutic response. As new therapies enter clinical trials, the role of Aβ imaging in vivo is becoming increasingly crucial. Aβ imaging allows the in vivo assessment of brain Aβ pathology and its changes over time, providing highly accurate, reliable, and reproducible quantitative statements of regional or global Aβ burden in the brain. As mentioned before, therapies, especially those targeting irreversible neurodegenerative processes, have a better chance to succeed if applied early, making early detection of the underlying pathological process so important. Therefore, Aβ imaging is an ideal tool for the selection of adequate candidates for anti-Aβ therapeutic trials while also monitoring—and potentially predicting—treatment response, thus aiding in reducing sample size and minimizing cost while maximizing outcomes. Studies are already showing the utility of this technique (Rinne et al. 2010; Ostrowitzki et al. 2011; Liu et al. 2015). These results, taken together with the results from longitudinal studies, support the growing consensus that anti-Aβ therapy to be effective may need to be given early in the course of the disease, perhaps even before symptoms appear (Sperling et al. 2011a, b, c), and that downstream mechanisms may also need to be addressed to successfully prevent the development of AD. Furthermore, the slow rate of Aβ deposition indicates that the time window for altering Aβ accumulation prior to the full manifestation of the clinical phenotype may be very wide (Villemagne et al. 2011a, b).

The introduction of radiotracers for the non-invasive in vivo quantification of Aβ burden in the brain has revolutionized the approach to the evaluation of AD. Aβ imaging has extended our insight into Aβ deposition in the brain, where Aβ burden as measured by PET matches histopathological reports of Aβ distribution in aging

and dementia, it appears more accurate than FDG for the diagnosis of AD, and it is an excellent aid in the differential diagnosis of AD from FTLD (Mathis et al. 2005; Johnson 2006; Mathis et al. 2007; Villemagne et al. 2008a; b; Jagust 2009; Rabinovici and Jagust 2009; Drzezga 2010; Klunk 2011; Villemagne et al. 2012a; b; c; d). APOE ε4 carriers, independent of diagnosis or disease severity, present with higher Aβ burden than non-ε4 carriers, and high retention of Aβ radiotracers closely corresponds with low CSF Aβ levels and increasing age (Reiman et al. 2009a; b; Fagan and Holtzman 2010; Morris et al. 2010; Rowe et al. 2010). Although Aβ burden as assessed by PET does not strongly correlate with cognitive impairment in AD, it does correlate with memory impairment and a higher risk for cognitive decline in the aging population and MCI subjects. This correlation with memory impairment, one of the earliest symptoms of AD, suggests that Aβ deposition is not part of normal aging, supporting the hypothesis that Aβ deposition occurs well before the onset of symptoms and it likely represents preclinical AD in asymptomatic individuals and prodromal AD in MCI. Further longitudinal observations, coupled with different disease-specific biomarkers to assess potential downstream effects of Aβ, are required to confirm this hypothesis and further elucidate the role of Aβ deposition in the course of Alzheimer's disease.

Acknowledgments We would like to thank Prof. Michael Woodward, Dr. Rachel Mulligan, Dr. Greg Savage, Dr. Joanne Robertson, Dr. Gordon Chan, Dr. Kenneth Young, Dr. Sylvia Gong, Mr. Ignatius Reilly, Ms. Fiona Lamb, Mrs. Svetlana Pejoska, and the Brain Research Institute for their assistance with this study.

This work was supported in part by Program Grant 1127007, Project Grant 1132604, and Research Fellowship 1046471 of the National Health and Medical Research Council of Australia and the Austin Hospital Medical Research Foundation.

References

Agdeppa ED, Kepe V, Liu J, Flores-Torres S, Satyamurthy N, Petric A, Cole GM, Small GW, Huang SC, Barrio JR (2001a) Binding characteristics of radiofluorinated 6-dialkylamino-2-naphthylethylidene derivatives as positron emission tomography imaging probes for beta-amyloid plaques in Alzheimer's disease. J Neurosci 21(24):RC189

Agdeppa ED, Kepe V, Shoghi-Jadid K et al (2001b) In vivo and in vitro labeling of plaques and tangles in the brain of an Alzheimer's disease patient: a case study. J Nucl Med 42(suppl 1):65

Aizenstein HJ, Nebes RD, Saxton JA, Price JC, Mathis CA, Tsopelas ND, Ziolko SK, James JA, Snitz BE, Houck PR, Bi W, Cohen AD, Lopresti BJ, Dekosky ST, Halligan EM, Klunk WE (2008) Frequent amyloid deposition without significant cognitive impairment among the elderly. Arch Neurol 65(11):1509–1517

Albert MS, Dekosky ST, Dickson D, Dubois B, Feldman HH, Fox NC, Gamst A, Holtzman DM, Jagust WJ, Petersen RC, Snyder PJ, Carrillo MC, Thies B, Phelps CH (2011) The diagnosis of mild cognitive impairment due to Alzheimer's disease: recommendations from the National Institute on Aging-Alzheimer's Association workgroups on diagnostic guidelines for Alzheimer's disease. Alzheimers Dement 7(3):270–279

Apostolova LG, Haider JM, Goukasian N, Rabinovici GD, Chetelat G, Ringman JM, Kremen S, Grill JD, Restrepo L, Mendez MF, Silverman DH (2016) Critical review of the appropriate use criteria for amyloid imaging: effect on diagnosis and patient care. Alzheimers Dement (Amst) 5:15–22

Apostolova LG, Hwang KS, Andrawis JP, Green AE, Babakchanian S, Morra JH, Cummings JL, Toga AW, Trojanowski JQ, Shaw LM, Jack CR Jr, Petersen RC, Aisen PS, Jagust WJ, Koeppe RA, Mathis CA, Weiner MW, Thompson PM (2010) 3D PIB and CSF biomarker associations with hippocampal atrophy in ADNI subjects. Neurobiol Aging 31(8):1284–1303

Archer HA, Edison P, Brooks DJ, Barnes J, Frost C, Yeatman T, Fox NC, Rossor MN (2006) Amyloid load and cerebral atrophy in Alzheimer's disease: an 11C-PIB positron emission tomography study. Ann Neurol 60(1):145–147

Armstrong RA, Cairns NJ, Lantos PL (2000) Beta-amyloid deposition in the temporal lobe of patients with dementia with Lewy bodies: comparison with non-demented cases and Alzheimer's disease. Dement Geriatr Cogn Disord 11(4):187–192

Arnold SE, Han LY, Clark CM, Grossman M, Trojanowski JQ (2000) Quantitative neurohistological features of frontotemporal degeneration. Neurobiol Aging 21(6):913–919

Backman L, Jones S, Berger AK, Laukka EJ, Small BJ (2005) Cognitive impairment in preclinical Alzheimer's disease: a meta-analysis. Neuropsychology 19(4):520–531

Bacskai BJ, Frosch MP, Freeman SH, Raymond SB, Augustinack JC, Johnson KA, Irizarry MC, Klunk WE, Mathis CA, Dekosky ST, Greenberg SM, Hyman BT, Growdon JH (2007) Molecular imaging with Pittsburgh compound B confirmed at autopsy: a case report. Arch Neurol 64(3):431–434

Barnes DE, Kaup A, Kirby KA, Byers AL, Diaz-Arrastia R, Yaffe K (2014) Traumatic brain injury and risk of dementia in older veterans. Neurology 83(4):312–319

Barrio JR, Huang SC, Cole G, Satyamurthy N, Petric A, Phelps ME, Small G (1999) PET imaging of tangles and plaques in Alzheimer disease with a highly hydrophobic probe. J Label Compd Radiopharm 42:S194–S195

Barrio JR, Small GW, Wong KP, Huang SC, Liu J, Merrill DA, Giza CC, Fitzsimmons RP, Omalu B, Bailes J, Kepe V (2015) In vivo characterization of chronic traumatic encephalopathy using [F-18]FDDNP PET brain imaging. Proc Natl Acad Sci U S A 112(16):E2039–E2047

Barthel H, Gertz HJ, Dresel S, Peters O, Bartenstein P, Buerger K, Hiemeyer F, Wittemer-Rump SM, Seibyl J, Reininger C, Sabri O (2011) Cerebral amyloid-beta PET with florbetaben ((18)F) in patients with Alzheimer's disease and healthy controls: a multicentre phase 2 diagnostic study. Lancet Neurol 10(5):424–435

Bateman RJ, Munsell LY, Morris JC, Swarm R, Yarasheski KE, Holtzman DM (2006) Human amyloid-beta synthesis and clearance rates as measured in cerebrospinal fluid in vivo. Nat Med 12(7):856–861

Bateman RJ, Xiong C, Benzinger TL, Fagan AM, Goate A, Fox NC, Marcus DS, Cairns NJ, Xie X, Blazey TM, Holtzman DM, Santacruz A, Buckles V, Oliver A, Moulder K, Aisen PS, Ghetti B, Klunk WE, McDade E, Martins RN, Masters CL, Mayeux R, Ringman JM, Rossor MN, Schofield PR, Sperling RA, Salloway S, Morris JC (2012) Clinical and biomarker changes in dominantly inherited Alzheimer's disease. N Engl J Med 367(9):795–804

Battle MR, Pillay LC, Lowe VJ, Knopman D, Kemp B, Rowe CC, Dore V, Villemagne VL, Buckley CJ (2018) Centiloid scaling for quantification of brain amyloid with [(18)F]flutemetamol using multiple processing methods. EJNMMI Res 8(1):107

Bauer M, Langer O, Dal-Bianco P, Karch R, Brunner M, Abrahim A, Lanzenberger R, Hofmann A, Joukhadar C, Carminati P, Ghirardi O, Piovesan P, Forloni G, Corrado ME, Lods N, Dudczak R, Auff E, Kletter K, Muller M (2006) A positron emission tomography microdosing study with a potential antiamyloid drug in healthy volunteers and patients with Alzheimer's disease. Clin Pharmacol Ther 80(3):216–227

Beach TG, Monsell SE, Phillips LE, Kukull W (2012) Accuracy of the clinical diagnosis of Alzheimer disease at National Institute on Aging Alzheimer disease centers, 2005–2010. J Neuropathol Exp Neurol 71(4):266–273

Becker JA, Hedden T, Carmasin J, Maye J, Rentz DM, Putcha D, Fischl B, Greve DN, Marshall GA, Salloway S, Marks D, Buckner RL, Sperling RA, Johnson KA (2011) Amyloid-beta associated cortical thinning in clinically normal elderly. Ann Neurol 69(6):1032–1042

Benzinger TL, Blazey T, Jack CR Jr, Koeppe RA, Su Y, Xiong C, Raichle ME, Snyder AZ, Ances BM, Bateman RJ, Cairns NJ, Fagan AM, Goate A, Marcus DS, Aisen PS, Christensen JJ, Ercole

L, Hornbeck RC, Farrar AM, Aldea P, Jasielec MS, Owen CJ, Xie X, Mayeux R, Brickman A, McDade E, Klunk W, Mathis CA, Ringman J, Thompson PM, Ghetti B, Saykin AJ, Sperling RA, Johnson KA, Salloway S, Correia S, Schofield PR, Masters CL, Rowe C, Villemagne VL, Martins R, Ourselin S, Rossor MN, Fox NC, Cash DM, Weiner MW, Holtzman DM, Buckles VD, Moulder K, Morris JC (2013) Regional variability of imaging biomarkers in autosomal dominant Alzheimer's disease. Proc Natl Acad Sci U S A 110(47):E4502–E4509

Berdyyeva T, Xia C, Taylor N, He Y, Chen G, Huang C, Zhang W, Kolb H, Letavic M, Bhattacharya A, Szardenings AK (2019) PET imaging of the P2X7 Ion Channel with a novel tracer [(18) F]JNJ-64413739 in a Rat model of Neuroinflammation. Mol Imaging Biol 21(5):871–878

Berg L, McKeel DW Jr, Miller JP, Storandt M, Rubin EH, Morris JC, Baty J, Coats M, Norton J, Goate AM, Price JL, Gearing M, Mirra SS, Saunders AM (1998) Clinicopathologic studies in cognitively healthy aging and Alzheimer's disease: relation of histologic markers to dementia severity, age, sex, and apolipoprotein E genotype. Arch Neurol 55(3):326–335

Bischof GN, Rodrigue KM, Kennedy KM, Devous MD Sr, Park DC (2016) Amyloid deposition in younger adults is linked to episodic memory performance. Neurology 87(24):2562–2566

Blennow K, Zetterberg H, Minthon L, Lannfelt L, Strid S, Annas P, Basun H, Andreasen N (2007) Longitudinal stability of CSF biomarkers in Alzheimer's disease. Neurosci Lett 419(1):18–22

Botha H, Mantyh WG, Murray ME, Knopman DS, Przybelski SA, Wiste HJ, Graff-Radford J, Josephs KA, Schwarz CG, Kremers WK, Boeve BF, Petersen RC, Machulda MM, Parisi JE, Dickson DW, Lowe V, Jack CR Jr, Jones DT (2018) FDG-PET in tau-negative amnestic dementia resembles that of autopsy-proven hippocampal sclerosis. Brain 141(4):1201–1217

Bourgeat P, Chetelat G, Villemagne VL, Fripp J, Raniga P, Pike K, Acosta O, Szoeke C, Ourselin S, Ames D, Ellis KA, Martins RN, Masters CL, Rowe CC, Salvado O (2010) Beta-amyloid burden in the temporal neocortex is related to hippocampal atrophy in elderly subjects without dementia. Neurology 74(2):121–127

Braak H, Braak E (1997) Frequency of stages of Alzheimer-related lesions in different age categories. Neurobiol Aging 18(4):351–357

Bresjanac M, Smid LM, Vovko TD, Petric A, Barrio JR, Popovic M (2003) Molecular-imaging probe 2-(1-[6-[(2-fluoroethyl)(methyl) amino]-2-naphthyl]ethylidene) malononitrile labels prion plaques in vitro. J Neurosci 23(22):8029–8033

Buckley RF, Maruff P, Ames D, Bourgeat P, Martins RN, Masters CL, Rainey-Smith S, Lautenschlager N, Rowe CC, Savage G, Villemagne VL, Ellis KA, AIBL study (2016) Subjective memory decline predicts greater rates of clinical progression in preclinical Alzheimer's disease. Alzheimers Dement 12(7):796–804

Buckner RL, Andrews-Hanna JR, Schacter DL (2008) The brain's default network: anatomy, function, and relevance to disease. Ann N Y Acad Sci 1124:1–38

Buckner RL, Snyder AZ, Shannon BJ, LaRossa G, Sachs R, Fotenos AF, Sheline YI, Klunk WE, Mathis CA, Morris JC, Mintun MA (2005) Molecular, structural, and functional characterization of Alzheimer's disease: evidence for a relationship between default activity, amyloid, and memory. J Neurosci 25(34):7709–7717

Burack MA, Hartlein J, Flores HP, Taylor-Reinwald L, Perlmutter JS, Cairns NJ (2010) In vivo amyloid imaging in autopsy-confirmed Parkinson disease with dementia. Neurology 74(1):77–84

Burnham SC, Bourgeat P, Dore V, Savage G, Brown B, Laws S, Maruff P, Salvado O, Ames D, Martins RN, Masters CL, Rowe CC, Villemagne VL, AIBL Research Group (2016) Clinical and cognitive trajectories in cognitively healthy elderly individuals with suspected non-Alzheimer's disease pathophysiology (SNAP) or Alzheimer's disease pathology: a longitudinal study. Lancet Neurol 15(10):1044–1053

Cairns NJ, Bigio EH, Mackenzie IR, Neumann M, Lee VM, Hatanpaa KJ, White CL 3rd, Schneider JA, Grinberg LT, Halliday G, Duyckaerts C, Lowe JS, Holm IE, Tolnay M, Okamoto K, Yokoo H, Murayama S, Woulfe J, Munoz DG, Dickson DW, Ince PG, Trojanowski JQ, Mann DM (2007) Neuropathologic diagnostic and nosologic criteria for frontotemporal lobar degeneration: consensus of the Consortium for Frontotemporal Lobar Degeneration. Acta Neuropathol 114(1):5–22

Cairns NJ, Ikonomovic MD, Benzinger T, Storandt M, Fagan AM, Shah AR, Reinwald LT, Carter D, Felton A, Holtzman DM, Mintun MA, Klunk WE, Morris JC (2009) Absence of Pittsburgh compound B detection of cerebral amyloid beta in a patient with clinical, cognitive, and cerebrospinal fluid markers of Alzheimer disease: a case report. Arch Neurol 66(12):1557–1562

Camus V, Payoux P, Barre L, Desgranges B, Voisin T, Tauber C, La Joie R, Tafani M, Hommet C, Chetelat G, Mondon K, de La Sayette V, Cottier JP, Beaufils E, Ribeiro MJ, Gissot V, Vierron E, Vercouillie J, Vellas B, Eustache F, Guilloteau D (2012) Using PET with (18)F-AV-45 (florbetapir) to quantify brain amyloid load in a clinical environment. Eur J Nucl Med Mol Imaging 39(4):621–631

Cappai R, White AR (1999) Amyloid beta. Int J Biochem Cell Biol 31(9):885–889

Carter SF, Scholl M, Almkvist O, Wall A, Engler H, Langstrom B, Nordberg A (2012) Evidence for astrocytosis in prodromal Alzheimer disease provided by 11C-deuterium-L-deprenyl: a multitracer PET paradigm combining 11C-Pittsburgh compound B and 18F-FDG. J Nucl Med 53(1):37–46

Ceccaldi M, Jonveaux T, Verger A, Krolak-Salmon P, Houzard C, Godefroy O, Shields T, Perrotin A, Gismondi R, Bullich S, Jovalekic A, Raffa N, Pasquier F, Semah F, Dubois B, Habert MO, Wallon D, Chastan M, Payoux P, Guedj E, Stephens A, NEUUS in AD study group (2018) Added value of (18)F-florbetaben amyloid PET in the diagnostic workup of most complex patients with dementia in France: a naturalistic study. Alzheimers Dement 14(3):293–305

Chang CY, Silverman DH (2004) Accuracy of early diagnosis and its impact on the management and course of Alzheimer's disease. Expert Rev Mol Diagn 4:63–69

Chen ST, Siddarth P, Merrill DA, Martinez J, Emerson ND, Liu J, Wong KP, Satyamurthy N, Giza CC, Huang SC, Fitzsimmons RP, Bailes J, Omalu B, Barrio JR, Small GW (2018) FDDNP-PET tau brain protein binding patterns in military personnel with suspected chronic traumatic Encephalopathy1. J Alzheimers Dis 65(1):79–88

Chetelat G, Desgranges B, de la Sayette V, Viader F, Berkouk K, Landeau B, Lalevee C, Le Doze F, Dupuy B, Hannequin D, Baron JC, Eustache F (2003) Dissociating atrophy and hypometabolism impact on episodic memory in mild cognitive impairment. Brain 126(Pt 9):1955–1967

Chetelat G, Eustache F, Viader F, De La Sayette V, Pelerin A, Mezenge F, Hannequin D, Dupuy B, Baron JC, Desgranges B (2005) FDG-PET measurement is more accurate than neuropsychological assessments to predict global cognitive deterioration in patients with mild cognitive impairment. Neurocase 11(1):14–25

Chetelat G, Villemagne VL, Bourgeat P, Pike KE, Jones G, Ames D, Ellis KA, Szoeke C, Martins RN, O'Keefe GJ, Salvado O, Masters CL, Rowe CC (2010a) Relationship between atrophy and beta-amyloid deposition in Alzheimer disease. Ann Neurol 67(3):317–324

Chetelat G, Villemagne VL, Pike KE, Baron JC, Bourgeat P, Jones G, Faux NG, Ellis KA, Salvado O, Szoeke C, Martins RN, Ames D, Masters CL, Rowe CC (2010b) Larger temporal volume in elderly with high versus low beta-amyloid deposition. Brain 133(11):3349–3358

Chetelat G, Villemagne VL, Villain N, Jones G, Ellis KA, Ames D, Martins RN, Masters CL, Rowe CC (2012) Accelerated cortical atrophy in cognitively normal elderly with high beta-amyloid deposition. Neurology 78(7):477–484

Choi SR, Golding G, Zhuang Z, Zhang W, Lim N, Hefti F, Benedum TE, Kilbourn MR, Skovronsky D, Kung HF (2009) Preclinical properties of 18F-AV-45: a PET agent for Abeta plaques in the brain. J Nucl Med 50(11):1887–1894

Clark CM, Davatzikos C, Borthakur A, Newberg A, Leight S, Lee VM, Trojanowski JQ (2008) Biomarkers for early detection of Alzheimer pathology. Neurosignals 16(1):11–18

Clark CM, Pontecorvo MJ, Beach TG, Bedell BJ, Coleman RE, Doraiswamy PM, Fleisher AS, Reiman EM, Sabbagh MN, Sadowsky CH, Schneider JA, Arora A, Carpenter AP, Flitter ML, Joshi AD, Krautkramer MJ, Lu M, Mintun MA, Skovronsky DM (2012) Cerebral PET with florbetapir compared with neuropathology at autopsy for detection of neuritic amyloid-beta plaques: a prospective cohort study. Lancet Neurol 11(8):669–678

Clark CM, Schneider JA, Bedell BJ, Beach TG, Bilker WB, Mintun MA, Pontecorvo MJ, Hefti F, Carpenter AP, Flitter ML, Krautkramer MJ, Kung HF, Coleman RE, Doraiswamy PM, Fleisher

AS, Sabbagh MN, Sadowsky CH, Reiman EP, Zehntner SP, Skovronsky DM (2011) Use of florbetapir-PET for imaging beta-amyloid pathology. JAMA 305(3):275–283

Cohen AD, McDade E, Christian B, Price J, Mathis C, Klunk W, Handen BL (2018) Early striatal amyloid deposition distinguishes down syndrome and autosomal dominant Alzheimer's disease from late-onset amyloid deposition. Alzheimers Dement 14(6):743–750

Cohen AD, Price JC, Weissfeld LA, James J, Rosario BL, Bi W, Nebes RD, Saxton JA, Snitz BE, Aizenstein HA, Wolk DA, Dekosky ST, Mathis CA, Klunk WE (2009) Basal cerebral metabolism may modulate the cognitive effects of Abeta in mild cognitive impairment: an example of brain reserve. J Neurosci 29(47):14770–14778

Cohen AD, Rabinovici GD, Mathis CA, Jagust WJ, Klunk WE, Ikonomovic MD (2012) Using Pittsburgh compound B for in vivo PET imaging of Fibrillar amyloid-Beta. Adv Pharmacol 64:27–81

Coleman RE (2005) Positron emission tomography diagnosis of Alzheimer's disease. Neuroimaging Clin N Am 15(4):837–846

Cordonnier C (2010) Brain microbleeds. Pract Neurol 10(2):94–100

Cselenyi Z, Jonhagen ME, Forsberg A, Halldin C, Julin P, Schou M, Johnstrom P, Varnas K, Svensson S, Farde L (2012) Clinical validation of 18F-AZD4694, an amyloid-beta-specific PET Radioligand. J Nucl Med 53(3):415–424

Cummings J (2019) The National Institute on Aging-Alzheimer's Association framework on Alzheimer's disease: application to clinical trials. Alzheimers Dement 15(1):172–178

Cummings JL, Vinters HV, Cole GM, Khachaturian ZS (1998) Alzheimer's disease: etiologies, pathophysiology, cognitive reserve, and treatment opportunities. Neurology 51(1):S2–S17; discussion S65–17

Curtis C, Gamez JE, Singh U, Sadowsky CH, Villena T, Sabbagh MN, Beach TG, Duara R, Fleisher AS, Frey KA, Walker Z, Hunjan A, Holmes C, Escovar YM, Vera CX, Agronin ME, Ross J, Bozoki A, Akinola M, Shi J, Vandenberghe R, Ikonomovic MD, Sherwin PF, Grachev ID, Farrar G, Smith AP, Buckley CJ, McLain R, Salloway S (2015) Phase 3 trial of flutemetamol labeled with radioactive fluorine 18 imaging and neuritic plaque density. JAMA Neurol 72(3):287–294

Dang C, Yassi N, Harrington KD, Xia Y, Lim YY, Ames D, Laws SM, Hickey M, Rainey-Smith S, Sohrabi HR, Doecke JD, Fripp J, Salvado O, Snyder PJ, Weinborn M, Villemagne VL, Rowe CC, Masters CL, Maruff P, A. R. Group (2019) Rates of age- and amyloid beta-associated cortical atrophy in older adults with superior memory performance. Alzheimers Dement (Amst) 11:566–575

Davies L, Wolska B, Hilbich C, Multhaup G, Martins R, Simms G, Beyreuther K, Masters CL (1988) A4 amyloid protein deposition and the diagnosis of Alzheimer's disease: prevalence in aged brains determined by immunocytochemistry compared with conventional neuropathologic techniques. Neurology 38(11):1688–1693

de Leon MJ, DeSanti S, Zinkowski R, Mehta PD, Pratico D, Segal S, Rusinek H, Li J, Tsui W, Saint Louis LA, Clark CM, Tarshish C, Li Y, Lair L, Javier E, Rich K, Lesbre P, Mosconi L, Reisberg B, Sadowski M, DeBernadis JF, Kerkman DJ, Hampel H, Wahlund LO, Davies P (2006) Longitudinal CSF and MRI biomarkers improve the diagnosis of mild cognitive impairment. Neurobiol Aging 27(3):394–401

de Leon MJ, Mosconi L, Blennow K, DeSanti S, Zinkowski R, Mehta PD, Pratico D, Tsui W, Saint Louis LA, Sobanska L, Brys M, Li Y, Rich K, Rinne J, Rusinek H (2007) Imaging and CSF studies in the preclinical diagnosis of Alzheimer's disease. Ann N Y Acad Sci 1097:114–145

de Wilde A, van der Flier WM, Pelkmans W, Bouwman F, Verwer J, Groot C, van Buchem MM, Zwan M, Ossenkoppele R, Yaqub M, Kunneman M, Smets EMA, Barkhof F, Lammertsma AA, Stephens A, van Lier E, Biessels GJ, van Berckel BN, Scheltens P (2018) Association of Amyloid Positron Emission Tomography with Changes in diagnosis and patient treatment in an unselected memory clinic cohort: the ABIDE project. JAMA Neurol 75(9):1062–1070

DeCarli C, Villeneuve S, Maillard P, Harvey D, Singh B, Carmichael O, Fletcher E, Olichney J, Farias S, Jagust W, Reed B, Mungas D (2019) Vascular burden score impacts cognition

independent of amyloid PET and MRI measures of Alzheimer's disease and vascular brain injury. J Alzheimers Dis 68(1):187–196

DeKosky ST, Ikonomovic MD, Styren SD, Beckett L, Wisniewski S, Bennett DA, Cochran EJ, Kordower JH, Mufson EJ (2002) Upregulation of choline acetyltransferase activity in hippocampus and frontal cortex of elderly subjects with mild cognitive impairment. Ann Neurol 51(2):145–155

Deshpande A, Mina E, Glabe C, Busciglio J (2006) Different conformations of amyloid beta induce neurotoxicity by distinct mechanisms in human cortical neurons. J Neurosci 26(22):6011–6018

Devanand DP, Jacobs DM, Tang MX, Del Castillo-Castaneda C, Sano M, Marder K, Bell K, Bylsma FW, Brandt J, Albert M, Stern Y (1997) The course of psychopathologic features in mild to moderate Alzheimer disease. Arch Gen Psychiatry 54(3):257–263

Dhollander I, Nelissen N, Van Laere K, Peeters D, Demaerel P, Van Paesschen W, Thijs V, Vandenberghe R (2011) In vivo amyloid imaging in cortical superficial siderosis. J Neurol Neurosurg Psychiatry 82(4):469–471

Dierksen GA, Skehan ME, Khan MA, Jeng J, Nandigam RN, Becker JA, Kumar A, Neal KL, Betensky RA, Frosch MP, Rosand J, Johnson KA, Viswanathan A, Salat DH, Greenberg SM (2010) Spatial relation between microbleeds and amyloid deposits in amyloid angiopathy. Ann Neurol 68(4):545–548

Donaghy PC, Firbank MJ, Thomas AJ, Lloyd J, Petrides G, Barnett N, Olsen K, O'Brien JT (2019) Amyloid imaging and longitudinal clinical progression in dementia with Lewy bodies. Am J Geriatr Psychiatry 28(5):573–577

Doody RS, Thomas RG, Farlow M, Iwatsubo T, Vellas B, Joffe S, Kieburtz K, Raman R, Sun X, Aisen PS, Siemers E, Liu-Seifert H, Mohs R, Alzheimer's Disease Cooperative Study Steering Committee; Solanezumab Study Group (2014) Phase 3 trials of solanezumab for mild-to-moderate Alzheimer's disease. N Engl J Med 370(4):311–321

Doraiswamy PM, Sperling RA, Coleman RE, Johnson KA, Reiman EM, Davis MD, Grundman M, Sabbagh MN, Sadowsky CH, Fleisher AS, Carpenter A, Clark CM, Joshi AD, Mintun MA, Skovronsky DM, Pontecorvo MJ (2012) Amyloid-beta assessed by florbetapir F 18 PET and 18-month cognitive decline: A multicenter study. Neurology 79(16):1636–1644

Dore V, Bullich S, Rowe CC, Bourgeat P, Konate S, Sabri O, Stephens AW, Barthel H, Fripp J, Masters CL, Dinkelborg L, Salvado O, Villemagne VL, De Santi S (2019) Comparison of (18)F-florbetaben quantification results using the standard Centiloid, MR-based, and MR-less CapAIBL((R)) approaches: validation against histopathology. Alzheimers Dement 15(6):807–816

Drago V, Babiloni C, Bartres-Faz D, Caroli A, Bosch B, Hensch T, Didic M, Klafki HW, Pievani M, Jovicich J, Venturi L, Spitzer P, Vecchio F, Schoenknecht P, Wiltfang J, Redolfi A, Forloni G, Blin O, Irving E, Davis C, Hardemark HG, Frisoni GB (2011) Disease tracking markers for Alzheimer's disease at the prodromal (MCI) stage. J Alzheimers Dis 26(Suppl 3):159–199

Driscoll I, Zhou Y, An Y, Sojkova J, Davatzikos C, Kraut MA, Ye W, Ferrucci L, Mathis CA, Klunk WE, Wong DF, Resnick SM (2010) Lack of association between (11)C-PiB and longitudinal brain atrophy in non-demented older individuals. Neurobiol Aging 32(12):2123–2130

Drzezga A (2010) Amyloid-plaque imaging in early and differential diagnosis of dementia. Ann Nucl Med 24(2):55–66

Drzezga A, Becker JA, Van Dijk KR, Sreenivasan A, Talukdar T, Sullivan C, Schultz AP, Sepulcre J, Putcha D, Greve D, Johnson KA, Sperling RA (2011) Neuronal dysfunction and disconnection of cortical hubs in non-demented subjects with elevated amyloid burden. Brain 134(Pt 6):1635–1646

Drzezga A, Grimmer T, Henriksen G, Stangier I, Perneczky R, Diehl-Schmid J, Mathis CA, Klunk WE, Price J, DeKosky S, Wester HJ, Schwaiger M, Kurz A (2008) Imaging of amyloid plaques and cerebral glucose metabolism in semantic dementia and Alzheimer's disease. NeuroImage 39(2):619–633

Drzezga A, Grimmer T, Riemenschneider M, Lautenschlager N, Siebner H, Alexopoulus P, Minoshima S, Schwaiger M, Kurz A (2005) Prediction of individual clinical outcome in MCI by means of genetic assessment and (18)F-FDG PET. J Nucl Med 46(10):1625–1632

Drzezga A, Lautenschlager N, Siebner H, Riemenschneider M, Willoch F, Minoshima S, Schwaiger M, Kurz A (2003) Cerebral metabolic changes accompanying conversion of mild cognitive impairment into Alzheimer's disease: a PET follow-up study. Eur J Nucl Med Mol Imaging 30(8):1104–1113

Dubois B, Feldman HH, Jacova C, Cummings JL, Dekosky ST, Barberger-Gateau P, Delacourte A, Frisoni G, Fox NC, Galasko D, Gauthier S, Hampel H, Jicha GA, Meguro K, O'Brien J, Pasquier F, Robert P, Rossor M, Salloway S, Sarazin M, de Souza LC, Stern Y, Visser PJ, Scheltens P (2010) Revising the definition of Alzheimer's disease: a new lexicon. Lancet Neurol 9(11):1118–1127

Dulamea A, Solomon E (2016) Role of the biomarkers for the diagnosis of Creutzfeldt-Jakob disease. J Med Life 9(2):211–215

Eckert A, Keil U, Marques CA, Bonert A, Frey C, Schussel K, Muller WE (2003) Mitochondrial dysfunction, apoptotic cell death, and Alzheimer's disease. Biochem Pharmacol 66(8):1627–1634

Edison P, Archer HA, Gerhard A, Hinz R, Pavese N, Turkheimer FE, Hammers A, Tai YF, Fox N, Kennedy A, Rossor M, Brooks DJ (2008a) Microglia, amyloid, and cognition in Alzheimer's disease: An [11C](R)PK11195-PET and [11C]PIB-PET study. Neurobiol Dis 32(3):412–419

Edison P, Archer HA, Hinz R, Hammers A, Pavese N, Tai YF, Hotton G, Cutler D, Fox N, Kennedy A, Rossor M, Brooks DJ (2007) Amyloid, hypometabolism, and cognition in Alzheimer disease: an [11C]PIB and [18F]FDG PET study. Neurology 68(7):501–508

Edison P, Rowe CC, Rinne JO, Ng S, Ahmed I, Kemppainen N, Villemagne VL, O'Keefe G, Nagren K, Chaudhury KR, Masters CL, Brooks DJ (2008b) Amyloid load in Parkinson's disease dementia and Lewy body dementia measured with [11C]PIB positron emission tomography. J Neurol Neurosurg Psychiatry 79(12):1331–1338

Egan MF, Kost J, Voss T, Mukai Y, Aisen PS, Cummings JL, Tariot PN, Vellas B, van Dyck CH, Boada M, Zhang Y, Li W, Furtek C, Mahoney E, Harper Mozley L, Mo Y, Sur C, Michelson D (2019) Randomized trial of Verubecestat for prodromal Alzheimer's disease. N Engl J Med 380(15):1408–1420

Ellis KA, Bush AI, Darby D, De Fazio D, Foster J, Hudson P, Lautenschlager NT, Lenzo N, Martins RN, Maruff P, Masters C, Milner A, Pike K, Rowe C, Savage G, Szoeke C, Taddei K, Villemagne V, Woodward M, Ames D (2009) The Australian imaging, biomarkers and lifestyle (AIBL) study of aging: methodology and baseline characteristics of 1112 individuals recruited for a longitudinal study of Alzheimer's disease. Int Psychogeriatr 21(4):672–687

Engler H, Forsberg A, Almkvist O, Blomquist G, Larsson E, Savitcheva I, Wall A, Ringheim A, Langstrom B, Nordberg A (2006) Two-year follow-up of amyloid deposition in patients with Alzheimer's disease. Brain 129(Pt 11):2856–2866

Engler H, Santillo AF, Wang SX, Lindau M, Savitcheva I, Nordberg A, Lannfelt L, Langstrom B, Kilander L (2008) In vivo amyloid imaging with PET in frontotemporal dementia. Eur J Nucl Med Mol Imaging 35(1):100–106

Fagan AM, Holtzman DM (2010) Cerebrospinal fluid biomarkers of Alzheimer's disease. Biomark Med 4(1):51–63

Fagan AM, Mintun MA, Mach RH, Lee SY, Dence CS, Shah AR, Larossa GN, Spinner ML, Klunk WE, Mathis CA, Dekosky ST, Morris JC, Holtzman DM (2006) Inverse relation between in vivo amyloid imaging load and cerebrospinal fluid Abeta(42) in humans. Ann Neurol 59(3):512–519

Fagan AM, Mintun MA, Shah AR, Aldea P, Roe CM, Mach RH, Marcus D, Morris JC, Holtzman DM (2009) Cerebrospinal fluid tau and ptau(181) increase with cortical amyloid deposition in cognitively normal individuals: implications for future clinical trials of Alzheimer's disease. EMBO Mol Med 1(8–9):371–380

Fagan AM, Roe CM, Xiong C, Mintun MA, Morris JC, Holtzman DM (2007) Cerebrospinal fluid tau/beta-amyloid(42) ratio as a prediction of cognitive decline in nondemented older adults. Arch Neurol 64(3):343–349

Fagan AM, Xiong C, Jasielec MS, Bateman RJ, Goate AM, Benzinger TL, Ghetti B, Martins RN, Masters CL, Mayeux R, Ringman JM, Rossor MN, Salloway S, Schofield PR, Sperling RA, Marcus D, Cairns NJ, Buckles VD, Ladenson JH, Morris JC, Holtzman DM, Dominantly

Inherited Alzheimer Network (2014) Longitudinal change in CSF biomarkers in autosomal-dominant Alzheimer's disease. Sci Transl Med 6(226):226ra230

Fandos N, Pérez-Grijalba V, Pesini P, Olmos S, Bossa M, Villemagne VL, Doecke J, Fowler C, Masters CL, Sarasa M (2017) Plasma amyloid β 42/40 ratios as biomarkers for amyloid β cerebral deposition in cognitively normal individuals. Alzheimers Dement (Amst) 8:179–187

Farrar G, Molinuevo JL, Zanette M (2019) Is there a difference in regional read [(18)F]flutemetamol amyloid patterns between end-of-life subjects and those with amnestic mild cognitive impairment? Eur J Nucl Med Mol Imaging 46(6):1299–1308

Farrer LA, Cupples LA, Haines JL, Hyman B, Kukull WA, Mayeux R, Myers RH, Pericak-Vance MA, Risch N, van Duijn CM (1997) Effects of age, sex, and ethnicity on the association between apolipoprotein E genotype and Alzheimer disease. A meta-analysis. APOE and Alzheimer disease meta analysis consortium. JAMA 278(16):1349–1356

Feldman HH, Maia LF, Mackenzie IR, Forster BB, Martzke J, Woolfenden A (2008) Superficial siderosis: a potential diagnostic marker of cerebral amyloid angiopathy in Alzheimer disease. Stroke 39(10):2894–2897

Fleisher AS, Chen K, Liu X, Roontiva A, Thiyyagura P, Ayutyanont N, Joshi AD, Clark CM, Mintun MA, Pontecorvo MJ, Doraiswamy PM, Johnson KA, Skovronsky DM, Reiman EM (2011) Using positron emission tomography and florbetapir F18 to image cortical amyloid in patients with mild cognitive impairment or dementia due to Alzheimer disease. Arch Neurol 68(11):1404–1411

Fletcher E, Filshtein TJ, Harvey D, Renaud A, Mungas D, DeCarli C (2018) Staging of amyloid beta, t-tau, regional atrophy rates, and cognitive change in a nondemented cohort: results of serial mediation analyses. Alzheimers Dement (Amst) 10:382–393

Fodero-Tavoletti MT, Brockschnieder D, Villemagne VL, Martin L, Connor AR, Thiele A, Berndt A, McLean CA, Krause S, Rowe CC, Masters CL, Dinkelborg L, Dyrks T, Cappai R (2012) In vitro characterisation of [18F]–florbetaben, an Aβ imaging radiotracer. Nucl Med Biol 39(7):1042–1048. https://doi.org/10.1016/j.nucmedbio.2012.1003.1001

Fodero-Tavoletti MT, Mulligan RS, Okamura N, Furumoto S, Rowe CC, Kudo Y, Masters CL, Cappai R, Yanai K, Villemagne VL (2009a) In vitro characterisation of BF227 binding to alpha-synuclein/Lewy bodies. Eur J Pharmacol 617(1–3):54–58

Fodero-Tavoletti MT, Okamura N, Furumoto S, Mulligan RS, Connor AR, McLean CA, Cao D, Rigopoulos A, Cartwright GA, O'Keefe G, Gong S, Adlard PA, Barnham KJ, Rowe CC, Masters CL, Kudo Y, Cappai R, Yanai K, Villemagne VL (2011) 18F-THK523: a novel in vivo tau imaging ligand for Alzheimer's disease. Brain 134(Pt 4):1089–1100

Fodero-Tavoletti MT, Rowe CC, McLean CA, Leone L, Li QX, Masters CL, Cappai R, Villemagne VL (2009b) Characterization of PiB binding to white matter in Alzheimer disease and other dementias. J Nucl Med 50(2):198–204

Fodero-Tavoletti MT, Smith DP, McLean CA, Adlard PA, Barnham KJ, Foster LE, Leone L, Perez K, Cortes M, Culvenor JG, Li QX, Laughton KM, Rowe CC, Masters CL, Cappai R, Villemagne VL (2007) In vitro characterization of Pittsburgh compound-B binding to Lewy bodies. J Neurosci 27(39):10365–10371

Formaglio M, Costes N, Seguin J, Tholance Y, Le Bars D, Roullet-Solignac I, Mercier B, Krolak-Salmon P, Vighetto A (2011) In vivo demonstration of amyloid burden in posterior cortical atrophy: a case series with PET and CSF findings. J Neurol 258(10):1841–1851

Forman MS, Mufson EJ, Leurgans S, Pratico D, Joyce S, Leight S, Lee VM, Trojanowski JQ (2007) Cortical biochemistry in MCI and Alzheimer disease: lack of correlation with clinical diagnosis. Neurology 68(10):757–763

Forsberg A, Almkvist O, Engler H, Wall A, Langstrom B, Nordberg A (2010) High PIB retention in Alzheimer's disease is an early event with complex relationship with CSF biomarkers and functional parameters. Curr Alzheimer Res 7(1):56–66

Forsberg A, Engler H, Almkvist O, Blomquist G, Hagman G, Wall A, Ringheim A, Langstrom B, Nordberg A (2008) PET imaging of amyloid deposition in patients with mild cognitive impairment. Neurobiol Aging 29(10):1456–1465

Forster S, Grimmer T, Miederer I, Henriksen G, Yousefi BH, Graner P, Wester HJ, Forstl H, Kurz A, Dickerson BC, Bartenstein P, Drzezga A (2012) Regional expansion of Hypometabolism in Alzheimer's disease follows amyloid deposition with temporal delay. Biol Psychiatry 71(9):792–797

Foster ER, Campbell MC, Burack MA, Hartlein J, Flores HP, Cairns NJ, Hershey T, Perlmutter JS (2010) Amyloid imaging of Lewy body-associated disorders. Mov Disord 25(15):2516–2523

Frisoni GB, Barkhof F, Altomare D, Berkhof J, Boccardi M, Canzoneri E, Collij L, Drzezga A, Farrar G, Garibotto V, Gismondi R, Gispert JD, Jessen F, Kivipelto M, Lopes Alves I, Molinuevo JL, Nordberg A, Payoux P, Ritchie C, Savicheva I, Scheltens P, Schmidt ME, Schott JM, Stephens A, van Berckel B, Vellas B, Walker Z, Raffa N (2019) AMYPAD diagnostic and patient management study: rationale and design. Alzheimers Dement 15(3):388–399

Frisoni GB, Fox NC, Jack CR Jr, Scheltens P, Thompson PM (2010) The clinical use of structural MRI in Alzheimer disease. Nat Rev Neurol 6(2):67–77

Furst AJ, Bigler ED (2016) Amyloid plaques in TBI: incidental finding or precursor for what is to come? Neurology 86(9):798–799

Furst AJ, Rabinovici GD, Rostomian AH, Steed T, Alkalay A, Racine C, Miller BL, Jagust WJ (2010) Cognition, glucose metabolism and amyloid burden in Alzheimer's disease. Neurobiol Aging 33(2):215–225

Furukawa K, Okamura N, Tashiro K, Furumoto S, Tomita N, Yanai K, Kudo Y, Arai H (2011) PET imaging with BF-227 in dementia with Lewy bodies. Alzheimers Dement 7(Suppl 1):S12–S13

Gatson JW, Stebbins C, Mathews D, Harris TS, Madden C, Batjer H, Diaz-Arrastia R, Minei JP (2016) Evidence of increased brain amyloid in severe TBI survivors at 1, 12, and 24 months after injury: report of 2 cases. J Neurosurg 124(6):1646–1653

Gomez-Isla T, West HL, Rebeck GW, Harr SD, Growdon JH, Locascio JJ, Perls TT, Lipsitz LA, Hyman BT (1996) Clinical and pathological correlates of apolipoprotein E epsilon 4 in Alzheimer's disease. Ann Neurol 39(1):62–70

Gomperts SN, Marquie M, Locascio JJ, Bayer S, Johnson KA, Growdon JH (2016) PET Radioligands reveal the basis of dementia in Parkinson's disease and dementia with Lewy bodies. Neurodegener Dis 16(1–2):118–124

Gomperts SN, Rentz DM, Moran E, Becker JA, Locascio JJ, Klunk WE, Mathis CA, Elmaleh DR, Shoup T, Fischman AJ, Hyman BT, Growdon JH, Johnson KA (2008) Imaging amyloid deposition in Lewy body diseases. Neurology 71(12):903–910

Gonneaud J, Arenaza-Urquijo EM, Mezenge F, Landeau B, Gaubert M, Bejanin A, de Flores R, Wirth M, Tomadesso C, Poisnel G, Abbas A, Desgranges B, Chetelat G (2017) Increased florbetapir binding in the temporal neocortex from age 20 to 60 years. Neurology 89(24):2438–2446

Grimmer T, Riemenschneider M, Forstl H, Henriksen G, Klunk WE, Mathis CA, Shiga T, Wester HJ, Kurz A, Drzezga A (2009) Beta amyloid in Alzheimer's disease: increased deposition in brain is reflected in reduced concentration in cerebrospinal fluid. Biol Psychiatry 65(11):927–934

Grimmer T, Tholen S, Yousefi BH, Alexopoulos P, Forschler A, Forstl H, Henriksen G, Klunk WE, Mathis CA, Perneczky R, Sorg C, Kurz A, Drzezga A (2010) Progression of cerebral amyloid load is associated with the apolipoprotein E epsilon4 genotype in Alzheimer's disease. Biol Psychiatry 68(10):879–884

Gurol ME, Dierksen G, Betensky R, Gidicsin C, Halpin A, Becker A, Carmasin J, Ayres A, Schwab K, Viswanathan A, Salat D, Rosand J, Johnson KA, Greenberg SM (2012) Predicting sites of new hemorrhage with amyloid imaging in cerebral amyloid angiopathy. Neurology 79(4):320–326

Hagens MHJ, Golla SSV, Janssen B, Vugts DJ, Beaino W, Windhorst AD, O'Brien-Brown J, Kassiou M, Schuit RC, Schwarte LA, de Vries HE, Killestein J, Barkhof F, van Berckel BNM, Lammertsma AA (2020) The P2X7 receptor tracer [(11)C]SMW139 as an in vivo marker of neuroinflammation in multiple sclerosis: a first-in man study. Eur J Nucl Med Mol Imaging 47(2):379–389

Halliday G, Hely M, Reid W, Morris J (2008) The progression of pathology in longitudinally followed patients with Parkinson's disease. Acta Neuropathol 115(4):409–415

Hampel H, Blennow K, Shaw LM, Hoessler YC, Zetterberg H, Trojanowski JQ (2010) Total and phosphorylated tau protein as biological markers of Alzheimer's disease. Exp Gerontol 45(1):30–40

Hanseeuw BJ, Betensky RA, Schultz AP, Papp KV, Mormino EC, Sepulcre J, Bark JS, Cosio DM, LaPoint M, Chhatwal JP, Rentz DM, Sperling RA, Johnson KA (2017) Fluorodeoxyglucose metabolism associated with tau-amyloid interaction predicts memory decline. Ann Neurol 81(4):583–596

Hansson O, Zetterberg H, Buchhave P, Andreasson U, Londos E, Minthon L, Blennow K (2007) Prediction of Alzheimer's disease using the CSF Abeta42/Abeta40 ratio in patients with mild cognitive impairment. Dement Geriatr Cogn Disord 23(5):316–320

Hardy J (1997) Amyloid, the presenilins and Alzheimer's disease. Trends Neurosci 20(4):154–159

Herholz K (1995) FDG PET and differential diagnosis of dementia. Alzheimer Dis Assoc Disord 9(1):6–16

Hill AF, Joiner S, Wadsworth JD, Sidle KC, Bell JE, Budka H, Ironside JW, Collinge J (2003) Molecular classification of sporadic Creutzfeldt-Jakob disease. Brain 126(Pt 6):1333–1346

Hodges JR, Patterson K (2007) Semantic dementia: a unique clinicopathological syndrome. Lancet Neurol 6(11):1004–1014

Hu X, Teunissen CE, Spottke A, Heneka MT, Duzel E, Peters O, Li S, Priller J, Buerger K, Teipel S, Laske C, Verfaillie SCJ, Barkhof F, Coll-Padros N, Rami L, Molinuevo JL, van der Flier WM, Jessen F (2019) Smaller medial temporal lobe volumes in individuals with subjective cognitive decline and biomarker evidence of Alzheimer's disease-data from three memory clinic studies. Alzheimers Dement 15(2):185–193

Hyman BT (2011) Amyloid-dependent and amyloid-independent stages of Alzheimer disease. Arch Neurol 68(8):1062–1064

Ikonomovic MD, Abrahamson EE, Isanski BA, Wuu J, Mufson EJ, DeKosky ST (2007) Superior frontal cortex cholinergic axon density in mild cognitive impairment and early Alzheimer disease. Arch Neurol 64(9):1312–1317

Ikonomovic MD, Abrahamson EE, Price JC, Hamilton RL, Mathis CA, Paljug WR, Debnath ML, Cohen AD, Mizukami K, Dekosky ST, Lopez OL, Klunk WE (2012) Early AD pathology in a [C-11]PiB-negative case: a PiB-amyloid imaging, biochemical, and immunohistochemical study. Acta Neuropathol 123(3):433–447

Ikonomovic MD, Klunk WE, Abrahamson EE, Mathis CA, Price JC, Tsopelas ND, Lopresti BJ, Ziolko S, Bi W, Paljug WR, Debnath ML, Hope CE, Isanski BA, Hamilton RL, DeKosky ST (2008) Post-mortem correlates of in vivo PiB-PET amyloid imaging in a typical case of Alzheimer's disease. Brain 131(Pt 6):1630–1645

Ikonomovic MD, Klunk WE, Abrahamson EE, Wuu J, Mathis CA, Scheff SW, Mufson EJ, DeKosky ST (2011) Precuneus amyloid burden is associated with reduced cholinergic activity in Alzheimer disease. Neurology 77(1):39–47

Inayathullah M, Teplow DB (2011) Structural dynamics of the DeltaE22 (Osaka) familial Alzheimer's disease-linked amyloid beta-protein. Amyloid 18(3):98–107

Isacson O, Seo H, Lin L, Albeck D, Granholm AC (2002) Alzheimer's disease and Down's syndrome: roles of APP, trophic factors and ACh. Trends Neurosci 25(2):79–84

Jack CR Jr, Bennett DA, Blennow K, Carrillo MC, Dunn B, Haeberlein SB, Holtzman DM, Jagust W, Jessen F, Karlawish J, Liu E, Molinuevo JL, Montine T, Phelps C, Rankin KP, Rowe CC, Scheltens P, Siemers E, Snyder HM, Sperling R, Contributors (2018) NIA-AA research framework: toward a biological definition of Alzheimer's disease. Alzheimers Dement 14(4):535–562

Jack CR Jr, Bennett DA, Blennow K, Carrillo MC, Feldman HH, Frisoni GB, Hampel H, Jagust WJ, Johnson KA, Knopman DS, Petersen RC, Scheltens P, Sperling RA, Dubois B (2016) A/T/N: An unbiased descriptive classification scheme for Alzheimer disease biomarkers. Neurology 87(5):539–547

Jack CR Jr, Knopman DS, Jagust WJ, Shaw LM, Aisen PS, Weiner MW, Petersen RC, Trojanowski JQ (2010) Hypothetical model of dynamic biomarkers of the Alzheimer's pathological cascade. Lancet Neurol 9(1):119–128

Jack CR Jr, Knopman DS, Weigand SD, Wiste HJ, Vemuri P, Lowe V, Kantarci K, Gunter JL, Senjem ML, Ivnik RJ, Roberts RO, Rocca WA, Boeve BF, Petersen RC (2012) An operational approach to National Institute on Aging-Alzheimer's Association criteria for preclinical Alzheimer disease. Ann Neurol 71(6):765–775

Jack CR Jr, Lowe VJ, Senjem ML, Weigand SD, Kemp BJ, Shiung MM, Knopman DS, Boeve BF, Klunk WE, Mathis CA, Petersen RC (2008a) 11C PiB and structural MRI provide complementary information in imaging of Alzheimer's disease and amnestic mild cognitive impairment. Brain 131(Pt 3):665–680

Jack CR Jr, Lowe VJ, Weigand SD, Wiste HJ, Senjem ML, Knopman DS, Shiung MM, Gunter JL, Boeve BF, Kemp BJ, Weiner M, Petersen RC (2009) Serial PIB and MRI in normal, mild cognitive impairment and Alzheimer's disease: implications for sequence of pathological events in Alzheimer's disease. Brain 132(Pt 5):1355–1365

Jack CR Jr, Weigand SD, Shiung MM, Przybelski SA, O'Brien PC, Gunter JL, Knopman DS, Boeve BF, Smith GE, Petersen RC (2008b) Atrophy rates accelerate in amnestic mild cognitive impairment. Neurology 70(19 Pt 2):1740–1752

Jack CR Jr, Wiste HJ, Lesnick TG, Weigand SD, Knopman DS, Vemuri P, Pankratz VS, Senjem ML, Gunter JL, Mielke MM, Lowe VJ, Boeve BF, Petersen RC (2013) Brain beta-amyloid load approaches a plateau. Neurology 80(10):890–896

Jack CR Jr, Wiste HJ, Weigand SD, Rocca WA, Knopman DS, Mielke MM, Lowe VJ, Senjem ML, Gunter JL, Preboske GM, Pankratz VS, Vemuri P, Petersen RC (2014) Age-specific population frequencies of cerebral beta-amyloidosis and neurodegeneration among people with normal cognitive function aged 50-89 years: a cross-sectional study. Lancet Neurol 13(10):997–1005

Jagust W (2009) Mapping brain beta-amyloid. Curr Opin Neurol 22(4):356–361

Jagust W, Reed B, Mungas D, Ellis W, Decarli C (2007) What does fluorodeoxyglucose PET imaging add to a clinical diagnosis of dementia? Neurology 69(9):871–877

Jagust WJ (2011) Amyloid imaging: liberal or conservative? Let the data decide. Arch Neurol 68(11):1377–1378

Jellinger, K. (1990). Morphology of Alzheimer disease and related disorders. Alzheimer disease: epidemiology, neuropathology, neurochemistry, and clinics. K. Maurer, P. Riederer and H. Beckmann. Berlin, Springer-Verlag: 61-77

Jellinger KA (2010) Con: can neuropathology really confirm the exact diagnosis? Alzheimers Res Ther 2(2):11

Jellinger KA, Attems J (2005) Prevalence and pathogenic role of cerebrovascular lesions in Alzheimer disease. J Neurol Sci 229–230:37–41

Jellinger KA, Bancher C (1998) Neuropathology of Alzheimer's disease: a critical update. J Neural Transm Suppl 54:77–95

Jessen F, Wiese B, Bachmann C, Eifflaender-Gorfer S, Haller F, Kolsch H, Luck T, Mosch E, van den Bussche H, Wagner M, Wollny A, Zimmermann T, Pentzek M, Riedel-Heller SG, Romberg HP, Weyerer S, Kaduszkiewicz H, Maier W, Bickel H, German Study on Aging, Cognition and Dementia in Primary Care Patients Study Group (2010) Prediction of dementia by subjective memory impairment: effects of severity and temporal association with cognitive impairment. Arch Gen Psychiatry 67(4):414–422

Johansson A, Savitcheva I, Forsberg A, Engler H, Langstrom B, Nordberg A, Askmark H (2008) [(11)C]-PIB imaging in patients with Parkinson's disease: preliminary results. Parkinsonism Relat Disord 14(4):345–347

Johnson AE, Jeppsson F, Sandell J, Wensbo D, Neelissen JA, Jureus A, Strom P, Norman H, Farde L, Svensson SP (2009) AZD2184: a radioligand for sensitive detection of beta-amyloid deposits. J Neurochem 108(5):1177–1186

Johnson KA (2006) Amyloid imaging of Alzheimer's disease using Pittsburgh compound B. Curr Neurol Neurosci Rep 6(6):496–503

Johnson KA, Gregas M, Becker JA, Kinnecom C, Salat DH, Moran EK, Smith EE, Rosand J, Rentz DM, Klunk WE, Mathis CA, Price JC, Dekosky ST, Fischman AJ, Greenberg SM (2007) Imaging of amyloid burden and distribution in cerebral amyloid angiopathy. Ann Neurol 62(3):229–234

Johnson KA, Minoshima S, Bohnen NI, Donohoe KJ, Foster NL, Herscovitch P, Karlawish JH, Rowe CC, Carrillo MC, Hartley DM, Hedrick S, Pappas V, Thies WH (2013) Appropriate use criteria for amyloid PET: a report of the Amyloid Imaging Task Force, the Society of Nuclear Medicine and Molecular Imaging, and the Alzheimer's Association. Alzheimers Dement 9(1):e1–e16

Johnson N, Davis T, Bosanquet N (2000) The epidemic of Alzheimer's disease. How can we manage the costs? PharmacoEconomics 18(3):215–223

Josephs KA, Holton JL, Rossor MN, Godbolt AK, Ozawa T, Strand K, Khan N, Al-Sarraj S, Revesz T (2004) Frontotemporal lobar degeneration and ubiquitin immunohistochemistry. Neuropathol Appl Neurobiol 30(4):369–373

Josephs KA, Whitwell JL, Ahmed Z, Shiung MM, Weigand SD, Knopman DS, Boeve BF, Parisi JE, Petersen RC, Dickson DW, Jack CR Jr (2008) Beta-amyloid burden is not associated with rates of brain atrophy. Ann Neurol 63(2):204–212

Jureus A, Swahn BM, Sandell J, Jeppsson F, Johnson AE, Johnstrom P, Neelissen JA, Sunnemark D, Farde L, Svensson SP (2010) Characterization of AZD4694, a novel fluorinated Abeta plaque neuroimaging PET radioligand. J Neurochem 114(3):784–794

Kadir A, Marutle A, Gonzalez D, Scholl M, Almkvist O, Mousavi M, Mustafiz T, Darreh-Shori T, Nennesmo I, Nordberg A (2011) Positron emission tomography imaging and clinical progression in relation to molecular pathology in the first Pittsburgh compound B positron emission tomography patient with Alzheimer's disease. Brain 134(Pt 1):301–317

Kalaitzakis ME, Walls AJ, Pearce RK, Gentleman SM (2011) Striatal Abeta peptide deposition mirrors dementia and differentiates DLB and PDD from other parkinsonian syndromes. Neurobiol Dis 41(2):377–384

Kambe T, Motoi Y, Ishii K, Hattori N (2010) Posterior cortical atrophy with [11C] Pittsburgh compound B accumulation in the primary visual cortex. J Neurol 257(3):469–471

Kantarci K, Lowe VJ, Chen Q, Przybelski SA, Lesnick TG, Schwarz CG, Senjem ML, Gunter JL, Jack CR Jr, Graff-Radford J, Jones DT, Knopman DS, Graff-Radford N, Ferman TJ, Parisi JE, Dickson DW, Petersen RC, Boeve BF, Murray ME (2020) Beta-amyloid PET and neuropathology in dementia with Lewy bodies. Neurology 94(3):e282–e291

Karran E, Mercken M, De Strooper B (2011) The amyloid cascade hypothesis for Alzheimer's disease: an appraisal for the development of therapeutics. Nat Rev Drug Discov 10(9):698–712

Kemppainen NM, Aalto S, Karrasch M, Nagren K, Savisto N, Oikonen V, Viitanen M, Parkkola R, Rinne JO (2008) Cognitive reserve hypothesis: Pittsburgh compound B and fluorodeoxyglucose positron emission tomography in relation to education in mild Alzheimer's disease. Ann Neurol 63(1):112–118

Kemppainen NM, Aalto S, Wilson IA, Nagren K, Helin S, Bruck A, Oikonen V, Kailajarvi M, Scheinin M, Viitanen M, Parkkola R, Rinne JO (2007) PET amyloid ligand [11C]PIB uptake is increased in mild cognitive impairment. Neurology 68(19):1603–1606

Kennedy AM, Frackowiak RS, Newman SK, Bloomfield P, Seaward J, Roques P, Lewington G, Cunningham VJ, Rossor MN (1995) Deficits in cerebral glucose metabolism demonstrated by positron emission tomography in individuals at risk of familial Alzheimer's disease. Neurosci Lett 186(1):17–20

Kepe V, Bordelon Y, Boxer A, Huang SC, Liu J, Thiede FC, Mazziotta JC, Mendez MF, Donoghue N, Small GW, Barrio JR (2013) PET imaging of neuropathology in tauopathies: progressive supranuclear palsy. J Alzheimers Dis 36(1):145–153

Khachaturian ZS (1985) Diagnosis of Alzheimer's disease. Arch Neurol 42(11):1097–1105

Kikuchi A, Takeda A, Okamura N, Tashiro M, Hasegawa T, Furumoto S, Kobayashi M, Sugeno N, Baba T, Miki Y, Mori F, Wakabayashi K, Funaki Y, Iwata R, Takahashi S, Fukuda H, Arai H, Kudo Y, Yanai K, Itoyama Y (2010) In vivo visualization of alpha-synuclein deposition by carbon-11-labelled 2-[2-(2-dimethylaminothiazol-5-yl)ethenyl]-6-[2-(fluoro)ethoxy]benzoxazole positron emission tomography in multiple system atrophy. Brain 133(Pt 6):1772–1778

Kim MJ, Shrestha SS, Cortes M, Singh P, Morse C, Liow JS, Gladding RL, Brouwer C, Henry K, Gallagher E, Tye GL, Zoghbi SS, Fujita M, Pike VW, Innis RB (2018) Evaluation of two potent

and selective PET Radioligands to image COX-1 and COX-2 in rhesus monkeys. J Nucl Med 59(12):1907–1912

Klunk W, Cohen AD, Bi W, Weissfeld L, Aizenstein H, McDade E, Mountz J, Nebes R, Saxton J, Snitz B, Lopez O, Price J, Mathis C (2012) Why we need two cutoffs for amyloid imaging: early versus Alzheimer's-like amyloid-positivity. Alzheimers Dement 8(4):P453–P454

Klunk WE (2011) Amyloid imaging as a biomarker for cerebral beta-amyloidosis and risk prediction for Alzheimer dementia. Neurobiol Aging 32(Suppl 1):S20–S36

Klunk WE, Engler H, Nordberg A, Wang Y, Blomqvist G, Holt DP, Bergstrom M, Savitcheva I, Huang GF, Estrada S, Ausen B, Debnath ML, Barletta J, Price JC, Sandell J, Lopresti BJ, Wall A, Koivisto P, Antoni G, Mathis CA, Langstrom B (2004) Imaging brain amyloid in Alzheimer's disease with Pittsburgh compound-B. Ann Neurol 55(3):306–319

Klunk WE, Koeppe RA, Price JC, Benzinger TL, Devous MD Sr, Jagust WJ, Johnson KA, Mathis CA, Minhas D, Pontecorvo MJ, Rowe CC, Skovronsky DM, Mintun MA (2015) The Centiloid Project: standardizing quantitative amyloid plaque estimation by PET. Alzheimers Dement 11(1):1–15. e11–14

Klunk WE, Lopresti BJ, Ikonomovic MD, Lefterov IM, Koldamova RP, Abrahamson EE, Debnath ML, Holt DP, Huang GF, Shao L, DeKosky ST, Price JC, Mathis CA (2005) Binding of the positron emission tomography tracer Pittsburgh compound-B reflects the amount of amyloid-beta in Alzheimer's disease brain but not in transgenic mouse brain. J Neurosci 25(46):10598–10606

Klunk WE, Price JC, Mathis CA, Tsopelas ND, Lopresti BJ, Ziolko SK, Bi W, Hoge JA, Cohen AD, Ikonomovic MD, Saxton JA, Snitz BE, Pollen DA, Moonis M, Lippa CF, Swearer JM, Johnson KA, Rentz DM, Fischman AJ, Aizenstein HJ, DeKosky ST (2007) Amyloid deposition begins in the striatum of presenilin-1 mutation carriers from two unrelated pedigrees. J Neurosci 27(23):6174–6184

Klunk WE, Wang Y, Huang GF, Debnath ML, Holt DP, Mathis CA (2001) Uncharged thioflavin-T derivatives bind to amyloid-beta protein with high affinity and readily enter the brain. Life Sci 69(13):1471–1484

Klunk WE, Wang Y, Huang GF, Debnath ML, Holt DP, Shao L, Hamilton RL, Ikonomovic MD, DeKosky ST, Mathis CA (2003) The binding of 2-(4′-methylaminophenyl)benzothiazole to postmortem brain homogenates is dominated by the amyloid component. J Neurosci 23(6):2086–2092

Knudsen KA, Rosand J, Karluk D, Greenberg SM (2001) Clinical diagnosis of cerebral amyloid angiopathy: validation of the Boston criteria. Neurology 56(4):537–539

Koeppe RA, Gilman S, Junck L, Wernette K, Frey KA (2008) Differentiating Alzheimer's disease from dementia with Lewy bodies and Parkinson's disease with (+)-[11C]dihydrotetrabenazine positron emission tomography. Alzheimers Dement 4(1 Suppl 1):S67–S76

Koivunen J, Pirttila T, Kemppainen N, Aalto S, Herukka SK, Jauhianen AM, Hanninen T, Hallikainen M, Nagren K, Rinne JO, Soininen H (2008a) PET amyloid ligand [C]PIB uptake and cerebrospinal fluid beta-amyloid in mild cognitive impairment. Dement Geriatr Cogn Disord 26(4):378–383

Koivunen J, Verkkoniemi A, Aalto S, Paetau A, Ahonen JP, Viitanen M, Nagren K, Rokka J, Haaparanta M, Kalimo H, Rinne JO (2008b) PET amyloid ligand [11C]PIB uptake shows predominantly striatal increase in variant Alzheimer's disease. Brain 131(Pt 7):1845–1853

Kreisl WC, Henter ID, Innis RB (2018) Imaging translocator protein as a biomarker of Neuroinflammation in dementia. Adv Pharmacol 82:163–185

Kreisl WC, Jenko KJ, Hines CS, Lyoo CH, Corona W, Morse CL, Zoghbi SS, Hyde T, Kleinman JE, Pike VW, McMahon FJ, Innis RB, Biomarkers Consortium PET Radioligand Project Team (2013) A genetic polymorphism for translocator protein 18 kDa affects both in vitro and in vivo radioligand binding in human brain to this putative biomarker of neuroinflammation. J Cereb Blood Flow Metab 33(1):53–58

Kuczynski B, Reed B, Mungas D, Weiner M, Chui HC, Jagust W (2008) Cognitive and anatomic contributions of metabolic decline in Alzheimer disease and cerebrovascular disease. Arch Neurol 65(5):650–655

Kudo Y (2006) Development of amyloid imaging PET probes for an early diagnosis of Alzheimer's disease. Minim Invasive Ther Allied Technol 15(4):209–213

Kudo Y, Okamura N, Furumoto S, Tashiro M, Furukawa K, Maruyama M, Itoh M, Iwata R, Yanai K, Arai H (2007) 2-(2-[2-Dimethylaminothiazol-5-yl]Ethenyl)-6- (2-[Fluoro]Ethoxy) Benzoxazole: a novel PET agent for in vivo detection of dense amyloid plaques in Alzheimer's disease patients. J Nucl Med 48(4):553–561

La Joie R, Ayakta N, Borys E, Boxer AL, deCarli C, Dore V, Grinberg LT, Huang EJ, Jack JCR, Jin LW, Klunk WE, Ikonomovic M, Lockhart SM, Lowe VL, Masters CL, Miller BL, Mungas DM, Murray ME, O'Neil J, Olichney JM, Petersen RC, Reed BR, Rowe CC, Seeley WW, Vemuri P, Villemagne VL, Jagust WJ, Rabinovici GD (2018). Multi-site study of PiB-PET imaging using the Centiloid method: relationships to pathological measures of β-amyloid pathology. 12th human amyloid imaging. Miami Beach, FL. 12: 148–149

La Joie R, Visani AV, Baker SL, Brown JA, Bourakova V, Cha J, Chaudhary K, Edwards L, Iaccarino L, Janabi M, Lesman-Segev OH, Miller ZA, Perry DC, O'Neil JP, Pham J, Rojas JC, Rosen HJ, Seeley WW, Tsai RM, Miller BL, Jagust WJ, Rabinovici GD (2020) Prospective longitudinal atrophy in Alzheimer's disease correlates with the intensity and topography of baseline tau-PET. Sci Transl Med 12(524):eaau5732

Landau SM, Fero A, Baker SL, Koeppe R, Mintun M, Chen K, Reiman EM, Jagust WJ (2015) Measurement of longitudinal beta-amyloid change with 18F-Florbetapir PET and standardized uptake value ratios. J Nucl Med 56(4):567–574

Landau SM, Harvey D, Madison CM, Koeppe RA, Reiman EM, Foster NL, Weiner MW, Jagust WJ (2009) Associations between cognitive, functional, and FDG-PET measures of decline in AD and MCI. Neurobiol Aging 32(7):1207–1218

Landau SM, Horng A, Jagust WJ, Alzheimer's Disease Neuroimaging Initiative (2018) Memory decline accompanies subthreshold amyloid accumulation. Neurology 90(17):e1452–e1460

Landau SM, Lu M, Joshi AD, Pontecorvo M, Mintun MA, Trojanowski JQ, Shaw LM, Jagust WJ, Alzheimer's Disease Neuroimaging (2013) Comparing positron emission tomography imaging and cerebrospinal fluid measurements of beta-amyloid. Ann Neurol 74(6):826–836

Landau SM, Villemagne VL (2020) Can amyloid PET differentiate "pure" LBD from AD with or without LBD copathology? Neurology 94(3):103–104

Larson EB, Edwards JK, O'Meara E, Nochlin D, Sumi SM (1996) Neuropathologic diagnostic outcomes from a cohort of outpatients with suspected dementia. J Gerontol A Biol Sci Med Sci 51(suppl 6):M313–M318

Laruelle M, Slifstein M, Huang Y (2003) Relationships between radiotracer properties and image quality in molecular imaging of the brain with positron emission tomography. Mol Imaging Biol 5(6):363–375

Leinonen V, Alafuzoff I, Aalto S, Suotunen T, Savolainen S, Nagren K, Tapiola T, Pirttila T, Rinne J, Jaaskelainen JE, Soininen H, Rinne JO (2008a) Assessment of β-amyloid in a frontal cortical brain biopsy specimen and by positron emission tomography with carbon 11-labeled Pittsburgh compound B. Arch Neurol 65(10):1304–1309

Leinonen V, Alafuzoff I, Aalto S, Suotunen T, Savolainen S, Nagren K, Tapiola T, Pirttila T, Rinne J, Jaaskelainen JE, Soininen H, Rinne JO (2008b) Assessment of beta-amyloid in a frontal cortical brain biopsy specimen and by positron emission tomography with carbon 11-labeled Pittsburgh compound B. Arch Neurol 65(10):1304–1309

Leuner K, Hauptmann S, Abdel-Kader R, Scherping I, Keil U, Strosznajder JB, Eckert A, Muller WE (2007) Mitochondrial dysfunction: the first domino in brain aging and Alzheimer's disease? Antioxid Redox Signal 9(10):1659–1675

Leuzy A, Savitcheva I, Chiotis K, Lilja J, Andersen P, Bogdanovic N, Jelic V, Nordberg A (2019) Clinical impact of [(18)F]flutemetamol PET among memory clinic patients with an unclear diagnosis. Eur J Nucl Med Mol Imaging 46(6):1276–1286

LeVine H 3rd (1999) Quantification of beta-sheet amyloid fibril structures with thioflavin T. Methods Enzymol 309:274–284

Levine H 3rd, Walker LC (2008) Molecular polymorphism of Abeta in Alzheimer's disease. Neurobiol Aging 31(4):542–548

Levine H 3rd, Walker LC (2010) Molecular polymorphism of Abeta in Alzheimer's disease. Neurobiol Aging 31(4):542–548

Leyton CE, Villemagne VL, Savage S, Pike KE, Ballard KJ, Piguet O, Burrell JR, Rowe CC, Hodges JR (2011) Subtypes of progressive aphasia: application of the international consensus criteria and validation using {beta}-amyloid imaging. Brain 134(Pt 10):3030–3043

Li QX, Villemagne VL, Doecke JD, Rembach A, Sarros S, Varghese S, McGlade A, Laughton KM, Pertile KK, Fowler CJ, Rumble RL, Trounson BO, Taddei K, Rainey-Smith SR, Laws SM, Robertson JS, Evered LA, Silbert B, Ellis KA, Rowe CC, Macaulay SL, Darby D, Martins RN, Ames D, Masters CL, Collins S, A. R. Group (2015) Alzheimer's disease normative cerebrospinal fluid biomarkers validated in PET amyloid-beta characterized subjects from the Australian imaging, biomarkers and lifestyle (AIBL) study. J Alzheimers Dis 48(1):175–187

Liberski PP (2004) Amyloid plaques in transmissible spongiform encephalopathies (prion diseases). Folia Neuropathol 42(Suppl B):109–119

Lin KS, Debnath ML, Mathis CA, Klunk WE (2009) Synthesis and beta-amyloid binding properties of rhenium 2-phenylbenzothiazoles. Bioorg Med Chem Lett 19(8):2258–2262

Lister-James J, Pontecorvo MJ, Clark C, Joshi AD, Mintun MA, Zhang W, Lim N, Zhuang Z, Golding G, Choi SR, Benedum TE, Kennedy P, Hefti F, Carpenter AP, Kung HF, Skovronsky DM (2011) Florbetapir f-18: a histopathologically validated Beta-amyloid positron emission tomography imaging agent. Semin Nucl Med 41(4):300–304

Liu E, Schmidt ME, Margolin R, Sperling R, Koeppe R, Mason NS, Klunk WE, Mathis CA, Salloway S, Fox NC, Hill DL, Les AS, Collins P, Gregg KM, Di J, Lu Y, Tudor IC, Wyman BT, Booth K, Broome S, Yuen E, Grundman M, Brashear HR, Bapineuzumab 301 and 302 Clinical Trial Investigators (2015) Amyloid-beta 11C-PiB-PET imaging results from 2 randomized bapineuzumab phase 3 AD trials. Neurology 85(8):692–700

LoBue C, Munro C, Schaffert J, Didehbani N, Hart J, Batjer H, Cullum CM (2019) Traumatic brain injury and risk of Long-term brain changes, accumulation of pathological markers, and developing dementia: a review. J Alzheimers Dis 70(3):629–654

Lockhart A, Lamb JR, Osredkar T, Sue LI, Joyce JN, Ye L, Libri V, Leppert D, Beach TG (2007) PIB is a non-specific imaging marker of amyloid-beta (Abeta) peptide-related cerebral amyloidosis. Brain 130(Pt 10):2607–2615

Lockhart A, Ye L, Judd DB, Merritt AT, Lowe PN, Morgenstern JL, Hong G, Gee AD, Brown J (2005) Evidence for the presence of three distinct binding sites for the thioflavin T class of Alzheimer's disease PET imaging agents on beta-amyloid peptide fibrils. J Biol Chem 280(9):7677–7684

Long JM, Holtzman DM (2019) Alzheimer disease: An update on pathobiology and treatment strategies. Cell 179(2):312–339

Lopresti BJ, Klunk WE, Mathis CA, Hoge JA, Ziolko SK, Lu X, Meltzer CC, Schimmel K, Tsopelas ND, DeKosky ST, Price JC (2005) Simplified quantification of Pittsburgh compound B amyloid imaging PET studies: a comparative analysis. J Nucl Med 46(12):1959–1972

Lowe VJ, Kemp BJ, Jack CR Jr, Senjem M, Weigand S, Shiung M, Smith G, Knopman D, Boeve B, Mullan B, Petersen RC (2009) Comparison of 18F-FDG and PiB PET in cognitive impairment. J Nucl Med 50(6):878–886

Lowe VJ, Lundt E, Knopman D, Senjem ML, Gunter JL, Schwarz CG, Kemp BJ, Jack CR Jr, Petersen RC (2017) Comparison of [(18)F]Flutemetamol and [(11)C]Pittsburgh compound-B in cognitively normal young, cognitively normal elderly, and Alzheimer's disease dementia individuals. Neuroimage Clin 16:295–302

Mackenzie IR, Foti D, Woulfe J, Hurwitz TA (2008) Atypical frontotemporal lobar degeneration with ubiquitin-positive, TDP-43-negative neuronal inclusions. Brain 131(Pt 5):1282–1293

Maeda J, Ji B, Irie T, Tomiyama T, Maruyama M, Okauchi T, Staufenbiel M, Iwata N, Ono M, Saido TC, Suzuki K, Mori H, Higuchi M, Suhara T (2007) Longitudinal, quantitative assessment of amyloid, neuroinflammation, and anti-amyloid treatment in a living mouse model of Alzheimer's disease enabled by positron emission tomography. J Neurosci 27(41):10957–10968

Maetzler W, Liepelt I, Reimold M, Reischl G, Solbach C, Becker C, Schulte C, Leyhe T, Keller S, Melms A, Gasser T, Berg D (2009) Cortical PIB binding in Lewy body disease is associated with Alzheimer-like characteristics. Neurobiol Dis 34(1):107–112

Maetzler W, Reimold M, Liepelt I, Solbach C, Leyhe T, Schweitzer K, Eschweiler GW, Mittelbronn M, Gaenslen A, Uebele M, Reischl G, Gasser T, Machulla HJ, Bares R, Berg D (2008) [11C]PIB binding in Parkinson's disease dementia. NeuroImage 39(3):1027–1033

Maezawa I, Hong HS, Liu R, Wu CY, Cheng RH, Kung MP, Kung HF, Lam KS, Oddo S, Laferla FM, Jin LW (2008) Congo red and thioflavin-T analogs detect Abeta oligomers. J Neurochem 104(2):457–468

Majocha RE, Reno JM, Friedland RP, Van Haight C, Lyle LR, Marotta CA (1992) Development of a monoclonal antibody specific for ß/A4 amyloid in Alzheimer's disease brain for application to in vivo imaging of amyloid angiopathy. J Nucl Med 33(12):2184–2189

Malkki H (2014) Traumatic brain injury: PET imaging detects amyloid deposits after TBI. Nat Rev Neurol 10(1):3

Manca C, Hopes L, Kearney-Schwartz A, Roch V, Karcher G, Baumann C, Marie PY, Malaplate-Armand C, Jonveaux TR, Verger A (2019) Assessment of 18F-Florbetaben amyloid PET imaging in patients with suspected Alzheimer's disease and isolated increase in cerebrospinal fluid tau proteins. J Alzheimers Dis 68(3):1061–1069

Marchant NL, Reed BR, Decarli CS, Madison CM, Weiner MW, Chui HC, Jagust WJ (2011) Cerebrovascular disease, beta-amyloid, and cognition in aging. Neurobiol Aging 33(5):1006.e25-36

Maruyama M, Maeda J, Ji B, Zhang MY, Okauchi T, Ono M, Hattori S, Trojanoswki JQ, Lee VM, Fukumura T, Higuchi M, Suhara T (2009) In-vivo optical and PET detections of fibrillar tau lesions in a mouse model of tauopathies. Alzheimers Dement 55(4, Supplement 1):P209–P210. [abstract]

Mashima K, Ito D, Kameyama M, Osada T, Tabuchi H, Nihei Y, Yoshizaki T, Noguchi E, Tanikawa M, Iizuka T, Date Y, Ogata Y, Nakahara T, Iwabuchi Y, Jinzaki M, Murakami K, Suzuki N (2017) Extremely low prevalence of amyloid positron emission tomography positivity in Parkinson's disease without dementia. Eur Neurol 77(5–6):231–237

Masliah E, Rockenstein E, Veinbergs I, Sagara Y, Mallory M, Hashimoto M, Mucke L (2001) Beta-amyloid peptides enhance alpha-synuclein accumulation and neuronal deficits in a transgenic mouse model linking Alzheimer's disease and Parkinson's disease. Proc Natl Acad Sci U S A 98(21):12245–12250

Masters CL (2005) Neuropathology of Alzheimer's disease. In: Burns A, O'Brien J, Ames D (eds) Dementia, 3rd edn. Hodder Arnold, London, pp 393–407

Masters CL, Beyreuther K (2005) The neuropathology of Alzheimer's disease in the year 2005. In: Beal MF, Lang AE, Ludolph AC (eds) Neurodegenerative diseases: neurobiology, pathogenesis and therapeutics. Cambridge University Press, Cambridge, pp 433–440

Masters CL, Beyreuther K (2006) Alzheimer's centennial legacy: prospects for rational therapeutic intervention targeting the Abeta amyloid pathway. Brain 129(Pt 11):2823–2839

Masters CL, Cappai R, Barnham KJ, Villemagne VL (2006) Molecular mechanisms for Alzheimer's disease: implications for neuroimaging and therapeutics. J Neurochem 97(6):1700–1725

Masters CL, Simms G, Weinman NA, Multhaup G, McDonald BL, Beyreuther K (1985) Amyloid plaque core protein in Alzheimer disease and down syndrome. Proc Natl Acad Sci U S A 82(12):4245–4249

Mathis CA, Bacskai BJ, Kajdasz ST, McLellan ME, Frosch MP, Hyman BT, Holt DP, Wang Y, Huang GF, Debnath ML, Klunk WE (2002) A lipophilic thioflavin-T derivative for positron emission tomography (PET) imaging of amyloid in brain. Bioorg Med Chem Lett 12(3):295–298

Mathis CA, Klunk WE, Price JC, DeKosky ST (2005) Imaging technology for neurodegenerative diseases: progress toward detection of specific pathologies. Arch Neurol 62(2):196–200

Mathis CA, Lopresti BJ, Klunk WE (2007) Impact of amyloid imaging on drug development in Alzheimer's disease. Nucl Med Biol 34(7):809–822

Matias-Guiu JA, Guerrero-Marquez C, Cabrera-Martin MN, Gomez-Pinedo U, Romeral M, Mayo D, Porta-Etessam J, Moreno-Ramos T, Carreras JL, Matias-Guiu J (2017) Amyloid- and FDG-PET in sporadic Creutzfeldt-Jakob disease: correlation with pathological prion protein in neuropathology. Prion 11(3):205–213

Mattsson N, Andreasson U, Persson S, Arai H, Batish SD, Bernardini S, Bocchio-Chiavetto L, Blankenstein MA, Carrillo MC, Chalbot S, Coart E, Chiasserini D, Cutler N, Dahlfors G, Duller S, Fagan AM, Forlenza O, Frisoni GB, Galasko D, Galimberti D, Hampel H, Handberg A, Heneka MT, Herskovits AZ, Herukka SK, Holtzman DM, Humpel C, Hyman BT, Iqbal K, Jucker M, Kaeser SA, Kaiser E, Kapaki E, Kidd D, Klivenyi P, Knudsen CS, Kummer MP, Lui J, Llado A, Lewczuk P, Li QX, Martins R, Masters C, McAuliffe J, Mercken M, Moghekar A, Molinuevo JL, Montine TJ, Nowatzke W, O'Brien R, Otto M, Paraskevas GP, Parnetti L, Petersen RC, Prvulovic D, de Reus HP, Rissman RA, Scarpini E, Stefani A, Soininen H, Schroder J, Shaw LM, Skinningsrud A, Skrogstad B, Spreer A, Talib L, Teunissen C, Trojanowski JQ, Tumani H, Umek RM, Van Broeck B, Vanderstichele H, Vecsei L, Verbeek MM, Windisch M, Zhang J, Zetterberg H, Blennow K (2011) The Alzheimer's Association external quality control program for cerebrospinal fluid biomarkers. Alzheimers Dement 7(4):386–395. e386

Mattsson N, Lonneborg A, Boccardi M, Blennow K, Hansson O, Geneva Task Force for the Roadmap of Alzheimer's Biomarkers (2017) Clinical validity of cerebrospinal fluid Abeta42, tau, and phospho-tau as biomarkers for Alzheimer's disease in the context of a structured 5-phase development framework. Neurobiol Aging 52:196–213

Mattsson N, Zetterberg H, Hansson O, Andreasen N, Parnetti L, Jonsson M, Herukka SK, van der Flier WM, Blankenstein MA, Ewers M, Rich K, Kaiser E, Verbeek M, Tsolaki M, Mulugeta E, Rosen E, Aarsland D, Visser PJ, Schroder J, Marcusson J, de Leon M, Hampel H, Scheltens P, Pirttila T, Wallin A, Jonhagen ME, Minthon L, Winblad B, Blennow K (2009) CSF biomarkers and incipient Alzheimer disease in patients with mild cognitive impairment. JAMA 302(4):385–393

Mawuenyega KG, Sigurdson W, Ovod V, Munsell L, Kasten T, Morris JC, Yarasheski KE, Bateman RJ (2010) Decreased clearance of CNS beta-amyloid in Alzheimer's disease. Science 330(6012):1774

McDade E, Wang G, Gordon BA, Hassenstab J, Benzinger TLS, Buckles V, Fagan AM, Holtzman DM, Cairns NJ, Goate AM, Marcus DS, Morris JC, Paumier K, Xiong C, Allegri R, Berman SB, Klunk W, Noble J, Ringman J, Ghetti B, Farlow M, Sperling RA, Chhatwal J, Salloway S, Graff-Radford NR, Schofield PR, Masters C, Rossor MN, Fox NC, Levin J, Jucker M, Bateman RJ, Dominantly Inherited Alzheimer Network (2018) Longitudinal cognitive and biomarker changes in dominantly inherited Alzheimer disease. Neurology 91(14):e1295–e1306

McKee AC, Abdolmohammadi B, Stein TD (2018) The neuropathology of chronic traumatic encephalopathy. Handb Clin Neurol 158:297–307

McKee AC, Stern RA, Nowinski CJ, Stein TD, Alvarez VE, Daneshvar DH, Lee HS, Wojtowicz SM, Hall G, Baugh CM, Riley DO, Kubilus CA, Cormier KA, Jacobs MA, Martin BR, Abraham CR, Ikezu T, Reichard RR, Wolozin BL, Budson AE, Goldstein LE, Kowall NW, Cantu RC (2013) The spectrum of disease in chronic traumatic encephalopathy. Brain 136(Pt 1):43–64

McKeith IG, Dickson DW, Lowe J, Emre M, O'Brien JT, Feldman H, Cummings J, Duda JE, Lippa C, Perry EK, Aarsland D, Arai H, Ballard CG, Boeve B, Burn DJ, Costa D, Del Ser T, Dubois B, Galasko D, Gauthier S, Goetz CG, Gomez-Tortosa E, Halliday G, Hansen LA, Hardy J, Iwatsubo T, Kalaria RN, Kaufer D, Kenny RA, Korczyn A, Kosaka K, Lee VM, Lees A, Litvan I, Londos E, Lopez OL, Minoshima S, Mizuno Y, Molina JA, Mukaetova-Ladinska EB, Pasquier F, Perry RH, Schulz JB, Trojanowski JQ, Yamada M (2005) Diagnosis and management of dementia with Lewy bodies: third report of the DLB consortium. Neurology 65(12):1863–1872

McKeith IG, Mosimann UP (2004) Dementia with Lewy bodies and Parkinson's disease. Parkinsonism Relat Disord 10(Suppl 1):S15–S18

McKhann GM, Knopman DS, Chertkow H, Hyman BT, Jack CR Jr, Kawas CH, Klunk WE, Koroshetz WJ, Manly JJ, Mayeux R, Mohs RC, Morris JC, Rossor MN, Scheltens P, Carrillo

MC, Thies B, Weintraub S, Phelps CH (2011) The diagnosis of dementia due to Alzheimer's disease: recommendations from the National Institute on Aging-Alzheimer's Association workgroups on diagnostic guidelines for Alzheimer's disease. Alzheimers Dement 7(3):263–269

McLean CA, Cherny RA, Fraser FW, Fuller SJ, Smith MJ, Beyreuther K, Bush AI, Masters CL (1999) Soluble pool of Aß amyloid as a determinant of severity of neurodegeneration in Alzheimer's disease. Ann Neurol 46(6):860–866

Michaelis ML, Dobrowsky RT, Li G (2002) Tau neurofibrillary pathology and microtubule stability. J Mol Neurosci 19(3):289–293

Mielke R, Herholz K, Grond M, Kessler J, Heiss WD (1992) Differences of regional cerebral glucose metabolism between presenile and senile dementia of Alzheimer type. Neurobiol Aging 13(1):93–98

Mintun MA, Larossa GN, Sheline YI, Dence CS, Lee SY, Mach RH, Klunk WE, Mathis CA, DeKosky ST, Morris JC (2006) [11C]PIB in a nondemented population: potential antecedent marker of Alzheimer disease. Neurology 67(3):446–452

Montine TJ, Phelps CH, Beach TG, Bigio EH, Cairns NJ, Dickson DW, Duyckaerts C, Frosch MP, Masliah E, Mirra SS, Nelson PT, Schneider JA, Thal DR, Trojanowski JQ, Vinters HV, Hyman BT (2012) National Institute on Aging-Alzheimer's Association guidelines for the neuropathologic assessment of Alzheimer's disease: a practical approach. Acta Neuropathol 123(1):1–11

Mormino EC, Brandel MG, Madison CM, Rabinovici GD, Marks S, Baker SL, Jagust WJ (2012) Not quite PIB-positive, not quite PIB-negative: slight PIB elevations in elderly normal control subjects are biologically relevant. NeuroImage 59(2):1152–1160

Mormino EC, Kluth JT, Madison CM, Rabinovici GD, Baker SL, Miller BL, Koeppe RA, Mathis CA, Weiner MW, Jagust WJ (2009) Episodic memory loss is related to hippocampal-mediated beta-amyloid deposition in elderly subjects. Brain 132(Pt 5):1310–1323

Morris JC (2012) Revised criteria for mild cognitive impairment may compromise the diagnosis of Alzheimer disease dementia. Arch Neurol 69(6):700–708. https://doi.org/10.1001/archneurol.2011.3152

Morris JC, Aisen PS, Bateman RJ, Benzinger TL, Cairns NJ, Fagan AM, Ghetti B, Goate AM, Holtzman DM, Klunk WE, McDade E, Marcus DS, Martins RN, Masters CL, Mayeux R, Oliver A, Quaid K, Ringman JM, Rossor MN, Salloway S, Schofield PR, Selsor NJ, Sperling RA, Weiner MW, Xiong C, Moulder KL, Buckles VD (2012) Developing an international network for Alzheimer research: the dominantly inherited Alzheimer network. Clin Investig (Lond) 2(10):975–984

Morris JC, Kimberly A, Quaid K, Holtzman DM, Kantarci K, Kaye J, Reiman EM, Klunk WE, Siemers ER (2005) Role of biomarkers in studies of presymptomatic Alzheimer's disease. Alzheimers Dement 1(2):145–151

Morris JC, Price AL (2001) Pathologic correlates of nondemented aging, mild cognitive impairment, and early-stage Alzheimer's disease. J Mol Neurosci 17(2):101–118

Morris JC, Roe CM, Grant EA, Head D, Storandt M, Goate AM, Fagan AM, Holtzman DM, Mintun MA (2009) Pittsburgh compound B imaging and prediction of progression from cognitive normality to symptomatic Alzheimer disease. Arch Neurol 66(12):1469–1475

Morris JC, Roe CM, Xiong C, Fagan AM, Goate AM, Holtzman DM, Mintun MA (2010) APOE predicts amyloid-beta but not tau Alzheimer pathology in cognitively normal aging. Ann Neurol 67(1):122–131

Mortimer JA (1997) Brain reserve and the clinical expression of Alzheimer's disease. Geriatrics 52(Suppl 2):S50–S53

Mosconi L, Sorbi S, de Leon MJ, Li Y, Nacmias B, Myoung PS, Tsui W, Ginestroni A, Bessi V, Fayyazz M, Caffarra P, Pupi A. (2006) Hypometabolism exceeds atrophy in presymptomatic early-onset familial Alzheimer'sdisease. J Nucl Med 47(11):1778–1786

Mosconi L, De Santi S, Li Y, Li J, Zhan J, Tsui WH, Boppana M, Pupi A, de Leon MJ (2006a) Visual rating of medial temporal lobe metabolism in mild cognitive impairment and Alzheimer's disease using FDG-PET. Eur J Nucl Med Mol Imaging 33(2):210–221

Mosconi L, Perani D, Sorbi S, Herholz K, Nacmias B, Holthoff V, Salmon E, Baron JC, De Cristofaro MT, Padovani A, Borroni B, Franceschi M, Bracco L, Pupi A (2004) MCI conversion to dementia and the APOE genotype: a prediction study with FDG-PET. Neurology 63(12):2332–2340

Mosconi L, Sorbi S, de Leon MJ, Li Y, Nacmias B, Myoung PS, Tsui W, Ginestroni A, Bessi V, Fayyazz M, Caffarra P, Pupi A (2006b) Hypometabolism exceeds atrophy in presymptomatic early-onset familial Alzheimer's disease. J Nucl Med 47(11):1778–1786

Mott RT, Dickson DW, Trojanowski JQ, Zhukareva V, Lee VM, Forman M, Van Deerlin V, Ervin JF, Wang DS, Schmechel DE, Hulette CM (2005) Neuropathologic, biochemical, and molecular characterization of the frontotemporal dementias. J Neuropathol Exp Neurol 64(5):420–428

Mountz JM, Laymon CM, Cohen AD, Zhang Z, Price JC, Boudhar S, McDade E, Aizenstein HJ, Klunk WE, Mathis CA (2015) Comparison of qualitative and quantitative imaging characteristics of [11C]PiB and [18F]flutemetamol in normal control and Alzheimer's subjects. Neuroimage Clin 9:592–598

Nakamura A, Kaneko N, Villemagne VL, Kato T, Doecke J, Doré V, Fowler C, Li Q-X, Martins R, Rowe C (2018) High performance plasma amyloid-β biomarkers for Alzheimer's disease. Nature 554(7691):249

Naslund J, Haroutunian V, Mohs R, Davis KL, Davies P, Greengard P, Buxbaum JD (2000) Correlation between elevated levels of amyloid beta-peptide in the brain and cognitive decline. JAMA 283(12):1571–1577

Navitsky M, Joshi AD, Kennedy I, Klunk WE, Rowe CC, Wong DF, Pontecorvo MJ, Mintun MA, Devous MD Sr (2018) Standardization of amyloid quantitation with florbetapir standardized uptake value ratios to the Centiloid scale. Alzheimers Dement 14(12):1565–1571

Nelissen N, Van Laere K, Thurfjell L, Owenius R, Vandenbulcke M, Koole M, Bormans G, Brooks DJ, Vandenberghe R (2009) Phase 1 study of the Pittsburgh compound B derivative 18F-flutemetamol in healthy volunteers and patients with probable Alzheimer disease. J Nucl Med 50(8):1251–1259

Nelson PT, Dickson DW, Trojanowski JQ, Jack CR, Boyle PA, Arfanakis K, Rademakers R, Alafuzoff I, Attems J, Brayne C, Coyle-Gilchrist ITS, Chui HC, Fardo DW, Flanagan ME, Halliday G, Hokkanen SRK, Hunter S, Jicha GA, Katsumata Y, Kawas CH, Keene CD, Kovacs GG, Kukull WA, Levey AI, Makkinejad N, Montine TJ, Murayama S, Murray ME, Nag S, Rissman RA, Seeley WW, Sperling RA, White Iii CL, Yu L, Schneider JA (2019) Limbic-predominant age-related TDP-43 encephalopathy (LATE): consensus working group report. Brain 142(6):1503–1527

Neumann M, Rademakers R, Roeber S, Baker M, Kretzschmar HA, Mackenzie IR (2009) A new subtype of frontotemporal lobar degeneration with FUS pathology. Brain 132(Pt 11):2922–2931

Neumann M, Sampathu DM, Kwong LK, Truax AC, Micsenyi MC, Chou TT, Bruce J, Schuck T, Grossman M, Clark CM, McCluskey LF, Miller BL, Masliah E, Mackenzie IR, Feldman H, Feiden W, Kretzschmar HA, Trojanowski JQ, Lee VM (2006) Ubiquitinated TDP-43 in frontotemporal lobar degeneration and amyotrophic lateral sclerosis. Science 314(5796):130–133

Newberg AB, Wintering NA, Plossl K, Hochold J, Stabin MG, Watson M, Skovronsky D, Clark CM, Kung MP, Kung HF (2006) Safety, biodistribution, and dosimetry of 123I-IMPY: a novel amyloid plaque-imaging agent for the diagnosis of Alzheimer's disease. J Nucl Med 47(5):748–754

Ng S, Villemagne VL, Berlangieri S, Lee ST, Cherk M, Gong SJ, Ackermann U, Saunder T, Tochon-Danguy H, Jones G, Smith C, O'Keefe G, Masters CL, Rowe CC (2007a) Visual assessment versus quantitative assessment of 11C-PIB PET and 18F-FDG PET for detection of Alzheimer's disease. J Nucl Med 48(4):547–552

Ng SY, Villemagne VL, Masters CL, Rowe CC (2007b) Evaluating atypical dementia syndromes using positron emission tomography with carbon 11 labeled Pittsburgh compound B. Arch Neurol 64(8):1140–1144

Ni R, Gillberg PG, Bergfors A, Marutle A, Nordberg A (2013) Amyloid tracers detect multiple binding sites in Alzheimer's disease brain tissue. Brain 136(Pt 7):2217–2227

Noda A, Murakami Y, Nishiyama S, Fukumoto D, Miyoshi S, Tsukada H, Nishimura S (2008) Amyloid imaging in aged and young macaques with [11C]PIB and [18F]FDDNP. Synapse 62(6):472–475

Nordberg A (2004) PET imaging of amyloid in Alzheimer's disease. Lancet Neurol 3(9):519–527

Nordberg A (2007) Amyloid imaging in Alzheimer's disease. Curr Opin Neurol 20(4):398–402

Nyberg S, Jonhagen ME, Cselenyi Z, Halldin C, Julin P, Olsson H, Freund-Levi Y, Andersson J, Varnas K, Svensson S, Farde L (2009) Detection of amyloid in Alzheimer's disease with positron emission tomography using [11C]AZD2184. Eur J Nucl Med Mol Imaging 36(11):1859–1863

O'Brien J, Ames D, Burns A (2000) Dementia, 2nd edn. Arnold, London

O'Brien JT, Colloby S, Fenwick J, Williams ED, Firbank M, Burn D, Aarsland D, McKeith IG (2004) Dopamine transporter loss visualized with FP-CIT SPECT in the differential diagnosis of dementia with Lewy bodies. Arch Neurol 61(6):919–925

Ojida A, Sakamoto T, Inoue MA, Fujishima SH, Lippens G, Hamachi I (2009) Fluorescent BODIPY-based Zn(II) complex as a molecular probe for selective detection of neurofibrillary tangles in the brains of Alzheimer's disease patients. J Am Chem Soc 131(18):6543–6548

Okamura N, Shiga Y, Furumoto S, Tashiro M, Tsuboi Y, Furukawa K, Yanai K, Iwata R, Arai H, Kudo Y, Itoyama Y, Doh-ura K (2010) In vivo detection of prion amyloid plaques using [(11) C]BF-227 PET. Eur J Nucl Med Mol Imaging 37(5):934–941

Okamura N, Suemoto T, Furumoto S, Suzuki M, Shimadzu H, Akatsu H, Yamamoto T, Fujiwara H, Nemoto M, Maruyama M, Arai H, Yanai K, Sawada T, Kudo Y (2005) Quinoline and benzimidazole derivatives: candidate probes for in vivo imaging of tau pathology in Alzheimer's disease. J Neurosci 25(47):10857–10862

Okamura N, Suemoto T, Shimadzu H, Suzuki M, Shiomitsu T, Akatsu H, Yamamoto T, Staufenbiel M, Yanai K, Arai H, Sasaki H, Kudo Y, Sawada T (2004) Styrylbenzoxazole derivatives for in vivo imaging of amyloid plaques in the brain. J Neurosci 24(10):2535–2541

Okello A, Edison P, Archer HA, Turkheimer FE, Kennedy J, Bullock R, Walker Z, Kennedy A, Fox N, Rossor M, Brooks DJ (2009a) Microglial activation and amyloid deposition in mild cognitive impairment: a PET study. Neurology 72(1):56–62

Okello A, Koivunen J, Edison P, Archer HA, Turkheimer FE, Nagren K, Bullock R, Walker Z, Kennedy A, Fox NC, Rossor MN, Rinne JO, Brooks DJ (2009b) Conversion of amyloid positive and negative MCI to AD over 3 years: an 11C-PIB PET study. Neurology 73(10):754–760

Omalu B, Small GW, Bailes J, Ercoli LM, Merrill DA, Wong KP, Huang SC, Satyamurthy N, Hammers JL, Lee J, Fitzsimmons RP, Barrio JR (2018) Postmortem autopsy-confirmation of Antemortem [F-18]FDDNP-PET scans in a football player with chronic traumatic encephalopathy. Neurosurgery 82(2):237–246

Ong K, Villemagne VL, Bahar-Fuchs A, Lamb F, Chetelat G, Raniga P, Mulligan RS, Salvado O, Putz B, Roth K, Masters CL, Reininger CB, Rowe CC (2013) (18)F-florbetaben Abeta imaging in mild cognitive impairment. Alzheimers Res Ther 5(1):4

Ong KT, Villemagne VL, Bahar-Fuchs A, Lamb F, Langdon N, Catafau AM, Stephens AW, Seibyl J, Dinkelborg LM, Reininger CB, Putz B, Rohde B, Masters CL, Rowe CC (2015) Abeta imaging with 18F-florbetaben in prodromal Alzheimer's disease: a prospective outcome study. J Neurol Neurosurg Psychiatry 86(4):431–436

Opazo C, Luza S, Villemagne VL, Volitakis I, Rowe C, Barnham KJ, Strozyk D, Masters CL, Cherny RA, Bush AI (2006) Radioiodinated clioquinol as a biomarker for beta-amyloid: Zn complexes in Alzheimer's disease. Aging Cell 5(1):69–79

Ossenkoppele R, Lyoo CH, Sudre CH, van Westen D, Cho H, Ryu YH, Choi JY, Smith R, Strandberg O, Palmqvist S, Westman E, Tsai R, Kramer J, Boxer AL, Gorno-Tempini ML, La Joie R, Miller BL, Rabinovici GD, Hansson O (2019) Distinct tau PET patterns in atrophy-defined subtypes of Alzheimer's disease. Alzheimers Dement 16(2):335–344

Ossenkoppele R, Tolboom N, Foster-Dingley JC, Adriaanse SF, Boellaard R, Yaqub M, Windhorst AD, Barkhof F, Lammertsma AA, Scheltens P, van der Flier WM, van Berckel BN (2012) Longitudinal imaging of Alzheimer pathology using [11C]PIB, [18F]FDDNP and [18F]FDG PET. Eur J Nucl Med Mol Imaging 39(6):990–1000

Ossenkoppele R, van Berckel BN, Prins ND (2011) Amyloid imaging in prodromal Alzheimer's disease. Alzheimers Res Ther 3(5):26

Ostrowitzki S, Deptula D, Thurfjell L, Barkhof F, Bohrmann B, Brooks DJ, Klunk WE, Ashford E, Yoo K, Xu ZX, Loetscher H, Santarelli L (2011) Mechanism of amyloid removal in patients with Alzheimer disease treated with Gantenerumab. Arch Neurol 69(2):198–207

Ovod V, Ramsey KN, Mawuenyega KG, Bollinger JG, Hicks T, Schneider T, Sullivan M, Paumier K, Holtzman DM, Morris JC (2017) Amyloid β concentrations and stable isotope labeling kinetics of human plasma specific to central nervous system amyloidosis. Alzheimers Dement 13(8):841–849

Palmqvist S, Insel PS, Stomrud E, Janelidze S, Zetterberg H, Brix B, Eichenlaub U, Dage JL, Chai X, Blennow K, Mattsson N, Hansson O (2019) Cerebrospinal fluid and plasma biomarker trajectories with increasing amyloid deposition in Alzheimer's disease. EMBO Mol Med 11(12):e11170

Pase MP, Satizabal CL, Seshadri S (2017) Role of improved vascular health in the declining incidence of dementia. Stroke 48(7):2013–2020

Perrotin A, La Joie R, de La Sayette V, Barre L, Mezenge F, Mutlu J, Guilloteau D, Egret S, Eustache F, Chetelat G (2017) Subjective cognitive decline in cognitively normal elders from the community or from a memory clinic: differential affective and imaging correlates. Alzheimers Dement 13(5):550–560

Petersen RC (2000) Mild cognitive impairment: transition between aging and Alzheimer's disease. Neurologia 15(3):93–101

Petersen RC, Smith GE, Ivnik RJ, Tangalos EG, Schaid DJ, Thibodeau SN, Kokmen E, Waring SC, Kurland LT (1995) Apolipoprotein E status as a predictor of the development of Alzheimer's disease in memory-impaired individuals. JAMA 273:1274–1278

Petersen RC, Smith GE, Waring SC, Ivnik RJ, Tangalos EG, Kokmen E (1999) Mild cognitive impairment: clinical characterization and outcome. Arch Neurol 56:303–308

Pettersen JA, Sathiyamoorthy G, Gao FQ, Szilagyi G, Nadkarni NK, St George-Hyslop P, Rogaeva E, Black SE (2008) Microbleed topography, leukoaraiosis, and cognition in probable Alzheimer disease from the Sunnybrook dementia study. Arch Neurol 65(6):790–795

Phelps ME (2000) PET: the merging of biology and imaging into molecular imaging. J Nucl Med 41(4):661–681

Pike KE, Ellis KA, Villemagne VL, Good N, Chetelat G, Ames D, Szoeke C, Laws SM, Verdile G, Martins RN, Masters CL, Rowe CC (2011) Cognition and beta-amyloid in preclinical Alzheimer's disease: data from the AIBL study. Neuropsychologia 49(9):2384–2390

Pike KE, Savage G, Villemagne VL, Ng S, Moss SA, Maruff P, Mathis CA, Klunk WE, Masters CL, Rowe CC (2007) Beta-amyloid imaging and memory in non-demented individuals: evidence for preclinical Alzheimer's disease. Brain 130(Pt 11):2837–2844

Pike VW (2009) PET radiotracers: crossing the blood-brain barrier and surviving metabolism. Trends Pharmacol Sci 30(8):431–440

Plassman BL, Havlik RJ, Steffens DC, Helms MJ, Newman TN, Drosdick D, Phillips C, Gau BA, Welsh-Bohmer KA, Burke JR, Guralnik JM, Breitner JC (2000) Documented head injury in early adulthood and risk of Alzheimer's disease and other dementias. Neurology 55(8):1158–1166

Pletnikova O, West N, Lee MK, Rudow GL, Skolasky RL, Dawson TM, Marsh L, Troncoso JC (2005) Abeta deposition is associated with enhanced cortical a-synuclein lesions in Lewy body diseases. Neurobiol Aging 26:1183–1192

Pontecorvo MJ, Arora AK, Devine M, Lu M, Galante N, Siderowf A, Devadanam C, Joshi AD, Heun SL, Teske BF, Truocchio SP, Krautkramer M, Devous MD Sr, Mintun MA (2017a) Quantitation of PET signal as an adjunct to visual interpretation of florbetapir imaging. Eur J Nucl Med Mol Imaging 44(5):825–837

Pontecorvo MJ, Siderowf A, Dubois B, Doraiswamy PM, Frisoni GB, Grundman M, Nobili F, Sadowsky CH, Salloway S, Arora AK, Chevrette A, Deberdt W, Dell'Agnello G, Flitter M, Galante N, Lowrey MJ, Lu M, McGeehan A, Devous MD Sr, Mintun MA (2017b) Effectiveness

of Florbetapir PET imaging in changing patient management. Dement Geriatr Cogn Disord 44(3–4):129–143

Price JC, Klunk WE, Lopresti BJ, Lu X, Hoge JA, Ziolko SK, Holt DP, Meltzer CC, DeKosky ST, Mathis CA (2005) Kinetic modeling of amyloid binding in humans using PET imaging and Pittsburgh compound-B. J Cereb Blood Flow Metab 25(11):1528–1547

Price JL, Morris JC (1999) Tangles and plaques in nondemented aging and "preclinical" Alzheimer's disease. Ann Neurol 45(3):358–368

Qu W, Kung MP, Hou C, Benedum TE, Kung HF (2007a) Novel styrylpyridines as probes for SPECT imaging of amyloid plaques. J Med Chem 50(9):2157–2165

Qu W, Kung MP, Hou C, Jin LW, Kung HF (2007b) Radioiodinated aza-diphenylacetylenes as potential SPECT imaging agents for beta-amyloid plaque detection. Bioorg Med Chem Lett 17(13):3581–3584

Rabinovici GD, Furst AJ, Alkalay A, Racine CA, O'Neil JP, Janabi M, Baker SL, Agarwal N, Bonasera SJ, Mormino EC, Weiner MW, Gorno-Tempini ML, Rosen HJ, Miller BL, Jagust WJ (2010) Increased metabolic vulnerability in early-onset Alzheimer's disease is not related to amyloid burden. Brain 133(Pt 2):512–528

Rabinovici GD, Furst AJ, O'Neil JP, Racine CA, Mormino EC, Baker SL, Chetty S, Patel P, Pagliaro TA, Klunk WE, Mathis CA, Rosen HJ, Miller BL, Jagust WJ (2007) 11C-PIB PET imaging in Alzheimer disease and frontotemporal lobar degeneration. Neurology 68(15):1205–1212

Rabinovici GD, Gatsonis C, Apgar C, Chaudhary K, Gareen I, Hanna L, Hendrix J, Hillner BE, Olson C, Lesman-Segev OH, Romanoff J, Siegel BA, Whitmer RA, Carrillo MC (2019) Association of Amyloid Positron Emission Tomography with Subsequent Change in clinical management among Medicare beneficiaries with mild cognitive impairment or dementia. JAMA 321(13):1286–1294

Rabinovici GD, Jagust WJ (2009) Amyloid imaging in aging and dementia: testing the amyloid hypothesis in vivo. Behav Neurol 21(1):117–128

Rabinovici GD, Jagust WJ, Furst AJ, Ogar JM, Racine CA, Mormino EC, O'Neil JP, Lal RA, Dronkers NF, Miller BL, Gorno-Tempini ML (2008) Abeta amyloid and glucose metabolism in three variants of primary progressive aphasia. Ann Neurol 64(4):388–401

Rabinovici GD, Miller BL (2010) Frontotemporal lobar degeneration: epidemiology, pathophysiology, diagnosis and management. CNS Drugs 24(5):375–398

Rabinovici GD, Rosen HJ, Alkalay A, Kornak J, Furst AJ, Agarwal N, Mormino EC, O'Neil JP, Janabi M, Karydas A, Growdon ME, Jang JY, Huang EJ, Dearmond SJ, Trojanowski JQ, Grinberg LT, Gorno-Tempini ML, Seeley WW, Miller BL, Jagust WJ (2011) Amyloid vs FDG-PET in the differential diagnosis of AD and FTLD. Neurology 77(23):2034–2042

Raniga P, Desmond P, Yates P, Salvado O, Bourgeat P, Fripp J, Pejoska S, Woodward M, Masters CL, Rowe CC, Villemagne VL (2017) Focal Ab-amyloid deposition precedes cerebral microbleeds and Superficial siderosis: a case report. J Neurosci Neurol Disord 1:039–044

Reiman EM, Caselli RJ, Yun LS, Chen K, Bandy D, Minoshima S, Thibodeau SN, Osborne D (1996) Preclinical evidence of Alzheimer's disease in persons homozygous for the epsilon 4 allele for apolipoprotein E. N Engl J Med 334(12):752–758

Reiman EM, Chen K, Liu X, Bandy D, Yu M, Lee W, Ayutyanont N, Keppler J, Reeder SA, Langbaum JB, Alexander GE, Klunk WE, Mathis CA, Price JC, Aizenstein HJ, Dekosky ST, Caselli RJ (2009a) Fibrillar amyloid-β burden in cognitively normal people at 3 levels of genetic risk for Alzheimer's disease. Proc Natl Acad Sci U S A 106:6820–6825

Reiman EM, Chen K, Liu X, Bandy D, Yu M, Lee W, Ayutyanont N, Keppler J, Reeder SA, Langbaum JB, Alexander GE, Klunk WE, Mathis CA, Price JC, Aizenstein HJ, DeKosky ST, Caselli RJ (2009b) Fibrillar amyloid-beta burden in cognitively normal people at 3 levels of genetic risk for Alzheimer's disease. Proc Natl Acad Sci U S A 106(16):6820–6825

Remes AM, Laru L, Tuominen H, Aalto S, Kemppainen N, Mononen H, Nagren K, Parkkola R, Rinne JO (2008) Carbon 11-labeled Pittsburgh compound B positron emission tomographic amyloid imaging in patients with APP locus duplication. Arch Neurol 65(4):540–544

Rentz DM, Locascio JJ, Becker JA, Moran EK, Eng E, Buckner RL, Sperling RA, Johnson KA (2010) Cognition, reserve, and amyloid deposition in normal aging. Ann Neurol 67(3):353–364

Resende R, Pereira C, Agostinho P, Vieira AP, Malva JO, Oliveira CR (2007) Susceptibility of hippocampal neurons to Abeta peptide toxicity is associated with perturbation of Ca^{2+} homeostasis. Brain Res 1143:11–21

Resnick SM, Sojkova J, Zhou Y, An Y, Ye W, Holt DP, Dannals RF, Mathis CA, Klunk WE, Ferrucci L, Kraut MA, Wong DF (2010) Longitudinal cognitive decline is associated with fibrillar amyloid-beta measured by [11C]PiB. Neurology 74(10):807–815

Riekse RG, Leverenz JB, McCormick W, Bowen JD, Teri L, Nochlin D, Simpson K, Eugenio C, Larson EB, Tsuang D (2004) Effect of vascular lesions on cognition in Alzheimer's disease: a community-based study. J Am Geriatr Soc 52(9):1442–1448

Rinne JO, Brooks DJ, Rossor MN, Fox NC, Bullock R, Klunk WE, Mathis CA, Blennow K, Barakos J, Okello AA, de Liano SRM, Liu E, Koller M, Gregg KM, Schenk D, Black R, Grundman M (2010) 11C-PiB PET assessment of change in fibrillar amyloid-beta load in patients with Alzheimer's disease treated with bapineuzumab: a phase 2, double-blind, placebo-controlled, ascending-dose study. Lancet Neurol 9(4):363–372

Roberts BR, Lind M, Wagen AZ, Rembach A, Frugier T, Li QX, Ryan TM, McLean CA, Doecke JD, Rowe CC, Villemagne VL, Masters CL (2017) Biochemically-defined pools of amyloid-beta in sporadic Alzheimer's disease: correlation with amyloid PET. Brain 140(5):1486–1498

Roder S, Danober L, Pozza MF, Lingenhoehl K, Wiederhold KH, Olpe HR (2003) Electrophysiological studies on the hippocampus and prefrontal cortex assessing the effects of amyloidosis in amyloid precursor protein 23 transgenic mice. Neuroscience 120(3):705–720

Rodriguez-Vieitez E, Nordberg A (2018) Imaging Neuroinflammation: quantification of Astrocytosis in a multitracer PET approach. Methods Mol Biol 1750:231–251

Rodriguez-Vieitez E, Saint-Aubert L, Carter SF, Almkvist O, Farid K, Scholl M, Chiotis K, Thordardottir S, Graff C, Wall A, Langstrom B, Nordberg A (2016) Diverging longitudinal changes in astrocytosis and amyloid PET in autosomal dominant Alzheimer's disease. Brain 139(Pt 3):922–936

Roe CM, Mintun MA, D'Angelo G, Xiong C, Grant EA, Morris JC (2008) Alzheimer disease and cognitive reserve: variation of education effect with carbon 11-labeled Pittsburgh compound B uptake. Arch Neurol 65(11):1467–1471

Rosen RF, Ciliax BJ, Wingo TS, Gearing M, Dooyema J, Lah JJ, Ghiso JA, LeVine H 3rd, Walker LC (2010) Deficient high-affinity binding of Pittsburgh compound B in a case of Alzheimer's disease. Acta Neuropathol 119(2):221–233

Rosendorff C, Beeri MS, Silverman JM (2007) Cardiovascular risk factors for Alzheimer's disease. Am J Geriatr Cardiol 16(3):143–149

Rossor MN, Kennedy AM, Frackowiak RS (1996) Clinical and neuroimaging features of familial Alzheimer's disease. Ann N Y Acad Sci 777:49–56

Rowe CC, Ackerman U, Browne W, Mulligan R, Pike KL, O'Keefe G, Tochon-Danguy H, Chan G, Berlangieri SU, Jones G, Dickinson-Rowe KL, Kung HP, Zhang W, Kung MP, Skovronsky D, Dyrks T, Holl G, Krause S, Friebe M, Lehman L, Lindemann S, Dinkelborg LM, Masters CL, Villemagne VL (2008) Imaging of amyloid beta in Alzheimer's disease with (18) F-BAY94-9172, a novel PET tracer: proof of mechanism. Lancet Neurol 7(2):129–135

Rowe CC, Bourgeat P, Ellis KA, Brown B, Lim YY, Mulligan R, Jones G, Maruff P, Woodward M, Price R, Robins P, Tochon-Danguy H, O'Keefe G, Pike KE, Yates P, Szoeke C, Salvado O, Macaulay SL, O'Meara T, Head R, Cobiac L, Savage G, Martins R, Masters CL, Ames D, Villemagne VL (2013a) Predicting Alzheimer disease with beta-amyloid imaging: results from the Australian imaging, biomarkers, and lifestyle study of ageing. Ann Neurol 74(6):905–913

Rowe CC, Dore V, Jones G, Baxendale D, Mulligan RS, Bullich S, Stephens AW, De Santi S, Masters CL, Dinkelborg L, Villemagne VL (2017) (18)F-Florbetaben PET beta-amyloid binding expressed in Centiloids. Eur J Nucl Med Mol Imaging 44(12):2053–2059

Rowe CC, Ellis KA, Rimajova M, Bourgeat P, Pike KE, Jones G, Fripp J, Tochon-Danguy H, Morandeau L, O'Keefe G, Price R, Raniga P, Robins P, Acosta O, Lenzo N, Szoeke C, Salvado

O, Head R, Martins R, Masters CL, Ames D, Villemagne VL (2010) Amyloid imaging results from the Australian imaging, biomarkers and lifestyle (AIBL) study of aging. Neurobiol Aging 31(8):1275–1283

Rowe CC, Jones G, Dore V, Pejoska S, Margison L, Mulligan RS, Chan JG, Young K, Villemagne VL (2016) Standardized expression of 18F-NAV4694 and 11C-PiB beta-amyloid PET results with the Centiloid scale. J Nucl Med 57(8):1233–1237

Rowe CC, Ng S, Ackermann U, Gong SJ, Pike K, Savage G, Cowie TF, Dickinson KL, Maruff P, Darby D, Smith C, Woodward M, Merory J, Tochon-Danguy H, O'Keefe G, Klunk WE, Mathis CA, Price JC, Masters CL, Villemagne VL (2007) Imaging beta-amyloid burden in aging and dementia. Neurology 68(20):1718–1725

Rowe CC, Pejoska S, Mulligan RS, Jones G, Chan JG, Svensson S, Cselenyi Z, Masters CL, Villemagne VL (2013b) Head-to-head comparison of 11C-PiB and 18F-AZD4694 (NAV4694) for beta-amyloid imaging in aging and dementia. J Nucl Med 54(6):880–886

Rowe CC, Villemagne VL (2011) Brain amyloid imaging. J Nucl Med 52(11):1733–1740

Rozga M, Bittner T, Hoglund K, Blennow K (2017) Accuracy of cerebrospinal fluid Abeta1-42 measurements: evaluation of pre-analytical factors using a novel Elecsys immunoassay. Clin Chem Lab Med 55(10):1545–1554

Sabbagh MN, Fleisher A, Chen K, Rogers J, Berk C, Reiman E, Pontecorvo M, Mintun M, Skovronsky D, Jacobson SA, Sue LI, Liebsack C, Charney AS, Cole L, Belden C, Beach TG (2011) Positron emission tomography and neuropathologic estimates of fibrillar amyloid-beta in a patient with down syndrome and Alzheimer disease. Arch Neurol 68(11):1461–1466

Sabbagh MN, Schauble B, Anand K, Richards D, Murayama S, Akatsu H, Takao M, Rowe CC, Masters CL, Barthel H, Gertz HJ, Peters O, Rasgon N, Jovalekic A, Sabri O, Schulz-Schaeffer WJ, Seibyl J (2017) Histopathology and Florbetaben PET in patients incorrectly diagnosed with Alzheimer's disease. J Alzheimers Dis 56(2):441–446

Sabri O, Sabbagh MN, Seibyl J, Barthel H, Akatsu H, Ouchi Y, Senda K, Murayama S, Ishii K, Takao M, Beach TG, Rowe CC, Leverenz JB, Ghetti B, Ironside JW, Catafau AM, Stephens AW, Mueller A, Koglin N, Hoffmann A, Roth K, Reininger C, Schulz-Schaeffer WJ, Florbetaben Phase 3 Study Group (2015) Florbetaben PET imaging to detect amyloid beta plaques in Alzheimer's disease: phase 3 study. Alzheimers Dement 11(8):964–974

Sair HI, Doraiswamy PM, Petrella JR (2004) In vivo amyloid imaging in Alzheimer's disease. Neuroradiology 46(2):93–104

Salloway S, Sperling R, Fox NC, Blennow K, Klunk W, Raskind M, Sabbagh M, Honig LS, Porsteinsson AP, Ferris S, Reichert M, Ketter N, Nejadnik B, Guenzler V, Miloslavsky M, Wang D, Lu Y, Lull J, Tudor IC, Liu E, Grundman M, Yuen E, Black R, Brashear HR, Bapineuzumab 301 and 302 Clinical Trial Investigators (2014) Two phase 3 trials of bapineuzumab in mild-to-moderate Alzheimer's disease. N Engl J Med 370(4):322–333

Salmon E, Sadzot B, Maquet P, Degueldre C, Lemaire C, Rigo P, Comar D, Franck G (1994) Differential diagnosis of Alzheimer's disease with PET. J Nucl Med 35(3):391–398

Sarro L, Senjem ML, Lundt ES, Przybelski SA, Lesnick TG, Graff-Radford J, Boeve BF, Lowe VJ, Ferman TJ, Knopman DS, Comi G, Filippi M, Petersen RC, Jack CR Jr, Kantarci K (2016) Amyloid-beta deposition and regional grey matter atrophy rates in dementia with Lewy bodies. Brain 139(Pt 10):2740–2750

Satizabal CL, Beiser AS, Chouraki V, Chene G, Dufouil C, Seshadri S (2016) Incidence of dementia over three decades in the Framingham heart study. N Engl J Med 374(6):523–532

Scheltens P, Rockwood K (2011) How golden is the gold standard of neuropathology in dementia? Alzheimers Dement 7(4):486–489

Schindler SE, Gray JD, Gordon BA, Xiong C, Batrla-Utermann R, Quan M, Wahl S, Benzinger TLS, Holtzman DM, Morris JC, Fagan AM (2018) Cerebrospinal fluid biomarkers measured by Elecsys assays compared to amyloid imaging. Alzheimers Dement 14(11):1460–1469

Schöll M, Almqvist O, Graff C, Nordberg A (2011) Amyloid imaging in members of a family harbouring the Arctic mutation. Alzheimers Dement 7(Suppl 1):303

Scholl M, Carter SF, Westman E, Rodriguez-Vieitez E, Almkvist O, Thordardottir S, Wall A, Graff C, Langstrom B, Nordberg A (2015) Early astrocytosis in autosomal dominant Alzheimer's disease measured in vivo by multi-tracer positron emission tomography. Sci Rep 5:16404

Schulz-Schaeffer WJ (2010) The synaptic pathology of alpha-synuclein aggregation in dementia with Lewy bodies, Parkinson's disease and Parkinson's disease dementia. Acta Neuropathol 120(2):131–143

Serdons, K., C. Terwinghe, P. Vermaelen, K. Van Laere, H. Kung, L. Mortelmans, G. Bormans and A. Verbruggen (2009a). "Synthesis and evaluation of (18)F-labeled 2-phenylbenzothiazoles as positron emission tomography imaging agents for amyloid plaques in Alzheimer's Disease." J Med Chem 52(5):1428-1437

Serdons K, Verduyckt T, Cleynhens J, Terwinghe C, Mortelmans L, Bormans G, Verbruggen A (2007) Synthesis and evaluation of a (99m)Tc-BAT-phenylbenzothiazole conjugate as a potential in vivo tracer for visualization of amyloid beta. Bioorg Med Chem Lett 17(22):6086–6090

Serdons K, Verduyckt T, Vanderghinste D, Cleynhens J, Borghgraef P, Vermaelen P, Terwinghe C, Van Leuven F, Van Laere K, Kung H, Bormans G, Verbruggen A (2009b) Synthesis of 18F-labelled 2-(4′-fluorophenyl)-1,3-benzothiazole and evaluation as amyloid imaging agent in comparison with [11C]PIB. Bioorg Med Chem Lett 19(3):602–605

Sevigny J, Chiao P, Bussiere T, Weinreb PH, Williams L, Maier M, Dunstan R, Salloway S, Chen T, Ling Y, O'Gorman J, Qian F, Arastu M, Li M, Chollate S, Brennan MS, Quintero-Monzon O, Scannevin RH, Arnold HM, Engber T, Rhodes K, Ferrero J, Hang Y, Mikulskis A, Grimm J, Hock C, Nitsch RM, Sandrock A (2016) The antibody aducanumab reduces Abeta plaques in Alzheimer's disease. Nature 537(7618):50–56

Shaw LM, Hansson O, Manuilova E, Masters CL, Doecke JD, Li QX, Rutz S, Widmann M, Leinenbach A, Blennow K (2019) Method comparison study of the Elecsys(R) beta-amyloid (1-42) CSF assay versus comparator assays and LC-MS/MS. Clin Biochem 72:7–14

Shaw LM, Korecka M, Clark CM, Lee VM, Trojanowski JQ (2007) Biomarkers of neurodegeneration for diagnosis and monitoring therapeutics. Nat Rev Drug Discov 6(4):295–303

Shih WJ, Markesbery WR, Clark DB, Goldstein S, Domstad PA, Coupal JJ, Kung H, DeKosky ST, DeLand FH (1987) Iodine-123 HIPDM brain imaging findings in subacute spongiform encephalopathy (Creutzfeldt-Jakob disease). J Nucl Med 28(9):1484–1487

Shoghi-Jadid K, Small GW, Agdeppa ED, Kepe V, Ercoli LM, Siddarth P, Read S, Satyamurthy N, Petric A, Huang SC, Barrio JR (2002) Localization of neurofibrillary tangles and beta-amyloid plaques in the brains of living patients with Alzheimer disease. Am J Geriatr Psychiatry 10(1):24–35

Siderowf A, Xie SX, Hurtig H, Weintraub D, Duda J, Chen-Plotkin A, Shaw LM, Van Deerlin V, Trojanowski JQ, Clark C (2010) CSF amyloid {beta} 1-42 predicts cognitive decline in Parkinson disease. Neurology 75(12):1055–1061

Silverman DH, Cummings JL, Small GW, Gambhir SS, Chen W, Czernin J, Phelps ME (2002) Added clinical benefit of incorporating 2-deoxy-2-[18F]fluoro-D-glucose with positron emission tomography into the clinical evaluation of patients with cognitive impairment. Mol Imaging Biol 4(4):283–293

Silverman DH, Small GW, Chang CY, Lu CS, Kung De Aburto MA, Chen W, Czernin J, Rapoport SI, Pietrini P, Alexander GE, Schapiro MB, Jagust WJ, Hoffman JM, Welsh-Bohmer KA, Alavi A, Clark CM, Salmon E, de Leon MJ, Mielke R, Cummings JL, Kowell AP, Gambhir SS, Hoh CK, Phelps ME (2001) Positron emission tomography in evaluation of dementia: regional brain metabolism and long-term outcome. JAMA 286(17):2120–2127

Slot RER, Sikkes SAM, Berkhof J, Brodaty H, Buckley R, Cavedo E, Dardiotis E, Guillo-Benarous F, Hampel H, Kochan NA, Lista S, Luck T, Maruff P, Molinuevo JL, Kornhuber J, Reisberg B, Riedel-Heller SG, Risacher SL, Roehr S, Sachdev PS, Scarmeas N, Scheltens P, Shulman MB, Saykin AJ, Verfaillie SCJ, Visser PJ, Vos SJB, Wagner M, Wolfsgruber S, Jessen F, Alzheimer's Disease Neuroimaging Initiative; DESCRIPA working group; INSIGHT-preAD study group; SCD-I working group; Wiesje M van der Flier (2019) Subjective cognitive decline and rates of incident Alzheimer's disease and non-Alzheimer's disease dementia. Alzheimers Dement 15(3):465–476

Small BJ, Gagnon E, Robinson B (2007) Early identification of cognitive deficits: preclinical Alzheimer's disease and mild cognitive impairment. Geriatrics 62(4):19–23

Small GW, Agdeppa ED, Kepe V, Satyamurthy N, Huang SC, Barrio JR (2002) In vivo brain imaging of tangle burden in humans. J Mol Neurosci 19(3):323–327

Small GW, Kepe V, Ercoli LM, Siddarth P, Bookheimer SY, Miller KJ, Lavretsky H, Burggren AC, Cole GM, Vinters HV, Thompson PM, Huang SC, Satyamurthy N, Phelps ME, Barrio JR (2006) PET of brain amyloid and tau in mild cognitive impairment. N Engl J Med 355(25):2652–2663

Small GW, Mazziotta JC, Collins MT, Baxter LR, Phelps ME, Mandelkern MA, Kaplan A, La Rue A, Adamson CF, Chang L et al (1995) Apolipoprotein E type 4 allele and cerebral glucose metabolism in relatives at risk for familial Alzheimer disease. JAMA 273(12):942–947

Smith EE, Egorova S, Blacker D, Killiany RJ, Muzikansky A, Dickerson BC, Tanzi RE, Albert MS, Greenberg SM, Guttmann CR (2008) Magnetic resonance imaging white matter hyperintensities and brain volume in the prediction of mild cognitive impairment and dementia. Arch Neurol 65(1):94–100

Snowden J, Neary D, Mann D (2007) Frontotemporal lobar degeneration: clinical and pathological relationships. Acta Neuropathol 114(1):31–38

Sojkova J, Driscoll I, Iacono D, Zhou Y, Codispoti KE, Kraut MA, Ferrucci L, Pletnikova O, Mathis CA, Klunk WE, O'Brien RJ, Wong DF, Troncoso JC, Resnick SM (2011a) In vivo fibrillar beta-amyloid detected using [11C]PiB positron emission tomography and neuropathologic assessment in older adults. Arch Neurol 68(2):232–240

Sojkova J, Resnick SM (2011) In vivo human amyloid imaging. Curr Alzheimer Res 8(4):366–372

Sojkova J, Zhou Y, An Y, Kraut MA, Ferrucci L, Wong DF, Resnick SM (2011b) Longitudinal patterns of beta-amyloid deposition in nondemented older adults. Arch Neurol 68(5):644–649

Song PJ, Bernard S, Sarradin P, Vergote J, Barc C, Chalon S, Kung MP, Kung HF, Guilloteau D (2008) IMPY, a potential beta-amyloid imaging probe for detection of prion deposits in scrapie-infected mice. Nucl Med Biol 35(2):197–201

Sperling R, Johnson K (2010) Pro: can biomarkers be gold standards in Alzheimer's disease? Alzheimers Res Ther 2(3):17

Sperling RA, Aisen PS, Beckett LA, Bennett DA, Craft S, Fagan AM, Iwatsubo T, Jack CR Jr, Kaye J, Montine TJ, Park DC, Reiman EM, Rowe CC, Siemers E, Stern Y, Yaffe K, Carrillo MC, Thies B, Morrison-Bogorad M, Wagster MV, Phelps CH (2011a) Toward defining the preclinical stages of Alzheimer's disease: recommendations from the National Institute on Aging-Alzheimer's Association workgroups on diagnostic guidelines for Alzheimer's disease. Alzheimers Dement 7(3):280–292

Sperling RA, Jack CR Jr, Aisen PS (2011b) Testing the right target and right drug at the right stage. Sci Transl Med 3(111):111cm133

Sperling RA, Jack CR Jr, Black SE, Frosch MP, Greenberg SM, Hyman BT, Scheltens P, Carrillo MC, Thies W, Bednar MM, Black RS, Brashear HR, Grundman M, Siemers ER, Feldman HH, Schindler RJ (2011c) Amyloid-related imaging abnormalities in amyloid-modifying therapeutic trials: recommendations from the Alzheimer's Association research roundtable workgroup. Alzheimers Dement 7(4):367–385

Sperling RA, Johnson KA, Doraiswamy PM, Reiman EM, Fleisher AS, Sabbagh MN, Sadowsky CH, Carpenter A, Davis MD, Lu M, Flitter M, Joshi AD, Clark CM, Grundman M, Mintun MA, Skovronsky DM, Pontecorvo MJ (2012) Amyloid deposition detected with florbetapir F 18 ((18)F-AV-45) is related to lower episodic memory performance in clinically normal older individuals. Neurobiol Aging 34(3):822–831

Sperling RA, Laviolette PS, O'Keefe K, O'Brien J, Rentz DM, Pihlajamaki M, Marshall G, Hyman BT, Selkoe DJ, Hedden T, Buckner RL, Becker JA, Johnson KA (2009) Amyloid deposition is associated with impaired default network function in older persons without dementia. Neuron 63(2):178–188

Sperling RA, Mormino EC, Schultz AP, Betensky RA, Papp KV, Amariglio RE, Hanseeuw BJ, Buckley R, Chhatwal J, Hedden T, Marshall GA, Quiroz YT, Donovan NJ, Jackson J, Gatchel JR, Rabin JS, Jacobs H, Yang HS, Properzi M, Kirn DR, Rentz DM, Johnson KA (2019) The

impact of amyloid-beta and tau on prospective cognitive decline in older individuals. Ann Neurol 85(2):181–193

Sperling RA, Rentz DM, Johnson KA, Karlawish J, Donohue M, Salmon DP, Aisen P (2014) The A4 study: stopping AD before symptoms begin? Sci Transl Med 6(228):228fs213

Stern Y (2002) What is cognitive reserve? Theory and research application of the reserve concept. J Int Neuropsychol Soc 8(3):448–460

Storandt M, Head D, Fagan AM, Holtzman DM, Morris JC (2012) Toward a multifactorial model of Alzheimer disease. Aging, Neurobiol

Strozyk D, Blennow K, White LR, Launer LJ (2003) CSF Abeta 42 levels correlate with amyloid-neuropathology in a population-based autopsy study. Neurology 60(4):652–656

Su Y, Flores S, Wang G, Hornbeck RC, Speidel B, Joseph-Mathurin N, Vlassenko AG, Gordon BA, Koeppe RA, Klunk WE, Jack CR Jr, Farlow MR, Salloway S, Snider BJ, Berman SB, Roberson ED, Brosch J, Jimenez-Velazques I, van Dyck CH, Galasko D, Yuan SH, Jayadev S, Honig LS, Gauthier S, Hsiung GR, Masellis M, Brooks WS, Fulham M, Clarnette R, Masters CL, Wallon D, Hannequin D, Dubois B, Pariente J, Sanchez-Valle R, Mummery C, Ringman JM, Bottlaender M, Klein G, Milosavljevic-Ristic S, McDade E, Xiong C, Morris JC, Bateman RJ, Benzinger TLS (2019) Comparison of Pittsburgh compound B and florbetapir in cross-sectional and longitudinal studies. Alzheimers Dement (Amst) 11:180–190

Sunderland T, Gur RE, Arnold SE (2005) The use of biomarkers in the elderly: current and future challenges. Biol Psychiatry 58(4):272–276

Sundgren-Andersson AK, Svensson SPS, Swahn BM, Juréus A, Sandell J, Johnson AE, Jeppsson F, Neelissen JAM, Halldin C, Johnström P, Schou M, Cselényi Z, Farde L (2009) AZD4694: Fluorinated Positron Emission Tomography (PET) radioligand for detection of beta-amyloid deposits. Alzheimers Dement 5(4, Supplement 1):P267–P268. [abstract]

Suo Z, Wu M, Citron BA, Wong GT, Festoff BW (2004) Abnormality of G-protein-coupled receptor kinases at prodromal and early stages of Alzheimer's disease: an association with early beta-amyloid accumulation. J Neurosci 24(13):3444–3452

Sur C, Zeng Z, Hostetler E, Connolly BM, Miller PJ, O'Malley S, Chen T, Culberson C, Harrison S, Mulhearn J, Wolkenberg S, Barrow J, Sanabria S, Cook JJ, Hargreaves R, Williams DL (2010) In vitro characterization of MK-3328: a novel fluorinated positron emission tomography tracer for beta-amyloid plaques. Alzheimers Dement 6(4):S40

Taniguchi S, McDonagh AM, Pickering-Brown SM, Umeda Y, Iwatsubo T, Hasegawa M, Mann DM (2004) The neuropathology of frontotemporal lobar degeneration with respect to the cytological and biochemical characteristics of tau protein. Neuropathol Appl Neurobiol 30(1):1–18

Tenovuo O, Kemppainen N, Aalto S, Nagren K, Rinne JO (2008) Posterior cortical atrophy: a rare form of dementia with in vivo evidence of amyloid-beta accumulation. J Alzheimers Dis 15(3):351–355

Thal DR, Beach TG, Zanette M, Heurling K, Chakrabarty A, Ismail A, Smith AP, Buckley C (2015) [(18)F]flutemetamol amyloid positron emission tomography in preclinical and symptomatic Alzheimer's disease: specific detection of advanced phases of amyloid-beta pathology. Alzheimers Dement 11(8):975–985

Thal DR, Beach TG, Zanette M, Lilja J, Heurling K, Chakrabarty A, Ismail A, Farrar G, Buckley C, Smith APL (2018) Estimation of amyloid distribution by [(18)F]flutemetamol PET predicts the neuropathological phase of amyloid beta-protein deposition. Acta Neuropathol 136(4):557–567

Thal DR, Del Tredici K, Braak H (2004) Neurodegeneration in normal brain aging and disease. Sci Aging Knowledge Environ 2004(23):pe26

Thal LJ, Kantarci K, Reiman EM, Klunk WE, Weiner MW, Zetterberg H, Galasko D, Pratico D, Griffin S, Schenk D, Siemers E (2006) The role of biomarkers in clinical trials for Alzheimer disease. Alzheimer Dis Assoc Disord 20(1):6–15

Thompson PW, Ye L, Morgenstern JL, Sue L, Beach TG, Judd DJ, Shipley NJ, Libri V, Lockhart A (2009) Interaction of the amyloid imaging tracer FDDNP with hallmark Alzheimer's disease pathologies. J Neurochem 109(2):623–630

Thurfjell L, Lotjonen J, Lundqvist R, Koikkalainen J, Soininen H, Waldemar G, Brooks DJ, Vandenberghe R (2012) Combination of biomarkers: PET [F]Flutemetamol imaging and structural MRI in dementia and mild cognitive impairment. Neurodegener Dis 10(1-4):246–249

Tolboom N, van der Flier WM, Yaqub M, Boellaard R, Verwey NA, Blankenstein MA, Windhorst AD, Scheltens P, Lammertsma AA, van Berckel BN (2009a) Relationship of cerebrospinal fluid markers to 11C-PiB and 18F-FDDNP binding. J Nucl Med 50(9):1464–1470

Tolboom N, Yaqub M, van der Flier WM, Boellaard R, Luurtsema G, Windhorst AD, Barkhof F, Scheltens P, Lammertsma AA, van Berckel BN (2009b) Detection of Alzheimer pathology in vivo using both 11C-PIB and 18F-FDDNP PET. J Nucl Med 50(2):191–197

Toledo JB, Bjerke M, Da X, Landau SM, Foster NL, Jagust W, Jack C Jr, Weiner M, Davatzikos C, Shaw LM, Trojanowski JQ, Alzheimer's Disease Neuroimaging Initiative Investigators (2015) Nonlinear association between cerebrospinal fluid and florbetapir F-18 beta-amyloid measures across the spectrum of Alzheimer disease. JAMA Neurol 72(5):571–581

Toledo JB, Xie SX, Trojanowski JQ, Shaw LM (2013) Longitudinal change in CSF tau and Abeta biomarkers for up to 48 months in ADNI. Acta Neuropathol 126(5):659–670

Tomiyama T, Nagata T, Shimada H, Teraoka R, Fukushima A, Kanemitsu H, Takuma H, Kuwano R, Imagawa M, Ataka S, Wada Y, Yoshioka E, Nishizaki T, Watanabe Y, Mori H (2008) A new amyloid beta variant favoring oligomerization in Alzheimer's-type dementia. Ann Neurol 63(3):377–387

Tosun D, Schuff N, Mathis CA, Jagust W, Weiner MW (2011) Spatial patterns of brain amyloid-beta burden and atrophy rate associations in mild cognitive impairment. Brain 134(Pt 4):1077–1088

Trojanowski JQ (2002) Emerging Alzheimer's disease therapies: focusing on the future. Neurobiol Aging 23(6):985–990

Tucker AM, Stern Y (2011) Cognitive reserve in aging. Curr Alzheimer Res 8(4):354–360

Vandenberghe R, Van Laere K, Ivanoiu A, Salmon E, Bastin C, Triau E, Hasselbalch S, Law I, Andersen A, Korner A, Minthon L, Garraux G, Nelissen N, Bormans G, Buckley C, Owenius R, Thurfjell L, Farrar G, Brooks DJ (2010) 18F-flutemetamol amyloid imaging in Alzheimer disease and mild cognitive impairment: a phase 2 trial. Ann Neurol 68(3):319–329

Vemuri P, Lesnick TG, Przybelski SA, Knopman DS, Lowe VJ, Graff-Radford J, Roberts RO, Mielke MM, Machulda MM, Petersen RC, Jack CR Jr (2017) Age, vascular health, and Alzheimer disease biomarkers in an elderly sample. Ann Neurol 82(5):706–718

Venneti S, Lopresti BJ, Wiley CA (2006) The peripheral benzodiazepine receptor (translocator protein 18kDa) in microglia: from pathology to imaging. Prog Neurobiol 80(6):308–322

Verfaillie SCJ, Timmers T, Slot RER, van der Weijden CWJ, Wesselman LMP, Prins ND, Sikkes SAM, Yaqub M, Dols A, Lammertsma AA, Scheltens P, Ossenkoppele R, van Berckel BNM, van der Flier WM (2019) Amyloid-beta load is related to worries, but not to severity of cognitive complaints in individuals with subjective cognitive decline: the SCIENCe project. Front Aging Neurosci 11:7

Verhoeff NP, Wilson AA, Takeshita S, Trop L, Hussey D, Singh K, Kung HF, Kung MP, Houle S (2004) In-vivo imaging of Alzheimer disease beta-amyloid with [11C]SB-13 PET. Am J Geriatr Psychiatry 12(6):584–595

Vernooij MW, van der Lugt A, Ikram MA, Wielopolski PA, Niessen WJ, Hofman A, Krestin GP, Breteler MM (2008) Prevalence and risk factors of cerebral microbleeds: the Rotterdam scan study. Neurology 70(14):1208–1214

Villain N, Chetelat G, Grassiot B, Bourgeat P, Jones G, Ellis KA, Ames D, Martins RN, Eustache F, Salvado O, Masters CL, Rowe CC, Villemagne VL (2012) Regional dynamics of amyloid-beta deposition in healthy elderly, mild cognitive impairment and Alzheimer's disease: a voxelwise PiB-PET longitudinal study. Brain 135(Pt 7):2126–2139

Villemagne VL, Ataka S, Mizuno T, Brooks WS, Wada Y, Kondo M, Jones G, Watanabe Y, Mulligan R, Nakagawa M, Miki T, Shimada H, O'Keefe GJ, Masters CL, Mori H, Rowe CC (2009a) High striatal amyloid beta-peptide deposition across different autosomal Alzheimer disease mutation types. Arch Neurol 66(12):1537–1544

Villemagne VL, Burnham S, Bourgeat P, Brown B, Ellis KA, Salvado O, Szoeke C, Macaulay SL, Martins R, Maruff P, Ames D, Rowe CC, Masters CL (2013) Amyloid beta deposition,

neurodegeneration, and cognitive decline in sporadic Alzheimer's disease: a prospective cohort study. Lancet Neurol 12(4):357–367

Villemagne VL, Cappai R, Barnham KJ, Cherny R, Opazo C, Novakovic KE, Rowe CC, Masters CL (2006) The Aβ centric pathway of Alzheimer's disease. In: Barrow CJ, Small BJ (eds) Abeta Peptide and Alzheimer's Disease. Springer-Verlag, London, pp 5–32

Villemagne VL, Dore V, Burnham SC, Masters CL, Rowe CC (2018) Imaging tau and amyloid-beta proteinopathies in Alzheimer disease and other conditions. Nat Rev Neurol 14(4):225–236

Villemagne VL, Fodero-Tavoletti MT, Masters CL, Rowe CC (2015) Tau imaging: early progress and future directions. Lancet Neurol 14(1):114–124

Villemagne VL, Fodero-Tavoletti MT, Pike KE, Cappai R, Masters CL, Rowe CC (2008a) The ART of loss: Aβ imaging in the evaluation of Alzheimer's disease and other dementias. Mol Neurobiol 38(1):1–15

Villemagne VL, Furumoto S, Fodero-Tavoletti MT, Mulligan RS, Hodges J, Piguet O, Pejoska S, Kudo Y, Masters CL, Yanai K, Rowe CC, Okamura N (2012a) In vivo tau imaging in Alzheimer's disease and other dementias. Alzheimers Dement 8(4):P9

Villemagne VL, Kim S, Rowe CC, Iwatsubo T (2014) Imago Mundi, Imago AD, Imago ADNI. Alzheimers Res Ther 6:62

Villemagne VL, Klunk WE, Mathis CA, Rowe CC, Brooks DJ, Hyman BT, Ikonomovic MD, Ishii K, Jack CR, Jagust WJ, Johnson KA, Koeppe RA, Lowe VJ, Masters CL, Montine TJ, Morris JC, Nordberg A, Petersen RC, Reiman EM, Selkoe DJ, Sperling RA, Van Laere K, Weiner MW, Drzezga A (2012b) Abeta imaging: feasible, pertinent, and vital to progress in Alzheimer's disease. Eur J Nucl Med Mol Imaging 39(2):209–219

Villemagne VL, McLean CA, Reardon K, Boyd A, Lewis V, Klug G, Jones G, Baxendale D, Masters CL, Rowe CC, Collins SJ (2009b) 11C-PiB PET studies in typical sporadic Creutzfeldt-Jakob disease. J Neurol Neurosurg Psychiatry 80(9):998–1001

Villemagne VL, Mulligan RS, Pejoska S, Ong K, Jones G, O'Keefe G, Chan JG, Young K, Tochon-Danguy H, Masters CL, Rowe CC (2012c) Comparison of (11)C-PiB and (18)F-florbetaben for Aβ imaging in ageing and Alzheimer's disease. Eur J Nucl Med Mol Imaging 39(6):983–989

Villemagne VL, Okamura N, Pejoska S, Drago J, Mulligan RS, Chetelat G, O'Keefe G, Jones G, Kung HF, Pontecorvo M, Masters CL, Skovronsky DM, Rowe CC (2012d) Differential diagnosis in Alzheimer's disease and dementia with Lewy bodies via VMAT2 and amyloid imaging. Neurodegener Dis 10(1–4):161–165

Villemagne VL, Ong K, Mulligan RS, Holl G, Pejoska S, Jones G, O'Keefe G, Ackerman U, Tochon-Danguy H, Chan JG, Reininger CB, Fels L, Putz B, Rohde B, Masters CL, Rowe CC (2011a) Amyloid imaging with 18F-Florbetaben in Alzheimer disease and other dementias. J Nucl Med 52(8):1210–1217

Villemagne VL, Pike K, Pejoska S, Boyd A, Power M, Jones G, Masters CL, Rowe CC (2010) ^{11}C-PiB PET ABri imaging in Worster-drought syndrome (familial British dementia): a case report. J Alzheimers Dis 19(2):423–428

Villemagne VL, Pike KE, Chetelat G, Ellis KA, Mulligan RS, Bourgeat P, Ackermann U, Jones G, Szoeke C, Salvado O, Martins R, O'Keefe G, Mathis CA, Klunk WE, Ames D, Masters CL, Rowe CC (2011b) Longitudinal assessment of Aβ and cognition in aging and Alzheimer disease. Ann Neurol 69(1):181–192

Villemagne VL, Pike KE, Darby D, Maruff P, Savage G, Ng S, Ackermann U, Cowie TF, Currie J, Chan SG, Jones G, Tochon-Danguy H, O'Keefe G, Masters CL, Rowe CC (2008b) Aβ deposits in older non-demented individuals with cognitive decline are indicative of preclinical Alzheimer's disease. Neuropsychologia 46(6):1688–1697

Villemagne VL, Rowe CC (2010) Amyloid ligands for dementia. PET Clin 5:33–53

Villemagne VL, Rowe CC, Macfarlane S, Novakovic KE, Masters CL (2005) Imaginem oblivionis: the prospects of neuroimaging for early detection of Alzheimer's disease. J Clin Neurosci 12(3):221–230

Viswanathan A, Rocca WA, Tzourio C (2009) Vascular risk factors and dementia: how to move forward? Neurology 72(4):368–374

Villemagne VL, Furumoto S., Fodero-Tavoletti MT, Harada R, Mulligan RS, Kudo T, Masters CL, Rowe CC, Okamura N (2012) The Challenges of Tau Imaging. Future Neurol 7(4) 409–421

Vlassenko AG, Mintun MA, Xiong C, Sheline YI, Goate AM, Benzinger TL, Morris JC (2011) Amyloid-beta plaque growth in cognitively normal adults: longitudinal [11C]Pittsburgh compound B data. Ann Neurol 70(5):857–861

Wahlund LO, Blennow K (2003) Cerebrospinal fluid biomarkers for disease stage and intensity in cognitively impaired patients. Neurosci Lett 339(2):99–102

Walker LC, Rosen RF, Levine H 3rd (2008) Diversity of Abeta deposits in the aged brain: a window on molecular heterogeneity? Romanian J Morphol Embryol 49(1):5–11

Wang G, Xiong C, McDade EM, Hassenstab J, Aschenbrenner AJ, Fagan AM, Benzinger TLS, Gordon BA, Morris JC, Li Y, Bateman RJ, Dominantly Inherited Alzheimer Network (DIAN) (2018) Simultaneously evaluating the effect of baseline levels and longitudinal changes in disease biomarkers on cognition in dominantly inherited Alzheimer's disease. Alzheimers Dement (N Y) 4:669–676

Weiner MW, Harvey D, Hayes J, Landau SM, Aisen PS, Petersen RC, Tosun D, Veitch DP, Jack CR Jr, Decarli C, Saykin AJ, Grafman J, Neylan TC, Department of Defense Alzheimer's Disease Neuroimaging Initiative (2017) Effects of traumatic brain injury and posttraumatic stress disorder on development of Alzheimer's disease in Vietnam veterans using the Alzheimer's disease neuroimaging initiative: preliminary report. Alzheimers Dement (N Y) 3(2):177–188

Weller RO, Preston SD, Subash M, Carare RO (2009) Cerebral amyloid angiopathy in the aetiology and immunotherapy of Alzheimer disease. Alzheimers Res Ther 1(2):6

Wermke M, Sorg C, Wohlschlager AM, Drzezga A (2008) A new integrative model of cerebral activation, deactivation and default mode function in Alzheimer's disease. Eur J Nucl Med Mol Imaging 35(Suppl 1):S12–S24

Wiley CA, Lopresti BJ, Venneti S, Price J, Klunk WE, DeKosky ST, Mathis CA (2009) Carbon 11-labeled Pittsburgh compound B and carbon 11-labeled (R)-PK11195 positron emission tomographic imaging in Alzheimer disease. Arch Neurol 66(1):60–67

Winblad B, Palmer K, Kivipelto M, Jelic V, Fratiglioni L, Wahlund LO, Nordberg A, Backman L, Albert M, Almkvist O, Arai H, Basun H, Blennow K, de Leon M, DeCarli C, Erkinjuntti T, Giacobini E, Graff C, Hardy J, Jack C, Jorm A, Ritchie K, van Duijn C, Visser P, Petersen RC (2004) Mild cognitive impairment--beyond controversies, towards a consensus: report of the international working group on mild cognitive impairment. J Intern Med 256(3):240–246

Wolk DA, Grachev ID, Buckley C, Kazi H, Grady MS, Trojanowski JQ, Hamilton RH, Sherwin P, McLain R, Arnold SE (2011) Association between in vivo fluorine 18-labeled flutemetamol amyloid positron emission tomography imaging and in vivo cerebral cortical histopathology. Arch Neurol 68(11):1398–1403

Wolk DA, Price JC, Madeira C, Saxton JA, Snitz BE, Lopez OL, Mathis CA, Klunk WE, Dekosky ST (2012a) Amyloid imaging in dementias with atypical presentation. Alzheimers Dement 8(5):389–398

Wolk DA, Price JC, Saxton JA, Snitz BE, James JA, Lopez OL, Aizenstein HJ, Cohen AD, Weissfeld LA, Mathis CA, Klunk WE, DeKosky ST (2009) Amyloid imaging in mild cognitive impairment subtypes. Ann Neurol 65(5):557–568

Wolk DA, Zhang Z, Boudhar S, Clark CM, Pontecorvo MJ, Arnold SE (2012b) Amyloid imaging in Alzheimer's disease: comparison of florbetapir and Pittsburgh compound-B positron emission tomography. J Neurol Neurosurg Psychiatry 83(9):923–926

Wong DF, Moghekar AR, Rigamonti D, Brasic JR, Rousset O, Willis W, Buckley C, Smith A, Gok B, Sherwin P, Grachev ID (2012) An in vivo evaluation of cerebral cortical amyloid with [(18)F]Flutemetamol using positron emission tomography compared with parietal biopsy samples in living Normal pressure hydrocephalus patients. Mol Imaging Biol 15(2):230–237

Wong DF, Rosenberg PB, Zhou Y, Kumar A, Raymont V, Ravert HT, Dannals RF, Nandi A, Brasic JR, Ye W, Hilton J, Lyketsos C, Kung HF, Joshi AD, Skovronsky DM, Pontecorvo MJ (2010) In vivo imaging of amyloid deposition in Alzheimer disease using the radioligand 18F-AV-45 (florbetapir [corrected] F 18). J Nucl Med 51(6):913–920

Yates PA, Sirisriro R, Villemagne VL, Farquharson S, Masters CL, Rowe CC (2011) Cerebral microhemorrhage and brain {beta}-amyloid in aging and Alzheimer disease. Neurology 77(1):48–54

Ye L, Morgenstern JL, Gee AD, Hong G, Brown J, Lockhart A (2005) Delineation of positron emission tomography imaging agent binding sites on beta-amyloid peptide fibrils. J Biol Chem 280(25):23599–23604

Ye L, Velasco A, Fraser G, Beach TG, Sue L, Osredkar T, Libri V, Spillantini MG, Goedert M, Lockhart A (2008) In vitro high affinity alpha-synuclein binding sites for the amyloid imaging agent PIB are not matched by binding to Lewy bodies in postmortem human brain. J Neurochem 105(4):1428–1437

Yee S, Mathis C, Klunk W, Weissfeld L, Lopresti B, Bi W, Ziolko S, Berginc M, DeKosky S, Price J (2007) Optimal time window for standardized uptake ratio as a simplified measure of PIB retention. J Nucl Med 48:404

Yokokura M, Mori N, Yagi S, Yoshikawa E, Kikuchi M, Yoshihara Y, Wakuda T, Sugihara G, Takebayashi K, Suda S, Iwata Y, Ueki T, Tsuchiya KJ, Suzuki K, Nakamura K, Ouchi Y (2011) In vivo changes in microglial activation and amyloid deposits in brain regions with hypometabolism in Alzheimer's disease. Eur J Nucl Med Mol Imaging 38(2):343–351

Zhang W, Oya S, Kung MP, Hou C, Maier DL, Kung HF (2005a) F-18 Polyethyleneglycol stilbenes as PET imaging agents targeting Abeta aggregates in the brain. Nucl Med Biol 32(8):799–809

Zhang W, Oya S, Kung MP, Hou C, Maier DL, Kung HF (2005b) F-18 stilbenes as PET imaging agents for detecting beta-amyloid plaques in the brain. J Med Chem 48(19):5980–5988

Zwan MD, Bouwman FH, Konijnenberg E, van der Flier WM, Lammertsma AA, Verhey FR, Aalten P, van Berckel BN, Scheltens P (2017) Diagnostic impact of [(18)F]flutemetamol PET in early-onset dementia. Alzheimers Res Ther 9(1):2

PET Imaging of the α4β2* Nicotinic Acetylcholine Receptors in Alzheimer's Disease

11

Osama Sabri, Philipp M. Meyer, Hermann-Josef Gertz, Solveig Tiepolt, Peter Brust, Henryk Barthel, and Swen Hesse

Contents

11.1 Introduction 347
11.2 Pathogenesis of AD 348
11.3 Radioligands for Imaging the Cholinergic System 348
11.4 Imaging of α4β2*-nAChRs 348
11.5 2-FA-PET to Assess α4β2*-nAChR Binding in AD: Findings of Monocentric Studies 349
11.5.1 2-FA-PET: Methods 350
11.5.2 2-FA-PET: Results and Discussion 351
11.6 Monocentre 2-FA-PET Data in Context with Other Available PET/SPECT Studies on α4β2*-nAChR Binding in AD/MCI 354
11.6.1 Own Data 354
11.6.2 Differences and Similarities Between the nAChR PET/SPECT Studies Conducted So Far in AD 355

The asterisk used in the receptor nomenclature indicates that the receptor complex may contain additional subunits.

Osama Sabri and Philipp M. Meyer contributed equally to this work.

O. Sabri (✉) · P. M. Meyer · S. Tiepolt · H. Barthel · S. Hesse
Department of Nuclear Medicine, University Hospital Leipzig, University of Leipzig, Leipzig, Germany
e-mail: osama.sabri@medizin.uni-leipzig.de; Philipp.Meyer@medizin.uni-leipzig.de; Solveig.Tiepolt@medizin.uni-leipzig.de; Henryk.Barthel@medizin.uni-leipzig.de; Swen.Hesse@medizin.uni-leipzig.de

H.-J. Gertz
Department of Psychiatry and Psychotherapy, University Hospital Leipzig, University of Leipzig, Leipzig, Germany
e-mail: Hermann-Josef.Gertz@medizin.uni-leipzig.de

P. Brust
Institute of Radiopharmacy, Helmholtz-Zentrum Dresden-Rossendorf, Leipzig, Germany
e-mail: P.Brust@HZDR.de

R. A. J. O. Dierckx et al. (eds.), *PET and SPECT in Neurology*,
https://doi.org/10.1007/978-3-030-53168-3_11

11.6.3 Possible Reasons for Discrepancies Between the Different PET/SPECT Studies..... 355
11.7 Second-Generation Radiotracers for Imaging α4β2*-nAChRs..... 356
11.8 Future Directions..... 359
11.9 Conclusions..... 360
References..... 360

Abstract

Alzheimer's disease (AD) is a progressive neurodegenerative disease and the most common form of dementia in the elderly. The subunits α4 and β2 of the nicotinic acetylcholine receptors (α4β2*-nAChRs) are widely abundant throughout the human brain and play an important role as neuromodulators in different neuronal systems. They are particularly important for cognitive functions and the loss of α4β2*-nAChRs, especially in cholinergic neurons may underlie memory loss in AD. Postmortem autoradiographic and immunohistochemical studies identified cortical and subcortical reductions in α4β2*-nAChR binding in patients with AD. Recently, the α4β2*-nAChR-specific PET and SPECT tracers 2-[^{18}F]FA-85380 (2-FA) and 5-[^{123}I]IA-85380 (5-IA) were developed enabling to study the α4β2*-nAChR availability in the living human brain. With such specific radioligands, α4β2*-nAChR binding and its association to cognitive symptoms can be quantitatively determined in patients with AD and mild cognitive impairment (MCI). Initial results show that α4β2*-nAChR availability is reduced in AD but also in amnestic MCI patients who progressed into AD. Hence, the prediction of conversion from MCI to AD seems to be feasible, and therefore, quantitative assessment of α4β2*-nAChR binding using 2-FA-PET or 5-IA-SPECT might become an early biomarker of mental dysfunction in AD. Novel, second-generation α4β2*-nAChR PET radioligands, characterized by faster kinetics, higher receptor affinity and selectivity, have been developed recently. Two first-in-human PET studies using the second-generation α4β2*-nAChR PET radioligands (-)[^{18}F]Flubatine and (+)[^{18}F]Flubatine, carried out successfully in patients with mild Alzheimer disease and healthy controls, showed promising results.

Abbreviations

2-FA	2-[^{18}F]F-A85380
5-IA	5-[^{123}I]I-A85380
AD	Alzheimer's disease
APP	β-amyloid-precursor protein
BP	Binding potential
CC	Corpus callosum

CERAD	Consortium to Establish a Registry for Alzheimer's Disease
CSF	Cerebrospinal fluid
DV	Distribution volume
DVR	Distribution volume ratio
DVS	Specific binding of the distribution volume
FWHM	Full width at half maximum
HC	Healthy controls
MCI	Mild cognitive impairment
MMSE	Mini-Mental State Examination
MRI	Magnetic resonance imaging
NINCDS-ADRDA	National Institute of Neurological and Communicative Disorders and Stroke and the Alzheimer's Disease and Related Disorders Association
NINDS-AIREN	National Institute of Neurological Disorder and Stroke-Association International pour la Recherche et l'Enseignement en Neurosciences
PET	Positron emission tomography
ROI	Region of interest
SPECT	Single-photon emission computed tomography
SPM	Statistical Parametric Mapping
VaD	Vascular dementia
α4β2*-nAChR	α4β2*-nicotinic acetylcholine receptor

11.1 Introduction

Clinical hallmarks of dementia are progressive memory loss and impairment of other cognitive functions such as aphasia, apraxia and agnosia, together with general cognitive symptoms significantly interfering with activities of daily living (Berti et al. 2011). Alzheimer's disease (AD) is a progressive neurodegenerative disorder, the most frequent form of dementia in the elderly causing 50–60% of all cases of dementia (Bohnen et al. 2012). The incidence of AD doubles in frequency every 5 years after 60 years of age, and therefore AD is becoming an increasingly important challenge for the healthcare systems as the elderly population grows (Cummings 2008). Late-onset AD is the most common form of AD (95%) with an onset older than 65 years of age. In contrast, early-onset AD with an onset younger than 65 years is much less common (5%) (van der Flier et al. 2011). According to a hypothetical model of biomarker dynamics in AD, new biomarkers, such as PET with β-amyloid-targeting radioligands, β-amyloid in the cerebrospinal fluid (CSF), [^{18}F]FDG-PET, structural MRI or tau-CSF, shift sensitivity to detect AD to the preclinical stage (Jack et al. 2010). In order to enhance the clinical diagnostic accuracy, these new biomarkers were implemented in the revised diagnostic guidelines for Alzheimer's disease recommended by the National Institute on Aging-Alzheimer's Association workgroups (NIA-AA; McKhann et al. 2011).

11.2 Pathogenesis of AD

The neurotransmitter acetylcholine appears to be particularly important for memory, and the loss of cholinergic neurons in particular in the basal forebrain may underlie the memory loss in AD (Francis et al. 1999). In AD, the cholinergic dysfunctions are accompanied by the occurrence of two major histopathological hallmarks of AD, the β-amyloid plaques and neurofibrillary tangles. Dysfunctional cholinergic neurotransmission may take part in the β-amyloid plaque pathology by compromising the β-amyloid-precursor protein (APP) processing in AD (Schliebs and Arendt 2011; Schliebs 2005). Preclinical data suggest that low levels of soluble β-amyloid modulate cholinergic synaptic function (e.g. nAChR) accompanied by impaired learning and memory before significant amyloid plaque loads occur (Schliebs 2005; Klingner et al. 2003; Lesné et al. 2006). The deposition of the amyloid plaques is followed by inflammatory reactions such as upregulation of interleukin-1 mediated by glia cells. This glial cell-mediated upregulation of interleukin-1 might again affect APP and lead to cholinergic dysfunction. Understanding the pathophysiology underlying the close association between cortical cholinergic dysfunction, β-amyloid processing and immunological mechanisms will help to find better treatment strategies in AD (Schliebs 2005). These findings suggest that PET and SPECT imaging of cholinergic deficits, in particular nAChR, may be more sensitive even than amyloid plaque PET and may serve as a predictor early in the course of AD (Klingner et al. 2003; Schliebs 2005; Lesné et al. 2006; Buckingham et al. 2009; Schliebs and Arendt 2011).

11.3 Radioligands for Imaging the Cholinergic System

The density of nAChR in the brain is rather low with highest density in the thalamus. More recently, suitable, high-affinity α4β2*-nAChR-specific radioligands, such as 5-[^{123}I]IA-85380 (5-IA) for SPECT and 6-[^{18}F]FA-85380 (6-FA) and 2-[^{18}F]FA-85380 (2-FA) for PET imaging, were developed, and the synthesis further improved (Mamede et al. 2004; Ding et al. 2004; Schildan et al. 2007; Kimes et al. 2003). In comparison, [^{11}C]nicotine is less suitable as a PET radioligand since it has high levels of nonspecific binding and blood flow dependence (Nordberg et al. 1995; Nordberg 2001). Radioligands targeting the vesicular acetylcholine transporter ([^{123}I]vesamicol) or acetylcholinesterase ([^{11}C]PMP) are likely to show reductions later than α4β2*-nAChRs in the time course of AD (Rinne et al. 2003; Kuhl et al. 1996).

11.4 Imaging of α4β2*-nAChRs

The α4β2*-nAChRs are ligand-gated channels, widely expressed throughout the brain, and play an important role as neuromodulators participating in a variety of cognitive functions such as attention, learning and memory (Dani and Bertrand

2007). There is evidence from postmortem autoradiographic and immunohistochemical studies that already early in AD, there is a substantial decline in α4β2*-nAChRs in cortical and subcortical brain areas (Perry et al. 1995; Rinne et al. 1991; Nordberg 2001). Accordingly, the pre- and post-synaptically located α4β2*-nAChRs, which are the most abundant subtypes in the brain, represent one of the major diagnostic and pharmacological targets for PET imaging studies. 2-FA and PET allow absolute quantitative assessment of the α4β2*-nAChR availability in the living human brain in AD and normal subjects. Using clinical scales to measure the severity of cognitive dysfunction, such as the Mini-Mental State Examination (MMSE), DemTect and CERAD, the association patterns of altered α4β2*-nAChR binding that may underlie cognitive dysfunction in AD can be determined in vivo (Sabri et al. 2008; Kendziorra et al. 2011).

11.5 2-FA-PET to Assess α4β2*-nAChR Binding in AD: Findings of Monocentric Studies

Using 2-FA-PET and clinical and cognitive measures, the authors aimed to investigate α4β2*-nAChR binding in AD, MCI and healthy controls (HC). The hypotheses were tested whether (1) there is a reduction of α4β2*-nAChRs in AD, (2) this reduction correlates with the clinical severity of dementia, (3) there is abnormal α4β2*-nAChR availability in MCI, (4) 2-FA-PET is sensitive to predict which of the MCI converts to AD in the clinical follow-up and (5) there is abnormal α4β2*-nAChR availability correlating to cognitive impairment in vascular dementia (communicated by Sabri et al. 1999) since cholinergic drugs, known to be effective in AD, can have similar beneficial effects in vascular dementia (Erkinjuntti et al. 2002).

Here we review previously published own studies: (1) results of a pilot cohort of three age-matched groups of mild to moderate AD (n = 9, age 66 ± 7 years, MMSE 18.3 ± 5.8, range 10–24), amnestic MCI (n = 8, age 61 ± 7 years, MMSE 26.8 ± 1.7, range 25–29) and healthy controls (HC; n = 7, age 61 ± 9 years, MMSE 29.6 ± 0.8, range 28–30) (Kendziorra et al. 2011) as well as (2) results of an extended cohort of mild to moderate AD (n = 17, age 70 ± 9 years, MMSE 16.8 ± 5.9, range 8–24), amnestic MCI (n = 6, age 62 ± 8 years, MMSE 26.5 ± 1.5, range 25–29) and HC (n = 10, age 54 ± 13 years, MMSE 29.7 ± 0.7, range 28–30) (Sabri et al. 2008), not age-adjusted yet, and further 2-FA-PET data of patients with amnestic MCI (n = 11), with vascular dementia (VaD, n = 4) and with mixed dementia (n = 4) of a large ongoing PET study. Patients with MCI were clinically followed up to 44 months in order to assess whether they progress to AD (Sabri et al. 2008; Kendziorra et al. 2011). Probable AD was diagnosed by clinical and neuropsychological criteria with the exclusion of other dementia causes (*NINCDS-ADRDA* criteria). MCI was defined according to the MCI consensus criteria by the *International Working Group on Mild Cognitive Impairment* (Winblad et al. 2004). The diagnosis of VaD was made according to published clinical and research criteria and when the lesion load as estimated by means of MRI within the deep white matter lesions was at least 40% (NINDS-AIREN,

National Institute of Neurological Disorder and Stroke-Association International pour la Recherche et l'Enseignement en Neurosciences 1993, Román et al. 1993; Erkinjuntti et al. 2002). All study subjects were nonsmokers and not taking any cholinergic drugs.

11.5.1 2-FA-PET: Methods

Dynamic PET (ECAT EXACT HR+) was performed from 0 to 2 h. Then, a late scan from 6 to 7 h was applied following a short-time bolus infusion (90 s) of 370 MBq 2-FA (Kendziorra et al. 2011; Meyer et al. 2009; Sabri et al. 2008). Of note, the bolus-infusion 2-FA technique has been introduced which is a reasonable alternative to the bolus 2-FA technique and provides valid regional nAChR data with a shorter procedure time (30 min) than bolus only. For accurate nAChR quantification, however, and due to the slow kinetics of 2-FA, PET acquisition time up to 8 h p.i. is still required (Kimes et al. 2008).

The MRI and neuropsychological assessments were performed between scans. To ensure exact repositioning and to avoid head movement artefacts between both PET studies, a thermoplastic mask system was used. The parametric images of the distribution volumes (2-FA-DV) were derived from the PET data applying the Logan plot (10 points between 1 and 7 h p.i.) with an arterial input function correcting for individual plasma protein binding and metabolites of the radioligand. Values of 2-FA-DV are the same as 2-FA-DV/f_p if the DV is computed according to Innis et al. (2007). f_p is the free fraction of the radioligand in the plasma (not bound to plasma proteins). The starting point of 1 h in the Logan plot analysis was utilized because linearity of the Logan plot was hit after 40–50 min in the thalamus, the region with the highest α4β2*-nAChR binding (Kendziorra et al. 2011; Sabri et al. 2008; Sorger et al. 2006, 2007). Both statistical parametric mapping (SPM) and region of interest (ROI) analyses were performed. For the ROI analysis, subcortical and cortical target regions were defined after coregistration of PET with the individual MRI on the overlaid images. The corpus callosum (CC) was used as a reference region, as the tracer uptake in this region is almost non-displaceable by nicotine and as this region contains the lowest density of α4β2*-nAChR in humans (Brody et al. 2006; Meyer et al. 2009). The binding potential (2-FA-BP) or the distribution volume ratio (2-FA-DVR) (used in the SPM analysis; see Figs. 11.1 and 11.2) as the most α4β2*-nAChR-specific measures were calculated as follows:

$$\text{2-FA-BP} = \frac{\left(\text{2-FA-DV}_{\text{target region}} - \text{2-FA-DV}_{\text{reference region}}\right)}{\text{2-FA-DV}_{\text{reference region}}}$$

$$\text{2-FA-DVR} = \frac{\text{2-FA-DV}_{\text{target region}}}{\text{2-FA-DV}_{\text{reference region}}}$$

For the SPM analysis, the 2-FA-DVR was calculated by scaling the 2-FA-DV to the corpus callosum (CC) or the cerebellum. To determine the 2-FA-DVR, 2-FA-DV values within the CC and the cerebellum were assessed by the ROI analysis. For the

SPM analysis brain images of the subjects were spatially normalized to the Talairach space using the [^{15}O]H_2O SPM PET template provided by SPM. The PET data were smoothed with a 12-mm FWHM Gaussian kernel in order to adapt the variation between the individual brains and heighten the signal-to-noise ratio (Kendziorra et al. 2011).

11.5.2 2-FA-PET: Results and Discussion

Both voxel-based (SPM) and ROI-based analyses revealed a widespread, significant reduction of 2-FA binding in the AD and MCI cohort comprising especially the posterior cingulate cortex/precuneus, the temporal cortex and the hippocampus, as well as the thalamus. The reduction pattern was found in both the pilot sample and the extended cohort in AD and MCI (Fig. 11.1). In the extended cohort of AD compared to the pilot cohort of AD, the pattern of lower α4β2*-nAChR binding relative to HC was more widespread, possibly due to the fact that the extended cohort of AD

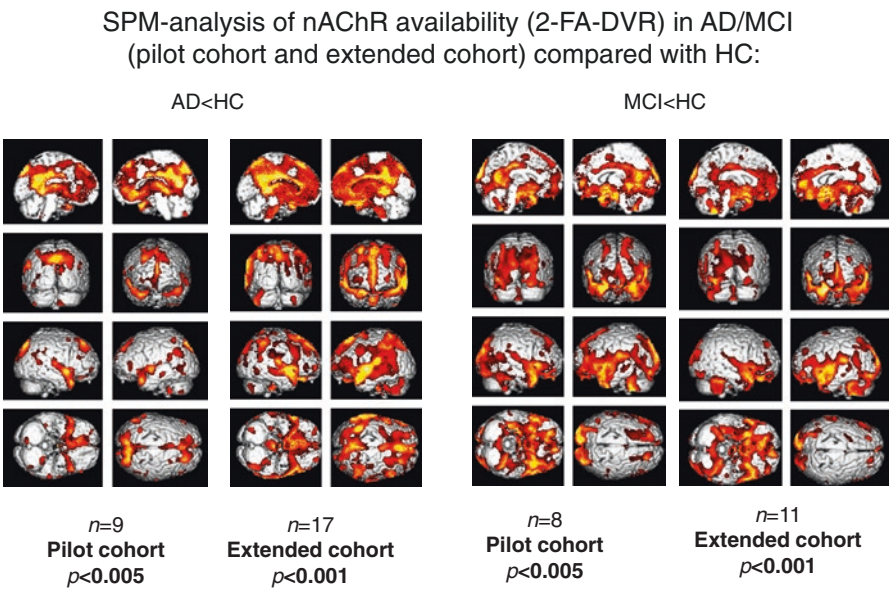

Fig. 11.1 In the SPM analysis the coloured clusters label the significantly lower α4β2*-nAChR availability by assessment of the 2-FA distribution volume ratio (2-FA-DVR) in AD and MCI patients (pilot cohort and extended cohort each) compared with healthy controls. For calculation of 2-FA-DVR, see 2-FA-PET – Methods. Unpaired *t*-test for group comparisons, significance at $p < 0.005$ and $p < 0.001$. Medial views (*top*), posterior view (*second row left*), anterior view (*second row right*), lateral views (*third row*), inferior view (*bottom left*) and superior view (*bottom right*). (Adopted from Kendziorra et al. (2011) with modifications—permission for reproduction by Springer-Verlag)

had a slightly higher degree of dementia as indicated by the lower MMSE (16.8 ± 5.9, $p < 0.05$) compared to the pilot cohort of AD (MMSE 18.3 ± 5.8) (Fig. 11.1, Kendziorra et al. 2011; Sabri et al. 2008). The nAChR reduction pattern corroborates postmortem data and points to a diagnostic capacity of high-affinity α4β2*-nAChR-specific PET radioligands such as 2-FA.

In order to assess whether amnestic MCI later progress to AD, patients were clinically followed with the mean follow-up of our cohorts of 33 months ranging from 24 to 44 months. From the pilot cohort, five out of eight with MCI converted into probably AD (MCI-C), whereas three remained stable (MCI-S; Fig. 11.2). In the extended study cohort, there were seven converters and four cognitively stable patients out of 11 with amnestic MCI (Fig. 11.1). Using 2-FA-PET, HC and AD clearly differed from each other with clear reduction of α4β2*-nAChR binding across the brain in typically AD-affected brain regions especially in the precuneus/posterior cingulate cortex, thalamus, (para)hippocampus, temporal cortex, frontal cortex and caudate nucleus in case of AD (Fig. 11.1). Whereas the cognitively stable MCI (non-converters, MCI-S; Fig. 11.2b) had α4β2*-nAChR binding in the range of HC, the MCI patients later progressing to AD showed a α4β2*-nAChR reduction pattern and values similar to AD (MCI-C; Fig. 11.2a, Kendziorra et al. 2011). This important finding suggests that 2-FA-PET is highly sensitive and capable to predict a later progression from amnestic MCI to AD.

Interestingly, using FDG-PET in amnestic MCI, we found less pronounced and less significant reduced FDG uptake especially in the precuneus/posterior cingulate (MCI-S) and parietotemporal (MCI-C) cortex, suggesting that 2-FA-PET might be more sensitive than FDG-PET to detect abnormalities in amnestic MCI. However, due to the small numbers of the study subjects, further multicentre investigations for verification would be needed (Sabri et al. 2008). Moreover, lower α4β2*-nAChR binding in AD and MCI was significantly related to the degree of cognitive symptoms as assessed by DemTect and MMSE in brain regions typically affected in AD such as the temporal cortex, anterior and posterior cingulate cortex, hippocampus, frontal cortex as well as caudate nucleus (Kendziorra et al. 2011; Sabri et al. 2008).

Also, preliminary analyses in VaD ($n = 4$) defined as having a lesion load greater than 40% of deep white matter indicate that there is a broad reduction of α4β2*-nAChR availability similar to AD. When compared with each other in a ROI analysis, cortical and subcortical grey matter α4β2*-nAChR reduction patterns are similar in AD, mixed dementia or VaD. In contrast, in the white matter, α4β2*-nAChR binding significantly differs between patient groups and compared to HC. In AD white matter, α4β2*-nAChR binding is not reduced; in mixed dementia white matter, there is interestingly a tendency for reduced α4β2*-nAChR binding ($p < 0.01$); and in pure VaD white matter, there is significantly lower α4β2*-nAChR binding. Thus, patients with vascular dementia have additionally significantly reduced α4β2*-nAChR binding in the deep white matter (which is not found in AD), indicating a disrupted integrity of distinct fibre bundles in the brain of VaD.

Cerebral atrophy, especially in patients with moderate AD, and successive atrophy-allocated effects on the 2-FA-PET data are critical and should be taken into

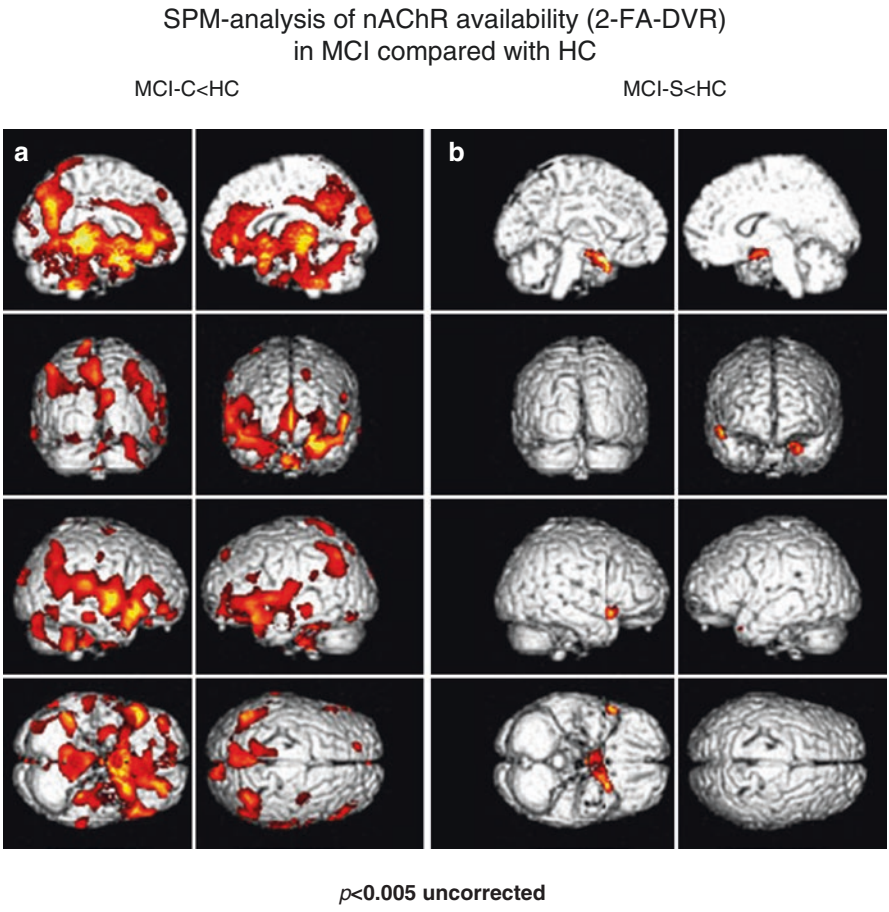

Fig. 11.2 In the SPM analysis, compared with healthy controls, the coloured clusters label the significantly lower α4β2*-nAChR availability by the assessment of the 2-FA distribution volume ratio (*2-FA-DVR*) in MCI who converted to AD (MCI-C, $n = 5$) (**a**) and in MCI who remain stable in the clinical follow-up period and show only minor *2-FA-DVR* changes (**b**) (MCI-S, $n = 3$). For calculation of *2-FA-DVR*, see 2-FA-PET – Methods. Unpaired *t*-test for group comparisons, significance at $p < 0.005$. Medial views (*top*), posterior view (*second row left*), anterior view (*second row right*), lateral views (*third row*), inferior view (*bottom left*) and superior view (*bottom right*). (Adopted from Kendziorra et al. (2011)—permission for reproduction by Springer-Verlag)

account for the interpretation of the PET results. Due to the fact that there is lower nAChR also in amnestic MCI, who have no or only mild brain atrophy, it is conceivable that the findings in AD patients are not primarily a result of atrophy (Kendziorra et al. 2011; Sabri et al. 2008). Also, to diminish atrophy-related effects, individual ROI analysis was performed and irregular, and only appropriate brain tissue-comprising ROIs were assessed by means of individual MRI following MRI/PET coregistration (Kendziorra et al. 2011; Sabri et al. 2008). However, it cannot be

ruled out that cerebral atrophy may contribute to the observed pattern of nAChR deficits especially in moderate AD compared to HC, and attempts to partial volume consideration shall be administered to clarify the influence of structural changes on the nAChR signal.

11.6 Monocentre 2-FA-PET Data in Context with Other Available PET/SPECT Studies on α4β2*-nAChR Binding in AD/MCI

There is some controversy regarding the question whether α4β2*-nAChRs are reduced, normal or even increased, for example, in the early stage of AD. Two studies using 5-[^{123}I]I-A85380 (5-IA)-SPECT in mild AD (n = 12), MCI (n = 10) vs. HC (n = 10) (Mitsis et al. 2009) and 2-[^{18}F]F-A85380 (2-FA)-PET in mild AD (n = 15) vs. HC (n = 14) (Ellis et al. 2008) assessed the distribution volume and did not find any significant differences of α4β2*-nAChR availability between groups. In contrast, using three different radioligands for the assessment of α4β2*-nAChR binding such as 5-IA, [^{11}C]nicotine, 2-FA and four different research groups (O'Brien et al. 2007; Terrière et al. 2010; Nordberg et al. 1995; Sabri et al. 2008; Kendziorra et al. 2011) consistently reported decreases in α4β2*-nAChR binding. Using 5-IA-SPECT, O'Brien et al. 2007, investigated mild to moderate AD (n = 16) which were compared to HC (n = 16). The cerebellum was used as reference region to normalize the data in order to account for interindividual variability. Lower α4β2*-nAChR binding was found in AD in frontotemporal cortices, striatum and pons. Terrière et al. (2010) performed a 5-IA-SPECT study in amnestic MCI (n = 9) and HC (n = 10). SPM analysis was performed and SPECT data was scaled to cerebellum as reference region. There was reduced nAChR binding in MCI in the medial temporal cortex. Nordberg et al. (1995) found lower nAChR availability using [^{11}C]nicotine PET in AD (n = 8) compared to HC (n = 3) in the cortical regions (frontal, temporal, hippocampal).

11.6.1 Own Data (Kendziorra et al. 2011; Sabri et al. 2008)

Parametric images of the 2-FA-DV were calculated using the Logan method, and the 2-FA-BP or 2-FA-DVR was assessed, normalizing the PET-DV data to the CC as unspecific reference region.

The major findings of these two studies were significantly lower nAChR binding in typically AD-affected brain regions in AD and amnestic MCI (pilot cohort and extended cohort) especially in the precuneus/posterior cingulate cortex, thalamus, (para)hippocampus, temporal cortex, frontal cortex and caudate nucleus. MCI were more mildly affected than AD. Of note, only MCI, who later converted to AD (MCI-C), demonstrated significantly lower nAChR binding. In contrast, MCI who were stable (MCI-S) during clinical follow-up did not show significant nAChR differences.

11.6.2 Differences and Similarities Between the nAChR PET/SPECT Studies Conducted So Far in AD

In two of the mentioned SPECT studies, Mitsis et al. (2009) and Ellis et al. (2008) did not find any differences between groups. For assessment of nAChR availability, the 2-FA-DV was calculated. The other five nAChR studies (O'Brien et al. 2007; Terrière et al. 2010; Nordberg et al. 1995; Kendziorra et al. 2011; Sabri et al. 2008) consistently find nAChR reductions, especially cortical in the cingulate cortex, frontotemporal cortices and hippocampus and also subcortical in the striatum. All these PET/SPECT studies used relative quantification normalizing the PET/SPECT data to a reference region (CC or cerebellum) in order to account for unspecific binding or interindividual variability. Furthermore, almost all nAChR PET/SPECT studies found a relationship between lower (especially) cortical nAChR binding and the degree of cognitive dysfunction in AD/MCI and HC (O'Brien et al. 2007; Terrière et al. 2010; Nordberg et al. 1995; Sabri et al. 2008; Kendziorra et al. 2011; Mitsis et al. 2009). In contrast, no correlations were demonstrated between nAChR availability in AD and cognitive symptoms by Ellis et al. (2008).

11.6.3 Possible Reasons for Discrepancies Between the Different PET/SPECT Studies

There are various possible reasons for the discrepancies between these studies. In general, PET is superior to SPECT regarding higher scanner resolution, sensitivity and specificity and allows absolute quantification of receptor availability. The negative findings of the two SPECT/PET studies (Mitsis et al. 2009; Ellis et al. 2008), however, may be mainly due to the fact that only the distribution volume was calculated to assess the nAChR availability. The relatively high amount of unspecific binding of 2-FA (and to a lesser amount of 5-IA) and interindividual variability can potentially influence data analysis and accuracy of the results. For between-group comparisons, therefore, it is favourable not only to calculate the parametric images of the DV but also to calculate the BP or DVR as the most specific measure of the α4β2*-nAChR availability (Sabri et al. 2008; Kendziorra et al. 2011). We demonstrated that the calculation of the 2-FA-BP or 2-FA-DVR using the CC as reference region is superior and more sensitive compared to another reference region, such as the cerebellum, which have been used in SPECT studies before. Since the cerebellum is not free of nAChR, it cannot be regarded as an optimal reference region. However, using the cerebellum as reference region may be helpful to account for interindividual variability when the CC cannot be assessed due to the limited resolution of SPECT (O'Brien et al. 2007; Kendziorra et al. 2011). However, discrepancies of the findings by the different study groups may also be a result of heterogeneity of (1) clinical parameters of the patient cohorts such as severity of dementia, (2) ApoE status, (3) age or (4) the relatively small number of patients in the study groups. Interestingly, it has been shown that early-onset AD has more cholinergic

brain abnormalities than late-onset AD, matched for clinical and cognitive parameters (Meyer et al. 2012; Kuhl et al. 1996). Further investigation in large patient groups is required to definitely clear this controversy.

11.7 Second-Generation Radiotracers for Imaging α4β2*-nAChRs

Due to the slow kinetics of 2-FA and 5-IA, long acquisition times up to 7 h are required for accurate quantification. Therefore, neither 2-FA nor 5-IA is an optimal radiotracer for clinical routine applications. Recently, new high-affinity α4β2*-nAChR PET tracers have been developed, and preclinical and first-in-human PET studies revealed promising results of faster tracer kinetics. In short, the most promising tracers for potential human application are (−)[^{18}F]NCFHEB, later called (−)[^{18}F]Flubatine (Brust et al. 2008; Sabri et al. 2008, 2015, 2018); (+)[^{18}F]Flubatine (Kranz et al. 2016; Ludwig et al. 2016, 2018; Tiepolt et al. 2018; Wilke et al. 2019); [^{18}F]AZAN (Kuwabara et al. 2012; Wong et al. 2013); [^{18}F]Nifene (Hillmer et al. 2011; Betthauser et al. 2017; Lao et al. 2017; Mukherjee et al. 2018); and [^{18}F]XTRA (Kuwabara et al. 2017; Coughlin et al. 2018). Among these second-generation radioligands for imaging of α4β2*-nAChRs, PET investigations in patients with AD are restricted to a first-in-human PET trial carried out by our group using (−)[^{18}F]Flubatine (Sabri et al. 2018). Furthermore, preliminary findings of our first-in-human PET study in AD patients, using the recently developed enantiomer (+)[^{18}F]Flubatine, were previously reported, showing suitable tracer characteristics, such as high stability and fast kinetics. In this (+)[^{18}F]Flubatine-PET study, there was a decrease of α4β2*-nAChR availability, especially within the mesial temporal cortex of patients with mild AD, as compared with HC. Interestingly, there was an inverse relationship between amyloid-β accumulation as assessed by [^{18}F]Florbetaben and α4β2*-nAChR binding, similar to previous PET findings in AD reported by Okada et al. using 2-FA and [^{11}C]PIB (Okada et al. 2013; Tiepolt et al. 2018; Wilke et al. 2019). (−)[^{18}F]Flubatine was developed, preclinically validated and initially applied to humans in a recent first-in-man trial by our group (Sabri et al. 2008, 2011a, b, c, d, 2015, 2018). Kinetic modelling analysis showed that (−)[^{18}F]Flubatine has fast brain kinetics and high in vivo stability, both characteristic of a suitable brain PET tracer (Sabri et al. 2015). There is a need for the development of PET biomarkers of neuroprogression in AD. These PET biomarkers should correlate with cognitive dysfunction in the early stage of AD and allow the prediction of disease progression and cognitive deterioration of AD. Thus, the primary objectives of our cross-sectional (−)[^{18}F]Flubatine PET study were to analyze whether α4β2*-nAChR availability as assessed by distribution volume (DV) or the specific binding part of the distribution volume using the corpus callosum as reference region (DVS; $DVS = DV - DV_{[corpus\ callosum]}$) were reduced in mild AD as compared to age-, education- and sex-matched healthy controls (HC) and whether alterations of α4β2*-nAChR binding in AD were associated with the dysfunction of five cognitive partial functions (memory, executive function/working memory, attention, language, and visuospatial function) which were calculated from findings of a large cognitive test

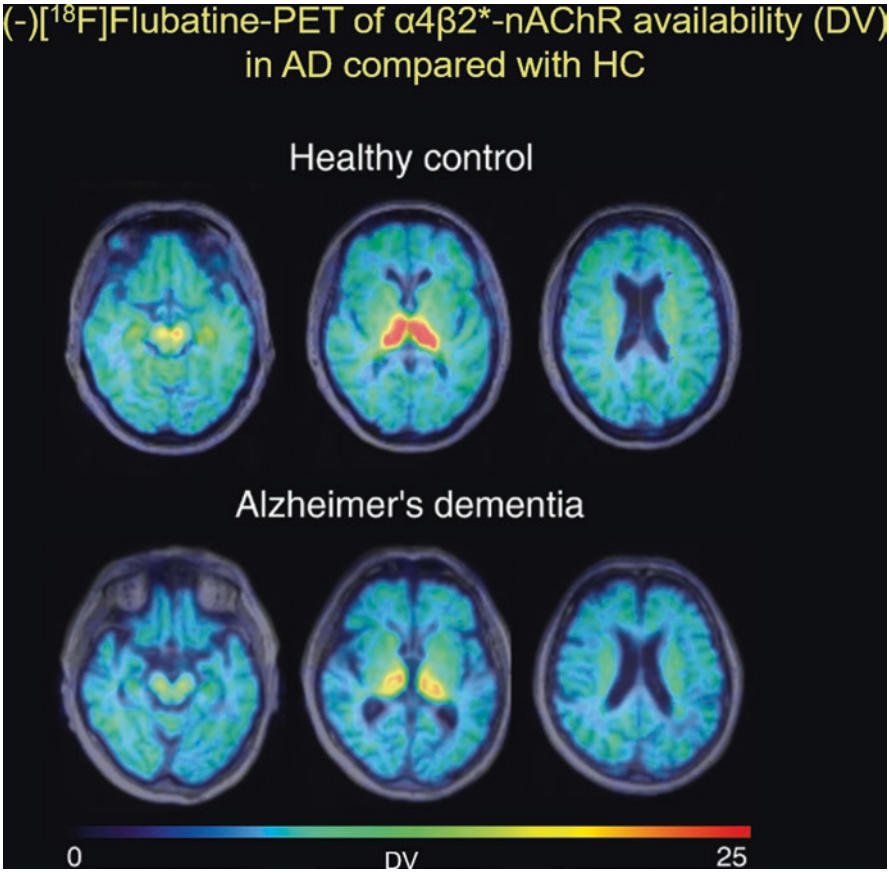

Fig. 11.3 Parametric (−)[^{18}F]Flubatine-PET images of α4β2*-nAChR availability (DV) in one patient with Alzheimer's disease (AD) and one healthy control (HC) are shown and exemplify lower cortical and subcortical α4β2*-nAChR availability (DV) in AD

battery (Sabri et al. 2018). In 14 non-smoking patients with mild AD compared to 15 HCs, the α4β2*-nAChR availability as assessed by the DV or DVS was significantly lower within 4 out of 5 a priori defined brain regions (i.e. hippocampus −10% or −23%, basal forebrain −10% or −34%, mean cortex −5% or −14%, frontal cortex −5% or −13%, $p < 0.05$ corrected; Figs. 11.3 and 11.4). These VOI-analysis findings were confirmed following partial volume effect correction. Using SPM, regression analysis in AD patients revealed a significant relationship between episodic memory and the α4β2*-nAChR availability (DV), especially within the basal forebrain ($p < 0.05$ corrected for multiple comparisons), frontal cortex, inferior temporal cortex and parahippocampus; between executive function/working memory and α4β2*-nAChR availability within the temporo-parietal cortices; between attention and α4β2*-nAChR availability within the thalamus, putamen and frontal white matter (Fig. 11.5); and between language and α4β2*-nAChR availability within the cerebellum (Fig. 11.5). Similar results were found for the relationship between the

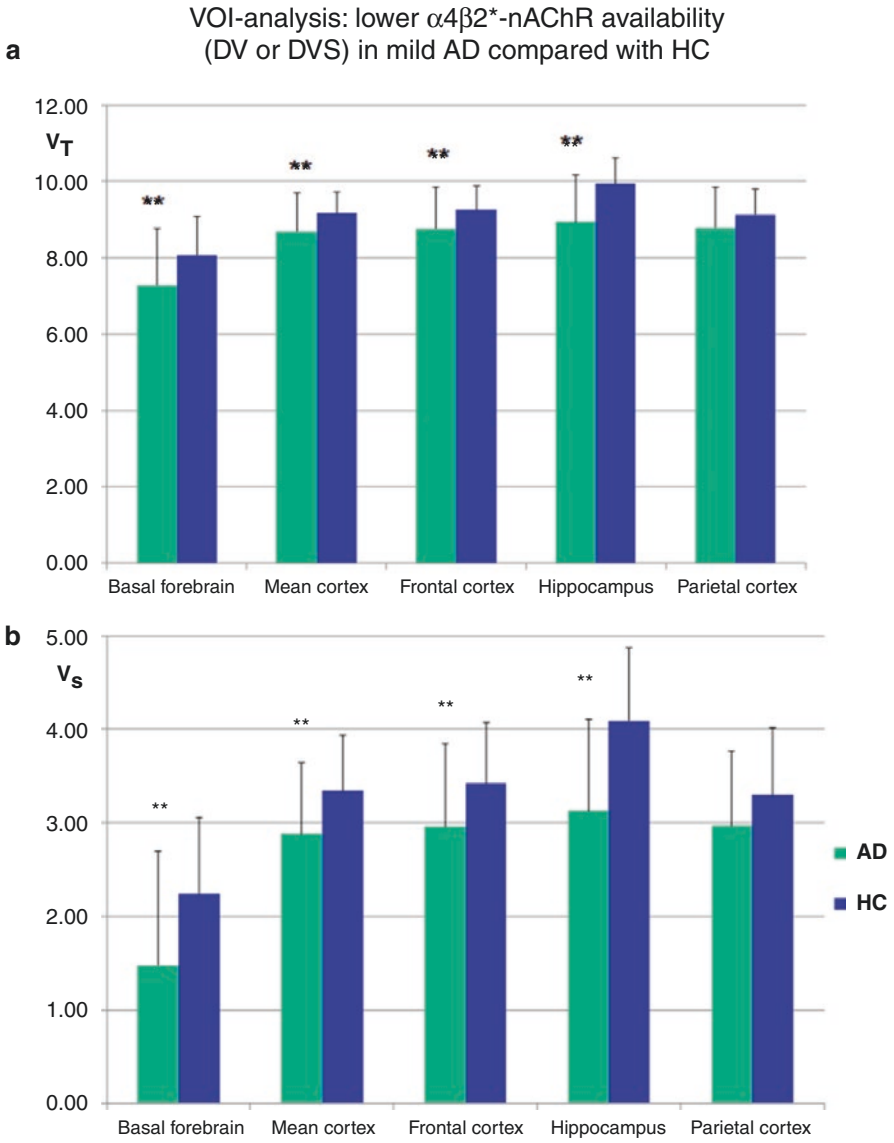

Fig. 11.4 (**a**, **b**) (−)[^{18}F]Flubatine-PET: VOI-analysis of α4β2*-nAChR availability (DV or DVS) within 5 a priori selected brain regions (basal forebrain, mean cortex, frontal cortex, hippocampus and parietal cortex) demonstrates significantly lower distribution volume (DV) or specific binding of the distribution volume (DVS), especially within the basal forebrain and hippocampus, in patients with Alzheimer's disease (AD, n = 14), compared with healthy controls (HC; n = 15). **ANCOVA (nuisance age and sex) for the comparison of AD with HC; significance at **$p < 0.05$ (corrected for multiple testing according to Benjamini-Hochberg)

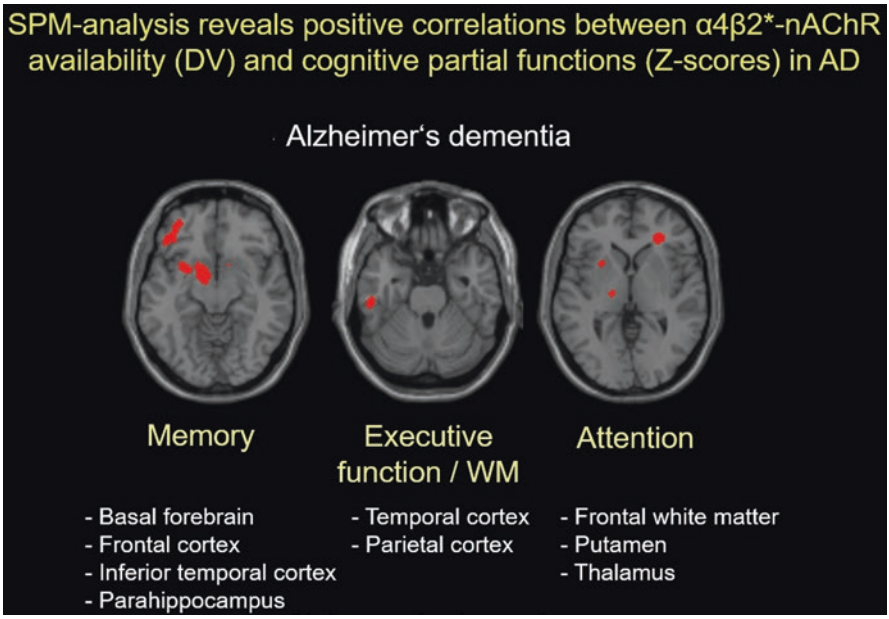

Fig. 11.5 (−)[^{18}F]Flubatine-PET: SPM-based regression analysis indicates significant, positive correlations between α4β2*-nAChR availability (DV) and episodic memory, executive function/working memory [WM], attention (*Z*-scores) in patients with mild AD (n = 14; MMSE 24 ± 3). Significance at $p < 0.001$ (uncorrected); $T > 3.9$; $k = 5$ voxels (basal forebrain: significance at $p < 0.05$ FWE-corrected)

partial cognitive functions and the α4β2*-nAChR availability as assessed by the DVS. Thus, according to these findings of our first-in-human (−)[^{18}F]Flubatine PET study, we suggested that (−)[^{18}F]Flubatine might have potential as a biomarker for cholinergic α4β2*-nAChR vulnerability, specific cognitive deterioration and progression of AD and other neurodegenerative disorders (Sabri et al. 2018). Preliminary findings of our first-in-human (+)[^{18}F]Flubatine PET study in AD patients and HC indicated that (+)[^{18}F]Flubatine, similar to (−)[^{18}F]Flubatine, is a very suitable ligand for imaging of α4β2*-nAChR availability in patients with neurodegenerative disorders such as AD (Tiepolt et al. 2018).

11.8 Future Directions

Neuroprogression is an important feature of neurodegenerative disorders such as AD. PET imaging of α4β2*-nAChRs demonstrated lower α4β2*-nAChR availability in early AD and a relationship between the impairment of several cognitive domains such as memory, attention, executive function/working memory, and

language and the reduction of α4β2*-nAChR availability in AD. Thus, PET imaging of α4β2*-nAChR availability might become a valuable biomarker of neuroprogression. However, to validate α4β2*-nAChR PET as a biomarker for neuroprogression in AD or other neurodegenerative disorders, longitudinal PET trials are required (Sabri et al. 2018). Preclinical and human PET studies on the relationship between the amyloid-β or tau-pathology and the availability of α4β2*-nAChR, or other subunits of nicotinic receptors such as α7-nAChR, in AD may help to improve our understanding of the AD pathophysiology and guide the development of novel drug therapies (Okada et al. 2013; Lombardo and Maskos 2015; Nishiyama et al. 2015; Samra et al. 2018; Tiepolt et al. 2018; Tiernan et al. 2018).

11.9 Conclusions

Using α4β2*-nAChR-specific radioligands such as 2-[^{18}F]FA-85380 (2-FA) and PET, reduced α4β2*-nAChR availability was not only found in mild to moderate AD patients but also in subjects with amnestic MCI who proceeded to AD within 3 years as well as in patients with VaD. Furthermore, lower α4β2*-nAChR binding in AD, MCI and aging was related to cognitive symptoms. However, although very sensitive for the assessment of α4β2*-nAChR reductions in the course of AD, the clinical use of 2-FA is hampered by its slow kinetics. Hence, suitable second-generation α4β2*-nAChR-specific radioligands such as (−)[^{18}F]Flubatine and (+)[^{18}F]Flubatine with fast kinetics and high stability in vivo were developed, preclinically tested, and first-in-human PET studies in AD patients and HC were successfully carried out. If proven in further clinical multicentre trials, α4β2*-nAChR-specific PET might become a pivotal biomarker for early diagnostics, course prediction and drug developments in patients with prodromal AD stages and possibly in other neurodegenerative diseases in daily diagnostic workflow. Combined PET investigations on the relationship between nicotinic receptor alterations and histopathological biomarkers such as amyloid-β or tau have become a highly interesting new field of nicotinic receptor research in AD in order to disentangle the molecular signature of the disease.

Acknowledgements We thank the cyclotron operators, PET physicists, chemists and technologists for their assistance. The studies were funded by *Interdisziplinäres Zentrum für Klinische Forschung (IZKF)* and *Bundesministerium für Bildung und Forschung (BMBF)* grants.

References

Berti V, Pupi A, Mosconi L (2011) PET/CT in diagnosis of dementia. Ann N Y Acad Sci 1228:81–92. Review

Betthauser TJ, Hillmer AT, Lao PJ, Ehlerding E, Mukherjee J, Stone CK, Christian BT (2017) Human biodistribution and dosimetry of [^{18}F]nifene, an α4β2* nicotinic acetylcholine receptor PET tracer. Nucl Med Biol 55:7–11. https://doi.org/10.1016/j.nucmedbio.2017.08.001

Bohnen NI, Djang DS, Herholz K, Anzai Y, Minoshima S (2012) Effectiveness and safety of ^{18}F-FDG PET in the evaluation of dementia: a review of the recent literature. J Nucl Med 53:59–71. Review

Brody AL, Mandelkern MA, London ED, Olmstead RE, Farahi J, Scheibal D, Jou J, Allen V, Tionqson E, Chefer SI, Koren AO, Mukhin AG (2006) Cigarette smoking saturates brain α4β2 nicotinic acetylcholine receptors. Arch Gen Psychiatry 63:907–915

Brust P, Patt JT, Deuther-Conrad W, Becker G, Patt M, Schildan A, Sorger D, Kendziorra K, Meyer P, Steinbach J, Sabri O (2008) In vivo measurement of nicotinic acetylcholine receptors with [^{18}F]norchloro-fluoro-homoepibatidine. Synapse 62:205–218

Buckingham SD, Jones AK, Brown LA, Sattelle DB (2009) Nicotinic acetylcholine receptor signalling: roles in Alzheimer's disease and amyloid neuroprotection. Pharmacol Rev 61:39–61. Review

Coughlin JM, Slania S, Du Y, Rosenthal HB, Lesniak WG, Minn I, Smith GS, Dannals RF, Kuwabara H, Wong DF, Wang Y, Horti AG, Pomper MG (2018) ^{18}F-XTRA PET for enhanced imaging of the extrathalamic α4β2 nicotinic acetylcholine receptor. J Nucl Med 59:1603–1608. https://doi.org/10.2967/jnumed.117.205492

Cummings JL (2008) The black book of Alzheimer's disease, part 1. Prim Psychiatry 15:66–76. Review

Dani JA, Bertrand D (2007) Nicotinic acetylcholine receptors and nicotinic cholinergic mechanisms of the central nervous system. Annu Rev Pharmacol Toxicol 47:699–729

Ding YS, Fowler JS, Logan J, Wang GJ, Telang F, Garza V, Biegon A, Pareto D, Rooney W, Shea C, Alexoff D, Volkow ND, Vocci F (2004) 6-[^{18}F]fluoro-A-85380, a new PET tracer for the nicotinic acetylcholine receptor: studies in the human brain and in vivo demonstration of specific binding in white matter. Synapse 53:184–189

Ellis JR, Villemagne VL, Nathan PJ, Mulligan RS, Gong SJ, Chan JG, Sachinidis J, O'Keefe GJ, Pathmaraj K, Wesnes KA, Savage G, Rowe CC (2008) Relationship between nicotinic receptors and cognitive function in early Alzheimer's disease: a 2-[18F]fluoro-A-85380 PET study. Neurobiol Learn Mem 90:404–412

Erkinjuntti T, Kurz A, Gauthier S, Bullock R, Lilienfeld S, Damaraju CV (2002) Efficacy of galantamine in probable vascular dementia and Alzheimer's disease combined with cerebrovascular disease: a randomised trial. Lancet 359:1283–1290

van der Flier WM, Pijnenburg YA, Fox NC, Scheltens P (2011) Early-onset versus late-onset Alzheimer's disease: the case of the missing APOE ε4 allele. Lancet Neurol 10:280–288. Review

Francis PT, Palmer AM, Snape M, Wilcock GK (1999) The cholinergic hypothesis of Alzheimer's disease: a review of progress. J Neurol Neurosurg Psychiatry 66:137–147

Hillmer AT, Wooten DW, Moirano JM, Slesarev M, Barnhart TE, Engle JW, Nickles RJ, Murali D, Schneider ML, Mukherjee J, Christian BT (2011) Specific α4β2 nicotinic acetylcholine receptor binding of [^{18}F]nifene in the rhesus monkey. Synapse 65:1309–1318

Innis RB, Cunningham VJ, Delforge J, Fujita M, Gjedde A, Gunn RN, Holden J, Houle S, Huang SC, Ichise M, Iida H, Ito H, Kimura Y, Koeppe RA, Knudsen GM, Knuuti J, Lammertsma AA, Laruelle M, Logan J, Maguire RP, Mintun MA, Morris ED, Parsey R, Price JC, Slifstein M, Sossi V, Suhara T, Votaw JR, Wong DF, Carson RE (2007) Consensus nomenclature for in vivo imaging of reversibly binding radioligands. J Cereb Blood Flow Metab 27:1533–1539

Jack CR Jr, Knopman DS, Jagust WJ, Shaw LM, Aisen PS, Weiner MW, Petersen RC, Trojanowski JQ (2010) Hypothetical model of dynamic biomarkers of the Alzheimer's pathological cascade. Lancet Neurol 9:119–128

Kendziorra K, Wolf H, Meyer PM, Barthel H, Hesse S, Becker GA, Luthardt J, Schildan A, Patt M, Sorger D, Seese A, Gertz HJ, Sabri O (2011) Decreased cerebral α4β2* nicotinic acetylcholine receptor availability in patients with mild cognitive impairment and Alzheimer's disease assessed with positron emission tomography. Eur J Nucl Med Mol Imaging 38:515–525

Kimes AS, Horti AG, London ED, Chefer SI, Contoreggi C, Ernst M, Friello P, Koren AO, Kurian V, Matochik JA, Pavlova O, Vaupel DB, Mukhin AG (2003) 2-[18F]F-A85380: PET imaging of brain nicotinic acetylcholine receptors and whole body distribution in humans. FASEB J 17:1331–1333

Kimes AS, Chefer SI, Matochik JA, Contoreggi CS, Vaupel DB, Stein EA, Mukhin AG (2008) Quantification of nicotinic acetylcholine receptors in the human brain with PET: bolus plus infusion administration of 2-[18F]F-A85380. NeuroImage 39:717–727

Klingner M, Apelt J, Kumar A, Sorger D, Sabri O, Steinbach J, Scheunemann M, Schliebs R (2003) Alterations in cholinergic and non-cholinergic neurotransmitter receptor densities in transgenic Tg2576 mouse brain with beta-amyloid plaque pathology. Int J Dev Neurosci 21:357–369

Kranz M, Sattler B, Tiepolt S, Wilke S, Deuther-Conrad W, Donat CK, Fischer S, Patt M, Schildan A, Patt J, Smits R, Hoepping A, Steinbach J, Sabri O, Brust P (2016) Radiation dosimetry of the α4β2 nicotinic receptor ligand (+)-[^{18}F]flubatine, comparing preclinical PET/MRI and PET/CT to first-in-human PET/CT results. EJNMMI Phys 3:25

Kuhl DE, Minoshima S, Fessler JA, Frey KA, Foster NL, Ficaro EP, Wieland DM, Koeppe RA (1996) In vivo mapping of cholinergic terminals in normal aging, Alzheimer's disease, and Parkinson's disease. Ann Neurol 40:399–410

Kuwabara H, Wong DF, Gao Y, Valentine H, Holt DP, Ravert HT, Dannalsand RF, Horti AG (2012) PET imaging of nicotinic acetylcholine receptors in baboons with ^{18}F-AZAN, a radioligand with improved brain kinetics. J Nucl Med 53:121

Kuwabara H, Gao Y, Stabin M, Coughlin J, Nimmagadda S, Dannals RF, Pomper MG, Horti AG (2017) Imaging α4β2 nicotinic acetylcholine receptors (nAChRs) in baboons with [^{18}F]XTRA, a radioligand with improved specific binding in extra-thalamic regions. Mol Imaging Biol 19:280–288. https://doi.org/10.1007/s11307-016-0999-9

Lao PJ, Betthauser TJ, Tudorascu DL, Barnhart TE, Hillmer AT, Stone CK, Mukherjee J, Christian BT (2017) [^{18}F]Nifene test-retest reproducibility in first-in-human imaging of α4β2* nicotinic acetylcholine receptors. Synapse 71(8). https://doi.org/10.1002/syn.21981

Lesné S, Koh MT, Kotilinek L, Kayed R, Glabe CG, Yang A, Gallagher M, Ashe KH (2006) A specific amyloid-beta protein assembly in the brain impairs memory. Nature 440(7082):352–357

Lombardo S, Maskos U (2015) Role of the nicotinic acetylcholine receptor in Alzheimer's disease pathology and treatment. Neuropharmacology 96(Pt B):255–262. https://doi.org/10.1016/j.neuropharm.2014.11.018. Review

Ludwig FA, Smits R, Fischer S, Donat CK, Hoepping A, Brust P, Steinbach J (2016) LC-MS supported studies on the in vitro metabolism of both enantiomers of Flubatine and the in vivo metabolism of (+)-[(^{18})F]Flubatine-a positron emission tomography radioligand for imaging α4β2 nicotinic acetylcholine receptors. Molecules 21(9):E1200. https://doi.org/10.3390/molecules21091200

Ludwig FA, Fischer S, Smits R, Deuther-Conrad W, Hoepping A, Tiepolt S, Patt M, Sabri O, Brust P (2018) Exploring the metabolism of (+)-[^{18}F]Flubatine in vitro and in vivo: LC-MS/MS aided identification of radiometabolites in a clinical PET study. Molecules 23(2):E464. https://doi.org/10.3390/molecules23020464

Mamede M, Ishizu K, Ueda M, Mukai T, Iida Y, Fukuyama H, Saga T, Saji H (2004) Quantification of human nicotinic acetylcholine receptors with ^{123}I-5-IA SPECT. J Nucl Med 45:1458–1470

McKhann GM, Knopman DS, Chertkow H, Hyman BT, Jack CR Jr, Kawas CH, Klunk WE, Koroshetz WJ, Manly JJ, Mayeux R, Mohs RC, Morris JC, Rossor MN, Scheltens P, Carrillo MC, Thies B, Weintraub S, Phelps CH (2011) The diagnosis of dementia due to Alzheimer's disease: recommendations from the National Institute on Aging-Alzheimer's Association workgroups on diagnostic guidelines for Alzheimer's disease. Alzheimers Dement 7:263–269

Meyer PM, Strecker K, Kendziorra K et al (2009) Reduced α4β2* Nicotinic acetylcholine receptor binding and its relationship to mild cognitive and depressive symptoms in Parkinson's disease. Arch Gen Psychiatry 66:866–877

Meyer PM, Gertz HJ, Schildan A, Luthardt J, Seese A, Sattler B, Barthel H, Hesse S, Sabri O (2012) Differentially decreased α4β2* nicotinic acetylcholine receptor availability (α4β2*-nAChR) in early-onset (EOAD) and late-onset Alzheimer's disease (LOAD). J Nucl Med 53(Suppl 1):39

Mitsis EM, Reech KM, Bois F, Tamagnan GD, Macavoy MG, Seibyl JP, Staley JK, van Dyck CH (2009) ^{123}I-5-IA-85380 SPECT imaging of nicotinic receptors in Alzheimer disease and mild cognitive impairment. J Nucl Med 50:1455–1463

Mukherjee J, Lao PJ, Betthauser TJ, Samra GK, Pan ML, Patel IH, Liang C, Metherate R, Christian BT (2018) Human brain imaging of nicotinic acetylcholine α4β2* receptors using [^{18}F]Nifene: selectivity, functional activity, toxicity, aging effects, gender effects, and extrathalamic pathways. J Comp Neurol 526(1):80–95. https://doi.org/10.1002/cne.24320

Nishiyama S, Ohba H, Kanazawa M, Kakiuchi T, Tsukada H (2015) Comparing α7 nicotinic acetylcholine receptor binding, amyloid-β deposition, and mitochondria complex-I function in living brain: a PET study in aged monkeys. Synapse 69(10):475–483. https://doi.org/10.1002/syn.21842

Nordberg A (2001) Nicotinic receptor abnormalities of Alzheimer's disease: therapeutic implications. Biol Psychiatry 49:200–210. Review

Nordberg A, Lundqvist H, Hartvig P, Lilja A, Långström B (1995) Kinetic analysis of regional (S) (-)^{11}C-nicotine binding in normal and Alzheimer brains – in vivo assessment using positron emission tomography. Alzheimer Dis Assoc Disord 9:21–27

O'Brien JT, Colloby SJ, Pakrasi S, Perry EK, Pimlott SL, Wyper DJ, McKeith IG, Williams ED (2007) α4β2 nicotinic receptor status in Alzheimer's disease using 123I-5-IA-85380 SPECT. J Neurol Neurosurg Psychiatry 78:356–362

Okada H, Ouchi Y, Ogawa M, Futatsubashi M, Saito Y, Yoshikawa E, Terada T, Oboshi Y, Tsukada H, Ueki T, Watanabe M, Yamashita T, Magata Y (2013) Alterations in α4β2 nicotinic receptors in cognitive decline in Alzheimer's aetiopathology. Brain 136(Pt 10):3004–3017. https://doi.org/10.1093/brain/awt195

Perry EK, Morris CM, Court JA et al (1995) Alteration in nicotine binding sites in Parkinson's disease, Lewy body dementia and Alzheimer's disease: possible index of early neuropathology. Neuroscience 64:385–395

Rinne JO, Myllykyla T, Lonnberg P, Marjamaki P (1991) A post mortem study of brain nicotinic receptors in Parkinson's and Alzheimer's disease. Brain Res 547:167–170

Rinne JO, Kaasinen V, Järvenpää T, Någren K, Roivainen A, Yu M, Oikonen V, Kurki T (2003) Brain acetylcholinesterase activity in mild cognitive impairment and early Alzheimer's disease. J Neurol Neurosurg Psychiatry 74:113–115

Román GC, Tatemichi TK, Erkinjuntti T, Cummings JL, Masdeu JC, Garcia JH, Amaducci L, Orgogozo JM, Brun A, Hofman A et al (1993) Vascular dementia: diagnostic criteria for research studies. Report of the NINDS-AIREN International Workshop. Neurology 43:250–260

Sabri O, Schneider R, Schreckenberger M, Hellwig D, Kaiser HJ, Wagenknecht G, Mull M, Ringelstein EB, Buell U (1999) Neuropsychological impairment correlates to hyperperfusion and hypometabolism but not to severity of white matter lesions on MRI in cerebral microangiopathy. In: Korczyn AD (ed) First International Congress on Vascular Dementia, Geneva, Switzerland, October 3–6, 1999. Monduzzi, Bologna

Sabri O, Kendziorra K, Wolf H, Gertz HJ, Brust P (2008) Acetylcholine receptors in dementia and mild cognitive impairment. Eur J Nucl Med Mol Imaging 35(Suppl 1):S30–S45. Review

Sabri O, Wilke S, Graef S, Schoenknecht P, Becker G, Patt M, Wagenknecht G, Hoepping A, Hegerl U, Brust P (2011a) Cerebral α4β2 nicotinic acetylcholine receptors (nAChRs) in early Alzheimer disease (AD) assessed with the new PET tracer (-)-[^{18}F]-norchloro-fluoro-homoepibatidine (NCFHEB). J Nucl Med 52(Suppl 1):1267

Sabri O, Wilke S, Graef S, Schoenknecht P, Habermann B, Becker G, Luthardt J, Patt M, Kendziorra K, Meyer P, Hesse S, Wagenknecht G, Hoepping A, Hegerl U, Brust P (2011b) PET imaging of cerebral nicotinic acetylcholine receptors (nAChRs) in early Alzheimer's disease (AD) assessed with the new radioligand (-)-[^{18}F]-NorChloro-Fluoro-HomoEpiBatidine (NCFHEB). In: Book of Abstracts, the XXVth International Symposium on Cerebral Blood Flow, Metabolism and Function and the Xth International Conference on Quantification of Brain Function with PET, Barcelona, Spain, May 25–28, 2011

Sabri O, Wilke S, Graef S, Lengler U, Gertz H-J, Schönknecht P, Habermann B, Becker G, Luthardt J, Patt M, Kendziorra K, Meyer P, Hesse S, Barthel H, Wagenknecht G, Hoepping A, Hegerl U, Brust P (2011c) First in man study to image α4β2 cerebral nicotinic acetylcholine receptors (nAChRs) in early Alzheimer's disease (AD) with the new radioligand (-)-[^{18}F]-norchloro-fluoro-homoepibatidine (NCFHEB) and PET. Alzheimers Dement 7(Suppl 1):S37

Sabri O, Wilke S, Gräf S, Gertz H, Schönknecht P, Becker G, Luthardt J, Patt M, Meyer P, Hesse S, Barthel H, Wagenknecht G, Höpping A, Hegerl U, Brust P (2011d) First in man study with the new radioligand (-)-[^{18}F]-norchloro-fluoro-homoepibatidine (NCFHEB) to image alpha4beta2 cerebral nicotinic acetylcholine receptors (nAChRs) in early Alzheimer's disease (AD) with PET. Eur J Nucl Med Mol Imaging 38(Suppl 2):S122

Sabri O, Becker GA, Meyer PM, Hesse S, Wilke S, Graef S, Patt M, Luthardt J, Wagenknecht G, Hoepping A, Smits R, Franke A, Sattler B, Habermann B, Neuhaus P, Fischer S, Tiepolt S, Deuther-Conrad W, Barthel H, Schönknecht P, Brust P (2015) First-in-human PET quantification study of cerebral α4β2* nicotinic acetylcholine receptors using the novel specific radioligand (-)-[(^{18})F]Flubatine. NeuroImage 118:199–208. https://doi.org/10.1016/j.neuroimage.2015.05.065

Sabri O, Meyer PM, Gräf S, Hesse S, Wilke S, Becker GA, Rullmann M, Patt M, Luthardt J, Wagenknecht G, Hoepping A, Smits R, Franke A, Sattler B, Tiepolt S, Fischer S, Deuther-Conrad W, Hegerl U, Barthel H, Schönknecht P, Brust P (2018) Cognitive correlates of α4β2 nicotinic acetylcholine receptors in mild Alzheimer's dementia. Brain 141(6):1840–1854. https://doi.org/10.1093/brain/awy099

Samra GK, Dang K, Ho H, Baranwal A, Mukherjee J (2018) Dual targeting agents for Aβ plaque/P-glycoprotein and Aβ plaque/nicotinic acetylcholine α4β2* receptors-potential approaches to facilitate Aβ plaque removal in Alzheimer's disease brain. Med Chem Res 27:1634–1646. https://doi.org/10.1007/s00044-018-2178-9

Schildan A, Patt M, Sabri O (2007) Synthesis procedure for routine production of 2-[^{18}F]fluoro-3-(2(S)-azetidinylmethoxy)pyridine (2-[^{18}F]FA-85380). Appl Radiat Isot 65:1244–1248

Schliebs R (2005) Basal forebrain cholinergic dysfunction in Alzheimer's disease – interrelationship with beta-amyloid, inflammation and neurotrophin signaling. Neurochem Res 30:895–908. Review

Schliebs R, Arendt T (2011) The cholinergic system in aging and neuronal degeneration. Behav Brain Res 221:555–563. Review

Sorger D, Becker GA, Hauber K, Schildan A, Patt M, Birkenmeier G, Otto A, Meyer P, Kluge M, Schliebs R, Sabri O (2006) Binding properties of the cerebral α4β2 nicotinic acetylcholine receptor ligand 2-[^{18}F]fluoro A85380 to plasma. Nucl Med Biol 33:899–906

Sorger D, Becker GA, Patt M, Schildan A, Grossmann U, Schliebs R, Seese A, Kendziorra K, Kluge M, Brust P, Mukhin AG, Sabri O (2007) Measurement of the α4β2* nicotinic acetylcholine receptor ligand 2-[^{18}F]Fluoro-A-85380 and its metabolites in human blood during PET investigation: a methodological study. Nucl Med Biol 34:331–342

Terrière E, Dempsey MF, Herrmann LL, Tierney KM, Lonie JA, O'Carroll RE, Pimlott S, Wyper DJ, Herholz K, Ebmeier KP (2010) 5-123I-A-85380 binding to the α4β2-nicotinic receptor in mild cognitive impairment. Neurobiol Aging 31:1885–1893

Tiepolt S, Becker GA, Wilke S, Cecchin D, Meyer PM, Barthel H, Hesse S, Patt M, Rullmann M, Wagenknecht G, Deuther-Conrad W, Ludwig FA, Wagner A, Gertz HJ, Smits R, Hoepping A, Brust P, Sabri O (2018) [(+)-[^{18}F]Flubatine ein neuer α4β2 nikotinischer Acetylcholin-Rezeptor (nAChR) PET Radioligand - Ergebnisse der First-In-Human Studie bei Patienten mit Alzheimer Demenz (AD) und gesunden Probanden (HC)]. Nuklearmedizin 57(Suppl):V103

Tiernan CT, Ginsberg SD, He B, Ward SM, Guillozet-Bongaarts AL, Kanaan NM, Mufson EJ, Counts SE (2018) Pretangle pathology within cholinergic nucleus basalis neurons coincides with neurotrophic and neurotransmitter receptor gene dysregulation during the progression of Alzheimer's disease. Neurobiol Dis 117:125–136. https://doi.org/10.1016/j.nbd.2018.05.021

Wilke S, Tiepolt S, Rullmann M, Meyer PM, Hesse S, Patt M, Luthardt J, Barthel H, Wagenknecht G, Smits R, Hoepping A, Sattler B, Deuther-Conrad W, Gertz HJ, Brust P, Becker GA, Sabri O (2019) Comparison of the novel α4β2 nicotinic acetylcholine receptor PET radioligands (-)-Flubatine and (+)-Flubatine in healthy controls. Nuklearmedizin (Suppl) 58:159–160. https://doi.org/10.1055/s-0039-1683635

Winblad B, Palmer K, Kivipelto M, Jelic V, Fratiglioni L, Wahlund LO, Nordberg A, Bäckman L, Albert M, Almkvist O, Arai H, Basun H, Blennow K, de Leon M, DeCarli C, Erkinjuntti T, Giacobini E, Graff C, Hardy J, Jack C, Jorm A, Ritchie K, van Duijn C, Visser P,

Petersen RC (2004) Mild cognitive impairment – beyond controversies, towards a consensus: report of the International Working Group on Mild Cognitive Impairment. J Intern Med 256:240–246. Review

Wong DF, Kuwabara H, Kim J, Brasic JR, Chamroonrat W, Gao Y, Valentine H, Willis W, Mathur A, McCaul ME, Wand G, Gean EG, Dannals RF, Horti AG (2013) PET imaging of high-affinity α4β2 nicotinic acetylcholine receptors in humans with ^{18}F-AZAN, a radioligand with optimal brain kinetics. J Nucl Med 54:1308–1314. https://doi.org/10.2967/jnumed.112.108001

Neuroimaging Findings in Mild Cognitive Impairment

12

Federico Massa, Matteo Bauckneht, Enrico Peira, Caterina Lapucci, Agnese Picco, Selene Capitanio, Dario Arnaldi, Luca Roccatagliata, Andrea Chincarini, and Flavio Nobili

Contents

12.1 Introduction 368
12.2 Morphological MRI 371
12.2.1 Principles 371
12.2.2 Utility in MCI 375
12.2.3 Combined Use of MRI and Other Biomarkers 378
12.3 Functional MRI, Arterial Spin Labeling (ASL), and Diffusion-Weighted Imaging 379
12.3.1 Blood-Oxygen-Level-Dependent (BOLD) Functional MRI (fMRI) Principles 379

F. Massa · C. Lapucci · A. Picco
Department of Neuroscience, Rehabilitation, Ophthalmology, Genetics, Maternal and Child Health (DiNOGMI), University of Genoa, Genoa, Italy

M. Bauckneht · S. Capitanio
IRCCS Ospedale Policlinico San Martino, Genoa, Italy
e-mail: Matteo.Bauckneht@hsanmartino.it; selene.capitanio@hsanmartino.it

E. Peira · A. Chincarini
Sezione di Genova, Istituto Nazionale di Fisica Nucleare, Genoa, Italy
e-mail: andrea.chincarini@ge.infn.it

D. Arnaldi · F. Nobili (✉)
Department of Neuroscience, Rehabilitation, Ophthalmology, Genetics, Maternal and Child Health (DiNOGMI), University of Genoa, Genoa, Italy

IRCCS Ospedale Policlinico San Martino, Genoa, Italy
e-mail: dario.arnaldi@unige.it; flaviomariano.nobili@hsanmartino.it

L. Roccatagliata
Department of Neuroscience, Rehabilitation, Ophthalmology, Genetics, Maternal and Child Health (DiNOGMI), University of Genoa, Genoa, Italy

IRCCS Ospedale Policlinico San Martino, Genoa, Italy

Department of Health Sciences (DiSSAL), University of Genoa, Genoa, Italy
e-mail: lroccatagliata@neurologia.unige.it

R. A. J. O. Dierckx et al. (eds.), *PET and SPECT in Neurology*,
https://doi.org/10.1007/978-3-030-53168-3_12

12.3.2 Utility in MCI..... 380
12.3.3 Arterial Spin Labeling (ASL)..... 383
12.3.4 Diffusion-Weighted Imaging (DWI) Principles..... 384
12.3.5 Utility in MCI..... 385
12.3.6 Combined Use of DTI and Other Biomarkers..... 388
12.4 Perfusion SPECT..... 389
12.4.1 Principles..... 389
12.4.2 Utility in MCI..... 389
12.4.3 Combined Use of SPECT and Other Biomarkers..... 392
12.5 ^{18}F-FDG-PET..... 392
12.5.1 Principles..... 392
12.5.2 Utility in MCI..... 393
12.5.3 Combined Use of FDG-PET and Other Biomarkers..... 398
12.6 Amyloid PET and Emerging Tracers..... 399
12.6.1 Amyloid PET Imaging..... 399
12.6.2 Utility in MCI..... 402
12.6.3 Combined Use of Amyloid PET and Other Biomarkers..... 404
12.6.4 Tau PET imaging..... 405
12.6.5 Receptor Imaging..... 406
12.7 Conclusions and Perspectives..... 407
References..... 408

Abstract

The clinical construct of mild cognitive impairment (MCI) identifies a syndrome of cognitive deficit which is not significant enough to interfere with daily activities, whose fate is unpredictable without establishing the underlying cause. Thus, MCI, though being the natural "reservoir" of subsequent dementing neurodegenerative diseases, can be provoked by a variety of psychiatric and systemic diseases as well as by drugs, alcohol, and substance abuse. In this context, morphological and, especially, functional neuroimaging by means of multitracer SPECT and PET are useful tools to provide clue information on the underlying pathological process. Both MRI and SPECT/PET have been included as indicative or supportive biomarkers in the diagnostic criteria of a variety of neurodegenerative conditions, already at the MCI stage, ranging from Alzheimer's disease to dementia with Lewy bodies and to frontotemporal dementia. New developments include MRI high-field equipment and functional techniques, fluorinated PET radiopharmaceuticals for protein Tau detection, and receptor studies. In the advanced memory clinics, appropriate use of neuroimaging is nowadays paramount for the correct diagnosis of cognitive disorders.

12.1 Introduction

The clinical construct of mild cognitive impairment (MCI), put forward at the end of the 1990s (Petersen et al. 1999), has bridged the gap between benign forgetfulness due to aging and dementia, a difficult to be interpreted "gray" area and

sometimes generating confusion in literature as well as in clinical practice. During the last decades, the efforts to elucidate the pathophysiological bases of MCI have matched the change in the conception of neurodegenerative diseases. Thus, the traditional diagnostic methods based only on clinical presentation, and eventually confirmed by postmortem neuropathological findings, have been replaced by a biomarker-based approach involving different biological measures able to reflect pathological changes in vivo.

Such approach is pivotal in understanding the underlying processes and in giving an insight in their pathological etiology, thus guiding clinicians in the differential diagnostic pathway of MCI as well as researchers in the development of new therapies. The MCI syndrome has been further classified, according to the cognitive profile of impairment, into "amnestic" (aMCI) and "non-amnestic" (naMCI) forms, with isolated (single-domain) or multiple (multi-domain) cognitive deficits (Petersen and Negash 2008). However, neuropsychological, cerebrospinal fluid (CSF), genetics, and neuroimaging studies have clarified that MCI is a clinical-neuropsychological syndrome and not a disease entity, as it may be underpinned by a myriad of neurological, psychiatric, and systemic disorders. In particular, one of the most attractive opportunities offered by the MCI construct is that it allows to track neurodegenerative disorders before the stage of dementia. Alzheimer's disease (AD) is the most common neurodegenerative disease of the elderly population and an aMCI syndrome, typically an episodic memory deficit not helped by semantic cues, antedates the onset of dementia by years. Instead, in the MCI stage of AD with presenile onset (i.e., before 65 years), memory function is often relatively spared and a neocortical deficit including apraxia, agnosia, aphasia, or their various combination, dominates the cognitive deficit. On the other hand, dementia with Lewy bodies (DLB), frontotemporal lobe degeneration (FTLD), and vascular cognitive impairment (VCI) patients more often exhibit a naMCI syndrome, although exceptions to this rule are frequent (Petersen and Negash 2008). Finally, depression, which is often under-detected in the elderly, further complicates the differential diagnosis, as it may present with either aMCI or naMCI (Ismail et al. 2017). Thus, the same neuropsychological profile considerably overlaps among different diseases causing cognitive impairment.

Within this framework, biomarkers have confirmed their relevance in understanding the pathophysiology which underpins cognitive deficit, thus paving the way to the correct diagnosis. The bulk of evidence has become so convincing that the proposed new lexicon for AD calls "prodromal" AD those MCI patients with firm biological (i.e., neuroimaging and/or CSF) evidence of the AD-neurodegenerative process and leaves the term MCI to collect all those cases in whom a definite evidence of AD or other specific processes is lacking (Dubois et al. 2010). Thus, nowadays, the definition of AD in living people is shifting from a syndromic to a biological construct, in which the cardinal neuropathological features must be present, i.e., amyloidosis and tauopathy, while signs of neurodegeneration and even more clinical symptoms may or may not coexist. Thus, even if β amyloid plaques and neurofibrillary tau deposits might not be causal in AD pathogenesis, these abnormal protein deposits define AD as a unique neurodegenerative disease among

different disorders leading to dementia (Jack et al. 2018). Similarly, in all the other neurodegenerative diseases, a biological rather than a syndromic approach has the goal to find unique neuropathological features and thus to distinguish one with the respect to another at the MCI stage. However, the clinical validation of all these biomarkers is still incomplete and needs further studies in longitudinal cohorts with adequate follow-up and pathological confirmation, with the evaluation of the impact they have on prognosis and outcome (Frisoni et al. 2017).

Structural neuroimaging by means of computed tomography (CT) opened the way to this concept, but after a while, it was replaced by magnetic resonance imaging (MRI) that nowadays is commonly performed by means of 1.5 T equipment but almost replaced by 3 T equipment in most advanced hospitals in the Western world, and experimental studies are now using 7 T equipment. MRI has led to a tremendous improvement of morphological imaging, helping the diagnostic procedure by the evidence of different topographical patterns of atrophy, vascular damage, and microbleeds/superficial siderosis. More recently, new MRI techniques have allowed to study the integrity of white matter fibers (diffusion tensor imaging, DTI), expanding the focus of the impact of neurodegenerative and cerebrovascular diseases at this level, too. Magnetic resonance is also able to investigate brain function during administration of cognitive paradigms. By means of "blood-oxygen-level-dependent" (BOLD) technique, increases in regional cerebral blood flow (rCBF) can be detected and mapped with "functional MRI" (fMRI), showing different patterns of activation between MCI subjects and healthy controls, who also differ in the so-called default mode network (DMN) of brain functioning as emerged from "resting-state" fMRI (Greicius et al. 2004).

Functional neuroimaging has become widely used thanks to perfusion ^{99m}Tc radiopharmaceuticals and SPECT technology that have largely contributed to our knowledge in dementia and then in MCI since the early 1990s. Peculiar dysfunction pictures in major brain regions for pre-dementia AD and FTLD have been identified, followed by interesting data in DLB. However, as spatial resolution is only about 1 cm or just a bit better (typically 7–8 mm), SPECT technology has been progressively replaced by PET technology, which ensure a much higher spatial resolution (typically about 3 mm), thus further improving detection of functional impairment even in small brain structures. Nowadays, ^{18}F-fluorodeoxyglucose PET (FDG-PET) is the cornerstone of brain functional assessment, but in the last years, tracers for brain amyloid load have opened a new field (Herholz and Ebmeier 2011), and new tracers for tau imaging are in an advanced stage of development (Leuzy et al. 2019). Moreover, neuroreceptor systems can be visualized by injecting specific radiopharmaceuticals binding to dopamine, acetylcholine, and serotonin receptors or transporters, and other tracers allow imaging of inflammation and synaptic function. The majority of these last tracers are still labeled with ^{11}C, which forces research centers to produce them in situ, while fluorinated (i.e., ^{18}F-labeled) transportable compounds are still limited in number.

In this chapter, major neuroimaging-provided clues to the understanding, classification, and clinical diagnosis of the composite MCI syndrome are critically reviewed.

12.2 Morphological MRI

12.2.1 Principles

Structural magnetic resonance imaging (MRI) is recognized as an important diagnostic tool for AD. Since it is one of the most widespread tools in the clinical practice, it can be used to assess in vivo the structural brain changes noninvasively and relatively cheaply. Thanks to these characteristics and the fact that clinical scanners have been around for some decades, MRI has become a dependable support in diagnosing early and prodromal AD which is important for both an appropriate patient management and a quick support to relatives and caregivers. Moreover, morphological MRI is important to exclude structural lesions potentially caused by tumors, subdural hematoma, arteriovenous malformations, and hydrocephalus (Harper et al. 2014). In addition, pathophysiological studies confirmed that cerebral atrophy and white matter changes in the living brain reflect underlying neuropathology and may be detectable using *ante mortem* MRI.

In AD, the neurobiological changes occur years before the onset of symptoms and are defined by the abnormal deposition of fibrillar amyloid-β and tau aggregates in the brain tissue leading to a progressive synaptic, neuronal, and axonal damage. Despite its lack of specificity for AD, the downstream neurodegeneration biomarkers, including morphological MRI, are incorporated in the 2018 research framework providing important pathologic staging information (Jack et al. 2018). Neurodegeneration signs associated to AD are observable both in white (WM) and gray (GM) matter (Jack 2012). Particularly, the cumulative loss and shrinkage of the neuropil are reflected in the atrophy measured by MRI (Zarow et al. 2005; Barkhof et al. 2007). Patterns of cortical atrophy may aid the differential diagnosis of neurodegenerative diseases beyond AD, including FTLD, corticobasal degeneration (CBD), progressive supranuclear palsy (PSP), and vascular dementia (VaD). However, the overlap between these diseases is consistent, and findings should always be considered along with clinical examination and taking aging into account (Harper et al. 2014).

The need of quantitative MRI processing and visualization derives from the fact that the human eye cannot perceive the subtle anatomical changes affecting the structures of the brain; thus, it detects atrophy after the brain has already undergone irreversible synaptic loss. The detailed spatial patterns of atrophy have been extensively studied, using methods such as voxel-based morphometry (VBM) and surface-based methods (with techniques such as the boundary shift integral) (Fox and Freeborough 1997).

In this context, current research heavily relies on sophisticated analysis techniques (including volume, thickness, shape, and texture analysis—see Table 12.1) where the patterns and the extent of cortical atrophy are key players for an accurate and effective usage of MRI in patients with cognitive impairment.

In AD, GM atrophy is first observed in medial temporal lobe (MTL) structures, especially in the hippocampus and the entorhinal cortex (Pennanen et al. 2004;

Table 12.1 Selected quantitative MRI studies in the classification of MCI and AD subject (modified by Leandrou et al. 2018)

Study	Region of interest (ROI)	Data type	Subjects	Classification	Accuracy	Sensitivity	Specificity
Kloppel et al. (2008)	GM	VBM	20 HC, 20 AD	HC vs. AD	0.9	0.85	0.95
Colliot et al. (2008)	Hippocampus	Volume	25 HC, 24 MCI, 25 AD	HC vs. AD HC vs. MCI MCI vs. AD	0.84 0.66 0.82	0.84 0.66 0.83	0.84 0.65 0.83
Juottonen et al. (1999)	Hippocampus and Entorhinal cortex	Volume	32 HC, 30 AD	HC vs. AD	Hp: 0.86 Erc: 0.87	0.8 0.80	0.91 0.94
Pennanen et al. (2004)	Hippocampus and entorhinal cortex	Volume	59 HC, 65 MCI, 48 AD	HC vs. AD HC vs. MCI MCI vs. AD	0.91 0.66 0.82	0.88 0.66 0.81	0.93 0.65 0.83
Desikan et al. (2009)	Entorhinal cortex supramarginal gyrus	Thickness	49 HC, 48 MCI 94 HC, 57 MCI	HC vs. AD	NA	0.74 0.90	0.94 0.91
Lerch et al. (2008)	Entire cortex Parahippocampal gyrus	Thickness	17 HC, 19 AD	HC vs. AD	0.75 0.94	0.79 0.94	0.71 0.95
Gerardin et al. (2009)	Hippocampus	Shape	23 HC, 23 MCI, 25 AD	HC vs. AD HC vs. MCI	0.94 0.83	0.96 0.83	0.92 0.84
Ferrarini et al. (2009)	Hippocampus	Shape	50 HC, 15 MCI-c, 15 MCI-non-c, 50 AD	HC vs. AD MCI vs. AD	0.9 0.8	0.92 0.8	NA NA
Freeborough and Fox (1998)	Whole brain	Texture	40 HC, 24 AD	HC vs. AD	0.91	0.79	1
Zhang et al. (2012a)	Hippocampus and entorhinal cortex and CSF	Texture	17 HC, 17 AD	HC vs. AD	0.64–0.96	NA	NA
Simões et al. (2012)	Whole brain	Statistical texture maps	15 HC, 15 MCI	HC vs. MCI	0.87	0.85	0.95

AUC area under curve *HC* healthy controls, *MCI* mild cognitive impairment, *MCI-non-c* MCI non-converters, *AD* Alzheimer's disease, *GM* gray matter, *CSF* cerebrospinal fluid, *Hip* Hippocampus, *Erc* entorhinal cortex, *VBM* voxel-based morphometry

Du et al. 2004). As the disease progresses, the damage extends to the remaining part of the MTL (Li et al. 2011) (i.e., medial temporal gyrus, parahippocampus, fusiform gyrus, and temporal pole) and then to the extratemporal regions including the posterior cingulate gyrus (PCG)/precuneus and the middle frontal gyrus (Wolk et al. 2011; Irish et al. 2013, 2012; Doré et al. 2013). Additional structures involved in AD are the amygdala, the olfactory bulb tract and the primary olfactory cortex, the putamen, and the basal forebrain cholinergic system; atrophy also spreads to frontal, parietal, and temporal brain areas and to the cerebellum, brainstem, and thalamus (Duarte et al. 2006; de Jong et al. 2008; Thomann et al. 2009; Guo et al. 2010; Cavedo et al. 2011; Kilimann et al. 2014; Lee et al. 2015; Tabatabaei-Jafari et al. 2017; Vasavada et al. 2017).

The hippocampal shrinkage is a key feature of AD (see Fig. 12.1); it is one of the most validated and easily accessed biomarkers of AD, and it has been associated to

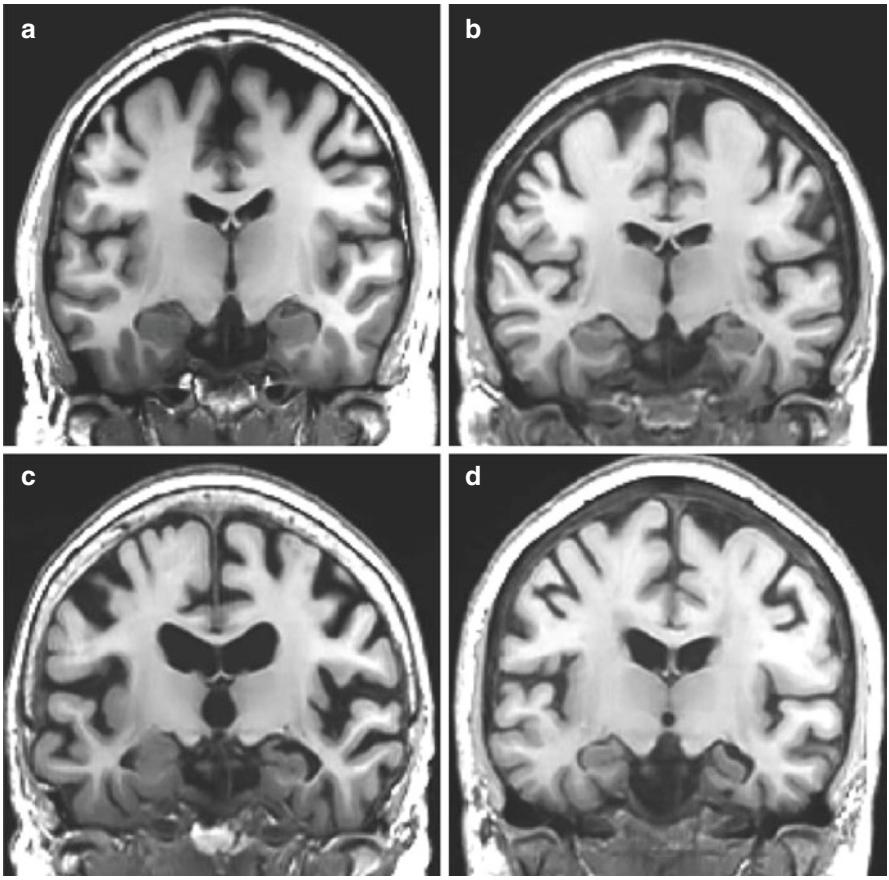

Fig. 12.1 Sample of MRI coronal sections showing regional atrophy. Subjective visual rating and linear measurements of the medial temporal lobe atrophy can be assessed on these MR films: (**a**) absent, (**b**) minimal, (**c**) moderate, and (**d**) severe

a variety of memory dysfunctions (Wolk et al. 2011; Doré et al. 2013; Lind et al. 2006; Dowell et al. 2016; Bonner-Jackson et al. 2015; Oosterman et al. 2012; Chetelat et al. 2003; Fujishima et al. 2014; Peter et al. 2016; Deweer et al. 1995; Kramer et al. 2005; Sarazin et al. 2010; Kerchner et al. 2012; Sexton et al. 2010; Molinuevo et al. 2011; Gomar et al. 2017). Several studies showed its effectiveness for demonstrating short-term clinical decline (Landau et al. 2010; Ewers et al. 2012; Lehmann et al. 2013; Jack et al. 2015) and for predicting conversion from the stage of MCI to the one of dementia (Jack et al. 2015; Holland et al. 2012; Leung et al. 2013). Especially, the hippocampal subfields are diversely affected by AD showing different sensitivity and specificity in distinguishing between AD dementia and MCI due to AD, as well as other dementias (La Joie et al. 2013; Li et al. 2013; Maruszak and Thuret 2014; Perrotin et al. 2015). In fact, a growing body of evidence suggests that the CA1 and subiculum subfields have the highest diagnostic power in detecting early AD (de Flores et al. 2015).

The combination of hippocampal and cortical features may also be used to differentiate pathologically defined subtypes of AD. For example, the greatest medial temporal lobe atrophy is observed with limbic-predominant AD, followed by typical AD and then hippocampal-sparing AD; conversely, the greatest cortical atrophy is seen in hippocampal-sparing AD, followed by typical AD and then limbic-predominant AD. So, the best discriminator of the three subtypes of AD is the ratio of hippocampal to cortical volumes (Whitwell et al. 2012).

With the advent of higher magnetic field strength scanners, the MTL remains an important target for imaging assessment at increased spatial resolution. Work at 3 T showed significant improvements due to the higher signal-to-noise ratio (SNR) and human studies at 7 T have again shown that improved SNR achieves greater reliability in visualization of the main hippocampal substructures (Theysohn et al. 2009; Kerchner et al. 2010) and at highest resolution begins to show finer details such as the dentate gyrus cell layer at only 0.1 mm in thickness (Kirov et al. 2013). However, the long duration of the scan and subject motion on a scale commensurate to—or often greater than—the size of the structures of interest hampers routine use of these techniques in clinical populations.

While AD is primarily associated with GM loss, WM may be concomitantly affected. It has been shown that MTL WM volume and integrity are positively related to memory performance in amnestic MCI (aMCI) and AD dementia (Sexton et al. 2010; Stoub et al. 2006; Zhuang et al. 2012; Meyer et al. 2013; Yakushev et al. 2010). Moreover, in APOE ε4 carriers, loss of entorhinal WM integrity was related to worse memory performance (Westlye et al. 2012), so that genetic status may mediate the relationship between MRI findings and cognition, too.

Besides these common MRI techniques, other approaches including diffusion kurtosis imaging, relaxometry, and magnetic transfer imaging may prove to be helpful in investigating WM integrity with high accuracy for whole brain mapping (Gouw et al. 2008; Struyfs et al. 2015). However, the number of studies using these approaches within the AD continuum is currently relatively small.

12.2.2 Utility in MCI

Image-based markers may be particularly interesting as they show a statistically significant prediction ability for those MCI subjects who will develop AD dementia. The prediction of conversion from MCI to AD dementia has been widely investigated (see Table 12.2), and there is agreement in imaging analysis being essential to this purpose. The most challenging task appears to be the distinction between normal controls (NC) and MCI subjects as the classification accuracy of most of the studies is lower compared to other groups of subjects (Leandrou et al. 2018).

Although hippocampal formation might be the most frequently used structure for the assessment of AD, the earlier involvement of the entorhinal cortex was proved by many studies and confirmed to be the relevant structure in the comparison of NC and MCI/AD (Juottonen et al. 1999; deToledo-Morrell et al. 2004; Killiany et al. 2002; Busatto et al. 2003; Tapiola et al. 2008; Gómez-Isla et al. 1997). Shape analysis appears to be a better technique compared to volume analysis, with similar results as voxel-based methods. While the entorhinal cortex is a better predictor compared to other structures, such as the hippocampus, the highest predictive accuracy (93.5% and 93%) was achieved when both were combined (deToledo-Morrell et al. 2004; Killiany et al. 2000). MTL atrophy also differentiates AD dementia from DLB and Parkinson's disease with dementia (PDD), as AD patients show the greatest reduction in hippocampal volume (Delli Pizzi et al. 2016; Tam et al. 2005).

Other studies focused on the other MTL and limbic structures besides hippocampus and entorhinal cortex and how MTL atrophy discriminates those who will convert from MCI to AD dementia from non-converter MCI patients (Nesteruk et al. 2015). In the former, decreased inferior frontal gyrus volume was associated with verbal memory decline (Defrancesco et al. 2014), suggesting extratemporal involvement as a predictor of disease progression. In addition, atrophy in MCI is found in the primary olfactory cortex (Kilimann et al. 2014), infratentorial brain areas including the cerebellum and brainstem (Lee et al. 2015; Tabatabaei-Jafari et al. 2017), and some basal forebrain cholinergic system structures (Duarte et al. 2006; Kilimann et al. 2014; Vasavada et al. 2017).

Outside the GM, WM studies suggested that precuneus WM volume reduction was also associated with worsened memory in aMCI (Meyer et al. 2013). In addition, periventricular white matter hyperintensities (WMHs) are predictive of progression from MCI to AD dementia, with an increase of one point in WMH rating associated with a 59% increased risk of phenoconversion (ECW et al. 2008). Similarly, increased number of WMHs in the bilateral periventricular regions, as expression of a more severe vascular impairment, was related to worse recall performance in MCI (Fujishima et al. 2014).

Table 12.2 Selected quantitative MRI studies assessing the prediction of the conversion from MCI to AD (modified by Leandrou et al. 2018)

Study	Region of interest (ROI)	Data type	Follow-up (months)	Converters/Total MCI	Accuracy	Sensitivity	Specificity
Davatzikos et al. (2011)	Whole brain	VBM	0–36	69/239	0.56	0.95	0.38
Misra et al. (2009)	Whole brain	VBM	0–36	27/103	0.82	NA	NA
Plant et al. (2010)	Whole brain	VBM	0–30	9/24	0.75	0.56	0.87
Duchesne et al. (2010)	MTL	VBM	0–28	11/31	0.81	0.7	1
Koikkalainen et al. (2011)	Whole brain	TBM	0–36	154/369	0.72	0.77	0.71
Chupin et al. (2009)	Hippocampus and amygdale	Volume	0–18	76/210	0.64	0.6	0.65
deToledo-Morrell et al. (2004)	Hippocampus and entorhinal cortex	Volume	0–36	10/27	0.93	NA	NA
Killiany et al. (2002)	Entorhinal cortex	Volume	0–36	13/73	0.84	NA	NA
Devanand et al. (2007)	Hippocampus and entorhinal cortex	Volume	0–36	37/139	0.88	0.83	NA
Killiany et al. (2000)	Entorhinal cortex	Volume	0–36	19/79	0.93	0.95	0.9
Querbes et al. (2009)	Cortex	Thickness	0–24	72/122	0.73	0.75	0.69
Eskildsen et al. (2013)	Cortex	Thickness	0–36	–	0.67–0.76	NA	NA
Bakkour et al. (2009)	Cortex	Thickness	0–30	20/49	NA	0.74	0.84
Desikan et al. (2010)	Neocortex	Thickness and volume	0–36	TC: 60/162 VC: 58/162	AUC: 0.82 AUC: 0.84	0.87	0.66
Ferrarini et al. (2009)	Hippocampus	Volume 3D shape	0–33	15/30	0.73 0.8	0.63 0.8	0.77 0.8

Costafreda et al. (2011)	Hippocampus	3D shape	0–12	22/103	0.8	0.77	0.8
Cuingnet et al. (2011)	Whole brain Hippocampus Cortex	VBM Atlas-based Thickness	– 0–18 –	– 76/210 –	0.71 0.67 0.7	0.77	0.78
Wolz et al. (2011)	Whole brain Whole brain Hippocampus Cortex Combination	TBM Manifold-based learning Atlas-based Thickness Combination	– – 0–48 – –	– – 167/405 – –	0.64 0.65 0.65 0.56 0.68	0.65 0.64 0.63 0.63 0.67	0.62 0.66 0.67 0.45 0.69
Sørensen et al. (2016)	Hippocampus	Texture Texture and volume	0–12 0–24	–	AUC: 0.74 AUC: 0.74	NA	NA

ROI region of interest, *MCI* mild cognitive impairment, *VBM* voxel-based morphometry, *TBM* tensor-based morphometry, *MTL* medial temporal lobe, *Hip* hippocampus, *Erc* entorhinal cortex, *STS* superior temporal sulcus, *TC* training cohort, *VC* validation cohort, *AUC* area under curve

12.2.3 Combined Use of MRI and Other Biomarkers

Nowadays, medical image analysis has become a computationally rich process that includes many intricate steps run on increasingly larger datasets with the use of many different tools and combined biomarkers. These biomarkers yield complementary information, as different modalities capture disease information from different perspectives and thus better reflect the neuropathological pattern than one single modality.

The combination of structural MRI, PET, and CSF biomarkers together with genetic data and neuropsychological status exam scores has been largely assessed. For example, the SPARE-AD score, summarizing brain atrophy patterns (Davatzikos et al. 2009; Fan et al. 2007) was combined with cognitive scores, APOE genotype, and CSF biomarkers (Da et al. 2014) to predict conversion from MCI to AD dementia. Similarly, Kohannim et al. (2010) found that the highest accuracy (82.2%) for AD classification was achieved when MRI hippocampal volume and ventricular summary, APOE genotype, and age were used together. Also, a benefit of combining MRI and FDG-PET in predicting conversion to AD dementia with respect to the single biomarker was reported (Walhovd et al. 2010) and was even higher when CSF was added (combinatorial accuracy of 92.1%) (Shaffer et al. 2013). However, other studies showed more modest results as adding CSF biomarkers to FDG-PET after MRI (i.e., CSF + MRI + FDG-PET) led to a 76.4% accuracy in distinguish MCI from healthy controls in a ADNI group, whereas the best biomarker taken alone (MRI) reached a 72% accuracy (Zhang et al. 2011). Moreover, just a 6% AUC value increase was demonstrated from the best single (t-Tau, AUC 0.77) to the best three-predictor combination model (t-Tau/HCV/CDR-sum of boxes, AUC = 0.83) in predicting conversion to AD dementia (Frölich et al. 2017). An overview of the possible approaches when combining biomarkers is shown in Fig. 12.2.

Concerning disease progression, morphometric measures derived from structural MRI can provide similar results with cellular or metabolic markers such as CSF, amyloid-Aβ, and FDG-PET (see (Schroeter et al. 2009) for a systematic and quantitative meta-analysis). Using images from the ADNI database with their corresponding segmentation masks (Heckemann et al. 2011), established regions of interest (ROIs) yielded an AUC of 0.79 in predicting progression to AD dementia in MCI patients (Martinez-Torteya et al. 2014). A similar performance was obtained with the combination of biomarkers derived from structural and functional imaging modalities (Jack et al. 2008a; Martínez-Torteya et al. 2015) as well as with the combination of MRI with genomic analysis. It was suggested that atrophy in the (trans-) entorhinal area/hippocampus and hypometabolism/hypoperfusion in the inferior parietal lobules could predict most reliably the progression from aMCI to AD dementia. However, according to a comprehensive meta-analysis (Yuan et al. 2009), FDG-PET was a better dementia predictor than morphological MRI.

Structural-based biomarkers are accurate predictors of outcome in symptomatic AD patients (Vemuri et al. 2009; Frisoni et al. 2010; Jack et al. 2009) and can be useful even in pre-symptomatic subjects (Pennanen et al. 2004; Killiany et al. 2002;

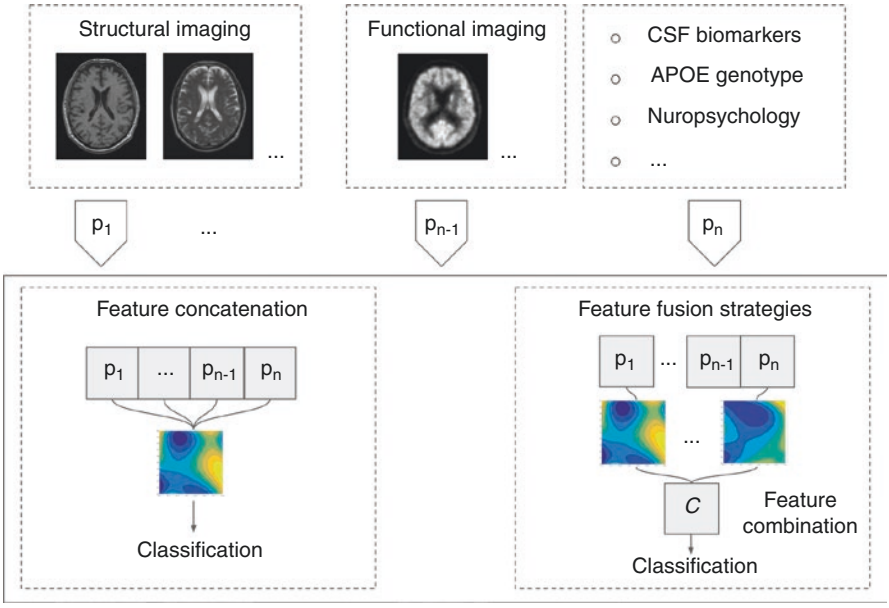

Fig. 12.2 A top-level breakdown of multimodality-based classification studies for AD classification

Davatzikos et al. 2008) even more than metabolic markers at least according to some studies (Desikan et al. 2010; Vemuri et al. 2009; Frisoni et al. 2010).

Of course, imaging as well as all other biomarkers has value only if properly embedded in the clinical context (Devanand et al. 2007; Jack et al. 2004; Julkunen et al. 2009). To date, however, there are very few studies that combine clinical variables with volume, thickness, shape, intensity, and texture in multivariate assessment of the disease, which in turn may result in better classification and prediction accuracies (Cuingnet et al. 2011; Wolz et al. 2011).

12.3 Functional MRI, Arterial Spin Labeling (ASL), and Diffusion-Weighted Imaging

12.3.1 Blood-Oxygen-Level-Dependent (BOLD) Functional MRI (fMRI) Principles

BOLD enables the assessment of hemodynamic changes associated with regional brain activity during a task (e.g., a motor or a cognitive task). Hemoglobin (Hb) in erythrocytes delivers oxygen to neurons. When neurons are activated, there is an increased demand for oxygen, eliciting an increase of rCBF to the brain regions involved in neural activity. Hb is diamagnetic when oxygenated, while it is paramagnetic when deoxygenated. This difference in magnetic properties is associated

with small differences in the magnetic resonance signal of blood, depending on the degree of oxygenation. Since blood oxygenation changes according to the neural activity, these differences can be used to explore brain activity. A detailed description of the neurophysiological basis of BOLD signal can be found in Logothetis (2002).

12.3.2 Utility in MCI

Performing fMRI studies in patients with cognitive impairment can be challenging. Even small head motions can compromise fMRI data quality and differences in task performance between patient and control groups, thus making the interpretation of data tricky or even misleading (Price and Friston 1999). Since the loss of memory is a key clinical feature of AD patients at all stages of the disease, anatomical regions and networks involved in memory have been explored by fMRI with appropriate tasks. Functional MRI has been utilized in normal subjects to investigate brain activity in memory processes in order to understand how neural activation differs, in memory tasks, for subsequently remembered or forgotten experiences. Successful retrieval of information is associated with fMRI evidence of activation in the MTL, prefrontal cortex, and ventral temporal cortex (Wagner et al. 1998; Kirchhoff et al. 2000; Brewer et al. 1998). Moreover, fMRI studies have demonstrated a brain network that "deactivates" during successful memory formation (Daselaar et al. 2004). These data evoke a theoretical model of memory formation that requires activation of the hippocampal nodes and concomitant deactivation of the retrosplenial-parietal nodes.

Functional MRI studies in MCI report different, and apparently conflicting, results when evaluating task-related BOLD signal changes. Many previous task-based fMRI studies showed a greater activity in MCI patients with respect to healthy controls in frontal and parietal regions across memory encoding and retrieval, working memory, executive function, and perception tasks (Bokde et al. 2010; Kaufmann et al. 2008; Poettrich et al. 2009). However, in a meta-analysis healthy elderly showed greater activity in MTL and frontal pole both in encoding and retrieval processing while an increased activation in ventral lateral prefrontal cortex, superior temporal gyrus was detected in AD patients (Schwindt and Black 2009). Browndyke et al. (2013) demonstrated a decreased activation in MTL and increased activation in prefrontal gyrus in both MCI and AD dementia patients with respect to healthy controls during memory encoding. Interestingly, other studies have found greater MTL activation in MCI with respect to controls, for instance, in an associative face-name encoding paradigm (Dickerson et al. 2005) or in an associative encoding of novel picture-word pair task (Hämäläinen et al. 2007). It seems that heterogeneity in patients' selection and methodological aspects cannot completely explain this variability in fMRI studies results. In fact, many authors hypothesize that there is a phase of increased MTL activation early in the course of MCI, most likely representing a compensatory response to AD pathology. Beyond this phase, as the disease progresses, there is a decrease in functional activation. This "compensatory" hypothesis is supported by data derived from studies in cognitively intact

APOE-epsilon4 allele carriers (Bookheimer et al. 2000). Such MTL hyperactivation could be useful to predict progression from MCI to AD dementia (Dickerson et al. 2005); however, a correct interpretation of fMRI hyperactivation with respect to particular brain regions and behavioral conditions is not always straightforward and might indeed pose interpretation problems. Considering a theoretical model with an "inverse U-shaped curve" of fMRI activation along the course of the disease, hyperactivation can be detected in the setting of minimal clinical impairment (and relatively little MTL atrophy) in the upgoing phase along the curve, while the same level of hyperactivation in the setting of more prominent clinical and memory impairment and MTL atrophy would be consistent with the downgoing phase of the curve. Thus, the same degree of fMRI hyperactivation may be associated with different biological stages of disease, a result that would make it difficult to use fMRI for clinical purposes at the MCI stage.

Recently, 39 task-based fMRI studies (697 MCI patients and 628 healthy controls) were included in MCI-related meta-analysis, while 36 task-based fMRI studies (421 AD patients and 512 healthy controls) were included in AD-related meta-analysis (Li et al. 2015). MCI and AD dementia patients showed abnormal regional brain activation but also alterations within large-scale brain networks. Relative to healthy controls, MCI patients showed hypoactivation in the default mode network (DMN) and in the frontoparietal and visual networks. AD-related hypoactivation was mainly located in visual, default, and ventral attention networks relative to healthy controls. Both MCI-related and AD dementia-related hyperactivation were identified in the frontoparietal, ventral attention, default, and motor networks with respect to healthy controls. Thus, it may be suggested that MCI and AD dementia share similar compensatory mechanisms in large-scale networks actuated in relation to different cognitive tasks.

Brain activation on fMRI may also be affected by cognitive training. Mnemonic strategies, frequently used as a part of cognitive rehabilitation programs, are effective in some patient populations (Cicerone et al. 2011) and result in increased prefrontal (Kondo et al. 2005; Miotto et al. 2006) and hippocampal (Nyberg et al. 2003) activity in healthy participants. Some authors have reported increased prefrontal activity accompanying behavioral improvement after cognitive training in MCI patients (Hampstead et al. 2011; Belleville et al. 2011) and a facilitation of hippocampal function (Hampstead et al. 2012). In conclusion, with increasing fMRI studies in AD, it has been demonstrated that some cortical regions are activated in a large variety of tasks. It may be suggested that AD is characterized by multiple and large-scale dysfunctional neuronal networks and not specifically by alterations in single brain regions.

Another field of research is represented by resting-state fMRI (rs-fMRI) and the study of "default mode" activity in people with MCI and AD. This fMRI modality has some advantages, particularly in the study of individuals with more severe cognitive impairment who may have difficulties performing a given task. Resting-state functional connectivity explores temporal correlations of BOLD signal between different brain regions and/or voxels. Studies examining rs-fMRI data have found low-frequency fluctuations of the measured cerebral hemodynamics

(Biswal et al. 1995). These signal variations, temporally correlated across the brain, correspond to functional resting-state networks that together characterize the neuronal baseline activity of the human brain in the absence of stimulated neuronal activity. The coherent resting fluctuations that have been identified include functionally relevant networks involved in motor function, visual processing, executive functioning, auditory processing, memory, and the DMN. This network is active during resting-state but has a decreased activity during the performance of cognitive tasks, which indicates that the DMN is fundamental for modulating cognitive processing. MCI patients are characterized by a disruption of functional connectivity within the DMN (Greicius et al. 2004; He et al. 2007; Wang and Su 2006; Han et al. 2011; Koch et al. 2015; Zhang et al. 2012b) that included the ventral medial prefrontal cortex, dorsal medial prefrontal cortex, posterior cingulate cortex (PCC), adjacent precuneus, lateral parietal cortex, hippocampus, and thalamus (Lin et al. 2018). Subsequent studies showed an increase in functional activity in the frontal cortex, besides a decrease in functional activity in the DMN regions (Jin et al. 2012). Hyperactivation in brain regions belonging to memory and cognitive circuits may possibly represent an attempted compensatory activity. Besides the methodological differences between the different studies, functional connectivity in the hippocampus and PCC has been demonstrated to be consistent with poor performance of neuropsychological tests in MCI, suggesting the potential role of functional connectivity as a predictor of cognitive decline (Han et al. 2011; Binnewijzend et al. 2012; Gardini et al. 2015). Considering that the brain is an intrinsically variable system, recently standard deviation of BOLD fluctuations (SD_{BOLD}) (instead of the mean value) has been proposed as a biomarker of AD, also to investigate the role of cerebrovascular status in determining BOLD variability (Scarapicchia et al. 2018), in the hypothesis that fluctuations on functional activity simply reflect vascular processes unrelated to neuronal function (Obrig et al. 2000; Wise et al. 2004).

Recently, more complex models, such as regional homogeneity (ReHo) (Zhang et al. 2012b; Lin et al. 2018; Zang et al. 2004; Bai et al. 2008), amplitude of low-frequency fluctuation (ALFF) (He et al. 2007; Pan et al. 2017), and graph theory have been used to explore the pathological process in MCI patients (Zhang et al. 2017) which is interesting in research but still far from being utilized in clinical practice.

The integration of task-free fMRI techniques able to identify the different networks involved in MCI and AD patients with tau PET and amyloid PET may be helpful to detect the interplay between tau and Aβ temporal and anatomical pattern of deposition across the brain with brain networks modifications and failure. Jones et al. (2017) demonstrated that younger age of disease onset was associated with tau deposition in nonclassical brain areas (“non-Braak-like” pattern), suggesting an association with atypical clinical phenotypes. Furthermore, the authors demonstrated that amyloid is a partial mediator of the relationship between functional network failure and tau deposition in functionally connected brain regions. While Aβ deposition reaches a plateau, tau deposition, which involves more specific functional networks related to AD, continues to increase over the time and correlates with clinical progression.

12.3.3 Arterial Spin Labeling (ASL)

Arterial spin labeling (ASL) is a noninvasive MRI technique able to reveal typical brain perfusion abnormalities in several neurological conditions without the need of injecting any contrast agent. In MRI-ASL inflowing arterial blood water is magnetically tagged proximally to the region of interest using a radiofrequency inversion pulse. Then, quantitative perfusion maps are obtained by subtracting the brain images without and with labeling of blood (Riederer et al. 2018).

ASL-MRI technique is known for human use for over a decade; in the last years, improvements in SNR and reliability have been achieved, and now several variants of ASL-MRI techniques are widely applied to neurodegenerative populations, including continuous ASL (CASL), pulsed ASL (pASL) (Xu et al. 2009; Ciarochi et al. 2016), and pseudo-continuous ASL (pCASL) (Ciarochi et al. 2016; Ferreira et al. 2011). The ISMRM perfusion study group and the European consortium for ASL in dementia recently provided a consensus including recommendations to optimize MRI-ASL images acquisition and analysis (Alsop et al. 2015).

Given the physiological coupling between metabolism and perfusion, in several studies about AD, both FDG-PET and MRI-ASL were acquired and compared to evaluate if the information provided by the different techniques is redundant or complementary (Chen et al. 2011a; Musiek et al. 2012; Verfaillie et al. 2015). ASL-MRI demonstrated that resting rCBF is able to predict conversion to MCI (Beason-Held et al. 2013) in adult healthy individuals; compared to individuals with preserved cognitive functions, adults that developed MCI showed hypoperfusion in parietal, temporal, and thalamic regions, suggesting that perfusion abnormalities take place years before the onset of cognitive symptoms. In accordance with FDG-PET literature, ASL-MRI performed in MCI patients (Johnson et al. 2005) reported decreased rCBF in posterior cingulate/precuneus and parietal regions, with a lesser extent than in AD dementia. A few longitudinal ASL-MRI studies have been performed in MCI patients (Chao et al. 2010); patients who converted to AD dementia showed greater hypoperfusion in the precuneus, middle cingulum, infero-parietal, and middle frontal cortices. When combined with measures of hippocampal volume at baseline, rCBF values provided additional predictive power.

In patients with AD dementia, regional CBF (rCBF) decrease was more prominent in the precuneus, posterior cingulate, and superior parietal cortex (Alsop et al. 2000); additional areas of hypoperfusion have been described in the lateral frontal lobe, orbitofrontal cortex, and temporal lobe including the parahippocampal gyrus and hippocampus (Wierenga et al. 2012). Interestingly, increased rCBF has been described in frontal regions and hypothesized to reflect compensatory or pathological elevation of neural activity, inflammation, or elevated production of vasodilators (Alsop et al. 2008). Also, the MTL has been reported to be relatively hyperperfused in early-stage AD patients with respect to controls (Chao et al. 2010). This feature is in contrast to a number of FDG-PET studies that have reported MTL hypometabolism (Chen et al. 2011a; Takahashi et al. 2014; Rodriguez et al. 2000). Time interval between MRI-ASL and FDG-PET scans has been hypothesized to be the cause of these concerns. Thus, in a very recent study (Riederer et al. 2018), integrated pulsed MRI-ASL and FDG-PET scan revealed similar findings in patients with AD dementia, while in MCI

patients, FDG-PET was more sensitive with respect to MRI-ASL in detecting quantitative hypometabolism in the precuneus. Future investigations based on MRI-ASL and on the association of MRI-ASL and FDG-PET in neurodegenerative disorders are necessary to evaluate the real role of this technique for early diagnosis and disease monitoring. This would be particularly meaningful using simultaneous PET-MRI acquisitions with dedicated PET-MRI scanners and might lead to clinical validation of ASL techniques in dementia diagnosis and prognosis.

12.3.4 Diffusion-Weighted Imaging (DWI) Principles

Diffusion-weighted imaging and related techniques, such as diffusion tensor imaging (DTI), are quantitative MRI modalities that measure water diffusion properties noninvasively and that have evolved as a reliable technology to probe central nervous system microstructure. DTI is highly sensitive to subtle structural changes in brain tissue, given the diffusion anisotropy characterizing WM. Thus, in normal WM, diffusion is not identical in all directions, but, for a given diffusion time, displacement of water molecules is on average greater along the length of axons than across the axons (Basser et al. 1994; Moseley et al. 1990). Several DTI-derived metrics can be obtained, including fractional anisotropy (FA) (Beaulieu 2002), mean diffusivity (MD), and parallel (i.e., axial diffusivity, DA) and perpendicular diffusivity (i.e., radial diffusivity, RD). In general, a decrease in anisotropy is considered a marker of loss of white matter integrity. Anisotropy can be reduced due to a decrease in parallel diffusivity and an increase in perpendicular diffusivity or some combination of these parameters. Even though inferring the histological contributors of anisotropy changes is not straightforward, experimental studies have shed some light on the biological basis of the different DTI-derived parameters. For instance, decreases in DA have been correlated with axonal loss, whereas increases in RD would indicate loss of myelin (Song et al. 2003). The diffusion measurements obtained in a DTI acquisition can be analyzed using different approaches. Among them, region-of-interest (ROI) analysis and voxel-based methods have been used in the study of MCI. Moreover, DTI can be used to isolate white matter pathways in vivo and thus enables diffusion measurements along a given anatomical structure. As an example, DTI can be used to obtain measurements within the voxels estimated to belong to a white matter bundle of interest.

Although DTI longitudinal reproducibility has been shown to be acceptable with different equipment used in healthy subjects (Jovicich et al. 2014), the use of different methodologies and equipment may account for the heterogeneous findings reported in different studies. Nonetheless, even studies that use the same methods of DTI data analysis may be difficult to compare. In fact, patients' characteristics may vary among studies; DTI acquisition parameters are often very different (the technical details of DTI are beyond the scope of this chapter, but many acquisition parameters such as "b" values and acquisition matrix can be dissimilar among studies). Also, when comparing "significant" findings among different studies, it must be noted that different statistical approaches can be utilized, and when comparing results from multiple ROIs, for example, more or less "liberal" statistical thresholds will lead to different results (Sexton et al. 2011). The single tensor DTI model

assumes a single tissue compartment per voxel, and this represents a limitation, thus leading to DTI metrics in voxels consisting of a mixture of WM and freely moving extracellular water molecules (Alexander et al. 2001; O'Donnell and Pasternak 2015). This may be particularly concerning in patients with neurodegenerative disease, since, along with brain atrophy, increase in water within a voxel may significantly influence diffusion derived metrics. Thus, multi-compartmental models were initially employed to detect water contamination within voxels but, as described below, also enable better characterization of tissue microstructure.

12.3.5 Utility in MCI

Using DTI, researchers have contributed to amplify the interest on WM pathology in MCI (and AD dementia) and added information to the debate on the relevance of WM pathology and on its pathogenesis. The most important question is whether WM pathological changes are related to GM pathology or not. WM pathology may occur as a consequence of GM pathology that first involves the hippocampus and the entorhinal cortex and then progresses to temporal and parietal association cortex; thus, WM microstructural damage would be the result of secondary degeneration. Other researchers hypothesize that WM and GM pathologies would be independent and would follow the myelogenesis pattern in a reverse order (Bartzokis 2004). Vascular changes may also contribute to WM pathology (Brun and Englund 1986).

DTI studies can be useful to better understand the relationship between GM and WM changes. For instance, an interesting study in AD patients found a significant regional correlation between FA within the corpus callosum and GM thickness in the lobes these fibers connect with (Sydykova et al. 2007); the authors concluded that decline of FA in the corpus callosum could be related to neuronal degeneration in corresponding cortical areas. Nevertheless, in the published DTI studies, there is no overall consensus, with some studies supporting secondary degeneration and others primary myelin pathology.

DTI studies have extensively showed, in vivo, the presence of WM changes in MCI patients with respect to control subjects. At first, studies using regional approaches reported changes in MD and anisotropy in the MTL, especially within the hippocampal formation (Wang and Su 2006; Kantarci et al. 2001), and higher baseline hippocampal MD has been reported useful in identifying patients with MCI who will progress to AD (Fellgiebel et al. 2006). WM disruption occurring in the preclinical stage of AD has been confirmed in more recent studies (Adluru et al. 2014; Fischer et al. 2015; Kantarci et al. 2014; Prescott et al. 2014), initially involving MTL association tracts and then spreading to the temporal and parietal white matter during clinical disease progression (Demirhan et al. 2015; Konukoglu et al. 2016). Other anatomical locations have then been assessed; using multiple ROIs, Zhang et al. (2007) identified the posterior cingulate, at the apex of the posterior curve of the tract, as the most suitable region in discerning between healthy controls and MCI or AD dementia. In that study, MTL volume was only 63% accurate for discriminating between healthy controls and MCI, but accuracy increased to 78% with the information derived from left posterior cingulate FA. An example of DTI findings in a patient with aMCI is reported in Fig. 12.3.

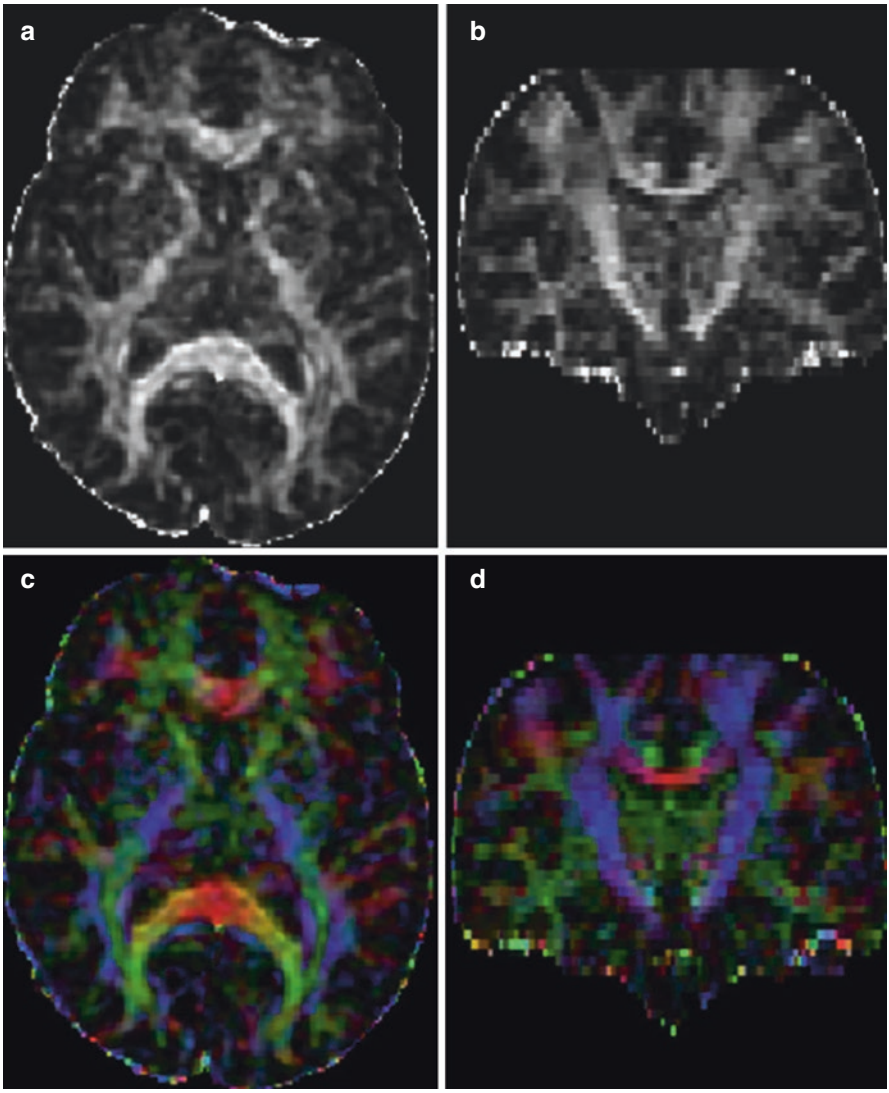

Fig. 12.3 Diffusion tensor imaging (*DTI*) acquisition in a 75-year-old female patient with MCI. Images (**a**, **b**) are axial and coronal reformats of fractional anisotropy (*FA*) maps, respectively. Image intensity reveals differences in anisotropy across different anatomical regions. (**c**, **d**) Color-coded maps. In color-coded maps, the principal direction of diffusion can be associated with the underlying white matter bundle orientation. The color *red*, for example, can be used to indicate diffusion along the left/right axis, *green* for diffusion along the anterior/posterior axis, and *blue* for diffusion along the superior/inferior axis (e.g., superior to inferior direction of corticospinal tracts can be seen in *blue*)

Voxel-based approaches can be utilized to overcome the limitation represented by the analysis of an individual ROI instead of the whole brain. Using the technique of tract-based spatial statistics, O'Dwyer et al. (2011) studied 19 patients with naMCI and 14 with aMCI subjects and found significantly higher DA in naMCI subjects compared to healthy controls in the right posterior cingulum/precuneus. They also found significantly higher DA in aMCI subjects compared to healthy controls in the left prefrontal cortex, particularly in the forceps minor and uncinate fasciculus. In a study of 96 aMCI and 69 naMCI subjects, Zhuang et al. (2010) found that the best discrimination between aMCI and controls was achieved by combining FA measures of the splenium of corpus callosum and crus of fornix, with accuracy of 74.8%.

The single tensor DTI model assumes a single tissue compartment per voxel, and this represents a limitation, thus leading to DTI metrics in voxels consisting of a mixture of WM and freely moving extracellular water molecules (Alexander et al. 2001; O'Donnell and Pasternak 2015). To overcome this concern, free water elimination (FWE) methods including an explicit compartment modeling free water have been proposed (Metzler-Baddeley et al. 2012; Baron and Beaulieu 2015), with interesting applications in longitudinal studies. Indeed, longitudinal changes in white matter microstructure may be related to brain slice positioning across MRI sessions, leading to different CSF-contamination-based partial volume effects (Metzler-Baddeley et al. 2012). Furthermore, the extracellular volume may be influenced by transient changes, such as dehydration, temperature, and stress, which may change between scans. In a recent study, longitudinal test-retest reproducibility of DTI metrics commonly used in clinical studies derived from the single tensor DTI model has been compared to those provided by a bi-tensor FWE diffusion model (Albi et al. 2017). In that study the authors demonstrated that FWE is characterized by a reduced reproducibility error in the majority of brain regions tested and by a better sensitivity in identifying more subtle changes, thus representing a promising tool for clinical applications.

Besides bi-tensor models, multi-shell diffusion MRI techniques have been developed in the last years, allowing an even more advanced analysis of the diffusion signal. The association between WM microstructure and performance on working memory tasks in healthy adults has been analyzed (Chung et al. 2018). Specific WM tract integrity (WMTI) metrics provided by multi-shell diffusion MRI analysis and diffusion tensor/kurtosis imaging (DTI/DKI) metrics have been used to describe microstructural characteristics in both the WM intra- and extra-axonal environments: axonal water fraction (AWF), intra-axonal diffusivity, extra-axonal axial, and radial diffusivities. These parameters allow a better biophysical interpretation of WM changes with respect to "conventional" DTI analysis. In that study, a positive correlation between AWF and letter-number sequencing (LNS) was demonstrated, suggesting that higher AWF may correspond to a greater axonal volume and myelination, leading to faster information processing.

Neurite orientation dispersion and density imaging (NODDI) (Zhang et al. 2012c) represents another possible application of multi-shell diffusion MRI techniques, able to provide tissue-specific microstructural information from multiple compartments within a voxel. The basic assumption of NODDI model comes down to the fact that water molecules in neuronal tissue may be placed in three different compartments: (a) free water, representing CSF; (b) restricted water, representing neurites; and (c) hindered water, representing diffusion within glial cells, neuronal cell bodies, and the extracellular environment. Through NODDI processing, different measures may be obtained, i.e., the neurite density index (NDI) (higher values reflect increased neurite density) and the orientation dispersion index (ODI), that give information about the degree of neurite dispersion. Furthermore, thanks to the capacity to estimate the free water fraction, the risk of partial volume effects due to the CSF is notably reduced with respect to the previous DTI models (Zhang et al. 2012b). In efforts to correlate diffusion derived metrics with pathology, differences in cortical NODDI measurements have been described in transgenic murine models of AD tauopathy (Colgan et al. 2016) finding a lower cortical ODI compared to wild type mice but increased cortical NDI that, interestingly, was associated with a greater tau immunoreactivity. This feature is discordant with a more recent study (Parker et al. 2018) in which a consistent decrease in NDI in early-onset AD (EOAD) patients compared to healthy controls was demonstrated in entorhinal, middle temporal, inferior temporal, fusiform, precuneus, and precentral areas and reductions in ODI in inferior temporal, middle temporal, fusiform, and precuneus regions. Interestingly, these findings persisted in the majority of regions after performing adjustment for cortical thickness, and, concerning NDI, abnormalities were detected also in the precentral gyrus, a region typically known to be spared of significant atrophy in AD. Furthermore, cortical NDI correlated with the Mini-Mental State Examination (MMSE) score.

12.3.6 Combined Use of DTI and Other Biomarkers

A few studies have tried to assess the relationship between cerebrovascular fluid biomarkers (CSF) and brain tissue microstructure using DTI indices (Bendlin et al. 2012; Gold et al. 2014). In a small group of adults with parental history of AD, CSF total tau and total tau/a$\beta_{1\text{-}42}$ ratio correlated with mean, axial, and radial diffusivity in WM regions next to GM areas affected in early AD, while there was no correlation between CSF biomarkers and GM volume (Bendlin et al. 2012). Similar results were described in another study that evaluated a group of adults at high risk of AD, as defined by parental history and APOE ε4 status and a group of subjects with preclinical AD pathology, assessed by CSF markers. By using DTI the authors identified an association between changes in MD with higher CSF hyperphosphorylated tau/a$\beta_{1\text{-}42}$ ratio, particularly in the temporal lobe WM, but not in hippocampal GM (Hoy et al. 2017). WM-DTI abnormalities have been also associated with imaging biomarkers suggestive of gray matter neurodegeneration such as cortical and hippocampal atrophy (Ouyang et al. 2015) and hypometabolism on FDG-PET (Kantarci

et al. 2014). Furthermore, WM degenerative changes provided by DTI analysis correlate with cognitive function and disease severity. Finally, Kantarci et al. (2017) correlated MD and FA values of the limbic projections and white matter regions that showed neurofibrillary tangles on neuropathological examination. They found that the higher cortical neurofibrillary tangle burden was associated with a higher MD and lower FA in the correspondent tracts and regions.

In conclusion, DTI studies indicate a pathological involvement of WM in MCI. The nature of these pathological changes, primary or secondary, is still a matter of debate. Thus, integrative studies including both DTI analysis in vivo and neuropathology *postmortem* may be of paramount importance to increase our knowledge about the biological correlates of microstructural parameters of tissue damage in MCI and AD dementia patients.

12.4 Perfusion SPECT

12.4.1 Principles

The most common radiopharmaceutical tracers used for brain perfusion SPECT are ^{99m}Tc hexamethylpropylene amine oxime (HMPAO) and ethylcysteinate dimer (ECD). ^{123}I-Iodoamphetamine (IMP) is also used, mainly in Japan. Those techniques measure the nonquantitative distribution of a perfusion tracer within the brain. Thus, even if the term "rCBF" is often used to report SPECT findings, the most appropriate term would be "brain perfusion," and "rCBF" should be reserved to "quantitative" measures, as obtained with $H_2{}^{15}O$ PET techniques.

General-purpose gamma cameras equipped with two or three head detectors and low-energy, high-resolution collimators are usually used, and such equipment is widely available. However, brain-dedicated cameras and fan-beam collimators, both yielding a higher spatial resolution, are less available. The newer SPECT-computed tomography (SPECT-CT) equipment has substantially increased image quality by improving attenuation correction computation. Three-dimensional imaging with fair spatial resolution (i.e., 6–8 mm) is allowed by reconstructing bidimensional projections. Moreover, to obtain reliable imaging, both acquisition and reconstruction protocols are crucial, and the procedural guidelines of the American Society (Juni et al. 2009) and of the European Association (Kapucu et al. 2009) of Nuclear Medicine should be strictly followed.

12.4.2 Utility in MCI

Patients with aMCI show hypoperfusion patterns that closely overlap FDG-PET patterns, even if the two modalities actually measure different parameters. However, literature studies have shown that both FDG and perfusion SPECT tracers mainly reflect the function of astrocytes that are closely connected to synaptic neurotransmission (Magistretti et al. 1999). Thus, the obtained imaging is similar, even if some

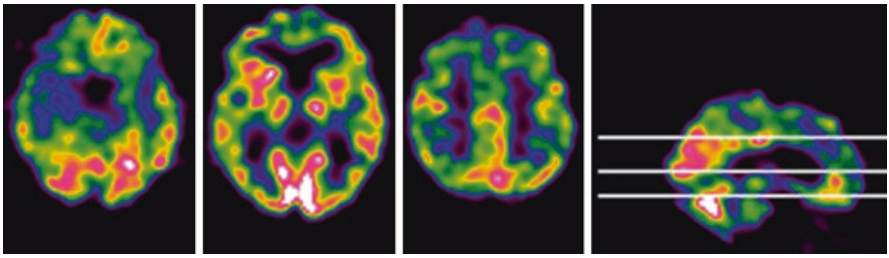

Fig. 12.4 Perfusion SPECT (^{99m}Tc-HMPAO) showed in three transaxial sections in an 82-year-old woman (15 years of full education) with aMCI (Mini-Mental State Examination score 27/30, no impairment in autonomy in everyday life activities). The scan shows reduced tracer uptake in the medial temporal lobe (on *left*), lateral temporal cortex (*middle*), and posterior cingulate cortex (*right*) in the right hemisphere

differences can be found, mainly between ^{99m}Tc-ECD and ^{99m}Tc-HMPAO (Koulibaly et al. 2003), whereas ^{99m}Tc-ECD images are more similar to FDG-PET ones.

The typical hypoperfusion pattern in aMCI patients includes the association portion of the parietal lobe, the posterolateral part of the temporal lobe, and the precuneus (Borroni et al. 2006; Encinas et al. 2003; Hirao et al. 2005; Høgh et al. 2004) (Fig. 12.4). Less frequently, hypoperfusion in the posterior cingulate has been reported in MCI patients, mainly in studies using ^{99m}Tc-HMPAO (Huang et al. 2003; Johnson et al. 2007) or ^{123}I-iodoamphetamine (Ishiwata et al. 2006). On the other hand, studies using ^{99m}Tc-ECD often failed in demonstrating posterior cingulate hypoperfusion (Borroni et al. 2006; Encinas et al. 2003; Nobili et al. 2008a). Then, when AD dementia develops, hypoperfusion becomes clearer in lateral frontal association cortex as well.

SPECT images at the aMCI stages of AD are often asymmetric reflecting "lateralization" of neuropsychological impairment, as language and visuospatial disturbances predominate in left and right hemisphere affection, respectively. Age at onset is a source of strong variability in AD. Indeed, in EOAD (i.e., <65 years) neocortical (i.e., posterior temporal-parietal) impairment predominates, whereas in late-onset AD (LOAD) dysfunction is more evident in MTL structures. Again, neuroimaging findings usually reflect neuropsychological profiles; thus, EOAD cases show a neocortical presentation with various combinations of symptoms within the triad aphasia-apraxia-agnosia and a relatively spared memory, while the opposite happens in LOAD cases. Brain perfusion pattern may be influenced by genetic traits. Thus, aMCI patients carrying at least one ε4 allele of the APOE gene have more evident hypoperfusion than severity-matched aMCI patients without ε4 alleles.

In patients with MCI, baseline SPECT hippocampal perfusion was able to predict conversion to AD dementia after 2 years of follow-up. Moreover, MCI patients with cognitive worsening over time showed hypoperfusion in inferior parietal lobule in comparison with stable MCI patients. In those patients, either baseline hippocampal or parietal perfusion was significantly correlated with verbal delayed

recall score at follow-up. Moreover, receiver operating characteristic (ROC) curves for hippocampal perfusion showed 0.81 sensitivity with 0.86 specificity in differentiating converters from non-converters. Thus, baseline SPECT can support outcome prediction in subjects with MCI (Nobili et al. 2009a). In order to study functional compensation in aMCI patients, MRI imaging co-registered with perfusion SPECT found relatively preserved perfusion in posterior cingulate, in the head of the hippocampus, in the amygdala, and in the insula bilaterally. Functional depression was instead disclosed in bilateral parahippocampal gyri. Thus, assessing functional compensation of neuronal loss as a phenomenon of brain reactivity could be helpful in order to understand those mechanisms counteracting the pathological changes of AD (Caroli et al. 2010). However, aMCI is not only a prerogative of patients later developing AD dementia, as it has been demonstrated in a part of patients with Parkinson's disease (PD) (Janvin et al. 2006). Even in PD patients with aMCI, perfusion SPECT is able to show mainly parieto-occipital hypoperfusion compared to aMCI patients without PD who instead show predominant MTL hypoperfusion (Nobili et al. 2009b). These findings may help identifying those PD patients with an amnestic syndrome who are therefore at higher risk of developing dementia in the short-to-medium term.

SPECT literature is less exhaustive in naMCI patients. One study disclosed statistically significant, reduced perfusion values in bilateral temporal cortex in naMCI patients compared to controls, but not significant with respect to aMCI or subjects with subjective memory complaints (Nobili et al. 2008b). Furthermore, naMCI patients showed hypoperfusion in right frontal cortex compared to all the other groups, significantly with respect to subjects with subjective memory complaints. Notably, naMCI patients had higher prevalence of arterial hypertension, depression, and white matter hyperintensities (WMHs) in MRI scan suggesting vascular damage and thus a non-neurodegenerative etiology of the cognitive impairment. In fact, executive dysfunction is thought to be driven especially by the activity of the dorsolateral prefrontal cortex and has been associated with WMHs in MCI patients (Reed et al. 2004). Also depression is associated with frontal hypoperfusion, with or without WHMs (Oda et al. 2003). Moreover, reduced rCBF in frontal and temporal areas is associated with hypertension, which frequently underpins chronic hypoperfusion and WMH (Rodriguez et al. 1987).

Though the lower spatial resolution makes subtle brain abnormalities less evident than with FDG-PET, perfusion SPECT could be more informative in MCI due to vascular disease, where glucose metabolism could be spared. Pros and cons of PET and SPECT have been well debated and analyzed in specialized reviews (Ishii and Minoshima 2005; Pupi and Nobili 2005), where also cost of PET has been evaluated; PET is indeed more expensive if FDG is bought from an external supplier, but price may be more affordable if it is produced in-house. Talking about brain blood perfusion, it should be reminded here that nowadays there is an increasing evidence that also early (postinjection) data acquisition of [^{18}F]-labeled amyloid PET tracers could be informative on brain perfusion distribution that is correlated with brain metabolic levels (Daerr et al. 2017).

12.4.3 Combined Use of SPECT and Other Biomarkers

Few studies have compared perfusion SPECT and MRI techniques (Takahashi et al. 2014; El Fakhri et al. 2003); notably, the diagnostic performance of ASL-MRI and SPECT in distinguishing AD from non-AD was almost equivalent, even though ASL-MRI was more influenced by hemodynamic factors (Takahashi et al. 2014). Furthermore, Habert et al. (2010) conducted a correlation study among brain perfusion SPECT and CSF biomarkers among patients with MCI, mild AD dementia, and a pooled population of control subjects. SPECT level of perfusion did not correlate with amyloidosis biomarker, such $A\beta_{1\text{-}42}$ levels. Instead, a significant correlation was found between brain perfusion in the left parietal cortex and either t-Tau or p-Tau concentrations. Thus, perfusion SPECT could be used as a marker of neurodegeneration, in agreement with Tau CSF level.

12.5 ^{18}F-FDG-PET

12.5.1 Principles

^{18}F-FDG-PET (or simply FDG-PET from now on) is able to estimate the local cerebral metabolic rate of glucose consumption (CMRgl), thus allowing in vivo evaluation of the distribution of neuronal death and synapse dysfunction (Herholz 2003). Indeed, glucose is phosphorylated by a hexokinase inside the neuron-astrocyte functional unit, and this is the first pivotal step of that metabolic pathway. At the synaptic terminals, energy is actively produced by the tricarboxylic acid pathway, using oxygen and leading to high ATP availability (aerobic glycolysis). On the other hand, astrocytes mainly utilize anaerobic glycolysis, which is faster but provides less energy. Therefore, glucose metabolism is closely related to both resting and active neuronal function (Magistretti 2000). FDG-PET is usually performed in a resting state and glucose uptake distribution is mainly driven by basal neuronal activity, representing general neuronal integrity (Herholz 2003). Thus, reduced glucose uptake basically reflects either reduced synaptic metabolic activity or a reduction in number of synapses. The specific molecular mechanisms of neuronal activity that are associated with energy metabolism have not been completely identified. However, the glucose metabolism measured by PET seems to be associated with glutamate-driven astrocytic glucose uptake (Magistretti et al. 1999; Mosconi 2005).

Radiolabeled glucose brain uptake takes about 20 min, thus FDG-PET has a very low temporal resolution. Therefore, any circumstance that alters "psychosensory resting" may significantly affect the results of the scan. The most relevant stimuli that must be avoided are speech and sensorial stimulation; however, also the vigilance state and anxiety should always be taken into account. Indeed, a significant inverse correlation between vigilance measures and FDG metabolism in bilateral frontal and temporal regions, bilateral cingulate gyrus, and right thalamus has been shown (Guenther et al. 2011).

12.5.2 Utility in MCI

AD and other types of dementia have been extensively studied with FDG-PET in the last 30 years (Mosconi 2005; Salmon et al. 2009). The research efforts moved then to pre-dementia stages and to MCI, mostly with the aim of identifying those patients suffering from AD in prodromal phase (Nobili et al. 2008a; Anchisi et al. 2005). Indeed, FDG-PET may provide useful information in this scenario, by showing (or not showing) specific disease patterns. A typical single or multi-domain aMCI patient with a clinical suspicion of AD has a high pretest probability to show typical brain metabolic abnormalities; thus the positive predictive value of FDG-PET is higher than 90%. Indeed, individual cases may show hypometabolism in posterior parieto-temporal cortex, lateral occipital cortex, precuneus, and PCC (Nobili et al. 2008a; Mosconi 2005; Morbelli et al. 2010). Among these, PCC hypometabolism is the most common finding in early AD patients (Minoshima et al. 1997); the reduced PCC activity found in prodromal AD patients may reflect decreased connectivity especially with entorhinal cortex and hippocampus, which are among the first regions affected by AD pathology (Meguro et al. 1999). The concept of metabolic disconnection of medial temporal cortex in early AD dementia was recently confirmed by the finding of lacking functional/metabolic connectivity between hippocampus and PC in prodromal AD patients, even without specific hippocampal hypometabolism (Morbelli et al. 2012). On the other hand, hippocampal hypometabolism is often not reported in FDG-PET studies, even if early hippocampal brain damage has been suggested to be related with hypofunction and likely reduced brain glucose metabolism. This is probably due to both limited spatial resolution of the first generations PET equipment and, particularly, to the use of the Statistical Parametric Mapping (SPM) analysis method (Mosconi 2005). To overcome the abovementioned issues in the evaluation of hippocampal hypometabolism, a different reorientation in SPECT clinical setting, the so-called Ohnishi transaxial plane (i.e., about 30° with the nose upward with respect to the bicommissural plane (Ohnishi et al. 1995)) has been successfully proposed for analyzing transaxial slices. In fact, the hippocampus is not parallel to the bicommissural line; thus the bicommissural plane is inadequate for hippocampus segmentation. This approach is appropriate for FDG-PET as well.

A very frequent FDG-PET finding in MCI patients is the strong asymmetric involvement, regardless of the cortical regions affected, and it is usually correlated with clinical symptoms and presentation. As already discussed for SPECT imaging, when left hemisphere hypometabolism is predominant, language impairment is more severe, whereas hypometabolism is predominantly right, visuospatial impairment is clearer. Therefore, visual analysis of scans strongly relies on evaluation of asymmetric abnormalities. Finally, the AD-related metabolic pattern, as identified by spatial covariance analysis, has been found in MCI patients, especially those converting to AD dementia (Meles et al. 2017).

Recently, the European Association of Nuclear Medicine (EANM) and the European Academy of Neurology (EAN) constituted a task force for the consensual

recommendations of clinical use of FDG-PET in dementing neurodegenerative disorders (Nobili et al. 2018). In particular, the clinical utility of FDG-PET in MCI has been explored (Arbizu et al. 2018). The incremental value of FDG-PET, as added to the clinical-neuropsychological examination, to ascertain the etiology of MCI has been investigated. Harmonized population, intervention, comparison, and outcome (PICO) questions were used to this end. The first PICO question was whether FDG-PET should be performed, as adding diagnostic value as compared to standard clinical/neuropsychological assessment alone, to detect prodromal AD, and a fair relative availability of evidence was achieved (Arbizu et al. 2018). This was because it was acknowledged that both the typical PCC and posterior temporoparietal hypometabolism in the majority of studies of MCI due to AD (Fig. 12.5) and a normal FDG-PET scan reasonably exclude neurodegeneration due to AD. Twenty-one papers were examined, showing a large range of sensitivity (38–98%), specificity (41–97%), and accuracy (58–100%) values for the identification of prodromal AD patients (Arbizu et al. 2018).

Most FDG-PET studies have focused on the investigation of clinical and etiological heterogeneity of MCI, mainly in the amnestic cognitive domain. Few FDG-PET studies have been conducted in naMCI (Seo et al. 2009; Raczka et al. 2010; Boeve 2012). Dementia with Lewy bodies (DLB) is the second most common cause of dementia after AD (Vieira et al. 2013) and is characterized by cognitive decline associated with a combination of attention fluctuations, visual hallucinations, rapid eye movement sleep behavior disorder (RBD), and parkinsonism (McKeith et al. 2017). However, little effort has been made for the identification of DLB patients in the pre-dementia stage. Three prototypical forms of prodromal DLB have been proposed, namely, an MCI variant, associated with early visuo-perceptual and attentional deficits, a delirium onset DLB with provoked or spontaneous delirium as the presenting features, and a psychiatric onset DLB with its primary presentation as a late-onset affective disorder or psychosis (McKeith et al. 2016). Indeed, DLB is a heterogeneous disease, with clinical core features being associated with more prominent hypometabolism in specific regions (Morbelli et al. 2019). As discussed, MCI syndrome may be associated with Lewy body pathology, regardless of the coexistence of parkinsonism, and the cognitive impairment is often accompanied or even preceded by RBD. Those patients can have hypometabolism in the occipital cortex, other than the known decreased basal ganglia uptake on dopamine transporter (DAT) imaging with either SPECT or PET tracers (Boeve 2012). Indeed, idiopathic RBD patients with cognitive impairment are likely to develop DLB over time (Postuma et al. 2019). A longitudinal study evaluating 30 either aMCI or naMCI patients showed that those patients converting to DLB at follow-up exhibited hypometabolism in the posterior and anterior cingulate gyrus and in the parietal lobe at baseline (Clerici et al. 2009) that, along with the presence of the posterior cingulate island sign (i.e., relatively preserved metabolism in the posterior cingulate area), closely overlap with the typical DLB pattern (Fig. 12.5). Therefore, the clinical use of FDG-PET to support the diagnosis of MCI due to DLB is recommended, mainly because of the potential clinical utility of the typical finding of hypometabolism in occipital cortex although the experts recognized that formal evidence to support its

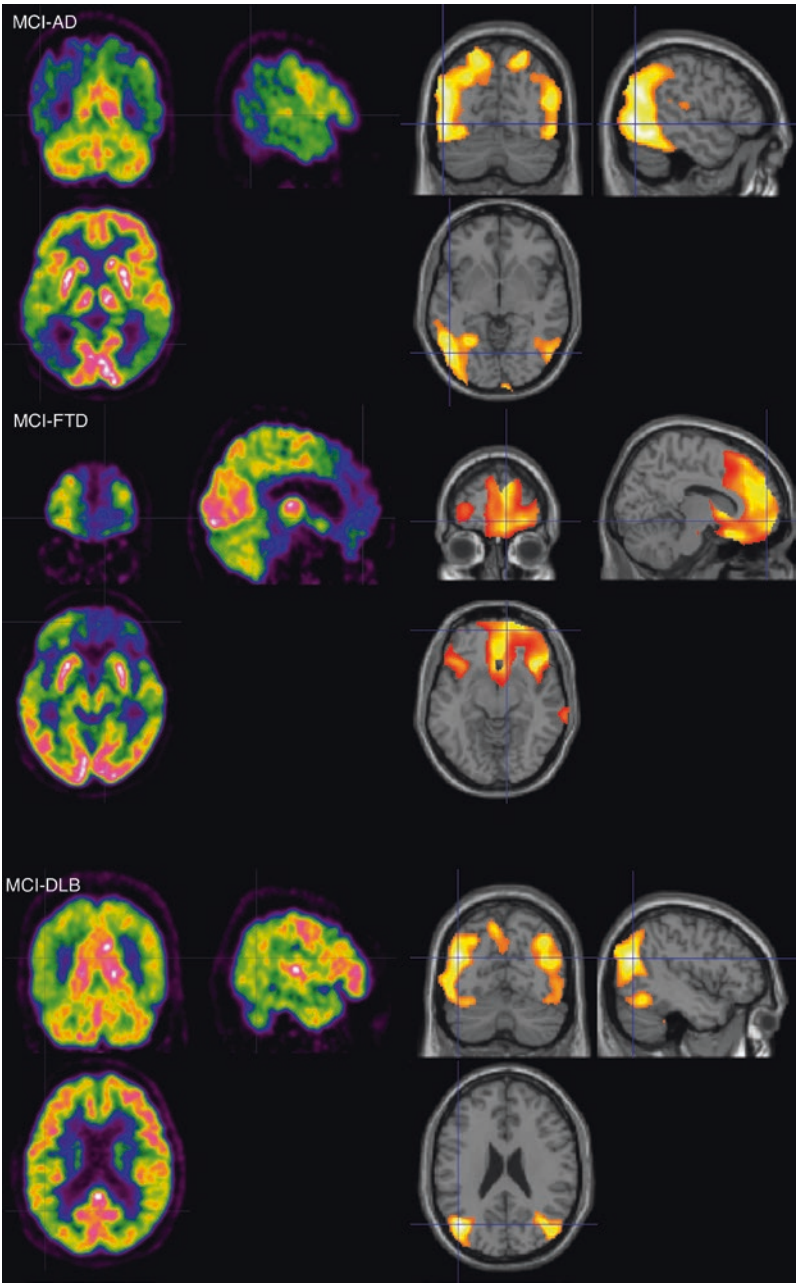

Fig. 12.5 Patterns of metabolism by means of FDG-PET in different neurodegenerative conditions (left). On the right, the results of voxel-based statistical comparison with respect to normal controls (SPM tool) with age as nuisance, in which statistical relevant relative hypometabolism is shown in yellow-to-red (uncorrected $p < 0.001$ at voxel level, $p < 0.05$ family-wise corrected for multiple comparisons at cluster level)

use in this condition is still poor (Arbizu et al. 2018). However, DAT SPECT, ^{18}F-DOPA PET, or ^{123}I-MIBG cardiac scintigraphy should be considered in first instance as being more informative investigations (Nobili et al. 2018).

Frontotemporal lobe degeneration (FTLD) is the third most common cause of dementia, following AD and DLB, and is a frequent type of early-onset dementia (Vieira et al. 2013). FTLD in its behavioral variant (bvFTLD) usually has an insidious onset, with progressive deficits in behavior, executive function, and language, and patients may be identified in the initial phases of the disease, before the emergence of dementia. In this group of patients, even at the MCI stage, FDG-PET usually shows orbitofrontal, frontal mesial and lateral, anterior cingulate, insular, and temporal lateral hypometabolism, while metabolism in medial temporal cortex and posterior cingulate is generally preserved (Raczka et al. 2010). These findings, sometimes associated with hypometabolism in the cerebellar hemisphere contralateral to the side of frontal damage (so-called crossed diaschisis), may be helpful in the differential diagnosis with AD dementia. However, in some case the differential diagnosis may be difficult, especially for the frontal variant of AD. Indeed, in these cases, FDG-PET may present the same pathophysiological ambiguity as the clinical symptoms. Amyloid PET may be a useful tool to achieve differential diagnosis, and it will be extensively discussed in the dedicated chapter.

Although full formal evidence on the clinical utility of FDG-PET to support the diagnosis of MCI due to bvFTLD is lacking (Arbizu et al. 2018), semiquantitative assessment of FDG-PET scans correctly identified MCI subjects who develop bvFTLD at follow-up (Perani et al. 2014), even if the number of subjects was very limited. Visual analysis of FDG-PET in MCI patients has been shown to be of limited use in differentiating between MCI patients developing AD and those developing bvFTLD (Grimmer et al. 2016). On the other hand, voxel-based analysis has shown high accuracy in correctly identifying MCI patients who later develop different neurodegenerative disease, including AD, bvFTLD, and DLB (Cerami et al. 2015). Thus, the clinical usefulness of FDG-PET to support the diagnosis of MCI due to bvFTLD has been recommended (Nobili et al. 2018), because of the presence of the known typical metabolic pattern in bvFTLD, already present at MCI stage, mainly including hypometabolism in at least one of the frontal lobes, the anterior temporal lobe, anterior cingulate gyrus, insula, amygdala, and caudate nuclei (Fig. 12.5). This is particularly relevant for the identification of the so-called bvFTLD phenocopies, i.e., patients with clinical symptoms that mimic bvFTLD (Gossink et al. 2016), usually of psychiatric pertinence, but with normal FDG-PET imaging (Kipps et al. 2009).

Vascular dementia (VaD) is a frequent form of dementia, even if several controversies remain, both for the terminology and the pathophysiological mechanisms. For instance, significant neuropathological and clinical overlap between AD and VaD has been found, especially in the early stages (Seo et al. 2009). FDG-PET may help confirm the vascular basis of cognitive impairment, mostly by excluding the presence of typical hypometabolism patterns of AD or of other types of degenerative dementia. However, patients with cognitive impairment of vascular origin may show scattered areas with reduced metabolism possibly extending over cortical and subcortical structures (Seo et al. 2009).

As discussed, FDG-PET has high accuracy in classifying MCI patients of different etiologies. However, the clinical application of research findings is still limited by the lack of standard analytical procedures. In each nuclear medicine unit around the world, scans are evaluated in very different ways, ranging from simple visual assessment to sophisticated computer-assisted comparisons with normal databases, either already available in workstations and supplied by the manufacturer or locally established. Several automatic software tools for the analysis of individual FDG-PET scans are freely available on the web (such as SPM and "Neurostat") or delivered by industry (such as BRASS®). "Neurostat" is based on "stereotactic surface projection" (SSP), and it has been developed and applied to patients with AD or questionable dementia (Minoshima et al. 1995) allowing very high accuracy in differentiating AD patients from controls. Topographic estimation of hypometabolic sites is allowed, showing the degree of hypometabolism in comparison with normal controls in terms of *Z* scores. The spatial normalization procedure is a critical step when using automatic software (such as "Neurostat" and SPM, for instance). Indeed, in order to compare a scan with others, individual's brain shape and structures must be distorted into a common topographical space. The best approach to achieve spatial normalization is to use a co-registered MRI of the same subject. However, this procedure may be time-consuming if the MRI has not been acquired simultaneously with the PET. New PET-MRI devices can overcome this limitation, allowing precise normalization also in clinical settings. Finally, predisposed normative databases embedded in common automatic tools may not be adequate for age span, number of subjects, or acquisition modalities. Moreover, the quality of locally prepared normal databases relies on selection criteria for normality, whose definition is not trivial.

AD-related hypometabolism can be objectively measured by voxel-by-voxel analysis, and global indices can be provided. The most common tools are the PMOD (PMOD Technologies) Alzheimer discrimination analysis tool (PALZ) (Haense et al. 2009), an AD-related hypometabolic convergence index (HCI) (Chen et al. 2011b), and an average metabolism computed on a set of meta-analytically derived ROIs reflecting an AD hypometabolism pattern (metaROI) (Landau et al. 2011). PALZ and HCI computation is based on the comparison of individual FDG-PET with a reference dataset of healthy controls by voxel-wise *t*-test. The PALZ score reflects the voxel-by-voxel sum of *t*-scores in a predefined AD-pattern mask. HCI represents the inner product of individual *z*-map in a predefined AD *z*-map. Both PALZ and HCI have shown good accuracy in differentiating AD patients from healthy age-matched controls (Haense et al. 2009; Chen et al. 2011b).

HCI may be able to predict the development of dementia in MCI patients, while metaROI was sensitive in detecting the longitudinal cognitive and functional modification in both MCI and AD patients (Landau et al. 2011). PALZ, HCI, and metaROI ability in distinguishing controls MCI and AD patients has been investigated, showing roughly comparable results between the three methods. Accuracy of classification in each clinical group varied more as a function of dataset than by technique. All techniques were differentially sensitive to disease severity, with a classification accuracy for MCI due to AD to moderate AD varying from 0.800 to 0.949 (PMOD Alzheimer tool), from 0.774 to 0.967 (metaROI), and from 0.801 to 0.983 (HCI) (Caroli et al. 2012).

Finally, support vector machine (SVM) analysis on FDG-PET meta-volumes of interest (metaVOI) has recently shown high accuracy in identifying MCI patients converting to AD (Pagani et al. 2017a, 2015; De Carli et al. 2019). Indeed, it has been proposed that automatic volumetric region-of-interest classifier, based on SVM approach, performs better than the voxel-based methods in differentiating patients with MCI due to AD from healthy controls (Brugnolo et al. 2019). Moreover, independent component analysis on FDG-PET metaVOIs has shown progressive disintegration of functional brain connectivity with progression of cognitive decline in MCI patients, especially those converting to AD dementia (Pagani et al. 2017b).

12.5.3 Combined Use of FDG-PET and Other Biomarkers

FDG-PET is one of the currently accepted imaging biomarkers for the pre-dementia diagnosis of AD, especially for its high sensitivity in the early diagnosis of AD (Salmon et al. 2009; Dubois et al. 2007). However, FDG-PET accuracy in detecting AD pathology in MCI patients is high but not complete; thus to combine it with other biomarkers or with neuropsychological (memory) test scores may be helpful. Good discriminative performance has been achieved by combining neuropsychology, PET and/or APOE genotype, and CSF biomarkers (Mosconi et al. 2008) and by combining neuropsychology and MRI atrophy analyses (Visser et al. 1999). Moreover, the combined use of neuropsychological testing (visuospatial construction skills), MRI-based hippocampal volume, and posterior cingulate hypometabolism resulted in 96% specificity and 92% sensitivity in identifying MCI patients developing dementia within 12 months (Ottoy et al. 2019).

A study with the combined use of FDG-PET, neuropsychology, and a memory complaint questionnaire has shown that patients with low awareness of memory deficit show a more severe hypometabolic pattern, typical of AD; thus they could have higher risk of developing dementia (Nobili et al. 2010). MCI patients with normal FDG-PET have a low risk of progression within 1 year, despite the presence of a severe memory deficit on neuropsychological testing (Anchisi et al. 2005), thus suggesting a very high negative predictive value of FDG-PET. However, aMCI patients showing a decline of cognitive performance over time, without developing dementia, had a more severe left MTL hypometabolism in comparison with cognitively stable aMCI (Pagani et al. 2010).

Subjects with prodromal AD may have FDG-PET heterogeneity. Similarly to what is shown by means of perfusion SPECT, LOAD patients exhibit more severe hypometabolism in MTL, while EOAD patients show more severe hypometabolism in posterior association neocortex (Kim et al. 2005). Usually, APOE ε4 allele carriers have more severe hypometabolism than noncarriers, despite a similar degree of cognitive impairment (Drzezga et al. 2005). Education has a protective role against symptoms onset in AD. However, when symptoms appear, patients with higher education show more severe hypometabolism in comparison with patients with lower education (Garibotto et al. 2008). A role for oxidative stress in brain glucose alteration in AD patients has been suggested. Indeed, in a mixed group of subjects

ranging from subjective memory complaints to mild AD dementia, a significant correlation between left temporal lobe glucose metabolism and plasma activities of extracellular superoxide dismutase, a measure of oxidative stress, has been found (Picco et al. 2014).

Topographical pattern of hypometabolism seems to follow brain amyloid deposition with temporal delay in AD patients (Förster et al. 2012). However, neither amyloid PET nor CSF amyloid marker is able to discriminate short-term converters from non-converters (Ottoy et al. 2019), although other studies assessing the combination of FDG-PET and CSF markers in AD (Landau et al. 2010; Choo et al. 2013; Fellgiebel et al. 2007) stated the utility of brain metabolism in adding a predictive information of conversion to CSF markers as taken alone. In fact, regarding the predictive value toward conversion to AD dementia, FDG-PET has the same value as total Tau (t-Tau) (Choo et al. 2013), as marker of neurodegeneration. Also, Lange et al. (2017) meaningfully followed a stepwise order of biomarkers (viz., ADAS-13 score, hippocampal volume (HV), CSF, and FDG-PET) and showed that CSF p-Tau provided the best incremental risk stratification when added to ADAS-13 score with respect to HV and FDG-PET; in the same study, FDG-PET used in the second step outperformed HV in MCI subjects with relatively preserved cognition (ADAS-13 score <18). Anyway, studies including ^{18}F-FDG-PET with CSF $A\beta_{1\text{-}42}$, and MRI, showed a very good prediction of AD dementia conversion in MCI patients, with FDG-PET having the highest added value to clinical and imaging parameters (Garibotto et al. 2017).

Taken together such findings suggest a role of ^{18}F-FDG-PET both as a diagnostic biomarker and as a predictor of conversion to AD dementia in MCI patients, with high correspondence with cognitive level and neurodegeneration and a moderate added value when combined with other imaging or fluid biomarkers.

12.6 Amyloid PET and Emerging Tracers

12.6.1 Amyloid PET Imaging

Although the etiology of AD has not been definitively established, converging evidence suggests that an amyloid precursor protein derivative, beta amyloid (Aβ), may play an important role in the pathogenesis of the disease and be an early event on the path to dementia. The pathogenetic pathways leading to AD are certainly very complex and involve different mechanisms such as the dysfunction in cholinergic neurons and the aberrant aggregation of hyperphosphorylated tau protein. However, the "amyloid cascade" hypothesis remains the most prominent one, according to which sufficient accumulation of Aβ carries significant biochemical, histological, and clinical changes in the pathogenesis of AD (Sanabria-Castro et al. 2017). Moreover, accumulation of Aβ fibrils in the form of "classic" (i.e., neuritic) amyloid plaques is one of the hallmarks of the disease and a key component of the neuropathological criteria for autopsy-based confirmation of diagnosis. Furthermore, assessment of brain Aβ amyloidosis has gained a pivotal role in the diagnosis of AD

in vivo, according to the last National Institute of Aging-Alzheimer Association (NIA-AA) (McKhann et al. 2011; Albert et al. 2011) and the International Working Group-2 (IWG-2) criteria (Dubois et al. 2014).

During the past two decades, major breakthroughs have focused on identifying diagnostic biomarkers able to demonstrate the presence of pathological mechanisms of AD and to predict further cognitive decline and dementia onset since the stage of MCI. In this setting, amyloid imaging has established itself as an important neuroimaging tool for the investigation of brain aging and dementia alongside MRI and FDG-PET. In contrast to techniques designed to indirectly estimate levels of brain amyloid plaques from Aβ levels in CSF or plasma, imaging techniques utilizing radiolabeled PET tracers that bind to the aggregated Aβ peptides in amyloid plaques have the potential to directly assess regional brain amyloid plaque pathology (Pontecorvo and Mintun 2011). In other words, amyloid imaging enables the detection and quantification of pathological protein aggregations in the brain.

Together with cerebrospinal fluid (CSF) amyloid-β_{1-42} reduction, brain amyloid accumulation identified by PET technology (AMY-PET) is considered one of the biomarkers able to identify the prodromal stage of AD (Jack et al. 2018).

AMY-PET results must be evaluated on the basis of the patient's medical history, physical examination, and cognitive testing because a positive scan identifies only the presence of brain amyloidosis and does not necessarily correspond to the presence of AD. In fact, amyloid deposition can also occur in normal aging (Aizenstein et al. 2008), and up to 35% of cognitively normal older people have positive AMY-PET. Pathological studies cannot provide information about events early in the disease process or determine how key events are temporally related to each other. The incidence of isolated amyloid-positive marker reaches its maximum at age 70, and then it lowers in older ages with the increase of combination of amyloid and neurodegenerative markers in normal subjects (Jack et al. 2017). Due to the absence of a proven effective disease-modifying drug for AD (Holmes et al. 2008; Cummings et al. 2019), the amyloid hypothesis is being increasingly challenged. Therefore, amyloid imaging allows to readdress questions about the relationship between Aβ aggregation and AD that have not been definitively answered by postmortem studies, such as the significance of Aβ aggregation in cognitively normal individuals and the relationship between the distribution and burden of amyloid pathology and clinical features of AD.

Various compounds have been developed for the imaging of amyloid: radiolabeled Aβ peptide antibodies and peptide fragments, small molecules (derivatives of Congo red, thioflavin, stilbene, and acridine) for PET and SPECT imaging, and putrescine-gadolinium-amyloid-β peptide for MRI. Nonetheless, these compounds failed to provide a direct visualization of amyloid and tau proteins in humans, in consideration of the poor passage across the blood–brain barrier, inadequate brain permeability, and/or low affinity to Aβ aggregates (Quigley et al. 2011). The most widely researched and best validated PET tracer imaging approach to date has utilized ^{11}C-PIB. PIB binds specifically to extracellular and intravascular fibrillar Aβ deposits. At PET tracer concentrations, PIB does not appreciably bind to other protein aggregates (e.g., neurofibrillary tangles), but it binds nonspecifically to WM,

likely due to delayed clearance of the lipophilic compound from WM (Quigley et al. 2011). Nonspecific WM retention, however, does not differ between AD and normal controls (Villemagne et al. 2012). PIB amyloid load shows a negative correlation with CSF levels of $A\beta_{1\text{-}42}$, the other in vivo marker of Aβ pathology, and a positive one with in vitro measures of Aβ pathology found at autopsy (plaques and vascular amyloid) (Rabinovici et al. 2008). PIB has proven to be a sensitive marker for underlying Aβ pathology in cognitively normal older individuals and patients with MCI due to AD or AD dementia. It can detect pathology in patients with early or atypical symptoms as well as in asymptomatic older adults, and it also provides in vivo insight about the dynamic relationship between amyloid deposition, clinical symptoms, and structural and functional brain changes in the continuum between normal aging and AD (Quigley et al. 2011). Nevertheless, more rigorous work is needed to establish the quantitative relationship between PIB binding and Aβ pathology at various disease stages. PIB binding may reach a ceiling at high plaque density and fail to capture the progression of pathology beyond a certain disease stage. Moreover, PIB binds only to fibrillar Aβ, and apparent dissociations between PIB uptake and other disease measures may be due to soluble forms of Aβ that are not detected by PiB-PET (Rabinovici et al. 2008).

A number of additional ^{11}C-labeled PET tracers have been studied in humans as potential amyloid imaging markers. However, the short half-life of ^{11}C is prohibitive in terms of adopting ^{11}C-PIB in clinical practice and limits its availability for research. In the last years, the large body of evidence available on the usefulness of ^{11}C-PIB has been followed by a growing number of publications on the ^{18}F-labeled compounds for amyloid PET imaging allowing broader application of amyloid imaging to clinical practice and research. In particular, three fluorinated tracers, the stilbene derivative ^{18}F-florbetaben (NeuraCeq®), ^{18}F-florbetapir (Amyvid®), and ^{18}F-flutemetamol (Vizamyl®), have been approved by both the US and the European authorities (Minoshima et al. 2016). All such tracers performed comparably to ^{11}C-PIB in preliminary studies in AD dementia, MCI, and control cohorts. In fact, despite a slight difference in retention in both GM and WM between these radiotracers, binding sites are substantially the same (Ni et al. 2013); thus all the radiopharmaceuticals may be considered similar in the estimation of cerebral amyloid plaques density.

With the precious support of semiquantitative measures, AMY-PET could assess not only brain amyloid load but could also provide tools for longitudinal assessment, progression, or therapeutic effects. To this purpose, the greatest accuracy and precision would be achieved by true quantification techniques. However, the acquisition times and arterial sampling make these methods scarcely applicable in clinical practice. As for semiquantification of amyloid tracer uptake within the brain, Lopresti et al. (2005) assessed a simplified normalization method, i.e., the standardized uptake value ratio (SUVR). SUVR involves the normalization of a standardized uptake value image to a reference region whereby the standardized uptake value image is divided by the mean uptake in the reference region. Cerebellar GM is used as a reference region for ^{11}C-PiB-PET normalization. SUVR normalization is performed on static or summed frames and does not require arterial sampling or

dynamic scans, providing similar discrimination between subjects diagnosed with AD and normal controls as compartmental and reference region-based graphic methods. SUVR has been validated both on visual reading and on autoptic studies (Thurfjell et al. 2014) and has become the most widespread technique for normalization of ^{11}C-PiB-PET because of its simplicity and ease of clinical implementation. However, SUVR is known to be affected by several intrinsic and technique-dependent factors such as scanning time window and blood flow (Cselényi and Farde 2015). Furthermore, a univocal agreement on the best method for drawing target ROIs and choosing reference ROIs for amyloid status evaluation has not been reached yet. With the "Centiloid Project" Klunk et al. (2015) tried to harmonize SUVR values on a common scale in order to standardize the method of analyzing PiB-PET data and facilitate direct comparison among different centers and different tracers. Moreover, in order to overcome SUVR limitations, alternative approaches have been attempted, such as the SUVR-independent approach named ELBA (EvaLuation of Brain Amyloidosis) which has been validated for ^{18}F-florbetapir (Chincarini et al. 2016). This more sophisticated technique uses a ROI-independent method designed to capture intensity distribution patterns rather than actual counts. Another semiquantitative method to measure β amyloid deposition that combines regional dual time-point amyloid PET and MRI data analysis through sophisticated post-processing steps has been recently proposed (Cecchin et al. 2017). In this case, amyloid information is not only corrected for atrophy and spillover errors but also, at least partially, for rCBF dependence. Actually, rCBF and regional cerebral metabolism seem to be tightly coupled in resting conditions, and rCBF and early-phase AMY-PET are highly correlated (Devous et al. 2014). For this reason, visual assessment and semiquantification techniques could be integrated with the information deriving from early AMY-PET acquisition as a proxy of brain perfusion images and a surrogate marker of neurodegeneration in order to obtain a single and more accurate index of brain amyloidosis.

Examples of amyloid PET scans with different tracers in patients with AD and control subjects are shown in Fig. 12.6.

12.6.2 Utility in MCI

Amyloid imaging studies support a model in which amyloid deposition is an early event on the path to dementia, beginning insidiously in cognitively normal individuals accompanied by subtle cognitive decline and functional and structural brain changes suggestive of incipient AD. As patients progress to dementia, clinical decline and neurodegeneration accelerate and proceed independently of amyloid accumulation, which has either reached a plateau or is increasing slowly (Quigley et al. 2011).

While there is considerable debate about the "amyloid hypothesis," in its traditional form, postulating that amyloid-β is the causative agent in AD, there is consensus that amyloid is a necessary, if not sufficient, condition to trigger downstream effects leading to symptoms of AD, years later (Musiek and Holtzman 2015).

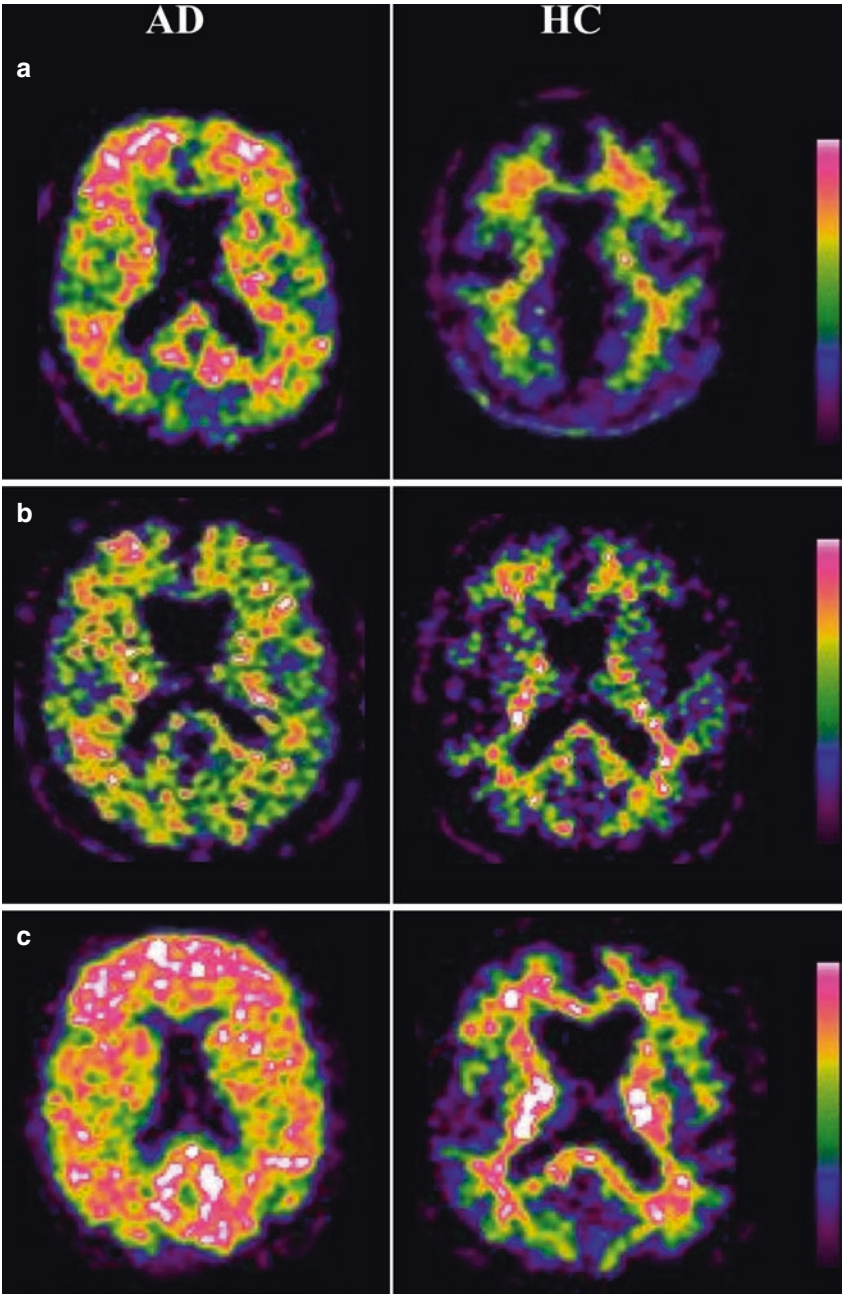

Fig. 12.6 PET scan with three different amyloid-binding radiotracers (**a**) ^{18}F-florbetaben, (**b**) ^{18}F-florbetapir (**c**) ^{18}F-flutemetamol in patients with AD (*left*) and in healthy elderly controls subject (HC) (*right*). Diffuse cortical uptake is shown in the AD patients, while HC show some non-specific uptake in deep white matter

AMY-PET imaging with ^{18}F-labeled compounds has been applied for predicting the probability of conversion from MCI to AD dementia. Doraiswamy et al. (2014) found that all MCI subjects with positive amyloid PET scan showed greater cognitive and global deterioration over a 3-year follow-up as compared with subjects with negative amyloid PET scan. These results were subsequently confirmed in a larger series of 618 patients with MCI possibly due to AD (Pontecorvo et al. 2017). Other authors (Jack et al. 2010) recommend the integrated use of AMY-PET and MRI to aid to predict progression to AD, combining the high sensitivity of hippocampal atrophy with the specificity of PiB-PET.

Amyloid imaging can also potentially identify patients with MCI who already show Aβ aggregation (thus, in the early clinical phase of AD) and separate them from patients with alternative causes for cognitive impairment (Morris et al. 2001). Such separation may have prognostic implications, assuming that people with MCI and an underlying AD pathology are at higher risk of progressing to dementia. Moreover, these patients may be good candidates for inclusion in clinical trials for AD-specific therapies, allowing these treatments to be tested when they may have a higher likelihood of success (Villemagne et al. 2012).

However, potential protective factors for AD, such as cognitive reserve, which may modulate the symptoms and modify the relationship between Aβ pathology and clinical expression of cognitive impairment, must be taken into account. If one considers average mean PIB uptake in MCI patient groups, they show intermediate values between AD patients and controls. However, this results from a bimodal distribution of PIB uptake in most studies, with a majority of patients demonstrating AD-like uptake levels, a minority showing low-control level binding, and a small number of patients in the intermediate range (Lopresti et al. 2005; Kemppainen et al. 2007; Pike et al. 2007; Rowe et al. 2007; Forsberg et al. 2008; Jack et al. 2008b; Mormino et al. 2009; Wolk et al. 2009). Patients meeting criteria for aMCI are more likely to be PIB-positive than patients with naMCI; PIB positivity is also more common in APOE ε4 carriers compared to noncarriers (Quigley et al. 2011). A meta-analysis (Ossenkoppele et al. 2015) showed that the prevalence of amyloid on PET decreased with age in participants diagnosed with AD (greatest in APOE ε4 noncarriers) and increased with age in most non-AD dementias suggesting that amyloid imaging could be most helpful for differential diagnosis in early-onset dementia, particularly if the goal is to rule in AD dementia. On the other hand, the high concordance between PET and pathology suggests that amyloid imaging might have the potential to be used to rule out AD dementia regardless of age. Furthermore, amyloid in non-AD dementia may be clinically important as amyloid positivity was associated with worse global cognition.

12.6.3 Combined Use of Amyloid PET and Other Biomarkers

The use of AD biomarkers in routine clinical practice should be chosen on the basis of both their diagnostic performances and cost-effective value. Despite CSF $A\beta_{1\text{-}42}$ levels and in particular $A\beta_{1\text{-}42/1\text{-}40}$ ratio well correlate with amyloid load on PET

(Niemantsverdriet et al. 2017; Hansson et al. 2018), CSF Aβ levels changes may precede brain amyloid deposition (Palmqvist et al. 2016). On the other hand, brain amyloid load on PET still continues to increase even after the onset of cognitive symptoms (Farrell et al. 2017); moreover, in the case of borderline CSF results, AMY-PET can provide a 35% added diagnostic value (Weston et al. 2016). In order to guide clinicians to accurately apply AMY-PET in cognitive decline clinical evaluation, Alzheimer's Association and the Society of Nuclear Medicine and Molecular Imaging (SNMMI) recommend the use of AMY-PET only in patients with clear cognitive deficits measured by a dementia specialist but in presence of diagnostic uncertainty (Johnson et al. 2013). International Working Group (IWG)-1 (Dubois et al. 2007) and IWG-2 (Dubois et al. 2014) and National Institute of Ageing Alzheimer Association (NIA-AA) criteria (Albert et al. 2011) proposed partially different sets of biomarker abnormalities to identify MCI at higher risk to convert to dementia. However, a univocal sequence order of biomarkers has not been fully established yet (Guerra et al. 2015) and is today matter of consensus conferences between experts (Boccardi et al. 2020).

Recently, NIA-AA diagnostic framework (Jack et al. 2018) grouped biomarkers—including imaging and biofluids—into those of β amyloid deposition (A), pathologic tau (T), and neurodegeneration (N). This ATN classification system shifted the definition of AD in living people from a syndromal to a biological construct and defined AD as a unique neurodegenerative disease characterized by abnormal protein deposits, among different disorders potentially leading to dementia. In this context, AMY-PET, FDG-PET, MRI, and CSF biomarkers ($A\beta_{1\text{-}42}$, T-tau and P-tau) play a complementary role in the complex field of AD biology and multifactorial etiology of dementia.

Future efforts should be focused on optimizing available resources in order to obtain a more appropriate patient treatment and management.

12.6.4 Tau PET imaging

The presence of neurofibrillary tangles (NFTs) is another pathological hallmark of AD. NFTs consist of abnormal tau protein which has several isoforms with different ultrastructural conformations participating to the development of intracellular tau aggregates.

Abnormal tau aggregation is mainly considered to be a downstream event after Aβ deposition in AD. Therefore, tau protein deposits are not frequent in the neocortex, even if widespread amyloid-β deposits in neocortex exist already in asymptomatic and very early stages of AD (Morris and Price 2001).

Pivotal studies conducted with tau PET imaging confirmed the already known spatiotemporal pattern of Tau deposition in AD, starting from entorhinal cortex to hippocampus and then extending to the rest of temporal lobe and eventually to neocortical regions (Braak and Braak 1997). Moreover, tau deposition has a close association with brain atrophy, cognitive decline, and severity of dementia symptoms, suggesting the high potential of tau PET imaging as a neuropathological imaging

biomarker able to provide not only diagnostic but also prognostic information (Ossenkoppele et al. 2016).

Recently, different Tau-selective PET tracers have been developed and used for human studies: ^{18}F-THK523, ^{18}F-THK5117, ^{18}FTHK5105, ^{18}F-THK5351, ^{18}F-AV1451 (T807), and ^{11}C-PBB3 (Okamura et al. 2016). However, functional imaging of NFTs has to face several technical problems including intracellular location and lower concentration of NFTs with respect to Aβ deposits; thus, by including large hydrophilic fractions in their structural formula, radiotracers are able to cross cell membranes and have high affinity in selectively binding tau isoforms, but not Aβ (Villemagne and Okamura 2014). Moreover, although some of these compounds have already been tested in clinical trials (up to phase 3), all the available tracers are currently still in an exploratory stage, and the available literature is limited. Current status and future directions of tau PET tracers in neurodegenerative conditions is summarized in Okamura et al. (2018).

12.6.5 Receptor Imaging

In the last years, several PET radiopharmaceuticals have been studied for receptor imaging in neurodegenerative diseases. PET tracers for acetylcholine (Ach) receptors and acetylcholinesterase (AchE) have been especially studied. Although interest toward the cholinergic hypothesis in AD has considerably decreased over the last decade because of the poor efficacy of the current AchE inhibitor treatments, evidences showing that cholinergic cell death in the basal forebrain could precede the formation and spreading of Aβ aggregates in the cortex (Schmitz et al. 2016), recently renewed the attention to Ach receptor imaging compounds in studying AD. C-11 labeled tracers, such as *N*-[^{11}C]methyl-piperidin-4-yl propionate (PMP) and *N*-[^{11}C]methylpiperidin-4-yl acetate (MP4A), have consistently showed reduced AchE activity in early AD in several cortical areas (Kuhl et al. 1999), further reduced by the acute administration of AchE inhibitors, such as donepezil (Bohnen et al. 2005) and galantamine (Darreh-Shori et al. 2008). These tracers have been proficiently used to demonstrate the severe cholinergic deficit also in Parkinson's disease, even before dementia, as well as in DLB (reviewed in (Nobili et al. 2011)). However, despite several attempts to identify a reliable tracer for clinical purpose, these tracers remain in the research domain and are mainly C-11 labeled radiopharmaceuticals.

More recently, the fluorinated tracer fluoroethoxybenzovesamicol (FEOBV) has been demonstrated to have an excellent binding specificity for the vesicular Ach transporter in vivo. PET imaging with ^{18}F-FEOBV allowed to quantify and map the brain cholinergic denervation at a single patient level, as a function of the clinical severity (Aghourian et al. 2017), in a cohort of AD patients. On the other hand, the postmortem observation that nicotinic rather than muscarinic Ach receptors are profoundly affected in AD (Flynn and Mash 1986), promoted the identification of selective nicotinic receptor imaging probes including ^{11}C-nicotine, the fluorinated

compound 2-[fluoro-3-(2(S)-azetidinylmethoxy) pyridine (^{18}F-2FA) or the newer ^{18}F-AZAN and ^{18}F-flubatine, showing promising results (see the review by (Bao et al. 2017)).

12.7 Conclusions and Perspectives

This review has tried to underline that there is no correct diagnosis in the field of MCI without the "rational" use of both morphological and functional neuroimaging. Thus, due to the current shift from a clinical to a biological conception in the diagnosis of neurodegenerative diseases, a biomarker-based approach involving different biological measures is paramount as it can reflect pathological changes in vivo. Yet, the areas of uncertainty remain in several instances. In the case of a healthy middle-age subject with brain amyloidosis but without signs of neurodegeneration, we still have too short follow-up studies to say whether all these subjects will develop AD dementia, or a part of them will never develop it, thanks to protective factors, such as brain plasticity/brain reserve, diet, lifestyle, etc. In other cases of MCI of suspected Alzheimer's disease nature, neuroimaging findings do not match CSF findings, and only the clinical follow-up (or new upcoming biomarkers) will disclose the fate of that individual. Such issues are even more complicated according to the most recent pathological evidences in which different proteinopathies, alone or in combination, might underlie the same clinical and even imaging presentation (Nelson et al. 2019).

Neuroimaging has now entered the routine practice, and further development will reinforce our diagnostic accuracy. Along with the validation of new radiotracers for receptor imaging, future efforts should be directed toward optimization of functional MRI techniques as well as quantitative and semiquantitative tools for PET imaging interpretation and to develop new tracers able to detect proteinopathies other than amyloidosis. Moreover, we hope we will have the new MRI-PET equipment available at reasonable costs. Also, we need the integration between neuroimaging findings and fluid biomarkers not just in Alzheimer's but also in other neurodegenerative diseases.

In conclusion, there is urgent need of worldwide harmonization and standardization of biomarkers, assessing and increasing their performance and accuracy in detecting early disease, and of the development of diagnostic algorithms comprising combinations of biomarkers; the final aim is to develop shared clinical guidelines to follow in advanced memory clinics facing the dilemma of etiologic diagnosis in MCI patients (Frisoni et al. 2017). We also need physicians able to dialogue on a common ground among neurologists, psychiatrists, and geriatricians, on the one hand, and neuroradiologists and nuclear medicine physicians, on the other hand. As the life expectancy of the western population is expected to increase, the field of cognitive disorders of the elderly will become a new medical specialty. This new "dementologist" should have advanced knowledge of neuroimaging tools and must be able to properly manage all available biomarkers.

References

Adluru N, Destiche DJ, Lu SY-F et al (2014) White matter microstructure in late middle-age: effects of apolipoprotein E4 and parental family history of Alzheimer's disease. NeuroImage Clin 4:730–742

Aghourian M, Legault-Denis C, Soucy J-P, Rosa-Neto P, Gauthier S, Kostikov A, Gravel P, Bédard M-A (2017) Quantification of brain cholinergic denervation in Alzheimer's disease using PET imaging with [18F]-FEOBV. Mol Psychiatry 22:1531–1538

Aizenstein HJ, Nebes RD, Saxton JA et al (2008) Frequent amyloid deposition without significant cognitive impairment among the elderly. Arch Neurol 65:1509

Albert MS, DeKosky ST, Dickson D et al (2011) The diagnosis of mild cognitive impairment due to Alzheimer's disease: recommendations from the National Institute on Aging-Alzheimer's Association workgroups on diagnostic guidelines for Alzheimer's disease. Alzheimers Dement 7:270–279

Albi A, Pasternak O, Minati L et al (2017) Free water elimination improves test-retest reproducibility of diffusion tensor imaging indices in the brain: a longitudinal multisite study of healthy elderly subjects. Hum Brain Mapp 38:12–26

Alexander AL, Hasan KM, Lazar M, Tsuruda JS, Parker DL (2001) Analysis of partial volume effects in diffusion-tensor MRI. Magn Reson Med 45:770–780

Alsop DC, Detre JA, Grossman M (2000) Assessment of cerebral blood flow in Alzheimer's disease by spin-labeled magnetic resonance imaging. Ann Neurol 47:93–100

Alsop DC, Casement M, de Bazelaire C, Fong T, Press DZ (2008) Hippocampal hyperperfusion in Alzheimer's disease. NeuroImage 42:1267–1274

Alsop DC, Detre JA, Golay X et al (2015) Recommended implementation of arterial spin-labeled perfusion MRI for clinical applications: a consensus of the ISMRM perfusion study group and the European consortium for ASL in dementia. Magn Reson Med 73:102–116

Anchisi D, Borroni B, Franceschi M et al (2005) Heterogeneity of brain glucose metabolism in mild cognitive impairment and clinical progression to Alzheimer disease. Arch Neurol 62:1728

Arbizu J, Festari C, Altomare D et al (2018) Clinical utility of FDG-PET for the clinical diagnosis in MCI. Eur J Nucl Med Mol Imaging 45:1497–1508

Bai F, Zhang Z, Yu H, Shi Y, Yuan Y, Zhu W, Zhang X, Qian Y (2008) Default-mode network activity distinguishes amnestic type mild cognitive impairment from healthy aging: a combined structural and resting-state functional MRI study. Neurosci Lett 438:111–115

Bakkour A, Morris JC, Dickerson BC (2009) The cortical signature of prodromal AD: regional thinning predicts mild AD dementia. Neurology 72:1048–1055

Bao W, Jia H, Finnema S, Cai Z, Carson RE, Huang YH (2017) PET imaging for early detection of Alzheimer's disease. PET Clin 12:329–350

Barkhof F, Polvikoski TM, van Straaten ECW et al (2007) The significance of medial temporal lobe atrophy: a postmortem MRI study in the very old. Neurology 69:1521–1527

Baron CA, Beaulieu C (2015) Acquisition strategy to reduce cerebrospinal fluid partial volume effects for improved DTI tractography. Magn Reson Med 73:1075–1084

Bartzokis G (2004) Age-related myelin breakdown: a developmental model of cognitive decline and Alzheimer's disease. Neurobiol Aging 25:5–18. Author reply 49–62

Basser PJ, Mattiello J, LeBihan D (1994) Estimation of the effective self-diffusion tensor from the NMR spin echo. J Magn Reson B 103:247–254

Beason-Held LL, Goh JO, An Y, Kraut MA, O'Brien RJ, Ferrucci L, Resnick SM (2013) Changes in brain function occur years before the onset of cognitive impairment. J Neurosci 33:18008–18014

Beaulieu C (2002) The basis of anisotropic water diffusion in the nervous system - a technical review. NMR Biomed 15:435–455

Belleville S, Clément F, Mellah S, Gilbert B, Fontaine F, Gauthier S (2011) Training-related brain plasticity in subjects at risk of developing Alzheimer's disease. Brain 134:1623–1634

Bendlin BB, Carlsson CM, Johnson SC et al (2012) CSF T-tau/Aβ42 predicts white matter microstructure in healthy adults at risk for Alzheimer's disease. PLoS One 7:e37720
Binnewijzend MAA, Schoonheim MM, Sanz-Arigita E et al (2012) Resting-state fMRI changes in Alzheimer's disease and mild cognitive impairment. Neurobiol Aging 33:2018–2028
Biswal B, Yetkin FZ, Haughton VM, Hyde JS (1995) Functional connectivity in the motor cortex of resting human brain using echo-planar MRI. Magn Reson Med 34:537–541
Boccardi M, Nicolosi V, Festari C et al (2020) Italian consensus recommendations for the biomarker-based etiological diagnosis in MCI patients. Eur J Neurol 27:475
Boeve BF (2012) Mild cognitive impairment associated with underlying Alzheimer's disease versus Lewy body disease. Parkinsonism Relat Disord 18:S41–S44
Bohnen NI, Kaufer DI, Hendrickson R et al (2005) Degree of inhibition of cortical acetylcholinesterase activity and cognitive effects by donepezil treatment in Alzheimer's disease. J Neurol Neurosurg Psychiatry 76:315–319
Bokde ALW, Karmann M, Born C et al (2010) Altered brain activation during a verbal working memory task in subjects with amnestic mild cognitive impairment. J Alzheimers Dis 21:103–118
Bonner-Jackson A, Mahmoud S, Miller J, Banks SJ (2015) Verbal and non-verbal memory and hippocampal volumes in a memory clinic population. Alzheimers Res Ther 7:61
Bookheimer SY, Strojwas MH, Cohen MS, Saunders AM, Pericak-Vance MA, Mazziotta JC, Small GW (2000) Patterns of brain activation in people at risk for Alzheimer's disease. N Engl J Med 343:450–456
Borroni B, Anchisi D, Paghera B et al (2006) Combined 99mTc-ECD SPECT and neuropsychological studies in MCI for the assessment of conversion to AD. Neurobiol Aging 27:24–31
Braak H, Braak E (1997) Frequency of stages of Alzheimer-related lesions in different age categories. Neurobiol Aging 18:351–357
Brewer JB, Zhao Z, Desmond JE, Glover GH, Gabrieli JD (1998) Making memories: brain activity that predicts how well visual experience will be remembered. Science 281:1185–1187
Browndyke JN, Giovanello K, Petrella J, Hayden K, Chiba-Falek O, Tucker KA, Burke JR, Welsh-Bohmer KA (2013) Phenotypic regional functional imaging patterns during memory encoding in mild cognitive impairment and Alzheimer's disease. Alzheimers Dement 9:284–294
Brugnolo A, De Carli F, Pagani M et al (2019) Head-to-head comparison among semi-quantification tools of brain FDG-PET to aid the diagnosis of prodromal Alzheimer's disease. J Alzheimers Dis 68:383–394
Brun A, Englund E (1986) A white matter disorder in dementia of the Alzheimer type: a pathoanatomical study. Ann Neurol 19:253–262
Busatto GF, Garrido GE, Almeida OP, Castro CC, Camargo CH, Cid CG, Buchpiguel CA, Furuie S, Bottino CM (2003) A voxel-based morphometry study of temporal lobe gray matter reductions in Alzheimer's disease. Neurobiol Aging 24:221–231
Caroli A, Geroldi C, Nobili F, Barnden LR, Guerra UP, Bonetti M, Frisoni GB (2010) Functional compensation in incipient Alzheimer's disease. Neurobiol Aging 31:387–397
Caroli A, Prestia A, Chen K et al (2012) Summary metrics to assess Alzheimer disease-related hypometabolic pattern with 18F-FDG PET: head-to-head comparison. J Nucl Med 53:592–600
Cavedo E, Boccardi M, Ganzola R, Canu E, Beltramello A, Caltagirone C, Thompson PM, Frisoni GB (2011) Local amygdala structural differences with 3T MRI in patients with Alzheimer disease. Neurology 76:727
Cecchin D, Barthel H, Poggiali D et al (2017) A new integrated dual time-point amyloid PET/MRI data analysis method. Eur J Nucl Med Mol Imaging 44:2060–2072
Cerami C, Della Rosa PA, Magnani G, Santangelo R, Marcone A, Cappa SF, Perani D (2015) Brain metabolic maps in Mild Cognitive Impairment predict heterogeneity of progression to dementia. NeuroImage Clin 7:187–194
Chao LL, Buckley ST, Kornak J, Schuff N, Madison C, Yaffe K, Miller BL, Kramer JH, Weiner MW (2010) ASL perfusion MRI predicts cognitive decline and conversion from MCI to dementia. Alzheimer Dis Assoc Disord 24:19–27

Chen Y, Wolk DA, Reddin JS et al (2011a) Voxel-level comparison of arterial spin-labeled perfusion MRI and FDG-PET in Alzheimer disease. Neurology 77:1977–1985

Chen K, Ayutyanont N, Langbaum JBS et al (2011b) Characterizing Alzheimer's disease using a hypometabolic convergence index. NeuroImage 56:52–60

Chetelat G, Desgranges B, de la Sayette V et al (2003) Dissociating atrophy and hypometabolism impact on episodic memory in mild cognitive impairment. Brain 126:1955–1967

Chincarini A, Sensi F, Rei L, Bossert I, Morbelli S, Guerra UP, Frisoni G, Padovani A, Nobili F, Alzheimer's Disease Neuroimaging Initiative (2016) Standardized uptake value ratio-independent evaluation of brain amyloidosis. J Alzheimers Dis 54:1437–1457

Choo IH, Ni R, Schöll M, Wall A, Almkvist O, Nordberg A (2013) Combination of 18F-FDG PET and cerebrospinal fluid biomarkers as a better predictor of the progression to Alzheimer's disease in mild cognitive impairment patients. J Alzheimers Dis 33:929–939

Chung S, Fieremans E, Kucukboyaci NE, Wang X, Morton CJ, Novikov DS, Rath JF, Lui YW (2018) Working memory and brain tissue microstructure: white matter tract integrity based on multi-shell diffusion MRI. Sci Rep 8:3175

Chupin M, Gérardin E, Cuingnet R, Boutet C, Lemieux L, Lehéricy S, Benali H, Garnero L, Colliot O, Alzheimer's Disease Neuroimaging Initiative and the ADN (2009) Fully automatic hippocampus segmentation and classification in Alzheimer's disease and mild cognitive impairment applied on data from ADNI. Hippocampus 19:579–587

Ciarochi JA, Calhoun VD, Lourens S et al (2016) Patterns of co-occurring gray matter concentration loss across the Huntington disease prodrome. Front Neurol 7:147

Cicerone KD, Langenbahn DM, Braden C et al (2011) Evidence-based cognitive rehabilitation: updated review of the literature from 2003 through 2008. Arch Phys Med Rehabil 92:519–530

Clerici F, Del Sole A, Chiti A, Maggiore L, Lecchi M, Pomati S, Mosconi L, Lucignani G, Mariani C (2009) Differences in hippocampal metabolism between amnestic and non-amnestic MCI subjects: automated FDG-PET image analysis. Q J Nucl Med Mol Imaging 53:646–657

Colgan N, Siow B, O'Callaghan JM et al (2016) Application of neurite orientation dispersion and density imaging (NODDI) to a tau pathology model of Alzheimer's disease. NeuroImage 125:739–744

Colliot O, Chételat G, Chupin M, Desgranges B, Magnin B, Benali H, Dubois B, Garnero L, Eustache F, Lehéricy S (2008) Discrimination between Alzheimer disease, mild cognitive impairment, and normal aging by using automated segmentation of the hippocampus. Radiology 248:194–201

Costafreda SG, Dinov ID, Tu Z et al (2011) Automated hippocampal shape analysis predicts the onset of dementia in mild cognitive impairment. NeuroImage 56:212–219

Cselényi Z, Farde L (2015) Quantification of blood flow-dependent component in estimates of beta-amyloid load obtained using quasi-steady-state standardized uptake value ratio. J Cereb Blood Flow Metab 35:1485–1493

Cuingnet R, Gerardin E, Tessieras J, Auzias G, Lehéricy S, Habert M-O, Chupin M, Benali H, Colliot O, Alzheimer's Disease Neuroimaging Initiative (2011) Automatic classification of patients with Alzheimer's disease from structural MRI: a comparison of ten methods using the ADNI database. NeuroImage 56:766–781

Cummings JL, Tong G, Ballard C (2019) Treatment combinations for Alzheimer's disease: current and future pharmacotherapy options. J Alzheimers Dis 67:779–794

Da X, Toledo JB, Zee J et al (2014) Integration and relative value of biomarkers for prediction of MCI to AD progression: spatial patterns of brain atrophy, cognitive scores, APOE genotype and CSF biomarkers. NeuroImage Clin 4:164–173

Daerr S, Brendel M, Zach C et al (2017) Evaluation of early-phase [18F]-florbetaben PET acquisition in clinical routine cases. NeuroImage Clin 14:77–86

Darreh-Shori T, Kadir A, Almkvist O, Grut M, Wall A, Blomquist G, Eriksson B, Långström B, Nordberg A (2008) Inhibition of acetylcholinesterase in CSF versus brain assessed by 11C-PMP PET in AD patients treated with galantamine. Neurobiol Aging 29:168–184

Daselaar SM, Prince SE, Cabeza R (2004) When less means more: deactivations during encoding that predict subsequent memory. NeuroImage 23:921–927

Davatzikos C, Fan Y, Wu X, Shen D, Resnick SM (2008) Detection of prodromal Alzheimer's disease via pattern classification of magnetic resonance imaging. Neurobiol Aging 29:514–523
Davatzikos C, Xu F, An Y, Fan Y, Resnick SM (2009) Longitudinal progression of Alzheimer's-like patterns of atrophy in normal older adults: the SPARE-AD index. Brain 132:2026–2035
Davatzikos C, Bhatt P, Shaw LM, Batmanghelich KN, Trojanowski JQ (2011) Prediction of MCI to AD conversion, via MRI, CSF biomarkers, and pattern classification. Neurobiol Aging 32:2322.e19–2322.e27
De Carli F, Nobili F, Pagani M et al (2019) Accuracy and generalization capability of an automatic method for the detection of typical brain hypometabolism in prodromal Alzheimer disease. Eur J Nucl Med Mol Imaging 46:334–347
Defrancesco M, Egger K, Marksteiner J, Esterhammer R, Hinterhuber H, Deisenhammer EA, Schocke M (2014) Changes in white matter integrity before conversion from mild cognitive impairment to Alzheimer's disease. PLoS One 9:e106062
Delli Pizzi S, Franciotti R, Bubbico G, Thomas A, Onofrj M, Bonanni L (2016) Atrophy of hippocampal subfields and adjacent extrahippocampal structures in dementia with Lewy bodies and Alzheimer's disease. Neurobiol Aging 40:103–109
Demirhan A, Nir TM, Zavaliangos-Petropulu A, Jack CR, Weiner MW, Bernstein MA, Thompson PM, Jahanshad N, Alzheimer's Disease Neuroimaging Initiative (ADNI) (2015) Feature selection improves the accuracy of classifying Alzheimer disease using diffusion tensor images. In: 2015 IEEE 12th International Symposium on Biomedical Imaging. IEEE, Washington, DC, pp 126–130
Desikan RS, Cabral HJ, Hess CP et al (2009) Automated MRI measures identify individuals with mild cognitive impairment and Alzheimer's disease. Brain 132:2048–2057
Desikan RS, Cabral HJ, Settecase F et al (2010) Automated MRI measures predict progression to Alzheimer's disease. Neurobiol Aging 31:1364–1374
deToledo-Morrell L, Stoub T, Bulgakova M, Wilson R, Bennett D, Leurgans S, Wuu J, Turner D (2004) MRI-derived entorhinal volume is a good predictor of conversion from MCI to AD. Neurobiol Aging 25:1197–1203
Devanand DP, Pradhaban G, Liu X et al (2007) Hippocampal and entorhinal atrophy in mild cognitive impairment: prediction of Alzheimer disease. Neurology 68:828–836
Devous MD, Joshi AD, Kennedy I, Navitsky M, Pontecorvo MJ, Skovronsky DJ, Mintun MA (2014) Employing early uptake data from F18-Florbetapir scans as an estimate of regional cerebral blood flow: comparison to F18-FDG. Alzheimers Dement 10:P102
Deweer B, Lehericy S, Pillon B, Baulac M, Chiras J, Marsault C, Agid Y, Dubois B, Agid B, Deweer B, Dubois S, Lehericy B, Pillon NY, Nouvelle B (1995) Memory disorders in probable Alzheimer's disease: the role of hippocampal atrophy as shown with MRI. J Neurol Neurosurg Psychiatry 58:590–597
Dickerson BC, Salat DH, Greve DN et al (2005) Increased hippocampal activation in mild cognitive impairment compared to normal aging and AD. Neurology 65:404–411
Doraiswamy PM, Sperling RA, Johnson K et al (2014) Florbetapir F 18 amyloid PET and 36-month cognitive decline: a prospective multicenter study. Mol Psychiatry 19:1044–1051
Doré V, Villemagne VL, Bourgeat P et al (2013) Cross-sectional and longitudinal analysis of the relationship between Aβ deposition, cortical thickness, and memory in cognitively unimpaired individuals and in Alzheimer disease. JAMA Neurol 70:903
Dowell NG, Evans SL, Tofts PS, King SL, Tabet N, Rusted JM (2016) Structural and resting-state MRI detects regional brain differences in young and mid-age healthy APOE-e4 carriers compared with non-APOE-e4 carriers. NMR Biomed 29:614–624
Drzezga A, Grimmer T, Riemenschneider M, Lautenschlager N, Siebner H, Alexopoulus P, Minoshima S, Schwaiger M, Kurz A (2005) Prediction of individual clinical outcome in MCI by means of genetic assessment and (18)F-FDG PET. J Nucl Med 46:1625–1632
Du AT, Schuff N, Kramer JH et al (2004) Higher atrophy rate of entorhinal cortex than hippocampus in AD. Neurology 62:422–427

Duarte A, Hayasaka S, Du A, Schuff N, Jahng G-H, Kramer J, Miller B, Weiner M (2006) Volumetric correlates of memory and executive function in normal elderly, mild cognitive impairment and Alzheimer's disease. Neurosci Lett 406:60–65

Dubois B, Feldman HH, Jacova C et al (2007) Research criteria for the diagnosis of Alzheimer's disease: revising the NINCDS–ADRDA criteria. Lancet Neurol 6:734–746

Dubois B, Feldman HH, Jacova C et al (2010) Revising the definition of Alzheimer's disease: a new lexicon. Lancet Neurol 9:1118–1127

Dubois B, Feldman HH, Jacova C et al (2014) Advancing research diagnostic criteria for Alzheimer's disease: the IWG-2 criteria. Lancet Neurol 13:614–629

Duchesne S, Bocti C, De Sousa K, Frisoni GB, Chertkow H, Collins DL (2010) Amnestic MCI future clinical status prediction using baseline MRI features. Neurobiol Aging 31:1606–1617

ECW S, Harvey D, Scheltens P, Barkhof F, Petersen RC, Thal LJ, Jack CR, DeCarli C, Alzheimer's Disease Cooperative Study Group (2008) Periventricular white matter hyperintensities increase the likelihood of progression from amnestic mild cognitive impairment to dementia. J Neurol 255:1302–1308

El Fakhri G, Kijewski MF, Johnson KA, Syrkin G, Killiany RJ, Becker JA, Zimmerman RE, Albert MS (2003) MRI-guided SPECT perfusion measures and volumetric MRI in prodromal Alzheimer disease. Arch Neurol 60:1066

Encinas M, de Juan R, Marcos A, Gil P, Barabash A, Fernández C, de Ugarte C, Cabranes JA (2003) Regional cerebral blood flow assessed with 99mTc-ECD SPET as a marker of progression of mild cognitive impairment to Alzheimer's disease. Eur J Nucl Med Mol Imaging 30:1473–1480

Eskildsen SF, Coupé P, García-Lorenzo D, Fonov V, Pruessner JC, Collins DL, Alzheimer's Disease Neuroimaging Initiative TADN (2013) Prediction of Alzheimer's disease in subjects with mild cognitive impairment from the ADNI cohort using patterns of cortical thinning. NeuroImage 65:511–521

Ewers M, Walsh C, Trojanowski JQ et al (2012) Prediction of conversion from mild cognitive impairment to Alzheimer's disease dementia based upon biomarkers and neuropsychological test performance. Neurobiol Aging 33:1203–1214.e2

Fan Y, Shen D, Gur RC, Gur RE, Davatzikos C (2007) COMPARE: classification of morphological patterns using adaptive regional elements. IEEE Trans Med Imaging 26:93–105

Farrell ME, Kennedy KM, Rodrigue KM, Wig G, Bischof GN, Rieck JR, Chen X, Festini SB, Devous MD, Park DC (2017) Association of longitudinal cognitive decline with amyloid burden in middle-aged and older adults. JAMA Neurol 74:830

Fellgiebel A, Dellani PR, Greverus D, Scheurich A, Stoeter P, Müller MJ (2006) Predicting conversion to dementia in mild cognitive impairment by volumetric and diffusivity measurements of the hippocampus. Psychiatry Res Neuroimaging 146:283–287

Fellgiebel A, Scheurich A, Bartenstein P, Müller MJ (2007) FDG-PET and CSF phospho-tau for prediction of cognitive decline in mild cognitive impairment. Psychiatry Res Neuroimaging 155:167–171

Ferrarini L, Frisoni GB, Pievani M, Reiber JHC, Ganzola R, Milles J (2009) Morphological hippocampal markers for automated detection of Alzheimer's disease and mild cognitive impairment converters in magnetic resonance images. J Alzheimers Dis 17:643–659

Ferreira LK, Diniz BS, Forlenza OV, Busatto GF, Zanetti MV (2011) Neurostructural predictors of Alzheimer's disease: a meta-analysis of VBM studies. Neurobiol Aging 32:1733–1741

Fischer FU, Wolf D, Scheurich A, Fellgiebel A, Alzheimer's Disease Neuroimaging Initiative (2015) Altered whole-brain white matter networks in preclinical Alzheimer's disease. NeuroImage Clin 8:660–666

de Flores R, La Joie R, Chételat G (2015) Structural imaging of hippocampal subfields in healthy aging and Alzheimer's disease. Neuroscience 309:29–50

Flynn DD, Mash DC (1986) Characterization of L-[3H]nicotine binding in human cerebral cortex: comparison between Alzheimer's disease and the normal. J Neurochem 47:1948–1954

Forsberg A, Engler H, Almkvist O, Blomquist G, Hagman G, Wall A, Ringheim A, Långström B, Nordberg A (2008) PET imaging of amyloid deposition in patients with mild cognitive impairment. Neurobiol Aging 29:1456–1465

Förster S, Grimmer T, Miederer I et al (2012) Regional expansion of hypometabolism in Alzheimer's disease follows amyloid deposition with temporal delay. Biol Psychiatry 71:792–797
Fox NC, Freeborough PA (1997) Brain atrophy progression measured from registered serial MRI: validation and application to alzheimer's disease. J Magn Reson Imaging 7:1069–1075
Freeborough PA, Fox NC (1998) MR image texture analysis applied to the diagnosis and tracking of Alzheimer's disease. IEEE Trans Med Imaging 17:475–478
Frisoni GB, Fox NC, Jack CR, Scheltens P, Thompson PM, Thompson PM (2010) The clinical use of structural MRI in Alzheimer disease. Nat Rev Neurol 6:67–77
Frisoni GB, Boccardi M, Barkhof F et al (2017) Strategic roadmap for an early diagnosis of Alzheimer's disease based on biomarkers. Lancet Neurol 16:661–676
Frölich L, Peters O, Lewczuk P et al (2017) Incremental value of biomarker combinations to predict progression of mild cognitive impairment to Alzheimer's dementia. Alzheimers Res Ther 9:84
Fujishima M, Maikusa N, Nakamura K, Nakatsuka M, Matsuda H, Meguro K (2014) Mild cognitive impairment, poor episodic memory, and late-life depression are associated with cerebral cortical thinning and increased white matter hyperintensities. Front Aging Neurosci 6:306
Gardini S, Venneri A, Sambataro F, Cuetos F, Fasano F, Marchi M, Crisi G, Caffarra P (2015) Increased functional connectivity in the default mode network in mild cognitive impairment: a maladaptive compensatory mechanism associated with poor semantic memory performance. J Alzheimers Dis 45:457–470
Garibotto V, Borroni B, Kalbe E et al (2008) Education and occupation as proxies for reserve in aMCI converters and AD: FDG-PET evidence. Neurology 71:1342–1349
Garibotto V, Herholz K, Boccardi M, Picco A, Varrone A, Nordberg A, Nobili F, Ratib O, Geneva Task Force for the Roadmap of Alzheimer's Biomarkers (2017) Clinical validity of brain fluorodeoxyglucose positron emission tomography as a biomarker for Alzheimer's disease in the context of a structured 5-phase development framework. Neurobiol Aging 52:183–195
Gerardin E, Chételat G, Chupin M et al (2009) Multidimensional classification of hippocampal shape features discriminates Alzheimer's disease and mild cognitive impairment from normal aging. NeuroImage 47:1476–1486
Gold BT, Zhu Z, Brown CA et al (2014) White matter integrity is associated with cerebrospinal fluid markers of Alzheimer's disease in normal adults. Neurobiol Aging 35:2263–2271
Gomar JJ, Ragland JD, Uluğ AM, Sousa A, Huey ED, Conejero-Goldberg C, Davies P, Goldberg TE (2017) Differential medial temporal lobe morphometric predictors of item- and relational-encoded memories in healthy individuals and in individuals with mild cognitive impairment and Alzheimer's disease. Alzheimer's Dement (New York, N Y) 3:238–246
Gómez-Isla T, Hollister R, West H, Mui S, Growdon JH, Petersen RC, Parisi JE, Hyman BT (1997) Neuronal loss correlates with but exceeds neurofibrillary tangles in Alzheimer's disease. Ann Neurol 41:17–24
Gossink FT, Dols A, Kerssens CJ, Krudop WA, Kerklaan BJ, Scheltens P, Stek ML, Pijnenburg YAL (2016) Psychiatric diagnoses underlying the phenocopy syndrome of behavioural variant frontotemporal dementia. J Neurol Neurosurg Psychiatry 87:64–68
Gouw AA, Seewann A, Vrenken H, van der Flier WM, Rozemuller JM, Barkhof F, Scheltens P, Geurts JJG (2008) Heterogeneity of white matter hyperintensities in Alzheimer's disease: post-mortem quantitative MRI and neuropathology. Brain 131:3286–3298
Greicius MD, Srivastava G, Reiss AL, Menon V (2004) Default-mode network activity distinguishes Alzheimer's disease from healthy aging: evidence from functional MRI. Proc Natl Acad Sci 101:4637–4642
Grimmer T, Wutz C, Alexopoulos P, Drzezga A, Forster S, Forstl H, Goldhardt O, Ortner M, Sorg C, Kurz A (2016) Visual versus fully automated analyses of 18F-FDG and amyloid PET for prediction of dementia due to Alzheimer disease in mild cognitive impairment. J Nucl Med 57:204–207
Guenther T, Schönknecht P, Becker G, Olbrich S, Sander C, Hesse S, Meyer PM, Luthardt J, Hegerl U, Sabri O (2011) Impact of EEG-vigilance on brain glucose uptake measured with [18F]FDG and PET in patients with depressive episode or mild cognitive impairment. NeuroImage 56:93–101

Guerra UP, Nobili FM, Padovani A, Perani D, Pupi A, Sorbi S, Trabucchi M (2015) Recommendations from the Italian Interdisciplinary Working Group (AIMN, AIP, SINDEM) for the utilization of amyloid imaging in clinical practice. Neurol Sci 36:1075–1081

Guo X, Wang Z, Li K, Li Z, Qi Z, Jin Z, Yao L, Chen K (2010) Voxel-based assessment of gray and white matter volumes in Alzheimer's disease. Neurosci Lett 468:146–150

Habert M-O, de Souza LC, Lamari F, Daragon N, Desarnaud S, Jardel C, Dubois B, Sarazin M (2010) Brain perfusion SPECT correlates with CSF biomarkers in Alzheimer's disease. Eur J Nucl Med Mol Imaging 37:589–593

Haense C, Herholz K, Jagust WJ, Heiss WD (2009) Performance of FDG PET for detection of Alzheimer's disease in two independent multicentre samples (NEST-DD and ADNI). Dement Geriatr Cogn Disord 28:259–266

Hämäläinen A, Pihlajamäki M, Tanila H, Hänninen T, Niskanen E, Tervo S, Karjalainen PA, Vanninen RL, Soininen H (2007) Increased fMRI responses during encoding in mild cognitive impairment. Neurobiol Aging 28:1889–1903

Hampstead BM, Stringer AY, Stilla RF, Deshpande G, Hu X, Moore AB, Sathian K (2011) Activation and effective connectivity changes following explicit-memory training for face–name pairs in patients with mild cognitive impairment. Neurorehabil Neural Repair 25:210–222

Hampstead BM, Stringer AY, Stilla RF, Giddens M, Sathian K (2012) Mnemonic strategy training partially restores hippocampal activity in patients with mild cognitive impairment. Hippocampus 22:1652–1658

Han Y, Wang J, Zhao Z, Min B, Lu J, Li K, He Y, Jia J (2011) Frequency-dependent changes in the amplitude of low-frequency fluctuations in amnestic mild cognitive impairment: a resting-state fMRI study. NeuroImage 55:287–295

Hansson O, Seibyl J, Stomrud E et al (2018) CSF biomarkers of Alzheimer's disease concord with amyloid-β PET and predict clinical progression: a study of fully automated immunoassays in BioFINDER and ADNI cohorts. Alzheimers Dement 14:1470–1481

Harper L, Barkhof F, Scheltens P, Schott JM, Fox NC (2014) An algorithmic approach to structural imaging in dementia. J Neurol Neurosurg Psychiatry 85:692–698

He Y, Wang L, Zang Y, Tian L, Zhang X, Li K, Jiang T (2007) Regional coherence changes in the early stages of Alzheimer's disease: a combined structural and resting-state functional MRI study. NeuroImage 35:488–500

Heckemann RA, Keihaninejad S, Aljabar P, Gray KR, Nielsen C, Rueckert D, Hajnal JV, Hammers A, Alzheimer's Disease Neuroimaging Initiative TADN (2011) Automatic morphometry in Alzheimer's disease and mild cognitive impairment. NeuroImage 56:2024–2037

Herholz K (2003) PET studies in dementia. Ann Nucl Med 17:79–89

Herholz K, Ebmeier K (2011) Clinical amyloid imaging in Alzheimer's disease. Lancet Neurol 10:667–670

Hirao K, Ohnishi T, Hirata Y et al (2005) The prediction of rapid conversion to Alzheimer's disease in mild cognitive impairment using regional cerebral blood flow SPECT. NeuroImage 28:1014–1021

Høgh P, Madsen Sjö N, Gade A, Waldemar G (2004) Temporal lobe hypoperfusion in isolated amnesia with slow onset: a single photon emission computer tomography study. Dement Geriatr Cogn Disord 18:15–23

Holland D, Desikan RS, Dale AM, McEvoy LK, Initiative for the ADN (2012) Rates of decline in Alzheimer disease decrease with age. PLoS One 7:e42325

Holmes C, Boche D, Wilkinson D et al (2008) Long-term effects of Aβ42 immunisation in Alzheimer's disease: follow-up of a randomised, placebo-controlled phase I trial. Lancet 372:216–223

Hoy AR, Ly M, Carlsson CM et al (2017) Microstructural white matter alterations in preclinical Alzheimer's disease detected using free water elimination diffusion tensor imaging. PLoS One 12:e0173982

Huang C, Wahlund L-O, Almkvist O, Elehu D, Svensson L, Jonsson T, Winblad B, Julin P (2003) Voxel- and VOI-based analysis of SPECT CBF in relation to clinical and psychological heterogeneity of mild cognitive impairment. NeuroImage 19:1137–1144

Irish M, Addis DR, Hodges JR, Piguet O (2012) Considering the role of semantic memory in episodic future thinking: evidence from semantic dementia. Brain 135:2178–2191
Irish M, Hodges JR, Piguet O (2013) Episodic future thinking is impaired in the behavioural variant of frontotemporal dementia. Cortex 49:2377–2388
Ishii K, Minoshima S (2005) PET is better than perfusion SPECT for early diagnosis of Alzheimer's disease. Eur J Nucl Med Mol Imaging 32:1463–1465
Ishiwata A, Sakayori O, Minoshima S, Mizumura S, Kitamura S, Katayama Y (2006) Preclinical evidence of Alzheimer changes in progressive mild cognitive impairment: a qualitative and quantitative SPECT study. Acta Neurol Scand 114:91–96
Ismail Z, Elbayoumi H, Fischer CE, Hogan DB, Millikin CP, Schweizer T, Mortby ME, Smith EE, Patten SB, Fiest KM (2017) Prevalence of depression in patients with mild cognitive impairment. JAMA Psychiatry 74:58
Jack CR (2012) Alzheimer disease: new concepts on its neurobiology and the clinical role imaging will play. Radiology 263:344–361
Jack CR, Shiung MM, Gunter JL et al (2004) Comparison of different MRI brain atrophy rate measures with clinical disease progression in AD. Neurology 62:591–600
Jack CR, Lowe VJ, Senjem ML et al (2008a) 11C PiB and structural MRI provide complementary information in imaging of Alzheimer's disease and amnestic mild cognitive impairment. Brain 131:665–680
Jack CR, Bernstein MA, Fox NC et al (2008b) The Alzheimer's disease neuroimaging initiative (ADNI): MRI methods. J Magn Reson Imaging 27:685–691
Jack CR, Lowe VJ, Weigand SD et al (2009) Serial PIB and MRI in normal, mild cognitive impairment and Alzheimer's disease: implications for sequence of pathological events in Alzheimer's disease. Brain 132:1355–1365
Jack CR, Wiste HJ, Vemuri P et al (2010) Brain beta-amyloid measures and magnetic resonance imaging atrophy both predict time-to-progression from mild cognitive impairment to Alzheimer's disease. Brain 133:3336–3348
Jack CR, Barnes J, Bernstein MA et al (2015) Magnetic resonance imaging in Alzheimer's Disease Neuroimaging Initiative 2. Alzheimers Dement 11:740–756
Jack CR, Wiste HJ, Weigand SD et al (2017) Age-specific and sex-specific prevalence of cerebral β-amyloidosis, tauopathy, and neurodegeneration in cognitively unimpaired individuals aged 50–95 years: a cross-sectional study. Lancet Neurol 16:435–444
Jack CR, Bennett DA, Blennow K et al (2018) NIA-AA Research Framework: toward a biological definition of Alzheimer's disease. Alzheimers Dement 14:535–562
Janvin CC, Larsen JP, Aarsland D, Hugdahl K (2006) Subtypes of mild cognitive impairment in parkinson's disease: progression to dementia. Mov Disord 21:1343–1349
Jin M, Pelak VS, Cordes D (2012) Aberrant default mode network in subjects with amnestic mild cognitive impairment using resting-state functional MRI. Magn Reson Imaging 30:48–61
Johnson NA, Jahng G-H, Weiner MW, Miller BL, Chui HC, Jagust WJ, Gorno-Tempini ML, Schuff N (2005) Pattern of cerebral hypoperfusion in Alzheimer disease and mild cognitive impairment measured with arterial spin-labeling MR imaging: initial experience. Radiology 234:851–859
Johnson KA, Moran EK, Becker JA, Blacker D, Fischman AJ, Albert MS (2007) Single photon emission computed tomography perfusion differences in mild cognitive impairment. J Neurol Neurosurg Psychiatry 78:240–247
Johnson KA, Minoshima S, Bohnen NI et al (2013) Appropriate use criteria for amyloid PET: a report of the Amyloid Imaging Task Force, the Society of Nuclear Medicine and Molecular Imaging, and the Alzheimer's Association. Alzheimers Dement 9:E1–E16
Jones DT, Graff-Radford J, Lowe VJ et al (2017) Tau, amyloid, and cascading network failure across the Alzheimer's disease spectrum. Cortex 97:143–159
de Jong LW, van der Hiele K, Veer IM, Houwing JJ, Westendorp RGJ, Bollen ELEM, de Bruin PW, Middelkoop HAM, van Buchem MA, van der Grond J (2008) Strongly reduced volumes of putamen and thalamus in Alzheimer's disease: an MRI study. Brain 131:3277–3285

Jovicich J, Marizzoni M, Bosch B et al (2014) Multisite longitudinal reliability of tract-based spatial statistics in diffusion tensor imaging of healthy elderly subjects. NeuroImage 101:390–403

Julkunen V, Niskanen E, Muehlboeck S et al (2009) Cortical thickness analysis to detect progressive mild cognitive impairment: a reference to Alzheimer's disease. Dement Geriatr Cogn Disord 28:404–412

Juni JE, Waxman AD, Devous MD, Tikofsky RS, Ichise M, Van Heertum RL, Carretta RF, Chen CC, Society for Nuclear Medicine (2009) Procedure guideline for brain perfusion SPECT Using 99mTc radiopharmaceuticals 3.0. J Nucl Med Technol 37:191–195

Juottonen K, Laakso MP, Partanen K, Soininen H (1999) Comparative MR analysis of the entorhinal cortex and hippocampus in diagnosing Alzheimer disease. AJNR Am J Neuroradiol 20:139–144

Kantarci K, Jack CR, Xu YC et al (2001) Mild cognitive impairment and Alzheimer disease: regional diffusivity of water. Radiology 219:101–107

Kantarci K, Schwarz CG, Reid RI et al (2014) White matter integrity determined with diffusion tensor imaging in older adults without dementia. JAMA Neurol 71:1547

Kantarci K, Murray ME, Schwarz CG et al (2017) White-matter integrity on DTI and the pathologic staging of Alzheimer's disease. Neurobiol Aging 56:172–179

Kapucu ÖL, Nobili F, Varrone A, Booij J, Vander Borght T, Någren K, Darcourt J, Tatsch K, Van Laere KJ (2009) EANM procedure guideline for brain perfusion SPECT using 99mTc-labelled radiopharmaceuticals, version 2. Eur J Nucl Med Mol Imaging 36:2093–2102

Kaufmann L, Ischebeck A, Weiss E, Koppelstaetter F, Siedentopf C, Vogel SE, Gotwald T, Marksteiner J, Wood G (2008) An fMRI study of the numerical Stroop task in individuals with and without minimal cognitive impairment. Cortex 44:1248–1255

Kemppainen NM, Aalto S, Wilson IA et al (2007) PET amyloid ligand [11C]PIB uptake is increased in mild cognitive impairment. Neurology 68:1603–1606

Kerchner GA, Hess CP, Hammond-Rosenbluth KE, Xu D, Rabinovici GD, Kelley DAC, Vigneron DB, Nelson SJ, Miller BL (2010) Hippocampal CA1 apical neuropil atrophy in mild Alzheimer disease visualized with 7-T MRI. Neurology 75:1381–1387

Kerchner GA, Deutsch GK, Zeineh M, Dougherty RF, Saranathan M, Rutt BK (2012) Hippocampal CA1 apical neuropil atrophy and memory performance in Alzheimer's disease. NeuroImage 63:194–202

Kilimann I, Grothe M, Heinsen H et al (2014) Subregional basal forebrain atrophy in Alzheimer's disease: a multicenter study. J Alzheimers Dis 40:687–700

Killiany RJ, Gomez-Isla T, Moss M, Kikinis R, Sandor T, Jolesz F, Tanzi R, Jones K, Hyman BT, Albert MS (2000) Use of structural magnetic resonance imaging to predict who will get Alzheimer's disease. Ann Neurol 47:430–439

Killiany RJ, Hyman BT, Gomez-Isla T, Moss MB, Kikinis R, Jolesz F, Tanzi R, Jones K, Albert MS (2002) MRI measures of entorhinal cortex vs hippocampus in preclinical AD. Neurology 58:1188–1196

Kim EJ, Cho SS, Jeong Y, Park KC, Kang SJ, Kang E, Kim SE, Lee KH, Na DL (2005) Glucose metabolism in early onset versus late onset Alzheimer's disease: an SPM analysis of 120 patients. Brain 128:1790–1801

Kipps CM, Hodges JR, Fryer TD, Nestor PJ (2009) Combined magnetic resonance imaging and positron emission tomography brain imaging in behavioural variant frontotemporal degeneration: refining the clinical phenotype. Brain 132:2566–2578

Kirchhoff BA, Wagner AD, Maril A, Stern CE (2000) Prefrontal-temporal circuitry for episodic encoding and subsequent memory. J Neurosci 20:6173–6180

Kirov II, Hardy CJ, Matsuda K et al (2013) In vivo 7Tesla imaging of the dentate granule cell layer in schizophrenia. Schizophr Res 147:362–367

Kloppel S, Stonnington CM, Chu C, Draganski B, Scahill RI, Rohrer JD, Fox NC, Jack CR, Ashburner J, Frackowiak RSJ (2008) Automatic classification of MR scans in Alzheimer's disease. Brain 131:681–689

Klunk WE, Koeppe RA, Price JC et al (2015) The centiloid project: standardizing quantitative amyloid plaque estimation by PET. Alzheimers Dement 11:1–15.e4

Koch K, Myers NE, Göttler J et al (2015) Disrupted intrinsic networks link amyloid-β pathology and impaired cognition in prodromal Alzheimer's disease. Cereb Cortex 25:4678–4688
Kohannim O, Hua X, Hibar DP, Lee S, Chou Y-Y, Toga AW, Jack CR, Weiner MW, Thompson PM, Alzheimer's Disease Neuroimaging Initiative (2010) Boosting power for clinical trials using classifiers based on multiple biomarkers. Neurobiol Aging 31:1429–1442
Koikkalainen J, Lötjönen J, Thurfjell L, Rueckert D, Waldemar G, Soininen H, Alzheimer's Disease Neuroimaging Initiative the ADN (2011) Multi-template tensor-based morphometry: application to analysis of Alzheimer's disease. NeuroImage 56:1134–1144
Kondo Y, Suzuki M, Mugikura S, Abe N, Takahashi S, Iijima T, Fujii T (2005) Changes in brain activation associated with use of a memory strategy: a functional MRI study. NeuroImage 24:1154–1163
Konukoglu E, Coutu J-P, Salat DH, Fischl B (2016) Multivariate statistical analysis of diffusion imaging parameters using partial least squares: application to white matter variations in Alzheimer's disease. NeuroImage 134:573–586
Koulibaly PM, Nobili F, Migneco O, Vitali P, Robert PH, Girtler N, Darcourt J, Rodriguez G (2003) 99m Tc-HMPAO and 99m Tc-ECD perform differently in typically hypoperfused areas in Alzheimer's disease. Eur J Nucl Med Mol Imaging 30:1009–1013
Kramer JH, Rosen HJ, Du A-T, Schuff N, Hollnagel C, Weiner MW, Miller BL, Delis DC (2005) Dissociations in hippocampal and frontal contributions to episodic memory performance. Neuropsychology 19:799–805
Kuhl DE, Koeppe RA, Minoshima S, Snyder SE, Ficaro EP, Foster NL, Frey KA, Kilbourn MR (1999) In vivo mapping of cerebral acetylcholinesterase activity in aging and Alzheimer's disease. Neurology 52:691–699
La Joie R, Perrotin A, de La Sayette V, Egret S, Doeuvre L, Belliard S, Eustache F, Desgranges B, Chételat G (2013) Hippocampal subfield volumetry in mild cognitive impairment, Alzheimer's disease and semantic dementia. NeuroImage Clin 3:155–162
Landau SM, Harvey D, Madison CM et al (2010) Comparing predictors of conversion and decline in mild cognitive impairment. Neurology 75:230–238
Landau SM, Harvey D, Madison CM, Koeppe RA, Reiman EM, Foster NL, Weiner MW, Jagust WJ, Alzheimer's Disease Neuroimaging Initiative (2011) Associations between cognitive, functional, and FDG-PET measures of decline in AD and MCI. Neurobiol Aging 32:1207–1218
Lange C, Suppa P, Pietrzyk U, Makowski MR, Spies L, Peters O, Buchert R, Alzheimer's Disease Neuroimaging Initiative (2017) Prediction of Alzheimer's dementia in patients with amnestic mild cognitive impairment in clinical routine: incremental value of biomarkers of neurodegeneration and brain amyloidosis added stepwise to cognitive status. J Alzheimers Dis 61:373–388
Leandrou S, Petroudi S, Kyriacou PA, Reyes-Aldasoro CC, Pattichis CS (2018) Quantitative MRI brain studies in mild cognitive impairment and Alzheimer's disease: a methodological review. IEEE Rev Biomed Eng 11:97–111
Lee JH, Ryan J, Andreescu C, Aizenstein H, Lim HK (2015) Brainstem morphological changes in Alzheimer's disease. Neuroreport 26:411–415
Lehmann M, Koedam EL, Barnes J, Bartlett JW, Barkhof F, Wattjes MP, Schott JM, Scheltens P, Fox NC, Alzheimer's Disease Neuroimaging Initiative (2013) Visual ratings of atrophy in MCI: prediction of conversion and relationship with CSF biomarkers. Neurobiol Aging 34:73–82
Lerch JP, Pruessner J, Zijdenbos AP, Collins DL, Teipel SJ, Hampel H, Evans AC (2008) Automated cortical thickness measurements from MRI can accurately separate Alzheimer's patients from normal elderly controls. Neurobiol Aging 29:23–30
Leung KK, Bartlett JW, Barnes J, Manning EN, Ourselin S, Fox NC, Alzheimer's Disease Neuroimaging Initiative (2013) Cerebral atrophy in mild cognitive impairment and Alzheimer disease: rates and acceleration. Neurology 80:648–654
Leuzy A, Chiotis K, Lemoine L, Gillberg P-G, Almkvist O, Rodriguez-Vieitez E, Nordberg A (2019) Tau PET imaging in neurodegenerative tauopathies—still a challenge. Mol Psychiatry 24:1112
Li X, Coyle D, Maguire L, Watson DR, McGinnity TM (2011) Gray matter concentration and effective connectivity changes in Alzheimer's disease: a longitudinal structural MRI study. Neuroradiology 53:733–748

Li Y-D, Dong H-B, Xie G-M, Zhang L (2013) Discriminative analysis of mild Alzheimer's disease and normal aging using volume of hippocampal subfields and hippocampal mean diffusivity. Am J Alzheimer's Dis Other Demen 28:627–633

Li H-J, Hou X-H, Liu H-H, Yue C-L, He Y, Zuo X-N (2015) Toward systems neuroscience in mild cognitive impairment and Alzheimer's disease: a meta-analysis of 75 fMRI studies. Hum Brain Mapp 36:1217–1232

Lin L, Xing G, Han Y (2018) Advances in resting state neuroimaging of mild cognitive impairment. Front Psychiatry 9:671

Lind J, Persson J, Ingvar M et al (2006) Reduced functional brain activity response in cognitively intact apolipoprotein E epsilon4 carriers. Brain 129:1240–1248

Logothetis NK (2002) The neural basis of the blood-oxygen-level-dependent functional magnetic resonance imaging signal. Philos Trans R Soc Lond Ser B Biol Sci 357:1003–1037

Lopresti BJ, Klunk WE, Mathis CA et al (2005) Simplified quantification of Pittsburgh Compound B amyloid imaging PET studies: a comparative analysis. J Nucl Med 46:1959–1972

Magistretti PJ (2000) Cellular bases of functional brain imaging: insights from neuron-glia metabolic coupling. Brain Res 886:108–112

Magistretti PJ, Pellerin L, Rothman DL, Shulman RG (1999) Energy on demand. Science 283:496–497

Martinez-Torteya A, Rodriguez-Rojas J, Celaya-Padilla JM, Galván-Tejada JI, Treviño V, Tamez-Peña J (2014) Magnetization-prepared rapid acquisition with gradient echo magnetic resonance imaging signal and texture features for the prediction of mild cognitive impairment to Alzheimer's disease progression. J Med Imaging 1:031005

Martínez-Torteya A, Treviño V, Tamez-Peña JG (2015) Improved diagnostic multimodal biomarkers for Alzheimer's disease and mild cognitive impairment. Biomed Res Int 2015:961314

Maruszak A, Thuret S (2014) Why looking at the whole hippocampus is not enough-a critical role for anteroposterior axis, subfield and activation analyses to enhance predictive value of hippocampal changes for Alzheimer's disease diagnosis. Front Cell Neurosci 8:95

McKeith I, Taylor J-P, Thomas A, Donaghy P, Kane J (2016) Revisiting DLB diagnosis: a consideration of prodromal DLB and of the diagnostic overlap with Alzheimer disease. J Geriatr Psychiatry Neurol 29:249–253

McKeith IG, Boeve BF, Dickson DW et al (2017) Diagnosis and management of dementia with Lewy bodies. Neurology 89:88–100

McKhann GM, Knopman DS, Chertkow H et al (2011) The diagnosis of dementia due to Alzheimer's disease: recommendations from the National Institute on Aging-Alzheimer's Association workgroups on diagnostic guidelines for Alzheimer's disease. Alzheimers Dement 7:263–269

Meguro K, Blaizot X, Kondoh Y, Le Mestric C, Baron JC, Chavoix C (1999) Neocortical and hippocampal glucose hypometabolism following neurotoxic lesions of the entorhinal and perirhinal cortices in the non-human primate as shown by PET. Implications for Alzheimer's disease. Brain 122(Pt 8):1519–1531

Meles SK, Pagani M, Arnaldi D, De Carli F, Dessi B, Morbelli S, Sambuceti G, Jonsson C, Leenders KL, Nobili F (2017) The Alzheimer's disease metabolic brain pattern in mild cognitive impairment. J Cereb Blood Flow Metab 37:3643–3648

Metzler-Baddeley C, O'Sullivan MJ, Bells S, Pasternak O, Jones DK (2012) How and how not to correct for CSF-contamination in diffusion MRI. NeuroImage 59:1394–1403

Meyer P, Feldkamp H, Hoppstädter M, King AV, Frölich L, Wessa M, Flor H (2013) Using voxel-based morphometry to examine the relationship between regional brain volumes and memory performance in amnestic mild cognitive impairment. Front Behav Neurosci 7:89

Minoshima S, Frey KA, Koeppe RA, Foster NL, Kuhl DE (1995) A diagnostic approach in Alzheimer's disease using three-dimensional stereotactic surface projections of fluorine-18-FDG PET. J Nucl Med 36:1238–1248

Minoshima S, Giordani B, Berent S, Frey KA, Foster NL, Kuhl DE (1997) Metabolic reduction in the posterior cingulate cortex in very early Alzheimer's disease. Ann Neurol 42:85–94

Minoshima S, Drzezga AE, Barthel H et al (2016) SNMMI procedure standard/EANM practice guideline for amyloid PET imaging of the brain 1.0. J Nucl Med 57:1316–1322
Miotto EC, Savage CR, Evans JJ, Wilson BA, Martins MGM, Iaki S, Amaro E (2006) Bilateral activation of the prefrontal cortex after strategic semantic cognitive training. Hum Brain Mapp 27:288–295
Misra C, Fan Y, Davatzikos C (2009) Baseline and longitudinal patterns of brain atrophy in MCI patients, and their use in prediction of short-term conversion to AD: results from ADNI. NeuroImage 44:1415–1422
Molinuevo JL, Gómez-Anson B, Monte GC, Bosch B, Sánchez-Valle R, Rami L (2011) Neuropsychological profile of prodromal Alzheimer's disease (Prd-AD) and their radiological correlates. Arch Gerontol Geriatr 52:190–196
Morbelli S, Piccardo A, Villavecchia G, Dessi B, Brugnolo A, Piccini A, Caroli A, Frisoni G, Rodriguez G, Nobili F (2010) Mapping brain morphological and functional conversion patterns in amnestic MCI: a voxel-based MRI and FDG-PET study. Eur J Nucl Med Mol Imaging 37:36–45
Morbelli S, Drzezga A, Perneczky R et al (2012) Resting metabolic connectivity in prodromal Alzheimer's disease. A European Alzheimer Disease Consortium (EADC) project. Neurobiol Aging 33:2533–2550
Morbelli S, Chincarini A, Brendel M et al (2019) Metabolic patterns across core features in dementia with lewy bodies. Ann Neurol 85:715–725
Mormino EC, Kluth JT, Madison CM et al (2009) Episodic memory loss is related to hippocampal-mediated-amyloid deposition in elderly subjects. Brain 132:1310–1323
Morris JC, Price JL (2001) Pathologic correlates of nondemented aging, mild cognitive impairment, and early-stage Alzheimer's disease. J Mol Neurosci 17:101–118
Morris JC, Storandt M, Miller JP, McKeel DW, Price JL, Rubin EH, Berg L (2001) Mild cognitive impairment represents early-stage Alzheimer disease. Arch Neurol 58:397–405
Mosconi L (2005) Brain glucose metabolism in the early and specific diagnosis of Alzheimer's disease. Eur J Nucl Med Mol Imaging 32:486–510
Mosconi L, Tsui WH, Herholz K et al (2008) Multicenter standardized 18F-FDG PET diagnosis of mild cognitive impairment, Alzheimer's disease, and other dementias. J Nucl Med 49:390–398
Moseley ME, Cohen Y, Kucharczyk J, Mintorovitch J, Asgari HS, Wendland MF, Tsuruda J, Norman D (1990) Diffusion-weighted MR imaging of anisotropic water diffusion in cat central nervous system. Radiology 176:439–445
Musiek ES, Holtzman DM (2015) Three dimensions of the amyloid hypothesis: time, space and "wingmen". Nat Neurosci 18:800–806
Musiek ES, Chen Y, Korczykowski M et al (2012) Direct comparison of fluorodeoxyglucose positron emission tomography and arterial spin labeling magnetic resonance imaging in Alzheimer's disease. Alzheimers Dement 8:51–59
Nelson PT, Dickson DW, Trojanowski JQ et al (2019) Limbic-predominant age-related TDP-43 encephalopathy (LATE): consensus working group report. Brain 142:1503–1527
Nesteruk M, Nesteruk T, Styczyńska M, Barczak A, Mandecka M, Walecki J, Barcikowska-Kotowicz M (2015) Predicting the conversion of mild cognitive impairment to Alzheimer's disease based on the volumetric measurements of the selected brain structures in magnetic resonance imaging. Neurol Neurochir Pol 49:349–353
Ni R, Gillberg P-G, Bergfors A, Marutle A, Nordberg A (2013) Amyloid tracers detect multiple binding sites in Alzheimer's disease brain tissue. Brain 136:2217–2227
Niemantsverdriet E, Ottoy J, Somers C et al (2017) The cerebrospinal fluid Aβ1–42/Aβ1–40 ratio improves concordance with amyloid-PET for diagnosing Alzheimer's disease in a clinical setting. J Alzheimers Dis 60:561–576
Nobili F, Salmaso D, Morbelli S, Girtler N, Piccardo A, Brugnolo A, Dessi B, Larsson SA, Rodriguez G, Pagani M (2008a) Principal component analysis of FDG PET in amnestic MCI. Eur J Nucl Med Mol Imaging 35:2191–2202
Nobili F, Frisoni GB, Portet F et al (2008b) Brain SPECT in subtypes of mild cognitive impairment. J Neurol 255:1344–1353

Nobili F, De Carli F, Frisoni GB et al (2009a) SPECT predictors of cognitive decline and Alzheimer's disease in mild cognitive impairment. J Alzheimers Dis 17:761–772
Nobili F, Abbruzzese G, Morbelli S et al (2009b) Amnestic mild cognitive impairment in Parkinson's disease: a brain perfusion SPECT study. Mov Disord 24:414–421
Nobili F, Mazzei D, Dessi B, Morbelli S, Brugnolo A, Barbieri P, Girtler N, Sambuceti G, Rodriguez G, Pagani M (2010) Unawareness of memory deficit in amnestic MCI: FDG-PET findings. J Alzheimers Dis 22:993–1003
Nobili F, Morbelli S, Arnaldi D, Ferrara M, Campus C, Brugnolo A, Mazzei D, Mehrdad N, Sambuceti G, Rodriguez G (2011) Radionuclide brain imaging correlates of cognitive impairment in Parkinson's disease (PD). J Neurol Sci 310:31–35
Nobili F, Arbizu J, Bouwman F, Drzezga A, Agosta F, Nestor P, Walker Z, Boccardi M, EANM-EAN Task Force for the Prescription of FDG-PET for Dementing Neurodegenerative Disorders (2018) European Association of Nuclear Medicine and European Academy of Neurology recommendations for the use of brain ^{18}F-fluorodeoxyglucose positron emission tomography in neurodegenerative cognitive impairment and dementia: Delphi consensus. Eur J Neurol 25:1201–1217
Nyberg L, Sandblom J, Jones S, Neely AS, Petersson KM, Ingvar M, Backman L (2003) Neural correlates of training-related memory improvement in adulthood and aging. Proc Natl Acad Sci 100:13728–13733
O'Donnell LJ, Pasternak O (2015) Does diffusion MRI tell us anything about the white matter? An overview of methods and pitfalls. Schizophr Res 161:133–141
O'Dwyer L, Lamberton F, Bokde ALW et al (2011) Using diffusion tensor imaging and mixed-effects models to investigate primary and secondary white matter degeneration in Alzheimer's disease and mild cognitive impairment. J Alzheimers Dis 26:667–682
Obrig H, Neufang M, Wenzel R, Kohl M, Steinbrink J, Einhäupl K, Villringer A (2000) Spontaneous low frequency oscillations of cerebral hemodynamics and metabolism in human adults. NeuroImage 12:623–639
Oda K, Okubo Y, Ishida R et al (2003) Regional cerebral blood flow in depressed patients with white matter magnetic resonance hyperintensity. Biol Psychiatry 53:150–156
Ohnishi T, Hoshi H, Nagamachi S, Jinnouchi S, Flores LG 2nd, Futami S, Watanabe K (1995) High-resolution SPECT to assess hippocampal perfusion in neuropsychiatric diseases. J Nucl Med 36:1163–1169
Okamura N, Harada R, Furukawa K, Furumoto S, Tago T, Yanai K, Arai H, Kudo Y (2016) Advances in the development of tau PET radiotracers and their clinical applications. Ageing Res Rev 30:107–113
Okamura N, Harada R, Ishiki A, Kikuchi A, Nakamura T, Kudo Y (2018) The development and validation of tau PET tracers: current status and future directions. Clin Transl Imaging 6:305–316
Oosterman JM, Oosterveld S, Rikkert MGO, Claassen JA, Kessels RPC (2012) Medial temporal lobe atrophy relates to executive dysfunction in Alzheimer's disease. Int Psychogeriatr 24:1474–1482
Ossenkoppele R, Cohn-Sheehy BI, La Joie R et al (2015) Atrophy patterns in early clinical stages across distinct phenotypes of Alzheimer's disease. Hum Brain Mapp 36:4421–4437
Ossenkoppele R, Schonhaut DR, Schöll M et al (2016) Tau PET patterns mirror clinical and neuroanatomical variability in Alzheimer's disease. Brain 139:1551–1567
Ottoy J, Niemantsverdriet E, Verhaeghe J et al (2019) Association of short-term cognitive decline and MCI-to-AD dementia conversion with CSF, MRI, amyloid- and 18F-FDG-PET imaging. NeuroImage Clin 22:101771
Ouyang X, Chen K, Yao L, Hu B, Wu X, Ye Q, Guo X, Alzheimer's Disease Neuroimaging Initiative (2015) Simultaneous changes in gray matter volume and white matter fractional anisotropy in Alzheimer's disease revealed by multimodal CCA and joint ICA. Neuroscience 301:553–562
Pagani M, Dessi B, Morbelli S et al (2010) MCI patients declining and not-declining at mid-term follow-up: FDG-PET findings. Curr Alzheimer Res 7:287–294

Pagani M, De Carli F, Morbelli S et al (2015) Volume of interest-based [18F]fluorodeoxyglucose PET discriminates MCI converting to Alzheimer's disease from healthy controls. A European Alzheimer's Disease Consortium (EADC) study. NeuroImage Clin 7:34–42

Pagani M, Nobili F, Morbelli S et al (2017a) Early identification of MCI converting to AD: a FDG PET study. Eur J Nucl Med Mol Imaging 44:2042–2052

Pagani M, Giuliani A, Öberg J et al (2017b) Progressive disintegration of brain networking from normal aging to Alzheimer disease: analysis of independent components of 18F-FDG PET data. J Nucl Med 58:1132–1139

Palmqvist S, Mattsson N, Hansson O, Alzheimer's Disease Neuroimaging Initiative (2016) Cerebrospinal fluid analysis detects cerebral amyloid-β accumulation earlier than positron emission tomography. Brain 139:1226–1236

Pan P, Zhu L, Yu T et al (2017) Aberrant spontaneous low-frequency brain activity in amnestic mild cognitive impairment: a meta-analysis of resting-state fMRI studies. Ageing Res Rev 35:12–21

Parker TD, Slattery CF, Zhang J et al (2018) Cortical microstructure in young onset Alzheimer's disease using neurite orientation dispersion and density imaging. Hum Brain Mapp 39:3005–3017

Pennanen C, Kivipelto M, Tuomainen S et al (2004) Hippocampus and entorhinal cortex in mild cognitive impairment and early AD. Neurobiol Aging 25:303–310

Perani D, Della Rosa PA, Cerami C et al (2014) Validation of an optimized SPM procedure for FDG-PET in dementia diagnosis in a clinical setting. NeuroImage Clin 6:445–454

Perrotin A, de Flores R, Lamberton F et al (2015) Hippocampal subfield volumetry and 3D surface mapping in subjective cognitive decline. J Alzheimers Dis 48:S141–S150

Peter J, Lahr J, Minkova L et al (2016) Contribution of the cholinergic system to verbal memory performance in mild cognitive impairment. J Alzheimers Dis 53:991–1001

Petersen RC, Negash S (2008) Mild cognitive impairment: an overview. CNS Spectr 13:45–53

Petersen RC, Smith GE, Waring SC, Ivnik RJ, Tangalos EG, Kokmen E (1999) Mild cognitive impairment: clinical characterization and outcome. Arch Neurol 56:303–308

Picco A, Polidori MC, Ferrara M et al (2014) Plasma antioxidants and brain glucose metabolism in elderly subjects with cognitive complaints. Eur J Nucl Med Mol Imaging 41:764–775

Pike KE, Savage G, Villemagne VL, Ng S, Moss SA, Maruff P, Mathis CA, Klunk WE, Masters CL, Rowe CC (2007) Beta-amyloid imaging and memory in non-demented individuals: evidence for preclinical Alzheimer's disease. Brain 130:2837–2844

Plant C, Teipel SJ, Oswald A, Böhm C, Meindl T, Mourao-Miranda J, Bokde AW, Hampel H, Ewers M (2010) Automated detection of brain atrophy patterns based on MRI for the prediction of Alzheimer's disease. NeuroImage 50:162–174

Poettrich K, Weiss PH, Werner A, Lux S, Donix M, Gerber J, von Kummer R, Fink GR, Holthoff VA (2009) Altered neural network supporting declarative long-term memory in mild cognitive impairment. Neurobiol Aging 30:284–298

Pontecorvo MJ, Mintun MA (2011) PET amyloid imaging as a tool for early diagnosis and identifying patients at risk for progression to Alzheimer's disease. Alzheimers Res Ther 3:11

Pontecorvo MJ, Siderowf A, Dubois B et al (2017) Effectiveness of florbetapir PET imaging in changing patient management. Dement Geriatr Cogn Disord 44:129–143

Postuma RB, Iranzo A, Hu M et al (2019) Risk and predictors of dementia and parkinsonism in idiopathic REM sleep behaviour disorder: a multicentre study. Brain 142:744–759

Prescott JW, Guidon A, Doraiswamy PM, Roy Choudhury K, Liu C, Petrella JR, Alzheimer's Disease Neuroimaging Initiative F the ADN (2014) The Alzheimer structural connectome: changes in cortical network topology with increased amyloid plaque burden. Radiology 273:175–184

Price CJ, Friston KJ (1999) Scanning patients with tasks they can perform. Hum Brain Mapp 8:102–108

Pupi A, Nobili FM (2005) PET is better than perfusion SPECT for early diagnosis of Alzheimer's disease. Eur J Nucl Med Mol Imaging 32:1466–1472

Querbes O, Aubry F, Pariente J, Lotterie J-A, Démonet J-F, Duret V, Puel M, Berry I, Fort J-C, Celsis P (2009) Early diagnosis of Alzheimer's disease using cortical thickness: impact of cognitive reserve. Brain 132:2036–2047

Quigley H, Colloby SJ, O'Brien JT (2011) PET imaging of brain amyloid in dementia: a review. Int J Geriatr Psychiatry 26:991–999

Rabinovici GD, Jagust WJ, Furst AJ et al (2008) Aβ amyloid and glucose metabolism in three variants of primary progressive aphasia. Ann Neurol 64:388–401

Raczka KA, Becker G, Seese A, Frisch S, Heiner S, Marschhauser A, Barthel H, Scheid R, Sabri O, Schroeter ML (2010) Executive and behavioral deficits share common neural substrates in frontotemporal lobar degeneration — a pilot FDG-PET study. Psychiatry Res Neuroimaging 182:274–280

Reed BR, Eberling JL, Mungas D, Weiner M, Kramer JH, Jagust WJ (2004) Effects of white matter lesions and lacunes on cortical function. Arch Neurol 61:1545

Riederer I, Bohn KP, Preibisch C, Wiedemann E, Zimmer C, Alexopoulos P, Förster S (2018) Alzheimer disease and mild cognitive impairment: integrated pulsed arterial spin-labeling MRI and ^{18}F-FDG PET. Radiology 288:198–206

Rodriguez G, Arvigo F, Marenco S, Nobili F, Romano P, Sandini G, Rosadini G (1987) Original contributions regional cerebral blood flow in essential hypertension: data evaluation by a mapping system. Stroke 18:13–20

Rodriguez G, Vitali P, Calvini P, Bordoni C, Girtler N, Taddei G, Mariani G, Nobili F (2000) Hippocampal perfusion in mild Alzheimer's disease. Psychiatry Res 100:65–74

Rowe CC, Ng S, Ackermann U et al (2007) Imaging-amyloid burden in aging and dementia. Neurology 68:1718–1725

Salmon E, Kerrouche N, Perani D, Lekeu F, Holthoff V, Beuthien-Baumann B, Sorbi S, Lemaire C, Collette F, Herholz K (2009) On the multivariate nature of brain metabolic impairment in Alzheimer's disease. Neurobiol Aging 30:186–197

Sanabria-Castro A, Alvarado-Echeverría I, Monge-Bonilla C (2017) Molecular pathogenesis of Alzheimer's disease: an update. Ann Neurosci 24:46–54

Sarazin M, Chauviré V, Gerardin E et al (2010) The amnestic syndrome of hippocampal type in Alzheimer's disease: an MRI study. J Alzheimers Dis 22:285–294

Scarapicchia V, Mazerolle EL, Fisk JD, Ritchie LJ, Gawryluk JR (2018) Resting state BOLD variability in Alzheimer's disease: a marker of cognitive decline or cerebrovascular status? Front Aging Neurosci 10:39

Schmitz TW, Nathan Spreng R, Alzheimer's Disease Neuroimaging Initiative (2016) Basal forebrain degeneration precedes and predicts the cortical spread of Alzheimer's pathology. Nat Commun 7:13249

Schroeter ML, Stein T, Maslowski N, Neumann J (2009) Neural correlates of Alzheimer's disease and mild cognitive impairment: a systematic and quantitative meta-analysis involving 1351 patients. NeuroImage 47:1196–1206

Schwindt GC, Black SE (2009) Functional imaging studies of episodic memory in Alzheimer's disease: a quantitative meta-analysis. NeuroImage 45:181–190

Seo SW, Cho SS, Park A, Chin J, Na DL (2009) Subcortical vascular versus amnestic mild cognitive impairment: comparison of cerebral glucose metabolism. J Neuroimaging 19:213–219

Sexton CE, Mackay CE, Lonie JA, Bastin ME, Terrière E, O'Carroll RE, Ebmeier KP (2010) MRI correlates of episodic memory in Alzheimer's disease, mild cognitive impairment, and healthy aging. Psychiatry Res Neuroimaging 184:57–62

Sexton CE, Kalu UG, Filippini N, Mackay CE, Ebmeier KP (2011) A meta-analysis of diffusion tensor imaging in mild cognitive impairment and Alzheimer's disease. Neurobiol Aging 32:2322.e5–2322.e18

Shaffer JL, Petrella JR, Sheldon FC, Choudhury KR, Calhoun VD, Coleman RE, Doraiswamy PM, Alzheimer's Disease Neuroimaging Initiative (2013) Predicting cognitive decline in subjects at risk for Alzheimer disease by using combined cerebrospinal fluid, MR imaging, and PET biomarkers. Radiology 266:583–591

Simões R, Slump C, van Walsum AMC (2012) Using local texture maps of brain MR images to detect mild cognitive impairment. In: Proceedings of the 21st International Conference on Pattern Recognition (ICPR2012); 2012 Nov 11–15, Tsukuba, Japan. IEEE, New York, NY, pp 153–156

Song S-K, Sun S-W, Ju W-K, Lin S-J, Cross AH, Neufeld AH (2003) Diffusion tensor imaging detects and differentiates axon and myelin degeneration in mouse optic nerve after retinal ischemia. NeuroImage 20:1714–1722

Sørensen L, Igel C, Liv Hansen N, Osler M, Lauritzen M, Rostrup E, Nielsen M, Alzheimer's Disease Neuroimaging Initiative and the Australian Imaging Biomarkers and Lifestyle Flagship Study of Ageing (2016) Early detection of Alzheimer's disease using MRI hippocampal texture. Hum Brain Mapp 37:1148–1161

Stoub TR, deToledo-Morrell L, Stebbins GT, Leurgans S, Bennett DA, Shah RC (2006) Hippocampal disconnection contributes to memory dysfunction in individuals at risk for Alzheimer's disease. Proc Natl Acad Sci 103:10041–10045

Struyfs H, Van Hecke W, Veraart J et al (2015) Diffusion kurtosis imaging: a possible MRI biomarker for AD diagnosis? J Alzheimers Dis 48:937–948

Sydykova D, Stahl R, Dietrich O, Ewers M, Reiser MF, Schoenberg SO, Moller H-J, Hampel H, Teipel SJ (2007) Fiber connections between the cerebral cortex and the corpus callosum in Alzheimer's disease: a diffusion tensor imaging and voxel-based morphometry study. Cereb Cortex 17:2276–2282

Tabatabaei-Jafari H, Walsh E, Shaw ME, Cherbuin N, Alzheimer's Disease Neuroimaging Initiative (ADNI) (2017) The cerebellum shrinks faster than normal ageing in Alzheimer's disease but not in mild cognitive impairment. Hum Brain Mapp 38:3141–3150

Takahashi H, Ishii K, Hosokawa C, Hyodo T, Kashiwagi N, Matsuki M, Ashikaga R, Murakami T (2014) Clinical application of 3D arterial spin-labeled brain perfusion imaging for Alzheimer disease: comparison with brain perfusion SPECT. AJNR Am J Neuroradiol 35:906–911

Tam CWC, Burton EJ, McKeith IG, Burn DJ, O'Brien JT (2005) Temporal lobe atrophy on MRI in Parkinson disease with dementia. Neurology 64:861–865

Tapiola T, Pennanen C, Tapiola M et al (2008) MRI of hippocampus and entorhinal cortex in mild cognitive impairment: a follow-up study. Neurobiol Aging 29:31–38

Theysohn JM, Kraff O, Maderwald S, Schlamann MU, de Greiff A, Forsting M, Ladd SC, Ladd ME, Gizewski ER (2009) The human hippocampus at 7 T-in vivo MRI. Hippocampus 19:1–7

Thomann PA, Dos Santos V, Toro P, Schönknecht P, Essig M, Schröder J (2009) Reduced olfactory bulb and tract volume in early Alzheimer's disease—a MRI study. Neurobiol Aging 30:838–841

Thurfjell L, Lilja J, Lundqvist R, Buckley C, Smith A, Vandenberghe R, Sherwin P (2014) Automated quantification of 18F-flutemetamol PET activity for categorizing scans as negative or positive for brain amyloid: concordance with visual image reads. J Nucl Med 55:1623–1628

Vasavada MM, Martinez B, Wang J, Eslinger PJ, Gill DJ, Sun X, Karunanayaka P, Yang QX (2017) Central olfactory dysfunction in Alzheimer's disease and mild cognitive impairment: a functional MRI study. J Alzheimers Dis 59:359–368

Vemuri P, Wiste HJ, Weigand SD, Shaw LM, Trojanowski JQ, Weiner MW, Knopman DS, Petersen RC, Jack CR, Alzheimer's Disease Neuroimaging Initiative (2009) MRI and CSF biomarkers in normal, MCI, and AD subjects: predicting future clinical change. Neurology 73:294–301

Verfaillie SCJ, Adriaanse SM, Binnewijzend MAA et al (2015) Cerebral perfusion and glucose metabolism in Alzheimer's disease and frontotemporal dementia: two sides of the same coin? Eur Radiol 25:3050–3059

Vieira RT, Caixeta L, Machado S, Silva AC, Nardi AE, Arias-Carrión O, Carta MG (2013) Epidemiology of early-onset dementia: a review of the literature. Clin Pract Epidemiol Ment Health 9:88–95

Villemagne VL, Okamura N (2014) In vivo tau imaging: obstacles and progress. Alzheimers Dement 10:S254–S264

Villemagne VL, Klunk WE, Mathis CA et al (2012) Aβ imaging: feasible, pertinent, and vital to progress in Alzheimer's disease. Eur J Nucl Med Mol Imaging 39:209–219

Visser PJ, Scheltens P, Verhey FR, Schmand B, Launer LJ, Jolles J, Jonker C (1999) Medial temporal lobe atrophy and memory dysfunction as predictors for dementia in subjects with mild cognitive impairment. J Neurol 246:477–485

Wagner AD, Schacter DL, Rotte M, Koutstaal W, Maril A, Dale AM, Rosen BR, Buckner RL (1998) Building memories: remembering and forgetting of verbal experiences as predicted by brain activity. Science 281:1188–1191

Walhovd KB, Fjell AM, Brewer J, McEvoy LK, Fennema-Notestine C, Hagler DJ, Jennings RG, Karow D, Dale AM, Alzheimer's Disease Neuroimaging Initiative (2010) Combining MR imaging, positron-emission tomography, and CSF biomarkers in the diagnosis and prognosis of Alzheimer disease. Am J Neuroradiol 31:347–354

Wang H, Su M-Y (2006) Regional pattern of increased water diffusivity in hippocampus and corpus callosum in mild cognitive impairment. Dement Geriatr Cogn Disord 22:223–229

Westlye ET, Hodneland E, Haász J, Espeseth T, Lundervold A, Lundervold AJ (2012) Episodic memory of APOE ε4 carriers is correlated with fractional anisotropy, but not cortical thickness, in the medial temporal lobe. NeuroImage 63:507–516

Weston PSJ, Paterson RW, Dickson J et al (2016) Diagnosing dementia in the clinical setting: can amyloid PET provide additional value over cerebrospinal fluid? J Alzheimers Dis 54:1297–1302

Whitwell JL, Dickson DW, Murray ME et al (2012) Neuroimaging correlates of pathologically defined subtypes of Alzheimer's disease: a case-control study. Lancet Neurol 11:868–877

Wierenga CE, Dev SI, Shin DD, Clark LR, Bangen KJ, Jak AJ, Rissman RA, Liu TT, Salmon DP, Bondi MW (2012) Effect of mild cognitive impairment and APOE genotype on resting cerebral blood flow and its association with cognition. J Cereb Blood Flow Metab 32:1589–1599

Wise RG, Ide K, Poulin MJ, Tracey I (2004) Resting fluctuations in arterial carbon dioxide induce significant low frequency variations in BOLD signal. NeuroImage 21:1652–1664

Wolk DA, Price JC, Saxton JA et al (2009) Amyloid imaging in mild cognitive impairment subtypes. Ann Neurol 65:557–568

Wolk DA, Dickerson BC, Alzheimer's Disease Neuroimaging Initiative (2011) Fractionating verbal episodic memory in Alzheimer's disease. NeuroImage 54:1530–1539

Wolz R, Julkunen V, Koikkalainen J, Niskanen E, Zhang DP, Rueckert D, Soininen H, Lötjönen J, Initiative the ADN (2011) Multi-method analysis of MRI images in early diagnostics of Alzheimer's disease. PLoS One 6:e25446

Xu L, Groth KM, Pearlson G, Schretlen DJ, Calhoun VD (2009) Source-based morphometry: the use of independent component analysis to identify gray matter differences with application to schizophrenia. Hum Brain Mapp 30:711–724

Yakushev I, Müller MJ, Lorscheider M, Schermuly I, Weibrich C, Dellani PR, Hammers A, Stoeter P, Fellgiebel A (2010) Increased hippocampal head diffusivity predicts impaired episodic memory performance in early Alzheimer's disease. Neuropsychologia 48:1447–1453

Yuan Y, Gu Z-X, Wei W-S (2009) Fluorodeoxyglucose–positron-emission tomography, single-photon emission tomography, and structural MR imaging for prediction of rapid conversion to Alzheimer disease in patients with mild cognitive impairment: a meta-analysis. Am J Neuroradiol 30:404–410

Zang Y, Jiang T, Lu Y, He Y, Tian L (2004) Regional homogeneity approach to fMRI data analysis. NeuroImage 22:394–400

Zarow C, Vinters HV, Ellis WG, Weiner MW, Mungas D, White L, Chui HC (2005) Correlates of hippocampal neuron number in Alzheimer's disease and ischemic vascular dementia. Ann Neurol 57:896–903

Zhang Y, Schuff N, Jahng G-H et al (2007) Diffusion tensor imaging of cingulum fibers in mild cognitive impairment and Alzheimer disease. Neurology 68:13–19

Zhang D, Wang Y, Zhou L, Yuan H, Shen D, Alzheimer's Disease Neuroimaging Initiative (2011) Multimodal classification of Alzheimer's disease and mild cognitive impairment. NeuroImage 55:856–867

Zhang J, Yu C, Jiang G, Liu W, Tong L (2012a) 3D texture analysis on MRI images of Alzheimer's disease. Brain Imaging Behav 6:61–69

Zhang Z, Liu Y, Jiang T, Zhou B, An N, Dai H, Wang P, Niu Y, Wang L, Zhang X (2012b) Altered spontaneous activity in Alzheimer's disease and mild cognitive impairment revealed by regional homogeneity. NeuroImage 59:1429–1440

Zhang H, Schneider T, Wheeler-Kingshott CA, Alexander DC (2012c) NODDI: practical in vivo neurite orientation dispersion and density imaging of the human brain. NeuroImage 61:1000–1016

Zhang Y-W, Zhao Z-L, Qi Z et al (2017) Local-to-remote cortical connectivity in amnestic mild cognitive impairment. Neurobiol Aging 56:138–149

Zhuang L, Wen W, Zhu W, Trollor J, Kochan N, Crawford J, Reppermund S, Brodaty H, Sachdev P (2010) White matter integrity in mild cognitive impairment: a tract-based spatial statistics study. NeuroImage 53:16–25

Zhuang L, Wen W, Trollor JN, Kochan NA, Reppermund S, Brodaty H, Sachdev P (2012) Abnormalities of the fornix in mild cognitive impairment are related to episodic memory loss. J Alzheimers Dis 29:629–639

Impact of the New Conceptual Framework of Alzheimer's Disease in Imaging Studies

13

Bruno Dubois, Nicolas Villain, Claudia Jacova, and Olga Uspenskaya

Contents

13.1 Alzheimer's Disease, History, and Evolution of Concepts . . . 428
13.2 The 1984 NINCDS-ADRDA Criteria for AD . . . 429
13.2.1 The MCI Construct . . . 430
13.2.2 Limitations of the 1984 NINCDS-ADRDA Criteria . . . 430
13.3 The IWG Conceptual Framework for AD . . . 432
13.3.1 The 2007 IWG Criteria . . . 432
13.3.2 Further Refinements of the 2007 IWG Criteria for AD . . . 433
13.3.3 The 2011 NIA-AA Criteria . . . 434
13.3.4 The 2015 Consensus on the Preclinical Stage of AD . . . 435
13.3.5 A/T/N/ Classification . . . 436
13.4 Perspectives . . . 438
13.4.1 General Considerations About a Biological Diagnosis of AD . . . 438
13.4.2 Diagnosing AD: Biomarkers Alone May Not Be Sufficient . . . 438
13.4.3 Preclinical AD and Normal Aging . . . 440
13.4.4 Asymptomatic Subjects and Risk Profiling . . . 441
13.4.5 Refining the IWG Framework . . . 441
13.4.6 The Proposal P+A+ T+ (at Least for Clinical Practice) . . . 442

B. Dubois (✉) · N. Villain
GRC no 21, Alzheimer Precision Medicine, Sorbonne Université, Paris, France

Alzheimer Research Centre (IM2A), Hôpital Pitié-Salpêtrière, AP-HP Sorbonne Université, Paris, France

Institut du Cerveau et de la Moelle Epinière – ICM, INSERM U1127, CNRS 7225, Sorbonne Université, Paris, France
e-mail: bruno.dubois@aphp.fr; nicolas.villain@aphp.fr

C. Jacova
Pacific University School of Graduate Psychology, Forest Grove, OR, USA
e-mail: cjacova@mail.ubc.ca

O. Uspenskaya
Prevail Therapeutics, New York, NY, USA
e-mail: olga.uspenskaya@prevailtherapeutics.com

R. A. J. O. Dierckx et al. (eds.), *PET and SPECT in Neurology*,
https://doi.org/10.1007/978-3-030-53168-3_13

13.5 Conclusion 444
Glossary 445
References 445

Abstract

For both research and clinical settings, the importance of an accurate diagnosis of AD is imperative given its much-feared consequences, which cannot be understated. The diagnosis of AD should be restricted to the presence of both: (1) a clinical phenotype, either typical (characterized by an amnestic syndrome of the hippocampal type) or atypical (including the posterior variant, the logopenic variant and the frontal variant, to which it may be possible to add the corticobasal syndrome), and (2) in vivo evidence of positive pathophysiological markers, acquired with molecular neuroimaging or with cerebrospinal fluid investigation. In the preclinical state of the disease, evidence reported in the last few years suggests that the presence of tau and amyloid positivity is not sufficient to definitively predict the invariable occurrence of symptoms. Therefore, measures of pathophysiological markers are not recommended in cognitively unimpaired individuals, in the absence of therapies or prevention programs showing efficacy on delaying onset of disease (although this may happen outside the clinical setting for specific reasons, for clinical trials, research projects or cohort studies).

In this chapter we propose an overview on the evolution of Alzheimer's disease definition and of its diagnostic approach in the medical and scientific community since 1907. Finally, we expose the latest data regarding this disease in order to propose a new framework for the diagnosis of Alzheimer's disease in a clinical setting.

13.1 Alzheimer's Disease, History, and Evolution of Concepts

Alois Alzheimer first described the disease that shares his name in it at the beginning of the twentieth century (Alzheimer 1907; Stelzmann et al. 1995). However, it was not until the last quarter of the twentieth century that Alzheimer's disease (AD) was recognized as the major cause of dementia in the general population by the medical and scientific community.

Since the beginning, AD was defined as a dementia. In an oral communication in 1906, published in 1907, Alzheimer reported the case of Auguste Deter, a 51-year-old woman. We have here the complete picture of AD as is currently defined: a progressive cognitive decline, primarily involving memory and leading to dementia, associated with neurofibrillary tangles (revealed later to be the result of hyperphosphorylated tau protein deposits) and a "special substance" that was found later to be an accumulation of amyloid β-proteins. Alzheimer thought this condition was "eine

eigenartige Erkrankung der Hirnrinde," i.e., an unusual illness of the cerebral cortex (Alzheimer 1907). Three years later, Kraepelin proposed to name after Alzheimer presenile dementia cases he identified as distinct from senile dementia, and this distinction remained predominant within the scientific and medical circles for much of the twentieth century (Kraepelin 1910). As a result of demographic, political, and scientific developments, senile dementia became increasingly recognized within the aging population, beyond what could be explained by the arteriosclerotic lesions or other known phenomena of old age. In April 1976, Robert Katzman sounded the call that awakened the world to the burden of Alzheimer's disease, with an editorial in the *Archives of Neurology* (Katzman 1976), in which he included the neurodegenerative condition among the world's greatest killers and Alzheimer's disease as the leading cause of dementia. A growing consensus around this call helped bring Alzheimer research into the modern era by "officially" acknowledging AD as a condition affecting patients in old age. Seven years later, the publication of the National Institute of Neurological and Communicative Disorders and Stroke-Alzheimer's Disease and Related Disorders Association (NINCDS-ADRDA) criteria confirmed AD as a disease, independent of age of presentation, and therefore as a cause of senile dementia (McKhann et al. 1984).

13.2 The 1984 NINCDS-ADRDA Criteria for AD

The publication of the NINCDS-ADRDA criteria in 1984 defined Alzheimer as a **dementia** (McKhann et al. 1984). Three major tenets of these criteria were that (1) the clinical diagnosis of AD could not be definitively made until there was a requisite postmortem confirmation; (2) consequently, the clinical diagnosis of AD could only be "probable"; and (3) the diagnosis could only be applied when the disease was advanced to the functional disability threshold of dementia. Based on the NINCDS-ADRDA criteria, the diagnosis of probable AD requires that a dementia syndrome is established by clinical examination, documented by mental status questionnaire, and confirmed by neuropsychological testing with evidence of deficit in two or more areas of cognition, including memory with a progressive worsening over time responsible for a significant impact on activities of daily living. Therefore, the clinical diagnosis of AD is made using a two-step procedure: (1) an initial identification of a dementia syndrome and then (2) the exclusion of other possible etiologies of dementia with blood/CSF investigations for ruling out infectious, inflammatory, or metabolic diseases and with brain neuroimaging (CT scan or MRI) for excluding small vessel diseases, strategic lacunar infarcts, large vessel infarcts, and/or cerebral hemorrhages, brain tumors, hydrocephalus, and similar disorders. These examinations were not indicated for identifying specific features of AD but only for excluding other diseases: AD was a default diagnostic.

With time, it became obvious that the established classification of AD as purely a dementia had important drawbacks, especially in dealing with the early and prodromal stages of the disease.

13.2.1 The MCI Construct

The early changes in cognition that precede the onset of dementia were not identified at that time. They were included in a vague age-related concept described by a wide range of nosological terms including age-associated memory impairment, age-related cognitive decline, age-associated cognitive decline, mild cognitive disorder, mild neurocognitive disorder, cognitively impaired not demented, and mild cognitive impairment (MCI) (Chételat and Baron 2003; Matthews et al. 2007; Reisberg et al. 2008; Petersen et al. 1999, 2001). This latter designation of MCI has been the most widely used diagnostic label referring to individuals who have objective memory and/or cognitive impairment and whose activities of daily living are considered to be generally normal. Progression to clinically diagnosable dementia occurs at a higher rate from MCI than from normal, but is clearly not the invariable clinical outcome at follow-up (Mitchell and Shiri-Feshki 2009; Petersen and Negash 2008; Palmer et al. 2008).

One of the proposed advantages of MCI has been its potential utility for clinical trials directed at delaying the time to onset of AD. The intention in these trials on MCI was to include a large number of patients at a predementia stage of AD. Unfortunately, the concept of MCI has a major limitation: collecting under a single label a variety of pathological entities (Dubois and Albert 2004). When the MCI inclusion criteria of these trials were applied to an observational cohort of memory clinic patients, they had diagnostic sensitivities of 46–88% and specificities of 37–90% in identifying future AD (Beach et al. 2012). Given these numbers, these trials have clearly treated a significant number of patients who do not have AD or are not going to progress to AD for a long time. This has diluted the potential for a significant treatment effect and may have contributed to the negative outcomes where none of the tested medications were successful at delaying the time to diagnosis of AD (Jelic et al. 2006). To decrease the clinical and pathological heterogeneity, sub-typing of amnestic and non-amnestic MCI has been proposed. However, only 70% of amnestic MCI cases that have progressed to dementia actually met neuropathological criteria for AD (Jicha et al. 2006).

13.2.2 Limitations of the 1984 NINCDS-ADRDA Criteria

In the early 2000s, two major considerations emphasized the need to revise the conceptual framework of AD:

1. The NINCDS-ADRDA criteria for AD have a low specificity against other dementias

   This is mainly due to the fact that, at the time of these criteria, i.e., 1984, the clinical phenotype of AD was not specified and no reference to biomarkers of AD was proposed. This explains why AD was frequently misdiagnosed with other neurodegenerative diseases that can fulfill the NINCDS-ADRDA criteria

(Varma et al. 1999). Since 1984, great progress had been made in several domains:

(a) The clinical phenotype of AD has been elucidated: in more than 85% of the cases, AD presents as a progressive amnestic disorder (Dubois and Albert 2004; Qiu et al. 2019). Postmortem studies of AD patients have shown a rather specific pattern of cortical neuronal lesions, which appear to begin within the medial temporal lobe structures (entorhinal cortex, hippocampal formations, parahippocampal gyrus) (Braak and Braak 1991; Delacourte et al. 1999), areas known to be critical for long-term episodic memory.

(b) Diagnostic accuracy of Alzheimer's disease (AD) has also been improved in the last years because of the characterization of new dementias through specific criteria, including the primary progressive aphasias, semantic dementia, cortico-basal degeneration, posterior cortical atrophy, and Lewy body dementia. The individualization of these diseases, which were previously confused with AD, has consequently decreased its apparent heterogeneity.

(c) Reliable biomarkers for AD have been isolated. Over the past three decades since the NINCDS-ADRDA criteria were published, great progress has been made in identifying the AD-associated structural and molecular changes in the brain and their biochemical footprints. MRI enables detailed visualization of medial temporal lobe structures implicated in the core diagnostic feature of AD (Scheltens et al. 1992; Seab et al. 1988). PET using fluorodeoxyglucose (FDG) has been approved in the USA for diagnostic purposes and has been shown to be sensitive and specific in detecting AD in early stages (Ferris et al. 1980; Chase et al. 1984; Choo et al. 2007). CSF biomarkers aimed at detecting the key molecular pathological features of AD in vivo (low Aβ and high total tau/phospho-tau levels) have become available and can be assessed reliably (Engelborghs et al. 2008). Their diagnostic predictability has been extended to prodromal stage (Hansson et al. 2006). In 2004, in vivo imaging of pathology-specific proteins (Pittsburgh compound B [PiB]) (Klunk et al. 2004) was discovered that makes possible to accurately identify AD brain lesions in demented patients and also in patients at prodromal and even preclinical stages of the disease. The growing body of evidence on AD biomarkers allows these to be now incorporated into new diagnostic research criteria for AD.

2. Diagnosing AD at the dementia stage is too late

AD is already at work when the patients express the first cognitive symptoms, and there is no reason to link the diagnosis of a disease to a certain threshold of severity and to exclude from diagnosis and treatment a large number of patients who are not yet expressing a full-blown dementia. At a time where clinical trials of disease-modifying treatments of AD dementia have failed to show efficacy, at least on meaningful clinical outcomes, identification of AD at a prodromal stage and recruiting patients several years before dementia was a critical next step. Individual clinicians' experience in dementia diagnosis and the quality of the information they receive on the cognitive and functional status of the patient impact significantly on the threshold of detection of the transition to AD

(Engelborghs et al. 2008). Therefore, it was timely to elaborate new criteria, at least for research purposes, with the idea of eliminating the MCI construct, thus bypassing issues in the clinical categorization process and consequent problems with reliability.

13.3 The IWG Conceptual Framework for AD

Earlier and more specific disease recognition were the two goals of the AD diagnostic framework proposed by the International Working Group (IWG) (Dubois et al. 2007, 2010).

13.3.1 The 2007 IWG Criteria

In 2007, the IWG provided a new conceptual framework according to which AD moves from a clinicopathological entity to a *clinico-biological entity* (Dubois et al. 2007). The new IWG criteria stipulate that AD can be recognized in vivo based on the presence of two associated features. The first is the evidence of an *amnestic syndrome of the hippocampal type* at least in the typical form of the disease (Dubois and Albert 2004). The importance of a specific memory pattern was highlighted because none of the other cognitive changes, which can be encountered in AD even at a prodromal stage, are specific of the disease. The second necessary feature is supportive evidence from biomarkers that were proposed for the first time for the diagnosis of AD. These include abnormalities on structural (medial temporal lobe atrophy on MRI) and molecular neuroimaging (abnormalities in glucose metabolism or amyloid burden on PET scanning) and in CSF protein concentrations. As a consequence, neuroimaging and CSF investigations are no longer proposed for excluding other etiologies of brain dysfunction but are primarily used for detecting AD-related changes. The added value of biomarkers and therefore the specificity of the IWG criteria for the diagnosis of AD were further confirmed (de Jager et al. 2010; Bouwman et al. 2010; Schoonenboom et al. 2008; Galluzzi et al. 2010). This is a requirement for research projects where a highly specific diagnosis is needed: (1) for the study of specific outcomes of AD that requires the follow-up of well-phenotyped cohorts of patients; (2) for the discovery or validation of new biomarkers which cannot be conducted on heterogeneous populations with a low/intermediate likelihood of diagnostic accuracy; or (3) for inclusion in clinical trials. The 2007 IWG criteria were successfully implemented in current Phase 2 clinical trials for prodromal AD with gamma secretase inhibitors and immunotherapies, and they have been qualified by the European Medicine Agency (EMA) for use in AD clinical trials (Isaac et al. 2011).

The use of biomarkers made it possible to extend the concept of AD to the *prodromal* (predementia) stage because biomarker changes are not completely linked to disease stages: their positivity reinforces the diagnosis of the disease at any stage.

Accordingly, the presence of a specific memory profile with a positive biomarker moves the patient from an undetermined MCI status to that of prodromal AD.

13.3.2 Further Refinements of the 2007 IWG Criteria for AD

1. *The first important refinements of these criteria came in 2010* where several clarifications were proposed (Dubois et al. 2010).
   (a) Typical versus atypical AD. The diagnostic framework introduced the concept of "atypical forms of AD." An amnestic presentation for AD may not always be the case, and other specific clinical phenotypes can be associated with postmortem evidence of AD pathology, in 15% of the cases. These specific clinical phenotypes include non-amnestic focal cortical syndromes, such as logopenic aphasia, bi-parietal atrophy, posterior cortical atrophy, and frontal variant AD. With the advent of biomarkers providing in vivo confirmation of Alzheimer's pathology, it is now possible to include these clinical disorders as atypical AD if there is convincing biomarker support.
   (b) Preclinical states. There was also an elaboration beyond symptomatic stages of AD. In approximately 20–30% of normal individuals over age 70, the presence of positive biomarkers (reduced CSF levels of Aβ 1-42 or increased deposits of Aβ in the brain as evaluated by amyloid PET) suggests an underlying AD pathology (Morris et al. 2009; Resnick et al. 2010; Stomrud et al. 2007). As the percentage of persons who will progress from this state to symptomatic clinical conditions within their life span was at that time unknown (some elderly with positive biomarkers will never develop AD symptoms), these individuals without clinical symptoms but with positive biomarkers of Alzheimer pathology were considered as *asymptomatic at risk of AD* (ARAD). Asymptomatic at risk for AD refers to subjects with a normal cognitive condition and evidence of amyloidosis in the brain (on PET amyloid) or Alzheimer pathologic changes in the CSF. Additionally, a designation of the stage of *presymptomatic AD* was reserved for individuals carrying autosomal dominant monogenic AD mutations as they will inevitably develop clinical AD if they live long enough. Since then the understanding of AD as a continuous clinical-biological entity encompassing both asymptomatic and symptomatic stages has grown in consensus.
2. *Data on the respective values of biomarkers were obtained*. No hierarchy between the biomarkers was proposed in the 2007 paper. Each biomarker was considered as having the same weight, in the absence of evidence for distinguishing between biomarker performance and accuracy at that time. However, new evidence had shown that biomarkers have different specificity properties. For instance, it appears that the specificity of hippocampal volume for AD may be influenced by several conditions, such as aging (Van De Pol et al. 2006), diabetes, sleep apnea, bipolar disorders (Fotuhi et al. 2012), and by other brain disorders including limbic age-related TDP-43 encephalopathy (LATE), Lewy-related pathology, argyrophilic grain disease, and frontotemporal dementia

(Barkhof et al. 2007; Galton et al. 2001). All these confounding factors make volumetric measure of medial temporal lobe structures less pertinent, at least on an individual level.

The 2010 revision of the IWG criteria divides biomarkers of AD into two groups: (1) *pathophysiological markers* which identify AD pathology since they are strongly correlated with postmortem AD histo-pathological changes. They are considered as markers of diagnosis and mainly consist of positive PET-amyloid scan results or CSF abnormalities; (2) *topographical markers* reflect downstream damage and are markers of progression, more targeted at assessing change over time and predicting outcomes. They mainly consist of hippocampal atrophy on volumetric MRI or hypometabolism on FDG-PET.

CSF changes were promising pathophysiological markers given their good correlations with postmortem AD changes (Buerger et al. 2006; Seppälä et al. 2012; Strozyk et al. 2003; Tapiola et al. 2009) reaching a sensitivity for AD detection of 96.4% (Shaw et al. 2009). However, Aβ alone may not be a sufficient marker given evidence of an overlap with other forms of dementias (such as diffuse Lewy body dementia and cerebral amyloid angiopathy) and because of its presence long before clinical AD. Numerous studies have shown that the combination of the three CSF biomarkers improves their discriminating accuracy (Blennow et al. 2010). Finally, Amyloid-PET imaging showed very high postmortem validation (Clark et al. 2011; Ikonomovic et al. 2008), good predictability for progression to AD dementia (Jack et al. 2010a; Koivunen et al. 2011), but low sensitivity to change in the clinical stages (Ossenkoppele et al. 2012).

3. *The 2014 IWG-2 criteria*: On the basis of these refinements, the IWG proposed in 2014 that the diagnosis of AD can be simplified, requiring the presence of an appropriate clinical AD phenotype (typical or atypical) and a pathophysiological biomarker consistent with the presence of Alzheimer's pathology (CSF Aβ and tau changes or Amyloid PET positivity) (Dubois et al. 2014). Downstream topographical biomarkers of the disease, such as volumetric MRI and fluorodeoxyglucose PET, might better serve in the measurement and monitoring of the course of disease (Dubois et al. 2014). In addition, the IWG introduced the notion of co-occurrence of pathologies in AD and proposed the diagnosis of mixed AD with Lewy body disease or cerebrovascular disease.

13.3.3 The 2011 NIA-AA Criteria

In line with the conceptual evolution in the field, the NIA/AA published diagnostic criteria in 2011 (Jack et al. 2011; Sperling et al. 2011; McKhann et al. 2011; Albert et al. 2011) that had the advantage of being applicable in both clinical and research settings. They similarly advanced from the NINCDS-ADRDA framework to broaden the coverage of stages of disease from the asymptomatic (preclinical), through the predementia stages (MCI due to AD) and through the most severe stages of dementia. They shared many features with the IWG criteria including recognition of an asymptomatic biomarker positive phase and of a predementia symptomatic

phase of AD. They also integrated biomarkers into the diagnostic process that were categorized into two types, one identifying amyloid abnormalities and one the downstream neurodegeneration. The most interesting contribution of the NIA/AA criteria was the one concerning the preclinical stages of the disease. Based on the biomarker model introduced by Jack and colleagues (2010b), it was proposed (Sperling et al. 2011) that (1) Aβ accumulation biomarkers become abnormal first and a substantial Aβ load accumulates before the appearance of clinical symptoms; (2) biomarkers of synaptic dysfunction, including FDG and functional MRI (fMRI), may demonstrate abnormalities very early, particularly in APOE ε4allele carriers, who may manifest functional abnormalities before detectable Aβ deposition (Reiman et al. 2004); (3) structural MRI is thought to become abnormal a bit later, as a marker of neuronal loss, and MRI retains a close relationship with cognitive performance through the clinical phases of MCI and dementia (Risacher et al. 2009); and (4) none of the biomarkers is static; rates of change in each biomarker change over time and follow a nonlinear time course.

The NIA/AA criteria differed conceptually from the IWG criteria in a number of important ways. At the preclinical stages, the position taken in this framework has been that the presence of Alzheimer pathologic changes indicates the diagnosis of AD and that this diagnosis is applicable at this "in situ" stage for research purposes. At the pre-dementia (MCI) stage, the framework is probabilistic and applies a likelihood of progression based on the presence of AD biomarkers, with designation either of biomarkers that reflect amyloidopathy (CSF Aβ or amyloid PET) or those that are "downstream" indicative of neuronal degeneration (CSF tau, FDG glucose, volumetric MRI). The likelihood of progression is determined by the specific combination of positive, negative, or indeterminate results on the "amyloid" and "downstream" biomarkers. Differently from the IWG criteria, the MCI stage of AD is formally distinguished from the dementia stage, which has its own diagnostic criteria. In the dementia stage, ten categories of dementia of the AD type are established including probable AD dementia, possible AD dementia, probable or possible AD dementia with evidence of the AD pathophysiological process, and pathophysiologically proven AD dementia. The later stage retains most of the features of the past diagnosis of probable AD (McKhann et al. 1984) despite the low specificity, the limited positive predictive value, and poor negative predictive value of these criteria (Varma et al. 1999).

13.3.4 The 2015 Consensus on the Preclinical Stage of AD

In 2015, a consensus meeting brought together experts from the International Working Group (IWG), the National Institute of Aging (NIA), and the Alzheimer Association (AA) for the definition, natural history, and diagnostic criteria of preclinical AD (Dubois et al. 2016). The fact that the disease process starts many years before the development of symptoms and that effective interventions could be initiated at this time in the future makes the definition of the preclinical stage necessary. Theoretically, the definition of preclinical AD would span from the first

neuropathological brain lesions to the onset of the first clinical symptoms of AD. In practice, however, these boundaries are challenging, and the definition also relies on a *low/high risk dichotomy* to further develop clinical AD. The risk—defined as the probability for a patient to develop the clinical symptoms during the remainder of his/her lifetime—is due to how fast the individual is progressing (determined by established risk enhancing modifiable or non-modifiable factors, such as age, modifying genes, cognitive reserve, and comorbidities) *and* how advanced the individual is on his/her curve of progression (stage of biomarker expression). Based on this classification, it was proposed to distinguish between: (1) an already developed AD pathology evidenced by the co-occurrence of amyloid AND tau pathology (that can be inferred in vivo with the use of pathophysiological biomarkers), whatever the stage (preclinical stage or symptomatic/prodromal and dementia stage), and (2) a situation at risk of AD (ARAD) mainly in asymptomatic individuals exhibiting an isolated brain amyloidopathy (asymptomatic A+) or tauopathy (asymptomatic T+). This reflects the separation between the disease itself and the presence of risk factors. Therefore, "preclinical AD" was defined by the presence of both Aβ and Tau markers beyond pathological thresholds.

13.3.5 A/T/N/ Classification

Rather than considering AD as a combination of symptomatic and neuropathological changes, Jack and a group of co-authors (Jack et al. 2016a, 2018a) recently proposed a descriptive, biomarker-based research framework of the disease, completely agnostic to clinical symptomatology. This "ATN" framework, developed by the NIA-AA working group, is centered around a biomarker definition of disease according to amyloid (A), tau (T), and neurodegeneration (N) status with an AD diagnosis characterized by the presence of both amyloid and tau positivity (A+T+). Therefore, even in the absence of any cognitive signs or symptoms, those subjects who have both abnormal amyloid and tau biomarkers (A+T+) are diagnosed as AD and those with abnormal amyloid biomarker only (A+T− or A+N−) are considered within an AD continuum. The A/T/N classification moved from a definition of AD as an illness with a phenotype to a definition of AD as a conjunction of pathological findings, which would cover all preclinical and clinical stages of the disease. In consequence, under this AD classification, there is an extended continuum from individuals who are cognitively normal to severely demented patients in the end stages of disease.

The NIA framework constitutes the summation of the previous works. It definitively disentangles the diagnosis of AD from the label dementia and opens up the possibility for research into the biological cause before symptoms occur, which is imperative to develop drugs for the earliest stage. For research purposes, the model

of dynamic biomarkers of Alzheimer's pathological cascade has the advantage of providing an unbiased framework useful for operationalizing the therapeutic roadmap by the identification of the sequence of biological events.

The "ATN" classification is easily applicable on an individual level, where "A+" corresponds to the presence of amyloid determined by amyloid PET or analysis of CSF Aβ42; "T+" is consistent with neurofibrillary tangles ascertained by tau PET or CSF phospho-tau; and "N+" is associated with a downstream neurodegeneration biomarker, such as hippocampal atrophy on structural MRI, hypometabolism in the brain as evidenced by FDG-PET, or CSF total tau. However, though relevant for research purposes, this "framework is not intended for general clinical practice," as underlined by the authors themselves (Alzheimer 1907).

These 2018 NIA AA criteria have engendered significant debate about the biomarker-based disease diagnosis, with clinical symptoms and phenotype being removed from the diagnostic framework and used only for staging. This debate has highlighted the need for clinical validation of this research (Garrett 2018; Glymour et al. 2018; Rabinovici and Carrillo 2019; Jack et al. 2019a; Jack 2020; Morris et al. 2018; Jagust et al. 2019; Louie 2019; McCleery et al. 2019a, b; Sweeney et al. 2019; Frisoni et al. 2019; Langa and Burke 2019). Recently Jack and co-authors have put ATN classification to the test (Jack et al. 2019b) and showed that 50% of cognitive changes with older age was associated with underlying AD pathology. However, it remained unclear what accounted for the other 50% of cognitive changes. While "ATN" classification may be relevant for use in secondary prevention clinical trials, allowing patients to be stratified based on their prognostic profile, it still remains purely a research construct and has several limitations. Evidence reported in the last few years suggests that the presence of tau and amyloid positivity is not sufficient to definitively predict the occurrence of symptoms (see below). Besides this limitation, several additional points should be raised. First, more work needs to be done to understand the role of age in the prediction of individual patients and prognosis. Second, while "ATN" classification incorporates neuroimaging advances in the AD field, such as amyloid and tau PET, its application may be cost-prohibitive in many research projects and clinical trials. Amyloid PET reimbursement remains limited to specific situations, while tau PET tracer approval by the regulatory authorities is still pending. Third, equating AD to solely the presence of neuropathological lesions could lead to the risk of marketing medicinal products, which decrease brain pathology without proof of their efficacy on clinical symptoms. Last but not least, "ATN" research criteria may not apply for the clinical practice, as underlined by the authors ("this framework is not intended for general clinical practice" (Reisberg et al. 2008)). This being said, "ATN" classification represents an important advancement in the conceptualization of AD, making a step further to the in vivo early biomarker-based diagnosis of AD and understanding of its biological continuum.

13.4 Perspectives

13.4.1 General Considerations About a Biological Diagnosis of AD

For both research and clinical settings, the importance of an accurate diagnosis of AD is imperative given its much-feared consequences, which cannot be understated.

1. *In clinical setting*—When there are no symptoms, reliance on a biomarker only diagnosis must require a very secure and tightly elaborated natural history connecting the biomarker with invariable subsequent expression of clinical symptoms. It is only with a high level of confidence in these parameters that a diagnosis is ready for disclosure to patients or to their families. Recent experience with the Sokrates study underscores some of the uncertainties that are inherent in revealing amyloid PET results alone (Mozersky et al. 2018).
2. *For research purposes*—The model of dynamic biomarkers of the Alzheimer's pathological cascade has the advantage of providing an unbiased framework useful for operationalizing the therapeutic roadmap by the identification of the sequence of biological events. In clinical trials, there is a trend today to target the earliest stages of the disease, and even the preclinical stage, because it is considered that patients with dementia are too advanced in the disease for hoping for a recovery or even a stabilization of their symptoms with therapy. The utility of applying biomarkers to clinical phenotype in prodromal AD has transformed clinical trials in the early symptomatic stages of disease and has been associated with the first preliminary evidence of benefits with monoclonal Aβ passive immunotherapy (Budd-Haeberlein et al. 2018; Swanson et al. 2018). However, for those who are asymptomatic at risk through biomarkers characterization, the evidence of invariable progression is still needed.

13.4.2 Diagnosing AD: Biomarkers Alone May Not Be Sufficient

Evidence reported in the last few years suggests that the presence of tau and amyloid positivity is not sufficient to definitively predict the invariable occurrence of symptoms:

- *Postmortem examinations* have long described significant AD brain lesions in cognitively normal subjects without signs of decline, adding weight to the early twentieth-century debate on the relevance of these lesions to the pathophysiology underlying cognitive decline (Alzheimer 1911; Katzman et al. 1988; Villain and Dubois 2019). This was reinforced by recent large postmortem cohorts using quantification and digital neuropathological methods, from the Baltimore Longitudinal Study of Aging and the Nun Study (Iacono et al. 2014; Mortimer 2012; Perez-Nievas et al. 2013; Boluda et al. 2014; Mufson et al. 2016), and by a study of Braak et al. (Braak et al. 2011) which, in a systematic postmortem

brain examination, showed that AD brain lesions (including both amyloid and tau lesions) are found in more than half of subjects aged 70 years and older, regardless of clinical status, i.e., well beyond the prevalence of having cognitive impairment, expected in up to 30% (Knopman et al. 2016). This pathological-clinical discrepancy is also found in cross-sectional molecular neuroimaging studies: for instance, 19% of 576 cognitively unimpaired elderly subjects (mean age 71 years) were found to have both amyloid and diffuse tau (i.e., outside the medial temporal lobe) pathologies (Knopman et al. 2016), i.e., with a probable signature of intermediate or high AD pathology according to neuropathological criteria (Lowe et al. 2018).

- Moreover, postmortem examinations have found neurofibrillary tangles (NFT) in the medial temporal regions in almost every cognitively normal individual over 70 years old (Braak et al. 2011; Hyman et al. 2012; Braak and Braak 1997; Duyckaerts and Hauw 1997). This primary age-related tauopathy (PART) is an age-related normal occurrence of tauopathy in the absence or with a low extent of Amyloid pathology (Thal Aβ Phase ≤2 (Katzman and Kawas 1994)). It is noteworthy that the cognitive decline of these patients (T+ A±) is significantly slower than that of patients with AD (Crary et al. 2014). This last finding indicates that low A(+) (i.e., Thal Aβ Phase ≤2) associated with T(+) does not necessarily lead to an accelerated cognitive decline and dementia.
- *Longitudinal molecular neuroimaging studies* are also inconsistent in predicting a reliable outcome at an individual level for those who are amyloid positive and unimpaired cognitively, even after long-term follow-up. A large majority of A+ subjects remain cognitively stable over time without progression even after several years (Jack et al. 2019b, 2016b; Bell et al. 2019; Clark et al. 2018; Sperling et al. 2019; Petersen et al. 2016; Mormino et al. 2014, 2017; Villemagne et al. 2013; Bilgel et al. 2018; Donohue et al. 2017; Monsell et al. 2014; Machulda et al. 2017; Lilamand et al. 2019; Burnham et al. 2016; Lim et al. 2018; Albert et al. 2018), although these studies do consistently report a significant group effect on cognitive decline. These later findings may have resulted from the admixture of a small proportion of progressors with those who were A+ nonprogressor subjects. In the INSIGHT-preAD study, 76 out of the 88 amyloid-positive subjects, with a mean age of 77 years at the entrance, had no changes in any cognitive, behavioral, and neuroimaging parameters when compared to baseline or to amyloid negative individuals after a 5-year follow-up (Bilgel et al. 2018). The same observations were reported in the Australian AIBL cohort, where only 19% (26/137) of amyloid-positive cognitive unimpaired elderly, with a mean age of 75 years old at the entrance, converted to MCI or AD dementia after a 6-year follow-up (Mormino et al. 2017). When data from 13 cohorts in the USA and Europe were pooled together, the lifetime risk of AD dementia for asymptomatic amyloid-positive individuals ranged between 5% and 23% according to age and sex (Dubois et al. 2018; Brookmeyer and Abdalla 2018). More recent studies show that a significant proportion of cognitively unimpaired A+T+ individuals also remain cognitively stable over time, even after several years: results from the ADNI cohort show that the A+T+ status increases moderately the 5-year risk

of clinical conversion (HR = 2.8) (Parnetti et al. 2019), and similar findings were observed in data from pooled cohorts (Yu et al. 2019). By the same token, a long-term longitudinal amyloid and tau PET study showed that, after 7 years of follow-up, only 35% (6/17) of amyloid-positive cognitive unimpaired elderly converted to MCI or AD dementia. It is noteworthy that there was no significant difference at baseline in term of tau lesions (mean SUVR) between the amyloid-positive converters and non-converters (Younes et al. 2019), indicating that baseline tau levels do not predict the evolution.

Furthermore, longitudinal Tau PET studies showed no or only minimal acceleration of Tau binding in the following 1 or 2 years in amyloid-positive compared to amyloid-negative cognitive unimpaired elderly participants (Hanseeuw et al. 2019; Jack et al. 2018b; Harrison et al. 2019), in contradiction with the prevalent model where the presence of brain amyloid lesions triggers a systematic spreading out of the tau lesions outside the medial temporal lobes (Cho et al. 2019; He et al. 2018). The relationships between co-occurrence of tau and amyloid pathology on the one hand and the development of cognitive decline and neurodegeneration on the other hand remain uncertain. This is confirmed, beyond all the studies devoted to this topic, by everyday practice during the follow-up of Amyloid-positive cognitively unimpaired subjects (Raj et al. 2015).

13.4.3 Preclinical AD and Normal Aging

The limitation of a biological definition of AD in clinical practice concerns the asymptomatic stage of the disease where, by definition, the pattern of cognitive changes does not support the presence of the disease. This is not the case for patients with cognitive/behavioral changes because the identification of specific clinical phenotypes is the expression of an illness that the biomarkers will ascertain. The assumption of equivalence between symptomatic and asymptomatic biomarker positive, in line with the linear amyloid cascade hypothesis, leads to the risk of considering all cognitively normal individuals with biomarker positivity as persons that are certain to experience subsequent cognitive decline, whereas a maximum of 5–42% will develop dementia in their lifetime (Dubois et al. 2018).

In the clinical setting, defining the disease by its lesions only—and no more to a clinical phenotype—exposes to the risk of confusion with aging in old subjects (where the risk of clinical progression despite AD lesions is low (Dubois et al. 2018)). This undermines the distinctions that have been worked out around well-identified specific clinical presentations supported by biomarkers. Publications in the field of dementia, which propose that the disease is a myth (Stanley et al. 2019) or a decoy (Whitehouse et al. 2008), illustrating the confusion between Alzheimer and old age, are worrying. Moreover, equating Alzheimer's disease with only the presence of neuropathological lesions might lead to the risk of marketing AD medicinal products that decrease brain pathology, with no more the need to prove their efficacy on clinical symptoms. Finally, diagnostic disclosure becomes more

challenging ethically when the physician should announce to an asymptomatic individual the diagnosis of an irreversible disease based on biomarkers even where the clinical trajectory is very uncertain (Saint Jean and Favereau 2018).

13.4.4 Asymptomatic Subjects and Risk Profiling

In line with this notion of a "risk of an illness" among patients with preclinical AD, it may be postulated that at early, asymptomatic stages, other contributing factors are needed for the occurrence of symptoms, in addition to AD neuropathological change. Occurrence of symptoms is a complex phenomenon, which has to be integrated in a network where modulating factors may aggravate or slow down the impact of the lesions (Schermer and Richard 2019). There is interplay between different factors (i.e., neuroinflammation, synergy between neuronal lesions, genetic/environmental risk/protective factors, cognitive/brain reserve, and comorbidities) whose final outcome is the occurrence of the illness or the resilience against it. The intervention of modulating factors in order to explain the inconsistency between pathological lesions and clinical symptoms has long been hypothesized and has given rise to the concept of "brain resilience" that encompasses the notion of "cognitive reserve," "brain reserve," and "brain maintenance" (Medina et al. 2017; Rothschild and Trainor 1937; Stern 2012; Arenaza-Urquijo and Vemuri 2018; Stern et al. 2018). This assumption has also received several evidences from basic neuroscience (Perneczky et al. 2019).

Therefore, it is possible that some asymptomatic biomarker-positive subjects may neither develop cognitive decline (Jack et al. 2019b, 2016b; Bell et al. 2019; Clark et al. 2018; Sperling et al. 2019; Petersen et al. 2016; Mormino et al. 2014, 2017; Villemagne et al. 2013; Bilgel et al. 2018; Donohue et al. 2017; Monsell et al. 2014; Machulda et al. 2017; Lilamand et al. 2019; Burnham et al. 2016; Lim et al. 2018; Albert et al. 2018; Brookmeyer and Abdalla 2018; Parnetti et al. 2019; Yu et al. 2019) nor demonstrate a frank acceleration of Tau lesions accumulation (Hanseeuw et al. 2019; Jack et al. 2018b; Harrison et al. 2019), an assumption theorized under the concept of "brain resistance" to AD pathology (Stern 2012), which is in line with observations of longitudinal cohorts.

13.4.5 Refining the IWG Framework

Given the nonlinear relationship between lesions and symptoms and the very high uncertainty of individual clinical trajectories, we propose (1) that the presence of both Amyloid and Tau lesions alone is insufficient for establishing the diagnosis of AD in cognitively normal subjects and (2) that we should distinguish in these cognitively normal subjects two subgroups for scientific, clinical, and ethical purposes:

- *Asymptomatic stable*: probably the most prevalent in numbers, refers to subjects stable over time, who may never (or very late in life) develop symptoms. Because

of not yet identified factors (including cognitive reserve, ApoE2 status, protective genetic predisposition, absence of synergy between neuronal lesions, and so forth), these individuals may (1) compensate and maintain a normal functioning despite the presence of an ongoing neurodegeneration process or (2) never develop the hallmarks of an accelerated degeneration of neurons, synapses, and cognitive functions.

- *Asymptomatic progressors*: another subgroup of subjects, less prevalent but more interesting for clinical trials, consists of progressors who demonstrate signs of accelerated neurodegeneration and whose compensatory mechanisms are overwhelmed. They are on the way to prodromal AD.

It is essential to separate the two groups in order to define the factors of prevention/compensation on the one hand and the algorithm of progression on the other hand.

13.4.6 The Proposal P+A+ T+ (at Least for Clinical Practice) (See Table 13.1)

Based on the current and aforementioned evidence:

1. *The diagnosis of AD* should be restricted to the presence of pathological evidence of disease in the presence of a clinical phenotype. The specific clinical phenotypes (typical and atypical AD) identified during the last 30 years have proved good sensitivity and specificity as markers of an ongoing accelerated cognitive decline (Matthews et al. 2007) and also proved to be a good surrogate marker of Tau pathology acceleration.

Table 13.1 The two categories of patients

1. Alzheimer's disease (P+A+T+)
2. Asymptomatic at risk for AD (ARAD) (P-):
(a) Asymptomatic with high risk: cognitively normal individuals subjects with
• CSF or PET A (+) and T (+)
• Tau PET (+) outside the limbic cortex (Braak ≥5)
• ApoE4 homozygous
(b) Asymptomatic with undefined risk*: cognitively normal individuals subjects with an incomplete biomarker pattern:
• A(+) and T(−)
• A(−) and T(+)
**to be worked out depending on the presence of modulating factors*
3. Genetic forms of AD

We define AD as a clinico-biological entity, characterized by:

(a) A clinical phenotype (P+): in the majority of cases (85%), this phenotype is described as *typical* when it combines memory disorders (an amnestic syndrome of the hippocampal type (Dubois and Albert 2004)) with other cognitive changes in language, visual recognition, spatiotemporal orientation, gestures, etc. (Qiu et al. 2019; Villain and Dubois 2019). Other cases may present with an *atypical phenotype*, and three different types have been well identified: the posterior variant, the logopenic variant, and the frontal variant (to which it may be possible to add the cortico-basal syndrome). It is noteworthy that (P+) refers to a specific cognitive phenotype of AD and not to subjective cognitive decline (SCD) as the more at risk are not always those who complain the more (Dourlen et al. 2019; Cacciamani et al. 2017).

(b) The presence of pathophysiological biomarkers: they reflect, in vivo, the underlying pathology (amyloid and tau lesions), present at any stage of the disease, even at the asymptomatic one. The positivity of both amyloid and tau biomarkers is required because, on the one hand, an isolated amnesic syndrome of the hippocampal type with only Amyloid positivity is not specific of AD and can be observed, for instance, in the case of a limbic-predominant age-related TDP-43 encephalopathy (LATE) with Amyloid co-pathology (Jack et al. 2018a) or in cases of cerebral amyloid angiopathy and amnestic vascular cognitive impairment (Hanseeuw et al. 2020). On the other hand, an isolated amnestic syndrome of the hippocampal type with only tau lesions can be observed in the case of primary age-related tauopathy (PART) or frontotemporal lobar degeneration (Villain and Dubois 2019; Katzman and Kawas 1994). CSF investigation is interesting by providing simultaneous information on the two types of biomarkers. However, CSF investigation only quantifies the level of tau changes but does not provide information on the topographical distribution of tau pathology (limbic only or neocortical), which can be relevant for certain stages of the disease (Jang et al. 1999). We recommend to take into account CSF P-tau or PET tau and not CSF T-tau due to its lack of specificity regarding the ongoing neurodegeneration process (Mattsson et al. 2018). Alternatively, a less invasive but expensive option can be the acquisition of two PET scans (amyloid and tau PET).

2. *Asymptomatic A+T+ subjects should not be diagnosed as AD*, but only at-risk for AD (ARAD), with different levels of risk (high or undefined), depending on the amount and aggressivity of the brain lesions and on the existence of modulating factors whose influence for each of them remains to be determined (see Table 13.2).
3. *Genetic forms of AD*: Separate from AD and ARAD, are carriers of autosomal dominant monogenic mutations for AD (APP, PSE1, PSE2, or T21) who can be A, T, P (+), or (-), depending on the natural history of their disease. They have an absolute risk to develop the disease.

Table 13.2 currently established modulating factors for a personalized risk profile

1. Factors that may increase the risk:
(a) Increased age
(b) Sex female
(c) Low education level
(d) ApoE status with an increased risk in case of heterozygous ApoE 4 status
(e) Familial history
(f) Memory complaints/SCD
(g) Presence of markers of neurodegeneration:
• Isolated hippocampal MRI atrophy
• FDG-PET hypometabolism; or elevated CSF NF-L
(h) Polygenic risk factors beyond ApoE
(i) Co-pathology α-synucleinopathy
(j) LATE
• Argyrophilic grain disease (AGD)
• Cortical aging-related tau astrogliopathy (ARTAG)
(k) Vascular pathology
2. Factors that may decrease the risk
(a) Protective genes, such as the presence of ApoE2 allele
(b) Higher education and cognitive reserve
3. Factors that need to be further confirmed:
(a) Pattern of neuroinflammation (e.g., using ^{18}F-DPA-714 PET)
(b) Occupation complexity
(c) Functional brain marker of cognitive reserve (e.g., using fMRI connectivity)

13.5 Conclusion

The major advance of the IWG Criteria and of the subsequent National Institute on Aging/Alzheimer's Association (NIA/AA) criteria (Jack et al. 2011; Sperling et al. 2011; McKhann et al. 2011; Albert et al. 2011) was to support the diagnosis of AD prior to the onset of dementia and integrate biomarkers of Alzheimer's pathology into the diagnostic framework.

The new framework establishes AD as a single disease on a continuum that includes different stages (preclinical, prodromal, and dementia stages) that are identified by a specific phenotype and supported by pathophysiological biomarkers. These criteria are particularly useful for research projects. However, for clinical practice we recommend to disclose an AD diagnosis only in the case of the presence of a specific phenotype and to mention a risk for AD to asymptomatic patients.

Glossary

AD dementia When cognitive symptoms interfere with activity of daily living.
Alzheimer's disease (AD) The whole clinical phase, no longer restricted to the dementia syndrome.
Alzheimer's pathology Underlying neurobiological changes responsible for AD
Asymptomatic at risk Cognitively normal individuals with positive pathophysiological biomarkers.
Atypical AD Less common but well-characterized clinical phenotypes that occur with Alzheimer's pathology. The diagnosis of AD needs in vivo evidence of pathophysiological markers.
Mild cognitive impairment (MCI) Patients for whom there is no disease clearly identified.
Mixed AD Patients who fulfill the criteria for AD and additionally present with clinical and biomarkers evidence of other comorbid disorders.
Pathophysiological markers Biological changes that reflect the underlying AD pathology (CSF changes; PET-amyloid). They are markers of diagnosis.
Prodromal AD The early symptomatic, predementia phase of AD.
Topographical biomarkers Downstream markers of neurodegeneration that can be structural (MRI) or metabolic (FDG-PET). They are markers of progression.
Typical AD The most common clinical phenotype of AD, characterized by an amnestic syndrome of the hippocampal type.

References

Albert MS, DeKosky ST, Dickson D et al (2011) The diagnosis of mild cognitive impairment due to Alzheimer's disease: recommendations from the National Institute on Aging-Alzheimer's Association workgroups on diagnostic guidelines for Alzheimer's disease. Alzheimers Dement 7:270–279

Albert M, Zhu Y, Moghekar A et al (2018) Predicting progression from normal cognition to mild cognitive impairment for individuals at 5 years. Brain 141:877–887

Alzheimer A (1907) Über eine eigenartige Erkrankung der Hirnrinde. Allg Zeitschrift fur Psychiatr und Psych Medizin 64:146–148

Alzheimer A (1911) Über eigenartige Krankheitsfälle des späteren Alters. Zbl Ges Neurol Psych 4:356–385

Arenaza-Urquijo EM, Vemuri P (2018) Resistance vs resilience to Alzheimer disease. Neurology 90:695–703

Barkhof F, Polvikoski TM, Van Straaten ECW et al (2007) The significance of medial temporal lobe atrophy: a postmortem MRI study in the very old. Neurology 69:1521–1527

Beach TG, Monsell SE, Phillips LE, Kukull W (2012) Accuracy of the clinical diagnosis of Alzheimer disease at National Institute on Aging Alzheimer Disease Centers, 2005-2010. J Neuropathol Exp Neurol 71:266–273

Bell WR, An Y, Kageyama Y et al (2019) Neuropathologic, genetic, and longitudinal cognitive profiles in primary age-related tauopathy (PART) and Alzheimer's disease. Alzheimers Dement 15:8–16

Bilgel M, An Y, Helphrey J et al (2018) Effects of amyloid pathology and neurodegeneration on cognitive change in cognitively normal adults. Brain 141:2475–2485

Blennow K, Hampel H, Weiner M, Zetterberg H (2010) Cerebrospinal fluid and plasma biomarkers in Alzheimer disease. Nat Rev Neurol 6:131–144

Boluda S, Toledo JB, Irwin DJ et al (2014) A comparison of Aβ amyloid pathology staging systems and correlation with clinical diagnosis. Acta Neuropathol 128:543–550

Bouwman FH, Verwey NA, Klein M et al (2010) New research criteria for the diagnosis of Alzheimer's disease applied in a memory clinic population. Dement Geriatr Cogn Disord 30:1–7

Braak H, Braak E (1991) Neuropathological stageing of Alzheimer-related changes. Acta Neuropathol 82:239–259

Braak H, Braak E (1997) Diagnostic criteria for neuropathologic assessment of Alzheimer's disease. Neurobiol Aging 18:S85–S88

Braak H, Thal DR, Ghebremedhin E, Del Tredici K (2011) Stages of the pathologic process in Alzheimer disease: age categories from 1 to 100 years. J Neuropathol Exp Neurol 70:960–969

Brookmeyer R, Abdalla N (2018) Estimation of lifetime risks of Alzheimer's disease dementia using biomarkers for preclinical disease. Alzheimers Dement 14:981–988

Budd-Haeberlein S, Castrillo-Viguera C, Gheuens S et al (2018) 24-month analysis of change from baseline in clinical dementia rating scale cognitive and functional domains in PRIME: a randomized phase 1b study of the anti–amyloid beta monoclonal antibody aducanumab. Alzheimers Dement 14:P242

Buerger K, Ewers M, Pirttilä T et al (2006) CSF phosphorylated tau protein correlates with neocortical neurofibrillary pathology in Alzheimer's disease. Brain 129:3035–3041

Burnham SC, Bourgeat P, Doré V et al (2016) Clinical and cognitive trajectories in cognitively healthy elderly individuals with suspected non-Alzheimer's disease pathophysiology (SNAP) or Alzheimer's disease pathology: a longitudinal study. Lancet Neurol 15:1044–1053

Cacciamani F, Tandetnik C, Gagliardi G et al (2017) Low cognitive awareness, but not complaint, is a good marker of preclinical Alzheimer's disease. J Alzheimers Dis 59:753–762

Chase TN, Foster NL, Fedio P, Brooks R, Mansi L, di Chiro G (1984) Regional cortical dysfunction in Alzheimer's disease as determined by positron emission tomography. Ann Neurol 15:170–174

Chételat G, Baron JC (2003) Early diagnosis of Alzheimer's disease: contribution of structural neuroimaging. NeuroImage 18:525–541

Cho H, Choi JY, Lee HS et al (2019) Progressive tau accumulation in Alzheimer disease: 2-year follow-up study. J Nucl Med 60:1611–1621

Choo IH, Lee DY, Youn JC et al (2007) Topographic patterns of brain functional impairment progression according to clinical severity staging in 116 Alzheimer disease patients: FDG-PET study. Alzheimer Dis Assoc Disord 21:77–84

Clark CM, Schneider JA, Bedell BJ et al (2011) Use of florbetapir-PET for imaging beta-amyloid pathology. JAMA 305:275–284

Clark LR, Berman SE, Norton D et al (2018) Age-accelerated cognitive decline in asymptomatic adults with csf β-amyloid. Neurology 90:E1306–E1315

Crary JF, Trojanowski JQ, Schneider JA et al (2014) Primary age-related tauopathy (PART): a common pathology associated with human aging. Acta Neuropathol 128:755–766

Delacourte A, David JP, Sergeant N et al (1999) The biochemical pathway of neurofibrillary degeneration in aging and Alzheimer's disease. Neurology 52:1158–1165

Donohue MC, Sperling RA, Petersen R, Sun CK, Weiner M, Aisen PS (2017) Association between elevated brain amyloid and subsequent cognitive decline among cognitively normal persons. JAMA 317:2305–2316

Dourlen P, Kilinc D, Malmanche N, Chapuis J, Lambert J-C (2019) The new genetic landscape of Alzheimer's disease: from amyloid cascade to genetically driven synaptic failure hypothesis? Acta Neuropathol 138:221–236

Dubois B, Albert ML (2004) Amnestic MCI or prodromal Alzheimer's disease? Lancet Neurol 3:246–248
Dubois B, Feldman HH, Jacova C et al (2007) Research criteria for the diagnosis of Alzheimer's disease: revising the NINCDS-ADRDA criteria. Lancet Neurol 6:734–746
Dubois B, Feldman HH, Jacova C et al (2010) Revising the definition of Alzheimer's disease: a new lexicon. Lancet Neurol 9:1118–1127
Dubois B, Feldman HH, Jacova C et al (2014) Advancing research diagnostic criteria for Alzheimer's disease: the IWG-2 criteria. Lancet Neurol 13:614–629
Dubois B, Hampel H, Feldman HH et al (2016) Preclinical Alzheimer's disease: definition, natural history, and diagnostic criteria. Alzheimers Dement 12:292–323
Dubois B, Epelbaum S, Nyasse F et al (2018) Cognitive and neuroimaging features and brain β-amyloidosis in individuals at risk of Alzheimer's disease (INSIGHT-preAD): a longitudinal observational study. Lancet Neurol 17:335–346
Duyckaerts C, Hauw JJ (1997) Prevalence, incidence and duration of Braak's stages in the general population: can we know? Neurobiol Aging 18:362–369
Engelborghs S, De Vreese K, Van de Casteele T et al (2008) Diagnostic performance of a CSF-biomarker panel in autopsy-confirmed dementia. Neurobiol Aging 29:1143–1159
Ferris SH, de Leon MJ, Wolf AP et al (1980) Positron emission tomography in the study of aging and senile dementia. Neurobiol Aging 1:127–131
Fotuhi M, Do D, Jack C (2012) Modifiable factors that alter the size of the hippocampus with ageing. Nat Rev Neurol 8:189–202
Frisoni GB, Ritchie C, Carrera E et al (2019) Re-aligning scientific and lay narratives of Alzheimer's disease. Lancet Neurol 18:918–919
Galluzzi S, Geroldi C, Ghidoni R et al (2010) The new Alzheimer's criteria in a naturalistic series of patients with mild cognitive impairment. J Neurol 257:2004–2014
Galton CJ, Gomez-Anson B, Antoun N et al (2001) Temporal lobe rating scale: application to Alzheimer's disease and frontotemporal dementia. J Neurol Neurosurg Psychiatry 70:165–173
Garrett MD (2018) A critique of the 2018 National Institute on Aging's. Research framework: toward a biological definition of Alzheimer's disease. Curr Neurobiol 9:49–58
Glymour MM, Brickman AM, Kivimaki M et al (2018) Will biomarker-based diagnosis of Alzheimer's disease maximize scientific progress? Evaluating proposed diagnostic criteria. Eur J Epidemiol 33:607–612
Hanseeuw BJ, Betensky RA, Jacobs HIL et al (2019) Association of amyloid and tau with cognition in preclinical Alzheimer disease: a longitudinal study. JAMA Neurol 76:915–924
Hanseeuw BJ, Scott MR, Sikkes S et al (2020) Evolution of anosognosia in Alzheimer's disease and its relationship to amyloid. Ann Neurol 87:267–280
Hansson O, Zetterberg H, Buchhave P, Londos E, Blennow K, Minthon L (2006) Association between CSF biomarkers and incipient Alzheimer's disease in patients with mild cognitive impairment: a follow-up study. Lancet Neurol 5:228–234
Harrison TM, La Joie R, Maass A et al (2019) Longitudinal tau accumulation and atrophy in aging and alzheimer disease. Ann Neurol 85:229–240
He Z, Guo JL, McBride JD et al (2018) Amyloid-β plaques enhance Alzheimer's brain tau-seeded pathologies by facilitating neuritic plaque tau aggregation. Nat Med 24:29–38
Hyman BT, Phelps CH, Beach TG et al (2012) National Institute on Aging-Alzheimer's Association guidelines for the neuropathologic assessment of Alzheimer's disease. Alzheimers Dement 8:1–13
Iacono D, Resnick SM, O'Brien R et al (2014) Mild cognitive impairment and asymptomatic Alzheimer disease subjects. J Neuropathol Exp Neurol 73:295–304
Ikonomovic MD, Klunk WE, Abrahamson EE et al (2008) Post-mortem correlates of in vivo PiB-PET amyloid imaging in a typical case of Alzheimer's disease. Brain 131:1630–1645
Isaac M, Vamvakas S, Abadie E, Jonsson B, Gispen C, Pani L (2011) Qualification opinion of novel methodologies in the predementia stage of Alzheimer's disease: cerebro-spinal-fluid related biomarkers for drugs affecting amyloid burden - regulatory considerations

by European Medicines Agency focusing in improving benefit/risk in regulatory trials. Eur Neuropsychopharmacol 21:781–788
Jack CR (2020) Preclinical Alzheimer's disease: a valid concept. Lancet Neurol 19:31
Jack CRJ, Wiste HJ, Vemuri P et al (2010a) Brain beta-amyloid measures and magnetic resonance imaging atrophy both predict time-to-progression from mild cognitive impairment to Alzheimer's disease. Brain 133:3336–3348
Jack CR, Knopman DS, Jagust WJ et al (2010b) Hypothetical model of dynamic biomarkers of the Alzheimer's pathological cascade. Lancet Neurol 9:119–128
Jack CRJ, Albert MS, Knopman DS et al (2011) Introduction to the recommendations from the National Institute on Aging-Alzheimer's Association workgroups on diagnostic guidelines for Alzheimer's disease. Alzheimer Dement J Alzheimer Assoc 7:257–262
Jack CR, Bennett DA, Blennow K et al (2016a) A/T/N: an unbiased descriptive classification scheme for Alzheimer disease biomarkers. Neurology 87:539–547
Jack CR, Therneau TM, Wiste HJ et al (2016b) Transition rates between amyloid and neurodegeneration biomarker states and to dementia: a population-based, longitudinal cohort study. Lancet Neurol 15:56–64
Jack CR, Bennett DA, Blennow K et al (2018a) NIA-AA research framework: toward a biological definition of Alzheimer's disease. Alzheimers Dement 14:535–562
Jack CR, Wiste HJ, Schwarz CG et al (2018b) Longitudinal tau PET in ageing and Alzheimer's disease. Brain 141:1517–1528
Jack C, Holtzman D, Sperling R (2019a) Dementia is not synonymous with Alzheimer's disease. Sci Transl Med 11:2–4
Jack CRJ, Wiste HJ, Therneau TM et al (2019b) Associations of amyloid, tau, and neurodegeneration biomarker profiles with rates of memory decline among individuals without dementia. JAMA 321:2316–2325
de Jager CA, Honey TE, Birks J, Wilcock GK (2010) Retrospective evaluation of revised criteria for the diagnosis of Alzheimer's disease using a cohort with post-mortem diagnosis. Int J Geriatr Psychiatry 25:988–997
Jagust W, Jack CR, Bennett DA et al (2019) "Alzheimer's disease" is neither "Alzheimer's clinical syndrome" nor "dementia". Alzheimers Dement 15:153–157
Jang KT, Choe GY, Suh YL, Chi JG (1999) Cerebral amyloid angiopathy: a report of two cases. Korean J Pathol 33:741–744
Jelic V, Kivipelto M, Winblad B (2006) Clinical trials in mild cognitive impairment: lessons for the future. J Neurol Neurosurg Psychiatry 77:429–438
Jicha GA, Parisi JE, Dickson DW et al (2006) Neuropathologic outcome of mild cognitive impairment following progression to clinical dementia. Arch Neurol 63:674
Katzman R (1976) The prevalence and malignancy of Alzheimer disease: a major killer. Arch Neurol 33:217–218
Katzman R, Kawas CH (1994) The epidemiology of dementia and Alzheimer disease. In: Terry RD, Katzman R, Bick KL (eds) Alzheimer disease. Ravens Press, New York, NY, pp 105–122
Katzman R, Terry R, DeTeresa R et al (1988) Clinical, pathological, and neurochemical changes in dementia: a subgroup with preserved mental status and numerous neocortical plaques. Ann Neurol 23:138–144
Klunk WE, Engler H, Nordberg A et al (2004) Imaging brain amyloid in Alzheimer's disease with Pittsburgh Compound-B. Ann Neurol 55:306–319
Knopman DS, Gottesman RF, Sharrett AR et al (2016) Mild cognitive impairment and dementia prevalence: The Atherosclerosis Risk in Communities neurocognitive study. Alzheimer Dement Diagnosis Assess Dis Monit 2:1–11
Koivunen J, Scheinin N, Virta JR et al (2011) Amyloid PET imaging in patients with mild cognitive impairment: a 2-year follow-up study. Neurology 76:1085–1090
Kraepelin E (1910) Psychiatrie. In: Ein Lehrbuch für Studierende und Ärzte. II. Bd., Klinische Psychiatrie, 8th edn. Barth, Leipzig
Langa KM, Burke JF (2019) Preclinical Alzheimer disease - early diagnosis or overdiagnosis? JAMA Intern Med 179:1161–1162

Lilamand M, Cesari M, Cantet C, Andrieu S (2019) Relation entre dépôts amyloïdes cérébraux et autonomie pour les activités instrumentales de la vie quotidienne des sujets âgés. Geriatr Psychol Neuropsychiatr Du Vieil 17(2):211

Lim YY, Kalinowski P, Pietrzak RH et al (2018) Association of ß-Amyloid and apolipoprotein e e4 with memory decline in preclinical Alzheimer disease. JAMA Neurol 75:488–494

Louie R (2019) The 2018 NIA-AA research framework: recommendation and comments. Alzheimers Dement 15:182–183

Lowe VJ, Bruinsma TJ, Min HK et al (2018) Elevated medial temporal lobe and pervasive brain tau-PET signal in normal participants. Alzheimer Dement Diagnosis Assess Dis Monit 10:210–216

Machulda MM, Hagen CE, Wiste HJ et al (2017) Practice effects and longitudinal cognitive change in clinically normal older adults differ by Alzheimer imaging biomarker status. Clin Neuropsychol 31:99–117

Matthews FE, Stephan BC, Bond J, McKeith I, Brayne C (2007) Operationalization of mild cognitive impairment: a graphical approach. PLoS Med 4:1615–1619

Mattsson N, Smith R, Strandberg O et al (2018) Comparing 18 F-AV-1451 with CSF t-tau and p-tau for diagnosis of Alzheimer disease. Neurology 90:E388–E395

McCleery J, Flicker L, Richard E, Quinn TJ (2019a) When is Alzheimer's not dementia - Cochrane commentary on the National Institute on Ageing and Alzheimer's Association Research Framework for Alzheimer's disease. Age Ageing 48:174–177

McCleery J, Flicker L, Richard E, Quinn TJ (2019b) The National Institute on Aging and Alzheimer's Association research framework: a commentary from the Cochrane Dementia and Cognitive Improvement Group. Alzheimers Dement 15:179–181

McKhann G, Drachman D, Folstein M, Katzman R, Price D, Stadlan EMM (1984) Clinical diagnosis of Alzheimer's disease: report of the NINCDS-ADRDA Work Group* under the auspices of Department of Health and Human Services Task Force on Alzheimer's Disease. Neurology 34:939–939

McKhann GM, Knopman DS, Chertkow H et al (2011) The diagnosis of dementia due to Alzheimer's disease: recommendations from the National Institute on Aging-Alzheimer's Association workgroups on diagnostic guidelines for Alzheimer's disease. Alzheimers Dement 7:263–269

Medina M, Khachaturian ZS, Rossor M, Avila J, Cedazo-Minguez A (2017) Toward common mechanisms for risk factors in Alzheimer's syndrome. Alzheimers Dement (N Y) 3:571. https://doi.org/10.1016/j.trci.2017.08.009

Mitchell AJ, Shiri-Feshki M (2009) Rate of progression of mild cognitive impairment to dementia--meta-analysis of 41 robust inception cohort studies. Acta Psychiatr Scand 119:252–265

Monsell SE, Mock C, Hassenstab J et al (2014) Neuropsychological changes in asymptomatic persons with Alzheimer disease neuropathology. Neurology 83:434–440

Mormino EC, Betensky RA, Hedden T et al (2014) Synergistic effect of β-amyloid and neurodegeneration on cognitive decline in clinically normal individuals. JAMA Neurol 71:1379–1385

Mormino EC, Papp KV, Rentz DM et al (2017) Early and late change on the preclinical Alzheimer's cognitive composite in clinically normal older individuals with elevated amyloid β. Alzheimers Dement 13:1004–1012

Morris JC, Roe CM, Grant EA et al (2009) Pittsburgh compound B imaging and prediction of progression from cognitive normality to symptomatic Alzheimer disease. Arch Neurol 66:1469–1475

Morris GP, Clark IA, Vissel B (2018) Questions concerning the role of amyloid-β in the definition, aetiology and diagnosis of Alzheimer's disease. Acta Neuropathol 136:663–689

Mortimer JA (2012) The Nun Study: risk factors for pathology and clinical-pathologic correlations. Curr Alzheimer Res 9:621–627

Mozersky J, Sankar P, Harkins K, Hachey S, Karlawish J (2018) Comprehension of an elevated amyloid positron emission tomography biomarker result by cognitively normal older adults. JAMA Neurol 75:44–50

Mufson EJ, Malek-Ahmadi M, Snyder N, Ausdemore J, Chen K, Perez SE (2016) Braak stage and trajectory of cognitive decline in noncognitively impaired elders. Neurobiol Aging 43:101–110

Ossenkoppele R, Tolboom N, Foster-Dingley JC et al (2012) Longitudinal imaging of Alzheimer pathology using [11C]PIB, [18F]FDDNP and [18F]FDG PET. Eur J Nucl Med Mol Imaging 39:990–1000

Palmer K, Backman L, Winblad B, Fratiglioni L (2008) Mild cognitive impairment in the general population: occurrence and progression to Alzheimer disease. Am J Geriatr Psychiatry 16:603–611

Parnetti L, Chipi E, Salvadori N, D'Andrea K, Eusebi P (2019) Prevalence and risk of progression of preclinical Alzheimer's disease stages: a systematic review and meta-analysis. Alzheimers Res Ther 11:1–13

Perez-Nievas BG, Stein TD, Tai HC et al (2013) Dissecting phenotypic traits linked to human resilience to Alzheimer's pathology. Brain 136:2510–2526

Perneczky R, Kempermann G, Korczyn AD et al (2019) Translational research on reserve against neurodegenerative disease: consensus report of the International Conference on Cognitive Reserve in the Dementias and the Alzheimer's Association Reserve, Resilience and Protective Factors Professional Interest Area Working Groups. BMC Med 17:1–15

Petersen RC, Negash S (2008) Mild cognitive impairment: an overview. CNS Spectr 13:45–53

Petersen RC, Smith GE, Waring SC, Ivnik RJ, Tangalos EG, Kokmen E (1999) Mild cognitive impairment: clinical characterization and outcome. Arch Neurol 56:303–308

Petersen RC, Doody R, Kurz A et al (2001) Current concepts in mild cognitive impairment. Arch Neurol 58:1985–1992

Petersen RC, Wiste HJ, Weigand SD et al (2016) Association of elevated amyloid levels with cognition and biomarkers in cognitively normal people from the community. JAMA Neurol 73:85–92

Qiu Y, Jacobs DM, Messer K, Salmon DP, Feldman HH (2019) Cognitive heterogeneity in probable Alzheimer disease: clinical and neuropathologic features. Neurology 93:E778–E790

Rabinovici GD, Carrillo MC (2019) Biomarker-informed treatment decisions in cognitively impaired patients do not apply to preclinical Alzheimer disease. JAMA Intern Med 179:1736–1737

Raj A, LoCastro E, Kuceyeski A, Tosun D, Relkin N, Weiner M (2015) Network diffusion model of progression predicts longitudinal patterns of atrophy and metabolism in Alzheimer's disease. Cell Rep 10:359–369

Reiman EM, Chen K, Alexander GE et al (2004) Functional brain abnormalities in young adults at genetic risk for late-onset Alzheimer's dementia. Proc Natl Acad Sci U S A 101:284–289

Reisberg B, Ferris SH, Kluger A, Franssen E, Wegiel J, de Leon MJ (2008) Mild cognitive impairment (MCI): a historical perspective. Int Psychogeriatr 20:18–31

Resnick SM, Sojkova J, Zhou Y et al (2010) Longitudinal cognitive decline is associated with fibrillar amyloid-beta measured by [11C]PiB. Neurology 74:807–815

Risacher SL, Saykin AJ, West JD, Shen L, Firpi HA, McDonald BC (2009) Baseline MRI predictors of conversion from MCI to probable AD in the ADNI cohort. Curr Alzheimer Res 6:347–361

Rothschild D, Trainor MA (1937) Pathologic changes in senile psychoses and their psychobiologic significance. Am J Psychiatr 93:757. https://doi.org/10.1176/ajp.93.4.757

Saint Jean O, Favereau E (2018) Alzheimer, le grand leurre. Michalon, Paris

Scheltens P, Leys D, Barkhof F et al (1992) Atrophy of medial temporal lobes on MRI in 'probable' Alzheimer's disease and normal ageing: diagnostic value and neuropsychological correlates. J Neurol Neurosurg Psychiatry 55:967–972

Schermer MHN, Richard E (2019) On the reconceptualization of Alzheimer's disease. Bioethics 33:138–145

Schoonenboom NSM, van der Flier WM, Blankenstein MA et al (2008) CSF and MRI markers independently contribute to the diagnosis of Alzheimer's disease. Neurobiol Aging 29:669–675

Seab JP, Jagust WJ, Wong STS, Roos MS, Reed BR, Budinger TF (1988) Quantitative NMR measurements of hippocampal atrophy in Alzheimer's disease. Magn Reson Med 8:200–208

Seppälä TT, Nerg O, Koivisto AM et al (2012) CSF biomarkers for Alzheimer disease correlate with cortical brain biopsy findings. Neurology 78:1568–1575

Shaw LM, Vanderstichele H, Knapik-Czajka M et al (2009) Cerebrospinal fluid biomarker signature in Alzheimer's disease neuroimaging initiative subjects. Ann Neurol 65:403–413

Sperling RA, Aisen PS, Beckett LA et al (2011) Toward defining the preclinical stages of Alzheimer's disease: recommendations from the National Institute on Aging-Alzheimer's Association workgroups on diagnostic guidelines for Alzheimer's disease. Alzheimers Dement 7:280–292

Sperling RA, Mormino EC, Schultz AP et al (2019) The impact of amyloid-beta and tau on prospective cognitive decline in older individuals. Ann Neurol 85:181–193

Stanley K, Stevens T, Walker Z (2019) The use of biomarkers in Alzheimer's disease: a case report. Prog Neurol Psychiatry 23:10–14

Stelzmann RA, Schnitzlein HN, Murtagh FR (1995) An English translation of Alzheimer's 1907 paper, 'Uber eine eigenartige Erkankung der Hirnrinde'. Clin Anat 8:429–431

Stern Y (2012) Cognitive reserve in ageing and Alzheimer's disease. Lancet Neurol 11:1006–1012

Stern Y, Arenaza-Urquijo EM, Bartrés-Faz D et al (2018) Whitepaper: defining and investigating cognitive reserve, brain reserve, and brain maintenance. Alzheimers Dement S1552–5260:33491–33495

Stomrud E, Hansson O, Blennow K, Minthon L, Londos E (2007) Cerebrospinal fluid biomarkers predict decline in subjective cognitive function over 3 years in healthy elderly. Dement Geriatr Cogn Disord 24:118–124

Strozyk D, Blennow K, White LR, Launer LJ (2003) CSF Aß 42 levels correlate with amyloid-neuropathology in a population-based autopsy study. Neurology 60:652–656

Swanson CJ, Zhang Y, Dhadda S et al (2018) Treatment of early AD subjects with BAN2401, an anti-Aβ protofibril monoclonal antibody, significantly clears amyloid plaque and reduces clinical decline. Alzheimers Dement 14:P1668

Sweeney MD, Montagne A, Sagare AP et al (2019) Vascular dysfunction—the disregarded partner of Alzheimer's disease. Alzheimers Dement 15:158–167

Tapiola T, Alafuzoff I, Herukka SK et al (2009) Cerebrospinal fluid β-amyloid 42 and tau proteins as biomarkers of Alzheimer-type pathologic changes in the brain. Arch Neurol 66:382–389

Van De Pol LA, Hensel A, Van Der Flier WM et al (2006) Hippocampal atrophy on MRI in frontotemporal lobar degeneration and Alzheimer's disease. J Neurol Neurosurg Psychiatry 77:439–442

Varma AR, Snowden JS, Lloyd JJ, Talbot PR, Mann DM, Neary D (1999) Evaluation of the NINCDS-ADRDA criteria in the differentiation of Alzheimer's disease and frontotemporal dementia. J Neurol Neurosurg Psychiatry 66:184–188

Villain N, Dubois B (2019) Alzheimer's disease including focal presentations. Semin Neurol 39:213–226

Villemagne VL, Burnham S, Bourgeat P et al (2013) Amyloid β deposition, neurodegeneration, and cognitive decline in sporadic Alzheimer's disease: a prospective cohort study. Lancet Neurol 12:357–367

Whitehouse PJ, George D, Daniel R (2008) The myth of Alzheimer's: what you aren't being told about today's most dreaded diagnosis. St. Martin's Press, New York, NY

Younes L, Albert M, Moghekar A, Soldan A, Pettigrew C, Miller MI (2019) Identifying change-points in biomarkers during the preclinical phase of Alzheimer's disease. Front Aging Neurosci 11:1–11

Yu JT, Li JQ, Suckling J et al (2019) Frequency and longitudinal clinical outcomes of Alzheimer's AT(N) biomarker profiles: a longitudinal study. Alzheimers Dement 15:1208–1217

14 Perfusion SPECT: Its Role in the Diagnosis and Differential Diagnosis of Alzheimer's Disease, with Particular Emphasis on Guidelines

Ronald W. J. van Rheenen, Gilles N. Stormezand, Jacoba P. van Amerongen, Andreas Otte, Peter Paul De Deyn, and Rudi A. J. O. Dierckx

Contents

14.1 Introduction 454
14.2 Guidelines 455
14.3 Accuracy of the *Clinical* Diagnosis of Alzheimer's Disease 456
14.4 Perfusion Pattern in AD 458
14.5 Accuracy of Perfusion SPECT for Alzheimer's Disease 460
14.6 SPECT in the Differential Diagnosis of Alzheimer's Disease 462
14.7 Status Praesens 463
References 465

R. W. J. van Rheenen · G. N. Stormezand (✉)
Department of Nuclear Medicine and Molecular Imaging, University Medical Center Groningen, University of Groningen, Groningen, The Netherlands
e-mail: r.van.rheenen@umcg.nl; g.n.stormezand01@umcg.nl

J. P. van Amerongen
Department of Neurology, Medisch Spectrum Twente, Enschede, The Netherlands

A. Otte
Faculty of Electrical Engineering, Medical Engineering and Computer Science, Offenburg University, Offenburg, Germany
e-mail: andreas.otte@hs-offenburg.de

P. P. De Deyn
Laboratory of Neurochemistry and Behavior, Department of Biomedical Sciences, Institute Born-Bunge, Born Bunge Foundation, University of Antwerp, Antwerp, Belgium

Department of Neurology, Alzheimer Research Center, University Medical Center Groningen, University of Groningen, Groningen, The Netherlands

R. A. J. O. Dierckx
Nuclear Medicine and Molecular Imaging, University Medical Center Groningen, Groningen, Groningen, The Netherlands
e-mail: r.a.dierckx@umcg.nl

R. A. J. O. Dierckx et al. (eds.), *PET and SPECT in Neurology*,
https://doi.org/10.1007/978-3-030-53168-3_14

Abstract

Dementia is a clinical diagnosis reflecting many possible underlying pathologies, for example, vascular dementia and neurodegenerative disorders such as frontotemporal dementia, Lewy body-type disorder or Alzheimer's disease (AD). The breakthrough of ^{99m}technetium-labelled perfusion tracers in the 1990s resulted in many SPECT studies of flow changes in AD. In the first decade of 2000, the role of perfusion SPECT was shifted from diagnosis towards differential diagnosis, parallel to the growing attention for diagnosing early stages of dementia. Previously a diagnosis based largely on a process of exclusion, new guidelines have emerged increasingly employing positive criteria to establish the diagnosis, including neuroimaging biomarkers. Nowadays, FDG PET has largely limited the role of perfusion SPECT, although it is still considered a valuable and cost-effective alternative when PET is not available.

14.1 Introduction

The development of perfusion tracers for brain imaging in the 1990s fuelled the interest in the potential role of perfusion SPECT for clinical questions related to dementia. Their theoretical utility relied on the results of PET perfusion studies using radioactive water. At that time, only a few centres worldwide disposed of PET scanners, radiochemical facilities, cyclotron and necessary expertise, hence, exist a clinical need, particularly in cerebrovascular disorders and dementia, for a commercially available SPECT equivalent enabling brain examinations on a larger scale. This need for SPECT perfusion tracers was rather urgent as morphological imaging techniques, such as CT scan and especially MRI, still were not widely available.

Imaging characteristics of ^{133}xenon and its logistical complexity hampered its breakthrough in a routine clinical environment at the benefit of iodine-123 and ^{99m}technetium-labelled pharmaceuticals. ^{123}I-labelled iodoamphetamine (IMP) was the first SPECT perfusion tracer with good imaging characteristics. Because of the relatively high cost of ^{123}iodine as a cyclotron-produced isotope, the use of ^{123}I-IMP remained limited (especially to Japan) and thus paved the way for development of the less expensive ^{99m}technetium-labelled pharmaceuticals, at first ^{99m}Tc-hexamethylpropylene amine oxime (HMPAO) and later on ^{99m}Tc-cysteinate dimer (^{99m}Tc-ethylene biyldicysteinate dimer; ECD). Commercialization of kits, allowing labelling with ^{99m}technetium, a cheap radionuclide available on a daily basis, gave a major boost to their accessibility and use (De Deyn et al. 1997).

Indications focused particularly on disorders such as dementia, in which morphological imaging did not provide all the requested clinical answers. Especially the presence of a distribution pattern considered to be typical for AD, which was developed from research, supported the clinician's confidence in establishing a diagnosis (De Deyn et al. 1997).

14.2 Guidelines

Already in 1994, the *Consensus development for producing diagnostic procedure guidelines on SPECT brain perfusion imaging* stated dementia explicitly as a 'widely accepted and suggested indication of SPECT in neuropsychiatry' (Fletcher et al. 1994).

Looking at the chronology of SPECT guidelines for dementia, it is noteworthy that they do not only reflect the development in thinking on dementia but also in evidence-based medical practice. These guidelines were at first often the result of clinical consensus amongst opinion leaders, while later on they were increasingly based on systematic reviews, meta-analyses and even health-economic evaluation. This evolution was a result of the rise and growth of electronic libraries and internet facilities, with their search engines and other functionalities.

The development of the European Association of Nuclear Medicine (EANM) guidelines started between 1998 and 2001 with a dedicated *Task Group on Quality Assurance and Standardization*. Clinical utility of investigations in terms of sensitivity and specificity was not considered in the guidelines of the EANM nor in those of the American College of Radiologists. These guidelines report indications for imaging that are positive and include dementias, but the emphasis of these guidelines was on procedure rather than on cost-effectiveness (Pimlott and Ebmeier 2007).

Despite large case-control studies that were available, the early guidelines stated that SPECT should only be used in specific recommended cases and should not be included in the routine evaluation of dementing patients (Waldemar et al. 2000; Knopman et al. 2001).

The *consensus paper of the European Alzheimer's disease consortium* recommended, on the basis of contemporary guidelines, that SPECT or PET should only be used in selected cases of diagnostic uncertainty, where these imaging modalities can provide significant incremental information (Waldemar et al. 2000; Knopman et al. 2001). Since the beginning of this century, larger and more clinically realistic studies have accumulated. These studies suggest that perfusion SPECT provides a higher specificity (91%) in the differential diagnosis of Alzheimer's dementia against other types of dementia than clinical diagnostic criteria (70%), although its sensitivity is limited (Pimlott and Ebmeier 2007).

Since 2007, consensus criteria published by Dubois and colleagues allowed neuroimaging tests to be used as a positive criterion for AD, whereas the diagnosis used to be based on a process of exclusion (Dubois et al. 2007). In this context, abnormalities on perfusion SPECT, as well as FDG PET and anatomic MRI may be viewed as an in vivo (progression) marker of the neuronal degeneration in AD. This feature, along with clinical evidence of an amnestic syndrome of the hippocampal type, could support the diagnosis of AD, both in the prodromal phase and in the dementia phase. It has to be stressed that to establish the diagnosis according to the novel framework, also pathophysiological or 'diagnostic' markers are required (e.g. increased tau levels in CSF, amyloid tracer retention on PET) (Dubois 2018).

Caution is warranted as the recent enthusiasm for evidence-based guidelines has led to the impression that they may replace physician's experience and expert opinion. While this is obviously not the case, the value of every opinion-based analysis could be improved if a formalized review of existing evidence was included. In summary, evidence-based guidelines should be seen as an additional tool, but not as the only tool in the clinicians' toolbox (Gronseth and French 2008).

Additionally, it is important to be aware of the fact that the classification of evidence does not pertain to a study, but rather to a question. Thus, the same study could provide a high level of evidence for one question but a low level for another (French and Gronseth 2008).

This same line of thought can be applied to the use of guidelines beyond the framework they were originally designed for. In recent years, guidelines have gained a more stringent character, sometimes even with legal implications or as a major weighting factor for reimbursement within a health insurance system. To counter this bias, some societies, such as the Dutch Society of Nuclear Medicine, have deliberately chosen to use the word 'recommendations' rather than 'guidelines' (Barneveld and van Urk 2007).

14.3 Accuracy of the *Clinical* Diagnosis of Alzheimer's Disease

Dementia is a clinical diagnosis reflecting many possible underlying pathologies, for example, vascular dementia and neurodegenerative disorders such as frontotemporal dementia, Lewy body-type disorder or Alzheimer's disease (AD). The latter is presently considered the number one pathology in dementia in terms of incidence and socioeconomic impact. Hebert et al. in 2001 reported in the United States 53 new Alzheimer's cases per 1000 people ageing from 65 to 74 years, 170 new cases per 1000 people ageing from 75 to 84 years and 231 new cases per 1000 people over the age of 85 (Hebert et al. 2001).

The first written description of AD in 1907 concerned a 55-year-old woman (initials A.D., 1850–1906), with prominent psychiatric symptoms, including agitation, paranoia and delusions (Alzheimer 1907). She died prematurely of a rapid downhill course of early-onset dementia. Upon neuropathological examination, Alois Alzheimer (1864–1915), a German psychiatrist and pathologist, noted a mass of disordered twisted protein fragments (Creutzfeldt 1920). Since the publication of a textbook by Kraepelin in 1910, this pathology was named Alzheimer's dementia.

However, in the course of time, focus of interest concerning the disease has shifted to higher ages, i.e. older than 65 years rather than younger, to predominantly cognitive changes (loss of episodic memory) rather than to psychiatric symptoms and to the extracellular accumulation of amyloid and the concomitant inflammation, rather than to the appearance of intracellular neurofibrillary tangles.

While 50–90% of patients go unrecognized in communities, this figure still amounts to 60% in the primary care setting (Thies and Bleiler 2013). In this context, diagnosis and differential diagnosis are the main clinical challenge, especially since

evaluation may be cost-effective even for the 2% of patients who are diagnosed with so-called 'treatable' dementia, for example, brain tumours (Degnan and Levy 2014). Moreover, in addition to relevance for adequate treatment options, accurate diagnosis has social and prognostic implications.

Meanwhile, it has also been recognized that AD pathology may exist almost 20 years before the onset of first symptoms, often consisting of mild cognitive impairment, especially the amnestic type. Mild cognitive impairment is four times more common than dementia and poses additional diagnostic problems as 15% per year convert to AD, while others remain stable or revert (Thies and Bleiler 2013).

Several studies in AD validating clinical diagnosis versus final histopathological diagnosis (golden standard) showed accuracy not to be 100%, resulting in false positives and false negatives (see Table 14.1). Table 14.1 summarizes sensitivity and specificity in approximately 200 persons. These older studies around the turn of the millennium made use of the available diagnostic criteria of the Diagnostic and Statistical Manual of Mental Disorders in psychiatry (DSM-III, revisited) and the criteria for possible and probable AD of the National Institute of Neurological and Communicative Diseases and Stroke/Alzheimer's Disease and Related Disorders Association in neurology.

Interestingly, using the DSM-IIIR criteria in the study by Jobst et al. resulted in the highest specificity, while the application of NINCDS-ADRDA criteria for possible AD yielded the highest sensitivity. Hence, in clinical practice a combined approach was advocated in which both criteria were applied in subsequent order, first aiming at sensitivity and subsequently at specificity.

However, Jobst et al. also pointed out the existence of different sets of neuropathological criteria, resulting in different sets of 'gold standards' (Khachaturian 1985; Tierney et al. 1986; Mirra et al. 1991).

A more recent article in 2004 by Silverman et al. reviewed the validity of clinical diagnosis. They concluded physicians frequently failed in making the diagnosis of AD when the disease is present, mostly due to additional atypical symptoms. Also physicians often failed in diagnosing early AD, when its clinical symptoms were subtle or almost absent (Silverman 2004).

Table 14.1 Studies validating diagnostic accuracy of AD versus histopathological conformation

Studies	Diagnosis	Sensitivity (%)	Specificity (%)	Accuracy (%)
Jobst et al. (1992a) (n = 118)	DSM-IIIR	51	97	66
	NINCDS-ADRDA Possible AD	93	61	77
	NINCDS-ADRDA Probable AD	49	100	66
	NINCDS-ADRDA Possible and probable AD combined	96	61	85
Jagust et al. (2001) (n = 70)	NINCDS-ADRDA Probable AD	59	87	71

The same review states that in the recent report of the *Quality Standards Subcommittee of the American Academy of Neurology*, only three class I studies were identified in which the diagnostic value of clinical assessment could meaningfully be measured. Only one of them focused on evaluating dementia at a relatively early stage (Silverman 2004).

Moreover, the Silverman review stresses that in these studies the reported sensitivities and specificities do not represent the diagnostic accuracy of an initial clinical evaluation but the diagnostic accuracy of an entire series of evaluations repeated over a period of years (Silverman 2004).

Depending on the expertise of the referring physician, more clinical accuracy may thus be expected, especially in case of specialized memory clinics. On the other hand, diagnostic accuracy declines in cases of early and/or atypical symptoms. In these cases with so-called intermediate probability, further arguments to confirm or exclude the diagnosis may be sought in additional imaging investigations.

In the workup of dementia patients, initial anatomical imaging allows, on the one hand, to exclude treatable disease, such as brain tumours, on the other hand, allows volumetric assessment of hippocampus. Already in the study of Jobst et al., CT scans pointed towards diagnostic AD-related volume losses in hippocampus, entorhinal cortex and less often parahippocampus, with medial temporal lobe atrophy at a rate ten times that observed in controls (Jobst et al. 1992b). These findings paved the way for imaging, not only to assess the presence of treatable disease but also to substantiate whether or not a patient suffers from a dementia disorder.

14.4 Perfusion Pattern in AD

There is a close relationship between brain metabolism and perfusion, as local metabolism is the driving force behind local microperfusion. This principle holds in physiology and most pathological conditions, such as degenerative disorders. It is used in perfusion SPECT and thus enables the imaging of neurodegenerative disorders, which may cause a decrease in metabolism and thus a decrease in microperfusion (Roy and Sherrington 1890; Lou et al. 1987; Kuschinsky 1991).

The first single-photon emitter used for evaluation of regional cerebral blood flow (rCBF) was ^{133}xenon (Lassen 1980). These early investigations showed a close coupling between rCBF and neuronal activity. A decrease in neural function due to Alzheimer's disease resulted in a decrease in rCBF. Calculations were performed using a wash-in and wash-out method, relying on the fact that ^{133}xenon is freely diffusible in brain tissue. Using planar imaging, the ^{133}xenon method received clinical attention, but after the SPECT technique emerged, interest declined because of poor image quality as compared to its upcoming competitors.

Tracers with improved kinetics were needed, which resulted in the synthesis of three new compounds: IMP, HMPAO and ECD. IMP is dependent on amine-binding sites, HMPAO is trapped within the cell by interaction of the lipophilic complex with glutathione and ECD is retained by metabolic transformation into an acid

product by specific enzymatic processes in brain tissue (Winchell et al. 1980; Ballinger et al. 1988; Walovitch et al. 1994; De Deyn et al. 1997). Because of differences in tracer kinetics, different regional tracer distributions were reported in several studies (Koyama et al. 1997; Inoue et al. 2003).

All of these tracers are intravenously injected; their biodistribution within the brain is proportional to the rCBF, whereafter they are trapped within the neurons. Studies have shown that this trapping is not affected in the majority of brain diseases, and thus a relatively low tracer uptake can be explained by a relatively low rCBF (Neirinckx et al. 1988). Imaging with ECD can be performed as early as 20 min after injection, but optimal image quality is obtained after 45 min. With HMPAO the minimal time interval is 40 min, with optimum imaging after 90 min (Juni et al. 1998).

In a landmark study in 1992, Holman provided a probability for a SPECT technical diagnosis of AD based on several distribution patterns. The highest probability of 82% was given to a pattern of bitemporal and biparietal hypoperfusion, decreasing to 77% for involvement of additional regions and 57% for unilateral temporal and parietal hypoperfusion. Major false positives consisted of vascular dementia, Parkinson's dementia and primary progressive aphasia. Moreover, solitary frontal lesions decreased probability further to 42% and proved to be attributable to progressive supranuclear palsy or HIV. Unfortunately, these figures were not validated on neuropathologically confirmed cases (Holman et al. 1992).

While studies in the 1990s used a region-of-interest technique (ROI), later studies introduced voxel analysis. The methodological drawback of selection of ROIs is that it depends on a priori hypotheses and leaves large brain areas unexplored. Voxel analysis is data driven and thus avoids the pitfall of subjectivity. Using such analysis in a longitudinal study in 1999, Kogure et al. demonstrated involvement of the posterior cingulate cortex and precuneus in early AD, reflecting functional deafferentation from entorhinal cortex. Subsequently, in moderate and severe AD, absolute rCBF decreases were noted in temporoparietal and medial temporal lobe cortices, which were further enhanced by atrophy (Kogure et al. 1999).

Finally, frontal lobe involvement may occur, but if isolated, other causes should be suspected (Hoffman et al. 2000). In time, larger areas of the brain get involved, and in parallel, hypometabolism also becomes more severe. On the other hand, specific brain regions remain spared and show normal perfusion and metabolism. These include sensorimotor and visual cortices, basal ganglia, thalamus, cerebellum and brainstem (Fig. 14.1).

Asymmetry often reflects neuropsychological findings, for example, visuospatial changes being related to more right-sided hypometabolism. Bilateral parietal hypometabolism was reported to occur in more severe cases of AD, early-onset AD and in men (Clarke et al. 2011). The increasing use of more specific (imaging) biomarkers has facilitated the identification of Alzheimer subtypes, including posterior cortical atrophy (PCA) and a logopenic variant of AD, grouped 'atypical AD' (Dubois et al. 2014). These may be accompanied by atypical findings on perfusion SPECT (Meyer and Hudock 2018).

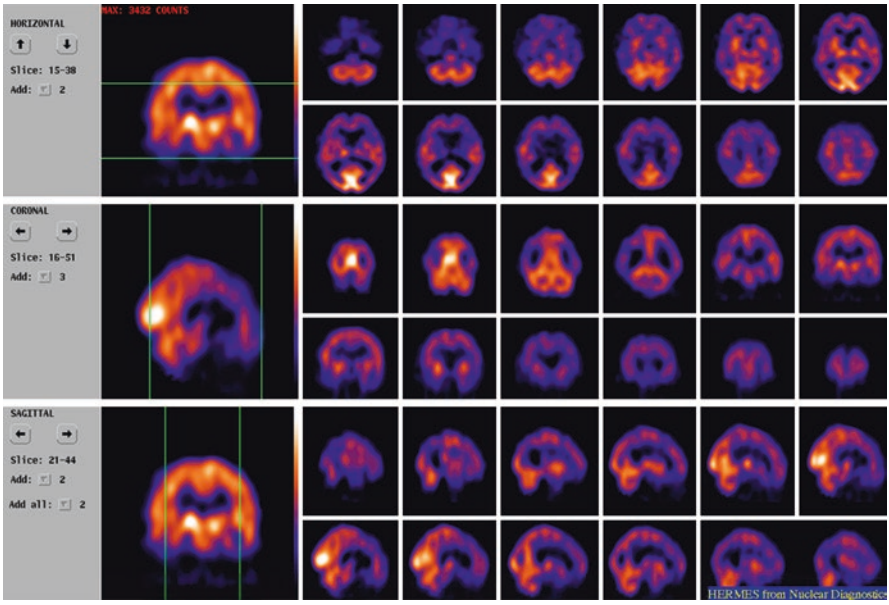

Fig. 14.1 ECD SPECT on a triple-headed gamma camera of a patient suffering from advanced AD, respective transaxial, coronal and sagittal slices. Extended hypoperfusion, especially of the posterior cortical regions, but sparing sensorimotor and visual cortices, basal ganglia, thalamus, cerebellum and brainstem

While accelerated atrophy occurs, it was shown that neocortical deficits (as observed in AD) reflect true metabolic reductions and are not just the result of atrophy (Ibáñez et al. 1998; de Santi et al. 2001).

Age-related hypoperfusion has been described and occurs more frontally as compared to temporal and parietal regions. Also small differences in perfusion patterns between men and women were suggested. Hence, age- and gender-stratified databases for different tracers were established, such as the *Ghent-Optimized Adult High-Resolution ECD Absolute Quantification Database* including 90 healthy volunteers (Slosman et al. 2001; van Laere et al. 2001; Silverman 2004).

It should be stressed, however, that distribution and hence use of such databases often remain limited to a few centres, mostly in the setting of research.

14.5 Accuracy of Perfusion SPECT for Alzheimer's Disease

Functional imaging such as HMPAO-SPECT or FDG-PET is requested to increase the diagnostic accuracy, the so-called incremental value of a diagnostic test.

In the 1990s, perfusion SPECT became indicated for the diagnosis of AD. In the 'consensus development for producing diagnostic procedure guidelines: SPECT brain perfusion imaging' published in 1994, Fletcher et al. reported on *widely accepted and suggested indications* of SPECT in neuropsychiatry. These

indications were ‘dementia, cerebrovascular pathology, seizure disorders’, while *accepted and suggested* indications consisted of ‘brain tumours, infectious disorders, brain injury, movement disorders and psychiatry’ (Fletcher et al. 1994).

The standard book on nuclear medicine at the time (Murray and Ell, first published in 1994) devoted already a chapter to SPECT and PET imaging in dementias, reflecting related interest and expectations. In 1996, the American Academy of Neurology assessed the role of brain SPECT to support the clinical diagnosis. The indication was rated as ‘established’, based on a class-II quality of evidence and strength of evidence type B (Altrocchi 1996).

In 1999, the Society of Nuclear Medicine released a procedure guideline for brain perfusion single-photon emission computed tomography (SPECT) using ^{99m}Tc radiopharmaceuticals. Evaluation of patients with suspected dementia was stated as a common indication (Juni et al. 1998).

An article by Catafau in 2001 aimed at providing fundamental knowledge on how and when to perform brain perfusion SPECT in clinical practice. Usefulness of perfusion SPECT in the differential diagnosis of dementia was explicitly mentioned as a good example (Catafau 2001).

The diagnostic value of perfusion SPECT in terms of specificity and sensitivity for the diagnosis of AD is presented in Table 14.2, which comprises three studies with validation against the gold standard of neuropathology.

Jobst and Jagust commented on the added value of SPECT as compared to clinical diagnosis. Jobst et al. concluded that combining HMPAO-SPECT and the temporal lobe-oriented X-ray CT scans resulted in a false-positive rate <10% instead of 25% for a clinical diagnosis (Jobst et al. 1992a).

In a similar study published later in 2001, Jagust et al. demonstrated that a positive SPECT increases the likelihood of clinical diagnosis of AD from 84% to 92%, while a negative SPECT decreases the likelihood to 70% (Jagust et al. 2001).

However, it must be stated that, for obvious reasons, these neuropathological studies did not investigate specifically the role of SPECT in *early* diagnosis. Often subgroup analysis in the aforementioned populations of AD was used to advocate perfusion SPECT in early AD, although clear figures on larger series for this indication are not available.

Using the Web of Science and PubMed for the period between 1988 and 2012, a limited number of references are found applying a search for ‘early and AD and sensitivity and SPECT’. Some articles published before 2004 give a positive indication, albeit cautiously (Prohovnik et al. 1988; Perani et al. 1988; Kogure et al. 1999).

Table 14.2 Diagnostic performance of perfusion SPECT versus neuropathological confirmation

Studies	Technique	Sensitivity (%)	Specificity (%)	Accuracy (%)
Bonte et al. (1997)	SPECT	86	73	–
Jagust et al. (2001)	SPECT	93	56	81
Jobst et al. (1992a)	SPECT	89	80	83
	CT	85	78	80
	SPECT + CT	80	93	88

Interestingly, in 1996, the American Academy of Neurology already stated that SPECT is an established technique for supporting the clinical diagnosis of AD. A relevant point in this regard was that perfusion changes may *precede* (or follow) neuropsychological changes.

Hence, in clinical practice it was not uncommon for patients to be referred for diagnosis of early AD. Indication for perfusion SPECT in this subgroup was then based on limited studies and a broad interpretation of the guidelines.

Finally, the accuracy of a diagnostic test is also largely related to the expertise of the interpreting physician. In an early publication, the interobserver agreement for HMPAO brain SPECT uptake patterns in 50 clinically diagnosed demented subjects (presumed AD, AD, vascular dementia) from four institutions was studied. The authors found significant reader agreement and a consensus sensitivity of 72% and specificity of 79% for identifying abnormalities in scans of demented subjects. In their final conclusion, they stated that interpretation of regional cerebral blood flow/SPECT images is concordant across multiple institutions and readers (Hellman et al. 1994).

14.6 SPECT in the Differential Diagnosis of Alzheimer's Disease

Another major clinical question was the contribution of SPECT to the clinical differential diagnosis. In a review in 2004 by Dougall et al., articles published between 1985 and 2002 were retrieved systematically from MEDLINE and EMBASE, cross-referencing with personal collections and 13 narrative reviews. Of 301 studies identified, 48 survived exclusion criteria and contained extractable data. Pathological verification studies suggest that clinical criteria may be more sensitive in detecting AD than brain SPECT (81% versus 74%). However, SPECT studies provide a higher specificity against other types of dementia than clinical criteria (91% versus 70%). Dougall et al. therefore concluded SPECT may be helpful in the differential diagnosis of AD (Dougall et al. 2004).

Pooling data in an exploratory manner from both the Bonte and Jagust studies gives a weighted sensitivity for brain SPECT against neuropathology of 74% and a weighted specificity of 91%.

Therefore, the use of pathological verification as a gold standard suggests that clinical criteria are more sensitive than brain SPECT (81% versus 74%) and that brain SPECT has a higher specificity than clinical criteria (91%, versus 70%) (Dougall et al. 2004).

Studies selected for this systematic review, however, were graded higher if ^{99m}Tc-HMPAO-SPECT brain images were assessed independently from clinical information to minimize bias. Of course, this does not reflect clinical practice, since clinicians routinely interpret ^{99m}Tc-HMPAO-SPECT images alongside clinical information (Dougall et al. 2004). The meta-analyses presented therefore provide a conservative estimate of the usefulness of ^{99m}Tc-HMPAO-SPECT as a standalone diagnostic instrument and do not accurately reflect the usefulness of the test as an adjunct to complementary clinical information (Dougall et al. 2004).

Several articles have demonstrated that SPECT provides useful positive information in dementia, particularly in the differentiation of AD and frontotemporal dementia. In a study from 1995, SPECT predicted pathologic diagnosis in 92.6% of 27 patients with dementia as compared with clinical diagnosis, which predicted 74.1%. Distinct patterns were associated with dementia caused by AD, frontotemporal dementia (FTD) and Creutzfeldt-Jakob disease (CJD) (Miller et al. 1991; Read et al. 1995).

In a publication concerning the discriminative use of SPECT in frontal lobe-type dementia (FLD) versus (senile) dementia of the Alzheimer's type, bifrontal hypoperfusion was found to be the most powerful predictor of clinical classification. Using the model described, 81% of the patients in the FLD group and 74% of the patients in the (S)DAT group were correctly classified (Pickut et al. 1997).

Another study confirmed the association of frontal or anterior perfusion deficits with frontotemporal dementia and not with AD (Miller and Gearhart 1999). Using a simple decision rule based on discriminant analysis of SPECT data, 20 patients with probable AD and 20 with probable frontotemporal dementia were evaluated. One hundred percent of patients with frontotemporal dementia and 90% of patients with AD were correctly classified (Miller and Gearhart 1999; Petrella et al. 2003).

An investigation reported a major increase in sensitivity when comparing consensus criteria versus MRI and SPECT/PET scan: 35.5% vs. 63.5% vs. 90.5%. The authors concluded that the clinical diagnosis of FTD needs to combine neuropsychiatric features with SPECT or PET findings and monitor changes in neuropsychological test scores (Mendez et al. 2007).

14.7 Status Praesens

SPECT has been the subject of major developments in terms of hard- and software, methodology, tracer developments and larger validations. Advances especially in voxel-based statistical analysis have markedly enhanced the value of brain perfusion SPECT in diagnosing early AD at the stage of mild cognitive impairment (Matsuda 2007).

On the other hand, nowadays the role of perfusion SPECT has been largely replaced by FDG-PET, with Medicare approval in 2004. The widespread availability of FDG-PET after its major breakthrough in oncology has also boosted its clinical use in AD. In the brain, FDG-PET shows mostly glutamate-driven astrocytic glucose uptake. Mean sensitivity for AD proved to be 90%, with lower specificity in differential diagnosis. Reviews by Yuan et al. and Bloudek et al. reported slightly superior diagnostic accuracy for FDG PET in comparison to perfusion SPECT with respect to conversion of MCI to AD and for diagnosing AD (Bloudek et al. 2011; Yuan et al. 2009). More recently, a systematic review pointed out that there were few head-to-head studies available comparing SPECT and PET and that the evidence to suggest the superiority of PET was limited (Davison and O'Brien 2014).

Neuroreceptor imaging using ^{11}C- or ^{18}F-labelled radioligands has become the playground of PET, because of the radiochemical success and possibilities for quantification.

A ^{11}C-labelled tracer, Pittsburgh B (^{11}C-PIB), has paved the way for ^{18}F-labelled tracers capable of visualizing amyloid deposition, one of the major histopathological hallmarks of AD, although critical reflection about their diagnostic value has been necessary (Silverman 2004; Schaller 2008; Bohnen et al. 2012). Amyloid deposition has raised a lot of discussion and confusion over the last decades, in the beginning focusing on uncertainties regarding its diagnostic consequences, and more recently on its place in the diagnostic algorithm. Although healthy subjects may have increased amyloid deposition, increased deposition may indicate Alzheimer's disease, but it was not known to what extent. One interesting publication showing no clear dependence of clinical dementia on amyloid deposition involved 678 nuns, the so-called Nun Study (Snowdon and Nun Study 2003). More recently, the diagnostic value of amyloid PET has become clearer, as more data became available. As a general rule of thumb, amyloid imaging may add most value in younger patients at higher risk for Alzheimer's disease. The relatively low prevalence of amyloid positivity in younger healthy adults in these cases would increase the positive predictive value of amyloid PET, while retaining the high negative diagnostic value (Bergeron et al. 2018).

Comparison of perfusion SPECT with FDG-PET points towards a 15–20% higher diagnostic accuracy for FDG-PET. It was also shown that FDG-PET has prognostic value (Silverman et al. 2001). An interesting development is the inclusion of additional examinations such as FDG-PET in the clinical diagnostic criteria.

In summary, the most recent guidelines issued by supranational societies such as the EANM and SNM indicate that perfusion SPECT still may be considered good practice in the workup of AD patients, especially when FDG-PET is not available.

A guideline published by the EANM in 2009 replaces a former version of 2001 which was inspired by the Society of Nuclear Medicine *Procedure Guideline for Brain Perfusion SPECT*, the views of the Society of Nuclear Medicine Brain Imaging Council and the individual experience of experts in European countries (Kapucu et al. 2009). The document states that in the evaluation of suspected dementia, indications include the early detection and differential diagnosis of various forms of dementia, such as Alzheimer's disease, Lewy body dementia, Parkinson's disease with dementia, vascular dementia and frontotemporal dementia (Kapucu et al. 2009). In the pre-dementia phase of these diseases, known as mild cognitive impairment, SPECT can detect a functional deficit and may thus guide prognosis and allow prodromal diagnosis (Sperling et al. 2011). Of note, a new conceptual framework of AD has proposed the category 'asymptomatic at risk of AD' in the *preclinical* phase based on the presence of specific biomarkers such as amyloid and tau, but not on perfusion abnormalities (Dubois 2018).

Unfortunately, the procedure guideline for brain perfusion SPECT using ^{99m}Tc radiopharmaceuticals (version 3.0, by the SNM) does not explicitly discuss indications and focuses more on the technical aspect of the investigation (Juni et al. 2009).

Last but not least, the final incremental value of perfusion SPECT strongly relies on the pretest probability, i.e. the clinical hypothesis, which has to be determined referring to the latest guidelines and should be based on thorough examination.

The official request of the referring physician should include not only the possible (differential) diagnosis but also all possible relevant information regarding clinical symptoms, results of MRI and/or CT scan and specific question, as they all allow better interpretation of the distribution pattern on SPECT or PET imaging. The nuclear medicine physician, on the other hand, has the obligation to check the justification of the indication for the examination, eventually to refuse it or point to better alternatives or suggest to acquire lacking information. Luckily, nowadays, much of the information needed may be found in electronic patient files.

As stated earlier, PET seems to have the edge over SPECT, but due to limited availability of PET, SPECT remains a sufficiently accurate, cost-effective and justified alternative, especially in the differential diagnosis of AD. In the context of new diagnostic criteria for AD, typical perfusion abnormalities on brain SPECT may be viewed of as a 'progression marker' of the disease, which may be interpreted along with pathologic markers of disease (e.g. increased tau levels in CSF, amyloid tracer retention on PET).

References

Altrocchi P (1996) Assessment of brain SPECT. Report of the therapeutics and technology assessment subcommittee of the American Academy of Neurology. Neurology 46:278–285

Alzheimer A (1907) Ueber eine eigenartige Erkrankung der Hirnrinde. Allgemeine Zeitschrift fur Psychiatrie und Psychisch-Gerichtliche Medizin 64:146–148

Ballinger JR, Reid RH, Gulenchyn KY (1988) Technetium-99m HM-PAO stereoisomers: differences in interaction with glutathione. J Nucl Med 29:1998–2000

Barneveld PC, van Urk P (2007) Aanbevelingen nucleaire geneeskunde 2007. Kloosterhof, Neer

Bergeron D, Ossenkoppele R, Laforce R Jr (2018) Evidence-based interpretation of amyloid-beta PET results: a clinician's tool. Alzheimer Dis Assoc Disord 32(1):28–34. https://doi.org/10.1097/WAD.0000000000000239

Bloudek LM, Spackman DE, Blankenburg M, Sullivan SD (2011) Review and meta-analysis of biomarkers and diagnostic imaging in Alzheimer's disease. J Alzheimers Dis 26(4):627–645. https://doi.org/10.3233/JAD-2011-110458

Bohnen NI, Djang DSW, Herholz K et al (2012) Effectiveness and safety of ^{18}F-FDG PET in the evaluation of dementia: a review of the recent literature. J Nucl Med 53:59–71. https://doi.org/10.2967/jnumed.111.096578

Bonte F, Weiner M, Bigio E, White C III (1997) Brain blood flow in the dementias: SPECT with histopathologic correlation in 54 patients. Radiology 202:793–797

Catafau A (2001) Brain SPECT in clinical practice. Part I: Perfusion. J Nucl Med 42:259–271

Clarke C, Howard R, Rossor M, Shorvon SD (2011) Neurology. Wiley-Blackwell, Hoboken, NJ

Creutzfeldt H (1920) Über eine eigenartige herdförmige Erkrankung des Zentralnervensystems (vorläufige Mitteilung). Z ges Neurol Psychiat 57:1–18

Davison CM, O'Brien JT (2014) A comparison of FDG-PET and blood flow SPECT in the diagnosis of neurodegenerative dementias: a systematic review. Int J Geriatr Psychiatry 29(6):551–561. https://doi.org/10.1002/gps.4036

De Deyn PP, Dierckx R, Alavi A, Pickut B et al (1997) A textbook of SPECT in neurology and psychiatry, 1st edn. John Libbey Eurotext Ltd, London. ISBN 0861965426

Degnan AJ, Levy LM (2014) Neuroimaging of rapidly progressive dementias, Part 2: Prion, inflammatory, neoplastic, and other etiologies. AJNR Am J Neuroradiol 35:424. https://doi.org/10.3174/ajnr.A3455

Dougall NJ, Bruggink S, Ebmeier KP (2004) Systematic review of the diagnostic accuracy of ^{99m}Tc-HMPAO-SPECT in dementia. Am J Geriatr Psychiatry 12:554–570. https://doi.org/10.1176/appi.ajgp.12.6.554

Dubois B (2018) The emergence of a new conceptual framework for Alzheimer's disease. J Alzheimers Dis 62(3):1059–1066. https://doi.org/10.3233/JAD-170536

Dubois B, Feldman HH, Jacova C, Dekosky ST, Barberger-Gateau P, Cummings J et al (2007) Research criteria for the diagnosis of Alzheimer's disease: revising the NINCDS-ADRDA criteria. Lancet Neurol 6(8):734–746. S1474-4422(07)70178-3 [pii]

Dubois B, Feldman HH, Jacova C, Hampel H, Molinuevo JL, Blennow K et al (2014) Advancing research diagnostic criteria for Alzheimer's disease: the IWG-2 criteria. Lancet Neurol 13(6):614–629. https://doi.org/10.1016/S1474-4422(14)70090-0

Fletcher JW, Woolf SH, Royal HD (1994) Consensus development for producing diagnostic procedure guidelines: SPECT brain perfusion imaging with exametazime. J Nucl Med 35:2003–2010

French J, Gronseth G (2008) Lost in a jungle of evidence: we need a compass. Neurology 71:1634–1638. https://doi.org/10.1212/01.wnl.0000336533.19610.1b

Gronseth G, French J (2008) Practice parameters and technology assessments: what they are, what they are not, and why you should care? Neurology 71:1639–1643. https://doi.org/10.1212/01.wnl.0000336535.27773.c0

Hebert LE, Beckett LA, Scherr PA (2001) Annual incidence of Alzheimer disease in the United States projected to the years 2000 through 2050. Alzheimer Dis Assoc Disord 15(4):169–173

Hellman R, Tikofsky R, Heertum R et al (1994) A multi-institutional study of interobserver agreement in the evaluation of dementia with rCBF/SPET ^{99m}Technetium- exametazime (HMPAO). Eur J Nucl Med 21:306–313

Hoffman J, Welsh-Bohmer K, Hanson M et al (2000) FDG PET imaging in patients with pathologically verified dementia. J Nucl Med 41:1920–1928

Holman B, Garada B, Johnson K et al (1992) A comparison of brain perfusion SPECT in cocaine abuse and AIDS dementia complex. J Nucl Med 33:1312–1315

Ibáñez V, Pietrini P, Alexander GE et al (1998) Regional glucose metabolic abnormalities are not the result of atrophy in Alzheimer's disease. Neurology 50:1585–1593

Inoue K, Nakagawa M, Goto R et al (2003) Regional differences between ^{99m}Tc-ECD and ^{99m}Tc-HMPAO SPET in perfusion changes with age and gender in healthy adults. Eur J Nucl Med Mol Imaging 30:1489–1497. https://doi.org/10.1007/s00259-003-1234-x

Jagust W, Thisted R, Devous MD et al (2001) SPECT perfusion imaging in the diagnosis of Alzheimer's disease a clinical-pathologic study. Neurology 56:950–956

Jobst K, Smith A, Barker C et al (1992a) Association of atrophy of the medial temporal lobe with reduced blood flow in the posterior parietotemporal cortex in patients with a clinical and pathological diagnosis of Alzheimer's disease. J Neurol Neurosurg Psychiatry 55:190–194

Jobst KA, Smith AD, Szatmari M et al (1992b) Detection in life of confirmed Alzheimer's disease using a simple measurement of medial temporal lobe atrophy by computed tomography. Lancet 340:1179–1183

Juni J, Waxman A, Devous M et al (1998) Procedure guideline for brain perfusion SPECT using technetium-99m radiopharmaceuticals. Soc Nucl Med 39:923–926

Juni JE, Waxman AD, Devous MD et al (2009) Procedure guideline for brain perfusion SPECT using (^{99m})Tc radiopharmaceuticals 3.0. J Nucl Med Technol 37:191–195. https://doi.org/10.2967/jnmt.109.067850

Kapucu O, Nobili F, Varrone A et al (2009) EANM procedure guideline for brain perfusion SPECT using ^{99m}Tc-labelled radiopharmaceuticals, version 2. Eur J Nucl Med Mol Imaging 36:2093–2102. https://doi.org/10.1007/s00259-009-1266-y

Khachaturian ZS (1985) Diagnosis of Alzheimer's disease. Arch Neurol 42:1097

Knopman DS, DeKosky ST, Cummings JL et al (2001) Practice parameter: diagnosis of dementia (an evidence-based review). Report of the Quality Standards Subcommittee of the American Academy of Neurology. Neurology 56:1143–1153

Kogure D, Matsuda H, Ohnishi T et al (1999) Longitudinal evaluation of early dementia of Alzheimer type using brain perfusion SPECT. Jpn J Nucl Med 36:91–101

Koyama M, Kawashima R, Ito H et al (1997) SPECT imaging of normal subjects with technetium-99m-HMPAO and technetium-99m-ECD. J Nucl Med 38:587–592

Kuschinsky W (1991) Coupling of function, metabolism, and blood flow in the brain. Neurosurg Rev 14:163–168

van Laere K, Versijpt J, Audenaert K et al (2001) ^{99m}Tc-ECD brain perfusion SPET: variability, asymmetry and effects of age and gender in healthy adults. Eur J Nucl Med Mol Imaging 28:873–887

Lassen NA (1980) Regional cerebral blood flow studied by xenon-133. Intra-arterial injection studies and inhalation studies using emission tomography. Bull Schweiz Akad Med Wiss 36:93–100

Lou HC, Edvinsson L, MacKenzie ET (1987) The concept of coupling blood flow to brain function: revision required? Ann Neurol 22:289–297. https://doi.org/10.1002/ana.410220302

Matsuda H (2007) Role of neuroimaging in Alzheimer's disease, with emphasis on brain perfusion SPECT. J Nucl Med 48:1289–1300. https://doi.org/10.2967/jnumed.106.037218

Mendez M, Shapira J, McMurtray A et al (2007) Accuracy of the clinical evaluation for frontotemporal dementia. Arch Neurol 64:830–835. https://doi.org/10.1001/archneur.64.6.830

Meyer MA, Hudock SA (2018) Posterior cortical atrophy: a rare variant of Alzheimer's disease. Neurol Int 10(2):7665. https://doi.org/10.4081/ni.2018.7665

Miller BL, Gearhart R (1999) Neuroimaging in the diagnosis of frontotemporal dementia. Dement Geriatr Cogn Disord 10:71–74

Miller BL, Cummings JL, Villanueva-Meyer J et al (1991) Frontal lobe degeneration: clinical, neuropsychological, and SPECT characteristics. Neurology 41:1374–1382

Mirra S, Heyman A, McKeel D et al (1991) The Consortium to Establish a Registry for Alzheimer's Disease (CERAD). Part II. Standardization of the neuropathologic assessment of Alzheimer's disease. Neurology 41:479–486

Murray IPC, Ell PJ (eds) (1994) Nuclear medicine in clinical diagnosis and treatment. Churchill and Livingstone, New York, NY. vols 2

Neirinckx RD, Burke JF, Harrison RC et al (1988) The retention mechanism of technetium-99m-HM-PAO: intracellular reaction with glutathione. J Cereb Blood Flow Metab 8:S4–S12. https://doi.org/10.1038/jcbfm.1988.27

Perani D, Piero V, Vallar G et al (1988) Technetium-99m HM-PAO-SPECT study of regional cerebral perfusion in early Alzheimer's disease. J Nucl Med 29:1507–1514

Petrella J, Coleman R, Doraiswamy P (2003) Neuroimaging and early diagnosis of Alzheimer disease: a look to the future. Radiology 226:315–336

Pickut BA, Saerens J, Mariën P et al (1997) Discriminative use of SPECT in frontal lobe-type dementia versus (senile) dementia of the Alzheimer's type. J Nucl Med 38:929–934

Pimlott SL, Ebmeier KP (2007) SPECT imaging in dementia. Br J Radiol 80(2):S153–S159. https://doi.org/10.1259/bjr/89285735

Prohovnik I, Mayeux R, Sackeim H et al (1988) Cerebral perfusion as a diagnostic marker of early Alzheimer's disease. Neurology 38:931–937

Read S, Miller B, Mena I et al (1995) SPECT in dementia: clinical and pathological correlation. J Am Geriatr Soc 43:1243–1247

Roy CS, Sherrington CS (1890) On the regulation of the blood-supply of the brain. J Physiol Lond 11:85–158. 17

de Santi S, de Leon MJ, Rusinek H et al (2001) Hippocampal formation glucose metabolism and volume losses in MCI and AD. Neurobiol Aging 22:529–539

Schaller BJ (2008) Strategies for molecular imaging dementia and neurodegenerative diseases. Neuropsychiatr Dis Treat 4:585

Silverman D (2004) Brain 18F-FDG PET in the diagnosis of neurodegenerative dementias: comparison with perfusion SPECT and with clinical evaluations lacking nuclear imaging. J Nucl Med 45:594–607

Silverman DH, Small GW, Chang CY et al (2001) Positron emission tomography in evaluation of dementia: regional brain metabolism and long-term outcome. JAMA 286:2120–2127

Slosman DO, Chicherio C, Ludwig C et al (2001) (133)Xenon-133 SPECT cerebral blood flow study in a healthy population: determination of T-scores. J Nucl Med 42:864–870

Snowdon DA, Nun Study (2003) Healthy aging and dementia: findings from the Nun Study. Ann Intern Med 139:450–454

Sperling RA, Aisen PS, Beckett LA et al (2011) Toward defining the preclinical stages of Alzheimer's disease: recommendations from the National Institute on Aging-Alzheimer's Association workgroups on diagnostic guidelines for Alzheimer's disease. Alzheimers Dement 7:280–292. https://doi.org/10.1016/j.jalz.2011.03.003

Thies W, Bleiler L (2013) 2013 Alzheimer's disease facts and figures. Alzheimers Dement 9:208–245. https://doi.org/10.1016/j.jalz.2013.02.003

Tierney M, Reid D, Zorzitto M et al (1986) The differential diagnosis of Alzheimer's disease: conceptual and methodological issues. Can J Neurol Sci 13:424–426

Waldemar G, Dubois B, Emre M et al (2000) Diagnosis and management of Alzheimer's disease and other disorders associated with dementia. The role of neurologists in Europe. European Federation of Neurological Societies. Eur J Neurol 7:133–144

Walovitch RC, Cheesman EH, Maheu LJ, Hall KM (1994) Studies of the retention mechanism of the brain perfusion imaging agent ^{99m}Tc-bicisate (^{99m} Tc-ECD). J Cereb Blood Flow Metab 14(Suppl 1):S4–S11

Winchell HS, Baldwin RM, Lin TH (1980) Development of I-123-labeled amines for brain studies: localization of I-123 iodophenylalkyl amines in rat brain. J Nucl Med 21:940–946

Yuan Y, Gu ZX, Wei WS (2009) Fluorodeoxyglucose-positron-emission tomography, single-photon emission tomography, and structural MR imaging for prediction of rapid conversion to Alzheimer disease in patients with mild cognitive impairment: a meta-analysis. AJNR Am J Neuroradiol 30(2):404–410. https://doi.org/10.3174/ajnr.A1357

Nuclear Imaging in Frontotemporal Dementia

15

Fransje E. Reesink, Gilles N. Stormezand, Rudi A. J. O. Dierckx, and Peter Paul De Deyn

Contents

15.1 Introduction 470
15.2 Nuclear Imaging 473
15.2.1 Regional Cerebral Blood Flow and Glucose Metabolism 473
15.2.2 Brain Perfusion Disease Pattern 474
15.2.3 Brain Glucose Metabolism Disease Pattern 475
15.2.4 Environmental Factors 479
15.2.5 Pharmacological Treatments 479
15.2.6 Longitudinal Studies 479
15.2.7 Correlation with Behaviour 480
15.3 Pathologic Markers 480

F. E. Reesink (✉)
Department of Neurology, Alzheimer Center, University Medical Center Groningen, University of Groningen, Groningen, The Netherlands
e-mail: f.e.reesink@umcg.nl

G. N. Stormezand
Department of Nuclear Medicine and Molecular Imaging, Alzheimer Research Center, University Medical Center Groningen, University of Groningen, Groningen, The Netherlands
e-mail: g.n.stormezand01@umcg.nl

R. A. J. O. Dierckx
Nuclear Medicine and Molecular Imaging, University Medical Center Groningen, Groningen, Groningen, The Netherlands
e-mail: r.a.dierckx@umcg.nl

P. P. De Deyn
Department of Neurology, Alzheimer Center, University Medical Center Groningen, University of Groningen, Groningen, The Netherlands

Laboratory of Neurochemistry and Behavior, Department of Biomedical Sciences, Institute Born-Bunge, Born Bunge Foundation, University of Antwerp, Antwerp, Belgium
e-mail: p.p.de.deyn@umcg.nl

R. A. J. O. Dierckx et al. (eds.), *PET and SPECT in Neurology*,
https://doi.org/10.1007/978-3-030-53168-3_15

15.4 Neurotransmitter Systems..... 482
15.4.1 Serotonergic System..... 483
15.4.2 Dopaminergic System..... 483
15.4.3 Cholinergic System..... 483
15.5 Conclusions..... 484
References..... 484

Abstract

Frontotemporal dementia (FTD) covers a range of heterogeneous neurodegenerative syndromes, predominantly affecting the frontal and temporal lobes (frontotemporal lobar degeneration or FTLD). Most patients present with behavioural deficits, executive dysfunction and language difficulties. FTD presents as clinically recognized subtypes with behavioural manifestation (FTD-b) and primary progressive aphasia (PPA), which can be divided into semantic dementia (SD), progressive nonfluent aphasia (PNFA) and logopenic aphasia (LPA). FTD is a common type of dementia, particularly at younger age. The underlying neuropathological process of FTLD leads to the clinical phenotype and can be characterized roughly in tauopathy (FTD-TAU) and TAR DNA-binding protein (TDP-43) pathology. Genetics is an important causal factor for FTD, and genetic heterogeneity is reflected by the identification of mutations in causative genes. Diagnostic criteria have modest sensitivity, and it may be challenging to differentiate FTD from psychiatric disorders or other types of dementia, especially AD. Advances in molecular imaging have increased the accuracy of FTD diagnosis, and nuclear imaging techniques improve the understanding of the molecular basis of FTD, which is important to develop rational therapies. Although currently no effective treatment is available for FTD, early and correct diagnosis is necessary for adequate clinical management, because of prognostic implications and for genetic counselling.

15.1 Introduction

Frontotemporal dementia (FTD), after Alzheimer's disease (AD), constitutes the major cause of young onset dementia. The prevalence of FTD ranges from 3% up to 26% of dementia, starting before the age of 65 years (Vieira et al. 2013). FTD is a heterogeneous neurodegenerative syndrome, predominantly affecting the frontal and temporal lobes (frontotemporal lobar degeneration or FTLD) (Ratnavalli et al. 2002; Neary et al. 1998; McKhann et al. 2001; Rosso et al. 2003). The clinical spectrum of FTD comprises an insidious onset and a progressive course, but with variable decline (Seelaar et al. 2011). FTD may manifest as two clinically recognized subtypes, based on the predominant features: behavioural and personality changes on the one hand and on the other hand language disturbances. The behavioural presentation (FTD-b) is characterized by severe changes in behaviour and personality,

Table 15.1 Diagnostic criteria FTD-b

Behavioural variant (FTD-b)
Inclusionary criteria: progressive deterioration of behaviour and/or cognition and *at least three* of the following symptoms (1–6)
1. Early (within the first 3 years) behavioural disinhibition (socially inappropriate behaviour, loss of decorum/impulsive or careless actions)
2. Early apathy or inertia
3. Early loss of sympathy or empathy (diminished response or interest to other people's needs and feelings)
4. Early perseverative, stereotyped or compulsive/ritualistic behaviours
5. Hyperorality and dietary changes
6. Neuropsychological profile: executive deficits with relative sparing of memory and visuospatial functions
Exclusionary criteria: 1 and 2 *must* be answered negatively for diagnosis. Criteria 3 *can* be positive for possible but *must* be negative for probable, FTLD-b
1. Pattern of deficits is better accounted for by other non-degenerative nervous system or medical disorders
2. Behavioural disturbance is better accounted for by a psychiatric diagnosis
3. Biomarkers strongly indicative of Alzheimer's disease or other neurodegenerative processes

Neary et al. (1998), Rascovsky et al. (2011)

such as disinhibition, apathy, loss of empathy, stereotypic behaviour, dietary changes and executive cognitive deficits (Table 15.1). FTD-b consensus criteria differentiate possible, probable and definite FTD-b with a sensitivity of 76–86% (Rascovsky et al. 2011). Because of the close similarity of behavioural changes in patients with psychiatric disorders, diagnosis is often challenging. Predominant language difficulties are classified as primary progressive aphasia (PPA) and may be divided into semantic dementia (SD) and progressive nonfluent aphasia (PNFA). SD presents with impaired comprehension and concomitant development of anomia, while speech production is spared. PNFA is characterized by effortful speech and grammatical errors, with sparing of language comprehension. A third presentation is described, the logopenic progressive aphasia (LPA), associated with a neuropathological diagnosis of Alzheimer's disease (Table 15.2) (Mesulam 2001; Gorno-Tempini et al. 2011). In the heterogeneous spectrum of FTD, there is also overlap with motor neuron disease (FTD-MND or FTD-ALS), as well as with parkinsonian syndromes such as progressive supranuclear palsy (PSP) and corticobasal degeneration (CBD) (Kertesz et al. 2005).

Neurodegenerative changes in the brain are characterized by various patterns of atrophy of frontal and temporal lobes. Clinical phenotypes have a strong correlation with anatomic pathology. FTD-b is associated with symmetric atrophy of the frontal lobes, insula, anterior cingulate and anterior lobes (Sieben et al. 2012). SD is associated with asymmetric atrophy of the left/linguistic dominant anterior inferior temporal lobe. In patients with PNFA, an asymmetric atrophy involving the anterior perisylvian cortex, mainly of the dominant hemisphere, is seen. The first patient with progressive aphasia and lobar atrophy was described by Arnold Pick in 1892 (Pick 1892). In 1911 Alois Alzheimer reported the presence of argyrophilic

Table 15.2 Diagnostic criteria PPA and variants

Inclusionary criteria. 1–3 *must* be present		
1. The most prominent clinical feature is difficulty with language		
2. These deficits are the principal cause of impaired daily living activity		
3. Aphasia should be the most prominent deficit at symptom onset and for the initial phases of the disease		
Exclusionary criteria. 1–4 *must* be answered negatively		
1. Pattern of deficits is better accounted for by other non-degenerative nervous system or medical disorders		
2. Cognitive disturbance is better accounted for by a psychiatric diagnosis		
3. Prominent initial episodic memory, visual memory and visuoperceptual impairments		
4. Prominent initial behavioural disturbance		
***SD* core features**	***PNFA* core features**	***LPA* core features**
Impaired confrontation naming and single-word comprehension	Agrammatism in language production and apraxia of speech	Impaired single-word retrieval in spontaneous speech and repetition of sentences and phrases
Other features	At least two of three other features	At least three other features
Impaired object knowledge, surface dyslexia or dysgraphia, spared repetition, spared speech production	Impaired comprehension of syntactically complex sentences, spared single-word comprehension, spared object knowledge	Phonologic errors in spontaneous speech and naming, spared single-word comprehension, spared motor speech, absence of frank agrammatism
Imaging supported	Imaging supported	Imaging supported
Predominant anterior temporal lobe atrophy, left greater than right, on MRI or hypoperfusion or hypometabolism on SPECT or PET	Predominant left fronto-insular atrophy on MRI or hypoperfusion or hypometabolism on SPECT or PET	Predominant left parietal and posterolateral temporal lobe atrophy on MRI or hypoperfusion or hypometabolism on SPECT or PET
Definite pathology—clinical diagnosis and either criterion 1 or 2 must be present		
1. Histopathologic evidence of specific neurodegenerative pathology		
2. Presence of known pathogenic mutation		

Neary et al. (1998), Mesulam (2001), Gorno-Tempini et al. (2011), Rabinovici et al. (2008)
PPA primary progressive aphasia, *SD* semantic dementia, *PNFA* progressive nonfluent aphasia, *LPA* logopenic progressive aphasia

neuronal inclusions at neuropathological examination, later known as 'Pick bodies' (Alzheimer 1911). Nowadays the neuropathology of FTD roughly can be divided in tauopathy (FTD-TAU) and ubiquitin pathology (FTD-U). Ubiquitin pathology is frequently combined with TAR DNA-binding protein (TDP-43) inclusions (FTD-TDP43). A considerable number of TDP43-negative FTD-U cases have inclusions of fused in sarcoma (FUS) protein, referred to as FTD-FUS (Mackenzie et al. 2010). Positive family history is observed in 30–40% of the FTD patients, most prominent in FTD-b (45%), and especially when concomitant symptoms of MND are present (60%) (Goldman et al. 2005; Greaves and Rohrer 2019). Genetic heterogeneity of FTD is reflected by the identification of mutations in the *MAPT* and *GRN* genes,

both linked at chromosome 17, in approximately 50% of familial cases. Mutations in the *valosin-containing protein (VCP)*, *charged multivesicular body protein (CHMP2B)*, TAR DNA-binding protein (TARDBP) and *fused in sarcoma (FUS)* genes are found in less than 5%. Mutations in progranulin (PGRN) gene are associated with ubiquitin pathology and TDP-43-positive inclusions (Cruts et al. 2006). Tauopathy is mostly caused by mutations in the *microtubule-associated protein tau (MAPT)* gene, but also *presenilin 1* mutations are reported (Dermaut et al. 2004). Also mutations were identificated on 9p21, *C9orf72 gene*, associated also with ubiquitin pathology and TDP-43-positive inclusions (DeJesus-Hernandez et al. 2011; Gijselinck et al. 2012; Simon-Sanchez et al. 2012). Increased knowledge about genetic FTD and clinical presymptomatic genetic testing could become more relevant as disease-modifying therapy trials will start in the genetic groups over the next few years (Greaves and Rohrer 2019). Structural neuroimaging is recommended in the diagnostic work-up, especially magnetic resonance imaging (MRI) scans, and visual rating scores from (MRI) improve diagnostic accuracy and can exclude other neurodegenerative diseases (Harper et al. 2016). Frontal scales distinguish best for FTLD-Tau group, while temporal scales were best to distinguish FTLD-TDP43 group.

15.2 Nuclear Imaging

15.2.1 Regional Cerebral Blood Flow and Glucose Metabolism

Nuclear imaging techniques using positron emission tomography (PET) or single-photon emission computed tomography (SPECT) tracers are able to visualize blood flow and oxygen and glucose consumption. Several SPECT and PET studies have detected functional deficits in FTD patients in comparison to controls. These perfusion or metabolic deficits may exist in a structurally normal brain. In 1977 Sokoloff et al. were the first to report that under physiological steady-state conditions, cerebral blood flow is coupled to the level of cerebral oxygen and glucose consumption (Sokoloff et al. 1977). Cerebral glucose metabolic activity is an index of synaptic function and density, and its loss is a characteristic feature of neurodegeneration (Liu et al. 1996; Bohnen et al. 2012). Stimulation of functional activity increases the local rate of glucose utilization, while reduced functional activity lowers it (Sokoloff 1977). The PET tracer [^{18}F]-fluorodeoxyglucose (FDG) allows the measurement of the cerebral metabolic rate of glucose (CMRglc) in vivo. Reivich et al. in 1979 were the first to study FDG-PET in man (Reivich et al. 1979). The clinical test used to rely on the qualitative visual interpretation of the scan images, on which areas with reduced metabolism were identified and interpreted along with the clinical context. Nowadays, software packages with quantitative aids such as database comparison and three-dimensional stereotactic surface projection (*3D-SSP*) analysis are available, which have led to an increase in diagnostic accuracy and confidence (Foster et al. 2007). FDG-PET imaging has been used extensively to identify characteristic disease-related patterns of regional glucose metabolism in patients with different variants of FTD (Josephs et al. 2010). Although SPECT has been more broadly

available, studies show PET has a higher diagnostic accuracy, suggesting that PET is superior to SPECT in its ability to separate healthy controls from patients with true dementing illnesses (Herholz et al. 2002).

15.2.2 Brain Perfusion Disease Pattern

SPECT studies usually have been performed using [^{99}Tc]-HMPAO, providing measurements of cerebral blood flow (CBF). According to the European Association of Nuclear Medicine Neuroimaging Committee (ENC) guidelines, brain perfusion SPECT can be used for early detection of various forms of dementia, including FTD (Kapucu et al. 2009). Early behavioural symptoms can precede the onset of dementia in FTD, and SPECT can predict diagnosis (Miller and Gearhart 1999; Read et al. 1995). SPECT in addition to clinical evaluation increases the diagnostic accuracy for neurodegenerative diseases (McNeill et al. 2007). FTD has typically been linked to a pattern of reduced cerebral blood flow (CBF) of symptomatic frontotemporal cortices (Fig. 15.1). Using voxel-based statistical methods, more specific areas of

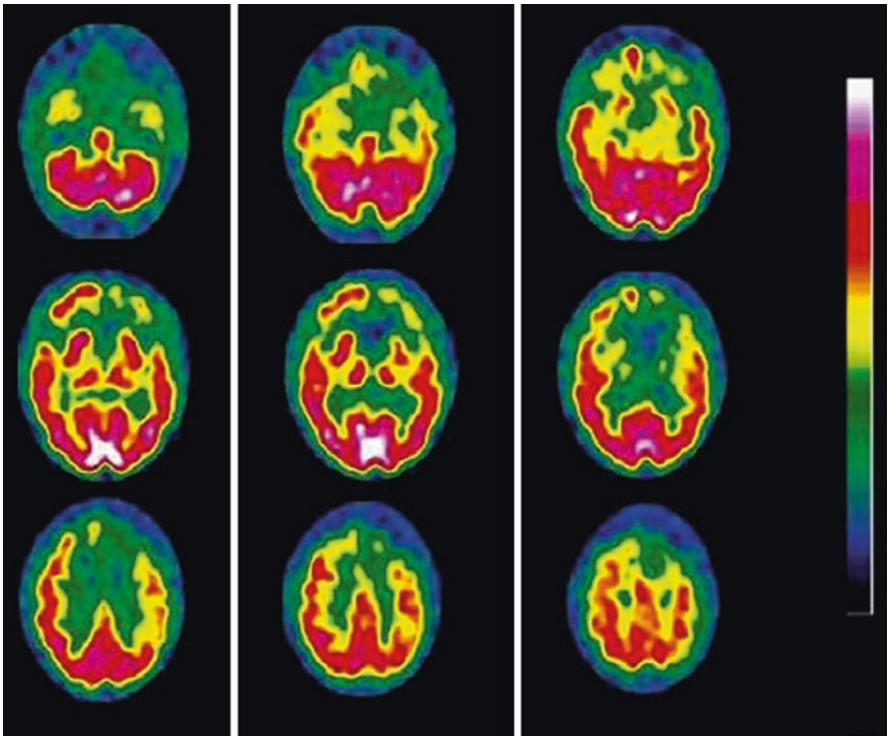

Fig. 15.1 Single-headed HMPAO SPECT study of a patient suffering from frontotemporal dementia. Transaxial slices from *bottom* to *top*. Moderate to severe cortical hypoperfusion of the frontal lobes, especially on the *left*, and slight hypoperfusion of the temporal poles

hypoperfusion were detected, affecting association cortices, including the hippocampus and amygdala, cingular and insular (Le Ber et al. 2006). SPECT provides useful information in differentiation of FTD subtypes; semantic dementia (SD) shows predominant hypoperfusion of the left temporal lobe (Diehl et al. 2004). SPECT imaging also aids in the differential diagnosis of patients with dementia. Numerous studies have been performed in patients with various forms of dementia, including AD, frontotemporal dementia and vascular dementia, with demonstration of unique uptake patterns. The presence of a frontal or anterior perfusion deficit has been associated with frontotemporal dementia and not with (early) AD, which is associated with a pattern of bitemporoparietal hypoperfusion (Varrone et al. 2002). In one study (Charpentier et al. 2000) in which a simple decision rule based on discriminant analysis of SPECT data was applied, 20 patients with probable AD and 20 with probable frontotemporal dementia were evaluated; 100% of patients with frontotemporal dementia and 90% of patients with AD were correctly classified. In a study of Pickut et al., using a model, 81% of the FTD and 74% of the AD were correctly classified (Pickut et al. 1997); bifrontal hypoperfusion was found to be the most powerful predictor of clinical classification. Patients showing bilateral anterior hypoperfusion are approximately 16 times more likely to suffer FTD than AD and are also considerably more likely to have FTD than vascular dementia or diffuse Lewy body-type disease (DLB) (Talbot et al. 1998). In another study (Sjogren et al. 2000) with 16 patients with frontotemporal dementia, 71 patients with other forms of dementia, 28 control subjects, an anterior-to-posterior ratio was successfully used to classify patients with frontotemporal dementia from those with other forms of dementia and from control subjects with a sensitivity of 87.5% and a specificity of 78.6%.

The effect of different SPECT uptake patterns at baseline on modification of the differential diagnosis was evaluated in a study (Talbot et al. 1998) with 363 patients followed up for a median of 3 years. Patients were classified into disease groups on the basis of clinical criteria. A bilateral posterior perfusion abnormality was associated with AD, whereas a bilateral anterior abnormality was associated with frontotemporal dementia. In 2015 a Cochrane Database Systemic review concluded that the routine use of SPECT to differentiate FTD from other dementia subtypes is not yet recommended in clinical practice (Archer et al. 2015). Further research is required, with standardized protocols and well described study populations.

15.2.3 Brain Glucose Metabolism Disease Pattern

In FTD, typically a frontotemporal pattern of hypometabolism may be found. Using voxel-based statistical methods, a more widespread pattern has been reported with involvement of the temporoparietal association cortex, basal ganglia and thalamus and marginally in the primary sensorimotor cortex and cerebellum (Ishii et al. 1998). Particularly, the ventromedial frontopolar cortex is known to be involved (Salmon et al. 2003; Garraux et al. 1999); this region is clinically related to decision-making, feelings of rightness and social knowledge. The behavioural variant-type FTD-b has been specifically related to hypometabolism of the right inferior frontal

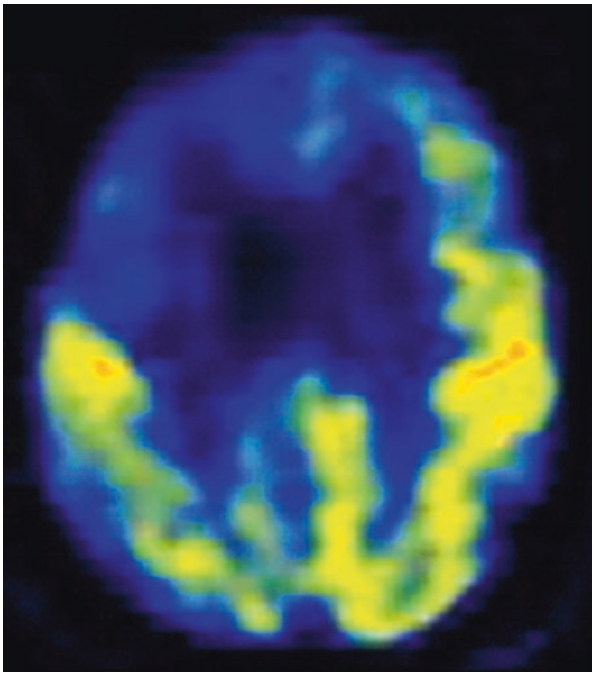

Fig. 15.2 [^{18}F]-FDG-PET in FTD-b, behaviour variant: right fronto (temporal) hypometabolism

lobe (Borroni et al. 2012) (Fig. 15.1). Three different clinical presentations of primary progressive aphasia (PPA) are associated with signature patterns of glucose metabolism (Fig. 15.2) (Rabinovici et al. 2008). Progressive nonfluent aphasia (PNFA) shows (sometimes subtle) asymmetric left frontal hypometabolism and semantic dementia (SD) prominent anterior temporal hypometabolism, left greater than right, whereas logopenic aphasia (LPA) shows metabolic lesions in the left parietal and posterolateral temporal lobes. A 2005 consensus report prepared by the Neuroimaging Work Group of the Alzheimer's Association concluded that FDG-PET is helpful for differentiating FTD from AD (Albert et al. 2005). This indication for FDG PET, among others (establishing diagnosis, differentiation from DLB), was again recommended by the European Association of Nuclear Medicine and European Academy of Neurology in 2018 (Nobili et al. 2018). In order to distinguish FTD from AD, detection of hippocampal hypometabolism may be particularly useful. Hippocampal hypometabolism is present in almost all AD cases, but only in a minority of FTD patients (Mosconi et al. 2008). Other regions which have specifically impaired glucose metabolism in FTD in comparison to AD include the (bi)lateral ventromedial frontal area, the left anterior insula and the inferior frontal cortex (Ibach et al. 2004). CBD, which shares clinical and pathologic features with FTD, has been associated with reduced metabolism of the primary sensorimotor region and/or basal ganglia and with asymmetric metabolic deficits in the hemispheres (Ishii et al. 1998). Disease-specific glucose metabolic patterns can differentiate FTD from other neurodegenerative brain diseases, like AD and DLB (Fig. 15.3, Teune et al. 2010).

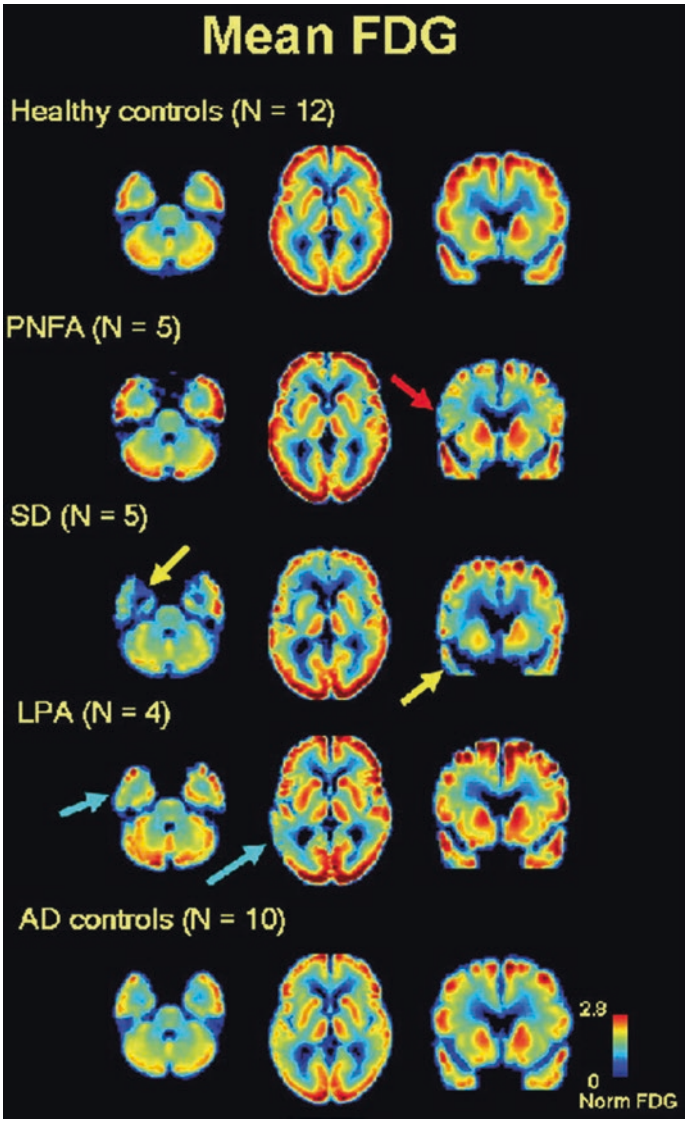

Fig. 15.3 [^{18}F]-FDG-PET in different types of FDG patterns. Axial (z = 9, z = 27) and coronal (y = 64) slices of mean atrophy-corrected FDG images from (*top* to *bottom*) normal controls (N = 12). PNFA (N = 5), SD (N = 5), LPA (N = 4) and AD (N = 10). PNFA is characterized by *left* frontal hypometabolism (*red arrow*), SD by left greater than right anterior temporal hypometabolism (*yellow arrows*) and LPA by asymmetric left temporoparietal hypometabolism (*light blue arrows*)

Besides FTD, metabolic or inflammatory diseases, such as neurodegeneration with brain iron accumulation (NBIA) (Santillo et al. 2009) and voltage-gated potassium channel encephalitis (Kotagal et al. 2012), may resemble FTD both clinically or using PET or SPECT (Fig. 15.4).

FDG-PET has been demonstrated to have higher sensitivity and specificity for the early detection of FTD when compared to perfusion SPECT (Dobert et al. 2005). In a community-based prospective study of patients suspected of early-onset dementia, sensitivity of PET to detect FTD was 53%, whereas specificity was 95% (Panegyres et al. 2009). An FDG-PET study of 45 patients with pathologically confirmed dementia showed that adding FDG-PET increased accuracy 11% compared to diagnoses based on clinical criteria alone (Foster et al. 2007). The sensitivities and specificities for the diagnosis of FTD were 36.5% and 100.0% for consensus criteria, 63.5% and 70.4% for magnetic resonance images and 90.5% and 74.6% for SPECT/PET scans, respectively. With a previous prevalence of nearly 50% for FTD, the positive predictive value was greatest for consensus criteria (100.0%), and the negative predictive value was greatest for SPECT/PET (89.8%) (Mendez et al. 2007). The initial neuropsychological results did not distinguish FTD, but the pattern of progression (worse naming and executive functions and preserved constructional ability) helped establish the diagnosis after 2 years. Right frontal lobe hypometabolism seems to have the highest predictive value for developing FTD. After 2 years of follow-up, patients showing hypoperfusion of this region at baseline were most likely to reach consensus criteria for FTD (McMurtray et al. 2006). A good diagnostic accuracy was found for additional FDG-PET with combined MRI for FTD-b patients with late onset behavioural changes (sensitivity 96%, specificity 73%), although caution should be taken in cases with a primary psychiatric differential diagnosis (Vijverberg et al. 2016). Recently, a number of studies have shown that the MRI-based perfusion technique arterial spin labelling (ASL) can potentially provide comparable diagnostic information to FDG-PET in FTD

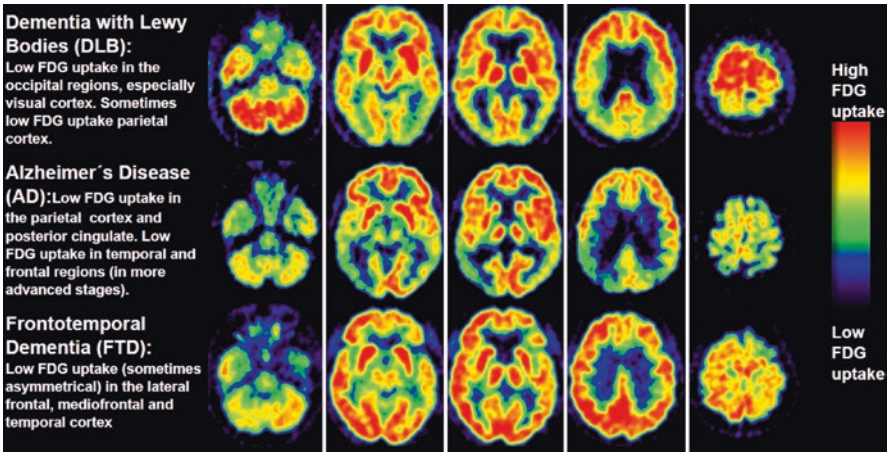

Fig. 15.4 [^{18}F]-FDG-PET in different types of dementia: DLB, AD and FTD (Teune et al. 2010)

(Fällmar et al. 2017; Verfaillie et al. 2015) patients due to the coupling of perfusion to glucose metabolism (Cha et al. 2013). However, sensitivity and specificity of FDG-PET for discriminant diagnosis of FTD patients from healthy individuals remains unmatched (Anazodo et al. 2017).

15.2.4 Environmental Factors

Using PET, a strong negative correlation has been found between the level of education and CMRglc, independent of demographics and the scores of the patients on cognitive testing in FTD (Perneczky et al. 2007). This finding suggests the presence of a cognitive reserve in highly educated FTD patients. A SPECT study showed a significant correlation between occupational attainments and hypoperfusion (Borroni et al. 2009). In addition, Spreng et al. assessed 161 occupational variables and found a predominantly verbal occupation to be associated with hypometabolism of the left-hemispheric pars triangularis of the inferior frontal gyrus, whereas a physical occupation was inversely correlated with CMRglc in the right-sided supplementary motor cortex (Spreng et al. 2011). These findings suggest that the translation of neuropathology into clinical symptoms may be influenced by environmental factors.

15.2.5 Pharmacological Treatments

FDG-PET also has been used to assess pharmacological treatment of FTD in small groups. Within a group treated with memantine, a noncompetitive *N*-methyl-D-aspartate and serotonin-3 receptor antagonist, an increase in glucose metabolism from baseline was observed, mainly in SD patients (Chow et al. 2011). However, this beneficial effect could not be correlated with an improvement in clinical symptoms. Other possible treatments have not been assessed using either PET or SPECT. Large natural history studies of presymptomatic genetic FTD are now underway (GENFI-the Genetic FTD Initiative and ARTFL/LEFFTDS study), in a collaborating effort under the banner of the FTD Prevention Initiative (FPI). These studies are taking forward the validation of biomarkers that aim to robustly measure disease onset, staging and progression in genetic FTD. Abnormal FDG-PET metabolism is seen at least 10 years before symptom onset, but the pattern and exact timing of changes differ between different genetic groups (Greaves and Rohrer 2019).

15.2.6 Longitudinal Studies

In the early stage of FTD, hypometabolism may be evident in the frontal lobes, mainly on the right, with sparing of the motor cortex (Diehl et al. 2004), while in the course of the disease, hypometabolism tends to progress more symmetrical and cross lobar borders (Diehl-Schmid et al. 2007). Worsening of metabolic deficits has

been reported specifically in the orbitofrontal parts of the frontal lobe as well as in subcortical structures (Grimmer et al. 2004). Another longitudinal study reported worsening of all hypometabolic structures at baseline and additional hypometabolism of the inferior frontal cortex, the inferior parietal lobe, the left precuneus and the inferior and middle temporal lobes (Diehl-Schmid et al. 2007). These regions may secondarily be affected as a consequence of impaired input from frontal areas via the *superior longitudinal fasciculus*, the *uncinate fasciculus* and the *cingulum bundle*. Involvement of more posterior regions has been described to occur after disease duration of more than 5 years (Le Ber et al. 2006).

15.2.7 Correlation with Behaviour

Initially studies made use of a region of interest (ROI) analysis in which certain regions which are expected to be involved in the disease are investigated. Voxel-based methods are used which allow detection of significantly altered brain regions without a priori hypothesis. These methods seem particularly useful in relating clinical symptoms to specific brain regions. Table 15.3 shows the relationship studies between clinical symptoms of FTD and functional imaging.

15.3 Pathologic Markers

Besides functional markers, specific markers of pathology are of interest in the evaluation of dementia. Advances in in vivo β-amyloid detection of AD allow further differentiation between FTD and AD. In the pathogenesis of AD, the depositions of amyloid-β are an early event in an amyloid cascade hypothesis (Hardy and Higgins 1992). The first tracer to selectively visualize amyloid-β in vivo is the Pittsburgh compound B *[^{11}C]-PiB* (Klunk et al. 2004). Nearly all AD patients show high retention of the [^{11}C]-PiB tracer, whereas retention in FTD is low or mild (Rabinovici et al. 2007; Rowe et al. 2007; Drzezga et al. 2008). Significant differences in retention of [^{11}C]-PiB between AD and FTD patients have been shown in frontal, parietal, temporal and occipital regions, as well as in the putamina (Engler et al. 2008). Correspondingly, inter-rater reliability is high, reflecting an on/off phenomenon for [^{11}C]-PiB retention (Rabinovici et al. 2007). Positive [^{11}C]-PiB scans in FTD are quite common (Engler et al. 2008; Burke et al. 2011), but [^{11}C]-PiB retention in supposedly FTD patients might also be reflective of concomitant AD pathology, e.g. in the logopedic variant of PPA (Leyton et al. 2011). With the introduction of fluorine-18-labelled amyloid tracers, such as *[^{18}F]-florbetaben*, distribution may be facilitated to medical centres without cyclotron. It has been shown in vitro that ^{18}F-florbetaben does not bind to τ-protein, associated with FTD, or to α-synuclein, associated with DLB (Fodero-Tavoletti et al. 2012). A recent in vivo study, using [^{18}F]-florbetaben, showed widespread cortical uptake in AD patients and only mild binding in one out of five FTLD

Table 15.3 Correlations between functional imaging and behavioural aspects of FTD

Author	Groups	Tracer	Statistics	Main results of hypometabolism or reduced blood flow
Mendez et al. (2006)	FTD ($n = 74$)	[^{99}Tc]-HMPAO SPECT	Visual assessment	Dysthymia and anxiety: R temporal lobe
				Frivolous behaviour: temporal lobes, particularly R
				Alterations in non-verbal behaviour: R frontal lobe
Le Ber et al. (2006)	FTD-b ($n = 68$: 25% inert, 19% disinhibit, 56% mixed)	[^{99}Tc]-HMPAO SPECT	Multicentre, voxel based, $p < 0.05$, corrected	Inertia: medial frontal cingulate gyrus
	Age-matched controls ($n = 28$)			Disinhibition: predominant ventromedial prefrontal and temporal
Raczka et al. (2010)	FTD ($n = 17$)	[^{18}F]-FDG-PET	Voxel based, $p < 0.001$, uncorrected	Executive dysfunction: anterior-mid cingulated gyrus, anterior medial frontal, L frontopolar and inferior/middle/superior frontal gyri, anterior and inferior part insula, globus pallidus, caudatum, thalamus
	Age-sex-matched controls ($n = 9$)			Behavioural impairment: L frontomedial inferior temporal gyrus and anterior/superior part of the insula
Bastin et al. (2012)	FTD-b ($n = 11$)	[^{18}F]-FDG-PET	Voxel based, $p < 0.05$, corrected	Severe loss of autonoetic consciousness[a]:
	Controls ($n = 26$)			L anterior medial frontal, L middle frontal cortex, near the superior frontal sulcus, L inferior parietal cortex and the posterior cingulate cortex, R postcentral sulcus
Borroni et al. (2012)	FTD-b ($n = 207$)	[^{99}Tc]-ECD SPECT	Confirmatory factor analysis, $p < 0.005$, uncorrected, minimum voxel size 25	Disinhibition: anterior cingulate, bilateral anterior temporal cortex hypoperfusion (R > L)
				Apathy: L dorsolateral frontal cortex
				Aggression: no region associated
				Language deficits: L frontotemporal lobes

R right side, *L* left side

[a]Autonoetic consciousness: ability to retrieve memories accompanied by recollection of encoding context

patients (Rowe et al. 2008). Another study in a larger group showed a similar pattern of increased uptake in nearly all AD patients and mild or low uptake in FTD patients (Villemagne et al. 2011). However, a majority of MCI subjects also demonstrated increased uptake. Especially in the elderly, the positive predictive value for AD of a positive amyloid scan may decrease because of the increased prevalence of positive amyloid positivity in the general population (Bergeron et al. 2018). A promising application is the use of early time frames of dynamic amyloid PET acquisitions as a surrogate for FDG PET, which could eliminate the need for two different scans (Asghar et al. 2019). Tau PET tracers as ^{18}F-flortaucipir (previously ^{18}F-T807 and ^{18}F-AV1451) bind in vitro with high affinity to neurofibrillary tangles in AD (Xia et al. 2013; Marquie et al. 2015; Lowe et al. 2016). This is promising for specific binding to FTD pathology (Maruyama et al. 2013), although in FTD and related tauopathies, in vivo findings with ^{18}F-flortaucipir have yielded conflicting results (Smith et al. 2016; Spina et al. 2017). The interpretation of in vivo retention in brain areas relevant to FTD tauopathies is further complicated by 'off-target' binding seen in normal controls in midbrain and basal ganglia, possibly reflecting a proclivity to bind to neuromelanin containing cells or mineralized tissue (Jang et al. 2018; Lockhart et al. 2017). Pathologic tau with three or four repeat microtubule binding domains aggregates intracellularly into paired helical filaments AD and twisted ribbons or straight filaments in a range of FTD syndromes (Crowther and Goedert 2000). Familial FTD can be caused by mutations in MAPT with resulting tau pathology or by mutations in GRN gene or C9ORF72, resulting in TDP-43 pathology (Ghetti et al. 2015; Hsiung et al. 2012; Mackenzie et al. 2006). TDP-43 pathology is seen in the majority of patients with semantic variant PPA and FTD-ALS (Spinelli et al. 2017). At present, ^{18}F-flortaucipir in patients with FTD and predicted tauopathy or TDP-43 pathology demonstrated limited sensitivity and specificity, and further postmortem pathological confirmation and development of FTD tau-specific ligands are needed (Tsai et al. 2019). Another area of interest in neurodegenerative diseases is a process often referred to as 'Glial activity', which was significantly increased in the frontal, occipital and posterior cingulate cortex compared to healthy controls (Miyoshi et al. 2010). Neuroinflammation may be a marker of τ-pathology in a presymptomatic state. However, the causal relationship between microglial activation and dementia pathogenesis still has not been fully established (Kreisl et al. 2018). Second-generation translocator protein (TSPO) PET imaging may shed more light on this issue in the future.

15.4 Neurotransmitter Systems

The involvement of different neurotransmitter systems varies between types of dementia, offering another possibility to differentiate FTD from other dementias. This could also have implications for pharmacotherapy. In this paragraph, findings in the serotonergic, dopaminergic and cholinergic system in FTD will be summarized.

15.4.1 Serotonergic System

Behavioural and psychological disorders are frequent in FTD, and many of them are related to serotonergic dysfunction (Salmon 2007). A study using [^{11}C]WAY-100635 showed that FTD patients had significantly decreased serotonin (5-HT$_{1A}$) binding potential (BP) compared with controls in all ten brain regions examined but most pronounced in frontal and temporal regions (Lanctot et al. 2007). The extent of BP reduction suggested that the potential of treatment with pharmacological agents, such as 5-HT$_{1A}$ receptor blockers and serotonin reuptake inhibitors, may be limited. However, this study was limited by small group size ($n = 4$) and further research is warranted.

15.4.2 Dopaminergic System

The prevalence of extrapyramidal symptoms in FTD is between 23% and 83% (Padovani et al. 2007). Akinesia, rigidity and a shuffling with a short stride are typical findings (Rinne et al. 2002). Neuropathological mechanisms responsible for these symptoms have been evaluated in FTD using radiotracers which bind to pre- or postsynaptic dopaminergic receptors. Using [^{123}I]-FP-CIT SPECT (DAT-scan), the presynaptic dopamine transporter has been assessed in FTD patients. Significantly reduced uptake was noted in both the right and left striatum. Therefore, reduced striatal uptake of a DAT-scan, considered characteristic for DLB, does not rule out FTD (Morgan et al. 2012). The pattern of striatal dopamine transporter (DAT) scans has prognostic value in determining whether patients with Parkinsonism and behavioural and/or language dysfunction will develop features of PSP or FTD later in the disease course (Yoo et al. 2018). In addition, there was a negative correlation between motor UPDRS scores in the right striatum and in the left striatum. These findings indicate functional loss of presynaptic dopamine transporters in FTD and underline the need for evaluation of dopamine drug treatment (Sedaghat et al. 2007). Impaired function of the dopamine transporter in FTD has also been demonstrated using [^{11}C]-CFT PET, both in the caudate nucleus and in the putamen when compared to controls (Rinne et al. 2002). This pattern of impaired nigrostriatal dopamine function is different from idiopathic Parkinson patients, in whom reduced uptake is usually more pronounced in the putamen, but may be similar to that observed in AD. Another PET ligand, [^{11}C]-DTBZ, can be used to visualize the distribution volume of the vesicular monoamine transporter type 2 (VMAT2) and has been demonstrated to provide additional information to [^{18}F]-FDG to facilitate differentiation between dementias, particularly between AD and DLB (Koeppe et al. 2005).

15.4.3 Cholinergic System

The cholinergic system has been investigated in FTD, CBD and PSP patients using the radiotracer [^{11}C]-MP4A. A distinct pattern of K3 values, reflecting acetylcholinesterase activity, was observed in each of these diseases. FTD patients did not show

significant differences in K3 values compared to controls. In PSP, reduction of acetylcholinesterase activity was mild in the cortex, but pronounced in the thalamus, whereas in CBD acetylcholinesterase activity reduction was moderate in the cortex, but absent in the thalamus (Hirano et al. 2010). However, in advanced stage FTD patients, reduced acetylcholinesterase activity has been shown, indicating the above patterns may not be disease specific (Hirano et al. 2006). Furthermore, both decreased and increased acetylcholinesterase activities have been reported in presymptomatic FTD-17 gene carriers (Miyoshi et al. 2010).

15.5 Conclusions

Neuroimaging, particularly functional brain studies, greatly increased the sensitivity of detecting FTD. Clinical diagnosis of FTD (consensus criteria) and neuropsychological and neuropsychiatric features combined with SPECT or PET findings increases accuracy of the diagnosis FTD. Frontotemporal hypometabolism is an early and specific sign and helps to differentiate from other forms of dementia, especially AD. FDG-PET has been demonstrated to have higher sensitivity and specificity for the early detection of FTD when compared to perfusion SPECT. In addition to metabolic markers, nuclear imaging techniques may be helpful to detect specific markers of pathology or deficits of different neurotransmitter systems, depending on degeneration of subcortical nuclei, and provide valuable insight in the pathophysiology of FTD.

References

Albert M, DeCarli CS, DeKosky ST, de Leon MJ, Foster NL, Fox NC, Frank R, Frackowiak RS, Jack CR, Jagust WJ, Knopman DS, Morris JC, Petersen RC, Reiman E, Scheltens P, Small G, Soininen H, Thal L, Wahlund L-O, Thies W, Weiner M, Khachaturian Z (2005) The use of MRI and PET for clinical diagnosis of dementia and investigation of cognitive impairment: a consensus report. In: Neuroimaging Work Group of the Alzheimer's Association Consensus Report, pp 1–15

Alzheimer A (1911) Über eigenartige krankheitsfälle des späteren alters. Zbl Ges Neurol Psych 4:356–385

Anazodo UC, Finger E, Yin Ming Kwan B, Pavlosky W, Warrington JC, Günther M, Prato FS, Thiessen JD, St. Lawrencea KS (2017) Using simultaneous PET/MRI to compare the accuracy of diagnosing frontotemporal dementia by arterial spin labelling MRI and FDG-PET. Neuroimage Clin 17:405–414

Archer HA, Smailagic N, John C, Holmes RB, Takwoingi Y, Coulthard EJ, Cullum S (2015) Regional cerebral blood flow single photon emission computed tomography for detection of Frontotemporal dementia in people with suspected dementia. Cochrane Database Syst Rev 6:CD010896

Asghar M, Hinz R, Herholz K, Carter SF (2019) Dual-phase [18F]florbetapir in frontotemporal dementia. Eur J Nucl Med Mol Imaging 46(2):304–311

Bastin C, Feyers D, Souchay C, Guillaume B, Pepin JL, Lemaire C et al (2012) Frontal and posterior cingulate metabolic impairment in the behavioral variant of frontotemporal dementia with impaired autonoetic consciousness. Hum Brain Mapp 33(6):1268–1278

Bergeron D, Ossenkoppele R, Jr Laforce R (2018) Evidence-based interpretation of amyloid-beta PET results: a clinician's tool. Alzheimer Dis Assoc Disord 32(1):28–34

Bohnen NI, Djang DS, Herholz K, Anzai Y, Minoshima S (2012) Effectiveness and safety of 18F-FDG PET in the evaluation of dementia: a review of the recent literature. J Nucl Med 53(1):59–71

Borroni B, Premi E, Agosti C, Alberici A, Garibotto V, Bellelli G et al (2009) Revisiting brain reserve hypothesis in frontotemporal dementia: evidence from a brain perfusion study. Dement Geriatr Cogn Disord 28(2):130–135

Borroni B, Grassi M, Premi E, Gazzina S, Alberici A, Cosseddu M et al (2012) Neuroanatomical correlates of behavioural phenotypes in behavioural variant of frontotemporal dementia. Behav Brain Res 235(2):124–129

Burke JF, Albin RL, Koeppe RA, Giordani B, Kilbourn MR, Gilman S et al (2011) Assessment of mild dementia with amyloid and dopamine terminal positron emission tomography. Brain 134(Pt 6):1647–1657

Cha Y-HK, Jog MA, Kim Y-C, Chakrapani S, Kraman SM, Wang DJ (2013) Regional correlation between resting state FDG PET and pCASL perfusion MRI. J Cereb Blood Flow Metab 33:1909–1914

Charpentier P, Lavenu I, Defebvre L, Duhamel A, Lecouffe P, Pasquier F et al (2000) Alzheimer's disease and frontotemporal dementia are differentiated by discriminant analysis applied to (99m) tc HmPAO SPECT data. J Neurol Neurosurg Psychiatry 69(5):661–663

Chow TW, Graff-Guerrero A, Verhoeff NP, Binns MA, Tang-Wai DF, Freedman M et al (2011) Open-label study of the short-term effects of memantine on FDG-PET in frontotemporal dementia. Neuropsychiatr Dis Treat 7:415–424

Crowther RA, Goedert M (2000) Abnormal tau-containing filaments in neurodegenerative diseases. J Struct Biol 130(2–3):271–279

Cruts M, Gijselinck I, van der Zee J, Engelborghs S, Wils H, Pirici D et al (2006) Null mutations in progranulin cause ubiquitin-positive frontotemporal dementia linked to chromosome 17q21. Nature 442(7105):920–924

DeJesus-Hernandez M, Mackenzie IR, Boeve BF, Boxer AL, Baker M, Rutherford NJ et al (2011) Expanded GGGGCC hexanucleotide repeat in noncoding region of C9ORF72 causes chromosome 9p-linked FTD and ALS. Neuron 72(2):245–256

Dermaut B, Kumar-Singh S, Engelborghs S, Theuns J, Rademakers R, Saerens J et al (2004) A novel presenilin 1 mutation associated with pick's disease but not beta-amyloid plaques. Ann Neurol 55(5):617–626

Diehl J, Grimmer T, Drzezga A, Riemenschneider M, Forstl H, Kurz A (2004) Cerebral metabolic patterns at early stages of frontotemporal dementia and semantic dementia. A PET study. Neurobiol Aging 25(8):1051–1056

Diehl-Schmid J, Grimmer T, Drzezga A, Bornschein S, Riemenschneider M, Forstl H et al (2007) Decline of cerebral glucose metabolism in frontotemporal dementia: a longitudinal 18F-FDG-PET-study. Neurobiol Aging 28(1):42–50

Dobert N, Pantel J, Frolich L, Hamscho N, Menzel C, Grunwald F (2005) Diagnostic value of FDG-PET and HMPAO-SPET in patients with mild dementia and mild cognitive impairment: metabolic index and perfusion index. Dement Geriatr Cogn Disord 20(2–3):63–70

Drzezga A, Grimmer T, Henriksen G, Stangier I, Perneczky R, Diehl-Schmid J et al (2008) Imaging of amyloid plaques and cerebral glucose metabolism in semantic dementia and Alzheimer's disease. NeuroImage 39(2):619–633

Engler H, Santillo AF, Wang SX, Lindau M, Savitcheva I, Nordberg A et al (2008) In vivo amyloid imaging with PET in frontotemporal dementia. Eur J Nucl Med Mol Imaging 35(1): 100–106

Fällmar D, Haller S, Lilja J, Danfors T, Kilander L, Tolboom N, Egger K, Kellner E, Croon PM, Verfaillie SCJ, van Berckel BNM, Ossenkoppele R, Barkhof F, Larsson E-M (2017) Arterial spin labeling-based Z-maps have high specificity and positive predictive value for neurodegenerative dementia compared to FDG-PET. Eur Radiol 27(10):4237–4246

Fodero-Tavoletti MT, Brockschnieder D, Villemagne VL, Martin L, Connor AR, Thiele A et al (2012) In vitro characterization of [18F]-florbetaben, an Abeta imaging radiotracer. Nucl Med Biol 39(7):1042–1048

Foster NL, Heidebrink JL, Clark CM, Jagust WJ, Arnold SE, Barbas NR et al (2007) FDG-PET improves accuracy in distinguishing frontotemporal dementia and Alzheimer's disease. Brain 130(Pt 10):2616–2635

Garraux G, Salmon E, Degueldre C, Lemaire C, Laureys S, Franck G (1999) Comparison of impaired subcortico-frontal metabolic networks in normal aging, subcortico-frontal dementia, and cortical frontal dementia. NeuroImage 10(2):149–162

Ghetti B, Oblak AL, Boeve BF, Johnson KA, Dickerson BC, Goedert M (2015) Invited review: frontotemporal dementia caused by microtubule-associated protein tau gene (MAPT) mutations: a chameleon for neuropathology and neuroimaging. Neuropathol Appl Neurobiol 41(1):24–46

Gijselinck I, Van Langenhove T, van der Zee J, Sleegers K, Philtjens S, Kleinberger G et al (2012) A C9orf72 promoter repeat expansion in a Flanders-Belgian cohort with disorders of the frontotemporal lobar degeneration-amyotrophic lateral sclerosis spectrum: a gene identification study. Lancet Neurol 11(1):54–65

Goldman JS, Farmer JM, Wood EM, Johnson JK, Boxer A, Neuhaus J et al (2005) Comparison of family histories in FTLD subtypes and related tauopathies. Neurology 65(11): 1817–1819

Gorno-Tempini ML, Hillis AE, Weintraub S, Kertesz A, Mendez M, Cappa SF et al (2011) Classification of primary progressive aphasia and its variants. Neurology 76(11):1006–1014

Greaves CV, Rohrer JD (2019) An update on genetic frontotemporal dementia. J Neurol 266(8):2075–2086

Grimmer T, Diehl J, Drzezga A, Forstl H, Kurz A (2004) Region-specific decline of cerebral glucose metabolism in patients with frontotemporal dementia: a prospective 18F-FDG-PET study. Dement Geriatr Cogn Disord 18(1):32–36

Hardy JA, Higgins GA (1992) Alzheimer's disease: the amyloid cascade hypothesis. Science 256(5054):184–185

Harper L, Fumagalli GG, Barkhof F, Scheltens P, O'Brien JT, Bouwman F et al (2016) MRI visual rating scales in the diagnosis of dementia: evaluation in 184 post-mortem confirmed cases. Brain 139:1211

Herholz K, Schopphoff H, Schmidt M, Mielke R, Eschner W, Scheidhauer K et al (2002) Direct comparison of spatially normalized PET and SPECT scans in Alzheimer's disease. J Nucl Med 43(1):21–26

Hirano S, Shinotoh H, Kobayashi T, Tsuboi Y, Wszolek ZK, Aotsuka A et al (2006) Brain acetylcholinesterase activity in FTDP-17 studied by PET. Neurology 66(8):1276–1277

Hirano S, Shinotoh H, Shimada H, Aotsuka A, Tanaka N, Ota T et al (2010) Cholinergic imaging in corticobasal syndrome, progressive supranuclear palsy and frontotemporal dementia. Brain 133(Pt 7):2058–2068

Hsiung GY, DeJesus-Hernandez M, Feldman HH, Sengdy P, Bouchard-Kerr P, Dwosh E et al (2012) Clinical and pathological features of familial frontotemporal dementia caused by C9ORF72 mutation on chromosome 9p. Brain 135(Pt 3):709–722

Ibach B, Poljansky S, Marienhagen J, Sommer M, Manner P, Hajak G (2004) Contrasting metabolic impairment in frontotemporal degeneration and early onset Alzheimer's disease. NeuroImage 23(2):739–743

Ishii K, Sakamoto S, Sasaki M, Kitagaki H, Yamaji S, Hashimoto M et al (1998) Cerebral glucose metabolism in patients with frontotemporal dementia. J Nucl Med 39(11):1875–1878

Jang YK, Lyoo CH, Park S, Oh SJ, Cho H, Oh M et al (2018) Head to head comparison of [(18) F] AV-1451 and [(18)F] THK5351 for tau imaging in Alzheimer's disease and frontotemporal dementia. Eur J Nucl Med Mol Imaging 45(3):432–442

Josephs KA, Duffy JR, Fossett TR, Strand EA, Claassen DO, Whitwell JL et al (2010) Fluorodeoxyglucose F18 positron emission tomography in progressive apraxia of speech and primary progressive aphasia variants. Arch Neurol 67(5):596–605

Kapucu OL, Nobili F, Varrone A, Booij J, Vander Borght T, Nagren K et al (2009) EANM procedure guideline for brain perfusion SPECT using 99mTc-labelled radiopharmaceuticals, version 2. Eur J Nucl Med Mol Imaging 36(12):2093–2102

Kertesz A, McMonagle P, Blair M, Davidson W, Munoz DG (2005) The evolution and pathology of frontotemporal dementia. Brain 128(Pt 9):1996–2005

Klunk WE, Engler H, Nordberg A, Wang Y, Blomqvist G, Holt DP et al (2004) Imaging brain amyloid in Alzheimer's disease with Pittsburgh compound-B. Ann Neurol 55(3):306–319

Koeppe RA, Gilman S, Joshi A, Liu S, Little R, Junck L et al (2005) 11C-DTBZ and 18F-FDG PET measures in differentiating dementias. J Nucl Med 46(6):936–944

Kotagal V, Lorincz MT, Bohnen NI (2012) A frontotemporal dementia-like syndrome mimicking postpartum depression detected by 18F fluorodeoxyglucose positron emission tomography. Clin Nucl Med 37(9):e223–e224

Kreisl WC, Henter ID, Innis RB (2018) Imaging translocator protein as a biomarker of neuroinflammation in dementia. Adv Pharmacol (San Diego, CA) 82:163–185

Lanctot KL, Herrmann N, Ganjavi H, Black SE, Rusjan PM, Houle S et al (2007) Serotonin-1A receptors in frontotemporal dementia compared with controls. Psychiatry Res 156(3):247–250

Le Ber I, Guedj E, Gabelle A, Verpillat P, Volteau M, Thomas-Anterion C et al (2006) Demographic, neurological and behavioural characteristics and brain perfusion SPECT in frontal variant of frontotemporal dementia. Brain 129(Pt 11):3051–3065

Leyton CE, Villemagne VL, Savage S, Pike KE, Ballard KJ, Piguet O, Hodges JR (2011) Subtypes of progressive aphasia: application of the international consensus criteria and validation using beta-amyloid imaging. Brain J Neurol 134(Pt 10):3030–3043

Liu X, Erikson C, Brun A (1996) Cortical synaptic changes and gliosis in normal aging, Alzheimer's disease and frontal lobe degeneration. Dementia 7(3):128–134

Lockhart SN, Ayakta N, Winer JR, La Joie R, Rabinovici GD, Jagust WJ (2017) Elevated (18)F-AV-1451 PET tracer uptake detected in incidental imaging findings. Neurology 88(11):1095–1097

Lowe VJ, Curran G, Fang P, Liesinger AM, Josephs KA, Parisi JE et al (2016) An autoradiographic evaluation of AV-1451 Tau PET in dementia. Acta Neuropathol Commun 4(1):58

Mackenzie IR, Baker M, Pickering-Brown S, Hsiung GY, Lindholm C, Dwosh E et al (2006) The neuropathology of frontotemporal lobar degeneration caused by mutations in the progranulin gene. Brain 129(Pt 11):3081–3090

Mackenzie IR, Rademakers R, Neumann M (2010) TDP-43 and FUS in amyotrophic lateral sclerosis and frontotemporal dementia. Lancet Neurol 9(10):995–1007

Marquie M, Normandin MD, Vanderburg CR, Costantino IM, Bien EA, Rycyna LG et al (2015) Validating novel tau positron emission tomography tracer [F-18]-AV-1451 (T807) on postmortem brain tissue. Ann Neurol 78(5):787–800

Maruyama M, Shimada H, Suhara T, Shinotoh H, Ji B, Maeda J et al (2013) Imaging of tau pathology in a tauopathy mouse model and in Alzheimer patients compared to normal controls. Neuron 79(6):1094–1108

McKhann GM, Albert MS, Grossman M, Miller B, Dickson D, Trojanowski JQ et al (2001) Clinical and pathological diagnosis of frontotemporal dementia: report of the work group on frontotemporal dementia and pick's disease. Arch Neurol 58(11):1803–1809

McMurtray AM, Chen AK, Shapira JS, Chow TW, Mishkin F, Miller BL et al (2006) Variations in regional SPECT hypoperfusion and clinical features in frontotemporal dementia. Neurology 66(4):517–522

McNeill R, Sare GM, Manoharan M, Testa HJ, Mann DM, Neary D et al (2007) Accuracy of single-photon emission computed tomography in differentiating frontotemporal dementia from Alzheimer's disease. J Neurol Neurosurg Psychiatry 78(4):350–355

Mendez MF, McMurtray A, Chen AK, Shapira JS, Mishkin F, Miller BL (2006) Functional neuroimaging and presenting psychiatric features in frontotemporal dementia. J Neurol Neurosurg Psychiatry 77(1):4–7

Mendez MF, Shapira JS, McMurtray A, Licht E, Miller BL (2007) Accuracy of the clinical evaluation for frontotemporal dementia. Arch Neurol 64(6):830–835

Mesulam MM (2001) Primary progressive aphasia. Ann Neurol 49(4):425–432
Miller BL, Gearhart R (1999) Neuroimaging in the diagnosis of frontotemporal dementia. Dement Geriatr Cogn Disord 10(Suppl 1):71–74
Miyoshi M, Shinotoh H, Wszolek ZK, Strongosky AJ, Shimada H, Arakawa R et al (2010) In vivo detection of neuropathologic changes in presymptomatic MAPT mutation carriers: a PET and MRI study. Parkinsonism Relat Disord 16(6):404–408
Morgan S, Kemp P, Booij J, Costa DC, Padayachee S, Lee L et al (2012) Differentiation of frontotemporal dementia from dementia with Lewy bodies using FP-CIT SPECT. J Neurol Neurosurg Psychiatry 83(11):1063–1070
Mosconi L, Tsui WH, Herholz K, Pupi A, Drzezga A, Lucignani G et al (2008) Multicenter standardized 18F-FDG PET diagnosis of mild cognitive impairment, Alzheimer's disease, and other dementias. J Nucl Med 49(3):390–398
Neary D, Snowden JS, Gustafson L, Passant U, Stuss D, Black S et al (1998) Frontotemporal lobar degeneration: a consensus on clinical diagnostic criteria. Neurology 51(6):1546–1554
Nobili F, Arbizu J, Bouwman F, Drzezga A, Agosta F, Nestor P, EANM-EAN Task Force for the Prescription of FDG-PET for Dementing Neurodegenerative Disorders (2018) European association of nuclear medicine and European academy of neurology recommendations for the use of brain (18) F-fluorodeoxyglucose positron emission tomography in neurodegenerative cognitive impairment and dementia: Delphi consensus. Eur J Neurol 25(10):1201–1217
Padovani A, Agosti C, Premi E, Bellelli G, Borroni B (2007) Extrapyramidal symptoms in frontotemporal dementia: prevalence and clinical correlations. Neurosci Lett 422(1):39–42
Panegyres PK, Rogers JM, McCarthy M, Campbell A, Wu JS (2009) Fluorodeoxyglucose-positron emission tomography in the differential diagnosis of early-onset dementia: a prospective, community-based study. BMC Neurol 9:41. 2377-9-41
Perneczky R, Diehl-Schmid J, Drzezga A, Kurz A (2007) Brain reserve capacity in frontotemporal dementia: a voxel-based 18F-FDG PET study. Eur J Nucl Med Mol Imaging 34(7):1082–1087
Pick A (1892) Über die beziehungen der senilen hirnatropie zur aphasie. Pragen Med Wochenschr 17:165–167
Pickut BA, Saerens J, Marien P, Borggreve F, Goeman J, Vandevivere J et al (1997) Discriminative use of SPECT in frontal lobe-type dementia versus (senile) dementia of the Alzheimer's type. J Nucl Med 38(6):929–934
Rabinovici GD, Furst AJ, O'Neil JP, Racine CA, Mormino EC, Baker SL et al (2007) 11C-PIB PET imaging in Alzheimer disease and frontotemporal lobar degeneration. Neurology 68(15):1205–1212
Rabinovici GD, Jagust WJ, Furst AJ, Ogar JM, Racine CA, Mormino EC et al (2008) Abeta amyloid and glucose metabolism in three variants of primary progressive aphasia. Ann Neurol 64(4):388–401
Raczka KA, Becker G, Seese A, Frisch S, Heiner S, Marschhauser A et al (2010) Executive and behavioral deficits share common neural substrates in frontotemporal lobar degeneration – a pilot FDG-PET study. Psychiatry Res 182(3):274–280
Rascovsky K, Hodges JR, Knopman D, Mendez MF, Kramer JH, Neuhaus J et al (2011) Sensitivity of revised diagnostic criteria for the behavioural variant of frontotemporal dementia. Brain 134(Pt 9):2456–2477
Ratnavalli E, Brayne C, Dawson K, Hodges JR (2002) The prevalence of frontotemporal dementia. Neurology 11;58(11):1615–1621.
Read SL, Miller BL, Mena I, Kim R, Itabashi H, Darby A (1995) SPECT in dementia: clinical and pathological correlation. J Am Geriatr Soc 43(11):1243–1247
Reivich M, Kuhl D, Wolf A, Greenberg J, Phelps M, Ido T et al (1979) The [18F]fluorodeoxyglucose method for the measurement of local cerebral glucose utilization in man. Circ Res 44(1):127–137
Rinne JO, Laine M, Kaasinen V, Norvasuo-Heila MK, Nagren K, Helenius H (2002) Striatal dopamine transporter and extrapyramidal symptoms in frontotemporal dementia. Neurology 58(10):1489–1493
Rosso SM, Donker Kaat L, Baks T, Joosse M, de Koning I, Pijnenburg Y et al (2003) Frontotemporal dementia in the Netherlands: patient characteristics and prevalence estimates from a population-based study. Brain 126(Pt 9):2016–2022

Rowe CC, Ng S, Ackermann U, Gong SJ, Pike K, Savage G et al (2007) Imaging beta-amyloid burden in aging and dementia. Neurology 68(20):1718–1725

Rowe CC, Ackerman U, Browne W, Mulligan R, Pike KL, O'Keefe G et al (2008) Imaging of amyloid beta in Alzheimer's disease with 18F-BAY94-9172, a novel PET tracer: proof of mechanism. Lancet Neurol 7(2):129–135

Salmon E (2007) A review of the literature on neuroimaging of serotoninergic function in Alzheimer's disease and related disorders. J Neural Transm 114(9):1179–1185

Salmon E, Garraux G, Delbeuck X, Collette F, Kalbe E, Zuendorf G et al (2003) Predominant ventromedial frontopolar metabolic impairment in frontotemporal dementia. NeuroImage 20(1):435–440

Santillo AF, Skoglund L, Lindau M, Eeg-Olofsson KE, Tovi M, Engler H et al (2009) Frontotemporal dementia-amyotrophic lateral sclerosis complex is simulated by neurodegeneration with brain iron accumulation. Alzheimer Dis Assoc Disord 23(3):298–300

Sedaghat F, Gotzamani-Psarrakou A, Dedousi E, Arnaoutoglou M, Psarrakos K, Baloyannis I et al (2007) Evaluation of dopaminergic function in frontotemporal dementia using I-FP-CIT single photon emission computed tomography. Neurodegener Dis 4(5):382–385

Seelaar H, Rohrer JD, Pijnenburg YA, Fox NC, van Swieten JC (2011) Clinical, genetic and pathological heterogeneity of frontotemporal dementia: a review. J Neurol Neurosurg Psychiatry 82(5):476–486

Sieben A, Van Langenhove T, Engelborghs S, Martin JJ, Boon P, Cras P et al (2012) The genetics and neuropathology of frontotemporal lobar degeneration. Acta Neuropathol 124(3):353–372

Simon-Sanchez J, Dopper EG, Cohn-Hokke PE, Hukema RK, Nicolaou N, Seelaar H et al (2012) The clinical and pathological phenotype of C9ORF72 hexanucleotide repeat expansions. Brain 135(Pt 3):723–735

Sjogren M, Gustafson L, Wikkelso C, Wallin A (2000) Frontotemporal dementia can be distinguished from Alzheimer's disease and subcortical white matter dementia by an anterior-to-posterior rCBF-SPET ratio. Dement Geriatr Cogn Disord 11(5):275–285

Smith R, Puschmann A, Scholl M, Ohlsson T, van Swieten J, Honer M et al (2016) 18F-AV-1451 tau PET imaging correlates strongly with tau neuropathology in MAPT mutation carriers. Brain 139(Pt 9):2372–2379

Sokoloff L (1977) Relation between physiological function and energy metabolism in the central nervous system. J Neurochem 29(1):13–26

Sokoloff L, Reivich M, Kennedy C, Des Rosiers MH, Patlak CS, Pettigrew KD et al (1977) The [14C]deoxyglucose method for the measurement of local cerebral glucose utilization: theory, procedure, and normal values in the conscious and anesthetized albino rat. J Neurochem 28(5):897–916

Spina S, Schonhaut DR, Boeve BF, Seeley WW, Ossenkoppele R, O'Neil JP et al (2017) Frontotemporal dementia with the V337M MAPT mutation: tau-PET and pathology correlations. Neurology 88(8):758–766

Spinelli EG, Mandelli ML, Miller ZA, Santos-Santos MA, Wilson SM, Agosta F et al (2017) Typical and atypical pathology in primary progressive aphasia variants. Ann Neurol 81(3):430–443

Spreng RN, Drzezga A, Diehl-Schmid J, Kurz A, Levine B, Perneczky R (2011) Relationship between occupation attributes and brain metabolism in frontotemporal dementia. Neuropsychologia 49(13):3699–3703

Talbot PR, Lloyd JJ, Snowden JS, Neary D, Testa HJ (1998) A clinical role for 99mTc-HMPAO SPECT in the investigation of dementia? J Neurol Neurosurg Psychiatry 64(3):306–313

Teune LK, Bartels AL, de Jomg BM, Willemsen ATM, Eshuis SA, de Vries JJ et al (2010) Typical cerebral metabolic patterns in neurodegenerative brain diseases. Mov Disord 25(14):2395–2404

Tsai RM, Bejanin A, Lesman-Segev O, LaJoie R, Visani A, Bourakova V (2019) ^{18}F-flortaucipir (AV-1451) tau PET in frontotemporal dementia syndromes. Alzheimers Res Ther 11:13

Varrone A, Pappata S, Caraco C, Soricelli A, Milan G, Quarantelli M et al (2002) Voxel-based comparison of rCBF SPET images in frontotemporal dementia and Alzheimer's disease highlights the involvement of different cortical networks. Eur J Nucl Med Mol Imaging 29(11):1447–1454

Verfaillie SCJ, Adriaanse SM, Binnewijzend MAA, Benedictus MR, Ossenkoppele R, Wattjes MP, Pijnenburg YAL, van der Flier WM, Lammertsma AA, Kuijer JPA, Boellaard R, Scheltens P, van Berckel BNM, Barkhof F (2015) 2015. Cerebral perfusion and glucose metabolism in Alzheimer's disease and frontotemporal dementia: two sides of the same coin? Eur Radiol 25(10):3050–3059

Vieira RT, Caixeta L, Machado S, Silva AC, Nardi AE et al. (2013) Epidemiology of early-onset dementia: a review of the literature. Clin Pract Epidemiol Ment Health 9:88–95.

Vijverberg EG, Wattjes MP, Dols A, Krudop WA, Möller C, Peters A, Kerssens CJ, Gossink F, Prins ND, Stek ML, Scheltens P, van Berckel BN, Barkhof F, Pijnenburg YA (2016) Diagnostic accuracy of MRI and additional [18F]FDG-PET for behavioral variant frontotemporal dementia in patients with late onset behavioral changes. J Alzheimers Dis 53(4):1287–1297

Villemagne VL, Ong K, Mulligan RS, Holl G, Pejoska S, Jones G et al (2011) Amyloid imaging with (18)F-florbetaben in Alzheimer disease and other dementias. J Nucl Med 52(8):1210–1217

Xia CF, Arteaga J, Chen G, Gangadharmath U, Gomez LF, Kasi D et al (2013) [(18)F]T807, a novel tau positron emission tomography imaging agent for Alzheimer's disease. Alzheimers Dement 9(6):666–676

Yoo HS, Chung SJ, Jong S, Kim SJ, Oh JS, Kim JS, Ye BS, Sohn YH, Lee PH (2018) The role of 18F-FP-CIT PET in differentiation of progressive supranuclear palsy and frontotemporal dementia in the early stage. Eur J Nucl Med Mol Imaging 45(9):1585–1595

Parkinsonian Dementias: PET Findings

16

Prabesh Kanel, Martijn L. T. M. Müller,
and Nicolaas I. Bohnen

Contents

16.1 Introduction 493
16.2 Glucose Metabolic Changes in Parkinsonian Dementia 494
16.3 Dopaminergic PET Imaging in Parkinsonian Dementia 496
16.4 Cholinergic PET Imaging in Parkinsonian Dementia 497
16.5 Multitracer PET Imaging Studies: Dopaminergic and Cholinergic Imaging Studies in PD and Parkinsonian Dementia 498
16.6 Fibrillary β-Amyloid PET Imaging in Parkinsonian Dementia 500
16.7 Tau PET Imaging in Parkinsonian Dementia 502
16.8 Neuroinflammation Imaging in Parkinsonian Dementia 505
16.9 Discussion 506
References 507

P. Kanel · M. L. T. M. Müller
Departments of Radiology, University of Michigan, Ann Arbor, MI, USA

Morris K. Udall Center of Excellence for Parkinson's Disease Research, University of Michigan, Ann Arbor, MI, USA
e-mail: prabeshk@umich.edu; mtmuller@umich.edu

N. I. Bohnen (✉)
Division of Nuclear Medicine, Department of Radiology, University of Michigan, Ann Arbor, MI, USA

Morris K. Udall Center of Excellence for Parkinson's Disease Research, University of Michigan, Ann Arbor, MI, USA

Department of Neurology, University of Michigan, Ann Arbor, MI, USA

Neurology Service and GRECC, Veterans Administration Ann Arbor Healthcare System, Ann Arbor, MI, USA
e-mail: nbohnen@umich.edu

R. A. J. O. Dierckx et al. (eds.), *PET and SPECT in Neurology*,
https://doi.org/10.1007/978-3-030-53168-3_16

Abstract

The etiology of cognitive decline in Lewy body parkinsonism, including Parkinson disease (PD), is not only multifactorial but also heterogeneous and likely related to cumulative and interactive effects between changes in neurotransmitter functions, proteinopathies (α-synuclein, β-amyloid, tau), neuroinflammation, and -, vascular-, metabolic-, and other changes. Glucose metabolic studies have shown mixed subcortical and cortical changes in Parkinson disease with dementia (PDD). For example, incident dementia in idiopathic PD is heralded by decreased metabolism of visual association (Brodmann area 18) and posterior cingulate cortices with additional involvement of the caudate nucleus. Subsequent progression to dementia is associated with mixed subcortical, especially thalamic, and widespread cortical changes that involve the mesiofrontal lobes also. Neurotransmitter-specific PET imaging shows early and prominent nigrostriatal dopaminergic losses in PD, with no major differences between PD and PDD. Therefore, caudate nucleus, limbic, and mesofrontal dopaminergic denervations do not appear alone sufficient for development of PDD. Cholinergic imaging studies have shown relatively mild losses in PD without dementia but more prominent decreases in PDD. This suggests significant cholinergic pathology underlying progressive cognitive decline in PD. Average dopaminergic and cholinergic denervation does not appear to differ between PDD and dementia with Lewy bodies (DLB), supporting the view that PDD and DLB lie on a common disease spectrum. In vivo PET imaging studies show variable β-amyloid binding in PDD with prevalence of pathologic amyloid deposition higher in DLB compared to PDD. However, despite the relatively lower binding levels compared to Alzheimer disease (AD), β-amyloid deposition contributes to cognitive impairment early in the course of cognitive decline in PD, suggesting a lower symptomatic threshold for amyloid deposition compared to normal aging and AD.

Emerging in vivo tau PET studies in Parkinsonian dementias show tau binding in cortical areas that have distinct distribution compared to AD. These preliminary tau imaging studies suggest a gradual increase of tau binding with appearance of absent/low binding in cognitively normal PD, low binding in cognitively impaired PD, intermediate binding in DLB, and highest binding in AD. Neuroinflammatory imaging studies shed new light on possible mechanistic factors underlying cognitive decline in Lewy body parkinsonism. Finally, medical comorbidities associated with systemic cardiovascular, metabolic, and inflammatory changes appear to contribute to the pathophysiological heterogeneity of the Lewy body dementias.

Abbreviations

AD	Alzheimer disease
DLB	Dementia with Lewy bodies
DTBZ	Dihydrotetrabenazine

FDG	Fluorodeoxyglucose
FDOPA	6-Fluorodopa
MP4A	Methyl-4-piperidyl acetate
PD	Parkinson disease
PDD	Parkinson disease with dementia
PET	Positron Emission Tomography
PMP	Methyl-4-piperidinyl propionate

16.1 Introduction

PD patients are at increased risk of developing dementia. The prevalence estimates of dementia in PD range from 24% to 31% (Aarsland et al. 2005), with over 80% of patients developing dementia after a disease duration of 20 years (Hely et al. 2008). Cognitive impairment in PD probably reflects several processes, including degeneration of subcortical neurotransmitter (esp. cholinergic and dopaminergic) projection systems and proteinopathies (including α-synuclein Lewy body and β-amyloid plaque and neurofibrillary tangles) (Hirsch et al. 1987; Zweig et al. 1989; Gibb 1989; Mahler and Cummings 1990; Churchyard and Lees 1997; Jellinger 2000, 2006). Lewy body dementias are a diverse entity for which clinical criteria attempt to define subtypes (McKeith et al. 1996; Bohnen et al. 2017). One of these, dementia with Lewy bodies (DLB) is the second most frequent type of all dementias, associated with a clinical phenotype including neuropsychiatric disturbances (prominent visual hallucinations, depression) and variability in arousal and attention, antedating or shortly following the onset of extrapyramidal motor symptoms (McKeith et al. 2005). An arbitrary but generally accepted distinction has been made in current International Consensus diagnostic criteria between patients presenting with developing parkinsonism and dementia concurrently (DLB) versus those with developing parkinsonism more than 1 year prior to the onset of dementia (PDD) (McKeith et al. 1996, 2005, 2017; Emre 2003). There is, however, substantial debate whether these two clinically defined diagnostic entities should be kept separately or not (McKeith et al. 2017; Postuma et al. 2015). For example, the recent Movement Disorder Society clinical diagnostic criteria do not consider the presence of dementia as an exclusion for the diagnosis of PD (regardless of when motor parkinsonism occurs relative to cognitive or behavioral changes) (Postuma et al. 2015, 2018). For example, clinically defined DLB patients could be labeled as "PDD with Lewy bodies subtype" (Postuma et al. 2015). In contrast, the 1-year rule has been upheld in recently updated consensus diagnostic criteria for DLB (McKeith et al. 2017). REM sleep behavior disorder is now also a core clinical feature. Furthermore, imaging biomarkers (cardiac [I-123]metaiodobenzylguanidine, MIBG, sympathetic myocardial scintigraphy dopamine transporter, DAT, SPECT, [F-18]fluorodeoxyglucose (FDG) PET) are now used as "indicative" biomarkers. If one of these is positive, only one out of the four core clinical features is needed to make the probable DLB diagnosis (McKeith et al. 2017).

The term Parkinsonian dementia will be used in this chapter to reflect both PDD and DLB, together, unless specified separately. The chapter will first review global cerebral changes in Parkinsonian dementia based on findings in [F-18]fluorodeoxyglucose (FDG) PET studies followed by a discussion of dopaminergic and cholinergic neurotransmitter studies, a summary of the in vivo imaging literature on proteinopathies in PD, particularly, deposition of fibrillary β-amyloid and tau, and ends with a review of neuroinflammatory PET studies.

16.2 Glucose Metabolic Changes in Parkinsonian Dementia

In vivo FDG-PET is a minimally invasive diagnostic imaging procedure used to evaluate the pattern of cerebral glucose metabolism. Resting-state FDG-PET studies have shown similar metabolic reductions in Parkinsonian dementia to those recognized in Alzheimer disease (AD), affecting the posterior cingulate and precuneus cortex as well as the association neocortices, including the temporoparietal more than the prefrontal regions (Albin et al. 1996). There is relative preservation of the primary sensorimotor cortex, basal ganglia, thalamus, and cerebellum (Minoshima et al. 1994; Womack et al. 2011). In PDD, the primary visual cortex in the occipital lobe may be reduced, whereas it is relatively unaffected in AD (Vander Borght et al. 1997). Metabolic reductions generally follow a similar topographic pattern in PDD and DLB (Albin et al. 1996). Figure 16.1 show typical topographic metabolic differences between the major types of dementia.

The consistent observation of a metabolic reduction in the medial occipital cortex in Parkinsonian dementia suggests the use of functional brain imaging as a potential clinical diagnostic aid to differentiate DLB from AD (Minoshima et al. 2001). Minoshima et al. found that the presence of occipital hypometabolism distinguished DLB from AD with 90% sensitivity and 80% specificity in a study using a post-mortem diagnostic validation (Minoshima et al. 2001). The sensitivity in discriminating DLB and AD using FDG PET was greater than using clinical diagnostic criteria that were applied retrospectively to the data from medical chart review (Minoshima et al. 2001; Luis et al. 1999). Glucose metabolic preservation of the mid or posterior cingulate gyrus (so-called cingulate island sign) may help to distinguish DLB from AD (Lim et al. 2009; Imabayashi et al. 2016).

Longitudinal studies in initially non-demented PD subjects offer an opportunity to study the metabolic pattern of incident dementia. We previously reported the results of a prospective cohort study where we compared changes in regional cerebral glucose metabolism in PD patients with incident dementia after 2–6 years of follow-up compared to patients who remained non-demented (Bohnen et al. 2011). We found that incident dementia in idiopathic PD initially presented as a predominant hypometabolic pathology in the visual association cortex (Brodmann area 18) and the posterior cingulum and precuneus. Although hypometabolism of the cuneus and precuneus remained most prominent, progression of dementia was associated with mixed subcortical and widespread cortical changes that also

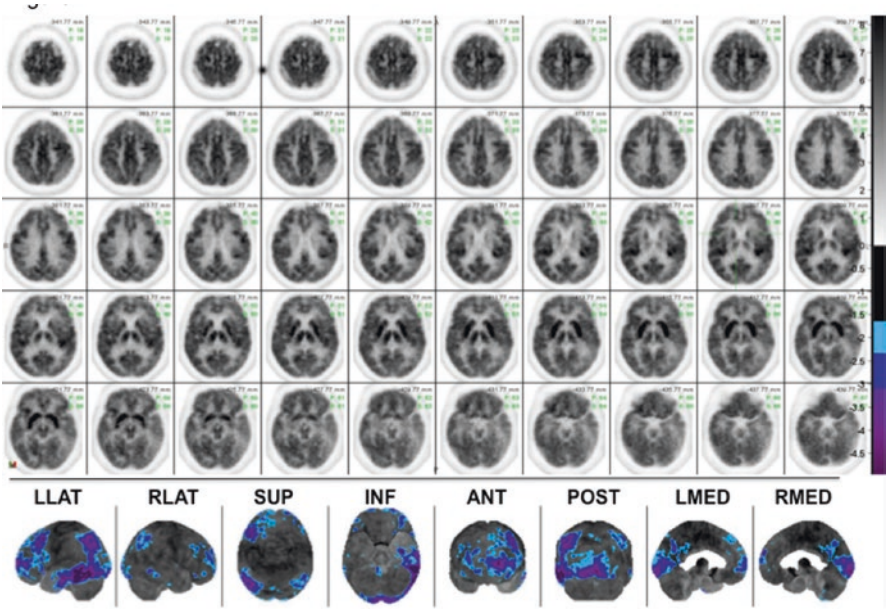

Fig. 16.1 FDG PET scan showing serial axial images and surface-rendered *z*-score maps of significant hypometabolism relative to a normal control database showing selective mesial occipital hypometabolism in a patient with DLB. Additional temporoparietal and mild frontal association cortical hypometabolism is typical both of DLB and of AD

involve the mesiofrontal lobes. The anterior cingulate cortex, which has distinct connections and behavioral attributes from the posterior cingulate, remained relatively spared. The PDD converter patients also demonstrated relative sparing of the primary sensorimotor cortex, a pattern similar to AD and DLB. Isolated occipital glucose hypometabolism is not specific for Parkinsonian dementia and can also be seen in non-demented PD patients (Bohnen et al. 1999). Recent longitudinal studies using FDG PET in PD consistently show hypometabolism in the posterior regions in early stage of cognitive normal PD that later converts from cognitively normal PD to PDD (Bohnen et al. 2011; Tard et al. 2015; Baba et al. 2017; Firbank et al. 2017).

Resting-state glucose metabolic imaging studies have been analyzed using voxel-based principal component analysis to characterize metabolic brain networks underlying cognitive dysfunction in PD (Huang et al. 2007). A specific factor, identified as the PD-related cognitive spatial covariance pattern (PDCP), is characterized by metabolic reductions in frontal and parietal association areas and relative increases in the cerebellar vermis and dentate nuclei. The PDCP can be quantitatively expressed as a numerical network score in individual subjects and will allow quantitative comparison of FDG PET scan findings over time to track progression of cognitive disease or response to treatment in PD (Mattis et al. 2016; Ko et al. 2017).

16.3 Dopaminergic PET Imaging in Parkinsonian Dementia

The basal ganglia and the neurotransmitter dopamine (DA) have been key targets for research exploring the pathophysiology underlying PD and its associated cognitive impairment. Several radiotracers have been employed previously to image nigrostriatal DA nerve terminals, including ligands metabolized by dopamine-synthetic enzymes such as [F-18]fluorodopa (FDOPA), synaptic vesicular monoamine transporter type 2 (VMAT2) ligands such as [C-11]dihydrotetrabenazine (DTBZ), and dopamine plasmalemmal DA reuptake transporter (DAT) ligands such as the cocaine analogue [C-11]WIN 35,428 (Garnett et al. 1978; Frey et al. 1996; Frost et al. 1993). The caudate nucleus has more prominent non-motor, cognitive, and affective connections, whereas the putamen plays a more direct role in motor functions (Alexander et al. 1986). Dopaminergic PET studies have shown prominent reductions of putaminal greater than caudate nucleus DA in PD (Fig. 16.2, top row) (Frey et al. 1996).

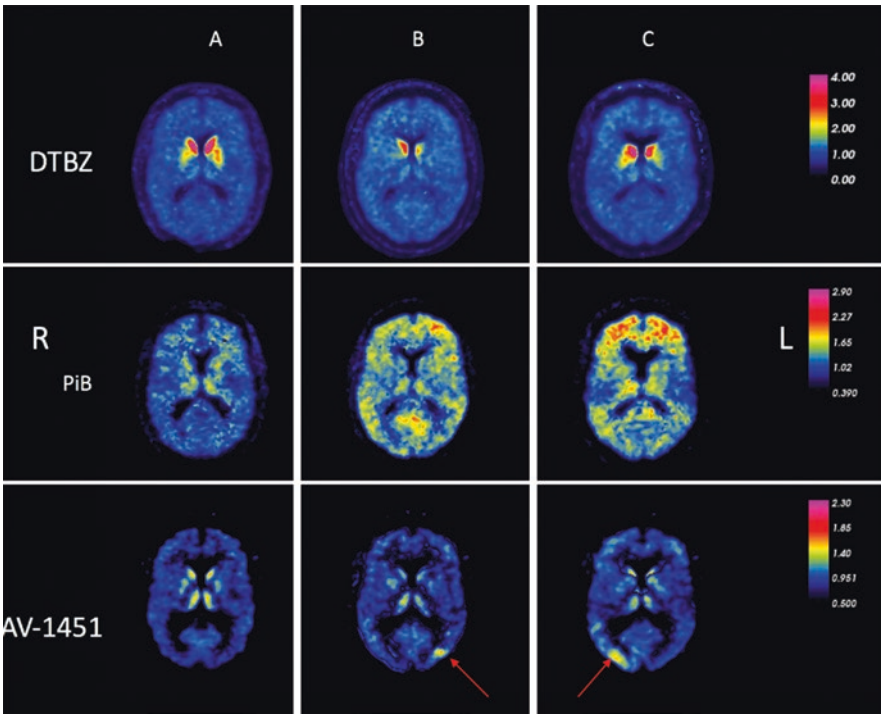

Fig. 16.2 Example of [C-11]dihydrotetrabenazine vesicular monoamine transporter type 2 (DTBZ VMAT2), [C-11]Pittsburgh compound B β-amyloid (PiB), and [F-18]AV-1451 tau PET scans for three Parkinsonian dementia subjects (columns A, B, and C). All scans are at the same transaxial slice. The top row shows nigrostriatal dopaminergic denervation patterns typical of Parkinsonian dementia. The middle-row shows variable cortical β-amyloid deposition with no significant deposition in Subject A and higher levels of increased amyloid deposition in subjects B and C. The bottom-row shows elevated levels of tau deposition in the occipital temporal junction cortex in Subjects B and C, with no appreciable binding in subject A. None of the amyloid and tau PET are at binding levels that can be typically observed in Alzheimer disease

Dopaminergic mesolimbic and mesocortical pathways that innervate parts of the limbic system and the mesiofrontal neocortex (Bjorklund and Lindvall 1984) may affect cognitive functions in PD (Kovari et al. 2003; Williams-Gray et al. 2009). An FDOPA study found relative differences in FDOPA uptake in the anterior cingulum, ventral striatum and right caudate nucleus in PDD compared to non-demented PD patients using voxel-based analysis (Nagano-Saito et al. 2004; Holthoff et al. 1994; Ito et al. 2002). These data suggest that dementia in PD is associated with impaired mesolimbic and caudate dopaminergic function. However, a subsequent FDOPA study also found evidence of significant reductions in the caudate nuclei, anterior cingulate, and mesolimbic and mesofrontal cortices in non-demented PD patients compared to normal control subjects (Klein et al. 2010). Furthermore, these authors did not find significant differences in striatal or extra-striatal cortical FDOPA activity between non-demented PD versus Parkinsonian dementia patients (Klein et al. 2010). Although striatal and limbofrontal dopaminergic denervation is involved in specific cognitive functions in PD (Christopher et al. 2014), other FDOPA PET studies have also failed to find differences in striatal activity between PDD and non-demented PD patients (Hilker et al. 2005). Similar findings were reported in a [F-18]FP-CIT dopamine transporter PET study, where patients with PDD did not differ from non-demented PD patients in caudate nucleus or putaminal activity (Song et al. 2013). Furthermore, a longitudinal dopamine transporter [F-18]FP-CIT study found progressive decreases in striatal dopaminergic activity that correlated with changes in metabolic motor network and clinical motor scores but not with metabolic cognitive network changes in PD (Huang et al. 2007). Therefore, caudate nucleus, limbic, and mesofrontal dopaminergic denervations alone do not appear sufficient for the development of dementia in PD (Klein et al. 2010). With respect to PDD versus DLB, Klein et al. did not find significant differences in striatal, limbic, or mesofrontal FDOPA uptake between the two clinical subtypes of Parkinsonian dementia (Klein et al. 2010). Patients with DLB have comparable VMAT2 nigrostriatal losses compared to PD, but there is no evidence of significant nigrostriatal denervation in AD (Villemagne et al. 2011, 2012). Therefore, findings of occipital hypometabolism, or the cingulate island sign on FDG PET, or of presynaptic nigrostriatal DA deficits can be used to distinguish PDD and DLB from AD (Lim et al. 2009; Imabayashi et al. 2016; Villemagne et al. 2011; Koeppe et al. 2005; Hu et al. 2000; Burke et al. 2011).

16.4 Cholinergic PET Imaging in Parkinsonian Dementia

Parkinson disease is viewed traditionally as a motor syndrome secondary to nigrostriatal dopaminergic denervation. However, some motor and non-motor impairments may result from an intricate interplay of comorbid pathology and neurotransmitter deficiencies that extend beyond the loss of dopaminergic nigral neurons (Muller and Bohnen 2013). For example, cholinergic denervation can occur early in PD, and progressive cholinergic denervation has been consistently associated with the presence of dementia in this disorder (Hilker et al. 2005; Shimada et al. 2009; Shinotoh et al. 1999; Bohnen et al. 2003). Imaging results are consistent

with post-mortem evidence that basal forebrain cholinergic system degeneration appears early in PD and worsens with the appearance of dementia (Ruberg et al. 1986; Roy et al. 2016). Impairment or degeneration of the cholinergic system plays a significant role in the progressive cognitive decline in PD (Perry et al. 1985).

There are two major sources of cholinergic projections in the brain. The nucleus basalis of Meynert/diagonal band of Broca/medial septum complex provides the principal cholinergic input to the entire cortical mantle and degenerates in PD (Mesulam and Geula 1988; Liu et al. 2015). The pedunculopontine nucleus, a brainstem locomotor center, provides cholinergic inputs to the basal ganglia, thalamus, cerebellum, several brainstem nuclei, and the spinal cord (Heckers et al. 1992) and also degenerates in PD (Lee et al. 2000). Acetylcholinesterase (AChE) PET imaging can assess cholinergic terminal integrity, with cortical activity reflecting basal forebrain projections and thalamic uptake reflecting pedunculopontine nucleus integrity.

Previous studies have found cognitive correlates of cortical cholinergic activity in PD (Shimada et al. 2009; Bohnen et al. 2006), whereas subcortical (pedunculopontine nucleus-thalamic) activity has been associated with a history of falls, sensory integration of postural control, and symptoms of REM sleep behavior disorder (Muller et al. 2013; Bohnen et al. 2009; Gilman et al. 2010; Kotagal et al. 2012).

We also found that low-range cholinergic activity in the thalamus, more robustly than the neocortex, was associated with symptoms of REM sleep behavior disorder (Kotagal et al. 2012). This finding provides a possible mechanism to explain to reported link between presence of REM sleep behavior disorder and risk of dementia in PD (Marion et al. 2008). In contrast to the degeneration of the basal forebrain complex in AD, the cholinergic innervation of the striatum (mainly originating from striatal interneurons) and of the thalamus (mainly originating from the brainstem) appears to remain relatively intact in AD (Mesulam 2004). The more selective cholinergic denervation of the cerebral cortex may explain the lower frequency of REM sleep behavior disorder in AD compared to Parkinsonian dementia (Gagnon et al. 2006). Cholinergic system degeneration may provide a conceptual framework to explain why PD patients with greater postural instability and gait disturbances are at an increased risk of developing dementia (Alves et al. 2006; Taylor et al. 2008). Our recent vesicular acetylcholine transporter [F-18]FEOBV-PET study confirmed subcortical reductions in DLB (Nejad-Davarani et al. 2019).

16.5 Multitracer PET Imaging Studies: Dopaminergic and Cholinergic Imaging Studies in PD and Parkinsonian Dementia

Several multitracer PET studies have been conducted to examine the combined effects of dopaminergic and cholinergic losses on clinical symptoms of Parkinsonian dementia. We reported findings of [C-11]dihydrotetrabenazine VMAT2 and AChE [C-11]PMP-PET studies in 101 patients with PD without dementia (Bohnen et al. 2012). We found that patients with lower cortical AChE activity had significantly

reduced cognitive performance scores for verbal learning, executive, and attention functions compared to patients with preserved cortical cholinergic activity. Analysis of covariance showed that global cognitive functions scores had independent regression with both cortical AChE activity and nigrostriatal VMAT2 binding. We did not find evidence either of exclusive cholinergic or dopaminergic substrates for specific cognitive domains to identify neurotransmitter-specific cognitive circuits. Although dopamine modulates corticostriatal circuits and performance on executive tasks such as working memory (Goldman-Rakic 1998) and attentional control (Williams-Gray et al. 2008), we found evidence of independent cholinergic and dopaminergic effects underlying these functions in PD. These findings indicate that multiple neurotransmitter deficits likely contribute in parallel to cognitive impairment in PD (Kehagia et al. 2010). Moreover, we also found evidence of an interactive effect (so-called "compensatory" hypothesis) between nigrostriatal and cholinergic changes in PD, where combined losses of these two neurotransmitter system result in more severe cognitive impairment, whereas cognition is relatively preserved in the setting of dopaminergic losses but preserved cholinergic integrity (Bohnen et al. 2015).

There are two studies that have directly compared FDOPA- and AChE-PET imaging studies in patients with PD and Parkinsonian dementia (Klein et al. 2010; Hilker et al. 2005). Hilker and colleagues performed MP4A AChE- and FDOPA-PET studies in 17 non-demented PD and 10 PDD patients (Hilker et al. 2005). Data were compared to 31 age-matched controls. Compared to normal controls, striatal FDOPA uptake was significantly decreased in PD and PDD; however, no differences in FDOPA uptake were observed between these two groups. Global cortical MP4A binding was severely reduced in PDD (29.7%, $p < 0.001$ versus controls), but only moderately decreased in PD (10.7%, $p < 0.01$ versus controls). The PDD group had lower cortical MP4A uptake rates than did patients with PD. In a subsequent study, this group of investigators also reported on FDOPA-, MP4A-, and FDG-PET findings in eight PDD, six DLB, and nine non-demented PD and age-matched control subjects (Klein et al. 2010). They reported reduced FDOPA uptake in the striatum and in limbic and associative prefrontal areas in all Parkinsonian patient groups. Patients with PDD and patients with DLB showed severe MP4A and FDG reductions in the neocortex with a gradient of worsening deficits from frontal to occipital regions. Significant differences between PDD and DLB were not found with any of the radioligands used. Patients with PD without dementia had mild cholinergic deficits and no significant FDG reductions versus controls. The authors concluded that patients with PDD and DLB share the same dopaminergic and cholinergic deficit profile, and that cholinergic deficits seem to be crucial for the development of Parkinsonian dementia.

We previously performed a triple ligand PET analysis in PD patients who were recruited based on risk factors for PDD and showed evidence of independent cognitive contributions of not only individual neurotransmitter changes (dopamine, acetylcholine) but also β-amyloidopathy (Shah et al. 2016). These data indicate that proteinopathy and neurotransmitter changes may make incremental and possibly

interactive contributions to cognitive impairment in PD at risk of dementia. It is plausible that heterogeneous combinations of neurotransmitter and proteinopathy changes may define endophenotypes within the cognitive dementia syndrome of PDD (Modreanu et al. 2017).

16.6 Fibrillary β-Amyloid PET Imaging in Parkinsonian Dementia

Neurodegenerative disorders are characterized by progressive dysfunction of specific populations of neurons. Neuronal loss is often associated with extra- and intracellular accumulations of misfolded proteins, typical of many neurodegenerative proteinopathies (Jellinger 2012). For example, extracellular fibrillary amyloid deposits characterize AD, and intracellular inclusions, such as Lewy bodies, containing α-synuclein, are characteristic of PD (Irvine et al. 2008). Although Parkinsonian dementia by definition is characterized by the presence of intraneuronal Lewy inclusion bodies, β-amyloid deposition can also be associated with Parkinsonian dementia, albeit to varying degree (Compta et al. 2011). The relative contributions of cortical and subcortical Aβ-amyloid deposition to cerebral dysfunction are unclear, and there are varying reports regarding the extent of β-amyloid depositions in PD versus PDD. Previous β-amyloid PET imaging studies using the Pittsburgh compound B (PiB) ligand have generally shown higher fibrillary β-amyloid burden in DLB compared to PDD (Rowe et al. 2007; Maetzler et al. 2009; Edison et al. 2008; Gomperts et al. 2008). For example, Johansson et al. did not find evidence of abnormal PiB retention in early stage PD subjects (Johansson et al. 2008). Maetzler and colleagues found abnormal cortical PiB binding in two out of ten PDD subjects (Maetzler et al. 2008). Edison et al. found high global cortical amyloid burden in DLB, but not in PDD (Edison et al. 2008). In the PDD patients, 2 out of 12 patients had both elevated cortical and striatal PiB retention. However, increased striatal PiB activity was also seen in two out of ten PDD patients who had no abnormal cortical retention. Interestingly, a post-mortem study found greater frequency of striatal β-amyloid deposition in PDD compared to PD (Kalaitzakis et al. 2008) and may imply a role of intrinsic striatal pathology in PDD. Gomperts et al. compared cortical PiB retention in PD, PDD, DLB, AD, and control groups and found higher cortical amyloid burden in DLB, at levels comparable to AD. Amyloid deposition in the PDD group was low, comparable to the PD and NC groups (Gomperts et al. 2008). However, a study by Foster and colleagues found no major differences in the degree of cortical nor caudate nucleus PiB binding between groups of PD (without or with mild cognitive impairment), PDD, or DLB (Foster et al. 2010) with the majority of subjects in each group having low-level PIB binding.

These observations are consistent with a literature review on in vivo β-amyloid PET imaging findings in Lewy body disorder that PD patients both without and with mild cognitive impairment (MCI) have a lower incidence (average 6% and 11%, respectively) of AD-range β-amyloid deposition compared to elderly normal

subjects (about 15% on average) and that PDD patients have a lower frequency of β-amyloid binding (average 27%, range 0–80%) compared to patients with DLB (mean of 57% with a range from 33% to 100%) (Frey and Petrou 2015). An [F-18]florbetaben β-amyloid PET study using visual assessment confirmed these observations of very low AD-range amyloidopathy in mild and non-demented PD (none out of 33) (Mashima et al. 2017). As is the case in AD, the degree of amyloidopathy may be a function of ApoE ε4 allele genotype status (Donaghy et al. 2015).

A post-mortem correlation study of in vivo amyloid imaging in three PDD subjects found that two subjects had abnormal cortical amyloid binding on PET imaging (Burack et al. 2010). At autopsy, all three patients had abundant cortical Lewy bodies but were classified as low-probability AD based on NIA-Reagan criteria. The two amyloid PET-positive individuals had abundant diffuse β-amyloid plaques but only sparse neuritic plaques and intermediate neurofibrillary tangle pathology. The amyloid PET-negative subject had rare diffuse plaques, no neuritic plaques, and low neurofibrillary tangle burden. These post-mortem correlates confirm that [^{11}C]PiB-PET is specific for fibrillar β-amyloid molecular pathology but may detect levels of deposition below thresholds for the pathological diagnosis of comorbid AD (Burack et al. 2010). Figure 16.2 (middle row) shows a pattern of mildly increased cortical β-amyloid activity in Parkinsonian dementia patients.

Findings of generally higher (or more frequently elevated) global cortical amyloid burden in DLB than in PDD suggest that cortical fibrillary β-amyloid deposition is not a requisite for PDD (Petrou et al. 2015). However, it may differentially contribute to the temporal manifestations and/or nature of the neurobehavioral phenotype of Parkinsonian dementia. Whether a combination of amyloid and Lewy body pathology exacerbates the memory and other cognitive problems in DLB is unclear, but it is likely it accelerates the dementia process, whereas Lewy body pathology alone may lead to a slower dementing process in PDD (Ballard et al. 2006; Petrou et al. 2012).

There are several studies that have directly correlated β-amyloid burden and cognitive performance in PD and PDD. We performed [C-11]PIB PET imaging in 40 patients with PD at high risk for development of dementia (Petrou et al. 2012). Detailed neuropsychological testing and [C-11]DTBZ VMAT2 PET imaging were also performed. We found that elevated cerebral PiB binding to levels seen in patients with AD were infrequent (only 6 of 40 subjects; 15%). Significant correlation was noted between cortical PiB binding and global composite cognitive function ($r = -0.55$, $p < 0.005$). Principal component analysis identified a factor with significant component loadings on cognitive parameters and PiB binding, but without significant striatal VMAT2 binding or other PD feature loadings. Although average cortical PIB binding in PD was in the range below than those commonly used to classify PiB-PET scans as typical of AD, these apparent low binding values have significant correlation with cognitive function. However, a subsequent literature review concluded inconsistent correlations between cognitive functions and β-amyloid deposition, at least in non-longitudinal analyses (Donaghy et al. 2015). In contrast, longitudinal cognitive analyses have shown that baseline amyloidopathy

in the precuneus at baseline was associated with more rapid progression to cognitive decline and Parkinsonian dementia (Gomperts et al. 2013, 2016a). Importantly, there may be a confounder in the literature where most in vivo β-amyloid PET imaging studies have focused on amyloid deposition in the cortex only. Neuropathological studies point to an important role for striatal amyloidopathy where striatal β-amyloid deposition is substantially greater in PDD compared to non-demented PD (Kalaitzakis et al. 2008, 2011; Halliday et al. 2011; Dugger et al. 2012). These post-mortem findings agree with our in vivo imaging observations showing that striatal amyloidopathy was present in about half of the patients who had abnormal cortical amyloid binding. We found significantly lower cognitive performance for combined cortical and striatal β-amyloid deposition compared to cortical-only binding (Shah et al. 2016). Subcortical amyloidopathy may be another modifying factor for the presence of cognitive decline in PD. More recently, we found that striatal, especially nucleus accumbens, and limbocortical amyloidopathy was a determinant of apathy ratings in PD (Zhou et al. 2020). These findings were independent from the degree of nigrostriatal denervation and clinical ratings of depression, anxiety, or cognitive impairment confirming our prior observations that even low levels of amyloidopathy in PD or PDD have significant cognitive and neurobehavioral consequences. The lower symptomatic threshold of amyloidopathy in Lewy body parkinsonism may reflect compounding effects of the co-existence of other neurodegenerations, such as α-synucleinopathy, monoaminergic, and cholinergic denervations, and underlie a decreased cognitive reserve capacity in PD.

16.7 Tau PET Imaging in Parkinsonian Dementia

In recent years several candidate radiotracers have been developed to assess in vivo the distribution pattern of *tau* neurofibrillary tangles pathology. This pathology is commonly seen in AD (Braak and Braak 1995). The most commonly used radiotracer is [F-18] AV-1451, which strongly correlates with post-mortem evidence of neurofibrillary tau tangles (Marquie et al. 2015; Smith et al. 2019). Several studies have performed tau PET imaging in PD and Parkinsonian dementia (Table 16.1).

Hansen and colleagues have detected absent to low [^{18}F] AV-1451 PET binding in PD subjects with or without mild cognitive impairment, but no binding among control subjects (Hansen et al. 2017). The investigators found no significant correlations between AV-1451 and cognitive dysfunction at this stage in the disease. In contrast, a [F-18]AV-1451 PET study in DLB patients found slightly higher AV-1451 binding in inferolateral temporal and parietal/precuneus in DLB compared to control subjects (Gomperts et al. 2016a). The increased tau binding in these regions correlated well with cognitive changes as measured by both the Mini-Mental State Examination (MMSE) and the Clinical Dementia Rating scale. In another AV-1451 PET study involving 18 AD subjects and 15 DLB patients, the AD subjects showed substantially higher AV-1451 uptake than the DLB group (Kantarci et al. 2017), with the former having the highest uptake in medial temporal and the DLB group having the lowest in this region. However, when compared to 90 healthy control

Table 16.1 Tau PET imaging studies in PD and PDD

Ligand	Study population	Major finding
[^{18}F] AV-1451 tau PET (Hansen et al. 2017)	PD (n = 26) without or with mild cognitive impairment; healthy controls (n = 23)	Tau pathology, as detected by AV-1451, absent in control to minimal tau binding in PD with or without mild cognitive impairment No significant correlation between cognitive dysfunction and AV-1451 uptake at this stage
[^{18}F] AV-1451 tau PET (Gomperts et al. 2016b)	DLB (n = 7) and PD cognitively impaired (n = 8) or cognitively normal (n = 9)	A combined group of DLB and cognitively impaired PD patients showed higher level of uptake of AV-1451 in inferolateral temporal gyrus and precuneus than the control group. Furthermore, increased binding in the region correlated well with cognitive impairment, as measured by MMSE and clinical Dementia Rating scale
[^{18}F] AV-1451 tau PET (Kantarci et al. 2017)	AD (n = 18); DLB (n = 15); controls (n = 90)	AD group showed substantially more severe and extensive AV-1451 uptake compared to DLB patients AV-1451 uptake within the medial temporal lobe completely distinguished AD dementia from probable DLB AV-1451 had higher level of retention among probable DLB subjects in their inferior, middle, and superior occipital, lingual, angular, fusiform, middle and inferior temporal gyri, and precuneus and cuneus than normal control subjects No significant cognitive or clinical correlations in AV-1451 binding
[^{18}F] AV-1451 tau PET (Mak et al. 2019).	DLB (n = 1) with confirmed parkinsonism, fluctuating cognition and RBD	Tau pattern in the DLB patient different from AD pattern Highest level of retention of V-1451 uptake in the primary visual cortex and the uptake in occipital cortices overlaps with the neuroinflammation binding as observed in [C-11]-PK11195 scans
[^{18}F] AV-1451 tau PET (Smith et al. 2018).	PD (n = 11); PDD (n = 18); DLB (n = 6); controls (n = 44)	AV-1451 higher level of retention in medial and lateral parietal lobes in DLB compared to controls AV-1451 higher uptake in medial parietal lobes in PDD than in PD PD group showed lower level of retention in inferior temporal lobes than in the controls and PDD Letter S-fluency and animal fluency score showed significant correlations of AV-1451 binding in medial and lateral parietal regions No correlations between cortical binding of AV-1451 and MMSE scores Decreased SUVR in substantia nigra correlated with UPDRS motor scale

(continued)

Table 16.1 (continued)

Ligand	Study population	Major finding
[^{18}F] AV-1451 tau PET (Nedelska et al. 2019)	DLB group (n = 33), PCA group (n = 18) and NC group (n = 100)	Higher level of uptake in entire cortical areas in PCA than in DLB and control DLB group showed moderate AV-1451 uptake compared to NC in temporal, parietal, occipital, and frontal cortices
[^{18}F] AV-1451 tau PET (Lee et al. 2018).	PD group with normal cognition (n = 12), PD group without normal cognition (n = 22), DLB group (n = 18), AD group (n = 25), NC group (n = 25)	AV-1451 binding level was higher in primary sensorimotor, visual cortices and the occipital and posterior parieto-temporal cortices in DLB-amyloid+ than in the control group AV-1451 binding level is higher for AD in middle and inferior temporal, entorhinal, parahippocampus, hippocampus and amygdala compared to DLB

subjects, the DLB patients showed higher AV-1451 uptake in the posterior temporoparietal and occipital cortex. However, there was no association between clinical measures (such as cognition, visual hallucination, motor Parkinsonism, and the presence of REM sleep behavior disorder) and AV-1451 retention in posterior temporoparietal and occipital regions (Kantarci et al. 2017). A subsequent larger AV-1451 PET imaging study from the same group compared 33 probable DLB patients, 18 posterior cortical atrophy (PCA) patients, and 100 control subjects (Nedelska et al. 2019). The DLB group showed overall moderate AV-1451 uptake in temporal, parietal, occipital, and frontal cortices compared to control subjects. These data also show that DLB patients have a different tau deposition pattern compared to prototypical AD.

Smith and colleagues evaluated AV-1451 retention in the substantia nigra and globus pallidus in 11 PD, 6 DLB, 18 PDD, and 44 control subjects and found significantly decreased binding in the substantia nigra in PDD compared to the other groups (PD, DLB, and controls) (Smith et al. 2019).

Interestingly, decreased uptake in the substantia nigra correlated with worse motor function in PD, PDD, and DLB. It should be noted that lower AV-1451 binding in the nigra reflects loss of neuromelanin, an off-target binding site for this radioligand (Hansen et al. 2016). Increased parietal tau binding was also associated with executive impairment in patients with synucleinopathies (Smith et al. 2018).

Lee and colleagues performed a multitracer PET study using AV-1451 tau and [F-18]florbetaben amyloid PET scans in 12 PD with normal cognition, 22 PD with cognitive impairment, 18 DLB, 25 AD patients, and 25 normal controls (Lee et al. 2018). These authors found that DLB subjects had higher level of binding of AV-1451 in the primary sensorimotor, visual cortices, and parietal-temporal cortices compared with the controls. Interestingly, when the analysis was limited to amyloid-positive DLB patients, AV-1451 binding in the same regions increased suggesting a possible interaction. Intriguingly, when compared to AD, amyloid-positive DLB patients had a higher level of binding in primary sensorimotor and visual cortices regions, and a lower in lateral and medial temporal cortices, parahippocampal

cortices, and hippocampus (Lee et al. 2018). Notably, there was no increased level of binding in any regions among amyloid-negative DLB when comparing to the AD group. Unlike significant correlations between tau binding and cognition in the AD group, tau binding in the DLB patients did not correlate significantly with cognitive or motor measures. However, a strong correlation was observed between all cortical regions in AV-1451 PET binding and MMSE scores in the cognitively impaired PD group.

Studies have suggested that AV-1451 binding appears to gradually increase from cognitively normal PD (none to lowest), cognitively impaired PD (low), DLB (intermediate) to AD (highest) (Hall et al. 2017). High tau burden can mostly be observed in the occipital visual association cortices, suggesting an atypical profile of tau progression in Parkinsonian dementia that deviates from the classical Braak AD staging. Figure 16.2 (bottom row) show examples of tau PET imaging findings in patients with Parkinsonian dementia.

16.8 Neuroinflammation Imaging in Parkinsonian Dementia

Neuroinflammation is an important factor in the pathophysiology of dementia, including Parkinsonian dementia (Mrak and Griffin 2007). Biomarkers of mitochondrial translocator protein (TSPO) functions, like [C-11]PK11195 PET, can be used to assess microglial activation in vivo. For example, microglial activation was found to be present in the substantia nigra and putamen in both PD and DLB patients using this PET measure (Iannaccone et al. 2013). Interestingly, there was higher uptake in the caudate and a more extended microglial activation pattern in the cerebellum and several cortical regions in DLB patients compared to PD. This may suggest a possible disease propagation pattern (Iannaccone et al. 2013). In a study in patients with PDD, increased PK11195 PET binding was seen in the cingulum (anterior and posterior), basal ganglia, and the occipital, parietal, temporal, and frontal cortical regions (Edison et al. 2013). Furthermore, microglial activation was less extensive in PD compared to PDD. Interestingly, there was a significant correlation between microglial activation and cognitive changes suggesting inflammation-induced neuronal dysfunction in the PDD patients (Edison et al. 2013). Multi-tracer studies have found inconsistent relationships between glucose metabolic or amyloidopathy changes and the extent of microglial activation in PDD (Iannaccone et al. 2013; Edison et al. 2013; Fan et al. 2015; Femminella et al. 2016).

Interesting observations came from a single-subject clinical and multi-modal imaging study concerning tau ([F-18]AV-1451), β-amyloid ([C-1111]-PIB), and neuroinflammation ([C-11]-PK11195) in a probable DLB patient, which showed an AD-like pattern in [C-11]-PIB images, but not in the tau and neuroinflammation study (Mak et al. 2019). High tau binding in the primary visual cortex overlapped with high TSPO binding as observed in the [C-11]-PK11195 PET scan (Mak et al. 2019).

Although microglial activation may be a driving factor in the disease process in PDD, it is also clear that neuroinflammatory mechanisms are complex and remain

poorly understood. For example, neuroinflammation could also be protective depending on the stage and condition of the dementing process (Stefaniak and O'Brien 2016). There is a clear need for longitudinal multi-modal imaging studies to help to disentangle the effects of inflammation across different stages of the disease and carefully relate these to clinical symptoms.

16.9 Discussion

Cognitive impairment in PD likely results from a combination of different pathologies in this pleomorphic neurodegeneration. Degeneration of subcortical systems, such as the dopaminergic nigrostriatal projection and the basal forebrain cholinergic corticopetal systems, plus neurodegeneration associated with cortical depositions of α-synuclein, intraneuronal hyperphosphorylated tau tangles, and β-amyloid are likely mutual contributors to cognitive impairment in PD (Kehagia et al. 2010; Compta et al. 2011). Glucose metabolic imaging studies have shown evidence of both posterior (parieto-occipital cortical) and anterior (frontal cortical and caudate nucleus) hypometabolism in PDD (Bohnen and Albin 2011). These regional changes may reflect distinct cognitive syndromes in PD with cognitive impairment. For example, Williams-Gray and colleagues reported that more posterior cortically-based cognitive defects evolved over time into dementia, whereas frontostriatal executive deficits were not associated with subsequent dementia risk per se (Williams-Gray et al. 2009). It is plausible that the glucose metabolic changes in the caudate nucleus and frontal cortex may in part be associated with dopaminergic denervation (Polito et al. 2012), whereas the more posterior cortical changes may in part be associated with cholinergic denervation or tau pathology (Klein et al. 2010; Williams-Gray et al. 2013). These data agree with dopaminergic PET studies showing that dopaminergic denervation of the caudate nucleus and fronto-limbic system alone is not sufficient for Parkinsonian dementia (Klein et al. 2010; Hilker et al. 2005). Cholinergic imaging studies agree with post-mortem evidence suggesting that primary basal forebrain cholinergic system degeneration significantly potentiates with the appearance of dementia. PET assessment of subcortical pedunculopontine nucleus-thalamic cholinergic denervation in PD has been associated with REM sleep behavior disorder (Kotagal et al. 2012). If basal forebrain cholinergic lesions develop in parallel, this may explain why RBD is a reported harbinger for the development of dementia in PD (Postuma et al. 2012). Furthermore, the association between a history of falls and subcortical cholinergic denervation in PD may in part provide additional insight into why PD patients with postural instability and gait disorders also appear at higher risk of developing dementia. The comorbid presence of two neurodegenerations (α-synuclein and β-amyloidopathy) in some patients with Parkinsonian dementia may suggest additive or even synergistic detrimental interactions of these proteinopathies (Tsigelny et al. 2008). This may explain findings that even low levels of cerebral amyloidopathy are significantly related to cognitive impairment in PD (Petrou et al. 2015, 2012). These data are further consistent with post-mortem findings that the presence of cortical amyloid pathology

may be associated with a shorter time to development of PDD (Compta et al. 2011). Cerebrospinal fluid amyloid β_{42} levels also have independent prediction of future cognitive decline in non-demented PD patients, supporting a significant role of Alzheimer pathology in the development of Parkinsonian dementia (Siderowf et al. 2010).

Emerging evidence of tau PET studies suggest a gradient of tau binding in Parkinsonian dementia from lowest in cognitively normal PD to low in cognitively impaired PD (low) to highest in DLB. The presence of amyloidopathy or neuroinflammation may be a possible driving force for tau deposition, at least in primary sensorimotor and visual cortices in Parkinsonian dementia.

Further studies are needed to determine the differential contributions of heterogeneous patterns of not only neurotransmitter changes and proteinopathies, but also neuroinflammation, to the cognitive and neurobehavioral phenotypes of the Parkinson syndrome. It is possible that neuroinflammation may be related to peripheral inflammation, systemic comorbidities, such as cardiovascular disease and insulin insensitivity, and impaired sleep (Surendranathan et al. 2018; Bohnen et al. 2014; Bohnen and Hu 2019). Finally, availability of new ligands that are specific for α-synuclein protein aggregates will be important to allow longitudinal prodromal studies that may shed light on this sequence of critical pathophysiological events across the spectrum of Parkinsonian dementias.

Acknowledgments The authors gratefully acknowledge research support from the NIH, the Department of Veterans Affairs and the Michael J. Fox Foundation.

References

Aarsland D, Zaccai J, Brayne C (2005) A systematic review of prevalence studies of dementia in Parkinson's disease. Mov Disord 20:1255–1263

Albin RL, Minoshima S, D'Amato CJ, Frey KA, Kuhl DE, Sima AAF (1996) Fluoro-deoxyglucose positron emission tomography in diffuse Lewy body disease. Neurology 47:462–466

Alexander GE, DeLong MR, Strick PL (1986) Parallel organization of functionally segregated circuits linking basal ganglia and cortex. Annu Rev Neurosci 9:357–381

Alves G, Larsen JP, Emre M, Wentzel-Larsen T, Aarsland D (2006) Changes in motor subtype and risk for incident dementia in Parkinson's disease. Mov Disord 21:1123–1130

Baba T, Hosokai Y, Nishio Y et al (2017) Longitudinal study of cognitive and cerebral metabolic changes in Parkinson's disease. J Neurol Sci 372:288–293

Ballard C, Ziabreva I, Perry R et al (2006) Differences in neuropathologic characteristics across the Lewy body dementia spectrum. Neurology 67:1931–1934

Bjorklund A, Lindvall O (1984) Dopamine-containing systems in the CNS. In: Bjorklund A, Hokfelt T (eds) Handbook of chemical neuroanatomy. Elsevier, Amsterdam, pp 55–122

Bohnen NI, Albin RL (2011) White matter lesions in Parkinson disease. Nat Rev Neurol 7:229–236

Bohnen NI, Hu MTM (2019) Sleep disturbance as potential risk and progression factor for Parkinson's disease. J Parkinsons Dis 9:603–614

Bohnen NI, Minoshima S, Giordani B, Frey KA, Kuhl DE (1999) Motor correlates of occipital glucose hypometabolism in Parkinson's disease without dementia. Neurology 52:541–546

Bohnen NI, Kaufer DI, Ivanco LS et al (2003) Cortical cholinergic function is more severely affected in parkinsonian dementia than in Alzheimer disease: an in vivo positron emission tomographic study. Arch Neurol 60:1745–1748

Bohnen NI, Kaufer DI, Hendrickson R et al (2006) Cognitive correlates of cortical cholinergic denervation in Parkinson's disease and parkinsonian dementia. J Neurol 253:242–247
Bohnen NI, Muller ML, Koeppe RA et al (2009) History of falls in Parkinson disease is associated with reduced cholinergic activity. Neurology 73:1670–1676
Bohnen NI, Koeppe RA, Minoshima S et al (2011) Cerebral glucose metabolic features of Parkinson disease and incident dementia: longitudinal study. J Nucl Med 52:848–855
Bohnen NI, Muller MLTM, Kotagal V et al (2012) Heterogeneity of cholinergic denervation in Parkinson's disease without dementia. J Cereb Blood Flow Metab 32:1609–1617
Bohnen NI, Kotagal V, Muller ML et al (2014) Diabetes mellitus is independently associated with more severe cognitive impairment in Parkinson disease. Parkinsonism Relat Disord 20:1394–1398
Bohnen NI, Albin RL, Muller ML et al (2015) Frequency of cholinergic and caudate nucleus dopaminergic deficits across the predemented cognitive spectrum of Parkinson disease and evidence of interaction effects. JAMA Neurol 72:194–200
Bohnen NI, Muller MLTM, Frey KA (2017) Molecular imaging and updated diagnostic criteria in Lewy body dementias. Curr Neurol Neurosci Rep 17:73
Braak H, Braak E (1995) Staging of Alzheimer's disease-related neurofibrillary changes. Neurobiol Aging 16:271–284
Burack MA, Hartlein J, Flores HP, Taylor-Reinwald L, Perlmutter JS, Cairns NJ (2010) In vivo amyloid imaging in autopsy-confirmed Parkinson disease with dementia. Neurology 74:77–84
Burke JF, Albin RL, Koeppe RA et al (2011) Assessment of mild dementia with amyloid and dopamine terminal positron emission tomography. Brain 134:1647–1657
Christopher L, Marras C, Duff-Canning S et al (2014) Combined insular and striatal dopamine dysfunction are associated with executive deficits in Parkinson's disease with mild cognitive impairment. Brain 137:565–575
Churchyard A, Lees A (1997) The relationship between dementia and direct involvement of the hippocampus and amygdala in Parkinson's disease. Neurology 49:1570–1576
Compta Y, Parkkinen L, O'Sullivan SS et al (2011) Lewy- and Alzheimer-type pathologies in Parkinson's disease dementia: which is more important? Brain 134:1493–1505
Donaghy P, Thomas AJ, O'Brien JT (2015) Amyloid PET imaging in lewy body disorders. Am J Geriatr Psychiatry 23:23–37
Dugger BN, Serrano GE, Sue LI et al (2012) Presence of striatal amyloid plaques in Parkinson's disease dementia predicts concomitant Alzheimer's disease: usefulness for amyloid imaging. J Parkinsons Dis 2:57–65
Edison P, Rowe CC, Rinne JO et al (2008) Amyloid load in Parkinson's disease dementia and Lewy body dementia measured with [^{11}C]PIB positron emission tomography. J Neurol Neurosurg Psychiatry 79:1331–1338
Edison P, Ahmed I, Fan Z et al (2013) Microglia, amyloid, and glucose metabolism in Parkinson's disease with and without dementia. Neuropsychopharmacology 38:938–949
Emre M (2003) Dementia associated with Parkinson's disease. Lancet Neurol 2:229–237
Fan Z, Aman Y, Ahmed I et al (2015) Influence of microglial activation on neuronal function in Alzheimer's and Parkinson's disease dementia. Alzheimers Dement 11:608–621.e607
Femminella GD, Ninan S, Atkinson R, Fan Z, Brooks DJ, Edison P (2016) Does microglial activation influence hippocampal volume and neuronal function in Alzheimer's disease and Parkinson's disease dementia? J Alzheimers Dis 51:1275–1289
Firbank MJ, Yarnall AJ, Lawson RA et al (2017) Cerebral glucose metabolism and cognition in newly diagnosed Parkinson's disease: ICICLE-PD study. J Neurol Neurosurg Psychiatry 88:310–316
Foster ER, Campbell MC, Burack MA et al (2010) Amyloid imaging of Lewy body-associated disorders. Mov Disord 25:2516–2523
Frey KA, Petrou M (2015) Imaging amyloidopathy in Parkinson disease and Parkinsonian dementia syndromes. Clin Transl Imaging 3:57–64
Frey KA, Koeppe RA, Kilbourn MR et al (1996) Presynaptic monoaminergic vesicles in Parkinson's disease and normal aging. Ann Neurol 40:873–884

Frost JJ, Rosier AJ, Reich SG et al (1993) Positron emission tomographic imaging of the dopamine transporter with ^{11}C-WIN 35,428 reveals marked declines in mild Parkinson's disease. Ann Neurol 34:423–431

Gagnon JF, Postuma RB, Mazza S, Doyon J, Montplaisir J (2006) Rapid-eye-movement sleep behaviour disorder and neurodegenerative diseases. Lancet Neurol 5:424–432

Garnett ES, Firnau G, Chan PKH, Sood S, Belbeck LW (1978) [^{18}F]fluoro-dopa, an analogue of dopa, and its use in direct measurement of storage, degeneration, and turnover of intracerebral dopamine. Proc Natl Acad Sci U S A 75:464–467

Gibb W (1989) Dementia and Parkinson's disease. Br J Psychiatry 154:596–614

Gilman S, Koeppe RA, Nan B et al (2010) Cerebral cortical and subcortical cholinergic deficits in parkinsonian syndromes. Neurology 74:1416–1423

Goldman-Rakic PS (1998) The cortical dopamine system: role in memory and cognition. Adv Pharmacol 42:707–711

Gomperts SN, Rentz DM, Moran E et al (2008) Imaging amyloid deposition in Lewy body diseases. Neurology 71:903–910

Gomperts SN, Locascio JJ, Rentz D et al (2013) Amyloid is linked to cognitive decline in patients with Parkinson disease without dementia. Neurology 80:85–91

Gomperts SN, Marquie M, Locascio JJ, Bayer S, Johnson KA, Growdon JH (2016a) PET radioligands reveal the basis of dementia in Parkinson's disease and dementia with lewy bodies. Neurodegener Dis 16:118–124

Gomperts SN, Locascio JJ, Makaretz SJ et al (2016b) Tau positron emission tomographic imaging in the lewy body diseases. JAMA Neurol 73:1334–1341

Hall B, Mak E, Cervenka S, Aigbirhio FI, Rowe JB, O'Brien JT (2017) In vivo tau PET imaging in dementia: pathophysiology, radiotracer quantification, and a systematic review of clinical findings. Ageing Res Rev 36:50–63

Halliday GM, Song YJ, Harding AJ (2011) Striatal beta-amyloid in dementia with Lewy bodies but not Parkinson's disease. J Neural Transm 118:713–719

Hansen AK, Knudsen K, Lillethorup TP et al (2016) In vivo imaging of neuromelanin in Parkinson's disease using 18F-AV-1451 PET. Brain 139:2039–2049

Hansen AK, Damholdt MF, Fedorova TD et al (2017) In vivo cortical tau in Parkinson's disease using 18F-AV-1451 positron emission tomography. Mov Disord 32:922–927

Heckers S, Geula C, Mesulam M (1992) Cholinergic innervation of the human thalamus: dual origin and differential nuclear distribution. J Comp Neurol 325:68–82

Hely MA, Reid WG, Adena MA, Halliday GM, Morris JG (2008) The Sydney multicenter study of Parkinson's disease: the inevitability of dementia at 20 years. Mov Disord 23:837–844

Hilker R, Thomas AV, Klein JC et al (2005) Dementia in Parkinson disease: functional imaging of cholinergic and dopaminergic pathways. Neurology 65:1716–1722

Hirsch EC, Graybiel AM, Duyckaerts C, Javoy-Agid F (1987) Neuronal loss in the pedunculopontine tegmental nucleus in Parkinson disease and in progressive supranuclear palsy. Proc Natl Acad Sci U S A 84:5976–5980

Holthoff VA, Vieregge P, Kessler J et al (1994) Discordant twins with Parkinson's disease: positron emission tomography and early signs of impaired cognitive circuits. Ann Neurol 36:176–182

Hu XS, Okamura N, Arai H et al (2000) ^{18}F-fluorodopa PET study of striatal dopamine uptake in the diagnosis of dementia with Lewy bodies. Neurology 55:1575–1577

Huang C, Tang C, Feigin A et al (2007) Changes in network activity with the progression of Parkinson's disease. Brain 130:1834–1846

Iannaccone S, Cerami C, Alessio M et al (2013) In vivo microglia activation in very early dementia with Lewy bodies, comparison with Parkinson's disease. Parkinsonism Relat Disord 19:47–52

Imabayashi E, Yokoyama K, Tsukamoto T et al (2016) The cingulate island sign within early Alzheimer's disease-specific hypoperfusion volumes of interest is useful for differentiating Alzheimer's disease from dementia with Lewy bodies. EJNMMI Res 6:67

Irvine GB, El-Agnaf OM, Shankar GM, Walsh DM (2008) Protein aggregation in the brain: the molecular basis for Alzheimer's and Parkinson's diseases. Mol Med 14:451–464

Ito K, Nagano-Saito A, Kato T et al (2002) Striatal and extrastriatal dysfunction in Parkinson's disease with dementia: a 6-[18F]fluoro-L-dopa PET study. Brain 125:1358–1365

Jellinger KA (2000) Morphological substrates of mental dysfunction in Lewy body disease: an update. J Neural Transm 59(Suppl):185–212

Jellinger KA (2006) The morphological basis of mental dysfunction in Parkinson's disease. J Neurol Sci 248:167–172

Jellinger KA (2012) Interaction between pathogenic proteins in neurodegenerative disorders. J Cell Mol Med 16:1166–1183

Johansson A, Savitcheva I, Forsberg A et al (2008) [(11)C]-PIB imaging in patients with Parkinson's disease: preliminary results. Parkinsonism Relat Disord 14:345–347

Kalaitzakis ME, Graeber MB, Gentleman SM, Pearce RK (2008) Striatal beta-amyloid deposition in Parkinson disease with dementia. J Neuropathol Exp Neurol 67:155–161

Kalaitzakis ME, Walls AJ, Pearce RK, Gentleman SM (2011) Striatal Abeta peptide deposition mirrors dementia and differentiates DLB and PDD from other Parkinsonian syndromes. Neurobiol Dis 41:377–384

Kantarci K, Lowe VJ, Boeve BF et al (2017) AV-1451 tau and beta-amyloid positron emission tomography imaging in dementia with Lewy bodies. Ann Neurol 81:58–67

Kehagia AA, Barker RA, Robbins TW (2010) Neuropsychological and clinical heterogeneity of cognitive impairment and dementia in patients with Parkinson's disease. Lancet Neurol 9:1200–1213

Klein JC, Eggers C, Kalbe E et al (2010) Neurotransmitter changes in dementia with Lewy bodies and Parkinson disease dementia in vivo. Neurology 74:885–892

Ko JH, Katako A, Aljuaid M et al (2017) Distinct brain metabolic patterns separately associated with cognition, motor function, and aging in Parkinson's disease dementia. Neurobiol Aging 60:81–91

Koeppe RA, Gilman S, Joshi A et al (2005) ^{11}C-DTBZ and ^{18}F-FDG PET measures in differentiating dementias. J Nucl Med 46:936–944

Kotagal V, Albin RL, Muller MLTM et al (2012) Symptoms of rapid eye movement sleep behavior disorder are associated with cholinergic denervation in Parkinson disease. Ann Neurol 71:560–568

Kovari E, Gold G, Herrmann FR et al (2003) Lewy body densities in the entorhinal and anterior cingulate cortex predict cognitive deficits in Parkinson's disease. Acta Neuropathol (Berl) 106:83–88

Lee MS, Rinne JO, Marsden CD (2000) The pedunculopontine nucleus: its role in the genesis of movement disorders. Yonsei Med J 41:167–184

Lee SH, Cho H, Choi JY et al (2018) Distinct patterns of amyloid-dependent tau accumulation in Lewy body diseases. Mov Disord 33:262–272

Lim SM, Katsifis A, Villemagne VL et al (2009) The 18F-FDG PET cingulate island sign and comparison to 123I-beta-CIT SPECT for diagnosis of dementia with Lewy bodies. J Nucl Med 50:1638–1645

Liu AK, Chang RC, Pearce RK, Gentleman SM (2015) Nucleus basalis of Meynert revisited: anatomy, history and differential involvement in Alzheimer's and Parkinson's disease. Acta Neuropathol 129:527–540

Luis CA, Barker WW, Gajaraj K et al (1999) Sensitivity and specificity of three clinical criteria for dementia with Lewy bodies in an autopsy-verified sample. Int J Geriatr Psychiatry 14:526–533

Maetzler W, Reimold M, Liepelt I et al (2008) [(11)C]PIB binding in Parkinson's disease dementia. NeuroImage 39:1027–1033

Maetzler W, Liepelt I, Reimold M et al (2009) Cortical PIB binding in Lewy body disease is associated with Alzheimer-like characteristics. Neurobiol Dis 34:107–112

Mahler ME, Cummings JL (1990) Alzheimer disease and the dementia of Parkinson disease: comparative investigations. Alzheimer Dis Assoc Disord 4:133–149

Mak E, Surendranathan A, Nicastro N, Aigbirhio F, Rowe J, O'Brien J (2019) Imaging tau, neuroinflammation, and abeta in dementia with lewy bodies: a deep-phenotyping case report. Mov Disord Clin Pract 6:77–80

Marion MH, Qurashi M, Marshall G, Foster O (2008) Is REM sleep behaviour disorder (RBD) a risk factor of dementia in idiopathic Parkinson's disease? J Neurol 255:192–196
Marquie M, Normandin MD, Vanderburg CR et al (2015) Validating novel tau positron emission tomography tracer [F-18]-AV-1451 (T807) on postmortem brain tissue. Ann Neurol 78:787–800
Mashima K, Ito D, Kameyama M et al (2017) Extremely low prevalence of amyloid positron emission tomography positivity in Parkinson's disease without dementia. Eur Neurol 77:231–237
Mattis PJ, Niethammer M, Sako W et al (2016) Distinct brain networks underlie cognitive dysfunction in Parkinson and Alzheimer diseases. Neurology 87:1925–1933
McKeith IG, Galasko D, Kosaka K et al (1996) Consensus guideline for the clinical and pathological diagnosis of dementia with Lewy bodies (LBD): report of the Consortium on DLB International Workshop. Neurology 47:1113–1124
McKeith IG, Dickson DW, Lowe J et al (2005) Diagnosis and management of dementia with Lewy bodies: third report of the DLB Consortium. Neurology 65:1863–1872
McKeith IG, Boeve BF, Dickson DW et al (2017) Diagnosis and management of dementia with Lewy bodies: fourth consensus report of the DLB Consortium. Neurology 89:88–100
Mesulam M (2004) The cholinergic lesion of Alzheimer's disease: pivotal factor or side show? Learn Mem 11:43–49
Mesulam MM, Geula C (1988) Nucleus basalis (Ch4) and cortical cholinergic innervation in the human brain: observations based on the distribution of acetylcholinesterase and choline acetyltransferase. J Comp Neurol 275:216–240
Minoshima S, Foster NL, Kuhl DE (1994) Posterior cingulate cortex in Alzheimer's disease. Lancet 344:895
Minoshima S, Foster NL, Sima AA, Frey KA, Albin RL, Kuhl DE (2001) Alzheimer's disease versus dementia with Lewy bodies: cerebral metabolic distinction with autopsy confirmation. Ann Neurol 50:358–365
Modreanu R, Cerquera SC, Marti MJ et al (2017) Cross-sectional and longitudinal associations of motor fluctuations and non-motor predominance with cerebrospinal tau and Abeta as well as dementia-risk in Parkinson's disease. J Neurol Sci 373:223–229
Mrak RE, Griffin WS (2007) Common inflammatory mechanisms in Lewy body disease and Alzheimer disease. J Neuropathol Exp Neurol 66:683–686
Muller ML, Bohnen NI (2013) Cholinergic dysfunction in Parkinson's disease. Curr Neurol Neurosci Rep 13:377
Muller ML, Albin RL, Kotagal V et al (2013) Thalamic cholinergic innervation and postural sensory integration function in Parkinson's disease. Brain 136:3282–3289
Nagano-Saito A, Kato T, Arahata Y et al (2004) Cognitive- and motor-related regions in Parkinson's disease: FDOPA and FDG PET studies. NeuroImage 22:553–561
Nedelska Z, Josephs KA, Graff-Radford J et al (2019) (18) F-AV-1451 uptake differs between dementia with lewy bodies and posterior cortical atrophy. Mov Disord 34:344–352
Nejad-Davarani S, Koeppe RA, Albin RL, Frey KA, Muller M, Bohnen NI (2019) Quantification of brain cholinergic denervation in dementia with Lewy bodies using PET imaging with [(18) F]-FEOBV. Mol Psychiatry 24:322
Perry EK, Curtis M, Dick DJ et al (1985) Cholinergic correlates of cognitive impairment in Parkinson's disease: comparisons with Alzheimer's disease. J Neurol Neurosurg Psychiatry 48:413–421
Petrou M, Bohnen NI, Muller ML, Koeppe RA, Albin RL, Frey KA (2012) Abeta-amyloid deposition in patients with Parkinson disease at risk for development of dementia. Neurology 79:1161–1167
Petrou M, Dwamena BA, Foerster BR et al (2015) Amyloid deposition in Parkinson's disease and cognitive impairment: a systematic review. Mov Disord 30:928
Polito C, Berti V, Ramat S et al (2012) Interaction of caudate dopamine depletion and brain metabolic changes with cognitive dysfunction in early Parkinson's disease. Neurobiol Aging 33:206.e229–206.e239

Postuma RB, Bertrand JA, Montplaisir J et al (2012) Rapid eye movement sleep behavior disorder and risk of dementia in Parkinson's disease: a prospective study. Mov Disord 27:720–726
Postuma RB, Berg D, Stern M et al (2015) MDS clinical diagnostic criteria for Parkinson's disease. Mov Disord 30:1591–1601
Postuma RB, Poewe W, Litvan I et al (2018) Validation of the MDS clinical diagnostic criteria for Parkinson's disease. Mov Disord 33:1601–1608
Rowe CC, Ng S, Ackermann U et al (2007) Imaging beta-amyloid burden in aging and dementia. Neurology 68:1718–1725
Roy R, Niccolini F, Pagano G, Politis M (2016) Cholinergic imaging in dementia spectrum disorders. Eur J Nucl Med Mol Imaging 43:1376–1386
Ruberg M, Rieger F, Villageois A, Bonnet AM, Agid Y (1986) Acetylcholinesterase and butyrylcholinesterase in frontal cortex and cerebrospinal fluid of demented and non-demented patients with Parkinson's disease. Brain Res 362:83–91
Shah N, Frey KA, Muller MLTM et al (2016) Striatal and cortical beta-amyloidopathy and cognition in Parkinson's Disease. Mov Disord 31:111–117
Shimada H, Hirano S, Shinotoh H et al (2009) Mapping of brain acetylcholinesterase alterations in Lewy body disease by PET. Neurology 73:273–278
Shinotoh H, Namba H, Yamaguchi M et al (1999) Positron emission tomographic measurement of acetylcholinesterase activity reveals differential loss of ascending cholinergic systems in Parkinson's disease and progressive supranuclear palsy. Ann Neurol 46:62–69
Siderowf A, Xie SX, Hurtig H et al (2010) CSF amyloid {beta} 1-42 predicts cognitive decline in Parkinson disease. Neurology 75:1055–1061
Smith R, Scholl M, Londos E, Ohlsson T, Hansson O (2018) (18)F-AV-1451 in Parkinson's disease with and without dementia and in dementia with lewy bodies. Sci Rep 8:4717
Smith R, Wibom M, Pawlik D, Englund E, Hansson O (2019) Correlation of in vivo [18F]Flortaucipir with postmortem Alzheimer disease tau pathology. JAMA Neurol 76:310–317
Song IU, Kim YD, Cho HJ, Chung SW, Chung YA (2013) An FP-CIT PET comparison of the differences in dopaminergic neuronal loss between idiopathic Parkinson disease with dementia and without dementia. Alzheimer Dis Assoc Disord 27:51
Stefaniak J, O'Brien J (2016) Imaging of neuroinflammation in dementia: a review. J Neurol Neurosurg Psychiatry 87:21–28
Surendranathan A, Su L, Mak E et al (2018) Early microglial activation and peripheral inflammation in dementia with Lewy bodies. Brain 141:3415–3427
Tard C, Demailly F, Delval A et al (2015) Hypometabolism in posterior and temporal areas of the brain is associated with cognitive decline in Parkinson's disease. J Parkinsons Dis 5:569–574
Taylor JP, Rowan EN, Lett D, O'Brien JT, McKeith IG, Burn DJ (2008) Poor attentional function predicts cognitive decline in patients with non-demented Parkinson's disease independent of motor phenotype. J Neurol Neurosurg Psychiatry 79:1318–1323
Tsigelny IF, Crews L, Desplats P et al (2008) Mechanisms of hybrid oligomer formation in the pathogenesis of combined Alzheimer's and Parkinson's diseases. PLoS One 3:e3135
Vander Borght T, Minoshima S, Giordani B et al (1997) Cerebral metabolic differences in Parkinson's and Alzheimer's disease matched for dementia severity. J Nucl Med 38:797–802
Villemagne VL, Okamura N, Pejoska S et al (2011) In vivo assessment of vesicular monoamine transporter type 2 in dementia with lewy bodies and Alzheimer disease. Arch Neurol 68:905–912
Villemagne VL, Okamura N, Pejoska S et al (2012) Differential diagnosis in Alzheimer's disease and dementia with lewy bodies via VMAT2 and amyloid imaging. Neurodegener Dis 10:161
Williams-Gray CH, Hampshire A, Barker RA, Owen AM (2008) Attentional control in Parkinson's disease is dependent on COMT val 158 met genotype. Brain 131:397–408
Williams-Gray CH, Evans JR, Goris A et al (2009) The distinct cognitive syndromes of Parkinson's disease: 5 year follow-up of the CamPaIGN cohort. Brain 132:2958–2969
Williams-Gray CH, Mason SL, Evans JR et al (2013) The CamPaIGN study of Parkinson's disease: 10-year outlook in an incident population-based cohort. J Neurol Neurosurg Psychiatry 84:1258–1264

Womack KB, Diaz-Arrastia R, Aizenstein HJ et al (2011) Temporoparietal hypometabolism in frontotemporal lobar degeneration and associated imaging diagnostic errors. Arch Neurol 68:329–337

Zhou Z, Muller M, Kanel P et al (2020) Apathy rating scores and beta-amyloidopathy in Parkinson disease patients at risk for cognitive decline. Neurology 94:e376

Zweig RM, Jankel WR, Hedreen JC, Mayeux R, Price DL (1989) The pedunculopontine nucleus in Parkinson's disease. Ann Neurol 26:41–46

SPECT/PET Findings in Dementia with Lewy Bodies

17

Sedigheh Zabihi, Tim Whitfield, and Zuzana Walker

Contents

17.1 Introduction 516
17.2 Metabolism in DLB 518
17.2.1 Hypometabolism and Differential Diagnosis of DLB Versus AD 518
17.2.2 Differential Diagnosis of DLB and Other Clinical Syndromes 521
17.2.3 Hypometabolism and Different Symptomatology 523
17.2.4 Correlation Between Hypometabolism and Pathology 525
17.2.5 Conclusion 526
17.3 Amyloid Deposition in DLB 526
17.3.1 Amyloid Frequency and Distribution 527
17.3.2 Amyloid Deposition Relative to Other Disorders and Healthy Controls 527
17.3.3 Amyloid and Clinical Correlates 532
17.3.4 Amyloid and Pathological Correlates 532
17.3.5 Tau Findings and Its Association with Amyloid in DLB 533
17.3.6 Conclusion 534
17.4 Microglial Activation in DLB 534
17.4.1 In Vitro Studies of DLB Patients 535
17.4.2 In Vivo Microglial Activation Studies 535
17.4.3 Conclusion 535
17.5 Dopaminergic Degeneration in DLB 536
17.5.1 Dopamine Transporter Imaging in DLB 537
17.5.2 Dopamine Turnover 546
17.5.3 Vesicular Monoamine Transporter Type 2 Imaging 546
17.5.4 Postsynaptic Dopaminergic Receptors 547
17.5.5 Conclusion 547

S. Zabihi · T. Whitfield (✉)
Division of Psychiatry, University College London, London, UK
e-mail: tim.whitfield@ucl.ac.uk

Z. Walker
Division of Psychiatry, University College London, London, UK

Essex Partnership University NHS Foundation Trust, Mental Health Unit, St Margaret's Hospital, Essex, UK

R. A. J. O. Dierckx et al. (eds.), *PET and SPECT in Neurology*,
https://doi.org/10.1007/978-3-030-53168-3_17

17.6 Cholinergic Deficits in DLB..... 548
17.6.1 Vesicular Acetylcholine Transporter Imaging..... 548
17.6.2 Imaging Acetylcholinesterase Activity..... 552
17.6.3 Imaging Muscarinic Receptors..... 553
17.6.4 Imaging Nicotinic Receptors..... 553
17.6.5 Conclusion..... 554
17.7 Conclusion..... 554
References..... 554

Abstract

Dementia with Lewy bodies (DLB) is the second most common form of degenerative dementia. However, it can be difficult to diagnose as it shares common features with both Alzheimer's disease (AD) and Parkinson's disease (PD). Early detection as well as accurate differentiation from other types of dementia are essential to inform management and treatment. Clinical diagnosis of DLB can be difficult, with up to 50% of cases being misdiagnosed (Walker et al., Lancet 386:1683–1697, 2015). The use of biomarkers, particularly imaging biomarkers, has greatly contributed to the accurate diagnosis of DLB. This chapter will give an overview of the contribution of PET and SPECT imaging modalities to the diagnosis of DLB and the better understanding of the underlying pathology. The areas covered include metabolic, amyloid, microglial activity, dopaminergic and cholinergic imaging in DLB. Some of these imaging methods are now well established and highly reliable at facilitating accurate diagnosis. In the future, others are likely to inform treatment or provide bases for the development of new drugs. New ligands are constantly being developed and are likely to focus on microglial activation and tau pathology in DLB.

17.1 Introduction

DLB is the second most common type of degenerative dementia and is responsible for up to 30% of cases (McKeith et al. 2004; Walker et al. 2015a). The term 'dementia with Lewy bodies' was the preferred name suggested by a consortium that met in 1995 to establish clinical and neuropathological diagnostic criteria for the disease (McKeith et al. 1996). The symptoms of DLB were identified through retrospective case note analysis of patients with proven Lewy body (LB) pathology at autopsy. The only neuropathological requirement for DLB was the presence of LB in the brain of a patient with a history of dementia. Since then, the consortium has issued three revisions of this report ((McKeith et al. 1999, 2005, 2017); see Table 17.1), the most recent of which suggested that AD pathology should be assessed alongside LB pathology in order to make a likelihood assessment that cortical LB pathology is responsible for the dementia. This is because many patients with AD also have LB pathology at autopsy, suggesting that LB are not always the primary substrate of dementia. At present, a clinical diagnosis of possible or probable DLB is made depending on the number of core clinical features and indicative biomarkers (see Table 17.1).

Table 17.1 Revised criteria for the clinical diagnosis of probable and possible DLB (reproduced from (McKeith et al. 2017) with permission from Wolters Kluwer Health, Inc.)

Essential for a diagnosis of DLB is dementia, defined as progressive cognitive decline of sufficient magnitude to interfere with normal social or occupational functions, or with usual daily activities. Prominent or persistent memory impairment may not necessarily occur in the early stages but is usually evident with progression. Deficits on tests of attention, executive function and visuoperceptual ability may be especially prominent and occur early.
Core clinical features (the first three typically occur early and may persist throughout the course.)
Fluctuating cognition with pronounced variations in attention and alertness
Recurrent visual hallucinations that are typically well formed and detailed
REM sleep behaviour disorder, which *may* precede cognitive decline
One or more spontaneous cardinal features of parkinsonism; these are bradykinesia (defined as slowness of movement and decrement in amplitude or speed), rest tremor or rigidity
Supportive clinical features
Severe sensitivity to antipsychotic agents; postural instability; repeated falls; syncope or other transient episodes of unresponsiveness; severe autonomic dysfunction, e.g. constipation, orthostatic hypotension, urinary incontinence; hypersomnia; hyposmia; hallucinations in other modalities; systematised delusions; apathy, anxiety and depression
Indicative biomarkers
Reduced dopamine transporter uptake in basal ganglia demonstrated by SPECT or PET
Abnormal (low uptake) ^{123}iodine-MIBG myocardial scintigraphy
Polysomnographic confirmation of REM sleep without atonia
Supportive biomarkers
Relative preservation of medial temporal lobe structures on CT/MRI scan
Generalised low uptake on SPECT/PET perfusion/metabolism scan with reduced occipital activity ± the cingulate island sign on FDG-PET imaging
Prominent posterior slow-wave activity on EEG with periodic fluctuations in the pre alpha/theta range
Probable DLB can be diagnosed if:
(a) Two or more core clinical features of DLB are present, with or without the presence of indicative biomarkers, or
(b) Only one core clinical feature is present but with one or more indicative biomarkers
Probable DLB should not be diagnosed on the basis of biomarkers alone
Possible DLB can be diagnosed if:
(a) Only one core clinical feature of DLB is present, with no indicative biomarker evidence, or
(b) One or more indicative biomarkers are present, but there are no core clinical features
DLB is less likely:
(a) In the presence of any other physical illness or brain disorder including cerebrovascular disease, sufficient to account in part or in total for the clinical picture, although these do not exclude a DLB diagnosis and may serve to indicate mixed or multiple pathologies contributing to the clinical presentation, or
(b) If parkinsonism features are the only core clinical feature and appear for the first time at a stage of severe dementia
DLB should be diagnosed when dementia occurs before or concurrently with parkinsonism. The term Parkinson disease dementia (PDD) should be used to describe dementia that occurs in the context of well-established Parkinson disease. In a practice setting, the term that is most appropriate to the clinical situation should be used, and generic terms such as Lewy body disease are often helpful. In research studies in which distinction needs to be made between DLB and PDD, the existing 1-year rule between the onset of dementia and parkinsonism continues to be recommended

At times, it can be difficult to differentiate DLB from AD, particularly in cases with mixed pathology. The differential diagnosis is important because optimal treatments vary between DLB and other disorders. Neuroleptic medications may be used to treat neuropsychiatric symptoms in AD but are contraindicated in DLB, as they can lead to worsening of Parkinsonian symptoms and acute confusion. Cautious treatment with dopaminergic agents can improve motor symptoms in DLB but can exacerbate psychiatric symptoms such as psychosis and impulsivity (Barbas 2006). Treatment options in DLB remain limited, and further research is needed in order to identify potential targets for intervention. There is also a need to address questions about the relevance of various neuropathological changes in DLB and how they relate to one another and clinical symptoms.

Nuclear molecular imaging has been applied to address some of these problems. Nuclear imaging studies have improved diagnostic accuracy, identified potential disease mechanisms and followed the progression of medicated and unmedicated patients. These studies have involved the identification of 'biomarkers'. Biomarkers can be defined as 'a characteristic that is objectively measured and evaluated as an indicator of normal biological processes, pathogenic processes, or pharmacological responses to a therapeutic intervention' (Atkinson et al. 2001, p. 91). The European Federation of the Neurological Societies offers guidance that there are two types of biomarkers. Biomarkers of *disease state* (i.e. indicators of diagnosis) and biomarkers of *disease stage* (i.e. the progression of the disease; (Filippi et al. 2012)).

This chapter reviews findings from positron emission tomography (PET) and single-photon emission computed tomography (SPECT) studies in DLB. We searched PubMed using broad topic terms to identify relevant papers. Considering the size of the literature, here we only report findings of the most pertinent papers. A summary is provided at the end of each section. We first discuss metabolism, followed by molecular pathology and deficits in neurotransmitter systems. Neuroimaging investigations using PET and SPECT have also allowed the relationship between brain pathology and symptoms to be studied, and this too will be outlined.

17.2 Metabolism in DLB

Brain metabolism in DLB has been studied extensively using ^{18}F-fluorodeoxyglucose (^{18}F-FDG) and PET. This has allowed researchers to investigate the regional cerebral metabolic rate of glucose (rCMRglc). Consistent patterns of metabolism have been identified, which are significantly different from those observed in both healthy controls and in patients with other neurodegenerative diseases (see Table 17.2).

17.2.1 Hypometabolism and Differential Diagnosis of DLB Versus AD

Albin and colleagues studied six patients with a neuropathologically confirmed diagnosis of DLB or DLB plus AD (Albin et al. 1996). Using ^{18}F-FDG PET, they identified diffuse cerebral hypometabolism in all patients relative to a database of

normal controls. They found that metabolism in sensorimotor and subcortical regions was relatively spared. The authors noted that these results constituted a metabolic pattern previously associated with AD, but that all their participants also had marked hypometabolism in the occipital cortex, a finding not previously observed in AD. A later study had similar results (Ishii et al. 1998), finding that metabolism across the cerebral cortex was generally lower in patients with DLB and AD than in normal controls. When compared directly, the only difference between DLB and AD was relative occipital hypometabolism in DLB. They noted that if the lowest absolute value for occipital metabolism from the control group was used as a cut-off, 8 of 12 patients with DLB fell below it, while this was true for only 1 of 12 patients with AD. This yielded a sensitivity of 67% and a specificity of 92% for differentiating DLB from AD. This study also identified that metabolism in the sensorimotor cortex did not differ between any of the groups and can thus be used as a reference region against which metabolic values from the rest of the brain can be normalised (Ishii et al. 1998). This procedure standardises inter-individual differences in metabolic rate. Using occipital metabolism normalised to the sensorimotor cortex, Ishii et al. (1998) demonstrated that patients with DLB could be differentiated from those with AD with a sensitivity and specificity of 92%.

In addition to occipital hypometabolism, Lim and colleagues (2009) showed that preservation of the mid or posterior cingulate gyrus relative to precuneus and cuneus had a very high specificity for a diagnosis of DLB (100%). This phenomenon is known as the cingulate island sign (CIS). More recently, another study (Graff-Radford et al. 2014) enrolled 39 patients with DLB and 39 with AD in addition to 78 matched healthy controls. The diagnosis of 10 participants was confirmed at autopsy. The patients underwent ^{18}F-FDG PET, amyloid imaging with PIB (Pittsburgh Compound B) and magnetic resonance imaging (MRI). The overall results indicated that the CIS ratio was higher in patients with DLB than in AD (median 0.97 versus 0.89). In the 10 cases that went to autopsy, the CIS ratio was 0.81 or greater in 7 DLB cases, while it was less than 0.81 in 3 AD cases, confirming that CIS ratio can help distinguish DLB from AD.

One study reported that the ratio of occipital to hippocampal metabolism was significantly reduced in patients with DLB compared to patients with AD or normal controls (Ishii et al. 2007). When applied, this ratio could be used to differentiate between individuals with DLB and AD with 87% accuracy.

Researchers have compared the diagnostic value of ^{18}F-FDG PET and ^{99m}Tc-HMPAO perfusion SPECT (O'Brien et al. 2014). They enrolled 30 DLB patients, 38 AD patients and 20 healthy controls. Based on previous research, the investigators considered visually rated patterns of CIS and reduced occipital uptake as DLB, reduced uptake in temporal and frontal lobes as AD and loss in the precuneus and lateral parietal lobes as an indicator of both. This study reported the number of negative and positive scans by each modality. The sensitivity and specificity of PET for detecting dementia cases (85% and 90%, respectively) were significantly higher than SPECT (sensitivity of 71% and specificity of 70%). For distinguishing DLB

Table 17.2 PET studies of metabolism in DLB

Study	Subjects						Findings in DLB
	DLB	AD	PD	PDD	Other	Control	
Mosconi et al. (2008)	27	199	–	–	212	110	Standardised disease-specific PET patterns correctly classified 92% of patients with DLB
Graff-Radford et al. (2014)	39	39	–	–	–	78	CIS ratio is highly specific for DLB and can distinguish it from AD
Huang et al. (2015)	25	–	–	–	–	9	The pattern of hypometabolism in DLB depends on the disease stage
O'Brien et al. (2014)	30	38	–	–	–	20	^{18}F-FDG PET has higher diagnostic accuracy than perfusion SPECT for differentiating neurodegenerative disorders
Nedelska et al. (2015)	30	30	–	–	–	60	White matter degeneration showed some overlap with hypometabolic regions in DLB
Firbank et al. (2016)	28	–	–	–	–	–	The occipital hypometabolism in DLB is associated with frequency and severity of VH
Iaccarino et al. (2016)	40	11	–	–	–	–	The hypometabolism in DLB patients with RBD was more severe in posterior cerebral regions, frontal regions and the amygdala
Iizuka and Kameyama (2016)	24	24	–	–	–	–	The CIS was associated with less MTL atrophy
Caminiti et al. (2017)	29	–	–	–	41	–	SPM t-map analysis of ^{18}F-FDG PET has high accuracy for differential diagnosis of atypical parkinsonian disorders
Whitwell et al. (2017)	13	–	–	–	16	29	DLB and PCA have overlapping patterns of hypometabolism but more severe and diffuse in DLB. Symmetric CIS more representative of DLB
Iaccarino et al. (2018)	38	–	–	–	–	38	DLB patients with VH show a metabolic connectivity pattern limited to the occipital-dorsal parietal regions

Table 17.2 (continued)

Study	Subjects						Findings in DLB
	DLB	AD	PD	PDD	Other	Control	
Caminiti et al. (2019)	72	60	36	–	–	–	The hypometabolic pattern of DLB can differentiate DLB from AD and PD with over 90% accuracy
Liguori et al. (2019)	10	55	28	–	54	35	The metabolic pattern of DLB is different from RBD
Morbelli et al. (2019)	171	–	–	–	–	–	Core features of DLB including parkinsonism, VH, RBD and cognitive fluctuations are associated with hypometabolic signatures
Sala et al. (2019)	72	–	–	–	–	–	Metabolic connectivity of posterior brain networks was disrupted in DLB. VH associated with changes in visual-attentional network connectivity; RBD was associated with alterations in attention and limbic networks

from AD, PET had 70% sensitivity and 74% specificity, while SPECT yielded a sensitivity of 67% and specificity of 54%.[1]

A systematic review evaluated the evidence for accuracy of ^{18}F-FDG PET for differential diagnosis among the main forms of dementia (Nestor et al. 2018). They identified a 'lack' of evidence for utility in distinguishing DLB from frontotemporal dementia (FTD). However, their analysis concluded there was 'good' evidence for ^{18}F-FDG PET in differentiating DLB from AD (see e.g. Fig. 17.1).

17.2.2 Differential Diagnosis of DLB and Other Clinical Syndromes

Mosconi and colleagues (2008) studied 548 patients with ^{18}F-FDG PET, including 110 controls, 114 individuals with mild cognitive impairment (MCI), 199 with AD, 98 with FTD and 27 with DLB. They investigated whether rCMRglc could differentiate the various dementia types, MCI and normal aging from one another. The researchers split their sample into two groups. They used the first 'training' cohort to identify specific patterns of rCMRglc associated with each group, and they used

[1] The authors of this chapter calculated the values for DLB versus AD sensitivity and specificity based on Table 4 in (O'Brien et al. 2014), taking only those with a correct imaging diagnosis of dementia (58 ^{18}F-FDG PET and 48 SPECT), as these values were not reported in the paper explicitly.

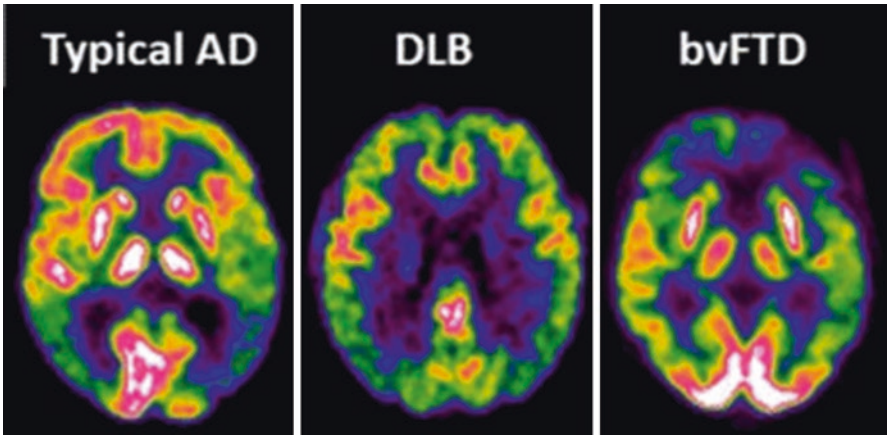

Fig. 17.1 Representative AD, DLB and behavioural variant of frontotemporal dementia (bvFTD) rCMRglc images. The global rCMRglc in DLB is lower than that of AD and bvFTD. The decreased occipital rCMRglc is characteristic for DLB. There is also a preserved pattern of metabolism in the posterior cingulate cortex, compared to AD. (Reproduced from Nestor et al. 2018 with permission from Springer Nature)

the second 'testing' cohort to assess the accuracy of these patterns for correctly diagnosing cases. In the training cohort, the researchers found that 10 of 14 individuals with DLB (71%) had hypometabolism in posterior brain regions preferentially involving the occipital cortex. The remaining four patients showed additional parietotemporal and posterior cingulate cortex hypometabolism. The authors noted prominent parietotemporal hypometabolism in patients with AD and prominent frontal or temporal hypometabolism in cases of FTD. In the training cohort, these criteria distinguished DLB from AD with 71% sensitivity and 99% specificity and DLB from FTD with 71% sensitivity and 65% specificity. If hippocampal metabolism was considered in addition to cortical evaluations, DLB could be distinguished from AD with 100% sensitivity and 98% specificity. This was due to hippocampal hypometabolism being present in 98 of 100 patients with AD but in only 3 of 14 individuals with DLB. Adding hippocampal hypometabolism to the criteria did not enhance diagnostic accuracy between DLB and FTD. Mosconi and colleagues (2008) then applied these findings to their testing cohort for validation of the diagnostic criteria. In this cohort, 12 of 13 individuals with DLB (92%) had occipitoparietal hypometabolism and were thus classified correctly. None of the other groups' patients were classified as DLB, giving the specific rCMRglc patterns 92% sensitivity and 100% specificity for differentiating DLB from AD, FTD, MCI and normal aging (Mosconi et al. 2008).

Patterns of hypometabolism in DLB and posterior cortical atrophy (PCA) have been compared using ^{18}F-FDG PET (Whitwell et al. 2017). Both PCA and DLB have been associated with occipital lobe hypometabolism, so finding other ways of differentiating these diseases is important. The authors recruited 13 DLB patients, 16 PCA patients and 29 healthy controls. DLB and PCA showed a largely similar

metabolic pattern, except that DLB showed greater hypometabolism in the medial occipital lobe, orbitofrontal cortex, anterior temporal lobe and basal ganglia. Hemispheric asymmetry in the occipital and parietal lobes was greater in PCA than DLB and controls. CIS was found in both conditions, though it was more asymmetrical in PCA. The authors concluded that, despite having overlap in patterns of hypometabolism, reduced metabolism in temporal and orbitofrontal cortices could differentiate DLB from PCA (Whitwell et al. 2017).

An Italian group investigated the diagnostic accuracy of metabolic imaging for differentiating DLB from other conditions using ^{18}F-FDG PET (Caminiti et al. 2019). They recruited 72 patients with a clinical diagnosis of DLB at 3-year follow-up in addition to 60 AD and 36 PD patients. Participants with DLB diagnosis at follow-up had various diagnoses at baseline (including various dementia subtypes and MCI). The ^{18}F-FDG PET was performed at 3 months follow-up. Independent raters blind to the initial diagnoses assessed the ^{18}F-FDG PET topographical features and identified a DLB metabolic pattern in 64 of 72 DLB patients, 3 AD and 5 PD patients. This pattern involved reduced metabolism in the lateral and medial occipital, temporoparietal and frontal cortices. The ^{18}F-FDG PET single-subject t-maps were also analysed using statistical parametric mapping (SPM). The latter analysis indicated a predictive accuracy of 89% against final clinical diagnosis at follow-up. The authors mentioned that among the hypometabolic regions involved in DLB, it was the degree of reduction in the occipital lobe that most accurately differentiated DLB from AD. An earlier study by the same group (Caminiti et al. 2017) examined the diagnostic accuracy of ^{18}F-FDG PET with SPM t-maps for distinguishing atypical Parkinsonian disorders from one another. The participants included 29 patients with DLB, 22 progressive supranuclear palsy, 11 corticobasal degeneration and 8 multiple system atrophy (MSA) patients. Compared to clinical diagnosis at follow-up, the SPM t-maps analysis of ^{18}F-FDG PET yielded 98% sensitivity and 99% specificity.

Another Italian group compared cerebral glucose metabolism in 10 patients with DLB, 54 with rapid eye movement sleep behaviour disorder (RBD), 28 with PD, 55 with AD and 35 healthy controls (Liguori et al. 2019). The individuals with RBD showed increased uptake of ^{18}F-FDG in temporal, parietal and occipital lobes but reduced uptake in anterior cingulate compared to DLB.

17.2.3 Hypometabolism and Different Symptomatology

Researchers have investigated if regional cerebral metabolic rates differ in DLB according to the specific clinical picture. A group based in Japan tested the hypothesis that occipital hypometabolism in PD/DLB is driven by nigrostriatal dysfunction (Imamura et al. 2001). They noted that an association between Parkinsonism and occipital hypometabolism in DLB would support this hypothesis. Their hypothesis followed earlier work, which found that PD patients had greater occipital hypometabolism in the hemisphere contralateral to their more affected side (Bohnen et al. 1999). However, the researchers did not confirm this—finding no difference in

occipital hypometabolism between patients with DLB with Parkinsonism, and DLB without Parkinsonism (Imamura et al. 2001). They also found that patients with DLB without Parkinsonism had significantly lower occipital metabolism compared to AD or controls. These observations suggest that the occipital hypometabolism observed in DLB is not primarily driven by nigrostriatal dysfunction.

Iaccarino and colleagues (2018) explored the association between metabolism and visual hallucinations (VH) in 19 DLB patients with VH, 19 DLB patients without VH and 38 healthy controls using ^{18}F-FDG PET. All participants with DLB showed a pattern of hypometabolism in posterior regions extending to medial and lateral parietal cortex, as well as in the prefrontal and temporal cortices. They also looked at connectivity between regions and assessed whether this was different according to the presence of VH. In DLB hallucinators, the metabolic connectivity pattern was limited to the occipital-dorsal parietal regions, while in DLB patients without VH, the pattern of connectivity originated from the occipitotemporal seed cluster and continued to the ventral visual stream. Researchers have identified associations between hypometabolism in the primary visual cortex and VH in DLB (Firbank et al. 2016), as well as between CIS and VH as well as amnestic impairment in DLB (Iizuka and Kameyama 2016).

Researchers have sought to establish the neural correlates of RBD in DLB. One study scanned 40 DLB patients and 11 AD patients with ^{18}F-FDG PET (Iaccarino et al. 2016). Half of the participants with DLB had RBD, while none with AD met the clinical criteria. All DLB patients showed posterior hypometabolism involving temporoparietal and occipital associative cortices. They found a more severe metabolic reduction in DLB patients with RBD in the dorsolateral and medial frontal regions, left precuneus, bilateral superior parietal lobule and rolandic operculum and the amygdala. Another difference was the broader hypometabolism in posterior regions in RBD.

Sala and colleagues (2019) studied 72 patients with probable DLB and 93 healthy controls, using ^{18}F-FDG PET. DLB patients with RBD had increased metabolic connectivity between the amygdala and the main brainstem nuclei. The result indicated that changes associated with RBD particularly affected the attention (dorsal attention and salience) and subcortical (limbic and basal ganglia) networks. VH in DLB patients were also associated with attention and visual networks. Furthermore, the most severe alterations in primary visual network connectivity were found in patients with the greatest impairment in visual selective attention and visuospatial/logical reasoning.

A recent multicentre study (Morbelli et al. 2019) investigated the association between hypometabolism and the core features of DLB in 171 patients with probable DLB. The study found that Parkinsonism covaried with metabolism in the parietal lobe and precuneus, while VH negatively covaried with dorsolateral frontal cortex metabolism. RBD negatively covaried with bilateral parietooccipital and precuneus metabolism. Cognitive fluctuations negatively covaried with occipital metabolism but positively with parietal lobe metabolic rate.

17.2.4 Correlation Between Hypometabolism and Pathology

There has been some discussion about the cause of the occipital hypometabolism observed in DLB. A group of researchers based in Japan studied the brains of 19 persons with AD, 17 with DLB and 11 controls at autopsy, with a further 11 individuals with AD, 7 with DLB and 10 controls studied using ^{18}F-FDG PET (Higuchi et al. 2000). They found that α-synuclein or ubiquitin-positive LB were least common in the occipital lobes of DLB cases compared to other brain regions. Conversely, they found extensive white matter (WM) spongiform changes in the DLB group most pronounced occipitally, with mild to moderate changes in the normal and AD groups. The authors also noted more severe WM gliosis in DLB relative to AD, with the greatest gliosis observed occipitally in DLB (Higuchi et al. 2000). The authors concluded that WM spongiform pathology and gliosis might be an important pathological substrate for the pattern of impaired glucose metabolism seen in DLB. The present authors note that LB and Lewy neurites are intracellular and may be lost during gliosis. This could account for the finding of minimal LB in occipital lobes.

In vivo studies have also tried to investigate the association between metabolism and pathology in DLB (Iizuka and Kameyama 2016). One group of investigators studied the association between CIS and temporal lobe atrophy in DLB. They studied 24 DLB, 24 AD and 48 controls with ^{18}F-FDG PET, ^{123}I-FP-CIT SPECT and MRI. The results showed that medial temporal lobe (MTL) atrophy is less pronounced in DLB compared to AD. The authors found that a higher CIS ratio correlated with less MTL atrophy in both DLB and AD.

Researchers have investigated the topographical overlap between WM changes, amyloid deposition and metabolism in DLB and AD relative to controls. One study recruited 30 patients with DLB, 30 with AD and 60 matched controls (Nedelska et al. 2015). The authors found reduced uptake of ^{18}F-FDG PET in temporal, posterior parietal and occipital cortices in DLB relative to controls. These decreases were more diffuse than WM alterations ascertained through diffusion tensor imaging (DTI), but hypometabolism overlapped with loss of WM integrity parietooccipitally. Loss of white matter integrity was not related to PIB uptake. A neuropathological study also found that higher CIS ratio on ante-mortem ^{18}F-FDG PET was strongly associated with lower Braak neurofibrillary tangle (NFT) stages ($r = -0.96$, $p < 0.001$) (Graff-Radford et al. 2014).

One study grouped patients with DLB according to their level of cognitive impairment, categorising them as mild or severe (Huang et al. 2015). ^{18}F-FDG PET imaging revealed hypometabolism in the temporal regions, anterior cingulate cortex, inferior orbital region, thalamus and caudate nucleus in mild DLB. Some of these structures overlapped with atrophic regions of grey matter. The authors argued that this finding showed cortical hypometabolism antecedes cortical atrophy.

17.2.5 Conclusion

The most reliable finding from the studies assessed is the relative occipital hypometabolism in DLB compared with AD and controls. Studies have demonstrated that this difference can separate DLB from AD and controls with high sensitivity and specificity. This procedure is reliable enough for use in clinical practice. Studies have also shown that CIS is more pronounced in DLB and is associated with less AD pathology. Occipital hypometabolism and CIS are associated with VH in DLB. One study suggests that hypometabolism is associated with spongiform pathology and gliosis rather than LB, but it is difficult to rule out a role for LB since they may be lost during gliosis. MTL atrophy is more frequently present in AD than DLB.

17.3 Amyloid Deposition in DLB

In recent years, there has been an increasing interest in the role of amyloid in the pathogenesis of dementia. Amyloid is a general term used to describe polypeptide filaments that are folded into a cross β-sheet structure (Lockhart et al. 2007). In the brain, β-amyloid typically aggregates in spherical senile plaques, which can be differentiated into neuritic or diffuse plaques. β-amyloid may also accumulate in the form of cerebrovascular amyloid. Post-mortem evidence of β-amyloid is necessary for the diagnosis of definite AD, and studies have observed extensive cortical β-amyloid deposition in AD. However, cerebral β-amyloid is not always associated with clinical dementia, since 20–30% of non-demented older adults have moderate to severe numbers of cortical neuritic plaques (Price and Morris 1999; Neuropathology Group. Medical Research Council Cognitive Function and Aging Study 2001). Researchers have postulated that amyloid deposition is an early event in the disease process and occurs before cognitive impairment becomes apparent (Villemagne et al. 2011).

Until the first decade of the twenty-first century, researchers could only measure cerebral β-amyloid at post-mortem or from a tissue biopsy. Thus, efforts were made to synthesise an ^{11}C-labelled version of the amyloid binding histological dye, thioflavin-T, for use with PET. These efforts culminated in the development of *N*-methyl-[^{11}C]2-(4′-methylaminophenyl)-6-hydroxybenzothiazole, which is known as 'Pittsburgh Compound B' (PIB). Klunk et al. (2004) injected 16 AD patients and 9 controls with PIB and scanned them with PET. They found that, compared to controls, the AD patients showed increased PIB retention. Notably, marked retention was observed in areas of association cortex known to contain large amounts of β-amyloid at post-mortem in AD. The researchers concluded that PET imaging with PIB can provide quantitative information on amyloid deposits in vivo. A multitude of similar studies ensued, and the original findings (Klunk et al. 2004) have been replicated extensively.

Although amyloid is most strongly associated with AD, autopsy series of adults with dementia report that 15–30% of brains show senile plaques *and* LB (Galasko

et al. 1996), suggesting that many patients with clinical DLB may also have cerebral β-amyloid. Shirvan and colleagues (2019) studied PIB PET scans of 18 patients with autopsy-confirmed diagnoses of DLB, PD-MCI and PDD. All cases bar one had significant Aβ deposits at autopsy. In the majority of cases, PIB retention accurately indicated the amount of amyloid plaques. Local PIB retention correlated with regional total amyloid burden in occipital and superior parietal lobes. PIB retention was associated with Braak NFT stage and Braak LB stage, with this association primarily driven by the DLB patients. The authors concluded that amyloid imaging is useful in the evaluation of patients with LB disorders (see, e.g. Fig. 17.2). This section discusses research that has used PET and PIB or newer ligands to image amyloid in vivo in patients with DLB. It will also briefly mention relevant imaging studies of tau in DLB.

17.3.1 Amyloid Frequency and Distribution

PET amyloid studies in DLB have reported variable rates of elevated radioligand uptake. These range from 29% (Villemagne et al. 2011) to 90% (Rowe et al. 2007) (see Table 17.3). Such great variation could be due to the source of patient recruitment. Maetzler and colleagues (2009), who recruited from movement clinics, found that a combined cohort of patients with DLB and PDD with raised amyloid (PIB+) did not differ in their Parkinsonism scores compared to those without (PIB−). They concluded that amyloid does not impact on motor scores. They suggested that patients seen at movement clinics with motor-related presentations are therefore less likely to display raised amyloid, whereas patients presenting at dementia clinics with more AD-like patterns of impairment will often have raised amyloid.

The pattern of raised amyloid distribution in DLB is largely similar to that seen in AD. However, the extent of amyloid is generally lower and varies greatly between individuals (Rowe et al. 2007). Across the literature assessed, the most common finding in DLB is raised amyloid in frontoparietal cortex and anterior and posterior cingulate (Kantarci et al. 2012; Rowe et al. 2007; Maetzler et al. 2009; Mak et al. 2019; Ishii et al. 2015) (see e.g. Fig. 17.3) although a number of these studies also reported raised amyloid in the temporal lobes and striatum. There was inconsistency regarding the occipital lobes, with several studies reporting raised amyloid (Rowe et al. 2007; Maetzler et al. 2009; Firbank et al. 2018), and one large study reporting no difference relative to controls (Kantarci et al. 2012).

17.3.2 Amyloid Deposition Relative to Other Disorders and Healthy Controls

At a group level, studies have frequently reported that patients with DLB show higher PIB retention than healthy controls but lower retention than patients with AD (Kantarci et al. 2012; Rowe et al. 2007; Firbank et al. 2018). Edison and colleagues (2008) reported that 11 of 13 patients with DLB were PIB+, compared to just 2 of

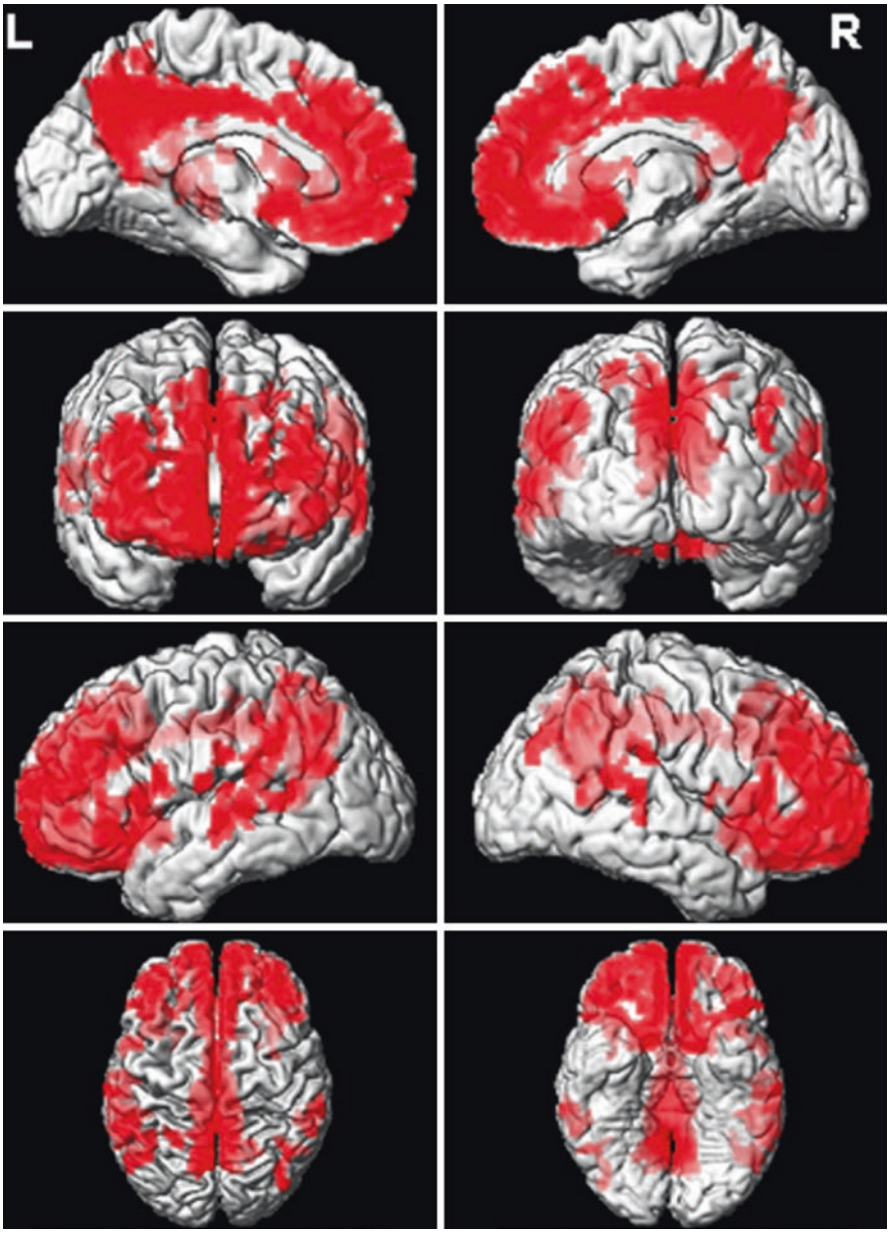

Fig. 17.2 Regional PIB retention in patients with DLB. Regional distribution of PIB retention in PIB-positive DLB patients ($n = 11$) was compared with PIB-negative cognitively normal subjects ($n = 33$). PIB retention was increased ($p < 0.05$; using family-wise error correction for multiple comparisons) in the frontal, parietal and superior temporal lobe association cortices (shown in red on the surface-render images). Inferior and medial temporal lobes, occipital lobes and pre- and postcentral gyri were typically spared in patients with DLB who were PIB positive. (Reproduced from Kantarci et al. 2012 with permission from Elsevier)

Table 17.3 PET and SPECT studies of amyloid deposition in DLB

Study	Subjects						Findings in DLB
	DLB	AD	PD	PDD	Other	Control	
Rowe et al. (2007)	10	17	–	–	15	27	Ninety percent of DLB patients had raised amyloid. Higher binding correlated with shorter time between onset of cognitive impairment and dementia
Edison et al. (2008)	13[a]	–	10	12	–	41	Eighty-five percent of DLB patients had raised amyloid. Maximum increases were in anterior or posterior cingulate followed by the frontal, parietal, temporal and occipital cortices
Maetzler et al. (2009)	9	–	14	12	–	–	4/9 (44.4%) of DLB patients had raised amyloid. Unlike PIB(−) patients, all PIB(+) patients had dementia
Kantarci et al. (2012)	21	21	–	–	–	42	11/21 (52.4%) of DLB patients had raised amyloid. The global cortical PIB retention ratio in patients with DLB was lower than in patients with AD but higher than normal controls
Gomperts et al. (2012)	18	–	29	12	14	85	Amyloid deposition was higher in DLB than PD, PD-MCI, PDD or controls. Amyloid deposition was associated with cognitive impairment in DLB only
Graff-Radford et al. (2014)	39	39	–	–	–	78	Amyloid deposition on PIB-PET was not associated with the cingulate island sing on FDG-PET
Siderowf et al. (2014)	11	10	5	–	–	5	Amyloid deposition in AD and DLB patients is significantly higher than PD patients and controls. MMSE scores in DLB patients are associated with uptake of ^{18}F-Florbetapir
Ishii et al. (2015)	10	10	–	–	–	–	Regional glucose metabolism in DLB patients is not associated with PIB retention
Nedelska et al. (2015)	30	30	–	–	–	60	White matter integrity in parietotemporal region is not associated with amyloid burden related to AD
Gomperts et al. (2016)	18	–	43[b]	12	–	–	Uptake of PIB in DLB is higher than PD and PDD. Combination of DAT and amyloid scan with PET is reliable for differentiating DLB from PD

(continued)

Table 17.3 (continued)

Study	Subjects						Findings in DLB
	DLB	AD	PD	PDD	Other	Control	
Sarro et al. (2016)	20	–	–	–	–	–	PIB uptake in DLB is associated with grey matter atrophy in posterior cingulate, temporal and occipital lobes and striatum
Kantarci et al. (2017)	19	19	–	–	–	95	Patients with AD have higher uptake of ^{18}F-AV-1451 especially in MTL, compared to DLB patients. Global cortical uptake of PIB is associated with ^{18}F-AV-1451 uptake in posterior temporoparietal and occipital cortices in DLB
Lee et al. (2018)	18	25	34[c]	–	–	25	DLB patients with amyloid deposition have a different pattern of ^{18}F-AV-1451 binding compared to AD
Donaghy et al. (2018)	37	20	–	–	–	20	Amyloid deposition is not associated with clinical and neuropsychological changes in DLB. However, it is associated with perfusion in MTL
Mak et al. (2019)	25	–	–	–	–	20	Amyloid deposition in DLB patients is associated with more severe atrophy in the hippocampus and subiculum
Nedelska et al. (2019)	33	–	–	–	18	100	^{18}F-AV-1451 uptake is higher in PCA compared to DLB and can differentiate these disorders with a sensitivity of over 97%
Shirvan et al. (2019)	10	–	4[d]	4	–	–	PET with PIB accurately shows the cortical amyloid depositions in patients with LB disease
Jack et al. (2019)	39	123	–	–	205	976	Most DLB patients did not have tau, and around half had high amyloid on PET

[a]10 of these 13 were patients from an earlier study (Rowe et al. 2007)
[b]14 PD with MCI
[c]22 PD with cognitive impairment
[d]PD with cognitive impairment

12 patients with PDD. Similar findings have been reported for the comparison between DLB and PD/PD-MCI (Gomperts et al. 2012). Some imaging studies have used other amyloid tracers. One study reported elevated uptake of ^{18}F-Florbetapir in dementia (highest in AD, followed by DLB) compared to PD and controls (Siderowf et al. 2014).

Regarding the usefulness of amyloid imaging to accurately differentiate between DLB and healthy controls or other neurodegenerative disorders, one study found

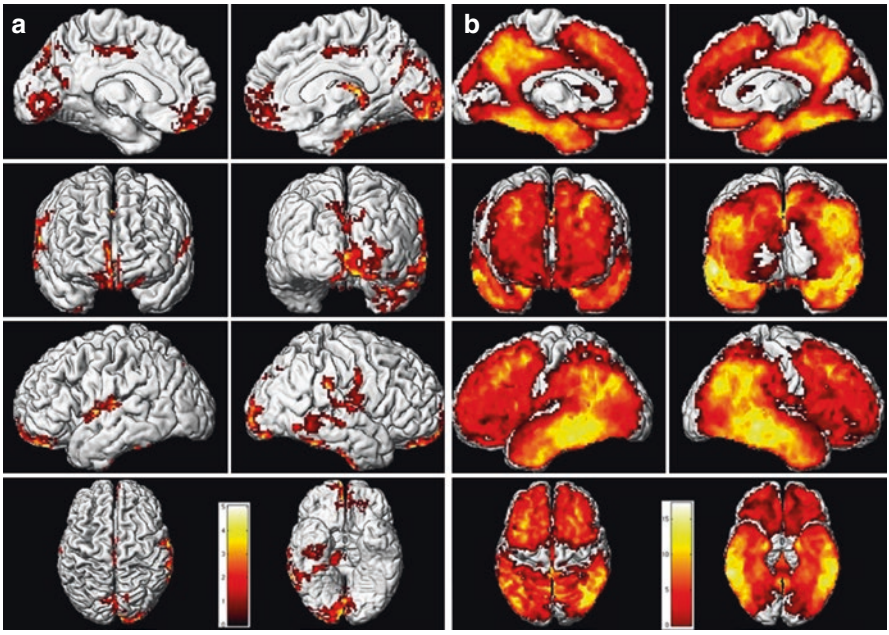

Fig. 17.3 Regional pattern of ^{18}F-AV-1451 uptake in probable DLB patients compared to the clinically normal controls and probable AD dementia. (**a**) Voxel-based analysis comparing patients with probable DLB to controls indicates greater uptake in DLB in the posterior and inferior temporoparietal lobes and medial frontal cortex. Higher uptake in the choroid plexus is seen on the left side ($p < 0.001$; uncorrected for multiple comparisons). Correction for multiple comparisons revealed no findings. (**b**) Voxel-based analysis comparing patients with probable DLB to AD dementia showed significantly greater uptake in AD throughout the brain relatively sparing the somatosensory and primary visual cortices ($p < 0.001$; family-wise error corrected for multiple comparisons). Colour bars show the *t*-value range. (Reproduced from Kantarci et al. 2017 with permission from John Wiley and Sons)

that scans were not able to reliably distinguish DLB from AD (Rowe et al. 2007). Kantarci and colleagues (2012) evaluated whether amyloid distribution differed between DLB and healthy controls but found no significant differences. However, that study reported that region of interest- and voxel-based analyses of global cortical PIB retention were useful in distinguishing patients with DLB from AD. The researchers also used MRI and ^{18}F-FDG PET (focussing on hippocampal volume and occipital metabolism) and found that the combination of amyloid imaging with either of the other two modalities was a better diagnostic predictor than amyloid imaging alone. Lastly, this study (Kantarci et al. 2012) reported no difference in metabolism between PIB+ and PIB− patients with DLB, despite PIB retention correlating inversely with metabolism in AD (Klunk et al. 2004). Gomperts and colleagues (2016) performed PET with altropane in addition to PIB and concluded that the combination of both modalities can discriminate DLB from PD and other disease groups.

17.3.3 Amyloid and Clinical Correlates

A number of studies have calculated correlation coefficients between amyloid deposition and clinical measures in patients with DLB. Rowe et al. (2007) reported that there was no significant relationship between amyloid deposition and mini mental state examination (MMSE) or Clinical Dementia Rating (CDR) scores in DLB. Maetzler and colleagues (2009) analysed a combined group of PDD and DLB patients and found that PIB+ patients had lower MMSE scores than PIB− patients, although amyloid did not affect Parkinsonian symptoms. Gomperts et al. (2012) found that amyloid deposition was associated with lower MMSE and worse semantic memory in DLB but not PD, PD-MCI or PDD. Conversely, this study found no association between amyloid burden and motor dysfunction in any group. Kantarci et al. (2012) found that amyloid deposition had no impact on functional impairment as measured with the CDR or Unified Parkinson's Disease Rating Scale (UPDRS). One study reported an association between lower MMSE scores and amyloid deposition in DLB (Siderowf et al. 2014). Donaghy and colleagues (2018) did not find any difference in clinical measures or cognitive scales between DLB patients with and without amyloid deposition. However, they found a negative correlation between cortical/striatal uptake and reaction time. The authors argued that their results could be due to ^{18}F-Florbetapir binding to both neuritic and diffuse plaques, while clinical symptoms are associated with neuritic plaques or NFT pathology only. Other studies reported associations between higher amyloid burden and more rapid development of core DLB features following patients' initial presentation (Rowe et al. 2007), as well as worsening CDR scores over time (Sarro et al. 2016).

All of the amyloid studies cited used ^{11}C-PIB as the ligand, with the exception of a study using ^{18}F-Florbetapir (Siderowf et al. 2014). ^{11}C-labelled ligands have a shorter (20-min) half-life, which limits their use to centres with an on-site cyclotron. As a result, access to ^{11}C-PIB is restricted, and the high cost of studies prohibits its routine use. This problem has been overcome with the development of ^{18}F-labelled ligands (including ^{18}F-Florbetaben, ^{18}F-Flutemetamol and ^{18}F-Florbetapir), which have a 110-min half-life. This allows the compounds to be synthesised off-site and delivered to research centres without on-site cyclotrons.

17.3.4 Amyloid and Pathological Correlates

Recently, studies have investigated the association between amyloid deposits and uptake of other ligands as well as changes on MRI in DLB. Graff-Radford and colleagues (2014) reported no difference in hypometabolism between DLB patients with and without PIB retention. Similarly, another study (Ishii et al. 2015) did not find a correlation between amyloid deposits and hypometabolism in parietotemporal and posterior cingulate. One study did not find an association between PIB retention and white matter integrity on DTI in DLB. However, that study identified overlap in parietooccipital lobes between decreased white matter integrity, grey matter alterations and hypometabolism (Nedelska et al. 2015). There is

inconsistency regarding the association between amyloid and grey matter in DLB. Mak and colleagues (2019) demonstrated modest overlap between global cortical thinning and Aβ, whereas a regional evaluation revealed an association between Aβ and hippocampal and subiculum atrophy. A UK-based team of researchers performed MRI and early- and late-phase PET with ^{18}F-Florbetapir (Donaghy et al. 2018). They did not find an association between amyloid deposition and grey matter atrophy. However, they reported an inverse association between amyloid deposition and perfusion in MTL. The authors argued that this association could be due to synergistic interactions between amyloid and α-synuclein. Sarro and colleagues (2016) scanned patients with DLB with PIB PET and MRI and found an association between amyloid deposition and greater grey matter loss over time in the posterior cingulate gyrus, temporal lobe and occipital lobe as well as the striatum. At present, there is early evidence of an association between amyloid deposition and grey matter changes in the temporal lobe in DLB; however, further studies are required to reach a more confident conclusion.

17.3.5 Tau Findings and Its Association with Amyloid in DLB

A number of studies have investigated tau pathology in DLB and its association with clinical profiles and amyloid deposits. The primarily used ligand for imaging tau with PET is ^{18}F-AV-1451. Kantarci and colleagues (2017) recruited 19 patients with DLB, 19 with AD and 95 healthy controls. They performed PET with ^{18}F-AV-1451 for tau and PIB for amyloid. Uncorrected voxel-based analyses showed higher uptake of ^{18}F-AV-1451 in the posterior and inferior temporoparietal and occipital lobes in DLB patients compared to controls. On the other hand, AD patients had higher binding of ^{18}F-AV-1451 compared to DLB patients, with the greatest difference in MTL. The investigators also found a correlation between higher uptake of ^{18}F-AV-1451 in posterior temporoparietal and occipital regions and higher cortical PIB uptake in DLB patients.

In a study imaging amyloid and tau in patients with DLB, PCA and controls, PCA showed higher uptake of ^{18}F-AV-1451 through the entire cortex, especially occipitally, compared to DLB (Nedelska et al. 2019). Compared to controls, DLB patients showed only moderate differences in ^{18}F-AV-1451 uptake. The authors concluded that the occipital uptake of the ^{18}F-AV-1451 is more than 97% sensitive for differentiating PCA from DLB.

Lee and colleagues (2018) recruited 18 patients with DLB, 25 with AD, 22 PD patients with cognitive impairment and 12 PD patients, as well as 25 healthy controls. PET scans were performed with ^{18}F-AV-1451 and ^{18}F-florbetaben. ^{18}F-AV-1451 binding in cortex tended to increase in patients across the LB spectrum (from PD, to PD-MCI, to DLB). Tau burden in cerebral cortex was increased in patients with LB disorders with a pattern similar to AD. However, DLB patients with amyloid deposition showed increased binding of ^{18}F-AV-1451 in a different pattern with increased involvement of primary cortices and less of the temporal cortex. The authors did not find an association between ^{18}F-AV-1451 regional binding with MMSE or motor

scores and concluded that tau accumulates differently in the cerebral cortex of DLB patients compared to AD.

Jack et al. (2019) reviewed PET scans of 39 patients with DLB, 23 with FTD, 123 with AD, 182 with MCI and 976 cognitively normal controls. They had previously performed PET with PIB and ^{18}F-AV-1451. The participants were grouped based on their scans: positive amyloid and negative tau scan (A+T−), negative amyloid and positive tau scan (A−T+), positive on both scans (A+T+) and negative on both scans (A−T−). The tau scans of the vast majority of DLB patients were negative with around half having a positive amyloid scan. The DLB patients with negative results on both scans probably represent more pure α-synuclein pathology, while the A+T− patients likely represented α-synuclein pathology as well as AD. The study authors concluded that the combination of amyloid and tau may help the clinician by indicating patients' staging on the Alzheimer's continuum (Jack et al. 2019).

17.3.6 Conclusion

In conclusion, across the studies reported, approximately 60% of patients with DLB had raised amyloid, though each study used different criteria for defining this. Studies typically report a higher rate of raised amyloid in AD, often at or near 100% (Rowe et al. 2007). It appears that patients with DLB have higher PIB retention than healthy controls but lower retention than patients with AD. Although amyloid is not associated with motor dysfunction in DLB, it may be associated with cognitive impairment (Gomperts et al. 2012). There is also evidence that increased amyloid is associated with a faster progression from onset of cognitive impairment to DLB (Rowe et al. 2007). Amyloid deposition does not appear reliable for differentiating DLB from healthy controls, AD, PD or PDD. However, its presence in patients with DLB suggests that use of anti-amyloid medication could be indicated, if this becomes available in the future. Tau in DLB is likely intermediate between healthy and AD.

17.4 Microglial Activation in DLB

Microglia are innate immune cells of the central nervous system. The activation of microglia reflects defence inflammation. Where microglial activation is prolonged, it can result in neuronal loss and neurodegeneration. The process of activation is rapid and occurs before other signs of tissue damage or cell death are detectable. Activation reflects disease activity rather than a specific aetiology (e.g. it is visible in patients with MCI prior to the development of AD; (Okello et al. 2009)). Interest is growing in this area, but results remain heterogeneous. Nevertheless, researchers have questioned if it might be possible to slow disease progression via inhibition of the inflammatory pathway, perhaps through the use of non-steroidal anti-inflammatory drugs or steroidal hormones like vitamin D (Hirohata et al. 2008; Jia et al. 2019). To date, however, very few in vivo studies have examined microglial activation in DLB.

17.4.1 In Vitro Studies of DLB Patients

An inflammatory mechanism has been extensively reported in AD (Eikelenboom and Stam 1982; Eikelenboom and Veerhuis 1996; McGeer et al. 1989), but results have been inconsistent in DLB. In post-mortem studies of DLB, researchers have observed levels of inflammation lower than AD or equivalent to controls (Shepherd et al. 2000; Szpak et al. 2001) and increased activation of microglia compared to controls, similar to PD patients (Power and Blumbergs 2009). Other researchers have observed significant inflammation in DLB patients even in the absence of Alzheimer's pathology, reporting a positive correlation between activated microglia and LB (Mackenzie 2000). One study found no difference in inflammatory responses between DLB, AD and controls (Gómez-Tortosa et al. 2003).

17.4.2 In Vivo Microglial Activation Studies

Activated microglia are linked to the 18-kDa translocator protein (TSPO). Increased TSPO is detectable in vivo by using PET with ^{11}C-PK11195, as it is specific for the peripheral benzodiazepine binding site (PBBS) which corresponds to the activation of microglia (see Fig. 17.4; (Banati et al. 2000)).

Surendranathan and colleagues (2018) studied central and peripheral inflammation in DLB. They enrolled 19 patients with DLB and 26 matched controls. All DLB patients and 16 controls underwent PET with ^{11}C-PK11195 and PIB. The authors categorised DLB patients into mild and moderate/severe DLB, based on the severity of their cognitive impairment. They observed that the inflammation in DLB does not have a linear progression. The uptake of ^{11}C-PK11195 as a marker for inflammation was higher in mild DLB compared to both moderate/severe DLB and controls. However, levels of inflammation were lower for moderate/severe DLB compared with controls. Furthermore, they investigated the correlations between clinical features and microglial activation. Greater microglial activation in the caudate, cuneus, anterior orbital gyrus and superior frontal gyrus was associated with more preserved cognition. Microglial activation in caudate was associated with lower Parkinsonism, but this did not survive correction for multiple comparisons. The authors concluded that microglial activation occurs early in DLB and decreases with cognitive deterioration.

17.4.3 Conclusion

Despite there being a paucity of studies investigating activated microglia in DLB patients in vivo, there has been significant progress in the development of new ligands for neuroinflammation. This may help improve our understanding of the role of inflammation in DLB and possibly facilitate the development of new treatment strategies in the future.

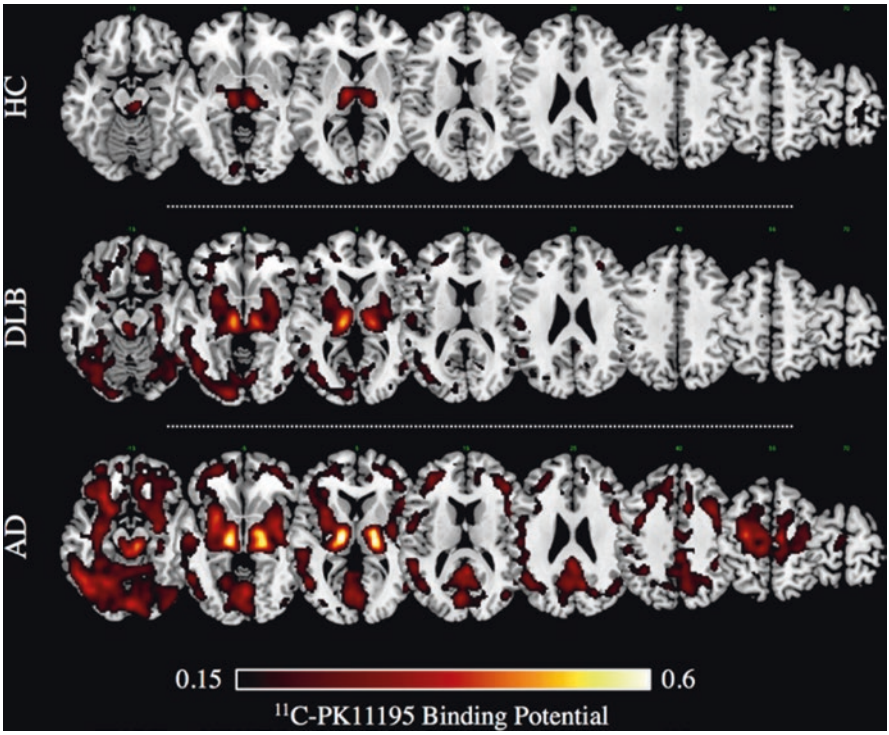

Fig. 17.4 Neuroinflammation imaging with PET. The image shows the binding of ^{11}C-PK11195 in a 74-year-old male with AD a 75-year-old male with DLB and an age-matched healthy control (HC). Neuroinflammation in DLB is scattered through several cortical regions, while it is more severe and widespread in the patient with AD. (Reproduced from Cerami et al. 2017 under the terms and conditions of the Creative Commons Attribution Licence)

17.5 Dopaminergic Degeneration in DLB

DLB is characterised by a significant dopamine deficiency in the striatum. This deficiency can be captured at different stages of the dopaminergic pathway (see Fig. 17.5). A neuropathological study (Piggott et al. 1999) compared dopaminergic activity along the rostrocaudal striatal axis between PD, DLB, AD and healthy controls. They identified 57% lower binding to presynaptic dopamine uptake sites in the putamen in DLB relative to controls, as well as a 72% reduction in dopamine. Additionally, patients with DLB had 17% lower binding to postsynaptic D2 receptors in the putamen relative to controls. Notably, patients with AD did not show deviations from normal across any of these measures. The reduced binding to dopamine uptake sites indicates reduced density of dopamine transporter (DAT), the membrane-spanning protein that pumps dopamine back into presynaptic cells. The loss of DAT is a consequence of the loss of nigrostriatal neurons which degenerate in DLB. The authors concluded that the distinct changes in the expression of striatal

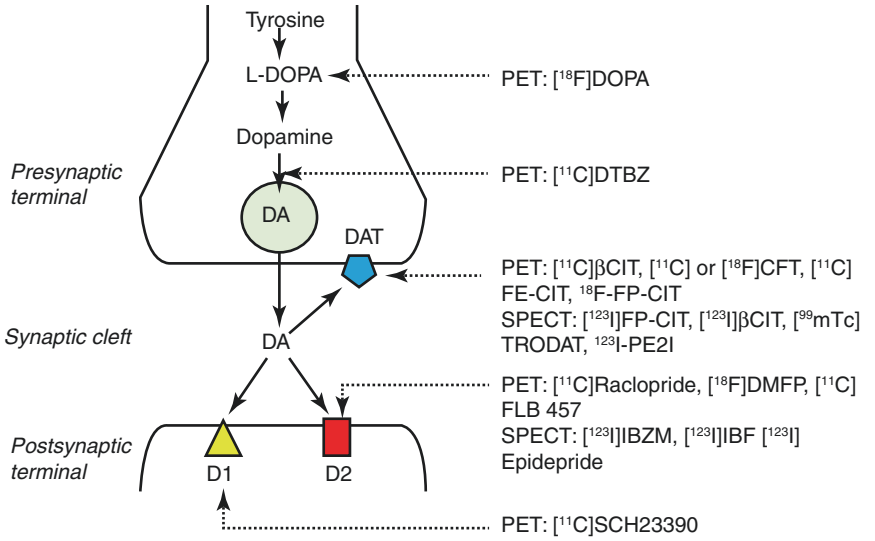

Fig. 17.5 Nigrostriatal dopaminergic synapse and targets of PET and SPECT ligands. Tyrosine is converted to L-DOPA by tyrosine hydroxylase. L-DOPA is then converted to dopamine (DA), which is gathered into vesicles by vesicular monoamine transporter and from which it is released into the synaptic cleft. Dopamine binds to D1 and D2 receptors on the postsynaptic membrane. Some dopamine re-enters the presynaptic terminal via dopamine transporters. (Reproduced from Walker and Rodda 2011 with permission from Cambridge University Press)

dopaminergic parameters might be relevant to the interpretation of in vivo imaging in DLB, especially regarding diagnosis (Piggott et al. 1999).

17.5.1 Dopamine Transporter Imaging in DLB

17.5.1.1 Discrimination of DLB Against AD

Although it is not currently possible to image the loss of nigrostriatal neurons in vivo in DLB, DAT may be used as a 'surrogate marker' for this neuronal degeneration and can be regionally quantified using appropriately labelled ligands and SPECT or PET (see Fig. 17.6; (Colloby et al. 2012)). The ligand most frequently used in these investigations has been the cocaine analogue ^{123}I-2β-carbomethoxy-3β-(4-iodophenyl)-*N*-(3-fluoropropyl)nortropane (^{123}I-FP-CIT). Walker and colleagues (2002) scanned patients with DLB, PD, AD and healthy controls with ^{123}I-FP-CIT and SPECT. They found that patients with DLB had lower mean binding bilaterally in posterior putamen, anterior putamen and caudate nucleus relative to AD and controls. Patients with AD did not differ in binding relative to controls. The authors noted that there was a clear separation of the AD and DLB groups with no overlap of the 95% confidence intervals for the means of radioactivity binding. The same lab subsequently reported on neuropathological data for the first 20 patients scanned and found that reduced striatal uptake of DAT was 88% sensitive and 100% specific

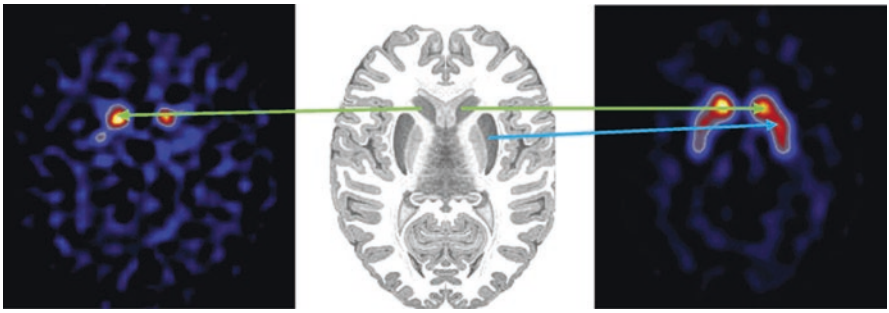

Fig. 17.6 ^{123}I-FP-CIT SPECT images from a healthy control (right) and a patient with neuropathologically confirmed DLB (left). In the control, there is good uptake throughout the bilateral caudate (green arrow) and putamen (blue arrow). In the DLB patient, there is reduced uptake of ^{123}I-FP-CIT SPECT in both the caudate and putamen. (Reproduced from Walker and Rodda 2011 with permission from Cambridge University Press)

for a post-mortem diagnosis of DLB (Walker et al. 2007). Initial clinical diagnosis of DLB in these patients (i.e. without the aid of imaging) had 75% sensitivity but only 42% specificity for a post-mortem diagnosis of DLB. The investigators noted that, on the basis of final diagnoses made at autopsy, scans facilitated a more accurate diagnosis than clinical criteria available at the time.

Following similar findings from an intervening study (O'Brien et al. 2004), McKeith and colleagues (2007) carried out a large, phase-III, multicentre study of the sensitivity and specificity of DAT imaging with ^{123}I-FP-CIT SPECT in DLB across 40 European sites. Three hundred and twenty-six patients with dementia were scanned and diagnosed blindly on the basis of these images by three nuclear medicine physicians. A panel of three expert clinicians assigned patients a consensus dementia diagnosis on the basis of clinical data alone. Inter-reader agreement between the three nuclear medicine physicians for rating scans as normal or abnormal was high (Cohen's $\kappa = 0.87$). The clinical diagnoses identified 88 patients as having probable DLB, 56 as having possible DLB and 144 with non-DLB dementia (90 probable AD, 34 possible AD, 9 vascular dementia and 11 with unspecified dementia). Measured against these clinical diagnoses, abnormal scans had a mean sensitivity of 78% for detecting probable DLB, with a specificity of 90% for excluding non-DLB dementia, which was predominantly due to AD. This study thus confirmed that there is a high correlation between abnormal DAT scans and a clinical diagnosis of probable DLB. The authors concluded that the diagnostic accuracy of ^{123}I-FP-CIT scans is sufficiently high for the technique to be clinically useful in distinguishing DLB from AD.

Differences in DAT uptake between DLB and AD have been well replicated. Swiss researchers reviewed ^{123}I-FP-CIT SPECT scans of 93 individuals with probable DLB and 18 with AD (Nicastro et al. 2017). They reported lower uptake in the striatum, caudate nucleus and putamen in DLB. Studies that used another ligand (^{11}C-altropane, a PET tracer for DAT) also found a reduction in striatal binding in patients with LB pathology compared to AD or healthy controls (Gomperts et al.

2016; Marquie et al. 2014). However, one study using ^{123}I-FP-CIT SPECT found no difference in binding in posterior putamen between DLB and AD (Shimizu et al. 2017a).

O'Brien and colleagues (2009) followed up the cohort from the phase-III study of ^{123}I-FP-CIT diagnostic accuracy (McKeith et al. 2007). They applied a second consensus clinical diagnosis to all patients 12 months after the first diagnosis. They were especially interested in the clinical status of patients originally diagnosed as having possible DLB at baseline. They found that, of 44 patients with possible DLB at baseline, 18 had the same diagnosis at follow-up (41%). However, 19 had converted to probable DLB (43%) and seven were diagnosed with AD (16%). Of the 19 who converted to probable DLB, 12 had abnormal scans at baseline (sensitivity 63%). All of the baseline possible DLB patients diagnosed as having AD at follow-up had normal scans (specificity 100%). The authors noted that overall, an abnormal ^{123}I-FP-CIT scan was predictive of an individual either keeping a diagnosis of probable DLB or the diagnosis becoming probable DLB. Their conclusion was that DAT imaging is of greatest diagnostic value for accurate and timely diagnosis in clinically uncertain cases of possible DLB. Consensus clinical diagnosis was used as the gold standard in these studies (McKeith et al. 2007; O'Brien et al. 2009). Clinical consensus diagnoses applied in research settings tend to be more accurate than those applied in clinical practice. Despite this approach, these studies are limited by the lack of neuropathological confirmation of diagnosis (Walker and Rodda 2011).

Walker and Walker (2009) increased the size of the previously reported autopsy cohort (Walker et al. 2007), bringing the total number of cases with ^{123}I-FP-CIT SPECT during life to 23. Ten cases met neuropathological criteria for DLB, 9 for AD and 4 for other dementia subtypes. In these 23 patients, the sensitivity of ^{123}I-FP-CIT SPECT scans for diagnosing DLB was 100%, and the specificity was 92%. The sensitivity of an initial clinical diagnosis of DLB was 80%, and the specificity was 46%. There were no false-negative scan results in this study. One false-positive diagnosis of DLB was given to a patient with extensive vascular disease. The patient had a vascular lesion in the substantia nigra which accounted for the abnormal scan result. This type of misinterpretation could be avoided in clinical practice by correlation with magnetic resonance imaging (MRI) data (Walker and Rodda 2011). More recently, researchers compared the diagnostic accuracy of ^{123}I-FP-CIT findings against autopsy diagnoses in an even larger cohort (Thomas et al. 2017). Recruiting from memory and dementia services, 33 patients with DLB and 22 with AD who had undergone ^{123}I-FP-CIT SPECT were included. The primary diagnosis was made based on consensus criteria. Independent clinicians blind to clinical information and other investigations rated the scans and neuropathological assessments. In order to evaluate the validity of ^{123}I-FP-CIT for detecting DLB, they pooled cases with pure DLB or mixed DLB + AD in one group and categorised all other cases as non-DLB. From 30 patients with autopsy confirmed diagnosis of DLB, 6 patients had normal ^{123}I-FP-CIT SPECT. Overall, their results indicated 80% sensitivity and 92% specificity of ^{123}I-FP-CIT, resulting in 86% balanced diagnostic accuracy. Of the 6 patients with DLB but normal scan, 3 cases had mixed DLB + AD, and 3 cases had pure DLB. Interestingly, the pure DLB cases with negative scan all had

limbic-only involvement. In sum, while an abnormal ^{123}I-FP-CIT SPECT scan is strongly predictive of a neuropathological diagnosis of DLB, a normal scan does not exclude DLB where this is associated with a minimally affected brainstem.

Walker and colleagues (2015b) randomised 170 patients with possible DLB into two groups: the 'active' arm underwent ^{123}I-FP-CIT SPECT imaging, and the controls were followed up without imaging. The authors explored the change in diagnosis (from possible DLB to probable DLB or non-DLB dementia) in each group at follow-up. In the imaging group, 49 patients (43%) had abnormal scans at baseline. After 8 weeks, the diagnosis of 70 participants (61%) of the scan group and two controls (4%) had changed. The corresponding numbers of patients with changed diagnosis were 77 (71%) and nine (16%) at 24 weeks follow-up (both time points $p < 0.01$). The results indicated that the diagnosis was changed more often if the scan was abnormal (82%) than if it was normal (46%). The authors concluded that an abnormal DAT SPECT in patients with dementia and some features of DLB indicate an increased likelihood of DLB diagnosis and highlights the importance of imaging in detecting cases that will progress to probable DLB.

17.5.1.2 DLB Compared to PD and PDD

Comparison of DAT scans between groups of patients with DLB, PD and PDD yields less notable differences than for DLB versus AD. This is because DLB, PD and PDD *all* feature nigrostriatal degeneration. This comparison also has less clinical relevance than that between DLB and AD, since PD and PDD are not common differential diagnoses of DLB. Nevertheless, researchers have identified subtle differences between some of the groups. One study scanned 21 patients with DLB, 19 drug naive patients with PD and 16 controls using ^{123}I-FP-CIT SPECT (Walker et al. 2004). Both DLB and PD groups had lower binding relative to controls bilaterally throughout the striatum. However, the DLB patients had lower binding than the PD patients in the caudate nucleus bilaterally. The authors concluded that their results suggested that DLB patients do not have the characteristic selective degeneration of ventrolateral nigral neurons consistently demonstrated in PD. The investigators also noted that there was a more marked asymmetry of binding in patients with PD in the posterior putamen compared to DLB and controls. This is concordant with the observation that patients with DLB present with more symmetric motor signs than patients with PD (Gnanalingham et al. 1997).

A study using an analogous design matched 53 DLB patients with 53 PD patients on gender, age and MMSE score (Joling et al. 2018). The patients underwent ^{123}I-FP-CIT SPECT and MR imaging. The analyses were adjusted for age and indicated that striatal DAT binding in bilateral posterior putamen was significantly lower in PD patients compared to DLB patients. Moreover, the caudate/putamen ratio was markedly lower in DLB compared to PD, consistent with earlier research (Walker et al. 2004). Although ^{123}I-FP-CIT has a high affinity for DAT, it is also highly selective for the serotonin transporter (SERT). The density of DAT is higher in basal ganglia, whereas SERT levels are higher in the thalamus and midbrain (their distributions do not overlap). The above study (Joling et al. 2018) also

investigated the differences in SERT between DLB and PD. They failed to find a difference in SERT binding between PD and DLB in the thalamus, amygdala or hippocampus. A subsequent similar study by the same investigators studied DLB, PD and healthy controls and found that only the DLB patients had reduced SERT in hypothalamus relative to controls (Joling et al. 2019). However, the authors stressed that both patient groups were at an early disease stage, which could account for the limited differences relative to controls.

Pilotto and colleagues (2019) also studied the striatal and extrastriatal uptake of ^{123}I-FP-CIT in DLB and PD using SPECT. They included 41 patients with DLB, 56 with PD and 54 healthy controls. At least 2 years of follow-up supported the clinical diagnoses of DLB and PD. They performed ^{123}I-FP-CIT SPECT and calculated specific binding ratios (SBR) for the cortex, striatum, thalamus and midbrain. They found lower SBRs in the caudate and putamen of subjects with PD and DLB compared to controls; however, there were no significant differences between the patient groups. This finding is unsurprising, since post-mortem studies do not support an arbitrary cut-off between PDD and DLB based on the neuropathologic and neurochemical gradation between them (Ballard et al. 2006). However, the above study found marked differences in extrastriatal SBRs between DLB and PD (Pilotto et al. 2019). The PD patients had lower SBRs in the insula and thalamus compared to healthy persons, while DLB patients showed additional reductions in the cingulate cortex. Further, the thalamic SBR in DLB was lower than in PD patients. The authors concluded that, despite sharing dopaminergic nigrostriatal and insular deficits, DLB and PD differentially involve monoaminergic cingulate and thalamic projections. Their findings are in line with the observed alpha-synuclein pathology in the insular and limbic systems and with the high prevalence of autonomic and affective dysfunction in patients with DLB and PD. Although these results are of interest, the clinical utility of SERT imaging is limited at present.

17.5.1.3 DLB Compared to FTD

Patients with FTD can usually be differentiated from DLB on clinical grounds; however, in some cases, the distinction is not straightforward. Both dementias may feature hallucinations, delusions, agitation and Parkinsonism. One study sought to establish whether striatal DAT binding varied amongst 9 patients with AD, 12 patients with FTD and 10 with DLB using ^{123}I-FP-CIT SPECT (Morgan et al. 2012). Their aim was to establish whether FTD and DLB could be differentiated on the basis of DAT imaging. In this study, one patient with AD (11%), four patients with FTD (33%) and nine patients with DLB (90%) had an abnormal scan. Dopaminergic scans were therefore 90% sensitive for a diagnosis of DLB. Compared to DLB, scans were 89% specific versus AD but only 67% specific versus FTD. The researchers noted that extrapyramidal motor signs (EPMS) were common in both FTD and DLB. They concluded that DAT scans are helpful in differentiating DLB from AD but that an abnormal ^{123}I-FP-CIT SPECT scan, even in patients with EPMS, does not exclude the diagnosis of FTD (Morgan et al. 2012).

17.5.1.4 Diagnostic Accuracy in DLB Versus Other Imaging Techniques

The sensitivity and specificity of an abnormal DAT scan compared to a clinical or neuropathological diagnosis of DLB are clearly high. Investigators have compared the diagnostic accuracy of dopamine imaging against other commonly used neuroimaging investigations. Shimizu and colleagues (2017b) compared the diagnostic value of ^{123}I-FP-CIT SPECT with MRI, perfusion SPECT and ^{123}I-metaiodobenzylguanidine (MIBG) myocardial scintigraphy for distinguishing between DLB and AD. They enrolled 32 patients with DLB and 32 patients with AD. ^{123}I-FP-CIT SPECT provided the most accurate differentiation of DLB from AD, followed by ^{123}I-MIBG. The diagnostic accuracy of MRI and perfusion SPECT were lower.

Kobayashi and colleagues (2017) recruited 34 patients with a clinical diagnosis of DLB and performed ^{99m}Tc-ECD perfusion SPECT, ^{123}I-MIBG and ^{123}I-FP-CIT SPECT. They first looked at the results of each method separately. ^{123}I-FP-CIT SPECT and ^{123}I-MIBG had the highest sensitivity (79%) compared to perfusion SPECT (53%). In the next step, the authors combined pairs of scans and assessed whether the combination performed better than individual investigations. The combination of ^{123}I-FP-CIT SPECT with perfusion SPECT or with ^{123}I-MIBG was able to detect 32 out of 34 patients. Finally, when they combined all three imaging modalities, all the patients had at least one abnormal scan, which resulted in 100% sensitivity for the combination of ^{123}I-MIBG, ^{123}I-FP-CIT SPECT and perfusion SPECT.

Shimizu and colleagues (2016) enrolled 133 patients (76 DLB and 57 AD), who underwent ^{123}I-FP-CIT SPECT and ^{123}I-MIBG. Although the diagnostic accuracy of ^{123}I-FP-CIT SPECT was slightly higher than ^{123}I-MIBG, this was not statistically significant. However, the combination of the two scans yielded a significantly improved sensitivity and specificity (96% and 91%, respectively). In sum, despite inconsistencies, DAT imaging seems to be the most accurate in vivo neuroimaging investigation for the diagnosis of DLB. However, combining two or more scans together yields higher diagnostic accuracy.

Most of the studies previously described are solely based on the visual assessment of ^{123}I-FP-CIT images. Recently, there have been efforts to develop quantitative methods to improve on this approach. In one report, researchers used BRASS™ software to calculate mean counts in striatal and background volumes of interest in patients with DLB and AD (Nicastro et al. 2017). The sensitivity and specificity of visual assessment were 97% and 94%, respectively. However, when combined with semi-quantitative analysis, the sensitivity for differentiating between AD and DLB increased to 100%. Distance-weighted histograms can also improve reproducibility of SBRs used to calculate DAT density (Okizaki et al. 2017).

On the other hand, quantitative analyses are not sufficient to be used in isolation, with one study reporting the sensitivity of semi-quantitative analysis as 98% but with a lower specificity of 72% (Nicastro et al. 2017). More recently, researchers used the Southampton method to re-analyse ^{123}I-FP-CIT SPECT scans from 99 patients (10 of whom had DLB; (Hayashi et al. 2019). They used a threshold method (TM) that corrected for brain atrophy in both the striatum and the whole-brain

reference region. The TM-corrected SBRs were lower than the conventional values, reflecting the adjustment for brain atrophy. The authors noted that, in a small number of cases, there was a change in the laterality of the SBR depending whether TM was used or not. They consequently concluded that even where quantitative analyses are available, the visual assessment of ^{123}I-FP-CIT SPECT is vital.

17.5.1.5 Correlation with Clinical Measures in DLB

Several studies have investigated the relationship between DAT and clinical and cognitive measures in DLB, yielding mixed results. Colloby and colleagues (2005) studied 20 patients with DLB, 20 with PD, 15 with PDD and 22 controls using serial ^{123}I-FP-CIT scans at a 1-year interval. Tracer binding in the caudate and posterior putamen of patients with DLB declined faster than in controls. Rates of decline were similar between DLB, PD and PDD. The researchers assessed the relationship between binding decline and clinicopathological measures in DLB and found that the initial binding value in the posterior putamen predicted annual percentage change in the same region (i.e. the higher the baseline uptake, the higher the rate of decline.) Additionally, cognitive decline was associated with greater loss of uptake in the posterior putamen ($r = -0.54$; $p = 0.02$).

Another group studied 18 patients with well-characterised DLB using ^{123}I-FP-CIT SPECT (Roselli et al. 2009). They investigated relationships between binding in the striatum and the severity of neuropsychiatric symptoms. They observed significant correlations between decreased striatal binding and VH. Additionally, when considering the caudate nucleus separately, delusions, depression and apathy were negatively correlated with caudate binding. The authors concluded that their results implicate dopaminergic deficits in the pathogenesis of neuropsychiatric symptoms in DLB.

One-hundred and thirty-three participants with DLB and 95 with AD were recruited and underwent ^{123}I-FP-CIT SPECT by Shimizu and colleagues (2017a). The authors did not observe a correlation between MMSE and DAT in any part of the striatum in patients with DLB. On the other hand, when comparing DLB patients with and without Parkinsonism, they found that participants with Parkinsonism had lower SBR in striatum and putamen.

Other groups have also investigated the association between clinical symptoms and DAT. Thirty-five patients with probable DLB underwent ^{123}I-FP-CIT SPECT (Siepel et al. 2016). Analyses indicated that there is a small yet significant negative association between motor severity and DAT uptake in putamen ($\beta = -0.02$; $p = 0.01$). Specifically, motor rigidity was negatively correlated with DAT uptake in putamen ($\beta = -0.05$; $p = 0.02$). This study also observed that executive functions were associated with DAT uptake in both caudate nucleus ($\beta = 0.26$; $p = 0.02$) and putamen ($\beta = 0.19$; $p = 0.04$). Importantly, in this study, the majority of diagnoses were confirmed by autopsy.

In a study by Ziebell and colleagues (2013), 51 patients with DLB and 28 healthy individuals were included. The investigators explored the association between the clinical severity of DLB and DAT binding in striatum using ^{123}I-PE2I SPECT. This study did not find an association between MMSE score and DAT binding in the

striatum, putamen or caudate nucleus, nor was there an association between DAT binding and the severity of Parkinsonism.

Although DAT SPECT has high diagnostic accuracy for DLB, some patients have normal scans. Researchers have sought to identify the clinical features in possible DLB that would predict an abnormal scan. In a large study (Walker et al. 2016), 170 participants with possible DLB were enrolled, of which 114 were randomised to undergo ^{123}I-FP-CIT SPECT. Diagnostic status was ascertained at 8 and 24 weeks from baseline. In the patients randomised to ^{123}I-FP-CIT SPECT, 43% had abnormal scans. The results indicated that only Parkinsonism could predict an abnormal scan ($p < 0.01$). However, only 27% of the participants had Parkinsonism at baseline. Furthermore, around a third of patients with only hallucinations or fluctuations but without Parkinsonism had an abnormal scan. The authors argued that if an abnormal DAT SPECT indicates DLB pathology, making a clinical diagnosis with only one DLB feature would be difficult without imaging. Moreover, they compared the progression of clinical features in patients with normal and abnormal scans. They found that frequency of clinical symptoms were stable over 24 weeks regardless of the scan. However, UPRDS scores increased compared to baseline in individuals with an abnormal ^{123}I-FP-CIT SPECT scan.

17.5.1.6 Dopaminergic Degeneration in Prodromal DLB

The interval between the appearance of initial symptoms and the full manifestation of DLB is termed the prodromal phase. At the time of writing, there are no published criteria for prodromal DLB diagnosis. However, there are a number of features that are thought to be associated with prodromal DLB. There is evidence that the prodromal phase of DLB may present as MCI in addition to the following: one or more core (vivid VH, marked fluctuation in cognition and attention, spontaneous Parkinsonism and RBD) or supportive clinical features; late-onset anxiety/depression or psychosis; recurrent delirium; hyposmia, constipation, orthostatic hypotension, urinary incontinence and hypersalivation; and primarily visuoperceptual and attentional deficits.

Kasanuki and colleagues (2017) used ^{123}I-FP-CIT SPECT to investigate prodromal DLB. They included 20 participants with prodromal DLB, 18 with probable DLB and 10 with probable AD. Inclusion criteria for prodromal DLB included MCI (measured by MMSE); intact activities of daily living; absence of cognitive fluctuations or VH; absent or mild Parkinsonism with onset after cognitive impairment; evidence of diffuse hypometabolism in the occipital lobe indicated by ^{18}F-FDG PET; having several non-motor symptoms associated with LB disease; and no family history of PD. Diagnosis of probable DLB was made according to consensus criteria. Their results showed that reductions in striatal DAT binding are marked in both DLB groups (regardless of the stage) compared to AD participants (see Fig. 17.7). However, their aim was to explore the association between DAT SPECT and clinical symptoms. They did not find a correlation between DAT density and cognitive function in patients with prodromal nor probable DLB. On the other hand, in patients with probable DLB as well as the total DLB group, there was a negative correlation between *SBR* scores and the severity of Parkinsonism. In prodromal

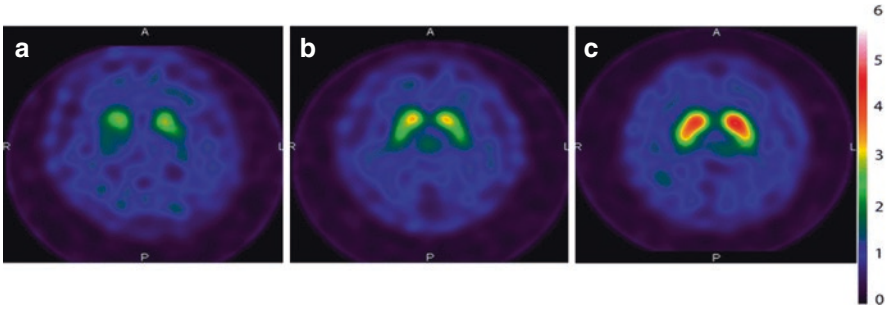

Fig. 17.7 Representative ^{123}I-FP-CIT SPECT scan of: (**a**) a 72-year-old man with DLB; (**b**) a 72-year-old woman with prodromal DLB and (**c**) a 74-year-old woman with AD. In both DLB and prodromal DLB, there is a significantly decreased uptake of tracer compared to AD. However, the difference between the two DLB patients is not significant. (Reproduced from Kasanuki et al. 2017 with permission from Springer Nature)

DLB, the SBR scores were negatively correlated with the duration of the olfactory dysfunction or RBD. The authors concluded that the associations between the reduction in DAT binding and clinical symptoms depend on the stage of DLB.

In another recent study, investigators further evaluated the diagnostic accuracy of DAT SPECT in prodromal DLB, also termed MCI with LB disease (MCI-LB) (Thomas et al. 2019). This study recruited 33 patients with probable MCI-LB, 15 with possible MCI-LB and 27 with MCI with Alzheimer's disease (MCI-AD). The participants underwent ^{123}I-FP-CIT. Their results showed that patients with prodromal DLB had more impaired scores on the UPDRS and instrumental activities of daily living compared to people with MCI-AD. They also had greater sleepiness and neuropsychiatric symptoms. Visually assessing the ^{123}I-FP-CIT results, 61% of people with probable MCI-LB and 40% of people with possible MCI-LB had abnormal scans. The frequency of abnormal scans was higher in the MCI-LB groups compared to MCI-AD. The study found that overall diagnostic accuracy of visually rated ^{123}I-FP-CIT scans for prodromal DLB was 67%, with 54% sensitivity and 89% specificity for detecting MCI-LB cases. The authors concluded that although the sensitivity is reduced due to less nigrostriatal degeneration relative to DLB, ^{123}I-FP-CIT SPECT can be used clinically in MCI patients where prodromal DLB is suspected.

RBD can, in some cases, represent prodromal DLB. One research group performed ^{123}I-FP-CIT on 87 patients with RBD and 20 healthy controls (Iranzo et al. 2017). Participants were followed for up to 7 years. After 3 years, from 51 patients with abnormal DAT SPECT at baseline, 13 patients developed DLB, 11 patients were diagnosed with PD and one patient received a diagnosis of MSA (Parkinsonian type). The rest of the patients remained disease free. Patients who developed synucleinopathies had more than 25% decreased uptake of ^{123}I-FP-CIT in putamen. Abnormal DAT SPECT identified synucleinopathies with 82% sensitivity and 52% specificity. The authors concluded that RBD patients with abnormal DAT SPECT are at increased risk of developing a synucleinopathy in the short term.

17.5.2 Dopamine Turnover

Although the majority of research investigating the nigrostriatal pathway in DLB has utilised ^{123}I-FP-CIT SPECT, other approaches have also been used. One is the use of 6-^{18}F-fluoro-L-3,4-dihydroxyphenylalanine (^{18}F-fluorodopa) and PET. This tracer images dopamine turnover in vivo. An early study scanned six patients with probable DLB, one with autopsy-confirmed DLB/AD, ten with probable AD and eight controls using ^{18}F-fluorodopa and PET (Hu et al. 2000). They calculated an influx rate constant (K_i) of ^{18}F-fluorodopa into selected striatal regions of interest for all participants. Hu et al. (2000) measured significantly lower mean K_i values in the caudate and putamen of the DLB group relative to the AD group. The K_i values for the AD group were not significantly different from controls. Putaminal K_i values differentiated DLB from AD with a sensitivity and specificity of 100% and 86%. K_i values in caudate yielded a sensitivity and specificity of 100% and 71%. These findings are in agreement with post-mortem findings of reduced striatal dopamine and degeneration of the nigrostriatal pathway in DLB (Piggott et al. 1999). The authors concluded that ^{18}F-flurodopa may be a useful diagnostic adjunct for distinguishing DLB from AD in vivo, but that a study using larger numbers would be necessary to confirm this.

17.5.3 Vesicular Monoamine Transporter Type 2 Imaging

Another line of investigation in DLB has been to assess the density of vesicular monoamine transporter type 2 (VMAT2) in vivo. VMAT2 is a protein found in monoaminergic neurons and is the only transporter that moves dopamine into presynaptic vesicles for subsequent exocytotic release (Zheng et al. 2006). VMAT2 binding has been assessed in vivo using PET and radiolabelled versions of the VMAT2 inhibitor tetrabenazine, which can be used as a marker for presynaptic terminal density. Koeppe and colleagues (2008) studied 25 patients with DLB, 30 with PD, 25 with AD and 57 controls using ^{11}C-DTBZ and PET. They quantified both blood-to-brain ligand transport (K_1) and striatal binding of the ligand, which enabled brain perfusion and monoaminergic presynaptic terminal density to be investigated using a single scan. The investigators observed markedly decreased VMAT2 binding in the striatum in the DLB and PD groups relative to the controls. Both DLB and PD groups had significantly greater interhemispheric asymmetry of striatal binding relative to AD and controls. The anterior-posterior striatal binding gradient was also steeper in DLB and PD relative to AD and controls, with the steepest gradient in PD. The researchers then compared the accuracy for distinguishing between patient groups on the basis of the two measures (perfusion and striatal binding). They found that for differentiation of DLB from AD, posterior putamen binding of ^{11}C-DTBZ was more accurate than assessment of occipital perfusion (99% accuracy versus 71%). Conversely, on the basis of combined assessment of asymmetry and rostrocaudal gradients in striatal binding, DLB can

reasonably be separated from PD, but not as well as on the basis of perfusion in the temporoparietal association cortex (88% accuracy versus 97%; (Koeppe et al. 2008)).

Siderowf and colleagues (2014) used the ^{18}F-labelled tetrabenazine derivative 9-fluoropropyl-(+)-dihydrotetrabenazine (^{18}F-AV-133) and PET to measure VMAT2 binding in 11 patients with DLB, 10 with AD, 5 with PD and 5 healthy controls. Participants also underwent amyloid imaging with ^{18}F-Florbetaben. Striatal VMAT2 densities were significantly reduced in DLB and PD relative to AD and controls. The greatest between-group difference was for lower posterior putamen. VMAT2 binding enabled DLB and PD to be accurately distinguished from AD or healthy, with a sensitivity of 88% and specificity of 100%. For the DLB group, MMSE scores correlated with ^{18}F-AV-133 binding in the caudate, but there was no association with posterior putamen. Across the studies surveyed, there are clear differences between DLB and AD/controls. There are reductions in VMAT2 binding in the striatum, least in caudate and greatest in posterior putamen. There is also greater interhemispheric striatal binding asymmetry in DLB relative to AD/controls. These data are concordant with neuropathological findings (Piggott et al. 1999).

17.5.4 Postsynaptic Dopaminergic Receptors

It has been noted that in PD, there is upregulation of postsynaptic D2 receptors in the putamen, but no abnormality in the caudate, leading to a reduced caudate/putamen D2 receptor ratio (Brooks 1993). Walker and colleagues (1997) investigated if this was also the case in DLB. They used ^{123}I-Iodobenzamide (^{123}I-IBZM) and SPECT to measure striatal postsynaptic D2 receptor availability in a sample of 16 patients with DLB, 13 with AD and 15 controls. The investigators found that DLB patients had a significantly lower mean caudate/putamen ratio than the AD group or controls. The decreased caudate/putamen D2 receptor ratio in DLB was due to upregulation of D2 receptors in the putamen as well as a marked decrease in binding sites in the caudate. These results contrast somewhat with an autopsy study reporting reduced D2 receptor density in both caudate and anterior putamen in DLB versus controls (Piggott et al. 1999). Furthermore, a later study scanned six patients with DLB with ^{123}I-IBZM and SPECT and found no difference in the density of striatal D2 receptors relative to a control group of patients with essential tremor (Plotkin et al. 2005). The studies discussed suggest that there may be reduced D2 receptor density in caudate in patients with DLB, but the evidence is inconclusive regarding the putamen. More research with a greater number of patients would help develop our understanding, though currently, there is no clear clinical role for D2 receptor imaging in DLB (Walker and Rodda 2011).

17.5.5 Conclusion

A wide range of dopaminergic PET and SPECT investigations have yielded abnormal results for patients with DLB relative to AD and controls. The most

commonly used investigation of ^{123}I-FP-CIT SPECT has reliably identified a reduction of striatal DAT in DLB. Measured against clinical criteria, these abnormal scans are 78% sensitive and 90% specific for DLB (McKeith et al. 2007). However, measured against the gold standard of neuropathological diagnosis, the scans are 80% sensitive and 92% specific for DLB, albeit demonstrated in a moderately sized sample (Thomas et al. 2017). Loss of DAT reflects degeneration of nigrostriatal neurons. The degeneration of these neurons also causes reduced density of VMAT2 (Koeppe et al. 2008). The loss of nigrostriatal neurons also affects dopamine turnover, which is significantly reduced in DLB compared to AD and controls (Hu et al. 2000). Dopaminergic imaging has clear utility for differentiating between DLB and AD, and a revision of the International Consensus Criteria for DLB has recommended low DAT radioligand uptake in the basal ganglia as an indicative biomarker for diagnosis (McKeith et al. 2017). However, dopaminergic imaging has limited utility when the differential diagnosis includes FTD (Morgan et al. 2012). The utility in prodromal DLB still needs to be established (Table 17.4).

17.6 Cholinergic Deficits in DLB

It is well documented that acetylcholine has an important role in attention, memory and cognition (Francis and Perry 2007; Perry et al. 1999). DLB is known to be associated with marked cholinergic deficits (Perry et al. 1993; Tiraboschi et al. 2000), and choline acetyltransferase activity in the neocortex has been shown to correlate with dementia severity in DLB (Samuel et al. 1997). In vivo studies have focused on acetylcholinesterase (AChE) activity as well as muscarinic and nicotinic receptors (see Table 17.5).

17.6.1 Vesicular Acetylcholine Transporter Imaging

Mazère and colleagues (2017) explored the role of the cholinergic system in DLB. They used ^{123}I-iodobenzovesamicol with SPECT in 11 patients with DLB (3 possible and 8 probable DLB) and 12 healthy controls. ^{123}I-iodobenzovesamicol traces the vesicular acetylcholine transporter, thus serving as an in vivo marker of presynaptic cholinergic terminal density. Compared to healthy participants, they found significant deterioration in the integrity of cholinergic pathways in DLB. In the Ch4 (innominatocortical) pathway, there was decreased ligand binding in the anterior cingulate (which was associated with apathy) and parietal cortices. They also observed reductions in the Ch5 terminal regions of the thalamus and striatum, reflecting changes to the pontothalamic cholinergic pathway. However, there were no differences in the Ch1 (septohippocampal) pathway between DLB and healthy controls. Their findings were in line with previous post-mortem and in vivo studies.

Table 17.4 PET and SPECT studies of dopaminergic function in DLB

Study	Subjects						Findings in DLB
	DLB	AD	PD	PDD	Other	Control	
^{123}I-FP-CIT SPECT							
Walker et al. (2002)	27	17	19	–	–	16	DLB and PD showed lower ligand uptake in all striatal areas relative to AD and controls
Walker et al. (2004)	21	–	19	–	–	16	DLB patients had lower binding in the caudate bilaterally compared to PD
Colloby et al. (2005)	20	–	20	15	–	22	Greater loss of uptake in the posterior putamen in patients with DLB was associated with cognitive decline over 1 year
McKeith et al. (2007)	144	124	–	–	20	–	Sensitivity of DAT imaging for a clinical diagnosis of probable DLB was 78% and specificity 90%
Walker et al. (2007)	8	9	–	–	3	–	Compared to neuropathological diagnosis, sensitivity and specificity of clinical DLB diagnosis were 75% and 42%. Sensitivity and specificity of DAT SPECT were 88% and 100%
O'Brien et al. (2009)	111	113	–	–	11	–	Of 19 possible DLB patients later diagnosed with probable DLB, 12 had abnormal scans at baseline (sensitivity 63%); all with AD at follow-up had normal scans (specificity 100%)
Siepel et al. (2016)	35	–	–	–	–	–	DAT uptake in putamen was associated with motor rigidity and executive functions
Walker et al. (2015b)	170[a]	–	–	–	–	–	SPECT imaging of DAT binding facilitated a more certain diagnosis at 8 and 24 weeks follow-up
Shimizu et al. (2016)	76	57	–	–	–	–	^{123}I-FP-CIT and MIBG myocardial scintigraphy are both diagnostically accurate, with their combination yielding even higher accuracy
Walker et al. (2016)	170[a]	–	–	–	–	–	UPDRS score increased in the abnormal scan group. Little evolution of other DLB features regardless of scan result
Iranzo et al. (2017)	–	–	–	–	87	20	RBD patients with abnormal DAT SPECT had increased risk of developing synucleinopathies in short term

(continued)

Table 17.4 (continued)

Study	Subjects						Findings in DLB
	DLB	AD	PD	PDD	Other	Control	
Kasanuki et al. (2017)	18 + 20[b]	10	–	–		–	DLB patients in all stages had severe DAT reduction compared to AD. In DLB, there was a negative correlation between DAT and parkinsonism
Kobayashi et al. (2017)	34	–	–	–	–	–	The combination of MIBG myocardial scintigraphy, perfusion SPECT and DAT SPECT correctly identified all DLB cases
Nicastro et al. (2017)	93	18	–	–	–	–	DAT uptake in striatum was lower in DLB than AD. Visual assessment had 97% sensitivity and semi-quantitative 98%. Combining both increased sensitivity to 100%
Shimizu et al. (2017c)	133	95	–	–	–	–	Both DaTView and DaTQUANT are useful in differentiating DLB from AD. Entire striatum was more useful than partial striatal regions
Shimizu et al. (2017a)	133	95	–	–	–	–	Parkinsonism severity correlated with striatal DAT uptake in DLB
Shimizu et al. (2017b)	32	32	–	–	–	–	DAT SPECT has the highest diagnostic accuracy for distinguishing DLB from AD, followed by MIBG
Thomas et al. (2017)	33	22	–	–	–	–	24 of 30 autopsy-confirmed DLB cases had abnormal scans (80% sensitivity). 23 of 25 non-DLB cases had normal imaging (92% specificity). Overall diagnostic accuracy was 86%
Hayashi et al. (2019)	10	39	15	–	28	7	Quantitative analysis of DAT-SPECT is affected by cerebral atrophy. Visual assessment remains crucial
Joling et al. (2019)	16	–	16	–	–	16	Loss of striatal DAT observed in both DLB and PD. DLB patients had lower hypothalamic SERT versus controls
Pilotto et al. (2019)	41	–	56	–	–	54	DLB and PD shared insular dopaminergic deficits, but only DLB had thalamic serotonergic impairment

Table 17.4 (continued)

Study	Subjects						Findings in DLB
	DLB	AD	PD	PDD	Other	Control	
Thomas et al. (2019)	48[b]	27[b]	–	–	–	–	DAT SPECT had high specificity for the prodromal stage of DLB and should be considered in clinical settings
^{18}F-fluorodopa PET							
Hu et al. (2000)	7	10	–	–	–	8	In the DLB group, K_i values were reduced in the caudate and putamen compared with AD
^{11}C-DTBZ or ^{18}F-AV-133 PET							
Koeppe et al. (2008)	25	25	30	–	–	57	In controls and AD, side-to-side asymmetry of striatal binding was less than in DLB and PD. The anterior-posterior gradient was steeper in DLB and PD
Siderowf et al. (2014)	11	10	5	–	–	5	Compared to controls and AD, VMAT2 density was lower in DLB and PD. VMAT2 density was associated with cognitive impairment in DLB
^{123}I-IBZM SPECT							
Walker et al. (1997)	16	13	–	–	–	15	DLB and PD patients had upregulation of postsynaptic D2 receptors in putamen and a marked decrease in binding sites in caudate
^{123}I-PE2I SPECT							
Ziebell et al. (2013)	51	–	–	–	–	28	No association between striatal DAT binding and DLB features
^{11}C-Altropane PET							
Marquie et al. (2014)	10	–	19	–	–	17	DAT concentration in putamen and caudate in PD and DLB lower than controls. Reduced DAT in caudate associated with worse global function and visual perception in DLB
Gomperts et al. (2016)	12	6	29	10	–	24	DAT in putamen could differentiate between DLB and AD. DAT in caudate could distinguish DLB from PD and was associated with functional impairment in DLB

[a]Possible DLB
[b]Prodromal stage

Table 17.5 PET and SPECT studies of cholinergic function in DLB

Study	Subjects					Findings in DLB
	DLB	AD	PD	PDD	Control	
Colloby et al. (2006)	14	–	25	–	24	Significant elevation of muscarinic ACh receptors in occipital lobe in DLB and PDD
O'Brien et al. (2008)	16	–	–	–	15	Reductions in frontal, striatal, temporal and cingulate binding. Elevated uptake in occipital cortex in DLB, more so in patients with VH
Shimada et al. (2009)	21[a]		18	–	26	Cholinergic dysfunction occurs in the medial occipital cortex
Shimada et al. (2015)	14	25	–	–	18	Cholinergic dysfunction in all regions in DLB, with diagnostic value for differentiating DLB from AD
Mazère et al. (2017)	11	–	–	–	12	There are cholinergic alterations in both cortical and subcortical regions in DLB. Cholinergic dysfunction in anterior cingulate associated with apathy

[a]Combined DLB and PDD

17.6.2 Imaging Acetylcholinesterase Activity

ACh that does not bind with a receptor or is released after reacting with a receptor is rapidly hydrolysed by AChE. One manifestation of cholinergic dysfunction in DLB is a reduction in AChE activity. Shimada and colleagues (2009) examined AChE activity amongst PD, PDD/DLB and age-matched controls using ^{11}C-labeled *N*-methyl-4-piperidyl-acetate (^{11}C-MP4A). They found that cholinergic dysfunction occurred in the cerebral cortex amongst the patient groups, with the medial occipital cortex showing more dysfunction in the PDD/DLB group. Additionally, lower AChE activity was associated with worse MMSE scores, suggesting that cholinergic deficits contribute to cognitive impairment in LB disorders.

In a subsequent study, the same authors scanned 14 DLB patients and 25 AD patients in addition to 18 healthy controls and scanned them with ^{11}C-MP4A and PET. AChE activity in the cortex was lower in both AD and DLB patients compared to controls. In DLB, the reduction was significant in all brain regions except for anterior cingulate gyri. The AD patients had significantly decreased activity compared to controls in the temporal cortex and posterior cingulate only. Lower AChE activity in the DLB relative to the AD group was observed in parietal, temporal and occipital regions of cortex, with the greatest difference in the posterior cingulate. The authors argued that cholinergic dysfunction in the posterior cingulate has high diagnostic value for distinguishing DLB from AD.

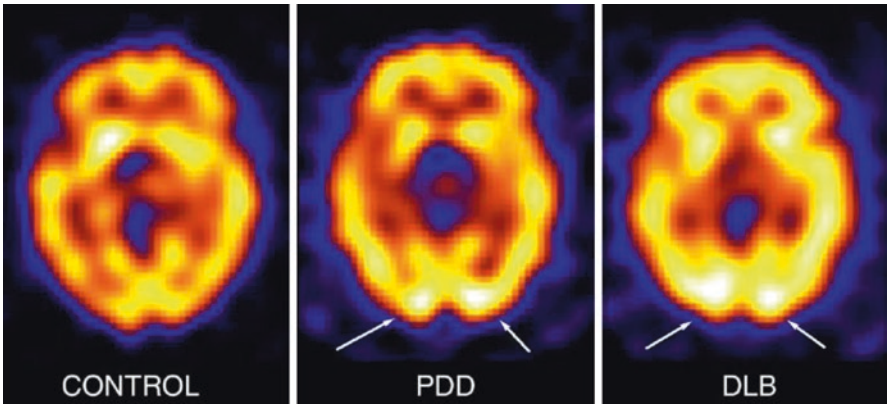

Fig. 17.8 Representative axial ^{123}I-QNB SPECT scans of an individual control, PDD and DLB patients. Notice the significant upregulation of ^{123}I-QNB binding in PDD and DLB relative to the control in the lingual and inferior occipital gyri (arrows). (Reproduced from Colloby et al. 2006 with permission from Elsevier)

17.6.3 Imaging Muscarinic Receptors

Colloby et al. (2006) scanned patients with ^{99m}Tc-exametazime and ^{123}iodo-quinuclidinyl benzilate (^{123}I-QNB) SPECT to investigate the relationship between rCBF and distribution of muscarinic acetylcholine (M1/M4) receptors. Comparisons were made between 14 DLB, 25 PDD and 24 age-matched controls. There was a significant elevation of ^{123}I-QNB binding in the right occipital lobe in DLB and right and left occipital lobes in PDD relative to controls (see Fig. 17.8). In addition, the PDD group uniquely showed significantly reduced uptake in frontal regions and bilateral temporal lobes. These patterns appeared to be independent of any corresponding rCBF changes. The higher binding in the occipital lobe may be related to visual disturbances in DLB.

17.6.4 Imaging Nicotinic Receptors

O'Brien and colleagues (2008) scanned 15 patients with DLB and 16 controls using ^{123}I-5IA-85380 and perfusion ^{99m}Tc-exametazime SPECT. The researchers examined in vivo differences in the distribution of α4β2 subtypes of nicotinic ACh receptors, as well as any possible association with perfusion. No relationship to perfusion was found. However, the ^{123}I-5IA-85380 results were consistent with previous post-mortem findings, as uptake was reduced in the frontal, striatal, temporal and cingulate regions in DLB relative to controls. However, there was elevation of uptake in occipital cortex in DLB, especially in patients with VH.

17.6.5 Conclusion

There is substantial evidence to support that cholinergic deficits are linked to cognitive deficits in LB disorders. Imaging the cholinergic system has shown that both AD and DLB have reduced AChE activity. This is more marked in DLB than in AD, and imaging the cholinergic dysfunction in the posterior cingulate could have some diagnostic value for distinguishing the two diseases. Imaging of nicotinic and muscarinic receptors suggests that there is upregulation in the occipital cortex and that this is related to VH in DLB.

17.7 Conclusion

New radiotracers are constantly being developed and tested, with recent studies also showing a continued role for well-established tracers. The most reliable finding from metabolic studies is the presence of occipital hypometabolism and relative preservation of the posterior cingulate cortex (the CIS). Amyloid imaging is becoming more established in the workup of dementia. Patients with DLB have higher amyloid tracer uptake than healthy controls but lower uptake than patients with AD. Likewise, imaging studies of DLB indicate that tau is intermediate between healthy and AD. The amount of amyloid and tau pathology in DLB suggests that in some cases specific disease-modifying drugs would be indicated where these become available.

The role of dopaminergic investigations has been further strengthened by autopsy studies showing that the most commonly used investigation of ^{123}I-FP-CIT SPECT is a reliable biomarker for degeneration of nigrostriatal neurons, which is typical for DLB and absent in AD. Research evaluating the utility of ^{123}I-FP-CIT SPECT in prodromal DLB is underway, though at present, the results are inconclusive.

There has been significant progress in the development of new ligands that capture inflammation in the brain in vivo. Preliminary research has given us some early insight about the role of inflammation in DLB. There is further evidence that cholinergic deficits have an important role in cognition in LB disorders with DLB having even more pronounced reduction of AChE activity than AD.

Dementia research is increasingly focused on prodromal disease phases, in order to facilitate early diagnosis and optimise therapeutic response. PET and SPECT studies have successfully identified diagnostic biomarkers that are sensitive and specific to the dementia stage of DLB. The emphasis of imaging studies at present is on the role of those biomarkers in prodromal disease.

References

Albin RL, Minoshima S, D'Amato CJ, Frey KA, Kuhl DA, Sima AA (1996) Fluoro-deoxyglucose positron emission tomography in diffuse Lewy body disease. Neurology 47(2):462–466

Atkinson J et al (2001) Biomarkers and surrogate endpoints: preferred definitions and conceptual framework. Clin Pharmacol Ther 69(3):89–95

Ballard C, Ziabreva I, Perry R, Larsen JP, O'Brien J, McKeith I et al (2006) Differences in neuropathologic characteristics across the Lewy body dementia spectrum. Neurology 67(11):1931–1934. https://doi.org/10.1212/01.wnl.0000249130.63615.cc

Banati RB, Newcombe J, Gunn RN, Cagnin A, Turkheimer F, Heppner F et al (2000) The peripheral benzodiazepine binding site in the brain in multiple sclerosis: quantitative in vivo imaging of microglia as a measure of disease activity. Brain 123(11):2321–2337. https://doi.org/10.1093/brain/123.11.2321

Barbas NR (2006) Cognitive, affective, and psychiatric features of Parkinson's disease. Clin Geriatr Med 22(4):773–796. https://doi.org/10.1016/j.cger.2006.06.004

Bohnen NI, Minoshima S, Giordani B, Frey KA, Kuhl DE (1999) Motor correlates of occipital glucose hypometabolism in Parkinson's disease without dementia. Neurology 52(3):541. https://doi.org/10.1212/wnl.52.3.541

Brooks DJ (1993) Functional imaging in relation to parkinsonian syndromes. J Neurol Sci 115(1):1–17. https://doi.org/10.1016/0022-510X(93)90061-3

Caminiti SP, Alongi P, Majno L, Volontè MA, Cerami C, Gianolli L et al (2017) Evaluation of an optimized [18F]fluoro-deoxy-glucose positron emission tomography voxel-wise method to early support differential diagnosis in atypical Parkinsonian disorders. Eur J Neurol 24(5):687–e26. https://doi.org/10.1111/ene.13269

Caminiti SP, Sala A, Iaccarino L, Beretta L, Pilotto A, Gianolli L et al (2019) Brain glucose metabolism in Lewy body dementia: implications for diagnostic criteria. Alzheimers Res Ther 11(1):20. https://doi.org/10.1186/s13195-019-0473-4

Cerami C, Iaccarino L, Perani D (2017) Molecular imaging of neuroinflammation in neurodegenerative dementias: the role of in vivo PET imaging. Int J Mol Sci 18(5):993

Colloby SJ, Williams ED, Burn DJ, Lloyd JJ, McKeith IG, O'Brien JT (2005) Progression of dopaminergic degeneration in dementia with Lewy bodies and Parkinson's disease with and without dementia assessed using 123I-FP-CIT SPECT. Eur J Nucl Med Mol Imaging 32(10):1176–1185. https://doi.org/10.1007/s00259-005-1830-z

Colloby SJ, Pakrasi S, Firbank MJ, Perry EK, Piggott MA, Owens J et al (2006) In vivo SPECT imaging of muscarinic acetylcholine receptors using (R,R) 123I-QNB in dementia with Lewy bodies and Parkinson's disease dementia. NeuroImage 33(2):423–429. https://doi.org/10.1016/j.neuroimage.2006.07.026

Colloby SJ, McParland S, O'Brien JT, Attems J (2012) Neuropathological correlates of dopaminergic imaging in Alzheimer's disease and Lewy body dementias. Brain 135(9):2798–2808. https://doi.org/10.1093/brain/aws211

Donaghy PC, Firbank MJ, Thomas AJ, Lloyd J, Petrides G, Barnett N et al (2018) Clinical and imaging correlates of amyloid deposition in dementia with Lewy bodies. Mov Disord 33(7):1130–1138. https://doi.org/10.1002/mds.27403

Edison P, Rowe CC, Rinne JO, Ng S, Ahmed I, Kemppainen N et al (2008) Amyloid load in Parkinson's disease dementia and Lewy body dementia measured with [11C]PIB positron emission tomography. J Neurol Neurosurg Psychiatry 79(12):1331–1338. https://doi.org/10.1136/jnnp.2007.127878

Eikelenboom P, Stam FC (1982) Immunoglobulins and complement factors in senile plaques. Acta Neuropathol 57(2):239–242. https://doi.org/10.1007/BF00685397

Eikelenboom P, Veerhuis R (1996) The role of complement and activated microglia in the pathogenesis of Alzheimer's disease. Neurobiol Aging 17(5):673–680

Filippi M, Agosta F, Barkhof F, Dubois B, Fox NC, Frisoni GB et al (2012) EFNS task force: the use of neuroimaging in the diagnosis of dementia. Eur J Neurol 19(12):1487–1501. https://doi.org/10.1111/j.1468-1331.2012.03859.x

Firbank MJ, Lloyd J, O'Brien JT (2016) The relationship between hallucinations and FDG-PET in dementia with Lewy bodies. Brain Imaging Behav 10(3):636–639. https://doi.org/10.1007/s11682-015-9434-0

Francis PT, Perry EK (2007) Cholinergic and other neurotransmitter mechanisms in Parkinson's disease, Parkinson's disease dementia, and dementia with Lewy bodies. Mov Disord 22(S17):S351–S3S7. https://doi.org/10.1002/mds.21683

Galasko D, Katzman R, Salmon DP, Hansen L (1996) Clinical and neuropathological findings in Lewy body dementias. Brain Cogn 31(2):166–175. https://doi.org/10.1006/brcg.1996.0040

Gnanalingham KK, Byrne EJ, Thornton A, Sambrook MA, Bannister P (1997) Motor and cognitive function in Lewy body dementia: comparison with Alzheimer's and Parkinson's diseases. J Neurol Neurosurg Psychiatry 62(3):243–252. https://doi.org/10.1136/jnnp.62.3.243

Gómez-Tortosa E, Gonzalo I, Fanjul S, Sainz MJ, Cantarero S, Cemillán C et al (2003) Cerebrospinal fluid markers in dementia with Lewy bodies compared with Alzheimer disease. JAMA Neurol 60(9):1218–1222. https://doi.org/10.1001/archneur.60.9.1218

Gomperts SN, Locascio JJ, Marquie M, Santarlasci AL, Rentz DM, Maye J et al (2012) Brain amyloid and cognition in Lewy body diseases. Mov Disord 27(8):965–973. https://doi.org/10.1002/mds.25048

Gomperts SN, Marquie M, Locascio JJ, Bayer S, Johnson KA, Growdon JH (2016) PET radioligands reveal the basis of dementia in Parkinson's disease and dementia with Lewy bodies. Neurodegener Dis 16(1–2):118–124. https://doi.org/10.1159/000441421

Graff-Radford J, Murray ME, Lowe VJ, Boeve BF, Ferman TJ, Przybelski SA et al (2014) Dementia with Lewy bodies: basis of cingulate island sign. Neurology 83(9):801–809. https://doi.org/10.1212/WNL.0000000000000734

Hayashi T, Mishina M, Sakamaki M, Sakamoto Y, Suda S, Kimura K (2019) Effect of brain atrophy in quantitative analysis of 123I-ioflupane SPECT. Ann Nucl Med 33(8):579–585. https://doi.org/10.1007/s12149-019-01367-4

Higuchi M, Tashiro M, Arai H, Okamura N, Hara S, Higuchi S et al (2000) Glucose hypometabolism and neuropathological correlates in brains of dementia with Lewy bodies. Exp Neurol 162(2):247–256. https://doi.org/10.1006/exnr.2000.7342

Hirohata M, Ono K, Morinaga A, Yamada M (2008) Non-steroidal anti-inflammatory drugs have potent anti-fibrillogenic and fibril-destabilizing effects for α-synuclein fibrils in vitro. Neuropharmacology 54(3):620–627. https://doi.org/10.1016/j.neuropharm.2007.11.010

Hu XS, Okamura N, Arai H, Higuchi M, Matsui T, Tashiro M et al (2000) ^{18}F-fluorodopa PET study of striatal dopamine uptake in the diagnosis of dementia with Lewy bodies. Neurology 55(10):1575–1577. https://doi.org/10.1212/wnl.55.10.1575

Huang S-H, Chang C-C, Lui C-C, Chen N-C, Lee C-C, Wang P-W et al (2015) Cortical metabolic and nigrostriatal abnormalities associated with clinical stage-specific dementia with Lewy bodies. Clin Nucl Med 40(1):26–31. https://doi.org/10.1097/rlu.0000000000000620

Iaccarino L, Marelli S, Iannaccone S, Magnani G, Ferini-Strambi L, Perani D (2016) Severe brain metabolic decreases associated with REM sleep behavior disorder in dementia with Lewy bodies. J Alzheimers Dis 52:989–997

Iaccarino L, Sala A, Caminiti SP, Santangelo R, Iannaccone S, Magnani G et al (2018) The brain metabolic signature of visual hallucinations in dementia with Lewy bodies. Cortex 108:13–24. https://doi.org/10.1016/j.cortex.2018.06.014

Iizuka T, Kameyama M (2016) Cingulate island sign on FDG-PET is associated with medial temporal lobe atrophy in dementia with Lewy bodies. Ann Nucl Med 30(6):421–429. https://doi.org/10.1007/s12149-016-1076-9

Imamura T, Ishii K, Hirono N, Hashimoto M, Tanimukai S, Kazui H et al (2001) Occipital glucose metabolism in dementia with Lewy bodies with and without parkinsonism: a study using positron emission tomography. Dement Geriatr Cogn Disord 12(3):194–197. https://doi.org/10.1159/000051257

Iranzo A, Santamaría J, Valldeoriola F, Serradell M, Salamero M, Gaig C et al (2017) Dopamine transporter imaging deficit predicts early transition to synucleinopathy in idiopathic rapid eye movement sleep behavior disorder. Ann Neurol 82(3):419–428. https://doi.org/10.1002/ana.25026

Ishii K, Imamura T, Sasaki M, Yamaji S, Kitagaki H, Hashimoto M et al (1998) Regional cerebral glucose metabolism in dementia with Lewy bodies and Alzheimer's disease. Neurology 51(1):125–130

Ishii K, Soma T, Kono AK, Sofue K, Miyamoto N, Yoshikawa T et al (2007) Comparison of regional brain volume and glucose metabolism between patients with mild dementia with Lewy bodies and those with mild Alzheimer's disease. J Nucl Med 48:704–711

Ishii K, Hosokawa C, Hyodo T, Sakaguchi K, Usami K, Shimamoto K et al (2015) Regional glucose metabolic reduction in dementia with Lewy bodies is independent of amyloid deposition. Ann Nucl Med 29(1):78–83. https://doi.org/10.1007/s12149-014-0911-0

Jack CR Jr, Wiste HJ, Botha H, Weigand SD, Therneau TM, Knopman DS et al (2019) The bivariate distribution of amyloid-β and tau: relationship with established neurocognitive clinical syndromes. Brain 142(10):3230–3242. https://doi.org/10.1093/brain/awz268

Jia J, Hu J, Huo X, Miao R, Zhang Y, Ma F (2019) Effects of vitamin D supplementation on cognitive function and blood Aβ-related biomarkers in older adults with Alzheimer's disease: a randomised, double-blind, placebo-controlled trial. J Neurol Neurosurg Psychiatry 90(12):1347–1352. https://doi.org/10.1136/jnnp-2018-320199

Joling M, Vriend C, van der Zande JJ, Lemstra AW, van den Heuvel OA, Booij J et al (2018) Lower 123I-FP-CIT binding to the striatal dopamine transporter, but not to the extrastriatal serotonin transporter, in Parkinson's disease compared with dementia with Lewy bodies. NeuroImage Clin 19:130–136. https://doi.org/10.1016/j.nicl.2018.04.009

Joling M, Vriend C, Raijmakers PGHM, van der Zande JJ, Lemstra AW, Berendse HW et al (2019) Striatal DAT and extrastriatal SERT binding in early-stage Parkinson's disease and dementia with Lewy bodies, compared with healthy controls: an 123I-FP-CIT SPECT study. NeuroImage Clin 22:101755. https://doi.org/10.1016/j.nicl.2019.101755

Kantarci K, Lowe VJ, Boeve BF, Weigand SD, Senjem ML, Przybelski SA et al (2012) Multimodality imaging characteristics of dementia with Lewy bodies. Neurobiol Aging 33(9):2091–2105. https://doi.org/10.1016/j.neurobiolaging.2011.09.024

Kantarci K, Lowe VJ, Boeve BF, Senjem ML, Tosakulwong N, Lesnick TG et al (2017) AV-1451 tau and beta-amyloid positron emission tomography imaging in dementia with Lewy bodies. Ann Neurol 81(1):58–67. https://doi.org/10.1002/ana.24825

Kasanuki K, Iseki E, Ota K, Kondo D, Ichimiya Y, Sato K et al (2017) 123I-FP-CIT SPECT findings and its clinical relevance in prodromal dementia with Lewy bodies. Eur J Nucl Med Mol Imaging 44(3):358–365. https://doi.org/10.1007/s00259-016-3466-6

Klunk WE, Engler H, Nordberg A, Wang Y, Blomqvist G, Holt DP et al (2004) Imaging brain amyloid in Alzheimer's disease with Pittsburgh compound-B. Ann Neurol 55(3):306–319. https://doi.org/10.1002/ana.20009

Kobayashi S, Makino K, Hatakeyama S, Ishii T, Tateno M, Iwamoto T et al (2017) The usefulness of combined brain perfusion single-photon emission computed tomography, dopamine-transporter single-photon emission computed tomography, and 123I-metaiodobenzylguanidine myocardial scintigraphy for the diagnosis of dementia with Lewy bodies. Psychogeriatrics 17(4):247–255. https://doi.org/10.1111/psyg.12227

Koeppe RA, Gilman S, Junck L, Wernette K, Frey KA (2008) Differentiating Alzheimer's disease from dementia with Lewy bodies and Parkinson's disease with (+)-[11C]dihydrotetrabenazine positron emission tomography. Alzheimers Dement 4(1 Suppl 1):S67–S76. https://doi.org/10.1016/j.jalz.2007.11.016

Lee SH, Cho H, Choi JY, Lee JH, Ryu YH, Lee MS et al (2018) Distinct patterns of amyloid-dependent tau accumulation in Lewy body diseases. Mov Disord 33(2):262–272. https://doi.org/10.1002/mds.27252

Liguori C, Ruffini R, Olivola E, Chiaravalloti A, Izzi F, Stefani A et al (2019) Cerebral glucose metabolism in idiopathic REM sleep behavior disorder is different from tau-related and α-synuclein-related neurodegenerative disorders: a brain [18F]FDG PET study. Parkinsonism Relat Disord 64:97–105. https://doi.org/10.1016/j.parkreldis.2019.03.017

Lim S, Katsifis A, Villemagne V, Best R, Jones G, Saling M et al (2009) The 18F-FDG PET cingulate island sign and comparison to 123I-beta-CIT SPECT for diagnosis of dementia with Lewy bodies. J Nucl Med 50(10):1638–1645

Lockhart A, Lamb JR, Osredkar T, Sue LI, Joyce JN, Ye L et al (2007) PIB is a non-specific imaging marker of amyloid-beta (Aβ) peptide-related cerebral amyloidosis. Brain 130(10):2607–2615. https://doi.org/10.1093/brain/awm191

Mackenzie IRA (2000) Activated microglia in dementia with Lewy bodies. Neurology 55(1):132–134. https://doi.org/10.1212/wnl.55.1.132

Maetzler W, Liepelt I, Reimold M, Reischl G, Solbach C, Becker C et al (2009) Cortical PIB binding in Lewy body disease is associated with Alzheimer-like characteristics. Neurobiol Dis 34(1):107–112. https://doi.org/10.1016/j.nbd.2008.12.008

Mak E, Donaghy PC, McKiernan E, Firbank MJ, Lloyd J, Petrides GS et al (2019) Beta amyloid deposition maps onto hippocampal and subiculum atrophy in dementia with Lewy bodies. Neurobiol Aging 73:74–81. https://doi.org/10.1016/j.neurobiolaging.2018.09.004

Marquie M, Locascio JJ, Rentz DM, Becker JA, Hedden T, Johnson KA et al (2014) Striatal and extrastriatal dopamine transporter levels relate to cognition in Lewy body diseases: an 11C altropane positron emission tomography study. Alzheimers Res Ther 6(5):52. https://doi.org/10.1186/s13195-014-0052-7

Mazère J, Lamare F, Allard M, Fernandez P, Mayo W (2017) 123I-Iodobenzovesamicol SPECT imaging of cholinergic systems in dementia with Lewy bodies. J Nucl Med 58:123–128

McGeer PL, Akiyama H, Itagaki S, McGeer EG (1989) Activation of the classical complement pathway in brain tissue of Alzheimer patients. Neurosci Lett 107(1):341–346. https://doi.org/10.1016/0304-3940(89)90843-4

McKeith IGGD, Kosaka K, Perry EK, Dickson DW, Hansen LA, Salmon DP et al (1996) Consensus guidelines for the clinical and pathological diagnosis of dementia with Lewy bodies (DLB): report of the consortium on DLB international workshop. Neurology 47(5):1113–1124

McKeith IG, Perry EK, Perry RH (1999) Report of the second dementia with Lewy body international workshop. Diagnosis and treatment. Neurology 53(5):902–905. https://doi.org/10.1212/wnl.53.5.902

McKeith I, Mintzer J, Aarsland D, Burn D, Chiu H, Cohen-Mansfield J et al (2004) Dementia with Lewy bodies. Lancet Neurol 3(1):19–28. https://doi.org/10.1016/S1474-4422(03)00619-7

McKeith IG, Dickson DW, Lowe J, Emre M, O'Brien JT, Feldman H et al (2005) Diagnosis and management of dementia with Lewy bodies. Third report of the DLB Consortium. Neurology 65(12):1863–1872. https://doi.org/10.1212/01.wnl.0000187889.17253.b1

McKeith I, O'Brien J, Walker Z, Tatsch K, Booij J, Darcourt J et al (2007) Sensitivity and specificity of dopamine transporter imaging with 123I-FP-CIT SPECT in dementia with Lewy bodies: a phase III, multicentre study. Lancet Neurol 6(4):305–313. https://doi.org/10.1016/S1474-4422(07)70057-1

McKeith IG, Boeve BF, Dickson DW, Halliday G, Taylor J-P, Weintraub D et al (2017) Diagnosis and management of dementia with Lewy bodies. Fourth consensus report of the DLB Consortium. Neurology 89(1):88–100. https://doi.org/10.1212/wnl.0000000000004058

Morbelli S, Chincarini A, Brendel M, Rominger A, Bruffaerts R, Vandenberghe R et al (2019) Metabolic patterns across core features in dementia with Lewy bodies. Ann Neurol 85(5):715–725. https://doi.org/10.1002/ana.25453

Morgan S, Kemp P, Booij J, Costa DC, Padayachee S, Lee L et al (2012) Differentiation of frontotemporal dementia from dementia with Lewy bodies using FP-CIT SPECT. J Neurol Neurosurg Psychiatry 83(11):1063–1070. https://doi.org/10.1136/jnnp-2012-302577

Mosconi L, Tsui WH, Herholz K, Pupi A, Drzezga A, Lucignani G et al (2008) Multicenter standardized 18F-FDG PET diagnosis of mild cognitive impairment, Alzheimer's disease, and other dementias. J Nucl Med 49(3):390–398. https://doi.org/10.2967/jnumed.107.045385

Nedelska Z, Schwarz CG, Boeve BF, Lowe VJ, Reid RI, Przybelski SA et al (2015) White matter integrity in dementia with Lewy bodies: a voxel-based analysis of diffusion tensor imaging. Neurobiol Aging 36(6):2010–2017. https://doi.org/10.1016/j.neurobiolaging.2015.03.007

Nedelska Z, Josephs KA, Graff-Radford J, Przybelski SA, Lesnick TG, Boeve BF et al (2019) 18F-AV-1451 uptake differs between dementia with Lewy bodies and posterior cortical atrophy. Mov Disord 34(3):344–352. https://doi.org/10.1002/mds.27603

Nestor PJ, Altomare D, Festari C, Drzezga A, Rivolta J, Walker Z et al (2018) Clinical utility of FDG-PET for the differential diagnosis among the main forms of dementia. Eur J Nucl Med Mol Imaging 45(9):1509–1525. https://doi.org/10.1007/s00259-018-4035-y

Neuropathology Group. Medical Research Council Cognitive Function and Aging Study (2001) Pathological correlates of late-onset dementia in a multicentre, community-based population in England and Wales. Neuropathology Group of the Medical Research Council Cognitive Function and Ageing Study (MRC CFAS). Lancet 357(9251):169–175. https://doi.org/10.1016/s0140-6736(00)03589-3

Nicastro N, Garibotto V, Allali G, Assal F, Burkhard PR (2017) Added value of combined semi-quantitative and visual [123I]FP-CIT SPECT analyses for the diagnosis of dementia with Lewy bodies. Clin Nucl Med 42(2):e96–e102. https://doi.org/10.1097/rlu.0000000000001477

O'Brien JT, Colloby S, Fenwick J, Williams ED, Firbank M, Burn D et al (2004) Dopamine transporter loss visualized with FP-CIT SPECT in the differential diagnosis of dementia with Lewy bodies. JAMA Neurol 61(6):919–925. https://doi.org/10.1001/archneur.61.6.919

O'Brien JT, Colloby SJ, Pakrasi S, Perry EK, Pimlott SL, Wyper DJ et al (2008) Nicotinic α4β2 receptor binding in dementia with Lewy bodies using 123I-5IA-85380 SPECT demonstrates a link between occipital changes and visual hallucinations. NeuroImage 40(3):1056–1063. https://doi.org/10.1016/j.neuroimage.2008.01.010

O'Brien JT, McKeith IG, Walker Z, Tatsch K, Booij J, Darcourt J et al (2009) Diagnostic accuracy of 123I-FP-CIT SPECT in possible dementia with Lewy bodies. Br J Psychiatry 194(1):34–39. https://doi.org/10.1192/bjp.bp.108.052050

O'Brien JT, Firbank MJ, Davison C, Barnett N, Bamford C, Donaldson C et al (2014) 18F-FDG PET and perfusion SPECT in the diagnosis of Alzheimer and Lewy body dementias. J Nucl Med 55:1959–1965

Okello A, Edison P, Archer HA, Turkheimer FE, Kennedy J, Bullock R et al (2009) Microglial activation and amyloid deposition in mild cognitive impairment. A PET study. Neurology 72(1):56–62. https://doi.org/10.1212/01.wnl.0000338622.27876.0d

Okizaki A, Nakayama M, Nakajima K, Katayama T, Uno T, Morikawa F et al (2017) Inter- and intra-observer reproducibility of quantitative analysis for FP-CIT SPECT in patients with DLB. Ann Nucl Med 31(10):758–763. https://doi.org/10.1007/s12149-017-1209-9

Perry EK, Irving D, Kerwin JM, McKeith IG, Thompson P, Collerton D et al (1993) Cholinergic transmitter and neurotrophic activities in Lewy body dementia: similarity to Parkinson's and distinction from Alzheimer disease. Alzheimer Dis Assoc Disord 7(2):69–79

Perry E, Walker M, Grace J, Perry R (1999) Acetylcholine in mind: a neurotransmitter correlate of consciousness? Trends Neurosci 22(6):273–280. https://doi.org/10.1016/S0166-2236(98)01361-7

Piggott MA, Marshall EF, Thomas N, Lloyd S, Court JA, Jaros E et al (1999) Striatal dopaminergic markers in dementia with Lewy bodies, Alzheimer's and Parkinson's diseases: rostrocaudal distribution. Brain 122(8):1449–1468. https://doi.org/10.1093/brain/122.8.1449

Pilotto A, Schiano di Cola F, Premi E, Grasso R, Turrone R, Gipponi S et al (2019) Extrastriatal dopaminergic and serotonergic pathways in Parkinson's disease and in dementia with Lewy bodies: a 123I-FP-CIT SPECT study. Eur J Nucl Med Mol Imaging 46(8):1642–1651. https://doi.org/10.1007/s00259-019-04324-5

Plotkin M, Amthauer H, Klaffke S, Kühn A, Lüdemann L, Arnold G et al (2005) Combined 123I-FP-CIT and 123I-IBZM SPECT for the diagnosis of parkinsonian syndromes: study on 72 patients. J Neural Transm 112(5):677–692. https://doi.org/10.1007/s00702-004-0208-x

Power JHT, Blumbergs PC (2009) Cellular glutathione peroxidase in human brain: cellular distribution, and its potential role in the degradation of Lewy bodies in Parkinson's disease and dementia with Lewy bodies. Acta Neuropathol 117(1):63–73. https://doi.org/10.1007/s00401-008-0438-3

Price JL, Morris JC (1999) Tangles and plaques in nondemented aging and "preclinical" Alzheimer's disease. Ann Neurol 45(3):358–368. https://doi.org/10.1002/1531-8249(199903)45:3<358::AID-ANA12>3.0.CO;2-X

Roselli F, Pisciotta NM, Perneczky R, Pennelli M, Aniello MS, De Caro MF et al (2009) Severity of neuropsychiatric symptoms and dopamine transporter levels in dementia with Lewy bodies: a 123I-FP-CIT SPECT study. Mov Disord 24(14):2097–2103. https://doi.org/10.1002/mds.22702

Rowe CC, Ng S, Ackermann U, Gong SJ, Pike K, Savage G et al (2007) Imaging β-amyloid burden in aging and dementia. Neurology 68(20):1718–1725. https://doi.org/10.1212/01.wnl.0000261919.22630.ea

Sala A, Caminiti SP, Iaccarino L, Beretta L, Iannaccone S, Magnani G et al (2019) Vulnerability of multiple large-scale brain networks in dementia with Lewy bodies. Hum Brain Mapp 40(15):4537–4550. https://doi.org/10.1002/hbm.24719

Samuel W, Alford M, Hofstetter CR, Hansen L (1997) Dementia with Lewy bodies versus pure Alzheimer disease: differences in cognition, neuropathology, cholinergic dysfunction, and synapse density. J Neuropathol Exp Neurol 56(5):499–508. https://doi.org/10.1097/00005072-199705000-00006

Sarro L, Senjem ML, Lundt ES, Przybelski SA, Lesnick TG, Graff-Radford J et al (2016) Amyloid-β deposition and regional grey matter atrophy rates in dementia with Lewy bodies. Brain 139(10):2740–2750. https://doi.org/10.1093/brain/aww193

Shepherd CE, Thiel E, McCann H, Harding AJ, Halliday GM (2000) Cortical inflammation in Alzheimer disease but not dementia with Lewy bodies. JAMA Neurol 57(6):817–822. https://doi.org/10.1001/archneur.57.6.817

Shimada H, Hirano S, Shinotoh H, Aotsuka A, Sato K, Tanaka N et al (2009) Mapping of brain acetylcholinesterase alterations in Lewy body disease by PET. Neurology 73(4):273–278. https://doi.org/10.1212/WNL.0b013e3181ab2b58

Shimada H, Hirano S, Sinotoh H, Ota T, Tanaka N, Sato K et al (2015) Dementia with Lewy bodies can be well-differentiated from Alzheimer's disease by measurement of brain acetylcholinesterase activity—a [11C]MP4A PET study. Int J Geriatr Psychiatry 30(11):1105–1113. https://doi.org/10.1002/gps.4338

Shimizu S, Hirao K, Kanetaka H, Namioka N, Hatanaka H, Hirose D et al (2016) Utility of the combination of DAT SPECT and MIBG myocardial scintigraphy in differentiating dementia with Lewy bodies from Alzheimer's disease. Eur J Nucl Med Mol Imaging 43(1):184–192. https://doi.org/10.1007/s00259-015-3146-y

Shimizu S, Hirose D, Namioka N, Kanetaka H, Hirao K, Hatanaka H et al (2017a) Correlation between clinical symptoms and striatal DAT uptake in patients with DLB. Ann Nucl Med 31(5):390–398. https://doi.org/10.1007/s12149-017-1166-3

Shimizu S, Kanetaka H, Hirao K, Fukasawa R, Namioka N, Hatanaka H et al (2017b) Neuroimaging for diagnosing dementia with Lewy bodies: what is the best neuroimaging technique in discriminating dementia with Lewy bodies from Alzheimer's disease? Geriatr Gerontol Int 17(5):819–824. https://doi.org/10.1111/ggi.12794

Shimizu S, Namioka N, Hirose D, Kanetaka H, Hirao K, Hatanaka H et al (2017c) Comparison of diagnostic utility of semi-quantitative analysis for DAT-SPECT for distinguishing DLB from AD. J Neurol Sci 377:50–54. https://doi.org/10.1016/j.jns.2017.03.040

Shirvan J, Clement N, Ye R, Katz S, Schultz A, Johnson KA et al (2019) Neuropathologic correlates of amyloid and dopamine transporter imaging in Lewy body disease. Neurology 93(5):e476–ee84. https://doi.org/10.1212/wnl.0000000000007855

Siderowf A, Pontecorvo MJ, Shill HA, Mintun MA, Arora A, Joshi AD et al (2014) PET imaging of amyloid with Florbetapir F18 and PET imaging of dopamine degeneration with 18F-AV-133 (florbenazine) in patients with Alzheimer's disease and Lewy body disorders. BMC Neurol 14:79. https://doi.org/10.1186/1471-2377-14-79

Siepel FJ, Dalen I, Grüner R, Booij J, Brønnick KS, Buter TC et al (2016) Loss of dopamine transporter binding and clinical symptoms in dementia with Lewy bodies. Mov Disord 31(1):118–125. https://doi.org/10.1002/mds.26327

Surendranathan A, Su L, Mak E, Passamonti L, Hong YT, Arnold R et al (2018) Early microglial activation and peripheral inflammation in dementia with Lewy bodies. Brain 141(12):3415–3427. https://doi.org/10.1093/brain/awy265

Szpak GM, Lechowicz W, Lewandowska E, Bertrand E, Wierzba-Bobrowicz T, Gwiazda E et al (2001) Neurones and microglia in central nervous system immune response to degenerative processes. Part 1: Alzheimer's disease and Lewy body variant of Alzheimer's disease. Quantitative study. Folia Neuropathol 39(3):181–192

Thomas AJ, Attems J, Colloby SJ, O'Brien JT, McKeith I, Walker R et al (2017) Autopsy validation of 123I-FP-CIT dopaminergic neuroimaging for the diagnosis of DLB. Neurology 88(3):276–283. https://doi.org/10.1212/WNL.0000000000003512

Thomas AJ, Donaghy P, Roberts G, Colloby SJ, Barnett NA, Petrides G et al (2019) Diagnostic accuracy of dopaminergic imaging in prodromal dementia with Lewy bodies. Psychol Med 49(3):396–402. https://doi.org/10.1017/S0033291718000995

Tiraboschi P, Hansen LA, Alford M, Sabbagh MN, Schoos B, Masliah E et al (2000) Cholinergic dysfunction in diseases with Lewy bodies. Neurology 54(2):407. https://doi.org/10.1212/wnl.54.2.407

Villemagne VL, Ong K, Mulligan RS, Holl G, Pejoska S, Jones G et al (2011) Amyloid imaging with (18)F-florbetaben in Alzheimer disease and other dementias. J Nucl Med 52(8):1210–1217

Walker Z, Rodda J (2011) Dopaminergic imaging: clinical utility now and in the future. Int Psychogeriatr 23(S2):S32–S40. https://doi.org/10.1017/S1041610211000883

Walker RWH, Walker Z (2009) Dopamine transporter single photon emission computerized tomography in the diagnosis of dementia with Lewy bodies. Mov Disord 24(S2):S754–S7S9. https://doi.org/10.1002/mds.22591

Walker Z, Costa DC, Janssen AG, Walker RWH, Livingstone G, Katona CLE (1997) Dementia with Lewy bodies: a study of post-synaptic dopaminergic receptors with iodine-123 iodobenzamide single-photon mission tomography. Eur J Nucl Med 24(6):609–614. https://doi.org/10.1007/BF00841397

Walker Z, Costa DC, Walker RWH, Shaw K, Gacinovic S, Stevens T et al (2002) Differentiation of dementia with Lewy bodies from Alzheimer's disease using a dopaminergic presynaptic ligand. J Neurol Neurosurg Psychiatry 73(2):134–140. https://doi.org/10.1136/jnnp.73.2.134

Walker Z, Costa DC, Walker RWH, Lee L, Livingston G, Jaros E et al (2004) Striatal dopamine transporter in dementia with Lewy bodies and Parkinson disease. A comparison. Neurology 62(9):1568–1572. https://doi.org/10.1212/01.wnl.0000123248.39847.1d

Walker Z, Jaros E, Walker RWH, Lee L, Costa DC, Livingston G et al (2007) Dementia with Lewy bodies: a comparison of clinical diagnosis, FP-CIT single photon emission computed tomography imaging and autopsy. J Neurol Neurosurg Psychiatry 78(11):1176–1181. https://doi.org/10.1136/jnnp.2006.110122

Walker Z, Possin KL, Boeve BF, Aarsland D (2015a) Lewy body dementias. Lancet 386(10004):1683–1697. https://doi.org/10.1016/S0140-6736(15)00462-6

Walker Z, Moreno E, Thomas A, Inglis F, Tabet N, Rainer M et al (2015b) Clinical usefulness of dopamine transporter SPECT imaging with 123I-FP-CIT in patients with possible dementia with Lewy bodies: randomised study. Br J Psychiatry 206(2):145–152. https://doi.org/10.1192/bjp.bp.114.148643

Walker Z, Moreno E, Thomas A, Inglis F, Tabet N, Stevens T et al (2016) Evolution of clinical features in possible DLB depending on FP-CIT SPECT result. Neurology 87(10):1045–1051. https://doi.org/10.1212/WNL.0000000000003076

Whitwell JL, Graff-Radford J, Singh TD, Drubach DA, Senjem ML, Spychalla AJ et al (2017) (18)F-FDG PET in posterior cortical atrophy and dementia with Lewy bodies. J Nucl Med 58(4):632–638. https://doi.org/10.2967/jnumed.116.179903

Zheng G, Dwoskin LP, Crooks PA (2006) Vesicular monoamine transporter 2: role as a novel target for drug development. AAPS J 8(4):E682–EE92. https://doi.org/10.1208/aapsj080478

Ziebell M, Andersen BB, Pinborg LH, Knudsen GM, Stokholm J, Thomsen G et al (2013) Striatal dopamine transporter binding does not correlate with clinical severity in dementia with Lewy bodies. J Nucl Med 54:1072–1076

SPECT and PET in Vascular Dementia

18

Yumin Zheng and Zhi Zhou

Contents

18.1 Introduction 564
18.2 SPECT 567
18.2.1 Tracers of SPECT 567
18.3 PET 568
18.3.1 Tracers of PET 568
References 571

Abstract

Vascular cognitive impairment (VCI) refers to the entire form of cognitive decline (from subjective cognitive decline to dementia) caused by the brain vascular pathology. Neuroimaging plays an important role in the diagnosis of VCI. Positron emission tomography (PET) and single photon emission computed tomography (SPECT) are widely used in the evaluation of the metabolism and perfusion change in VCI. Recent advancements in molecular imaging allow the in vivo visualization of deposition of abnormal proteins, including amyloid β and tau. In this chapter, we will briefly describe the characteristics of commonly used radio ligand tracers in VCI. And we will discuss the utility of PET and SPECT in the clinical and research field of VCI.

Y. Zheng
Department of Nuclear Medicine, China-Japan Friendship Hospital, Beijing, China

Z. Zhou (✉)
Department of Neurology, China-Japan Friendship Hospital, Beijing, China

R. A. J. O. Dierckx et al. (eds.), *PET and SPECT in Neurology*,
https://doi.org/10.1007/978-3-030-53168-3_18

Abbreviations

AD	Alzheimer's disease
aMCI	Amnestic mild cognitive impairment
Aβ	Amyloid β
CBD	Corticobasal degeneration
CBF	Cerebral blood flow
CBV	Cerebral blood volume
DLB	Dementia with Lewy bodies
ECD	Ethyl-cysteinate-dimer
FDG	Fluoro-deoxy-glucose
FTLD	Frontotemporal lobar degeneration
HMPAO	Hexa methyl propyleneamine oxime
IMP	I-Isopropylamphetamine
MRI	Magnetic resonance imaging
NFT	Neurofibrillary tangles
OEF	Oxygen extraction fraction
PET	Positron emission tomography
PIB	Pittsburgh compound B
PSD	Post stroke dementia
PSP	Progressive supranuclear palsy
rCMRGlc	Regional cerebral metabolic rate for glucose
$rCMRO_2$	Regional cerebral metabolic rate for oxygen
SPECT	Single-photon emission computed tomography
SVCI	Subcortical vascular cognitive impairment
VaD	Vascular dementia
VBM	Voxel-based morphometry
VCI	Vascular cognitive impairment
VICCCS	Vascular Impairment of Cognition Classification Consensus Study
WMH	White matter hyperintensities

18.1 Introduction

Vascular cognitive impairment (VCI), which is defined as a clinical-radiological-pathological syndrome, refers to the entire form of cognitive decline (from subjective cognitive decline to dementia) caused by the brain vascular pathology (van der Flier et al. 2018).

Till now, numerous terms and diagnostic criteria had been used to describe the conception. The terms included vascular dementia (VaD), vascular cognitive impairment (VCI), subcortical (ischemic) VaD/VCI, and vascular cognitive disorder (Skrobot et al. 2017). It's still controversial which term is more appropriate. There are also a number of diagnostic criteria, including the American Heart Association/American Stroke Association (Gorelick et al. 2011), the Vascular Impairment of

Cognition Classification Consensus Study (VICCCS) criteria (Skrobot et al. 2017), the VASCOG criteria (Sachdev et al. 2019), and so on.

Several reasons made the diagnosis of VCI difficult. One is the lack of consistency of the diagnostic criteria, which hamper the progress in investigating the pathophysiology and clinical features of VCI. Second, though VaD is the second most prevalent dementia (15–30%) in epidemiological studies (Goodman et al. 2017), comorbidities between vascular pathology and the other types of pathology frequently occur. Indeed, cognitive impairment solely due to cerebrovascular disease is not common in both the pathological and clinical studies (Barker et al. 2002; Hejl et al. 2002). Specifically, vascular pathology alone probably accounts for only less than 10% of dementia cases (Schneider et al. 2007), while 78% of dementia patients at autopsy had vascular pathological change (Neuropathology Group. Medical Research Council Cognitive and Aging 2001). Therefore, dementia due to mixed pathology is common.

In this chapter, according to the VICCCS criteria (Skrobot et al. 2017), we will use the term of VCI. However, as the term VaD is used in most previous literature, we could not avoid the use of both the terms of VaD and VCI. Figure 18.1 describes the classification of VCI in the VICCCS criteria. The VCI is divided into the subtype of mild VCI and major VCI (VaD) according to the level of cognitive impairment (Skrobot et al. 2017). Major VCI (VaD) is further classified into four subtypes:

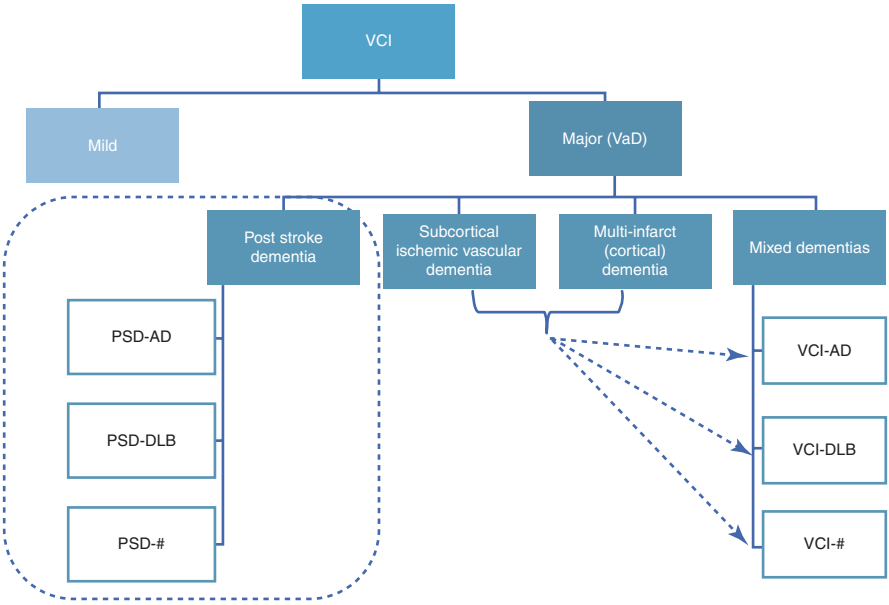

Fig. 18.1 Revised conceptualization of VCI in VICCCS. (Reproduced with permission from Skrobot et al. 2017). *DLB* dementia with Lewy bodies, *PSD* post-stroke dementia, *VaD* vascular dementia, *VCI* vascular cognitive impairment, *VICCCS* Vascular Impairment of Cognition Classification Consensus Study

post stroke dementia (PSD), subcortical ischemic VaD, multi-infarct (cortical) dementia, and mixed dementia. The PSD is differentiated from other forms of major VCI (VaD) by a 6-month interval between cognitive decline and stroke. Cases with multiple cortical and subcortical infarcts, strategic infarcts, subcortical ischemic vascular dementia, and various forms of neurodegenerative pathology, including Alzheimer's disease (AD), which develop within 6 months of stroke are considered as the PSD. Subcortical ischemic VaD is mainly caused by the cerebral small vessel disease. Lacunar infarcts and ischemic white matter lesions, located predominantly in the subcortical region, are the main type of brain lesions. Multi-infarct dementia refers to multiple large cortical infarcts and their possible contribution to cognitive impairment. "Mixed dementia" is used to indicate the combination of vascular and other neurodegenerative pathologies, including VCI-AD, VCI-dementia with Lewy bodies (DLB), and so on. Mild VCI is not further subdivided in this framework.

Neuroimaging plays an important role in the diagnosis of VCI (Wardlaw et al. 2013). In VICCCS, magnetic resonance imaging (MRI) is a "gold standard" requirement for the clinical diagnosis of VCI. Although there are numerous diagnostic criteria, the main pathological features of cerebrovascular VCI are the infarction, hemorrhage, and white matter lesions due to ischemia (Gorelick et al. 2011). MRI has a high sensitivity for the white matter hyperintensities (WMHs), cerebral infarction, and hemorrhage. Therefore, MRI plays an important role in assessing the type, location, and extent of vascular lesions for patients with suspected VCI.

Functional neuroimaging, including positron emission tomography (PET) and single-photon emission computed tomography (SPECT), is widely used for the evaluation of the metabolism and perfusion change in dementia. The regional cerebral metabolic rate of oxygen ($rCMRO_2$) is maintained by continuous oxygen delivery, adjusted to the metabolic demand by variations of regional cerebral blood flow (rCBF), oxygen extraction fraction (OEF), and cerebral blood volume (CBV) and can be assessed with [$^{15}O_2$] and PET. And with ^{18}F-labeled 2-fluoro-2-deoxy-D-glucose (^{18}F-FDG), we can measure the utilization of glucose. In addition, with the advancement of molecular imaging, a broad range of molecular targets, including the abnormal proteins, enzyme activity, and neurotransmitter receptors and transporters, can be imaged with various PET tracers in vivo. PET had been widely used in the research work to explore the underlying pathophysiological mechanisms of disease. The strategies of diagnosis and treatment in dementia are increasingly based on the underlying neuropathological characteristics these days. In longitudinal study, repeated measurement can reflect the disease progression and demonstrate the efficiency of the newly developed treatment strategies. The commonly used tracers are summarized in Table 18.1.

Though PET and SPECT are not the routine examination in the clinical practice of VCI, they can provide additional information to increase the diagnostic accuracy compared with MRI. Furthermore, recent studies use the multimodal strategies, combining the SPECT/PET and MRI, to investigate the molecular mechanism of the brain functional networks.

Table 18.1 Synopsis of vascular dementia relevant tracers

Physiologic variable	Method	Tracers
Cerebral blood flow (CBF)	PET	^{15}O-Carbon dioxide; ^{15}O-water; ^{15}O-Butanol; ^{13}N-ammonia
	SPECT	^{133}Xe; ^{99m}Tc-hydroxy-methyl-propyleneamine oxime (HMPAO); ^{99m}Tc-ethyl-cysteinate-dimer (ECD); ^{123}I-isopropyl-*p*-iodoamphetamine (IPM)
Oxygen extraction fraction (OEF) and metabolism ($CMRO_2$)	PET	^{15}O-Oxygen ($CMRO_2$ is calculated by multiplying CBF by OEF)
Glucose metabolism	PET	^{18}F-Fluoro-deoxy-glucose (^{18}F-FDG)
Blood volume	PET	^{15}O-Carbon monoxide
	SPECT	^{99m}Tc-Labeled red blood cells
Amyloid deposits	PET	^{11}C-2-(4-Methylaminophenyl)-6-hydroxybenzothiazole (Pittsburgh compound-B, PIB); ^{11}C-4-*N*-methylamino-4′-hydroxystilbene (SB13); ^{18}F-1,1-dicyano-2-[6-(dimethylamino)-2-naphthalenyl] propene (FDNNP); ^{18}F-flutemetamol (GE-067, AH110690); ^{18}F-florbetaben (BAY94-9172, AV-1); ^{18}F-florbetapir (AV-45)
Tau deposits	PET	^{11}C-PBB3, ^{18}F-AV-1451, ^{18}F-THK-523, ^{18}F-THK-5117, ^{18}F-THK-5105, ^{18}F-THK-5351

18.2 SPECT

18.2.1 Tracers of SPECT

18.2.1.1 ^{133}Xe Gas

^{133}Xe Gas was originally used for ventilation studies of the lungs (Suga et al. 1998) and also for the assessment of cerebral blood flow (Ogasawara et al. 2002; Tran Dinh et al. 1997). Xenon-133 also crosses the *BBB* but is not trapped. The dynamic transit of ^{133}Xe can be used in a quantitative rCBF measurement (ml/min/100 g) (Devous Sr. et al. 1986).

18.2.1.2 ^{99m}Tc-Hexamethylpropylene Amine Oxime (^{99m}Tc-HMPAO)

The clinical use of ^{99m}Tc-HMPAO is mainly for brain perfusion imaging. ^{99m}Tc-HMPAO is also applied for brain scintigraphy for diagnosis and differentiation of AD and VCI (Park et al. 2014; Radic et al. 2019).

18.2.1.3 ^{99m}Tc-Ethyl Cysteinate Dimer (^{99m}Tc-ECD)

The clinical use of ^{99m}Tc-ECD is mainly for quantitative measurement of rCBF (Tsuchida et al. 1997). ^{99m}Tc-ECD is mainly used in brain scintigraphy for diagnosis

of acute cerebral ischemia, epilepsy, head trauma, and dementia (Dormehl et al. 1997; Nocun et al. 2011).

18.2.1.4 ^{123}I-Isopropyl-*p*-Iodoamphetamine (^{123}I-IMP)

^{123}I-isopropyl-*p*-iodoamphetamine (^{123}I-IMP) is one of the most suitable SPECT tracers for the measurement of rCBF. ^{123}I-IMP has a good linear correlation between its accumulation in cerebral tissue and rCBF. Researchers recently developed a simple noninvasive ^{123}I-IMP microsphere method using chest dynamic planar images and brain SPECT (Ofuji et al. 2016).

18.2.1.5 ^{99m}Tc-Labeled Red Blood Cells (^{99m}Tc-RBC)

^{99m}Tc-Labeled erythrocytes (^{99m}Tc-RBC) have also been used for CBV measurement in SPECT (Reinstrup et al. 2001; Sabatini et al. 1991). The regional radioactivity measured by ^{99m}Tc-RBC was converted to CBV level by division with the radioactivity per volume in the blood tests and was expressed as a percentage of the corresponding brain volume (Blatter et al. 1995).

Overall, with SPECT we can evaluate the perfusion and the local hemodynamics in the ischemic territories. It could also be used in the investigation of the crossed cerebellar diaschisis (CCD), which is the remote effect of supratentorial dysfunction of the brain in the unilateral hemisphere inducing contralateral cerebellar hypoperfusion and hypometabolism (Lin 1997). The mechanism of CCD implies the involvement of cortico-ponto-cerebellar fibers. However, whether the focal change in the cerebellum is a form of Wallerian degeneration or the result of accumulation of pathological substrates in the cerebellum itself is still unknown. Though the role of SPECT in the diagnosis and research of VCI has gradually decreased, it still can be used as an option to increase the diagnostic accuracy (Radic et al. 2019).

18.3 PET

18.3.1 Tracers of PET

18.3.1.1 ^{15}O-Labeled Gases and ^{15}O-Water

^{15}O-Labeled radiotracers can be used for quantitative cerebral blood flow (CBF), OEF, and $CMRO_2$ images. However, most of these techniques require an additional C^{15}O scan to correct for changes of CBV. Therefore, a formula had been developed to eliminate the need for the CBV information. This computational improvement for the dual-tracer method has been done using the dual basis function method (DBFM) (Hattori et al. 2004; Kudomi et al. 2005).

18.3.1.2 ^{15}O-Butanol

^{15}O-Butanol can also be used for quantitative rCBF images (Herzog et al. 1996). Compared with ^{15}O-water, ^{5}O-butanol is a better perfusion agent because its partition coefficient is nearly 1.0 compared to 0.9 for water.

18.3.1.3 ^{13}N-Ammonia (^{13}N-NH_3)

^{13}N-NH_3 is a useful PET imaging agent for assessing regional blood flow in tissues (Phelps et al. 1977). The linear relationship between distribution of ^{13}N-NH_3 and the regional perfusion makes it feasible for measuring CBF.

18.3.1.4 ^{18}F-FDG

As glucose is the main substance for brain energy metabolism, regional cerebral metabolic rate for glucose (rCMRGlc) as measured by PET can be applied for detecting changes in regional brain function induced by different diseases. With ^{18}F-FDG PET we can measure the cerebral utilization of glucose by PET. Measurement of rCMRGlc by ^{18}F-FDG PET has become a standard technique during the past decade. Many studies have documented a close relationship between rCMRGlc and cognitive functions (Bohnen et al. 2012; Herholz et al. 2002).

18.3.1.5 Amyloid and Tau Imaging Tracers

The accumulation of misfolded protein is a common pathogenic mechanism in neurodegenerative diseases. The presence of amyloid β (Aβ) and NFT is a neuropathological hallmark of AD (Jack Jr. et al. 2013). Several PET ligands have been developed to provide a method for noninvasive visualization of pathological protein deposition in human brains.

The PET ligands, which have a high binding affinity for Aβ, were developed based on the structure of two different histopathology stains, thioflavin T and Congo red. ^{11}C-2-(4-Methylaminophenyl)-6-hydroxybenzothiazole, also known as 11C-Pittsburgh Compound-B (PIB), is the most widely used tracer, which has a high sensitive for detecting the fibrillar form of amyloid-β (Bacskai et al. 2003). ^{11}C-4-*N*-Methylamino-4′-hydroxystilbene (SB13) is also an effective PET tracer for detecting fibrillar Aβ plaques (Verhoeff et al. 2004). However, because of the short radioactive half-life (about 20 min) of ^{11}C-labeled tracers, they can only be used in fully equipped PET centers with on-site cyclotron and radiopharmacy, which limit their application. Therefore, the ^{18}F-labeled amyloid ligands with a longer radioactive half-life (about 110 min) have also been developed for broader clinical applications. ^{18}F-1,1-Dicyano-2-[6-(dimethylamino)-2-naphthalenyl]propene (FDDNP) (Small et al. 2006) attaches to a different receptor on Aβ and also binds to NFT (Shoghi-Jadid et al. 2002). Other potential agents being investigated are ^{18}F-AH110690 (a 3′-fluoro analogue of PIB), the stilbene derivative ^{18}F-BAY94-9172, and ^{18}F-AV-45 (Nelissen et al. 2009; Klunk and Mathis 2008; Nordberg 2008; Rowe et al. 2008).

Tauopathies refer to the neurodegenerative diseases characterized by the accumulation of tau protein (Lee et al. 2001). There are six tau isoforms classified according to their tubulin-biding domains as three repeat domains (3R) tau and four repeat domains (4R) tau (Goedert et al. 1992). In normal brains, equal amounts of 3R and 4R tau isoforms exist. The changes in the 3R and 4R tau ratio lead to tauopathies. In FTLD, Pick's disease is related with 3R tau, and PSP and CBD are related with 4R tau (Flament et al. 1991; Kato and Nakamura 1990; Ksiezak-Reding et al.

1994). ^{18}F-THK523 was the first tau-selective ligand (Kudomi et al. 2005; Okamura et al. 2005). Other THK compounds (including ^{18}F-THK5105, ^{18}F-THK5117, and ^{18}F-THK5351), which have higher affinity for tau compared to ^{18}F-THK523, have been developed since then (Hall et al. 2017). More recently, benzimidazole pyrimidines derivatives have also been identified as tau tracers (Xia et al. 2013). ^{18}F-AV1451 (formerly known as T807) is the most widely used tracer. ^{11}C-PBB3 is another tau radiotracer developed by Maruyama and colleagues (2013).

18.3.1.6 The Utility of FDG-PET

AD is the most prevalent form of dementia. Though most patients have a combination of both AD and VCI, it is still important to distinguish patients with predominantly VCI and patients with predominantly AD. FDG-PET measuring the rCMRGlc can show the metabolic pattern. Compared with the typical metabolic pattern of AD (the hypometabolism in neocortical association areas, but relative preserved in the primary visual and sensorimotor cortical area, basal ganglia, and cerebellum), the VCI patients showed a significant metabolic reduction in scattered areas of focal cortical and subcortical regions (Benson et al. 1983; Heiss and Zimmermann-Meinzingen 2012). Another study showed that the metabolic reduction in VaD was less affected in primary sensorimotor and association cortex, but more severe in subcortical areas than in AD (Mielke et al. 1992). Studies using voxel-based morphometry (VBM) also provide similar findings: VaD patients had lower metabolism in deep gray nuclei, cerebellum, primary cortex, middle temporal gyrus, and anterior cingulate cortex, while AD patients showed reductions in hippocampal area, orbitofrontal cortex, posterior cingulate cortex, and posterior parietal cortex (Kerrouche et al. 2006).

As the prodromal phase of AD, amnestic mild cognitive impairment (aMCI) has a high incidence of conversion to AD (Petersen et al. 2001). The hypometabolism pattern in aMCI was in the bilateral parahippocampal, bilateral posterior cingulate cortex, left superior temporal cortex, left inferior parietal lobule, and right inferior frontal cortex, whereas the hypometabolism in VCI affected the thalamus, insula, superior temporal gyrus, cingulate cortex, right basal ganglia, cerebellum and brainstem, and the differentiation in the thalamus, brainstem, and cerebellum was the most significant (Seo et al. 2009).

18.3.1.7 The Utility of Aβ and Tau PET

Recent studies have shown the strong association between AD pathology, including the Aβ plaques and NFTs, and cerebrovascular pathology (Schneider et al. 2007). However, whether Aβ and tau deposits play a role in the cognitive impairment in VCI is unknown. With the rapid advancement of molecular imaging, the visualization of AD pathology in vivo is possible.

The relationship between Aβ and cognitive impairment have been well established in AD. However, more evidence suggested that Aβ might also contribute to deterioration in cognitive performance in VCI. Previous studies reported that 30% of all patients with subcortical ischemic vascular damage have Aβ pathology deposition on PET (Lee et al. 2011, 2014). Rabin et al. also observed synergistic effects

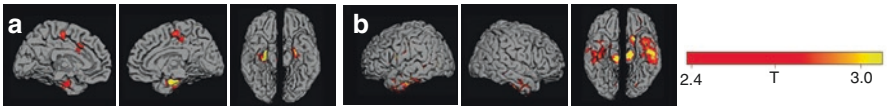

Fig. 18.2 Independent association of amyloid β (Aβ) (**a**) or cerebral small vessel disease (CSVD) score (**b**) with AV1451 uptake in subcortical VCI after controlling for age. (Reproduced with permission from Kim et al. 2018)

of higher levels of vascular risk and elevated Aβ deposition in the reduction of cognitive function (Rabin et al. 2018).

In the classical amyloid cascade model of AD, the NFT spreading is trigged by the Aβ accumulation (Jack Jr. et al. 2013). However, whether the Aβ or the ischemic lesion is the trigger of tau accumulation in subcortical VCI is still uncertain.

Using ^{18}F-AV1451 PET, Kim et al. found that in patients with subcortical VCI, Aβ and cerebral small vessel disease burden were independently associated with increased tau accumulation in the medial temporal and inferior temporal regions, respectively (Fig. 18.2). Moreover, they also found that the tau pathology played an important role in the cognitive decline of subcortical VCI (Kim et al. 2018). Consistent with the finding, Franzmeier et al. showed elevated tau levels in VCI in the absence of Aβ (Franzmeier et al. 2019). Recently, a post-mortem study showed that the higher systolic blood pressure, which is a risk factor for VCI, is associated with higher NFT density but no Aβ (Arvanitakis et al. 2018). These results may support the hypothesis that the tau accumulation is triggered by the chronic hypoperfusion or ischemia independent of Aβ.

Jang et al. applied the AT (Aβ/tau) classification system to patients with subcortical VCI, according to the recently developed biomarker-based diagnostic criteria of AD. They found that the frequency of tau deposition were 25.9% and 70.0% in Aβ-positive subcortical VCI and Aβ-positive AD, respectively. Moreover, subcortical VCI subgroup with both Aβ and tau positive is associated with the fastest decline of brain volume and cognitive function, followed by subgroup with Aβ positive but tau negative and then the subgroup with Aβ negative. The results proved that the new AT system could also be effectively applied to the subcortical VCI research framework and provide new pathology targeted therapy options for the subgroups of subcortical VCI in the future (Jang et al. 2019).

References

Arvanitakis Z, Capuano AW, Lamar M, Shah RC, Barnes LL, Bennett DA, Schneider JA (2018) Late-life blood pressure association with cerebrovascular and Alzheimer disease pathology. Neurology 91(6):e517–e525. https://doi.org/10.1212/WNL.0000000000005951

Bacskai BJ, Hickey GA, Skoch J, Kajdasz ST, Wang Y, Huang GF et al (2003) Four-dimensional multiphoton imaging of brain entry, amyloid binding, and clearance of an amyloid-beta ligand in transgenic mice. Proc Natl Acad Sci U S A 100(21):12462–12467. https://doi.org/10.1073/pnas.2034101100

Barker WW, Luis CA, Kashuba A, Luis M, Harwood DG, Loewenstein D et al (2002) Relative frequencies of Alzheimer disease, Lewy body, vascular and frontotemporal dementia, and hippocampal sclerosis in the State of Florida Brain Bank. Alzheimer Dis Assoc Disord 16(4):203–212

Benson DF, Kuhl DE, Hawkins RA, Phelps ME, Cummings JL, Tsai SY (1983) The fluorodeoxyglucose 18F scan in Alzheimer's disease and multi-infarct dementia. Arch Neurol 40(12):711–714. https://doi.org/10.1001/archneur.1983.04050110029003

Blatter DD, Bigler ED, Gale SD, Johnson SC, Anderson CV, Burnett BM et al (1995) Quantitative volumetric analysis of brain MR: normative database spanning 5 decades of life. AJNR Am J Neuroradiol 16(2):241–251

Bohnen NI, Djang DS, Herholz K, Anzai Y, Minoshima S (2012) Effectiveness and safety of 18F-FDG PET in the evaluation of dementia: a review of the recent literature. J Nucl Med 53(1):59–71. https://doi.org/10.2967/jnumed.111.096578

Devous MD Sr, Stokely EM, Chehabi HH, Bonte FJ (1986) Normal distribution of regional cerebral blood flow measured by dynamic single-photon emission tomography. J Cereb Blood Flow Metab 6(1):95–104. https://doi.org/10.1038/jcbfm.1986.12

Dormehl IC, Oliver DW, Langen KJ, Hugo N, Croft SA (1997) Technetium-99m-HMPAO, technetium-99m-ECD and iodine-123-IMP cerebral blood flow measurements with pharmacological interventions in primates. J Nucl Med 38(12):1897–1901

Flament S, Delacourte A, Verny M, Hauw JJ, Javoy-Agid F (1991) Abnormal tau proteins in progressive supranuclear palsy. Similarities and differences with the neurofibrillary degeneration of the Alzheimer type. Acta Neuropathol 81(6):591–596. https://doi.org/10.1007/bf00296367

Franzmeier N, Rubinski A, Neitzel J, Kim Y, Damm A, Na DL et al (2019) Functional connectivity associated with tau levels in ageing, Alzheimer's, and small vessel disease. Brain 142(4):1093–1107. https://doi.org/10.1093/brain/awz026

Goedert M, Spillantini MG, Cairns NJ, Crowther RA (1992) Tau proteins of Alzheimer paired helical filaments: abnormal phosphorylation of all six brain isoforms. Neuron 8(1):159–168. https://doi.org/10.1016/0896-6273(92)90117-v

Goodman RA, Lochner KA, Thambisetty M, Wingo TS, Posner SF, Ling SM (2017) Prevalence of dementia subtypes in United States Medicare fee-for-service beneficiaries, 2011–2013. Alzheimers Dement 13(1):28–37. https://doi.org/10.1016/j.jalz.2016.04.002

Gorelick PB, Scuteri A, Black SE, Decarli C, Greenberg SM, Iadecola C et al (2011) Vascular contributions to cognitive impairment and dementia: a statement for healthcare professionals from the American Heart Association/American Stroke Association. Stroke 42(9):2672–2713. https://doi.org/10.1161/STR.0b013e3182299496

Hall B, Mak E, Cervenka S, Aigbirhio FI, Rowe JB, O'Brien JT (2017) In vivo tau PET imaging in dementia: pathophysiology, radiotracer quantification, and a systematic review of clinical findings. Ageing Res Rev 36:50–63. https://doi.org/10.1016/j.arr.2017.03.002

Hattori N, Bergsneider M, Wu HM, Glenn TC, Vespa PM, Hovda DA et al (2004) Accuracy of a method using short inhalation of (15)O-O(2) for measuring cerebral oxygen extraction fraction with PET in healthy humans. J Nucl Med 45(5):765–770

Heiss WD, Zimmermann-Meinzingen S (2012) PET imaging in the differential diagnosis of vascular dementia. J Neurol Sci 322(1–2):268–273. https://doi.org/10.1016/j.jns.2012.09.023

Hejl A, Hogh P, Waldemar G (2002) Potentially reversible conditions in 1000 consecutive memory clinic patients. J Neurol Neurosurg Psychiatry 73(4):390–394. https://doi.org/10.1136/jnnp.73.4.390

Herholz K, Salmon E, Perani D, Baron JC, Holthoff V, Frolich L et al (2002) Discrimination between Alzheimer dementia and controls by automated analysis of multicenter FDG PET. NeuroImage 17(1):302–316

Herzog H, Seitz RJ, Tellmann L, Rota Kops E, Julicher F, Schlaug G et al (1996) Quantitation of regional cerebral blood flow with 15O-butanol and positron emission tomography in humans. J Cereb Blood Flow Metab 16(4):645–649. https://doi.org/10.1097/00004647-199607000-00015

Jack CR Jr, Knopman DS, Jagust WJ, Petersen RC, Weiner MW, Aisen PS et al (2013) Tracking pathophysiological processes in Alzheimer's disease: an updated hypothetical model of dynamic biomarkers. Lancet Neurol 12(2):207–216. https://doi.org/10.1016/S1474-4422(12)70291-0

Jang H, Kim HJ, Park S, Park YH, Choe Y, Cho H et al (2019) Application of an amyloid and tau classification system in subcortical vascular cognitive impairment patients. Eur J Nucl Med Mol Imaging 47:292. https://doi.org/10.1007/s00259-019-04498-y

Kato S, Nakamura H (1990) Cytoplasmic argyrophilic inclusions in neurons of pontine nuclei in patients with olivopontocerebellar atrophy: immunohistochemical and ultrastructural studies. Acta Neuropathol 79(6):584–594. https://doi.org/10.1007/bf00294235

Kerrouche N, Herholz K, Mielke R, Holthoff V, Baron JC (2006) 18FDG PET in vascular dementia: differentiation from Alzheimer's disease using voxel-based multivariate analysis. J Cereb Blood Flow Metab 26(9):1213–1221. https://doi.org/10.1038/sj.jcbfm.9600296

Kim HJ, Park S, Cho H, Jang YK, San Lee J, Jang H et al (2018) Assessment of extent and role of tau in subcortical vascular cognitive impairment using 18F-AV1451 positron emission tomography imaging. JAMA Neurol 75(8):999–1007. https://doi.org/10.1001/jamaneurol.2018.0975

Klunk WE, Mathis CA (2008) The future of amyloid-beta imaging: a tale of radionuclides and tracer proliferation. Curr Opin Neurol 21(6):683–687. https://doi.org/10.1097/WCO.0b013e3283168e1a

Ksiezak-Reding H, Morgan K, Mattiace LA, Davies P, Liu WK, Yen SH et al (1994) Ultrastructure and biochemical composition of paired helical filaments in corticobasal degeneration. Am J Pathol 145(6):1496–1508

Kudomi N, Hayashi T, Teramoto N, Watabe H, Kawachi N, Ohta Y et al (2005) Rapid quantitative measurement of CMRO(2) and CBF by dual administration of (15)O-labeled oxygen and water during a single PET scan-a validation study and error analysis in anesthetized monkeys. J Cereb Blood Flow Metab 25(9):1209–1224. https://doi.org/10.1038/sj.jcbfm.9600118

Lee VM, Goedert M, Trojanowski JQ (2001) Neurodegenerative tauopathies. Annu Rev Neurosci 24:1121–1159. https://doi.org/10.1146/annurev.neuro.24.1.1121

Lee JH, Kim SH, Kim GH, Seo SW, Park HK, Oh SJ et al (2011) Identification of pure subcortical vascular dementia using 11C-Pittsburgh compound B. Neurology 77(1):18–25. https://doi.org/10.1212/WNL.0b013e318221acee

Lee MJ, Seo SW, Na DL, Kim C, Park JH, Kim GH et al (2014) Synergistic effects of ischemia and beta-amyloid burden on cognitive decline in patients with subcortical vascular mild cognitive impairment. JAMA Psychiat 71(4):412–422. https://doi.org/10.1001/jamapsychiatry.2013.4506

Lin WY (1997) Crossed cerebellar diaschisis: related to lesion location or disease duration? J Nucl Med 38(12):2006

Maruyama M, Shimada H, Suhara T, Shinotoh H, Ji B, Maeda J et al (2013) Imaging of tau pathology in a tauopathy mouse model and in Alzheimer patients compared to normal controls. Neuron 79(6):1094–1108. https://doi.org/10.1016/j.neuron.2013.07.037

Mielke R, Herholz K, Grond M, Kessler J, Heiss WD (1992) Severity of vascular dementia is related to volume of metabolically impaired tissue. Arch Neurol 49(9):909–913. https://doi.org/10.1001/archneur.1992.00530330031011

Nelissen N, Van Laere K, Thurfjell L, Owenius R, Vandenbulcke M, Koole M et al (2009) Phase 1 study of the Pittsburgh compound B derivative 18F-flutemetamol in healthy volunteers and patients with probable Alzheimer disease. J Nucl Med 50(8):1251–1259. https://doi.org/10.2967/jnumed.109.063305

Neuropathology Group. Medical Research Council Cognitive Function and Aging Study (2001) Pathological correlates of late-onset dementia in a multicentre, community-based population in England and Wales. Neuropathology Group of the Medical Research Council Cognitive Function and Ageing Study (MRC CFAS). Lancet 357(9251):169–175. https://doi.org/10.1016/s0140-6736(00)03589-3

Nocun A, Wilczynski M, Wronski J, Chrapko B (2011) Usefulness of 99mTc-ECD brain SPECT with voxel-based analysis in evaluation of perfusion changes early after carotid endarterectomy. Med Sci Monit 17(5):CR297–CR303. https://doi.org/10.12659/msm.881771

Nordberg A (2008) Amyloid imaging in Alzheimer's disease. Neuropsychologia 46(6):1636–1641. https://doi.org/10.1016/j.neuropsychologia.2008.03.020

Ofuji A, Mimura H, Yamashita K, Takaki A, Sone T, Ito S (2016) Development of a simple non-invasive microsphere quantification method for cerebral blood flow using I-123-IMP. Ann Nucl Med 30(3):242–249. https://doi.org/10.1007/s12149-015-1053-8

Ogasawara K, Ogawa A, Yoshimoto T (2002) Cerebrovascular reactivity to acetazolamide and outcome in patients with symptomatic internal carotid or middle cerebral artery occlusion: a xenon-133 single-photon emission computed tomography study. Stroke 33(7):1857–1862. https://doi.org/10.1161/01.str.0000019511.81583.a8

Okamura N, Suemoto T, Furumoto S, Suzuki M, Shimadzu H, Akatsu H et al (2005) Quinoline and benzimidazole derivatives: candidate probes for in vivo imaging of tau pathology in Alzheimer's disease. J Neurosci 25(47):10857–10862. https://doi.org/10.1523/JNEUROSCI.1738-05.2005

Park SY, Yoon H, Lee N, Oh JK, Yoo Ie R, Kim SH, Chung YA (2014) Analysis of cerebral blood flow with single photon emission computed tomography in mild subcortical ischemic vascular dementia. Nucl Med Mol Imaging 48(4):272–277. https://doi.org/10.1007/s13139-014-0287-z

Petersen RC, Stevens JC, Ganguli M, Tangalos EG, Cummings JL, DeKosky ST (2001) Practice parameter: early detection of dementia: mild cognitive impairment (an evidence-based review). Report of the Quality Standards Subcommittee of the American Academy of Neurology. Neurology 56(9):1133–1142. https://doi.org/10.1212/wnl.56.9.1133

Phelps ME, Hoffman EJ, Raybaud C (1977) Factors which affect cerebral uptake and retention of 13NH3. Stroke 8(6):694–702. https://doi.org/10.1161/01.str.8.6.694

Rabin JS, Schultz AP, Hedden T, Viswanathan A, Marshall GA, Kilpatrick E et al (2018) Interactive associations of vascular risk and beta-amyloid burden with cognitive decline in clinically normal elderly individuals: findings from the Harvard Aging Brain Study. JAMA Neurol 75(9):1124–1131. https://doi.org/10.1001/jamaneurol.2018.1123

Radic B, Petrovic R, Golubic A, Bilic E, Borovecki F (2019) EEG analysis and SPECT imaging in Alzheimer's disease, vascular dementia and mild cognitive impairment. Psychiatr Danub 31(1):111–115. https://doi.org/10.24869/psyd.2019.111

Reinstrup P, Ryding E, Ohlsson T, Dahm PL, Uski T (2001) Cerebral blood volume (CBV) in humans during normo- and hypocapnia: influence of nitrous oxide (N(2)O). Anesthesiology 95(5):1079–1082. https://doi.org/10.1097/00000542-200111000-00009

Rowe CC, Ackerman U, Browne W, Mulligan R, Pike KL, O'Keefe G et al (2008) Imaging of amyloid beta in Alzheimer's disease with 18F-BAY94-9172, a novel PET tracer: proof of mechanism. Lancet Neurol 7(2):129–135. https://doi.org/10.1016/S1474-4422(08)70001-2

Sabatini U, Celsis P, Viallard G, Rascol A, Marc-Vergnes JP (1991) Quantitative assessment of cerebral blood volume by single-photon emission computed tomography. Stroke 22(3):324–330. https://doi.org/10.1161/01.str.22.3.324

Sachdev PS, Lipnicki DM, Crawford JD, Brodaty H (2019) The vascular behavioral and cognitive disorders criteria for vascular cognitive disorders: a validation study. Eur J Neurol 26(9):1161–1167. https://doi.org/10.1111/ene.13960

Schneider JA, Arvanitakis Z, Bang W, Bennett DA (2007) Mixed brain pathologies account for most dementia cases in community-dwelling older persons. Neurology 69(24):2197–2204. https://doi.org/10.1212/01.wnl.0000271090.28148.24

Seo SW, Cho SS, Park A, Chin J, Na DL (2009) Subcortical vascular versus amnestic mild cognitive impairment: comparison of cerebral glucose metabolism. J Neuroimaging 19(3):213–219. https://doi.org/10.1111/j.1552-6569.2008.00292.x

Shoghi-Jadid K, Small GW, Agdeppa ED, Kepe V, Ercoli LM, Siddarth P et al (2002) Localization of neurofibrillary tangles and beta-amyloid plaques in the brains of living patients with Alzheimer disease. Am J Geriatr Psychiatry 10(1):24–35

Skrobot OA, O'Brien J, Black S, Chen C, DeCarli C, Erkinjuntti T et al (2017) The vascular impairment of cognition classification consensus study. Alzheimers Dement 13(6):624–633. https://doi.org/10.1016/j.jalz.2016.10.007

Small GW, Kepe V, Ercoli LM, Siddarth P, Bookheimer SY, Miller KJ et al (2006) PET of brain amyloid and tau in mild cognitive impairment. N Engl J Med 355(25):2652–2663. https://doi.org/10.1056/NEJMoa054625

Suga K, Kume N, Nishigauchi K, Kawakami Y, Kawamura T, Matsumoto T, Matsunaga N (1998) Three-dimensional surface display of dynamic pulmonary xenon-133 SPECT in patients with obstructive lung disease. J Nucl Med 39(5):889–893

Tran Dinh YR, Ille O, Guichard JP, Haguenau M, Seylaz J (1997) Cerebral postischemic hyperperfusion assessed by Xenon-133 SPECT. J Nucl Med 38(4):602–607

Tsuchida T, Sadato N, Yonekura Y, Yamamoto K, Waki A, Sugimoto K et al (1997) Quantification of regional cerebral blood flow with continuous infusion of technetium-99m-ethyl cysteinate dimer. J Nucl Med 38(11):1699–1702

van der Flier WM, Skoog I, Schneider JA, Pantoni L, Mok V, Chen CLH, Scheltens P (2018) Vascular cognitive impairment. Nat Rev Dis Primers 4:18003. https://doi.org/10.1038/nrdp.2018.3

Verhoeff NP, Wilson AA, Takeshita S, Trop L, Hussey D, Singh K et al (2004) In-vivo imaging of Alzheimer disease beta-amyloid with [11C]SB-13 PET. Am J Geriatr Psychiatry 12(6):584–595. https://doi.org/10.1176/appi.ajgp.12.6.584

Wardlaw JM, Smith EE, Biessels GJ, Cordonnier C, Fazekas F, Frayne R et al (2013) Neuroimaging standards for research into small vessel disease and its contribution to ageing and neurodegeneration. Lancet Neurol 12(8):822–838. https://doi.org/10.1016/S1474-4422(13)70124-8

Xia CF, Arteaga J, Chen G, Gangadharmath U, Gomez LF, Kasi D et al (2013) [(18)F]T807, a novel tau positron emission tomography imaging agent for Alzheimer's disease. Alzheimers Dement 9(6):666–676. https://doi.org/10.1016/j.jalz.2012.11.008

Value of MIBG in the Differential Diagnosis of Neurodegenerative Disorders

19

Mitsuhiro Yoshita

Contents

19.1 Introduction 578
19.2 Evaluation of Cardiac Sympathetic Nerve Activity 579
19.3 Pathology in Lewy Body Disease 580
19.4 *Meta*iodobenzylguanidine Imaging in Lewy Body Disease 580
19.4.1 Parkinson's Disease 581
19.4.2 Dementia with Lewy Bodies 582
19.4.3 Pure Autonomic Failure 584
19.5 Differential Diagnosis of Lewy Body Disease Using ^{123}I-MIBG Cardiac Scintigraphy 584
19.6 Conclusion 586
References 587

Abstract

^{123}I-*Meta*iodobenzylguanidine (MIBG) has a history of 30 years as a marker of myocardial sympathetic activity and has been used for assessment of various cardiac diseases. Reduced cardiac MIBG uptake in myocardial scintigraphy has been reported in patients with Parkinson's disease (PD), dementia with Lewy bodies (DLB), pure autonomic failure (PAF), rapid eye movement sleep behavior disorder (RBD), and familial PD linked to *SNCA* duplication. In 2005, the Dementia with Lewy Bodies Consortium considered ^{123}I-MIBG myocardial scintigraphy a "supportive" diagnostic tool. Recently, reliable and clear evidence for the usefulness of ^{123}I-MIBG scintigraphy in the diagnosis of Lewy body disorders has been accumulated, and it has become increasingly popular, whereas reduction of cardiac MIBG accumulation was reported in some cases of atypical

M. Yoshita (✉)
Department of Neurology, Institute for Clinical Research, Dementia Medical Center, Hokuriku National Hospital, National Hospital Organization, Nanto, Toyama, Japan
e-mail: yoshita.mitsuhiro.tv@mail.hosp.go.jp; http://researchmap.jp/read0109633

R. A. J. O. Dierckx et al. (eds.), *PET and SPECT in Neurology*,
https://doi.org/10.1007/978-3-030-53168-3_19

parkinsonian syndromes such as progressive supranuclear palsy and multiple system atrophy. In ^{123}I-*N*-ω-fluoropropyl-2β-carbomethoxy-3β-(4-iodophenyl) nortropan (FP-CIT) SPECT-supplemented MIBG scintigraphy of PD and DLB, FP-CIT binding in basal ganglia is closely related to cardiac MIBG uptake. Based on the high diagnostic specificity in our multicenter study with standardized techniques, weighting of ^{123}I-MIBG myocardial scintigraphy was upgraded in the revised criteria for the clinical diagnosis of DLB.

Abbreviations

^{123}I-IMP	*N*-Isopropyl-*p*-[^{123}I]-iodoamphetamine
AD	Alzheimer's-type dementia
CBD	Corticobasal degeneration
DLB	Dementia with Lewy bodies
DOPS	Dihydroxyphenylserine
ECD	Ethyl cysteinate dimer
FDG	Fluorodeoxyglucose
FP-CIT	*N*-ω-Fluoropropyl-2β-carbomethoxy-3β-(4-iodophenyl)nortropan
HMPAO	Hexamethyl-propylene-amine-oxine
LBD	Lewy body disease
MAO	Monoamine oxidase
MIBG	*Meta*iodobenzylguanidine
PAF	Pure autonomic failure
PD	Parkinson's disease
PSP	Progressive supranuclear palsy

19.1 Introduction

*Meta*iodobenzylguanidine (MIBG) is a physiologic analog of norepinephrine, used to determine the location, integrity, and function of postganglionic noradrenergic neurons. ^{123}I-MIBG cardiac scintigraphy is a noninvasive tool for estimating local myocardial sympathetic nerve damage in various myocardial and neurological diseases (Glowniak et al. 1989; Merlet et al. 1992; Yoshita 1998). Noradrenergic postganglionic sympathetic denervation is a common feature of Parkinson's disease (PD) and related Lewy body disorders. Patients with PD can exhibit reduced cardiac ^{123}I-MIBG accumulation without other evidence of autonomic failure, whereas those with dementia with Lewy bodies (DLB) can have reduced cardiac ^{123}I-MIBG uptake without evidence of parkinsonism (Yoshita et al. 1998, 2006). In this chapter, usefulness of ^{123}I-MIBG myocardial scintigraphy is reviewed with special emphasis on diagnostic issues in neurodegenerative disorders.

19.2 Evaluation of Cardiac Sympathetic Nerve Activity

After subjects have been in a supine position for 20 min, 111 MBq ^{123}I-MIBG is injected intravenously. The energy discrimination is centered on 159 keV with a 20% window. Early and delayed planar images are obtained at 20–30 min and 3–4 h, respectively. Acquisition conditions and normal values are reported elsewhere (Nakajima et al. 1990). A single-photon emission computed tomography (SPECT) scan is also obtained in both early and delayed imaging. Anterior planar imaging is required for the quantification of the heart-to-mediastinum (H/M) ratio.

Relative organ uptake is determined by setting the region of interest (ROI) on the anterior view. A polygonal ROI is manually drawn over the whole heart, including the left ventricular cavity, and a rectangular ROI is set on the mediastinum (Fig. 19.1). The H/M ratio is calculated by dividing the count density of the ventricular ROI by that of the mediastinum ROI. The washout rate (WR) is calculated as follows: $WR = 100 \times (Ec - Dc)/Ec$, where Ec is the early cardiac count density and Dc is the decay-corrected delayed cardiac count density. Recently, a method for standardization of H/M ratios was developed to avoid the influence of different acquisition conditions (Nakajima et al. 2012).

Though several medications can interfere with MIBG uptake, among anti-Parkinson drugs, particularly L-threo-DOPS and MAO-B inhibitors may reduce the cardiac MIBG uptake (Solanki et al. 1992) (Table 19.1). For reliable results, the use of these drugs should be avoided.

It is well-known that various type of cardiac diseases and diabetes mellitus exhibited low MIBG uptake. In those cases, distribution pattern of MIBG accumulation may help the differential diagnosis. Three-dimensional evaluation using SPECT and echocardiographic assessment for cardiac wall motion is recommended to confirm the cause of MIBG uptake reduction (Nakajima et al. 2008).

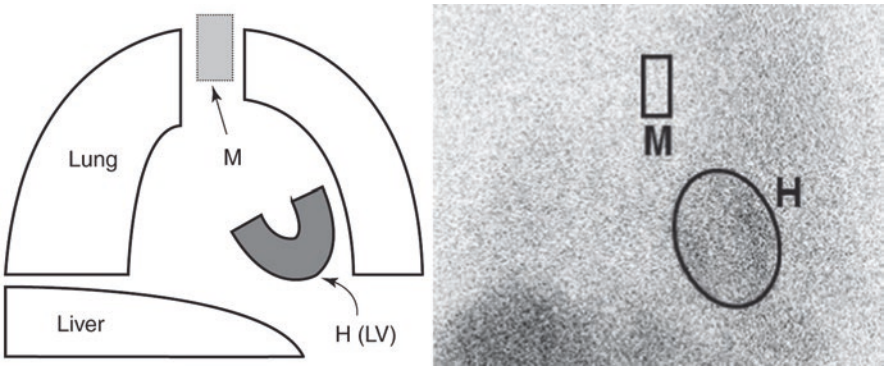

Fig. 19.1 Example of mediastinal and cardiac region of interest (ROI) on anterior planar image. The left ventricular ROI was drawn including the ventricular cavity (H), and a rectangular ROI was set on the middle mediastinum (M)

Table 19.1 Drugs interacting with MIBG

Antidepressants
Amitriptyline, amoxapine, clomipramine, desipramine, imipramine, trazodone, mianserin, etc.
α- and β-blocker
Labetalol, phenoxybenzamine, etc.
Sympathomimetics and sympatholytics
L-Threo-DOPS, norepinephrine, dobutamine, dopamine, phenylephrine, phenylpropanolamine, salbutamol, selegiline, brimonidine, etc.
Antipsychotics
Chlorpromazine, trazodone, haloperidol, droperidol, clozapine, quetiapine, risperidone, etc.
CNS stimulants
Cocaine, caffeine, amphetamine, etc.
Calcium channel blocker
Diltiazem, isradipine, nicardipine, nifedipine, nimodipine, verapamil, etc.

19.3 Pathology in Lewy Body Disease

Pathological assessment of Lewy body disease (LBD) reveals aggregates of α-synuclein, referred to as Lewy bodies, found in neurons and glia. Their presence is required for the pathological diagnosis of LBD. Lewy bodies are present not only in the brain stem but also in the limbic system and neocortex in relation to their phenotypes. In addition to central nervous system involvement, variable amounts of Lewy body burden are found in the peripheral nervous system and autonomic nervous system (Wakabayashi and Takahashi 1997). A postmortem study reported cardiac plexus was more heavily involved than the sympathetic ganglia in a patient with PD (Mitsui et al. 2006). On the other hand, other movement disorders and dementia syndromes, such as progressive supranuclear palsy (PSP), multiple system atrophy (MSA), essential tremor, frontotemporal dementia, and Alzheimer's-type dementia (AD), generally found no sympathetic ganglionic changes. Accordingly, Lewy body disease is not specific to the brain but instead is a generalized neuronal disorder.

19.4 *Meta*iodobenzylguanidine Imaging in Lewy Body Disease

PD, DLB, and pure autonomic failure (PAF) are recognized as LBD. Among all neurological diseases, they are characterized by a significant reduction in MIBG uptake. Recently, a markedly reduced cardiac MIBG uptake was also reported in idiopathic rapid eye movement sleep behavior disorder (RBD), consistent with the loss of sympathetic terminals and suggesting an association of RBD with Lewy body pathology (Miyamoto et al. 2006) (Fig. 19.2). It was revealed that cardiac MIBG uptake for early and delayed images was correlated with the proportion of residual cardiac sympathetic TH-positive nerve fibers at autopsy (Takahashi et al.

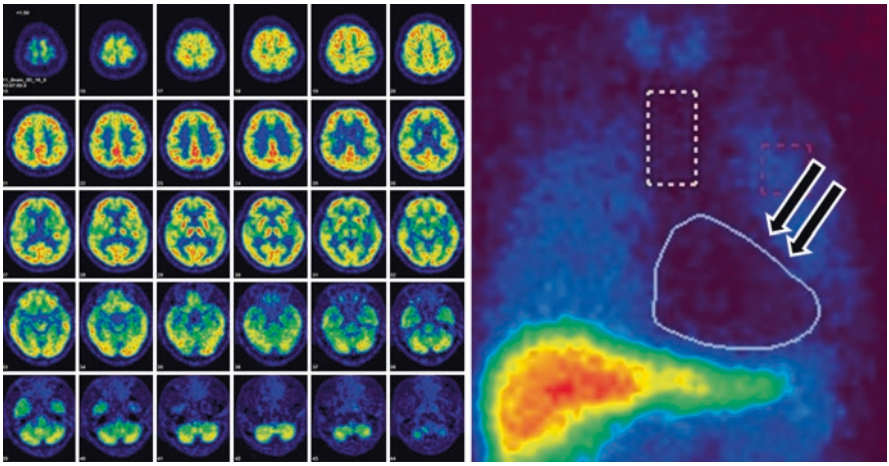

Fig. 19.2 Brain ^{18}F-FDG-PET and anterior planar MIBG image of patients with REM sleep behavior disorder. ^{18}F-FDG-PET shows normal brain metabolism, but no cardiac MIBG uptake (arrows)

Table 19.2 FP-CIT SPECT and MIBG scintigraphy in discrimination of DLB from AD

Tracer	Diagnostic significance (McKeith et al. 2017)	Subject	Method	Sensitivity/ specificity (%)
FP-CIT	Indicative biomarkers	Probable DLB vs. non DLB	Multicenter	77.7/90.4 (McKeith et al. 2007)
MIBG	Indicative biomarkers	Probable DLB vs. probable AD	Multicenter	69–77/89–97 (Yoshita et al. 2015; Komatsu et al. 2018)

FP-CIT N-ω-fluoropropyl-2β-carbomethoxy-3β-(4-iodophenyl)nortropan, *MIBG meta*iodobenzylguanidine

2015). As ^{123}I-*N*-ω-fluoropropyl-2β-carbomethoxy-3β-(4-iodophenyl)nortropan (FP-CIT) SPECT successfully visualizes presynaptic dopaminergic degeneration of the nigrostriatal tract, the finding of reduced tracer uptake in basal ganglia is recognized as a "indicative biomarker" of DLB (Mckeith et al. 2017) (Table 19.2). A study aimed at differentiation of PD from atypical parkinsonian disorder revealed that ^{123}I-FP-CIT SPECT and MIBG scintigraphy have similar diagnostic accuracy (Südmeyer et al. 2011).

19.4.1 Parkinson's Disease

MIBG studies for PD began in 1994 (Hakusui et al. 1994; Yoshita et al. 1996; Iwasa et al. 1998). Their clinical value has become recognized by an increasing number of reports and experiences (Yoshita 1998; Braune et al. 1998; Orimo et al. 1999; Reinhardt et al. 2000; Druschky et al. 2000; Takatsu et al. 2000a, b; Taki et al.

2000). A characteristic feature of MIBG imaging in PD has been shown to be an impressively low uptake in the whole myocardium. The severely depressed cardiac MIBG uptake in PD seems to occur in a disease-specific manner among related movement disorders. Based on a meta-analysis of studies, the overall sensitivity and specificity for correct discrimination of patients with PD were both about 90% (Braune 2001; Orimo et al. 2012; Treglia et al. 2012).

Although the H/M ratio tends to decrease with disease progression, many PD patients in Hoehn and Yahr stage I have decreased cardiac MIBG uptake. The H/M ratio is not suitable as an index of the disease severity. Tremor-dominant patients with PD had higher MIBG uptake than those with postural instability and gait disorder, while reduced MIBG uptake was linked to greater bradykinesia, higher age at onset, and longer disease duration (Saiki et al. 2004; Spiegel et al. 2007).

Cardiac MIBG uptake is not correlated with dysautonomic clinical symptoms in patients with PD, though some cardiac autonomic tests showed a negative correlation of MIBG uptake and cardiac sympathetic denervation (Oka et al. 2011). The use of different methods for evaluation of cardiac MIBG uptake or early occurrence of sympathetic nerve fiber loss in LBD might explain such poor correlations (Iwanaga et al. 1999; Taki et al. 2004).

In genetically identified cases of PD, cardiac MIBG uptake findings are not consistent. MIBG or fluorodopamine uptake in the heart decreased in some patients with PARK1, PARK4, PARK6, PARK7, and PARK 8 mutations (Quattrone et al. 2008; Valldeoriola et al. 2011; Tijero et al. 2010). On the contrary, patients with PARK2 mutations showed no difference in H/M ratios as compared to controls (Orimo et al. 2005).

19.4.2 Dementia with Lewy Bodies

Antemortem diagnosis of DLB and differentiation of DLB from AD is important, because some patients with DLB may show an accelerated disease progression, life-threatening adverse reaction to antipsychotic medications, and a good response to anticholinesterase inhibitors. Clinical utility of MIBG scintigraphy in differentiating DLB from AD has been reported (Watanabe et al. 2001; Yoshita et al. 2001, 2006; Treglia and Gason 2012). Although the diagnosis of DLB may be confounded by the absence of parkinsonism, DLB patients without parkinsonism had a decreased MIBG accumulation in the heart as well as those with parkinsonism (Yoshita et al. 2006) (Fig. 19.3). The MIBG uptake reduction does not correlate with disease duration. To increase diagnostic weighting of MIBG in the criteria (McKeith et al. 2005), standardization of the MIBG techniques and multicenter study with standardized MIBG were performed. First, differences between collimators in institutions were standardized by using a calibration phantom (Nakajima et al. 2012, 2014). Setting of ROIs for heart and mediastinum was semi-automated by using “smart MIBG” (standardized method for automatic ROI setting in MIBG study) (Okuda et al. 2011). These methods made it possible to obtain standardized data of the H/M ratio from different institutions. Second, a prospective multicenter

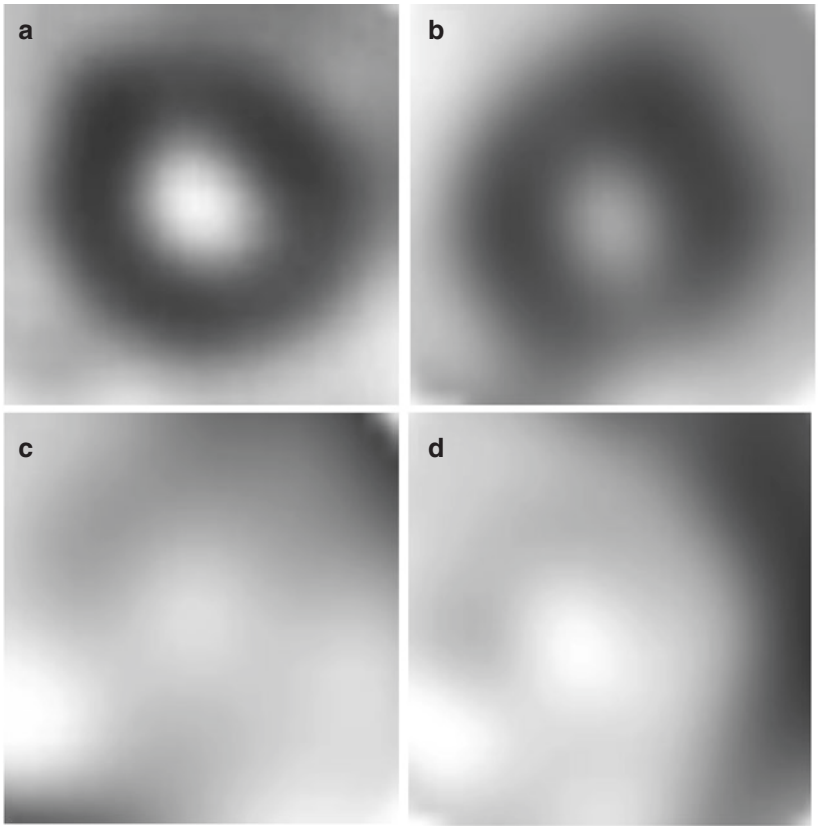

Fig. 19.3 Cardiac radioactivity in delayed short axis view after injection of ^{123}I-MIBG in a control subject, a patient with *AD*, a patient with DLB with parkinsonism, and a patient with DLB without parkinsonism. Both patients with DLB have undetectable myocardial ^{123}I-MIBG radioactivity. (**a**) Control, (**b**) AD, (**c**) DLB with parkinsonism, (**d**) DLB without parkinsonism

study for evaluation of cardiac sympathetic function for the diagnosis of DLB, involving ten institutions in Japan, was performed. Independent committees performed clinical and MIBG assessment. One hundred and thirty-three patients were registered, including probable DLB, possible DLB, and probable AD cases. This multicenter study to date found a sensitivity of 69% and specificity of 89% (Yoshita et al. 2015). The diagnostic accuracy of MIBG in this study improved when compared with clinical diagnosis 3 years after the scan (sensitivity 77%, specificity 97%) (Komatsu et al. 2018). Consensus guidelines for the clinical and pathologic diagnosis of DLB were published in 2017 (McKeith et al. 2017). In this guideline, clinical features and diagnostic biomarkers were clearly distinguished. Significant new evidence about previously reported aspects of DLB has been incorporated, with increased diagnostic weighting given to RBD and ^{123}I-MIBG myocardial scintigraphy.

Table 19.3 Discriminating DLB from AD using brain perfusion SPECT

Tracer	Subjects	Sensitivity/specificity (%)
^{99m}Tc-HMPAO	23 DLB (definite 4, probable 17, possible 2) vs. 50 AD (definite 2, probable 21, possible 27)	65/87 (Lobotesis et al. 2001)
^{123}I-IMP	19 probable DLB vs. 39 probable AD	74/82 (Hanyu et al. 2006)
^{99m}Tc-ECD	23 probable DLB vs. 23 probable AD	65/75 (Yoshita and Yamada 2003)

HMPAO hexamethyl-propylene-amine-oxine, *^{123}I-IMP* *N*-isopropyl-*p*-[^{123}I]-iodoamphetamine, *ECD* ethyl cysteinate dimer

Occipital hypoperfusion on brain perfusion SPECT is a "suggestive biomarker" of DLB as well as less severe medial temporal lobe atrophy on structural imaging (McKeith et al. 2017). When the MIBG study was compared with brain perfusion SPECT with ^{99m}Tc-ethylene cysteine dimer or ^{123}I-*N*-isopropyl-iodoamphetamine, the MIBG study seemed to be more accurate as a means of discriminating DLB from AD (Yoshita and Yamada 2003; Hanyu et al. 2006) (Table 19.3). Although brain perfusion SPECT failed to demonstrate significant hypoperfusion in the occipital region in some patients with DLB, a marked reduction of MIBG uptake was found in most of the patients with DLB.

19.4.3 Pure Autonomic Failure

PAF is a rare phenotype of Lewy body disease in which patients have prominent autonomic disturbance thought to be associated with a diffuse loss of sympathetic terminal innervations. PET with 6-^{18}F-flurodopamine as well as MIBG studies revealed a loss of cardiac tracer uptake, indicating cardiac denervation in PAF (Goldstein et al. 2000; Yoshida et al. 1997). ^{123}I-MIBG cardiac scintigraphy should be able to distinguish MSA and PAF (Hirayama et al. 1995; Kashihara et al. 2006).

19.5 Differential Diagnosis of Lewy Body Disease Using ^{123}I-MIBG Cardiac Scintigraphy

In general, a neurological differential diagnosis in the early stages between PD, MSA, PSP, and corticobasal degeneration (CBD) is important because of differences in prognosis and therapy among these diseases. In contrast with PD, central and preganglionic neurons are predominantly affected, while postganglionic neurons are usually spared in MSA. Therefore, cardiac MIBG uptake might not be impaired. In MSA, cardiac MIBG uptake is higher than that in PD, irrespective of the severity of autonomic dysfunction (Yoshita 1998; Braune et al. 1999; Orimo et al. 1999). Although 77–95% discrimination specificity between PD and MSA has been proposed (Braune 2001; Treglia et al. 2011), the Quality Standards Subcommittee of the American Academy of Neurology found insufficient evidence

Table 19.4 Demographic and clinical data

	PSP	CBD	PD	DLB	CN	*p* value
N (M/F)	19 (13/6)	7 (2/5)	19 (8/11)	11 (5/6)	13 (6/7)	NA
Duration (months)	29.4 ± 20.9	18.4 ± 12.5	67.4 ± 61.6	36.3 ± 24.6	NA	<0.01[a]
Age (years)	69.6 ± 6.7	65.6 ± 10.2	68.7 ± 5.9	75.1 ± 5.6	69.6 ± 6.7	<0.05[b]
HY stage	3.2 ± 0.4	2.9 ± 1.2	2.7 ± 1.3	2.6 ± 0.7	NA	0.33
MMSE	24.3 ± 4.9	24.3 ± 4.5	26.3 ± 1.7	20.8 ± 6.0	NA	0.078

Values are expressed as the mean ± SD
PSP progressive supranuclear palsy, *CBD* corticobasal degeneration, *PD* Parkinson's disease, *DLB* dementia with Lewy body, *CN* control, *HY stage* Hoehn and Yahr stage, *MMSE* Mini-Mental State Examination, *NA* not applicable
Post hoc comparison of significant group differences:
[a]PD vs. CBD
[b]DLB vs. CBD

to recommend MIBG cardiac imaging for differentiating PD from MSA (Suchowersky et al. 2006). A few cases of patient with MSA showed decreased cardiac MIBG uptake (Yoshita 1998, 2000). A small number of patients with MSA have postmortem evidence of postganglionic cardiac denervation which may account for the reported decreased cardiac MIBG uptake (Orimo et al. 2007). These cases of MSA may have involvement of both glial cytoplasmic inclusion in the brain and Lewy bodies in sympathetic ganglia.

PSP, classified as tauopathy, is a degenerative disorder causing supranuclear gaze palsy, bradykinesia, muscular rigidity with progressive axial dystonia, pseudobulbar palsy, and subcortical dementia. The H/M ratio of this disease entity is within normal range or slightly reduced (Yoshita 1998; Taki et al. 2000). However, we have noted a markedly low MIBG uptake in about 20% of patients with PSP (Yoshita et al. 2008) (Table 19.4, Figs. 19.4 and 19.5). These cases of PSP may have concomitant Lewy bodies (Mori et al. 2002).

CBD, also classified as tauopathy, shows asymmetric akinetic-rigid syndrome, cortical signs, and cognitive decline. MIBG imaging showed normal uptake which could be used to differentiate CBD from Lewy body diseases (Taki et al. 2000; Orimo et al. 2003; Kashihara et al. 2006; Yoshita et al. 2008), whereas autopsy-proven CBD cases which had decreased myocardial uptake of MIBG were reported. In one case, Lewy bodies, which were not seen in the central nervous system, were seen only in the sympathetic ganglia, and a severe loss of nerve fibers was apparent in the sympathetic nerve endings in the heart (Mori et al. 2012). In another case, there were no Lewy pathologies in both the central nervous system and the sympathetic ganglia (Yoshimura et al. 2018). There might be other mechanisms such as norepinephrine transporter dysfunction to reduce cardiac MIBG accumulation besides pathologically proven cardiac sympathetic damage (Yoshita 1998).

Nagayama et al. reported that nearly 70% of the patients without PD also had low uptake, and there were considerable overlaps in the H/M ratio (2005). Although reduced cardiac accumulation of MIBG represents a pathological change in the sympathetic nerve endings in the heart, the distribution of Lewy bodies cannot be

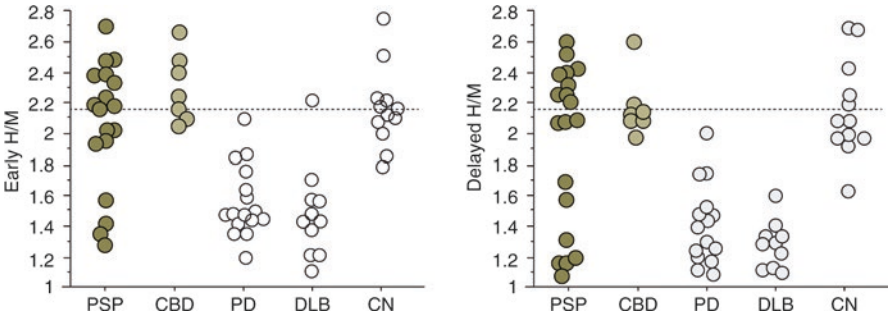

Fig. 19.4 Individual values for the H/M ratio in the study of LBD, PSP, and CBD. The dashed line indicates the mean value in the control (CN) group. Significantly reduced H/M ratios in both the early and the delayed images were observed in the Lewy body disease (LBD) group in comparison with progressive supranuclear palsy (PSP), corticobasal degeneration (CBD), and CN groups. Four of the early and five of the delayed images of the patients with PSP have a reduced H/M ratio

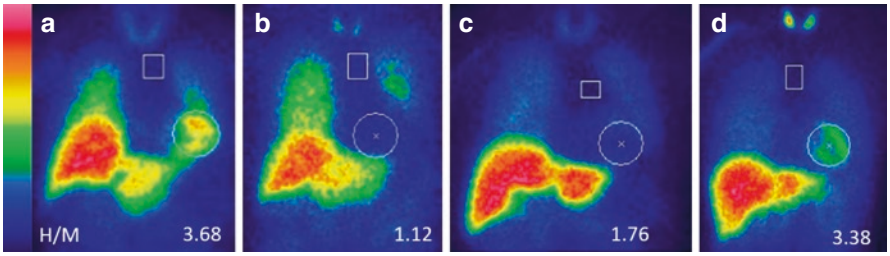

Fig. 19.5 smartMIBG (Okuda et al. 2011) view of delayed planar images in AD, PSP, and DLB patients. Patients with AD (**a**) and PSP (**d**) show significant cardiac accumulation. Patients with DLB (**b**) and another PSP (**c**) have no cardiac uptake and reduced H/M ratio

determined from this finding. Thus, MIBG cardiac scintigraphy should not be used alone to confirm a diagnosis of PD. With respect to this, combining other neuroimaging method such as brain MRI, ^{123}I-FP-CIT SPECT, or transcranial sonography measurement to MIBG scintigraphy may improve diagnostic accuracy of PD in comparison with MIBG scintigraphy alone (Kollensperger et al. 2007; Kajimoto et al. 2009; Rascol and Schelosky 2009; Südmeyer et al. 2011).

A few data show that ^{123}I-MIBG cardiac scintigraphy is useful to distinguish LBD from other movement disorder and dementia syndromes, such as essential tremor, drug-induced parkinsonism, vascular parkinsonism, and frontotemporal dementia (Orimo et al. 1999; Lee et al. 2007; Movellino et al. 2010).

19.6 Conclusion

In Lewy body disease, both central and peripheral autonomic nervous systems are involved. The myocardial MIBG defects reflect a pathological progression of the disease process involving extensive autonomic involvement. Considering all the

data together, severe myocardial MIBG uptake reduction seems to be a specific marker of Lewy body disease. If these ^{123}I-MIBG findings reflect cardiac Lewy body pathology and precede CNS involvement, ^{123}I-MIBG myocardial scintigraphy may have the potential to diagnose Lewy body disease in its preclinical stages, which could be useful in evaluating the impact of disease-modifying and preventive interventions.

References

Braune S (2001) The role of cardiac metaiodobenzylguanidine uptake in the differential diagnosis of parkinsonian syndromes. Clin Auton Res 11:351–355

Braune S, Reinhardt M, Bathmann J et al (1998) Impaired cardiac uptake of meta-[123I]iodobenzylguanidine in Parkinson's disease with autonomic failure. Acta Neurol Scand 97:307–314

Braune S, Reinhardt M, Schnitzer R et al (1999) Cardiac uptake of [123I]MIBG separates Parkinson's disease from multiple system atrophy. Neurology 53:1020–1025

Druschky A, Hilz MJ, Platsch G et al (2000) Differentiation of Parkinson's disease and multiple system atrophy in early disease stages by means of I-123-MIBG- SPECT. J Neurol Sci 175:3–12

Glowniak JV, Turner FE, Gray LL et al (1989) Iodine-123 metaiodobenzylguanidine imaging of the heart in idiopathic congestive cardiomyopathy and cardiac transplants. J Nucl Med 30:1182–1191

Goldstein DS, Holmes C, Li ST, Bruce S et al (2000) Cardiac sympathetic denervation in Parkinson disease. Ann Intern Med 133:338–347

Hakusui S, Yasuda T, Yanagi T et al (1994) A radiological analysis of heart sympathetic functions with meta-[123I]iodobenzylguanidine in neurological patients with autonomic failure. J Auton Nerv Syst 49:81–84

Hanyu H, Shimizu S, Hirao K et al (2006) Comparative value of brain perfusion SPECT and [123I]MIBG myocardial scintigraphy in distinguishing between dementia with Lewy bodies and Alzheimer's disease. Eur J Nucl Med Mol Imaging 33:248–253

Hirayama M, Hakusui S, Koike Y et al (1995) A scintigraphical qualitative analysis of peripheral vascular sympathetic function with meta-[123I]iodobenzylguanidine in neurological patients with autonomic failure. J Auton Nerv Syst 53:230–234

Iwanaga K, Wakabayashi K, Yoshimoto M et al (1999) Lewy body type degeneration in cardiac plexus in Parkinson's and incidental Lewy body diseases. Neurology 52:1269–1271

Iwasa K, Nakajima K, Yoshikawa H (1998) Decreased myocardial ^{123}I-MIBG uptake in Parkinson's disease. Acta Neurol Scand 97:303–306

Kajimoto Y, Miwa H, Okawa-Izawa M et al (2009) Transcranial sonography of the substantia nigra and MIBG myocardial scintigraphy: complementary role in the diagnosis of Parkinson's disease. Parkinsonism Relat Disord 15:270–272

Kashihara K, Ohno M, Kawada S et al (2006) Reduced cardiac uptake and enhanced washout of 123I-MIBG in pure autonomic failure occurs conjointly with Parkinson's disease and dementia with Lewy bodies. J Nucl Med 47:1099–1101

Kollensperger M, Seppi K, Liener C et al (2007) Diffusion weighted imaging best discriminates PD from MSA-P: a comparison with tilt table testing and heart MIBG scintigraphy. Mov Disord 22:1771–1776

Komatsu J, Samuraki M, Nakajima K et al (2018). ^{123}I-MIBG myocardial scintigraphy for the diagnosis of DLB: a multicentre 3-year follow-up study J Neurol Neurosurg Psychiatry 89(11):1167–1173

Lee PH, Yeo SH, Yong SW et al (2007) Odour identification test and its relation to cardiac 123I-metaiodobenzylguanidine in patients with drug induced parkinsonism. J Neurol Neurosurg Psychiatry 78:1250–1252

Lobotesis K, Fenwick JD, Phipps A et al (2001) Occipital hypoperfusion on SPECT in dementia with Lewy bodies but not AD. Neurology 56:643–649

McKeith IG, Dickson DW, Lowe J et al (2005) Diagnosis and management of dementia with Lewy bodies: third report of the DLB Consortium. Neurology 65:1863–1872
McKeith I, O'Brien J, Walker Z et al (2007) Sensitivity and specificity of dopamine transporter imaging with 123I-FP-CIT SPECT in dementia with Lewy bodies: a phase III, multicentre study. Lancet Neurol 6:305–313
McKeith IG, Boeve BF, Dickson DW et al (2017) Diagnosis and management of dementia with Lewy bodies: fourth consensus report of the DLB Consortium. Neurology 89:88–100
Merlet P, Valette H, Dubois-Rande JL et al (1992) Prognostic value of cardiac metaiodobenzylguanidine imaging in patients with heart failure. J Nucl Med 33:471–477
Mitsui J, Saito Y, Momose T et al (2006) Pathology of the sympathetic nervous system corresponding to the decreased cardiac uptake in ^{123}I-metaiodobenzylguanidine (MIBG) scintigraphy in a patient with Parkinson's disease. J Neurol Sci 243:101–104
Miyamoto T, Miyamoto M, Inoue Y et al (2006) Reduced cardiac ^{123}I-MIBG scintigraphy in idiopathic REM sleep behavior disorder. Neurology 67:2236–2238
Mori H, Oda M, Komori T et al (2002) Lewy bodies in progressive supranuclear palsy. Acta Neuropathol 104:273–278
Mori K, Iwasaki Y, Ito M et al (2012) Decreased myocardial uptake of meta-iodobenzylguanidine in an autopsy-confirmed case of corticobasal degeneration with Lewy bodies restricted to the sympathetic ganglia. Clin Neurol 52:405–410
Movellino F, Bagnato A, Salsone M et al (2010) Myocardial ^{123}I-MIBG scintigraphy for differentiation of Lewy bodies disease from FTD. Neurobiol Aging 31:1903–1933
Nagayama H, Hirayama M et al (2005) Reliability of MIBG myocardial scintigraphy in the diagnosis of Parkinson's disease. J Neurol Neurosurg Psychiatry 76:249–251
Nakajima K, Bunko H, Taki J et al (1990) Quantitative analysis of 123I-meta-iodobenzylguanidine (MIBG) uptake in hypertrophic cardiomyopathy. Am Heart J 119:1329–1337
Nakajima K, Yoshita M, Matsuo S et al (2008) Iodine-123-MIBG sympathetic imaging in Lewy-body diseases and related movement disorders. Q J Nucl Mol Imaging 52:378–387
Nakajima K, Okuda K, Matsuo S et al (2012) Standardization of metaiodobenzylguanidine heart to mediastinum ratio using a calibration phantom: effects of correction on normal databases and a multicentre study. Eur J Nucl Med Mol Imaging 39:113–119
Nakajima K, Okuda K, Yoshimura M et al (2014) Multicenter cross-calibration of I-123 metaiodobenzylguanidine heart-to-mediastinum ratios to overcome camera-collimator variations. J Nucl Cardiol 21:970–978
Oka H, Toyoda C, Yogo M et al (2011) Reduced cardiac 123I-MIBG uptake reflects sympathetic dysfunction in de novo Parkinson's disease. J Neural Transm 118:1323–1327
Okuda K, Nakajima K, Hosoya T et al (2011) Semi-automated algorithm for calculating heart-to-mediastinum ratio in cardiac Iodine-123 MIBG imaging. J Nucl Cardiol 18:82–89
Orimo S, Ozawa E, Nakade S et al (1999) ^{123}I-metaiodobenzylguanidine myocardial scintigraphy in Parkinson's disease. J Neurol Neurosurg Psychiatry 67:189–194
Orimo S, Ozawa E, Nakade S et al (2003) [123I] meta-iodobenzylguanidine myocardial scintigraphy differentiates corticobasal degeneration from Parkinson's disease. Intern Med 42:127–128
Orimo S, Amino T, Yokouchi M et al (2005) Preserved cardiac sympathetic nerve accounts for normal cardiac uptake of MIBG in PARK2. Mov Disord 20:1350–1353
Orimo S, Kanazawa T, Nakamura A et al (2007) Degeneration of cardiac sympathetic nerve can occur in multiple system atrophy. Acta Neuropathol 113:81–86
Orimo S, Suzuki M, Inaba A et al (2012) ^{123}I-MIBG myocardial scintigraphy for differentiating Parkinson's disease from other neurodegenerative parkinsonism: a systematic review and meta-analysis. Parkinsonism Relat Disord 18:494–500
Quattrone A, Bangnato A, Annesi G et al (2008) Myocardial ^{123}I-metaiodobenzylguanidine uptake in genetic Parkinson's disease. Mov Disord 23:21–27
Rascol O, Schelosky L (2009) ^{123}I-metaiodobezylguanidine scintigraphy in Parkinson's disease and related disorders. Mov Disord 24(Suppl 2):S732–S741

Reinhardt MJ, Jungling FD, Krause TM et al (2000) Scintigraphic differentiation between two forms of primary dysautonomia early after onset of autonomic dysfunction: value of cardiac and pulmonary iodine-123 MIBG uptake. Eur J Nucl Med 27:595–600

Saiki S, Hirose G, Sakai K et al (2004) Cardiac ^{123}I-MIBG scintigraphy can assess the disease severity and phenotype of PD. J Neurol Sci 220:105–111

Solanki KK, Bomanji J, Moyes J et al (1992) A pharmacological guide to medicines which interfere with the biodistribution of radiolabelled meta-iodobenzylguanidine (MIBG). Nucl Med Commun 13:513–521

Spiegel J, Hellwig D, Farmakis G et al (2007) Myocardial sympathetic degeneration correlates with clinical phenotype of Parkinson's disease. Mov Disord 22:1004–1008

Suchowersky O, Reich S, Perlmutter J et al (2006) Practice parameter: diagnosis and prognosis of new onset Parkinson disease (an evidence-based review): report of the Quality Standards Subcommittee of the American Academy of Neurology. Neurology 66:968–975

Südmeyer M, Antke C, Zizek T et al (2011) Diagnostic accuracy of combined FP-CIT, IBZM, and MIBG scintigraphy in the differential diagnosis of degenerative parkinsonism: a multidimensional statistical approach. J Nucl Med 52:733–740

Takahashi M, Ikemura M, Oka T et al (2015) Quantitative correlation between cardiac MIBG uptake and remaining axons in the cardiac sympathetic nerve in Lewy body disease. J Neurol Neurosurg Psychiatry 86:939–944

Takatsu H, Nagashima K, Murase M et al (2000a) Differentiating Parkinson disease from multiple-system atrophy by measuring cardiac iodine-123 metaiodobenzylguanidine accumulation. JAMA 284:44–45

Takatsu H, Nishida H, Matsuo H et al (2000b) Cardiac sympathetic denervation from the early stage of Parkinson's disease: clinical and experimental studies with radio-labeled MIBG. J Nucl Med 41:71–77

Taki J, Nakajima K, Hwang EH et al (2000) Peripheral sympathetic dysfunction in patients with Parkinson's disease without autonomic failure is heart selective and disease specific. Eur J Nucl Med 27:566–573

Taki J, Yoshita M, Yamada M et al (2004) Significance of ^{123}IMIBG scintigraphy as a pathophysiological indicator in the assessment of Parkinson's disease and related disorders: it can be a specific marker for Lewy body disease. Ann Nucl Med 18:453–461

Tijero B, Gomez-Esteban JC, Llorens V et al (2010) Cardiac sympathetic denervation precedes nigrostrial loss in the E46K mutation of the alpha-synuclein gene (SNCA). Clin Auton Res 20:267–269

Treglia G, Gason E (2012) Diagnostic performance of myocardial innervation imaging using MIBG scintigraphy in differential diagnosis between dementia with Lewy bodies and other dementias: a systematic review and a meta-analysis. J Neuroimaging 22:111–117

Treglia G, Stefanelli A, Gason E et al (2011) Diagnostic performance of iodine-123-metaiodobenzylguanidine scintigraphy in differential diagnosis between Parkinson's disease and multiple-system atrophy: a systematic review and a meta-analysis. Clin Neurol Neurosurg 113:823–829

Treglia G, Cason E, Stefanelli A et al (2012) MIBG scintigraphy in differential diagnosis of parkinsonism: a meta-analysis. Clin Auton Res 22:43–55

Valldeoriola F, Gaig C, Muxi A et al (2011) ^{123}I-MIBG cardiac uptake and smell identification in parkinsonian patients with LRRK2 mutations. J Neurol 258:1126–1132

Wakabayashi K, Takahashi H (1997) Neuropathology of autonomic nervous system in Parkinson's disease. Eur Neurol 38(Suppl 2):2–7

Watanabe H, Ieda T, Katayama T et al (2001) Cardiac ^{123}I-meta-iodobenzylguanidine (MIBG) uptake in dementia with Lewy bodies: comparison with Alzheimer's disease. J Neurol Neurosurg Psychiatry 70:781–783

Yoshida M, Fukumoto Y, Kuroda Y et al (1997) Sympathetic denervation of myocardium demonstrated by ^{123}I-MIBG scintigraphy in pure autonomic failure. Eur Neurol 38:291–296

Yoshimura N, Homma T, Uchihara T et al (2018) Decreased uptake of metaiodobenzylguanidine (MIBG) myocardial scintigraphy in a 64-year-old female, who was diagnosed as a progressive supranuclear palsy. Brain Nerve 70:929–936

Yoshita M (1998) Differentiation of idiopathic Parkinson's disease from striatonigral degeneration and progressive supranuclear palsy using iodine-123 meta-iodobenzylguanidine myocardial scintigraphy. J Neurol Sci 155:60–67

Yoshita M (2000) Cardiac uptake of [123I]MIBG separates PD from multiple system atrophy. Neurology 54:1877–1878

Yoshita M, Yamada M (2003) Occipital cerebral hypoperfusion and cardiac sympathetic dysfunction in dementia with Lewy bodies and MIBG scintigraphy in patients with dementia of the Alzheimer's type. Neurology 60(Suppl 1):A208

Yoshita M, Matsubara S, Tada A (1996) Decreased accumulation of ^{123}I-metaiodobenzylguanidine myocardial scintigraphy in Parkinson's disease. Neurol Med 45:221–225

Yoshita M, Hayashi M, Hirai S (1998) Decreased myocardial accumulation of ^{123}I-meta-iodobenzyl guanidine in Parkinson's disease. Nucl Med Commun 19:137–142

Yoshita M, Taki J, Yamada M (2001) A clinical role for [(123)I]MIBG myocardial scintigraphy in the distinction between dementia of the Alzheimer's-type and dementia with Lewy bodies. J Neurol Neurosurg Psychiatry 71:583–588

Yoshita M, Taki J, Yokoyama K et al (2006) Value of ^{123}I-MIBG radioactivity in the differential diagnosis of DLB from AD. Neurology 66:1850–1854

Yoshita M, Noto D, Takahashi K et al (2008) ^{123}I-MIBG scintigraphy in PSP, CBD and IPD. Clin Auton Res 18:281

Yoshita M, Arai H, Arai T et al (2015) Diagnostic accuracy of ^{123}I-meta-iodobenzylguanidine myocardial scintigraphy in dementia with Lewy bodies: a multicenter study. PLoS One 10:e012054

Part III

Cerebrovascular Disorders

Perfusion Imaging in Healthy Human Aging

20

Sabine L. Collette, Auke P. Appelman, and Reinoud P. H. Bokkers

Contents

20.1 Introduction . . . 594
20.2 Cerebral Perfusion . . . 594
20.2.1 Cerebral Autoregulation . . . 595
20.2.2 Hemodynamic Impairment . . . 595
20.3 Age-Related Perfusion Changes . . . 596
20.3.1 Development of Perfusion in Infants and Adolescence . . . 596
20.3.2 Age-Induced Changes in CBF . . . 597
20.3.3 Vascular Cognitive Impairment . . . 598
20.4 Perfusion Imaging . . . 599
20.4.1 Single-Photon Emission CT . . . 599
20.4.2 PET . . . 601
20.5 Conclusions . . . 602
References . . . 603

Abstract

Healthy aging is the process of developing and maintaining the functional ability that enables well-being in older age. For brain diseases, such as cognitive decline and stroke, age is one of the most important risk factors. Increasing evidence shows that functional impairment of the cerebral microvasculature and perfusion plays a critical role in these various age-related medical conditions.

In this chapter, we will discuss cerebral perfusion, the effect of aging upon cerebral perfusion, and the potential mechanisms involved in age-related cerebrovascular dysfunction. Second, we will discuss the clinical application of positron emission tomography (PET) and single-photon emission computed tomography (SPECT) imaging for evaluation cerebral perfusion and age-related changes.

S. L. Collette · A. P. Appelman · R. P. H. Bokkers (✉)
Department of Radiology, Medical Imaging Center, University Medical Center Groningen, University of Groningen, Groningen, The Netherlands
e-mail: s.l.collette@umcg.nl; a.appelman@umcg.nl; r.p.h.bokkers@umcg.nl

R. A. J. O. Dierckx et al. (eds.), *PET and SPECT in Neurology*,
https://doi.org/10.1007/978-3-030-53168-3_20

20.1 Introduction

Healthy aging is the process of developing and maintaining the functional ability that enables well-being in older age (Beard et al. 2016). This ongoing interaction between the individual and its surrounding environment may lead to a long life with a high level of maintained functionality.

Improvements in public health, education, and health care have resulted in a steep increase in global life expectancy over the past several decades. As the global population aged over 60 years is expected to double within the next 30 years, the incidence of age-related injuries and diseases will increase with medical and economic consequences. Effective intervention strategies are therefore needed in order to prevent and delay the progression of these age-related conditions.

For brain diseases, such as cognitive decline and stroke, age is one of the most important risk factors. Increasing evidence shows that functional impairment of the cerebral microvasculature and perfusion plays a critical role in various age-related medical conditions.

The purpose of this chapter is twofold. First, we will discuss cerebral perfusion, the effect of aging upon cerebral perfusion, and the potential mechanisms involved in age-related cerebrovascular dysfunction. Second, we will discuss the clinical application of positron emission tomography (PET) and single-photon emission computed tomography (SPECT) imaging for evaluation of cerebral perfusion and age-related changes.

20.2 Cerebral Perfusion

Cerebral perfusion is the delivery of blood to the brain tissue parenchyma. A steady supply of oxygen- and nutrients-enriched blood is needed, as the brain has a high energy demand, but however a limited capacity to store intracellular energy substrates. Basic physiological functions of the CNS, such as synaptic transmission, the membrane ion pump, and energy metabolism, consume 20% of the total body oxygen output and 25% of glucose (Kety and Schmidt 1948). To fulfill the energy demand, approximately 750 ml/min of freshly oxygenated blood is delivered to the brain by arterial vessels. Consequently, the brain receives roughly 15% of the cardiac output, while it only constitutes 2% of the total body weight.

The blood volume passing through the brain per time unit can be expressed as cerebral blood flow (CBF). The standard unit of measurement for CBF is milliliters of blood per 100 g of tissue per minute. Normal gray matter is perfused at a rate of roughly 60 ml/100 g/min and white matter at a rate of 20 ml/100 g/min. In some literature, CBF is expressed as flow per unit of volume of brain tissue. It is important to recognize that these values are not comparable to flow per 100 g of tissue per minute, as brain tissue weighs on average between 1.04 and 1.06 g/ml (Barber et al. 1970).

The two main factors that determine CBF are the cerebral perfusion pressure (CPP) and vascular resistance within the brain. CPP is the main pressure gradient

causing blood to flow from the supplying vasculature to the brain (Lassen 1959). It is defined as the difference between the mean arterial pressure (MAP), which is the weighted average of the systolic and diastolic pressure, and the intracranial pressure (ICP), which is the pressure of the cerebrospinal fluid (CSF) in the subarachnoid space. The vascular resistance is the accumulative effect of the resistance within the cerebrovasculature, from the large cervical arteries up to the smallest cerebral arterioles.

20.2.1 Cerebral Autoregulation

Cerebral autoregulation refers to the physiological mechanisms that aim to maintain stable cerebral blood flow despite changes in the systemic blood flow. Under normal conditions, CBF is primarily determined by the amount of resistance within cerebral blood vessels, which is directly related to their diameter. Through transitory dilatation and constriction of the small artery and arteriole walls, the vascular resistance of the brain tissue can be varied within seconds to minimize the effect of systemic blood pressure variations (Lassen 1959; Aaslid et al. 1989).

The concept of cerebral autoregulation was first described by Lassen in 1959, after evidence was found of changes of vascular diameter of the cerebral vessels in animal studies (Lassen 1959). Initially thought to be only controlled by carbon dioxide and changes in the cerebral perivascular nerves, three different mechanisms have been found to contribute to the process of autoregulation. These mechanisms are myogenic, neurogenic, and metabolic (Rapela and Green 1964; MacKenzie et al. 1979; McHedlishvili 1980). Myogenic regulation is the detection of changes in blood pressure through a stress sensing mechanism in the large arteries and arterioloes. An increase in the transmural pressure causes depolarization of vascular smooth muscle cells, increasing intracellular Ca^{2+} levels and promoting vasoconstriction. Because the large proximal arteries take up to 40% of the total cerebral resistance into account, this response plays an important role in preventing high pressure from reaching the distal cerebral circulation (Toth et al. 2017). For the neurogenic mechanism, the perivascular neurons exert an autoregulatory effect controlled via sympathetic innervation from the brainstem. The metabolic mechanism is driven by differences in concentrations of vasoactive metabolites, such as adenosine, caused by differences in cerebral metabolism and oxygen delivery (Fantini et al. 2016).

20.2.2 Hemodynamic Impairment

CBF is stable under normal conditions; however, a number of physiological and biochemical mechanisms, such as extreme changes in cardiac output or stenoocclusive lesions in the arteries feeding the brain, may lead to fluctuations that are beyond the autoregulatory limits. In 1954, Finnerty and colleagues studied the effect of systemic hypotension on brain function and CBF in awake subjects using the

nitrous oxide Kety-Schmidt method (Finnerty Jr et al. 1954). This method was the first to provide quantitative measures of CBF by assessing the area between the arterial and venous washout curves of a diffusible tracer. With this method, they were the first to describe that whenever CBF was below 29 ml/100 g/min, neurological signs would appear. Shortly thereafter, Jennett and colleagues studied the effect of CBF decrease in a study in which the carotid artery was clamped during surgical revascularization of the carotid artery (Jennett et al. 1966). By means of intra-arterial injection of ^{133}Xe into the carotid artery, they observed that hemiparesis developed if cortical CBF dropped 30% from the pre-occlusion level.

Hemodynamic impairment is classically divided in three stages (Powers et al. 1985). In the first stage, CBF is maintained through the vasodilatory response. This results in an increase in the volume of cerebral blood in the brain, while CBF may decrease up to 18%. Stage 2 of hemodynamic compromise occurs when the vasodilatory capacity is overcome. In this stage, CBF will decrease passively with the decline in perfusion pressure. In order to sustain oxygen metabolism, the oxygen extracted from blood will increase to its maximum. This phase, in which flow reduction is balanced by an increased oxygen extraction fraction (OEF) from the blood to maintain the cerebral metabolic rate of oxygen ($CMRO_2$), is called oligemia. A further decline, described in stage 3, leads to a fall of both the cerebral metabolic rate of oxygen ($CMRO_2$), CBV and possibly also OEF (Nemoto et al. 2003),eventually resulting in cellular ischemia and permanent brain tissue damage. Interestingly, animal studies have shown that before this phase occurs, the cerebral metabolic rate of glucose transiently increases, potentially caused by an increase in anaerobic metabolism to maintain ATP levels (Paschen et al. 1992).

20.3 Age-Related Perfusion Changes

Changes in cerebral perfusion occur throughout the various stages of development and aging of the brain. This is caused by altered blood flow, autoregulation, neurovascular coupling, and endothelial permeability.

20.3.1 Development of Perfusion in Infants and Adolescence

In infants born before 37 completed weeks of gestation (preterm), the CBF is substantially lower than in infants born between 37 and 42 weeks (term), due to ongoing development of the cerebral vasculature. In humans, the arterial development starts in the brain stem and cerebellum between 20 and 24 weeks, before developing in the basal ganglia and diencephalon by week 24–28 and lastly in the cortex. Initially, a single vascular plexus covers the cerebral surface to form the vasculature. By the 24th week of gestation, penetrating vessels descend from the pial surface down toward the ventricles to form arterial end zones (Brew et al. 2014). Where normal gray matter is perfused at a rate of roughly 60 ml/100 g/min in adolescents, studies using Xenon clearance techniques and PET have shown that the CBF in

preterm range between 5 and 19 ml/100 g/min (Greisen 1986; Altman et al. 1993). Animal studies in lambs have furthermore shown that the autoregulation takes longer to develop and is not fully functional until 19 weeks of gestation in lambs, which corresponds to approximately 36 weeks in humans (Helou et al. 1994). Using transcranial Doppler (TCD), this has also been demonstrated in human studies, where the autoregulatory function was found to develop between 23 and 33 weeks of gestation (Rhee et al. 2014). Using near-infrared spectroscopy (NIRS), studies have shown that impairment of these autoregulatory mechanisms significantly increase the risk of death and intraventricular hemorrhage (Tsuji et al. 2000; Alderliesten et al. 2013; Wong et al. 2012).

20.3.2 Age-Induced Changes in CBF

Large cohort studies have shown that in middle-aged and elderly adults, there is a decrease of 4–5% in global CBF per decade (Lu et al. 2011). This decline is thought to be caused by a multitude of factors, of which arterial stiffness and an increase in blood pressure, a decrease in cardiac output, and impairment of autoregulatory mechanisms play a role (Nagata et al. 2016).

Arterial stiffness refers to the reduction of elasticity of conduit arteries, such as the aorta and carotid arteries, due to an increase of calcium depositions and collagen in particularly the intima (Bergsneider et al. 1998; Kovacic et al. 2011). As a result, the pulsatile flow from the heart cannot be adequately damped to a continuous blood flow before it reaches the capillary bed (Scuteri et al. 2011). Therefore, the arterial stiffness is associated with increased amplitude of the systolic pressure in the aorta (Phan et al. 2016). The inclined central pulse pressure may lead to damage of the large cerebral vessels and deep microvasculature, resulting in (micro) hemorrhages, endothelial injury, and blood-brain barrier disruption due to damage to the neurovascular unit. Thickening and weakening of the arterial wall may furthermore result in activation of platelets and the clotting cascade causing ischemic lesions due to thrombotic obstructions. As a consequence, vascular cognitive impairment may develop (Gorelick et al. 2011).

As mentioned above, the CBF partly depends on the MAP and thus on the cardiac output. Therefore, age-related decline in cardiac output may play a role in the decrease of CBF during aging (Tarumi and Zhang 2018; Meng et al. 2015). Xing et al. investigated this possible relationship by determining a CBF/cardiac output ratio index in 139 healthy adults between 21 and 80 years and found that this ratio declined by 1.3% per decade. There was however no association between both variables, as the cardiac output remained constant during aging, while the CBF decreased (Xing et al. 2017).

The CBF is tightly regulated by the arterial carbon dioxide tension ($PaCO_2$). Under healthy conditions, an increase of $PaCO_2$ results an incline of CBF by vasodilatation and a decrease of $PaCO_2$ in a decline of CBF by vasoconstriction (Kanno et al. 1988). The relationship between the CBF and $PaCO_2$ is called the cerebral vasomotor reactivity (CVMR). Studies show different outcomes with regard to the

effect of aging on the CVMR due to lack of a standardized protocol to measure the CMVR (Riecker et al. 2003; Bakker et al. 2004; Kastrup et al. 1998; Ito et al. 2002; Zhu et al. 2013; Thomas et al. 2013). Overall, the CMVR seems to decrease during aging. In the Rotterdam study, it declined with 0.6%/kPa up to 90 years of age (Bakker et al. 2004). Furthermore, sex seems to be associated with the CMVR, women developing a greater decline in vasomotor reactivity during aging (Bakker et al. 2004; Kastrup et al. 1998). In vascular dementia, the vasomotor reactivity is impaired due to dilated vessels caused by the ischemia of multiple cerebral infarctions. It is unclear whether CMVR is also affected by Alzheimer's disease because the discovered associations could have been biased by coexisting vascular lesions (Nagata et al. 2000; Bonte et al. 1989).

Neurovascular coupling is the mechanism that adjusts the regional CBF in response to neuronal activity to fulfill the high energetic demand of neurons (Haydon and Carmignoto 2006). During aging, the connection between CBF and neurons weakens due to increased production of reactive oxygen species (Park et al. 2007; Csiszar et al. 2002; Fabiani et al. 2014). This uncoupling is expected to affect the neuronal function of the brain leading to cognitive decline (Fabiani et al. 2014; Sorond et al. 2005). Furthermore, it can aggravate the outcome of patients with Alzheimer's disease (Hock et al. 1997; Janik et al. 2016). The reduced response of CBF to neuronal activity may, however, be reversible as a decreased production of reactive oxygen species was found in aged mice treated with resveratrol (Toth et al. 2014).

20.3.3 Vascular Cognitive Impairment

Epidemiological, clinical, and experimental studies are increasingly showing that these age-related changes to neurovascular function and CBF play a critical role in the pathogenesis of many types of cognitive impairment. The concept of vascular cognitive impairment and dementia (VCI or VCID) was introduced to capture the wide spectrum of age-related vascular pathologies that disrupts normal brain function and may cause cognitive impairment through brain ischemia or loss of vascular integrity with hemorrhage. Given the etiologic complexity and wide clinical heterogeneity, the Vascular Impairment of Cognition Classification Consensus Study was designed to achieve a consensus on the conceptualization of impairment in cognition (Skrobot et al. 2017). In this recent guideline, severity of impairment is divided into mild and major. In mild VCI, there is at least impairment in one cognitive domain and mild to no impairment in instrumental activities of daily living. In major VCI (also called vascular dementia), there are clinically significant deficits of sufficient severity in at least one cognitive domain (deficits may be present in multiple domains) and severe disruption in daily living. Major VCI (also called Vascular Dementia) can furthermore be classified in four subtypes; post-stroke dementia, mixed dementia, subcortical ischemic vascular dementia, and multi-infarct dementia.

A requirement for the diagnosis of mild and major VCI is that there is imaging evidence of cerebrovascular disease. Despite the underlying vascular etiology, the diagnosis is made based on structural changes in terms of brain atrophy, white matter lesions of vascular origin, prior ischemic lesions, and (micro)hemorrhages. Imaging of perfusion and age-related changes to the vascular tree may in the future help to improve phenotyping and to investigate the etiology of VCI (Skrobot et al. 2018).

20.4 Perfusion Imaging

Throughout the last decades there have been vast improvements in the techniques for imaging brain perfusion. Seminal work in the 1950s by Seymour Kety and Carl Schmidt paved the way for development of a wide variety of methods for measuring CBF. The Kety/Schmidt method provided a quantitative value of CBF by measuring the uptake of nitrous oxide after inhalation and measuring the difference between the area of the arterial and venous washout curve (Kety and Schmidt 1948).

Since this early research, many different imaging techniques have developed, such as PET, SPECT, Xenon-enhanced computed tomography (XeCT), Doppler ultrasound, CT, and magnetic resonance imaging (MRI). These methods can be broadly categorized as "direct" or "indirect" measures. Direct techniques measure cerebral perfusion and tissue level. These techniques include, but are not limited to, PET, SPECT, Xenon-enhanced computed tomography, dynamic perfusion computed tomography (CT), magnetic resonance susceptibility contrast imaging, and arterial spin labeling magnetic resonance imaging (MRI). Indirect techniques provide information regarding the flow velocity in the afferent arteries (TCD and phase-contrast MRI) or measure various tissue properties that are related to cerebral perfusion, such as NIRS where regional hemoglobin oxygenation and deoxygenation are measured (Wintermark et al. 2005). While the direct techniques provide similar information regarding hemodynamics and are based on the measurement of the amount of a tracer delivered to the human brain tissue by blood, the principles underlying each technique differ, as do their relative strengths and weaknesses.

20.4.1 Single-Photon Emission CT

Perfusion imaging with SPECT is performed by generating tomographic images of the distribution of a flow tracer or a receptor binding substance tagged with a radionuclide. Proportionately to the rate of delivery of nutrients to the brain tissue, these radionuclide-labeled agents pass the blood-brain barrier and are then metabolized and retained intracellularly. Using a gamma camera and the technique of CT, the distribution of the radionuclide is visualized. Depending on the nature of the tracer,

a number of minutes are allowed to pass prior to imaging. Historically inhaled ^{133}Xe gas was the most used method for assessing cerebral perfusion; however the gamma rays emitted by this radionuclide are of low energy, resulting in poor spatial resolution and abundant scatter. Currently, flow tracers such as hexamethylpropyleneamine oxime (HMPAO), ethyl cysteinate dimer (ECD), and nisopropyl-*p*-iodoamphetamine (IMP), labeled with the radioisotope technetium-99m (^{99m}Tc), are the most common clinically used gamma ray producing radiopharmaceuticals. The doses used in adults are typically 20 mCi for HMPAO, 30 mCi for ECD, and 5 mCi for IMP. These amounts of radioactivity represent effective doses of 6.88, 2.21 and 3.53 mSv, respectively (Wintermark et al. 2005).

Rather than being able to provide absolute CBF values, SPECT provides brain perfusion indices of regional cerebral blood flow, which can be used to determine the presence of hypo- and hyperperfusion. Its clinical applicability lies in a variety of neurologic disorders, where qualitative assessment of perfusion is of importance, varying from (sub)acute stroke for perfusion-deficit detection to identifying hypoperfusion in cognitive decline (Fig. 20.1) seizures and neoplasms. An advantage of SPECT is that the radionuclide-labelled agents distribution remains relatively stable from 20 min to 6 h after the injection, depending on the specific agent (Assessment of brain SPECT report of the Therapeutics and Technology Assessment Subcommittee of the American Academy of Neurology 1996). This allows the

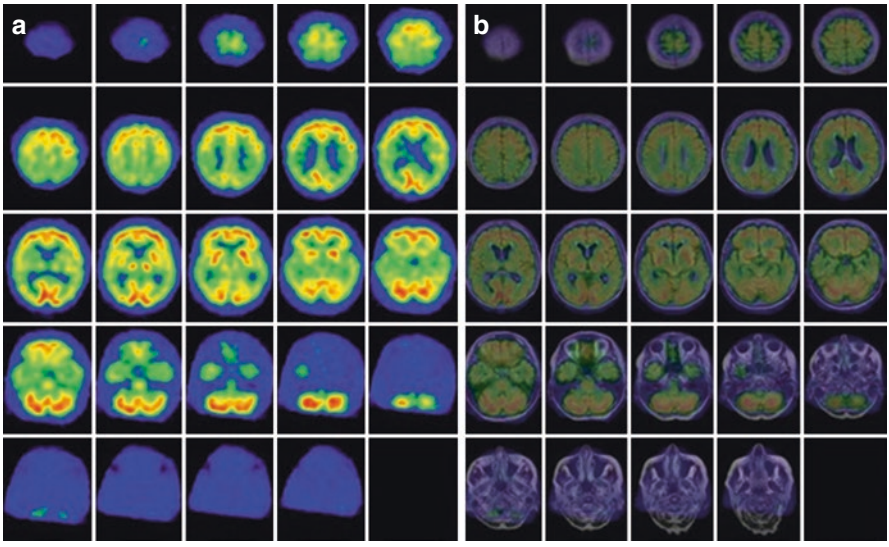

Fig. 20.1 ^{99m}Tc-HMPAO SPECT derived image of an 81-year-old woman with progressive cognitive decline: (**a**) axial ^{99m}Tc-HMPAO SPECT images show severe hypoperfusion in the temporoparietal association cortices and posterior cingulate, with sparing of the occipital cortex, sensorimotor cortex, basal ganglia, thalamus, and cerebellum, consistent with a diagnosis of Alzheimer's disease, (**b**) Fusion of SPECT with MRI confirms the above findings and demonstrates mild gross cerebral atrophy and white matter changes suggestive of concomitant microvascular disease, a common comorbidity in this population. (From Elman et al. (2014) with permission)

clinician or researcher to make a snapshot of the activity that can be assessed at a later stage. This is especially beneficial in conditions where the clinical situation does not allow for direct measurement, such as in the investigating of early reperfusion after stroke or in episodic phenomena such as seizures.

20.4.2 PET

PET can be applied for studying a myriad of cerebral processes and can also provide quantitative parameters of various aspects of hemodynamics. Imaging of cerebral perfusion is possible by using tracers which enter the brain tissue through diffusion. The distribution of these radionuclides is imaged by the coincidence detection of photons emitted from the decay of positron-emitting radionuclides. The tracers used are $H_2{}^{15}O$, carbon dioxide ($C^{15}O_2$), or ^{15}O-labeled oxygen ($^{15}O_2$). As these tracers are metabolically inert and freely diffusible in the brain, a single-tissue compartment model can be used to quantify CBF, as also previously detailed in this book (Leenders et al. 1990). Furthermore, PET can provide quantitative parameters of various other aspects of hemodynamics, such as regional oxygen extraction fraction, cerebral blood volume (CBV), cell viability, and also metabolic activity, including the regional cerebral metabolic rate of oxygen, glucose consumption, and processes of neurotransmission (Wintermark et al. 2005). The radiation dose of a PET perfusion examination ranges usually between 0.5 and 2 mSv per scan, depending on the quality of the PET camera and protocol. A disadvantage of this form of perfusion imaging is that the PET radiopharmaceuticals have a very short half-life and require a cyclotron in the near vicinity.

Besides steady-state CBF, PET is also able to assess hemodynamic impairment through repeated CBF measurements in combination with a vasodilatory challenge or quantification of the OEF (Weber et al. 2004). For the first stage of hemodynamic impairment, the vasodilatory capacity of the cerebral vasculature can be tested by intravenous injection of acetazolamide. Acetazolamide penetrates the blood-brain barrier and inhibits carbonic anhydrase, a protein that has been detected widely in cerebral tissue. This induces acidosis and consequently blocks the vasoreaction to CO_2 (Okudaira et al. 1995; Hartkamp et al. 2016). Stage 2 of hemodynamic impairment, where the vasodilatory capacity has been depleted, can be assessed by measuring the OEF. In patients with a symptomatic carotid artery occlusion, the St. Louis Carotid Occlusion Study found that increased OEF was associated with an increased risk of subsequent stroke (Fig. 20.2) (Grubb Jr. et al. 1998). Based on these findings, Powers and colleagues designed a prospective blinded-adjudication treatment trial, where PET was used to identify patients with decreased OEF (Powers et al. 2011). These patient then received best medical treatment or an extracranial-to-intracranial bypass in order to improve the perfusion on the side of the occlusion. This study was however terminated early as the bypass surgery in combination with medical therapy did not reduce the risk of recurrent ischemic stroke. Other clinical applications have been focused on the field of brain tumors, cognitive decline, and dementia.

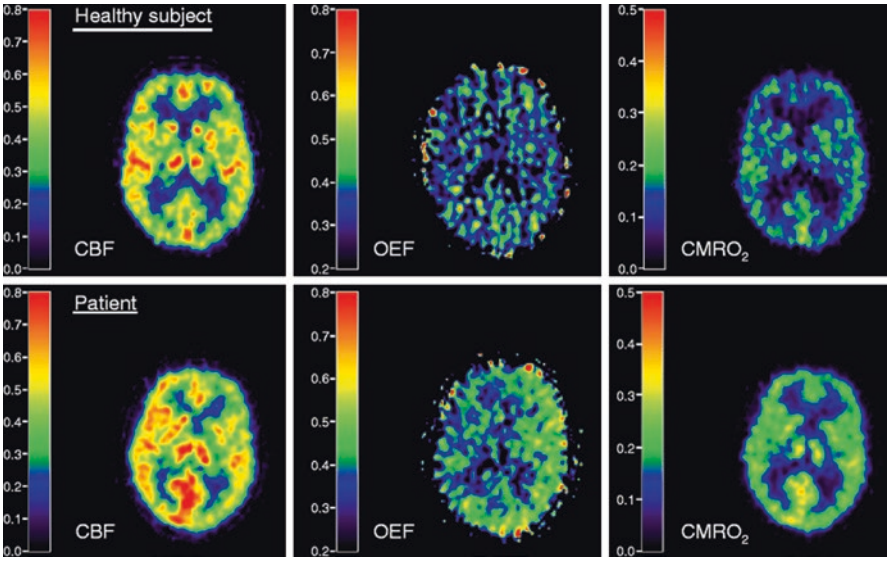

Fig. 20.2 PET-derived CBF, OEF, and $CMRO_2$ parametric maps of a healthy volunteer (top row) and a patient who had recurrent TIAs associated with a left internal carotid artery occlusion (bottom row). The PET images show decreased CBF and increased OEF in the hemisphere ipsilateral to the occlusion when compared to the contralateral hemisphere. (From Bremmer et al. (2010) with permission)

20.5 Conclusions

The downside of healthy aging, which refers to the process of developing and maintaining the functional ability that enables well-being in advanced age, is the increasing incidence of age-related injuries. In brain disorders such as cerebrovascular disease, cognitive decline, and dementia, decreased perfusion of brain tissue plays a central role. Although cerebral perfusion is stable under normal conditions, there are a number of physiological and biochemical mechanisms that may lead to an age-induced reduction in cerebral perfusion. Effective intervention strategies are therefore needed in order to prevent and delay the progression of these age-related conditions in which impairment of the cerebral microvasculature and perfusion may play a role. Perfusion imaging can play a vital role, both in identifying potential mechanisms involved in this process and providing imaging biomarkers for early health-care interventions.

Disclosures The authors report that they have no relevant relationships to disclose.

References

Aaslid R, Lindegaard KF, Sorteberg W, Nornes H (1989) Cerebral autoregulation dynamics in humans. Stroke 20:45–52

Alderliesten T, Lemmers PM, Smarius JJ, van de Vosse RE, Baerts W, van Bel F (2013) Cerebral oxygenation, extraction, and autoregulation in very preterm infants who develop peri-intraventricular hemorrhage. J Pediatr 162:698–704.e2. https://doi.org/10.1016/j.jpeds.2012.09.038

Altman DI, Perlman JM, Volpe JJ, Powers WJ (1993) Cerebral oxygen metabolism in newborns. Pediatrics 92(1):99–104

(1996) Assessment of brain SPECT report of the Therapeutics and Technology Assessment Subcommittee of the American Academy of Neurology. Neurology 46(1):278–85

Bakker SL, de Leeuw FE, den Heijer T, Koudstaal PJ, Hofman A, Breteler MM (2004) Cerebral haemodynamics in the elderly: the Rotterdam study. Neuroepidemiology 23:178–184

Barber TW, Brockway JA, Higgins LS (1970) The density of tissues in and about the head. Acta Neurol Scand 46:85–92

Beard JR, Officer A, de Carvalho IA, Sadana R, Pot AM, Michel JP et al (2016) The World report on ageing and health: a policy framework for healthy ageing. Lancet 387:2145–2154. https://doi.org/10.1016/S0140-6736(15)00516-4

Bergsneider M, Alwan AA, Falkson L, Rubinstein EH (1998) The relationship of pulsatile cerebrospinal fluid flow to cerebral blood flow and intracranial pressure: a new theoretical model. Acta Neurochir Suppl 1998(Suppl. 71):266–268

Bonte FJ, Devous MD Sr, Reisch JS, Ajmani AK, Weiner MF, Hom J et al (1989) The effect of acetazolamide on regional cerebral blood flow in patients with Alzheimer's disease or stroke as measured by single-photon emission computed tomography. Investig Radiol 24:99–103

Brew N, Walker D, Wong FY (2014) Cerebral vascular regulation and brain injury in preterm infants. Am J Physiol Regul Integr Comp Physiol 306:R773–R786. https://doi.org/10.1152/ajpregu.00487.2013

Csiszar A, Ungvari Z, Edwards JG, Kaminski P, Wolin MS, Koller A et al (2002) Aging-induced phenotypic changes and oxidative stress impair coronary arteriolar function. Circ Res 90:1159–1166

Fabiani M, Gordon BA, Maclin EL, Pearson MA, Brumback-Peltz CR, Low KA et al (2014) Neurovascular coupling in normal aging: a combined optical, ERP and fMRI study. NeuroImage 85:592–607. https://doi.org/10.1016/j.neuroimage.2013.04.113

Fantini S, Sassaroli A, Tgavalekos KT, Kornbluth J (2016) Cerebral blood flow and autoregulation: current measurement techniques and prospects for noninvasive optical methods. Neurophotonics 3:031411. https://doi.org/10.1117/1.NPh.3.3.031411

Finnerty FA Jr, Witkin L, Fazekas JF (1954) Cerebral hemodynamics during cerebral ischemia induced by acute hypotension. J Clin Invest 33:1227–1232

Gorelick PB, Scuteri A, Black SE, Decarli C, Greenberg SM, Iadecola C et al (2011) Vascular contributions to cognitive impairment and dementia: a statement for healthcare professionals from the American Heart Association/American Stroke Association. Stroke 42:2672–2713. https://doi.org/10.1161/STR.0b013e3182299496

Greisen G (1986) Cerebral blood flow in preterm infants during the first week of life. Acta Paediatr Scand 75(1):43–51

Grubb RL Jr, Derdeyn CP, Fritsch SM, Carpenter DA, Yundt KD, Videen TO et al (1998) Importance of hemodynamic factors in the prognosis of symptomatic carotid occlusion. JAMA 280(12):1055–1060. http://jama.jamanetwork.com/article.aspx?articleid=188003

Hartkamp NS, Hendrikse J, Bokkers R (2016) Perfusion in chronic carotid artery disease, Ch. 49. In: Bammer R (ed) MR and CT perfusion and pharmacokinetic imaging: clinical applications and theoretical principles, 1st edn. Elsevier, Amsterdam

Haydon PG, Carmignoto G (2006) Astrocyte control of synaptic transmission and neurovascular coupling. Physiol Rev 86:1009–1031

Helou S, Koehler RC, Gleason CA, Jones MD Jr, Traystman RJ (1994) Cerebrovascular autoregulation during fetal development in sheep. Am J Phys 266:H1069–H1074

Hock C, Villringer K, Müller-Spahn F, Wenzel R, Heekeren H, Schuh-Hofer S et al (1997) Decrease in parietal cerebral hemoglobin oxygenation during performance of a verbal fluency task in patients with Alzheimer's disease monitored by means of near-infrared spectroscopy (NIRS)—correlation with simultaneous rCBF-PET measurements. Brain Res 755:293–303

Ito H, Kanno I, Ibaraki M, Hatazawa J (2002) Effect of aging on cerebral vascular response to $PaCO_2$ changes in humans as measured by positron emission tomography. J Cereb Blood Flow Metab 22:997–1003

Janik R, Thomason LA, Chaudhary S, Dorr A, Scouten A, Schwindt G et al (2016) Attenuation of functional hyperemia to visual stimulation in mild Alzheimer's disease and its sensitivity to cholinesterase inhibition. Biochim Biophys Acta 1862:957–965. https://doi.org/10.1016/j.bbadis.2015.10.023

Jennett WB, Harper AM, Gillespie FC (1966) Measurement of regional cerebral blood-flow during carotid ligation. Lancet 2:1162–1163

Kanno I, Uemura K, Higano S, Murakami M, Iida H, Miura S et al (1988) Oxygen extraction fraction at maximally vasodilated tissue in the ischemic brain estimated from the regional CO_2 responsiveness measured by positron emission tomography. J Cereb Blood Flow Metab 8:227–235

Kastrup A, Dichgans J, Niemeier M, Schabet M (1998) Changes of cerebrovascular CO_2 reactivity during normal aging. Stroke 29:1311–1314

Kety SS, Schmidt CF (1948) The nitrous oxide method for the quantitative determination of cerebral blood flow in man; theory, procedure and normal values. J Clin Invest 27:476–483

Kovacic JC, Moreno P, Nabel EG, Hachinski V, Fuster V (2011) Cellular senescence, vascular disease, and aging: part 2 of a 2-part review: clinical vascular disease in the elderly. Circulation 123:1900–1910. https://doi.org/10.1161/CIRCULATIONAHA.110.009118

Lassen NA (1959) Cerebral blood flow and oxygen consumption in man. Physiol Rev 39:183–238

Leenders KL, Perani D, Lammertsma AA, Heather JD, Buckingham P, Jones T et al (1990) Cerebral blood flow, blood volume and oxygen utilization: normal values and effect of age. Brain 113(1):27–47

Lu H, Xu F, Rodrigue KM, Kennedy KM, Cheng Y, Flicker B et al (2011) Alterations in cerebral metabolic rate and blood supply across the adult lifespan. Cereb Cortex 21:1426–1434. https://doi.org/10.1093/cercor/bhq224

MacKenzie ET, Farrar JK, Fitch W, Graham DI, Gregory PC, Harper AM (1979) Effects of hemorrhagic hypotension on the cerebral circulation. I. Cerebral blood flow and pial arteriolar caliber. Stroke 10:711–718

McHedlishvili G (1980) Physiological mechanisms controlling cerebral blood flow. Stroke 11:240–248

Meng L, Hou W, Chui J, Han R, Gelb AW (2015) Cardiac output and cerebral blood flow: the integrated regulation of brain perfusion in adult humans. Anesthesiology 123:1198–1208. https://doi.org/10.1097/ALN.0000000000000872

Nagata K, Kondoh Y, Atchison R, Sato M, Satoh Y, Watahiki Y et al (2000) Vascular and metabolic reserve in Alzheimer's disease. Neurobiol Aging 21:301–307

Nagata K, Yamazaki T, Takano D, Maeda T, Fujimaki Y, Nakase T et al (2016) Cerebral circulation in aging. Ageing Res Rev 30:49–60. https://doi.org/10.1016/j.arr.2016.06.001

Nemoto EM, Yonas H, Chang Y (2003) Stages and thresholds of hemodynamic failure. Stroke 34:2–3

Okudaira Y, Bandoh K, Arai H, Sato K (1995) Evaluation of the acetazolamide test. Vasoreactivity and cerebral blood volume. Stroke 26(7):1234–1239

Park L, Anrather J, Girouard H, Zhou P, Iadecola C (2007) Nox2-derived reactive oxygen species mediate neurovascular dysregulation in the aging mouse brain. J Cereb Blood Flow Metab 27:1908–1918

Paschen W, Mies G, Hossmann KA (1992) Threshold relationship between cerebral blood flow, glucose utilization, and energy metabolites during development of stroke in gerbils. Exp Neurol 117:325–333

Phan TS, Li JKJ, Segers P, Chirinos JA (2016) Misinterpretation of the determinants of elevated forward wave amplitude inflates the role of the proximal aorta. J Am Heart Assoc 5(2):1–12

Powers WJ, Grubb RL Jr, Darriet D, Raichle ME (1985) Cerebral blood flow and cerebral metabolic rate of oxygen requirements for cerebral function and viability in humans. J Cereb Blood Flow Metab 5:600–608

Powers WJ, Clarke WR, Grubb RL Jr, Videen TO, Adams HP Jr, Derdeyn CP (2011) Extracranial-intracranial bypass surgery for stroke prevention in hemodynamic cerebral ischemia: the Carotid Occlusion Surgery Study randomized trial. JAMA 306(18):1983–1992. http://www.ncbi.nlm.nih.gov/pmc/articles/PMC3601825/pdf/nihms450325.pdf

Rapela CE, Green HD (1964) Autoregulation of canine cerebral blood flow. Circ Res 15:205–212

Rhee CJ, Fraser CD III, Kibler K, Easley RB, Andropoulos DB, Czosnyka M et al (2014) The ontogeny of cerebrovascular pressure autoregulation in premature infants. J Perinatol 34:926–931. https://doi.org/10.1038/jp.2014.122

Riecker A, Grodd W, Klose U, Schulz JB, Gröschel K, Erb M et al (2003) Relation between regional functional MRI activation and vascular reactivity to carbon dioxide during normal aging. J Cereb Blood Flow Metab 23:565–573

Scuteri A, Nilsson PM, Tzourio C, Redon J, Laurent S (2011) Microvascular brain damage with aging and hypertension: pathophysiological consideration and clinical implications. J Hypertens 29:1469–1477

Skrobot OA, O'Brien J, Black S, Chen C, DeCarli C, Erkinjuntti T et al (2017) The vascular impairment of cognition classification consensus study. Alzheimers Dement 13:624–633. https://doi.org/10.1016/j.jalz.2016.10.007

Skrobot OA, Black SE, Chen C, DeCarli C, Erkinjuntti T, Ford GA et al (2018) Progress toward standardized diagnosis of vascular cognitive impairment: guidelines from the Vascular Impairment of Cognition Classification Consensus Study. Alzheimers Dement 14:280–292. https://doi.org/10.1016/j.jalz.2017.09.007

Sorond FA, Khavari R, Serrador JM, Lipsitz LA (2005) Regional cerebral autoregulation during orthostatic stress: age-related differences. J Gerontol A Biol Sci Med Sci 60(11):1484–1487

Tarumi T, Zhang R (2018) Cerebral blood flow in normal aging adults: cardiovascular determinants, clinical implications, and aerobic fitness. J Neurochem 144:595–608

Thomas BP, Yezhuvath US, Tseng BY, Liu P, Levine BD, Zhang R et al (2013) Life-long aerobic exercise preserved baseline cerebral blood flow but reduced vascular reactivity to CO_2. J Magn Reson Imaging 38:1177–1183. https://doi.org/10.1002/jmri.24090

Toth P, Tarantini S, Tucsek Z, Ashpole NM, Sosnowska D, Gautam T et al (2014) Resveratrol treatment rescues neurovascular coupling in aged mice: role of improved cerebromicrovascular endothelial function and downregulation of NADPH oxidase. Am J Physiol Heart Circ Physiol 306:H299–H308. https://doi.org/10.1152/ajpheart.00744.2013

Toth P, Tarantini S, Csiszar A, Ungvari Z (2017) Functional vascular contributions to cognitive impairment and dementia: mechanisms and consequences of cerebral autoregulatory dysfunction, endothelial impairment, and neurovascular uncoupling in aging. Am J Physiol Heart Circ Physiol 312:H1–H20. https://doi.org/10.1152/ajpheart.00581.2016

Tsuji M, Saul JP, du Plessis A, Eichenwald E, Sobh J, Crocker R et al (2000) Cerebral intravascular oxygenation correlates with mean arterial pressure in critically ill premature infants. Pediatrics 106:625–632

Weber B, Westera G, Treyer V, Burger C, Khan N, Buck A (2004) Constant-infusion H215O PET and acetazolamide challenge in the assessment of cerebral perfusion status. J Nucl Med 45(8):1344–1350

Wintermark M, Sesay M, Barbier E, Borbély K, Dillon WP, Eastwood JD et al (2005) Comparative overview of brain perfusion imaging techniques. Stroke 36:e83–e99

Wong FY, Silas R, Hew S, Samarasinghe T, Walker AM (2012) Cerebral oxygenation is highly sensitive to blood pressure variability in sick preterm infants. PLoS One 7:e43165. https://doi.org/10.1371/journal.pone.0043165

Xing CY, Tarumi T, Liu J, Zhang Y, Turner M, Riley J et al (2017) Distribution of cardiac output to the brain across the adult lifespan. J Cereb Blood Flow Metab 37:2848–2856. https://doi.org/10.1177/0271678X16676826

Zhu YS, Tarumi T, Tseng BY, Palmer DM, Levine BD, Zhang R (2013) Cerebral vasomotor reactivity during hypo- and hypercapnia in sedentary elderly and Masters athletes. J Cereb Blood Flow Metab 33:1190–1196. https://doi.org/10.1038/jcbfm.2013.66

Carotid Plaque Imaging with SPECT/CT and PET/CT

21

Riemer H. J. A. Slart, Hendrikus H. Boersma, and Clark J. Zeebregts

Contents

21.1 Introduction 608
21.2 Background of Plaque Vulnerability 609
21.3 Functional Imaging of Carotid Artery Plaque with SPECT/CT and PET/CT 610
21.3.1 Inflammation 612
21.3.2 Lipid Accumulation 615
21.3.3 Proteolysis 615
21.3.4 Apoptosis 616
21.3.5 Angiogenesis 617
21.3.6 Thrombosis 618
21.3.7 Plaque Calcification 619
21.4 Future Perspectives 620
References 623

R. H. J. A. Slart (✉)
Department of Nuclear Medicine and Molecular Imaging, University Medical Center Groningen, University of Groningen, Groningen, The Netherlands
e-mail: r.h.j.a.slart@umcg.nl

H. H. Boersma
Department of Nuclear Medicine and Molecular Imaging, University Medical Center Groningen, University of Groningen, Groningen, The Netherlands

Hospital and Clinical Pharmacy, University Medical Center Groningen, University of Groningen, Groningen, The Netherlands
e-mail: h.h.boersma@umcg.nl

C. J. Zeebregts
Surgery, Division of Vascular Surgery, University Medical Center Groningen, University of Groningen, Groningen, The Netherlands
e-mail: c.j.a.m.zeebregts@umcg.nl

R. A. J. O. Dierckx et al. (eds.), *PET and SPECT in Neurology*,
https://doi.org/10.1007/978-3-030-53168-3_21

Abstract

A major contributor to the occurrence of ischemic stroke is the existence of carotid atherosclerosis. A vulnerable carotid atherosclerotic plaque may rupture or erode, thus causing a thrombotic event. Currently, clinical decision-making with regard to carotid endarterectomy or stenting is still primarily based on the extent of luminal stenosis, estimated with CT angiography and/or (duplex) ultrasonography. However, there is growing evidence that the anatomic impact of stenosis alone has limited value in predicting the exact consequences of plaque vulnerability. Various molecular processes have, independently of degree of stenosis, shown to be importantly associated with the plaque's capability to cause thrombotic events. These molecular processes can be visualized with nuclear medicine techniques allowing the identification of vulnerable patients by non-invasive in vivo SPECT(/CT) and PET(/CT) imaging. This chapter provides an overview of SPECT(/CT) and PET(/CT) imaging with specific radiotracers that have been evaluated for the detection of plaques together with a future perspective in this field of imaging.

21.1 Introduction

Cerebral infarction and transient ischemic attacks (TIAs) are frequently caused by embolism from an atherothrombotic plaque or thrombosis at the site of plaque rupture (Bamford et al. 1991). Although the degree of anatomic lumen obstruction is a relevant marker of the risk of stroke (Halliday et al. 2004), the recognition of the role of the vulnerable plaque has opened new avenues in the field of atherothrombotic stroke. Vulnerability is caused in part by the plaques' tissue structure, which, in turn, is influenced by pathophysiologic mechanisms at the cellular and molecular level. All types of atherosclerotic plaques with a high chance on thrombotic complications and rapid progression should be considered as vulnerable plaques causing part of clinical events (Naghavi et al. 2006). However, not all (vulnerable) plaques become symptomatic and will result in a stroke or a TIA. Removal of carotid artery stenosis by surgical endarterectomy or treatment with stenting will reduce stroke incidence markedly. On the other hand, approximately 3–9% of patients undergoing such an interventional treatment will suffer from stroke or even death as a complication from it. Stenting procedures are generating a higher risk for major complications than carotid endarterectomy (van der Vaart et al. 2008). Current selection criteria for intervention are determined by the grade of stenosis and symptomatology. It is generally accepted to be more aggressive in a high-grade symptomatic carotid stenosis. Invasive interventions in lower-grade stenosis/low frequency of symptomatology are still a matter of debate. Currently conventional available imaging modalities, such as ultrasound, angiography, CT angiography, or MR angiography, can delineate vascular wall anatomy and the severity of stenosis. However, evidence is growing that stenosis severity

alone has limited value in predicting plaque vulnerability and its associated risk for cerebral ischemic events (Sanidas et al. 2012). Furthermore, various pathological processes have, independent of the degree of stenosis, shown to be importantly associated with plaque vulnerability. Imaging the target biologic processes is important in the evaluation of plaque evolution and plaque (in)stability. Expansion of the vessel wall involving remodeling of the extracellular matrix can be imaged, as can angiogenesis of the vasa vasorum, plaque inflammation, proteolysis, lipid accumulation, apoptosis, and fibrin deposits in early non-occlusive atherosclerosis. Several imaging platforms are available for targeted vascular imaging to acquire information on both anatomy and pathobiology. This can be achieved in the same imaging session using hybrid technology with novel tracers targeting processes identified by molecular biology to be of importance. In this chapter we focus on visualizing molecular processes with nuclear medicine/molecular imaging techniques allowing the identification of vulnerable plaques by non-invasive in vivo SPECT(/CT) and PET(/CT) imaging.

21.2 Background of Plaque Vulnerability

Atherosclerotic lesions arise from focal thickenings of the intima of arteries of any size. It is initiated by a process of inflammatory damage, existing of lipid accumulation, inflammatory and smooth muscle cells, as well as connective tissue systematically deposited in these lesions (Fig. 21.1). Low-density lipoprotein (LDL) particles in excess infiltrate the artery wall and are retained in the intima, predominantly at sites of hemodynamic stress flow (Skalen et al. 2002). Local oxidative and enzymatic modifications of LDL particles lead to the release of inflammatory

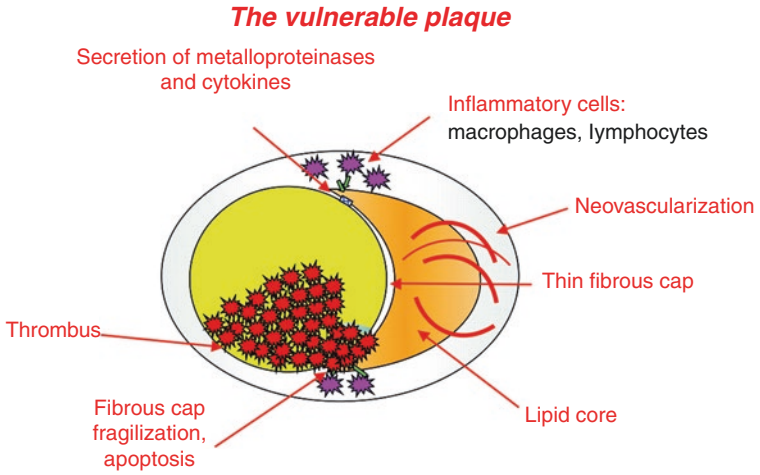

Fig. 21.1 Biological factors supporting plaque vulnerability (Nighoghossian et al. 2005). (Permission to use figure and legend granted by Lippincott, Williams & Wilkins; http://lww.com)

lipids that induce endothelial cells to express leukocyte adhesion molecules such as vascular cell adhesion molecule like (VCAM)-1, E-selectin, and P-selectin. These in turn facilitate the recruitment as well as the subsequent attachment to the artery wall of various white blood cell types, such as T lymphocytes and monocytes (Falk 2006; Hansson 2005). Monocytes differentiate into macrophages, a process described to be associated with the upregulation of pattern recognition receptors including scavenger receptors and Toll-like receptors. These processes lead to foam cell formation. In turn, these release growth factors, cytokines, metalloproteinases, and reactive oxygen species which have their particular influence on the vascular remodeling process. During the atherosclerotic process, endothelial cells, macrophages, and smooth muscle cells die from apoptosis or necrosis (Littlewood and Bennett 2003). Disintegration of foam cells, loss of smooth muscle cells, and production of matrix metalloproteinases by activated leukocytes have detrimental consequences. These processes will finally lead to the formation of destabilizing lipid-rich cores and fragile and rupture-prone fibrous caps (Falk 2006; Jones et al. 2003). The occurrence of VEGF is also linked to advanced atherosclerosis and is probably a marker of ongoing pathologic activity, resulting in high-risk plaques. Also, the progression of atherosclerotic plaques is associated with the appearance and growth of vasa vasorum (Hansson 2005; Barger et al. 1984). In human plaques, microvessel content increases with plaque progression and is likely to be stimulated by plaque hypoxia, hypoxia-inducible factor (HIF) signalling, reactive oxygen species, and other inflammatory signals (Sluimer and Daemen 2009). The presence of plaque hypoxia is primarily determined by plaque inflammation (increasing oxygen demand), while the contribution of plaque thickness (reducing oxygen supply) seems to be a minor factor. Plaque microvessels are immature and fragile, and the distorted integrity of microvessel endothelium likely leads to intraplaque hemorrhage and plaques at increased risk for rupture (Sluimer et al. 2009).

These various stages of atherosclerotic plaque development, with specific histopathologic characteristics, may result in clinically recognizable events.

Further in this chapter, we will categorize the nuclear imaging techniques using different radiopharmaceuticals that are currently available to visualize these various stages. We will discuss their specific properties with regard to visualization of the different pathways associated with vulnerability, including inflammation, proteolysis, apoptosis, angiogenesis, and lipid accumulation in carotid plaque formation.

21.3 Functional Imaging of Carotid Artery Plaque with SPECT/CT and PET/CT

Nuclear imaging modalities are capable of visualizing molecular processes. Clinical positron emission tomography (PET) has a 2–3 times better spatial resolution than single-photon emission computed tomography (SPECT) and does not require the presence of a collimator.

The spatial resolution for PET is approximately 5 mm and is only useful in large arteries. Also PET has shown to be capable of quantifying tracer activity in the region of interest. Restricted resolution can be partially counteracted by coregistration of scintigraphic images with CT (SPECT/CT and PET/CT hybrid camera systems) or with MRI. CT and MRI will be helpful for partial volume correction, but most importantly the advantage of coregistration is precise anatomic information concerning tracer uptake and to visualize aspects that are not depicted by PET and SPECT, such as stenosis and the plaque extent. If PET and SPECT are to gain a position as a clinical instrument in the search for the vulnerable plaque, specific tracers will be needed to image components which play an important role in the formation and progression of vulnerable plaques (Table 21.1) (Glaudemans et al. 2010).

Table 21.1 Radiopharmaceuticals for imaging atherosclerosis

Radiopharmaceutical	Target
	Lipid accumulation
^{99m}Tc-LDL/oxLDL/ac-LDL	Foam cells
^{99m}Tc-LOX-1-mAb	Foam cells
^{99m}Tc-β-VLDL	Lipoproteins
^{125}I/^{99m}Tc-MDA2, ^{125}I-IK17	Lipids
	Inflammation
^{99m}Tc/^{125}I-MCP-1	Macrophages and monocytes
^{68}Ga-SST-2 receptor	Macrophages
^{99m}Tc/^{123}I-IL-8	Neutrophils
^{123}I-IL-1 RA	Monocytes and lymphocytes
^{123}I- or ^{99m}Tc-IL-2	Lymphocytes
^{99m}Tc-Fucoidan	P-selectin
^{18}F-FDG	Glucose activity
	Calcification
^{18}F-Sodium fluoride	Active mineral deposition
	Thrombosis
^{111}In-Platelets	Platelets
^{99m}Tc-Apcitide/P280	Activated platelets
^{99m}Tc-DMP444	Activated platelets
^{99m}Tc-Fibrin-binding domain (FBD)	Fibrins
^{99m}Tc-labelled fibrin α-chain peptide	Fibrins
	Apoptosis
^{99m}Tc-Annexin A5	Apoptotic cells
	Angiogenesis
^{111}In-Bevacizumab	VEGF activity
^{123}I-VEGF$_{165}$	VEGF receptor
^{99m}Tc-Endothelin	Smooth muscle cells
^{11}C-L-159,884	Angiotensin 1 receptor
^{89}Zr-Bevacizumab	VEGF activity
^{18}F-Galacto-RGD	αvβ3 integrin receptor
^{99m}Tc-MMP-tracers	Metalloproteinase (several subtypes)

21.3.1 Inflammation

Inflammation plays a key role in early atherosclerotic plaque development and in plaque destabilization. Especially, macrophages play a central role in plaque pathogenesis. By ingesting lipids, they transform into foam cells and produce a large array of pro- and anti-inflammatory cytokines. The highly inflammatory vulnerable plaque is characterized by an abundance of inflammatory cells and proteins that are all potential targets for molecular imaging tracers. Therefore, molecular imaging of inflammatory activity in the plaque may predict vulnerability and stroke risk. The most widely studied imaging method to identify inflammatory processes in carotid artery plaques is radionuclide scintigraphic imaging by PET. Radionuclide tracers for macrophage metabolism, macrophage recruitment, and inflammatory markers have also been developed and have potential to image inflammatory activity (Masteling et al. 2011). ^{18}F-Fluorodeoxyglucose (FDG) is a glucose analogue that is taken up by glucose-using cells and accumulates in proportion to metabolic activity. FDG-PET has extensively been used in cancer patients. Some cancer patients undergoing FDG-PET showed uptake of FDG in the large arteries, and they were retrospectively identified as having risk factors for atherosclerosis (Yun et al. 2002). This suggested that atherosclerotic plaques may be detectable by FDG-PET imaging. In atherosclerosis, FDG-PET is thought to identify only those plaques that are most actively inflamed and at highest risk for instability and is therefore a potential method for non-invasive identification of an unstable carotid plaque (Fig. 21.2). An early clinical study using FDG-PET in carotid artery plaques was performed in 2002, showing more accumulation of FDG in unstable plaques (Rudd et al. 2002). FDG-PET signals have also shown to correlate with histological macrophage staining or macrophage markers in human atherosclerotic plaques (Masteling et al. 2011). In another clinical study, 12 patients with a recent TIA underwent FDG-PET and high-resolution MRI. FDG uptake was high in 83% of patients with lesions that were compatible with the patients' presenting symptoms (Davies et al. 2005). In

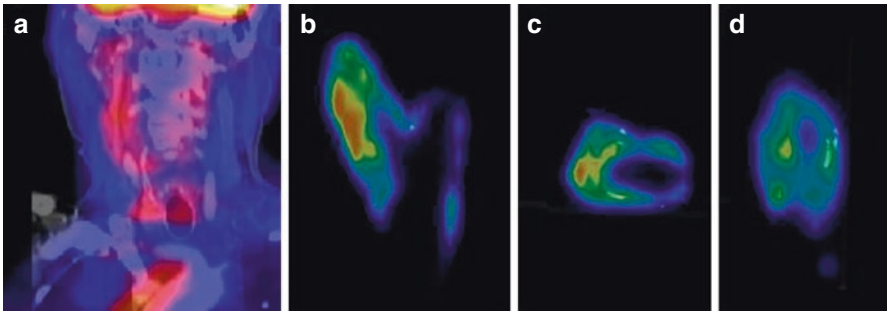

Fig. 21.2 Clinical fused PET-CT image from a patient showing FDG uptake in the affected right carotid artery (**a**). Coronal (**b**), transverse (**c**), and sagittal plane (**d**) of corresponding μPET images in the same patient showing also patchy FDG uptake and calcified areas (white depositions) (Masteling et al. 2011)

another study, concerning new symptomatic carotid stenosis, inflammation-related FDG uptake was associated with early stroke recurrence, independent of the degree of stenosis. FDG-PET may identify patients at highest risk for stroke recurrence, who may be selected for immediate revascularization or intensive medical treatment (Marnane et al. 2012). Bucerius et al. showed that carotid inflammation as revealed by FDG-PET is also highly prevalent in the coronary artery disease population and is associated with obesity, age over 65 years, history of hypertension, smoking, and male gender. Artery wall FDG uptake increased when components of the metabolic syndrome clustered (Bucerius et al. 2011). In a large cohort of 932 cancer patients, increased FDG uptake in major arteries emerged as the strongest predictor of a subsequent vascular event. Concomitant severe vascular calcifications seemed to impart a particularly high risk (Rominger et al. 2009). FDG uptake within an arterial wall or plaque can be quantified in several ways, but there is always a partial volume error (PVE), depending on the spatial resolution of the imaging technique that is being used (Rousset et al. 1998), even though PET has a 2–3 times better spatial resolution than SPECT. Izquierdo-Garcia et al. studied the reproducibility of methods of quantification by MR-guided FDG-PET in symptomatic carotid artery plaques and compared quantification methods to a gold standard technique using the Patlak analysis (Izquierdo-Garcia et al. 2009; Patlak et al. 1983). MR-guided FDG-PET proved to be a highly reproducible technique. A recent meta-analysis includes 14 articles where comparing FDG-PET uptake in symptomatic versus asymptomatic disease yielded a standard mean difference of 94 (95% CI 0.58–1.130; $P < 0.0001$, $I^2 = 65\%$) (Chowdhury et al. 2018). A major disadvantage of FDG imaging is its non-specificity. A FDG-positive scan of the carotid area may indicate plaque formation but may also reflect physiological tracer uptake in muscle or brown fat. CT and MRI may be helpful to distinguish vascular from extravascular uptake. However, there is still a need for more specific PET tracers which are suitable for the detection of the unstable carotid plaque.

While ample data exist about the pattern of FDG uptake in the arterial tree and its colocalization with plaque calcification, only limited data exist for choline and fluorocholine. ^{18}F-labelled fluorocholine (^{18}F-fluorocholine) has been introduced for imaging of the brain and diagnosis of prostate cancer. Choline is taken up into cells by specific transport mechanisms and is phosphorylated by choline kinase. Afterward, it is metabolized to phosphatidylcholine and eventually incorporated into cell and organelle membranes. Increased choline uptake has been shown in tumor cells and activated macrophages.

Bucerius et al. reported the first data correlating ^{18}F-fluorocholine uptake and morphological wall alterations in aortic and common iliac arteries of five patients (Bucerius et al. 2008).

Their observations suggested that fluorocholine uptake and calcification sites are mostly not colocated, similar to the findings of previous studies with FDG (Fig. 21.3).

Another study found out that ^{11}C-choline uptake and calcification in the aortic and common carotid arterial walls are common in elderly men (Kato et al. 2009). Radiotracer uptake and calcification are, however, only rarely colocalized.

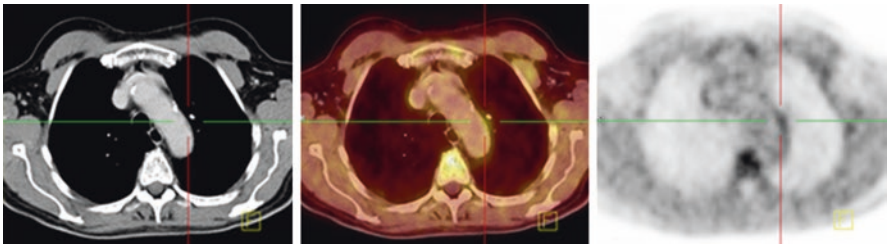

Fig. 21.3 Example of arterial ^{18}F-choline uptake and calcifications representative transaxial ^{18}F-choline-PET/CT results: partially calcified atherosclerotic plaque within the aortic arch which accumulates ^{18}F-choline mainly in the non-calcified part in a 62-year-old (Forster et al. 2010). (**a**) (From left to right) CT image; (**b**) PET/CT fusion; (**c**) PET image

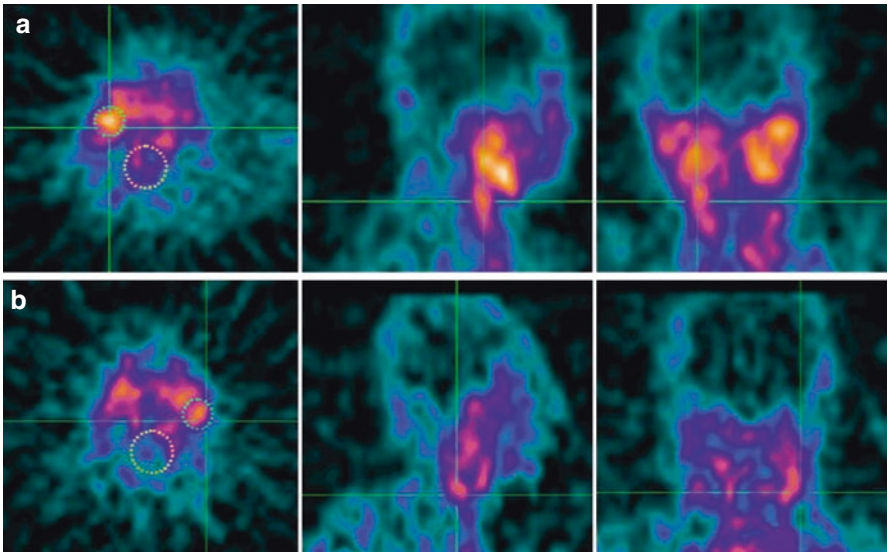

Fig. 21.4 ^{99m}Tc-IL2 scintigraphy in two patients with a plaque in the right (**a**) and the left (**b**) carotid. Images are transaxial, sagittal, and coronal views at the level of the carotid bifurcation. Circles are drawn on the carotid region (small), and larger circles are drawn on the vertebral regions, serving as background to calculate the uptake ratio (carotid/background) (Annovazzi et al. 2006)

^{11}C-choline has the potential to provide information about atherosclerotic plaques independent of calcification measurement with CT.

Another radionuclide tracer that has been used in carotid artery patients is ^{99m}technetium-interleukin-2 (^{99m}Tc-IL-2) SPECT. Higher serum IL-2 levels are associated with increased carotid artery intima-media thickness (IMT), a predictor of stroke and vascular disease (Elkind et al. 2005). ^{99m}Tc-IL-2 is therefore also used for imaging carotid atherosclerosis in humans (Fig. 21.4). Fourteen patients (16 plaques) eligible for endarterectomy underwent ^{99m}Tc-IL-2 scintigraphy before surgery. Another 9 patients (13 plaques) received atorvastatin or a standard

hypocholesterolemic diet, and scintigraphy was performed before and after 3 months of treatment. ^{99m}Tc-IL-2 accumulated in vulnerable carotid plaques, and the accumulation correlated with the amount of IL-2R+ cells within the plaque (measured ex vivo by histology). Also, the amount of ^{99m}Tc-IL-2 within the plaque was influenced by lipid-lowering treatment with a statin (Annovazzi et al. 2006). ^{99m}Tc-IL-2 seems a promising tracer that could provide useful information for the selection of infiltrated vulnerable plaques at risk of rupture. However, it is not yet commercially available, and a major drawback is the complexity and duration of the labelling procedure (Signore et al. 2003). Furthermore, development of the PET tracer ^{18}F-IL-2 for clinical use could be of additional importance since it offers higher resolution (Di Gialleonardo et al. 2012). A new agent for more specific macrophage imaging is the somatostatin receptor subtype-2 (SST2) binding PET tracer. ^{68}Ga-DOTATATE ligand binding to SST2 receptors occurred in CD68-positive macrophage-rich carotid plaque regions. Tarkin et al. validated ^{68}Ga-DOTATATE PET as a novel marker of atherosclerotic inflammation and confirmed that ^{68}Ga-DOTATATE offers superior coronary imaging, excellent macrophage specificity, and better power to discriminate high-risk versus low-risk coronary lesions than FDG (Tarkin et al. 2017). In conclusion, of all radionuclide tracers, ^{18}FDG has currently the most validated and greatest clinical potential to identify inflamed plaques in patients with carotid artery disease, although target binding is not very specific.

21.3.2 Lipid Accumulation

Lipid accumulation not only plays a role in the initial phases of atherogenesis but also is important in the stability of the atherosclerotic plaque. Unstable lesions were shown to have a much greater area occupied by lipids (Dangas et al. 1998). In addition, elevated oxidized low-density lipoprotein (LDL) levels play a role in the transition from stable to unstable plaques and are associated with a higher risk for atherosclerotic complications. In carotid artery disease, technetium-99m labelled LDL (^{99m}Tc-LDL) was used for identification of plaque and appeared to accumulate depending on plaque composition (Lees et al. 1988). Another study in carotid artery plaques compared ^{99m}Tc-oxLDL uptake between normal carotid arteries and patients with a carotid artery stenosis. They found significantly higher uptake of ^{99m}Tc-oxLDL in carotid plaques compared with normal carotid arteries. However, the relationship between ^{99m}Tc-oxLDL uptake and plaque vulnerability by comparison between stable and unstable plaques was not assessed (Iuliano et al. 1996). Although the clinical experience in imaging lipid accumulation is limited, some results suggest that at-risk plaques with high lipid content may be detected by non-invasive imaging in the future.

21.3.3 Proteolysis

Release of proteolytic enzymes such as matrix metalloproteinases (MMPs) and cathepsin cysteine proteases (CCPs) has been suggested as a mechanism of cap

erosion and thus plaque destabilization. Several studies in atherosclerotic plaques have shown proteolytic activity in relation to plaque instability (Loftus et al. 2000; Morgan et al. 2004). Therefore, non-invasive visualization and quantification of MMP and CCP activity is of great potential in risk assessment of carotid artery pathology. Radiolabelled molecules designed to specifically target proteolytic activity have been developed for SPECT and PET. For example, radiolabelled MMP inhibitors that bind to a broad spectrum of MMPs have been studied in mice and showed higher uptake in carotid artery stenosis compared to normal arteries (Schafers et al. 2004). Histological analysis showed colocalization of the specific tracer and MMP-9. In rabbits, MMP activity could be detected by non-invasive SPECT imaging and correlated well with immunohistochemically verified macrophage infiltration and presence of MMP-2 and MMP-9 within the atherosclerotic plaque. In addition, statin therapy and dietary modification were shown to decrease MMP activity as visualized by SPECT, and again immunohistochemical correlations were high (Fujimoto et al. 2008). This indicates that SPECT may be an important tool for monitoring the effects of new therapeutic strategies. However, most of the tracers have only been validated in animal studies, and only ^{111}In-DTPA-N-TIMP-2 has been tested in humans (Van de Wiele and Oltenfreiter 2006). The development of new tracers for atherosclerotic plaques is complicated by a poor target-to-background ratio, which means that background activity makes it hard to distinguish plaque uptake from surrounding healthy tissue.

21.3.4 Apoptosis

Apoptosis also plays an important role in human atherosclerotic plaque progression. The risk of plaque rupture depends in part upon the presence of a necrotic core, containing lipids, dead cells, and debris with a thin fibrous cap (Libby and Theroux 2005). Carotid artery plaques with an increased necrotic core and a thin fibrous cap due to apoptosis of macrophages or smooth muscle cells are known to be instable and are at high risk for rupture.

Imaging of apoptosis in carotid artery plaques has mainly been performed in animal models by targeting markers of apoptosis such as annexin A5. In a rabbit model, Technetium-99m-labelled annexin A5 showed a higher uptake in atherosclerotic lesions compared with controls (Kolodgie et al. 2003). In another rabbit study, annexin A5 (^{111}In-labelled annexin A5) was imaged in combination with MMP activity (^{99m}Tc-labelled matrix metalloproteinase inhibitor (MPI)) using SPECT/CT (Haider et al. 2009). Annexin A5 and MPI uptake were both visualized in atherosclerotic animals and were interrelated.

In a clinical pilot study of four patients with a history of TIA caused by symptomatic carotid artery stenosis, annexin A5 uptake corresponded well with histopathological characterization of vulnerability of the endarterectomy specimens (Fig. 21.5) (Kietselaer et al. 2004). Unstable plaques showed higher uptake of annexin A5, while in stable plaques no uptake of annexin A5 was seen after SPECT imaging. Although obviously more clinical studies in apoptotic markers are needed,

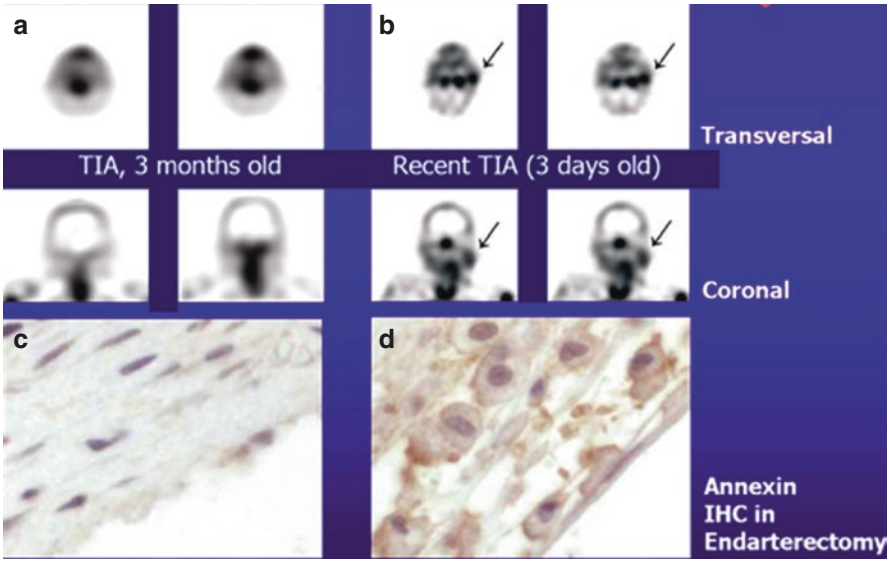

Fig. 21.5 Panel **a** shows transverse and coronal views obtained by single-photon emission computed tomography (SPECT) in a patient who had had a right-sided TIA 3 months before imaging, but did not show evidence of annexin A5 uptake in the carotid-artery region on either side. Doppler ultrasonography revealed a clinically significant obstructive lesion on the affected side. Histopathological analysis of an endarterectomy specimen from this patient (Panel **c**; polyclonal rabbit anti-annexin A5 antibody, ×400) shows a lesion rich in smooth muscle cells, with negligible binding of annexin A5. Panel **b**, a patient who had a left-sided transient ischemic attack (TIA) 3 days before imaging. Although this patient had clinically significant stenosis of both carotid arteries, uptake of radiolabelled annexin A5 is evident only in the culprit lesion (arrows). Immunohistology analysis of an endarterectomy specimen from this patient (Panel **d**; polyclonal rabbit anti-annexin A5 antibody, ×400) shows substantial infiltration of macrophages into the neointima, with extensive binding of annexin A5 (brown) (Kietselaer et al. 2004)

so far ^{99m}Tc-annexin A5 is one of the few tracers that have been used in the clinical setting of acute vascular disease. It should be mentioned that Annexin V is not specific for apoptosis, as many forms of vascular stress may lead to an Annexin V signal. Caspase-3-dependent pathways play also an important role in the apoptosis process. Specific targeting of caspase-3 may lead to a more specific PET signal, but this approach has not yet been validated in humans (Faust et al. 2007).

21.3.5 Angiogenesis

In atherosclerotic plaques, the formation of microvessels has been studied as a possible contributing factor to plaque destabilization and rupture. Neo-vessels in carotid artery plaques are fragile and prone to rupture and may cause plaque growth and intraplaque hemorrhage, resulting in a high-risk plaque (Takaya et al. 2005). Several angiogenic cytokines, such as vascular endothelial growth factor (VEGF), integrins,

or angiotensin, may be potential targets for molecular imaging of angiogenesis during plaque formation (Holm et al. 2009; Slart et al. 2008). Angiotensin 1 receptor (Szabo et al. 2001) and VEGF radionuclide tracers (Nagengast et al. 2007) have already been used in other diseases in which angiogenesis plays an important role, but not in atherosclerosis. For example, non-invasive imaging of angiogenesis by radionuclide VEGF tracers (Blankenberg et al. 2006) has been performed.

Hypoxic conditions in atherosclerotic angiogenesis can be imaged with radiolabelled 2-nitroimidazoles, ^{18}F-FAZA, ^{18}F-MISO, and ^{61}Cu-ATSM (Kurihara et al. 2012). To date, it is unclear if the concentration of hypoxia in plaques will be sufficient to visualize hypoxia. VEGF and VEGF-receptor expression is also induced in response to hypoxia, and therefore these VEFG receptors represent reasonable targets for imaging of mediators of ischemia-induced angiogenesis, also in atherosclerotic plaques (Virmani et al. 2005). Previous studies used ^{111}In-VEGF121 in different animal models, for example, in rabbits (Lu et al. 2003). The anti-VEGF monoclonal antibody VG76e has been labelled with the PET tracer ^{124}I, following successful validation in a mouse model (Collingridge et al. 2002). A humanized monoclonal antibody, bevacizumab, binds strongly to VEGF by the tyrosine kinase receptor and neutralizes all isoforms of the ligand VEGF-A (Ferrara and Davis-Smyth 1997; Gerber and Ferrara 2005). This makes bevacizumab also an interesting antibody to visualize angiogenesis. ^{111}In-bevacizumab and ^{89}Zr-bevacizumab reveal high uptake in vascularized tissues (Nagengast et al. 2007). It is also feasible to visualize VEGF expression within carotid endarterectomy specimens using ^{89}Zr-bevacizumab PET. ^{89}Zr-bevacizumab accumulation in plaques is specific, and tissue-to-background ratio correlates with immunohistochemistry scores (Golestani et al. 2013) (Fig. 21.6). Also radiolabelled RGD peptides as integrin alpha(v)beta3-targeted PET tracers may play an important role for the imaging of angiogenesis (Laitinen et al. 2009). Integrin alpha(v)beta3 is expressed on the plasma membrane in an active status in which it binds its ligands and transduces signals when exposed, activating external stimuli of angiogenesis in atherosclerosis such as VEGF (Laitinen et al. 2009).

Microvessels in atherosclerotic plaque can also show an overexpression of VCAM-1 and ICAM-1 (Boyle et al. 2000). However, no radiolabelled VCAM-1 tracer is produced until now. ^{64}Cu-(anti-ICAM)NPs have been used in a previous study to analyze endothelial inflammation (Rossin et al. 2008).

21.3.6 Thrombosis

In carotid artery plaques, thrombotic activity is associated with stroke and TIAs (Sayed et al. 2009). Unstable carotid artery plaques express a variety of thrombomodulatory factors, and expression of these factors is higher in unstable plaques compared to stable plaques (Spagnoli et al. 2004). In a large series of carotid endarterectomy specimens, thrombotic activity was seen in 74% and 35% of patients with

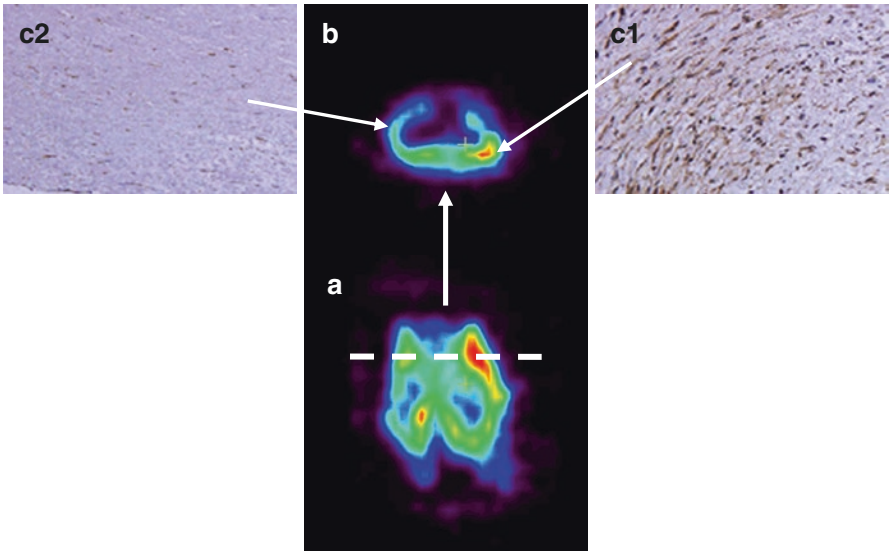

Fig. 21.6 (**a**) Coronal view of carotid endarterectomy specimen incubated with ^{89}Zr-bevacizumab using μPET. (**b**) Dashed lines show the levels of transverse views. (**c1**) Immunohistochemistry of a slide with high ^{89}Zr-bevacizumab uptake shows intense staining of VEGF (c1) in CEA specimens. (**c2**) Immunohistochemistry of a slide with low ^{89}Zr-bevacizumab uptake shows diminished VEGF staining (c2) (Golestani et al. 2013). *VEGF* vascular endothelial growth factor

ischemic stroke and TIAs, respectively, and only in 14% of asymptomatic patients. In stroke patients, thrombotic activity was seen until several months after the first cerebrovascular event (Sayed et al. 2009). These findings suggest that thrombotic activity plays a crucial role in plaque rupture and the pathogenesis of stroke (Hermus et al. 2010). Several nuclear tracers are available to image thrombus activity (Table 21.1); however most are evaluated in dated studies.

21.3.7 Plaque Calcification

Calcification may play a role in stabilizing the plaque but is also related to cardiovascular risk (Mauriello et al. 2011). The association of aortic calcification with cardiovascular events and all-cause mortality has been emphasized in several reports. Arterial calcification has been traditionally determined by CT, whereas inflammation mainly mediated by macrophage activity has been assessed by FDG-PET over the last few years. The increasing use of ^{18}F-sodium fluoride (^{18}F-NaF) PET has raised the theoretical possibility of studying active mineral deposition in the atherosclerotic plaque perhaps years or even decades earlier than they become visible on conventional imaging, such as CT. To date there have been some clinical

studies (Derlin et al. 2010, 2011a, b; Dweck et al. 2012) that have explored the feasibility of using ^{18}F-NaF PET/CT in assessing the calcification component of atherosclerosis. Derlin et al., in a retrospective study (2011a), evaluated the correlation of ^{18}F-NaF accumulation in the common carotid arteries of neurologically asymptomatic patients with cardiovascular risk factors. ^{18}F-NaF accumulation in the common carotid arteries was analyzed both qualitatively and semiquantitatively by measuring the blood-pool-corrected standardized uptake value (target-to-background ratio) and comparing it with cardiovascular risk factors and calcified plaque burden. ^{18}F-NaF uptake was observed at 141 sites in 94 (34.9%) patients. Radiotracer accumulation was colocalized with calcification in all atherosclerotic lesions. ^{18}F-NaF uptake was significantly associated with age ($P < 0.0001$), male sex ($P < 0.0001$), hypertension ($P < 0.002$), and hypercholesterolemia ($P < 0.05$). The presence of calcified plaque correlated significantly with these risk factors but also with diabetes ($P < 0.0001$), history of smoking ($P = 0.03$), and prior cardiovascular events ($P < 0.01$). There was a highly significant correlation between the presence of ^{18}F-NaF and the number of cardiovascular risk factors that were present ($r = 0.30$, $P < 0.0001$). It was concluded that carotid ^{18}F-NaF uptake is a surrogate measure of calcifying carotid plaque, correlates with cardiovascular risk factors, and is more frequent in patients with a high-risk profile for atherothrombotic events but demonstrates a weaker correlation with risk factors than does calcified plaque burden. A more recent study demonstrated comparable results in carotid patients and stated that ^{18}F-NaF PET represents a different stage in the calcification process than CT (Hop et al. 2019). They observed a similar PET assessed ^{18}F-NaF uptake and pattern in culprit and non-culprit plaques of high-risk patients, indicating that this method may be of more value in early atherosclerotic stenosis development. These studies provide a rationale to conduct further prospective studies to determine whether ^{18}F-NaF uptake can predict vascular events, or if it may be used to monitor pharmacologic therapy.

^{18}F-NaF PET/CT is also a promising new approach for the assessment of coronary artery plaque biology. Prospective studies with clinical outcomes are however needed to assess whether coronary ^{18}F-NaF uptake represents a novel marker of plaque vulnerability, recent plaque rupture, and future cardiovascular risk (Dweck et al. 2012). Active molecular calcification may be assessed by ^{18}F-NaF PET/CT much earlier than the detectable calcification identified by CT and, hence, provides clinically relevant information in the individual patient at an early stage when medical intervention is likely to have a correspondingly greater effect.

21.4 Future Perspectives

The identification of major, causal risk factors for the development of atherosclerosis provides physicians reliable tools to identify individuals who are at high risk for atherosclerosis-related clinical events. However, the quantitative risk assessment would be significantly improved if atherosclerotic plaque vulnerability could

be assessed more directly. The emerging area of nuclear imaging techniques can provide measures to evaluate the vulnerability of atherosclerotic plaques, thereby improving the prediction of clinical events. Important is the need to learn which of the different morphological, molecular, biological, or mechanical features of vulnerable plaques are clinically relevant to the outcome of patients. It is likely that more than one plaque feature will be needed to make a clinically useful assessment. In this regard, combined imaging will be necessary. SPECT/CT and PET/CT offer the possibility to combine morphology and pathophysiological processes. PET and SPECT are able to accurately detect the tracer in very low concentrations (pg/mL). Anatomical detail is however warranted; therefore effort must be invested to reach an optimal resolution. Clinical PET has a far better resolution than SPECT and is in matter of quality a method of first choice but more expensive. A more recent study highlights the importance of standardizing all aspects of methodological approaches to ensure accuracy and reproducibility (Giannotti et al. 2017). They found statistically significant differences in FDG SUV measurements in 101 carotid patients between 2 software packages, ranging from 9% to 21.8%, depending on ROI location. In 79% ($n = 23$) of the ROI locations, the differences between the SUV measurements from each software package were found to be statistically significant. The time taken to perform the analyses and export data from the software packages also varied considerably. Physicians must be aware that when a PET-CT data set is analyzed, with the same software package should be used or cross-calibration between packages should be performed. The use of radionuclide tracers is associated with ionizing radiation, and this potentially may limit their clinical application. Much effort has been directed toward reducing the radiation dose and the effective dose equivalent, and organ doses are now comparable or lower than the radiation dose used in CT examinations, depending on the CT acquisition protocol (Huang et al. 2009). With modern equipment even lower activities of the tracer are required, and a safe total radiation dose can be achieved. For molecular imaging, MRI can also be used in conjunction with PET, using a hybrid PET-MRI system (Pichler et al. 2010). In contrast to PET and CT, MRI offers excellent soft-tissue contrast in combination with high spatial resolution, but it gives little functional information. Simultaneous acquisition of PET and MRI under identical physiological circumstances and optimal matching of both images could overcome the shortcomings of both separate techniques. They can provide quantitative functional information about the atherosclerotic lesion, with more accurate localization and motion correction. Taken together, this could improve the overall differential diagnosis and guide treatment strategies, resulting in better medical care. MRI allows for the characterization of plaque composition, i.e., the discrimination of lipid core, fibrosis, and intraplaque hemorrhage deposits; however identification of calcification is difficult. A further important focus of research is the development of specific MRI probes (targeted molecular imaging), which can be combined with PET probes to obtain complementary information simultaneously. The combination of different modalities (PET and MRI), imaging different targets, allows useful synergies for non-invasive in vivo imaging. Molecular

MRI probes for fibrin, macrophages, and high-density lipoprotein (HDL) have been tested at the preclinical level to visualize thrombotic material, inflammation, or transport of HDL metabolism within atherosclerotic plaques in vivo (Frias et al. 2004; Skajaa et al. 2010). A variety of magnetic nanoparticles (MNPs) have been developed to detect aspects of inflammation in the atherosclerotic plaque. Nanoparticles are digested by macrophages and accumulate in macrophages that are present in the carotid artery plaque. MNPs are detectable in vivo by high-resolution MRI. The ability to image the presence or biological activity of specific molecules ("molecular imaging") in atherosclerotic plaques in vivo is of considerable interest. Assessment of molecular information in vivo requires high-affinity, target-specific contrast agents, with marked signal amplification, and high-resolution imaging modalities, such as magnetic resonance. Most of the available paramagnetic magnetic MRI contrast agent constructs, however, are not capable of delivering a large amount of gadolinium ions to induce a large MRI signal. Moreover, some of the MRI contrast agent molecules may be too large to have free access to biochemical epitopes within the vascular subendothelium of atherosclerotic plaques. The role of specific enhancers deserves therefore further investigation (Corti and Fuster 2011).

Another new and promising technique to image biological plaque activity in atherosclerotic plaques is near-infrared fluorescence (NIRF) imaging. This technique operates in the near-infrared spectrum of light and uses activatable probes that provide fluorescent images to detect enzymatic action of proteolytic enzymes such as MMPs and CCPs. Probes, such as gelatinase-activated (Deguchi et al. 2006) or cathepsin B-sensitive agents (Chen et al. 2002), are conjugated with NIRF fluorochromes. These probes produce very low background fluorescence and after activation produce a profound amplification of fluorescence. This way, vulnerable plaques with high proteolytic activity can be identified—at this stage only ex vivo or in animal studies. The first NIRF application in human carotid artery plaques was reported by Wallis de Vries et al. who detected MMP-2 and MMP-9 in a carotid endarterectomy specimen (Fig. 21.7) (Wallis de Vries et al. 2009). Other targets, like the inflammatory molecule vascular cell adhesion molecule-1 (VCAM-1) receptor expression in carotid artery plaques, can be imaged in vivo with fluorescence imaging, but their value is unknown (Nahrendorf et al. 2006). It will take technical developments and preclinical toxicity testing before in vivo studies in humans can be performed with NIRF. Furthermore, the reporter capabilities and specific cellular distribution in vivo need to be understood, and technical aspects, such as dose-finding studies of a fluorescent tracer and timing of imaging, need to be improved to obtain optimal fluorescence signals of a plaque in situ.

In conclusion, several radiopharmaceuticals are available to image different processes of the vulnerable plaque. Hybrid imaging will increase the accuracy of plaque identification. New technique developments will support this.

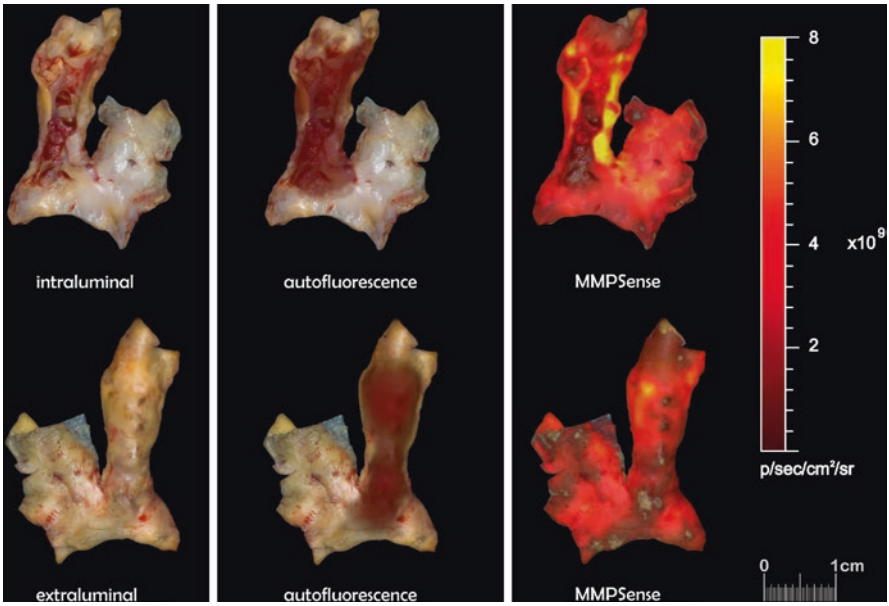

Fig. 21.7 MMPSense 680 fluorescence probe enables mapping of differential MMP activity in endarterectomized atherosclerotic plaques. Carotid endarterectomy specimen in white light (left), near-infrared fluorescence signal before (autofluorescence, middle) and after incubation with MMP-sensitive activatable fluorescent probe (MMPSense, right) within the IVIS Spectrum (bioluminescence and fluorescence in vivo imaging system). After incubation with MMPSense, highlighted hot spots were identified both at the intraluminal and extraluminal side, most present in the origin of the internal carotid artery and at the level of the common carotid bulb. Spots indicated by the frames were excised and processed for in situ zymography, real-time reverse-transcriptase polymerase chain reaction, and morphological analysis. The intensity of the NIRF signals obtained throughout the plaque is expressed as number of photons/s/cm^2/steradian (Wallis de Vries et al. 2009)

References

Annovazzi A, Bonanno E, Arca M, D'Alessandria C, Marcoccia A, Spagnoli LG et al (2006) 99mTc-interleukin-2 scintigraphy for the in vivo imaging of vulnerable atherosclerotic plaques. Eur J Nucl Med Mol Imaging 33(2):117–126

Bamford J, Sandercock P, Dennis M, Burn J, Warlow C (1991) Classification and natural history of clinically identifiable subtypes of cerebral infarction. Lancet 337(8756):1521–1526

Barger AC, Beeuwkes R III, Lainey LL, Silverman KJ (1984) Hypothesis: vasa vasorum and neovascularization of human coronary arteries. A possible role in the pathophysiology of atherosclerosis. N Engl J Med 310(3):175–177

Blankenberg FG, Backer MV, Levashova Z, Patel V, Backer JM (2006) In vivo tumor angiogenesis imaging with site-specific labeled (99m)Tc-HYNIC-VEGF. Eur J Nucl Med Mol Imaging 33(7):841–848

Boyle JJ, Wilson B, Bicknell R, Harrower S, Weissberg PL, Fan TP (2000) Expression of angiogenic factor thymidine phosphorylase and angiogenesis in human atherosclerosis. J Pathol 192(2):234–242

Bucerius J, Schmaljohann J, Bohm I, Palmedo H, Guhlke S, Tiemann K et al (2008) Feasibility of 18F-fluoromethylcholine PET/CT for imaging of vessel wall alterations in humans—first results. Eur J Nucl Med Mol Imaging 35(4):815–820

Bucerius J, Duivenvoorden R, Mani V, Moncrieff C, Rudd JH, Calcagno C et al (2011) Prevalence and risk factors of carotid vessel wall inflammation in coronary artery disease patients: FDG-PET and CT imaging study. JACC Cardiovasc Imaging 4(11):1195–1205

Chen J, Tung CH, Mahmood U, Ntziachristos V, Gyurko R, Fishman MC et al (2002) In vivo imaging of proteolytic activity in atherosclerosis. Circulation 105(23):2766–2771

Chowdhury MM, Tarkin JM, Evans NR, Le E, Warburton EA, Hayes PD et al (2018) 18F-FDG uptake on PET/CT in symptomatic versus asymptomatic carotid disease: a meta-analysis. Eur J Vasc Endovasc Surg 56(2):172–179

Collingridge DR, Carroll VA, Glaser M, Aboagye EO, Osman S, Hutchinson OC et al (2002) The development of [(124)I]iodinated-VG76e: a novel tracer for imaging vascular endothelial growth factor in vivo using positron emission tomography. Cancer Res 62(20):5912–5919

Corti R, Fuster V (2011) Imaging of atherosclerosis: magnetic resonance imaging. Eur Heart J 32(14):1709–1719

Dangas G, Mehran R, Harpel PC, Sharma SK, Marcovina SM, Dube G et al (1998) Lipoprotein(a) and inflammation in human coronary atheroma: association with the severity of clinical presentation. J Am Coll Cardiol 32(7):2035–2042

Davies JR, Rudd JH, Fryer TD, Graves MJ, Clark JC, Kirkpatrick PJ et al (2005) Identification of culprit lesions after transient ischemic attack by combined 18F fluorodeoxyglucose positron-emission tomography and high-resolution magnetic resonance imaging. Stroke 36(12):2642–2647

Deguchi JO, Aikawa M, Tung CH, Aikawa E, Kim DE, Ntziachristos V et al (2006) Inflammation in atherosclerosis: visualizing matrix metalloproteinase action in macrophages in vivo. Circulation 114(1):55–62

Derlin T, Richter U, Bannas P, Begemann P, Buchert R, Mester J et al (2010) Feasibility of 18F-sodium fluoride PET/CT for imaging of atherosclerotic plaque. J Nucl Med 51(6):862–865

Derlin T, Wisotzki C, Richter U, Apostolova I, Bannas P, Weber C et al (2011a) In vivo imaging of mineral deposition in carotid plaque using 18F-sodium fluoride PET/CT: correlation with atherogenic risk factors. J Nucl Med 52(3):362–368

Derlin T, Toth Z, Papp L, Wisotzki C, Apostolova I, Habermann CR et al (2011b) Correlation of inflammation assessed by 18F-FDG PET, active mineral deposition assessed by 18F-fluoride PET, and vascular calcification in atherosclerotic plaque: a dual-tracer PET/CT study. J Nucl Med 52(7):1020–1027

Di Gialleonardo V, Signore A, Glaudemans AW, Dierckx RA, De Vries EF (2012) N-(4-18F-Fluorobenzoyl)Interleukin-2 for PET of human-activated T lymphocytes. J Nucl Med 53(5):679–686

Dweck MR, Chow MW, Joshi NV, Williams MC, Jones C, Fletcher AM et al (2012) Coronary arterial 18F-sodium fluoride uptake: a novel marker of plaque biology. J Am Coll Cardiol 59(17):1539–1548

Elkind MS, Rundek T, Sciacca RR, Ramas R, Chen HJ, Boden-Albala B et al (2005) Interleukin-2 levels are associated with carotid artery intima-media thickness. Atherosclerosis 180(1):181–187

Falk E (2006) Pathogenesis of atherosclerosis. J Am Coll Cardiol 47(8 Suppl):C7–C12

Faust A, Wagner S, Law MP, Hermann S, Schnockel U, Keul P et al (2007) The nonpeptidyl caspase binding radioligand (S)-1-(4-(2-[18F]Fluoroethoxy)-benzyl)-5-[1-(2-methoxymethylpyrrolidinyl)sulfonyl]isatin ([18F]CbR) as potential positron emission tomography-compatible apoptosis imaging agent. Q J Nucl Med Mol Imaging 51(1):67–73

Ferrara N, Davis-Smyth T (1997) The biology of vascular endothelial growth factor. Endocr Rev 18(1):4–25

Forster S, Rominger A, Saam T, Wolpers S, Nikolaou K, Cumming P et al (2010) 18F-fluoroethylcholine uptake in arterial vessel walls and cardiovascular risk factors: correlation in a PET-CT study. Nuklearmedizin 49(4):148–153

Frias JC, Williams KJ, Fisher EA, Fayad ZA (2004) Recombinant HDL-like nanoparticles: a specific contrast agent for MRI of atherosclerotic plaques. J Am Chem Soc 126(50):16316–16317

Fujimoto S, Hartung D, Ohshima S, Edwards DS, Zhou J, Yalamanchili P et al (2008) Molecular imaging of matrix metalloproteinase in atherosclerotic lesions: resolution with dietary modification and statin therapy. J Am Coll Cardiol 52(23):1847–1857

Gerber HP, Ferrara N (2005) Pharmacology and pharmacodynamics of bevacizumab as monotherapy or in combination with cytotoxic therapy in preclinical studies. Cancer Res 65(3):671–680

Giannotti N, O'Connell MJ, Foley SJ, Kelly PJ, McNulty JP (2017) Carotid atherosclerotic plaques standardised uptake values: software challenges and reproducibility. EJNMMI Res 7(1):39

Glaudemans AW, Slart RH, Bozzao A, Bonanno E, Arca M, Dierckx RA et al (2010) Molecular imaging in atherosclerosis. Eur J Nucl Med Mol Imaging 37(12):2381–2397

Golestani R, Zeebregts CJ, Terwisscha van Scheltinga AG, Lub-de Hooge MN, van Dam GM, Glaudemans AW et al (2013) Feasibility of VEGF imaging in human atherosclerotic plaque using ^{89}Zr-bevacizumab positron emission tomography. Mol Imaging 12(4):235–243

Haider N, Hartung D, Fujimoto S, Petrov A, Kolodgie FD, Virmani R et al (2009) Dual molecular imaging for targeting metalloproteinase activity and apoptosis in atherosclerosis: molecular imaging facilitates understanding of pathogenesis. J Nucl Cardiol 16(5):753–762

Halliday A, Mansfield A, Marro J, Peto C, Peto R, Potter J et al (2004) Prevention of disabling and fatal strokes by successful carotid endarterectomy in patients without recent neurological symptoms: randomised controlled trial. Lancet 363(9420):1491–1502

Hansson GK (2005) Inflammation, atherosclerosis, and coronary artery disease. N Engl J Med 352(16):1685–1695

Hermus L, Lefrandt JD, Tio RA, Breek JC, Zeebregts CJ (2010) Carotid plaque formation and serum biomarkers. Atherosclerosis 213(1):21–29

Holm PW, Slart RH, Zeebregts CJ, Hillebrands JL, Tio RA (2009) Atherosclerotic plaque development and instability: a dual role for VEGF. Ann Med 41(4):257–264

Hop H, de Boer SA, Reijrink M, Kamphuisen PW, de Borst MH, Pol RA et al (2019) 18F-sodium fluoride positron emission tomography assessed microcalcifications in culprit and non-culprit human carotid plaques. J Nucl Cardiol 26(4):1064–1075

Huang B, Law MW, Khong PL (2009) Whole-body PET/CT scanning: estimation of radiation dose and cancer risk. Radiology 251(1):166–174

Iuliano L, Signore A, Vallabajosula S, Colavita AR, Camastra C, Ronga G et al (1996) Preparation and biodistribution of 99m technetium labelled oxidized LDL in man. Atherosclerosis 126(1):131–141

Izquierdo-Garcia D, Davies JR, Graves MJ, Rudd JH, Gillard JH, Weissberg PL et al (2009) Comparison of methods for magnetic resonance-guided [18-F]fluorodeoxyglucose positron emission tomography in human carotid arteries: reproducibility, partial volume correction, and correlation between methods. Stroke 40(1):86–93

Jones CB, Sane DC, Herrington DM (2003) Matrix metalloproteinases: a review of their structure and role in acute coronary syndrome. Cardiovasc Res 59(4):812–823

Kato K, Schober O, Ikeda M, Schafers M, Ishigaki T, Kies P et al (2009) Evaluation and comparison of 11C-choline uptake and calcification in aortic and common carotid arterial walls with combined PET/CT. Eur J Nucl Med Mol Imaging 36(10):1622–1628

Kietselaer BL, Reutelingsperger CP, Heidendal GA, Daemen MJ, Mess WH, Hofstra L et al (2004) Noninvasive detection of plaque instability with use of radiolabeled annexin A5 in patients with carotid-artery atherosclerosis. N Engl J Med 350(14):1472–1473

Kolodgie FD, Petrov A, Virmani R, Narula N, Verjans JW, Weber DK et al (2003) Targeting of apoptotic macrophages and experimental atheroma with radiolabeled annexin V: a technique with potential for noninvasive imaging of vulnerable plaque. Circulation 108(25):3134–3139

Kurihara H, Honda N, Kono Y, Arai Y (2012) Radiolabelled agents for PET imaging of tumor hypoxia. Curr Med Chem 19(20):3282–3289

Laitinen I, Saraste A, Weidl E, Poethko T, Weber AW, Nekolla SG et al (2009) Evaluation of alphavbeta3 integrin-targeted positron emission tomography tracer 18F-galacto-RGD for imaging of vascular inflammation in atherosclerotic mice. Circ Cardiovasc Imaging 2(4):331–338

Lees AM, Lees RS, Schoen FJ, Isaacsohn JL, Fischman AJ, Mckusick KA et al (1988) Imaging human atherosclerosis with 99mTc-labeled low density lipoproteins. Arteriosclerosis 8(5):461–470

Libby P, Theroux P (2005) Pathophysiology of coronary artery disease. Circulation 111(25):3481–3488

Littlewood TD, Bennett MR (2003) Apoptotic cell death in atherosclerosis. Curr Opin Lipidol 14(5):469–475

Loftus IM, Naylor AR, Goodall S, Crowther M, Jones L, Bell PR et al (2000) Increased matrix metalloproteinase-9 activity in unstable carotid plaques. A potential role in acute plaque disruption. Stroke 31(1):40–47

Lu E, Wagner WR, Schellenberger U, Abraham JA, Klibanov AL, Woulfe SR et al (2003) Targeted in vivo labeling of receptors for vascular endothelial growth factor: approach to identification of ischemic tissue. Circulation 108(1):97–103

Marnane M, Merwick A, Sheehan OC, Hannon N, Foran P, Grant T et al (2012) Carotid plaque inflammation on 18F-fluorodeoxyglucose positron emission tomography predicts early stroke recurrence. Ann Neurol 71(5):709–718

Masteling MG, Zeebregts CJ, Tio RA, Breek JC, Tietge UJ, de Boer JF et al (2011) High-resolution imaging of human atherosclerotic carotid plaques with micro 18F-FDG PET scanning exploring plaque vulnerability. J Nucl Cardiol 18(6):1066–1075

Mauriello A, Servadei F, Sangiorgi G, Anemona L, Giacobbi E, Liotti D et al (2011) Asymptomatic carotid plaque rupture with unexpected thrombosis over a non-canonical vulnerable lesion. Atherosclerosis 218(2):356–362

Morgan AR, Rerkasem K, Gallagher PJ, Zhang B, Morris GE, Calder PC et al (2004) Differences in matrix metalloproteinase-1 and matrix metalloproteinase-12 transcript levels among carotid atherosclerotic plaques with different histopathological characteristics. Stroke 35(6):1310–1315

Nagengast WB, de Vries EG, Hospers GA, Mulder NH, de Jong JR, Hollema H et al (2007) In vivo VEGF imaging with radiolabeled bevacizumab in a human ovarian tumor xenograft. J Nucl Med 48(8):1313–1319

Naghavi M, Falk E, Hecht HS, Jamieson MJ, Kaul S, Berman D et al (2006) From vulnerable plaque to vulnerable patient--Part III: Executive summary of the Screening for Heart Attack Prevention and Education (SHAPE) Task Force report. Am J Cardiol 98(2A):2H–15H

Nahrendorf M, Jaffer FA, Kelly KA, Sosnovik DE, Aikawa E, Libby P et al (2006) Noninvasive vascular cell adhesion molecule-1 imaging identifies inflammatory activation of cells in atherosclerosis. Circulation 114(14):1504–1511

Nighoghossian N, Derex L, Douek P (2005) The vulnerable carotid artery plaque: current imaging methods and new perspectives. Stroke 36(12):2764–2772

Patlak CS, Blasberg RG, Fenstermacher JD (1983) Graphical evaluation of blood-to-brain transfer constants from multiple-time uptake data. J Cereb Blood Flow Metab 3(1):1–7

Pichler BJ, Kolb A, Nagele T, Schlemmer HP (2010) PET/MRI: paving the way for the next generation of clinical multimodality imaging applications. J Nucl Med 51(3):333–336

Rominger A, Saam T, Wolpers S, Cyran CC, Schmidt M, Foerster S et al (2009) 18F-FDG PET/CT identifies patients at risk for future vascular events in an otherwise asymptomatic cohort with neoplastic disease. J Nucl Med 50(10):1611–1620

Rossin R, Muro S, Welch MJ, Muzykantov VR, Schuster DP (2008) In vivo imaging of 64Cu-labeled polymer nanoparticles targeted to the lung endothelium. J Nucl Med 49(1):103–111

Rousset OG, Ma Y, Evans AC (1998) Correction for partial volume effects in PET: principle and validation. J Nucl Med 39(5):904–911

Rudd JHF, Warburton EA, Fryer TD, Jones HA, Clark JC, Antoun N et al (2002) Imaging atherosclerotic plaque inflammation with [F-18]-fluorodeoxyglucose positron emission tomography. Circulation 105(23):2708–2711

Sanidas EA, Mintz GS, Maehara A, Cristea E, Wennerblom B, Iniguez A et al (2012) Adverse cardiovascular events arising from atherosclerotic lesions with and without angiographic disease progression. JACC Cardiovasc Imaging 5(3 Suppl):S95–S105

Sayed S, Cockerill GW, Torsney E, Poston R, Thompson MM, Loftus IM (2009) Elevated tissue expression of thrombomodulatory factors correlates with acute symptomatic carotid plaque phenotype. Eur J Vasc Endovasc Surg 38(1):20–25

Schafers M, Riemann B, Kopka K, Breyholz HJ, Wagner S, Schafers KP et al (2004) Scintigraphic imaging of matrix metalloproteinase activity in the arterial wall in vivo. Circulation 109(21):2554–2559

Signore A, Capriotti G, Scopinaro F, Bonanno E, Modesti A (2003) Radiolabelled lymphokines and growth factors for in vivo imaging of inflammation, infection and cancer. Trends Immunol 24(7):395–402

Skajaa T, Cormode DP, Falk E, Mulder WJ, Fisher EA, Fayad ZA (2010) High-density lipoprotein-based contrast agents for multimodal imaging of atherosclerosis. Arterioscler Thromb Vasc Biol 30(2):169–176

Skalen K, Gustafsson M, Rydberg EK, Hulten LM, Wiklund O, Innerarity TL et al (2002) Subendothelial retention of atherogenic lipoproteins in early atherosclerosis. Nature 417(6890):750–754

Slart RH, Zeebregts CJ, Tio RA (2008) Can nuclear medicine shed light on the dark side of angiogenesis in cardiovascular disease? Nucl Med Commun 29(7):585–587

Sluimer JC, Daemen MJ (2009) Novel concepts in atherogenesis: angiogenesis and hypoxia in atherosclerosis. J Pathol 218(1):7–29

Sluimer JC, Kolodgie FD, Bijnens AP, Maxfield K, Pacheco E, Kutys B et al (2009) Thin-walled microvessels in human coronary atherosclerotic plaques show incomplete endothelial junctions relevance of compromised structural integrity for intraplaque microvascular leakage. J Am Coll Cardiol 53(17):1517–1527

Spagnoli LG, Mauriello A, Sangiorgi G, Fratoni S, Bonanno E, Schwartz RS et al (2004) Extracranial thrombotically active carotid plaque as a risk factor for ischemic stroke. JAMA 292(15):1845–1852

Szabo Z, Speth RC, Brown PR, Kerenyi L, Kao PF, Mathews WB et al (2001) Use of positron emission tomography to study AT1 receptor regulation in vivo. J Am Soc Nephrol 12(7):1350–1358

Takaya N, Yuan C, Chu B, Saam T, Polissar NL, Jarvik GP et al (2005) Presence of intraplaque hemorrhage stimulates progression of carotid atherosclerotic plaques: a high-resolution magnetic resonance imaging study. Circulation 111(21):2768–2775

Tarkin JM, Joshi FR, Evans NR, Chowdhury MM, Figg NL, Shah AV et al (2017) Detection of atherosclerotic inflammation by 68Ga-DOTATATE PET compared to [^{18}F]FDG PET imaging. J Am Coll Cardiol 69(14):1774–1791

Van de Wiele C, Oltenfreiter R (2006) Imaging probes targeting matrix metalloproteinases. Cancer Biother Radiopharm 21(5):409–417

van der Vaart MG, Meerwaldt R, Reijnen MM, Tio RA, Zeebregts CJ (2008) Endarterectomy or carotid artery stenting: the quest continues. Am J Surg 195(2):259–269

Virmani R, Kolodgie FD, Burke AP, Finn AV, Gold HK, Tulenko TN et al (2005) Atherosclerotic plaque progression and vulnerability to rupture: angiogenesis as a source of intraplaque hemorrhage. Arterioscler Thromb Vasc Biol 25(10):2054–2061

Wallis de Vries B, Hillebrands JL, van Dam GM, Tio RA, de Jong JS et al (2009) Images in cardiovascular medicine. Multispectral near-infrared fluorescence molecular imaging of matrix metalloproteinases in a human carotid plaque using a matrix-degrading metalloproteinase-sensitive activatable fluorescent probe. Circulation 119(20):e534–e536

Yun M, Jang S, Cucchiara A, Newberg AB, Alavi A (2002) 18F FDG uptake in the large arteries: a correlation study with the atherogenic risk factors. Semin Nucl Med 32(1):70–76

PET in Brain Arteriovenous Malformations and Cerebral Proliferative Angiopathy

22

J. Marc C. van Dijk, Timo Krings, Janine Doorduin, and Riemer H. J. A. Slart

Contents

22.1 Introduction 630
22.2 Brain Arteriovenous Malformation 631
22.2.1 Clinical Presentation 631
22.2.2 Natural History 631
22.2.3 Treatment Options 633
22.3 Cerebral Proliferative Angiopathy 634
22.3.1 Clinical Presentation 635
22.3.2 Natural History 635
22.3.3 Treatment Options 636
22.4 Radiological Imaging 636
22.4.1 Cross-Sectional Imaging 636
22.4.2 Cerebral Catheter Angiography 637
22.5 PET Imaging of Brain AVM 638
22.5.1 Cerebral Blood Flow (CBF) 639
22.5.2 Cerebral Blood Volume (CBV) 641
22.5.3 Cerebral Metabolic Rate for Oxygen ($CRMO_2$) 642
22.5.4 Oxygen Extraction Factor (OEF) 642
22.5.5 Cerebral Metabolic Rate for Glucose (CMRGlc) 643
22.5.6 Effect of Treatment of BAVMs 643
22.5.7 Conclusion of the PET Imaging Findings 643

J. M. C. van Dijk (✉)
Department of Neurosurgery, University Medical Center Groningen, University of Groningen, Groningen, The Netherlands

T. Krings
Department of Medical Imaging, Toronto Western Hospital, University Health Network, Toronto, ON, Canada
e-mail: timo.krings@uhn.ca

J. Doorduin · R. H. J. A. Slart
Department of Nuclear Medicine and Molecular Imaging, University Medical Center Groningen, University of Groningen, Groningen, The Netherlands
e-mail: j.doorduin@umcg.nl; r.h.j.a.slart@umcg.nl

R. A. J. O. Dierckx et al. (eds.), *PET and SPECT in Neurology*,
https://doi.org/10.1007/978-3-030-53168-3_22

22.6 PET for Differentiation Between BAVM and CPA..... 644
22.6.1 Glucose Metabolism..... 644
22.6.2 Inflammation..... 646
22.6.3 Angiogenesis..... 648
References..... 648

Abstract

A brain arteriovenous malformation (BAVM) is a neurovascular entity that consists of a localized dense network of abnormal blood vessels (a nidus) that hold arteries shunting directly into veins in the absence of a capillary bed. In their natural history, BAVMs carry a risk of hemorrhage or other neurological complications, for which reason they are frequently treated. Cerebral proliferative angiopathy (CPA) is a different type of neurovascular malformation with distinct angiographic and clinical features that can be used to differentiate it from a classical BAVM. The basic difference between CPA and a BAVM is that CPA has normal brain tissue intermingled in-between its network of vessels. Treatment of CPA by surgery, radiosurgery, or embolization consequently harbors a high risk of neurological complications. As such, reliable diagnostic discrimination between CPA and BAVM is crucial to adequately treat patients. However, despite the fact that CPA has some characteristic imaging features, the differentiation between CPA and a brain AVM may be difficult. PET imaging as a technique that reveals functional brain tissue is therefore likely to be of additional diagnostic value.

22.1 Introduction

Vascular pathology in the central nervous system is subdivided on biological grounds into neurovascular neoplasms (hemangiomas) and true nonneoplastic neurovascular diseases. The latter group comprises a wide range of diseases, displaying a spectrum from the arterial aneurysms via the arteriovenous and capillary malformations to the venous and lymphatic disorders (Mulliken and Glowacki 1982).

This chapter focuses on pial arteriovenous (AV) malformations that corresponding to their definition shows an abnormal shunt between the supplying high-pressure arterial system and the draining low-pressure venous system, bypassing the standard intermediate capillary network of the brain parenchyma. Based on the nidus architecture, one may differentiate two types of AV malformations: a nidus type that shows a tangle of abnormal, thin-walled vessels in-between the arterial feeder and the venous draining system shunting the arterialized blood to the veins (AVM) and a fistulous type in which the artery directly joins the vein in the absence of a transitional network (AVF). Since AVFs in the brain are rare and nearly always related to hereditary hemorrhagic telangiectasia (Rendu-Osler-Weber syndrome), which is beyond the scope of this chapter, the emphasis will be on the pial nidus-type brain

AVM (BAVM) and an important differential diagnosis that may resemble an AVM but does indeed represent a different disease concerning angioarchitecture, pathomechanism, natural history, and treatment, the so-called cerebral proliferative angiopathy (CPA).

22.2 Brain Arteriovenous Malformation

A brain arteriovenous malformation (BAVM) is a congenital nonneoplastic neurovascular lesion that gives rise to—often high-flow—arteriovenous shunting, through a newly created subpial nidus of small pathological vessels (Fleetwood and Steinberg 2002). Its prevalence is approximately 18 per 100,000 in the adult population, giving rise to a yearly incidence of about 1 per 100,000. In comparison, intracranial aneurysms occur in a tenfold frequency. Bleeding from a BAVM accounts for 1–2% of all strokes and for 9% of spontaneous subarachnoid hemorrhages (Al-Shahi and Warlow 2001).

22.2.1 Clinical Presentation

Although a BAVM is considered a congenital lesion, the development of the malformation occurs during life. Clinical presentation is typically between 10 and 40 years of age. Most commonly, a BAVM presents with hemorrhage (~60%), followed by seizures (~34%), chronic headache (~31%), and focal neurological deficit (~15%) (Mast et al. 1995). The percentage of presentation with hemorrhage is found to be higher in the pediatric population than in adults (Fullerton et al. 2005). Also, the percentage of asymptomatic presentation is mounting due to the increasing application of advanced cross-sectional imaging (CT/MRI, Fig. 22.1).

22.2.2 Natural History

After the clinical presentation of a BAVM, the most important issue is the estimate of the natural disease course during the rest of the life of the patient. The choice of treatment modality is dependent on this estimate, as the success rate, and the risk of complications of the procedure should outweigh the risk of the BAVM in its natural history. However, studying the natural history poses a problem, since true observation prescribes the complete withdrawal of medical intervention, while medical ethics mandate every patient to be entitled to the best available care. Nevertheless, many studies have been performed over the decades, since in older days conservative management was the only treatment available.

The retrospective literature reports from the late twentieth century by Graf, Crawford, and Brown et al. (mean follow-up 4.8–10.2 years) revealed an overall hemorrhage risk of 2–3% per year regardless of the mode of presentation. In contrast to Crawford and Brown, the report by Graf pointed out a doubled hemorrhage

Fig. 22.1 Typical MR image of a BAVM

risk during the first year following presentation with a bleeding. None of these studies revealed a predictor for a differentiated natural history (Brown et al. 1988; Crawford et al. 1986; Graf et al. 1983).

Ondra et al. reported the first prospectively collected data in 1990, describing a series of 166 unoperated symptomatic patients with a mean follow-up of 23.7 years. The constant rate of (recurrent) hemorrhage was 4.0% per year, with a combined incidence of major morbidity and mortality of 2.7% (annual mortality rate 1.0%). There was no difference in the frequency of bleeding or death regardless of the way of presentation. Nevertheless, despite its design, this study also had significant limitations: the study inclusion dates were between 1942 and 1975, well before tomographic brain imaging was available, and in line with currently known annual hemorrhage rates, it is estimated that there has been a considerable under-detection of cases; probably only one-third of the cases were identified (262 reported versus 825 estimated) (Ondra et al. 1990).

Nowadays, the knowledge of the natural history of BAVMs is dictated by large prospectively kept databases, e.g., the Columbia AVM Databank, the Kaiser Permanente Medical Care Program Cohort, the Scottish Intracranial Vascular Malformation Study, and the Toronto BAVM Study Group. At the time of the 2006 publication by Stapf et al., the Columbia database covered 622 consecutive patients that during follow-up had an average annual hemorrhage rate of 2.8%. However, increasing age, hemorrhagic presentation, deep brain location, and exclusively deep venous drainage were recognized as independent predictors for hemorrhagic events

during natural history follow-up. Without risk factors the average annual hemorrhage risk was calculated 0.9%, while all risk factors together show a cumulative hemorrhage risk of 34.3% per year (Stapf et al. 2006). In 2009, Da Costa et al. reported the Toronto database to contain 759 patients, of which 678 patients had sufficient information for analysis. He calculated an overall annual hemorrhage rate of 4.6% for the entire cohort during follow-up. However, he as well found hemorrhagic presentation to be a significant independent predictor of future hemorrhage, whereas the presence of associated aneurysms and deep venous drainage showed a trend toward significance (da Costa et al. 2009). Based on these figures, the Columbia group launched a global multicenter randomized controlled trial aiming to include 800 adult patients with an unruptured BAVM to further elucidate its natural history (Fiehler and Stapf 2008).

22.2.3 Treatment Options

If conservative management of a BAVM is considered having a higher overall risk compared to active treatment, then several modalities are available. The main goal of BAVM treatment is the prevention of hemorrhage, which can be achieved by microsurgical resection of the nidus, endovascular embolization, radiosurgery, or a combination of these techniques.

Typical for a BAVM is that the brain tissue within the nidus is either absent or highly gliotic and nonfunctional (Anderson and Korbin 1958). This feature is eminent for a complete removal of the nidus without the risk for neurological complications. Partial treatment (obliteration less than 90%) has been reported to be insufficient to prevent hemorrhage, although partial endovascular embolization targeted toward intranidal aneurysms and larger fistulas may be beneficial (Meisel et al. 2002; Wikholm et al. 2001).

The selection of the optimal treatment modality is usually made by multidisciplinary consensus and based on the experience of the local treating team, for which recommendations have been published by the American Stroke Association (Ogilvy et al. 2001). These recommendations are based upon classification by the Spetzler-Martin grading scale that appreciates the size of the nidus, the pattern of venous drainage, and the eloquence of the surrounding parenchyma (Table 22.1).

Table 22.1 Spetzler-Martin grading scale for BAVMs. The grade is calculated by adding up the points for each feature (Spetzler and Martin 1986)

Feature	Appreciation
Nidus size	<3 cm—1 point
	3–6 cm—2 points
	>6 cm—3 points
Venous drainage	Superficial—0 point
	Deep—1 point
Nidus location	Not eloquent—0 point
	Eloquent—1 point

22.2.3.1 ASA Recommendations

- Surgical extirpation should be considered the primary mode of therapy for low-grade BAVMs (Spetzler-Martin grades I and II). Radiosurgery should be considered for small lesions when surgery may be associated with increased risk based on anatomical location or angioarchitecture.
- Multimodality treatment with endovascular embolization followed by surgical resection may be used in intermediate-grade BAVMs (Spetzler-Martin grade III).
- Invasive treatment of high-grade BAVMs (Spetzler-Martin grades IV and V) is associated with a high risk. Such BAVMs are generally managed conservatively.

Of course treatment decisions should be made on an individual basis and based on locally available expertise. For example, in the Toronto Western Hospital, single-compartment BAVMs (with a low Spetzler-Martin grade) are primarily treated by endovascular means.

The management of BAVM-associated aneurysms is a matter of debate and dependent on their size and location. We do not advocate the treatment of pre-nidal aneurysms as they are flow-related and regress following obliteration of the brain AVM. Intranidal aneurysms, on the other hand, are often the source of hemorrhage in acutely ruptured brain AVMs and may therefore represent an angioarchitectural point of weakness in an unruptured AVM warranting treatment.

22.3 Cerebral Proliferative Angiopathy

In 1989, Lasjaunias et al. launched the term cerebral proliferative angiopathy (CPA) for a peculiar type of large cerebral vascular malformations that demonstrated distinctive angiographic and clinical features discriminating it from a classical BAVM. In the Bicêtre neurovascular database of 1434 BAVMs, a subgroup of 49 patients (3.4%) with CPA was identified. It is more common in females (2:1) and presents at a mean age of 20 years (Lasjaunias et al. 2008).

Similar to a BAVM, CPA presents as a diffuse network of densely enhancing vascular although distinct angiographic characteristics:

- Discrepancy between the large size of the nidus and a relatively small shunting volume
- Absence of flow-related aneurysms
- Presence of diffuse angiogenesis
- Small caliber of a multitude of arteries and draining veins

The most striking difference between CPA and a BAVM is the existence of normal neural tissue intermingled with the abnormal vascular channels in CPA (Fig. 22.2). Since normally functioning brain is interspersed with abnormal vascular channels, the risk of neurological deficit in the surgical, radiosurgical, or endovascular obliterative treatment of CPA is highly increased compared to BAVM (Chin et al. 1992).

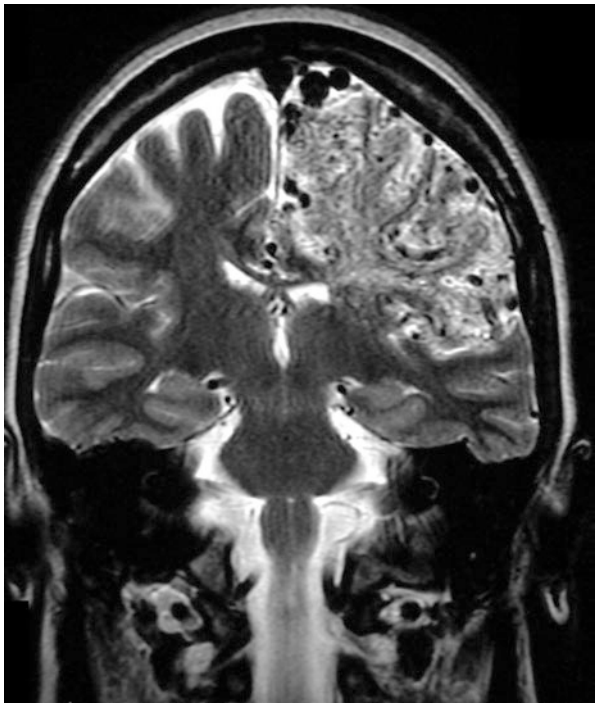

Fig. 22.2 The diffuse aspect of CPA on MRI with its characteristic lobar involvement

22.3.1 Clinical Presentation

Seizures, headaches, and transient ischemic attacks are far more frequent in CPA than in classical AVMs, while hemorrhages are exceedingly rare. Patients may present with progressive neurological deficits or with TIA-like symptoms indicating that hypoperfusion may be an important underlying pathological mechanism (Lasjaunias et al. 2008).

22.3.2 Natural History

The pathophysiology of CPA is unknown, but it is assumed to be an acquired condition induced by tissue hypoxemia related to local hypoperfusion. As such, transdural supply is a well-known feature of CPA, likely to be provoked by local hypoxemia. Ducreux et al. applied perfusion-weighted MRI in seven CPA patients to demonstrate hypoperfusion throughout the affected hemisphere (Ducreux et al. 2004). Therefore, stroke-like symptoms, e.g., TIAs and nonhemorrhagic neurological deficits, are likely to occur during the natural disease course. Hemorrhage occurs much less frequently as a presenting symptom than in a BAVM, but once a hemorrhage has occurred, there is a high risk for further hemorrhages (Lasjaunias et al. 2008).

22.3.3 Treatment Options

Since the typical gliotic plane of a BAVM nidus with the surrounding normal white matter is nonexistent in CPA, the surgical resection or endovascular embolization of CPA is impossible without damaging healthy brain parenchyma. As such, obliterative treatment possibilities of CPA carry a high risk of neurological deficits. In patients presenting with hemorrhages, partial targeted embolization may be employed if a target (i.e., an intranidal aneurysm) can be identified. Since the pathological mechanism is related to local hypoxemia, treatment should be targeted at increasing the blood supply to the affected hemisphere. Both in the series of Lasjaunias and in a recent case report by Ellis et al., the treatment of these lesions by pial synangiosis (burr hole treatment) leads to an increase in blood supply to the affected hemisphere and an amelioration of symptoms (including seizures, headaches, and TIA-like symptoms) (Ducreux et al. 2002a; Ellis et al. 2011).

22.4 Radiological Imaging

The differentiation between BAVM and CPA has large implications for the choice of the management strategy. Since it is not always possible to diagnose CPA on clinical grounds in the individual patient, but pathological specimens have proven a clear anatomical and functional difference between the disorders, determination is largely dependent on imaging techniques.

22.4.1 Cross-Sectional Imaging

With CT and MRI, the presence of a vascular malformation in the brain is well identifiable, but further discrimination between BAVM and CPA may be problematic. On CT and MRI, CPA presents as a diffuse network of densely enhancing vascular spaces intermingled with normal brain parenchyma. T1- and T2-WI show small, widely distributed flow voids that may involve multiple lobes or the entire hemisphere. In most cases, the primary lesion extends from the surface into the basal ganglia and thalamus and involves more than one vascular territory. Compared to the size of the nidus, relatively few draining vessels are seen on CT or MRI, and these are only moderately enlarged. Perfusion-weighted MRI (p-MRI) demonstrates perfusion abnormalities far beyond the boundaries of the morphological malformation seen on conventional MR sequences, so the disease actually affects the entire hemisphere. The nidus shows increased cerebral blood volume, slightly decreased TTP (time to peak), and prolonged mean transit time (MTT). Remote from the nidus, in normal-appearing cortical and subcortical areas, the TTP is increased, and the blood volume is decreased, indicating remote, widespread hypoperfusion. Lasjaunias et al. reported that in the majority (67%) of CPA cases, its localization was in-between the different vascular territories (watershed zone). In addition he noticed that in comparison with the size of the CPA nidus, there was a relative

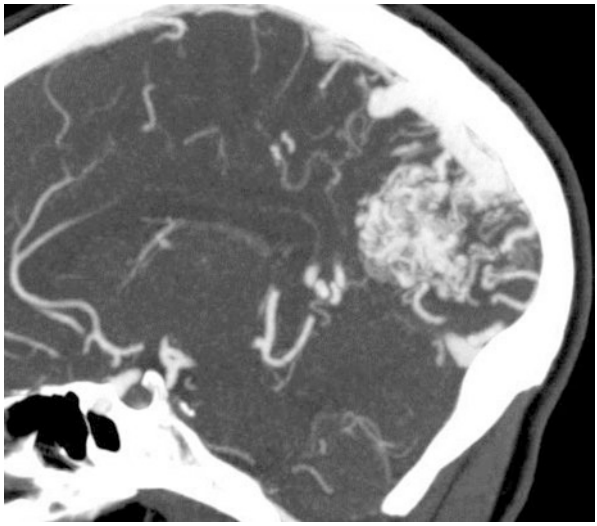

Fig. 22.3 CTA can depict the compact nidus of a BAVM but lacks the dynamic features

paucity of draining veins that were often only moderately enlarged (Lasjaunias et al. 2008). Another finding indicative of CPA is that both on CT and MRI, most vessels densely enhance with intravenous contrast because of relatively slow flow, while in BAVM, most vessels do not enhance due to the high flow and turbulence (Vargas and Castillo 2011).

A BAVM usually has a more or less compact nidus (Fig. 22.3). T2-WI shows punctate to linear flow voids in the subarachnoid space over the brain reflecting the dilated surface vessels. Within the brain, the punctate flow voids often lie within hyperintense, gliotic parenchyma. This gliosis may extend to the surrounding brain tissue. T1-WI shows highly variable signal within the AVM, due to turbulent flow, blood degradation products, and the variable flow rate in the veins. Different from CPA, the perfusion abnormalities do not extend far beyond the boundaries of the nidus (Ducreux et al. 2002b, 2004; Vargas and Castillo 2011; Lasjaunias et al. 2008). Recent studies by the Toronto group with BOLD-MRI have demonstrated a severely impaired cerebrovascular reserve in patients with CPA, which was also demonstrated in BAVMs in combination with seizures, although functional imaging with the BOLD technique in the past by Ducreux et al. failed to point out the functional aspect of the brain tissue in-between the CPA nidus (Ducreux et al. 2002a; Fierstra et al. 2010, 2011).

22.4.2 Cerebral Catheter Angiography

Lasjaunias et al. described the characteristics of cerebral catheter angiography in CPA in his launching paper in 2008. In BAVM pathognomonic dominant arterial feeders are present, while CPA is fed by multiple arteries that are not enlarged or are only moderately enlarged. Unlike classical AVMs, all arteries of the affected region

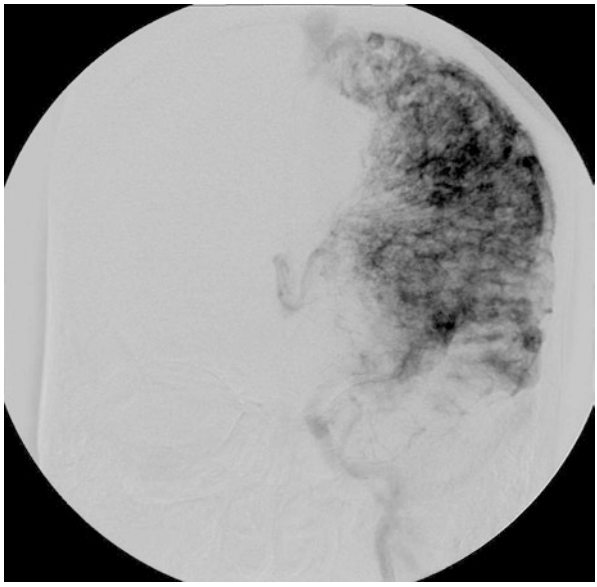

Fig. 22.4 Classical appearance of a CPA nidus on conventional X-ray angiography

contribute equally to the malformation. Stenosis of the proximal arteries is present in 40% and affects the internal carotid artery (ICA) and the proximal horizontal segments of the middle cerebral artery (M1) and anterior cerebral artery (A1). Flow-related proximal aneurysms can be present in BAVM but are not seen in CPA. The nidus has a classical appearance with scattered areas of "puddling" of contrast within what looks like capillary ectasias (Fig. 22.4). These persist into the late arterial and early venous phase. The nidus is usually fuzzy, poorly circumscribed, and >6 cm in diameter. Intranidal vessels show a capillary ectasia. Perinidal angiogenesis is often present and difficult to distinguish from the nidus proper. There is no high-flow fistulous component to the arteriovenous shunt, so early opacification of draining veins is uncommon. The size of the draining veins, the "shunt volume," and the time until the veins are visualized never "correspond" to the size of the nidus. CPA has a higher tendency for transdural supply from the external carotid circulation than BAVM (Lasjaunias et al. 2008).

22.5 PET Imaging of Brain AVM

The current classifications of BAVM are based on surgical anatomical features, such as the location and size of the nidus and the pattern of the venous drainage. However, as these attributes are mainly focused on the difficulty for interventional assessment of the vascular lesion, they do not allow for a functional-dynamic differentiation between a genuine BAVM and CPA. Nevertheless, as stated before, the distinction between BAVM and CPA is of great importance, since there are different therapeutic indications. With conventional radiological imaging techniques, i.e., CT, MRI,

and angiography, it is difficult to distinguish between BAVM and CPA. PET imaging though can be a useful adjunct, allowing for visualization of specific molecular processes, i.e., processes that are different in BAVM and CPA.

To date, PET imaging of BAVM has mainly been focused on the hemodynamic and metabolic effects of BAVMs. The first study on PET imaging of BAVM was published in 1977 and was a case report on a patient with a BAVM in the right posterior frontal region of the brain. Using [^{68}Ga]-EDTA, an early focal filling of the radioligand was found in the right frontal region, which was followed by a deep spreading pattern. The average distribution of the radioligand showed a rapid blood flow rate in the nidus as well as in adjacent tissue. The blood flow rate was (visually) found to be impaired in the area behind the nidus (Yamamoto et al. 1977).

After this first study on BAVM in the early days of PET research, most of the later PET studies focused on imaging of the cerebral blood flow (CBF), the cerebral blood volume (CBV), the cerebral metabolic rate for oxygen ($CMRO_2$), the oxygen extraction fraction (OEF), and cerebral metabolic rate for glucose (CMRGlc) using the radioligands [^{15}O]H_2O, [^{15}O]O_2, [^{15}O]CO_2, [^{15}O]CO, and [^{18}F]FDG (summarized in Table 22.2).

22.5.1 Cerebral Blood Flow (CBF)

In 1989, in a [^{15}O]O_2 study of two patients with a BAVM, it was shown that CBF was decreased in areas perifocal to the BAVM. This reduction was found to be close to the malformation in the patient that presented with seizures and was found at more distance of the malformation in the patient that suffered from repeated attacks of right hemiparesis (De Reuck et al. 1989). The finding of regionally decreased CBF was confirmed in a larger study by Iwama et al. in 2002. In a group of 24 patients with a BAVM, they studied CBF in a brain region perifocal to the BAVM and compared to both a contralateral brain region and an ipsilateral brain region distant from the BAVM. When comparing the average CBF of all 24 patients, no significant difference was found between the three brain regions. However, when patients were divided in two groups, i.e., with either high or low BAVM flow based on angiographic findings, a decreased CBF was found in those patients with a high BAVM flow in comparison with the contralateral brain region and, to a lesser extent, the ipsilateral brain region. Additionally, CBF was found to be increased in comparison with the contralateral brain region for medium- to large-sized (>5 cm) BAVMs (Iwama et al. 2002).

Nevertheless, two other studies reported that CBF was not affected by a BAVM, neither in the brain of the patient nor in comparison with control values. Sollevi et al. studied the effect of adenosine on CBF by PET in seven patients with a BAVM. The PET scan performed prior to the infusion of adenosine showed lower or similar CBF perifocal to the AVM compared to the contralateral hemisphere. The patients were however anesthetized (normoventilation), which may have interfered with the measurements of CBF (Sollevi et al. 1987). Though, an unaltered CBF was also demonstrated in patients with BAVMs that were non-anesthetized. When

Table 22.2 PET studies on metabolic and hemodynamic parameters in BAVM

Measure	Author	PET tracer	Finding	remark	
CBF	Sollevi et al. (1987)	$[^{15}O]H_2O$	↓/=	Perifocal to BAVM	Patients were under anesthesia during PET scan
	Tyler et al. (1989)	$[^{15}O]O_2$, $[^{15}O]CO_2$, $[^{15}O]CO$	=	Ipsilateral and contralateral to BAVM	In comparison with control values
	De Reuck et al. (1989)	$[^{15}O]O_2$	↓	Behind/distant from BAVM	
	Kaminaga et al. (1999)	$[^{15}O]O_2$	↓	In territory of the carotid artery, ipsilateral to BAVM	
	Iwama et al. (2002)	$[^{15}O]O_2$, $[^{15}O]CO_2$, $[^{15}O]CO$	↓	Perifocal to BAVM	Only in BAVM with high flow
	Kuroda et al. (2004)	$[^{15}O]O_2$	↓	Perifocal to BAVM	
CBV	Tyler et al. (1989)	$[^{15}O]O_2$, $[^{15}O]CO_2$, $[^{15}O]CO$	↑	Ipsilateral and contralateral to BAVM	In comparison with control values
	Fink (1992)	$[^{15}O]CO_2$	↑	Perifocal to BAVM	In both high- and low-flow perifocal tissue
	Iwama et al. (2002)	$[^{15}O]O_2$, $[^{15}O]CO_2$, $[^{15}O]CO$	↑	Perifocal to BAVM	
	Kuroda et al. (2004)	$[^{15}O]O_2$	↑	Perifocal to BAVM	
$CMRO_2$	Tyler et al. (1989)	$[^{15}O]O_2$, $[^{15}O]CO_2$, $[^{15}O]CO$	=	Ipsilateral and contralateral to BAVM	In comparison with control values
	De Reuck et al. (1989)	$[^{15}O]O_2$	↓	Behind BAVM	
	Fink (1992)	$[^{15}O]O_2$	↓	Perifocal to BAVM	In low-flow perifocal tissue
		$[^{15}O]O_2$	↑	Perifocal to BAVM	In high-flow perifocal tissue
	Kaminaga et al. (1999)	$[^{15}O]O_2$	=	In territory of the carotid artery, ipsilateral to BAVM	
	Iwama et al. (2002)	$[^{15}O]O_2$, $[^{15}O]CO_2$, $[^{15}O]CO$	=	Perifocal to BAVM	
	Kuroda et al. (2004)	$[^{15}O]O_2$	↓	Perifocal to BAVM	

Table 22.2 (continued)

Measure	Author	PET tracer	Finding	remark	
OEF	Tyler et al. (1989)	[^{15}O]O_2, [^{15}O]CO_2, [^{15}O]CO	=	Ipsilateral and contralateral to BAVM	In comparison with control values
	Fink (1992)	[^{15}O]O_2	↓	Perifocal to BAVM	In low-flow perifocal tissue
		[^{15}O]O_2	↑	Perifocal to BAVM	In high-flow perifocal tissue
	Kaminaga et al. (1999)	[^{15}O]O_2	=	In territory of the carotid artery, ipsilateral to BAVM	
	Iwama et al. (2002)	[^{15}O]O_2, [^{15}O]CO_2, [^{15}O]CO	↑	Perifocal to BAVM	
	Kuroda et al. (2004)	[^{15}O]O_2	↑	Perifocal to BAVM	
CMRGlc	Tyler et al. (1989)	[^{18}F]FDG	↓	Ipsilateral and contralateral to BAVM	Contralateral CMRGlc only decreased in case of large BAVM size
	Fink (1992)	[^{18}F]FDG	↓	Perifocal to BAVM	In low-flow perifocal tissue
		[^{18}F]FDG	=	Perifocal to BAVM	In high-flow perifocal tissue

compared to control values, CBF in both the ipsilateral and the contralateral hemisphere was found to be unaffected by BAVMs of small (<6 cm), medium (6–11 cm), or large size (>11 cm). In this study, the ipsilateral CBF was calculated as an average of four different regions in the hemisphere—excluding the BAVM—while the studies that report decreased CBF mainly included perifocal brain regions. Since the largest effect on CBF is expected in brain areas close to the BAVM, averaging different regions might explain why no decrease was found (Tyler et al. 1989).

22.5.2 Cerebral Blood Volume (CBV)

In contrast to CBF, CBV was unanimously found to be increased by three separate studies. Tyler et al. reported an increase in CBV in both the ipsilateral and contralateral hemisphere in small (<6 cm), medium (6–11 cm), and large (>11 cm) BAVMs. They additionally calculated the ratio of CBV to CBF and found that the ratios in both the ipsilateral and contralateral hemisphere were not different from control values for small-sized BAVMs but was increased for large-sized BAVMs. For medium-sized BAVMs, the ratio was only increased in the ipsilateral

hemisphere (Tyler et al. 1989). This finding was confirmed by Iwama et al., reporting that the CBV was increased in comparison with both a contralateral brain region and an ipsilateral brain region distant from the BAVM, for both small (<5 cm) and medium (>5 cm) BAVMs. It was also shown that the increased CBV did not depend on the BAVM flow, i.e., there was no difference in CBV between high- and low-flow BAVMs (as based on angiographic findings) (Iwama et al. 2002). Fink et al. also studied the effect of CBF on CBV, but they divided the patients in two groups according to the CBF in the perifocal brain region, measured by PET. They found that CBV was increased in both perifocal brain regions with high and low CBF when compared to a contralateral reference region (Fink 1992).

22.5.3 Cerebral Metabolic Rate for Oxygen ($CRMO_2$)

All but one of the PET studies mentioned above also measured the $CMRO_2$, reporting various results. The study by Tyler et al. reported no changes in CBF and an increase in CBV and found that the $CRMO_2$ in patients with a BAVM was not different from controls in either the ipsilateral or the contralateral hemisphere. $CRMO_2$ was unaffected by the size of the BAVM (Tyler et al. 1989). Similar findings for $CMRO_2$ were reported by Iwama et al., showing that $CRMO_2$ in the brain perifocal to the BAVM was not different from the contralateral brain and ipsilateral brain distant from the BAVM, despite the decrease in CBF and increase in CBV. The size of the BAVM or the flow within the BAVM (as based on angiographic findings) did not affect the $CMRO_2$ (Iwama et al. 2002). The group of Fink et al. did find changes in the $CRMO_2$ in patients with a BAVM that were divided into two groups according to the CBF in the perifocal brain region measured by PET. Patients with a low perifocal CBF showed a decreased perifocal $CMRO_2$ compared to the contralateral reference region. A perifocally increased $CMRO_2$ was however found in patients with high perifocal CBF (Fink 1992).

A decrease in $CRMO_2$ in brain regions perifocal to the BAVM was also found by De Reuck et al. in a small study with two patients (De Reuck et al. 1989).

22.5.4 Oxygen Extraction Factor (OEF)

In addition to the $CRMO_2$, the OEF was determined. Tyler et al. reported that the OEF in patient was comparable with controls (Tyler et al. 1989). Fink et al. showed that the changes in OEF were similar to those found for $CMRO_2$, i.e., perifocal to the BAVM, OEF was decreased and increased in patients with low- and high-flow BAVMs, respectively (Fink 1992). In contrast, although Iwama et al. did not find any changes in $CRMO_2$, an increase was found in the brain region perifocal to the BAVM compared to the contralateral brain region. This decrease was mainly found for patients with a high flow in the BAVM (as based on angiographic findings) and with a medium- to large-sized (>5 cm) BAVM (Iwama et al. 2002).

22.5.5 Cerebral Metabolic Rate for Glucose (CMRGlc)

So far, only two studies reported on CMRGlc in patients with a BAVM and both reported a decrease. In comparison with control values, Tyler et al. showed that the CMRGlc was decreased in the ipsilateral hemisphere in patients with small- (<6 cm), medium- (6–11 cm), and large (>11 cm)-sized BAVMs and in the contralateral hemisphere in patients with large-sized BAVMs only (Tyler et al. 1989). Fink et al. found that the CMRGlc was decreased in the brain region perifocal to the BAVM, as compared to a contralateral reference region, in patients with low CBF in the perifocal brain region (as measured by PET), but was not affected in patients with high CBF (Fink 1992).

22.5.6 Effect of Treatment of BAVMs

In addition to determining the effect of BAVMs on hemodynamics and metabolism, two studies focused on changes after treatment of the BAVM. Kaminaga et al. studied CBF, $CMRO_2$, and OEF in six patients with a BAVM before and after embolization, mainly to evaluate the effectiveness of this treatment. Before embolization the CBF in the ipsilateral territory of the internal carotid artery was decreased when compared to the contralateral territory. No differences between the ipsilateral and contralateral territories were found for $CMRO_2$ and OEF. Five to 20 weeks after embolization, CBF was found to be increased in the ipsilateral territory in all patients. The contralateral territory also showed increased CBF, although to a lesser extent. In contrast to the increase in CBF, $CMRO_2$ and OEF were not affected by embolization. Despite the increase in CBF, clinical symptoms were only found to be improved in three of the six patients (Kaminaga et al. 1999).

A similar study was performed by Kuroda et al. in a group of eight patients with a dural AVF. The CBF was decreased in all patients, CBV was increased in seven patients, $CMRO_2$ was decreased in seven patients, and OEF was increased in three patients, in the area that had been drained by the involved cortical veins. The eight patients underwent transvenous embolization, direct packing, or surgical excision, and a post-treatment scan was performed 4–8 weeks later. CBF and $CMRO_2$ were increased and decreased, respectively, in seven of the eight patients; CBV was decreased in all patients; and OEF was not affected by treatment. Clinical symptoms disappeared or improved in all eight patients (Kuroda et al. 2004).

22.5.7 Conclusion of the PET Imaging Findings

All literature reports taken together, the findings of PET imaging show a decreased CBF and an increased CBV in brain regions perifocal to the BAVM. While the decrease in perifocal CBF seems to be dependent on the flow in the BAVMs and their size, the CBV was increased independently from both flow and size. The

findings on $CRMO_2$ and OEF are inconclusive, which is at least in part due to the limited number of studies performed so far. Possibly, the latter measurements are more sensitive to methodological differences than CBF and CBV. The CMRGlc was measured in a limited number of studies, showing a consistent decrease.

The decrease in CBF—hypoperfusion—in areas perifocal to the BAVMs can be explained by multiple factors. First of all, it should be pointed out that the immediate perinidal regions are gliotic with an appropriate reduction in CBF and metabolism due to neuronal loss. Another mentioned possibility is the so-called steal phenomenon. This is thought to occur especially in large BAVMs where the intranidal vascular resistance is much lower than the resistance of vessels surrounding the BAVM. As a consequence the volume of blood directed to the BAVM increases (i.e., the BAVM "steals" the blood), and the normal vessels are deprived of CBF. This might lead to insufficient perfusion of brain tissue perifocal to the AVMs and as such to seizures or neurological deficits. In the literature the discussion about the existence of the steal phenomenon is ongoing. Other factors that may cause the decreased CBF are diffuse secondary vasospasms after hemorrhage, hydrocephalus, and dilatation of the veins due to impaired venous drainage. Independent of the cause of decreased CBF, the CBV can increase due to the small resistance in the nidus. Reduced $CMRO_2$ and CMRGlc might be a consequence of the decreased CBF and/or the presence of gliotic tissue surrounding the BAVM.

Note: Although PET imaging studies have found that CBF, CBV, $CMRO_2$, OEF, and CMRGlc are affected by the BAVM in perifocal and distant brain regions, none of the studies report on differentiation of the BAVMs. It might thus be the case that part of the patients studied presented with CPA rather than a classical BAVM.

22.6 PET for Differentiation Between BAVM and CPA

So far, PET imaging studies have focused on the hemodynamics and metabolism in BAVM, disregarding any subclassification. Nonetheless, PET techniques harbor the strong potential to differentiate between a classical BAVM and CPA.

22.6.1 Glucose Metabolism

One of the most important differences between classical BAVMs and CPA is the presence of identifiable neurons and normal brain tissue in-between the dense network of vessels in CPA, whereas in classical BAVMs, the nidus is surrounded by neuronal loss and gliosis. Loss of neurons and gliosis leads to a decreased function of brain tissue, and therefore a reduced CMRGlc can be expected in and directly surrounding the nidus. The normal brain tissue associated with CPA is expected to function normally, resulting in a normal CMRGlc. As such, although no studies have been performed so far, [^{18}F]FDG PET can be used as a method to distinguish between classical BAVM and CPA (Cases 22.1 and 22.2, Figs. 22.8 and 22.9).

Case 22.1

An otherwise healthy 51-year-old male patient complained of tinnitus and dizziness for several years. A vascular malformation with characteristics of CPA occupying the left cerebellar hemisphere was seen on MRI (Fig. 22.5) and DSA (Fig. 22.6).

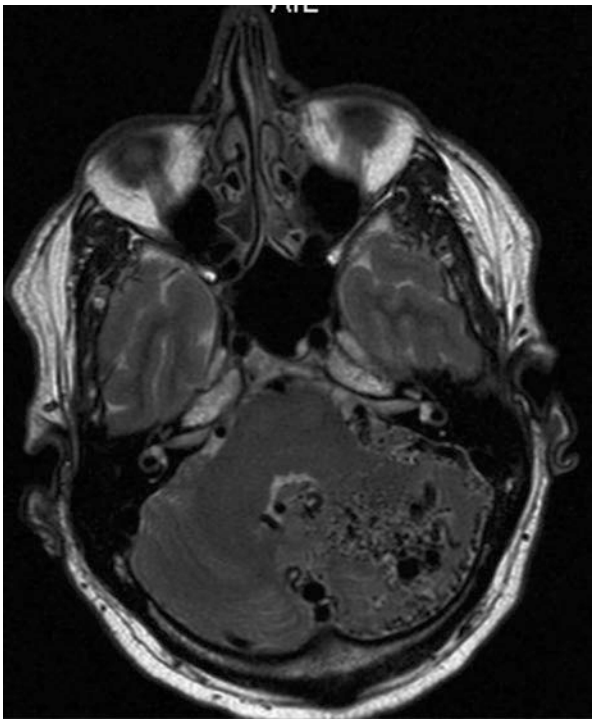

Fig. 22.5 T2-weighted image. Extensive vascular malformation consisting of a diffuse network of densely vascular spaces in the left cerebellar hemisphere

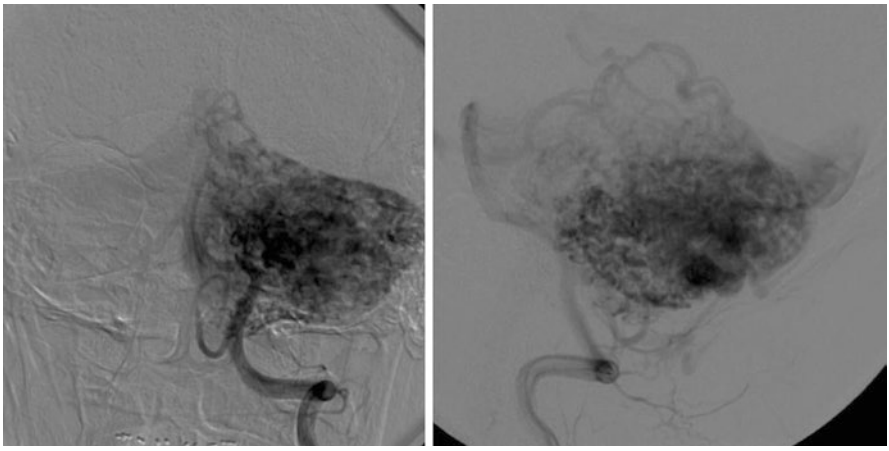

Fig. 22.6 Same case as in Fig. 22.5 with DSA. Left cerebellar vascular malformation, predominant arterial supply by vertebrobasilar arteries but also transdurally by left occipital artery. Note relatively small shunting volume and concomitant volume of draining veins

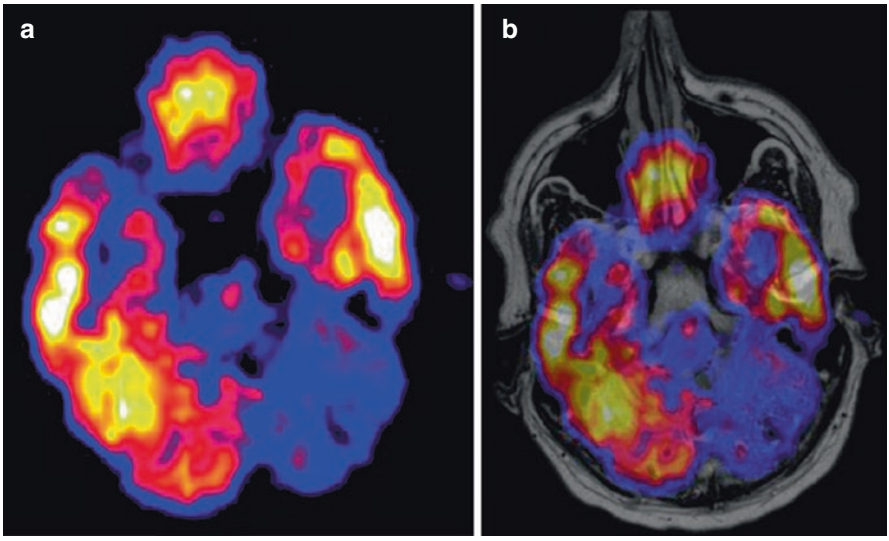

Fig. 22.7 Same case as in Fig. 22.5 showing hypometabolism in the left cerebellar hemisphere and supratentorial hypometabolism in the right (temporal) hemisphere on [^{18}F]FDG PET (**a**). Fusion of [^{18}F]FDG PET-MRI (**b**)

[^{18}F]FDG PET showed increased perfusion and decrease metabolism in the left hemisphere (Fig. 22.7). Symptoms show no progression to date and the patient remains untreated.

Case 22.2
See Figs. 22.8 and 22.9.

22.6.2 Inflammation

The neuronal loss and gliosis in the nidus of a classical BAVM may cause activation of the brain immune system. Inflammation in the brain triggers the activation of microglia (the macrophages of the brain that provide the first line of defense against invading pathogens or neuronal damage), the activation of astrocytes, and the infiltration of macrophages and lymphocytes. In histological specimens of a BAVM, it has been shown that macrophages, monocytes, and microglia are scattered around the vascular wall and brain parenchyma. In contrast, T- and B-lymphocytes were found to be rare in the BAVM tissue (Chen et al. 2008). The presence of macrophages, monocytes, and microglia may be a potential target for the differentiation between BAVMs and CPA, since in the absence of neuronal loss and gliosis, inflammation is most likely less prominent in CPA, if present at all. Upon activation, microglia shows an increased expression of the translocator protein (TSPO) that is located in the outer mitochondrial membrane. Infiltrating macrophages express the same receptor. The PET tracer [^{11}C]PK11195 binds to the TSPO and can thus be used for imaging of microglia activation and infiltrating macrophages. [^{11}C]PK11195

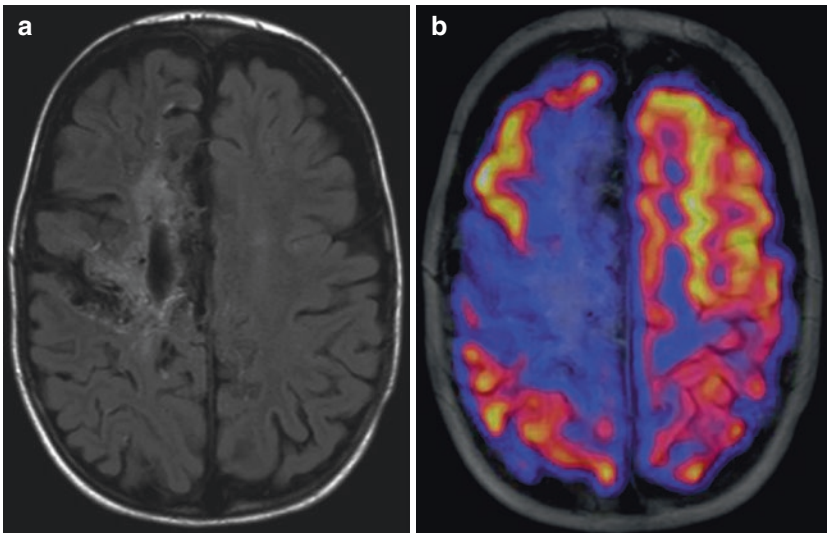

Fig. 22.8 Case of a 5-year-old boy with CPA. T2-weighted FLAIR MRI transaxial slide (**a**), and fused [^{18}F]FDG PET-MRI (**b**), showing a more extended area of hypometabolism of the right cortex, especially at the frontal cortex compared to the MRI

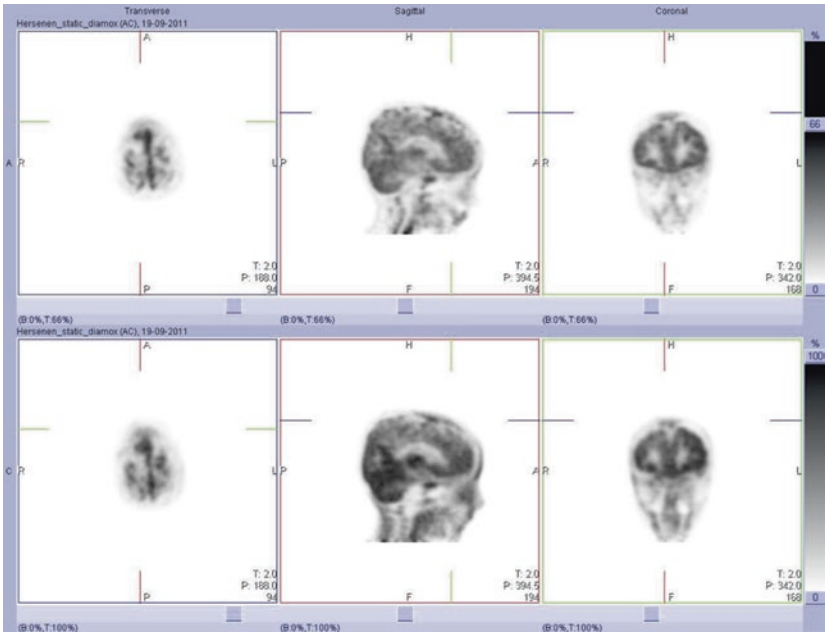

Fig. 22.9 Same case as in Fig. 22.8: [^{15}O]H_2O PET brain image. Upper row shows water perfusion during rest. The lower row shows water perfusion 10 min after acetazolamide i.v., to quantify stress-induced ischemia. During rest reduced perfusion is noticed in the right frontal and medial cortex. During acetazolamide stress the perfusion is further reduced in this cortical area, especially in relation to the increased perfusion of the normal left cortex

PET has been used to assess the role of neuroinflammation in many neurological and also psychiatric disorders (Doorduin et al. 2008) and might therefore be a potent tool for distinguishing CPA from BAVMs.

22.6.3 Angiogenesis

Another feature that distinguishes CPA from BAVMs is the formation of new blood vessels, i.e., angiogenesis (Lasjaunias et al. 2008). The exact reason why angiogenesis takes place in CPA is not known, but it is probably induced in response to cortical ischemia. This ischemia is not related to a previous hemorrhagic or traumatic event, which makes the angiogenesis a pathognomical feature of CPA. PET imaging of angiogenesis is thus a potential tool to distinguish CPA from a classical BAVM. One of the signal proteins that are produced by cells to stimulate angiogenesis is vascular endothelial growth factor (VEGF). The ischemic brain tissue in CPA is likely producing VEGF that can be used as a target for PET imaging. VEGF is known for its important role in tumor angiogenesis. In order to stop tumor growth or stimulate tumor necrosis, antibodies against VEGF have been developed. One the most widely used humanized monoclonal antibody is bevacizumab that has been shown to inhibit tumor growth. Bevacizumab has been labeled with the PET isotope [^{89}Zr] and was found to visualize VEGF expression in tumors in mice (Nagengast et al. 2007, 2010). Also, [^{111}In]bevacizumab for SPECT studies could visualize melanoma lesions in patients with stage III/IV melanoma (Nagengast et al. 2011) or even for the detection of angiogenetic-mediated atherosclerosis (Golestani et al. 2013). In theory, [^{89}Zr]bevacizumab PET can as such provide a tool for distinguishing CPA from classical BAVMs and play a role in the decision for optimal treatment, preventing the risk for treatment-induced damage to the healthy brain damage in CPA. On that basis, another promising PET tracer is [^{18}F]-labeled RGD, which can visualize the $\alpha_v\beta_3$ integrin expression as a marker of vascular endothelium activity (Beer et al. 2011).

References

Al-Shahi R, Warlow C (2001) A systematic review of the frequency and prognosis of arteriovenous malformations of the brain in adults. Brain 124:1900–1926

Anderson FM, Korbin MA (1958) Arteriovenous anomalies of the brain; a review and presentation of 37 cases. Neurology 8:89–101

Beer AJ, Kessler H, Wester H-J, Schwaiger M (2011) PET imaging of integrin αVβ3 expression. Theranostics 1:48–57

Brown RD, Wiebers DO, Forbes G et al (1988) The natural history of unruptured intracranial arteriovenous malformations. J Neurosurg 68:352–357. https://doi.org/10.3171/jns.1988.68.3.0352

Chen Y, Zhu W, Bollen AW et al (2008) Evidence of inflammatory cell involvement in brain arteriovenous malformations. Neurosurgery 62:1340–1349; discussion 1349–1350. https://doi.org/10.1227/01.neu.0000333306.64683.b5

Chin LS, Raffel C, Gonzalez-Gomez I et al (1992) Diffuse arteriovenous malformations: a clinical, radiological, and pathological description. Neurosurgery 31:863–868; discussion 868–869

Crawford PM, West CR, Chadwick DW, Shaw MD (1986) Arteriovenous malformations of the brain: natural history in unoperated patients. J Neurol Neurosurg Psychiatry 49:1–10

da Costa L, Wallace MC, ter Brugge KG et al (2009) The natural history and predictive features of hemorrhage from brain arteriovenous malformations. Stroke 40:100–105. https://doi.org/10.1161/STROKEAHA.108.524678

De Reuck J, Van Aken J, Van Landegem W, Vakaet A (1989) Positron emission tomography studies of changes in cerebral blood flow and oxygen metabolism in arteriovenous malformation of the brain. Eur Neurol 29:294–297

Doorduin J, de Vries EFJ, Dierckx RA, Klein HC (2008) PET imaging of the peripheral benzodiazepine receptor: monitoring disease progression and therapy response in neurodegenerative disorders. Curr Pharm Des 14:3297–3315

Ducreux D, Petit-Lacour MC, Marsot-Dupuch K et al (2002a) Functional MRI in symptomatic proliferative angiopathies. Neuroradiology 44:883–892. https://doi.org/10.1007/s00234-002-0871-2

Ducreux D, Petit-Lacour MC, Marsot-Dupuch K et al (2002b) MR perfusion imaging in a case of cerebral proliferative angiopathy. Eur Radiol 12:2717–2722. https://doi.org/10.1007/s00330-001-1293-y

Ducreux DD, Meder JFJ, Fredy DD et al (2004) MR perfusion imaging in proliferative angiopathy. Neuroradiology 46:105–112. https://doi.org/10.1007/s00234-003-1045-6

Ellis MJ, Armstrong D, Dirks PB (2011) Large vascular malformation in a child presenting with vascular steal phenomenon managed with pial synangiosis. J Neurosurg Pediatr 7:15–21. https://doi.org/10.3171/2010.10.PEDS10388

Fiehler J, Stapf C (2008) ARUBA–beating natural history in unruptured brain AVMs by intervention. Neuroradiology 50:465–467. https://doi.org/10.1007/s00234-008-0380-z

Fierstra J, Conklin J, Krings T et al (2010) Impaired peri-nidal cerebrovascular reserve in seizure patients with brain arteriovenous malformations. Brain 134:100–109. https://doi.org/10.1093/brain/awq286

Fierstra J, Spieth S, Tran L et al (2011) Severely impaired cerebrovascular reserve in patients with cerebral proliferative angiopathy. J Neurosurg Pediatr 8:310–315. https://doi.org/10.3171/2011.6.PEDS1170

Fink GR (1992) Effects of cerebral angiomas on perifocal and remote tissue: a multivariate positron emission tomography study. Stroke 23:1099–1105

Fleetwood IG, Steinberg GK (2002) Arteriovenous malformations. Lancet 359:863–873. https://doi.org/10.1016/S0140-6736(02)07946-1

Fullerton HJ, Achrol AS, Johnston SC et al (2005) Long-term hemorrhage risk in children versus adults with brain arteriovenous malformations. Stroke 36:2099–2104. https://doi.org/10.1161/01.STR.0000181746.77149.2b

Golestani R, Zeebregts CJ, Terwisscha van Scheltinga AG et al (2013) Feasibility of VEGF imaging in human atherosclerotic plaque using ^{89}Zr-bevacizumab positron emission tomography. Mol Imaging 12(4):235–243

Graf CJ, Perret GE, Torner JC (1983) Bleeding from cerebral arteriovenous malformations as part of their natural history. J Neurosurg 58:331–337. https://doi.org/10.3171/jns.1983.58.3.0331

Iwama T, Hayashida K, Takahashi JC et al (2002) Cerebral hemodynamics and metabolism in patients with cerebral arteriovenous malformations: an evaluation using positron emission tomography scanning. J Neurosurg 97:1314–1321. https://doi.org/10.3171/jns.2002.97.6.1314

Kaminaga T, Hayashida K, Iwama T, Nishimura T (1999) Hemodynamic changes around cerebral arteriovenous malformation before and after embolization measured with PET. J Neuroradiol 26:236–241

Kuroda S, Furukawa K, Shiga T et al (2004) Pretreatment and posttreatment evaluation of hemodynamic and metabolic parameters in intracranial dural arteriovenous fistulae with cortical venous reflux. Neurosurgery 54:585–591; discussion 591–2

Lasjaunias PL, Landrieu P, Rodesch G et al (2008) Cerebral proliferative angiopathy: clinical and angiographic description of an entity different from cerebral AVMs. Stroke 39:878–885. https://doi.org/10.1161/STROKEAHA.107.493080

Mast H, Mohr JP, Osipov A et al (1995) “Steal” is an unestablished mechanism for the clinical presentation of cerebral arteriovenous malformations. Stroke 26:1215–1220

Meisel HJ, Mansmann U, Alvarez H et al (2002) Effect of partial targeted N-butyl-cyano-acrylate embolization in brain AVM. Acta Neurochir 144:879–887; , discussion 888. https://doi.org/10.1007/s00701-002-0978-6

Mulliken JB, Glowacki J (1982) Hemangiomas and vascular malformations in infants and children: a classification based on endothelial characteristics. Plast Reconstr Surg 69:412–422

Nagengast WB, de Vries EG, Hospers GA et al (2007) In vivo VEGF imaging with radiolabeled bevacizumab in a human ovarian tumor xenograft. J Nucl Med 48:1313–1319. https://doi.org/10.2967/jnumed.107.041301

Nagengast WB, de Korte MA, Oude Munnink TH et al (2010) 89Zr-bevacizumab PET of early antiangiogenic tumor response to treatment with HSP90 inhibitor NVP-AUY922. J Nucl Med 51:761–767. https://doi.org/10.2967/jnumed.109.071043

Nagengast WB, Hooge MNL-D, van Straten EME et al (2011) VEGF-SPECT with ^{111}In-bevacizumab in stage III/IV melanoma patients. Eur J Cancer 47:1595–1602. https://doi.org/10.1016/j.ejca.2011.02.009

Ogilvy CS, Stieg PE, Awad I et al (2001) AHA scientific statement: recommendations for the management of intracranial arteriovenous malformations: a statement for healthcare professionals from a Special Writing Group of the Stroke Council, American Stroke Association. Stroke 32:1458–1471

Ondra SL, Troupp H, George ED, Schwab K (1990) The natural history of symptomatic arteriovenous malformations of the brain: a 24-year follow-up assessment. J Neurosurg 73:387–391. https://doi.org/10.3171/jns.1990.73.3.0387

Sollevi A, Ericson K, Eriksson L et al (1987) Effect of adenosine on human cerebral blood flow as determined by positron emission tomography. J Cereb Blood Flow Metab 7:673–678. https://doi.org/10.1038/jcbfm.1987.121

Spetzler RF, Martin NA (1986) A proposed grading system for arteriovenous malformations. J Neurosurg 65:476–483. https://doi.org/10.3171/jns.1986.65.4.0476

Stapf C, Mast H, Sciacca RR et al (2006) Predictors of hemorrhage in patients with untreated brain arteriovenous malformation. Neurology 66:1350–1355. https://doi.org/10.1212/01.wnl.0000210524.68507.87

Tyler JL, Leblanc R, Meyer E et al (1989) Hemodynamic and metabolic effects of cerebral arteriovenous malformations studied by positron emission tomography. Stroke 20:890–898

Vargas MC, Castillo M (2011) Magnetic resonance perfusion imaging in proliferative cerebral angiopathy. J Comput Assist Tomogr 35:33–38. https://doi.org/10.1097/RCT.0b013e3181ff1e79

Wikholm G, Lundqvist C, Svendsen P (2001) The Göteborg cohort of embolized cerebral arteriovenous malformations: a 6-year follow-up. Neurosurgery 49:799–805; discussion 805–806

Yamamoto YL, Thompson CJ, Meyer E et al (1977) Dynamic positron emission tomography for study of cerebral hemodynamics in a cross section of the head using positron-emitting 68Ga-EDTA and 77Kr. J Comput Assist Tomogr 1:43–56

PET Reveals Pathophysiology in Ischemic Stroke

23

Wolf-Dieter Heiss and Olivier Zaro-Weber

Contents

23.1 Introduction 652
23.2 The Concept of the Ischemic Penumbra in Patients with Ischemic Stroke 653
23.3 Penumbra Defined by PET 654
23.4 Comparison of PET and PW/DW-MRI 658
23.5 PET as a Surrogate Marker for Treatment Efficiency 660
23.6 PET for Prediction of "Malignant Infarction" 661
23.7 Microglia Activation as an Indicator of Inflammation 662
23.8 Complex Activation Studies 665
23.9 Conclusion 667
References 667

Abstract

The concepts of pathophysiology of ischemic brain damage as the basis for therapeutic strategies are derived from results of experiments in animal models. For their transfer into clinical application methods are required which permit repeated noninvasive quantitative determination of regional cerebral blood flow, oxygen consumption, and energy metabolism in patients after acute ischemic stroke. The method of choice for this purpose is still positron emission tomography (PET) which can be applied for high-resolution quantitative imaging of various parameters—cerebral blood flow, oxygen consumption, and glucose metabolism but

W.-D. Heiss (✉)
Max Planck Institute for Neurological Research, Cologne, Germany
e-mail: wdh@nf.mpg.de

O. Zaro-Weber
Max Planck Institute for Neurological Research, Cologne, Germany

Department of Neurology and Center for Stroke Research Berlin (CSB), Charité – Universitätsmedizin, Berlin, Germany
e-mail: zaroweber@nf.mpg.de

R. A. J. O. Dierckx et al. (eds.), *PET and SPECT in Neurology*,
https://doi.org/10.1007/978-3-030-53168-3_23

also of molecular events and of functional states—in humans as well as small animals. In this review some examples of PET applications for translational research in stroke are described.

One successful application of PET was regarding the transfer of the concept of the penumbra into the clinical management of acute ischemic stroke. Experiments in baboons and cats in the 1970s and 1980s defined blood flow values for functional disturbance and irreversible morphological damage, which could also be established by PET in patients with acute stroke. The progression of irreversible damage, the core of ischemia, into the functionally impaired area, the penumbra, could be followed in experimental models. Also the potential for recovery of these areas with reperfusion within the time window was demonstrated in these models, a result which formed the basis for thrombolysis and other reperfusion therapies. In animal models tracers for neuronal integrity were tested which are useful for early detection of irreversible tissue damage. These tracers can help in therapeutic decisions and in the prediction of malignant course after occlusion of large arteries. In the assessment of subacute and chronic pathophysiological changes after stroke, results from animal experiments indicated the importance of neuroinflammation, which can be visualized as microglia activation, for progression of damage into areas primarily not affected by ischemia and for prognosis of functional deficits. These inflammatory changes might also play an important role in increased amyloid deposition and might therefore be involved in the development of poststroke dementia. PET can also help to prove experimental concepts for improving recovery, e.g., by demonstrating the effect of repetitive transmagnetic stimulation for inhibiting contralateral overactivated cortex areas in rehabilitation therapy.

All these examples underline the role PET has played for translational research in stroke in the last 30 years. Its impact might even be increased by the advent of combined MR/PET equipment and the introduction of more sophisticated molecular tracers into clinical application.

23.1 Introduction

The energy demands of the nervous tissue are very high, and therefore sufficient blood supply to the brain must be maintained consistently. A normal adult male's brain containing approx. 130 billion neurons (21.5 billion in the neocortex) (Pakkenberg and Gundersen 1997) comprises only 2% of total body mass yet consumes at rest approximately 20% of the body's total basal oxygen consumption supplied by 16% of the cardiac blood output. The brain's oxygen consumption is almost entirely for the oxidative metabolism of glucose, which in normal physiological conditions is the almost exclusive substrate for the brain's energy metabolism (Clarke and Sokoloff 1999). It must be kept in mind that the glucose metabolized in neuronal cell bodies is mainly to support cellular vegetative and house-keeping functions, e.g., axonal transport, biosynthesis of nucleic acids, proteins, lipids, as

well as other energy-consuming processes not related directly to action potentials. Therefore, the rate of glucose consumption of neuronal cell bodies is essentially unaffected by neuronal functional activation. Increases in glucose consumption (and regional blood flow) evoked by functional activation are confined to synapse-rich regions, i.e., neuropil which contains axonal terminals, dendritic processes, and also the astrocytic processes that envelop the synapses. The magnitudes of these increases are linearly related to the frequency of action potentials in the afferent pathways, and increases in the projection zones occur regardless of whether the pathway is excitatory or inhibitory. Energy metabolism by functional activation is due mostly to stimulation of the Na^+K^+-ATPase activity to restore the ionic gradients across the cell membrane and the membrane potentials that were degraded by the spike activity and is rather high compared to the demand of neuronal cell bodies (Sokoloff 1999). Overall, 87% of the total energy consumed is required by signaling, mainly action potential propagation and postsynaptic ion fluxes, and only 13% is expended in maintaining membrane resting potential (Laughlin and Attwell 2001).

23.2 The Concept of the Ischemic Penumbra in Patients with Ischemic Stroke

Experimental work on the ischemic flow thresholds of brain tissue demonstrated the existence of two critical levels of decreased perfusion: first, a level representing the flow threshold for reversible functional failure (functional threshold); second, a lower threshold below which irreversible membrane failure and morphological damage occur (Astrup et al. 1977). The range of perfusion values between those limits was called the "ischemic penumbra" (Astrup et al. 1981), which was characterized by the potential for functional recovery without morphological damage, provided that local blood flow can be reestablished at a sufficient level and within a certain time window.

Whereas neuronal function is impaired immediately when blood flow drops below the threshold, the development of irreversible morphological damage is time dependent. Numerous studies were performed to investigate for how long brain tissue or individual cells tolerate ischemia of a given density. The interaction of severity and duration of ischemia in the development of irreversible cell damage can be studied by simultaneous recordings of cortical neuronal activity and local blood flow (Heiss and Rosner 1983). On the basis of a large number of neurons assessed during and after ischemia of varying degree and duration, it was possible to construct a discriminant curve representing the worst possible constellations of residual blood flow and duration of ischemia still permitting neuronal recovery. Typical points on this curve are blood flow rates of almost 0, 10, or 15 ml/100 g/min maintained for periods of 25, 40, and 80 min, respectively. Between 17 and 18 ml/100 g/min, the duration of ischemia tends to infinity, thus indicating that this low-flow state can lead to morphological damage when maintained for very long but still ill-defined periods of time. These results broaden the concept of ischemic penumbra: the potential for post-ischemic recovery of functionally impaired cells is determined

not only by the level of residual flow in the ischemic phase but also by the duration of the flow disturbance. Furthermore, a number of biological factors differing from neuron to neuron obviously govern the specific ischemic vulnerability of each cell.

Many interrelated biochemical mechanisms are involved in or contribute to ischemic cell damage, and therefore various markers can be used as indicators of ischemic thresholds and of reversible or irreversible functional deficits in animal experiments (reviews in (Heiss 1992; Hossmann 1994)).

23.3 Penumbra Defined by PET

The concept of the penumbra is based on neurophysiological and functional studies in experimental models of focal ischemia. The transfer of this concept into imaging modalities is difficult as most markers used in experimental studies necessitate invasive procedures, e.g., the detection of the mismatch between tissue ATP-depletion (for the definition of the infarction) and any biochemical disturbance that evolves at flow values in the penumbral range, such as lactic acidosis, inhibition of protein synthesis, or expression of the stress protein hsp 72 (Hossmann 2006; Hata et al. 1998). These invasive autoradiographic procedures can also not be applied to demonstrating the gradual disappearance of penumbra with increasing times of ischemia, the progression of the irreversible damage, or the recovery of functionally impaired tissue after reperfusion. In order to follow these pathophysiologic changes, noninvasive imaging modalities are required, which provide quantitative maps of several important physiologic variables, including regional cerebral blood flow (rCBF), regional cerebral blood volume (rCBV), regional oxygen extraction fraction (rOEF), and regional cerebral metabolic rate of oxygen ($rCMRO_2$) and of glucose (rCMRGlc). Even though there are approaches to implement these measurements in MRI (review in Lin and Powers 2018), up to now only positron emission tomography (PET) is able to measure these quantitative variables repeatedly.

Early PET studies in stroke have identified various tissue compartments within a brain territory compromised by ischemia (Ackerman et al. 1981; Baron et al. 1981a; Lenzi et al. 1982; Powers et al. 1985). Tissue with rCBF < 12 ml/100 g/min or $rCMRO_2$ < 65 μmol/100 g/min at the time of measurement (usually several hours after stroke) was found to be infarcted on late CTs. Relatively preserved $CMRO_2$ was an indicator of maintained neuronal integrity in regions with severely reduced CBF. This pattern, coined misery perfusion (Baron et al. 1981b), served as a definition of the penumbra that is characterized as the area of an increased oxygen extraction fraction (up to >80% from the normal value of approximately 40%). Regions with CBF between 12 and 22 ml/100 g/min have an unstable metabolic situation; infarction might develop if low-flow values persist. These PET studies allow the classification of three regions within the disturbed vascular territory: the core of ischemia with a flow <12 ml/100 g/min usually showing a transition into necrosis; a penumbra region with a flow between 12 and 22 ml/100 g/min of still viable tissue but with uncertain chances for infarction or recovery; and a hypoperfused area

(>22 ml/100 g/min) not primarily damaged by the lack of blood supply. It has to be kept in mind that the condition of the tissue is changing with time; the extent of the penumbra and its conversion into infarction is a dynamic process, and irreversible damage spreads from the core of ischemia to its border. This can be followed directly with advanced PET equipment, by which changes in the physiologic variables were studied after occlusion of the middle cerebral artery (MCA) in baboons and cats (review in Heiss 2000). A description of the experimental results, therefore, may help to understand findings in humans.

In the cat, changes after MCAO are immediate and severe. Sequential studies of rCBF, rCBV, rOEF, $rCMRO_2$, and rCMRGlc from a control before to the end point 24 h after MCA occlusion recorded an immediate decrease in CBF within the MCA territory to <30% of control upon arterial occlusion. $rCMRO_2$ was less diminished and was preserved at an intermediate level. Consequently, OEF was increased, indicating misery perfusion. In most instances, the misery perfusion condition was followed by a marked decrease in OEF, reflecting progressive impairment of metabolism and suggesting a transition to necrosis spreading from the core to the periphery of the ischemic territory. The infarcts were more or less complete 18–24 h after MCAO.

Reversible MCAO was studied in cats by reopening the MCA after 60 min. If OEF remained elevated throughout the ischemic episode, reperfusion prevented large infarcts involving cortical areas. In contrast, if the initial OEF increase disappeared during ischemia, extended post-ischemic hyperperfusion accompanied large reductions in $CMRO_2$ and rCMRGlc, large infarcts developed, and intracranial pressure increased fatally. These experimental findings from sequential studies and clinical investigations at different time-points after the attack (Fig. 23.1) (Heiss et al. 1992; Baron 1999) imply that the extent of the penumbra, i.e., of morphologically intact but functionally impaired tissue, depends on the time of measurement, relative to the onset of ischemia. The volume is large, and the flow values are low if the penumbra is defined in the first hours of ischemia; at this point of time, reperfusion strategies are most effective. The volume is small if defined later, limiting the efficacy of treatment.

Flow measurements in the first hours after a stroke permitted to identify various compartments of tissue and their contribution to the final infarct on CT and MRI. If the threshold for probable infarction was set to the conventional value of 12 ml/100 g/min and that for the upper limit of penumbra to 18 ml/100 g/min, a large compartment of the final infarct (70%) was perfused below 12 ml/100 g/min, i.e., at the level predicting necrosis; a smaller portion (18%) had flow values in the penumbra range (12–18 ml/100 g/min), and a fairly small compartment (12%) had perfusion at a higher level (Heiss et al. 1999a).

Measurement of blood flow values and determination of oxygen extraction fraction by PET require arterial blood sampling, and the clinical applicability is further limited by the complex logistics and instrumentation involved; isolated flow determinations at a single time-point might be confusing as long as the pattern over time is not known. A marker of neuronal integrity is needed that can identify irreversibly damaged tissue irrespective of the time elapsed since the vascular attack and irrespective of the variations in the blood flow over time, which also does not require

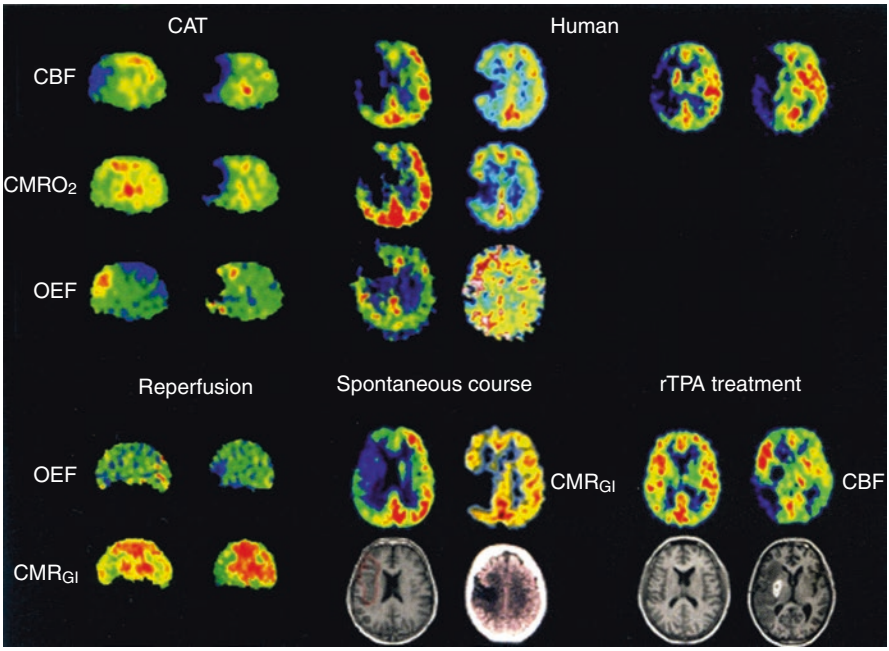

Fig. 23.1 Sequential PET images of CBF, $CMRO_2$, and OEF of MCA occlusion in cats compared to images of patients after stroke. Left columns: in the left cat, the progressive decrease of $CMRO_2$ and the reduction of OEF predict infarction and cannot benefit from reperfusion. Only if OEF is increased until start of reperfusion it can be salvaged (right cat). Middle columns: in the patient, the areas with preserved OEF are not infarcted and can survive in spontaneous course (posterior part of ischemic cortex in left, anterior part in right patient as indicated on late MRI and CT). Right columns: in patients receiving rtPA treatment, measurements of $CMRO_2$ and OEF are not feasible, but flow determinations show the effect. If reperfusion occurs early enough and before tissue damage, tissue can be salvaged (left patient). If reperfusion is achieved too late, tissue cannot be salvaged despite hyperperfusion in some parts (right patient)

arterial blood sampling. The central benzodiazepine receptor ligand flumazenil (FMZ) binds to the GABA receptor abundant in the cerebral cortex. These receptors are sensitive to ischemic damage and can therefore identify early neuronal loss. In transient MCA occlusion in cats, irrespective of the level of reperfusion, deficits in FMZ binding 2–3 h after MCAO were closely related to areas with severely depressed oxygen consumption and predicted the size of the final infarcts, whereas preserved FMZ binding indicated an intact cortex (Fig. 23.2a) (Heiss et al. 1997). Using FMZ as a marker of neuronal integrity and $H_2{}^{15}O$ for flow determinations, the pathophysiological changes early after ischemic stroke could be accurately specified: 55% of the volume of the final infarct had FMZ uptake decreased below the limit of 95% probability for infarction in the first hours after stroke; 21% of the final infarct had flow below 14 ml/100 g/min, the 95% probability threshold for survival in this study, but FMZ uptake above the critical value, thereby indicating penumbra tissue (Fig. 23.2b). In only 13% of the final infarct, neuronal integrity was indicated

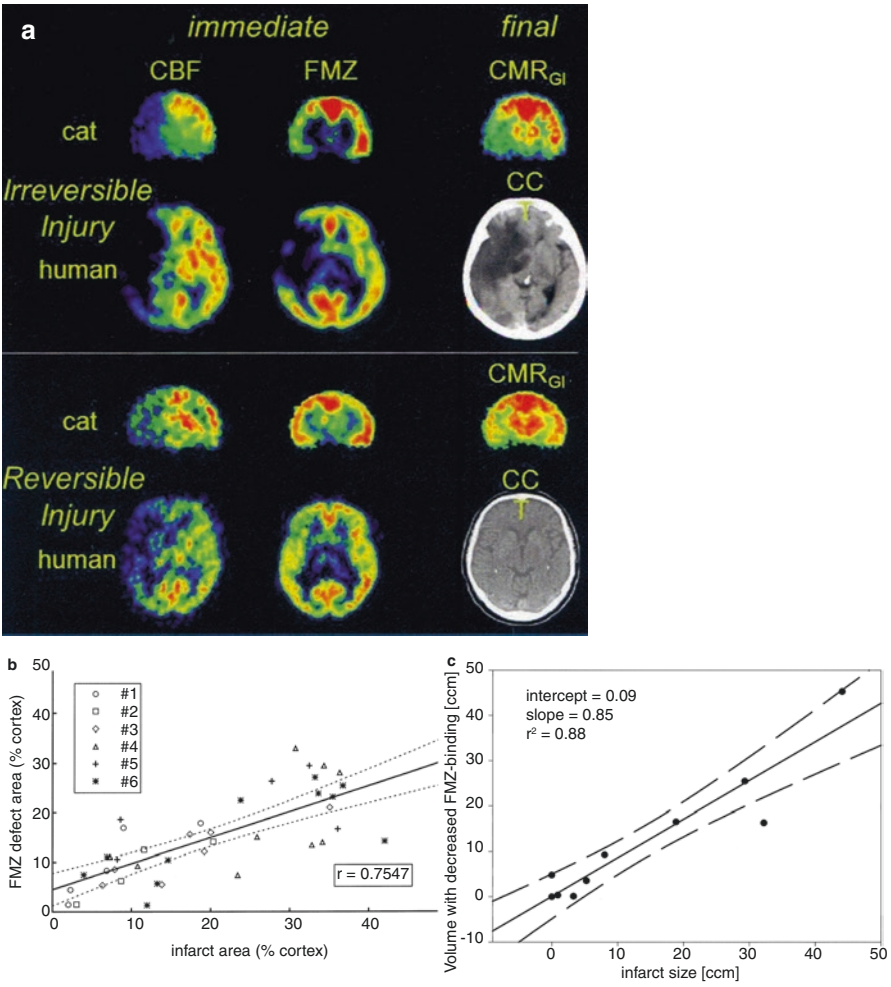

Fig. 23.2 Flumazenil as a molecular marker of neuronal integrity and for prediction of effect of reperfusion therapy. (**a**) PET images of early CBF and FMZ binding immediately following 1-h transient occlusion in cats or just before the start of thrombolysis in patients. Upper trace: both the cat and the human study demonstrate good correspondence of early deficits detected in FMZ images with final deficits depicted in CMR_{glc} and CCT images, respectively. Lower trace: in both cat ischemia and human stroke, moderate perfusional disturbance does not lead to severe deficits in FMZ binding in the early stage. Consequently, only minor final deficits, depicted in CMR_{glc} and CCT images, develop. (**b**) Linear regression between final infarct volume on MRI/CT and volume of decreased FMZ binding on initial PET. Broken lines indicate 95% confidence limits. (**c**) Comparison between size of infarct ~15 h after MCAO and extent of defect in FMZ uptake 2–3 h after reperfusion following 1-h MCAO. Size of altered regions in relation to entire cortical regions of respective hemisphere (% cortex) is shown (number of compared regions per individual cat depends on histological sections that could be matched to PET images)

by FMZ, and CBF values were above the penumbra range. These results indicate the potential and the limits of therapy in acute stroke: early reperfusion cannot reverse already developed infarction but is crucial for salvaging the penumbra; the small compartment which is sufficiently perfused might be damaged by delayed mechanisms and might benefit from neuroprotective measures. Another PET study (Morris et al. 2018) performed ^{11}C-FMZ PET in acute stroke patients (n = 13) to investigate selective neuronal loss (SNL) in penumbral tissue. This study demonstrated the presence of selective neuronal loss in the surviving penumbra which might represent a novel therapeutic target of acute stroke therapy.

23.4 Comparison of PET and PW/DW-MRI

Although PET remains the imaging gold standard for identification of the penumbra in stroke patients, MR studies using diffusion and perfusion imaging might provide a differentiation between the core and the penumbra: the early diffusion-weighted imaging (DWI) lesion might define the ischemic core, and adjacent critically hypoperfused tissue might be identified with perfusion-weighted imaging (PWI) (Warach et al. 1996; Sorensen et al. 1996). Therefore, brain regions with hypoperfusion assessed by PWI but without restricted diffusion (PWI/DWI mismatch) were assumed to represent the penumbra (Schlaug et al. 1999).

This surrogate definition of the penumbra has several uncertainties (Kidwell et al. 2003): the initial diffusion lesion does not only consist of irreversibly infarcted tissue; diffusion lesions may be reversed if blood flow is restored at an early time-point. However, DWI lesions detected at later time-points, when the PW/DWI mismatch might be used for therapeutic decisions in ischemic stroke, seem to reflect final infarct more reliably (Campbell et al. 2012; Nagaraja et al. 2020). Critical perfused tissue (i.e., penumbra) cannot be clearly differentiated from tissue experiencing oligemia; the PWI abnormality often overestimated the amount of tissue at risk.

Several studies were performed in order to validate mismatch as a surrogate of penumbra on PET-derived discrimination of irreversibly damaged, critically perfused “at risk” and oligemic “not at risk” tissue. The studies demonstrated that the early DWI lesion predicts more or less the finally infarcted tissue (Fig. 23.3) (Heiss et al. 2004) but contains up to 25% false positive, i.e., surviving tissue. The degree of disturbance of oxygen consumption was variable within individual DWI lesions suggesting variable potential for recovery (Guadagno et al. 2006).

The inaccuracy in defining the penumbra with PWI/DWI mismatch is thought to be mainly related to PWI data acquisition, which is a complex process, and the parameters used to estimate perfusion are variable and somewhat arbitrary (Ostergaard 2005). As a consequence, perfusion lesion size differs markedly depending on the parameters calculated (Kane et al. 2007) and usually is overestimated and extends into considerable areas with non-critical oligemia especially when short delays are used (Olivot et al. 2009). Time to peak (TTP) delays of 4 and 6 s reliably identified hypoperfused and excluded normoperfused tissue (threshold arbitrarily set to 20 ml/100 g/min) but still overestimated the size of the critically

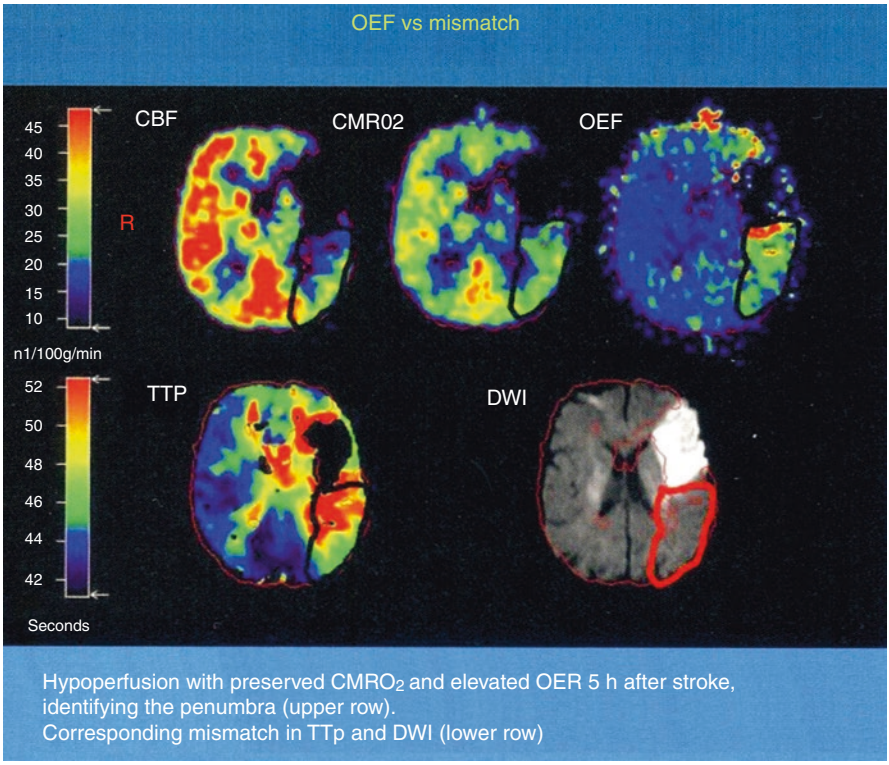

Fig. 23.3 Coregistered images of multitracer PET (upper row) and PW/DW-MRI (lower row) in a patient with right-sided hemiparesis and expressive aphasia 5 h after symptom onset. The penumbra is characterized by hypoperfusion (CBF), preserved $CMRO_2$, and elevated OEF. These findings correspond grossly to the mismatch between DWI hyperintensity and a TTP delay of 4 s compared with the unaffected hemisphere

perfused tissue (Sobesky et al. 2004) and therefore overestimated the volume of critically perfused but salvageable tissue, i.e., the penumbra (Sobesky et al. 2005): of 13 patients showing considerable PW-DWI mismatch, only 8 had areas with elevated OEF typical for penumbra tissue, and these areas were always smaller on PET than on PWI/DWI.

Overall, the mismatch volume in PW/DWI as conventionally calculated does not reliably reflect misery perfusion, i.e., the penumbra as defined by PET. Therefore several validation studies of various perfusion parameters calculated from PW-MRI on full quantitative ^{15}O-PET were performed (Takasawa et al. 2008; Zaro-Weber et al. 2019, 2010, 2017) and resulted in corrections permitting reliable classification of critical but potentially reversible ischemia (e.g., Tmax and TTP) (Fig. 23.4). These thresholds have been implemented into recent clinical stroke trials in order to improve efficiency of therapeutic interventions (EXTEND and DEFUSE-3) (Ma et al. 2019; Albers et al. 2018).

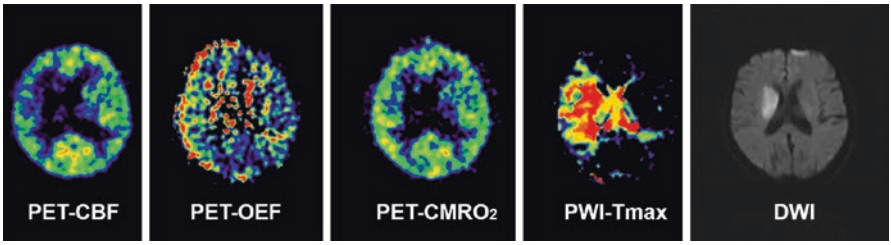

Fig. 23.4 Coregistered images of multitracer ^{15}O-positron emission tomography (PET), magnetic resonance perfusion-weighted imaging (PWI) time to maximum (Tmax) and diffusion-weighted imaging (DWI) in a patient with acute ischemic stroke. The images show penumbral tissue on PET with reduced cerebral blood flow (CBF), elevated oxygen extraction fraction (OEF), and normal cerebral metabolic rate of oxygen ($CMRO_2$)

With the advance of arterial spin labeling (ASL) MR techniques (Hernandez et al. 2012) and of CT perfusion studies for determination of cerebral perfusion (Campbell et al. 2011), it will be necessary to validate the results on flow values from fully quantitative methods.

23.5 PET as a Surrogate Marker for Treatment Efficiency

The efficacy of treatment in ischemic stroke can only be proven by controlled randomized double blind clinical trials, as successfully performed for thrombolysis with iv rtPA and thrombectomy (review in Heiss and Zaro-Weber 2019). Since such controlled trials require large patients' populations collected in many stroke centers and therefore usually take long time and considerable funds, surrogate markers are applied to predict potential therapeutic effects in small groups of patients. It has to be kept in mind that proven effects on surrogate markers always must be confirmed in controlled trials based on sufficient patients' populations. In recent years identification of salvageable tissue by neuroimaging has gained much interest as a surrogate marker for treatment efficiency in stroke.

The effect of the thrombolytic therapy for acute ischemic stroke was established also in imaging studies, in which reperfusion to penumbral tissue was followed by improvement in neurological deficits: reperfusion was significantly increased in rtPA treated patients compared to controls (Grotta and Alexandrov 1998). The volume of tissue salvaged by reperfusion was established in a study in which CBF, as determined by $H_2{}^{15}$O-PET within 3 h of stroke onset, was compared to the volume of infarction determined on MRI 3 weeks after the ictus (Heiss et al. 1998). The percentage of initially critically ischemic voxels (i.e., with a flow below the threshold of 12 ml/100 g/min) that became reperfused at almost normal levels clearly predicted the degree of clinical improvement achieved within 3 weeks. Overall, only 22.7% of the gray matter that was initially perfused at rates below the conventional threshold of critical ischemia became necrotic after thrombolytic therapy in this small sample of 12 patients. This means that a considerable portion of the

critically hypoperfused tissue was probably salvaged by the reperfusion therapy. Another PET study in 11 patients (Heiss et al. 2000) indicated that hypoperfused tissue could benefit from reperfusion only as long as cortical flumazenil binding was not reduced to or below 3.4 times the mean uptake in white matter. This marker of neuronal integrity can therefore serve as an indicator for irreversibly damaged tissue that is not amenable to treatment.

23.6 PET for Prediction of "Malignant Infarction"

A multitude of electrical and biological disturbances interact in the progression of irreversible cell damage in ischemia (review in Hossmann 2006). Peri-infarct spreading depression like depolarizations (PIDs) plays an important role in triggering and continuously stimulating this pathogenic molecular/biochemical cascade of cell injury (Dreier et al. 2017), they are related to stepwise increases in irreversible damage, and their frequency correlates to size of ischemic lesions in experimental ischemia (Nakamura et al. 2010). Their occurrence might predict a malignant course with large space occupying infarcts in patients (Dohmen et al. 2008). Such malignant brain infarcts develop in about 10% of patients with ischemic stroke in the middle cerebral artery (MCA) territory. Invasive treatment strategies, especially decompressive hemicraniectomy, might improve mortality and morbidity of these patients (Juttler et al. 2011, 2014; Dasenbrock et al. 2017; Goedemans et al. 2020). The selection of patients who can benefit and the determination of the best time for these interventions however are still controversial and require a better assessment of the extent of irreversible ischemic damage (review in Heiss 2016a). In experimental MCA occlusion in cats, a malignant course was indicated by severe ischemia in 55–75% of the hemisphere at the end of 3 h occlusion. Hyperperfusion after reopening of the MCA turned into hypoperfusion and finally led to severe global ischemia with transtentorial herniation. In the animals with a non-malignant course, severe ischemia only covered 10–44% of the hemisphere, and recirculation only induced moderate hyperperfusion and delayed hypoperfusion. Intracranial pressure continued to rise in the malignant group throughout the observation period and reached values above 70 mmHg.

In 34 patients with ischemic changes of >50% of the MCA territory in early cerebral CT scans, PET was performed with ^{11}C-FMZ to assess CBF and irreversible neuronal damage. Thereafter, probes for microdialysis and for measurement of intercranial pressure and tissue oxygen pressure were placed into the ipsilateral frontal lobe (Dohmen et al. 2003). PET measurements within 24 h after stroke showed larger volumes of ischemic core (mean, 144.5 versus 62.2 cm^3) and larger volumes of irreversible neuronal damage (157.9 versus 47.0 cm^3) in patients with malignant course (i.e., edema formation with midline shift) than in patients with benign course (Fig. 23.5). Mean cerebral blood flow values within the ischemic core were significantly lower, and the volume of the ischemic penumbra was smaller in the malignant than in the benign group. In patients with malignant course, cerebral perfusion pressure dropped to <50 to 60 mmHg 22 to 72 h (mean, 52.0 h) after onset of symptoms; subsequently, tissue oxygen tension (PtO_2) dropped, and glutamate

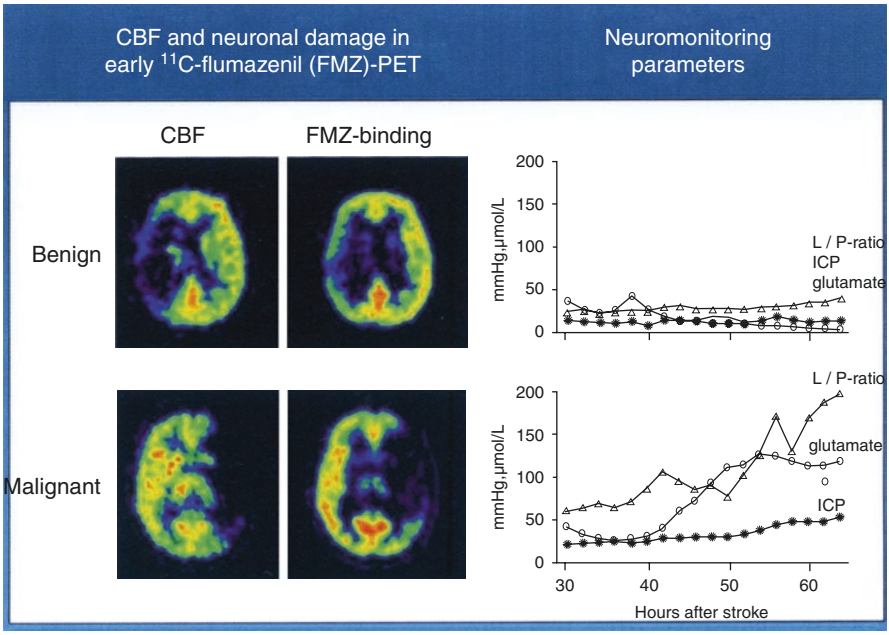

Fig. 23.5 FMZ distribution and FMZ binding in patients with large MCA infarcts: in benign infarcts, volume of severe hypoperfusion and reduced FMZ binding, i.e., neuronal damage, were smaller than in patients with malignant course. Neuromonitoring did not reveal significant deflections of variables, whereas in malignant patients, substrate concentrations and intracranial pressure rose progressively

increased, indicating secondary ischemia. Maximal changes in the monitored variables reached significant levels for glutamate, aspartate, GABA, glycerol, lactate-to-pyruvate ratio, hypoxanthine, intracranial pressure, cerebral perfusion pressure, and PtO_2 (Fig. 23.5). Corresponding to the experimental results, PET allowed prediction of malignant MCA infarction within the time window suggested for hemicraniectomy. Neuromonitoring helped to classify the clinical courses by characterizing pathophysiological sequelae of malignant edema formation. In contrast to PET, however, it did not predict fatal outcome early enough for successful implementation of invasive therapies.

23.7 Microglia Activation as an Indicator of Inflammation

Microglia constitutes up to 10% of the total cell population of the brain. As resident macrophages of the central nervous system, microglia phagocytose cellular debris, present foreign antigens and are sensors of pathological events including ischemia (Hanisch and Kettenmann 2007). Microglia changes from a resting to an activated state in response to central nervous system insults that stimulate them to function as phagocytes. In this activation process, they undergo a shift in their effector program

by transforming their morphology, proliferating, releasing proinflammatory compounds, and increasing expression of immunomodulatory surface antigens (Weinstein et al. 2010). As one of the consequences, the translocator protein 18 kDa (TSPO), formerly known as the peripheral benzodiazepine receptor (PBR), is upregulated in mitochondria of activated microglia and may thus serve as a biomarker of inflammation. Several radioligands have been developed to image the activation of microglia in experimental models and in various diseases of the central nervous system (e.g., ^{11}C-PK11195, ^{11}C-DPA-713, and ^{18}F-GE-180) (Thiel and Heiss 2011). Early studies in ischemia models using ^{3}H-PK 11195 autoradiography demonstrated increased binding sites in the area of infarction and in the boundary zones between major arteries in hypertensive animals, which were associated with reactive glia cells and macrophages and reached a maximum 4–8 days after the induction of local ischemia. Applying high-resolution microPET to imaging expression of TSPO/PBR in transient experimental ischemia, a high signal was detected in the core of ischemia starting on Day 4 and increasing to Day 7, and this strong signal was related to microglia/macrophages. A less prominent signal indicating elevated TSPO expression was observed in the region surrounding the infarct at Day 7, which could be attributed to reactive astrocytes. These results demonstrate cellular heterogeneity for TSPO/PBR expression depending on intrinsic features of inflammatory cells (Rojas et al. 2007; Demerle-Pallardy et al. 1991). In permanent ischemia in rats induced by macrosphere injection into the middle cerebral artery, no increase in ^{3}H-PK 11195 binding was found in the infarct core 7 days after the attack, but the permanent middle cerebral artery ischemia caused increased tracer binding in the normoperfused peri-infarct zone, which was colocalized with an increased glucose metabolism and accumulated microglia and macrophages. This peri-infarct neuroinflammation might contribute to the extension of tissue damage (Schroeter et al. 2009). However, a recent PET study (Morris et al. 2018) performed ^{11}C-PK11195 PET and ^{11}C-FMZ PET in acute human stroke to investigate microglial activation (PK11195) and selective neuronal loss (FMZ) in penumbral tissue. This study demonstrated the presence of microglia activation in the non-penumbral part of the non-infarcted MCA territory distant from the lesion, indicating remote degeneration after stroke (Thiel et al. 2010), but failed to show increased microglia activation in the surviving penumbral tissue. This study indicated that microglia activation is unlikely to contribute to neuronal loss within the rescued penumbra.

Another study (Chaney et al. 2019) directly compared two promising second-generation TSPO tracers,^{11}C-DPA-713 and ^{18}F-GE-180, in ischemic stroke in mice. They found ^{11}C-DPA-713 to detect microglia activation in infarcted tissue more accurately than ^{18}F-GE-180.

One clinical PET study (Visi et al. 2020) investigated the potential rule of anti-neuroinflammatory therapy on microglia activation in acute ischemic stroke. In this PET study, microglia activation was detected using the recently developed radiopharmaceutical ^{18}F-GE-180 with positron emission tomography as well as the gold standard ^{11}C-PK11195. However due to the limited clinical applicability of ^{18}F-GE-180 in acute stroke, the study failed to show a link between brain inflammation and clinical recovery.

Many histological studies have documented the presence of activated microglia in the ischemic brain after stroke in humans. Abundant reactive microglia/macrophages have been found in the ischemic core within 1–2 days after ischemic infarction. Over time, they extended from the ischemic core into the peri-infarct zones (Weinstein et al. 2010). In several imaging studies, increased binding of ^{11}C-PK11195 was observed around the outer border of ischemic lesions after several days (Fig. 23.6) but also in areas distant from the lesion (review in Thiel and Heiss 2011). Increased tracer binding was also detected in the thalamus ipsilateral to the stroke and in the subcortical white matter tracts. This possible relationship between neuroinflammatory reaction and integrity of white matter tracts has recently been investigated more systematically by combining microglia positron emission tomography with diffusion tensor imaging (Radlinska et al. 2009). Diffusion tensor imaging acquires information about the anisotropic diffusion of water molecules along white matter fiber tracts, giving detailed information about tissue microstructure. Using diffusion tensor imaging-based definitions of the pyramidal tract, Radlinska et al. (2009) demonstrated in a prospective controlled study that microglia activation occurs along the pyramidal tract anterograde to the lesion only in those patients with acute subcortical stroke, where the pyramidal tract was affected. These anterograde tract portions are that who will undergo Wallerian degeneration in the weeks and months after stroke. This relationship was further investigated in a similarly designed but longitudinal study (Thiel et al. 2010), in which the extent of anterograde microglia activity in the brain stem was found to be linearly related to the extent of pyramidal tract damage. This remote inflammatory activity was

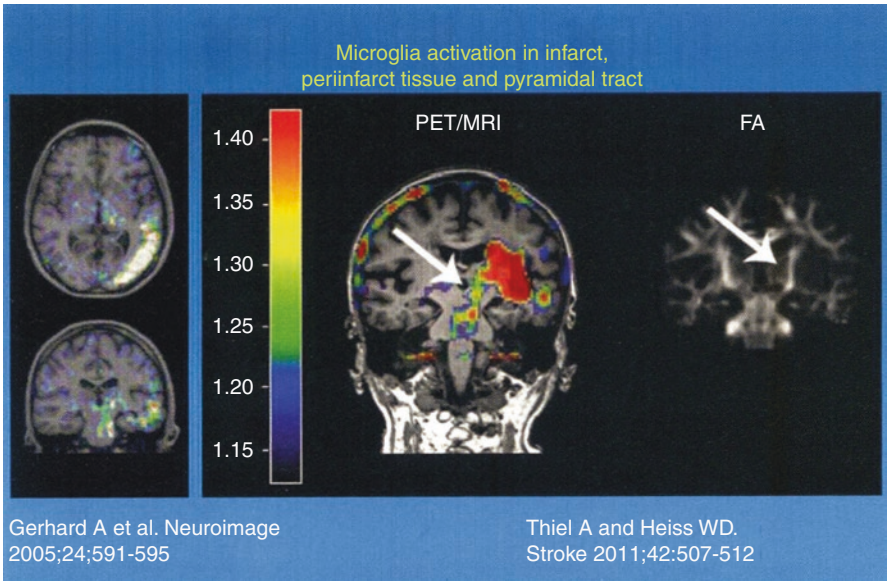

Fig. 23.6 Microglia activation in infarct, peri-infarct areas (left; modified from Gerhard et al. 2005), and in remote fiber tracts imaged by ^{11}C-PK11195-PET (right; from Thiel and Heiss 2011): ^{11}C-PK11195-PET overlaid on T1-weighted MRI (left) and fractional anisotropy image showing fiber tracts (right). Tracer binding is high in the infarct but also follows the pyramidal tract (white arrows) in an anterograde direction to the level of the pons (scale indicates uptake ratios)

positively related with outcome, indicating a possible neuroprotective role or repair function of microglia cells along the tract portions undergoing Wallerian degeneration. In contrast, local microglia activity in the area of the infarct was only related to persisting tract damage in the chronic phase and correlated negatively with clinical outcome.

On the other hand, the activation of microglia in the vicinity and in distant areas of an infarct might go along with increased deposition of amyloid leading to post-stroke dementia. Experimental findings have identified a probable link between ischemia, inflammation, and amyloid deposition (Whitehead et al. 2007). This interaction is now investigated in a cooperative multitracer study in stroke patients applying ^{11}C-PK11195 and ^{11}C-PIB (Heiss et al. 2011).

23.8 Complex Activation Studies

Regional cerebral metabolism and blood flow are dependent on the functional state of the brain tissue. This has been well established in animal experiments using autoradiography (review in Sokoloff et al. 1975); a direct coupling of neuronal activity and focal blood flow could be demonstrated directly by simultaneous recordings with microelectrodes (Heiss et al. 1979). The transfer to human studies was achieved by the 133 Xenon clearance method for measurement of regional cerebral blood flow (Ingvar 1976), by which two dimensional cortical activation patterns for various tasks including speech and memory could be obtained. With the advance of PET, three-dimensional regional activation studies became feasible in healthy controls and in patients with various CNS disorders (review (Phelps and Mazziotta 1985)). Due to the radiation exposure and the complex logistics required by PET, these activation studies were taken over by fMRI with the availability of high-resolution MR equipment (Raichle 1998). However, PET activation studies are still required and justified for the detection of changes in complex patterns elicited by stimulation procedures not feasible in MRI.

Our group has a long-lasting experience with activation studies in aphasia (review in Heiss 2016b; Heiss 2009a). In the brain of healthy right-handers and the majority of left-handers language is a function of the left, dominant hemisphere. This asymmetry is established during language acquisition and actively maintained in the adult brain by fiber bundles connecting both hemispheres across the corpus callosum. These fibers are glutaminergic and are connected to inhibitory inter-neurons in the non-dominant hemisphere. This means that language areas active in the dominant hemisphere (e.g., Broca's area) suppress activity in homologous areas of the non-dominant hemisphere (transcallosal inhibition). The existence of these inhibitory mechanisms has been deducted from imaging studies in patients with brain lesions and has directly been demonstrated in normal subjects using imaging-guided repetitive transcranial magnetic stimulation (rTMS) (Thiel et al. 2006a). A unilateral and focal brain lesion (such as a stroke) to language areas of the dominant hemisphere does not only reduce activity in the affected hemisphere thus causing aphasia but also releases activity in the unaffected hemisphere, via interruption of those transcallosal fibers (transcallosal disinhibition) (Thiel et al. 2006b). This activity of brain regions in the non-dominant hemisphere in the first days and weeks after a stroke has

repeatedly been demonstrated in sequential brain imaging studies (Saur et al. 2006). In the following weeks and months of recovery, brain activation shifts back to the dominant hemisphere. The extent of this backward shift to the dominant hemisphere varies from patient to patient and appears to be a major factor for successful recovery of language function (Heiss et al. 1999b) in the acute and subacute phase. Reestablishing functional networks of the affected dominant hemisphere early in the course of recovery seems to be the superior strategy over recruiting homologous brain regions in the unaffected non-dominant hemisphere in order to achieve good rehabilitation results. In chronic aphasics right-hemispheric regions can be compensatory (Richter et al. 2008), but this seems to be only the second-line long-term strategy if additional recruitment of left-hemisphere areas is no longer possible. Based on this evidence, a reasonable strategy for improvement of language function would seek to actively suppress right hemisphere and to enhance left-hemisphere activity in the early phase after stroke and possibly use techniques more targeted at the right-hemisphere in the chronic stage. Results from a feasibility study in post-stroke aphasia show that activity of the non-lesioned hemisphere is decreased by inhibitory rTMS. This shift of activation is related to an improvement in language function by speech therapy combined to inhibitory rTMS of the Broca homologous area of the non-dominant hemisphere (Fig. 23.7) (Weiduschat et al. 2011).

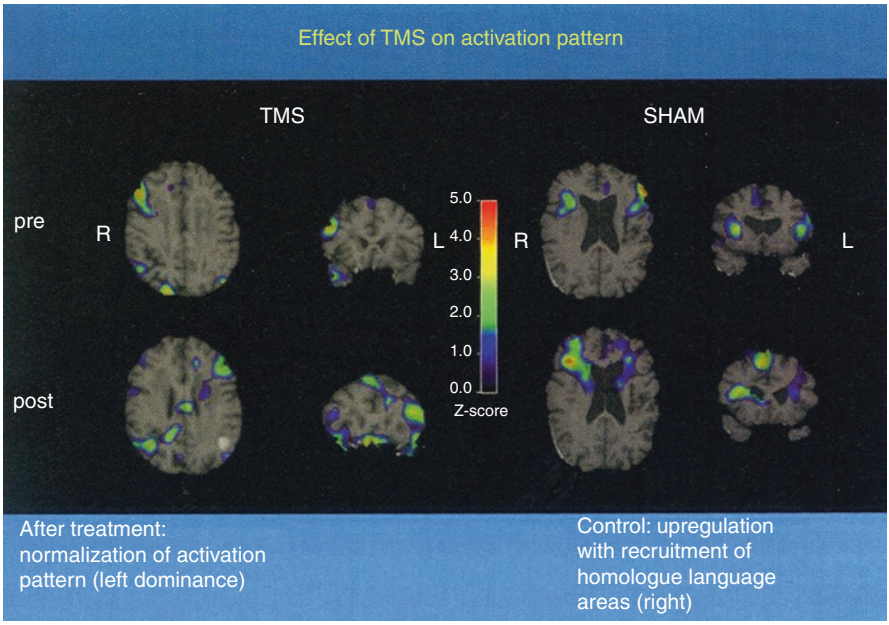

Fig. 23.7 Illustrative single subject activation during verb generation in one subject of the TMS group (*patient 7*) and the sham group (*patient 6*), respectively, before and after the 2-week rehabilitation period. Although there is a reactivation of the left-hemispheric structures in the patient of the intervention group, the patient of the sham group presents with increasing right-hemispheric activity. (From Weiduschat et al. 2011)

A randomized, blinded, and sham-controlled proof-of-principle study in subacute ischemic stroke (Thiel et al. 2013) tested the effect of an inhibitory rTMS protocol over the right posterior inferior frontal gyrus in combination with speech and language therapy. This study could prove a significant improvement of language recovery in subacute ischemic stroke and showed an improved recruitment of left-hemispheric language networks.

23.9 Conclusion

Over the years PET has been the most efficient technique to provide accurate quantitative in vivo regional measurements of cerebral blood flow, cerebral metabolism, and cerebral molecular activities in human subjects. It therefore played a prominent role in the translation of research concepts from experimental models into clinical application, which is fundamental for understanding the pathophysiology and for developing treatment strategies in various brain diseases including stroke. With the advent of high-resolution integrated PET/MRI facilities, simultaneous investigations of several molecular, metabolic, perfusional, and morphological parameters are feasible (Sauter et al. 2010; Heiss 2009b) which might enhance our insights into brain function and disorders.

Disclosures Wolf-Dieter Heiss and Olivier Zaro-Weber were funded by the WDH Foundation and the Marga and Walter Boll Foundation.

References

Ackerman RH, Correia JA, Alpert NM, Baron JC, Gouliamos A, Grotta JC et al (1981) Positron imaging in ischemic stroke disease using compounds labeled with oxygen 15. Initial results of clinicophysiologic correlations. Arch Neurol 38(9):537–543

Albers GW, Marks MP, Kemp S, Christensen S, Tsai JP, Ortega-Gutierrez S et al (2018) Thrombectomy for stroke at 6 to 16 hours with selection by perfusion imaging. N Engl J Med 378(8):708–718

Astrup J, Symon L, Branston NM, Lassen NA (1977) Cortical evoked potential and extracellular K+ and H+ at critical levels of brain ischemia. Stroke 8(1):51–57

Astrup J, Siesjö BK, Symon L (1981) Thresholds in cerebral ischemia - the ischemic penumbra. Stroke 12(6):723–725

Baron JC (1999) Mapping the ischaemic penumbra with PET: implications for acute stroke treatment. Cerebrovasc Dis 9:193–201

Baron JC, Bousser MG, Comar D, Soussaline F, Castaigne P (1981a) Noninvasive tomographic study of cerebral blood flow and oxygen metabolism in vivo. Potentials, limitations, and clinical applications in cerebral ischemic disorders. Eur Neurol 20(3):273–284

Baron JC, Bousser MG, Rey A, Guillard A, Comar D, Castaigne P (1981b) Reversal of focal "misery-perfusion syndrome" by extra-intracranial arterial bypass in hemodynamic cerebral ischemia. A case study with 15O positron emission tomography. Stroke 12(4):454–459

Campbell BC, Christensen S, Levi CR, Desmond PM, Donnan GA, Davis SM et al (2011) Cerebral blood flow is the optimal CT perfusion parameter for assessing infarct core. Stroke 42(12):3435–3440

Campbell BC, Purushotham A, Christensen S, Desmond PM, Nagakane Y, Parsons MW et al (2012) The infarct core is well represented by the acute diffusion lesion: sustained reversal is infrequent. J Cereb Blood Flow Metab 32(1):50–56

Chaney A, Cropper HC, Johnson EM, Lechtenberg KJ, Peterson TC, Stevens MY et al (2019) (11) C-DPA-713 versus (18)F-GE-180: a preclinical comparison of translocator protein 18 kDa PET tracers to visualize acute and chronic neuroinflammation in a mouse model of ischemic stroke. J Nucl Med 60(1):122–128

Clarke DD, Sokoloff L (1999) Circulation and energy metabolism of the brain. In: Siegel G, Agranoff B, Albers RW, Fisher S (eds) Basic neurochemistry: molecular, cellular, and medical aspects, 6th edn. Lippincott-Raven, Philadelphia, pp 637–669

Dasenbrock HH, Robertson FC, Vaitkevicius H, Aziz-Sultan MA, Guttieres D, Dunn IF et al (2017) Timing of decompressive hemicraniectomy for stroke: a nationwide inpatient sample analysis. Stroke 48(3):704–711

Demerle-Pallardy C, Duverger D, Spinnewyn B, Pirotzky E, Braquet P (1991) Peripheral type benzodiazepine binding sites following transient forebrain ischemia in the rat: effect of neuroprotective drugs. Brain Res 565(2):312–320

Dohmen C, Bosche B, Graf R, Staub F, Kracht L, Sobesky J et al (2003) Prediction of malignant course in MCA infarction by PET and microdialysis. Stroke 34(9):2152–2158

Dohmen C, Sakowitz OW, Fabricius M, Bosche B, Reithmeier T, Ernestus RI et al (2008) Spreading depolarizations occur in human ischemic stroke with high incidence. Ann Neurol 63(6):720–728

Dreier JP, Fabricius M, Ayata C, Sakowitz OW, Shuttleworth CW, Dohmen C et al (2017) Recording, analysis, and interpretation of spreading depolarizations in neurointensive care: review and recommendations of the COSBID research group. J Cereb Blood Flow Metab 37(5):1595–1625

Gerhard A, Schwarz J, Myers R, Wise R, Banati RB (2005) Evolution of microglial activation in patients after ischemic stroke: a 11CR-PK11195 PET study. Neuroimage 24(2): 591–595

Goedemans T, Verbaan D, Coert BA, Kerklaan B, van den Berg R, Coutinho JM et al (2020) Outcome after decompressive craniectomy for middle cerebral artery infarction: timing of the intervention. Neurosurgery 86(3):E318–EE25

Grotta JC, Alexandrov AV (1998) tPA-associated reperfusion after acute stroke demonstrated by SPECT. Stroke 29(2):429–432

Guadagno JV, Warburton EA, Jones PS, Day DJ, Aigbirhio FI, Fryer TD et al (2006) How affected is oxygen metabolism in DWI lesions?: a combined acute stroke PET-MR study. Neurology 67(5):824–829

Hanisch UK, Kettenmann H (2007) Microglia: active sensor and versatile effector cells in the normal and pathologic brain. Nat Neurosci 10(11):1387–1394

Hata R, Mies G, Wiessner C, Fritze K, Hesselbarth D, Brinker G et al (1998) A reproducible model of middle cerebral artery occlusion in mice: hemodynamic, biochemical, and magnetic resonance imaging. J Cereb Blood Flow Metab 18(4):367–375

Heiss WD (1992) Experimental evidence of ischemic thresholds and functional recovery. Stroke 23(11):1668–1672

Heiss WD (2000) Ischemic penumbra: evidence from functional imaging in man. J Cereb Blood Flow Metab 20(9):1276–1293

Heiss W-D (2009a) WSO Leadership in Stroke Medicine Award Lecture Vienna, September 26, 2008: functional imaging correlates to disturbance and recovery of language function. Int J Stroke 4:129–136

Heiss W-D (2009b) The potential of PET/MR for brain imaging. Eur J Nucl Med Mol Imaging 36(Suppl 1):105–112

Heiss WD (2016a) Malignant MCA infarction: pathophysiology and imaging for early diagnosis and management decisions. Cerebrovasc Dis 41(1–2):1–7

Heiss WD (2016b) Imaging effects related to language improvements by rTMS. Restor Neurol Neurosci 34(4):531–536

Heiss WD, Rosner G (1983) Functional recovery of cortical neurons as related to degree and duration of ischemia. Ann Neurol 14(3):294–301

Heiss WD, Zaro-Weber O (2019) Extension of therapeutic window in ischemic stroke by selective mismatch imaging. Int J Stroke 14(4):351–358

Heiss WD, Turnheim M, Vollmer R, Rappelsberger P (1979) Coupling between neuronal activity and focal blood flow in experimental seizures. Electroencephr Clin Neurophysiol 47(4):396–403

Heiss WD, Huber M, Fink GR, Herholz K, Pietrzyk U, Wagner R et al (1992) Progressive derangement of periinfarct viable tissue in ischemic stroke. J Cereb Blood Flow Metab 12(2):193–203

Heiss WD, Graf R, Fujita T, Ohta K, Bauer B, Löttgen J et al (1997) Early detection of irreversibly damaged ischemic tissue by flumazenil positron emission tomography in cats. Stroke 28(10):2045–2051

Heiss WD, Grond M, Thiel A, von Stockhausen HM, Rudolf J, Ghaemi M et al (1998) Tissue at risk of infarction rescued by early reperfusion: a positron emission tomography study in systemic recombinant tissue plasminogen activator thrombolysis of acute stroke. J Cereb Blood Flow Metab 18(12):1298–1307

Heiss WD, Thiel A, Grond M, Graf R (1999a) Which targets are relevant for therapy of acute ischemic stroke? Stroke 30(7):1486–1489

Heiss WD, Kessler J, Thiel A, Ghaemi M, Karbe H (1999b) Differential capacity of left and right hemispheric areas for compensation of poststroke aphasia. Ann Neurol 45(4):430–438

Heiss WD, Kracht L, Grond M, Rudolf J, Bauer B, Wienhard K et al (2000) Early [11C]flumazenil/H_2O positron emission tomography predicts irreversible ischemic cortical damage in stroke patients receiving acute thrombolytic therapy. Stroke 31(2):366–369

Heiss WD, Sobesky J, Smekal U, Kracht LW, Lehnhardt FG, Thiel A et al (2004) Probability of cortical infarction predicted by flumazenil binding and diffusion-weighted imaging signal intensity: a comparative positron emission tomography/magnetic resonance imaging study in early ischemic stroke. Stroke 35(8):1892–1898

Heiss W-D, Radlinska B, Soucy J-P, Schirrmacher R, Thiel A, Hachinski V (2011) Is poststroke dementia related to amyloid deposition and microglia activation. Ann Neurol 70(Suppl):T1510

Hernandez DA, Bokkers RP, Mirasol RV, Luby M, Henning EC, Merino JG et al (2012) Pseudocontinuous arterial spin labeling quantifies relative cerebral blood flow in acute stroke. Stroke 43(3):753–758

Hossmann KA (1994) Viability thresholds and the penumbra of focal ischemia. Ann Neurol 36(4):557–565

Hossmann KA (2006) Pathophysiology and therapy of experimental stroke. Cell Mol Neurobiol 26(7–8):1057–1083

Ingvar DH (1976) Functional landscapes of the dominant hemisphere. Brain Res 107(1):181–197

Juttler E, Bosel J, Amiri H, Schiller P, Limprecht R, Hacke W et al (2011) DESTINY II: DEcompressive Surgery for the Treatment of malignant INfarction of the middle cerebral arterY II. Int J Stroke 6(1):79–86

Juttler E, Unterberg A, Woitzik J, Bosel J, Amiri H, Sakowitz OW et al (2014) Hemicraniectomy in older patients with extensive middle-cerebral-artery stroke. N Engl J Med 370(12):1091–1100

Kane I, Carpenter T, Chappell F, Rivers C, Armitage P, Sandercock P et al (2007) Comparison of 10 different magnetic resonance perfusion imaging processing methods in acute ischemic stroke: effect on lesion size, proportion of patients with diffusion/perfusion mismatch, clinical scores, and radiologic outcomes. Stroke 38(12):3158–3164

Kidwell CS, Alger JR, Saver JL (2003) Beyond mismatch: evolving paradigms in imaging the ischemic penumbra with multimodal magnetic resonance imaging. Stroke 34(11):2729–2735

Laughlin SB, Attwell D (2001) The metabolic cost of neural information: from fly eye to mammalian cortex. In: Frackowiak RSJ, Magistretti PJ, Shulman RG, Altman JS, Adams M (eds) Neuroenergetics: relevance for functional brain imaging. HFSP - Workshop XI, Strasbourg, pp 54–64

Lenzi GL, Frackowiak RSJ, Jones T (1982) Cerebral oxygen metabolism and blood flow in human cerebral ischemic infarction. J Cereb Blood Flow Metab 2:321–335

Lin W, Powers WJ (2018) Oxygen metabolism in acute ischemic stroke. J Cereb Blood Flow Metab 38(9):1481–1499

Ma H, Campbell BCV, Parsons MW, Churilov L, Levi CR, Hsu C et al (2019) Thrombolysis guided by perfusion imaging up to 9 hours after onset of stroke. N Engl J Med 380(19):1795–1803

Morris RS, Simon Jones P, Alawneh JA, Hong YT, Fryer TD, Aigbirhio FI et al (2018) Relationships between selective neuronal loss and microglial activation after ischaemic stroke in man. Brain 141(7):2098–2111

Nagaraja N, Forder JR, Warach S, Merino JG (2020) Reversible diffusion-weighted imaging lesions in acute ischemic stroke: a systematic review. Neurology 94:571

Nakamura H, Strong AJ, Dohmen C, Sakowitz OW, Vollmar S, Sue M et al (2010) Spreading depolarizations cycle around and enlarge focal ischaemic brain lesions. Brain 133(Pt 7):1994–2006

Olivot JM, Mlynash M, Thijs VN, Kemp S, Lansberg MG, Wechsler L et al (2009) Optimal Tmax threshold for predicting penumbral tissue in acute stroke. Stroke 40(2):469–475

Ostergaard L (2005) Principles of cerebral perfusion imaging by bolus tracking. J Magn Reson Imaging 22(6):710–717

Pakkenberg B, Gundersen HJ (1997) Neocortical neuron number in humans: effect of sex and age. J Comp Neurol 384(2):312–320

Phelps ME, Mazziotta JC (1985) Positron emission tomography: human brain function and biochemistry. Science 228:799–809

Powers WJ, Grubb RL Jr, Darriet D, Raichle ME (1985) Cerebral blood flow and cerebral metabolic rate of oxygen requirements for cerebral function and viability in humans. J Cereb Blood Flow Metab 5:600–608

Radlinska BA, Ghinani SA, Lyon P, Jolly D, Soucy JP, Minuk J et al (2009) Multimodal microglia imaging of fiber tracts in acute subcortical stroke. Ann Neurol 66(6):825–832

Raichle ME (1998) Behind the scenes of functional brain imaging: a historical and physiological perspective. Proc Natl Acad Sci U S A 95(3):765–772

Richter M, Miltner WH, Straube T (2008) Association between therapy outcome and right-hemispheric activation in chronic aphasia. Brain 131(5):1391–1401

Rojas S, Martin A, Arranz MJ, Pareto D, Purroy J, Verdaguer E et al (2007) Imaging brain inflammation with [(11)C]PK11195 by PET and induction of the peripheral-type benzodiazepine receptor after transient focal ischemia in rats. J Cereb Blood Flow Metab 27(12):1975–1986

Saur D, Lange R, Baumgaertner A, Schraknepper V, Willmes K, Rijntjes M et al (2006) Dynamics of language reorganization after stroke. Brain 129(6):1371–1384

Sauter AW, Wehrl HF, Kolb A, Judenhofer MS, Pichler BJ (2010) Combined PET/MRI: one step further in multimodality imaging. Trends Mol Med 16(11):508–515

Schlaug G, Benfield A, Baird AE, Siewert B, Lovblad KO, Parker RA et al (1999) The ischemic penumbra: operationally defined by diffusion and perfusion MRI. Neurology 53(7):1528–1537

Schroeter M, Dennin MA, Walberer M, Backes H, Neumaier B, Fink GR et al (2009) Neuroinflammation extends brain tissue at risk to vital peri-infarct tissue: a double tracer [11C]PK11195- and [18F]FDG-PET study. J Cereb Blood Flow Metab 29(6):1216–1225

Sobesky J, Zaro-Weber O, Lehnhardt FG, Hesselmann V, Thiel A, Dohmen C et al (2004) Which time-to-peak threshold best identifies penumbral flow? Stroke 35:2843–2847

Sobesky J, Zaro-Weber O, Lehnhardt FG, Hesselmann V, Neveling M, Jacobs A et al (2005) Does the mismatch match the penumbra? Magnetic resonance imaging and positron emission tomography in early ischemic stroke. Stroke 36(5):980–985

Sokoloff L (1999) Energetics of functional activation in neural tissues. Neurochem Res 24(2):321–329

Sokoloff L, Ingvar DH, Lassen NA (1975) Influence of functional activity on local cerebral glucose utilization. Brain work. Munksgaard, Copenhagen, pp 385–388

Sorensen AG, Buonanno FS, Gonzalez RG, Schwamm LH, Lev MH, Huang-Hellinger FR et al (1996) Hyperacute stroke: evaluation with combined multisection diffusion-weighted and hemodynamically weighted echo planar MR imaging. Radiology 199(2):391–401

Takasawa M, Jones PS, Guadagno JV, Christensen S, Fryer TD, Harding S et al (2008) How reliable is perfusion MR in acute stroke? Validation and determination of the penumbra threshold against quantitative PET. Stroke 39(3):870–877

Thiel A, Heiss WD (2011) Imaging of microglia activation in stroke. Stroke 42(2):507–512

Thiel A, Schumacher B, Wienhard K, Gairing S, Kracht LW, Wagner R et al (2006a) Direct demonstration of transcallosal disinhibition in language networks. J Cereb Blood Flow Metab 26(9):1122–1127

Thiel A, Habedank B, Herholz K, Kessler J, Winhuisen L, Haupt WF et al (2006b) From the left to the right: how the brain compensates progressive loss of language function. Brain Lang 98:57–65

Thiel A, Radlinska BA, Paquette C, Sidel M, Soucy JP, Schirrmacher R et al (2010) The temporal dynamics of poststroke neuroinflammation: a longitudinal diffusion tensor imaging-guided PET study with 11C-PK11195 in acute subcortical stroke. J Nucl Med 51(9):1404–1412

Thiel A, Hartmann A, Rubi-Fessen I, Anglade C, Kracht L, Weiduschat N et al (2013) Effects of noninvasive brain stimulation on language networks and recovery in early poststroke aphasia. Stroke 44(8):2240–2246

Visi E, Hinz R, Punter M, Majid A, Gerhard A, Herholz K (2020) Positron emission tomography to image cerebral neuroinflammation in ischaemic stroke: a pilot study. Efficacy Mech Evaluat 7:1

Warach S, Dashe JF, Edelman RR (1996) Clinical outcome in ischemic stroke predicted by early diffusion-weighted and perfusion magnetic resonance imaging: a preliminary analysis. J Cereb Blood Flow Metab 16(1):53–59

Weiduschat N, Thiel A, Rubi-Fessen I, Hartmann A, Kessler J, Merl P et al (2011) Effects of repetitive transcranial magnetic stimulation in aphasic stroke: a randomized controlled pilot study. Stroke 42(2):409–415

Weinstein JR, Koerner IP, Moller T (2010) Microglia in ischemic brain injury. Future Neurol 5(2):227–246

Whitehead SN, Cheng G, Hachinski VC, Cechetto DF (2007) Progressive increase in infarct size, neuroinflammation, and cognitive deficits in the presence of high levels of amyloid. Stroke 38(12):3245–3250

Zaro-Weber O, Moeller-Hartmann W, Heiss W-D, Sobesky J (2010) Maps of time to maximum and time to peak for mismatch definition in clinical stroke studies validated with positron emission tomography. Stroke 41(12):2817–2821

Zaro-Weber O, Moeller-Hartmann W, Siegmund D, Kandziora A, Schuster A, Heiss WD et al (2017) MRI-based mismatch detection in acute ischemic stroke: optimal PWI maps and thresholds validated with PET. J Cereb Blood Flow Metab 37(9):3176–3183

Zaro-Weber O, Fleischer H, Reiblich L, Schuster A, Moeller-Hartmann W, Heiss WD (2019) Penumbra detection in acute stroke with perfusion magnetic resonance imaging: validation with (15)O-positron emission tomography. Ann Neurol 85(6):875–886

Part IV

Movement Disorders

Parkinson's Disease

24

Michele Matarazzo, Andre C. Felicio, and A. Jon Stoessl

Contents

24.1 Introduction 676
24.1.1 Parkinson's Disease Burden 676
24.1.2 Clinical Manifestations 676
24.1.3 Brain Pathology 677
24.1.4 Neurochemical Pathology 678
24.2 Brain Dopaminergic Imaging in PD 679
24.2.1 Targeting Dopaminergic Function 679
24.2.2 Tracers for the Assessment of Presynaptic Dopamine Function 681
24.2.3 Tracers for the Assessment of Postsynaptic Dopamine Function 683
24.3 Brain Non-dopaminergic Sites 684
24.3.1 Other Neurotransmitters 684
24.3.2 Brain Metabolism and Perfusion 687
24.3.3 Protein Aggregation 688
24.3.4 Neuroinflammation 689
24.3.5 Phosphodiesterase 10A 690
24.4 Peripheral Nuclear Imaging 691
24.5 Clinical Implications 692
24.5.1 Diagnosis and Differential Diagnosis 692
24.5.2 Tracking Disease Progression 693
24.5.3 Monitoring Therapeutic Effects 695
References 696

M. Matarazzo · A. J. Stoessl (✉)
Pacific Parkinson's Research Center, University of British Columbia, Vancouver, BC, Canada
e-mail: jon.stoessl@ubc.ca

A. C. Felicio
Hospital Israelita Albert Einstein, São Paulo, Brazil

R. A. J. O. Dierckx et al. (eds.), *PET and SPECT in Neurology*,
https://doi.org/10.1007/978-3-030-53168-3_24

Abstract

A growing body of evidence supports the importance of functional imaging studies using single-photon emission tomography (SPECT) or positron emission tomography (PET) in neurology. In particular, Parkinson's disease (PD) and other neurodegenerative disorders are useful disease models to understand the contribution of modern functional neuroimaging techniques. In this chapter, our aim is to address the principles of molecular imaging and also its pitfalls, with a focus on PD motor and nonmotor symptoms. From brain pathology to neurochemical pathology, from clinically unclear cases of parkinsonism to non-dopaminergic ligands and, finally, taking into account experimental tracers, we hope to cover key issues regarding the contribution of SPECT and PET in PD.

24.1 Introduction

24.1.1 Parkinson's Disease Burden

Parkinson's disease (PD) is the second most prevalent neurodegenerative disorder after Alzheimer's disease (AD) worldwide. Recent epidemiological studies have shown an increase of its prevalence that has more than doubled in less than 30 years, affecting more than six million people worldwide in 2016 (GBD 2016 Parkinson's Disease Collaborators 2018). With the growing ageing population, along with potential contributions from other factors, the prevalence and worldwide burden of PD is estimated to increase even more in future years, with an expected doubling between 2010 and 2030 (Marras et al. 2018). This will boost the already very high social and economic burden of the disease with huge impact on the quality of life of millions of people and of their caregivers.

24.1.2 Clinical Manifestations

Currently, the diagnosis of PD is based on the combination of clinical manifestations, including bradykinesia and at least one other cardinal motor sign (rest tremor, rigidity, postural instability) (Gibb and Lees 1988; Postuma et al. 2015). However, the manifestations of PD extend beyond this spectrum, encompassing a wide variety of nonmotor symptoms, including neuropsychiatric disorders, autonomic dysfunction, olfactory loss and sleep disturbance, some of which may be present even before the onset of motor manifestations (Chaudhuri et al. 2011; Goldman and Postuma 2014; Postuma et al. 2015).

Additionally, at the time an affected PD patient is diagnosed, it is estimated that 30–50% of the nigrostriatal neurons are lost, associated with striatal dopamine loss of 50–80% (Bernheimer et al. 1973; Fearnley and Lees 1991; Kordower et al. 2013).

Despite the recent adoption of newer diagnostic criteria, such as the Movement Disorder Society Clinical Diagnostic Criteria for PD, the accuracy of the diagnosis is still suboptimal, with an estimated accuracy around 90% after extended clinical follow-up (lower at earlier stages), even though definitive clinicopathological validation is still strikingly lacking (Hughes et al. 2001; Postuma et al. 2018). The misdiagnosis in clinical practice, more so in a non-movement disorder specialized setting, is estimated to be even higher (Hughes et al. 1992, 2001).

Further, the high degree of variability in the clinical manifestations of PD and its long-term prognosis represent a major issue in clinical practice, with pragmatic consequences related to the unpredictability of the disease progression, at least at an individual level. To overcome this challenge, different phenotyping methods have been developed over time based on motor symptoms or, more recently, on a combination of motor and nonmotor symptoms (Fereshtehnejad et al. 2017; Hoehn and Yahr 1967; Stebbins et al. 2013). Additionally, early- versus late-onset PD may be associated with different epidemiological, clinical and genetic characteristics (Schrag and Schott 2006), which can also be assessed in part by in vivo studies using SPECT (Shih et al. 2007) and PET (de la Fuente-Fernández et al. 2011) ligands.

24.1.3 Brain Pathology

It is now known that clinical parkinsonism is just the tip of the iceberg in the complex cascade of events that takes place before the onset of motor symptoms in PD (Langston 2006). Indeed, long before the involvement of the substantia nigra *pars compacta* (SNc) and the loss of striatal dopamine, there is an ongoing neurodegenerative process. While the origin of the disease is still unclear, the prevailing hypothesis suggests a caudal-to-rostral spread of misfolded alpha-synuclein pathology that may start in the peripheral nervous system. The olfactory bulb is involved early, and the disease may actually onset in peripheral autonomic ganglia (Braak et al. 2003). Other theories have been recently proposed, and there is no definite evidence on the actual pathophysiological mechanism, especially in the earlier stages (Foffani and Obeso 2018). Even the toxic role of alpha-synuclein is now questioned, as this may represent a compensatory or even protective physiological reaction to an underlying neurodegenerative process (Espay et al. 2019). However, the hallmark pathology of this disease still relies on the identification of Lewy bodies in the SNc, which corresponds to intra-cytoplasmatic alpha-synuclein-positive staining inclusions (Spillantini et al. 1997).

The understanding of PD pathology is very important, especially when one considers the anticipated reality of disease-modifying therapies to come. Therefore, identifying individuals at earlier disease stages and preferably preclinical subjects would provide better therapeutic windows. Currently, there are available biomarkers, though with some drawbacks, but liable to be useful in identifying those subjects most likely to benefit from neuroprotective therapies, as well as in monitoring the effects of these interventions (Agarwal and Stoessl 2013; Merchant et al. 2019).

24.1.4 Neurochemical Pathology

Not only dopamine but also non-dopaminergic neurotransmitters such as acetylcholine, serotonin, GABA and glutamate are involved in the pathophysiology of PD and can potentially be assessed with in vivo molecular imaging approaches (Politis et al. 2017; Stoessl 2012; Stoessl et al. 2014). Additionally, other molecular targets that may shed insight into disease pathogenesis, such as aggregation of proteins known to participate in neurodegenerative processes (e.g. tau) and markers of neuroinflammation, may be of interest in PD, as well as other neurological conditions (Ghadery et al. 2019; Hammes et al. 2018; Narayanaswami et al. 2018).

24.1.4.1 Dopaminergic Dysfunction

Striatal dopamine denervation is the major neurochemical outcome of the relentless neurodegenerative process in PD, as it underlies the major clinical findings and it is the theoretical base for most of the treatment currently used. The dopaminergic denervation happens in the context of dysfunction in direct and indirect loops of the cortico-striato-pallido-thalamo-cortical pathway with secondary neurochemical, neurophysiological and functional changes in the brain at several anatomical network levels (Wichmann 2019; Wichmann et al. 2011).

Changes in dopamine metabolism are also related to changes in dopamine receptors and transporters during the course of PD. For example, in early PD at the presynaptic level, while dopamine transporters are downregulated, there is an upregulation in dopa-decarboxylase activity associated with a decrease in vesicular monoamine transporter type 2. However, at the postsynaptic level, D2 dopamine receptors are initially increased/upregulated, with a subsequent normalization, as disease progresses and dopamine-substitutive therapy is introduced (Antonini et al. 1997; Au et al. 2005). However, the interpretation of this latter finding might be biased by the reduced receptor occupancy due to reduced dopamine released at presynaptic level.

The equilibrium between the cellular and neuronal terminal loss and the compensatory mechanisms, likely influenced also by the treatment administered, undergoes a continuous biological adaptation over the course of the disease, which is more pronounced in the early phase. As a consequence, the neurophysiological and neurobiological profiles change in different stages of the disease.

24.1.4.2 Cholinergic Dysfunction

The main sources of cholinergic projection fibres in the forebrain are the *nucleus basalis* of Meynert and the septal nuclei. In the brainstem, the pedunculopontine and laterodorsal tegmental nuclei provide important cholinergic projections to the thalamus, hypothalamus, midbrain dopaminergic nuclei and the basal forebrain (Holmstrand and Sesack 2011). Both regions may be affected in PD (Rogers et al. 1985), with resulting cognitive impairment (Yarnall et al. 2011) and possible contributions to sleep disturbances. It is estimated that almost 85% of 20-year PD survivors are demented, pointing to the importance of cholinergic dysfunction in late stages of PD (Hely et al. 2008). The pedunculopontine tegmental nucleus

(PPN) involvement in PD has been established in neuropathological studies and represents the theoretical basis for the use of cholinesterase inhibitors in PD-related gait disorders, as well as for the trials of PPN deep brain stimulation (DBS), again for improving the gait dysfunction in people with advanced PD (Henderson et al. 2016; Moro et al. 2010). Also, symptoms of rapid eye movement (REM) sleep behaviour disorder (RBD) are associated with cholinergic denervation in PD (Kotagal et al. 2012), therefore showing the importance of the cholinergic system in nonmotor symptoms.

24.1.4.3 Serotonergic Dysfunction

Serotonin neurons have widespread projections in the brain, particularly in the brainstem, striatum, thalamus, hypothalamus, amygdala and cingulate cortex. A relationship between mood and serotonin deficiency is widely assumed, based on the response to tricyclic, tetracyclic, selective serotonin reuptake inhibitor and monoamine oxidase inhibitor antidepressants (Hung et al. 2011). However, serotonin has many other functions besides its effects on mood, and these rely in part on the 14 distinct serotonin receptors evident in mammals (Saulin et al. 2012). For example, body mass index changes and fatigue, both of which may be therapeutically challenging problems in PD, may be affected by serotonergic function (Pavese et al. 2010; Politis et al. 2011).

In addition, there is animal and human evidence showing the role of serotonin dysfunction in PD-related dyskinesias (Rylander et al. 2010). The machinery of a serotonergic neuron resembles that of the dopaminergic one. They both share dopadecarboxylase and the vesicular monoamine transporter type 2. Therefore, it is proposed that dopamine may be released as a false neurotransmitter by serotonin terminals in PD patients. It is suggested that the absence of dopamine autoreceptors or dopamine transporters results in excessive nonphysiological and nonregulated dopamine release within the synaptic cleft, which contributes to the pathogenesis and expression of dyskinesias (Carta et al. 2007).

24.2 Brain Dopaminergic Imaging in PD

24.2.1 Targeting Dopaminergic Function

Molecular imaging studies depend on quantifying the distribution of radiotracers that bind to specific receptor sites or that reflect the activity of a particular enzyme or biochemical pathway, with minimal non-specific binding. These tracers are labelled with positron emitting or single-photon emitting radioisotopes. Radioisotopes labelled for PET have a much shorter half-life compared to those used in SPECT. This may permit studies using multiple tracers or multiple doses of the same tracer before and after a variety of interventions but on the other hand will also require a more well-structured dedicated facility, usually including an on-site cyclotron. Table 24.1 shows general characteristics of PET and SPECT techniques and their application in PD.

Table 24.1 General characteristics of positron emission tomography (PET) and single-photon emission tomography (SPECT) techniques and their application to Parkinson's disease

Technique	Pros	Cons	Radioisotopes	Application in Parkinson's disease
PET	– Unlimited depth penetration – Whole-body imaging – Co-registering with MRI or CT	– Irradiation exposure – Expensive – Intermediate spatial resolution (2–8 mm) – Long acquisition time	^{11}C ^{18}F ^{15}O	– Research – Dopamine-specific tracers not commercially available, fluorodeoxyglucose and amyloid tracers are
SPECT	– Unlimited depth penetration – Whole-body imaging – Co-registering with MRI or CT – Can combine imaging and radiotherapy	– Irradiation exposure – Low spatial resolution (5–10 mm) – Long acquisition time	^{99m}Tc ^{123}I	– Research – Commercially available to help with clinically unclear cases of parkinsonism, e.g. differentiation from essential tremor

Adapted from Pysz et al. (2010)

Both PET and SPECT techniques are capable of measuring the in vivo biodistribution of minute ($<10^{-10}$ M) concentrations of radiolabelled biomolecules with resolution of a few millimetres and, with the application of appropriate models, of quantifying the molecular kinetic processes in which they participate (Felicio et al. 2009).

SPECT is similar to PET in its use of radioactive tracer material and detection of gamma rays (Pysz et al. 2010). In contrast with PET, however, the tracers used in SPECT emit single gamma rays, whereas PET tracers emit positrons that annihilate with electrons up to a few millimetres away, resulting in the emission of two gamma photons in opposite directions, whose simultaneous detection is required in order to be identified as an event.

The additional correction for degrading factors such as attenuation, scatter, random detection events, detector efficiencies and dead time allows for a quantitative image of the radiolabelled ligand's concentration to be generated. Spatial resolution is limited (SPECT > PET), but either the SPECT or PET data can be co-registered with structural data from computed tomography (CT) or MRI images to provide additional anatomical context to the functional PET data (Aiello et al. 2018; Owen et al. 2011; Sossi 2018; Tondo et al. 2019).

PET or SPECT data can be acquired and analysed using a variety of different approaches, including a simple ratio of target to background activity obtained from a single (static) image, or more complex analyses applied to dynamically acquired data. The application of tracer kinetic models to these data allows for the determination of quantitative measures of specific binding, which is aided by the presence of a reference region devoid of specific binding. If present, such 'reference regions'

also facilitate modelling and may allow the investigator to bypass the requirement for arterial blood sampling (Tatsch and Poepperl 2012). Figure 24.1 shows the dopamine-related tracers most widely available and their binding sites.

24.2.2 Tracers for the Assessment of Presynaptic Dopamine Function

There are different binding sites at the presynaptic level, which can be assessed either by PET or SPECT ligands. This set of targets is of major interest in PD and parkinsonian disorders, as dopaminergic presynaptic terminals in the striatum presumably reflect the loss of nigrostriatal neurons, the pathophysiological hallmark of PD. Overall, these tracers provide useful information about the function of dopamine neurons while addressing key steps in dopamine turnover: dopamine synthesis, storage, release and reuptake (Stoessl 2011).

24.2.2.1 L-Aromatic Acid Decarboxylase (L-AADC)

The assessment of L-AADC through PET tracers such as ^{18}F-fluorodopa allows the estimate of dopamine synthesis and storage. Information derived from activity measured over the first 90–120 min of radiotracer administration provides evaluation of the uptake and conversion of fluorodopa to fluorodopamine by L-AADC (Martin et al. 1989). However, by measuring activity over a prolonged time (4 h following tracer administration), one can estimate the distribution volume and its inverse, dopamine turnover (Sossi et al. 2002). Hence, these prolonged scans can also be used to assess dopamine turnover.

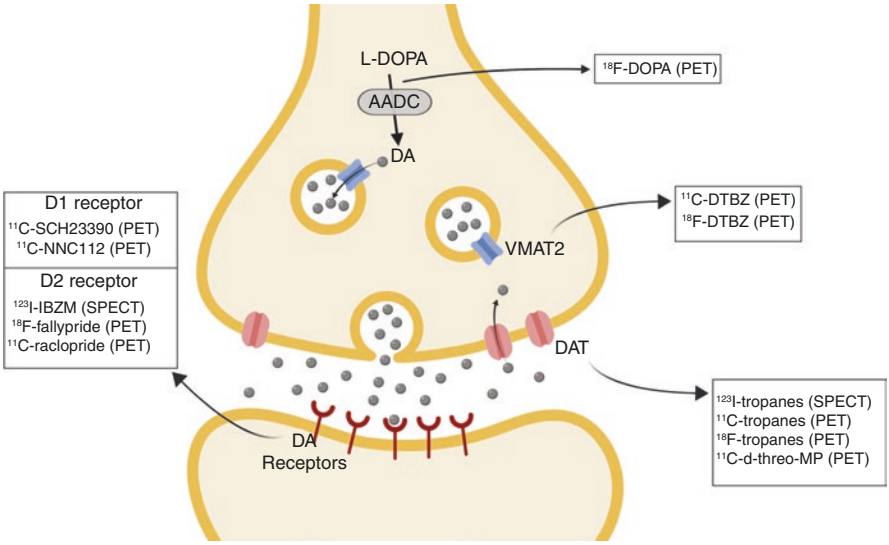

Fig. 24.1 Dopamine nerve terminal and dopaminergic radiotracer binding sites

AADC may be subject to compensatory upregulation, particularly in early PD, and F-dopa uptake is accordingly increased relative to dopamine nerve terminal density as assessed by vesicular monoamine transporter type 2 (VMAT2) binding (Lee et al. 2000; Nandhagopal et al. 2011). Hence, fluorodopa uptake may underestimate the degree of dopaminergic denervation, particularly in earlier stages of disease. Additionally, AADC is not specific to the dopaminergic neuron but is also expressed by serotonergic neurons, and F-dopa uptake is accordingly seen in non-dopaminergic regions (Moore et al. 2003, 2008; Pavese et al. 2012). In line with this, experimental evidence shows that dopamine may be released as a false neurotransmitter by serotonergic nerve terminals in parkinsonian rats (Carlsson et al. 2009; Carta et al. 2010; Muñoz et al. 2009, 2008; Rylander et al. 2010).

Another drawback of F-dopa scans is that some of its metabolites, which are formed by the action of the ubiquitous enzyme catechol-*O*-methyltransferase (COMT), can enter the brain and diminish image contrast. Therefore, an alternative agent is the related tracer 6-^{18}F-fluoro-meta-tyrosine (FMT). FMT is also a good substrate for L-AADC but is not metabolized by COMT and therefore has a higher sensitivity to represent L-AADC activity compared to F-dopa. However, FMT cannot be used to assess dopamine turnover (Asari et al. 2011; DeJesus et al. 1992, 2005; Doudet et al. 1999).

24.2.2.2 Vesicular Monoamine Transporter Type 2 (VMAT2)

VMAT2 promotes the transport of biogenic monoamines, such as serotonin and dopamine, from the cytoplasm to synaptic vesicles. It is assessed by PET with ^{11}C-dihydrotetrabenazine (^{11}C-DTBZ). While the VMAT2 is expressed by all monoaminergic neurons, striatal binding of DTBZ reflects mainly dopaminergic projections, and DTBZ PET is accordingly very useful to assess the density of dopamine nerve terminals. Although DTBZ binding is thought to be less subject to pharmacological effects (Vander Borght et al. 1995) or compensatory changes than either DAT ligands or fluorodopa, it is nonetheless subject to competition from endogenous intra-vesicular dopamine and may accordingly be increased in states of profound DA deficiency such as dopa-responsive dystonia (De La Fuente-Fernández et al. 2003) and early methamphetamine abstinence (Boileau et al. 2008a) and is reduced following levodopa administration in patients with advanced PD (de la Fuente-Fernández et al. 2009).

24.2.2.3 Dopamine Transporter (DAT)

The plasmalemmal DAT is located on the presynaptic terminals of dopaminergic neurons and is responsible for the reuptake of dopamine released into the synaptic cleft. In the healthy brain, this is the leading mechanism responsible for the termination of the actions of DA (Varrone and Halldin 2010). DAT imaging can be assessed using both PET and SPECT tracers as presented in Table 24.2. While the majority of DAT SPECT tracers are iodine- or technetium-labelled, DAT PET tracers are generally carbon- or fluorine-labelled.

Although DAT imaging is frequently used in PD as a surrogate imaging method to assess dopaminergic dysfunction, one should recognize the potential caveats of

Table 24.2 Commercially and research-available dopamine transporter ligands in Parkinson's disease studies

Binding site	SPECT	PET
DAT	^{99m}Tc-TRODAT-1[a]	^{11}C-dMP (d-threo-Methylphenidate)
	^{99m}Tc-Technepine	^{11}C-Cocaine
	^{123}I-FP-CIT[b]	^{11}C-Altropane
	^{123}I-PE2I	^{11}C/^{18}F-β-CFT
	^{123}I-β-CIT	^{11}C-RTI-32
	^{123}I-β-CIT-FE	^{11}C-β-CIT-FE
	^{123}I-Altropane	^{11}C-PE2I
		^{18}F-FE-PE2I

Adapted from Piccini (2003)
PET positron emission tomography, *SPECT* single-photon emission tomography
[a]Commercially available, non-FDA-approved
[b]Commercially available, FDA-approved

this methodology (Piccini 2003). Firstly, age-associated physiological DAT decline is estimated to range from 3% to 8% per decade and corresponds to nigrostriatal cell loss. This is substantially lower than the ~8% per year pathological DAT loss seen in PD (Volkow et al. 1994). Another major confounder is that DAT is subject to pharmacological regulation according to different medication intake, such as dopamine reuptake inhibitors (bupropion) or methylphenidate (Kägi et al. 2010). While this is an important theoretical concern, the significance of this in clinical trials with imaging outcome measures is less clear. Finally, DAT is also subject to compensatory changes, such as may occur in the early stages of PD. Downregulation of DAT should allow dopamine to interact for a longer time with pre- and postsynaptic receptors, by preventing its rapid reuptake (Lee et al. 2000). While several tracers are available for assessing DAT binding, it should be noted that their specificity for the DAT (as opposed to other plasmalemmal monoamine transporters) is variable, as are their pharmacokinetic properties.

24.2.3 Tracers for the Assessment of Postsynaptic Dopamine Function

Dopamine receptors are the primary targets in the treatment of many disorders such as PD, Huntington's chorea and schizophrenia. There are several radiotracers that can be used to access D1-like and D2-like dopamine receptors. ^{18}F-fallypride and ^{11}C-FLB-457, which are PET ligands, and ^{11}C-epidepride, a SPECT ligand, are ultrahigh affinity dopamine receptor antagonist radioligands, which allow quantification and visualization of low-density dopamine extrastriatal D2/D3 receptors as well as striatal receptors (de Paulis 2003). On the other hand, the radioligands ^{11}C-raclopride (or ^{11}C-RAC) for PET and ^{123}I-IBZM for SPECT are widely employed to assess striatal DA receptor availability. In contrast to the former, these ligands

have lower D2/D3 receptor affinity; hence, quantification of extrastriatal receptors is not possible (Pinborg et al. 2007). However, RAC and IBZM are subject to competition from endogenous DA for in vivo binding to D2 receptors and can therefore be used to infer alterations in synaptic DA concentration, using multiple scans before and after a given intervention or, more recently, using models to dynamically quantify the synaptic dopamine in a single scan (Lippert et al. 2019).

Similar to DAT ligands, dopamine receptor binding is also influenced by age and, to a lesser extent, the stage of PD and therapy. While increased tracer binding is observed in the more affected putamen in early PD, probably reflecting a compensatory upregulation of dopamine receptors (Antonini et al. 1997), advanced PD and chronic treatment result in normalization of binding in the putamen and decreased binding in the caudate (Thobois et al. 2004). In contrast, D1 binding as assessed by ^{11}C-SCH23390 and PET is normal in PD (Rinne et al. 1990) but may be decreased in conditions characterized by loss of striatal neurons, such as multiple system atrophy (Shinotoh et al. 1993).

24.3 Brain Non-dopaminergic Sites

24.3.1 Other Neurotransmitters

24.3.1.1 Serotoninergic Tracers

5-Hydroxytryptamine (5-HT, serotonin) is a neurotransmitter widely distributed in the brain, and both pre- and postsynaptic tracers have been developed to study its involvement in vivo in different types of disorders, including PD.

Most studies of the serotonergic system in PD have focused on tracers that bind to the presynaptic serotonin reuptake transporter (SERT). The first SERT ligand developed in humans has been the ^{11}C-(+)-6β-(4-methylthiophenyl)-1,2,3,5,6α,10β-hexahydropyrrolo[2,1-a]isoquinoline (^{11}C-McN 5652) (Szabo et al. 1995). Over the next years, a second generation of ligands was developed to overcome some of the limitations of the ^{11}C-McN 5652, such as the relatively high non-specific binding and the protracted brain uptake (Frankle et al. 2004). The ^{11}C-3-amino-4-(2-dimethylaminomethylphenylthio)benzonitrile (^{11}C-DASB) has been vastly used in human studies in different neurological and psychiatric disorders. In PD, the analysis of ^{11}C-DASB binding has permitted the study of the role of serotonin in motor symptoms and complications as well as nonmotor symptoms, such as fatigue and mood disorders.

SERT binding has been found to be reduced in several areas (caudate, putamen, raphe nuclei, thalamus and cortical areas) of PD subjects with tremor-dominant phenotype as compared to the akinetic-rigid subtype, with a correlation with postural and action tremor, even though interestingly resting tremor was not correlated with DASB binding (Loane et al. 2013). The implication of serotonin in the tremor has been also suggested by a PET study using the $5HT_{1A}$ receptor ligand ^{11}C-WAY 100635 (^{3}H-(*N*-(2-(1-(4-(2-methoxyphenyl)-1-piperazinyl)ethyl)-*N*-(2-pyridyl) cyclohexane-carboxamide) that showed a reduction in PD subjects compared to

healthy controls in the midbrain raphe, which correlated with the severity of resting tremor (Doder et al. 2003). As midbrain $5HT_{1A}$ receptors are somatodendritic autoreceptors, this is compatible with a loss of 5HT neurons. The role of serotonin in levodopa-induced dyskinesias finds its pathophysiological explanation in the possible aberrant levodopa uptake and unregulated dopamine release by serotonin terminals in the dopamine-denervated striatum (Carta et al. 2007). PET and SPECT studies have found an elevated SERT-to-DAT ratio in subjects with dyskinesias (Lee et al. 2015; Roussakis et al. 2016), as well as higher SERT preservation in the *globus pallidus* (Smith et al. 2015). The compensatory role of serotonin in the premotor stages of PD has also been hypothesized, as ^{11}C-DASB binding was found to be increased in premanifest *LRRK2* mutation carriers, compared to idiopathic PD subjects (hypothalamus and striatum) and to *LRRK2*-related PD (hypothalamus and brainstem) (Wile et al. 2017). In contrast, in premanifest *SNCA* A53T mutation carriers, ^{11}C-DASB binding was reduced even in the presence of normal SPECT dopaminergic imaging (Wilson et al. 2019). This difference between *LRRK2*-PD and *SNCA*-PD may be related to mutation-specific biological mechanisms, and therefore, particularly in the case of *LRRK2* mutations, the results might not be generalizable to idiopathic PD.

Serotonin innervation changes have been studied also in nonmotor symptoms related to PD. Correlation between ^{11}C-DASB binding and several nonmotor manifestations of the disease has been found, such as depression (increased SERT in limbic structures and raphe nuclei; Boileau et al. 2008b; Politis et al. 2010), body weight changes (Politis et al. 2011), fatigue, apathy and sleep problems (reduced SERT in basal ganglia and diencephalon; Maillet et al. 2016; Pavese et al. 2010; Wilson et al. 2018).

24.3.1.2 Cholinergic Tracers

The cholinergic system can be imaged with tracers for both SPECT and PET that bind to different targets related to acetylcholine storage and metabolism, including ligands for acetylcholinesterase (AChE), the presynaptic vesicular acetylcholine transporter (VAChT) and muscarinic or nicotinic acetylcholine receptors (Table 24.3).

The study of the cholinergic system is currently restricted to research, with limited clinical value on an individual basis. The interest for imaging this neurotransmitter originally derived from its implication in cognition, mainly to study in vivo the cholinergic neuronal loss in Alzheimer's disease. Along with the evidence of cognitive dysfunction and of implication of the cholinergic system in PD in neuropathological studies, starting from relatively early stages, several studies have focused on the role of the acetylcholine in PD. Acetylcholinesterase imaging shows widespread deficits in cortical and thalamic function in PD, more marked in those with cognitive impairment, but also associated with postural instability, REM sleep behaviour disorder and olfactory loss (Bohnen et al. 2003, 2009, 2012; Gilman et al. 2010; Hilker et al. 2005b; Hiraoka et al. 2012; Klein et al. 2010; Kotagal et al. 2012; Shimada et al. 2009; Shinotoh et al. 1999), even though the binding decline can vary significantly between subjects, and up to one third of the non-demented PD subjects

Table 24.3 Research-available acetylcholine transporter ligands in Parkinson's disease studies

Binding site	SPECT	PET
VAChT	(−)-5-^{123}I-Iodobenzovesamicol (^{123}I-IBVM)	^{18}F-Fluoroethoxybenzovesamicol (^{18}F-FEOBV)
AChE		^{11}C-Methyl-4-piperidyl acetate (^{11}C-MP4A)
		^{11}C-Methyl-4-piperidinyl propionate (^{11}C-PMP)
		^{11}C-Donepezil
Nicotinic receptors	5-^{123}I-Iodo-3-[2(*S*)-2-azetidinylmethoxy]pyridine (5-^{123}I-5-IA-85380)	2-^{18}F-FA-85380
		^{18}F-Flubatine
		^{11}C-Nicotine
		^{18}F-ASEM
Muscarinic receptors	^{123}I-Iodo-quinuclidinylbenzilate (^{123}I-QNB)	^{11}C-*N*-Methyl-4-piperidyl benzilate (^{11}C-NMPB)
		^{11}C-Benztropine

PET positron emission tomography, *SPECT* single-photon emission tomography, *VAChT* vesicular acetylcholine transporter, *AChE* acetylcholinesterase

may have values within the normal range (Bohnen et al. 2012). Interestingly, in subjects with *LRRK2* mutations (in whom cognitive impairment and RBD are less common), an increased AchE hydrolysis rate was shown compared to idiopathic PD, with higher values in non-manifesting carriers, suggesting a compensatory role at least in this subset of individuals (Liu et al. 2018).

Widespread cortical and subcortical reduction in nicotinic receptors has been observed in PD (Fujita et al. 2006; Kas et al. 2009; Meyer et al. 2009; Oishi et al. 2007), while the few muscarinic receptor-based studies have shown increased cortical binding, presumably reflecting upregulation in the face of cholinergic denervation (Asahina et al. 1995, 1998; Colloby et al. 2006). VAChT binding is decreased in PD dementia compared with PD subjects and in Lewy body dementia compared to healthy control (Kuhl et al. 1996; Mazère et al. 2017). A more recent study has shown a reduction of ^{18}F-FEOBV binding in PD with freezing of gait (striatum and limbic cortex) and falls (thalamus) compared to PD without gait impairment (Bohnen et al. 2019).

24.3.1.3 Noradrenergic Tracers

The lack until recently of a selective noradrenergic tracer that could cross the blood-brain barrier has limited the possibility of studying the role of the noradrenergic system in vivo. Only a few studies using non-selective monoaminergic synthesis or monoaminergic transporter-binding tracers have focused on this important neurotransmitter (Pavese et al. 2011; Remy et al. 2005).

More recently, selective reboxetine-based tracers that cross the blood-brain barrier and bind to the noradrenaline transporter (NET) have become available for the evaluation of the noradrenergic system in vivo. The (*S*,*S*)-^{11}C-2-(α-(2-methoxyphenoxy)

benzyl)morpholine (^{11}C-MeNER) has been studied in PD showing BP reduction in several cortical (Sommerauer et al. 2018b) and subcortical regions, with higher reduction in PD subjects with RBD (Nahimi et al. 2018; Sommerauer et al. 2018a), confirming previous in vitro literature findings.

24.3.2 Brain Metabolism and Perfusion

The study of brain glucose metabolism and cerebral blood flow can provide valuable information in different diseases. Different SPECT tracers are used to measure brain perfusion, including ^{99m}Tc-ECD, ^{99m}Tc-HMPAO and ^{123}I-IMP. Usual findings show decreased perfusion in cortical regions in PD compared to controls, while subcortical perfusion is relatively increased in subcortical structures, including the basal ganglia (Imon et al. 1999). A relatively large number of studies have investigated the glucose metabolism in PD using the tracer ^{18}F-fluorodeoxyglucose (FDG). Similarly to the brain perfusion, a metabolism reduction has been observed in cortical regions, and it has been associated also with cognitive deficits. A diffuse involvement of lateral frontal, temporo-parietal and occipital cortex has been described in PD dementia (PDD), while no clear differences between PDD and dementia with Lewy bodies (DLB) are usually observed. Interestingly, the hypometabolism is correlated with neurocognitive measures and is significantly more pronounced in posterior regions in PDD compared with PD-related mild cognitive impairment (PD-MCI), and one study showed that lower values at diagnosis have prognostic value to predict lower cognition at 18 months (Firbank et al. 2017; Garcia-Garcia et al. 2012; Vander Borght et al. 1997; Wu et al. 2018). Relative hypermetabolism in cerebellum, pons, thalamus, paracentral gyrus and lentiform nucleus has also been described. Using FDG PET, Eidelberg et al. have developed an algorithm based on principal component analysis (PCA) to define a so-called PD-related pattern (PDRP) that has been proven to be accurate in the discrimination of PD from healthy controls, and, interestingly, it also has shown to be specific for PD, not being present in other types of parkinsonism (Fukuda et al. 2001; Tomše et al. 2017). Therefore, it has been suggested that it could be helpful in the differential diagnosis of parkinsonisms, especially at early stages. Also, the PDRP has been shown to correlate with disease progression (i.e. with clinical evaluations and with disease duration) and to be responsive to levodopa therapy and circuit-based treatment, such as STN DBS (Asanuma et al. 2006; Feigin et al. 2001). This algorithm-based approach has been used by the same group to define other neurometabolic network patterns, specifically associated with different aspects of the disease, such as tremor (PD tremor-related metabolic network, PDTP) and cognition (PD-related cognitive pattern, PDCP). The PDTP shows only a partial overlap with the PDRP, being mainly a different independent network, manifesting with a relative increased metabolic activity in the primary motor cortex, anterior cerebellum/dorsal pons and the caudate/putamen. In one study, it was significantly associated with tremor in PD subjects and responded to STN DBS, as well as DBS of the ventral intermediate nucleus (Vim) of the thalamus, while the PDRP responded only to STN DBS but not to

stimulation of the Vim (which is a DBS target for tremor but not for other parkinsonian features) (Mure et al. 2011). The PDCP is characterized by hypometabolism in premotor and supplementary motor areas and posterior parietal regions and relative hypermetabolism of the cerebellar vermis and dentate nuclei. Its expression is increased in PDD and PD-MCI, and, contrary to the PDRP, it does not change significantly with dopaminergic or DBS treatment (Huang et al. 2007a, 2008).

24.3.3 Protein Aggregation

Parkinson's disease pathology is characterized by the accumulation of alpha-synuclein in the brain, but, as is the case in other neurodegenerative conditions, aggregation of other misfolded proteins, as well as mixed pathology, is well recognized (Constantinides et al. 2017; Irwin et al. 2013; Winer et al. 2017). To date, there is still no radiolabeled tracer available that binds selectively and consistently to alpha-synuclein that has been tested in humans, but other tracers that bind to other misfolded proteins, such as tau and amyloid beta, have been assessed. The possible role of this type of imaging in PD is to clarify the effect of mixed pathology in the phenotype of the disease, to be used as a predictor of specific characteristics or symptoms and to assess disease progression and the impact of disease-modifying therapies. Also, this may help in clinical practice for the differential diagnosis of doubtful cases, where there are overlapped or mixed symptoms.

24.3.3.1 Tau Imaging

Tau protein, in its different isoforms, is the pathological hallmark of different neurodegenerative diseases, including atypical parkinsonian syndromes. Tau imaging has been used especially to study the most common neurodegenerative disorder, Alzheimer's disease (AD), but it has also been investigated in tau-related forms of parkinsonism, such as PSP and corticobasal degeneration (CBD), in which the aggregated tau is in a different isoform compared to AD (Buée et al. 2000).

The tracer ^{18}F-AV1451, also known as flortaucipir, has been intensively studied in different conditions, including PD. Interestingly, it was shown that the binding in the substantia nigra is decreased in PD compared to controls and likely related to off-target binding of this ligand to neuromelanin that is reduced in PD subjects compared to controls. Also, flortaucipir, as well as other tau tracers, has off-target binding to monoamine oxidase enzymes, which may alter the interpretation of the results, especially when the tau load is not very high, as in AD (Murugan et al. 2019). A more recent ligand, called ^{11}C-PBB3 (2-((1*E*,3*E*)-4-(6-(^{11}C-methylamino) pyri-din-3-yl)buta-1,3-dienyl)benzo[d]thiazol-6-ol), has shown a higher affinity for pure 4R isoforms of tau, which may be beneficial in non-AD tauopathies. However, it appears to have off-target binding to alpha-synuclein both in vitro (Koga et al. 2017) and in vivo (Perez-Soriano et al. 2017). This tracer could therefore potentially be used to study alpha-synuclein aggregation and could be a potential biomarker for PD, even though this dual protein-binding may complicate the interpretation of the results.

24.3.3.2 Amyloid Beta Imaging

Amyloid beta (Aβ) PET imaging has been proposed as a biomarker for Alzheimer's disease (AD). Neuropathological studies have reported varying amounts of amyloid pathology in PDD and more so in DLB (Hughes et al. 1993; Hurtig et al. 2000; Jellinger 2003). Therefore, PET with amyloid ligands has been used to investigate its relationship with the clinical phenotype of Lewy body-related disorders in vivo.

The ^{11}C-Pittsburgh compound B (PiB) is the most investigated Aβ tracer. Other tracers include ^{18}F-florbetaben (FBB), ^{18}F-florbetapir, ^{18}F-flutemetamol and fluoroethyl-methylamino-2-naphthylethylidene malononitrile (^{18}F-FDDNP). Studies in subjects with PD, PD-related mild cognitive impairment (PD-MCI) and PDD have shown variable results, ranging from no differences compared to healthy controls in all PD groups (PD, PD-MCI and PDD) to increase binding in up to 37% of the PD sample, with cortical and striatal involvement (Akhtar et al. 2017; Jokinen et al. 2010; Mashima et al. 2017; Melzer et al. 2019; Petrou et al. 2015; Shah et al. 2016).

The negative results in most PD subjects, even with cognitive dysfunction, have suggested that the cognitive decline in PD is not mainly driven by Aβ deposition. Furthermore, the cases of positive PET studies may be related with a mixed pathology with overlap of Lewy bodies and AD-type pathology (Maetzler et al. 2008), showing the typical AD CSF characteristics and a higher prevalence of ApoE4 genotype, and therefore probably represent the manifestation of a different coincident pathological condition (Maetzler et al. 2009).

24.3.4 Neuroinflammation

Neuroinflammation has been implicated in the process of neurodegeneration in PD and in other neurodegenerative disorders. The interest in this area has grown in the last years, linked to the hope that this may result in new therapeutic targets that could potentially alter the progression of the disease. Having reliable in vivo data on neuroinflammation is vital to further explore the role of this process in the progression of the disease, possibly also in its premotor phase, and as a biomarker to study new drugs.

The main molecular target for the study of neuroinflammation with molecular imaging has been the mitochondrial translocator protein (TSPO), which is upregulated in activated microglia (but is also expressed in astrocytes). A large number of studies have assessed the expression of this protein in vivo, in several neurological conditions, but several problems have limited the interpretation of the findings achieved with tracers that target this protein. The first-generation tracer ^{11}C-(R) PK11195 shows a high level of non-specific binding, with a relatively poor signal-to-noise ratio, and reduced penetration of the brain-blood barrier. Also, the second-generation radioligands (e.g. ^{11}C-PBR28, ^{18}F-PBR-111) have shown high between-subject binding variability in healthy controls as well as people with PD, reflecting a variable binding affinity related to a polymorphism (rs6971) in the gene encoding *TSPO*. This complicates the interpretation of the findings, despite

adjusting the results according to the genetic status (Owen et al. 2014). Thirdly, there is no consistently good reference region for TSPO binding, which further complicates scan analysis. Despite these limitations, some studies have shown an increase in TSPO binding (measured with ^{11}C-PK 11195) in PD compared to healthy controls in different brain regions, including midbrain, substantia nigra, striatum and cortical regions (Gerhard et al. 2006; Iannaccone et al. 2013; Terada et al. 2016), with midbrain binding inversely correlated with striatal dopaminergic denervation (measured by ^{11}C-CFT PET) (Ouchi et al. 2005), and cortical binding inversely correlated with hippocampal volume and metabolism and with cognitive scores (Edison et al. 2013; Fan et al. 2015; Femminella et al. 2016). Increased ^{11}C-PK 11195 binding has also been demonstrated in the substantia nigra of patients with idiopathic REM sleep behaviour disorder (Stokholm et al. 2017). However, studies performed with second-generation TSPO ligands such as ^{18}F-FEPPA (Koshimori et al. 2015) or ^{11}C-PBR28 (Varnäs et al. 2019) have failed to demonstrate a consistent increase in PD brain.

To overcome some of the limitations of the TSPO imaging, newer neuroinflammation tracers that target different molecules, such as the P2X7 receptor, reactive oxygen species or the colony-stimulating factor-1 receptor, are under investigation (Horti et al. 2019; Narayanaswami et al. 2018). In a pilot study, ^{11}C-JNJ54173717, a radioligand that binds to the P2X7 receptor, found no differences between PD subjects and healthy controls. Furthermore, the investigators observed a relationship between total volume of distribution (V_T) and a polymorphism of the *P2X7R* gene, raising the question of whether genotyping will also be needed with this target (Van Weehaeghe et al. 2019).

24.3.5 Phosphodiesterase 10A

Phosphodiesterase 10A (PDE10A) is an intracellular enzyme highly expressed in the medium spiny neurons of the striatum, involved in several neuronal functions through the hydrolysis of the cyclic nucleotides adenosine monophosphate (cAMP) and guanosine monophosphate (cGMP) (Bollen and Prickaerts 2012). It has a role in the signalling of dopamine receptors in the striatum (Nishi et al. 2008), and mutations in the *PDE10A* gene have been associated with genetically driven movement disorders, including childhood-onset chorea and one case of adult-onset parkinsonism (Mencacci et al. 2016). Furthermore, a downregulation of PDE10A has been demonstrated in the striatum of animal models of parkinsonism (Sancesario et al. 2014). For these reasons, there has been an increasing interest in the study of this pathway, which has also been postulated as a possible therapeutic target for diseases that affect the basal ganglia, including Huntington's disease and PD. Its evaluation in vivo is therefore considered of high relevance in this subset of diseases, and a relatively high number of ligands have been tested in human studies (Boscutti et al. 2019). In PD subjects, the ligand ^{11}C-IMA107 has reduced binding compared to

controls in the striatum but also in the GP, correlating positively with disease duration and motor severity (Niccolini et al. 2015). Indeed, longer disease duration and increased motor deficit correlate with reduced PDE10A binding in both caudate and putamen, whereas in the case of dopamine transporter binding, this correlation is seen in putamen only (Pagano et al. 2019). Another study did not find significant differences in caudate or putamen binding between PD subjects and healthy controls, using a different tracer (^{18}F-JNJ42259152), but this could be due to the small sample size and to the relatively early stage of the disease of the subjects scanned. Interestingly, though, the same study found that PD but also PSP patients had a lower caudate-to-putamen binding ratio compared to healthy controls (Koole et al. 2017). Further investigation is needed to define the utility of this interesting target as a biomarker and to understand its potential role in the therapy of the disease, and the molecular imaging is certainly an ideal way to study it.

24.4 Peripheral Nuclear Imaging

Parkinson's disease is a multisystemic disorder that affects the CNS but also the peripheral and enteric nervous system. An increasing body of evidence has shown the peripheral involvement in the early stages of the disease, even before the first motor symptoms are detected that may be responsible of some of the nonmotor features, such as the gastrointestinal and genitourinary symptoms. It has been hypothesized that the disease may even start in the peripheral nervous system and then spread to the CNS, as alpha-synuclein deposits have been detected in the gastrointestinal tract and other peripheral tissues. Nuclear imaging in PD has mainly focused on the brain, but some recent studies have shown the usefulness of imaging the periphery both for clinical purposes and also in research for better understanding of the progression of the disease.

Cardiac sympathetic denervation has been detected using ^{123}I-metaiodobenzylguanidine (^{123}I-MIBG) scintigraphy and SPECT. About 80–90% of PD and DLB subjects have reduced uptake compared to controls (Chung and Kim 2015; Orimo et al. 1999, 2012). Interestingly, this feature is specific of PD, while there is no uptake decline in PSP or MSA subjects (Tateno et al. 2011; Yoshita et al. 1998). As a consequence, this test can be used in clinical practice to help differentiate the PD from other non-Lewy body parkinsonisms. It is necessary to keep in mind that the cardiac sympathetic denervation is not specific for PD, but it can be observed also in diabetes and chronic heart failure, and therefore the interpretation of results must be cautious in this subset of subjects.

A cholinergic tracer, ^{11}C-donepezil, has been used to study AChE density in peripheral organs, as a surrogate to quantify in vivo vagal innervation by one group. A reduced cholinergic innervation has been observed in colon, small intestine and pancreas of early PD subjects, possibly reflecting the parasympathetic involvement of PD (Fedorova et al. 2017; Gjerløff et al. 2015).

24.5 Clinical Implications

24.5.1 Diagnosis and Differential Diagnosis

In clinical practice, the diagnosis of PD is still based on clinical criteria (Postuma et al. 2018), with no required investigations in the vast majority of cases. In some clinically doubtful cases, though, the differential diagnosis may benefit from objective tests. This is especially useful to differentiate secondary parkinsonisms (e.g. iatrogenic parkinsonism) or cases of tremor with mixed characteristics or overlapped mild parkinsonism. In these cases, several approaches have been suggested to help the differential diagnosis, including smell tests, SN ultrasound and molecular neuroimaging. PET and SPECT dopaminergic imaging are able to show dopaminergic denervation that follows the typical posterior-to-anterior pattern and is usually asymmetric (Fig. 24.2). SPECT DAT imaging is probably the most commonly used investigation in Europe and North America and has consistently shown its usefulness in this specific setting.

Unfortunately, DAT imaging performance in differentiating PD from other types of neurodegenerative parkinsonism, such as progressive supranuclear palsy (PSP), multiple system atrophy (MSA) or dementia with Lewy bodies (LBD), is low, and therefore it is not useful in clinical practice. For this problem, multiple-step approaches have been suggested, in which a DAT imaging for the initial diagnosis of a neurodegenerative parkinsonism is followed by a dopaminergic postsynaptic imaging or by FDG PET, which shows better results in differentiating PD from other non-Lewy body parkinsonisms (Hellwig et al. 2012). The cardiac MIBG imaging has also been proposed as a useful test to differentiate PD from other

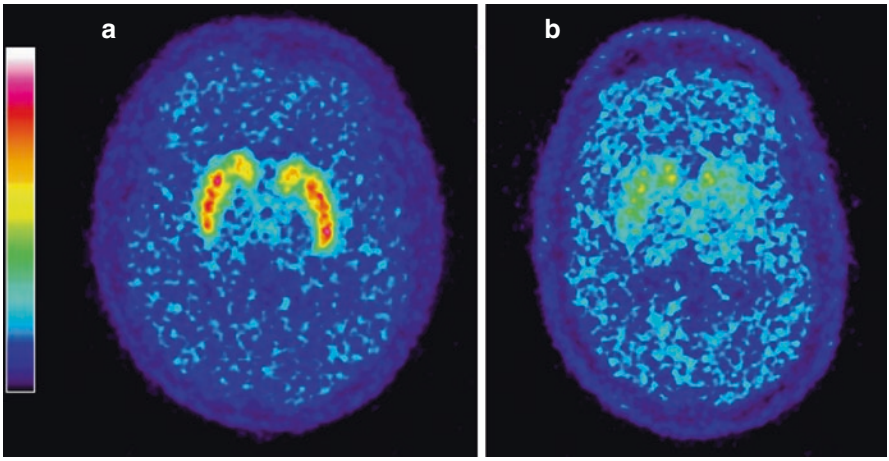

Fig. 24.2 ^{11}C-DTBZ imaging in PD. The figure shows normal striatal binding of the ^{11}C-DTBZ in a healthy subject (**a**) and the striatal binding reduction in a PD subject, which follows the typical posterior-to-anterior pattern of involvement in the putamen, in an asymmetric fashion (**b**)

clinically similar conditions, as the cardiac sympathetic denervation is seen in PD but is usually absent in other types of parkinsonism. In the future, we may envision the use of tau protein-based tracers to diagnose tauopathies, but they still need further validation, and therefore their role in the clinical practice is still to be defined.

At present, these investigations have several limitations. First of all, they are not widely available, and their cost is high when compared to possible clinical benefit. Also, their usefulness is mostly in the early stages of the disease, as the longitudinal progression and the response to medication are usually sufficient to define an operational diagnosis. And finally, in the absence of disease-modifying drugs for any of these diseases, the importance of a specific and early diagnosis is limited, as it does not imply a different management of the patients in clinical practice.

24.5.2 Tracking Disease Progression

Molecular neuroimaging would be an ideal biomarker to track disease progression, as it is a relatively noninvasive technique and it can provide an insight at multiple functional and molecular levels (Strafella et al. 2017). In the earliest stages of PD, presynaptic dopamine tracer uptake is most severely decreased in the dorsal part of the caudal putamen, but a significant reduction of uptake is also seen throughout the striatum. The rate of loss of FD uptake is much higher in PD than in age-matched normal controls (Nurmi et al. 2001; Vingerhoets et al. 1994). In patients with unilateral disease, the clinically unaffected putamen is still abnormal, as one would expect with a subclinical loss of dopaminergic function (Marek et al. 1996).

A posterior-to-anterior gradient of dopaminergic dysfunction has been demonstrated in the putamen, with side-to-side asymmetry in tracer uptake between the less and more severely affected striatal structures that normally correspond to the clinical findings (more severely affected side contralateral to clinically most affected limbs). This asymmetry is also a supporting feature in the diagnosis of PD, when compared to other forms of parkinsonism, or normal ageing. As disease progresses, the antero-posterior gradient is maintained, suggesting a similar relative rate of decline throughout the putamen, while the degree of asymmetry between less and more severely affected putamen diminishes (Brück et al. 2009; Nandhagopal et al. 2009). Thus, when ^{18}F-dopa PET was used to assess the annual rate of decline of tracer uptake in different striatal subregions over a 5-year period, the annual reduction in uptake was found to be 10.3% in posterior putamen, 8.3% in anterior putamen and 5.9% in caudate compared to baseline values. However, the absolute rate of decline was similar in all striatal subregions (Nurmi et al. 2001). Other studies have found similar results (Brück et al. 2006).

These findings are consistent with the view that while factors responsible for the initiation of PD affect striatal subregions in a differential fashion, once disease has started, progression may occur due to non-specific mechanisms such as oxidative stress/free radical elaboration, excitotoxicity, mitochondrial damage and inflammation (Muchowski 2002; Schapira et al. 1998) that would affect striatal subregions to a similar degree.

Analysis of longitudinal data with multitracer PET has revealed that at symptom onset, there is a substantially greater loss of putaminal DTBZ binding in younger, compared with older, PD patients. Further, the rate of reduction in tracer uptake is slower in younger compared to older patients, and the estimated presymptomatic disease phase spans more than 20 years in younger patients compared to one decade in older cases. This suggests that younger PD patients' symptoms progress more slowly and they are able to endure more damage to the dopaminergic system before the appearance of motor symptoms, both possibly due to more efficient compensatory mechanisms (de la Fuente-Fernández et al. 2011).

Autopsy studies in PD have shown a 45% decrease in nigral cell counts during the first 10 years of PD, ten times greater than the loss associated with normal ageing, with a tendency to approach the normal age-related linear decline in the later stages. A number of PET studies support this non-linear pattern of nigral cell loss (Brück et al. 2009; Nandhagopal et al. 2009). Dopaminergic hypofunction in the putamen, as demonstrated by decline in uptake of dopaminergic tracers, is more rapid in early disease than in later stages, supporting the hypothesis of negative exponential decline (Kuramoto et al. 2013; Nandhagopal et al. 2009) as also shown in neuropathological post-mortem analysis of loss of striatal TH staining (Kordower et al. 2013).

Estimation of preclinical duration in PD based on FD PET studies varies according to the model that is used as well as other technical factors but is approximately 6 years with estimated losses ranging from approximately 30% (Hilker et al. 2005a; Morrish et al. 1998) to 55% (Lee et al. 2000) of normal putaminal FD uptake at the time of symptom onset, in general agreement with post-mortem studies. Longitudinal analysis of DTBZ data also suggests that the preclinical interval varies depending on the age of onset, with longer duration in subjects with a younger age of onset. For DTBZ, this preclinical interval is approximately 17 years (for age of onset 53), but at this same age of onset, the interval is shorter when other tracers are used (13 years for DAT binding, 6 years for FD uptake; de la Fuente-Fernández et al. 2011).

PET with DA tracers is a sensitive means of detecting striatal DA dysfunction. This has been used in clinically unaffected mutation carriers from families with LRRK2 mutations (Adams et al. 2005), and progression in these families has been associated with further decline in dopaminergic tracer uptake, with clinical involvement appearing to correspond to progression of impaired FD uptake (Nandhagopal et al. 2008). Interestingly, abnormalities of DA turnover can be seen very early in LRRK2 mutation carriers, many years prior to the expected age of disease onset and earlier than changes in other markers of DA function (Sossi et al. 2010). Once PD becomes manifest in LRRK2 mutation carriers, the rate of decline in presynaptic dopaminergic tracer uptake is indistinguishable from that seen in sporadic disease (Wile et al. 2017).

Changes in metabolic network activity can also be used to track PD progression (Huang et al. 2007b). PDRP expression has been found to be elevated at baseline relative to healthy control subjects and to increase linearly with disease progression, with increasing metabolism in the STN, GPi, dorsal pons and primary motor cortex and declining metabolism in prefrontal and inferior parietal regions with

advancement of disease. Changes in PDRP activity correlated with concurrent declines in striatal DAT binding and increases in motor ratings. However, PDRP is also expressed in the asymptomatic striatum in patients with unilateral disease and progresses symmetrically and in parallel with the symptomatic striatum, with no difference in values between the two sides. A relatively short preclinical period is indicated, in which dissociation of the normal relation between metabolic activity and age occurred about 5 years prior to the onset of PD symptoms (Tang et al. 2010).

24.5.3 Monitoring Therapeutic Effects

Imaging has been used as an in vivo biomarker to assess the effect of treatment on disease progression in various clinical trials. These studies include the comparison of the agonist pramipexole with levodopa on motor complications of Parkinson's disease (CALM-PD) study (Parkinson Study Group 2000) which used ^{123}I-β-CIT SPECT (a measure of DAT binding) to compare the effects of L-dopa versus pramipexole in early PD, REAL-PET (Whone et al. 2003) that compared ropinirole and L-dopa in de novo PD patients with FD PET as the primary outcome measure and the earlier versus later levodopa in Parkinson's disease (ELLDOPA) study (Fahn 1999) in which the effects of L-dopa on clinical progression of PD were studied, and ^{123}I-β-CIT SPECT was included, and studies on foetal nigral transplantation and intraputaminal glial cell line-derived neurotrophic factor (GDNF) on clinical and imaging end points have also been reported with FD PET as a secondary outcome measure (Gill et al. 2003; Lang et al. 2006; Nakamura et al. 2001; Olanow et al. 2003; Whone et al. 2019).

All the above studies found discordance in results between clinical outcome and estimated disease progression, as determined by SPECT or PET. Imaging findings suggested a slower rate of disease progression with pramipexole in the CALM-PD study and with ropinirole in REAL-PET. However, clinical improvement, as measured by the unified Parkinson's disease rating scale (UPDRS), was more in the levodopa treatment group. In ELLDOPA, the L-dopa treatment group had a slower rate of clinical progression compared with the placebo group when clinical assessments were performed after a washout period of two weeks. Although this probably reflects inadequate washout of symptomatic effects, a more rapid rate of decline in DAT binding was noted with imaging in the L-dopa treatment group. In the studies of foetal nigral transplantation and intraputaminal GDNF, although there was a significant increase in striatal FD uptake, there was no significant change in the clinical outcomes.

This discrepancy between clinical progression and imaging findings could reflect many factors, including potentially confounding effects of dopaminergic medication or other therapy on the imaging biomarkers rather than on the disease process. Levodopa may act to depress DAT binding and AADC activity relative to DA agonists. Also, if DA agonists are indeed neuroprotective or levodopa neurotoxic, this effect might be masked by the higher symptomatic efficacy of levodopa, especially when using short washout periods. It must also be noted that clinical progression

was measured using the UPDRS that reflects a composite of dopaminergic and non-dopaminergic dysfunction in PD; the clinical sign that best reflects the severity of the nigrostriatal lesion is bradykinesia. Clinical rating scales also remain vulnerable to both patient and evaluator subjectivity. In the case of cell-based therapy such as transplantation, grafts may survive but fail to form synaptic connections with the host striatum, there may be other deficits in reintegration of a repaired nigrostriatal system into the cortico-striato-pallido-thalamo-cortical network and, finally, many of the deficits of advanced PD may be related to non-dopaminergic abnormalities. Thus, assessment of the nigrostriatal DA system alone may be inadequate to assess the overall disease progression in PD.

Further trials are hence needed to define the contribution of possible confounding factors and to better validate imaging outcomes as biomarkers of PD progression (Agarwal and Stoessl 2013). Attention to study design and analysis are imperative, and functional imaging outcomes must be interpreted with caution and in the context of the clinical result.

The above concerns notwithstanding, functional imaging still offers an objective method of assessing disease progression in PD. In trials of implantation of foetal DA cells (Brundin et al. 2000) into putamen, ^{18}F-dopa PET provided proof of mechanism by detecting increased DA storage capacity after treatment. Similarly, changes in glucose metabolism with PET, while not providing a direct evaluation of DA function, can also be used to infer re-establishment of physiological connections. This approach has been successfully used to study the effects of STN DBS, response to levodopa and glutamic acid decarboxylase (GAD) gene transfer in the STN (Kaplitt et al. 2007). The disadvantage of this approach is that while it may track the outcome of a therapy, it is related to its symptomatic effect, and it may therefore be difficult to determine the degree to which it reflects a disease-modifying component.

Acknowledgements Dr. M. Matarazzo was supported by a Clinical Research Fellowship Award from Parkinson Canada. Dr. A. J. Stoessl is supported by the Michael J. Fox Foundation, the Weston Brain Institute and the Canada Research Chairs Program. We gratefully acknowledge the assistance of Nasim Vafai for the image processing and generating the figures.

References

Adams JR, van Netten H, Schulzer M, Mak E, Mckenzie J, Strongosky A et al (2005) PET in LRRK2 mutations: comparison to sporadic Parkinson's disease and evidence for presymptomatic compensation. Brain 128(Pt 12):2777–2785. https://doi.org/10.1093/brain/awh607

Agarwal PA, Stoessl AJ (2013) Biomarkers for trials of neuroprotection in Parkinson's disease. Mov Disord 28(1):71–85. https://doi.org/10.1002/mds.25065

Aiello M, Cavaliere C, Marchitelli R, D'Albore A, De Vita E, Salvatore M (2018) Hybrid PET/MRI methodology. Int Rev Neurobiol 141:97–128. https://doi.org/10.1016/bs.irn.2018.07.026

Akhtar RS, Xie SX, Chen YJ, Rick J, Gross RG, Nasrallah IM et al (2017) Regional brain amyloid-β accumulation associates with domain-specific cognitive performance in Parkinson disease without dementia. PLoS One 12(5):e0177924. https://doi.org/10.1371/journal.pone.0177924

Antonini A, Schwarz J, Oertel WH, Pogarell O, Leenders KL (1997) Long-term changes of striatal dopamine D2 receptors in patients with Parkinson's disease: a study with positron emission tomography and [11C]raclopride. Mov Disord 12(1):33–38. https://doi.org/10.1002/mds.870120107

Asahina M, Shinotoh H, Hirayama K, Suhara T, Shishido F, Inoue O, Tateno Y (1995) Hypersensitivity of cortical muscarinic receptors in Parkinson's disease demonstrated by PET. Acta Neurol Scand 91(6):437–443

Asahina M, Suhara T, Shinotoh H, Inoue O, Suzuki K, Hattori T (1998) Brain muscarinic receptors in progressive supranuclear palsy and Parkinson's disease: a positron emission tomographic study. J Neurol Neurosurg Psychiatry 65(2):155–163. https://doi.org/10.1136/jnnp.65.2.155

Asanuma K, Tang C, Ma Y, Dhawan V, Mattis P, Edwards C et al (2006) Network modulation in the treatment of Parkinson's disease. Brain 129(Pt 10):2667–2678. https://doi.org/10.1093/brain/awl162

Asari S, Fujimoto K, Miyauchi A, Sato T, Nakano I, Muramatsu S (2011) Subregional 6-[18F]fluoro-L-m-tyrosine uptake in the striatum in Parkinson's disease. BMC Neurol 11:35. https://doi.org/10.1186/1471-2377-11-35

Au WL, Adams JR, Troiano AR, Stoessl AJ (2005) Parkinson's disease: in vivo assessment of disease progression using positron emission tomography. Brain Res Mol Brain Res 134(1):24–33. https://doi.org/10.1016/j.molbrainres.2004.09.028

Bernheimer H, Birkmayer W, Hornykiewicz O, Jellinger K, Seitelberger F (1973) Brain dopamine and the syndromes of Parkinson and Huntington. Clinical, morphological and neurochemical correlations. J Neurol Sci 20(4):415–455. https://doi.org/10.1016/0022-510X(73)90175-5

Bohnen NI, Kaufer DI, Ivanco LS, Lopresti B, Koeppe RA, Davis JG et al (2003) Cortical cholinergic function is more severely affected in parkinsonian dementia than in Alzheimer disease: an in vivo positron emission tomographic study. Arch Neurol 60(12):1745–1748. https://doi.org/10.1001/archneur.60.12.1745

Bohnen NI, Müller MLTM, Koeppe RA, Studenski SA, Kilbourn MA, Frey KA, Albin RL (2009) History of falls in Parkinson disease is associated with reduced cholinergic activity. Neurology 73(20):1670–1676. https://doi.org/10.1212/WNL.0b013e3181c1ded6

Bohnen NI, Müller MLTM, Kotagal V, Koeppe RA, Kilbourn MR, Gilman S et al (2012) Heterogeneity of cholinergic denervation in Parkinson's disease without dementia. J Cereb Blood Flow Metab 32(8):1609–1617. https://doi.org/10.1038/jcbfm.2012.60

Bohnen NI, Kanel P, Zhou Z, Koeppe RA, Frey KA, Dauer WT et al (2019) Cholinergic system changes of falls and freezing of gait in Parkinson's disease. Ann Neurol 85(4):538–549. https://doi.org/10.1002/ana.25430

Boileau I, Rusjan P, Houle S, Wilkins D, Tong J, Selby P et al (2008a) Increased vesicular monoamine transporter binding during early abstinence in human methamphetamine users: is VMAT2 a stable dopamine neuron biomarker? J Neurosci 28(39):9850–9856. https://doi.org/10.1523/JNEUROSCI.3008-08.2008

Boileau I, Warsh JJ, Guttman M, Saint-Cyr JA, McCluskey T, Rusjan P et al (2008b) Elevated serotonin transporter binding in depressed patients with Parkinson's disease: a preliminary PET study with [11C]DASB. Mov Disord 23(12):1776–1780. https://doi.org/10.1002/mds.22212

Bollen E, Prickaerts J (2012) Phosphodiesterases in neurodegenerative disorders. IUBMB Life 64(12):965–970. https://doi.org/10.1002/iub.1104

Boscutti GA, Rabiner E, Plisson C (2019) PET radioligands for imaging of the PDE10A in human: current status. Neurosci Lett 691:11–17. https://doi.org/10.1016/j.neulet.2018.08.006

Braak H, Del Tredici K, Rüb U, de Vos RAI, Jansen Steur ENH, Braak E (2003) Staging of brain pathology related to sporadic Parkinson's disease. Neurobiol Aging 24(2):197–211. https://doi.org/10.1016/S0197-4580(02)00065-9

Brück A, Aalto S, Nurmi E, Vahlberg T, Bergman J, Rinne JO (2006) Striatal subregional 6-[18F]fluoro-L-dopa uptake in early Parkinson's disease: a two-year follow-up study. Mov Disord 21(7):958–963. https://doi.org/10.1002/mds.20855

Brück A, Aalto S, Rauhala E, Bergman J, Marttila R, Rinne JO (2009) A follow-up study on 6-[18F]fluoro-L-dopa uptake in early Parkinson's disease shows nonlinear progression in the putamen. Mov Disord 24(7):1009–1015. https://doi.org/10.1002/mds.22484

Brundin P, Pogarell O, Hagell P, Piccini P, Widner H, Schrag A et al (2000) Bilateral caudate and putamen grafts of embryonic mesencephalic tissue treated with lazaroids in Parkinson's disease. Brain 123(Pt 7):1380–1390. https://doi.org/10.1093/brain/123.7.1380

Buée L, Bussière T, Buée-Scherrer V, Delacourte A, Hof PR (2000) Tau protein isoforms, phosphorylation and role in neurodegenerative disorders. Brain Res Brain Res Rev 33(1):95–130. https://doi.org/10.1016/S0165-0173(00)00019-9

Carlsson T, Carta M, Muñoz A, Mattsson B, Winkler C, Kirik D, Björklund A (2009) Impact of grafted serotonin and dopamine neurons on development of L-DOPA-induced dyskinesias in parkinsonian rats is determined by the extent of dopamine neuron degeneration. Brain 132(Pt 2):319–335. https://doi.org/10.1093/brain/awn305

Carta M, Carlsson T, Kirik D, Björklund A (2007) Dopamine released from 5-HT terminals is the cause of L-DOPA-induced dyskinesia in parkinsonian rats. Brain 130(Pt 7):1819–1833. https://doi.org/10.1093/brain/awm082

Carta M, Carlsson T, Muñoz A, Kirik D, Björklund A (2010) Role of serotonin neurons in the induction of levodopa- and graft-induced dyskinesias in Parkinson's disease. Mov Disord 25(Suppl 1):S174–S179. https://doi.org/10.1002/mds.22792

Chaudhuri KR, Odin P, Antonini A, Martinez-Martin P (2011) Parkinson's disease: the non-motor issues. Parkinsonism Relat Disord 17(10):717–723. https://doi.org/10.1016/j.parkreldis.2011.02.018

Chung EJ, Kim SJ (2015) (123)I-Metaiodobenzylguanidine myocardial scintigraphy in lewy body-related disorders: a literature review. J Mov Disord 8(2):55–66. https://doi.org/10.14802/jmd.15015

Colloby SJ, Pakrasi S, Firbank MJ, Perry EK, Piggott MA, Owens J et al (2006) In vivo SPECT imaging of muscarinic acetylcholine receptors using (R,R) 123I-QNB in dementia with Lewy bodies and Parkinson's disease dementia. NeuroImage 33(2):423–429. https://doi.org/10.1016/j.neuroimage.2006.07.026

Constantinides VC, Paraskevas GP, Emmanouilidou E, Petropoulou O, Bougea A, Vekrellis K et al (2017) CSF biomarkers β-amyloid, tau proteins and a-synuclein in the differential diagnosis of Parkinson-plus syndromes. J Neurol Sci 382(September):91–95. https://doi.org/10.1016/j.jns.2017.09.039

De La Fuente-Fernández R, Furtado S, Guttman M, Furukawa Y, Lee CS, Calne DB et al (2003) VMAT2 binding is elevated in dopa-responsive dystonia: visualizing empty vesicles by PET. Synapse (New York, NY) 49(1):20–28. https://doi.org/10.1002/syn.10199

de la Fuente-Fernández R, Sossi V, McCormick S, Schulzer M, Ruth TJ, Stoessl AJ (2009) Visualizing vesicular dopamine dynamics in Parkinson's disease. Synapse (New York, NY) 63(8):713–716. https://doi.org/10.1002/syn.20653

de la Fuente-Fernández R, Schulzer M, Kuramoto L, Cragg J, Ramachandiran N, Au WL et al (2011) Age-specific progression of nigrostriatal dysfunction in Parkinson's disease. Ann Neurol 69(5):803–810. https://doi.org/10.1002/ana.22284

de Paulis T (2003) The discovery of epidepride and its analogs as high-affinity radioligands for imaging extrastriatal dopamine D(2) receptors in human brain. Curr Pharm Des 9(8):673–696

DeJesus OT, Holden JE, Endres C, Murali D, Oakes TR, Shelton S et al (1992) Visualization of dopamine nerve terminals by positron tomography using [18F]fluoro-beta-fluoromethylene-m-tyrosine. Brain Res 597(1):151–154. https://doi.org/10.1016/0006-8993(92)91518-j

DeJesus OT, Flores LG, Murali D, Converse AK, Bartlett RM, Barnhart TE et al (2005) Aromatic L-amino acid decarboxylase turnover in vivo in rhesus macaque striatum: a microPET study. Brain Res 1054(1):55–60. https://doi.org/10.1016/j.brainres.2005.06.086

Doder M, Rabiner EA, Turjanski N, Lees AJ, Brooks DJ, 11C-WAY 100635 PET Study (2003) Tremor in Parkinson's disease and serotonergic dysfunction: an 11C-WAY 100635 PET study. Neurology 60(4):601–605

Doudet DJ, Chan GL, Jivan S, DeJesus OT, McGeer EG, English C et al (1999) Evaluation of dopaminergic presynaptic integrity: 6-[18F]fluoro-L-dopa versus 6-[18F]fluoro-L-m-tyrosine. J Cereb Blood Flow Metab 19(3):278–287. https://doi.org/10.1097/00004647-199903000-00006

Edison P, Ahmed I, Fan Z, Hinz R, Gelosa G, Ray Chaudhuri K et al (2013) Microglia, amyloid, and glucose metabolism in Parkinson's disease with and without dementia. Neuropsychopharmacology 38(6):938–949. https://doi.org/10.1038/npp.2012.255

Espay AJ, Vizcarra JA, Marsili L, Lang AE, Simon DK, Merola A et al (2019) Revisiting protein aggregation as pathogenic in sporadic Parkinson and Alzheimer diseases. Neurology 92(7):329–337. https://doi.org/10.1212/WNL.0000000000006926

Fahn S (1999) Parkinson disease, the effect of levodopa, and the ELLDOPA trial. Earlier vs later L-DOPA. Arch Neurol 56(5):529–535. https://doi.org/10.1001/archneur.56.5.529

Fan Z, Aman Y, Ahmed I, Chetelat G, Landeau B, Ray Chaudhuri K et al (2015) Influence of microglial activation on neuronal function in Alzheimer's and Parkinson's disease dementia. Alzheimers Dement 11(6):608–21.e7. https://doi.org/10.1016/j.jalz.2014.06.016

Fearnley JM, Lees AJ (1991) Ageing and Parkinson's disease: substantia nigra regional selectivity. Brain 114(Pt 5):2283–2301. https://doi.org/10.1136/jnnp.2007.131045

Fedorova TD, Seidelin LB, Knudsen K, Schacht AC, Geday J, Pavese N et al (2017) Decreased intestinal acetylcholinesterase in early Parkinson disease: an 11C-donepezil PET study. Neurology 88(8):775–781. https://doi.org/10.1212/WNL.0000000000003633

Feigin A, Fukuda M, Dhawan V, Przedborski S, Jackson-Lewis V, Mentis MJ et al (2001) Metabolic correlates of levodopa response in Parkinson's disease. Neurology 57(11):2083–2088. https://doi.org/10.1212/wnl.57.11.2083

Felicio AC, Shih MC, Godeiro-Junior C, Andrade LAF, Bressan RA, Ferraz HB (2009) Molecular imaging studies in Parkinson disease: reducing diagnostic uncertainty. Neurologist 15(1):6–16. https://doi.org/10.1097/NRL.0b013e318183fdd8

Femminella GD, Ninan S, Atkinson R, Fan Z, Brooks DJ, Edison P (2016) Does microglial activation influence hippocampal volume and neuronal function in Alzheimer's disease and Parkinson's disease dementia? J Alzheimers Dis 51(4):1275–1289. https://doi.org/10.3233/JAD-150827

Fereshtehnejad S, Zeighami Y, Dagher A, Postuma RB (2017) Clinical criteria for subtyping Parkinson's disease: biomarkers and longitudinal progression. Brain 140(7):1959–1976. https://doi.org/10.1093/brain/awx118

Firbank MJ, Yarnall AJ, Lawson RA, Duncan GW, Khoo TK, Petrides GS et al (2017) Cerebral glucose metabolism and cognition in newly diagnosed Parkinson's disease: ICICLE-PD study. J Neurol Neurosurg Psychiatry 88(4):310–316. https://doi.org/10.1136/jnnp-2016-313918

Foffani G, Obeso JA (2018) A cortical pathogenic theory of Parkinson's disease. Neuron 99(6):1116–1128. https://doi.org/10.1016/j.neuron.2018.07.028

Frankle WG, Huang Y, Hwang D, Talbot PS, Slifstein M, Van Heertum R et al (2004) Comparative evaluation of serotonin transporter radioligands 11C-DASB and 11C-McN 5652 in healthy humans. J Nucl Med 45(4):682–694

Fujita M, Ichise M, Zoghbi SS, Liow J-S, Ghose S, Vines DC et al (2006) Widespread decrease of nicotinic acetylcholine receptors in Parkinson's disease. Ann Neurol 59(1):174–177. https://doi.org/10.1002/ana.20688

Fukuda M, Mentis MJ, Ma Y, Dhawan V, Antonini A, Lang AE et al (2001) Networks mediating the clinical effects of pallidal brain stimulation for Parkinson's disease: a PET study of resting-state glucose metabolism. Brain 124(Pt 8):1601–1609. https://doi.org/10.1093/brain/124.8.1601

Garcia-Garcia D, Clavero P, Gasca Salas C, Lamet I, Arbizu J, Gonzalez-Redondo R et al (2012) Posterior parietooccipital hypometabolism may differentiate mild cognitive impairment from dementia in Parkinson's disease. Eur J Nucl Med Mol Imaging 39(11):1767–1777. https://doi.org/10.1007/s00259-012-2198-5

GBD 2016 Parkinson's Disease Collaborators (2018) Global, regional, and national burden of Parkinson's disease, 1990–2016: a systematic analysis for the Global Burden of Disease Study 2016. Lancet Neurol 17(11):939–953. https://doi.org/10.1016/S1474-4422(18)30295-3

Gerhard A, Pavese N, Hotton G, Turkheimer F, Es M, Hammers A et al (2006) In vivo imaging of microglial activation with [11C](R)-PK11195 PET in idiopathic Parkinson's disease. Neurobiol Dis 21(2):404–412. https://doi.org/10.1016/j.nbd.2005.08.002

Ghadery C, Best LA, Pavese N, Tai YF, Strafella AP (2019) PET evaluation of microglial activation in non-neurodegenerative brain diseases. Curr Neurol Neurosci Rep 19(7):38. https://doi.org/10.1007/s11910-019-0951-x

Gibb WR, Lees AJ (1988) The relevance of the Lewy body to the pathogenesis of idiopathic Parkinson's disease. J Neurol Neurosurg Psychiatry 51(6):745–752. https://doi.org/10.1136/jnnp.51.6.745

Gill SS, Patel NK, Hotton GR, O'Sullivan K, McCarter R, Bunnage M et al (2003) Direct brain infusion of glial cell line-derived neurotrophic factor in Parkinson disease. Nat Med 9(5):589–595. https://doi.org/10.1038/nm850

Gilman S, Koeppe RA, Nan B, Wang C-N, Wang X, Junck L et al (2010) Cerebral cortical and subcortical cholinergic deficits in parkinsonian syndromes. Neurology 74(18):1416–1423. https://doi.org/10.1212/WNL.0b013e3181dc1a55

Gjerløff T, Fedorova T, Knudsen K, Munk OL, Nahimi A, Jacobsen S et al (2015) Imaging acetylcholinesterase density in peripheral organs in Parkinson's disease with 11C-donepezil PET. Brain 138(Pt 3):653–663. https://doi.org/10.1093/brain/awu369

Goldman JG, Postuma R (2014) Premotor and nonmotor features of Parkinson's disease. Curr Opin Neurol 27(4):434–441. https://doi.org/10.1097/WCO.0000000000000112

Hammes J, Drzezga A, van Eimeren T (2018) The role of Tau imaging in parkinsonian disorders. Curr Neurol Neurosci Rep 18(12):86. https://doi.org/10.1007/s11910-018-0898-3

Hellwig S, Amtage F, Kreft A, Buchert R, Winz OH, Vach W et al (2012) [^{18}F]FDG-PET is superior to [^{123}I]IBZM-SPECT for the differential diagnosis of parkinsonism. Neurology 79(13):1314–1322. https://doi.org/10.1212/WNL.0b013e31826c1b0a

Hely MA, Reid WGJ, Adena MA, Halliday GM, Morris JGL (2008) The Sydney multicenter study of Parkinson's disease: the inevitability of dementia at 20 years. Mov Disord 23(6):837–844. https://doi.org/10.1002/mds.21956

Henderson EJ, Lord SR, Brodie MA, Gaunt DM, Lawrence AD, Close JCT et al (2016) Rivastigmine for gait stability in patients with Parkinson's disease (ReSPonD): a randomised, double-blind, placebo-controlled, phase 2 trial. Lancet Neurol 15(3):249–258. https://doi.org/10.1016/S1474-4422(15)00389-0

Hilker R, Schweitzer K, Coburger S, Ghaemi M, Weisenbach S, Jacobs AH et al (2005a) Nonlinear progression of Parkinson disease as determined by serial positron emission tomographic imaging of striatal fluorodopa F18 activity. Arch Neurol 62(3):378–382. https://doi.org/10.1001/archneur.62.3.378

Hilker R, Thomas AV, Klein JC, Weisenbach S, Kalbe E, Burghaus L et al (2005b) Dementia in Parkinson disease: functional imaging of cholinergic and dopaminergic pathways. Neurology 65(11):1716–1722. https://doi.org/10.1212/01.wnl.0000191154.78131.f6

Hiraoka K, Okamura N, Funaki Y, Hayashi A, Tashiro M, Hisanaga K et al (2012) Cholinergic deficit and response to donepezil therapy in Parkinson's disease with dementia. Eur Neurol 68(3):137–143. https://doi.org/10.1159/000338774

Hoehn MM, Yahr MD (1967) Parkinsonism: onset, progression and mortality. Neurology 17(5):427–442

Holmstrand EC, Sesack SR (2011) Projections from the rat pedunculopontine and laterodorsal tegmental nuclei to the anterior thalamus and ventral tegmental area arise from largely separate populations of neurons. Brain Struct Funct 216(4):331–345. https://doi.org/10.1007/s00429-011-0320-2

Horti AG, Naik R, Foss CA, Minn I, Misheneva V, Du Y et al (2019) PET imaging of microglia by targeting macrophage colony-stimulating factor 1 receptor (CSF1R). Proc Natl Acad Sci U S A 116(5):1686–1691. https://doi.org/10.1073/pnas.1812155116

Huang C, Mattis P, Tang C, Perrine K, Carbon M, Eidelberg D (2007a) Metabolic brain networks associated with cognitive function in Parkinson's disease. NeuroImage 34(2):714–723. https://doi.org/10.1016/j.neuroimage.2006.09.003

Huang C, Tang C, Feigin A, Lesser M, Ma Y, Pourfar M et al (2007b) Changes in network activity with the progression of Parkinson's disease. Brain 130(Pt 7):1834–1846. https://doi.org/10.1093/brain/awm086

Huang C, Mattis P, Perrine K, Brown N, Dhawan V, Eidelberg D (2008) Metabolic abnormalities associated with mild cognitive impairment in Parkinson disease. Neurology 70(16 Pt 2):1470–1477. https://doi.org/10.1212/01.wnl.0000304050.05332.9c

Hughes AJ, Daniel SE, Kilford L, Lees AJ (1992) Accuracy of clinical diagnosis of idiopathic Parkinson's disease: a clinico-pathological study of 100 cases. J Neurol Neurosurg Psychiatry 55(3):181–184. https://doi.org/10.1136/jnnp.55.3.181

Hughes AJ, Daniel SE, Blankson S, Lees AJ (1993) A clinicopathologic study of 100 cases of Parkinson's disease. Arch Neurol 50(2):140–148. https://doi.org/10.1001/archneur.1993.00540020018011

Hughes AJ, Daniel SE, Lees AJ (2001) Improved accuracy of clinical diagnosis of Lewy body Parkinson's disease. Neurology 57(8):1497–1499. https://doi.org/10.1212/WNL.57.8.1497

Hung ASM, Tsui TYM, Lam JCY, Wai MSM, Chan WM, Yew DT (2011) Serotonin and its receptors in the human CNS with new findings - a mini review. Curr Med Chem 18(34):5281–5288

Hurtig HI, Trojanowski JQ, Galvin J, Ewbank D, Schmidt ML, Lee VM et al (2000) Alpha-synuclein cortical Lewy bodies correlate with dementia in Parkinson's disease. Neurology 54(10):1916–1921. https://doi.org/10.1212/wnl.54.10.1916

Iannaccone S, Cerami C, Alessio M, Garibotto V, Panzacchi A, Olivieri S et al (2013) In vivo microglia activation in very early dementia with Lewy bodies, comparison with Parkinson's disease. Parkinsonism Relat Disord 19(1):47–52. https://doi.org/10.1016/j.parkreldis.2012.07.002

Imon Y, Matsuda H, Ogawa M, Kogure D, Sunohara N (1999) SPECT image analysis using statistical parametric mapping in patients with Parkinson's disease. J Nucl Med 40(10):1583–1589

Irwin DJ, Lee VM-Y, Trojanowski JQ (2013) Parkinson's disease dementia: convergence of α-synuclein, tau and amyloid-β pathologies. Nat Rev Neurosci 14(9):626–636. https://doi.org/10.1038/nrn3549

Jellinger KA (2003) Neuropathological spectrum of synucleinopathies. Mov Disord 18(S6):S2–S12. https://doi.org/10.1002/mds.10557

Jokinen P, Scheinin N, Aalto S, Någren K, Savisto N, Parkkola R et al (2010) [(11)C]PIB-, [(18)F]FDG-PET and MRI imaging in patients with Parkinson's disease with and without dementia. Parkinsonism Relat Disord 16(10):666–670. https://doi.org/10.1016/j.parkreldis.2010.08.021

Kägi G, Bhatia KP, Tolosa E (2010) The role of DAT-SPECT in movement disorders. J Neurol Neurosurg Psychiatry 81(1):5–12. https://doi.org/10.1136/jnnp.2008.157370

Kaplitt MG, Feigin A, Tang C, Fitzsimons HL, Mattis P, Lawlor PA et al (2007) Safety and tolerability of gene therapy with an adeno-associated virus (AAV) borne GAD gene for Parkinson's disease: an open label, phase I trial. Lancet (London, England) 369(9579):2097–2105. https://doi.org/10.1016/S0140-6736(07)60982-9

Kas A, Bottlaender M, Gallezot JD, Vidailhet M, Villafane G, Grégoire MC et al (2009) Decrease of nicotinic receptors in the nigrostriatal system in Parkinson's disease. J Cereb Blood Flow Metab 29(9):1601–1608. https://doi.org/10.1038/jcbfm.2009.74

Klein JC, Eggers C, Kalbe E, Weisenbach S, Hohmann C, Vollmar S et al (2010) Neurotransmitter changes in dementia with Lewy bodies and Parkinson disease dementia in vivo. Neurology 74(11):885–892. https://doi.org/10.1212/WNL.0b013e3181d55f61

Koga S, Ono M, Sahara N, Higuchi M, Dickson DW (2017) Fluorescence and autoradiographic evaluation of tau PET ligand PBB3 to α-synuclein pathology. Mov Disord 32(6):884–892. https://doi.org/10.1002/mds.27013

Koole M, Van Laere K, Ahmad R, Ceccarini J, Bormans G, Vandenberghe W (2017) Brain PET imaging of phosphodiesterase 10A in progressive supranuclear palsy and Parkinson's disease. Mov Disord 32(6):943–945. https://doi.org/10.1002/mds.27005

Kordower JH, Olanow CW, Dodiya HB, Chu Y, Beach TG, Adler CH et al (2013) Disease duration and the integrity of the nigrostriatal system in Parkinson's disease. Brain 136(Pt 8):2419–2431. https://doi.org/10.1093/brain/awt192

Koshimori Y, Ko J-H, Mizrahi R, Rusjan P, Mabrouk R, Jacobs MF et al (2015) Imaging striatal microglial activation in patients with Parkinson's disease. PLoS One 10(9):e0138721. https://doi.org/10.1371/journal.pone.0138721

Kotagal V, Albin RL, Müller MLTM, Koeppe RA, Chervin RD, Frey KA, Bohnen NI (2012) Symptoms of rapid eye movement sleep behavior disorder are associated with cholinergic denervation in Parkinson disease. Ann Neurol 71(4):560–568. https://doi.org/10.1002/ana.22691

Kuhl DE, Minoshima S, Fessler JA, Frey KA, Foster NL, Ficaro EP et al (1996) In vivo mapping of cholinergic terminals in normal aging, Alzheimer's disease, and Parkinson's disease. Ann Neurol 40(3):399–410. https://doi.org/10.1002/ana.410400309

Kuramoto L, Cragg J, Nandhagopal R, Mak E, Sossi V, de la Fuente-Fernández R et al (2013) The nature of progression in Parkinson's disease: an application of non-linear, multivariate, longitudinal random effects modelling. PLoS One 8(10):e76595. https://doi.org/10.1371/journal.pone.0076595

Lang AE, Gill S, Patel NK, Lozano A, Nutt JG, Penn R et al (2006) Randomized controlled trial of intraputamenal glial cell line-derived neurotrophic factor infusion in Parkinson disease. Ann Neurol 59(3):459–466. https://doi.org/10.1002/ana.20737

Langston JW (2006) The Parkinson's complex: parkinsonism is just the tip of the iceberg. Ann Neurol 59(4):591–596. https://doi.org/10.1002/ana.20834

Lee CS, Samii A, Sossi V, Ruth TJ, Schulzer M, Holden JE et al (2000) In vivo positron emission tomographic evidence for compensatory changes in presynaptic dopaminergic nerve terminals in Parkinson's disease. Ann Neurol 47(4):493–503. https://doi.org/10.1002/1531-8249(200004)47:4<493::AID-ANA13>3.0.CO;2-4

Lee J-Y, Seo S, Lee JS, Kim H-J, Kim YK, Jeon BS (2015) Putaminal serotonergic innervation: monitoring dyskinesia risk in Parkinson disease. Neurology 85(10):853–860. https://doi.org/10.1212/WNL.0000000000001909

Lippert RN, Cremer AL, Edwin Thanarajah S, Korn C, Jahans-Price T, Burgeno LM et al (2019) Time-dependent assessment of stimulus-evoked regional dopamine release. Nat Commun 10(1):336. https://doi.org/10.1038/s41467-018-08143-4

Liu S-Y, Wile DJ, Fu JF, Valerio J, Shahinfard E, McCormick S et al (2018) The effect of LRRK2 mutations on the cholinergic system in manifest and premanifest stages of Parkinson's disease: a cross-sectional PET study. Lancet Neurol 17(4):309–316. https://doi.org/10.1016/S1474-4422(18)30032-2

Loane C, Wu K, Bain P, Brooks DJ, Piccini P, Politis M (2013) Serotonergic loss in motor circuitries correlates with severity of action-postural tremor in PD. Neurology 80(20):1850–1855. https://doi.org/10.1212/WNL.0b013e318292a31d

Maetzler W, Reimold M, Liepelt I, Solbach C, Leyhe T, Schweitzer K et al (2008) [11C]PIB binding in Parkinson's disease dementia. NeuroImage 39(3):1027–1033. https://doi.org/10.1016/j.neuroimage.2007.09.072

Maetzler W, Liepelt I, Reimold M, Reischl G, Solbach C, Becker C et al (2009) Cortical PIB binding in Lewy body disease is associated with Alzheimer-like characteristics. Neurobiol Dis 34(1):107–112. https://doi.org/10.1016/j.nbd.2008.12.008

Maillet A, Krack P, Lhommée E, Météreau E, Klinger H, Favre E et al (2016) The prominent role of serotonergic degeneration in apathy, anxiety and depression in de novo Parkinson's disease. Brain 139(Pt 9):2486–2502. https://doi.org/10.1093/brain/aww162

Marras C, Beck JC, Bower JH, Roberts E, Ritz B, Ross GW et al (2018) Prevalence of Parkinson's disease across North America. NPJ Parkinsons Dis 4(1):21. https://doi.org/10.1038/s41531-018-0058-0

Martin WR, Palmer MR, Patlak CS, Calne DB (1989) Nigrostriatal function in humans studied with positron emission tomography. Ann Neurol 26(4):535–542. https://doi.org/10.1002/ana.410260407

Mashima K, Ito D, Kameyama M, Osada T, Tabuchi H, Nihei Y et al (2017) Extremely low prevalence of amyloid positron emission tomography positivity in Parkinson's disease without dementia. Eur Neurol 77(5–6):231–237. https://doi.org/10.1159/000464322

Mazère J, Lamare F, Allard M, Fernandez P, Mayo W (2017) 123I-Iodobenzovesamicol SPECT imaging of cholinergic systems in dementia with lewy bodies. J Nucl Med 58(1):123–128. https://doi.org/10.2967/jnumed.116.176180

Melzer TR, Stark MR, Keenan RJ, Myall DJ, MacAskill MR, Pitcher TL et al (2019) Beta amyloid deposition is not associated with cognitive impairment in Parkinson's disease. Front Neurol 10(April):391. https://doi.org/10.3389/fneur.2019.00391

Mencacci NE, Kamsteeg E-J, Nakashima K, R'Bibo L, Lynch DS, Balint B et al (2016) De novo mutations in PDE10A cause childhood-onset chorea with bilateral striatal lesions. Am J Hum Genet 98(4):763–771. https://doi.org/10.1016/j.ajhg.2016.02.015

Merchant KM, Cedarbaum JM, Brundin P, Dave KD, Eberling J, Espay AJ et al (2019) A proposed roadmap for Parkinson's disease proof of concept clinical trials investigating compounds targeting alpha-synuclein. J Parkinsons Dis 9(1):31–61. https://doi.org/10.3233/JPD-181471

Marek KL, Seibyl JP, Zoghbi SS, Zea-Ponce Y, Baldwin RM, Fussell B, Charney DS, van Dyck C, Hoffer PB, Innis RP (1996) [123I] beta-CIT/SPECT imaging demonstrates bilateral loss of dopamine transporters in hemi-Parkinson's disease. Neurology 46:231–237

Meyer PM, Strecker K, Kendziorra K, Becker G, Hesse S, Woelpl D et al (2009) Reduced alpha4beta2*-nicotinic acetylcholine receptor binding and its relationship to mild cognitive and depressive symptoms in Parkinson disease. Arch Gen Psychiatry 66(8):866–877. https://doi.org/10.1001/archgenpsychiatry.2009.106

Moore RY, Whone AL, McGowan S, Brooks DJ (2003) Monoamine neuron innervation of the normal human brain: an 18F-DOPA PET study. Brain Res 982(2):137–145. https://doi.org/10.1016/s0006-8993(03)02721-5

Moore RY, Whone AL, Brooks DJ (2008) Extrastriatal monoamine neuron function in Parkinson's disease: an 18F-dopa PET study. Neurobiol Dis 29(3):381–390. https://doi.org/10.1016/j.nbd.2007.09.004

Moro E, Hamani C, Poon Y-Y, Al-Khairallah T, Dostrovsky JO, Hutchison WD, Lozano AM (2010) Unilateral pedunculopontine stimulation improves falls in Parkinson's disease. Brain 133(Pt 1):215–224. https://doi.org/10.1093/brain/awp261

Morrish PK, Rakshi JS, Bailey DL, Sawle GV, Brooks DJ (1998) Measuring the rate of progression and estimating the preclinical period of Parkinson's disease with [18F]dopa PET. J Neurol Neurosurg Psychiatry 64(3):314–319. https://doi.org/10.1136/jnnp.64.3.314

Muchowski PJ (2002) Protein misfolding, amyloid formation, and neurodegeneration: a critical role for molecular chaperones? Neuron 35(1):9–12

Muñoz A, Li Q, Gardoni F, Marcello E, Qin C, Carlsson T et al (2008) Combined 5-HT1A and 5-HT1B receptor agonists for the treatment of L-DOPA-induced dyskinesia. Brain 131(Pt 12):3380–3394. https://doi.org/10.1093/brain/awn235

Muñoz A, Carlsson T, Tronci E, Kirik D, Björklund A, Carta M (2009) Serotonin neuron-dependent and -independent reduction of dyskinesia by 5-HT1A and 5-HT1B receptor agonists in the rat Parkinson model. Exp Neurol 219(1):298–307. https://doi.org/10.1016/j.expneurol.2009.05.033

Mure H, Hirano S, Tang CC, Isaias IU, Antonini A, Ma Y et al (2011) Parkinson's disease tremor-related metabolic network: characterization, progression, and treatment effects. NeuroImage 54(2):1244–1253. https://doi.org/10.1016/j.neuroimage.2010.09.028

Murugan NA, Chiotis K, Rodriguez-Vieitez E, Lemoine L, Ågren H, Nordberg A (2019) Cross-interaction of tau PET tracers with monoamine oxidase B: evidence from in silico modelling and in vivo imaging. Eur J Nucl Med Mol Imaging 46(6):1369–1382. https://doi.org/10.1007/s00259-019-04305-8

Nahimi A, Sommerauer M, Kinnerup MB, Østergaard K, Winterdahl M, Jacobsen J et al (2018) Noradrenergic deficits in Parkinson disease imaged with 11C-MeNER. J Nucl Med 59(4):659–664. https://doi.org/10.2967/jnumed.117.190975

Nakamura T, Dhawan V, Chaly T, Fukuda M, Ma Y, Breeze R et al (2001) Blinded positron emission tomography study of dopamine cell implantation for Parkinson's disease. Ann Neurol 50(2):181–187

Nandhagopal R, Mak E, Schulzer M, McKenzie J, McCormick S, Sossi V et al (2008) Progression of dopaminergic dysfunction in a LRRK2 kindred: a multitracer PET study. Neurology 71(22):1790–1795. https://doi.org/10.1212/01.wnl.0000335973.66333.58

Nandhagopal R, Kuramoto L, Schulzer M, Mak E, Cragg J, Lee CS et al (2009) Longitudinal progression of sporadic Parkinson's disease: a multi-tracer positron emission tomography study. Brain 132(Pt 11):2970–2979. https://doi.org/10.1093/brain/awp209

Nandhagopal R, Kuramoto L, Schulzer M, Mak E, Cragg J, McKenzie J et al (2011) Longitudinal evolution of compensatory changes in striatal dopamine processing in Parkinson's disease. Brain 134(Pt 11):3290–3298. https://doi.org/10.1093/brain/awr233

Narayanaswami V, Dahl K, Bernard-Gauthier V, Josephson L, Cumming P, Vasdev N (2018) Emerging PET radiotracers and targets for imaging of neuroinflammation in neurodegenerative diseases: outlook beyond TSPO. Mol Imaging 17:1536012118792317. https://doi.org/10.1177/1536012118792317

Niccolini F, Foltynie T, Reis Marques T, Muhlert N, Tziortzi AC, Searle GE et al (2015) Loss of phosphodiesterase 10A expression is associated with progression and severity in Parkinson's disease. Brain 138(Pt 10):3003–3015. https://doi.org/10.1093/brain/awv219

Nishi A, Kuroiwa M, Miller DB, O'Callaghan JP, Bateup HS, Shuto T et al (2008) Distinct roles of PDE4 and PDE10A in the regulation of cAMP/PKA signaling in the striatum. J Neurosci 28(42):10460–10471. https://doi.org/10.1523/JNEUROSCI.2518-08.2008

Nurmi E, Ruottinen HM, Bergman J, Haaparanta M, Solin O, Sonninen P, Rinne JO (2001) Rate of progression in Parkinson's disease: a 6-[18F]fluoro-L-dopa PET study. Mov Disord 16(4):608–615. https://doi.org/10.1002/mds.1139

Oishi N, Hashikawa K, Yoshida H, Ishizu K, Ueda M, Kawashima H et al (2007) Quantification of nicotinic acetylcholine receptors in Parkinson's disease with (123)I-5IA SPECT. J Neurol Sci 256(1–2):52–60. https://doi.org/10.1016/j.jns.2007.02.014

Olanow CW, Goetz CG, Kordower JH, Stoessl AJ, Sossi V, Brin MF et al (2003) A double-blind controlled trial of bilateral fetal nigral transplantation in Parkinson's disease. Ann Neurol 54(3):403–414. https://doi.org/10.1002/ana.10720

Orimo S, Ozawa E, Nakade S, Sugimoto T, Mizusawa H (1999) (123)I-metaiodobenzylguanidine myocardial scintigraphy in Parkinson's disease. J Neurol Neurosurg Psychiatry 67(2):189–194. https://doi.org/10.1136/jnnp.67.2.189

Orimo S, Suzuki M, Inaba A, Mizusawa H (2012) 123I-MIBG myocardial scintigraphy for differentiating Parkinson's disease from other neurodegenerative parkinsonism: a systematic review and meta-analysis. Parkinsonism Relat Disord 18(5):494–500. https://doi.org/10.1016/j.parkreldis.2012.01.009

Ouchi Y, Yoshikawa E, Sekine Y, Futatsubashi M, Kanno T, Ogusu T, Torizuka T (2005) Microglial activation and dopamine terminal loss in early Parkinson's disease. Ann Neurol 57(2):168–175. https://doi.org/10.1002/ana.20338

Owen DRJ, Piccini P, Matthews PM (2011) Towards molecular imaging of multiple sclerosis. Mult Scler 17(3):262–272. https://doi.org/10.1177/1352458510390070

Owen DR, Guo Q, Kalk NJ, Colasanti A, Kalogiannopoulou D, Dimber R et al (2014) Determination of [(11)C]PBR28 binding potential in vivo: a first human TSPO blocking study. J Cereb Blood Flow Metab 34(6):989–994. https://doi.org/10.1038/jcbfm.2014.46

Pagano G, Niccolini F, Wilson H, Yousaf T, Khan NL, Martino D et al (2019) Comparison of phosphodiesterase 10A and dopamine transporter levels as markers of disease burden in early Parkinson's disease. Mov Disord 34(10):1505–1515. https://doi.org/10.1002/mds.27733

Parkinson Study Group (2000) Pramipexole vs levodopa as initial treatment for Parkinson disease: a randomized controlled trial. Parkinson Study Group. JAMA 284(15):1931–1938. https://doi.org/10.1001/jama.284.15.1931

Pavese N, Metta V, Bose SK, Chaudhuri KR, Brooks DJ (2010) Fatigue in Parkinson's disease is linked to striatal and limbic serotonergic dysfunction. Brain 133(11):3434–3443. https://doi.org/10.1093/brain/awq268

Pavese N, Rivero-Bosch M, Lewis SJ, Whone AL, Brooks DJ (2011) Progression of monoaminergic dysfunction in Parkinson's disease: a longitudinal 18F-dopa PET study. NeuroImage 56(3):1463–1468. https://doi.org/10.1016/j.neuroimage.2011.03.012

Pavese N, Simpson BS, Metta V, Ramlackhansingh A, Chaudhuri KR, Brooks DJ (2012) [^{18}F]FDOPA uptake in the raphe nuclei complex reflects serotonin transporter availability. A combined [^{18}F]FDOPA and [^{11}C]DASB PET study in Parkinson's disease. NeuroImage 59(2):1080–1084. https://doi.org/10.1016/j.neuroimage.2011.09.034

Perez-Soriano A, Arena JE, Dinelle K, Miao Q, McKenzie J, Neilson N et al (2017) PBB3 imaging in Parkinsonian disorders: evidence for binding to tau and other proteins. Mov Disord 32(7):1016–1024. https://doi.org/10.1002/mds.27029

Petrou M, Dwamena BA, Foerster BR, Maceachern MP, Bohnen NI, Müller ML et al (2015) Amyloid deposition in Parkinson's disease and cognitive impairment: a systematic review. Mov Disord 30(7):928–935. https://doi.org/10.1002/mds.26191

Piccini PP (2003) Dopamine transporter: basic aspects and neuroimaging. Mov Disord 18(Suppl. 7):S3–S8. https://doi.org/10.1002/mds.10571

Pinborg LH, Videbaek C, Ziebell M, Mackeprang T, Friberg L, Rasmussen H et al (2007) [123I]Epidepride binding to cerebellar dopamine D2/D3 receptors is displaceable: implications for the use of cerebellum as a reference region. NeuroImage 34(4):1450–1453. https://doi.org/10.1016/j.neuroimage.2006.11.003

Politis M, Wu K, Loane C, Turkheimer FE, Molloy S, Brooks DJ, Piccini P (2010) Depressive symptoms in PD correlate with higher 5-HTT binding in raphe and limbic structures. Neurology 75(21):1920–1927. https://doi.org/10.1212/WNL.0b013e3181feb2ab

Politis M, Loane C, Wu K, Brooks DJ, Piccini P (2011) Serotonergic mediated body mass index changes in Parkinson's disease. Neurobiol Dis 43(3):609–615. https://doi.org/10.1016/j.nbd.2011.05.009

Politis M, Pagano G, Niccolini F (2017) Imaging in Parkinson's disease. Int Rev Neurobiol 132(C):233–274. https://doi.org/10.1016/bs.irn.2017.02.015

Postuma RB, Berg D, Stern M, Poewe W, Olanow CW, Oertel WH et al (2015) MDS clinical diagnostic criteria for Parkinson's disease. Mov Disord 30(12):1591–1601. https://doi.org/10.1002/mds.26424

Postuma RB, Poewe W, Litvan I, Lewis S, Lang AE, Halliday G et al (2018) Validation of the MDS clinical diagnostic criteria for Parkinson's disease. Mov Disord 33(10):1601–1608. https://doi.org/10.1002/mds.27362

Pysz MA, Gambhir SS, Willmann JK (2010) Molecular imaging: current status and emerging strategies. Clin Radiol 65(7):500–516. https://doi.org/10.1016/j.crad.2010.03.011

Remy P, Doder M, Lees A, Turjanski N, Brooks D (2005) Depression in Parkinson's disease: loss of dopamine and noradrenaline innervation in the limbic system. Brain 128(Pt 6):1314–1322. https://doi.org/10.1093/brain/awh445

Rinne JO, Laihinen A, Någren K, Bergman J, Solin O, Haaparanta M et al (1990) PET demonstrates different behaviour of striatal dopamine D-1 and D-2 receptors in early Parkinson's disease. J Neurosci Res 27(4):494–499. https://doi.org/10.1002/jnr.490270409

Rogers JD, Brogan D, Mirra SS (1985) The nucleus basalis of Meynert in neurological disease: a quantitative morphological study. Ann Neurol 17(2):163–170. https://doi.org/10.1002/ana.410170210

Roussakis A-A, Politis M, Towey D, Piccini P (2016) Serotonin-to-dopamine transporter ratios in Parkinson disease: relevance for dyskinesias. Neurology 86(12):1152–1158. https://doi.org/10.1212/WNL.0000000000002494

Rylander D, Parent M, O'Sullivan SS, Dovero S, Lees AJ, Bezard E et al (2010) Maladaptive plasticity of serotonin axon terminals in levodopa-induced dyskinesia. Ann Neurol 68(5):619–628. https://doi.org/10.1002/ana.22097

Sancesario G, Morrone LA, D'Angelo V, Castelli V, Ferrazzoli D, Sica F et al (2014) Levodopa-induced dyskinesias are associated with transient down-regulation of cAMP and cGMP in the caudate-putamen of hemiparkinsonian rats: reduced synthesis or increased catabolism? Neurochem Int 79:44–56. https://doi.org/10.1016/j.neuint.2014.10.004

Saulin A, Savli M, Lanzenberger R (2012) Serotonin and molecular neuroimaging in humans using PET. Amino Acids 42(6):2039–2057. https://doi.org/10.1007/s00726-011-1078-9

Schapira AH, Gu M, Taanman JW, Tabrizi SJ, Seaton T, Cleeter M, Cooper JM (1998) Mitochondria in the etiology and pathogenesis of Parkinson's disease. Ann Neurol 44(3 Suppl 1):S89–S98

Schrag A, Schott JM (2006) Epidemiological, clinical, and genetic characteristics of early-onset parkinsonism. Lancet Neurol 5(4):355–363. https://doi.org/10.1016/S1474-4422(06)70411-2

Shah N, Frey KA, Müller MLTM, Petrou M, Kotagal V, Koeppe RA et al (2016) Striatal and cortical β-amyloidopathy and cognition in Parkinson's disease. Mov Disord 31(1):111–117. https://doi.org/10.1002/mds.26369

Shih MC, Felicio AC, de Oliveira Godeiro-Junior C, de Carvalho Aguiar P, de Andrade LAF, Ferraz HB, Bressan RA (2007) Molecular imaging in hereditary forms of parkinsonism. Eur J Neurol 14(4):359–368. https://doi.org/10.1111/j.1468-1331.2007.01691.x

Shimada H, Hirano S, Shinotoh H, Aotsuka A, Sato K, Tanaka N et al (2009) Mapping of brain acetylcholinesterase alterations in Lewy body disease by PET. Neurology 73(4):273–278. https://doi.org/10.1212/WNL.0b013e3181ab2b58

Shinotoh H, Inoue O, Hirayama K, Aotsuka A, Asahina M, Suhara T et al (1993) Dopamine D1 receptors in Parkinson's disease and striatonigral degeneration: a positron emission tomography study. J Neurol Neurosurg Psychiatry 56(5):467–472. https://doi.org/10.1136/jnnp.56.5.467

Shinotoh H, Namba H, Yamaguchi M, Fukushi K, Nagatsuka S, Iyo M et al (1999) Positron emission tomographic measurement of acetylcholinesterase activity reveals differential loss of ascending cholinergic systems in Parkinson's disease and progressive supranuclear palsy. Ann Neurol 46(1):62–69. https://doi.org/10.1002/1531-8249(199907)46:1<62::AID-ANA10>3.0.CO;2-P

Smith R, Wu K, Hart T, Loane C, Brooks DJ, Björklund A et al (2015) The role of pallidal serotonergic function in Parkinson's disease dyskinesias: a positron emission tomography study. Neurobiol Aging 36(4):1736–1742. https://doi.org/10.1016/j.neurobiolaging.2014.12.037

Sommerauer M, Fedorova TD, Hansen AK, Knudsen K, Otto M, Jeppesen J et al (2018a) Evaluation of the noradrenergic system in Parkinson's disease: an 11C-MeNER PET and neuromelanin MRI study. Brain 141(2):496–504. https://doi.org/10.1093/brain/awx348

Sommerauer M, Hansen AK, Parbo P, Fedorova TD, Knudsen K, Frederiksen Y et al (2018b) Decreased noradrenaline transporter density in the motor cortex of Parkinson's disease patients. Mov Disord 33(6):1006–1010. https://doi.org/10.1002/mds.27411

Sossi V (2018) Advances in PET methodology. In: International review of neurobiology, vol 141, 1st edn. Elsevier Inc., Amsterdam, pp 3–30. https://doi.org/10.1016/bs.irn.2018.07.034

Sossi V, de La Fuente-Fernández R, Holden JE, Doudet DJ, McKenzie J, Stoessl AJ, Ruth TJ (2002) Increase in dopamine turnover occurs early in Parkinson's disease: evidence from a new modeling approach to PET 18 F-fluorodopa data. J Cereb Blood Flow Metab 22(2):232–239. https://doi.org/10.1097/00004647-200202000-00011

Sossi V, de la Fuente-Fernández R, Nandhagopal R, Schulzer M, McKenzie J, Ruth TJ et al (2010) Dopamine turnover increases in asymptomatic LRRK2 mutations carriers. Mov Disord 25(16):2717–2723. https://doi.org/10.1002/mds.23356

Spillantini MG, Schmidt ML, Lee VM, Trojanowski JQ, Jakes R, Goedert M (1997) Alpha-synuclein in Lewy bodies. Nature 388(6645):839–840. https://doi.org/10.1038/42166

Stebbins GT, Goetz CG, Burn DJ, Jankovic J, Khoo TK, Tilley BC (2013) How to identify tremor dominant and postural instability/gait difficulty groups with the movement disorder society unified Parkinson's disease rating scale: comparison with the unified Parkinson's disease rating scale. Mov Disord 28(5):668–670. https://doi.org/10.1002/mds.25383

Stoessl AJ (2011) Neuroimaging in Parkinson's disease. Neurotherapeutics 8(1):72–81. https://doi.org/10.1007/s13311-010-0007-z

Stoessl AJ (2012) Neuroimaging in Parkinson's disease: from pathology to diagnosis. Parkinsonism Relat Disord 18(Suppl 1):S55–S59. https://doi.org/10.1016/S1353-8020(11)70019-0

Stoessl AJ, Lehericy S, Strafella AP (2014) Imaging insights into basal ganglia function, Parkinson's disease, and dystonia. Lancet (London, England) 384(9942):532–544. https://doi.org/10.1016/S0140-6736(14)60041-6

Stokholm MG, Iranzo A, Østergaard K, Serradell M, Otto M, Svendsen KB et al (2017) Assessment of neuroinflammation in patients with idiopathic rapid-eye-movement sleep behaviour disorder: a case-control study. Lancet Neurol 16(10):789–796. https://doi.org/10.1016/S1474-4422(17)30173-4

Strafella AP, Bohnen NI, Perlmutter JS, Eidelberg D, Pavese N, Van Eimeren T et al (2017) Molecular imaging to track Parkinson's disease and atypical parkinsonisms: new imaging frontiers. Mov Disord 32(2):181–192. https://doi.org/10.1002/mds.26907

Szabo Z, Kao PF, Scheffel U, Suehiro M, Mathews WB, Ravert HT et al (1995) Positron emission tomography imaging of serotonin transporters in the human brain using [11C](+)McN5652. Synapse (New York, NY) 20(1):37–43. https://doi.org/10.1002/syn.890200107

Tang CC, Poston KL, Dhawan V, Eidelberg D (2010) Abnormalities in metabolic network activity precede the onset of motor symptoms in Parkinson's disease. J Neurosci 30(3):1049–1056. https://doi.org/10.1523/JNEUROSCI.4188-09.2010

Tateno F, Sakakibara R, Kishi M, Ogawa E, Terada H, Ogata T, Haruta H (2011) Sensitivity and specificity of metaiodobenzylguanidine (MIBG) myocardial accumulation in the diagnosis of Lewy body diseases in a movement disorder clinic. Parkinsonism Relat Disord 17(5):395–397. https://doi.org/10.1016/j.parkreldis.2011.02.001

Tatsch K, Poepperl G (2012) Quantitative approaches to dopaminergic brain imaging. Q J Nucl Med Mol Imaging 56(1):27–38

Terada T, Yokokura M, Yoshikawa E, Futatsubashi M, Kono S, Konishi T et al (2016) Extrastriatal spreading of microglial activation in Parkinson's disease: a positron emission tomography study. Ann Nucl Med 30(8):579–587. https://doi.org/10.1007/s12149-016-1099-2

Thobois S, Vingerhoets F, Fraix V, Xie-Brustolin J, Mollion H, Costes N et al (2004) Role of dopaminergic treatment in dopamine receptor down-regulation in advanced Parkinson disease: a positron emission tomographic study. Arch Neurol 61(11):1705–1709. https://doi.org/10.1001/archneur.61.11.1705

Tomše P, Jensterle L, Grmek M, Zaletel K, Pirtošek Z, Dhawan V et al (2017) Abnormal metabolic brain network associated with Parkinson's disease: replication on a new European sample. Neuroradiology 59(5):507–515. https://doi.org/10.1007/s00234-017-1821-3

Tondo G, Esposito M, Dervenoulas G, Wilson H, Politis M, Pagano G (2019) Hybrid PET-MRI applications in movement disorders. Int Rev Neurobiol 144:211–257. https://doi.org/10.1016/bs.irn.2018.10.003

Van Weehaeghe D, Koole M, Schmidt ME, Deman S, Jacobs AH, Souche E et al (2019) [11C]JNJ54173717, a novel P2X7 receptor radioligand as marker for neuroinflammation: human biodistribution, dosimetry, brain kinetic modelling and quantification of brain P2X7 receptors in patients with Parkinson's disease and healthy volunteers. Eur J Nucl Med Mol Imaging 46(10):2051–2064. https://doi.org/10.1007/s00259-019-04369-6

Vander Borght TM, Kilbourn MR, Koeppe RA, DaSilva JN, Carey JE, Kuhl DE, Frey KA (1995) In vivo imaging of the brain vesicular monoamine transporter. J Nucl Med 36(12):2252–2260. https://doi.org/10.1096/fj.00-0204rev

Vander Borght T, Minoshima S, Giordani B, Foster NL, Frey KA, Berent S et al (1997) Cerebral metabolic differences in Parkinson's and Alzheimer's diseases matched for dementia severity. J Nucl Med 38(5):797–802

Varnäs K, Cselényi Z, Jucaite A, Halldin C, Svenningsson P, Farde L, Varrone A (2019) PET imaging of [11C]PBR28 in Parkinson's disease patients does not indicate increased binding to TSPO despite reduced dopamine transporter binding. Eur J Nucl Med Mol Imaging 46(2):367–375. https://doi.org/10.1007/s00259-018-4161-6

Varrone A, Halldin C (2010) Molecular imaging of the dopamine transporter. J Nucl Med 51(9):1331–1334. https://doi.org/10.2967/jnumed.109.065656

Vingerhoets FJG, Snow BJ, Lee CS, Schulzer M, Mak E, Calne DB (1994) Longitudinal fluorodopa positron emission tomographic studies of the evolution of idiopathic parkinsonism. Ann Neurol 36(5):759–764. https://doi.org/10.1002/ana.410360512

Volkow ND, Fowler JS, Wang GJ, Logan J, Schlyer D, MacGregor R et al (1994) Decreased dopamine transporters with age in health human subjects. Ann Neurol 36(2):237–239. https://doi.org/10.1002/ana.410360218

Whone AL, Watts RL, Stoessl AJ, Davis M, Reske S, Nahmias C et al (2003) Slower progression of Parkinson's disease with ropinirole versus levodopa: the REAL-PET study. Ann Neurol 54(1):93–101. https://doi.org/10.1002/ana.10609

Whone A, Luz M, Boca M, Woolley M, Mooney L, Dharia S et al (2019) Randomized trial of intermittent intraputamenal glial cell line-derived neurotrophic factor in Parkinson's disease. Brain 142(3):512–525. https://doi.org/10.1093/brain/awz023

Wichmann T (2019) Changing views of the pathophysiology of Parkinsonism. Mov Disord 34(8):1130–1143. https://doi.org/10.1002/mds.27741

Wichmann T, DeLong MR, Guridi J, Obeso JA (2011) Milestones in research on the pathophysiology of Parkinson's disease. Mov Disord 26(6):1032–1041. https://doi.org/10.1002/mds.23695

Wile DJ, Agarwal PA, Schulzer M, Mak E, Dinelle K, Shahinfard E et al (2017) Serotonin and dopamine transporter PET changes in the premotor phase of LRRK2 parkinsonism: cross-sectional studies. Lancet Neurol 16(5):351–359. https://doi.org/10.1016/S1474-4422(17)30056-X

Wilson H, Giordano B, Turkheimer FE, Chaudhuri KR, Politis M (2018) Serotonergic dysregulation is linked to sleep problems in Parkinson's disease. NeuroImage Clin 18:630–637. https://doi.org/10.1016/j.nicl.2018.03.001

Wilson H, Dervenoulas G, Pagano G, Koros C, Yousaf T, Picillo M et al (2019) Serotonergic pathology and disease burden in the premotor and motor phase of A53T α-synuclein parkinsonism: a cross-sectional study. Lancet Neurol 18(8):748–775. https://doi.org/10.1016/S1474-4422(19)30140-1

Winer JR, Maass A, Pressman P, Stiver J, Schonhaut DR, Baker SL et al (2017) Associations between tau, β-amyloid, and cognition in Parkinson disease. JAMA Neurol 94702:1–9. https://doi.org/10.1001/jamaneurol.2017.3713

Wu L, Liu F-T, Ge J-J, Zhao J, Tang Y-L, Yu W-B et al (2018) Clinical characteristics of cognitive impairment in patients with Parkinson's disease and its related pattern in 18F-FDG PET imaging. Hum Brain Mapp 39(12):4652–4662. https://doi.org/10.1002/hbm.24311

Yarnall A, Rochester L, Burn DJ (2011) The interplay of cholinergic function, attention, and falls in Parkinson's disease. Mov Disord 26(14):2496–2503. https://doi.org/10.1002/mds.23932

Yoshita M, Hayashi M, Hirai S (1998) Decreased myocardial accumulation of 123I-meta-iodobenzyl guanidine in Parkinson's disease. Nucl Med Commun 19(2):137–142

Computer-Aided Diagnosis of Parkinson's Disease, Based on SPECT Scans of the Dopamine Transporter

25

Francisco P. M. Oliveira and Durval C. Costa

Contents

25.1 Introduction 710
25.2 ^{123}I-FP-CIT SPECT 711
25.3 Striatal Uptake Indices and Shape Extraction 712
25.4 How Classifiers Work 713
25.5 Classification Methods Based Only on DaT SPECT 715
25.5.1 Hypothesis-Driven Classification Methods 718
25.5.2 Data-Driven Classification Methods 720
25.6 Classification Methods Combining DaT SPECT and Other Data 722
25.7 Discussion and Conclusions 722
References 724

Abstract

Computer-aided diagnosis (CAD) tools have been, more and more frequently, proposed as a complement to the visual evaluation of dopamine transporter (DaT) single-photon emission computed tomography (SPECT) scans. Classification accuracies up to 98% have been reported in the differentiation between healthy control (HC) subjects and patients with Parkinson's disease (PD) based on DaT SPECT. CAD systems have also been used to differentiate between different types of Parkinsonism, but the accuracies are not as high as for the classification of PD patients versus HC subjects. When compared with cutoff-based classification techniques or visual classification, the CAD originated higher accuracy. The works reported in the literature on CAD systems of DaT SPECT have some limitations, with the lack of postmortem diagnosis the most

F. P. M. Oliveira (✉) · D. C. Costa
Nuclear Medicine – Radiopharmacology, Champalimaud Centre for the Unknown, Champalimaud Foundation, Lisbon, Portugal
e-mail: francisco.oliveira@fundacaochampalimaud.pt; durval.costa@fundacaochampalimaud.pt

R. A. J. O. Dierckx et al. (eds.), *PET and SPECT in Neurology*,
https://doi.org/10.1007/978-3-030-53168-3_25

important of them. The lack of consistency in the definition of the groups of patients and overlap of datasets used are also significant limitations. Despite all limitations and inconsistencies found in the published works, there is evidence that CAD based on DaT SPECT can effectively help in the clinics and is surely a better solution than the cutoff-based techniques only. Therefore, we believe CAD should be used in clinics as a complement to the visual and quantitative evaluation.

25.1 Introduction

Parkinson's disease is a progressive neurological disorder characterized by tremor, rigidity, and bradykinesia associated with progressive dopaminergic neuronal loss projecting into the striatum originated from the substantia nigra and other brain structures (Tolosa et al. 2006). DaT integrity assessment is frequently done using ^{123}I-FP-CIT (DaTscan™, GE Healthcare) with SPECT. Besides the visual evaluation, quantitative analysis is recommended (Darcourt et al. 2010).

Other radiopharmaceuticals have been developed for DaT integrity assessment with SPECT, namely, ^{123}I-β-CIT and ^{99m}Tc-TRODAT-1 (Van Laere et al. 2004). For positron emission tomography (PET), ^{11}C-FE-CIT (Antonini et al. 2001) and ^{11}C-PE2I (Appel et al. 2015) have been reported as successful with similar sensitivity and specificity values.

CAD has been emerging in different areas of medicine with increasing utility. Basically, it takes a set of features or characteristics of the subject, organ, tumor, exam, etc., and based on that and a previously built model, an output is obtained, usually claiming a binary decision or probability.

The idea of classifying a new case based on a previously built model is the oldest in medicine. The physician takes his/her decision based on a mental or written model or set of rules he/she has learned with experience. In the simplest CAD systems, the classification model may be similar to the rule or set of rules the clinicians use, taking advantage of the automated computation and therefore hopefully reducing the probability of error and increasing performance.

The CAD systems used in DaT SPECT can be broadly divided in two types: hypothesis driven and data driven. In the first case, the features or data extracted from the subjects are predefined based on the knowledge about the disease and how the disease is represented in the scan. Frequently, in the particular case of DaT SPECT, the features are related to the uptake in the striatum. Fully data-driven methods make no assumption on the features. Frequently, the selection of the features and the building of the model are optimized simultaneously.

Several different machine learning algorithms have been used for the classification task. In the literature survey done in the scope of this work, support vector machines (SVM) were the most often used. But decision trees, artificial neural networks (ANN), convolutional neural networks (CNN), k-nearest neighbors (k-NN),

nearest mean classifier (NMC), logistic regression, and discriminant analysis techniques were also employed.

The construction of well-documented and validated databases has given a boost in the development of CAD systems for DaT SPECT. The most frequently referred and utilized in the literature, regarding this subject, is the Parkinson's Progression Markers Initiative (PPMI) (Marek et al. 2011, 2018).

25.2 ^{123}I-FP-CIT SPECT

^{123}I-FP-CIT is an analogue of cocaine and therefore binds selectively to the dopamine (and catecholamine) presynaptic transporter. Used with SPECT technology, ^{123}I-FP-CIT imaging is the most popular imaging method to confirm dopaminergic neuronal degeneration in vivo, mainly of the nigrostriatal pathway. It is therefore used in clinics to confirm the diagnosis of neurodegenerative Parkinsonism distinguishing bilateral from mainly unilateral disease. It is also of value in clearly distinguishing patients with drug-induced Parkinsonism (DIP) and essential tremor (ET), where there is no significant dopaminergic degeneration, from those with true Parkinsonism due to dopaminergic degeneration. Although envisaged as difficult and frequently doubtful, in some occasions, it is possible to demonstrate more cortico-striatal degeneration than nigrostriatal degeneration, in particular in patients with corticobasal ganglionic degeneration whose SPECT data with ^{123}I-FP-CIT reveal more often reduced uptake in the caudate nucleus compared to reduced putaminal uptake. Asymmetrical putaminal uptake reduction is the most frequent characteristic found in patients with PD of the idiopathic type. This is associated with less marked volumetric reduction as measured with high-resolution X-ray computed tomography (CT) and/or magnetic resonance imaging (MRI). In patients with very early signs of PD, the uptake reduction is so asymmetric that one of the striata (and particularly the putamen) appears with normal or almost normal uptake, either visually or quantitatively. Patients with other Parkinsonism types, such as multiple system atrophy (MSA) and progressive supranuclear palsy (PSP), frequently show clearly bilateral (symmetrical or slightly asymmetrical) reduced uptake from early stages of the disease.

The majority of data available for disease classification are based on clinical diagnosis and patient follow-up. However, the work of Walker et al. (2002) on correlation of clinical diagnosis with ^{123}I-FP-CIT SPECT imaging results and autopsy confirmatory diagnosis emphasizes shortcomings in the accuracy of the clinical diagnostic criteria that show a tendency to overdiagnose dementia with Lewy bodies (DLB). Consequently, the semiquantitative binding measures for the DLB group were all made somewhat narrower, after autopsy diagnosis, and more importantly the separation of the DLB group from the Alzheimer's disease (AD) group became larger. Due to difficulties inherent to the time it takes to obtain autopsy data from AD, DLB, PD patients, and also normal volunteers, this work is still ongoing to try and obtain a larger cohort possible of postmortem data.

It is clear that inaccuracies concerning clinical criteria in the final (autopsy data) diagnosis may be reduced with time and longitudinal clinical follow-up. However, it is highly likely that relatively early quantitative DaT SPECT will be able to tease out AD from DLB and PD, in addition to normal volunteer controls. Autopsy confirmatory diagnosis will improve group separation and therefore diagnostic classification.

We think that it is paramount to try and emphasize the importance of DaT SPECT data quantification by promoting several types of data extraction as described in this chapter.

25.3 Striatal Uptake Indices and Shape Extraction

Striatal uptake indices are frequently based on ratios between the counts in the striatal regions of interest and the counts in the reference region (a region without specific uptake). Striatal regions are computed separately for the left and right hemisphere and frequently are divided into whole striatum, caudate, and putamen (sometimes divided into two or three regions). The common reference regions are situated in the occipital lobe with possible partial inclusion of the cerebellum or other regions of the brain excluding the striatum and neighbor regions (Costa et al. 1988; Habraken et al. 1999; Tossici-Bolt et al. 2006; Oliveira et al. 2018). Ratios between the caudate and putamen uptake and left-right asymmetry coefficient are also occasionally used (Morton et al. 2005; Prashanth et al. 2016; Oliveira et al. 2018).

Geometric features extracted from the shape of the striatal uptake have been used in recent works (Augimeri et al. 2016; Prashanth et al. 2016; Oliveira et al. 2018). These features are assessed only in the striatal region with high uptake, at least higher than the background. They do not measure the real shape of the striatum. Examples of shape features are striatal volume, length (anterior-posterior), width (left-right), thickness (inferior-superior), and orientation-related features (Augimeri et al. 2016; Oliveira et al. 2018).

Nowadays, there are several software solutions to extract striatal uptake indices or shape descriptors. In many cases, it is possible to compare the measures with a database of normal scans. Examples are, for instance:

- BasGan software (Calvini et al. 2007) starts by a manual rigid preregistration, followed by an automatic affine registration with a template. Then, the uptake in the left and right caudate and putamen is extracted independently and automatically. Uptake in an occipital region is also extracted to be used as reference region.
- Hermes Brass™ is a commercial software that has a tool for automatic ^{123}I-FP-CIT analysis. It automatically quantifies uptake in the striatum and compares it with a normal database.
- PMOD software is a commercial tool that has been used in many research works found in the literature. It is a general tool but with some adaptation can be used for the quantification of DaT SPECT.

As some other groups, our group has its own solution to extract relevant features from the DaT SPECT (Oliveira et al. 2014, 2018). Our solution starts by automatic rigid or affine registration with a template. Then, predefined striatal regions of interest are optimally positioned. From that, uptake in the left and right caudate and putamen is extracted independently and automatically. The reference region is automatically defined. It can be an occipital region or whole brain except a region around the basal ganglia and ventricles. Volume, length, width, and thickness of left and right striatal regions with normal uptake are also automatically measured.

25.4 How Classifiers Work

To build a classifier, two fundamental things are necessary: a dataset of observations (or measurements or features), labeled by class, and a theoretical classification model. The features are the independent variables, and the known classification labels are the dependent variable. Then, in most of the classifiers, an optimization algorithm is used to optimize the parameters of the model, i.e., the parameters that make the model as accurate as possible in predicting the classification. This optimization step is usually known as training or learning. After optimizing the model, it can be used to predict the classification of new cases. To assess the accuracy of the model, a dataset of cases not used in the training process are classified by the model, and the output is compared with the known gold standard classification.

There are several conceptually different models that can be used, each one with several variants. Here, we briefly explain the foundation of the models found in the literature regarding the classification of patients with Parkinsonism based on DaT SPECT. As previously referred, in all cases, the input is a set of features describing the case. These may be discrete or continuous variables or even the images themselves. The final output is always a discrete variable, i.e., the predicted label.

A SVM classifier is a linear model, like linear regression, i.e., the output is a linear combination of the input variables. The main difference is the goal of the optimization. In linear regression, the goal is to fit the model to the data, while in the SVM the goal is to find the optimal model (usually a hyperplane) that best separates the two classes of the training data. With adequate transformation of the input variables, nonlinear behavior of the input variables may be modulated to a linear one. The output of the SVM model is a continuous variable that needs to be binarized. If it is higher than zero, the case is classified in one way (positive, for instance); otherwise, it is classified in the other way.

Logistic regression is a well-known technique used in statistics. The output is the probability of a case to be positive, for instance. Thus, defining a threshold, usually 0.5, the output is binarized. The classification model is obtained by optimizing the parameters of the model (a logistic function) with the goal to fit the model to the training data.

Naive Bayes is other technique to build classifiers. It assumes the features are independent of each other, regardless if possible correlations between the features may exist. The idea is to compute the probability of an observation that occurs

assuming that observation belongs to a predefined class (Bayes theorem). Using, for instance, the method of maximum likelihood, the optimal parameters of the model can be estimated. Usually, the decision rule is based on the hypothesis that is most probable (maximum a posterior rule).

Decision tree is a conceptually simple classifier. In its basic formulation, it starts by the feature that best separates the cases. It splits "optimally" the cases in two groups based on that feature, creating two branches. Then, for each branch, a new split is done based on other feature and so on. The optimal cutoffs are optimally defined during the training process. The final classification model is the rule with the cutoffs that optimally classify the training dataset.

The ANN classifiers are based on the idea of the connections between neurons. It may have several neurons and layers. In the basic implementation, all neurons of the first layer have as inputs the original features. Then, each neuron computes an output measure, usually a real number, based on the features and a specific mathematical model for that neuron. The outputs of the neurons of the first layer are then passed as inputs to the neurons of the second layer and so on till the last layer. The neurons and the connections between neurons ("synapses") have weights that are optimized in the training process. By reducing or increasing the weight of a synapse, that synapse may be reinforced or eliminated. The same happens with neurons.

The CNN is a type of ANN. In very short, the input is the image or a patch of the image. The first layer is a convolutional layer, i.e., a set of convolution filters are applied to the image. The kernels of the filters are not static; they are optimized/learned during the process. Next layers may be convolutional or not. In a CNN, there is no need for feature extraction, since this process is incorporated in the convolution layers.

Discriminant analysis is a classical statistics technique. It assumes the distribution of the features is normally distributed in each class. It tries to find a linear combination of the features that best describe or separate the classes of objects based on some threshold. It is related to regression analysis.

The NMC is very simple. The training dataset is used to compute the mean feature vector of each class (centroid of each class). Then, a new case gets the classification of the nearest centroid.

The k-NN classifier is almost as simple as the NMC. A case is classified based on its k most "closed" cases in the training dataset by voting of closeness. The distance is taken from the values of the features extracted from the cases. This is the only classifier here presented that always needs the full training dataset. The other classifiers here presented only need the training dataset to optimize the classification model or to obtain the centroids of the classes, and then only the model or the centroids are needed.

There are several measures that can be used to report the quality of a binary classifier. In this work, we opted to use the simplest measures for a nonexpert in classification/statistics area. The simplest one is the accuracy (Acc), which is defined by the ratio of number of correct classifications (true positive plus true negative) and the number of cases (see Fig. 25.1). The sensitivity and specificity are also very useful, the first being the ratio of the number of true positive and the number of positives and the second being the ratio between the number of true negative and the

		Gold standard	
		Positive	Negative
Classifier outcome	Predicted positive	True positive (TP)	False positive (FP)
	Predicted negative	False negative (FN)	True negative (TN)

Fig. 25.1 General binary confusion matrix

number of negatives. The balanced accuracy (BAcc) is the mean of the sensitivity and specificity, which makes it very suitable as a measure of the classifier quality. Besides that, the balanced accuracy is more informative in unbalanced datasets than the accuracy. For this reason, in this work, whenever possible, we use the balanced accuracy.

For multiclass classifiers, i.e., more than two classes, the accuracy can always be computed. The sensitivity and specificity may also be computed for the classification of each class against all the others together.

25.5 Classification Methods Based Only on DaT SPECT

As referred before, the PD pathology hallmark is characterized by a progressive dopaminergic neuronal loss projecting into the striatum originated from the substantia nigra and other brain structures. This causes a decrease of the DaT ligand uptake in the striatum, mostly in the putamen in the initial stages of the disease. This uptake pattern led to the appearing of classification techniques based on cutoffs. If a single measure is taken from the striatum, there is no need for a computer to assess if the measure is above or below the cutoff. This type of classification has been used for a long time. For instance, Costa et al. (1988) defined a striatal binding index (SBI) related to the uptake in whole striatum. Then, the patients that had an SBI inferior to the cutoff at least in one side of the striatum were considered as having striatal DaT degeneration. The cutoff-based approaches are still very common and used in many clinical sites.

Nowadays, most common uptake indices are computed separately in the caudate and putamen. Figure 25.2 shows two examples of the delineation of the caudate and putamen nucleus on a transaxial slice. The indices may be simply the ratio of the mean counts per voxel in the specific region and the mean counts per voxel in the reference region or the binding potential (BP) in the specific regions:

$$\left(\mathrm{BP} = \frac{\text{Mean counts per voxel in the specific region}}{\text{Mean counts per voxel in the reference region}} - 1 \right)$$

Other four uptake indices frequently used in quantification and classification problems are shown in Fig. 25.3 with their distribution in the differential diagnosis between healthy controls and patients with PD. They are the specific binding ratio

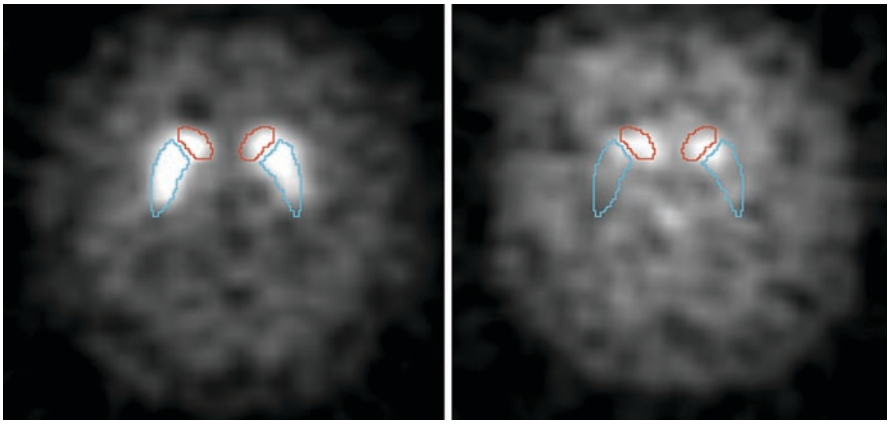

Fig. 25.2 Two transaxial slice images taken from two DaT SPECT examinations of two different patients. On the left, there is a typical normal uptake distribution throughout the striatum (including caudate and putamen) from a patient with no dopaminergic degeneration. On the right, very abnormal uptake is demonstrated within both striata of a patient (more intensely reduced in the putamen) with bilateral nigrostriatal degeneration. The red and blue contours delineate the caudate and putamen, respectively

(SBR) (Tossici-Bolt et al. 2006), caudate binding potential (CBP), putamen binding potential (PBP), and striatum binding potential (SBP) (Oliveira et al. 2018). Data represented were obtained from the analysis of 209 HC subjects and 443 PD patients based on the work of Oliveira et al. (2018). It is clear that all indices separate well, but not perfectly, the PD patients from the HC subjects.

Many research works found in the literature measured the discriminative power of a feature based on the area under the receiver operating characteristic (ROC) curve. The ROC curve is a graphical representation of the false positive rate (1 − specificity) versus the true positive rate (sensitivity) for different cutoffs of the feature. If there is a cutoff value that separates perfectly the cases in two classes, then the area under the ROC curve is 1. This technique allows obtaining a measure of the feature classification discriminative power (area under the ROC curve) on the training dataset. It does not give the expected classification accuracy if the "optimal" cutoff chosen were applied to a different dataset. It does not involve validation. Yet, it was frequently used in many works (Staff et al. 2009; Skanjeti et al. 2014, 2015; Iwabuchi et al. 2018). Figure 25.4 shows four ROC curves obtained from the same data as in Fig. 25.3.

Currently, several uptake indices can be extracted from the scans. Thus, establishing a cutoff for each one is not the ideal solution because frequently there are disagreements among them, especially for the borderline cases. A better solution is using optimization to build a classification model based on all known relevant features available. This is the fundamental idea behind the hypothesis-driven classifiers.

In the next subsections, a compilation of published papers that use a CAD strategy on DaT SPECT images for differential diagnosis of Parkinsonism is presented.

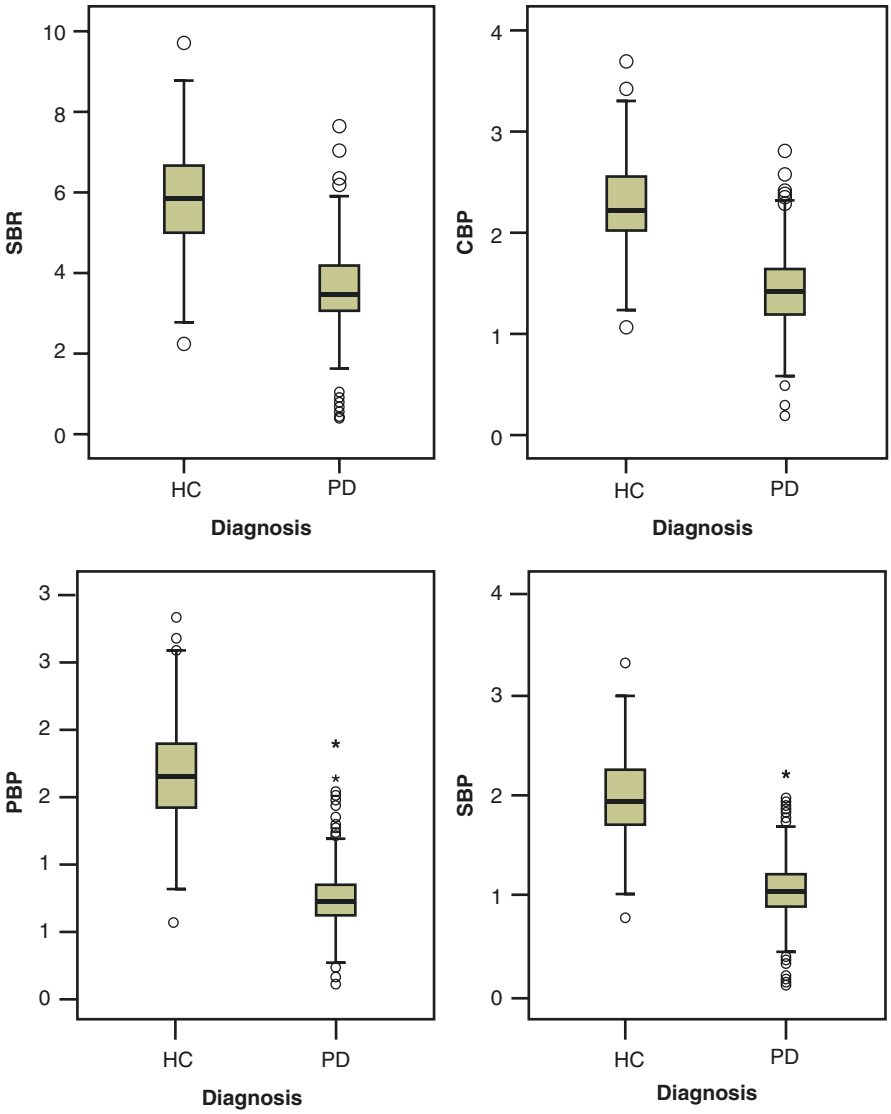

Fig. 25.3 Four boxplots representing the distribution of the SBR, CBP, PBP, and SBP when analyzing 209 HC subjects and 443 PD patients based on the work of Oliveira et al. (2018). For each subject, only the minimum value of both hemispheres was considered

Most common classifiers classify PD patients versus HC subjects; however, groups of patients with ET, corticobasal degeneration (CBD), DLB, DIP, PSP, MSA, and vascular Parkinsonism (VP) were also included in some works. In addition, some research works divided the PD patients into early PD (ePD) and advanced PD (aPD). In some works, the authors defined a Parkinsonian syndrome (PS) group

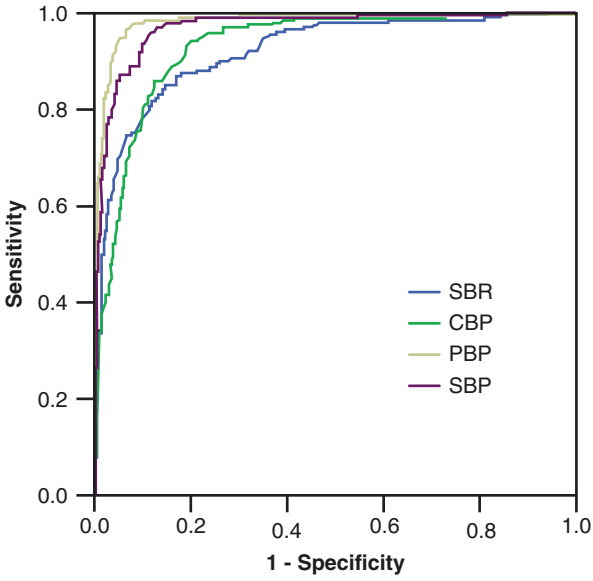

Fig. 25.4 Four ROC curves from the analysis of 209 HC subjects and 443 PD patients based on the work of Oliveira et al. (2018). The ROC curves are shown for the uptake indices SBR, CBP, PBP, and SBP. For each subject/patient, only the minimum value of both hemispheres was considered. Areas under the curves are 0.922, 0.933, 0.982, and 0.971 for the SBR, CBP, PBP, and SBP, respectively. Based on these values, the PBP index can separate better the HC subjects from the PD patients than the other indices

including all Parkinsonism cases with evidence of dopaminergic deficit. Other works did not have a class of healthy controls; instead, they included a category of controls containing the scans without evidence of dopaminergic deficit (SWEDD).

Only works that used cross-validation or an independent dataset for validation and described the dataset used are here presented. There are works that have tested different classifiers and/or different sets of features. In these cases, only the best result per classifier is presented.

Based on the survey done, there are works that also compared the classification accuracy obtained with the CAD systems against the cutoff-based techniques. In all cases, the CAD gave higher accuracy (see, for instance, Taylor and Fenner (2017) and Oliveira et al. (2018)).

25.5.1 Hypothesis-Driven Classification Methods

A compilation of the works found in the literature survey that used hypothesis-driven CAD based only on DaT SPECT images for differential diagnosis of Parkinsonism is presented in Table 25.1. ^{123}I-FP-CIT was the radiopharmaceutical used in all studies, except one that reports to have used ^{99m}Tc-TRODAT-1 instead. The extraction of the indices was fully automated in some of them and observer dependent in others. Examples of both cases are included. At least two uptake indices were used in all the works, one related to the uptake in the caudate and the other in the putamen.

Table 25.1 Papers found in the literature using hypothesis-driven classifiers based on DaT SPECT

Paper	Features used	Groups of subjects or images (total including training and validation)	Type of classifier	Main results
Van Laere et al. (2004)	Striatal uptake indices	PD (n = 47), controls (n = 10)	Discriminant analysis	BAcc: 91% (PD vs. controls)
	Striatal uptake indices (^{99m}Tc-TRODAT-1)	PD (n = 47), controls (n = 10)	Discriminant analysis	BAcc: 81% (PD vs. controls)
Van Laere et al. (2006)	Striatal uptake indices	PD (n = 58), ET (n = 27), MSA (n = 24), PSP (n = 12), DLB (n = 8)	Discriminant analysis	BAcc: 93% (PD + MSA + PSP + DLB vs. ET)
Hamilton et al. (2006)	Striatal uptake indices	PD (n = 13), ET (n = 5)	ANN	BAcc: 100% (PD vs. ET)
Palumbo et al. (2010)	Striatal uptake indices	ET (n = 89), ePD (n = 64), aPD (n = 63)	ANN	Acc: 82% ePD, 79% aPD, 97% ET (ePD vs. aPD vs. ET)
Palumbo et al. (2014)	Striatal uptake indices	PD (n = 56), ET + DIP (n = 34)	SVM	BAcc: 90% (PD vs. DIP)
Prashanth et al. (2014)	Striatal uptake indices	PD (n = 396), HC (n = 179)	SVM	BAcc: 96% (PD vs. HC)
			Logistic regression	BAacc: 87% (PD vs. HC) (no cross-validation reported)
Huertas-Fernández et al. (2015)	Striatal uptake indices	PD (n = 164), VP (n = 80)	SVM	BAcc: 87% (PD vs. VP)
			Discriminant analysis	BAcc: 87% (PD vs. VP)
			Logistic regression	BAcc: 87% (PD vs. VP)
Prashanth et al. (2016)	Striatal uptake indices and uptake shape	PD (n = 427), HC (n = 208), SWEDD (n = 80)	SVM	BAcc: 97% (PD vs. HC + SWEDD)
			Boosted trees (a type of decision trees)	BAcc: 97% (PD vs. HC + SWEDD)
			Random forest (a multitude of decision trees)	BAcc: 97% (PD vs. HC + SWEDD)
			Naive Bayes	BAcc: 96% (PD vs. HC + SWEDD)

(continued)

Table 25.1 (continued)

Paper	Features used	Groups of subjects or images (total including training and validation)	Type of classifier	Main results
Taylor and Fenner (2017))	Striatal uptake indices	PPMI dataset: PD (n = 448), HC (n = 209)	SVM	BAcc: 97% (PD vs. HC)
		Local dataset: PD (n = 191), non-PD patients (n = 191)	SVM	BAcc: 91% (PD vs. non-PD)
Oliveira et al. (2018)	Striatal uptake indices and uptake shape	PD (n = 443), HC (n = 209)	SVM	BAcc: 98% (PD vs. HC)
			Logistic regression	BAcc: 96% (PD vs. HC)
			KNN	BAcc: 97% (PD vs. HC)
Nicastro et al. (2019)	Striatal uptake indices	PD (n = 280), CBD (n = 28), MSA-P (n = 21), PSP (n = 41), HC (n = 208)	SVM	BAcc: 93% (HC vs. CBD + MSA-P + PSP)
			SVM	BAcc: range from 61% (PD vs. MSA-P) to 84% (CBD vs. MSA-P)
Wenzel et al. (2019))	Specific binding ratio	PPMI dataset: PD (n = 438), HC (n = 207)	Based on optimal cutoff	BAcc: 97% (PD vs. HC)
		Local dataset: PS (n = 149), controls (n = 149)	Based on optimal cutoff	BAcc: 97% (PS vs. controls)

25.5.2 Data-Driven Classification Methods

In Table 25.2, a compilation of published papers that used a data-driven approach to classify patients based on DaT SPECT is presented. By definition, data-driven methods do not make any assumption on the uptake pattern of the scan. They should use all image content to search for the features and/or regions that best separate the cases. In some works, as are, for instance, Martínez-Murcia et al. (2014) and Oliveira and Castelo-Branco (2015), only a striatal region was used to feed the classifier. Illán et al. (2012) also assumed previous knowledge on the DaT SPECT, in this case to do the intensity normalization of the scans. Even though these types of methods are not truly data driven because they assume that the relevant information is in the striatum, they are included in Table 25.2.

The simpler approach for the data-driven methods is the voxel-as-feature (VAF) approach, i.e., each voxel is an independent feature. However, as for other approaches, this method may not be robust if the number of cases is not much higher than the number of features, ideally at least 6–12 times higher. Thus, a

Table 25.2 Papers found in the literature using data-driven classifiers based on DaT SPECT. In all cases, the ^{123}I-FP-CIT radiopharmaceutical was used

Paper	Features and reduction strategy	Groups of subjects or images (total including training and validation)	Type of classifier	Main results
Towey et al. (2011)	All voxels followed by SVD	PS (n = 79), controls (n = 37)	Naive Bayes	BAcc: 96% (PS vs. controls)
			NMC	BAcc: 94% (PS vs. controls)
Illán et al. (2012)	Voxels in a striatal region	PS (n = 100), controls (n = 108)	SVM	BAcc: 91% (PS vs. controls)
			KNN	BAcc: 86% (PS vs. controls)
			NMC	BAcc: 87% (PS vs. controls)
Segovia et al. (2012)	Voxels in a striatal region followed by PLS	PS (n = 95), controls (n = 94)	SVM	BAcc: 93% (PD vs. controls)
Rojas et al. (2013)	Voxels in a striatal region followed by PCA or ICA	PS (n = 41), controls (n = 39)	SVM	BAcc: 95% (PS vs. controls)
Martínez-Murcia et al. (2014)	Voxels in a striatal region followed by PCA	PD (n = 222), controls (n = 275)	SVM	BAcc: 91% to 95% (PD vs. controls)
Oliveira and Castelo-Branco (2015)	Voxels in a striatal region	PD (n = 445), HC (n = 209)	SVM	BAcc: 98% (PD vs. HC)
Brahim et al. (2015)	Voxels in a striatal region	PS (n = 95), controls (n = 94)	SVM	BAcc: 91% (PS vs. controls)
	Voxels in a striatal region followed by PCA		SVM	BAcc: 93% (PS vs. controls)
Huertas-Fernández et al. (2015)	Voxels in a striatal region	PD (n = 164), VP (n = 80)	SVM	BAcc: 88% (PD vs. VP)
			Discriminant analysis	BAcc: 86% (PD vs. VP)
			Logistic regression	BAcc: 84% (PD vs. VP)
Tagare et al. (2017)	Voxels in a striatal region; feature selection was done together with the optimization	PD (n = 448), HC (n = 210)	Logistic regression	BAcc: 97% (PD vs. HC)
Zhang and Kagen (2017))	All voxels	PD (n = 1171), HC (n = 211), SWEDD (n = 131)	ANN	BAcc: 90% (PD vs. HC + SWEDD)

(continued)

Table 25.2 (continued)

Paper	Features and reduction strategy	Groups of subjects or images (total including training and validation)	Type of classifier	Main results
Taylor and Fenner (2017)	All voxels followed by PCA	PPMI dataset: PD (n = 448), HC (n = 209)	SVM	BAcc: 98% (PD vs. HC)
		Local dataset: PD (n = 191), non-PD patients (n = 191)	SVM	BAcc: 91% (PD vs. non-PD)
Choi et al. (2017)	All voxels	PD (n = 431), HC (n = 193)	CNN	BAcc: 97% (PD vs. HC)
Martinez-Murcia et al. (2018)	All voxels	PD (n = 448), HC (n = 194)	CNN	BAcc: 95% (PD vs. HC)
Wenzel et al. (2019)	Voxels of the slices containing the striatum	PPMI dataset: PD (n = 438), HC (n = 207)	CNN	BAcc: 97% (PD vs. HC)
		Local dataset: PS (n = 149), controls (n = 149)	CNN	BAcc: 98% (PS vs. controls)

technique of feature reduction should be used. Singular value decomposition (SVD), principal component analysis (PCA), or partial least squares (PLS) are used in some works. These three techniques are similar; they try to explain a set of variables by a smaller number of variables that explain as much as possible the total variability contained in the original variables. Feature reduction based on independent component analysis (ICA) was also found.

25.6 Classification Methods Combining DaT SPECT and Other Data

The DaT SPECT is a valuable tool to assist on the differential diagnosis of neurodegenerative and non-neurodegenerative Parkinsonism. However, DaT SPECT may not be conclusive regarding the type of neurodegenerative Parkinsonism. In the survey done, two works were found that developed CAD systems using perfusion SPECT as complement to DaT SPECT. They are presented in Table 25.3.

25.7 Discussion and Conclusions

Several CAD strategies and classifiers have been implemented to classify any single DaT SPECT examination. SVM classifiers have been the most frequent choice for hypothesis-driven classification methodologies, giving also the best results.

Table 25.3 Papers found in the literature combining features from DaT SPECT and features from other SPECT scans

Paper	Features and reduction strategy	Groups of subjects or images (total including training and validation)	Type of classifier	Main results
Van Laere et al. (2006))	^{123}I-FP-CIT—striatal uptake indices ^{99m}Tc-Ethylcysteinate dimer SPECT (perfusion imaging)—cortical regions	PD (n = 58), ET (n = 27), MSA (n = 24), PSP (n = 12), DLB (n = 8)	Discriminant analysis	Acc: 98% (PD + MSA + PSP + DLB vs. ET), 82% (PD vs. MSA vs. PSP vs. DLB)
Takaya et al. (2018)	^{123}I-FP-CIT—several brain regions [^{123}I] Iodoamphetamine SPECT (perfusion imaging)—several brain regions	PD (n = 44), DLB (n = 2), PSP (n = 10), CBD (n = 8), MSA (n = 15)	Logistic regression	Acc: 86% (PD + DLB vs. PSP + CBD + MSA), 95% (DLB vs. PSP), 87% (DLB vs. CBD), 80% (DLB vs. MSA), 91% (CBD vs. MSA), 88% (MSA vs. PSP)

Balanced accuracy in the binary classification of PD patients versus HC subjects has reached 98% based on a PPMI cohort.

CAD of different types of neurodegenerative Parkinsonism has also been tested. However, the accuracies are lower, and the inconsistencies among studies are much higher than those found during the distinction between PD patients and HC. This is mainly because the datasets used in these cases are small and the confirmatory clinical diagnosis is harder to find than for the PD patients. Thus, there are no conclusive results.

Based on DaT SPECT, data-driven methods are less frequently used than hypothesis-driven methods. Both of them achieve similar accuracies according to what can be encountered in the published literature. Most of the classifiers here identified as data-driven methods are, in reality, mixed methods, since they assume a priori the striatum to be the relevant area, and for this reason only the voxels inside and in its vicinity are included. Fully data-driven methods have an apparent advantage over the others since feature extraction is already incorporated within themselves. However, if they do not support their classification results with understandable language and characteristics for the physician, their implementation must be considered with extreme caution.

The works found in the literature on CAD systems of DaT SPECT have a fundamental limitation: the gold standard diagnoses are clinical; thus, they are not true gold standard. Besides that, the DaT SPECT has been used to aid the clinical diagnosis. Another issue is related to the definition of the control group. In the papers

based on PPMI database, there is a clear healthy control group. However, in other works, the control group is sometimes made of patients with a visually normal DaT SPECT.

In our survey, we only included works where an independent dataset or cross-validation technique had been used to assess the classification accuracy. However, in most of the selected work, the authors tested different approaches for the feature selection and classification. This increases the risk of obtaining high accuracies by chance.

Some research works reported classification results obtained using simultaneous features extracted from DaT SPECT and clinical or demographic features to build the classifiers. These results were not included because they diverge from the main focus of this work.

Other limitation of the results found in the literature survey is the overlap of datasets used. Most commonly, there is a partial overlap of datasets extracted from PPMI database, but there is also overlap in some non-PPMI-based works. In addition, some PPMI dataset-based works included more than one DaT SPECT of the same patients, in particular follow-up examinations.

Only one work tested the robustness of the CAD systems according to the reconstruction protocols/parameters/algorithms (Wenzel et al. 2019). Authors conclude the CNN classifier is more robust than the SBR optimal cutoff. This result was expected since the SBR optimal cutoff is influenced by the reconstruction protocol. Besides that, in the CNN classifier, authors optimized approximately 2.87 million parameters, which obviously may have more potential to separate two classes than a single uptake index. These issues need to be better addressed in future work; otherwise, each classifier may only be valid for a specific protocol or a specific setting.

Despite all limitations and inconsistencies found in the published works related to CAD of DaT SPECT, there is evidence that CAD can effectively help in the clinics. Irrespective of the author, when comparing the classification accuracy obtained with the CAD systems against the cutoff techniques based on uptake indices, the CAD gave always higher accuracy that is on its own better than the accuracy based on qualitative visual evaluation (Badiavas et al. 2011).

In conclusion, CAD of DaT SPECT has been increasingly used in research. We believe it is now mature enough to be used in clinics as a complement to the visual and quantitative evaluation. It should, at least, serve as quality control and guide for experienced clinicians from now on. In addition, it may also be used to help train less experienced clinicians.

References

Antonini A, Moresco RM, Gobbo C, De Notaris R et al (2001) The status of dopamine nerve terminals in Parkinson's disease and essential tremor: a PET study with the tracer [11-C]FE-CIT. Neurol Sci 22(1):47–48. https://doi.org/10.1007/s100720170040

Appel L, Jonasson M, Danfors T, Nyholm D et al (2015) Use of ^{11}C-PE2I PET in differential diagnosis of Parkinsonian disorders. J Nucl Med 56(2):234–242. https://doi.org/10.2967/jnumed.114.148619

Augimeri A, Cherubini A, Cascini GL, Galea D et al (2016) CADA-computer-aided DaTSCAN analysis. EJNMMI Phys 3(1):4–4. https://doi.org/10.1186/s40658-016-0140-9

Badiavas K, Molyvda E, Iakovou I, Tsolaki M et al (2011) SPECT imaging evaluation in movement disorders: far beyond visual assessment. Eur J Nucl Med Mol Imaging 38(4):764–773. https://doi.org/10.1007/s00259-010-1664-1

Brahim A, Ramírez J, Górriz JM, Khedher L, Salas-Gonzalez D (2015) Comparison between different intensity normalization methods in ^{123}I-ioflupane imaging for the automatic detection of Parkinsonism. PLoS One 10(6):e0130274–e0130274. https://doi.org/10.1371/journal.pone.0130274

Calvini P, Rodriguez G, Inguglia F, Mignone A et al (2007) The basal ganglia matching tools package for striatal uptake semi-quantification: description and validation. Eur J Nucl Med Mol Imaging 34(8):1240–1253. https://doi.org/10.1007/s00259-006-0357-2

Choi H, Ha S, Im HJ, Paek SH, Lee DS (2017) Refining diagnosis of Parkinson's disease with deep learning-based interpretation of dopamine transporter imaging. NeuroImage Clin 16:586–594. https://doi.org/10.1016/j.nicl.2017.09.010

Costa DC, Walker Z, Dizdarevic S, Ionnides C et al (1988) Striatal binding of FP-CIT: a simple method to separate Parkinson's disease patients and normal controls. Paper presented at the Joint Congress of the European Association of Nuclear Medicine and the World Federation of Nuclear Medicine and Biology, Berlin, Germany, 30 Aug to 4 Sep

Darcourt J, Booij J, Tatsch K, Varrone A et al (2010) EANM procedure guidelines for brain neurotransmission SPECT using ^{123}I-labelled dopamine transporter ligands, version 2. Eur J Nucl Med Mol Imaging 37(2):443–450. https://doi.org/10.1007/s00259-009-1267-x

Habraken JBA, Booij J, Slomka P, Sokole EB, Royen EAV (1999) Quantification and visualization of defects of the functional dopaminergic system using an automatic algorithm. J Nucl Med 40:1091–1097

Hamilton D, List A, Butler T, Hogg S, Cawley M (2006) Discrimination between parkinsonian syndrome and essential tremor using artificial neural network classification of quantified DaTSCAN data. Nucl Med Commun 27(12):939–944. https://doi.org/10.1097/01.mnm.0000243369.80765.24

Huertas-Fernández I, García-Gómez FJ, García-Solís D, Benítez-Rivero S et al (2015) Machine learning models for the differential diagnosis of vascular parkinsonism and Parkinson's disease using [^{123}I]FP-CIT SPECT. [journal article]. Eur J Nucl Med Mol Imaging 42(1):112–119. https://doi.org/10.1007/s00259-014-2882-8

Illán IA, Górriz JM, Ramírez J, Segovia F et al (2012) Automatic assistance to Parkinson's disease diagnosis in DaTSCAN SPECT imaging. Med Phys 39(10):5971–5980. https://doi.org/10.1118/1.4742055

Iwabuchi Y, Nakahara T, Kameyama M, Yamada Y et al (2018) Quantitative evaluation of the tracer distribution in dopamine transporter SPECT for objective interpretation. Ann Nucl Med 32(5):363–371. https://doi.org/10.1007/s12149-018-1256-x

Marek K, Jennings D, Lasch S, Siderowf A et al (2011) The Parkinson progression marker initiative (PPMI). Prog Neurobiol 95(4):629–635. https://doi.org/10.1016/j.pneurobio.2011.09.005

Marek K, Chowdhury S, Siderowf A, Lasch S et al (2018) The Parkinson's progression markers initiative (PPMI) – establishing a PD biomarker cohort. Ann Clin Transl Neurol 5(12):1460–1477. https://doi.org/10.1002/acn3.644

Martínez-Murcia FJ, Górriz JM, Ramírez J, Illán IA et al (2014) Automatic detection of Parkinsonism using significance measures and component analysis in DaTSCAN imaging. Neurocomputing 126:58–70. https://doi.org/10.1016/j.neucom.2013.01.054

Martinez-Murcia FJ, Górriz JM, Ramírez J, Ortiz A (2018) Convolutional neural networks for neuroimaging in Parkinson's disease: is preprocessing needed? Int J Neural Syst 28(10):1850035. https://doi.org/10.1142/s0129065718500351

Morton RJ, Guy MJ, Clauss R, Hinton PJ et al (2005) Comparison of different methods of DatSCAN quantification. Nucl Med Commun 26(12):1139–1146

Nicastro N, Wegrzyk J, Preti MG, Fleury V et al (2019) Classification of degenerative parkinsonism subtypes by support-vector-machine analysis and striatal ^{123}I-FP-CIT indices. J Neurol 266(7):1771–1781. https://doi.org/10.1007/s00415-019-09330-z

Oliveira FPM, Castelo-Branco M (2015) Computer-aided diagnosis of Parkinson's disease based on [^{123}I]FP-CIT SPECT binding potential images, using the voxels-as-features approach and support vector machines. J Neural Eng 12(2):026008. https://doi.org/10.1088/1741-2560/12/2/026008

Oliveira FPM, Faria DB, Costa DC, Tavares JMRS (2014) A robust computational solution for automated quantification of a specific binding ratio based on [^{123}I]FP-CIT SPECT images. Q J Nucl Med Mol Imaging 58(1):74–84

Oliveira FPM, Faria DB, Costa DC, Castelo-Branco M, Tavares JMRS (2018) Extraction, selection and comparison of features for an effective automated computer-aided diagnosis of Parkinson's disease based on [^{123}I]FP-CIT SPECT images. Eur J Nucl Med Mol Imaging 45(6):1052–1062. https://doi.org/10.1007/s00259-017-3918-7

Palumbo B, Fravolini ML, Nuvoli S, Spanu A et al (2010) Comparison of two neural network classifiers in the differential diagnosis of essential tremor and Parkinson's disease by ^{123}I-FP-CIT brain SPECT. Eur J Nucl Med Mol Imaging 37(11):2146–2153. https://doi.org/10.1007/s00259-010-1481-6

Palumbo B, Fravolini ML, Buresta T, Pompili F et al (2014) Diagnostic accuracy of Parkinson disease by support vector machine (SVM) analysis of ^{123}I-FP-CIT brain SPECT data: implications of putaminal findings and age. Medicine 93(27):e228–e228. https://doi.org/10.1097/md.0000000000000228

Prashanth R, Roy SD, Mandal PK, Ghosh S (2014) Automatic classification and prediction models for early Parkinson's disease diagnosis from SPECT imaging. Expert Syst Appl 41(7):3333–3342. https://doi.org/10.1016/j.eswa.2013.11.031

Prashanth R, Roy SD, Mandal PK, Ghosh S (2016) High accuracy classification of Parkinson's disease through shape analysis and surface fitting in ^{123}I-Ioflupane SPECT imaging. IEEE J Biomed Health Inform. https://doi.org/10.1109/JBHI.2016.2547901

Rojas A, Górriz JM, Ramírez J, Illán IA et al (2013) Application of empirical mode decomposition (EMD) on DaTSCAN SPECT images to explore Parkinson disease. Expert Syst Appl 40(7):2756–2766. https://doi.org/10.1016/j.eswa.2012.11.017

Segovia F, Górriz JM, Ramírez J, Álvarez I et al (2012) Improved Parkinsonism diagnosis using a partial least squares based approach. Med Phys 39(7):4395–4403. https://doi.org/10.1118/1.4730289

Skanjeti A, Angusti T, Iudicello M, Dazzara F et al (2014) Assessing the accuracy and reproducibility of computer-assisted analysis of ^{123}I-FP-CIT SPECT using BasGan (V2). J Neuroimaging 24(3):257–265. https://doi.org/10.1111/jon.12008

Skanjeti A, Castellano G, Elia BO, Zotta M et al (2015) Multicenter semiquantitative evaluation of ^{123}I-FP-CIT brain SPECT. J Neuroimaging 25(6):1023–1029. https://doi.org/10.1111/jon.12242

Staff R, Ahearn T, Wilson K, Counsell C et al (2009) Shape analysis of ^{123}I-N-omega-fluoropropyl-2-beta-carbomethoxy-3beta-(4-iodophenyl) nortropane single-photon emission computed tomography images in the assessment of patients with parkinsonian syndromes. Nucl Med Commun 30(3):194–201. https://doi.org/10.1097/MNM.0b013e328314b863

Tagare HD, DeLorenzo C, Chelikani S, Saperstein L, Fulbright RK (2017) Voxel-based logistic analysis of PPMI control and Parkinson's disease DaTscans. NeuroImage 152:299–311. https://doi.org/10.1016/j.neuroimage.2017.02.067

Takaya S, Sawamoto N, Okada T, Okubo G et al (2018) Differential diagnosis of parkinsonian syndromes using dopamine transporter and perfusion SPECT. Parkinsonism Relat Disord 47:15–21. https://doi.org/10.1016/j.parkreldis.2017.11.333

Taylor JC, Fenner JW (2017) Comparison of machine learning and semi-quantification algorithms for (I123)FP-CIT classification: the beginning of the end for semi-quantification? EJNMMI Phys 4(1):29. https://doi.org/10.1186/s40658-017-0196-1

Tolosa E, Wenning G, Poewe W (2006) The diagnosis of Parkinson's disease. Lancet Neurol 5:75–86. https://doi.org/10.1016/S1474-4422(05)70285-4

Tossici-Bolt L, Hoffmann SMA, Kemp PM, Mehta RL, Fleming JS (2006) Quantification of [^{123}I]FP-CIT SPECT brain images: an accurate technique for measurement of the specific

binding ratio. Eur J Nucl Med Mol Imaging 33(12):1491–1499. https://doi.org/10.1007/s00259-006-0155-x

Towey DJ, Bain PG, Nijran KS (2011) Automatic classification of ^{123}I-FP-CIT (DaTSCAN) SPECT images. Nucl Med Commun 32(8):699–707. https://doi.org/10.1097/MNM.0b013e328347cd09

Van Laere K, De Ceuninck L, Dom R, Van den Eynden J et al (2004) Dopamine transporter SPECT using fast kinetic ligands: ^{123}I-FP-β-CIT versus ^{99m}Tc-TRODAT-1. Eur J Nucl Med Mol Imaging 31(8):1119–1127. https://doi.org/10.1007/s00259-004-1480-6

Van Laere K, Casteels C, Ceuninck LD, Vanbilloen B et al (2006) Dual-tracer dopamine transporter and perfusion SPECT in differential diagnosis of Parkinsonism using template-based discriminant analysis. J Nucl Med 47(3):384–392

Walker Z, Costa DC, Walker RWH, Shaw K et al (2002) Differentiation of dementia with Lewy bodies from Alzheimer's disease using a dopaminergic presynaptic ligand. J Neurol Neurosurg Psychiatry 73(2):134–140. https://doi.org/10.1136/jnnp.73.2.134

Wenzel M, Milletari F, Krüger J, Lange C et al (2019) Automatic classification of dopamine transporter SPECT: deep convolutional neural networks can be trained to be robust with respect to variable image characteristics. Eur J Nucl Med Mol Imaging. https://doi.org/10.1007/s00259-019-04502-5

Zhang YC, Kagen AC (2017) Machine learning interface for medical image analysis. J Digit Imaging 30(5):615–621. https://doi.org/10.1007/s10278-016-9910-0

PET and SPECT Imaging in Atypical Parkinsonian Syndromes

26

Martin Niethammer, Yoon Young Choi, Chris C. Tang, and David Eidelberg

Contents

26.1 Atypical Parkinsonian Syndromes (APS) 731
26.1.1 Clinical Features 731
26.1.2 Structural Imaging 732
26.2 Functional Imaging 733
26.2.1 Dopaminergic Imaging 733
26.2.2 Perfusion Imaging 736
26.2.3 Metabolic Imaging 737
26.2.4 Microglial Imaging 745
26.3 Future Directions 748
References 749

Abstract

Parkinson's disease and parkinsonian disorders can present with a variety of symptoms, and there is often a significant overlap between the different disorders. Diagnosis typically relies on clinical examination, especially at follow-up visits, which has limitations. Neuroimaging has played a major role in the eluci-

M. Niethammer · D. Eidelberg (✉)
Center for Neurosciences, The Feinstein Institutes for Medical Research, Manhasset, NY, USA

Department of Neurology, North Shore University Hospital, Northwell Health, Manhasset, NY, USA
e-mail: mniethamme@northwell.edu; deidelbe@northwell.edu

Y. Y. Choi · C. C. Tang
Center for Neurosciences, The Feinstein Institutes for Medical Research, Manhasset, NY, USA
e-mail: ychoi3@northwell.edu; ctang@northwell.edu

R. A. J. O. Dierckx et al. (eds.), *PET and SPECT in Neurology*,
https://doi.org/10.1007/978-3-030-53168-3_26

dation of anatomical and functional abnormalities in different parkinsonian disorders. Various imaging techniques have been investigated for their potential to aid in diagnosis during routine clinical practice. In this chapter, we describe the use of functional imaging with PET and SPECT in the research of atypical parkinsonian syndromes (APS), including multiple system atrophy, progressive supranuclear palsy, and corticobasal degeneration. We focus on the utility of these imaging techniques to facilitate differential diagnosis and assess disease progression in patients with APS, especially in the early stages of disease.

Abbreviations

^{11}C-(R)-PK11195	^{11}C(R)-1-(2-Chlorophenyl)-N-methyl-N-(1-methylpropyl)-3-isoquinolinecarboxamide
^{11}C-DPA713	(N,N-Diethyl-2-[2-(4-methoxyphenyl)-5,7-dimethylpyrazolo[1,5-a]pyrimidin-3-yl]acetamide
^{11}C-PBR28	*N*-Acetyl-N-(2-[11C] methoxybenzyl)-2-phenoxy-5-pyridinamine
^{123}I-IBF	^{123}I-Iodolisuride
^{123}I-IBZM	^{123}I-Iodobenzamide
6-OHDA	6-Hydroxydopamine
^{99m}Tc-ECD	Technetium-99m ethyl cysteinate dimer
ADRP	Alzheimer's disease-related pattern
APS	Atypical parkinsonian syndromes
CBD	Corticobasal degeneration
CBDRP	Corticobasal degeneration-related pattern
CIT	Carboxymethyoxy-3-β-(4-iodophenyl) tropane
COX-2	Cyclooxygenase-2
CVLT	California Verbal Learning Test
DAT	Dopamine transporter
DLB	Dementia with Lewy bodies
DWI	Diffusion-weighted imaging
FDG	^{18}F-Fluorodeoxyglucose
FP	Fluoropropyl
HVLT	Hooper Verbal Learning Test
MCI	Mild cognitive impairment
MIBG	Meta-^{123}I-iodobenzylguanidine
MR	Magnetic resonance
MRI	Magnetic resonance imaging
MSA	Multiple system atrophy
MSA-C	Multiple system atrophy—cerebellar
MSA-P	Multiple system atrophy—parkinsonian
MSARP	Multiple system atrophy-related pattern
PAGF	Pure akinesia with gait freezing

PBBS	Peripheral benzodiazepine binding site
PCA	Principal component analysis
PD	Parkinson's disease
PDCP	Parkinson's disease-related cognitive pattern
PDRP	Parkinson's disease-related motor pattern
PDTP	Parkinson's disease tremor-related pattern
PET	Positron emission tomography
PPV	Positive predictive value
PSP	Progressive supranuclear palsy
PSPRP	Progressive supranuclear palsy-related pattern
RVM	Relevance vector machine analysis
SPECT	Single-photon emission computed tomography
TCS	Transcranial sonography
TSPO	Translocator protein 18 kDa
UPDRS	Unified Parkinson's Disease Rating Scale

26.1 Atypical Parkinsonian Syndromes (APS)

26.1.1 Clinical Features

Parkinsonism is characterized clinically by a combination of features that include tremor, bradykinesia, rigidity, and postural instability. Syndromes with parkinsonism can be divided into neurodegenerative (sporadic and hereditary) and secondary parkinsonism. Idiopathic Parkinson's disease (PD) is the most common cause of neurodegenerative parkinsonism. Additionally, multiple system atrophy (MSA), progressive supranuclear palsy (PSP), and corticobasal degeneration (CBD) represent as much as 15% of parkinsonian syndromes seen in specialty practice.

MSA is characterized by a combination of autonomic dysfunction and varying degrees of parkinsonism or cerebellar symptoms (Gilman et al. 2008). Historically, patients with these symptoms were classified as having Shy-Drager syndrome, striatonigral degeneration, or spontaneous olivopontocerebellar atrophy, depending on the predominant symptomatology. Once a common underlying pathology was identified, these syndromes were grouped as MSA and later subdivided by the predominant motor symptoms into cerebellar (MSA-C, 20% of cases) and parkinsonian (MSA-P, 80% of cases) subtypes (Gilman et al. 2008; Papp et al. 1989; Wenning and Stefanova 2009).

Similar to PD, MSA is characterized pathologically by intracytoplasmic α-synuclein inclusions, albeit in oligodendroglia. In contrast, the pathology of both PSP and CBD involves tau filaments. Clinically, PSP is characterized by marked postural instability with early falls, coupled with vertical supranuclear gaze palsy, frontal subcortical dementia, and levodopa unresponsiveness (Williams and Lees 2009). In addition to this constellation of symptoms, termed Richardson's syndrome, clinical variants have recently been identified. These include PSP-parkinsonism,

which includes patients with asymmetric onset, limited response to levodopa, and pure akinesia with gait freezing (PAGF) (Williams et al. 2005, 2007). Asymmetry is the principal feature of CBD, in addition to rigidity, bradykinesia, limb apraxia, and stimulus-induced myoclonus (Litvan et al. 1997; Boeve et al. 2003), though cognitive dysfunction can also predominate early in the disease and may confound the diagnosis (Litvan 2003; Mahapatra et al. 2004; Hu et al. 2009; Boeve 2011).

Diagnosis of these atypical parkinsonian syndromes (APS) and differentiation from PD is made following clinical examination and is based on established consensus criteria (Gilman et al. 2008; Armstrong et al. 2013; Postuma et al. 2015; Hoglinger et al. 2017). Nevertheless, postmortem studies show only 76–80% accuracy in the diagnosis of PD at initial presentation (Hughes et al. 2002; Rizzo et al. 2016). Though this accuracy does increase with longer follow-up and evaluations by movement disorders specialists, it remains under 90% for PD and significantly lower for atypical syndromes (Hughes et al. 2002; Rizzo et al. 2016; Josephs and Dickson 2003).

Thus, one important aim of neuroimaging is to provide increased diagnostic accuracy, which would allow for better selection of appropriate treatments and a more accurate prognosis. Multiple imaging modalities have been investigated in this regard, though the majority of studies to date have utilized patient cohorts with established diagnoses, i.e., later in the disease course.

26.1.2 Structural Imaging

Magnetic resonance imaging (MRI) has been a standard imaging technique in neurology for nearly 30 years. Perhaps the most important role of conventional MRI is the identification of cases of secondary parkinsonism that result from structural lesions, including neoplasms, multiple sclerosis, hydrocephalus, and vascular parkinsonism (Benamer and Grosset 2009; Winikates and Jankovic 1999). The role of conventional MRI in the diagnosis of neurodegenerative parkinsonism continues to evolve. Atrophy in the substantia nigra may be evident, but these findings do not rise to a level of specificity that allows for differentiation of PD from other forms of neurodegeneration or even from healthy controls, especially early in the disease (Linder et al. 2009; Jesse et al. 2012). In patients with MSA, PSP, or CBD, several characteristic findings have been described, though practical application is often hampered by the need for quantitative measurements that are not readily available in clinical practice (Schott et al. 2007; Paviour et al. 2005; Watanabe et al. 2002; Soliveri et al. 1999). Other MR modalities such as morphometric MR, diffusion-weighted imaging (DWI), or MR spectroscopy have shown promise in the differentiation of these parkinsonian syndromes (Minnerop et al. 2007; Seppi and Schocke 2005; Nicoletti et al. 2006; Kanazawa et al. 2004; Quattrone et al. 2008; Paviour et al. 2006, 2007; Albrecht et al. 2017, 2019; Sako et al. 2019). While these measures can distinguish APS and PD, they often are of low sensitivity (Mueller et al. 2018), and most have not been applied prospectively to patients in the early stages of disease (Holtbernd and Eidelberg 2014; Heim et al. 2018).

Transcranial sonography (TCS) is another imaging technique that is widely available and does not require radiotracers. TCS has the potential to aid in the diagnosis of PD and to distinguish APS from PD. Hyperechogenicity is detected in the substantia nigra (SN) in most PD patients (Berg et al. 2001, 2011; Richter et al. 2017), with normal echogenicity being more suggestive of MSA (Behnke et al. 2005; Walter et al. 2007), whereas hyperechogenicity of the lentiform nucleus (LN) is identified in the majority of patients with MSA, PSP, or CBD (Walter et al. 2004, 2003), albeit with low sensitivity or specificity (Gaenslen et al. 2008). Overall, the literature suggests that the diagnostic accuracy of TCS is high for differentiating PD from patients with essential tremor (ET) or APS but relatively low for the different types of APS in early parkinsonian patients (Tao et al. 2019).

26.2 Functional Imaging

Functional imaging techniques with single-photon emission computed tomography (SPECT) and positron emission tomography (PET) use different radioligands or radiotracers to quantitatively measure brain glucose metabolism, blood perfusion, and functional changes in neural pathways in neurodegenerative disorders. PET provides higher resolution than SPECT but at a higher cost. Both SPECT and PET are commonly applied in clinical diagnosis of parkinsonian patients as well as in the study of functional abnormalities in these disorders. These imaging techniques have proven to be particularly useful in investigating the underlying disease processes and improving the diagnostic accuracy for MSA, PSP, and CBD.

26.2.1 Dopaminergic Imaging

Radioligands for SPECT imaging, such as ^{123}I-β-CIT and ^{123}I-FP-CIT, are typically derivatives of cocaine that bind to the dopamine transporter (DAT) for measurement of dopamine reuptake. SPECT imaging with these radiotracers for DAT is used to detect presynaptic neural degeneration. In comparison, SPECT imaging with radiotracers for the dopamine D_2 receptor, such as ^{123}I-iodobenzamide (^{123}I-IBZM) and ^{123}I-iodolisuride (^{123}I-IBF), assesses the density of postsynaptic neuronal loss in the brain, particularly in the basal ganglia where these radiotracers are highly concentrated. Using PET, ^{18}F-DOPA provides measures of dopa-decarboxylase activity and integrity of presynaptic terminals, while ^{11}C-raclopride is used as a postsynaptic dopaminergic radiotracer.

SPECT imaging is a useful method for assessing nigrostriatal degeneration in patients with parkinsonism (Benamer et al. 2003; Marshall et al. 2009). In the striatum of PD patient, there is a marked decrease in DAT binding, which correlates with clinical measures of disease severity (Benamer et al. 2000; Spiegel et al. 2005), as well as an upregulation of postsynaptic D_2 receptors in this region (Ichise et al. 1999). The SPECT technique is particularly sensitive in detecting subtle functional abnormalities in PD, contributing to a better assessment of disease progression and

more accurate diagnosis in early-stage patients (Pirker et al. 2002). SPECT has also proven useful in differentiating PD patients from healthy controls (Eshuis et al. 2006), vascular parkinsonism (Gerschlager et al. 2002), or between early and advanced PD patients (Eshuis et al. 2009).

Likewise, DAT SPECT imaging has proven to be a useful tool to study the progression and differential diagnosis of patients with APS. In a longitudinal ^{123}I-β-CIT SPECT study, baseline striatal binding was found to be less reduced in APS patients (−36% of age-corrected normal values) than in PD patients with short (−42%) or long (−51%) disease duration (Pirker et al. 2002). However, striatal binding declined significantly over time in APS (14.9% per year) at a faster rate than for both short- (7.1% per year) and long-duration (no significant change) PD. These results suggest that striatal ^{123}I-β-CIT binding may be more sensitive in measuring the progression of APS than PD (Pirker et al. 2002). In cases of CBD, initial SPECT imaging may be normal early in the disease, only to become abnormal on follow-up scan, suggesting delayed substantia nigra neuronal loss compared to other APS (Ceravolo et al. 2013; O'Sullivan et al. 2008).

While there is general consensus that presynaptic dopaminergic imaging (SPECT or PET) cannot reliably distinguish between PD and APS or between the different APS (Bajaj et al. 2013; Thobois et al. 2019), regional differences can be seen with DAT imaging. Unlike PD, ^{123}I-β-CIT SPECT studies have further shown reduced and symmetrical DAT binding in the striatum in patients with MSA.

A study comparing 26 MSA patients with 157 PD patients found that there was a substantial reduction of striatal DAT binding in both PD and MSA groups (Varrone et al. 2001). Likewise, studying 51 subjects with PD and 127 with APS, Ko et al. (2017) found significant reductions of putaminal DAT binding in all subjects except those with MSA-C. In all patient groups with the exception of MSA-C and CBD, DAT binding correlated with disease duration and severity measures.

Although the magnitude of DAT loss does differentiate between the MSA and PD, MSA patients may exhibit less asymmetric loss in the striatum relative to the PD patients, thought to be compatible with the less asymmetric symptoms in MSA (Varrone et al. 2001). These findings were substantiated in another ^{123}I-β-CIT SPECT study (Knudsen et al. 2004), in which MSA patients were also found to have less asymmetry in striatal binding than PD patients (with the exception of one MSA patient who had high asymmetry). Furthermore, a 15% hemispheric difference in binding value was suggested as the cutoff for differentiating PD (>15%) from MSA (5–15%), relative to healthy controls (<5%) (Knudsen et al. 2004). Nevertheless, other SPECT studies have reported that the asymmetry in striatal binding was either not significantly different between MSA and PD (Pirker et al. 2000) or even greater in patients with MSA (Perju-Dumbrava et al. 2012). Indeed, Perju-Dumbrava and colleagues found that there was a trend of greater asymmetry of striatal DAT binding in MSA compared with PD. Among the six MSA cases studied, two patients had been misdiagnosed during their lifetime; in particular, one patient with pronounced asymmetry in striatal DAT binding and clear asymmetry of clinical symptoms had been misdiagnosed as CBD. Based on these data and the relatively low accuracy of clinical diagnosis in MSA reported in literature (Hughes et al. 2002), the authors

pointed out that because MSA patients with clear clinical asymmetry were more likely to have been misdiagnosed or excluded from prior imaging studies, the striatal binding asymmetry could have been underestimated for MSA resulting in a possible bias of patient selection. Thus, they concluded that individual MSA and PD patients cannot be differentiated accurately by subregional analysis of striatal DAT binding (Perju-Dumbrava et al. 2012).

DAT reduction has also been observed in the midbrain of MSA patients. In an ^{123}I-β-CIT SPECT study of 15 patients with early-stage MSA, 15 early PD patients, and 13 healthy control subjects, both MSA and PD patients showed significant loss of striatal DAT binding, while only MSA patients had binding loss in the midbrain. More interestingly, binding values in the caudate and midbrain together provided an accurate classification (95.2%) of subjects as MSA, PD, or normal controls. Although it is perhaps more clinically relevant to exclude the normal controls from this discriminant analysis, the data underscore the potential importance of applying midbrain DAT binding to the differential diagnosis of patients with uncertain parkinsonism (Scherfler et al. 2005). Other extrastriatal regions may also prove to be useful in the differential diagnosis of parkinsonism. Employing a region-of-interest (ROI) approach to parkinsonian patients (30 PD, 9 MSA-P, 7 MSA-C, 13 PSP), extrastriatal ^{123}I-FP-CIT SPECT binding ratios in the hypothalamus (presumed to be to serotonin transporters) were found to be significantly lower in PSP than MSA-C subjects (Joling et al. 2017). Furthermore, binding ratios in the caudate nucleus of PSP patients were lower than those of both PD and MSA-C patients, and in the posterior putamen, binding ratios were significantly lower in MSA-P, PSP, and PD than MSA-C patients. Thus, striatal ^{123}I-FP-CIT binding and hypothalamic ^{123}I-FP-CIT binding are significantly lower in MSA-P and PSP than in PD and MSA-C patients and might therefore be of interest for differential diagnosis (Joling et al. 2017).

More recently, Badoud and colleagues applied voxel-wise univariate statistical parametric mapping and multivariate pattern recognition to the DAT scans of 392 consecutive patients with degenerative parkinsonism (Badoud et al. 2016). MSA and PSP showed less tracer uptake in the head of caudate nucleus relative to PD and CBD, and CBD had higher uptake in both putamen relative to PD, MSA, and PSP. Classification was significant for PD versus APS ($p < 0.05$) and between APS subtypes (MSA vs. CBD, $p < 0.05$; MSA vs. PSP, $p < 0.05$; CBD vs. PSP, $p < 0.05$). While both striatal and extrastriatal regions contained classification information, the combination of both regions did not significantly improve classification accuracy (Badoud et al. 2016). Building on this, support-vector-machine analysis applied to DAT scans from 370 patients with degenerative parkinsonism was able to reliably distinguish parkinsonism from controls, as well as between different parkinsonian syndromes with sensitivities and specificities between 60% and 80%, with particularly good separation of CBD from other parkinsonian syndromes (Nicastro et al. 2019).

In general, metabolic imaging has proven to be more useful in the differentiation of APS (see below) than dopaminergic imaging. However, cerebral perfusion and metabolism generally are linked, and early phase dopaminergic imaging does contain information related to perfusion (Koeppe et al. 2005). Using dynamic PET data

acquired during the first 10 minutes after ^{18}F-FP-CIT administration in 67 subjects with parkinsonism (23 PD, 27 MSA-C, 12 MSA-P, 5 PSP), Jin et al. were able to show correlation between the CIT images and FDG PET images from the same subjects (Jin et al. 2017). Visual concordance between the two modalities was high (86.2–93.1% diagnostic), and both MSA subtypes showed different regional uptake patterns compared to PD. Thus, it may be possible to use images acquired in the first 10 minutes of CIT imaging in the differential diagnosis of APS, though this will need to be confirmed in further studies, as well as with ^{123}I-β-CIT SPECT imaging for greater clinical utility.

In addition, SPECT imaging with dopamine D_2 receptor radioligands (e.g., ^{123}I-IBZM) has been used to study postsynaptic cell loss in patients with APS. In contrast to upregulated binding in the striatum of early PD (Kaasinen et al. 2000; Leenders 2003), striatal D_2 binding was found to be markedly reduced in MSA and PSP (Knudsen et al. 2004; Kim et al. 2002) while relatively preserved in CBD (Klaffke et al. 2006; Plotkin et al. 2005). Nonetheless, the role of ^{123}I-IBZM SPECT on differential diagnosis of parkinsonism remains controversial. In a ^{123}I-IBZM SPECT study, Vlaar et al. reported a low accuracy in differentiating between PD and APS (Vlaar et al. 2008). This result is in contrast with another SPECT study suggesting that a combination of ^{123}I-FP-CIT, ^{123}I-IBZM, and meta-^{123}I-iodobenzylguanidine (MIBG) scintigraphy resulted in high accuracy of 94% sensitivity and 94% specificity in differentiating PD from APS (Sudmeyer et al. 2011). More studies are needed to investigate the utility of these imaging tracers in the diagnosis of APS.

26.2.2 Perfusion Imaging

Technetium-99m ethyl cysteinate dimer (^{99m}Tc-ECD) perfusion SPECT has also been used in the differentiation of PD and MSA. One study found that the putamen was the only region where there was a significant difference in uptake between MSA and PD (Bosman et al. 2003). Using the putamen uptake value as the discriminating factor, an accuracy of 83.6% was achieved in classifying MSA patients against a combined group of PD and healthy controls but decreased to 67% in a three-group analysis of MSA, PD, and healthy volunteers. Furthermore, dual-tracer brain SPECT with ^{99m}Tc-ECD/^{123}I-FP-CIT, which allows for simultaneous assessment of blood perfusion and dopamine transporter function in parkinsonian patients, was applied to the differential diagnosis of parkinsonism, allowing for differentiation of PD and MSA, as well as PSP and CBD (El Fakhri et al. 2006; El Fakhri and Ouyang 2011). There was significantly lower perfusion in the striatum in MSA compared to PD, while striatal DAT binding was higher in MSA than PD (El Fakhri et al. 2006). Using statistical parametric mapping in ECD SPECT scans of PD and MSA patients, Van Laere et al. (2004) were able to separate PD from MSA and healthy controls, finding symmetric hypoperfusion in the thalamus and putamen of MSA subjects, whereas PD patients had additional cortical hypoperfusion. In a second study, discriminant analysis revealed that the two imaging measures together

improved the overall classification accuracy to 82.4% in differentiating patients with PD, MSA, PSP, or dementia with Lewy bodies (DLB) over either imaging measure alone (DAT, 58.8%; perfusion, 67.6%) (Van Laere et al. 2006). After excluding PD subjects from the analysis, a striking 100% separation was achieved among MSA, PSP, and DLB (Van Laere et al. 2006). Although these results require rigorous validation in independent patient populations, dual-tracer DAT and perfusion SPECT may be a potentially useful approach for accurate differentiation between the most common APS in clinically uncertain cases.

26.2.3 Metabolic Imaging

26.2.3.1 Metabolic Imaging Networks

Functional imaging with ^{18}F-fluorodeoxyglucose (FDG) positron emission tomography (PET) can be applied to measure glucose utilization of neurons, which in turn provides an estimate of rest-state regional and global metabolism in the brain. Prior PET studies have shown hypometabolism in the striatum and cerebellum with increased metabolism in the frontal cortex in MSA (Eckert et al. 2005), while in PSP, hypometabolism was present in the supplementary motor area (SMA), anterior cingulate, thalamus, and striatum (Eckert et al. 2005; Bartels et al. 2006; Park et al. 2009; Teune et al. 2010). Moreover, regional hypometabolism in the striatum was found to be a common feature in both MSA and PSP (Ghaemi et al. 2002), in contrast to the increased metabolic activity in this region in PD (Bosman et al. 2003; Eckert et al. 2005; Eidelberg et al. 1993). In addition, profound asymmetric hypometabolism in the frontal and parietal areas is a unique feature in CBD (Eckert et al. 2005; Teune et al. 2010).

The use of spatial covariance analysis on FDG PET imaging data has led to the discovery of abnormal brain metabolic networks specifically related to neurodegenerative diseases such as PD and APS (Eckert et al. 2005; Eidelberg 2009; Poston and Eidelberg 2009; Schindlbeck and Eidelberg 2018). The technical details of the spatial covariance analysis (or network analysis) have been previously described in detail (Eidelberg 2009; Spetsieris et al. 2013). Briefly, a multivariate method utilizing principal component analysis (PCA) is employed to analyze voxel-wise metabolic imaging data in FDG PET scans from a combined group of patients and healthy subjects. This approach allows for the identification of spatial covariance patterns of brain regions in which metabolic abnormalities can be quantified as subject scores, used to differentiate between the patient and healthy control groups (Feigin et al. 2007; Habeck et al. 2008; Ma et al. 2007). After a disease-related metabolic pattern is identified in the original derivation cohort, the expression of this pattern (i.e., subject score) can be computed prospectively in individual scans of new subjects. In each individual scan, the subject score of the disease-related pattern can be viewed as a quantitative representation of the whole-brain metabolic abnormality for this subject at the time of imaging. Because of their quantitative nature, subject scores can be used to examine group separation, disease progression,

treatment responses, and even individual correlations of imaging changes with clinical or neuropsychological measures in neurodegenerative disorders.

26.2.3.2 PD-Related Networks

In PD, FDG PET with network analysis has proven useful in identifying abnormal metabolic networks associated with motor and cognitive manifestations in PD. The motor-related pattern, termed PDRP, is characterized by pallido-thalamic metabolic increases and concurrent metabolic decreases in the premotor cortex, supplementary motor area, and parietal association areas (Nicastro et al. 2019; Schindlbeck and Eidelberg 2018; Niethammer et al. 2012).

PDRP has been extensively studied in numerous independent populations around the world. It has proven to be highly reproducible and stable, both at a single imaging center (Ma et al. 2007) and in independent PD populations scanned with different scanners. Indeed, in six independent cohorts, individual PDRP expression was consistently elevated in PD patients compared to healthy controls, when scanned at rest at least 12 hours after their last medication dose (i.e., in the off-state) (Eidelberg 2009; Wu et al. 2013; Holtbernd et al. 2015; Teune et al. 2013; Tripathi et al. 2016).

Individual PDRP expression scores reliably correlate with the Unified Parkinson's Disease Rating Scale (UPDRS) motor ratings (Asanuma et al. 2006; Lozza et al. 2004; Eidelberg et al. 1994, 1995; Niethammer and Eidelberg 2012), and PDRP expression declines (i.e., normalizes) with treatment, either dopaminergic medication or deep brain stimulation (DBS) (Asanuma et al. 2006; Pourfar et al. 2009).

Additional distinct PD-related patterns that correlate with tremor (PDTP; Mure et al. 2011) and cognition (PDCP; Huang et al. 2007) have also been identified. PDTP is characterized by increased metabolic activity of the cerebellum/dentate nucleus and primary motor cortex and, to a lesser degree, the caudate/putamen (Mure et al. 2011). At baseline, PDTP expression was abnormally elevated in PD patients with DBS implanted electrodes. When tremor was effectively improved by stimulation, this led to reductions of PDTP expression.

PDCP is characterized by metabolic reductions in the rostral supplementary motor area (pre-SMA), prefrontal cortex, precuneus, and parietal association regions, with metabolic increases in the cerebellar vermis and dentate nuclei. PDCP expression was correlated with performance on neuropsychological tests of executive functioning, such as the California and Hopkins Verbal Learning Tests (CVLT/HVLT), in the original derivation and in prospective groups of non-demented PD patients with or without mild cognitive impairment (MCI) (Huang et al. 2008). Importantly, PDCP does not simply reflect cognitive decline regardless of the cause and is specific to cognitive dysfunction in PD, as its topography is distinct from the independently characterized Alzheimer's disease-related patterns (ADRP) (Ma et al. 2003; Mattis et al. 2016; Teune et al. 2014).

Compared to PDRP, PDCP is expressed later in the disease course. In a 4-year longitudinal study of early PD patients (Huang et al. 2007; Tang et al. 2010a), both PDRP and PDCP expressions were found to increase with disease progression over time in the whole brain and in the two hemispheres independently, although PDCP expression reached abnormal levels approximately 4 years later than PDRP expression.

26.2.3.3 Networks Related to APS

This network-based approach has also been employed to identify specific disease-related metabolic patterns for MSA, PSP, and CBD. The MSA-related pattern (MSARP) is characterized by metabolic decreases in the putamen and cerebellum (Fig. 26.1a); the PSP-related pattern (PSPRP) is characterized by metabolic reductions in the upper brainstem, medial prefrontal cortex, and medial thalamus (Fig. 26.1b); and the CBD-related pattern (CBDRP) is characterized by bilateral, asymmetric metabolic reductions involving frontal and parietal cortex, thalamus, and caudate nucleus (Fig. 26.1c) (Eckert et al. 2008; Spetsieris et al. 2009; Poston et al. 2012; Ge et al. 2018; Niethammer et al. 2014). In accordance with the clinical picture of these disorders, MSARP and PSPRP were relatively symmetric, while in CDBRP, these pattern-related changes were greater in magnitude in the cerebral hemisphere opposite the more clinically affected body side (reflecting the marked asymmetry seen in CBD (Poston 2010)). CBDRP and PSPRP are not abnormally elevated in MSA patients, whereas the expression of both patterns is abnormally elevated in both PSP and CBD cohorts, and there is overlap (~24%) in the topography of the two patterns (Niethammer et al. 2014). Pathologically, PSP and CBD are distinct, but both diseases are classified as tauopathies (Dickson et al. 2007), suggesting that these patterns capture regional overlap in the pathologies of these diseases. Nevertheless, CBDRP is more asymmetric than PSPRP, a feature that may be helpful in using PSPRP and CBDRP for clinical diagnosis (see Sect. 2.3.4).

MSARP and PSPRP have recently been reproduced and validated in independent cohorts of MSA and PSP patients from the Netherlands (Teune et al. 2013). Like PDRP, the expression of each of these patterns accurately discriminated between patients and healthy controls on an individual basis in the original pattern derivation cohort. These data demonstrated that the atypical parkinsonian syndromes are indeed associated with distinct patterns of abnormal metabolic activity.

Additionally, MSARP, but not PDRP expression, is correlated with clinical severity and disease duration in MSA patients (Fig. 26.2) (Poston et al. 2012). In this study, two MSA patients who were clinically followed for up to 7 years exhibited continuous increases in MSARP expression over time, while their PDRP scores fluctuated within the normal range over the same time period (Poston et al. 2012). Clinically, MSA is further subdivided into cerebellar (MSA-C) and parkinsonian (MSA-P) subtypes. Remarkably, while patients in the two subgroups displayed some difference in regional metabolism, MSARP elevations were remarkably similar. Thus, these covariance networks provide descriptors based on underlying disease pathology rather than specific clinical features (Poston et al. 2012).

Moreover, the correlation between MSARP scores and disease duration suggests that these metabolic networks may also be used as potential imaging biomarkers for disease progression in APS (Poston et al. 2012). Although this potential association between pattern expression and disease progression needs to be further examined in prospective longitudinal studies of larger populations, especially for early-stage patients, the present findings suggest that the MSARP could be a sensitive biomarker for disease severity and progression in patients with MSA. Likewise, the investigation of progressive changes of metabolic networks in other parkinsonian syndromes will need to be the focus of future PET studies.

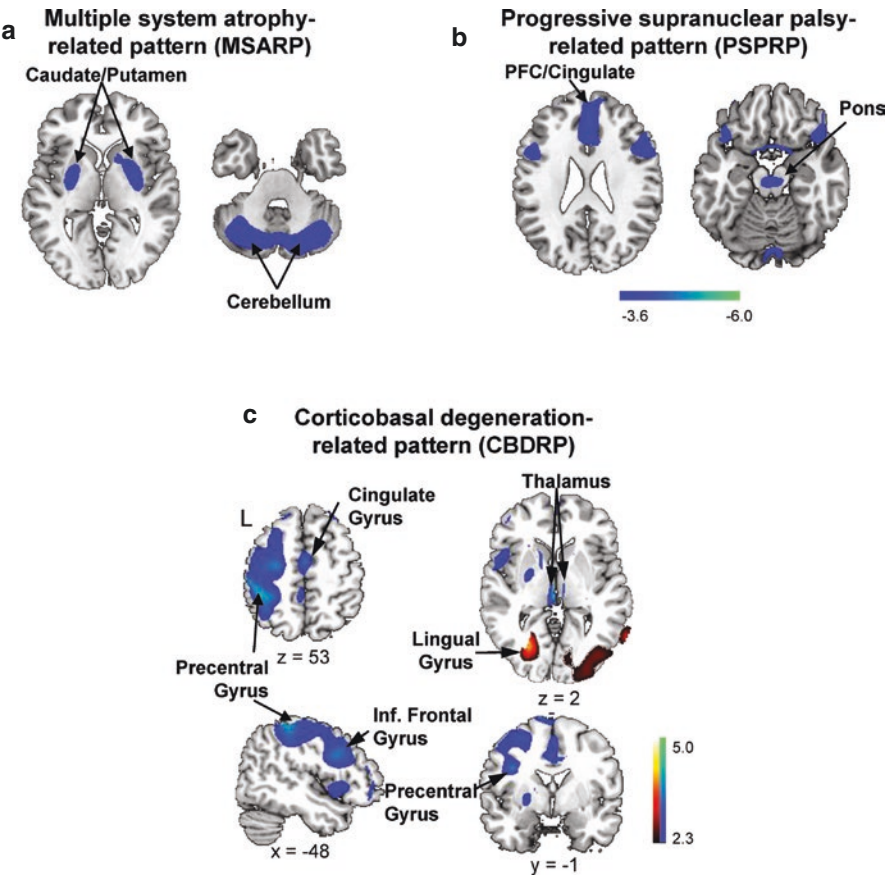

Fig. 26.1 Abnormal networks in atypical parkinsonian disorders. (**a**) Multiple system atrophy-related metabolic pattern (MSARP) identified by spatial covariance analysis of FDG PET scans from ten MSA patients and ten healthy volunteer subjects (Eckert et al. 2008; Poston et al. 2012). (Adapted from *Mov Disord*, 23, Eckert T, Tang C, Ma Y, Brown N, Lin T, Frucht S, Feigin A, Eidelberg D, Abnormal metabolic networks in atypical parkinsonism, pp. 727–733, Copyright (2008), with permission from John Wiley and Sons.) (**b**) Progressive supranuclear palsy-related metabolic pattern (PSPRP) identified by spatial covariance analysis of FDG PET scans from ten PSP patients and ten healthy volunteer subjects (Eckert et al. 2008). (Adapted from *Mov Disord*, 23, Eckert T, Tang C, Ma Y, Brown N, Lin T, Frucht S, Feigin A, Eidelberg D, Abnormal metabolic networks in atypical parkinsonism, pp. 727–733, Copyright (2008), with permission from John Wiley and Sons.) (**c**) Corticobasal degeneration-related pattern (CBDRP) identified by spatial covariance analysis of FDG PET scans from a derivation cohort of ten patients with CBD and ten healthy volunteer subjects scanned at the North Shore University Hospital (eight CBD and ten control subjects) and Stanford University (two CBD subjects) (Niethammer et al. 2014). (Displays of the MSARP and PSPRP covariance maps are thresholded at $Z = 3.61$, $p < 0.001$, and overlaid on T1-weighted magnetic resonance template images. The display of CBDRP represents regions that contributed significantly to the network thresholded at $Z = 2.33$ ($p < 0.01$). Voxels with positive region weights (metabolic increases) are color-coded red, and those with negative region weights (metabolic decreases) are color-coded blue. Left hemisphere is labeled as "L.") (From Niethammer M, Tang CC, Feigin A, Allen PJ, Heinen L, Hellwig S, Amtage F, Hanspal E, Vonsattel JP, Poston KL, Meyer PT, Leenders KL, Eidelberg D, A disease-specific metabolic brain network associated with corticobasal degeneration, *Brain*, 2014, 137, pp. 3036–46, by permission of Oxford University Press.)

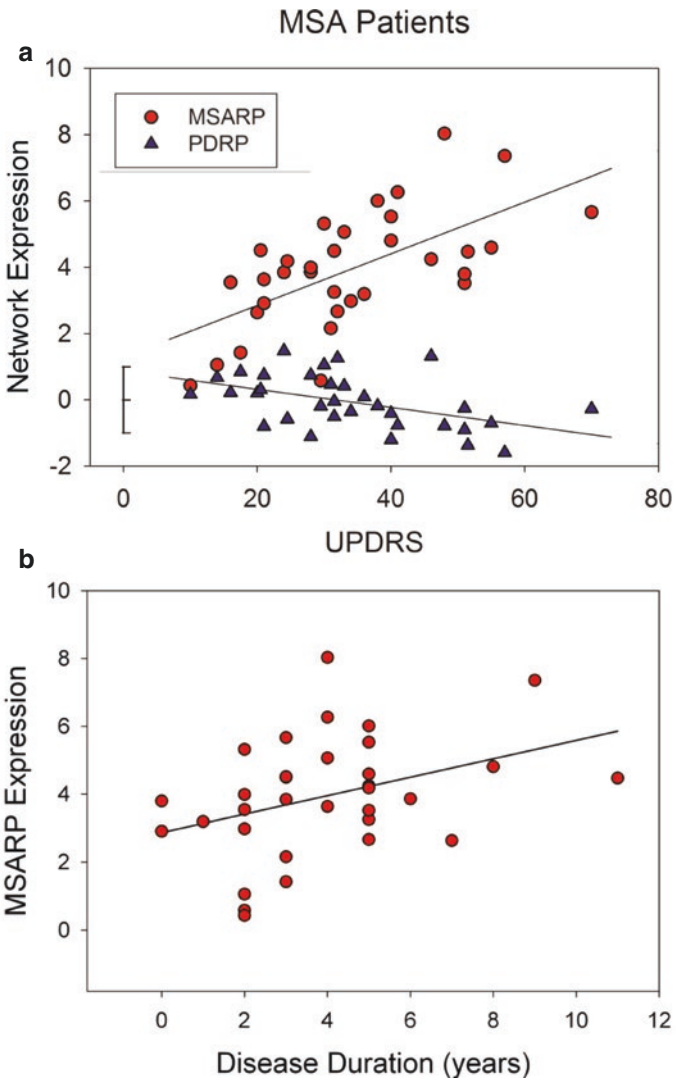

Fig. 26.2 MSARP expression correlates with disease severity and duration. (**a**) In MSA patients, increased MSARP expression (*red circles*) correlated with greater clinical disability as measured by increased Unified Parkinson's Disease Rating Scale (UPDRS) motor ratings (r = 0.57, $p < 0.001$). In contrast, increased motor disability in these subjects was associated with lower PDRP expression values (*blue triangles*; $r = 0.53$, $p < 0.002$). (**b**) In the MSA patients, there was a linear correlation between MSARP expression and symptom duration (r = 0.38, p = 0.03). (Reprinted with permission from Poston KL, Tang CC, Eckert T, Dhawan V, Frucht S, Vonsattel JP, Fahn S, Eidelberg D, Network correlates of disease severity in multiple system atrophy, *Neurology*, 2012, 78, pp.1237–1244.)

Potentially, metabolic networks may also be of use in the premotor stages of parkinsonian disorders. While REM sleep behavior disorder (RBD) can occur in isolation, many individuals develop a neurodegenerative syndrome within 5 years of diagnosis, and it is considered a strong risk factor for the future development of PD (Berg et al. 2015; Postuma et al. 2012). Most often, phenoconversion is a manifestation of underlying synuclein pathology as seen in idiopathic PD, DLB, and MSA (Boeve 2010). Indeed, PDRP expression is elevated in many RBD patients. However, in a longitudinal study of RBD subjects, those with low PDRP scores appeared more likely to phenoconvert to MSA, though this finding will need to be confirmed in larger cohorts and with inclusion of MSARP (Holtbernd et al. 2014).

26.2.3.4 Differential Diagnosis

As mentioned above, the diagnosis of PD and parkinsonian disorders can be challenging, especially early in the disease course. This uncertainty necessitates better diagnostic criteria, especially in the clinical trial setting when participant numbers may be small or subjects early in the diseases are being enrolled. In addition to providing unique information on disease progression, metabolic imaging and network analysis may be valuable in facilitating differential diagnosis in patients with APS.

Visual inspection of FDG PET images, aided by standard templates based on statistical parametric mapping, has typically been used to facilitate clinical diagnosis in patients with parkinsonism (Eckert et al. 2005) and is superior to DAT imaging, though the two measures may provide complementary information (Ko et al. 2017). In a study of 78 patients with APS, the area under the receiver-operating-characteristic (ROC) curve for discrimination between APS and Lewy body disease (PD and DLB) was significantly larger for FDG PET (0.94) than for IBZM SPECT (0.74; $p < 0.001$), with a sensitivity and specificity of 86% and 91%, respectively, for diagnosing APS with FDG PET (Hellwig et al. 2012). However, this approach may be difficult to scale due to the need for trained readers and does not yield quantifiable measures.

To automate the differential diagnosis procedure, a computerized algorithm was developed based on network analysis of FDG PET scans of 167 patients with uncertain parkinsonism who were referred for PET (Tang et al. 2010b). These patients were then followed by movement disorders specialists for over 2 years to obtain a final clinical diagnosis. For each patient, subject scores of different metabolic patterns related to PD, MSA, and PSP were computed and used to calculate the probability of each disease. The algorithm is a fully automated two-level classification procedure. At the first level, a logistic regression model was utilized to discriminate between the PD group and a combined group of MSA and PSP patients and to compute the probabilities of having PD and APS for each subject. At the second level, logistic regression analysis was also used to further discriminate MSA and PSP patients by computing the probabilities of these two diseases for each subject. At both levels, image-based classification was determined for individual patients based on each subject's disease probabilities with reference to the diagnostic criteria that were established from the ROC curve analysis of the probabilities of all subjects.

Finally, the image-based classifications of individual patients were compared to their follow-up clinical diagnosis. It was found that the image-based algorithm achieved highly accurate classification results (91–98% positive predictive value (PPV), 94–96% specificity, and 84–88% of sensitivity) for differential diagnosis of PD, MSA, and PSP. In addition, the classification results remained accurate in a subset of early patients with very short symptom durations (i.e., <2 years) at the time of PET as well as in a small subgroup of subjects whose clinical diagnoses were confirmed at autopsy.

This approach was recently validated in an independent cohort of 129 parkinsonian patients with uncertain diagnosis (Fig. 26.3) (Tripathi et al. 2016, 2012). Of

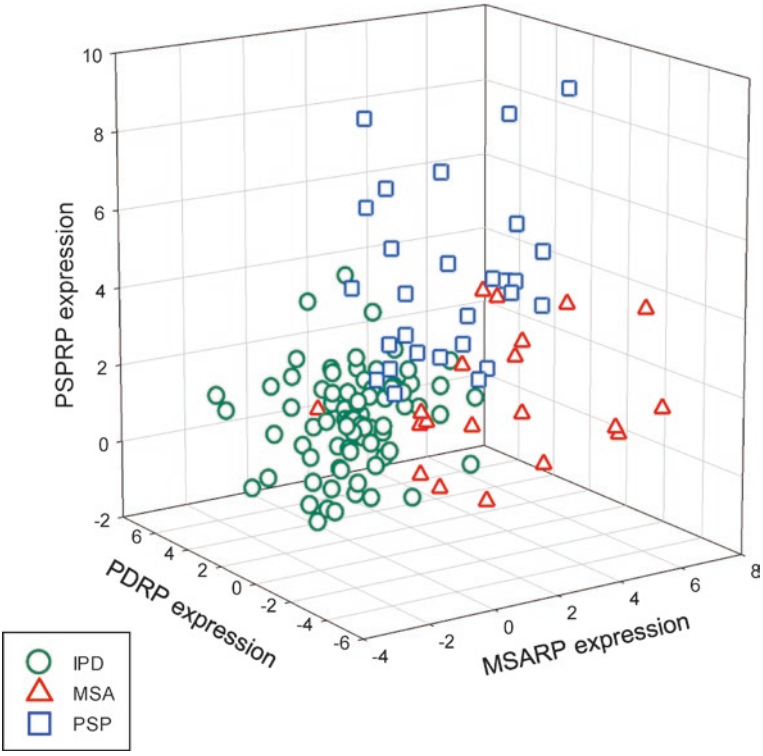

Fig. 26.3 Using network analysis for differential diagnosis. Three-dimensional plot of pattern expression. Expression values for PDRP (*x*-axis), MSARP (*y*-axis), and PSPRP (*z*-axis) topographies are shown for Indian validation cohort (Tripathi et al. 2016). This group comprised 129 parkinsonian patients with uncertain clinical diagnosis. On the basis of serial clinical examinations by movement disorders specialists blind to scan data, 81 of these subjects were subsequently diagnosed with idiopathic PD (IPD) and 48 subjects with APS (20 with MSA and 28 with PSP). Pattern expression values were computed in FDG PET scans from these subjects acquired 2.2 ± 0.4 years (mean ± SD) before final clinical diagnosis. (Reprinted from Tripathi M, Tang CC, Feigin A, De Lucia I, Nazem A, Dhawan V, Eidelberg D, Automated differential diagnosis of early parkinsonism using metabolic brain networks: A validation study, *J Nucl Med*, 2016, 57, pp. 60–66.)

these patients, 60% had disease duration of under 2 years. Nevertheless, idiopathic PD subjects were distinguished from APS with 94% specificity and 96% PPV. The algorithm achieved 90% specificity and 85% PPV for MSA and 94% specificity and 94% PPV for PSP. Diagnostic accuracy was similarly high (specificity and PPV > 90%) for parkinsonian subjects with short symptom duration, underlining the possible utility of this approach early in the disease course.

It is worthwhile to point out that in the study by Tang et al. (2010b), a small proportion (14%) of subjects could not be definitively classified as having either PD or APS and were classified into an indeterminate parkinsonism category. These indeterminate cases may not have developed sufficient metabolic abnormalities at the time of PET, thus requiring clinical follow-up to reach a definitive diagnosis, or they may have had other atypical parkinsonian syndromes such as CBD. Indeed, based on a small study, a similar approach can be used to distinguish patients with CBD from those with other APS (Niethammer et al. 2014). However, an additional step was required in this case. While increased PDRP and MSARP values are seen predominantly in their respective diseases, CBDRP and PSPRP are both abnormally elevated in both CBD and PSP cohorts (Ko et al. 2017; Niethammer et al. 2014). In order to differentiate the two diseases, the algorithm used expression of PSPRP, as well as an index of asymmetry in CBDRP expression. Of note, preliminary results did not find elevated CBDRP expression in patients with AD, which has a different tau pathology. To date, CBDRP has not been incorporated into the larger algorithm for PD and APS, and it is not clear which (if any) pattern would be elevated in patients with pathologically proven CBD who have a different clinical syndrome in life (Litvan et al. 1997; Hu et al. 2009; Boeve 2011; Hassan et al. 2011). Though these preliminary results are promising, this pattern was derived from a small group of patients and has not been validated in independent patient cohorts. Nonetheless, once a specific network for CBD is confirmed, it can be incorporated into the present automated algorithm for differential diagnosis of this disease.

Other automated methods for the differential diagnosis of PD and APS have been reported, such as relevance vector machine analysis (RVM) (Garraux et al. 2013) and decision trees applied to covariance patterns (Mudali et al. 2015), with promising results (Fig. 26.4). Using RVM on 120 FDG PET scans from patients with parkinsonism (42 PD, 31 MSA, 26 PSP, 21 CBD), classification sensitivity, specificity, and positive and negative predictive values for PD were 93%, 83%, 75%, and 96%, respectively, for distinguishing PD from APS (Garraux et al. 2013). Multiclass RVM achieved 45%, 55%, and 62% classification accuracy for, MSA, PSP, and CBS, respectively. The decision tree method employed by Mudali et al. on FDG PET scans from parkinsonian patients (20 PD, 21 MSA, 17 PSP) and 18 healthy controls was able to separate MSA and PSP relatively well from healthy controls, but PD less well from healthy controls (Mudali et al. 2015). Differentiation between the different parkinsonian syndromes was promising, but larger subject numbers are needed to further refine this approach. Likewise, prospective validation studies, preferably comparing multiple methods in larger cohorts, will be needed before the relative utility of these methods can be determined.

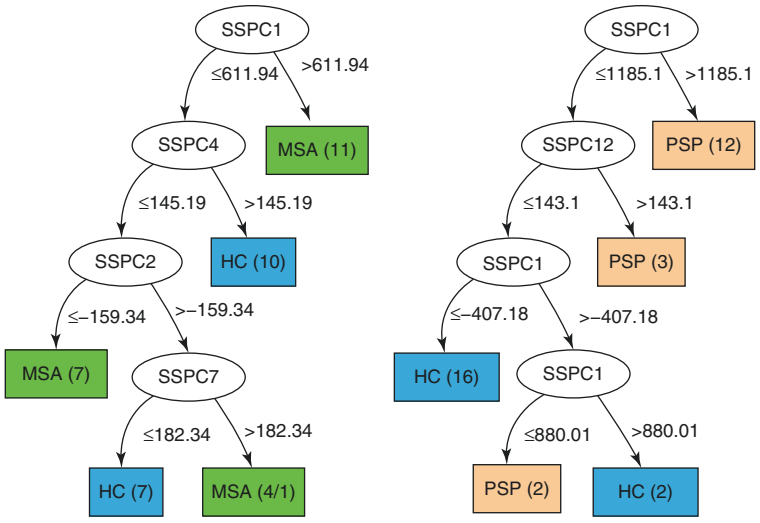

Fig. 26.4 Classification of APS using decision tree analysis. Example of discrimination tree applied to FDG PET scan between MSA subjects ($n = 21$) and healthy controls (HC, $n = 18$) (*left*) and between PSP ($n = 17$) and HC ($n = 18$) (*right*) (Mudali et al. 2015). The subject scores derived from 38 principal components are the attributes on which decisions are made and are represented as oval-shaped nodes in the tree. The threshold values used to split the dataset are shown next to the arrows. The leaf nodes are represented as rectangles and show the final class or decision made at that level of the tree. The numbers in the rectangles show the total number of cases classified at that leaf. Additionally, the number after the slash (if present) represents the number of misclassified cases at that leaf. (Reprinted from Mudali M, Teune LK, Renken RJ, Leenders KL, Roerdink JBTM, Classification of parkinsonian syndromes from FDG-PET brain data using decision trees with SSM/PCA features, *Comput Math Methods Med*, 2015, 136921.)

These data have demonstrated that the imaging classification approach based on disease-related metabolic networks can assist in accurate differential diagnosis for parkinsonian patients several years before a final diagnosis is made. Before its application to clinical cases, the automated differential diagnosis algorithm needs to be prospectively tested in independent patient populations with rigorously ascertained follow-up diagnosis in multicenter longitudinal studies. The algorithm may also prove useful as a screening test for the recruitment of participants in clinical trials for APS. The identification of misdiagnosed subjects and even "indeterminate" cases before enrollment provides a distinct advantage of the image-based classification procedure for identifying appropriate candidates in clinical studies.

26.2.4 Microglial Imaging

Neuropathological studies have demonstrated that neuroinflammation associated with increased microglial activation is present in PD (Imamura et al. 2003, 2005), MSA (Ishizawa et al. 2004), and PSP and CBD (Ishizawa and Dickson 2001),

suggesting that activated microglia play a role in the pathogenesis of these neurodegenerative disorders. ^{11}C-(R)-PK11195 is a specific ligand for the mitochondrial translocator protein 18 kDa (TSPO, previously also known as the peripheral benzodiazepine binding site, PBBS) which is highly expressed in activated microglial cells (Papadopoulos et al. 2006). While specific for TSPO, ^{11}C-(R)-PK11195 exhibits low signal-to-noise ratio; accordingly, several newer TSPO radioligands with improved signal have been developed, including ^{11}C-PBR28, ^{11}C-DPA713, ^{18}F-FEPPA, and ^{11}C-DAA1106 (Venneti et al. 2006; Varnas et al. 2019). The majority of TSPO imaging studies have been performed in PD patients, though ^{11}C-(R)-PK11195 has been utilized to investigate microglial activation in APS.

In a 6-hydroxydopamine (6-OHDA)-induced PD rat model, increased ^{11}C-(R)-PK11195 binding was found in the substantia nigra and striatum, indicating marked microglial activation in these areas, further confirmed by postmortem immunohistochemical evidence of regional neuroinflammatory responses (Cicchetti et al. 2002). PD patients with established diagnosis also exhibited significantly increased ^{11}C-(R)-PK11195 binding in the basal ganglia, as well as in the pons and frontal/temporal cortical regions. The binding levels, however, were not correlated with clinical severity and remain stable over time (Gerhard et al. 2006a). Using a second-generation TSPO radioligand, ^{11}C-PBR28, Real and colleagues reported increased tracer uptake in the striatum 10 days after 6-OHDA injection, though this increase reversed by 30 days, perhaps suggesting that the microglial activation is an acute process accompanying nigral neurodegeneration (Real et al. 2019). In early drug-naïve PD patients, microglial activation in the midbrain has been found to be correlated with clinical severity and dopamine loss in the putamen (Ouchi et al. 2005). Likewise, in PD patients with and without dementia, ^{11}C-(R)-PK11195 binding correlates with lower cognitive scores and cortical metabolism (Edison et al. 2013; Fan et al. 2015).

It has been postulated that neuroinflammation with microglial activation contributes to the early neurodegenerative process of the disease and that, theoretically, early treatment with anti-inflammatory or neuroprotective drugs may be beneficial to patients with PD (Bartels and Leenders 2007). This hypothesis was explored in a small pilot study of ^{11}C-(R)-PK11195 PET imaging in five PD patients treated with celecoxib—a cyclooxygenase-2 (COX-2) inhibitor (Bartels et al. 2010). COX-2 inhibition did not result in significant posttreatment changes in the putamen and midbrain binding levels in this small sample, suggesting that the neuroinflammation is likely to be a persistent neuropathological process in PD that is not easily altered by the conventional anti-inflammatory therapy.

However, at least one study with ^{11}C-PBR28 of 16 PD patients could not demonstrate increased TSPO binding or any relationship between TSPO binding and DAT binding (Varnas et al. 2019). Indeed, studies with both ^{11}C-PBR28 and ^{18}F-FEPPA suggest that TSPO polymorphisms strongly influence ligand binding, which may affect the utility of these tracers as biomarkers in PD and parkinsonism (Ghadery et al. 2017; Koshimori et al. 2015; Owen et al. 2012; Mizrahi et al. 2012).

Only a small number of studies have focused on investigating neuroinflammatory changes with ^{11}C-(R)-PK11195 PET in APS patients. In MSA, compared to healthy controls, increased binding has been found in the substantia nigra, putamen, pallidum, pons, and dorsolateral prefrontal cortex in one study (Gerhard et al. 2003), with another reporting widespread increased binding in the caudate nucleus, putamen, pallidum, precentral gyrus, orbitofrontal cortex, pre-subgenual anterior cingulate cortex, and the superior parietal gyrus (Fig. 26.5) (Kubler et al. 2019). However, this increased binding did not correlate with clinical measures such as age, disease duration, motor scores, and Schwab and England Scale (Kubler et al. 2019). In a clinical trial on MSA patients treated with minocycline, a second-generation tetracycline that has anti-inflammatory effects, two of the three patients scanned with ^{11}C-(R)-PK11195 PET showed decreased binding at 24 weeks after the treatment, in contrast to a longitudinal increase in binding in the placebo group (Dodel et al. 2010).

Increased binding and microglial activation was also evident in the basal ganglia and cortical/subcortical regions in patients with PSP (Gerhard et al. 2006b) or CBD

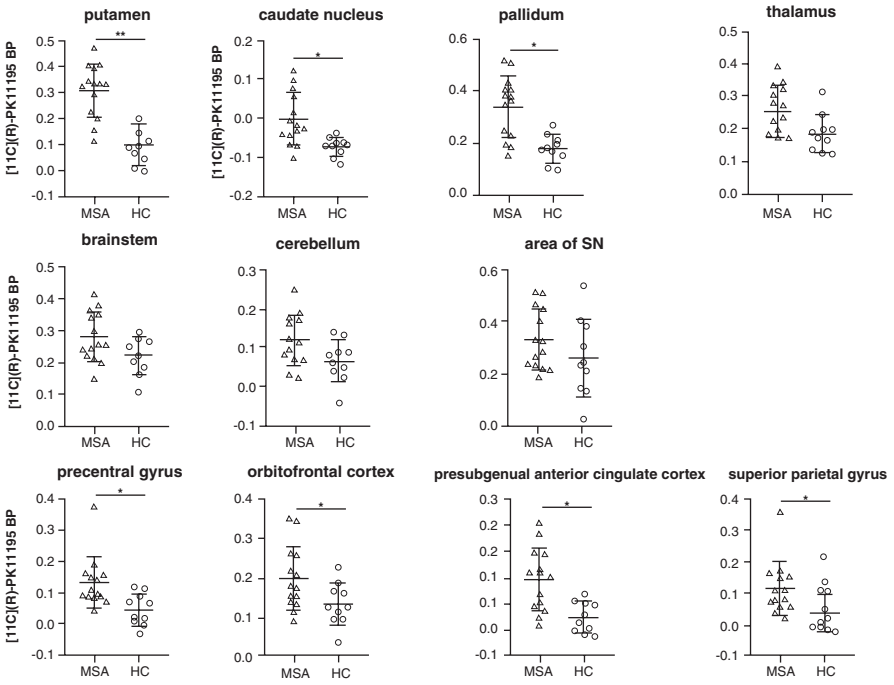

Fig. 26.5 Microglial activation in multiple system atrophy. Comparison of ^{11}C-(R)-PK11195 binding potential (BP) values of MSA patients (n = 14) and healthy controls (HC, n = 10) in selected volumes of interest (VOI) (Kubler et al. 2019). Horizontal bars indicate mean and standard deviation. *$p < 0.01$, **$p \leq 0.001$ (Reprinted from Kubler D, Wachter T, Cabanel N, Su Z, Turkheimer FE, Dodel R, Brooks DJ, Oertel WH, Gerhard A, Widespread microglial activation in multiple system atrophy, *Mov Disord*, 2019, 34, pp. 564–568.)

(Gerhard et al. 2004; Henkel et al. 2004), in accordance with the neuropathological changes in these disorders. In a study of patients with Alzheimer's disease (AD) or PSP, Passamonti et al. found increased ^{11}C-(R)-PK11195 binding in the medial temporal lobe and occipital, temporal, and parietal cortices in AD patients, relative both to patients with PSP and to controls (Passamonti et al. 2018). In PSP patients, compared to controls, there was elevated ^{11}C-(R)-PK11195 binding in the thalamus, putamen, and pallidum. ^{11}C-(R)-PK11195 binding in the cuneus/precuneus correlated with episodic memory impairment in AD, while ^{11}C-(R)-PK11195 binding in the pallidum, midbrain, and pons correlated with disease severity in PSP.

Kobylecki and colleagues studied the relation between microglial activation (measured by ^{11}C-(R)-PK11195 binding) and regional microstructural changes (measured by regional apparent diffusion coefficient, rADC) in patients with PD or APS (MSA and PSP) (Kobylecki et al. 2013). In APS, ^{11}C-(R)-PK11195 binding correlated with rADC in the pons, but not the basal ganglia, suggesting the microglial activation does not contribute to microstructural damage in all regions.

These findings, though based on studies of small patient cohorts, support the notion that neuroinflammation and associated microglial activation contribute to the pathogenesis of APS, regardless of the underlying pathology. Large-scale studies on APS patients and healthy controls are needed to confirm these results and, importantly, examine the relationship between changes in microglial activation and disease progression. Whether anti-inflammatory therapy is an effective strategy for APS is also a topic of further investigation.

26.3 Future Directions

In this chapter, we have briefly reviewed recent advances in SPECT and PET imaging in the study of the progression and differential diagnosis of APS. We discussed the use of various presynaptic and postsynaptic radioligands with SPECT in the research of MSA, PSP, and CBD, as well as the latest FDG PET findings of brain metabolic networks associated with these disorders. A distinct advantage of network analysis over conventional imaging analytical techniques, such as group-mean-based statistical parametric mapping analysis, is its prospective application on individual subjects. That is, once a disease-specific pattern has been identified and validated, the expression of this pattern in a given subject can be computed prospectively from that individual's scan. The resulting pattern expression values for individual subjects can be used to discriminate between groups, assess the progression of the disease, or correlate with other measures/biomarkers in cross-sectional or longitudinal datasets (Eidelberg 2009; Schindlbeck and Eidelberg 2018).

Although the disease-specific patterns identified were derived originally from FDG PET scans using spatial covariance analysis, the application of these patterns is not limited to metabolic imaging. Eckert et al. have demonstrated that the expression of the disease-related metabolic pattern (i.e., PDRP) derived from FDG PET scans can be quantified prospectively in ECD SPECT or early phase CIT SPECT images (Jin et al. 2017; Eckert et al. 2007). This proof-of-principle study indicates

that network analysis can be applied to SPECT scans of parkinsonian patients and that the disease-related brain networks represent the underlying pathology of respective disorders rather than the imaging modality per se. Thus, it is conceivable that spatial covariance analysis may be utilized in future SPECT imaging studies to identify abnormal functional networks specific to each parkinsonian disorder.

For differential diagnosis of APS, we focused on the development and application of an automated algorithm integrating multiple disease-related networks for accurate classification of individual patients with PD, MSA, or PSP at early disease stages when the clinical diagnosis is still uncertain. This algorithm for differential diagnosis can be further developed to include other less common APS, such as CBD, after the disease-related patterns for these disorders are validated. Needless to say, this method may have a profound impact on the research of parkinsonism as it can be used as an objective screening tool that, in addition to improving clinical diagnosis, can identify ideal candidates in clinical trials of APS. It may also help general neurologists and even the specialists to achieve higher accuracy in recognizing and diagnosing APS in routine clinical practice.

References

Albrecht F, Bisenius S, Morales Schaack R, Neumann J, Schroeter ML (2017) Disentangling the neural correlates of corticobasal syndrome and corticobasal degeneration with systematic and quantitative ALE meta-analyses. NPJ Parkinsons Dis 3:12

Albrecht F, Bisenius S, Neumann J, Whitwell J, Schroeter ML (2019) Atrophy in midbrain & cerebral/cerebellar pedunculi is characteristic for progressive supranuclear palsy – a double-validation whole-brain meta-analysis. Neuroimage Clin 22:101722

Armstrong MJ, Litvan I, Lang AE, Bak TH, Bhatia KP, Borroni B et al (2013) Criteria for the diagnosis of corticobasal degeneration. Neurology 80(5):496–503

Asanuma K, Tang C, Ma Y, Dhawan V, Mattis P, Edwards C et al (2006) Network modulation in the treatment of Parkinson's disease. Brain 129(Pt 10):2667–2678

Badoud S, Van De Ville D, Nicastro N, Garibotto V, Burkhard PR, Haller S (2016) Discriminating among degenerative parkinsonisms using advanced (123)I-ioflupane SPECT analyses. Neuroimage Clin 12:234–240

Bajaj N, Hauser RA, Grachev ID (2013) Clinical utility of dopamine transporter single photon emission CT (DaT-SPECT) with (123I) ioflupane in diagnosis of parkinsonian syndromes. J Neurol Neurosurg Psychiatry 84(11):1288–1295

Bartels AL, Leenders KL (2007) Neuroinflammation in the pathophysiology of Parkinson's disease: evidence from animal models to human in vivo studies with [11C]-PK11195 PET. Mov Disord 22(13):1852–1856

Bartels AL, de Jong BM, Giladi N, Schaafsma JD, Maguire RP, Veenma L et al (2006) Striatal dopa and glucose metabolism in PD patients with freezing of gait. Mov Disord 21(9):1326–1332

Bartels AL, Willemsen AT, Doorduin J, de Vries EF, Dierckx RA, Leenders KL (2010) [11C]-PK11195 PET: quantification of neuroinflammation and a monitor of anti-inflammatory treatment in Parkinson's disease? Parkinsonism Relat Disord 16(1):57–59

Behnke S, Berg D, Naumann M, Becker G (2005) Differentiation of Parkinson's disease and atypical parkinsonian syndromes by transcranial ultrasound. J Neurol Neurosurg Psychiatry 76(3):423–425

Benamer H, Grosset D (2009) Vascular parkinsonism: a clinical review. Eur Neurol 61(1):11–15

Benamer HT, Patterson J, Wyper DJ, Hadley DM, Macphee GJ, Grosset DG (2000) Correlation of Parkinson's disease severity and duration with 123I-FP-CIT SPECT striatal uptake. Mov Disord 15(4):692–698

Benamer HT, Oertel WH, Patterson J, Hadley DM, Pogarell O, Hoffken H et al (2003) Prospective study of presynaptic dopaminergic imaging in patients with mild parkinsonism and tremor disorders: part 1. Baseline and 3-month observations. Mov Disord 18(9):977–984

Berg D, Siefker C, Becker G (2001) Echogenicity of the substantia nigra in Parkinson's disease and its relation to clinical findings. J Neurol 248(8):684–689

Berg D, Seppi K, Behnke S, Liepelt I, Schweitzer K, Stockner H et al (2011) Enlarged substantia nigra hyperechogenicity and risk for Parkinson disease: a 37-month 3-center study of 1847 older persons. Arch Neurol 68(7):932–937

Berg D, Postuma RB, Adler CH, Bloem BR, Chan P, Dubois B et al (2015) MDS research criteria for prodromal Parkinson's disease. Mov Disord 30(12):1600–1611

Boeve BF (2010) REM sleep behavior disorder: updated review of the core features, the REM sleep behavior disorder-neurodegenerative disease association, evolving concepts, controversies, and future directions. Ann N Y Acad Sci 1184:15–54

Boeve BF (2011) The multiple phenotypes of corticobasal syndrome and corticobasal degeneration: implications for further study. J Mol Neurosci 45(3):350–353

Boeve BF, Lang AE, Litvan I (2003) Corticobasal degeneration and its relationship to progressive supranuclear palsy and frontotemporal dementia. Ann Neurol 54(Suppl 5):S15–S19

Bosman T, Van Laere K, Santens P (2003) Anatomically standardised 99mTc-ECD brain perfusion SPET allows accurate differentiation between healthy volunteers, multiple system atrophy and idiopathic Parkinson's disease. Eur J Nucl Med Mol Imaging 30(1):16–24

Ceravolo R, Rossi C, Cilia R, Tognoni G, Antonini A, Volterrani D et al (2013) Evidence of delayed nigrostriatal dysfunction in corticobasal syndrome: a SPECT follow-up study. Parkinsonism Relat Disord 19(5):557–559

Cicchetti F, Brownell AL, Williams K, Chen YI, Livni E, Isacson O (2002) Neuroinflammation of the nigrostriatal pathway during progressive 6-OHDA dopamine degeneration in rats monitored by immunohistochemistry and PET imaging. Eur J Neurosci 15(6):991–998

Dickson DW, Rademakers R, Hutton ML (2007) Progressive supranuclear palsy: pathology and genetics. Brain Pathol 17(1):74–82

Dodel R, Spottke A, Gerhard A, Reuss A, Reinecker S, Schimke N et al (2010) Minocycline 1-year therapy in multiple-system-atrophy: effect on clinical symptoms and [(11)C] (R)-PK11195 PET (MEMSA-trial). Mov Disord 25(1):97–107

Eckert T, Barnes A, Dhawan V, Frucht S, Gordon MF, Feigin AS et al (2005) FDG PET in the differential diagnosis of parkinsonian disorders. NeuroImage 26(3):912–921

Eckert T, Van Laere K, Tang C, Lewis DE, Edwards C, Santens P et al (2007) Quantification of Parkinson's disease-related network expression with ECD SPECT. Eur J Nucl Med Mol Imaging 34(4):496–501

Eckert T, Tang C, Ma Y, Brown N, Lin T, Frucht S et al (2008) Abnormal metabolic networks in atypical parkinsonism. Mov Disord 23(5):727–733

Edison P, Ahmed I, Fan Z, Hinz R, Gelosa G, Ray Chaudhuri K et al (2013) Microglia, amyloid, and glucose metabolism in Parkinson's disease with and without dementia. Neuropsychopharmacology 38(6):938–949

Eidelberg D (2009) Metabolic brain networks in neurodegenerative disorders: a functional imaging approach. Trends Neurosci 32(10):548–557

Eidelberg D, Takikawa S, Moeller JR, Dhawan V, Redington K, Chaly T et al (1993) Striatal hypometabolism distinguishes striatonigral degeneration from Parkinson's disease. Ann Neurol 33(5):518–527

Eidelberg D, Moeller J, Dhawan V, Spetsieris P, Takikawa S, Ishikawa T et al (1994) The metabolic topography of parkinsonism. J Cereb Blood Flow Metab 14(5):783–801

Eidelberg D, Moeller JR, Ishikawa T, Dhawan V, Spetsieris P, Chaly T et al (1995) Assessment of disease severity in parkinsonism with fluorine-18-fluorodeoxyglucose and PET. J Nucl Med 36(3):378–383

El Fakhri G, Ouyang J (2011) Dual-radionuclide brain SPECT for the differential diagnosis of parkinsonism. Methods Mol Biol 680:237–246

El Fakhri G, Habert MO, Maksud P, Kas A, Malek Z, Kijewski MF et al (2006) Quantitative simultaneous (99m)Tc-ECD/123I-FP-CIT SPECT in Parkinson's disease and multiple system atrophy. Eur J Nucl Med Mol Imaging 33(1):87–92

Eshuis SA, Maguire RP, Leenders KL, Jonkman S, Jager PL (2006) Comparison of FP-CIT SPECT with F-DOPA PET in patients with de novo and advanced Parkinson's disease. Eur J Nucl Med Mol Imaging 33(2):200–209

Eshuis SA, Jager PL, Maguire RP, Jonkman S, Dierckx RA, Leenders KL (2009) Direct comparison of FP-CIT SPECT and F-DOPA PET in patients with Parkinson's disease and healthy controls. Eur J Nucl Med Mol Imaging 36(3):454–462

Fan Z, Aman Y, Ahmed I, Chetelat G, Landeau B, Ray Chaudhuri K et al (2015) Influence of microglial activation on neuronal function in Alzheimer's and Parkinson's disease dementia. Alzheimers Dement 11(6):608–21.e7

Feigin A, Tang C, Ma Y, Mattis P, Zgaljardic D, Guttman M et al (2007) Thalamic metabolism and symptom onset in preclinical Huntington's disease. Brain 130(Pt 11):2858–2867

Gaenslen A, Unmuth B, Godau J, Liepelt I, Di Santo A, Schweitzer KJ et al (2008) The specificity and sensitivity of transcranial ultrasound in the differential diagnosis of Parkinson's disease: a prospective blinded study. Lancet Neurol 7(5):417–424

Garraux G, Phillips C, Schrouff J, Kreisler A, Lemaire C, Degueldre C et al (2013) Multiclass classification of FDG PET scans for the distinction between Parkinson's disease and atypical parkinsonian syndromes. Neuroimage Clin 2:883–893

Ge J, Wu J, Peng S, Wu P, Wang J, Zhang H et al (2018) Reproducible network and regional topographies of abnormal glucose metabolism associated with progressive supranuclear palsy: multivariate and univariate analyses in American and Chinese patient cohorts. Hum Brain Mapp 39(7):2842–2858

Gerhard A, Banati RB, Goerres GB, Cagnin A, Myers R, Gunn RN et al (2003) [11C](R)-PK11195 PET imaging of microglial activation in multiple system atrophy. Neurology 61(5):686–689

Gerhard A, Watts J, Trender-Gerhard I, Turkheimer F, Banati RB, Bhatia K et al (2004) In vivo imaging of microglial activation with [11C](R)-PK11195 PET in corticobasal degeneration. Mov Disord 19(10):1221–1226

Gerhard A, Pavese N, Hotton G, Turkheimer F, Es M, Hammers A et al (2006a) In vivo imaging of microglial activation with [11C](R)-PK11195 PET in idiopathic Parkinson's disease. Neurobiol Dis 21(2):404–412

Gerhard A, Trender-Gerhard I, Turkheimer F, Quinn NP, Bhatia KP, Brooks DJ (2006b) In vivo imaging of microglial activation with [11C](R)-PK11195 PET in progressive supranuclear palsy. Mov Disord 21(1):89–93

Gerschlager W, Bencsits G, Pirker W, Bloem BR, Asenbaum S, Prayer D et al (2002) [123I]beta-CIT SPECT distinguishes vascular parkinsonism from Parkinson's disease. Mov Disord 17(3):518–523

Ghadery C, Koshimori Y, Coakeley S, Harris M, Rusjan P, Kim J et al (2017) Microglial activation in Parkinson's disease using [(18)F]-FEPPA. J Neuroinflammation 14(1):8

Ghaemi M, Hilker R, Rudolf J, Sobesky J, Heiss WD (2002) Differentiating multiple system atrophy from Parkinson's disease: contribution of striatal and midbrain MRI volumetry and multitracer PET imaging. J Neurol Neurosurg Psychiatry 73(5):517–523

Gilman S, Wenning G, Low P, Brooks D, Mathias C, Trojanowski J et al (2008) Second consensus statement on the diagnosis of multiple system atrophy. Neurology 71(9):670–676

Habeck C, Foster N, Perneczky R, Kurz A, Alexopoulos P, Koeppe R et al (2008) Multivariate and univariate neuroimaging biomarkers of Alzheimer's disease. NeuroImage 40(4):1503–1515

Hassan A, Whitwell JL, Josephs KA (2011) The corticobasal syndrome-Alzheimer's disease conundrum. Expert Rev Neurother 11(11):1569–1578

Heim B, Krismer F, Seppi K (2018) Structural imaging in atypical parkinsonism. Int Rev Neurobiol 142:67–148

Hellwig S, Amtage F, Kreft A, Buchert R, Winz OH, Vach W et al (2012) [(1)(8)F]FDG-PET is superior to [(1)(2)(3)I]IBZM-SPECT for the differential diagnosis of parkinsonism. Neurology 79(13):1314–1322

Henkel K, Karitzky J, Schmid M, Mader I, Glatting G, Unger JW et al (2004) Imaging of activated microglia with PET and [11C]PK 11195 in corticobasal degeneration. Mov Disord 19(7):817–821

Hoglinger GU, Respondek G, Stamelou M, Kurz C, Josephs KA, Lang AE et al (2017) Clinical diagnosis of progressive supranuclear palsy: the movement disorder society criteria. Mov Disord 32(6):853–864

Holtbernd F, Eidelberg D (2014) The utility of neuroimaging in the differential diagnosis of parkinsonian syndromes. Semin Neurol 34(2):202–209

Holtbernd F, Gagnon JF, Postuma RB, Ma Y, Tang CC, Feigin A et al (2014) Abnormal metabolic network activity in REM sleep behavior disorder. Neurology 82(7):620–627

Holtbernd F, Ma Y, Peng S, Schwartz F, Timmermann L, Kracht L et al (2015) Dopaminergic correlates of metabolic network activity in Parkinson's disease. Hum Brain Mapp 36(9):3575–3585

Hu WT, Rippon GW, Boeve BF, Knopman DS, Petersen RC, Parisi JE et al (2009) Alzheimer's disease and corticobasal degeneration presenting as corticobasal syndrome. Mov Disord 24(9):1375–1379

Huang C, Mattis P, Tang C, Perrine K, Carbon M, Eidelberg D (2007) Metabolic brain networks associated with cognitive function in Parkinson's disease. NeuroImage 34(2):714–723

Huang C, Mattis P, Perrine K, Brown N, Dhawan V, Eidelberg D (2008) Metabolic abnormalities associated with mild cognitive impairment in Parkinson disease. Neurology 70(16 Pt 2):1470–1477

Hughes A, Daniel S, Ben-Shlomo Y, Lees A (2002) The accuracy of diagnosis of parkinsonian syndromes in a specialist movement disorder service. Brain 125(Pt 4):861–870

Ichise M, Kim YJ, Ballinger JR, Vines D, Erami SS, Tanaka F et al (1999) SPECT imaging of pre- and postsynaptic dopaminergic alterations in L-dopa-untreated PD. Neurology 52(6):1206–1214

Imamura K, Hishikawa N, Sawada M, Nagatsu T, Yoshida M, Hashizume Y (2003) Distribution of major histocompatibility complex class II-positive microglia and cytokine profile of Parkinson's disease brains. Acta Neuropathol 106(6):518–526

Imamura K, Hishikawa N, Ono K, Suzuki H, Sawada M, Nagatsu T et al (2005) Cytokine production of activated microglia and decrease in neurotrophic factors of neurons in the hippocampus of Lewy body disease brains. Acta Neuropathol 109(2):141–150

Ishizawa K, Dickson DW (2001) Microglial activation parallels system degeneration in progressive supranuclear palsy and corticobasal degeneration. J Neuropathol Exp Neurol 60(6):647–657

Ishizawa K, Komori T, Sasaki S, Arai N, Mizutani T, Hirose T (2004) Microglial activation parallels system degeneration in multiple system atrophy. J Neuropathol Exp Neurol 63(1):43–52

Jesse S, Kassubek J, Muller HP, Ludolph AC, Unrath A (2012) Signal alterations of the basal ganglia in the differential diagnosis of Parkinson's disease: a retrospective case-controlled MRI data bank analysis. BMC Neurol 12:163

Jin S, Oh M, Oh SJ, Oh JS, Lee SJ, Chung SJ et al (2017) Additional value of early-phase 18F-FP-CIT PET image for differential diagnosis of atypical parkinsonism. Clin Nucl Med 42(2):e80–ee7

Joling M, Vriend C, van den Heuvel OA, Raijmakers P, Jones PA, Berendse HW et al (2017) Analysis of extrastriatal (123)I-FP-CIT binding contributes to the differential diagnosis of parkinsonian diseases. J Nucl Med 58(7):1117–1123

Josephs K, Dickson D (2003) Diagnostic accuracy of progressive supranuclear palsy in the Society for Progressive Supranuclear Palsy brain bank. Mov Disord 18(9):1018–1026

Kaasinen V, Ruottinen HM, Nagren K, Lehikoinen P, Oikonen V, Rinne JO (2000) Upregulation of putaminal dopamine D2 receptors in early Parkinson's disease: a comparative PET study with [11C] raclopride and [11C]N-methylspiperone. J Nucl Med 41(1):65–70

Kanazawa M, Shimohata T, Terajima K, Onodera O, Tanaka K, Tsuji S et al (2004) Quantitative evaluation of brainstem involvement in multiple system atrophy by diffusion-weighted MR imaging. J Neurol 251(9):1121–1124

Kim YJ, Ichise M, Ballinger JR, Vines D, Erami SS, Tatschida T et al (2002) Combination of dopamine transporter and D2 receptor SPECT in the diagnostic evaluation of PD, MSA, and PSP. Mov Disord 17(2):303–312

Klaffke S, Kuhn AA, Plotkin M, Amthauer H, Harnack D, Felix R et al (2006) Dopamine transporters, D2 receptors, and glucose metabolism in corticobasal degeneration. Mov Disord 21(10):1724–1727

Knudsen GM, Karlsborg M, Thomsen G, Krabbe K, Regeur L, Nygaard T et al (2004) Imaging of dopamine transporters and D2 receptors in patients with Parkinson's disease and multiple system atrophy. Eur J Nucl Med Mol Imaging 31(12):1631–1638

Ko JH, Lee CS, Eidelberg D (2017) Metabolic network expression in parkinsonism: clinical and dopaminergic correlations. J Cereb Blood Flow Metab 37(2):683–693

Kobylecki C, Counsell SJ, Cabanel N, Wachter T, Turkheimer FE, Eggert K et al (2013) Diffusion-weighted imaging and its relationship to microglial activation in parkinsonian syndromes. Parkinsonism Relat Disord 19(5):527–532

Koeppe RA, Gilman S, Joshi A, Liu S, Little R, Junck L et al (2005) 11C-DTBZ and 18F-FDG PET measures in differentiating dementias. J Nucl Med 46(6):936–944

Koshimori Y, Ko JH, Mizrahi R, Rusjan P, Mabrouk R, Jacobs MF et al (2015) Imaging striatal microglial activation in patients with Parkinson's disease. PLoS One 10(9):e0138721

Kubler D, Wachter T, Cabanel N, Su Z, Turkheimer FE, Dodel R et al (2019) Widespread microglial activation in multiple system atrophy. Mov Disord 34(4):564–568

Leenders KL (2003) Significance of non-presynaptic SPECT tracer methods in Parkinson's disease. Mov Disord 18(Suppl 7):S39–S42

Linder J, Birgander R, Olsson I, Riklund K, Larsson A, Edstrom M et al (2009) Degenerative changes were common in brain magnetic resonance imaging in patients with newly diagnosed Parkinson's disease in a population-based cohort. J Neurol 256(10):1671–1680

Litvan I (2003) Update on epidemiological aspects of progressive supranuclear palsy. Mov Disord 18(Suppl 6):S43–S50

Litvan I, Agid Y, Goetz C, Jankovic J, Wenning GK, Brandel JP et al (1997) Accuracy of the clinical diagnosis of corticobasal degeneration: a clinicopathologic study. Neurology 48(1):119–125

Lozza C, Baron JC, Eidelberg D, Mentis MJ, Carbon M, Marie RM (2004) Executive processes in Parkinson's disease: FDG-PET and network analysis. Hum Brain Mapp 22(3):236–245

Ma Y, Feigin A, Okulski J, Dhawan V, Chaly T, Eidelberg D (2003) Implementation of atrophy correction in metabolic mapping studies of presymptomatic Huntington's disease. J Cereb Blood Flow Metab 2003:S629

Ma Y, Tang C, Spetsieris P, Dhawan V, Eidelberg D (2007) Abnormal metabolic network activity in Parkinson's disease: test-retest reproducibility. J Cereb Blood Flow Metab 27(3):597–605

Mahapatra RK, Edwards MJ, Schott JM, Bhatia KP (2004) Corticobasal degeneration. Lancet Neurol 3(12):736–743

Marshall VL, Reininger CB, Marquardt M, Patterson J, Hadley DM, Oertel WH et al (2009) Parkinson's disease is overdiagnosed clinically at baseline in diagnostically uncertain cases: a 3-year European multicenter study with repeat [123I]FP-CIT SPECT. Mov Disord 24(4):500–508

Mattis PJ, Niethammer M, Sako W, Tang CC, Nazem A, Gordon ML et al (2016) Distinct brain networks underlie cognitive dysfunction in Parkinson and Alzheimer diseases. Neurology 87(18):1925–1933

Minnerop M, Specht K, Ruhlmann J, Schimke N, Abele M, Weyer A et al (2007) Voxel-based morphometry and voxel-based relaxometry in multiple system atrophy-a comparison between clinical subtypes and correlations with clinical parameters. NeuroImage 36(4):1086–1095

Mizrahi R, Rusjan PM, Kennedy J, Pollock B, Mulsant B, Suridjan I et al (2012) Translocator protein (18 kDa) polymorphism (rs6971) explains in-vivo brain binding affinity of the PET radioligand [(18)F]-FEPPA. J Cereb Blood Flow Metab 32(6):968–972

Mudali D, Teune LK, Renken RJ, Leenders KL, Roerdink JB (2015) Classification of Parkinsonian syndromes from FDG-PET brain data using decision trees with SSM/PCA features. Comput Math Methods Med 2015:136921

Mueller C, Hussl A, Krismer F, Heim B, Mahlknecht P, Nocker M et al (2018) The diagnostic accuracy of the hummingbird and morning glory sign in patients with neurodegenerative parkinsonism. Parkinsonism Relat Disord 54:90–94

Mure H, Hirano S, Tang CC, Isaias IU, Antonini A, Ma Y et al (2011) Parkinson's disease tremor-related metabolic network: characterization, progression, and treatment effects. NeuroImage 54(2):1244–1253

Nicastro N, Wegrzyk J, Preti MG, Fleury V, Van de Ville D, Garibotto V et al (2019) Classification of degenerative parkinsonism subtypes by support-vector-machine analysis and striatal (123) I-FP-CIT indices. J Neurol 266(7):1771–1781

Nicoletti G, Lodi R, Condino F, Tonon C, Fera F, Malucelli E et al (2006) Apparent diffusion coefficient measurements of the middle cerebellar peduncle differentiate the Parkinson variant of MSA from Parkinson's disease and progressive supranuclear palsy. Brain 129(Pt 10):2679–2687

Niethammer M, Eidelberg D (2012) Metabolic brain networks in translational neurology: concepts and applications. Ann Neurol 72(5):635–647

Niethammer M, Feigin A, Eidelberg D (2012) Functional neuroimaging in Parkinson's disease. Cold Spring Harb Perspect Med 2(5):a009274

Niethammer M, Tang CC, Feigin A, Allen PJ, Heinen L, Hellwig S et al (2014) A disease-specific metabolic brain network associated with corticobasal degeneration. Brain 137(Pt 11):3036–3046

O'Sullivan SS, Burn DJ, Holton JL, Lees AJ (2008) Normal dopamine transporter single photon-emission CT scan in corticobasal degeneration. Mov Disord 23(16):2424–2426

Ouchi Y, Yoshikawa E, Sekine Y, Futatsubashi M, Kanno T, Ogusu T et al (2005) Microglial activation and dopamine terminal loss in early Parkinson's disease. Ann Neurol 57(2):168–175

Owen DR, Yeo AJ, Gunn RN, Song K, Wadsworth G, Lewis A et al (2012) An 18-kDa translocator protein (TSPO) polymorphism explains differences in binding affinity of the PET radioligand PBR28. J Cereb Blood Flow Metab 32(1):1–5

Papadopoulos V, Baraldi M, Guilarte TR, Knudsen TB, Lacapere JJ, Lindemann P et al (2006) Translocator protein (18kDa): new nomenclature for the peripheral-type benzodiazepine receptor based on its structure and molecular function. Trends Pharmacol Sci 27(8):402–409

Papp M, Kahn J, Lantos P (1989) Glial cytoplasmic inclusions in the CNS of patients with multiple system atrophy (striatonigral degeneration, olivopontocerebellar atrophy and Shy-Drager syndrome). J Neurol Sci 94(1–3):79–100

Park HK, Kim JS, Im KC, Oh SJ, Kim MJ, Lee JH et al (2009) Functional brain imaging in pure akinesia with gait freezing: [18F] FDG PET and [18F] FP-CIT PET analyses. Mov Disord 24(2):237–245

Passamonti L, Rodriguez PV, Hong YT, Allinson KSJ, Bevan-Jones WR, Williamson D et al (2018) [(11)C]PK11195 binding in Alzheimer disease and progressive supranuclear palsy. Neurology 90(22):e1989–e1e96

Paviour D, Price S, Stevens J, Lees A, Fox N (2005) Quantitative MRI measurement of superior cerebellar peduncle in progressive supranuclear palsy. Neurology 64(4):675–679

Paviour DC, Price SL, Jahanshahi M, Lees AJ, Fox NC (2006) Regional brain volumes distinguish PSP, MSA-P, and PD: MRI-based clinico-radiological correlations. Mov Disord 21(7):989–996

Paviour DC, Thornton JS, Lees AJ, Jager HR (2007) Diffusion-weighted magnetic resonance imaging differentiates Parkinsonian variant of multiple-system atrophy from progressive supranuclear palsy. Mov Disord 22(1):68–74

Perju-Dumbrava LD, Kovacs GG, Pirker S, Jellinger K, Hoffmann M, Asenbaum S et al (2012) Dopamine transporter imaging in autopsy-confirmed Parkinson's disease and multiple system atrophy. Mov Disord 27(1):65–71

Pirker W, Asenbaum S, Bencsits G, Prayer D, Gerschlager W, Deecke L et al (2000) [123I]beta-CIT SPECT in multiple system atrophy, progressive supranuclear palsy, and corticobasal degeneration. Mov Disord 15(6):1158–1167

Pirker W, Djamshidian S, Asenbaum S, Gerschlager W, Tribl G, Hoffmann M et al (2002) Progression of dopaminergic degeneration in Parkinson's disease and atypical parkinsonism: a longitudinal beta-CIT SPECT study. Mov Disord 17(1):45–53

Plotkin M, Amthauer H, Klaffke S, Kuhn A, Ludemann L, Arnold G et al (2005) Combined 123I-FP-CIT and 123I-IBZM SPECT for the diagnosis of parkinsonian syndromes: study on 72 patients. J Neural Transm (Vienna) 112(5):677–692

Poston KL (2010) Overview of rare movement disorders. Continuum (Minneap Minn) 16(1 Movement Disorders):49–76

Poston KL, Eidelberg D (2009) Network biomarkers for the diagnosis and treatment of movement disorders. Neurobiol Dis 35(2):141–147

Poston K, Tang C, Eckert T, Dhawan V, Frucht S, Vonsattel J et al (2012) Network correlates of disease severity in multiple system atrophy. Neurology 78(16):1237–1244

Postuma RB, Gagnon JF, Montplaisir JY (2012) REM sleep behavior disorder: from dreams to neurodegeneration. Neurobiol Dis 46:553–558

Postuma RB, Berg D, Stern M, Poewe W, Olanow CW, Oertel W et al (2015) MDS clinical diagnostic criteria for Parkinson's disease. Mov Disord 30(12):1591–1601

Pourfar M, Tang C, Lin T, Dhawan V, Kaplitt MG, Eidelberg D (2009) Assessing the microlesion effect of subthalamic deep brain stimulation surgery with FDG PET. J Neurosurg 110(6):1278–1282

Quattrone A, Nicoletti G, Messina D, Fera F, Condino F, Pugliese P et al (2008) MR imaging index for differentiation of progressive supranuclear palsy from Parkinson disease and the Parkinson variant of multiple system atrophy. Radiology 246(1):214–221

Real CC, Doorduin J, Kopschina Feltes P, Vallez Garcia D, de Paula FD, Britto LR et al (2019) Evaluation of exercise-induced modulation of glial activation and dopaminergic damage in a rat model of Parkinson's disease using [(11)C]PBR28 and [(18)F]FDOPA PET. J Cereb Blood Flow Metab 39(6):989–1004

Richter D, Woitalla D, Muhlack S, Gold R, Tonges L, Krogias C (2017) Coronal transcranial sonography and M-mode tremor frequency determination in Parkinson's disease and essential tremor. J Neuroimaging 27(5):524–530

Rizzo G, Copetti M, Arcuti S, Martino D, Fontana A, Logroscino G (2016) Accuracy of clinical diagnosis of Parkinson disease: a systematic review and meta-analysis. Neurology 86(6):566–576

Sako W, Abe T, Haji S, Murakami N, Osaki Y, Izumi Y et al (2019) "One line": a method for differential diagnosis of parkinsonian syndromes. Acta Neurol Scand 140(3):229–235

Scherfler C, Seppi K, Donnemiller E, Goebel G, Brenneis C, Virgolini I et al (2005) Voxel-wise analysis of [123I]beta-CIT SPECT differentiates the Parkinson variant of multiple system atrophy from idiopathic Parkinson's disease. Brain 128(Pt 7):1605–1612

Schindlbeck KA, Eidelberg D (2018) Network imaging biomarkers: insights and clinical applications in Parkinson's disease. Lancet Neurol 17(7):629–640

Schott J, Williams D, Butterworth R, Janssen J, Larner A, Holton J et al (2007) Shunt responsive progressive supranuclear palsy? Mov Disord 22(6):902–903

Seppi K, Schocke M (2005) An update on conventional and advanced magnetic resonance imaging techniques in the differential diagnosis of neurodegenerative parkinsonism. Curr Opin Neurol 18(4):370–375

Soliveri P, Monza D, Paridi D, Radice D, Grisoli M, Testa D et al (1999) Cognitive and magnetic resonance imaging aspects of corticobasal degeneration and progressive supranuclear palsy. Neurology 53(3):502–507

Spetsieris P, Ma Y, Dhawan V, Eidelberg D (2009) Differential diagnosis of parkinsonian syndromes using PCA-based functional imaging features. NeuroImage 45(4):1241–1252

Spetsieris P, Ma Y, Peng S, Ko JH, Dhawan V, Tang CC et al (2013) Identification of disease-related spatial covariance patterns using neuroimaging data. J Vis Exp 76:e50319

Spiegel J, Mollers MO, Jost WH, Fuss G, Samnick S, Dillmann U et al (2005) FP-CIT and MIBG scintigraphy in early Parkinson's disease. Mov Disord 20(5):552–561

Sudmeyer M, Antke C, Zizek T, Beu M, Nikolaus S, Wojtecki L et al (2011) Diagnostic accuracy of combined FP-CIT, IBZM, and MIBG scintigraphy in the differential diagnosis of degenerative parkinsonism: a multidimensional statistical approach. J Nucl Med 52(5):733–740

Tang CC, Poston KL, Dhawan V, Eidelberg D (2010a) Abnormalities in metabolic network activity precede the onset of motor symptoms in Parkinson's disease. J Neurosci 30(3):1049–1056

Tang CC, Poston KL, Eckert T, Feigin A, Frucht S, Gudesblatt M et al (2010b) Differential diagnosis of parkinsonism: a metabolic imaging study using pattern analysis. Lancet Neurol 9(2):149–158

Tao A, Chen G, Deng Y, Xu R (2019) Accuracy of transcranial sonography of the substantia nigra for detection of Parkinson's disease: a systematic review and meta-analysis. Ultrasound Med Biol 45(3):628–641

Teune LK, Bartels AL, de Jong BM, Willemsen AT, Eshuis SA, de Vries JJ et al (2010) Typical cerebral metabolic patterns in neurodegenerative brain diseases. Mov Disord 25(14):2395–2404

Teune LK, Renken RJ, Mudali D, De Jong BM, Dierckx RA, Roerdink JB et al (2013) Validation of parkinsonian disease-related metabolic brain patterns. Mov Disord 28(4):547–551

Teune LK, Strijkert F, Renken RJ, Izaks GJ, de Vries JJ, Segbers M et al (2014) The Alzheimer's disease-related glucose metabolic brain pattern. Curr Alzheimer Res 11(8):725–732

Thobois S, Prange S, Scheiber C, Broussolle E (2019) What a neurologist should know about PET and SPECT functional imaging for parkinsonism: a practical perspective. Parkinsonism Relat Disord 59:93–100

Tripathi M, Tang C, Peng S, Dhawan V, Sharma R, Jaimini A et al (2012) Metabolic image-based algorithm for accurate differential diagnosis of parkinsonism: prospective validation in Indian patient population. J Nucl Med 53(Suppl 1):1974

Tripathi M, Tang CC, Feigin A, De Lucia I, Nazem A, Dhawan V et al (2016) Automated differential diagnosis of early parkinsonism using metabolic brain networks: a validation study. J Nucl Med 57(1):60–66

Van Laere K, Santens P, Bosman T, De Reuck J, Mortelmans L, Dierckx R (2004) Statistical parametric mapping of (99m)Tc-ECD SPECT in idiopathic Parkinson's disease and multiple system atrophy with predominant parkinsonian features: correlation with clinical parameters. J Nucl Med 45(6):933–942

Van Laere K, Casteels C, De Ceuninck L, Vanbilloen B, Maes A, Mortelmans L et al (2006) Dual-tracer dopamine transporter and perfusion SPECT in differential diagnosis of parkinsonism using template-based discriminant analysis. J Nucl Med 47(3):384–392

Varnas K, Cselenyi Z, Jucaite A, Halldin C, Svenningsson P, Farde L et al (2019) PET imaging of [(11)C]PBR28 in Parkinson's disease patients does not indicate increased binding to TSPO despite reduced dopamine transporter binding. Eur J Nucl Med Mol Imaging 46(2):367–375

Varrone A, Marek KL, Jennings D, Innis RB, Seibyl JP (2001) [(123)I]beta-CIT SPECT imaging demonstrates reduced density of striatal dopamine transporters in Parkinson's disease and multiple system atrophy. Mov Disord 16(6):1023–1032

Venneti S, Lopresti BJ, Wiley CA (2006) The peripheral benzodiazepine receptor (translocator protein 18 kDa) in microglia: from pathology to imaging. Prog Neurobiol 80(6):308–322

Vlaar AM, de Nijs T, Kessels AG, Vreeling FW, Winogrodzka A, Mess WH et al (2008) Diagnostic value of 123I-ioflupane and 123I-iodobenzamide SPECT scans in 248 patients with parkinsonian syndromes. Eur Neurol 59(5):258–266

Walter U, Niehaus L, Probst T, Benecke R, Meyer BU, Dressler D (2003) Brain parenchyma sonography discriminates Parkinson's disease and atypical parkinsonian syndromes. Neurology 60(1):74–77

Walter U, Dressler D, Wolters A, Probst T, Grossmann A, Benecke R (2004) Sonographic discrimination of corticobasal degeneration vs progressive supranuclear palsy. Neurology 63(3):504–509

Walter U, Dressler D, Probst T, Wolters A, Abu-Mugheisib M, Wittstock M et al (2007) Transcranial brain sonography findings in discriminating between parkinsonism and idiopathic Parkinson disease. Arch Neurol 64(11):1635–1640

Watanabe H, Saito Y, Terao S, Ando T, Kachi T, Mukai E et al (2002) Progression and prognosis in multiple system atrophy: an analysis of 230 Japanese patients. Brain 125(Pt 5):1070–1083

Wenning G, Stefanova N (2009) Recent developments in multiple system atrophy. J Neurol 256(11):1791–1808

Williams D, Lees A (2009) Progressive supranuclear palsy: clinicopathological concepts and diagnostic challenges. Lancet Neurol 8(3):270–279

Williams D, de Silva R, Paviour D, Pittman A, Watt H, Kilford L et al (2005) Characteristics of two distinct clinical phenotypes in pathologically proven progressive supranuclear palsy: Richardson's syndrome and PSP-parkinsonism. Brain 128(6):1247–1258

Williams D, Holton J, Strand K, Revesz T, Lees A (2007) Pure akinesia with gait freezing: a third clinical phenotype of progressive supranuclear palsy. Mov Disord 22(15):2235–2241

Winikates J, Jankovic J (1999) Clinical correlates of vascular parkinsonism. Arch Neurol 56(1):98–102

Wu P, Wang J, Peng S, Ma Y, Zhang H, Guan Y et al (2013) Metabolic brain network in the Chinese patients with Parkinson's disease based on 18F-FDG PET imaging. Parkinsonism Relat Disord 19(6):622–627

Amyotrophic Lateral Sclerosis

27

Martin R. Turner and Marco Pagani

Contents

27.1 Introduction 761
27.2 Single-Photon Emission Computed Tomography 761
27.3 PET 769
27.3.1 Blood Flow and Metabolism 769
27.3.2 Ligand Studies 771
27.3.3 The Future 775
References 776

Abstract

The core of the clinical syndrome of amyotrophic lateral sclerosis (ALS) is a progressive and typically rapid and uniformly fatal disintegration of the motor system, comprising upper motor neurons (UMNs) of the primary motor cortex and corticospinal tract (CST), brainstem nuclei and the lower motor neurons (LMNs) arising from the anterior horns of the spinal cord. While the spinal anterior horns and corticospinal tract superficially appear to bear the brunt of histopathology in ALS, it is clear that neurodegeneration extends to involve the extra-motor brain, preferentially involving the frontal and temporal lobes having clinical, histopathological and genetic overlap with frontotemporal dementia

M. R. Turner (✉)
Nuffield Department of Clinical Neurosciences, John Radcliffe Hospital, Oxford University, Oxford, UK
e-mail: martin.turner@ndcn.ox.ac.uk

M. Pagani
Institute of Cognitive Sciences and Technologies, CNR, Rome, Italy

Medical Radiation Physics and Nuclear Medicine, Karolinska University Hospital, Stockholm, Sweden
e-mail: marco.pagani@istc.cnr.it

R. A. J. O. Dierckx et al. (eds.), *PET and SPECT in Neurology*,
https://doi.org/10.1007/978-3-030-53168-3_27

(FTD). There is a profound microglial and astrocytic component to pathology, with cortical hyperexcitability thought to be underpinned by changes in the balance of cortical inhibitory interneuronal influences. The marked clinical heterogeneity of the ALS-FTD spectrum, frequent diagnostic delay and reliance of therapeutic trials on survival as the primary outcome measure have made biomarker development a research priority. PET, in particular, continues to provide key mechanistic insights into pathogenesis at a unique systems level.

Abbreviations

5-HT	5-Hydroxytriptamine (serotonin)
ALS	Amyotrophic lateral sclerosis
ALSFRS-R	Revised amyotrophic lateral sclerosis functional rating scale
ATSM	Diacetyl-bis(N4-methylthiosemicarbazone)
CBF	Cerebral blood flow
CST	Corticospinal tract
DA	Discriminant analysis
DLPFC	Dorsolateral prefrontal cortex
ECD	Ethyl cysteinate dimer
FA	Fractional anisotropy
fALS	Familial ALS
FDG	Fluorodeoxyglucose
FMZ	Flumazenil
FTD	Frontotemporal dementia
FU	Follow-up
GABA	γ-Aminobutyric acid
HC	Healthy controls
HMPAO	Hexamethylpropyleneamine oxime
IMP	Iodoamphetamine
KD	Kennedy's disease
LMN	Lower motor neuron
mI/Cr	Myoinositol-creatinine ratio
MMSE	Mini-mental state examination
NAA/Cr	N-Acetylaspartate-creatinine ratio
PBB3	2-([1E,3E]-4-[6-([11C]Methylamino)pyridin-3-yl]buta-1,3-dienyl) benzo[d]thiazol-6-ol
PBR	Peripheral benzodiazepine receptor
PLS	Primary lateral sclerosis
PMA	Progressive muscular atrophy
PMC	Primary motor cortex
SOD1	Superoxide dismutase (ps, presymptomatic; hom, homozygous)
SVM	Support vector machine
TARDBP	Transactive region DNA-binding protein
UMN	Upper motor neuron
UMNB	Upper motor neuron burden

27.1 Introduction

The core of the clinical syndrome of amyotrophic lateral sclerosis (ALS) is a progressive and typically rapid degeneration of a previously normally functioning motor system, comprising upper motor neurons (UMNs) of the primary motor cortex and corticospinal tract (CST), brainstem nuclei and the lower motor neurons (LMNs) arising from the anterior horns of the spinal cord. Weakness, with variable wasting, of the musculature of the limbs and of speech and swallowing ensues, with involvement of the diaphragm resulting in respiratory insufficiency and a median survival of 3 years (van Es et al. 2017). The marked clinical heterogeneity, frequent diagnostic delay and reliance of therapeutic trials on survival as the primary outcome measure have made the discovery of biomarkers across the ALS-FTD spectrum a research priority (Turner et al. 2009).

While the spinal anterior horns and corticospinal tract superficially appear to bear the brunt of histopathology in ALS, it has been known for several decades that neurodegeneration extends to involve the extra-motor brain (Smith 1960), preferentially involving areas of the frontal and temporal lobes having clinical (Phukan et al. 2007) and genetic (DeJesus-Hernandez et al. 2011; Renton et al. 2011) overlap with some forms of frontotemporal dementia (FTD) (Giordana et al. 2011). Variable motor and extra-motor neuronal cytoplasmic inclusions of the transactive region DNA-binding protein TDP-43 are the unifying pathological feature (Neumann et al. 2006). Thus, involvement of the central nervous system has become a core feature of ALS pathogenesis, even in those with no clinical signs of UMN pathology (cases sometimes termed progressive muscular atrophy, PMA) (Brownell et al. 1970; Ince et al. 2003). The development of neuroimaging has revealed a range of novel aspects of ALS pathogenesis (Turner and Verstraete 2015). SPECT and particularly PET were the first tools to demonstrate this wider extra-motor involvement in vivo and to lay the foundation for the modern understanding of ALS as a broad system failure, revealing extra-motor involvement (and related cognitive impairment) in patients unable to comply with standard neuropsychological testing because of physical disability. The individual studies in ALS (and related clinical subtypes) are listed in Table 27.1.

27.2 Single-Photon Emission Computed Tomography

Early SPECT in ALS used the tracer N-isopropyl-p-^{123}I-iodoamphetamine (^{123}I-IMP). This revealed widespread cortical reductions, pronounced in those with longer disease duration (Ludolph et al. 1989) (Fig. 27.1). Soon afterwards, ^{99m}Tc-HMPAO (hexamethylpropyleneamine oxime) SPECT revealed frontotemporal changes in four ALS cases with dementia (Neary et al. 1990), the same group proffering the now accepted concept of a continuum between ALS and FTD (Talbot et al. 1995). A comparative study involving patients with a slowly progressive LMN 'mimic' of ALS, Kennedy's disease (KD, X-linked spinobulbar muscular atrophy), showed no equivalent decreases in cerebral blood flow (CBF) observed in the

Table 27.1 Radionuclide studies in ALS and related disorders

Scan type	Radiotracer	Participants	Main findings	Reference
SPECT	^{123}I-IMP	1 ALS-FTD 1 HC	Marked loss of frontotemporal uptake	Sawada et al. (1988)
		17 ALS (1 FU after 9 months); 15 disease controls	Widespread uptake reduction, correlated with disease severity and duration	Ludolph et al. (1989)
		1 ALS (16-month FU)	Extension of uptake reduction from PMC to frontal lobes over scan interval	Waragai et al. (1997)
	^{99m}Tc-HMPAO	4 ALS-dementia	Reduced frontal lobe uptake (*postmortem* details included)	Neary et al. (1990)
		14 ALS; 14 HC	8/14 prominently reduced frontal lobe uptake (3 with dementia, 1 with aphasia)	Waldemar et al. (1992)
		18 ALS; 8 disease controls	Categorisation into four groups by reduced uptake: frontal + motor, mainly motor, just motor and no reductions, which then correlated with the spectrum of cognitive impairment	Abe et al. (1993)
		19 ALS; 8 ALS-dementia; 29 FTD; 10 HC	Frontal and anterior temporal reduced uptake in all groups, greater in those with ALS-dementia and FTD	Talbot et al. (1995)
		26 ALS; 26 HC	Reduced frontal uptake in those with cognitive impairment (*postmortem* details included)	Abe et al. (1997)
	^{99m}Tc-ECD	35 ALS; 12 KD; 88 HC	Reduced frontal uptake in those with progressive bulbar palsy (correlated with bulbar functional scores); no change in KD patients compared with controls	Morimoto et al. (2012)
		1 *C9ORF72* fALS-FTD; 3 FTD	Hypoperfusion in regions overlapping with the resting-state functional MRI-derived 'salience network'	Boeve et al. (2012)

Table 27.1 (continued)

Scan type	Radiotracer	Participants	Main findings	Reference
PET blood flow/ metabolism	^{18}FDG	12 ALS (5 FU); 3 poliomyelitis; 11 HC	Widespread and progressively reduced cerebral metabolism (not cerebellum) in those with clinical UMN signs	Dalakas et al. (1987)
		3 PLS	Reduced uptake in pericentral cortex	Garnett et al. (1990)
		18 ALS	Reduced glucose metabolism over entire cortex and frontal lobes. Some correlation with neuropsychological impairments	Ludolph et al. (1992)
		3 PLS	Reduced uptake in pericentral cortex in 2/3 patients	Pringle et al. (1992)
		7 ALS (3 FU); 1 PMA; 11 HC	No overall group difference. Progressive decrease in glucose metabolism in precentral gyrus but *increase* in middle frontal gyrus with progression	Hoffman et al. (1992)
		3 PLS with parkinsonian signs; control database	Precentral, prefrontal and cingulate uptake reductions	Mabuchi et al. (2004)
		3 *TARDBP* fALS-FTD	Hypometabolism in frontal associative areas	Chio et al. (2010)
		3 PLS	Focal hypometabolism in the precentral gyri—the 'stripe sign'	Claassen et al. (2010)
		32 ALS 22 HC	*Increased* metabolism in brainstem, amygdalae and cerebellum in all patients. Decreased metabolism in frontal and parietal regions in bulbar versus spinal onset	Cistaro et al. (2012)
		6 ALS; 4 ALS-FTD	More extensive hypometabolism in ALS, including orbitofrontal cortex; relative *preservation* of anterolateral frontal metabolism in ALS patients and perirolandic region in ALS-FTD	Renard et al. (2012)

(continued)

Table 27.1 (continued)

Scan type	Radiotracer	Participants	Main findings	Reference
		1 ALS-dementia	FTD-like hypometabolism despite clinical Alzheimer-like dementia; *C9ORF72* hexanucleotide expansion later identified	Adeli et al. (2014)
		9 ALS;4 ALS-dementia; 13 HC	Hypoperfusion and hypometabolism in anterior cerebral hemispheres (and cerebellar hypoperfusion) in ALS-dementia	Tanaka et al. (1993)
		30 ALS; 12 ALS-FTD; 15 C9ORF72-ALS; 40 HC	Hypometabolism in *C9ORF72*-ALS in anterior and posterior cingulate cortex, insula, caudate and thalamus more widespread than in ALS-FTD	Cistaro et al. (2014)
		70 ALS; 7 PLS; 4 PMA; 20 HC	Perirolandic and prefrontal hypometabolism in ALS and PLS patients. DA correctly classified 95% of ALS cases	Van Laere et al. (2014)
		195 ALS; 40 HC	Hypometabolism in frontal, motor and occipital cortex. Hypermetabolism in midbrain, temporal pole and CST in ALS patients. DA correctly classified 95% of ALS cases	Pagani et al. (2014)
		175 ALS; 10 PLS; 4 PMA; 20 HC	Frontal hypometabolism and cerebellar-occipital hypermetabolism in ALS and PLS patients. SVM approach predicted 100% of the new ALS cases. Extensive frontotemporal hypometabolism was predictive for a lower survival	Van Weehaeghe et al. (2016)

Table 27.1 (continued)

Scan type	Radiotracer	Participants	Main findings	Reference
		259 ALS; 40 HC	Eight independent components discriminated ALS patients with 99.0% accuracy. Bilateral cerebellum/midbrain alone discriminated 96.3% of ALS patients	Pagani et al. (2016)
		94 ALS-Cn; 20 ALS-FTD; 37 ALS-Ci	Frontal and prefrontal hypometabolism and cerebellar, midbrain and CST hypermetabolism progressively more severe proportionally with cognitive impairment	Canosa et al. (2016)
		30 ALS; 30 HC	Spinal cord hypermetabolism in ALS patients	Marini et al. (2016)
		10 ALS; 10 HC	Spinal cord hypermetabolism correlated in ALS patients with the progression of the ALS FRS. No changes in 11C-FMZ uptake	Yamashita et al. (2017)
		10 ALS	The extent of hypometabolism in primary motor cortex correlated with symptom duration	Endo et al. (2017)
		SET 1: 175 ALS 20 HC; SET 2: 195 ALS 40 HC	ALS pattern consistency between the two sets. Frontal hypometabolism in HC of SET 2 as compared to HC SET 1	D'hulst et al. (2018)
		70 ALS; 33 PP; 29 HC	DA correctly classified 82% of ALS and PP, 85% for disease-specific pattern expression scores	Devrome et al. (2018)
		44 ALS; 44 HC	Cervical and dorsal spinal cord hypermetabolism and frontal-dorsolateral cortex hypometabolism in ALS patients	Marini et al. (2018)
		265 ALS; 60 HC	Good evidence for FDG-PET utility to support the diagnosis also if not justified as a routine investigation	Agosta et al. (2018)

(continued)

Table 27.1 (continued)

Scan type	Radiotracer	Participants	Main findings	Reference
		95 ALS (60 spinal-onset, 35 bulbar-onset); 112 HC	Hypometabolism in primary motor cortex and hypermetabolism in cerebellum discriminated spinal versus bulbar symptom onset with 63% accuracy	Sala et al. (2019)
		159 ALS	Positive correlation in prefrontal and anterior cingulate cortex between metabolism and *APOE* with lower metabolism towards the ε2/ε2 extreme	Canosa et al. (2019)
	$^{15}O_2$ and $C^{15}O_2$	12 ALS; 6 HC	Widespread impairment of activation, with expanded region of activation in response to movement task	Kew et al. (1993b)
		10 ALS; 5 HC	Widespread reductions in blood flow in response to motor task, greatest in those with cognitive impairment (reduced verbal fluency)	Kew et al. (1993a)
		12 ALS; 6 HC	Those with cognitive impairment (reduced verbal fluency) showed reduced frontal (insula and thalamic) reductions in rCBF in response to cognitive task	Abrahams et al. (1995)
	$H_2{}^{15}{}_O$	17 ALS; 17 HC	Widespread reductions in cortical binding	Lloyd et al. (2000)
PET ligand	^{11}C-Flumazenil ($GABA_A$ receptor)	5 PLS	Regional cerebral blood flow reductions in fronto-opercular region, mainly precentral gyrus, extending to ventrolateral prefrontal region and anterior cingulate cortex	Le Forestier et al. (2001)
		24 ALS; 10 homozygous 'D90' *SOD1* fALS; 2 presymptomatic homozygous 'D90' *SOD1* carriers; 24 HC	Distinct less motor, more frontal reductions in binding in more slowly progressive 'D90A' (including two presymptomatics) compared with sporadic ALS patients	Turner et al. (2005b)

Table 27.1 (continued)

Scan type	Radiotracer	Participants	Main findings	Reference
		4 PLS; 24 ALS; 10 hom 'D90' *SOD1* fALS 24 HC	Similar pattern of reduced binding in PLS and sporadic ALS patients. Preserved orbitofrontal binding in PLS versus both ALS groups	Turner et al. (2007a)
		12 ALS	Reduced binding in right inferior frontal and superior temporal gyri plus insula with poorer verbal fluency. Reduced left middle frontal gyrus and left cuneus with poorer confrontation naming	Wicks et al. (2008)
		10 ALS	Reduced binding in anterior cingulate gyrus related to writing errors	Yabe et al. (2012)
		10 ALS 10 HC	Widespread binding, including CST, DLPFC, thalamus (linked to clinical UMN signs)	Turner et al. (2004)
	11C-PK11195 (peripheral BZP receptor on activated microglia)	5 FTD 8 HC	Increased binding in frontotemporal regions	Cagnin et al. (2004)
		1 PLS and 1 Mills' syndrome patient with predominant right hemiparesis	Binding predominantly in left hemisphere	Turner et al. (2005a)
	18 F-DPA-714 (TSPO ligand expressed on activated microglia)	10 ALS 10 HC	Significantly increased binding in primary motor, supplementary motor and temporal lobe cortices	Corcia et al. (2012)
	11C-WAY100635 (5-HT1A receptor)	21 ALS (nondepressed); 19 HC	Marked frontotemporal reductions in binding	Turner et al. (2005c)
		21 ALS (nondepressed); 11 homozygous (nondepressed) 'D90A' fALS; 19 HC	Proportionately increased regional binding in more slowly progressive familial ALS patients	Turner et al. (2007b)
		4 FTD (nondepressed); 8 HC	Marked frontotemporal reductions in binding	Lanctot et al. (2007)

(continued)

Table 27.1 (continued)

Scan type	Radiotracer	Participants	Main findings	Reference
	18 F-6-Fluorodopa (presynaptic dopamine receptor)	12 ALS-parkinsonism-dementia complex of Guam; 7 HC	Intermediate presynaptic dopaminergic deficit in ALS-predominant patients ($n = 4$)	Snow et al. (1990)
		16 ALS; 13 HC	Progressive decline in dopaminergic function with disease duration	Takahashi et al. (1993)
	11C-Raclopride (postsynaptic dopamine receptor)	1 *FUS* fALS; HC	Decreased putamenal binding (no clinical parkinsonian features)	Kono et al. (2012)
	11C-PBR28 (peripheral benzodiazepine receptors)	10 ALS; 10 HC	Higher uptake in precentral gyrus positively correlated with UMNB scores and negatively with ALSFRS-R	Zürcher et al. (2015)
		10 ALS; 10 HC	Higher uptake in motor cortex colocalised and correlated negatively with reduced FA and cortical thinning. All correlated with UMNB	Alshikho et al. (2016)
		40 ALS	In precentral gyrus, positive correlation with mI/Cr and UMNB and negative correlations with NAA/Cr and FA	Ratai et al. (2018)
		10 ALS; 10 HC	Higher uptake in motor regions colocalises with reduced cortical thickness and FA	Paganoni et al. (2018)
	62Cu-ATSM (over-reductive mitochondrial state)	12 ALS; 9 HC	Increased uptake in bilateral motor cortex negatively correlated with ALSFRS-R	Ikawa et al. (2015)
	11C PBB (Tau protein tracer)	5 ALS/ Parkinson; 13 HC	Deposition of 11C PBB in cerebral cortex, white matter and CST correlating in frontal, temporal and parietal cortex with MMSE	Shinotoh et al. (2019)
	18F-Fluorbetaben (amyloid tracer); 18F-FDG	18 ALS; 24 HC	Three ALS patients were 18F-fluorbetaben positive. Hypometabolism in frontal cortex and hypermetabolism in cerebellum	Matías-Guiu et al. (2016)

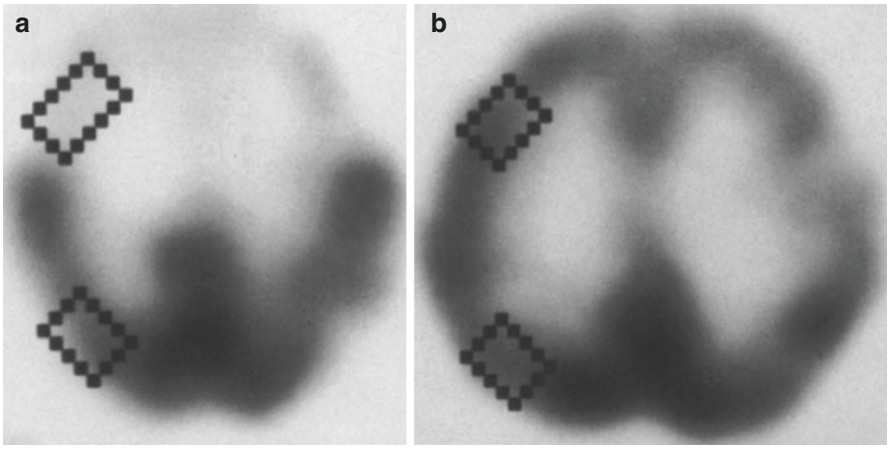

Fig. 27.1 ^{123}I-IMP SPECT in an ALS patient with dementia (**a**) compared to a healthy control (**b**). There is a clear loss of frontotemporal uptake in keeping with the understanding of extra-motor spread of pathology (Adapted from Sawada et al. (1988) with kind permission of Springer Science+Business Media; superimposed boxes show quantitative sampling regions)

frontal lobes of the larger ALS patient group (when compared to healthy controls) (Morimoto et al. 2012).

At least one third of cases with a family history of ALS are linked to an intronic hexanucleotide repeat expansion within *C9ORF72*, and carriers within the same pedigree may manifest 'pure' (usually behavioural variant) FTD, ALS or mixed ALS-FTD (Majounie et al. 2012). A SPECT study in affected gene carriers showed a similar frontal hypometabolism in the single ALS-FTD subject to those with pure FTD, with the overall pattern showing overlap with the 'salience network' as defined by resting-state functional MRI (Boeve et al. 2012).

27.3 PET

27.3.1 Blood Flow and Metabolism

The initial application of PET to ALS was in studies of cerebral blood flow and metabolism, though superseded by noninvasive functional MRI (Turner et al. 2012). Early and longitudinal studies with PET in ALS using ^{18}F-fluorodeoxyglucose (FDG) as a surrogate for cerebral metabolism (regional cerebral metabolic rate for glucose—rCMRGlc) confirmed widespread and progressive reductions in those ALS patients with clinical UMN signs (Dalakas et al. 1987). This was linked to neuropsychological deficits of a frontal lobe nature in ALS patients, particularly verbal fluency (Ludolph et al. 1992), in keeping with the predilection of ALS to cause a dysexecutive syndrome (Phukan et al. 2012). Alternative tracers $H_2{}^{15}{}_O$ and $C^{15}O_2$ were used to measure similar reductions in regional cerebral blood flow

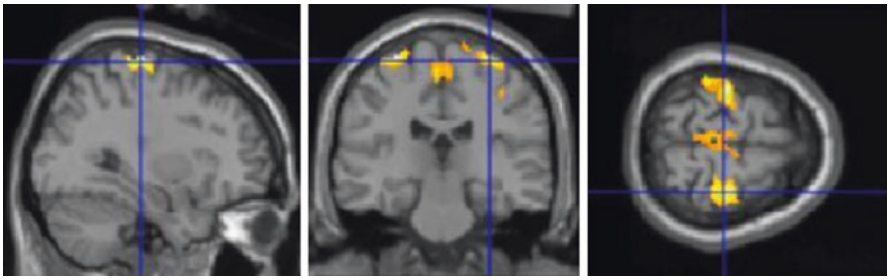

Fig. 27.2 FDG-PET findings in an ALS patient with spinal onset compared with 40 control subjects. Statistically significant hypometabolic clusters (SPM8, $p < 0.05$ $FDR_{corrected}$) are highlighted on a MRI T1 template. Left sagittal view; middle, coronal view; right, transverse view

(rCBF) in ALS patients with dementia (Tanaka et al. 1993) and were also linked to abnormalities of verbal fluency in ALS patients without overt dementia (Kew et al. 1993a). Some studies of patients with the UMN-only, consistently slowly progressive and related disorder primary lateral sclerosis (PLS) have demonstrated a strikingly focal, though inconsistent, hypometabolism of the precentral gyri (the 'stripe sign'), in keeping with the frequent observation of atrophy in this region (Pringle et al. 1992; Claassen et al. 2010).

The increasing availability and low cost of FDG-PET have increased its application to both research and clinical practice in ALS (Fig. 27.2). Studies in which the number of recruited ALS patients dramatically increased were able to delineate metabolic patterns of patients with spinal versus bulbar onset to symptoms (Cistaro et al. 2012) and between patients carrying the *C9ORF72* expansion mutation and apparently sporadic cases (Cistaro et al. 2014). Two studies recruiting a very large number of patients set a well-defined metabolic pattern for ALS. Frontal, prefrontal and pre- and post-central hypometabolism coupled to cerebellar, midbrain and corticospinal tract hypermetabolism, the latter originating by extensive astrocytosis in these areas, characterised ALS patients and allowed up to a 95% discrimination at the single patient level (Van Laere et al. 2014; Pagani et al. 2014). Further studies underscored the impact of frontal hypometabolism on survival (Van Weehaeghe et al. 2016), identified independent components able to discriminate ALS patients with an accuracy of 99% (Pagani et al. 2016) and cross-validated these findings comparing the respective datasets (D'hulst et al. 2018). Further FDG-PET studies have investigated metabolic differences between ALS patients and Parkinson-plus syndromes (Devrome et al. 2018), the association between hypometabolism extension and disease progression (Endo et al. 2017) and the correlation between metabolism and *APOE* genotypes, strengthening the role for ε2 as a risk factor for cognitive impairment in ALS (Canosa et al. 2019).

With potential for more routine clinical applications, FDG-PET focused on the detection of cognitive impairment in ALS patients and spinal cord pathology. Using a much higher sample size than the original investigations, the cerebral hypometabolic pattern was noted to progressively spread towards the prefrontal cortex in

relation to executive cognitive impairment and frontotemporal dementia (Canosa et al. (2016). Spinal cord hypermetabolism in ALS has been noted in three FDG-PET investigations (Yamashita et al. 2017; Marini et al. 2016, 2018), though univariate analysis failed to discriminate ALS patients with spinal versus bulbar onset to symptoms (Sala et al. 2019). The overall clinical value of FDG-PET in ALS was evaluated by a panel of expert neurologists and nuclear medicine physicians, concluding that although the methodology has a good utility to support the diagnosis, it is not yet justified as a routine investigation (Agosta et al. 2018).

27.3.2 Ligand Studies

PET ligands have probed specific molecular pathways and provided unique in vivo insight into ALS pathogenesis (Fig. 27.3).

27.3.2.1 An Inhibitory Interneuronal Deficit

A variety of clinical and pathological evidence supports a potentially fundamental loss of cortical inhibitory influence with or without concomitant cortical hyperexcitability in the pathogenesis of ALS (Turner and Douaud 2012; Turner and Kiernan 2012). Cortical hyperexcitability is a consistent feature of ALS, across phenotypes (Van den Bos et al. 2018). The 'boundary shift' in cortical activation seen in response to a joystick task led to the initial hypothesis of a loss of cortical inhibitory interneuronal circuits (Kew et al. 1993b) (Fig. 27.4). Widespread extra-motor cortical changes were then seen using the inhibitory neurotransmitter γ-aminobutyric acid $(GABA)_A$ receptor ligand ^{11}C-flumazenil, providing further evidence for loss of inhibitory influences (Lloyd et al. 2000).

Subsequent comparative ^{11}C-flumazenil PET studies were carried out in familial cases associated with a rare recessive mutation in the superoxide dismutase-1 gene (*SOD1*) linked to a consistently slowly progressive form of ALS. These demonstrated relative preservation of tracer binding in motor regions, in patients matched for disability and UMN signs, supporting the view that preservation of inhibitory influence might have prognostic significance (Turner et al. 2005b).

Comparative studies in PLS revealed preservation of inhibitory influences frontally (Turner et al. 2007a), in keeping with the generally lower incidence of overt cognitive impairment in this group.

27.3.2.2 Neuroinflammation

A key role for neuroinflammatory mechanisms in the pathogenesis of ALS remains the subject of active research (Philips and Robberecht 2011; Evans et al. 2013). The PET ligand ^{11}C-PK11195 binds to the peripheral benzodiazepine receptor expressed by activated microglia. A study in ALS patients provided in vivo evidence of widespread corticospinal tract and extra-motor microglial activation (Turner et al. 2004). A particularly tight correlation between thalamic ^{11}C-PK11195 binding and clinical UMN burden scores in this study may reflect the widespread connectivity of this structure and its disease-related disconnection in ALS. Cortical binding was notably

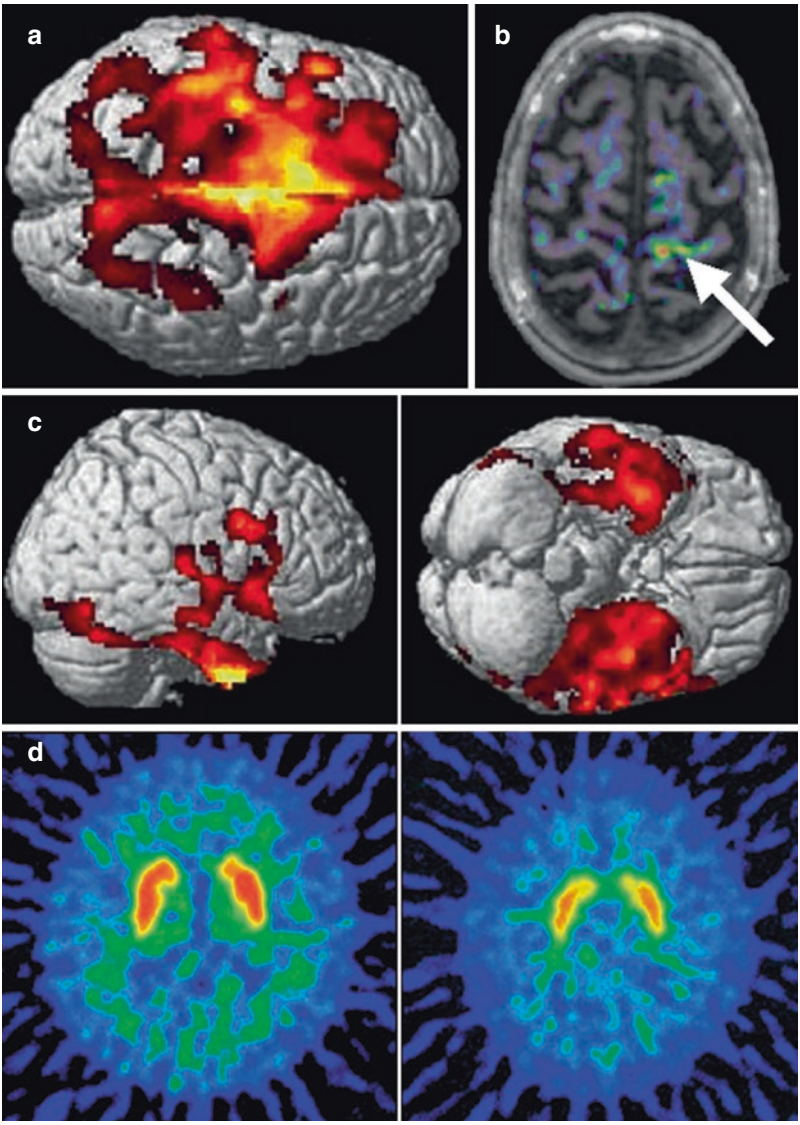

Fig. 27.3 Composite image from ligand PET studies in ALS, revealing different aspects of pathogenesis. A large area of motor and premotor cortex with reduced binding of the $GABA_A$ receptor ligand ^{11}C-flumazenil in ALS patients compared with healthy controls (**a**) supporting a loss of interneuronal inhibitory influence. Evidence of activated microglia, as demonstrated by binding of the peripheral benzodiazepine receptor ^{11}C-PK11195 (**b**), was localised to the left motor cortex (*arrow*) of a patient with weakness lateralised to the right-sided limbs. Right and inferior views of the brain show strikingly frontotemporal localisation of reduced binding of the serotonin $5\text{-}HT_{1A}$ receptor ligand ^{11}C-WAY100635 (**c**) in keeping with the pathological links between ALS and FTD. Reduced ^{11}C-raclopride binding to the striatal postsynaptic dopamine D2 receptor (**d**) (control subject on *left*, *FUS* fALS patient on the *right*) may reflect the occasional observation of parkinsonian signs in those with ALS (Adapted from Turner et al. (2012) with permission of Future Medicine Ltd., and Kono et al. (2012), with kind permission of Springer Science+Business Media)

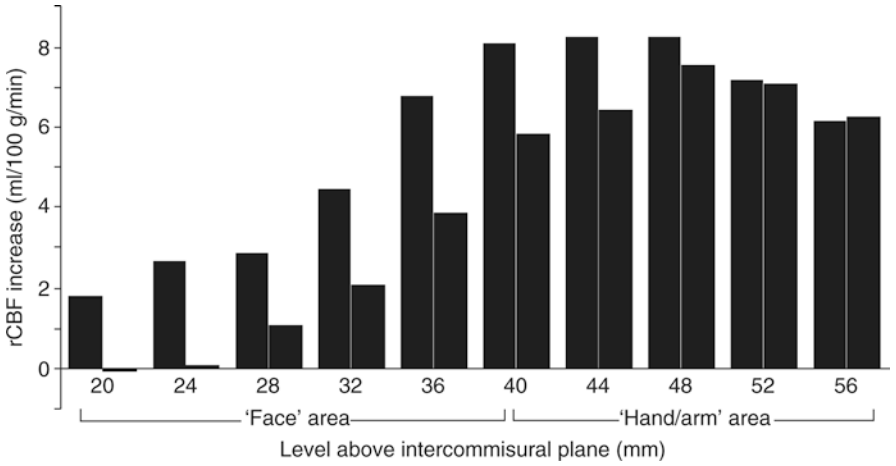

Fig. 27.4 Paired histogram showing mean regional CBF increases at ten points along the motor cortex in ALS (left column of each pair) and healthy controls (right column of each pair) in response to a motor task using hand-held joystick. The ALS patients demonstrated a 'boundary shift' in activation spreading to involve the face as well as hand motor areas. Loss of local inhibitory neuronal circuits was hypothesised (Adapted from Kew et al. (1993b), with permission of Oxford University Press)

lateralised within the hemisphere contralateral to the most affected body side in individuals with rare forms of motor neuron disease (Turner et al. 2005a). Immunohistochemistry studies have subsequently confirmed extensive microglial activation in the CST (Brettschneider et al. 2012). A new ligand for the translocator protein (TSPO) expressed by activated microglia—^{18}F-DPA-714—shows promise for future human ALS studies, with significantly increased binding in primary motor, supplementary motor and temporal lobe cortices, though with marked overlap between healthy control and patient distribution volume ratios (Corcia et al. 2012).

Previous ALS studies have described a significant proliferation and activation of astrocytes as well as activated microglia, in pyramidal cells of the motor cortex and in their projections to the spinal cord (Barbeito et al. 2004). Such reactive proliferation has been investigated by ^{11}C-PBR28, a radiotracer with 80 times greater binding specificity than ^{11}C-PK11195 for peripheral benzodiazepine receptors in the outer mitochondrial membrane of microglia and astrocytes. Increase of ^{11}C-PBR28 intensity in motor cortex and corticospinal tracts was similarly correlated with the clinical UMN burden scores (Zürcher et al. 2015, Fig. 27.5), and additionally reported to colocalise with cortical thinning and decreased fractional anisotropy (Alshikho et al. 2016; Paganoni et al. 2017), and correlated with precentral gyrus with markers of gliosis as detected by magnetic resonance spectroscopy (Ratai et al. 2018).

A PET oxidative stress marker, ^{62}Cu-ATSM, was found to accumulate in regions around the central sulcus in proportion to decreased motor function, underscoring a role of mitochondrial dysfunction in motor neuron degeneration (Ikawa et al. 2015).

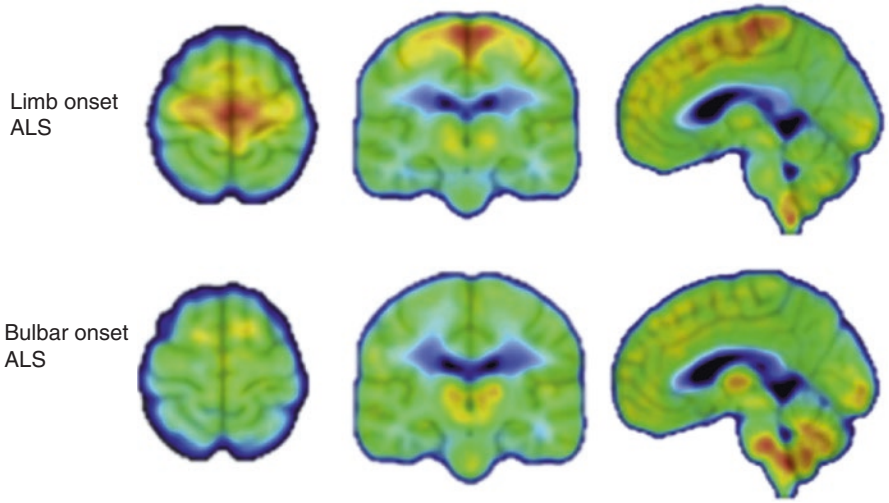

Fig. 27.5 [^{11}C]-PBR28 PET images from ALS patients showing areas of microglial activation (binding potential shown as a heat map). The top row is based on a group of ALS patients with limb onset to symptoms, with the signal predominantly located in motor cortex. The bottom row shows a group of bulbar-onset patients where there is signal more concentrated in the pons and cerebellum. Figure adapted from Zürcher et al. 2015

Finally, deposits of fibrillar amyloid were found in some ALS patients suggesting comorbid Alzheimer's disease (Matías-Guiu et al. 2016).

27.3.2.3 Serotonergic Neuronal Involvement

A serotonin 5-HT$_{1A}$ receptor PET ligand ^{11}C-WAY100635 revealed unexpectedly marked reductions in binding in a group of (importantly) nondepressed ALS patients (Turner et al. 2005c), with proportionately greater regional binding seen in those with a more slowly progressive form of familial ALS (Turner et al. 2007b). Loss of binding was located mainly in frontotemporal regions and was strikingly similar in distribution to a subsequent study in patients with pure FTD (Lanctot et al. 2007), later also confirmed histologically (Bowen et al. 2008). Ostensibly assumed to be a surrogate marker of cerebral pyramidal cell loss in ALS (DeFelipe et al. 2001), this transmitter system has a number of other potential roles in ALS pathogenesis (Sandyk 2006), including the regulation of motoneuronal excitability, neurotrophic actions and spasticity (Dentel et al. 2013), and warrants further study.

27.3.2.4 Parkinsonian Overlap

With the emerging theme of a multisystem cerebral degeneration, and the long-standing observation of extrapyramidal signs among some ALS patients (Hudson 1981), PET studies using ligands previously applied to Parkinson's disease (PD) patients have been applied to ALS. Both pre- and postsynaptic dopamine receptors, namely, ^{18}F-6-fluorodopa and ^{11}C-raclopride, have provided evidence for involvement of the dopaminergic system in cases of ALS, even in the absence of clinical

signs (Takahashi et al. 1993; Kono et al. 2012). In contrast, cases of PLS with marked parkinsonian features clinically showed no changes in nigrostriatal regions with either ligand but hypometabolism in the precentral gyrus, extending to prefrontal and cingulate regions using FDG PET (Mabuchi et al. 2004). The same held true for ALS patients with parkinsonian signs in which 123I-ioflupane SPECT was normal in 17/19 patients but metabolism relatively decreased in left cerebellum and increased in right insula and frontal regions (Calvo et al. 2019). Tau protein imaging in patients with the ALS-PD-dementia complex found in inhabitants of the Kii Peninsula, using ^{11}C-PBB3 PET, revealed (unsurprisingly) widespread grey and white matter distribution, including corticospinal tracts, pons and cerebellum (Shinotoh et al. 2019).

27.3.3 The Future

Cerebral radionuclide studies in ALS were prescient of the current era in which ALS and FTD are accepted to have fundamental overlap. Advanced MRI-based techniques, including resting-state functional and network-based analysis of whole-brain structural connectivity, may ultimately offer greater specificity but currently lack application at the individual patient level (Menke et al. 2017).

Ligand PET offers great potential to explore disease mechanisms, particularly with advances in statistical methods for whole-brain analysis that are not reliant on a priori region-of-interest definition, which may be difficult to define in early disease. However, this has typically required short-lived radionuclides to date, entailing a local cyclotron, and so access has been restricted to a few centres with appropriate experience. Moreover, the precise pharmacodynamic properties required for a successful radioligand lie within a narrow range, so that an active radiochemistry research and development programme, including quality control processes, places further restrictions on the availability of this kind of PET research.

It seems likely that, as for other neurodegenerative disorders, the emergence of symptoms in ALS occurs years, perhaps decades, after the earliest cellular changes. There is a consistent diagnostic delay of up to 1 year after symptom onset in ALS, and studies of individuals soon after symptoms are all too rare as a result. The identification of familial ALS cases (~5%) with common and highly penetrant genetic mutations such as those in *SOD1* gene and the *C9ORF72* repeat expansion offers a potential window on such events, through the study of presymptomatic carriers (Benatar and Wuu 2012). Flumazenil PET was one of the first applications of this approach, in which two presymptomatic individuals showed some evidence for an early deficit in $GABA_A$ receptor function in the left operculum region (Turner et al. 2005b). Novel $GABA_A$ receptor radioligands with longer half-lives may offer broader applicability of PET to study at least one potentially important pathogenic mechanism (Jackson et al. 2013). Re-evaluation of the serotonergic system using PET in the post-FTD-linked era of ALS, as well as the application of novel neuroinflammatory target ligands, might also identify novel therapeutic targets. PET ligands might then serve as pharmacodynamic markers for drug discovery, providing proof of mechanism in the early stages of drug development. Finally, with the accumulation of aggregated protein as a common theme across neurodegenerative

disorders, the development of PET ligands for *intracellular* targets has been anticipated. Tau imaging is the exemplar, which has made a major contribution to advancing Alzheimer's disease research (Wang and Edison 2019). It has been interesting to note that the tau ligand 18F-AV-1451 has shown increased binding in areas associated with TDP-43 pathology (Bevan-Jones et al. 2018a, b), suggesting it may have wider potential in ALS. The challenges of detecting TDP-43 as a biomarker in biofluid studies are already recognised (Feneberg et al. 2018). Significant technical challenges notwithstanding (Skotland 2012), TDP-43 PET imaging would have the potential to detect many more presymptomatic individuals and provide a readout for the neuroprotective therapies of the future.

References

Abe K, Fujimura H, Toyooka K, Hazama T, Hirono N, Yorifuji S, Yanagihara T (1993) Single-photon emission computed tomographic investigation of patients with motor neuron disease. Neurology 43:1569–1573

Abe K, Fujimura H, Toyooka K, Sakoda S, Yorifuji S, Yanagihara T (1997) Cognitive function in amyotrophic lateral sclerosis. J Neurol Sci 148:95–100

Abrahams S, Leigh PN, Kew JJ, Goldstein LH, Lloyd CM, Brooks DJ (1995) A positron emission tomography study of frontal lobe function (verbal fluency) in amyotrophic lateral sclerosis. J Neurol Sci 129(Suppl):44–46

Adeli A, Savica R, Lowe VJ, Vemuri P, Knopman DS, Dejesus-Hernandez M, Rademakers R, Fields JA, Crum BA, Jack CR, Petersen RC, Boeve BF (2014) The GGGGCC repeat expansion in C9ORF72 in a case with discordant clinical and FDG-PET findings: PET trumps syndrome. Neurocase 20:110–120

Agosta F, Altomare D, Festari C et al (2018) Clinical utility of FDG-PET in amyotrophic lateral sclerosis and Huntington's disease. Eur J Nucl Med Mol Imaging 45:1546–1556

Alshikho MJ, Zürcher NR, Loggia ML et al (2016) Glial activation colocalizes with structural abnormalities in amyotrophic lateral sclerosis. Neurology 87:2554–2561

Barbeito LH, Pehar M, Cassina P, Vargas MR, Peluffo H, Viera L et al (2004) A role for astrocytes in motor neuron loss in amyotrophic lateral sclerosis. Brain Res Rev 47(1–3):263–274

Benatar M, Wuu J (2012) Presymptomatic studies in ALS: rationale, challenges, and approach. Neurology 79:1732–1739

Bevan-Jones RW, Cope TE, Jones SP, Passamonti L, Hong YT, Fryer T et al (2018a) [(18) F]AV-1451 binding is increased in frontotemporal dementia due to C9orf72 expansion. Ann Clin Transl Neurol 5(10):1292–1296

Bevan-Jones WR, Cope TE, Jones PS, Passamonti L, Hong YT, Fryer TD et al (2018b) [(18) F]AV-1451 binding in vivo mirrors the expected distribution of TDP-43 pathology in the semantic variant of primary progressive aphasia. J Neurol Neurosurg Psychiatry 89(10):1032–1037

Boeve BF, Boylan KB, Graff-Radford NR, DeJesus-Hernandez M, Knopman DS, Pedraza O, Vemuri P, Jones D, Lowe V, Murray ME, Dickson DW, Josephs KA, Rush BK, Machulda MM, Fields JA, Ferman TJ, Baker M, Rutherford NJ, Adamson J, Wszolek ZK, Adeli A, Savica R, Boot B, Kuntz KM, Gavrilova R, Reeves A, Whitwell J, Kantarci K, Jack CR Jr, Parisi JE, Lucas JA, Petersen RC, Rademakers R (2012) Characterization of frontotemporal dementia and/or amyotrophic lateral sclerosis associated with the GGGGCC repeat expansion in C9ORF72. Brain 135:765–783

Bowen DM, Procter AW, Mann DM, Snowden JS, Esiri MM, Neary D, Francis PT (2008) Imbalance of a serotonergic system in frontotemporal dementia: implication for pharmacotherapy. Psychopharmacology 196:603–610

Brettschneider J, Toledo JB, Van Deerlin VM, Elman L, McCluskey L, Lee VM, Trojanowski JQ (2012) Microglial activation correlates with disease progression and upper motor neuron clinical symptoms in amyotrophic lateral sclerosis. PLoS One 7:e39216

Brownell B, Oppenheimer DR, Hughes JT (1970) The central nervous system in motor neurone disease. J Neurol Neurosurg Psychiatry 33:338–357

Cagnin A, Rossor M, Sampson EL, Mackinnon T, Banati RB (2004) In vivo detection of microglial activation in frontotemporal dementia. Ann Neurol 56:894–897

Calvo A, Chiò A, Pagani M et al (2019) Parkinsonian traits in amyotrophic lateral sclerosis (ALS): a prospective population-based study. J Neurol 266:1633–1642

Canosa A, Pagani M, Cistaro A et al (2016) 18F-FDG-PET correlates of cognitive impairment in ALS. Neurology 86:44–49

Canosa A, Pagani M, Brunetti M et al (2019) Correlation between apolipoprotein E genotype and brain metabolism in amyotrophic lateral sclerosis. Eur J Neurol 26:306–312

Chio A, Calvo A, Moglia C, Restagno G, Ossola I, Brunetti M, Montuschi A, Cistaro A, Ticca A, Traynor BJ, Schymick JC, Mutani R, Marrosu MG, Murru MR, Borghero G (2010) Amyotrophic lateral sclerosis-frontotemporal lobar dementia in 3 families with p. Ala382Thr TARDBP mutations. Arch Neurol 67:1002–1009

Cistaro A, Valentini MC, Chio A, Nobili F, Calvo A, Moglia C, Montuschi A, Morbelli S, Salmaso D, Fania P, Carrara G, Pagani M (2012) Brain hypermetabolism in amyotrophic lateral sclerosis: a FDG PET study in ALS of spinal and bulbar onset. Eur J Nucl Med Mol Imaging 39:251–259

Cistaro A, Pagani M, Montuschi A, Calvo A, Moglia C, Canosa A, Restagno G, Traynor BJ, Nobili F, Carrara G, Fania PC, Lopiano L, Valentini MC, Chiò A (2014) The metabolic signature of C9ORF72-related ALS, compared to non-mutated patients: a FDG PET study. Eur J Nucl Med Mol Imaging 41:844–852

Claassen DO, Josephs KA, Peller PJ (2010) The stripe of primary lateral sclerosis: focal primary motor cortex hypometabolism seen on fluorodeoxyglucose F18 positron emission tomography. Arch Neurol 67:122–125

Corcia P, Tauber C, Vercoullie J, Arlicot N, Prunier C, Praline J, Nicolas G, Venel Y, Hommet C, Baulieu JL, Cottier JP, Roussel C, Kassiou M, Guilloteau D, Ribeiro MJ (2012) Molecular imaging of microglial activation in amyotrophic lateral sclerosis. PLoS One 7:e52941

D'hulst L, Van Weehaeghe D, Chiò A et al (2018) Multicenter validation of [18F]-FDG PET and support-vector machine discriminant analysis in automatically classifying patients with amyotrophic lateral sclerosis versus controls. Amyotroph Lateral Scler Frontotemporal Degener 2018:1–8. https://doi.org/10.1080/21678421.2018.1476548

Dalakas MC, Hatazawa J, Brooks RA, Di Chiro G (1987) Lowered cerebral glucose utilization in amyotrophic lateral sclerosis. Ann Neurol 22:580–586

DeFelipe J, Arellano JI, Gomez A, Azmitia EC, Munoz A (2001) Pyramidal cell axons show a local specialization for GABA and 5-HT inputs in monkey and human cerebral cortex. J Comp Neurol 433:148–155

DeJesus-Hernandez M, Mackenzie IR, Boeve BF, Boxer AL, Baker M, Rutherford NJ, Nicholson AM, Finch NA, Flynn H, Adamson J, Kouri N, Wojtas A, Sengdy P, Hsiung GY, Karydas A, Seeley WW, Josephs KA, Coppola G, Geschwind DH, Wszolek ZK, Feldman H, Knopman DS, Petersen RC, Miller BL, Dickson DW, Boylan KB, Graff-Radford NR, Rademakers R (2011) Expanded GGGGCC hexanucleotide repeat in noncoding region of C9ORF72 causes chromosome 9p-linked FTD and ALS. Neuron 72:245–256

Dentel C, Palamiuc L, Henriques A, Lannes B, Spreux-Varoquaux O, Gutknecht L, Rene F, Echaniz-Laguna A, Gonzalez de Aguilar JL, Lesch KP, Meininger V, Loeffler JP, Dupuis L (2013) Degeneration of serotonergic neurons in amyotrophic lateral sclerosis: a link to spasticity. Brain 136:483–493

Devrome M, Van Weehaeghe D, De Vocht J et al (2018) Glucose metabolic brain patterns to discriminate amyotrophic lateral sclerosis from Parkinson plus syndromes. EJNMMI Res 8:110

Endo H, Sekiguchi K, Ueda T et al (2017) Regional glucose hypometabolic spread within the primary motor cortex is associated with amyotrophic lateral sclerosis disease progression: a fluoro-deoxyglucose positron emission tomography study. eNeurol Sci 6:74–79

Evans MC, Couch Y, Sibson N, Turner MR (2013) Inflammation and neurovascular changes in amyotrophic lateral sclerosis. Mol Cell Neurosci 53:34–41

Feneberg E, Gray E, Ansorge O, Talbot K, Turner MR (2018) Towards a TDP-43-Based Biomarker for ALS and FTLD. Mol Neurobiol 55(10):7789–7801

Garnett ES, Chirakal R, Firnau G, Nahmias C, Hudson AJ (1990) Recent developments in PET scanning related to amyotrophic lateral sclerosis and primary lateral sclerosis. In: Hudson AJ (ed) Amyotrophic lateral sclerosis: concepts in pathogenesis and etiology. University of Toronto Press, Toronto, ON, pp 358–370

Giordana MT, Ferrero P, Grifoni S, Pellerino A, Naldi A, Montuschi A (2011) Dementia and cognitive impairment in amyotrophic lateral sclerosis: a review. Neurol Sci 32:9–16

Hoffman JM, Mazziotta JC, Hawk TC, Sumida R (1992) Cerebral glucose utilization in motor neuron disease. Arch Neurol 49:849–854

Hudson AJ (1981) Amyotrophic lateral sclerosis and its association with dementia, parkinsonism and other neurological disorders: a review. Brain 104:217–247

Ikawa M, Okazawa H, Tsujikawa T et al (2015) Increased oxidative stress is related to disease severity in the ALS motor cortex: a PET study. Neurology 84:2033–2039

Ince PG, Evans J, Knopp M, Forster G, Hamdalla HH, Wharton SB, Shaw PJ (2003) Corticospinal tract degeneration in the progressive muscular atrophy variant of ALS. Neurology 60:1252–1258

Jackson A, Guilbert BB, Plant SD, Goggi J, Battle MR, Woodcraft JL, Gaeta A, Jones CL, Bouvet DR, Jones PA, O'Shea DM, Zheng PH, Brown SL, Ewan AL, Trigg W (2013) The development of potential new fluorine-18 labelled radiotracers for imaging the GABA (A) receptor. Bioorg Med Chem Lett 23:821–826

Kew JJ, Goldstein LH, Leigh PN, Abrahams S, Cosgrave N, Passingham RE, Frackowiak RS, Brooks DJ (1993a) The relationship between abnormalities of cognitive function and cerebral activation in amyotrophic lateral sclerosis. A neuropsychological and positron emission tomography study. Brain 116(Pt 6):1399–1423

Kew JJ, Leigh PN, Playford ED, Passingham RE, Goldstein LH, Frackowiak RS, Brooks DJ (1993b) Cortical function in amyotrophic lateral sclerosis. A positron emission tomography study. Brain 116(Pt 3):655–680

Kono S, Ouchi Y, Terada T, Suzuki M, Yagi S, Miyajima H (2012) Combined FDG and raclopride PET study in a case of ALS with the R521C FUS gene mutation. J Neurol 259:367–369

Lanctot KL, Herrmann N, Ganjavi H, Black SE, Rusjan PM, Houle S, Wilson AA (2007) Serotonin-1A receptors in frontotemporal dementia compared with controls. Psychiatry Res 156:247–250

Le Forestier N, Maisonobe T, Spelle L, Lesort A, Salachas F, Lacomblez L, Samson Y, Bouche P, Meininger V (2001) Primary lateral sclerosis: further clarification. J Neurol Sci 185:95–100

Lloyd CM, Richardson MP, Brooks DJ, Al Chalabi A, Leigh PN (2000) Extramotor involvement in ALS: PET studies with the GABA (A) ligand [(11) C] flumazenil. Brain 123(Pt 11):2289–2296

Ludolph AC, Elger CE, Bottger IW, Kuttig AG, Lottes G, Brune GG (1989) N-isopropyl-p-123I-amphetamine single photon emission computer tomography in motor neuron disease. Eur Neurol 29:255–260

Ludolph AC, Langen KJ, Regard M, Herzog H, Kemper B, Kuwert T, Bottger IG, Feinendegen L (1992) Frontal lobe function in amyotrophic lateral sclerosis: a neuropsychologic and positron emission tomography study. Acta Neurol Scand 85:81–89

Mabuchi N, Watanabe H, Atsuta N, Hirayama M, Ito H, Fukatsu H, Kato T, Ito K, Sobue G (2004) Primary lateral sclerosis presenting parkinsonian symptoms without nigrostriatal involvement. J Neurol Neurosurg Psychiatry 75:1768–1771

Majounie E, Renton AE, Mok K, Dopper EG, Waite A, Rollinson S, Chio A, Restagno G, Nicolaou N, Simon-Sanchez J, van Swieten JC, Abramzon Y, Johnson JO, Sendtner M, Pamphlett R, Orrell RW, Mead S, Sidle KC, Houlden H, Rohrer JD, Morrison KE, Pall H, Talbot K, Ansorge O, Hernandez DG, Arepalli S, Sabatelli M, Mora G, Corbo M, Giannini F, Calvo A, Englund

E, Borghero G, Floris GL, Remes AM, Laaksovirta H, McCluskey L, Trojanowski JQ, Van Deerlin VM, Schellenberg GD, Nalls MA, Drory VE, Lu CS, Yeh TH, Ishiura H, Takahashi Y, Tsuji S, Le Ber I, Brice A, Drepper C, Williams N, Kirby J, Shaw P, Hardy J, Tienari PJ, Heutink P, Morris HR, Pickering-Brown S, Traynor BJ (2012) Frequency of the C9orf72 hexanucleotide repeat expansion in patients with amyotrophic lateral sclerosis and frontotemporal dementia: a cross-sectional study. Lancet Neurol 11:323–330

Marini C, Cistaro A, Campi C et al (2016) A PET/CT approach to spinal cord metabolism in amyotrophic lateral sclerosis. Eur J Nucl Med Mol Imaging 43:2061–2071

Marini C, Morbelli S, Cistaro A et al (2018) Interplay between spinal cord and cerebral cortex metabolism in amyotrophic lateral sclerosis. Brain 141:2272–2279

Matías-Guiu JA, Pytel V, Cabrera-Martín MN, Galán L, Valles-Salgado M, Guerrero A, Moreno-Ramos T, Matías-Guiu J, Carreras JL (2016) Amyloid- and FDG-PET imaging in amyotrophic lateral sclerosis. Eur J Nucl Med Mol Imaging 43:2050–2060

Menke RA, Agosta F, Grosskreutz J, Filippi M, Turner MR (2017) Neuroimaging endpoints in amyotrophic lateral sclerosis. Neurotherapeutics 14(1):11–23

Morimoto N, Kurata T, Sato K, Ikeda Y, Sato S, Abe K (2012) Frontal dysfunctions of ALS-PBP patients in relation to their bulbar symptoms and rCBF decline. J Neurol Sci 319:96–101

Neary D, Snowden JS, Mann DM, Northen B, Goulding PJ, Macdermott N (1990) Frontal lobe dementia and motor neuron disease. J Neurol Neurosurg Psychiatry 53:23–32

Neumann M, Sampathu DM, Kwong LK, Truax AC, Micsenyi MC, Chou TT, Bruce J, Schuck T, Grossman M, Clark CM, McCluskey LF, Miller BL, Masliah E, Mackenzie IR, Feldman H, Feiden W, Kretzschmar HA, Trojanowski JQ, Lee VM (2006) Ubiquitinated TDP-43 in frontotemporal lobar degeneration and amyotrophic lateral sclerosis. Science 314:130–133

Pagani M, Chiò A, Valentini MC et al (2014) Functional pattern of brain FDG-PET in amyotrophic lateral sclerosis. Neurology 83:1067–1074

Pagani M, Öberg J, De Carli F et al (2016) Metabolic connectivity in amyotrophic lateral sclerosis as revealed by independent component analysis. Hum Brain Mapp 37:942–953

Paganoni S, Alshikho MJ, Zürcher NR, Cernasov P, Babu S, Loggia ML, Chan J, Chonde DB, Garcia DI, Catana C, Mainero C, Rosen BR, Cudkowicz ME, Hooker JM, Atassi N (2017) Imaging of glia activation in people with primary lateral sclerosis. Neuroimage Clin 17:347–353

Philips T, Robberecht W (2011) Neuroinflammation in amyotrophic lateral sclerosis: role of glial activation in motor neuron disease. Lancet Neurol 10:253–263

Phukan J, Pender NP, Hardiman O (2007) Cognitive impairment in amyotrophic lateral sclerosis. Lancet Neurol 6:994–1003

Phukan J, Elamin M, Bede P, Jordan N, Gallagher L, Byrne S, Lynch C, Pender N, Hardiman O (2012) The syndrome of cognitive impairment in amyotrophic lateral sclerosis: a population-based study. J Neurol Neurosurg Psychiatry 83:102–108

Pringle CE, Hudson AJ, Munoz DG, Kiernan JA, Brown WF, Ebers GC (1992) Primary lateral sclerosis. Clinical features, neuropathology and diagnostic criteria. Brain 115(Pt 2):495–520

Ratai EM, Alshikho MJ, Zürcher NR et al (2018) Integrated imaging of [11C]-PBR28 PET, MR diffusion and magnetic resonance spectroscopy 1H-MRS in amyotrophic lateral sclerosis. Neuroimage Clin 20:357–364

Renard D, Collombier L, Castelnovo G, Fourcade G, Kotzki PO, LaBauge P (2012) Brain FDG-PET changes in ALS and ALS-FTD. Acta Neurol Belg 111:306–309

Renton AE, Majounie E, Waite A, Simon-Sanchez J, Rollinson S, Gibbs JR, Schymick JC, Laaksovirta H, van Swieten JC, Myllykangas L, Kalimo H, Paetau A, Abramzon Y, Remes AM, Kaganovich A, Scholz SW, Duckworth J, Ding J, Harmer DW, Hernandez DG, Johnson JO, Mok K, Ryten M, Trabzuni D, Guerreiro RJ, Orrell RW, Neal J, Murray A, Pearson J, Jansen IE, Sondervan D, Seelaar H, Blake D, Young K, Halliwell N, Callister JB, Toulson G, Richardson A, Gerhard A, Snowden J, Mann D, Neary D, Nalls MA, Peuralinna T, Jansson L, Isoviita VM, Kaivorinne AL, Holtta-Vuori M, Ikonen E, Sulkava R, Benatar M, Wuu J, Chio A, Restagno G, Borghero G, Sabatelli M, Heckerman D, Rogaeva E, Zinman L, Rothstein JD, Sendtner M, Drepper C, Eichler EE, Alkan C, Abdullaev Z, Pack SD, Dutra A, Pak E, Hardy J, Singleton A, Williams NM, Heutink P, Pickering-Brown S, Morris HR, Tienari PJ, Traynor

BJ (2011) A hexanucleotide repeat expansion in C9ORF72 is the cause of chromosome 9p21-linked ALS-FTD. Neuron 72:257–268
Sala A, Iaccarino L, Fania PC et al (2019) Testing the diagnostic accuracy of [18F]FDG-PET in discriminating spinal- and bulbar-onset amyotrophic lateral sclerosis. Eur J Nucl Med Mol Imaging 46:1117–1131
Sandyk R (2006) Serotonergic mechanisms in amyotrophic lateral sclerosis. Int J Neurosci 116:775–826
Sawada H, Udaka F, Kishi Y, Seriu N, Mezaki T, Kameyama M, Honda M, Tomonobu M (1988) Single photon emission computed tomography in motor neuron disease with dementia. Neuroradiology 30:577–578
Shinotoh H, Shimada H, Kokubo Y et al (2019) Tau imaging detects distinctive distribution of tau pathology in ALS/PDC on the Kii Peninsula. Neurology 92:e136–e147
Skotland T (2012) Molecular imaging: challenges of bringing imaging of intracellular targets into common clinical use. Contrast Media Mol Imaging 7:1–6
Smith MC (1960) Nerve fibre degeneration in the brain in amyotrophic lateral sclerosis. J Neurol Neurosurg Psychiatry 23:269–282
Snow BJ, Peppard RF, Guttman M, Okada J, Martin WR, Steele J, Eisen A, Carr G, Schoenberg B, Calne D (1990) Positron emission tomographic scanning demonstrates a presynaptic dopaminergic lesion in Lytico-Bodig. The amyotrophic lateral sclerosis-parkinsonism-dementia complex of Guam. Arch Neurol 47:870–874
Takahashi H, Snow BJ, Bhatt MH, Peppard R, Eisen A, Calne DB (1993) Evidence for a dopaminergic deficit in sporadic amyotrophic lateral sclerosis on positron emission scanning. Lancet 342:1016–1018
Talbot PR, Goulding PJ, Lloyd JJ, Snowden JS, Neary D, Testa HJ (1995) Inter-relation between "classic" motor neuron disease and frontotemporal dementia: neuropsychological and single photon emission computed tomography study. J Neurol Neurosurg Psychiatry 58:541–547
Tanaka M, Kondo S, Hirai S, Sun X, Yamagishi T, Okamoto K (1993) Cerebral blood flow and oxygen metabolism in progressive dementia associated with amyotrophic lateral sclerosis. J Neurol Sci 120:22–28
Turner MR, Douaud G (2012) Faulty brakes: an inhibitory neuronal deficit in the pathogenesis of motor neuron disease. Adv Clin Neurosci Rehabil 12:10–11
Turner MR, Kiernan MC (2012) Does interneuronal dysfunction contribute to neurodegeneration in amyotrophic lateral sclerosis? Amyotroph Lateral Scler 13:245–250
Turner MR, Verstraete E (2015) What does imaging reveal about the pathology of amyotrophic lateral sclerosis? Curr Neurol Neurosci Rep 15(7):569
Turner MR, Cagnin A, Turkheimer FE, Miller CC, Shaw CE, Brooks DJ, Leigh PN, Banati RB (2004) Evidence of widespread cerebral microglial activation in amyotrophic lateral sclerosis: an [(11) C]®-PK11195 positron emission tomography study. Neurobiol Dis 15:601–609
Turner MR, Gerhard A, Al-Chalabi A, Shaw CE, Hughes RAC, Banati RB, Brooks DJ, Leigh PN (2005a) Mills' and other isolated upper motor neuron syndromes: in vivo study with [11C]-PK11195 PET. J Neurol Neurosurg Psychiatry 76:871–874
Turner MR, Hammers A, Al-Chalabi A, Shaw CE, Andersen PM, Brooks DJ, Leigh PN (2005b) Distinct cerebral lesions in sporadic and 'D90A' SOD1 ALS: studies with [11C] flumazenil PET. Brain 128:1323–1329
Turner MR, Rabiner EA, Hammers A, Al-Chalabi A, Grasby PM, Shaw CE, Brooks DJ, Leigh PN (2005c) [11C]-WAY100635 PET demonstrates marked 5-HT1A receptor changes in sporadic ALS. Brain 128:896–905
Turner MR, Hammers A, Al-Chalabi A, Shaw CE, Andersen PM, Brooks DJ, Leigh PN (2007a) Cortical involvement in four cases of primary lateral sclerosis using [(11) C]-flumazenil PET. J Neurol 254:1033–1036
Turner MR, Rabiner EA, Al-Chalabi A, Shaw CE, Brooks DJ, Leigh PN, Andersen PM (2007b) Cortical 5-HT1A receptor binding in patients with homozygous D90A SOD1 vs sporadic ALS. Neurology 68:1233–1235

Turner MR, Kiernan MC, Leigh PN, Talbot K (2009) Biomarkers in amyotrophic lateral sclerosis. Lancet Neurol 8:94–109

Turner MR, Agosta F, Bede P, Govind V, Lule D, Verstraete E (2012) Neuroimaging in amyotrophic lateral sclerosis. Biomark Med 6:319–337

Van den Bos MAJ, Higashihara M, Geevasinga N, Menon P, Kiernan MC, Vucic S (2018) Imbalance of cortical facilitatory and inhibitory circuits underlies hyperexcitability in ALS. Neurology 91(18):e1669–e1e76

van Es MA, Hardiman O, Chio A, Al-Chalabi A, Pasterkamp RJ, Veldink JH et al (2017) Amyotrophic lateral sclerosis. Lancet 390(10107):2084–2098

Van Laere K, Vanhee A, Verschueren J et al (2014) Value of 18fluorodeoxyglucose-positron-emission tomography in amyotrophic lateral sclerosis: a prospective study. JAMA Neurol 71:553–561

Van Weehaeghe D, Ceccarini J, Delva A et al (2016) Prospective validation of 18F-FDG brain PET discriminant analysis methods in the diagnosis of amyotrophic lateral sclerosis. J Nucl Med 57:1238–1243

Waldemar G, Vorstrup S, Jensen TS, Johnsen A, Boysen G (1992) Focal reductions of cerebral blood flow in amyotrophic lateral sclerosis: a [99mTc]-d, l-HMPAO SPECT study. J Neurol Sci 107:19–28

Wang YT, Edison P (2019) Tau imaging in neurodegenerative diseases using positron emission tomography. Curr Neurol Neurosci Rep 19(7):45

Waragai M, Takaya Y, Hayashi M (1997) Serial MRI and SPECT in amyotrophic lateral sclerosis: a case report. J Neurol Sci 148:117–120

Wicks P, Turner MR, Abrahams S, Hammers A, Brooks DJ, Leigh PN, Goldstein LH (2008) Neuronal loss associated with cognitive performance in amyotrophic lateral sclerosis: an (11C)-flumazenil PET study. Amyotroph Lateral Scler 9:43–49

Yabe I, Tsuji-Akimoto S, Shiga T, Hamada S, Hirata K, Otsuki M, Kuge Y, Tamaki N, Sasaki H (2012) Writing errors in ALS related to loss of neuronal integrity in the anterior cingulate gyrus. J Neurol Sci 315:55–59

Yamashita T, Hatakeyama T, Sato K et al (2017) Flow-metabolism uncoupling in the cervical spinal cord of ALS patients. Neurol Sci 38:659–665

Zürcher NR, Loggia ML, Lawson R et al (2015) Increased in vivo glial activation in patients with amyotrophic lateral sclerosis: assessed with [(11)C]-PBR28. Neuroimage Clin 7:409–414

PET in Huntington's Disease

28

H. P. H. (Berry) Kremer

Contents

28.1 Introduction 784
28.2 Clinical Features and Neuropathology of HD 784
28.3 Structural Defects Are Associated with Metabolic Defects 786
28.4 Dopamine Receptor Imaging: A Way to Establish Neuronal Integrity? 788
28.5 Imaging of Other Neurotransmitter Receptors 789
28.6 Other Intraneuronal Markers of Neurodegeneration 790
28.7 Inflammation as an Indicator of Neurodegeneration 791
28.8 PET Imaging as a Biomarker in Experimental Therapeutics 792
28.9 Conclusions 793
References 793

Abstract

From the 1980s onward, PET molecular imaging has yielded a wealth of information on the molecular and structural biology of neurodegeneration in patients with Huntington's disease. While currently not in use for day-to-day diagnostic or predictive clinical purposes in patients, it may acquire new relevance. In this review, I will outline its applications to the study of human preclinical and clinical disease, to our understanding of the neurobiology of Huntington's, as well as in the field of experimental therapeutics.

H. P. H. (Berry) Kremer (✉)
Department of Neurology AB51, University Medical Center Groningen, University of Groningen, Groningen, The Netherlands
e-mail: h.p.h.kremer@umcg.nl

R. A. J. O. Dierckx et al. (eds.), *PET and SPECT in Neurology*,
https://doi.org/10.1007/978-3-030-53168-3_28

28.1 Introduction

PET imaging has contributed considerably to our understanding of the biology of Huntington's disease (HD). It did confirm *in vivo*—in patients—molecular observations that had been made previously in human postmortem brains, and it has introduced novel concepts regarding the pathophysiology of the clinical manifestations as well as the neurodegenerative process itself. Moreover, PET imaging has been developed as a valuable biomarker that can be used in experimental therapeutics.

This chapter reviews how PET molecular imaging has been used in HD research. It focuses on how it has helped to delineate the extent of the neuropathology, on how molecular changes underlie the disease, and on how this has helped to better understand the clinical disease phenotype. Then, the role of PET in experimental therapeutics will be addressed. A discussion of how PET can be used in HD (dys) functional network analysis and how it has been used in animal models of the disease will be omitted, as will a consideration of differences and similarities between PET and SPECT molecular imaging.

28.2 Clinical Features and Neuropathology of HD

Huntington's disease is a hereditary autosomal dominant neurodegenerative disorder that was first described by George Huntington in 1872. The end of his now classical three-page paper in *The Medical and Surgical Reporter*, "On Chorea," still summarizes, almost in passing, concisely the core clinical features of the disease: motor, cognitive, and behavioral impairment (Lanska 2000). In George Huntington's own and sometimes dramatic words:

> The hereditary chorea as I shall call it is confined to certain and fortunately few families and has been transmitted to them as an heirloom from generations way back in the dim past. It is spoken of by those in whose veins the seeds of the disease are known to exist with a kind of horror and not at all alluded to except through dire necessity with it being mentioned as 'that disorder.' It is attended generally by all the symptoms of common chorea only in an aggravated degree, hardly ever manifesting itself until adult or middle life and then coming on gradually but surely, increasing by degrees and often occupying years in its development until the hapless sufferer is but a quivering wreck of his former self. There are three marked peculiarities in this disease; (1) its hereditary nature, (2) a tendency to insanity and suicide, and (3) its manifesting itself as a grave disease only in adult life.

The best known motor feature is chorea, but dystonia, myoclonus, bradykinesia, general clumsiness, and motor impairment can all be observed in various stages in various patients. Cognitive impairment initially manifests in attentional and executive deficits—primarily a frontal type of dysfunction. Over the course of the disease, more global and massive deficits develop. As to the behavioral or psychiatric alterations, mood disorders, apathy, and loss of impulse control are among the most common manifestations. Rarely, psychosis, mania, and paranoid delusions develop late in the disease. These neuropsychiatric impairments lead to the gradual and

surprisingly linear decrease over time of total functional capacity. From a genetic point of view, HD is the archetypical autosomal dominant adult-onset disease with complete penetrance. Each child of an affected parent has 50% chance of developing the disease, irrespective of sex. Patients who are homozygous (i.e., have two mutated alleles instead of one) have a disease that cannot be differentiated from the heterozygous state (one mutated allele), although they may experience a more severe disease course (Squitieri et al. 2003).

In 1983, the gene for HD was found to be linked to a locus on the short arm of chromosome 4. In 1993, the actual gene and its causative mutation were identified (Gusella et al. 1983; MacDonald et al. 1993). This mutation turned out to be an expanded CAG trinucleotide repeat in what is now called the *Huntingtin* gene. The repeat in this gene is highly polymorphic in the normal population, varying between 10 and 29 repeats. In HD patients, the repeat contains 36 or more CAG trinucleotides (Kremer et al. 1994). CAG size correlates strongly (typically $r = 0.7$) with age at onset of the disease (Andrew et al. 1993). Thus, CAG repeat length assessment not only allows the establishment of an unambiguous diagnosis but also an estimate of the time when the motor manifestations will occur (Kremer et al. 1994; Langbehn et al. 2004).

The function of the gene is still unknown, although in its mutated, CAG expanded form, it may interfere with such diverse cellular processes as energy metabolism, transcriptional regulation, intracellular transport, vesicular trafficking, proteasome function, or excitatory amino acid toxicity (Landles and Bates 2004; Lieberman et al. 2018). These toxic effects are mediated by protein fragments derived from the full-length Huntingtin that contain an expanded polyglutamine stretch encoded by the genomic expanded CAG triplet repeat stretch.

Whatever the exact effects of Huntingtin in its wild-type and mutated forms, on a neuropathological level, the effects are quite specific and can be summarized as follows: early and profound loss of striatal (caudate nuclear and putaminal) GABAergic medium-sized spiny projection neurons, followed by cortical neurons in layers 3, 5, and 6, as well as neuronal loss in various subcortical areas such as the thalamus and the hypothalamus (Vonsattel et al. 1985; Rüb et al. 2016). Intraneuronal inclusions consist of Huntingtin-derived protein aggregates that are found in the nucleus and the cytoplasm, sometimes extending into the axonal and dendritic tree (Vonsattel and Keller 2011). The macroscopic alterations such as striatal and cortical atrophy can also be observed with structural imaging such as MRI (Tabrizi et al. 2012).

The pattern of neurodegeneration in HD is commonly considered "regionally selective," but this implies temporal selectivity, more so than "many regions not being affected." Different regions pursue different temporal neurodegenerative trajectories. Moreover, while specific neuronal populations degenerate earlier and faster than others, at any time in the course of the disease, complex changes in neuronal structure and molecular makeup should be expected. Neuronal markers such as glucose metabolism, neurotransmitters, their pre- and postsynaptic receptors, and inflammation-associated markers will change over time in a complex pattern that reflects the interwoven and interdependent molecular networks. PET imaging of these changes may teach us a lot about the underlying neurobiology.

28.3 Structural Defects Are Associated with Metabolic Defects

The first studies of dynamic and quantitative (Kuwert et al. 1993) FDG-PET in HD patients were published in the early 1980s. They described a strong and consistent reduction in glucose utilization in the caudate nucleus and the putamen, not only in more or less advanced symptomatic patients but also in some persons who were at 50% risk for the disease but did not (yet) display any signs. (At that time, an unambiguous molecular diagnosis was not yet possible.) Moreover, this local hypometabolism might precede striatal shrinkage as revealed by CT or MRI. This led to the concept of a regional metabolic defect that precedes actual structural changes (Kuhl et al. 1982; Hayden et al. 1986; Young et al. 1986; Mazziotta et al. 1987).

Based on these findings, it was proposed to use dynamic (Kuwert et al. 1993) FDG-PET as a way to identify very early or even preclinical disease and to identify the carriers of the mutated gene (Hayden et al. 1986; Mazziotta et al. 1987; Kuwert et al. 1993). This last application has become obsolete since the identification of the HD gene itself in 1993 (MacDonald et al. 1993), which allowed direct molecular testing.

In subsequent (Kuwert et al. 1993) FDG-PET studies of presymptomatic mutation carriers, as identified by CAG repeat analysis, it turned out that such definitely presymptomatic individuals may have normal striatal glucose utilization during an extended period before becoming symptomatic. A few years prior to converting from presymptomatic to symptomatic, the striatal glucose metabolism goes down (Mazziotta et al. 1992; Antonini et al. 1996). This transition may probably occur as early as 10 years prior to onset of the movement disorder (López-Mora et al. 2016). Repeat examinations of initially asymptomatic persons after follow-up of 58–83 months suggested that in those who converted to the symptomatic state, initial striatal glucose metabolism may be a predictor of time to conversion, independent from CAG size (Ciarmiello et al. 2012).

Basal ganglia local metabolic rates correlated surprisingly strong with total functional capacity; with measures of motor performance, such as chorea, bradykinesia, and rigidity, fine motor control, and oculomotor impairment; and with neuropsychological performance on tests for verbal learning and memory (Young et al. 1986; Berent et al. 1988).

Not only the basal ganglia but also various cortical areas showed a decline of local metabolic rates of glucose consumption in HD patients (Kuwert et al. 1990). The application of network analysis, for example, by establishing metabolic covariance pattern models, has further refined our understanding of large-scale alterations in (early or pre-) symptomatic patients. Thus, medial temporal hypometabolism and occipital hypermetabolism could be defined in relation to the striatal hypometabolism (Feigin et al. 2001). Network analysis also revealed that in presymptomatic gene carriers, thalamic metabolism may initially be somewhat increased but will decline later, concurrent with clinical progression (Feigin et al. 2007). Spatial covariance network analysis of FDG data from presymptomatic gene carriers, acquired at baseline, after follow-up of 1.5 years, 4 years, and in some after 7 years, revealed

a distinct and linear, monotonous metabolic progression pattern that could be confirmed in an independent group of premanifest subjects (Tang et al. 2013). Regions in which metabolism declined were the caudate/putamen, the mediodorsal thalamus, and the posterior cingulate, prefrontal, insular, and medial occipital cortices. Metabolic activity was found increased in the pons, the cerebellum, the hippocampus, and temporal, orbitofrontal, and lateral occipital cortices (Tang et al. 2013).

Although these findings and resulting applications were considered to be completely in line with what was known from neuropathology, conceptual problems remained. Particularly, the question what the decrease in metabolism really represents—intrinsic neuronal loss or loss of synapses of neurons that project into the striatum—was never definitely answered. Moreover, it has always been an issue which part of the metabolic signal decrease should be attributed to concurrent nerve cell loss and which part is due to a true metabolic defect that precedes neuronal fallout. It should also be pointed out that the way to analyze these FDG measurements has mostly been through delineation of "regions of interest" (ROIs) or later "voxels of interest" (VOIs). Presenting single ROI/VOI values for regional cerebral metabolic rates of glucose consumption—rCMRglc—introduced methodological issues of local tissue inhomogeneities, partial volume effects, and the effects of ROI size (Kuwert et al. 1992a, b). However, reliable partial volume correction algorithms have been established using co-registered MRI data, and they were applied in studies since the late 1990s (Rousset et al. 1998; Müller-Gärtner et al. 1992). Using such methods, the view has gradually emerged that both regional structural loss and regional metabolic decline are indeed very early features in the brains of HD gene carriers who do not yet display clinical signs of the disease (Ciarmiello et al. 2006).

Results consistent with the concept of basal ganglia and cortical hypometabolism, and similar to FDG-PET results, have been obtained with 99mTc-HMPAO SPECT perfusion imaging in HD patients, but the method, due to its limited quantifiability, as well as its likely inferiority to FDG-PET, has never gained wide acceptance as a diagnostic or disease-monitoring biomarker (Botsch et al. 1987; Reid et al. 1988; Hasselbalch et al. 1992; Kuwert et al. 1993; Boecker et al. 1994; Harris et al. 1996).

From a clinical point of view, neither PET nor SPECT is currently of any use for routine clinical care in terms of early demonstration of decreased metabolism. Making a definite diagnosis can be done by DNA testing of individuals with specific clinical manifestations, and the same applies for predictive testing of at-risk individuals. Tracking progress of the disease is primarily done by using standardized clinical assessments, while MRI structural imaging may be gaining increasing significance (Tabrizi et al. 2012). On the other hand, measurements of local metabolic rates may turn out to be useful as a specific biomarker for disease-modifying intervention trials, e.g., in drug trials that aim at stimulation of mitochondrial function (discussed below). It should be mentioned here that FDG-PET has also been used as a way to unravel the functional connectivity of cognitive performance in (pre)clinical HD patients. As this subject is outside the scope of this chapter, with results to be discussed in relation to many subsequent fMRI studies, I refer to a slightly older but still excellent review (Paulsen 2009).

28.4 Dopamine Receptor Imaging: A Way to Establish Neuronal Integrity?

A second approach to reveal neuronal damage, and one that attempts to measure structural neuronal integrity as opposed to metabolic impairment, has been post- and presynaptic receptor imaging. The implicit assumption is that a measured loss of receptors is related to a loss of receptor carrying structures such as neurites or neurons. The problem here is that receptor up- or downregulation may occur in structurally intact neurons, either as a result of molecular pathology in the neuron itself, as a result of altered input from connected systems, or as a result of general factors such as drugs. Despite these caveats, receptor imaging in HD patients has provided a wealth of biological and clinical insights.

Most work has been done on postsynaptic dopamine receptor imaging, particularly using D1 and D2 ligands as tracers. These two receptors are highly enriched in the mammalian caudate and putamen and therefore of particular interest as markers of HD pathology. The first attempt at dopaminergic molecular imaging in HD was made using IBZM-SPECT. This already allowed the visualization of a decrease in striatal receptor binding (Brucke et al. 1991). ^{123}I-epidepride turned out to be an alternative for SPECT studies (Leslie et al. 1996, 1999; Pirker et al. 1997).

But PET allows for better quantification of this phenomenon. The first published PET study used the D1-receptor benzazepine PET ligand C-SCH 23390. A decrease in both calculated receptor density and total number of D1 receptors was found that equaled (for density) or exceeded (for total number) the magnitude of the 50% striatal volume loss as measured by MRI (Sedvall et al. 1994; Rüb et al. 2016).

The most widely used D2-receptor tracer has been ^{11}C-raclopride (which has also high affinity for D3 receptors, e.g., those localized in the nucleus accumbens). Binding studies, sometimes combining multiple ligands, have revealed a consistent and strong decrease in striatal D2-receptor binding of 50% or more, similar to D1 binding reduction, in all symptomatic and some but not in all presymptomatic subjects (Turjanski et al. 1995; Andrews et al. 1999). Their decline was related to the duration of the disease, with disease progression over the years being accompanied by a progressive receptor binding decline in both symptomatic patients and presymptomatic individuals who converted to symptomatic status (Antonini et al. 1996; Andrews et al. 1999; Ginovart et al. 1997; Pavese et al. 2003; Van Oostrom et al. 2005, 2009). Reduced striatal metabolism as revealed by FDG correlated with reduced raclopride binding (Antonini et al. 1996), but D2 binding may be a more sensitive and earlier marker of striatal damage in presymptomatic patients (Van Oostrom et al. 2005).

In statistical models that used D2-receptor density as a dependent variable, in both presymptomatic and symptomatic patients, CAG size was found to be an independent explanatory variable among others such as measures of tissue atrophy (Van Oostrom et al. 2005; Antonini et al. 1998).

Dopamine receptors can also be detected in the human cortex. Decreases in temporal cortical D1 binding and in temporal, frontal, and amygdalar D2 binding in HD patients suggest that D1 and D2 ligands may be markers for cortical neuronal

damage (Ginovart et al. 1997; Pavese et al. 2003, 2010). No such decrease in cortical nor thalamic binding could be demonstrated in one study with the D2/D3 ligand ^{11}C-FLB 457 (Esmaeilzadeh et al. 2011a). Dopamine receptor binding correlates with clinical symptoms. Strong correlations between performance in cognitive tasks that assessed executive function and aspects of visuospatial ability, episodic memory, verbal fluency, perceptual speed, and reasoning on the one hand and D1, D2, and dopamine transporter (DAT) tracer binding on the other hand were found (Bäckman et al. 1997; Lawrence et al. 1998). This was not only true for symptomatic individuals but also for presymptomatic gene carries near their estimated age of onset (Lawrence et al. 1998). Similar correlations between neuropsychological performance and striatal D2 binding were confirmed by some but not by others (Pavese et al. 2003; Sanchez-Pernaute et al. 2000).

In symptomatic patients, a decrease in cortical raclopride binding correlated with measures of impaired executive functions and attention, apparently independent of striatal D2 binding reduction (Pavese et al. 2010). An important additional and significantly contributing covariable in these studies, however, was striatal volume as assessed by MRI.

All these data are consistent with the hypothesis that D1- and D2-receptor densities offer a measure of local neuronal loss. In general, it can be summarized that all HD symptomatic patients have decreased striatal D2-receptor densities, while a variable portion of presymptomatic gene carriers—depending on the number of years prior to projected onset—display a similar biomarker pattern.

Moreover, many correlations between motor and cognitive performance on the one hand with receptor binding have been reported. But before inferring neurobiological conclusions from correlations between such regional receptor binding changes (or, for that part, FDG changes) with specific neuropsychological alterations, one should be aware of the huge collinearity in the data. HD is a generalized brain disease, and over the course of the disease, everything goes down.

Presynaptic nigrostriatal dopamine transporter density has been studied using ^{11}C-βCIT SPECT or α-^{11}C-dihydrotetrabenazine (DTBZ) PET. These ligands reflect nigrostriatal terminal integrity; their derived transporter densities were also found to be decreased in patients, either as a consequence of loss of nerve terminals or as a result of downregulated expression (Ginovart et al. 1997; Gamez et al. 2010; Kiferle et al. 2013). Nigrostriatal integrity may be particularly compromised in akinetic-rigid (often juvenile) HD patients (Bohnen et al. 2000). Thus, not only the striatum itself is affected but also, as in Parkinson's disease, the nigrostriatal dopaminergic projections. Anatomical correlates have been reported in postmortem brain samples of HD patients (Yohrling et al. 2003).

28.5 Imaging of Other Neurotransmitter Receptors

GABA is the main neurotransmitter of many striatal efferents, while GABA receptors can be found in high density in most basal ganglia components. Cannabinoid CB1 and adenosine A2A receptors are abundant as well, the latter colocalizing with

dopamine receptors in the striatum (Jamwal and Kumar 2018; Glass et al. 2000). These properties have invited *in vivo* ligand-receptor interaction studies in HD patients using either PET or SPECT.

^{11}C-Flumazenil, a non-subtype-selective central benzodiazepine/GABA-receptor ligand, binds with strong regional specificity to neurons in the basal ganglia and the thalamus. Decreased ^{11}C-flumazenil binding has been found in the caudate nucleus of HD patients but not in the putamen (Holthoff et al. 1993; Künig et al. 2000). An inverse correlation between putaminal D2-receptor density and flumazenil binding has been described and interpreted as indicating GABA-receptor upregulation in early disease (Künig et al. 2000). The results of a SPECT study using ^{123}I-iomazenil to calculate flumazenil affinity constants (K_d) demonstrated distribution volumes in the unblocked state that were in line with the degree of basal ganglia degeneration, while flumazenil K_d was similar in the patients and controls. The study concluded that the benzodiazepine receptor must be functionally intact (Pinborg et al. 2001).

Imaging of cannabinoid CB1 receptors was performed in 20 symptomatic HD patients and 14 healthy controls, using a novel highly selective high-affinity CB1 radioligand ^{18}F-MK-9470 (Casteels et al. 2010). A significant decrease in CB1 availability was found in many regions. This decrease occurred also in regions that were macroscopically intact and affected early HD patients and more advanced patients equally (Van Laere et al. 2010).

28.6 Other Intraneuronal Markers of Neurodegeneration

Any intraneuronal structural molecule or neuronal membrane-bound molecule that can be targeted by a radiotracer may potentially be used to evaluate neurodegeneration. Tracers that measure intraneuronal enzymatic activity may demonstrate either structural neuronal demise or metabolic alterations that precede actual structural changes. FDG is the prime example of this principle in *in vivo* PET studies.

Phosphodiesterase10A offers another example. The enzyme's substrates are cyclic adenosine and guanosine monophosphate (cAMP, cGMP). PDE10A is highly enriched in the brain, particularly in the striatum, where it plays an important role in intracellular cyclic nucleotide-mediated signaling and thus in many downstream signaling cascades that are involved in gene transcription, growth, differentiation, and neurotransmitter-mediated signaling (Wilson and Brandon 2014). Striatal PDE10A levels were found significantly reduced in R6/1 and R6/2 mice, which are accepted transgenic models for HD (Hebb et al. 2004). Mutations in the PDE10A gene have been found associated with childhood-onset chorea with striatal abnormalities (Mencacci et al. 2016; Narayanan et al. 2018).

The first study in five HD patients and 11 controls, using ^{18}F-JNJ42259152 in dynamic scans, found 60–70% reduction in striatal ligand binding potential in all patients, even in two patients who were only mildly affected (Ahmad et al. 2014). A similar magnitude of basal ganglia binding potential decrease, using the ligand ^{18}F-MNI-659, was replicated in eight affected individuals with early motor manifestations. Three premanifest gene carriers showed decreased binding that was

intermediate between affected and controls (Russell et al. 2014). A second scan in 8 of these 11 individuals, 1 year later, revealed 5–6% deterioration in binding potential (Russell et al. 2016). Significant changes in PDE10A binding up to 34% could even be detected in gene carriers who were estimated to be 17–43 years before onset, with a decrease in basal ganglia binding but an increase in motor thalamus binding (Niccolini et al. 2015). It should be noted that such individuals have no discernable macroscopic striatal volume loss on MRI, which argues in favor of a very early neuronal dysfunction signal. PDE10A expression was also found decreased in the insular and occipital fusiform cortex of early presymptomatic gene carriers (Wilson et al. 2016).

The adenosine A_1A receptor (A_1AR) was visualized with ^{18}F-CPFPX in a cross-sectional study of 13 presymptomatic mutation carriers and eight symptomatic persons. A decrease in striatal and orbitofrontal cortical binding potential was observed from those who were >10 years from estimated disease onset to those who had symptomatic disease. Presymptomatic individuals far away from disease onset displayed 13% higher whole brain binding than controls; those who were close to symptom onset had binding similar to controls, while symptomatic subjects had lowest values, particularly in the striatum (up to 19%). Regional differences were quite outspoken. Considering that the magnitude of these changes is smaller than that of, for example, dopamine receptor binding and that A_1AR regulation is complex, with various molecular signaling systems being involved, the current role of A_1AR imaging may be primarily in experimental pharmacotherapy (Matusch et al. 2014).

28.7 Inflammation as an Indicator of Neurodegeneration

A true challenge is imaging the mechanisms of the neurodegenerative process itself. Several theories consider neuro-inflammation as a key component of neurodegeneration, not only in Alzheimer's and in Parkinson's disease but also in Huntington's disease (Crotti and Glass 2015). This hypothesis was examined by PET imaging using ^{11}C-PK11195 as an intracerebral microglial marker. Formerly known as the peripheral benzodiazepine receptor ligand, PK11195 is now considered to bind to a translocator protein (TSPO) that is expressed by the mitochondria of activated microglia, indicating the transition of microglia from a resting to an activated state. PK11195 binding was found to be increased in the striatum of HD patients, as well as in the prefrontal and anterior cingulate cortex (Pavese et al. 2006). Moreover, the binding correlated with disease severity as indicated by clinical measures and decreased raclopride binding (Tomasi et al. 2011).

PK11195 binding was found to be also increased in both the striatum and the cortex of presymptomatic gene carriers, in whom it correlated inversely with striatal raclopride D2 binding (Tai et al. 2007). In the hypothalamus, one of the affected extrastriatal areas, similar changes appear to present very early in the disease (Politis et al. 2008). A more detailed study in 32 subjects was able to demonstrate very early increases in PK11195 binding in cortical and subcortical areas that are involved in various motor, cognitive, and behavioral functions (Politis et al. 2011).

28.8 PET Imaging as a Biomarker in Experimental Therapeutics

Perhaps the greatest contribution of PET imaging to HD research and care may turn out to be in the field of experimental therapeutics (Kuwert et al. 1993). FDG imaging has proven to be valid as a biomarker of disease progression. It was used in a drug trial which assessed the efficacy of lamotrigine (a sodium-channel blocker with glutamate release-inhibiting properties) in retarding disease progression. No outcome differences were found in the two treatment groups, but over the 30-month treatment period of the study, FDG metabolic rates declined detectably. Significant decreases were found in the basal ganglia, the frontal cortex, the temporal cortex, and the thalamus. In contrast, neither the parietal nor the cerebellar metabolic rates decreased over this time span. The most profound decrease in metabolic rates occurred in the basal ganglia, with a decrease of approximately 7% per year (Kremer et al. 1999).

In a later small trial using riluzole as a potential neuroprotective agent, FDG-PET in combination with MRI was used in a similar way to assess neuroprotective efficacy (Squitieri et al. 2009). Although this study claimed a more rapid decline for the placebo-treated group, potential clinical efficacy of riluzole had previously already been excluded in a very large European multicenter trial (Landwehrmeyer et al. 2007).

In an open-label trial with pridopidine (ACR16), a compound that can both enhance and counteract ("stabilize") central dopamine functions, eight treated HD patients were examined by two successive FDG scans at a 2-week interval. An increase in metabolic activity in the precuneus bilaterally, the left superior temporal gyrus and the left middle frontal gyrus, and the left mediodorsal thalamic nucleus was found. The relevance of this finding, however, is currently unknown (Esmaeilzadeh et al. 2011b).

Yet another application of ^{18}FDG-PET has been in the field of experimental neuronal grafting in the striatum of animal models and human HD patients. The first animal models were obtained by intrastriatal injection of excitotoxins in rodents and nonhuman primates. Grafting of intra- or cross-species fetal striatal cells into the lesioned areas was able to partially restore resulting motor and behavioral abnormalities. FDG-PET was able to demonstrate local graft metabolism, as well as graft rejection (Schumacher et al. 1992).

The most remarkable results of this approach were demonstrated in a French trial in which five patients received fetal striatoneuronal allografts. After 1–2-year follow-up, increased metabolism in functioning grafts in three patients could be contrasted with hypometabolism in presumably nonfunctioning grafts in two patients, and these assessments correlated with clinical improvement in the motor, cognitive, and general functional domains (Bachoud-Lévi et al. 2000). Functioning striatal grafts did not only improve striatal hypometabolism but also cortical hypometabolism, thus demonstrating improvement of striatocortical connections (Gaura et al. 2004). In an Italian study in which four patients were grafted and followed up for 2 years, similar FDG-PET results of patients with either metabolically active or

inactive grafts were reported (Paganini et al. 2010). In this study, D2-receptor imaging was done by IBZM-SPECT. An initial increase in D2 binding was interpreted as indicating newly generated tissue. In a North American study of seven patients who were examined at a 2-year follow-up after intrastriatal fetal neuronal grafts, lack of clinical benefit was associated with persisting and unaltered striatal glucose hypometabolism. D1-receptor density (SCH23390) was unchanged after 2 years, but D2-receptor density (raclopride) had decreased significantly. This was interpreted as either loss of graft viability or disease progression (Furtado et al. 2005).

28.9 Conclusions

These data illustrate several points. Both metabolic FDG studies and dopamine receptor-binding studies and PDEA10 are sensitive in detecting neurodegeneration in vivo in HD patients. They are able to track the progression of the disease, from the truly presymptomatic to the clearly affected stages. They provide correlations with clinical measures of neurological impairment, and they may be used as surrogate outcome measures in experimental therapeutics. Moreover, basic aspects of the neurodegenerative process, e.g., inflammation, are not beyond reach of in vivo imaging. But perhaps the most remarkable point is how much has *not* yet been accomplished in HD PET research. Many receptor systems, e.g., serotoninergic or noradrenergic, have remained untouched. Examining the relation of neurotransmitter alterations with psychiatric and behavioral symptoms is an area largely unexplored. The visualization and measurement of the massive corticostriatal glutamatergic projections remain a daunting challenge (Gruber and Ametamey 2017). Also the molecular imaging of the underlying intracellular Huntingtin aggregation is a highly desirable target—probably not out of reach (Mestre and Sampaio 2017). Thus, many opportunities for novel PET molecular imaging applications exist.

References

Ahmad R, Bourgeois S, Postnov A, Schmidt ME, Bormans G, Van Laere K et al (2014) PET imaging shows loss of striatal PDE10A in patients with Huntington disease. Neurology 82:279–281

Andrew SE, Goldberg YP, Kremer B, Telenius H, Theilmann J, Adam S et al (1993) The relationship between trinucleotide (CAG) repeat length and clinical features of Huntington's disease. Nat Genet 4:398–403

Andrews TC, Weeks RA, Turjanski N, Gunn RN, Watkins LHA, Sahakian B et al (1999) Huntington's disease progression. PET and clinical observations. Brain 122:2353–2363

Antonini A, Leenders KL, Spiegel R, Meier D, Vontobel P, Weigell-Weber M et al (1996) Striatal glucose metabolism and dopamine D2 receptor binding in asymptomatic gene carriers and patients with Huntington's disease. Brain 119:2085–2095

Antonini A, Leenders KL, Eidelberg D (1998) [11C]Raclopride-PET studies of the Huntington's disease rate of progression: relevance of the trinucleotide repeat length. Ann Neurol 43:253–255

Bachoud-Lévi AC, Rémy P, Nǵuyen JP, Brugières P, Lefaucheur JP, Bourdet C et al (2000) Motor and cognitive improvements in patients with Huntington's disease after neural transplantation. Lancet 356:1975–1979

Bäckman L, Robins-Wahlin TB, Lundin A, Ginovart N, Farde L (1997) Cognitive deficits in Huntington's disease are predicted by dopaminergic PET markers and brain volumes. Brain 120:2207–2217

Berent S, Giordani B, Lehtinen S, Markel D, Penney JB, Buchtel HA et al (1988) Positron emission tomographic scan investigations of Huntington's disease: cerebral metabolic correlates of cognitive function. Ann Neurol 23:541–546

Boecker H, Kuwert T, Langen KJ, Lange HW, Czech N, Ziemons K et al (1994) SPECT with HMPAO compared to PET with FDG in Huntington disease. J Comput Assist Tomogr 18:542–548

Bohnen NI, Koeppe RA, Meyer P, Ficaro E, Wernette K, Kilbourn MR et al (2000) Decreased striatal monoaminergic terminals in huntington disease. Neurology 54:1753–1759

Botsch H, Oepen G, Deuschl G, Wolff G (1987) SPECT-Untersuchungen mit 99m Tc-HMPAO bei Patienten mit Huntingtonscher Chorea. RöFo Fortschritte auf dem Gebiet der Röntgenstrahlen und der Bildgeb Verfahren 147:666–668

Brucke T, Podreka I, Angelberger P, Wenger S, Topitz A, Kufferle B et al (1991) Dopamine D2 receptor imaging with SPECT: studies in different neuropsychiatric disorders. J Cereb Blood Flow Metab 11:220–228

Casteels C, Martinez E, Bormans G, Camon L, De Vera N, Baekelandt V et al (2010) Type 1 cannabinoid receptor mapping with [18F]MK-9470 PET in the rat brain after quinolinic acid lesion: a comparison to dopamine receptors and glucose metabolism. Eur J Nucl Med Mol Imaging 37:2354–2363

Ciarmiello A, Cannella M, Lastoria S, Simonelli M, Frati L, Rubinsztein DC et al (2006) Brain white-matter volume loss and glucose hypometabolism precede the clinical symptoms of Huntington's disease. J Nucl Med 47:215–222

Ciarmiello A, Giovacchini G, Orobello S, Bruselli L, Elifani F, Squitieri F (2012) 18F-FDG PET uptake in the pre-Huntington disease caudate affects the time-to-onset independently of CAG expansion size. Eur J Nucl Med Mol Imaging 39:1030–1036

Crotti A, Glass CK (2015) The choreography of neuroinflammation in Huntington's disease. Trends Immunol 36:364–373

Esmaeilzadeh M, Farde L, Karlsson P, Varrone A, Halldin C, Waters S et al (2011a) Extrastriatal dopamine D 2 receptor binding in Huntington's disease. Hum Brain Mapp 32:1626–1636

Esmaeilzadeh M, Kullingsjö J, Ullman H, Varrone A, Tedroff J (2011b) Regional cerebral glucose metabolism after pridopidine (ACR16) treatment in patients with huntington disease. Clin Neuropharmacol 34:95–100

Feigin A, Leenders KL, Moeller JR, Missimer J, Kuenig G, Spetsieris P et al (2001) Metabolic network abnormalities in early Huntington's disease: an [(18)F]FDG PET study. J Nucl Med 42:1591–1595

Feigin A, Tang C, Ma Y, Mattis P, Zgaljardic D, Guttman M et al (2007) Thalamic metabolism and symptom onset in preclinical Huntington's disease. Brain 130:2858–2867

Furtado S, Sossi V, Hauser RA, Samii A, Schulzer M, Murphy CB et al (2005) Positron emission tomography after fetal transplantation in Huntington's disease. Ann Neurol 58:331–337

Gallina P, Paganini M, Lombardini L, Mascalchi M, Porfirio B, Gadda D et al (2010) Human striatal neuroblasts develop and build a striatal-like structure into the brain of Huntington's disease patients after transplantation. Exp Neurol 222:30–41

Gamez J, Lorenzo-Bosquet C, Cuberas-Borrós G, Carmona F, Hernández-Vara J, Castilló J et al (2010) Does reduced [123I]-FP-CIT binding in Huntington's disease suggest pre-synaptic dopaminergic involvement? Clin Neurol Neurosurg 112:870–875

Gaura V, Bachoud-Lévi AC, Ribeiro MJ, Nguyen JP, Frouin V, Baudic S et al (2004) Striatal neural grafting improves cortical metabolism in Huntington's disease patients. Brain 127:65–72

Ginovart N, Lundin A, Farde L, Halldin C, Bäckman L, Swahn CG et al (1997) PET study of the pre- and post-synaptic dopaminergic markers for the neurodegenerative process in Huntington's disease. Brain 120:503–514

Glass M, Dragunow M, Faull RLM (2000) The pattern of neurodegeneration in Huntington's disease: a comparative study of cannabinoid, dopamine, adenosine and GABA(A) receptor alterations in the human basal ganglia in Huntington's disease. Neuroscience 97:505–519

Gruber S, Ametamey SM (2017) Imaging the glutamate receptor subtypes—much achieved, and still much to do. Drug Discov Today Technol 25:27–36

Gusella JF, Wexler NS, Conneally PM, Naylor SL, Anderson MA, Tanzi RE et al (1983) A polymorphic DNA marker genetically linked to Huntington's disease. Nature 306:234–238

Harris GJ, Aylward EH, Peyser CE, Pearlson GD, Brandt J, Roberts-Twillie JV et al (1996) Single photon emission computed tomographic blood flow and magnetic resonance volume imaging of basal ganglia in Huntington's disease. Arch Neurol 53:316–324

Hasselbalch SG, Øberg G, Sørensen SA, Andersen AR, Waldemar G, Schmidt JF et al (1992) Reduced regional cerebral blood flow in Huntington's disease studied by SPECT. J Neurol Neurosurg Psychiatry 55:1018–1023

Hayden MR, Martin WRW, Stoessl AJ, Clark C, Hollenberg S, Adam MJ et al (1986) Positron emission tomography in the early diagnosis of Huntington's disease. Neurology 36:888–894

Hebb ALO, Robertson HA, Denovan-Wright EM (2004) Striatal phosphodiesterase mRNA and protein levels are reduced in Huntington's disease transgenic mice prior to the onset of motor symptoms. Neuroscience 123:967–981

Holthoff VA, Koeppe RA, Frey KA, Penney JB, Markel DS, Kuhl DE et al (1993) Positron emission tomography measures of benzodiazepine receptors in Huntington's disease. Ann Neurol 34:76–81

Jamwal S, Kumar P (2018) Insight into the emerging role of striatal neurotransmitters in the pathophysiology of Parkinson's disease and Huntington's disease: a review. Curr Neuropharmacol 17:165–175

Kiferle L, Mazzucchi S, Unti E, Pesaresi I, Fabbri S, Nicoletti V et al (2013) Nigral involvement and nigrostriatal dysfunction in Huntington's disease: evidences from an MRI and SPECT study. Parkinsonism Relat Disord 19:800–805

Kremer B, Goldberg P, Andrew SE, Theilmann J, Telenius H, Zeisler J et al (1994) A worldwide study of the Huntington's disease mutation: the sensitivity and specificity of measuring CAG repeats. N Engl J Med 330:1401–1406

Kremer B, Clark CM, Almqvist EW, Raymond LA, Graf P, Jacova C et al (1999) Influence of lamotrigine on progression of early Huntington disease: a randomized clinical trial. Neurology 53:1000–1011

Kuhl DE, Phelps ME, Markham CH, Metter EJ, Riege WH, Winter J (1982) Cerebral metabolism and atrophy in Huntington's disease determined by 18FDG and computed tomographic scan. Ann Neurol 12:425–434

Künig G, Leenders KL, Sanchez-Pernaute R, Antonini A, Vontobel P, Verhagen A et al (2000) Benzodiazepine receptor binding in Huntington's disease: [11C]flumazenil uptake measured using positron emission tomography. Ann Neurol 47:644–648

Kuwert T, Lange HW, Langen KJ, Herzog H, Aulich A, Feinendegen LE (1990) Cortical and subcortical glucose consumption measured by pet in patients with Huntington's disease. Brain 113:1405–1423

Kuwert T, Sures T, Herzog H, Loken M, Hennerici M, Langen KJ et al (1992a) On the influence of spatial resolution and of the size and form of regions of interest on the measurement of regional cerebral metabolic rates by positron emission tomography. J Neural Transm Suppl 37:53–66

Kuwert T, Ganslandt T, Jansen P, Jülicher F, Lange H, Herzog H et al (1992b) Influence of size of regions of interest on PET evaluation of caudate glucose consumption. J Comput Assist Tomogr 16:789–794

Kuwert T, Lange HW, Boecker H, Titz H, Herzog H, Aulich A et al (1993) Striatal glucose consumption in chorea-free subjects at risk of Huntington's disease. J Neurol 241:31–36

Landles C, Bates GP (2004) Huntingtin and the molecular pathogenesis of Huntington's disease. EMBO Rep 5:958–963

Landwehrmeyer GB, Dubois B, De Yébenes JG, Kremer B, Gaus W, Kraus PH et al (2007) Riluzole in Huntington's disease: a 3-year, randomized controlled study. Ann Neurol 62:262–272

Langbehn DR, Brinkman RR, Falush D, Paulsen JS, Hayden MR (2004) A new model for prediction of the age of onset and penetrance for Huntington's disease based on CAG length. Clin Genet 65:267–277

Lanska DJ (2000) George Huntington (1850–1916) and hereditary chorea. J Hist Neurosci 2000:76–89

Lawrence AD, Weeks RA, Brooks DJ, Andrews TC, Watkins LHA, Harding AE et al (1998) The relationship between striatal dopamine receptor binding and cognitive performance in Huntington's disease. Brain 121:1343–1355

Leslie WD, Abrams DN, Greenberg CR, Hobson D (1996) Comparison of iodine-123-epidepride and iodine-123-IBZM for dopamine D2 receptor imaging. J Nucl Med 37:1589–1591

Leslie WD, Greenberg CR, Abrams DN, Hobson D (1999) Clinical deficits in Huntington disease correlate with reduced striatal uptake on iodine-123 epidepride single-photon emission tomography. Eur J Nucl Med 26:1458–1464

Lieberman AP, Shakkottai VG, Albin RL (2018) Polyglutamine repeats in neurodegenerative diseases. Annu Rev Pathol Mech Dis 14:1–27

López-Mora DA, Camacho V, Pérez-Pérez J, Martínez-Horta S, Fernández A, Sampedro F et al (2016) Striatal hypometabolism in premanifest and manifest Huntington's disease patients. Eur J Nucl Med Mol Imaging 43:2183–2189

MacDonald ME, Ambrose CM, Duyao MP, Myers RH, Lin C, Srinidhi L et al (1993) A novel gene containing a trinucleotide repeat that is expanded and unstable on Huntington's disease chromosomes. Cell 72:971–983

Matusch A, Saft C, Elmenhorst D, Kraus PH, Gold R, Hartung HP et al (2014) Cross sectional PET study of cerebral adenosine A1 receptors in premanifest and manifest Huntington's disease. Eur J Nucl Med Mol Imaging 41:1210–1220

Mazziotta JC, Phelps ME, Pahl JJ, Huang S-C, Baxter LR, Riege WH et al (1987) Reduced Cerebral glucose metabolism in asymptomatic subjects at risk for Huntington's disease. N Engl J Med 316:357–362

Mazziotta JC, Baxter LR, Phelps ME, Haines JL, Gusella J, Grafton ST et al (1992) Serial changes of cerebral glucose metabolism and caudate size in persons at risk for Huntington's disease. Arch Neurol 49:1161–1167

Mencacci NE, Kamsteeg EJ, Nakashima K, R'Bibo L, Lynch DS, Balint B et al (2016) De novo mutations in PDE10A cause childhood-onset chorea with bilateral striatal lesions. Am J Hum Genet 98:763–771

Mestre TA, Sampaio C (2017) Huntington disease: linking pathogenesis to the development of experimental therapeutics. Curr Neurol Neurosci Rep 17:18

Müller-Gärtner HW, Links JM, Prince JL, Bryan RN, McVeigh E, Leal JP et al (1992) Measurement of radiotracer concentration in brain gray matter using positron emission tomography: MRI-based correction for partial volume effects. J Cereb Blood Flow Metab 12:571–583

Narayanan DL, Deshpande D, Das Bhowmik A, Varma DR, Dalal A (2018) Familial choreoathetosis due to novel heterozygous mutation in PDE10A. Am J Med Genet Part A 176:146–150

Niccolini F, Haider S, Reis Marques T, Muhlert N, Tziortzi AC, Searle GE et al (2015) Altered PDE10A expression detectable early before symptomatic onset in Huntington's disease. Brain 138:3016–3029

Paulsen JS (2009) Functional imaging in Huntington's disease. Exp Neurol 216:272–277

Pavese N, Andrews TC, Brooks DJ, Ho AK, Rosser AE, Barker RA et al (2003) Progressive striatal and cortical dopamine receptor dysfunction in Huntington's disease: a PET study. Brain 126:1127–1135

Pavese N, Gerhard A, Tai YF, Ho AK, Turkheimer F, Barker RA et al (2006) Microglial activation correlates with severity in Huntington disease: a clinical and PET study. Neurology 66:1638–1643

Pavese N, Politis M, Tai YF, Barker RA, Tabrizi SJ, Mason SL et al (2010) Cortical dopamine dysfunction in symptomatic and premanifest Huntington's disease gene carriers. Neurobiol Dis 37:356–361

Pinborg LH, Videbæk C, Hasselbalch SG, Paulson OB, Knudsen GM, Sørensen SA et al (2001) Benzodiazepine receptor quantification in Huntington's disease with [123I]iomazenil and SPECT. J Neurol Neurosurg Psychiatry 70:657–661

Pirker W, Asenbaum S, Wenger S, Kornhuber J, Angelberger P, Deecke L et al (1997) Iodine-123-epidepride-SPECT: studies in Parkinson's disease, multiple system atrophy and Huntington's disease. J Nucl Med 38:1711–1717

Politis M, Pavese N, Tai YF, Tabrizi SJ, Barker RA, Piccini P (2008) Hypothalamic involvement in Huntington's disease: an in vivo PET study. Brain 131:2860–2869

Politis M, Pavese N, Tai YF, Kiferle L, Mason SL, Brooks DJ et al (2011) Microglial activation in regions related to cognitive function predicts disease onset in Huntington's disease: a multimodal imaging study. Hum Brain Mapp 32:258–270

Reid IC, Besson JAO, Best PV, Sharp PF, Gemmell HG, Smith FW (1988) Imaging of cerebral blood flow markers in Huntington's disease using single photon emission computed tomography. J Neurol Neurosurg Psychiatry 51:1264–1268

Rousset OG, Ma Y, Evans AC (1998) Correction for partial volume effects in PET: principle and validation. J Nucl Med 39:904–911

Rüb U, Seidel K, Heinsen H, Vonsattel JP, den Dunnen WF, Korf HW (2016) Huntington's disease (HD): the neuropathology of a multisystem neurodegenerative disorder of the human brain. Brain Pathol 26:726–740

Russell DS, Barret O, Jennings DL, Friedman JH, Tamagnan GD, Thomae D et al (2014) The phosphodiesterase 10 positron emission tomography tracer, [18F]MNI-659, as a novel biomarker for early Huntington disease. JAMA Neurol 71:1520–1528

Russell DS, Jennings DL, Barret O, Tamagnan GD, Carroll VM, Caillé F et al (2016) Change in PDE10 across early Huntington disease assessed by [18 F]MNI-659 and PET imaging. Neurology 86:748–754

Sanchez-Pernaute R, Kunig G, del Barrio AA, de Yebenes JG, Vontobel P, Leenders KL (2000) Bradykinesia in early Huntington's disease. Neurology 54:119–125

Schumacher JM, Hantraye P, Brownell AL, Riche D, Madras BK, Davenport PD et al (1992) A primate model of Huntington's disease: functional neural transplantation and CT-guided stereotactic procedures. Cell Transplant 1:313–322

Sedvall G, Karlsson P, Lundin A, Anvret M, Suhara T, Halldin C et al (1994) Dopamine D1 receptor number—a sensitive PET marker for early brain degeneration in Huntington's disease. Eur Arch Psychiatry Clin Neurosci 243:249–255

Squitieri F, Gellera C, Cannella M, Mariotti C, Cislaghi G, Rubinsztein DC et al (2003) Homozygosity for CAG mutation in Huntington disease is associated with a more severe clinical course. Brain 126:946–955

Squitieri F, Orobello S, Cannella M, Martino T, Romanelli P, Giovacchini G et al (2009) Riluzole protects Huntington disease patients from brain glucose hypometabolism and grey matter volume loss and increases production of neurotrophins. Eur J Nucl Med Mol Imaging 36:1113–1120

Tabrizi SJ, Reilmann R, Roos RAC, Durr A, Leavitt B, Owen G et al (2012) Potential endpoints for clinical trials in premanifest and early Huntington's disease in the TRACK-HD study: analysis of 24 month observational data. Lancet Neurol 11:42–53

Tai YF, Pavese N, Gerhard A, Tabrizi SJ, Barker RA, Brooks DJ et al (2007) Microglial activation in presymptomatic Huntington's disease gene carriers. Brain 130:1759–1766

Tang CC, Feigin A, Ma Y, Habeck C, Paulsen JS, Leenders KL et al (2013) Metabolic network as a progression biomarker of premanifest Huntington's disease. J Clin Invest 123:4076–4088

Tomasi G, Bertoldo A, Cobelli C, Pavese N, Tai YF, Hammers A et al (2011) Global-two-stage filtering of clinical PET parametric maps: application to [11 C]-(R)-PK11195. Neuroimage 55:942–953

Turjanski N, Weeks R, Dolan R, Harding AE, Brooks DJ (1995) Striatal D1 and D2 receptor binding in patients with Huntington's disease and other choreas A PET study. Brain 118:689–696

Van Laere K, Casteels C, Dhollander I, Goffin K, Grachev I, Bormans G et al (2010) Widespread decrease of type 1 cannabinoid receptor availability in Huntington disease in vivo. J Nucl Med 51:1413–1417

Van Oostrom JCH, Maguire RP, Verschuuren-Bemelmans CC, Veenma-Van Der Duin L, Pruim J, RAC R et al (2005) Striatal dopamine D2 receptors, metabolism, and volume in preclinical Huntington disease. Neurology 65:941–943

Van Oostrom JCH, Dekker M, Willemsen ATM, De Jong BM, Roos RAC, Leenders KL (2009) Changes in striatal dopamine D2 receptor binding in pre-clinical Huntington's disease. Eur J Neurol 16:226–231

Vonsattel JP, Myers RH, Stevens TJ, Ferrante RJ, Bird ED, Richardson EP (1985) Neuropathological classification of Huntington's disease. J Neuropathol Exp Neurol 44:559–577

Vonsattel JPG, Keller C, Cortes Ramirez EP (2011) Huntington's disease – neuropathology. In: William J, Weiner ET (eds) Handbook on clinical neurology, vol 100. Elsevier, Amsterdam, pp 83–100

Wilson L, Brandon N (2014) Emerging biology of PDE10A. Curr Pharm Des 21:378–388

Wilson H, Niccolini F, Haider S, Marques TR, Pagano G, Coello C et al (2016) Loss of extrastriatal phosphodiesterase 10A expression in early premanifest Huntington's disease gene carriers. J Neurol Sci 368:243–248

Yohrling GJ, Jiang GC-T, DeJohn MM, Miller DW, Young AB, Vrana KE et al (2003) Analysis of cellular, transgenic and human models of Huntington's disease reveals tyrosine hydroxylase alterations and substantia nigra neuropathology. Brain Res Mol Brain Res 119:28–36

Young AB, Penney JB, Starosta-Rubinstein S, Markel DS, Berent S, Giordani B et al (1986) PET scan investigations of Huntington's disease: cerebral metabolic correlates of neurological features and functional decline. Ann Neurol 20:296–303

PET and SPECT Imaging in Dystonia

29

Evelien Zoons, Jan Booij, Bauke de Jong,
and Marina A. J. Tijssen

Contents

29.1 General Introduction.. 801
29.1.1 Historical Background.. 801
29.1.2 Epidemiology.. 801
29.1.3 Classification, Clinical Features, and Etiology.. 801
29.1.4 Pathophysiology.. 805
29.1.5 Treatment.. 805
29.2 Imaging with PET and SPECT in Different Forms of Dystonia.. 805
29.3 Focal Dystonia.. 806
29.3.1 Glucose Metabolism PET.. 806
29.3.2 Regional Cerebral Blood Flow PET.. 809
29.3.3 Dopamine Receptor Imaging with PET and SPECT.. 810
29.3.4 Receptor Imaging of Other Neurotransmitter Systems with PET and SPECT.. 811
29.4 Inherited Generalized Dystonia.. 812
29.4.1 Glucose Metabolism and Regional Cerebral Blood Flow.. 813
29.4.2 Receptor Imaging with PET.. 814
29.5 Dopamine-Responsive Dystonia.. 815
29.6 Myoclonus-Dystonia.. 816

E. Zoons
Department of Neurology, Zaans Medisch Centrum, Zaandam, The Netherlands
e-mail: zoons.e@zaansmc.nl

J. Booij
Department of Radiology and Nuclear Medicine, Academic Medical Center, Amsterdam, The Netherlands
e-mail: j.booij@amsterdamumc.nl

B. de Jong · M. A. J. Tijssen (✉)
Department of Neurology, University Medical Center Groningen, Groningen, The Netherlands
e-mail: b.de.jong@umcg.nl; m.a.j.de.koning-tijssen@umcg.nl

R. A. J. O. Dierckx et al. (eds.), *PET and SPECT in Neurology*,
https://doi.org/10.1007/978-3-030-53168-3_29

29.7 Rapid-Onset Dystonia-Parkinsonism..... 816
29.8 Paroxysmal Dystonia..... 816
29.9 Conclusion..... 817
References..... 817

Abstract

Dystonia is a syndrome characterized by involuntary, sustained muscle contractions causing twisting movements and abnormal postures. It is a common movement disorder with different forms that can be classified based on different clinical characteristics. Idiopathic focal dystonia (dystonia in one body part with no known cause) is the most common form. The more generalized (throughout the body) forms of dystonia have a younger age of onset and usually an underlying genetic defect. The mode of inheritance is usually autosomal dominant. Of these, the most common are DYT-TOR1A and DYT-THAP1 dystonia. In combined dystonia syndromes, also autosomal dominantly inherited disorders, dystonia patients have additional neurological symptoms (e.g., parkinsonism or myoclonus). This group includes dopamine-responsive dystonia, myoclonus-dystonia, rapid-onset dystonia-parkinsonism, and paroxysmal dystonia. In this chapter, we describe results from positron emission tomography (PET) and single-photon emission computed tomography (SPECT) studies in the different forms of dystonia.

Three different kinds of PET and SPECT techniques have been used in patients with dystonia: glucose metabolism scans, regional cerebral blood flow studies, and receptor imaging. Increased glucose metabolism was found in the basal ganglia, thalamus, and cerebellum of patients with different forms of focal dystonia and in DYT1 dystonia. Patients with DYT6 dystonia showed decreased glucose metabolism in the putamen. Results from regional cerebral blood flow (rCBF)-activation studies differed extensively among different studies and different patient groups, mainly because of study design. Overall, the primary and secondary motor and sensory cortices were found to be abnormal in almost all forms of dystonia, although the direction of the abnormalities differed. Dopamine was found to play a role in dystonia reflected by decreased dopamine D2/3 receptor binding in the striatum of patients with almost all forms of dystonia. In recent years, it has been established that other neurotransmitter systems, such as serotonin and gamma aminobutyric acid (GABA) also play a role in dystonia. In conclusion, dystonia is likely to be a network disorder with abnormalities in a large number of cortical and subcortical areas. There might be a central role for the basal ganglia with abnormalities in dopamine receptor binding, as well as other neurotransmitter systems.

29.1 General Introduction

29.1.1 Historical Background

Dystonia was first described in 1911 by Hermann Oppenheim, a renowned German neurologist, as a disorder causing variable muscle tone and recurrent muscle spasm and was initially called "dystonia musculorum deformans." Two neurologists from Poland, Flatau and Sterling, objected to the term dystonia, since they did not consider the varying muscle tone to be the clinical hallmark. They proposed the term "progressive torsion spasm," as patients showed torsion spasms of unknown origin. The two terms were combined and the term "primary torsion dystonia" became widely accepted (Grundmann 2005; Tarsy and Simon 2006). The etiology has been a matter of debate over the years. Especially in the time of Sigmund Freud, several patients with dystonia were described and considered to suffer from hysteria. In 1959, the hereditary nature of primary torsion dystonia was demonstrated. Since then, dystonia is considered to be a neurologic condition, although case reports of psychogenic dystonia have been published over the years (Munts and Koehler 2010).

29.1.2 Epidemiology

Dystonia is the third most common movement disorder (annual incidence: 15–25 per 100,000; ESDE 2000; Le et al. 2003) after Parkinson's disease (PD; von Campenhausen et al. 2005) and tremor (Louis and Ferreira 2010). Idiopathic cervical dystonia (CD; dystonia of the neck) is the most common form of dystonia. The estimated prevalence of CD in the Netherlands (total population: 16.9 million) is 8000 patients, although less than half of these patients are regularly seen by a neurologist (ESDE 2000; Le et al. 2003).

29.1.3 Classification, Clinical Features, and Etiology

Dystonia is a syndrome characterized by involuntary, sustained muscle contractions causing twisting movements and abnormal postures (Tarsy and Simon 2006). Dystonia can be classified based on different characteristics. A frequently used classification is based on topographic distribution, including focal dystonia (one body region), segmental dystonia (two or more adjacent regions), multifocal dystonia (two or more nonadjacent regions), hemidystonia (ipsilateral arm and leg), and generalized dystonia (Tarsy and Simon 2006). Another important division is made in associated features: isolated dystonia, combined dystonia (dystonia with another movement disorder), and dystonia associated with other neurological and systemic manifestations. The third commonly used classification is based on etiology:

nervous system pathology (neurodegenerative disorders and structural lesions), inherited dystonia, acquired dystonia, and idiopathic dystonia. In idiopathic dystonia, there is no underlying disorder recognized causing the dystonia (Albanese et al. 2013). A small proportion of these patients has an inherited form of dystonia. Combined dystonia syndromes are genetic syndromes with dystonia and another movement disorder, for example myoclonus (jerks) or parkinsonism. Acquired dystonia can be caused by a large number of neurological and other conditions, medication, and intoxications. Imaging today has a small role in clinical practice and is mainly used to exclude acquired dystonia in young patients or patients with an atypical disease course (Tarsy and Simon 2006). For an overview and classification of the different forms of dystonia, see Table 29.1.

Idiopathic focal dystonia is dystonia of unknown origin in one body part. The most common form of focal dystonia is CD. Other forms are for example blepharospasm (BLS; dystonia of the eyelids), writer's cramp (WC) or focal hand dystonia, oromandibular dystonia (dystonia of the jaw), and spasmodic dysphonia (dystonia of the vocal cords). Most forms of focal dystonia debut around the age of 50 years. One of the most extraordinary features of focal dystonia is that it can be action specific, a feature that is often used in imaging studies. The most well-known form of action-specific dystonia is WC where patients get a dystonic posture of the hand while trying to write, but not in rest or during other hand movements. Action-specific dystonia has been described in other body parts than the hands as well, for example in the mouth in musicians playing a wind instrument (embouchure dystonia). There usually is no identifiable genetic cause in focal dystonia, although in 20–30% of patients the family history is positive for dystonia (Tarsy and Simon 2006; Lohmann and Klein 2017). Over the years, many loci have been linked to dystonia; however, the precise role of these genetic risk factors remains to be determined (Lohmann and Klein 2017).

Patients with generalized dystonia usually develop dystonia in childhood or during adolescence. These patients frequently have a genetic cause for dystonia and most of these familial syndromes have been allocated a DYT number based on clinical characteristics. The combined dystonia syndromes are included in the DYT numbering as well (Muller 2009). Over the years, it has become clear that several DYT syndromes were caused by one gene, while in other DYT syndromes multiple genes were responsible for one phenotype. Recently, the DYT classification has therefore been changed to a system where DYT is now followed by the causative gene. For example, DYT1 is now named DYT-TOR1A (Lohmann and Klein 2017).

Two forms of generalized dystonia that have been well studied are DYT-TOR1A (formerly DYT1) and DYT-THAP1 (formerly DYT6) dystonia. Onset of dystonia in DYT-TOR1A is usually in childhood and first symptoms are typically in the limbs. Dystonia generalizes over the course of a few years in most cases. DYT-TOR1A dystonia is caused by a mutation in the TorsinA gene. The penetrance of the mutation is 30% meaning that only 30% of gene carriers develop dystonia during their lifetime (Muller 2009).

DYT-THAP1 is the second most common genetic cause of inherited dystonia. Age at onset is more variable than in DYT-TOR1A dystonia, varying from onset in

Table 29.1 Classification of dystonia

Type of dystonia	Prominent symptoms	Etiology
Focal dystonia		
Cervical	Dystonia of the neck muscles	Mostly idiopathic, some cases due to DYT-ANO3
Blepharospasm	Dystonia of the eyelids	Unknown
Writer's cramp	Action-specific dystonia of the hands	Unknown
Focal hand dystonia	Nonaction-specific dystonia of the hands	Unknown
Oromandibular dystonia	Dystonia of the jaw and tongue	Unknown
Spasmodic dysphonia	Dystonia of the vocal cords	Unknown
Segmental dystonia		
Meige syndrome	Blepharospasm with dystonia of the jaw or lower face muscles	Unknown
Inherited form of adult-onset segmental dystonia	Craniocervical dystonia with or without dystonia of one arm	DYT-GNAL
Multifocal dystonia		
Hemidystonia		
Post-stroke dystonia	Dystonia of the arm and leg on one side of the body	Usually post-stroke
Generalized dystonia		
Acquired	Generalized dystonia	Usually post-anoxia, e.g., birth trauma
DYT-TOR1A	Generalized dystonia starting in the limbs	TorsinA gene mutation
DYT-THAP1	Focal or generalized dystonia starting in the cranial or cervical muscles	THAP1 gene mutation
Combined dystonia		
Dopamine-responsive dystonia	Generalized dystonia starting in one leg that responds to levodopa	GCH1 gene or SRG gene mutation
Myoclonus-dystonia	Myoclonus, dystonia, and psychiatric symptoms	SGCE gene mutation
Rapid-onset dystonia-parkinsonism	Acute-onset dystonia and parkinsonism	ATP1A3 gene mutation
Paroxysmal dystonia		
Paroxysmal kinesigenic dystonia	Attacks of generalized dystonia triggered by sudden movements	Most commonly PRRT2 gene mutation, however several other genes described
Paroxysmal non-kinesigenic dystonia (DYT8 and 20)	Spontaneous attacks of generalized dystonia	Most commonly PNKD1 gene mutation
Paroxysmal exercise-induced dystonia (DYT18)	Attacks of generalized dystonia triggered by prolonged exercise	GLUT1 gene mutation

childhood to adult onset. Dystonia typically starts in cranial or cervical muscles after which it slowly progresses. Dysphonia is a common symptom in DYT-THAP1 dystonia. DYT-THAP1 dystonia is caused by a mutation in the THAP1 gene. This mutation also has reduced penetrance: 60% of gene carriers develop dystonia (Muller 2009).

The combined dystonia dopamine-responsive dystonia (DRD, also known as Segawa syndrome) has been named DYT-GCH1 dystonia (formerly DYT5). DRD usually starts in childhood with dystonia of a leg. After this, dystonia usually progresses and patients also develop parkinsonian features. Typical features of DRD are worsening of symptoms after sustained action and reduction of symptoms after rest or sleep (Muller 2009). DRD is most commonly (~80% of cases) caused by a mutation in the GCH1 gene encoding GTP-cyclohydrolase-1, an enzyme necessary for the production of dopamine. This mutation is transmitted in an autosomal dominant fashion with a penetrance of ~30%. The second most commonly affected gene is the sepiapterine reductase gene (SRG), another enzyme used in the production of dopamine. Both mutations lead to reduced production of endogenous dopamine (Muller 2009).

Myoclonus-dystonia (MD; DYT-SCGE formerly DYT11) is a form of combined dystonia. Patients exhibit both dystonia and myoclonic jerks. Onset is usually in childhood or adolescence with myoclonic jerks, later followed by a relatively mild form of dystonia. Patients with MD often also exhibit psychiatric symptoms, mainly depression, anxiety, and obsessive-compulsive syndrome. Motor symptoms in MD are highly responsive to alcohol. MD is caused by a mutation in the epsilon-sarcoglycan gene (SGCE gene) and is transmitted in an autosomal dominant matter with reduced penetrance and maternal imprinting. The latter means that only gene carriers inheriting the gene from their father can get the disease. This is largely true, but a small percentage of patients inheriting the gene from their mother also has (mild) symptoms (Muller 2009).

Rapid-onset dystonia-parkinsonism (RDP; DYT-ATP1A3 formerly DYT12) is an autosomal dominant disease with abrupt onset of dystonia and parkinsonism over days to weeks, followed by little or no improvement. Permanent and disabling dystonia presents acutely after physical or psychological stress, fever, or alcohol excess. RDP is caused by mutations in the α3 subunit of the Na/K-ATPase, the ATP1A3 gene (Muller 2009).

Paroxysmal dystonia is a group of disorders that is characterized by attacks of dystonic movements and postures with sometimes chorea or myoclonus. The disorders that can be distinguished are paroxysmal kinesigenic dystonia (PKD; attacks of several seconds triggered by sudden movements), paroxysmal non-kinesigenic dystonia (PNKD; spontaneous attacks lasting minutes to several hours), and exercise-induced dystonia (PED; Muller 2009). The most common form, PKD, was shown to be caused by mutations in the *PRRT2* gene (Wang et al. 2011). Exercise-induced dystonia is found to be caused by a mutation in the *GLUT1* gene, encoding a glucose transporter in the blood-brain barrier. Due to the mutation in this gene, there is reduced glucose transport to the brain (Muller 2009). Recent studies suggest that the phenotypes of the different genes are overlapping and there are even nongenetic disorders that can present with paroxysmal dystonia (Erro and Bhatia 2019).

29.1.4 Pathophysiology

The pathophysiology of dystonia is still largely unknown even for the inherited forms of dystonia. In the last few years, evidence has been gathered that suggests that TorsinA is needed for neuronal cell membrane stability and architecture, nuclear export, and protein trafficking (Gonzalez-Alegre 2019). It is still unclear what the function of the THAP1, GCH, SRG, and SGCE gene is and what happens at a cellular level when these genes are mutated. For focal dystonia, a combination of genetic and environmental factors is hypothesized to play a role (Tarsy and Simon 2006). Imaging studies with positron emission tomography (PET) and single-photon emission computed tomography (SPECT), though also with varying magnetic resonance imaging (MRI) techniques, have been performed over the years to try to unravel the pathophysiology of dystonia. Dopamine is believed to play an important role in the pathophysiology of all forms of dystonia and has been one of the points of focus in PET and SPECT imaging. One argument for the role of dopamine is DRD, which can successfully be treated with levodopa (Naumann et al. 1997). Other important arguments are the coexistence of dystonia in patients with Parkinson's disease, especially in patients who develop PD at a young age and patients who have been treated with levodopa for longer periods (Wickremaratchi et al. 2009) and the possibility of developing dystonia after use of antipsychotics (dopamine $D_{2/3}$ receptor blockers; Haddad and Dursun 2008). We will collaborate more on results from PET and SPECT studies below.

29.1.5 Treatment

Treatment differs for the different types of dystonia. Most forms of focal dystonia are treated locally with intramuscular botulinum toxin (BTX) injections (Zoons et al. 2012). BTX can also be used in patients with generalized dystonia or MD in the body part that is most affected or causes most disability. Usually patients with generalized dystonia are treated with drugs, for example, trihexyphenidyl (Artane), benzodiazepines, or baclofen, or with deep brain stimulation (DBS). Patients with DRD are treated with small amounts of levodopa with dramatic treatment response. The treatment for paroxysmal dystonia consists of anti-epileptics, for example, carbamazepine (Tarsy and Simon 2006).

29.2 Imaging with PET and SPECT in Different Forms of Dystonia

PET and SPECT studies have been performed in patients with different forms of dystonia. The studies that have been performed can roughly be divided into three types: PET studies for glucose metabolism, PET studies for regional cerebral blood flow (rCBF-activation studies), and PET and SPECT studies for receptor imaging, mainly dopamine; however, the serotonin, gamma aminobutyric acid (GABA), and opioid systems have also been studied. The information in this chapter is divided by

forms of dystonia, starting with focal dystonia and followed by generalized dystonia and combined dystonia: DRD, MD, RDP, and paroxysmal dystonia. We will not discuss the results in acquired dystonia. As mentioned above, the causes for acquired dystonia are numerous and the abnormalities found with imaging are usually a result of the underlying condition and not of dystonia per se. A general overview of findings is presented in Table 29.2.

29.3 Focal Dystonia

Several PET and SPECT studies have been performed over the years trying to unravel the pathophysiology of focal dystonia (for a review, see Zoons et al. 2011)

29.3.1 Glucose Metabolism PET

Using [18F]-fluorodeoxyglucose (FDG) PET, increases and decreases in FDG uptake have been found in the basal ganglia, cerebellum, and sensorimotor cortex (SMC) of patients with focal dystonia. A bilateral increase in glucose metabolism in the basal ganglia, thalamus, lentiform nucleus, premotor-motor cortex, and cerebellum has been found in patients with CD compared to controls (Galardi et al. 1996; Magyar-Lehmann et al. 1997). There was an increase in glucose metabolism in the striatum and thalamus of patients with BLS and Meige syndrome (combined dystonia of the eyes and mouth/jaw) compared to controls (Esmaeli-Gutstein et al. 1999) and in the cerebellum and pons in patients with BLS compared to controls (Hutchinson et al. 2000). During induced sleep, patients with BLS showed glucose hypometabolism in the superior-medial aspect of Brodmann area 8 compared to controls. This region is associated with supranuclear control of eyelid opening (Hutchinson et al. 2000). The glucose hypermetabolism in the cerebellum and the pons has been replicated in a study that examined patients with BLS after treatment with BTX. A bilateral glucose hypermetabolism in the thalamus and the pons of patients with BLS was found compared to controls as well as a trend toward glucose hypermetabolism in the putamen bilaterally. Patients with incomplete suppression of BLS on BTX had glucose hypermetabolism in the cerebellum and the pons compared to patients with complete suppression (Suzuki et al. 2007). Furthermore, a complex network of cortical and subcortical regions with increased and decreased metabolism was found in patients with BLS compared to controls. There was increased metabolism in the inferior frontal gyri, right posterior cingulated gyrus, left middle occipital gyrus, fusiform gyrus of the right temporal lobe, left anterior cingulate gyrus, and the caudate nucleus. Decreased glucose metabolism was found in the inferior frontal gyri, left cerebellar hemisphere, and thalamus. Lateralization of activation of the frontal and temporal cortex to the right with contralateral deactivation of the left cerebellum suggests a connection mediated by the corticopontocerebellar pathway (Kerrison et al. 2003). One study compared untreated patients with various forms of isolated focal dystonia (mainly CD and WC) to patients with

Table 29.2 Results of PET and SPECT imaging in dystonia

Type of dystonia	Glucose metabolism	Regional cerebral blood flow	Receptor imaging
Focal			
Cervical	↑ Basal ganglia, thalamus, lentiform nucleus, premotor-motor cortex, cerebellum ↓ Caudate nucleus, thalamus, lentiform nucleus, and temporal, frontal, prefrontal, and parietal cortices	↓ SMA, precentral gyrus, SMC and ↑ ipsilateral parietal cortex, and bilateral occipital cortex (during sensory trick)	↓ Striatal D2/3R binding = DAT binding ↓ Striatal VAChT binding ↓ Midbrain SERT binding (SPECT) = SERT binding (PET) ↑ GABA right precentral gyrus, left parahippocampal gyrus
Blepharospasm	↑ Striatum, thalamus, cerebellum, pons ↓ Brodmann area 8 (supranuclear control of eyelid opening; during induced sleep) *Network*: ↑ inf frontal gyri, r post-cingulated gyrus, l mid-occipital gyrus, fusiform gyrus of the r temp lobe, l ant cingulated gyrus and caudate nucleus and ↓ inf frontal gyri, l cerebellar hemisphere and thalamus	↓ PMC (in response to facial vibration; patients with OMD were also included)	↓ D2/3R binding
Writer's cramp/ focal hand dystonia	↓ Caudate nucleus, thalamus, lentiform nucleus, and temporal, frontal, prefrontal, and parietal cortices	↓ PMC, ↑ frontal and parietal association areas, PSC, SMA (while writing) ↓ SMC and premotor structures (during tasks) ↑ Inferior prefrontal cortex (rest) ↑ Contralateral thalamus, SMC and premotor cortex, and ipsilateral cerebellum (while writing)	↓ D2/3R binding ↓ GABA right cerebellum, left sensorimotor cortex ↑ GABA inferior prefrontal cortex
Segmental dystonia			
Meige syndrome	↑ striatum, thalamus	ND	ND

(continued)

Table 29.2 (continued)

Type of dystonia	Glucose metabolism	Regional cerebral blood flow	Receptor imaging
Inherited generalized dystonia			
DYT-TOR1A	↑ Sup frontal gyrus (incl pre-SMA), precuneus, inf parietal cortex ↑ Putamen ↑ Cerebellum	↑ l premotor area, SMA, ant cingulate cortex, l DLPFC, cerebellum, putamen, gyrus frontalis medialis, sup frontal gyrus, fronto-orbital cortex, and thalamus (during right-hand movements)	↓ D2/3R binding ↓ GABAa receptor binding in PMC, premotor cortex, PSC, SSC, posterior insula, l ant cingulate gyrus = Opioid receptor binding
DYT-THAP1	↑ Sup frontal gyrus (incl pre-SMA), precuneus, inf parietal cortex ↓ Putamen = Cerebellum	ND	↓ D2/3R binding
Combined dystonia			
Dopamine-responsive dystonia	ND	ND	↑ D2/3R binding = DAT binding = D1R binding ↑ VMAT2 binding
Myoclonus-dystonia	ND	ND	↓ D2/3R binding (stabilizes after GPi DBS)
Rapid-onset dystonia-parkinsonism	ND	=	↑ DAT binding = DAT binding ↓ DAT binding
Paroxysmal dystonia			
Paroxysmal kinesigenic dystonia (DYT9 and 10)	ND	↓ Basal ganglia and thalamus	ND
Paroxysmal non-kinesigenic dystonia (DYT8 and 20)	ND	ND	= VMAT2 binding
Paroxysmal exercise-induced dystonia (DYT18)	ND	↓ Cerebellum	ND

↑ increase, ↓ decrease; = no abnormalities, *ant* anterior, *D2/3R* dopamine D2/3 receptors, *DAT* dopamine transporter, *DBS* deep brain stimulation, *DLPFC* dorsolateral prefrontal cortex, *GPi* globus pallidus interna, *incl* including, *inf* inferior, *l* left, *mid* middle, *ND* not done, *OMD* oromandibular dystonia, *PET* positron emission tomography, *PMC* primary motor cortex, *post* posterior, *PSC* primary sensory cortex, *r* right, *SMA* supplementary motor area, *SMC* sensorimotor cortex, *SPECT* single-photon emission computed tomography, *SSC* secondary sensory cortex, *sup* superior, *VAChT* vesicular acetylcholine transporter, *VMAT2* vesicular monoamine transporter type 2

essential tremor (ET) and found that both groups show hypometabolism in the caudate nucleus, thalamus, lentiform nucleus, and temporal, frontal, prefrontal, and parietal cortices. There was a significant difference in the extent of decrease in glucose metabolism between these two groups in the left thalamus, right lentiform nucleus, cingulate gyrus, and pons. The authors propose that quantification of glucose metabolism in these areas can be used to differentiate between the two disorders; however, these results have not been replicated yet (Belenky et al. 2018).

In summary, both patients with CD and BLS showed hypermetabolism in basal ganglia, thalamus, and cerebellum. A network of other cortical and subcortical areas could also be affected in patients with BLS. There could be a difference in glucose metabolism between isolated focal dystonia and ET.

29.3.2 Regional Cerebral Blood Flow PET

Where the above-described studies using [18F]-FDG found abnormalities in glucose metabolism mainly in the basal ganglia, the abnormalities in regional cerebral blood flow-activation studies (rCBF-activation studies) as measured with [15O]-H_2O are mainly cortically localized. [15O]-H_2O PET is often used in task-related studies on WC patients. Due to the short half-life of [15O] (2 min), repeated studies can be performed in a short time period. rCBF-activation PET is essentially the prelude of functional MRI (fMRI) and can still be used in research especially in patients in whom movement artifacts are a problem, for example, dystonia patients (Mishina 2008).

One study showed impaired activation of the primary motor cortex (PMC) and greater activation in frontal and parietal association areas in WC patients compared to controls while writing. BTX treatment failed to normalize the impaired activation of primary motor cortex, but did enhance activation of parietal cortex and accessory motor areas (Ceballos-Baumann et al. 1997). Patients with WC also showed reduced rCBF-activation in sensorimotor and premotor structures in different tasks compared to controls. Certain regions were significantly abnormal for specific tasks. Patients showed significantly less rCBF-activation in the contralateral versus ipsilateral primary sensorimotor cortex, during sustained flexion or extension of the wrist. There was a significant decrease in rCBF-activation in the left premotor cortex with writing, but there were no differences during tapping (Ibanez et al. 1999). A significant increase was found in rCBF-activation of the primary sensory cortex and decrease in rCBF-activation of the supplementary motor area (SMA) in patients with WC during writing and tapping compared to controls. Increased activation of the primary sensory cortex found in this study might reflect more intense processing of the sensory information or possibly expanded cortical representation of the hand area. The investigators also found increased activation of the right cerebellum of patients with WC compared to controls (Lerner et al. 2004). In patients with CD using a sensory trick, a significant decrease in motor cortical activation contralateral to the side toward which the head tends to rotate was found. This modulation includes the SMA (anterior part), part of the precentral gyrus, and the primary

sensorimotor cortex (SMC). In addition, the sensory trick leads to an increased activation of the parietal cortex ipsilateral to the direction of dystonic head rotation and bilateral occipital cortex (Naumann et al. 2000). A study of patients with facial dystonia (blepharospasm and oromandibular dystonia) showed a significantly reduced primary sensorimotor area (PSA) activation response to vibration of the lower face in patients with facial dystonia compared to healthy controls. The peak activations the authors observed in this study were centered in the precentral gyrus, adjacent to the central sulcus, consistent with the primary motor cortex (Feiwell et al. 1999). The only study using [15O]-butanol in patients with WC found increased blood flow in the contralateral thalamus and primary sensorimotor and premotor cortical areas, though also in the ipsilateral cerebellum as the patients with WC invoked progressively greater dysfunction by a longer duration of writing (Odergren et al. 1998). Concluding, abnormalities in rCBF-activation were less consistent than those in glucose metabolism. The most consistent findings included a decreased rCBF-activation in the PMC, SMC, SMA, and PSA and an increase in rCBF-activation in frontal and parietal association areas.

29.3.3 Dopamine Receptor Imaging with PET and SPECT

Two PET studies looked at $D_{2/3}$ receptor (D2/3R) availability in patients with focal dystonia. Leenders and coworkers found no difference in striatal [11C]-*N*-methylspiperone (NMSP) binding to D2-like receptors in patients with mainly CD when compared to healthy controls. A trend was observed regarding the side to side differences: specific binding of the tracer tended to be higher in the striatum contralateral to the side to which the head was turning to (Leenders et al. 1993). Another study showed decreased [18F]-spiperone (SP; another D2-like receptor tracer) binding in the putamen of patients with hand and facial dystonia. There was no significant difference between patients with hand and facial dystonia (Perlmutter et al. 1997).

In patients with CD, the average specific striatal binding to D2/3Rs, measured with [123I]-iodobenzamide ([123I]-IBZM) SPECT, was not significantly different from a group of healthy controls. However, patients exhibited a more asymmetric striatal binding compared to controls and 50% of the patient group did show a higher receptor binding in the striatum contralateral to the direction of head rotation. The difference in binding was statistically significant for this patient group (Hierholzer et al. 1994). This is in accordance with the increased dopamine receptor binding in the contralateral striatum found in the PET study in patients with CD mentioned above and has also been found in other SPECT studies (Leenders et al. 1993). For example, a tendency for a reduced iodobenzamide (IBZM) binding in the dorsal portion and an increase in the ventral parts of the striatum contralateral to the side of head rotation was found by Becker et al. (1997) in CD patients, but these results did not reach statistical significance, probably because of small study size (n = 10). The low IBZM binding contralateral to the side of head deviation may indicate a reduced postsynaptic D2/3R density within the lentiform nucleus. These

findings may point toward the medial lentiform nucleus or pallidothalamic pathway as the site of pathology in CD (Becker et al. 1997). Another study evaluated both the pre- and postsynaptic dopaminergic system in patients with CD, using [123I]-epidepride (a tracer for D2/3R) and [123I]-β-CIT (a tracer for the presynaptic dopamine transporter, DAT). Striatal D2/3R binding was bilaterally significantly reduced in patients compared to controls, but there was no difference in striatal DAT binding (Naumann et al. 1998). A similar design has been used in a more recent study using [123I]-IBZM and [123I]-FP-CIT (DAT tracer) in 27 patients with CD and 15 controls. This study found no difference in striatal DAT binding overall and only a trend toward lower striatal IBZM binding. However, both striatal DAT and D2/3R binding correlated significantly with depressive symptoms, which are common in CD. Both striatal DAT and D2/3R binding were significantly lower in depressed CD patients compared to nondepressed CD patients (Zoons et al. 2017a). Previous dopamine imaging studies in patients with CD and other forms of focal dystonia did not correct for depressive symptoms, which could have caused the difference in results.

In a study evaluating patients with WC, the striatal D2/3R binding was bilaterally decreased in patients compared to controls (Horstink et al. 1997). Another SPECT study evaluated patients with WC pre- and post-biofeedback-based sensorimotor training with [123I]-IBZM SPECT and also found decreased striatal binding. The training made patients more confident to write with a relaxed limb, writing improved, and striatal D2R-binding restored to nearly normal levels (Berger et al. 2007).

In summary, the findings in PET and SPECT studies implicate a role for the striatal dopaminergic system and the basal ganglia in the pathophysiology of focal dystonia. However, it can be debated whether dopamine plays a more important role in the pathophysiology of motor or non-motor symptoms in patients with focal dystonia.

29.3.4 Receptor Imaging of Other Neurotransmitter Systems with PET and SPECT

Recently, other neurotransmitter systems than the dopamine systems have received more attention. One study evaluated the integrity of cholinergic nerve terminals in patients with CD using [123I]-iodobenzavesamicol ([123I]-IBVM), a SPECT tracer that binds to the vesicular acetylcholine transporter (VAChT). They found a reduced IBVM binding in the putamen as well as in the whole striatum in patients with CD compared to controls (Albin et al. 2003).

One PET and one SPECT study have evaluated the presynaptic serotonin transporter (SERT) in patients with CD. In the SPECT study, the nonselective tracer [123I], FP-CIT (this tracer binds predominantly to the DAT in the striatum, and to the SERT in extrastriatal brain areas; Booij et al. 2007) was used and consequently only SERT binding in the diencephalon/midbrain area could be evaluated in patients with CD. A clear trend toward lower SERT binding in CD patients with psychiatric symptoms (mainly depression and anxiety) was found compared to controls.

Furthermore, in CD patients with head jerks or tremor, there was a significant positive correlation between extrastriatal SERT binding and striatal DAT binding that was absent in CD patients without head jerks or tremor (Zoons et al. 2017b). In the PET study, the selective SERT tracer [11C]-DASB was used that allowed a more extensive evaluation of SERT binding throughout the brain and more detailed imaging of small brain regions, which showed a completely different picture. No significant difference was found in SERT binding between CD patients and controls before or after correction for psychiatric symptoms. However, higher SERT binding in the dorsal raphe nucleus was statistically significantly correlated with motor symptom severity and to a lesser extent also to pain and sleep disturbances. There was also a significant relationship between SERT binding in the medial raphe nucleus and fatigue as well as a significant relationship between SERT binding in the caudate nucleus and sleep disturbances (Smit et al. 2018).

In two molecular imaging studies in patients with focal dystonia, the GABA system has been investigated. In a study in patients with CD, using the PET tracer [11C]-flumazenil (FMZ), increased $GABA_A$ availability was found in the right precentral gyrus and in the left parahippocampal gyrus. Furthermore, the side of head turning correlated to a specific pattern in $GABA_A$ availability in several motor regions. Disease severity positively correlated to $GABA_A$ availability in the cerebellar hemispheres and disease duration correlated negatively to several brain regions including cerebellum, thalamus, and basal ganglia (Berman et al. 2018). In a study in patients with focal hand dystonia using both [11C]-flumazenil and [15O]-H2O to measure perfusion, different results were found. In this study, a decreased GABA availability was found in the right cerebellum and left sensorimotor cortex. Increased GABA availability was found in the inferior prefrontal cortex, which also showed an increase in perfusion. These findings correlated negatively to disease duration (Gallea et al. 2018). Both PET studies hypothesize that the areas that show reduced GABA availability are a result of loss of inhibition.

Several studies have implicated a role for the acetylcholine, serotonin, and GABA systems. However, the number of studies is limited and the results vary too much to draw definitive conclusions about the precise role of these neurotransmitter systems.

29.4 Inherited Generalized Dystonia

The discovery of the DYT-TOR1A and DYT-THAP1 genes gave the opportunity to perform imaging studies in both manifesting gene carriers and non-manifesting gene carriers. It is believed that abnormalities found in non-manifesting gene carriers are related to genotype, whereas abnormalities found in patients but not in non-manifesting gene carriers are consistent with phenotype and are either caused by the dystonia or have been the trigger that caused dystonia. On the other hand, abnormalities that have only been found in non-manifesting gene carriers and not in patients or controls could be a physical protection system (Carbon et al. 2004a).

29.4.1 Glucose Metabolism and Regional Cerebral Blood Flow

Differences in glucose metabolism have been found between patients with DYT-TOR1A, DYT-THAP1, and controls. Both the DYT-TOR1A and the DYT-THAP1 patients showed a bilateral increase in glucose metabolism in the superior frontal gyrus, including the pre-SMA, precuneus, and the inferior parietal cortex compared to controls. This increase is a similarity between DYT-TOR1A and DYT-THAP1, but overall there are more differences between the two groups. When comparing DYT-TOR1A carriers, both manifesting and non-manifesting, to controls, there is an increased glucose metabolism in the putamen. In DYT-THAP1 carriers, there is a decreased glucose metabolism in the putamen compared to controls. This decrease is more pronounced in DYT-THAP1 patients than in non-manifesting carriers. Another difference between DYT-TOR1A and DYT-THAP1 is the activation of the cerebellum. In DYT-TOR1A carriers, there is an increased cerebellar glucose metabolism compared to controls; however, the metabolism in the cerebellum of DYT-THAP1 carriers is normal. These differences also become apparent when directly comparing DYT-TOR1A and DYT-THAP1 carriers. DYT-TOR1A carriers have a bilateral increased metabolism in the inferior cerebellum and putamen compared to DYT-THAP1 carriers. DYT-THAP1 carriers have an increased metabolism in the anterior cingulate cortex bilaterally including the subgenual region, the ventral prefrontal cortex, and the middle and superior temporal gyri compared to DYT-TOR1A carriers. Thus far, it is unclear why these patients have different activation patterns in the brain, while they have overlapping symptomatology (Carbon et al. 2004b). In an earlier FDG-PET study, there was no difference in global and regional metabolism between patients with idiopathic torsion dystonia with mainly right-sided symptoms (DYT-TOR1A phenotype) and controls. However, a brain network was identified consisting of increased metabolic activity in the lateral frontal and paracentral cortices, associated with relative covariate hypermetabolism of the contralateral lentiform nucleus, pons, and midbrain. The presence of this network was associated with severity of dystonia. These findings suggest that dystonia is a network disorder (Eidelberg et al. 1995).

In another PET study, rCBF-activation in patients with generalized torsion dystonia (mostly DYT-TOR1A) was compared to that of controls during rest and during a joystick task with their right hand. There was little or no dystonia during task execution. There were no differences in rCBF-activation during rest, but during right-hand movements patients showed more rCBF-activation in the left premotor area, SMA, anterior cingulate cortex, and left dorsolateral prefrontal cortex (DLPFC) compared to controls. Also, some subcortical areas were more active during the joystick task. There was an increase in rCBF-activation in cerebellum and putamen in patients compared to controls. There was a decrease in rCBF-activation in the sensorimotor cortex contralateral to the hand that was executing the task in patients compared to controls (Playford et al. 1998). The overactivation of the DLPFC has been replicated in patients with generalized dystonia and globus pallidus interna (GPi) DBS when they were OFF stimulation. In these patients, other

areas that were overactivated were the gyrus frontalis medialis, superior frontal gyrus, fronto-orbital cortex, and thalamus. Turning the DBS stimulators ON reduced the activation in these areas, as well as in the putamen, but not to the level of controls (Detante et al. 2004).

Most abnormalities that have been found in patients with DYT-TOR1A dystonia have also been found in non-manifesting DYT-TOR1A carriers. In non-manifesting DYT-TOR1A carriers, there was reduced rCBF-activation during a sequence learning task bilateral in DLPFC, in the left dorsal premotor cortex, left ventral prefrontal cortex, and lateral cerebellum. DYT-TOR1A carriers deactivated their left cingulate cortex and activated the right inferotemporal areas during the task. This was opposite to the activation pattern in controls. In controls, there was activation of the left cingulate cortex and deactivation of the right inferotemporal areas (Carbon et al. 2011, 2008; Ghilardi et al. 2003). During a motor task with the right hand, non-manifesting DYT-TOR1A carriers showed increased activation of the left premotor cortex and right SMA and decreased activation of the posterior medial cerebellum compared to controls (Carbon et al. 2011, 2008; Ghilardi et al. 2003). As with FDG-PET, rCBF-activation PET has also been used to assess brain networks in generalized dystonia. A motor-related activation pattern was identified both in controls and DYT-TOR1A gene carriers consisting of covarying neural activity in the sensorimotor cortex, dorsal premotor cortex, SMA, and cerebellum. This network was hyperactive in manifesting DYT-TOR1A gene carriers compared to controls during movement, but not in asymptomatic gene carriers. In rest, there was increased activation of this network both in manifesting and non-manifesting DYT-TOR1A gene carriers compared to controls with the non-manifesting gene carriers showing activation levels between those of the patients and controls (Carbon et al. 2010).

In summary, glucose metabolism differs between patients with DYT-TOR1A and DYT-THAP1 dystonia, with increased metabolism in putamen and cerebellum in DYT-TOR1A dystonia and decreased metabolism in putamen and normal cerebellar metabolism in DYT-THAP1 dystonia. Large numbers of brain areas show abnormal rCBF-activation in patients with DYT-TOR1A, but the significance of these findings is uncertain. Both FDG-PET and rCBF-activation studies have indicated that DYT-TOR1A dystonia is likely to be a network disorder.

29.4.2 Receptor Imaging with PET

Different neurotransmitter systems have been imaged with PET in patients with inherited generalized dystonia. With [11C]-raclopride (RAC; a D2/3 receptor tracer), both manifesting and non-manifesting DYT-TOR1A and DYT-THAP1 carriers have been compared to healthy controls. Both DYT-TOR1A and DYT-THAP1 carriers had reduced RAC binding in the caudate nucleus, putamen, and right ventrolateral thalamus compared to controls (Asanuma et al. 2005; Carbon et al. 2009). In DYT-THAP1 carriers, RAC binding was more reduced than in DYT-TOR1A carriers. This finding combined with the abnormalities in glucose metabolism may indicate that DYT-THAP1 dystonia is associated with striatal receptor loss, while

DYT-TOR1A dystonia is associated with high levels of endogenous dopamine. Thus far, there is no clear evidence for this hypothesis (Carbon and Eidelberg 2009). Although the hypothesis was that RAC binding in non-manifesting carriers was between that of patients and controls, there were no differences in RAC binding between manifesting and non-manifesting carriers in either genotype (Asanuma et al. 2005; Carbon et al. 2009).

Besides dopamine, other neurotransmitters have been studied including GABA, since one hypothesis is that dystonia is a condition of disturbed inhibition. Patients with generalized dystonia (DYT-TOR1A carriers and sporadic cases) showed reduced binding of [11C]-flumazenil (FMZ), a selective $GABA_A$ receptor PET ligand, bilateral in the primary motor and premotor cortex compared to controls. FMZ binding was also reduced in the primary and secondary somatosensory cortex, posterior insula, and in the motor component of the left anterior cingulate gyrus of patients with generalized dystonia compared to controls (Garibotto et al. 2011).

The opioid system has also been investigated in patients with DYT-TOR1A dystonia with [11C]-diprenorphine and PET, but no differences were found cortically or subcortically in DYT-TOR1A patients compared to controls (Whone et al. 2004).

In summary, dopamine is likely to play a role in the pathophysiology of both DYT-TOR1A and DYT-THAP1 dystonia, as GABA in DYT-TOR1A dystonia.

29.5 Dopamine-Responsive Dystonia

Because of the extraordinary treatment effect of levodopa on DRD, molecular imaging studies have focused on dopaminergic neurotransmission.

One of the most consistent findings in DRD is an increased tracer binding to D2/3R in caudate nucleus and putamen measured with RAC (Kishore et al. 1998; Kunig et al. 1998; Rinne et al. 2004). This could be consistent with reduced endogenous dopamine or altered receptor characteristics due to chronic dopamine depletion (Kunig et al. 1998). Increased RAC binding has also been found in asymptomatic DYT-GCH1 carriers and is therefore probably a genotypic and not a phenotypic feature (Kishore et al. 1998). There are no abnormalities in tracer binding to the dopamine transporter (DAT) or dopamine D1 receptors between patients with DRD and controls (Rinne et al. 2004). However, one study using SPECT and the DAT tracer [99mTc]-TRODAT found that striatal uptake correlated to clinical heterogeneity. More specifically, in one family the family members with a predominant parkinsonian phenotype had reduced uptake compared to the family members with a predominant dystonia phenotype (Lin et al. 2018). Abnormalities have been found in [11C]-dihydrotetrabenazine (DTBZ) binding in DRD patients. DTBZ is a tracer that binds to the vesicular monoamine transporter type 2 (VMAT2). In the striatum, VMAT2 is believed to mainly transport dopamine. Patients with DRD showed an increased DTBZ binding compared to controls. This could have been caused by reduced competition because of low concentrations of intravesicular dopamine or by upregulation of VMAT2 (De La Fuente-Fernandez et al. 2003). Finally, one report on a case with DRD and a

mutation in the SRG gene also showed no loss of striatal DAT and D2/3R (Abeling et al. 2006).

As expected from the levodopa response, dopamine plays an important role in the pathophysiology of DRD. This is characterized by increased tracer binding to D2R and VMAT2 and normal tracer binding to DAT and D1R.

29.6 Myoclonus-Dystonia

Imaging results in myoclonus-dystonia (MD) only consist of two SPECT studies with [123I]-iodobenzamide (IBZM), a selective D2/3R SPECT tracer. Both MD patients and asymptomatic DYT-SCGE carriers show reduced IBZM binding compared to controls. This is consistent with the theory that a high level of endogenous dopamine causes downregulation of D2 receptors and leads to more occupied receptors, limiting IBZM binding potential (Beukers et al. 2009). After globus pallidus interna (GPi) DBS, IBZM binding in MD patients remains stable over time, whereas in patients who did not receive DBS, IBZM binding decreased further over time. This may mean that DBS in the GPi stabilizes the dopaminergic system in these patients (Beukers et al. 2012).

29.7 Rapid-Onset Dystonia-Parkinsonism

Because of the relation between dystonia and parkinsonism in this rare form of combined dystonia, most studies evaluated the dopamine system, more specifically the DAT, and compared the results to normal controls and patients with idiopathic Parkinson's disease. Tracer binding to DAT in three reports in a total of five patients yielded different results. One study in three patients showed a slight increase in tracer binding to striatal DAT (Brashear et al. 1999), while two other case reports showed normal DAT binding (Svetel et al. 2010) and a slight reduction in DAT binding (Zanotti-Fregonara et al. 2008), respectively. A perfusion SPECT scan in one patient showed no abnormalities (Zanotti-Fregonara et al. 2008).

Overall, gross abnormalities in dopaminergic neurotransmission are unlikely in RDP.

29.8 Paroxysmal Dystonia

In PKD, interictal perfusion SPECT showed regional hypoperfusion of the basal ganglia and the thalamus (Tsai et al. 2005). In PNKD, no abnormalities were found in VMAT2 binding in the striatum (Bohnen et al. 1999). Patients with exercise-induced dystonia showed reduced perfusion to the frontal cortex and basal ganglia and increased perfusion to the cerebellum during an attack using [99mTc]-ethyl cysteinate dimer (ECD) and SPECT (Kluge et al. 1998).

29.9 Conclusion

PET and SPECT studies have been performed in different forms of dystonia. Surprisingly, found abnormalities are quite similar in patients with idiopathic focal dystonia and DYT-TOR1A inherited generalized dystonia. Both focal and DYT-TOR1A dystonia patients show increased glucose metabolism in the basal ganglia, the cerebellum, and premotor structures. The areas in which rCBF-activation is abnormal are also comparable in focal and DYT-TOR1A dystonia, with increased rCBF-activation in premotor structures, frontal areas including DLPFC and cerebellum, and decreased activation in sensorimotor cortex. The found abnormalities indicate that dystonia is a circuit disorder and that the underlying cause lies somewhere in the cortico-striato-thalamo-cortical loop. The dopamine system plays an important role in both focal and DYT-TOR1A dystonia, with decreased D2R binding in the striatum pointing toward a hyperdopaminergic system. The precise role of other neurotransmitter systems, such as acetylcholine, serotonin, and GABA, remains to be determined.

DYT-THAP1 dystonia seems to be a different condition, since the reported abnormalities are different from other forms of dystonia. Striking are the decreased rCBF-activation in the putamen and normal rCBF-activation in the cerebellum, in contrast to increased rCBF-activation in the putamen and cerebellum of patients with DYT-TOR1A dystonia. The only similarity between DYT-THAP1 dystonia and other forms of dystonia is the decreased D2/3R binding. Thus far, it is still unclear what causes the differences between DYT-THAP1 dystonia and other forms of dystonia.

D2/3R binding is also decreased in MD, but is increased in DRD. Patients with DRD have a problem with the synthesis of dopamine and are therefore hypodopaminergic. The studies in different forms of paroxysmal dystonia are too limited and diverse to draw any definite conclusions.

References

Abeling NG, Duran M, Bakker HD et al (2006) Sepiapterin reductase deficiency an autosomal recessive DOPA-responsive dystonia. Mol Genet Metab 89:116–120

Albanese A, Bhatia K, Bressman SB et al (2013) Phenomenology and classification of dystonia: a consensus update. Mov Disord 28:863–873

Albin RL, Cross D, Cornblath WT et al (2003) Diminished striatal [123I]iodobenzovesamicol binding in idiopathic cervical dystonia. Ann Neurol 53:528–532

Asanuma K, Ma Y, Okulski J et al (2005) Decreased striatal D2 receptor binding in non-manifesting carriers of the DYT1 dystonia mutation. Neurology 64:347–349

Becker G, Naumann M, Scheubeck M et al (1997) Comparison of transcranial sonography, magnetic resonance imaging, and single photon emission computed tomography findings in idiopathic spasmodic torticollis. Mov Disord 12:79–88

Belenky V, Stanzhevsky A, Klicenko O, Skoromets A (2018) Brain positron emission tomography with 2-(18)F-2-deoxi-D-glucose of patients with dystonia and essential tremor detects differences between these disorders. Neuroradiol J 31:60–68

Berger HJ, van der Werf SP, Horstink CA, Cools AR, Oyen WJ, Horstink MW (2007) Writer's cramp: restoration of striatal D2-binding after successful biofeedback-based sensorimotor training. Parkinsonism Relat Disord 13:170–173

Berman BD, Pollard RT, Shelton E, Karki R, Smith-Jones PM, Miao Y (2018) GABAA receptor availability changes underlie symptoms in isolated cervical dystonia. Front Neurol 9:188

Beukers RJ, Booij J, Weisscher N, Zijlstra F, van Amelsvoort TA, Tijssen MA (2009) Reduced striatal D2 receptor binding in myoclonus-dystonia. Eur J Nucl Med Mol Imaging 36:269–274

Beukers RJ, Contarino MF, Speelman JD, Schuurman PR, Booij J, Tijssen MA (2012) Deep brain stimulation of the pallidum is effective and might stabilize striatal D(2) receptor binding in myoclonus-dystonia. Front Neurol 3:22

Bohnen NI, Albin RL, Frey KA, Fink JK (1999) (+)-alpha-[11C]Dihydrotetrabenazine PET imaging in familial paroxysmal dystonic choreoathetosis. Neurology 52:1067–1069

Booij J, de Jong J, de Bruin K, Knol R, de Win MM, van Eck-Smit BL (2007) Quantification of striatal dopamine transporters with 123I-FP-CIT SPECT is influenced by the selective serotonin reuptake inhibitor paroxetine: a double-blind, placebo-controlled, crossover study in healthy control subjects. J Nucl Med 48:359–366

Brashear A, Mulholland GK, Zheng QH, Farlow MR, Siemers ER, Hutchins GD (1999) PET imaging of the pre-synaptic dopamine uptake sites in rapid-onset dystonia-parkinsonism (RDP). Mov Disord 14:132–137

Carbon M, Eidelberg D (2009) Abnormal structure-function relationships in hereditary dystonia. Neuroscience 164:220–229

Carbon M, Kingsley PB, Su S et al (2004a) Microstructural white matter changes in carriers of the DYT1 gene mutation. Ann Neurol 56:283–286

Carbon M, Su S, Dhawan V, Raymond D, Bressman S, Eidelberg D (2004b) Regional metabolism in primary torsion dystonia: effects of penetrance and genotype. Neurology 62:1384–1390

Carbon M, Ghilardi MF, Argyelan M, Dhawan V, Bressman SB, Eidelberg D (2008) Increased cerebellar activation during sequence learning in DYT1 carriers: an equiperformance study. Brain 131:146–154

Carbon M, Niethammer M, Peng S et al (2009) Abnormal striatal and thalamic dopamine neurotransmission: genotype-related features of dystonia. Neurology 72:2097–2103

Carbon M, Argyelan M, Habeck C et al (2010) Increased sensorimotor network activity in DYT1 dystonia: a functional imaging study. Brain 133:690–700

Carbon M, Argyelan M, Ghilardi MF et al (2011) Impaired sequence learning in dystonia mutation carriers: a genotypic effect. Brain 134:1416–1427

Ceballos-Baumann AO, Sheean G, Passingham RE, Marsden CD, Brooks DJ (1997) Botulinum toxin does not reverse the cortical dysfunction associated with writer's cramp. A PET study. Brain 120(Pt 4):571–582

De La Fuente-Fernandez R, Furtado S, Guttman M et al (2003) VMAT2 binding is elevated in dopa-responsive dystonia: visualizing empty vesicles by PET. Synapse 49:20–28

Detante O, Vercueil L, Thobois S et al (2004) Globus pallidus internus stimulation in primary generalized dystonia: a H215O PET study. Brain 127:1899–1908

Eidelberg D, Moeller JR, Ishikawa T et al (1995) The metabolic topography of idiopathic torsion dystonia. Brain 118(Pt 6):1473–1484

Erro R, Bhatia KP (2019) Unravelling of the paroxysmal dyskinesias. J Neurol Neurosurg Psychiatry 90:227–234

ESDE (2000) A prevalence study of primary dystonia in eight European countries. J Neurol 247:787–792

Esmaeli-Gutstein B, Nahmias C, Thompson M, Kazdan M, Harvey J (1999) Positron emission tomography in patients with benign essential blepharospasm. Ophthal Plast Reconstr Surg 15:23–27

Feiwell RJ, Black KJ, McGee-Minnich LA, Snyder AZ, MacLeod AM, Perlmutter JS (1999) Diminished regional cerebral blood flow response to vibration in patients with blepharospasm. Neurology 52:291–297

Galardi G, Perani D, Grassi F et al (1996) Basal ganglia and thalamo-cortical hypermetabolism in patients with spasmodic torticollis. Acta Neurol Scand 94:172–176
Gallea C, Herath P, Voon V et al (2018) Loss of inhibition in sensorimotor networks in focal hand dystonia. Neuroimage Clin 17:90–97
Garibotto V, Romito LM, Elia AE et al (2011) In vivo evidence for GABA(A) receptor changes in the sensorimotor system in primary dystonia. Mov Disord 26:852–857
Ghilardi MF, Carbon M, Silvestri G et al (2003) Impaired sequence learning in carriers of the DYT1 dystonia mutation. Ann Neurol 54:102–109
Gonzalez-Alegre P (2019) Advances in molecular and cell biology of dystonia: focus on torsinA. Neurobiol Dis 127:233–241
Grundmann K (2005) Primary torsion dystonia. Arch Neurol 62:682–685
Haddad PM, Dursun SM (2008) Neurological complications of psychiatric drugs: clinical features and management. Hum Psychopharmacol 23(Suppl 1):15–26
Hierholzer J, Cordes M, Schelosky L et al (1994) Dopamine D2 receptor imaging with iodine-123-iodobenzamide SPECT in idiopathic rotational torticollis. J Nucl Med 35:1921–1927
Horstink CA, Praamstra P, Horstink MW, Berger HJ, Booij J, van Royen EA (1997) Low striatal D2 receptor binding as assessed by [123I]IBZM SPECT in patients with writer's cramp. J Neurol Neurosurg Psychiatry 62:672–673
Hutchinson M, Nakamura T, Moeller JR et al (2000) The metabolic topography of essential blepharospasm: a focal dystonia with general implications. Neurology 55:673–677
Ibanez V, Sadato N, Karp B, Deiber MP, Hallett M (1999) Deficient activation of the motor cortical network in patients with writer's cramp. Neurology 53:96–105
Kerrison JB, Lancaster JL, Zamarripa FE et al (2003) Positron emission tomography scanning in essential blepharospasm. Am J Ophthalmol 136:846–852
Kishore A, Nygaard TG, de la Fuente-Fernandez R et al (1998) Striatal D2 receptors in symptomatic and asymptomatic carriers of dopa-responsive dystonia measured with [11C]-raclopride and positron-emission tomography. Neurology 50:1028–1032
Kluge A, Kettner B, Zschenderlein R et al (1998) Changes in perfusion pattern using ECD-SPECT indicate frontal lobe and cerebellar involvement in exercise-induced paroxysmal dystonia. Mov Disord 13:125–134
Kunig G, Leenders KL, Antonini A, Vontobel P, Weindl A, Meinck HM (1998) D2 receptor binding in dopa-responsive dystonia. Ann Neurol 44:758–762
Le KD, Nilsen B, Dietrichs E (2003) Prevalence of primary focal and segmental dystonia in Oslo. Neurology 61:1294–1296
Leenders K, Hartvig P, Forsgren L et al (1993) Striatal [11C]-N-methyl-spiperone binding in patients with focal dystonia (torticollis) using positron emission tomography. J Neural Transm Park Dis Dement Sect 5:79–87
Lerner A, Shill H, Hanakawa T, Bushara K, Goldfine A, Hallett M (2004) Regional cerebral blood flow correlates of the severity of writer's cramp symptoms. NeuroImage 21:904–913
Lin JJ, Lu CS, Tsai CH (2018) Variability of presynaptic nigrostriatal dopaminergic function and clinical heterogeneity in a dopa-responsive dystonia family with GCH-1 gene mutation. J Neurol 265:478–485
Lohmann K, Klein C (2017) Update on the genetics of dystonia. Curr Neurol Neurosci Rep 17:26
Louis ED, Ferreira JJ (2010) How common is the most common adult movement disorder? Update on the worldwide prevalence of essential tremor. Mov Disord 25:534–541
Magyar-Lehmann S, Antonini A, Roelcke U et al (1997) Cerebral glucose metabolism in patients with spasmodic torticollis. Mov Disord 12:704–708
Mishina M (2008) Positron emission tomography for brain research. J Nippon Med Sch 75:68–76
Muller U (2009) The monogenic primary dystonias. Brain 132:2005–2025
Munts AG, Koehler PJ (2010) How psychogenic is dystonia? Views from past to present. Brain 133:1552–1564
Naumann M, Pirker W, Reiners K, Lange K, Becker G, Brucke T (1997) [123I]beta-CIT single-photon emission tomography in DOPA-responsive dystonia. Mov Disord 12:448–451

Naumann M, Pirker W, Reiners K, Lange KW, Becker G, Brucke T (1998) Imaging the pre- and postsynaptic side of striatal dopaminergic synapses in idiopathic cervical dystonia: a SPECT study using [123I] epidepride and [123I] beta-CIT. Mov Disord 13:319–323

Naumann M, Magyar-Lehmann S, Reiners K, Erbguth F, Leenders KL (2000) Sensory tricks in cervical dystonia: perceptual dysbalance of parietal cortex modulates frontal motor programming. Ann Neurol 47:322–328

Odergren T, Stone-Elander S, Ingvar M (1998) Cerebral and cerebellar activation in correlation to the action-induced dystonia in writer's cramp. Mov Disord 13:497–508

Perlmutter JS, Stambuk MK, Markham J et al (1997) Decreased [18F]spiperone binding in putamen in idiopathic focal dystonia. J Neurosci 17:843–850

Playford ED, Passingham RE, Marsden CD, Brooks DJ (1998) Increased activation of frontal areas during arm movement in idiopathic torsion dystonia. Mov Disord 13:309–318

Rinne JO, Iivanainen M, Metsahonkala L et al (2004) Striatal dopaminergic system in dopa-responsive dystonia: a multi-tracer PET study shows increased D2 receptors. J Neural Transm (Vienna) 111:59–67

Smit M, Vallez Garcia D, de Jong BM et al (2018) Relationships between serotonin transporter binding in the raphe nuclei, basal ganglia, and hippocampus with clinical symptoms in cervical dystonia: a [(11)C]DASB Positron Emission Tomography Study. Front Neurol 9:88

Suzuki Y, Mizoguchi S, Kiyosawa M et al (2007) Glucose hypermetabolism in the thalamus of patients with essential blepharospasm. J Neurol 254:890–896

Svetel M, Ozelius LJ, Buckley A et al (2010) Rapid-onset dystonia-parkinsonism: case report. J Neurol 257:472–474

Tarsy D, Simon DK (2006) Dystonia. N Engl J Med 355:818–829

Tsai JD, Chou IC, Tsai FJ, Kuo HT, Tsai CH (2005) Clinical manifestation and carbamazepine treatment of patients with paroxysmal kinesigenic choreoathetosis. Acta Paediatr Taiwan 46:138–142

von Campenhausen S, Bornschein B, Wick R et al (2005) Prevalence and incidence of Parkinson's disease in Europe. Eur Neuropsychopharmacol 15:473–490

Wang JL, Cao L, Li XH et al (2011) Identification of PRRT2 as the causative gene of paroxysmal kinesigenic dyskinesias. Brain 134:3493–3501

Whone AL, Von Spiczak S, Edwards M et al (2004) Opioid binding in DYT1 primary torsion dystonia: an 11C-diprenorphine PET study. Mov Disord 19:1498–1503

Wickremaratchi MM, Ben-Shlomo Y, Morris HR (2009) The effect of onset age on the clinical features of Parkinson's disease. Eur J Neurol 16:450–456

Zanotti-Fregonara P, Vidailhet M, Kas A et al (2008) [123I]-FP-CIT and [99mTc]-HMPAO single photon emission computed tomography in a new sporadic case of rapid-onset dystonia-parkinsonism. J Neurol Sci 273:148–151

Zoons E, Booij J, Nederveen AJ, Dijk JM, Tijssen MA (2011) Structural, functional and molecular imaging of the brain in primary focal dystonia—a review. NeuroImage 56:1011–1020

Zoons E, Dijkgraaf MG, Dijk JM, van Schaik IN, Tijssen MA (2012) Botulinum toxin as treatment for focal dystonia: a systematic review of the pharmaco-therapeutic and pharmaco-economic value. J Neurol 259(12):2519–2526

Zoons E, Tijssen MA, Dreissen YE, Speelman JD, Smit M, Booij J (2017a) The relationship between the dopaminergic system and depressive symptoms in cervical dystonia. Eur J Nucl Med Mol Imaging 44:1375–1382

Zoons E, Booij J, Speelman JD, Dreissen YEM, Smit M, Tijssen MAJ (2017b) Lower serotonin transporter binding in patients with cervical dystonia is associated with psychiatric symptoms. EJNMMI Res 7:87

PET and SPECT Imaging in Hyperkinetic Movement Disorders

30

Evelien Zoons, Sarvi Sharifi, Jan Booij, Bauke de Jong, and Marina A. J. Tijssen

Contents

30.1 General Introduction 823
30.2 Tremor 824
30.2.1 Historical Background 824
30.2.2 Classification, Clinical Features, Etiology, and Pathophysiology 824
30.2.3 Treatment 825
30.2.4 Imaging with PET and SPECT 825
30.2.5 Orthostatic Tremor 827
30.3 Gilles de la Tourette Syndrome and Tics 828
30.3.1 Historical Background 828
30.3.2 Clinical Features and Etiology 829

E. Zoons
Department of Neurology, Zaans Medisch Centrum, Zaandam, The Netherlands
e-mail: zoons.e@zaansmc.nl

S. Sharifi
Department of Neurology, Amsterdam University Medical Center, Amsterdam, The Netherlands
e-mail: s.sharifi@amsterdamumc.nl

J. Booij
Department of Radiology and Nuclear Medicine, Amsterdam University Medical Center, Amsterdam, The Netherlands
e-mail: j.booij@amsterdamumc.nl

B. de Jong · M. A. J. Tijssen (✉)
Department of Neurology, University Medical Center Groningen, Groningen, The Netherlands
e-mail: b.de.jong@umcg.nl; m.a.j.de.koning-tijssen@umcg.nl

R. A. J. O. Dierckx et al. (eds.), *PET and SPECT in Neurology*,
https://doi.org/10.1007/978-3-030-53168-3_30

30.3.3 Pathophysiology..... 830
30.3.4 Treatment..... 830
30.3.5 Imaging with PET and SPECT..... 830
30.4 Myoclonus..... 834
30.4.1 Historical Background..... 834
30.4.2 Classification, Clinical Features, and Etiology..... 834
30.4.3 Pathophysiology..... 835
30.4.4 Treatment..... 835
30.4.5 Imaging..... 836
30.5 Restless Legs Syndrome and Periodic Limb Movements in Sleep..... 839
30.5.1 Historical Background..... 839
30.5.2 Clinical Features and Etiology..... 839
30.5.3 Pathophysiology..... 840
30.5.4 Treatment..... 840
30.5.5 Imaging..... 840
30.6 General Conclusion..... 842
References..... 842

Abstract

Movement disorders can be classified in hypokinetic (e.g., Parkinson's disease, PD) and hyperkinetic disorders (e.g., dystonia, chorea, tremor, tics, myoclonus, and restless legs syndrome). In this chapter, we will discuss results from positron emission tomography (PET) and single photon emission computed tomography (SPECT) imaging studies in patients with tremor, tics, myoclonus, and restless legs syndrome.

Most studies in patients with tremor included patients with essential tremor (ET): a bilateral, largely symmetric, postural or kinetic tremor mainly involving the upper limbs and sometimes the head. Other studies evaluated patients with orthostatic tremor (OT): an unusually high frequent tremor in the legs that mainly occurs when patients are standing still. Increased regional cerebral blood flow (rCBF) and increased glucose metabolism have been found in the cerebellum, sensorimotor cortex, and thalamus in both patients with ET and OT compared to controls. Both PET and SPECT studies have evaluated the dopamine system in patients with ET and OT. Most imaging studies in patients with ET showed no, or only subtle loss of striatal tracer binding to the dopamine transporter indicating that ET is not characterized by nigrostriatal cell loss. The serotonin and/or gamma-aminobutyric acid (GABA) systems may play a role in the pathophysiology of ET. PET and SPECT imaging of the dopamine and serotonin system in patients with OT showed no abnormalities.

Tics, the clinical hallmark of Gilles de la Tourette syndrome (TS), are relatively brief and intermittent involuntary movements (motor tic) and sounds (phonic tic). The essential features of tics are that (1) they can be temporarily suppressed; after suppression a rebound usually occurs with a flurry of tics; (2) the patient experiences an urge to tic, and (3) the tic is followed by a short moment of relief. Using ^{18}F-FDG PET, it was shown that TS is a network disor-

der where multiple brain areas are active or inactive at the same time. The exact composition of this network is yet to be determined. Using rCBF PET and SPECT many brain regions were found to be abnormal, however, tics mostly correlated with hypoperfusion of the caudate nucleus and cingulate cortex. Both dopamine and serotonin are likely to play a role in the pathophysiology of TS. It is hypothesized that TS is characterized by low serotonin levels that modulate increased phasic dopamine release.

Myoclonus is defined as a brief muscle jerk and occurs in many neurologic and non-neurologic disorders. Imaging with PET and SPECT in patients with myoclonus mainly showed abnormalities consistent with the underlying disorder. We described PET and SPECT imaging results in patients in which myoclonus was a prominent symptom. Hypoperfusion and/or hypometabolism of the frontoparietal cortex was found in patients with negative epileptic myoclonus, Alzheimer's disease, corticobasal degeneration, Creutzfeldt–Jakob disease, fatal familiar insomnia, and posthypoxic myoclonus. Other findings that were frequently reported were decreased rCBF and/or glucose metabolism in the cerebellum and thalamus and abnormalities in the dopamine system.

Restless legs syndrome (RLS) is defined as an urge to move the legs accompanied with an unpleasant sensation in the legs or in another body part that is especially present during the evening and night and that can be accompanied by periodic limb movements in sleep (PLMS). Imaging studies in these patients have mainly focused on the dopamine system. Most PET studies found decreased tracer binding to the dopamine transporter, although this was not found in SPECT studies. Both PET and SPECT studies showed conflicting results regarding dopamine $D_{2/3}$ receptor binding: both increased and decreased tracer binding was reported. Furthermore, it is likely that the serotonin and opioid systems also play a role in the pathophysiology of RLS.

30.1 General Introduction

Movement disorders can be classified in hypo- and hyperkinetic disorders. The hypokinetic movement disorders include Parkinson's disease and other syndromes with parkinsonian features, for example, bradykinesia (slowness of movements). The hyperkinetic movement disorders form a large group of disorders including dystonia, chorea, myoclonus, tremor, tics, restless legs syndrome, and other rarer movement disorders (Fahn 2011). PET and SPECT findings in dystonia and chorea are dealt with in separate chapters. In this chapter, we will discuss PET and SPECT imaging in the more jerky movement disorders: tremor, tics, myoclonus, and restless legs syndrome. Every section on a specific movement disorder will start with an introduction, including historical background, phenomenology and clinical features, epidemiology, etiology, pathophysiology, and treatment. After this, results from studies using PET and SPECT are discussed.

30.2 Tremor

30.2.1 Historical Background

The first comprehensive summary of different tremor syndromes was made as late as 1998 by the Movement Disorder Society (MDS) (Deuschl et al. 1998). It was recognized that many different disorders could cause tremor. In most patients, tremor is located in the upper limbs, present during posture and is not evidently associated with other neurological symptoms, so-called essential tremor (ET). In 1981, Marsden and co-workers separated postural hand tremor into four types based on its severity. Type 1 was defined as enhanced physiological tremor, and therefore not considered pathological. Type 4 was regarded an ET-like action tremor as a symptom of another disorder (e.g., Parkinson's disease, dystonic tremor, or neuropathic tremor). Types 2 and 3 were considered to be mild and severe "pure" ET, respectively. These two types are now considered to be one disorder, namely, ET. Several rare tremor syndromes, such as orthostatic tremor (OT) and palatal tremor, were not included in this classification, but are of interest (Elble and Deuschl 2011). In this chapter, we will discuss ET and OT.

30.2.2 Classification, Clinical Features, Etiology, and Pathophysiology

ET was defined in the 1998 MDS consensus statement as a bilateral, largely symmetric postural, or kinetic tremor involving the hands and forearms that are visible and persistent. An additional or isolated tremor of the head may occur in the absence of abnormal posturing and other causes for tremor must be excluded (Deuschl et al. 1998; Elble and Deuschl 2011). The overall prevalence of ET is estimated to be 0.4–0.9% in the general population, however, can be as high as 4.8% in patients over 60 years of age (Louis and Ferreira 2010). Most patients with ET have their first symptoms in early adulthood, and the disease is characterized by slow progression and usually does not lead to disability until older age (Elble and Deuschl 2011). The tremor is highly responsive to alcohol and tends to increase after alcohol withdrawal (Crawford and Zimmerman 2011). ET has always been thought to be a monogenic disorder inherited in an autosomal dominant manner. However, current thinking is that the pathophysiology is more complex. Besides monogenic forms of ET, which can have incomplete penetrance, there are also patients in which multiple genes in combination with environmental factors contribute to disease etiology (Louis 2018). So far, genetic studies have revealed three genes to be linked to ET. These include the FUS gene (16p11.2), one of the genes implicated in the pathophysiology of hereditary amyotrophic lateral sclerosis, which accounts for a small proportion of both familial and sporadic cases of ET (Merner et al. 2012). Furthermore, mutations in the LINGO1 and TENM4 gene have been linked to ET (Louis 2018). Most of the pathophysiology of ET is unclear. ET has been associated mainly with (GABAergic) cerebellar dysfunction and disturbance of cerebello-thalamo-cortical network (Zhang and Santaniello 2019). ET is probably not linked

to neurodegeneration but to abnormalities of central oscillators arising within the olivocerebellar and thalamocortical loops (Deuschl et al. 2000; Jenkins and Frackowiak 1993). Case reports where ET disappears after a stroke in cerebellum, the pons, or the thalamus suggest that interruption in central neural networks affects this type of tremor (Duncan et al. 1988; Dupuis et al. 1989, 2010; Nagaratnam and Kalasabail 1997). Postmortem studies have mainly found cerebellar pathology, more specifically Purkinje cell changes regarding their number, dendritic fields, and axons in a large proportion of ET patients (Mavroudis et al. 2019; Louis et al. 2006; Louis and Vonsattel 2008). Other findings included increased number of Lewy bodies in the brainstem and cell loss in the locus ceruleus (Mavroudis et al. 2019).

OT is a tremor of unusual high frequency (13–18 Hz) that mainly occurs in the legs when patients are standing still (Elble and Deuschl 2011). Onset of complaints is mainly around 50 years of age (Gerschlager et al. 2004). Little is known of the epidemiology of this disorder. The tremor causes a feeling of discomfort and unsteadiness that is reduced by sitting or walking (Gerschlager et al. 2004). OT is palpable as a tremulous contraction of the muscle and is audible when a stethoscope is placed on the leg (Elble and Deuschl 2011). OT can be primary or occur as a symptom of another disorder (e.g., Parkinson's disease, RLS, tardive dyskinesias) (Gerschlager et al. 2004). In this chapter, we only describe studies in patients with primary OT. In OT, there is probably a common cerebral drive causing coherent tremor activity through widespread synchronous oscillation, but the location of this drive is unknown (Elble and Deuschl 2011).

30.2.3 Treatment

Several types of medication can be used for the treatment of ET. The nonselective beta-blocker propranolol and the antiepileptic drug primidone have proven to be efficient in reducing limb tremor and should therefore be considered treatment of first choice. Propranolol is probably also effective in reducing head tremor. If these therapies fail or yield too much side effects, other drugs (mainly other beta blockers, antiepileptics, or benzodiazepines) that are probably effective are alprazolam, atenolol, gabapentin, sotalol, or topiramate. In severe cases, where medication fails, deep brain stimulation (DBS) in the ventral intermediate nucleus (Vim) of the thalamus can be considered (Zesiewicz et al. 2011). There are a few treatment options in patients with OT, but most of them tend to be unsuccessful in the majority of patients. Drugs that can be tested are gabapentin, primidone, and clonazepam. Some patients have been treated with DBS in the thalamus (Elble and Deuschl 2011).

30.2.4 Imaging with PET and SPECT

PET and SPECT studies that have been performed in tremor syndromes can roughly be divided in three types: ^{18}F-fluorodeoxyglucose (FDG) PET studies to assess brain glucose metabolism, PET, and SPECT studies for regional cerebral blood flow (rCBF) and PET and SPECT studies for receptor imaging, mainly focusing on the dopamine and GABA systems.

30.2.4.1 Essential Tremor

Regional Cerebral Blood Flow and Glucose Metabolism

RCBF has been measured both with PET and SPECT in patients with ET. The most consistent finding was increased rCBF bilaterally in the cerebellum of patients with ET. This increased rCBF was seen when patients with ET were in rest as compared to healthy controls (Jenkins and Frackowiak 1993; Boecker et al. 1996; Czarnecki et al. 2011; Wills et al. 1994) as well as when patients were maintaining a posture that induced tremor compared to a resting condition (Jenkins and Frackowiak 1993; Boecker et al. 1996; Wills et al. 1994; Colebatch et al. 1990). After ethanol administration, rCBF in cerebellum reduces and the rCBF in the inferior olivary nucleus increases (Boecker et al. 1996). Other findings included increased rCBF in the sensorimotor cortex contralateral to the arm maintaining a tremor-inducing posture (Jenkins and Frackowiak 1993; Czarnecki et al. 2011; Colebatch et al. 1990) and in the thalamus (Jenkins and Frackowiak 1993; Wills et al. 1994). The thalamus was also found to be overactive at rest in patients with ET compared to controls (Wills et al. 1994). Furthermore, patients with ET showed increased rCBF in the contralateral primary motor cortex (Czarnecki et al. 2011; Colebatch et al. 1990), supplementary motor area (SMA) (Czarnecki et al. 2011), contralateral striatum (Jenkins and Frackowiak 1993), and midbrain (Wills et al. 1994) during the posture compared to resting state. The only decrease in rCBF was found in the inferior temporal and occipital areas in patients with ET during tremor compared to controls (Wills et al. 1994).

One study evaluated glucose metabolism with PET in patients with ET during rest and found increased metabolism in the inferior olivary nucleus and thalamus compared to controls (Hallett and Dubinsky 1993). A more recent study showed decreased glucose metabolism in the medial frontal lobe, medial temporal lobe, and the precuneus of the parietal lobe in 17 male ET patients compared to controls (Ha et al. 2015). No abnormalities in metabolism of the cerebellum were found in both studies. Another study did find decreased glucose metabolism in the cerebellum when comparing ET patients to healthy controls, as well as decreased glucose metabolism in the frontal, temporal and occipital lobes, and the precuneus of the right parietal lobe (Song et al. 2015). In the same study, ET patients with a good response to propranolol were compared to ET patients that did not respond to propranolol. The responders had lower tremor scores and decreased glucose metabolism in the left basal ganglia (Song et al. 2015).

In summary, results from perfusion and metabolism scans of a heterogeneous ET group implicate in rest and posture the cerebellum, sensorimotor cortex, and thalamus (implicating the cerebello-thalamo-cortical network) as well as other areas in the pathophysiology of ET.

Receptor Imaging

Receptor imaging has mainly focused on the dopamine system and in many studies patients with ET were compared to controls as well as to patients with Parkinson's disease (PD). Patients with PD also frequently suffer from tremor in the hands and the two disorders can be mistaken for each other early in the disease course.

Most studies found slightly diminished tracer binding to the dopamine transporter (DAT) in the striatum of patients with ET compared to controls (Gerasimou et al. 2012; Group PS 2000; Isaias et al. 2008a; Lee et al. 1999; Schwartz et al. 2004; Waln et al. 2015). Patients with PD in these studies had a far more distinct reduction in striatal DAT tracer binding and DAT SPECT and DOPA PET scans were able to distinguish patients with PD and ET (Gerasimou et al. 2012; Lee et al. 1999; Waln et al. 2015; Brooks et al. 1992; Isaias and Antonini 2010; Isaias et al. 2008b; Roselli et al. 2010). Three of these studies reporting reduced striatal DAT binding have not included "pure" ET patients, but patients with parkinsonism-like isolated rest tremor and visual-motor coordination failure (Lee et al. 1999; Schwartz et al. 2004; Waln et al. 2015). Other studies did not find any difference in tracer binding to DAT in patients with ET compared to controls (Brooks et al. 1992; Isaias and Antonini 2010; Roselli et al. 2010). Two of the largest studies including ET patients fulfilling official criteria without any parkinsonism showed normal DAT binding in ET (Asenbaum et al. 1998; Benamer et al. 2000). It is possible that the heterogeneity of the groups included is the cause that some studies found (slightly) reduced tracer binding and others did not. Overall, it can be concluded that ET is likely associated with normal DAT binding. One SPECT study using ^{123}I-FP-CIT as a radiotracer found increased tracer binding in the midbrain of patients with ET compared to controls as well as compared to patients with PD and other parkinsonian syndromes (progressive supranuclear palsy and dementia with Lewy bodies) (Roselli et al. 2010). FP-CIT binding in the midbrain area reflects predominant binding to the serotonin transporter (SERT) (Booij et al. 2007) but it is unclear if these finding reflect a disturbance in serotonergic neurotransmission (Roselli et al. 2010).

One study used ^{11}C-flumazenil and PET to evaluate GABAergic neurotransmission in patients with ET and found increased tracer binding in the cerebellum in patients with ET compared to controls. This may indicate reduced GABAergic function and therefore overactivity of cerebellothalamic circuits. These findings, however, await replication (Boecker et al. 2010).

Concluding, most imaging studies in pure ET showed no, or only subtle loss of striatal DAT binding/DOPA uptake, indicating that ET is not characterized by loss of nigrostriatal cells. However, preliminary results of imaging studies may indicate a possible role of disturbances of the serotonin and/or GABA systems in the pathophysiology of ET.

30.2.5 Orthostatic Tremor

As mentioned in the introductory section, the discussed studies included patients with primary OT. RCBF has been evaluated with PET in patients with OT both during rest and while maintaining a posture with the right arm that induced arm tremor. In comparison to rest state, during action there was increased rCBF in the cerebellum bilaterally and contralateral in the lentiform nucleus and thalamus. During rest, patients with OT had increased rCBF bilaterally in the cerebellum compared to

controls. These findings are comparable to those in patients with other forms of tremor (Wills et al. 1996). In one patient with medication refractory OT, FDG PET scans were acquired before the implantation of deep brain stimulation in the Vim of the thalamus and afterward both OFF and ON stimulations. Scans were acquired after repeated periods of standing that induced OT. The FDG-PET scans before DBS and OFF stimulation showed hypermetabolism of the primary motor cortex and cerebellar vermis compared to the scan ON stimulation (Guridi et al. 2008). This study was later repeated in a group of ten OT patients compared to controls, where all subjects had to stand for 10 min prior to scanning. Patients showed an increase in glucose metabolism in the pontine brainstem tegmentum, bilateral posterior lobes of the cerebellum (dentate nuclei and paravermal areas), thalamus and bilateral primary motor cortex after resting (lying down). A decrease in glucose metabolism was found in the mesiofrontal cortex in OT patients after resting compared to controls. The same differences were found when comparing OT patients and controls after standing, with the only exception that a decrease in glucose metabolism was also found in the bilateral anterior insula and posterior cingulate cortex in OT (Schoberl et al. 2017).

Other studies have focused on (dopamine) receptor imaging with varying results. Some studies compared patients with OT not only with healthy controls, but also with patients with PD. Most studies found no differences in tracer binding to DAT or dopamine $D_{2/3}$ receptors (D2/3R) between patients with OT and healthy controls (Guridi et al. 2008; Raudino et al. 2009; Trocello et al. 2008; Wegner et al. 2008). Striatal DAT binding in patients with OT did also not show differences in caudate-to-putamen ratio or asymmetry index compared to controls. In contrast to most studies, 1 study in 11 patients with OT showed reduced DAT binding in the striatum compared to controls. Binding was equally reduced in the caudate nucleus and the putamen and was higher and more symmetrical compared to patients with PD. There was no correlation between tracer binding and age, severity of OT symptoms or disease duration (Katzenschlager et al. 2003). It is unclear why reduced DAT binding was found in this study and not in other studies, but it could be that some of the OT patients in the latter study had a premorbid form of PD. One study found no differences in SERT binding between patients with OT and healthy controls (Wegner et al. 2008).

Concluding, the cerebellum probably plays an important role in the pathophysiology of OT, as it does in other tremor syndromes. The results of molecular imaging studies may indicate that dopaminergic and serotonergic disturbances are unlikely to be important.

30.3 Gilles de la Tourette Syndrome and Tics

30.3.1 Historical Background

Tourette syndrome (TS) was defined in 1885 by Gilles de la Tourette (1885). This was probably not the first description of this syndrome, but it was the first clear and

comprehensive overview. Gilles de la Tourette described his observations in nine patients with a condition that started in childhood. He suspected the disorder to be degenerative and caused by an inherited weakened nervous system. Since Gilles de la Tourette's description, little has changed in the definition of the syndrome that still bears his name (McNaught and Mink 2011).

30.3.2 Clinical Features and Etiology

TS is a neurodevelopmental disorder that starts in childhood. It is a hereditary condition characterized by motor and/or vocal tics. Motor tics are sudden, rapid, recurrent, nonrhythmic movements, while vocal tics are sounds or words. Both motor and vocal tics can be simple or complex. Simple tics involve only one group of muscles and occur rapidly and jerky (eye blinking, jerking of head, neck of limbs, throat clearing, and grunting) or slowly and dystonic. Where simple tics usually look involuntary, complex tics are more coordinated movements or verbalizations and seem intentional (bending, gyrating, echolalia (repeating someone else's words), palilalia (repeating one's own words), and coprolalia (saying obscene or socially offensive words)). The first symptoms in a patient with TS are usually simple motor tics and become apparent between the age of 4 and 6 years, after which they slowly become worse. Symptoms peak between the age of 10 and 12 years. Tics are usually preceded by a premonitory urge or inner tension and followed by a short period of relief. Most patients are able to suppress their tics for a short period of time, after which a worsening of tics occurs: rebound phenomenon. The diagnosis of TS can only be made when multiple motor tics and at least one vocal tic are present before the age of 18 years and last for more than 1 year from onset. The prevalence of TS in children is estimated to be between 0.3% and−0.8%. TS is present in every ethnic group, although African-American and sub-Saharan black African populations seem to be less affected. TS is three times more common in boys than it is in girls. Isolated tics are suggested to occur in up to 24% of children. In most children, simple isolated tics disappear in adolescence, but patients with TS will usually continue to have some tics (McNaught and Mink 2011). Next to motor and vocal tics, 50–90% of patients with TS suffer from psychiatric comorbidity, especially attention-deficit hyperactivity disorder (ADHD) and obsessive–compulsive disorder (OCD) (McNaught and Mink 2011). It is very likely that TS is a multifactorial disorder. It is clear that genetic variation plays a major role in the development of TS, considering its hereditary nature. The incidence of tics and TS is up to 100 times greater in first-degree relatives of a patient with TS compared to the general population. Recently, some vulnerability genes have been identified, but they are rare variants that only contribute to etiology in a small proportion of patients (Dale 2017). Next to genetic vulnerability, several environmental factors have been implicated in the development of TS, for example, tobacco smoking, stress, infections and autoimmune conditions prenatally, perinatally, or during early postnatal development. The exact role of these factors has not been determined yet (McNaught and Mink 2011).

30.3.3 Pathophysiology

The pathophysiology of TS is largely unclear and complex. The basal ganglia play an important role in the pathophysiology of TS. There is a reduction of ~60% of GABAergic and cholinergic neurons in the caudate nucleus and putamen of patients with TS at autopsy compared to control data. Studies also showed a decreased number of GABAergic neurons in the globus pallidus externa and an increased number of these neurons in the globus pallidus interna. These anatomic alterations could have been caused by disturbed neuronal cell migration in the central nervous system during development and could lead to reduced sensory and motor inhibition in turn leading to the urge to perform inappropriate or excessive vocal and motor activities. Furthermore, it is likely that dopaminergic neurotransmission plays an important role in the pathophysiology of TS. This is likely because dopamine blocking medication is effective on tics (see below), and dopaminergic medication, such as Levodopa, can aggravate tics. PET and SPECT studies have also shown alterations in the dopaminergic neurotransmission in these patients (see below) (McNaught and Mink 2011).

30.3.4 Treatment

Treatment in patients with TS consists of multiple options. Educating patients and surroundings about the nature of the syndrome is important and can lead to understanding and respect. Behavioral therapy is used quite often in patients with TS; teaching the patient how to modify the environmental factors that influence the severity of their tics, as well as optimizing the patients' management of his symptoms. Besides behavioral therapy, there are several pharmacologic options. First treatment choice usually consists of alpha-adrenergic agonists, such as clonidine. If ineffective, antipsychotics can be used. Antipsychotics are usually divided in typical antipsychotics that are dopamine D_2 receptor antagonists, such as haloperidol, and atypical antipsychotics that are dopamine and serotonin antagonists, such as risperidone. Atypical antipsychotics are preferred, since they have a lower risk on inducing extrapyramidal side effects. Other medications include benzodiazepines, injections with botulinum toxin, and tetrabenazine. If both behavioral and medical therapy fail, patients can sometimes receive deep brain stimulation. Thus far, it is unclear in which nucleus the stimulators have to be placed and how the stimulator settings should be for an optimal treatment effect, therefore DBS currently remains an experimental therapy (McNaught and Mink 2011).

30.3.5 Imaging with PET and SPECT

Many PET and SPECT studies have been performed in patients with tics and TS. We divided the information in PET studies investigating glucose metabolism, PET and

SPECT studies investigating regional cerebral blood flow, and PET and SPECT studies investigating receptor binding.

30.3.5.1 Glucose Metabolism

Using FDG-PET, patients with TS have been investigated. Global and regional metabolic rates were found to be normal in patients with TS compared to controls (Eidelberg et al. 1997). Later studies have mainly focused on brain networks: regions that simultaneously show an increase or decrease in metabolism in patients, but not in controls. Simultaneous increases in metabolism were found bilaterally in the premotor cortex, supplementary motor area (SMA), midbrain and cerebellum in patients with TS compared to controls (Eidelberg et al. 1997; Jeffries et al. 2002; Pourfar et al. 2011). Simultaneous decreases in metabolism were found in the striatum, primary motor cortex, somatosensory association areas, insula, orbitofrontal cortex, thalamus, lentiform nucleus, and hippocampus compared to controls (Eidelberg et al. 1997; Jeffries et al. 2002; Pourfar et al. 2011). All these brain regions have been implicated in other movement disorders as well, and are therefore considered as aspecific (Eidelberg et al. 1997). In both patients with TS and controls, there was a connection between the activity of the motor cortex and the lateral orbitofrontal cortex, but the interaction pattern between these areas may differ. In patients with TS, there was a positive interaction in these areas meaning they were both active or inactive at the same time, but in controls there was a negative interaction. In controls, either the motor cortex was active or the orbitofrontal cortex, but they were not active at the same time (Jeffries et al. 2002). In patients with TS and comorbid OCD, an additional network correlating with the severity of OCD consisted of reduced metabolic activity in the anterior cingulate cortex and dorsolateral prefrontal cortex (DLPFC) with increased activity in the primary motor cortex and precuneus (Pourfar et al. 2011).

In summary, TS is likely to be a network disorder, but the exact composition of the affected circuits is not clear yet.

30.3.5.2 Regional Cerebral Blood Flow

The first studies investigating rCBF in patients with tics and TS used [^{99m}Tc-D,L]-hexamethylpropyleneamine-oxime (HMPAO) and SPECT. Increased rCBF was found in the right frontal cortex in patients with TS, of which a part also had OCD, compared to controls. There was no difference between patients with and without OCD (George et al. 1992). Reduced rCBF was found in the right basal ganglia, orbitofrontal and medial frontal cortex, temporal lobes, left caudate nucleus, anterior cingulate cortex, and left DLPFC in patients with TS compared to controls (Klieger et al. 1997; Lampreave et al. 1998; Moriarty et al. 1995). The severity of tics was correlated to the hypoperfusion of the left caudate nucleus, anterior cingulate cortex, and a medial temporal region. Hypoperfusion of the DLPFC was correlated to mood in patients (Moriarty et al. 1995). The reduced rCBF in the orbitofrontal and medial frontal cortex and in the temporal lobes in patients increased after treatment with neuropsychotics, but not to the same level as controls (Lampreave et al. 1998).

A study with another SPECT tracer to assess rCBF, [^{99m}Tc]-ethylene cysteinate dimer (ECD), found comparable results in children with TS as the above-named studies. Children with TS had reduced rCBF in the left caudate nucleus, cingulate cortex, right cerebellum, left DLPFC, and left orbitofrontal cortex compared to controls. There was a correlation between the severity of the vocal tics and rCBF in cerebellum and bilateral DLPFC. Patients did not have psychiatric comorbidity, but scores on depression and OCD were negatively correlated to rCBF values, especially in temporal regions (Diler et al. 2002).

An event-related PET study with ^{15}O-H_2O showed activation of cerebellum, insula, SMA, motor cortex, thalamus, and putamen during tics (Lerner et al. 2007). In one study, five severely affected TS patients were compared to healthy controls and rescanned after implantation of DBS electrodes both in the globus pallidus pars interna (GPi) and the thalamus. After surgery, GPi, thalamus, and sham stimulation were applied in a random order each for 3 months and ECD SPECT was made at the end of each 3-month period. Preoperative TS patients had decreased rCBF in the right pre- and postcentral cortex, left paracentral cortex, bilateral SMA, bilateral superior frontal cortex, right middle frontal gyrus, and parietal cortex compared to healthy controls. rCBF was increased in the left temporal cortex and bilaterally in the cerebellum. After surgery, both GPi and thalamic stimulation resulted in significant decreases in rCBF in basal ganglia and cerebellum and increases in rCBF in the frontal cortex compared to sham stimulation. A relation to symptom improvement was not reported (Haense et al. 2016).

Concluding, the perfusion of many brain regions was found to be abnormal in patients with Tourette syndrome, but tics mostly correlated with hypoperfusion of the caudate nucleus and cingulate cortex. Treatment with medication and DBS can alter rCBF in TS patients.

30.3.5.3 Receptor Imaging

PET and SPECT studies investigating receptor binding in patients with tics and TS have mainly focused on the dopamine system, although some studies looked at the serotonin system.

One PET study found increased tracer binding to dopamine $D_{2/3}$ receptors (D2/3R) (Wong et al. 2008), where others did not (Abi-Jaoude et al. 2015; Turjanski et al. 1994; Wong et al. 1997). Increased dopamine release was found after administration of the dopamine releaser amphetamine or the neuroleptic haloperidol (Wong et al. 2008, 1997). There was a trend toward a correlation of D2/3R binding and severity of vocal tics (Wong et al. 1997). There were no differences in tracer binding to striatal DATs (Wong et al. 2008; Turjanski et al. 1994) or striatal vesicular monoamine transporters 2 (VMAT2) (Albin et al. 2009; Meyer et al. 1999). These results were confirmed by a large meta-analysis (Hienert et al. 2018). One study using ^{18}F-fallypride, a PET tracer which can be used to also assess extrastriatal dopamine D2/3R, found reduced binding in the orbitofrontal cortex, primary motor cortex, anterior cingulate gyrus, mediodorsal nucleus of the thalamus, and hippocampus. These areas are concerned with motivation, reward, sensory gating,

movement, and attention, and also showed abnormalities in PET studies investigating glucose metabolism and rCBF (Gilbert et al. 2006).

Results from SPECT studies investigating the dopamine system in tics and TS varied. Most studies found increased DAT binding in the striatum of patients with TS compared to controls (Cheon et al. 2004; Heinz et al. 1998; Liu et al. 2010; Muller-Vahl et al. 2000; Serra-Mestres et al. 2004), although in some studies no difference in DAT binding was found (Hwang et al. 2008; Stamenkovic et al. 2001; Yeh et al. 2006). It is unclear what caused these varying results. One study found an association between DAT binding and self-injurious behavior and impulse control problems (Muller-Vahl et al. 2000). However, it appears that behavioral and psychiatric symptoms in TS are not directly related to measurable abnormalities in striatal DAT activity. Another study found a negative correlation between DAT binding and disease duration (Liu et al. 2010). DAT could be hyperfunctional during the first years of disease, after which some form of adaptation takes place (Liu et al. 2010; Yeh et al. 2006). This could explain the reduction of tics that is usually seen during puberty (Muller-Vahl et al. 2000). One SPECT study compared striatal DAT binding before and after a methylphenidate challenge. This study showed less reduction in DAT binding (reflecting occupancy of the DAT by methylphenidate) in patients with TS compared to controls, after phasic administration of methylphenidate (Yeh et al. 2007). If this theory of a hyperfunctional DAT system followed by adaptation is true, this could have contributed to the different results in the PET and SPECT studies investigating DAT binding in patients with Tourette syndrome. Other explanations for the discrepancies between studies could be sample size, age of patients (some studies investigated children, while others looked at adults), and use of dopamine blocking medication. In all SPECT studies, medication was stopped prior to scanning, but rest effect of medication cannot be completely ruled out. SPECT studies looking at the (postsynaptic) D2/3R did not find differences between patients with TS and controls (Muller-Vahl et al. 2000; Hwang et al. 2008; George et al. 1994), although one study found decreased tracer binding to these receptors in patients who had TS for more than 15 years compared to patients who had complaints less than 15 years and controls (Muller-Vahl et al. 2000). This could also be consistent with some form of adaptation of the dopamine system. One study in monozygotic twins with different levels of tic severity found a correlation between D2R binding in the caudate nucleus and severity of tics (Wolf et al. 1996).

Some PET and SPECT studies looked into the serotonin system. Tracer binding to the SERT in the midbrain and thalamus was decreased in patients with TS compared to controls (Wong et al. 2008; Muller-Vahl et al. 2005). There was a negative correlation between SERT binding and severity of tics (Heinz et al. 1998; Muller-Vahl et al. 2005), as well as a negative correlation between SERT binding and the severity of comorbid obsessive–compulsive symptoms (Muller-Vahl et al. 2005). Tracer binding to the serotonin receptor ($5\text{-}HT_{2A}$) was increased in the anterior cingulate cortex, orbitofrontal cortex, medial inferior frontal cortex, superior frontal cortex, and putamen in patients with TS compared to controls in one study (Haugbol et al. 2007), while another study only found weakly increased binding in patients

with TS and comorbid OCD compared to controls in prefrontal, temporal, and cingulate cortices (Wong et al. 2008). Only one molecular imaging study compared SERT binding in TS patients with OCD (TS + OCD), TS patients without OCD (TS − OCD), and OCD patients without TS (OCD) to healthy controls using SPECT. SERT binding (measured with the selective SERT tracer ^{123}I-ADAM) was normal in patients with OCD and TS-OCD, but significantly increased in caudate nucleus, hypothalamus, and midbrain in TS + OCD. In TS patients with and without OCD, SERT binding in the pons was negatively correlated with tic severity (Muller-Vahl et al. 2019). One PET study used alfa-^{11}C-methyl-L-tryptophan (AMT) and PET to examine serotonin synthesis in children with TS compared to controls. AMT uptake was bilaterally reduced in the DLPFC and bilaterally increased in the thalamus (Behen et al. 2007). Altogether, these studies indicate that serotonin may play a role in the pathophysiology of Tourette syndrome (Heinz et al. 1998; Haugbol et al. 2007; Behen et al. 2007).

One PET study used ^{18}F-fluoroethoxybenzovesamicol in patients with TS to evaluate striatal cholinergic interneuron density and found no differences compared to healthy controls (Albin et al. 2017).

Concluding, both dopamine and serotonin are likely to play a role in the pathophysiology of TS. One of the current hypotheses is that TS is characterized by increased phasic dopamine release modulated by low serotonin levels. The low concentration of serotonin could explain the high percentages of comorbid psychiatric disorders, such as OCD (Wong et al. 2008). The role of acetylcholine has to be further investigated.

30.4 Myoclonus

30.4.1 Historical Background

Friedreich was the first to describe myoclonus in 1881 in a patient with possible myoclonic epilepsy (Faught 2003). Myoclonus is defined as brief muscle jerks and occurs in many neurologic and non-neurologic disorders. Over the years, most of the attention was on cortical myoclonus, in which Grinker in 1938 reported trains of electroencephalographic discharges coinciding with myoclonus in patients with familial myoclonus epilepsy. Since then different forms of myoclonus have been discovered as well as numerous underlying disorders (see below) (Shibasaki and Thompson 2011).

30.4.2 Classification, Clinical Features, and Etiology

There are three generally accepted classifications for myoclonus that are based on clinical characteristics, etiology, and anatomic localization. These three classifications are highly interrelated (Dijk and Tijssen 2010). When classifying myoclonus on clinical signs, it is important to note the distribution: focal, segmental, axial, or generalized. Myoclonus can sometimes be induced by action, especially in patients with posthypoxic

encephalopathy, or by a tactile stimulus (stimulus-sensitive or reflex myoclonus). Furthermore, myoclonus can occur as muscle contractions (positive myoclonus) or as interruption of muscle tone (negative myoclonus) (Dijk and Tijssen 2010).

There are many disorders that can cause myoclonus, but they can roughly be divided into four etiological groups: physiological, symptomatic, epileptic, and essential. Physiological myoclonus is common in healthy individuals and consists of sleep jerks, hiccups, and other nonpathological forms of myoclonus. Symptomatic myoclonus accounts for approximately 70% of cases with a pathological origin. Underlying disorders that can cause myoclonus are for example, posthypoxic syndrome, Alzheimer's disease, drug-induced, and toxic–metabolic conditions. Epileptic myoclonus is the second most common pathological etiological category. Epileptic myoclonus can be the only symptom of epilepsy or can be a component of a seizure of any type. In essential myoclonus, myoclonus is the only or most important symptom. Most disorders in this category are hereditary and the most prevalent one is myoclonus-dystonia (see Chapter 29). One of the most prevalent causes of myoclonus is not included in this classification: psychogenic myoclonus. Approximately 8.5% of patients with myoclonus have psychogenic myoclonus and 17.2% of patients with a psychogenic movement disorder have myoclonus (Dijk and Tijssen 2010).

Anatomically myoclonus can be divided by electrophysiological tests in cortical (e.g., posthypoxic, epileptic, or in patients with neurodegenerative diseases), subcortical (e.g., myoclonus-dystonia), brainstem (e.g., hyperekplexia, opsoclonus-myoclonus syndrome), spinal (e.g., segmental or propriospinal myoclonus, the latter almost always has a psychogenic origin) or peripheral (e.g., hemifacial spasm) (Shibasaki and Thompson 2011).

The incidence and prevalence of myoclonus are mainly dependent on the incidence and prevalence of disorders causing myoclonus. The lifetime prevalence of pathological and persistent myoclonus was 8.6 cases per 100,000 population in a large study in the United States. In nursing homes, 0.5% of patients suffer from myoclonus. Transient (e.g., drug-induced) myoclonus is not included in this lifetime prevalence, but represents 27.6% of all patients with myoclonus who visit an emergency room for a movement disorder (Dijk and Tijssen 2010).

30.4.3 Pathophysiology

The pathophysiology of myoclonus is dependent on both the anatomical origin as well as the etiological cause of dystonia. It is beyond the scope of this chapter to deal with all the different pathophysiological processes that can eventually lead to myoclonus.

30.4.4 Treatment

Treatment of myoclonus mainly depends on the anatomical origin. Treatment of myoclonus is difficult and time-consuming. It often requires several drug trials before a drug with a beneficiary effect is found and most drugs only partly relieve

symptoms, while at the same time causing side effects. In cortical myoclonus, first choice is the antiepileptic levetiracetam or piracetam, but the benzodiazepine clonazepam can also be used, especially in patients with posthypoxic cortical reflex myoclonus. Clonazepam is also the first choice in patients with myoclonus-dystonia, as well as most other forms of subcortical myoclonus and spinal myoclonus. Patients with peripheral myoclonus can be locally treated with botulinum toxin injections and patients with myoclonic epilepsy have to be treated with antiepileptics. This is only an indication for therapy and not an exhaustive overview. For this, we would like to refer to some of the excellent reviews on this topic (Dijk and Tijssen 2010).

30.4.5 Imaging

Imaging in some forms of myoclonus is dealt with in other chapters (e.g., myoclonus dystonia in the chapter on dystonia, and restless legs syndrome below). In this section, we will discuss findings in epileptic myoclonus, myoclonus in degenerative diseases (Alzheimer's disease and corticobasal degeneration), in prion disease (Creutzfeldt–Jakob disease and fatal familial insomnia), posthypoxic myoclonus, and opsoclonus-myoclonus syndrome.

30.4.5.1 Epileptic Myoclonus

In epilepsy two different forms of myoclonus can occur. Positive myoclonic jerks usually occur as focal seizures in patients with different forms of progressive myoclonus epilepsy. These patients often also suffer from generalized seizures. Another form is epileptic negative myoclonus, which is a short loss of muscle tone due to epilepsy. This causes, for example, the hands to drop when the arms and hands are extended. Both forms have been investigated with PET and SPECT.

In two patients with Lafora disease, a form of progressive myoclonus epilepsy, FDG PET imaging showed occipital hypometabolism. This is consistent with the visual hallucinations and visual agnosia these patients usually also have and is probably unrelated with the myoclonus or epilepsy (Jennesson et al. 2010). In four patients with Unverricht–Lundborg disease, another form of progressive myoclonus-epilepsy, tracer binding to D2/3R was evaluated with ^{11}C-raclopride and PET. Tracer binding was increased in the thalamus and striatum in patients compared to controls (Korja et al. 2007).

In patients with epileptic negative myoclonus on the right side of the body, hyperperfusion of the left premotor area, parietal cortex, and putamen were found using perfusion SPECT (Baumgartner et al. 1996; Yu et al. 2009). Surprisingly, FDG-PET in one of these patients showed hypometabolism of the left frontoparietal cortex (Yu et al. 2009). In one patient, ^{123}I-iomazenil (IMZ; a selective GABA-A receptor tracer) and SPECT showed reduced tracer binding in the premotor cortex (Usui et al. 2010).

In summary, imaging results in epileptic myoclonus are too limited to draw any definite conclusions.

30.4.5.2 Degenerative Diseases

Perfusion has been evaluated using SPECT in two important degenerative diseases that frequently cause myoclonus: Alzheimer's disease (AD) and corticobasal degeneration (CBD). We will only discuss results from studies that explicitly reported on patients with myoclonus. In patients with AD hypoperfusion was found in the frontal and parietal lobes (Hu et al. 2009; Kobayashi et al. 2000). In one study, this frontoparietal hypoperfusion was contralateral to the arm with the most severe myoclonus (Kobayashi et al. 2000).

In patients with CBD, more extensive hypoperfusion was found. The most consistent findings were frontoparietal and thalamus hypoperfusion (Hu et al. 2009; Huang et al. 2007; Storey et al. 1995). Areas that were implicated were the temporal lobe and cerebellum (Hu et al. 2009; Lu et al. 1998). Hypoperfusion was more prominent in the hemisphere contralateral to the most affected arm, with additional hypoperfusion in the interconnected ipsilateral cerebellum (Huang et al. 2007; Storey et al. 1995; Lu et al. 1998). Patients with CBD also have generalized cerebral atrophy, but hypoperfusion was found to be more extensive than would be expected based on atrophy (Storey et al. 1995). DAT binding was found to be reduced contralateral to the most affected arm or bilateral in the striatum (Huang et al. 2007).

Concluding, myoclonus in degenerative diseases like AD and CBD is correlated to frontoparietal hypoperfusion. Dopamine possibly plays a role in the pathophysiology of myoclonus in CBD. However, most of these findings have also been described in patients with AD or CBD, but without myoclonus.

30.4.5.3 Prion Disease

Creutzfeldt–Jakob disease (CJD) is a condition caused by misfolded prion proteins. CJD can be sporadic or hereditary. The misfolded prion proteins can cause varying symptoms of which the most prominent are memory and cognitive decline, and movement disorders including myoclonus, ataxia, and visual disturbances. The disease has a dramatic disease course and is uniformly fatal within months to years (Imran and Mahmood 2011). FDG PET imaging in a group of patients with CJD showed extensive hypometabolism that was most prominent in the temporal and parietal regions. Other affected areas included the occipital lobe, cerebellum, and basal ganglia. Myoclonus correlated to hypometabolism of the contralateral parietal lobe and basal ganglia (Henkel et al. 2002). In another patient, an FDG-PET scan showed hypermetabolism in the right frontoparietal cortex and left cerebellum early in the disease course. After the disease progressed, the patient developed seizures. A perfusion SPECT scan showed hypoperfusion of the right frontoparietal cortex, consistent with the study by Henkel and colleagues (Nagasaka et al. 2011). DAT binding was bilaterally reduced in the striatum of patients with CJD (Chen et al. 2010; Ragno et al. 2009) and tracer binding to the GABA-A receptor was reduced throughout the entire cerebral cortex, but not in the cerebellum (Itoh et al. 1998).

Fatal familial insomnia (FFI) is a genetic prion disease characterized by insomnia, oneiric stupor with autonomic and motor hyperactivity, pyramid tract symptoms, myoclonus, dysarthria, dysphagia, and ataxia. Like CJD, it has a fatal disease course within months to a few years (Imran and Mahmood 2011). With FDG-PET,

a prominent hypometabolism of the thalamus with less extensive hypometabolism of the basal ganglia, frontotemporal cingulate cortex, and the cerebellum has been found in patients with FFI. The amount of hypometabolism correlates with the disease duration. SERT binding was reduced in the thalamus and hypothalamic regions in patients with FFI compared to controls, implicating the serotonin system in this rare disease (Montagna 2005; Montagna et al. 2003). As in degenerative diseases, these findings do not seem to be specific for myoclonus as the same results have been described in patients with prion diseases, but without myoclonus.

30.4.5.4 Posthypoxic Myoclonus

Posthypoxic myoclonus (Lance-Adams syndrome) is a form of cortical myoclonus that predominantly occurs during action. In patients with Lance-Adams syndrome increased metabolism of the pontine tegmentum spreading to the mesencephalon, ventrolateral thalamus, and medial temporal lobes, and decreased metabolism of the bilateral frontal lobes was found using FDG and PET (Frucht et al. 2004; Zhang et al. 2007). A perfusion SPECT scan in one patient showed hypoperfusion of the left temporal lobe (Zhang et al. 2007).

30.4.5.5 Opsoclonus-Myoclonus Syndrome

Opsoclonus-myoclonus syndrome (OMS) is a syndrome that usually occurs during or after a systemic infection or as a paraneoplastic phenomenon and is characterized by myoclonus of the limbs and myoclonic movements of the eyes (opsoclonus) (Dijk and Tijssen 2010). Perfusion SPECT scans in two patients with a recently developed OMS showed hyperperfusion of the cerebellum, mainly in the vermis (Oguro et al. 1997; van Toorn et al. 2005). Surprisingly, in a patient who already suffered more than 3 years from OMS a perfusion SPECT scan showed hypoperfusion of the cerebellum (Oguro et al. 1997). It could be that OMS is characterized by inflammation and hyperperfusion in the early stage, followed by hypoperfusion caused by cell death and gliosis (Oguro et al. 1997). Similar results were shown in one patient with an adnexal teratoma and paraneoplastic OMS using FDG-PET. In the acute stage, there was an increased glucose metabolism in the cerebellum that decreased after symptoms diminished with treatment of the teratoma. Twelve months after symptom onset, symptoms had completely resolved and there was a decrease in glucose metabolism of the visual cortex and still a slight increase of glucose metabolism in the deep cerebellar nuclei, albeit metabolism was lower than in the acute phase (Oh et al. 2017).

30.4.5.6 General Remarks on Imaging in Patients with Myoclonus

Imaging studies have been performed in patients with different underlying causes of myoclonus and it is interesting to see what the similarities are, as they could teach us more about the underlying brain abnormalities that lead to myoclonus. Hypoperfusion and/or hypometabolism of the frontoparietal cortex are found in different conditions with myoclonus. This has been found in patients with negative epileptic myoclonus, Alzheimer's disease, CBD, Creutzfeldt–Jakob disease, fatal familiar insomnia, and posthypoxic myoclonus. In several studies, the reduced

perfusion or metabolism in the frontoparietal cortex was described to be contralateral to the most affected arm. Other areas that were often found to have abnormalities in perfusion or metabolism were the thalamus and the cerebellum. In most cases, there was reduced perfusion or metabolism in these regions. A third common factor was the involvement of the dopamine system in the striatum. D2/3R binding was increased in progressive myoclonus epilepsy and striatal DAT binding was reduced in corticobasal degeneration and Creutzfeldt–Jakob disease. However, thus far, results from different studies are too limited and too diverse to draw any hard conclusions on the origin of myoclonic jerks. Furthermore, most results merely seem to reflect abnormalities caused by the underlying condition and not by the myoclonus.

30.5 Restless Legs Syndrome and Periodic Limb Movements in Sleep

30.5.1 Historical Background

Restless legs syndrome (RLS) was first described in detail by Professor Ekbom, a Swedish neurologist, in his doctoral thesis in 1944. However, the first description of RLS dates back to 1685 in a publication by Sir Thomas Willis, who describes people who are so restless in bed that it looks as if they are being tortured (Teive et al. 2009). After this first description, several cases were published, most of which were thought to be psychogenic at that time, although the hereditary nature of the condition had also been noted. It was not until Ekbom published his first paper on RLS that it was recognized as a distinct neurological syndrome (Teive et al. 2009). Phillips et al. showed in 2000 that RLS occurs in up to 10% of the population and is heavenly underdiagnosed (Phillips et al. 2000; Shepard Jr. et al. 2005).

30.5.2 Clinical Features and Etiology

RLS is considered both a movement disorder as well as a sleep disorder. RLS is defined as an urge to move the legs accompanied with an unpleasant sensation in the legs or in another body part. Complaints are aggravated by rest, alleviated by movement and are worse in the evening or night (Avidan 2009). The incidence of RLS increases with age. Population prevalence of RLS varies between 1% and 15% in different studies and it is twice as common in females as males (Yeh et al. 2012).

RLS can be either primary or secondary. Primary RLS occurs early in life, with a peak at age 20, has a strong genetic component and family history is usually positive (Yeh et al. 2012). Secondary RLS develops later in life and is usually sporadic. Secondary RLS is often associated with another disorder, for example, peripheral neuropathy. There are some risk factors for developing RLS, for example, pregnancy, low serum iron, lower socioeconomic status, and poor medical as well as mental health and PD (Yeh et al. 2012).

Periodic limb movements in sleep (PLMS) are characteristic limb movements that occur at a typical rate of 0.5- to 5- or 10-s duration and recur periodically (5- to 90-s period) in a series (four or more) in any sleep state. The movements usually consist of extension of the big toe with partial flexion of the ankle, knee, and sometimes hip. These movements can be associated with a partial arousal or awakening; however, the patient is usually unaware of this. Patients can complain of excessive daytime sleepiness, headaches, and psychiatric symptoms, due to disturbed sleep. PLMS is estimated to occur in 4–11% of adults and is most common in patients with other sleep disorders, especially RLS (Avidan 2009).

30.5.3 Pathophysiology

The pathophysiology of RLS is largely unclear; however, there is some evidence for a role of the dopamine system in the pathophysiology of RLS. Higher concentrations of dopamine and homovanillic acid have been found in cerebrospinal fluid during daytime compared to nighttime in patients with RLS. This could indicate that a disturbed circadian rhythm of dopaminergic function is responsible for RLS symptoms. No genes have been identified yet, although some loci have been linked to RLS complaints in families with primary RLS (Avidan 2009).

30.5.4 Treatment

There are several different medical treatments for RLS, but they almost all share the risk of augmentation, which is the recurrence and worsening of symptoms after an initial period of improvement with treatment. Major classes of drugs that are being used in the treatment of RLS are dopamine agonists such as ropinirole and pramipexole, benzodiazepines such as clonazepam, anticonvulsants such as carbamazepine and gabapentin, opioids such as codeine, propoxyphene or oxycodone, bupropion and iron supplementation (Avidan 2009; Yeh et al. 2012). Treatment of PLMS is the same as for RLS, although one should be careful with prescribing benzodiazepines or opioids in patients with PLMS because of the high incidence of obstructive sleep apnea (Avidan 2009).

30.5.5 Imaging

Because of the proposed role of dopamine in the pathophysiology of RLS and PLMS, PET and SPECT imaging focused on the dopamine system. PET studies in patients with RLS showed decreased DAT binding in the caudate nucleus and putamen of patients compared to controls (Earley et al. 2011; Ruottinen et al. 2000; Turjanski et al. 1999). This was found in patients with and without comorbid PLMS and was found on scans both acquired at daytime and in the evening (Earley et al. 2011; Ruottinen et al. 2000). DAT binding in the striatum was not decreased,

however, and there was no correlation between striatal DAT binding and severity of complaints (Earley et al. 2011). There were no differences in DAT binding between patients treated with levodopa at the time of scanning and patients without medical treatment (Turjanski et al. 1999). Results for PET tracer binding to D2/3R were somewhat conflicting. Two PET studies found decreased binding to D2/3R in the caudate nucleus, putamen, and nucleus accumbens of patients with RLS compared to controls (Turjanski et al. 1999; Oboshi et al. 2012). In these studies, there was no difference between patients with RLS treated with levodopa and patients without medical treatment (Turjanski et al. 1999). There was a negative correlation between D2/3R binding and severity of RLS symptoms and a positive correlation between D2/3R binding and the amount of improvement after treatment with the dopamine agonist pramipexole (Oboshi et al. 2012). In another PET study, D2/3R binding was however increased in the striatum, thalamus, and anterior cingulate cortex in patients with RLS compared to controls. This increased D2/3R binding was found both at daytime and in the evening (Cervenka et al. 2006). It is unclear what caused this difference in D2/3R binding; however, it might be partly explained by medication effects. In the studies, finding decreased D2/3R binding at least part of the patients had been exposed to dopaminergic medication, while in the study that found increased D2R binding all patients were medication-naïve (Cervenka et al. 2006).

SPECT studies also studied the dopamine system in patients with RLS and PLMS. Most SPECT studies found no difference in DAT binding between patients with RLS and PLMS compared to controls (Eisensehr et al. 2001; Linke et al. 2004; Michaud et al. 2002; Mrowka et al. 2005). One of these studies did find a lower putamen to caudate nucleus ratio in patients with RLS as compared to controls. In controls tracer binding in putamen was comparable to binding in caudate nucleus (Mrowka et al. 2005). One SPECT study found increased DAT binding in caudate nucleus, posterior putamen, and total striatum in elderly patients with moderately to severe RLS (Kim et al. 2012). Like the results from PET studies, results from SPECT studies looking at D2/3R binding were conflicting. Three SPECT studies found no difference in D2/3R binding in patients with RLS compared to controls (Eisensehr et al. 2001; Kim et al. 2012; Tribl et al. 2004), while two other studies found decreased D2/3R binding in the striatum of patients with RLS compared to controls (Michaud et al. 2002; Staedt et al. 1995). Both the studies with decreased D2R binding were performed in patients with RLS and PLMS (Michaud et al. 2002; Staedt et al. 1995), but so was one of the studies that did not find a difference in D2/3R binding (Tribl et al. 2004). Overall, most studies are consistent with the theory of central dopaminergic dysfunction as part of the pathophysiology in RLS and PLMS.

A few imaging studies did not focus on the dopamine system. One study used ^{123}I-beta-CIT and SPECT to evaluate the SERT in patients with RLS. There were no differences in SERT binding between patients with RLS and controls, but there was a negative correlation between scores on the International RLS Study Group Severity Scale and SERT binding in the pons and medulla. The authors hypothesized that an increase of serotonergic neurotransmission in the brainstem could cause deterioration of RLS symptoms through an effect on dopaminergic

neurotransmission or through a direct effect on the activity of spinal and sensory neurons (Jhoo et al. 2010). Another study looked at the opioid system in patients with RLS using ^{11}C-diprenorphine (a nonselective opioid receptor ligand) and PET. There were no differences between tracer binding in patients with RLS and controls. There was, however, a negative correlation between severity of RLS symptoms and tracer binding in the medial pain system (medial thalamus, amygdala, caudate nucleus, anterior cingulate gyrus, insular cortex, and orbitofrontal cortex) in patients with RLS. Pain scores correlated negatively to tracer binding in the orbitofrontal cortex and anterior cingulate gyrus in patients with RLS (von Spiczak et al. 2005).

The only study using FDG and PET found no differences in regional glucose metabolism between patients with RLS and controls (Trenkwalder et al. 1999).

Concluding, imaging studies suggest that both the serotonin and the opioid system seem to play a role in the pathophysiology of RLS as does the dopamine system.

30.6 General Conclusion

PET and SPECT studies have been used extensively to unravel the pathophysiology of hyperkinetic movement disorders. As expected, results from these studies differ between different conditions, but it is interesting to see that there are also similarities between the different movement disorders. The most important difference lies in the areas of abnormal perfusion or metabolism in the different disorders. In tremor, the cerebellum is most implicated, while in myoclonus there is mainly abnormal perfusion or metabolism in the frontoparietal regions, and in TS a neuronal network including the basal ganglia, motor cortex, thalamus, and hippocampus may be implicated. The most outstanding similarity is that abnormalities of the dopaminergic system, and probably the serotonergic system as well, are likely to play a role in almost all hyperkinetic movement disorders. How changes in dopamine levels can lead to such diversity in symptomatology is yet to be discovered.

References

Abi-Jaoude E, Segura B, Obeso I et al (2015) Similar striatal D2/D3 dopamine receptor availability in adults with Tourette syndrome compared with healthy controls: a [(11) C]-(+)-PHNO and [(11) C]raclopride positron emission tomography imaging study. Hum Brain Mapp 36:2592–2601

Albin RL, Koeppe RA, Wernette K et al (2009) Striatal [11C]dihydrotetrabenazine and [11C]methylphenidate binding in Tourette syndrome. Neurology 72:1390–1396

Albin RL, Minderovic C, Koeppe RA (2017) Normal striatal vesicular acetylcholine transporter expression in Tourette syndrome. eNeuro 4(4):ENEURO.0178-17.2017

Asenbaum S, Pirker W, Angelberger P, Bencsits G, Pruckmayer M, Brucke T (1998) [123I]beta-CIT and SPECT in essential tremor and Parkinson's disease. J Neural Transm (Vienna) 105:1213–1228

Avidan AY (2009) Parasomnias and movement disorders of sleep. Semin Neurol 29:372–392

Baumgartner C, Podreka I, Olbrich A et al (1996) Epileptic negative myoclonus: an EEG-single-photon emission CT study indicating involvement of premotor cortex. Neurology 46:753–758
Behen M, Chugani HT, Juhasz C et al (2007) Abnormal brain tryptophan metabolism and clinical correlates in Tourette syndrome. Mov Disord 22:2256–2262
Benamer TS, Patterson J, Grosset DG et al (2000) Accurate differentiation of parkinsonism and essential tremor using visual assessment of [123I]-FP-CIT SPECT imaging: the [123I]-FP-CIT study group. Mov Disord 15:503–510
Boecker H, Wills AJ, Ceballos-Baumann A et al (1996) The effect of ethanol on alcohol-responsive essential tremor: a positron emission tomography study. Ann Neurol 39:650–658
Boecker H, Weindl A, Brooks DJ et al (2010) GABAergic dysfunction in essential tremor: an 11C-flumazenil PET study. J Nucl Med 51:1030–1035
Booij J, de Jong J, de Bruin K, Knol R, de Win MM, van Eck-Smit BL (2007) Quantification of striatal dopamine transporters with 123I-FP-CIT SPECT is influenced by the selective serotonin reuptake inhibitor paroxetine: a double-blind, placebo-controlled, crossover study in healthy control subjects. J Nucl Med 48:359–366
Brooks DJ, Playford ED, Ibanez V et al (1992) Isolated tremor and disruption of the nigrostriatal dopaminergic system: an 18F-dopa PET study. Neurology 42:1554–1560
Cervenka S, Palhagen SE, Comley RA et al (2006) Support for dopaminergic hypoactivity in restless legs syndrome: a PET study on D2-receptor binding. Brain 129:2017–2028
Chen JC, Hsu YT, Chiou TS et al (2010) Cortical and non-cortical myoclonus of Creutzfeldt-Jakob disease. Eur Neurol 64:265–267
Cheon KA, Ryu YH, Namkoong K, Kim CH, Kim JJ, Lee JD (2004) Dopamine transporter density of the basal ganglia assessed with [123I]IPT SPECT in drug-naive children with Tourette's disorder. Psychiatry Res 130:85–95
Colebatch JG, Findley LJ, Frackowiak RS, Marsden CD, Brooks DJ (1990) Preliminary report: activation of the cerebellum in essential tremor. Lancet 336:1028–1030
Crawford P, Zimmerman EE (2011) Differentiation and diagnosis of tremor. Am Fam Physician 83:697–702
Czarnecki K, Jones DT, Burnett MS, Mullan B, Matsumoto JY (2011) SPECT perfusion patterns distinguish psychogenic from essential tremor. Parkinsonism Relat Disord 17:328–332
Dale RC (2017) Tics and Tourette: a clinical, pathophysiological and etiological review. Curr Opin Pediatr 29:665–673
Deuschl G, Bain P, Brin M (1998) Consensus statement of the Movement Disorder Society on Tremor. Ad Hoc Scientific Committee. Mov Disord 13(Suppl 3):2–23
Deuschl G, Wenzelburger R, Loffler K, Raethjen J, Stolze H (2000) Essential tremor and cerebellar dysfunction clinical and kinematic analysis of intention tremor. Brain 123(Pt 8):1568–1580
Dijk JM, Tijssen MA (2010) Management of patients with myoclonus: available therapies and the need for an evidence-based approach. Lancet Neurol 9:1028–1036
Diler RS, Reyhanli M, Toros F, Kibar M, Avci A (2002) Tc-99m-ECD SPECT brain imaging in children with Tourette's syndrome. Yonsei Med J 43:403–410
Duncan R, Bone I, Melville ID (1988) Essential tremor cured by infarction adjacent to the thalamus. J Neurol Neurosurg Psychiatry 51:591–592
Dupuis MJ, Delwaide PJ, Boucquey D, Gonsette RE (1989) Homolateral disappearance of essential tremor after cerebellar stroke. Mov Disord 4:183–187
Dupuis MJ, Evrard FL, Jacquerye PG, Picard GR, Lermen OG (2010) Disappearance of essential tremor after stroke. Mov Disord 25:2884–2887
Earley CJ, Kuwabara H, Wong DF et al (2011) The dopamine transporter is decreased in the striatum of subjects with restless legs syndrome. Sleep 34:341–347
Eidelberg D, Moeller JR, Antonini A et al (1997) The metabolic anatomy of Tourette's syndrome. Neurology 48:927–934
Eisensehr I, Wetter TC, Linke R et al (2001) Normal IPT and IBZM SPECT in drug-naive and levodopa-treated idiopathic restless legs syndrome. Neurology 57:1307–1309
Elble R, Deuschl G (2011) Milestones in tremor research. Mov Disord 26:1096–1105

Fahn S (2011) Classification of movement disorders. Mov Disord 26:947–957
Faught E (2003) Clinical presentations and phenomenology of myoclonus. Epilepsia 44(Suppl 11):7–12
Frucht SJ, Trost M, Ma Y, Eidelberg D (2004) The metabolic topography of posthypoxic myoclonus. Neurology 62:1879–1881
George MS, Trimble MR, Costa DC, Robertson MM, Ring HA, Ell PJ (1992) Elevated frontal cerebral blood flow in Gilles de la Tourette syndrome: a 99Tcm-HMPAO SPECT study. Psychiatry Res 45:143–151
George MS, Robertson MM, Costa DC et al (1994) Dopamine receptor availability in Tourette's syndrome. Psychiatry Res 55:193–203
Gerasimou G, Costa DC, Papanastasiou E et al (2012) SPECT study with I-123-Ioflupane (DaTSCAN) in patients with essential tremor. Is there any correlation with Parkinson's disease? Ann Nucl Med 26:337–344
Gerschlager W, Munchau A, Katzenschlager R et al (2004) Natural history and syndromic associations of orthostatic tremor: a review of 41 patients. Mov Disord 19:788–795
Gilbert DL, Christian BT, Gelfand MJ, Shi B, Mantil J, Sallee FR (2006) Altered mesolimbocortical and thalamic dopamine in Tourette syndrome. Neurology 67:1695–1697
Gilles de la Tourette G (1885) Étude sur une affection nerveuse caracterisée par l'incoordination motrice accompagnée d'écholalie et de coprolalie. Arch Neurol 9:19–42. et 158–200
Group PS (2000) A multicenter assessment of dopamine transporter imaging with DOPASCAN/SPECT in parkinsonism. Neurology 55:1540–1547
Guridi J, Rodriguez-Oroz MC, Arbizu J et al (2008) Successful thalamic deep brain stimulation for orthostatic tremor. Mov Disord 23:1808–1811
Ha SW, Yang YS, Song IU, Chung YA, Oh JK, Chung SW (2015) Changes in regional brain glucose metabolism measured with F-18-FDG-PET in essential tremor. Acta Radiol 56:482–486
Haense C, Muller-Vahl KR, Wilke F et al (2016) Effect of deep brain stimulation on regional cerebral blood flow in patients with medically refractory Tourette syndrome. Front Psych 7:118
Hallett M, Dubinsky RM (1993) Glucose metabolism in the brain of patients with essential tremor. J Neurol Sci 114:45–48
Haugbol S, Pinborg LH, Regeur L et al (2007) Cerebral 5-HT2A receptor binding is increased in patients with Tourette's syndrome. Int J Neuropsychopharmacol 10:245–252
Heinz A, Knable MB, Wolf SS et al (1998) Tourette's syndrome: [I-123]beta-CIT SPECT correlates of vocal tic severity. Neurology 51:1069–1074
Henkel K, Zerr I, Hertel A et al (2002) Positron emission tomography with [(18)F]FDG in the diagnosis of Creutzfeldt-Jakob disease (CJD). J Neurol 249:699–705
Hienert M, Gryglewski G, Stamenkovic M, Kasper S, Lanzenberger R (2018) Striatal dopaminergic alterations in Tourette's syndrome: a meta-analysis based on 16 PET and SPECT neuroimaging studies. Transl Psychiatry 8:143
Hu WT, Rippon GW, Boeve BF et al (2009) Alzheimer's disease and corticobasal degeneration presenting as corticobasal syndrome. Mov Disord 24:1375–1379
Huang KJ, Lu MK, Kao A, Tsai CH (2007) Clinical, imaging and electrophysiological studies of corticobasal degeneration. Acta Neurol Taiwanica 16:13–21
Hwang WJ, Yao WJ, Fu YK, Yang AS (2008) [99mTc]TRODAT-1/[123I]IBZM SPECT studies of the dopaminergic system in Tourette syndrome. Psychiatry Res 162:159–166
Imran M, Mahmood S (2011) An overview of human prion diseases. Virol J 8:559
Isaias IU, Antonini A (2010) Single-photon emission computed tomography in diagnosis and differential diagnosis of Parkinson's disease. Neurodegener Dis 7:319–329
Isaias IU, Alterman RL, Tagliati M (2008a) Outcome predictors of pallidal stimulation in patients with primary dystonia: the role of disease duration. Brain 131:1895–1902
Isaias IU, Canesi M, Benti R et al (2008b) Striatal dopamine transporter abnormalities in patients with essential tremor. Nucl Med Commun 29:349–353
Itoh Y, Amano T, Shimizu T, Hashimoto J, Kubo A, Fukuuchi Y (1998) Single-photon emission computed tomography image of benzodiazepine receptors in a patient with Creutzfeldt-Jakob disease. Intern Med 37:896–900

Jeffries KJ, Schooler C, Schoenbach C, Herscovitch P, Chase TN, Braun AR (2002) The functional neuroanatomy of Tourette's syndrome: an FDG PET study III: functional coupling of regional cerebral metabolic rates. Neuropsychopharmacology 27:92–104
Jenkins IH, Frackowiak RS (1993) Functional studies of the human cerebellum with positron emission tomography. Rev Neurol (Paris) 149:647–653
Jennesson M, Milh M, Villeneuve N et al (2010) Posterior glucose hypometabolism in Lafora disease: early and late FDG-PET assessment. Epilepsia 51:708–711
Jhoo JH, Yoon IY, Kim YK et al (2010) Availability of brain serotonin transporters in patients with restless legs syndrome. Neurology 74:513–518
Katzenschlager R, Costa D, Gerschlager W et al (2003) [123I]-FP-CIT-SPECT demonstrates dopaminergic deficit in orthostatic tremor. Ann Neurol 53:489–496
Kim KW, Jhoo JH, Lee SB et al (2012) Increased striatal dopamine transporter density in moderately severe old restless legs syndrome patients. Eur J Neurol 19:1213–1218
Klieger PS, Fett KA, Dimitsopulos T, Kurlan R (1997) Asymmetry of basal ganglia perfusion in Tourette's syndrome shown by technetium-99m-HMPAO SPECT. J Nucl Med 38:188–191
Kobayashi K, Shimoda K, Higashima M et al (2000) Report of three cases of Alzheimer's disease with focal motor symptoms: clinical correlates of neuroimaging findings. World J Biol Psychiatry 1:164–169
Korja M, Kaasinen V, Lamusuo S, Parkkola R, Nagren K, Marttila RJ (2007) Substantial thalamostriatal dopaminergic defect in Unverricht-Lundborg disease. Epilepsia 48:1768–1773
Lampreave JL, Molina V, Mardomingo MJ et al (1998) Technetium-99m-HMPAO in Tourette's syndrome on neuroleptic therapy and after withdrawal. J Nucl Med 39:624–628
Lee MS, Kim YD, Im JH, Kim HJ, Rinne JO, Bhatia KP (1999) 123I-IPT brain SPECT study in essential tremor and Parkinson's disease. Neurology 52:1422–1426
Lerner A, Bagic A, Boudreau EA et al (2007) Neuroimaging of neuronal circuits involved in tic generation in patients with Tourette syndrome. Neurology 68:1979–1987
Linke R, Eisensehr I, Wetter TC et al (2004) Presynaptic dopaminergic function in patients with restless legs syndrome: are there common features with early Parkinson's disease? Mov Disord 19:1158–1162
Liu H, Dong F, Meng Z, Zhang B, Tan J, Wang Y (2010) Evaluation of Tourette's syndrome by (99m)Tc-TRODAT-1 SPECT/CT imaging. Ann Nucl Med 24:515–521
Louis ED (2018) Essential tremor then and now: how views of the most common tremor diathesis have changed over time. Parkinsonism Relat Disord 46(Suppl 1):S70–S74
Louis ED, Ferreira JJ (2010) How common is the most common adult movement disorder? Update on the worldwide prevalence of essential tremor. Mov Disord 25:534–541
Louis ED, Vonsattel JP (2008) The emerging neuropathology of essential tremor. Mov Disord 23:174–182
Louis ED, Vonsattel JP, Honig LS, Ross GW, Lyons KE, Pahwa R (2006) Neuropathologic findings in essential tremor. Neurology 66:1756–1759
Lu CS, Ikeda A, Terada K et al (1998) Electrophysiological studies of early stage corticobasal degeneration. Mov Disord 13:140–146
Mavroudis I, Petridis F, Kazis D (2019) Neuroimaging and neuropathological findings in essential tremor. Acta Neurol Scand 139:491–496
McNaught KS, Mink JW (2011) Advances in understanding and treatment of Tourette syndrome. Nat Rev Neurol 7:667–676
Merner ND, Girard SL, Catoire H et al (2012) Exome sequencing identifies FUS mutations as a cause of essential tremor. Am J Hum Genet 91:313–319
Meyer P, Bohnen NI, Minoshima S et al (1999) Striatal presynaptic monoaminergic vesicles are not increased in Tourette's syndrome. Neurology 53:371–374
Michaud M, Soucy JP, Chabli A, Lavigne G, Montplaisir J (2002) SPECT imaging of striatal pre- and postsynaptic dopaminergic status in restless legs syndrome with periodic leg movements in sleep. J Neurol 249:164–170
Montagna P (2005) Fatal familial insomnia: a model disease in sleep physiopathology. Sleep Med Rev 9:339–353

Montagna P, Gambetti P, Cortelli P, Lugaresi E (2003) Familial and sporadic fatal insomnia. Lancet Neurol 2:167–176
Moriarty J, Costa DC, Schmitz B, Trimble MR, Ell PJ, Robertson MM (1995) Brain perfusion abnormalities in Gilles de la Tourette's syndrome. Br J Psychiatry 167:249–254
Mrowka M, Jobges M, Berding G, Schimke N, Shing M, Odin P (2005) Computerized movement analysis and beta-CIT-SPECT in patients with restless legs syndrome. J Neural Transm (Vienna) 112:693–701
Muller-Vahl KR, Berding G, Brucke T et al (2000) Dopamine transporter binding in Gilles de la Tourette syndrome. J Neurol 247:514–520
Muller-Vahl KR, Meyer GJ, Knapp WH et al (2005) Serotonin transporter binding in Tourette syndrome. Neurosci Lett 385:120–125
Muller-Vahl KR, Szejko N, Wilke F et al (2019) Serotonin transporter binding is increased in Tourette syndrome with obsessive compulsive disorder. Sci Rep 9:972
Nagaratnam N, Kalasabail G (1997) Contralateral abolition of essential tremor following a pontine stroke. J Neurol Sci 149:195–196
Nagasaka T, Nagasaka K, Ohta E et al (2011) Cerebral hypermetabolism demonstrated by FDG PET in familial Creutzfeldt-Jakob disease. Clin Nucl Med 36:725–727
Oboshi Y, Ouchi Y, Yagi S et al (2012) In vivo mesolimbic D2/3 receptor binding predicts post-therapeutic clinical responses in restless legs syndrome: a positron emission tomography study. J Cereb Blood Flow Metab 32:654–662
Oguro K, Kobayashi J, Aiba H, Hojo H (1997) Opsoclonus-myoclonus syndrome with abnormal single photon emission computed tomography imaging. Pediatr Neurol 16:334–336
Oh SY, Boegle R, Eulenburg PZ, Ertl M, Kim JS, Dieterich M (2017) Longitudinal multi-modal neuroimaging in opsoclonus-myoclonus syndrome. J Neurol 264:512–519
Phillips B, Young T, Finn L, Asher K, Hening WA, Purvis C (2000) Epidemiology of restless legs symptoms in adults. Arch Intern Med 160:2137–2141
Pourfar M, Feigin A, Tang CC et al (2011) Abnormal metabolic brain networks in Tourette syndrome. Neurology 76:944–952
Ragno M, Scarcella MG, Cacchio G et al (2009) Striatal [123I] FP-CIT SPECT demonstrates dopaminergic deficit in a sporadic case of Creutzfeldt-Jakob disease. Acta Neurol Scand 119:131–134
Raudino F, Muscia F, Osio M (2009) Orthostatic tremor and I-123-FP-CIT-SPECT: report of a case. Neurol Sci 30:365–366
Roselli F, Pisciotta NM, Pennelli M et al (2010) Midbrain SERT in degenerative parkinsonisms: a 123I-FP-CIT SPECT study. Mov Disord 25:1853–1859
Ruottinen HM, Partinen M, Hublin C et al (2000) An FDOPA PET study in patients with periodic limb movement disorder and restless legs syndrome. Neurology 54:502–504
Schoberl F, Feil K, Xiong G et al (2017) Pathological ponto-cerebello-thalamo-cortical activations in primary orthostatic tremor during lying and stance. Brain 140:83–97
Schwartz M, Groshar D, Inzelberg R, Hocherman S (2004) Dopamine-transporter imaging and visuo-motor testing in essential tremor, practical possibilities for detection of early stage Parkinson's disease. Parkinsonism Relat Disord 10:385–389
Serra-Mestres J, Ring HA, Costa DC et al (2004) Dopamine transporter binding in Gilles de la Tourette syndrome: a [123I]FP-CIT/SPECT study. Acta Psychiatr Scand 109:140–146
Shepard JW Jr, Buysse DJ, Chesson AL Jr et al (2005) History of the development of sleep medicine in the United States. J Clin Sleep Med 1:61–82
Shibasaki H, Thompson PD (2011) Milestones in myoclonus. Mov Disord 26:1142–1148
Song IU, Ha SW, Yang YS, Chung YA (2015) Differences in regional glucose metabolism of the brain measured with F-18-FDG-PET in patients with essential tremor according to their response to beta-blockers. Korean J Radiol 16:967–972
Staedt J, Stoppe G, Kogler A et al (1995) Nocturnal myoclonus syndrome (periodic movements in sleep) related to central dopamine D2-receptor alteration. Eur Arch Psychiatry Clin Neurosci 245:8–10

Stamenkovic M, Schindler SD, Asenbaum S et al (2001) No change in striatal dopamine re-uptake site density in psychotropic drug naive and in currently treated Tourette's disorder patients: a [(123)I]-beta-CIT SPECt-study. Eur Neuropsychopharmacol 11:69–74

Storey E, Lichtenstein M, Desmond P, Lloyd J (1995) Clinical features and SPECT scanning in presumed cortico-basal ganglionic degeneration. J Clin Neurosci 2:321–328

Teive HA, Munhoz RP, Barbosa ER (2009) Professor Karl-Axel Ekbom and restless legs syndrome. Parkinsonism Relat Disord 15:254–257

Trenkwalder C, Walters AS, Hening WA et al (1999) Positron emission tomographic studies in restless legs syndrome. Mov Disord 14:141–145

Tribl GG, Asenbaum S, Happe S, Bonelli RM, Zeitlhofer J, Auff E (2004) Normal striatal D2 receptor binding in idiopathic restless legs syndrome with periodic leg movements in sleep. Nucl Med Commun 25:55–60

Trocello JM, Zanotti-Fregonara P, Roze E et al (2008) Dopaminergic deficit is not the rule in orthostatic tremor. Mov Disord 23:1733–1738

Turjanski N, Sawle GV, Playford ED et al (1994) PET studies of the presynaptic and postsynaptic dopaminergic system in Tourette's syndrome. J Neurol Neurosurg Psychiatry 57:688–692

Turjanski N, Lees AJ, Brooks DJ (1999) Striatal dopaminergic function in restless legs syndrome: 18F-dopa and 11C-raclopride PET studies. Neurology 52:932–937

Usui K, Matsuda K, Terada K et al (2010) Epileptic negative myoclonus: a combined study of EEG and [123I]iomazenil (123I-IMZ) single photon emission computed tomography indicating involvement of medial frontal area. Epilepsy Res 89:220–226

van Toorn R, Rabie H, Warwick JM (2005) Opsoclonus-myoclonus in an HIV-infected child on antiretroviral therapy—possible immune reconstitution inflammatory syndrome. Eur J Paediatr Neurol 9:423–426

von Spiczak S, Whone AL, Hammers A et al (2005) The role of opioids in restless legs syndrome: an [11C]diprenorphine PET study. Brain 128:906–917

Waln O, Wu Y, Perlman R, Wendt J, Van AK, Jankovic J (2015) Dopamine transporter imaging in essential tremor with and without parkinsonian features. J Neural Transm (Vienna) 122:1515–1521

Wegner F, Strecker K, Boeckler D et al (2008) Intact serotonergic and dopaminergic systems in two cases of orthostatic tremor. J Neurol 255:1840–1842

Wills AJ, Jenkins IH, Thompson PD, Findley LJ, Brooks DJ (1994) Red nuclear and cerebellar but no olivary activation-associated with essential tremor – a positron emission tomographic study. Ann Neurol 36:636–642

Wills AJ, Thompson PD, Findley LJ, Brooks DJ (1996) A positron emission tomography study of primary orthostatic tremor. Neurology 46:747–752

Wolf SS, Jones DW, Knable MB et al (1996) Tourette syndrome: prediction of phenotypic variation in monozygotic twins by caudate nucleus D2 receptor binding. Science 273:1225–1227

Wong DF, Singer HS, Brandt J et al (1997) D2-like dopamine receptor density in Tourette syndrome measured by PET. J Nucl Med 38:1243–1247

Wong DF, Brasic JR, Singer HS et al (2008) Mechanisms of dopaminergic and serotonergic neurotransmission in Tourette syndrome: clues from an in vivo neurochemistry study with PET. Neuropsychopharmacology 33:1239–1251

Yeh CB, Lee CH, Chou YH, Chang CJ, Ma KH, Huang WS (2006) Evaluating dopamine transporter activity with 99mTc-TRODAT-1 SPECT in drug-naive Tourette's adults. Nucl Med Commun 27:779–784

Yeh CB, Lee CS, Ma KH, Lee MS, Chang CJ, Huang WS (2007) Phasic dysfunction of dopamine transmission in Tourette's syndrome evaluated with 99mTc TRODAT-1 imaging. Psychiatry Res 156:75–82

Yeh P, Walters AS, Tsuang JW (2012) Restless legs syndrome: a comprehensive overview on its epidemiology, risk factors, and treatment. Sleep Breath 16:987–1007

Yu HY, Kwan SY, Lirng JF, Liao KK, Chu YK, Liao SQ (2009) Epileptic negative myoclonus: SPECT, PET, and video/EEG studies and the dramatic effects of levetiracetam. Epilepsy Behav 14:687–690

Zesiewicz TA, Elble RJ, Louis ED et al (2011) Evidence-based guideline update: treatment of essential tremor: report of the Quality Standards Subcommittee of the American Academy of Neurology. Neurology 77:1752–1755

Zhang X, Santaniello S (2019) Role of cerebellar GABAergic dysfunctions in the origins of essential tremor. Proc Natl Acad Sci U S A 116:13592–13601

Zhang YX, Liu JR, Jiang B et al (2007) Lance-Adams syndrome: a report of two cases. J Zhejiang Univ Sci B 8:715–720

Clinical Applications of [^{123}I]FP-CIT SPECT Imaging

31

Jan Booij, Marina A. J. Tijssen, and Henk W. Berendse

Contents

31.1 Introduction 850
31.2 Dopamine Transporter Imaging in Healthy Controls with [^{123}I]FP-CIT SPECT 851
31.3 [^{123}I]FP-CIT SPECT Imaging in Parkinson's Disease and Atypical Parkinsonian Syndromes 852
31.3.1 [^{123}I]FP-CIT SPECT Imaging in Parkinson's Disease 852
31.3.2 [^{123}I]FP-CIT SPECT Imaging in Multiple System Atrophy and Progressive Supranuclear Palsy 855
31.3.3 [^{123}I]FP-CIT SPECT Imaging in Corticobasal Degeneration 856
31.3.4 [^{123}I]FP-CIT SPECT Imaging in Vascular Parkinsonism and Traumatic Brain Injury 857
31.3.5 [^{123}I]FP-CIT SPECT Imaging in DLB 859
31.4 Methods to Analyse [^{123}I]FP-CIT SPECT Studies in Routine Clinical Practice 861
31.5 Extrastriatal [^{123}I]FP-CIT Binding 862
31.6 Concluding Remarks 863
References 863

J. Booij (✉)
Department of Radiology and Nuclear Medicine, Amsterdam University Medical Centers. Academic Medical Center, University of Amsterdam, Amsterdam, The Netherlands
e-mail: j.booij@amsterdamumc.nl

M. A. J. Tijssen
Department of Neurology, University Medical Center Groningen, University of Groningen, Groningen, The Netherlands
e-mail: m.a.j.de.koning-tijssen@umcg.nl

H. W. Berendse
Department of Neurology, Amsterdam University Medical Centers, VU University Medical Center, Amsterdam, The Netherlands
e-mail: h.berendse@amsterdamumc.nl

R. A. J. O. Dierckx et al. (eds.), *PET and SPECT in Neurology*,
https://doi.org/10.1007/978-3-030-53168-3_31

Abstract

Dopamine transporter (DAT) imaging with [^{123}I]*N*-ω-fluoropropyl-2β-carbomethoxy-3β-(4-iodophenyl)nortropane ([^{123}I]FP-CIT) single-photon emission computed tomography (SPECT) is commonly used in routine clinical studies to exclude or detect a loss of striatal DATs in individual patients with a movement disorder or dementia. In this chapter, we describe the clinical applications of [^{123}I]FP-CIT SPECT imaging. To facilitate the interpretation of [^{123}I]FP-CIT SPECT images, we first describe the results of [^{123}I]FP-CIT SPECT studies in healthy controls. Thereafter, we describe the typical findings when applying this technique in movement disorders and dementia characterised by a loss of striatal DATs (e.g. Parkinson's disease and dementia with Lewy bodies). We will also describe the possibilities to analyse [^{123}I]FP-CIT SPECT scans in the setting of routine clinical practice. Finally, we briefly discuss the characterisation of extrastriatal [^{123}I]FP-CIT binding and its potential role in future studies.

31.1 Introduction

As described extensively in another chapter of this book series (Booij et al. 2020), the dopamine transporter (DAT) is mainly located in the membrane of presynaptic dopaminergic neurons (see Fig. 1 of Booij et al. 2020). Several radioligands for the DAT have been developed successfully for both positron emission tomography (PET) and single-photon emission computed tomography (SPECT) imaging (for details see Booij et al. 2020). Yet, only a single radiotracer for the DAT has been licensed both by the Federal Drug Administration (FDA) and the European Medicines Agency (EMA). This radiotracer is [^{123}I]*N*-ω-fluoropropyl-2β-carbomethoxy-3β-(4-iodophenyl)nortropane ([^{123}I]FP-CIT), which is marketed as DaTSCAN and DaTscan in Europe and the United States, respectively. [^{123}I]FP-CIT is a cocaine derivative that was first synthesised by the chemist John L. Neumeyer in the early 1990s (Neumeyer et al. 1994).

Currently, [^{123}I]FP-CIT SPECT is often used in routine clinical practice to exclude or detect the loss of nigrostriatal neurons in individual patients (Booij et al. 2001; Løkkegaard et al. 2002; Kupsch et al. 2012; Catafau et al. 2004).

In this chapter, we will discuss the potential clinical applications of [^{123}I]FP-CIT SPECT. We will first describe the results of studies performed in healthy control subjects and then discuss the role of [^{123}I]FP-CIT SPECT in differentiating between degenerative and non-degenerative movement disorders in clinical practice as well as its potential role in dementia. We will also discuss how [^{123}I]FP-CIT SPECT images can be analysed optimally as part of a routine clinical procedure. Finally, we will touch upon the potential role of extrastriatal [^{123}I]FP-CIT binding in future imaging studies.

31.2 Dopamine Transporter Imaging in Healthy Controls with [123I]FP-CIT SPECT

In routine clinical studies, it is important to recognise abnormalities of striatal [123I]FP-CIT binding on SPECT scans. Therefore, it is essential to be aware of the range of normal binding levels against which abnormal binding needs to be recognised. This will increase the diagnostic accuracy of [123I]FP-CIT SPECT imaging in routine clinical practice. In this paragraph, we will discuss the results of [123I]FP-CIT SPECT studies in healthy control subjects.

Autopsy studies in humans have shown a reduction in the number of pigmented neurons in the pars compacta of the substantia nigra with advancing age (McGeer et al. 1977; Fearnley and Lees 1991). In addition, autopsy studies showed that the concentration of striatal DATs declines with natural ageing (Allard and Marcusson 1989; De Keyser et al. 1990). In line with these pathological observations, [123I]FP-CIT SPECT studies performed in healthy controls revealed decreases in striatal DAT binding with age, ranging from 3.3% up to 9.6% per decade (Ishikawa et al. 1996; Lavalaye et al. 2000; Tissingh et al. 1998; Eusebio et al. 2012; van de Giessen et al. 2013; Kaasinen et al. 2015; Yamamoto et al. 2017). The two largest [123I]FP-CIT SPECT studies on this topic so far included 139 healthy controls (age range 20–83 years) and 256 healthy controls (age range 20–83 years), respectively, and reported an average decline of striatal DAT availability of 5.5–6.3% per decade (Varrone et al. 2013; Matsuda et al. 2018). Interestingly, one study included mainly Caucasians (Varrone et al. 2013), while the other included Asian subjects (Matsuda et al. 2018). Since the age-related decline in striatal DATs was comparable in both cohorts, this suggests that ageing effects on striatal DAT expression may be unrelated to race. Importantly, ageing had no effect on the caudate-to-putamen ratio of DAT binding (Fig. 31.1). This is in line with another large study in healthy controls

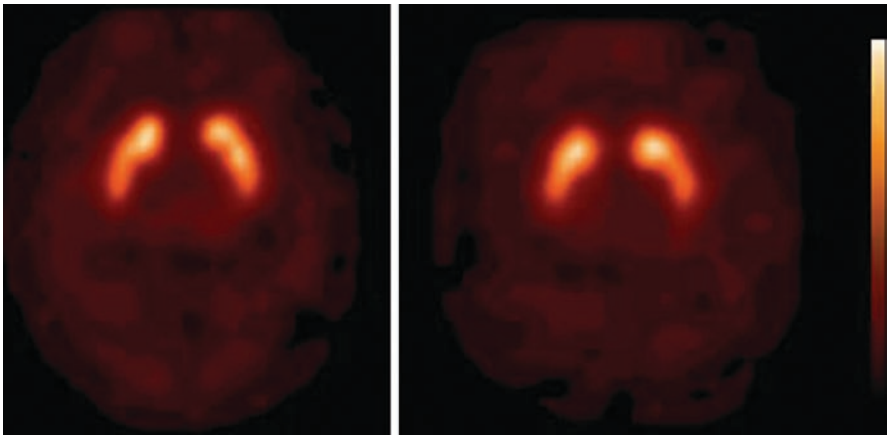

Fig. 31.1 [123I]FP-CIT SPECT scan obtained (3 h after injection) in a 21-year-old healthy female control (*left side*) and in a 78-year-old healthy female control (*right side*). Striatal binding of [123I]FP-CIT is symmetrical and clearly visible in both the caudate nucleus and putamen, in the young as well as the aged healthy control

using [^{123}I]β-CIT (a well-validated SPECT DAT tracer that is structurally closely related to [^{123}I]FP-CIT) and SPECT, which made clear that the rate of decline of DAT binding in the caudate nucleus and putamen with ageing was comparable (van Dyck et al. 2002). These findings suggest that it is important in routine clinical studies to take into account the effect of natural ageing on striatal DAT binding. A useful parameter, that is not influenced by natural ageing, is the caudate-to-putamen [^{123}I]FP-CIT binding ratio (Fig. 31.1).

Some [^{123}I]FP-CIT SPECT studies reported higher striatal binding ratios in women than in men (Lavalaye et al. 2000; Eusebio et al. 2012; Yamamoto et al. 2017; Matsuda et al. 2018), and this effect was more pronounced in younger than older controls (Lavalaye et al. 2000; Varrone et al. 2013; Matsuda et al. 2018), although this gender effect was not observed in all [^{123}I]FP-CIT studies (Pak et al. 2018). Also, an [^{123}I]β-CIT SPECT study performed in a large cohort of healthy controls (70 males and 52 females) did not find a significant effect of gender on striatal binding ratios (Best et al. 2005). Taken together, these data suggest that the diagnostic accuracy of [^{123}I]FP-CIT SPECT in routine clinical studies may be improved by taking gender effects into account, which may be particularly relevant in younger individuals.

[^{123}I]β-CIT SPECT studies in healthy controls demonstrated that the level of striatal DAT availability in the human brain may be associated with polymorphisms in the gene encoding for the DAT (van de Giessen et al. 2009; van Dyck et al. 2005; Jacobsen et al. 2000). However, a meta-analysis failed to establish a significant relationship between in vivo striatal DAT availability and polymorphisms in the gene encoding for the DAT in healthy controls (Costa et al. 2011). In a more recent meta-analysis, Faraone and co-workers concluded that the findings of SPECT studies on this topic were highly heterogeneous, and that the significant relationship between striatal DAT availability and polymorphisms in the gene encoding for the DAT may be limited to [^{123}I]β-CIT SPECT studies (Faraone et al. 2014). Also, to our knowledge no [^{123}I]FP-CIT SPECT study has been performed to look into this topic in a large group of healthy controls. Consequently, as it stands now, there is insufficient support to take gene effects into account in a setting in which [^{123}I]FP-CIT SPECT imaging is used for routine diagnostic purposes.

31.3 [^{123}I]FP-CIT SPECT Imaging in Parkinson's Disease and Atypical Parkinsonian Syndromes

31.3.1 [^{123}I]FP-CIT SPECT Imaging in Parkinson's Disease

An important neuropathological characteristic of Parkinson's disease (PD) is a severe loss of nigrostriatal dopamine neurons and consequently a decrease in striatal DATs (Kish et al. 1988; Kaufman and Madras 1991).

Several studies have established that [^{123}I]FP-CIT SPECT scanning can detect a loss of striatal DAT binding even in the early motor phase of PD (Eshuis et al. 2009; Isaias et al. 2007; Booij et al. 1997b; Tissingh et al. 1998; Pagano et al. 2018).

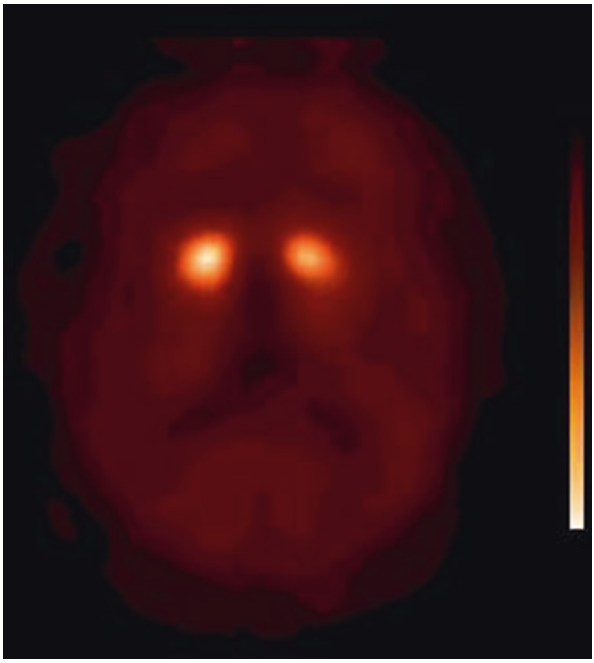

Fig. 31.2 [123I]FP-CIT SPECT scan (3 h after injection) of a hemi-parkinsonian patient. Note the asymmetry of binding, as well as the severe loss of binding bilaterally in the putamen

Typically, the reduction in striatal DAT binding is stronger in the putamen than in the caudate nucleus and has an asymmetrical pattern (Fig. 31.2). Most often, DAT binding is lowest in the contralateral putamen (i.e. the side contralateral to the most affected side of the body). However, in individual PD patients, the decrease in DAT binding can be rather symmetrical or even lower on the ipsilateral than on the contralateral side. It has been suggested that this last phenomenon may be particularly true for PD patients with tremor-dominant features (Isaias et al. 2007). Interestingly, in many patients with clinically unilateral PD, there is a bilateral loss of putamen DAT binding (Tissingh et al. 1998; Filippi et al. 2005), which is consistent with studies in hemi-PD patients using [123I]β-CIT as a ligand (Marek et al. 1996) (Fig. 31.2). However, for routine clinical studies, it is important to be aware of the fact that in some patients with unilateral PD, the loss of DAT binding may be restricted to one side of the brain (Fig. 31.3).

In early-stage PD patients, using age-corrected data, an approximately 60–65% loss of DAT availability can be found in the contralateral putamen (Booij et al. 2001; Tissingh et al. 1998). Additionally, recent studies have suggested that [123I]FP-CIT SPECT scanning is sensitive enough to detect a loss of striatal DAT binding in the premotor phase of PD (Iranzo et al. 2010, 2017; Stiasny-Kolster et al. 2005; Doppler et al. 2017), consistent with findings from earlier [123I]β-CIT SPECT studies (Berendse et al. 2001; Ponsen et al. 2004, 2010). Finally, the loss of striatal [123I]FP-CIT binding in PD correlates with the degree of rigidity and hypokinesia, but not with the severity of resting or postural tremor (Spiegel et al. 2007; Isaias et al. 2007).

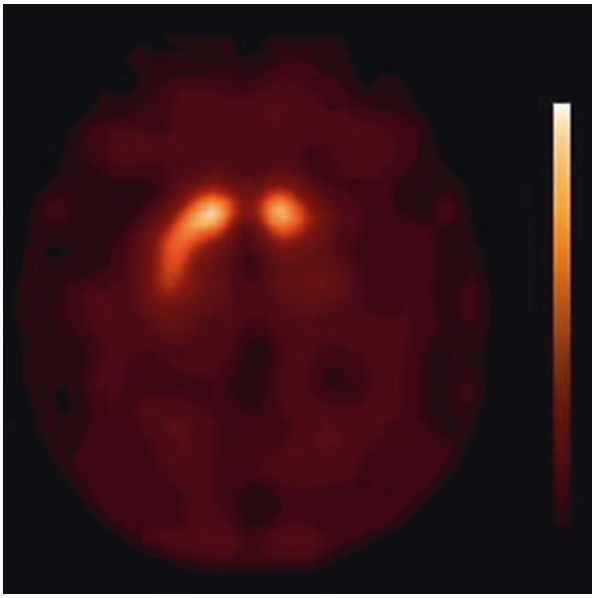

Fig. 31.3 [^{123}I]FP-CIT SPECT scan (3 h after injection) of an early-stage PD patient. Note that in this hemi-parkinsonian patient (motor signs only on the right side of the body), the loss of striatal binding is restricted to the contralateral (*left*) striatum

Although, in most studies in PD, loss of striatal DAT binding does not correlate with tremor scores (Spiegel et al. 2007; Isaias et al. 2007), it has, however, been suggested that a widespread degeneration of the nigrostriatal dopaminergic pathway might still play a role in the aetiology of rest tremor in PD (Isaias et al. 2007). Interestingly, tremor-dominant PD patients can have significantly lower DAT binding in the striatum *ipsilateral* to the rest tremor as compared to akinetic-rigid PD patients (Isaias et al. 2007). Moreover, in some patients with a strictly unilateral resting tremor (without bradykinesia and rigidity), reduced DAT binding may be restricted to the *ipsilateral* (instead of the contralateral) side of the striatum (Aguirregomozcorta et al. 2013; Lin and Chang 1997; Spiegel et al. 2007). These observations may be explained by degeneration/damage of 'crossed' dopaminergic fibres (Aguirregomozcorta et al. 2013).

In some large clinical trials into which patients were enrolled based on a clinical diagnosis of PD, 11–15% of patients showed no degeneration of the nigrostriatal pathway. In the ELLDOPA study, 15% of the included PD patients who were scanned with [^{123}I]β-CIT SPECT had normal baseline scans (Parkinson study group 2002). Importantly, the follow-up scans remained normal in the patients who were rescanned 4 year later. These patients have since been referred to as scans without evidence of dopaminergic deficit (SWEDD; Fahn 2005). Also, a more recent [^{123}I]FP-CIT SPECT study of 16 SWEDD cases showed that after a mean follow-up of 5.4 years, repeat DAT imaging was normal in 14 of these cases (87.5%) (Batla et al. 2014). Recent studies suggest that many of these patients do not suffer from PD but from other conditions including dystonic tremor, parkinsonism associated with fragile X mental retardation 1 gene expansions or even non-neurological

diseases (Bajaj et al. 2010; Hall et al. 2010; Schneider et al. 2007; Sixel-Döring et al. 2011). These data emphasise the diagnostic power of DAT imaging.

In routine clinical studies, [123I]FP-CIT SPECT is commonly used in inconclusive cases to differentiate PD from syndromes not characterised by nigrostriatal loss, for example, essential tremor or drug-induced parkinsonism (DIP) (Booij et al. 2001; Benamer et al. 2000; Marshall and Grosset 2003; Bajaj et al. 2013). In particular, the differentiation of PD from drug-induced parkinsonism (DIP) may present a diagnostic challenge to clinicians. Recent studies have shown that in this clinical situation, an abnormal [123I]FP-CIT SPECT scan is indicative of an underlying neurodegenerative process as is common in PD (Bovi et al. 2010; Diaz-Corrales et al. 2010; Kägi et al. 2010; Tinazzi et al. 2009; Lim et al. 2013; Morley et al. 2016). DIP may persist beyond 6–9 months from the time of neuroleptic withdrawal, as was demonstrated in a recent report on two patients in whom DAT binding was normal (Lim et al. 2013). Importantly, for an accurate interpretation of [123I]FP-CIT SPECT studies, it is not necessary to withdraw neuroleptics prior to the scanning procedure (Booij and Kemp 2008; Booij et al. 2010). Finally, a recent meta-analysis reported that [123I]FP-CIT SPECT may be a useful imaging tool to differentiate PD from DIP (Brigo et al. 2014).

In summary, these findings suggest that [123I]FP-CIT SPECT is a sensitive means to detect a loss of striatal DAT binding in PD. In routine clinical studies, [123I]FP-CIT SPECT can be used to differentiate PD from other forms of parkinsonism that are not characterised by a loss of presynaptic dopaminergic neurons (e.g. essential tremor, psychogenic parkinsonism or DIP), in particular in clinically uncertain cases (Booij et al. 2001; Løkkegaard et al. 2002; Catafau et al. 2004; Cummings et al. 2011; Kägi et al. 2010; Marshall and Grosset 2003; Marshall et al. 2009; Kupsch et al. 2012; Bajaj et al. 2013).

31.3.2 [123I]FP-CIT SPECT Imaging in Multiple System Atrophy and Progressive Supranuclear Palsy

Multiple system atrophy (MSA) and progressive supranuclear palsy (PSP) are neurodegenerative disorders associated with parkinsonism that are also characterised neuropathologically by a loss of nigrostriatal cells and consequently a loss of DATs (Kish et al. 1985; Ruberg et al. 1985; Warren et al. 2007; González et al. 2000).

[123I]FP-CIT SPECT has been used in several studies to demonstrate a loss of striatal DATs in MSA-P (MSA with predominantly parkinsonian signs) and PSP versus healthy controls (Antonini et al. 2003; El Fakhri et al. 2006; Plotkin et al. 2005; van Laere et al. 2006; Bae et al. 2016; Kim et al. 2016). Generally speaking, the results obtained using [123I]FP-CIT as a ligand in MSA-P are in line with findings in studies using [123I]β-CIT (Scherfler et al. 2005; Knudsen et al. 2004; Varrone et al. 2001; Seppi et al. 2006; Joling et al. 2017). In a prospective study, [123I]FP-CIT SPECT scanning was sensitive enough to detect MSA-P in the premotor phase (Iranzo et al. 2010). A subject with rapid eye movement sleep behaviour disorder

but without parkinsonian signs had an abnormal [^{123}I]FP-CIT SPECT scan and developed MSA-P 2.5 years later.

Even in MSA-C (MSA-cerebellar subtype) patients without parkinsonian signs, a significant loss of striatal DAT binding compared to controls has been demonstrated using [^{123}I]FP-CIT SPECT (Muñoz et al. 2011). However, in comparison to patients with PD, MSA-P or PSP patients, the reported decrease in striatal DAT binding was relatively mild (an average loss of 20% of putamen DAT binding). Interestingly, the results of this SPECT study suggest that most but not all MSA-C patients without parkinsonism do have some degree of nigrostriatal dopaminergic denervation. The observation that a loss of DAT binding does not occur in all MSA-C cases (Bae et al. 2016; Joling et al. 2017; Vergnet et al. 2019) was confirmed by a post-mortem study in an autopsy-proven MSA-C case (Kolenc et al. 2012).

In most MSA-P and PSP patients, DAT binding in the putamen is lower than in the caudate nucleus. However, particularly in PSP, some studies suggested a more uniform loss of DATs in the putamen and caudate nucleus (Antonini et al. 2003), but this could not be reproduced by others (Seppi et al. 2006). Furthermore, some studies have shown that striatal DAT binding may differentiate MSA and/or PSP patients from PD patients at a group level (Goebel et al. 2011; Stoffers et al. 2005; Joling et al. 2017), although this is not a consistent finding in SPECT studies (Seppi et al. 2006). In any case, there is considerable overlap in striatal DAT binding values between groups, which suggests that in a routine clinical setting DAT imaging cannot be used to differentiate PD from MSA-P or PSP in individual cases (Stoffers et al. 2005). A recent post-mortem study of PD and MSA-P cases confirmed that the loss of striatal DAT was not significantly different between MSA and PD patients and also that the asymmetry of DAT binding was not significantly different between the two groups of patients (Perju-Dumbrava et al. 2012).

In summary, the results of the above-discussed studies suggest that [^{123}I]FP-CIT SPECT is a sensitive means to detect a loss of striatal DAT in MSA-P and PSP. However, it is important to emphasise that DAT imaging cannot be used to differentiate individual PD patients from MSA-P or PSP patients. Furthermore, striatal [^{123}I]FP-CIT binding can be normal in some MSA-C patients.

31.3.3 [^{123}I]FP-CIT SPECT Imaging in Corticobasal Degeneration

Corticobasal degeneration (CBD) is a rare syndrome, also characterised by nigrostriatal degeneration at autopsy (Oyanagi et al. 2001; Dickson et al. 2002). Indeed, an [^{123}I]FP-CT SPECT study that included the largest cohort of patients with a clinical diagnosis of probable CBD showed a loss of striatal DAT binding in 32 out of the 36 included patients (Cilia et al. 2011). In line with this observation, [^{123}I]β-CIT SPECT and other [^{123}I]FP-CIT SPECT studies in smaller groups of patients have also shown a loss of striatal DAT binding in CBD (Klaffke et al. 2006; Plotkin et al. 2005; Hammesfahr et al. 2016).

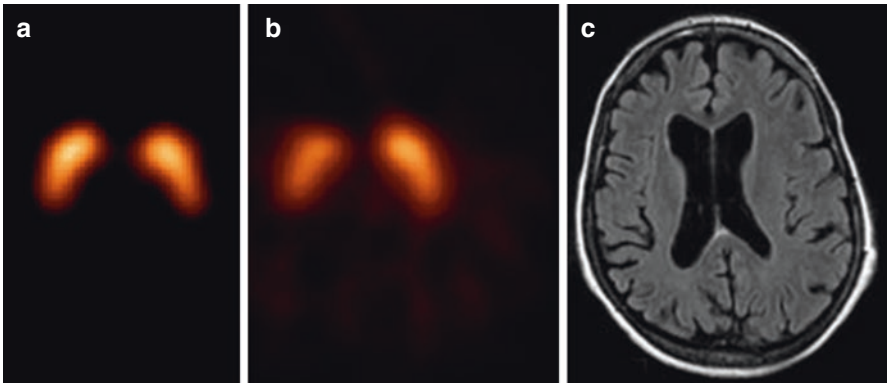

Fig. 31.4 [123I]β-CIT SPECT scan of a healthy control (A) and a patient suffering from corticobasal degeneration (B), as well as an MR image of the same patient (C). The corticobasal degeneration has led to an asymmetrical degeneration of the nigrostriatal pathway (B) and a unilateral atrophy of the brain (C), both contralateral to the body side that showed clinical motor signs (Reprinted from 'Bewegingsstoornissen'; editors ECh Wolters and T van Laar, Amsterdam, 2002, The Netherlands)

Intriguingly, Cilia et al. (2011) demonstrated that the loss of striatal [123I]FP-CIT binding in their sample of CBD patients was characterised by a larger variability, more uniform striatal reduction and a greater asymmetry of binding than in PD patients. Indeed, DAT SPECT images in some CBD patients may be quite characteristic for CBD (Fig. 31.4), whereas in many other CBD cases the [123I]FP-CIT SPECT images may look similar to the images obtained in PD patients. Even of more interest, in some sporadic autopsy-proven CBD cases an ante-mortem [123I]FP-CIT SPECT scan showed no evidence of a reduction in striatal DAT binding (O'Sullivan et al. 2008; Walker et al. 2002). In the study by Cilia et al. (2011), there were no remarkable differences in clinical or neuropsychological characteristics between CBD subjects with or without abnormal striatal [123I]FP-CIT binding. Apparently, extrapyramidal motor symptoms in CBD may not always be associated with nigrostriatal degeneration and could involve supranigral factors (Cilia et al. 2011).

For routine clinical studies, it is important to underline that in many, but not all CBD cases, an [123I]FP-CIT SPECT scan is abnormal (Hammesfahr et al. 2016). In some cases, the pattern of striatal DAT loss may even be characteristic for CBD (Fig. 31.4).

31.3.4 [123I]FP-CIT SPECT Imaging in Vascular Parkinsonism and Traumatic Brain Injury

Significant vascular lesions in the striatum or in the substantia nigra pars compacta can be associated with a loss of striatal [123I]FP-CIT binding (Marshall and Grosset 2003; Zijlmans et al. 2002; Booij et al. 2018; Fig. 31.5), although initial [123I]β-CIT

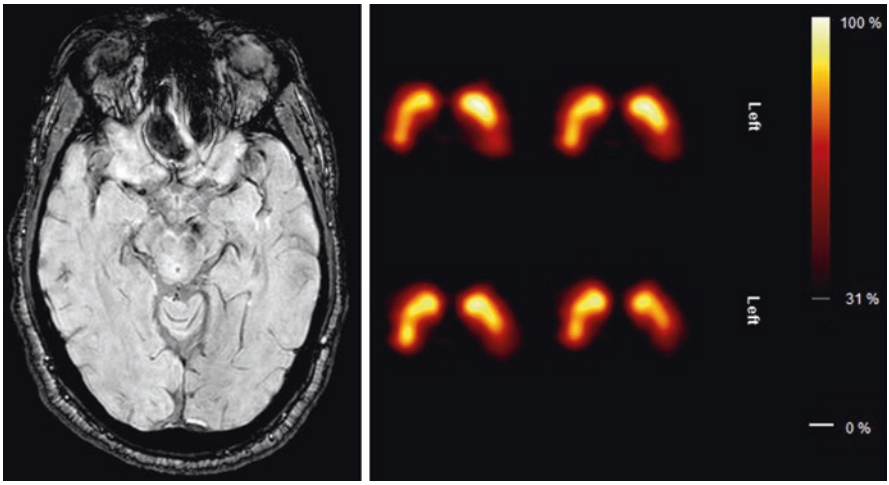

Fig. 31.5 MRI (susceptibility-weighted imaging) and [^{123}I]FP-CIT SPECT scan of the brain in a patient with vascular parkinsonism. The small lesion (hematoma) at the level of the substantia nigra (left panel) induced the abnormal SPECT scan. Please note that the [^{123}I]FP-CIT binding is normal in the right striatum, and abnormal in the posterior part of the left putamen. This pattern is atypical for Parkinson's disease since there is no gradual posterior-to-anterior loss of binding (reprinted from Booij et al. Imago 2018)

SPECT studies suggested that the vast majority of patients suffering from vascular parkinsonism had a normal [^{123}I]β-CIT SPECT scan (Gerschlager et al. 2002).

In a hallmark paper by Zijlmans and co-workers (Zijlmans et al. 2007), even patients fulfilling clinical criteria for vascular parkinsonism and without vascular lesions in the striatum could have an abnormal [^{123}I]FP-CIT SPECT scan, with bilateral loss of DAT binding, particularly in the putamen. A [^{123}I]FP-CIT SPECT study in a large cohort of PD patients and patients with vascular parkinsonism confirmed these findings and showed that around 60–70% of SPECT scans were abnormal in vascular parkinsonism (Benítez-Rivero et al. 2013). Importantly, scores based on visual pattern recognition discriminated better between PD and vascular parkinsonism cases than semi-quantitative scores based on the positioning of regions of interest. Lastly, in another [^{123}I]FP-CIT SPECT study in PD patients and patients with vascular parkinsonism, a significant number of patients with vascular lesions in the basal ganglia had a normal SPECT scan, which indicates that vascular lesions in the basal ganglia do not always cause abnormal striatal DAT binding (Antonini et al. 2012). In the same study, a normal [^{123}I]FP-CIT SPECT scan was associated with a lack of benefit from dopaminomimetic treatment in over 90% of these subjects (Antonini et al. 2012). Finally, a recent meta-analysis concluded that [^{123}I]FP-CIT SPECT may be a useful imaging tool to differentiate PD from vascular parkinsonism (Brigo et al. 2014).

All in all, a substantial number of patients with vascular parkinsonism have an abnormal [^{123}I]FP-CIT SPECT. Frequently, it is possible to differentiate vascular parkinsonism from PD using [^{123}I]FP-CIT SPECT. To do so, it may be of utmost

importance to perform an careful visual inspection of the SPECT images (including structural images), and to recognise patterns of striatal DAT loss which are atypical for PD, but could support the diagnosis of vascular parkinsonism.

A recent study examined the effects of traumatic brain injury (TBI) on DAT binding (Jenkins et al. 2018). Forty-two moderate-severe TBI patients with cognitive impairments but without motor parkinsonism were examined. Around 20% of these patients had evidence of reduced DAT binding in the striatum as measured with [123I]FP-CIT SPECT. Importantly, the caudate nucleus was affected more consistently than other striatal regions. Also, 11 patients had small, but visible, lesions in the striatum demonstrated by magnetic resonance imaging. Importantly, patients with lesions in these structures did not have different striatal DAT binding ratios compared to patients without lesions. These findings suggest that in the majority of patients with moderate/severe TBI, but without parkinsonism, the [123I]FP-CIT SPECT scan is normal; in patients in whom such scans are rated as abnormal, the pattern of DAT loss may differ from what is typical for PD; and small lesions in the striatum may not influence significantly DAT loss as assessed by [123I]FP-CIT SPECT.

In an older study, a severe reduction in striatal DAT binding, as measured by [123I]β-CIT SPECT, was observed in a group of ten patients who were in a vegetative state or had persistent parkinsonism (Donnemiller et al. 2000).

31.3.5 [123I]FP-CIT SPECT Imaging in DLB

Like other diseases characterised by Lewy body pathology (i.e. PD), also dementia with Lewy bodies (DLB) is associated with a loss of dopamine neurons and striatal DATs (Perry et al. 1998). By contrast, the loss of striatal DATs appears to be only subtle in patients suffering from Alzheimer's disease (Perry et al. 1998). In line with these autopsy findings, hallmark studies by Walker and colleagues demonstrated that ante-mortem DAT imaging with [123I]FP-CIT SPECT substantially enhanced the accuracy of a diagnosis of DLB by comparison with clinical criteria alone (Walker et al. 2002, 2007). Many subsequent [123I]FP-CIT SPECT studies confirmed the loss of striatal DATs in DLB (Auning et al. 2011; McKeith et al. 2007; Morgan et al. 2012; Roselli et al. 2009; van Laere et al. 2006; O'Brien et al. 2004; Siepel et al. 2013, 2016; Thomas et al. 2017; Jung et al. 2018). [123I]FP-CIT SPECT may even detect a loss of striatal DAT binding in the preclinical phase of DLB (Iranzo et al. 2010; Thomas et al. 2019). Importantly, the results of [123I]FP-CIT SPECT imaging may predict which patients with a clinical diagnosis of possible DLB will convert to probable DLB or to Alzheimer's disease (O'Brien et al. 2009). Finally, a meta-analysis indicated that the diagnostic accuracy of [123I]FP-CIT SPECT in the diagnosis of DLB is high (Papathanasiou et al. 2012).

In most DLB patients, loss of striatal DAT binding is stronger in the putamen than in the caudate nucleus. Also, the loss of striatal DAT binding can be asymmetrical. However, in line with autopsy findings (Perry et al. 1998), the loss of striatal [123I]FP-CIT binding can also be symmetrical with a relatively strong involvement

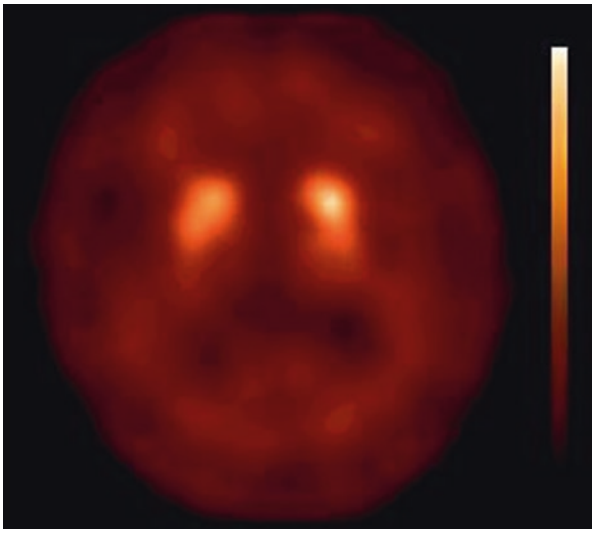

Fig. 31.6 [^{123}I]FP-CIT SPECT scan obtained (3 h after injection) in a DLB patient. Note that due to the strong reduction in specific binding of [^{123}I]FP-CIT in the striatum, the contrast between specific and non-specific binding is low. Also, the loss of binding is relatively symmetrical and involves both the caudate nucleus and putamen

of the caudate nucleus as compared to PD cases (Walker et al. 2004; Joling et al. 2018) (Fig. 31.6).

Although [^{123}I]FP-CIT SPECT appears to be very sensitive in differentiating between DLB and Alzheimer's disease, the role in the differential diagnosis between PD with dementia (PDD), frontotemporal dementia and DLB is probably limited, since a recent study showed that a third of frontotemporal dementia cases had an abnormal [^{123}I]FP-CIT SPECT scan (Morgan et al. 2012). Similarly, although at a group level loss of striatal DATs may be greater in PDD than DLB, the abnormalities on individual [^{123}I]FP-CIT SPECT scans (i.e. lower DAT binding in the putamen than caudate nucleus) in PDD may be similar to the abnormalities observed in DLB (O'Brien et al. 2004; Colloby et al. 2012).

Importantly, an autopsy study in DLB, PDD and Alzheimer's cases showed that ante-mortem DAT imaging was associated with post-mortem nigral dopaminergic neuronal density (but not α-synuclein, tau or amyloid burden) in demented patients (Colloby et al. 2012). This observation may cast doubt on the potential of DAT imaging to differentiate DLB patients without parkinsonism from Alzheimer's disease cases. Nevertheless, most DLB patients without parkinsonism have abnormal DAT SPECT scans (O'Brien et al. 2004; McKeith et al. 2007). On the other hand, Alzheimer's disease patients with parkinsonism may have normal scans (McKeith et al. 2007; Ceravolo et al. 2004).

The results of recent studies suggest that in a subgroup of probable DLB patients the [^{123}I]FP-CIT SPECT scan may be rated as normal initially, but becomes abnormal over time (Colloby et al. 2012; van der Zande et al. 2016; Thomas et al. 2017). This subgroup may consist of approximately 10% of DLB cases (van der Zande et al. 2016; Thomas et al. 2017), and the concept is that in these patients the Lewy bodies are expressed predominantly in the cortex, with initially only minimal involvement of the brainstem.

To summarise, there is evidence that [123I]FP-CIT SPECT is helpful in differentiating DLB from Alzheimer's disease, but its role in differentiating DLB from frontotemporal dementia may be limited.

31.4 Methods to Analyse [123I]FP-CIT SPECT Studies in Routine Clinical Practice

In routine clinical practice, many departments of nuclear medicine evaluate [123I]FP-CIT SPECT scans by visual inspection only. Major reasons are a lack of age-matched control data and the fact that it is a simple way to analyse images. Although a visual qualitative analysis may seem inaccurate, this approach can in fact be very effective in excluding or confirming a loss of striatal DATs (Benamer et al. 2000; O'Brien et al. 2004; McKeith et al. 2007; Booij et al. 2017). An important advantage of visual analysis over a quantitative approach is that an abnormal pattern can be recognised rapidly. A recent study showed that a visual analysis approach was even more accurate in differentiating vascular parkinsonism from PD than a semi-quantitative approach (Benítez-Rivero et al. 2013). In addition, another large study on the diagnostic performance of [123I]FP-CIT SPECT in patients with movement disorders or dementia showed that the results of combined reading (visual reading plus quantitative [123I]FP-CIT SPECT data available to the reader) were not inferior to the results of the visual reading analysis, but the combined reading offered an increase in reader confidence (Booij et al. 2017). Moreover, the visual interpretation of [123I]FP-CIT SPECT images can be further improved by visual rating of parametric distribution volume ratio images (Meyer et al. 2011). However, a visual analysis of [123I]FP-CIT SPECT images may be less accurate in patients in which the degeneration is quite symmetrical and the involvement of the caudate nucleus and putamen more uniform. This type of pattern has been described in some DLB, PSP and MSA-C patients.

Even though visual assessment of [123I]FP-CIT SPECT images remains an integral part of the study report, it is nowadays frequently supplemented by a quantification method (Tatsch and Poepperl 2012; Badiavas et al. 2011). Quantification does not only offer a more objective adjunct to an individual subjective judgement but also has the potential to detect subtle changes that can elude the human eye (Tatsch and Poepperl 2012) and may increase the reader confidence (Booij et al. 2017) and consistency between reporters (Taylor et al. 2018). In routine clinical DAT SPECT studies, semi-quantitative techniques using ROIs are commonly used due to their simplicity. Striatal ROIs were initially defined by manually drawing an irregular contour around the caudate nucleus and putamen and around a region devoid of DATs (occipital cortex or cerebellum). However, this method is strongly influenced by the intensity of striatal DAT binding. In other words, if there is decreased striatal [123I]FP-CIT binding (e.g. in a PD case), the reader tends to draw smaller ROIs over striatal regions than in cases with more intense striatal [123I]FP-CIT binding. Therefore, fixed (or predefined) ROIs are now used more frequently. These ROIs are derived from anatomical atlases or MR images and have led to a better

standardisation. However, this technique is still investigator dependent and does not take into account interindividual differences in striatal volumes. From this perspective, it is of interest that several (semi)automated quantification tools have been developed and several methods have been proposed to quantify DAT studies by (semi)automated positioning of ROIs or volumes of interest (VOIs) (Badiavas et al. 2011; Habraken et al. 1999). Examples are BasGan (Calvini et al. 2007), BRASS (Radau et al. 2000) and DaTQUANT (Brogley 2019) (for a comprehensive review, see Tatsch and Poepperl 2012). Voxel-based analysis, for example, using statistical parametric mapping (SPM), has also been used to analyse [^{123}I]FP-CIT SPECT studies (Kas et al. 2007; van de Giessen et al. 2013). Automated voxel-based image analyses may increase the diagnostic accuracy of DAT imaging in differentiating between PD and other parkinsonian syndromes (Goebel et al. 2011). Finally, in recent years, machine learning paradigms have been developed and evaluated successfully to classify [^{123}I]FP-CIT SPECT studies (Taylor and Fenner 2017; Taylor et al. 2018; Iwabuchi et al. 2019). However, future studies are needed to evaluate the feasibility of voxel-based techniques as well as machine learning paradigms in routine clinical practice.

As mentioned before, for an optimal interpretation of [^{123}I]FP-CIT SPECT images, ageing effects should be taken into account, and gender effects may be relevant in younger subjects. However, it may be difficult for departments of nuclear medicine to acquire [^{123}I]FP-CIT SPECT data in healthy controls and to build their own control database. The Neuroimaging Committee of the EANM understood this problem and decided to initiate a programme to overcome it by setting up an investigator-initiated multicentre trial using EARL (EANM Research Ltd) as a platform (Tatsch 2012). This initiative resulted in a highly standardised European database which is available to allow correction of quantitative DAT binding for age and gender, mostly independent of the equipment used and the centre performing the scan (Dickson et al. 2012; Tatsch 2012; Varrone et al. 2013).

For an optimal interpretation of [^{123}I]FP-CIT SPECT images, it is important to take into account the potential effects of the medication used on [^{123}I]FP-CIT binding to the DAT (for a review see Booij and Kemp 2008). Luckily, most dopaminergic drugs that are commonly used by patients suffering from parkinsonian or dementia syndromes (e.g. levodopa, dopamine agonists or acetylcholinesterase inhibitors) will not significantly influence [^{123}I]FP-CIT binding to the DAT and therefore do not have to be discontinued prior to routine [^{123}I]FP-CIT SPECT studies (Booij and Kemp 2008). On the other hand, selective serotonin reuptake inhibitors may increase striatal [^{123}I]FP-CIT binding ratios.

31.5 Extrastriatal [^{123}I]FP-CIT Binding

In vitro experiments have shown that [^{123}I]FP-CIT has a high affinity for the DAT (low nanomolar range), a moderate affinity for the serotonin transporter (SERT) and a negligible affinity for the norepinephrine transporter (Abi-Dargham et al. 1996;

Scheffel et al. 1997). It is well accepted that striatal [123I]FP-CIT binding predominantly reflects binding to the DAT (Booij et al. 1997a; Andringa et al. 2005).

In recent years, extrastriatal [123I]FP-CIT binding has gained attention (Booij et al. 2007; Eusebio et al. 2012; Hesse et al. 2009; Koopman et al. 2012; Roselli et al. 2010; Kaasinen et al. 2015; Joling et al. 2017, 2018; Joutsa et al. 2015). For example, [123I]FP-CIT binding in the SERT-rich midbrain and diencephalon can be blocked with a selective serotonin reuptake inhibitor (SSRI) in healthy volunteers (Booij et al. 2007). In addition to the severe loss of striatal [123I]FP-CIT binding, there is significantly lower midbrain [123I]FP-CIT binding in DLB and PSP compared to PD patients (Roselli et al. 2010), and lower hypothalamic binding in PSP and MSA-p than in PD (Joling et al. 2017). Future studies will have to determine whether analysis of extrastriatal [123I]FP-CIT binding is helpful in routine clinical studies.

31.6 Concluding Remarks

[123I]FP-CIT SPECT is a very sensitive means to detect a loss of striatal DAT binding. This tool is particularly helpful in uncertain clinical cases with slight parkinsonian features, as well as in the differential diagnosis between syndromes characterised by nigrostriatal neuronal loss (e.g. PD or DLB) and syndromes in which the nigrostriatal system is spared (e.g. essential tremor or Alzheimer's disease).

References

Abi-Dargham A, Gandelman MS, DeErausquin GA et al (1996) SPECT imaging of dopamine transporters in human brain with iodine-123-fluoroalkyl analogs of β-CIT. J Nucl Med 37:1129–1133

Aguirregomozcorta M, Stamelou M, Antonini A et al (2013) Patients with rest-tremor and scans with ipsilateral dopaminergic deficit. J Neurol 260:1132–1135

Allard P, Marcusson JO (1989) Age-correlated loss of dopamine uptake sites with [3H]GBR-12935 in human putamen. Neurobiol Aging 10:661–664

Andringa G, Drukarch B, Bol JG et al (2005) Pinhole SPECT imaging of dopamine transporters correlates with dopamine transporter immunohistochemical analysis in the MPTP mouse model of Parkinson's disease. NeuroImage 26:1150–1158

Antonini A, Benti R, De Notaris R et al (2003) 123I-Ioflupane/SPECT binding to striatal dopamine transporter (DAT) uptake in patients with Parkinson's disease, multiple system atrophy, and progressive supranuclear palsy. Neurol Sci 24:149–150

Antonini A, Vitale C, Barone P et al (2012) The relationship between cerebral vascular disease and parkinsonism: the VADO study. Parkinsonism Relat Disord 18:775–780

Auning E, Rongve A, Fladby T et al (2011) Early and presenting symptoms of dementia with Lewy bodies. Dement Geriatr Cogn Disord 32:202–208

Badiavas K, Molyvda E, Iakovou I, Tsolaki M, Psarrakos K, Karatzas N (2011) SPECT imaging evaluation in movement disorders: far beyond visual assessment. Eur J Nucl Med Mol Imaging 38:764–773

Bae YJ, Kim JM, Kim E et al (2016) Loss of nigral hyperintensity on 3 Tesla MRI of parkinsonism: comparison with 123I-FP-CIT SPECT. Mov Disord 31:684–692

Bajaj NP, Gontu V, Birchall J, Patterson J, Grosset DG, Lees AJ (2010) Accuracy of clinical diagnosis in tremulous parkinsonian patients: a blinded video study. J Neurol Neurosurg Psychiatry 81:1223–1228

Bajaj N, Hauser RA, Grachev ID (2013) Clinical utility of dopamine transporter single photon emission CT (DaT-SPECT) with (123I) ioflupane in diagnosis of parkinsonian syndromes. J Neurol Neurosurg Psychiatry 84:1288–1295

Batla A, Erro R, Stamelou M, Schneider SA, Schwingenschuh P, Ganos C, Bhatia KP (2014) Patients with scans without evidence of dopaminergic deficit: a long-term follow-up study. Mov Disord 29:1820–1825

Benamer TS, Patterson J, Grosset DG et al (2000) Accurate differentiation of parkinsonism and essential tremor using visual assessment of [123I]-FP-CIT SPECT imaging: the [123I]-FP-CIT study group. Mov Disord 15:503–510

Benítez-Rivero S, Marín-Oyaga VA et al (2013) Clinical features and 123I-FP-CIT SPECT imaging in vascular parkinsonism and Parkinson's disease. J Neurol Neurosurg Psychiatry 84:122–129

Berendse HW, Booij J, Francot CM, Bergmans PL, Hijman R, Stoof JC, Wolters EC (2001) Subclinical dopaminergic dysfunction in asymptomatic Parkinson's disease patients' relatives with a decreased sense of smell. Ann Neurol 50:34–41

Best SE, Sarrel PM, Malison RT et al (2005) Striatal dopamine transporter availability with [123I]β-CIT SPECT is unrelated to gender or menstrual cycle. Psychopharmacology 183:181–189

Booij J, Kemp P (2008) Dopamine transporter imaging with [123I]FP-CIT SPECT: potential effects of drugs. Eur J Nucl Med Mol Imaging 35:424–438

Booij J, Andringa G, Rijks LJ et al (1997a) [^{123}I]FP-CIT binds to the dopamine transporter as assessed by biodistribution studies in rats and SPECT studies in MPTP-lesioned monkeys. Synapse 27:183–190

Booij J, Tissingh G, Boer GJ et al (1997b) [123I]FP-CIT SPECT shows a pronounced decline of striatal dopamine transporter labelling in early and advanced Parkinson's disease. J Neurol Neurosurg Psychiatry 62:133–140

Booij J, Speelman JD, Horstink MW, Wolters EC (2001) The clinical benefit of imaging striatal dopamine transporters with [123I]FP-CIT SPET in differentiating patients with presynaptic parkinsonism from those with other forms of parkinsonism. Eur J Nucl Med 28:266–272

Booij J, de Jong J, de Bruin K, Knol R, de Win MM, van Eck-Smit BL (2007) Quantification of striatal dopamine transporters with 123I-FP-CIT SPECT is influenced by the selective serotonin reuptake inhibitor paroxetine: a double-blind, placebo-controlled, crossover study in healthy control subjects. J Nucl Med 48:359–366

Booij J, van Amelsvoort T, Boot E (2010) Co-occurrence of early-onset Parkinson disease and 22q11.2 deletion syndrome: potential role for dopamine transporter imaging. Am J Med Genet A 152A:2937–2938

Booij J, Dubroff J, Pryma D, Yu J, Agarwal R, Lakhani P, Kuo PH (2017) Diagnostic performance of the visual reading of $_{123}$I-ioflupane SPECT images with or without quantification in patients with movement disorders or dementia. J Nucl Med 58:1821–1826

Booij J, Reneman L, Adriaanse S, de Bie R (2018) Dopaminetransporterscintigrafie bij patiënten met parkinsonisme. Image 2:37–42

Booij J, van Wieringen JP, van de Giessen EM, Knol RJJ, Finnema SJ (2020) PET and SPECT imaging of the central dopamine system in humans. In: Dierckx RAJO, Otte A, de Vries EFJ, van Waarde A, Lammertsma AA (eds) PET and SPECT of neurobiological systems. Springer, New York, NY

Bovi T, Antonini A, Ottaviani S et al (2010) The status of olfactory function and the striatal dopaminergic system in drug-induced parkinsonism. J Neurol 257:1882–1889

Brigo F, Matinella A, Erro R, Tinazzi M (2014) [^{123}I]FP-CIT SPECT (DaTSCAN) may be a useful tool to differentiate between Parkinson's disease and vascular or drug-induced parkinsonisms: a meta-analysis. Eur J Neurol 21:1369–1376

Brogley JE (2019) DaTQUANT: the future of diagnosing Parkinson's disease. J Nucl Med Technol 47:21–26

Calvini P, Rodriguez G, Inguglia F, Mignone A, Guerra UP, Nobili F (2007) The basal ganglia matching tools package for striatal uptake semi-quantification: description and validation. Eur J Nucl Med Mol Imaging 34:1240–1253

Catafau AM, Tolosa E, DaTSCAN Clinically Uncertain Parkinsonian Syndromes Study Group (2004) Impact of dopamine transporter SPECT using 123I-Ioflupane on diagnosis and management of patients with clinically uncertain Parkinsonian syndromes. Mov Disord 19:1175–1182

Ceravolo R, Volterrani D, Gambaccini G et al (2004) Presynaptic nigro-striatal function in a group of Alzheimer's disease patients with parkinsonism: evidence from a dopamine transporter imaging study. J Neural Transm 111:1065–1073

Cilia R, Rossi C, Frosini D, Volterrani D et al (2011) Dopamine transporter SPECT imaging in corticobasal syndrome. PLoS One 6:e18301

Colloby SJ, McParland S, O'Brien JT, Attems J (2012) Neuropathological correlates of dopaminergic imaging in Alzheimer's disease and Lewy body dementias. Brain 135:2798–2808

Costa A, Riedel M, Müller U, Möller HJ, Ettinger U (2011) Relationship between SLC6A3 genotype and striatal dopamine transporter availability: a meta-analysis of human single photon emission computed tomography studies. Synapse 65:998–1005

Cummings JL, Henchcliffe C, Schaier S, Simuni T, Waxman A, Kemp P (2011) The role of dopaminergic imaging in patients with symptoms of dopaminergic system neurodegeneration. Brain 134:3146–3166

De Keyser JD, Ebinger G, Vauquelin G (1990) Age-related changes in the human nigrostriatal dopaminergic system. Ann Neurol 27:157–161

Diaz-Corrales FJ, Sanz-Viedma S, Garcia-Solis D, Escobar-Delgado T, Mir P (2010) Clinical features and 123I-FP-CIT SPECT imaging in drug-induced parkinsonism and Parkinson's disease. Eur J Nucl Med Mol Imaging 37:556–564

Dickson DW, Bergeron C, Chin SS et al (2002) Neuropathologic criteria for corticobasal degeneration. J Neuropathol Exp Neurol 61:935–946

Dickson JC, Tossici-Bolt L, Sera T et al (2012) Proposal for the standardisation of multi-centre trials in nuclear medicine imaging: prerequisites for a European 123I-FP-CIT SPECT database. Eur J Nucl Med Mol Imaging 39:188–197

Donnemiller E, Brenneis C, Wissel J, Scherfler C, Poewe W, Riccabona G, Wenning GK (2000) Impaired dopaminergic neurotransmission in patients with traumatic brain injury: a SPECT study using 123I-beta-CIT and 123I-IBZM. Eur J Nucl Med 27:1410–1414

Doppler K, Jentschke HM, Schulmeyer L et al (2017) Dermal phospho-alpha-synuclein deposits confirm REM sleep behaviour disorder as prodromal Parkinson's disease. Acta Neuropathol 133:535–545

El Fakhri G, Habert MO, Maksud P, Kas A, Malek Z, Kijewski MF, Lacomblez L (2006) Quantitative simultaneous 99mTc-ECD/123I-FP-CIT SPECT in Parkinson's disease and multiple system atrophy. Eur J Nucl Med Mol Imaging 33:87–92

Eshuis SA, Jager PL, Maguire RP, Jonkman S, Dierckx RA, Leenders KL (2009) Direct comparison of FP-CIT SPECT and F-DOPA PET in patients with Parkinson's disease and healthy controls. Eur J Nucl Med Mol Imaging 36:454–462

Eusebio A, Azulay JP, Ceccaldi M, Girard N, Mundler O, Guedj E (2012) Voxel-based analysis of whole-brain effects of age and gender on dopamine transporter SPECT imaging in healthy subjects. Eur J Nucl Med Mol Imaging 39:1778–1783

Fahn S (2005) Does levodopa slow or hasten the rate of progression of Parkinson's disease? J Neurol 252(Suppl 4):IV37–IV42

Faraone SV, Spencer TJ, Madras BK, Zhang-James Y, Biederman J (2014) Functional effects of dopamine transporter gene genotypes on in vivo dopamine transporter functioning: a meta-analysis. Mol Psychiatry 19:880–889

Fearnley JM, Lees AJ (1991) Ageing and Parkinson's disease: substantia nigra regional selectivity. Brain 114:2283–2301

Filippi L, Manni C, Pierantozzi M et al (2005) 123I-FP-CIT semi-quantitative SPECT detects preclinical bilateral dopaminergic deficit in early Parkinson's disease with unilateral symptoms. Nucl Med Commun 26:421–426

Gerschlager W, Bencsits G, Pirker W et al (2002) [123I]beta-CIT SPECT distinguishes vascular parkinsonism from Parkinson's disease. Mov Disord 17:518–523

Goebel G, Seppi K, Donnemiller E et al (2011) A novel computer-assisted image analysis of [123I]β-CIT SPECT images improves the diagnostic accuracy of parkinsonian disorders. Eur J Nucl Med Mol Imaging 38:702–710

González AM, Berciano J, Figols J, Pazos A, Pascual J (2000) Loss of dopamine uptake sites and dopamine D2 receptors in striatonigral degeneration. Brain Res 852:228–232

Habraken JB, Booij J, Slomka P, Sokole EB, van Royen EA (1999) Quantification and visualization of defects of the functional dopaminergic system using an automatic algorithm. J Nucl Med 40:1091–1097

Hall DA, Jennings D, Seibyl J, Tassone F, Marek K (2010) FMR1 gene expansion and scans without evidence of dopaminergic deficits in parkinsonism patients. Parkinsonism Relat Disord 16:608–611

Hammesfahr S, Antke C, Mamlins E et al (2016) FP-CIT- and IBZM-SPECT in corticobasal syndrome: results from a clinical follow-up study. Neurodegener Dis 16:342–347

Hesse S, Meyer PM, Strecker K et al (2009) Monoamine transporter availability in Parkinson's disease patients with or without depression. Eur J Nucl Med Mol Imaging 36:428–435

Iranzo A, Lomeña F, Stockner H et al (2010) Decreased striatal dopamine transporter uptake and substantia nigra hyperechogenicity as risk markers of synucleinopathy in patients with idiopathic rapid-eye-movement sleep behaviour disorder: a prospective study. Lancet Neurol 9:1070–1077

Iranzo A, Santamaría J, Valldeoriola F et al (2017) Dopamine transporter imaging deficit predicts early transition to synucleinopathy in idiopathic rapid eye movement sleep behavior disorder. Ann Neurol 82:419–428

Isaias IU, Benti R, Cilia R et al (2007) [123I]FP-CIT striatal binding in early Parkinson's disease patients with tremor vs. akinetic-rigid onset. Neuroreport 18:1499–1502

Ishikawa T, Dhawan V, Kazumata K et al (1996) Comparative nigrostriatal dopaminergic imaging with iodine-123-bCIT-FP/SPECT and fluorine-18-FDOPA/PET. J Nucl Med 37:1760–1765

Iwabuchi Y, Nakahara T, Kameyama M et al (2019) Impact of a combination of quantitative indices representing uptake intensity, shape, and asymmetry in DAT SPECT using machine learning: comparison of different volume of interest settings. EJNMMI Res 9:7

Jacobsen LK, Staley JK, Zoghbi SS et al (2000) Prediction of dopamine transporter binding availability by genotype: a preliminary report. Am J Psychiatry 157:1700–1703

Jenkins PO, De Simoni S, Bourke NJ (2018) Dopaminergic abnormalities following traumatic brain injury. Brain 141:797–810

Joling M, Vriend C, van den Heuvel OA et al (2017) Analysis of extrastriatal 123I-FP-CIT binding contributes to the differential diagnosis of parkinsonian diseases. J Nucl Med 58:1117–1123

Joling M, Vriend C, van der Zande JJ et al (2018) Lower 123I-FP-CIT binding to the striatal dopamine transporter, but not to the extrastriatal serotonin transporter, in Parkinson's disease compared with dementia with Lewy bodies. Neuroimage Clin 19:130–136

Joutsa J, Johansson J, Seppänen M, Noponen T, Kaasinen V (2015) Dorsal-to-ventral shift in midbrain dopaminergic projections and increased thalamic/raphe serotonergic function in early Parkinson disease. J Nucl Med 56:1036–1041

Jung Y, Jordan LG 3rd, Lowe VJ et al (2018) Clinicopathological and ^{123}I-FP-CIT SPECT correlations in patients with dementia. Ann Clin Transl Neurol 5:376–381

Kaasinen V, Joutsa J, Noponen T, Johansson J, Seppänen M (2015) Effects of aging and gender on striatal and extrastriatal [123I]FP-CIT binding in Parkinson's disease. Neurobiol Aging 36:1757–1763

Kägi G, Bhatia KP, Tolosa E (2010) The role of DAT-SPECT in movement disorders. J Neurol Neurosurg Psychiatry 81:5–12

Kas A, Payoux P, Habert MO et al (2007) Validation of a standardized normalization template for statistical parametric mapping analysis of 123I-FP-CIT images. J Nucl Med 48:1459–1467

Kaufman MJ, Madras BK (1991) Severe depletion of cocaine recognition sites associated with the dopamine transporter in Parkinson's-diseased striatum. Synapse 9:43–49

Kim JM, Jeong HJ, Bae YJ et al (2016) Loss of substantia nigra hyperintensity on 7 Tesla MRI of Parkinson's disease, multiple system atrophy, and progressive supranuclear palsy. Parkinsonism Relat Disord 26:47–54

Kish SJ, Chang LJ, Mirchandani L (1985) Progressive supranuclear palsy: relationship between extrapyramidal disturbances, dementia, and brain neurotransmitter markers. Ann Neurol 18:530–536

Kish SJ, Shannak K, Hornykiewicz O (1988) Uneven pattern of dopamine loss in the striatum of patients with idiopathic Parkinson's disease. Pathophysiologic and clinical implications. N Engl J Med 318:876–880

Klaffke S, Kuhn AA, Plotkin M, Amthauer H, Harnack D, Felix R, Kupsch A (2006) Dopamine transporters, D2 receptors, and glucose metabolism in corticobasal degeneration. Mov Disord 21:1724–1727

Knudsen GM, Karlsborg M, Thomsen G et al (2004) Imaging of dopamine transporters and D2 receptors in patients with Parkinson's disease and multiple system atrophy. Eur J Nucl Med Mol Imaging 31:1631–1638

Kolenc M, Popović M, Grmek M, Pirtošek Z, Trošt M (2012) A case of multiple system atrophy with normal dopamine transporter imaging. J Neurol 259:2719–2731

Koopman KE, la Fleur SE, Fliers E, Serlie MJ, Booij J (2012) Assessing the optimal time point for the measurement of extrastriatal serotonin transporter binding with 123I-FP-CIT SPECT in healthy, male subjects. J Nucl Med 53:1087–1090

Kupsch AR, Bajaj N, Weiland F et al (2012) Impact of DaTscan SPECT imaging on clinical management, diagnosis, confidence of diagnosis, quality of life, health resource use and safety in patients with clinically uncertain parkinsonian syndromes: a prospective 1-year follow-up of an open-label controlled study. J Neurol Neurosurg Psychiatry 83:620–628

Lavalaye J, Booij J, Reneman L, Habraken JB, van Royen EA (2000) Effect of age and gender on dopamine transporter imaging with [123I]FP-CIT SPET in healthy volunteers. Eur J Nucl Med 27:867–869

Lim TT, Ahmed A, Itin I, Gostkowski M, Rudolph J, Cooper S, Fernandez HH (2013) Is 6 months of neuroleptic withdrawal sufficient to distinguish drug-induced parkinsonism from Parkinson's disease? Int J Neurosci 123:170–174

Lin JJ, Chang DC (1997) Tremor caused by ipsilateral chronic subdural hematoma. Case illustration. J Neurosurg 87:474

Løkkegaard A, Werdelin LM, Friberg L (2002) Clinical impact of diagnostic SPET investigations with a dopamine re-uptake ligand. Eur J Nucl Med Mol Imaging 29:1623–1629

Marek KL, Seibyl JP, Zoghbi SS et al (1996) [123I]beta-CIT/SPECT imaging demonstrates bilateral loss of dopamine transporters in hemi-Parkinson's disease. Neurology 46:231–237

Marshall V, Grosset D (2003) Role of dopamine transporter imaging in routine clinical practice. Mov Disord 18:1415–1423

Marshall VL, Reininger CB, Marquardt M et al (2009) Parkinson's disease is overdiagnosed clinically at baseline in diagnostically uncertain cases: a 3-year European multicenter study with repeat [123I]FP-CIT SPECT. Mov Disord 24:500–508

Matsuda H, Murata M, Mukai Y et al (2018) Japanese multicenter database of healthy controls for [123I]FP-CIT SPECT. Eur J Nucl Med Mol Imaging 45:1405–1416

McGeer PL, McGeer EG, Suzuki J (1977) Aging and extrapyramidal function. Arch Neurol 34:33–35

McKeith I, O'Brien J, Walker Z et al (2007) Sensitivity and specificity of dopamine transporter imaging with 123I-FP-CIT SPECT in dementia with Lewy bodies: a phase III, multicentre study. Lancet Neurol 6:305–313

Meyer PT, Winz OH, Dafotakis M, Werner CJ, Krohn T, Schäfer WM (2011) Improved visual [123I]FP-CIT SPECT interpretation for evaluation of parkinsonism by visual rating of parametric distribution volume ratio images. Q J Nucl Med Mol Imaging 55:301–309

Morgan S, Kemp P, Booij J et al (2012) Differentiation of frontotemporal dementia from dementia with Lewy bodies using FP-CIT SPECT. J Neurol Neurosurg Psychiatry 83:1063–1070

Morley JF, Cheng G, Dubroff JG, Wood S, Wilkinson JR, Duda JE (2016) Olfactory impairment predicts underlying dopaminergic deficit in presumed drug-induced parkinsonism. Mov Disord Clin Pract 28:603–606

Muñoz E, Iranzo A, Rauek S et al (2011) Subclinical nigrostriatal dopaminergic denervation in the cerebellar subtype of multiple system atrophy (MSA-C). J Neurol 258:2248–2253

Neumeyer JL, Wang S, Gao Y et al (1994) N-ω-fluoroalkyl analogs of (1R)-2β-carbomethoxy-3β-(4-iodophenyl)-tropane (β-CIT): radiotracers for positron emission tomography and single photon emission computed tomography imaging of dopamine transporters. J Med Chem 37:1558–1561

O'Brien JT, Colloby S, Fenwick J et al (2004) Dopamine transporter loss visualized with FP-CIT SPECT in the differential diagnosis of dementia with Lewy bodies. Arch Neurol 61:919–925

O'Brien JT, McKeith IG, Walker Z et al (2009) Diagnostic accuracy of 123I-FP-CIT SPECT in possible dementia with Lewy bodies. Br J Psychiatry 194:34–39

O'Sullivan SS, Burn DJ, Holton JL, Lees AJ (2008) Normal dopamine transporter single photon-emission CT scan in corticobasal degeneration. Mov Disord 23:2424–2426

Oyanagi K, Tsuchiya K, Yamazaki M, Keda K (2001) Substantia nigra in progressive supranuclear palsy, corticobasal degeneration, and parkinsonism-dementia complex of Guam: specific pathological features. J Neuropathol Exp Neurol 60:393–402

Pagano G, De Micco R, Yousaf T, Wilson H, Chandra A, Politis M (2018) REM behavior disorder predicts motor progression and cognitive decline in Parkinson disease. Neurology 91:894–905

Pak K, Nam HY, Shin S et al (2018) Effects of rs591323 on serotonin transporter availability in healthy male subjects. Ann Nucl Med 32:431–436

Papathanasiou ND, Boutsiadis A, Dickson J, Bomanji JB (2012) Diagnostic accuracy of $^{123I\text{-}FP\text{-}CIT}$ (DaTSCAN) in dementia with Lewy bodies: a meta-analysis of published studies. Parkinsonism Relat Disord 18:225–229

Parkinson Study Group (2002) Dopamine transporter brain imaging to assess the effects of Pramipexole vs levodopa Parkinson disease progression. JAMA 287:1653–1661

Perju-Dumbrava LD, Kovacs GG, Pirker S, Jellinger K, Hoffmann M, Asenbaum S, Pirker W (2012) Dopamine transporter imaging in autopsy-confirmed Parkinson's disease and multiple system atrophy. Mov Disord 27:65–71

Perry E, Court J, Goodchild R et al (1998) Clinical neurochemistry: developments in dementia research based on brain bank material. J Neural Transm 105:915–933

Plotkin M, Amthauer H, Klaffke S et al (2005) Combined 123I-FP-CIT and 123I-IBZM SPECT for the diagnosis of parkinsonian syndromes: study on 72 patients. J Neural Transm 112:677–692

Ponsen MM, Stoffers D, Booij J, van Eck-Smit BL, Wolters EC, Berendse HW (2004) Idiopathic hyposmia as a preclinical sign of Parkinson's disease. Ann Neurol 56:173–181

Ponsen MM, Stoffers D, Wolters EC, Booij J, Berendse HW (2010) Olfactory testing combined with dopamine transporter imaging as a method to detect prodromal Parkinson's disease. J Neurol Neurosurg Psychiatry 81:396–399

Radau PE, Linke R, Slomka PJ, Tatsch K (2000) Optimization of automated quantification of 123I-IBZM uptake in the striatum applied to parkinsonism. J Nucl Med 41:220–227

Roselli F, Pisciotta NM, Perneczky R et al (2009) Severity of neuropsychiatric symptoms and dopamine transporter levels in dementia with Lewy bodies: a 123I-FP-CIT SPECT study. Mov Disord 24:2097–2103

Roselli F, Pisciotta NM, Pennelli M et al (2010) Midbrain SERT in degenerative parkinsonisms: a 123I-FP-CIT SPECT study. Mov Disord 25:1853–1859

Ruberg M, Javoy-Agid F, Hirsch E et al (1985) Dopaminergic and cholinergic lesions in progressive supranuclear palsy. Ann Neurol 18:523–529

Scheffel U, Lever JR, Abraham P et al (1997) N-substituted phenyltropanes as in vivo binding ligands for rapid imaging studies of the dopamine transporter. Synapse 25:345–349

Scherfler C, Seppi K, Donnemiller E et al (2005) Voxel-wise analysis of [123I]beta-CIT SPECT differentiates the Parkinson variant of multiple system atrophy from idiopathic Parkinson's disease. Brain 128:1605–1612

Schneider SA, Edwards MJ, Mir P, Cordivari C, Hooker J, Dickson J, Quinn N, Bhatia KP (2007) Patients with adult-onset dystonic tremor resembling parkinsonian tremor have scans without evidence of dopaminergic deficit (SWEDDs). Mov Disord 22:2210–2215

Seppi K, Scherfler C, Donnemiller E et al (2006) Topography of dopamine transporter availability in progressive supranuclear palsy: a voxelwise [123I]beta-CIT SPECT analysis. Arch Neurol 63:1154–1160

Siepel FJ, Rongve A, Buter TC, Beyer MK, Ballard CG, Booij J, Aarsland D (2013) (123I) FP-CIT SPECT in suspected dementia with Lewy bodies: a longitudinal case study. BMJ Open 3(4):pii: e002642

Siepel FJ, Dalen I, Grüner R, Booij J, Brønnick KS, Buter TC, Aarsland D (2016) Loss of dopamine transporter binding and clinical symptoms in dementia with Lewy bodies. Mov Disord 31:118–125

Sixel-Döring F, Liepe K, Mollenhauer B, Trautmann E, Trenkwalder C (2011) The role of 123I-FP-CIT-SPECT in the differential diagnosis of Parkinson and tremor syndromes: a critical assessment of 125 cases. J Neurol 258:2147–2154

Spiegel J, Hellwig D, Samnick S et al (2007) Striatal FP-CIT uptake differs in the subtypes of early Parkinson's disease. J Neural Transm 114:331–335

Stiasny-Kolster K, Doerr Y, Möller JC et al (2005) Combination of 'idiopathic' REM sleep behaviour disorder and olfactory dysfunction as possible indicator for alpha-synucleinopathy demonstrated by dopamine transporter FP-CIT-SPECT. Brain 128:126–137

Stoffers D, Booij J, Bosscher L, Winogrodzka A, Wolters EC, Berendse HW (2005) Early-stage [123I]beta-CIT SPECT and long-term clinical follow-up in patients with an initial diagnosis of Parkinson's disease. Eur J Nucl Med Mol Imaging 32:689–695

Tatsch K (2012) Standardisation and harmonisation boost the credibility of nuclear medicine procedures. Eur J Nucl Med Mol Imaging 39:186–187

Tatsch K, Poepperl G (2012) Quantitative approaches to dopaminergic brain imaging. Q J Nucl Med Mol Imaging 56:27–38

Taylor JC, Fenner JW (2017) Comparison of machine learning and semi-quantification algorithms for (I123)FP-CIT classification: the beginning of the end for semi-quantification? EJNMMI Phys 4:29

Taylor JC, Romanowski C, Lorenz E, Lo C, Bandmann O, Fenner J (2018) Computer-aided diagnosis for (123I)FP-CIT imaging: impact on clinical reporting. EJNMMI Res 8:36

Thomas AJ, Attems J, Colloby SJ et al (2017) Autopsy validation of 123I-FP-CIT dopaminergic neuroimaging for the diagnosis of DLB. Neurology 88:276–283

Thomas AJ, Donaghy P, Roberts G et al (2019) Diagnostic accuracy of dopaminergic imaging in prodromal dementia with Lewy bodies. Psychol Med 49:396–402

Tinazzi M, Antonini A, Bovi T et al (2009) Clinical and [123I]FP-CIT SPET imaging follow-up in patients with drug-induced parkinsonism. J Neurol 256:910–915

Tissingh G, Booij J, Bergmans P et al (1998) Iodine-123-N-omega-fluoropropyl-2beta-carbomethoxy-3beta-(4-iodophenyl)tropane SPECT in healthy controls and early-stage, drug-naive Parkinson's disease. J Nucl Med 39:1143–1148

van de Giessen E, de Win MM, Tanck MW, van den Brink W, Baas F, Booij J (2009) Striatal dopamine transporter availability associated with polymorphisms in the dopamine transporter gene SLC6A3. J Nucl Med 50:45–52

van de Giessen EV, Hesse S, Caan MW et al (2013) No association between striatal dopamine transporter binding and body mass index: a multi-center European study in healthy volunteers. NeuroImage 64:61–67

van der Zande JJ, Booij J, Scheltens P, Raijmakers PG, Lemstra AW (2016) [123]FP-CIT SPECT scans initially rated as normal became abnormal over time in patients with probable dementia with Lewy bodies. Eur J Nucl Med Mol Imaging 43:1060–1066

van Dyck CH, Seibyl JP, Malison RT et al (2002) Age-related decline in dopamine transporters: analysis of striatal subregions, nonlinear effects, and hemispheric asymmetries. Am J Geriatr Psychiatry 10:36–43

van Dyck CH, Malison RT, Jacobsen LK et al (2005) Increased dopamine transporter availability associated with the 9-repeat allele of the SLC6A3 gene. J Nucl Med 46:745–751

Van Laere K, Casteels C, De Ceuninck L et al (2006) Dual-tracer dopamine transporter and perfusion SPECT in differential diagnosis of parkinsonism using template-based discriminant analysis. J Nucl Med 47:384–392

Varrone A, Marek KL, Jennings D, Innis RB, Seibyl JP (2001) [(123)I]beta-CIT SPECT imaging demonstrates reduced density of striatal dopamine transporters in Parkinson's disease and multiple system atrophy. Mov Disord 16:1023–1032

Varrone A, Dickson JC, Tossici-Bolt L et al (2013) European multicentre database of healthy controls for [123I]FP-CIT SPECT (ENC-DAT): age-related effects, gender differences and evaluation of different methods of analysis. Eur J Nucl Med Mol Imaging 40:213–227

Vergnet S, Hives F, Foubert-Samier A (2019) Dopamine transporter imaging for the diagnosis of multiple system atrophy cerebellar type. Parkinsonism Relat Disord 63:199–203

Walker Z, Costa DC, Walker RW et al (2002) Differentiation of dementia with Lewy bodies from Alzheimer's disease using a dopaminergic presynaptic ligand. J Neurol Neurosurg Psychiatry 73:134–140

Walker Z, Costa DC, Walker RW et al (2004) Striatal dopamine transporter in dementia with Lewy bodies and Parkinson disease: a comparison. Neurology 62:1568–1572

Walker Z, Jaros E, Walker RW et al (2007) Dementia with Lewy bodies: a comparison of clinical diagnosis, FP-CIT single photon emission computed tomography imaging and autopsy. J Neurol Neurosurg Psychiatry 78:1176–1181

Warren NM, Piggott MA, Greally E, Lake M, Lees AJ, Burn DJ (2007) Basal ganglia cholinergic and dopaminergic function in progressive supranuclear palsy. Mov Disord 22:1594–1600

Yamamoto H, Arimura S, Nakanishi A et al (2017) Age-related effects and gender differences in Japanese healthy controls for [^{123}I] FP-CIT SPECT. Ann Nucl Med 31:407–412

Zijlmans J, Booij J, Valk J, Lees A, Horstink M (2002) Posttraumatic tremor without parkinsonism in a patient with complete contralateral loss of the nigrostriatal pathway. Mov Disord 17:1086–1088

Zijlmans J, Evans A, Fontes F, Katzenschlager R, Gacinovic S, Lees AJ, Costa D (2007) [123I]FP-CIT spect study in vascular parkinsonism and Parkinson's disease. Mov Disord 22:1278–1285

Part V

Inflammatory Disorders

PET Imaging of Microglia Activation and Infection in Neuropsychiatric Disorders with Potential Infectious Origin

32

Hans Christiaan Klein, Lot de Witte, Robert Bransfield, and Peter Paul De Deyn

Contents

32.1 General Introduction 874
32.2 Establishment of CNS Infection 875
32.2.1 Neuroinvasive Species 876
32.2.2 Neuroinvasion Mechanisms 876
32.2.3 Pathogen Reservoirs 877
32.2.4 Response to Pathogens 877
32.3 Inflammatory Response to CNS Infection 878
32.3.1 Functions of the Blood–Brain Barrier 878
32.3.2 Functions of Microglia 879

H. C. Klein (✉)
Medical Imaging Centre, University Medical Hospital Groningen, University of Groningen, Groningen, The Netherlands

Lentis Mental Health and VNN Addiction Care, Groningen, The Netherlands

L. de Witte
Department of Psychiatry, University Medical Center Utrecht, University of Utrecht, Utrecht, The Netherlands

Department of Psychiatry, Icahn School of Medicine, New York, NY, USA

Mental Illness Research, Education and Clinical Center (MIRECC), James J Peters VA Medical Center, Bronx, NY, USA
e-mail: lotje.dewitte@mssm.edu

R. Bransfield
Department of Psychiatry, Rutgers-Robert Wood Johnson Medical School, Piscataway, NJ, USA

P. P. De Deyn
Department of Neurology, Alzheimer Center Groningen, University Medical Center Groningen, University of Groningen, Groningen, The Netherlands

Laboratory of Neurochemistry and Behavior, Department of Biomedical Sciences, Institute Born-Bunge, University of Antwerp, Born Bunge Foundation, Antwerp (Wilrijk), Belgium
e-mail: p.p.de.deyn@umcg.nl

R. A. J. O. Dierckx et al. (eds.), *PET and SPECT in Neurology*,
https://doi.org/10.1007/978-3-030-53168-3_32

32.3.3 Microglia Activation: Imaging with [11C]PK11195 880
32.4 Microglia Activation in Neuropsychiatric Disorders 881
32.4.1 Neurodegenerative Disorders 881
32.4.2 Vitamin Deficiency 883
32.4.3 Encephalopathy 883
32.4.4 Psychiatric Disorders 883
32.5 Microglia Activation in Neuroinfectious Disorders 884
32.5.1 Herpes Simplex Virus Infection 884
32.5.2 HIV 885
32.5.3 Neuroborreliosis 885
32.6 Neuroinfection Imaging 886
32.7 Clinical Note 887
32.8 Conclusion 887
References 887

Abstract

The central nervous system (CNS) is an immunoprivileged location for the possible sequestration of latent infections. The presence of pathogens may be involved in the etiology of neuropsychiatric diseases by inducing classical inflammatory responses, hypersensitivity, cellular toxicity, or direct alteration of cellular processes. Infection, persistence, and activation of microbes in the brain are not easy to assess in vivo, and the relation with clinical disease is very difficult to prove. An elegant way to determine an inflammatory response in the brain in vivo is by molecular imaging of microglia activation with [11C]PK11195 and other radiopharmaceuticals that target the translocator protein (TSPO). In this chapter, we summarize the neuroimaging studies that target the TSPO in patients with neuropsychiatric diseases, and we propose positron emission tomography (PET) imaging with radiopharmaceuticals that target the metabolism of infectious agents directly.

32.1 General Introduction

During World War I, an epidemic of psychiatric disorders with a probable infectious origin occurred. This epidemic of "encephalitis lethargica" was meticulously described by Constantin von Economo, regarding the psychiatric, neurological, epidemiological, and postmortem microscopical phenomena of the disease (Dickman 2001; Triarhou 2006). In those days, 50% or more of the patients referred to mental hospitals appeared to have suffered from the epidemic (Economo 1929). Many patients subsequently acquired neurological symptoms such as parkinsonism, oculogyric crises, and lethargy. The inflammatory changes in the brain parenchyma (particularly in the midbrain) were also meticulously described. Von Economo showed that transmission of brain specimens of patients to small animals caused similar neuropathological and behavioral changes. The agent of transmission was nonfilterable; it passed filters that blocked the transmission of the bacterial diseases known at that time.

The dementia paralytica of the insane (DPI) is another example of an infectious neuropsychiatric disease. DPI is caused by the sexually transmitted spirochete *Treponema pallidum*. *T. pallidum* is a genus in the family of Spirochaetaceae. CNS infection (neurospirochetosis) was designated "the great imitator" of psychiatric disorders, and sequelae of obsessive–compulsive behavior, classical manic episodes, and paranoid delusional psychoses were frequent. Paralytic death ensued in nearly all patients suffering from DPI. A treatment was discovered by the 1927 Nobel laureate (Physiology and Medicine) Wagner Jauregg, which involved transmission of the *Plasmodium falciparum* parasite to the patient, inducing recurring malaria fevers. The working mechanism of fever therapy is probably immune modulation to eradicate the spirochete (Whitrow 1990). The therapy was lifesaving, and quite some patients regained full functioning after the therapy, although not all recovered, and in some, recovery was observed only during a certain period of time.

Borrelia genera are structurally similar to *Treponema* genera and both are part of the family of Spirochaetaceae. In contrast to sexual transmission of *Treponema* species, the *Borrelia* species is predominantly transmitted by ticks. *Borrelia burgdorferi* infections present as an erythema migrans skin lesion, and incidence of this primary lesions is increasing in many endemic areas, for example, in the Netherlands. There is some evidence that transmission of the spirochete by ticks is increasing and transmission of the spirochete to the brain of the human host is becoming more prevalent (Hildenbrand et al. 2009; Steere et al. 2004). Similar to DPI and encephalitis lethargica, a variety of symptoms can occur associated with neuroborreliosis (Markeljević et al. 2011; Almodovar et al. 2012; Miklossy 2008).

The degree of involvement of infections in neuropsychiatric diseases is currently a subject of debate. The difficulty in clarifying this issue is mainly due to the scarcity of methods to directly detect pathogens in the CNS in vivo. In comparison to peripheral tissue, biopsies of the brain are contraindicated presently and performed only in extremely rare case such as brain tumors. Infection of the brain parenchyma is not necessarily associated with detection of the pathogen in the cerebrospinal fluid (CSF). PET imaging may offer a solution to pursue infectious inflammatory changes in the living brain parenchyma. Uptake of the radiopharmaceutical [^{11}C]PK11195 is indicative of brain inflammation, and the number of studies with this imaging agent and second-generation radiopharmaceuticals targeting neuroinflammation is growing. Radiopharmaceuticals derived from antibiotics are available for imaging purposes, but not yet applied broadly for infection imaging. We propose a role for radiopharmaceuticals derived from—among others—nitroimidazole antibiotics as promising tools for imaging of infection of the CNS.

32.2 Establishment of CNS Infection

This first paragraph discusses the mechanisms involved in the dissemination of the pathogens to the brain and the mechanisms involved in the establishment of latent infection.

32.2.1 Neuroinvasive Species

The brain is often viewed as a sterile organ unless incidentally infected leading to diseases such as encephalitis. However, it is now known that the brain parenchyma is not pathogen free.

Using sensitive molecular techniques, it has been shown that respiratory viruses, herpes simplex viruses (HSV), *Borrelia* spirochetes, and many other pathogens can be present in brain tissue postmortem (Lakeman and Whitley 1995; Schmutzhard 2001).

Neuroinvasive microbes are microbes that can enter the CNS easily. Some microbes primarily reside within the CNS; others only incidentally invade the CNS. *Neurovirulent* microbes are pathogens that can cause diseases of the CNS. These include diseases established by direct infection of the CNS, such as viral and bacterial encephalitis, neuroborreliosis, and neurosyphilis, but also subacute sclerosing panencephalitis after measles infection. Furthermore, it is thought that the interaction between neurovirulent pathogens and the host may be involved in the pathophysiology of various neuropsychiatric diseases, such as Alzheimer's disease, depression, and schizophrenia.

Several classes of neurovirulent microbes have been described and include:

1. Viruses: human herpes viruses (herpes simplex virus, cytomegalovirus, etc.), polyomaviruses (JC/BK virus), flaviviruses (West Nile virus, Japanese encephalitis virus, etc.), human retroviruses (HIV, etc.), measles virus, influenza virus, rabies virus, and poliovirus.
2. Bacteria: *Treponema pallidum*, *B. burgdorferi*.
3. Parasites: *P. falciparum*, *Toxoplasma gondii*.
4. Fungi: *Cryptococcus neoformans*.
5. Human endogenous retroviruses: These viruses are not "real" neuroinvasive microbes, but are retroviruses that have infected the germline in the recent or ancient past and integrated their viral sequences in the human genome. In this way, the viral sequences also reach the CNS. These sequences have been implicated in various neuropsychiatric diseases, such as schizophrenia (Yolken et al. 2000) and multiple sclerosis (Anderton et al. 2011).

32.2.2 Neuroinvasion Mechanisms

Due to the blood–brain barrier (BBB), the brain is relatively protected from invading pathogens. However, microbes have evolved various strategies to invade the brain:

1. Although the BBB provides a barrier to most pathogens, some pathogens can invade the brain by this hematogenous route. The pathogen may penetrate the endothelium directly (transcytosis) or may first produce a productive infection in the endothelial cells. High levels of viremia/bacteremia are thought to be required

for direct spread via the hematogenous route; however, as a result of systemic infection, the permeability of the BBB can be increased (Moriarty et al. 2008).
2. In addition, certain pathogens can spread from the circulation into the brain via infiltration of leukocytes. HIV is thought to hide in leukocytes to spread throughout the body, including the CNS by passing the BBB to cause neuro-HIV ("Trojan horse") (Lindl et al. 2010).
3. The olfactory route is used by several pathogens to invade the brain. After a local infection in the skin or nasal mucosa, these pathogens spread by the olfactory nerve or by the perineuronal (cerebrospinal fluid) route to the CNS (Mori et al. 2005; Sips et al. 2011). Viruses also use other peripheral and cranial nerves for retrograde axonal transport to invade the CNS. For example, HSV uses the axons to the trigeminal nucleus to spread to the CNS (Theil et al. 2004).

32.2.3 Pathogen Reservoirs

Some microbes that have gained access to the brain transform into a state of relative inactivity. Only proteins are expressed that keep the microbe viable, but present in a latent state. Microbes may reside intracellularly (with, e.g., DNA as epigenome in the nucleus of the cell) or extracellularly (e.g., cysts of fungi), creating a reservoir, from which reactivations may occur. Various reservoirs in the brain are available for neuroinvasive pathogens:

1. HIV dementia is a disease, in which brain macrophages are loaded with viral RNA (Alexaki et al. 2008), but the virus often replicates at low speed.
2. HSV is "resting" in a latent form in many individuals without overt clinical symptoms in neurons of the sensory ganglia (especially trigeminal) (Theil et al. 2003). A continuous immune surveillance with cytotoxic-type T cells is necessary to keep the virus in latency and prevent it from replicating and disseminating (Posavad et al. 2003; Derfuss et al. 2007). Interestingly, HSV DNA can not only be detected in the trigeminal ganglion but can also be detected by PCR in the brain (Gordon et al. 1996). Intraparenchymal replication in HSV encephalitis predominantly affects the temporal lobes, cortex, and hippocampus, inducing bizarre behavior, language impairment, headache, paralysis, and memory deficits that can partly remain after resolution of the infection (Kapur et al. 1994).
3. It is clear that spirochetes of the *Borrelia* species can be present but latent in the brain. However, the reservoir is still unknown. A variety of possibilities exist: intracellular or extracellular and in defective cyst form or in replication competent spirochetal form (Miklossy et al. 2008).

32.2.4 Response to Pathogens

Although we now know that neurons can be partly regenerated after CNS injury, the CNS environment is in an anti-inflammatory state compared to other organs to

protect against immune-mediated brain damage. The severity of infection, virulence factors of the microbe, but also host factors are thought to play an important role in directing the level and nature of how the immune system responds. Microbial invasion may be followed by an absence of a response, mild to severe classical inflammatory responses, but also hypersensitivity reactions and direct cellular toxicity. Since most neuropsychiatric diseases are at least partly dependent on genetic factors, it is likely that the infectious disease phenotype is modified by genetic factors, both of the host and the pathogens. Examples of responses to various neurotropic pathogens are as follows:

1. Infection of the CNS by HIV may lead to an inflammatory response, including production of cytokines, excitotoxic neurotransmitters, and oxygen radicals (Lindl et al. 2010). Combined administration of various therapeutic drugs may be necessary to acquire a good response of patients with neuro-HIV.
2. Despite the fact that HSV is present in a latent state in the majority of people, HSV encephalitis is very rare. It is thought that the virus is kept under control and trapped in the neuron by local T cells and macrophage-like cells. This cellular response occurs in the ganglion to prevent the virus from replicating and disseminating. Interesting is the fact that psychotropic drugs, such as lithium, may also improve resistance against HSV infections (Amsterdam 1990). Probably the immune-modulating properties of psychotropic drugs explain these favorable actions on viral diseases (Lieb 2002).
3. The immune response to spirochetal diseases is noteworthy. Seronegativity in serum and cerebrospinal fluid (CSF) does not rule out neurospirochetosis and can lead to a fatal outcome (Oksi et al. 1996). Immune responses in the periphery may also be absent in *Treponema pallidum* infection while the spirochete is actively moving within the ocular tissue (Smith and Israel 1967). Thus, immune responses toward spirochetes in the CNS are either restricted to the CNS or actively suppressed in the periphery.

32.3 Inflammatory Response to CNS Infection

This paragraph discusses the specialized cells in the brain that respond to the dissemination and establishment of infection of pathogens. Functions of cells in the blood–brain barrier, in the circumventricular organs, and in the brain, parenchyma shall be addressed. Immune response is orchestrated by microglia and the activation of microglia can be imaged with [^{11}C]PK11195.

32.3.1 Functions of the Blood–Brain Barrier

The brain parenchyma is protected from direct influx of compounds from the blood by the blood–brain barrier (BBB). The BBB is impermeable for diffusion of polar molecules such as cytokines and immune globulins due to the presence of tight

junctions between the endothelial cells of the capillaries (Pardridge 1999). However, specific carriers can transport some molecules across the BBB. Carrier-mediated transport of polar molecules is heavily dependent on the expression of specific carriers for solutes in the blood (Kusuhara and Sugiyama 2005). Transcytosis (penetration through the cell, by phagocytosis and intracellular transport and exocytosis) is an "emergent" specialized property of the BBB (Hervé et al. 2008), modified by mostly unknown factors. The BBB creates a unique immune milieu in the brain parenchyma, dependent on the immune molecules and cells that are allowed to traverse the BBB.

An exception to the tightly controlled transport from the circulation to the CNS is the circumventricular organ. In the circumventricular organs of the brain, the capillary endothelium is fenestrated, giving direct access of cytokines and immune globulins into the parenchyma (although then barred by the next barrier, the basement membrane), and only in these regions can peripheral proteins and microbes enter the parenchyma directly (Sisó et al. 2010). Specialized "leaky barriers" in the hypothalamus provide the possibility to specifically sense blood milieu and CSF milieu (Rodríguez et al. 2010).

32.3.2 Functions of Microglia

Early during embryogenesis, myeloid cells of the macrophage/monocyte lineage seed the CNS, where they find residency (Monier et al. 2007). In the brain, these cells differentiate into microglia. The roles of microglia have only partly been unraveled. Microglia have important functions in neurodevelopment, neuroinflammation, and CNS repair. During embryogenesis, microglia are essential for neuronal synaptogenesis and neurogenesis (Tremblay and Majewska 2011). In adulthood, these trophic functions probably continue, and microglia are activated in regions of the brain that are experiencing remodeling, for example, after peripheral nerve lesions (Moneta et al. 1993). Recent murine studies demonstrated the importance of functional microglia in synaptic pruning (Paolicelli et al. 2011).

Microglia can reside in both resting and more activated state. Activated microglia may take part in the following:

1. Rescuing response
2. Response to remove debris
3. Toxic response (release of nitric oxide (NO) by microglia is detrimental)

A local response by microglia is not necessarily mirrored by changes in serum or cerebrospinal fluid, because of the BBB and brain–CSF barrier. It may be safely assumed that in the early prodromal phase of a subtle infectious process in the brain, no detectable immune changes occur in the periphery. The BBB restricts the diffusion into plasma, and the brain–CSF barrier restricts diffusion into the CSF of cytokines as potential markers of inflammation of the brain parenchyma.

Therefore, in vivo imaging techniques for inflammation are needed that combine the property of effective penetration through the BBB and of sufficient binding to microglia in the brain parenchyma. In this chapter, we will focus on the most applied radiopharmaceutical for detecting microglia activation, [^{11}C]PK11195.

32.3.3 Microglia Activation: Imaging with [^{11}C]PK11195

Radiopharmaceuticals—when sufficiently lipophilic and not a substrate for efflux pumps—easily penetrate the lipid biomembranes of the BBB. To image inflammation, the intermediately lipophilic isoquinolone PK11195 is available (log $P = 3.4$) among others (Doorduin et al. 2009b). This compound binds to the translocator protein (TSPO) of mitochondria in activated microglia cells and other immune cells and increases during inflammation (Cosenza-Nashat et al. 2009). In noninflammatory conditions, expression in brain is low, thereby offering "contrast" between inflamed and noninflamed tissues. Microglia activation as imaged with TSPO ligand is usually designated as "neuroinflammation." However, neuroinflammation reflects the sum of activation of glia, microglia, and perivascular macrophages in the brain, increasing numbers of glia, microglia, and perivascular macrophages (by influx from the periphery or cell division). All of these activations are reflected by increased expression of TSPO and subsequently increased trapping of [^{11}C]PK11195 in tissue, and the microglia provide the major uptake of [^{11}C]PK11195 (Cosenza-Nashat et al. 2009). In the last years, many radiopharmaceuticals alternative to [^{11}C]PK11195 were developed and applied in human research. Drawbacks of the alternatives are that binding is dependent on frequent gene polymorphisms in man that prevent reliable binding of the radiopharmaceutical in all carriers of the polymorphism (Song 2019). Clinical relevance of the carrier is not known and selecting only noncarrier for imaging hampers conclusions from the studies. The most classic way of neuroinflammation imaging with [^{11}C]PK11195 and arterial input normalization—by coregistration of arterial [^{11}C]PK11195 concentration during the scanning procedure—is still the most robust (Plavén-Sigray et al. 2018). Despite the promises of new radiopharmaceuticals, major caveats appeared and [^{11}C]PK11195 remains the most reliable (Best et al. 2019). Therefore, we limited the description of studies on neuroinflammation in brain diseases to [^{11}C]PK11195 imaging.

Activated microglia are either involved in proinflammatory responses, such as production of cytokines and cytotoxic compounds and NO, or involved in anti-inflammatory responses and excretion of growth factors such as brain-derived neurotropic factor (BDNF). Activated microglia can be divided in M1 and M2 phenotypes with inflammatory switch functions in the brain (Durafourt et al. 2012). Microglia with the M1 phenotype have in vitro destructive capacities as opposed to M2 phenotype microglia, which are protective/anti-inflammatory. To our knowledge, no radiopharmaceuticals have as yet been developed to target these receptors specifically.

32.4 Microglia Activation in Neuropsychiatric Disorders

Microglia activation imaging with [^{11}C]PK11195 has been helpful in gaining knowledge of the mechanisms of many neuropsychiatric disorders. The association between loss of function of brain regions and elevation of [^{11}C]PK11195 uptake supports the role of inflammation in the disease. The inflammation may be related to tissue loss and debris removal, neuroplasticity/remodeling, autoimmunity, presence of toxic metabolites, hypovitaminosis, or antimicrobial response. This paragraph summarizes the results of [^{11}C]PK11195 imaging studies in neuropsychiatric disorders in general, without direct proof of a specific infectious origin. In the next paragraph, the studies with [^{11}C]PK11195 in patients suffering from infectious disorders are summarized.

32.4.1 Neurodegenerative Disorders

It is well known that in many neurodegenerative diseases, inflammation is part of the pathophysiological process. Microglial activation has, for example, been found in gray matter of postmortem brain from patients with multiple sclerosis (MS). A study shows that MS in patients with active disease is reflected by increased [^{11}C]PK11195 uptake in gray matter of regions that correspond to disease symptomatology of individual patients (Politis et al. 2012). More recently, two studies show enhanced uptake in MS lesions that reduce 12.3% upon treatment with fingolimod (Sucksdorff et al. 2017) and 26.8% on natalizumab (Kaunzner et al. 2017). Also, in Parkinson's disease, with destruction of neurons in the substantia nigra and projecting areas such as striatum, increased uptake was found in basal ganglia, pons, and cortical regions. Elevated [^{11}C]PK11195 uptake was present chronically and not associated with loss of dopaminergic neurons nor with clinical symptoms (Gerhard et al. 2006). In Huntington's disease, caused by accumulation of huntingtin in neurons, the striatum is affected in the inflammatory process. The accumulation of [^{11}C]PK11195 is significantly associated with the number of CAG repeats and symptom severity (Pavese et al. 2006). Asymptomatic carriers of the CAG repeat already show profound microglial activation (and loss of dopaminergic terminals) which is correlated to the number of CAG repeats of the huntingtin gene (Tai et al. 2007). In corticobasal degeneration (CBD), the inflammatory changes also involve striatum, one of the major structures involved in the neurodegenerative process (Gerhard et al. 2004). The diagnosis of upper motor neuron disease is difficult to confirm by clinical investigation. [^{11}C]PK11195 PET imaging may help confirm the diagnosis by showing inflammatory lesions in specific areas of the cerebral cortex that correspond to the clinical signs (Turner et al. 2005). Also, in amyotrophic lateral sclerosis, the uptake of [^{11}C]PK11195 is increased in the regions of the brain that are responsible for clinical symptoms in patients and predictive of function loss (Turner et al. 2004). In the first microglia PET study in Alzheimer's disease patients, increases of [^{11}C]PK11195 were found in the parietotemporal and cingulate cortex,

and also the entorhinal cortex was affected (Cagnin et al. 2001a, b). Cortical involvement of neuroinflammation was confirmed in a later study showing the frontal, temporoparietal, and cingulated regions affected. A positive correlation between cognitive impairment (MMSE) and microglia activation was elegantly shown (Edison et al. 2008). In other studies, subtle microglia activation was found in occipital cortex (Schuitemaker et al. 2013). In this and another study (Wiley et al. 2009), the patients with mild cognitive impairment showed no significant elevation of [^{11}C]PK11195 binding. A study involving consecutive imaging with the amyloid radiopharmaceutical [^{11}C]PiB (Pittsburg compound) for amyloid foci and [^{11}C]PK11195 for neuroinflammation showed that specifically the amyloid lesions in early MCI were subject to inflammation. An increase of the average binding potential by 0.18 was noted in the amyloid foci (Parbo et al. 2017). Later, in the transition toward full-blown Alzheimer Disease, the association between amyloid accumulation and neuroinflammation is less clear (Chaney et al. 2019). Therefore, the neuroinflammation within PiB positive amyloid plaques provides an early denominator of the MCI phase, and may reflect the early or triggering pathophysiology of Alzheimer disease progression.

In neurodegenerative diseases, microglia activation specifically in the afflicted brain regions is a more common finding. The localization of inflammatory lesions corresponds to the localization of the disease process: motor cortex in ALS, dispersed focal inflammatory sites in MS, parietotemporal lesions in Alzheimer's disease, alterations in the basal ganglia in Parkinson's disease, Huntington's disease, and corticobasal degeneration. The timing of neuroinflammation in these diseases appears to be dependent on the stage of the disease. In Parkinson's disease, the microglia activation occurs early in the disease, but does not correspond further to clinical stage. In Huntington's disease, neuroinflammatory changes occur very early, already in the symptom-free phase of aberrant gene carriers. In Alzheimer's disease, microglia activation appears as a more subtle and late general phenomenon, but focal in the MCI stage.

These examples illustrate that the imaging studies did not resolve the exact role of the microglia response, which is probably very dependent on the underlying pathophysiology, which may be autoimmune/infectious/toxic/genetic, or combinations of these factors. For example, the late response in Alzheimer's disease might correspond to tissue remodeling and clearing of cellular debris, while in the early MCI stage microglia activation, that is only detectable in the PiB positive amyloid foci, might represent a protective, even anti-inflammatory response. This focal tracer accumulation might, for example, represent a protective response in the early phase, which precedes conversion to full-blown dementia and could predict which patients will and will not convert to full-blown Alzheimer dementia. The results of neuroinflammation scanning in Huntington's carriers is also illustrative. In these patients, microglia activation is found very early, already in the symptom-free phase. In Huntington's disease, microglia activation might also represent a protective/adaptive response opposing toxic accumulation of huntingtin in neurons. The major limitation of [^{11}C]PK11195 imaging is that it does not differentiate between protective and detrimental activities of microglia. Development of specific

radiopharmaceuticals that target only M1 (destructive) or M2 (protective) microglia may resolve this issue.

32.4.2 Vitamin Deficiency

Thiamine (vitamin B1) deficiency causes increased uptake of [^{3}H]PK11195 in autoradiography slices of specific nuclei (Leong et al. 1994) associated with the human syndrome of Korsakoff's dementia. Microglia activation is a core feature of thiamine-deficiency induced brain damage (Wang and Hazell 2010). Immediate supply of high-dose thiamine partially restores the histological changes of microglia and neurons in vulnerable nuclei (Ke et al. 2003). To our knowledge, no human studies have been performed studying in vivo microglia activation with positron emission tomography (PET) in thiamine deficiency and Korsakoff syndrome in man.

32.4.3 Encephalopathy

Liver infections of hepatitis C virus (HCV) may induce encephalopathy with emotional disorders and cognitive decline. The mechanism of this encephalopathic syndrome is unknown. Peripheral accumulation of ammonia (in cirrhosis), effect of peripheral cytokines released by the infection in the liver, and direct infection of the brain parenchyma with HCV are potential mechanisms. In vivo imaging with [^{11}C]PK11195 showed an increased binding in the caudate nucleus (Grover et al. 2012). This binding was associated with impaired metabolism (magnetic resonance spectroscopy, choline–creatine ratio increase) and impaired cognition, as was also shown in a more recent study (Pflugrad et al. 2016). HCV infection of the brain might be causing these metabolic and inflammatory changes.

Traumatic brain injury may also induce a prolonged encephalopathy associated with neuroinflammation. Prolonged activation of microglia in the thalamus was shown to persist for years after brain injury in some patients. Microglia activation is associated with ongoing suffering from encephalopathy in these subjects (Ramlackhansingh et al. 2011).

32.4.4 Psychiatric Disorders

In major psychiatric disorders, such as schizophrenia and depression, many studies showed reduction of hippocampal volume. In schizophrenia, hippocampal volume reduction occurs quite early in the disease, already before the occurrence of psychosis (Hurlemann et al. 2008). In major depression, hippocampal volume reductions are associated with recurrence of depressions (MacQueen et al. 2003). Interestingly, the hippocampus shows elevated uptake of [^{11}C]PK11195 in patients during psychotic episodes (Doorduin et al. 2009a), and uptake is insignificantly elevated in patients with resolved psychosis (Van Berckel et al. 2008). These

studies were most reliable, because they employed an arterial input function for determination of specific binding of [^{11}C]PK11195 to the brain regions of interest. Reduction of hippocampal volume in patients with schizophrenia probably occurs during or soon after a psychosis and is detectable in prospective magnetic resonance imaging (MRI) studies. This may imply that the hippocampus is especially prone to volume reductions during the psychotic phase of schizophrenia, and this vulnerability is reflected by neuroinflammation. Regrettably, more recent studies (Holmes et al. 2016; Di Biase et al. 2017) used the reference tissue model, which compares the specific binding of [^{11}C]PK11195 to the region of interest with binding to cerebellar tissue, which is not neutral, not by definition free from inflammation and therefore prone to more variation than arterial input. The question in which stage—in our opinion during psychotic symptom phase with active inflammation—hippocampal volume reduction takes place in the disease process, is therefore not completely resolved yet. In patients with major depression, microglia activation appears to be globally occurring in brain, and is not limited to the hippocampus as we found in psychotic patients (Doorduin et al. 2009a), and in bipolar disorder patients (Haarman et al. 2014). Interesting results from [^{11}C]PK11195 study in depression is that microglia activation was limited to the patients with suicidal thought, implicating a neuroinflammatory component to suicidality (Holmes et al. 2018).

32.5 Microglia Activation in Neuroinfectious Disorders

Very little research is performed on imaging of infectious diseases directly and also studies with neuroinflammation imaging in patients during infection are scarce. This is peculiar, because PET imaging of neuroinflammation is relatively noninvasive and may support the diagnostic process of encephalitis before CSF alterations are found. Robust PK11195 imaging has some disadvantages, for example, arterial input necessity, and elaborate data analysis (cluster analysis) when the input function is not used. In this chapter, we will show some pioneering studies on neuroinflammation in the herpes encephalitis model and some research in HIV patients and suggest to apply [^{11}C]PK11195 imaging in the diagnosis of neuroborreliosis. Despite the disadvantages of PK11195, we did not yet succeed in finding a better tracer for neuroinflammation imaging of infection (Doorduin et al. 2009b, 2010).

32.5.1 Herpes Simplex Virus Infection

Herpes simplex virus encephalitis (HSE) is a classic example of an infection of the brain with a major impact on human behavior, emotion, and cognition. HSV is a common pathogen in man, is known to produce bizarre behavioral disturbances after brain infection, and can be diagnosed reliably with the detection of HSV antibodies or DNA in CSF. We used an HSE model in rats and studied changes in

[^{11}C]PK11195 trapping. We showed a signal of neuroinflammation in the affected areas, with highest signal at the entrance site of infection (olfactory bulbs, in olfactory route infection). Interestingly, also in the midbrain nuclei, a signal was found: Possibly the infection of this locus explains part of the behavioral changes, such as manic-like behavior in the open field in these rats. Interestingly, after administration of antipsychotics, the manic-like behavior and the neuroinflammatory changes in the brain were attenuated (Doorduin 2010).

HSE in humans is rare, and to our knowledge only one study with [^{11}C]PK11195 imaging has been performed. In this study, predominantly the temporal lobe and the hippocampus were affected. A follow-up MRI after 1 year clearly showed disappearance of hippocampus tissue in the inflamed area (Cagnin et al. 2001a). Microglia activation might reflect an adaptive response of the host after infection that results in the removal of dysfunctional neurons and circuitry.

32.5.2 HIV

In primate models of neuroAIDS, the retention of [^{11}C]PK11195 was proportional to the number of activated macrophages/microglia in the brain (Venneti et al. 2008). Two early studies in patients with HIV in comparison with healthy controls were performed with [^{11}C]PK11195 and yielded different results. In one study (Wiley et al. 2006), no difference in brain uptake was found between HIV patients and healthy controls. In the other study, a significantly elevated uptake of [^{11}C]PK11195 was found in five regions in the brain of HIV dementia patients as compared to healthy controls (Hammoud et al. 2005). Further research of microglia activation in HIV patients with [^{11}C]DPA-713 as TSPO tracer showed that microglia activation is related to dementia signs of the disease (Rubin et al. 2018).

32.5.3 Neuroborreliosis

It is quite surprising that no [^{11}C]PK11195 studies have been performed in neuroborreliosis patients. A case study with brain stem involvement of the *Borrelia* infection shows a [^{18}F]FDG PET hot spot in the brain stem (Plotkin et al. 2005). This spot resolved after successful antibiotic treatment. After treatment of neuroborreliosis and residual cognitive symptoms, on perfusion single-photon emission computed tomography (SPECT) images, a left frontal hypometabolism was shown. The hypometabolism was normalized in patients that gained relief from the cognitive symptoms. In the patients that remained symptomatic, the hypometabolism did not resolve (Logigian et al. 1997). A study with [^{11}C]DPA-713 as TSPO tracer showed increased TSPO binding in eight brain regions in post-Lyme treatment symptomatic patients, excluding the patients with the low affinity T/T polymorphism of TSPO (Coughlin et al. 2018).

32.6 Neuroinfection Imaging

This section addresses an emerging technique for neuropsychiatric research: imaging of infectious pathogens in the CNS with PET in the living brain. Two examples of infection imaging in the CNS are briefly discussed. It is beyond the scope of this section to allude to all further efforts for development of tracers for infection. The examples in this chapter show how specific radiopharmaceuticals were chosen, derived from antiviral or antibiotic drugs.

Nucleoside analogs are used for treatment of viral infections. Examples are the thymidine analogs that are used in clinical practice to inhibit replication of herpes viruses. These compounds bind irreversibly to the herpes virus thymidine kinase (TK) enzyme and thereby inhibit the enzyme to phosphorylate thymidine, which is essential for DNA replication of virus in nondividing neuronal cells. Acyclovir and penciclovir are examples of these thymidine analogs. Fluorinated penciclovir ([^{18}F]FHBG) is available as a radiotracer to image presence of HSV-TK. Fluorinated ganciclovir ([^{18}F]FHPG) is an alternative for the detection of TK in tissues using PET imaging (De Vries et al. 2006). These compounds have been successfully applied to determine efficacious gene therapy (insertion of TK gene in solid tumors for subsequent killing with acyclovir). We also showed that HSV-TK imaging was feasible in a rat model of HSE (Buursma et al. 2005). We showed that in patients with schizophrenia, uptake of [^{18}F]FHBG was significantly higher in the temporal lobe of patients with severe symptoms of psychosis (Doorduin 2010). Nucleoside radiopharmaceuticals are polar compounds and penetrate the intact BBB rather slowly, and the absolute uptake of [^{18}F]FHBG was very low.

Antibiotics could be used as base material for synthesis of radiopharmaceuticals aimed at detecting bacterial infections. The advantages of some antibiotics are their lipophilic character and easy penetration of the BBB. Interesting compounds to image bacterial infections might be [^{18}F]FMISO or [^{18}F]FAZA. These radiopharmaceuticals are derived from the antibiotic misonidazole and azomycin, respectively, and belong to the group of nitroimidazoles. Nitroimidazoles are active against a broad spectrum of gram-negative bacteria. Therefore, nitroimidazole accumulation may be an indicator of infection of all sensitive microbes. Because[^{18}F]FMISO is trapped in the mitochondrial electron transport chain in the host during conditions of hypoxia, [^{18}F]FMISO is in use as a hypoxia imaging radiopharmaceutical (Lee and Scott 2007).] [^{18}F]FMISO infection imaging has been described in a study with patients experiencing periodontal spirochetal infections (Liu et al. 1996) and [^{18}F]FAZA imaging in Echinococcus infections (Rolle et al. 2015). The extent of accumulation of [^{18}F]FMISO and [^{18}F]FAZA in infected pockets may reflect infectious burden. Nitroimidazole imaging has also been suggested to be promising in assessing the number of bacilli in tuberculosis granuloma (Ankrah et al. 2016).

It is a challenge with profound opportunities to study presence of viruses or bacteria in the CNS with specific radiopharmaceuticals. The nucleosides [^{18}F]FHPG and [^{18}F]FHBG and the nitroimidazoles [^{18}F]FMISO and [^{18}F]FAZA are promising probes to elucidate if specific neuropsychiatric diseases might have an infectious cause.

32.7 Clinical Note

If a clinician is confronted with a patient experiencing a neuropsychiatric syndrome of potential infectious origin, and a lesion on brain MRI does not discriminate between infection/malignancy and neurodegenerative disorders, PET imaging may already be useful. [^{11}C]PK11195 imaging has been performed in herpes encephalitis patients (Cagnin et al. 2001a). Although it is not feasible to apply PET imaging in the acute phase of the disease, it could be used to demonstrate ongoing inflammation and necessitate extended prescription of antiviral medication.

Infection imaging is used in clinical practice by infusing labeled leucocytes or by using an inflammation analysis algorithm for [^{18}F]FDG. PET imaging is of limited use in parenchymal brain infections because resting glucose metabolism in brain is high, which limits the contrast between inflamed tissue and surrounding healthy tissue. The clinician could regard a whole-body inflammation [^{18}F]FDG scan, as this may reveal any peripheral infectious site which disseminates, for example, to a brain abscess (Haroon et al. 2012). The pattern of distribution of peripheral foci of [^{18}F]FDG may give a cue to the type of infection. For example, if neuropsychiatric symptoms are associated with joint pains and occur in patients with an infection history of tick bite and the patient is seropositive for Borrelia species, then one might expect that [^{18}F]FDG whole body scans reveal hot spots in the affected joints.

32.8 Conclusion

Microglia activation occurs in the brains of patients suffering from schizophrenia, Parkinson's disease, Alzheimer's disease, and Korsakoff's dementia. It is very important to clarify the causes of this inflammatory process, and this requires intelligent use of available molecular imaging techniques. The brain is quite accessible for pathogens that acquire latency in the brain. Examples are HSV and *B. burgdorferi*. Pathogens in the brain are a neglected element in the etiopathogenesis of neuropsychiatric disorders, since access to the brain for biopsy is normally not possible. The application of PET imaging with nucleoside and nitroimidazole radiopharmaceuticals to determine virus and spirochete infection of the brain is a logical and promising avenue for further research.

Acknowledgments The intellectual and financial support from the Stanley Medical Research Institute and the Virgo consortium, funded by the Dutch Government project number FES0908 and the Netherlands Genomics Initiative (NGI) project number 050-060-452, is kindly acknowledged.

References

Alexaki A, Liu Y, Wigdahl B (2008) Cellular reservoirs of HIV-1 and their role in viral persistence. Curr HIV Res 6(5):388–400

Almodovar JL, Hehir MK, Nicholson KA, Stommel EW (2012) Acute bilateral painless radiculitis with abnormal Borrelia burgdorferi immunoblot. J Clin Neuromuscul Dis 14(2):75–77. https://doi.org/10.1097/CND.0b013e318279d634

Amsterdam J (1990) A possible antiviral action of lithium carbonate in herpes simplex virus infections. Biol Psychiatry 27(4):447–453. https://doi.org/10.1016/0006-3223(90)90555-G

Anderton JA, Bose S, Vockerodt M, Vrzalikova K, Wei W, Kuo M, Helin K et al (2011) The H3K27me3 demethylase, KDM6B, is induced by Epstein-Barr virus and over-expressed in Hodgkin's lymphoma. Oncogene 30(17):2037–2043. https://doi.org/10.1038/onc.2010.579

Ankrah AO, Glaudemans AWJM, Sathekge MM, Klein HC (2016) Imaging latent tuberculosis infection with radiolabeled nitroimidazoles. Clin Transl Imaging 4:157–159

Best L, Ghadery C, Pavese N, Tai YF, Strafella AP (2019) New and Old TSPO PET radioligands for imaging brain microglial activation in neurodegenerative disease. Curr Neurol Neurosci Rep 19(5):24. https://doi.org/10.1007/s11910-019-0934-y

Buursma AR, De Vries EFJ, Garssen J, Kegler D, Van Waarde A, Schirm J, Hospers GAP et al (2005) [18F]FHPG positron emission tomography for detection of herpes simplex virus (HSV) in experimental HSV encephalitis. J Virol 79(12):7721–7727. https://doi.org/10.1128/JVI.79.12.7721-7727.2005

Cagnin A, Myers R, Gunn RN, Lawrence AD, Stevens T, Kreutzberg GW, Jones T et al (2001a) In vivo visualization of activated glia by [11C] (R)-PK11195-PET following herpes encephalitis reveals projected neuronal damage beyond the primary focal lesion. Brain 124(Pt 10):2014–2027. http://www.ncbi.nlm.nih.gov/pubmed/11571219

Cagnin A, Brooks DJ, Kennedy AM, Gunn RN, Myers R, Turkheimer FE, Jones T et al (2001b) In-vivo measurement of activated microglia in dementia. Lancet 358(9280):461–467. https://doi.org/10.1016/S0140-6736(01)05625-2

Chaney A, Williams SR, Boutin H (2019) In vivo molecular imaging of neuroinflammation in Alzheimer's disease. J Neurochem 149(4):438–451. https://doi.org/10.1111/jnc.14615

Cosenza-Nashat M, Zhao M-L, Suh H-S, Morgan J, Natividad R, Morgello S, Lee SC (2009) Expression of the translocator protein of 18 kDa by microglia, macrophages and astrocytes based on immunohistochemical localization in abnormal human brain. Neuropathol Appl Neurobiol 35(3):306–328. https://doi.org/10.1111/j.1365-2990.2008.01006.x

Coughlin JM, Yang T, Rebman AW, Bechtold KT, Du Y, Mathews WB et al (2018) Imaging glial activation in patients with post-treatment Lyme disease symptoms: a pilot study using [11C]DPA-713 PET. J Neuroinflammation 15(1):346. https://doi.org/10.1186/s12974-018-1381-4

De Vries EFJ, Dierckx RA, Klein HC (2006) Nuclear imaging of inflammation in neurologic and psychiatric disorders. Curr Clin Pharmacol 1(3):229–242. http://www.ncbi.nlm.nih.gov/pubmed/18666748

Derfuss T, Segerer S, Herberger S, Sinicina I, Hüfner K, Ebelt K, Knaus H-G et al (2007) Presence of HSV-1 immediate early genes and clonally expanded T-cells with a memory effector phenotype in human trigeminal ganglia. Brain Pathol 17(4):389–398. https://doi.org/10.1111/j.1750-3639.2007.00088.x

Di Biase MA, Zalesky A, O'keefe G, Laskaris L, Baune BT, Weickert CS et al (2017) PET imaging of putative microglial activation in individuals at ultra-high risk for psychosis, recently diagnosed and chronically ill with schizophrenia. Transl Psychiatry 7(8):e1225. https://doi.org/10.1038/tp.2017.193

Dickman MS (2001) von Economo encephalitis. Arch Neurol 58(10):1696–1698. http://www.ncbi.nlm.nih.gov/pubmed/11594935

Doorduin J (2010) Herpes viruses and neuroinflammation: PET imaging and implication in schizophrenia. Dissertations, University of Groningen

Doorduin J, De Vries EFJ, Willemsen ATM, De Groot JC, Dierckx RA, Klein HC (2009a) Neuroinflammation in schizophrenia-related psychosis: a PET study. J Nucl Med 50(11):1801–1807. https://doi.org/10.2967/jnumed.109.066647

Doorduin J, Klein HC, Dierckx RA, James M, Kassiou M, De Vries EFJ (2009b) [11C]-DPA-713 and [18F]-DPA-714 as new PET tracers for TSPO: a comparison with [11C]-(R)-PK11195 in a rat model of herpes encephalitis. Mol Imaging Biol 11(6):386–398. https://doi.org/10.1007/s11307-009-0211-6

Doorduin J, Klein HC, De Jong JR, Dierckx RA, De Vries EFJ (2010) Evaluation of [11C]-DAA1106 for imaging and quantification of neuroinflammation in a rat model of herpes encephalitis. Nucl Med Biol 37(1):9–15. https://doi.org/10.1016/j.nucmedbio.2009.09.002

Durafourt BA, Moore CS, Zammit DA, Johnson TA, Zaguia F, Guiot M-C, Bar-Or A et al (2012) Comparison of polarization properties of human adult microglia and blood-derived macrophages. Glia 60(5):717–727. https://doi.org/10.1002/glia.22298

Economo C (1929) Die Encephalitis Lethargica, ihre Nachkrankheiten und ihre Behandlung. Engl J Med 201:708

Edison P, Archer HA, Gerhard A, Hinz R, Pavese N, Turkheimer FE, Hammers A et al (2008) Microglia, amyloid, and cognition in Alzheimer's disease: an [11C](R)PK11195-PET and [11C]PIB-PET study. Neurobiol Dis 32(3):412–419. https://doi.org/10.1016/j.nbd.2008.08.001

Gerhard A, Watts J, Trender-Gerhard I, Turkheimer F, Banati RB, Bhatia K, Brooks DJ (2004) In vivo imaging of microglial activation with [11C](R)-PK11195 PET in corticobasal degeneration. Mov Disord 19(10):1221–1226. https://doi.org/10.1002/mds.20162

Gerhard A, Trender-Gerhard I, Turkheimer F, Quinn NP, Bhatia KP, Brooks DJ (2006) In vivo imaging of microglial activation with [11C](R)-PK11195 PET in progressive supranuclear palsy. Mov Disord 21(1):89–93. https://doi.org/10.1002/mds.20668

Gordon L, McQuaid S, Cosby SL (1996) Detection of herpes simplex virus (types 1 and 2) and human herpesvirus 6 DNA in human brain tissue by polymerase chain reaction. Clin Diagn Virol 6(1):33–40. http://www.ncbi.nlm.nih.gov/pubmed/15566888

Grover VPB, Pavese N, Koh S-B, Wylezinska M, Saxby BK, Gerhard A, Forton DM et al (2012) Cerebral microglial activation in patients with hepatitis C: in vivo evidence of neuroinflammation. J Viral Hepat 19(2):e89–e96. https://doi.org/10.1111/j.1365-2893.2011.01510.x

Haarman BCMB, Riemersma-Van der Lek RF, de Groot JC, Ruhé HGE, Klein HC, Zandstra TE et al (2014) Neuroinflammation in bipolar disorder – a [(11)C]-(R)-PK11195 positron emission tomography study. Brain Behav Immun 40:219–225. https://doi.org/10.1016/j.bbi.2014.03.016

Hammoud DA, Endres CJ, Chander AR, Guilarte TR, Wong DF, Sacktor NC, McArthur JC et al (2005) Imaging glial cell activation with [11C]-R-PK11195 in patients with AIDS. J Neurovirol 11(4):346–355. https://doi.org/10.1080/13550280500187351

Haroon A, Zumla A, Bomanji J (2012) Role of fluorine 18 fluorodeoxyglucose positron emission tomography-computed tomography in focal and generalized infectious and inflammatory disorders. Clin Infect Dis 54(9):1333–1341. https://doi.org/10.1093/cid/cis193

Hervé F, Ghinea N, Scherrmann J-M (2008) CNS delivery via adsorptive transcytosis. AAPS J 10(3):455–472. https://doi.org/10.1208/s12248-008-9055-2

Hildenbrand P, Craven DE, Jones R, Nemeskal P (2009) Lyme neuroborreliosis: manifestations of a rapidly emerging zoonosis. AJNR Am J Neuroradiol 30(6):1079–1087. https://doi.org/10.3174/ajnr.A1579

Holmes SE, Hinz R, Drake RJ, Gregory CJ, Conen S, Matthews JC et al (2016) In vivo imaging of brain microglial activity in antipsychotic-free and medicated schizophrenia: a [11C](R)-PK11195 positron emission tomography study. Mol Psychiatry 21(12):1672–1679

Holmes SE, Hinz R, Conen S, Gregory CJ, Matthews JC, Anton-Rodriguez JM et al (2018) Elevated translocator protein in anterior cingulate in major depression and a role for inflammation in suicidal thinking: a positron emission tomography study. Biol Psychiatry 83(1):61–69. https://doi.org/10.1016/j.biopsych.2017.08.005

Hurlemann R, Jessen F, Wagner M, Frommann I, Ruhrmann S, Brockhaus A, Picker H et al (2008) Interrelated neuropsychological and anatomical evidence of hippocampal pathology in the at-risk mental state. Psychol Med 38(6):843–851. https://doi.org/10.1017/S0033291708003279

Kapur N, Barker S, Burrows EH, Ellison D, Brice J, Illis LS, Scholey K et al (1994) Herpes simplex encephalitis: long term magnetic resonance imaging and neuropsychological profile. J Neurol Neurosurg Psychiatry 57(11):1334–1342

Kaunzner UW, Kang Y, Monohan E, Kothari PJ, Nealon N, Perumal J et al (2017) Reduction of PK11195 uptake observed in multiple sclerosis lesions after natalizumab initiation. Mult Scler Relat Disord 15(6):27–33. https://doi.org/10.1016/j.msard.2017.04.008

Ke Z-J, DeGiorgio LA, Volpe BT, Gibson GE (2003) Reversal of thiamine deficiency-induced neurodegeneration. J Neuropathol Exp Neurol 62(2):195–207

Kusuhara H, Sugiyama Y (2005) Active efflux across the blood-brain barrier: role of the solute carrier family. NeuroRx 2(1):73–85. https://doi.org/10.1602/neurorx.2.1.73

Lakeman FD, Whitley RJ (1995) Diagnosis of herpes simplex encephalitis: application of polymerase chain reaction to cerebrospinal fluid from brain-biopsied patients and correlation with disease. J Infect Dis 171(4):857–863

Lee ST, Scott AM (2007) Hypoxia positron emission tomography imaging with 18f-fluoromisonidazole. Semin Nucl Med 37(6):451–461. https://doi.org/10.1053/j.semnuclmed.2007.07.001

Leong DK, Le O, Oliva L, Butterworth RF (1994) Increased densities of binding sites for the "peripheral-type" benzodiazepine receptor ligand [3H]PK11195 in vulnerable regions of the rat brain in thiamine deficiency encephalopathy. J Cereb Blood Flow Metab 14(1):100–105. https://doi.org/10.1038/jcbfm.1994.14

Lieb J (2002) Lithium and antidepressants: inhibiting eicosanoids, stimulating immunity, and defeating microorganisms. Med Hypotheses 59(4):429–432. https://doi.org/10.1016/S0306-9877(02)00148-2

Lindl KA, Marks DR, Kolson DL, Jordan-Sciutto KL (2010) HIV-associated neurocognitive disorder: pathogenesis and therapeutic opportunities. J Neuroimmune Pharmacol 5(3):294–309. https://doi.org/10.1007/s11481-010-9205-z

Liu RS, Chu LS, Yen SH, Chang CP, Chou KL, Wu LC, Chang CW et al (1996) Detection of anaerobic odontogenic infections by fluorine-18 fluoromisonidazole. Eur J Nucl Med 23(10):1384–1387. http://www.ncbi.nlm.nih.gov/pubmed/8781145

Logigian EL, Johnson KA, Kijewski MF, Kaplan RF, Becker JA, Jones KJ, Garada BM et al (1997) Reversible cerebral hypoperfusion in Lyme encephalopathy. Neurology 49(6):1661–1670. http://www.ncbi.nlm.nih.gov/pubmed/9409364

MacQueen GM, Campbell S, McEwen BS, Macdonald K, Amano S, Joffe RT, Nahmias C et al (2003) Course of illness, hippocampal function, and hippocampal volume in major depression. Proc Natl Acad Sci U S A 100(3):1387–1392. https://doi.org/10.1073/pnas.0337481100

Markeljević J, Sarac H, Rados M (2011) Tremor, seizures and psychosis as presenting symptoms in a patient with chronic lyme neuroborreliosis (LNB). Coll Antropol 35(Suppl 1):313–318. http://www.ncbi.nlm.nih.gov/pubmed/21648354

Miklossy J (2008) Biology and neuropathology of dementia in syphilis and Lyme disease. In: Duyckaerts C, Litvan I (eds) Handbook of clinical neurology (3rd series). Dementias, vol 89. Elsevier, Amsterdam, pp 825–844

Miklossy J, Kasas S, Zurn AD, McCall S, Yu S, McGeer PL (2008) Persisting atypical and cystic forms of Borrelia burgdorferi and local inflammation in Lyme neuroborreliosis. J Neuroinflammation 5:40. https://doi.org/10.1186/1742-2094-5-40

Moneta ME, Gehrmann J, Töpper R, Banati RB, Kreutzberg GW (1993) Cell adhesion molecule expression in the regenerating rat facial nucleus. J Neuroimmunol 45(1–2):203–206. http://www.ncbi.nlm.nih.gov/pubmed/8101190

Monier A, Adle-Biassette H, Delezoide A-L, Evrard P, Gressens P, Verney C (2007) Entry and distribution of microglial cells in human embryonic and fetal cerebral cortex. J Neuropathol Exp Neurol 66(5):372–382. https://doi.org/10.1097/nen.0b013e3180517b46

Mori I, Nishiyama Y, Yokochi T, Kimura Y (2005) Olfactory transmission of neurotropic viruses. J Neurovirol 11(2):129–137. https://doi.org/10.1080/13550280590922793

Moriarty TJ, Norman MU, Colarusso P, Bankhead T, Kubes P, Chaconas G (2008) Real-time high resolution 3D imaging of the Lyme disease spirochete adhering to and escaping from the vasculature of a living host. PLoS Pathog 4(6):e1000090. https://doi.org/10.1371/journal.ppat.1000090

Oksi J, Kalimo H, Marttila RJ, Marjamäki M, Sonninen P, Nikoskelainen J, Viljanen MK (1996) Inflammatory brain changes in Lyme borreliosis. A report on three patients and review of literature. Brain 119(Pt 6):2143–2154. http://www.ncbi.nlm.nih.gov/pubmed/9010017

Paolicelli RC, Bolasco G, Pagani F, Maggi L, Scianni M, Panzanelli P, Giustetto M et al (2011) Synaptic pruning by microglia is necessary for normal brain development. Science 333(6048):1456–1458. https://doi.org/10.1126/science.1202529

Parbo P, Ismail R, Hansen KV, Amidi A, Mårup FH, Gottrup H et al (2017) Brain inflammation accompanies amyloid in the majority of mild cognitive impairment cases due to Alzheimer's disease. Brain 140(7):2002–2011

Pardridge WM (1999) Blood-brain barrier biology and methodology. J Neurovirol 5(6):556–569. https://doi.org/10.3109/13550289909021285

Pavese N, Gerhard A, Tai YF, Ho AK, Turkheimer F, Barker RA, Brooks DJ et al (2006) Microglial activation correlates with severity in Huntington disease: a clinical and PET study. Neurology 66(11):1638–1643. https://doi.org/10.1212/01.wnl.0000222734.56412.17

Pflugrad H, Meyer G-J, Dirks M, Raab P, Tryc AB, Goldbecker A et al (2016) Cerebral microglia activation in hepatitis C virus infection correlates to cognitive dysfunction. J Viral Hepat 23(5):348–357. https://doi.org/10.1111/jvh.12496

Plavén-Sigray P, Matheson GJ, Cselényi Z, Jucaite A, Farde L, Cervenka S (2018) Test-retest reliability and convergent validity of (R)-[11C]PK11195 outcome measures without arterial input function. EJNMMI Res 8. https://doi.org/10.1186/s13550-018-0455-8

Plotkin M, Hautzel H, Krause BJ, Mohr S, Langen KJ, Müller H-W (2005) Fluorine-18-labeled fluorodeoxyglucose-positron emission tomography studies of acute brainstem Lyme neuroborreliosis [corrected] case report. J Neurosurg 102(5):927–929. https://doi.org/10.3171/jns.2005.102.5.0927

Politis M, Giannetti P, Su P, Turkheimer F, Keihaninejad S, Wu K, Waldman A et al (2012) Increased PK11195 PET binding in the cortex of patients with MS correlates with disability. Neurology 79(6):523–530. https://doi.org/10.1212/WNL.0b013e3182635645

Posavad CM, Wald A, Hosken N, Huang ML, Koelle DM, Ashley RL, Corey L (2003) T cell immunity to herpes simplex viruses in seronegative subjects: silent infection or acquired immunity? J Immunol 170(8):4380–4388. http://www.ncbi.nlm.nih.gov/pubmed/12682275

Ramlackhansingh AF, Brooks DJ, Greenwood RJ, Bose SK, Turkheimer FE, Kinnunen KM, Gentleman S et al (2011) Inflammation after trauma: microglial activation and traumatic brain injury. Ann Neurol 70(3):374–383. https://doi.org/10.1002/ana.22455

Rodríguez EM, Blázquez JL, Guerra M (2010) The design of barriers in the hypothalamus allows the median eminence and the arcuate nucleus to enjoy private milieus: the former opens to the portal blood and the latter to the cerebrospinal fluid. Peptides 31(4):757–776. https://doi.org/10.1016/j.peptides.2010.01.003

Rolle A-M, Soboslay PT, Reischl G, Hoffmann WH, Pichler BJ, Wiehr S (2015) Evaluation of the metabolic activity of Echinococcus multilocularis in rodents using positron emission tomography tracers. Mol Imaging Biol 17(4):512–520

Rubin LH, Sacktor N, Creighton J, Du Y, Endres CJ, Pomper MG, Coughlin JM (2018) Microglial activation is inversely associated with cognition in individuals living with HIV on effective antiretroviral therapy. AIDS (London, England) 32(12):1661–1667

Schmutzhard E (2001) Viral infections of the CNS with special emphasis on herpes simplex infections. J Neurol 248(6):469–477. http://www.ncbi.nlm.nih.gov/pubmed/11499636

Schuitemaker A, Kropholler MA, Boellaard R, Van der Flier WM, Kloet RW, Van der Doef TF, Knol DL et al (2013) Microglial activation in Alzheimer's disease: an (R)-[^{11}C]PK11195 positron emission tomography study. Neurobiol Aging 34(1):128–136. https://doi.org/10.1016/j.neurobiolaging.2012.04.021

Sips GJ, Wilschut J, Smit JM (2011) Neuroinvasive flavivirus infections. Rev Med Virol. https://doi.org/10.1002/rmv.712

Sisó S, Jeffrey M, González L (2010) Sensory circumventricular organs in health and disease. Acta Neuropathol 120:689–705. https://doi.org/10.1007/s00401-010-0743-5

Smith JL, Israel CW (1967) Spirochetes in the aqueous humor in seronegative ocular syphilis. Persistence after penicillin therapy. Arch Ophthalmol 77(4):474–477

Song YS (2019) Perspectives in TSPO PET imaging for neurologic diseases. Nucl Med Mol Imaging 53(6):382–385. https://doi.org/10.1007/s13139-019-00620-y

Steere AC, Coburn J, Glickstein L (2004) The emergence of Lyme disease. J Clin Invest 113(8):1093–1101. https://doi.org/10.1172/JCI21681

Sucksdorff M, Rissanen E, Tuisku J, Nuutinen S, Paavilainen T, Rokka J et al (2017) Evaluation of the effect of fingolimod treatment on microglial activation using serial PET imaging in multiple sclerosis. J Nucl Med 58(10):1646–1651. https://doi.org/10.2967/jnumed.116.183020

Tai YF, Pavese N, Gerhard A, Tabrizi SJ, Barker RA, Brooks DJ, Piccini P (2007) Microglial activation in presymptomatic Huntington's disease gene carriers. Brain 130(Pt 7):1759–1766. https://doi.org/10.1093/brain/awm044

Theil D, Derfuss T, Paripovic I, Herberger S, Meinl E, Schueler O, Strupp M et al (2003) Latent herpesvirus infection in human trigeminal ganglia causes chronic immune response. Am J Pathol 163(6):2179–2184. http://www.pubmedcentral.nih.gov/articlerender.fcgi?artid=1892378&tool=pmcentrez&rendertype=abstract

Theil D, Horn AKE, Derfuss T, Strupp M, Arbusow V, Brandt T (2004) Prevalence and distribution of HSV-1, VZV, and HHV-6 in human cranial nerve nuclei III, IV, VI, VII, and XII. J Med Virol 74(1):102–106. https://doi.org/10.1002/jmv.20152

Tremblay M-È, Majewska AK (2011) A role for microglia in synaptic plasticity? Commun Integr Biol 4(2):220–222. https://doi.org/10.4161/cib.4.2.14506

Triarhou LC (2006) The signalling contributions of Constantin von Economo to basic, clinical and evolutionary neuroscience. Brain Res Bull 69(3):223–243. https://doi.org/10.1016/j.brainresbull.2006.02.001

Turner MR, Cagnin A, Turkheimer FE, Miller CCJ, Shaw CE, Brooks DJ, Leigh PN et al (2004) Evidence of widespread cerebral microglial activation in amyotrophic lateral sclerosis: an [11C](R)-PK11195 positron emission tomography study. Neurobiol Dis 15(3):601–609. https://doi.org/10.1016/j.nbd.2003.12.012

Turner MR, Gerhard A, Al-Chalabi A, Shaw CE, Hughes RAC, Banati RB, Brooks DJ et al (2005) Mills' and other isolated upper motor neurone syndromes: in vivo study with 11C-(R)-PK11195 PET. J Neurol Neurosurg Psychiatry 76(6):871–874. https://doi.org/10.1136/jnnp.2004.047902

Van Berckel BN, Bossong MG, Boellaard R, Kloet R, Schuitemaker A, Caspers E, Luurtsema G et al (2008) Microglia activation in recent-onset schizophrenia: a quantitative (R)-[11C]PK11195 positron emission tomography study. Biol Psychiatry 64(9):820–822. https://doi.org/10.1016/j.biopsych.2008.04.025

Venneti S, Bonneh-Barkay D, Lopresti BJ, Bissel SJ, Wang G, Mathis CA, Piatak M et al (2008) Longitudinal in vivo positron emission tomography imaging of infected and activated brain macrophages in a macaque model of human immunodeficiency virus encephalitis correlates with central and peripheral markers of encephalitis and areas of synaptic degeneration. Am J Pathol 172(6):1603–1616. https://doi.org/10.2353/ajpath.2008.070967

Wang D, Hazell AS (2010) Microglial activation is a major contributor to neurologic dysfunction in thiamine deficiency. Biochem Biophys Res Commun 402(1):123–128. https://doi.org/10.1016/j.bbrc.2010.09.128

Whitrow M (1990) Wagner-Jauregg and fever therapy. Med Hist 34(3):294–310. http://www.pubmedcentral.nih.gov/articlerender.fcgi?artid=1036142&tool=pmcentrez&rendertype=abstract

Wiley CA, Lopresti BJ, Becker JT, Boada F, Lopez OL, Mellors J, Meltzer CC et al (2006) Positron emission tomography imaging of peripheral benzodiazepine receptor binding in human immunodeficiency virus-infected subjects with and without cognitive impairment. J Neurovirol 12(4):262–271. https://doi.org/10.1080/13550280600873868

Wiley CA, Lopresti BJ, Venneti S, Price J, Klunk WE, DeKosky ST, Mathis CA (2009) Carbon 11-labeled Pittsburgh compound B and carbon 11-labeled (R)-PK11195 positron emission tomographic imaging in Alzheimer disease. Arch Neurol 66(1):60–67. https://doi.org/10.1001/archneurol.2008.511

Yolken RH, Karlsson H, Yee F, Johnston-Wilson NL, Torrey EF (2000) Endogenous retroviruses and schizophrenia. Brain Res Brain Res Rev 31(2–3):193–199. http://www.ncbi.nlm.nih.gov/pubmed/10719148

PET Imaging in Multiple Sclerosis

33

Chris W. J. van der Weijden, Jan F. Meilof, and Erik F. J. de Vries

Contents

33.1 Introduction 894
33.2 PET Tracers Used to Assess MS Pathology 896
33.3 PET Imaging to Assess Neuro-Inflammation 897
33.4 PET Imaging to Assess Myelin Integrity 903
33.5 PET Imaging to Assess Neuronal Integrity 905
33.6 PET Imaging as a Tool to Aid in Differential Diagnosis 908
33.7 PET Imaging to Assess Treatment Effects in MS 908
33.8 Clinical Notes 911
33.9 Conclusion 911
References 911

Abstract

Multiple sclerosis (MS) pathology is associated with inflammation and demyelination in the central nervous system (CNS), which leads to neurodegeneration. Various positron emission tomography (PET) tracers have been employed to image these processes. PET tracers for 18-kD translocator protein (TSPO) receptors, which are overexpressed on activated microglia, macrophages, and astrocytes, have been used to assess neuro-inflammation. PET imaging of TSPO expression depicted an increased activation of inflammatory cells in normal

C. W. J. van der Weijden (✉) · E. F. J. de Vries
Department of Nuclear Medicine and Molecular Imaging, University Medical Center Groningen, University of Groningen, Groningen, The Netherlands
e-mail: c.w.j.van.der.weijden@umcg.nl; e.f.j.de.vries@umcg.nl

J. F. Meilof
Department of Biomedical Sciences of Cells and Systems, University Medical Center Groningen, University of Groningen, Groningen, The Netherlands

Department of Neurology, Martini Ziekenhuis, Groningen, The Netherlands
e-mail: j.f.meilof@umcg.nl

R. A. J. O. Dierckx et al. (eds.), *PET and SPECT in Neurology*,
https://doi.org/10.1007/978-3-030-53168-3_33

appearing white matter (NAWM), grey matter (GM), and MS lesions. A reduction in inflammation in MS lesions was found to be a main determinant of treatment efficacy. Recently, advances have been made in myelin visualisation with PET. The first clinical studies to visualise myelin with PET show promising results. As for other neurodegenerative diseases, [^{18}F]FDG is still the main PET tracer used to assess neuronal damage. Current clinical use of PET in MS is mainly restricted to aiding in differential diagnosis or for determining the efficacy of immune suppressive treatments. Once myelin imaging has been validated as a reliable method for characterisation of myelin integrity, it would enable the evaluation of the efficacy of a new line of therapies that aim to repair myelin.

33.1 Introduction

Multiple sclerosis (MS) is the most common neurodegenerative disease in young adults (Ramagopalan et al. 2010). MS pathology is characterised by immune attacks on the myelin sheath covering the axon (Traugott et al. 1983). The initiation of the immune response seems to be driven by peripheral activation of the adaptive immune system (Dendrou et al. 2015). After migration to the central nervous system (CNS), activated T cells cause activation of antigen presenting cells, like microglia and macrophages, which then initiate recruitment of additional inflammatory cells (Fig. 33.1). During this process, myelin-specific antibodies are produced and together with cytotoxic cytokines, excitotoxins, reactive oxygen, and nitric oxide, which are released by activated microglia and macrophages, they cause the damage to myelin (Dendrou et al. 2015; Lassmann et al. 2012). Oligodendrocytes are able to repair the myelin sheaths of axons (remyelination) and thereby restore the protective and signal enhancement function of myelin (Prineas and Connell 1979). However, when myelin damage is too severe, it will be beyond the restoration capacity of oligodendrocytes. Damaged myelin makes axons vulnerable for any exposure to environmental effects and ultimately leads to neurodegeneration (Ferguson et al. 1997; Franklin and Ffrench-Constant 2008). All these processes (i.e. inflammation, myelin degradation, and neurodegeneration) are part of the MS pathology and are involved in relapses (episodes with a temporary increase in severity of symptoms) and disease progression.

When a patient presents with a history of only one relapse, this is called a clinically isolated syndrome (CIS). Subjects with CIS have an increased risk to develop MS, and therefore CIS is considered to be a prodromal stage of MS (Baecher-Allan et al. 2018). Almost all patients with CIS develop relapsing remitting MS (RRMS), although this may take many years. RRMS is with an 85% occurrence, the most prevalent form of MS. The remaining 15% of patients have a slowly progressive disease course from disease onset without relapses, which is called primary progressive MS (PPMS). In RRMS, clinical symptoms emerge during relapses, but subsequently diminish over time during remission due to reduction of inflammation and recovery of the myelin sheaths. Incomplete repair of myelin damage leads to

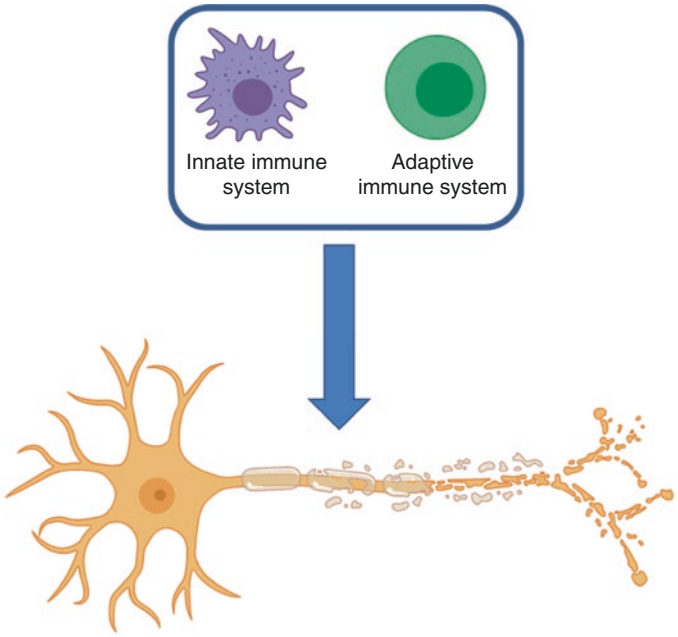

Fig. 33.1 Current view of the MS pathogenesis pathway. Inflammatory cells cause demyelination, which ultimately results in neurodegeneration

increased axonal damage and disease progression. When remissions no longer occur and axonal damage increases more gradually, MS patients are considered to have entered the secondary progressive (SP) stage of MS.

Due to the random location of inflammatory lesions occurring in the CNS, clinical symptoms in MS are highly diverse. The most typical symptoms are the ones involving the optic nerve, the urinary tract, and those resulting in sensory and motor symptoms (Huang et al. 2017; Miljković and Spasojević 2013). Disease severity is often expressed using the Expanded Disability Status Scale (EDSS) (Kurtzke 1983). The EDSS is scored from 0 (no disability or other impairments) to 10 (death due to MS). With a score of 5, the patient is hampered in his daily activities and walking distance due to symptoms of MS, and is not capable of completing full work days without special precautions.

A diagnosis of MS is based on the combination of clinical symptoms, the presence of typical lesions on MRI, and, if necessary, analysis of cerebrospinal fluid (Thompson et al. 2018). The mainstay in diagnosing MS is the demonstration of dissemination of lesions in place and in time clinically or with MRI. Current MRI protocols are very effective in supporting a diagnosis of MS and excluding other diseases. On MRI scans, the damage caused by inflammation is visualised as white matter lesions, which are hyper-intense on T2 fluid-attenuated inversion recovery (T2-FLAIR) images (Biediger et al. 2014). The visually non-affected white matter is typically called normal appearing white matter (NAWM), which does not mean

biological changes are absent. Gadolinium (Gd) contrast enhancement is a marker for blood–brain barrier breakdown. This makes it possible to distinguish with MRI between active (Gd-enhanced) and non-active (non-enhanced) lesions (Kaunzner and Gauthier 2017). However, irrespective of their activity status, these lesions depict a combination of processes including inflammation, gliosis, demyelination, and axonal loss. MRI is therefore currently not able to visualise alterations in individual biological processes. The availability of highly specific ligands would enable distinguishing between individual biological alterations in MS pathology with molecular imaging techniques, in particular positron emission tomography (PET).

33.2 PET Tracers Used to Assess MS Pathology

PET imaging can enable imaging of individual biological processes. However, it is only possible to visualise one biological process per scan. Many tracers have been developed for specific biological processes. MS is best described using the three major biological processes involving inflammation, demyelination, and neurodegeneration. Within these processes, there are multiple aspects that can be visualised, and hence a wide variety of tracers have been used in MS. An overview of the tracers used in MS is displayed in Table 33.1. A more thorough discussion of the relevance of these tracers within MS pathology is provided in the following sections.

Table 33.1 PET tracers currently being employed for the visualisation of biological processes in MS pathology

Tracer	Imaging target	Relevant structures/cells
[^{11}C]PK11195	TSPO	Activated microglia, macrophages, astrocytes
[^{11}C]PBR28	TSPO	Activated microglia, macrophages, astrocytes
[^{18}F]PBR06	TSPO	Activated microglia, macrophages, astrocytes
[^{18}F]PBR111	TSPO	Activated microglia, macrophages, astrocytes
[^{18}F]GE-180	TSPO	Activated microglia, macrophages, astrocytes
[^{11}C]DPA713	TSPO	Activated microglia, macrophages, astrocytes
[^{18}F]DPA714	TSPO	Activated microglia, macrophages, astrocytes
[^{11}C]acetate	MCT	Activated astrocytes
[^{11}C]TMSX	Adenosine A_{2A} receptor	Cerebral stress coping mechanisms
[^{11}C]PiB	Amyloid beta and MBP	In MS pathology, assessment of myelin integrity
[^{18}F] Florbetaben	Amyloid beta and MBP	In MS pathology, assessment of myelin integrity
[^{18}F] Florbetapir	Amyloid beta and MBP	In MS pathology, assessment of myelin integrity
[^{11}C] flumazenil	Benzodiazepine receptor	Synaptic integrity
[^{11}C]DASB	Serotonin transporters	Neuronal presynaptic membrane
[^{18}F]FDG	Glucose consumption	Neurodegeneration
[^{11}C] methionine	Protein synthesis	Differential diagnosis between MS and brain tumours

MBP myelin basic protein, *MCT* monocarboxylate transporter, *MS* multiple sclerosis, *TSPO* 18-kDa translocator protein

33.3 PET Imaging to Assess Neuro-Inflammation

MS is characterised by neuro-inflammation aimed at the myelin layers around the axons. The 18-kD translocator protein (TSPO) is upregulated in activated inflammatory cells in the brain (Fig. 33.2), especially in microglia, but also in macrophages and to a lesser extent in astrocytes (Chechneva and Deng 2016). TSPO is found on mitochondrial membranes and has many functions, including the mediation of cholesterol transport from the cytosol into the mitochondria (Papadopoulos et al. 2006) and regulation of mitochondrial energy metabolism (Gut 2015). The latter function could be the reason why TSPO is upregulated in activated inflammatory cells. Thus, determination of TSPO expression is used to assess the amount of activated inflammatory cells (Fig. 33.3). Traditionally, [^{11}C]PK11195 PET imaging was the primary method for the evaluation of TSPO expression (Vowinckel et al. 1997). [^{11}C]PK11195 is currently still regularly used (Table 33.2), although a new generation of TSPO tracers with higher affinity has been developed as well. A major disadvantage of the new so-called "second generation" tracers is the genotype-dependent binding affinity. The second-generation tracers require therefore classification of patients into low- (LAB), medium- (MAB), and high-affinity binding (HAB) individuals. A single-nucleotide polymorphism in the TSPO gene (rs6971), which replaces alanine with threonine (Ala147Thr), was shown to be responsible for the variation in binding affinity resulting in LAB for homozygotes of this single nucleotide permutation (SNP) (Owen et al. 2012). A study assessing the frequency of the different TSPO binding affinities showed that 66% were HAB, 29% MAB, and 5% LAB (Owen et al. 2012). This means that, aside from the PET scan, also genotyping has to be performed for a correct analysis of the acquired images. In contrast, [^{11}C]PK11195 binding is not affected by this SNP and is therefore still a regularly used PET tracer for inflammation.

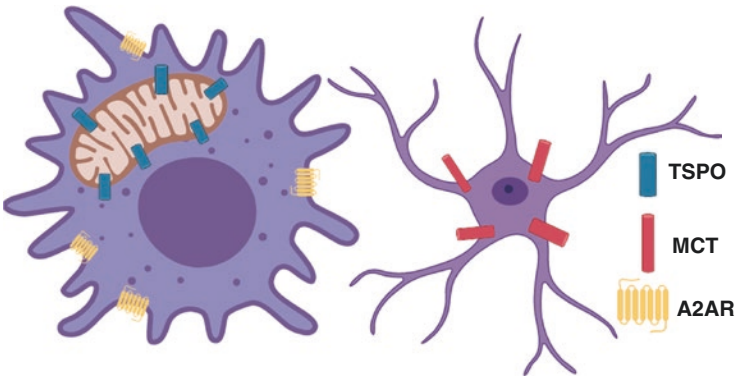

Fig. 33.2 PET imaging targets on inflammatory cells used in MS research. TSPO and monocarboxylate transporter (MCT) are markers for neuro-inflammation. Within activated inflammatory cells, TSPO is upregulated. Many PET tracers that bind TSPO have been developed to enable the visualisation of this upregulation and thus the activation status of inflammatory cells. A more specific method is imaging of MCT expression, which is upregulated in activated astrocytes. Microglial A2AR expression is supposed to modulate the inflammatory response

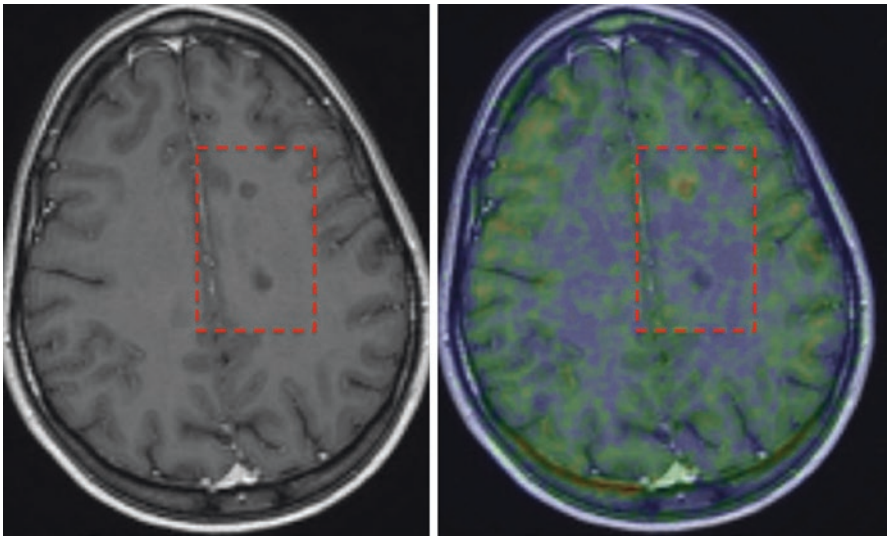

Fig. 33.3 Differentiation of two non-enhanced lesions on T1 MRI and [^{11}C]PK11195 PET. The upper lesion clearly depicts an increase in [^{11}C]PK11195 uptake, which means inflammatory activation, and thus depicts an active lesion. In contrast, the lower lesion does not show increased tracer uptake, and therefore is an inactive lesion (permission for the use of the images was obtained; source: DOI: https://doi.org/10.1007/s40336-015-0147-6) (Airas et al. 2015)

Studies assessing TSPO expression in MS with [^{11}C]PK11195 PET imaging displayed increased tracer uptake in NAWM, cortical grey matter (GM), and thalamus, which was associated with a longer disease duration and higher age (Giannetti et al. 2015; Politis et al. 2012; Rissanen et al. 2014). Other studies found only a significantly increased uptake in the whole brain, but not in individual regions (Sucksdorff et al. 2017). These findings illustrate that with advancing disease duration and age, more activated inflammatory cells are observed. More detailed analysis of the lesions themselves resulted in differential results for Gd-contrast-enhanced lesions vs. non-contrast-enhanced lesions. In general, lesions have a higher tracer uptake than NAWM, with contrast-enhanced lesions having an even higher [^{11}C]PK11195 uptake than non-enhanced lesions, supporting the concept that MRI contrast enhancement is a marker for inflammation (Vowinckel et al. 1997; Giannetti et al. 2015; Kaunzner et al. 2017). Increased [^{11}C]PK11195 uptake in cortical GM has also been observed in MS patients and was significantly correlated (r = 0.84, p = 0.0089) with EDSS scores (Politis et al. 2012). In RRMS patients, a higher [^{11}C]PK11195 uptake has been associated with smaller total black hole volumes, which are supposed to represent inactive non-remyelinated lesions with extensive axonal damage (Giannetti et al. 2014). In short, these studies show a global cerebral increase of activated inflammatory cells with disease progression, duration, and age, which corresponds to increased clinical disability. Furthermore, an increase of [^{11}C]PK11195 uptake in MS lesions corresponds with disease activity. As depicted in Table 33.2, there are also studies that do not show an increased uptake in GM

Table 33.2 Overview of the main results per study using [^{11}C]PK11195 PET to image inflammatory response in MS patients

Study	Tracer	Subjects	GM	NAWM	Non-enhanced lesions	Enhanced lesions
Giannetti et al. (2015)	[^{11}C] PK11195	8 HC 18 CIS	No differences observed	Increased [^{11}C] PK11195 uptake	n.a.	n.a.
Politis et al. (2012)	[^{11}C] PK11195	8 HC 10 RRMS	Increased [^{11}C] PK11195 uptake	Increased [^{11}C] PK11195 uptake	n.a.	n.a.
		8 SPMS	More increased [^{11}C] PK11195 uptake than in RRMS	More increased [^{11}C] PK11195 uptake than in RRMS		
E. Rissanen et al. (2014)	[^{11}C] PK11195	8 HC 10 SPMS	No differences observed	Increased [^{11}C] PK11195 uptake		Increased [^{11}C] PK11195 uptake
Sucksdorff et al. (2017)	[^{11}C] PK11195	8 HC 10 RRMS	No differences observed	No differences observed	n.a.	n.a.
Kaunzner et al. (2017)	[^{11}C] PK11195	5 HC 18 MS	n.a.	n.a.	Increased [^{11}C] PK11195 uptake	More increased [^{11}C] PK11195 uptake than non-enhanced lesions
Vowinckel et al. (1997)	[^{11}C] PK11195	2 MS	n.a.	n.a.	[^{11}C] PK11195 uptake not increased	Increased [^{11}C] PK11195 uptake

CIS clinically isolated syndrome, *HC* healthy control, *MS* multiple sclerosis, *n.a.* not applicable, *SPMS* secondary progressive MS, *RRMS* relapse remitting MS

(Giannetti et al. 2015; Rissanen et al. 2014; Sucksdorff et al. 2017), Sucksdorff et al. (2017) did not observe differences in NAWM, and Vowinckel et al. (1997) found only an increased uptake in contrast-enhanced lesions, but not in non-enhanced lesions. Giannetti et al. (2015) investigated CIS, which is a group early in the spectrum of the MS disease course, so it is logical that they found less differences in inflammation. This is in line with the findings of Politis et al. (2012) that observed increased tracer uptake in RRMS, which was further increased in secondary progressive MS (SPMS). Aside from that, the inconsistencies most likely arise from the extreme heterogeneous aspect of MS pathology and the small sample sizes in the

studies. The amount and severity of inflammation vary per person and the low affinity of [^{11}C]PK11195 for TSPO makes it difficult to find uniform group-based differences.

The most frequently studied second-generation TSPO tracer is [^{11}C]PBR28 (Table 33.3). Increased [^{11}C]PBR28 uptake has been generally observed in MS patients, including in the whole cortex, thalamus, hippocampus, basal ganglia, NAWM, lesions, and more specifically in contrast-enhanced lesions (Oh et al. 2011;

Table 33.3 Overview of the main results of studies using second-generation TSPO tracers

Study	Tracer	Subjects	GM	NAWM	Non-enhanced lesions	Enhanced lesions
Herranz et al. (2016)	[^{11}C] PBR28	11 HC 12 RRMS	Increased tracer uptake	Increased tracer uptake	n.a.	n.a.
		15 SPMS	More increased tracer uptake than for RRMS	More increased tracer uptake than for RRMS		
Oh et al. (2011)	[^{11}C] PBR28	7 HC 11 MS	No differences observed	No differences observed	Tracer uptake not increased	Increased tracer uptake
Singhal et al. (2018)	[^{11}C] PBR28	6 RRMS	n.a.	Increased tracer uptake	n.a.	n.a.
	[^{18}F] PBR06			Increased tracer uptake		
Datta et al. (2017b)	[^{11}C] PBR28	20 HC 24 MS	n.a.	Increased tracer uptake	Increased tracer uptake	Increased tracer uptake
	[^{18}F] PBR111	10 HC 10 MS	n.a.	Increased tracer uptake	Increased tracer uptake	Increased tracer uptake
Colasanti et al. (2014)	[^{18}F] PBR111	11 HC 11 RRMS	n.a.	Increased	Lesional uptake increased (enhancement not specified)	
Unterrainer et al. (2018)	[^{18}F] GE-180	19 RRMS	n.a.	n.a.	Increased tracer uptake	Tracer uptake increased more than non-enhanced
Bunai et al. (2018)	[^{11}C] DPA713	6 HC 6 RRMS	Increased	n.a.	n.a.	n.a.
Hagens et al. (2018)	[^{18}F] DPA714	7 HC 3 SPMS 5 PPMS	n.a.	n.a.	Tracer uptake increased (enhancement not specified)	

GM grey matter, *HC* healthy control, *MS* multiple sclerosis, *n.a.* not applicable, *NAWM* normal appearing white matter, *RRMS* relapse remitting MS, *SPMS* secondary progressive MS

Herranz et al. 2016). This increased [^{11}C]PBR28 uptake also appeared to increase with disability and disease duration (Oh et al. 2011; Herranz et al. 2016). In addition, a higher uptake of [^{11}C]PBR28 in NAWM and GM has been observed in SPMS compared to RRMS, which might be explained by the relation between increased tracer uptake and disease duration and/or elevated immune cell activation in SPMS as compared to RRMS patients in a remission phase (Herranz et al. 2016). Furthermore, [^{11}C]PBR28 uptake in both NAWM and lesions were positively correlated with T2 lesion volumes in RRMS, indicating that a higher tracer uptake corresponds with a larger total T2 lesion volume in RRMS (Datta et al. 2017a). In SPMS, a higher activation of inflammatory cells (tracer uptake) was positively correlated with brain atrophy, illustrating that neurodegenerative effects are accompanying the increased activation of inflammatory cells and further explaining the relation between disease duration and EDSS score (Datta et al. 2017a). Thus, like [^{11}C]PK11195, increased [^{11}C]PBR28 uptake, corresponding with increased activated inflammatory cells, is related to disease progression, duration, and clinical disability and an increase of [^{11}C]PBR28 uptake in MS lesions corresponds with disease activity. As stated in the previous section about [^{11}C]PK11195, inconsistencies in the literature are also found for the higher affinity second-generation TSPO tracers (Table 33.3). Oh et al. (2011) did not find any differences in tracer uptake for GM and NAWM non-enhanced lesions, but did for contrast-enhanced lesions. This is, however, the only study showing discrepancies with other studies, and illustrates the relative uniformity in the data with higher affinity TSPO tracers compared with the first-generation tracers. Heterogeneity in MS pathology may explain the remaining inconsistencies between studies.

Direct comparisons of [^{11}C]PBR28 with [^{18}F]PBR06, [^{18}F]PBR111, and [^{18}F]GE-180 have been performed, but not with [^{11}C]PK11195 (Table 33.3). Both [^{11}C]PBR28 and [^{18}F]PBR06 have a high tracer uptake in NAWM; however, only [^{18}F]PBR06 uptake was correlated to EDSS score, meaning that [^{18}F]PBR06 could be more sensitive to slight changes in immune activation in the specific population studied (Singhal et al. 2018). A comparison of [^{11}C]PBR28 with [^{18}F]PBR111 showed that [^{11}C]PBR28 has a higher binding in thalamus compared to [^{18}F]PBR111, aside from that, both tracers showed an increased uptake in NAWM, and both showed a higher tracer uptake in both contrast and non-contrast-enhanced lesions (Datta et al. 2017b). The other study analysing solely [^{18}F]PBR111 TSPO binding confirmed the higher tracer uptake in both NAWM and lesions (Colasanti et al. 2014). [^{11}C]PBR28 and [^{18}F]GE-180 TSPO binding are highly comparable (Sridharan et al. 2019). Like [^{11}C]PBR28, [^{18}F]GE-180 tracer uptake is also increased in lesions, especially in contrast-enhanced lesions (Unterrainer et al. 2018). According to these findings, all tracers seem to perform comparable, although [^{18}F]PBR06 might be slightly more and [^{18}F]PBR111 slightly less sensitive than [^{11}C]PB28.

Other second-generation TSPO tracers are [^{11}C]DPA713 and [^{18}F]DPA714 (Table 33.3). [^{11}C]DPA713 showed a global cortical increase of tracer uptake in MS patients (Bunai et al. 2018). For [^{18}F]DPA714, an increased uptake was observed in lesions compared to NAWM, and specifically for HAB patients. [^{18}F]DPA714

Table 33.4 Studies assessing MCT to image neuro-inflammation

Study	Tracer	Subjects	GM	NAWM	Non-enhanced lesions	Enhanced lesions
Takata et al. (2014)	[^{11}C] acetate	6 HC 6 RRMS	Increased tracer uptake	Increased tracer uptake	n.a.	n.a.

GM grey matter, *HC* healthy control, n.a. not applicable, *NAWM* normal appearing white matter, *RRMS* relapse remitting MS

showed also an increased tracer binding in NAWM when compared to NAWM of HAB healthy subjects (Hagens et al. 2018). These findings indicate that with [^{11}C]DPA713 PET, a global increase of activated inflammatory cells is observed in MS, and with [^{18}F]DPA714 the increase in activated immune cells was only visible in NAWM of HAB patients. This suggests that [^{11}C]DPA713 might be more suitable for visualising inflammatory changes in MS than [^{18}F]DPA714. The fact that [^{18}F]DPA714 is a TSPO agonist, whereas the other TSPO tracers are antagonists may also play a role in explaining this difference in binding.

Despite the upregulation of TSPO in microglia, macrophages, and astrocytes, TSPO imaging is primarily used to assess microglial activation (Fig. 33.2). However, astrocytes also play a role in MS pathology. In MS, there is an increased cerebral expression of the monocarboxylate transporter (MCT) (Nijland et al. 2014). MCT functions as a transporter for monocarboxylates, such as acetate. Acetate is preferentially absorbed into astrocytes by MCT (Waniewski and Martin 1998). Therefore, [^{11}C]acetate could be used to assess astrocyte activation, due to the upregulation of MCT by activated astrocytes (Table 33.4). Using [^{11}C]acetate, increased tracer uptake was observed in both WM and GM in MS patients compared to healthy subjects, and the amount of [^{11}C]acetate uptake was positively correlated to the number of lesions (Takata et al. 2014). This suggests that aside from microglia, also astrocytes are activated in MS pathology, and the amount of activation increases with disease severity. Whether the increased activation of astrocytes in MS pathology is supporting repair of neuronal damage still remains to be investigated.

Following degradation of the myelin sheaths, axons are susceptible to adverse environmental impact, such as exposure to oxidative stress, ultimately leading to neurodegeneration. The inflammation in MS pathology is a major source of oxidative stress. Upon neuronal damage, adenosine is released leading to the attraction of microglia. One intrinsic manner to cope with inflammation and corresponding tissue damage is the microglial upregulation of adenosine signalling via the adenosine A_{2A} receptor (A2AR) (Garcia et al. 2007). Upregulation of A2AR results in attenuation of inflammation (Fig. 33.2) and thereby limits the damage caused by inflammation (Blackburn et al. 2009). In MS, A2AR upregulation has been demonstrated by PET imaging with the A2AR tracer [^{11}C]TMSX (Rissanen et al. 2013). This indicates that in MS, microglial upregulation of A2AR expression might attenuate the inflammation, thereby reducing tissue damage and enhancing axonal survival.

33.4 PET Imaging to Assess Myelin Integrity

One of the main characteristics of MS pathology is the degradation of myelin. However, a validated and specific imaging method to directly visualise myelin in vivo and therefore to assess its integrity is still lacking. Because of high binding of amyloid tracers to white matter in healthy subjects, amyloid tracers have been recently applied for assessment of myelin integrity (Matías-Guiu et al. 2015). Amyloid tracers are designed to bind amyloid-beta deposits in the brain, which is one of the hallmarks of Alzheimer's disease pathology. More specifically, amyloid tracers bind to the beta sheets in amyloid-beta depositions (Wu et al. 2011). Myelin basic protein (MBP), one of the most prominent protein in the myelin lipid layers, also contains beta sheet structures (Ridsdale et al. 2002). Therefore, the high uptake of amyloid tracers in white matter of healthy subjects is hypothesised to correspond with binding to MBP, and thus might be used as a measurement for assessing myelin integrity (Fig. 33.4).

Amyloid tracers for assessing myelin integrity generally display a decreased uptake in the white matter lesions compared to NAWM (Table 33.5). However, none of the studies also assessed the perfusion rate of lesions. Diminished perfusion in lesions could also lead to a lower tracer uptake in the lesions, even without demyelination. Current research with amyloid tracers leads to conflicting results regarding differentiation between NAWM in MS patients and WM of healthy subjects. [^{18}F]Florbetaben, for instance, showed differences between tracer uptake in NAWM

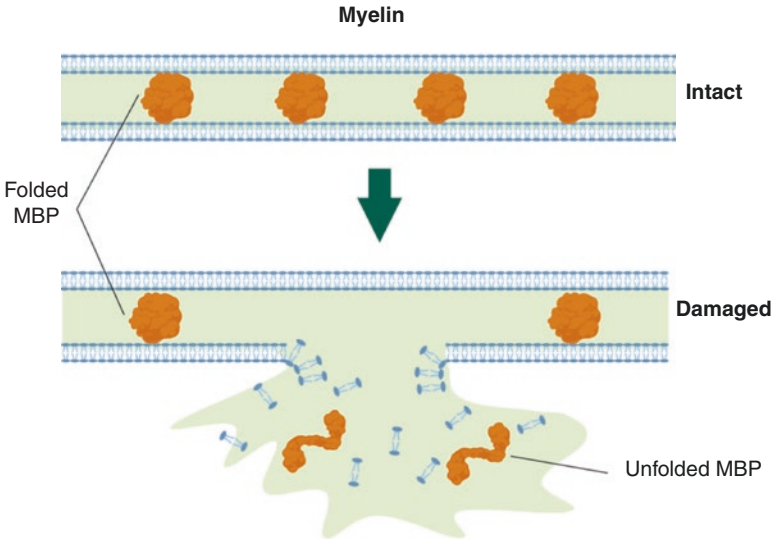

Fig. 33.4 Mechanism of action for myelin visualisation. The main target for myelin visualisation is supposedly myelin basic protein (MBP). The tracers bind to the beta sheets of intact MBP. When myelin is damaged, MBP loses its structure and thereby the tracer binding site (the figure is inspired by Stapulionis et al. (2008); Source: DOI: https://doi.org/10.4049/jimmunol.180.6.3946)

Table 33.5 Overview of studies with amyloid tracers employed for myelin imaging

Study	Tracer	Subjects	GM	NAWM	Non-enhanced lesions	Enhanced lesions
Bodini et al. (2016)	[^{11}C]PiB	8 HC 20 RRMS	No differences in tracer uptake	No differences in tracer uptake	Decreased tracer uptake	Decreased tracer uptake
Grecchi et al. (2017)	[^{11}C]PiB	20 RRMS	n.a.	n.a.	Decreased tracer uptake	Decreased tracer uptake
Zeydan et al. (2018)	[^{11}C]PiB	80 HC 12 MS	No differences in tracer uptake	No differences in tracer uptake	n.a.	n.a.
Matías-Guiu et al. (2015)	[^{18}F] Florbetaben	3 HC 5 RRMS 5 SPMS 2 PPMS	n.a.	Decreased tracer uptake	Decreased tracer uptake (enhancement not specified)	
Matías-Guiu et al. (2017)	[^{18}F] Florbetaben	1 MS	n.a.	n.a.	Decreased tracer uptake (enhancement not specified)	
Pietroboni et al. (2019)	[^{18}F] Florbetapir	7 RRMS 3 SPMS 2 PPMS	n.a.	n.a.	Decreased tracer uptake (enhancement not specified)	

GM grey matter, *HC* healthy control, *MS* multiple sclerosis, *n.a.* not applicable, *NAWM* normal appearing white matter, *PPMS* primary progressive MS, *RRMS* relapse remitting MS, *SPMS* secondary progressive MS

and WM, whereas [^{11}C]PiB did not (Matías-Guiu et al. 2015; Bodini et al. 2016). [^{18}F]Florbetaben, [^{18}F]Florbetapir, as well as [^{11}C]PiB, all showed a decreased tracer uptake in lesions relative to NAWM (Matías-Guiu et al. 2015, 2017; Bodini et al. 2016; Pietroboni et al. 2019; Zeydan et al. 2018; Grecchi et al. 2017). Furthermore, [^{11}C]PiB has shown to be able to capture remyelination and demyelination processes (Bodini et al. 2016). In contrast, [^{18}F]Florbetaben displayed differences in tracer uptake in lesions between different MS disease types, while no significant differences were observed in T2-weighted total lesion volumes between MS types (Matías-Guiu et al. 2015). This difference in [^{18}F]Florbetaben uptake in lesions between MS types might illustrate possible remyelination processes of lesions that occur in RRMS, which might not be detectable with T2 imaging. An example of [^{18}F]Florbetaben PET employed for myelin imaging is displayed in Fig. 33.5. Aside from the repurposing of amyloid tracers, recently the tracer [^{11}C]MeDAS has been specifically developed for the visualisation of myelin (Wu et al. 2010). PET studies with [^{11}C]MeDAS in preclinical models show that the tracer binds more specifically to MBP than other tracers (De Paula et al. 2014a, 2014b). Currently, the first clinical study with [^{11}C]MeDAS is still in progress (Trial register no. NL7262).

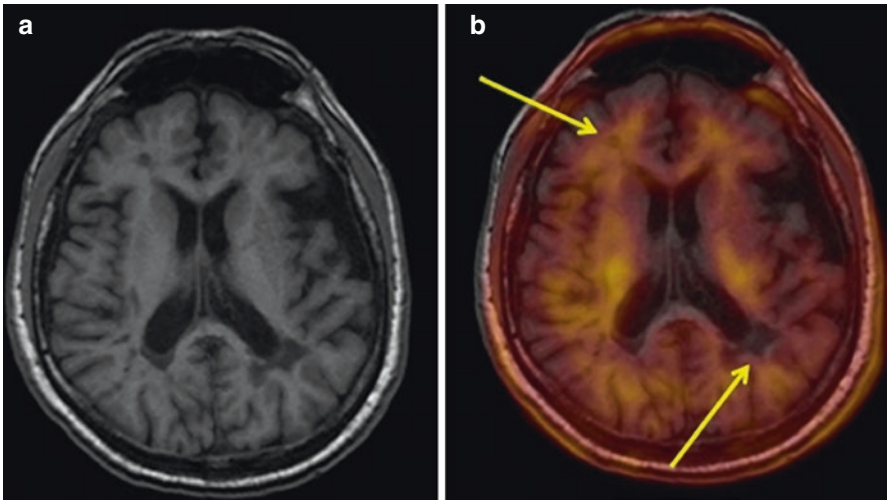

Fig. 33.5 A [^{18}F]Florbetaben PET image illustrating its ability to depict demyelination. On the left, a T1 MRI scan is displayed, with on the right a PET-MRI fusion image, illustrating both normal tracer uptake (left top corner) and a decreased tracer uptake (right bottom corner) at the lesion location as detected by T1 MRI (permission for the use of the images was obtained; Source: DOI: https://doi.org/10.1186/s12883-015-0502-2) (Matías-Guiu et al. 2015)

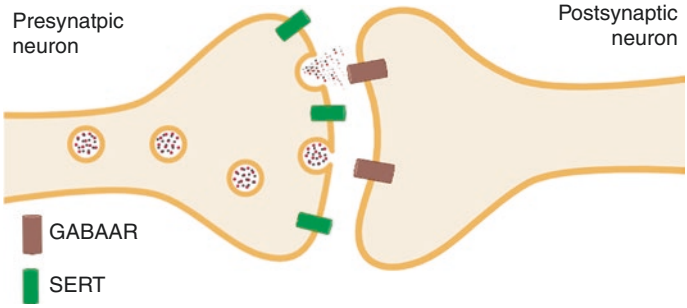

Fig. 33.6 Neuronal targets used for PET imaging in MS. $GABA_A$ receptor is essential for the propagation of action potentials, a reduced expression indicates a reduced synaptic density. SERT upregulation increases serotonin re-uptake and thereby enhances depressive symptoms

33.5 PET Imaging to Assess Neuronal Integrity

As a result of neurodegeneration, the amount of synapses decreases. One of the most important synaptic receptors is the γ-aminobutyric $acid_A$ ($GABA_A$) receptor. $GABA_A$ receptors (Fig. 33.6) are essential for propagating action potentials, and thus responsible for signal transduction (Mohler 2009). One of the sub-components of the $GABA_A$ receptor is the benzodiazepine receptor. Benzodiazepines enhance the effect of GABA binding to the $GABA_A$ receptor (Sigel and Ernst 2018). In MS, imaging with [^{11}C]flumazenil, an antagonist for the benzodiazepine receptor,

resulted in a lower cortical tracer uptake compared to healthy subjects, indicating a reduction of synapses in MS (Freeman et al. 2015).

Depression and mood disorders can occur in MS, possibly as a direct result of the disease. Depression is associated with a decreased availability of serotonin. Serotonin is a major contributor to feelings of well-being and happiness (Mitchell and Phillips 2007). One cause for the decreased availability of serotonin is an increase of serotonin transporters (Fakhoury 2016). Serotonin transporters transport serotonin from the synaptic cleft to the presynaptic neuron, and thereby counteract the effects of serotonin (Fig. 33.6). Therefore, a decrease or inhibition of serotonin transporters increases serotonin concentrations in the synapses and thus stimulates serotonin functions. [^{11}C]DASB is a tracer binding to serotonin transporters. In MS, a study with [^{11}C]DASB showed a reduced tracer uptake in the cingulate cortex, the thalamus, and the insula and an increased uptake in the orbitofrontal cortex (Hesse et al. 2014). This indicates a reduction of serotonin transporters in limbic and paralimbic regions and an increase in frontal regions. This study also assessed the correlation between [^{11}C]DASB uptake and depression. In line with expectations, there was a positive correlation between insular tracer uptake and depression, which means the higher the amount of serotonin transporters in the insula, the more prominent the depressive symptoms.

Like in all other neurodegenerative diseases, [^{18}F]FDG, a tracer for imaging glucose consumption is also used in MS to study neuronal integrity (Roelcke et al. 1997). As neurons are the major consumers of glucose in the brain, a decreased uptake of [^{18}F]FDG depicts dysfunction or degeneration of neurons. Reduced cortical [^{18}F]FDG uptake has also been found to be associated with a reduced cortical *N*-acetylaspartate concentration normalised to creatine (NAA/Cr) in RRMS (Blinkenberg et al. 2011). NAA/Cr is another method to assess neuronal deterioration and thus further illustrates the ability of [^{18}F]FDG to capture neurodegenerative processes in MS. However, as MS is a quite heterogeneous disease, there is a wide variety of regions showing neurodegeneration (Table 33.6). The hypometabolism in those regions was also positively correlated with both the duration and severity of MS (Bakshi et al. 1998). The clinical effects of neurodegeneration studied with [^{18}F]FDG in MS are mostly related to mobility or fatigue, but also to some extent to cognition.

Several brain regions are involved in the initiation of movement, and therefore neurodegeneration in any of those regions can affect mobility. The combination of regions responsible for movement is called the motor network. For the initiation of movement, first the parietal and temporal lobes receive sensory information and then initiate the motor network by stimulation of the prefrontal cortex (Gray and Bjorklund 2014). The prefrontal cortex then creates a general plan of action, which is then converted by the premotor area into neural programmes for movement. The primary motor cortex propagates this to the cerebellum and basal ganglia for fine tuning. The optimised plan of action is then sent down the spinal cord for execution of the movement.

Table 33.6 Overview of studies assessing CNS glucose metabolism in MS using [^{18}F]FDG PET

Study	Subjects	Metabolism quantification method	Hypermetabolism
Bakshi et al. (1998)	6 HC 25 MS	Absolute	Whole brain, cortex, WM, subcortical
Derache et al. (2013)	17 RRMS	CMRglu	Negative correlations with fatigue
Roelcke et al. (1997)	16 HC 47 MS	Normalised to mean uptake (CMRglu)	Whole brain, prefrontal cortex, premotor cortex, putamen, supplementary motor area, basal ganglia
Kindred et al. (2014)	8 HC 8 RRMS	SUVmean	Spinal cord
Blinkenberg et al. (2001)	9 HC 23 MS	CMRglu	Cortex, prefrontal cortex, orbitofrontal cortex, caudatus, putamen, thalamus, hippocampus

CMRglu cerebral metabolic rate of glucose, *HC* healthy control, *MS* multiple sclerosis, *RRMS* relapse remitting MS, *SUVmean* mean standardised uptake value, *WM* white matter

Several studies found changes in metabolism in regions of the motor network (Table 33.6). For instance, a reduction in cortical glucose uptake was found to be associated with disease severity expressed as fatigue (Roelcke et al. 1997; Derache et al. 2013). This might be explained by the increased muscular demands caused by a decreased CNS efficacy, and therefore leads to earlier muscular exhaustion, hence fatigue (Rudroff et al. 2014). Also negative correlations have been observed between physical score and metabolism in left parietal regions, right frontal regions, and right temporal regions (Derache et al. 2013). This means the higher physical score, the lower the [^{18}F]FDG uptake in those regions, which might illustrate network disruptions in patients with fatigue. In addition, a decreased [^{18}F]FDG uptake was observed in the spinal cord of MS patients (Kindred et al. 2014). This might indicate that the autonomic nervous system and walking/motor dysfunctions that are often seen in patients with MS could originate from spinal cord neurodegeneration.

While assessing cognitive effects of MS pathology, a negative correlation was observed between cognition and metabolism in thalamus (Derache et al. 2013). This means lower cognitive performance, relates to higher [^{18}F]FDG uptake in the thalamus, and thus may illustrate cerebral compensation for maintaining cognitive function. A more thorough assessment of the effects of MS pathology on cognition revealed a relation between lesion-affected regions, adjacent cortical hypometabolism, and corresponding diminished cognitive performance (Blinkenberg et al. 2001). This study found no other clinical deterioration aside from cognition and therefore illustrates that cognitive deterioration may occur without any other signs of disease progression, most likely resulting from white matter lesion-induced neurodegeneration.

33.6 PET Imaging as a Tool to Aid in Differential Diagnosis

MRI lesions can show a pattern specific for MS. In some cases, lesions seem to resemble tumours, both radiologically and clinically (Di Patre et al. 2003). This type of MS is therefore called tumefactive MS. For the differentiation of the lesions of tumefactive MS from brain tumours, [^{11}C]methionine PET imaging might be employed. Tumours are associated with a high proliferation and protein synthesis (Waarde and Elsinga 2008). For PET imaging of protein synthesis, radiolabelled amino acids, like [^{11}C]methionine, are used. Methionine was shown to have a low uptake in the healthy brain, but in tumours methionine uptake is increased (Jager et al. 2001; Coope et al. 2007). Therefore, [^{11}C]Methionine PET is widely used to aid in the diagnosis of brain tumours, and thus might be used to differentiate between tumefactive MS and cerebral tumours. However, at the moment there is only evidence from case studies to support this concept.

For instance, in a case for which it was not possible to differentiate between a tumefactive MS lesion and a tumour with MRI, [^{11}C]methionine PET displayed no significant uptake in the lesion (Ninomiya et al. 2015). The diagnosis of this specific patient was therefore tumefactive MS, which significantly influenced the selection of treatment strategies. In another case, [^{11}C]methionine PET was used to differentiate a low-grade glioma from a suspected diagnosis of tumefactive MS (Tarkkonen et al. 2016). In this patient there was actually significant [^{11}C]methionine uptake in the lesion, which suggested a possible tumour (Fig. 33.7). In addition, a [^{11}C]PK11195 PET scan was performed, which showed no increased uptake, arguing against MS and leading ultimately to a glioma diagnosis. These cases clearly illustrate that the important contribution PET could potentially have in differential diagnosis in cases where other techniques are inconclusive.

33.7 PET Imaging to Assess Treatment Effects in MS

To study therapy effects on MS pathology, PET imaging can play an important role due to visualisation of alterations in individual biological processes (Table 33.7). Currently, the primary treatment strategy of MS is inhibition of the immune attacks on the myelin sheaths. Current disease modifying therapies are all anti-inflammatory. For example, treatment with fingolimod inhibits the migration of lymphocytes from the lymph nodes (Matloubian et al. 2004; Mandala et al. 2002). Due to the reduction of lymphocytes, the severity of inflammatory responses in MS is reduced. In a [^{11}C]PK11195 PET imaging study, increased tracer uptake in NAWM and GM areas was observed in MS patients prior to fingolimod treatment, as compared to healthy subjects (Sucksdorff et al. 2017). After 6 months of fingolimod treatment patients displayed a decrease in tracer uptake in lesions, but not in other brain areas. Therefore, the inhibition of lymphocyte migration by fingolimod has globally limited effects on the activation of microglia and macrophages outside of the lesions. The observed clinical improvements are therefore probably primarily caused by the reduction of activation of inflammatory cells within the lesions. This illustrates the

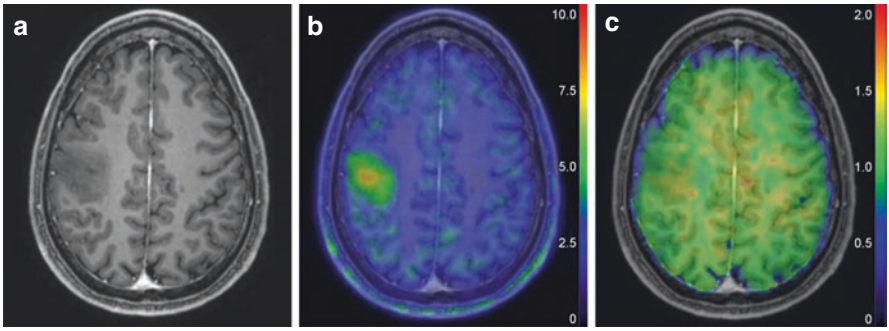

Fig. 33.7 MS differential diagnosis with PET imaging. (**a**) depicts a T1 MRI image with a hypointense lesion. (**b**) is a [^{11}C]methionine PET image, which clearly illustrates an increased uptake at the lesion. (**c**) [^{11}C]PK11195 PET image, illustrating no significant differences in uptake, and thus supported glioma diagnosis, which was confirmed by brain biopsy (permission for the use of the images was obtained; Source: DOI: https://doi.org/10.1016/j.msard.2016.07.016) (Tarkkonen et al. 2016)

Table 33.7 Overview of studies using PET to analyse therapy effects in MS

Study	Tracer	Subjects	Treatment	Treatment response
Sucksdorff et al. (2017)	[^{11}C] PK11195	10 RRMS	Fingolimod	Reduced lesional tracer uptake after 6 months of treatment, but not in other brain areas
Baumgartner et al. (2018)	[^{18}F]FDG	10 HC 9 RRMS	Interferon beta therapy	6 months IFN-beta. After treatment, decreased metabolism in cerebellum, increased metabolism in left inferior parietal cortex, right insula, left temporo-occipital cortex, left frontal cortex, and left striatum
Bunai et al. (2018)	[^{11}C] DPA713	6 HC 4 RRMS	Fingolimod	After 1 year treatment, a broad increased tracer uptake, especially in temporal and parietal cortex
		2 RRMS	Interferon beta therapy	
Ratchford et al. (2012)	[^{11}C] PK11195	9 RRMS	Glatiramer acetate	After 1 year of treatment, whole brain tracer uptake decreased, cerebral white matter, cortical grey matter. No change in binding in lesions
Kaunzner et al. (2017)	[^{11}C] PK11195	5 HC 18 MS	Natalizumab	After 6 months of treatment, decreased tracer uptake in both non- and enhanced lesions. No changes observed in NAWM, thalamus, and cortex

HC healthy control, *IFN-beta* interferon beta, *MS* multiple sclerosis, *NAWM* normal appearing white matter, *RRMS* relapse remitting MS

importance of reducing the inflammatory status within lesions. In another study on the effect of interferon (IFN)-beta therapy, [^{18}F]FDG PET showed no differences between patients and healthy subjects at baseline (Baumgartner et al. 2018). However, after 6 months of treatment, using relative regional glucose metabolism (rCMRglu) as outcome measure, a decreased [^{18}F]FDG uptake was observed in the cerebellum and an increased [^{18}F]FDG uptake in various brain regions in MS patients compared to healthy subjects. Although this might suggest that IFN-beta would lead to a decrease in cerebellar neuronal integrity, due to the use of relative measurements instead of absolute, this effect could also represent a global increase in cerebral metabolic rate of glucose (CMRglu), combined with no increase in cerebellum and, thus, a relative decrease in cerebellum. Nevertheless, these results do not depict any effects of the efficacy of IFN-beta therapy on modulation of the inflammatory response. Another study, which analysed the effects of both fingolimod and IFN-beta, showed an increased [^{11}C]DPA713 uptake at baseline in patients, which was even further increased at follow-up (Bunai et al. 2018). Traditionally, TSPO tracers are used to visualise activated inflammatory cells, however, aside from the pro-inflammatory status (e.g. M1 microglia), activated inflammatory cells can also have a protective function (e.g. M2 microglia) and thus depict protective mechanisms. Nevertheless, the results of these studies show the complexity of disentangling the mechanisms of action of disease modifying therapies in MS.

[^{11}C]PK11195 PET has also been used for the analysis of the effects of glatiramer acetate, which is commonly used in MS treatment. Glatiramer acetate putatively binds to the major histocompatibility complex receptors and thereby inhibits the T-cell response to myelin antigens (Schrempf and Ziemssen 2007). The reduction of adaptive immune system activation should also reduce the activation of the innate immune system. A study analysing the effects of glatiramer acetate with [^{11}C]PK11195 displayed a decreased tracer uptake after 1 year of treatment compared to baseline (Ratchford et al. 2012). Therefore, these results support the concept of a decreased activation of the innate immune system over time due to glatiramer acetate treatment and thus illustrate its mechanism of action.

Antibodies are also commonly used in the treatment of MS. One of these antibodies is natalizumab, which very specifically binds to integrins expressed on the cerebral vasculature, and strongly decreases the influx of lymphocytes into the CNS (Peterson et al. 2002; Yednock et al. 1992). The influx reduction limits the effects of the adaptive immune system in the CNS and subsequently the activation of innate immune cells (Del Pilar Martin et al. 2008). [^{11}C]PK11195 PET imaging showed a decrease of tracer uptake in lesions after 6 months of treatment with natalizumab, but no changes were detected in NAWM, the thalamus, and GM (Kaunzner et al. 2017). These results illustrate that natalizumab treatment also has its main effect on inflammation in lesions compared to non-lesional tissue. While both fingolimod and natalizumab have proven clinical efficacy, this seems to be mainly caused by the reduction of the inflammation within lesions. Therefore, a more thorough assessment of the lesions with PET imaging instead of whole brain analysis would be more indicative for the efficacy of therapies.

33.8 Clinical Notes

The clinical application of PET scanning in MS at this moment is restricted to aiding diagnosis in difficult cases. PET imaging in MS has been mainly used in a research setting so far. If myelin binding ligands can deliver on their promise and quantifying myelin loss in lesions becomes feasible, such scan techniques can probably be used in phase II and III trials to aid in identifying drugs promoting myelin repair. Further down the road, myelin imaging using PET may be used to inform clinicians and patients about the individual treatment effect of myelin restoring treatment protocols. The place of inflammation imaging using PET in MS is more difficult to predict. MRI protocols are already capable of imaging inflammation in MS and do not have the disadvantage of using ionising radiation.

33.9 Conclusion

The use of PET imaging in MS is increasing, in particular, in a research setting. Currently, its primary role in clinical practice is in aiding with differential diagnosis between MS and brain tumours. PET imaging of activation of the innate immune system could be of particular interest in drug development, as the technique would enable objective efficacy evaluation of immune suppressive therapies. Due to the increasing interests in myelin imaging, a method to assess myelin integrity may soon become available. As myelin repair is likely the next target of interest in the treatment of MS, myelin PET could initially be used to determine the efficacy of various remyelination therapies, and in the end to monitor individual remyelination treatment responses.

References

Airas L, Rissanen E, Rinne JO (2015) Imaging neuroinflammation in multiple sclerosis using TSPO-PET. Clin Transl Imaging 3(6):461–473. https://doi.org/10.1007/s40336-015-0147-6

Baecher-Allan C, Kaskow BJ, Weiner HL (2018) Multiple sclerosis: mechanisms and immunotherapy. Neuron 97(4):742–768. https://doi.org/10.1016/j.neuron.2018.01.021

Bakshi R, Miletrch RS, Kinkel PR, Emmet ML, Kinkel WR (1998) High-resolution fluorodeoxyglucose positron emission tomography shows both global and regional cerebral hypometabolism in multiple sclerosis. J Neuroimaging 8(4):228–234. https://doi.org/10.1111/jon199884228

Baumgartner A, Frings L, Schiller F, Stich O, Mix M, Egger K, Schluh G, Rauer S, Meyer PT (2018) Regional neuronal activity in patients with relapsing remitting multiple sclerosis. Acta Neurol Scand 138(6):466–474. https://doi.org/10.1111/ane.13012

Biediger D, Collet C, Armspach J (2014) Multiple sclerosis lesion detection with local multimodal Markovian analysis and cellular automata 'GrowCut.' J Comput Surg. https://doi.org/10.1186/2194-3990-1-3

Blackburn MR, Vance CO, Morschl E, Wilson CN (2009) Adenosine receptors and inflammation. Handb Exp Pharmacol (193):215–269. https://doi.org/10.1007/978-3-540-89615-9_8

Blinkenberg M, Rune K, Jensen CV, Ravnborg MH, Kyllingsbaek S, Holm S, Paulson OB, Sørensen PS (2001) [Reduced metabolism in cerebral cortex correlates with MRI changes and cognitive dysfunction in patients with disseminated sclerosis]. Ugeskr Laeger 63(27):3788–3792

Blinkenberg M, Mathiesen HK, Tscherning T, Jønsson A, Svarer C, Holm S, Sellebjerg F, Paulson OB, Hanson LG, Sorensen PS (2011) Cerebral metabolism, magnetic resonance spectroscopy and cognitive dysfunction in early multiple sclerosis: an exploratory study. Neurol Res 34(1):52–58. https://doi.org/10.1179/1743132811y.0000000059

Bodini B, Veronese M, García-Lorenzo D, Battaglini M, Poirion E, Chardain A, Freeman L, Louapre C, Tchikviladze M, Papeix C, Dollé F, Zalc B, Lubetzki C, Bottlaender M, Turkheimer F, Stankoff B (2016) Dynamic imaging of individual remyelination profiles in multiple sclerosis. Ann Neurol 79:726–738. https://doi.org/10.1002/ana.24620

Bunai T, Terada T, Kono S, Yokokura M, Yoshikawa E, Futatsubashi M, Miyajima H, Ouchi Y (2018) Neuroinflammation following disease modifying therapy in multiple sclerosis: a pilot positron emission tomography study. J Neurol Sci 385:30–33. https://doi.org/10.1016/j.jns.2017.12.004

Chechneva O, Deng W (2016) Mitochondrial translocator protein (TSPO), astrocytes and neuroinflammation. Neural Regen Res 11(7):1056–1057. https://doi.org/10.4103/1673-5374.187027

Colasanti A, Guo Q, Muhlert N, Giannetti P, Onega M, Newbould RD, Ciccarelli O, Rison S, Thomas C, Nicholas R, Muraro PA, Malik O, Owen DR, Piccini P, Gunn RN, Rabiner EA, Matthews PM (2014) In vivo assessment of brain white matter inflammation in multiple sclerosis with 18F-PBR111 PET. J Nucl Med 55(7):1112–1118. https://doi.org/10.2967/jnumed.113.135129

Coope DJ, Cizek J, Eggers C, Vollmar S, Heiss W-D, Herholz K (2007) Evaluation of primary brain tumors using 11C-methionine PET with reference to a normal methionine uptake map. J Nucl Med 48(12):1971–1980. https://doi.org/10.2967/jnumed.107.043240

Datta G, Colasanti A, Kalk N, Owen D, Scott G, Rabiner EA, Gunn RN, Lingford-Hughes A, Malik O, Ciccarelli O, Nicholas R, Nei L, Battaglini M, Stefano ND, Matthews PM (2017a) 11 C-PBR28 and 18 F-PBR111 detect white matter inflammatory heterogeneity in multiple sclerosis. J Nucl Med 58(9):1477–1482. https://doi.org/10.2967/jnumed.116.187161

Datta G, Colasanti A, Rabiner EA, Gunn RN, Malik O, Ciccarelli O, Nicholas R, Van Vlierberghe E, Van Hecke W, Searle G, Santos-Ribeiro A, Matthews PM (2017b) Neuroinflammation and its relationship to changes in brain volume and white matter lesions in multiple sclerosis. Brain 140(11):2927–2938. https://doi.org/10.1093/brain/awx228

De Paula Faria D, Copray S, Sijbesma JWA, Willemsen ATM, Buchpiguel CA, Dierckx RAJO, De Vries EFJ (2014a) PET imaging of focal demyelination and remyelination in a rat model of multiple sclerosis: comparison of [11C]MeDAS, [11C]CIC and [11C]PIB. Eur J Nucl Med Mol Imaging 41(5):995–1003. https://doi.org/10.1007/s00259-013-2682-6

De Paula Faria D, De Vries EFJ, Sijbesma JWA, Dierckx RAJO, Buchpiguel CA, Copray S (2014b) PET imaging of demyelination and remyelination in the cuprizone mouse model for multiple sclerosis: a comparison between [11C]CIC and [11C]MeDAS. NeuroImage 87:395–402. https://doi.org/10.1016/j.neuroimage.2013.10.057

Del Pilar Martin M, Cravens PD, Winger R, Frohman EM, Racke MK, Eagar TN, Zamvil SS, Weber MS, Hemmer B, Karandikar NJ, Kleinschmidt-DeMasters BK, Stüve O (2008) Decrease in the numbers of dendritic cells and CD4 + T cells in cerebral perivascular spaces due to natalizumab. Arch Neurol 65(12):1596–1603. https://doi.org/10.1001/archneur.65.12.noc80051

Dendrou CA, Fugger L, Friese MA (2015) Immunopathology of multiple sclerosis. Nat Rev Immunol 5(9):545–558. https://doi.org/10.1038/nri3871

Derache N, Grassiot B, Mézenge F, Emmanuelle Dugué A, Desgranges B, Constans JM, Defer GL (2013) Fatigue is associated with metabolic and density alterations of cortical and deep gray matter in relapsing-remitting-multiple sclerosis patients at the earlier stage of the disease: a PET/MR study. Mult Scler Relat Disord 2(4):362–369. https://doi.org/10.1016/j.msard.2013.03.005

Di Patre PL, Castillo V, Delavelle J, Vuillemoz S, Picard F, Landis T (2003) "Tumor-mimicking" multiple sclerosis. Clin Neuropathol 22(5):235–239

Fakhoury M (2016) Revisiting the serotonin hypothesis: implications for major depressive disorders. Mol Neurobiol 53:2778–2786. https://doi.org/10.1007/s12035-015-9152-z

Ferguson B, Matyszak MK, Esiri MM, Perry VH (1997) Axonal damage in acute multiple sclerosis lesions. Brain 120(Pt 3):393–399. https://doi.org/10.1093/brain/120.3.393

Franklin RJM, Ffrench-Constant C (2008) Remyelination in the CNS: from biology to therapy. Nat Rev Neurosci 9(11):839–855. https://doi.org/10.1038/nrn2480

Freeman L, Garcia-Lorenzo D, Bottin L, Leroy C, Louapre C, Bodini B, Papeix C, Assouad R, Granger B, Tourbah A, Dollé F, Lubetzki C, Bottlaender M, Stankoff B (2015) The neuronal component of gray matter damage in multiple sclerosis: a [11C]flumazenil positron emission tomography study. Ann Neurol 78(4):554–567. https://doi.org/10.1002/ana.24468

Garcia GE, Truong LD, Li P, Zhang P, Du J, Chen J-F, Feng L (2007) Adenosine A 2A receptor activation and macrophage-mediated experimental glomerulonephritis. FASEB J 22(2):445–454. https://doi.org/10.1096/fj.07-8430com

Giannetti P, Politis M, Su P, Turkheimer F, Malik O, Keihaninejad S, Wu K, Reynolds R, Nicholas R, Piccini P (2014) Microglia activation in multiple sclerosis black holes predicts outcome in progressive patients: an in vivo [(11)C](R)-PK11195-PET pilot study. Neurobiol Dis 65:203–210. https://doi.org/10.1016/j.nbd.2014.01.018

Giannetti P, Politis M, Su P, Turkheimer FE, Malik O, Keihaninejad S, Wu K, Waldman A, Reynolds R, Nicholas R, Piccini P (2015) Increased PK11195-PET binding in normal-appearing white matter in clinically isolated syndrome. Brain 138(1):110–119. https://doi.org/10.1093/brain/awu331

Gray P, Bjorklund DF (2014) Psychology. Worth, New York

Grecchi E, Veronese M, Bodini B, García-Lorenzo D, Battaglini M, Stankoff B, Turkheimer FE (2017) Multimodal partial volume correction: application to [11C]PIB PET/MRI myelin imaging in multiple sclerosis. J Cereb Blood Flow Metab 37(12):3803–3817. https://doi.org/10.1177/0271678X17712183

Gut P (2015) Targeting mitochondrial energy metabolism with TSPO ligands. Biochem Soc Trans 43(4):537–542. https://doi.org/10.1042/bst20150019

Hagens MHJ, Golla SV, Wijburg MT, Yaqub M, Heijtel D, Steenwijk MD, Schober P, Brevé JJP, Schuit RC, Reekie TA, Kassiou M, van Dam AM, Windhorst AD, Killestein J, Barkhof F, van Berckel BNM, Lammertsma AA (2018) In vivo assessment of neuroinflammation in progressive multiple sclerosis: a proof of concept study with [18F]DPA714 PET. J Neuroinflammation 15(1):314. https://doi.org/10.1186/s12974-018-1352-9

Herranz E, Giannì C, Louapre C, Treaba CA, Govindarajan ST, Ouellette R, Loggia ML, Sloane JA, Madigan N, Izquierdo-Garcia D, Ward N, Mangeat G, Granberg T, Klawiter EC, Catana C, Hooker JM, Taylor N, Ionete C, Kinkel RP, Mainero C (2016) Neuroinflammatory component of gray matter pathology in multiple sclerosis. Ann Neurol 80(5):776–790. https://doi.org/10.1002/ana.24791

Hesse S, Moeller F, Petroff D, Lobsien D, Luthardt J, Regenthal R, Becker GA, Patt M, Thomae E, Seese A, Meyer PM, Bergh FT, Sabri O (2014) Altered serotonin transporter availability in patients with multiple sclerosis. Eur J Nucl Med Mol Imaging 41(5):827–835. https://doi.org/10.1007/s00259-013-2636-z

Huang WJ, Chen WW, Zhang X (2017) Multiple sclerosis: pathology, diagnosis and treatments (review). Exp Ther Med 13(6):3163–3166. https://doi.org/10.3892/etm.2017.4410

Jager PL, Vaalburg W, Pruim J, de Vries EG, Langen KJ, Piers DA (2001) Radiolabeled amino acids: basic aspects and clinical applications in oncology. J Nucl Med 42(3):432–445

Kaunzner UW, Gauthier SA (2017) MRI in the assessment and monitoring of multiple sclerosis: an update on best practice. Ther Adv Neurol Disord 10(6):247–261. https://doi.org/10.1177/1756285617708911

Kaunzner UW, Kang Y, Monohan E, Kothari PJ, Nealon N, Perumal J, Vartanian T, Kuceyeski A, Vallabhajosula S, Mozley PD, Riley CS, Newman SM, Gauthier SA (2017) Reduction of PK11195 uptake observed in multiple sclerosis lesions after natalizumab initiation. Mult Scler Relat Disord 15:27–33. https://doi.org/10.1016/j.msard.2017.04.008

Kindred JH, Koo PJ, Rudroff T (2014) Glucose uptake of the spinal cord in patients with multiple sclerosis detected by 18f-fluorodeoxyglucose PET/CT after walking. Spinal Cord 52(Suppl 3):S11–S13. https://doi.org/10.1038/sc.2014.130

Kurtzke JF (1983) Rating neurologic impairment in multiple sclerosis: an expanded disability status scale (EDSS). Neurology 33(11):1444–1452

Lassmann H, Van Horssen J, Mahad D (2012) Progressive multiple sclerosis: pathology and pathogenesis. Nat Rev Neurol 8:647–656. https://doi.org/10.1038/nrneurol.2012.168

Mandala S, Hajdu R, Bergstrom J, Quackenbush E, Xie J, Milligan J, Thornton R, Shei GJ, Card D, Keohane CA, Rosenbach M, Hale J, Lynch CL, Rupprecht K, Parsons W, Rosen H (2002) Alteration of lymphocyte trafficking by sphingosine-1-phosphate receptor agonists. Science 296(5566):346–349. https://doi.org/10.1126/science.1070238

Matías-Guiu JA, Cabrera-Martín MN, Matías-Guiu J, Oreja-Guevara C, Riola-Parada C, Moreno-Ramos T, Arrazola J, Carreras JL (2015) Amyloid PET imaging in multiple sclerosis: an 18F-florbetaben study. BMC Neurol 15:243. https://doi.org/10.1186/s12883-015-0502-2

Matías-Guiu JA, Cabrera-Martín MN, Cortés-Martínez A, Pytel V, Moreno-Ramos T, Oreja-Guevara C, Carreras JL, Matías-Guiu J (2017) Amyloid PET in pseudotumoral multiple sclerosis. Mult Scler Relat Disord 15:15–17. https://doi.org/10.1016/j.msard.2017.05.002

Matloubian M, Lo CG, Cinamon G, Lesneski MJ, Xu Y, Brinkmann V, Allende ML, Proia RL, Cyster JG (2004) Lymphocyte egress from thymus and peripheral lymphoid organs is dependent on S1P receptor 1. Nature 427(6972):355–360. https://doi.org/10.1038/nature02284

Miljković D, Spasojević I (2013) Multiple sclerosis: molecular mechanisms and therapeutic opportunities. Antioxid Redox Signal 19(18):2286–2334. https://doi.org/10.1089/ars.2012.5068

Mitchell RLC, Phillips LH (2007) The psychological, neurochemical and functional neuroanatomical mediators of the effects of positive and negative mood on executive functions. Neuropsychologia 45(4):617–629. https://doi.org/10.1016/j.neuropsychologia.2006.06.030

Mohler H (2009) Role of GABAA receptors in cognition. Biochem Soc Trans 37(Pt 6):1328–1333. https://doi.org/10.1042/BST0371328

Nijland PG, Michailidou I, Witte ME, Mizee MR, Van Der Pol SMA, Van Het Hof B, Reijerkerk A, Pellerin L, van der Valk P, de Vries HE, van Horssen J (2014) Cellular distribution of glucose and monocarboxylate transporters in human brain white matter and multiple sclerosis lesions. Glia 62(7):1125–1141. https://doi.org/10.1002/glia.22667

Ninomiya S, Hara M, Morita A, Teramoto H, Momose M, Takahashi T, Kamei S (2015) Tumefactive demyelinating lesion differentiated from a brain tumor using a combination of magnetic resonance imaging and ^{11}C-methionine positron emission tomography. Intern Med 54(11):1411–1414. https://doi.org/10.2169/internalmedicine.54.3712

Oh U, Fujita M, Ikonomidou VN, Evangelou IE, Matsuura E, Harberts E, Ohayon J, Pike VW, Zhang Y, Zoghbi SS, Innis RB, Jacobson S (2011) Translocator protein PET imaging for glial activation in multiple sclerosis. J Neuroimmune Pharmacol 6(3):354–361. https://doi.org/10.1007/s11481-010-9243-6

Owen DR, Yeo AJ, Gunn RN, Song K, Wadsworth G, Lewis A, Rhodes C, Pulford DJ, Bennacef I, Parker CA, Stjean PL, Cardon LR, Mooser VE, Matthews PM, Rabiner EA, Rubio JP (2012) An 18-kDa translocator protein (TSPO) polymorphism explains differences in binding affinity of the PET radioligand PBR28. J Cereb Blood Flow Metab 32(1):1–5. https://doi.org/10.1038/jcbfm.2011.147

Papadopoulos V, Baraldi M, Guilarte TR, Knudsen TB, Lacapère JJ, Lindemann P, Norenberg MD, Nutt D, Weizman A, Zhang MR, Gavish M (2006) Translocator protein (18 kDa): new nomenclature for the peripheral-type benzodiazepine receptor based on its structure and molecular function. Trends Pharmacol Sci 27(8):402–409. https://doi.org/10.1016/j.tips.2006.06.005

Peterson JW, Bö L, Mörk S, Chang A, Ransohoff RM, Trapp BD (2002) VCAM-1-positive microglia target oligodendrocytes at the border of multiple sclerosis lesions. J Neuropathol Exp Neurol 61(6):539–546. https://doi.org/10.1093/jnen/61.6.539

Pietroboni AM, Carandini T, Colombi A, Mercurio M, Ghezzi L, Giulietti G, Scarioni M, Arighi A, Fenoglio C, De Riz MA, Fumagalli GG, Basilico P, Serpente M, Bozzali M, Scarpini E, Galimberti D, Marotta G (2019) Amyloid PET as a marker of normal-appearing white matter

early damage in multiple sclerosis: correlation with CSF β-amyloid levels and brain volumes. Eur J Nucl Med Mol Imaging 46(2):280–287. https://doi.org/10.1007/s00259-018-4182-1

Politis M, Giannetti P, Su P, Turkheimer F, Keihaninejad S, Wu K, Waldman A, Malik O, Matthews PM, Reynolds R, Nicholas R, Piccini P (2012) Increased PK11195 PET binding in the cortex of patients with MS correlates with disability. Neurology 79(6):523–530. https://doi.org/10.1212/WNL.0b013e3182635645

Prineas JW, Connell F (1979) Remyelination in multiple sclerosis. Ann Neurol 5(1):22–31. https://doi.org/10.1002/ana.410050105

Ramagopalan SV, Dobson R, Meier UC, Giovannoni G (2010) Multiple sclerosis: risk factors, prodromes, and potential causal pathways. Lancet Neurol 9(7):727–739. https://doi.org/10.1016/S1474-4422(10)70094-6

Ratchford JN, Endres CJ, Hammoud DA, Pomper MG, Shiee N, McGready J, Pham DL, Calabresi PA (2012) Decreased microglial activation in MS patients treated with glatiramer acetate. J Neurol 259(6):1199–1205. https://doi.org/10.1007/s00415-011-6337-x

Ridsdale RA, Beniac DR, Tompkins TA, Moscarello MA, Harauz G (2002) Three-dimensional structure of myelin basic protein. J Biol Chem 272:4269–4275. https://doi.org/10.1074/jbc.272.7.4269

Rissanen E, Virta JR, Paavilainen T, Tuisku J, Helin S, Luoto P, Parkkola R, Rinne JO, Airas L (2013) Adenosine A2A receptors in secondary progressive multiple sclerosis: a [11C]TMSX brain PET study. J Cereb Blood Flow Metab 33(9):1394–1401. https://doi.org/10.1038/jcbfm.2013.85

Rissanen E, Tuisku J, Rokka J, Paavilainen T, Parkkola R, Rinne JO, Airas L (2014) In vivo detection of diffuse inflammation in secondary progressive multiple sclerosis using PET imaging and the radioligand 11C-PK11195. J Nuclar Med 55(6):939–944. https://doi.org/10.2967/jnumed.113.131698

Roelcke U, Kappos L, Lechner-Scott J, Brunnschweiler H, Huber S, Ammann W, Plohmann A, Dellas S, Maguire RP, Missimer J, Radü EW, Steck A, Leenders KL (1997) Reduced glucose metabolism in the frontal cortex and basal ganglia of multiple sclerosis patients with fatigue: a 18 F-fluorodeoxyglucose positron emission tomography study. Neurology 48(6):1566–1571. https://doi.org/10.1212/WNL.48.6.1566

Rudroff T, Kindred JH, Koo PJ, Karki R, Hebert JR (2014) Asymmetric glucose uptake in leg muscles of patients with multiple sclerosis during walking detected by [18F]-FDG PET/CT. NeuroRehabilitation 35(4):813–823. https://doi.org/10.3233/NRE-141179

Schrempf W, Ziemssen T (2007) Glatiramer acetate: mechanisms of action in multiple sclerosis. Autoimmun Rev 6(7):469–475. https://doi.org/10.1016/j.autrev.2007.02.003

Sigel E, Ernst M (2018) The benzodiazepine binding sites of GABAA receptors. Trends Pharmacol Sci 39(7):659–671. https://doi.org/10.1016/j.tips.2018.03.006

Singhal T, O'Connor K, Dubey S, Belanger AP, Hurwitz S, Chu R, Tauhid S, Kijewski MF, Dicarli MF, Weiner HL, Bakshi R (2018) 18F-PBR06 versus 11C-PBR28 PET for assessing white matter translocator protein binding in multiple sclerosis. Clin Nucl Med 43(9):e289–e295. https://doi.org/10.1097/RLU.0000000000002179

Sridharan S, Raffel J, Nandoskar A, Record C, Brooks DJ, Owen D, Sharp D, Muraro PA, Gunn R, Nicholas R (2019) Confirmation of specific binding of the 18-kDa translocator protein (TSPO) radioligand [18F]GE-180: a blocking study using XBD173 in multiple sclerosis normal appearing white and grey matter. Mol Imaging Biol 21(5):935–944. https://doi.org/10.1007/s11307-019-01323-8

Stapulionis R, Oliveira CLP, Gjelstrup MC, Pedersen JS, Hokland ME, Hoffmann SV, Poulsen K, Jacobsen C, Vorup-Jensen T (2008) Structural insight into the function of myelin basic protein as a ligand for integrin alpha M beta 2. J Immunol 180(6):3946–3956

Sucksdorff M, Rissanen E, Tuisku J, Nuutinen S, Paavilainen T, Rokka J, Rinne J, Airas L (2017) Evaluation of the effect of fingolimod treatment on microglial activation using serial PET imaging in multiple sclerosis. J Nucl Med 58(10):1646–1651. https://doi.org/10.2967/jnumed.116.183020

Takata K, Kato H, Shimosegawa E, Okuno T, Koda T, Sugimoto T, Mochizuki H, Hatazawa J, Nakatsuji Y (2014) 11C-Acetate PET imaging in patients with multiple sclerosis. PLoS One 9(11):e111598. https://doi.org/10.1371/journal.pone.0111598

Tarkkonen A, Rissanen E, Tuokkola T, Airas L (2016) Utilization of PET imaging in differential diagnostics between a tumefactive multiple sclerosis lesion and low-grade glioma. Mult Scler Relat Disord 9:147–149. https://doi.org/10.1016/j.msard.2016.07.016

Thompson AJ, Banwell BL, Barkhof F, Carroll WM, Coetzee T (2018) Diagnosis of multiple sclerosis: 2017 revisions of the McDonald criteria. Lancet Neurol 17(2):162–173. https://doi.org/10.1016/s1474-4422(17)30470-2

Traugott U, Reinherz EL, Raine CS (1983) Multiple sclerosis. Distribution of T cells, T cell subsets and Ia-positive macrophages in lesions of different ages. J Neuroimmunol 4(3):201–221. https://doi.org/10.1016/0165-5728(83)90036-X

Unterrainer M, Mahler C, Vomacka L, Lindner S, Havla J, Brendel M, Böning G, Ertl-Wagner B, Kümpfel T, Milenkovic VM, Rupprecht R, Kerschensteiner M, Bartenstein P, Albert NL (2018) TSPO PET with [18F]GE-180 sensitively detects focal neuroinflammation in patients with relapsing–remitting multiple sclerosis. Eur J Nucl Med Mol Imaging 45(8):1423–1431. https://doi.org/10.1007/s00259-018-3974-7

Vowinckel E, Reutens D, Becher B, Verge G, Evans A, Owens T, Antel JP (1997) PK11195 binding to the peripheral benzodiazepine receptor as a marker of microgila activation in multiple sclerosis and experimental autoimmune encephalomyelitis. J Neurosci Res 50(2):345–353. https://doi.org/10.1002/(SICI)1097-4547(19971015)50:2<345::AID-JNR22>3.0.CO;2-5

Waarde A, Elsinga P (2008) Proliferation markers for the differential diagnosis of tumor and inflammation. Curr Pharm Des 14(31):3326–3339. https://doi.org/10.2174/138161208786549399

Waniewski RA, Martin DL (1998) Preferential utilization of acetate by astrocytes is attributable to transport. J Neurosci 18(14):5225–5233. https://doi.org/10.1523/jneurosci.18-14-05225.1998

Wu C, Wang C, Popescu DC, Zhu W, Somoza EA, Zhu J, Condie AG, Flask CA, Miller RH, MacKlin W, Wang Y (2010) A novel PET marker for in vivo quantification of myelination. Bioorg Med Chem 18(24):8592–8599. https://doi.org/10.1016/j.bmc.2010.10.018

Wu C, Bowers MT, Shea JE (2011) On the origin of the stronger binding of PIB over thioflavin T to protofibrils of the Alzheimer Amyloid-β peptide: a molecular dynamics study. Biophys J 100(5):1316–1324. https://doi.org/10.1016/j.bpj.2011.01.058

Yednock TA, Cannon C, Fritz LC, Sanchez-Madrid F, Steinman L, Karin N (1992) Prevention of experimental autoimmune encephalomyelitis by antibodies against α4βl integrin. Nature 356(6364):63–66. https://doi.org/10.1038/356063a0

Zeydan B, Lowe VJ, Schwarz CG, Przybelski SA, Tosakulwong N, Zuk SM, Senjem ML, Gunter JL, Roberts RO, Mielke MM, Benarroch EE, Rodriguez M, Machulda MM, Lesnick TG, Knopman DS, Petersen RC, Jack CR, Kantarci K, Kantarci OH (2018) Pittsburgh compound-B PET white matter imaging and cognitive function in late multiple sclerosis. Mult Scler J 24(6):739–749. https://doi.org/10.1177/1352458517707346

PET and SPECT Imaging of Neurotoxicity

34

Erik F. J. de Vries, Rudi A. J. O. Dierckx,
and Didima M. G. de Groot

Contents

34.1 Introduction 918
34.1.1 Exposure to Neurotoxins 919
34.1.2 Developmental Neurotoxicity 920
34.1.3 Assessment of Neurotoxicity 921
34.1.4 Imaging of Neurotoxicity 922
34.2 Intrauterine Imaging of Exposure to Xenobiotics 923
34.2.1 Imaging of the Blood–Placenta Barrier 923
34.2.2 Imaging Intrauterine Fetal Accumulation of Neurotoxins 924
34.2.3 Imaging Pharmacological Response to Intrauterine Fetal Exposure 925
34.3 Developmental Neurotoxicity After Maternal Exposure to Xenobiotics 926
34.3.1 Methodology 926
34.3.2 Methylazoxymethanol 927
34.3.3 Methylmercury 927
34.4 Neurotoxicity After Adulthood Intoxication 929
34.4.1 Organic Solvents 929
34.4.2 Metals 933
34.4.3 Pesticides 936
34.4.4 Dioxins and PCBs 937

E. F. J. de Vries (✉)
Nuclear Medicine and Molecular Imaging, University Medical Center Groningen, University of Groningen, Groningen, The Netherlands
e-mail: e.f.j.de.vries@umcg.nl

R. A. J. O. Dierckx
Nuclear Medicine and Molecular Imaging, University Medical Center Groningen, Groningen, The Netherlands

Department of Radiology and Nuclear Medicine, Ghent University, Ghent, Belgium
e-mail: r.a.dierckx@umcg.nl

D. M. G. de Groot
Netherlands Organization for Applied Scientific Research (TNO), Zeist, The Netherlands

Neurotoxicology|Safety Pharmacology, Stevensbeek, The Netherlands

R. A. J. O. Dierckx et al. (eds.), *PET and SPECT in Neurology*,
https://doi.org/10.1007/978-3-030-53168-3_34

34.5 Neurotoxicity in Suicide Survivors..... 938
34.5.1 Cyanide..... 938
34.5.2 Carbon Monoxide..... 939
34.5.3 Pesticides..... 939
34.5.4 Drug Overdose..... 940
34.6 Concluding Remarks..... 940
References..... 941

Abstract

From conception until death, we are exposed to neurotoxins that can potentially induce toxic encephalopathy. Neurotoxins can cause acute adverse effects or show delayed symptoms. They can even induce impaired brain development in the offspring of exposed pregnant females. Both in patients and in animals, it can be difficult to establish the effects of toxins on the (developing) brain. Functional imaging with positron emission tomography (PET) or single-photon emission computed tomography (SPECT) could provide useful tools for preclinical testing of (developmental) neurotoxicity of potential toxic substances. These techniques could also aid clinicians in determining the damage that was done to brain functioning by exposure to a neurotoxin, and they may provide insight in the mechanisms that are involved in the intoxication. This book chapter reviews the potential applications of PET and SPECT imaging in (developmental) neurotoxicity testing and in the evaluation of functional deficits in the brain after exposure to neurotoxins.

Abbreviations

[^{11}C]DOPA	L-[^{11}C]-3,4-dihydroxyphenylalanine
[^{18}F]FDG	2′-[^{18}F]fluoro-2′-deoxyglucose
[^{18}F]FDOPA	L-6-[^{18}F]fluoro-3,4-dihydroxyphenylalanine
BBB	Blood–brain barrier
LPS	Lipopolysaccharide
MAM	Methylazoxymethanol
MPTP	1-Methyl-4-phenyl-1,2,3,6-tetrahydropyridine
MRI	Magnetic resonance imaging
PCBs	Polychlorinated biphenyls
PET	Positron emission tomography
SPECT	Single-photon emission computed tomography
TCDD	2,3,7,8-tetrachlorodibenzo-*p*-dioxin

34.1 Introduction

In our daily lives, we are continuously exposed to chemicals and toxins from the environment, medication, drinking water, and food (Prüss-Ustün et al. 2011). In most cases, exposure does not have any detrimental effect, because the human body

has several defense mechanisms against potentially harmful substances. Examples of such effective protection mechanisms are the immune system and the liver that support detoxification and excretion of harmful substances. In addition to the central defense mechanisms, some critical organs have their own firewall. The brain, for example, is well protected behind the blood–brain barrier (BBB), which prevents brain entry by pathogens, particles, and large hydrophilic molecules. In addition, the BBB contains several efflux pumps that actively extrude xenobiotics from the brain (Leslie et al. 2005). These defense mechanisms, however, are not perfect. Occasionally, a toxic substance can penetrate the BBB and interfere with neurotransmission or cause damage to the brain. This can culminate in the destruction of neurons and eventually in loss of function. This process is called neurotoxicity and can be defined as the ability of substances to exert a destructive or poisonous effect upon nervous tissue. The common perception is that neurotoxicity is induced by exposure to harmful substances that originate outside the body. However, several compounds produced by our own body are also capable of inflicting brain injury. These endogenous toxic substances include glutamate, reactive oxygen species, and beta-amyloid. The production of these harmful endogenous substances and the neurotoxicity induced by them play an important role particularly in neurodegenerative diseases but also in psychiatric disorders that are associated with inflammation and/or brain atrophy. Imaging of these diseases has already been discussed in other chapters of this book series. This chapter will therefore focus only on neurotoxicity induced by exposure to exogenous substances.

34.1.1 Exposure to Neurotoxins

Whether a potentially harmful substance will actually induce neurotoxicity depends on numerous factors. The nature and importance of these factors can strongly differ between individual substances. In general, however, the dose, duration, and time window of exposure determine the severity of adverse effects (Tennekes and Sánchez-Bayo 2013). Neurotoxins can have an immediate effect after acute exposure to high levels of a hazardous compound. The cause of an acute toxic exposure can be either accidental in case of calamities or intentional, for example, as a result of a suicide attempt by a drug overdose. In case of acute exposure, the cause of neurotoxicity can easily be ascribed to a particular neurotoxin and as a result it may sometimes be possible to take specific countermeasures to reverse or reduce the (long-term) damage. In contrast to acute neurotoxicity, chronic exposure to low doses of a xenobiotic may remain asymptomatic for an extended period of time. During this latency period, brain injury accumulates until a threshold is reached and delayed symptoms of neurotoxicity become overt. At this stage, damage to the brain is often already irreversible. Some evidence indicates that neurotoxicity can even develop into neurodegenerative diseases like Alzheimer's disease and Parkinson's disease (Bartels 2011). In many cases, chronic exposure to a potential neurotoxin is unintentional, and therefore it can be difficult to correlate delayed neurotoxicity to a specific cause. Retrospective studies may give an indication of the potential culprit(s), but these studies may be prone to bias and therefore the

results should be interpreted with care (Lees-Haley and Williams 1997). In some situations, the cause–effect relationship between a specific xenobiotic and neurological symptoms has been indisputably proven. A notorious example is the neurological syndrome, called Minamata disease, which is caused by methyl mercury poisoning (Ekino et al. 2007). This syndrome was first discovered in 1953 in the Minamata Bay region (Japan), where polluted industrial wastewater caused bioaccumulation of high levels of methyl mercury in fish and shellfish. The seafood was subsequently consumed by the local population, resulting in high uptake of methyl mercury. More recently, Spencer and coworkers reported evidence for a causal relationship between environmental chemicals and Western Pacific amyotrophic lateral sclerosis–Parkinson dementia (ALS–PD) complex in three genetically isolated areas (Guam, Kii, W. Papua). What these regions had in common was that the locals used cycad seed kernels for food consumption and medical care. Metabolites in the cycad seed kernels with genotoxic and neurotoxic properties like cycasin and methylazoxymethanol (MAM) appeared to cause ALS–PD (Kisby and Spencer 2011). Not only environmental pollution but also chronic occupational exposure to potentially harmful substances presents a serious risk of neurotoxicity. Workers in particular occupations (e.g., painters, industrial workers, and farmers) are frequently exposed to hazardous compounds, such as organic solvents, chemicals, pesticides, and herbicides, that potentially can be causatives of neurotoxicity (Meyer-Baron et al. 2012). Chronic exposure to harmful substances, however, can also be voluntary. Especially abuse of recreational drugs can be a potential risk factor for neurotoxicity, because of either the drug itself or contaminations in the drug. For example, long-term use of XTC was found to seriously impair brain functioning (Sarkar and Schmued 2010). Because of the addictive nature of recreational drugs, it is often difficult to convince users of the potential risk. Brain imaging in addiction will be covered by another chapter in this book series, and therefore neurotoxicity as a result of the chronic use of drugs of abuse will not be addressed in detail in this chapter.

34.1.2 Developmental Neurotoxicity

Not only the level and duration of exposure to harmful substances are important for the development of neurotoxicity, but also the specific phase in life at which the exposure occurs is a crucial factor. The brain is particularly vulnerable during development. Different brain regions have different functions and develop at different moments of time by specific processes of proliferation, migration, and differentiation. Moreover, the capacity of the blood–brain barrier to protect the brain from xenobiotics is low in the immature brain (Ek et al. 2012). Neurotoxins can not only induce direct damage to the immature brain but also interfere with normal development of the brain (Bondy and Campbell 2005). Exposure of pregnant and lactating women to chemicals, pharmaceuticals, or toxins can therefore be potentially harmful to their own brain, as well as to the development of the brain of their children. Moreover, brain development is still incomplete when a child is born. The brain

continues to develop until early adulthood; brain development ends approximately at the age of 20–25 years. As a consequence, exposure to hazardous compounds presents a higher risk for (developmental) neurotoxicity to the fetus and infants than to adults. Despite the differences in vulnerability between infants and adults, existing international guidelines for toxicity testing mainly focus on exposure of adult animals and on physical malformations of the newborn after in utero exposure. However, the safety information from adults does not always adequately predict the safety profiles for pediatric groups, especially for immature systems such as the developing brain (Coecke et al. 2006).

34.1.3 Assessment of Neurotoxicity

Currently, several in vitro and in vivo methods are used to assess the neurotoxicity of a specific compound (Bull 2006). In vitro tests are usually performed on primary brain cells isolated from rodents or on cell lines, which can be of various origin. Cytotoxicity can be used as a general endpoint, but also more specific parameters, like morphology and electrophysiology, are applied (De Groot et al. 2013). Although these in vitro tests may give a first indication of the neurotoxicity potential of a specific compound, the predictive value of these assays is often limited. In vivo evaluation of neurotoxicity is usually performed in rodents, especially when referring to regulatory testing of chemicals for (developmental) neurotoxicity, although more recently the use of zebra fish embryos and larvae is explored (De Esch et al. 2012). In vivo tests in general comprise assessment of structural hallmarks by neuropathology and a series of functional tests addressing different domains of the nervous system to assess behavioral, physiological, and neurological endpoints, including impaired motor, sensory, and cognitive function. An important limitation of the behavioral tests is that they can only show symptoms of toxicity, rather than directly reveal neurotoxicity in the brain itself. As a consequence, the observed behavioral effects could as well originate from other factors than impaired brain functioning. Moreover, most behavioral tests were only validated for adult animals and may therefore not be suitable to assess *developmental* neurotoxicity. Both the behavioral tests and the proposed morphological tests are not very sensitive (De Groot et al. 2005). Besides these shortcomings, the existing neurotoxicity tests are also extremely laborious and require the sacrifice of hundreds of animals. As a result, the potential to cause detrimental effects on the (developing) brain has been investigated for only a limited number of chemicals, for example for organic solvents (De Groot 2017). For hazard identification and risk assessment of potentially harmful substances, more sensitive tests that could detect abnormalities directly in the brain would be highly advantageous (Radonjic et al. 2013).

Information about neurotoxicity in humans is scarce. Well-designed prospective studies in humans are not possible for ethical reasons. Most data originate from retrospective evaluation of accidents or incidents. Large epidemiological studies have provided relevant information on the detrimental effects of chemicals on the

developing brain (i.e., effects in fetuses, children, and adolescents), but only for a limited number of compounds: heavy metals (lead, methylmercury, cadmium), dioxins, and dioxin-like polychlorinated biphenyls (PCBs), organochlorines (DDT/DDE/HCB), organophosphates, carbamates, and some others (bisphenol A, OH-PCBs, phthalates, flame retardants, perfluoro compounds). Epidemiological studies in humans concerning the neurotoxic potency of compounds on the developing brain are by definition long-lasting and very costly, as they involve the study of more than one generation. Supportive evidence is obtained from animal studies, which increasingly employ a combination of modern technologies like in vivo imaging, microdosing, sensor technologies, modern statistics, and various -omics.

In case of suspected neurotoxicity, a patient will first be assessed by clinical evaluation, including standard neurological examination (Bull 2006). When necessary, the examination can be extended with neuropsychological, electrophysiological, and behavioral tests. Imaging can also be added, as it enables investigation of neurotoxicity-related effects on brain structure and function in a noninvasive manner. The results of structural or functional neuroimaging investigations can be integrated with the data from the neurobehavioral evaluation to get better insight into the extent of the neurotoxicity and the affected brain structures, which can provide a better understanding of the observed symptoms.

34.1.4 Imaging of Neurotoxicity

Magnetic resonance imaging (MRI) is the most frequently applied neuroimaging technique to assess neurotoxicity. Structural MRI can provide high-resolution anatomical information about (changes in) individual brain structures. Special MRI techniques, such as BOLD, diffusion tensor imaging, and magnetic resonance spectroscopy, can also provide some insight in functional brain parameters. PET and SPECT are highly sensitive functional brain imaging techniques that are largely complementary to MRI. PET and SPECT are based on measurement of the kinetics and distribution of radiolabeled diagnostic probes (tracers) that participate in a specific biochemical or physiological process. Processes that can be monitored by PET and SPECT include receptor expression and occupancy, transporter and enzyme activity, blood flow, glucose metabolism. To measure a specific target or process of interest with PET or SPECT, a suitable tracer is required. When suitable tracers are available, PET and SPECT can not only give insight in the extent of neurodegeneration but also detect impairment of neurotransmission. Despite the potential advantages, the use of PET and SPECT in neurotoxicity assessment is still limited. In preclinical studies, toxicologists still largely rely on behavioral tests and histopathology of postmortem tissues. If neuroimaging is performed in humans, MRI is often selected as the method of choice. This chapter aims to give the reader insight in some opportunities that PET and SPECT may offer for assessment of neurotoxicity after exposure to exogenous neurotoxins. Exposure during different episodes of our lifetime, from fetus to adult, will be addressed.

34.2 Intrauterine Imaging of Exposure to Xenobiotics

34.2.1 Imaging of the Blood–Placenta Barrier

The developing fetus is connected to the outside world via the placenta, which is responsible for oxygen supply, nutrient uptake, and waste excretion. Since there is no direct intermingling between maternal and fetal blood, the placenta also serves as an efficient barrier protecting the fetus from microbes and many (but not all) xenobiotic substances. Still, maternal exposure to harmful chemicals and drugs may affect brain development of the fetus, if neurotoxins can cross the placenta and accumulate in the fetal brain. Part of the defense system of the placenta is formed by a series of efflux pumps that actively remove many harmful substances from the placenta back into the maternal blood pool (Leslie et al. 2005). One of these efflux pumps is the P-glycoprotein pump. Chung and coworkers investigated the activity of the P-glycoprotein pump in the blood–placenta barrier in pregnant macaques using PET imaging with the P-glycoprotein substrate [^{11}C]verapamil (Chung et al. 2010). The macaques were imaged twice: at day 75 (mid-gestation) and day 150 (late gestation) after conception. If P-glycoprotein in the placenta functions properly, the efflux pump prevents accumulation of the PET tracer in the fetus. Cyclosporine A is a competitive inhibitor of the P-glycoprotein pump and thus hampers the efflux of the PET tracer, resulting in an increase in tracer uptake in the fetus. In their study, Chung et al. used the cyclosporine A-induced increase in [^{11}C]verapamil uptake in the fetal liver (relative to maternal blood) as a measure for P-glycoprotein activity. At late gestation, cyclosporine induced a significantly larger increase in [^{11}C]verapamil uptake in the fetal liver than at mid-gestation, suggesting that P-glycoprotein activity was higher at late gestation. These results would implicate that at mid-gestation, the fetus is more vulnerable towards toxic compounds that are substrate of P-glycoprotein than at late gestation.

The P-glycoprotein pump in the placenta can also be affected by external factors, like infections. Wang and coworkers (Wang et al. 2005) showed that in the placenta of pregnant female rats, *mdr1a* and *mdr1b* RNA levels (encoding P-glycoprotein) were strongly downregulated 24 hours after intraperitoneal administration of the *E. coli* endotoxin lipopolysaccharide (LPS). Ex vivo biodistribution with ^{99m}Tc-sestamibi, a SPECT tracer for P-glycoprotein, confirmed the endotoxin-induced reduction in P-glycoprotein efflux activity. Four hours after tracer injection, the ratio of radioactivity concentration in the fetus to that in the placenta was 3.5-fold higher in LPS-treated rats than in saline-treated controls. LPS also caused an increased retention of the tracer in several maternal organs. The results of this study indicate that inflammation causes a suppression of P-glycoprotein activity, resulting in an increased permeability of the blood–placenta barrier for potentially harmful substances. As a consequence, maternal infection during pregnancy could lead to an increased risk of exposure of the fetus to potentially harmful neurotoxins.

34.2.2 Imaging Intrauterine Fetal Accumulation of Neurotoxins

Toxic substances may be able to penetrate the blood–placenta barrier, despite the presence of efflux pumps in the placenta. To assess the potential risk of maternal exposure to a particular substance, it would be helpful to estimate the exposure of the fetus. Therefore, it is essential to determine whether a particular compound can cross the placenta and to what extent it accumulates in the fetus. Accurate determination of fetal accumulation of a compound can be done by postmortem analysis after miscarriage or—in case of animal studies—after sacrifice of the animal. PET imaging can provide a means to measure the fetal exposure to a harmful substance in a noninvasive manner. For this purpose, it is required to radiolabel the particular compound with a PET isotope. Hartvig and coworkers provided proof of concept for this approach (Hartvig et al. 1989). To assess the transfer of drugs from the mother to the fetus, they radiolabeled [^{11}C]morphine and [^{11}C]heroin. The radiolabeled drugs were administered to pregnant rhesus monkeys, and radioactivity was measured over time in maternal blood, placenta, and fetal liver. Both drugs showed rapid accumulation in the fetus, followed by rapid washout. A noteworthy observation was that fetal plasma concentrations of [^{11}C]morphine could even exceed the maternal plasma concentration. This result would implicate that the risk for the fetus can be substantially higher than estimated based on the maternal blood levels.

Although the study by Hartvig et al. demonstrated that PET can be used to assess the intra-utero exposure of a fetus to a harmful substance, it did not specifically investigate the exposure of the fetal brain (Hartvig et al. 1989). Benveniste and coworkers injected pregnant bonnet macaques intravenously with [^{11}C]cocaine and investigated the accumulation of the tracer in the fetal brain with PET (Benveniste et al. 2005). In order to anatomically localize tracer accumulation, PET images were coregistered with the corresponding MRI images. Uptake of [^{11}C]cocaine in the fetal brain gradually increased over a period of 15–20 minutes after tracer injection. Tracer uptake in the fetal brain was slower and lower (11–22% lower distribution volume ratio) than uptake in the maternal brain. Uptake in fetal striatum was higher than that in cerebellum, reflecting the differential expression of binding sites (dopamine transporters) in these brain regions. Since PET only measures radioactivity, fetal brain uptake likely comprises a mixture of intact [^{11}C]cocaine and its metabolites. Still, this study nicely demonstrated the concomitant exposure of the fetal brain after maternal administration of the drug cocaine and thus provides supportive evidence for a causative relationship between cocaine use by pregnant women and the behavioral and cognitive deficits observed in their offspring (Buckingham-Howes et al. 2013).

Paraquat is a herbicide that has structural similarities with the neurotoxin 1-methyl-4-phenyl-1,2,3,6-tetrahydropyridine (MPTP). Paraquat has been shown to be toxic to dopaminergic cells in vitro (Gómez-Sánchez et al. 2010) and was therefore suspected to be a potential neurotoxin that could be implicated in the induction of Parkinson's disease. Bartlett and colleagues radiolabeled paraquat and used PET/CT (computed tomography) to investigate the exposure of the fetal brain to [^{11}C]paraquat in two rhesus monkeys (Bartlett et al. 2011). The CT images were

used to delineate the fetal skull and subsequently to define the outline of the fetal brain. PET images at later time points showed that [^{11}C]paraquat did indeed accumulate in the fetus. However, uptake of [^{11}C]paraquat in the fetal brain was minimal (K_is 0.0016 min^{-1}) and not significantly different from uptake in the maternal brain (K_is 0.0009 min^{-1}). Thus, this imaging study suggests that prenatal exposure to the herbicide paraquat is unlikely to induce any neurotoxicity that could evolve in Parkinson's disease.

Metformin is an antidiabetic drug that has been widely used during pregnancy. Overgaard and coworkers used PET imaging with ^{11}C-labeled metformin in pregnant chinchilla to investigate the accumulation of this antidiabetic drug in the fetus (Overgaard et al. 2019). They demonstrated that [^{11}C]metformin did not accumulate in the chinchilla fetus. These results are in sharp contrast to the available evidence that indicates that the drug can readily pass the placenta in pregnant women (Charles et al. 2006). Analysis of placental mRNA, however, revealed that chinchilla and human expressed different subtypes of organic cation transporters. This family of transporters is involved in the transport of metformin across the blood–placenta barrier. These results clearly show that extrapolation of the findings from animal studies to humans should be done with extreme care.

34.2.3 Imaging Pharmacological Response to Intrauterine Fetal Exposure

The aforementioned studies demonstrated that PET can be a suitable tool to investigate the exposure of the fetal brain to a potential neurotoxin. However, a major disadvantage of the aforementioned approaches is that the toxic compound under investigation needs to be labeled with a PET isotope. This can be a time-consuming process and may not even be possible in some cases. As an alternative, a surrogate biomarker could be used to demonstrate the fetal brain exposure to a neurotoxin. Measurement of fetal brain glucose metabolism by PET with the glucose analogue 2′-[^{18}F]fluoro-2′-deoxyglucose ([^{18}F]FDG) could be an attractive approach, since this PET tracer is widely available. Benveniste and coworkers showed that [^{18}F]FDG PET could be used to assess fetal brain metabolism in pregnant bonnet macaques, if the PET images are properly coregistered with MRI images for anatomical localization (Benveniste et al. 2003). [^{18}F]FDG readily crosses the placenta and shows a distribution in the fetus that is comparable to that in adult animals. [^{18}F]FDG uptake in maternal brain was 23% higher than [^{18}F]FDG uptake in fetal brain (standardized uptake value 1.95 vs. 1.58). The [^{18}F]FDG PET approach seems feasible to investigate the in utero exposure of potential neurotoxins. In fact, the same group used [^{18}F]FDG PET to study the pharmacological effects of cocaine on brain metabolism of the fetus (Benveniste et al. 2010). Thus, pregnant bonnet macaques were intravenously (i.v.) injected with 1 mg/kg cocaine at the time of [^{18}F]FDG injection. In unchallenged control animals, brain glucose metabolism was twofold higher in the maternal brain than in the fetal brain (10.1 ± 7.6 vs. 5.1 ± 3.1 μg/100 g per minute). Exposure of the pregnant animals to cocaine increased the glucose metabolism in

both maternal and fetal brains by approximately 100%. So, this study demonstrates that cocaine abuse during pregnancy can have a direct pharmacological effect on both maternal and fetal brain. This could affect the normal development of the fetal brain and result in detrimental effects in the offspring.

So far, all PET imaging studies on the accumulation of xenobiotics in the fetus have been carried out in animals, usually monkeys. An important reason for the lack of intrauterine PET imaging studies in humans is the radiation burden to the fetus that is intrinsically associated with PET imaging. A recent PET-MRI study showed that the absorbed dose to the fetus for [^{18}F]FDG PET is highly variable between subjects and is substantially higher in early pregnancies (Zanotti-Fregonara et al. 2015). Yet, the authors concluded that the absorbed dose is "below the threshold for noncancer health effects," although it remains a matter of debate whether the radiation exposure of the fetus is within acceptable limits. A potential way to overcome this hurdle is provided by the development of total-body PET (Cherry et al. 2018). The concept of this latest generation PET camera is to extend the number of detector rings in order to cover the entire body (or at least most of it). The extension of the field-of-view results in an increase in sensitivity of up to 40-fold compared to a conventional PET camera. Consequently, the injected tracer dose could be reduced 40 times, which would result in an absorbed radiation dose to the fetus that would be in the same range as other sources of radioactivity a pregnant woman is exposed to (e.g., an intercontinental flight). At such a low radiation burden, intrauterine PET imaging in humans may become feasible in the near future.

34.3 Developmental Neurotoxicity After Maternal Exposure to Xenobiotics

34.3.1 Methodology

PET can not only be used to assess the acute effect of a neurotoxin to the fetal brain, but it may also be used as a tool to evaluate the long-term effects of perinatal exposure on brain development. As PET is a noninvasive technique, it allows repetitive imaging of the same animals between birth and adulthood. Moreover, PET can measure neurotoxic effects directly in the brain and thus will likely have more statistical power than indirect methods like behavioral tests. As a consequence, implementation of PET in neurotoxicity testing paradigms may result in a strong reduction in the number of laboratory animals required. When a certain neurotoxic effect is expected, a specific process in the brain can be monitored by PET, provided that a dedicated PET tracer is available. However, in most cases the effect of a neurotoxin is not known in advance or the required PET tracer is not available. In these cases, PET imaging of a generic process that is likely affected by many neurotoxins should still be feasible. [^{18}F]FDG PET imaging can be used as a surrogate biomarker for brain glucose metabolism (and thus brain activity). As brain activity is likely to be affected by direct neurotoxicity and by inappropriate brain development, [^{18}F]FDG PET could be a valuable, generally applicable tool to assess developmental neurotoxicity. However, standardization of the imaging protocol is essential. For accurate

determination of the glucose metabolism with [^{18}F]FDG PET, arterial blood sampling and pharmacokinetic modeling are required, but arterial blood sampling precludes any longitudinal studies. Moreover, conscious animals should preferably be used in these studies, because brain activity—and thus [^{18}F]FDG uptake—in awake animals is higher than in anesthetized animals. To overcome these potential hurdles, Schiffer and coworkers investigated different simplified procedures to estimate cerebral glucose metabolism in conscious animals (Schiffer et al. 2007). They developed a practical procedure that allowed good estimation of glucose metabolism in conscious animals. Thus, awake rats were intraperitoneally injected with [^{18}F]FDG. After 60 minutes of tracer distribution, animals were anesthetized and a 30-minute static scan was acquired. During the distribution time, a behavioral test can be performed. Best results are obtained if the tracer concentration in brain is corrected for radioactivity and glucose concentration in a blood sample that is taken 60 minutes after tracer injection.

34.3.2 Methylazoxymethanol

In a feasibility study, we have tested the potential of [^{18}F]FDG PET as a tool for developmental neurotoxicity testing, using the known proliferation inhibitor methylazoxymethanol (MAM) as the developmental neurotoxin (De Vries et al. 2008). Pregnant female rats were exposed to MAM (5 mg/kg body weight/day) on gestation days 13–15, which was known to cause reduced neuron numbers in brain areas under proliferation, the effects being larger at adolescent age (postnatal day [PND] 21) compared to young adult age (PND 61), suggesting a delay in structural brain development (De Groot et al. 2005). The offspring was subjected to serial [^{18}F]FDG PET imaging between postnatal days 18 and 61. On postnatal day 18, [^{18}F]FDG brain uptake was 24–32% reduced in the MAM-treated group as compared to saline-treated control animals (Fig. 34.1). Cerebral [^{18}F]FDG uptake remained lower in the MAM treatment group until day 61, although the difference between groups gradually diminished (10% reduction at day 61). Thus, in this study functional [^{18}F]FDG PET could clearly reveal a delay in structural brain development after in utero exposure of the pups to MAM. Interestingly, [^{18}F]FDG PET could already detect significant differences in brain glucose metabolism between the treatment group and the control group when only four animals per group were used, whereas a conventional open-field assay—also representing brain functioning—could not detect any significant effect in motor activity, even when ten animals per group were used. This indicates that PET could provide a more sensitive functional endpoint for developmental neurotoxicity than the behavioral test indicated by international guidelines for developmental neurotoxicity testing (OECD 2007; US EPA 1998).

34.3.3 Methylmercury

After this successful feasibility study, [^{18}F]FDG PET imaging—together with field potential analysis and microarray gene expression profiling—was

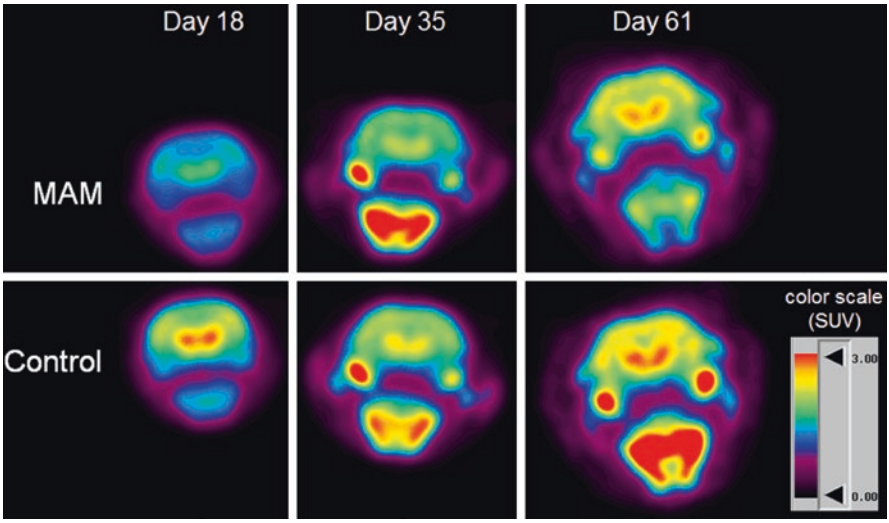

Fig. 34.1 [^{18}F]FDG PET imaging of the brain in the offspring of female rats that were exposed to methylazoxymethanol (MAM) during pregnancy. PET images were acquired between postnatal day 18 and 61. Images show a cross section of the brain that includes striatum

supplemented to a regulatory developmental toxicity study with methylmercury (according to US Environmental Protection Agency: Health Effects Test Guidelines OPPTS 870.6300 Developmental Neurotoxicity Study, EPA 712-C-98-239 1998). The aim was to investigate the added value of the imaging technique and to help unravel the mechanism of action of the neurotoxin (Radonjic et al. 2013). Four [^{18}F]FDG PET scans (postnatal days 18, 22, 37, and 61) were performed on control animals and on a group of animals that was exposed to 1.5 mg/kg methylmercury per day from gestation day 6 until lactation day 10. In the methylmercury-treated group, a trend towards a reduced glucose metabolism was observed in the hippocampus and cerebellum ($0.05 < p < 0.1$), whereas a trend towards increased tracer uptake in these brain regions was observed on day 22. On postnatal day 37, [^{18}F]FDG PET revealed significantly reduced tracer uptake in the hippocampus and cerebellum of methylmercury-treated animals as compared to healthy control animals. At day 61, the difference in tracer uptake between groups was largely diminished and—although still apparent—no longer statistically significant. Interestingly, the curves of [^{18}F]FDG uptake as a function of age (PND) had exactly the same shape, but the curve of the methylmercury-treated group was shifted by 15 days. This result suggests that maternal exposure to methylmercury induced a delay in brain development in the offspring. PET imaging data were in agreement with microarray gene expression profiling results, which also pointed towards a delayed brain development in the exposed animals. These effects were not detected by the classical tests in the developmental neurotoxicity testing guidelines, confirming the sensitivity of [^{18}F]FDG PET as a neurodevelopmental endpoint.

We have shown that this imaging methodology is widely applicable in neurotoxicity studies. Besides the aforementioned studies, we have also used the same study design to investigate developmental neurotoxicity effects of maternal and juvenile exposure to organotin compounds (De Groot et al. 2011, 2012b) and to ethanol (De Groot et al. 2012a). In both studies, [^{18}F]FDG PET could detect abnormalities in brain glucose metabolism, whereas conventional tests appeared far less sensitive or failed to show any effect of the neurotoxin. Thus, these studies strongly support the use of imaging endpoints in developmental toxicity testing.

34.4 Neurotoxicity After Adulthood Intoxication

PET and SPECT imaging have not been applied often to investigate neurotoxicity after adulthood exposure to neurotoxins; especially the number of animal studies is limited. Most studies describe the imaging findings of encephalopathy of workers after occupational intoxication, although some studies also investigated the effects of neurotoxicity after environmental exposure. The main neurotoxins involved are organic solvents and metals. The studies are in general retrospective in nature, as patients are usually studied only after the clinical diagnosis has already been established.

34.4.1 Organic Solvents

So far only a few case reports have been published on the use of [^{18}F]FDG PET for imaging the detrimental effects of chronic exposure to organic solvents, but these reports clearly show the strength of PET. Morrow and coworkers (Morrow et al. 1990) described a patient who was accidentally exposed to tetrabromoethane and experienced somatic, cognitive, and personality disorders. [^{18}F]FDG PET was performed, because neurological examination, CT, electroencephalogram (EEG), and electromyography (EMG) could not detect any abnormalities. PET showed decreased tracer uptake in the temporal and parietal cortices, basal ganglia, amygdala, and hippocampus, when compared to reference values of 24 healthy volunteers. This reduction in tracer uptake was consistent with neurobehavioral abnormalities (memory, motor function, and emotional reaction). A similar case report was published by Varney and coworkers, who performed [^{18}F]FDG PET on a worker who developed an encephalopathy after more than 750 occupational exposures to organic solvents over a period of 15 years (Varney et al. 1998). Despite multiple neurological abnormalities, findings from EEG and MRI appeared normal. Yet, the patient showed a marked reduction in brain glucose metabolism in the hippocampus and frontal and parietal cortices, even after 4 years of cessation of exposure. Both these case studies showed that [^{18}F]FDG PET can clearly identify an organic cause for neurological complaints, even when findings from EEG and MRI are normal. This could have important consequences for the workers involved, as it may help them obtain financial compensation for their work-related illness.

Solvent-induced encephalopathy has also been investigated by SPECT, which is more widely available and cheaper than PET. Hagstadius and colleagues used ^{133}Xe SPECT to measure resting state cerebral blood flow in 28 men who developed mild toxic encephalopathy after extensive exposure to organic solvents for 7–50 years and compared the results with 72 normal volunteers and with 50 male paint factory workers without complaints (Hagstadius et al. 1989). At diagnosis, the patients had significantly reduced cerebral blood flow in both hemispheres, as compared to controls. The largest reductions were observed in the prefrontal, frontotemporal, and inferior temporal regions. At follow-up after 24–84 months, the difference in cerebral blood flow was largely resolved, suggesting that some improvement in brain function occurred after cessation of exposure. Callender and coworkers investigated 33 workers who developed clinical toxic encephalopathy after exposure to a variety of neurotoxins, of which the majority was exposed to organic solvents (Callender et al. 1993). Cerebral blood flow measured with ^{99m}Tc-HMPAO SPECT showed abnormal findings in 94% (31/33) of the workers. Reduced flow was mainly observed in the frontal and temporal lobes, basal ganglia, and thalamus. The location of the abnormal cerebral blood flow was in agreement with the observed symptoms and behavioral effects. EEG and structural imaging were substantially less sensitive than SPECT, as abnormalities were observed in only 8, 7, and 29% of the patients with EEG, CT, and MRI, respectively. Neuropsychological evaluation showed abnormalities in only 79% of the patients and thus was less sensitive than SPECT as well. In two patients, both SPECT and [^{18}F]FDG PET were performed. In one patient, PET and SPECT showed the same abnormalities, whereas in the other patient, PET detected more abnormal brain regions than SPECT. These results were confirmed by Fincher et al., who used ^{99m}Tc-HMPAO SPECT to investigate cerebral blood flow in 25 subjects exposed to mixed organic solvents and 25 controls (Fincher et al. 1997). They observed reduced early phase tracer uptake in temporal, frontal, and thalamic brain regions of solvent-exposed subjects, suggestive of impaired cerebral blood flow. Taken together, these data indicate that ^{99m}Tc-HMPAO SPECT is a very sensitive tool to detect pathological effects of exposure to chemicals. [^{18}F]FDG PET might even be more sensitive, but an adequate head-to-head comparison between the two nuclear imaging techniques in a larger group of patients is still required.

Haut and colleagues used [^{15}O]water PET to measure the cerebral blood flow in six patients with toxic encephalopathy as a result of exposure to organic solvents and six age- and education-matched healthy controls (Haut et al. 2000). Since the symptoms of the patients were related to their verbal working memory, subjects were instructed to perform a verbal working memory task during the PET scan. The performance on the tasks was comparable for patients and controls. Patients showed a normal blood flow pattern in the posterior brain regions typical for the verbal working memory tasks but an abnormal blood flow pattern in the frontal lobe, which was ascribed to frontal dysfunction. Although this study nicely showed abnormal brain activation associated with a specific task, these types of studies are now largely

being replaced by fMRI studies, which do not require the exposure of patients to radiation.

Measurement of metabolism and blood flow with PET or SPECT can provide general information about abnormalities that are induced by exposure to organic solvents. PET and SPECT can also give more specific information, for example, about the involvement of a specific circuitry or neurotransmitter system. Visser and coworkers investigated the frontal lobe–striatum–thalamus circuitry with SPECT, magnetic resonance spectroscopy, and diffusion tensor imaging (Visser et al. 2008). Three groups were investigated: 10 patients with chronic solvent-induced encephalopathy, 10 asymptomatic solvent-exposed house painters, and 11 nonexposed carpenters. SPECT with the tracer [^{123}I]iodobenzamide was used to measure the postsynaptic dopamine D_2 receptor binding (expressed as striatal-to-occipital uptake ratios). Remarkably, both solvent-induced encephalopathy patients and asymptomatic solvent-exposed painters showed a strong reduction in dopamine D_2 receptor binding in striatum, as compared to nonexposed controls. Dopamine D_2 receptor binding was negatively correlated with the solvent exposure index. In encephalopathy patients, but not in solvent-exposed workers, dopamine D_2 receptor binding was inversely correlated with attention and simple psychomotor speed performance. These results implicate that the striatal dopaminergic system is already affected by solvent exposure before symptoms become overt and that these effects in presymptomatic subjects can already be detected by [^{123}I]iodobenzamide SPECT. Edling and colleagues also investigated the dopaminergic system in the striatum of 17 male patients with neuropsychiatric symptoms after long-term (23 ± 8 years) occupational exposure to organic solvents (8 with and 9 without the final diagnosis toxic encephalopathy) and 11 healthy controls (Edling et al. 1997a). No presymptomatic exposed subjects were included. In this study, PET imaging with the tracers L-[^{11}C]-3,4-dihydroxyphenylalanine ([^{11}C]DOPA), [^{11}C]nomifensine, and [^{11}C]raclopride was used to evaluate dopamine synthesis, presynaptic dopaminergic terminals (more precisely presynaptic dopamine reuptake), and postsynaptic D_2 receptors, respectively. There were no differences in the striatal uptake of [^{11}C]DOPA, [^{11}C]nomifensine, or [^{11}C]raclopride between patients with or without the diagnosis toxic encephalopathy. After correction for age differences, the dopamine synthesis in patients was 25% higher than that in healthy controls. The number of presynaptic dopaminergic nerve terminals was not affected in patients. Unfortunately, the paper did not report any comparison of the postsynaptic D_2 receptors between patients and controls. However, when the results of these studies are combined, one could speculate that exposure to organic solvents results in a downregulation in postsynaptic D_2 receptor expression, or a reduction of D_2 receptor affinity, which causes an increase in dopamine production as a compensatory response.

Caseni and coworkers investigated dopamine transporter density in striatum of Parkinson patients with a history of exposure to hydrocarbon solvents, nonexposed Parkinson patients and controls using [^{123}I]Ioflupane SPECT (Canesi et al. 2007). Patients in the exposed group were subjected to exposure to solvents for more than 10 hours per week for at least 10 years. Both groups of Parkinson patients

showed striatal tracer uptake well below that in healthy controls. In Parkinson patients chronically exposed to hydrocarbon solvents, the uptake of [^{123}I]Ioflupane in striatum was significantly more reduced than in nonexposed patients. The decrease in tracer binding was greater in putamen than in caudate. This study shows that occupational exposure to organic solvents results in an increased decrease in dopamine transporter density in striatum of Parkinson patients.

Edling et al. also investigated the acute effect of short-term exposure to toluene on dopamine synthesis and presynaptic dopaminergic nerve terminals (Edling et al. 1997b). Eleven male healthy volunteers were exposed to 100 ppm toluene while performing light exercise (pedaling on a bicycle ergometer at a workload of 50 W). [^{11}C]DOPA and [^{11}C]nomifensine PET were performed before and immediately after the acute exposure to toluene. None of the tracers showed any significant differences between baseline and postexposure PET scans. Thus, it was concluded that short exposure to toluene does not have an acute effect on dopamine synthesis or the number of presynaptic dopaminergic nerve terminals. Schiffer and coworkers used [^{18}F]FDG PET to study both the acute and long-term effects of toluene on brain metabolism in rats (Schiffer et al. 2006). Thus, adolescent rats were six times exposed to 5000 ppm toluene for 30 minutes on every other day. [^{18}F]FDG PET scans of the brain were made at baseline and 2 hours, 24 hours, 3 weeks, and 2 months after the last exposure. Tracer injection and distribution occurred in conscious animals. Toluene immediately induced a significant reduction in [^{18}F]FDG uptake (−21%) in all brain regions, although more pronounced in the subcortical regions. Abnormalities in tracer uptake were in agreement with the known distribution of toluene in the brain. The reduction in tracer uptake persisted throughout the experiment (−39%), although some recovery was observed after 2 months (−31%). The recovery was stronger in thalamus, hippocampus, and midbrain than in the cortical regions.

Airas and coworkers reported the use of L-6-[^{18}F]fluoro-3,4-dihydroxyphenylalanine ([^{18}F]FDOPA) PET in a case of methanol intoxication (Airas et al. 2008). The patient had consumed two cups of windshield washer containing methanol and developed blindness and severe extrapyramidal symptoms, such as hypokinesia and rigidity. [^{18}F]FDOPA PET was acquired 3.5 months after the intoxication and showed strongly reduced tracer uptake in striatum (putamen −60%; caudate −40%), indicating severely impaired dopamine synthesis. PET was in accordance with MRI findings that revealed substantial necrosis in the putamen. These results point towards severely injured dopaminergic neurostriatal neurons, causing the extrapyramidal symptoms in this patient. The patient responded well on treatment with L-DOPA.

Taken together, these studies indicate that PET and SPECT imaging can play an important role in identifying neurotoxic effects that are induced by exposure to organic solvents. In fact, PET and SPECT appear more sensitive than EEG and structural imaging with CT and MRI. Despite wide variability in exposure, most studies indicate that predominantly the frontal and temporal cortical regions and the dopaminergic system are affected by organic solvents. In general, imaging findings could well explain the neurobehavioral effects.

34.4.2 Metals

34.4.2.1 Manganese

Several studies have been published on the use of PET or SPECT for imaging of neurotoxicity after exposure to manganese dust. Manganese intoxication can lead to extrapyramidal symptoms that might mimic Parkinsonism.

Wooten and coworkers investigated the biodistribution and pharmacokinetics of manganese(II) in mice after intravenous injection or inhalation of a [^{52}Mn]manganese chloride solution (Wooten et al. 2017). Ex vivo analysis and PET imaging showed that substantial amounts of manganese accumulate inside the brain after both intravenous injection and inhalation of aerosols (0.9% ID/g and 0.3% ID/g after 24 hours, respectively). These results demonstrate that manganese salts can indeed cross the blood–brain barrier and may support findings of manganese-induced neurotoxicity.

Wolters et al. investigated dopamine synthesis and cerebral glucose metabolism in four workers exposed to manganese, using [^{18}F]FDOPA PET and [^{18}F]FDG PET, respectively (Wolters et al. 1989). [^{18}F]FDOPA PET did not show any abnormalities in striatal dopamine synthesis, whereas [^{18}F]FDG PET revealed a reduction in cortical glucose metabolism. In another study, four patients with Parkinsonian symptoms after chronic occupational exposure to manganese dust received both a [^{11}C]raclopride and a [^{18}F]FDOPA PET scan (Shinotoh et al. 1997). [^{18}F]FDOPA PET was normal in all patients, indicating normal presynaptic dopamine synthesis. In contrast, [^{11}C]raclopride PET showed reduced postsynaptic dopamine D_2 receptor binding in caudate (−12%) and putamen (−11%), although this effect was only statistically significant for caudate. The patients in this study did not respond to treatment with L-DOPA, which is in agreement with the observation that manganese causes postsynaptic damage. These results were partly confirmed by studies in monkeys (Shinotoh et al. 1995). [^{18}F]FDOPA, [^{11}C]raclopride, and [^{18}F]FDG PET were performed on three rhesus monkeys that were exposed to manganese by seven intravenous injections of 10–14 mg/kg $MnCl_2$. [^{18}F]FDOPA PET did not show any abnormalities, indicating that dopamine synthesis is not affected. [^{11}C]raclopride uptake in striatum was slightly reduced in one out of three animals 4 days after the last manganese administration, but returned to normal levels 4 days later. In contrast to the study by Wolters, [^{18}F]FDG PET did not reveal any effects on glucose metabolism in striatum or cerebral cortex in these monkeys, which could be ascribed to the shorter duration of the exposure to manganese. A subsequent study in these rhesus monkeys showed that animals that develop Parkinsonian symptoms after manganese intoxication do not respond to L-DOPA (Olanow et al. 1996), as was also observed in patients. Autopsy revealed gliosis in globus pallidus and substantia nigra pars reticularis, whereas the dopaminergic nigrostriatal system remains unaffected. Taken together, these studies show that the mild Parkinsonian symptoms induced by manganese intoxication in humans and monkeys are likely mainly due to downstream effects in the nigrostriatal pathway.

Despite similarities in clinical presentation of patients with chronic manganese intoxication and patients with idiopathic Parkinsonism, imaging can be used in the

differential diagnosis between the two pathologies, as was nicely shown in two case reports by Kim and coworkers (Kim et al. 1998). The first case was a worker who was occupationally exposed to manganese in the production of welding rods and presented with Parkinsonian features. [^{18}F]FDOPA PET showed normal uptake in striatum and it was concluded that this patient suffered from manganese-induced Parkinsonism, rather than from idiopathic Parkinsonism (Kim et al. 1998). The second case consisted of a welder who also presented Parkinsonian features. Because of suspected chronic manganese intoxication, [^{18}F]FDOPA PET was performed. PET images showed reduced tracer uptake in left putamen, indicating presynaptic damage. It was therefore concluded that this patient had idiopathic Parkinsonism (Kim et al. 1999).

With the availability of newer generation PET-CT systems with better resolution, the effects of manganese intoxication on subregions of the presynaptic dopaminergic system have also been evaluated. Criswell et al. performed [^{18}F]FDOPA PET in 20 asymptomatic welders exposed to manganese fumes and compared them with 20 idiopathic Parkinson patients and 20 healthy controls (Criswell et al. 2011). They observed a small, but significant reduction in [^{18}F]FDOPA consumption in the caudate of welders when compared to controls. In asymptomatic welders, caudate was more affected than anterior putamen, which was in turn more affected than posterior putamen. Interestingly, this regional pattern of reduced [^{18}F]FDOPA uptake was distinct from Parkinson patients, in which the reversed order was observed. Thus, the authors suggested that reduced [^{18}F]FDOPA uptake in caudate may be an early marker of manganese neurotoxicity. In a subsequent publication, the same group investigated presynaptic striatal [^{18}F]FDOPA uptake in 27 manganese-exposed welders, 14 other manganese exposed workers, and 31 nonexposed controls (Criswell et al. 2018a). Both manganese-exposed groups showed lower [^{18}F]FDOPA uptake in caudate than controls. However, the reduced [^{18}F]FDOPA uptake in caudate was not associated with the manganese exposure dose or with clinical Parkinsonism symptoms, according to the Unified Parkinson Disease Rating Scale motor subscore 3 (UPDRS3).

Huang et al. used PET imaging with the type 2 vesicle monoamine transporter ligand [^{18}F]FP-(+)-DTBZ to investigate presynaptic dopaminergic dysfunction in four manganism patients, eight Parkinson patients, and eight healthy controls (Huang et al. 2015). PET Imaging indicated that nigrostriatal tracer uptake was reduced in Parkinson patients, but not in chronic manganism patients, indicating that presynaptic neurons in striatum are not degenerated in patients suffering from manganese exposure.

Huang and colleagues investigated the integrity of the presynaptic dopamine transporter function with ^{99m}Tc-TRODAT-1 SPECT in 4 patients with manganese-induced Parkinsonian features, 12 patients with Parkinson's disease, and 12 healthy controls (Huang et al. 2003). The ^{99m}Tc-TRODAT-1 uptake in putamen was only mildly reduced in manganese-exposed patients, as compared to healthy controls, whereas the uptake in caudate and total striatum was not significantly affected. In contrast, both caudate and putamen were strongly affected in patients with Parkinson's disease, who had much lower tracer uptake in total striatum and in

caudate and putamen individually, as compared to manganese-exposed patients. This study demonstrated that presynaptic dopamine transporter activity is strongly reduced in Parkinson's disease but remains largely unaffected after chronic manganese exposure, thus confirming the results of [^{18}F]FDOPA PET studies. Therefore, the authors suggest that ^{99m}Tc-TRODAT-1 SPECT could be a relatively cheap and reliable tool to discriminate Parkinson's disease from manganese-induced neurotoxicity.

Criswell et al. also investigated the postsynaptic D2 receptor density in manganese-exposed welders and other workers using PET with the tracer *N*-[^{11}C]methylbenperidol (Criswell et al. 2018b). This tracer is insensitive to variation in dopamine level, as it cannot be displaced by the endogenous ligand. After correction for age, the binding potential of *N*-[^{11}C]methylbenperidol in substantia nigra was significantly greater in manganese-exposed workers than in nonexposed controls. Tracer binding in substantia nigra increased with increasing duration of manganese exposure and UPDRS3 score. These results suggest that D2 receptors in substantia nigra are involved in manganese-induced Parkinsonism.

34.4.2.2 Thallium

Acute thallium poisoning can cause polyneuropathy that is associated with myelin damage and axonal degeneration (Kuo et al. 2005). Recently, [^{18}F]FDG PET was applied to investigate cerebral glucose metabolism in two patients with acute thallium poisoning via the drinking water (Liu et al. 2013). Both patients showed severe cognitive impairment, which partially recovered during the 18-month follow-up. [^{18}F]FDG PET at month 5 (patient 1) and month 2 (patient 2) after intoxication showed a marked reduction in glucose metabolism in the cingulate gyrus and frontal and parietal lobes, as compared to healthy controls. Patient 2 received a follow-up scan 2 months after the first scan, showing partial recovery of the abnormalities in glucose metabolism. In contrast to PET, structural MRI did not reveal any abnormalities.

34.4.2.3 Arsenic

In the Japanese city of Kamisu, many inhabitants were intoxicated with diphenylarsinic acid by drinking water from a contaminated well. Diphenylarsinic intoxication mainly caused cerebellar and brainstem symptoms, such as ataxic gait, titubation, scanning speech, and tremors, but in some subjects also cerebral symptoms such as insomnia, visual and memory impairment (Ishii et al. 2004). To investigate diphenylarsinic acid-induced neurotoxicity, cerebral blood flow was assessed with *N*-isopropyl-*p*-[^{123}I]iodoamphetamine SPECT in 35 symptomatic and 43 asymptomatic subjects drinking contaminated well water for at least 1 year and 38 in healthy controls (Ishii et al. 2019). The asymptomatic group did not show any significant differences in cerebral blood flow, when compared to healthy controls. However, symptomatic exposed subjects revealed a significant reduction in cerebral blood flow in inferior occipital gyrus and cuneus as compared to healthy controls, and significantly lower cerebral blood flow in superior frontal gyrus as compared to the asymptomatic group. Moreover, cerebral blood flow in inferior occipital gyrus

was negatively correlated with diphenylarsinic acid concentrations in hair and nails. This study was nicely able to link exposure to an environmental poison to adverse physiological effects in the brain, in particular reduced blood flow in the occipital lobe.

34.4.2.4 Mercury

Chronic exposure to metallic mercury can cause neurological symptoms like ataxia, tremor, coordination problems, and memory impairment (Bose-O'Reilly et al. 2017). Since these symptoms are also observed in Parkinson's disease, Lin and coworkers used ^{99m}Tc-TRODAT SPECT to investigate dopamine transporter concentrations in lamp factory workers who were exposed to mercury vapors and age- and gender-matched controls (Lin et al. 2011). ^{99m}Tc-TRODAT SPECT revealed a moderate but significant negative correlation between mercury levels in urine and the tracer uptake in striatum, caudate, and putamen. Cumulative mercury exposure was also negatively correlated with ^{99m}Tc-TRODAT uptake in striatum and caudate. Consequently, mercury-exposed workers exhibited significantly lower ^{99m}Tc-TRODAT uptake in striatum, caudate, and putamen than age-matched controls. Yet, the mercury-exposed workers did not show any clinical manifestation of Parkinsonism yet. These results suggest that ^{99m}Tc-TRODAT SPECT could provide an early indicator for mercury-induced neurotoxicity.

34.4.3 Pesticides

Pesticides, such as paraquat, rotenone, and maneb, have been associated with neurotoxicity and increased risk of Parkinson's disease. In fact, these pesticides were shown to cause degeneration of dopaminergic neurons in animals and were therefore used to generate animal models for Parkinson's disease (Uversky 2004). To investigate whether similar effects could be found in humans, Lewis et al. studied the integrity of striatal dopaminergic terminals in agricultural workers exposed to these pesticides by assessing dopamine transporter density with [^{123}I]ioflupane SPECT (Lewis et al. 2017). [^{123}I]ioflupane SPECT, however, did not reveal any significant difference in dopamine transporter binding in any striatal subregion between controls, low- and high-exposure agricultural workers. Dopamine transporter binding also did not correlate with the days of pesticide exposure. This study therefore could not demonstrate any degenerative effect of pesticide exposure on dopaminergic neurons in humans.

Another group of pesticides that are associated with neurotoxicity are organophosphates, such as glyphosate ("Roundup") and diisopropylfluorophosphate. Intoxication with these organophosphates can lead to inhibition of acetylcholinesterase and cause convulsions, recurrent seizures, affective disorders, and cognitive deficits (Glusczak et al. 2006; Chen 2012). Flannery and coworkers longitudinally investigated the neuroinflammatory response after acute intoxication of adult rats with [^{11}C]PK11195 PET (Flannery et al. 2016). The PET tracer [^{11}C]PK11195 binds

to the 18-kDa mitochondrial membrane translocator protein, which is overexpressed on activated microglia, the resident macrophages of the brain. PET imaging showed an increased uptake of [^{11}C]PK11195 in animals that were exposed to diisopropylfluorophosphate. The increase in tracer uptake was highest on day 7, but some increased uptake was still present on day 21 after exposure. These results indicate that the pesticide induced persistent inflammatory response in the brain. Interestingly, the three animals with least severe seizures in this study did not show this temporal pattern of increased [^{11}C]PK11195 uptake in the PET images, indicating that neuroinflammation is positively correlated with seizure severity. However, PET imaging results did not correlate with cognitive impairment, suggesting that the observed cognitive impairment is not dependent on the diisopropylfluorophosphate-induced neuroinflammatory response.

34.4.4 Dioxins and PCBs

Dioxins and polychlorinated biphenyls (PCBs) are members of the family of polychlorinated aromatic hydrocarbons. Dioxins and PCBs are side products of the incomplete burning of waste containing chlorinated organic compounds. Dioxins are also formed in forest fires and volcanic eruptions, whereas PCBs have also been produced for industrial applications. Dioxins and PCBs are persistent in the environment and accumulate in the food chain. Human exposure occurs mainly via consumption of fatty food, especially meat, fish, dairy products, and eggs. Dioxins and PCB have been associated with a wide range of toxic effects, including immune toxicity, carcinogenicity, and developmental toxicity (Larsen 2006). Whether these compounds also induce neurotoxicity is a matter of discussion. To gain more insight in the effect of dioxins on the brain, Urban and coworkers performed ^{99m}Tc-ECD SPECT to assess abnormalities in cerebral blood flow in a cohort of 15 workers who were accidentally exposed to 2,3,7,8-tetrachlorodibenzo-*p*-dioxin (TCDD) in a chemical plant 35 years before (Urban et al. 2007). Nine of these patients showed signs of polyneuropathy and had more than 2× higher TCDD plasma concentrations than the other exposed subjects. Yet, SPECT showed abnormalities in cerebral blood flow in 14 of 15 patients, of which 4 had unilateral and 10 had bilateral foci of reduced cerebral blood flow. Patients had on average 2.5 perfusion defects, which were predominantly located in the region of the middle cerebral artery. In a follow-up study, the last eight survivors of this cohort were investigated again 50 years after the exposure to TCDD (Pelclova et al. 2018). All subjects showed impairment in neurological tests, and four subjects showed clinical signs of polyneuropathy and two subjects of mononeuropathy in the upper extremities. ^{99m}Tc-HMPAO SPECT revealed foci with decreased cerebral blood flow in both hemispheres in all patients. In six out of eight patients the cerebral blood flow defects had worsened since the previous follow-up 6 years before. These data suggest that the dioxin TCDD can induce chronic and progressive damage that is still measurable with SPECT 50 years after the fact.

On the basis of the results of preclinical studies, Seegal and coworkers hypothesized that PCBs could have a detrimental effect on the dopaminergic system in the brain. Therefore, they performed [^{123}I]β-CIT SPECT scans to assess the dopamine transporter density in a group of 89 workers who were occupationally exposed to PCBs in a capacitor factory (Seegal et al. 2010). SPECT showed that striatal dopamine transporter density was inversely correlated with serum PCB concentrations in women, whereas no such correlation was observed in men. Similar correlations were observed in caudate and putamen, independent of the subclass of PCBs subjects were exposed to. All women in this study were postmenopausal and the authors suggest that the gender difference observed in this study could be due to the fact the women have lost the neuroprotective effect of estrogens after menopause. These findings stress the need to take gender into consideration when exploring the effect of environmental factors on the brain.

34.5 Neurotoxicity in Suicide Survivors

34.5.1 Cyanide

A few case reports have been published that describe PET imaging of neurotoxicity in survivors of suicide attempts. A case report described the use of PET imaging of a survivor of a suicide attempt by ingestion of 1.5 g of potassium cyanide (Rosenberg et al. 1989). After treatment, the patient developed a severe Parkinsonian syndrome. MRI and PET imaging demonstrated that cyanide intoxication caused severe injury to dopaminergic neurons. [^{18}F]FDOPA PET showed reduced tracer uptake in striatum, indicating that dopamine synthesis is impaired, as is also observed in patients with Parkinson's disease. These results were in agreement with another case report, in which postmortem analysis of the brains of a survivor of a suicide attempt with cyanide showed major destruction of globus pallidus and putamen (Uitti et al. 1985). Zaknun et al. described the case of a 35-year-old woman who survived the ingestion of a lethal dose of potassium cyanide (Zaknun et al. 2005). ^{99m}Tc-HMPAO SPECT revealed reduced perfusion in frontal and striatal brain regions 9 days after intoxication and an additional perfusion defect in the precentral cortex after 7 weeks. [^{123}I]β-CIT SPECT showed reduced uptake in striatum on day 18 and a further reduction on day 54 after cyanide intoxication. [^{18}F]FDG PET showed reduced glucose metabolism, especially in striatum, frontal and anterior temporal lobes 19 days after cyanide ingestion. In line with these findings, another case report described a 20-year-old male surviving a suicide attempt with cyanide, who developed Parkinsonian syndrome (Sarikaya et al. 2006). [^{18}F]FDG PET of this patient revealed virtually no tracer uptake in putamen and reduced uptake in caudate and cerebellum. Taken together, the imaging findings in these case reports indicate that cyanide intoxication causes progressive degeneration of presynaptic nigrostriatal dopaminergic nerve terminals, which could be accompanied by frontal and cerebellar hypometabolism and/or hypoperfusion.

34.5.2 Carbon Monoxide

Carbon monoxide intoxication is a frequently applied suicide method. In Taiwan and Hong Kong, the number of suicides by inhalation of burning charcoal gasses, resulting in carbon monoxide poisoning, is strongly increasing since 1998 (Liu et al. 2007). A substantial fraction (10–30%) of the patients who were intoxicated with carbon monoxide develops delayed neuropsychiatric problems. Since the neuropsychiatric symptoms of carbon monoxide intoxication can resemble those of Parkinson's disease, Yang and coworkers hypothesized that the nigrostriatal dopaminergic neurons are more affected in patients with delayed neuropsychological abnormalities. Therefore, they used ^{99m}Tc-TRODAT SPECT to assess the striatal dopamine transporter density in 27 charcoal burning suicide patients (Yang et al. 2011). SPECT showed that dopamine transporter binding was lower in striatum of patients with neuropsychiatric symptoms than in patients without symptoms. Interestingly, when the initial loss of consciousness was included as a variable, the predictive value of dopamine transporter binding for neuropsychiatric effects was largely increased. In a subsequent study by the same group, ^{99m}Tc-TRODAT SPECT was performed in the first week after carbon monoxide intoxication and again 6 months later (Yang et al. 2015). Striatal dopamine transporter binding at baseline and after 6 months' follow-up was significantly lower in carbon monoxide poisoning patients than in healthy controls. There was no significant difference between baseline and follow-up SPECT, indicating that striatal degeneration did not progress any further after the acute intoxication phase. Changes in striatal dopamine transporter binding between baseline and follow-up were found to positively correlate with scores on the Wisconsin Card Sorting Test, a test for executive function.

Chen et al. analyzed networks of neurodegeneration with MRI and [^{18}F]FDG PET in 49 suicide survivors exposed to carbon monoxide by charcoal burning and 15 age-matched controls (Chen et al. 2015). [^{18}F]FDG PET demonstrated a pattern of hypometabolism in anterior brain regions, including prefrontal, cingulate, insular and temporal regions, caudate, and thalamus. These regions largely overlapped with gray matter atrophy as detected by MRI. The metabolic rate defects were more severe and extended for patients with higher clinical dementia rating scores. [^{18}F]FDG uptake in the orbital–frontal and dorsolateral prefrontal regions, anterior insular, temporal–parietal, and posterior cingulate cortex was significantly correlated with the Mini-Mental State Examination scores. Verbal memory learning, Stroop test, digit backward, and clinical dementia rating sum of box scores were also correlated with [^{18}F]FDG uptake in inferior and lateral frontal regions. These results indicate that carbon monoxide intoxication caused a specific degeneration pattern mainly in anterior brain regions that is associated with cognitive impairment in neuropsychological tests.

34.5.3 Pesticides

Wang et al. reported the imaging findings of two patients who were intoxicated with organophosphates, resulting in blindness of the patients (Wang et al. 1999). One patient tried to commit suicide by drinking a bottle of insecticide (Phosdrin R); the

other patient was attacked by her boyfriend and injected with another insecticide (*O*-ethyl-*O*-nitrophenyl phenylphosphonate). In both patients, the finding from MRI of the visual areas was normal. In contrast, PET showed decreased glucose metabolism in the visual cortex areas in both patients and thus provided an organic cause for their blindness.

Mittal and coworkers investigated the cerebral blood flow in patients acutely exposed to organophosphate (chlorpyrifos, dichlorvos, phorate) poisoning, either by ingestion due to a suicide attempt (n = 17) or by accidental exposure due to a spraying accident (n = 11). ^{99m}Tc-ECD SPECT were acquired between days 5 and 13 after admission and revealed abnormal cerebral blood flow in 96% of the patients (Mittal et al. 2011). More perfusion defects were observed in men than in women and blood flow deficits were most common in the occipital lobes. However, abnormal cerebral blood flow observed by SPECT could not predict cognitive decline, as blood flow deficits did not correlate with neurocognitive dysfunction, either in the admission phase or at 3 months' follow-up.

34.5.4 Drug Overdose

Recently, a case report was published that described the use of [^{18}F]FDG PET in a survivor of a suicide attempt with an overdose of the antidepressant fluoxetine (Szólics et al. 2012). An overdose of the selective serotonin reuptake inhibitor fluoxetine (Prozac) causes serotonin toxicity, resulting in necrosis in the globus pallidus and white matter ischemia, was observed by MRI. [^{18}F]FDG PET was performed 37 years after the suicide attempt, but still showed reduced tracer uptake in the frontal, temporal, and parietal cortices and caudate.

Thus, these reports show that PET can provide sensitive functional information about the brain regions that are affected by the neurotoxin, even a long time after exposure. This information may help the clinician explain the neurobehavioral abnormalities of the patient.

34.6 Concluding Remarks

Neurotoxicity has long been a research area primarily for neurologists, pathologists, and toxicologists. Imaging of neurotoxicity has mainly been restricted to evaluation of structural abnormalities by MRI or CT. So far, the role of nuclear medicine in this field has been limited. Still, several studies have demonstrated the potential of PET and SPECT imaging. Since prospective clinical trials on the potential neurotoxicity of agents are ethically unacceptable, the neurotoxic effect of compounds is generally tested in animals, if at all. In preclinical studies, PET and SPECT seem to be especially attractive for evaluation of the developmental neurotoxicity effects of potential neurotoxins. Not only can PET be applied to assess the intrauterine exposure of a fetus to a neurotoxin, but PET also promises to be a very sensitive endpoint for developmental neurotoxicity testing. Several studies have already shown that [^{18}F]FDG PET can detect functional brain abnormalities after pre- or perinatal

exposure to a toxin, when standard tests according to international guidelines for toxicity testing fail to show any effect. Because of its noninvasive nature, PET allows longitudinal testing, which, in addition to the high sensitivity of the technique, can result in a strong reduction of the number of animals required for the evaluation of the developmental neurotoxic potency of a substance. Because of the potential reduction in animals and workload, PET may even be cost-effective. The clinical application of PET and SPECT has mainly remained restricted to retrospective evaluation of patients who developed neurological symptoms after occupational, environmental, or accidental exposure to neurotoxins, mainly organic solvents and heavy metals, and to survivors of suicide attempts. Most studies show that PET and SPECT can detect functional abnormalities, even when EEG, CT, and MRI are normal. Thus, PET and SPECT are often able to detect an organic cause where other modalities fail. For patients, this can be of great importance when disputes on establishing the cause of the disorder and financial compensation are involved. Furthermore, functional PET and SPECT imaging can help to elucidate the extent of the encephalopathy and the mechanism responsible for intoxication-induced pathology. For mechanistic studies, back-translation to animal studies using functional imaging can provide additional information or confirmation of clinical results. So, functional imaging can help the clinician to better understand the cognitive, behavioral, and functional deficits of the patient. In some particular cases, PET and SPECT imaging can even provide a useful tool for the differential diagnosis between toxic encephalopathy and neurodegenerative diseases, as was nicely demonstrated for manganese intoxication and Parkinson's disease. Despite the potential of PET and SPECT imaging of neurotoxicity, the supporting evidence for the application of these imaging techniques in the clinic is still limited and mainly restricted to case reports and studies on small patient samples. Ideally, large clinical trials should be performed to establish the added value of PET and SPECT. However, this will be extremely difficult, since the number of patients who are acutely or chronically exposed to a particular neurotoxic substance and develop neurological deficits is fortunately very low, due to increasingly strict regulations.

Innovative technologies like microdosing in combination with PET or SPECT imaging may play an important role in the near future to explore the toxic potential of new medicines, as the effect of very low dosages of a compound in individual subjects can be measured in a very sensitive way. Combinations of imaging and -omics in such studies are very promising as they can help to unravel underlying neurotoxicity pathways which, in turn, will support the translation of results from animal to human and vice versa. A significant role for PET and SPECT in the science of (developmental) neurotoxicology seems warranted.

References

Airas L, Paavilainen T, Marttila RJ, Rinne J (2008) Methanol intoxication-induced nigrostriatal dysfunction detected using 6-[^{18}F]fluoro-L-dopa PET. Neurotoxicology 29:671–674

Bartels AL (2011) Blood-brain barrier P-glycoprotein function in neurodegenerative disease. Curr Pharm Des 17:2771–2777

Bartlett RM, Murali D, Nickles RJ, Barnhart TE, Holden JE, DeJesus OT (2011) Assessment of fetal brain uptake of paraquat in utero using in vivo PET/CT imaging. Toxicol Sci 122:551–556

Benveniste H, Fowler JS, Rooney WD, Moller DH, Backus WW, Warner DA, Carter P, King P, Scharf B, Alexoff DA, Ma Y, Vaska P, Schlyer D, Volkow ND (2003) Maternal-fetal in vivo imaging: a combined PET and MRI study. J Nucl Med 44:1522–1530

Benveniste H, Fowler JS, Rooney W, Ding YS, Baumann AL, Moller DH, Du C, Backus W, Logan J, Carter P, Coplan JD, Biegon A, Rosenblum L, Scharf B, Gatley JS, Volkow ND (2005) Maternal and fetal ^{11}C-cocaine uptake and kinetics measured in vivo by combined PET and MRI in pregnant nonhuman primates. J Nucl Med 46:312–320

Benveniste H, Fowler JS, Rooney WD, Scharf BA, Backus WW, Izrailtyan I, Knudsen GM, Hasselbalch SG, Volkow ND (2010) Cocaine is pharmacologically active in the nonhuman primate fetal brain. Proc Natl Acad Sci U S A 107:1582–1587

Bondy SC, Campbell A (2005) Developmental neurotoxicology. J Neurosci Res 81:605–612

Bose-O'Reilly S, Bernaudat L, Siebert U, Roider G, Nowak D, Drasch G (2017) Signs and symptoms of mercury-exposed gold miners. Int J Occup Med Environ Health 30:249–269

Buckingham-Howes S, Berger SS, Scaletti LA, Black MM (2013) Systematic review of prenatal cocaine exposure and adolescent development. Pediatrics 131:e1917–e1936

Bull S (2006) Review of environmental chemicals and toxicity. Focus on neurological diseases. Health Protection Agency publication HPA-ChaPD-001. http://www.hpa.org.uk/webc/HPAwebFile/HPAweb_C/1194947320712

Callender TJ, Morrow L, Subramanian K, Duhon D, Ristovv M (1993) Three-dimensional brain metabolic imaging in patients with toxic encephalopathy. Environ Res 60:295–319

Canesi M, Benti R, Marotta G, Cilia R, Isaias IU, Gerundini P, Pezzoli G, Antonini A (2007) Striatal dopamine transporter binding in patients with Parkinson's disease and severe occupational hydrocarbon exposure. Eur J Neurol 14:297–299

Charles B, Norris R, Xiao X, Hague W (2006) Population pharmacokinetics of metformin in late pregnancy. Ther Drug Monit 28:67–72

Chen Y (2012) Organophosphate-induced brain damage: mechanisms, neuropsychiatric and neurological consequences, and potential therapeutic strategies. Neurotoxicology 33:391–400

Chen NC, Huang CW, Huang SH, Chang WN, Chang YT, Lui CC, Lin PH, Lee CC, Chang YH, Chang CC (2015) Cognitive severity-specific neuronal degenerative network in charcoal burning suicide-related carbon monoxide intoxication: a multimodality neuroimaging study in Taiwan. Medicine (Baltimore) 94:e783

Cherry SR, Jones T, Karp JS, Qi J, Moses WW, Badawi RD (2018) Total-body PET: maximizing sensitivity to create new opportunities for clinical research and patient care. J Nucl Med 59:3–12

Chung FS, Eyal S, Muzi M, Link JM, Mankoff DA, Kaddoumi A, O'Sullivan F, Hsiao P, Unadkat JD (2010) Positron emission tomography imaging of tissue P-glycoprotein activity during pregnancy in the non-human primate. Br J Pharmacol 159:394–404

Coecke S, Eskes C, Gartlon J, Kinsner A, Price A, Van Vliet E, Prieto P, Boveri M, Bremer S, Adler S, Pellizzer C, Wendel A, Hartung T (2006) The value of alternative testing for neurotoxicity in the context of regulatory needs. Environ Toxicol Pharmacol 21:153–167

Criswell SR, Perlmutter JS, Videen TO, Moerlein SM, Flores HP, Birke AM, Racette BA (2011) Reduced uptake of [^{18}F]FDOPA PET in asymptomatic welders with occupational manganese exposure. Neurology 76:1296–1301

Criswell SR, Nielsen SS, Warden M, Perlmutter JS, Moerlein SM, Flores HP, Huang J, Sheppard L, Seixas N, Checkoway H, Racette BA (2018a) [^{18}F]FDOPA positron emission tomography in manganese-exposed workers. Neurotoxicology 64:43–49

Criswell SR, Warden MN, Searles Nielsen S, Perlmutter JS, Moerlein SM, Sheppard L, Lenox-Krug J, Checkoway H, Racette BA (2018b) Selective D2 receptor PET in manganese-exposed workers. Neurology 91:e1022–e1030

De Esch C, Slieker R, Wolterbeek A, Woutersen R, De Groot DM (2012) Zebrafish as potential model for developmental neurotoxicity testing: a mini review. Neurotoxicol Teratol 34:545–553

De Groot DMG (2017) Scientific review on the link between the narcotic effects of solvents and (developmental) neurotoxicity. Final report. Prepared for ECHA. Contract

Number: ECHA.6677-E3. March 2017; 241p. https://echa.europa.eu/de/publications/technical-scientific-reports

De Groot DM, Bos-Kuijpers MH, Kaufmann WS, Lammers JH, O'Callaghan JP, Pakkenberg B, Pelgrim MT, Waalkens-Berendsen ID, Waanders MM, Gundersen HJ (2005) Regulatory developmental neurotoxicity testing: a model study focussing on conventional neuropathology endpoints and other perspectives. Environ Toxicol Pharmacol 19:745–755

De Groot DM, Heerschap A, Krul C, Radonjic M, De Vries EF (2011) PET and MRI improve safety testing with far less animals (<50%). ALTEX 28:256

De Groot DM, Bogaart M, Nederlof R, Slieker RC, Wolterbeek AP, Dierckx RA, Van Waarde A, De Vries EF (2012a) In vivo [^{18}F]FDG microPET imaging in developmental neurotoxicity: a feasibility study in rat with ethanol. Reprod Toxicol 34:160–161

De Groot DM, Kuper CF, Radonjic M, Stierum R, Wolterbeek A, Heerschap A, Veltien A, Dierckx RA, De Vries EF (2012b) Imaging and omics in developing and juvenile rats after exposure to TBTO. Toxicol Lett 211:S155

De Groot MWGDM, Westerink RHS, Dingemans MML (2013) Don't judge a neuron only by its cover: neuronal function in *in vitro* developmental neurotoxicity testing. Toxicol Sci 132(1):1–7

De Vries EFJ, Van Waarde A, Willemsen ATM, Dierckx RA, Wolterbeek A, Wesselius A, De Groot DMG (2008) Protection of the unborn child from harmful drugs: a role for PET? Eur J Nucl Med Mol Imaging 35(suppl 2):S141

Edling C, Hellman B, Arvidson B, Andersson J, Hartvig P, Lilja A, Valind S, Långström B (1997a) Do organic solvents induce changes in the dopaminergic system? Positron emission tomography studies of occupationally exposed subjects. Int Arch Occup Environ Health 70:180–186

Edling C, Hellman B, Arvidson B, Johansson G, Andersson J, Hartvig P, Valind S, Långström B (1997b) Positron emission tomography studies of healthy volunteers—no effects on the dopamine terminals and synthesis after short-term exposure to toluene. Hum Exp Toxicol 16:171–176

Ek CJ, Dziegielewska KM, Habgood MD, Saunders NR (2012) Barriers in the developing brain and neurotoxicology. Neurotoxicology 33:586–604

Ekino S, Susa M, Ninomiya T, Imamura K, Kitamura T (2007) Minamata disease revisited: an update on the acute and chronic manifestations of methyl mercury poisoning. J Neurol Sci 262:131–144

Fincher CE, Chang TS, Harrell EH, Kettelhut MC, Rea WJ, Johnson A, Hickey DC, Simon TR (1997) Comparison of single photon emission computed tomography findings in cases of healthy adults and solvent-exposed adults. Am J Ind Med 31:4–14

Flannery BM, Bruun DA, Rowland DJ, Banks CN, Austin AT, Kukis DL, Li Y, Ford BD, Tancredi DJ, Silverman JL, Cherry SR, Lein PJ (2016) Persistent neuroinflammation and cognitive impairment in a rat model of acute diisopropylfluorophosphate intoxication. J Neuroinflammation 13:267

Glusczak L, dos Santos Miron D, Crestani M, Braga da Fonseca M, de Araújo Pedron F, Duarte MF, Vieira VL (2006) Effect of glyphosate herbicide on acetylcholinesterase activity and metabolic and hematological parameters in piava (Leporinus obtusidens). Ecotoxicol Environ Saf 65:237–241

Gómez-Sánchez R, Bravo-San Pedro JM, Niso-Santano M, Soler G, Fuentes JM, González-Polo RA (2010) The neuroprotective effect of talipexole from paraquat-induced cell death in dopaminergic neuronal cells. Neurotoxicology 31:701–708

Hagstadius S, Orbaek P, Risberg J, Lindgren M (1989) Regional cerebral blood flow at the time of diagnosis of chronic toxic encephalopathy induced by organic-solvent exposure and after the cessation of exposure. Scand J Work Environ Health 15:130–135

Hartvig P, Lindberg BS, Lilja A, Lundqvist H, Långström B, Rane A (1989) Positron emission tomography in studies on fetomaternal disposition of opioids. Dev Pharmacol Ther 12:74–80

Haut MW, Leach S, Kuwabara H, Whyte S, Callahan T, Ducatman A, Lombardo LJ, Gupta N (2000) Verbal working memory and solvent exposure: a positron emission tomography study. Neuropsychology 14:551–558

Huang CC, Weng YH, Lu CS, Chu NS, Yen TC (2003) Dopamine transporter binding in chronic manganese intoxication. J Neurol 250:1335–1339

Huang CY, Liu CH, Tsao E, Hsieh CJ, Weng YH, Hsiao IT, Yen TC, Lin KJ, Huang CC (2015) Chronic manganism: A long-term follow-up study with a new dopamine terminal biomarker of 18F-FP-(+)-DTBZ (18F-AV-133) brain PET scan. J Neurol Sci 353:102–106

Ishii K, Tamaoka A, Otsuka F, Iwasaki N, Shin K, Matsui A, Endo G, Kumagai Y, Ishii T, Shoji S, Ogata T, Ishizaki M, Doi M, Shimojo N (2004) Diphenylarsinic acid poisoning from chemical weapons in Kamisu, Japan. Ann Neurol 56:741–745

Ishii K, Nemoto K, Iwasaki N, Takeda T, Masuda T, Shibata Y, Tamaoka A (2019) Decreased regional cerebral blood flow in patients with diphenylarsinic acid intoxication. Eur J Neurol 26:136–141

Kim JW, Kim Y, Cheong HK, Ito K (1998) Manganese induced parkinsonism: a case report. J Korean Med Sci 13:437–439

Kim Y, Kim JW, Ito K, Lim HS, Cheong HK, Kim JY, Shin YC, Kim KS, Moon Y (1999) Idiopathic parkinsonism with superimposed manganese exposure: utility of positron emission tomography. Neurotoxicology 20:249–252

Kisby GE, Spencer PS (2011) Is neurodegenerative disease a long-latency response to early-life genotoxin exposure? Int J Environ Res Public Health 10:3889–3921

Kuo HC, Huang CC, Tsai YT, Chu CC, Hsieh ST, Chu NS (2005) Acute painful neuropathy in thallium poisoning. Neurology 65:302–304

Larsen JC (2006) Risk assessments of polychlorinated dibenzo- p-dioxins, polychlorinated dibenzofurans, and dioxin-like polychlorinated biphenyls in food. Mol Nutr Food Res 50:885–896

Lees-Haley PR, Williams CW (1997) Neurotoxicity of chronic low-dose exposure to organic solvents: a skeptical review. J Clin Psychol 53:699–712

Leslie EM, Deeley RG, Cole SP (2005) Multidrug resistance proteins: role of P-glycoprotein, MRP1, MRP2, and BCRP (ABCG2) in tissue defense. Toxicol Appl Pharmacol 204:216–237

Lewis MM, Sterling NW, Du G, Lee EY, Shyu G, Goldenberg M, Allen T, Stetter C, Kong L, Snipes SA, Jones BC, Chen H, Mailman RB, Huang X (2017) Lateralized basal ganglia vulnerability to pesticide exposure in asymptomatic agricultural workers. Toxicol Sci 159:170–178

Lin CY, Liou SH, Hsiech CM, Ku MC, Tsai SY (2011) Dose-response relationship between cumulative mercury exposure index and specific uptake ratio in the striatum on Tc-99m TRODAT SPECT. Clin Nucl Med 36:689–693

Liu KY, Beautrais A, Caine E, Chan K, Chao A, Conwell Y, Law C, Lee D, Li P, Yip P (2007) Charcoal burning suicides in Hong Kong and urban Taiwan: an illustration of the impact of a novel suicide method on overall regional rates. J Epidemiol Community Health 61:248–253

Liu CH, Lin KJ, Wang HM, Kuo HC, Chuang WL, Weng YH, Shih TS, Huang CC (2013) Brain fluorodeoxyglucose positron emission tomography (^{18}FDG-PET) in patients with acute thallium intoxication. Clin Toxicol 51:167–173

Meyer-Baron M, Kim EA, Nuwayhid I, Ichihara G, Kang SK (2012) Occupational exposure to neurotoxic substances in Asian countries - challenges and approaches. Neurotoxicology 33:853–861

Mittal T, Gupta N, Kohli A, Bhalla A, Singh B, Singh S (2011) Correlation of defects in regional cerebral blood flow determined by 99mTc SPECT with residual neurocognitive testing abnormalities during and 3 months post exposure in acutely poisoned patients with organophosphates. Clin Toxicol (Phila) 49:464–470

Morrow LA, Callender T, Lottenberg S, Buchsbaum MS, Hodgson MJ, Robin N (1990) PET and neurobehavioral evidence of tetrabromoethane encephalopathy. J Neuropsychiatry Clin Neurosci 2:431–435

Olanow CW, Good PF, Shinotoh H, Hewitt KA, Vingerhoets F, Snow BJ, Beal MF, Calne DB, Perl DP (1996) Manganese intoxication in the rhesus monkey: a clinical, imaging, pathologic, and biochemical study. Neurology 46:492–498

Organisation for Economic Co-operation and Development (OECD) (2007) OECD guidelines for the testing of chemicals, section 4: health effects test no.426: developmental neurotoxicity study. https://doi.org/10.1787/9789264067394

Overgaard MD, Duvald CS, Vendelbo MH, Pedersen SB, Jakobsen S, Alstrup AKO, Mikkelsen E, Ovesen PG, Pedersen M (2019) Biodistribution of [^{11}C]-Metformin and mRNA expression of placentae metformin transporters in the pregnant chinchilla. Contrast Media Mol Imaging 2019:9787340

Pelclova D, Urban P, Fenclova Z, Vlckova S, Ridzon P, Kupka K, Meckova Z, Bezdicek O, Navratil T, Rosmus J, Zakharov S (2018) Neurological and neurophysiological findings in workers with chronic 2,3,7,8-tetrachlorodibenzo-p-dioxin intoxication 50 years after exposure. Basic Clin Pharmacol Toxicol 122:271–277

Prüss-Ustün A, Vickers C, Haefliger P, Bertollini R (2011) Knowns and unknowns on burden of disease due to chemicals: a systematic review. Environ Health 10:9

Radonjic M, Cappaert NL, De Vries EF, De Esch CE, Kuper FC, Van Waarde A, Dierckx RA, Wadman WJ, Wolterbeek AP, Stierum RH, De Groot DM (2013) Delay and impairment in brain development and function in rat offspring after maternal exposure to methylmercury. Toxicol Sci 133:112–124

Rosenberg NL, Myers JA, Martin WR (1989) Cyanide-induced parkinsonism: clinical, MRI, and 6-fluorodopa PET studies. Neurology 39:142–144

Sarikaya I, Apaydin H, Topal U, Karaoglan O (2006) Cyanide-induced parkinsonism and F-18 FDG PET/CT findings. Clin Nucl Med 31:363–364

Sarkar S, Schmued L (2010) Neurotoxicity of ecstasy (MDMA): an overview. Curr Pharm Biotechnol 11:460–469

Schiffer WK, Lee DE, Alexoff DL, Ferrieri R, Brodie JD, Dewey SL (2006) Metabolic correlates of toluene abuse: decline and recovery of function in adolescent animals. Psychopharmacology (Berl) 186:159–167

Schiffer WK, Mirrione MM, Dewey SL (2007) Optimizing experimental protocols for quantitative behavioral imaging with ^{18}F-FDG in rodents. J Nucl Med 48:277–287

Seegal RF, Marek KL, Seibyl JP, Jennings DL, Molho ES, Higgins DS, Factor SA, Fitzgerald EF, Hills EA, Korrick SA, Wolff MS, Haase RF, Todd AC, Parsons P, McCaffrey RJ (2010) Occupational exposure to PCBs reduces striatal dopamine transporter densities only in women: a beta-CIT imaging study. Neurobiol Dis 38:219–225

Shinotoh H, Snow BJ, Hewitt KA, Pate BD, Doudet D, Nugent R, Perl DP, Olanow W, Calne DB (1995) MRI and PET studies of manganese-intoxicated monkeys. Neurology 45:1199–1204

Shinotoh H, Snow BJ, Chu NS, Huang CC, Lu CS, Lee C, Takahashi H, Calne DB (1997) Presynaptic and postsynaptic striatal dopaminergic function in patients with manganese intoxication: a positron emission tomography study. Neurology 48:1053–1056

Szólics M, Chaudhry M, Ljubisavljevic M, Corr P, Samir HA, Van Gorkom KN (2012) Neuroimaging findings in a case of fluoxetine overdose. J Neuroradiol 39:254–257

Tennekes HA, Sánchez-Bayo F (2013) The molecular basis of simple relationships between exposure concentration and toxic effects with time. Toxicology 309:39–51

Uitti RJ, Rajput AH, Ashenhurst EM, Rozdilsky B (1985) Cyanide-induced parkinsonism: a clinicopathologic report. Neurology 35:921–925

Urban P, Pelclová D, Lukás E, Kupka K, Preiss J, Fenclová Z, Smerhovský Z (2007) Neurological and neurophysiological examinations on workers with chronic poisoning by 2,3,7,8-TCDD: follow-up 35 years after exposure. Eur J Neurol 14:213–218

US Environmental Protection Agency (US EPA) (1998) Health effect test guidelines OPPTS 870.6300 developmental neurotoxicity study. Docket ID:EPA 712-C-98-239

Uversky VN (2004) Neurotoxicant-induced animal models of Parkinson's disease: understanding the role of rotenone, maneb and paraquat in neurodegeneration. Cell Tissue Res 318:225–241

Varney NR, Morrow LA, Pinkston JB, Wu JC (1998) PET scan findings in a patient with a remote history of exposure to organic solvents. Appl Neuropsychol 5:100–106

Visser I, Lavini C, Booij J, Reneman L, Majoie C, De Boer AG, Wekking EM, De Joode EA, Van der Laan G, Van Dijk FJ, Schene AH, Den Heeten GJ (2008) Cerebral impairment in chronic solvent-induced encephalopathy. Ann Neurol 63:572–580

Wang AG, Liu RS, Liu JH, Teng MM, Yen MY (1999) Positron emission tomography scan in cortical visual loss in patients with organophosphate intoxication. Ophthalmology 106:1287–1291

Wang JH, Scollard DA, Teng S, Reilly RM, Piquette-Miller M (2005) Detection of P-glycoprotein activity in endotoxemic rats by ^{99m}Tc-sestamibi imaging. J Nucl Med 46:1537–1545

Wolters EC, Huang CC, Clark C, Peppard RF, Okada J, Chu NS, Adam MJ, Ruth TJ, Li D, Calne DB (1989) Positron emission tomography in manganese intoxication. Ann Neurol 26:647–651

Wooten AL, Aweda TA, Lewis BC, Gross RB, Lapi SE (2017) Biodistribution and PET imaging of pharmacokinetics of manganese in mice using Manganese-52. PLoS One 12:e0174351

Yang KC, Ku HL, Wu CL, Wang SJ, Yang CC, Deng JF, Lee MB, Chou YH (2011) Striatal dopamine transporter binding for predicting the development of delayed neuropsychological sequelae in suicide attempters by carbon monoxide poisoning: A SPECT study. Psychiatry Res 194:219–223

Yang KC, Wang SJ, Hsieh WC, Lirng JF, Yang CC, Deng JF, Lin CL, Chou YH (2015) Longitudinal changes in the dopamine transporter and cognition in suicide attempters with charcoal burning. Psychiatry Res 231:160–167

Zaknun JJ, Stieglbauer K, Trenkler J, Aichner F (2005) Cyanide-induced akinetic rigid syndrome: clinical, MRI, FDG-PET, beta-CIT and HMPAO SPECT findings. Parkinsonism Relat Disord 11:125–129

Zanotti-Fregonara P, Laforest R, Wallis JW (2015) Fetal radiation dose from 18F-FDG in pregnant patients imaged with PET, PET/CT, and PET/MR. J Nucl Med 56:1218–1222

PET and SPECT in Hepatic and Uraemic Encephalopathy

35

Georg Berding, Frank Bengel, and Karin Weissenborn

Contents

35.1 Introduction 948
35.2 Hepatic Encephalopathy 948
35.2.1 Pathophysiology 948
35.2.2 Regional Cerebral Blood Flow: SPECT and PET 949
35.2.3 Ammonia: PET 953
35.2.4 Energy Metabolism: PET 954
35.2.5 Neuroinflammation: PET 954
35.2.6 Neurotransmission: PET and SPECT 955
35.2.7 Open Questions: PET and SPECT in Hepatic Encephalopathy 957
35.3 Uraemic Encephalopathy 958
35.3.1 Pathophysiology and Symptomatology 958
35.3.2 Blood Flow: SPECT and PET 958
35.3.3 Energy Metabolism: PET 960
35.3.4 PET and SPECT in Uraemic Encephalopathy With Parkinsonism 960
35.3.5 Open Questions: PET and SPECT in Uraemic Encephalopathy 961
References 961

Abstract

Liver or kidney failure can disturb brain function to a variable extent. If organ failure is treated successfully, brain function is normally, at least in part, restored. A broad spectrum of radiotracer imaging methods has been employed to measure correlates of brain function and thereby elucidate the pathophysiology of hepatic or uraemic encephalopathy. Measurements of regional cerebral perfusion as well

G. Berding (✉) · F. Bengel
Department of Nuclear Medicine, Hannover Medical School, Hannover, Germany
e-mail: berding.georg@mh-hannover.de; Bengel.Frank@mh-hannover.de

K. Weissenborn
Department of Neurology, Hannover Medical School, Hannover, Germany
e-mail: Weissenborn.Karin@mh-hannover.de

R. A. J. O. Dierckx et al. (eds.), *PET and SPECT in Neurology*,
https://doi.org/10.1007/978-3-030-53168-3_35

as energy metabolism in hepatic encephalopathy (HE) mostly revealed reductions in areas (particularly the frontal cortex and cingulum) relevant for the typically observed functional deficits (e.g. in attention or movement initiation). Positron emission tomography (PET) studies demonstrated that in HE, brain uptake of the neurotoxic ammonia increases with its plasma concentration. Some studies using the biomarker C-11-PK11195 indicate the presence of neuroinflammation in HE. Different neuroreceptor systems have been studied in HE throughout demonstrating reduced binding—particularly to central gamma-aminobutyric acid (GABA)-A receptors and dopamine as well as serotonin transporters. In patients with chronic renal failure and particularly those with depressive mood, reductions of cerebral blood flow and energy metabolism have been demonstrated, primarily located in the frontal cortex.

35.1 Introduction

Both the liver and kidneys are required to maintain human homeostasis in particular by preventing accumulation of toxic molecules with potentially detrimental effects on the central nervous system (CNS). Failure of these organs can therefore be the pathophysiologic basis of brain dysfunction ranging from mild subclinical impairments to devastating, potentially life-threatening complications. In contrast to degenerative brain diseases, there are quite effective treatment options available, for example, transplantation to tackle the underlying cause (organ failure) and thereby brain dysfunction. Nevertheless, these treatment options are demanding and sometimes accompanied by serious side effects themselves. As a consequence, it is of major importance to improve an understanding of the pathophysiology of brain disease caused by liver or renal failure for optimisation of therapy management with regard to minimal collateral brain damage. In this context, functional molecular imaging of the brain using radiotracer methods can give crucial information. Changes in regional brain perfusion, substrate and energy metabolism or in specific neurotransmission systems as well as neuroinflammatory response can be detected. Either single-photon emission computed tomography (SPECT) or positron emission tomography (PET) can be employed for this purpose. The aim of this review is to summarise the present knowledge on the use of these methods with regard to brain alterations in patients with failure or at least substantial dysfunction of the liver or kidneys.

35.2 Hepatic Encephalopathy

35.2.1 Pathophysiology

Major players in the pathogenesis of hepatic encephalopathy (HE) are (1) ammonia, (2) neuroinflammation, (3) GABAergic neurotransmission and (4) branched-chain

amino acids (Gillmann et al. 2012; McPhail et al. 2010; Patel et al. 2012). It is assumed that in patients with liver failure, increased ammonia levels in the blood result into increased levels in the brain and specifically in astrocytes where ammonia is converted to glutamine. Moreover, it has been suggested that increased glutamine levels are associated with oxidative stress, astrocyte swelling and consequently brain oedema. A second important factor is a neuroinflammatory reaction in the brain, in the frame of a systemic inflammatory response syndrome, triggered by pro-inflammatory cytokines including tumour necrosis factor (α) and interleukins (1β and 6) originating from the liver. Changes in neurotransmission include particularly the GABA- and glutamatergic pathways (Llansola et al. 2015). Finally, the composition of amino acids in the blood has been related to the pathophysiology and prognosis of HE. In particular, reductions in valine concentrations and the ratio between branched-chain and aromatic amino acids (Fischer's ratio) have been demonstrated to be associated with HE. Low concentrations of branched chain amino acids were linked to sarcopenia and thus a reduction of muscular metabolism of ammonia (Kinny-Köster et al. 2016). Consequently, supplementation of branched-chain amino acids is used to suppress this route of HE pathogenesis. All of the four aforementioned factors in the pathophysiology of HE have been addressed in radiotracer imaging studies by some means or other. Table 35.1 gives an overview in the employed radiopharmaceuticals, addressed patient groups and main results.

35.2.2 Regional Cerebral Blood Flow: SPECT and PET

Studies of brain perfusion using SPECT tracers require limited resources and provide nevertheless a robust insight into cerebrovascular changes and regional functional activity. PET enables absolute measurements of regional cerebral blood flow (CBF), but it is technically more complex, for example, requiring an onsite cyclotron and invasive blood sampling, and higher priced. Both methods allow to assess treatment effects on the brain with an objective measure and correlate this to clinical symptoms and neuropsychological testing.

The comparability of SPECT studies on resting-state brain perfusion in patients with liver disease is sometimes limited by the fact that presence and extent of HE are not properly documented. Nevertheless, in the spectrum of patients with liver cirrhosis, if documented without HE, with minimal HE or overt HE, mostly relative regional hypoperfusion of cerebral cortex has been observed with SPECT (Catafau et al. 2000; Ohta et al. 1998; Iwasa et al. 2000, 2005; Nakagawa et al. 2004; Trzepacz et al. 1994; Yazgan et al. 2003). Some studies report (coexisting) hyperperfusion in areas of the limbic system, for example, the basal ganglia (Catafau et al. 2000; Ohta et al. 1998; Kohira et al. 1994; Yazgan et al. 2003). Hypoperfusion involves most frequently parts of the frontal cortex (Iwasa et al. 2000; Nakagawa et al. 2004), particularly prefrontal (Catafau et al. 2000; Nakagawa et al. 2004); parietal cortex (Ohta et al. 1998; Iwasa et al. 2000; Nakagawa et al. 2004); cingulum (Nakagawa et al. 2004), particularly the anterior cingulate (Iwasa et al. 2005), and sometimes the temporal cortex (Iwasa et al. 2000; Trzepacz et al. 1994). PET studies obtaining

Table 35.1 Overview of the results of brain imaging studies with SPECT or PET in hepatic encephalopathy reported in the literature

Imaging procedure	Author, year	Patients	Key finding
Tc-99m-HMPAO-, Tc-99m-ECD-, I-123-IMP- or I-133-xenon-SPECT	Catafau et al. (2000)	Subclinical HE	Regional hypo-/ hyperperfusion
	Ikeda et al. (2001)	Before and after liver transplantation	No change in perfusion
	Iwasa et al. (2000, 2005)	Liver cirrhosis	Regional hypoperfusion
	Iwasa et al. (2003)	Liver cirrhosis	Hypoperfusion improved after BCAA therapy
	Jalan et al. (2003)	Liver cirrhosis	Regional hypoperfusion after amino acid load
	Kohira et al. (1994)	HE	Regional hyperperfusion
	Nakagawa et al. (2004)	Minimal HE	Regional hypoperfusion
	Ohta et al. (1998)	Portal–systemic encephalopathy	Regional hypo-/ hyperperfusion improved after therapy
	Strauss et al. (1999)	Fulminant hepatic failure	Reduced anterior-to-posterior perfusion ratio
	Trzepacz et al. (1994)	Subclinical HE	Regional hypoperfusion
	Yazgan et al. (2003)	Subclinical HE	Regional hypo-/ hyperperfusion
O-15-water with/ without N-13-ammonia PET	Ahl et al. (2004)	Liver cirrhosis, minimal HE	Reduced regional CBF in lenticular nucleus and cerebellar vermis, no change in PS product
	Dam et al. (2013)	Liver cirrhosis, acute HE	Reduced global CBF, normalised after recovery from HE
	Goldbecker et al. (2010)	Liver fibrosis, no HE	No changes in global or regional CBF and PS product
	Iversen et al. (2009)	Liver cirrhosis, acute HE	Reduced global and regional CBF (frontal, parietal, temporal and occipital cortices, striatum and thalamus)
	Keiding et al. (2006)	Liver cirrhosis, acute HE	Correlation between ammonia in blood and trapping in brain, no change in PS product
	Lockwood et al. (1979)	Liver disease	Correlation between ammonia in blood and trapping in brain
	Lockwood et al. (1991)	Minimal HE	Increased PS product

Table 35.1 (continued)

Imaging procedure	Author, year	Patients	Key finding
F-18-fluorodeoxy-glucose (FDG) or O-15-oxygen PET	Kato et al. (2000)	Subclinical HE	Reduced regional glucose metabolism
	Giewekemeyer et al. (2007)	Early HE	Reduced regional glucose metabolism
	Iversen et al. (2009)	Overt HE	Reduced regional oxygen metabolism
	Senzolo et al. (2009)	Before and after liver transplantation	Improvement of glucose metabolism
	Vankadari et al. (2018)	Decompensated liver cirrhosis	Glucose metabolism reduced in cerebral cortex, increased in basal ganglia
	Zhang et al. (2019)	Cirrhosis without overt HE	Glucose metabolism reduced in cerebral cortex, increased in basal ganglia
C-11-PK11195 PET	Berding et al. (2010)	HCV-infected	Increased marker binding
	Berding et al. (2012)	Alcohol-toxic cirrhosis	No increased marker binding
	Cagnin et al. (2006)	HE	Increased marker binding
	Iversen et al. (2006)	HE	No increased marker binding
C-11-flumazenil PET	Jalan et al. (2000)	HE	Increased radioligand binding
	MacDonald et al. (1997)	HE	Increased radioligand binding
	Samson et al. (1987)	HE	Increased radioligand binding
I-123-β-CIT or I-123-IBZM SPECT	Weissenborn et al. (2000)	HE	Reduced dopamine transporter and receptor binding
I-123-β-CIT SPECT	Weissenborn et al. (2006)	HCV-infected	Reduced dopamine and serotonin transporter binding
	Heeren et al. (2011)	HCV-infected	
F-18-CPFPX PET	Boy et al. (2008)	Liver cirrhosis	Reduced adenosine receptor binding

HE hepatic encephalopathy, *BCAA* branched-chain amino acid, *CBF* cerebral blood flow, *PS product* blood–brain barrier permeability surface area product, *HCV* hepatitis C virus

absolute measures of cerebral blood flow in patients with liver disease substantiate the presence of flow impairments (Ahl et al. 2004; Dam et al. 2013; Goldbecker et al. 2010; Iversen et al. 2009; Keiding et al. 2006; Lockwood et al. 1991). Ahl et al. (2004) found in liver cirrhosis patients with HE compared with those without HE reduced CBF within lenticular nucleus and cerebellar vermis. Widespread reductions of regional CBF were observed in cirrhotic patients with an acute

episode of HE compared with healthy subjects—encompassing areas within the frontal, parietal, temporal and occipital cortices as well as striatum and thalamus (Iversen et al. 2009). With respect to global changes of CBF in patients with liver disease, findings are consistently pointing to a decrease. Not significant decreases of 7% in patients with liver fibrosis without HE (Goldbecker et al. 2010) and around 20% in minimal or early HE (Ahl et al. 2004; Lockwood et al. 1991) were reported. A significant decrease of 35–40% in global CBF was found during acute episodes of HE, reversing to an insignificant decrease of 11% after recovery from HE (Dam et al. 2013; Iversen et al. 2009).

A positive correlation between regional cerebral perfusion assessed by SPECT imaging and scores obtained in neuropsychological testing has been reported by some authors (Catafau et al. 2000; Iwasa et al. 2005; Trzepacz et al. 1994). Results of brain perfusion measurements in general might suggest the possibility of a higher susceptibility of phylogenetically younger brain regions in particular the frontal cortex to pathophysiologic changes induced by late-stage liver disease which is in line with observed neuropsychological deficits in attention and visuopractic domains observed in neuropsychological testing (Trzepacz et al. 1994; Strauss et al. 1999).

Two interventional studies have focused on acute changes of brain (patho)physiology in patients with advanced liver disease. Jalan et al. (2003) simulated in patients with liver cirrhosis a gastrointestinal bleeding by oral administration of amino acids (mimicking haemoglobin). This resulted into a significant increase of blood ammonia levels and deterioration in neuropsychological test results. Sequential SPECT studies prior to administration of amino acids and 4 hours later revealed reduced perfusion in both temporal lobes, left superior frontal gyrus, right parietal and cingulate gyrus. The study stresses the relevance of ammonia and the time course of the pathophysiology. Strauss et al. (1999) studied in patients with fulminant hepatic failure whether the use of hyperventilation to prevent or postpone the development of cerebral oedema and intracranial hypertension has an influence on cerebral perfusion. They employed xenon-133 and Tc-99-HMPAO SPECT for that purpose. No significant difference between perfusion during normoventilation vs. hyperventilation was observed. Nevertheless, perfusion was impaired in the frontal cortex of patients compared with healthy controls and was restored to normal in patients after hepatic recovery and disappearance of HE.

Effects of treatment for liver failure on HE and brain perfusion have been investigated as well. In a study of patients with liver cirrhosis without overt HE, treatment with branched-chain amino acids resulted in a 13–20% increase of blood flow as demonstrated using sequential brain perfusion SPECT (Iwasa et al. 2003). PET has been used to study the impact of transjugular intrahepatic portosystemic shunting (TIPS) as a therapy option for end-stage liver disease, which is carrying a risk for the development of HE. No change of cerebral blood flow before and after TIPS was found—although flow values varied considerably preinterventionally (Iversen et al. 2011). Moreover, a study of patients with citrullinaemia type II brain perfusion SPECT before and 6–36 months after liver transplantation failed to show significant changes—however, no marked decreases of perfusion had been present preoperatively (Ikeda et al. 2001). Finally, a recent meta-analysis of studies on CBF in HE

including non-emission tomographic methods as well (like magnetic resonance imaging [MRI] arterial spin labelling and nitrogen oxide (N_2O) based measurements) revealed a considerable degree of variation across studies (Bjerring et al. 2018). However, predominantly reductions of CBF in HE were reported, with the exemption of HE following portocaval shunting with a tendency towards increased CBF and the observation that MRI and N_2O-based methods resulted in higher CBF during HE.

35.2.3 Ammonia: PET

Due to the central role of ammonia in the pathophysiology of HE, N-13-labelled ammonia has been employed to further elucidate the pathogenesis. If N-13 ammonia is used in conjunction with measurements of blood flow using O-15-water, the permeability of the blood–brain barrier (BBB) for ammonia can be assessed by calculation of the so-called permeability surface (PS) product (Berding et al. 2009).

This concept has been applied in the context of HE first by Lockwood et al. (1991) in patients with minimal HE. They reported a globally increased permeability supporting a key role of ammonia in HE pathogenesis and even relevance in cases with moderately or a lack of increased ammonia blood levels. This paper had a major impact on the conception of pathophysiology in HE; however, the results have not been reproduced and criticised for methodological reasons. Two points of criticism have been addressed: (1) the lack of measuring metabolites in this study might disregard radioactive metabolites entering the brain and (2) the lack of dynamic acquisition eliminated the possibility to apply full bio-kinetic modelling including consideration of backflux of tracer to the blood (Sørensen and Ott 2012).

Ahl et al. (2004) found no significant difference in global PS product between liver cirrhosis patients with and without minimal HE. However, the PS product in the thalamus was even increased in patients without HE, possibly implicating that increased permeability of the blood–brain barrier might be an early phenomenon of disease. Nevertheless, a later study of the same group comparing the PS product in patients with liver fibrosis with that in healthy controls revealed no significant difference (Goldbecker et al. 2010). Likewise, studies of patients with liver cirrhosis carried out at the University Hospital Aarhus did not show significant changes of the PS product in patients without HE and those with acute overt HE during the episode as well as after recovery compared to healthy control subjects (Dam et al. 2013; Keiding et al. 2006).

Interestingly, with respect to ammonia trapping in the brain, studies comparing ammonia concentration in the blood and the metabolic rate of ammonia in the brain (derived by multiplication of net ammonia influx and arterial ammonia concentration) demonstrated a linear correlation (Keiding et al. 2006; Lockwood et al. 1979). Proceeding from the lack of specific change in blood–brain barrier permeability for ammonia shown by the aforementioned studies using a state-of-the-art approach for quantification, this implies that the pathophysiologically relevant concentration of ammonia in the brain is simply driven by the blood ammonia concentration.

35.2.4 Energy Metabolism: PET

Measurements of energy metabolism have been employed to improve an understanding of pathophysiology and therapy effects in HE. First, Kato et al. (2000) demonstrated hypometabolism in the frontal and temporal cortices as well as the basal ganglia of patients with subclinical HE compared to control subjects. Partly divergent, in more recent studies (as far as declared also in patients with subclinical HE), extended cortical hypometabolism (particularly parietal and occipital) but hypermetabolism in the basal ganglia was found (Vankadari et al. 2018, Zhang et al. 2019). A study of Giewekemeyer et al. (2007) aimed to identify brain regions relevant for bradykinesia, as an early sign of HE. They performed F-18-flurodeoxyglucose (FDG) PET studies at rest in patients with normal neurological status and either no or minimal HE according to portosystemic encephalopathy (PSE) syndrome test. Significant correlations between motor function (finger and hand tapping) and glucose metabolism could be demonstrated for brain areas relevant for movement initiation (cingulate gyrus, frontomedial, frontodorsal and parietal cortices). Iversen et al. (2009) studied oxygen consumption using oxygen-15 (O-15) PET in patients with cirrhosis without HE and with an acute episode of HE. They reported a clear reduction during the acute episode but not in patients without HE. Moreover, oxygen consumption was negatively correlated to plasma concentrations of ammonia. The authors conclude that the reduction is associated with the pathophysiology of HE and not the cirrhosis as such. Interestingly the authors published a few years later data of oxidative metabolisms that have been obtained in the same patients using C-11-acetate always after the O-15 PET studies reported earlier (Iversen et al. 2014). This elegant approach allows to disentangle the oxidative metabolism of neurons and astrocytes, since in the brain, acetate is metabolised in the astrocytes because the only monocarboxylate transporter (MCT) of neurons, MCT2, fails to recognise acetate to the same extent as MCT1 located in endothelial cells and astrocytes. The net rate constant of oxidation of C-11-acetate was not different between patients with cirrhosis and HE and control subjects, implicating that the observed reduction observed in patients based on O-15 is related to changes in neurons.

The impact of therapy for end-stage liver disease on brain energy metabolism was investigated by Senzolo et al. (2009). He studied in cirrhotic patients without overt HE but neuropsychological deficits cerebral glucose metabolism using F-18-FDG PET before and 1 year after liver transplantation. Significant beneficial effects of transplantation on initially impaired metabolism in most of the cortical (frontal, temporal, occipital) and subcortical regions corresponding with improvements in neuropsychological testing could be demonstrated.

35.2.5 Neuroinflammation: PET

In patients with hepatic disorders affecting the brain, a widely used first-generation marker of activated microglia (C-11-PK11195) has been applied. However, this marker has certain limitations, such as a relatively high non-specific uptake/low signal-to-noise ratio and complexity of quantification. Therefore, intense search for

alternative markers is going on (Chauveau et al. 2008; Owen and Matthews 2011). The target for these radiotracers is the 18-kDa translocator protein (TSPO), which is present at very low levels in the normal healthy CNS but shows highly enhanced expression in the neuroinflammatory state. TSPO is located intracellularly at the mitochondrial membrane. Due to TSPO presence in peripheral tissues like the kidney and high affinity to benzodiazepines, it has originally been named as peripheral benzodiazepine receptor. Its functions are not fully understood, but they include the control of cholesterol transport, neurosteroid synthesis and maybe also the release of pro-inflammatory cytokines (Politis et al. 2012; Venneti et al. 2013).

Results of experimental studies imply an involvement of TSPO in the pathogenesis of encephalopathy in hepatic disease. Exposure of cultured astrocytes to ammonia results in increased TSPO expression. Exposure of mice to ammonia results in increased H-3-PK11195 binding/TSPO expression in the brain (Desjardins and Butterworth 2002). Consequently, C-11-PK11195 has been applied in patients with HE—nevertheless, results reported in the literature so far are ambiguous. Cagnin et al. (2006) observed in patients with minimal HE significantly increased C-11-PK11195 binding in the basal ganglia and the prefrontal cortex. In contrast, Iversen et al. (2006) found in patients with alcoholic liver cirrhosis during an acute episode of clinically overt HE no significant difference in C-11-PK11195 binding compared to healthy control subjects. Controversial findings might be related to different inclusion criteria, encompassing patients with hepatitis (3 out of 5) in the study of Cagnin et al. (2006), while this condition is not declared in the paper of Iversen et al. (2006). In a study employing C-11-PK11195 in a homogeneous group of hepatitis C-infected patients with fatigue, significantly increased binding was observed in the basal ganglia (thalamus) and frontal cortex (Berding et al. 2010). A study from the same group comparing liver cirrhosis patients according to the cause of liver disease, patients with cirrhosis due to hepatitis C showed increased C-11-PK11195 binding in frontal and occipital cortices, while no increase was found in those with alcoholic cirrhosis (Berding et al. 2012). Figure 35.1 displays results of C-11-PK11195 PET obtained in patients with hepatitis C, alcoholic cirrhosis and healthy control subjects. Patients with hepatitis C were also studied by Grover et al. (2012). They observed no change of C-11-PK11195 binding in the cerebral cortex but increased binding in the caudate and the thalamus. More recently, Pflugrad et al. (2016) described increased C-11-PK11195 binding in putamen, caudate, thalamus and (right) frontal cortex of hepatitis C-infected patients without deficits in a combined score of cognitive domains, including attention, concentration, learning ability and memory. Thus, in summary, the presently available data suggest that neuroinflammation in the brain depends on the cause of liver cirrhosis and is specifically driven by hepatitis C virus infection.

35.2.6 Neurotransmission: PET and SPECT

Specific detection of molecular processes in signal transduction between neurons is one of the exclusive goals for radiotracer studies. With respect to HE, there are hypotheses for preferential damage of specific neurotransmission systems.

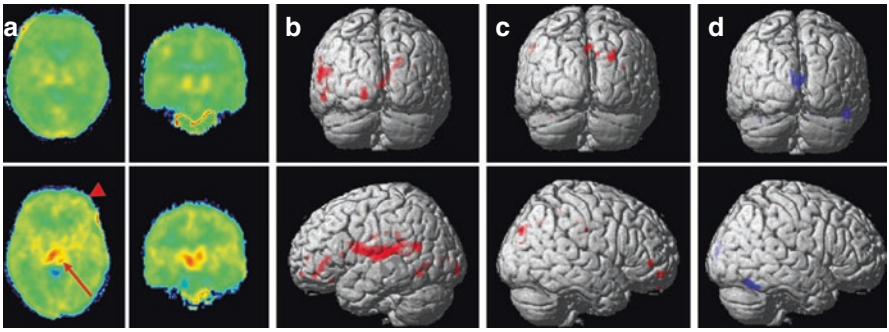

Fig. 35.1 C-11-PK11195 PET imaging of neuroinflammation in hepatic encephalopathy indicates the relevance of underlying liver disease. In panel (**a**), results of individual PET studies in a healthy control subject (upper row) and a patient with hepatitis C and fatigue symptomatology (lower row) are displayed. In the patient, increased binding in thalamus (red arrow) and frontal cortex (arrowhead) can be seen. Panels (**b**–**d**) show group comparisons with statistical parametric mapping. Regionally increased tracer binding ($p < 0.001$, uncorrected) is evident in hepatitis C-infected patients with cirrhosis vs. normal controls (**b**) and vs. patients with alcohol-toxic cirrhosis (**c**). The comparison between patients with alcohol-toxic cirrhosis and normal controls revealed reduced activity in the first group (**d**)

Particularly, the gamma-aminobutyric acid (GABA)/central benzodiazepine receptor system has been implicated to play a role in HE pathophysiology. The assumption of an increased GABAergic tone has primarily been based on the observation of beneficial effects of benzodiazepine antagonists such as flumazenil in patients with HE and animal models of HE (Albrecht and Jones 1999). Several partly controversial explanations for this increased tone have been given. A decrease in hepatic metabolism of benzodiazepines and an increase in benzodiazepine precursors provided by the intestinal flora (both resulting into increased natural benzodiazepines in the brain), an increased permeability of the blood–brain barrier for GABA and a modulation of the GABA-A receptors by ammonia or neurosteroids (Albrecht and Jones 1999; Ahboucha and Butterworth 2004; Patel et al. 2012).

In line with pathophysiological concepts, the first PET study employing C-11-flumazenil as tracer for benzodiazepine receptor binding in patients with HE showed a two- to threefold increase in uptake (Samson et al. 1987). In another study using the same radioligand along with blood sampling and bio-kinetic modelling in patients with recurrent HE, significant increases in benzodiazepine receptor binding in the thalamus, cerebellum and pons as well as minor and statistically insignificant increases in the cerebral cortex, putamen and whole brain could be demonstrated (MacDonald et al. 1997). This has been confirmed in a study by Jalan et al. (2000), observing significantly increased C-11-flumazenil binding in the cerebral cortex, basal ganglia and cerebellum of HE patients compared to control subjects.

With respect to other neurotransmission systems, the available imaging data are less sound. The monoaminergic systems (dopaminergic, serotonergic) have been thought to be afflicted in the pathophysiology of motor and cognitive deficits observed in HE patients. First evidence for an involvement of the dopaminergic system came from a post-mortem study (Mousseau et al. 1993). Corresponding

results were obtained in an in vivo case study demonstrating impaired pre- and postsynaptic striatal dopaminergic transmission (Weissenborn et al. 2000). In patients with hepatitis C infection and fatigue, reduced dopamine and serotonin transporter binding was found (Weissenborn et al. 2006; Heeren et al. 2011). Patients with transporter binding below the normal reference range showed reduced performance in neuropsychological testing. However, with respect to serotonin, experimental findings indicate increased synthesis as well as metabolism of this transmitter (Lozeva-Thomas 2004). Nevertheless, the precise changes expected in HE at serotonin transporter/receptor level still have to be defined.

A major importance with respect to the pathophysiology of HE is assumed for the glutamatergic system. It has been shown experimentally that ammonia increases glutamate release resulting in overstimulation of glutamate receptors specifically *N*-methyl-D-aspartate (NMDA) receptors. This has been proposed as a potential background for seizures in HE. Beneficial effects of a NMDA receptor antagonists (MK-801) have been demonstrated by in vivo model of HE. The chronic state of HE is believed to result in a downregulation of glutamatergic NMDA receptors (Albrecht and Jones 1999). In vivo imaging studies of glutamatergic receptors in HE patients are lacking so far. In part difficulties in finding a suitable radioligand in the past decades are responsible for this; however, new options are foreseeable (Sobrio et al. 2010).

A solitary study has investigated adenosine receptors in the brains of patients with liver cirrhosis (Boy et al. 2008). The authors expected an alteration of this neuromodulatory receptor system contributing to neurotransmitter imbalance observed in these patients. As a matter of fact, they observed widely distributed significant reductions of adenosine receptor binding in the cortical and subcortical regions ranging between 20 and 50% compared to control subjects.

35.2.7 Open Questions: PET and SPECT in Hepatic Encephalopathy

As laid out earlier, the pathophysiology of HE has been widely reviewed using radiotracer methods. Nevertheless, basically new aspects remain to be addressed. Three main points might be taken into consideration. (1) The effects of liver transplantation on brain function are not well investigated. Only two studies have been performed so far. One study demonstrated no effect on brain perfusion in contrast to the clinically known beneficial effects and the other study demonstrated beneficial effects on brain metabolism (Ikeda et al. 2001; Senzolo et al. 2009). Of importance would be prognostic information. (2) There is a large body of experimental evidence for neuroinflammation to play a key role in HE. The in vivo data in patients generated with C-11-PK11195 so far produced partly conflicting results. New second-generation markers of neuroinflammation are available but have not been employed in HE so far. (3) Finally, data on in vivo changes in neurotransmission systems occurring in HE patients are fragmentary. Especially with respect to the glutamatergic systems, further insights might hold promise even for the development of new drug therapies.

35.3 Uraemic Encephalopathy

35.3.1 Pathophysiology and Symptomatology

Renal failure is associated with a broad spectrum of neurological complications, including encephalopathy, movement disorders, neuropathy, myelinolysis, myopathy, atherosclerosis and cerebrovascular accidents (Brouns and De Deyn 2004; Seifter and Samuels 2011). The pathophysiology of these complications is assumed to base on an accumulation of uraemic toxins, disturbances of intermediary metabolism and hormonal regulation. In conjunction with specific therapies of renal failure, additional pathogenetic factors have to be considered. For example, the disequilibrium syndrome in conjunction with haemodialysis, which is presumed to result from the fast reversion of urea plasma concentration and an intracellular acidosis in the cerebral cortex—or in the context of renal transplantation: toxicity of immunosuppressive drugs and opportunistic infections (Brouns and De Deyn 2004). More recently, the important role of organic anion transporters (OAT-3) came into focus. These transporters are located at the blood–brain and blood–cerebrospinal fluid barriers (BBB, BCSPFB) (Seifter and Samuels 2011; Hosoya and Tachikawa 2011). Dysfunction of these transporters by uraemic toxins is assumed to cause an accumulation of uraemic toxins itself, for example, guanidine compounds. Inhibitory effects of these compounds on GABA-A receptors and activating effects on NMDA receptors might explain enhanced cortical excitability and play in general an important role in the pathogenesis of uraemic encephalopathy (UE) (De Deyn et al. 2009; Hosoya and Tachikawa 2011; Seifter and Samuels 2011). Some of the aforementioned factors in the pathophysiology of UE have been addressed in radiotracer imaging studies. Table 35.2 gives an overview of the employed radiopharmaceuticals, addressed patient groups and main results.

35.3.2 Blood Flow: SPECT and PET

Since there is a strong indication for a pathophysiologic relevance of changes in the cerebrovascular system, blood flow has been one of the main targets in imaging studies of UE using either SPECT or PET. A number of SPECT studies focus on patients with end-stage renal failure before or on haemodialysis with depression. Particularly, frontal and/or temporal hypoperfusions have been identified in these patients (Fazekas et al. 1996; Kim et al. 2008; Nam et al. 2011; Song et al. 2009). However, one of these studies showed that hypoperfusion can be present even in non-depressed pre-dialytic patients, and another study showed that perfusion deficits are reversed in pre-dialytic patients after initiation of haemodialysis (Song et al. 2009; Nam et al. 2011). Furthermore, end-stage renal failure can be associated with movement disturbances. In this context, a case report of Lee et al. (2006) indicates a possible affection of the basal ganglia, specifically hyperperfusion. However, other researchers report, in contrast, hypoperfusion in the basal ganglia in patients

Table 35.2 Overview of the results of brain imaging studies with SPECT or PET in uraemic encephalopathy reported in the literature

Imaging procedure	Author, year	Patients	Key finding
Tc-99m-HMPAO- or Tc-99m-ECD-SPECT	Fazekas et al. (1996)	Haemodialysis	Regional hypoperfusion
	Kim et al. (2008)	Pre-dialytic and depressive	Regional hypoperfusion
	Lass et al. (1999)	End-stage renal failure	Multiple infarct pattern
	Lee et al. (2006)	Renal failure and movement disorder	Regional hyperperfusion in basal ganglia
	Nam et al. (2011)	Pre-dialytic and depressive	Increased perfusion after dialysis if depression reduced
	Nishikawa et al. (2000)	Haemolytic uraemic syndrome	No abnormalities
	Song et al. (2009)	Pre-dialytic and depressive	Regional hypoperfusion
	Choi et al. (2015)	Uraemic syndrome and parkinsonism	Hypoperfusion in basal ganglia
O-15-water PET	Kuwabara et al. (2002)	Chronic renal failure and anaemia	Reduced cerebrovascular perfusion reserve
	Moore et al. (2002)	Renal failure in Fabry disease	Increased cerebrovascular perfusion reserve
	Moore et al. (2001)	Renal failure in Fabry disease	Enzyme replacement reversed increased perfusion
Oxygen-15 PET	Kanai et al. (2001)	Chronic renal failure	Oxygen metabolism reduced, extraction increased
F-18-fluorodeoxy-glucose (FDG) PET	Minamimoto et al. (2007)	Suspected renal failure	Reduced regional glucose metabolism
	Song et al. (2008)	Pre-dialytic chronic kidney disease	Reduced regional glucose metabolism
	Wang et al. (2004)	Diabetic uraemia	Reduced regional glucose metabolism
C-11-CFT (2-carbomethoxy-3-(4-fluorophenyl) tropane), C-11-raclopride	Ishii et al. (2016)	Diabetic uraemic syndrome and parkinsonism	Reduced pre- and postsynaptic dopaminergic function

with renal failure (Song et al. 2009; Fazekas et al. 1996). In a case study of a patient with haemolytic uraemic syndrome (HUS), no abnormalities in brain perfusion were detected (Nishikawa et al. 2000). Lass et al. (1999) described a pattern of multiple discrete cortical perfusion defects as typical for patients in end-stage renal failure rather than involvement of more extended brain regions.

A PET study of cerebrovascular perfusion reserve revealed a general reduction of this parameter in patients with chronic renal failure (CRF) (Kuwabara et al. 2002). Reversely, in Fabry disease, an X-linked enzyme deficiency of alpha-galactosidase associated with renal failure, an increase of flow reserve was observed (Moore et al. 2002). Moreover, increased resting blood flow observed in the latter group was observed to be significantly lowered after enzyme replacement therapy (Moore et al. 2001).

35.3.3 Energy Metabolism: PET

Oxygen metabolism and glucose utilisation have been studied in patients with chronic renal failure (CRF) using PET. CRF patients showed in the hemisphere significantly reduced regional cortical metabolic rate of oxygen ($rCMRO_2$) and significantly increased regional oxygen extraction fraction (rOEF) (Kanai et al. 2001). There was a tendency of lowest values in the frontal cortex. Minamimoto et al. (2007) selected during a period of 2.5 years out of patients receiving F-18-FDG PET scans for cancer a subgroup of 20 patients with suspected renal failure (i.e. blood serum creatinine level in excess of 1.1 mg/dL). They found significantly reduced standardised uptake values (SUV) in the brain cortex and white matter of patients as compared to healthy volunteers. Song et al. (2008) studied patients with pre-dialytic chronic kidney disease using F-18-FDG brain scans. They observed significant decreases in glucose metabolism primarily in the prefrontal cortex and additionally in the anterior cingulate and the temporal and parietal cortices. Metabolism in the orbitofrontal cortex was inversely correlated with the Hamilton Depression Rating Scale. Finally, Wang et al. (2004) performed F-18-FDG PET brain scans in two patients with diabetic uraemia. Tracer uptake in patients was significantly reduced compared to a control group of healthy subjects in the striatum and in the cerebral cortex (with occipital predominance in one and frontal in the other case).

35.3.4 PET and SPECT in Uraemic Encephalopathy With Parkinsonism

The pathophysiology of parkinsonism in uraemic encephalopathy has been addressed in two case studies. Choi et al. (2015) demonstrated hypoperfusion in the basal ganglia—as known to be present in atypical Parkinson syndromes—by means of Tc-99m-HMPAO SPECT. Ishii et al. (2016) observed decreased binding to striatal dopamine transporters as well as dopamine D_2 receptors using specific PET radioligands in a patient with diabetic uraemic syndrome presenting with parkinsonism—again a constellation of findings characteristic for atypical Parkinson syndromes (Brooks 2012). The case studies illustrate the potential of SPECT and PET to objectivise regional specific neuronal damage according to clinical symptomatology in encephalopathy, for example, of uraemic origin.

35.3.5 Open Questions: PET and SPECT in Uraemic Encephalopathy

Brain effects of renal failure are studied to a much lesser extent using emission tomographic methods when compared to the effects of liver failure. Particularly, studies of neuroinflammatory changes in vivo are lacking. Nevertheless, the current knowledge on the pathophysiology of brain-related symptoms in patients with renal failure strongly implies a relevance of such processes, which can be targeted by radiotracers. This would be specifically of interest in patients receiving immunosuppression or with respect to GABAergic or glutamatergic neurotransmission.

References

Ahboucha S, Butterworth RF (2004) Pathophysiology of hepatic encephalopathy: a new look at GABA from the molecular standpoint. Metab Brain Dis 19:331–343

Ahl B, Weissenborn K, van den Hoff J, Fischer-Wasels D, Köstler H, Hecker H, Burchert W (2004) Regional differences in cerebral blood flow and cerebral ammonia metabolism in patients with cirrhosis. Hepatology 40:73–79

Albrecht J, Jones EA (1999) Hepatic encephalopathy: molecular mechanisms underlying the clinical syndrome. J Neurol Sci 170:138–146

Berding G, Banati RB, Buchert R, Chierichetti F, Grover VPBB, Kato A, Keiding S, Taylor-Robinson SD (2009) Radiotracer imaging studies in hepatic encephalopathy: ISHEN practice guidelines. Liver Int 29:621–628

Berding G, Boellaard R, Wilke F, Pflugrad H, Fitz E, Meyer GJ, Buchert R, Knapp WH, Geworski L, Weissenborn K (2010) Evidence for a relevance of neuroinflammation in the pathogenesis of fatigue in hepatitis C infected patients. Eur J Nucl Med Mol Imaging 37(suppl 2):S209

Berding G, Afshar K, Boellaard R, Wilke F, Pflugrad H, Meyer GJ, Geworski L, Bengel F, Weissenborn K, Tryc A (2012) Cerebral C-11-PK11195 binding is significantly increased in patients with hepatitis C-cirrhosis but not in alcohol toxic. J Nucl Med 53(Suppl 1):1946

Bjerring PN, Gluud LL, Larsen FS (2018) Cerebral blood flow and metabolism in hepatic encephalopathy - a meta-analysis. J Clin Exp Hepatol 8:286–293

Boy C, Meyer PT, Kircheis G, Holschbach MH, Herzog H, Elmenhorst D, Kaiser HJ, Coenen HH, Haussinger D, Zilles K, Bauer A (2008) Cerebral A1 adenosine receptors (A1AR) in liver cirrhosis. Eur J Nucl Med Mol Imaging 35:589–597

Brooks DJ (2012) Parkinson's disease: diagnosis. Parkinsonism Relat Disord 18:S31–S33

Brouns R, De Deyn PP (2004) Neurological complications in renal failure: a review. Clin Neurol Neurosurg 107:1–16

Cagnin A, Taylor-Robinson SD, Forton DM, Banati RB (2006) In vivo imaging of cerebral "peripheral benzodiazepine binding sites" in patients with hepatic encephalopathy. Gut 55:547–553

Catafau AM, Kulisevsky J, Berna L, Pujol J, Martin JC, Otermin P, Balanzo J, Carrio I (2000) Relationship between cerebral perfusion in frontal-limbic-basal ganglia circuits and neuropsychologic impairment in patients with subclinical hepatic encephalopathy. J Nucl Med 41:405–410

Chauveau F, Boutin H, Van Camp N, Dollé F, Tavitian B (2008) Nuclear imaging of neuroinflammation: a comprehensive review of [^{11}C]PK11195 challengers. Eur J Nucl Med Mol Imaging 35:2304–2319

Choi EK, Oh JK, Chung YA, Song IU (2015) Brain SPECT and MRI findings in a uremic patient with parkinsonism. Clin Nucl Med 40:e453–e454

Dam G, Keiding S, Munk OL, Ott P, Vilstrup H, Bak LK, Waagepetersen HS, Schousboe A, Sørensen M (2013) Hepatic encephalopathy is associated with decreased cerebral oxygen metabolism and blood flow, not increased ammonia uptake. Hepatology 57:258–265

De Deyn PP, Vanholder R, Eloot S, Glorieux G (2009) Guanidino compounds as uremic (neuro) toxins. Semin Dial 22:340–345

Desjardins P, Butterworth RF (2002) The "peripheral-type" benzodiazepine (omega 3) receptor in hyperammonemic disorders. Neurochem Int 41:109–114

Fazekas G, Fazekas F, Schmidt R, Flooh E, Valetitsch H, Kapeller P, Krejs GJ (1996) Pattern of cerebral blood flow and cognition in patients undergoing chronic haemodialysis treatment. Nucl Med Commun 17:603–608

Giewekemeyer K, Berding G, Ahl B, Ennen JC, Weissenborn K (2007) Bradykinesia in cirrhotic patients with early hepatic encephalopathy is related to a decreased glucose uptake of frontomesial cortical areas relevant for movement initiation. J Hepatol 46:1034–1039

Gillmann A, Gerharz CD, Müssig K (2012) Diagnostics and treatment of hepatic encephalopathy. Dtsch Med Wochenschr 137:29–33

Goldbecker A, Buchert R, Berding G, Bokemeyer M, Lichtinghagen R, Wilke F, Ahl B, Weissenborn K (2010) Blood-brain barrier permeability for ammonia in patients with different grades of liver fibrosis is not different from healthy controls. J Cereb Blood Flow Metab 30:1384–1393

Grover VP, Pavese N, Koh SB, Wylezinska M, Saxby BK, Gerhard A, Forton DM, Brooks DJ, Thomas HC, Taylor-Robinson SD (2012) Cerebral microglial activation in patients with hepatitis C: in vivo evidence of neuroinflammation. J Viral Hepat 19:e89–e96

Heeren M, Weissenborn K, Arvanitis D, Bokemeyer M, Goldbecker A, Tountopoulou A, Peschel T, Grosskreutz J, Hecker H, Buchert R, Berding G (2011) Cerebral glucose utilisation in hepatitis C virus infection-associated encephalopathy. J Cereb Blood Flow Metab 31:2199–2208

Hosoya K, Tachikawa M (2011) Roles of organic anion/cation transporters at the blood-brain and blood-cerebrospinal fluid barriers involving uremic toxins. Clin Exp Nephrol 15:478–485

Ikeda S, Yazaki M, Takei Y, Ikegami T, Hashikura Y, Kawasaki S, Iwai M, Kobayashi K, Saheki T (2001) Type II (adult onset) citrullinaemia: clinical pictures and the therapeutic effect of liver transplantation. J Neurol Neurosurg Psychiatry 71:663–670

Ishii K, Ishii K, Shioya A, Nemoto K, Tamaoka A (2016) Decreased dopamine transporter and receptor ligand binding in Parkinsonism with diabetic uremic syndrome. Ann Nucl Med 30:320–324

Iversen P, Hansen DA, Bender D, Rodell A, Munk OL, Cumming P, Keiding S (2006) Peripheral benzodiazepine receptors in the brain of cirrhosis patients with manifest hepatic encephalopathy. Eur J Nucl Med Mol Imaging 33:810–816

Iversen P, Sørensen M, Bak LK, Waagepetersen HS, Vafaee MS, Borghammer P, Mouridsen K, Jensen SB, Vilstrup H, Schousboe A, Ott P, Gjedde A, Keiding S (2009) Low cerebral oxygen consumption and blood flow in patients with cirrhosis and an acute episode of hepatic encephalopathy. Gastroenterology 136:863–871

Iversen P, Keiding S, Mouridsen K, Ott P, Vilstrup H (2011) Transjugular intrahepatic portosystemic shunt does not alter cerebral blood flow. Clin Gastroenterol Hepatol 9:1001–1003

Iversen P, Mouridsen K, Hansen MB, Jensen SB, Sorensen M, Bak LK, Waagepetersen HS, Schousboe A, Ott P, Vilstrup H, Keiding S, Gjedde A (2014) Oxidative metabolism of astrocytes is not reduced in hepatic encephalopathy: a PET study with [^{11}C]acetate in humans. Front Neurosci 8:353

Iwasa M, Matsumura K, Kaito M, Ikoma J, Kobayashi Y, Nakagawa N, Watanabe S, Takeda K, Adachi Y (2000) Decrease of regional cerebral blood flow in liver cirrhosis. Eur J Gastroenterol Hepatol 12:1001–1006

Iwasa M, Matsumura K, Watanabe Y, Yamamoto M, Kaito M, Ikoma J, Gabazza EC, Takeda K, Adachi Y (2003) Improvement of regional cerebral blood flow after treatment with branched-chain amino acid solutions in patients with cirrhosis. Eur J Gastroenterol Hepatol 15:733–737

Iwasa M, Matsumura K, Nakagawa Y, Yamamoto M, Tanaka H, Horiike S, Ikoma J, Kaito M, Takeda K, Adachi Y (2005) Evaluation of cingulate gyrus blood flow in patients with liver cirrhosis. Metab Brain Dis 20:7–17

Jalan R, Turjanski N, Taylor-Robinson SD, Koepp MJ, Richardson MP, Wilson JA, Bell JD, Brooks DJ (2000) Increased availability of central benzodiazepine receptors in patients with chronic hepatic encephalopathy and alcohol related cirrhosis. Gut 46:546–552

Jalan R, Olde Damink SW, Lui HF, Glabus M, Deutz NE, Hayes PC, Ebmeier K (2003) Oral amino acid load mimicking hemoglobin results in reduced regional cerebral perfusion and deterioration in memory tests in patients with cirrhosis of the liver. Metab Brain Dis 18:37–49

Kanai H, Hirakata H, Nakane H, Fujii K, Hirakata E, Ibayashi S, Kuwabara Y (2001) Depressed cerebral oxygen metabolism in patients with chronic renal failure: a positron emission tomography study. Am J Kidney Dis 38(4 suppl 1):S129–S133

Kato A, Suzuki K, Kaneta H, Obara H, Fujishima Y, Sato S (2000) Regional differences in cerebral glucose metabolism in cirrhotic patients with subclinical hepatic encephalopathy using positron emission tomography. Hepatol Res 17:237–245

Keiding S, Sørensen M, Bender D, Munk OL, Ott P, Vilstrup H (2006) Brain metabolism of ^{13}N-ammonia during acute hepatic encephalopathy in cirrhosis measured by positron emission tomography. Hepatology 43:42–50

Kim SJ, Song SH, Kim JH, Kwak IS (2008) Statistical parametric mapping analysis of the relationship between regional cerebral blood flow and symptom clusters of the depressive mood in patients with pre-dialytic chronic kidney disease. Ann Nucl Med 22:201–206

Kinny-Köster B, Bartels M, Becker S, Scholz M, Thiery J, Ceglarek U, Kaiser T (2016) Plasma amino acid concentrations predict mortality in patients with end-stage liver disease. PLoS One 11(7):e0159205

Kohira I, Matsuo E, Shiro Y, Uemura N, Matsumoto S, Kitamura Y, Matsumoto Y, Ishizu H, Sakai K, Kuroda S et al (1994) Hepatic encephalopathy with increased cerebral blood flow in SPECT and MRI abnormalities in the basal ganglia. Jpn J Psychiatry Neurol 48:33–36

Kuwabara Y, Sasaki M, Hirakata H, Koga H, Nakagawa M, Chen T, Kaneko K, Masuda K, Fujishima M (2002) Cerebral blood flow and vasodilatory capacity in anemia secondary to chronic renal failure. Kidney Int 61:564–569

Lass P, Buscombe JR, Harber M, Davenport A, Hilson AJ (1999) Cognitive impairment in patients with renal failure is associated with multiple-infarct dementia. Clin Nucl Med 24:561–565

Lee PH, Shin DH, Kim JW, Song YS, Kim HS (2006) Parkinsonism with basal ganglia lesions in a patient with uremia: evidence of vasogenic edema. Parkinsonism Relat Disord 12:93–96

Llansola M, Montoliu C, Agusti A, Hernandez-Rabaza V, Cabrera-Pastor A, Gomez-Gimenez B, Malaguarnera M, Dadsetan S, Belghiti M, Garcia-Garcia R, Balzano T, Taoro L, Felipo V (2015) Interplay between glutamatergic and GABAergic neurotransmission alterations in cognitive and motor impairment in minimal hepatic encephalopathy. Neurochem Int 88:15–19

Lockwood AH, McDonald JM, Reiman R, Gelbard AS, Laughlin JS, Duffy TE, Plum F (1979) The dynamics of ammonia metabolism in man. Effects of liver disease and hyperammonemia. J Clin Invest 63:449–460

Lockwood AH, Yap EW, Wong WH (1991) Cerebral ammonia metabolism in patients with severe liver disease and minimal hepatic encephalopathy. J Cereb Blood Flow Metab 11(2):337–341

Lozeva-Thomas V (2004) Serotonin brain circuits with a focus on hepatic encephalopathy. Metab Brain Dis 19:413–420

Macdonald GA, Frey KA, Agranoff BW, Minoshima S, Koeppe RA, Kuhl DE, Shulkin BL, Lucey MR (1997) Cerebral benzodiazepine receptor binding in vivo in patients with recurrent hepatic encephalopathy. Hepatology 26:277–282

McPhail MJ, Bajaj JS, Thomas HC, Taylor-Robinson SD (2010) Pathogenesis and diagnosis of hepatic encephalopathy. Expert Rev Gastroenterol Hepatol 4:365–378

Minamimoto R, Takahashi N, Inoue T (2007) FDG-PET of patients with suspected renal failure: standardized uptake values in normal tissues. Ann Nucl Med 21:217–222

Moore DF, Scott LT, Gladwin MT, Altarescu G, Kaneski C, Suzuki K, Pease-Fye M, Ferri R, Brady RO, Herscovitch P, Schiffmann R (2001) Regional cerebral hyperperfusion and nitric oxide pathway dysregulation in Fabry disease: reversal by enzyme replacement therapy. Circulation 104:1506–1512

Moore DF, Altarescu G, Herscovitch P, Schiffmann R (2002) Enzyme replacement reverses abnormal cerebrovascular responses in Fabry disease. BMC Neurol 2:4

Mousseau DD, Perney P, Layrargues GP, Butterworth RF (1993) Selective loss of pallidal dopamine D2 receptor density in hepatic encephalopathy. Neurosci Lett 162:192–196

Nakagawa Y, Matsumura K, Iwasa M, Kaito M, Adachi Y, Takeda K (2004) Single photon emission computed tomography and statistical parametric mapping analysis in cirrhotic patients with and without minimal hepatic encephalopathy. Ann Nucl Med 18:123–129

Nam HY, Song SH, Kim SJ, Kwak IS, Kim IJ, Lee SB, Lee DW, Kim BS, Pak K, Kim YK, Yun HS (2011) Effect of dialysis on cerebral blood flow in depressive end-stage renal disease patients. Ann Nucl Med 25:165–171

Nishikawa M, Hayashi T, Yoshitomi T, Inoue T, Ichiyama T, Furukawa S (2000) Perioperative evaluation of cerebral hemodynamics by transcranial Doppler ultrasonography in patient with hemolytic uremic syndrome. No To Hattatsu 32:520–523

Ohta H, Matsumoto R, Kato T, Tomono N, Shimizu T (1998) Tc-99m HMPAO brain perfusion SPECT images in a patient with portal-systemic encephalopathy. Clin Nucl Med 23:634–636

Owen DR, Matthews PM (2011) Imaging brain microglial activation using positron emission tomography and translocator protein-specific radioligands. Int Rev Neurobiol 101:19–39

Patel D, McPhail MJ, Cobbold JF, Taylor-Robinson SD (2012) Hepatic encephalopathy. Br J Hosp Med (Lond) 73:79–85

Pflugrad H, Meyer GJ, Dirks M, Raab P, Tryc AB, Goldbecker A, Worthmann H, Wilke F, Boellaard R, Yaqub M, Berding G, Weissenborn K (2016) Cerebral microglia activation in hepatitis C virus infection correlates to cognitive dysfunction. J Viral Hepat 23:348–357

Politis M, Su P, Piccini P (2012) Imaging of microglia in patients with neurodegenerative disorders. Front Pharmacol 3:96

Samson Y, Bernuau J, Pappata S, Chavoix C, Baron JC, Maziere MA (1987) Cerebral uptake of benzodiazepine measured by positron emission tomography in hepatic encephalopathy. N Engl J Med 316:414–415

Seifter JL, Samuels MA (2011) Uremic encephalopathy and other brain disorders associated with renal failure. Semin Neurol 31:139–143

Senzolo M, Pizzolato G, Ferronato C, Chierichetti F, Boccagni P, Dam M, Burra P (2009) Long-term evaluation of cognitive function and cerebral metabolism in liver transplanted patients. Transplant Proc 41:1295–1296

Sobrio F, Gilbert G, Perrio C, Barré L, Debruyne D (2010) PET and SPECT imaging of the NMDA receptor system: an overview of radiotracer development. Mini Rev Med Chem 10:870–886

Song SH, Kim IJ, Kim SJ, Kwak IS, Kim YK (2008) Cerebral glucose metabolism abnormalities in patients with major depressive symptoms in pre-dialytic chronic kidney disease: statistical parametric mapping analysis of F-18-FDG PET, a preliminary study. Psychiatry Clin Neurosci 62:554–561

Song SH, Kwak IS, Kim SJ, Kim YK, Kim IJ (2009) Depressive mood in pre-dialytic chronic kidney disease: statistical parametric mapping analysis of Tc-99m ECD brain SPECT. Psychiatry Res 173:243–247

Sørensen M, Ott P (2012) Cerebral ammonia metabolism in cirrhosis. In: Keiding S, Sørensen M (eds) Functional molecular imaging in hepatology. Bentham Science Publishers, Sharjah, pp 153–159. eISBN: 978-1-60805-290-5

Strauss GI, Høgh P, Møller K, Knudsen GM, Hansen BA, Larsen FS (1999) Regional cerebral blood flow during mechanical hyperventilation in patients with fulminant hepatic failure. Hepatology 30:1368–1373

Trzepacz PT, Tarter RE, Shah A, Tringali R, Faett DG, Van Thiel DH (1994) SPECT scan and cognitive findings in subclinical hepatic encephalopathy. J Neuropsychiatry Clin Neurosci 6:170–175

Vankadari K, Mittal BR, Kumar R, Singh H, Bhattacharya A, Dhiman RK (2018) Detection of hepatic encephalopathy on ^{18}F-FDG PET/CT brain images in a patient with decompensated liver cirrhosis. Clin Nucl Med 43:e486–e4e7

Venneti S, Lopresti BJ, Wiley CA (2013) Molecular imaging of microglia/macrophages in the brain. Glia 61:10–23

Wang HC, Hsu JL, Shen YY (2004) Acute bilateral basal ganglia lesions in patients with diabetic uremia: an FDG-PET study. Clin Nucl Med 29:475–478

Weissenborn K, Berding G, Köstler H (2000) Altered striatal dopamine D_2 receptor density and dopamine transport in a patient with hepatic encephalopathy. Metab Brain Dis 15:173–178

Weissenborn K, Ennen JC, Bokemeyer M, Ahl B, Wurster U, Tillmann HL, Trebst C, Hecker H, Berding G (2006) Monoaminergic neurotransmission is altered in hepatitis C virus infected patients with chronic fatigue and cognitive impairment. Gut 55:1624–1630

Yazgan Y, Narin Y, Demirturk L, Saracoglu M, Ercan M, Akyatan N, Dalkanat N, Ozel AM, Cetin M (2003) Value of regional cerebral blood flow in the evaluation of chronic liver disease and subclinical hepatic encephalopathy. J Gastroenterol Hepatol 18:1162–1167

Zhang W, Ning N, Li X, Li M, Duan X, Guo Y, Dang Y, Li Y, Gao J, Ye J, Yang J (2019) Impaired brain glucose metabolism in cirrhosis without overt hepatic encephalopathy: a retrospective ^{18}F-FDG PET/CT study. Neuroreport 30:776–782

Part VI

Epilepsy

PET in Epilepsy

36

Matthias Koepp, Marian Galovic,
and Maria Ilyas-Feldmann

Contents

36.1 Clinical Impact of PET in Epilepsy 970
36.2 Impact of Novel PET Ligands 971
36.2.1 Imaging GABAergic Neurotransmission 972
36.2.2 Imaging Serotonergic Neurotransmission 973
36.2.3 Imaging Opioid Neurotransmission 974
36.2.4 Imaging P-gp Function 975
36.2.5 Imaging NMDA Receptor Function 978
36.2.6 Imaging Dopaminergic Neurotransmission 978
36.2.7 Imaging Inflammation 979
36.3 Outlook 979
References 979

M. Koepp (✉)
Department of Clinical and Experimental Epilepsy, Institute of Neurology, University College London, London, UK
e-mail: m.koepp@ucl.ac.uk

M. Galovic
Department of Clinical and Experimental Epilepsy, Institute of Neurology, University College London, London, UK

Department of Neurology, University Hospital Zurich, Zurich, Switzerland
e-mail: Marian.Galovic@usz.ch

M. Ilyas-Feldmann
Department of Clinical and Experimental Epilepsy, Institute of Neurology, University College London, London, UK

Epilepsy-Center Berlin-Brandenburg, Department of Neurology, Charité—Universitätsmedizin Berlin, Berlin, Germany
e-mail: m.feldmann@alumni.ucl.ac.uk

R. A. J. O. Dierckx et al. (eds.), *PET and SPECT in Neurology*,
https://doi.org/10.1007/978-3-030-53168-3_36

Abstract

The major drawback in clinical positron emission tomography (PET) imaging is that of specificity: in epilepsy, PET shows both the cause and consequence of seizure activity in the focus and projection area of the seizure onset. This can make treatment decisions for resective surgery difficult.

18F-Fluorodeoxyglucose ([^{18}F]FDG) PET has been long integrated in presurgical neuroimaging in many centres and proved to be clinically useful in identifying focal glucose metabolic abnormalities.

[^{11}C]Flumazenil, which delineates γ-aminobutyric acid receptor A (GABA-A) availability, may provide a biochemical marker of epileptogenicity and strengthens the hypothesis that inhibitory mechanisms are disturbed in the epileptic focus. Although [^{11}C]flumazenil, and other novel PET ligands for opioid and serotonin neurotransmission, showed great potential in selected patient subgroups, these tracers have not yet reached the stage of routine clinical application.

Ultimately, the challenge for PET imaging in epilepsy, like for most central nervous system (CNS) diseases, is overcoming drug-resistance due to poor delivery and/or retention of pharmaceuticals across the blood-brain barrier. There is the potential of PET to be relevant for the selection of certain novel treatment strategies, beyond the localisation of the focus for resective surgery.

36.1 Clinical Impact of PET in Epilepsy

Deoxyglucose radiolabelled with 18-fluorine ([^{18}F]FDG) administered to patients interictally is the sole application of PET in widespread routine clinical use in epilepsy. The technique provides a measure of cerebral glucose metabolism, which is reduced in the epileptogenic region interictally, in 60–90% of patients with temporal lobe epilepsy (TLE). Ictal [^{18}F]FDG PET is unhelpful as cerebral uptake of the radioligand takes place over many minutes post-injection.

Unfortunately, the area of hypometabolism demonstrated with [^{18}F]FDG PET is usually considerably larger than the pathological abnormality, site of neuronal loss and epileptogenic zone. In those patients with definitive magnetic resonance imaging (MRI) lesions, the technique adds little. However, its place remains in the presurgical evaluation of patients with non-definitive MRI abnormalities and/or discordant data, in particular patients with normal MRI—both in temporal and neocortical epilepsies and subtle focal cortical dysplasia. Imaging with [^{18}F]FDG PET has shown that patients with TLE who were seizure-free after temporal lobe resection had a greater proportion of hypometabolic area surgically removed than individuals who continued to have seizures (Willmann et al. 2007). This finding raises the possibility of tailoring the extent of resection according to the area of hypometabolism, especially in anatomically complex cases. Such a tailored approach would be challenging, however, as the volume of hypometabolism is often extensive and

frequently extends into eloquent cerebral areas. The findings in patients with TLE might simply reflect the possibility that the greater the extent of resection, the greater the chance of seizure remission.

The available evidence for clinical effectiveness of PET is inadequate to reliably inform clinical practice. This is astonishing considering that since the 1980s, [^{18}F]FDG PET has been the imaging workhorse of presurgical evaluations in patients with epilepsy, although over the past 20 years, these imaging techniques have been largely superseded by high-quality MRI. Indeed, FDG PET is redundant if a lesion shown on MRI is concordant with clinical and electroencephalogram (EEG) data (Willmann et al. 2007). The value of FDG PET data is enhanced by voxel-based comparisons of individual patient scans with normative data and coregistration of PET images with MRI scans (Salamon et al. 2008). These advances have helped to decide on placement of intracranial EEG electrodes, but have not yet been shown to improve surgical outcomes. There is a lack of studies evaluating the impact of these tests on clinical decision-making and patient outcomes; only one such study meets this criterion, reporting the impact of imaging (FDG PET) on the decision-making process (O'Brien et al. 2008). Of the 110 patients who received FDG PET, the decision for or against surgery was considered to be influenced by the results of the FDG PET scan in 78 patients (71%): 48 influenced the decision in favour of surgery and 28 in favour of no surgery, and 2 patients had doubt cast on prior decisions and eligibility for surgery became uncertain. The positive decision predictive value for PET was 65% (95% CI 53–77%) and negative decision predictive value was 60% (95% CI 45–72%). It showed that if the FDG PET result does not lead to a positive or negative decision to undertake surgery, invasive EEG is offered. This strategy appeared the most cost-effective at conventional cost-effectiveness thresholds of £20,000–30,000. When the additional benefits conferred over the longer term for patients who received surgery compared to medical management alone (i.e. the benefits over and above those attributed to the additional success rate of surgery in increasing the probability of patients becoming seizure-free at 1 year) were excluded, medical management appeared to be the more appropriate management strategy for patients in whom the decision to proceed to surgery was still unclear following the results of FDG PET.

36.2 Impact of Novel PET Ligands

The development of specific PET ligands to identify focal abnormalities and, hence, to inform surgical treatment has been a long-term aspiration in epilepsy surgery. Several PET receptor ligands have been used to investigate the neurochemical basis of the epilepsies and have partially entered clinical routine. The aim is to assess neurotransmitter systems that are directly responsible for modulating synaptic activity, specific ligand–receptor relationships that seem to be important for epileptogenesis and spread of epileptic activity and generic mechanisms relevant for the development of pharmaco-resistance.

36.2.1 Imaging GABAergic Neurotransmission

[^{11}C]Flumazenil (FMZ) binds to the γ-aminobutyric acid receptor complex and can identify occult surgically relevant abnormalities. In the context of identifying epileptogenic tissue, binding of [^{11}C]FMZ was significantly lower in the epileptic focus than in the contralateral homotopic reference region and the remaining neocortex (Savic et al. 1988). It identified occult but surgically relevant abnormalities of benzodiazepine receptors (Ryvlin et al. 1998), and in malformations of cortical development, abnormalities were more extensive than subtle structural abnormality revealed with MRI (Hammers et al. 2001). Reduced binding can be seen at the epileptogenic focus and the seizure onset region, however, in a more restricted distribution than the corresponding area of [^{18}F]FDG hypometabolism, and sometimes also in projection areas (Savic et al. 1995). In addition, the degree of GABA receptor reduction showed a positive correlation with seizure frequency (Laufs et al. 2011). Furthermore, there was a close correlation between time since last seizure and magnitude of change in FMZ binding (Bouvard et al. 2005). Therefore, this method may not only be suitable for noninvasive localisation of the seizure focus but also provides a biochemical marker of epileptogenicity, strengthening the hypothesis that inhibitory mechanisms are disturbed in the epileptic focus. In unilateral hippocampal sclerosis, reduction of binding of [^{11}C]FMZ has been shown to be confined to the hippocampus (Koepp et al. 1996) and to be over and above that caused by neuron loss and hippocampal atrophy (Koepp et al. 1998a). In malformations of cortical development, abnormalities of benzodiazepine receptors, as demonstrated with [^{11}C]FMZ PET, were more extensive than the structural abnormality revealed with MRI (Hammers et al. 2001). Moreover, [^{11}C]FMZ PET was shown to be more accurate than [^{18}F]FDG PET for the detection of cortical regions of seizure onset and frequent spiking in patients with extra-TLE (Muzik et al. 2000), whereas both [^{18}F]FDG and [^{11}C]FMZ PET showed low sensitivity in the detection of cortical areas of rapid seizure spread (Koepp et al. 2000).

Currently, the clinical role of [^{11}C]FMZ for the detection of temporal and extratemporal foci is viewed controversially. Even though [^{11}C]FMZ binding has revealed focal abnormalities in 80% of patients with refractory TLE and normal high-quality MRI, this method has not been considered consistently helpful in localising epileptic foci (Koepp et al. 2000). In addition, the short half-time of ^{11}C (20 min) hampers the wide use of [^{11}C]FMZ for clinical routine. The possible implementation of [^{18}F]FMZ in clinical routine will most probably provide a more definite answer about the clinical benefit of benzodiazepine receptor imaging (Vivash et al. 2013).

The use of interictal [^{11}C]FMZ PET in patients with idiopathic generalised epilepsy, together with voxel-based morphometry MRI studies, has truly challenged the concept of generalised epilepsies revealing predominantly frontal increases in FMZ binding suggestive of focal microdysgenesis (Koepp et al. 1997; Savic et al. 1994). In a similar vein, the prevailing concept in focal epilepsies of epileptogenic zones, defined ‘posthum’ through seizure freedom following complete resection, has been challenged in a recent analysis of FMZ PET studies. Laufs and colleagues averaged both PET and functional MRI (fMRI) data across a group of patients with

different sites of seizure onset and identified an area in the human piriform (primary olfactory) cortex that was active in association with interictal EEG spikes and showed reduced FMZ binding associated with increased seizure frequency (Laufs et al. 2011). This region was located in close proximity to the physiologically defined deep piriform cortex from which convulsants are known to initiate temporal lobe seizures, and blockade of glutamate receptors or application of a GABA receptor agonist reduces limbic motor seizures in rodents and nonhuman primates (Piredda and Gale 1985).

36.2.2 Imaging Serotonergic Neurotransmission

One major drawback in clinical imaging is that of specificity. MRI, FDG and FMZ PET all show both the cause and consequence of seizure activity, in the focus and projection area of the seizure onset. Furthermore, often multiple lesions are detected, and the significance of these changes is unclear.

Alpha[^{11}C]methyl-L-tryptophan (AMT) is an analogue of the essential amino acid tryptophan, the precursor of serotonin. AMT PET was originally developed to study abnormalities of brain serotonin synthesis. Preliminary studies in patients with neocortical epilepsy demonstrated that epileptogenic cortical areas show increased AMT uptake in some patients, even if MRI or FDG PET are non-localising (Fedi et al. 2001; Juhász et al. 2003). An increase in alpha [^{11}C]AMT uptake has been suggested to indicate the epileptic focus in situations where more than one possible focus is present, such as in patients with tuberous sclerosis. In one study, 25% of children with refractory focal epilepsy and normal MRI had a focal increase in AMT binding, and positive findings had a high specificity for the identification of the epileptic focus (Wakamoto et al. 2008). The sensitivity of AMT PET appears to be below 50% in non-lesional epilepsy, but its high specificity for detecting the lobe of seizure onset makes it an attractive imaging modality when other, more conventional imaging techniques fail to provide a clear localising information and also in presurgical evaluation of patients for reoperation after a failed surgery (Juhász et al. 2003). Recent studies suggested that increased AMT uptake may be relatively common in patients with epileptogenic cortical malformations (Chugani et al. 2013).

Experimental data in animals indicate that 5-HT$_{1A}$ receptors are located predominantly in limbic areas and that serotonin, via these receptors, mediates an antiepileptic and anticonvulsant effect. The literature on 5-HT$_{1A}$ receptor binding has recently been reviewed in detail (Hammers 2012). 5-HT$_{1A}$ receptors have been investigated with [^{18}F]FCWAY (Toczek et al. 2003). Twelve patients with TLE were correctly lateralised but not localised, including three patients with normal hippocampal volumes. Asymmetry indices for [^{18}F]fluorocyclohexanecarboxylic acid (FCWAY) were greater than those for FDG PET or hippocampal volumes.

Another study used the novel 5-HT$_{1A}$ radioligand [^{18}F]MPPF (20-methoxyphenyl-(*N*-20-pyridinyl)-*p*-[18F]fluorobenzamidoethylpiperazine), an antagonist of the 5-HT$_{1A}$ receptors, to assess the extent of 5-HT$_{1A}$ receptor binding changes in patients with TLE and hippocampal ictal onset. Patients had TLE of various aetiologies, and

all underwent video-EEG evaluation with depth electrodes implanted. Binding was reduced in the epileptogenic areas, and magnitude of decrease was related to both electrophysiological data (greatest in areas of ictal onset and spread) and structural data (greatest in lesions with volume loss, followed by lesions). Binding potential (BP) reductions were found in all nine patients; they corresponded to or included the ictal onset zone in five and propagation areas in two and were maximal in the onset areas but failed to reach significance in two. In four patients, contralateral abnormalities were seen; in one of these patients who was explored with contralateral depth electrodes, one seizure did start contralaterally. [^{18}F]MPPF PET correctly indicated lateralisation in all three patients without lesions on MRI. In patients with normal hippocampal volume, the BP decrease was restricted to the temporal pole (Merlet et al. 2004a). The decrease was more pronounced in the seizure onset zone and in regions where the discharge propagated than in regions where only interictal paroxysms or no epileptic activity was recorded (Merlet et al. 2004b). Therefore, these results indicate that [^{18}F]MPPF binding not only reflects structural changes but also reflects neuronal loss.

The reduction in 5-HT$_{1A}$ BP in patients with mesial TLE may be explained, on the one hand, by a decrease in receptor density due to downregulation due to hyperexcitability or, on the other hand, by an increase in endogenous serotonin as a reactional process to modulate hyperexcitability.

Comparison between [^{18}F]FDG and [^{18}F]MPPF PET data showed the clear-cut superiority of the latter for localising visually the epileptogenic area in patients with mesial TLE. The specificity of [^{18}F]FDG PET was lower than that of [^{18}F]MPPF PET, with only 23% of patients showing hypometabolism restricted to the hippocampus, amygdala and temporal pole, versus 38% demonstrating such abnormalities with [^{18}F]MPPF PET (Didelot et al. 2008). Taken together, these studies suggest that 5-HT$_{1A}$ receptor PET could play a role in lateralising TLE when other imaging modalities are nonconclusive.

36.2.3 Imaging Opioid Neurotransmission

PET studies using opioid receptor ligands with different selectivity support findings from animal experiments suggesting a predominantly anticonvulsant effect of opioid peptides. The earliest human PET study indicating selective modulation of the opiate system in partial epilepsy was that of Frost et al. (1988), who demonstrated, with the μ-selective ligand [^{11}C]carfentanil, increased μ-opioid receptor availability in the areas of the epileptogenic temporal lobe exhibiting interictal hypometabolism. Increased receptor availability could point either to a decreased interictal tone of endogenous opioids, to an increased number of μ-opioid receptors, or both. In contrast to this finding, no comparable asymmetry was detectable with the nonspecific opioid receptor ligand [^{11}C] diprenoprhine (DPN) and the κ- and μ-selective ligand [^{18}F]carfentanil (CFX) (Mayberg et al. 1991; Theodore et al. 1992). A study with the δ-selective opioid receptor ligand [^{11}C]methylnaltrindole also showed increased receptor availability in the epileptogenic temporal lobe, but with a different regional pattern (Madar et al. 1997).

The in vivo demonstration in humans of selective regional alterations of κ- and μ-receptor binding in TLE supports the hypothesis derived from animal studies that endogenous ligand binding to these receptor subtypes plays a role in the tonic anticonvulsive mechanism that limits the spread of seizure activity from the epileptogenic focus. One important advantage of PET is that it allows for localising changes in neurotransmitter levels that accompany changes in neural activity. All the studies listed so far were performed in the interictal (between seizure) state. A limitation of the aforementioned studies is that they do not provide evidence for dynamic changes in opioid receptor availability, which would form a more compelling argument for the relevance of opioid receptor-mediated neurotransmission in epilepsy. Some studies used frequency of seizures and time since last seizure as indirect marker for epileptogenicity, as ictal (during seizure) investigations are difficult to perform due to the paroxysmal nature of the epilepsies. Seizure provocation is possible for some generalised epilepsies and reflex epilepsies, such as reading epilepsy, which is an ideal model to study functional changes that occur at or around the time of seizures.

Our group addressed the issue by demonstrating decreased [^{11}C]DPN binding in the left parietal–temporal–occipital cortex, a reading-associated area, during reading-induced seizures, in patients with reading epilepsy (Koepp et al. 1998b). Extrapolating this finding suggests the release of endogenous peptides during the ictal period in the epileptogenic (or at least, symptomatogenic) region, that is, the temporal lobe in TLE. Further evidence is provided by the finding of increased elimination of diprenorphine from the association cortex during hyperventilation-induced absence seizures and also by the finding of decreased [^{18}F]CFX binding in the presumed epileptogenic zone during a fortuitous ictal scan (Theodore et al. 1992; personal communication). More recently, our group demonstrated increased opioid peptide receptor binding postictally (i.e. within 24 h after a seizure) in the ipsilateral fusiform gyrus and temporal pole in patients with TLE (Hammers et al. 2007). Opioid receptor binding, which was also elevated relative to that of healthy controls, returned to baseline within the interictal period (6–56 days).

In summary, there is evidence for a dynamic relationship between opioid peptide receptor availability and seizures. Interictal studies suggest increased μ- and δ-opiate receptor availability in the ipsilateral temporal lobe during the interictal period in TLE. Ictal studies of reading-induced and absence epilepsies suggest decreased μ-, δ- and κ-opiate receptor availability during seizures. Postictal opioid peptide receptor binding is increased in the ipsilateral temporal lobe in TLE. The finding of changes in opioid receptor availability over a time course of hours following spontaneous seizures suggests an important role of the endogenous opioid receptor-mediated neurotransmission in temporal lobe seizures.

36.2.4 Imaging P-gp Function

The challenge in treating most CNS diseases is overcoming drug-resistance due to poor delivery and/or retention of pharmaceuticals. In epilepsy, about one third of patients are drug-resistance. The drug transporter hypothesis proposes that drug-resistance is related to increased expression of multidrug efflux transporter proteins

such as P-glycoprotein (P-gp). These proteins are thought to prevent antiepileptic drug (AED) entry by actively extruding AEDs from their target site (Sisodiya et al. 2002). Multidrug efflux transporters are highly expressed in capillary endothelial cells and astrocytic foot processes that form the blood brain barrier (BBB). They limit intracellular concentration of substrates by pumping them out of the cell through an active energy-dependent mechanism. Epilepsy was the first CNS disorder for which drug-resistance was associated with enhanced expression of P-gp in the brain (Tishler et al. 1995). Pathologically elevated expression of P-gp has been found in resected brain tissue of patients with drug-resistant TLE undergoing surgery (Sisodiya et al. 2002) as well as in limbic brain regions of mouse and rat models of TLE (Loscher and Potschka 2005a). It is not clear whether the endothelial and parenchymal overexpression of P-gp is a consequence of epilepsy, of uncontrolled seizures or of chronic treatment with AEDs or whether it is constitutive, that is, present before the onset of epilepsy (Loscher and Potschka 2005b). Noninvasive brain imaging of multidrug efflux transporter function in drug-resistant and seizure-free epilepsy patients are a strategy to evaluate whether the overexpression of multidrug efflux transporters at the BBB as postulated in the transporter hypothesis have any functional consequences that underlie drug-resistance in epilepsy. Additionally, PET tracers for multidrug efflux transporters could be useful to identify epilepsy patients with increased multidrug efflux transporter activity who will benefit from treatment with multidrug efflux transporter modulation drugs and therefore hold great promises for individualised medicine (Sisodiya and Bates 2006).

P-gp function at the BBB of healthy humans has been imaged and quantified using the high-affinity P-gp substrates [(^{11})C]-verapamil and [^{11}C]-*N*-desmethyl-loperamide, which are very effectively transported by P-gp at the BBB. This results in low brain uptake of this radiotracer thus making it difficult to identify regional differences in cerebral P-gp function. A possible strategy to overcome the limitation of the low brain uptake of these P-gp substrate radiotracers is to perform PET scans after partial blockade by P-gp-modulating drugs, such as cyclosporine A (CsA) or tariquidar (Loscher and Langer 2010). The third-generation P-gp inhibitor tariquidar is safer than the non-selective CsA for use in human subjects and was shown to lack interaction with metabolism and plasma protein binding of (R)-[^{11}C]verapamil (Bankstahl et al. 2008; Wagner et al. 2009). Blocking P-gp with an inhibitor allows the radiotracer to enter the BBB and hence increase its uptake and signal in the brain. A proof of concept study was performed in rats 48 h after pilocarpine-induced status epilepticus (SE), supporting the hypothesis of regionally increased cerebral P-gp function in epilepsy. Both control and post-SE rats underwent (R)-[^{11}C]verapamil PET scans after administration of tariquidar at 3 mg/kg (Bankstahl et al. 2011). Regional PET data was analysed, and P-gp expression was independently quantified in the same brain regions using immunohistochemical staining (Bankstahl et al. 2011). In brain regions with increased P-gp expression (cerebellum, thalamus and hippocampus) in SE rats, the influx rate constants from blood to brain (K_1-values) of (R)-[^{11}C]verapamil were significantly decreased relative to control animals.

The caveat in the interpretation of (R)-[^{11}C]verapamil is that the peripheral metabolism of the radiotracer is significantly faster in epilepsy patients compared to

healthy controls. This is most likely caused by hepatic cytochrome P450 enzyme induction of AEDs (Abrahim et al. 2008). The difficulty is that these radiometabolites which are generated from the (R)-[^{11}C]verapamil are also taken up into the brain tissue independent of P-gp function and compromise the quantitative measurement of P-gp function especially when comparing different study groups such as patient and healthy controls. To limit the effect of radio-labelled metabolites, a kinetic analysis with a single-tissue compartment model on the first 10 min of dynamic PET data should be used (Muzi et al. 2009).

A pilot study by Langer et al. (2007) used PET and the radiotracer (R)-[^{11}C]verapamil to test for differences in P-gp activity between epileptogenic and non-epileptogenic brain regions of patients with drug-resistant unilateral TLE. Although statistical significance was not reached, the findings were in-line with the hypothesis of P-gp overexpression. Influx rate constants from the blood to brain (K_1) and efflux rate constants from the brain to blood (K_2) were increased ipsilateral to the seizure focus in several temporal lobe regions known to be involved in seizure generation and propagation. Additionally, asymmetries were most prominent in the parahippocampal and ambient gyrus, amygdala, medial anterior temporal lobe and lateral anterior temporal lobe. In contrast to temporal lobe volumes of interest, asymmetries were minimal in regions located outside the temporal lobe.

Our recent voxel-based data revealed that at baseline K_1 was significantly reduced in drug-resistance compared to seizure-free TLE in temporal lobe regions and higher P-gp activity was associated with higher seizure frequency. After TQD, whole-brain K_1 increases were significantly reduced in drug-resistance TLE patients compared to controls (21.9% vs. 56.8% after 2 mg/kg TQD and 42.6% vs. 57.9% after 3 mg/kg TQD) which was most pronounced in the sclerotic hippocampus (24.5% vs. 65%, $p < 0.0001$). The reduced K_1 at baseline and reduced increases in K_1 after TQD in pharmacoresistant TLE compared to seizure-free TLE patients and controls support the hypothesis of P-gp overexpression in drug-resistant epilepsy (Feldmann et al. 2013). A follow-up (R)-[^{11}C]verapamil PET study analysed P-gp activity in seven patients undergoing epilepsy surgery (Bauer et al. 2014). They showed that optimal surgical outcome was associated with higher temporal lobe P-gp function before surgery, higher P-gp-positive staining in surgically resected hippocampal specimens, and reduction in global P-gp function postoperatively, compared with nonoptimal surgery outcome. Their result also indicated that P-gp expression is dynamic and changes with seizure frequency or AED treatment.

Our results were externally reproduced in a study using (R)-[^{11}C]verapamil PET and the non-selective P-gp inhibitor CsA in six patients with drug-resistant epilepsy and five patients with drug-sensitive epilepsy compared to eight healthy controls (Shin et al. 2016). All patients with drug-resistant epilepsy had significantly different asymmetry from the healthy controls, whereas all patients with drug-sensitive epilepsy had an asymmetry similar to that in healthy controls. In the temporal lobe, the asymmetry indices of patients with left temporal lobe drug-resistant epilepsy were more positive than those of healthy controls (healthy controls: 4.0413 ± 1.7452; patients: 7.2184 ± 1.8237; $p = 0.048$), and those of patients with right temporal drug-resistant epilepsy were more negative (patients: -1.6496 ± 3.4136; $p = 0.044$).

In addition, specific regions that had significant asymmetry were different between the lateral and medial temporal lobe epilepsy groups (Shin et al. 2016). By using this imaging technique with (R)-[^{11}C]verapamil PET we can identify individual patients where drug-resistance is caused by P-gp overactivity and potentially individualise treatment. Moreover, comparative studies between drug-resistant and seizure-free epilepsy patients can enable testing for a correlation between P-gp function and the pharmacoresponse. This imaging technique can also guide patient selection for future clinical studies. In particular, PET imaging of P-gp function may allow individualised application of approaches to overcome P-gp-associated drug-resistance.

36.2.5 Imaging NMDA Receptor Function

The *N*-methyl-D-aspartate (NMDA) receptor complex binds glutamate, the most important excitatory neurotransmitter in the brain. NMDA receptors have been showed to be involved in epileptogenesis and antagonists of the NMDA receptor have been used to treat seizures, particularly refractory status epilepticus. Developing a suitable ligand for in vivo imaging in humans has, however, proven difficult.

One study detected reduced binding of [^{11}C]-labelled ketamine in the ipsilateral temporal lobe of patients with TLE (Kumlien et al. 1999). This could reflect either reduced NMDA receptor density, reduced perfusion or focal atrophy.

More recently [^{18}F]GE-179, a novel ligand binding to activated (i.e. open) NMDA receptors, has been successfully employed in people with epilepsy (McGinnity et al. 2015). Its longer half-life makes it potentially more broadly available and might increase its clinical applicability. Increased activation of NMDA receptors was demonstrated in 8 people with epilepsy using this tracer. This could reflect ongoing epileptogenesis in these refractory cases. Conversely, tracer uptake was reduced in three epilepsy patients taking antidepressants. This could point to an interaction of antidepressants with the NMDA receptor. Further studies of this ligand are currently ongoing.

36.2.6 Imaging Dopaminergic Neurotransmission

The dopaminergic system is tough to play a role in seizure termination by modulating thalamo-cortical connections. Thus, alterations of the dopaminergic system in epilepsy could point to a disturbed mechanism of ictal termination.

Several PET studies demonstrated reduced dopaminergic neurotransmission in the basal ganglia of people with epilepsy. A variety of different radioligands were employed and a broad mix of clinical syndromes were examined, adding support to the robustness of the findings. These observations included presynaptic dopaminergic deficits using [^{18}F]fluoro-L-DOPA (Bouilleret et al. 2005, 2008), decreased D2/D3-receptor binding using [^{18}F]fallypride (Werhahn et al. 2006; Yakushev et al. 2010; Landvogt et al. 2010; Bernedo Paredes et al. 2015), decreased D1-receptor binding using [^{11}C]SCH23390 (Fedi et al. 2008), and reduced dopamine transporter

activity with [^{11}C]PE2I (Ciumas et al. 2008, 2010; Odano et al. 2012). The syndromes studied included not only TLE, but also juvenile myoclonic epilepsy, idiopathic generalised epilepsy and autosomal dominant nocturnal frontal lobe epilepsy. Studying regions outside of the basal ganglia is difficult because of a low concentration of dopaminergic synapses in the neocortex. However, two studies also found reduced tracer uptake in the epileptogenic zone of TLE patients (Werhahn et al. 2006, Landvogt et al. 2010).

36.2.7 Imaging Inflammation

Measuring inflammation in epilepsy using PET focused on the translocator protein (TSPO), a marker that is overexpressed on activated microglia and reactive astrocytes. Three studies from the same research group demonstrated increased TSPO tracer binding ([^{11}C]PBR28 and [^{11}C]DPA-713) in the epileptogenic zone of people with mesial TLE and neocortical epilepsy (Hirvonen et al. 2012; Gershen et al. 2015; Dickstein et al. 2019). In one of these studies, the authors also found increased binding in the hemisphere contralateral to the epileptogenic zone, whereas it was less pronounced than on the ipsilateral side (Gershen et al. 2015). In one patient studied longitudinally, significantly increased tracer uptake was observed 36 h after a seizure compared to an interictally rescan (Butler et al. 2013). Overall, these findings point to increased inflammation and microglia activation in people with epilepsy, particularly within the epileptic focus and shortly after seizures. Another case series observed increased TSPO expression using [^{11}C]PK11195 PET in two patients with histologically confirmed Rasmussen's encephalitis (Banati et al. 1999), substantiating the role of neuroinflammation in this syndrome.

36.3 Outlook

Future research needs to be considered in relation to how the research informs the different levels of the diagnostic evaluation framework and ultimately how this links to the decision problem(s) faced by clinicians. It is integral to the evaluation of diagnostic technologies in the workup for epilepsy surgery that their impact on clinical decision-making, and on further treatment decisions, is considered; findings from these studies should be used alongside assessments of the long-term clinical effects and of costs of such treatments.

References

Abrahim A, Luurtsema G, Bauer M, Karch R, Lubberink M, Pataraia E, Joukhadar C, Kletter K, Lammertsma A, Baumgartner C, Muller M, Langer O (2008) Peripheral metabolism of (R)-[11C]verapamil in epilepsy patients. Eur J Nucl Med Mol Imaging 35:116–123

Banati RB, Goerres GW, Myers R et al (1999) [11C](R)-PK11195 positron emission tomography imaging of activated microglia in vivo in Rasmussen's encephalitis. Neurology 53(9):2199–2203

Bankstahl JP, Kuntner C, Abrahim A, Karch R, Stanek J, Wanek T, Wadsak W, Kletter K, Muller M, Loscher W, Langer O (2008) Tariquidar-induced P-glycoprotein inhibition at the rat blood-brain barrier studied with (R)-11C-verapamil and PET. J Nucl Med 49:1328–1335

Bankstahl JP, Bankstahl M, Kuntner C, Stanek J, Wanek T, Meier M, Ding XQ, Muller M, Langer O, Loscher W (2011) A novel positron emission tomography imaging protocol identifies seizure-induced regional overactivity of P-glycoprotein at the blood-brain barrier. J Neurosci 31:8803–8811

Bauer M, Karch R, Zeitlinger M, Liu J, Koepp MJ, Asselin M-C, Sisodiya SM et al (2014) In vivo P-glycoprotein function before and after epilepsy surgery. Neurology 83:1326–1331

Bernedo Paredes VE, Buchholz H-G, Gartenschläger M, Breimhorst M, Schreckenberger M, Werhahn KJ (2015) Reduced D2/D3 receptor binding of Extrastriatal and striatal regions in temporal lobe epilepsy. PLoS One 10(11):e0141098. https://doi.org/10.1371/journal.pone.0141098

Bouilleret V, Semah F, Biraben A et al (2005) Involvement of the basal ganglia in refractory epilepsy: an 18F-fluoro-L-DOPA PET study using 2 methods of analysis. J Nucl Med 46(3):540–547

Bouilleret V, Semah F, Chassoux F et al (2008) Basal ganglia involvement in temporal lobe epilepsy: a functional and morphologic study. Neurology 70(3):177–184. https://doi.org/10.1212/01.wnl.0000297514.47695.48

Bouvard et al (2005) Seizure-related short-term plasticity of benzodiazepine receptors in partial epilepsy: a [11C]flumazenil-PET study. Brain 128:1330–1343

Butler T, Ichise M, Teich AF et al (2013) Imaging inflammation in a patient with epilepsy due to focal cortical dysplasia. J Neuroimaging 23(1):129–131

Chugani HT, Luat AF, Kumar A, Govindan R, Pawlik K, Asano E (2013) α-[11C]-Methyl-L-tryptophan-PET in 191 patients with tuberous sclerosis complex. Neurology 81(7):674–680

Ciumas C, Wahlin T-BR, Jucaite A, Lindstrom P, Halldin C, Savic I (2008) Reduced dopamine transporter binding in patients with juvenile myoclonic epilepsy. Neurology 71(11):788–794

Ciumas C, Wahlin T-BR, Espino C, Savic I (2010) The dopamine system in idiopathic generalized epilepsies: identification of syndrome-related changes. NeuroImage 51(2):606–615

Dickstein LP, Liow J-S, Austermuehle A et al (2019) Neuroinflammation in neocortical epilepsy measured by PET imaging of translocator protein. Epilepsia 313(3):285–287

Didelot A, Ryvlin P, Lothe A, Merlet I, Hammers A, Mauguiere F (2008) PET imaging of brain 5-HT1A receptors in the preoperative evaluation of temporal lobe epilepsy. Brain 131:2751–2764

Fedi M, Reutens D, Okazawa H et al (2001) Localizing value of alpha-methyl-L-tryptophan PET in intractable epilepsy of neocortical origin. Neurology 57:1629–1636

Fedi M, Berkovic SF, Scheffer IE et al (2008) Reduced striatal D1 receptor binding in autosomal dominant nocturnal frontal lobe epilepsy. Neurology 71(11):795–798

Feldmann M, Asselin MC, Liu J, Wang S, McMahon A, Anton-Rodriguez J, Walker M, Symms M, Brown G, Hinz R, Matthews J, Bauer M, Langer O, Thom M, Jones T, Vollmar C, Duncan JS, Sisodiya SM, Koepp MJ (2013) P-glycoprotein expression and function in patients with temporal lobe epilepsy: a case-control study. Lancet Neurol 12(8):777–785

Frost JJ, Mayberg HS, Fisher RS et al (1988) Mu-opiate receptors measured by positron emission tomography are increased in temporal lobe epilepsy. Ann Neurol 23:231–237

Gershen LD, Zanotti-Fregonara P, Dustin IH et al (2015) Neuroinflammation in temporal lobe epilepsy measured using positron emission tomographic imaging of Translocator protein. JAMA Neurol 72(8):882–888

Hammers A (2012) Epilepsy. NeuroMethods. https://doi.org/10.1007/7657_2012_58

Hammers A, Koepp MJ, Richardson MP et al (2001) Central benzodiazepine receptors in malformations of cortical development: a quantitative study. Brain 124:1555–1565

Hammers A, Asselin MC, Hinz R et al (2007) Upregulation of opioid receptor binding following spontaneous epileptic seizures. Brain 130:1009–1016

Hirvonen J, Kreisl WC, Fujita M et al (2012) Increased in vivo expression of an inflammatory marker in temporal lobe epilepsy. J Nucl Med 53(2):234–240

Juhász C, Chugani DC, Muzik O et al (2003) Alpha-methyl-L-tryptophan PET detects epileptogenic cortex in children with intractable epilepsy. Neurology 60:960–968
Koepp MJ, Richardson MP, Brooks DJ, Poline JB, Van Paesschen W, Friston KJ et al (1996) Cerebral benzodiazepine receptors in hippocampal sclerosis. An objective in vivo analysis. Brain 119:1677–1687
Koepp MJ, Richardson MP, Brooks DJ, Cunningham VJ, Duncan JS (1997) Central benzodiazepine/gamma-aminobutyric acid A receptors in idiopathic generalized epilepsy: an [11C]flumazenil positron emission tomography study. Epilepsia 38:1089–1097
Koepp MJ, Hand KS, Labbé C, Richardson MP, Van Paesschen W, Baird VH et al (1998a) In vivo [11C]flumazenil-PET correlates with ex vivo [3H]flumazenil autoradiography in hippocampal sclerosis. Ann Neurol 43:618–626
Koepp MJ, Richardson MP, Brooks DJ, Duncan JS (1998b) Focal cortical release of endogenous opioids during reading-induced seizures. Lancet 352:952–955
Koepp MJ, Hammers A, Labbe C, Woermann FG, Brooks DJ, Duncan JS (2000) 11CFlumazenil PET in patients with refractory temporal lobe epilepsy and normal MRI. Neurology 54:332–339
Kumlien E, Hartvig P, Valind S, Oye I, Tedroff J, Långström B (1999) NMDA-receptor activity visualized with (S)-[N-methyl-11C]ketamine and positron emission tomography in patients with medial temporal lobe epilepsy. Epilepsia 40(1):30–37
Landvogt C, Buchholz H-G, Bernedo V, Schreckenberger M, Werhahn KJ (2010) Alteration of dopamine D2/D3 receptor binding in patients with juvenile myoclonic epilepsy. Epilepsia 51(9):1699–1706
Langer O, Bauer M, Hammers A, Karch R, Pataraia E, Koepp MJ, Abrahim A, Luurtsema G, Brunner M, Sunder-Plassmann R, Zimprich F, Joukhadar C, Gentzsch S, Dudczak R, Kletter K, Muller M, Baumgartner C (2007) Pharmacoresistance in epilepsy: a pilot PET study with the P-glycoprotein substrate R-[11C]verapamil. Epilepsia 48:1774–1784
Laufs et al (2011) Converging PET and fMRI evidence for a common area involved in human focal epilepsies. Neurology 77(9):904–910
Loscher W, Langer O (2010) Imaging of P-glycoprotein function and expression to elucidate mechanisms of pharmacoresistance in epilepsy. Curr Top Med Chem 10(17):1785–1791
Loscher W, Potschka H (2005a) Drug resistance in brain diseases and the role of drug efflux transporters. Nat Rev Neurosci 6:591–602
Loscher W, Potschka H (2005b) Role of drug efflux transporters in the brain for drug disposition and treatment of brain diseases. Prog Neurobiol 76:22–76
Madar I, Lesser RP, Krauss G et al (1997) Imaging of delta- and mu-opioid receptors in temporal lobe epilepsy by positron emission tomography. Ann Neurol 41:358–367
Mayberg HS, Sadzot B, Meltzer CC et al (1991) Quantification of mu and non-mu opiate receptors in temporal lobe epilepsy using positron emission tomography. Ann Neurol 30:3–11
McGinnity CJ, Koepp MJ, Hammers A et al (2015) NMDA receptor binding in focal epilepsies. J Neurol Neurosurg Psychiatry 86(10):1150–1157
Merlet I, Ryvlin P, Costes N et al (2004a) Statistical parametric mapping of 5-HT1A receptor binding in temporal lobe epilepsy with hippocampal ictal onset on intracranial EEG. NeuroImage 22:886–896
Merlet I, Ostrowsky K, Costes N et al (2004b) 5-HT1A receptor binding and intracerebral activity in temporal lobe epilepsy: an [18F]MPPF-PET study. Brain 127:900–913
Muzi M, Mankoff DA, Link JM, Shoner S, Collier AC, Sasongko L, Unadkat JD (2009) Imaging of cyclosporine inhibition of P-glycoprotein activity using 11C-verapamil in the brain: studies of healthy humans. J Nucl Med 50:1267–1275
Muzik O, da Silva EA, Juhasz C et al (2000) Intracranial EEG versus flumazenil and glucose PET in children with extratemporal lobe epilepsy. Neurology 54:171–179
O'Brien TJ et al (2008) The cost-effective use of 18F-FDG PET in the presurgical evaluation of medically refractory focal epilepsy. J Nucl Med 49:931–937
Odano I, Varrone A, Savic I et al (2012) Quantitative PET analyses of regional [11C]PE2I binding to the dopamine transporter--application to juvenile myoclonic epilepsy. NeuroImage 59(4):3582–3593

Piredda S, Gale K (1985) A crucial epileptogenic site in the deep prepiriform cortex. Nature 317:623–625
Ryvlin P et al (1998) Clinical utility of flumazenil-PET versus [18F]fluorodeoxyglucose-PET and MRI in refractory partial epilepsy. A prospective study in 100 patients. Brain 121:2067–2081
Salamon N et al (2008) FDG-PET/MRI coregistration improves detection of cortical dysplasia in patients with epilepsy. Neurology 71:1594–1601
Savic I, Persson A, Roland P, Pauli S, Sedvall G, Widen L (1988) In-vivo demonstration of reduced benzodiazepine receptor binding in human epileptic foci. Lancet 2:863–866
Savic I, Pauli S, Thorell JO, Blomqvist G (1994) In vivo demonstration of altered benzodiazepine receptor density in patients with generalised epilepsy. J Neurol Neurosurg Psychiatry 57:797–804
Savic I, Thorell JO, Roland P (1995) [11C]Flumazenil positron emission tomography visualizes frontal epileptogenic regions. Epilepsia 36:1225–1232
Shin J-W, Chu K, Shin SA, Jung K-H, Lee S-T, Lee Y-S, Moon J et al (2016) Clinical applications of simultaneous PET/MR imaging using (R)-[11 C]-verapamil with Cyclosporin a: preliminary results on a surrogate marker of drug-resistant epilepsy. Am J Neuroradiol 37:600–606
Sisodiya SM, Bates SE (2006) Treatment of drug resistance in epilepsy: one step at a time. Lancet Neurol 5:380–381
Sisodiya SM, Lin WG, Harding BN, Squier MV, Thom M (2002) Drug resistance in epilepsy: expression of drug resistance proteins in common causes of refractory epilepsy. Brain 125:22–31
Theodore WH, Carson RE, Andreasen P et al (1992) PET imaging of opiate receptor binding in human epilepsy using [18F]cyclofoxy. Epilepsy Res 13:129–139
Tishler DM, Weinberg KI, Hinton DR, Barbaro N, Annett GM, Raffel C (1995) MDR1 gene expression in brain of patients with medically intractable epilepsy. Epilepsia 36:1–6
Toczek MT, Carson RE, Lang L et al (2003) PET imaging of 5-HT1A receptor binding in patients with temporal lobe epilepsy. Neurology 60(5):749–756
Vivash L, Gregoire MC, Lau EW, Ware RE, Binns D, Roselt P, Bouilleret V, Myers DE, Cook MJ, Hicks RJ, O'Brien TJ (2013) 18F-flumazenil: a γ-aminobutyric acid A-specific PET radiotracer for the localization of drug-resistant temporal lobe epilepsy. J Nucl Med 54(8):1270–1277
Wagner CC et al (2009) A pilot study to assess the efficacy of tariquidar to inhibit P-glycoprotein at the human blood-brain barrier with (R)–11C-verapamil and PET. J Nucl Med 50:1954–1961
Wakamoto H et al (2008) Alpha-methyl-l-tryptophan positron emission tomography in epilepsy with cortical developmental malformations. Pediatr Neurol 39:181–188
Werhahn KJ, Landvogt C, Klimpe S et al (2006) Decreased dopamine D2/D3-receptor binding in temporal lobe epilepsy: an [18F]fallypride PET study. Epilepsia 47(8):1392–1396
Willmann O, Wennberg R, May T, Woermann FG, Pohlmann-Eden B (2007) The contribution of 18F-FDG PET in preoperative epilepsy surgery evaluation for patients with temporal lobe epilepsy: a meta-analysis. Seizure 16:509–520
Yakushev IY, Dupont E, Buchholz H-G et al (2010) In vivo imaging of dopamine receptors in a model of temporal lobe epilepsy. Epilepsia 51(3):415–422

Imaging Evaluation of Epilepsy: Functional and Structural Approaches

37

Sara K. Inati and William H. Theodore

Contents

37.1 Overview . . . 984
37.2 Hypometabolism in Focal Epilepsy Using FDG-PET . . . 987
37.3 The Role of FDG-PET for Localization in Focal Epilepsy . . . 987
37.4 Comparison with Other Imaging Methods in Focal Epilepsy . . . 989
37.5 FDG-PET in Non-focal Epilepsy Syndromes . . . 992
37.6 Neuroinflammation . . . 993
37.7 P-gp Imaging: Mechanisms of Drug Resistance . . . 994
37.8 Benzodiazepine Receptors . . . 995
37.9 Serotonin Receptors . . . 995
37.10 Excitatory Amino Acid Receptors . . . 997
37.11 Conclusions . . . 998
References . . . 998

Abstract

Carefully selected patients with drug-resistant epilepsy may be candidates for resective surgery. Neuroimaging, including positron emission tomography (PET), magnetic resonance imaging (MRI), and ictal single-photon emission computed tomography (SPECT), are important clinical tools for presurgical seizure focus localization. MRI is an essential part of evaluation for patients with epilepsy. Structural studies may show focal abnormalities such as mesial temporal sclerosis or focal cortical dysplasia, which are the pathological substrates of seizure initiation. Functional localization data from arterial spin labeling for cerebral blood flow and spike-triggered or resting-state signal acquisition are potentially valuable as well. PET and SPECT usually only are performed for patients being considered for surgery. PET may show decreased interictal glu-

S. K. Inati · W. H. Theodore (✉)
National Institute of Neurological Disorders and Stroke, Bethesda, MD, USA
e-mail: Sara.inati@nih.gov; theodorw@ninds.nih.gov

R. A. J. O. Dierckx et al. (eds.), *PET and SPECT in Neurology*,
https://doi.org/10.1007/978-3-030-53168-3_37

cose metabolism in the epileptogenic zone. PET may also contribute to understanding the pathophysiology of epilepsy through the use of ligands for neurotransmitter receptors and neuroinflammation. Reduced benzodiazepine receptor binding may have occasional clinical relevance. Ictal SPECT may show increased blood flow if the tracer is injected soon after seizure onset, particularly if an interictal scan is subtracted and the image co-registered with structural MRI. When interpreting imaging in epilepsy, it is important to consider the clinical context, ictal semiology, and electrographic studies.

37.1 Overview

Positron emission tomography (PET) is relatively unique as a neuroimaging tool given the variety of radioligands that can be used to investigate different aspects of metabolic processes underlying normal brain function and diseases. Since the initial studies in the 1980s, PET using [^{18}F]2-fluoro-2-deoxy-D-glucose ([^{18}F]FDG) for measurement of the cerebral metabolic rate of glucose consumption (CMRglc) has become an established clinical tool for the evaluation of patients with epilepsy. Its most important clinical application is in seizure focus localization to aid with presurgical planning in patients with drug-resistant epilepsy (Fig. 37.1). In addition, FDG-PET can be used to study the pathophysiology of epilepsy and its comorbidities and the effects of antiepileptic drugs and other treatments and may have some diagnostic utility in conditions such as autoimmune encephalitis. PET ligands used

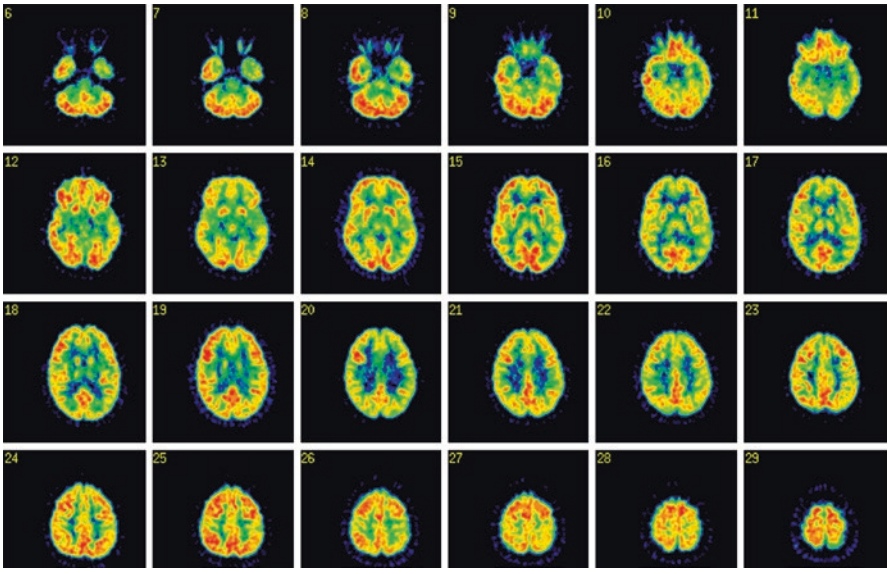

Fig. 37.1 FDG-PET scan showing left temporal hypometabolism in a patient with focal dyscognitive seizures of left mesial temporal onset

to image neuroreceptor binding and inflammation thus far have less clinical importance than FDG but have provided important data on basic mechanisms of epilepsy and can link human epilepsy with experimental models. Recent reviews have summarized the findings to date in the field of PET imaging in epilepsy for [^{18}F]FDG as well as a wide variety of other tracers (Kumar et al. 2012; Theodore 2017; Galovic and Koepp 2016; Juhasz and John 2020; Sidhu et al. 2018).

PET imaging is a fundamentally dynamic process, and there are several aspects of timing that must be taken into account. First, each PET modality involves production of a positron emitter followed by a radiochemistry procedure to bind it to a biologically active molecule. Each of these positron-emitting radioligands has a different half-life, which limits the amount of time available between production of the ligand and the detection of the ligand in a scanner. Since fluorine-18, used in FDG, has a half-life of 110 min, production at a central facility for transport to a scanner is practical. Carbon-11, however, which is used for many neurotransmitter receptor ligands, has a half-life of only 20 min and must be produced onsite; the radiochemistry procedures are thus more time-sensitive than for FDG. Second, uptake of the biologically active molecule that is part of the radioligand is a dynamic functional process. It is thus critical to be aware of the state of the patient during and before scanning. For example, the "metabolic window" measured by FDG lasts 30–40 min after isotope injection; the "time resolution" of PET is therefore significantly wider than for Electroencephalography (EEG) or fMRI. Moreover, there may be effects of recent seizure frequency on hypometabolism, even if no seizure activity occurs during the uptake period. This was demonstrated in a study using the benzodiazepine receptor ligand [11C]flumazenil, in which binding reduction in the seizure focus was partially reversed in the setting of more recent seizures (Bouvard et al. 2005).

Analysis methods for FDG-PET include traditional visual radiologic inspection of the images, region-of-interest-based templates used to measure relative asymmetries in CMRglc, and statistical approaches such as statistical parametric mapping. Some studies suggest that relative measurement of asymmetry indices is superior to pure visual interpretation, but more formal approaches including calculation of FDG kinetic parameters have not shown clear advantages (Theodore et al. 1992; Kim et al. 2003; van't Klooster et al. 2014; Mayoral et al. 2019; Tang et al. 2018). In addition to these analysis approaches, neurotransmitter receptor ligands require more complex tracer kinetic modeling. Some ligands may also be substrates for brain efflux transporters, further complicating binding measurements (Liow et al. 2016). PET imaging has relatively lower spatial resolution than structural MRI (the best current resolution for PET/CT and PET/MRI is ~4.5 mm). This leads to partial volume effects that may be particularly important in analysis of relatively small structures or when neuronal loss is present; these effects can be somewhat reduced by using MRI-based correction procedures (Figs. 37.2 and 37.3).

It is worth noting that many PET studies in epilepsy suffer from small subject numbers as well as methodologic limitations, including insufficient delineation of study populations, retrospective data collection, lack of blinding, and, for surgical outcome studies, inconsistent grading and limited follow-up (Gaillard et al. 2011). Large-scale multicenter studies would be much more efficient and provide a more solid basis for attempting to clarify the uses of PET in epilepsy.

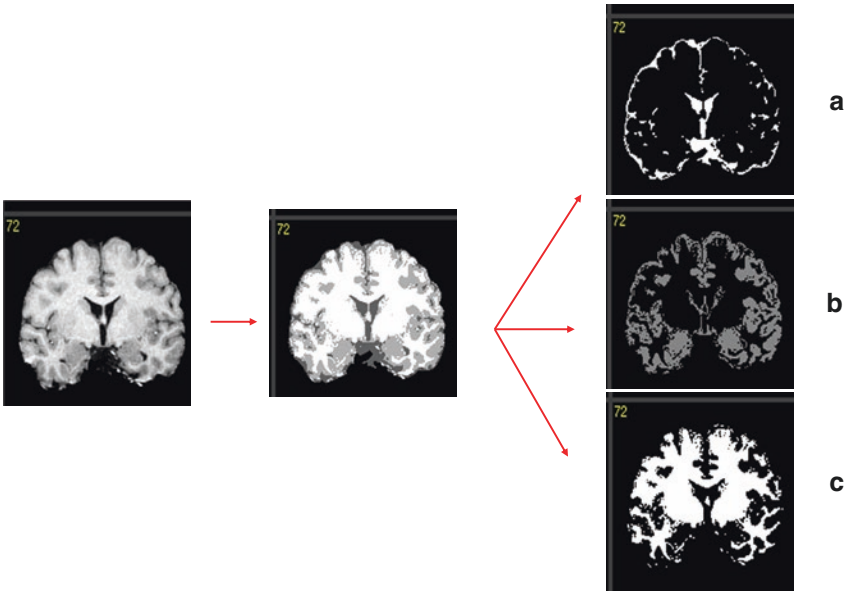

Fig. 37.2 Segmentation for partial volume correction. After skull stripping, the image is parceled into cerebrospinal fluid (**a**), gray matter (**b**), and whiter matter (**c**) spaces

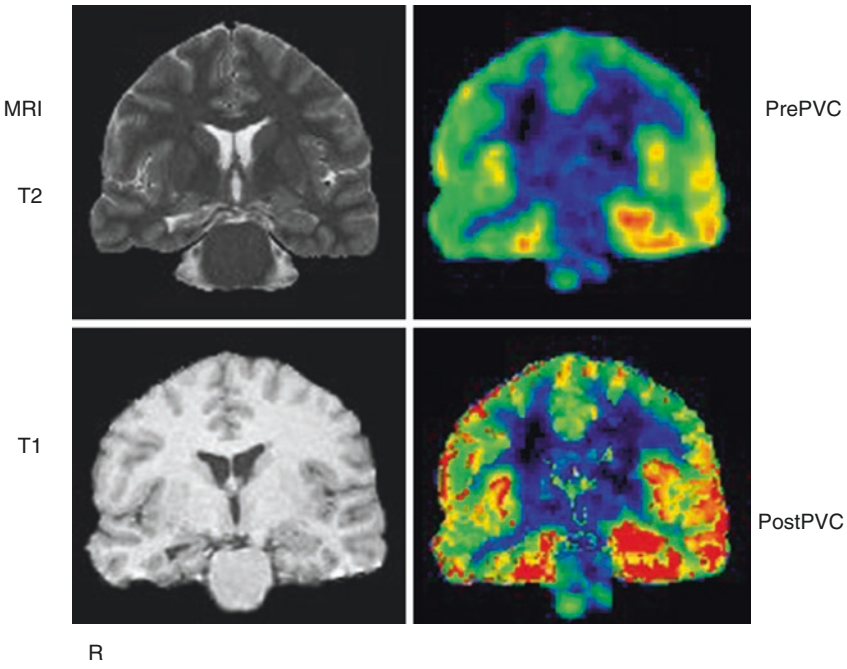

Fig. 37.3 Partial volume correction of FDG-PET scan in a patient with mesial temporal sclerosis. After application of the gray matter mask, apparent glucose metabolism is increased throughout. However, the relative hypometabolism in the right temporal cortex is preserved

37.2 Hypometabolism in Focal Epilepsy Using FDG-PET

FDG-PET has been shown in a large number of studies to detect hypometabolism interictally in patients with focal epilepsy, as well as in some patients with generalized epilepsy. Several factors likely contribute to this finding. The main energy consumption of the brain is dedicated to maintaining ionic gradients such as the Na^+/K^+ pump and neurotransmitter release and reuptake (Bazzigaluppi et al. 2017). Subsidiary uses are related to neurotransmitter synthesis, axonal transport, and biochemical syntheses. During seizures, there appears to be a sudden shift from hypo- to hypermetabolism. Although the mechanisms underlying such shifts are unclear, altered interictal Na^+/K^+ pump activity due to hypometabolism may lead to membrane instability and hyperexcitability. Several studies in experimental animals using the pilocarpine (Guo et al. 2009) and kainic acid models (Jupp et al. 2012) showed that limbic hypometabolism develops in concert with epileptogenesis and precedes the appearance of spontaneous seizures. Several studies suggest that the degree of initial hypometabolism at epilepsy diagnosis may predict prognosis (Gaillard et al. 2007). The extent of hypometabolism may subsequently fluctuate in relation to seizure frequency (Benedek et al. 2006). Over time, hypometabolic regions in children with focal epilepsy may increase in extent and be associated with persistent seizures (Govil-Dalela et al. 2018).

In addition to the mechanisms of neuronal dysfunction and altered metabolism, it appears that neuronal loss also plays a contributing role; it does not, however, account completely for the observations, as shown by studies using partial volume correction. This is also supported by studies in patients with clear unilateral seizure foci, in whom hypometabolism often extends beyond anatomic limits and may be bilateral. Additionally, in focal cortical dysplasia, hypometabolism can extend beyond the observed structural MRI findings and has been hypothesized to reflect reduced mitochondrial complex IV function to a greater degree than the extent of the structural abnormality (Tenney et al. 2014). The extent of seizure spread, in addition to metabolic dysfunction, may also be a contributing factor to the hypometabolism observed in FDG-PET imaging in epilepsy (Chassoux et al. 2016).

37.3 The Role of FDG-PET for Localization in Focal Epilepsy

Accurate identification of seizure foci is critical to the success of epilepsy surgery in treating drug-resistant epilepsy. This can be relatively straightforward in the setting of clear structural lesions on MRI with concordant interictal and ictal EEG findings; patients with lesional epilepsy on MRI have been shown to have improved postoperative seizure outcomes compared to those without lesions (Tellez-Zenteno et al. 2010; Tonini et al. 2004). Mesial temporal lobe epilepsy (mTLE) is one of the most common forms of drug-resistant epilepsy that is treated surgically. In mTLE, a large number of studies have shown that FDG-PET can detect hypometabolism in about 70–80% of patients (Theodore 2017). In these patients, PET hypometabolism appears to be regional, rather than localizing. It is common for patients to have lateral temporal neocortical as well as mesial hypometabolism, and hypometabolism

may extend beyond the temporal lobe to include the ipsilateral frontal lobes, insular, and thalamus. These findings, when ipsilateral, do not appear to affect surgical outcome; in a meta-analysis of 46 PET studies from 1992 to 2006, ipsilateral PET hypometabolism was found to have an 86% predictive value for "good" (variably defined in the studies included) surgical outcome (Willmann et al. 2007). While it was unclear whether PET added much of value for patients with lesional MRI, unilateral PET hypometabolism is a favorable prognostic factor in cases in which the MRI is "normal." In a retrospective study of MRI-negative TLE, the presence of focal hypometabolism increased seizure-free outcome from 45 to 82% (Mariani et al. 2019). In contrast, bilateral hypometabolism, associated with bilateral EEG findings, more frequent secondary generalization, and more severe neuropsychological deficits, is associated with worse surgical outcome (Kumar et al. 2012; Cahill et al. 2019).

Results vary more widely for extratemporal epilepsy. In a study of 194 patients, PET was helpful for surgical decision-making in 63% with temporal lobe epilepsy, compared with 38% with frontal lobe epilepsy (Rathore et al. 2014). In a review of 11 studies with normal MRI, reports of localized FDG-PET hypometabolism ranged from 36 to 93% of patients, with a mean of 71% (Juhasz and John 2020). A prospective study of 130 patients found that about 20% of TLE patients had extratemporal, and extratemporal patients temporal, hypometabolism, which was an adverse surgical prognostic factor for both groups (Tomas et al. 2019). Unilobar hypometabolism within the resection zone was a good prognostic factor, with an odds ratio of 5.4 for complete seizure control. For patients with extratemporal seizure foci, hypometabolism that was "remote" from the electrophysiologic seizure focus (contralateral or in a non-contiguous lobe) was an adverse prognostic finding (Wong et al. 2012).

One of the most common causes of non-lesional epilepsy appears to be focal cortical dysplasia (FCD), which is found on pathological examination in approximately 50% of non-lesional epilepsy patients undergoing surgery (Chapman et al. 2005; McGonigal et al. 2007). Conversely, it is estimated that approximately 1/3 of FCDs are not apparent using conventional radiological visual inspection of the MRI (Chassoux et al. 2012). One approach in these cases has been to use quantitative MR image post-processing techniques to aid in identification of subtle FCDs (Adler et al. 2017; Ahmed et al. 2015; Thesen et al. 2011; Wang et al. 2016; Hong et al. 2014). Another approach is to incorporate information from additional imaging modalities, and FDG-PET has been shown to provide additional diagnostic utility in increasing the detection rate or confirming the presence of lesions in apparently MR-negative cases, as well as having some prognostic value in predicting seizure outcomes (Juhasz and John 2020). In some studies, detection of hypometabolism, particularly when co-registered with three-dimensional MRI reconstruction, improved identification of focal cortical dysplasia and surgical outcome. In a study of 48 children, FDG-PET showed a clear advantage over MRI alone in detecting mild malformations of cortical development, which were missed in about 2/3 of the cases using MRI but detected by PET in 77% (Kim et al. 2011). In a study of [18F]FDG-PET scans from 103 consecutive patients with histologically proven FCD type II, visual analysis showed focal or regional hypometabolism

corresponding to the FCD in 44%; the main factors influencing positive PET localization were the grade of hypometabolism and the size of the lesion (Desarnaud et al. 2018). MRI was localizing in 59%. However, FDG was able to localize the lesion in 83% of the patients for whom MRI was unrevealing.

37.4 Comparison with Other Imaging Methods in Focal Epilepsy

In non-lesional patients, or in patients with discordant noninvasive studies, invasive electrode studies are often used to identify the seizure-onset zone (SOZ) and currently are the gold standard for seizure focus localization. The presence of focal hypometabolism using FDG-PET is clearly associated with seizure-onset zone localization using invasive electrode studies, at least at the regional level (Montaz-Rosset et al. 2019; Juhasz et al. 2000a, b; Alkonyi et al. 2009). In 16 patients with periventricular nodular heterotopias, there was 84% concordance between hypometabolic and epileptiform nodules on SEEG, and unresected hypometabolic nodules predicted worse surgical outcome (Popescu et al. 2019).

Single-photon emission computed tomography (SPECT) is another tool that has been used for seizure focus localization and will be discussed in detail in this volume in a subsequent chapter. Subtraction ictal SPECT images co-registered to MRI (SISCOM), in which the interictal is subtracted from the ictal SPECT image, was found in a meta-analysis to be localizing in ~50% of FCD-related surgical patients (Lerner et al. 2009) and has been found in multiple studies to predict seizure outcome in both temporal and extratemporal lobe epilepsies (Theodore 2017). In addition to exposure to radiation (as with PET), this modality requires inpatient hospitalization and significant expertise for the injection to occur within 15 s of seizure onset, which is necessary for optimal localization of the seizure focus; late injections can be associated with falsely localizing or non-localizing results (O'Brien et al. 1998). Additionally, other studies have suggested that ictal SPECT may not alter surgical outcomes (Velasco et al. 2011; Noe et al. 2013; Lascano et al. 2016) and can lead to significant additional expense (Sun et al. 2015). In studies directly comparing FDG-PET and SISCOM, these modalities appear overall to be comparable in terms of both localization of the seizure focus and prediction of surgical outcomes, with some studies suggesting that FDG-PET may be more sensitive in TLE, while SPECT may be more sensitive in ETLE (see review in Theodore (2017)). In other multimodality studies, PET hypometabolism was found more frequently than ictal hyperperfusion using SISCOM (Fernandez et al. 2015), and cases with concordance between EEG, MRI, PET, and SISCOM localization had significantly improved seizure outcomes compared to cases with discordant localization results across modalities (Chandra et al. 2014; Perry et al. 2017).

Arterial spin labeling (ASL) is an MRI-based technique that allows for visualization of brain perfusion using magnetically labeled arterial blood water molecules as an endogenous contrast agent. This technique is potentially advantageous in comparison to SISCOM and PET imaging as it does not involve exposure to

radioactivity and MRI scanners are widely available. Several studies have reported interictal hypoperfusion in seizure foci, mostly in patients with mesial temporal lobe epilepsy, usually co-localizing with areas of hypometabolism seen using FDG-PET (Lim et al. 2008; Pendse et al. 2010; Pizzini et al. 2013; Wissmeyer et al. 2010; Altrichter et al. 2009; Guo et al. 2015). Several studies have reported hyperperfusion using ASL in the setting of frequent seizures associated with focal cortical dysplasia (Wintermark et al. 2013) or status epilepticus (Matsuura et al. 2015). Other studies have reported variable hypo- and hyperperfusion on ASL in presumed seizure foci, presumably with hypoperfusion seen interictally and hyperperfusion occurring peri-ictally (Storti et al. 2014; Sierra-Marcos et al. 2016; Kim et al. 2016). In total, these findings would be consistent with perfusion changes reported using SPECT, with increased cerebral blood flow seen in ictal in comparison to interictal studies, due either to simple increased blood flow in the setting of increased activity or possibly due to focal inflammation and damage to the blood-brain barrier either due to epileptiform activity or due to epileptogenic lesions such as low-grade tumors (O'Brien et al. 1998; Pizzini et al. 2013; Fabene et al. 2008).

In comparison with other imaging modalities, altered perfusion on ASL tends to co-localize with MRI and PET findings; in a small study of nine children with FCD on MRI, co-localized decreases in cerebral blood flow were observed in all nine children, with PET hypometabolism observed in 5/6 cases (Blauwblomme et al. 2014). In a study of patients with neocortical epilepsy, 15/25 showed alterations in ASL, generally concordant with structural MRI findings (Sierra-Marcos et al. 2016). In this same study, 17/25 patients underwent both ASL and FDG-PET; 9 had PET hypometabolism, of which 5 showed hypoperfusion, 2 hyperperfusion, and 2 no perfusion changes using ASL. In 17/18 patients with hyperperfusion on SISCOM, only 6 showed perfusion abnormalities on ASL. In a study of 20 patients with MR-negative refractory focal epilepsy, PET and ASL were acquired simultaneously using a hybrid PET/MR system, allowing for comparison of the 2 modalities in the identical pathophysiological state. Hypometabolism on PET and hypoperfusion using ASL were found in the same hemisphere in 18/20 patients and were completely concordant in 14/18 (Boscolo Galazzo et al. 2016). In a subsequent study using simultaneous PET and ASL in 12 patients with hippocampal sclerosis and unilateral mTLE based on SEEG, relative hypoperfusion and hypometabolism were seen in all patients in the ipsilateral hippocampus as determined using SEEG, with Engel 1 outcomes in 10/12 patients with 4–13-month follow-up (Wang et al. 2018).

Functional MRI (fMRI) is another technique that has been used to assist with localization of seizure foci and to map epileptogenic networks. Simultaneous EEG-fMRI recordings have been used to detect transient changes in cerebral blood flow (hemodynamic responses) that occur in response to interictal epileptiform discharges (IEDs) on EEG. In focal epilepsy, IED-related blood oxygen level dependent (BOLD) signal changes have been found to be concordant with other metrics of estimating the SOZ, although they are often more widely distributed, with BOLD changes frequently identified in the contralateral homologous cortex and in default mode network areas in temporal lobe epilepsy (see review in Centeno and Carmichael (2014); Pittau et al. (2017)). The cluster with the maximal hemodynamic response

has been found to often overlap with intracranial EEG (iEEG) markers of epileptogenicity, including the high-frequency oscillations, the IED spike-onset zone, and the SOZ (Khoo et al. 2018, 2017a; Gonzalez Otarula et al. 2018). Areas demonstrating IED-related hemodynamic responses in the gray matter have also been shown to demonstrate synchronous iEEG IED activity (Khoo et al. 2017b). This suggests that there is consistent spread of epileptiform activity observed using fMRI and iEEG, as is the observation that focal fMRI activations tend to precede more widely distributed network effects associated with the late spike component on EEG (Walz et al. 2017). Propagation of interictal activity may also help to explain the findings of high although not complete concordance between simultaneous intracranial EEG spiking and BOLD responses (Aghakhani et al. 2015). In addition to interictal activity, seizures are occasionally recorded during fMRI-EEG studies. Seizures during EEG-fMRI were described in one study of 20 patients, with significant seizure-related BOLD changes in all patients; in 6 cases that underwent subsequent invasive monitoring, the most significant cluster was found to be within 3.5 cm from the invasively defined SOZ (Chaudhary et al. 2012). Finally, concordance between the maximal IED-related cluster and the area of resection appears to predict a favorable postoperative seizure outcome (PPV 70%), while discordance predicts a poor outcome (NPV 90.95) (An et al. 2013). Similar findings have been described in focal cortical dysplasia, in which discordant or widespread responses were found to be markers of poor prognosis (Thornton et al. 2011; Aubert et al. 2009).

Changes in the underlying patterns of resting-state fMRI activity have also been described in focal epilepsy. Such changes have been most well-described in temporal lobe epilepsy, with altered connectivity found within ipsilateral and contralateral mesial temporal structures and also between medial temporal structures and lateral temporal neocortex, regions involved in the default mode network, and subcortical areas such as the thalamus and brainstem (see reviews in Centeno and Carmichael (2014); Caciagli et al. (2014); Reyes et al. (2016)). These alterations in connectivity appear to change over time, with initial inter-hippocampal disruptions evolving to increased connectivity over years (Morgan et al. 2015). Changes in connectivity have also been described in patients with focal cortical dysplasia, with FCD type IIB lesions appearing to lead to hypo-connectivity and type IIA lesions to hyperconnectivity (Hong et al. 2019). In frontal lobe epilepsy, epileptogenic regions appear to have increased overall functional connections and higher laterality of these connections, with increased local and decreased distant connections (Luo et al. 2014). Changes in dynamic functional connectivity are less well characterized; changes have been described in dynamic regional phase synchrony (Omidvarnia et al. 2017; Pedersen et al. 2017) and in the autocorrelation function, a measure of entropy, with increased local and decreased long-range connectivity in a group of patients with left mesial temporal lobe epilepsy (Nedic et al. 2015).

Some studies have attempted to use these resting-state abnormalities to attempt to identify seizure foci in individual patients with epilepsy. In an early small study, 5/6 patients with focal epilepsy were found to have statistically significant increases in local connectivity compared to 300 control subjects in areas that were later found to be epileptogenic using iEEG (Stufflebeam et al. 2011). Dansereau et al. developed

a method to identify abnormal resting-state networks (RSNs) in individual patients and were able to detect abnormalities in 5/6 patients that were "closely related" to the epileptogenic focus as defined by seizure freedom following surgical resection (Dansereau et al. 2014). Lee et al. identified alterations in functional connectivity by measuring differences between intrahemispheric and interhemispheric ICC; concordance was found between the iEEG SOZ and this measure in 21/29 (72.4) of patients, with higher concordance in patients with good surgical outcome (Lee et al. 2014). A different approach is to use visual identification of abnormal independent components obtained from resting-state fMRI data; in 40 evaluated pediatric patients, concordance of these components with the iEEG SOZ was 90%; of 33 patients with at least 1 rs-fMRI EZ concordant with the iEEG SOZ, only 25% with unresected rs-fMRI EZs became seizure-free; in comparison, 76% patients with fully concordant rs-fMRI and iEEG SOZs obtained seizure freedom (Boerwinkle et al. 2017). Additionally, normalization of the identified SOZ resting-state networks (RSNs) postoperatively was found to significantly correlate with seizure outcome, with 97% with SOZ RSN normalization becoming seizure-free, versus 5% seizure freedom in those without SOZ RSN normalization (Boerwinkle et al. 2019).

37.5 FDG-PET in Non-focal Epilepsy Syndromes

Lennox-Gastaut syndrome (LGS) is a rare, severe childhood epilepsy syndrome with a variety of underlying etiologies, characterized by multiple generalized and focal seizure types, cognitive impairment, and characteristic EEG findings. FDG-PET has been shown to have variable patterns of metabolism in LGS, including unilateral focal, unilateral diffuse, and bilateral diffuse hypometabolism and normal metabolism (Kumar et al. 2012). In rare cases, focal hypometabolism can lead to consideration of surgical treatment when consistent with clinical and electrophysiologic data. In children with epileptic spasms, the presence of focal areas of hypometabolism on PET has also helped to provide targets for surgical interventions that can lead to significant improvements in outcome (Chugani et al. 2015; Asarnow et al. 1997). In another rare pediatric epilepsy syndrome caused by mutations in SCN1A, progressive hypometabolism has been reported 1–6 years after diagnosis. Scans were normal initially, followed by development of diffuse cortical hypometabolism (Kumar et al. 2018; Haginoya et al. 2018). Studies of patients with primary generalized epilepsy, which usually has a more benign prognosis, have been reported to have increased ictal with normal interictal metabolism (Kumar et al. 2012).

In autoimmune encephalitis, FDG-PET can identify hypometabolism and may be more sensitive for detection of focal abnormalities than MRI, particularly in early disease stages and for patients with NMDA receptor antibodies (Solnes et al. 2017; Guerin et al. 2019). Occipital hypometabolism has also been reported in these patients (Probasco et al. 2018). A study of 12 patients with new-onset refractory status epilepticus, 9 of whom had antineuronal antibodies, found a combination of hyper- and hypometabolism, predominantly in the mesial temporal region; hypometabolism was predictive of worse outcome (Strohm et al. 2019).

37.6 Neuroinflammation

Neuroinflammation plays a role in epilepsy and can be imaged with PET ligands for translocator protein 18 kDa (TSPO), which is highly expressed in microglia and reactive astrocytes (Alam et al. 2017). An early study using [^{11}C]PK11195 found increased binding in Rasmussen's encephalitis but not in TLE (Banati et al. 1999). [^{11}C]PK11195 binding was also reported to be increased in a patient with presumed focal cortical dysplasia and was greater when a second scan was performed 36 h after a seizure than during a seizure-free period (Butler et al. 2016). Studies in patients with temporal lobe epilepsy using a newer ligand, [^{11}C]PBR28, found increased uptake ipsilateral to seizure foci (Hirvonen et al. 2012; Gershen et al. 2015) (Fig. 37.4). Patients with mesial temporal sclerosis had higher binding

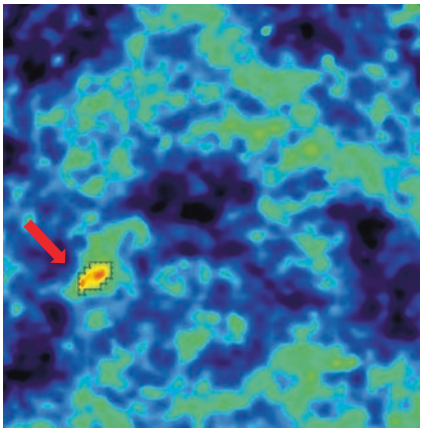

^{11}C-PBR28 PET (TLE_04)

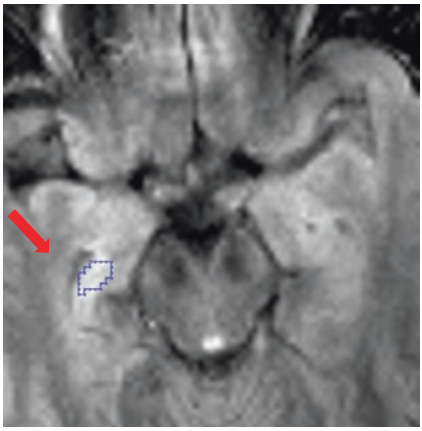

FLAIR MRI (TLE_04)

Fig. 37.4 Increased binding of a ligand for the translocator protein 18 kilodalton, expressed in activated microglia and reactive astrocytes, is present in a region of mesial temporal increased flare signal in a patient with mesial temporal sclerosis. This suggests the presence of inflammation

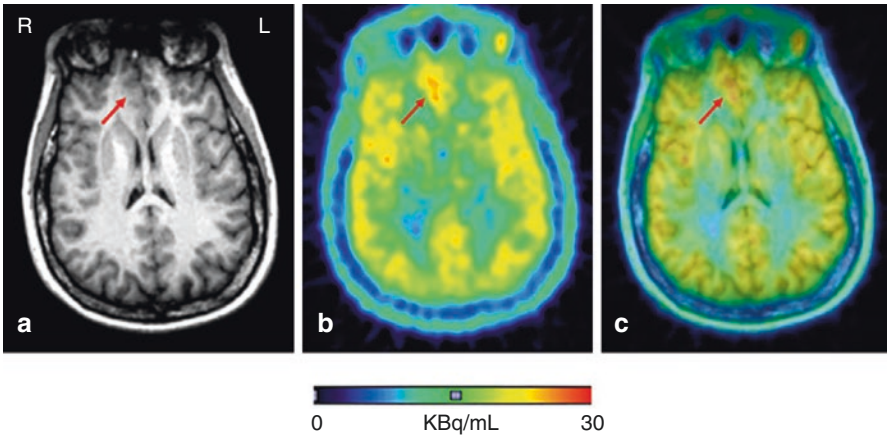

Fig. 37.5 (**a**) Structural MRI showing region of increased right frontal signal suggestive of focal cortical dysplasia. (**b**) TSPO-PET scan showing increased ligand binding. In the same region consistent with inflammation, (**c**) merged images. Reprinted from Dickstein et al. Epilepsia 2019;60:1248–1254

compared to the contralateral hippocampus than those with normal MRI. When full quantitation was carried out, bilateral, although asymmetrical, increases were found compared with healthy volunteers (Gershen et al. 2015). Similarly, in patients with neocortical foci, increased binding was observed ipsilateral to the seizure focus in 9 of 12 patients, 3 with normal MRI and 6 with FCD (Dickstein et al. 2019) (Fig. 37.5).

Inflammation during epileptogenesis has been studied in the mouse unilateral intrahippocampal kainic acid model using PET with another TSPO ligand, [^{18}F]DPA-714, which allowed for tracking of the development of hippocampal sclerosis at 7 days, 14 days, 1 month, and 6 months (Nguyen et al. 2018). PET TSPO binding was observed to peak at 7 days in concert with microglial activation; by 14 days, reactive astrocytes were the main TSPO-expressing cells. Both of these cell types are present in human MTS.

Cannabinoid receptors have also been implicated in inflammatory mechanisms in the hippocampus (Ativie et al. 2018). During electrical amygdala kindling in nonhuman primates, type I cannabinoid receptors (CB1R) were imaged with [^{18}F]MK-9470 PET binding in addition to [^{18}F]FDG-PET. The seizure-onset zone showed increased CB1R binding and decreased glucose metabolism, becoming more marked in extent and intensity during kindling; the ipsilateral thalamus and insula showed transiently increased CB1R binding (Cleeren et al. 2018).

37.7 P-gp Imaging: Mechanisms of Drug Resistance

Several studies have investigated the potential role of P-glycoprotein (P-gp)-mediated drug efflux at the blood-brain barrier in drug-resistant epilepsy using PET imaging with [^{11}C]verapamil. No differences were found between regions ipsilateral

and contralateral to the focus in seven patients (Langer et al. 2007). The plasma-to-brain transport rate constant, K1, was investigated before and after administration of the P-glycoprotein inhibitor tariquidar in 16 patients with TLE and 17 healthy controls (Feldmann et al. 2013). Pharmacoresistant epilepsy patients had lower baseline K1 values and lower increases in K1 after administration of tariquidar than healthy controls, suggesting increased P-glycoprotein activity in regions both ipsilateral and contralateral to their seizure foci. Additionally, six patients with drug-resistant epilepsy had increased binding ipsilateral to their temporal lobe seizure focus compared to five patients with drug-responsive epilepsy, as well as eight healthy controls (Shin et al. 2016), supporting a possible role for P-gp-mediated drug efflux in pharmacoresistance in these patients.

37.8 Benzodiazepine Receptors

The benzodiazepine receptor tracer [^{11}C]flumazenil (FMZ) has had more consistent clinical application for epilepsy than any other ligand apart from FDG. Several studies showed that FMZ-PET appeared to have greater sensitivity, but not necessarily specificity, for detecting mesial temporal sclerosis than FDG-PET (Kumar et al. 2012; Komoto et al. 2015). Increased binding reported in some studies may be related to malformations of cortical development and appears to predict poor surgical outcome if these regions are not resected (Yankam Njiwa et al. 2015). FMZ-PET may be more sensitive to seizure recency effects than FDG-PET (Bouvard et al. 2005). An alternative ligand, [^{18}F]flumazenil, may have practical advantages due to its longer half-life (Vivash et al. 2013).

In addition to its use in identification of the seizure focus, [^{11}C]FMZ-PET has been used to investigate the pharmacology of epilepsy. The antiepileptic drug vigabatrin blocks GABA catabolism, increasing synaptic GABA. [^{11}C]FMZ binding volume of distribution was lower in patients taking vigabatrin than other antiepileptic drugs, confirming increased occupation of binding sites due to vigabatrin (Juhasz et al. 2001). Patients with succinic semialdehyde dehydrogenase deficiency, a disorder in which increased GABA is present due to reduced catabolic activity, have also been found to have decreased [^{11}C]FMZ binding due to binding site occupation by GABA, while their parents, obligate heterozygotes, do not (Pearl et al. 2009) (Fig. 37.6).

37.9 Serotonin Receptors

Activation of 5HT1A receptors has been shown to have anti-seizure effects in several animal models. Studies using several 5HT1A receptor ligands have shown reduced binding in mesial temporal seizure foci, including the hippocampus and amygdala, as well as the parahippocampal and fusiform gyri (Kumar et al. 2012) (Fig. 37.7). These findings persisted after MRI-based partial volume correction, suggesting that they are independent of the presence of MRI lesions and related

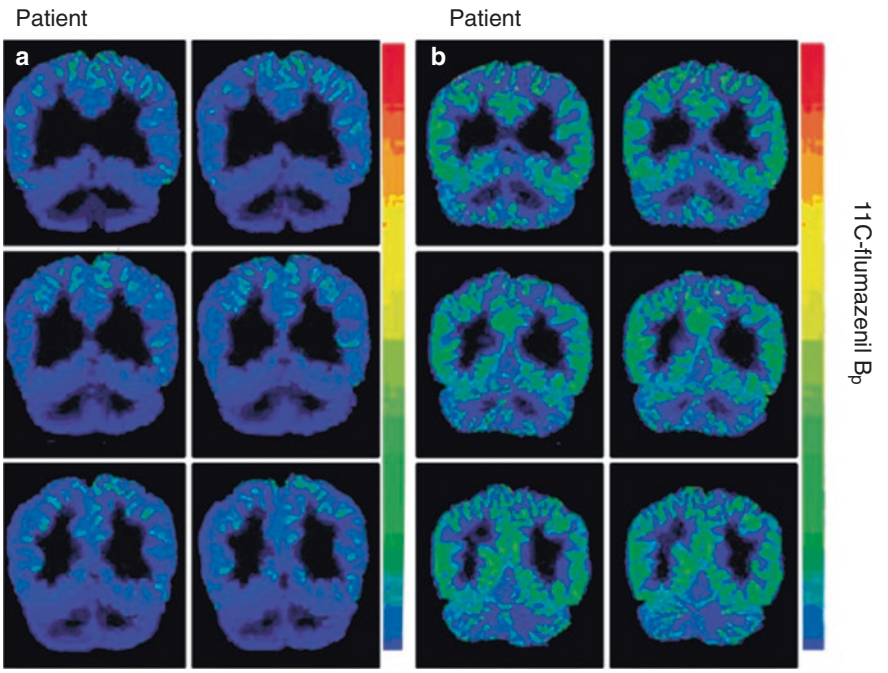

Fig. 37.6 Succinic semialdehyde dehydrogenase deficiency: [^{11}C]flumazenil PET imaging of benzodiazepine receptors. Reduced binding in patients, but normal binding in parents, who are obligate heterozygotes. Reprinted from Pearl et al. Neurology 2009; 73: 423–429

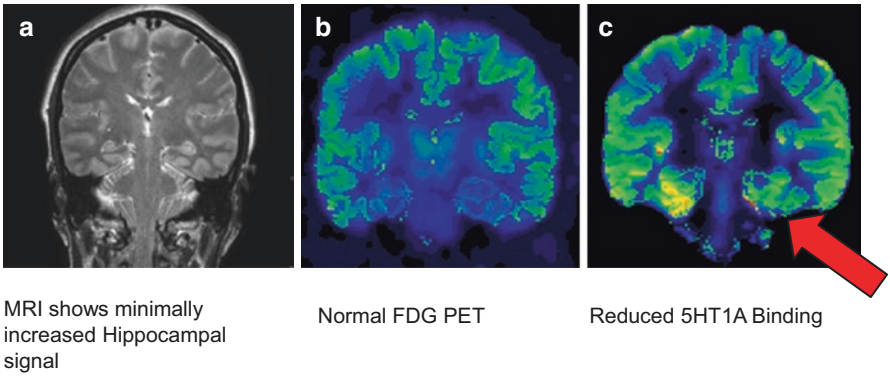

Fig. 37.7 A 44-year-old patient with a history of drug-resistant seizures; surface electroencephalography revealed left temporal seizure onset. (**a**) Normal MRI result. (**b**) Normal [^{18}F]FDG-PET result. (**c**) [^{18}F]FCWAY PET shows relatively decreased left temporal [^{18}]FCWAY binding, indicating reduced 5HT1A receptor availability. Reproduced from Theodore et al. Journal of Nuclear Medicine 2012; 53:1375–1382

neuronal loss. In addition, the combination of [^{18}F]FCWAY 5HT1A receptor imaging and [^{18}F]FDG-PET improved prediction of seizure-free outcome after temporal lobectomy compared with the use of either tracer alone (Theodore et al. 2012). In tuberous sclerosis, a PET ligand for a serotonin precursor, [^{11}C]alpha-methyl tryptophan, has been used to identify epileptogenic tubers (Kumar et al. 2012).

Mood disorders are a frequent and significant comorbidity in patients with drug-resistant focal epilepsy. Reduced 5HT1A receptors have been reported in patients with primary major depressive disorders (Drevets et al. 2007). Studies using [^{11}C]FCWAY and [^{18}F]FCWAY showed correlations between reduced binding and depression rating scales (Savic et al. 2004; Theodore et al. 2007). Patients with a diagnosis of major depressive disorder, based on the Structured Clinical Interview for the Diagnostic and Statistical Manual for Mental Disorders, fourth edition (DSM-IV), had lower binding in limbic regions than those with epilepsy alone (Hasler et al. 2007). In contrast, a study using 2′-methoxyphenyl-(*N*-2′-pyridinyl)-*p*-F-fluoro-benzamidoethylpiperazine ([^{18}F]MPPF) found a positive correlation between Beck Depression Inventory scores and binding in several regions (Lothe et al. 2008). This dichotomy can be explained by the greater sensitivity of MPPF than FCWAY to reduced synaptic serotonin levels, which could lead to apparently increased MPPF binding even in the presence of reduced receptor availability. A study using [^{11}C]DASB, a ligand for serotonin transport, found relatively reduced activity ipsilateral to temporal lobe foci in patients with both seizures and depression compared to subjects with TLE alone, implying additional alteration in synaptic 5HT availability in epilepsy patients in the presence of comorbid depression (Martinez et al. 2013). In kindled rats, [18F]MPPF binding was increased with no change in receptors measured by autoradiography, consistent with the effect of decreased synaptic serotonin (Bascunana et al. 2019). These data underline the importance of understanding the kinetics of specific receptor ligands when interpreting PET neurotransmitter studies.

37.10 Excitatory Amino Acid Receptors

Several recent studies have investigated alterations of excitatory amino acid receptors in epilepsy. The mGLUR5 ligand [^{11}C]ABP688 showed reduced binding in epileptogenic mesial temporal regions after partial volume correction in 31 patients (Lam et al. 2019). The investigators suggested that reductions might be due to receptor internalization or conformational changes in response to excessive extracellular glutamate. Seven of ten patients with FCD studied with [^{11}C]ABP688 had reduced binding in the dysplastic region (DuBois et al. 2016). Balloon cells tended to show lower binding compared with surrounding tissue. Eleven patients had PET with the open-channel *N*-methyl-D-aspartate (NMDA) receptor ligand ([^{18}F]GE-179) (McGinnity et al. 2015). Four had a cluster with increased focal binding, including two with normal MRIs. Interestingly, patients not taking antidepressants had globally increased [^{18}F]GE-179 binding, while three patients taking an antidepressant

drug had decreased binding. Taken together, these results could be explained by differences in underlying pathology, in the receptors being imaged, or the vagaries of small PET studies.

This literature continues to grow, with increasing numbers of ligands being investigated. Other tracers studied in patients with epilepsy to date include ligands for several opiate and dopamine receptors, as well as nicotinic acetylcholine receptors (Galovic and Koepp 2016).

37.11 Conclusions

Epilepsy is recognized increasingly as a "spectrum disorder," characterized not only by seizures but neuropsychological and psychiatric comorbidities. Both PET and MRI have made important contributions to evaluation of patients, as well as to our understanding of pathophysiology. Imaging techniques, in concert with genetic and clinical data, may lead to new classification systems based on disease mechanisms that will facilitate more carefully planned and directed treatment.

References

van't Klooster MA, Huiskamp G, Zijlmans M, Debets RM, Comans EF, Bouvard S et al (2014) Can we increase the yield of FDG-PET in the preoperative work-up for epilepsy surgery? Epilepsy Res 108(6):1095–1105

Adler S, Wagstyl K, Gunny R, Ronan L, Carmichael D, Cross JH et al (2017) Novel surface features for automated detection of focal cortical dysplasias in paediatric epilepsy. Neuroimage Clin 14:18–27

Aghakhani Y, Beers CA, Pittman DJ, Gaxiola-Valdez I, Goodyear BG, Federico P (2015) Co-localization between the BOLD response and epileptiform discharges recorded by simultaneous intracranial EEG-fMRI at 3 T. Neuroimage Clin 7:755–763

Ahmed B, Brodley CE, Blackmon KE, Kuzniecky R, Barash G, Carlson C et al (2015) Cortical feature analysis and machine learning improves detection of "MRI-negative" focal cortical dysplasia. Epilepsy Behav 48:21–28

Alam MM, Lee J, Lee SY (2017) Recent progress in the development of TSPO PET ligands for neuroinflammation imaging in neurological diseases. Nucl Med Mol Imaging 51(4):283–296

Alkonyi B, Juhasz C, Muzik O, Asano E, Saporta A, Shah A et al (2009) Quantitative brain surface mapping of an electrophysiologic/metabolic mismatch in human neocortical epilepsy. Epilepsy Res 87(1):77–87

Altrichter S, Pendse N, Wissmeyer M, Jagersberg M, Federspiel A, Viallon M et al (2009) Arterial spin-labeling demonstrates ictal cortical hyperperfusion in epilepsy secondary to hemimegalencephaly. J Neuroradiol 36(5):303–305

An D, Fahoum F, Hall J, Olivier A, Gotman J, Dubeau F (2013) Electroencephalography/functional magnetic resonance imaging responses help predict surgical outcome in focal epilepsy. Epilepsia 54(12):2184–2194

Asarnow RF, LoPresti C, Guthrie D, Elliott T, Cynn V, Shields WD et al (1997) Developmental outcomes in children receiving resection surgery for medically intractable infantile spasms. Dev Med Child Neurol 39(7):430–440

Ativie F, Komorowska JA, Beins E, Albayram O, Zimmer T, Zimmer A et al (2018) Cannabinoid 1 receptor signaling on hippocampal GABAergic neurons influences microglial activity. Front Mol Neurosci 11:295

Aubert S, Wendling F, Regis J, McGonigal A, Figarella-Branger D, Peragut JC et al (2009) Local and remote epileptogenicity in focal cortical dysplasias and neurodevelopmental tumours. Brain 132(pt 11):3072–3086

Banati RB, Goerres GW, Myers R, Gunn RN, Turkheimer FE, Kreutzberg GW et al (1999) [11C](R)-PK11195 positron emission tomography imaging of activated microglia in vivo in Rasmussen's encephalitis. Neurology 53(9):2199–2203

Bascunana P, Garcia-Garcia L, Javela J, Fernandez de la Rosa R, Shiha AA, Kelly J et al (2019) PET neuroimaging reveals serotonergic and metabolic dysfunctions in the hippocampal electrical kindling model of epileptogenesis. Neuroscience 409:101–110

Bazzigaluppi P, Ebrahim Amini A, Weisspapir I, Stefanovic B, Carlen PL (2017) Hungry neurons: metabolic insights on seizure dynamics. Int J Mol Sci 18(11):2269

Benedek K, Juhasz C, Chugani DC, Muzik O, Chugani HT (2006) Longitudinal changes in cortical glucose hypometabolism in children with intractable epilepsy. J Child Neurol 21(1):26–31

Blauwblomme T, Boddaert N, Chemaly N, Chiron C, Pages M, Varlet P et al (2014) Arterial spin Labeling MRI: a step forward in non-invasive delineation of focal cortical dysplasia in children. Epilepsy Res 108(10):1932–1939

Boerwinkle VL, Mohanty D, Foldes ST, Guffey D, Minard CG, Vedantam A et al (2017) Correlating resting-state functional magnetic resonance imaging connectivity by independent component analysis-based epileptogenic zones with intracranial electroencephalogram localized seizure onset zones and surgical outcomes in prospective Pediatric intractable epilepsy study. Brain Connect 7(7):424–442

Boerwinkle VL, Cediel EG, Mirea L, Williams K, Kerrigan JF, Lam S et al (2019) Network-targeted approach and postoperative resting-state functional magnetic resonance imaging are associated with seizure outcome. Ann Neurol 86(3):344–356

Boscolo Galazzo I, Mattoli MV, Pizzini FB, De Vita E, Barnes A, Duncan JS et al (2016) Cerebral metabolism and perfusion in MR-negative individuals with refractory focal epilepsy assessed by simultaneous acquisition of (18)F-FDG PET and arterial spin labeling. Neuroimage Clin 11:648–657

Bouvard S, Costes N, Bonnefoi F, Lavenne F, Mauguiere F, Delforge J et al (2005) Seizure-related short-term plasticity of benzodiazepine receptors in partial epilepsy: a [11C]flumazenil-PET study. Brain 128(pt 6):1330–1343

Butler T, Li Y, Tsui W, Friedman D, Maoz A, Wang X et al (2016) Transient and chronic seizure-induced inflammation in human focal epilepsy. Epilepsia 57(9):e191–e194

Caciagli L, Bernhardt BC, Hong SJ, Bernasconi A, Bernasconi N (2014) Functional network alterations and their structural substrate in drug-resistant epilepsy. Front Neurosci 8:411

Cahill V, Sinclair B, Malpas CB, McIntosh AM, Chen Z, Vivash LE et al (2019) Metabolic patterns and seizure outcomes following anterior temporal lobectomy. Ann Neurol 85(2):241–250

Centeno M, Carmichael DW (2014) Network connectivity in epilepsy: resting state fMRI and EEG-fMRI contributions. Front Neurol 5:93

Chandra PS, Vaghania G, Bal CS, Tripathi M, Kuruwale N, Arora A et al (2014) Role of concordance between ictal-subtracted SPECT and PET in predicting long-term outcomes after epilepsy surgery. Epilepsy Res 108(10):1782–1789

Chapman K, Wyllie E, Najm I, Ruggieri P, Bingaman W, Luders J et al (2005) Seizure outcome after epilepsy surgery in patients with normal preoperative MRI. J Neurol Neurosurg Psychiatry 76(5):710–713

Chassoux F, Landre E, Mellerio C, Turak B, Mann MW, Daumas-Duport C et al (2012) Type II focal cortical dysplasia: electroclinical phenotype and surgical outcome related to imaging. Epilepsia 53(2):349–358

Chassoux F, Artiges E, Semah F, Desarnaud S, Laurent A, Landre E et al (2016) Determinants of brain metabolism changes in mesial temporal lobe epilepsy. Epilepsia 57(6):907–919

Chaudhary UJ, Carmichael DW, Rodionov R, Thornton RC, Bartlett P, Vulliemoz S et al (2012) Mapping preictal and ictal haemodynamic networks using video-electroencephalography and functional imaging. Brain 135(pt 12):3645–3663

Chugani HT, Ilyas M, Kumar A, Juhasz C, Kupsky WJ, Sood S et al (2015) Surgical treatment for refractory epileptic spasms: the Detroit series. Epilepsia 56(12):1941–1949

Cleeren E, Casteels C, Goffin K, Koole M, Van Laere K, Janssen P et al (2018) Positron emission tomography imaging of cerebral glucose metabolism and type 1 cannabinoid receptor availability during temporal lobe epileptogenesis in the amygdala kindling model in rhesus monkeys. Epilepsia 59(5):959–970

Dansereau CL, Bellec P, Lee K, Pittau F, Gotman J, Grova C (2014) Detection of abnormal resting-state networks in individual patients suffering from focal epilepsy: an initial step toward individual connectivity assessment. Front Neurosci 8:419

Desarnaud S, Mellerio C, Semah F, Laurent A, Landre E, Devaux B et al (2018) (18)F-FDG PET in drug-resistant epilepsy due to focal cortical dysplasia type 2: additional value of electroclinical data and coregistration with MRI. Eur J Nucl Med Mol Imaging 45(8):1449–1460

Dickstein LP, Liow JS, Austermuehle A, Zoghbi S, Inati SK, Zaghloul K et al (2019) Neuroinflammation in neocortical epilepsy measured by PET imaging of translocator protein. Epilepsia 60(6):1248–1254

Drevets WC, Thase ME, Moses-Kolko EL, Price J, Frank E, Kupfer DJ et al (2007) Serotonin-1A receptor imaging in recurrent depression: replication and literature review. Nucl Med Biol 34(7):865–877

DuBois JM, Rousset OG, Guiot MC, Hall JA, Reader AJ, Soucy JP et al (2016) Metabotropic glutamate receptor type 5 (mGluR5) cortical abnormalities in focal cortical dysplasia identified in vivo with [11C]ABP688 positron-emission tomography (PET) imaging. Cereb Cortex 26(11):4170–4179

Fabene PF, Navarro Mora G, Martinello M, Rossi B, Merigo F, Ottoboni L et al (2008) A role for leukocyte-endothelial adhesion mechanisms in epilepsy. Nat Med 14(12):1377–1383

Feldmann M, Asselin MC, Liu J, Wang S, McMahon A, Anton-Rodriguez J et al (2013) P-glycoprotein expression and function in patients with temporal lobe epilepsy: a case-control study. Lancet Neurol 12(8):777–785

Fernandez S, Donaire A, Seres E, Setoain X, Bargallo N, Falcon C et al (2015) PET/MRI and PET/MRI/SISCOM coregistration in the presurgical evaluation of refractory focal epilepsy. Epilepsy Res 111:1–9

Gaillard WD, Weinstein S, Conry J, Pearl PL, Fazilat S, Fazilat S et al (2007) Prognosis of children with partial epilepsy: MRI and serial 18FDG-PET. Neurology 68(9):655–659

Gaillard WD, Cross JH, Duncan JS, Stefan H, Theodore WH (2011) Epilepsy imaging study guideline criteria: commentary on diagnostic testing study guidelines and practice parameters. Epilepsia 52(9):1750–1756

Galovic M, Koepp M (2016) Advances of molecular imaging in epilepsy. Curr Neurol Neurosci Rep 16(6):58

Gershen LD, Zanotti-Fregonara P, Dustin IH, Liow JS, Hirvonen J, Kreisl WC et al (2015) Neuroinflammation in temporal lobe epilepsy measured using positron emission tomographic imaging of translocator protein. JAMA Neurol 72(8):882–888

Gonzalez Otarula KA, Khoo HM, von Ellenrieder N, Hall JA, Dubeau F, Gotman J (2018) Spike-related haemodynamic responses overlap with high frequency oscillations in patients with focal epilepsy. Brain 141(3):731–743

Govil-Dalela T, Kumar A, Behen ME, Chugani HT, Juhasz C (2018) Evolution of lobar abnormalities of cerebral glucose metabolism in 41 children with drug-resistant epilepsy. Epilepsia 59(7):1307–1315

Guerin J, Watson RE, Carr CM, Liebo GB, Kotsenas AL (2019) Autoimmune epilepsy: findings on MRI and FDG-PET. Br J Radiol 92(1093):20170869

Guo Y, Gao F, Wang S, Ding Y, Zhang H, Wang J et al (2009) In vivo mapping of temporospatial changes in glucose utilization in rat brain during epileptogenesis: an 18F-fluorodeoxyglucose-small animal positron emission tomography study. Neuroscience 162(4):972–979

Guo X, Xu S, Wang G, Zhang Y, Guo L, Zhao B (2015) Asymmetry of cerebral blood flow measured with three-dimensional pseudocontinuous arterial spin-labeling mr imaging in temporal lobe epilepsy with and without mesial temporal sclerosis. J Magn Reson Imaging 42(5):1386–1397

Haginoya K, Togashi N, Kaneta T, Hino-Fukuyo N, Ishitobi M, Kakisaka Y et al (2018) [(18) F]fluorodeoxyglucose-positron emission tomography study of genetically confirmed patients with Dravet syndrome. Epilepsy Res 147:9–14

Hasler G, Bonwetsch R, Giovacchini G, Toczek MT, Bagic A, Luckenbaugh DA et al (2007) 5-HT1A receptor binding in temporal lobe epilepsy patients with and without major depression. Biol Psychiatry 62(11):1258–1264

Hirvonen J, Kreisl WC, Fujita M, Dustin I, Khan O, Appel S et al (2012) Increased in vivo expression of an inflammatory marker in temporal lobe epilepsy. J Nucl Med 53(2):234–240

Hong SJ, Kim H, Schrader D, Bernasconi N, Bernhardt BC, Bernasconi A (2014) Automated detection of cortical dysplasia type II in MRI-negative epilepsy. Neurology 83(1):48–55

Hong SJ, Lee HM, Gill R, Crane J, Sziklas V, Bernhardt BC et al (2019) A connectome-based mechanistic model of focal cortical dysplasia. Brain 142(3):688–699

Juhasz C, John F (2020) Utility of MRI, PET, and ictal SPECT in presurgical evaluation of nonlesional pediatric epilepsy. Seizure 77:15–28

Juhasz C, Chugani DC, Muzik O, Watson C, Shah J, Shah A et al (2000a) Electroclinical correlates of flumazenil and fluorodeoxyglucose PET abnormalities in lesional epilepsy. Neurology 55(6):825–835

Juhasz C, Chugani DC, Muzik O, Watson C, Shah J, Shah A et al (2000b) Is epileptogenic cortex truly hypometabolic on interictal positron emission tomography? Ann Neurol 48(1):88–96

Juhasz C, Behen ME, Muzik O, Chugani DC, Chugani HT (2001) Bilateral medial prefrontal and temporal neocortical hypometabolism in children with epilepsy and aggression. Epilepsia 42(8):991–1001

Jupp B, Williams J, Binns D, Hicks RJ, Cardamone L, Jones N et al (2012) Hypometabolism precedes limbic atrophy and spontaneous recurrent seizures in a rat model of TLE. Epilepsia 53(7):1233–1244

Khoo HM, Hao Y, von Ellenrieder N, Zazubovits N, Hall J, Olivier A et al (2017a) The hemodynamic response to interictal epileptic discharges localizes the seizure-onset zone. Epilepsia 58(5):811–823

Khoo HM, von Ellenrieder N, Zazubovits N, Dubeau F, Gotman J (2017b) Epileptic networks in action: synchrony between distant hemodynamic responses. Ann Neurol 82(1):57–66

Khoo HM, von Ellenrieder N, Zazubovits N, He D, Dubeau F, Gotman J (2018) The spike onset zone: the region where epileptic spikes start and from where they propagate. Neurology 91(7):e666–ee74

Kim YK, Lee DS, Lee SK, Kim SK, Chung CK, Chang KH et al (2003) Differential features of metabolic abnormalities between medial and lateral temporal lobe epilepsy: quantitative analysis of (18)F-FDG PET using SPM. J Nucl Med 44(7):1006–1012

Kim YH, Kang HC, Kim DS, Kim SH, Shim KW, Kim HD et al (2011) Neuroimaging in identifying focal cortical dysplasia and prognostic factors in pediatric and adolescent epilepsy surgery. Epilepsia 52(4):722–727

Kim BS, Lee ST, Yun TJ, Lee SK, Paeng JC, Jun J et al (2016) Capability of arterial spin labeling MR imaging in localizing seizure focus in clinical seizure activity. Eur J Radiol 85(7):1295–1303

Komoto D, Iida K, Higaki T, Kaichi Y, Takauchi K, Arihiro K et al (2015) Diagnostic performance of positron emission tomography for the presurgical evaluation of patients with non-lesional intractable partial epilepsy: comparison among 18F-FDG, 11C-flumazenil, and 11C-flumazenil binding potential imaging using statistical imaging analysis. Hiroshima J Med Sci 64(4):51–57

Kumar A, Semah F, Chugani HT, Theodore WH (2012) Epilepsy diagnosis: positron emission tomography. Handb Clin Neurol 107:409–424

Kumar A, Juhasz C, Luat A, Govil-Dalela T, Behen ME, Hicks MA et al (2018) Evolution of brain glucose metabolic abnormalities in children with epilepsy and SCN1A gene variants. J Child Neurol 33(13):832–836

Lam J, DuBois JM, Rowley J, Gonzalez-Otarula KA, Soucy JP, Massarweh G et al (2019) In vivo metabotropic glutamate receptor type 5 abnormalities localize the epileptogenic zone in mesial temporal lobe epilepsy. Ann Neurol 85(2):218–228

Langer O, Bauer M, Hammers A, Karch R, Pataraia E, Koepp MJ et al (2007) Pharmacoresistance in epilepsy: a pilot PET study with the P-glycoprotein substrate R-[(11)C]verapamil. Epilepsia 48(9):1774–1784

Lascano AM, Perneger T, Vulliemoz S, Spinelli L, Garibotto V, Korff CM et al (2016) Yield of MRI, high-density electric source imaging (HD-ESI), SPECT and PET in epilepsy surgery candidates. Clin Neurophysiol 127(1):150–155

Lee HW, Arora J, Papademetris X, Tokoglu F, Negishi M, Scheinost D et al (2014) Altered functional connectivity in seizure onset zones revealed by fMRI intrinsic connectivity. Neurology 83(24):2269–2277

Lerner JT, Salamon N, Hauptman JS, Velasco TR, Hemb M, Wu JY et al (2009) Assessment and surgical outcomes for mild type I and severe type II cortical dysplasia: a critical review and the UCLA experience. Epilepsia 50(6):1310–1335

Lim YM, Cho YW, Shamim S, Solomon J, Birn R, Luh WM et al (2008) Usefulness of pulsed arterial spin labeling MR imaging in mesial temporal lobe epilepsy. Epilepsy Res 82(2–3):183–189

Liow JS, Zoghbi SS, Hu S, Hall MD, Hines CS, Shetty HU et al (2016) (18)F-FCWAY, a serotonin 1A receptor radioligand, is a substrate for efflux transport at the human blood-brain barrier. NeuroImage 138:134–140

Lothe A, Didelot A, Hammers A, Costes N, Saoud M, Gilliam F et al (2008) Comorbidity between temporal lobe epilepsy and depression: a [18F]MPPF PET study. Brain 131(pt 10):2765–2782

Luo C, An D, Yao D, Gotman J (2014) Patient-specific connectivity pattern of epileptic network in frontal lobe epilepsy. Neuroimage Clin 4:668–675

Mariani V, Revay M, D'Orio P, Rizzi M, Pelliccia V, Nichelatti M et al (2019) Prognostic factors of postoperative seizure outcome in patients with temporal lobe epilepsy and normal magnetic resonance imaging. J Neurol 266(9):2144–2156

Martinez A, Finegersh A, Cannon DM, Dustin I, Nugent A, Herscovitch P et al (2013) The 5-HT1A receptor and 5-HT transporter in temporal lobe epilepsy. Neurology 80(16):1465–1471

Matsuura K, Maeda M, Okamoto K, Araki T, Miura Y, Hamada K et al (2015) Usefulness of arterial spin-labeling images in periictal state diagnosis of epilepsy. J Neurol Sci 359(1–2):424–429

Mayoral M, Ninerola-Baizan A, Marti-Fuster B, Donaire A, Perissinotti A, Rumia J et al (2019) Epileptogenic zone localization with (18)FDG PET using a new dynamic parametric analysis. Front Neurol 10:380

McGinnity CJ, Koepp MJ, Hammers A, Riano Barros DA, Pressler RM, Luthra S et al (2015) NMDA receptor binding in focal epilepsies. J Neurol Neurosurg Psychiatry 86(10):1150–1157

McGonigal A, Bartolomei F, Regis J, Guye M, Gavaret M, Trebuchon-Da Fonseca A et al (2007) Stereoelectroencephalography in presurgical assessment of MRI-negative epilepsy. Brain 130(pt 12):3169–3183

Montaz-Rosset MS, Scholly J, Voulleminot P, Severac F, Hirsch E, Valenti-Hirsch MP et al (2019) Comparison of functional deficit zone defined by FDG PET to the epileptogenic zones described in stereo-electroencephalograph in drug-resistant epileptic patients treated by surgery. Clin Nucl Med 44(7):526–531

Morgan VL, Abou-Khalil B, Rogers BP (2015) Evolution of functional connectivity of brain networks and their dynamic interaction in temporal lobe epilepsy. Brain Connect 5(1):35–44

Nedic S, Stufflebeam SM, Rondinoni C, Velasco TR, dos Santos AC, Leite JP et al (2015) Using network dynamic fMRI for detection of epileptogenic foci. BMC Neurol 15:262

Nguyen DL, Wimberley C, Truillet C, Jego B, Caille F, Pottier G et al (2018) Longitudinal positron emission tomography imaging of glial cell activation in a mouse model of mesial temporal lobe epilepsy: toward identification of optimal treatment windows. Epilepsia 59(6):1234–1244

Noe K, Sulc V, Wong-Kisiel L, Wirrell E, Van Gompel JJ, Wetjen N et al (2013) Long-term outcomes after nonlesional extratemporal lobe epilepsy surgery. JAMA Neurol 70(8):1003–1008

O'Brien TJ, So EL, Mullan BP, Hauser MF, Brinkmann BH, Bohnen NI et al (1998) Subtraction ictal SPECT co-registered to MRI improves clinical usefulness of SPECT in localizing the surgical seizure focus. Neurology 50(2):445–454

Omidvarnia A, Pedersen M, Vaughan DN, Walz JM, Abbott DF, Zalesky A et al (2017) Dynamic coupling between fMRI local connectivity and interictal EEG in focal epilepsy: a wavelet analysis approach. Hum Brain Mapp 38(11):5356–5374

Pearl PL, Gibson KM, Quezado Z, Dustin I, Taylor J, Trzcinski S et al (2009) Decreased GABA-A binding on FMZ-PET in succinic semialdehyde dehydrogenase deficiency. Neurology 73(6):423–429

Pedersen M, Omidvarnia A, Curwood EK, Walz JM, Rayner G, Jackson GD (2017) The dynamics of functional connectivity in neocortical focal epilepsy. Neuroimage Clin 15:209–214

Pendse N, Wissmeyer M, Altrichter S, Vargas M, Delavelle J, Viallon M et al (2010) Interictal arterial spin-labeling MRI perfusion in intractable epilepsy. J Neuroradiol 37(1):60–63

Perry MS, Bailey L, Freedman D, Donahue D, Malik S, Head H et al (2017) Coregistration of multimodal imaging is associated with favourable two-year seizure outcome after paediatric epilepsy surgery. Epileptic Disord 19(1):40–48

Pittau F, Ferri L, Fahoum F, Dubeau F, Gotman J (2017) Contributions of EEG-fMRI to assessing the Epileptogenicity of focal cortical dysplasia. Front Comput Neurosci 11:8

Pizzini FB, Farace P, Manganotti P, Zoccatelli G, Bongiovanni LG, Golay X et al (2013) Cerebral perfusion alterations in epileptic patients during peri-ictal and post-ictal phase: PASL vs DSC-MRI. Magn Reson Imaging 31(6):1001–1005

Popescu CE, Mai R, Sara R, Lizio D, Zanni D, Rossetti C et al (2019) The role of FDG-PET in patients with epilepsy related to periventricular nodular heterotopias: diagnostic features and Long-term outcome. J Neuroimaging 29(4):512–520

Probasco JC, Solnes L, Nalluri A, Cohen J, Jones KM, Zan E et al (2018) Decreased occipital lobe metabolism by FDG-PET/CT: an anti-NMDA receptor encephalitis biomarker. Neurol Neuroimmunol Neuroinflamm 5(1):e413

Rathore C, Dickson JC, Teotonio R, Ell P, Duncan JS (2014) The utility of 18F-fluorodeoxyglucose PET (FDG PET) in epilepsy surgery. Epilepsy Res 108(8):1306–1314

Reyes A, Thesen T, Wang X, Hahn D, Yoo D, Kuzniecky R et al (2016) Resting-state functional MRI distinguishes temporal lobe epilepsy subtypes. Epilepsia 57(9):1475–1484

Savic I, Lindstrom P, Gulyas B, Halldin C, Andree B, Farde L (2004) Limbic reductions of 5-HT1A receptor binding in human temporal lobe epilepsy. Neurology 62(8):1343–1351

Shin JW, Chu K, Shin SA, Jung KH, Lee ST, Lee YS et al (2016) Clinical applications of simultaneous PET/MR imaging using (R)-[11C]-verapamil with Cyclosporin A: preliminary results on a surrogate marker of drug-resistant epilepsy. AJNR Am J Neuroradiol 37(4):600–606

Sidhu MK, Duncan JS, Sander JW (2018) Neuroimaging in epilepsy. Curr Opin Neurol 31(4):371–378

Sierra-Marcos A, Carreno M, Setoain X, Lopez-Rueda A, Aparicio J, Donaire A et al (2016) Accuracy of arterial spin labeling magnetic resonance imaging (MRI) perfusion in detecting the epileptogenic zone in patients with drug-resistant neocortical epilepsy: comparison with electrophysiological data, structural MRI, SISCOM and FDG-PET. Eur J Neurol 23(1):160–167

Solnes LB, Jones KM, Rowe SP, Pattanayak P, Nalluri A, Venkatesan A et al (2017) Diagnostic value of (18)F-FDG PET/CT versus MRI in the setting of antibody-specific autoimmune encephalitis. J Nucl Med 58(8):1307–1313

Storti SF, Boscolo Galazzo I, Del Felice A, Pizzini FB, Arcaro C, Formaggio E et al (2014) Combining ESI, ASL and PET for quantitative assessment of drug-resistant focal epilepsy. NeuroImage 102(pt 1):49–59

Strohm T, Steriade C, Wu G, Hantus S, Rae-Grant A, Larvie M (2019) FDG-PET and MRI in the evolution of new-onset refractory status epilepticus. AJNR Am J Neuroradiol 40(2):238–244

Stufflebeam SM, Liu H, Sepulcre J, Tanaka N, Buckner RL, Madsen JR (2011) Localization of focal epileptic discharges using functional connectivity magnetic resonance imaging. J Neurosurg 114(6):1693–1697

Sun PY, Wyatt K, Nickels KC, Wong-Kisiel LC, Mandrekar J, Wirrell E (2015) Predictors of length of stay in children admitted for presurgical evaluation for epilepsy surgery. Pediatr Neurol 53(3):207–210

Tang Y, Liow JS, Zhang Z, Li J, Long T, Li Y et al (2018) The evaluation of dynamic FDG-PET for detecting epileptic foci and Analyzing reduced glucose phosphorylation in refractory epilepsy. Front Neurosci 12:993

Tellez-Zenteno JF, Hernandez Ronquillo L, Moien-Afshari F, Wiebe S (2010) Surgical outcomes in lesional and non-lesional epilepsy: a systematic review and meta-analysis. Epilepsy Res 89(2–3):310–318

Tenney JR, Rozhkov L, Horn P, Miles L, Miles MV (2014) Cerebral glucose hypometabolism is associated with mitochondrial dysfunction in patients with intractable epilepsy and cortical dysplasia. Epilepsia 55(9):1415–1422

Theodore WH (2017) Presurgical focus localization in epilepsy: PET and SPECT. Semin Nucl Med 47(1):44–53

Theodore WH, Sato S, Kufta C, Balish MB, Bromfield EB, Leiderman DB (1992) Temporal lobectomy for uncontrolled seizures: the role of positron emission tomography. Ann Neurol 32(6):789–794

Theodore WH, Hasler G, Giovacchini G, Kelley K, Reeves-Tyer P, Herscovitch P et al (2007) Reduced hippocampal 5HT1A PET receptor binding and depression in temporal lobe epilepsy. Epilepsia 48(8):1526–1530

Theodore WH, Martinez AR, Khan OI, Liew CJ, Auh S, Dustin IM et al (2012) PET of serotonin 1A receptors and cerebral glucose metabolism for temporal lobectomy. J Nucl Med 53(9):1375–1382

Thesen T, Quinn BT, Carlson C, Devinsky O, DuBois J, McDonald CR et al (2011) Detection of epileptogenic cortical malformations with surface-based MRI morphometry. PLoS One 6(2):e16430

Thornton R, Vulliemoz S, Rodionov R, Carmichael DW, Chaudhary UJ, Diehl B et al (2011) Epileptic networks in focal cortical dysplasia revealed using electroencephalography-functional magnetic resonance imaging. Ann Neurol 70(5):822–837

Tomas J, Pittau F, Hammers A, Bouvard S, Picard F, Vargas MI et al (2019) The predictive value of hypometabolism in focal epilepsy: a prospective study in surgical candidates. Eur J Nucl Med Mol Imaging 46(9):1806–1816

Tonini C, Beghi E, Berg AT, Bogliun G, Giordano L, Newton RW et al (2004) Predictors of epilepsy surgery outcome: a meta-analysis. Epilepsy Res 62(1):75–87

Velasco TR, Wichert-Ana L, Mathern GW, Araujo D, Walz R, Bianchin MM et al (2011) Utility of ictal single photon emission computed tomography in mesial temporal lobe epilepsy with hippocampal atrophy: a randomized trial. Neurosurgery 68(2):431–436; discussion 436

Vivash L, Gregoire MC, Lau EW, Ware RE, Binns D, Roselt P et al (2013) 18F-flumazenil: a gamma-aminobutyric acid A-specific PET radiotracer for the localization of drug-resistant temporal lobe epilepsy. J Nucl Med 54(8):1270–1277

Walz JM, Pedersen M, Omidvarnia A, Semmelroch M, Jackson GD (2017) Spatiotemporal mapping of epileptic spikes using simultaneous EEG-functional MRI. Brain 140(4):998–1010

Wang ZI, Suwanpakdee P, Jones SE, Jaisani Z, Moosa AN, Najm IM et al (2016) Re-review of MRI with post-processing in nonlesional patients in whom epilepsy surgery has failed. J Neurol 263(9):1736–1745

Wang YH, An Y, Fan XT, Lu J, Ren LK, Wei PH et al (2018) Comparison between simultaneously acquired arterial spin labeling and (18)F-FDG PET in mesial temporal lobe epilepsy assisted by a PET/MR system and SEEG. Neuroimage Clin 19:824–830

Willmann O, Wennberg R, May T, Woermann FG, Pohlmann-Eden B (2007) The contribution of 18F-FDG PET in preoperative epilepsy surgery evaluation for patients with temporal lobe epilepsy a meta-analysis. Seizure 16(6):509–520

Wintermark P, Lechpammer M, Warfield SK, Kosaras B, Takeoka M, Poduri A et al (2013) Perfusion imaging of focal cortical dysplasia using arterial spin Labeling: correlation with histopathological vascular density. J Child Neurol 28(11):1474–1482

Wissmeyer M, Altrichter S, Pereira VM, Viallon M, Federspiel A, Seeck M et al (2010) Arterial spin-labeling MRI perfusion in tuberous sclerosis: correlation with PET. J Neuroradiol 37(2):127–130

Wong CH, Bleasel A, Wen L, Eberl S, Byth K, Fulham M et al (2012) Relationship between preoperative hypometabolism and surgical outcome in neocortical epilepsy surgery. Epilepsia 53(8):1333–1340

Yankam Njiwa J, Gray KR, Costes N, Mauguiere F, Ryvlin P, Hammers A (2015) Advanced [(18) F]FDG and [(11)C]flumazenil PET analysis for individual outcome prediction after temporal lobe epilepsy surgery for hippocampal sclerosis. Neuroimage Clin 7:122–131

SISCOM (Subtraction Ictal SPECT with Coregistration to MRI)

38

Hwareung Lee, Jung Sik Kim, Ji Hyun Kim, and Seung Bong Hong

Contents

38.1 Introduction 1008
38.2 Image Processing for SISCOM 1008
38.3 Interpretation of SISCOM 1010
38.4 Clinical Significance and Research Applications of SISCOM 1011
References 1022

Abstract

Brain single-photon emission computed tomography (SPECT) is a functional nuclear imaging technique that can provide a regional map of cerebral blood flow (CBF) changes during the interictal or ictal period in patients with epilepsy and other neurological disorders. The radiotracer for brain SPECT is rapidly taken up by the brain within 30–60 s after its injection. The radiotracer injection during

H. Lee
Department of Neurology, Samsung Medical Center, Samsung Biomedical Research Institute, Sungkyunkwan University, Seoul, Republic of Korea

Severnace Hospital, Yonsei University, Seoul, South Korea

J. S. Kim · S. B. Hong (✉)
Department of Neurology, Samsung Medical Center, Samsung Biomedical Research Institute, Sungkyunkwan University, Seoul, Republic of Korea
e-mail: sbhong@skku.edu

J. H. Kim
The David S. Olton Behavioral Biology Program, Krieger School of Arts and Sciences, Johns Hopkins University, Baltimore, MD, USA

R. A. J. O. Dierckx et al. (eds.), *PET and SPECT in Neurology*,
https://doi.org/10.1007/978-3-030-53168-3_38

seizure activity (ictal SPECT) can show a snapshot of regional CBF (rCBF) changes during seizure. The sensitivity of ictal SPECT is high in temporal lobe epilepsy but relatively lower in extratemporal epilepsy. SISCOM is an imaging technique to subtract ictal and interictal SPECT images and to coregister them on brain MRI. SISCOM significantly improves the sensitivity of ictal SPECT and can further localize epileptic focus. But the successful localization of epileptic focus can be affected by the time of radiotracer injection, seizure duration, and propagation pattern of ictal EEG. Ictal hypoperfusion as well as ictal hyperperfusion is an important finding. Thus, ictal SPECT and SISCOM should be carefully interpreted by simultaneous review with seizure semiology, clinical information, features, injection time, duration of seizure, and ictal EEG pattern at the injection times. SISCOM is also useful for localizing brain structure generating specific feature of seizures and studying propagation pathways of epileptic seizures and pathomechanism of other neurological disorders and sleep disorders.

38.1 Introduction

Ictal SPECT (single-photon emission computed tomography) has been used successfully for localizing mesial temporal lobe epilepsy and has been reported to be less sensitive but more specific in extratemporal lobe epilepsy (O'Brien et al. 1998a; Spanaki et al. 1999; Lee et al. 2000; Valenti et al. 2002; Kaiboriboon et al. 2005). The low sensitivity of ictal SPECT in neocortical epilepsy may be related to various clinical factors such as inhomogeneous and various perfusion patterns in brain regions, difficulty in detection of subtle perfusion changes, differences in the amount of radioisotope delivered to the brain and time taken to inject radioisotope, different slice levels and orientation arising from different patient positioning during the interictal and ictal SPECT scans, and lack of quantitative assessment of the difference between interictal and ictal SPECT images. To solve these problems arising from qualitative analysis, quantitative analysis methods were developed by calculating the perfusion difference between ictal and interictal SPECTs. SPECT difference images can be calculated by subtraction of ictal and interictal SPECT scans (Zubal et al. 1995) or subtraction ictal SPECT with coregistration to MRI (SISCOM) (O'Brien et al. 1998a).

38.2 Image Processing for SISCOM

Subtraction ictal SPECT with coregistration to MRI (SISCOM) procedure consists of the following steps (Fig. 38.1):

Ictal–interictal SPECT registration: Before subtracting each voxel value of the ictal and interictal SPECT images, three-dimensional position of the interictal SPECT is transformed to the ictal SPECT using a chamfer surface matching algorithm. In all cases, root mean square distance is within one voxel. It is crucial to

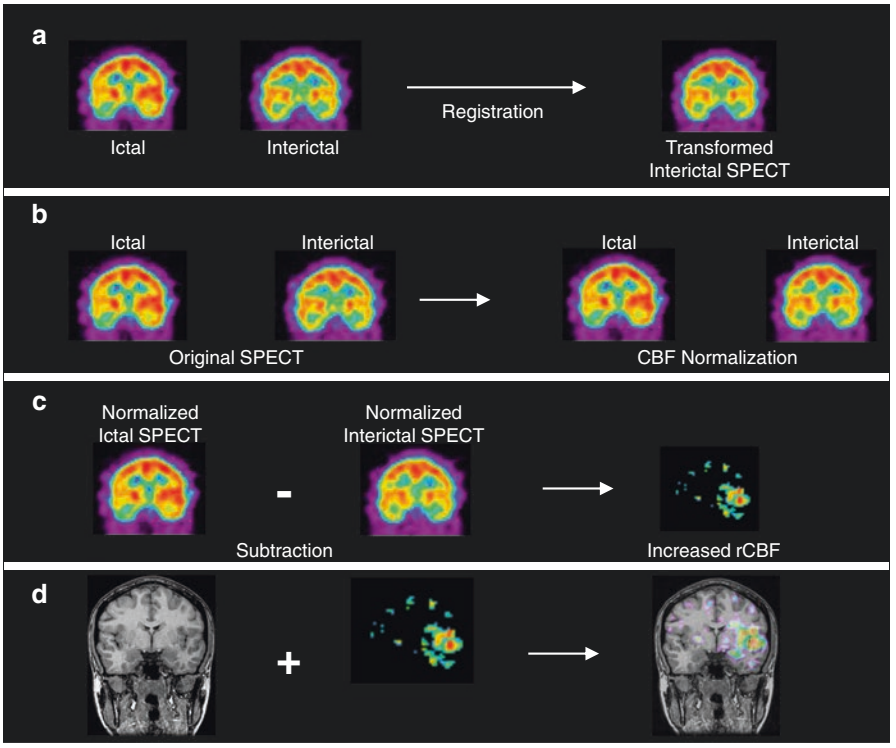

Fig. 38.1 The process of subtraction ictal SPECT with coregistration to MRI. Interictal SPECT is linearly transformed to the same patient's ictal SPECT using chamfer surface matching algorithm (**a**). The total intensity levels of ictal and transformed interictal SPECTs are normalized (**b**). The difference of two corresponding pixel values of ictal and interictal SPECTs is calculated and separated into positive (increased rCBF) and negative difference (decreased rCBF) images (**c**). Finally, subtracted SPECT is overlaid to MRI for anatomical localization (**d**)

make an accurate interictal-to-ictal SPECT registration both for improving the sensitivity of the SPECT subtraction and for preventing false-negative or false-positive perfusion differences.

Normalization of differences in pixel intensities: Ictal and interictal cerebral pixel intensities are rescaled to constant mean pixel intensities to normalize different levels of radioisotope uptake, retention, and decay. A normalization factor is calculated based on total pixel counts in the whole brain (global normalization), but sometimes this method can produce false-positive or false-negative findings especially when the areas of perfusion changes are extensive. In that case, regional normalization using the cerebellum, white matter, non-epileptic hemisphere, or brain stem may be a better normalization scheme (Zubal et al. 1995).

Ictal-transformed interictal SPECT subtraction: To obtain the cerebral perfusion difference, transformed and normalized interictal SPECT is subtracted from ictal SPECT pixel by pixel. Thus, brain regions of increased rCBF (with positive pixel

values) and regions of decreased rCBF (with negative pixel values) are separately identified.

Intensity thresholding: To eliminate scattered and non-interest region from the subtracted images, it is required to calculate the standard deviation (SD) of subtracted SPECT pixels. It may be possible to use varying thresholds (1.0–3.0 SD) according to SISCOM results. In clinical purpose, it is commonly used for 2 SD to localize seizure-onset zone. Placing the significance level at 3 SD increases specificity, but decreases sensitivity. If no significant rCBF change is observed in subtracted SPECT, one can consider reducing the threshold to 1 SD and searching for (nonsignificant) tendencies of ictal rCBF changes.

MRI-subtracted SPECT registration: For the localization of difference images, the subtracted SPECT is coregistered with a structural brain MRI. In most cases, the error ranges of SPECT–MRI registration for clinical use are within 5 mm (O'Brien et al. 1998a).

38.3 Interpretation of SISCOM

Ictal hyperperfusion and hypoperfusion in subtracted SPECT are generally considered significant when the difference of rCBF in each pixel is greater than 2 SD. The location of significant ictal hyperperfusion is visually decided on MRI by SPECT–MRI coregistration. For the determination of significant rCBF changes, only brain regions showing three and more voxels (3.56 mm × 3 = 10.68 mm) with significantly different intensity values between ictal and interictal SPECT images are included. Because the subtracted SPECT may reflect the peri-ictal or postictal state when the injection of radioisotope was delayed or seizures were very short-lasting, the subtracted SPECT should be interpreted with considering the interval between radioisotope injection and seizure onset, duration of seizure, and time of seizure end. The propagation pattern of ictal EEG discharges at the time of radiotracer injection is also very important because it may affect the final result of subtracted SPECT. Frontal lobe seizures show a tendency of more rapid propagation compared to temporal lobe seizures. The interpretation of SISCOM should include careful simultaneous review of seizure semiology, sequences of ictal EEG patterns, injection time in relation to seizure duration, structural lesion, and other clinical information. SISCOM reflects only cerebral perfusion changes (significantly different from the interictal state) at the time of tracer injection, not always the zone of seizure onset.

Recent two studies assessed the optimal *z*-score threshold of SISCOM to localize seizure-onset zone (Newey et al. 2013; Coster et al. 2018). One study (2013) examined 4 thresholding values (1, 1.5, 2, and 2.5) for the optimal SISCOM analysis to localize a seizure-onset zone in 26 epilepsy patients who underwent epilepsy surgery with at least 6-month seizure-free after surgery and found a slightly improved localization accuracy with a *z*-score threshold of 1.5 compared to evaluation at the *z*-score threshold of 1 and 2. Other study (2018) investigated the robustness of *z*-score threshold in 80 patients with drug-resistant epilepsy in whom the exact

location of the ictal-onset zone was known after successful epilepsy surgery. This study showed no difference in correct seizure localization between the two thresholds (1.5 SD, 70%; 2 SD, 72%). They suggested that the *z*-score threshold of 2 SD should be used in a routine clinical setting since 2 SD threshold shows higher inter-rater agreement and observer confidence rates than 1.5 SD threshold.

38.4 Clinical Significance and Research Applications of SISCOM

The first study using subtracted SPECT was published by Zubal et al. (1995). From this difference image technique, the epileptic focus was localized in five of six temporal lobe focus patients and in four of six for extratemporal seizure patients. This result was superior to visual analysis, and the difference images provided more precise information regarding location of seizure focus.

Subtraction of interictal from ictal SPECT coregistered to three-dimensional MRI (SISCOM) is an improved and better validated technique for ictal and interictal SPECT subtraction. Various clinical studies have been performed using this SISCOM technique in the field of epilepsy (O'Brien et al. 1998a, b, 1999; Lee et al. 2000). In the first study on patients with intractable partial epilepsy (O'Brien et al. 1998a), SISCOM was able to localize the epileptic focus in 45 out of 51 (88.2%) patients, while the traditional side-by-side inspection of ictal and interictal SPECT images localized 20 out of 51 (39.2%). However, late injection of the radiotracer (>45 s after seizure onset) but not secondary generalization was associated with a falsely localizing or non-localizing SISCOM. To overcome the problem of delayed injection, automated equipment for self-injection was developed which improved the sensitivity of ictal SPECT (Van Paesschen et al. 2000). To circumvent the difficulty of early injection during seizures, a postictal SPECT study was performed (O'Brien et al. 1999). The combined interpretation of hyperperfusion (positive values) and hypoperfusion (negative values) of SISCOM showed a better concordance rate with the final diagnosis than the analysis of either the hyperperfusion or hypoperfusion SISCOM image alone. In a similar study (Lee et al. 2000), the sensitivity of the combined hyperperfusion and hypoperfusion SISCOM (91.8%) was superior to only hyperperfusion SISCOM (85.2%) and visual inspection of ictal SPECT (68.9%). Ictal hypoperfusion at the epileptic focus was first reported in that study. Figure 38.2e demonstrated that a patient with an epileptic focus at the left posterior lateral temporal cortex showed ictal hypoperfusion at the epileptic focus, while ictal hyperperfusion was seen at the left anterior temporal region where ictal discharges propagated rapidly at the time of radiotracer injection. Rapid propagation of ictal discharges to other brain regions with early postictal state of the epileptic focus despite persistence of clinical seizures is the probable explanation for ictal hypoperfusion. In cases where early radiotracer injection is difficult, postictal SPECT subtraction can also be helpful in the evaluation and localization of the epileptic focus (Zubal et al. 1999).

Other study compared the ability of MSI, FDG-PET, and ictal SPECT to predict seizure-free outcome after epilepsy surgery with intracranial EEG monitoring. The

odds ratios of MSI (magnetic source imaging), FDG-PET, and ictal SPECT for prediction of seizure outcome were 4.4, 7.1, and 9.1, respectively, although the number of patients who had MSI, FDG-PET, or ictal SPECT was different (Knowlton et al. 2008).

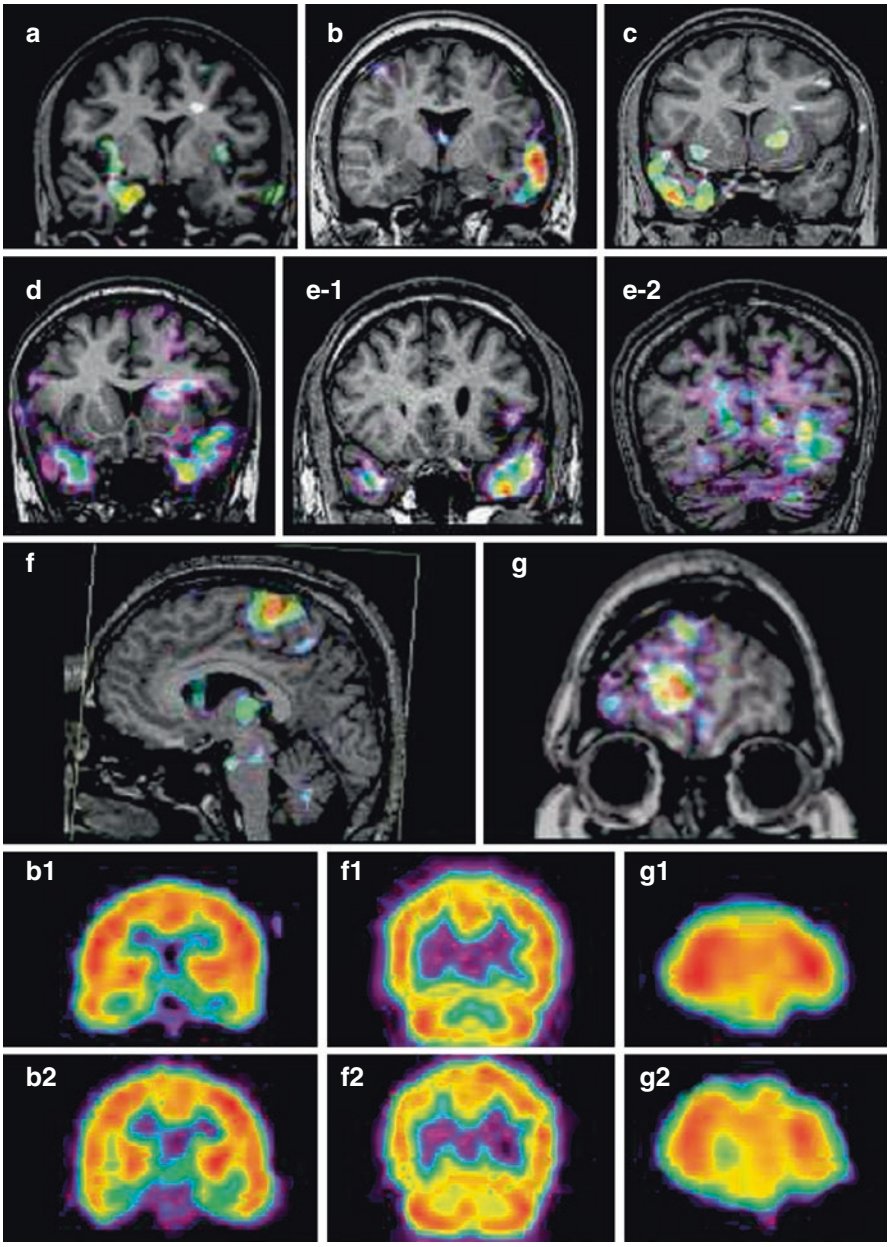

Another study compared different diagnostic tools in the prognostic factors for surgical outcome in neocortical epilepsy patients. Diagnostic sensitivities of interictal EEG, ictal scalp EEG, FDG-PET, and subtraction ictal single-photon emission computed tomography were 37.1%, 70.8%, 44.3%, and 41.1%, respectively. Localization by FDG-PET and interictal EEG was correlated with a seizure-free outcome. Concordance with two or more presurgical evaluations was significantly related to a seizure-free outcome. But this study showed lower sensitivity of SISCOM compared to other studies (Lee et al. 2005). So there are many factors affecting the result of ictal SPECT and SISCOM including seizure type and duration, radiotracer type, injection time, epilepsy monitoring unit setting, experience of technicians, and the method of SISCOM.

Ahnlide et al. (2007) analyzed SISCOM in 26 patients who had intracranial EEG monitoring and epilepsy surgery. SISCOM findings altered and extended the strategy for electrode placement at invasive recording in 15 patients. In this study, SISCOM was a prerequisite for seizure outcome in all six patients with favorable outcomes, and SISCOM is valuable for the identification of the epileptogenic zone in patients with drug-resistant epilepsy scheduled for invasive video-EEG.

Other two studies also indicated that SISCOM may have an impact on surgical decision (Tan et al. 2008; von Oertzen et al. 2011) (Fig. 38.3).

A previous study with 95 pediatric epilepsy patients investigated impact of timing of radiotracer injection, MRI findings, and seizure characteristics on SISCOM results (Stamoulis et al. 2017). This study showed that the SISCOM results were correlated with the radioisotope injection delay ($p < 0.01$) and cerebral lobe of seizure onset (specifically frontal vs. temporal, $p = 0.02$) but not with MRI findings ($p = 0.33$), epilepsy etiology ($p = 0.27$), or seizure duration ($p = 0.20$).

Repeated ictal SPECTs ictal SPECT with SISCOM analysis was shown to be helpful for localizing an epileptic focus in patients with partial epilepsy who had a non-localized first ictal SPECT and SISCOM (Lee et al. 2011). The SISCOM results of the second ictal SPECT were further localized in 43 (62.3%) patients. In the second ictal SPECT, radiotracer injection time from seizure onset was significantly

Fig. 38.2 Various perfusion patterns of subtracted SPECT in TLE (temporal lobe epilepsy) and ETLE (extratemporal lobe epilepsy) patients. The perfusion patterns of subtracted SPECT in TLE are (**a**) hyperperfusion in only mesial temporal region of the right mesial TLE, (**b**) hyperperfusion in lateral temporal region of the left neocortical TLE, (**c**) hyperperfusion in both mesial and lateral temporal areas in the right mesial TLE, and (**d**) hyperperfusion-plus pattern of subtracted SPECT: bilateral temporal hyperperfusion with left predominance in the left neocortical TLE. (*e-1* and *e-2*) Combined hyperperfusion–hypoperfusion pattern of subtracted SPECT in a patient with an epileptic focus at the left posterior lateral temporal cortex; *e-1* is a positive image showing hyperperfusion in the left anterior temporal region, and *e-2* is a negative image showing hypoperfusion in the left posterior lateral and basal temporal cortex from the same interictal and ictal SPECT images. (**f** and **g**) Perfusion patterns of subtracted SPECT in ETLE patients: (**f**) focal hyperperfusion in a left supplementary motor area seizure and (**g**) focal hypoperfusion in the right frontal lobe epilepsy. *b-2*, *f-2*, and *g-2* are conventional ictal SPECT of patients *b*, *f*, and *g*, while *b-1*, *f-1*, and *g-1* are conventional interictal SPECT of patients *b*, *f*, and *g*. All images are presented in radiological view

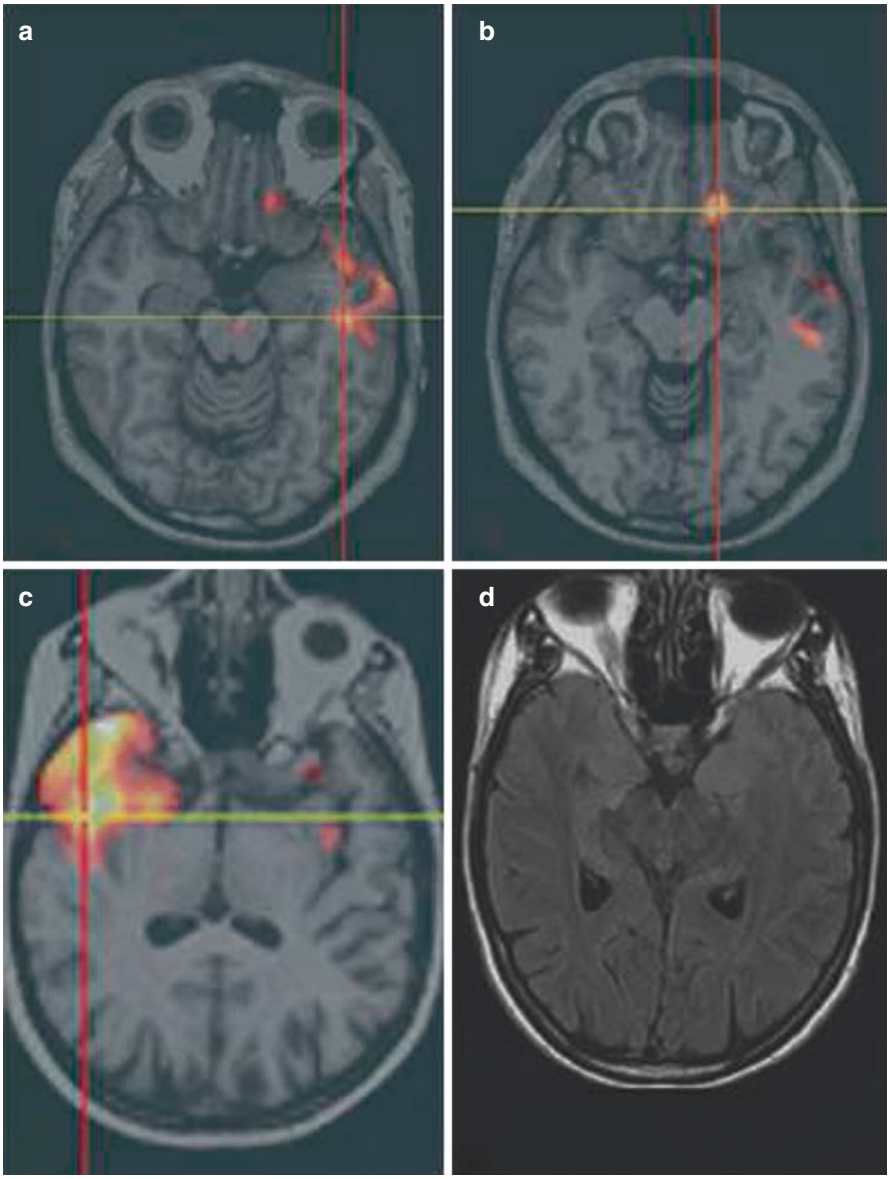

Fig. 38.3 (**a**, **b**) Example of multiple SISCOM hyperperfusions which are concordant to multifocal ECoG (electrocorticography) seizure onsets: a 22-year-old male patient with drug-refractory epilepsy had two types of seizures. (**c**, **d**) Example of nonlesional MRI with SISCOM concordant to site of surgery and seizure-free outcome

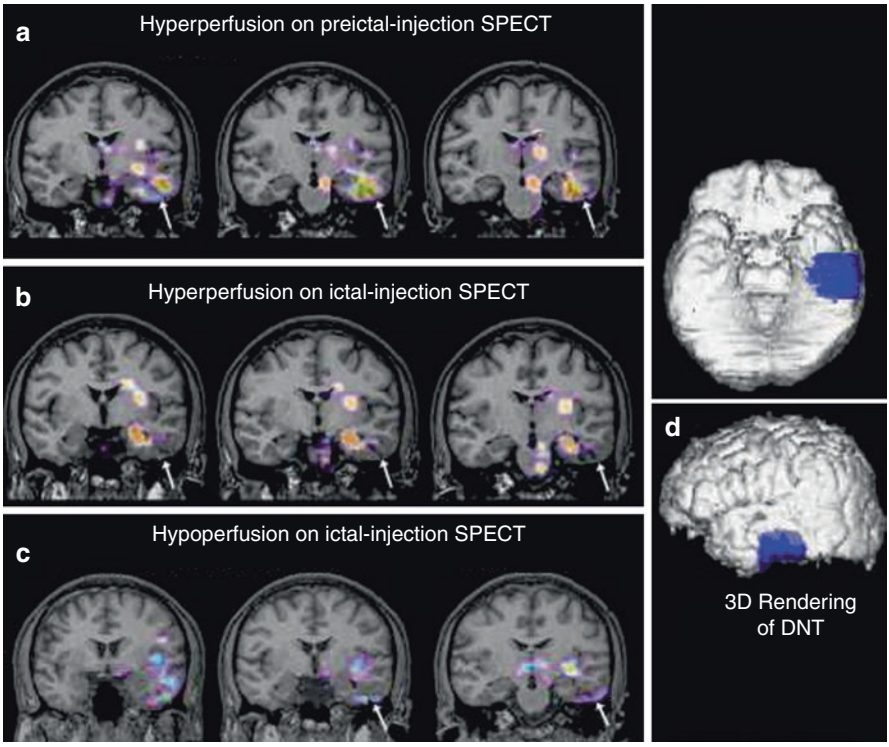

Fig. 38.4 Preictal SISCOM results. (**a**) SISCOM with preictal-injection SPECT shows hyperperfusion on the tumor lesion located at the left inferior–basal temporal area, ipsilateral midbrain, and thalamus. ^{99m}Tc-ECD injection was completed 11 s before the seizure began. (**b**) SISCOM with ictal-injection SPECT shows hyperperfusion at the ipsilateral amygdala–hippocampus, basal ganglia, and pons. The ^{99m}Tc-ECD injection was completed after 25 s (out of a 47 s seizure duration). (**c**) SISCOM with ictal-injection SPECT shows hypoperfusion at the tumor lesion and adjacent temporal lobe tissue. (**d**) A three-dimensional rendering view of the patient's brain MRI and tumor (*blue color*). **White arrows* indicate the location of the tumor

shorter in the localized group (25.1 ± 8.9 s) than the non-localized group (49.2 ± 55.8 s) ($p = 0.008$).

Since the time of radiotracer injection greatly affects ictal SPECT and SISCOM, preictal SPECT has been reported (Hong et al. 2008). We injected the radiotracer for SPECT study two times (one was injected during seizure and the other was 11 s prior to clinical seizure). While SISCOM with ictal SPECT showed focal hyperperfusion in ipsilateral hippocampus, SISCOM with preictal SPECT revealed early ictal hyperperfusion in an ipsilateral tumor located in the inferior temporal lobe (Fig. 38.4). So we presumed seizure started from the tumor itself and then rapidly propagated to the hippocampus. The patient had a resection of the tumor with

preservation of the hippocampus and became seizure-free without memory deficit postsurgically. Indeed, if we are able to inject radiotracer preictally, SISCOM will theoretically show early changes of CBF during seizures.

SISCOM is also useful in guiding the location and extent of resection in the surgery of intractable extratemporal lobe epilepsy. The extent of resection according to the cortical region of the SISCOM focus is significantly associated with the rate of excellent outcome (100% with complete resection, 60% with partial resection, and 20% with non-resection) (O'Brien et al. 2000). But another study reported inferior sensitivity of subtracted SPECT compared to visual inspection of ictal and interictal SPECT (Koh et al. 1998). The reasons for this difference of sensitivity may be the differences in study design, the technical method of SPECT subtraction, the rapidity of radiotracer injection in each laboratory, and the way of subtracted SPECT interpretation.

In 2016, Jalota et al. (2016) assessed the positive predictive value of surgical outcomes obtained by presurgical SISCOM in 44 patients with lesional (MRI-positive) and nonlesional (MRI-negative) refractory ETLE and TLE (Jalota et al. 2016). Concordance between one or more regions of SISCOM hyperperfusion with ECoG and at least partial resection of the dominant SISCOM signal provided additional useful information for predicting long-term surgical outcomes. The authors suggested that such regions are likely critical nodes in more extensive, active, epileptogenic circuits.

A meta-analysis study demonstrated the role of SISCOM in presurgical evaluation for patients who had epilepsy surgery in 11 SISCOM studies (Chen and Guo 2016). The authors assessed the value of SISCOM in identifying the epileptogenic zone and predicting postoperative outcomes. This study indicates that SISCOM has moderate sensitivity in localizing the epileptogenic zone and can provide complementary information when MRI is negative.

SISCOM is useful not only for localizing an epileptic focus but also for localizing the brain structure producing specific features of seizures or other paroxysmal neurological disorders. TLE seizure associated with or without contralateral dystonia showed different CBF changes during seizures (Joo et al. 2004). SISCOM showed that TLE seizures with dystonia were associated with significantly higher incidences of ictal hyperperfusion in the caudate nucleus, putamen, and thalamus compared to those without dystonia (Fig. 38.5). Other study showed that temporal lobe seizure presenting dystonic posturing are associated with ictal hyperperfusion on contralateral basal ganglia (Shin et al. 2002).

SISCOM revealed ictal hyperperfusion in the right amygdala, hippocampus, insula, and anterior temporal lobe during musicogenic seizures, which was concordant to the brain regions with hypometabolism in FDG-PET (Fig. 38.6) (Cho et al. 2007). Two complex partial seizures were provoked by listening to a ballad.

The patient experienced palpitation and an unpleasant feeling 1–2 min after listening to a song and then progressed to a complex partial seizure.

A SISCOM of apneic seizures showed ictal hyperperfusion in the left, posterior, mid-lateral temporal cortex. This finding supports the previous theory that apneic

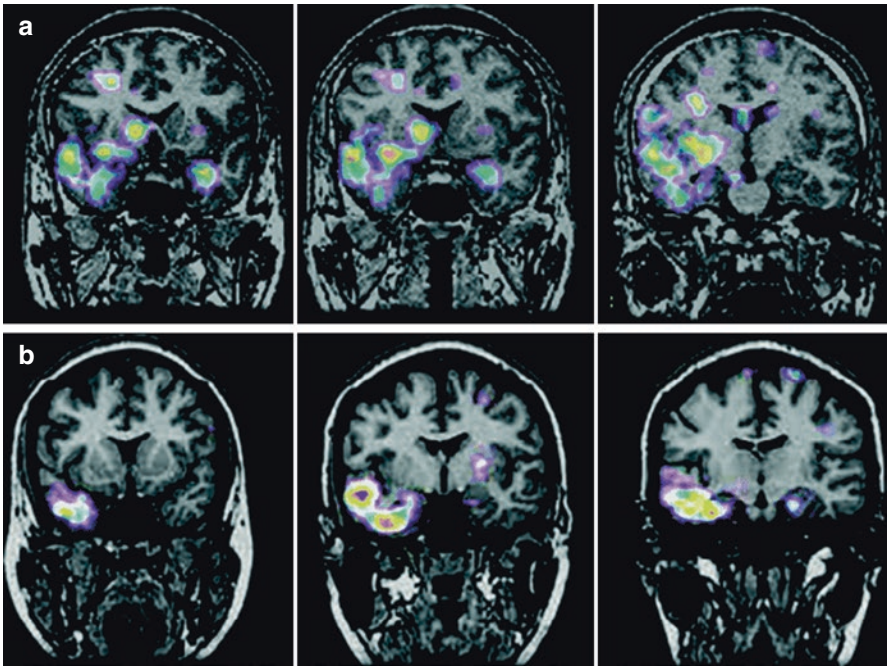

Fig. 38.5 (**a**) SISCOM of a patient with dystonic posturing during seizure. Ictal hyperperfusion on the right temporal lobe with ipsilateral caudate nucleus and putamen in a 24-year-old woman with right mesial temporal lobe epilepsy (TLE). (**b**) SISCOM of a patient without dystonic posturing. Ictal hyperperfusion on the right temporal lobe without basal ganglia hyperperfusion in a 31-year-old man with right mesial TLE

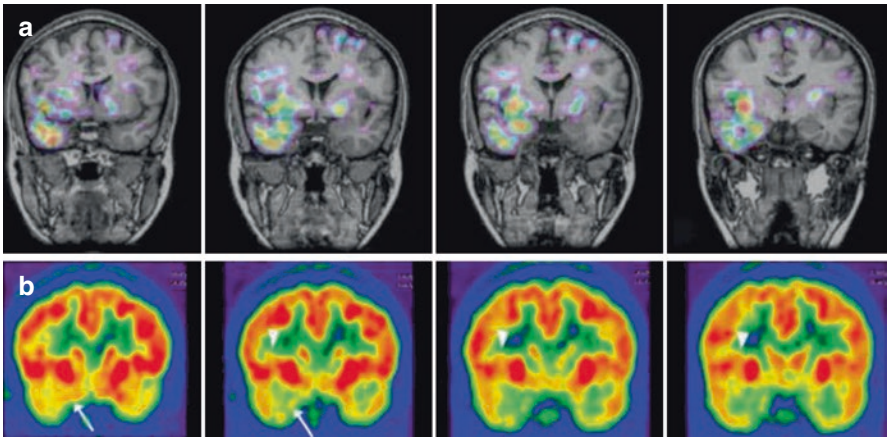

Fig. 38.6 SISCOM and FDG-PET. SISCOM images show the hyperperfusion in the right anterior mesial temporal regions, amygdala, hippocampal head, and insula (**a**). FDG-PET demonstrates interictal hypometabolism in the right amygdala (*arrow*), hippocampal head, and insula (*arrow heads*) (**b**)

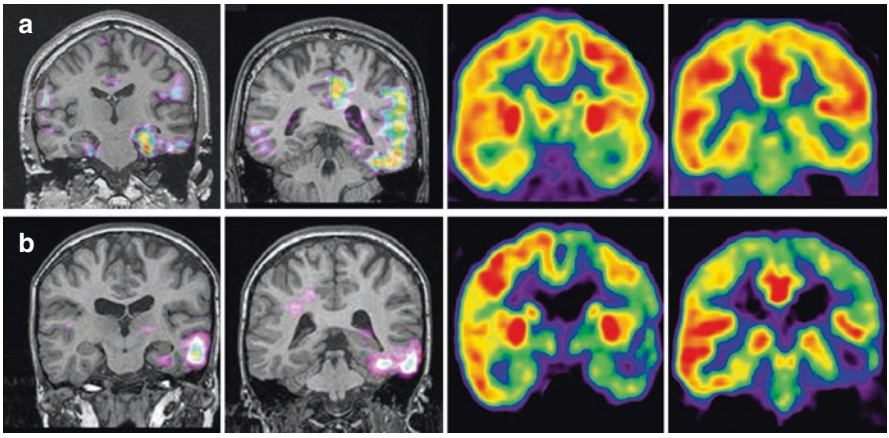

Fig. 38.7 SISCOM and FDG-PET findings in a MLTLE and a LTLE patient. (**a**) Left upper two SISCOM images show ictal hyperperfusion in left mesial and lateral temporal regions during seizure, and right upper two FDG-PET images depict interictal hypometabolism in the left mesial and lateral temporal regions in a MLTLE patient. (**b**) Lower row shows ictal hyperperfusion in left middle–inferior temporal gyrus and posterior basal temporal regions (left two SISCOM images) and interictal hypometabolism in the left hemisphere, especially in the lateral and basal temporal and frontoparietal regions (right two FDG-PET images) in a LTLE patient

seizures might be mediated through the limbic and associated cortical systems (Lee et al. 1999).

Our study demonstrated the usefulness of SISCOM and FDG-PET analyses for differentiating between two subtypes of TLE (mesio-lateral TLE (MLTLE) and lateral TLE (LTLE)) (Joo et al. 2015). We investigated the differences of the functional neuroimaging features (FDG-PET hypometabolism and ictal SPECT hyperperfusion) in addition to clinical, electrophysiological, and neuropsychological findings between MLTLE ($n = 31$) and LTLE ($n = 41$) groups. Our study showed that MLTLE group was more likely to have FDG-PET hypometabolism and SISCOM hyperperfusion restricted to the temporal areas, compared to the LTLE group (Fig. 38.7). Interestingly, no significant differences were found in scalp EEG, MRI, and Wada asymmetry between the two groups. The overall seizure-free rate was good (73.8%, mean follow-up = 9.7 years), which was not different in MLTLE (Engel class I, 74.3%) vs. LTLE (73.6%). Memory function after surgery was spared in LTLE patients, while visual memory was impaired in MLTLE patients when their mesial temporal structures were sufficiently resected.

SISCOM can be very helpful in refractory epilepsy patients with a normal MRI for intracranial electrode implantation to map a seizure-onset zone. In 26 MRI-negative refractory TLE or ETLE patients, SISCOM images in 92% of the patients had a focus of abnormal perfusion detected by blinded reviewers (O'Brien et al. 1998a). They also evaluated the usefulness of SISCOM in the presurgical evaluation of 17 patients with MRI-negative ETLE (O'Brien et al. 2000). Seventy-seven percent of them showed a correct localization in SISCOM results by blinded reviewers.

Concordance of the SISCOM localization with the site of surgical resection was associated with a significantly better chance of excellent surgery outcome than those in whom the SISCOM results were either non-concordant or non-localizing (55% vs. 0%, $p < 0.05$). In 33 MRI-negative TLE patients who underwent SISCOM studies and surgery (Bell et al. 2009), the SISCOM abnormality localized to the resection site was found to be significantly associated with postsurgical seizure-free outcome. Another study in 85 patients with MRI-negative ETLE showed that SISCOM was localizing in 68% (58/85) of the patients (Noe et al. 2013). However, 38% of only 24 patients who had a resective surgery were seizure-free after 10 more years after surgery.

SISCOM can be used for studies of propagation pathways of epileptic seizures in human brain. To investigate ictal hyperperfusion patterns during semiologic progression of seizures, we performed ictal SPECT and SISCOM in 50 patients with mesial TLE (Shin et al. 2002). The patients were categorized into five groups according to semiologic progression during ictal SPECT (Group 1 had aura only; Group 2 had motionless staring with or without aura; Group 3 had motionless staring and then automatism with or without aura; Group 4 had motionless staring and then dystonic posturing with or without aura and automatism; and Group 5 had motionless staring, automatism, and then head version and generalized seizures with or without aura and dystonic posturing). The semiologic progression in TLE seizures were related to the propagation of hyperperfusion from ipsilateral temporal lobe to contralateral temporal lobe, insula, basal ganglia, and frontal lobe (Fig. 38.8).

By SISCOM analysis, we studied ictal hyperperfusion in the cerebellum and basal ganglia in TLE (Shin et al. 2001). During TLE seizures, hemispheric cerebellar hyperperfusion occurred not only in contralateral but also in ipsilateral or bilateral cerebellar hemispheres to the side of seizure origin. Although temporal lobe origin seizures associated with additional frontal hyperperfusion produced more frequent hemispheric cerebellar hyperperfusion, seizures showing only temporal hyperperfusion without frontal hyperperfusion could produce hyperperfusion of the basal ganglia and cerebellar hyperperfusion.

Another study showed that impairment of consciousness showed a strong association with secondary hyperperfusion in the thalamic/upper brain stem region. The authors suggest that the spread of epileptic discharges or a transsynaptic activation (diaschisis) of these structures is an important mechanism in the alteration of consciousness during seizures (Lee et al. 2002).

A recent SISCOM study in 31 consecutive focal epilepsy patients who underwent an intracranial electrode implantation investigated whether ictal perfusion changes correspond to electrically connected brain networks (Tousseyn et al. 2017). In all patients, cortico-cortical evoked potential examinations were performed after repetitive electrical stimulation of an ictal-onset zone. The authors concluded that strong connectivity was demonstrated between the ictal-onset zone and hyperperfused SISCOM regions, while connectivity was weaker in the direction of baseline-perfused or hypoperfused SISCOM areas, and suggested that one should consider the contribution of all hyperperfused regions, as these are likely not random but represent an electrically connected epileptic network.

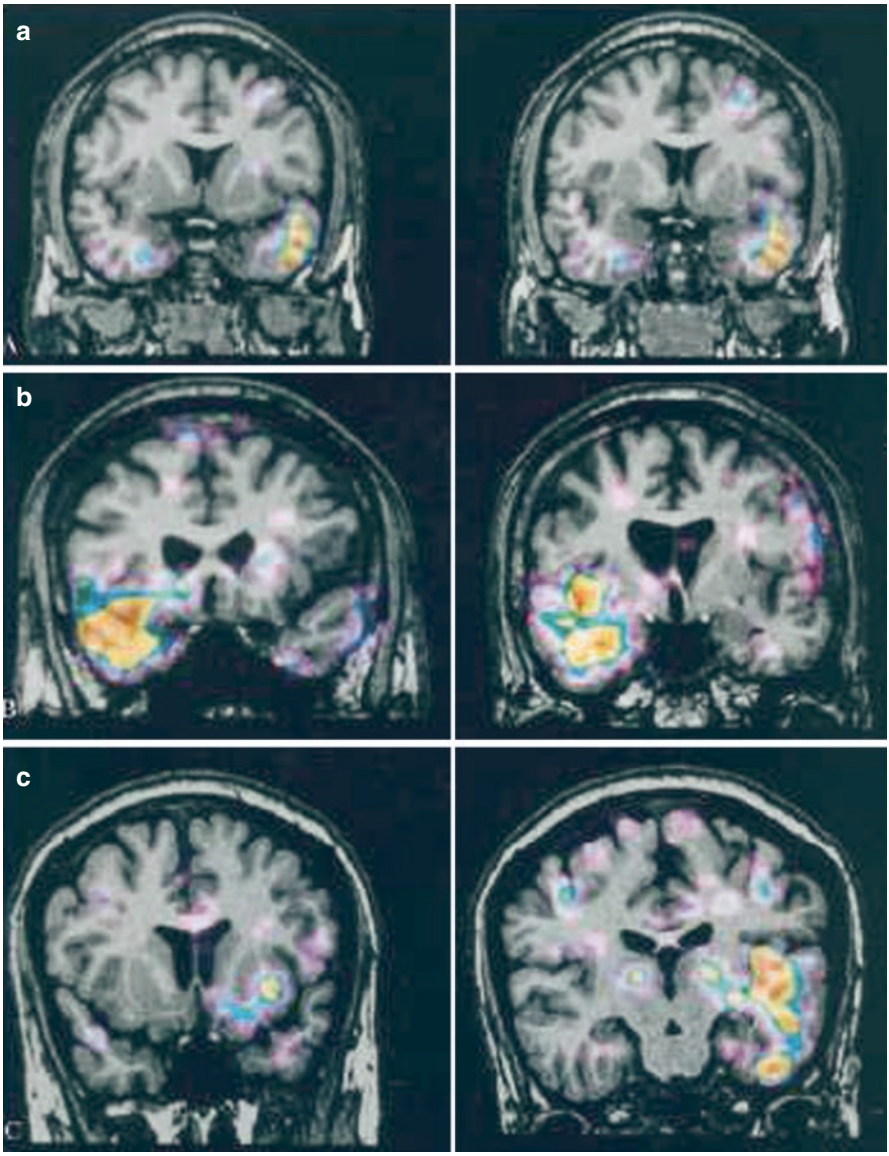

Fig. 38.8 Images of subtracted SPECT with MRI coregistration in each group. (**a**) Ictal hyperperfusion on the left temporal lobe with subtle right temporal change in a 37-year-old woman with left temporal lobe epilepsy (Group 1). (**b**) Ictal hyperperfusion on the right temporal lobe and ipsilateral insular cortex in a 25-year-old man with right temporal lobe epilepsy (Group 2). (**c**) A 42-year-old man with left temporal lobe epilepsy showing ictal hyperperfusion of the left temporal lobe, its adjacent insula, and small portions of basal ganglia (Group 3). (**d**) Ictal hyperperfusion on the left temporal lobe, basal ganglia, and insula in a 34-year-old man with left temporal lobe epilepsy (Group 4). (**e**) A 28-year-old man with right temporal lobe epilepsy showing ictal hyperperfusion on bilateral multiple brain regions with right temporal predominance (Group 5)

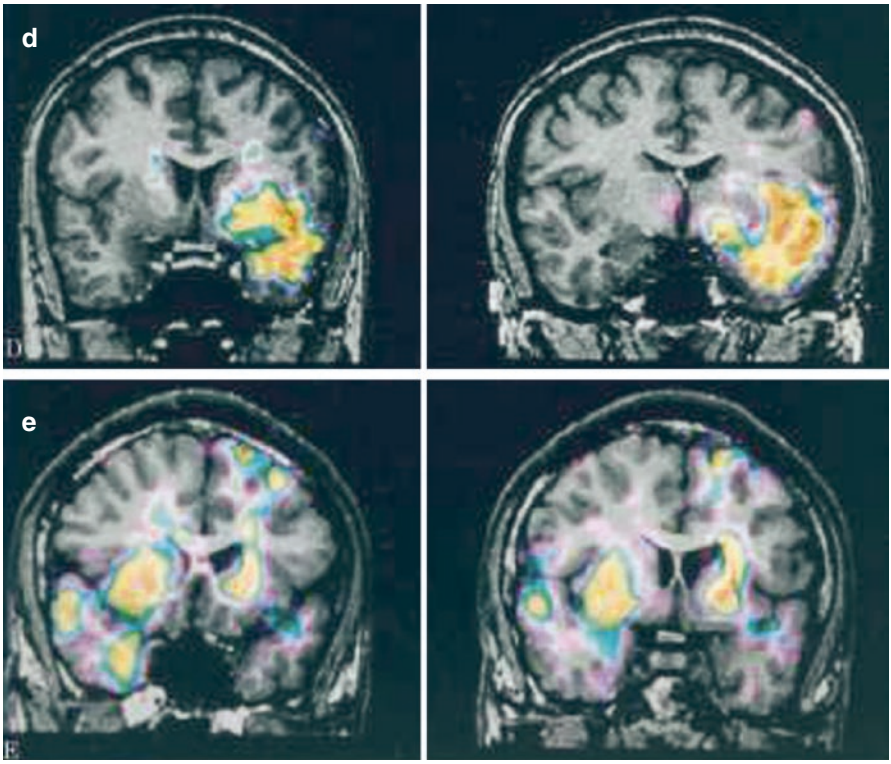

Fig. 38.8 (continued)

SISCOM can be used for the study of other paroxysmal neurological disorders. SISCOM with ictal SPECT during cataplectic attack in a narcolepsy patient showed ictal hyperperfusion in the right amygdala, bilateral cingulate gyri, basal ganglia, thalami, premotor cortices, sensorimotor cortices, right insula, and brain stem and hypoperfusion in the prefrontal cortex and occipital lobe (Hong et al. 2006a). A SISCOM study during the symptomatic period of Kleine–Levin syndrome revealed significant hypoperfusion in the left hypothalamus, bilateral thalami, basal ganglia, bilateral medial and dorsolateral frontal regions, and left temporal lobe during the hypersomnia period compared to the asymptomatic period (Hong et al. 2006b).

In summary, SISCOM is a useful tool for presurgical evaluation of patients with drug-resistant partial epilepsy. SISCOM improves the sensitivity of ictal SPECT for localizing an epileptic focus, but the time of radiotracer injection, seizure semiology and duration, and ictal EEG pattern at injection time may affect the result. SISCOM is also useful for clinical research aimed at examining the brain structure–semiology relationship, seizure propagation pathways, and brain pathomechanisms of other neurological disorders and sleep disorders.

References

Ahnlide JA, Rosén I, Lindén-Mickelsson Tech P, Källén K (2007) Does SISCOM contribute to favorable seizure outcome after epilepsy surgery? Epilepsia 48(3):579–588

Bell M, Rao S, So E et al (2009) Epilepsy surgery outcomes in temporal lobe epilepsy with a normal MRI. Epilepsia 50:2053–2060

Chen T, Guo L (2016) The role of SISCOM in preoperative evaluation for patients with epilepsy surgery: a meta-analysis. Seizure 41:43–50

Cho JW, Seo DW, Joo EY et al (2007) Neural correlates of musicogenic epilepsy: SISCOM and FDG-PET. Epilepsy Res 77(2–3):169–173

Coster LD, Laere KV, Cleeren E et al (2018) On the optimal z-score threshold for SISCOM analysis to localize the ictal onset zone. EJNMMI Res 8(1):34

Hong SB, Tae WS, Joo EY (2006a) Cerebral perfusion changes during cataplexy in narcolepsy patients. Neurology 66(11):1747–1749

Hong SB, Joo EY, Tae WS et al (2006b) Episodic diencephalic hypoperfusion in Kleine-Levin syndrome. Sleep 29(8):1091–1093

Hong SB, Joo EY, Tae WS et al (2008) Preictal versus ictal injection of radiotracer for SPECT study in partial epilepsy: SISCOM. Seizure 17(4):383–386

Jalota A, Rossi MA, Pylypyuk V et al (2016) Resecting critical nodes from an epileptogenic circuit in refractory focal-onset epilepsy patients using subtraction ictal SPEC coregistered to MRI. J Neurosurg 125:1565–1576

Joo YE, Hong SB, Lee EK et al (2004) Regional cerebral hyperperfusion with ictal dystonic posturing: ictal-interictal SPECT subtraction. Epilepsia 45(6):686–689

Joo EY, Seo DW, Hong SC et al (2015) Functional neuroimaging findings in patients with lateral and mesio-lateral temporal lobe epilepsy; FDG-PET and ictal SPECT studies. J Neurol 262:1120–1129

Kaiboriboon K, Bertrand ME, Osman MM, Hogan RE (2005) Quantitative analysis of cerebral blood flow patterns in mesial temporal lobe epilepsy using composite SISCOM. J Nucl Med 46:38–43

Knowlton RC, Elgavish RA, Bartolucci A, Ojha B, Limdi N, Blount J, Burneo JG, Ver Hoef L, Paige L, Faught E, Kankirawatana P, Riley K, Kuzniecky R (2008) Functional imaging: II. Prediction of epilepsy surgery outcome. Ann Neurol 64(1):35

Koh CS, Lee MC, Chung JK, Lee DS, Lee SK, Seo JM, Lee JS, Kim HJ (1998) Diagnosis of ictal hyperperfusion using subtraction image of ictal and interictal brain perfusion SPECT. Korean J Nucl Med 32(1):20–31

Lee HW, Hong SB, Tae WS et al (1999) Partial seizures manifesting as apnea only in an adult. Epilepsia 40:1828–1831

Lee HW, Hong SB, Tae WS (2000) Opposite ictal perfusion patterns of subtracted SPECT. Hyperperfusion and hypoperfusion. Brain 123:2150–2159

Lee KH, Meador KJ, Park YD et al (2002) Pathophysiology of altered consciousness during seizures: subtraction SPECT study. Neurology 59:841–846

Lee SK, Lee SY, Kim KK, Hong KS, Lee DS, Chung CK (2005) Surgical outcome and prognostic factors of cryptogenic neocortical epilepsy. Ann Neurol 58(4):525–532

Lee JY, Joo EY, Park HS et al (2011) Repeated ictal SPECT in partial epilepsy patients: SISCOM analysis. Epilepsia 52(12):2249–2256

Newey CR, Wong C, Wang ZI et al (2013) Optimizing SPECT SISCOM analysis to localize seizure-onset zone by using varying z scores. Epilepsia 54(5):793–800

Noe K, Sulc V, Wong-Kisiel L et al (2013) Long-term outcomes after nonlesional extratemporal lobe epilepsy surgery. JAMA Neurol 70:1003–1008

O'Brien TJ, So EL, Mullan BP et al (1998a) Subtraction ictal SPECT co-registered to MRI improves clinical usefulness of SPECT in localizing the surgical seizure focus. Neurology 50:445–454

O'Brien TJ, O'Connor MK, Mullan BP et al (1998b) Subtraction ictal SPET co-registered to MRI in partial epilepsy: description and technical validation of the method with phantom and patient studies. Nucl Med Commun 19:31–45

O'Brien TJ, So EL, Mullan BP et al (1999) Subtraction SPECT co-registered to MRI improves postictal SPECT localization of seizure foci. Neurology 52:137–146

O'Brien TJ, So EL, Mullan BP et al (2000) Subtraction peri-ictal SPECT is predictive of extratemporal epilepsy surgery outcome. Neurology 55:1668–1677

von Oertzen TJ, Mormann F, Urbach H, Reichmann K, Koenig R, Clusmann H, Biersack HJ, Elger CE (2011) Prospective use of subtraction ictal SPECT coregistered to MRI (SISCOM) in presurgical evaluation of epilepsy. Epilepsia 52(12):2239–2248

Shin WC, Hong SB, Tae WS et al (2001) Ictal hyperperfusion of cerebellum and basal ganglia in temporal lobe epilepsy: SPECT subtraction with MRI coregistration. J Nucl Med 42:853–858

Shin WC, Hong SB, Tae WS et al (2002) Ictal hyperperfusion patterns according to the progression of temporal lobe seizures. Neurology 58:373–380

Spanaki MV, Spencer SS, Corsi M et al (1999) Sensitivity and specificity of quantitative difference SPECT analysis in seizure localization. J Nucl Med 40:730–736

Stamoulis C, Verma N, Kaulas H et al (2017) The promise of subtraction ictal SPECT co-registered to MRI for improved seizure localization in pediatric epilepsies: affecting factors and relationship to the surgical outcome. Epilepsy Res 129:59–66

Tan KM, Britton JW, Buchhalter JR, Worrell GA, Lagerlund TD, Shin C, Cascino GD, Meyer FB, So EL (2008) Influence of subtraction ictal SPECT on surgical management in focal epilepsy of indeterminate localization: a prospective study. Epilepsy Res 82(2–3):190–193

Tousseyn S, Krishnan B, Wang ZI et al (2017) Connectivity in ictal single photon emission computed tomography perfusion: a cortico-cortical evoked potential study. Brain 140:1872–1884

Valenti MP, Froelich S, Armspach JP et al (2002) Contribution of SISCOM imaging in the presurgical evaluation of temporal lobe epilepsy related to dysembryoplastic neuroepithelial tumors. J Nucl Med 43:991–998

Van Paesschen W, Dupont P, Van Heerden B et al (2000) Self-injection ictal SPECT during partial seizures. Neurology 54:1994–1997

Zubal IG, Spencer SS, Imam K et al (1995) Difference images calculated from ictal and interictal technetium-99 m-HMPAO SPECT scans of epilepsy. J Nucl Med 36:684–689

Zubal IG, Spanaki MV, MacMullan J et al (1999) Influence of technetium-99m-hexamethylpropylene amine oxime injection time on single-photon emission tomography perfusion changes in epilepsy. Eur J Nucl Med 26:12–17

Part VII

Tumors of the Nervous System

Gliomas

39

Karl Herholz

Contents

39.1 Introduction . . . 1028
39.2 Glioma Grading and Detection of Malignant Transformation . . . 1029
39.3 Vascular and Blood-Brain Barrier Changes . . . 1030
39.3.1 Vascular Proliferation . . . 1030
39.3.2 Blood-Brain Barrier . . . 1030
39.3.3 Metabolic Changes . . . 1032
39.4 Biopsy Targeting . . . 1035
39.5 Guiding and Monitoring Therapy . . . 1035
39.5.1 Planning Surgical Resection . . . 1036
39.5.2 Planning Radiotherapy . . . 1037
39.5.3 Monitoring of Therapy . . . 1038
39.5.4 Detection of Recurrent Glioma . . . 1038
39.6 Summary and Conclusion . . . 1039
References . . . 1040

Abstract

Positron emission tomography (PET) is increasingly contributing to diagnosis and management decision in patients with brain tumours and especially gliomas. Through the use of FDG, amino acid tracers ([^{11}C]-methionine, [^{18}F]-fluoro-ethyl-tyrosine and [^{18}F]-fluorodopa) and [^{18}F]-fluorothymidine, PET contributes to diagnosis as well as planning and monitoring of therapy. Amino acid tracers are particularly sensitive for delineating the extent of gliomas and detection of recurrence. They are also being investigated for planning of resection and conformal radiation therapy. Further PET applications include the monitoring and outcome prediction in radiotherapy and chemotherapy and the identification of hypoxic tissue.

K. Herholz (✉)
The University of Manchester, Division of Neuroscience and Experimental Psychology, Manchester, UK
e-mail: karl.herholz@manchester.ac.uk

R. A. J. O. Dierckx et al. (eds.), *PET and SPECT in Neurology*,
https://doi.org/10.1007/978-3-030-53168-3_39

39.1 Introduction

Imaging methods have made enormous progress in the past decades. For instance, magnetic resonance imaging (MRI) provides excellent sensitivity for detection of brain tumours, even for low-grade gliomas that do not exhibit enhancement after application of contrast material. However, even though detection is no longer a major issue, many other problems of diagnosis and management remain unresolved. This is particularly true for gliomas as the most frequent type of intrinsic brain tumours.

Gliomas occur in a wide range of malignancy grades (1–4; see Table 39.1) and different histological subtypes, which are associated with substantial differences in prognosis and require different therapeutic strategies. The recent revision of the WHO histopathological classification (Louis et al. 2016) now also includes molecular markers. Gliomas with the wild-type isocitrate dehydrogenase (IDH) gene are most aggressive. They typically progress to the most malignant type, glioblastoma, even when initially presenting as grade 2 or 3 astrocytomas. IDH-mutant astrocytomas have longer survival times but ultimately also mostly recur and progress. In contrast to astrocytomas, oligodendrogliomas are characterised by 1p19q codeletion.

Gliomas of grade 1, such as pilocytic astrocytoma, most frequently occur in children. Their imaging features, biological characteristics and treatment options are different in many respects from gliomas of grades 2–4 (Galldiks et al. 2010a, Kumar et al. 2010, Dunkl et al. 2015). Therefore, pilocytic astrocytoma and other childhood brain tumours have not been included in this review.

PET and SPECT as imaging techniques in brain tumours have been reviewed recently (Herholz et al. 2012, Herholz 2017), and PET guidelines have been published by a joint working group for the European Associations of Nuclear Medicine and Neuro-Oncology (Law et al. 2019). Therefore, I will concentrate this review on the potential and perspectives of these methods to address frequent clinical questions in the diagnosis and treatment of gliomas.

Table 39.1 Glioma grades

WHO grade	Mean age	Typical survival time	Main histological types	Surgical therapy	Medical therapy
1	Children	Cure possible	Pilocytic astrocytoma	Total resection	Not required (if resected)
2	35	10–16 years	Oligodendroglioma	Gross total resection (when possible)	Individual decision
	35	6–8 years	Astrocytoma		
3	50	3 years	Anaplastic astrocytoma or oligodendroglioma		Radiotherapy and chemotherapy
4	>60	3–24 months	Glioblastoma		

39.2 Glioma Grading and Detection of Malignant Transformation

Grading and classification of gliomas have been improved substantially in recent years by use of molecular markers (Louis et al. 2016). Still, imaging is essential for treatment planning. Tumour heterogeneity is a big challenge, as different parts of gliomas frequently exhibit different degrees of malignancy, and for correct grading of the tumour, the most malignant part is relevant. However, if only parts of the tumour were accessible to surgical intervention or only few small tumour samples have been taken, as in stereotactic biopsies, the most malignant part may not even be available for histological examination.

Grade 2 gliomas pose a particular therapeutic dilemma, as aggressive therapy may do more harm than good (Douw et al. 2009), while a "wait-and-see" strategy may allow progression and malignant degeneration of the tumour that could possibly be prevented by earlier intervention. Also, recurrent tumours may present with a more malignant grade than seen in the original histopathologic sample. Therefore, imaging techniques are often required for accurate grading of gliomas and detection of areas progressing to a higher grade.

Malignant transformation of gliomas is associated with many changes that are accessible to imaging (Table 39.2). This provides many diagnostic possibilities but

Table 39.2 Aspects of malignant degeneration and associated imaging techniques in brain tumours

• Vascular changes
– Increase of blood volume and blood flow
Dynamic CT, perfusion-/diffusion-weighted MRI
Perfusion PET and SPECT ([^{15}O]-water, [^{99m}Tc]-HMPAO, [^{99m}Tc]-ECD)
– Endothelial activation and proliferation
Amino acid PET/SPECT (MET, FET, FDOPA and others)
PET of endothelial markers (e.g., [^{18}F]-galacto-RGD: αVβ3-integrin)
– BBB breakdown
MRI/CT contrast enhancement
PET and SPECT (^{201}Tl, ^{82}Rb, [^{68}Ga]-EDTA, FLT)
• Cellular changes
– Increase of glycolysis
FDG PET
MRS (lactate)
– Increase of proliferation
FLT (also requiring BBB breakdown)
– Changes of lipid metabolism
[^{11}C]-choline (possibly also [^{18}F]-fluorocholine)
MRS (choline, phospholipids)

is also a source of considerable uncertainty about their relative merits as only few of these imaging techniques have been directly compared with each other in large and representative samples. Most likely malignant degeneration is the consequence of cumulative genetic and biochemical changes that facilitate each other but do not necessarily occur in a regular order (Masui et al. 2012).

39.3 Vascular and Blood-Brain Barrier Changes

39.3.1 Vascular Proliferation

Gliomas show multiple alterations of vasculature and blood-brain barrier (BBB). Malignant transformation is associated with vascular proliferation, which may result in an increase in blood volume and blood flow, while it is also associated with tissue hypoxia. Cerebral blood flow (CBF) has been studied mostly by SPECT and PET, but the impact has been limited by variability of results and poor relation to tumour grade (Langen et al. 1988). The advent of functional MRI techniques to measure blood volume and perfusion (Waldman et al. 2009) has renewed the interest in this topic. Apparently, blood volume is subject to less physiological variability than blood flow and may thus provide a more reliable diagnostic marker. Several studies indicate that an increase in blood volume is related to expression of endothelial growth factor (Maia et al. 2005, Ludemann et al. 2006, Kapoor et al. 2009).

Imaging molecular markers of vascular proliferation directly has been the goal of several research studies. For instance, [^{18}F]-galacto-RGD images correlated with immunohistochemical alpha(v)beta(3) integrin expression of corresponding tumour samples in glioblastoma (Schnell et al. 2009). This receptor has also been targeted in experimental studies by other tracers labelled with ^{18}F, ^{68}Ga or ^{64}Cu. However, a multicentre clinical trial of [^{18}F]-fluciclatide (GE-135-03) showed only weak correlation with expression of alpha(v)beta(3) integrin in glioma (Sharma et al. 2015). Studies often were motivated by the advent of antiangiogenic therapy with bevacizumab, which even has been labelled with ^{89}Zr to identify patients who would most likely benefit from that therapy (Jansen et al. 2017).

39.3.2 Blood-Brain Barrier

The BBB prevents the transfer of many drugs, including radiopharmaceuticals, from blood to brain. It is modified in glioma, most prominently in the most malignant manifestation as glioblastoma (Dimberg 2014), but more subtle changes are also present at lower grades.

The standard techniques for imaging of BBB breakdown, allowing leakage of large molecules, in malignant gliomas and most other brain tumours are contrast-enhanced CT and MRI. By dynamic scanning, these techniques also allow quantitation of BBB permeability (Haroon et al. 2004, Herholz et al. 2007). Corresponding nuclear medicine techniques, such as 201Tl SPECT (Dierckx et al. 1994), have

attracted only limited interest because of their relatively low resolution, even though the sensitivity of the potassium analogue 201Tl for BBB changes may be higher than the large inert molecules used as contrast agents with CT and MRI (Gomez-Rio et al. 2008).

The main motivation for imaging of BBB permeability with PET is investigating functional BBB alterations, which may be present already in low-grade gliomas, and to assess the transfer of labelled therapeutic drugs (van Tellingen et al. 2015). There is an increased transport of amino acids by specific transporter enzymes, which is widely utilised with PET for imaging gliomas (Herholz et al. 2012) as described in subsequent sections.

In relation to therapeutic drugs, studies have been performed to assess the activity of enzymes that may help in delivering drugs or reducing efflux. These include studies of ABCB1 and ABCG2 transporters with [^{11}C]-erlotinib (Verheijen et al. 2018) and p-glycoprotein activity (Hendrikse et al. 1999).

Imaging with PET and SPECT tracers in the brain generally depends on tracer delivery to tissue. Blood flow is the limiting factor for freely diffusible tracers, which are rarely used in brain tumours. FDG uptake is provided by a high-capacity glucose transporter, while uptake of other tracers depends to some degree on BBB alterations. Thus, it is often difficult to demonstrate that in vivo uptake is related to specific binding in gliomas, especially for tracers which do not pass the intact BBB. For instance, the capacity of their transporters at the BBB is very limited for [^{18}F]-fluorothymidine (FLT), and tumours without substantial BBB damage are negative on a FLT scan (Tripathi et al. 2009). Dependency of tracer uptake on BBB damage but lack of correlation with somatostatin receptor expression was also observed in glioblastoma with ^{68}Ga-DOTA-peptides (Kiviniemi et al. 2015). Unfortunately, this problem is also largely preventing clinical translation of experimental PET studies using labelled macromolecules.

39.3.2.1 Amino Acid Tracers

An essential function of the endothelial cells in the cerebral vasculature is the active transport of amino acids from blood to tissue, and endothelial proliferation is associated with an increase of transporter expression and activity (Verrey et al. 2004). Several amino acids are being used as PET tracers, and increased uptake in gliomas has been demonstrated clinically (see reviews by Herholz et al. 2012, Herholz 2017 and Parent et al. 2019) and in experimental studies (Miyagawa et al. 1998, Viel et al. 2012). When compared to FDG, amino acid tracers provide higher sensitivity for tumour detection (Dunet et al. 2015).

For many years since 1980, [^{11}C]-methionine (MET) has been the most widely used amino acid tracer. Compared to normal brain, the uptake is increased in most gliomas, including the majority of low-grade gliomas with intact blood-brain barrier (BBB) (Herholz et al. 1998). On average, uptake is higher in high-grade than in low-grade gliomas, but the difference is quantitatively less pronounced than with tracers and contrast agents that depend on BBB breakdown, which is present in the majority of high-grade but absent in the majority of low-grade gliomas. In cross-sectional studies, there is no consensus about the utility of MET for glioma grading

(Moulin-Romsee et al. 2007). This may partially be due to the quantitatively small mean difference between grades and is potentially confounded by the fact that oligodendrogliomas have significantly higher uptake than astrocytomas of the same WHO grade (Derlon et al. 1997, Herholz et al. 1998, Ribom and Smits 2005, Shinozaki et al. 2011), even though they tend to have longer survival times. Nevertheless, longitudinal studies demonstrate that malignant progression of gliomas is associated with a significant increase of MET uptake that is absent in non-progressing tumours (Ullrich et al. 2009).

The very short physical half-life of carbon-11 (20 min) restricts the application of MET to PET research centres with own cyclotron and thus prevents wider clinical use. Therefore, fluorine-18-labelled amino acid tracers have found broad interest for clinical application. In recent years, [^{18}F]-fluoro-ethyl-tyrosine (FET) has been used by many clinical research groups and has been included in multiple clinical trials. Similar to MET, it is also a substrate for large neutral amino acid transporters LAT1 (Habermeier et al. 2015) and LAT2 (Langen et al. 2006), while, in contrast to MET, it is not incorporated into proteins. Interestingly, studies comparing the clinical properties of these two tracers directly (Weber et al. 2000) found similar tumour-to-background ratios (while overall tissue uptake of FET is somewhat lower than MET), suggesting that the activated transport is the process that dominates the signal (rather than further metabolism and protein synthesis) even for MET. Correspondingly, it was also found that the magnitude of FET uptake is not a particularly strong indicator of tumour grade. This limitation can be overcome by dynamic FET scans, because the early phase of tracer uptake provides a better differentiation between high- and low-grade gliomas than late uptake (Popperl et al. 2007, Jansen et al. 2012).

As an alternative to FET, FDOPA has also been used for imaging of gliomas (Heiss et al. 1996, Ledezma et al. 2009, Tripathi et al. 2009, Walter et al. 2012, Nioche et al. 2013, Villani et al. 2015, Chiaravalloti et al. 2019). Clinical results are similar to FET, while there is more variable background than with FET because of the high physiological accumulation of FDOPA in the basal ganglia. Another alternative is [^{11}C]-alpha-methyltryptophan, which also relates to the kynurenic pathway and has been used in promising clinical research studies (Juhasz et al. 2011, 2014, Bosnyak et al. 2016).

Cyclic amino acids, most notably anti-[^{18}F]FACBC ([^{18}F]-fluciclovine), accumulate in tumours by Na^+-dependent transporters, while there is little uptake in normal brain. Few studies have been performed in glioma, demonstrating even better tumour-to-background contrast in recurrent glioma than MET (Michaud et al. 2019) and good discrimination between low- and high-grade glioma (Parent et al. 2018).

39.3.3 Metabolic Changes

Malignant degeneration of gliomas is associated with many changes in their metabolism. Imaging these changes is particularly attractive if it can be done without interference by BBB damage. The situation in that respect is best for FDG, because

of the relatively rapid kinetics and large capacity of the glucose transporter. Freely diffusible tracers, the uptake of which also does not depend on BBB disruption, are not available for targeting metabolic processes. An exception may be the blood flow marker [^{13}N]-NH_3, which is trapped in tissue by glutamine synthase and has successfully been used in glioma (Shi et al. 2013, Khangembam et al. 2014).

39.3.3.1 FDG

Several studies demonstrated that FDG uptake in gliomas is related to prognosis (Patronas et al. 1985, Holzer et al. 1993, Kaschten et al. 1998, De Witte et al. 2001, Padma et al. 2003, Pardo et al. 2004, Van Laere et al. 2005, Pauleit et al. 2009, Colavolpe, Metellus, Mancini, Barrie, Bequet-Boucard, Figarella-Branger, Mundler, Chinot, and Guedj 2012b). The main limitation for putting that into broader clinical use has probably been the difficulty to identify gliomas on FDG PET scans. FDG uptake in normal grey matter is similar to that of malignant gliomas, resulting in poor contrast. White matter FDG uptake is lower (typically about 40–50% of grey matter on a FDG PET scan), and FDG uptake of low-grade gliomas is usually only slightly higher than white matter uptake. Thus, the regional heterogeneity of normal brain metabolism is comparable to the difference between low- and high-grade gliomas. Thus, in most studies comparing FDG with amino acid tracers (Fig. 39.1), the latter appear to provide the more sensitive and distinct signal (Derlon et al. 2000, Kim et al. 2005, Van Laere et al. 2005, Potzi et al. 2007, Pauleit et al. 2009, Li et al. 2012).

The limitations caused by poor image contrast can be overcome by PET-MRI coregistration (Padma et al. 2003, Leiva-Salinas et al. 2017), which achieves an accuracy of 1–2 mm and thus considerably better than actual PET scan spatial resolution (Cizek et al. 2004). On hybrid PET/MRI scanners, PET can even be combined directly with multiparametric MRI assessment of glioma (Sacconi et al. 2016). Reliable classification of FDG uptake in tumour, as localised on the coregistered MRI, can be achieved by a grading scale in relation to normal brain tissue, e.g. 0 = no uptake; 1 = uptake less or equal to contralateral white matter; 2 = uptake greater than contralateral white matter and less than grey matter; and 3 = equal to or greater than contralateral grey matter (Padma et al. 2003). Rather than relying on a plain SUV only, semiquantitative assessment of lesion uptake should be done in the tissue volume that is suspect of tumour on the MRI scan and divided by uptake in a contralateral mirror region, providing a SUV ratio (SUVR) which is equivalent to a simple activity ratio. Normal brain glucose metabolism is reduced in patients with aggressive tumours (DeLaPaz et al. 1983, Holzer et al. 1993), thus enhancing the contrast between malignant gliomas with high FDG uptake and normal brain background. An improvement of the contrast can also be achieved by delayed scanning, which may demonstrate continuing accumulation of FDG in the tumour (Spence et al. 2004, Prieto et al. 2011).

39.3.3.2 Proliferation

The most important factors being considered in histological grading of gliomas are the degree of cellular anaplasia and indicators of cellular proliferation. Initial work

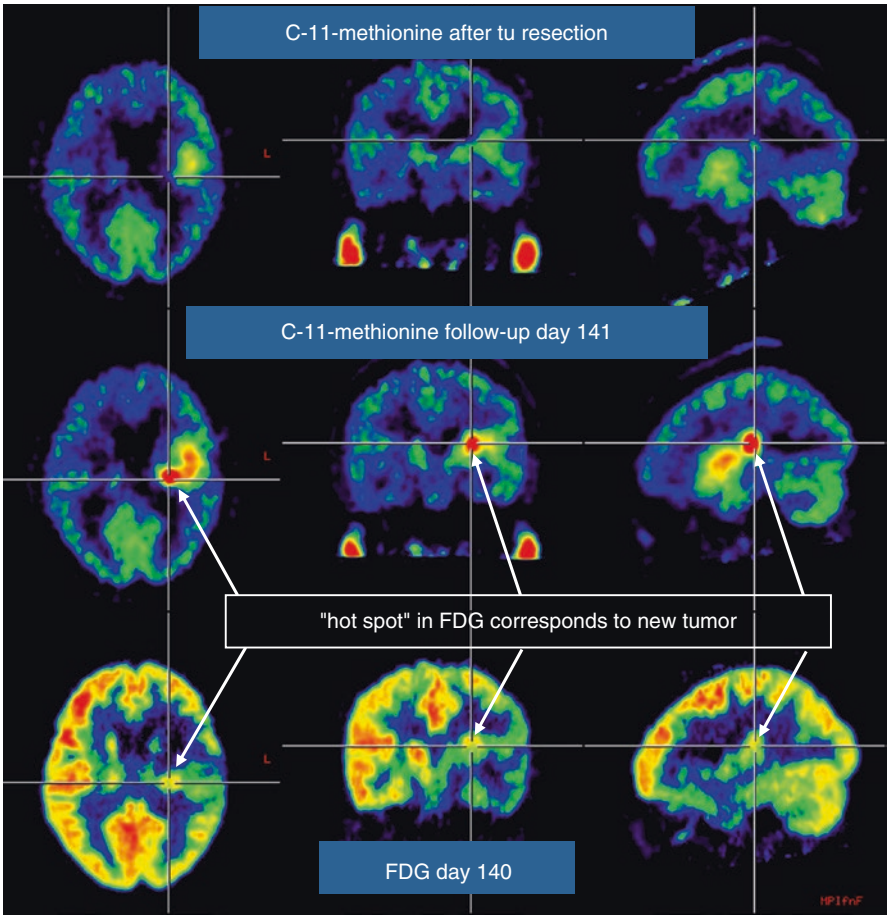

Fig. 39.1 Comparison of MET PET and FDG in recurrent glioblastoma. Within a few weeks after macroscopically complete tumour resection, MET PET is already showing increased uptake in the resection area (top row), which increases in intensity during the next 3 months (middle row), when the recurrence is also identified with less signal intensity on FDG PET (bottom row)

with [^{11}C]-thymidine demonstrated in vitro and in vivo that the activity of thymidine kinase 1 (TK-1) is associated with cellular accumulation of the tracer and tumour proliferation (Eary et al. 1999). To facilitate more widespread applicability, the fluorine-18-labelled thymidine analogue FLT has been developed for imaging of tumour proliferation (Shields et al. 1998). Although its affinity to cellular nucleoside transporters and TK-1 is less than that of thymidine (Krohn et al. 2005), a correlation between tracer uptake kinetics and proliferation markers has been demonstrated in malignant glioma (Ullrich et al. 2008, Price et al. 2009). Volume and intensity of FLT uptake predicted survival in patients with recurrent malignant

glioma (Zhao et al. 2014). FLT does not cross the intact BBB (at least not at an amount that would allow clinical PET imaging); thus it provides a negative finding in most low-grade gliomas (Chen et al. 2005) and is not suitable for measuring proliferation rates in this tumour group (Tripathi et al. 2009).

Another potential proliferation marker is choline. Magnetic resonance spectroscopy has demonstrated significant differences with respect to the phospholipid and choline signal between low- and high-grade gliomas (Tedeschi et al. 1997). Correspondingly, there is also interest whether this could also be achieved by [^{11}C]-choline (Shinoura et al. 1997). Ohtani et al. (2001) demonstrated increased uptake in high-grade gliomas and extra-axial tumours lacking the BBB, while uptake in most low-grade gliomas was comparable to background. While initial experience with [^{18}F]-fluorocholine was limited (Lam et al. 2011) and tracer uptake is affected by BBB disruption, a subsequent study indicated high sensitivity for detection of recurrent glioma (Gomez-Rio et al. 2015).

Recently, expression of the mitochondrial translocator protein (TSPO) by glioma cells has been identified as a potential proliferation marker (Janczar et al. 2015). It has been imaged using [^{11}C]-PK11195 (Su et al. 2015), demonstrating increased binding to TSPO in high-grade glioma, and with [^{18}F]-GE180 (Unterrainer et al. 2019) which, however, does not cross the intact BBB in normal brain.

39.4 Biopsy Targeting

Unfortunately, none of the currently available PET tracers are absolutely specific for tumours. For instance, FDG uptake is also increased in inflammation, and increased amino acid uptake has been observed in various acute brain lesions (Floeth et al. 2006). Thus histological tissue examination remains the ultimate tool for accurate diagnosis, and PET can contribute to accurate diagnosis by guiding neurosurgeons towards the most active glioma parts (Pirotte et al. 2004a, b, Kunz et al. 2011). Areas of increased FDG and methionine uptake tend to correspond with each other (Pirotte et al. 2004a, b). There is also some correlation with increased CBV in gliomas, but focal increases of tracer uptake and CBF are often not co-localised (Fig. 39.2) (Filss et al. 2017).

39.5 Guiding and Monitoring Therapy

There is currently no definitive therapy for gliomas in adults. Diffuse tissue infiltration is the primary reason for glioma recurrence (Scherer 1940), preventing curative resection (with the exception of pilocytic astrocytoma) and probably also contributing to ultimate failure of regional radiotherapy. Furthermore, at recurrence, gliomas often progress to a higher grade. Imaging is essential to tailor therapy individually for each patient at each stage of progression.

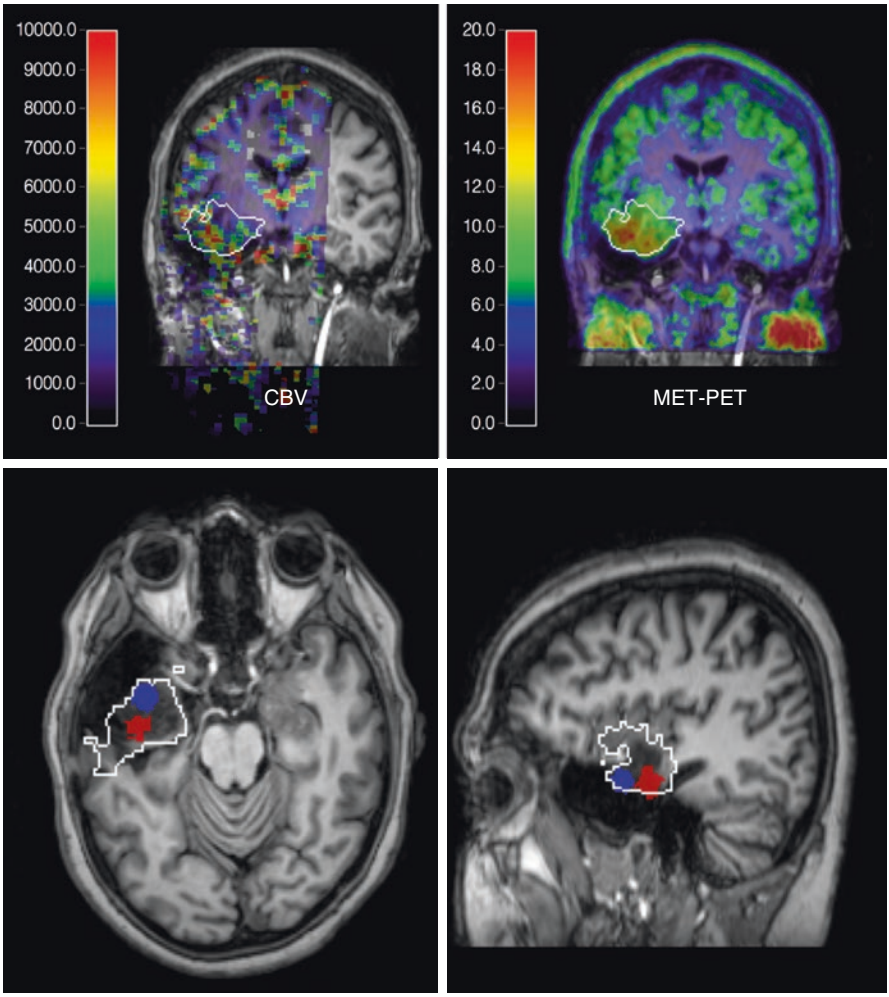

Fig. 39.2 Low-grade glioma with focal increases of CBV (Dynamic susceptibility contrast-enhanced MRI) and amino acid uptake (MET PET) indicating beginning focal dedifferentiation. Images are shown in coregistration and fusion with T1-weighted contrast-enhanced MRI; the white outline indicates the extent of the lesion on FLAIR MRI. On the coronal cuts (top row), there is some correspondence between CBV and MET PET within the tumour, while the transaxial and sagittal slices (bottom row) demonstrate that peaks are actually not in the same position (peak MET uptake marked blue, peak CBV red)

39.5.1 Planning Surgical Resection

There are some issues that need to be considered when using PET for therapy planning. Diffuse infiltration does not have sharp borders, and in order to prevent recurrence, one would rather treat as large a volume as possible, in principle irrespective of any imaging guidance. The very narrow limit to that approach is the need to

minimise treatment side effects and especially treatment-induced neurological deficits. Therefore "eloquent areas", i.e. brain areas that are crucial for particular neurological function, need to be excluded from resection or intense irradiation. The individual location of these areas can vary considerably, and therefore functional imaging methods to localise eloquent areas are increasingly being used for therapy planning. This work has initially been pioneered with ^{15}O-water PET (Herholz et al. 1997) and has been continued and expanded with functional MRI techniques. Coregistration of structural, functional and molecular images can then provide the comprehensive information delineating macroscopic anatomy, eloquent brain areas and tumour extent to maximise the radicality of intervention to improve prognosis while minimising side effects and maintaining neurological function.

Amino acid tracers are prime candidates for guiding resection because of their excellent sensitivity for delineation of glioma including parts that do not take up contrast material (Galldiks et al. 2010b). Studies have demonstrated that radiolabelled amino acids detect the solid mass of gliomas and metabolically active tumour areas more reliably than either CT or MRI (Mosskin et al. 1989, Goldman et al. 1997, Kracht et al. 2004, Pirotte et al. 2004a, b, Pauleit et al. 2005). Pirotte et al. (2009) demonstrated that total resection of tumour guided by amino acid tracer uptake was associated with a significantly longer survival in patients with malignant gliomas.

39.5.2 Planning Radiotherapy

While surgery is aiming at removal of solid tumour, radiotherapy also is also aiming at stopping tumour infiltration of healthy tissue. Thus, irradiation fields typically include a "safety margin" around resected and solid tumour. Studies have been initiated to clarify whether amino acid PET can improve radiation planning and ultimate outcome of radiotherapy (Piroth et al. 2016, Oehlke and Grosu 2017, Poulsen et al. 2017, Hirata et al. 2019). However, there is no clear limit of infiltration, and there is also some variation of the background signal with lower normal uptake of amino acids in white than in grey matter (Coope et al. 2007). Depending on the chosen thresholds, resulting target volumes for conformal radiotherapy may vary considerably, and there is a need for standardisation based on proven improvement of outcome.

Hypoxic tumour tissue is relatively resistant to irradiation, asking for individual adjustment of radiotherapy protocols to overcome resistance while keeping side effects under control. Macroscopic and microscopic heterogeneity of vascular proliferation and hypoxia pose substantial challenges to imaging. Imaging of hypoxic tissue can be provided by [^{18}F]-fluoromisonidazole (FMISO) (Valk et al. 1992) and related tracers (Koch et al. 2010, Shibahara et al. 2010, Mapelli et al. 2017). Several recent studies indicate that this may provide a clinically useful tool for detection of hypoxia (Spence et al. 2008) and diagnosis of glioblastoma (Hirata et al. 2012). Increased binding of hypoxia markers is often found close to areas with BBB damage and contrast enhancement (Swanson et al. 2009, Kawai et al. 2011) but does not correspond to areas with vascular deoxygenation, as measured by MRI oxygen imaging (Preibisch et al. 2017).

39.5.3 Monitoring of Therapy

There is a clinical need for monitoring of therapy in gliomas. As with most tumours, a definitive assessment of response based on clinical symptoms or structural imaging is possible only after several months, and it is even more difficult for low-grade gliomas because of their slow natural progression (Reardon et al. 2011). Furthermore, there is the problem with possible pseudoprogression and pseudoresponse on CT and standard MRI (Brandsma and van den Bent 2009), and there is considerable interindividual variability of gliomas in the response to therapy. Especially with the rapidly progressing glioblastomas, one would want to leave any inefficient chemotherapy as soon as possible and switch to an alternative regimen to avoid unnecessary side effects and loss of the bone marrow reserve that is needed for more intense protocols. Thus, reliable early response markers are needed.

Consistent early responses to radiotherapy and chemotherapy have been observed with amino acid tracers (Galldiks et al. 2006, 2012, Wyss et al. 2009, Hutterer et al. 2011). The critical distinction between tumour progression and pseudoprogression with necrosis has also been addressed by amino acid PET, most successfully with more than 80% accuracy by dynamic imaging or combination with perfusion MRI (Galldiks et al. 2017). FET PET has been used for evaluation of emerging new therapies, such as TTFields (Ceccon et al. 2018), and detailed recommendations for amino acid PET in clinical oncology have been published (Albert et al. 2016).

While FDG may also serve as a response marker in radiotherapy (Tralins et al. 2002) and chemotherapy (Charnley et al. 2006, Colavolpe et al. 2012a), it is potentially complicated by the "flare" effect (Trigonis and Jackson 2010), which has been observed as an initial response to radiotherapy before ultimately FDG uptake declines as the viability of tumour cells decreases. Its clinical significance is not clear, and it may be associated with radiological pseudoprogression (Hygino da Cruz et al. 2011).

Expectations have been high for FLT as an early response marker, and indeed a study by Chen et al. (2007) demonstrated a large and early reduction of uptake after therapy that included the antiangiogenic drug bevacizumab, predicting later response on structural imaging. However, a subsequent study demonstrated that FLT did not predict overall survival, while this was achieved by FDOPA (Harris et al. 2012).

39.5.4 Detection of Recurrent Glioma

Recurrent glioma poses specific diagnostic problems because treatment, especially surgery and radiotherapy, can induce alterations in non-tumour tissue that can be indistinguishable from recurrent tumour using standard contrast-enhanced CT and MRI (Rachinger et al. 2005). In particular, radiation-induced necrosis needs to be distinguished from recurrent tumour, while both lesions may show contrast enhancement. Studies demonstrate that FDG, FLT and amino acid tracers have the potential to provide that differentiation (see Table 39.3 and de Zwart et al. (2019) for

Table 39.3 Discrimination between recurrent glioma and necrosis (modified from Herholz et al. (2012))

Tracer	*n*	Sensitivity	Specificity	Lesion type	References
FDG	47	75% (21/28)	81% (13/16)	Malignant tumour	Chao et al. (2001)
FDG	15	43% (6/14)	100% (1/1)	Glioma	Thompson et al. (1999)
FDG	84	73%	56%	Malignant tumour	Ricci et al. (1998)
FDG	38	88% (15/17)	81% (17/21)	Glioma	Valk et al. (1988)
FDG	21	81% (13/16)	40% (2/5)	Tumour	Kahn et al. (1994)
FDG	9	80% (4/5)	100% (4/4)	Tumour[a]	Ogawa et al. (1991)
FDG	30	95%	50%	Glioma	Van Laere et al. (2005)
MET	30	75%	70%	Glioma	Van Laere et al. (2005)
MET	12	100% (5/5)	86% (6/7)	Glioma[a]	Sonoda et al. (1998)
MET	32	75%	75%	Glioma[a]	Terakawa et al. (2008)
MET	11	100% (6/6)	60% (3/5)	Glioma[a]	Tsuyuguchi et al. (2004)
FET	53	100% (42/42)	100% (11/11)	Glioma	Popperl et al. (2004)
FET	127	70%	71%	Glioma	Maurer et al. (2020)
FLT[b]	19	100% (15/15)	100% (4/4)	Glioma	Spence et al. (2009)

[a]With histopathological verification in all tumour cases
[b]Dynamic scans with tracer kinetic analysis

overview). There are also reports that assessments of CBV by dynamic MRI (Kim et al. 2010) or measures derived from MRS (Smith et al. 2009) may provide similar information, but interpretation of amino acid PET is easier due to better separation of tumour from background (Cicone et al. 2015). Amino acid PET also provides very high sensitivity to detect recurrent or residual glioma (Galldiks et al. 2015). Patient survival with recurrent malignant glioma can also be predicted by FLT (Zhao et al. 2014).

39.6 Summary and Conclusion

PET can make major contributions to management of glioma patients (Table 39.4). Of the most frequently used tracer types, the amino acids (mainly MET, FET and FDOPA) are most versatile because they show better tumour-to-background contrast than FDG and uptake is increased even in most low-grade gliomas, whereas FLT uptake depends on BBB damage. Thus, amino acid PET is increasingly recognised in clinical guidelines as a sensitive and relatively specific marker for planning and monitoring of glioma therapy. It is also useful for distinction between gliomas and benign brain lesions. Oligodendrogliomas show higher amino acid uptake than astrocytomas of the same grade, which needs to be kept in mind when using amino acid PET for tumour grading. Multiple radiopharmaceuticals and dynamic contrast-enhanced MRI techniques are being used to assess changes in tumour vasculature, which are also related to tumour malignancy and progression. More research is needed to evaluate the potential of nucleoside, choline and hypoxia markers in clinical glioma management.

Table 39.4 Contribution of PET tracers to management of gliomas

Management issue	FDG	AA	FLT
Grading	x	(1)	x
Targeting biopsy	x	x	(2)
Determining extent and infiltration		x	
Detecting residual/recurrent tumour		x	
Monitoring therapy		x	(2)

AA amino acids (MET, FET, FDOPA)
(1) Low grading accuracy with static scanning
(2) Contrast enhancing tumours only; dynamic data analysis may be required

References

Albert NL, Weller M, Suchorska B, Galldiks N, Soffietti R, Kim MM, la Fougere C, Pope W, Law I, Arbizu J, Chamberlain MC, Vogelbaum M, Ellingson BM, Tonn JC (2016) Response assessment in Neuro-Oncology working group and European Association for Neuro-Oncology recommendations for the clinical use of PET imaging in gliomas. Neuro-Oncology 18(9):1199–1208

Bosnyak E, Kamson DO, Robinette NL, Barger GR, Mittal S, Juhasz C (2016) Tryptophan PET predicts spatial and temporal patterns of post-treatment glioblastoma progression detected by contrast-enhanced MRI. J Neuro-Oncol 126(2):317–325

Brandsma D, van den Bent MJ (2009) Pseudoprogression and pseudoresponse in the treatment of gliomas. Curr Opin Neurol 22(6):633–638

Ceccon G, Lazaridis L, Stoffels G, Rapp M, Weber M, Blau T, Lohmann P, Kebir S, Herrmann K, Fink GR, Langen K-J, Glas M, Galldiks N (2018) Use of FET PET in glioblastoma patients undergoing neurooncological treatment including tumour-treating fields: initial experience. Eur J Nucl Med Mol Imaging 45(9):1626–1635

Chao ST, Suh JH, Raja S, Lee SY, Barnett G (2001) The sensitivity and specificity of FDG PET in distinguishing recurrent brain tumor from radionecrosis in patients treated with stereotactic radiosurgery. Int J Cancer 96(3):191–197

Charnley N, West CM, Barnett CM, Brock C, Bydder GM, Glaser M, Newlands ES, Swindell R, Matthews J, Price P (2006) Early change in glucose metabolic rate measured using FDG-PET in patients with high-grade glioma predicts response to temozolomide but not temozolomide plus radiotherapy. Int J Radiat Oncol Biol Phys 66(2):331–338

Chen W, Cloughesy T, Kamdar N, Satyamurthy N, Bergsneider M, Liau L, Mischel P, Czernin J, Phelps ME, Silverman DH (2005) Imaging proliferation in brain tumors with 18F-FLT PET: comparison with 18F-FDG. J Nucl Med 46(6):945–952

Chen W, Delaloye S, Silverman DH, Geist C, Czernin J, Sayre J, Satyamurthy N, Pope W, Lai A, Phelps ME, Cloughesy T (2007) Predicting treatment response of malignant gliomas to bevacizumab and irinotecan by imaging proliferation with [18F] fluorothymidine positron emission tomography: a pilot study. J Clin Oncol 25(30):4714–4721

Chiaravalloti A, Esposito V, Ursini F, Di Giorgio E, Zinzi M, Calabria F, Cimini A, Schillaci O (2019) Overall survival and progression-free survival in patients with primary brain tumors after treatment: is the outcome of [^{18}F] FDOPA PET a prognostic factor in these patients? Ann Nucl Med 33(7):471–480

Cicone F, Filss CP, Minniti G, Rossi-Espagnet C, Papa A, Scaringi C, Galldiks N, Bozzao A, Shah NJ, Scopinaro F, Langen KJ (2015) Volumetric assessment of recurrent or progressive gliomas: comparison between F-DOPA PET and perfusion-weighted MRI. Eur J Nucl Med Mol Imaging 42(6):905–915

Cizek J, Herholz K, Vollmar S, Schrader R, Klein J, Heiss WD (2004) Fast and robust registration of PET and MR images of human brain. NeuroImage 22(1):434–442

Colavolpe C, Chinot O, Metellus P, Mancini J, Barrie M, Bequet-Boucard C, Tabouret E, Mundler O, Figarella-Branger D, Guedj E (2012a) FDG-PET predicts survival in recurrent high-grade gliomas treated with bevacizumab and irinotecan. Neuro-Oncology 14(5):649–657

Colavolpe C, Metellus P, Mancini J, Barrie M, Bequet-Boucard C, Figarella-Branger D, Mundler O, Chinot O, Guedj E (2012b) Independent prognostic value of pre-treatment 18-FDG-PET in high-grade gliomas. J Neuro-Oncol 107(3):527–535

Coope DJ, Cizek J, Eggers C, Vollmar S, Heiss W-D, Herholz K (2007) Evaluation of primary brain tumors using 11C-methionine PET with reference to a normal methionine uptake map. J Nucl Med 48:1971–1980

De Witte O, Lefranc F, Levivier M, Salmon I, Brotchi J, Goldman S (2001) FDG-PET as a prognostic factor in high-grade astrocytoma. JNeurooncol 49(2):157–163

DeLaPaz RL, Patronas NJ, Brooks RA, Smith BH, Kornblith PL, Milam H, Di Chiro G (1983) Positron emission tomographic study of suppression of gray-matter glucose utilization by brain tumors. AJNR Am J Neuroradiol 4(3):826–829

Derlon JM, Petit-Taboue MC, Chapon F, Beaudouin V, Noel MH, Creveuil C, Courtheoux P, Houtteville JP (1997) The in vivo metabolic pattern of low-grade brain gliomas: a positron emission tomographic study using 18F-fluorodeoxyglucose and 11C-L-methylmethionine. Neurosurgery 40(2):276–288

Derlon JM, Chapon F, Noel MH, Khouri S, Benali K, Petit-Taboue MC, Houtteville JP, Chajari MH, Bouvard G (2000) Non-invasive grading of oligodendrogliomas: correlation between in vivo metabolic pattern and histopathology. Eur J Nucl Med 27(7):778–787

Dierckx RA, Martin JJ, Dobbeleir A, Crols R, Neetens I, De Deyn PP (1994) Sensitivity and specificity of thallium-201 single-photon emission tomography in the functional detection and differential diagnosis of brain tumours. Eur J Nucl Med 21(7):621–633

Dimberg A (2014) The glioblastoma vasculature as a target for cancer therapy. Portland Press, London

Douw L, Klein M, Fagel SS, van den Heuvel J, Taphoorn MJ, Aaronson NK, Postma TJ, Vandertop WP, Mooij JJ, Boerman RH, Beute GN, Sluimer JD, Slotman BJ, Reijneveld JC, Heimans JJ (2009) Cognitive and radiological effects of radiotherapy in patients with low-grade glioma: long-term follow-up. Lancet Neurol 8(9):810–818

Dunet V, Pomoni A, Hottinger A, Nicod-Lalonde M, Prior JO (2015) Performance of 18F-FET versus 18F-FDG-PET for the diagnosis and grading of brain tumors: systematic review and meta-analysis. Neuro-Oncology 18(3):426–434

Dunkl V, Cleff C, Stoffels G, Judov N, Sarikaya-Seiwert S, Law I, Bogeskov L, Nysom K, Andersen SB, Steiger HJ, Fink GR, Reifenberger G, Shah NJ, Coenen HH, Langen KJ, Galldiks N (2015) The usefulness of dynamic O-(2-18F-fluoroethyl)-L-tyrosine PET in the clinical evaluation of brain tumors in children and adolescents. J Nucl Med 56(1):88–92

Eary JF, Mankoff DA, Spence AM, Berger MS, Olshen A, Link JM, O'Sullivan F, Krohn KA (1999) 2-[C-11]thymidine imaging of malignant brain tumors. Cancer Res 59(3):615–621

Filss CP, Cicone F, Shah NJ, Galldiks N, Langen K-J (2017) Amino acid PET and MR perfusion imaging in brain tumours. Clin Transl Imaging 3(5):209–223

Floeth FW, Pauleit D, Sabel M, Reifenberger G, Stoffels G, Stummer W, Rommel F, Hamacher K, Langen KJ (2006) 18F-FET PET differentiation of ring-enhancing brain lesions. J Nucl Med 47(5):776–782

Galldiks N, Kracht LW, Burghaus L, Thomas A, Jacobs AH, Heiss WD, Herholz K (2006) Use of 11C-methionine PET to monitor the effects of temozolomide chemotherapy in malignant gliomas. Eur J Nucl Med Mol Imaging 33(5):516–524

Galldiks N, Kracht LW, Berthold F, Miletic H, Klein JC, Herholz K, Jacobs AH, Heiss WD (2010a) [11C]-L-methionine positron emission tomography in the management of children and young adults with brain tumors. J Neuro-Oncol 96(2):231–239

Galldiks N, Ullrich R, Schroeter M, Fink G, Kracht L (2010b) Volumetry of [11C]-methionine PET uptake and MRI contrast enhancement in patients with recurrent glioblastoma multiforme. Eur J Nucl Med Mol Imaging 37(1):84–92

Galldiks N, Langen KJ, Holy R, Pinkawa M, Stoffels G, Nolte KW, Kaiser HJ, Filss CP, Fink GR, Coenen HH, Eble MJ, Piroth MD (2012) Assessment of treatment response in patients with glioblastoma using O-(2-18F-fluoroethyl)-L-tyrosine PET in comparison to MRI. J Nucl Med 53(7):1048–1057

Galldiks N, Stoffels G, Filss C, Rapp M, Blau T, Tscherpel C, Ceccon G, Dunkl V, Weinzierl M, Stoffel M, Sabel M, Fink GR, Shah NJ, Langen KJ (2015) The use of dynamic O-(2-18F-fluoroethyl)-l-tyrosine PET in the diagnosis of patients with progressive and recurrent glioma. Neuro-Oncology 17(9):1293–1300

Galldiks N, Law I, Pope WB, Arbizu J, Langen K-J (2017) The use of amino acid PET and conventional MRI for monitoring of brain tumor therapy. NeuroImage Clin 13:386–394

Goldman S, Levivier M, Pirotte B, Brucher JM, Wikler D, Damhaut P, Dethy S, Brotchi J, Hildebrand J (1997) Regional methionine and glucose uptake in high-grade gliomas: a comparative study on PET-guided stereotactic biopsy. J Nucl Med 38(9):1459–1462

Gomez-Rio M, Rodriguez-Fernandez A, Ramos-Font C, Lopez-Ramirez E, Llamas-Elvira JM (2008) Diagnostic accuracy of 201Thallium-SPECT and 18F-FDG-PET in the clinical assessment of glioma recurrence. Eur J Nucl Med Mol Imaging 35(5):966–975

Gomez-Rio M, Testart Dardel N, Santiago Chinchilla A, Rodriguez-Fernandez A, Olivares Granados G, Luque Caro R, Zurita Herrera M, Chamorro Santos CE, Lardelli-Claret P, Llamas-Elvira JM (2015) 18F-Fluorocholine PET/CT as a complementary tool in the follow-up of low-grade glioma: diagnostic accuracy and clinical utility. Eur J Nucl Med Mol Imaging 42(6):886–895

Habermeier A, Graf J, Sandhofer BF, Boissel JP, Roesch F, Closs EI (2015) System L amino acid transporter LAT1 accumulates O-(2-fluoroethyl)-L-tyrosine (FET). Amino Acids 47(2):335–344

Haroon HA, Buckley DL, Patankar TA, Dow GR, Rutherford SA, Baleriaux D, Jackson A (2004) A comparison of Ktrans measurements obtained with conventional and first pass pharmacokinetic models in human gliomas. J Magn Reson Imaging 19(5):527–536

Harris RJ, Cloughesy TF, Pope WB, Nghiemphu PL, Lai A, Zaw T, Czernin J, Phelps ME, Chen W, Ellingson BM (2012) 18F-FDOPA and 18F-FLT positron emission tomography parametric response maps predict response in recurrent malignant gliomas treated with bevacizumab. Neuro-Oncology 14(8):1079–1089

Heiss WD, Wienhard K, Wagner R, Lanfermann H, Thiel A, Herholz K, Pietrzyk U (1996) F-Dopa as an amino acid tracer to detect brain tumors. J Nucl Med 37:1180–1182

Hendrikse NH, de Vries EG, Eriks-Fluks L, van der Graaf WT, Hospers GA, Willemsen AT, Vaalburg W, Franssen EJ (1999) A new in vivo method to study P-glycoprotein transport in tumors and the blood-brain barrier. Cancer Res 59(10):2411–2416

Herholz K (2017) Brain tumors: an update on clinical PET research in gliomas. Semin Nucl Med 47(1):5–17

Herholz K, Reulen HJ, von Stockhausen HM, Thiel A, Ilmberger J, Kessler J, Eisner W, Yousry TA, Heiss WD (1997) Preoperative activation and intraoperative stimulation of language-related areas in glioma patients. Neurosurgery 41:1253–1262

Herholz K, Holzer T, Bauer B, Schroder R, Voges J, Ernestus RI, Mendoza G, Weber-Luxenburger G, Lottgen J, Thiel A, Wienhard K, Heiss WD (1998) 11C-Methionine PET for differential diagnosis of low-grade gliomas. Neurology 50(5):1316–1322

Herholz K, Coope D, Jackson A (2007) Metabolic and molecular imaging in neuro-oncology. Lancet Neurol 6(8):711–724

Herholz K, Langen KJ, Schiepers C, Mountz JM (2012) Brain tumors. Semin Nucl Med 42(6):356–370

Hirata K, Terasaka S, Shiga T, Hattori N, Magota K, Kobayashi H, Yamaguchi S, Houkin K, Tanaka S, Kuge Y, Tamaki N (2012) (18)F-Fluoromisonidazole positron emission tomography may differentiate glioblastoma multiforme from less malignant gliomas. Eur J Nucl Med Mol Imaging 39(5):760–770

Hirata T, Kinoshita M, Tamari K, Seo Y, Suzuki O, Wakai N, Achiha T, Umehara T, Arita H, Kagawa N, Kanemura Y, Shimosegawa E, Hashimoto N, Hatazawa J, Kishima H, Teshima T,

Ogawa K (2019) 11C-methionine-18F-FDG dual-PET-tracer-based target delineation of malignant glioma: evaluation of its geometrical and clinical features for planning radiation therapy. J Neurosurg 131:676–686

Holzer T, Herholz K, Jeske J, Heiss WD (1993) FDG-PET as a prognostic indicator in radiochemotherapy of glioblastoma. J Comput Assist Tomogr 17(5):681–687

Hutterer M, Nowosielski M, Putzer D, Waitz D, Tinkhauser G, Kostron H, Muigg A, Virgolini IJ, Staffen W, Trinka E, Gotwald T, Jacobs AH, Stockhammer G (2011) O-(2-18F-fluoroethyl)-L-tyrosine PET predicts failure of antiangiogenic treatment in patients with recurrent high-grade glioma. J Nucl Med 52(6):856–864

Hygino da Cruz LC Jr, Rodriguez I, Domingues RC, Gasparetto EL, Sorensen AG (2011) Pseudoprogression and pseudoresponse: imaging challenges in the assessment of posttreatment glioma. AJNR Am J Neuroradiol 32(11):1978–1985

Janczar K, Su Z, Raccagni I, Anfosso A, Kelly C, Durrenberger PF, Gerhard A, Roncaroli F (2015) The 18-kDa mitochondrial translocator protein in gliomas: from the bench to bedside. Biochem Soc Trans 43(4):579–585

Jansen NL, Graute V, Armbruster L, Suchorska B, Lutz J, Eigenbrod S, Cumming P, Bartenstein P, Tonn JC, Kreth FW, la Fougere C (2012) MRI-suspected low-grade glioma: is there a need to perform dynamic FET PET? Eur J Nucl Med Mol Imaging 39(6):1021–1029

Jansen MH, van Zanten SEMV, Van Vuurden DG, Huisman MC, Vugts DJ, Hoekstra OS, van Dongen GA, Kaspers G-JL (2017) Molecular drug imaging: 89Zr-bevacizumab PET in children with diffuse intrinsic pontine glioma. J Nucl Med 58(5):711–716

Juhasz C, Muzik O, Chugani DC, Chugani HT, Sood S, Chakraborty PK, Barger GR, Mittal S (2011) Differential kinetics of alpha-[(11)C]methyl-L-tryptophan on PET in low-grade brain tumors. J Neuro-Oncol 102(3):409–415

Juhasz C, Dwivedi S, Kamson DO, Michelhaugh SK, Mittal S (2014) Comparison of amino acid positron emission tomographic radiotracers for molecular imaging of primary and metastatic brain tumors. Mol Imaging 13. https://doi.org/10.2310/7290.2014.00015

Kahn D, Follett KA, Bushnell DL, Nathan MA, Piper JG, Madsen M, Kirchner PT (1994) Diagnosis of recurrent brain tumor: value of 201Tl SPECT vs 18F- fluorodeoxyglucose PET. AJR 163(6):1459–1465

Kapoor GS, Gocke TA, Chawla S, Whitmore RG, Nabavizadeh A, Krejza J, Lopinto J, Plaum J, Maloney-Wilensky E, Poptani H, Melhem ER, Judy KD, O'Rourke DM (2009) Magnetic resonance perfusion-weighted imaging defines angiogenic subtypes of oligodendroglioma according to 1p19q and EGFR status. J Neuro-Oncol 92(3):373–386

Kaschten B, Stevenaert A, Sadzot B, Deprez M, Degueldre C, Del FG, Luxen A, Reznik M (1998) Preoperative evaluation of 54 gliomas by PET with fluorine-18-fluorodeoxyglucose and/or carbon-11-methionine. J Nucl Med 39(5):778–785

Kawai N, Maeda Y, Kudomi N, Miyake K, Okada M, Yamamoto Y, Nishiyama Y, Tamiya T (2011) Correlation of biological aggressiveness assessed by 11C-methionine PET and hypoxic burden assessed by 18F-fluoromisonidazole PET in newly diagnosed glioblastoma. Eur J Nucl Med Mol Imaging 38(3):441–450

Khangembam BC, Karunanithi S, Sharma P, Kc SS, Kumar R, Julka PK, Bal C (2014) Perfusion-metabolism coupling in recurrent gliomas: a prospective validation study with 13N-ammonia and 18F-fluorodeoxyglucose PET/CT. Neuroradiology 56(10):893–902

Kim S, Chung JK, Im SH, Jeong JM, Lee DS, Kim DG, Jung HW, Lee MC (2005) 11C-methionine PET as a prognostic marker in patients with glioma: comparison with 18F-FDG PET. Eur J Nucl Med Mol Imaging 32(1):52–59

Kim YH, Oh SW, Lim YJ, Park CK, Lee SH, Kang KW, Jung HW, Chang KH (2010) Differentiating radiation necrosis from tumor recurrence in high-grade gliomas: assessing the efficacy of 18F-FDG PET, 11C-methionine PET and perfusion MRI. Clin Neurol Neurosurg 112(9):758–765

Kiviniemi A, Gardberg M, Frantzen J, Pesola M, Vuorinen V, Parkkola R, Tolvanen T, Suilamo S, Johansson J, Luoto P, Kemppainen J, Roivainen A, Minn H (2015) Somatostatin receptor subtype 2 in high-grade gliomas: PET/CT with (68)Ga-DOTA-peptides, correlation to prognostic markers, and implications for targeted radiotherapy. EJNMMI Res 5:25

Koch CJ, Scheuermann JS, Divgi C, Judy KD, Kachur AV, Freifelder R, Reddin JS, Karp J, Stubbs JB, Hahn SM, Driesbaugh J, Smith D, Prendergast S, Evans SM (2010) Biodistribution and dosimetry of (18)F-EF5 in cancer patients with preliminary comparison of (18)F-EF5 uptake versus EF5 binding in human glioblastoma. Eur J Nucl Med Mol Imaging 37(11):2048–2059

Kracht LW, Miletic H, Busch S, Jacobs AH, Voges J, Hoevels M, Klein JC, Herholz K, Heiss WD (2004) Delineation of brain tumor extent with [11C]L-methionine positron emission tomography: local comparison with stereotactic histopathology. Clin Cancer Res 10(21):7163–7170

Krohn KA, Mankoff DA, Muzi M, Link JM, Spence AM (2005) True tracers: comparing FDG with glucose and FLT with thymidine. Nucl Med Biol 32(7):663–671

Kumar AJ, Leeds NE, Kumar VA, Fuller GN, Lang FF, Milas Z, Weinberg JS, Ater JL, Sawaya R (2010) Magnetic resonance imaging features of pilocytic astrocytoma of the brain mimicking high-grade gliomas. J Comput Assist Tomogr 34(4):601–611

Kunz M, Thon N, Eigenbrod S, Hartmann C, Egensperger R, Herms J, Geisler J, la Fougere C, Lutz J, Linn J, Kreth S, von Deimling A, Tonn JC, Kretzschmar HA, Popperl G, Kreth FW (2011) Hot spots in dynamic (18)FET-PET delineate malignant tumor parts within suspected WHO grade II gliomas. Neuro-Oncology 13(3):307–316

Lam WW, Ng DC, Wong WY, Ong SC, Yu SW, See SJ (2011) Promising role of [18F] fluorocholine PET/CT vs [18F] fluorodeoxyglucose PET/CT in primary brain tumors-early experience. Clin Neurol Neurosurg 113(2):156–161

Langen KJ, Herzog H, Kuwert T, Roosen N, Rota E, Kiwit JC, Bock WJ, Feinendegen LE (1988) Tomographic studies of rCBF with [99mTc]-HM-PAO SPECT in patients with brain tumors: comparison with C15O2 continuous inhalation technique and PET. J Cereb Blood Flow Metab 8(6):S90–S94

Langen KJ, Hamacher K, Weckesser M, Floeth F, Stoffels G, Bauer D, Coenen HH, Pauleit D (2006) O-(2-[18F]fluoroethyl)-L-tyrosine: uptake mechanisms and clinical applications. Nucl Med Biol 33(3):287–294

Law I, Albert NL, Arbizu J, Boellaard R, Drzezga A, Galldiks N, la Fougere C, Langen KJ, Lopci E, Lowe V, McConathy J, Quick HH, Sattler B, Schuster DM, Tonn JC, Weller M (2019) Joint EANM/EANO/RANO practice guidelines/SNMMI procedure standards for imaging of gliomas using PET with radiolabelled amino acids and [(18)F]FDG: version 1.0. Eur J Nucl Med Mol Imaging 46(3):540–557

Ledezma CJ, Chen W, Sai V, Freitas B, Cloughesy T, Czernin J, Pope W (2009) 18F-FDOPA PET/MRI fusion in patients with primary/recurrent gliomas: initial experience. Eur J Radiol 71(2):242–248

Leiva-Salinas C, Schiff D, Flors L, Patrie JT, Rehm PK (2017) FDG PET/MR imaging coregistration helps predict survival in patients with glioblastoma and radiologic progression after standard of care treatment. Radiology 283(2):508–514

Li DL, Xu YK, Wang QS, Wu HB, Li HS (2012) 11C-methionine and 18F-fluorodeoxyglucose positron emission tomography/CT in the evaluation of patients with suspected primary and residual/recurrent gliomas. Chin Med J 125(1):91–96

Louis DN, Perry A, Reifenberger G, Von Deimling A, Figarella-Branger D, Cavenee WK, Ohgaki H, Wiestler OD, Kleihues P, Ellison DW (2016) The 2016 World Health Organization classification of tumors of the central nervous system: a summary. Acta Neuropathol 131(6):803–820

Ludemann L, Grieger W, Wurm R, Wust P, Zimmer C (2006) Glioma assessment using quantitative blood volume maps generated by T1-weighted dynamic contrast-enhanced magnetic resonance imaging: a receiver operating characteristic study. Acta Radiol 47(3):303–310

Maia AC Jr, Malheiros SM, da Rocha AJ, da Silva CJ, Gabbai AA, Ferraz FA, Stavale JN (2005) MR cerebral blood volume maps correlated with vascular endothelial growth factor expression and tumor grade in nonenhancing gliomas. AJNR Am J Neuroradiol 26(4):777–783

Mapelli P, Incerti E, Bettinardi V, Conte GM, Fallanca F, Bailo M, Vuozzo M, Callea M, Gianolli L, Picchio M (2017) Hypoxia 18F-FAZA PET/CT imaging in lung cancer and high-grade glioma: open issues in clinical application. Clin Transl Imaging 4(5):389–397

Masui K, Cloughesy TF, Mischel PS (2012) Review: molecular pathology in adult high-grade gliomas: from molecular diagnostics to target therapies. Neuropathol Appl Neurobiol 38(3):271–291

Maurer GD, Brucker DP, Stoffels G, Filipski K, Filss CP, Mottaghy FM, Langen KJ (2020) ^{18}F-FET PET Imaging in differentiating glioma progression from treatment-related changes: a single-center experience. J Nucl Med. 61(4):505–511

Michaud L, Beattie BJ, Akhurst T, Dunphy M, Zanzonico P, Finn R, Mauguen A, Schöder H, Weber WA, Lassman AB, Blasberg R (2019) 18F-Fluciclovine (^{18}F-FACBC) PET imaging of recurrent brain tumors. Eur J Nucl Med Mol Imaging 47(6):1353–1367

Miyagawa T, Oku T, Uehara H, Desai R, Beattie B, Tjuvajev J, Blasberg R (1998) "Facilitated" amino acid transport is upregulated in brain tumors. J Cereb Blood Flow Metab 18(5):500–509

Mosskin M, Ericson K, Hindmarsh T, von Holst H, Collins VP, Bergstrom M, Eriksson L, Johnstrom P (1989) Positron emission tomography compared with magnetic resonance imaging and computed tomography in supratentorial gliomas using multiple stereotactic biopsies as reference. Acta Radiol 30(3):225–232

Moulin-Romsee G, D'Hondt E, de Groot T, Goffin J, Sciot R, Mortelmans L, Menten J, Bormans G, Van Laere K (2007) Non-invasive grading of brain tumours using dynamic amino acid PET imaging: does it work for 11C-methionine? Eur J Nucl Med Mol Imaging 34(12):2082–2087

Nioche C, Soret M, Gontier E, Lahutte M, Dutertre G, Dulou R, Capelle L, Guillevin R, Foehrenbach H, Buvat I (2013) Evaluation of quantitative criteria for glioma grading with static and dynamic 18F-FDopa PET/CT. Clin Nucl Med 38(2):81–87

Oehlke O, Grosu A-L (2017) PET/MRI and brain tumors: focus on radiation oncology treatment planning. Clin Transl Imaging 5(2):159–167

Ogawa T, Kanno I, Shishido F, Inugami A, Higano S, Fujita H, Murakami M, Uemura K, Yasui N, Mineura K, Kowada M (1991) Clinical value of PET with 18F-fluorodeoxyglucose and L-methyl- 11C-methionine for diagnosis of recurrent brain tumor and radiation injury. Acta Radiol 32(3):197–202

Ohtani T, Kurihara H, Ishiuchi S, Saito N, Oriuchi N, Inoue T, Sasaki T (2001) Brain tumour imaging with carbon-11 choline: comparison with FDG PET and gadolinium-enhanced MR imaging. Eur J Nucl Med 28(11):1664–1670

Padma MV, Said S, Jacobs M, Hwang DR, Dunigan K, Satter M, Christian B, Ruppert J, Bernstein T, Kraus G, Mantil JC (2003) Prediction of pathology and survival by FDG PET in gliomas. J Neuro-Oncol 64(3):227–237

Pardo FS, Aronen HJ, Fitzek M, Kennedy DN, Efird J, Rosen BR, Fischman AJ (2004) Correlation of FDG-PET interpretation with survival in a cohort of glioma patients. Anticancer Res 24(4):2359–2365

Parent EE, Benayoun M, Ibeanu I, Olson JJ, Hadjipanayis CG, Brat DJ, Adhikarla V, Nye J, Schuster DM, Goodman MM (2018) [18 F]-Fluciclovine PET discrimination between high- and low-grade gliomas. EJNMMI Res 8(1):67

Parent EE, Sharma A, Jain M (2019) Amino acid PET imaging of glioma. Curr Radiol Rep 7(5):14

Patronas NJ, Di Chiro G, Kufta C, Bairamian D, Kornblith PL, Simon R, Larson SM (1985) Prediction of survival in glioma patients by means of positron emission tomography. J Neurosurg 62(6):816–822

Pauleit D, Floeth F, Hamacher K, Riemenschneider MJ, Reifenberger G, Muller HW, Zilles K, Coenen HH, Langen KJ (2005) O-(2-[18F]fluoroethyl)-L-tyrosine PET combined with MRI improves the diagnostic assessment of cerebral gliomas. Brain 128(pt 3):678–687

Pauleit D, Stoffels G, Bachofner A, Floeth FW, Sabel M, Herzog H, Tellmann L, Jansen P, Reifenberger G, Hamacher K, Coenen HH, Langen KJ (2009) Comparison of (18)F-FET and (18)F-FDG PET in brain tumors. Nucl Med Biol 36(7):779–787

Piroth MD, Galldiks N, Pinkawa M, Holy R, Stoffels G, Ermert J, Mottaghy FM, Shah NJ, Langen KJ, Eble MJ (2016) Relapse patterns after radiochemotherapy of glioblastoma with FET PET-guided boost irradiation and simulation to optimize radiation target volume. Radiat Oncol 11:87

Pirotte B, Goldman S, Massager N, David P, Wikler D, Lipszyc M, Salmon I, Brotchi J, Levivier M (2004a) Combined use of 18F-fluorodeoxyglucose and 11C-methionine in 45 positron emission tomography-guided stereotactic brain biopsies. J Neurosurg 101(3):476–483

Pirotte B, Goldman S, Massager N, David P, Wikler D, Vandesteene A, Salmon I, Brotchi J, Levivier M (2004b) Comparison of 18F-FDG and 11C-methionine for PET-guided stereotactic brain biopsy of gliomas. J Nucl Med 45(8):1293–1298

Pirotte BJ, Levivier M, Goldman S, Massager N, Wikler D, Dewitte O, Bruneau M, Rorive S, David P, Brotchi J (2009) Positron emission tomography-guided volumetric resection of supratentorial high-grade gliomas: a survival analysis in 66 consecutive patients. Neurosurgery 64(3):471–481, discussion 481

Popperl G, Gotz C, Rachinger W, Gildehaus FJ, Tonn JC, Tatsch K (2004) Value of O-(2-[18F]fluoroethyl)- L-tyrosine PET for the diagnosis of recurrent glioma. Eur J Nucl Med Mol Imaging 31(11):1464–1470

Popperl G, Kreth FW, Mehrkens JH, Herms J, Seelos K, Koch W, Gildehaus FJ, Kretzschmar HA, Tonn JC, Tatsch K (2007) FET PET for the evaluation of untreated gliomas: correlation of FET uptake and uptake kinetics with tumour grading. Eur J Nucl Med Mol Imaging 34(12):1933–1942

Potzi C, Becherer A, Marosi C, Karanikas G, Szabo M, Dudczak R, Kletter K, Asenbaum S (2007) [11C] methionine and [18F] fluorodeoxyglucose PET in the follow-up of glioblastoma multiforme. J Neuro-Oncol 84(3):305–314

Poulsen SH, Urup T, Grunnet K, Christensen IJ, Larsen VA, Jensen ML, Af Rosenschold PM, Poulsen HS, Law I (2017) The prognostic value of FET PET at radiotherapy planning in newly diagnosed glioblastoma. Eur J Nucl Med Mol Imaging 44(3):373–381

Preibisch C, Shi K, Kluge A, Lukas M, Wiestler B, Göttler J, Gempt J, Ringel F, Al Jaberi M, Schlegel J, Meyer B, Zimmer C, Pyka T, Förster S (2017) Characterizing hypoxia in human glioma: a simultaneous multimodal MRI and PET study. NMR Biomed 30(11). https://doi.org/10.1002/nbm.3775

Price SJ, Fryer TD, Cleij MC, Dean AF, Joseph J, Salvador R, Wang DD, Hutchinson PJ, Clark JC, Burnet NG, Pickard JD, Aigbirhio FI, Gillard JH (2009) Imaging regional variation of cellular proliferation in gliomas using 3′-deoxy-3′-[18F]fluorothymidine positron-emission tomography: an image-guided biopsy study. Clin Radiol 64(1):52–63

Prieto E, Marti-Climent JM, Dominguez-Prado I, Garrastachu P, Diez-Valle R, Tejada S, Aristu JJ, Penuelas I, Arbizu J (2011) Voxel-based analysis of dual-time-point 18F-FDG PET images for brain tumor identification and delineation. J Nucl Med 52(6):865–872

Rachinger W, Goetz C, Popperl G, Gildehaus FJ, Kreth FW, Holtmannspotter M, Herms J, Koch W, Tatsch K, Tonn JC (2005) Positron emission tomography with O-(2-[18F]fluoroethyl)-l-tyrosine versus magnetic resonance imaging in the diagnosis of recurrent gliomas. Neurosurgery 57(3):505–511, discussion 505–511

Reardon DA, Galanis E, DeGroot JF, Cloughesy TF, Wefel JS, Lamborn KR, Lassman AB, Gilbert MR, Sampson JH, Wick W, Chamberlain MC, Macdonald DR, Mehta MP, Vogelbaum MA, Chang SM, Van den Bent MJ, Wen PY (2011) Clinical trial end points for high-grade glioma: the evolving landscape. Neuro-Oncology 13(3):353–361

Ribom D, Smits A (2005) Baseline 11C-methionine PET reflects the natural course of grade 2 oligodendrogliomas. Neurol Res 27(5):516–521

Ricci PE, Karis JP, Heiserman JE, Fram EK, Bice AN, Drayer BP (1998) Differentiating recurrent tumor from radiation necrosis: time for re-evaluation of positron emission tomography? [see comments]. AJNR Am J Neuroradiol 19(3):407–413

Sacconi B, Raad RA, Lee J, Fine H, Kondziolka D, Golfinos JG, Babb JS, Jain R (2016) Concurrent functional and metabolic assessment of brain tumors using hybrid PET/MR imaging. J Neuro-Oncol 127(2):287–293

Scherer HJ (1940) The forms of growth in gliomas and their practical significance. Brain 63(1):1–35

Schnell O, Krebs B, Carlsen J, Miederer I, Goetz C, Goldbrunner RH, Wester HJ, Haubner R, Popperl G, Holtmannspotter M, Kretzschmar HA, Kessler H, Tonn JC, Schwaiger M, Beer AJ

(2009) Imaging of integrin {alpha}v{beta}3 expression in patients with malignant glioma by [18F]galacto-RGD positron emission tomography. Neuro Oncol 11(6):861–870
Sharma R, Kallur KG, Ryu JS, Parameswaran RV, Lindman H, Avril N, Gleeson FV, Lee JD, Lee KH, O'Doherty MJ, Groves AM, Miller MP, Somer EJ, Coombes CR, Aboagye EO (2015) Multicenter reproducibility of 18F-fluciclatide PET imaging in subjects with solid tumors. J Nucl Med 56(12):1855–1861
Shi X, Liu Y, Zhang X, Yi C, Wang X, Chen Z, Zhang B (2013) The comparison of 13N-ammonia and 18F-FDG in the evaluation of untreated gliomas. Clin Nucl Med 38(7):522–526
Shibahara I, Kumabe T, Kanamori M, Saito R, Sonoda Y, Watanabe M, Iwata R, Higano S, Takanami K, Takai Y, Tominaga T (2010) Imaging of hypoxic lesions in patients with gliomas by using positron emission tomography with 1-(2-[18F] fluoro-1-[hydroxymethyl]ethoxy)methyl-2-nitroimidazole, a new 18F-labeled 2-nitroimidazole analog. J Neurosurg 113(2):358–368
Shields AF, Grierson JR, Dohmen BM, Machulla HJ, Stayanoff JC, Lawhorn-Crews JM, Obradovich JE, Muzik O, Mangner TJ (1998) Imaging proliferation in vivo with [F-18]FLT and positron emission tomography. Nat Med 4(11):1334–1336
Shinoura N, Nishijima M, Hara T, Haisa T, Yamamoto H, Fujii K, Mitsui I, Kosaka N, Kondo T, Hara T (1997) Brain tumors: detection with C-11 choline PET. Radiology 202(2):497–503
Shinozaki N, Uchino Y, Yoshikawa K, Matsutani T, Hasegawa A, Saeki N, Iwadate Y (2011) Discrimination between low-grade oligodendrogliomas and diffuse astrocytoma with the aid of 11C-methionine positron emission tomography. J Neurosurg 114(6):1640–1647
Smith EA, Carlos RC, Junck LR, Tsien CI, Elias A, Sundgren PC (2009) Developing a clinical decision model: MR spectroscopy to differentiate between recurrent tumor and radiation change in patients with new contrast-enhancing lesions. AJR Am J Roentgenol 192(2):W45–W52
Sonoda Y, Kumabe T, Takahashi T, Shirane R, Yoshimoto T (1998) Clinical usefulness of 11C-MET PET and 201T1 SPECT for differentiation of recurrent glioma from radiation necrosis. Neurol Med Chir (Tokyo) 38(6):342–347
Spence AM, Muzi M, Mankoff DA, O'Sullivan SF, Link JM, Lewellen TK, Lewellen B, Pham P, Minoshima S, Swanson K, Krohn KA (2004) 18F-FDG PET of gliomas at delayed intervals: improved distinction between tumor and normal gray matter. J Nucl Med 45(10):1653–1659
Spence AM, Muzi M, Swanson KR, O'Sullivan F, Rockhill JK, Rajendran JG, Adamsen TC, Link JM, Swanson PE, Yagle KJ, Rostomily RC, Silbergeld DL, Krohn KA (2008) Regional hypoxia in glioblastoma multiforme quantified with [18F]fluoromisonidazole positron emission tomography before radiotherapy: correlation with time to progression and survival. Clin Cancer Res 14(9):2623–2630
Spence AM, Muzi M, Link JM, O'Sullivan F, Eary JF, Hoffman JM, Shankar LK, Krohn KA (2009) NCI-sponsored trial for the evaluation of safety and preliminary efficacy of 3′-deoxy-3′-[18F]fluorothymidine (FLT) as a marker of proliferation in patients with recurrent gliomas: preliminary efficacy studies. Mol Imaging Biol 11(5):343–355
Su Z, Roncaroli F, Durrenberger PF, Coope DJ, Karabatsou K, Hinz R, Thompson G, Turkheimer FE, Janczar K, Du Plessis D, Brodbelt A, Jackson A, Gerhard A, Herholz K (2015) The 18-kDa mitochondrial translocator protein in human gliomas: an 11C-(R)PK11195 PET imaging and neuropathology study. J Nucl Med 56(4):512–517
Swanson KR, Chakraborty G, Wang CH, Rockne R, Harpold HL, Muzi M, Adamsen TC, Krohn KA, Spence AM (2009) Complementary but distinct roles for MRI and 18F-fluoromisonidazole PET in the assessment of human glioblastomas. J Nucl Med 50(1):36–44
Tedeschi G, Lundbom N, Raman R, Bonavita S, Duyn JH, Alger JR, Di Chiro G (1997) Increased choline signal coinciding with malignant degeneration of cerebral gliomas: a serial proton magnetic resonance spectroscopy imaging study. J Neurosurg 87(4):516–524
van Tellingen O, Yetkin-Arik B, de Gooijer MC, Wesseling P, Wurdinger T, de Vries HE (2015) Overcoming the blood-brain tumor barrier for effective glioblastoma treatment. Drug Resist Updat 19:1–12
Terakawa Y, Tsuyuguchi N, Iwai Y, Yamanaka K, Higashiyama S, Takami T, Ohata K (2008) Diagnostic accuracy of 11C-methionine PET for differentiation of recurrent brain tumors from radiation necrosis after radiotherapy. J Nucl Med 49(5):694–699

Thompson TP, Lunsford LD, Kondziolka D (1999) Distinguishing recurrent tumor and radiation necrosis with positron emission tomography versus stereotactic biopsy. StereotactFunctNeurosurg 73(1–4):9–14

Tralins KS, Douglas JG, Stelzer KJ, Mankoff DA, Silbergeld DL, Rostomily RC, Hummel S, Scharnhorst J, Krohn KA, Spence AM (2002) Volumetric analysis of 18F-FDG PET in glioblastoma multiforme: prognostic information and possible role in definition of target volumes in radiation dose escalation. J Nucl Med 43(12):1667–1673

Trigonis I, Jackson A (2010) Imaging pharmacodynamics in oncology: the potential significance of "flares". Ann Nucl Med 24(3):137–147

Tripathi M, Sharma R, D'Souza M, Jaimini A, Panwar P, Varshney R, Datta A, Kumar N, Garg G, Singh D, Grover RK, Mishra AK, Mondal A (2009) Comparative evaluation of F-18 FDOPA, F-18 FDG, and F-18 FLT-PET/CT for metabolic imaging of low grade gliomas. Clin Nucl Med 34(12):878–883

Tsuyuguchi N, Takami T, Sunada I, Iwai Y, Yamanaka K, Tanaka K, Nishikawa M, Ohata K, Torii K, Morino M, Nishio A, Hara M (2004) Methionine positron emission tomography for differentiation of recurrent brain tumor and radiation necrosis after stereotactic radiosurgery--in malignant glioma. Ann Nucl Med 18(4):291–296

Ullrich R, Backes H, Li H, Kracht L, Miletic H, Kesper K, Neumaier B, Heiss WD, Wienhard K, Jacobs AH (2008) Glioma proliferation as assessed by 3′-fluoro-3′-deoxy-L-thymidine positron emission tomography in patients with newly diagnosed high-grade glioma. Clin Cancer Res 14(7):2049–2055

Ullrich RT, Kracht L, Brunn A, Herholz K, Frommolt P, Miletic H, Deckert M, Heiss WD, Jacobs AH (2009) Methyl-L-11C-methionine PET as a diagnostic marker for malignant progression in patients with glioma. J Nucl Med 50(12):1962–1968

Unterrainer M, Fleischmann DF, Diekmann C, Vomacka L, Lindner S, Vettermann F, Brendel M, Wenter V, Ertl-Wagner B, Herms J, Wetzel C, Rupprecht R, Tonn JC, Belka C, Bartenstein P, Niyazi M, Albert NL (2019) Comparison of (18)F-GE-180 and dynamic (18)F-FET PET in high grade glioma: a double-tracer pilot study. Eur J Nucl Med Mol Imaging 46(3):580–590

Valk PE, Budinger TF, Levin VA, Silver P, Gutin PH, Doyle WK (1988) PET of malignant cerebral tumors after interstitial brachytherapy. Demonstration of metabolic activity and correlation with clinical outcome. J Neurosurg 69(6):830–838

Valk PE, Mathis CA, Prados MD, Gilbert JC, Budinger TF (1992) Hypoxia in human gliomas: demonstration by PET with fluorine-18-fluoromisonidazole. J Nucl Med 33(12):2133–2137

Van Laere K, Ceyssens S, Van Calenbergh F, de Groot T, Menten J, Flamen P, Bormans G, Mortelmans L (2005) Direct comparison of 18F-FDG and 11C-methionine PET in suspected recurrence of glioma: sensitivity, inter-observer variability and prognostic value. Eur J Nucl Med Mol Imaging 32(1):39–51

Verheijen RB, Yaqub M, Sawicki E, van Tellingen O, Lammertsma AA, Nuijen B, Schellens JHM, Beijnen JH, Huitema ADR, Hendrikse NH (2018) Molecular imaging of ABCB1 and ABCG2 inhibition at the human blood–brain barrier using Elacridar and 11C-Erlotinib PET. J Nucl Med 59(6):973–979

Verrey F, Closs EI, Wagner CA, Palacin M, Endou H, Kanai Y (2004) CATs and HATs: the SLC7 family of amino acid transporters. Pflugers Arch 447(5):532–542

Viel T, Talasila KM, Monfared P, Wang J, Jikeli JF, Waerzeggers Y, Neumaier B, Backes H, Brekka N, Thorsen F, Stieber D, Niclou SP, Winkeler A, Tavitian B, Hoehn M, Bjerkvig R, Miletic H, Jacobs AH (2012) Analysis of the growth dynamics of angiogenesis-dependent and -independent experimental glioblastomas by multimodal small-animal PET and MRI. J Nucl Med 53(7):1135–1145

Villani V, Carapella CM, Chiaravalloti A, Terrenato I, Piludu F, Vidiri A, Schillaci O, Floris R, Marzi S, Fabi A, Pace A (2015) The role of PET [18F]FDOPA in evaluating low-grade glioma. Anticancer Res 35(9):5117–5122

Waldman AD, Jackson A, Price SJ, Clark CA, Booth TC, Auer DP, Tofts PS, Collins DJ, Leach MO, Rees JH (2009) Quantitative imaging biomarkers in neuro-oncology. Nat Rev Clin Oncol 6(8):445–454

Walter F, Cloughesy T, Walter MA, Lai A, Nghiemphu P, Wagle N, Fueger B, Satyamurthy N, Phelps ME, Czernin J (2012) Impact of 3,4-dihydroxy-6-18F-fluoro-L-phenylalanine PET/CT on managing patients with brain tumors: the referring physician's perspective. J Nucl Med 53(3):393–398

Weber WA, Wester HJ, Grosu AL, Herz M, Dzewas B, Feldmann HJ, Molls M, Stocklin G, Schwaiger M (2000) O-(2-[18F]fluoroethyl)-L-tyrosine and L-[methyl-11C]methionine uptake in brain tumours: initial results of a comparative study. Eur J Nucl Med 27(5):542–549

Wyss M, Hofer S, Bruehlmeier M, Hefti M, Uhlmann C, Bartschi E, Buettner UW, Roelcke U (2009) Early metabolic responses in temozolomide treated low-grade glioma patients. J Neuro-Oncol 95(1):87–93

Zhao F, Cui Y, Li M, Fu Z, Chen Z, Kong L, Yang G, Yu J (2014) Prognostic value of 3′-deoxy-3′-18F-fluorothymidine ([(18)F] FLT PET) in patients with recurrent malignant gliomas. Nucl Med Biol 41(8):710–715

de Zwart PL, van Dijken BRJ, Holtman GA, Stormezand GN, Dierckx RA, van Laar PJ, van der Hoorn A (2019) Diagnostic accuracy of positron emission tomography tracers for the differentiation of tumor progression from treatment-related changes in high-grade glioma: a systematic review and meta-analysis. J Nucl Med 61(4):498–504

Single-Photon Emission Computed Tomography [Neuro-SPECT] Imaging of Brain Tumors

40

George A. Alexiou, Spyridon Tsiouris, and Andreas D. Fotopoulos

Contents

40.1 Introduction 1052
40.2 SPECT Radiotracers 1055
40.3 Clinical Applications 1056
40.3.1 Characterization of Intracranial Masses: Differentiation of Brain Tumors from Nonneoplastic Lesions 1056
40.3.2 Differentiate Glioma Recurrence from Treatment-Induced Necrosis (TIN) 1058
40.3.3 Assessment of Glioma Aggressiveness 1059
40.3.4 Assessment of Meningioma Aggressiveness 1060
40.3.5 Assessment of Patient Prognosis 1061
40.4 Conclusion 1061
References 1062

Abstract

Primary brain tumors have an annual incidence rate of 7–19.1 cases per 100,000 population. Metastatic tumors to the brain are more common with more than 100,000 patients per year in the United States. Gliomas are the most common primary brain tumor. CT and MRI are necessary to characterize the tumor type, size, and extension. Nevertheless, in patients with brain lesions, it is not uncommon for CT and MRI to provide nonspecific information, even after contrast or gadolinium infusion. Imaging of intracranial space-occupying lesions by nuclear medicine techniques such as SPECT and PET has also been introduced as a method providing information about the metabolic status of various brain tumors. Although PET constitutes the most sophisticated modality of nuclear medicine

G. A. Alexiou (✉)
Department of Neurosurgery, University of Ioannina Medical School, Ioannina, Greece

S. Tsiouris · A. D. Fotopoulos
Department of Nuclear Medicine, University of Ioannina, Medical School, Ioannina, Greece

R. A. J. O. Dierckx et al. (eds.), *PET and SPECT in Neurology*,
https://doi.org/10.1007/978-3-030-53168-3_40

imaging, SPECT has a lower cost, worldwide availability, and gained practical experience. The primary role of SPECT in brain tumor patients lies on the non-invasive assessment of tumor aggressiveness, differentiation of treatment-induced necrosis from tumor recurrence, assessment of response to treatment, and estimation of overall prognosis.

40.1 Introduction

The incidence rate of primary brain tumors is ranging between 7 and 19 cases per 100,000 person-years. In persons over 40 years, the annual average age-adjusted incidence for brain and other central nervous system tumors (CNS) was 40.82 per 100,000 population, and the median age at diagnosis was 59 years. Nearly 42% of all brain and CNS tumors occur in males and 58% in females. These malignancies are more common in the white race (Ostrom et al. 2017). Brain metastases from systemic cancer are up to ten times more common than primary brain malignancies (Figs. 40.1, 40.2, 40.3, and 40.4).

Primary brain tumors can be benign or malignant. According to the World Health Organization (WHO) grading system, they are classified into four grades (I–IV). The latest WHO 2016 CNS tumor classification uses molecular parameters in addition to histology to define several tumor entities (Louis et al. 2016). There are many types of primary intracranial tumors; meningiomas are the most common, accounting for 34% of all, followed by gliomas (32%). Glioblastoma (WHO Grade IV) is the most malignant primary brain tumor, accounting for 14.9% of all CNS tumors.

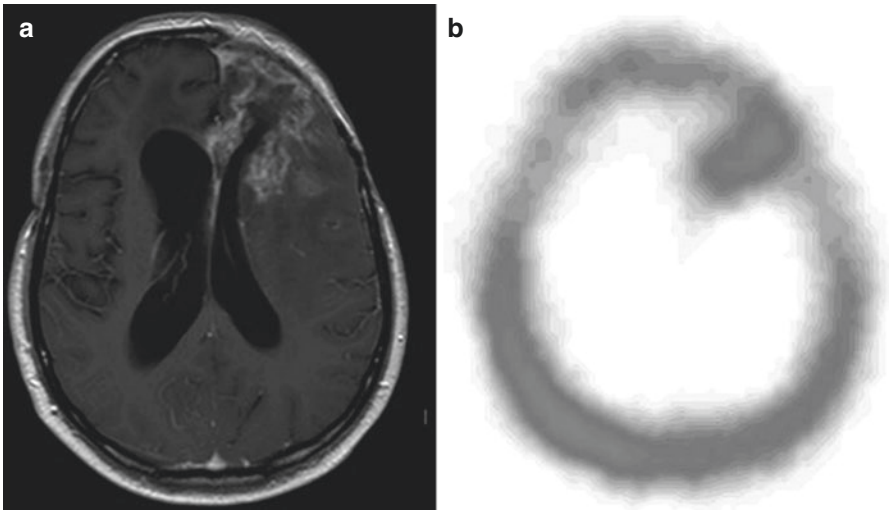

Fig. 40.1 (**a**) Gadolinium-enhanced T1-weighted MRI revealing recurrence of an anaplastic oligoastrocytoma. (**b**) ^{99m}Tc-tetrofosmin brain SPECT revealing increased tracer uptake in the corresponding area

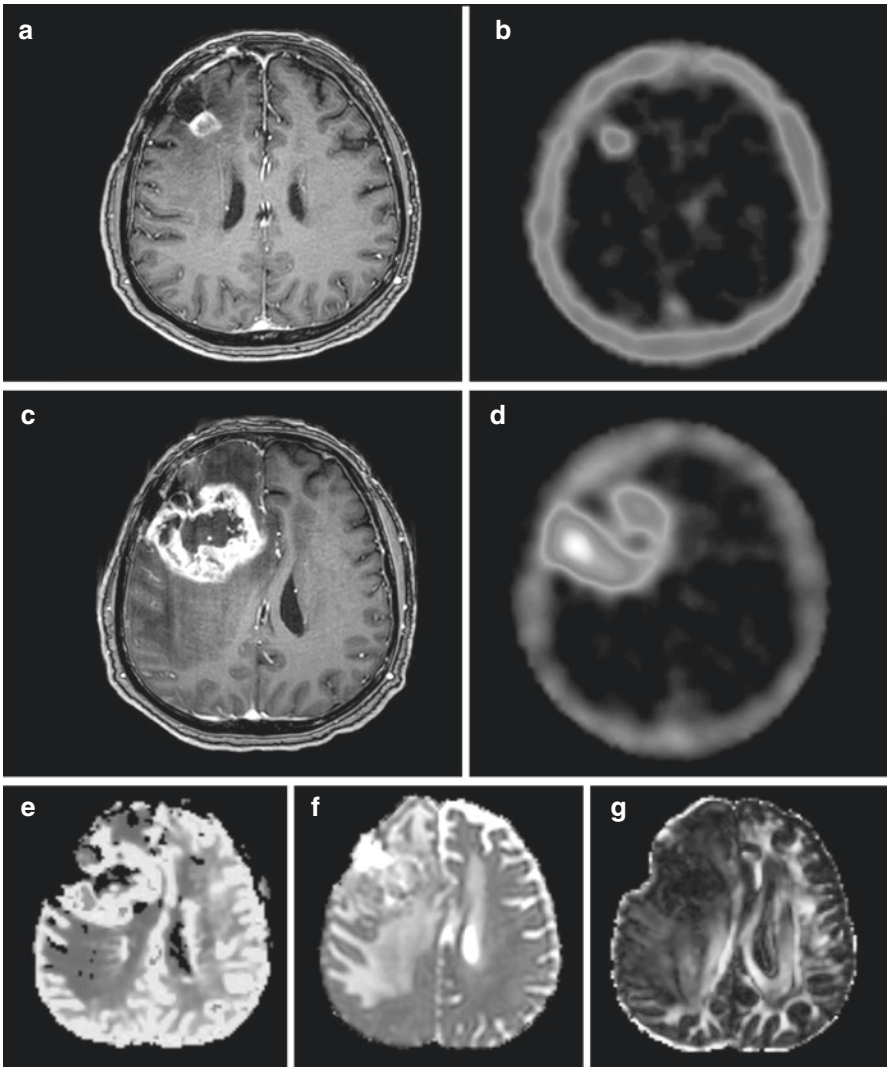

Fig. 40.2 A 66-year-old male with glioblastoma of the right frontal lobe diagnosed 21 months earlier and treated by surgery and radiochemotherapy (temozolomide). (**a**) Gadolinium-enhanced T1-weighted MRI revealed a postsurgical cavity with an adjacent enhancing dense area that raised the question of tumor recurrence versus radiation necrosis. (**b**) A few days later, ^{99m}Tc-tetrofosmin SPECT revealed intense tracer uptake (tumor-to-background ratio [TBR] = 11) in the corresponding area of gadolinium enhancement suggesting recurrence. (**c**) Eight months later—a new surgery in the meantime verified recurrent glioblastoma—Gd-T1w MRI revealed tumor progression. (**d**) The corresponding SPECT image at the time was also typical of tumor progression (TBR > 20) with a central photopenic necrotic area. (**e**) Further investigation by advanced MRI techniques showed an increased relative cerebral blood volume (rCBV) in the corresponding areas of profound radiotracer uptake, indicating intense angiogenesis. (**f**) The apparent diffusion coefficient (ADC) map showed highly irregular water diffusivity throughout the lesion that was surrounded by extensive edema. (**g**) Diffusion tensor imaging (DTI) with fractional anisotropy (FA) mapping revealed abrupt white matter fiber disruption by the lesion consistent with a high-grade recurrent tumor

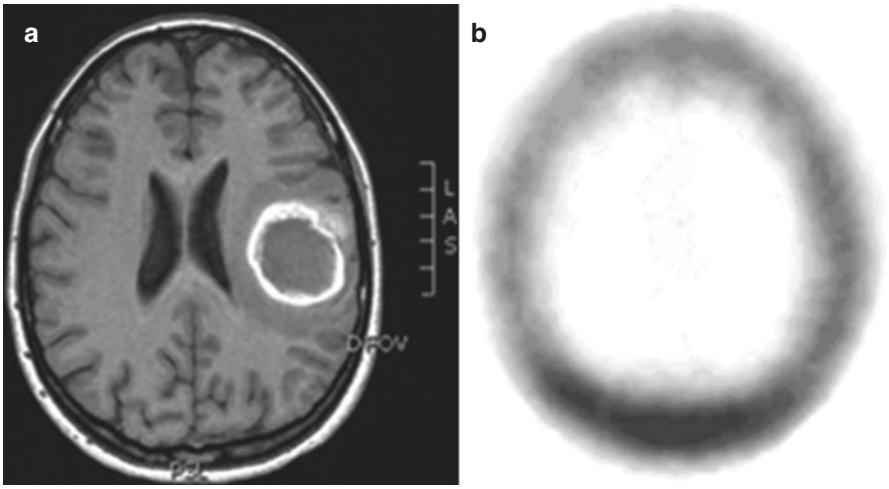

Fig. 40.3 (**a**) T1-weighted MRI in a patient with an intracerebral hemorrhage. The neoplastic hemorrhagic origin could not be ruled out. (**b**) Brain SPECT demonstrating no tracer uptake suggesting nonneoplastic hemorrhagic origin

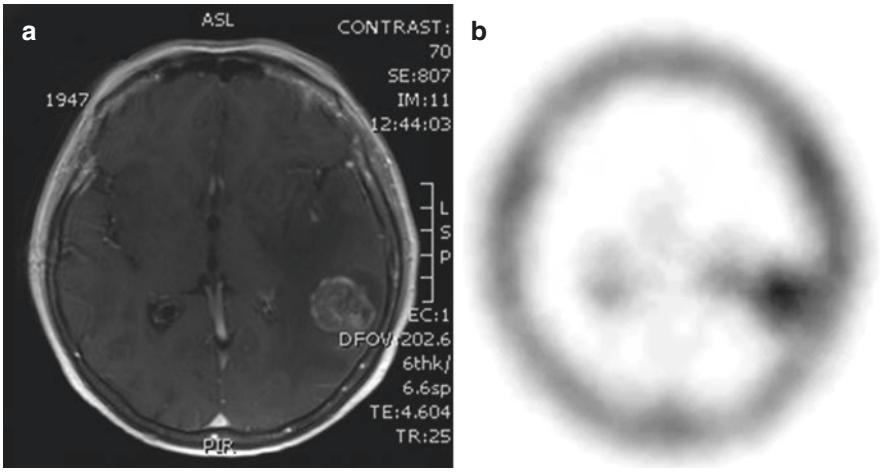

Fig. 40.4 (**a**) T1-weighted MRI after gadolinium infusion in a patient with a metastatic lesion. (**b**) ^{99m}Tc-tetrofosmin brain SPECT revealing increased tracer uptake in the corresponding area

Other types are pituitary adenomas (13.1%), neuroepithelial tumors (5.1%), lymphoma (2.4%), oligodendrogliomas (2%), ependymomas (1.8%), embryonal tumors (1%), and craniopharyngioma (0.7%).

Causes and risk factors can be environmental and genetic. The most common presenting symptoms of brain tumors are due to increased intracranial pressure (headache, nausea, vomiting), seizures, focal neurological deficits, and possibly cognitive deterioration (Perry and Schmidt 2006). Treatment depends on tumor

aggressiveness. Radical surgical excision is usually curative in benign tumor. Treatment options for high-grade lesions are surgery, radiation therapy, and chemotherapy. The majority of patients get a combination of treatments (Alexiou et al. 2009).

With regard to imaging, the most commonly used method for diagnosis and follow-up is magnetic resonance imaging (MRI). Nevertheless, in patients with brain lesions, it is not uncommon for MRI to provide nonspecific information, even after contrast administration. Advanced MRI techniques, including diffusion, perfusion (dynamic susceptibility contrast, dynamic contrast enhanced, and arterial spin labeling), and spectroscopy, offer important diagnostic advantages over conventional imaging in the assessment of patients with brain tumors. Imaging modalities used in nuclear medicine, namely, positron emission tomography (PET) and single-photon emission computed tomography (SPECT), have also been employed toward the evaluation of brain tumors. At present, PET constitutes the most sophisticated modality of nuclear medicine imaging for brain tumor evaluation, owing to higher resolution compared to SPECT. Nevertheless, SPECT has a lower cost, worldwide availability, and gained practical experience. The more sophisticated hybrid SPECT-CT scanners provide both functional and anatomic imaging to be acquired simultaneously (Hasegawa et al. 2002). Various SPECT radiotracers have been used to date and are presented in detail.

40.2 SPECT Radiotracers

Various SPECT radiotracers have been evaluated toward noninvasive assessment of brain lesions, with image acquisition usually performed 20 min after intravenous radiotracer administration. Among them, thallium-201 (^{201}Tl) was one of the first tracers that were widely employed (physical half-life 73 h, emitting γ-rays at 135 and 167 keV, and X-rays at ~70–80 keV, administered activity 148 MBq). The precise cellular uptake process is still questioned, but the sodium-potassium ATPase pump is probably involved, at least in part.

Technetium-99m-labeled compounds (physical half-life 6 h, emitting γ-rays at 140 keV) have also been studied and were proven advantageous over ^{201}Tl due to higher photon flux, better spatial resolution, and less radiation burden to the patient (Benard et al. 2002; Soler et al. 1998). Among them, ^{99m}Tc-hexamethypropyleneamine oxime (HMPAO) (administered activity 1110 MBq) and more extensively ^{99m}Tc-hexakis-2-methoxy isobutyl isonitrile (^{99m}Tc-sestamibi or ^{99m}Tc-MIBI) and ^{99m}Tc-tetrofosmin (^{99m}Tc-TF) (administered activity 700 MBq for both) have also been studied. ^{99m}Tc-MIBI diffuses passively into the cell through the intact cellular membrane, driven by the membrane negative electric potential, and an estimated 95% of the tracer is localized in the mitochondria. ^{99m}Tc-TF enters viable cells similar to sestamibi, and mostly localizes within the cytosol, with only a small fraction passing into the mitochondria. Although both ^{99m}Tc-TF and ^{99m}Tc-MIBI have been found in vitro to be substrates of P-gp, the fact that ^{99m}Tc-TF uptake in glioma cells is not particularly influenced by the

expression of their multidrug resistance proteins (MDR) protein genotype substantiates a plausible clinical superiority over ^{99m}Tc-MIBI, which is prone to extracellular excretion by P-gp. Pentavalent Tc-99m dimercaptosuccinic acid (^{99m}Tc-(V) DMSA) (administered activity 700 MBq) is another tumor-seeking SPECT tracer, being a possible $PO4^{3-}$ anion analogue. Its proliferative imaging potential in gliomas has been suggested in vitro and sporadically reported in vivo. Tsiouris et al. stated that mounting evidence indicates that ^{99m}Tc-(V)DMSA is a credible noninvasive proliferation depicter and its cellular accumulation linked closely to phosphate uptake and kinase pathway activation (Denoyer et al. 2004, 2005; Tsiouris et al. 2007; Amin et al. 2012). ^{99m}Tc-methionine and ^{99m}Tc-glucoheptonate have also been utilized, but are not easily available and not commonly used.

Radiolabeled amino acids have been evaluated and proved tracers for the delineation of tumors, particularly brain neoplasms. These tracers are not taken up by normal brain and provide a greater target-to-background contrast, thus allowing better characterization and differentiation of the tumor from the normal brain. L-3-[Iodine-123]-iodo-alpha-methyl-L-tyrosine (^{123}I-IMT) is well established for SPECT imaging of gliomas, and p-[iodine-123]-iodo-L-phenylalanine (^{123}I-IPA) has been also used. The latter may prove promising for therapeutic use in gliomas after labeling with iodine-131 (Hellwig et al. 2008).

40.3 Clinical Applications

The primary role of SPECT in brain tumor patients lies on the noninvasive assessment of tumor's aggressiveness, differentiation of treatment-induced necrosis from tumor recurrence, assessment of response to treatment, and estimation of overall prognosis.

40.3.1 Characterization of Intracranial Masses: Differentiation of Brain Tumors from Nonneoplastic Lesions

The noninvasive assessment of the nature of an intracranial lesion is of paramount importance for patient's management. Differentiation of high-grade from low-grade gliomas may not be always possible on conventional MRI, since non-enhancing high-grade gliomas exist. Furthermore, a ring-enhanced lesion may be a brain tumor, an abscess, tumefactive multiple sclerosis, or other nonneoplastic pathologies such as an intracerebral hemorrhage. The above problems are encountered in everyday practice.

^{99m}Tc-TF brain SPECT was evaluated in 106 patients with intracranial lesion suspicious of tumor on conventional radiological imaging. Ninety patients suffered from neoplastic lesions, and 16 harbored nonneoplastic pathologies (abscesses, nonmalignant hemorrhages, radiation necroses). A lesion-to-normal (L/N) tracer uptake ratio of 2.8 could differentiate high-grade gliomas from low-grade lesions

(Fotopoulos et al. 2011). Similar findings have been reported by other authors (Choi et al. 2000). Furthermore, ^{99m}Tc-TF differentiated effectively high- and low-grade gliomas from nonneoplastic lesions. Nonetheless, differentiation between primary gliomas (low or high grade) and metastases was not feasible on the basis of quantitative scintigraphic criteria.

Thallium-201, one of the most commonly used tracers for brain tumor imaging, showed promise for the differentiation of malignant from benign brain tumors. ^{201}Tl brain SPECT could increase confidence in the diagnosis of intracranial lesions with ring-like contrast enhancement when conventional MRI was not able to differentiate between benign and malignant disease. A brain tumor would show avid tracer uptake compared to the low uptake of a brain abscess (Kita et al. 2007). Another important issue that has been addressed is the optimal lesion size for an accurate diagnosis. In a study comparing ^{201}Tl uptake between primary CNS lymphoma and abscess, the authors reported that lesion size is a significant determinant of the accuracy of this tracer, which should be the initial diagnostic tool for lesions over 2 cm (Young et al. 2005). Furthermore, the location of a lesion is important, since infratentorial lesions may tend to display lower tracer uptake (Scott et al. 1994).

^{99m}Tc-(V)DMSA has been proven valuable for brain tumor characterization. Hirano et al. compared ^{99m}Tc-(V)DMSA and ^{201}Tl in 100 patients with various brain pathologies. They found that early uptake ratios of both radiopharmaceuticals were closely related to tumor vascularity, but could not differentiate benign from malignant disease. The delayed tracer uptake ratio, retention ratio, and retention index were higher in malignant tumors than benign ones on ^{99m}Tc(V)-DMSA; however, there was no statistically significant difference between benign and malignant tumors on ^{201}Tl. They concluded that ^{99m}Tc(V)DMSA is superior in imaging primary and metastatic brain tumors and differentiating their histological malignancy grade noninvasively (Hirano et al. 1997a).

^{99m}Tc-MIBI has been evaluated in various brain pathologies. If performed within 5 days of symptom onset, it has been found capable to differentiate neoplastic from nonneoplastic intracerebral hematomas (Minutoli et al. 2005). When compared to ^{201}Tl, it proved superior for differentiating intracranial lymphoma from nonmalignant lesions, exhibiting similar sensitivity but higher specificity (Naddaf et al. 1998).

Somatostatin receptors (SSRs) are expressed in 70–100% of meningiomas and can be used to image the radiolabeled tumors for maximizing resection, detection of residual, or early recurrent tumors or for therapeutic purposes (Dammers et al. 2009). Brain SPECT by the radiolabeled SSR-agonist peptide indium-111 (^{111}In)-pentetreotide (^{111}In-DTPA-octreotide) may provide important information for the noninvasive differentiation of meningiomas from other cranial dural-based pathology in conjugation with conventional MRI. This method provided high-negative predictive value (100%) for the diagnosis of meningiomas (Nathoo et al. 2007). Yttrium-90 (^{90}Y)-DOTA-Phe1-Tyr3-octreotide (^{90}Y-SMT 487, OctreoTher™) has shown potential for effectively treating patients with neuroendocrine tumors (Bushnell et al. 2004).

40.3.2 Differentiate Glioma Recurrence from Treatment-Induced Necrosis (TIN)

Malignant gliomas are the most common type of primary brain tumors and carry a dismal prognosis. Glioblastoma multiforme (GBM) usually has a rapid and fatal clinical course. The standard of care for newly diagnosed GBM includes maximal surgical resection when possible, followed by radiotherapy and concomitant and adjuvant temozolomide. Nevertheless, high-grade gliomas usually recur despite treatment, whereas radiotherapy may cause post-radiation damage (Alexiou et al. 2009). The incidence of treatment-related necrosis in GBM patients treated with concomitant temozolomide and radiotherapy reaches 30%. Furthermore, apart from radiation necrosis, new posttreatment entities such as pseudoprogression and pseudoresponse have been recognized (Zikou et al. 2018). Differentiation between TIN and recurrent glioma on the basis of CT and conventional MRI is not always possible. Nuclear medicine/molecular imaging has also been actively implicated in the detection of recurrent tumor by SPECT and PET. Among the SPECT tracers, the most extensively studied are ^{201}Tl and ^{99m}Tc-MIBI.

Recurrent disease exhibits increased ^{201}Tl uptake compared to necrosis. Early and delayed postinjection imaging has been used to calculate the radiotracer retention index (RI) (i.e., the ratio of delayed L/N uptake ratio to early L/N uptake ratio); RI has been suggested as a significant diagnostic marker by Matsunaga et al. (2013). Even in the follow-up of low-grade gliomas by ^{201}Tl, a tracer uptake index value of 1.25 as cutoff for detecting recurrent tumor activity resulted in 90% sensitivity and 80% specificity (Gómez-Río et al. 2004).

^{99m}Tc-MIBI has also been extensively evaluated, with good reported results and a significant diagnostic advantage over contrast-enhanced MRI (Soler et al. 1998). In a study that included 81 patients, the sensitivity for tumor recurrence was 90%, specificity 91.5%, and accuracy 90.5% (Le Jeune et al. 2006a). H-MRS proved equal to ^{99m}Tc-MIBI SPECT with 90% sensitivity, 100% specificity, 93% accuracy, 83% negative predictive value, and 100% positive predictive value (Palumbo et al. 2006).

Apart from ^{201}Tl and ^{99m}Tc-MIBI, ^{99m}Tc-TF has been also evaluated toward the detection of recurrent tumor, having the advantage of not being influenced by glioma MDR phenotype (P-gp expression). A cutoff L/N value of 4.8 was found as the most accurately discriminating recurrence from postirradiation damage (Alexiou et al. 2007). In a comparative study between relative cerebral blood volume (rCBV) by perfusion MRI and ^{99m}Tc-TF brain SPECT, they were found of similar diagnostic accuracy. Furthermore, a significant correlation between tracer uptake ratio and rCBV was verified (Alexiou et al. 2014). However, it must be kept in mind that ^{99m}Tc-TF SPECT exhibits suboptimal sensitivity in the detection of recurrent tumors located supratentorially in the posterior fossa (Barai et al. 2003).

^{99m}Tc-(V)DMSA also proved useful for the detection of glioma recurrence. In a comparative study between ^{99m}Tc-(V)DMSA SPECT and H-MRS, the first was more accurate for the detection of tumor residual tissues or recurrence in glioma

patients with previous radiotherapy. ^{99m}Tc-(V)DMSA allowed an early and noninvasive differentiation of residual tumor or recurrence from TIN (Amin et al. 2012).

Imaging protein synthesis with the use of radiolabeled amino acids is another approach that has been employed toward the noninvasive detection of tumor recurrence. Amino acid uptake in normal brain tissue is low; thus recurrent gliomas can be readily distinguished from their surrounding normal tissue. The majority of labeled amino acid tracers have been developed for PET imaging; however, SPECT tracers may be a cost-effective alternative. ^{99m}Tc-methionine can be a possible substitute to ^{11}C-MET PET and was compared to F-FDG PET/CT and contrast-enhanced MRI for the detection of recurrent glioma. The specificity of ^{99m}Tc-methionine SPECT/CT proved to be higher than MRI but not of F-FDG PET/CT (Arora et al. 2018).

^{99m}Tc DTPA-bismethionine (^{99m}Tc-MDM) has been also evaluated for the detection of recurrent/residual glioma. This tracer was found comparable to contrast-enhanced MRI and ^{18F}FLT-PET for the postsurgical follow-up period (Singh et al. 2015). ^{123}I-IMT has been validated in SPECT studies. Samnick et al. studied 78 glioma patients after primary therapy and possible tumor recurrence and found that ^{123}I-IMT had 100% sensitivity for the detection of high-grade glioma recurrence and 84% and 92% for Grade II and Grade III glioma recurrence, respectively (Samnick et al. 2002). In a comparative study between single-voxel H-MRS at 3.0 T and ^{123}I-IMT SPECT, a tracer uptake cutoff value of 1.62 proved superior to MRS (sensitivity 95%, specificity 100%, and accuracy 96% vs. 89%, 83%, and 88%, respectively) (Plotkin et al. 2004).

40.3.3 Assessment of Glioma Aggressiveness

Assessing the proliferative potential of tumor cells is of paramount importance for predicting their biological behavior, response to therapy, and prognosis. Noninvasive imaging modalities that could reliably assess the proliferative potential of intracranial space-occupying lesions in vivo would be of obvious significance (Alexiou et al. 2010a). Various methods have been proposed to estimate proliferation in tissue samples. The most extensively studied are flow cytometry, bromodeoxyuridine (BrdU) labeling index, MIB-1 antibody staining to the nuclear antigen Ki-67, staining to the proliferating cell nuclear antigen (PCNA), and argyrophilic staining to nucleolar organizing regions (AgNOR) (Prayson 2005). Among these, the MIB-1/Ki-67 assay can be easily applied, is considered as the most reliable method, and is performed routinely.

A significant correlation between L/N ^{201}Tl uptake and BrdU labeling index in glioma was first reported by Oriuchi et al. (1993). Subsequent studies using the PCNA as proliferation marker also reported a positive correlation. Both ^{99m}Tc-MIBI and ^{99m}Tc-TF depicted a significant positive correlation with both Ki-67 index and S-phase estimated by flow cytometry cell-cycle analysis. ^{99m}Tc-(V)DMSA enters cancer cells via the Na^+-Pi co-transporter like the phosphate ion, this uptake being

directly linked to the cellular levels of phosphorylated (activated) focal adhesion kinase protein, a keypoint of increased proliferation. In a study of glioma cell lines, 99mTc-(V)DMSA reflected Pi3-K and protein kinase C (PKC) activity and correlated with tumor aggressiveness (Le Jeune et al. 2006b). In the clinical setting of primary brain tumors, ^{99m}Tc-(V)DMSA SPECT could noninvasively differentiate histological malignancy and tumor grade (Hirano et al. 1997b). With regard to amino acid imaging, a study with ^{123}I-IMT in 27 glioma patients revealed a significant correlation between tracer uptake and Ki-67 (Kuwert et al. 1997).

40.3.4 Assessment of Meningioma Aggressiveness

Meningiomas are the most common benign intracranial tumors arising from the dural coverings of the brain at any site, most commonly the skull vault and the skull base. Although meningiomas typically exhibit benign histological features and total resection is associated with favorable prognosis, atypical (WHO Grade II) or anaplastic (WHO Grade III) tumors can be found in 6% of cases and are associated with increased risk of recurrence (Alexiou et al. 2010b).

^{201}Tl uptake in meningiomas was thought mainly to be related to lesional vascularity. Tracer RI may provide clues to differentiate meningothelial from transitional or fibroplastic tumors. Although these meningioma subtypes are benign variants, transitional and fibrous meningiomas have different chromosomal abnormalities (Maillo et al. 2001). The delayed ^{201}Tl uptake index of atypical meningiomas is significantly higher than that of the benign subtypes. A significant correlation between delayed ^{201}Tl uptake index, MIB-1/Ki-67 labeling index, and vascular endothelial growth factor (VEGF) expression has been described (Takeda et al. 2011).

^{99m}Tc-MIBI has not been extensively evaluated in meningiomas and few reports exist. A small-scale study found no correlation between Ki-67 index and tracer uptake; still ^{99m}Tc-MIBI could predict anticancer drug resistance related to the expression of MDR-1 mRNA and its gene product P-gp (Kunishio et al. 2003). Tumor ^{99m}Tc-TF uptake is not influenced by MDR phenotype expression and has been proven suitable for discriminating malignant from benign meningiomas, with an L/N tracer uptake value of 9.6 being the optimal threshold (Fotopoulos et al. 2008). Furthermore, L/N correlated significantly with both meningioma grade and Ki-67 expression. These initial results were supported by a subsequent study that aimed to correlate meningioma ^{99m}Tc-TF uptake with its proliferative profile, as assessed by cell-cycle analysis with flow cytometry. This study revealed a significant correlation of radiotracer uptake with both the S-phase fraction and the level of DNA aneuploidy (Alexiou et al. 2008). DNA ploidy and S-phase, as assessed by flow cytometry, are useful indicators of tumors with different biological behavior. Nuclear DNA content has been reported to predict risk of recurrence and clinical outcome for several brain tumors (Alexiou et al. 2008; Coons et al. 1994). Coons et al. found three groups of astrocytoma patients with significantly different survival, based on S-phase fraction ranges of <3.0%, 3.0–5.9%, and ≥6% (Coons et al. 1994).

40.3.5 Assessment of Patient Prognosis

Assessing prognosis and predicting patient outcome is of paramount importance in gliomas and more notably in GBM. Although the mean survival of GBM is 15 months, a subset of patients demonstrate long-term survival that may exceed 3 years (Liu et al. 2010). Thus, the identification of prognostic variables is important to identify patients that could benefit from more aggressive treatment schemes.

The prognostic value of tumoral ^{201}Tl uptake has been evaluated in glioma patients and was found associated with worse survival for lesions located supratentorially (Oriuchi et al. 1993). Recently, Vos et al. (2012) reported that ^{201}Tl uptake correlated with overall survival in glioma patients treated with temozolomide. Even in low-grade glioma, ^{201}Tl SPECT is useful for the prediction of early tumor progression, not only in resected low-grade astrocytomas (LGAs) but also in biopsy-proven lesions. Thus, patients with biopsy-proven LGAs should be considered as high-risk groups for early progression, if the tumor exhibits a high ^{201}Tl uptake (Park et al. 2012).

Postirradiation ^{99m}Tc-MIBI uptake has also been described to comprise prognostic implications in high-grade gliomas, and similar results have been reported for ^{123}I-IMT (Beauchesne et al. 2004; Weber et al. 2001). Pretreatment ^{99m}Tc-TF uptake was well correlated with overall survival in patients with glioblastoma. Patients with an L/N index exceeding 4.7 bore significantly worse survival than those with lower uptake values (Alexiou et al. 2010c). ^{99m}Tc-(V)DMSA also showed promise for the evaluation of glioblastoma patients' prognosis in a study of 40 patients. In the multivariate analysis, ^{99m}Tc-(V)DMSA SPECT was an independent prognostic factor for survival (Amin et al. 2015).

40.4 Conclusion

Although brain imaging by conventional MRI and CT is of paramount importance in identifying structural abnormalities secondary to the development of space-occupying lesions, especially when those pathologies disrupt the blood-brain barrier and give rise to contrast enhancement, edema, and mass effects, the true nature of each visible lesion may lie well beyond gross structural patterns, down in the cellular and molecular level. It is therefore of paramount importance to identify noninvasively the true nature of any visible lesion, and this is where functional metabolic imaging by SPECT, PET, and modern MRI techniques come into play and excel their role.

SPECT can provide accurate and important information for proper patient management, having the advantages of lower cost and excellent availability compared to PET. Various radiotracers are available in clinical practice that can accurately characterize brain tumor metabolism. The results of several studies thus far justify further research on the clinical utility of this imaging modality, entailing additional comparative studies with PET and functional MR techniques.

References

Alexiou GA, Fotopoulos AD, Papadopoulos A, Kyritsis AP, Polyzoidis KS, Tsiouris S (2007) Evaluation of brain tumor recurrence by ^{99m}Tc-tetrofosmin SPECT: a prospective pilot study. Ann Nucl Med 21:293–298

Alexiou GA, Tsiouris S, Goussia A, Papadopoulos A, Kyritsis AP, Polyzoidis KS, Fotopoulos AD (2008) Evaluation of glioma proliferation by ^{99m}Tc-Tetrofosmin. Neuro-Oncology 10:104–105

Alexiou GA, Tsiouris S, Kyritsis AP, Voulgaris S, Argyropoulou MI, Fotopoulos AD (2009) Glioma recurrence versus radiation necrosis: accuracy of current imaging modalities. J Neuro-Oncol 95:1–11

Alexiou GA, Tsiouris S, Kyritsis AP, Argyropoulou MI, Voulgaris S, Fotopoulos AD (2010a) Assessment of glioma proliferation using imaging modalities. J Clin Neurosci 17:1233–1238

Alexiou GA, Gogou P, Markoula S, Kyritsis AP (2010b) Management of meningiomas. Clin Neurol Neurosurg 112:177–182

Alexiou GA, Tsiouris S, Kyritsis AP, Fotakopoulos G, Goussia A, Voulgaris S, Fotopoulos AD (2010c) The value of ^{99m}Tc-tetrofosmin brain SPECT in predicting survival in patients with glioblastoma multiforme. J Nucl Med 51:1923–1926

Alexiou GA, Zikou A, Tsiouris S et al (2014) Comparison of diffusion tensor, dynamic susceptibility contrast MRI and (99m)Tc-Tetrofosmin brain SPECT for the detection of recurrent high-grade glioma. Magn Reson Imaging 32:854–859

Amin A, Moustafa H, Ahmed E, El-Toukhy M (2012) Glioma residual or recurrence versus radiation necrosis: accuracy of pentavalent technetium-99 m-dimercaptosuccinic acid [Tc-99 m (V) DMSA] brain SPECT compared to proton magnetic resonance spectroscopy (1H-MRS): initial results. J Neuro-Oncol 106:579–587

Amin A, Mustafa M, Abd El-Hadi E, Monier A, Badwey A, Saad E (2015) Pentavalent technetium-99m-dimercaptosuccinic acid [Tc-99m (V) DMSA] brain SPECT: does it have a place in predicting survival in patients with glioblastoma multiforme? J Neuro-Oncol 121:303–309

Arora G, Sharma P, Sharma A et al (2018) 99mTc-methionine hybrid SPECT/CT for detection of recurrent glioma: comparison with 18F-FDG PET/CT and contrast-enhanced MRI. Clin Nucl Med 43:e132–e138

Barai S, Bandopadhayaya GP, Julka PK, Haloi AK, Seith A, Malhotra A (2003) Evaluation of single photon emission computerised tomography (SPECT) using Tc99m-tetrofosmin as a diagnostic modality for recurrent posterior fossa tumours. J Postgrad Med 49:316–320

Beauchesne P, Pedeux R, Boniol M, Soler C (2004) ^{99m}Tc-sestamibi brain SPECT after chemoradiotherapy is prognostic of survival in patients with high-grade glioma. J Nucl Med 3:409–413

Benard F, Romsa J, Hustinx R (2002) Imaging gliomas with positron emission tomography and single-photon emission computed tomography. Semin Nucl Med 33:148–162

Bushnell D, Menda Y, O'Dorisio T, Madsen M, Miller S, Carlisle T, Squires S, Kahn D, Walkner W, Connolly M, O'Dorisio S, Karwal M, Ponto J, Bouterfa H (2004) Effects of intravenous amino acid administration with Y-90 DOTA-Phe1-Tyr3-Octreotide [SMT487(OctreoTher)] treatment. Cancer Biother Radiopharm 19:35–41

Choi JY, Kim SE, Shin HJ, Kim BT, Kim JH (2000) Brain tumor imaging with 99mTc-tetrofosmin: comparison with 201Tl, 99mTc-MIBI, and 18F-fluorodeoxyglucose. J Neuro-Oncol 46:63–70

Coons SW, Johnson PC, Pearl DK (1994) Prognostic significance of flow cytometry deoxyribonucleic acid analysis of human astrocytomas. Neurosurgery 35:119–125

Dammers R, Hsu SP, Krisht AF (2009) Radioguided improved resection of a cranial base meningioma. Neurosurgery 64:84–85

Denoyer D, Perek N, Le Jeune N, Frere D, Dubois F (2004) Evidence that 99mTc-(V)- DMSA uptake is mediated by NaPi cotransporter type III in tumour cell lines. Eur J Nucl Med Mol Imaging 31:77–84

Denoyer D, Perek N, Le Jeune N, Cornillon J, Dubois F (2005) Correlation between 99mTc-(V)-DMSA uptake and constitutive level of phosphorylated focal adhesion kinase in an in vitro model of cancer cell lines. Eur J Nucl Med Mol Imaging 32:820–827

Fotopoulos AD, Alexiou GA, Goussia A, Papadopoulos A, Kyritsis AP, Polyzoidis KS, Voulgaris S, Tsiouris S (2008) ^{99m}Tc-Tetrofosmin brain SPECT in the assessment of meningiomas-correlation with histological grade and proliferation index. J Neuro-Oncol 89:225–230

Fotopoulos AD, Kyritsis AP, Tsiouris S, Al-Boucharali J, Papadopoulos A, Voulgaris S, Alexiou GA (2011) Characterization of intracranial space-occupying lesions by ^{99m}Tc-Tetrofosmin SPECT. J Neuro-Oncol 101:83–89

Gómez-Río M, Martínez Del Valle Torres D, Rodríguez-Fernández A, Llamas-Elvira JM, Lozano SO, Font CR, López Ramírez E, Katati M (2004) (201)Tl-SPECT in low-grade gliomas: diagnostic accuracy in differential diagnosis between tumour recurrence and radionecrosis. Eur J Nucl Med Mol Imaging 31:1237–1243

Hasegawa BH et al (2002) Dual-modality imaging of cancer with SPECT/CT. Technol Cancer Res Treat 1:449–458

Hellwig D, Romeike BF, Ketter R, Moringlane JR, Kirsch CM, Samnick S (2008) Intra-individual comparison of p-[123I]-iodo-L-phenylalanine and L-3-[123I]-iodo-alpha-methyl-tyrosine for SPECT imaging of gliomas. Eur J Nucl Med Mol Imaging 35:24–31

Hirano T, Otake H, Kazama K, Wakabayashi K, Zama A, Shibasaki T, Tamura M, Endo K (1997a) Technetium-99 m(V)-DMSA and thallium-201 in brain tumor imaging: correlation with histology and malignant grade. J Nucl Med 38:1741–1749

Hirano T, Otake H, Shibasaki T, Tamura M, Endo K (1997b) Differentiating histologic malignancy of primary brain tumors: pentavalent technetium-99 m-DMSA. J Nucl Med 38:20–26

Kita T, Hayashi K, Yamamoto M, Kawauchi T, Sakata I, Iwasaki Y, Kosuda S (2007) Does supplementation of contrast MR imaging with thallium-201 brain SPECT improve differentiation between benign and malignant ring-like contrast-enhanced cerebral lesions? Ann Nucl Med 21:251–256

Kunishio K, Morisaki K, Matsumoto Y, Nagao S, Nishiyama Y (2003) Technetium-99m sestamibi single photon emission computed tomography findings correlated with P-glycoprotein expression, encoded by the multidrug resistance gene-1 messenger ribonucleic acid, in intracranial meningiomas. Neurol Med Chir (Tokyo) 43:573–580

Kuwert T, Probst-Cousin S, Woesler B et al (1997) Iodine-123-alpha-methyl tyrosine in gliomas: correlation with cellular density and proliferative activity. J Nucl Med 38:1551–1555

Le Jeune FP, Dubois F, Blond S, Steinling M (2006a) Sestamibi technetium-99 m brain single-photon emission computed tomography to identify recurrent glioma in adults: 201 studies. J Neuro-Oncol 77:177–183

Le Jeune N, Perek N, Dubois F (2006b) Influence of Pi3-K and PKC activity on 99mTc-(V)-DMSA uptake: correlation with tumour aggressiveness in an in vitro malignant glioblastoma cell line model. Eur J Nucl Med Mol Imaging 33:1206–1213

Liu Y, Shete S, Etzel CJ et al (2010) Polymorphisms of LIG4, BTBD2, HMGA2, and RTEL1 genes involved in the double-strand break repair pathway predict glioblastoma survival. J Clin Oncol 28:2467–2474

Louis DN, Perry A, Reifenberger G et al (2016) The 2016 World Health Organization classification of tumors of the central nervous system: a summary. Acta Neuropathol 131:803–820

Maillo A, Diaz P, Sayagues JM, Blanco A, Tabernero MD, Ciudad J, Lopez A, Goncalves JM, Orfao A (2001) Gains of chromosome 22 by fluorescence in situ hybridization in the context of an hyperdiploid karyotype are associated with aggressive clinical features in meningioma patients. Cancer 92:377–385

Matsunaga S, Shuto T, Takase H, Ohtake M, Tomura N, Tanaka T, Sonoda M (2013) Semiquantitative analysis using thallium-201 SPECT for differential diagnosis between tumor recurrence and radiation necrosis after gamma knife surgery for malignant brain tumors. Int J Radiat Oncol Biol Phys 85(1):47–52

Minutoli F, Angileri FF, Conti A, Herberg A, Aricò D, Baldari S, Cardali S, de Divitiis O, Germanò A, Baldari S (2005) Timing of examination affects reliability of 99mTc-methoxyisobutylisonitrile SPECT in distinguishing neoplastic from nonneoplastic brain hematomas. J Nucl Med 46:574–579

Naddaf SY, Akisik MF, Aziz M, Omar WS, Hirschfeld A, Masdeu J, Donnenfeld H, Abdel-Dayem HM (1998) Comparison between 201Tl-chloride and 99Tc(m)-sestamibi SPET brain imaging for differentiating intracranial lymphoma from non-malignant lesions in AIDS patients. Nucl Med Commun 19:47–53

Nathoo N, Ugokwe K, Chang AS, Li L, Ross J, Suh JH, Vogelbaum MA, Barnett GH (2007) The role of 111indium-octreotide brain scintigraphy in the diagnosis of cranial, dural-based meningiomas. J Neuro-Oncol 81:167–174

Oriuchi N, Tamura M, Shibazaki T et al (1993) Clinical evaluation of thallium-201 SPECT in supratentorial gliomas: relationship to histologic grade, prognosis and proliferative activities. J Nucl Med 34:2085–2089

Ostrom QT, Gittleman H, Liao P et al (2017) CBTRUS statistical report: primary brain and other central nervous system tumors diagnosed in the United States in 2010-2014. Neuro-Oncology 6:v1–v88

Palumbo B, Lupattelli M, Pelliccioli GP, Chiarini P, Moschini TO, Palumbo I, Siepi D, Buoncristiani P, Nardi M, Giovenali P, Palumbo R (2006) Association of 99mTc-MIBI brain SPECT and proton magnetic resonance spectroscopy (1H-MRS) to assess glioma recurrence after radiotherapy. Q J Nucl Med Mol Imaging 50:88–93

Park KJ, Kang SH, Park DH, Cho TH, Choe JG, Chung YG (2012) Usefulness of thallium-201 SPECT for prediction of early progression in low-grade astrocytomas diagnosed by stereotactic biopsy. Clin Neurol Neurosurg 114:223–229

Perry A, Schmidt RE (2006) Cancer therapy-associated CNS neuropathology: an update and review of the literature. Acta Neuropathol 111:197–212

Plotkin M, Eisenacher J, Bruhn H, Wurm R, Michel R, Stockhammer F, Feussner A, Dudeck O, Wust P, Felix R, Amthauer H (2004) 123I-IMT SPECT and 1H MR-spectroscopy at 3.0 T in the differential diagnosis of recurrent or residual gliomas: a comparative study. J Neuro-Oncol 70:49–58

Prayson R (2005) The utility of MIB-1/Ki-67 immunostaining in the evaluation of central nervous system neoplasms. Adv Anat Pathol 12:144–148

Samnick S, Bader JB, Hellwig D, Moringlane JR, Alexander C, Romeike BF, Feiden W, Kirsch CM (2002) Clinical value of iodine-123-alpha-methyl-L-tyrosine single-photon emission tomography in the differential diagnosis of recurrent brain tumor in patients pretreated for glioma at follow-up. J Clin Oncol 20:396–404

Scott AM, Macapinlac H, Zhang JJ et al (1994) Clinical applications of fusion imaging in oncology. Nucl Med Biol 21:775–784

Singh B, Kumar N, Sharma S et al (2015) 99mTc-MDM brain SPECT for the detection of recurrent/remnant glioma-comparison with ceMRI and 18F-FLT PET imaging: initial results. Clin Nucl Med 40:e475–e479

Soler C, Beauchesne P, Maatougui K, Schmitt T, Barral FG, Michel D, Dubois F, Brunon J (1998) Technetium-99 m sestamibi brain single-photon emission tomography for detection of recurrent gliomas after radiation therapy. Eur J Nucl Med 25:1649–1657

Takeda T, Nakano T, Asano K, Shimamura N, Ohkuma H (2011) Usefulness of thallium-201 SPECT in the evaluation of tumor natures in intracranial meningiomas. Neuroradiology 53:867–873

Tsiouris S, Pirmettis I, Chatzipanagiotou T, Ptohis N, Papantoniou V (2007) Pentavalent technetium-99 m dimercaptosuccinic acid 99mTc-(V) DMSA brain scintitomography a plausible non-invasive depicter of glioblastoma proliferation and therapy response. J Neuro-Oncol 85:291–295

Vos MJ, Berkhof J, Hoekstra OS, Bosma I, Sizoo EM, Heimans JJ, Reijneveld JC, Sanchez E, Lagerwaard FJ, Buter J, Noske DP, Postma TJ (2012) MRI and thallium-201 SPECT in the prediction of survival in glioma. Neuroradiology 54:539–546

Weber WA, Dick S, Reidl G et al (2001) Correlation between postoperative 3-[(123)I]iodo-L-alpha-methyltyrosine uptake and survival in patients with gliomas. J Nucl Med 8:1144–1150

Young RJ, Ghesani MV, Kagetsu NJ, Derogatis AJ (2005) Lesion size determines accuracy of thallium-201 brain single-photon emission tomography in differentiating between intracranial malignancy and infection in AIDS patients. AJNR Am J Neuroradiol 26:1973–1979

Zikou A, Sioka C, Alexiou GA, Fotopoulos A, Voulgaris S, Argyropoulou MI (2018) Radiation necrosis, pseudoprogression, pseudoresponse, and tumor recurrence: imaging challenges for the evaluation of treated gliomas. contrast media. Mol Imaging 2018:6828396

41 The Value of Positron Emission Tomography for Differentiating Brain Tumor Progression and Treatment-Induced Changes

Bart R. J. van Dijken, Roelien H. Enting, Hanne-Rinck Jeltema, Miranda C. A. Kramer, Rudi A. J. O. Dierckx, and Anouk van der Hoorn

Contents

41.1 Introduction 1068
41.1.1 Primary Brain Tumors 1068
41.1.2 Brain Metastases 1070
41.2 Imaging: Role and Dilemma 1070
41.2.1 Role of Magnetic Resonance Imaging 1070
41.2.2 Role of Positron Emission Tomography 1071
41.2.3 Dilemma of Treatment-Induced Changes 1074
41.3 Opportunities of Neuroimaging in Differentiating Tumor Progression and Treatment-Induced Changes 1076
41.3.1 Advanced MRI 1076
41.3.2 PET 1076

B. R. J. van Dijken (✉) · A. van der Hoorn
Department of Radiology, Medical Imaging Center (MIC), University Medical Center Groningen, University of Groningen, RB, Groningen, The Netherlands
e-mail: b.r.j.van.dijken@umcg.nl

R. H. Enting
Department of Neurology, University Medical Center Groningen, University of Groningen, RB, Groningen, The Netherlands

H.-R. Jeltema
Department of Neurosurgery, University Medical Center Groningen, University of Groningen, RB, Groningen, The Netherlands

M. C. A. Kramer
Department of Radiotherapy, University Medical Center Groningen, University of Groningen, RB, Groningen, The Netherlands

R. A. J. O. Dierckx
Department of Nuclear Medicine and Molecular Imaging, Medical Imaging Center (MIC), University Medical Center Groningen, University of Groningen, RB, Groningen, The Netherlands

R. A. J. O. Dierckx et al. (eds.), *PET and SPECT in Neurology*,
https://doi.org/10.1007/978-3-030-53168-3_41

41.4 Limitations and Future Perspectives of MRI and PET..... 1077
41.5 Summary..... 1078
References..... 1078

Abstract

Accurate differentiation of tumor progression and treatment-induced changes is the key to treatment decision in brain tumors. Several new tracer options are promising, of which [^{11}C]-methyl-L-methionine (MET) and O-(2-[^{18}F]-fluoroethyl)-L-tyrosine (FET) positron emission tomography (PET) are the most used. This chapter provides a clinical overview of important issues of treatment evaluation in primary brain tumors and brain metastases. The role and dilemmas in neuroimaging, including magnetic resonance imaging (MRI) and PET, are discussed. An overview is given of the role of MRI and PET in brain tumor follow-up with special focus on available literature in the role of amino acid PET to differentiate between tumor progression and treatment-induced changes.

41.1 Introduction

Malignant brain tumors are relatively uncommon tumors in adults, making up less than 2% of all cancer cases (DeAngelis 2001; Miranda-Filho et al. 2017). The two major groups are a heterogeneous group of primary brain tumors and cerebral metastases from systemic cancer, with the latter being more common (DeAngelis 2001). Brain tumors are responsible for a significant loss of healthy life years and impaired quality of life. Treatment is often aggressive trying to improve this outcome. During and after treatment, patients are monitored with imaging to assess treatment response and to decide whether the current treatment should be continued or not.

41.1.1 Primary Brain Tumors

Primary intra-axial brain tumors are most commonly gliomas (in approximately 80% of the cases), with the majority being grade IV glioblastoma (Ostrom et al. 2019). Less frequent intra-axial primary brain tumors are lymphomas (6% of cases) and embryonal tumors (in about 3%) (Ostrom et al. 2019; Louis et al. 2016). In this chapter, we focus on gliomas.

To determine the tumor grade of gliomas, historically, the WHO grading system is used, representing a malignancy scale varying from I to IV. Grade I lesions are regarded as benign tumors due to their low proliferative potential and curative intent of surgical resection alone. Grade II tumors represent low-grade tumors, and grade III and IV tumors are high-grade tumors, often associated with rapid disease evolution and a dismal survival.

Recently, the WHO grading system for brain tumors has been revised. Genetic and molecular markers have now become integral to the grading (Louis et al. 2016). Survival has been shown to be greatly dependent upon these molecular markers (Rogers et al. 2018; Bell et al. 2018; Binabaj et al. 2018). Diffuse gliomas, being astrocytomas and oligodendrogliomas, are defined based on their molecular profile. Currently, the most important molecular markers are mutations in the isocitrate dehydrogenase (IDH) genes, most often IDH-1 and sometimes IDH-2. They are associated with a better prognosis in lower-grade gliomas or secondary glioblastomas (Rogers et al. 2018). Low-grade gliomas are diffusely infiltrating and slow-growing. Low-grade astrocytomas are currently defined as IDH-1- or IDH-2-mutated tumors without a 1p/19q co-deletion (Louis et al. 2016). Oligodendrogliomas are both IDH-mutant and 1p/19q-co-deleted (Louis et al. 2016).

High-grade gliomas usually lack the aforementioned IDH mutations. Another important prognostic marker for high-grade gliomas is O6-methylguanine methyltransferase (MGMT) gene methylation status. Patients with an MGMT-methylated tumor are more susceptible to alkalizing chemotherapy such as temozolomide and thus have a better survival (Bell et al. 2018; Binabaj et al. 2018).

Patients with IDH-mutant grade II tumors or co-deleted gliomas have a median survival of 10+ years, and patients with a non-co-deleted WHO grade III tumor have a median survival of 5 years (van den Bent et al. 2017), in contrast with patients with IDH wild-type grade IV tumors with a median survival of 1 year. Unfortunately, high-grade gliomas account for over 70% of newly diagnosed gliomas (Ostrom et al. 2019).

Peak incidence of low-grade gliomas occurs in patients aged between 35 and 45 years (Weller et al. 2017). It is assumed that all low-grade gliomas will transform into high-grade gliomas. Current clinical practice of low-grade gliomas recommends early surgical resection when safely possible. This is followed by both radiotherapy and chemotherapy or a wait-and-scan policy. The latter is usually chosen in completely resected young patients (Weller et al. 2017).

Patients with glioblastoma have a median age of onset of approximately 60 years. Prognosis of patients with high-grade gliomas has remained poor for the last decades. Glioblastomas, as all gliomas, are infiltrating in nature, often involving eloquent structures, and extend beyond visual borders on imaging, making complete resection without unacceptable damage impossible (Boonzaier et al. 2017; Yan et al. 2019). Nevertheless, surgery remains the cornerstone in glioblastoma treatment. Patients with high-grade gliomas benefit from a greater extent of resection in terms of survival (Sanai and Berger 2008; Yan et al. 2017). The standard adjuvant treatment in patients in good general and neurological condition, aged up to 70 years, is 60 Gy radiotherapy with concomitant temozolomide chemotherapy followed by a six-course regimen of maintenance temozolomide chemotherapy (Stupp et al. 2005). Recurrence, however, is inevitable due to the inability of radical resection and subsequent resistance to chemoradiation therapy. Currently the median survival after standard treatment of chemoradiation is 14.9 months, with the biggest gain for patients with a methylated MGMT tumor (Stupp et al. 2005). A lack of standard of care for patients with recurrent glioblastoma further contributes to the poor prognosis for these patients.

41.1.2 Brain Metastases

In adults, brain metastases are by far the most common cause of intracranial neoplasms. Brain metastases occur in approximately 20% of the patients with systemic cancer (Achrol et al. 2019). The incidence of brain metastases has increased over the years due to therapeutic advances for patients with metastatic cancer that are associated with prolonged survival.

Brain metastases originate most commonly, in order of cumulative incidence, from lung, breast, and skin (melanoma) cancers (Tabouret et al. 2012). Although the highest numbers of brain metastases arise from the lung, melanoma has the highest propensity to metastasize to the brain (Tabouret et al. 2012).

The distribution of brain metastases correlates with blood flow and tissue volume, with 80% detected in the cerebral hemispheres, 15% in the cerebellum, and 5% in the brain stem (Delattre et al. 1988). Often, brain metastases are asymptomatic and are seen on staging brain scans. Most patients (80%) present with multiple brain metastases, and only a minority of patients (10–20%) have a solitary metastasis (Tabouret et al. 2012).

Therapeutic approaches for brain metastases are resection, radiotherapy, and systemic treatment, including immunotherapy (Hardesty and Nakaji 2016; Soffietti et al. 2017; Chen et al. 2018). Radiotherapy options can be differentiated into whole-brain radiation therapy (WBRT), which is used less frequently in recent years, and stereotactic radiotherapy (SRT), the primary choice if possible.

41.2 Imaging: Role and Dilemma

Neuroimaging is essential in the follow-up and treatment evaluation in brain tumors. Regular follow-up through neuroimaging aids clinical decision-making (Dhermain et al. 2010). Treatment is continued in patients responsive to treatment. For patient unresponsive to treatment, the treatment should be stopped. However, (beneficial) treatment reaction may appear similar to recurrent disease on conventional imaging, greatly complicating treatment decisions.

41.2.1 Role of Magnetic Resonance Imaging

41.2.1.1 Conventional MRI

Magnetic resonance imaging (MRI) is the gold standard for treatment response imaging due to its high spatial resolution, allowing detailed visualization of lesions in relation to brain anatomy. Low-grade gliomas (>90%) usually demonstrate no or limited contrast enhancement on T1-weighted imaging after gadolinium administration and are best evaluated on fluid-attenuated inversion recovery (FLAIR) and T2-weighted MRI; on the contrary, high-grade gliomas usually have contrast enhancement and are surrounded by extensive vasogenic edema (Dhermain et al. 2010). Brain metastases usually present as contrast-enhancing lesion on T1-weighted

MRI with peritumoral edema visualized on FLAIR/T2-weighted MRI. Microlesions <5 mm can already be detected with the current 1.5 and 3.0 T MRI scanners.

41.2.1.2 Advanced MRI

The rationale behind advanced MRI sequences is a better visualization of biological processes (Dhermain et al. 2010; van Dijken et al. 2017). The increased cellularity of brain tumors causes impaired diffusivity of water molecules, which is detectable by diffusion-weighted imaging. Tissue perfusion is measurable with perfusion-weighted imaging through means of detectable cerebral blood flow and volume parameters (van Dijken et al. 2019). Neovascularization, which is a hallmark of neoplasms, generally causes a measurable increase in blood flow and volume on perfusion-weighted imaging. Finally, concentrations of specific metabolites can be calculated with MR spectroscopy. Detectable metabolites include N-acetylaspartate (NAA), a marker of neuronal viability and thus intact brain tissue, choline which marks increased cellular proliferation, and lactate which demonstrates anaerobic metabolism and cell death. Increases in choline and lactate with simultaneous decrease in NAA are suggestive of tumor.

41.2.2 Role of Positron Emission Tomography

Positron emission tomography (PET) has recently been recommended by the Response Assessment in Neuro-oncology (RANO) working group to be of added value in oncological neuroimaging, thereby complementing MRI (Albert et al. 2016; Langen et al. 2017; Galldiks et al. 2019; Law et al. 2019).

41.2.2.1 FDG PET

[^{18}F]-2-fluoro-2-deoxy-D-glucose (FDG) is glucose-based and to date remains the most widely employed tracer in oncology based on an increased glucose consumption of tumors. Despite the fact that FDG is the most available tracer worldwide, its use in oncological neuroimaging is limited due to the relatively high physiological glucose metabolism of normal brain tissue (Fig. 41.1).

41.2.2.2 Amino Acid PET

Cellular proliferation associated with malignant tumors activates increased protein synthesis. Amino acids function as essential compounds of proteins, and thus amino acid transport and protein synthesis are vastly increased in malignant proliferating cells and higher compared to normal healthy tissue. Radiolabeled amino acids and amino acid analogs have different metabolic fates depending on their chemical structures (van Waarde and Elsinga 2008). Amino acid tracers are predominantly based on L-type amino acid transporters (LAT), LAT-1 and LAT-2. The most frequently used radiolabeled amino acids are [^{11}C]-methyl-L-methionine (MET) (Figs. 41.2 and 41.3), O-(2-[^{18}F]-fluoroethyl)-L-tyrosine (FET), and 3,4-dihydroxy-6-[^{18}F]-fluoro-L-phenylalanine (FDOPA) (Fig. 41.4) (Glaudemans et al. 2013; de Zwart et al. 2019).

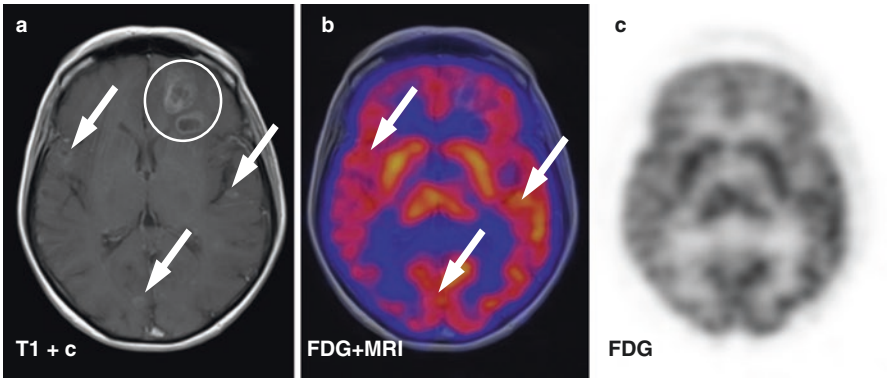

Fig. 41.1 Treatment follow-up with FDG PET in a patient with multiple brain metastases. A 62-year-old female patient with multiple brain metastases of a small cell lung cancer. Gadolinium-enhanced MRI (**a**) was performed after WBRT and demonstrated multiple contrast-enhancing lesions, with two larger lesions frontally on the left side (white circle) and several smaller lesions (white arrows). FDG PET (**b**, **c**) demonstrated high physiological uptake throughout the brain but failed to clearly localize most contrast-enhancing MRI lesions as demonstrated by the white arrows on co-registration of FDG PET images with MRI (**b**). This case demonstrates the lack of diagnostic sensitivity of FDG PET for treatment response evaluation in brain tumors

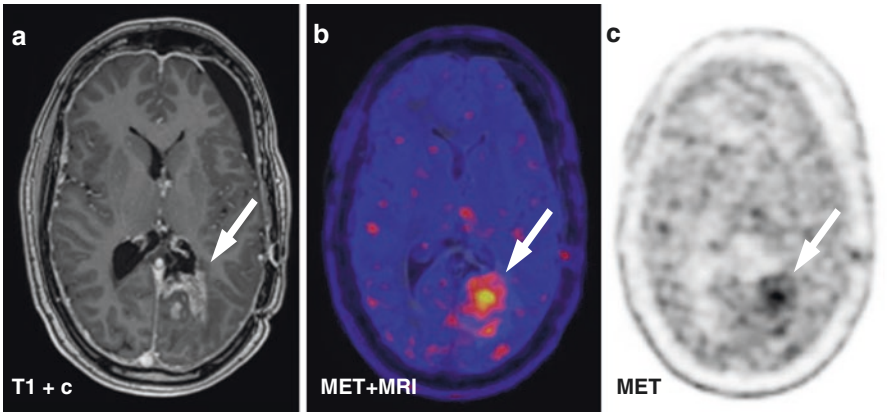

Fig. 41.2 Example of MET PET follow-up in a patient with an anaplastic astrocytoma. Case of a 49-year-old patient with an anaplastic astrocytoma (WHO grade III) after treatment with surgical resection followed by radiotherapy and temozolomide chemotherapy. One year after surgery, follow-up gadolinium-enhanced MRI (**a**) showed new contrast enhancement (white arrow). The differentiation between tumor progression and radionecrosis could not be made, and MET PET was performed (**b**, **c**). MET PET (**c**) demonstrated high tracer uptake (white arrow) suggestive of tumor progression. Co-registration of MET PET images with MRI (**b**) shows good agreement of the contrast-enhancing lesion and increased tracer uptake

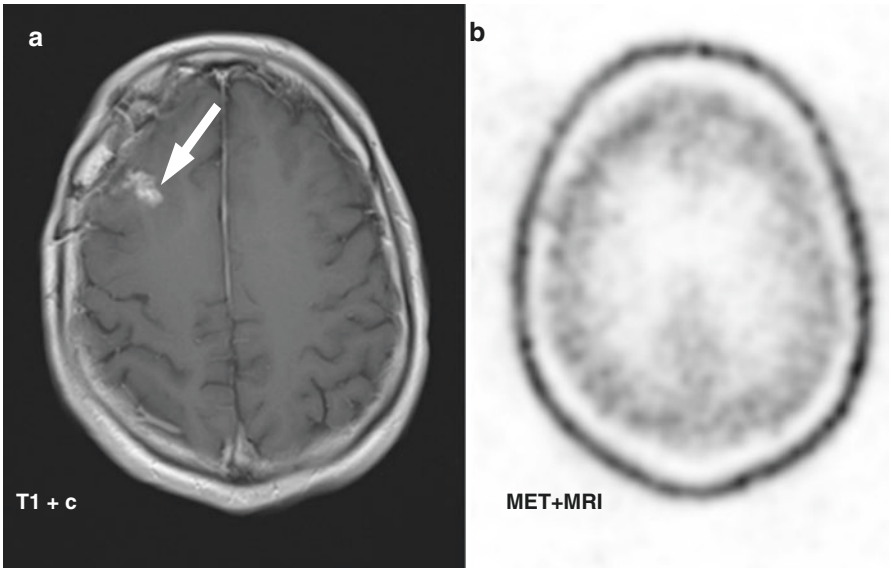

Fig. 41.3 Example of MET PET follow-up in a patient with a brain metastasis. Case of a 54-year-old male with right frontal solitary brain metastasis from a fibrosarcoma. The patient was treated with surgical resection and stereotactic radiosurgery. After treatment, follow-up gadolinium-enhanced MRI showed a new contrast-enhancing lesion (white arrow). MET PET was performed which did not demonstrate increased tracer uptake at the lesion site. The contrast enhancement was in this case shown to be due to treatment-induced changes

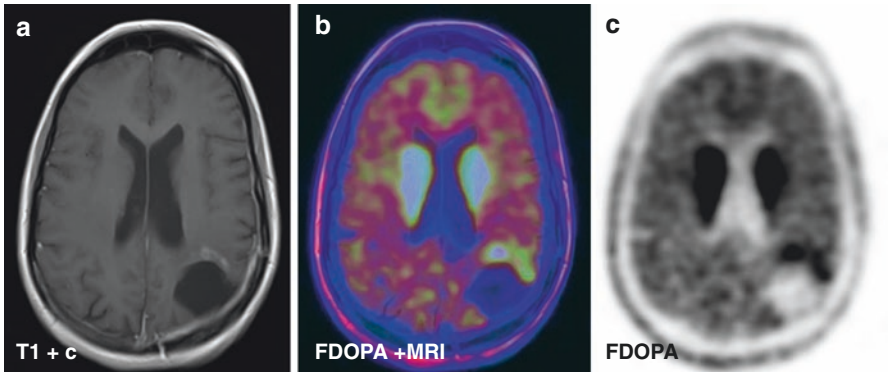

Fig. 41.4 Example of FDOPA PET follow-up in a patient with a glioblastoma. Follow-up imaging of a 26-year-old female glioblastoma patient, after surgical resection and chemoradiotherapy. Gadolinium-enhanced T1-weighted MRI (left image) 5 months after surgery was suggestive of tumor progression (white arrow). FDOPA PET was performed for other reasons (middle and right images) and demonstrated increased uptake (white arrows), also suggesting tumor progression. Co-registration of FDOPA PET and MRI (middle image) showed increased uptake at the site of enhancement on MRI. Subsequent follow-up MRI later showed further growth, confirming this case of tumor progression. The patient deceased within a year after the FDOPA PET scan

Physiological uptake of amino acid tracers in the brain is generally low, depending on anatomical region and age (Coope et al. 2007; Nagata et al. 2011). The high tumor uptake in combination with low background uptake is associated with straightforward visual assessment of amino acid PET tracers (Glaudemans et al. 2013). Therefore, the tumor detection rate and tumor delineation are thought to be better compared to FDG (Albert et al. 2016; Langen et al. 2017; Galldiks et al. 2019; de Zwart et al. 2019). Images can be interpreted visually or quantitatively. The most often used calculation method is the tumor-to-normal background ratio (T/N ratio) that compares tumor uptake to physiological uptake in the contralateral hemisphere. Uptake may also be defined by the standardized uptake value (SUV), a unit normalized to injected tracer dose per kilogram of body weight.

41.2.2.3 Other PET Tracers

In addition to amino acid PET tracers, other tracers have also been advanced. These tracers are markers of cell proliferation, such as 3′-deoxy-3′-[^{18}F]-fluorothymidine (FLT), or of the synthesis of membrane phospholipids, such as [^{11}C]-choline or [^{18}F]-fluorocholine (de Zwart et al. 2019). Both processes displayed by these tracers are active in brain tumors, thus leading to increased tracer uptake. However, these tracers are not capable of crossing an intact blood-brain barrier (BBB) (Galldiks et al. 2019). Although the BBB is usually disrupted in tumors, this is not always the case for the full extent of the tumor. To this end, only limited literature exists on these tracers. In this chapter, we will focus on amino acid PET only.

41.2.3 Dilemma of Treatment-Induced Changes

The extensive treatment regimen of malignant brain tumors, especially high-dose radiotherapy with or without concomitant chemotherapy, can produce adverse events. Damage to healthy brain tissue may lead to radiological suspicion of tumor progression (Fig. 41.3) which can even be accompanied by clinical symptoms indistinguishable from tumor progression (Brandsma et al. 2008; Thust et al. 2018). It is important to timely identify the nature of the radiological changes. True progression is indicative of failing treatment, while treatment-induced changes in fact conform with a desired response to the given treatment.

These treatment-induced changes, often called pseudoprogression in literature, are resulting from blood-brain barrier dysfunction, vasodilation, and subsequent vasogenic edema due to damage from given radiotherapy with or without chemotherapy (Brandsma et al. 2008; Thust et al. 2018). Typically, these changes occur within 3 months after treatment and will ultimately stabilize or decrease in size (Brandsma et al. 2008). Therefore, early posttreatment progression should not automatically lead to interruption of current treatment and start of second-line regimens. Delayed and longer-lasting effects, 6 months to several years after treatment, can sometimes also be seen and are then referred to as radiation necrosis.

Pseudoprogression and radiation necrosis are different clinical entities, although within the same pathological spectrum.

In high-grade gliomas, the incidence of treatment-induced changes is as high as 36% (Abbasi et al. 2018). Advances in radiotherapy planning techniques enable a high conformal dose distribution around the target volume; however, radiation dose to healthy brain tissue is unavoidable due to the infiltrative behavior of gliomas. Furthermore, treatment-induced changes are more frequent in IDH wild-type and MGMT-methylated tumors (van Dijken et al. 2019).

The incidence of treatment-induced changes in brain metastases after hypofractionated stereotactic radiotherapy (HFSRT) or stereotactic radiosurgery (SRS) is approximately 15% (Sneed et al. 2015), but some studies have suggested higher percentages (Donovan et al. 2019). Factors related to the development of radiation necrosis, especially after SRS, include dose, treated volume, and volume of the brain receiving a specific dose. An increase in the occurrence of treatment-induced changes is also expected with immunotherapy. The first studies have shown that immunotherapy alone or in addition to radiotherapy can lead to pseudoprogression and pose a new challenge for follow-up of brain metastases (Galldiks et al. 2020).

Conventional MRI cannot reliably differentiate between tumor recurrence and treatment-induced changes (van Dijken et al. 2017). Both tumor progression (Figs. 41.2 and 41.4) and treatment-induced changes (Fig. 41.3) demonstrate contrast enhancement on T1-weighted MRI with surrounding FLAIR/T2 hyperintensities. Conventional MRI, to date still the gold standard for brain tumor treatment response imaging, reached a pooled sensitivity and specificity of 68% (95% CI 51–81) and 77% (95% CI 45–93), respectively, for the detection of tumor progression in a recent meta-analysis for gliomas (van Dijken et al. 2017). Robust meta-analyses similar to those for gliomas are currently lacking for MRI in brain metastases.

To assist the clinician in the problematic differentiation of tumor progression and treatment-induced changes, the RANO criteria for gliomas and for brain metastases have been established (Wen et al. 2010; Lin et al. 2015). According to the RANO criteria, progression on conventional imaging within 3 months after chemoradiotherapy is only certain if there is new enhancement outside of the radiation field or after pathological confirmation (Wen et al. 2010). These criteria are similar for gliomas and metastases (Wen et al. 2010; Lin et al. 2015). However, in clinical practice, pathological confirmation is often not acquired in asymptomatic patients since this requires a neurosurgical intervention with a chance of morbidity. As a consequence, follow-up with imaging is usually chosen. However, this is time-consuming and can potentially expose a patient to a failing, but possibly toxic, treatment or delay the start of a second-line treatment. More advanced MRI sequences and PET tracers have therefore extensively been studied to overcome the limitations of conventional MRI (Dhermain et al. 2010; van Dijken et al. 2017, 2019; Langen et al. 2017; Galldiks et al. 2019; de Zwart et al. 2019).

41.3 Opportunities of Neuroimaging in Differentiating Tumor Progression and Treatment-Induced Changes

41.3.1 Advanced MRI

Advanced MRI sequences that have been studied for the aforementioned differentiation include diffusion-weighted imaging, detecting changes in cellular density; perfusion-weighted imaging, visualizing increased blood flow and neovascularization; and MR spectroscopy, an imaging technique capable of detecting changes in metabolites. All these advanced MRI techniques outperformed conventional MRI. Meta-analysis in high-grade gliomas showed a sensitivity and specificity for diffusion-weighted imaging of 71% (95% CI 60–80) and 86% (95% CI 76–92), respectively (van Dijken et al. 2017). For perfusion-weighted imaging, this was 87% (95% CI 82–91) and 86% (95% CI 77–91) (van Dijken et al. 2017). MR spectroscopy demonstrated the highest diagnostic accuracy with a sensitivity of 91% (95% CI 79–97) and specificity of 95% (95% CI 65–99) (van Dijken et al. 2017). As MR spectroscopy is time-consuming, with risk of movement artifacts, diffusion-weighted imaging and perfusion-weighted imaging are most often used to aid in the differentiation of tumor progression from treatment-induced changes.

Studies on the diagnostic value of advanced MRI in brain metastases after treatment are limited. Perfusion-weighted imaging and MR spectroscopy demonstrate the most promising results thus far (Chuang et al. 2016). Diagnostic accuracy seems to be in a similar good range as seen for gliomas. However, a drawback of MR spectroscopy is the relatively large voxel size, making differentiation of tumor progression from treatment-induced changes in smaller metastases difficult.

41.3.2 PET

The uptake of PET tracers is physiologically different in tumor progression and treatment-induced changes. In progressive tumors, the uptake is caused by active uptake of tracer in the tumor cells (Figs. 41.2 and 41.4). On the other hand, in treatment-induced changes, uptake is caused by passive diffusion across a disrupted BBB (Fig. 41.3). Theoretically, the uptake in tumor cells should thus exceed the uptake after radiation injury; however, there is an overlap between these uptakes. The value of PET for differentiating tumor progression from treatment-induced changes has been extensively studied in high-grade gliomas (de Zwart et al. 2019).

Recently, a meta-analysis has been conducted (de Zwart et al. 2019). This meta-analysis included 39 studies and confirmed a lower diagnostic accuracy for FDG (Fig. 41.1) than for the two most common amino acid tracers. FDG reached a sensitivity of 84% (95%CI 72–92) and specificity of 84% (95%CI 69–93), while FET, with a sensitivity of 90% (95%CI 81–95) and a specificity of 85% (95%CI 71–93), and MET (Figs. 41.2 and 41.3), with a sensitivity and specificity of 93% (95%CI 80-98) and 82% (95%CI 68-91), respectively, performed significantly better (de Zwart et al. 2019). FDOPA is a less studied tracer (Fig. 41.4), with only four known

studies being published, but demonstrates comparable diagnostic accuracy with a sensitivity ranging from 85% to 100% and specificity ranging from 72% to 100% (Lapa et al. 2014; Karunanithi et al. 2013; Paquet et al. 2017; Herrmann et al. 2014).

The usefulness of FDG PET is very limited in brain metastases (Fig. 41.1). Studies have shown that FDG PET only marginally improves accurate differentiation between tumor progression and treatment-induced changes after ambiguous MRI (Chao et al. 2001; Belohlávek et al. 2003). As expected, the accuracy of amino acid PET is superior to FDG PET.

Several studies have confirmed that a difference in FET T/N ratios can quantitatively distinguish metastatic progression from treatment-induced changes (Galldiks et al. 2012; Romagna et al. 2016; Ceccon et al. 2017). However, the number of patients studied with FET PET ($N = 126$) is much smaller than for MET PET.

For MET PET, most studies had a relatively high sensitivity, specificity, and diagnostic accuracy (>85%) in common, with advantages over conventional imaging (Figs. 41.2 and 41.3) (Terakawa et al. 2008; Yomo and Oguchi 2017; Okamoto et al. 2010; Yamane et al. 2010; Tsuyuguchi et al. 2003). However, a considerable overlap in the uptake values of methionine in progressing tumor and treatment-induced change occurs (Minamimoto et al. 2015).

A visual analysis of 83 lesions in 32 patients also demonstrated positive results for FDOPA (Lizarraga et al. 2014). In another study, among 13 patients of whom 3 had histologically confirmed treatment-induced changes, there was a visual difference in FDOPA uptake between recurrent or progressive metastases and treatment-induced changes (Papin-Michault et al. 2016). This study additionally demonstrated a difference in LAT-1 expression between tumor progression cases and treatment-induced changes, explaining the difference in FDOPA uptake (Papin-Michault et al. 2016). Interestingly, FDOPA outperformed perfusion-weighted imaging in a study among 42 patients with brain metastases after SRS (Cicone et al. 2015).

41.4 Limitations and Future Perspectives of MRI and PET

MRI and PET seem to perform similar in the differentiation of treatment-induced changes from tumor progression. However, only few studies have compared MRI and PET directly.

A study by Kim et al. (2010) stated that perfusion-weighted MRI is superior in distinguishing a recurrence of high-grade glioma from radiation necrosis compared to MET. Dandois et al. (2010) also found that perfusion-weighted MRI had an at least similar diagnostic accuracy to MET in differentiating tumor recurrence and treatment-induced changes. However, FDOPA was suggested to outperform perfusion-weighted MRI (Cicone et al. 2015), and another study also demonstrated that amino acid PET is possibly superior over perfusion-weighted MRI (Tomura et al. 2017).

The diagnostic accuracy of the different amino acid PET tracers seems comparable, although FDOPA is somewhat understudied compared to MET and FET PET. Most experience is gathered with MET. However, MET is impractical since it

demands a cyclotron due to its very short half-life (20 min). Fluorine-18-labeled FET has gained ground due to its longer half-life (109.7 min).

There is an urgent need for uniform scanning protocols and quantification methods for both advanced MRI and amino acid PET. Furthermore, few data are available on interobserver agreement in the interpretation of these advanced MRI sequences and PET studies. Amino acid PET can usually relatively easily be interpreted visually, but there is a lack of consensus on the used reference region for calculation of T/N ratios. Local variations in tracer uptake between different reference regions may significantly alter results. With T/N ratios still being the most reported quantitative parameter, this is troublesome. Future studies should thus focus on establishing robust guidelines for analysis and quantification methods for amino acid PET in brain tumors.

It has been suggested that the recent development of hybrid PET/MRI cameras could lead to a jump forward in the imaging of brain tumors. Combining both modalities might overcome a number of individual limitations and avoids the necessity of additional scanning. This would enable an absolute match between tissue information of both modalities under the same physiological conditions and may thus lead to better localization of the PET signal within the soft tissues. However, the economic cost of hybrid PET/MRI scanners is substantial. The first studies have been published and indeed demonstrate the feasibility of using combined PET/MRI machines (Hojjati et al. 2018; Deuschl et al. 2018). However, these studies are limited to FDG PET (Hojjati et al. 2018), which has insufficient value in brain tumor imaging, and carbon-bound MET PET (Deuschl et al. 2018), which is not feasible in many centers. Therefore, more PET/MRI studies with emphasis on treatment evaluation of gliomas and brain metastases using fluorine-bound amino tracers are desired.

41.5 Summary

Treatment-induced changes are a common phenomenon among both treated gliomas and brain metastases. Conventional MRI is not able to differentiate tumor progression and treatment-induced changes. Both advanced MRI techniques and amino acid PET provide additional information that can aid the clinician in decision-making following treatment. Combining all evidence that we presented in this chapter, there does not seem to be a preferred advanced MRI or PET imaging method to differentiate tumor progression from treatment-induced changes.

References

Abbasi AW, Westerlaan HE, Holtman GA, Aden KM, van Laar PJ, van der Hoorn A (2018) Incidence of tumour progression and pseudoprogression in high-grade gliomas: a systematic review and meta- analysis. Clin Neuroradiol 28:401–411

Achrol A, Rennert R, Anders C et al (2019) Brain metastases. Nat Rev Dis Primers 5(1):5

Albert NL, Weller M, Suchorska B et al (2016) Response assessment in neuro-oncology working group and european association for neuro-oncology recommendations for the clinical use of PET imaging in gliomas. Neuro-Oncology 18:1199–1208

Bell EH, Zhang P, Fisher BJ et al (2018) Association of MGMT promoter methylation status with survival outcomes in patients with high-risk glioma treated with radiotherapy and temozolomide: an analysis from the NRG oncology/RTOG 0424 trial. JAMA Oncol 4(10):1405–1409

Belohlávek O, Simonová G, Kantorová I, Novotný J Jr, Liscák R (2003) Brain metastases after stereotactic radiosurgery using the leksell gamma knife: can FDG PET help to differentiate radionecrosis from tumour progression? Eur J Nucl Med Mol Imaging 30(1):96–100

Binabaj MM, Bahrami A, ShahidSales S et al (2018) The prognostic value of MGMT promoter methylation in glioblastoma: a meta-analysis of clinical trials. J Cell Physiol 233(1):378–386

Boonzaier NR, Larkin TJ, Matys T et al (2017) Multiparametric MR imaging of diffusion and perfusion in contrast-enhancing and nonenhancing components in patients with glioblastoma. Radiology 284(1):180–190

Brandsma D, Stalpers L, Taal W, Sminia P, van den Bent MJ (2008) Clinical features, mechanisms, and management of pseudoprogression in malignant gliomas. Lancet Oncol 9:453–461

Ceccon G, Lohmann P, Stoffels G et al (2017) Dynamic O-(2-18F-fluoroethyl)-L-tyrosine positron emission tomography differentiates brain metastasis recurrence from radiation injury after radiotherapy. Neuro-Oncology 19(2):281–288

Chao ST, Suh JH, Raja S, Lee SY, Barnett G (2001) The sensitivity and specificity of FDG PET in distinguishing recurrent brain tumor from radionecrosis in patients treated with stereotactic radiosurgery. Int J Cancer 96(3):191–197

Chen L, Douglass J, Kleinberg L et al (2018) Concurrent immune checkpoint inhibitors and stereotactic radiosurgery for brain metastases in non-small cell lung cancer, melanoma, and renal cell carcinoma. Int J Radiat Oncol Biol Phys 100(4):916–925

Chuang MT, Liu YS, Tsai YS, Chen YC, Wang CK (2016) Differentiating radiation-induced necrosis from recurrent brain tumor using MR perfusion and spectroscopy: a meta-analysis. PLoS One 11(1):e0141438

Cicone F, Minniti G, Romano A et al (2015) Accuracy of F-DOPA PET and perfusion-MRI for differentiating radionecrotic from progressive brain metastases after radiosurgery. Eur J Nucl Med Mol Imaging 42(1):103–111

Coope DJ, Cizek J, Eggers C et al (2007) Evaluation of primary brain tumors using 11C-methionine PET with reference to a normal methionine uptake map. J Nucl Med 48(12):1971–1980

Dandois V, Rommel D, Renard L, Jamart J, Cosnard G (2010) Substitution of 11C-methionine PET by perfusion MRI during the follow-up of treated high-grade gliomas: preliminary results in clinical practice. Neuroradiology 37:89–97

de Zwart PL, van Dijken BRJ, Holtman GA et al (2019) Diagnostic accuracy of positron emission tomography tracers for the differentiation of tumor progression from treatment-related changes in high-grade glioma: a systematic review and meta-analysis. J Nucl Med 119:233809

DeAngelis LM (2001) Brain tumors. N Engl J Med 344:114–123

Delattre JY, Krol G, Thaler HT, Posner JB (1988) Distribution of brain metastases. Arch Neurol 45(7):741–744

Deuschl C, Kirchner J, Poeppel TD et al (2018) 11C-MET PET/MRI for detection of recurrent glioma. Eur J Nucl Med Mol Imaging 45(4):593–601

Dhermain FG, Hau P, Lanfermann H, Jacobs AH, van den Bent MJ (2010) Advanced MRI and PET imaging for assessment of treatment response in patients with gliomas. Lancet Neurol 9:906–920

Donovan EK, Parpia S, Greenspoon JN (2019) Incidence of radionecrosis in single-fraction radiosurgery compared with fractionated radiotherapy in the treatment of brain metastasis. Curr Oncol 26(3):e328–e333

Galldiks N, Stoffels G, Fills CP et al (2012) Role of O-(2-(18)F-fluoroethyl)-L-tyrosine PET for differentiation of local recurrent brain metastasis from radiation necrosis. J Nucl Med 53(9):1367–1374

Galldiks N, Lohmann P, Albert NL et al (2019) Current status of PET imaging in neuro-oncology. Neuro-Oncol Adv 1(1):vdz010

Galldiks N, Kocher M, Ceccon G et al (2020) Imaging challenges of immunotherapy and targeted therapy in patients with brain metastases: response, progression, and pseudoprogression. Neuro-Oncology 22(1):17–30

Glaudemans AWJM, Enting RH, Heesters MAAM et al (2013) Value of 11C-methionine PET in imaging brain tumours and metastases. Eur J Nucl Med Mol Imaging 40:615–635
Hardesty D, Nakaji P (2016) The current and future treatment of brain metastases. Front Surg 3(30):1–7
Herrmann K, Czernin J, Cloughesy T et al (2014) Comparison of visual and semiquantitative analysis of 18F-FDOPA- PET/CT for recurrence detection in glioblastoma patients. Neuro-Oncology 16:603–609
Hojjati M, Badve C, Garg V et al (2018) Role of FDG-PET/MRI, FDG-PET/CT, and dynamic susceptibility contrast perfusion mri in differentiating radiation necrosis from tumor recurrence in glioblastomas. J Neuroimaging 28:118–125
Karunanithi S, Sharma P, Kumar A et al (2013) Comparative diagnostic accuracy of contrast-enhanced MRI and 18F-FDOPA PET-CT in recurrent glioma. Eur Radiol 23:2628–2635
Kim YH, Oh SW, Lim YJ et al (2010) Differentiating radiation necrosis from tumor recurrence in high-grade gliomas: assessing the efficacy of 18F-FDG PET, 11C-methionine PET and perfusion MRI. Clin Neurol Neurosurg 112(9):758–765
Langen KJ, Galldiks N, Hattingen E, Shah NJ (2017) Advances in neuro-oncology imaging. Nat Rev Neurol 13:279–289
Lapa C, Linsenmann T, Monoranu CM et al (2014) Comparison of the amino acid tracers 18F-FET and 18F-DOPA in high-grade glioma patients. J Nucl Med 55:1611–1616
Law I, Albert NL, Arbizu J et al (2019) Joint EANM/EANO/RANO practice guidelines/SNMMI procedure standards for imaging of gliomas using PET with radiolabelled amino acids and [18F]FDG: version 1.0. Eur J Nucl Med Mol Imaging 46:540–557
Lin NU, Lee EQ, Aoyama H et al (2015) Response assessment criteria for brain metastases: proposal from the RANO group. Lancet Oncol 16(6):e270–e278. https://doi.org/10.1016/S1470-2045(15)70057-4
Lizarraga KJ, Allen-Auerbach M, Czernin J et al (2014) (18)F-FDOPA PET for differentiating recurrent or progressive brain metastatic tumors from late or delayed radiation injury after radiation treatment. J Nucl Med 55(1):30–36
Louis DN, Perry A, Reifenberger G et al (2016) The 2016 World Health Organization classification of tumors of the central nervous system: a summary. Acta Neuropathol 131:803–820
Minamimoto R, Saginoya T, Kondo C, Tomura N, Ito K, Matsuo Y et al (2015) Differentiation of brain tumor recurrence from post-radiotherapy necrosis with 11C-methionine PET: visual assessment versus quantitative assessment. PLoS One 10(7):e0132515
Miranda-Filho A, Pineros M, Soerjomataram I et al (2017) Cancers of the brain and CNS: global patterns and trends in incidence. Neuro-Oncology 19(2):270–280
Nagata T, Tsuyuguchi N, Uda T et al (2011) Examination of 11C-methionine metabolism by the standardized uptake value in the normal brain of children. J Nucl Med 52:201–205
Okamoto S, Shiga T, Hattori N, Kubo N, Takei T, Katoh N et al (2010) Semiquantitative analysis of C-11 methionine PET may distinguish brain tumor recurrence from radiation necrosis even in small lesions. Ann Nucl Med 25(3):213–220
Ostrom QT, Cioffi G, Gittleman H et al (2019) BTRUS statistical report: primary brain and other central nervous system tumors diagnosed in the United States in 2012–2016. Neuro Oncol 21(Suppl 5):v1–v100
Papin-Michault C, Bonnetaud C, Dufour M et al (2016) Study of LAT1 expression in brain metastases: towards a better understanding of the results of positron emission tomography using amino acid tracers. PLoS One 11(6):e0157139
Paquet M, Doyen J, Mondot L et al (2017) Value of early and delayed imaging for 18F-FDOPA PET high grade gliomas evaluation [abstract]. Eur J Nucl Med Mol Imaging 44:S642–S643
Rogers TW, Toor G, Drummond K et al (2018) The 2016 revision of the WHO classification of central nervous system tumours: retrospective application to a cohort of diffuse gliomas. J Neuro-Oncol 137(1):181–189
Romagna A, Unterrainer M, Schmid-Tannwald C et al (2016) Suspected recurrence of brain metastases after focused high dose radiotherapy: can [18F]FET- PET overcome diagnostic uncertainties? Radiat Oncol 11(1):139

Sanai N, Berger MS (2008) Glioma extent of resection and its impact on patient outcome. Neurosurgery 62(4):753–764

Sneed P, Mendez J, Vemer-van den Hoek J et al (2015) Adverse radiation effect after stereotactic radiosurgery for brain metastases: incidence, time course, and risk factors. J Neurosurg 123(2):373–386

Soffietti R, Abacioglu U, Baumert B et al (2017) Diagnosis and treatment of brain metastases from solid tumors: guidelines from the European Association of Neuro-Oncology (EANO). Neuro-Oncology 19(2):162–174

Stupp R, Mason WP, van den Bent MJ et al (2005) Radiotherapy plus concomitant and adjuvant temozolomide for glioblastoma. N Engl J Med 352:987–996

Tabouret E et al (2012) Recent trends in epidemiology of brain metastases: an overview. Anticancer Res 32:4655–4662

Terakawa Y, Tsuyuguchi N, Iwai Y, Yamanaka K, Higashiyama S, Takami T et al (2008) Diagnostic accuracy of 11C-methionine PET for differentiation of recurrent brain tumors from radiation necrosis after radiotherapy. J Nucl Med 49(5):694–699

Thust SC, Van Den Bent MJ, Smits M (2018) Pseudoprogression of brain tumors. J Magn Reson Imaging 48:571–589

Tomura N, Kokubun M, Saginoya T et al (2017) Differentiation between treatment-induced necrosis and recurrent tumors in patients with metastatic brain tumors: comparison among 11C-methionine-PET, FDG-PET, MR permeability imaging, and MRI-ADC—preliminary results. AJNR 38(8):1520–1527

Tsuyuguchi N, Sunada I, Iwai Y et al (2003) Methionine positron emission tomography of recurrent metastatic brain tumor and radiation necrosis after stereotactic radiosurgery: is a differential diagnosis possible? J Neurosurg 98(5):1056–1064

van den Bent MJ, Baumert B, Erridge SC et al (2017) Interim results from the CATNON trial (EORTC study 26053-22054) of treatment with concurrent and adjuvant temozolomide for 1p/19q non-co-deleted anaplastic glioma: a phase 3, randomised, open-label intergroup study. Lancet 390(10103):1645–1653

van Dijken BRJ, van Laar PJ, Holtman GA, van der Hoorn A (2017) Diagnostic accuracy of magnetic resonance imaging techniques for treatment response evaluation in patients with high-grade glioma, a systematic review and meta-analysis. Eur Radiol 27:4129–4144

van Dijken BRJ, van Laar PJ, Smits M et al (2019) Perfusion MRI in treatment evaluation of glioblastomas: clinical relevance of current and future techniques. J Magn Reson Imaging 49:11–22

van Waarde A, Elsinga PH (2008) Proliferation markers for the differential diagnosis of tumor and inflammation. Curr Pharm Des 14(31):3326–3339

Weller M, van den Bent MJ, Tonn JC et al (2017) European Association for Neuro-Oncology (EANO) guideline on the diagnosis and treatment of adult astrocytic and oligodendroglial gliomas. Lancet Oncol 18(6):e315–e329

Wen PY, Macdonald DR, Reardon DA et al (2010) Updated response assessment criteria for high-grade gliomas: response assessment in neuro-oncology working group. J Clin Oncol 28:1963–1972

Yamane T, Sakamoto S, Senda M (2010) Clinical impact of 11C-methionine PET on expected management of patients with brain neoplasm. Eur J Nucl Med Mol Imaging 37(4):685–690

Yan JL, van der Hoorn A, Larkin TTJ et al (2017) Extent of resection of peritumoral diffusion tensor imaging-detected abnormality as a predictor of survival in adult glioblastoma patients. J Neurosurg 126(1):234–241

Yan JL, Li C, Boonzaier NR et al (2019) Multimodal MRI characteristics of the glioblastoma infiltration beyond contrast enhancement. Ther Adv Neurol Disord 12:1756286419844664

Yomo S, Oguchi K (2017) Prospective study of 11C-methionine PET for distinguishing between recurrent brain metastases and radiation necrosis: limitations of diagnostic accuracy and long-term results of salvage treatment. BMC Cancer 17(1):713

Imaging Brain Metastases of Neuroendocrine Tumors

42

Klaas Pieter Koopmans and A. H. Brouwers

Contents

42.1 Introduction 1084
42.2 Incidence 1085
42.3 Origin of Neuroendocrine Brain Metastases 1085
42.4 Growth Patterns of Neuroendocrine Brain Metastases 1085
42.5 Clinical Presentation 1086
42.6 Imaging 1087
42.7 Somatostatin Receptor Imaging 1087
42.8 Metabolic Imaging 1089
42.8.1 Catecholamine Pathway 1089
42.8.2 Serotonin Pathway 1090
42.9 Conclusion 1091
References 1091

Abstract

Neuroendocrine tumors (NETs) are rare tumors with a low incidence, characterized by a slow growth with often an indolent course. These tumors can arise in nearly all organs, with gastrointestinal and bronchopulmonary sites being the most common primary sites. The occurrence of primary neuroendocrine brain tumors is very rare, but metastases of NET to the brain are more common. The incidence of brain metastasis in patients with NET is approximately 1.5–5% with a median age of diagnosis of 60 years. Detection of NET brain metastases occurs

K. P. Koopmans (✉)
Department of Radiology and Nuclear Medicine, Martini Hospital Groningen, Groningen, The Netherlands
e-mail: k.koopmans@mzh.nl

A. H. Brouwers
Department of Nuclear Medicine and Molecular Imaging, University of Groningen, University Medical Center Groningen, Groningen, The Netherlands

R. A. J. O. Dierckx et al. (eds.), *PET and SPECT in Neurology*,
https://doi.org/10.1007/978-3-030-53168-3_42

with a median of 1.5 years after diagnosis of primary NET with a likely underdiagnosis. Brain metastases most commonly develop in patients with bronchopulmonary NET. Brain metastases grow globoid with a microglial boundary and are often surrounded by vasogenic edema. Metastatic brain lesions are made up of a subgroup of cells with a different biological behavior compared to the primary NET and other metastases which can be explained by the difficulties these cells have to face before being able to successfully grow within the brain. These patients suffer from a more aggressive NET behavior, and in many patients, carcinoid syndrome is also present. Clinical presentation is mostly characterized by headaches, personality changes, and gait disturbances.

According to the European Neuroendocrine Tumor Society (ENETS) consensus guidelines, MRI is the preferred modality for detection of NET brain metastases. However, PET has gained a very important role in the staging of NET, and it is likely that PET will become very helpful for the detection of neuroendocrine brain tumors and metastases. Several tracers are available at this moment, of which somatostatin receptor PET and 18F-DOPA PET seem the most promising at this moment. Due to the high background uptake in the brain and the relatively low glucose metabolism in NET cells, the indication of 18F-FDG PET seems very limited for the detection of neuroendocrine brain tumors.

However, due to the rarity of NET overall and thus especially for NET brain metastases, data on these tumors is limited, and additional research is warranted.

42.1 Introduction

Neuroendocrine tumors are a unique group of slow-growing tumors arising from neuroendocrine cells. Neuroendocrine cells are widely dispersed within the body. These neuroendocrine cells are characterized by a common phenotype which consists of the expression of hormonal products and general protein markers which are specific for each cell type (Reubi 1995). Neuroendocrine cells regulate many different body functions through paracrine signalling with dedicated amines and peptides. The most commonly produced are the biogenic amines, of which serotonin and catecholamines are the most prominent. Other well-known biogenic amines produced by neuroendocrine cells are, for example, adrenocorticotropic hormone, growth hormone, neuropeptide K, substance P, bradykinin, kallikrein, and prostaglandins (Kloppel et al. 1996; Schnirer et al. 2003). Neuroendocrine tumors have a low incidence, which has been estimated to be approximately 1–2 cases per 100,000 individuals in the United States (Godwin 1975; Modlin et al. 2003). Although these tumors can arise in nearly all organs, the most common primary sites are the gastrointestinal (56–64%) and bronchopulmonary tracts (12–20%) (Modlin et al. 2003; Soga 2003). Generally, neuroendocrine tumors are characterized by a slow growth, which accounts for the long time span before these tumors become symptomatic. Although neuroendocrine tumors often follow an indolent course, in 12–69% of

patients, dependent on tumor differentiation, metastatic disease was already evident at first diagnosis (Lepage et al. 2013; Modlin et al. 2003). Generally neuroendocrine tumors metastasize to the liver, lungs, and bone. Other sites, such as the brain, are much rarer.

42.2 Incidence

Metastases of neuroendocrine tumors to the central nervous system constitute approximately 1.3–1.4% of all patients presenting with brain metastases (Cho et al. 1998; Maiuri et al. 2004). Conversely, it is estimated that the incidence of brain metastases in patients with neuroendocrine tumors is approximately 1.5–5% (Hlatky et al. 2004; Krug et al. 2019; Patchell and Posner 1986; Pavel et al. 2010). The median age at the time of diagnosis of brain metastasis is 60 years, but the time course after which these brain metastases occur varies. The time between detection of the primary site and brain metastases ranges from 0 months to 16.3 years from a median of 1.5 years (Hlatky et al. 2004; Patchell and Posner 1986). However, data on brain metastases of neuroendocrine tumors are rare. Consequently, it is likely that the reported incidence is an underestimation of the true incidence of neuroendocrine tumor brain metastases, since dedicated brain imaging is not routinely performed to assess metastatic spread in these patients (Pavel et al. 2010). Additional imaging of the brain is usually only performed when patients present with neurological symptoms caused by the intracranial mass.

42.3 Origin of Neuroendocrine Brain Metastases

Brain metastases of neuroendocrine tumors have been reported with several neuroendocrine primary tumor locations. Most commonly primary neuroendocrine tumors of the lungs give brain metastasis (Hlatky et al. 2004; Krug et al. 2019; Pavel et al. 2010). The development of brain metastasis of neuroendocrine tumors can be explained by two separate mechanisms. The first is direct hematogenous spread from lung tumors/metastases, and the second is spread from pelvic neuroendocrine tumor metastases via Batson's venous plexus. Batson's venous plexus is a venous plexus system, which directly connects pelvic structures with the brain via valveless veins running in the spinal epidural space (Batson 1940; Hlatky et al. 2004).

42.4 Growth Patterns of Neuroendocrine Brain Metastases

Generally, brain metastases grow as well-circumscribed globoid lesions. Activated microglial cells form a distinct boundary between the tumor mass and brain tissue (He et al. 2006; Sul and Posner 2007). This boundary may account for the well-circumscribed appearance of brain metastases. Vasogenic edema often surrounds

metastatic brain lesions. This edema is caused by intratumoral leakage of protein-rich fluids through the disrupted blood-brain barrier. These fluids then diffuse into the surrounding brain, increasing the local fluid content of the brain.

Brain metastases are formed by a subset of cells which have detached from the primary tumor. During their passage through the extracellular environment, into the bloodstream, and finally to their place of growth, these metastatic cells will have encountered and successfully counteracted or "fooled" a huge number of host defense mechanisms. Hence, this collection of cells must have specific properties which make them suitable for metastasizing. Especially metastatic tumor cells in the brain, which is a difficult environment for free circulating tumor cells to successfully grow out to a metastatic lesion, can have a greatly different biological behavior as compared to the cells constituting the primary lesion. Additionally, brain tumor lesions may be constituted from different subsets of tumor cells. This also explains why several brain lesions can differ in behavior from each other (Klein et al. 2002; Sul and Posner 2007). Unfortunately, only series with small numbers of patients with neuroendocrine tumor metastasis to the brain have been described. From the available literature, it has become clear that both well- and poorly differentiated neuroendocrine tumors can give rise to metastatic brain lesions. From data limited to pulmonary neuroendocrine tumors, it has been reported that typical carcinoids (Granberg et al. 2000), atypical carcinoids (Nakamura et al. 2001), and large cell neuroendocrine tumors (Doddoli et al. 2004) can all lead to metastatic brain lesions. Only 1.3–1.4% of patients with neuroendocrine tumors present with neurological symptoms caused by brain lesions as first presentation of their disease (Maiuri et al. 2004; Nakamura et al. 2001; Porter et al. 2000).

42.5 Clinical Presentation

Hlatky et al. found in their series of 24 patients with brain metastases from carcinoid tumors that most patients with neuroendocrine brain metastases experience symptoms directly related to the brain metastases (96%). These symptoms consisted of headaches (96%), personality changes (25%), gait disturbances (21%), cranial nerve deficits (13%), seizures (8%), nausea (8%), motor deficits (4%), and memory deficits (4%) (Hlatky et al. 2004). In their patient group, only one patient (4%) was asymptomatic, and the metastatic brain lesion was found during a regular metastatic work-up. In 50% of these patients, carcinoid syndrome was present.

From the data of the study of Krug et al. in a retrospective study comprising 51 patients with brain metastasis from NET, it appeared that most patients suffered from a more aggressive behavior of the NET. These patients also showed a shorter overall median survival compared to patients without brain metastases with a median survival time of 11 months (Krug et al. 2019).

42.6 Imaging

Generally, due to the low incidence of brain metastases from neuroendocrine tumors, patients with neuroendocrine tumors are not routinely screened for brain metastases during the metastatic work-up. The European Neuroendocrine Tumor Society (ENETS) published a consensus guideline for brain metastases in neuroendocrine tumors which dates from 2010, titled "ENETS consensus guidelines for the management of brain, cardiac and ovarian metastases from neuroendocrine tumors" (Pavel et al. 2010). In these guidelines, they also described the position of the currently used nuclear medicine imaging techniques. They stated that, due to the inadequate data on nuclear imaging techniques for the detection of neuroendocrine brain metastasis, MRI thus far has the highest sensitivity for the detection of single and multiple brain metastases and should be recommended as part of the diagnostic work-up in patients with neuroendocrine carcinoma of the lung.

It is unfortunate that there is inadequate data to support clinical applicability of nuclear medicine imaging techniques for the detection of neuroendocrine brain metastases. However, from evidence from case reports and on metastases outside the brain, it can be argued that nuclear medicine techniques may be applicable for the detection of neuroendocrine brain metastases. Much research on the position of nuclear medicine imaging techniques for neuroendocrine brain metastases is however warranted.

42.7 Somatostatin Receptor Imaging

For the regulation of several functions in both body and brain, regulatory peptides play an important role. Several receptors for regulatory peptides are overexpressed on the cellular membranes of neuroendocrine tumors and their metastases with an increased density as compared with normal tissue. Somatostatin (SST) is a cyclic hormone, of which two forms have been identified, SST-14 and SST-28. SST acts as an inhibitor for the release of many hormones by neuroendocrine cells in the body and brain, such as growth hormone, glucagon, and insulin, by binding to G-coupled SST receptors (SSTr) (Weckbecker et al. 2003). Five different subtypes of these receptors have thus far been identified in humans, named SSTr1–SSTr5. Generally, neuroendocrine tumor cells express the highest density of the SSTr2 subtype (Khan and Beck-Sickinger 2008). Somatostatin binds to SSTr and is subsequently transported to the intracellular environment where these hormone-receptor complexes are metabolized in lysosomes (Hofland and Lamberts 2003). Historically somatostatin receptor scintigraphy has played a very important role in the staging of neuroendocrine tumors for the last 20 years (Koopmans et al. 2009; Krenning et al. 1992; Lamberts et al. 1993). In 2001, somatostatin analogues have been coupled to positron-emitting isotopes, enabling the use of PET camera systems (Henze et al. 2001; Hofmann et al. 2001). Provided that the primary neuroendocrine tumor is

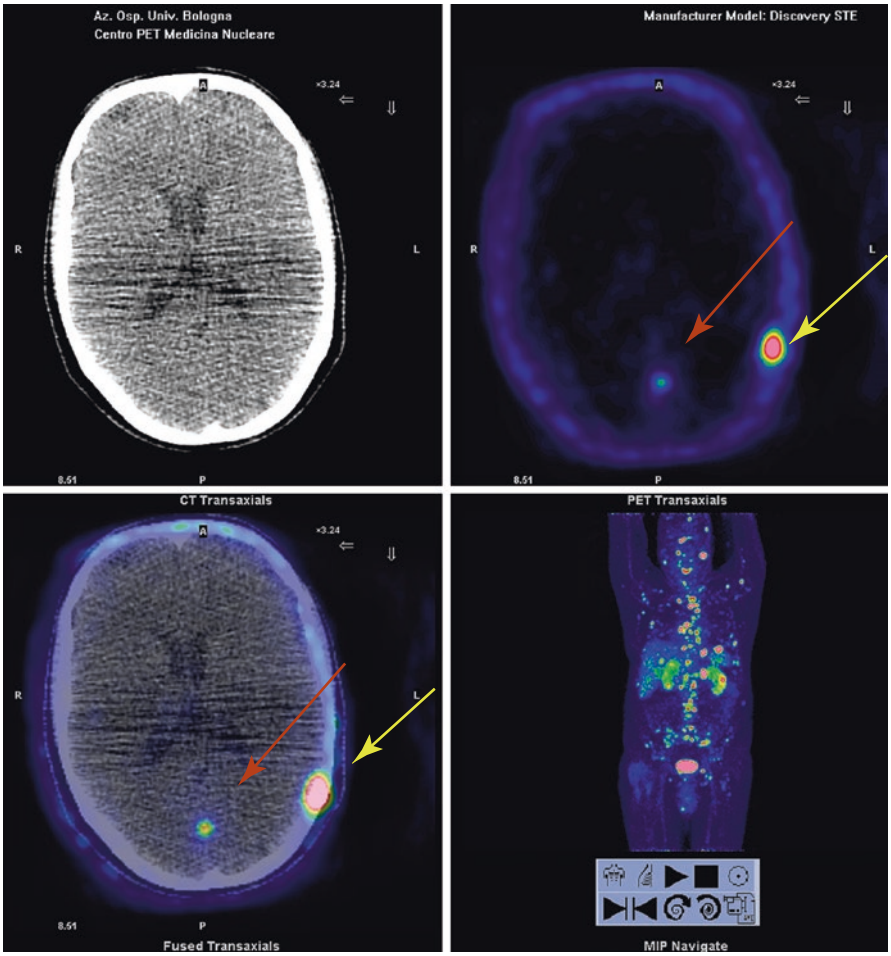

Fig. 42.1 ^{68}Ga-DOTATOC PET scan of a patient with extensively metastasized neuroendocrine lung tumor, who also had a small brain metastasis (red arrow) as well as an ossal lesion in the skull (yellow arrow). (Courtesy of Valentina Ambrosini, Nuclear Medicine, Azienda Ospedaliero-Universitaria di Bologna, Policlinico S. Orsola-Malpighi, Bologna, Italy)

well differentiated and has shown pathologically increased tracer uptake of ^{111}Indium somatostatin analogues or ^{68}Ga-labelled somatostatin analogues, these tracers might be helpful for the diagnosis of neuroendocrine brain metastasis. An example of ^{68}Ga-somatostatin PET is provided in Fig. 42.1. In a publication, ^{68}Ga-somatostatin receptor PET/CT was able to identify 6 metastatic brain lesions in 4210 scans in patients with neuroendocrine tumors (Carreras et al. 2013). Many case reports have been published in the last 10 years, in which the role of PET imaging with somatostatin analogues seems to perform a pivotal role. However, false-positive ^{68}Ga-SSTr uptake can be caused by other tumors such as non-Hodgkin lymphoma, metastatic meningioma, breast cancer, thyroid adenoma, and papillary carcinoma resulting in a positive PET/CT scan (Yamagi et al. 2017).

42.8 Metabolic Imaging

^{18}F-Fluorodeoxyglucose (^{18}FDG), which is important in oncology, has a limited role for the detection of brain metastasis due to the high glucose metabolism of the brain (Kruger et al. 2011). The potential role of ^{18}FDG PET scanning for the detection of neuroendocrine brain metastasis will very likely be even more limited. In contrast to many other malignancies, well-differentiated gastroenteropancreatic (GEP neuroendocrine tumors (NETs) generally have a low glucose metabolism (Adams et al. 1998; Belhocine et al. 2002). For the primary staging of neuroendocrine tumors, ^{18}F-fluorodeoxyglucose (^{18}FDG) PET scanning has limited value due to the only moderately increased glucose metabolism of most GEP NET. Therefore, as a staging tool, ^{18}FDG PET is most likely not suited for the detection of suspected brain metastasis in patients with neuroendocrine tumors (Adams et al. 1998; Pasquali et al. 1998).

Many neuroendocrine tumors and their metastasis have an increased synthesis and secretion of hormones and neurotransmitters. Serotonin, catecholamine, and histamine are the most common examples of secreted hormones by these tumors (Jager et al. 2008). The increased biosynthesis of catecholamines and serotonin in neuroendocrine tumors enables imaging with specific amine precursors. In this chapter, we will shortly discuss 6-^{18}F-L-3,4-dihydroxyphenylalanine (^{18}F-DOPA), a PET tracer for the catecholamine pathway, and β-[^{11}C]-5-hydroxy-L-tryptophan (^{11}C-5-HTP), a PET tracer for the serotonin pathway.

42.8.1 Catecholamine Pathway

In the brain, catecholamines, such as adrenaline, act as neurotransmitters or as hormones, via α- and β-adrenergic receptors located on vessels and internal organs.

For the synthesis of catecholamines, phenylalanine and intermediate products such as L-3,4-dihydroxyphenylalanine (L-DOPA) are taken up via system L large amino acid transporters (LAT). These precursors are decarboxylated to dopamine intracytoplasmatically via the enzyme aromatic amino acid decarboxylase (AADC). The resulting products are then taken up by vesicular monoamine transporters (VMAT) for intravesicular storage. Intravesicularly, dopamine can, depending on the activity of specific enzymes, be further metabolized to noradrenaline and adrenaline. These vesicles are capable to release the end products dopamine, noradrenaline, and adrenaline in the extracellular environment. Selective re-uptake transporter systems, e.g., dopamine and noradrenaline transporters, are capable to transport these hormones back into the cell.

For the catecholamine pathway, both 6-^{18}F-L-3,4-dihydroxyphenylalanine (^{18}F-DOPA) and 6-^{18}F-dopamine are available as tracers. However, currently no data exist on the use of 6-^{18}F-dopamine for brain tumors or metastases in general, so this chapter will be limited to ^{18}F-DOPA.

^{18}F-DOPA can be produced via two different synthesis routes: regioselective fluorodestannylation (electrophilic fluorination) and nucleophilic fluorination, which is a multistep procedure. This last synthesis procedure is more

time-consuming but has the advantage of having readily available large quantities of no-carrier-added ^{18}F-fluoride (Jager et al. 2008; Lemaire et al. 1994).

The tracer ^{18}F-DOPA was developed and first studied in men at McMaster University, Hamilton, Canada, during the 1970s and 1980s of the last century (Garnett et al. 1983). In the first years after development of this tracer, it was solely used for imaging of the dopaminergic system of the brain. Several years later, the first whole-body scans in patients with NETs and other brain tumors were published (Heiss et al. 1996; Hoegerle et al. 2001).

Although data on the performance of ^{18}F-DOPA PET(/CT) imaging for the detection of neuroendocrine metastases outside the brain shows a high potential, unfortunately, no data are reported on the use of ^{18}F-DOPA for the detection of brain metastases of these tumors (Koopmans et al. 2008). For other brain tumors, like glioma, ^{18}F-DOPA has proven to be of value (Chen et al. 2006).

Since ^{18}F-DOPA is already commercially available in many countries, the increased availability may lead to a better understanding of the place of ^{18}F-DOPA PET in clinical decision-making for brain metastases of NETs.

42.8.2 Serotonin Pathway

Serotonin is a monoamine neurotransmitter present in the brain, blood platelets, and intestinal wall. In the brain, it acts as a neurotransmitter and plays a role in feelings of well-being.

The serotonin pathway shares the LAT and VMAT systems with the catecholamine pathway for transport and synthesis. In both pathways, the enzyme AADC plays a key role in the final step for the synthesis to a functional hormone, which is serotonin in the serotonin pathway.

After uptake via the LAT system, the amino acid tryptophan and the intermediate product 5-hydroxytryptophan (5-HTP) are used as precursors for the serotonin pathway. These precursors are decarboxylated to serotonin via the enzyme AADC. Serotonin is taken up via VMAT transporters into storage vesicles for future extracellular release. After release, serotonin is eventually metabolized to 5-hydroxyindole acetic acid (5-HIAA) which is secreted in the urine. The serotonin pathway is overactive in many NETs, which makes this pathway a good candidate for imaging with PET tracers (Koopmans et al. 2009).

The carbon-11-labelled tracer β-[^{11}C]-5-hydroxy-L-tryptophan (^{11}C-5-HTP) has been developed in the 1980s in the last century in Uppsala, Sweden, and is thus far the only suitable tracer for the serotonin pathway. The synthesis of this tracer is complex, demanding an on-site cyclotron for the production of the ^{11}C isotope which has a half-life of only 20 min. The synthesis requires two multi-enzyme steps (Bjurling et al. 1989; Neels et al. 2006). ^{11}C-5-HTP is therefore only produced by a few centers in the world. Image interpretation in the brain is mostly easy due to a very low background uptake and, at least in extracranial tumor localizations, a high tumor tracer uptake (Koopmans et al. 2008).

Due to the low worldwide tracer availability of ^{11}C-5-HTP, and the limited number of patients scanned with this tracer, no published data exist on the efficacy of ^{11}C-5-HTP PET for the detection of neuroendocrine tumor metastasis to the brain. Due to the biodistribution, however, it can be expected that this tracer likely results in good uptake in brain metastasis. Synthesis of this tracer is very difficult, which hampers widespread use and experience.

42.9 Conclusion

Due to the low incidence of neuroendocrine tumors and metastatic brain lesions of neuroendocrine tumors, inadequate data is available to determine the relative efficacy of nuclear medicine imaging techniques such as ^{68}Ga-DOTATOC PET, ^{18}F-DOPA PET, or, for example, ^{11}C-HTP for the detection of brain metastasis of neuroendocrine tumors. Although the incidence of brain metastasis in NET is rare, it appears that these patients show a worse survival compared to patients without brain metastases. More and more case reports published thus far mention the accidental finding of brain metastasis with PET techniques. From the data available and these case reports, it can be argued that it could be worthwhile to screen for brain metastases in patients conforming to the ENETS guidelines, to start appropriate treatment early. Nevertheless, MRI is still the recommended imaging modality for the detection of neuroendocrine brain metastasis. Research is warranted, although due to the low incidence, we can only hope for better data.

References

Adams S, Baum R, Rink T, Schumm-Drager PM, Usadel KH, Hor G (1998) Limited value of fluorine-18 fluorodeoxyglucose positron emission tomography for the imaging of neuroendocrine tumours. Eur J Nucl Med 25(1):79–83

Batson OV (1940) The function of the vertebral veins and their role in the spread of metastases. Ann Surg 112(1):138–149

Belhocine T, Foidart J, Rigo P, Najjar F, Thiry A, Quatresooz P, Hustinx R (2002) Fluorodeoxyglucose positron emission tomography and somatostatin receptor scintigraphy for diagnosing and staging carcinoid tumours: correlations with the pathological indexes p53 and Ki-67. Nucl Med Commun 23(8):727–734

Bjurling P, Watanabe Y, Tokushige M, Oda T, Långström B (1989) Syntheses of β-11C-labelled L-tryptophan and 5-hydroxy-L-tryptophan using a multi-enzymatic reaction route. J Chem Soc Perkin Trans 1(7):1331–1334

Carreras C, Kulkarni HR, Baum RP (2013) Rare metastases detected by (68)Ga-somatostatin receptor PET/CT in patients with neuroendocrine tumors. Recent Results Cancer Res 194:379–384. https://doi.org/10.1007/978-3-642-27994-2_20

Chen W, Silverman DH, Delaloye S, Czernin J, Kamdar N, Pope W et al (2006) 18F-FDOPA PET imaging of brain tumors: comparison study with 18F-FDG PET and evaluation of diagnostic accuracy. J Nucl Med 47(6):904–911

Cho KH, Hall WA, Gerbi BJ, Higgins PD, Bohen M, Clark HB (1998) Patient selection criteria for the treatment of brain metastases with stereotactic radiosurgery. J Neurooncol 40(1):73–86

Doddoli C, Barlesi F, Chetaille B, Garbe L, Thomas P, Giudicelli R, Fuentes P (2004) Large cell neuroendocrine carcinoma of the lung: an aggressive disease potentially treatable with surgery. Ann Thorac Surg 77(4):1168–1172. https://doi.org/10.1016/j.athoracsur.2003.09.049

Garnett ES, Firnau G, Nahmias C (1983) Dopamine visualized in the basal ganglia of living man. Nature 305(5930):137–138

Godwin JD II (1975) Carcinoid tumors. An analysis of 2,837 cases. Cancer 36(2):560–569

Granberg D, Wilander E, Oberg K, Skogseid B (2000) Prognostic markers in patients with typical bronchial carcinoid tumors. J Clin Endocrinol Metab 85(9):3425–3430

He BP, Wang JJ, Zhang X, Wu Y, Wang M, Bay BH, Chang AY (2006) Differential reactions of microglia to brain metastasis of lung cancer. Mol Med 12(7–8):161–170. https://doi.org/10.2119/2006-00033.He

Heiss WD, Wienhard K, Wagner R, Lanfermann H, Thiel A, Herholz K, Pietrzyk U (1996) F-Dopa as an amino acid tracer to detect brain tumors. J Nucl Med 37(7):1180–1182

Henze M, Schuhmacher J, Hipp P, Kowalski J, Becker DW, Doll J et al (2001) PET imaging of somatostatin receptors using [68GA]DOTA-D-Phe1-Tyr3-octreotide: first results in patients with meningiomas. J Nucl Med 42(7):1053–1056

Hlatky R, Suki D, Sawaya R (2004) Carcinoid metastasis to the brain. Cancer 101(11):2605–2613. https://doi.org/10.1002/cncr.20659

Hoegerle S, Altehoefer C, Ghanem N, Koehler G, Waller CF, Scheruebl H et al (2001) Whole-body 18F dopa PET for detection of gastrointestinal carcinoid tumors. Radiology 220(2):373–380

Hofland LJ, Lamberts SW (2003) The pathophysiological consequences of somatostatin receptor internalization and resistance. Endocr Rev 24(1):28–47

Hofmann M, Maecke H, Borner R, Weckesser E, Schoffski P, Oei L et al (2001) Biokinetics and imaging with the somatostatin receptor PET radioligand (68)Ga-DOTATOC: preliminary data. Eur J Nucl Med 28(12):1751–1757. https://doi.org/10.1007/s002590100639

Jager PL, Chirakal R, Marriott CJ, Brouwers AH, Koopmans KP, Gulenchyn KY (2008) 6-L-18F-fluorodihydroxyphenylalanine PET in neuroendocrine tumors: basic aspects and emerging clinical applications. J Nucl Med 49(4):573–586. https://doi.org/10.2967/jnumed.107.045708

Khan IU, Beck-Sickinger AG (2008) Targeted tumor diagnosis and therapy with peptide hormones as radiopharmaceuticals. Anti Cancer Agents Med Chem 8(2):186–199

Klein CA, Blankenstein TJ, Schmidt-Kittler O, Petronio M, Polzer B, Stoecklein NH, Riethmuller G (2002) Genetic heterogeneity of single disseminated tumour cells in minimal residual cancer. Lancet 360(9334):683–689. https://doi.org/10.1016/S0140-6736(02)09838-0

Kloppel G, Heitz PU, Capella C, Solcia E (1996) Pathology and nomenclature of human gastrointestinal neuroendocrine (carcinoid) tumors and related lesions. World J Surg 20(2):132–141

Koopmans KP, Neels OC, Kema IP, Elsinga PH, Sluiter WJ, Vanghillewe K et al (2008) Improved staging of patients with carcinoid and islet cell tumors with 18F-dihydroxy-phenyl-alanine and 11C-5-hydroxy-tryptophan positron emission tomography. J Clin Oncol 26(9):1489–1495. https://doi.org/10.1200/JCO.2007.15.1126

Koopmans KP, Neels ON, Kema IP, Elsinga PH, Links TP, de Vries EG, Jager PL (2009) Molecular imaging in neuroendocrine tumors: molecular uptake mechanisms and clinical results. Crit Rev Oncol Hematol 71(3):199–213. https://doi.org/10.1016/j.critrevonc.2009.02.009

Krenning EP, Bakker WH, Kooij PP, Breeman WA, Oei HY, de Jong M et al (1992) Somatostatin receptor scintigraphy with indium-111-DTPA-D-Phe-1-octreotide in man: metabolism, dosimetry and comparison with iodine-123-Tyr-3-octreotide. J Nucl Med 33(5):652–658

Krug S, Teupe F, Michl P, Gress TM, Rinke A (2019) Brain metastases in patients with neuroendocrine neoplasms: risk factors and outcome. BMC Cancer 19(1):362. https://doi.org/10.1186/s12885-019-5559-7

Kruger S, Mottaghy FM, Buck AK, Maschke S, Kley H, Frechen D et al (2011) Brain metastasis in lung cancer. Comparison of cerebral MRI and 18F-FDG-PET/CT for diagnosis in the initial staging. Nuklearmedizin 50(3):101–106. https://doi.org/10.3413/Nukmed-0338-10-07

Lamberts SW, Reubi JC, Krenning EP (1993) Validation of somatostatin receptor scintigraphy in the localization of neuroendocrine tumors. Acta Oncol 32(2):167–170

Lemaire C, Damhaut P, Plenevaux A, Comar D (1994) Enantioselective synthesis of 6-[fluorine-18]-fluoro-L-dopa from no-carrier-added fluorine-18-fluoride. J Nucl Med 35(12):1996–2002

Lepage C, Bouvier AM, Faivre J (2013) Endocrine tumours: epidemiology of malignant digestive neuroendocrine tumours. Eur J Endocrinol 168(4):R77–R83. https://doi.org/10.1530/EJE-12-0418

Maiuri F, Cappabianca P, Del Basso De Caro M, Esposito F (2004) Single brain metastases of carcinoid tumors. J Neurooncol 66(3):327–332

Modlin IM, Lye KD, Kidd M (2003) A 5-decade analysis of 13,715 carcinoid tumors. Cancer 97(4):934–959. https://doi.org/10.1002/cncr.11105

Nakamura Y, Shimokawa S, Ishibe R, Ikee T, Taira A (2001) Pulmonary carcinoid found in a patient who presented with initial symptoms of brain metastasis: report of a case. Surg Today 31(6):510–512

Neels OC, Jager PL, Koopmans KP, Eriks E, de Vries EGE, Kema IP, Elsinga PL (2006) Development of a reliable remote-controlled synthesis of β-[11C]-5-hydroxy-L-tryptophan on a Zymark robotic system. J Label Compd Radiopharm 49:889–895

Pasquali C, Rubello D, Sperti C, Gasparoni P, Liessi G, Chierichetti F et al (1998) Neuroendocrine tumor imaging: can 18F-fluorodeoxyglucose positron emission tomography detect tumors with poor prognosis and aggressive behavior? World J Surg 22(6):588–592

Patchell RA, Posner JB (1986) Neurologic complications of carcinoid. Neurology 36(6):745–749

Pavel M, Grossman A, Arnold R, Perren A, Kaltsas G, Steinmuller T et al (2010) ENETS consensus guidelines for the management of brain, cardiac and ovarian metastases from neuroendocrine tumors. Neuroendocrinology 91(4):326–332. https://doi.org/10.1159/000287277

Porter DG, Chakrabarty A, McEvoy A, Bradford R (2000) Intracranial carcinoid without evidence of extracranial disease. Neuropathol Appl Neurobiol 26(3):298–300

Reubi JC (1995) Neuropeptide receptors in health and disease: the molecular basis for in vivo imaging. J Nucl Med 36(10):1825–1835

Schnirer II, Yao JC, Ajani JA (2003) Carcinoid—a comprehensive review. Acta Oncol 42(7):672–692

Soga J (2003) Carcinoids and their variant endocrinomas. An analysis of 11842 reported cases. J Exp Clin Cancer Res 22(4):517–530

Sul J, Posner JB (2007) Brain metastases: epidemiology and pathophysiology. Cancer Treat Res 136:1–21

Weckbecker G, Lewis I, Albert R, Schmid HA, Hoyer D, Bruns C (2003) Opportunities in somatostatin research: biological, chemical and therapeutic aspects. Nat Rev Drug Discov 2(12):999–1017. https://doi.org/10.1038/nrd1255

Yamagi, L.Y.I., Wagner, J., Funari M.B.G. (2017)68Ga-DOTATATE PET/CT in nonneuroendocrine tumors: a pictorial essay. Clin Nucl Med 42(6):e313-e316

Traumatic Brain Injury: Nuclear Medicine Neuroimaging

43

Carlos A. Sanchez-Catasus, Gilles N. Stormezand, David Vállez García, Eloísa Le Riverend Morales, Reinaldo Galvizu Sánchez, and Rudi A. J. O. Dierckx

Contents

43.1 Introduction 1097
43.2 PET 1098
43.2.1 ^{18}F-FDG PET in the Acute Phase of Brain Trauma 1099
43.2.2 ^{18}F-FDG PET in the Chronic Phase of Brain Trauma 1103
43.2.3 PET Imaging of Specific Cellular Process in Brain Trauma 1108

C. A. Sanchez-Catasus (✉)
Division of Nuclear Medicine, Department of Radiology, University of Michigan, Ann Arbor, MI, USA

Department of Nuclear Medicine and Molecular Imaging, University Medical Center Groningen, Groningen, The Netherlands
e-mail: carlosas@umich.edu

G. N. Stormezand · D. Vállez García
Department of Nuclear Medicine and Molecular Imaging, University Medical Center Groningen, Groningen, The Netherlands
e-mail: g.n.stormezand01@umcg.nl; d.vallez-garcia@umcg.nl

E. Le Riverend Morales
Department of Vaccine Regulation, Finlay Institute, Havana, Cuba
e-mail: lochy@infomed.sld.cu

R. Galvizu Sánchez
Department of Nuclear Medicine, Center for Neurological Restoration (CIREN), Havana, Cuba
e-mail: rgalvizu@neuro.ciren.cu

R. A. J. O. Dierckx
Department of Nuclear Medicine and Molecular Imaging, University Medical Center Groningen, Groningen, The Netherlands

Department of Radiology and Nuclear Medicine, Ghent University, Ghent, Belgium
e-mail: r.a.dierckx@umcg.nl

R. A. J. O. Dierckx et al. (eds.), *PET and SPECT in Neurology*,
https://doi.org/10.1007/978-3-030-53168-3_43

43.3 Single-Photon Emission Computed Tomography (SPECT)..... 1113
43.4 Conclusions..... 1115
References..... 1115

Abstract

This chapter provides an up-to-date review of nuclear medicine neuroimaging in traumatic brain injury (TBI). Although the role of FDG PET may be limited in the acute phase due to the more rapid availability of CT or MRI, ^{18}F-FDG PET could remain a valuable tool in researching complex mechanisms associated with early metabolic dysfunction in TBI, particularly in the absence of structurally apparent brain damage. $^{15}O_2$-PET is also a solid technique for research in acute TBI, but in contrast to ^{18}F-FDG PET, it is not widely available due to its high cost. In the chronic TBI phase, most ^{18}F-FDG PET studies converge to identify a diffuse cortical–subcortical hypometabolism involving key regions for cognitive function. In these cases, FDG PET may also be used for the evaluation of therapeutic interventions. More recently, research has focused on the imaging of specific pathological processes, such as neuroinflammation and accumulation of tau, as well as on distinct entities as chronic traumatic encephalopathy and the post-concussion syndrome. In this light, the in vivo demonstration of tau deposits in athletes exposed to repetitive head injury has gained special interest. These techniques may provide useful information, especially in situations where structural damage typically fails to show a pathologic substrate. Despite a paucity of recent research publications, SPECT may still be regarded a valid alternative for the study of TBI.

Abbreviations

AChE	Acetylcholinesterase
BP	Binding potential
BP_{ND}	Non-displaceable binding potential
BZR	Central-type benzodiazepine receptor
C-(R)-PK11195	1-[2-Chlorophenyl]-*N*-methyl-*N*-[1-methylpropyl]-3-isoquinoline carboxamide
CBF	Cerebral blood flow
C-MP4A	[Methyl-^{11}C]*N*-methylpiperidyl-4-acetate
CMRFDG	Cerebral metabolic rate of FDG
CMRglc	Cerebral metabolic rate of glucose
$CMRO_2$	Cerebral metabolic rate of oxygen
C-NMSP	^{11}C-*N*-methylspiperone
CT	Computed tomography
CTE	Chronic traumatic encephalopathy
D_2	Dopamine receptor type 2
DAI	Diffuse axonal injury

DTI	Diffusion tensor imaging
FIQ	Full-scale intelligence quotient
FMZ	Flumazenil
GCS	Glasgow Coma Scale
GM	Gray matter
GOS	Glasgow Outcome Scale
L/N ratio	Lesion-to-normal contralateral ratio
MRI	Magnetic resonance imaging
NSC	Neural stem cell
OEF	Oxygen extraction fraction
OGR	Oxygen-to-glucose metabolic ratio
ROI	Regions of interest
SPM	Statistical parametric mapping
TBI	Traumatic brain injury
TSPO	Translocator protein
V/C ratio	Vermis-to-cerebellum ratio
WM	White matter

43.1 Introduction

Traumatic brain injury (TBI) is described as a traumatically induced disruption of the brain, in the presence of one of the following symptoms: loss of consciousness, anterograde or retrograde memory loss, alterations of the mental state at the time of the incident, or focal neurological deficits. The worldwide prevalence of TBI demands global attention and effective actions involving all levels of society. The annual incidence of TBI has been estimated to be up to 500 per 100,000 inhabitants in the European Union and the United States, causing 200 out of every 100,000 hospital admissions (Faul et al. 2010; Stryke et al. 2007; Tagliaferri et al. 2006). Worldwide incidence is growing mainly due to traffic accidents, with a higher increase in developing countries (WHO/OMS 2009). Not less important is the rise of the social and economic TBI burden because of military conflicts and civilian exposure in war zones. TBI as a consequence of sports practice and recreational activities should not be underestimated either. TBI has devastating effects on patients and their families due to death or chronic disabilities, with high socioeconomic cost throughout the world. Therefore, a widespread international effort is necessary to reduce TBI causes as much as possible and at the same time to increase knowledge on this complex disease that will allow mitigating or reverting short- and long-term outcomes.

TBI includes a wide and heterogeneous spectrum of pathologies ranging from focal damage caused by contusion (with or without cranial fracture) to diffuse axonal injury (DAI), including complex secondary pathophysiological processes (Zasler et al. 2007), which could be aggravated by systemic events, patient age, or preexisting chronic disease. In many cases, TBI may secondarily lead to epilepsy

(Frey 2003), and after aging, it is the most important nongenetic factor that increases the risk of dementia (McKee et al. 2009), including chronic traumatic encephalopathy.

Immediate clinical TBI consequences are directly related to the severity, mechanism, location, and duration of the impact (Maas et al. 2008). Conventional computed tomography (CT) is the technique of choice for the initial evaluation of TBI patients because it enables detection of fractures and helps to decide whether the patient requires an immediate surgical intervention, when focal injury with hematomas is suspected (Kubal 2012). When results on CT are unclear or negative, MRI may be performed to demonstrate occult traumatically induced injury, such as microhemorrhages (Haller et al. 2018). After the initial examination, secondary damage—indirect consequences of trauma—may contribute significantly to short- and long-term impairment, which is especially due to cell and inflammatory damage (Park et al. 2008). Secondary damage is a key concept, since it opens doors to treatment methods for preventing and limiting secondary injury. Neuroimaging using nuclear medicine techniques also has great potential for studying secondary damage and may serve as a guide to evaluate several therapeutic approaches.

In this chapter, a review of several relevant contributions of nuclear medicine neuroimaging toward improved understanding of TBI is presented, using both positron emission tomography (PET) and single-photon emission computed tomography (SPECT). Various articles published in the last years, which summarize current knowledge on the roles of PET and SPECT, could be considered starting points for new research and clinical applications. The molecular basis of both techniques, especially PET, provides unique possibilities for studying complex cellular processes that take place in TBI, which are not yet fully understood.

43.2 PET

Despite the large number of studies using PET in TBI, in which the usefulness of this technique was shown in several clinical settings, there is no meta-analysis clarifying the importance of this technique either by itself or by complementary to structural neuroimaging. This is mostly due to the clinical heterogeneity and complexity of TBI, reflected in the diversity of studies published with regard to several aspects: first, differences in the time elapsed between the moment of injury and image acquisition; second, differences in patient characteristics with respect to TBI severity; third, differences in PET radiotracers; fourth, differences in methodological designs; and fifth, the use of different image analysis methodologies. In addition, no prospective randomized, blinded clinical trials have been conducted for obtaining major evidence, which can partly be explained by the high cost of such studies that require several years of follow-up. It is not surprising that such studies are scarce in medical imaging, including conventional CT and MRI (Medina et al. 2011).

43.2.1 ^{18}F-FDG PET in the Acute Phase of Brain Trauma

The first ^{18}F-FDG PET studies in TBI patients appeared in the 1980s and 1990s (Rao et al. 1984; Langfitt et al. 1986; Alavi 1989; Alavi et al. 1997; Tenjin et al. 1990; Yamaki et al. 1996; Fontaine et al. 1999). They pointed out that abnormalities detected by ^{18}F-FDG PET were more extensive than those observed by CT and that it was possible to detect them very early when structural modalities could still be negative. In those years, PET was still restricted to very few centers in the world. This situation began to change after the beginning of the present century. One of the predominant issues from the 1990s to date has been the study of brain metabolism in the acute phase of TBI. Findings of Bergsneider et al. (1997, 2000, 2001) suggested the existence of a triphasic pattern in the cerebral metabolic rate of glucose (CMRglc) measured by ^{18}F-FDG PET. This pattern had been previously observed in animal models. The first and brief hyperacute phase is characterized by an increase of metabolic activity and followed by a second, relatively prolonged, period of reduced metabolism (for a month approximately), until a stable level within normal limits is achieved again. However, later studies have found that regional diffuse deficits may persist chronically (this will be discussed in Sect. 43.2). These studies also suggested that during the intermediate phase, there was disassociation between the global CMRglc and the level of consciousness measured by the Glasgow Coma Scale (GCS) (Bergsneider et al. 2000). The paper published by this group in 2001 is particularly interesting (Bergsneider et al. 2001). Fifty-four patients in acute phase (2–39 days post onset), with the three degrees of severity defined by the GCS (34 severe and 20 moderate or mild), were studied. ^{18}F-FDG PET scan was repeated in 13 patients during trauma evolution (6–15 months after the onset of injury). In the whole sample, the authors found the previously mentioned triphasic pattern, independent of the degree of TBI severity, suggesting that the degree of TBI severity does not affect the time course of CMRglc changes. In a follow-up study on 13 patients with ^{18}F-FDG PET, no relationship was found between CMRglc changes and neurological state changes measured by the disability rating scale. The authors concluded that ^{18}F-FDG PET should not be used as a surrogate marker to estimate the degree of functional recovery following TBI.

On the other hand, Hattori et al. (2003) using a new generation of PET scanners with better spatial resolution, capable of identifying smaller brain regions, demonstrated in 23 acute-phase patients (5 days post onset) that, unlike global CMRglc, there was a direct association between level of consciousness measured by GCS and CMRglc values for the thalamus, brain stem, and cerebellum. This study significantly contributed to a better understanding of how the level of consciousness and brain glucose metabolism measured by ^{18}F-FDG PET are related.

Three articles published by the UCLA group in 2004 made the role of ^{18}F-FDG PET in the acute phase of TBI even clearer (Hattori et al. 2004; Wu et al. 2004a, b). The first of these papers was a thorough characterization of brain tissue ^{18}F-FDG kinetics during the acute phase (Hattori et al. 2004). In this study, the authors characterized ^{18}F-FDG uptake, transport, and hexokinase activity using kinetic

modeling. The study group comprised 21 TBI patients with cerebral contusions. Cerebral blood flow (CBF) was also evaluated by dynamic $H_2{}^{15}O$-PET. Results demonstrated that hexokinase activity was reduced in the entire brain, including apparently undamaged brain cortex, while glucose transport and CBF were reduced only in pericontusional areas. Seven patients showed regionally increased ^{18}F-FDG uptake in pericontusional areas, probably associated with residual regional increase of hexokinase activity during the hyperacute phase (first phase of the triphasic pattern).

Hypotheses taken into account to explain focal pericontusional hyperglycolysis were anaerobic glycolysis, ionic disturbance, release of excitatory amino acids, and glycolysis due to increased glutamate activity. Bearing in mind that glycolysis takes place mainly in glial cells, authors suggested that an increase in glial metabolic activity was a possible cause of hyperglycolysis.

The following study was inspired by an important observation (Wu et al. 2004a) concerning the fact that gray matter (GM) to white matter (WM) contrast in ^{18}F-FDG PET images is reduced in patients with acute TBI, with or without focal damage, compared to normal healthy controls. Interestingly, this reduction was not observed in $H_2{}^{15}O$-PET of CBF in the same patients. For this reason, the authors hypothesized that changes of glucose metabolism in the acute phase were different in GM and WM. They studied 14 patients with severe to moderate TBI (0–4 days post onset), all with structural focal abnormalities by CT. In all subjects, ^{18}F-FDG PET, triple dynamic ^{15}O-PET ($C^{15}O$, $O^{15}O$, $H_2{}^{15}O$), and MRI were carried out. Initial GCS at onset and the Glasgow Outcome Scale (GOS) 12 months post onset were also evaluated. Peri-hemorrhagic regions were excluded from the analysis. For comparison, a control group of 18 healthy subjects was studied. The results showed that the GM-to-WM ratio in ^{18}F-FDG PET images was significantly reduced in the TBI group. Although a global reduction of CMRglc was observed in the patients, as expected from the previous study (Hattori et al. 2004), CMRglc and hexokinase activity were selectively reduced in the GM and not in the WM. Significant changes of global CBF were not found in GM or in WM, corroborating that glucose supply to the brain was not limited. Even more interesting was the finding that the GM-to-WM ratio was positively correlated with the initial GCS and patients with higher GM-to-WM ratio showed better recovery (GOS) after 12 months. Before this study, physiological changes occurring in WM after TBI had received less attention compared to changes in GM. Based on prior observations in animal models, the authors considered several hypotheses to explain the unexpected finding that there were no significant changes in CMRglc in WM (or that it was increased with respect to the global CMRglc). One of these hypotheses is that in WM there was a combination of infiltration of inflammatory cells and reactive gliosis after TBI, which was probably associated with DAI.

The third article of the UCLA group (Wu et al. 2004b) was a direct consequence of the aforementioned study. The authors examined the relationship between glucose and oxygen metabolism in WM in the acute phase to determine the nature, extension, and degree of abnormalities in regions remote from hemorrhagic lesions. The study sample was essentially the previous one and using the same image

acquisitions (PET and MRI). Five types of quantitative images were generated: CMRglc, CBF, cerebral metabolic rate of oxygen ($CMRO_2$), oxygen extraction fraction (OEF), and oxygen-to-glucose metabolic ratio (OGR). The results corroborated that CMRglc was reduced only in GM. CBF and OEF were preserved, while $CMRO_2$ was reduced in both GM and WM. The main result was that OGR was selectively reduced in WM. Thus, this study showed that acute metabolic changes in WM had a particular feature, characterized by $CMRO_2$ depression, without parallel depression of CMRglc, suggesting a nonoxidative use of glucose in this region during the acute phase. These findings were present throughout WM, even in regions without evidence of DAI based on conventional MRI images, thus suggesting that DAI detected by multimodal PET was much more extensive and subtle than that detected by conventional MRI. As possible explanations for these findings, authors indicated an increase in inflammatory cells during the acute phase, especially in the WM, which are more prone to anaerobic glycolytic metabolism. Combining results published by the UCLA group between 2003 and 2004 (Hattori et al. 2003, 2004; Wu et al. 2004a, b), the state of coma was shown to involve a thalamocortical disconnection with a clearly defined metabolic substrate, and a prognostic value of ^{18}F-FDG PET was suggested (Wu et al. 2004a).

Complexity of metabolic dysfunction during the acute phase continues to be the object of current research and debate. Findings from the Cambridge University group, combining microdialysis and ^{18}F-FDG PET studies, did not support the hypothesis of nonoxidative metabolism associated with an increase in glucose cerebral metabolism in the acute phase (Hutchinson et al. 2009; O'Connell et al. 2005).

On the other hand, another study indicated that early dysfunction of nonischemic oxidative metabolism in the acute phase leads to chronic brain atrophy in TBI patients (Xu et al. 2010). This study showed that both cortical CMRglc and $CMRO_2$ were reduced in the acute phase, even in apparently normal areas by MRI. However, the extent of regional brain atrophy 6 months after TBI correlated better with $CMRO_2$ and CBF, particularly in the frontal and temporal lobes ($N = 32$). CMRglc correlated with atrophy only in the frontal lobe. They also found that OEF was not in the ischemic range and did not correlate with chronic brain atrophy. These results emphasized the fact that chronic brain atrophy is related with early metabolic changes, especially in brain areas not directly damaged during TBI.

Another work carried out a longitudinal study in vivo that identified and traced the spatial and temporal metabolic and structural changes in an experimental TBI model in rats (Liu et al. 2010). Images were acquired 1 week and 1, 3, and 6 months post TBI by micro^{18}F-FDG PET and microMRI in 16 rats with lateral fluid percussion injury and 11 control rats (sham procedure). Using several methods of image analysis, including statistical parametric mapping (SPM), the authors found that regions with hypometabolism at 1 week and 1 month after TBI were essentially the same that subsequently showed progressive atrophy by microMRI. Hypometabolism was highest at 1 month but persisted in the study at 6 months in the ipsilateral amygdala. Disagreement was also found between structural and metabolic changes. Hypometabolism decreased or resolved at 6 months and preceded atrophy. Atrophy continued progressing for up to 6 months. Hippocampi changed shape with

reduction in volume, and both sides showed different patterns of change. The most interesting observation in this study was that both structural and functional changes seemed to consolidate between 3 and 6 months, suggesting that the temporal window to intervene and limit secondary neurodegenerative damage (atrophy) may be wider than expected.

In our view, ^{18}F-FDG PET will remain a valuable tool in researching complex mechanisms associated with early metabolic dysfunction in TBI, presently not well understood. Future research may benefit from more stringent inclusion of patients based on the timing and the type of trauma. From a clinical point of view, although appropriate clinical trials are still needed to provide more evidence, ^{18}F-FDG PET in the TBI acute phase appeared to be more useful and to show incremental validity (prognostic information) in those patients in whom CT (or MRI) failed to show damage explaining their neurological state. Of note, as has been addressed in a critical review in 2014, CMRglc values may be less reproducible in patients with traumatic brain injury, as the lumped constant—CMRFDG divided by CMRglc—could be altered after traumatic brain injury (Byrnes et al. 2014). With the growing number of hybrid PET–CT and PET/MRI systems and ^{18}F-FDG availability, combined studies of both structural and functional damage are now more feasible. This could facilitate acquisition of multicenter databases to carry out evidence-based imaging studies that enable demonstration of incremental validity of ^{18}F-FDG PET. Cost-effectiveness analysis is also necessary to compare ^{18}F-FDG PET with MRI-based techniques, such as diffusion tensor imaging (DTI), magnetization transfer imaging, magnetic resonance spectroscopy, and functional magnetic resonance (Hunter et al. 2012).

43.2.1.1 $^{15}O_2$-PET

TBI consequences are not only determined by primary injury but also by subsequent neuronal death due to secondary damage, which already starts during the acute phase. For this reason, the main strategy in TBI patient management, especially those in critical neurological state, is to prevent or limit secondary damage as much as possible (Park et al. 2008). Secondary damage can be initiated or aggravated by hypoperfusion, arterial hypotension, hypoxemia, autoregulation failure, as well as metabolic, immunologic, and biochemical changes. Although delayed ischemia is one of the routes of secondary damage, reperfusion can also take place, elevating intracranial pressure, reducing perfusion pressure, and finally reducing CBF again.

Triple dynamic $^{15}O_2$-PET is the best technique for determining true ischemia because it is the only one that can simultaneously measure CBF, $CMRO_2$, and OEF globally and regionally. To demonstrate true ischemia, it is not enough to demonstrate that CBF is reduced, since this could be a response to $CMRO_2$ decrease (flow metabolism coupling). Therefore, it is essential to demonstrate that CBF is also inadequate for the oxygen demand, which means confirming a significant OEF increase in the ischemic range.

Since the beginning of this century, several articles have been published about triple $^{15}O_2$-PET studies that have allowed a deepened understanding of regional

ischemia mechanisms in acute TBI. Some studies have demonstrated significant regional ischemia in the first hours after TBI (Coles et al. 2004a; Coles and Fryer 2004; Abate et al. 2008), while in other studies, ischemia has been less evident (Wu et al. 2004b; Vespa et al. 2005; Kawai et al. 2008; Xu et al. 2010). This apparent contradiction could be due to the heterogeneity and complexity of TBI. Another explanation for these contradictory results has been provided by triple $^{15}O_2$-PET studies (Cunningham et al. 2005). The authors found that unlike classical acute ischemia (stroke), the quantitative CBF threshold that defines irreversible ischemia did not discriminate correctly between surviving and irreversibly damaged tissue acutely post TBI ($N = 14$). Although the quantitative $CMRO_2$ threshold was comparable to the threshold reported for brain infarction, extensive overlapping was found for both tissues. From this study, the hypothesis emerged that selective neuronal death could be present in apparently surviving regions, which are not visible in conventional MR images that better identify regions with pan-necrosis. Studies using ^{11}C-flumazenil (FMZ) seem to corroborate this idea. ^{11}C-FMZ PET studies in TBI patients are examined in the next subsection of this chapter.

Other $^{15}O_2$-PET studies have allowed examination of new hypotheses about additional mechanisms of hypoxia and energetic failure, such as metabolic suppression, mitochondrial dysfunction, and microvascular disease in the acute phase of TBI (Menon et al. 2004; Vespa et al. 2005; Robertson 2004). Other studies have proven useful to evaluate the impact of therapeutic interventions in critical state patients (Coles et al. 2004b, 2006; Johnston et al. 2005; Diringer et al. 2007, 2011; Nortje et al. 2008) and in animal models of TBI (Ley et al. 2009; Ley and Park 2010). $^{15}O_2$-PET studies also validated and refined bedside monitoring technologies, which facilitate continuous monitoring of cerebrovascular physiology (Hutchinson et al. 2002; Gupta et al. 2002; Coles et al. 2004b). Bedside monitoring has the advantage of continuous temporal monitoring of CBF, autoregulation, and metabolic state of the patient (Dagal and Lam 2011). The main difficulty is that it can only monitor a small area of the brain, unlike $^{15}O_2$-PET which allows studying the whole brain in a more quantitative way. The main disadvantages of $^{15}O_2$-PET are that continuous monitoring is not possible and the patient must be moved from the intensive care unit to the scanner and the high cost of the cyclotron. In our opinion, $^{15}O_2$-PET is a solid technique for research into the complex pathophysiology of acute TBI, but in contrast to ^{18}F-FDG PET, it is not widely available due to its high cost. Also it presents a more logistical challenge, when compared to perfusion CT or MRI. Therefore, it is used mainly in research and less in clinical practice.

43.2.2 ^{18}F-FDG PET in the Chronic Phase of Brain Trauma

In the last years, there have been important advances in the care of neurocritical patients after TBI, resulting in a significant decrease of mortality (Bullock et al. 2007). However, TBI survivors frequently suffer from a wide variety of chronic cognitive, emotional, and behavioral disorders that hinder return to normal social and work life. Persistent vegetative state is the worst final outcome.

Neural networks connecting brain cortical and subcortical regions are crucial to maintain normal cognitive function (Bassett and Bullmore 2009). TBI damages, both primary and secondary, can impair not only particular nodes of these networks (focal damage) but also the wiring (DAI). Focal damage is easily identifiable both in structural and functional neuroimages, unlike DAI which can be underestimated by routine structural imaging in many patients.

Findings of the UCLA group in acute TBI using ^{18}F-FDG PET already suggested a thalamocortical disconnection as the cause of coma (Hattori et al. 2004; Wu et al. 2004a, b). Cortical–subcortical disconnection may persist to a larger or lesser extent in many patients in the chronic phase after TBI. ^{18}F-FDG PET studies in chronic TBI patients have allowed characterization and unveiling of many aspects of this cortical–subcortical disconnection. The use of voxel-based image analysis methods, especially SPM (Friston 1994), is common in several of these studies. Unlike the methods based on regions of interest (ROI), SPM enables analysis of the whole-brain volume voxel by voxel, without prior spatial hypothesis. In this regard, the exploration range is considerably broadened, giving in many cases unexpected results that reveal subtle information contained in the images, which are very difficult to extract using the visual qualitative method or ROI analysis. Table 43.1 summarizes the findings of FDG PET in the chronic phase of traumatic brain injury. Taken together, studies point toward the presence of corticothalamic deficits which carry an association with the neurological outcome, even without structural abnormalities. In addition to neuronal loss, altered ionic states, protein synthesis inhibition, CBF reduction, and alterations of the neurotransmitter systems could be involved to explain these findings (Marklund et al. 2009). Preliminary studies indicated that abnormalities at baseline may be monitored using FDG PET to evaluate the effectivity of treatment regimens. Kraus et al. (2005) evaluated the effects of amantadine. Amantadine is a dopaminergic agent and *N*-methyl-D-aspartate (NMDA) receptor antagonist. The results showed significant improvement of the executive function in a group of patients after amantadine therapy ($N = 22$). Analysis of ^{18}F-FDG PET images also showed a significant increase in the metabolism of the left prefrontal cortex. This region correlated positively with the executive function in the patient group.

Two more recent studies evaluated the effects of donepezil, an acetylcholinesterase inhibitor, and memantine, a noncompetitive NMDA receptor antagonist (Kim et al. 2009, 2010). The study using donepezil (Kim et al. 2009) included two groups of patients with cognitive impairment after TBI (mean interval after injury = 5.2 months). The control group was treated only with rehabilitation ($N = 13$). The other group received rehabilitation plus donepezil medication ($N = 13$). In the donepezil-treated group, ^{18}F-FDG PET and neuropsychological test studies were carried out at treatment onset and completion. In the control group, only neuropsychological tests were performed. ^{18}F-FDG PET images were analyzed by SPM. At the beginning of the study, no significant differences in cognitive function of both groups were observed. At the end, the group given donepezil showed a significant improvement in cognitive functions compared with controls and a significant bilateral increase of cortical metabolism in the frontal, parietal, occipital, and temporal regions.

Table 43.1 FDG PET in chronic phase of traumatic brain injury

Authors	Subjects	Design/methods	Main results	Specifications
Nakayama et al. (2006)	Chronic TBI patients (higher dysfunction) ($N = 22$), minimally conscious state ($N = 13$), persistent vegetative state ($N = 17$), controls ($N = 30$)	Cross-sectional, SPM analysis	Bilateral hypometabolism pattern involving prefrontal medial region, medial frontobasal region, anterior and posterior regions of the cingulate gyrus, and thalamus	This pattern was more extensive and prominent in the group in persistent vegetative state and less in the group with higher brain dysfunction, with an intermediate level in the group with minimally conscious state
Kato et al. (2007)	Patients with clinical DAI ($N = 32$), controls ($N = 30$)	Cross-sectional, SPM, correlation analysis between regional metabolism and neuropsychological variables in the patient group	Full-scale intelligence quotient (FIQ) was found to correlate positively with metabolism in the right cingulate gyrus and the bilateral medial frontal region	
Nakashima et al. (2007)	DAI patients with neurological deficits ($N = 12$) and controls ($N = 32$)	Cross-sectional, SPM, case-by-case analysis using 3D stereotactic surface projection (SSP)	Group comparison revealed hypometabolism in the cingulate, lingual, and cuneus gyrus. Case-by-case analysis showed differences regarding the site and extension of hypometabolism in the cingulate gyrus, although hypometabolism was more frequent in the medial region of the cingulate gyrus (six patients)	
Lupi et al. (2007)	Chronic TBI ($N = 57$) and controls ($N = 57$)	Cross-sectional, visual and ROI analysis	Results showed that in most patients, there was visually increased ^{18}F-FDG uptake in the cerebellar vermis. V/C also showed a significant increase in the patients compared to controls	The time elapsed between the acute phase and the ^{18}F-FDG PET was highly variable in the patient sample (15 days–4 years)
Lupi et al. (2011)			Strong correlation between V/C ratio and the severity of TBI as determined by cognitive and performance testings. Good correlation between V/C ratio determined shortly after TBI and the clinical outcome	Findings suggest that V/C ratio may be considered an index of brain suffering

(continued)

Table 43.1 (continued)

Authors	Subjects	Design/methods	Main results	Specifications
Zhang et al. (2010)	Chronic TBI patients ($N = 81$) and controls ($N = 68$), subgroups with ($N = 35$) and without ($N = 40$) structural abnormalities	Cross-sectional, SPM analysis.	Group comparison showed extensive bilateral hypometabolism in the cerebral cortex (including the frontal and temporal lobes) and the thalamus. Cluster counting analysis showed that patients with TBI (with or without structural lesion) had a higher proportion of large clusters of hypometabolism, and they were closer to the brain edge when compared with controls	One of the most interesting findings was that the cortical–subcortical hypometabolism was similar in patients with or without structural lesion, suggesting that abnormal patterns of metabolism are similar in patients with focal or diffuse TBI
Lull et al. (2010)	Controls ($N = 10$), a group with minimally conscious or persistent vegetative state ($N = 17$), a group with posttraumatic amnesia ($N = 12$), and a group with patients emerging from posttraumatic amnesia ($N = 20$)	Cross-sectional, SPM	Hypometabolism in the thalamus was directly related to the neurological outcome	This region was the most sensitive structure when patients in different neurological states were compared, despite the small percentage of patients with structural thalamic lesions in the three groups
Garcia-Panach et al. (2011)	Same groups as Lull et al.	Cross-sectional, SPM	Significant correlation between neurological outcome and glucose metabolism in all brain regions analyzed (precuneus, frontal and temporal lobes, and thalamus); there was also a direct relationship between hypometabolism and disease severity	
Ito et al. (2016)	Patients with chronic mild/moderate traumatic brain injury ($N = 90$), with ($N = 50$) and without ($N = 40$) visible lesions on MRI	Cross-sectional, SPM	Significant decrease of metabolisms in the orbital gyrus, cingulate gyrus, and medial thalamus but increased in the parietal and occipital convexity in subjects with MRI abnormalities, but not in those without	

In the memantine study (Kim et al. 2010), a group of 17 TBI patients were evaluated (mean post-onset duration = 6.8 months). ^{18}F-FDG PET was done at the beginning and after completion of the treatment. Furthermore, a covariance analysis was performed to assess if metabolic enhancement correlated with increases in mini-mental status examination (MMSE) scores. ^{18}F-FDG PET image analysis was performed by SPM. Results showed that MMSE scores were significantly improved after memantine treatment. When ^{18}F-FDG PET data acquired before and after treatment were compared, a significant increase of metabolism in the prefrontal region and the parietal association cortex was observed. A significant correlation was also found between MMSE and metabolism in the prefrontal regions and the association parietal cortex of the left hemisphere.

Distinct mechanisms may be at play in two entities we will briefly address in the next two subsections: chronic traumatic encephalopathy and the post-concussion syndrome.

43.2.2.1 Chronic Traumatic Encephalopathy

Chronic traumatic encephalopathy is a neurodegenerative disease resulting from repetitive head injury, which involves the development of long-term neuropsychiatric sequelae. Since the neuropathological studies of Omalu et al. in American football players (Omalu et al., 2010)—which became the subject of the popular movie "Concussion"—the impact of repetitive head injury in sports and associated chronic traumatic encephalopathy has gained attention, both in research and in society. Symptoms vary according to the stage but may be related to behavior, mood, or cognition. Neuropathologically, it is characterized by deposition of hyperphosphorylated tau (p-tau) protein as neurofibrillary tangles, astrocytic tangles, and neurites in clusters around small blood vessels of the cortex, preferentially located around small vessels in the depths of sulci (McKee et al. 2016). In recent years, tau PET ligands have become available allowing in vivo identification of tauopathies. Stern and colleagues demonstrated increased Standardized Uptake Value Ratios (SUVRs) using flortaucipir PET in the former American Football League players, a population particularly prone to CTE, primarily in the bilateral superior frontal, bilateral medial temporal, and left parietal regions (Stern et al. 2019). Takahata et al. using another tau ligand, ^{11}C-PBB3, determined the "binding capacity" in patients with a history of severe TBI of repetitive head injury ($n = 30$) and controls ($n = 16$). Binding capacity was significantly increased in widespread brain regions in patients, whereas clinical symptoms (diagnosis of traumatic encephalopathy syndrome) in the patient group were related to increased binding capacity in the white matter (Takahata et al. 2019). This group also demonstrated PBB3 binding to neurofibrillary tangles in cortical gray matter by means of PBB3 fluorescence labelling and immunofluorescence of autopsied TBI brains, albeit not in the same group of patients. These results seem to confirm the potential of PET to detect tauopathy in vivo in chronic TBI patients, although it is generally noted that the tau load is significantly less when compared to Alzheimer's disease. In the context of cognitive decline after repetitive head injury, additional amyloid positivity may be demonstrated using ^{11}C-PIB scanning (Okonkwo et al. 2019).

43.2.2.2 Post-concussion Syndrome

The "post-concussion syndrome" is a complex disorder in which symptoms—such as headaches and dizziness—may persist for weeks of months after a mild traumatic brain injury. These symptoms are often present in the absence of structural brain damage, which has also been described as "complicated" mild traumatic brain injury (Lange et al. 2009). Komura and colleagues studied 89 patients who suffered a single blunt mild traumatic brain injury without structural abnormalities and persistent mental and cognitive problems (Komura et al. 2019). Reduced metabolism was reported in the bilateral prefrontal area and significantly increased around the limbic system in the patient group compared with normal controls, which is different from patterns typically implicated in DAI. Mild chronic TBI due to cerebral concussion caused by repeated blast exposure in war zones has also been evaluated using ^{18}F-FDG PET (Peskind et al. 2011). The study included a group of Iraq war veterans ($N = 12$) and a control group ($N = 12$). The patient group showed hypometabolism in the cerebellum, vermis, pons, and medial region of the temporal lobe. The patients had mild cognitive dysfunction similar to that reported for patients with cerebellar lesions.

43.2.3 PET Imaging of Specific Cellular Process in Brain Trauma

Since the mid-2000s, several papers of great interest using other PET radiotracers to study specific cellular processes in TBI pathophysiology have been published. An example of these is ^{11}C-flumazenil (FMZ), which is a marker of central-type benzodiazepine receptor (BZR). FMZ binding, i.e., coupling of BZRs with GABA-A receptors, can be used as a marker of neuronal viability. The first study using $^{15}O_2$-PET and ^{11}C-FMZ PET (the binding potential of FMZ) investigated the relation between $CMRO_2$ abnormalities and loss of neuronal integrity in symptomatic patients with chronic TBI ($N = 10$), without structural abnormalities detected by MRI (Shiga et al. 2006). The study included a control group ($N = 10$). Image evaluation was done using ROI analysis. $CMRO_2$ abnormalities were observed in all patients, while reduced uptake in ^{11}C-FMZ BP images was only found in six patients. Reduced uptake in ^{11}C-FMZ BP images was accompanied by abnormalities in $CMRO_2$ images. In 15 lesions observed in $CMRO_2$ images, no abnormalities were found in ^{11}C-FMZ BP images, suggesting that ^{11}C-FMZ PET can be useful for differentiating hypometabolism caused by selective neuronal loss from hypometabolism caused by other factors. A more recent study using ^{11}C-FMZ PET aimed at identifying regional neuronal damage occurring in chronic diffuse TBI patients with neuropsychological impairment ($N = 8$) (Kawai et al. 2010). The study included a control group ($N = 20$). 3D SSP group comparisons showed significant bilateral reductions of ^{11}C-FMZ uptake in the frontal medial gyrus, anterior cingulate gyrus, and thalamus. Case-by-case analysis also found reduced ^{11}C-FMZ uptake in these regions, although the distribution and extent were different in each case. Furthermore, FIQ and performance IQ were negatively correlated with the degree of ^{11}C-FMZ BP

reduction in the right thalamus. Likewise, FIQ, verbal IQ, and performance IQ were negatively correlated with the degree of ^{11}C-FMZ BP reduction in the left frontal medial gyrus.

We consider that even though these results are promising for detection of selective neuronal loss in patients with chronic diffuse TBI, they still require validation in larger patient samples and improvement of quantification methods. A recent study was aimed at validating reference tissue kinetic modeling of ^{11}C-FMZ PET within a group of patients with TBI (Geeraerts et al. 2011). ^{11}C-FMZ PET imaging were performed on controls (N = 16) and patients (N = 11) at least 6 months after TBI. Regional non-displaceable binding potentials (BP_{ND}) were estimated from five reference tissue models and compared to BP_{ND} from arterial input models. Total distribution volume of the pons was not significantly different between controls and patients. BP_{ND} from all the reference tissue approaches significantly correlated with BP_{ND} from the plasma input models for control and patient groups. Thus this study demonstrated the validity of the pons as a reference region for calculating ^{11}C-FMZ BP in apparently normal and perilesional regions in patients with chronic TBI.

More recently, adenosine receptor imaging has been used in an effort to identify neuronal and axonal injury in patients in the chronic phase of DAI. Hayashi and colleagues used A_1 receptor (A1R) [1-methyl-^{11}C] 8-dicyclopropylmethyl-1-methyl-3-propylxanthine (MPDX) PET in ten patients in the chronic phase of DAI and reported increased BPs in the lower frontal lobe, posterior cingulate cortex, and rolandic cortex, without any apparent decreases in BP (Hayashi et al. 2018). These areas did not correlate with regions of decreased ^{11}C-FMZ binding in the same patients, suggesting that the observed alterations using MPDX PET reflect neuroprotective effects rather than neuronal loss.

Another specific cell process recently examined in chronic TBI is the activity of the cholinergic system (Östberg et al. 2011). This preliminary study was carried out in a group of patients with chronic diffuse TBI with cognitive deficit (N = 17) and a control group (N = 12). PET studies were performed with [methyl-^{11}C]*N*-methylpiperidyl-4-acetate (^{11}C-MP4A). ^{11}C-MP4A reflects acetylcholinesterase (AChE) activity. Group comparisons by SPM showed a significant bilateral reduction of AChE in several areas of the neocortex in the TBI group, more pronounced in the parietal–occipital regions. ROI analysis also showed a significant reduction of AChE in all ROIs examined, except in the medial temporal region, probably associated with the relatively small size of the sample. Since the study sample only represents a certain type of TBI, we agree with the authors that it would be interesting to study larger and more varied samples. Moreover, it would be interesting to study what percentage of cases with TBI shows cholinergic dysfunction and whether this dysfunction correlates with clinical symptoms and outcome. This methodology could also be useful to clarify differences between patients with chronic TBI who respond to treatment with AChE inhibitors and those that do not respond.

The outcome of ^{11}C-NMSP/^{18}F-FDG microPET studies aimed at evaluating the effects of neural stem cell (NSC) transplantation in a TBI model in rats was recently published (Zhang et al. 2008). ^{11}C-NMSP (^{11}C-*N*-methylspiperone) is a radioligand for the dopamine receptor subtype 2 (D_2). The combination of microPET and a

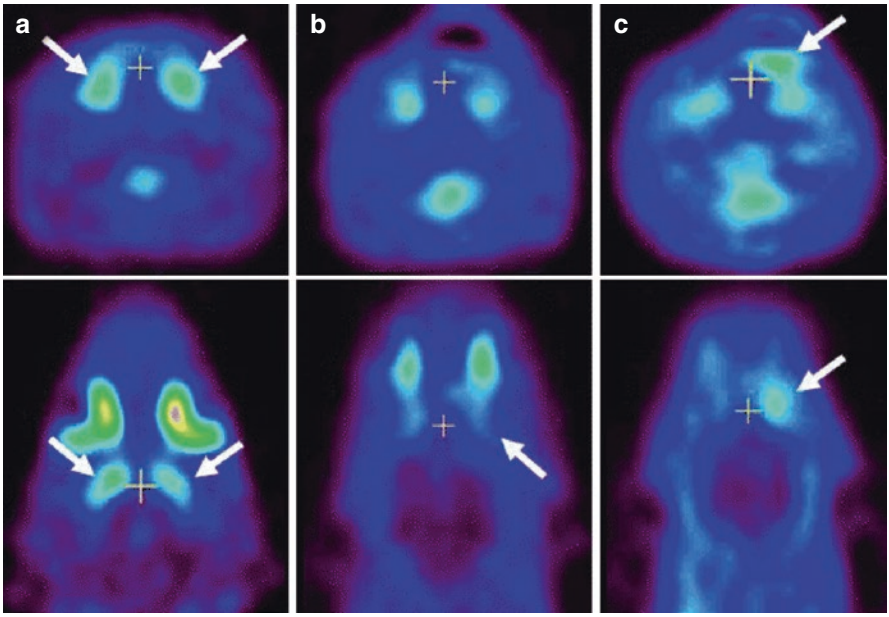

Fig. 43.1 Typical examples of ^{11}C-NMSP microPET imaging in various conditions. Coronal and axial sections of rat brain are shown. White cross markers in the coronal and axial sections indicate the same position in a scan. (**a**) Typical image of ^{11}C-NMSP microPET in normal rat brain showing high ^{11}C-NMSP accumulation in the striatum. (**b**) L/N ratio of ^{11}C-NMSP decreased after traumatic brain injury. (**c**) High accumulation of ^{11}C-NMSP indicated the existence of transplanted DRD2-positive NSCs. (From Zhang et al. (2008); with permission)

reporter gene system to track transplanted stem cells in animal experiments has allowed researchers to trace reporter gene carrying cells in vivo. The study was performed in a group of 18 rats with focal TBI in the right parietal lobe, later randomly assigned to a group that received a transplant ($N = 10$) and a control group ($N = 8$). In the former group, NSCs were transplanted in the brain lesion. ^{11}C-NMSP and ^{18}F-FDG microPET images were used to monitor changes in D_2 expression and glucose metabolism in the brain lesion before and after transplantation. Behavioral neurological function was also evaluated. Histological analysis identified viable NSCs at the transplantation site. The lesion-to-normal contralateral ratio (L/N ratio) of ^{11}C-NMSP in the brain lesion decreased from 97 to 68% after TBI, increasing to 137% 1 day after transplantation (Fig. 43.1) and later decreasing gradually. On the other hand, L/N ratio of glucose metabolism decreased to 35% in the brain lesion and then increased to 87% 2 weeks after transplantation (Fig. 43.2). The behavioral neurological function significantly improved in the transplanted group compared to the control group. Thus, this study demonstrates the feasibility of using microPET and a reporter gene system to evaluate NSC-induced D_2 expression in rat models, which could prove useful in future clinical trials of NSC transplantation therapy in TBI patients.

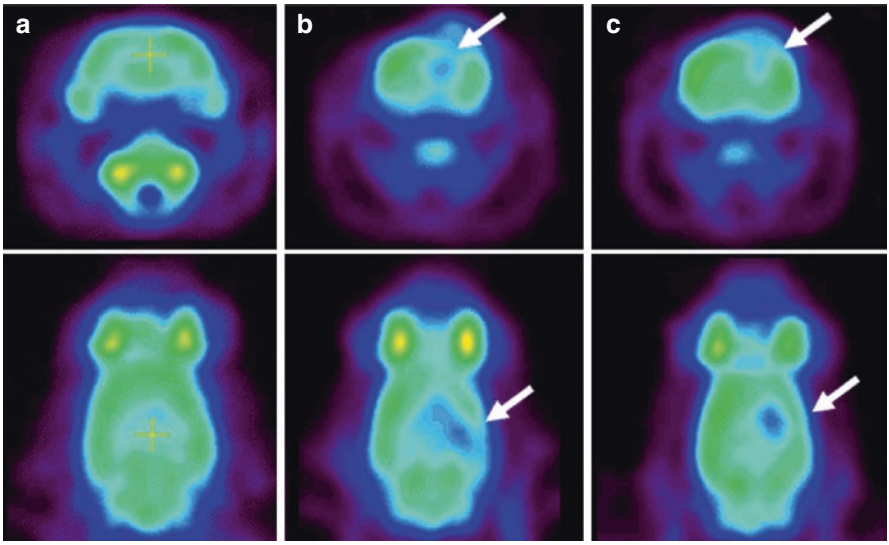

Fig. 43.2 Typical examples of ^{18}F-FDG microPET imaging in various conditions. Coronal and axial sections of rat brain are shown. (**a**) Typical image of ^{18}F-FDG microPET in normal rat brain. (**b**) As shown with *arrows*, the focal traumatic lesion appeared as a hypometabolic area in the right parietal cortex. (**c**) The regional glucose metabolism of the focal traumatic lesion recovered 14 days after NSC transplantation. (From Zhang et al. (2008); with permission)

43.2.3.1 PET Imaging of Neuroinflammation

Cellular processes that have received much attention lately are those involved in TBI neuroinflammation. Microglial, astrocyte, and neuron cells resident in the central nervous system begin to react in the acute TBI phase and eventually may be chronically activated. The role of activated microglia is to serve as the most important antigen-presenting cells and to synthesize inflammatory mediators and complement, which are crucial in the neuroinflammatory cascade after TBI. Microglia functions are very complex, since they have both neurotoxic and neuroprotective roles. In the acute phase, it may be involved in the restauration of the homeostasis in the brain. It has been hypothesized that chronic neuroinflammation may drive neurodegeneration after (repetitive) traumatic brain injury, which could be related to the release of pro-inflammatory cytokines, reactive oxygen species, nitrogen species, and excitatory neurotransmitters (Donat et al. 2017). Previous studies in TBI animal models have demonstrated that the inflammatory process may persist for at least a year, especially in the thalamus (Nagamoto-Combs et al. 2007, 2010). Human postmortem studies have also found microglial activation many years after TBI (Gentleman et al. 2004).

The neuroinflammatory response can be studied in vivo with PET using the radioligand ^{11}C-(R)-PK11195 (1-[2-chlorophenyl]-*N*-methyl-*N*-[1-methylpropyl]-3-isoquinoline carboxamide), which is a selective marker for activated microglia.

(R)-PK11195 binds to the 18 kDa translocator protein (TSPO), expressed in the mitochondria of activated microglia. ^{11}C-(R)-PK11195 PET has previously been used to study neuroinflammation in several neurodegenerative diseases.

The first studies using ^{11}C-(R)-PK11195 PET in TBI patients have been published recently (Folkersma et al. 2011; Ramlackhansingh et al. 2011). In the paper by Folkersma and coworkers, a patient group in chronic stage with moderate or severe TBI ($N = 8$) and a control group ($N = 7$) were studied. ^{11}C-(R)-PK11195 PET and MR images were acquired 6 months after TBI. ^{11}C-(R)-PK11195 BP_{ND} parametric images were generated. To generate a reference tissue input, the authors used supervised cluster analysis (Boellaard et al. 2008). Evaluation of the ^{11}C-(R)-PK11195 BP_{ND} was done in the whole brain and regionally. Group comparisons showed a significant increase of whole-brain ^{11}C-(R)-PK11195 BP_{ND} in the TBI group. This increase was not only observed in structurally affected brain regions (MRI) but also in apparently normal regions. On the other hand, there was no correlation between TBI severity (GCS) or neurological outcome (GOS) and whole-brain ^{11}C-(R)-PK11195 BP_{ND}. Although microglial activation is mostly a diffuse event in TBI, brain regions showing significant increases of ^{11}C-(R)-PK11195 BP_{ND} were the left and right frontal lobe, left and right thalamus, left parietal lobe, right temporal lobe, hippocampus and putamen, midbrain, and pons. An interesting finding was that ^{11}C-(R)-PK11195 BP_{ND} was maximal in the thalamus in six out of eight patients.

The study by Ramlackhansingh et al. (2011) investigated whether the inflammatory response persists in patients with chronic TBI and if this response was related to structural abnormalities and cognitive dysfunction. This paper included a group of patients with moderate to severe chronic TBI ($N = 10$). Five patients had focal damage visible in MR images, while the other five did not show abnormalities. ^{11}C-(R)-PK11195 PET was performed on all patients at least 11 months after TBI. Like in the previous study, ^{11}C-(R)-PK11195 BP_{ND} parametric images were generated using supervised cluster analysis. Volumetric MRI and DTI were done to evaluate focal damage and the disruption of WM. Cognitive function was also evaluated. Group comparisons showed that ^{11}C-(R)-PK11195 BP_{ND} was increased in the thalami, putamen, occipital cortices, and posterior limb of the internal capsules in the patient group compared with controls (Fig. 43.3). Unlike the study by Folkersma and coworkers, they found no increase in ^{11}C-(R)-PK11195 BP_{ND} at the original site of focal brain injury, which is probably due to the different intervals which had elapsed after TBI in both studies. In the patient sample, a positive correlation was observed between ^{11}C-(R)-PK11195 BP_{ND} in the thalamus and the degree of cognitive impairment. ^{11}C-(R)-PK11195 BP_{ND} increase was not associated with structural damage found by volumetric MRI and DTI or the time elapsed after TBI. Like in the article by Folkersma, persistent microglial activation in chronic TBI patients was confirmed especially in subcortical regions. Taking into account the long intervals after injury in the patient sample, this paper also suggests that therapeutic interventions can be beneficial even for a long time after TBI.

Over the past decades, new TSPO PET ligands have been developed with higher signal-to-noise ratios, including second- and third-generation ligands. After it

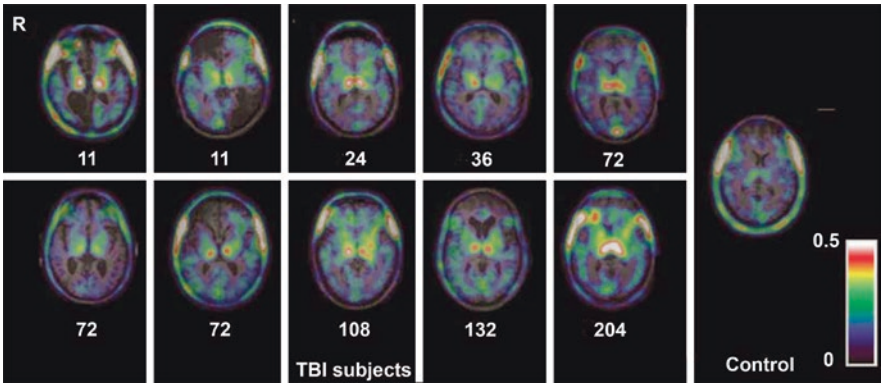

Fig. 43.3 Chronic microglial activation is present following traumatic brain injury (*TBI*). Overlay images of the transverse T1 magnetic resonance imaging at the level of the thalamus superimposed with ^{11}C-(R)-PK11195 (*PK*) images of all TBI subjects and a representative control subject. Numbers indicate time in months from the time of TBI to positron emission tomography scanning. Images illustrate the greater binding of PK in the thalami of all TBI subjects. *R* right. (From Ramlackhansingh et al. (2011); with permission)

became apparent that the binding of second-generation ligands was influenced by the rs6971 polymorphism (Ala147Thr) in the TSPO gene, efforts using third-generation ligands have shown promise to reduce this issue (Ikawa et al. 2017). Although its clinical value still has to be determined, these developments may eventually facilitate the use of TSPO PET as a biomarker after traumatic brain injury.

43.3 Single-Photon Emission Computed Tomography (SPECT)

Perfusion SPECT using ^{99m}Tc-hexamethyl-propyleneamine oxime (HMPAO) or ^{99m}Tc-ethylene cysteine dimer (ECD) has been extensively used in TBI. Reviews of this neuroimaging modality have appeared regularly in the last years (Davalos and Bennett 2002; Cihangiroglu et al. 2002; Belanger et al. 2007; Tikofsky 2010; Tong et al. 2011). These reviews coincide in pointing out that perfusion SPECT has high negative predictive value during the acute phase in mild TBI. They also agree that perfusion SPECT, like ^{18}F-FDG PET, is more sensitive than CT for identifying abnormalities in TBI during the first hours, detecting them in very early stages, when CT (or MRI) scans may still be negative. Abnormalities detected by perfusion SPECT are more extensive than those observed by structural neuroimaging. A recent study shows that the combination of structural neuroimages, such as CT, with perfusion SPECT using ^{99m}Tc-ECD is useful to determine the extent and severity of TBI lesions and tissue viability in core, edema, and perilesional tissue (Pifarré et al. 2011). Figure 43.4 shows CT and SPECT perfusion imaging of a patient with left frontal primarily brain trauma.

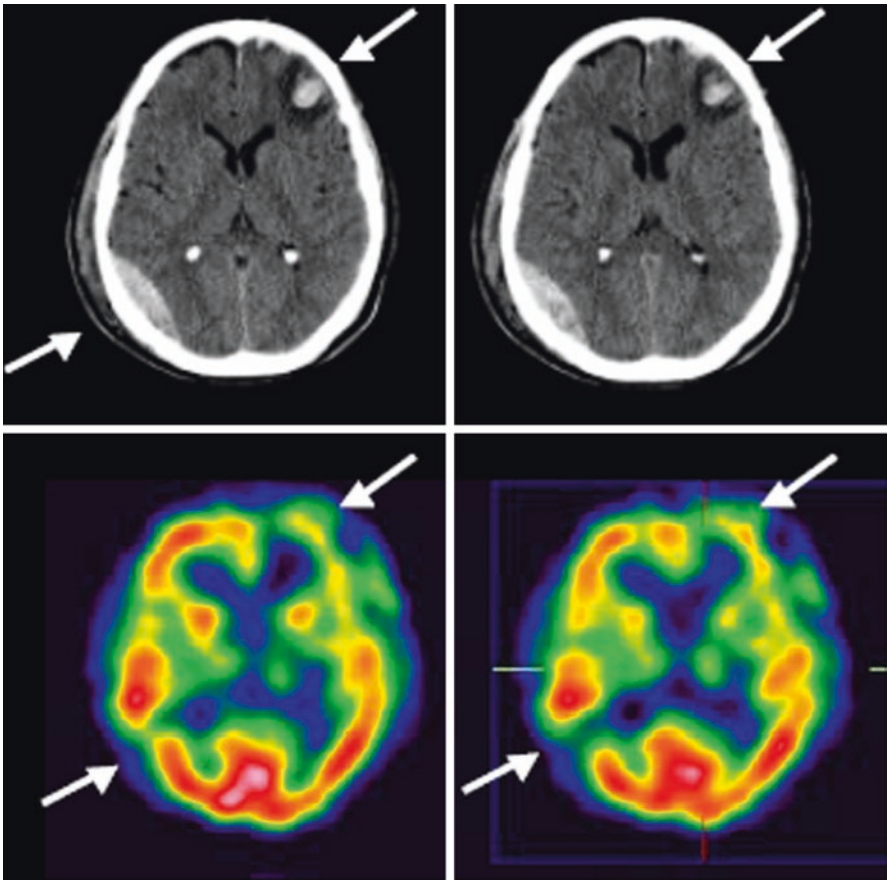

Fig. 43.4 CT and SPECT perfusion imaging of a patient with left frontal primarily brain trauma. In the hemorrhagic lesion seen on the CT in the right posterior temporal region, SPECT images show an absence of perfusion. (From Pifarré et al. (2011))

Furthermore, using SPECT, it is possible to study cell-specific processes related to TBI pathophysiology. Studies combining ^{123}I-2-β-carbomethoxy-3-β-(4-iodophenyl) tropane (β-CIT) and ^{123}I-iodobenzamide (IBZM) found nigrostriatal dysfunction in TBI patients, although the striatum was structurally relatively preserved, suggesting these studies may be useful in the evaluation of therapies directed toward reducing parkinsonian symptoms in TBI patients (Donnemiller et al. 2000). Another very recent animal study used *N*′,*N*′-diethyl-6-chloro-(4′-[^{123}I]iodophenyl) imidazo[1,2-*a*]pyridine-3-acetamide (^{123}I-CLINDE) for the in vivo monitoring of neuroinflammation by SPECT (Mattner et al. 2011). ^{123}I-CLINDE is a highly specific radioligand for TSPO. A recent perfusion SPECT activation study investigated cognitive fatigue mechanisms in patients with mild TBI (Hattori et al. 2009). In this study, it was possible to show that there is a frontocerebellar dissociation in patients with mild TBI that may explain cognitive impairment and cognitive fatigue in the chronic phase.

Technological advances in SPECT detector systems, hybrid SPECT–CT, continuous development of new gamma-emitting radioligands, and the application of modern methods of image analysis make the SPECT technique a valid alternative for the study of TBI, both for clinical practice and for research. Nevertheless, like ^{18}F-FDG PET, evidence-based imaging studies are required to demonstrate its incremental validity in TBI. The main advantage of SPECT is that it is much less costly and is still more widely available on a worldwide scale in comparison to PET.

43.4 Conclusions

In the acute TBI phase, ^{18}F-FDG PET seems to be more useful and has prognostic value in patients whose neurological state cannot be explained by structural neuroimages. However, evidence-based imaging studies are necessary to demonstrate the incremental validity of ^{18}F-FDG PET together with cost-effectiveness analysis to appropriately compare ^{18}F-FDG PET with other neuroimaging techniques. Whichever the results of these studies, ^{18}F-FDG PET and $^{15}O_2$-PET will remain very valuable tools for research of the complex and not yet fully understood pathophysiology of acute-phase TBI. In chronic TBI patients, most of the ^{18}F-FDG PET studies coincide in indicating a diffuse cortical–subcortical pattern of hypometabolism associated with cognitive impairment, even in patients without evident structural abnormalities. Preliminary studies also suggest the usefulness of ^{18}F-FDG PET for the evaluation of different therapeutic approaches for improving cognitive function in chronic TBI. In recent years, interest in studying cell-specific processes involved in TBI pathophysiology with PET is growing. Most considerably, tau PET ligands became available, which have allowed in vivo imaging of tauopathy in subjects who were exposed to (repetitive) traumatic brain injury. Another interesting application has been the imaging of markers of neuroinflammation using TSPO PET. Neuroinflammation imaging could become very attractive for detecting secondary damage after TBI, possibly with higher sensitivity than ^{18}F-FDG PET. Furthermore, it could serve in the evaluation of different therapeutic approaches, especially with the arrival of more sensitive third-generation TSPO ligands Finally, SPECT is a valid alternative for the study of TBI. However, as with PET, evidence-based imaging studies are required to demonstrate its incremental validity. SPECT is much less expensive and more widely available on a global scale.

References

Abate M, Trivedi M, Fryer TD et al (2008) Early derangements in oxygen and glucose metabolism following head injury: the ischemic penumbra and pathophysiological heterogeneity. Neurocrit Care 9:319–325

Alavi A (1989) Functional and anatomic studies of head injury. J Neuropsychiatry Clin Neurosci 1:S45–S50

Alavi A, Mirot A, Newberg A et al (1997) Fluorine-18-FDG evaluation of crossed cerebellar diaschisis in head injury. J Nucl Med 38:1717–1720

Bassett DS, Bullmore ET (2009) Human brain networks in health and disease. Curr Opin Neurol 22:340–347

Belanger HG, Vanderploeg RD, Curtiss G et al (2007) Recent neuroimaging techniques in mild traumatic brain injury. J Neuropsychiatry Clin Neurosci 19:5–20

Bergsneider M, Hovda DA, Shalmon E et al (1997) Cerebral hyperglycolysis following severe traumatic brain injury in humans: a positron emission tomography study. J Neurosurg 86:241–251

Bergsneider M, Hovda DA, Lee SM et al (2000) Dissociation of cerebral glucose metabolism and level of consciousness during the period of metabolic depression following human traumatic brain injury. J Neurotrauma 17:389–401

Bergsneider M, Hovda DA, McArthur DL et al (2001) Metabolic recovery following human traumatic brain injury based on FDG-PET: time course and relationship to neurological disability. J Head Trauma Rehabil 16:135–148

Boellaard R, Turkheimer F, Hinz R et al (2008) Performance of a modified supervised cluster algorithm for extracting reference region input function from [11C](R)-PK11195 brain PET studies. In IEEE Nucl Sci Symp Conf Rec 5400–5402

Bullock R, Chestnut RM, Clifton G et al (2007) Guidelines for the management of severe traumatic brain injury, 3rd ed. J Neurotrauma 24(Suppl 1):S26–S31

Byrnes KR, Wilson CM, Brabazon F, von Leden R, Jurgens JS, Oakes TR, Selwyn RG (2014) FDG-PET imaging in mild traumatic brain injury: a critical review. Front Neuroenerg 5:13

Cihangiroglu M, Ramsey RG, Dohrmann GJ (2002) Brain injury: analysis of imaging modalities. Neurol Res J24:7–18

Coles J, Fryer T (2004) ^{15}O PET imaging of cerebral metabolism and ischaemia following traumatic brain injury: defining the ischaemic brain volume. J Cereb Blood Flow Metab 24:191–201

Coles JP, Fryer TD, Smielewski P et al (2004a) Incidence and mechanisms of cerebral ischemia in early clinical head injury. J Cereb Blood Flow Metab 24:202–211

Coles JP, Steiner LA, Johnston AJ et al (2004b) Does induced hypertension reduce cerebral ischaemia within the traumatized human brain? Brain 127:2479–2490

Coles JP, Fryer TD, Coleman MR et al (2006) Hyperventilation following head injury: effect on ischemic burden and cerebral oxidative metabolism. Crit Care Med 35:568–578

Cunningham AS, Salvador R, Coles JP et al (2005) Physiological thresholds for irreversible tissue damage in contusional regions following traumatic brain injury. Brain 128:1931–1942

Dagal A, Lam AM (2011) Cerebral blood flow and the injured brain: how should we monitor and manipulate it? Curr Opin Anaesthesiol 24:131–137

Davalos DB, Bennett TL (2002) A review of the use of single-photon emission computerized tomography as a diagnostic tool in mild traumatic brain injury. Appl Neuropsychol 9:92–105

Diringer MN, Aiyagari V, Zazulia AR et al (2007) Effect of hyperoxia on cerebral metabolic rate for oxygen measured using positron emission tomography in patients with acute severe head injury. J Neurosurg 106:526–529

Diringer MN, Scalfani M, Zazulia A et al (2011) Effect of mannitol on cerebral blood volume in patients with head injury. Neurosurgery 70(5):1215–1219. https://doi.org/10.1227/NEU.0b013e3182417bc2

Donat CK, Scott G, Gentleman SM, Sastre M (2017) Microglial activation in traumatic brain injury. Front Aging Neurosci 9:208

Donnemiller E, Brenneis C, Wissel J et al (2000) Impaired dopaminergic neurotransmission in patients with traumatic brain injury: a SPET study using (123)I-beta-CIT and (123)I-IBZM. Eur J Nucl Med Mol Imaging 27:1410–1414

Faul M, Xu L, Wald MM et al (2010) Traumatic brain injury in the United States: Emergency Department Visits, Hospitalizations and Deaths 2002–2006. Centers for Disease Control and Prevention, National Center for Injury Prevention and Control, Atlanta. http://cdc.gov/TraumaticBrainInjury

Folkersma H, Boellaard R, Yaqub M et al (2011) Widespread and prolonged increase in (R)-(^{11})C-PK11195 binding after traumatic brain injury. J Nucl Med 52:1235–1239

Fontaine A, Azouvi P, Remy P et al (1999) Functional anatomy of neuropsychological deficits after severe traumatic brain injury. Neurology 53:1963–1968

Frey LC (2003) Epidemiology of posttraumatic epilepsy: a critical review. Epilepsia 44:11–17
Friston KJ (1994) Statistical parametric mapping. In: Thatcher RW, Hallet M, Zeffiro T, John ER, Huerta M (eds) Functional neuroimaging. Academic, New York
Garcia-Panach J, Lull N, Jose Lull J et al (2011) A voxel-based analysis of FDG-PET in traumatic brain injury: regional metabolism and relationship between the thalamus and cortical areas. J Neurotrauma 28:1707–1717
Geeraerts T, Coles JP, Aigbirhio FI et al (2011) Validation of reference tissue modelling for [(11)C]flumazenil positron emission tomography following head injury. Ann Nucl Med 25:396–405
Gentleman SM, Leclercq PD, Moyes L et al (2004) Long-term intracerebral inflammatory response after traumatic brain injury. Forensic Sci Int 146:97–104
Gupta AK, Hutchinson PJ, Fryer T et al (2002) Measurement of brain tissue oxygenation performed using positron emission tomography scanning to validate a novel monitoring method. J Neurosurg 96:263–268
Haller S, Vernooij MW, Kuijer JPA, Larsson EM, Jager HR, Barkhof F (2018) Cerebral microbleeds: imaging and clinical significance. Radiology 287(1):11–28
Hattori N, Huang SC, Wu HM et al (2003) Correlation of regional metabolic rates of glucose with Glasgow Coma Scale after traumatic brain injury. J Nucl Med 44:1709–1716
Hattori N, Huang SC, Wu HM et al (2004) Acute changes in regional cerebral ^{18}F-FDG kinetics in patients with traumatic brain injury. J Nucl Med 45:775–783
Hattori N, Swan M, Stobbe GA et al (2009) Differential SPECT activation patterns associated with PASAT performance may indicate frontocerebellar functional dissociation in chronic mild traumatic brain injury. J Nucl Med 50:1054–1061
Hayashi S, Inaji M, Nariai T, Oda K, Sakata M, Toyohara J, Ishii K, Ishiwata K, Maehara T (2018) Increased binding potential of brain adenosine A1 receptor in chronic stages of patients with diffuse axonal injury measured with [1-methyl-(11)C] 8-dicyclopropylmethyl-1-methyl-3-propylxanthine Positron Emission Tomography Imaging. J Neurotrauma 35(1):25–31
Hunter JV, Wilde EA, Tong KA et al (2012) Emerging imaging tools for use with traumatic. Brain Injury Res J Neurotrauma 29:654–671
Hutchinson PJ, Gupta AK, Fryer TF et al (2002) Correlation between cerebral blood flow, substrate delivery, and metabolism in head injury: a combined microdialysis and triple oxygen positron emission tomography study. J Cereb Blood Flow Metab 22:735–745
Hutchinson PJ, O'Connell MT, Seal A et al (2009) A combined microdialysis and FDG-PET study of glucose metabolism in head injury. Acta Neurochir 151:51–61
Ikawa M, Lohith TG, Shrestha S, Telu S, Zoghbi SS, Castellano S, Taliani S, Da Settimo F, Fujita M, Pike VW, Innis RB, Biomarkers Consortium Radioligand Project Team (2017) 11C-ER176, a radioligand for 18-kDa translocator protein, has adequate sensitivity to robustly image all three affinity genotypes in human brain. J Nucl Med 58(2):320–325
Ito K, Asano Y, Ikegame Y, Shinoda J (2016) Differences in brain metabolic impairment between chronic mild/moderate TBI patients with and without visible brain lesions based on MRI. BioMed Res Int 2016:3794029
Johnston AJ, Steiner LA, Coles JP et al (2005) Effect of cerebral perfusion pressure augmentation on regional oxygenation and metabolism after head injury. Crit Care Med 33:189–195
Kato T, Nakayama N, Yasokawa Y et al (2007) Statistical image analysis of cerebral glucose metabolism in patients with cognitive impairment following diffuse traumatic brain injury. J Neurotrauma 24:919–926
Kawai N, Nakamura T, Tamiya T et al (2008) Metabolic disturbance without brain ischemia in traumatic brain injury: a positron emission tomography study. Acta Neurochir Suppl 102:241–245
Kawai N, Maeda Y, Kudomi N et al (2010) Focal neuronal damage in patients with neuropsychological impairment after diffuse traumatic brain injury: evaluation using (11)C-flumazenil positron emission tomography with statistical image analysis. J Neurotrauma 27:2131–2138
Kim YW, Kim DY, Shin JC et al (2009) The changes of cortical metabolism associated with the clinical response to donepezil therapy in traumatic brain injury. Clin Neuropharmacol 32:63–68
Kim Y, Shin JC, Ys A (2010) Changes in cerebral glucose metabolism in patients with posttraumatic cognitive impairment after memantine therapy: a preliminary study. Ann Nucl Med 24:363–369

Komura A, Kawasaki T, Yamada Y, Uzuyama S, Asano Y, Shinoda J (2019) Cerebral glucose metabolism in patients with chronic mental and cognitive sequelae after a single blunt mild traumatic brain injury without visible brain lesions. J Neurotrauma 36(5):641–649

Kraus MF, Smith GS, Butters M et al (2005) Effects of the dopaminergic agent and NMDA receptor antagonist amantadine on cognitive function, cerebral glucose metabolism and D2 receptor availability in chronic traumatic brain injury: a study using positron emission tomography (PET). Brain Inj 19:471–479

Kubal WS (2012) Updated imaging of traumatic brain injury. Radiol Clin N Am 50:15–41

Lange RT, Iverson GL, Franzen MD (2009) Neuropsychological functioning following complicated vs. uncomplicated mild traumatic brain injury. Brain Injury 23(2):83–91

Langfitt TW, Obrist WD, Alavi A et al (1986) Computerized tomography, magnetic resonance imaging, and positron emission tomography in the study of brain trauma. J Neurosurg 64:760–767

Ley E, Park R (2010) In vivo effect of propranolol dose and timing on cerebral perfusion after traumatic brain injury. J Trauma 68:353–356

Ley EJ, Scehnet J, Park R et al (2009) The in vivo effect of propranolol on cerebral perfusion and hypoxia after traumatic brain injury. J Trauma 66:154–161

Liu YR, Cardamone L, Hogan R et al (2010) Progressive metabolic and structural cerebral perturbations after traumatic brain injury: an in vivo imaging study in the rat. J Nucl Med 51:1788–1795

Lull N, Noe E, Jose Lull J et al (2010) Voxel-based statistical analysis of thalamic glucose metabolism in traumatic brain injury: relationship with consciousness and cognition. Brain Inj 24:1098–1107

Lupi A, Bertagnoni G, Salgarello M et al (2007) Cerebellar vermis relative hypermetabolism: an almost constant PET finding in an injured brain. Clin Nucl Med 32:445–451

Lupi A, Bertagnoni G, Borghero A et al (2011) Relative hypermetabolism of vermis cerebelli in traumatic brain injured patients studied with 18FDG PET: a descriptor of brain damage and a possible predictor of outcome. Curr Radiopharm 4:167–175

Maas AI, Stocchetti N, Bullock R (2008) Moderate and severe traumatic brain injury in adults. Lancet Neurol 7:728–741

Marklund N, Sihver S, Hovda D et al (2009) Increased cerebral uptake of [18F]fluoro-deoxyglucose but not [1-14c]glucose early following traumatic brain injury in rats. J Neurotrauma 26:1281–1293

Mattner F, Bandin DL, Staykova M et al (2011) Evaluation of [(123)I]-CLINDE as a potent SPECT radiotracer to assess the degree of astroglia activation in cuprizone-induced neuroinflammation. Eur J Nucl Med Mol Imaging 38:1516–1528

McKee AC, Cantu RC, Nowinski CJ et al (2009) Chronic traumatic encephalopathy in athletes: progressive tauopathy after repetitive head injury. J Neuropathol Exp Neurol 68:709–735

McKee AC, Cairns NJ, Dickson DW, Folkerth RD, Keene CD, Litvan I, Perl DP, Stein TD, Vonsattel JP, Stewart W, Tripodis Y, Crary JF, Bieniek KF, Dams-O'Connor K, Alvarez VE, Gordon WA, TBI/CTE group (2016) The first NINDS/NIBIB consensus meeting to define neuropathological criteria for the diagnosis of chronic traumatic encephalopathy. Acta Neuropathologica 131(1):75–86

Medina LS, Blackmore CC, Applegate KE et al (2011) Principles of evidence-based imaging. In: Medina LS, Blackmore CC (eds) Evidence-based imaging: improving the quality of imaging in patient care. Springer, New York

Menon DKP, Coles JPP, Gupta AKF et al (2004) Diffusion limited oxygen delivery following head injury. Crit Care Med 32:1384–1390

Nagamoto-Combs K, Mcneal DW, Morecraft RJ et al (2007) Prolonged microgliosis in the rhesus monkey central nervous system after traumatic brain injury. J Neurotrauma 24:1719–1742

Nagamoto-Combs K, Morecraft RJ, Darling WG et al (2010) Long-term gliosis and molecular changes in the cervical spinal cord of the rhesus monkey after traumatic brain injury. J Neurotrauma 27:565–585

Nakashima T, Nakayama N, Miwa K et al (2007) Focal brain glucose hypometabolism in patients with neuropsychologic deficits after diffuse axonal injury. AJNR Am J Neuroradiol 28:236–242

Nakayama N, Okumura A, Shinoda J et al (2006) Relationship between regional cerebral metabolism and consciousness disturbance in traumatic diffuse brain injury without large focal lesions: an FDG-PET study with statistical parametric mapping analysis. J Neurol Neurosurg Psychiatry 77:856–862

Nortje J, Coles JP, Timofeev I et al (2008) Effect of hyperoxia on regional oxygenation and metabolism after severe traumatic brain injury: preliminary findings. Crit Care Med 36:273–281

O'Connell MT, Seal A, Nortje J et al (2005) Glucose metabolism in traumatic brain injury: a combined microdialysis and [(18)F]-2-fluoro-2-deoxy-D-glucose-positron emission tomography (FDG-PET) study. Acta Neurochir Suppl 95:165–168

Okonkwo DO, Puffer RC, Minhas DS, Beers SR, Edelman KL, Sharpless J, Laymon CM, Lopresti BJ, Benso S, Puccio AM, Pathak S, Ikonomovic MD, Mettenburg JM, Schneider W, Mathis CA, Mountz JM (2019) [(18)F]FDG, [(11)C]PiB, and [(18)F]AV-1451 PET imaging of neurodegeneration in two subjects with a history of repetitive trauma and cognitive decline. Front Neurol 10:831

Omalu BI, Hamilton RL, Kamboh MI, DeKosky ST, Bailes J (2010) Chronic traumatic encephalopathy (CTE) in a National Football League Player: case report and emerging medicolegal practice questions. J Forensic Nurs 6(1):40–46

Östberg A, Virta J, Rinne JO et al (2011) Cholinergic dysfunction after traumatic brain injury: preliminary findings from a PET study. Neurology 76:1046–1050

Park E, Bell JD, Baker AJ (2008) Traumatic brain injury: can the consequences be stopped? CMAJ 178:1163–1170

Peskind ER, Petrie EC, Cross DJ et al (2011) Cerebrocerebellar hypometabolism associated with repetitive blast exposure mild traumatic brain injury in 12 Iraq war Veterans with persistent post-concussive symptoms. NeuroImage 54(Suppl 1):S76–S82

Pifarré P, Cuberas G, Benejam B et al (2011) Cerebral blood flow measurement in the assessment of post-traumatic cerebral contusions. Open J Radiol 1:21–27

Ramlackhansingh AF, Brooks DJ, Greenwood RJ et al (2011) Inflammation after trauma: microglial activation and traumatic brain injury. Ann Neurol 70:374–383

Rao N, Turski PA, Polcyn RE et al (1984) F-18 positron emission computed-tomography in closed head-injury. Arch Phys Med Rehabil 65:780–785

Robertson C (2004) Mitochondrial dysfunction contributes to cell death following traumatic brain injury in adult and immature animals. J Bioenerg Biomembr 36:363–368

Shiga T, Ikoma K, Katoh C et al (2006) Loss of neuronal integrity: a cause of hypometabolism in patients with traumatic brain injury without MRI abnormality in the chronic stage. Eur J Nucl Med Mol Imaging 33:817–822

Stern RA, Adler CH, Chen K, Navitsky M, Luo J, Dodick DW, Alosco ML, Tripodis Y, Goradia DD, Martin B, Mastroeni D, Fritts NG, Jarnagin J, Devous MD, Mintun MA, Pontecorvo MJ, Shenton ME, Reiman EM (2019) Tau Positron-Emission Tomography in Former National Football League Players. N Engl J Med 380(18):1716–1725

Stryke J, Stalnacke B, Sojka P et al (2007) Traumatic brain injuries in a well-defined population: epidemiological aspects and severity. J Neurotrauma 24:1425–1436

Tagliaferri F, Compagnone C, Korsic M et al (2006) A systematic review of brain injury epidemiology in Europe. Acta Neurochir 148:255–268

Takahata K, Kimura Y, Sahara N, Koga S, Shimada H, Ichise M, Saito F, Moriguchi S, Kitamura S, Kubota M, Umeda S, Niwa F, Mizushima J, Morimoto Y, Funayama M, Tabuchi H, Bieniek KF, Kawamura K, Zhang MR, Dickson DW, Mimura M, Kato M, Suhara T, Higuchi M (2019) PET-detectable tau pathology correlates with long-term neuropsychiatric outcomes in patients with traumatic brain injury. Brain 142(10):3265–3279

Tenjin H, Ueda S, Mizukawa N et al (1990) Positron emission tomographic studies on cerebral hemodynamics in patients with cerebral contusion. Neurosurgery 26:971–979

Tikofsky RS (2010) Traumatic brain injury: SPECT and PET. In: Van Heertum RL, Tikofsky RS, Ichise M (eds) Functional cerebral SPECT and PET imaging, 4th edn. Wolters Kluwer Lippincott Williams & Wilkins, Philadelphia

Tong KA, Oyoyo UE, Holshouser BA et al (2011) Neuroimaging for traumatic brain injury. In: Medina LS, Blackmore CC (eds) Evidence-based imaging: improving the quality of imaging in patient care. Springer, New York

Vespa P, Bergsneider M, Hattori N et al (2005) Metabolic crisis without brain ischemia is common after traumatic brain injury: a combined microdialysis and positron emission tomography study. J Cereb Blood Flow Metab 25:763–774

WHO/OMS (2009) Global status report on road safety: time for action. World Health Organisation, Geneva. http://whqlibdoc.who.int/publications/2009/9789241563840_eng.pdf

Wu HM, Huang SC, Hattori N et al (2004a) Selective metabolic reduction in gray matter acutely following human traumatic brain injury. J Neurotrauma 21:149–161

Wu HM, Huang SC, Hattori N et al (2004b) Subcortical white matter metabolic chances remote from focal hemorrhagic lesions suggest diffuse injury after human traumatic brain injury. Neurosurgery 55:1306–1317

Xu Y, McArthur DL, Alger JR et al (2010) Early nonischemic oxidative metabolic dysfunction leads to chronic brain atrophy in traumatic brain injury. J Cereb Blood Flow Metab 30:883–894

Yamaki T, Yoshino E, Fujimoto M et al (1996) Chronological positron emission tomographic study of severe diffuse brain injury in the chronic stage. J Trauma 40:50–56

Zasler ND, Katz D, Zafonte RD (2007) Brain injury medicine: principles and practice. Demos Medical Publishing, New York

Zhang H, Zheng X, Yang X et al (2008) ^{11}C-NMSP/18F-FDG microPET to monitor neural stem cell transplantation in a rat model of traumatic brain injury. Eur J Nucl Med Mol Imaging 35:1699–1708

Zhang J, Mitsis EM, Chu K et al (2010) Statistical parametric mapping and cluster counting analysis of [(18)F] FDG-PET imaging in traumatic brain injury. J Neurotrauma 27:35–49

Part VIII

Other Subjects

Anaesthesia and PET of the Brain

44

Anthony Absalom and Ram Adapa

Contents

44.1 Introduction 1124
44.2 Consciousness and Unconsciousness 1124
44.3 Definition of Anaesthesia 1125
44.4 Why Study Anaesthesia? 1126
44.5 Available Tools for Studying Anaesthesia 1127
44.6 Early Theories of the Molecular Mechanism of Anaesthetic Action 1129
44.7 Current Theories of the Molecular Mechanism of Anaesthetic Action 1129
44.8 Early PET Studies of the Global and Regional Changes in Cerebral Glucose Metabolism Caused by Anaesthetic Agents 1131
44.9 PET and Propofol 1132
44.10 PET and Ketamine 1135
44.11 PET and Alpha2 Agonists 1137
44.12 PET and Volatile Anaesthetic Agents 1139
44.13 PET and Nitrous Oxide 1141
44.14 PET and Xenon 1142
44.15 Summary and Conclusion 1143
References 1144

Abstract

Although drugs have been used to administer general anaesthesia for more than a century and a half, relatively little was known until recently about the molecular and cellular effects of the anaesthetic agents and the neurobiology of anaes-

A. Absalom (✉)
Department of Anesthesiology, University Medical Center Groningen, Groningen University, Groningen, The Netherlands
e-mail: a.r.absalom@umcg.nl

R. Adapa
Anaesthetic Department, Addenbrooke's Hospital, Cambridge, UK
e-mail: ra342@cam.ac.uk

R. A. J. O. Dierckx et al. (eds.), *PET and SPECT in Neurology*,
https://doi.org/10.1007/978-3-030-53168-3_44

thesia. Positron emission tomography (PET) and single-photon emission computed tomography (SPECT) studies have played a valuable role in improving this knowledge. PET studies using ^{11}C-flumazenil binding have been used to demonstrate that the molecular action of some, but not all, of the current anaesthetic agents is mediated via the $GABA_A$ receptor. Using different tracers labelled with ^{18}F, ^{11}C and ^{15}O, PET studies have shown the patterns of changes in cerebral metabolism and blood flow associated with different intravenous and volatile anaesthetic agents. Within classes of volatile agents, there are minor variations in patterns. More profound differences are found between classes of agents. Interestingly, all agents cause alterations in the blood flow and metabolism of the thalamus, providing strong support for the hypothesis that the anaesthetic agents interfere with consciousness by interfering with thalamocortical communication.

44.1 Introduction

Every day, around the world, a large number of patients receive sedative and anaesthetic agents for sedation and anaesthesia in intensive care units, in operating theatres and in other centres where diagnostic and therapeutic procedures are performed. Despite this and the fact that anaesthetic drugs have been used regularly since the 1840s, surprisingly, little is known about the state of anaesthesia, the mechanism and site of action of the anaesthetic agents and the longer-term consequences of sedation and anaesthesia. In the early 1990s, so little was known about the state of anaesthesia that Christof Koch co-wrote a serious article discussing the basic question 'Does anaesthesia cause loss of consciousness?' (Kulli and Koch 1991). In the decades since, significant progress has been made, thanks mostly to developments in technologies for functional imaging, such as PET, but still many fundamental questions remain unanswered! Part of the reason for slow progress is the current limited understanding of the neurobiology of consciousness.

Although anaesthesia is sometimes required for clinical PET scanning of the brain and other organs, the anaesthetic management of patients undergoing scanning will not be discussed here. Rather, this chapter will focus on the application of PET brain scanning techniques to studies of the neurobiology of anaesthesia.

44.2 Consciousness and Unconsciousness

One of the aims of anaesthesia is to induce loss of consciousness and prevent return of consciousness during a surgical procedure. Consciousness is an ethereal concept, whose nature and meaning have been debated for centuries. Today, most people believe it to be a subjective experience resulting from the electrical activity of the neurons in the brain (or more accurately the co-ordinated activity of assemblies or networks of neurons). Generally, we infer that an individual is conscious on the

basis of his behaviour, his interactions with his environment and his reports of his experiences.

Medically, we define unconsciousness as an absence of wakefulness, alertness and awareness, but inferences that these are absent are usually based on the absence of behavioural responses to external stimuli. There are several circumstances when such inferences may not be true, as in patients with the 'locked-in' syndrome. In anaesthetic practice, we commonly administer doses of opioid drugs that obtund responses to stimuli (but do not necessarily by themselves prevent consciousness), and in patients presumed to be unconscious, we often administer drugs that paralyze the muscles but do not alter consciousness.

The literature contains a wide range of published incidences of the so-called problem of accidental awareness of general anaesthesia with subsequent recall of intraoperative events (AAGA). The differences arise mostly from differences in study population and methodology. The reported incidence also appears to be higher when structured postoperative interviews are used to test for explicit recall (Mashour et al. 2013; Walker et al. 2016), with incidences in large trials of the 1–2 out of every 1000 patients undergoing anaesthesia (Sandin et al. 2000; Sebel et al. 2004). A recent large UK national audit project (NAP5) indicated that the incidence of spontaneous complaints of AAGA is much lower (~1: 19,000 patients) but higher in specific patient populations and a wide range of psychological consequences (Pandit et al. 2014). The incidence of awareness during surgery without subsequent recall is not known but is likely to be much higher (Absalom and Green 2013).

44.3 Definition of Anaesthesia

Due to the combined problems of a poor understanding of consciousness and of the effects of anaesthetic drugs on the brain, anaesthesia has been very difficult to define and has largely been defined on the basis of the absence of features of consciousness. For most of the history of the practice of anaesthesia, anaesthesiologists have tended to define adequate clinical anaesthesia as a triad of 'hypnosis', analgesia and muscle relaxation. In anaesthetic jargon, anaesthetic-induced loss of consciousness is referred to as 'hypnosis' and anaesthesia-inducing drugs as 'hypnotics'. The term 'analgesia' was previously used to refer more generally to the (desired) loss of autonomic responses to painful stimuli, and muscle relaxation referred to the desire of the surgeon for a lack of patient movement and for some operations a reduction in muscle tone. Early volatile anaesthetic agents were able to suppress consciousness and, in sufficiently large doses, were able to suppress autonomic responses (tachycardia, hypertension) and reduce muscular tone. These latter effects are mediated by separate actions of the drugs on different parts of the nervous system and on the cardiovascular system and are not part of a single spectrum of effects at a single site (Prys-Roberts 1987; Kissin 1993). Thus, modern clinical practice involves administration of different 'purer' agents targeted at different elements of this triad—modest doses of hypnotic agents for suppression of consciousness, local and systemic analgesic drugs for suppression of autonomic responses and neuromuscular

blocking agents for muscle relaxation or paralysis where that is required. With this approach, more attention is now focused on the cognitive aspects of anaesthesia, with anaesthesia being defined as a drug-induced reversible state of unconsciousness principally characterized by a lack of awareness of, and subsequent memory for, intraoperative events.

Thus, this chapter will focus on the use of PET technology to understand the main component of anaesthesia, 'hypnosis', and will not deal with functional imaging of pain perception and analgesia.

44.4 Why Study Anaesthesia?

In current clinical practice, many anaesthesiologists err on the side of deeper anaesthesia in the hope of avoiding the problem of anaesthetic awareness. This is not an ideal approach since all the anaesthetic agents in current use possess dose-related adverse effects, such as depression of the cardiovascular and immune systems.

Earlier studies suggested an association between excessive depth of anaesthesia (i.e. an excessive dose) and mortality within 1 and 2 years (Monk et al. 2005; Lindholm et al. 2009). A recent large randomized controlled trial however indicated that there was no difference in 1-year mortality between light general anaesthesia and deep general anaesthesia in elderly patients (Short et al. 2019).

Animal evidence suggests that in the extremes of age (i.e. in the very young and the elderly), anaesthetic agents may be neurotoxic.

There is a plethora of evidence that exposure of a wide variety of animals to the commonly used anaesthetic agents during the neonatal period results in neuronal injury and associated cognitive changes (Jevtovic-Todorovic et al. 2013). Epidemiological studies of neonatal exposure to anaesthetic agents have shown conflicting results, whereas a randomized controlled trial in human neonates showed no evidence of changes in cognitive function at 3 and 5 years after exposure (Davidson et al. 2016; McCann et al. 2019).

While there is some in vitro evidence that anaesthetic agents may promote Alzheimer's disease-type changes (Mandal and Fodale 2009; Whittington et al. 2011), so far, there is no convincing clinical evidence that anaesthetic exposure enhances neurodegenerative processes in the ageing brain.

Studies of the molecular mechanisms of action of the anaesthetic agents offer much more than simply satisfying the curiosity of anaesthesiologists. Better knowledge of the molecular mechanism may inform the development of newer agents, specifically designed to have a broader therapeutic range and fewer adverse effects.

Furthermore, studies of the mechanism of action of the anaesthetic agents may provide information about the nature of, and the mechanisms of, consciousness itself. Here, the hypnotics or sedatives used could be regarded as probes, by which investigators can interfere with different cognitive functions, to help shed light on functions such as speech processing and memory functions (Davis et al. 2007; Adapa et al. 2014; Naci et al. 2018), alertness, wakefulness, awareness and

consciousness itself (Arhem et al. 2003; Lydic and Baghdoyan 2005; Hameroff 2006; Mashour 2006; Franks 2008; Alkire et al. 2008b; Brown et al. 2010; Varley et al. 2019). Once again, this knowledge has practical relevance, since a better understanding of memory function, and of the interactions among anaesthetic agents and stress on awareness and memory function, may inform methods of detecting and preventing inadvertent awareness with subsequent recall of intraoperative events.

44.5 Available Tools for Studying Anaesthesia

To fully understand anaesthesia, multiple layers and domains of knowledge are required, starting with the molecular effects (or possibly at submolecular level), explaining how these influence the function of individual neurons and how these influence the interactions or communication among networks or assemblies of other neurons, before making the jump to explain how the perturbed electrical and other activities in these assemblies or networks of neurons eventually result in impairment or absence of consciousness.

Different techniques lend themselves to study of different parts of this chain of events. Molecular biology laboratory techniques (such as identification and isolation of specific receptor types and patch-clamp techniques to measure the effects of ion fluxes in response to application of different agonists and antagonists) have been the basis for much of our improved understanding of the molecular actions of our agents. However, as will be seen below, in recent years, PET-based techniques have also been used to study receptor effects.

Cellular function is also commonly studied by molecular biology techniques and by recordings of local field potentials, usually in animals (Imas et al. 2006). PET techniques have been used very successfully to describe the indirect neurophysiological effects of anaesthetic agents such as changes in regional blood flow and metabolism secondary to changes in neuronal (electrical) activity. Occasionally, clever designs have been used to link these regional changes with specific neuronal populations.

Changes in regional neurophysiology are also detectable with functional MRI techniques, in which the scanner sequences are chosen so that regional changes in blood oxyhaemoglobin levels are detectable. This so-called BOLD or blood oxygen level-dependent signal relies on the fact that deoxyhaemoglobin is paramagnetic, whereas oxyhaemoglobin is not. When regional neuronal electrical activity increases, local blood flow and oxygen delivery increase in excess of the increase in oxygen requirements, thereby causing a reduction in the regional concentration of deoxyhaemoglobin and the MRI signal. These fMRI techniques have the benefit of superior temporal resolution compared with PET but suffer from the disadvantage of worse spatial resolution. There is also sometimes debate about the validity of fMRI techniques when anaesthetic agents are used, since, although the anaesthetic agents generally cause matched reductions in cerebral electrical activity,

metabolism and flow, they can also have direct vasodilatory effects which result in oxygen delivery in excess of requirements and thus produce BOLD signal changes unrelated to changes in neuronal activity.

We assume that cognitive functions are mediated by electrical activity in networks of neurons, and so perhaps electroencephalography (EEG) can be said to be the most direct and objective measure of brain activity. It has excellent temporal resolution but only reflects cortical activity and represents the summed activity of millions of cortical pyramidal neurons in the vicinity of each electrode. Nonetheless, EEG-based monitors of anaesthetic depth have been developed and shown to assist with rational and patient-individualized titration of anaesthetic dose. These monitoring techniques suffer from the disadvantage that at best, their output correlates with the probability of consciousness but seldom gives an absolute indication of whether consciousness is present or absent. Although there are EEG patterns associated with wakefulness and also with very deep anaesthesia, there is currently no known EEG signal that can clearly detect the transition between consciousness and unconsciousness. Some early efforts have been made to integrate information obtained from electroencephalography with that from PET-based assessments of changes in regional neurophysiology (Noirhomme et al. 2009). Others have combined transcranial magnetic stimulation and EEG recording to yield insights into differences in signal transmission during wakefulness and natural sleep (Massimini et al. 2005, 2007). Finally, studies of the regional correlations in electrical activity, and in particular coherence analyses, are beginning to yield interesting insights into how anaesthetic agents might interfere with the transfer of information between regions (Lee et al. 2009).

Ultimately though, the aim of anaesthesia is to induce loss of consciousness and prevent return of consciousness during a surgical procedure. To understand how the molecular, cellular and neuronal network effects of the anaesthetic agents finally result in a change of consciousness and memory functions is possibly the most challenging step, since it remains to be explained how molecular, cellular and electrical activity generates conscious experiences at all.

In anaesthetic studies, a common aim is to correlate drug-induced regional neurophysiological changes with cognitive function changes. This can be difficult to achieve, even with the time-honoured behavioural testing techniques of cognitive neuroscience and experimental psychology. At lower, sedative doses, when some cognitive functions are still intact, behavioural and memory testing is informative. However, when the end point is loss of consciousness, observations of behaviour and memory are only partially informative. Firstly, assessment of behavioural responses usually involves application of a verbal or painful stimulus that may itself alter the state of consciousness. Secondly, the absence of behavioural responses does not always imply lack of consciousness, but may only indicate a failure of volition or motor control, and in some circumstances, movement in response to pain can occur without the presence of consciousness. Likewise, reliance on explicit memory is not always informative, since sub-sedative doses of several anaesthetic agents are associated with profound amnesia.

44.6 Early Theories of the Molecular Mechanism of Anaesthetic Action

The range of possible types of theories for the mechanism of action is from so-called unitary theories, proposing a single neuronal target, to hypotheses that propose multiple neuronal targets per drug. For most of the twentieth century, the Meyer-Overton hypothesis—a unitary theory—held sway. It was noted that the potency of the anaesthetic agents correlated with their lipid solubility, and this combined with the observation that increases in ambient pressure could reverse anaesthesia leads to the conclusion that anaesthetic effects were mediated by a non-specific physical effect on the lipid bilayer of neuronal cell membranes. It was thought that the physical presence of anaesthetic molecules within this layer caused alterations in membrane volume and fluidity, resulting in dose-dependent dysfunction of all exposed neurons.

Towards the end of the twentieth century, evidence mounted against the Meyer-Overton hypothesis. Studies showed that membrane volume changes were in fact negligible. Other evidence against a non-specific mechanism came from increasing knowledge of exceptions to the rule and biochemical experiments with known anaesthetic agents where small alterations in structure were associated with loss of anaesthetic potency. Further evidence against a simple physical mechanism came from studies showing that current flows along giant squid axons (mediated by voltage-gated Na and K channels) were insensitive to anaesthetic agents (Haydon and Urban 1983, 1986). A major breakthrough came when Franks and Lieb produced the first strong evidence that known anaesthetic agents exhibited dose-dependent effects on proteins, leading to the suggestion that anaesthetic agents acted on membrane receptors (Franks and Lieb 1984). Nonetheless, the academic community was slow to accept this, and it was only with growing evidence against non-specific membrane effects (such as the demonstration of differences in potency among optical isomers of known anaesthetic agents (Franks and Lieb 1993)) and growing evidence of specific effects at receptors (Hales and Lambert 1991; Franks and Lieb 1997) that the Meyer-Overton hypothesis was gradually rejected.

44.7 Current Theories of the Molecular Mechanism of Anaesthetic Action

Most workers in the field now agree that anaesthetic agents act to hyperpolarize neurons by either potentiating inhibitory circuits or inhibiting excitatory pathways and that they do so by specific actions at ligand-gated receptors (Franks 2008; Alkire et al. 2008b; Franks and Lieb 2004). In the case of the commonly used intravenous anaesthetic agent propofol, and for the less commonly used agents such as the barbiturates and etomidate, the chief molecular effect seems to be potentiation at the $GABA_A$ receptor. Gene knockout studies in animals suggest that the different components of the clinical effects of these agents, such as amnesia and sedation, are

mediated by different $GABA_A$ receptor subtypes. In fact, sensitivity to the different anaesthetic effects may be strongly modulated by single nucleotide substitutions (Belelli et al. 1997; Mihic et al. 1997; Reynolds et al. 2003), suggesting a potential genetic basis for some of the pharmacodynamic variability seen in clinical practice. Although the $GABA_A$ receptor is posited to be the main molecular site of action, there is also evidence for effects at an array of other sites, such as at nicotinic ACh receptors and voltage-gated potassium channels, although the significance of these effects is unclear (Fig. 44.1).

Two less commonly used intravenous anaesthetic agents that have not yet been mentioned are ketamine and dexmedetomidine. Ketamine causes potent analgesia, and when used as the sole hypnotic, it causes a dissociated state (in which the patient may appear conscious but is dissociated from the environment and applied stimuli). Both effects are mediated via an antagonist effect at the NMDA glutamate receptor (Franks 2008; Alkire et al. 2008b). Dexmedetomidine also has some weaker analgesic effects and at low doses causes arousable sedation not dissimilar to a natural sleep state, with general anaesthesia occurring at much higher doses. These effects are mediated by an agonist effect at α2 adrenergic receptors, with sedative and hypnotic effects probably mediated by actions on these receptors in the locus coeruleus.

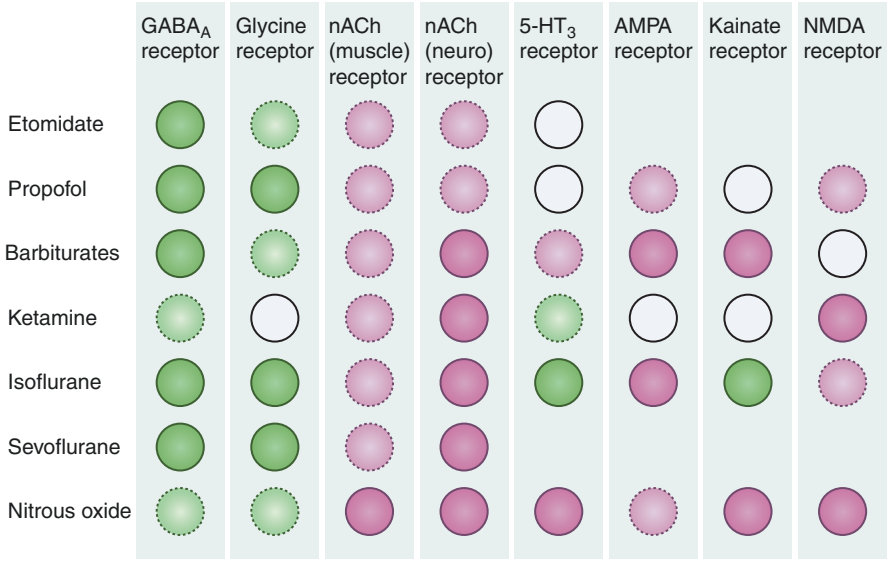

Fig. 44.1 Ligand-gated ion channels are probably the most relevant targets for general anaesthetics. A *dark green* or *pink spot* indicates significant potentiation or inhibition, respectively, of agonist actions at the receptor by the anaesthetic with an *EC50* or *IC50* that is no greater than three times higher than the EC50 for producing immobility. A *light green* or *light pink spot* indicates little potentiation or inhibition, respectively, at concentrations that were less than three times the EC50 for immobility; an *empty spot* indicates no effect at any concentration tested. (From Rudolph and Antkowiak (2004) used with permission)

For the volatile anaesthetic agents, agonist effects at the $GABA_A$ receptor appear to be important (Alkire et al. 2008b) but with binding of the agents to different binding sites than those for propofol and the barbiturates. The molecular mechanism of action of the volatile agents may also include significant potentiating effects at two-pore potassium and glycine channels and inhibitory effects at NMDA receptors (Franks 2008).

44.8 Early PET Studies of the Global and Regional Changes in Cerebral Glucose Metabolism Caused by Anaesthetic Agents

The earliest PET studies of anaesthesia were performed in rats, in which ^{18}FDG was used during propofol anaesthesia, and showed dose-dependent global reductions in cerebral glucose utilization (Ori et al. 1986; Dam et al. 1990; Cavazzuti et al. 1991). These studies led Dr Michael Alkire to perform the first PET studies of anaesthesia in humans. In that, ^{18}FDG was used before and during propofol anaesthesia, and as in the rat studies, it was found that anaesthesia caused reductions in glucose metabolism in all measured cortical and subcortical areas (Alkire et al. 1995). In this study, marked regional differences in tracer uptake were noted, with a greater suppression of cortical than subcortical activity. At this time, it was just becoming apparent that the molecular mechanism of action of propofol was mediated by the $GABA_A$ receptor. These regional differences even led Alkire and colleagues to speculate that differences in the regional distribution of $GABA_A$ receptors were responsible for the regional variations in metabolic activity.

Alkire and his group then went on to study the influence of isoflurane anaesthesia on glucose metabolism, again using the ^{18}FDG tracer (Alkire et al. 1997). Although they found a similar degree of global reduction in metabolic activity to propofol, they found less regional variability with isoflurane. They found similar reductions in cortical and subcortical activity and widespread, fairly uniform reductions in activity across all cortical and subcortical areas. This widely quoted study was taken to provide support for a non-specific, physical explanation of the mechanism of action of the anaesthetic agents.

A subsequent study with an older volatile anaesthetic agent, halothane, showed similar global reductions in metabolic activity to isoflurane and propofol (40% vs. 46% and 55%, respectively) (Alkire et al. 1999). In general, the pattern of regional metabolic effects was similar to that found with isoflurane, with the exception of the cerebellum, where metabolism was more suppressed by halothane. As with isoflurane, midbrain metabolism was more suppressed than with propofol, and here, the authors speculated that this is because the volatile anaesthetics have a strong influence on cholinergic transmission, whereas propofol does not.

Each of the above three studies involved only a small number of subjects, in whom anaesthetic dose was titrated to loss of consciousness, with concurrent EEG monitoring, using the bispectral index (BIS) monitor (Covidien, USA), a monitor of depth of anaesthesia, which gives an output of between 0 and 100, where zero

indicates no brain electrical activity and 100 the completely awake state and values between 40 and 60 are taken to represent adequate anaesthesia. The authors combined the data to show that the degree of global reduction in glucose metabolism correlated strongly with the bispectral index (Alkire 1998).

Although the above findings were sometimes taken to provide evidence of a non-specific mechanism of anaesthetic activity, they also indicated differences between anaesthetic agents and regional variations in metabolic suppression, providing evidence against the theory of a single non-specific mechanism of action. In the subsequent years, the evidence against this theory continued to mount up, particularly as investigators designed more sophisticated studies, combined imaging modalities and compared the results of different drugs and modalities. PET methodology played an important role in this. Indeed, by 2005, there was sufficient evidence from studies involving PET measures of cerebral blood flow and metabolism with different anaesthetic agents for Alkire to perform a conjunction analysis. This analysis highlighted the considerable regional differences among different agents, thereby providing strong evidence for specific anaesthetic effects (Alkire and Miller 2005). Further, despite differences in molecular mechanisms and in regional neurophysiological effects, all agents with anaesthetic effects had in common a significant effect on the thalamus (see Fig. 44.2). Based on this work and on previous animal findings (Angel 1993), Alkire became a strong proponent of the 'thalamocortical switch hypothesis', the theory that thalamocortical resonant loops are essential for consciousness and that all anaesthetic agents interrupt consciousness by interrupting the thalamocortical interactions and interrupting onward transmission of ascending electrical signals (Alkire et al. 2000).

Subsequent work using PET has assessed various combinations of cerebral metabolism, blood flow, blood volume and receptor occupancy, for different drugs (sometimes in combination). To simplify the findings, they will be subdivided by drug type, starting with the intravenous agents (propofol, ketamine and the alpha2 agonists) and finishing with the inhaled agents (volatile anaesthetic agents, nitrous oxide, xenon).

44.9 PET and Propofol

The early work by Alkire et al. (1995) has already been mentioned. Although this showed global reductions in glucose metabolism, the effects of propofol on relative glucose metabolism were different for different areas (where regional metabolism as a proportion of global metabolism is considered). Thus, whereas the relative glucose metabolism decreased for most cortical areas and the thalamus, there were relative increases for the temporal lobe, hippocampus, basal ganglia, midbrain and cerebellum.

Fiset and colleagues used $H_2{}^{15}O$ PET to study changes in global and regional cerebral blood flow (rCBF) associated with mild sedation, deep sedation and unconsciousness induced by propofol (Fiset et al. 1999). Concordant with the findings of Alkire, they found dose-related decreases in global CBF. Further, they identified

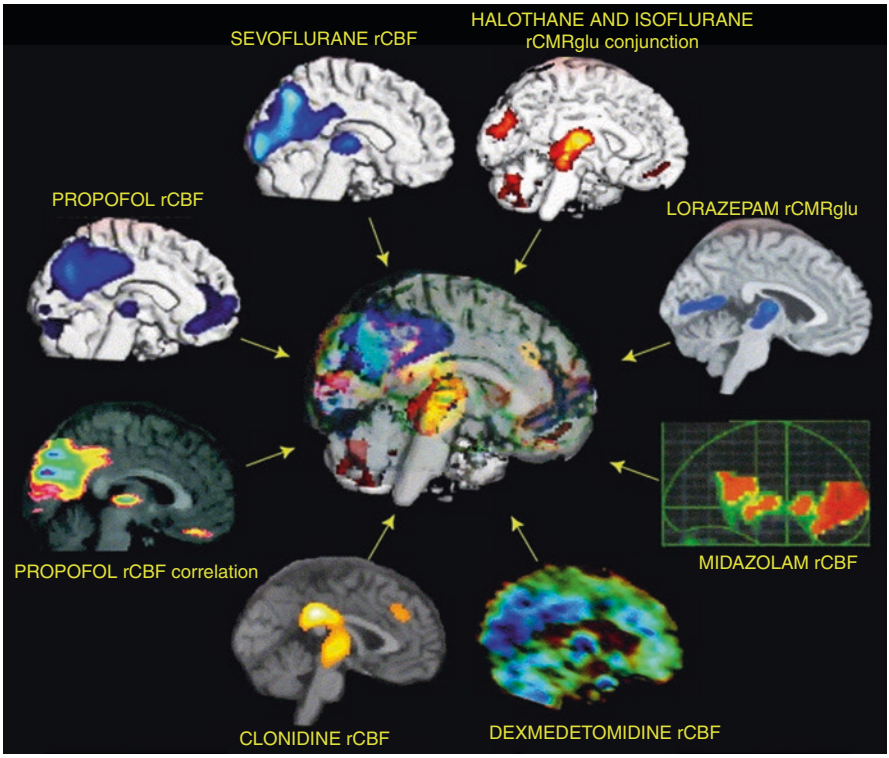

Fig. 44.2 The regional effects of anaesthetics on brain function in humans who were given various anaesthetic agents at doses that altered the level of consciousness. The data are from seven different groups of investigators and encompass the study of eight different agents. The regional effects were measured using blood-flow- or glucose-metabolism-based techniques. All images show regional decreases in activity caused by anaesthesia compared to the awake state, except the propofol correlation image, which shows increasing anaesthetic dose correlates with decreasing blood flow. The figure identifies that altered blood flow and metabolism in the thalamus are a common finding associated with anaesthetic-induced unconsciousness. (From Alkire and Miller (2005) used with permission)

evidence supporting specific molecular effects of propofol. They found that propofol preferentially decreased rCBF in brain regions involved in arousal, autonomic functions and associative functions, such as the medial thalamus, midbrain, cuneus and precuneus, posterior cingulate cortex and orbitofrontal regions. Interestingly, there were strong correlations in rCBF in the midbrain and thalamus, indicating strong functional interactions between the arousal systems of these regions.

In a more sophisticated study, this group measured CBF responses (using $H_2{}^{15}O$ PET) to vibrotactile stimulation during graded sedation and anaesthesia (Bonhomme et al. 2001). In general, this study demonstrated that propofol caused dose-dependent decreases in rCBF in the thalamus, bilateral precuneus and bilateral posterior cingulate gyri. During unconsciousness, there were widespread increases in rCBF when $PaCO_2$ was increased by 20%, which can be explained by the fact that CO_2

reactivity is preserved with propofol. In the awake state, vibrotactile stimulation produced a predicted pattern of rCBF changes—increases in relative rCBF in the left thalamus and primary somatosensory cortex (S1) and left superior frontal gyrus and bilateral secondary somatosensory (S2) cortices. Most interesting was the finding that propofol produced dose-dependent, selective regional effects on the responses to vibrotactile stimulation. At low sedative doses, the S1 responses were abolished, and at moderate sedative doses, the S2 responses were abolished (and accompanied by changes in sensory perception), whereas thalamic responses were only abolished when consciousness was lost.

Scheinin et al. in Finland used $H_2{}^{15}O$ PET to assess changes in absolute and relative CBF during graded general anaesthesia (from moderate to deep levels) with propofol and sevoflurane (Kaisti et al. 2002). Propofol caused a significant global decrease in absolute rCBF but with a ceiling effect at the lowest anaesthetic concentration studied (a target plasma concentration of 6 μg/mL, which is approximately the concentration required to suppress movement responses to pain in 50% of patients). The transition from the awake state to that at EC50 was associated with relative rCBF decreases in the thalamus, midbrain, cuneus, precuneus, posterior limbic system and parietal and frontal cortices. The lack of absolute changes in rCBF with propofol, even at 2 × EC50, suggested that flow-metabolism coupling is maintained during propofol anaesthesia. In a subsequent study by the same group, also involving propofol anaesthesia, but at a lower dose (mean measured concentration 3.7 μg/mL), similar changes in rCBF, regional oxygen metabolism and regional cerebral blood volume (assessed by $H_2{}^{15}O$, $^{15}O_2$ and $C_{15}O$ tracers, respectively) were found (Kaisti et al. 2003). This provided evidence of intact flow-metabolism coupling at this low dose, which suggests that low-dose propofol anaesthesia does not produce direct vasodilatory effects. Another group administered a similar level of propofol anaesthesia (targeting a BIS of 35–40) to volunteers and found similarly matched changes in flow and metabolism (in this case, metabolism was assessed with ^{18}FDG PET) (Schlunzen et al. 2012).

Most studies of the influence of propofol metabolism have assessed glucose or oxygen metabolism. One study, however, has assessed regional cerebral protein synthesis rates using the tracer L-[1-^{11}C]leucine (Bishu et al. 2009). No effect of propofol on protein synthesis was found (measured propofol concentrations were in the range 4.2–8.1 μg/mL).

The remaining studies to be discussed in this section were focused on receptor effects of propofol. Alkire and Haier performed a study in which they correlated their findings concerning regional cerebral glucose metabolism rates under propofol and isoflurane anaesthesia, with data previously published by other investigators on the regional distributions of different neurotransmitter systems (Alkire and Haier 2001). The latter data were acquired from post-mortem immunochemistry investigations (Braestrup et al. 1977; Zezula et al. 1988; Enna and Snyder 1977). They were able to show that there were significant correlations between regional reductions in glucose metabolism during propofol anaesthesia and the regional distribution of benzodiazepine binding sites (from studies using ^{3}H-diazepam which binds to both neuronal and mitochondrial benzodiazepine receptors and ^{3}H-flunitrazepam

which binds only to neuronal benzodiazepine binding sites on $GABA_A$ receptors). There were also weaker correlations with the distribution of opioid binding sites but no correlations with distribution densities of adrenergic, muscarinic and serotonin binding sites.

Salmi and colleagues later showed that propofol increases ^{11}C-flumazenil binding, indicating that propofol enhances the affinity of GABA for $GABA_A$ receptors (Salmi et al. 2004). At around the same time, another group found that propofol anaesthesia was associated with a reduction in muscarinic receptor binding by the tracer [*N*-^{11}C-methyl]-benztropine (Xie et al. 2004), but this finding was difficult to interpret. Although it may have indicated binding of propofol to muscarinic receptors, it could also have been the result of a change of affinity of the receptor for benztropine or an increase in benztropine metabolism caused by propofol. Several years later, members of the same group performed an intriguing study in which they measured CBF with a $H_2{}^{15}O$ technique at baseline, after loss of consciousness with propofol and administration of the cholinesterase inhibitor, physostigmine (Xie et al. 2011). Some, but not all, volunteers regained consciousness after physostigmine administration, despite constant blood and brain concentrations of propofol. The authors found that loss of consciousness was associated with decreases in rCBF in the thalamus and precuneus and that among those that regained consciousness after physostigmine, restoration of consciousness was associated with increases in rCBF in these same structures. It is assumed that the increased ACh levels caused by physostigmine result in activation of cholinergic pathways and an increase in thalamic throughput of electrical signals sufficient to cause a return of consciousness.

Taken together, these studies indicate that propofol causes a specific pattern of changes in regional metabolic activity and CBF but with a key effect at the thalamus and that loss of consciousness is associated with interruption of thalamocortical signalling. Finally, the work from the past decade and a half supports the hypothesis that propofol acts at specific protein targets, most notably at the $GABA_A$ receptor.

44.10 PET and Ketamine

Ketamine is an older anaesthetic agent than propofol but is seldom used alone for inducing or maintaining surgical anaesthesia because of a propensity to cause troublesome psychiatric adverse effects. It remains interesting clinically and is being used with increasing frequency as an adjunct during propofol anaesthesia. Known and potential beneficial effects include improved cardiovascular stability, neuroprotection, reduced acute post-operative pain, potent antidepressant activity and attenuation of post-operative hyperalgesia and chronic pain.

Ketamine is also of scientific interest because it acts as an antagonist at the NMDA receptor and causes different neurophysiological changes to the other hypnotics. When used alone, it causes impaired consciousness but with cortical electrical activation accompanied by increases in glucose metabolism (Vollenweider et al. 1997) and rCBF. The reasons behind these effects are not clear. The drug antagonizes an excitatory pathway, but presumably, this results in activation of other

excitatory pathways. Impaired consciousness is probably the result of impaired connectivity or communication between regions of the brain important for consciousness.

Långsjö and colleagues studied the effects of sub-anaesthetic doses of **racemic ketamine** on rCBF, regional oxygen metabolism ($rCMRO_2$) and regional cerebral blood volume (rCBV) using the PET tracers $H_2{}^{15}O$, $^{15}O_2$ and C ^{15}O (Långsjö et al. 2003). Ketamine caused global dose-dependent changes in absolute rCBF, with the biggest changes in the anterior cingulate, insula and frontal cortex (areas involved in pain processing) and also in the thalamus and putamen. As expected, mean systemic arterial pressures were increased. There were no significant changes in $rCMRO_2$, and hence, the oxygen extraction fraction was reduced. rCBV was only increased in the frontal cortex. Taken together, these findings were consistent with known behavioural and electrophysiological changes seen with ketamine sedation but did give rise to a suggestion of altered flow-metabolism coupling. The authors performed a follow-up study, this time using ^{18}FDG to assess regional changes in glucose metabolism (rCMRG) associated with sub-sedative racemic ketamine doses (at the highest dose used in the previous study) (Långsjö et al. 2004). Region of interest analyses showed global absolute increases in rCMRG but with the greatest changes in the thalamus and frontal and parietal cortex. Voxel-based analyses showed increases in relative rCMRG in frontal, temporal and parietal cortices. These changes occurred in a similar distribution and magnitude to the rCBF findings of the previous study (Långsjö et al. 2003), suggesting maintenance of flow-metabolism coupling. The authors suggested that the absence of $rCMRO_2$ changes was the result of non-oxidative glucose metabolism in response to ketamine-induced glutamate release. A recent study by Laaksonen and colleagues comparing the effects of dexmedetomidine, propofol and *S*-ketamine also identified no significant changes in rCMRG in the ketamine cohort (Laaksonen et al. 2018).

The Långsjö group also studied the effects of ***S*-ketamine** on cerebral blood flow and metabolism, using a complex study design (Långsjö et al. 2005). $H_2{}^{15}O$ and $^{15}O_2$ scans were performed during one session, at three moments: awake, during low-dose sub-sedative *S*-ketamine administration and during much higher dose of *S*-ketamine anaesthesia. ^{18}FDG scans were performed 3 weeks before the main study and finally also towards the end of the *S*-ketamine anaesthesia. The authors found dose-dependent increases in total CBF and in absolute rCBF in almost all regions studied. During low-dose *S*-ketamine administration, the greatest increases were in the anterior cingulate, whereas at anaesthetic doses, the largest increase (86.5%) was in the insula. At low doses, there were no significant increases in $rCMRO_2$, whereas at anaesthetic doses, $rCMRO_2$ was increased only in the frontal cortex (by 15.7%). During anaesthesia, rCMRG was only increased in the thalamus, and CBV was increased >50%. These findings show that CBF is increased in excess of metabolic needs, suggesting a disturbance of flow-metabolism coupling. While the excess flow may be perceived to be protective, these findings confirmed the long-held views of anaesthesiologists (based on the work of others using different methodologies) that ketamine is not a suitable agent for use during neurosurgery, where the increases in CBF and CBV can cause increased brain volume, increased intracranial pressure and impaired surgical access.

Finally, the same group studied the influence of sub-anaesthetic doses of ketamine on ^{11}C-flumazenil binding (Salmi et al. 2005). They showed no interference in binding, thereby confirming that ketamine has minimal effects on the $GABA_A$ receptor.

The antidepressant effect of ketamine has also been explored using PET scanning in recent years. Using [^{11}C]DASB PET in healthy volunteers, it was demonstrated that the antidepressant effect was not mediated by ketamine binding to the serotonin transporter (Spies et al. 2018). More recently, the radiotracer ^{18}F-FPEB was used to establish that ketamine leads to a downregulation of the metabotropic glutamate receptor 5 (mGluR5) (Holmes et al. 2019). These two studies highlight how PET imaging can be used to probe existing (serotonin reuptake) and novel (mGluR5) treatment targets for psychiatric disorders.

44.11 PET and Alpha2 Agonists

PET technology has only been used a few times to study the alpha2 agonists, among which clonidine and dexmedetomidine are the two agents available for clinical use. Although clonidine has been available for a long time, it has mainly been used intravenously for its antihypertensive effects. More recently, it has been used as a preoperative oral sedative premedication and perioperatively as an intravenous analgesic adjunct. Dexmedetomidine has been in use for almost 20 years in the USA. Initially, it was mostly used for ICU sedation; more recently, it has been used as a sedative during surgical procedures such as awake craniotomy. It was first registered in Europe in late 2011.

Prielipp used $H_2{}^{15}O$ scans to assess the changes in rCBF during and after low and high sedative dose infusions of dexmedetomidine. The agent caused marked reductions in global CBF and also reductions in absolute rCBF in 13 out of 14 regions of interest studied. There were no significant differences in patterns of rCBF between low and high sedative doses. Despite the rapid pharmacokinetics of dexmedetomidine, CBF remained decreased when assessed 30 min after the end of the dexmedetomidine infusion (Prielipp et al. 2002). This reduction of CBF in the absence of concomitant reduction in $CMRO_2$ raised concerns about the potential for cerebral ischaemia with dexmedetomidine. More recently however, the abovementioned comparative study by Laaksonen et al. revealed that volunteers sedated with dexmedetomidine showed the lowest rCMRG in almost all brain regions compared to other anaesthetics (Fig. 44.3).

More recent reports have studied healthy volunteers sedated with dexmedetomidine in an attempt to explore disruptions in brain functional connectivity with combined PET-fMRI studies. Unconsciousness was associated with reduced regional blood flow and CMRG in the thalamus, the default mode network (DMN) and the bilateral frontoparietal networks (FPNs) (Akeju et al. 2014). Importantly, functional connectivity within these networks was preserved, while internetwork connectivity was disrupted. As reported above, recovery from unconsciousness was associated with sustained reduction in CBF and restored DMN thalamocortical functional connectivity. Other studies have identified greater functional connectivity between the

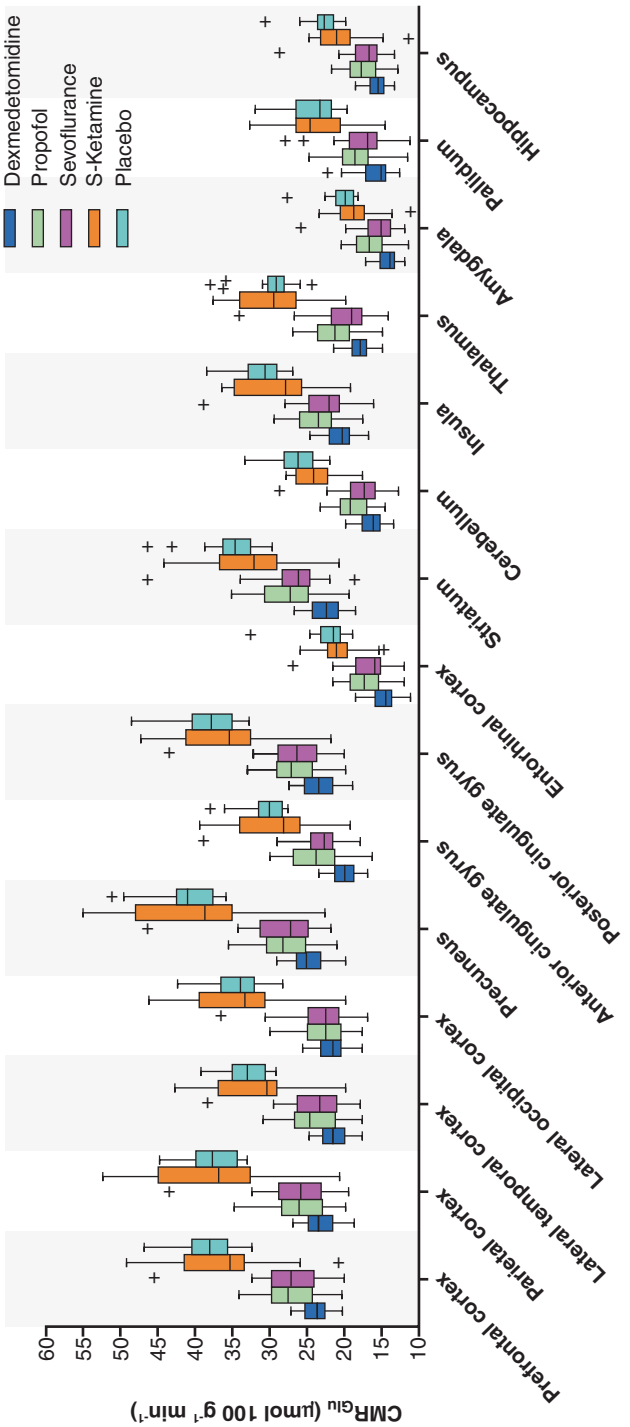

Fig. 44.3 Boxplots of regional cerebral metabolic rate of glucose (CMR_{glu}) in the 15 analyzed regions of interest (ROIs) during dexmedetomidine, propofol, sevoflurane, *S*-ketamine and placebo administration in 160 healthy subjects ($P < 0.001$ between the treatments in all ROIs). Lowest CMR_{glu} values were observed in the dexmedetomidine group. Boxes represent lower quartiles and medians and upper quartiles; whiskers represent 1.5 × interquartile ranges below and above the lower and upper quartiles, respectively. Outlying values are marked with symbols

parietal and anterior cingulate cortex upon emergence from anaesthesia, prompting suggestions of a functional network that activates with restored consciousness (Långsjö et al. 2012).

Another group studied the influence of clonidine infusions on rCBF (assessed by $H_2{}^{15}O$ PET), clinical status and EEG (Bonhomme et al. 2008). Clonidine caused rousable sedation and on the EEG spindle patterns similar to those found during non-rapid eye movement sleep. There was a negative correlation between measured plasma clonidine concentration and rCBF in a network of regions including the thalamus, prefrontal cortex, orbital and parietal association cortex, posterior cingulate cortex and precuneus. Changes in these regions are associated with natural sleep. These regions also form part of the default mode network, whose component areas show strong correlations in activity (assessed by fMRI) during the resting state, but not during task performance conditions (Mason et al. 2007; Stamatakis et al. 2010).

44.12 PET and Volatile Anaesthetic Agents

Volatile anaesthetic agents have been the subject of many PET studies. These have mainly focused on the neurophysiological changes in flow and metabolism and have shown generally concordant findings, with only minor variations between studies, possibly related to differences in dose. Minor variations were found according to drug, despite some chemical differences between the agents studied, such as structure, molecular weight, degree of halogenations and water and lipid solubility. Halothane is a halogenated hydrocarbon that is now seldom used in the First World. Isoflurane, sevoflurane and desflurane are halogenated ethers. The latter two agents are the most commonly used inhalational anaesthetic agents, although there are few PET studies involving desflurane.

The early work by Alkire, showing that isoflurane anaesthesia caused a 46% reduction in rCMRG with fairly uniform regional distribution, has already been mentioned (Alkire et al. 1997). Alkire then studied the effects of halothane on rCMRG, since this agent had been shown in earlier studies to cause less uniform rCMRG reductions (Alkire et al. 1999). Halothane anaesthesia was found to cause a 40% reduction in global rCMRG, but in keeping with the prior animal work, there were some regional differences, with the greater metabolic reductions being found in the basal forebrain, thalamus, limbic system, cerebellum and occipital cortex.

In the above studies, halothane and isoflurane were administered until an end point of loss of consciousness (the mean concentrations administered were 30% and 60% less than the concentrations required to prevent a response to a surgical incision—the so-called MAC value, a measure of potency). Kaisti studied the effects of surgical levels of sevoflurane anaesthesia—at concentrations that were 1.0, 1.5 and 2.0 multiples of the MAC value—on rCBF using $H_2{}^{15}O$ (Kaisti et al. 2002). At 1.0 MAC, sevoflurane caused global decreases in absolute rCBF (regional decreases were between 36% and 53% of baseline). Increasing doses caused a redistribution

of flow, with increases in rCBF in the thalamus and cerebellum, suggesting a disturbance of flow-metabolism coupling.

In a follow-up study, using $H_2{}^{15}O$, $^{15}O_2$ and C ^{15}O to study rCBF, $rCMRO_2$ and CBV, respectively, Kaisti titrated sevoflurane and propofol anaesthesia (with and without N_2O) to a moderate depth of anaesthesia, guided by the BIS (Kaisti et al. 2003). Sevoflurane concentrations were thus lower than in the previous study—0.75 × MAC without N_2O and 0.6 MAC with 70% N_2O. Sevoflurane without N_2O reduced the total CBF but only caused rCBF decreases in some areas (the occipital cortex, cerebellum, caudate and thalamus). The most significant changes in relative rCBF were in the thalamus, cuneus, frontoparietal cortex and cerebellum. Addition of N_2O caused a global return to baseline rCBF values, with the most significant relative rCBF increases in the occipital cortex and pons. With regard to $CMRO_2$, sevoflurane caused a global reduction, with absolute decreases in $rCMRO_2$ in all areas studied. The greatest reductions in relative $rCMRO_2$ were in the thalamus, cuneus, frontoparietal cortex and cerebellum. Addition of N_2O increased $rCMRO_2$ in the parieto-occipital region and cerebellum, but not quite to baseline/awake levels. At the doses studied, sevoflurane with and without N_2O did not alter rCBV. It was associated with a tendency towards reduced oxygen extraction fraction, more marked in the presence of N_2O, indicating that metabolism was more suppressed than flow, suggesting a degree of disturbed flow-metabolism coupling.

The above findings were generally confirmed by Schlunzen et al., although some increases in rCBF were found at lower doses (Schlunzen et al. 2004). The study involved use of $H_2{}^{15}O$ to study changes in rCBF associated with sub-anaesthetic to anaesthetic doses of sevoflurane (0.2, 0.35 and 1.0 MAC multiples). At all doses, sevoflurane increased rCBF in the anterior cingulate and decreased rCBF in the cerebellum. Compared with the baseline state, 0.2 MAC sevoflurane decreased rCBF in the inferior temporal cortex and lingual gyrus. 0.35 MAC increased rCBF in the middle temporal cortex and lingual gyrus while decreasing rCBF in the thalamus. The latter finding is unsurprising given that some volunteers displayed no response to a verbal stimulus, whereas other showed only sluggish responses. Finally, compared with 0.35 MAC, 1 MAC increased rCBF in the insula and decreased rCBF in the posterior cingulated, lingual gyrus, precuneus and frontal cortex. Similar patterns of changes were found in subsequent study, using similar methodology and equipotent isoflurane doses (Schlunzen et al. 2006).

When administering anaesthesia to patients with raised intracranial pressure who require surgical excision of space-occupying lesions, anaesthesiologists often employ a degree of hyperventilation in order to reduce CBF and intracranial pressure. Schlunzen thus studied the influence of hyperventilation on rCBF in volunteers subjected to surgical levels of sevoflurane anaesthesia (1 MAC) (Schlunzen et al. 2010). A reduction of the mean $PaCO_2$ from 5.5 to 3.8 kPa reduced the total CBF by 44%. The largest reductions in rCBF were found in the thalamus, medial occipitotemporal gyrus, cerebellum, precuneus, putamen and insula. This work clearly showed that under surgical levels of sevoflurane anaesthesia, CO_2 reactivity is maintained, with stronger responses in some areas than others.

Finally, this group also studied the effects of surgical levels of sevoflurane anaesthesia (1 MAC) on $rCMRO_2$ (Schlunzen et al. 2010). Total CMRG was reduced by 56%, and absolute rCMRG was decreased in all areas studied. The most significant relative rCMRG decreases were found in the lingual gyrus, occipital lobe and thalamus.

A few studies have addressed the molecular biology of the volatile agents. Among five subjects subjected to isoflurane anaesthesia, Alkire showed that the regional distribution of changes in rCBF correlated best with ex vivo-demonstrated muscarinic acetylcholine binding density, suggesting that the molecular action of isoflurane may involve antagonism of central acetylcholine pathways (Alkire and Haier 2001). On the other hand, Salmi showed that sevoflurane increased the distribution volume of ^{11}C-flumazenil in all areas studied (except pons and white matter), suggesting the involvement of $GABA_A$ receptors in the mechanism of action of sevoflurane (Salmi et al. 2004). This was concordant with a previous study of isoflurane, which showed a dose-dependent increase in distribution volume of ^{11}C-flumazenil (Gyulai et al. 2001).

Alkire and colleagues used PET to study the effects of sevoflurane at a higher system level (Alkire et al. 2008a). In the first step, they determined that exposure to low doses of sevoflurane—0.1% and 0.2% (0.05 and 0.1 MAC, respectively)—provided a subsequent mnemonic boost for emotional arousal but not neutral stimuli, presented during the sevoflurane exposure. This mnemonic boost was absent in volunteers administered with 0.25% sevoflurane. In the second step, ^{18}FDG PET was used to assess regional changes in glucose metabolism associated with 0.25% sevoflurane. Using structural equation modelling, they demonstrated that this dose blocked emotional memory by interfering with the amygdala to hippocampal connectivity.

44.13 PET and Nitrous Oxide

Nitrous oxide used to be commonly administered concomitantly with volatile anaesthetics. Although this practice is common, it is declining in frequency as environmental concerns have resulted in some departments no longer having inbuilt nitrous oxide supplies. On its own, the gas is a weak anaesthetic (administration of a partial pressure > 1 atm is required for general anaesthesia) but a reasonably strong analgesic, thanks to the fact that the drug acts as an antagonist at the NDMA receptor.

Few studies have used PET to study the neurophysiological changes associated with administration of nitrous oxide. Reinstrup used ^{133}Xe SPECT to study CBF changes associated with inhalation of 50% N_2O (Reinstrup et al. 1994). They found global increases in CBF, which were fairly uniform during normocapnia, although it remains possible that these changes were partly the result of Xe administration. It was also unclear whether these changes were the result of direct cerebral vasodilatation or from increases in metabolism. Later, the same group used ^{18}FDG to study

changes in glucose metabolism (Reinstrup et al. 2008). Inhalation of 50% nitrous oxide did not change global rCMRG, but did change the relative distribution of glucose metabolism, with 14% and 22% increases in the basal ganglia and thalamus, respectively.

In a study focused on sevoflurane and propofol, Kaisti and colleagues studied the effects of adjunct administration of 70% N_2O and found that N_2O counteracted some of the $rCMRO_2$ and rCBF reductions seen when propofol or sevoflurane was used alone (Kaisti et al. 2003). The findings all corroborated the findings of previous animal and human studies, in which other methods were used to study the cerebral blood flow and metabolic responses to N_2O.

44.14 PET and Xenon

Xenon is a rare (and expensive) noble gas and also a weak anaesthetic. Exposure to a 70% Xe will prevent purposeful movements in response to a surgical stimulus in 50% of volunteers (for comparison, the MAC of sevoflurane is 2.0%). The molecule is interesting because, like N_2O, it is also an NMDA antagonist, and it is probably for this reason that it may be neuroprotective.

PET studies of changes in rCBF have shown that in contrast to ketamine (also an NMDA antagonist), anaesthetic concentrations of Xe cause widespread decreases in rCBF, mostly marked in the cerebellum, thalamus and parietal cortex (Laitio et al. 2007). Findings for changes in rCMRG induced by Xe anaesthesia were also contrary to expectations, based on findings for N_2O and ketamine. Rex and colleagues found that Xe reduced total CMRG by 26% and decreased rCMRG in all areas studied (Rex et al. 2006). In a subsequent study, this group measured changes in rCBF associated with Xe anaesthesia, using $H_2{}^{15}O$ PET (Rex et al. 2008). Relative decreases in several cortical, subcortical and cerebellar areas were shown, with relative increases in white matter. These findings matched well with the previous pattern of findings with regard to rCBF, suggesting that flow-metabolism coupling is maintained with Xe.

Laitio and colleagues used ^{18}FDG and ^{15}O PET to study combined changes in rCMRG and rCBF associated with 67% Xe (Laitio et al. 2009). While the patterns of changes were broadly similar to those of Rex and colleagues, they found that the decreases in metabolism exceeded those of blood flow. When they calculated the rCBF/rCMRG ratio, they found that this was particularly increased in the insula, anterior and posterior cingulated and somatosensory cortex.

Although the patterns of changes in blood flow and metabolism are not too dissimilar to those found with the volatile anaesthetic agents, Xe does not influence ^{11}C-flumazenil binding, suggesting that the molecular mechanism of action of Xe does not involve an effect on the $GABA_A$ receptor (Salmi et al. 2008).

44.15 Summary and Conclusion

Early studies on the regional distribution of changes in cerebral metabolism associated with anaesthetic doses of isoflurane seemed to suggest uniform changes in keeping with a unitary hypothesis of a non-specific, physical molecular mechanism of action of the anaesthetic drugs. A limited number of studies have specifically studied the molecular mechanisms and site of action of the anaesthetic agents. In general, these studies have confirmed the findings of laboratory work using molecular biology techniques.

More recent PET studies have shown that the anaesthetic agents cause regionally specific effects on metabolism and flow and that these are probably the result of regionally specific distributions of neuronal $GABA_A$, NMDA and muscarinic ACh receptors. Most groups report global CBF and metabolic rate findings, absolute changes in rCBF and rCMRG or $rCMRO_2$ and then also changes in relative rCBF and rCMRG or $rCMRO_2$. The assumption inherent in the latter approach is that the greatest relative changes will happen in the regions where key anaesthetic effects are mediated. Different anaesthetic agents cause slightly different patterns of regional effects, but all cause an alteration in flow and/or metabolism in the thalamus. Anaesthetic-induced loss of consciousness appears to be associated with a significant reduction in blood flow and metabolism in the thalamus. While some investigators argue that this provides evidence that the thalamus is a key site of action of these agents (Alkire et al. 2000), caution is required, since these reductions in blood flow and metabolism may be the result of reduced cortical activity and thus reduced cortical input to the thalamus. EEG and electrocorticography studies suggest that the primary effect of anaesthetic agents is at the cortex, rather than at subcortical structures (Velly et al. 2007). EEG and fMRI studies provide contradictory evidence, with some suggesting that thalamocortical connectivity is maintained despite loss of consciousness (Boveroux et al. 2010; Boly et al. 2012), and others that preserved thalamocortical connectivity are a necessary prerequisite for consciousness (Barttfeld et al. 2015; Malekmohammadi et al. 2019).

Generally, the findings from PET studies of regional changes in blood flow and metabolism are in keeping with the known molecular sites of action. Xenon is one exception, since it has the same site of action as nitrous oxide and ketamine (NMDA receptor) yet has regional effects on blood flow and metabolism similar to those caused by the volatile anaesthetic agents (whose effects are mediated by action at $GABA_A$ and muscarinic Ach receptors and possibly also at K channels).

Much work remains to be done to understand how these molecular effects result in regional changes in activity and connectivity and changes in communication among distributed areas and how each of changes mediates alterations in consciousness.

References

Absalom AR, Green D (2013) NAP5: the tip of the iceberg, or all we need to know? Br J Anaesth 113(4):527–530

Adapa RM, Davis MH, Stamatakis EA, Absalom AR, Menon DK (2014) Neural correlates of successful semantic processing during propofol sedation. Hum Brain Mapp 35:2935–2949

Akeju O, Loggia ML, Catana C, Pavone KJ, Vazquez R, Rhee J et al (2014) Disruption of thalamic functional connectivity is a neural correlate of dexmedetomidine-induced unconsciousness. elife 4:e04499

Alkire MT (1998) Quantitative EEG correlations with brain glucose metabolic rate during anesthesia in volunteers. Anesthesiology 89(2):323–333

Alkire MT, Haier RJ (2001) Correlating in vivo anaesthetic effects with ex vivo receptor density data supports a GABAergic mechanism of action for propofol, but not for isoflurane. Br J Anaesth 86(5):618–626

Alkire MT, Miller J (2005) General anesthesia and the neural correlates of consciousness. Prog Brain Res 150:229–244

Alkire MT, Haier RJ, Barker SJ, Shah NK, Wu JC, Kao YJ (1995) Cerebral metabolism during propofol anesthesia in humans studied with positron emission tomography. Anesthesiology 82(2):393–403

Alkire MT, Haier RJ, Shah NK, Anderson CT (1997) Positron emission tomography study of regional cerebral metabolism in humans during isoflurane anesthesia. Anesthesiology 86(3):549–557

Alkire MT, Pomfrett CJ, Haier RJ, Gianzero MV, Chan CM, Jacobsen BP, Fallon JH (1999) Functional brain imaging during anesthesia in humans: effects of halothane on global and regional cerebral glucose metabolism. Anesthesiology 90(3):701–709

Alkire MT, Haier RJ, Fallon JH (2000) Toward a unified theory of narcosis: brain imaging evidence for a thalamocortical switch as the neurophysiologic basis of anesthetic-induced unconsciousness. Conscious Cogn 9(3):370–386

Alkire MT, Gruver R, Miller J, McReynolds JR, Hahn EL, Cahill L (2008a) Neuroimaging analysis of an anesthetic gas that blocks human emotional memory. Proc Natl Acad Sci U S A 105(5):1722–1727

Alkire MT, Hudetz AG, Tononi G (2008b) Consciousness and anesthesia. Science 322(5903):876–880

Angel A (1993) Central neuronal pathways and the process of anaesthesia. Br J Anaesth 71(1):148–163

Arhem P, Klement G, Nilsson J (2003) Mechanisms of anesthesia: towards integrating network, cellular, and molecular level modeling. Neuropsychopharmacology 28(Suppl 1):S40–S47

Barttfeld P, Bekinschtein TA, Salles A, Stamatakis EA, Adapa R, Menon DK, Sigman M (2015) Factoring the brain signatures of anesthesia concentration and level of arousal across individuals. NeuroImage Clin 9:385–391

Belelli D, Lambert JJ, Peters JA, Wafford K, Whiting PJ (1997) The interaction of the general anesthetic etomidate with the gamma-aminobutyric acid type A receptor is influenced by a single amino acid. Proc Natl Acad Sci U S A 94(20):11031–11036

Bishu S, Schmidt KC, Burlin TV, Channing MA, Horowitz L, Huang T, Liu ZH, Qin M, Vuong BK, Unterman AJ, Xia Z, Zametkin A, Herscovitch P, Quezado Z, Smith CB (2009) Propofol anesthesia does not alter regional rates of cerebral protein synthesis measured with L-[1-(11) C]leucine and PET in healthy male subjects. J Cereb Blood Flow Metab 29(5):1035–1047

Boly M, Moran R, Murphy M, Boveroux P, Bruno MA, Noirhomme Q, Ledoux D, Bonhomme V, Brichant JF, Tononi G, Laureys S, Friston K (2012) Connectivity changes underlying spectral EEG changes during propofol-induced loss of consciousness. J Neurosci 32(20):7082–7090

Bonhomme V, Fiset P, Meuret P, Backman S, Plourde G, Paus T, Bushnell MC, Evans AC (2001) Propofol anesthesia and cerebral blood flow changes elicited by vibrotactile stimulation: a positron emission tomography study. J Neurophysiol 85(3):1299–1308

Bonhomme V, Maquet P, Phillips C, Plenevaux A, Hans P, Luxen A, Lamy M, Laureys S (2008) The effect of clonidine infusion on distribution of regional cerebral blood flow in volunteers. Anesth Analg 106(3):899–909, table of contents

Boveroux P, Vanhaudenhuyse A, Bruno MA, Noirhomme Q, Lauwick S, Luxen A, Degueldre C, Plenevaux A, Schnakers C, Phillips C, Brichant JF, Bonhomme V, Maquet P, Greicius MD, Laureys S, Boly M (2010) Breakdown of within- and between-network resting state functional magnetic resonance imaging connectivity during propofol-induced loss of consciousness. Anesthesiology 113(5):1038–1053

Braestrup C, Albrechtsen R, Squires RF (1977) High densities of benzodiazepine receptors in human cortical areas. Nature 269(5630):702–704

Brown EN, Lydic R, Schiff ND (2010) General anesthesia, sleep, and coma. N Engl J Med 363(27):2638–2650, no. 1533-4406; 0028-4793

Cavazzuti M, Porro CA, Barbieri A, Galetti A (1991) Brain and spinal cord metabolic activity during propofol anaesthesia. Br J Anaesth 66(4):490–495

Dam M, Ori C, Pizzolato G, Ricchieri GL, Pellegrini A, Giron GP, Battistin L (1990) The effects of propofol anesthesia on local cerebral glucose utilization in the rat. Anesthesiology 73(3):499–505

Davidson AJ, Disma N, de Graaff JC et al (2016) Neurodevelopmental outcome at 2 years of age after general anaesthesia and awake-regional anaesthesia in infancy (GAS): an international multicentre, randomised controlled trial. Lancet 387(10015):239–250

Davis MH, Coleman MR, Absalom AR, Rodd JM, Johnsrude IS, Matta BF, Owen AM, Menon DK (2007) Dissociating speech perception and comprehension at reduced levels of awareness. Proc Natl Acad Sci U S A 104(41):16032–16037

Enna SJ, Snyder SH (1977) GABA receptor binding in frog spinal cord and brain. J Neurochem 28(4):857–860

Fiset P, Paus T, Daloze T, Plourde G, Meuret P, Bonhomme V, Hajj-Ali N, Backman SB, Evans AC (1999) Brain mechanisms of propofol-induced loss of consciousness in humans: a positron emission tomographic study. J Neurosci 19(13):5506–5513

Franks NP (2008) General anaesthesia: from molecular targets to neuronal pathways of sleep and arousal. Nat Rev Neurosci 9(5):370–386

Franks NP, Lieb WR (1984) Do general anaesthetics act by competitive binding to specific receptors? Nature 310(5978):599–601, no. 0028-0836; 0028-0836

Franks NP, Lieb WR (1993) Selective actions of volatile general anaesthetics at molecular and cellular levels. Br J Anaesth 71(1):65–76

Franks NP, Lieb WR (1997) Inhibitory synapses. Anaesthetics set their sites on ion channels. Nature 389(6649):334–335

Franks NP, Lieb WR (2004) Seeing the light: protein theories of general anesthesia. 1984. Anesthesiology 101(1):235–237

Gyulai FE, Mintun MA, Firestone LL (2001) Dose-dependent enhancement of in vivo GABA(A)-benzodiazepine receptor binding by isoflurane. Anesthesiology 95(3):585–593, no. 0003-3022; 0003-3022

Hales TG, Lambert JJ (1991) The actions of propofol on inhibitory amino acid receptors of bovine adrenomedullary chromaffin cells and rodent central neurones. Br J Pharmacol 104(3):619–628

Hameroff SR (2006) The entwined mysteries of anesthesia and consciousness: is there a common underlying mechanism? Anesthesiology 105(2):400–412

Haydon DA, Urban BW (1983) The effects of some inhalation anaesthetics on the sodium current of the squid giant axon. J Physiol 341:429–439

Haydon DA, Urban BW (1986) The actions of some general anaesthetics on the potassium current of the squid giant axon. J Physiol 373:311–327

Holmes SE, Gallezot JD, Davis MT et al (2019) Measuring the effects of ketamine on mGluR5 using [(18)F]FPEB and PET. J Cereb Blood Flow Metab. https://doi.org/10.1177/271678X19886316

Imas OA, Ropella KM, Wood JD, Hudetz AG (2006) Isoflurane disrupts anterio-posterior phase synchronization of flash-induced field potentials in the rat. Neurosci Lett 402(3):216–221

Jevtovic-Todorovic V, Absalom AR, Blomgren K, Brambrink A, Crosby G, Culley DJ et al (2013) Anaesthetic neurotoxicity and neuroplasticity: an expert group report and statement based on the BJA Salzburg Seminar. Br J Anaesth 111(2):143–151

Kaisti KK, Metsahonkala L, Teras M, Oikonen V, Aalto S, Jaaskelainen S, Hinkka S, Scheinin H (2002) Effects of surgical levels of propofol and sevoflurane anesthesia on cerebral blood flow in healthy subjects studied with positron emission tomography. Anesthesiology 96(6):1358–1370

Kaisti KK, Langsjo JW, Aalto S, Oikonen V, Sipila H, Teras M, Hinkka S, Metsahonkala L, Scheinin H (2003) Effects of sevoflurane, propofol, and adjunct nitrous oxide on regional cerebral blood flow, oxygen consumption, and blood volume in humans. Anesthesiology 99(3):603–613

Kissin I (1993) General anesthetic action: an obsolete notion? Anesth Analg 76(2):215–218

Kulli J, Koch C (1991) Does anesthesia cause loss of consciousness? Trends Neurosci 14(1):6–10

Laaksonen L, Kallioinen M, Långsjö J et al (2018) Comparative effects of dexmedetomidine, propofol, sevoflurane, and S-ketamine on regional cerebral glucose metabolism in humans: a positron emission tomography study. Br J Anaesth 121(1):281–290

Laitio RM, Kaisti KK, Långsjö JW, Aalto S, Salmi E, Maksimow A, Aantaa R, Oikonen V, Sipila H, Parkkola R, Scheinin H (2007) Effects of xenon anesthesia on cerebral blood flow in humans: a positron emission tomography study. Anesthesiology 106(6):1128–1133

Laitio RM, Långsjö JW, Aalto S, Kaisti KK, Salmi E, Maksimow A, Aantaa R, Oikonen V, Viljanen T, Parkkola R, Scheinin H (2009) The effects of xenon anesthesia on the relationship between cerebral glucose metabolism and blood flow in healthy subjects: a positron emission tomography study. Anesth Analg 108(2):593–600

Långsjö JW, Kaisti KK, Aalto S, Hinkka S, Aantaa R, Oikonen V, Sipila H, Kurki T, Silvanto M, Scheinin H (2003) Effects of subanesthetic doses of ketamine on regional cerebral blood flow, oxygen consumption, and blood volume in humans. Anesthesiology 99(3):614–623

Långsjö JW, Salmi E, Kaisti KK, Aalto S, Hinkka S, Aantaa R, Oikonen V, Viljanen T, Kurki T, Silvanto M, Scheinin H (2004) Effects of subanesthetic ketamine on regional cerebral glucose metabolism in humans. Anesthesiology 100(5):1065–1071

Långsjö JW, Maksimow A, Salmi E, Kaisti K, Aalto S, Oikonen V, Hinkka S, Aantaa R, Sipila H, Viljanen T, Parkkola R, Scheinin H (2005) S-ketamine anesthesia increases cerebral blood flow in excess of the metabolic needs in humans. Anesthesiology 103(2):258–268

Långsjö JW, Alkire MT, Kaskinoro K, Hayama H, Maksimow A, Kaisti KK, Aalto S, Aantaa R, Jääskeläinen SK, Revonsuo A, Scheinin H (2012) Returning from oblivion: imaging the neural core of consciousness. J Neurosci 32(14):4935–4943

Lee U, Kim S, Noh GJ, Choi BM, Hwang E, Mashour GA (2009) The directionality and functional organization of frontoparietal connectivity during consciousness and anesthesia in humans. Conscious Cogn 18(4):1069–1078

Lindholm ML, Traff S, Granath F, Greenwald SD, Ekbom A, Lennmarken C, Sandin RH (2009) Mortality within 2 years after surgery in relation to low intraoperative bispectral index values and preexisting malignant disease. Anesth Analg 108(2):508–512, no. 1526-7598

Lydic R, Baghdoyan HA (2005) Sleep, anesthesiology, and the neurobiology of arousal state control. Anesthesiology 103(6):1268–1295

Malekmohammadi M, Price CM, Hudson AE, DiCesare JAT, Pouratian N (2019) Propofol-induced loss of consciousness is associated with a decrease in thalamocortical connectivity in humans. Brain 142(8):2288–2302

Mandal PK, Fodale V (2009) Isoflurane and desflurane at clinically relevant concentrations induce amyloid beta-peptide oligomerization: an NMR study. Biochem Biophys Res Commun 379(3):716–720

Mashour GA (2006) Integrating the science of consciousness and anesthesia. Anesth Analg 103(4):975–982

Mashour GA, Kent C, Picton P, Ramachandran SK, Tremper KK, Turner CR, Shanks A, Avidan MS (2013) Assessment of intraoperative awareness with explicit recall: a comparison of 2 methods. Anesth Analg 116:889–891

Mason MF, Norton MI, Van Horn JD, Wegner DM, Grafton ST, Macrae CN (2007) Wandering minds: the default network and stimulus-independent thought. Science (New York, NY) 315(5810):393–395

Massimini M, Ferrarelli F, Huber R, Esser SK, Singh H, Tononi G (2005) Breakdown of cortical effective connectivity during sleep. Science 309(5744):2228–2232

Massimini M, Ferrarelli F, Esser SK, Riedner BA, Huber R, Murphy M, Peterson MJ, Tononi G (2007) Triggering sleep slow waves by transcranial magnetic stimulation. Proc Natl Acad Sci U S A 104(20):8496–8501

McCann ME, de Graaff JC, Dorris L et al (2019) Neurodevelopmental outcome at 5 years of age after general anaesthesia or awake-regional anaesthesia in infancy (GAS): an international, multicentre, randomised, controlled equivalence trial. Lancet 393(10172):664–677

Mihic SJ, Ye Q, Wick MJ, Koltchine VV, Krasowski MD, Finn SE, Mascia MP, Valenzuela CF, Hanson KK, Greenblatt EP, Harris RA, Harrison NL (1997) Sites of alcohol and volatile anaesthetic action on GABA(A) and glycine receptors. Nature 389(6649):385–389

Monk TG, Saini V, Weldon BC, Sigl JC (2005) Anesthetic management and one-year mortality after noncardiac surgery. Anesth Analg 100(1):4–10, no. 0003-2999; 0003-2999

Naci L, Haugg A, MacDonald A, Anello M, Houldin E, Naqshbandi G-LL, Arango M, Harle C, Cusack R, Owen A (2018) Functional diversity of brain networks supports consciousness and verbal intelligence. Sci Rep 8:13259

Noirhomme Q, Boly M, Bonhomme V, Boveroux P, Phillips C, Peigneux P, Soddu A, Luxen A, Moonen G, Maquet P, Laureys S (2009) Bispectral index correlates with regional cerebral blood flow during sleep in distinct cortical and subcortical structures in humans. Arch Ital Biol 147(1–2):51–57

Ori C, Dam M, Pizzolato G, Battistin L, Giron G (1986) Effects of isoflurane anesthesia on local cerebral glucose utilization in the rat. Anesthesiology 65(2):152–156

Pandit JJ, Andrade J, Bogod DG, Hitchman JM et al (2014) 5th National Audit Project (NAP5) on accidental awareness during general anaesthesia: summary of main findings and risk factors. Br J Anaesth 113(4):549–559

Prielipp RC, Wall MH, Tobin JR, Groban L, Cannon MA, Fahey FH, Gage HD, Stump DA, James RL, Bennett J, Butterworth J (2002) Dexmedetomidine-induced sedation in volunteers decreases regional and global cerebral blood flow. Anesth Analg 95(4):1052–1059, table of contents

Prys-Roberts C (1987) Anaesthesia: a practical or impractical construct? Br J Anaesth 59:1341–1345

Reinstrup P, Ryding E, Algotsson L, Berntman L, Uski T (1994) Effects of nitrous oxide on human regional cerebral blood flow and isolated pial arteries. Anesthesiology 81(2):396–402

Reinstrup P, Ryding E, Ohlsson T, Sandell A, Erlandsson K, Ljunggren K, Salford LG, Strand S, Uski T (2008) Regional cerebral metabolic rate (positron emission tomography) during inhalation of nitrous oxide 50% in humans. Br J Anaesth 100(1):66–71

Rex S, Schaefer W, Meyer PH, Rossaint R, Boy C, Setani K, Bull U, Baumert JH (2006) Positron emission tomography study of regional cerebral metabolism during general anesthesia with xenon in humans. Anesthesiology 105(5):936–943

Rex S, Meyer PT, Baumert JH, Rossaint R, Fries M, Bull U, Schaefer WM (2008) Positron emission tomography study of regional cerebral blood flow and flow-metabolism coupling during general anaesthesia with xenon in humans. Br J Anaesth 100(5):667–675

Reynolds DS, Rosahl TW, Cirone J, O'Meara GF, Haythornthwaite A, Newman RJ, Myers J, Sur C, Howell O, Rutter AR, Atack J, Macaulay AJ, Hadingham KL, Hutson PH, Belelli D, Lambert JJ, Dawson GR, McKernan R, Whiting PJ, Wafford KA (2003) Sedation and anesthesia mediated by distinct GABA(A) receptor isoforms. J Neurosci 23(24):8608–8617

Rudolph U, Antkowiak B (2004) Molecular and neuronal substrates for general anaesthetics. Nat Rev Neurosci 5(9):709–720

Salmi E, Kaisti KK, Metsahonkala L, Oikonen V, Aalto S, Nagren K, Hinkka S, Hietala J, Korpi ER, Scheinin H (2004) Sevoflurane and propofol increase 11C-flumazenil binding to gamma-aminobutyric acid A receptors in humans. Anesth Analg 99(5):1420–1426

Salmi E, Langsjo JW, Aalto S, Nagren K, Metsahonkala L, Kaisti KK, Korpi ER, Hietala J, Scheinin H (2005) Subanesthetic ketamine does not affect 11C-flumazenil binding in humans. Anesth Analg 101(3):722–725

Salmi E, Laitio RM, Aalto S, Maksimow AT, Langsjo JW, Kaisti KK, Aantaa R, Oikonen V, Metsahonkala L, Nagren K, Korpi ER, Scheinin H (2008) Xenon does not affect gamma-aminobutyric acid type A receptor binding in humans. Anesth Analg 106(1):129–134

Sandin RH, Enlund G, Samuelsson P, Lennmarken C (2000) Awareness during anaesthesia: a prospective case study. Lancet 355(9205):707–711

Schlunzen L, Vafaee MS, Cold GE, Rasmussen M, Nielsen JF, Gjedde A (2004) Effects of subanaesthetic and anaesthetic doses of sevoflurane on regional cerebral blood flow in healthy volunteers. A positron emission tomographic study. Acta Anaesthesiol Scand 48(10):1268–1276

Schlunzen L, Cold GE, Rasmussen M, Vafaee MS (2006) Effects of dose-dependent levels of isoflurane on cerebral blood flow in healthy subjects studied using positron emission tomography. Acta Anaesthesiol Scand 50(3):306–312

Schlunzen L, Vafaee MS, Juul N, Cold GE (2010) Regional cerebral blood flow responses to hyperventilation during sevoflurane anaesthesia studied with PET. Acta Anaesthesiol Scand 54(5):610–615

Schlunzen L, Juul N, Hansen KV, Cold GE (2012) Regional cerebral blood flow and glucose metabolism during propofol anaesthesia in healthy subjects studied with positron emission tomography. Acta Anaesthesiol Scand 56(2):248–255

Sebel PS, Bowdle TA, Ghoneim MM, Rampil IJ, Padilla RE, Gan TJ, Domino KB (2004) The incidence of awareness during anesthesia: a multicenter United States study. Anesth Analg 99(3):833–839

Short TG, Campbell D, Frampton C et al (2019) Anaesthetic depth and complications after major surgery: an international, randomised controlled trial. Lancet 394(10212):1907–1914

Spies M, James GM, Berroterán-Infante N, Ibeschitz H, Kranz GS, Unterholzner J, Godbersen M, Gryglewski G, Hienert M, Jungwirth J et al (2018) Assessment of ketamine binding of the serotonin transporter in humans with positron emission tomography. Int J Neuropsychopharmacol 21:145–153

Stamatakis EA, Adapa RM, Absalom AR, Menon DK (2010) Changes in resting neural connectivity during propofol sedation. PLoS One 5(12):e14224, no. 1932-6203; 1932-6203

Varley TF, Luppi A, Pappas I, Naci L, Adapa R, Owen A, Menon DK, Stamatakis EA (2019) Consciousness and brain functional complexity in propofol anaesthesia. bioRxiv: 680447

Velly LJ, Rey MF, Bruder NJ, Gouvitsos FA, Witjas T, Regis JM, Peragut JC, Gouin FM (2007) Differential dynamic of action on cortical and subcortical structures of anesthetic agents during induction of anesthesia. Anesthesiology 107(2):202–212

Vollenweider FX, Leenders KL, Oye I, Hell D, Angst J (1997) Differential psychopathology and patterns of cerebral glucose utilisation produced by (S)- and (R)-ketamine in healthy volunteers using positron emission tomography (PET). Eur Neuropsychopharmacol 7(1):25–38

Walker EM, Bell M, Cook TM, Grocott MP, Moonesinghe SR (2016) SNAP-1 investigator group. Patient reported outcome of adult perioperative anaesthesia in the United Kingdom: a cross-sectional observational study. Br J Anaesth 117:758–766

Whittington RA, Virag L, Marcouiller F et al (2011) Propofol directly increases tau phosphorylation. PLoS One 6(1):e16648

Xie G, Gunn RN, Dagher A, Daloze T, Plourde G, Backman SB, Diksic M, Fiset P (2004) PET quantification of muscarinic cholinergic receptors with [N-11C-methyl]-benztropine and application to studies of propofol-induced unconsciousness in healthy human volunteers. Synapse 51(2):91–101

Xie G, Deschamps A, Backman SB, Fiset P, Chartrand D, Dagher A, Plourde G (2011) Critical involvement of the thalamus and precuneus during restoration of consciousness with physostigmine in humans during propofol anaesthesia: a positron emission tomography study. Br J Anaesth 106(4):548–557

Zezula J, Cortes R, Probst A, Palacios JM (1988) Benzodiazepine receptor sites in the human brain: autoradiographic mapping. Neuroscience 25(3):771–795

PET Imaging in Altered States of Consciousness: Coma, Sleep, and Hypnosis

45

Estelle A. C. Bonin, Géraldine Martens, Helena Cassol, Camille Chatelle, Steven Laureys, and Aurore Thibaut

Contents

45.1 Introduction 1150
45.2 Disorders of Consciousness Following a Brain Injury 1154
45.3 PET Scan and Disorders of Consciousness 1159
45.3.1 Measuring the Brain at "Rest" 1159
45.3.2 Measuring the Brain During Sensory Stimulation 1163
45.4 PET Scan and Sleep 1164
45.5 PET Scan and Hypnosis 1166
45.6 Conclusion 1169
References 1169

Abstract

Positron emission tomography (PET) allows studies of cerebral metabolism and blood flow and has been widely used to investigate physiological mechanisms underlying altered states of consciousness. Consciousness is characterized by two components: wakefulness and awareness. In this chapter, we review the current literature on brain metabolism during pathological loss of consciousness (vegetative/unresponsive or minimally conscious states), sleep (in healthy subjects and in patients with insomnia), and under hypnosis. By identifying brain areas specifically involved in conscious processing, these studies have contrib-

E. A. C. Bonin · G. Martens · H. Cassol · C. Chatelle · S. Laureys · A. Thibaut (✉)
Coma Science Group, GIGA-Consciousness, University of Liège, Liège, Belgium

Centre du Cerveau (C2), University Hospital of Liège, Liège, Belgium
e-mail: Estelle.Bonin@uliege.be; Geraldine.Martens@chuliege.be; hcassol@uliege.be; Steven.Laureys@uliege.be; athibaut@uliege.be

R. A. J. O. Dierckx et al. (eds.), *PET and SPECT in Neurology*,
https://doi.org/10.1007/978-3-030-53168-3_45

uted to our understanding of the underlying physiology of consciousness. The precuneal and cingulate cortices, for example, seem to be key areas for maintaining conscious awareness. FDG-PET further allowed the identification of the minimal energetic requirement for conscious awareness in this population, which corresponds to 42% of normal cortical activity. Up to now, it is the most accurate neuroimaging tool regarding the diagnosis of patients with disorders of consciousness. In the future, its use as part of multimodal assessment could improve diagnosis and prognosis in this challenging population. In sleep, a greater activity of the precuneus/posterior cingulate cortex and the frontoparietal areas during non-rapid eye movement sleep also seems to play a role in disorders such as insomnia. Other areas such as the hypothalamus, amygdala, or temporo-occipital cortex seem to play a role in different states such as rapid eye movement sleep and hypnosis. PET studies permit a better comprehension of the neural correlates of consciousness and identify the implication of specific neural areas and networks in altered states of consciousness in post-comatose patients, sleep, and induced hypnosis.

45.1 Introduction

There is at present no validated objective definition of consciousness (Noirhomme and Laureys 2011). Numerous definitions abound in the literature (Nagel et al. 1979; Searle 2000; Dehaene and Naccache 2001; Tononi 2004; Baars 2005); for a review, see Damasio and Kaspar (2009). Consciousness is a multifaceted concept described as comprising two major components: arousal and awareness (Zeman 2001). This dichotomous terminology provides a practical approach, which corresponds well to clinical settings (Posner et al. 2007). Arousal refers to the degree of wakefulness or the level of consciousness. It is clinically manifested by spontaneous eye opening (indicating wakefulness and rest cycles) and controlled mainly by the ascending reticular system in the brainstem, midbrain, and thalamus. Awareness is a term used to describe the capacity to perceive and to experience something—that is, the phenomenological experience of being (Nagel et al. 1979) or the contents of consciousness. Evidence from functional neuroimaging studies suggests that there are two anticorrelated cortical systems that mediate conscious awareness: an "extrinsic" network that encompasses lateral frontoparietal areas and has been linked with processes of external input (external awareness) and an "intrinsic" network which includes mainly medial brain areas and has been associated with internal processes (internal awareness) (Vanhaudenhuyse et al. 2011). The clinical quantification of awareness is limited to evaluating patients' motor responsiveness to commands and nonreflex behaviors, such as visual pursuit or localization to pain (Noirhomme and Laureys 2011; for a review, see Gosseries et al., 2014).

Awareness is believed to be a phenomenon emerging from cortical activity and supported by subcortical connections in particular to the thalamus. Even if awareness normally follows from arousal, the two qualities are dissociable. Hence,

preserved arousal does not necessarily imply awareness (Laureys 2005). As the anatomical and physiological correlates of consciousness are complex, the interplay of arousal and awareness is incompletely understood, and a plethora of questions remain unsolved, limiting our understanding of the human consciousness.

During the last decade, researchers began to investigate brain activity in patients with disorders of consciousness (DOC) following severe brain injury. Other studies focused on hypnosis and sleep, and in conjunction, these investigations contributed to our current understanding of the minimal neural correlates of conscious awareness in both physiological and pathological states.

One way to study brain activity is by positron emission tomography (PET), measuring regional increases in cerebral blood flow (rCBF) with [^{18}F]-fluorodeoxyglucose (FDG) or using ^{15}O-labeled water (H_2O^{15}). PET imaging allows studies of regional brain functionality at rest, without the patients' active participation. The aim of this chapter is to provide an overview of the neural correlates of altered consciousness, identified by PET studies, in both physiological and pathological conditions (for summary, see Tables 45.1, 45.2, 45.3, and 45.4). We will first discuss studies on

Table 45.1 Summary of FDG-PET studies on disorders of consciousness during resting state

Authors	*N*	Diagnosis	Time since injuries	Main findings
Levy et al. (1987)	*7*	UWS	1–72	60% (53–67%) decrease in metabolism
DeVolder et al. (1990)	*7*	UWS	1–4	53% (43–65%) decrease in metabolism
Tommasino et al. (1995)	*10*	UWS	2–24	56% decrease in metabolism
Plum et al. (1998)	*3*	UWS		50% decrease in metabolism with significant regional variations
Laureys et al. (1999a)	*4*	UWS	<1–60	Frontoparietal hypometabolism and disconnections
Laureys et al. (1999b)	*1*	UWS	1	38% decrease in metabolism; recovery of consciousness = frontoparietal recovery
Rudolf et al. (1999a)	*24*	UWS	<1–6	25% decrease in metabolism (17% for acute patients (<3 months) and 33% for chronic patients (>3 months))
Schiff and Plum (1999)	*1*	UWS	240	50% decrease in metabolism with significant regional variations
Laureys et al. (2000b)	*1*	UWS	4	Recovery of consciousness = thalamocortical reconnections
Rudolf et al. (2000)	*9*	UWS	<1	Decrease in benzodiazepine receptor density in VS/UWS
Laureys et al. (2002a)	*30*	UWS	1–5	56% (37–72%) decrease in metabolism

(continued)

Table 45.1 (continued)

Authors	*N*	Diagnosis	Time since injuries	Main findings
Schiff et al. (2002)	*5*	UWS	6–240	50% (31–87%) decrease in metabolism with regional variations
Beuthien-Baumann et al. (2003)	*16*	UWS	2–12	58% decrease in metabolism; frontoparietal hypometabolism
Tengvar et al. (2004)	*1*	MCS	6	47–65% frontoparietal hypometabolism
Juengling et al. (2005)	*5*	UWS	1–48	Frontoparietal and thalamic hypometabolism
Nakayama et al. (2006)	*30*	17 UWS 13 MCS	6–60	Frontoparietal and thalamic hypometabolism in VS/UWS
				Less impaired in MCS
Majerus et al. (2009)	*36*	MCS	1–265	Hypometabolism in language-processing regions (left superior, middle and inferior temporal gyri, left inferior frontal gyrus, and the right inferior temporal gyri)
Schnakers et al. (2008)	*1*	MCS	24	Changes in the fronto-temporoparietal network and the sensorimotor area
Silva et al. (2010)	*10*	UWS	2–24	Frontoparietal hypometabolism
Lull et al. (2010)	*17*	UWS and MCS	12	Thalamus hypometabolism
Bruno et al. (2010)	*10*	UWS	3	Frontoparietal hypometabolism (VS/UWS without fixation = patients with fixation)
Phillips et al. (2011)	*13 8*	UWS LIS	<1–290	Automatic classification between VS/UWS and healthy subjects or LIS using the "relevance vector machine"
Garcia-Panach et al. (2011)	*17*	UWS and MCS	12	Cortico-thalamocortical hypometabolism correlates with less favorable outcomes
Bruno et al. (2012)	*27*	13 MCS	1–70	Left-sided metabolism MCS+ (command following) > MCS− (low level of nonreflexive behaviors)
		14 MCS+		Broca's region disconnection from language network, mesiofrontal, and cerebellar areas in MCS−
Thibaut et al. (2012)	*70*	24 UWS	<1–270	Extrinsic and intrinsic network hypometabolism in VS/UWS
Studies using resting state FDG-PET to evaluate the effects of pharmacological treatment				
Chatelle et al. (2014)	3	MCS	18 months to 7 years	Metabolism increase in bilateral dorsolateral prefrontal and mesiofrontal cortices after the administration of zolpidem
Studies using resting state FDG-PET to evaluate the effects of pharmacological treatment and as a diagnostic tool				
Stender et al. (2014)	112	UWS, MCS, LIS	<1 month to >1 year	85% of diagnosis agreement between CRS-R and FDG-PET for MCS (67% for UWS). 74% good outcome prediction

Table 45.1 (continued)

Authors	*N*	Diagnosis	Time since injuries	Main findings
Stender et al. (2015)	41	UWS, MCS, eMCS	10 days to 9 years	Regional differences between VS/UWS and MCS more pronounced in the frontoparietal cortex. In the brainstem and thalamus, metabolism declined equally in both VS/UWS and MCS
Stender et al. (2016)	131	UWS, MCS, eMCS	622–1299 days	Use of extracerebral tissue normalization. 42% of normal cortical activity = minimal energetic requirement for conscious awareness
Studies using resting state FDG-PET as part of multimodal assessment				
Soddu et al. (2016)	15	UWS, LIS	NA	High correlation between resting state fMRI total neuronal activity and PET cerebral metabolism. UWS vs. HS = decrease in lateral and medial frontoparietal networks for both techniques
Annen et al. (2016)	25	UWS, MCS, eMCS	30 days to 1.8 years	Association between functional metabolism (inferior parietal, precuneus, and frontal regions) and structural integrity of the DMN (frontal-inferior parietal, precuneus-inferior parietal, thalamo-inferior parietal, and thalamofrontal tracts)
Di Perri et al. (2016)	58	UWS, MCS, eMCS	27 months	Correlation between FDG-PET brain metabolism and fMRI connectivity. Brain metabolism increase in the thalamus, basal ganglia, and lateral frontoparietal, parieto-occipital, and temporal cortices. Correlation between brain metabolisms and CRS-R scores in the lateral frontoparietal and superior temporal regions
Bodart et al. (2017)	24	UWS, MCS, eMCS, LIS	5–1116 weeks	FDG-PET and PCI revealed preserved metabolic rates and high complexity levels in four patients who were behaviorally unresponsive.
Golkowski et al. (2017)	20	UWS, MCS	116–170 days	Glucose metabolism in the occipital lobe higher in MCS as compared to VS/UWS. FDG-PET values in the occipital cortex correlated with CRS-R on the day of measurement
Annen et al. (2018)	12	UWS, MCS	7.5–50 months	Preservation in the region of the right dorsolateral prefrontal cortex, the inferior parietal junction, and the inferior temporal gyrus in patient with signs of "covert command following"

VS/UWS vegetative state/unresponsive wakefulness syndrome, *MCS* minimally conscious state, *MCS+* patients in "MCS plus" (showing command following), *MCS−* patients in "MCS minus" (showing minimal level of behavioral interactions without command following), *LIS* locked-in syndrome, *EMCS* emergence from the minimally conscious state, *HS* healthy subject, *DMN* default mode network, *CRS-R* Coma Recovery Scale-Revised, *EEG* electroencephalogram, *fMRI* functional magnetic resonance imaging, *PCI* perturbational complexity index

Table 45.2 Summary of PET-H_2O^{15} studies in patients with disorders of consciousness during sensory stimulations

Authors	*N*	Diagnosis	Time since insult (day(s) and month(s))	Passive stimulation	Level of activation
De Jong et al. (1997)	1	UWS	2 months	Auditory (familiar voice)	High
Menon et al. (1998)	1	UWS	3 months	Visual (familiar face)	Low
Laureys et al. (2000a)	5	UWS	3–38 days	Auditory (click)	Low
Laureys et al. (2002b)	15	UWS	1 month	Pain (electrical stimulation)	Low
Schiff et al. (2002)	5	3 UWS, 2 UWS	6–300 months	Auditory (click), tactile	Low/high
Owen et al. (2002)	3	1 UWS, 2 UWS	4 months	Visual (familiar face), auditory (noise, words)	Low/high
Kassubek et al. (2003)	7	UWS	3–48 months	Pain (electrical stimulation)	High
Boly et al. (2004)	20	15 UWS, 5 MCS	1–4 months	Auditory (click)	Low/high
Laureys et al. (2004b)	1	MCS	6 months	Auditory (noise, cries, own name)	High
Owen et al. (2005)	1	UWS	4 months	Auditory (speech)	High
Giacino et al. (2006)	5	UWS	1–3 months	Visual (flash)	Low
Boly et al. (2008a)	20	15 UWS, 5 MCS	1–4 months	Pain (electrical stimulation)	Low/high
Silva et al. (2010)	5	UWS	2–22 months	Tactile	Low

UWS unresponsive wakefulness syndrome, *MCS* minimally conscious state, *LIS* locked-in syndrome

patients with disorders of consciousness, in resting state condition and during passive stimulation paradigms. We will then give an overview of sleep and hypnosis studies and discuss the clinical implications of these findings.

45.2 Disorders of Consciousness Following a Brain Injury

Following severe brain damage with loss of consciousness, patients usually evolve through different clinical stages before fully or partially recovering consciousness. Coma is defined as complete absence of arousal and awareness, with no eye opening

Table 45.3 Summary of PET studies on healthy subjects during sleep

Authors	*N*		Stage	Main findings
Maquet et al. (1990)	11	FDG	SWS	Metabolism decrease 40% (>thalami)
			REMS	Metabolism = wakefulness
Maquet et al. (1996)	7	FDG	REMS	Metabolism increase in the tegmentum, left thalamus, amygdala, ACC, and right parietal operculum
				Metabolism decrease in dorsolateral prefrontal and parietal cortices, PCC, and the precuneus
Braun et al. (1997)	37	H_2O^{15}	SWS/REMS	Metabolism decrease in centrencephalic and heteromodal association regions and increase in S1–S2
				Metabolism increase in centrencephalic and S1–S2 and decrease in the frontoparietal association cortices
Hofle et al. (1997)	11	H_2O^{15}	SWS	rCBF negatively correlates with sigma power (EEG) in the thalamus bilaterally
Maquet (1997)	11	H_2O^{15}	SWS	Metabolism decrease in the dorsal pons and mesencephalon, thalami, basal ganglia, basal forebrain/hypothalamus, orbitofrontal cortex, anterior cingulate cortex, and precuneus
Andersson et al. (1998)	19	H_2O^{15}	SWS	Metabolism decrease in the thalamus and the frontal and parietal association areas and increase in the cerebellum
Kajimura et al. (1999)	18	H_2O^{15}	SWS	Metabolism decrease in midbrain tegmentum, cerebellar vermis, basal forebrain, caudate nucleus, posterior cingulate gyrus, and neocortical regions
Nofzinger et al. (1997)	8	FDG	REMS	Metabolism increase in limbic regions and orbitofrontal, cingulate, entorhinal, and insular cortices
Peigneux et al. (2001)	12	H_2O^{15}	REMS	Correlation during REMS between the density of REMS and rCBF in the occipital and the lateral geniculate bodies of the thalamus
Nofzinger et al. (2002)	14	FDG	SWS	Metabolism decrease in frontal, parietal, temporal and occipital cortices and the thalamus
				Increases in the dorsal pontine tegmentum, hypothalamus, basal forebrain, ventral striatum, anterior cingulate cortex, and mesial temporal lobe
Dang-Vu et al. (2005)	23	H_2O^{15}	SWS	Association between rCBF in the ventromedial prefrontal regions and delta power (EEG)
Maquet et al. (2005)	207	H_2O^{15}	REMS	Metabolism decrease in frontal and parietal areas

(continued)

Table 45.3 (continued)

Authors	*N*		Stage	Main findings
Wilckens et al. (2016)	52	FDG	Wakefulness	Higher relative slow-wave activity associated with greater dorsolateral prefrontal metabolism in healthy subjects. Negative correlation between age and wake metabolism in the dorsolateral prefrontal cortex
Kay et al. (2016)	44 PI, 40 GS	FDG	Wakefulness, SWS/NREM	Insomnia associated with impaired disengagement of theleft frontoparietal and the left middle frontal cortices, the precuneus/ posterior cingulate, and the fusiform/lingual gyri during NREM sleep and impaired engagement of these regions during wakefulness
Kay et al. (2019)	17 PI, 19 GS	FDG	Wakefulness, SWS/NREM	Individuals with insomnia and good sleepers showed similar relative rCMRglc responses to acute sleep restriction (lower relative rCMRglc in the left frontoparietal cortex, medial frontal cortex, posterior cingulate cortex, and thalamus)

FDG fluorodeoxyglucose, *SWS* slow-wave sleep, *REMS* rapid eye movement sleep, *NREMS* non-rapid eye movement sleep, *rCBF* regional cerebral blood flow, *ACC* anterior cingulate cortex, *S1–S2* primary and secondary sensorimotor areas, *EEG* electroencephalography, *GS* good sleeper, *PI* primary insomnia, *rCMRglc* regional cerebral metabolic rate for glucose

and only presenting reflexive behavior, in other words an "unarousable unresponsiveness" (Posner et al. 2007). When eye opening and rest-wake cycles are reestablished but the patients still only exhibit reflexive behaviors, they are said to be in a vegetative state (VS), now called unresponsive wakefulness syndrome (UWS) (The Multi-Society Task Force on PVS 1994; Laureys et al. 2010). Progression from VS/UWS usually leads to the minimally conscious state, where reproducible but fluctuating signs of consciousness are present, such as eye tracking motion or response to verbal or tactile stimuli (Giacino et al. 2002), but these patients are, by definition, unable to effectively communicate. We recently proposed a subcategorization of MCS patients based on the complexity of their behavior in two entities: "MCS −" and "MCS +." "MCS −" describes patients with minimal level of behavioral interactions without command following (e.g., visual pursuit, localization of noxious stimulation, and/or smiling/crying in contingent relationship to external stimuli). "MCS +" patients show higher-level behavioral responses such as command following (Fig. 45.1) (Bruno et al. 2012). The emergence of the MCS is characterized by the recovery of functional communication (verbal or nonverbal) or functional use of objects (Giacino et al. 2002). In rare cases, following brainstem lesions, patients can fully recover consciousness but remain totally paralyzed and aphonic, in the aptly named locked-in syndrome (Laureys et al. 2005a). These patients are able to communicate only with small eye movements (American Congress of Rehabilitation Medicine 1995). The difficulty in disentangling reflexive from voluntary responses, the fluctuation of vigilance, and the additional cognitive or sensory deficits lead to a

Table 45.4 PET studies on hypnosis, at rest, and during pain stimulation in healthy subjects

Authors	*N*	PET	Paradigm	State	Main findings
Maquet (1999)	9	H_2O^{15}	Rest	Hypnotic state	Widespread metabolism increase, mainly left sided (occipital, parietal, precentral, premotor, and ventrolateral prefrontal cortices)
Rainville et al. (1999b)	10	H_2O^{15}	Pain	Hypnotic suggestion	Increased metabolism in ACC and in the inferior frontal gyri
					Decreased metabolism in the right inferior parietal lobule, the left precuneus, and the posterior cingulate gyrus
Rainville et al. (1997)	11	H_2O^{15}	Pain	Hypnotic suggestion	Increase in ACC
Rainville et al. (1999a)	22	H_2O^{15}	Pain	Hypnotic state	Increase in ACC, insula, S1 and S2
Faymonville et al. (2000)	11	H_2O^{15}	Pain	Hypnotic state	Metabolism increase in right-sided extrastriate area and the ACC
Hofbauer et al. (2001)	10	H_2O^{15}	Pain	(a) Hypnotic state	(a) Activation of S1 and S2, ACC, and insula
				(b) Hypnotic suggestion	(b) Significant increase in pain-evoked activity within S1 and ACC
Rainville et al. (2002)	10	H_2O^{15}	Rest	Hypnotic state	Metabolism increase in the ACC, thalamus, and pontomesencephalic brainstem
					Decrease in the inferior parietal lobule, the precuneus, and the posterior temporal cortices
Faymonville et al. (2003)	19	H_2O^{15}	Pain	Hypnotic state	Increased functional connectivity between midcingulate cortex and insula, pregenual and frontal areas, pre-SMA, brainstem, thalamus, and basal ganglia
Derbyshire et al. (2004)	33	H_2O^{15}	Rest	Hypnotic suggestion	Both pain and hypnotically induced pain experience and pain stimulation induced metabolic modulations within the thalamus, ACC, insula, and prefrontal and parietal cortices
Nusbaum et al. (2011)	14	H_2O^{15}	Rest (patients with chronic low-back pain)	Hypnotic suggestion	Metabolism increase in frontotemporal area, insula, caudate, acumens, lenticular nuclei, and ACC

ACC anterior cingulate cortex, *S1–S2* primary and secondary sensorimotor cortex, *SMA* supplementary motor area

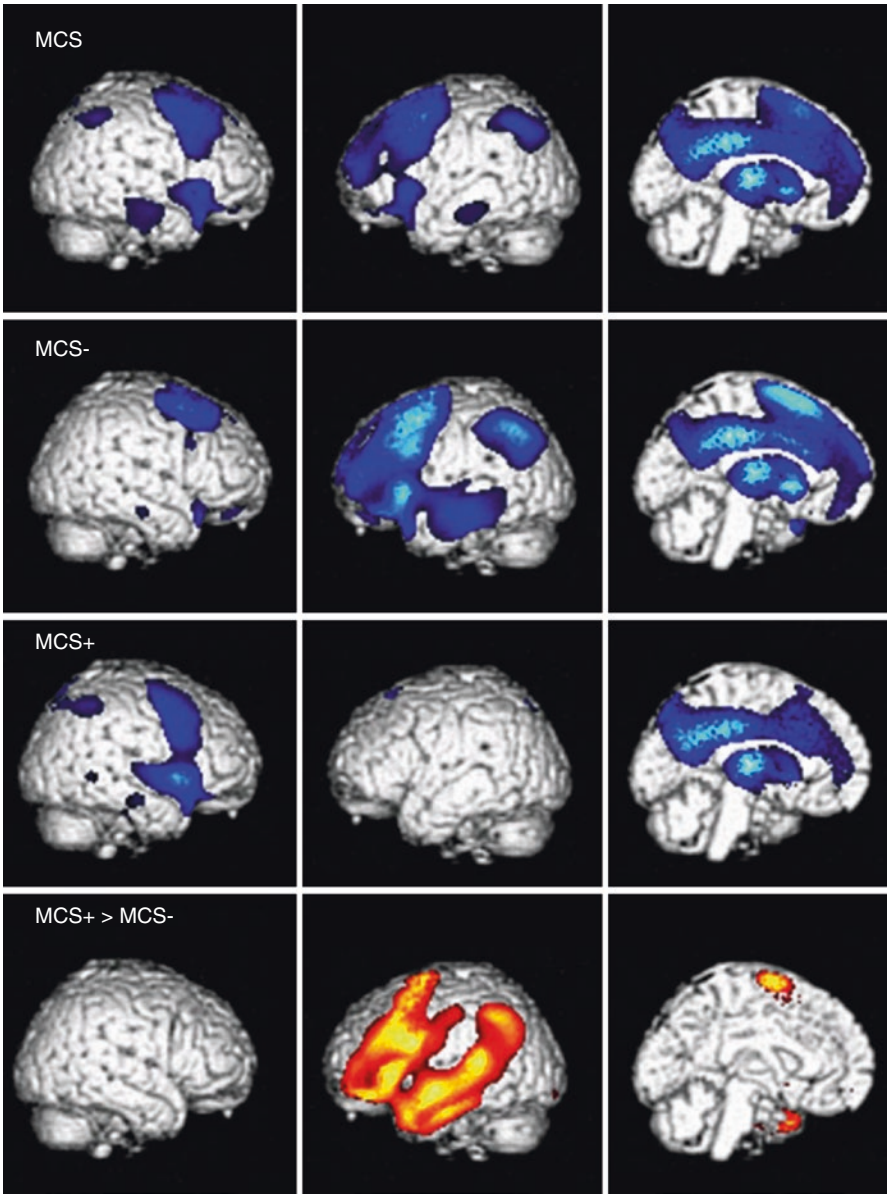

Fig. 45.1 Areas with impaired metabolism (shown in *blue*) in patients in a minimally conscious state (*MCS*), MCS− (showing nonreflex behavior), and MCS+ (showing command following). The *lowest panel* illustrates areas with higher metabolism in MCS+ as compared to MCS− (shown in *orange*). All results are shown on a 3D MRI template and thresholded at false discovery rate corrected $p < 0.05$ (from Bruno et al. (2012))

high rate of misdiagnosis between VS/UWS and MCS (Andrews et al. 1996; Childs and Mercer 1996; Schnakers et al. 2009) and locked-in syndrome (Bruno et al. 2009). The diagnosis may influence decisions about the patients' care, regarding crucial matters such as end-of-life decisions (Demertzi et al. 2011) or pain management (Demertzi et al. 2009). In this context, objective measures independent of the integrity of the motor pathways are needed to supplement behavioral assessments at the bedside. Neuroimaging provides a promising means to this end (for a review, see Schiff (2006) and Laureys and Schiff (2012)).

45.3 PET Scan and Disorders of Consciousness

45.3.1 Measuring the Brain at "Rest"

In 1987, the first FDG-PET study on VS/UWS patients showed a global decrease in brain metabolism of about 40–50% (Levy et al. 1987). These results were reproduced in several studies (DeVolder et al. 1990; Tommasino et al. 1995; Laureys et al. 1999b; Rudolf et al. 1999b; Stender et al. 2015). FDG-PET was suggested to be a good tool to complement bedside examination and reduce misdiagnosis (Schnakers et al. 2009). Indeed, regarding the diagnosis of MCS patients, FDG-PET showed 85% of good congruence with the score of the Coma Recovery Scale-Revised (i.e., CRS-R, this behavioral scale is the gold standard for the diagnosis of DOC patient) with a sensitivity to identify MCS patients of 93%. It is also a good tool to predict patient outcomes (i.e., 74% of VS/UWS and MCS patients diagnosed by FDG-PET remained respectively unconscious and conscious at follow-up) (Stender et al. 2014). Even if the diagnostic and prognostic usefulness of this technique has been shown, they still lack clear guidelines regarding the assessment of changes in brain metabolism due to the use of nonquantitative methods (i.e., visual examination). More recent studies (Table. 45.2) reported an average of 42% of global cerebral metabolism rate of glucose (CMRglc) in VS/UWS and 55% in MCS patients with more pronounced difference in the frontoparietal and precuneal cortices (Stender et al. 2015), highlighting that a minimum of 42% of global brain metabolism preservation is needed for the emergence of consciousness in post-comatose patients. In another study using an objective method to quantify FDG-PET images (i.e., by normalizing the images to extracerebral tissue and not the brainstem which could be impaired and bias the results), they confirmed that 42% of normal cortical hemispheric activity represents the minimal energetic requirement for sustained awareness (Stender et al. 2016). Moreover, in this study, all the FDG-PET images of MCS patients were normalized to their global best-hemisphere mean in order to investigate the effect of regional variation relative to resting baseline metabolism on cognitive and sensory function. The results showed an increase of this regional metabolism variation relative to resting baseline (i.e., 10–30% of increase) in response to sensory and cognitive tasks reflecting a preservation of some specific cognitive and sensory functions in MCS patients.

Regarding patients in locked-in syndrome, brain metabolism levels are closer to normal than VS/UWS patients (Levy et al. 1987). Results from studies by Laureys et al. indicated that no supratentorial cortical areas show significantly lower metabolism in acute and chronic locked-in patients when compared to age-matched healthy subjects (Laureys et al. 2003, 2004a, 2005a). However, the global brain metabolism is not directly correlated with the level of consciousness. A recovery from VS/UWS does not always imply substantial changes in global brain metabolism (Laureys et al. 1999b). Moreover, some healthy subjects show metabolic rates of glucose comparable to VS/UWS patients (Laureys 2005). Those results suggest that some brain areas are more important for the emergence of consciousness than others (Laureys et al. 1999b, 2000c, 2004a). Studies on regional brain metabolism were performed to identify areas specifically involved in loss of consciousness, comparing brain metabolism of VS/UWS and MCS patients with age-matched healthy subjects. Results highlighted a widespread impairment of the frontoparietal network, encompassing midline (i.e., anterior cingulate cortex (ACC)/mesiofrontal and posterior cingulate cortex (PCC)/precuneus) and lateral (i.e., prefrontal and posterior parietal) associative cortices being associated with a decreased level of consciousness (Laureys et al. 1999a, b; Beuthien-Baumann et al. 2003; Juengling et al. 2005; Nakayama et al. 2006; Lull et al. 2010; Silva et al. 2010; Bruno et al. 2012; Thibaut et al. 2012). Preserved areas were the midbrain and brainstem structures, known to be involved in autonomous functions such as sleep-wake cycles, thermoregulation, and respiration (Laureys et al. 2002a). Moreover, functional connectivity studies also highlighted a cortico-cortical (Laureys et al. 1999a, 2000b, 2002b) and thalamocortical (Laureys et al. 2000b) disconnection syndrome in VS/UWS patients. A recent study showed that a cortico-thalamocortical hypometabolism seems to be correlated with less favorable outcome (Garcia-Panach et al. 2011). These observations led to the hypothesis that consciousness is an emergent property of frontoparietal functional connectivity (Baars et al. 2003; Laureys 2005).

A clinical trial (Giacino et al. 2012) has shown effects of amantadine, a mixed noradrenergic and dopaminergic agonist, toward improving the speed of recovery from disorders of consciousness. A case study reported by Schnakers et al. highlighted effects on brain metabolism of the drug, in a widespread frontotemporoparietal network and the sensorimotor area (Schnakers et al. 2008). These data suggest a modulation of polymodal associative cortical metabolism and motor function by amantadine. Alongside, they underline the behavioral improvements associated with amantadine treatment (e.g., recovery of command following). Within this frontoparietal network, the precuneus seems to be a critical region (Vogt and Laureys 2005). This area is the most active in conscious resting states (Raichle and Snyder 2007) and seems to be the most widely impaired in patients with disorders of consciousness (Laureys et al. 2005b). Studies, based on the mesocircuit hypothesis (Schiff 2010), investigated the effect of zolpidem in DOC patients (Whyte and Myers 2009). Indeed, in rare cases, this non-benzodiazepine agent usually used to treat insomnia (Langtry and Benfield 1990; Sanger 2004) results in a paradoxical increase in responsiveness at bedside (Clauss and Nel 2006; Shames and Ring 2008). A case study using FDG-PET was performed in three zolpidem

responders that were MCS and showed an increased metabolism in the dorsolateral prefrontal and mesiofrontal cortices following zolpidem administration (Chatelle et al. 2014). According to the mesocircuit hypothesis, zolpidem could increase thalamic activity by disinhibiting the globus pallidus interna and thereby restoring thalamocortical connectivity, preferentially with the prefrontal cortex, and, thus, induce increase in prefrontal activity. After zolpidem intake, an impaired brain metabolism was observed in the thalami and the left precuneus/posterior cingulated. These impaired brain areas did not show structural lesions, suggesting that neurologic deficits in responders are not due to brain lesions in these areas but could rather be linked to an inhibitory functional effect of the fronto-thalamic connectivity.

A study on traumatic brain-injured patients found a hypometabolism in the ACC and PCC, the medial frontobasal regions, and the thalamus. The metabolism in these regions was mostly impaired in VS/UWS patients compared to MCS. Moreover, hypometabolism was more widespread and prominent in the MCS group as compared to patients who had emerged from the MCS (Nakayama et al. 2006). Within this network, it seems possible to distinguish areas involved in external (related to external/sensory awareness) or internal consciousness (related to internal/self-awareness) (Laureys et al. 1999a; Tian et al. 2007; Boly et al. 2008b; Vanhaudenhuyse et al. 2011). These results demonstrated that both external (encompassing lateral frontoparietal cortices) and internal (midline areas) networks were impaired in VS/UWS patients, while MCS patients only had decreased metabolism in the internal network, even less affected in patients emerging from the MCS (Thibaut et al. 2012).

Cerebral PET imaging has also been employed to disentangle reflexive from nonreflexive movements. International guidelines seem to disagree whether visual fixation is compatible with the diagnosis of VS/UWS (i.e., automatic subcortical process (Royal College of Physicians 2003)) or is a sufficient sign of awareness by mandating a higher-order cortical processing (Giacino et al. 2002). It was shown that anoxic VS/UWS patients with or without visual fixation presented identical brain metabolism and cortico-cortical functional disconnections, indicating that visual fixation does not necessarily reflect awareness in anoxic patients (Bruno et al. 2010). PET scan was also used to explore other cognitive dysfunctions, such as aphasia, which could induce an underestimation of cognitive capabilities of patients with disorders of consciousness. A study by Majerus and collaborators highlights that brain metabolism in language-processing regions (left superior, middle, and inferior temporal gyri, left inferior frontal gyrus, and right inferior temporal gyri) was shown to be particularly impaired in MCS patients whatever the etiology (Majerus et al. 2009), suggesting that a significant part of this population could suffer from language disorders such as aphasia. It was further investigated whether the differences in brain metabolism supported the subcategorization of the MCS into MCS− and MCS + (Bruno et al. 2012). Patients in MCS+ showed a higher cerebral metabolism in left-sided cortical areas encompassing the language network, premotor, pre-supplementary motor, and sensorimotor cortices as compared to patients in MCS− (Fig. 45.1). FDG-PET studies also allow development of machine-learning classifiers for clinical use, by automatic assessment of the functional integrity in this

frontoparietal network and calculation of a probability for a patient to be conscious or not (Phillips et al. 2011). The development of automated methods could help in the future to improve the accuracy of the diagnosis of these patients on a single-subject level.

Recently, several studies focused on the use of multimodal assessment to improve diagnostic precision in DOC patients (Table. 45.1). Indeed, transcranial magnetic stimulation combined with electroencephalography (i.e., TMS-EEG; Bodart et al. 2017) and P3-based brain-computer interface (Annen et al. 2016) showed good congruence with FDG-PET diagnosis. The combined use of FDG-PET and these techniques seems to be a reliable way to increase diagnostic accuracy in DOC patients. In the first case, TMS-EEG could be used to assess the effective connectivity of cortical neurons in patients for whom an accurate diagnosis is needed for important clinical decisions (Bodart et al. 2017). In the second case, P3-based brain-computer interface (BCI) paradigm allows the identification of patients with "covert command following" (i.e., presenting an appropriate cortical activation—measured by EEG—in response to a command, without being able to respond to command at the bedside). PET images of these patients with "covert command following" showed a higher glucose metabolism in brain regions involved in language and a good agreement with the diagnosis of MCS (Annen et al. 2018). The use of resting state functional magnetic resonance imaging (i.e., fMRI) as a complementary technique has also been investigated in several recent studies. A study comparing functional MRI neuronal activity maps and FDG-PET cerebral metabolic maps found a high correlation between these two techniques. Results suggest that resting state fMRI maps could allow the estimation of relative levels of FDG-PET metabolic activity and could be useful for clinical centers with no FDG-PET (Soddu et al. 2016). Other studies investigated the relationship between functional brain activity and structural connectivity in DOC patients by combining FDG-PET and fMRI. The results showed an association between functional metabolism (i.e., the inferior parietal, precuneus, and frontal regions) and structural integrity of the default mode network (i.e., DMN including frontal-inferior parietal, precuneus-inferior parietal, thalamo-inferior parietal, and thalamofrontal tracts) (Annen et al. 2016; Di Perri et al. 2016). Even if FDG-PET seems to have a better diagnostic precision than mental imagery fMRI, this last one could be a good complement when further investigation about preserved cognitive abilities is needed (Stender et al. 2014). A recent case series using simultaneously EEG-PET-fMRI techniques confirmed that the use of multimodal assessment could improve diagnosis and prognosis of DOC patients (Golkowski et al. 2017). Multimodal assessment could also help for the management of pharmaceutical and non-pharmacological treatment trials such as amantadine, zolpidem, and apomorphine or tDCS and DBS and to assess the effect of such therapeutic interventions on brain activity of DOC patients (Table. 45.1) (Lemaire et al. 2018; Sanz et al. 2019; Schnakers et al. 2008; for a review, see Thibaut et al., 2019).

45.3.2 Measuring the Brain During Sensory Stimulation

Since the 1990s, functional neuroimaging studies have investigated regional increases in rCBF in response to passive external stimulation (auditory, visual, or somatosensory) using ^{15}O-labeled water PET (see Table 45.3). The first studies on brain metabolism in VS/UWS patients during sensory stimulation found a residual subcortical neural activation but also gray matter region activation encompassing primary auditory (De Jong et al. 1997; Laureys et al. 2000a; Owen et al. 2002; Schiff et al. 2002; Boly et al. 2004), somatosensory (Laureys et al. 2002b; Boly et al. 2008a), or visual cortices (Menon et al. 1998; Giacino et al. 2006), depending on the stimulation. However, these studies also highlighted a functional disconnection from associative cortical areas encompassing ACC, insular, prefrontal, and posterior parietal cortices reported to be necessary for awareness (Schiff et al. 2002). These results suggest that brain processing following a stimulus is insufficient to induce a conscious integration of the stimulation in VS/UWS population (Laureys et al. 1999a, 2002b; Boly et al. 2004). In contrast, brain activation and connectivity were significantly higher in MCS than in VS/UWS patients following an auditory stimulus, suggesting that MCS patients can reach a certain level of sensory and affective perception (Boly et al. 2004). Other studies investigated the impact of an emotional auditory stimulus, such as the voice of a relative or the patients' own name. These studies demonstrated that emotional stimuli in MCS, as compared to VS/UWS, induced a higher level of activation in the internal network (i.e., ACC/mesiofrontal and PCC/precuneus) areas known to be involved in self-awareness (Laureys and Boly 2007). Modification of blood flow in response to different auditory relevant modalities, such as meaningful stories told by a relative (Bekinschtein et al. 2004) or self-referential stimuli (i.e., patients' own name) (Laureys 2004; Qin et al. 2010), also showed an activation within this network. Moreover, a linear correlation between the level of consciousness and activation of the ACC in MCS patients was identified (Qin et al. 2010). These results suggest a relative preservation of emotional perception in MCS, as compared to VS/UWS.

Differential pain sensitivity—a matter with important ethical implications—was investigated using PET imaging during nociceptive stimulation. Boly et al. reported an activation and preservation of the connectivity within the "pain matrix" in MCS patients, including ACC and insular areas, thought to be important in the affective emotional perception of pain (Kupers et al. 2005; Boly et al. 2008a). These observations should encourage physicians to systematically use analgesic treatment in MCS, even if (by definition) they cannot communicate their feelings (Demertzi et al. 2009, 2012; Schnakers et al. 2012). However, these neuroimaging data are shown at the group level and should be used with caution regarding clinical or ethical decisions at the single level.

45.4 PET Scan and Sleep

Normal sleep can be considered as a physiological state of reduction of consciousness. It is characterized by the absence of arousal and different stages of awareness—from alteration (rapid eye movement sleep, REMS) to loss of awareness (slow-wave sleep, SWS). Slow-wave activity is a part of non-rapid eye movement sleep (NREMS). During NREMS, a decrease in cerebral blood flow and glucose metabolism is observed in regions involved in cognitive, affective, and arousal system (Braun et al. 1997; Buchsbaum 2001; Nofzinger et al. 2002). A recent study in young and middle-age (i.e., range from 25 to 61 years old) healthy adults showed that greater encephalographic slow-wave activity during NREMS was related to a greater prefrontal metabolic rate during wakefulness, suggesting that neural synchrony underlying slow-wave activity leads to the restoration of waking function (Wilckens et al. 2016). In contrast, age was related to a lower semiquantitative whole-brain metabolism and superior frontal metabolism during wakefulness, but this effect was moderated by the presence of slow-wave activity. During SWS, overall brain metabolism decreases to approximately 60% of normal waking values (Maquet et al. 1997), whereas in REMS, metabolism returns to nearly normal waking values (Maquet 2000) (Table 45.4, Fig. 45.2). Further studies have investigated the related changes to regional brain metabolism and highlighted cerebral deactivations in a wide frontoparietal network encompassing the polymodal associative cortices, bilateral frontal regions, parietotemporal and posterior parietal areas, PCC,

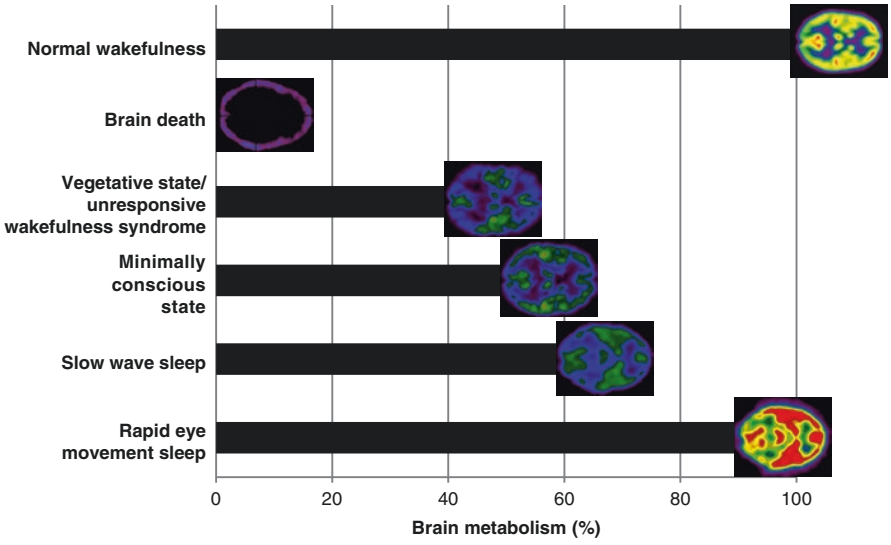

Fig. 45.2 Mean decrease in global cerebral metabolism (in percentage of normal conscious waking values) in pathological (brain death, vegetative state/unresponsive wakefulness syndrome, minimally conscious state) and physiological (sleep—slow-wave and rapid eye movement sleeps) altered states of consciousness. (Adapted from Laureys et al. (2004a) and Maquet (2000))

and mesiofrontal and precuneal cortices, while primary sensory cortices were still active (Maquet et al. 1996, 1997; Braun et al. 1997; Nofzinger et al. 2002). These frontoparietal associative cortical areas are called the "default mode network" and were shown to be mostly active in resting non-stimulated waking conditions in a functional magnetic resonance imaging study (Raichle and Mintun 2006). This network is known to be important in various functions relating to consciousness, such as attention, memory, and language (Baars et al. 2003), and its deactivation could explain the alteration of consciousness during SWS. FDG-PET studies on patients with insomnia confirmed the importance of these regions in sleep regulation. Indeed, a recent study aimed to compare regional cerebral metabolic rate of glucose in patients with insomnia and good sleepers. In good sleepers, the greater NREMS vs. wake differences were observed in the cerebellum and the prefrontal and parietal cortices. Compared to good sleepers, patients with insomnia also showed a smaller glucose metabolism difference during NREMS and wakefulness in regions involved in conscious awareness (i.e., left frontoparietal and the left middle frontal cortices, the precuneus/posterior cingulate, and the fusiform gyri). This smaller NREMS vs. wake difference could reflect a greater metabolic rate of glucose during NREMS that could explain a hyperarousal during sleep leading to insomnia (Kay et al. 2016). Another FDG-PET study investigated the impact of acute sleep deprivation on cerebral glucose metabolism during NREMS in people with insomnia and good sleepers. In good sleepers, sleep restriction leads to a decrease in whole-brain glucose metabolism during recovery of NREMS (i.e., after one night of sleep restriction) compared to baseline NREMS. In people with insomnia, no change in glucose metabolism was observed at the whole-brain level, but there was a decrease in regional glucose metabolism in the left hemisphere and the DMN (left frontoparietal cortex, right precuneus/posterior cingulate cortex, and right lingual/fusiform gyri). These results suggest that sleep deprivation, by reducing brain activity in regions involved in conscious awareness, could improve quality of sleep in people with insomnia (Kay et al. 2019). Dang-Vu et al. investigated the neural correlates of delta activity during SWS (Dang-Vu et al. 2005). The analysis characterized the cerebral correlates of delta waves (between 0 and 4 Hz; registered by electroencephalography) in areas where rCBF decreases during SWS (Maquet et al. 1997). An association was observed between rCBF in the ventromedial prefrontal regions and delta power. However, no correlation was observed with the thalamus, highlighting the importance of an extra-thalamic delta rhythm among the synchronous SWS oscillations. Therefore, rCBF could be a reflection of the cellular processes involved in cortical delta waves during SWS. These results confirm the frontal predominance of slow-wave activity during human SWS, as demonstrated by scalp electroencephalography studies (Finelli et al. 2001). On the other hand, activity in the thalamus seems to be negatively correlated with the rCBF during SWS (Hofle et al. 1997). This negative correlation may reflect the neural substrates underlying the progressive decrease in sensory awareness, motor responsiveness, and arousal that occur during SWS. Nevertheless, specific areas were found less activated, such as frontal and parietal areas encompassing the PCC, dorsolateral prefrontal and inferior parietal cortices, and precuneus (Maquet et al. 1996, Maquet et al. 2005;

Braun et al. 1997). Significant increases in rCBF were found in the pontine tegmentum, thalamus, basal forebrain, amygdala, hippocampus, and ACC (Maquet et al. 1996; Braun et al. 1997). An activation of posterior cortices (i.e., temporo-occipital areas) and a modification in connectivity in this network were also observed (Braun et al. 1998). These studies could explain the relationship between consciousness during REMS and regional patterns of brain hypometabolism in the frontal and parietal areas and the precuneus/PCC, areas known to be involved in internal and external consciousness (Laureys et al. 1999a; Boly et al. 2008b; Vanhaudenhuyse et al. 2011). Metabolic increases in regions such as the pontine tegmentum, thalamic nuclei, and limbic areas might correlate with some features of cognition, as reflected in dream reports (Maquet et al. 2005).

Functional neuroimaging has offered an increasingly refined description of brain activity across the sleep-wake cycle, from regional patterns of sleep stages to transient activations during sleep oscillations. Reports using PET demonstrated a specialized network of deactivated brain areas during SWS (i.e., the ACC, thalamus, frontal and parietal association areas) and activated/deactivated structures (i.e., decrease in frontal and parietal areas and PCC/precuneus; activation of the pontine tegmentum, thalamus, basal forebrain, amygdale, hippocampus, and ACC) during REMS.

45.5 PET Scan and Hypnosis

In 1994, hypnosis was defined as "a procedure during which a health professional or researcher suggests that a patient or subject experiences changes in sensations, perceptions, thoughts, or behavior" (The Executive Committee of the American Psychological Association – Division of Psychological Hypnosis 1994). However, this definition was criticized as being too long and presenting a theoretical limitation (i.e., concept such as "state" and "self-hypnosis" was not mentioned, and the use of hypnosis in hospital does not appear in the list of application). Eventually, hypnosis has been redefined in 2014 as "a state of consciousness involving focused attention and reduced peripheral awareness characterized by an enhanced capacity for response to suggestion" (Elkins et al. 2016). This procedure induces an altered state of awareness which could be explained by specific cortical changes (i.e., dynamic properties and neural correlates) (Maquet et al. 1999; Rainville et al. 2002; Cardeña et al. 2013). Hypnosis can be considered as an appropriate means to transiently modulate conscious cognition in healthy subjects because it does not lead to general unconsciousness (compared to pharmacological anesthesia or sleep) and does not have long-term effects on neuroplasticity (compared to meditation techniques (Holzel et al. 2008)). Even more, it is well documented to induce an altered conscious state (Oakley and Halligan 2009). The hypnotic process has three main components: absorption, dissociation, and suggestibility (Spiegel 1991). Absorption is the ability to be fully involved in a thought experiment. Dissociation can be defined as the separation of mental behavior that usually goes together (e.g., in the case of dreams where we are at the same time the actor and the observer). This

condition can also cause a sensation of driving or uncontrollable feelings of discontinuity of a body part compared to others. Finally, suggestibility is the ability of the person to comply with the instructions of the professional practicing hypnosis. These processes could diminish the tendency to judge and censor, whereas hypnosis could reduce spontaneous thoughts and give the feeling of one's own response as automatic (Rainville and Price 2003; Terhune and Cardeña 2010). However, a study showed that individuals do not display a uniform response to a hypnotic induction (Terhune and Cardeña 2010).

It is important to emphasize that people under hypnosis do not lose complete control of their behavior. They are aware of their identity and their actual location, and unless amnesia is induced, they keep a souvenir of the experience during the hypnotic process. Another important thing to note is that not all individuals respond to hypnosis. There are low and highly suggestible subjects. A study conducted by Terhune and collaborators (2011) using EEG showed that highly suggestible participants reliably experienced greater state of dissociation and exhibited lower frontoparietal phase synchrony in the α-2 frequency band during hypnosis than low-suggestible participants. These findings suggest that highly suggestible individuals exhibit a disruption of the frontoparietal network that is only observable following a hypnotic induction. At the same time, the fact that cerebral responses to hypnosis are different between subjects points to the difficulty of generalizing obtained results.

Hypnosis has for many years been used, among other things, in the treatment of both somatic and psychological disorders (such as pain, gastrointestinal and dermatological diseases, depression, anxiety, stress, and addictions). In addition to its clinical application, the study of hypnosis is thought to provide leverage to investigate not only the contents of consciousness but also the neural correlates of its background states. Functional neuroimaging studies have been performed as a means of investigation of the phenomenon, mainly using PET imaging. The earliest studies found a modulation of ACC activity and highlighted changes in connectivity between ACC and prefrontal areas during hypnosis (Maquet et al. 1999; Faymonville et al. 2003, 2006) and hypnotic suggestion (Rainville et al. 1997, 1999b; Hofbauer et al. 2001). The activation in the ACC could reflect the attentional effort necessary for the subject to internally generate mental imagery, while the connectivity between ACC and prefrontal areas may indicate a modification in distributed associative processes of cognitive appraisal, attention, or memory of perceived noxious stimuli (Rainville et al. 1997, 1999a, 2002; Faymonville et al. 2000; Hofbauer et al. 2001).

Mental imagery appears to play a role in hypnosis. This notion is supported by the activation of the occipital and temporal cortices, precuneus, and other extrastriate visual areas during hypnotic state and hypnotic suggestion, which account for the altered perception of reality (Maquet 1999; Rainville et al. 1999b; Faymonville et al. 2006). This is further stressed by the fact that motor commands are processed differently than in the normal conscious state, with activity deviating toward the precuneus and extrastriate visual areas (Casale et al. 2012). After induction of a hypotonic state, an increase in rCBF was observed in the ACC, the thalami, and the mesencephalic brainstem, while brain metabolism decreased in the precuneus, the

parietal lobule, and the posterior temporal cortex (Rainville et al. 2002). The hypometabolism of the precuneus during hypnosis supports the correlation between awareness and precuneal integration. The induction of a hypotonic state produced the expected increases in both mental relaxation and absorption. Regression analyses between rCBF and self-ratings confirm the hypothesized involvement of the ACC, the thalamus, and the pontomesencephalic brainstem in the generation of hypnotic states. Hypnotic relaxation further involved an increase in occipital rCBF, consistent with previous interpretation that hypnotic states are characterized by a decrease in cortical arousal and a reduction in cross-modality suppression (disinhibition). In contrast, increases in mental absorption during hypnotic state were associated with rCBF increases in a distributed network of cortical and subcortical structures described as the brain's attentional system (Rainville et al. 2002).

Because of its analgesic effects, hypnosis is increasingly used in anesthesia for several minor surgeries (such as scar correction, tooth extraction, thyroidal lobectomy, or face lifting) (Vanhaudenhuyse et al. 2008). This technique is called hypnosedation. Neuroimaging—especially PET studies—was conducted trying to understand the mechanisms underlying the anesthetic effects of hypnosis. The results showed an activation of a widespread set of cortical areas involving occipital, parietal, precentral, premotor, and ventrolateral, as well as the ACC and the prefrontal cortex during hypnotic state (Rainville et al. 1997; Faymonville et al. 2000, 2003, 2006; Hofbauer et al. 2001;). The ACC is known to be involved in interaction processes between cognitive and emotional perceptions related to changes in attentional and emotional states (Devinsky et al. 1995; Bush et al. 2000). Decrease in pain perception during hypnosedation was shown to be related to increases in connectivity between ACC and a large neural cortical and subcortical network, known to be involved in pain perception and integration (i.e., the prefrontal cortex, supplementary and premotor area, insula, striatum, thalamus, and brainstem) (Faymonville et al. 2006). These changes in connectivity between the ACC and prefrontal brain regions induced by hypnosis might reflect a change in the associative processes of judgment, attention, or memory of perceived nociceptive stimuli. In contrast with these studies, Derbyshire and collaborators used hypnosis to induce pain (Derbyshire et al. 2004). They found that both real pain-heating stimuli and hypnosis-induced pain experience modulated the activity within the thalamus, ACC, insula, and prefrontal and parietal cortices. This study showed that hypnosis is able to induce cerebral activations as real pain stimuli.

PET studies highlighted an activation of a widespread set of cortical areas involving ACC and occipital, parietal, precentral, premotor, and ventrolateral prefrontal cortices related to the hypnotic state. This pattern of activation shares some similarities with mental imagery tasks, from which it mainly differs by the relative deactivation of the precuneus. This deactivation could explain the alteration of awareness induced by hypnosis. Indeed, hypometabolism of the precuneus seems to be highly correlated with modified state of consciousness (Maquet et al. 1996, 2005; Braun et al. 1997; Laureys et al. 1999a, b; Vogt and Laureys, 2005). Nevertheless, results could be confounded, because of the differences between high- and low-suggestible individuals in terms of neuronal processes underlying hypnosis induction.

Comparing the brain activation patterns associated with the analgesic effect of hypnosis and the resting state, a reduction of affective and sensory responses to noxious stimulation was found, which is modulated by the activity in the midcingulate cortex and especially the ACC.

45.6 Conclusion

Recent advances in functional neuroimaging techniques are beginning to open the black box of altered consciousness. PET studies facilitate a better understanding of the mechanisms underlying the altered state of consciousness and highlight the involvement of specific neural areas and networks in pathologically altered states of consciousness (VS/UWS and MCS), in sleep, and under hypnosis. Results from several studies point to the importance of the precuneus and cingulate cortices in altered states of consciousness in all of these conditions. Clinically, these findings may prove important in facilitating precise differential diagnostic tools to distinguish low levels of awareness in unresponsive patient populations. Currently, FDG-PET is the most robust paraclinical technique for differential diagnosis in DOC patients. However, the use and the development of multimodal assessment could be a good complement for the examination/diagnosis and management of this sensitive population. Taken together, the frontoparietal network which is hypometabolic during SWS and mostly impaired in patients with disorders of consciousness—but not during REMS or hypnosis—could reflect the preservation of brain activity in correlation with different brain processes such as dreaming, memory consolidation (sleep), or motor imagery (hypnosis).

Acknowledgments This update is based on the work of previous authors whom we would like to thank: Johan Stender, Athena Demertzi, Claire Bernard, Roland Hustinx, and Marie-Aurélie Bruno.

References

American Congress of Rehabilitation Medicine (1995) Recommendations for use of uniform nomenclature pertinent to patients with severe alterations of consciousness. Arch Phys Med Rehabil 76:205–209

Andersson JL, Onoe H, Hetta J, Lidstrom K, Valind S, Lilja A, Sundin A, Fasth KJ, Westerberg G, Broman JE, Watanabe Y, Langstrom B (1998) Brain networks affected by synchronized sleep visualized by positron emission tomography. J Cereb Blood Flow Metab 18:701–715

Andrews K, Murphy L, Munday R, Littlewood C (1996) Misdiagnosis of the vegetative state: retrospective study in a rehabilitation unit. BMJ 313:13–16

Annen J, Heine L, Ziegler E et al (2016) Function-structure connectivity in patients with severe brain injury as measured by MRI-DWI and FDG-PET: function-structure connectivity in DOC. Hum Brain Mapp 37:3707–3720

Annen J, Blandiaux S, Lejeune N et al (2018) BCI performance and brain metabolism profile in severely brain-injured patients without response to command at bedside. Front Neurosci 12:370

Baars BJ (2005) Global workspace theory of consciousness: toward a cognitive neuroscience of human experience. Prog Brain Res 150:45–53

Baars BJ, Ramsoy TZ, Laureys S (2003) Brain, conscious experience and the observing self. Trends Neurosci 26:671–675

Bekinschtein T, Leiguarda R, Armony J, Owen A, Carpintiero S, Niklison J, Olmos L, Sigman L, Manes F (2004) Emotion processing in the minimally conscious state. J Neurol Neurosurg Psychiatry 75:788

Beuthien-Baumann B, Handrick W, Schmidt T, Burchert W, Oehme L, Kropp J, Schackert G, Pinkert J, Franke WG (2003) Persistent vegetative state: evaluation of brain metabolism and brain perfusion with PET and SPECT. Nucl Med Commun 24:643–649

Bodart O, Gosseries O, Wannez S et al (2017) Measures of metabolism and complexity in the brain of patients with disorders of consciousness. NeuroImage Clin 14:354–362

Boly M, Faymonville ME, Peigneux P, Lambermont B, Damas P, Del Fiore G, Degueldre C, Franck G, Luxen A, Lamy M, Moonen G, Maquet P, Laureys S (2004) Auditory processing in severely brain injured patients: differences between the minimally conscious state and the persistent vegetative state. Arch Neurol 61:233–238

Boly M, Faymonville ME, Schnakers C, Peigneux P, Lambermont B, Phillips C, Lancellotti P, Luxen A, Lamy M, Moonen G, Maquet P, Laureys S (2008a) Perception of pain in the minimally conscious state with PET activation: an observational study. Lancet Neurol 7:1013–1020

Boly M, Phillips C, Tshibanda L, Vanhaudenhuyse A, Schabus M, Dang-Vu TT, Moonen G, Hustinx R, Maquet P, Laureys S (2008b) Intrinsic brain activity in altered states of consciousness: how conscious is the default mode of brain function? Ann N Y Acad Sci 1129:119–129

Braun AR, Balkin TJ, Wesenten NJ, Carson RE, Varga M, Baldwin P, Selbie S, Belenky G, Herscovitch P (1997) Regional cerebral blood flow throughout the sleep-wake cycle. An H2(15)O PET study. Brain J Neurol 120(Pt 7):1173–1197

Braun AR, Balkin TJ, Wesensten NJ, Gwadry F, Carson RE, Varga M, Baldwin P, Belenky G, Herscovitch P (1998) Dissociated pattern of activity in visual cortices and their projections during human rapid eye movement sleep. Science 279:91–95

Bruno MA, Schnakers C, Damas F, Pellas F, Lutte I, Bernheim J, Majerus S, Moonen G, Goldman S, Laureys S (2009) Locked-in syndrome in children: report of five cases and review of the literature. Pediatr Neurol 41:237–246

Bruno MA, Vanhaudenhuyse A, Schnakers C, Boly M, Gosseries O, Demertzi A, Majerus S, Moonen G, Hustinx R, Laureys S (2010) Visual fixation in the vegetative state: an observational case series PET study. BMC Neurol 10:35

Bruno MA, Majerus S, Boly M, Vanhaudenhuyse A, Schnakers C, Gosseries O, Boveroux P, Kirsch M, Demertzi A, Bernard C, Hustinx R, Moonen G, Laureys S (2012) Functional neuroanatomy underlying the clinical subcategorization of minimally conscious state patients. J Neurol 259:1087–1098

Buchsbaum M (2001) Positron emission tomography with deoxyglucose-F18 imaging of sleep. Neuropsychopharmacology 25:50–56

Bush G, Luu P, Posner MI (2000) Cognitive and emotional influences in anterior cingulate cortex. Trends Cogn Sci 4:215–222

Cardeña E, Jonsson P, Terhune DB, Marcusson-Clavertz D (2013) The neurophenomenology of neutral hypnosis. Cortex 49(2):375–385

Casale AD, Ferracuti S, Rapinesi C, Serata D, Sani G, Savoja V, Kotzalidis GD, Tatarelli R, Girardi P (2012) Neurocognition under hypnosis: findings from recent functional neuroimaging studies. Int J Clin Exp Hypn 60:286–317

Chatelle C, Thibaut A, Gosseries O et al (2014) Changes in cerebral metabolism in patients with a minimally conscious state responding to zolpidem. Front Hum Neurosci 8:917

Childs NL, Mercer WN (1996) Misdiagnosing the persistent vegetative state. Misdiagnosis certainly occurs. BMJ 313:944

Clauss R, Nel W (2006) Drug induced arousal from the permanent vegetative state. NeuroRehabilitation 21(1):23–28

Damasio A, Kaspar M (2009) Consciousness: an overview of the phenomenon and of its possible neural basis. In: Laureys S, Tononi J (eds) The neurology of consciousness. Elsevier, London

Dang-Vu TT, Desseilles M, Laureys S, Degueldre C, Perrin F, Phillips C, Maquet P, Peigneux P (2005) Cerebral correlates of delta waves during non-REM sleep revisited. NeuroImage 28:14–21

De Jong B, Willemsen A, Paans A (1997) Regional cerebral blood flow changes related to affective speech presentation in persistent vegetative state. Clin Neurol Neurosurg 47:197–204

Dehaene S, Naccache L (2001) Towards a cognitive neuroscience of consciousness: basic evidence and a workspace framework. Cognition 79:1–37

Demertzi A, Schnakers C, Ledoux D, Chatelle C, Bruno MA, Vanhaudenhuyse A, Boly M, Moonen G, Laureys S (2009) Different beliefs about pain perception in the vegetative and minimally conscious states: a European survey of medical and paramedical professionals. Prog Brain Res 177:329–338

Demertzi A, Ledoux D, Bruno MA, Vanhaudenhuyse A, Gosseries O, Soddu A, Schnakers C, Moonen G, Laureys S (2011) Attitudes towards end-of-life issues in disorders of consciousness: a European survey. J Neurol 258:1058–1065

Demertzi A, Racine E, Bruno M, Ledoux D, Gosseries O, Vanhaudenhuyse A, Thonnard M, Soddu A, Moonen G, Laureys S (2012) Pain perception in disorders of consciousness: neuroscience, clinical care, and ethics in dialogue. Neuroethics 6:1–14

Derbyshire SW, Whalley MG, Stenger VA, Oakley DA (2004) Cerebral activation during hypnotically induced and imagined pain. NeuroImage 23:392–401

Devinsky O, Morrell MJ, Vogt BA (1995) Contributions of anterior cingulate cortex to behaviour. Brain 118(Pt 1):279–306

DeVolder AG, Goffinet AM, Bol A, Michel C, de Barsy T, Laterre C (1990) Brain glucose metabolism in postanoxic syndrome. Positron emission tomographic study. Arch Neurol 47:197–204

Di Perri C, Bahri MA, Amico E et al (2016) Neural correlates of consciousness in patients who have emerged from a minimally conscious state: a cross-sectional multimodal imaging study. Lancet Neurol 15:830–842

Elkins GR, Barabasz AF, Council JR, Spiegel D (2016) Advancing research and practice: the revised APA division 30 definition of hypnosis. Int J Clin Exp Hypn 63:1–9

Faymonville ME, Laureys S, Degueldre C, DelFiore G, Luxen A, Franck G, Lamy M, Maquet P (2000) Neural mechanisms of antinociceptive effects of hypnosis. Anesthesiology 92:1257–1267

Faymonville ME, Roediger L, Del Fiore G, Delgueldre C, Phillips C, Lamy M, Luxen A, Maquet P, Laureys S (2003) Increased cerebral functional connectivity underlying the antinociceptive effects of hypnosis. Brain Res Cogn Brain Res 17:255–262

Faymonville ME, Boly M, Laureys S (2006) Functional neuroanatomy of the hypnotic state. J Physiol Paris 99:463–469

Finelli LA, Borbely AA, Achermann P (2001) Functional topography of the human nonREM sleep electroencephalogram. Eur J Neurosci 13:2282–2290

Garcia-Panach J, Lull N, Lull JJ, Ferri J, Martinez C, Sopena P, Robles M, Chirivella J, Noe E (2011) A voxel-based analysis of FDG-PET in traumatic brain injury: regional metabolism and relationship between the thalamus and cortical areas. J Neurotrauma 28:1707–1717

Giacino JT, Ashwal S, Childs N, Cranford R, Jennett B, Katz DI, Kelly JP, Rosenberg JH, Whyte J, Zafonte RD, Zasler ND (2002) The minimally conscious state: definition and diagnostic criteria. Neurology 58:349–353

Giacino JT, Hirsch J, Schiff N, Laureys S (2006) Functional neuroimaging applications for assessment and rehabilitation planning in patients with disorders of consciousness. Arch Med Rehab 87:S67–S76

Giacino JT, Whyte J, Bagiella E, Kalmar K, Childs N, Khademi A, Eifert B, Long D, Katz DI, Cho S, Yablon SA, Luther M, Hammond FM, Nordenbo A, Novak P, Mercer W, Maurer-Karattup P, Sherer M (2012) Placebo-controlled trial of amantadine for severe traumatic brain injury. N Engl J Med 366:819–826

Golkowski D, Merz K, Mlynarcik C et al (2017) Simultaneous EEG–PET–fMRI measurements in disorders of consciousness: an exploratory study on diagnosis and prognosis. J Neurol 264:1986–1995

Gosseries O, Zasler ND, Laureys S (2014) Recent advances in disorders of consciousness: focus on the diagnosis. Brain Inj 28:1141–1150

Hofbauer RK, Rainville P, Duncan GH, Bushnell MC (2001) Cortical representation of the sensory dimension of pain. J Neurophys 86:402–411

Hofle N, Paus T, Reutens D, Fiset P, Gotman J, Evans AC, Jones BE (1997) Regional cerebral blood flow changes as a function of delta and spindle activity during slow wave sleep in humans. J Neurosci 17:4800–4808

Holzel BK, Ott U, Gard T, Hempel H, Weygandt M, Morgen K, Vaitl D (2008) Investigation of mindfulness meditation practitioners with voxel-based morphometry. Soc Cogn Affect Neurosci 3:55–61

Juengling FD, Kassubek J, Huppertz HJ, Krause T, Els T (2005) Separating functional and structural damage in persistent vegetative state using combined voxel-based analysis of 3-D MRI and FDG-PET. J Neurol Sci 228:179–184

Kajimura N, Uchiyama M, Takayama Y, Uchida S, Uema T, Kato M, Sekimoto M, Watanabe T, Nakajima T, Horikoshi S, Ogawa K, Nishikawa M, Hiroki M, Kudo Y, Matsuda H, Okawa M, Takahashi K (1999) Activity of midbrain reticular formation and neocortex during the progression of human non-rapid eye movement sleep. J Neurosci 19:10065–10073

Kassubek J, Juengling FD, Els T, Spreer J, Herpers M, Krause T, Moser E, Lucking CH (2003) Activation of a residual cortical network during painful stimulation in long-term postanoxic vegetative state: a 15O-H2O PET study. J Neurol Sci 212:85–91

Kay DB, Karim HT, Soehner AM et al (2016) Sleep-wake differences in relative regional cerebral metabolic rate for glucose among patients with insomnia compared with good sleepers. Sleep 39:1779–1794

Kay DB, Karim HT, Hasler BP et al (2019) Impact of acute sleep restriction on cerebral glucose metabolism during recovery non-rapid eye movement sleep among individuals with primary insomnia and good sleeper controls. Sleep Med 55:81–91

Kupers R, Faymonville ME, Laureys S (2005) The cognitive modulation of pain: hypnosis- and placebo-induced analgesia. Prog Brain Res 150:251–269

Langtry HD, Benfield P (1990) Zolpidem: a review of its pharmacodynamic and pharmacokinetic properties and therapeutic potential. Drugs 40:291–313

Laureys S (2004) Functional neuroimaging in the vegetative state. NeuroRehabilitation 19:335–341

Laureys S (2005) The neural correlate of (un)awareness: lessons from the vegetative state. Trends Cogn Sci 9:556–559

Laureys S, Boly M (2007) What is it like to be vegetative or minimally conscious? Curr Opin Neurol 20:609–613

Laureys S, Schiff ND (2012) Coma and consciousness: paradigms (re)framed by neuroimaging. NeuroImage 61:478–491

Laureys S, Goldman S, Phillips C, Van Bogaert P, Aerts J, Luxen A, Franck G, Maquet P (1999a) Impaired effective cortical connectivity in vegetative state: preliminary investigation using PET. NeuroImage 9:377–382

Laureys S, Lemaire C, Maquet P, Phillips C, Franck G (1999b) Cerebral metabolism during vegetative state and after recovery to consciousness. J Neurol Neurosurg Psychiatry 67:121

Laureys S, Faymonville ME, Degueldre C, Fiore GD, Damas P, Lambermont B, Janssens N, Aerts J, Franck G, Luxen A, Moonen G, Lamy M, Maquet P (2000a) Auditory processing in the vegetative state. Brain J Neurol 123(Pt 8):1589–1601

Laureys S, Faymonville ME, Luxen A, Lamy M, Franck G, Maquet P (2000b) Restoration of thalamocortical connectivity after recovery from persistent vegetative state. Lancet 355:1790–1791

Laureys S, Faymonville ME, Moonen G, Luxen A, Maquet P (2000c) PET scanning and neuronal loss in acute vegetative state. Lancet 355:1825–1826; author reply 1827

Laureys S, Antoine S, Boly M, Elincx S, Faymonville ME, Berre J, Sadzot B, Ferring M, De Tiege X, van Bogaert P, Hansen I, Damas P, Mavroudakis N, Lambermont B, Del Fiore G, Aerts J, Degueldre C, Phillips C, Franck G, Vincent JL, Lamy M, Luxen A, Moonen G, Goldman S, Maquet P (2002a) Brain function in the vegetative state. Acta Neurol Belg 102:177–185

Laureys S, Faymonville ME, Peigneux P, Damas P, Lambermont B, Del Fiore G, Degueldre C, Aerts J, Luxen A, Franck G, Lamy M, Moonen G, Maquet P (2002b) Cortical processing of noxious somatosensory stimuli in the persistent vegetative state. NeuroImage 17:732–741

Laureys S, Van Eeckhout P, Ferring M, Faymonville M, Mavroudakis N, Berre J, Van Bogaert P, Pellas F, Cornu P, Luxen A, Vincent J, Moonen G, Maque P, Goldman S (2003) Brain function in acute and chronic locked-in syndrome. In 9th annual meeting of the Organisation for Human Brain Mapping (OHBM), vol 19 NY, USA

Laureys S, Owen AM, Schiff ND (2004a) Brain function in coma, vegetative state, and related disorders. Lancet Neurol 3:537–546

Laureys S, Perrin F, Faymonville ME, Schnakers C, Boly M, Bartsch V, Majerus S, Moonen G, Maquet P (2004b) Cerebral processing in the minimally conscious state. Neurology 63:916–918

Laureys S, Pellas F, Van Eeckhout P, Ghorbel S, Schnakers C, Perrin F, Berre J, Faymonville ME, Pantke KH, Damas F, Lamy M, Moonen G, Goldman S (2005a) The locked-in syndrome : what is it like to be conscious but paralyzed and voiceless? Prog Brain Res 150:495–511

Laureys S, Piret S, Ledoux D (2005b) Quantifying consciousness. Lancet Neurol 4:789–790

Laureys S, Celesia GG, Cohadon F, Lavrijsen J, Leon-Carrion J, Sannita WG, Sazbon L, Schmutzhard E, von Wild KR, Zeman A, Dolce G (2010) Unresponsive wakefulness syndrome: a new name for the vegetative state or apallic syndrome. BMC Med 8:68

Lemaire J-J, Sontheimer A, Pereira B et al (2018) Deep brain stimulation in five patients with severe disorders of consciousness. Ann Clin Transl Neurol 5:1372–1384

Levy DE, Sidtis JJ, Rottenberg DA, Jarden JO, Strother SC, Dhawan V, Ginos JZ, Tramo MJ, Evans AC, Plum F (1987) Differences in cerebral blood flow and glucose utilization in vegetative versus locked-in patients. Ann Neurol 22:673–682

Lull N, Noe E, Lull JJ, Garcia-Panach J, Chirivella J, Ferri J, Lopez-Aznar D, Sopena P, Robles M (2010) Voxel-based statistical analysis of thalamic glucose metabolism in traumatic brain injury: relationship with consciousness and cognition. Brain Inj 24:1098–1107

Majerus S, Bruno MA, Schnakers C, Giacino JT, Laureys S (2009) The problem of aphasia in the assessment of consciousness in brain-damaged patients. Prog Brain Res 177:49–61

Maquet P (1997) Positron emission tomography studies of sleep and sleep disorders. J Neurol 244:S23–S28

Maquet P (1999) Brain mechanisms of sleep: contribution of neuroimaging techniques. J Psychopharmacol 13:S25–S28

Maquet P (2000) Functional neuroimaging of normal human sleep by positron emission tomography. J Sleep Res 9:207–231

Maquet P, Dive D, Salmon E, Sadzot B, Franco G, Poirrier R, von Frenckell R, Franck G (1990) Cerebral glucose utilization during sleep-wake cycle in man determined by positron emission tomography and [18F] 2-fluoro-2-deoxy-D-glucose method. Brain Res 513:136–143

Maquet P, Peters J, Aerts J, Delfiore G, Degueldre C, Luxen A, Franck G (1996) Functional neuroanatomy of human rapid-eye-movement sleep and dreaming. Nature 383:163–166

Maquet P, Degueldre C, Delfiore G, Aerts J, Peters JM, Luxen A, Franck G (1997) Functional neuroanatomy of human slow wave sleep. J Neurosci 17:2807–2812

Maquet P, Faymonville ME, Degueldre C, Delfiore G, Franck G, Luxen A, Lamy M (1999) Functional neuroanatomy of hypnotic state. Biol Psychiatry 45:327–333

Maquet P, Ruby P, Maudoux A, Albouy G, Sterpenich V, Dang-Vu T, Desseilles M, Boly M, Perrin F, Peigneux P, Laureys S (2005) Human cognition during REM sleep and the activity profile within frontal and parietal cortices: a reappraisal of functional neuroimaging data. Prog Brain Res 150:219–227

Menon DK, Owen AM, Williams EJ, Minhas PS, Allen CM, Boniface SJ, Pickard JD (1998) Cortical processing in persistent vegetative state. Wolfson Brain Imaging Centre Team. Lancet 352:200

Nagel T et al (1979) What is it like to be a bad? In: Mortal questions. Cambridge University Press, Cambridge, pp 165–180

Nakayama N, Okumura A, Shinoda J, Nakashima T, Iwama T (2006) Relationship between regional cerebral metabolism and consciousness disturbance in traumatic diffuse brain injury

without large focal lesions: an FDG-PET study with statistical parametric mapping analysis. J Neurol Neurosurg Psychiatry 77:856–862
Nofzinger EA, Mintun MA, Wiseman M, Kupfer DJ, Moore RY (1997) Forebrain activation in REM sleep: an FDG PET study. Brain Res 770:192–201
Nofzinger EA, Buysse DJ, Miewald JM, Meltzer CC, Price JC, Sembrat RC, Ombao H, Reynolds CF, Monk TH, Hall M, Kupfer DJ, Moore RY (2002) Human regional cerebral glucose metabolism during non-rapid eye movement sleep in relation to waking. Brain J Neurol 125:1105–1115
Noirhomme Q, Laureys S (2011) Altering consciousness and neuropathology. In: Winkelman E, Cardeña AM (eds) Altering consciousness: multidisciplinary perspectives, vol 2. Praeger, Santa Barbara
Nusbaum F, Redoute J, Le Bars D, Volckmann P, Simon F, Hannoun S, Ribes G, Gaucher J, Laurent B, Sappey-Marinier D (2011) Chronic low-back pain modulation is enhanced by hypnotic analgesic suggestion by recruiting an emotional network: a PET imaging study. Int J Clin Exp Hypn 59:27–44
Oakley DA, Halligan PW (2009) Hypnotic suggestion and cognitive neuroscience. Trends Cogn Sci 13:264–270
Owen AM, Menon DK, Johnsrude IS, Bor D, Scott SK, Manly T, Williams EJ, Mummery C, Pickard JD (2002) Detecting residual cognitive function in persistent vegetative state. Neurocase 8:394–403
Owen AM, Coleman MR, Menon DK, Berry EL, Johnsrude IS, Rodd JM, Davis MH, Pickard JD (2005) Using a hierarchical approach to investigate residual auditory cognition in persistent vegetative state. Prog Brain Res 150:457–471
Peigneux P, Laureys S, Delbeuck X, Maquet P (2001) Sleeping brain, learning brain. The role of sleep for memory systems. Neuroreport 12:A111–A124
Phillips CL, Bruno MA, Maquet P, Boly M, Noirhomme Q, Schnakers C, Vanhaudenhuyse A, Bonjean M, Hustinx R, Moonen G, Luxen A, Laureys S (2011) "Relevance vector machine" consciousness classifier applied to cerebral metabolism of vegetative and locked-in patients. NeuroImage 56:797–808
Plum F, Schiff N, Ribary U, Llinas R (1998) Coordinated expression in chronically unconscious persons. Philos Trans R Soc B-Biol Sci 353:1929–1933
Posner J, Saper C, Schiff N, Plum F (2007) Plum and Posner's diagnosis of stupor and coma. Oxford University Press, New York
Qin P, Di H, Liu Y, Yu S, Gong Q, Duncan N, Weng X, Laureys S, Northoff G (2010) Anterior cingulate activity and the self in disorders of consciousness. Hum Brain Mapp 31:1993–2002
Raichle ME, Mintun MA (2006) Brain work and brain imaging. Ann Rev Neurosci 29:449–476
Raichle ME, Snyder AZ (2007) A default mode of brain function: a brief history of an evolving idea. NeuroImage 37:1083–1090, discussion 1097–1089
Rainville P, Price DD (2003) Hypnosis phenomenology and the neurobiology of consciousness. Int J Clin Exp Hypn 51:105–129
Rainville P, Duncan GH, Price DD, Carrier B, Bushnell MC (1997) Pain affect encoded in human anterior cingulate but not somatosensory cortex. Science 277:968–971
Rainville P, Carrier B, Hofbauer RK, Bushnell MC, Duncan GH (1999a) Dissociation of sensory and affective dimensions of pain using hypnotic modulation. Pain 82:159–171
Rainville P, Hofbauer RK, Paus T, Duncan GH, Bushnell MC, Price DD (1999b) Cerebral mechanisms of hypnotic induction and suggestion. J Cogn Neurosci 11:110–125
Rainville P, Hofbauer RK, Bushnell MC, Duncan GH, Price DD (2002) Hypnosis modulates activity in brain structures involved in the regulation of consciousness. J Cogn Neurosci 14:887–901
Royal College of Physicians (2003) The vegetative state: guidance on diagnosis and management. Clin Med 3:249–254
Rudolf J, Ghaemi M, Haupt WF, Szelies B, Heiss WD (1999a) Cerebral glucose metabolism in acute and persistent vegetative state. J Neurosurg Anesthesiol 11:17–24
Rudolf J, Grond M, Schindler D, Heiss WD, Desnick RJ (1999b) Cerebral glucose metabolism in type I alpha-N-acetylgalactosaminidase deficiency: an infantile neuroaxonal dystrophy. J Child Neurol 14:543–547

Rudolf J, Sobesky J, Grond M, Heiss WD (2000) Identification by positron emission tomography of neuronal loss in acute vegetative state. Lancet 355:115–116
Sanger DJ (2004) The pharmacology and mechanisms of action of new generation, non-benzodiazepine hypnotic agents. CNS Drugs 18:9–15
Sanz LRD, Lejeune N, Blandiaux S et al (2019) Treating disorders of consciousness with apomorphine: protocol for a double-blind randomized controlled trial using multimodal assessments. Front Neurol 10:240
Schiff ND (2006) Multimodal neuroimaging approaches to disorders of consciousness. J Head Trauma Rehabil 21:388–397
Schiff ND (2010) Recovery of consciousness after brain injury: a mesocircuit hypothesis. Trends Neurosci 33(1):1–9
Schiff ND, Plum F (1999) Cortical function in the persistent vegetative state. Trends Cogn Sci 3:43–44
Schiff ND, Ribary U, Moreno DR, Beattie B, Kronberg E, Blasberg R, Giacino J, McCagg C, Fins JJ, Llinas R, Plum F (2002) Residual cerebral activity and behavioural fragments can remain in the persistently vegetative brain. Brain J Neurol 125:1210–1234
Schnakers C, Hustinx R, Vandewalle G, Majerus S, Moonen G, Boly M, Vanhaudenhuyse A, Laureys S (2008) Measuring the effect of amantadine in chronic anoxic minimally conscious state. J Neurol Neurosurg Psychiatry 79:225–227
Schnakers C, Vanhaudenhuyse A, Giacino J, Ventura M, Boly M, Majerus S, Moonen G, Laureys S (2009) Diagnostic accuracy of the vegetative and minimally conscious state: clinical consensus versus standardized neurobehavioral assessment. BMC Neurol 9:35
Schnakers C, Chatelle C, Demertzi A, Majerus S, Laureys S (2012) What about pain in disorders of consciousness? AAPS J 14:437–444
Searle JR (2000) Consciousness. Ann Rev Neurosci 23:557–578
Shames JL, Ring H (2008) Transient reversal of anoxic brain injury−related minimally conscious state after zolpidem administration: a case report. Arch Phys Med Rehabil 89:386–388
Silva S, Alacoque X, Fourcade O, Samii K, Marque P, Woods R, Mazziotta J, Chollet F, Loubinoux I (2010) Wakefulness and loss of awareness: brain and brainstem interaction in the vegetative state. Neurology 74:313–320
Soddu A, Gómez F, Heine L et al (2016) Correlation between resting state fMRI total neuronal activity and PET metabolism in healthy controls and patients with disorders of consciousness. Brain Behav 6(1):e00424
Spiegel D (1991) Neurophysiological correlates of hypnosis and dissociation. J Neuropsychiatr Clin Neurosci 3:440–445
Stender J, Gosseries O, Bruno M-A et al (2014) Diagnostic precision of PET imaging and functional MRI in disorders of consciousness: a clinical validation study. Lancet 384:514–522
Stender J, Kupers R, Rodell A et al (2015) Quantitative rates of brain glucose metabolism distinguish minimally conscious from vegetative state patients. J Cereb Blood Flow Metab 35:58–65
Stender J, Mortensen KN, Thibaut A et al (2016) The minimal energetic requirement of sustained awareness after brain injury. Curr Biol 26:1494–1499
Tengvar C, Johansson B, Sorensen J (2004) Frontal lobe and cingulate cortical metabolic dysfunction in acquired akinetic mutism: a PET study of the interval form of carbon monoxide poisoning. Brain Inj 18:615–625
Terhune DB, Cardeña E (2010) Differential patterns of spontaneous experiential response to a hypnotic induction: a latent profile analysis. Conscious Cogn 19:1140–1150
Terhune DB, Cardeña E, Lindgren M (2011) Differential frontal-parietal phase synchrony during hypnosis as a function of hypnotic suggestibility. Psychophysiology 48:1444–1447
The Executive Committee of the American Psychological Association – Division of Psychological Hypnosis (1994) Definition and description of hypnosis. Contemp Hypn 11:142–162
The Multi-Society Task Force on PVS (1994) Medical aspects of the persistent vegetative state (1). N Engl J Med 330:1499–1508
Thibaut A, Bruno MA, Chatelle C, Gosseries O, Vanhaudenhuyse A, Demertzi A, Schnakers C, Thonnard M, Charland-Verville V, Bernard C, Bahri MA, Phillips C, Boly M, Hustinx R,

Laureys S (2012) Metabolic activity in external and internal awareness networks in severely brain-damaged patients. J Rehab Med 44(6):487–494
Thibaut A, Schiff N, Giacino J et al (2019) Therapeutic interventions in patients with prolonged disorders of consciousness. Lancet Neurol 18:600–614
Tian L, Jiang T, Liu Y, Yu C, Wang K, Zhou Y, Song M, Li K (2007) The relationship within and between the extrinsic and intrinsic systems indicated by resting state correlational patterns of sensory cortices. NeuroImage 36:684–690
Tommasino C, Grana C, Lucignani G, Torri G, Fazio F (1995) Regional cerebral metabolism of glucose in comatose and vegetative state patients. J Neurosurg Anesthesiol 7:109–116
Tononi G (2004) An information integration theory of consciousness. BMC Neurosci 5:42
Vanhaudenhuyse A, Boveroux P, Boly M, Schnakers C, Bruno MA, Kirsch M, Demertzi A, Lamy M, Maquet P, Laureys S, Faymonville ME (2008) Hypnosis and pain perception. Rev Med Liege 63:424–428
Vanhaudenhuyse A, Demertzi A, Schabus M, Noirhomme Q, Bredart S, Boly M, Phillips C, Soddu A, Luxen A, Moonen G, Laureys S (2011) Two distinct neuronal networks mediate the awareness of environment and of self. J Cogn Neurosci 23:570–578
Vogt BA, Laureys S (2005) Posterior cingulate, precuneal and retrosplenial cortices: cytology and components of the neural network correlates of consciousness. Prog Brain Res 150:205–217
Whyte J, Myers R (2009) Incidence of clinically significant responses to zolpidem among patients with disorders of consciousness: a preliminary placebo controlled trial. Am J Phys Med Rehabil 88:410–418
Wilckens KA, Aizenstein HJ, Nofzinger EA et al (2016) The role of non-rapid eye movement slow-wave activity in prefrontal metabolism across young and middle-aged adults. J Sleep Res 25:296–306
Zeman A (2001) Consciousness. Brain J Neurol 124:1263–1289

Modulation of CNS Functions by Deep Brain Stimulation: Insights Provided by Molecular Imaging

46

Alexandre Boutet, Mehr Jain, Dave Gwun, Pablo Rusjan, Clemens Neudorfer, Gavin J. B. Elias, Jürgen Germann, Alexander Bilbily, Walter Kucharczyk, Alfonso Fasano, Gwenn S. Smith, and Andres M. Lozano

A. Boutet · W. Kucharczyk
University Health Network, Toronto, ON, Canada

Joint Department of Medical Imaging, University of Toronto, Toronto, ON, Canada
e-mail: alexandre.boutet@mail.utoronto.ca; w.kucharczyk@utoronto.ca

M. Jain · D. Gwun · C. Neudorfer · G. J. B. Elias · J. Germann
University Health Network, Toronto, ON, Canada
e-mail: mjain030@uottawa.ca

P. Rusjan
Research and Imaging Centre and Campbell Family Mental Health Research Institute at the Centre for Addiction and Mental Health, Toronto, ON, Canada
e-mail: pablo.rusjan@camhpet.ca

A. Bilbily
University Health Network, Toronto, ON, Canada

Joint Department of Medical Imaging, University of Toronto, Toronto, ON, Canada

16 Bit Inc., Toronto, ON, Canada
e-mail: alexander@16bit.ai

A. Fasano
University Health Network, Toronto, ON, Canada

Edmond J. Safra Program in Parkinson's Disease, Morton and Gloria Shulman Movement Disorders Clinic, Toronto Western Hospital, UHN, Division of Neurology, University of Toronto, Toronto, ON, Canada

Krembil Brain Institute, Toronto, ON, Canada
e-mail: alfonso.fasano@uhn.ca

G. S. Smith
Department of Psychiatry and Behavioral Sciences, John Hopkins University School of Medicine, Baltimore, MD, USA
e-mail: gsmith95@jhmi.edu

A. M. Lozano (✉)
University Health Network, Toronto, ON, Canada

Division of Neurosurgery, Toronto Western Hospital, Toronto, ON, Canada
e-mail: lozano@uhnresearch.ca

R. A. J. O. Dierckx et al. (eds.), *PET and SPECT in Neurology*,
https://doi.org/10.1007/978-3-030-53168-3_46

Contents

46.1 Introduction . . . 1179
46.1.1 Electrophysiology and Functional Neuroimaging . . . 1183
46.2 Methods . . . 1186
46.3 DBS-Specific Experimental Variables . . . 1186
46.4 Molecular Neuroimaging Tracers . . . 1187
46.5 Review of PET and SPECT Studies . . . 1188
46.6 Movement Disorders . . . 1188
46.6.1 Parkinson's Disease . . . 1188
46.6.2 Other Movement Disorders . . . 1209
46.7 Psychiatric Disorders . . . 1212
46.7.1 Major Depressive Disorder . . . 1212
46.7.2 Obsessive-Compulsive Disorder . . . 1218
46.7.3 Other Psychiatric Disorders . . . 1220
46.8 Cognitive Disorders . . . 1221
46.8.1 Alzheimer's Disease . . . 1221
46.9 Other DBS Indications . . . 1224
46.10 Limitations . . . 1227
46.11 Future Directions . . . 1228
46.12 Conclusion . . . 1230
Appendix . . . 1231
Abbreviations Used in Tables . . . 1231
References . . . 1233

Abstract

Deep brain stimulation (DBS) is a neurosurgical intervention that allows probing and recalibration of dysfunctional brain circuits using electrical current delivered via implanted electrodes. While predominantly used in the treatment of Parkinson's disease and other movement disorders, DBS is increasingly being studied for its application to psychiatric diseases (e.g., major depressive disorder and obsessive-compulsive disorder) and cognitive disorders (e.g., Alzheimer's disease). Despite these growing applications of DBS, the mechanisms of action underlying DBS are poorly understood. Molecular neuroimaging modalities such as positron emission tomography (PET) and single-photon emission computed tomography (SPECT) provide a unique window into the neural changes induced by electrical stimulation; as such, they constitute invaluable research tools, with the potential to dramatically enhance both our understanding of this technology and its therapeutic impact. This chapter aims to provide an up-to-date review of insights gleaned from PET and SPECT studies in DBS patients.

Abbreviations

[^{11}C]dMP	[^{11}C]d-Threo-methylphenidate
[^{11}C]DTBZ	[^{11}C]Dihydrotetrabenazine
[^{11}C]NEM	[^{11}C]Nemonapride
[^{11}C]RACLO	[^{11}C]Raclopride

[^{123}I]FP-CIT	*N*-ω-Fluoropropyl-2β-carboxymethoxy-3β-(4-iodophenyl)tropane
[^{123}I]IBZM	[^{123}I]Iodobenzamide
[^{123}I]IMP	*N*-Isopropyl-*p*-(iodine-123)-iodoamphetamine
[^{18}F]FDG	18-Fluoro-2-deoxyglucose
[^{18}F]FDOPA	L-6-[^{18}F]Fluoro-3,4-dihydroxyphenylalanine
[^{18}F]FP	[^{18}F]Fallypride
[^{99m}Tc]ECD	^{99m}Technetium-ethylene biyldicysteinate dimer
[^{99m}Tc]HMPAO	^{99m}Technetium hexamethyl
ACC	Anterior cingulate cortex
AD	Alzheimer's disease
BOLD	Blood-oxygenation-level-dependent
CSTC	Cortico-striato-thalamo-cortical
DBS	Deep brain stimulation
fMRI	Functional magnetic resonance imaging
GPi	Globus pallidus internus
MDD	Major depressive disorder
MRI	Magnetic resonance imaging
NAcc	Nucleus accumbens
OCD	Obsessive-compulsive disorder
PCC	Posterior cingulate cortex
PD	Parkinson's disease
PDRP	Parkinson's disease-related pattern
PET	Positron emission tomography
SGC	Subgenual cingulate cortex
SMA	Supplementary motor area
SPECT	Single-photon emission computed tomography
STN	Subthalamic nucleus

46.1 Introduction

DBS is a neurosurgical procedure that involves electrical stimulation of structures deep within the brain using implanted electrodes. Since its inception in the early 1960s, the field of DBS has undergone rapid advancements, shaping how we understand and treat brain disorders today. An estimated 150,000 patients have received DBS treatment to date (Hariz 2017). While initially employed in the treatment of pain and movement disorders such as Parkinson's disease (PD), essential tremor (ET), and dystonia (DY), DBS has seen its spectrum of applications expand considerably in recent years. Today, DBS is being investigated for its therapeutic potential in psychiatric disorders such as obsessive-compulsive disorder (OCD), treatment-refractory major depressive disorder (MDD), Tourette's syndrome, and anorexia nervosa (Lozano et al. 2019). Currently ongoing clinical trials are also investigating its utility in cognitive disorders, such as Alzheimer's disease (AD), as well as

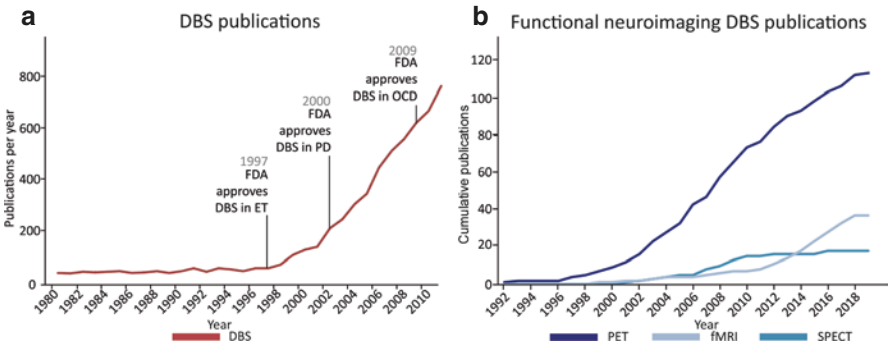

Fig. 46.1 DBS studies over time. (**a**) Cumulative number of deep brain stimulation studies published from 1980 to 2011 (modified from Neuron, 77/3, Lozano AM, Lipsman N, Probing and Regulating Dysfunctional Circuits Using Deep Brain Stimulation, 406–424, 2013, with permission from Elsevier). (**b**) Cumulative publications of positron emission tomography (PET), single-photon emission computed tomography (SPECT), and functional magnetic resonance imaging (fMRI) deep brain stimulation studies published from 1992 to 2019. Note the relative increase of PET and, more recently, fMRI studies as compared to SPECT investigations, which plateaued from 2010. *DBS* deep brain stimulation, *ET* essential tremor, *FDA* Food and Drug Administration, *fMRI* functional magnetic resonance imaging, *MRI* magnetic resonance imaging, *OCD* obsessive-compulsive disorder, *PET* positron emission tomography, *PD* Parkinson's disease, *SPECT* single-photon emission computed tomography

conditions such as morbid obesity. DBS interventions have yielded encouraging results in the treatment of chronic pain syndromes, cluster headache, and traumatic brain injury (Lozano and Lipsman 2013; Lozano et al. 2019). Due to its established and potential benefits for a broad spectrum of indications, both the number of DBS procedures conducted worldwide and the number of published DBS-related studies are rapidly increasing every year (Lozano and Lipsman 2013) (Fig. 46.1a).

DBS surgery entails the insertion of electrodes into deep brain structures through burr holes that enable access to the desired brain target. For accurate and safe electrode placement, the neurosurgeon relies on both preoperative and intraoperative imaging modalities. These typically entail multimodal, high-resolution MRI scans that allow visualization of brain structures and surrounding blood vessels (Boutet et al. 2019a). During preoperative stereotactic planning, the electrode trajectory is adjusted to accurately target the desired brain region while avoiding surrounding blood vessels and eloquent cortical areas such as the motor cortex. Following trajectory planning, electrodes are surgically implanted under local or general anesthesia. To confirm ideal electrode placement and ensure patient benefit, electrophysiological monitoring (i.e., microelectrode recordings), stimulation testing, and cranial imaging are commonly performed intraoperatively. In the final step of the surgery, an extension wire is tunneled under the skin in order to connect the electrodes to an implantable pulse generator commonly positioned in the upper chest wall (Lozano and Lipsman 2013) (Fig. 46.2a). Of note, DBS surgery is reversible; the device can be removed without long-term brain damage other than the formation of mild scar-like tissue along the implantation tracts (Erasmi et al. 2018).

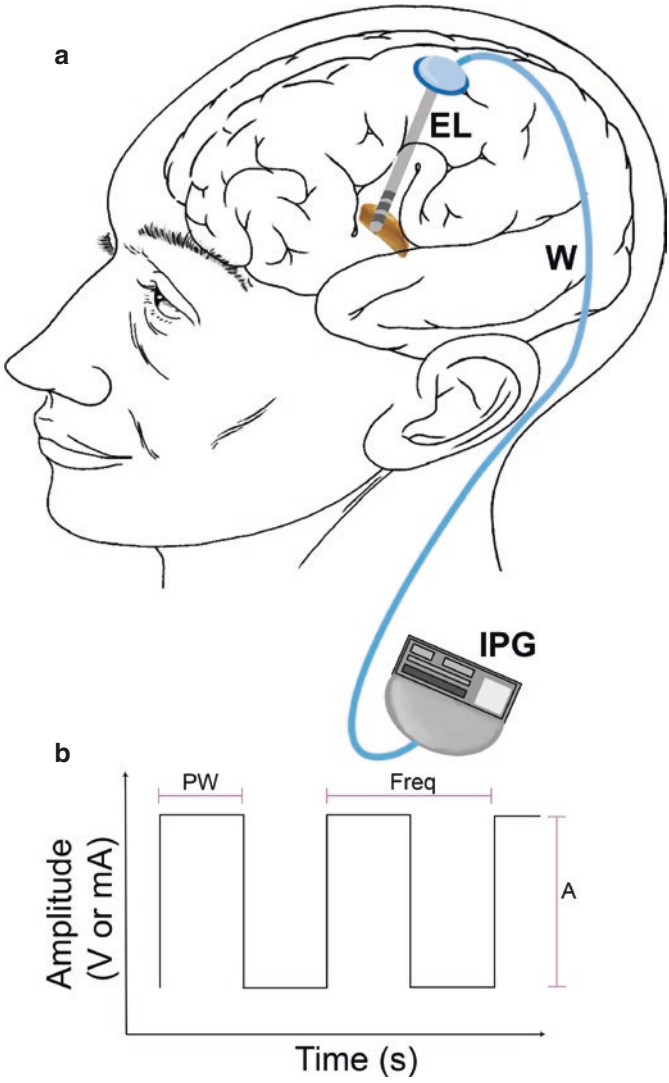

Fig. 46.2 DBS neuromodulation system. (**a**) The device consists of three components: electrode (EL), extension wire (W), and implantable pulse generator (IPG). The stimulating contacts of the electrode are placed within specific areas of the brain and receive power from the IPG that is typically placed subcutaneously in the right upper chest area. Electrode and IPG are connected via an extension wire that is tunneled under the skin. (**b**) Representation of the employed stimulation parameters during chronic DBS. Waveforms typically consist of square pulses that are applied at a predefined amplitude (A), pulse width (PW), and frequency (Freq). Parameters can be titrated individually to maximize clinical efficacy and reduce adverse effects to a minimum. V, volts; mA, milliamp; s: seconds

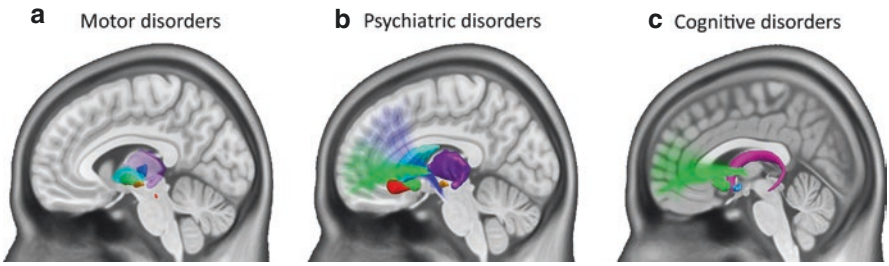

Fig. 46.3 Common DBS targets. 3D representation of brain targets overlaid on sagittal MRI (T1-weighted standard Montreal Neurological Institute brain). Apart from the caudate nucleus, only targets which have been investigated with molecular neuroimaging are displayed (Tables 46.1, 46.2, 46.3, 46.4, 46.5, 46.6, and 46.7). (**a**) Motor disorder targets: the globus pallidus externa (light blue), globus pallidus internus (green), pedunculopontine nucleus (red), subthalamic nucleus (yellow), thalamus (purple), and ventral intermediate nucleus of the thalamus (dark blue). (**b**) Psychiatric disorders targets: the caudate nucleus (light blue), middle forebrain bundle (dark blue), subgenual cingulate gyrus (red), subthalamic nucleus (yellow), thalamus (purple), and ventral capsule/ventral striatum and relevant tracts (green). (**c**) Cognitive disorder targets: the fornix (pink), nucleus basalis (blue), and ventral capsule/ventral striatum and relevant tracts (green)

To achieve maximum benefit, DBS electrodes are strategically placed within gray and white matter structures that are considered important in the pathophysiology of the respective disease. Targets are manifold and have mostly been adapted from the lesional era of neurosurgery (Miocinovic et al. 2013). In the treatment of movement disorders, established targets include the subthalamic nucleus (STN), globus pallidus internus (GPi), and ventral intermediate nucleus of the thalamus. These targets are part of a common motor circuit that processes and regulates the planning and execution of movements. In contrast, the major hubs and related white matter connections implicated—and therefore stimulated—in psychiatric diseases include structures such as the nucleus accumbens (NAcc), anterior limb of the internal capsule, anterior cingulate cortex (ACC), and medial forebrain bundle (Lozano et al. 2019). Common hubs of the major circuits targeted by DBS are shown in Fig. 46.3.

Electrical stimulation is usually not initiated immediately following electrode implantation but typically commences days to weeks after surgery, after the acute surgical effects have resolved. Local inflammatory changes of brain tissue occur surrounding the leads, which may induce temporary improvement of patients' symptoms that are unrelated to electrical stimulation (commonly referred to as "insertional effect"). Electrical stimulation is typically initiated by a physician specialized in DBS programming (Picillo et al. 2016). The stimulation parameters (i.e., voltage, frequency, and pulse width) are gradually adjusted and customized toward the patient's specific symptom constellation (Fig. 46.2b). The goal of the titration process is to maximize symptom control while reducing undesired adverse effects (e.g., speech impairment, paresthesia) that may arise from stimulation of adjacent brain structures. Stimulation programming is typically performed empirically and often involves selection of parameters on a trial-and-error basis with respect to exhibited symptoms. When adjusted properly, striking clinical improvements may be observed.

46.1.1 Electrophysiology and Functional Neuroimaging

DBS not only holds therapeutic potential for various neurological and psychiatric conditions but also offers a unique opportunity to monitor and probe neural activity in close vicinity to the chosen target structure (Lozano et al. 2018). This is accomplished, in part, through the intraoperative brain mapping techniques that are used to identify DBS target locations. Specifically, electrophysiological recordings provide insight into the dynamics of brain activity at the level of cell populations (in the case of local field potential—LFP—recordings) or individual neurons (in the case of single-unit recordings) (Rosa et al. 2013). While LFP and single-unit recordings feature a high spatial and temporal resolution, their utility is limited to confined areas in close proximity to the recording device; inferences regarding functional changes across distributed neural networks are not usually possible. To overcome these limitations, functional neuroimaging techniques such as molecular neuroimaging (e.g., positron emission tomography (PET), single-photon emission computed tomography (SPECT)), and functional magnetic resonance imaging (fMRI) have evolved that allow the study of network-level changes in response to DBS (Ko et al. 2013).

Functional neuroimaging techniques have found increasing application as research and targeting tool in DBS in recent years (Fig. 46.1b). They have provided valuable insights into how cortical and subcortical activity changes in response to different DBS paradigms (e.g., ON vs. OFF stimulation) and have gone a considerable way toward elucidating the mechanisms of DBS in movement disorders and psychiatric and neurodegenerative diseases (Ko et al. 2013). Notably, PET data have also contributed to the identification of new DBS targets for MDD and cluster headaches pinpointing key network hubs whose activity is altered in disease (May et al. 1998; Mayberg et al. 2005) (Fig. 46.4).

The selection of the appropriate functional neuroimaging modality largely depends on the experimental hypothesis and technical specifications (Friston 2009). PET and SPECT can provide information on tissue glucose consumption and cerebral blood flow and hence can be used to assess regional brain function. While these tracers measure brain activity, it is not possible to infer whether said activity is caused by the recruitment of excitatory or inhibitory neuron populations as the measurements reflect a final common pathway of brain activity (Dale and Halgren 2001; Friston 2009). As such, these methods can identify changes in neural function, but the results are not mechanistically specific. Importantly, there are established PET and SPECT radiotracers that can provide mechanistic information on specific neurotransmitter pathways (e.g., metabolism, transporters, and receptors), neuromodulators, pathological processes (e.g., inflammation), and proteins involved in neurodegenerative diseases (e.g., beta amyloid and tau proteins; Hooker and Carson 2019). Among the most commonly studied radiotracer targets of this kind are those related to monoaminergic neurotransmission (dopamine and serotonin) metabolism, receptors, and transporters. While there are several limitations of PET and SPECT imaging, mainly related to spatial and temporal resolution, these remain the only techniques available for in vivo imaging of a broad range of neurobiological mechanisms.

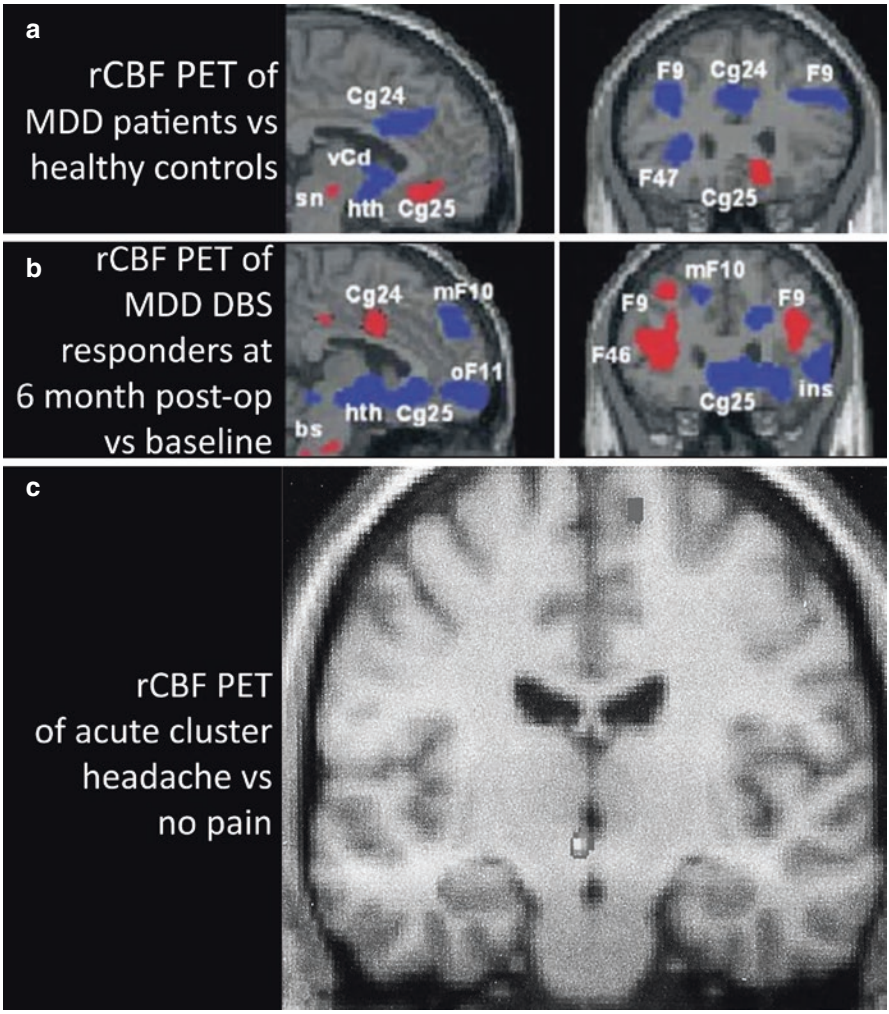

Fig. 46.4 Examples of insights from molecular neuroimaging. (**a**) In therapy-refractory major depressive disorder (MDD), PET [^{15}O]H_2O data have indicated increased blood flow within the subgenual cingulate cortex (SGC or Cg25), which has led to the investigation of this area as a potential DBS target. (**b**) Reversal of increased blood flow during SGC-DBS was associated with alleviation of depressive symptoms (**a** and **b** modified from Neuron, 45/5, Mayberg HS, Lozano AM, Voon V, McNeely HE, Seminowicz D, Hamani C, Schwalb JM, Kennedy SH, 651–660, 2005, with permission from Elsevier). (**c**) Acute episodes of headache were associated with increased hypothalamic blood flow ([^{15}O]H_2O), opening the door to hypothalamic modulation for cluster headaches (reprinted from The Lancet, 352, May A, Bahra A, Buchel C, Frackowiak RSJ, Goadsby PJ, Hypothalamic activation in cluster headache attacks, 275–278, 1998, with permission from Elsevier). *Bs* brain stem, *Cg24* anterior cingulate, *Cg 25* subgenual cingulate, *F9* dorsolateral prefrontal, *F46* prefrontal, *F47* ventrolateral prefrontal, *hth* hypothalamus, *ins* anterior insula, *mF10* medial frontal, *oF11* orbital frontal, and *vCd* ventral caudate

As neuroimaging techniques permit in vivo investigation of brain activity, PET and SPECT are often compared to magnetic resonance imaging (MRI). Compared to magnetic resonance imaging (MRI), PET and SPECT imaging technology is less widely available. The spatial (1–2 mm) and temporal resolution of MRI are superior to that of PET and SPECT imaging. The latest-generation PET scanners have reached the theoretical limit of resolution for PET (2.5 mm) (Turner and Jones 2003). The spatial resolution of PET and SPECT limits the ability to accurately quantitate radiotracer binding in small structures due to partial-volume effect that creates spillover of signal leading to less accurate signal quantification (Soret et al. 2007). MRI techniques for measuring brain function include fMRI that measures blood-oxygenation-level-dependent (BOLD) signal and arterial spin labelling that quantify blood flow, both thought to be a correlate of brain activity. MRI's signal-to-noise ratio for subcortical structures may be suboptimal, which is relevant as most DBS electrodes are placed in deep brain structures. Compared to PET, fMRI is also limited by the lack of absolute quantification (Dale and Halgren 2001; Friston 2009). In terms of participant burden, MRI involves no radiation compared to PET and SPECT. As MRI relies on strong magnetic fields and radio-frequency pulses, its application to DBS has historically been hamstrung by the risk of interference with metallic implants (Boutet et al. 2019b). Also, compared to PET and SPECT, MRI data in patients receiving DBS will be hampered to a greater extent by the metallic susceptibility artefact and associated image distortion (Fig. 46.5). Experimental designs will strongly benefit from weighting pros and cons of these modalities.

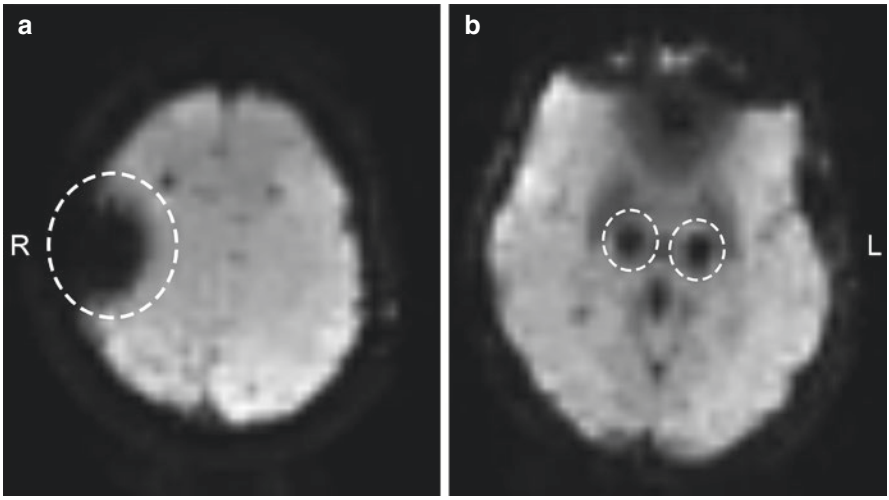

Fig. 46.5 fMRI artifacts related to the DBS device. Select axial GRE-EPI images acquired with 3 T MRI in a patient with Parkinson's disease receiving subthalamic nucleus (STN) DBS. (**a**) Artifact related to the coiled DBS extension wire under the scalp (dotted line circle). (**b**) Artifact related to the DBS leads (dotted line circle). *L* left, *R* right. *GRE-EPI* gradient recalled echo-echo planar imaging

In this chapter, we review the state-of-the-art of PET and SPECT applications in the field of DBS. First, DBS-specific experimental variables for neuroimaging studies are reviewed to guide study findings interpretation. Then, we summarize the insights gained from PET and SPECT studies in the field and provide an overview of the limitations. Finally, we provide an overview of future directions of the application of functional neuroimaging to the study of the neurobiology of DBS. Despite their potential relevance, fMRI studies were excluded as they exceed the scope of this review on molecular imaging. fMRI is briefly touched upon in Sect. 46.11.

46.2 Methods

Peer-reviewed literature pertaining to molecular neuroimaging in DBS was surveyed by searching the publicly accessible database MEDLINE. Search terms included "deep brain stimulation," "DBS," "electrical stimulation," "positron emission tomography," "PET," "PET scan," "CT PET scan," "positron emission tomography computed tomography," "single-photon emission computed tomography," "SPECT," "single-photon emission CAT scan," "single-photon emission CT scan," "single-photon emission computer assisted tomography," and "single photon emission computed radionuclide tomography." Relevant articles and reviews from other sources were included as well. We only reviewed papers published in English that involved human subjects. Data extraction from the studies is presented in the appendix and includes the following variables: study year, number of DBS patients, time of PET or SPECT after the surgery, tracer, contrast, and brain areas showing tracer increase or decrease. To remain concise, we aimed to report molecular neuroimaging findings pertaining to a single comparison (i.e., contrast representing a unique contribution) per study. In order of priority, we reported long-term changes (i.e., neuroimaging data acquired postop vs. preoperative with DBS-ON (i.e., DBS turned on) or DBS-OFF (i.e., DBS turned off)), acute changes (i.e., DBS-ON vs. DBS-OFF), and, finally, other comparisons such as OFF vs. preoperative or DBS patients vs. healthy controls.

46.3 DBS-Specific Experimental Variables

Several considerations must be kept in mind when reviewing and interpreting the results of functional neuroimaging studies involving DBS patients (Vitek et al. 2010). First, PET and SPECT findings depend on the timing between surgery and acquisition of imaging data. Indeed, inflammatory reactions as well as local swelling of brain tissue along the electrode path may confound imaging results in the immediate postoperative course. Second, changes in the medication regimen after DBS (as is done in PD patients for levodopa and dopamine agonists) and adjustment of stimulation settings prior to the imaging session (which would affect whether patients were scanned after a period of stable, optimal stimulation) have to be taken into account when investigating DBS effects. These variables may change the

interpretation of the clinical and functional neuroimaging outcomes. Programming optimization is particularly problematic for psychiatric disorders for which we lack objective markers to quantify maximal symptom improvement. Third, when comparing DBS-ON and DBS-OFF, a washout period between programming and data acquisition is recommended to ensure that the prior stimulation condition does not interfere with data acquisition. Washout periods vary greatly across diseases and are determined by considerations of patient tolerability and the time course of both the re-emergence of symptoms and of the neurobiological effects. Fourth, interpretation of neuroimaging data is often complicated by the lack of information regarding electrode position. Variations in position across patients, surgeons, and institutions inevitably result in heterogeneous targeting and should ideally be assessed and accounted for to allow meaningful statements in the context of patient benefit and neuroimaging findings (Butson et al. 2007). At a single institution, the number of patients receiving DBS can be low, which results in small sample sizes unless multisite collaboration is undertaken.

46.4 Molecular Neuroimaging Tracers

For the purpose of this chapter, PET and SPECT will be grouped under the umbrella terms "molecular neuroimaging" or "functional neuroimaging" modalities. Changes in brain activity in neural circuits upon stimulation have been the most commonly studied aspect across the DBS functional neuroimaging literature using various tracers (Fig. 46.6). In this chapter, PET (e.g., [^{18}F]FDG, [^{15}O]H_2O) and SPECT (e.g., [^{99m}Tc]ECD, [^{123}I]IMP, and [^{99m}Tc]HMPAO) tracers will be considered markers of brain "activity" or "function." However, while tracers such as [^{18}F]FDG, [^{15}O]H_2O, and [^{99m}Tc]ECD all serve to index brain function, they do so in different ways; [^{18}F]FDG, for instance, measures glucose consumption, while [^{15}O]H_2O and

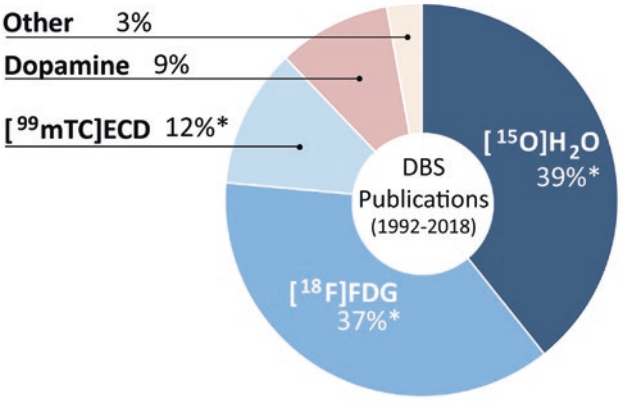

Fig. 46.6 PET and SPECT tracers commonly used in DBS studies. From 1992 to 2019, tracers used to measure brain activity (indicated by asterisk) were most commonly used. Dopaminergic tracers were also used mostly in Parkinson's disease studies

[^{99m}Tc]ECD measure cerebral blood flow. These differences should be kept in mind when comparing studies. A smaller number of PD studies have used tracers for the dopamine system, including tracers for dopamine synthesis and turnover (PET: [^{18}F]FDOPA), dopamine transporters (PET: [^{11}C]dMP; SPECT: [^{123}I]FP-CIT), vesicular monoamine transporter (PET: [^{11}C]DTBZ), and dopamine D2 receptors (PET: [^{11}C]RAC, [^{11}C]NEM, [^{18}F]FP; SPECT: [^{123}I]IBZM) (Lammertsma 2001; Shen et al. 2012).

46.5 Review of PET and SPECT Studies

The following sections provide an overview of PET and SPECT studies in DBS; studies pertaining to movement disorders, psychiatric disorders, and cognitive disorders are addressed in turn. Each section is divided into "molecular neuroimaging findings" and "contributions of molecular neuroimaging." The former summarizes the results of the literature, whereas the latter identifies insights to the field provided by these results.

46.6 Movement Disorders

Movement disorders constitute the most common indication for DBS surgery today. This is owing to the rapid and striking clinical benefits that electrical stimulation elicits in conditions such as PD, essential tremor, and dystonia (Lozano et al. 2019). The brain regions targeted in the treatment of movement disorders are subcortical motor circuit hubs that play a crucial role in the planning and execution of movement (Fig. 46.3a). Below, we will review the molecular neuroimaging findings that have provided insights into the neural substrates underlying the clinical changes that occur with DBS mainly in Parkinson's disease and, to a lesser extent, in other movement disorders.

46.6.1 Parkinson's Disease

Parkinson's disease (PD) is the second most common neurodegenerative disorder with a rapidly increasing incidence after the age of 50 (Lozano et al. 2019; Poewe et al. 2017). The disease is defined by a number of hallmark symptoms, including akinesia or bradykinesia, rigidity, and tremor. Typically, postural instability and gait issues occur in later stages of the disease. Autonomic dysfunctions including orthostatic hypotension, sweating, and bladder and bowel dysfunctions are also usually seen in late PD. More recently, studies have investigated the poorly understood nonmotor manifestations of PD, namely, cognitive dysfunction (from mild executive dysfunction to distinct manifestations of dementia) and psychiatric manifestations (e.g., depression, anxiety, and psychosis) (Jankovic 2008; Rodriguez-Oroz et al. 2009).

PD is characterized by the degeneration of dopamine-rich neurons within the substantia nigra pars compacta as well as widespread accumulation of intracellular α-synuclein throughout the brain. Neurodegeneration and a-synuclein accumulation follow stages of severity known as the Braak stages: initially, the lower brain stem (including the substantia nigra compacta) undergoes pathological changes, followed by the midbrain and basal forebrain, and finally the limbic system and neocortex (Poewe et al. 2017).

The cortico-striato-thalamo-cortical (CSTC) circuit is the principal functional network for the regulation of motor activity and complex behavior in the brain. Within the circuit, information is conveyed from the cortex to major subcortical nodes such as the striatum, globus pallidus, STN, substantia nigra, and thalamus. These structures process incoming information and relay the output back to the cortex, forming a feedback loop (Albin et al. 1989; DeLong 1990) (Fig. 46.7a). For effective information processing, an equilibrium must be maintained within the circuit that readily allows adaptation to external stimuli. To this end, antagonistic regulatory subpathways have evolved within the CSTC circuit, namely, "direct," "indirect," and "hyperdirect" pathways (Fig. 46.7b). The "direct" pathway exerts inhibitory effects on the internal segment of the globus pallidus (GPi) and facilitates cortical activation via disinhibition of the thalamus. In contrast, the "indirect" pathway reduces thalamic output. This is achieved by a cascade of inhibitory and excitatory relays that promote GPi output and eventually arrest thalamic activity

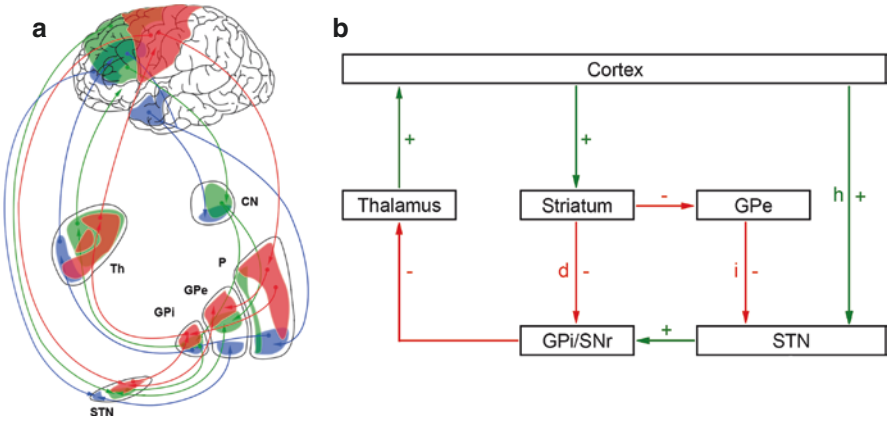

Fig. 46.7 Cortico-striato-thalamo-cortical (CSTC) circuit. (**a**) Network-wide-level representation of the CSTC circuit depicting the functional parallel reentrant loops that reside within segregated basal ganglia territories (red, sensorimotor; blue, associative; green, limbic). (**b**) Classic model of the CSTC circuit featuring direct (d) and indirect (i) and hyperdirect (h) pathway and their influence (+, excitatory; −, inhibitory) on downstream basal ganglia territories (**a** and **b** modified with permission from Springer Nature Customer Service Centre GmbH: Springer Nature, Brain Structure and Function, Neuroanatomical background and functional considerations for stereotactic interventions in the H fields of Forel, Neudorfer C, Maarouf M, 2017). *CN* caudate nucleus, *GPe* globus pallidus externa, *GPi* globus pallidus internus, *P* putamen, *SNr* substantia nigra reticulata, *STN* subthalamic nucleus, *Th* thalamus

(Chevalier and Deniau 1990; Rodriguez-Oroz et al. 2009). The "hyperdirect" pathway has only been described recently and incorporates fibers that bypass the inhibitory relay stations of the striatum and directly project to STN (Nambu et al. 2002). Functionally, the circuit is comparable to the "indirect" pathway; the projections, however, allow direct transmission of cortical input into downstream basal ganglia territories on a shorter temporal scale.

Aberrant and dysfunctional processing of information within functionally isolated loops has been associated with neurological conditions and led to the characterization of many disorders as "circuitopathies." Disruption of normal function of the basal ganglia and CSTC circuit secondary to pathological changes has been hypothesized to play a key role in PD pathophysiology (Rodriguez-Oroz et al. 2009). The classic CSTC circuit model suggests that the lack of nigrostriatal dopaminergic input secondary to neuronal loss causes aberrant processing of neural information within basal ganglia loops, leading to a disequilibrium within subpathways. Neurosurgical intervention, namely, deep brain stimulation (DBS), recalibrates dysfunctional activity by recruiting neuron populations within anatomically confined areas (Lozano and Lipsman 2013).

Molecular neuroimaging, in particular PET, has provided key insights into the functional status of the CSTC circuit in PD and other movement disorders. PET studies of cerebral glucose metabolism have defined the so-called Parkinson's disease-related pattern (PDRP) which consists of a spatial pattern of abnormal activity consistently found in PD patients (Eidelberg 2009; Ma et al. 2007). Specifically, the premotor and parieto-occipital cortical regions show relative metabolism reductions compared to the hyperactive pallidothalamic and pontine areas. In comparison to healthy controls, the expression of the PDRP is increased with disease progression and decreased with PD treatments, including levodopa and DBS. Hyperactivity of the indirect pathway causing an increase in inhibitory pallidal outflow to the thalamus and pons has, in turn, been hypothesized to underlie this pathological pattern of activity (Eidelberg 2009; Ma et al. 2007).

As mentioned, PD accounts for the largest proportion of DBS patients by far. When selected properly, the majority of PD patients highly benefit from this treatment (Okun 2012). Although multiple structures may be targeted, the STN and, to a lesser extent, GPi are most often stimulated (Fig. 46.3a). The target choice will be informed by discussion within a multidisciplinary team and dictated by the patient's unique clinical profile and needs. For example, GPi is sometimes recommended for patients with cognitive or psychiatric impairments due to the possible negative adverse effects of STN stimulation on these functions. Some symptoms such as tremor and rigidity tend to improve more than other PD manifestations including gait and speech, which may in fact worsen with stimulation. Over the years, empiric postoperative DBS programming algorithms have improved and can achieve individually optimized stimulation (Picillo et al. 2016). Immediate clinical feedback (e.g., tremor or rigidity reduction) in response to stimulation in PD patients makes DBS programming slightly easier. However, this optimization process still takes up to a year to complete. As such, clinical benefits can generally be maximized and adverse effects minimized for each patient (Lozano and Lipsman 2013; Picillo et al. 2016).

46.6.1.1 Molecular Neuroimaging Findings

Molecular neuroimaging studies have mainly focused on one of the following experimental designs to evaluate the impact of DBS on PD symptoms: (1) investigating the main effects of acute stimulation (by comparing ON and OFF stimulation conditions) or chronic stimulation (by comparing postoperative and preoperative imaging data) while the patients are at rest ("resting experiments") and (2) comparison between performance on particular tasks in ON and OFF stimulation conditions ("task experiments"). The most frequent focus of PD studies has been changes in brain function, as assessed using various PET (e.g., [^{18}F]FDG and [^{15}O]H_2O) and SPECT (e.g., [^{99m}Tc]ECD) tracers. Other PET tracers investigating dopamine metabolism ([^{11}C]NEM, [^{18}F]fallypride, [^{123}I]FP-CIT, [^{18}F]FDOPA, and [^{11}C]DTBZ) and SPECT ([^{123}I]FP-CIT and [^{123}I]IBZM) have also been used to investigate DBS mechanism of action and change in disease progression.

STN-DBS studies contrasting ON vs. OFF stimulation conditions have consistently shown changes in metabolism predominantly within major hubs of the motor circuits, although the directionality of metabolic changes is fairly heterogeneous Table 46.1. In general, STN and the neighboring thalamus show increased activity in response to STN stimulation (Asanuma et al. 2006; Garraux et al. 2011; Hershey et al. 2003; Hilker et al. 2004; 2008; Hill et al. 2013; Karimi et al. 2008; Volonte et al. 2012). Interestingly, the pallidum, which receives input from the STN, has inconsistently shown change in activity characterized by mixed directionality changes either with [^{18}F]FDG or [^{15}O]H_2O (Asanuma et al. 2006; Bradberry et al. 2012; Garraux et al. 2011; Hilker et al. 2004; 2008; Hill et al. 2013; Wang et al. 2010). Brain activity within the precentral gyrus most commonly decreases during STN-DBS, which is in line with the CSTC circuit concept (Asanuma et al. 2006; Hershey et al. 2003; Hilker et al. 2002; Trost et al. 2006). However, one study has reported increased metabolism in the motor cortex (Garraux et al. 2011). Conversely, prefrontal areas tend to preferentially show increased activity (Bradberry et al. 2012; Garraux et al. 2011; Hilker et al. 2004; Trost et al. 2006). In a few instances, the precuneus and the occipitotemporal cortex have also shown increased brain activity (Asanuma et al. 2006; Bradberry et al. 2012; Hilker et al. 2002; Trost et al. 2006). The cerebellum, an important relay of the motor network, also demonstrated mixed activity patterns with STN-DBS whether the studies were measuring metabolism or regional cerebral blood flow (rCBF) (Asanuma et al. 2006; Bradberry et al. 2012; Garraux et al. 2011; Hershey et al. 2003; Hilker et al. 2002, 2004; Nagaoka et al. 2007; Trost et al. 2006; Volonte et al. 2012; Wang et al. 2010). When investigating the effects of stimulation at the network level, resting studies have shown acute reduction (and thus normalization) of the PDRP activity with STN-DBS (Asanuma et al. 2006; Trost et al. 2006; Wang et al. 2010).

To compare across studies, we diagrammatically represented the brain areas showing changes in brain function (i.e., metabolic tracers including [^{18}F]FDG, [^{15}O]H_2O) and SPECT (e.g., [^{99m}Tc]ECD, [^{123}I]IMP, and [^{99m}Tc]HMPAO) in studies employing more conservative statistics using any method of multiple comparison corrections (e.g., family-wise error, Bonferroni, or threshold cluster corrections) (Asanuma et al. 2006; Garraux et al. 2011; Hershey et al. 2003; Hilker et al. 2004;

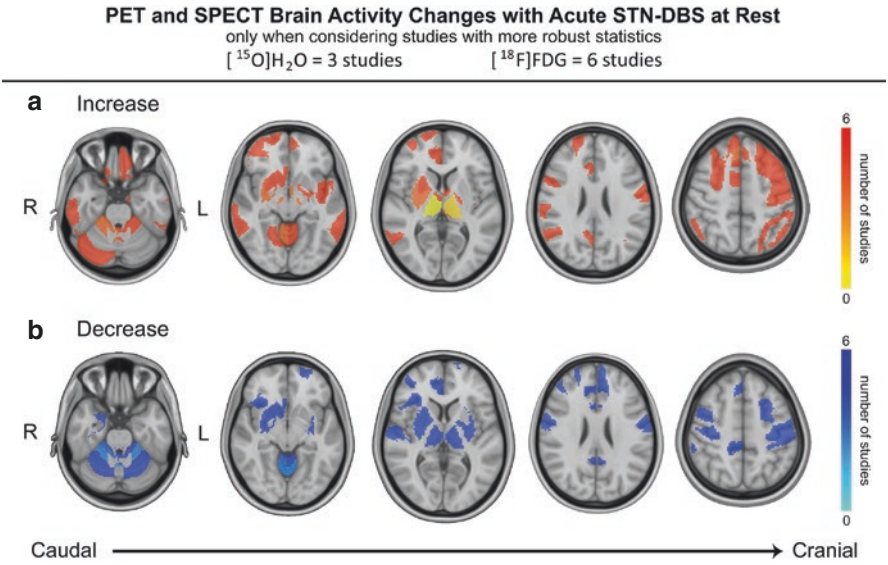

Fig. 46.8 Diagrammatic summary of activity changes with acute STN-DBS at rest. Only studies assessing acute changes with stimulation (studies with ON vs. OFF in Table 46.1) and using a form of multiple comparison correction were included to maintain robustness of reported brain regions (studies labeled with [b] in Table 46.1). First, brain regions were obtained from spatial parcellation according to published atlases (cortical, An Atlas of Intrinsic Connectivity of Homotopic Areas (Joliot et al. 2015); subcortical, Ewert et al. (2018); brain stem, Harvard Ascending Arousal Network Atlas (Edlow et al. 2012); cerebellum, Diedrichsen et al. (2009)). Then, regions were weighted according to the number of studies reporting significant changes in each region. To decide which parcellated brain areas from the atlases would be selected, we used in order of priority (1) visual representation, (2) reported coordinates, and (3) naming of areas with activation available in studies. For large activation areas, multiple parcellated brain areas were selected. Areas of brain activity changes were then overlaid on select MRI (T1-weighted Montreal Neurological Institute brain) axial images. Across studies, brain regions with an increase in activity (hot colors) are shown in (**a**), whereas brain regions with significant decrease in activity (cool colors) are shown in (**b**). Color bars represent the number of studies

Hill et al. 2013; Karimi et al. 2008; Nagaoka et al. 2007; Volonte et al. 2012; Wang et al. 2010) (Fig. 46.8).

A subset of studies have focused on *long-term changes (postop vs. preop)* associated with STN stimulation Table 46.1. The follow-up times for long-term PD studies ranged from 1 month to 20 months post operation. Interestingly, the areas demonstrating changes here differ from those linked to acute stimulation changes. Long-term changes predominantly appear to involve the frontal lobes and, to a lesser extent, the parietal and temporal lobes (Antonini et al. 2003; Cilia et al. 2009; Le Jeune et al. 2010a; Sestini et al. 2002, 2005, 2007). The direction of changes is inconsistent across studies. In contrast to ON vs. OFF stimulation studies, hubs of the motor circuit such as the STN, thalamus, GPi, and precentral gyrus seldom showed significant changes in most studies. A few studies, however, reported

increased (Cilia et al. 2009; Le Jeune et al. 2010a; Peron et al. 2010; Pourfar et al. 2009; Sestini et al. 2005; Tanei et al. 2009) and decreased (Cao et al. 2017) brain activity in the cerebellum. Finally, Cao et al. (2017) reported a decrease in PDRP activity 8 months after STN-DBS surgery. When only considering more statistically stringent studies (i.e., those using any method of multiple comparison corrections), further insights into the directionality of changes in cortical areas are gleaned: the posterior parietal cortex most commonly showed increased brain activity, whereas prefrontal areas usually demonstrated decreased brain function (Antonini et al. 2003; Cao et al. 2017; Cilia et al. 2009; Le Jeune et al. 2008; 2010a; Li et al. 2006; Peron et al. 2010; Pourfar et al. 2009; Sestini et al. 2002, 2005, 2007; Smith et al. 2019; Tanei et al. 2009) (Fig. 46.9).

A subset of STN-DBS studies have investigated the functional changes associated with motor and non-motor (usually cognitive or emotional) tasks during

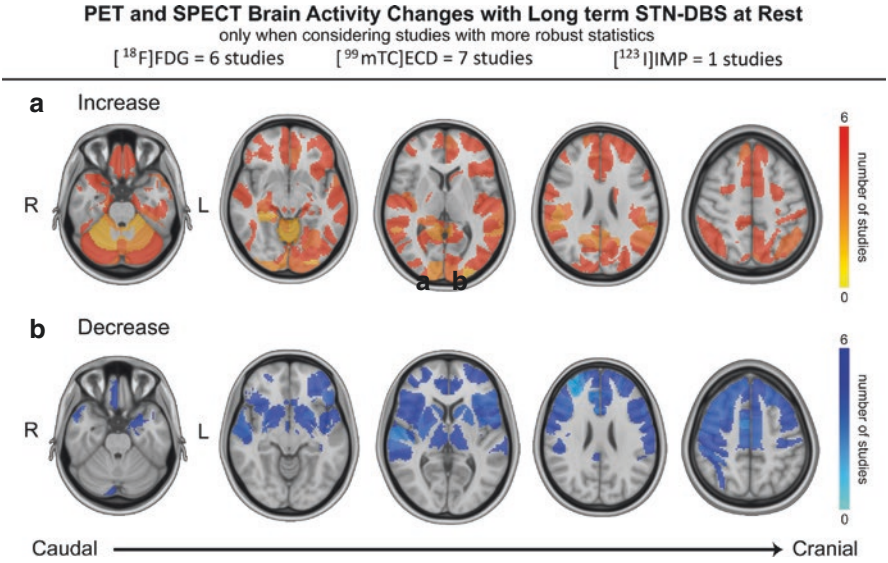

Fig. 46.9 Diagrammatic summary of activity changes with long-term STN-DBS at rest. Only studies assessing long-term changes with stimulation (studies with postop vs. preop in Table 46.1) and using a form of multiple comparison correction were included to maintain robustness of reported brain regions (studies labeled with [b] in Table 46.1). First, brain regions were obtained from spatial parcellation according to published atlases (cortical, An Atlas of Intrinsic Connectivity of Homotopic Areas (Joliot et al. 2015); subcortical, Ewert et al. (2018); brain stem, Harvard Ascending Arousal Network Atlas (Edlow et al. 2012); cerebellum, Diedrichsen et al. (2009)). Then, regions were weighted according to the number of studies reporting significant changes in each region. To decide which parcellated brain areas from the atlases would be selected, we used in order of priority (1) visual representation, (2) reported coordinates, and (3) naming of areas with activation available in studies. For large activation areas, multiple parcellated brain areas were selected. Areas of brain activity changes were then overlaid on select MRI (T1-weighted Montreal Neurological Institute brain) axial images. Across studies, brain regions with an increase in activity (hot colors) are shown in (**a**), whereas brain regions with significant decrease in activity (cool colors) are shown in (**b**). Color bars represent the number of studies

stimulation (Table 46.2). For the purpose of this chapter, task-based studies reported in conjunction with changes in behavior are discussed; these studies most often studied the effect of stimulation (DBS-ON vs. DBS-OFF) on tasks. Similar to resting studies, there are also inconsistencies in the results of studies using motor tasks. A likely explanation is the additional issue of variation in the motor tasks employed: motor tasks may have involved internally generated or externally cued movements as well as repetitive, random or sequential, and unilateral or bimanual movements. Modulation of motor task by STN-DBS was commonly associated with primary motor cortex and supplementary motor area (SMA) regional cerebral blood flow (rCBF) changes (Ceballos-Baumann et al. 1999; Limousin et al. 1997; Park et al. 2015; Strafella et al. 2003a). Similar to motor task studies, those using non-motor cognitive or emotional tasks provided task-specific results, with limited generalizability to other studies. In cognitive task studies (e.g., Stroop task or random number generation) investigating the effect of stimulation on cognition (i.e., interaction term), the prefrontal areas and ACC were engaged (Schroeder et al. 2002, 2003; Thobois et al. 2002, 2007; Ventre-Dominey et al. 2014). A study investigating the effect of stimulation during executive functions (spatial working memory tasks) found increased rCBF in the ACC and insula as well as decreased rCBF in the parietal lobes (Ventre-Dominey et al. 2014). Some studies also investigated the effect of motor imagery tasks. They showed rCBF changes in hubs of the motor circuit such as the precentral gyrus and SMA as well as the prefrontal cortex (Thobois et al. 2002). Specifically, Weiss et al. (2015) demonstrated that STN-DBS is associated with an increase in pedunculopontine nucleus rCBF when patients perform a gait imagination task. Interestingly, this nucleus is a DBS target for gait disturbances (Thevathasan and Moro 2019). Motor speech abilities often do not respond or respond negatively to STN-DBS (Narayana et al. 2009). A study reported decreased verbal fluency with stimulation in conjunction with decreased rCBF in the right orbitofrontal cortex, the left inferior temporal gyrus, and the left inferior frontal/insular cortex (Schroeder et al. 2003). Since a left frontotemporal network implicated in verbal fluency has been defined, this effect of STN-DBS could be related to decreased blood flow in these areas. Similarly, stuttering was worsened with STN-DBS, while the precentral gyrus, SMA, and cerebellum showed increased rCBF (Burghaus et al. 2006). Yet, a study also reported improved dysarthria in PD patients with STN stimulation causing normalization of brain activity in the motor cortex, SMA, and cerebellum (Pinto et al. 2004). These different effects of STN-DBS on various aspects of speech could be related to electrode placement, stimulation spillover on adjacent neural, and possibly related to separate circuits governing different speech facets. Various other non-motor tasks have been studied in the context of STN-DBS, such as urge to void (Herzog et al. 2006, 2008), change in pain (Dellapina et al. 2012) and smell (Cury et al. 2018; Fonoff et al. 2010), and response conflict decisions (Schroeder et al. 2002; Thobois et al. 2007) (Table 46.2). These studies usually show less engagement of the motor circuit hubs and rather changes of brain function in areas such as the thalamus, ACC, and prefrontal cortices.

A few resting studies have performed correlations with emotional changes with STN-DBS. Interestingly, worsening manic symptoms with STN-DBS have been

consistently linked to increased prefrontal and ACC rCBF (Schilbach et al. 2012; Ulla et al. 2006, 2011). Worse performance in fear recognition, feeling of disgust, and worsening depression symptoms was all associated with increased (Bejjani et al. 1999) and decreased activity (Le Jeune et al. 2008; Ory et al. 2017) in the orbitofrontal cortex with STN-DBS. The STN has motor, associative, and limbic components, which explain the motor benefits and also the cognitive and emotional changes seen with DBS. These less desirable symptoms may be associated with stimulation spillover to the less desirable associative and limbic subdivisions.

As discussed, DBS electrodes may be placed in other brain targets when treating PD patients. A minority of studies have investigated PET and SPECT changes with stimulation of motor targets other than STN (Table 46.3). As with STN-DBS, GPi stimulation provides motor benefits and seems to also engage motor areas such as the motor cortex and SMA (Fukuda et al. 2001a; Valalik et al. 2009). Interestingly, one study also reported reduction (and thus normalization) of the PDRP activity with GPi-DBS (Fukuda et al. 2001b). This suggests that both STN and GPi targets provide benefits by modulating similar circuits. Additional targets are usually engaged for specific symptoms. For example, pedunculopontine nucleus (PPN) stimulation has been attempted to improve gait, while VIM stimulation is typically conducted to help patients suffering from therapy-refractory tremor (Lozano and Lipsman 2013; Lozano et al. 2019).

46.6.1.2 Studies of Dopaminergic Mechanisms

Given that degeneration of dopamine neurons within the substantia nigra is the pathophysiological hallmark of PD, investigators have used dopamine tracers to understand the role of dopamine in the mechanism of action of DBS (Poewe et al. 2017) (Tables 46.1, 46.2 and 46.3).

Dopamine tracers have been used to understand the *acute effects of STN stimulation on dopamine*. Apart from Nimura et al. (2005), most studies investigating dopamine receptor D2/3 availabilities have failed to show an acute change in striatal dopamine levels with STN stimulation whether patients were concomitantly off (Abosch et al. 2003; Arai et al. 2008; Thobois et al. 2003) or on (Strafella et al. 2003b) dopaminergic pharmacotherapy, regardless of the time duration after the stimulation was turned off. A recent study using [^{11}C]DTBZ showed a reduction in vesicular monoamine transporter 2 (VMAT2) availability which may be related to an increase of vesicular dopamine in the caudate nucleus, putamen, and some cortical and limbic regions (Smith et al. 2019). The inability of D2/3 studies to show dopamine changes with STN stimulation may be related (1) to its lack of sensitivity for detecting changes in endogenous dopamine; (2) to the slow washout of dopamine after stimulation cessation, which could last up to 12 h; and (3) to other neurotransmitters which may be involved (e.g., serotonin, gamma-aminobutyric acid (GABA), and glutamate) (Smith et al. 2019). A study comparing metabolic changes with STN-DBS and levodopa pharmacotherapy found that both treatments increased activity in SMA and decreased activity in the primary motor cortex. However, differences were seen: increased putaminal metabolism was only seen with levodopa, whereas prefrontal areas showed increased metabolism with STN-DBS

Table 46.1 STN-DBS studies in Parkinson's disease patients at rest

Studies	*n*	Postop time (month)	PD Med	Tracer	Contrast	Increase	Decrease
Hilker et al. (2002)	1	3 weeks	ON	[^{18}F]FDG	ON vs. OFF	B: MeFG, PCC, PCUN/OC, STG R: SMA, cCereb, iCereb L: PMC	B: PrG, rCereb L: Thal, hThal
Sestini et al. (2002)[a,b]	10	4.8	OFF	[^{99}mTc]ECD	ON vs. preop	B: MeFG, ACC, DLPFC, FPC; R: SFG	None
Antonini et al. (2003)[a,b]	13	6	NA	[^{99}mTc]ECD	ON (responder) vs. HC	Normalization of cortical areas	None
Hershey et al. (2003)[b]	13	2	OFF	[^{15}O]H_2O	ON vs. OFF	L: SN, RN, STN, Thal	B: SMA, PFC, MeFG R: STG, MTG, SPL, aCereb L: PrG, PoG, Cl, SFG
Hilker et al. (2003)	6	>4	OFF	[^{11}C]RACLO	ON vs. OFF	None	None
Hilker et al. (2004)[b]	8	4	NA	[^{18}F]FDG	ON vs. OFF	B: VL, STN R: DLPFC, OFC, IPL, MTG, LenN, Cereb, PCC L: ACC	L: Cereb
Haslinger et al. (2005)	6	16	OFF	[^{15}O]H_2O	Correlation between DBS frequencies (5–190 Hz) and metabolism	(Positive correlation) B: STN	(Negative correlation) B: PrG, MeFG, PMC
Hilker et al. (2005)	30	16	OFF	FDOPA	ON vs. preop	None	Unknown: CdN, Pu
Nimura et al. (2005)	3	6	ON	[^{11}C]RACLO	ON vs. preop	None	None
Sestini et al. (2005)[a–c]	10	5	OFF	[^{99}mTc]ECD	ON (5 mo) vs. ON (42 mo)	B: MeFG, SFG, aCereb, Po, SN, Thal, GPe; L: MFG, PrG, PoG	None

Asanuma et al. (2006)[b]	9	NA	ON	[^{18}F]FDG	ON vs. OFF	R: PCUN L: Thal, STN	B: mCereb, PrG, PoG R: Pu L: GPi, PFC (PDRP)
Li et al. (2006)[b]	5	1	OFF	[^{18}F]FDG	ON vs. preop	B: LG R: MFG, MidB L: PCUN, GP	B: IFG L: pHi
Trost et al. (2006)	6	6	OFF	[^{18}F]FDG	ON vs. OFF	Ips: PAC, PFC	Ips, contra: rPo, rMidB Ips: PrG, SMA, cerebellar vermis (PDRP)
Cilia et al. (2007)[a]	20	12	ON	[^{99}mTc]ECD	Correlation between verbal fluency performance and brain metabolism (stim ON)	(Positive correlation) L: DLPFC, ACC, CdN R: PMC	No negative correlation
Lokkegaard et al. (2007)[a]	35	12	ON	[^{123}I]FP-CIT	ON vs. preop	None	Unknown: Str
Lyoo et al. (2007)	18	2	OFF	[^{18}F]FDG	1. Correction between UPDRS score during DBS-ON and metabolism	(Positive correlation) unknown: SMA, ACC, PFC	(Negative correlation) none
Nagaoka et al. (2007)[b]	8	1	ON	[^{18}F]FDG	ON vs. OFF	R: PMC, Cereb	None
Sestini et al. (2007)[a–c]	10	5	OFF	[^{99}mTc]ECD	OFF vs. preop (5 months postop) OFF vs. preop (42 months postop)	L: SMA, PMC, PoG, MFG	None
Arai et al. (2008)	8	>4	OFF	[^{18}F]FDG, FDOPA	1. ON vs. OFF ([^{18}F]FDG) 2. ON vs. OFF (FDOPA)	1. Ips: Thal 2. None	1. Contra: GPi 2. None

(continued)

Table 46.1 (continued)

Studies	*n*	Postop time (month)	PD Med	Tracer	Contrast	Increase	Decrease
Campbell et al. (2008)	29	>2	OFF	[^{15}O]H_2O	ON vs. OFF	None	None
Hesse et al. (2008)[a]	18	12	OFF	[^{123}I]FP-CIT, [^{123}I]IBZM	1. ON vs. preop ([123I]FP-CIT) 2. ON vs. preop ([123I]IBZM)	1. None 2. Ips: Pu, CdN	1. None 2. None
Hilker et al. (2008)	12	6	OFF	[^{18}F]FDG	ON vs. OFF	Ips: STN Contra: GP	None
Hirano et al. (2008)	11	NA	OFF	[^{18}F]FDG, [^{15}O]H_2O	ON vs. OFF	None	None
Le Jeune et al. (2008)[b]	13	3	ON	[^{18}F]FDG	ON vs. preop	B: Cereb R: FG	B: LC, CC R SFG, PrG, MFG, STG
Karimi et al. (2008)[b]	48	>4	OFF	[^{15}O]H_2O	ON vs. OFF	B: Thal R: MidB	R: PMC
Cilia et al. (2009)[a,b]	40	12	ON	[^{99}mTc]ECD	ON vs. preop	B: OC, pHi R: Hi, PCUN, Cereb L: MTG	B: PMC, PrG, IFG, ACC, MFG R: SMA, SFG, PoG, GPe L: MeFG, Thal
Kalbe et al. (2009)	9	6	OFF	[^{18}F]FDG	ON vs. preop	None	B: vACC L: dACC
Pourfar et al. (2009)[b]	6	20	OFF	[^{18}F]FDG	OFF vs. preop	L: OC, PCUN R: SMC, pCereb, PoG	R: Pu, GP, Thal No change in PDRP expression
Tanei et al. (2009)[a,b]	7	10	ON	[^{123}I]IMP	ON vs. preop	B: CC, Cereb	B: MFG L: STG
Haegelen et al. (2010)[a]	6	3	ON	[^{18}F]FDG, HMPAO	1. ON vs. Preop ([^{18}F]FDG) 2. ON vs. Preop (HMPAO)	1. None 2. None	1. B: SFG 2. None

Le Jeune et al. (2010a)[b]	20	3	ON	[^{18}F]FDG	ON vs. preop	B: PCC, IFG, FG, Cereb L: MTG, pHi, MFG, OC	B: ACC, IFG, PrG, STG, PoG, MFG R: SFG, INS, MeFG L: CdN
Peron et al. (2010)[b]	13	3	ON	[^{18}F]FDG	ON vs. preop	B: Cereb R: IPL	B: ACC L: SFG
Wang et al. (2010)[b]	5	6	NA	[^{18}F]FDG	ON vs. OFF	L: MidB, Po	B: Thal, PCUN R: GPi, pCereb, SMG (PDRP)
Garraux et al. (2011)[b]	8	24	OFF	[^{18}F]FDG	ON vs. OFF	B: FPC, IFG, MFG, SFG, PrG, MTG, TPJ, IPL, PoG, CdN, Thal R: OFC, FO, pINS, AnG, SFG, MeFG, ACC, PPN L: TPo, STG, ITG, FuG, LG, MCC, CUN, GP, Cereb	None
Volonte et al. (2012)[b]	14	6	OFF	[^{18}F]FDG	ON vs. OFF	B: STN, Thal	B: Cereb
Bradberry et al. (2012)	11	24	ON	[^{15}O]H_2O	ON vs. OFF	B: SFG, OFC, OC, PCUN, FuG, INS, GP, Amy, Hi, Thal R: MeFG L: pCereb, IFG, PoG, Pu, MTG	B: pCereb, mCereb, PrG, SMA, MFG, PoG, SMG, Pu R: OC L: SFC, IFG, FuG, ITG, MTG, ACC
Hill et al. (2013)[b]	37	22.4	OFF	[^{15}O]H_2O	1. Ventral STN ON vs. ventral STN OFF 2. Dorsal STN ON vs. dorsal STN OFF	1. Ips, contra: GPi, STN, Thal 2. Ips, contra: STN, GPi	1. None 2. None

(continued)

Table 46.1 (continued)

Studies	*n*	Postop time (month)	PD Med	Tracer	Contrast	Increase	Decrease
Cao et al. (2017)[b]	8	12	OFF	[^{18}F]FDG	ON vs. preop	B: PMC, PoG, OC, SMG	B: Cereb, MFG, SFG, MeFG L: IFG, Pu (PDRP)
Smith et al. (2019)[b]	7	4–6	OFF	1. [^{11}C]DTBZ 2. [^{18}F]FDG	ON vs. preop	1. None 2. B: STG, PCUN, FG, Cereb R: pHi L: INS, IPL	1. B: PrG, Pu L: INS, STG, Amy, PCUN, IPL, CdN, Pu 2. B: CdN, STN R: Thal, Pu L: GP

Studies investigating acute (i.e., ON vs. OFF stimulation states) and long-term (i.e., postop vs. preop) effects of stimulation are listed. Clinical benefits for most patients are implicit in STN-DBS studies. *n* represents the number of patients with DBS who underwent neuroimaging. Brain areas reported to exhibit significant changes by the authors are mentioned as increase and decrease in reference to the listed contrast. However, to limit the number of abbreviations, similar areas described by different nomenclature may have been grouped under a single abbreviation with slightly less spatial specificity (e.g., middle temporal cortex was grouped under middle temporal gyrus, and thalamic subnuclei were grouped under thalamus). Most commonly, the nomenclature used to describe the areas corresponds to the terms used in the studies. *NA* not available. *PD Med* Parkinson's disease medication

[a]SPECT studies (the remainder were PET studies)

[b]This study reported a form of multiple comparison correction and was used in Figs. 46.8 and 46.9

[c]Patient overlap between these two studies

Table 46.2 Task STN-DBS studies in Parkinson's disease patients

Studies	*n*	Postop time (month)	PD Med	Tracer	Contrast	Increase	Decrease	DBS behavioral changes
Limousin et al. (1997)[a]	12	NA	OFF	$[^{15}O]H_2O$	Joystick task: effective vs. ineffective stimulation	Unknown: SMA, CC, DLPFC	None	Improvement in elbow flexion movement time
Ceballos-Baumann et al. (1999)[a]	9	>4	OFF	$[^{15}O]H_2O$	Joystick task: ON vs. OFF	Ips, contra: rSMA Ips: PMC	Ips: PrG, cSMA	Improved reaction and movement time
Strafella (2003)[a]	5	NA	OFF	$[^{15}O]H_2O$	Joystick task: Bilateral ON vs. OFF	*Contra or Ips to stimulation Ips, contra: cSMA, rSMA, GP Ips: DLPFC Contra: cACC, rACC	None	Decreased motor latency during bilateral and contralateral stimulation
Payoux et al. (2004)[a]	7	>10	OFF	$[^{15}O]H_2O$	Fist clench task: High-freq ON vs. OFF	L: STN	R: Cereb L: ACC, PrG, PoG	Improved motor symptoms (high freq)
Grafton et al. (2006)	6	4	OFF	NA	Tracking task: effective vs. ineffective stimulation	(Normalization)B: ACC R: VPMC, pCereb, IFG, SFG, CC, Pu, GP, Thal L: MeSFG, SFG, SPL, PrG, PoG, PPO	NA	Increase in extent and velocity of movement
Ballanger et al. (2009)[a]	7	47	Off	$[^{15}O]H_2O$	Go/No-Go task: ON vs. OFF	None	None	Improved motor symptoms

(continued)

Table 46.2 (continued)

Studies	*n*	Postop time (month)	PD Med	Tracer	Contrast	Increase	Decrease	DBS behavioral changes
Nozaki et al. (2013)[a]	12	32.8	OFF	[^{11}C] RACLO	Foot motion: ON vs. OFF	None	B: NAcc, CdN	Improved motor task (foot movement)
Park et al. (2015)	10		ON	[^{15}O]H_2O	1. ON: finger opposition vs. at rest 2. OFF: finger opposition vs. at rest	1. B: PrG, PoG, Cereb, CC 2. B: PrG, PoG R: SMA L: Cereb	1. Unknown: pHi 2. R: PCUN L: ITG	No difference in motor performance
Atkinson-Clement et al. (2017)	12	NA	OFF	[^{15}O]H_2O	1. Hand motion: ON vs. OFF 2. Speech production task: ON vs. OFF	1. L: PoG, IPL 2. None	1. R: Cereb L: MeFG 2. None	Improved speech and hand motion combined tasks (not in individual tasks)
Hagelweide et al. (2018)	8	NA	OFF	[^{15}O]H_2O	Serial prediction task: ON vs. OFF	R: Thal, MeOFC	None	No improvement in task
Schroeder et al. (2002)[a]	10	5	OFF	[^{15}O]H_2O	Stroop task: ON vs. OFF	L: AnG	R: ACC, Pu	Prolonged reaction time (increased Stroop effect)
Thobois et al. (2002)[a]	7	3	OFF	[^{15}O]H_2O	1. Motor imagery task: ON vs. OFF 2. Motor execution task: ON vs. OFF	1. Contra: DLPFC 2. Contra: DLPFC	1. Ips: PrG, SMA 2. Contra: SMA, PrG, IPL	Nonsignificant improvement in completion times
Schroeder et al. (2003)[a]	7	NA	NA	[^{15}O]H_2O	Fluency task: ON vs. OFF	None	R: OFC, CdN ITG, IFG, INS	Decreased verbal fluency

Burghaus et al. (2006)	1	>3	OFF	[^{15}O]H_2O	Stuttering task: ON vs. OFF	B: ACC, Cereb R: PrG L: rSMA, BA, SMA, ACC	B: PrG, SMA, DLPFC R: WA, Cereb L: BA, aINS, ACC, rSMA	Worsening stutter (bilateral stimulation)
Geday et al. (2006)	10	NA	OFF	[^{15}O]H_2O	1. ON: emotional faces vs. neutral visual stimuli 2. OFF: emotional situations vs. neutral visual stimuli	1. R: PFC 2. L: ACC	1. R: FuG, Pu, ITG L: INS2. R: ITG	Patients scored facial images as less pleasant
Herzog et al. (2006)[a]	11	NA	OFF	[^{15}O]H_2O	Full bladder: ON vs. OFF	None	L: LFG	Increased urge to void volume
Thobois et al. (2007)[a]	6	>3	OFF	[^{15}O]H_2O	Random number generation task: ON vs. OFF	R: GPi	R: ACC L: DLPFC	Decreased random number generation
Herzog et al. (2008)[a]	9	22	OFF	[^{15}O]H_2O	Full bladder: ON vs. OFF	R: INS, Thal	None	Improved urge to void (determined by self-report scales)
Narayana et al. (2009)	1	24	NA	[^{15}O]H_2O	1. ON: speech task vs. rest 2. OFF: speech task vs. rest	1. B: ACC, PCC, INS, Thal, BG, Cereb, pAuC/sAuC, OC R: SMA 2. B: PrG, ACC Unknown: SMA, PCC, INS, Thal, BG, Cereb, pAuC/sAuC, OC	1. L: SMA, PrG 2. None	Decrease in speech production perceptual ratings
Fonoff et al. (2010)	1	> 6	ON	[^{18}F]FDG	Odor exposure: ON vs. OFF	B: Thal, Str, ACC, Amy, STN L: RG	None	Return of hyposmia when stimulation turned off

(continued)

Table 46.2 (continued)

Studies	*n*	Postop time (month)	PD Med	Tracer	Contrast	Increase	Decrease	DBS behavioral changes
Dellapina et al. (2012)	8	>3	OFF	$[^{15}O]H_2O$	Pain: ON vs. OFF	R: PoG	None	Decreased VAS and NPSI score
Ventre-Dominey et al. (2014)[a]	14	>6	OFF	$[^{15}O]H_2O$	1. Spatial working memory task: ON vs. OFF 2. Nonspatial working memory task: ON vs. OFF	1. R: ACC L: INS, OFC 2. R: MTG, STG	1. R: IPL, SPL, AnG L: PCUN 2 R: pHi, IPFC L: MTG	No difference in response time in all tasks
Weiss et al. (2015)[a]	10	NA	OFF	$[^{15}O]H_2O$	Gait imagination: ON vs. OFF	L: PPN	None	Increase in walking distance, gait velocity, and stride length
(Cury et al. (2018)	12	12	ON	$[^{18}F]FDG$	Smell task improvement: ON vs. OFF	R: PMC, SMA, IPL/SMG L: MidB, aCereb	None	Improved olfactory function
Mubeen et al. (2018)	7	>2	OFF	$[^{15}O]H_2O$	Speech task: ON vs. OFF	Unknown: Cereb Global CBF	None	CBF did not have a direct role in motor speech control

Studies investigating the effects of stimulation for a given task. For task studies, behavioral changes related to the task upon stimulation are reported, and the effect of stimulation on behavioral task (i.e., interaction term) was reported if available (i.e., $(Task_{on} - Rest_{on}) - (Task_{off} - Rest_{off})$). *n* represents the number of patients with DBS who underwent neuroimaging. Brain areas reported to exhibit significant changes by the authors are mentioned as increase and decrease in reference to the listed contrast. However, to limit the number of abbreviations, similar areas described by different nomenclature may have been grouped under a single abbreviation with slightly less spatial specificity (e.g., middle temporal cortex was grouped under middle temporal gyrus, and thalamic subnuclei were grouped under thalamus). Most commonly, the nomenclature used to describe the areas corresponds to the terms used in the studies. Double line separates motor vs. non-motor tasks. *NA* not available. *PD Med* Parkinson's disease medication

[a]Studies reporting interaction term

Table 46.3 DBS studies in Parkinson's disease patients using other targets

Studies	DBS target	*n*	Postop time (month)	PD Med	Tracer	Contrast	Increase	Decrease	DBS behavioral changes
Deiber et al. (1993)	VIM	6	>4	NA	$[^{15}O]H_2O$	Effective stimulation: contra vs. Ips electrode	Contra: PrG, Thal	Contra: CC	NA
Fukuda et al. (2001a)	GPi	6	NA	OFF	$[^{15}O]H_2O$	Motor task: ON vs. OFF	B: SMA R: ACC L: PrG, PoG	None	Improved kinematic parameters of motor task
Fukuda et al. (2001b)	GPi	7	NA	OFF	$[^{18}F]$FDG	ON vs. OFF	Ips, contra: pCereb Ips: PMC	Ips: PDRP	NA
Nakajima et al. (2003)	GPi	6	NA	OFF	$[^{11}C]$NEM	Postop DBS or PVP vs. HC	None	Unknown: ACC	NA
Carbon and Eidelberg (2006)[a]	GPi	14	>12	NA	$[^{15}O]H_2O$ and $[^{123}I]$ FP-CIT	1. Correlation between motor learning and metabolism (PD, HC) 2. Correlation between motor learning and dopamine transporter (DAT) binding (PD)	1. B: BG, DLPFC, PMC, ACC, PL, OL L vPFC 2. L: DLPFC, vPFC	1. None 2. None	Improved motor learning and reference task performance
Valalik et al. (2009)	GPi	5	>6	ON	$[^{15}O]H_2O$	ON (joystick task) vs. OFF (rest)	R: SMA, PMC, aINS	L: PrG, PoG	Decrease in reaction time and movement time postop (DBS-ON and DBS-OFF). Reaction time: OFF > ON

(continued)

Table 46.3 (continued)

Studies	DBS target	*n*	Postop time (month)	PD Med	Tracer	Contrast	Increase	Decrease	DBS behavioral changes
Parker et al. (1992)	VIM	7	4	NA	$[^{15}O]H_2O$	Tremor: ON vs. OFF	Ips, contra: mCereb Contra: PrG, SMA, PrG, PoG, CdN,	None	NA
Wielepp et al. (2001)[a]	VIM	4	>1	NA	$[^{99}mTc]$ ECD	ON vs. HC	None	Ips, contra: PFC, ACC Ips: CdN, SMA, PrG	NA
Fukuda et al. (2004)	VIM	8	>12	OFF	$[^{15}O]H_2O$	ON vs. OFF	L: Br, Thal, OC, CUN, PCUN	R: aCereb, mCereb L: PrG, PoG	NA
Mure et al. (2011)	VIM	9	NA	OFF	$[^{18}F]$FDG	ON vs. OFF	B: CC R: aCereb L: Pu Unknown: CdN, PrG	R: PrG, PoG (PDRP)	NA
Strafella et al. (2008)	PPN	1	3	NA	$[^{15}O]H_2O$	ON vs. OFF	Ips, contra: Thal Ips: INS, Pu, Cereb	None	NA
Stefani et al. (2010)	PPN	6	>12	NA	$[^{18}F]$FDG	ON vs. OFF	B: IFG, DLPFC, OFC, ACC, SFG, IPL, SMG, SMA R: INS, STG L: vStr, SMA	R: PCC L: aCereb	NA

Davis et al. (1997)	GPi, VIM	9	>1	OFF	[^{15}O]H_2O	1. GPi: ON vs. OFF 2. VIM: ON vs. OFF	1. Ips: SMA, Pu, GPe, pHi 2. Ips: OC, DMPFC Contra: DLPFC	1. Contra: ACC 2. Ips: SAA Contra: mCereb, ACC, SMA	NA
Payoux et al. (2009)	GPi, GPe	5	>26	OFF	[^{15}O]H_2O	1. GPe ON vs. OFF (independent of motor task) 2. GPi ON vs. OFF (independent of motor task)	1. None 2. Ips: Pu	1. Ips: Cereb, PMC 2. Ips: PrG, PoG, PMC, SMA, SMA, ACC	Decreased rigidity and akinesia UPDRS scores (GPe) and decreased rigidity UPDRS score (GPi)
Velasco et al. (2015)	Raprl	5	>3	OFF	[^{18}F]FDG	ON vs. preop	Ips, contra: OFC, Cereb Unknown: Pu, SMA, Thal	None	NA
Mo et al. (2016)[a]	cZI	6	1 year	ON	[^{123}I] FP-CIT	1. PD DBS vs. PD control	None	Ips: CdN, Pu	No difference

Studies investigating the effects of stimulation at rest or during a task are listed. For rest studies, clinical benefits for most patients are implicit and no behavioral changes are reported. For task studies, behavioral changes related to the task upon stimulation are reported, and the effect of stimulation on behavioral task (i.e., interaction term) was reported if available (i.e., $(Task_{on} - Rest_{on}) - (Task_{off} - Rest_{off})$). *n* represents the number of patients with DBS who underwent neuroimaging. Brain areas reported to exhibit significant changes by the authors are mentioned as increase and decrease in reference to the listed contrast. However, to limit the number of abbreviations, similar areas described by different nomenclature may have been grouped under a single abbreviation with slightly less spatial specificity (e.g., middle temporal cortex was grouped under middle temporal gyrus, and thalamic subnuclei were grouped under thalamus). Most commonly, the nomenclature used to describe the areas corresponds to the terms used in the studies. Double lines separate DBS targets. *NA* not available. *PD Med* Parkinson's disease medication

[a]SPECT studies (the remainder were PET studies)

and decreased metabolism with levodopa (Hilker et al. 2002). These findings suggest that the dopamine system may be involved in the mechanisms of action of DBS.

Long-term dopamine changes from STN-DBS have also been studied with molecular neuroimaging. One study of the dopamine transporter failed to show a difference over time in dopaminergic function between PD patients with DBS and those treated medically (Lokkegaard et al. 2007). A second study similarly found annual rates of dopamine function decline in the caudate and putamen with STN-DBS to be comparable to other studies in PD patients treated medically (Hilker et al. 2005). However, a single D2 receptor study ([^{123}I]IBZM) reported an increase in receptor binding in the caudate nucleus and putamen with subthalamic stimulation between preop and 12 months after surgery (Hesse et al. 2008). This finding was confounded by the fact that many patients underwent changes in their dopaminergic medication regimen after surgery. The magnitude of the dopamine (or dopaminergic receptors) change over time due to DBS could be too small to detect in humans (Volkow et al. 1993). However, animal studies suggest that the dopamine increase with STN-DBS should be large enough to be detected with molecular neuroimaging (Bruet et al. 2001; Meissner et al. 2002). So far, dopaminergic molecular neuroimaging studies have not found evidence of a neuroprotective effect of STN-DBS on the dopamine system.

46.6.1.3 Contributions of Molecular Neuroimaging

PET and SPECT studies conducted in PD patients have confirmed distributed motor circuit engagement for various DBS targets. Prior literature reviews emphasized the inconsistency in the directionality of change in these areas, asserting this pattern of results supports the notion that DBS modulation is not merely inhibitory or excitatory (Boertien et al. 2011; Obeso et al. 2011). We have separated studies investigating acute (ON vs. OFF) from chronic (postop vs. preop) stimulation effects in order to disentangle these inconsistencies. Interestingly, our analysis revealed different patterns of activity changes: acute stimulation predominantly engaged primary motor hubs of the CSTC circuit, whereas chronic stimulation primarily induced changes in the frontoparietal cortex and cerebellum.

Acute changes with stimulation consistently engaged the motor hubs of the CSTC circuit including the precentral gyrus, thalamus, STN, and to a lesser extent the pallidum. In agreement with findings from PET and SPECT studies, increased brain activity of the STN and thalamus as well as pallidal activation support increased afferent inhibitory pallidothalamic tract activation (Hill et al. 2013; Volonte et al. 2012). Brain function changes in the CSTC circuit may be explained in the context of the direct and indirect pathways but may also arise from the hyperdirect pathway (Haslinger et al. 2005) (Fig. 46.7). Given the key role of the indirect pathway, the lack of consistent activity changes in the pallidum is surprising because STN and GPi modulation were demonstrated with electrophysiology upon STN stimulation (Hashimoto et al. 2003; Windels et al. 2000). Functional neuroimaging studies represent a final common pathway of neurochemical and other molecular mechanisms and may not be able to differentiate afferent and/or local inhibitory and/or excitatory synaptic activity. Combining PET and SPECT findings with

electrophysiology or study employing radiotracers for GABA or glutamate would be informative.

Chronic metabolic changes with STN-DBS conform to a fairly different pattern. Instead of changes within motor CSTC hubs, diffuse changes of cortical activity were observed; specifically, decreased activity in prefrontal areas and increased activity in posterior parietal areas were shown. Contrary to acute stimulation changes, subcortical structures less commonly showed chronic changes in metabolism and displayed decreased metabolism when changes were observed. Posterior parietal increase and subcortical decrease in activity are in effect normalization of the abnormal PDRP pattern in PD patients (Asanuma et al. 2006). The decrease seen in the prefrontal areas may be a result of the STN stimulation-induced decrease in compensatory striatal hyperactivity seen in PD patients (Poston et al. 2016; Smith et al. 2019). Prefrontal decreases could also be related to the known executive impairment associated with STN-DBS (Jahanshahi et al. 2000). The posterior parietal function changes may be related to the complex interplay between the prefrontal and parietal areas as well as the caudate nucleus, which are all part of the CSTC associative loop (Alexander and Crutcher 1990). Notably, the cerebellum also commonly displayed increased activity with chronic STN-DBS. Since cerebellar lesions are known to disrupt motor planning, it is plausible that the cerebellar increases seen with long-term stimulation are a result of yet another compensatory mechanism (Manto et al. 2012).

46.6.2 Other Movement Disorders

Only a handful of studies have investigated molecular neuroimaging correlates of DBS in non-PD movement disorders; these studies most often target the motor thalamus or GPi. Table 46.4 provides a comprehensive summary of published studies in DBS for dystonia, essential tremor, and other neurodegenerative disorders. The internal segment of the globus pallidus (GPi) is the most often chosen target for DBS in dystonia (Lozano et al. 2019). As observed in PD, pallidal stimulation in dystonia patients seems to engage motor cortex and SMA (Katsakiori et al. 2009; Kefalopoulou et al. 2010; Kumar et al. 1999). Owing to the lack of studies, the overall heterogeneity of the disease etiology, and different tracers used, clear statements regarding functional changes in dystonia DBS are not possible. Indeed, dystonia studies have used [^{15}O]H_2O (Detante et al. 2004; Kumar et al. 1999; Thobois et al. 2008), [^{99}mTc]ECD (Katsakiori et al. 2009; Kefalopoulou et al. 2010), and [^{123}I]IBZM (Beukers et al. 2012). Also, they used different experimental designs such as DBS-ON vs. DBS-OFF (Katsakiori et al. 2009; Kefalopoulou et al. 2010; Thobois et al. 2008) and task-based assessments (Detante et al. 2004; Kumar et al. 1999). In essential tremor, the cerebello-thalamo-cortical tremor network is thought to be dysfunctional (Hallett 2014). Molecular neuroimaging studies have primarily reported increased rCBF in the precentral gyrus, thalamus, and cerebellum, with less involvement of diffuse cortical areas such as seen with STN-DBS (Ceballos-Baumann et al. 2001; Haslinger et al. 2003; Perlmutter et al. 2002; Reich et al. 2016).

Table 46.4 DBS studies for other movement disorders

Study	Disease	*n*	DBS target	Postop time (month)	Tracer	Contrast	Increase	Decrease
Kumar et al. (1999)[a]	Dystonia	1	GPi	12 month	[^{15}O] H_2O	Joy task: ON vs. OFF	B: OC	B: DLPFC, LPMC, PrG, PoG, VLPFC, SMA, PCUN, ACC, MeTG L: STG, GP
Detante et al. (2004)	Dystonia	6	GPi	>3	[^{15}O] H_2O	Execution task: ON vs. OFF	Ips: PrG, PoG, cSMA, PL Contra: mCereb	None
Thobois et al. (2008)	Tardive dystonia (depression)	5	GPi	>6	[^{15}O] H_2O	ON vs. OFF	B: Cereb R: OC L: SPL	B: SMA L: PrG, ACC
Katsakiori et al. (2009)[b]	Dystonia	8	GPi, Voa	NA	[^{99}mTc] ECD	ON vs. OFF	None	Unknown: PrG, SMA, ACC, DLPFC, FPC
Kefalopoulou et al. (2010)[b]	Dystonia	6	GPi, Voa	6	[^{99}mTc] ECD	ON vs. OFF	None (increase seen in one patient in PrG, PMC, SMA)	Unknown: PrG, PFC
Beukers et al. (2012)[b]	Myoclonus-dystonia	3	GPi	2 years	[^{123}I] IBZM	Postop vs. preop	None	None
Moro et al. (2004)[a]	HD-chorea	1	GPi	NA	[^{15}O] H_2O	1. Low frequency: ON vs. OFF 2. High frequency: ON vs. OFF	1. B: SMA, ACC R: Cereb L: PrG, PoG, PMC 2. B: SMA, ACC R: Cereb L: PrG, PoG	1. None 2. None
Yianni et al. (2004)[b]	Senile chorea	1	GPi, Vop	>5	[^{99}mTc] ECD	1. ON (GPi) vs. OFF 2. ON (Vop) vs. OFF	1. None 2. None	1. L: Pu, CdN, upper Br 2. L: Pu, STN, upper Br

Li et al. (2012)	Chorea-acanthocytosis	2	GPi	>1	[^{18}F] FDG	Postop vs. preop	None	None
Ceballos-Baumann et al. (2001)	ET	6	VIM	>4	[^{15}O] H_2O	Effective vs. ineffective stimulation	Ips, contra: CC Ips: PrG	Ips: IFG Contra: OC
Perlmutter et al. (2002)	ET	10	VIM	15	[^{15}O] H_2O	ON vs. OFF	Ips: Thal, SMA, PrG Contra: PPL, Cereb	None
Haslinger et al. (2003)	ET	4	VIM	9.7	[^{15}O] H_2O	1. Correlation between amplitude and blood flow 2. Correlation between frequency and blood flow	(Positive correlation) 1. B: Thal, PrG, PoG 2. B: Thal, PrG, PoG	(Negative correlation) None
Reich et al. (2016)	ET	10	Thal	23	[^{18}F] FDG	Ataxia: ON vs. OFF	B: Thal R: Cereb	None
Kefalopoulou et al. (2009)[b]	TD	1	GPi	3	[^{99}mTc] ECD	ON vs. OFF	None	Unknown: PrG, PMC, SMA
Wilcox et al. (2011)	PPFG	1	PPN	5	[^{18}F] FDG	ON vs. HC	(Normalization) B: Br, Cereb	None

Studies investigating the effects of stimulation at rest or during a task are listed. For rest studies, clinical benefits for most patients are implicit and no behavioral changes are reported. For task studies, behavioral changes related to the task upon stimulation are reported, and the effect of stimulation on behavioral task (i.e., interaction term) was reported if available (i.e., $(Task_{on} - Rest_{on}) - (Task_{off} - Rest_{off})$). *n* represents the number of patients with DBS who underwent neuroimaging. Brain areas reported to exhibit significant changes by the authors are mentioned as increase and decrease in reference to the listed contrast. However, to limit the number of abbreviations, similar areas described by different nomenclature may have been grouped under a single abbreviation with slightly less spatial specificity (e.g., middle temporal cortex was grouped under middle temporal gyrus, and thalamic subnuclei were grouped under thalamus). Most commonly, the nomenclature used to describe the areas corresponds to the terms used in the studies. Double lines separate movement disorders. *NA* not available. *PPFG* primary progressive freezing of gait, *TD* tardive dyskinesia

[a]Studies reporting interaction term

[b]SPECT studies (the remainder were PET studies)

46.7 Psychiatric Disorders

The striking clinical benefits seen in movement disorder patients have provided an impetus for applying DBS to non-motor—especially psychiatric—conditions. Neuroanatomical insights have led to the expansion of the circuit-based concept of brain function to psychiatric disease, with an emphasis on major limbic hubs and connecting white matter such as the ACC, NAcc, anterior limb of the internal capsule, subcallosal region, and medial forebrain bundle. In particular, MDD, OCD, and to a lesser extent anorexia nervosa and Tourette's syndrome have been explored as potential indications for DBS intervention (Lozano et al. 2019). The brain structures targeted in each case have been selected based on animal models, neuropathology, and functional neuroimaging studies that have characterized the neuronal circuitry associated with each disorder (Fig. 46.3b). To date, the two most common psychiatric disorders studied in the context of DBS using functional neuroimaging are MDD and OCD.

46.7.1 Major Depressive Disorder

MDD encompasses the largest cohort of psychiatric patients receiving DBS. Subgenual cingulate cortex (SGC) has been targeted in the greatest number of patients to date (Hamani et al. 2011; Mayberg et al. 2005). PET neuroimaging, particularly findings laid out in a series of seminal papers showing hypermetabolism of SGC in depression and low mood states, was instrumental in defining the SGC as a DBS target for MDD (Fig. 46.4a) (Drevets et al. 1997; Mayberg et al. 1999, 2005). Although open-label studies in general have reported meaningful clinical response in 50% of SGC-DBS patients, a recent multicenter randomized sham-controlled trial of patients who were evaluated in the first 6 months of treatment did not detect statistically significant antidepressant efficacy (Holtzheimer et al. 2017). This negative outcome may have been related to clinical features of the patient population (e.g., severe chronic depression) or heterogeneous electrode positions.

46.7.1.1 Molecular Neuroimaging Findings

Most MDD functional neuroimaging studies in DBS patients have used PET [^{18}F]FDG and [^{15}O]H_2O in the resting state to investigate brain function changes associated with stimulation (Table 46.5). The majority of these molecular neuroimaging findings were reported in conjunction with behavioral assessments, which facilitates data interpretation.

Out of eight MDD studies (Table 46.5), two studies assessed acute stimulation effects by contrasting ON and OFF stimulation states (Martin-Blanco et al. 2015; Millet et al. 2014), whereas the remaining studies investigated chronic changes, typically from 3 to 12 months after surgery (Bewernick et al. 2010; Conen et al. 2018; Fenoy et al. 2018; Lozano et al. 2008; Mayberg et al. 2005; Schlaepfer et al. 2008). Both SGC and NAcc chronic stimulation yielded changes in brain activity in the cingulate cortex, thalamus, and prefrontal cortex (Bewernick et al. 2010; Conen

Table 46.5 DBS studies for psychiatric disorders

Study	Disease	*n*	DBS target	Postop time (month)	PET tracer	Contrast	Increase	Decrease	DBS behavioral changes
Mayberg et al. (2005)[a]	MDD	3 responders	SCG	6	$[^{15}O]H_2O$	Postop vs. preop	B: PrG, AnG, DLPFC R: PAG L: CC	B: SGC, hThal, INS, SFG L OFC	Reduced HDRS-17
Lozano et al. (2008)	MDD	8 responders	SCG	>3	$[^{15}O]H_2O$, $[^{18}F]$FDG	1. ON (FDG) vs. preop 2. ON (H_2O) vs. preop	1. Unknown: PFC, midCC, PCC 2. Unknown: PCC	1. B: MeFG, OFC, INS 2. B: OFC R: MeFG L: DLPFC Unknown: SGC	Improved HDRS-17
Schlaepfer et al. (2008)[a]	MDD	3	NAcc	1 week	$[^{18}F]$FDG	Postop vs. preop	B: NAcc, DLPFC, DMPFC, CC, Amy R: MTG, Hi, FuG, AnG L: Pu, aCereb	B: VLPFC, VMPFC R: SN, Thal, ITG, SMG L: ACC, aINS, CdN	Improved depression ratings
Bewernick et al. (2010)[a]	MDD	7	NAcc	7	$[^{18}F]$FDG	ON vs. preop	R: PrG	R: vsFS, MeFG, SGCC, PCC, dsFS L: PFC, Thal, CdN, Cereb	Improved HDRS-28, MADRS, and IDS-SR scores
Millet et al. (2014)[a]	MDD	4	NAcc	5	$[^{18}F]$FDG	ON vs. OFF	B: SFG R: ACC L: MeFG	B: Cereb R: PCC L: SFG, MeFG	Decrease in HDRS score in some patients

(continued)

Table 46.5 (continued)

Study	Disease	*n*	DBS target	Postop time (month)	PET tracer	Contrast	Increase	Decrease	DBS behavioral changes
Martin-Blanco et al. (2015)[a]	MDD	7	SCG	6	[^{18}F]FDG	ON vs. OFF	None	R: ACC, PMC, Pu	None
Conen et al. (2018)[a]	MDD	7	SCG/VAC/ NAcc	>3	[^{15}O]H_2O	OFF vs. preop	R: ACC	R: MeFG L: ACC, MTG, OC, STG	Some patients remitted
Fenoy et al. (2018)[a]	MDD	6	Medial forebrain bundle	>12	[^{18}F]FDG	Postop vs. preop	None	CdN	Reduced CGI scores in all patients
Nuttin et al. (2003)[a]	OCD	3 responders	ALIC	>3	[^{18}F]FDG	ON vs. preop	B: Str, OC R: FG, MTG, STG	B: FG	Reduced Y-BOCS
Abelson et al. (2005)	OCD	3	ALIC	3 weeks	[^{18}F]FDG	ON vs. OFF	Unknown: OFC	None	Improvement in OCD and depression symptoms (Y-BOCS and HAM-D)
Rauch et al. (2006)[a]	OCD	6	VC/VS	3	[^{15}O]H_2O	ON high frequency vs. OFF	R: MeOFC, CC, Pu L: GP	None	Improved Y-BOCS
Le Jeune et al. (2010b)[a]	OCD	10	STN	6	[^{18}F]FDG	ON vs. OFF	None	L: CC, MeFG	Improved Y-BOCS
Tsai et al. (2012)	OCD	4	VC/VS	3	[^{18}F]FDG	ON vs. HC	B: VS R: SN	B: pHi L: ACC, Cereb	Improved OCD, HAM-D, and GAF scores
Figee et al. (2014)[b]	OCD	15	NAcc	12	[^{123}I] IBZM	ON vs. OFF	B: Pu	None	Improved Y-BOCS, HDRS, HARS scores

Suetens et al. (2014)[a]	OCD	16	VC/VS	68 days	[^{18}F]FDG	OFF vs. preop	R: CdN, Thal	None	Improved Y-BOCS and HAM-D
Dougherty et al. (2016)[a]	OCD	6	VC/VS	5 years	[^{15}O]H_2O	1. Ventral ON vs. OFF 2. Dorsal ON vs. OFF	1. R: dACC 2. B: GP R: Str L: Thal	None	Reduced depressive symptom severity
Goethals et al. (2008)[b]	TS	1	Thal	12	[^{99}mTc] ECD	ON vs. OFF	Ips, contra: APFC, OFC Con: DLPFC, VLPFC, LTG	None	NA
Kuhn et al. (2012)	TS	3	Thal	6 month	[^{18}F]FP	ON vs. OFF	Ips: Thal Unknown: Pu	Contra: Thal	Improved YGTSS score
Haense et al. (2016)[b]	TS	5	GPi or CM/Voi	>3	[^{99}mTc] ECD	1. GPi vs. preop 2. CM/Voi vs. preop	1. None 2. R: SMG L: PrG, PoG, MFG	1. B: MTG, Pu, Cereb R: Thal, CdN, INS, IFG, Hi L: PAL2. R: CdN, STG, MTG L: IFG	Improved YGTSS score in stimulation and sham groups
Vernaleken et al. (2009)	TS	1	STN	6 month	[^{18}F]FP	ON vs. OFF	None	B: Thal	Improved YGTSS score
Lipsman et al. (2013)	AN	6	SCG	6	[^{18}F]FDG	Postop vs. preop	R: MTG, ITG, PCUN, SMG, IPL L: PoG, CUN	B: MeFG, INS R: ACC, SGC L: CdN, Cl, mCereb	Decreased BMI
Zhang et al. (2013)	AN	4	NAcc	>3	[^{18}F]FDG	ON vs. preop	None	B: LenN, Hi, IFG	NA

(continued)

Table 46.5 (continued)

Study	Disease	*n*	DBS target	Postop time (month)	PET tracer	Contrast	Increase	Decrease	DBS behavioral changes
Heldmann et al. (2012)	AA	1	NAcc	18	[^{15}O]H_2O	ON vs. OFF	B: IFG, Cereb, FG R: Thal, OC, PoG, CUN L: MeGP, MTG, STG, TG, OC, FuG, OC, MFG	None	Slower and less risky choices
Giordano et al. (2016)	IED	1	VC/VS	22	[^{18}F]FDG	ON vs. preop	L: IFG	L: IFG, DLPFC, ITG, Un, FuG, TG, Amy	Reduced rage attacks

Studies investigating acute (i.e., ON vs. OFF stimulation states) and long-term (i.e., postop vs. preop) effects of stimulation are listed. Behavioral changes from stimulation are reported. *n* represents the number of patients with DBS who underwent neuroimaging. Brain areas reported to exhibit significant changes by the authors are mentioned as increase and decrease in reference to the listed contrast. However, to limit the number of abbreviations, similar areas described by different nomenclature may have been grouped under a single abbreviation with slightly less spatial specificity (e.g., middle temporal cortex was grouped under middle temporal gyrus, and thalamic subnuclei were grouped under thalamus). Most commonly, the nomenclature used to describe the areas corresponds to the terms used in the studies. Double lines separate psychiatric disorders. *AA* alcohol addiction, *AN* anorexia nervosa, *IED* intermittent explosive disease, *NA* not available

[a]This study reported a form of multiple comparison correction and was used in Fig. 46.10 and 46.11

[b]SPECT studies (the remainder were PET studies)

et al. 2018; Lozano et al. 2008; Mayberg et al. 2005; Schlaepfer et al. 2008). In one study (n = 6) that stimulated the medial forebrain bundle, significant metabolism decrease in the caudate nucleus was found when comparing ON and OFF stimulation conditions (Fenoy et al. 2018). MDD studies with stringent statistics showed a similar pattern, as well as highlighted the predominant prefrontal increase in brain function (Bewernick et al. 2010; Conen et al. 2018; Fenoy et al. 2018; Martin-Blanco et al. 2015; Mayberg et al. 2005; Millet et al. 2014; Schlaepfer et al. 2008) (Fig. 46.10).

46.7.1.2 Contributions of Molecular Neuroimaging

Functional neuroimaging studies following DBS for MDD have demonstrated that local stimulation—similar to DBS for movement disorders—exerts much of its

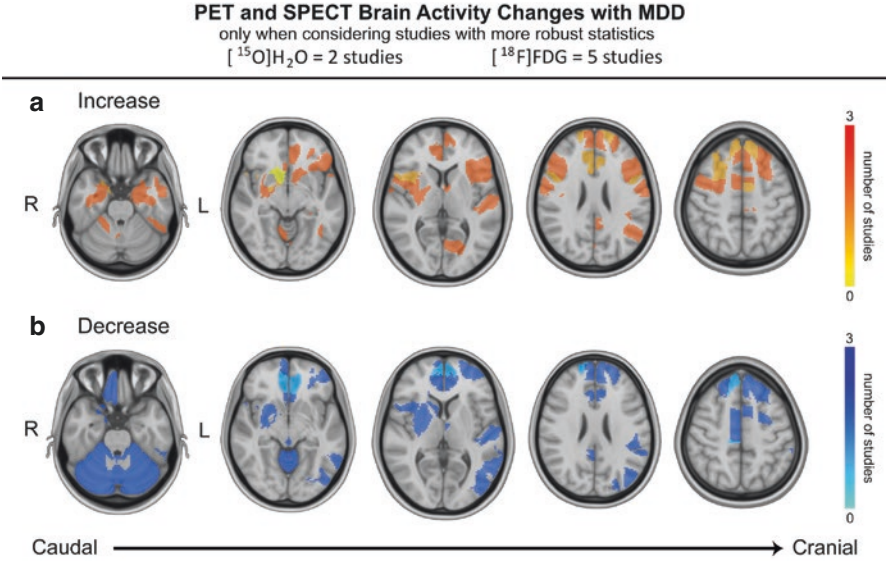

Fig. 46.10 Diagrammatic summary of activity changes in MDD. Only studies assessing either acute or long-term changes with stimulation (studies with ON vs. OFF or postop vs. preop in Table 46.5) and using a form of multiple comparison correction were included to maintain robustness of reported brain regions (studies labeled with [c] in Table 46.5). First, brain regions were obtained from spatial parcellation according to published atlases (cortical, An Atlas of Intrinsic Connectivity of Homotopic Areas (Joliot et al. 2015); subcortical, Ewert et al. (2018); brain stem, Harvard Ascending Arousal Network Atlas (Edlow et al. 2012); cerebellum, Diedrichsen et al. (2009)). Then, regions were weighted according to the number of studies reporting significant changes in each region. To decide which parcellated brain areas from the atlases would be selected, we used in order of priority (1) visual representation, (2) reported coordinates, and (3) naming of areas with activation available in studies. For large activation areas, multiple parcellated brain areas were selected. Areas of brain activity changes were then overlaid on select MRI (T1-weighted Montreal Neurological Institute brain) axial images. Across studies, brain regions with an increase in activity (hot colors) are shown in (**a**), whereas brain regions with significant decrease in activity (cool colors) are shown in (**b**). Color bars represent the number of studies

effect at the network level. The specificity of the engaged network is reflected by metabolic changes in a number of regions implicated in the disorders in question.

In MDD, increased SGC activity has been associated with sadness. Reduction of SGC metabolic activity is seen in response to effective pharmacological treatment with antidepressants (Mayberg et al. 2000). SGC-DBS also decreases metabolism in SGC, supporting the concept that DBS normalizes aberrant circuitry (Lozano et al. 2008; Mayberg et al. 2005). The ACC is a key player in emotional processing; its ventral aspect, the SGC, is primarily implicated in negative affect, while its dorsal section has been associated with positive emotional processing (Amodio and Frith 2006; Koski and Paus 2000; Margulies et al. 2007). Monoamine dysregulation, especially of the serotonin system, has also been implicated in MDD pathogenesis. In some studies, serotonin receptor binding (5-HT1A) is decreased in the mesiotemporal cortex in depressed patients (Savitz and Drevets 2013). In general, a visceromotor network comprising the prefrontal cortex, ACC, thalamus, caudate, and putamen demonstrates a relative hypermetabolism in the depressed state relative to the treated state (Drevets 2007; Drevets et al. 2008). Pharmacological and electroconvulsive therapy both tend to normalize metabolism in these areas (Goldapple et al. 2004; Mayberg et al. 2000; Nobler et al. 2001). Most PET and SPECT studies show that DBS for MDD also engages these aforementioned brain regions.

46.7.2 Obsessive-Compulsive Disorder

Although less commonly treated with DBS than MDD, OCD was among the first psychiatric indication to be investigated for DBS. While capsulotomy was aimed at the destruction of fronto-striatal and fronto-thalamic fibers, DBS of the anterior limb of the internal capsule was proposed as a reversible alternative (Nuttin et al. 1999). Interestingly, this target has now been refined to be more ventral (i.e., ventral striatum) and posterior (i.e., anterior commissure) than the originally defined target (Greenberg et al. 2010; Raymaekers et al. 2017). Other groups have also targeted the ventromedial associative region of the STN (Mallet et al. 2008). Most of these targets have demonstrated efficacy to some degree, although randomized, sham-controlled trials have not yet been completed. Although mostly the anterior limb of the internal capsule, thalamus, STN, and NAcc have been studied with PET and SPECT, many other brain structures including the medial forebrain bundle (Coenen et al. 2017), inferior thalamic peduncle (Lee et al. 2019), and bed nucleus of stria terminalis (Nuttin et al. 2013) have been targeted in OCD patients.

46.7.2.1 Molecular Neuroimaging Findings

Similar to MDD studies, most OCD functional neuroimaging studies in DBS patients have investigated brain activity changes associated with stimulation and provided behavioral outcomes (Table 46.5).

Increased activity in the striatum and frontal lobes was generally associated with thalamic stimulation in patients with OCD (Dougherty et al. 2016; Nuttin

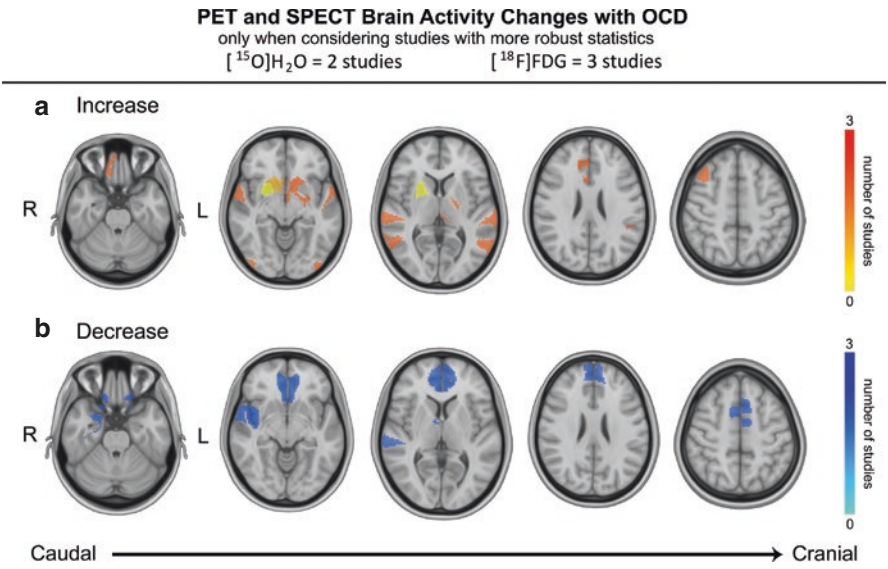

Fig. 46.11 Diagrammatic summary of activity changes with long-term OCD. Only studies assessing either acute or long-term changes with stimulation (studies with ON vs. OFF or postop vs. preop in Table 46.5) and using a form of multiple comparison correction were included to maintain robustness of reported brain regions (studies labeled with [a] in Table 46.5). First, brain regions were obtained from spatial parcellation according to published atlases (cortical, An Atlas of Intrinsic Connectivity of Homotopic Areas (Joliot et al. 2015); subcortical, Ewert et al. (2018); brain stem, Harvard Ascending Arousal Network Atlas (Edlow et al. 2012); cerebellum, Diedrichsen et al. (2009)). Then, regions were weighted according to the number of studies reporting significant changes in each region. To decide which parcellated brain areas from the atlases would be selected, we used in order of priority (1) visual representation, (2) reported coordinates, and (3) naming of areas with activation available in studies. For large activation areas, multiple parcellated brain areas were selected. Areas of brain activity changes were then overlaid on select MRI (T1-weighted Montreal Neurological Institute brain) axial images. Across studies, brain regions with an increase in activity (hot colors) are shown in (**a**), whereas brain regions with significant decrease in activity (cool colors) are shown in (**b**). Color bars represent the number of studies

et al. 2003; Suetens et al. 2014). A study with NAcc stimulation in patients with OCD found an increase in the level of striatal dopamine as well as clinical improvement with stimulation (Figee et al. 2014). Studies with robust statistics generally demonstrated frontal lobe decrease in activity, albeit less diffuse than in MDD, involving mostly the medial and basal frontal areas. These studies also showed changes in metabolism in the striatum (Dougherty et al. 2016; Le Jeune et al. 2010b; Nuttin et al. 2003; Rauch et al. 2006; Suetens et al. 2014) (Fig. 46.11). Rather than activity changes, a single study investigated striatal dopamine changes with NAcc-DBS. The authors found an increase in striatal dopamine release with acute and chronic stimulation (1 year after DBS surgery) suggested by decreased D2/3 receptor availability and increased plasma levels of homovanillic acid (Figee et al. 2014).

46.7.2.2 Contributions of Molecular Neuroimaging

Regions including the thalamus, ACC, and frontal lobes that have been implicated in OCD are also regions being modulated by DBS (Graybiel and Rauch 2000; Saxena et al. 1998; Whiteside et al. 2004). The hypermetabolic orbitofrontal cortex, which is a hallmark of OCD, is reduced with DBS (Robbins et al. 2019; Saxena et al. 1998) (Fig. 46.11).These findings support a major role for the dysfunction of the limbic circuit in OCD pathophysiology and show that DBS effectively modulates this pathway.

PET and SPECT findings in OCD (and other psychiatric disorders) support the notion that various DBS targets for psychiatric disorders represent key nodes in the same affective regulatory circuit. This concept of modulating different hubs belonging to the same circuit to achieve similar benefits was suggested in PD with STN and GPi-DBS. The more numerous and diversified DBS targets for psychiatric disorders reinforce this emerging idea. Stimulation of different brain targets for OCD seems to provide clinical benefits and modulate brain activity in similar areas such as the striatum, CC, and frontal lobes. Although different targets engaged similar areas to some degree, it is also plausible that each target provides slightly different benefits. For example, stimulation of most OCD targets seems to improve OCD symptoms as measured by commonly used scales such as Yale-Brown Obsessive-Compulsive Scale. Including other scales (e.g., Hamilton Depression Rating Scale), measuring different aspects of the disorder phenotypes (i.e., depression in OCD) may help inform the detailed benefits provided by each target. A thorough knowledge of symptom-specific networks could open the door to individualized phenotype-based DBS targeting.

46.7.3 Other Psychiatric Disorders

Findings in other psychiatric disorders including Tourette's syndrome and anorexia nervosa are summarized in Table 46.5. A study using [^{99}mTc]ECD to investigate brain function changes in Tourette's syndrome demonstrated increased activity in the superior and middle temporal gyri with either thalamic or GPi stimulation; this was associated with clinical improvements (Haense et al. 2016). Increased prefrontal activity was also noticed with thalamic stimulation inducing alternate personality state in a Tourette's syndrome patient (Goethals et al. 2008). Increased thalamic dopaminergic transmission was suggested in two studies due to decrease D2/3 receptor availability (Kuhn et al. 2012; Vernaleken et al. 2009). Interestingly, thalamic stimulation was used in one study, whereas STN stimulation was used in the second study. Both anorexia nervosa PET [^{18}F]FDG studies showed that DBS normalizes the activity in disease-implicated areas: SGC-DBS was shown to reverse the abnormalities seen in the anterior cingulate, insula, and parietal lobe (Lipsman et al. 2013), whereas hypermetabolism in the frontal lobe, hippocampus, and lentiform nucleus was decreased after NAcc-DBS (Zhang et al. 2013).

46.8 Cognitive Disorders

46.8.1 Alzheimer's Disease

Alzheimer's disease (AD) is the most common neurodegenerative disease and has a significant socioeconomic burden (Scheltens et al. 2016). Our understanding of its genetics and neuropathological hallmarks has improved in recent years. Furthermore, neuroimaging findings have identified the topography of dysfunctional brain areas in AD as well as characterize abnormalities which may eventually be used as biomarkers (Femminella et al. 2018). Although the structures of the memory circuits are affected most severely, pathological changes such as brain atrophy and change in brain metabolism can be seen globally in AD. Despite these advances, the therapeutic options remain limited. Pharmacotherapies augmenting acetylcholine availability are the mainstay of treatment. Additional experimental therapies aiming at reversing neuropathological abnormalities including amyloid plaques and tau protein accumulation are subject to extensive preclinical and clinical investigations (Graham et al. 2017).

Therapeutic modulation of the limbic and memory circuits has been a recent focus of DBS studies. Several targets have been investigated in humans including the fornix, entorhinal cortex, and nucleus basalis of Meynert (NBM) (Kuhn et al. 2015; Lozano et al. 2016) (Fig. 46.3c). The majority of studies have involved the fornix and have consistently shown sustained cortical metabolic activity in AD patients (Laxton et al. 2010; Lozano et al. 2016). The one randomized, double-blind study targeting the fornix (the main hippocampal inflow and outflow tract) identified an interaction between patient age and treatment outcomes, suggesting that older patients may be more likely to benefit from this treatment (Lozano et al. 2016). As with other DBS indications, AD patient selection (including such variables as age and severity of pathology) will likely be of paramount importance for optimizing treatment outcomes.

46.8.1.1 Molecular Neuroimaging Findings

Functional neuroimaging studies in AD DBS have used PET [18F]FDG to investigate the biological underpinnings of electrical stimulation in patients in the resting state (Table 46.6). Fornix stimulation increased metabolism mainly in the parietal and temporal lobes. Mesial temporal lobe structures such as the hippocampus also demonstrated increased metabolic activity (Fontaine et al. 2013; Lozano et al. 2016). Areas of the default mode network including the posterior cingulate cortex and precuneus also showed increased activity (Laxton et al. 2010; Smith et al. 2012). Importantly, the increase in metabolism was correlated with less decline in cognitive function. Also, increased functional connectivity in cortical-limbic networks was observed. A correlation between the nucleus basalis metabolism and cognitive scores was found when that structure was stimulated; no other significant change in metabolic activity was reported (Kuhn et al. 2015). Given that few studies listed in Table 46.6 used a form of multiple comparison correction, no diagrammatic representation was generated for cognitive disorders. To date, no molecular imaging human studies assessed the effects of stimulation on amyloid plaques or tau proteins.

Table 46.6 DBS studies for cognitive disorders

Study	Disease	*n*	DBS target	Postop time (month)	Tracer	Contrast	Increase	Decrease	DBS behavioral changes
Scharre et al. (2018)	AD	3	VC/VS	>4 weeks	[^{18}F] FDG	ON vs. OFF	Unknown: OFC, VMPFC, DLPFC	None	Activation only seen in responders (2/3 patients)
Laxton et al. (2010)[a]	AD	6	Fornix	>1	[^{18}F] FDG	ON vs. preop	B: PrG, PoG, STG, PCUN, IPL, mCereb R: PrG, LG L: MTG, PCC, Cl, Cereb	R: IFG L: ACC, MFG	Worsening of ADAS-cog score over 12 months
Smith et al. (2012)	AD	6	Fornix	>1	[^{18}F] FDG	Correlation between ADAS-cog score and metabolism	(Positive correlation) B: PrG, OC, Pu, Thal, cuneus R: PoG	(Negative correlation) B: ACC, SFG, MeFG, STG, PCUN, PCC, mCereb R: IFG, INS, IPL, SMG L: MTG, FuG	Worsening of ADAS-cog score
Fontaine et al. (2013)	AD	1	Fornix	6	[^{18}F] FDG	ON vs. preop	B: MeTG	None	Husband reported improvement in daily functioning, behavior, and mood
Kuhn et al. (2015)	AD	4	Nucleus basalis	12	[^{18}F] FDG	Correlation between ADAS-cog and MMSE score and metabolism	(Positive correlation) R: NuB	None	Nonsignificant worsening of ADAS-cog score after 12 months

Lozano et al. (2016)[a]	AD	42	Fornix	6	[^{18}F] FDG	1. ON (6 months postop) vs. OFF 2. ON (12 months postop) vs. OFF	1. Unknown: PrG, PoG, TAC, Hi, PAC, OC, Cereb 2. None	1. None 2. None	No difference in ADAS-cog 13 and CDR-SB sores

Studies investigating acute (i.e., ON vs. OFF stimulation states) and long-term (i.e., postop vs. preop) effects of stimulation are listed. Behavioral changes from stimulation are reported. *n* represents the number of patients with DBS who underwent neuroimaging. Brain areas reported to exhibit significant changes by the authors are mentioned as increase and decrease in reference to the listed contrast. However, to limit the number of abbreviations, similar areas described by different nomenclature may have been grouped under a single abbreviation with slightly less spatial specificity (e.g., middle temporal cortex was grouped under middle temporal gyrus, and thalamic subnuclei were grouped under thalamus). Most commonly, the nomenclature used to describe the areas corresponds to the terms used in the studies. *NA* not available

46.8.1.2 Contributions of Molecular Neuroimaging

Insights provided by PET [^{18}F]FDG have been instrumental in identifying the functional neuroanatomical changes associated with AD and monitoring the effects of DBS as a treatment for AD. Neuroimaging findings have consistently demonstrated a pattern of functional and morphometric change in patients with AD involving primarily the parietal and temporal lobes. These changes include temporal-parietal hypometabolism, decreased functional connectivity, and atrophy (Ferreira and Busatto 2011; Frisoni et al. 2010). PET findings associated with DBS of the hippocampal outflow tract (i.e., the fornix) demonstrated network-wide metabolic effects including persistent (1 year after DBS surgery) increased metabolism in the parietal and temporal lobes as well as in the mesial temporal lobe structures which are crucial components of the memory circuit (Laxton et al. 2010; Lozano et al. 2016; Smith et al. 2012). These PET findings confirm network engagement and target specificity. Interestingly, fornix-DBS also seems to increase default mode network (DMN) activity, which is known to be dysfunctional in AD patients (Greicius et al. 2004; Sperling et al. 2009). Similar to psychiatric disorders, molecular neuroimaging was able to substantiate stimulation-induced metabolic changes within the faulty circuits that seem to be of relevance in AD DBS (viz., the memory circuit). Understanding DBS mechanism of action with selective radiotracers (e.g., beta-amyloid, tau, muscarinic, or nicotinic receptors) may also inform the development of more effective treatments. Furthermore, identifying pattern of metabolic changes in AD may help refine patient selection and serve as predictors of response (Smith et al. 2012).

As beta-amyloid plaque and tau protein accumulation are neuropathological hallmarks of AD and radiotracers for these proteins are available, studies could be performed to determine whether DBS decreases or stabilizes their accumulation over time. Preclinical studies have shown the neurobiological effects of DBS on temporal lobe structures and AD pathology. Chronic entorhinal cortex stimulation in a mouse model of AD decreased beta-amyloid plaque and tau protein accumulation in the hippocampus and prefrontal cortex (Mann et al. 2018). Further, rodent studies reported rapid modulation of neurotrophic factors and markers of synaptic plasticity in the hippocampus with fornix-DBS (Gondard et al. 2015).

46.9 Other DBS Indications

Since DBS has shown therapeutic modulation of specific circuits hypothesized to underlie neurobiological disorders, it is being investigated for multiple other disorders. Indications include chronic pain, traumatic brain injury, and headache. Notably, hypothalamic DBS for cluster headache provides significant improvement in headache frequency, and the selection of the target was informed by PET studies that identify areas of increased hypothalamic metabolism during induced headaches (May et al. 1998) (Fig. 46.4c). For these less common indications and targets, the sample sizes are usually small and heterogeneous. Table 46.7 summarizes the molecular neuroimaging studies for these indications.

Table 46.7 DBS studies for other disorders

Study	Disease	*n*	DBS target	Postop time (month)	PET tracer	Contrast	Increase	Decrease	DBS behavioral changes
Duncan et al. (1998)	Pain	5	Thal	>36	$[^{15}O]H_2O$	ON vs. preop	Ips: aINS, Thal, LenN, IC	None	Satisfactory pain relief following DBS
Davis et al. (2000)	Pain	5	Thal	>4	$[^{15}O]H_2O$	ON vs. OFF	Ips: GP, IC Contra: ACC	Ips, contra: IPL Ips: OC, ITG, PrG Contra: sAuC, OC, Cereb	None
Kupers et al. (2000)	Pain	1	Thal	NA	$[^{15}O]H_2O$	ON vs. OFF	R: VMPFC L: Amy, aINS	None	Complete reduction of pain following DBS
Pereira et al. (2007)	Pain	3	VPL, PVG	5	HMPAO	1. VPL-ON vs. VPL-OFF 2. PVG-ON vs. PVG-OFF 3. VPL, PVG-ON vs. PVG-OFF	1. Ips, contra: PVG, Thal Contra: OC 2. Ips, contra: PVG, Thal Ips: INS, LenN Contra: LTG, anterior subcortical area 3. Ips, contra: PVG, Thal, OC	1. Ips, contra: LenN, PTC Ips: LTG, OC, SPL, OFC Contra: PrG, PoG 2. Ips, contra: PrG, PoG, Po, MidB, Thal Ips: LenN Contra: LTG, PVG, anterior subcortical area, DFG 3. Ips, contra: LTG, PVG Ips: SPL, LTG, INS Contra: anterior subcortical area, PTC, OC, ACC	Reduced pain

(continued)

Table 46.7 (continued)

Study	Disease	*n*	DBS target	Postop time (month)	PET tracer	Contrast	Increase	Decrease	DBS behavioral changes
Sims-Williams et al. (2017)	Pain	5	PAG	7	[^{11}C]DPN, [^{15}O]H_2O	1. ON vs. OFF [^{11}C] DPN 2. ON vs. OFF [^{15}O] H_2O	1. None 2. None	1. PAG 2. None	None
Rezai et al. (2016)	TBI	4	NAcc	2 years	[^{18}F]FDG	Correlation between cognitive score and brain metabolism	None	(Negative correlation) B: MeFG, aINS, NAcc R: Thal L: OFC, MFG, IFG, ACC, ITG	Negative correlation between cognitive score and brain metabolism
Lemaire et al. (2018)	TBI	5	mPal	5	[^{18}F]FDG	ON vs. preop	Unknown: DMN	None	Increased internally oriented cortex activation following low-frequency DBS
May et al. (2006)	HA	10	hThal	>2 years	[^{15}O]H_2O	ON vs. OFF	Contra: aINS Ips: hThal, Thal, primary PoG, PCUN, ACC, TN Unknown: ITG, PCC, aINS, mCereb, MTG	Ips, contra: ITG Unknown: SFG, MTG, PCC	Improved headache frequency

Studies investigating acute (i.e., ON vs. OFF stimulation states) and long-term (i.e., postop vs. preop) effects of stimulation are listed. Behavioral changes from stimulation are reported. *n* represents the number of patients with DBS who underwent neuroimaging. Brain areas reported to exhibit significant changes by the authors are mentioned as increase and decrease in reference to the listed contrast. However, to limit the number of abbreviations, similar areas described by different nomenclature may have been grouped under a single abbreviation with slightly less spatial specificity (e.g., middle temporal cortex was grouped under middle temporal gyrus, and thalamic subnuclei were grouped under thalamus). Most commonly, the nomenclature used to describe the areas corresponds to the terms used in the studies. Double lines separate the disorders. *HA* headache, *NA* not available. *TBI* traumatic brain injury

46.10 Limitations

The DBS literature has several limitations. Patient demographics, etiology, disease duration, and dominant disease phenotype vary considerably across studies. Moreover, selection of appropriate patient candidates is particularly challenging in psychiatric disorders as there is a lack of consensus on the definition of treatment resistance in many conditions. Patient selection is also challenging in AD in which the optimal target population is still being established. Also, the medication status varies across studies, which is particularly relevant in PD studies given the striking clinical improvements after dopaminergic medication intake and the dose reductions observed after DBS surgery. Most studies involving PD patients include an OFF-medication period of 12 h before neuroimaging data acquisition. However, it is also plausible that chronic pharmacotherapy has long-lasting influences on brain responses. Cross-study comparisons of imaging findings are thus hampered by considerable differences between study populations and the limited number and small sample size of studies conducted to date.

Data regarding electrode position and the circuitry being stimulated is not typically reported and represents an important limitation when interpreting DBS clinical and neuroimaging studies. This data is of paramount importance as targets are often in close proximity to other eloquent structures that might account for symptom improvements. For example, SGC (an MDD target) is surrounded by many white matter bundles including the forceps minor and uncinate fasciculus (Riva-Posse et al. 2018). A detailed description of electrode position is particularly pertinent in psychiatric conditions because—unlike in the case of movement disorder DBS—intraoperative electrophysiological monitoring (i.e., microelectrode recordings) is not generally conducted during psychiatric DBS surgery. Detailed position of the active contact (and DBS settings) will provide a detailed understanding of the neural structures being stimulated (Boutet et al. 2019a).

Another issue is the insufficient details regarding the stimulation programming. Optimization of stimulation parameters in psychiatric DBS is particularly challenging owing to the lack of objective biomarkers to verify patient response and the delayed onset of response which may take several weeks or months (Lozano and Lipsman 2013). Programming algorithms and whether or not patients are deemed optimized based on established scales should be included in publications. In fact, the limited successes in clinical trials for psychiatric disorders have been partly attributed to suboptimal programming. In psychiatric and cognitive disorders, the outcomes are more complex, and approaches are being developed to determine sensitive outcome measures (Kucewicz et al. 2018). While optimization status is seldom reported in PD studies, presumably because most patients benefit from the treatment, the programming process can also take months to achieve optimal symptom control. There may be variability in symptom control between patients, all of which should thus be reported in detail (Picillo et al. 2016). In addition, the lack of comparisons between effective and ineffective stimulation is a limitation. Indeed, it becomes difficult to differentiate areas with artifactual metabolic changes that are not clinically relevant from those providing clinical benefits.

Neuroimaging data in response to stimulation would be highly informative if multiple clinical outcomes were reported to untangle the meaning of the pattern of changes seen. Indeed, the common sole assessment of motor changes in PD studies is problematic since STN stimulation is known to have widespread connections and effects. Similarly, psychiatric and cognitive disorders are known to have multiple comorbidities that should be taken into account into clinical outcomes. In other words, neuroimaging findings may not be entirely attributable to a single measured behavioral change. Including multidimensional clinical outcomes (e.g., motor, mood, cognition assessments) would help with data interpretation.

Finally, there is a specific caveat when interpreting functional neuroimaging data for PD and movement disorders in general. DBS leads to a change in clinical state (e.g., decreased rigidity or tremor), introducing a possible confound for signal interpretation. It is therefore difficult to differentiate whether the observed brain response was a direct DBS-driven effect rather than a consequence of clinical improvement due to the stimulation itself.

46.11 Future Directions

As emphasized throughout this chapter, DBS studies are associated with experimental variables that should be taken into consideration when reporting the results (e.g., medication status, electrode location, programming optimization status). Guidelines to standardize data in DBS publications have been published (Vitek et al. 2010). Similarly, we also recommend a minimal set of required data specific to DBS studies including neuroimaging, which are necessary to facilitate the interpretation and comparison of results across DBS studies (Fig. 46.12).

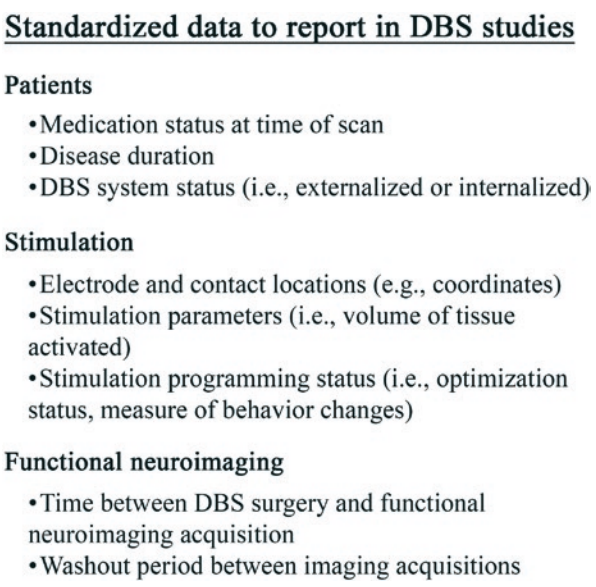

Fig. 46.12 Guidelines for data reporting in DBS neuroimaging studies. Standardized data reporting in DBS neuroimaging studies should be followed to improve experimental design, data interpretation, and comparison across studies

Most DBS patient samples from a single institution are unlikely to be sufficient to permit recruitment of an ideal and homogeneous patient cohort. Experiments are thus usually associated with numerous limitations related to sample size that constrain their generalizability. As the number of patients with DBS grows and as large-scale clinical trials are increasingly incorporating functional neuroimaging, the enabled larger sample size should enhance data analysis and interpretation. Also, multidimensional outcome assessments and novel network analysis methods (e.g., scaled subprofile modeling and partial least squares) should also be entertained to improve our ability to detect results and improve reproducibility across studies (Krishnan et al. 2011; Spetsieris and Eidelberg 2011). Furthermore, methodological guidelines have been developed (e.g., the Alzheimer's Disease Neuroimaging Initiative) to standardize imaging acquisition and to combine data for analysis across institutions.

Reporting precise electrode location will inform the slight variation of neural substrates being stimulated across patients. Commercially available and open-source software offer a method pipeline to accurately locate electrodes on CT or MRI (Horn et al. 2019). Importantly, recent neuroimaging advances have also enabled comparison of stimulation across patients: (1) precise transformation of patients' brain into standardized brain space (i.e., nonlinear normalization to Montreal Neurological Institute brain template), (2) DBS electrode localization, and (3) estimation of the volume of tissue activated (VTA) (Ewert et al. 2019; Horn et al. 2019; McIntyre et al. 2004) (Fig. 46.13). Easy-to-use imaging analysis

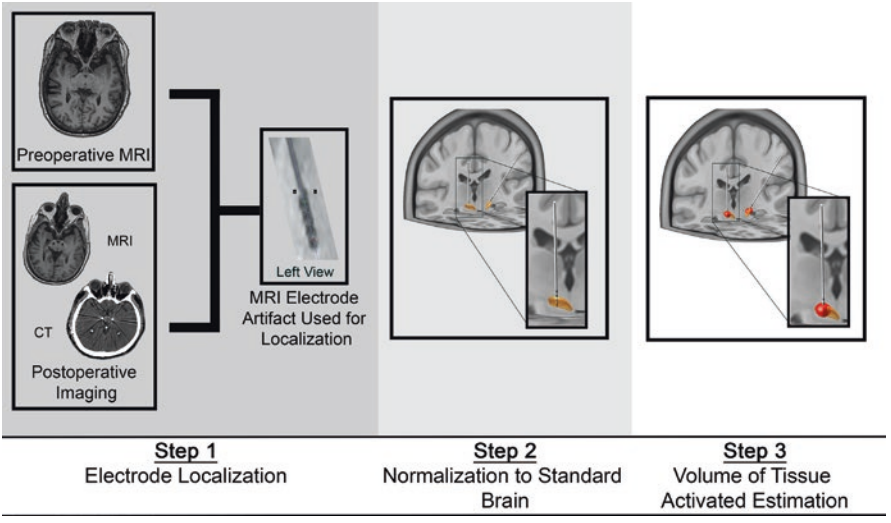

Fig. 46.13 Pipeline for electrode localization. Step 1: The electrodes are localized on postoperative imaging using the metallic artifact. Step 2: To enable group analysis, electrode positions are transformed into standardized brain space (Montreal Neurological Institute brain) using preoperative imaging (i.e., normalization). The subthalamic nucleus is shown in shaded orange. Step 3: Volume of tissue activated (shaded red) is computed based on the programming settings

pipelines have been developed to streamline this process. The variations in stimulated neural substrates across patients can be taken into account by incorporating electrode positions or alternatively distance to a target as covariates may improve the analysis. Alternatively, recent studies tend to compute VTA, thought to be a more accurate measure to compare differences of stimulation across patients.

In summary, the majority of functional neuroimaging studies have focused on PET glucose metabolism studies as an outcome. One of the main advantages of PET and SPECT is the experimental versatility that is afforded by the wide range of tracers available. Future MDD or anorexia studies investigating network-level serotonin changes (e.g., 5-HTR tracers) upon stimulation would further inform DBS mechanism of action as well as pathophysiology.

Owing to technological advancements in neuroimaging and DBS hardware, many challenges of performing MRI in patients with neurostimulators have been partially overcome. Recent studies, however, have demonstrated the feasibility of safe 3 T MRI (and fMRI) using a high-resolution body-transmit coil—the contemporary gold standard for clinical and research MRI—in patients receiving DBS, under specific conditions (Boutet et al. 2019b, c; Hancu et al. 2019). These studies potentially open the door to PET-MRI imaging in DBS patients. It should be noted that, due to the intense radio-frequency pulses required, arterial spin labelling cannot be performed safely in patients with DBS (Boutet et al. 2019b). While PET and SPECT have the major advantages of assessing specific molecules, fMRI may investigate changes in brain circuitry with a superior spatial-temporal resolution. As new fMRI studies are emerging, it will be interesting to compare BOLD changes with PET/SPECT findings; this new data should further inform DBS mechanism of action.

46.12 Conclusion

This chapter emphasizes the importance of molecular neuroimaging techniques, namely, PET and SPECT. The symbiotic relationship between DBS and neuroimaging research has to date led to the identification of new stimulation targets, the validation of current targets, and the confirmation of disease-relevant circuit engagement. In this way, functional neuroimaging has been critical for furthering our understanding of the network mechanisms underlying DBS. In particular, distinct patterns of metabolic and blood flow changes associated with stimulation of different targets can be appreciated. Standardized reporting of DBS studies and larger sample sizes would go a long way toward elucidating them. In addition, insights from other emerging neuroimaging modalities such as fMRI can and should be integrated in order to further our understanding and interpretation of PET and SPECT data. Continued functional neuroimaging research will likely contribute to improved patient selection and surgical targeting as well as to the identification of biomarkers of treatment efficacy.

Conflicts of Interest Dr. Bilbily is the co-founder and CEO of 16 Bit Inc. Dr. Fasano reports grants, personal fees, and nonfinancial support from AbbVie; grants, personal fees, and nonfinancial support from Medtronic; grants and personal fees from Boston Scientific; personal fees from Sunovion; personal fees from Chiesi Farmaceutici, personal fees from UCB; and grants and personal fees from Ipsen, outside the submitted work. Dr. Lozano serves as a consultant for Medtronic, Abbott, Boston Scientific, and Functional Neuromodulation, during the conduct of the study, and reports grants from GE Healthcare, outside the submitted work. Other authors report no conflict of interest.

Funding: This chapter was supported by the RR Tasker Chair in Functional Neurosurgery at University Health Network and a Tier 1 Canada Research Chair in Neuroscience and the German Research Foundation (Deutsche Forschungsgemeinschaft, DFG NE 2276/1-1) (C.N.). The corresponding author confirms that he had full access to all the data in the study and had final responsibility for the decision to submit for publication.

Appendix

Abbreviations Used in Tables

a	Anterior
Amy	Amygdala
AnG	Angular gyrus
BA	Broca's area
BG	Basal ganglia
Br	Brain stem
c	Caudal
CC	Cingulate cortex
CdN	Caudate nucleus
Cereb	Cerebellum
Cl	Claustrum
CUN	Cuneus
d	Dorsal
DMN	Default mode network
FG	Frontal gyrus
FO	Frontal operculum
FPC	Frontopolar cortex
FS	Frontal sulcus
FuG	Fusiform gyrus
GP	Globus pallidus
GPe	Globus pallidus externus
GPi	Globus pallidus internus
Hi	Hippocampus
hThal	Hypothalamus
i	Inferior
IC	Internal capsule
INS	Insula
l	Lateral
LC	Limbic cortex

LenN	Lentiform nucleus
LG	Lingual gyrus
m	Middle
me	Medial
MidB	Midbrain
NAcc	Nucleus accumbens
NuB	Nucleus basalis
OC	Occipital cortex
OFC	Orbitofrontal cortex
p	Posterior
PAC	Parietal association cortex
PAG	Periaqueductal gray
PAL	Pallidum
pAuC/sAuC	Primary/secondary auditory cortex
PCUN	Precuneus
PFC	Prefrontal cortex
pHi	Parahippocampus
PL	Parietal lobe
PMC	Premotor cortex
Po	Pons
PoG	Postcentral gyrus
PPN	Pedunculopontine nucleus
PPO	Postcentral parietal operculum
PrG	Precentral gyrus
PTC	Parietotemporal cortex
Pu	Putamen
PVG	Periventricular gray
r	Rostral
RC	Retrosplenial cortex
RN	Red nucleus
s	Superior
SAA	Sensory association area
SG	Subgenual
SMA	Supplementary motor cortex
SMG	Supramarginal gyrus
SN	Substantia nigra
Str	Striatum
TAC	Temporal association cortex
TG	Temporal gyrus
Thal	Thalamus (includes all parts of the thalamus)
TN	Trigeminal nucleus
TPJ	Temporoparietal junction
TPo	Temporal pole
Un	Uncus
v	Ventral
WA	Wernicke's area

References

Abelson JL et al (2005) Deep brain stimulation for refractory obsessive-compulsive disorder. Biol Psychiatry 57:510–516. https://doi.org/10.1016/j.biopsych.2004.11.042

Abosch A et al (2003) Stimulation of the subthalamic nucleus in Parkinson's disease does not produce striatal dopamine release. Neurosurgery 53:1095–1102. , discussion 1095–1102. https://doi.org/10.1227/01.neu.0000088662.69419.1b

Albin RL, Young AB, Penney JB (1989) The functional anatomy of basal ganglia disorders. Trends Neurosci 12:366–375

Alexander GE, Crutcher MD (1990) Functional architecture of basal ganglia circuits: neural substrates of parallel processing. Trends Neurosci 13:266–271

Amodio DM, Frith CD (2006) Meeting of minds: the medial frontal cortex and social cognition. Nat Rev Neurosci 7:268–277. https://doi.org/10.1038/nrn1884

Antonini A et al (2003) Brain flow changes before and after deep brain stimulation of the subthalamic nucleus in Parkinson's disease. Neurol Sci 24:151–152. https://doi.org/10.1007/s10072-003-0104-4

Arai N et al (2008) Mechanisms of unilateral STN-DBS in patients with Parkinson's disease: a PET study. J Neurol 255:1236–1243. https://doi.org/10.1007/s00415-008-0906-7

Asanuma K et al (2006) Network modulation in the treatment of Parkinson's disease. Brain 129:2667–2678. https://doi.org/10.1093/brain/awl162

Atkinson-Clement C et al (2017) Subthalamic nucleus stimulation effects on single and combined task performance in Parkinson's disease patients: a PET study. Brain Imaging Behav 11:1139–1153. https://doi.org/10.1007/s11682-016-9588-4

Ballanger B et al (2009) Stimulation of the subthalamic nucleus and impulsivity: release your horses. Ann Neurol 66:817–824. https://doi.org/10.1002/ana.21795

Bejjani BP et al (1999) Transient acute depression induced by high-frequency deep-brain stimulation. N Engl J Med 340:1476–1480. https://doi.org/10.1056/NEJM199905133401905

Beukers RJ, Contarino MF, Speelman JD, Schuurman PR, Booij J, Tijssen MA (2012) Deep brain stimulation of the pallidum is effective and might stabilize striatal D(2) receptor binding in myoclonus-dystonia. Front Neurol 3:22. https://doi.org/10.3389/fneur.2012.00022

Bewernick BH et al (2010) Nucleus accumbens deep brain stimulation decreases ratings of depression and anxiety in treatment-resistant depression. Biol Psychiatry 67:110–116. https://doi.org/10.1016/j.biopsych.2009.09.013

Boertien T et al (2011) Functional imaging of subthalamic nucleus deep brain stimulation in Parkinson's disease. Mov Disord 26:1835–1843. https://doi.org/10.1002/mds.23788

Boutet A et al (2019a) Neuroimaging technological advancements for targeting in functional neurosurgery. Curr Neurol Neurosci Rep 19:42. https://doi.org/10.1007/s11910-019-0961-8

Boutet A et al (2019b) 3-Tesla MRI of deep brain stimulation patients: safety assessment of coils and pulse sequences. J Neurosurg 32(2):586–594. https://doi.org/10.3171/2018.11.JNS181338

Boutet A et al (2019c) Functional MRI safety and artifacts during deep brain stimulation: experience in 102 patients. Radiology 293(1):174–183. https://doi.org/10.1148/radiol.2019190546

Bradberry TJ et al (2012) Common and unique responses to dopamine agonist therapy and deep brain stimulation in Parkinson's disease: an H(2)(15)O PET study. Brain Stimul 5:605–615. https://doi.org/10.1016/j.brs.2011.09.002

Bruet N, Windels F, Bertrand A, Feuerstein C, Poupard A, Savasta M (2001) High frequency stimulation of the subthalamic nucleus increases the extracellular contents of striatal dopamine in normal and partially dopaminergic denervated rats. J Neuropathol Exp Neurol 60:15–24. https://doi.org/10.1093/jnen/60.1.15

Burghaus L et al (2006) Deep brain stimulation of the subthalamic nucleus reversibly deteriorates stuttering in advanced Parkinson's disease. J Neural Transm (Vienna) 113:625–631. https://doi.org/10.1007/s00702-005-0341-1

Butson CR, Cooper SE, Henderson JM, CC MI (2007) Patient-specific analysis of the volume of tissue activated during deep brain stimulation. Neuroimage 34:661–670. https://doi.org/10.1016/j.neuroimage.2006.09.034

Campbell MC et al (2008) Neural correlates of STN DBS-induced cognitive variability in Parkinson disease. Neuropsychologia 46:3162–3169. https://doi.org/10.1016/j.neuropsychologia.2008.07.012

Cao C et al (2017) Modified fluorodeoxyglucose metabolism in motor circuitry by subthalamic deep brain stimulation. Stereotact Funct Neurosurg 95:93–101. https://doi.org/10.1159/000455930

Carbon M, Eidelberg D (2006) Functional imaging of sequence learning in Parkinson's disease. J Neurol Sci 248:72–77. https://doi.org/10.1016/j.jns.2006.05.005

Ceballos-Baumann AO et al (1999) A positron emission tomographic study of subthalamic nucleus stimulation in Parkinson disease: enhanced movement-related activity of motor-association cortex and decreased motor cortex resting activity. Arch Neurol 56:997–1003. https://doi.org/10.1001/archneur.56.8.997

Ceballos-Baumann AO et al (2001) Thalamic stimulation for essential tremor activates motor and deactivates vestibular cortex. Neurology 56:1347–1354. https://doi.org/10.1212/wnl.56.10.1347

Chevalier G, Deniau JM (1990) Disinhibition as a basic process in the expression of striatal functions. Trends Neurosci 13:277–280

Cilia R et al (2007) Brain networks underlining verbal fluency decline during STN-DBS in Parkinson's disease: an ECD-SPECT study parkinsonism. Relat Disord 13:290–294. https://doi.org/10.1016/j.parkreldis.2006.11.011

Cilia R et al (2009) Clinical and cerebral activity changes induced by subthalamic nucleus stimulation in advanced Parkinson's disease: a prospective case-control study. Clin Neurol Neurosurg 111:140–146. https://doi.org/10.1016/j.clineuro.2008.09.018

Coenen VA et al (2017) The medial forebrain bundle as a target for deep brain stimulation for obsessive-compulsive disorder. CNS Spectr 22:282–289. https://doi.org/10.1017/S1092852916000286

Conen S, Matthews JC, Patel NK, Anton-Rodriguez J, Talbot PS (2018) Acute and chronic changes in brain activity with deep brain stimulation for refractory depression. J Psychopharmacol 32:430–440. https://doi.org/10.1177/0269881117742668

Cury RG et al (2018) Effects of subthalamic stimulation on olfactory function in Parkinson disease. World Neurosurg 114:e559–e564. https://doi.org/10.1016/j.wneu.2018.03.033

Dale AM, Halgren E (2001) Spatiotemporal mapping of brain activity by integration of multiple imaging modalities. Curr Opin Neurobiol 11:202–208

Davis KD, Taub E, Houle S, Lang AE, Dostrovsky JO, Tasker RR, Lozano AM (1997) Globus pallidus stimulation activates the cortical motor system during alleviation of parkinsonian symptoms. Nat Med 3:671–674

Davis KD, Taub E, Duffner F, Lozano AM, Tasker RR, Houle S, Dostrovsky JO (2000) Activation of the anterior cingulate cortex by thalamic stimulation in patients with chronic pain: a positron emission tomography study. J Neurosurg 92:64–69. https://doi.org/10.3171/jns.2000.92.1.0064

Deiber MP et al (1993) Thalamic stimulation and suppression of parkinsonian tremor. Evidence of a cerebellar deactivation using positron emission tomography. Brain 116(Pt 1):267–279. https://doi.org/10.1093/brain/116.1.267

Dellapina E et al (2012) Effect of subthalamic deep brain stimulation on pain in Parkinson's disease. Pain 153:2267–2273. https://doi.org/10.1016/j.pain.2012.07.026

DeLong MR (1990) Primate models of movement disorders of basal ganglia origin. Trends Neurosci 13:281–285

Detante O et al (2004) Globus pallidus internus stimulation in primary generalized dystonia: a H215O PET study. Brain 127:1899–1908. https://doi.org/10.1093/brain/awh213

Diedrichsen J, Balsters JH, Flavell J, Cussans E, Ramnani N (2009) A probabilistic MR atlas of the human cerebellum. Neuroimage 46:39–46. https://doi.org/10.1016/j.neuroimage.2009.01.045

Dougherty DD et al (2016) Acute deep brain stimulation changes in regional cerebral blood flow in obsessive-compulsive disorder. J Neurosurg 125:1087–1093. https://doi.org/10.3171/2015.9.JNS151387

Drevets WC (2007) Orbitofrontal cortex function and structure in depression. Ann N Y Acad Sci 1121:499–527. https://doi.org/10.1196/annals.1401.029

Drevets WC, Price JL, Simpson JR Jr, Todd RD, Reich T, Vannier M, Raichle ME (1997) Subgenual prefrontal cortex abnormalities in mood disorders. Nature 386:824–827. https://doi.org/10.1038/386824a0

Drevets WC, Price JL, Furey ML (2008) Brain structural and functional abnormalities in mood disorders: implications for neurocircuitry models of depression. Brain Struct Funct 213:93–118. https://doi.org/10.1007/s00429-008-0189-x

Duncan GH, Kupers RC, Marchand S, Villemure JG, Gybels JM, Bushnell MC (1998) Stimulation of human thalamus for pain relief: possible modulatory circuits revealed by positron emission tomography. J Neurophysiol 80:3326–3330. https://doi.org/10.1152/jn.1998.80.6.3326

Edlow BL et al (2012) Neuroanatomic connectivity of the human ascending arousal system critical to consciousness and its disorders. J Neuropathol Exp Neurol 71:531–546. https://doi.org/10.1097/NEN.0b013e3182588293

Eidelberg D (2009) Metabolic brain networks in neurodegenerative disorders: a functional imaging approach. Trends Neurosci 32:548–557. https://doi.org/10.1016/j.tins.2009.06.003

Erasmi R, Granert O, Zorenkov D, Falk D, Wodarg F, Deuschl G, Witt K (2018) White matter changes along the electrode lead in patients treated with deep brain stimulation. Front Neurol 9:983. https://doi.org/10.3389/fneur.2018.00983

Ewert S et al (2018) Toward defining deep brain stimulation targets in MNI space: a subcortical atlas based on multimodal MRI, histology and structural connectivity. Neuroimage 170:271–282. https://doi.org/10.1016/j.neuroimage.2017.05.015

Ewert S, Horn A, Finkel F, Li N, Kuhn AA, Herrington TM (2019) Optimization and comparative evaluation of nonlinear deformation algorithms for atlas-based segmentation of DBS target nuclei. Neuroimage 184:586–598. https://doi.org/10.1016/j.neuroimage.2018.09.061

Femminella GD, Thayanandan T, Calsolaro V, Komici K, Rengo G, Corbi G, Ferrara N (2018) Imaging and molecular mechanisms of Alzheimer's disease: a review. Int J Mol Sci 19(12):3702. https://doi.org/10.3390/ijms19123702

Fenoy AJ et al (2018) A longitudinal study on deep brain stimulation of the medial forebrain bundle for treatment-resistant depression. Transl Psychiatry 8:111. https://doi.org/10.1038/s41398-018-0160-4

Ferreira LK, Busatto GF (2011) Neuroimaging in Alzheimer's disease: current role in clinical practice and potential future applications. Clinics (Sao Paulo) 66(Suppl 1):19–24. https://doi.org/10.1590/s1807-59322011001300003

Figee M et al (2014) Deep brain stimulation induces striatal dopamine release in obsessive-compulsive disorder. Biol Psychiatry 75:647–652. https://doi.org/10.1016/j.biopsych.2013.06.021

Fonoff ET et al (2010) Pet findings in reversible improvement of olfactory dysfunction after STN stimulation in a Parkinson's disease patient. Mov Disord 25:2466–2468. https://doi.org/10.1002/mds.23253

Fontaine D, Deudon A, Lemaire JJ, Razzouk M, Viau P, Darcourt J, Robert P (2013) Symptomatic treatment of memory decline in Alzheimer's disease by deep brain stimulation: a feasibility study. J Alzheimers Dis 34:315–323. https://doi.org/10.3233/JAD-121579

Frisoni GB, Fox NC, Jack CR Jr, Scheltens P, Thompson PM (2010) The clinical use of structural MRI in Alzheimer disease. Nat Rev Neurol 6:67–77. https://doi.org/10.1038/nrneurol.2009.215

Friston KJ (2009) Modalities, modes, and models in functional neuroimaging. Science 326:399–403. https://doi.org/10.1126/science.1174521

Fukuda M et al (2001a) Functional correlates of pallidal stimulation for Parkinson's disease. Ann Neurol 49:155–164

Fukuda M et al (2001b) Networks mediating the clinical effects of pallidal brain stimulation for Parkinson's disease: a PET study of resting-state glucose metabolism. Brain 124:1601–1609. https://doi.org/10.1093/brain/124.8.1601

Fukuda M et al (2004) Thalamic stimulation for parkinsonian tremor: correlation between regional cerebral blood flow and physiological tremor characteristics. Neuroimage 21:608–615. https://doi.org/10.1016/j.neuroimage.2003.09.068

Garraux G, Bahri MA, Lemaire C, Degueldre C, Salmon E, Kaschten B (2011) Brain energization in response to deep brain stimulation of subthalamic nuclei in Parkinson's disease. J Cereb Blood Flow Metab 31:1612–1622. https://doi.org/10.1038/jcbfm.2011.41

Geday J, Ostergaard K, Gjedde A (2006) Stimulation of subthalamic nucleus inhibits emotional activation of fusiform gyrus. Neuroimage 33:706–714. https://doi.org/10.1016/j.neuroimage.2006.06.056

Giordano F et al (2016) Deep brain stimulation of the anterior limb of the internal capsule may be efficacious for explosive aggressive behaviour. Stereotact Funct Neurosurg 94:371–378. https://doi.org/10.1159/000449171

Goethals I, Jacobs F, Van der Linden C, Caemaert J, Audenaert K (2008) Brain activation associated with deep brain stimulation causing dissociation in a patient with Tourette's syndrome. J Trauma Dissociation 9:543–549

Goldapple K, Segal Z, Garson C, Lau M, Bieling P, Kennedy S, Mayberg H (2004) Modulation of cortical-limbic pathways in major depression: treatment-specific effects of cognitive behavior therapy. Arch Gen Psychiatry 61:34–41. https://doi.org/10.1001/archpsyc.61.1.34

Gondard E, Chau HN, Mann A, Tierney TS, Hamani C, Kalia SK, Lozano AM (2015) Rapid modulation of protein expression in the rat hippocampus following deep brain stimulation of the fornix. Brain Stimul 8:1058–1064. https://doi.org/10.1016/j.brs.2015.07.044

Grafton ST, Turner RS, Desmurget M, Bakay R, Delong M, Vitek J, Crutcher M (2006) Normalizing motor-related brain activity: subthalamic nucleus stimulation in Parkinson disease. Neurology 66:1192–1199. https://doi.org/10.1212/01.wnl.0000214237.58321.c3

Graham WV, Bonito-Oliva A, Sakmar TP (2017) Update on Alzheimer's disease therapy and prevention strategies. Annu Rev Med 68:413–430. https://doi.org/10.1146/annurev-med-042915-103753

Graybiel AM, Rauch SL (2000) Toward a neurobiology of obsessive-compulsive disorder. Neuron 28:343–347

Greenberg BD et al (2010) Deep brain stimulation of the ventral internal capsule/ventral striatum for obsessive-compulsive disorder: worldwide experience. Mol Psychiatry 15:64–79. https://doi.org/10.1038/mp.2008.55

Greicius MD, Srivastava G, Reiss AL, Menon V (2004) Default-mode network activity distinguishes Alzheimer's disease from healthy aging: evidence from functional MRI. Proc Natl Acad Sci U S A 101:4637–4642. https://doi.org/10.1073/pnas.0308627101

Haegelen C et al (2010) SPECT and PET analysis of subthalamic stimulation in Parkinson's disease: analysis using a manual segmentation. J Neurol 257:375–382. https://doi.org/10.1007/s00415-009-5327-8

Haense C et al (2016) Effect of deep brain stimulation on regional cerebral blood flow in patients with medically refractory tourette syndrome. Front Psychiatry 7:118. https://doi.org/10.3389/fpsyt.2016.00118

Hagelweide K, Schonberger AR, Kracht LW, Grundler TOJ, Fink GR, Schubotz RI (2018) Motor cognition in patients treated with subthalamic nucleus deep brain stimulation: limits of compensatory overactivity in Parkinson's disease. Neuropsychologia 117:491–499. https://doi.org/10.1016/j.neuropsychologia.2018.07.007

Hallett M (2014) Tremor: pathophysiology parkinsonism. Relat Disord 20(Suppl 1):S118–S122. https://doi.org/10.1016/S1353-8020(13)70029-4

Hamani C, Mayberg H, Stone S, Laxton A, Haber S, Lozano AM (2011) The subcallosal cingulate gyrus in the context of major depression. Biol Psychiatry 69:301–308. https://doi.org/10.1016/j.biopsych.2010.09.034

Hancu I et al (2019) On the (non-)equivalency of monopolar and bipolar settings for deep brain stimulation fMRI studies of Parkinson's disease patients. J Magn Reson Imaging 49:1736–1749. https://doi.org/10.1002/jmri.26321

Hariz M (2017) My 25 stimulating years with DBS in Parkinson's disease. J Parkinsons dis 7:S35–S43. https://doi.org/10.3233/JPD-179007

Hashimoto T, Elder CM, Okun MS, Patrick SK, Vitek JL (2003) Stimulation of the subthalamic nucleus changes the firing pattern of pallidal neurons. J Neurosci 23:1916–1923

Haslinger B et al (2003) Differential modulation of subcortical target and cortex during deep brain stimulation. NeuroImage 18:517–524
Haslinger B, Kalteis K, Boecker H, Alesch F, Ceballos-Baumann AO (2005) Frequency-correlated decreases of motor cortex activity associated with subthalamic nucleus stimulation in Parkinson's disease. Neuroimage 28:598–606. https://doi.org/10.1016/j.neuroimage.2005.06.034
Heldmann M et al (2012) Deep brain stimulation of nucleus accumbens region in alcoholism affects reward processing. PLoS One 7:e36572. https://doi.org/10.1371/journal.pone.0036572
Hershey T et al (2003) Cortical and subcortical blood flow effects of subthalamic nucleus stimulation in PD. Neurology 61:816–821. https://doi.org/10.1212/01.wnl.0000083991.81859.73
Herzog J et al (2006) Subthalamic stimulation modulates cortical control of urinary bladder in Parkinson's disease. Brain 129:3366–3375. https://doi.org/10.1093/brain/awl302
Herzog J et al (2008) Improved sensory gating of urinary bladder afferents in Parkinson's disease following subthalamic stimulation. Brain 131:132–145. https://doi.org/10.1093/brain/awm254
Hesse S et al (2008) Effects of subthalamic nucleus stimulation on striatal dopaminergic transmission in patients with Parkinson's disease within one-year follow-up. J Neurol 255:1059–1066. https://doi.org/10.1007/s00415-008-0849-z
Hilker R, Voges J, Thiel A, Ghaemi M, Herholz K, Sturm V, Heiss WD (2002) Deep brain stimulation of the subthalamic nucleus versus levodopa challenge in Parkinson's disease: measuring the on- and off-conditions with FDG-PET. J Neural Transm (Vienna) 109:1257–1264. https://doi.org/10.1007/s00702-002-0696-5
Hilker R et al (2003) Deep brain stimulation of the subthalamic nucleus does not increase the striatal dopamine concentration in parkinsonian humans. Mov Disord 18:41–48. https://doi.org/10.1002/mds.10297
Hilker R et al (2004) Subthalamic nucleus stimulation restores glucose metabolism in associative and limbic cortices and in cerebellum: evidence from a FDG-PET study in advanced Parkinson's disease. J Cereb Blood Flow Metab 24:7–16. https://doi.org/10.1097/01.WCB.0000092831.44769.09
Hilker R et al (2005) Disease progression continues in patients with advanced Parkinson's disease and effective subthalamic nucleus stimulation. J Neurol Neurosurg Psychiatry 76:1217–1221. https://doi.org/10.1136/jnnp.2004.057893
Hilker R et al (2008) STN-DBS activates the target area in Parkinson disease: an FDG-PET study. Neurology 71:708–713. https://doi.org/10.1212/01.wnl.0000312380.01852.77
Hill KK et al (2013) Cerebral blood flow responses to dorsal and ventral STN DBS correlate with gait and balance responses in Parkinson's disease. Exp Neurol 241:105–112. https://doi.org/10.1016/j.expneurol.2012.12.003
Hirano S et al (2008) Dissociation of metabolic and neurovascular responses to levodopa in the treatment of Parkinson's disease. J Neurosci 28:4201–4209. https://doi.org/10.1523/JNEUROSCI.0582-08.2008
Holtzheimer PE et al (2017) Subcallosal cingulate deep brain stimulation for treatment-resistant depression: a multisite, randomised, sham-controlled trial. Lancet Psychiatry 4:839–849. https://doi.org/10.1016/S2215-0366(17)30371-1
Hooker JM, Carson RE (2019) Human positron emission tomography neuroimaging. Annu Rev Biomed Eng 21:551–581. https://doi.org/10.1146/annurev-bioeng-062117-121056
Horn A et al (2019) Lead-DBS v2: towards a comprehensive pipeline for deep brain stimulation imaging. Neuroimage 184:293–316. https://doi.org/10.1016/j.neuroimage.2018.08.068
Jahanshahi M et al (2000) The impact of deep brain stimulation on executive function in Parkinson's disease. Brain 123(Pt 6):1142–1154. https://doi.org/10.1093/brain/123.6.1142
Jankovic J (2008) Parkinson's disease: clinical features and diagnosis. J Neurol Neurosurg Psychiatry 79:368–376. https://doi.org/10.1136/jnnp.2007.131045
Joliot M et al (2015) AICHA: an atlas of intrinsic connectivity of homotopic areas. J Neurosci Methods 254:46–59. https://doi.org/10.1016/j.jneumeth.2015.07.013
Kalbe E et al (2009) Frontal FDG-PET activity correlates with cognitive outcome after STN-DBS in Parkinson disease. Neurology 72:42–49. https://doi.org/10.1212/01.wnl.0000338536.31388.f0

Karimi M et al (2008) Subthalamic nucleus stimulation-induced regional blood flow responses correlate with improvement of motor signs in Parkinson disease. Brain 131:2710–2719. https://doi.org/10.1093/brain/awn179

Katsakiori PF et al (2009) Deep brain stimulation for secondary dystonia: results in 8 patients. Acta Neurochir (Wien) 151:473–478.; ; discussion 478. https://doi.org/10.1007/s00701-009-0281-x

Kefalopoulou Z, Paschali A, Markaki E, Vassilakos P, Ellul J, Constantoyannis C (2009) A double-blind study on a patient with tardive dyskinesia treated with pallidal deep brain stimulation. Acta Neurol Scand 119:269–273. https://doi.org/10.1111/j.1600-0404.2008.01115.x

Kefalopoulou Z, Paschali A, Markaki E, Ellul J, Chroni E, Vassilakos P, Constantoyannis C (2010) Regional cerebral blood flow changes induced by deep brain stimulation in secondary dystonia. Acta Neurochir (Wien) 152:1007–1014. https://doi.org/10.1007/s00701-010-0612-y

Ko JH, Tang CC, Eidelberg D (2013) Brain stimulation and functional imaging with fMRI and PET. Handb Clin Neurol 116:77–95. https://doi.org/10.1016/B978-0-444-53497-2.00008-5

Koski L, Paus T (2000) Functional connectivity of the anterior cingulate cortex within the human frontal lobe: a brain-mapping meta-analysis. Exp Brain Res 133:55–65. https://doi.org/10.1007/s002210000400

Krishnan A, Williams LJ, McIntosh AR, Abdi H (2011) Partial Least Squares (PLS) methods for neuroimaging: a tutorial and review. Neuroimage 56:455–475. https://doi.org/10.1016/j.neuroimage.2010.07.034

Kucewicz MT et al (2018) Evidence for verbal memory enhancement with electrical brain stimulation in the lateral temporal cortex. Brain 141:971–978. https://doi.org/10.1093/brain/awx373

Kuhn J et al (2012) In vivo evidence of deep brain stimulation-induced dopaminergic modulation in Tourette's syndrome. Biol Psychiatry 71:e11–e13. https://doi.org/10.1016/j.biopsych.2011.09.035

Kuhn J et al (2015) Deep brain stimulation of the nucleus basalis of Meynert in Alzheimer's dementia. Mol Psychiatry 20:353–360. https://doi.org/10.1038/mp.2014.32

Kumar R, Dagher A, Hutchison WD, Lang AE, Lozano AM (1999) Globus pallidus deep brain stimulation for generalized dystonia: clinical and PET investigation. Neurology 53:871–874. https://doi.org/10.1212/wnl.53.4.871

Kupers RC, Gybels JM, Gjedde A (2000) Positron emission tomography study of a chronic pain patient successfully treated with somatosensory thalamic stimulation. Pain 87:295–302

Lammertsma AA (2001) PET/SPECT: functional imaging beyond flow. Vision Res 41:1277–1281. https://doi.org/10.1016/s0042-6989(00)00262-5

Laxton AW et al (2010) A phase I trial of deep brain stimulation of memory circuits in Alzheimer's disease. Ann Neurol 68:521–534. https://doi.org/10.1002/ana.22089

Le Jeune F et al (2008) Subthalamic nucleus stimulation affects orbitofrontal cortex in facial emotion recognition: a PET study. Brain 131:1599–1608. https://doi.org/10.1093/brain/awn084

Le Jeune F et al (2010a) Subthalamic nucleus stimulation affects limbic and associative circuits: a PET study. Eur J Nucl Med Mol Imaging 37:1512–1520. https://doi.org/10.1007/s00259-010-1436-y

Le Jeune F et al (2010b) Decrease of prefrontal metabolism after subthalamic stimulation in obsessive-compulsive disorder: a positron emission tomography study. Biol Psychiatry 68:1016–1022. https://doi.org/10.1016/j.biopsych.2010.06.033

Lee DJ et al (2019) Inferior thalamic peduncle deep brain stimulation for treatment-refractory obsessive-compulsive disorder: a phase 1 pilot trial. Brain Stimul 12:344–352. https://doi.org/10.1016/j.brs.2018.11.012

Lemaire JJ et al (2018) Deep brain stimulation in five patients with severe disorders of consciousness. Ann Clin Transl Neurol 5:1372–1384. https://doi.org/10.1002/acn3.648

Li D, Zuo C, Guan Y, Zhao Y, Shen J, Zan S, Sun B (2006) FDG-PET study of the bilateral subthalamic nucleus stimulation effects on the regional cerebral metabolism in advanced Parkinson disease. Acta Neurochir Suppl 99:51–54

Li P et al (2012) Deep brain stimulation of the globus pallidus internal improves symptoms of chorea-acanthocytosis. Neurol Sci 33:269–274. https://doi.org/10.1007/s10072-011-0741-y

Limousin P, Greene J, Pollak P, Rothwell J, Benabid AL, Frackowiak R (1997) Changes in cerebral activity pattern due to subthalamic nucleus or internal pallidum stimulation in Parkinson's disease. Ann Neurol 42:283–291. https://doi.org/10.1002/ana.410420303

Lipsman N et al (2013) Subcallosal cingulate deep brain stimulation for treatment-refractory anorexia nervosa: a phase 1 pilot trial. Lancet 381:1361–1370. https://doi.org/10.1016/S0140-6736(12)62188-6

Lokkegaard A et al (2007) Dopamine transporter imaging and the effects of deep brain stimulation in patients with Parkinson's disease. Eur J Nucl Med Mol Imaging 34:508–516. https://doi.org/10.1007/s00259-006-0257-5

Lozano AM, Lipsman N (2013) Probing and regulating dysfunctional circuits using deep brain stimulation. Neuron 77:406–424. https://doi.org/10.1016/j.neuron.2013.01.020

Lozano AM, Mayberg HS, Giacobbe P, Hamani C, Craddock RC, Kennedy SH (2008) Subcallosal cingulate gyrus deep brain stimulation for treatment-resistant depression. Biol Psychiatry 64:461–467. https://doi.org/10.1016/j.biopsych.2008.05.034

Lozano AM et al (2016) A phase II study of fornix deep brain stimulation in mild Alzheimer's disease. J Alzheimers Dis 54:777–787. https://doi.org/10.3233/JAD-160017

Lozano CS, Ranjan M, Boutet A, Xu DS, Kucharczyk W, Fasano A, Lozano AM (2018) Imaging alone versus microelectrode recording-guided targeting of the STN in patients with Parkinson's disease. J Neurosurg:1–6. https://doi.org/10.3171/2018.2.JNS172186

Lozano AM et al (2019) Deep brain stimulation: current challenges and future directions. Nat Rev Neurol 15(Suppl 1):1. https://doi.org/10.1038/s41582-018-0128-2

Lyoo CH, Aalto S, Rinne JO, Lee KO, Oh SH, Chang JW, Lee MS (2007) Different cerebral cortical areas influence the effect of subthalamic nucleus stimulation on parkinsonian motor deficits and freezing of gait. Mov Disord 22:2176–2182. https://doi.org/10.1002/mds.21609

Ma Y, Tang C, Spetsieris PG, Dhawan V, Eidelberg D (2007) Abnormal metabolic network activity in Parkinson's disease: test-retest reproducibility. J Cereb Blood Flow Metab 27:597–605. https://doi.org/10.1038/sj.jcbfm.9600358

Mallet L et al (2008) Subthalamic nucleus stimulation in severe obsessive-compulsive disorder. N Engl J Med 359:2121–2134. https://doi.org/10.1056/NEJMoa0708514

Mann A et al (2018) Chronic deep brain stimulation in an Alzheimer's disease mouse model enhances memory and reduces pathological hallmarks. Brain Stimul 11:435–444. https://doi.org/10.1016/j.brs.2017.11.012

Manto M et al (2012) Consensus paper: roles of the cerebellum in motor control--the diversity of ideas on cerebellar involvement in movement. Cerebellum 11:457–487. https://doi.org/10.1007/s12311-011-0331-9

Margulies DS, Kelly AM, Uddin LQ, Biswal BB, Castellanos FX, Milham MP (2007) Mapping the functional connectivity of anterior cingulate cortex. Neuroimage 37:579–588. https://doi.org/10.1016/j.neuroimage.2007.05.019

Martin-Blanco A et al (2015) Immediate cerebral metabolic changes induced by discontinuation of deep brain stimulation of subcallosal cingulate gyrus in treatment-resistant depression. J Affect Disord 173:159–162. https://doi.org/10.1016/j.jad.2014.10.035

May A, Bahra A, Buchel C, Frackowiak RS, Goadsby PJ (1998) Hypothalamic activation in cluster headache attacks. Lancet 352:275–278. https://doi.org/10.1016/S0140-6736(98)02470-2

May A, Leone M, Boecker H, Sprenger T, Juergens T, Bussone G, Tolle TR (2006) Hypothalamic deep brain stimulation in positron emission tomography. J Neurosci 26:3589–3593. https://doi.org/10.1523/JNEUROSCI.4609-05.2006

Mayberg HS et al (1999) Reciprocal limbic-cortical function and negative mood: converging PET findings in depression and normal sadness. Am J Psychiatry 156:675–682. https://doi.org/10.1176/ajp.156.5.675

Mayberg HS, Brannan SK, Tekell JL, Silva JA, Mahurin RK, McGinnis S, Jerabek PA (2000) Regional metabolic effects of fluoxetine in major depression: serial changes and relationship to clinical response. Biol Psychiatry 48:830–843

Mayberg HS et al (2005) Deep brain stimulation for treatment-resistant depression. Neuron 45:651–660. https://doi.org/10.1016/j.neuron.2005.02.014

McIntyre CC, Grill WM, Sherman DL, Thakor NV (2004) Cellular effects of deep brain stimulation: model-based analysis of activation and inhibition. J Neurophysiol 91:1457–1469. https://doi.org/10.1152/jn.00989.2003

Meissner W, Harnack D, Paul G, Reum T, Sohr R, Morgenstern R, Kupsch A (2002) Deep brain stimulation of subthalamic neurons increases striatal dopamine metabolism and induces contralateral circling in freely moving 6-hydroxydopamine-lesioned rats. Neurosci Lett 328:105–108. https://doi.org/10.1016/s0304-3940(02)00463-9

Millet B et al (2014) Limbic versus cognitive target for deep brain stimulation in treatment-resistant depression: accumbens more promising than caudate. Eur Neuropsychopharmacol 24:1229–1239. https://doi.org/10.1016/j.euroneuro.2014.05.006

Miocinovic S, Somayajula S, Chitnis S, Vitek JL (2013) History, applications, and mechanisms of deep brain stimulation. JAMA Neurol 70:163–171. https://doi.org/10.1001/2013.jamaneurol.45

Mo SJ, Linder J, Blomstedt P, Granasen G, Forsgren L, Hariz M (2016) Long-term dopamine transporter imaging in Parkinson's disease treated with zona incerta stimulation. Nucl Med Commun 37:499–508. https://doi.org/10.1097/MNM.0000000000000469

Moro E et al (2004) Bilateral globus pallidus stimulation for Huntington's disease. Ann Neurol 56:290–294. https://doi.org/10.1002/ana.20183

Mubeen AM, Ardekani B, Tagliati M, Alterman R, Dhawan V, Eidelberg D, Sidtis JJ (2018) Global and multi-focal changes in cerebral blood flow during subthalamic nucleus stimulation in Parkinson's disease. J Cereb Blood Flow Metab 38:697–705. https://doi.org/10.1177/0271678X17705042

Mure H et al (2011) Parkinson's disease tremor-related metabolic network: characterization, progression, and treatment effects. Neuroimage 54:1244–1253. https://doi.org/10.1016/j.neuroimage.2010.09.028

Nagaoka T, Katayama Y, Kano T, Kobayashi K, Oshima H, Fukaya C, Yamamoto T (2007) Changes in glucose metabolism in cerebral cortex and cerebellum correlate with tremor and rigidity control by subthalamic nucleus stimulation in Parkinson's disease: a positron emission tomography study. Neuromodulation 10:206–215. https://doi.org/10.1111/j.1525-1403.2007.00110.x

Nakajima T, Nimura T, Yamaguchi K, Ando T, Itoh M, Yoshimoto T, Shirane R (2003) The impact of stereotactic pallidal surgery on the dopamine D2 receptor in Parkinson disease: a positron emission tomography study. J Neurosurg 98:57–63. https://doi.org/10.3171/jns.2003.98.1.0057

Nambu A, Tokuno H, Takada M (2002) Functional significance of the cortico-subthalamo-pallidal 'hyperdirect' pathway. Neurosci Res 43:111–117

Narayana S et al (2009) A noninvasive imaging approach to understanding speech changes following deep brain stimulation in Parkinson's disease. Am J Speech Lang Pathol 18:146–161. https://doi.org/10.1044/1058-0360(2008/08-0004)

Nimura T et al (2005) Attenuation of fluctuating striatal synaptic dopamine levels in patients with Parkinson disease in response to subthalamic nucleus stimulation: a positron emission tomography study. J Neurosurg 103:968–973. https://doi.org/10.3171/jns.2005.103.6.0968

Nobler MS, Oquendo MA, Kegeles LS, Malone KM, Campbell CC, Sackeim HA, Mann JJ (2001) Decreased regional brain metabolism after ECT. Am J Psychiatry 158:305–308. https://doi.org/10.1176/appi.ajp.158.2.305

Nozaki T et al (2013) Effect of subthalamic nucleus stimulation during exercise on the mesolimbocortical dopaminergic region in Parkinson's disease: a positron emission tomography study. J Cereb Blood Flow Metab 33:415–421. https://doi.org/10.1038/jcbfm.2012.183

Nuttin B, Cosyns P, Demeulemeester H, Gybels J, Meyerson B (1999) Electrical stimulation in anterior limbs of internal capsules in patients with obsessive-compulsive disorder. Lancet 354:1526. https://doi.org/10.1016/S0140-6736(99)02376-4

Nuttin BJ et al (2003) Long-term electrical capsular stimulation in patients with obsessive-compulsive disorder. Neurosurgery 52:1263–1272.; ; discussion 1272-1264. https://doi.org/10.1227/01.neu.0000064565.49299.9a

Nuttin B et al (2013) Targeting bed nucleus of the stria terminalis for severe obsessive-compulsive disorder: more unexpected lead placement in obsessive-compulsive disorder than in surgery

for movement disorders. World Neurosurg 80:S30 e11–S30 e36. https://doi.org/10.1016/j.wneu.2012.12.029

Obeso I, Ray NJ, Antonelli F, Cho SS, Strafella AP (2011) Combining functional imaging with brain stimulation in Parkinson's disease. Int Rev Psychiatry 23:467–475. https://doi.org/10.3109/09540261.2011.621414

Okun MS (2012) Deep-brain stimulation for Parkinson's disease. N Engl J Med 367:1529–1538. https://doi.org/10.1056/NEJMct1208070

Ory S et al (2017) Pre-frontal-insular-cerebellar modifications correlate with disgust feeling blunting after subthalamic stimulation: a positron emission tomography study in Parkinson's disease. J Neuropsychol 11:378–395. https://doi.org/10.1111/jnp.12094

Park HJ et al (2015) A network analysis of (1)(5)O-H(2)O PET reveals deep brain stimulation effects on brain network of Parkinson's disease. Yonsei Med J 56:726–736. https://doi.org/10.3349/ymj.2015.56.3.726

Parker F, Tzourio N, Blond S, Petit H, Mazoyer B (1992) Evidence for a common network of brain structures involved in parkinsonian tremor and voluntary repetitive movement. Brain Res 584:11–17. https://doi.org/10.1016/0006-8993(92)90872-7

Payoux P et al (2004) Subthalamic nucleus stimulation reduces abnormal motor cortical overactivity in Parkinson disease. Arch Neurol 61:1307–1313. https://doi.org/10.1001/archneur.61.8.1307

Payoux P et al (2009) Contrasting changes in cortical activation induced by acute high-frequency stimulation within the globus pallidus in Parkinson's disease. J Cereb Blood Flow Metab 29:235–243. https://doi.org/10.1038/jcbfm.2008.107

Pereira EA, Green AL, Bradley KM, Soper N, Moir L, Stein JF, Aziz TZ (2007) Regional cerebral perfusion differences between periventricular grey, thalamic and dual target deep brain stimulation for chronic neuropathic pain. Stereotact Funct Neurosurg 85:175–183. https://doi.org/10.1159/000101296

Perlmutter JS et al (2002) Blood flow responses to deep brain stimulation of thalamus. Neurology 58:1388–1394. https://doi.org/10.1212/wnl.58.9.1388

Peron J et al (2010) Subthalamic nucleus stimulation affects theory of mind network: a PET study in Parkinson's disease. PLoS One 5:e9919. https://doi.org/10.1371/journal.pone.0009919

Picillo M, Lozano AM, Kou N, Puppi Munhoz R, Fasano A (2016) Programming deep brain stimulation for Parkinson's disease: the Toronto Western Hospital Algorithms. Brain Stimul 9:425–437. https://doi.org/10.1016/j.brs.2016.02.004

Pinto S et al (2004) Subthalamic nucleus stimulation and dysarthria in Parkinson's disease: a PET study. Brain 127:602–615. https://doi.org/10.1093/brain/awh074

Poewe W et al (2017) Parkinson disease. Nat Rev Dis Primers 3:17013. https://doi.org/10.1038/nrdp.2017.13

Poston KL et al (2016) Compensatory neural mechanisms in cognitively unimpaired Parkinson disease. Ann Neurol 79:448–463. https://doi.org/10.1002/ana.24585

Pourfar M, Tang C, Lin T, Dhawan V, Kaplitt MG, Eidelberg D (2009) Assessing the microlesion effect of subthalamic deep brain stimulation surgery with FDG PET. J Neurosurg 110:1278–1282. https://doi.org/10.3171/2008.12.JNS08991

Rauch SL et al (2006) A functional neuroimaging investigation of deep brain stimulation in patients with obsessive-compulsive disorder. J Neurosurg 104:558–565. https://doi.org/10.3171/jns.2006.104.4.558

Raymaekers S, Vansteelandt K, Luyten L, Bervoets C, Demyttenaere K, Gabriels L, Nuttin B (2017) Long-term electrical stimulation of bed nucleus of stria terminalis for obsessive-compulsive disorder. Mol Psychiatry 22:931–934. https://doi.org/10.1038/mp.2016.124

Reich MM et al (2016) Progressive gait ataxia following deep brain stimulation for essential tremor: adverse effect or lack of efficacy? Brain 139:2948–2956. https://doi.org/10.1093/brain/aww223

Rezai AR et al (2016) Improved function after deep brain stimulation for chronic, severe traumatic brain injury. Neurosurgery 79:204–211. https://doi.org/10.1227/NEU.0000000000001190

Riva-Posse P et al (2018) A connectomic approach for subcallosal cingulate deep brain stimulation surgery: prospective targeting in treatment-resistant depression. Mol Psychiatry 23:843–849. https://doi.org/10.1038/mp.2017.59

Robbins TW, Vaghi MM, Banca P (2019) Obsessive-compulsive disorder: puzzles and prospects. Neuron 102:27–47. https://doi.org/10.1016/j.neuron.2019.01.046

Rodriguez-Oroz MC, Jahanshahi M, Krack P, Litvan I, Macias R, Bezard E, Obeso JA (2009) Initial clinical manifestations of Parkinson's disease: features and pathophysiological mechanisms. Lancet Neurol 8:1128–1139. https://doi.org/10.1016/S1474-4422(09)70293-5

Rosa M, Marceglia S, Barbieri S, Priori A (2013) Local field potential and deep brain stimulation (DBS). In: Jaeger D, Jung R (eds) Encyclopedia of computational neuroscience. Springer, New York, pp 1–20. https://doi.org/10.1007/978-1-4614-7320-6_547-1

Savitz JB, Drevets WC (2013) Neuroreceptor imaging in depression. Neurobiol Dis 52:49–65. https://doi.org/10.1016/j.nbd.2012.06.001

Saxena S, Brody AL, Schwartz JM, Baxter LR (1998) Neuroimaging and frontal-subcortical circuitry in obsessive-compulsive disorder. Br J Psychiatry Suppl:26–37

Scharre DW et al (2018) Deep brain stimulation of frontal lobe networks to treat Alzheimer's disease. J Alzheimers Dis 62:621–633. https://doi.org/10.3233/JAD-170082

Scheltens P, Blennow K, Breteler MM, de Strooper B, Frisoni GB, Salloway S, Van der Flier WM (2016) Alzheimer's disease. Lancet 388:505–517. https://doi.org/10.1016/S0140-6736(15)01124-1

Schilbach L, Weiss PH, Kuhn J, Timmermann L, Klosterkotter J, Huff W (2012) Pharmacological treatment of deep brain stimulation-induced hypomania leads to clinical remission while preserving motor benefits. Neurocase 18:152–159. https://doi.org/10.1080/13554794.2011.568502

Schlaepfer TE et al (2008) Deep brain stimulation to reward circuitry alleviates anhedonia in refractory major depression. Neuropsychopharmacology 33:368–377. https://doi.org/10.1038/sj.npp.1301408

Schroeder U et al (2002) Subthalamic nucleus stimulation affects striato-anterior cingulate cortex circuit in a response conflict task: a PET study. Brain 125:1995–2004. https://doi.org/10.1093/brain/awf199

Schroeder U et al (2003) Subthalamic nucleus stimulation affects a frontotemporal network: a PET study. Ann Neurol 54:445–450. https://doi.org/10.1002/ana.10683

Sestini S, Scotto di Luzio A, Ammannati F, De Cristofaro MT, Passeri A, Martini S, Pupi A (2002) Changes in regional cerebral blood flow caused by deep-brain stimulation of the subthalamic nucleus in Parkinson's disease. J Nucl Med 43:725–732

Sestini S, Ramat S, Formiconi AR, Ammannati F, Sorbi S, Pupi A (2005) Brain networks underlying the clinical effects of long-term subthalamic stimulation for Parkinson's disease: a 4-year follow-up study with rCBF SPECT. J Nucl Med 46:1444–1454

Sestini S, Pupi A, Ammannati F, Silvia R, Sorbi S, Castagnoli A (2007) Are there adaptive changes in the human brain of patients with Parkinson's disease treated with long-term deep brain stimulation of the subthalamic nucleus? A 4-year follow-up study with regional cerebral blood flow SPECT. Eur J Nucl Med Mol Imaging 34:1646–1657. https://doi.org/10.1007/s00259-007-0428-z

Shen LH, Liao MH, Tseng YC (2012) Recent advances in imaging of dopaminergic neurons for evaluation of neuropsychiatric disorders. J Biomed Biotechnol 2012:259349. https://doi.org/10.1155/2012/259349

Sims-Williams H, Matthews JC, Talbot PS, Love-Jones S, Brooks JC, Patel NK, Pickering AE (2017) Deep brain stimulation of the periaqueductal gray releases endogenous opioids in humans. Neuroimage 146:833–842. https://doi.org/10.1016/j.neuroimage.2016.08.038

Smith GS, Laxton AW, Tang-Wai DF, McAndrews MP, Diaconescu AO, Workman CI, Lozano AM (2012) Increased cerebral metabolism after 1 year of deep brain stimulation in Alzheimer disease. Arch Neurol 69:1141–1148. https://doi.org/10.1001/archneurol.2012.590

Smith GS et al (2019) Effect of STN DBS on vesicular monoamine transporter 2 and glucose metabolism in Parkinson's disease. Parkinsonism Relat Disord 64:235–241. https://doi.org/10.1016/j.parkreldis.2019.04.006

Soret M, Bacharach SL, Buvat I (2007) Partial-volume effect in PET tumor imaging. J Nucl Med 48:932–945. https://doi.org/10.2967/jnumed.106.035774

Sperling RA et al (2009) Amyloid deposition is associated with impaired default network function in older persons without dementia. Neuron 63:178–188. https://doi.org/10.1016/j.neuron.2009.07.003

Spetsieris PG, Eidelberg D (2011) Scaled subprofile modeling of resting state imaging data in Parkinson's disease: methodological issues. Neuroimage 54:2899–2914. https://doi.org/10.1016/j.neuroimage.2010.10.025

Stefani A, Pierantozzi M, Ceravolo R, Brusa L, Galati S, Stanzione P (2010) Deep brain stimulation of pedunculopontine tegmental nucleus (PPTg) promotes cognitive and metabolic changes: a target-specific effect or response to a low-frequency pattern of stimulation? Clin EEG Neurosci 41:82–86. https://doi.org/10.1177/155005941004100207

Strafella AP, Dagher A, Sadikot AF (2003a) Cerebral blood flow changes induced by subthalamic stimulation in Parkinson's disease. Neurology 60:1039–1042. https://doi.org/10.1212/01.wnl.0000052691.48076.92

Strafella AP, Sadikot AF, Dagher A (2003b) Subthalamic deep brain stimulation does not induce striatal dopamine release in Parkinson's disease. Neuroreport 14:1287–1289. https://doi.org/10.1097/00001756-200307010-00020

Strafella AP, Lozano AM, Ballanger B, Poon YY, Lang AE, Moro E (2008) rCBF changes associated with PPN stimulation in a patient with Parkinson's disease: a PET study. Mov Disord 23:1051–1054. https://doi.org/10.1002/mds.22055

Suetens K, Nuttin B, Gabriels L, Van Laere K (2014) Differences in metabolic network modulation between capsulotomy and deep-brain stimulation for refractory obsessive-compulsive disorder. J Nucl Med 55:951–959. https://doi.org/10.2967/jnumed.113.126409

Tanei T, Kajita Y, Nihashi T, Kaneoke Y, Takebayashi S, Nakatsubo D, Wakabayashi T (2009) Changes in regional blood flow induced by unilateral subthalamic nucleus stimulation in patients with Parkinson's disease. Neurol Med Chir (Tokyo) 49:507–513. https://doi.org/10.2176/nmc.49.507

Thevathasan W, Moro E (2019) What is the therapeutic mechanism of pedunculopontine nucleus stimulation in Parkinson's disease? Neurobiol Dis 128:67–74. https://doi.org/10.1016/j.nbd.2018.06.014

Thobois S et al (2002) Effects of subthalamic nucleus stimulation on actual and imagined movement in Parkinson's disease: a PET study. J Neurol 249:1689–1698. https://doi.org/10.1007/s00415-002-0906-y

Thobois S et al (2003) Chronic subthalamic nucleus stimulation and striatal D2 dopamine receptors in Parkinson's disease--a [(11)C]-raclopride PET study. J Neurol 250:1219–1223. https://doi.org/10.1007/s00415-003-0188-z

Thobois S, Hotton GR, Pinto S, Wilkinson L, Limousin-Dowsey P, Brooks DJ, Jahanshahi M (2007) STN stimulation alters pallidal-frontal coupling during response selection under competition. J Cereb Blood Flow Metab 27:1173–1184. https://doi.org/10.1038/sj.jcbfm.9600425

Thobois S et al (2008) Globus pallidus stimulation reduces frontal hyperactivity in tardive dystonia. J Cereb Blood Flow Metab 28:1127–1138. https://doi.org/10.1038/sj.jcbfm.9600610

Trost M et al (2006) Network modulation by the subthalamic nucleus in the treatment of Parkinson's disease. Neuroimage 31:301–307. https://doi.org/10.1016/j.neuroimage.2005.12.024

Tsai HC, Chang CH, Pan JI, Hsieh HJ, Tsai ST, Hung HY, Chen SY (2012) Pilot study of deep brain stimulation in refractory obsessive-compulsive disorder ethnic Chinese patients. Psychiatry Clin Neurosci 66:303–312. https://doi.org/10.1111/j.1440-1819.2012.02352.x

Turner R, Jones T (2003) Techniques for imaging neuroscience. Br Med Bull 65:3–20. https://doi.org/10.1093/bmb/65.1.3

Ulla M et al (2006) Manic behaviour induced by deep-brain stimulation in Parkinson's disease: evidence of substantia nigra implication? J Neurol Neurosurg Psychiatry 77:1363–1366. https://doi.org/10.1136/jnnp.2006.096628

Ulla M et al (2011) Contact dependent reproducible hypomania induced by deep brain stimulation in Parkinson's disease: clinical, anatomical and functional imaging study. J Neurol Neurosurg Psychiatry 82:607–614. https://doi.org/10.1136/jnnp.2009.199323

Valalik I, Emri M, Lengyel Z, Mikecz P, Tron L, Csokay A, Marian T (2009) Pallidal deep brain stimulation and L-dopa effect on PET motor activation in advanced Parkinson's disease. J Neuroimaging 19:253–258. https://doi.org/10.1111/j.1552-6569.2008.00304.x

Velasco F et al (2015) Metabolic changes induced by electrical stimulation of prelemniscal radiations for the treatment of Parkinson disease. Stereotact Funct Neurosurg 93:333–341. https://doi.org/10.1159/000438997

Ventre-Dominey J, Bourret S, Mollion H, Broussolle E, Dominey PF (2014) Dissociable dorsal and ventral frontostriatal working memory circuits: evidence from subthalamic stimulation in Parkinson's disease. Hum Brain Mapp 35:552–566. https://doi.org/10.1002/hbm.22205

Vernaleken I et al (2009) Bithalamical deep brain stimulation in tourette syndrome is associated with reduction in dopaminergic transmission. Biol Psychiatry 66:e15–e17. https://doi.org/10.1016/j.biopsych.2009.06.025

Vitek JL et al (2010) Standard guidelines for publication of deep brain stimulation studies in Parkinson's disease (Guide4DBS-PD). Mov Disord 25:1530–1537. https://doi.org/10.1002/mds.23151

Volkow ND et al (1993) Reproducibility of repeated measures of carbon-11-raclopride binding in the human brain. J Nucl Med 34:609–613

Volonte MA et al (2012) Changes in brain glucose metabolism in subthalamic nucleus deep brain stimulation for advanced Parkinson's disease. Parkinsonism Relat Disord 18:770–774. https://doi.org/10.1016/j.parkreldis.2012.03.016

Wang J, Ma Y, Huang Z, Sun B, Guan Y, Zuo C (2010) Modulation of metabolic brain function by bilateral subthalamic nucleus stimulation in the treatment of Parkinson's disease. J Neurol 257:72–78. https://doi.org/10.1007/s00415-009-5267-3

Weiss PH et al (2015) Subthalamic nucleus stimulation improves parkinsonian gait via brainstem locomotor centers. Mov Disord 30:1121–1125. https://doi.org/10.1002/mds.26229

Whiteside SP, Port JD, Abramowitz JS (2004) A meta-analysis of functional neuroimaging in obsessive-compulsive disorder. Psychiatry Res 132:69–79. https://doi.org/10.1016/j.pscychresns.2004.07.001

Wielepp JP, Burgunder JM, Pohle T, Ritter EP, Kinser JA, Krauss JK (2001) Deactivation of thalamocortical activity is responsible for suppression of parkinsonian tremor by thalamic stimulation: a 99mTc-ECD SPECT study. Clin Neurol Neurosurg 103:228–231

Wilcox RA, Cole MH, Wong D, Coyne T, Silburn P, Kerr G (2011) Pedunculopontine nucleus deep brain stimulation produces sustained improvement in primary progressive freezing of gait. J Neurol Neurosurg Psychiatry 82:1256–1259. https://doi.org/10.1136/jnnp.2010.213462

Windels F, Bruet N, Poupard A, Urbain N, Chouvet G, Feuerstein C, Savasta M (2000) Effects of high frequency stimulation of subthalamic nucleus on extracellular glutamate and GABA in substantia nigra and globus pallidus in the normal rat. Eur J Neurosci 12:4141–4146

Yianni J et al (2004) Senile chorea treated by deep brain stimulation: a clinical, neurophysiological and functional imaging study. Mov Disord 19:597–602. https://doi.org/10.1002/mds.10716

Zhang HW, Li DY, Zhao J, Guan YH, Sun BM, Zuo CT (2013) Metabolic imaging of deep brain stimulation in anorexia nervosa: a 18F-FDG PET/CT study. Clin Nucl Med 38:943–948. https://doi.org/10.1097/RLU.0000000000000261

Radionuclide Imaging Studies in Pediatric Neurology

47

Ajay Kumar, Csaba Juhasz, and Harry T. Chugani

Contents

47.1 Introduction 1246
47.2 Epileptic Disorders 1247
47.2.1 Epilepsy 1250
47.2.2 Pediatric Epilepsy Syndromes 1258
47.3 Other Neurological Disorders 1266
47.3.1 Perinatal Hypoxic Ischemic Brain Injury and Cerebral Palsy 1266
47.3.2 Autism 1267
47.3.3 Developmental Dyslexia 1270
47.3.4 Landau-Kleffner Syndrome 1271
47.3.5 Tourette Syndrome 1272
47.3.6 Neuronal Ceroid Lipofuscinosis or Spielmeyer-Vogt (or Batten) Disease 1274
47.4 Multimodal Imaging with Simultaneous PET-MR 1275
References 1276

Abstract

Functional imaging modalities, such as positron emission tomography (PET) and single-photon emission computed tomography (SPECT), can noninvasively provide very useful qualitative (visual) and quantitative information about a variety of physiological and biological processes in the brain, which may be altered during disease conditions. The use of these techniques not only can shed light upon the underlying pathology but also can provide biomarkers to aid in the

A. Kumar (✉) · C. Juhasz
Departments of Pediatrics and Neurology, PET Center, Children's Hospital of Michigan, Detroit Medical Center, Wayne State University School of Medicine, Detroit, MI, USA
e-mail: ajaykumar@med.wayne.edu

H. T. Chugani
Department of Neurology, NYU School of Medicine, New York, NY, USA

R. A. J. O. Dierckx et al. (eds.), *PET and SPECT in Neurology*,
https://doi.org/10.1007/978-3-030-53168-3_47

diagnosis, localization, follow-up, treatment development, and/or treatment response evaluation and prognostication in various diseases. PET and SPECT have been used clinically in the evaluation of medically refractory epilepsy to select candidates for surgical intervention, especially when structural imaging (CT, MRI, etc.) is normal or discordant with other localizing information. In addition, functional neuroimaging can assist evaluation of some specific epileptic syndromes, such as tuberous sclerosis, to identify noninvasively the epileptic tuber, as well as conditions like infantile spasms or Lennox-Gastaut syndrome, to reveal a focal region for surgical resection in otherwise cryptogenic cases. Similarly, these techniques are instrumental to investigate the underlying basis for various neurocognitive and behavioral abnormalities in children, where other imaging modalities are often normal or reveal only subtle and nonspecific changes. Even when structural imaging is abnormal, PET and SPECT abnormalities may precede or extend beyond the structural changes, which can have immense therapeutic and prognostic implications.

47.1 Introduction

Functional imaging modalities, such as positron emission tomography (PET) and single-photon emission computed tomography (SPECT), can provide noninvasively qualitative (visual) and quantitative information about a variety of physiological and biological processes in the brain. These techniques not only allow in vivo visualization of these processes but also have revolutionized our understanding of various brain functions and etiopathogenesis of several neurological disorders. PET and SPECT imaging techniques use gamma ray emission from the *nuclear* disintegration of radioisotopes or radiolabeled molecules to study the perfusion or function of an organ. With both methods, a very small amount of a selected radiotracer is injected into the patient. The radiotracer is selected on the basis of the desired purpose, i.e., which organs and what functions are of interest. Once inside the body, these radiotracers become distributed in a specific way depending upon the nature of the radiotracer and the function of the targeted organs. The gamma rays emitted by the radiotracers are detected externally with the help of detectors, and an image of the spatial distribution of these radiotracers is generated. Theoretically, any organ or its function can be studied, provided appropriate and suitable radiotracers are available. The reason for applying PET and SPECT in neurology is based on the fact that the metabolism (particularly of glucose), neurochemical production/distribution, receptor density/expression, or cerebral blood flow may be altered in various neurological disorders, and these events can be visualized or quantified using PET or SPECT. Therefore, the use of these techniques not only can shed some light upon the underlying pathology but also can help in the diagnosis, localization, follow-up, treatment development, and/or treatment response evaluation and prognostication, once these pathologies are

known/established. In this chapter, we will discuss the role and application of PET and SPECT in various pediatric neurological disorders.

47.2 Epileptic Disorders

Presently, neither PET nor SPECT is used in the primary diagnosis or evaluation of recent-onset epilepsy; however, they play a very unique and important role in certain specific situations, such as in the evaluation of medically refractory cases for epilepsy surgery, particularly when structural imaging (CT, MRI, etc.) is normal, or in the evaluation of some specific epileptic syndromes, such as tuberous sclerosis. As of now, neither PET nor SPECT can identify precisely the epileptogenic zone to be resected; however, they can help in the general identification of these regions, including functional deficit zone, and quite often can provide some information related to the observed neurocognitive and behavioral abnormalities.

PET in pediatric epilepsy is performed using 2-deoxy-2(^{18}F)-fluoro-D-glucose (FDG), which shows hypometabolism or decreased glucose consumption in the epileptic cortex in the interictal state. The hypometabolism can result from a variety of mechanisms, including neuronal loss, diaschisis, or reduction in synaptic density. It appears that cortical hypometabolism may be associated with duration, frequency, and severity of the seizures, as focal hypometabolism is found in only one-fifth of children with new-onset epilepsy compared to 80–85% of adults with intractable seizures (Gaillard et al. 2002). Persistent or increased seizure frequency may lead to enlargement of the hypometabolic area, whereas seizure control may be associated with decrease in the size of hypometabolic cortex or even its resolution, as demonstrated by longitudinal PET studies (Benedek et al. 2006). The time interval between PET acquisition and the most recent seizure also may affect the extent and severity of the cortical abnormality, with shorter duration leading to larger extent or severity of the hypometabolism on FDG PET scan (Bouvard et al. 2005). Pure ictal PET is rarely possible, as seizures usually last for a few seconds to minutes, whereas FDG PET shows cumulative FDG uptake over a period of 30–45 min; thus, the metabolic pattern usually reflects a summation of interictal, ictal, and postictal metabolic changes and is difficult to interpret in patients who had coincidental seizure(s) during the tracer uptake period. While a rare finding, interictal PET **hypermetabolism** does occur and may help identify epileptogenic zones with careful analysis (Schur et al. 2018).

FDG PET usually shows larger areas of hypometabolism compared to the abnormality shown on MRI (if there is one), and ictal or intracranial subdural EEG-determined epileptogenic region. An early study from our group compared the exact locations of objectively defined cortical hypometabolic regions on PET to ictal and interictal epileptiform abnormalities from subdural EEG recordings (Juhasz et al. 2000a). We found that the overlap between hypometabolic areas and seizure-onset electrodes was only partial, with seizure onset extending beyond the hypometabolic cortex, while glucose metabolic abnormalities incorporated non-epileptogenic regions also. This observation was subsequently confirmed in other studies (Alkonyi

et al. 2009; Jeong et al. 2017; Tomás et al. 2019). Therefore, FDG PET abnormalities cannot be solely relied upon to determine the surgical margin; however, they can help in lateralization or *general* localization of the epileptic focus, which can facilitate surgical planning and subsequent placement of intracranial electrodes, particularly in cases of normal MRI and non-localizing scalp EEG. Various co-registration and objective analytic methods, such as statistical parametric mapping (SPM), a voxel-based whole-brain analysis, or SPM extent analysis with asymmetry index, can be quite helpful in these cases (Van Bogaert et al. 2000; Kim et al. 2006; Akman et al. 2010; Kumar et al. 2010).

It has been shown that the sensitivity of FDG PET can be increased by co-registration of PET images with structural MRI, particularly in patients with cortical dysplasia (Lerner et al. 2009). Co-registration can lead to detection of mild type I cortical dysplasia in up to 98% of the cases and can add useful localizing value in one-third of patients with non-concordant EEG and MRI findings (Salamon et al. 2008). FDG PET has a clear advantage over MRI in detecting mild malformations of cortical development, which can be missed in about 2/3 of the cases (Kim et al. 2011). Use of higher-strength MRI (3 T) images co-registered with FDG PET can further increase the detection of focal abnormalities (Ding et al. 2018). A recent study showed the utility of quantitative PET processing in combination with morphometric analysis to automatically and objectively identify epileptogenic abnormalities in the cohort of MRI-negative epilepsy patients (Lin et al. 2018). It demonstrated that the complete resection of MRI/PET-positive regions was associated with seizure-free outcome, and this effect was more robust in the extratemporal subgroup as compared to those with temporal lobe epilepsy. Another study found that hypometabolism confined to the epileptogenic zone as defined by EEG and MRI is associated with a favorable postoperative outcome in both temporal lobe and extratemporal lobe epilepsy patients (Tomás et al. 2019).

Sometimes, hypometabolism can be quite extensive and may even extend into the contralateral hemisphere, perhaps depending upon the type, location, duration, and severity of the seizure and maturity of the brain (Kumar et al. 2010). Long-standing severe seizures, particularly in the immature pediatric brain, may show extensive areas of hypometabolism, likely involving seizure propagation pathways, or the seizure effect on connected brain regions. FDG PET is particularly useful in the evaluation of the functional status of the rest of the brain when an epileptogenic lesion is considered for surgical resection, as postsurgical neurocognitive outcome will also depend upon the integrity of the remaining (unresected) cortex. This is particularly important in children, because brain plasticity following resection is more likely to involve functionally intact regions.

Several other PET tracers, such as ^{11}C-flumazenil (FMZ) and ^{11}C-alpha-methyl-L-tryptophan (AMT), used for the evaluation of gamma-aminobutyric acid type A ($GABA_A$) receptors and serotonin/kynurenine metabolism, respectively, have also been investigated in epilepsy and have been found to be useful in certain situations. FMZ PET may be clinically useful in cases of temporal lobe epilepsy (Ryvlin et al. 1998), particularly in identifying medial temporal lobe involvement (Henry et al. 1993; Koepp et al. 1996). AMT PET is very useful in patients with tuberous

sclerosis and certain types of epileptogenic cortical malformations (Chugani et al. 1998a, b; Asano et al. 2000; Fedi et al. 2003; Chugani et al. 2011, 2013a, b). These applications are discussed in further detail below. Several other PET tracers, such as radioligands for opiate, histamine, NMDA, acetylcholine, dopamine, and other neuro-receptors, have been investigated in epilepsy. PET imaging using these tracers shows either increased (^{11}C-carfentanyl (μ-opioid receptor agonist), ^{11}C-methylnaltrindole (δ-opioid receptor antagonist), ^{18}F-cyclofoxy (μ-, κ-opioid receptor antagonist), ^{11}C-doxepin (H1 receptor antagonist), and ^{11}C-L-deprenyl (MAO-B inhibitor)) or decreased (^{11}C-diprenorphine (μ-, δ-, κ-opioid receptor antagonist), ^{11}C/^{18}F-FCWAY ($5HT_{1A}$ receptor antagonist), ^{18}F-MPPF ($5HT_{1A}$ receptor antagonist), ^{18}F-altanserin ($5HT_{2A}$ receptor antagonist), ^{11}C-(S)-[*N-methyl*]-ketamine (NMDA receptor antagonist), ^{11}C-NMBP ($_{m}$Ach receptor antagonist), and ^{123}I-iododexetimide ($_{m}$Ach receptor antagonist)) binding in the presumed epileptogenic region. However, only a limited number of studies are available regarding these tracers, and the clinical role and additional value of these tracers in epilepsy evaluation are yet to be established.

For epilepsy evaluation, SPECT is usually performed using ^{99m}Tc-labeled ethylcysteinate dimer (ECD) or hexamethylpropylene amine oxime (HMPAO) and demonstrates increased or decreased cerebral perfusion in the epileptic cortex when performed in the ictal or interictal state, respectively. During the ictal phase, blood flow in the epileptic region can increase up to 300%, which can be seen as an area of hyperperfusion on *ictal* SPECT (Hougaard et al. 1976). *Interictal* SPECT shows hypoperfusion or normal perfusion in the epileptogenic region; however, hypoperfusion may be very mild and sometimes difficult to distinguish from the surrounding normal brain on visual examination. The main role of interictal SPECT at present is to assist in the evaluation of ictal SPECT, visually or quantitatively, using statistical parametric mapping (SPM) or subtraction ictal SPECT co-registered to MRI (SISCOM), by providing a baseline blood flow image. Use of these registration techniques can increase the sensitivity and specificity of ictal SPECT. Studies have shown that SPM can increase the sensitivity of SPECT (and also PET) scan over visual analysis (Lee et al. 2000; Bruggemann et al. 2004; Tae et al. 2005). However, lack of age-matched controls can make its use difficult, particularly in children less than 6 years of age (Muzik et al. 2000a). SISCOM, on the other hand, appears to be very useful in children. The probability of localizing an ictal-onset zone is reported to be higher with SISCOM, compared to ictal EEG and MRI (O'Brien et al. 1998, 1999). Use of SISCOM can help in the detection of subtle MRI changes, initially reported as normal (Chiron et al. 1999a; Lawson et al. 2000). Recent pediatric studies demonstrated the complementary value of SISCOM, especially in localizing extratemporal foci (Kim et al. 2009). Outcome studies have also shown that the area of the resected SISCOM abnormality is associated with the surgical result; the larger the area of resected SISCOM abnormality, the better the outcome (O'Brien et al. 1998, 1999, 2000; von Oertzen et al. 2011). Simultaneous use of FDG PET and iomazenil SPECT may be particularly useful in patients with non-lesional epilepsy in identifying the seizure focus and predicting a seizure-free outcome (Fujimoto et al. 2018). The major limitation of SPECT in children is

difficulty in acquiring a good ictal study because children may have very frequent and short-lasting seizures (such as infantile spasms or myoclonic epilepsy) so the ictal phase is missed. Another limitation is the poor spatial resolution (10–15 mm) of SPECT, compared to FDG PET (about 5–6 mm), which becomes even more crucial in small pediatric brains. Overall, the performance of ictal SPECT versus FDG PET has been variable, depending on the patient population and study design (Sturm et al. 2000; Kim et al. 2001; Seo et al. 2011; Jalota et al. 2016).

47.2.1 Epilepsy

47.2.1.1 Temporal Lobe Epilepsy

As stated above, FDG PET does not have much role in temporal lobe epilepsy evaluation if MRI is positive and concordant with localization suggested by EEG and seizure semiology. However, MRI is negative in a large number of patients, particularly in the pediatric population. Many times, the EEG can be noncontributory, generalized, or bilateral, depending upon various factors, such as seizure duration, seizure severity, or location of a seizure focus close to the midline (Lamusuo et al. 2001). PET can play an important role in these conditions, particularly considering that almost a quarter of epileptic patients become refractory and may have normal MRI and sometimes equivocal EEG (Fig. 47.1). FDG PET can help to identify the epileptic temporal lobe in almost half of the patients with noncontributory EEG (Theodore et al. 1997). It can be particularly helpful in cases with dual pathology

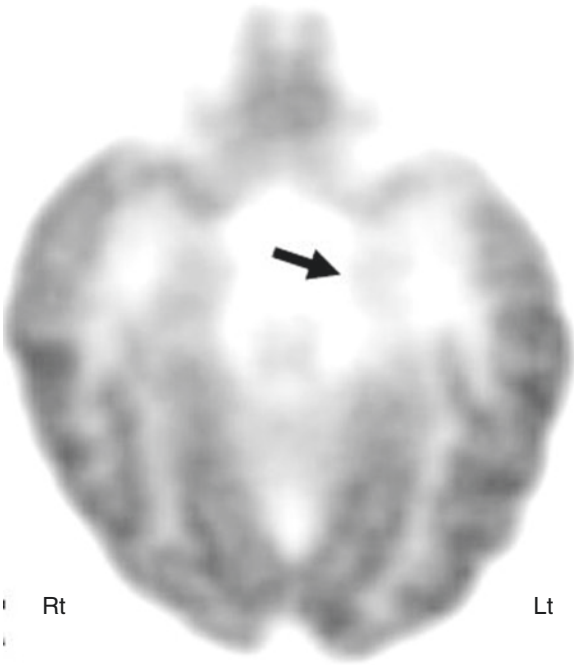

Fig. 47.1 Axial 2-deoxy-2(^{18}F)-fluoro-D-glucose PET scan in a child with intractable temporal lobe epilepsy and normal MRI. EEG changes were occasionally bilateral or equivocal. PET scan showed hypometabolism in the left medial temporal region (*arrow*) and increased the confidence for epilepsy surgery. The child underwent surgery, which showed mild sclerotic changes in the medial temporal lobe on histopathology, and is seizure-free after the surgery

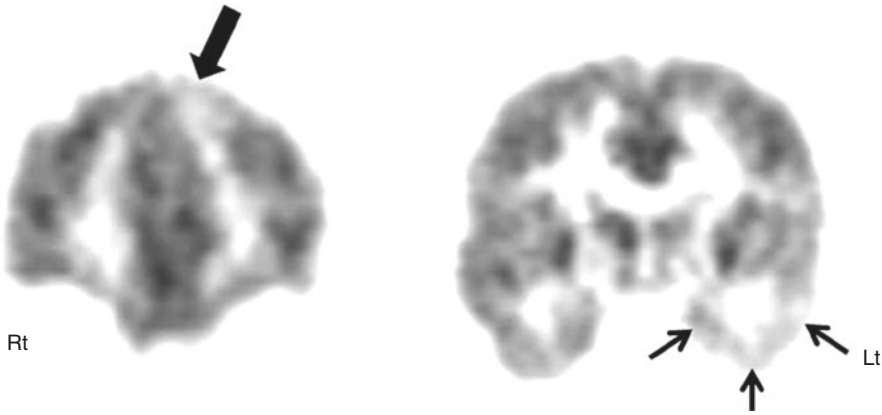

Fig. 47.2 2-Deoxy-2(^{18}F)-fluoro-D-glucose PET in a child with dual pathology. Coronal PET showing an area of decreased glucose metabolism in the left medial frontal cortex (*thick arrow*), in addition to hypometabolic left temporal lobe (*small thin arrows*) in a child with intractable temporal lobe epilepsy and bilateral epileptiform discharges on EEG. The child underwent epilepsy surgery with simultaneous resection of the left medial frontal cortex and hippocampus and is seizure-free

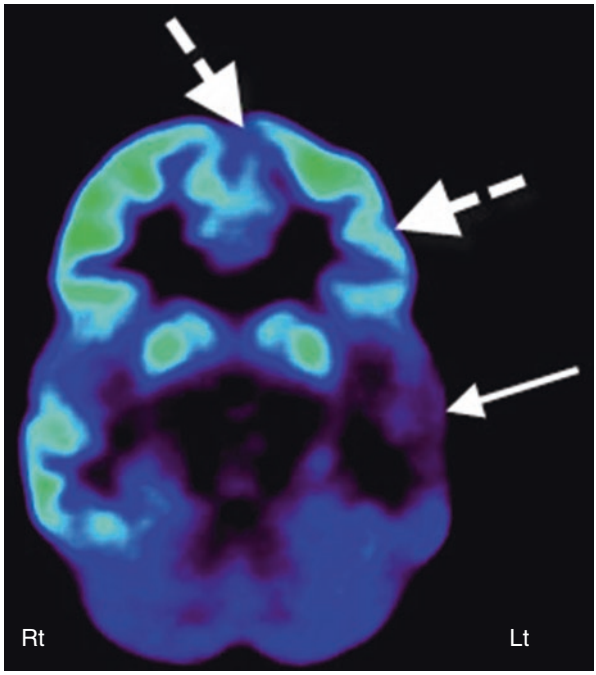

Fig. 47.3 2-Deoxy-2(^{18}F)-fluoro-D-glucose PET scan in a case of suspected secondary epileptic focus. A child with long-standing temporal lobe epilepsy (primary seizure focus) developed a change in seizure semiology with independent epileptiform discharges from frontal regions. PET scan showed severe hypometabolism of the left temporal lobe (*arrow*) along with reduced glucose metabolism in the left inferior frontal lobe (*broken arrows*), suggesting a possible secondary epileptic focus presumably due to persistent kindling through the uncinate fasciculus

(Fig. 47.2) or secondary epileptic foci (Fig. 47.3). The overall sensitivity of FDG PET in identifying the epileptic temporal lobe is in the range of 85–90% (Swartz et al. 1989; Gaillard et al. 1995; Knowlton et al. 1997; Ryvlin et al. 1998). Importantly, FDG PET can provide additional information about the epileptic focus

in many patients, affecting ultimate surgical decision-making in 50–70% of patients (Ollenberger et al. 2005; Uijl et al. 2007), with it alone being the basis of surgical decision in almost 17% of patients (Uijl et al. 2007). FDG PET also has prognostic value, as unilateral PET hypometabolism appears to predict a good surgical outcome, even in patients with negative MRI or equivocal EEG (Willmann et al. 2007). An odds ratio of 7.1 has been reported for FDG PET in predicting a seizure-free outcome (Knowlton et al. 2008). It has been recently proposed that the difference in metabolic patterns, depending on the lateralization of medial temporal lobe epilepsy, may represent distinct epileptic networks in patients with right versus left medial temporal lobe epilepsy and can guide preoperative counseling and surgical planning (Cahill et al. 2019).

Another PET tracer, FMZ, has been investigated by quite a few centers. FMZ binds to the $GABA_A$ receptors, the main binding sites of the inhibitory neurotransmitter γ-aminobutyric acid (GABA). Since neurons in the normal hippocampus and amygdala have strong $GABA_A$ receptor expression, FMZ PET has been found to be particularly useful in detecting medial temporal lobe epileptic foci, which often show decreased FMZ binding, and may sometimes delineate abnormalities, either not seen or appearing subtle on FDG PET (Fig. 47.4). FMZ PET can also show decreased $GABA_A$ receptor binding in the epileptogenic neocortex, and the extent of abnormality is usually less than that seen on FDG PET scan (Henry et al. 1993; Savic et al. 1993; Szelies et al. 1996; Ryvlin et al. 1998). FMZ PET is almost 100% sensitive in cases of hippocampal sclerosis and can reveal contralateral abnormality

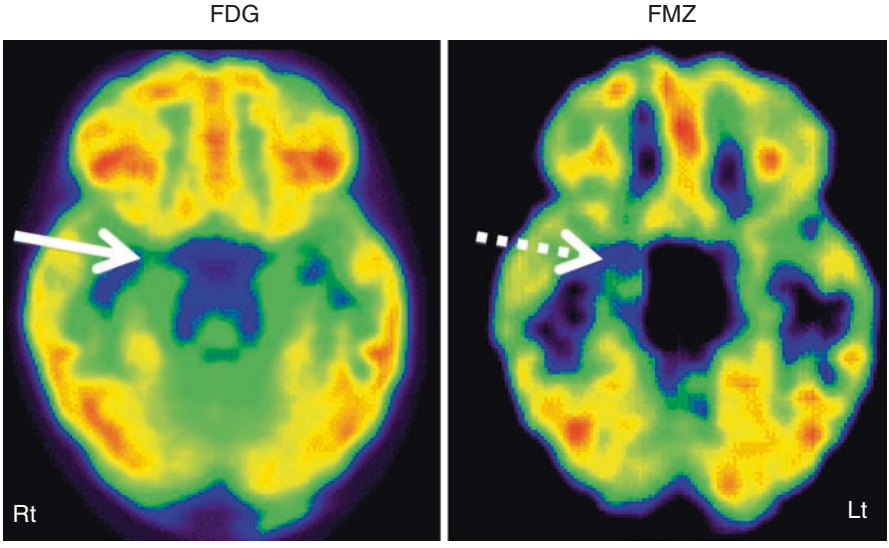

Fig. 47.4 ^{11}C-Flumazenil PET (*right image*) showing better delineation of right hippocampal abnormality (*broken arrow*) in a child with medial temporal lobe epilepsy, compared to 2-deoxy-2(^{18}F)-fluoro-D-glucose PET (*left image*) which showed only subtle changes (*solid arrow*) in this region

in almost one-third of patients with apparently unilateral hippocampal sclerosis on MRI (Henry et al. 1993; Koepp et al. 1996). FMZ PET can sometimes show increased FMZ binding in cases of cortical developmental malformations (Koepp et al. 1997) or microdysgenesis in the white matter (Hammers et al. 2002). Still, clinical use of FMZ PET in temporal lobe epilepsy is not established. Increasing availability of novel, ^{18}F-labeled (thus, longer half-life) flumazenil tracers may facilitate further exploration of this technique as a clinical tool.

Several other PET tracers have been tested in temporal lobe epilepsy for receptor imaging with variable results. AMT PET has been reported to be somewhat useful in identifying the epileptic foci in patients with temporal lobe epilepsy and normal hippocampal volume, but not in those with hippocampal sclerosis (Natsume et al. 2003); however, the added clinical value in individual cases remains uncertain. Studies of opiate receptor PET imaging have reported both increased (Frost et al. 1988; Madar et al. 1997) and normal (Mayberg et al. 1991; Theodore et al. 1992) receptor density in patients with temporal lobe epilepsy. Similarly, the level of monoamine oxidase B has been found to be both high (Kumlien et al. 1992) and low (Kumlien et al. 2001) in temporal lobe epilepsy. While significantly reduced dopamine receptor binding has been reported in the epileptogenic temporal lobe (Werhahn et al. 2006), no binding alterations were found in PET studies using ^{11}C-verapamil, a P-glycoprotein substrate (Langer et al. 2007). Patients with temporal lobe epilepsy have also been shown to have reduced NMDA receptor binding (Kumlien et al. 1999) but increased ^{11}C-doxepine uptake (Iinuma et al. 1993) in the epileptogenic temporal cortex. Recently, evidence of inflammatory changes was found in the hippocampus, parahippocampal gyrus, amygdala, and fusiform gyrus, ipsilateral to the epileptic focus in patients with temporal lobe epilepsy who underwent PET scanning with the translocator protein (TSPO) tracer ^{11}C-PBR28 (Hirvonen et al. 2012). A subsequent study also using ^{11}C-PBR28 found increased binding in temporal lobe regions both ipsilateral and contralateral to the epileptic focus, suggesting that inflammation may be an important pathophysiological mechanism in temporal lobe epilepsy (Gershen et al. 2015). In patients with neocortical epilepsy, ^{11}C-PBR28 PET revealed both focal and more distributed inflammation, as well as significant variability, thus limiting its role in clinical application (Dickstein et al. 2019).

Although limited SPECT data exist in the pediatric epilepsy population, it has been reported to be consistent with other noninvasive presurgical examinations in up to 95% of patients (O'Brien et al. 1998; Chiron et al. 1999a; Vera et al. 1999; Lawson et al. 2000; Kaminska et al. 2003; Lee et al. 2005; Kurian et al. 2007). Interictal SPECT has very low sensitivity (less than 50%) in the detection of epileptogenic regions in temporal lobe epilepsy, with false-positive or false-negative findings in 20–75% of cases. In contrast, ictal SPECT can correctly localize the epileptic foci in 70–90% of cases with unilateral temporal lobe epilepsy (Fig. 47.5) (Rowe et al. 1991; Harvey et al. 1993; Lee et al. 2005; Benifla et al. 2006). Various registration techniques, such as SPM or subtraction ictal SPECT co-registered to MRI (SISCOM), can further increase the sensitivity and specificity of ictal SPECT but require two separate SPECT studies including interictal and ictal scans. In children,

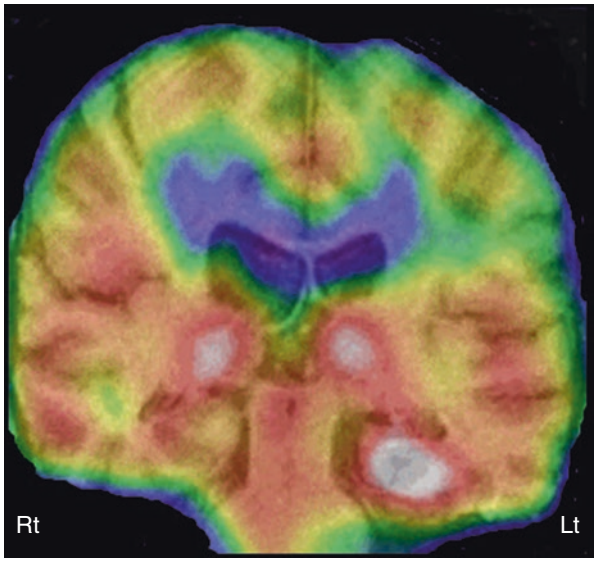

Fig. 47.5 Ictal ^{99m}Tc-ethyl cysteinate dimer SPECT (coronal view, co-registered onto the corresponding MRI slice) in a child with temporal lobe epilepsy showing increased perfusion in the left hippocampus, suggesting an epileptic focus. Also noted is increased perfusion in bilateral thalami, which can be seen during the ictal phase

SISCOM has been reported to be helpful in identifying the epileptogenic region in up to 95% of cases (Chiron et al. 1999b). In comparison to intracranial EEG findings, ictal ECD SPECT was found to correctly localize the seizure-onset zone in 80% of children with intractable epilepsy (Kaminska et al. 2003). In addition, in the majority of children with favorable outcome following resective epilepsy surgery, the surgical margin coincided with the SPECT focus. Postictal SPECT is also more sensitive (70–90%) than interictal SPECT, and its accuracy also can improve further with the use of SISCOM (Rowe et al. 1989; O'Brien et al. 1999). SISCOM can be particularly useful in cases of dysembryoplastic neuroepithelial tumor (DNET), which is often located in the temporal lobe and most prevalent in the pediatric population. SISCOM can demonstrate some additional dysplastic cortical areas around the DNET, and removal of these areas is essential for better surgical outcome. The use of SISCOM can increase the focus detection rate up to 93%, compared to 74% without it (Chiron et al. 1999b; Vera et al. 1999; Valenti et al. 2002). More rigorous studies in 113 children show less favorable results, with overall sensitivity of 64.8% and specificity of 40.7% in identifying the epileptogenic region (Aungaroon et al. 2018). Recently, a new approach PET interictal subtracted ictal SPECT co-registered with MRI (PISCOM) has been explored, and preliminary studies suggest promising results, but more data are required (Perissinotti et al. 2018).

47.2.1.2 Extratemporal Lobe Epilepsy

FDG PET plays a relatively more important role in extratemporal lobe epilepsy in children, compared to adults, due to its higher incidence in children with a large majority having noncontributory MRI (Wyllie et al. 1998). Normal MRI is perhaps due to the higher incidence of subtle cortical dysplasia in children compared to the adults, as these lesions are often difficult to detect on MRI. Here, FDG PET can play

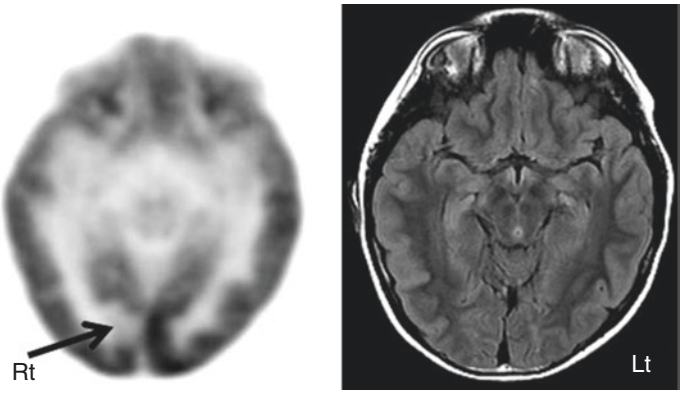

Fig. 47.6 2-Deoxy-2(^{18}F)-fluoro-D-glucose PET (*left image*) in a child with intractable epilepsy, normal fluid-attenuated inversion recovery (FLAIR) MRI (*right image*), and bilateral synchrony on EEG showed a very focal area of hypometabolism (*arrow*), which is strongly suspected to be cortical dysplasia

a valuable role, as the dysplastic cortex is usually hypometabolic (Fig. 47.6). Even when MRI is positive, it does not provide the full extent of the dysplasia, which is more obvious on FDG PET scan. FDG PET can also sometimes reveal additional epileptic foci, which can have a huge impact on surgical planning. Although a variable sensitivity of 45–92% has been reported for FDG PET in extratemporal lobe epilepsy, usually, it is less sensitive than in temporal lobe epilepsy (Henry et al. 1991; Swartz et al. 1995; da Silva et al. 1997; Kim et al. 2002; Honbolygo et al. 2006; Patil et al. 2007). The wide range of sensitivity is likely due to the variable patient populations studied and the lack of standardized analytic techniques across studies. Presurgical evaluation by co-registration of FDG PET and MRI could improve the identification of the epileptogenic focus and may further guide the surgical decision-making and improve the outcome of the refractory extratemporal lobe epilepsy with normal MRI (Ding et al. 2018). It seems that the combination of morphometric analysis, magnetoencephalography (MEG), and subtraction ictal SPECT co-registered to MRI (SISCOM) can be further useful, with morphometric analysis providing the highest yield of unique information when other tests are negative or non-localizing (Wang et al. 2019).

FMZ PET has a sensitivity of 60–100% for detecting the epileptogenic cortex in extratemporal epilepsy (Savic et al. 1995; Ryvlin et al. 1998; Muzik et al. 2000b), although most studies included a highly biased surgical population. FMZ PET abnormalities tend to be smaller than the area of FDG hypometabolism and sometimes may show better concordance with intracranial EEG findings (Arnold et al. 2000; Juhasz et al. 2000b; Szelies et al. 2002) (Fig. 47.7). FMZ PET can reveal abnormality even in patients with normal MRI (Muzik et al. 2000a; Koepp and Woermann 2005), and the complete surgical resection of FMZ abnormality has been found to be associated with good seizure outcome (Muzik et al. 2000b; Juhasz et al. 2001). The use of SPM can further increase the usefulness of FMZ PET, providing objective detection

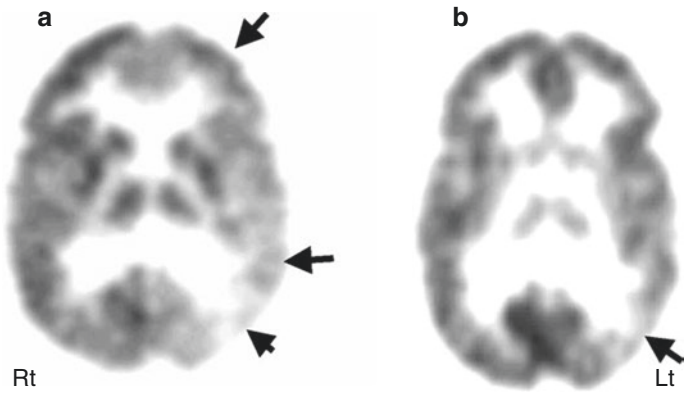

Fig. 47.7 ^{11}C-flumazenil PET (**b**) showing much smaller area of reduced flumazenil binding (*arrow*) compared to the extensive area of reduced glucose uptake in 2-deoxy-2(^{18}F)-fluoro-D-glucose PET scan (**a**) in the left temporal and frontal lobe, which was more consistent with predominantly posterior quadrant epileptiform activity on EEG

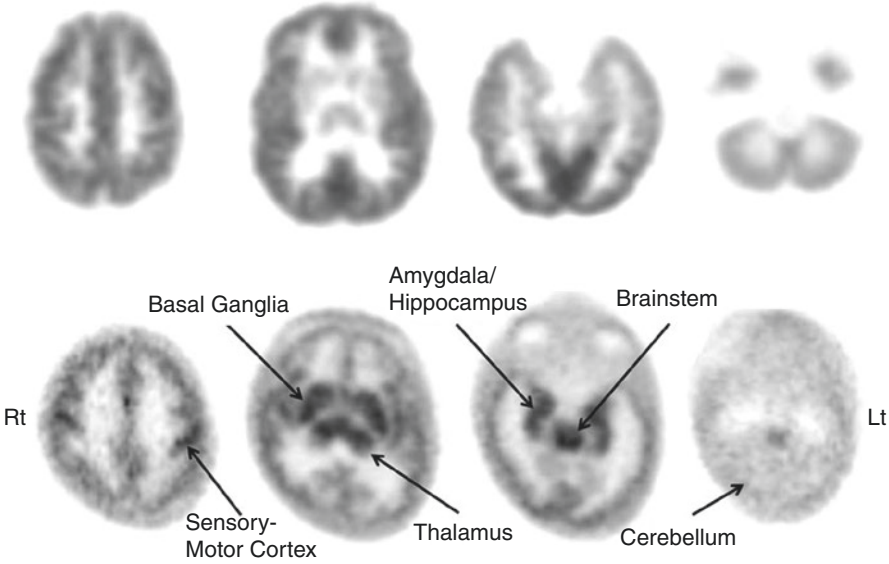

Fig. 47.8 ^{11}C-Flumazenil PET scan in an adult (upper row) and newborn (lower row) showing different pattern of FMZ-receptor binding in the newborn compared to the adult. In the newborn, highest receptor binding is seen in the amygdala-hippocampus, sensory-motor cortex, thalamus, brain stem, and basal ganglia, in that order; whereas the cerebellum and most of the cerebral cortex show relatively low binding, receptor binding is higher in the cortex compared to the basal ganglia and thalamus in normal adults

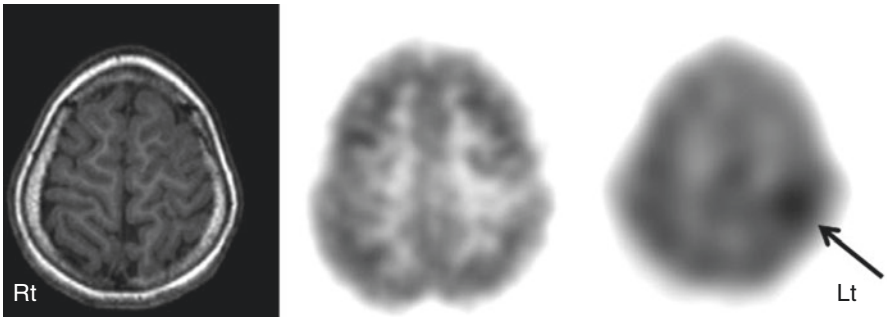

Fig. 47.9 T1-weighted MRI (*left image*), 2-deoxy-2(^{18}F)-fluoro-D-glucose (*middle image*), and ^{11}C-alpha-methyl tryptophan PET scan (*right image*) in a child with intractable epilepsy and a left frontal epileptic focus on the EEG. Whereas MRI was normal and 2-deoxy-2(^{18}F)-fluoro-D-glucose PET showed only mild hypometabolism in the left frontal region, ^{11}C-alpha-methyl tryptophan PET scan showed a focal area of increased tracer uptake interictally in this region (*arrow*). Postsurgical histopathology revealed focal cortical dysplasia

of cortical $GABA_A$ receptor abnormalities in those with or without normal MRI (Richardson et al. 1998, 2001). It should be emphasized that interpretation of FMZ PET images in very young children must take into account the normal developmental patterns seen at this age (Chugani et al. 2013a, b; Chugani 2018) (Fig. 47.8).

Another PET tracer, AMT, a ^{11}C-labeled tryptophan tracer, appears to have an important role in tuberous sclerosis (see below) and some role in selected cases, particularly in patients with cortical dysplasia and normal MRI and mild FDG changes (Juhasz et al. 2003; Wakamoto et al. 2008; Kumar et al. 2011). In these cases, AMT PET sometimes shows increased tracer uptake, particularly in patients with cortical dysplasia type IIB, who usually have very good surgical outcome (Chugani et al. 2011) (Fig. 47.9). This is an important development as it demonstrates, for the first time, that an in vivo imaging technique appears to be able to predict pathologic subtype and thus may provide presurgical prognostic information. Although the *specificity* of AMT PET is very high for detecting the seizure-onset lobe in both lesional (97%) and non-lesional neocortical epilepsies (up to 100%), its *sensitivity* is much lower (47% in lesional vs. 29% in non-lesional cases) (Wakamoto et al. 2008).

There have been a few studies which have evaluated various other brain receptors in extratemporal epilepsy. Lower opiate receptor availability was reported in the left parietal-temporal-occipital cortex in patients with reading epilepsy (Koepp et al. 1998). While reduced dopamine receptor binding in the right putamen was reported in autosomal dominant nocturnal frontal lobe epilepsy (Fedi et al. 2008), another group of investigators found increased tracer binding to nicotinic acetylcholine receptors in the midbrain, pons, and cerebellum and reduced binding in the dorsolateral prefrontal cortex in this condition (Picard et al. 2006).

Obtaining useful SPECT in pediatric extratemporal epilepsy is often difficult, as seizures are usually of short duration and propagate rapidly (such as infantile spasms

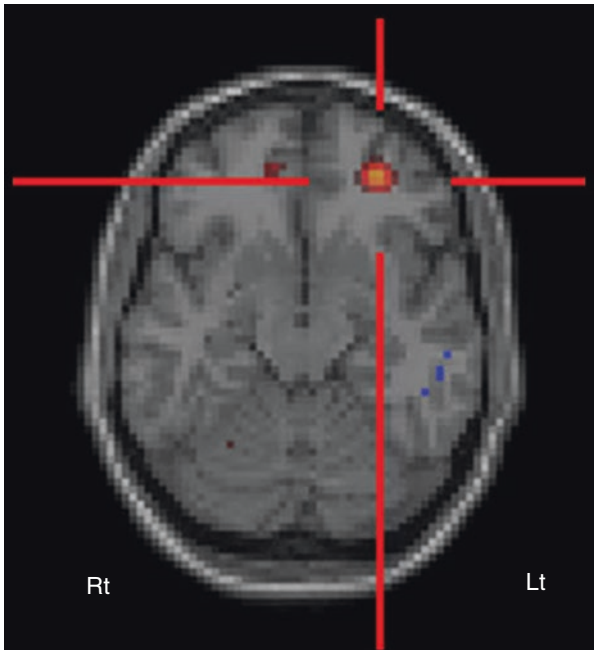

Fig. 47.10 Subtraction ictal SPECT co-registered to MRI (SISCOM) image in a patient with intractable epilepsy, normal MRI, and non-localizing surface EEG. SISCOM revealed a focal area of hyperperfusion in the left inferior frontal cortex (*red cross*)

or myoclonic epilepsy), thus making it difficult to acquire an ictal SPECT study. Postictal scans also appear less helpful because, unlike in temporal lobe epilepsy, seizure-induced perfusion changes do not always extend into the postictal phase. However, a success rate of 70% has been reported for ictal HMPAO SPECT in localizing epileptic foci (Hwang et al. 2001), and under certain conditions, it can be very useful, particularly in children with non-localizing EEG (Marks et al. 1992). Again, the use of SISCOM can further increase its localizing value (O'Brien et al. 1998; Vera et al. 1999) (Fig. 47.10). In two studies, ictal SPECT and SISCOM were found to be more sensitive than FDG PET in the detection of epileptic foci (Sturm et al. 2000; Seo et al. 2011). However, in another study of occipital lobe epilepsy, ictal HMPAO SPECT was found to be less sensitive than FDG PET (Kim et al. 2001). The use of SISCOM appears to increase the diagnostic yield in extratemporal lobe epilepsy also and correlates better with postsurgical outcome (O'Brien et al. 2000; Knowlton et al. 2008). Nevertheless, a multimodal imaging approach may provide the most benefit in children with non-lesional epilepsy (Seo et al. 2011).

47.2.2 Pediatric Epilepsy Syndromes

47.2.2.1 Infantile Spasms or West Syndrome

PET can play an important role in the evaluation of patients with infantile spasms, particularly those diagnosed with cryptogenic infantile spasms (Chugani et al. 1990, 1993). For example, uni- or multifocal cortical metabolic abnormalities were found

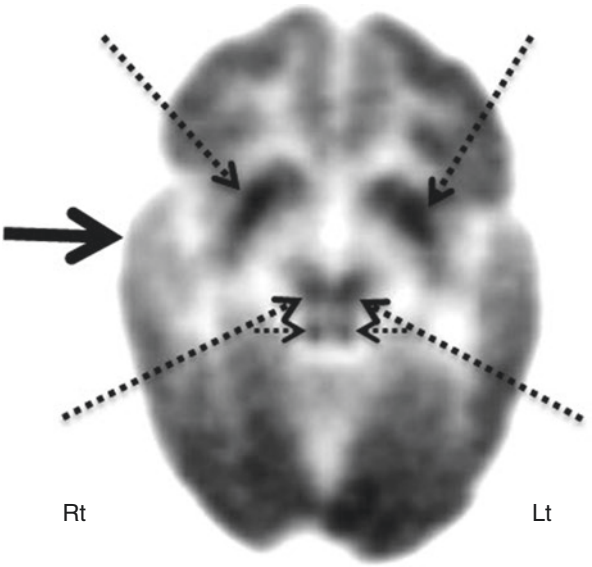

Fig. 47.11 2-Deoxy-2 (^{18}F)-fluoro-D-glucose PET showed focal hypometabolism in the right temporal cortex (*solid arrow*) in a child with infantile spasms and normal MRI. This child may be considered for focal cortical resection for possible seizure control and cognitive improvement. Also noted is hypermetabolism in the bilateral basal ganglia and brain stem nuclei (*dotted arrows*), likely implicating their role in spasm generation

in 95% of children with an initial diagnosis of cryptogenic infantile spasms (Chugani and Conti 1996). Four different patterns of FDG hypometabolism were observed: unifocal in 20%, multifocal in 65%, diffuse in 5%, and bitemporal hypometabolism in 10% of children (Chugani and Conti 1996). Out of these, the patients with unifocal lesion can be considered for epilepsy surgery if they have uncontrolled spasms with the majority of EEG changes corresponding to the PET-defined lesion, as the surgical removal of focal brain lesion leads not only to cessation of the spasms but also to improved neurocognitive outcome (Fig. 47.11) (Branch and Dyken 1979; Mimaki et al. 1983; Palm et al. 1988; Ruggieri et al. 1989; Uthman et al. 1991; Chugani et al. 1993, Chugani et al. 2015; Asarnow et al. 1997; Jonas et al. 2005; Yum et al. 2011). Occasionally, patients with a multifocal pattern can also be considered for palliative surgery, with improved quality of life but guarded developmental outcome, if the majority of seizures originate from one region (Chugani et al. 2010; Ilyas et al. 2014). The diffuse metabolic pattern is likely associated with underlying metabolic, genetic, or neurodegenerative pathology, and these patients are unlikely to be surgical candidates. Interestingly, children with bitemporal hypometabolism show a distinct clinical phenotype characterized by severe developmental delay, particularly in the language domain, and autism or pervasive developmental disorder (Chugani et al. 1996). These children are unlikely to become surgical candidates. Longitudinal studies have shown that the PET abnormalities are not always static, but may evolve as the brain matures (Sakaguchi et al. 2018).

FDG PET can also shed some light on the possible pathomechanism of epileptic spasms. For example, these patients may show a focal cortical hypometabolism along with prominent glucose metabolism in the lenticular nuclei and brain stem, suggesting complex cortical-subcortical interactions (Fig. 47.11) (Chugani et al. 1992). Basal ganglia and brain stem involvement likely suggests their role in the

secondary generalization of focal cortical discharges, resulting in spasms. It appears that the spasms result primarily from focal or diffuse cortical abnormalities interacting with the brain stem and lenticular nuclei and that this type of generalization accounts for the bilateral motor involvement and relative symmetry of the majority of spasms even in the presence of a discrete focal lesion (Chugani et al. 1992). Ictal and interictal brain SPECT can also provide some interesting clues regarding the probable origin and propagation of electrical events responsible for spasms. Interictal SPECT studies have shown perfusion abnormalities, ranging from cortical hypoperfusion (Chiron et al. 1993; Miyazaki et al. 1994; Hwang et al. 1996; Sztriha et al. 1997; Haginoya et al. 1998, 2001) to cortical hyperperfusion (Chiron et al. 1993). Ictal SPECT has shown areas of cortical hyperperfusion with occasional hyperperfusion of the subcortical structures (Haginoya et al. 1998, 2001), consistent with FDG PET findings. Recent studies, using a combination of interictal and ictal SPECT, found ictal *hyper*perfusion of a cortical lesion and basal ganglia, supporting the notion that secondary generalization from a cortical focus may account for the spasms (Mori et al. 2007; Kakisaka et al. 2009). The finding of localized cortical perfusion defects in some children with West syndrome confirms that focal cortical lesions play an important role in its development (Haginoya et al. 2000). Interestingly, in infants, hyperperfusion has been found interictally in the area of cortical dysgenesis and appears to be specific for this young population (Hwang et al. 1996; Haginoya et al. 2000). These findings corroborate the notion that infantile spasms result from complex cortical-subcortical interaction with age and brain maturity playing an important role. Rapid involvement of the basal ganglia and brain stem likely results in the secondary generalization of a seemingly partial seizure, arising from a focal cortical lesion (Chugani et al. 1992). What leads to this interaction is yet to be elucidated.

47.2.2.2 Tuberous Sclerosis

Tuberous sclerosis complex (TSC) is an autosomal dominant neurocutaneous disorder characterized by multiple cortical tubers, caused by inactivating mutations in the TSC genes. Epilepsy is the main manifestation of this condition, with a prevalence of 80–90% (Osborne et al. 1991), becoming refractory to medical treatment in 50–80% of cases, as early as 2 years of age (Evans et al. 2012). As intractable seizures have a detrimental effect on neurocognitive development, these patients often benefit from epilepsy surgery (Perot et al. 1966). However, many times it is difficult to localize the epileptic focus, due to multifocal EEG changes and multiplicity of cortical tubers, even though a single tuber may be epileptogenic. In these cases, PET can play a valuable role by noninvasively lateralizing and localizing the epileptic focus *interictally* and rendering these patients surgical candidates. FDG PET can show the tubers (Asano et al. 2000, 2005; Ohta et al. 2001; Karenfort et al. 2002; Chandra et al. 2006; Weiner et al. 2006; Moshel et al. 2010; Wu et al. 2010; Carlson et al. 2011); however, it cannot identify the epileptogenic one, as all tubers appear hypometabolic (Fig. 47.12). AMT PET has been reported to be very useful in this condition, as it shows increased tracer uptake in epileptogenic tubers only (Fig. 47.12) (Chugani et al. 1998a, 2013a, b; Asano et al. 2000; Fedi et al. 2003;

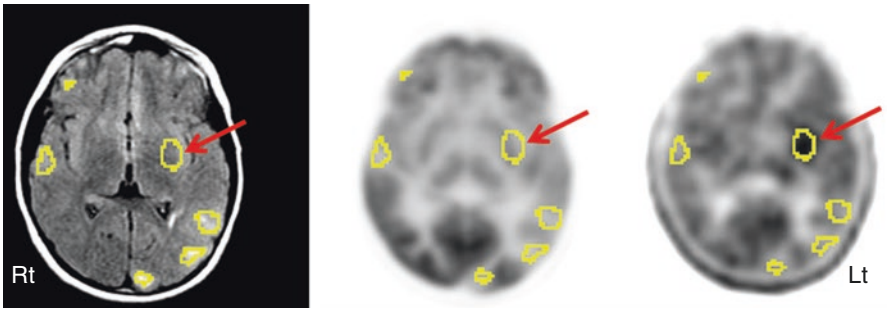

Fig. 47.12 FLAIR MRI (*left image*), 2-deoxy-2(^{18}F)-fluoro-D-glucose (*middle image*), and ^{11}C-alpha-methyl tryptophan PET (*right image*) scan in a patient with multiple tubers (*encircled* with "region of interests"), intractable seizures, and non-localizing scalp EEG. While 2-deoxy-2(^{18}F)-fluoro-D-glucose PET showed hypometabolism in all the tubers and overlying cortices, interictal ^{11}C-alpha-methyl tryptophan PET scan revealed increased alpha-methyl tryptophan uptake in an insular tuber (*arrow*)

Rubí et al. 2013), sometimes at one of its edges only with some involvement of the adjacent apparently normal cortex; such cortical regions usually turn out to be dysplastic on histopathological examination (Kagawa et al. 2005). The increased AMT uptake appears to be due to the activation of the kynurenine pathway, leading to the production of quinolinic acid, a proconvulsant, in the tuber and dysplastic cortex (Chugani et al. 1998a). AMT PET with quantitative evaluation of lesional uptake levels can identify epileptogenic tuber(s) in almost two-thirds of children with tuberous sclerosis and intractable epilepsy and is almost 100% specific (Chugani et al. 1998a; Asano et al. 2000; Fedi et al. 2003). Tubers with at least 10% increase of AMT uptake appear to be invariably epileptogenic, and a cutoff threshold of 1.02 for AMT uptake ratio provides 83% accuracy for detecting tubers that need to be resected to achieve a seizure-free outcome (Asano et al. 2000; Kagawa et al. 2005). The high specificity of increased AMT uptake is also suggested by the good correlation between resections of epileptogenic tubers, showing increased AMT uptake and seizure outcome (Kagawa et al. 2005). However, its sensitivity is suboptimal, likely depending upon the underlying pathology and method of data analysis. It appears that MRI-based quantitative assessment can increase the sensitivity of AMT PET to 79% from 44% with visual assessment (Juhasz et al. 2002). This may be related to the fact that non-epileptic tubers show decreased AMT uptake and the epileptogenic ones with relatively increased AMT uptake but still close to the surrounding normal cortex, and therefore, these increases might appear subtle and be missed on visual analysis. SPECT can also play an important role in identifying epileptic tubers, by showing them hyperperfused during ictal phase (Koh et al. 1999; Romanelli et al. 2002; Weiner et al. 2006; Moshel et al. 2010; Aboian et al. 2011; Carlson et al. 2011). A good correlation has been reported between ictal SPECT and ictal scalp EEG (Koh et al. 1999; Mori et al. 2007). SISCOM further increases the usefulness of SPECT in identifying the epileptogenic zone and in guiding the location and extent of epilepsy surgery in children with tuberous

sclerosis complex and multifocal abnormalities (Aboian et al. 2011). Complete resection of the SISCOM hyperperfusion abnormality was found to be associated with seizure freedom. SPECT, using ^{123}I-iomazenil, has been used to evaluate benzodiazepine receptor status in patients with tuberous sclerosis (Kuki et al. 2008, 2012; Mori et al. 2012). GABA receptor binding was found to be decreased in cortical tubers (Mori et al. 2012), suggesting that decreased neuronal inhibition might have a role in epileptogenesis in this condition.

47.2.2.3 Lennox-Gastaut Syndrome

FDG PET can help in the metabolic characterization of the brain in *Lennox-Gastaut syndrome*, a triad of multiple seizure types including tonic seizures, developmental delay, and 1–2.5 Hz generalized "slow" spike-and-wave EEG pattern, which may have implication for prognosis, as well as treatment planning (Gur et al. 1982; Chugani et al. 1987b; Iinuma et al. 1987; Theodore et al. 1987; Miyauchi et al. 1988; Ferrie et al. 1996; You et al. 2007; Zhai et al. 2010; Hur et al. 2011). These patients may show four metabolic patterns on FDG PET scan: unilateral focal hypometabolism, unilateral diffuse hypometabolism, bilateral diffuse hypometabolism, and normal patterns (Chugani et al. 1987b). Interictal SPECT usually shows multiple areas of hypoperfusion (Heiskala et al. 1993). Patients with unilateral focal pattern may be occasionally considered for cortical resection provided there is good concordance between PET and ictal EEG findings (You et al. 2007; Hur et al. 2011).

47.2.2.4 Sturge-Weber Syndrome

In children with *Sturge-Weber syndrome* (*SWS*), FDG PET reveals hypometabolism in the involved cortex and usually identifies additional areas of abnormal cortex extending beyond the abnormality seen on MRI (Chugani et al. 1989; Juhasz et al. 2007). However, affected infants may show a paradoxical pattern of *increased* glucose metabolism interictally in the cortex underlying the leptomeningeal angioma; as the disease progresses, the hypermetabolic area becomes hypometabolic (Fig. 47.13) (Chugani et al. 1989). The presence of early cortical hypermetabolism on PET may be an imaging marker of subsequent severe epilepsy, requiring surgery (Alkonyi et al. 2011). In some young patients, serial FDG PET scans show rapidly progressing and severe hypometabolism in the affected area, probably because of rapid demise of the brain tissue associated with the angioma: these patients will have improvement in seizure status and paradoxical preservation of cognitive function and therefore may not require surgical intervention (Behen et al. 2011). Early and rapid progression in unilateral cases of SWS leads to early and more efficient reorganization in the contralateral cortex. On the other hand, persistent mild hypometabolism of the lesion may indicate ongoing functional disturbance, and these patients may show persistent seizures and developmental arrest (Lee et al. 2001b; Behen et al. 2011). These are the patients who require surgical intervention for seizure control and possible cognitive improvement by promoting effective reorganization in the contralateral hemisphere while brain plasticity is still at a maximum during development. In SWS, detrimental metabolic changes mostly occur before 3–4 years of age (Juhasz et al. 2007), coinciding with a sharp increase in

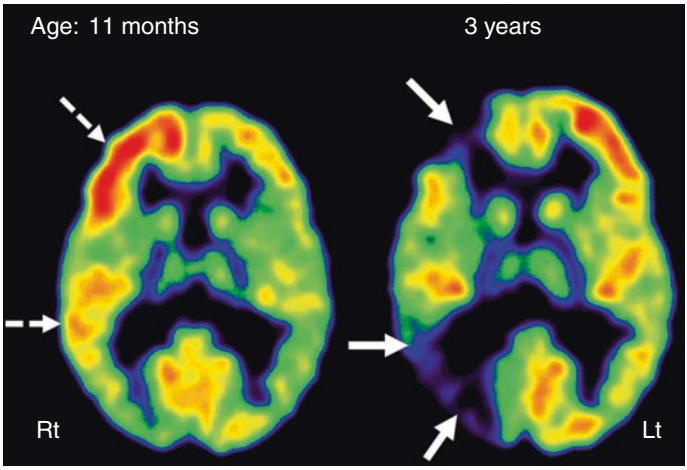

Fig. 47.13 Serial 2-deoxy-2(^{18}F)-fluoro-D-glucose PET scan showing progression of glucose metabolic abnormalities in the affected right hemisphere (MRI showed extensive leptomeningeal enhancement on that side) in a child with Sturge-Weber syndrome. PET scan at 11 months of age showed a transient increase of metabolism, most prominent in the frontal lobe and mild in the temporal cortex (*dashed arrows*). Repeat PET at 3 years of age showed severe hypometabolism in the right frontal and temporal cortices (*solid arrows*)

developmentally regulated cerebral metabolic demand (Chugani et al. 1987a). Progressive hypometabolism is associated with high seizure frequency in these children. However, metabolic abnormalities may remain limited or even partially recover later in some children with well-controlled seizures. Metabolic recovery accompanied by neurological improvement suggests a critical window for therapeutic intervention in children with unilateral SWS (Juhasz et al. 2007). FDG PET can also be used to assess for cognitive function and regional functional reorganization (Bosnyák et al. 2016; Kim et al. 2018).

Perfusion SPECT, using xenon-133, showed hyperperfusion in the lesion even before seizure onset (Pinton et al. 1997), analogous to the transient hypermetabolism seen on PET (Chugani et al. 1989; Juhasz et al. 2007). After 1 year of age, these areas typically show hypoperfusion, as revealed by another xenon-133 SPECT study (Chiron et al. 1989). In a single case report on a patient with failed functional hemispherectomy, ictal ECD SPECT showed hyperperfusion in the residual lesion with falsely lateralized EEG; further surgery resulted in seizure freedom (Bilgin et al. 2008). In recent years, SPECT studies have been largely replaced by perfusion MRI, which can be performed in conjunction with conventional clinical MRI and provide quantitative maps of blood volume and blood flow in children with Sturge-Weber syndrome (Alkonyi et al. 2012).

47.2.2.5 Hemimegalencephaly

Hemimegalencephaly is a severe congenital malformation of hemispheric development with a unilateral enlarged and defectively developed hemisphere and

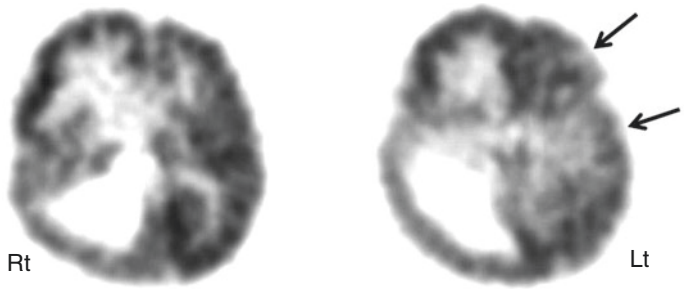

Fig. 47.14 2-Deoxy-2(^{18}F)-fluoro-D-glucose PET scan in a child with right hemimegalencephaly showing an enlarged right hemisphere with increased glucose metabolism in the right frontal lobe because of epileptic activity during the radiotracer uptake period. Also noted are mildly hypometabolic areas in the frontal and temporal regions of the left hemisphere (*arrows*), indicating functional impairment of this hemisphere, which appeared to be normal on MRI. Although right hemispherectomy resulted in seizure freedom, the child remained developmentally delayed because of an abnormal left hemisphere

intractable seizures. PET and SPECT usually show variable appearance in the involved hemisphere: hypo- and/or hypermetabolism on the FDG PET and hypo- and/or hyperperfusion on HMPAO or ECD SPECT, depending upon the seizure status at the time of scanning. Early hemisphere disconnection in these children may lead to seizure control and improved cognitive development, provided the other hemisphere is normal. Therefore, the main role of PET or SPECT is the evaluation of the apparently normal hemisphere (Fig. 47.14). In children with hemimegalencephaly, FDG PET often shows additional less pronounced abnormalities in the opposite hemisphere, which probably accounts for the suboptimal cognitive outcome even with complete seizure control after surgical removal of the profoundly abnormal hemisphere (Rintahaka et al. 1993). Thus, FDG PET can be useful in such cases to assess the functional integrity of the contralateral hemisphere prior to hemispherectomy and help predict cognitive outcome.

47.2.2.6 Rasmussen's Encephalitis and Epilepsy of Suspected Inflammatory Origin

FDG PET can show both hyper- or hypometabolism in cases of Rasmussen's encephalitis, depending upon the seizure status during the scan (Tien et al. 1992; Fiorella et al. 2001; Lee et al. 2001a). It can particularly help in the unequivocal identification of the affected cerebral hemisphere in patients whose MR imaging findings are subtle or distributed bilaterally (Fiorella et al. 2001). FDG PET can further help in guiding the site of biopsy when indicated, thus assisting in earlier diagnosis. Interictal hypometabolism expands over time and usually precedes the anatomical changes, thus further helping in clarifying the equivocal cases or assessing the functional impairment and its evolution (Lee et al. 2001a). Perfusion SPECT also shows hyper- or hypometabolism of the affected cortex, depending upon the seizure status during the tracer injection, and can guide the histopathological evaluation or surgical planning (Yacubian et al. 1997; Burneo et al. 2006). It appears that

benzodiazepine SPECT and FDG PET can detect the ictal-onset area efficiently even in the absence of MRI abnormalities (Kuki et al. 2018).

Neuroinflammation is the underlying cause for intractable epilepsy in Rasmussen's encephalitis, as well as some other epileptic conditions. Neuroinflammation is mediated by activated microglia, which secrete a number of proinflammatory molecules such as cytokines, chemokines, and neurotoxins, free radicals, nitric oxide, proteinases, eicosanoids, and excitotoxins, which may play a role in epileptogenesis. Although the exact mechanisms are unclear, it appears that the inflammatory mediators act by increasing glutamatergic neurotransmission, decreasing GABA-mediated currents and inducing neovascularization, and damaging the blood-brain barrier. Detection of microglia is not possible with current radiological methods or biochemical techniques; however, they can be imaged with PET tracers binding to the activated microglia. ^{11}C-PK11195 is the most commonly used radioligand which binds specifically to the translocator protein receptors, predominantly expressed by the activated microglia in cases of neuroinflammation, thus making the in vivo detection of neuroinflammation possible (Banati et al. 1999). PET scanning using ^{11}C-PK11195 can help in the early diagnosis of Rasmussen's syndrome or other inflammatory conditions with intractable seizures, where CT and MRI are often normal for several months after the

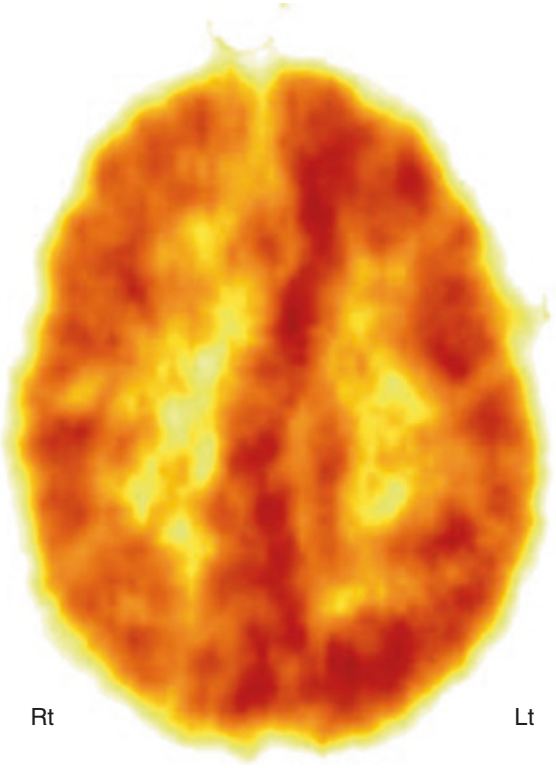

Fig. 47.15 ^{11}C-PK11195 PET scan showing increased radiotracer binding in the left hemisphere, indicating neuroinflammation mediated by activated microglia, in a child with Rasmussen's encephalitis

clinical manifestation of the disease (Fig. 47.15). Localization of the most affected brain regions may also provide a guide in deciding the site of brain biopsy in order to avoid sampling errors and can help in the surgical removal of that region (Kumar et al. 2008).

Autoimmune encephalitis is increasingly being recognized as an important cause of intractable epilepsy in adults and children, and a number of antibodies targeting brain proteins have been identified (reviewed in Spatola and Dalmau 2017). Depending upon the specific antibody, different brain regions may be involved, but in general, FDG PET shows hypermetabolism in the acute stages and hypometabolism in the chronic stages (Guerin et al. 2019). Further studies with PET and SPECT using radioligands targeting microglia (neuroinflammation) in autoimmune encephalitis will be potentially useful clinically, but a major obstacle in performing such studies is the rapid availability of the tracer in the acute setting when anti-inflammatory treatment cannot be withheld ethically.

47.3 Other Neurological Disorders

47.3.1 Perinatal Hypoxic Ischemic Brain Injury and Cerebral Palsy

PET scanning of cerebral glucose metabolism can be helpful to assess severity of brain damage in infants with hypoxic ischemic encephalopathy (HIE) and brain injury. Early FDG PET studies found areas of hypometabolism, extending beyond the affected regions shown by CT scan (Doyle et al. 1983). Cerebral perfusion PET showed relative hypoperfusion in the parasagittal regions in full-term neonates with perinatal asphyxia (Volpe et al. 1985). In preterm infants with intraventricular and intracerebral hemorrhage, large areas of hypoperfusion were reported in the affected hemisphere (Volpe et al. 1983). Subsequent studies suggested that persistently low cerebral glucose metabolism is associated with delayed development in children with HIE (Suhonen-Polvi et al. 1993). Total brain glucose metabolic rates (CMRglc) were found to be inversely correlated with the severity of HIE: neonates with the lowest CMRglc subsequently developed permanent neurological symptoms and cerebral palsy (Thorngren-Jerneck et al. 2001). A transient increase of glucose metabolic rates has been also observed in the basal ganglia in the neonatal period, followed by severe hypometabolism in the lenticular nuclei and thalami, in some newborns who suffered HIE and subsequently developed dystonic cerebral palsy (Fig. 47.16) (Batista et al. 2007).

Cerebral palsy is a heterogeneous neurological condition that sometimes may be related to perinatal brain injury. FDG PET studies of these children with cerebral palsy due to birth injury have shown that the distribution of metabolic impairment almost invariably extends beyond the apparent anatomical involvement seen on MRI. PET also can help in identifying the location and severity of functional involvement of cortical and subcortical structures in the major subtypes of cerebral palsy in the chronic stages. Analysis of these different subtypes demonstrated focal areas of cortical hypometabolism in spastic diplegic patients, without any obvious

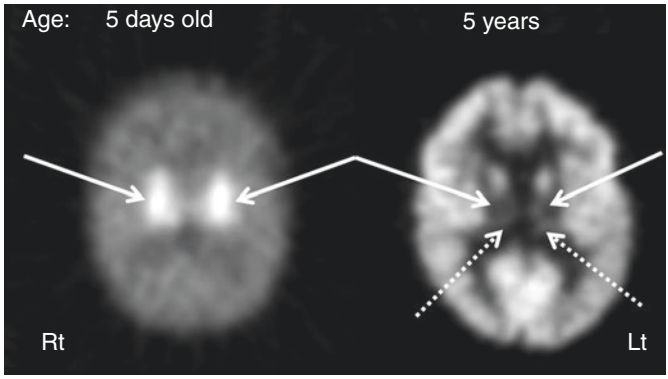

Fig. 47.16 2-Deoxy-2(^{18}F)-fluoro-D-glucose PET scans of a child who suffered hypoxic ischemic encephalopathy at birth and later developed dystonic/choreoathetoid cerebral palsy. The *left image* from the newborn period showed intense hypermetabolism in the basal ganglia (*solid arrows*). The *right image* at 5 years of age showed severe hypometabolism in the lenticular nuclei (*solid arrows*) and thalami (*dotted arrows*). Note the relative preservation of metabolism in the cerebral cortex

cortical lesion on structural imaging; in contrast, a relatively normal pattern of cortical metabolism is seen in some children with choreoathetoid cerebral palsy, who often show hypometabolism in the thalamus and lenticular nuclei (Kerrigan et al. 1991). Relative sparing of the cerebral cortex is consistent with the clinical observation that many of these children have good cognitive function despite suffering from severe motor impairment. Use of FMZ PET has demonstrated increased GABA receptor binding in the bilateral motor and visual cortex and decreased binding in the brain stem, suggesting a role of abnormal GABA mechanisms in poor motor control (Lee et al. 2007). In addition, recent studies with a rabbit model of intrauterine brain injury suggested that PET imaging of activated microglia in newborns, using ^{11}C-PK11195, can detect neuroinflammatory changes in the white matter that later develops severe structural damage causing symptoms of cerebral palsy (Kannan et al. 2007).

47.3.2 Autism

Functional neuroimaging in autism is currently a clinical research tool and has been utilized to identify neuroanatomic substrates involved in various symptoms associated with the disease. In early studies with PET scanning, increased glucose metabolic rates were reported in multiple brain regions in autistic adults, but no common regional abnormality could be identified (Rumsey et al. 1985). In a subsequent study involving 18 autistic children, neither the rates nor the regional distribution of brain glucose metabolism was different from those in control subjects (De Volder et al. 1987). Similarly, no significant abnormality in regional cerebral blood flow, oxygen consumption, and metabolism was reported in six adult autistic subjects (Herold et al. 1988). However, another study found some reversed (left > right)

asymmetry of glucose metabolism in the anterior rectal gyrus (Siegel et al. 1992). A combined MRI and PET study in high-functioning autistic patients reported volume loss and associated hypometabolism in the anterior and posterior cingulate (Haznedar et al. 1997, 2000). Perfusion PET studies using radiolabeled water found hypoperfusion in the right dentate nucleus and left frontal cortex during verbal auditory and expressive language tasks (Muller et al. 1998) and hypoperfusion of the superior temporal cortex during acoustic stimulation and the cerebellum during nonverbal auditory perception task (Muller et al. 1999). Subsequently, lower glucose metabolism was reported in the medial frontal cortex and cingulate (Hazlett et al. 2004) and in the ventral caudate, putamen, and thalamus (Haznedar et al. 2006) during verbal memory task in autistic subjects.

Simultaneously with glucose PET studies, several SPECT studies attempted to find global or focal cerebral perfusion abnormalities in autistic subjects in the 1990s; most early studies were small, and the results were mixed. One study found no regional perfusion abnormalities in 21 autistic children on xenon-133 SPECT (Zilbovicius et al. 1992). Another smaller HMPAO SPECT study found global hypoperfusion as well as regions with hypoperfusion, including the right lateral temporal lobe and frontal lobes in four autistic adults (George et al. 1992). In a subsequent longitudinal study, the same group reported frontal hypoperfusion in autistic children at ages 3–4 years, which disappeared by the ages of 6–7 years, suggesting a delayed frontal maturation in childhood autism. Yet another HMPAO SPECT study showed decreased blood flow in the temporoparietal region in six autistic patients between 9 and 21 years of age, without any apparent clinical correlation (Mountz et al. 1995). A relatively larger ECD SPECT study, including 23 children with infantile autism compared to 26 non-autistic controls (matched for age and IQ), reported decreased regional blood flow in the bilateral insula, superior temporal gyri, and left prefrontal cortices and found several clinico-imaging correlations (Ohnishi et al. 2000). First, altered perfusion in the medial prefrontal cortex and anterior cingulate gyrus was associated with impairments in communication and social interaction (related to deficits in the theory of mind), and second, altered perfusion in the right medial temporal lobe was related to the obsessive desire for sameness. Thus, these findings pointed to specific locations of brain dysfunction underlying abnormal behavioral patterns in autistic patients. More recent studies have utilized objective analytic approaches such as SPM to identify abnormal cerebral blood flow patterns in autism. One such study, using ECD SPECT, also reported both global reductions and an increased right-left perfusion asymmetry in 11 autistic children, as compared to age-matched healthy children; the asymmetries were particularly prominent in the temporoparietal areas associated with language and comprehension of music and sound (Burroni et al. 2008). Another study, using a similar approach in 23 children with autistic spectrum disorder (mostly boys), found bilateral frontal, temporal, and basal ganglia hypoperfusion in autistic children (Yang et al. 2011). Interestingly, there were greater asymmetries in children with Asperger syndrome than autism, suggesting different neurobiological mechanisms. Recently, cerebral hypoperfusion using functional neuroimaging in autism subjects has been reviewed (Bjørklund et al. 2018).

PET imaging with various radiotracers allows the study of global and regional cerebral abnormalities of specific neurotransmitter systems and their potential roles in the pathophysiology of autism. These studies have been designed based on previous work demonstrating alterations in neurotransmitters, hormones, and their metabolites in the blood, cerebrospinal fluid (CSF), and urine of autistic patients. In a PET study using [^{18}F]-labeled fluorodopa (F-DOPA, a precursor of dopamine, accumulated in dopaminergic terminals) in 14 medication-free autistic children, decreased dopaminergic activity was found only in the anterior medial prefrontal cortex in the autistic group, suggesting that decreased dopaminergic function in the prefrontal cortex may contribute to the cognitive impairment seen in autism (Ernst et al. 1997). A subsequent study of 20 adults with autism also demonstrated increased dopamine transporter binding in the orbitofrontal cortex, and these abnormalities were inversely correlated with serotonin transporter binding, suggesting a potential interplay between the dopaminergic and serotonergic systems in affected brain regions (Nakamura et al. 2010).

Abnormalities of the serotonergic system have been long implicated in the pathophysiology of autism. Tryptophan depletion, leading to decreased serotonin levels, resulted in an exacerbation of symptoms in autistic subjects (McDougle et al. 1996b). Conversely, serotonin reuptake inhibitors may result in the improvement of compulsive symptoms, repetitive movements, and social difficulties in autistic adults (Cook et al. 1992; Gordon et al. 1993; McDougle et al. 1996a). Chugani et al. (1997) used AMT PET scanning to study children with autism and their healthy non-autistic siblings. AMT PET demonstrated robust AMT uptake asymmetries in the frontal cortex, thalamus, and cerebellum in seven autistic boys (Fig. 47.17); however, this pattern was not seen in one autistic girl and in four of the five siblings. Specifically, decreased AMT accumulation was seen in the left frontal cortex and

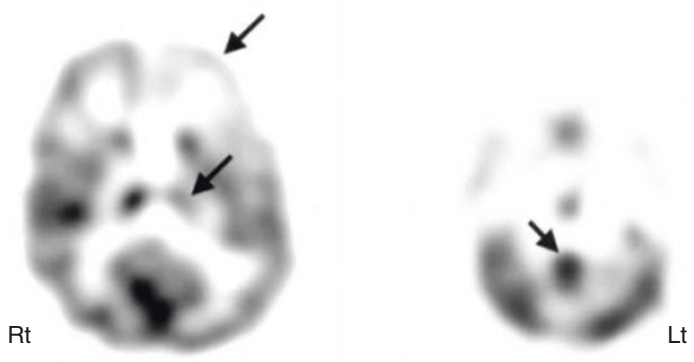

Fig. 47.17 ^{11}C-Alpha-methyl tryptophan PET showing asymmetric alpha-methyl tryptophan uptake in the frontal cortex, thalamus, and dentate nucleus of the cerebellum in a boy with autism spectrum disorder, with decreased uptake in the ipsilateral frontal cortex and thalamus and with increased uptake in the contralateral dentate nucleus (*arrows*), suggesting the involvement of dentato-thalamo-cortical pathway in autism

thalamus in five of seven autistic boys, while elevated AMT accumulation was present in the right cerebellum, in the dentate nucleus. The same children showed a normal pattern of brain glucose metabolism and normal MRI on visual evaluation, supporting that the observed novel focal cerebral abnormalities on AMT PET were specific for serotonergic abnormalities. In a subsequent larger study, Chugani et al. (1999) also reported global brain values for serotonin synthesis capacity of 54 children: 30 healthy seizure-free autistic children (24 males, 2–15 years), eight healthy non-autistic siblings (six males, 2–14 years), and 16 epileptic children without autism (nine males, 3 months–13 years). Non-autistic children showed a nonlinear change in global serotonin synthesis capacity: their values reached >200% of adult values until the age of about 5 years and then gradually declined toward adult values. In autistic children, a different developmental pattern was found: serotonin synthesis capacity increased gradually between the ages of 2 and 15 years to values 1.5 times of the adult normal values. The data indicated a period of relatively high brain serotonin synthesis capacity during childhood and that the normal developmental process is disrupted in autistic children. These results prompted further larger-scale imaging studies of the serotonergic system of the developing brain in autism. When data of a larger group (n = 117) of autistic children were analyzed, additional focal patterns were recognized, including right cortical and left cortical decreases and a subgroup with no abnormal asymmetry (Chandana et al. 2005). Children with left cortical AMT uptake decreases showed a higher prevalence of severe language impairment, whereas right cortical decreases were associated with left and mixed handedness. These studies, altogether, suggested that both global and focal asymmetric development in the serotonergic system may be implicated in abnormal "wiring" of neural circuits related to hemispheric specialization. Therefore, restoration of serotonin levels pharmacologically in a critical age window may alter developmental trajectory and improve symptoms of autistic children. Indeed, molecular imaging using various radiotracers may provide important biomarkers and pave the way for new therapeutic interventions (Hwang et al. 2017).

47.3.3 Developmental Dyslexia

Dyslexia is a specific learning disability that manifests primarily with difficulty in written language, particularly with reading and spelling. Various PET studies have shown the predominant involvement of bilateral posterior temporal and parietal cortices. Initial cerebral blood flow studies, using Xe-133, found increased left more than right asymmetry and reduced anterior to posterior difference (Rumsey et al. 1987), as well as hypoperfusion in the left superior temporal region with hyperperfusion in the more posterior temporoparietal region (Flowers et al. 1991). Subsequently, PET studies using ^{15}O-labeled water in dyslexic subjects showed a failure to activate the left temporoparietal cortex during a rhyme detection task and reduced activation/unusual deactivation in the mid- and posterior temporal cortex bilaterally and also in inferior parietal cortex, predominantly on the left side (Rumsey et al. 1992, 1997). Other PET studies showed less activation in the right

superior temporal and right postcentral gyri and left cerebellum (McCrory et al. 2000) or in the right cerebellar cortex and left cingulate gyrus (Nicolson et al. 1999). Functional disconnection of the left angular gyrus from other parts of the reading network has also been reported in adults with persistent developmental dyslexia (Horwitz et al. 1998). A recent ^{15}O PET study of the learning of phoneme categorization found a less strongly left-lateralized activation involving the superior temporal, inferior parietal, and inferior lateral frontal cortex during the speech mode (Dufor et al. 2007). Frontal and parietal subparts of these left-sided regions were found to be significantly less activated in the dyslexic subjects. However, larger activations in the right frontal cortex for both speech and acoustic modes compared to the rest and an unexpected large deactivation in the medial occipital cortex for the acoustic mode were noted in the dyslexic subjects. Subsequently, the same group found activity enhancement in left premotor cortex, likely related to the persistence of motor coding for allophonic representations of speech (Dufor et al. 2009).

FDG PET studies have shown diminished asymmetry in glucose metabolism in prefrontal and lingual (inferior) regions of the occipital lobe during reading in dyslexic subjects, indicating that brain regions are activated differently in this disorder (Gross-Glenn et al. 1991). Another FDG PET study showed significantly higher absolute and relative brain metabolism along an anterior-posterior gradient, including the medial temporal lobe, in dyslexic subjects, during an auditory syllable discrimination task, suggesting more effortful processing in dyslexia (Hagman et al. 1992). Perfusion SPECT has also shown hypoperfusion in areas involved in the reading and writing processes, predominantly in the temporal lobe (Kaneko et al. 1998; Arduini et al. 2006; Sauer et al. 2006).

47.3.4 Landau-Kleffner Syndrome

Landau-Kleffner syndrome (LKS) is characterized by the sudden or gradual development of aphasia in children who had previously developed typically with normal language until disease onset. While many of the affected children have clinical seizures, some may have only electrographic seizures. FDG PET usually shows bilateral temporal lobe involvement, in the form of hyper- or hypometabolism depending upon the electrographic status of this region, particularly of the superior and medial part (Maquet et al. 1990; Rintahaka et al. 1995; da Silva et al. 1997; Honbolygo et al. 2006; Shiraishi et al. 2007). During the phase of aphasia, frequent epileptiform spiking is seen in these regions, associated with glucose hypermetabolism on FDG PET, which becomes quiescent during remission, manifested as hypometabolism on FDG PET scan. FDG PET can also show the possible involvement of temporal lobes in the generation of continuous spike waves during slow-wave sleep (Maquet et al. 1990, 1995; Rintahaka et al. 1995). FDG PET can be further useful to monitor dynamic changes of glucose metabolism in the temporal lobe during episodes of aphasia and remission, where it shows hyper- and hypometabolism, likely related to presence or absence of continuous spiking on scalp EEG, respectively, during these periods (Fig. 47.18) (Luat et al. 2006). Using ^{15}O-labeled water PET, posterior

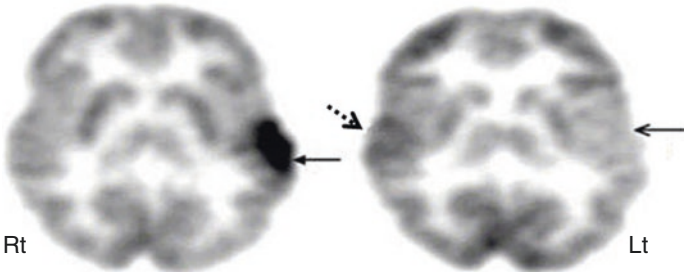

Fig. 47.18 2-Deoxy-2(^{18}F)-fluoro-D-glucose PET scan in a child with Landau-Kleffner syndrome showing marked hypermetabolism in the left temporal region (*arrow*) during the peak of his aphasic episode. EEG, performed during PET scan, showed frequent spike-and-wave activity from this region. A repeat PET scan during his remission state showed hypometabolism in the same region (*arrow*). Interestingly, a mildly increased glucose metabolism is noted in the second PET scan on the other side (right superior temporal cortex—*broken arrow*), which corresponded to some spike-and-wave discharges from this region

superior temporal gyri were found to have decreased perfusion/activation, long after remission was achieved in patients with LKS, and residual impairment in verbal short-term memory, suggesting an important role played by the temporal lobe in this condition (Majerus et al. 2003). FMZ PET revealed a deficit in benzodiazepine receptor binding at the tip of the left temporal lobe in a child affected by LKS, suggesting that the tip of the left temporal lobe might play an important role in the pathogenesis of this disease (Shiraishi et al. 2007). SPECT studies have also shown variable perfusion abnormalities, predominantly in uni- or bilateral temporal lobes, ranging from hypo- to hyperperfusion, likely related to the timing of the SPECT (Hu et al. 1989; O'Tuama et al. 1992; Guerreiro et al. 1996; Harbord et al. 1999; Sayit et al. 1999; Sinclair and Snyder 2005; Shiraishi et al. 2007).

47.3.5 Tourette Syndrome

Tourette syndrome is an inherited neuropsychiatric disorder with onset in childhood and is characterized by the presence of multiple motor tics and at least one vocal tic for more than 1 year. Initial studies using FDG PET, in a limited number of children with Tourette syndrome, failed to show any consistent glucose metabolic abnormalities. Decreased metabolic rates were reported in various regions, including paralimbic and ventral prefrontal cortices (Braun et al. 1993). Decreases were also observed in subcortical regions, including the ventral striatum (nucleus accumbens/ventromedial caudate) and in the midbrain. These changes were more robust and occurred with greater frequency in the left hemisphere and were associated with bilateral increases in metabolic activity of the supplementary motor, lateral premotor, and Rolandic cortices. Subsequently, cerebral perfusion PET studies were used for the investigation of neuronal circuits involved in tic generation. An ^{15}O PET

cerebral blood flow study showed widely distributed tic-associated activation in the medial and lateral premotor cortices, anterior cingulate cortex, dorsolateral rostral prefrontal cortex, inferior parietal cortex, putamen, and caudate, as well as the primary motor cortex, Broca's area, superior temporal gyrus, insula, and claustrum (Stern et al. 2000). Another ^{15}O PET study showed robust activation of the cerebellum, insula, thalamus, and putamen during tic release (Lerner et al. 2007). Based on these studies, it can be postulated that aberrant activity in the interrelated sensorimotor, language, executive, and paralimbic circuits may account for the initiation and execution of diverse motor and vocal behaviors in Tourette syndrome.

Imaging studies of dopaminergic transmission sought to determine the potential contribution of abnormalities in the dopaminergic system to the pathophysiology of Tourette syndrome. Several aspects of dopaminergic abnormalities have been studied, including striatal dopamine transporter levels, which were elevated (Krause et al. 2002); presynaptic DOPA decarboxylase activity (Ernst et al. 1999); and D2 receptor availability, which was found to be decreased (Gilbert et al. 2006). These abnormalities again could be detected in widespread cortical and subcortical regions (e.g., the orbitofrontal cortex, primary motor cortex, anterior cingulate gyrus, mediodorsal nucleus of thalamus, and hippocampus), suggesting abnormalities in brain networks important for motivation and reward, sensory gating, movement, and attention. Another study also demonstrated increased dopamine release in the striatum, particularly the putamen, of Tourette patients (Singer et al. 2002; Wong et al. 2008). A recent meta-analysis of 16 PET and SPECT studies in Tourette subjects showed trends but no significant findings in dopaminergic alterations. While the studies supported the general notion of dopamine mechanism involvement in the pathophysiology of Tourette syndrome, the lack of significant findings was attributed to the heterogeneity of this disorder (Hienert et al. 2018). Imaging data using AMT PET appear to support the role of abnormal serotonergic neurotransmission in the pathophysiology of Tourette syndrome and some of its comorbid conditions, such as ADHD and OCD (Behen et al. 2007). Increased serotonin receptor binding was found not only in regions closely related to subcortical regions in patients with Tourette syndrome but also in most other brain regions (Haugbol et al. 2007). Decreased AMT uptake in bilateral dorsolateral prefrontal cortical and bilaterally increased uptake in the thalamus with bilateral increased ratio of AMT uptake in subcortical structures to dorsolateral prefrontal cortex was reported in Tourette syndrome children (Behen et al. 2007). However, thalamic and basal ganglia asymmetry in AMT uptake is also frequently found in these children (Fig. 47.19). Recent studies have suggested that alterations in the serotonergic system in Tourette syndrome may be related to comorbid obsessive-compulsive disorder rather than the primary cause of the disease (Müller-Vahl et al. 2019).

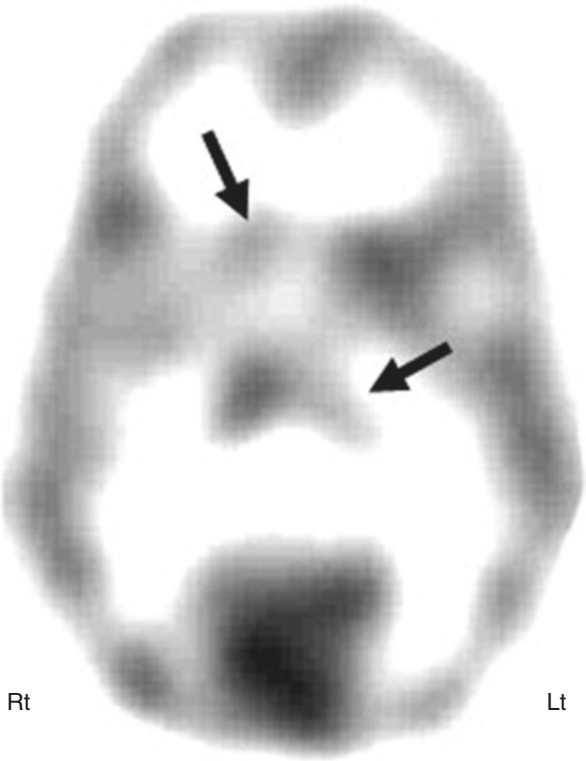

Fig. 47.19 A unique pattern of abnormality seen on ^{11}C-alpha-methyl tryptophan PET scan in a child with Tourette syndrome, with decreased alpha-methyl tryptophan uptake in the basal ganglia and contralateral thalamus (*arrows*)

47.3.6 Neuronal Ceroid Lipofuscinosis or Spielmeyer-Vogt (or Batten) Disease

The neuronal ceroid lipofuscinoses are a group of autosomal recessive neurodegenerative disorders, resulting from excessive accumulation of lipopigments (lipofuscin) in the tissue. The disorder is generally characterized by seizures, developmental regression, and progressive visual impairment. MRI can show nonspecific cortical and cerebellar atrophy and T2 hyperintensities of the white matter (D'Incerti 2000). On PET imaging, children with the juvenile form (CLN-3) or Spielmeyer-Vogt (or Batten) disease show decreased glucose metabolism in the calcarine cortex early in the course of the disease, while children with late infantile neuronal ceroid lipofuscinosis (CLN-2, Jansky-Bielschowsky disease with curvilinear inclusions) show rapid degeneration with generalized cortical and subcortical hypometabolism (De Volder et al. 1990; Iannetti et al. 1994; Philippart et al. 1994, 1997; Philippart and Chugani 1995). As the juvenile form of the disease progresses, a rostral spread of glucose hypometabolism to other cortical areas is observed (Philippart et al. 1994). Therefore, FDG PET can play a role in the early diagnosis, follow-up, and monitoring of the disease progression. PET studies have also shown reduced dopamine D1

receptors in both the caudate and putamen in juvenile neuronal ceroid lipofuscinosis (Ruottinen et al. 1997; Rinne et al. 2002).

An exhaustive review of PET imaging in the many rare neurodegenerative disorders of childhood is beyond the scope of this chapter. Suffice it to say that a recent review of the topic found adequate evidence to indicate that glucose metabolism PET scans are clinically useful in children with neurodegenerative disorders. In addition, PET imaging provides biomarkers which will be important as treatments become available for these rare disorders (Chugani 2019).

47.4 Multimodal Imaging with Simultaneous PET-MR

Both MRI and PET are powerful imaging tools used to study structure and function in pediatric neurological disorders, yet they offer complementary imaging perspectives. The simultaneous use of these tools in a single setting with recently available PET-MR scanners offers many research and clinical advantages. This new technology is a significant advancement to biomedical research because it allows simultaneously acquired noninvasive and quantitative comparisons of anatomical, functional, and metabolic tissue measures. Indeed, the fundamental advantages of simultaneous acquisition of PET and MR data reach far beyond simple co-registration of PET and MR image volumes. Important issues for children include automated motion correction for PET dynamic studies using MR navigator sequences; both structural and functional image acquisition at the same time requiring only one sedation (if necessary); image-derived arterial input function, thus eliminating the need for arterial blood sampling for quantitative modeling; and lower radioactivity exposure as the need for a transmission CT for attenuation correction used by current PET/CT technology is eliminated.

When using the PET-MR, scanning time is dictated more by MRI acquisition (approximately 40 min depending on desired sequences) than PET (approximately 10 min). We have taken advantage of this, particularly in children, by reducing the FDG dose by more than 50% and increasing PET acquisition time

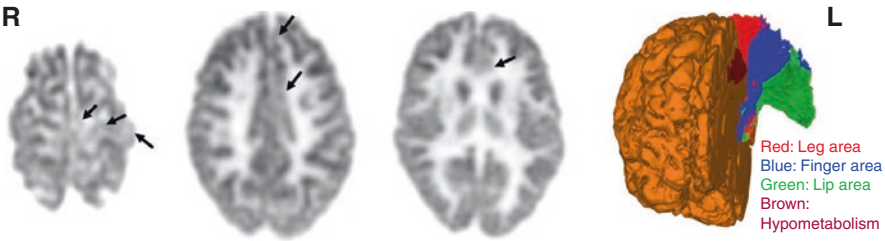

Fig. 47.20 FDG PET in a 14-year-old girl with uncontrolled seizures for 8 years, beginning with right leg shaking, nonlateralized EEG, and normal MRI, showing hypometabolism in the left motor cortex, extending into left anteromedial frontal cortex (*arrows*). The diffusion tensor analysis showing superimposition of hypometabolic region upon corticospinal tract

to equal that required for the MRI. In epilepsy surgery patients, we routinely include diffusion tensor imaging (DTI) in order to study the location of motor or language fibers in relation to the PET and MRI abnormalities (Fig. 47.20) in order to minimize damage to these vital regions during resection. PET-MR is also rapidly becoming an important research tool in the study of epilepsy by allowing a powerful approach to study anatomical-functional relationships or dual functional relationships, e.g., MR spectroscopy or functional MRI in relation to PET molecular imaging.

References

Aboian MS, Wong-Kisiel LC, Rank M, Wetjen NM, Wirrell EC, Witte RJ (2011) SISCOM in children with tuberous sclerosis complex-related epilepsy. Pediatr Neurol 45:83–88

Akman CI, Ichise M, Olsavsky A, Tikofsky RS, Van Heertum RL, Gilliam F (2010) Epilepsy duration impacts on brain glucose metabolism in temporal lobe epilepsy: results of voxel-based mapping. Epilepsy Behav 17:373–380

Alkonyi B, Juhasz C, Muzik O, Asano E, Saporta A, Shah A, Chugani HT (2009) Quantitative brain surface mapping of an electrophysiologic/metabolic mismatch in human neocortical epilepsy. Epilepsy Res 87:77–87

Alkonyi B, Chugani HT, Juhasz C (2011) Transient focal cortical increase of interictal glucose metabolism in Sturge-Weber syndrome: implications for epileptogenesis. Epilepsia 52:1265–1272

Alkonyi B, Miao Y, Wu J, Cai Z, Hu J, Chugani HT, Juhasz C (2012) A perfusion-metabolic mismatch in Sturge-Weber syndrome: a multimodality imaging study. Brain Dev 34:553–562

Arduini RG, Capellini SA, Ciasca SM (2006) Comparative study of the neuropsychological and neuroimaging evaluations in children with dyslexia. Arq Neuropsiquiatr 64:369–375

Arnold S, Berthele A, Drzezga A, Tolle TR, Weis S, Werhahn KJ, Henkel A, Yousry TA, Winkler PA, Bartenstein P, Noachtar S (2000) Reduction of benzodiazepine receptor binding is related to the seizure onset zone in extratemporal focal cortical dysplasia. Epilepsia 41:818–824

Asano E, Chugani DC, Muzik O, Shen C, Juhasz C, Janisse J, Ager J, Canady A, Shah JR, Shah AK, Watson C, Chugani HT (2000) Multimodality imaging for improved detection of epileptogenic foci in tuberous sclerosis complex. Neurology 54:1976–1984

Asano E, Juhasz C, Shah A, Muzik O, Chugani DC, Shah J, Sood S, Chugani HT (2005) Origin and propagation of epileptic spasms delineated on electrocorticography. Epilepsia 46:1086–1097

Asarnow RF, LoPresti C, Guthrie D, Elliott T, Cynn V, Shields WD, Shewmon DA, Sankar R, Peacock WJ (1997) Developmental outcomes in children receiving resection surgery for medically intractable infantile spasms. Dev Med Child Neurol 39:430–440

Aungaroon G, Trout A, Radhakrishnan R, Horn PS, Arya R, Tenney JR, Arthur TM, Holland KD, Mangano FT, Leach JL, Rozhkov L, Greiner HM (2018) Impact of radiotracer injection latency and seizure duration on subtraction ictal SPECT co-registered to MRI (SISCOM) performance in children. Clin Neurophysiol 129(9):1842–1848

Banati RB, Goerres GW, Myers R, Gunn RN, Turkheimer FE, Kreutzberg GW, Brooks DJ, Jones T, Duncan JS (1999) [11C](R)-PK11195 positron emission tomography imaging of activated microglia in vivo in Rasmussen's encephalitis. Neurology 53:2199–2203

Batista CE, Chugani HT, Juhasz C, Behen ME, Shankaran S (2007) Transient hypermetabolism of the basal ganglia following perinatal hypoxia. Pediatr Neurol 36:330–333

Behen M, Chugani HT, Juhasz C, Helder E, Ho A, Maqbool M, Rothermel RD, Perry J, Muzik O (2007) Abnormal brain tryptophan metabolism and clinical correlates in Tourette syndrome. Mov Disord 22:2256–2262

Behen ME, Juhasz C, Wolfe-Christensen C, Guy W, Halverson S, Rothermel R, Janisse J, Chugani HT (2011) Brain damage and IQ in unilateral Sturge-Weber syndrome: support for a "fresh start" hypothesis. Epilepsy Behav 22:352–357

Benedek K, Juhasz C, Chugani DC, Muzik O, Chugani HT (2006) Longitudinal changes in cortical glucose hypometabolism in children with intractable epilepsy. J Child Neurol 21:26–31

Benifla M, Otsubo H, Ochi A, Weiss SK, Donner EJ, Shroff M, Chuang S, Hawkins C, Drake JM, Elliott I, Smith ML, Snead OC III, Rutka JT (2006) Temporal lobe surgery for intractable epilepsy in children: an analysis of outcomes in 126 children. Neurosurgery 59:1203–1213; discussion 1213–1214

Bilgin O, Vollmar C, Peraud A, la Fougere C, Beleza P, Noachtar S (2008) Ictal SPECT in Sturge-Weber syndrome. Epilepsy Res 78:240–243

Bjørklund G, Kern JK, Urbina MA, Saad K, El-Houfey AA, Geier DA, Chirumbolo S, Geier MR, Mehta JA, Aaseth J (2018) Cerebral hypoperfusion in autism spectrum disorder. Acta Neurobiol Exp (Wars) 78(1):21–29

Bosnyák E, Behen ME, Guy WC, Asano E, Chugani HT, Juhasz C (2016) Predictors of cognitive functions in children with Sturge-Weber syndrome: a longitudinal study. Pediatr Neurol 61:38–45

Bouvard S, Costes N, Bonnefoi F, Lavenne F, Mauguiere F, Delforge J, Ryvlin P (2005) Seizure-related short-term plasticity of benzodiazepine receptors in partial epilepsy: a [11C]flumazenil-PET study. Brain 128:1330–1343

Branch CE, Dyken PR (1979) Choroid plexus papilloma and infantile spasms. Ann Neurol 5:302–304

Braun AR, Stoetter B, Randolph C, Hsiao JK, Vladar K, Gernert J, Carson RE, Herscovitch P, Chase TN (1993) The functional neuroanatomy of Tourette's syndrome: an FDG-PET study. I Regional changes in cerebral glucose metabolism differentiating patients and controls. Neuropsychopharmacology 9:277–291

Bruggemann JM, Som SS, Lawson JA, Haindl W, Cunningham AM, Bye AM (2004) Application of statistical parametric mapping to SPET in the assessment of intractable childhood epilepsy. Eur J Nucl Med Mol Imaging 31:369–377

Burneo JG, Hamilton M, Vezina W, Parrent A (2006) Utility of Ictal SPECT in the presurgical evaluation of Rasmussen's encephalitis. Can J Neurol Sci 33:107–110

Burroni L, Orsi A, Monti L, Hayek Y, Rocchi R, Vattimo AG (2008) Regional cerebral blood flow in childhood autism: a SPET study with SPM evaluation. Nucl Med Commun 29:150–156

Cahill V, Sinclair B, Malpas CB, McIntosh AM, Chen Z, Vivash LE, O'Shea MF, Wilson SJ, Desmond PM, Berlangieri SU, Hicks RJ, Rowe CC, Morokoff AP, King JA, Fabinyi GC, Kaye AH, Kwan P, Berkovic SF, O'Brien TJ (2019) Metabolic patterns and seizure outcomes following anterior temporal lobectomy. Ann Neurol 85(2):241–250

Carlson C, Teutonico F, Elliott RE, Moshel YA, LaJoie J, Miles D, Devinsky O, Weiner HL (2011) Bilateral invasive electroencephalography in patients with tuberous sclerosis complex: a path to surgery? J Neurosurg Pediatr 7:421–430

Chandana SR, Behen ME, Juhasz C, Muzik O, Rothermel RD, Mangner TJ, Chakraborty PK, Chugani HT, Chugani DC (2005) Significance of abnormalities in developmental trajectory and asymmetry of cortical serotonin synthesis in autism. Int J Dev Neurosci 23:171–182

Chandra PS, Salamon N, Huang J, Wu JY, Koh S, Vinters HV, Mathern GW (2006) FDG-PET/MRI coregistration and diffusion-tensor imaging distinguish epileptogenic tubers and cortex in patients with tuberous sclerosis complex: a preliminary report. Epilepsia 47:1543–1549

Chiron C, Raynaud C, Tzourio N, Diebler C, Dulac O, Zilbovicius M, Syrota A (1989) Regional cerebral blood flow by SPECT imaging in Sturge-Weber disease: an aid for diagnosis. J Neurol Neurosurg Psychiatry 52:1402–1409

Chiron C, Dulac O, Bulteau C, Nuttin C, Depas G, Raynaud C, Syrota A (1993) Study of regional cerebral blood flow in West syndrome. Epilepsia 34:707–715

Chiron C, Vera P, Kaminska A, Hollo A, Cieuta C, Ville D, Dulac O (1999a) Single-photon emission computed tomography: ictal perfusion in childhood epilepsies. Brain Dev 21:444–446

Chiron C, Vera P, Kaminska A, Cieuta C, Hollo A, Ville D, Gardin I, Stievenart JL, Dulac O (1999b) Ictal SPECT in the epileptic child. Contribution of subtraction interictal images and superposition of with MRI. Rev Neurol (Paris) 155:477–481

Chugani HT (2018) Imaging brain metabolism in the newborn. J Child Neurol 33(13):851–860

Chugani HT (2019) Positron Emission Tomography in Pediatric Neurodegenerative Disorders. Pediatr Neurol 100:12–25

Chugani HT, Conti JR (1996) Etiologic classification of infantile spasms in 140 cases: role of positron emission tomography. J Child Neurol 11:44–48

Chugani HT, Phelps ME, Mazziotta JC (1987a) Positron emission tomography study of human brain functional development. Ann Neurol 22:487–497

Chugani HT, Mazziotta JC, Engel J Jr, Phelps ME (1987b) The Lennox-Gastaut syndrome: metabolic subtypes determined by 2-deoxy-2[18F]fluoro-D-glucose positron emission tomography. Ann Neurol 21:4–13

Chugani HT, Mazziotta JC, Phelps ME (1989) Sturge-Weber syndrome: a study of cerebral glucose utilization with positron emission tomography. J Pediatr 114:244–253

Chugani HT, Shields WD, Shewmon DA, Olson DM, Phelps ME, Peacock WJ (1990) Infantile spasms: I. PET identifies focal cortical dysgenesis in cryptogenic cases for surgical treatment. Ann Neurol 27:406–413

Chugani HT, Shewmon DA, Sankar R, Chen BC, Phelps ME (1992) Infantile spasms: II. Lenticular nuclei and brain stem activation on positron emission tomography. Ann Neurol 31:212–219

Chugani HT, Shewmon DA, Shields WD, Sankar R, Comair Y, Vinters HV, Peacock WJ (1993) Surgery for intractable infantile spasms: neuroimaging perspectives. Epilepsia 34:764–771

Chugani HT, Da Silva E, Chugani DC (1996) Infantile spasms: III. Prognostic implications of bitemporal hypometabolism on positron emission tomography. Ann Neurol 39:643–649

Chugani DC, Muzik O, Rothermel R, Behen M, Chakraborty P, Mangner T, da Silva EA, Chugani HT (1997) Altered serotonin synthesis in the dentatothalamocortical pathway in autistic boys. Ann Neurol 42:666–669

Chugani DC, Muzik O, Chakraborty P, Mangner T, Chugani HT (1998a) Human brain serotonin synthesis capacity measured in vivo with alpha-[C-11]methyl-L-tryptophan. Synapse 28:33–43

Chugani DC, Chugani HT, Muzik O, Shah JR, Shah AK, Canady A, Mangner TJ, Chakraborty PK (1998b) Imaging epileptogenic tubers in children with tuberous sclerosis complex using alpha-[11C]methyl-L-tryptophan positron emission tomography. Ann Neurol 44:858–866

Chugani DC, Muzik O, Behen M, Rothermel R, Janisse JJ, Lee J, Chugani HT (1999) Developmental changes in brain serotonin synthesis capacity in autistic and nonautistic children. Ann Neurol 45:287–295

Chugani HT, Asano E, Sood S (2010) Infantile spasms: who are the ideal surgical candidates? Epilepsia 51(Suppl 1):94–96

Chugani HT, Kumar A, Kupsky W, Asano E, Sood S, Juhasz C (2011) Clinical and histopathologic correlates of (11) C-alpha-methyl-L-tryptophan (AMT) PET abnormalities in children with intractable epilepsy. Epilepsia 52(9):1692–1698

Chugani HT, Kumar A, Muzik O (2013a) GABA(A) receptor imaging with positron emission tomography in the human newborn: a unique binding pattern. Pediatr Neurol 48(6):459–462

Chugani HT, Luat AF, Kumar A, Govindan R, Pawlik K, Asano E (2013b) α-[11C]-Methyl-L-tryptophan-PET in 191 patients with tuberous sclerosis complex. Neurology 81:674–680

Chugani HT, Ilyas M, Kumar A, Juhász C, Kupsky WJ, Sood S, Asano E (2015) Surgical treatment for refractory epileptic spasms: The Detroit series. Epilepsia 56(12):1941–1949

Cook EH Jr, Rowlett R, Jaselskis C, Leventhal BL (1992) Fluoxetine treatment of children and adults with autistic disorder and mental retardation. J Am Acad Child Adolesc Psychiatry 31:739–745

D'Incerti L (2000) MRI in neuronal ceroid lipofuscinosis. Neurol Sci 21:S71–S73

da Silva EA, Chugani DC, Muzik O, Chugani HT (1997) Identification of frontal lobe epileptic foci in children using positron emission tomography. Epilepsia 38:1198–1208

De Volder A, Bol A, Michel C, Congneau M, Goffinet AM (1987) Brain glucose metabolism in children with the autistic syndrome: positron tomography analysis. Brain Dev 9:581–587

De Volder AG, Cirelli S, de Barsy T, Brucher JM, Bol A, Michel C, Goffinet AM (1990) Neuronal ceroid-lipofuscinosis: preferential metabolic alterations in thalamus and posterior association cortex demonstrated by PET. J Neurol Neurosurg Psychiatry 53:1063–1067

Dickstein LP, Liow JS, Austermuehle A, Zoghbi S, Inati SK, Zaghloul K, Zanotti-Fregonara P, Theodore WH (2019) Neuroinflammation in neocortical epilepsy measured by PET imaging of translocator protein. Epilepsia 60(6):1248–1254

Ding Y, Zhu Y, Jiang B, Zhou Y, Jin B, Hou H (2018) 18F-FDG PET and high-resolution MRI co-registration for pre-surgical evaluation of patients with conventional MRI-negative refractory extra-temporal lobe epilepsy. Eur J Nucl Med Mol Imaging 45:1567–1572

Doyle LW, Nahmias C, Firnau G, Kenyon DB, Garnett ES, Sinclair JC (1983) Regional cerebral glucose metabolism of newborn infants measured by positron emission tomography. Dev Med Child Neurol 25:143–151

Dufor O, Serniclaes W, Sprenger-Charolles L, Demonet JF (2007) Top-down processes during auditory phoneme categorization in dyslexia: a PET study. NeuroImage 34:1692–1707

Dufor O, Serniclaes W, Sprenger-Charolles L, Demonet JF (2009) Left premotor cortex and allophonic speech perception in dyslexia: a PET study. NeuroImage 46:241–248

Ernst M, Zametkin AJ, Matochik JA, Pascualvaca D, Cohen RM (1997) Low medial prefrontal dopaminergic activity in autistic children. Lancet 350:638

Ernst M, Zametkin AJ, Jons PH, Matochik JA, Pascualvaca D, Cohen RM (1999) High presynaptic dopaminergic activity in children with Tourette's disorder. J Am Acad Child Adolesc Psychiatry 38:86–94

Evans LT, Morse R, Roberts DW (2012) Epilepsy surgery in tuberous sclerosis: a review. Neurosurg Focus 32:E5

Fedi M, Reutens DC, Andermann F, Okazawa H, Boling W, White C, Dubeau F, Nakai A, Gross DW, Andermann E, Diksic M (2003) alpha-[11C]-Methyl-L-tryptophan PET identifies the epileptogenic tuber and correlates with interictal spike frequency. Epilepsy Res 52:203–213

Fedi M, Berkovic SF, Scheffer IE, O'Keefe G, Marini C, Mulligan R, Gong S, Tochon-Danguy H, Reutens DC (2008) Reduced striatal D1 receptor binding in autosomal dominant nocturnal frontal lobe epilepsy. Neurology 71:795–798

Ferrie CD, Maisey M, Cox T, Polkey C, Barrington SF, Panayiotopoulos CP, Robinson RO (1996) Focal abnormalities detected by 18FDG PET in epileptic encephalopathies. Arch Dis Child 75:102–107

Fiorella DJ, Provenzale JM, Coleman RE, Crain BJ, Al-Sugair AA (2001) (18)F-fluorodeoxyglucose positron emission tomography and MR imaging findings in Rasmussen encephalitis. AJNR Am J Neuroradiol 22:1291–1299

Flowers DL, Wood FB, Naylor CE (1991) Regional cerebral blood flow correlates of language processes in reading disability. Arch Neurol 48:637–643

Frost JJ, Mayberg HS, Fisher RS, Douglass KH, Dannals RF, Links JM, Wilson AA, Ravert HT, Rosenbaum AE, Snyder SH et al (1988) Mu-opiate receptors measured by positron emission tomography are increased in temporal lobe epilepsy. Ann Neurol 23:231–237

Fujimoto A, Okanishi T, Kanai S, Sato K, Itamura S, Baba S, Nishimura M, Masui T, Enoki H (2018) Double match of (18)F-fluorodeoxyglucose-PET and iomazenil-SPECT improves outcomes of focus resection surgery. Acta Neurochir 160(9):1875–1882

Gaillard WD, Bhatia S, Bookheimer SY, Fazilat S, Sato S, Theodore WH (1995) FDG-PET and volumetric MRI in the evaluation of patients with partial epilepsy. Neurology 45:123–126

Gaillard WD, Kopylev L, Weinstein S, Conry J, Pearl PL, Spanaki MV, Fazilat S, Venzina LG, Dubovsky E, Theodore WH (2002) Low incidence of abnormal (18)FDG-PET in children with new-onset partial epilepsy: a prospective study. Neurology 58:717–722

George MS, Costa DC, Kouris K, Ring HA, Ell PJ (1992) Cerebral blood flow abnormalities in adults with infantile autism. J Nerv Ment Dis 180:413–417

Gershen LD, Zanotti-Fregonara P, Dustin IH, Liow JS, Hirvonen J, Kreisl WC, Jenko KJ, Inati SK, Fujita M, Morse CL, Brouwer C, Hong JS, Pike VW, Zoghbi SS, Innis RB, Theodore WH (2015) Neuroinflammation in temporal lobe epilepsy measured using positron emission tomographic imaging of translocator protein. JAMA Neurol 72(8):882–888

Gilbert DL, Christian BT, Gelfand MJ, Shi B, Mantil J, Sallee FR (2006) Altered mesolimbocortical and thalamic dopamine in Tourette syndrome. Neurology 67:1695–1697

Gordon CT, State RC, Nelson JE, Hamburger SD, Rapoport JL (1993) A double-blind comparison of clomipramine, desipramine, and placebo in the treatment of autistic disorder. Arch Gen Psychiatry 50:441–447

Gross-Glenn K, Duara R, Barker WW, Loewenstein D, Chang JY, Yoshii F, Apicella AM, Pascal S, Boothe T, Sevush S et al (1991) Positron emission tomographic studies during serial word-reading by normal and dyslexic adults. J Clin Exp Neuropsychol 13:531–544

Guerin J, Watson RE, Carr CM, Liebo GB, Kotsenas AL (2019) Autoimmune epilepsy: findings on MRI and FDG-PET. Br J Radiol 92(1093):20170869

Guerreiro MM, Camargo EE, Kato M, Menezes Netto JR, Silva EA, Scotoni AE, Silveira DC, Guerreiro CA (1996) Brain single photon emission computed tomography imaging in Landau-Kleffner syndrome. Epilepsia 37:60–67

Gur RC, Sussman NM, Alavi A, Gur RE, Rosen AD, O'Connor M, Goldberg HI, Greenberg JH, Reivich M (1982) Positron emission tomography in two cases of childhood epileptic encephalopathy (Lennox-Gastaut syndrome). Neurology 32:1191–1194

Haginoya K, Kon K, Takayanagi M, Yoshihara Y, Kato R, Tanaka S, Yokoyama H, Munakata M, Nagai M, Maruoka S, Yamazaki T, Abe Y, Iinuma K (1998) Heterogeneity of ictal SPECT findings in nine cases of West syndrome. Epilepsia 39(Suppl 5):26–29

Haginoya K, Kon K, Yokoyama H, Tanaka S, Kato R, Munakata M, Yagi T, Takayanagi M, Yoshihara Y, Nagai M, Yamazaki T, Maruoka S, Iinuma K (2000) The perfusion defect seen with SPECT in West syndrome is not correlated with seizure prognosis or developmental outcome. Brain Dev 22:16–23

Haginoya K, Munakata M, Yokoyama H, Kato R, Tanaka S, Hirose M, Ishitobi M, Kon K, Yoshihara Y, Takayanagi M, Yamazaki T, Iinuma K (2001) Mechanism of tonic spasms in West syndrome viewed from ictal SPECT findings. Brain Dev 23:496–501

Hagman JO, Wood F, Buchsbaum MS, Tallal P, Flowers L, Katz W (1992) Cerebral brain metabolism in adult dyslexic subjects assessed with positron emission tomography during performance of an auditory task. Arch Neurol 49:734–739

Hammers A, Koepp MJ, Hurlemann R, Thom M, Richardson MP, Brooks DJ, Duncan JS (2002) Abnormalities of grey and white matter [11C]flumazenil binding in temporal lobe epilepsy with normal MRI. Brain 125:2257–2271

Harbord MG, Singh R, Morony S (1999) SPECT abnormalities in Landau-Kleffner syndrome. J Clin Neurosci 6:9–16

Harvey AS, Bowe JM, Hopkins IJ, Shield LK, Cook DJ, Berkovic SF (1993) Ictal 99mTc-HMPAO single photon emission computed tomography in children with temporal lobe epilepsy. Epilepsia 34:869–877

Haugbol S, Pinborg LH, Regeur L, Hansen ES, Bolwig TG, Nielsen FA, Svarer C, Skovgaard LT, Knudsen GM (2007) Cerebral 5-HT2A receptor binding is increased in patients with Tourette's syndrome. Int J Neuropsychopharmacol 10:245–252

Hazlett EA, Buchsbaum MS, Hsieh P, Haznedar MM, Platholi J, LiCalzi EM, Cartwright C, Hollander E (2004) Regional glucose metabolism within cortical Brodmann areas in healthy individuals and autistic patients. Neuropsychobiology 49:115–125

Haznedar MM, Buchsbaum MS, Metzger M, Solimando A, Spiegel-Cohen J, Hollander E (1997) Anterior cingulate gyrus volume and glucose metabolism in autistic disorder. Am J Psychiatry 154:1047–1050

Haznedar MM, Buchsbaum MS, Wei TC, Hof PR, Cartwright C, Bienstock CA, Hollander E (2000) Limbic circuitry in patients with autism spectrum disorders studied with positron emission tomography and magnetic resonance imaging. Am J Psychiatry 157:1994–2001

Haznedar MM, Buchsbaum MS, Hazlett EA, LiCalzi EM, Cartwright C, Hollander E (2006) Volumetric analysis and three-dimensional glucose metabolic mapping of the striatum and thalamus in patients with autism spectrum disorders. Am J Psychiatry 163:1252–1263

Heiskala H, Launes J, Pihko H, Nikkinen P, Santavuori P (1993) Brain perfusion SPECT in children with frequent fits. Brain Dev 15:214–218

Henry TR, Sutherling WW, Engel J Jr, Risinger MW, Levesque MF, Mazziotta JC, Phelps ME (1991) Interictal cerebral metabolism in partial epilepsies of neocortical origin. Epilepsy Res 10:174–182

Henry TR, Frey KA, Sackellares JC, Gilman S, Koeppe RA, Brunberg JA, Ross DA, Berent S, Young AB, Kuhl DE (1993) In vivo cerebral metabolism and central benzodiazepine-receptor binding in temporal lobe epilepsy. Neurology 43:1998–2006

Herold S, Frackowiak RS, Le Couteur A, Rutter M, Howlin P (1988) Cerebral blood flow and metabolism of oxygen and glucose in young autistic adults. Psychol Med 18:823–831

Hienert M, Gryglewski G, Stamenkovic M, Kasper S, Lanzenberger R (2018) Striatal dopaminergic alterations in Tourette's syndrome: a meta-analysis based on 16 PET and SPECT neuroimaging studies. Transl Psychiatry 8(1):143

Hirvonen J, Kreisl WC, Fujita M, Dustin I, Khan O, Appel S, Zhang Y, Morse C, Pike VW, Innis RB, Theodore WH (2012) Increased in vivo expression of an inflammatory marker in temporal lobe epilepsy. J Nucl Med 53:234–240

Honbolygo F, Csepe V, Fekeshazy A, Emri M, Marian T, Sarkozy G, Kalmanchey R (2006) Converging evidences on language impairment in Landau-Kleffner Syndrome revealed by behavioral and brain activity measures: a case study. Clin Neurophysiol 117:295–305

Horwitz B, Rumsey JM, Donohue BC (1998) Functional connectivity of the angular gyrus in normal reading and dyslexia. Proc Natl Acad Sci U S A 95:8939–8944

Hougaard K, Oikawa T, Sveinsdottir E, Skinoj E, Ingvar DH, Lassen NA (1976) Regional cerebral blood flow in focal cortical epilepsy. Arch Neurol 33:527–535

Hu SX, Wu XR, Lin C, Hao SY (1989) Landau-Kleffner syndrome with unilateral EEG abnormalities–two cases from Beijing, China. Brain Dev 11:420–422

Hur YJ, Kang HC, Kim DS, Choi SR, Kim HD, Lee JS (2011) Uncovered primary seizure foci in Lennox-Gastaut syndrome after corpus callosotomy. Brain Dev 33:672–677

Hwang PA, Otsubo H, Koo BK, Gilday DL, Chuang SH, Jay V, Hoffman HJ (1996) Infantile spasms: cerebral blood flow abnormalities correlate with EEG, neuroimaging, and pathologic findings. Pediatr Neurol 14:220–225

Hwang SI, Kim JH, Park SW, Han MH, Yu IK, Lee SH, Lee DS, Lee SK, Chung CK, Chang KH (2001) Comparative analysis of MR imaging, positron emission tomography, and ictal single-photon emission CT in patients with neocortical epilepsy. AJNR Am J Neuroradiol 22:937–946

Hwang BJ, Mohamed MA, Brašić JR (2017) Molecular imaging of autism spectrum disorder. Int Rev Psychiatry 29(6):530–554

Iannetti P, Messa C, Spalice A, Lucignani G, Fazio F (1994) Positron emission tomography in neuronal ceroid lipofuscinosis (Jansky-Bielschowsky disease): a case report. Brain Dev 16:459–462

Iinuma K, Yanai K, Yanagisawa T, Fueki N, Tada K, Ito M, Matsuzawa T, Ido T (1987) Cerebral glucose metabolism in five patients with Lennox-Gastaut syndrome. Pediatr Neurol 3:12–18

Iinuma K, Yokoyama H, Otsuki T, Yanai K, Watanabe T, Ido T, Itoh M (1993) Histamine H1 receptors in complex partial seizures. Lancet 341:238

Ilyas M, Sivaswamy L, Asano E, Sood S, Zidan M, Chugani H (2014) Seizure control following palliative resective surgery for intractable epilepsy-a pilot study. Pediatr Neurol 51(3):330–335

Jalota A, Rossi MA, Pylypyuk V, Stein M, Stoub T, Balabanov A (2016) Resecting critical nodes from an epileptogenic circuit in refractory focal-onset epilepsy patients using subtraction ictal SPECT coregistered to MRI. J Neurosurg 125:1565–1576

Jeong JW, Asano E, Pilli V, Nakai Y, Chugani HT, Juhasz C (2017) Objective 3D surface evaluation of intracranial electrophysiologic correlates of cerebral glucose metabolic abnormalities in children with focal epilepsy. Hum Brain Mapp 38:3098–3112

Jonas R, Asarnow RF, LoPresti C, Yudovin S, Koh S, Wu JY, Sankar R, Shields WD, Vinters HV, Mathern GW (2005) Surgery for symptomatic infant-onset epileptic encephalopathy with and without infantile spasms. Neurology 64:746–750

Juhasz C, Chugani DC, Muzik O, Watson C, Shah J, Shah A, Chugani HT (2000a) Is epileptogenic cortex truly hypometabolic on interictal positron emission tomography? Ann Neurol 48:88–96

Juhasz C, Chugani DC, Muzik O, Watson C, Shah J, Shah A, Chugani HT (2000b) Electroclinical correlates of flumazenil and fluorodeoxyglucose PET abnormalities in lesional epilepsy. Neurology 55:825–835

Juhasz C, Chugani DC, Muzik O, Shah A, Shah J, Watson C, Canady A, Chugani HT (2001) Relationship of flumazenil and glucose PET abnormalities to neocortical epilepsy surgery outcome. Neurology 56:1650–1658

Juhasz C, Chugani DC, Asano E, Shah A, Shah J, Muzik O, Sood S, Chugani HT (2002) Alpha[11C]methyl-L-tryptophan positron emission tomography scanning in 176 patients with intractable epilepsy. Ann Neurol 52:S118. (abstract)

Juhasz C, Chugani DC, Muzik O, Shah A, Asano E, Mangner TJ, Chakraborty PK, Sood S, Chugani HT (2003) Alpha-methyl-L-tryptophan PET detects epileptogenic cortex in children with intractable epilepsy. Neurology 60:960–968

Juhasz C, Batista CE, Chugani DC, Muzik O, Chugani HT (2007) Evolution of cortical metabolic abnormalities and their clinical correlates in Sturge-Weber syndrome. Eur J Paediatr Neurol 11:277–284

Kagawa K, Chugani DC, Asano E, Juhasz C, Muzik O, Shah A, Shah J, Sood S, Kupsky WJ, Mangner TJ, Chakraborty PK, Chugani HT (2005) Epilepsy surgery outcome in children with tuberous sclerosis complex evaluated with alpha-[11C]methyl-L-tryptophan positron emission tomography (PET). J Child Neurol 20:429–438

Kakisaka Y, Haginoya K, Ishitobi M, Togashi N, Kitamura T, Wakusawa K, Sato I, Hino-Fukuyo N, Uematsu M, Munakata M, Yokoyama H, Iinuma K, Kaneta T, Higano S, Tsuchiya S (2009) Utility of subtraction ictal SPECT images in detecting focal leading activity and understanding the pathophysiology of spasms in patients with West syndrome. Epilepsy Res 83:177–183

Kaminska A, Chiron C, Ville D, Dellatolas G, Hollo A, Cieuta C, Jalin C, Delalande O, Fohlen M, Vera P, Soufflet C, Dulac O (2003) Ictal SPECT in children with epilepsy: comparison with intracranial EEG and relation to postsurgical outcome. Brain 126:248–260

Kaneko M, Uno A, Kaga M, Matsuda H, Inagaki M, Haruhara N (1998) Cognitive neuropsychological and regional cerebral blood flow study of a developmentally dyslexic Japanese child. J Child Neurol 13:457–461

Kannan S, Saadani-Makki F, Muzik O, Chakraborty P, Mangner TJ, Janisse J, Romero R, Chugani DC (2007) Microglial activation in perinatal rabbit brain induced by intrauterine inflammation: detection with 11C-(R)-PK11195 and small-animal PET. J Nucl Med 48:946–954

Karenfort M, Kruse B, Freitag H, Pannek H, Tuxhorn I (2002) Epilepsy surgery outcome in children with focal epilepsy due to tuberous sclerosis complex. Neuropediatrics 33:255–261

Kerrigan JF, Chugani HT, Phelps ME (1991) Regional cerebral glucose metabolism in clinical subtypes of cerebral palsy. Pediatr Neurol 7:415–425

Kim SK, Lee DS, Lee SK, Kim YK, Kang KW, Chung CK, Chung JK, Lee MC (2001) Diagnostic performance of [18F]FDG-PET and ictal [99mTc]-HMPAO SPECT in occipital lobe epilepsy. Epilepsia 42:1531–1540

Kim YK, Lee DS, Lee SK, Chung CK, Chung JK, Lee MC (2002) (18)F-FDG PET in localization of frontal lobe epilepsy: comparison of visual and SPM analysis. J Nucl Med 43:1167–1174

Kim MA, Heo K, Choo MK, Cho JH, Park SC, Lee JD, Yun M, Park HJ, Lee BI (2006) Relationship between bilateral temporal hypometabolism and EEG findings for mesial temporal lobe epilepsy: analysis of 18F-FDG PET using SPM. Seizure 15:56–63

Kim JT, Bai SJ, Choi KO, Lee YJ, Park HJ, Kim DS, Kim HD, Lee JS (2009) Comparison of various imaging modalities in localization of epileptogenic lesion using epilepsy surgery outcome in pediatric patients. Seizure 18:504–510

Kim YH, Kang HC, Kim DS, Kim SH, Shim KW, Kim HD (2011) Neuroimaging in identifying focal cortical dysplasia and prognostic factors in pediatric and adolescent epilepsy surgery. Epilepsia 52:722–727

Kim JA, Jeong JW, Behen ME, Pilli VK, Luat A, Chugani HT, Juhasz C (2018) Metabolic correlates of cognitive function in children with unilateral Sturge-Weber syndrome: evidence for regional functional reorganization and crowding. Hum Brain Mapp 39(4):1596–1606

Knowlton RC, Laxer KD, Ende G, Hawkins RA, Wong ST, Matson GB, Rowley HA, Fein G, Weiner MW (1997) Presurgical multimodality neuroimaging in electroencephalographic lateralized temporal lobe epilepsy. Ann Neurol 42:829–837

Knowlton RC, Elgavish RA, Bartolucci A, Ojha B, Limdi N, Blount J, Burneo JG, Ver Hoef L, Paige L, Faught E, Kankirawatana P, Riley K, Kuzniecky R (2008) Functional imaging: II. Prediction of epilepsy surgery outcome. Ann Neurol 64:35–41

Koepp MJ, Woermann FG (2005) Imaging structure and function in refractory focal epilepsy. Lancet Neurol 4:42–53

Koepp MJ, Richardson MP, Brooks DJ, Poline JB, Van Paesschen W, Friston KJ, Duncan JS (1996) Cerebral benzodiazepine receptors in hippocampal sclerosis. An objective in vivo analysis. Brain 119(Pt 5):1677–1687

Koepp MJ, Labbe C, Richardson MP, Brooks DJ, Van Paesschen W, Cunningham VJ, Duncan JS (1997) Regional hippocampal [11C]flumazenil PET in temporal lobe epilepsy with unilateral and bilateral hippocampal sclerosis. Brain 120(Pt 10):1865–1876

Koepp MJ, Richardson MP, Brooks DJ, Duncan JS (1998) Focal cortical release of endogenous opioids during reading-induced seizures. Lancet 352:952–955

Koh S, Jayakar P, Resnick T, Alvarez L, Liit RE, Duchowny M (1999) The localizing value of ictal SPECT in children with tuberous sclerosis complex and refractory partial epilepsy. Epileptic Disord 1:41–46

Krause KH, Dresel S, Krause J, Kung HF, Tatsch K, Lochmuller H (2002) Elevated striatal dopamine transporter in a drug naive patient with Tourette syndrome and attention deficit//hyperactivity disorder: positive effect of methylphenidate. J Neurol 249:1116–1118

Kuki I, Kawawaki H, Oba S, Okazaki S, Ikeda H, Tomiwa K (2008) 123I iomazenil SPECT and identification of the epileptogenic tubers in patients with tuberous sclerosis. No To Hattatsu 40:54–56

Kuki I, Kawawaki H, Okazaki S, Inoue T, Nukui M, Tomiwa K, Amou K, Togawa M, Shiomi M (2012) Usefulness of 123I-iomazenil SPECT in pediatric patients with neurological disease. No To Hattatsu 44:5–12

Kuki I, Matsuda K, Kubota Y, Fukuyama T, Takahashi Y, Inoue Y, Shintaku H (2018) Functional neuroimaging in Rasmussen syndrome. Epilepsy Res 140:120–127

Kumar A, Chugani HT, Luat A, Asano E, Sood S (2008) Epilepsy surgery in a case of encephalitis: use of 11C-PK11195 positron emission tomography. Pediatr Neurol 38:439–442

Kumar A, Juhasz C, Asano E, Sood S, Muzik O, Chugani HT (2010) Objective detection of epileptic foci by 18F-FDG PET in children undergoing epilepsy surgery. J Nucl Med 51:1901–1907

Kumar A, Asano E, Chugani HT (2011) alpha-[(1)(1)C]-methyl-L-tryptophan PET for tracer localization of epileptogenic brain regions: clinical studies. Biomark Med 5:577–584

Kumlien E, Hilton-Brown P, Spannare B, Gillberg PG (1992) In vitro quantitative autoradiography of [3H]-L-deprenyl and [3H]-PK 11195 binding sites in human epileptic hippocampus. Epilepsia 33:610–617

Kumlien E, Hartvig P, Valind S, Oye I, Tedroff J, Langstrom B (1999) NMDA-receptor activity visualized with (S)-[N-methyl-11C]ketamine and positron emission tomography in patients with medial temporal lobe epilepsy. Epilepsia 40:30–37

Kumlien E, Nilsson A, Hagberg G, Langstrom B, Bergstrom M (2001) PET with 11C-deuterium-deprenyl and 18F-FDG in focal epilepsy. Acta Neurol Scand 103:360–366

Kurian M, Spinelli L, Delavelle J, Willi JP, Velazquez M, Chaves V, Habre W, Meagher-Villemure K, Roulet E, Villeneuve JG, Seeck M (2007) Multimodality imaging for focus localization in pediatric pharmacoresistant epilepsy. Epileptic Disord 9:20–31

Lamusuo S, Jutila L, Ylinen A, Kalviainen R, Mervaala E, Haaparanta M, Jaaskelainen S, Partanen K, Vapalahti M, Rinne J (2001) [18F]FDG-PET reveals temporal hypometabolism in patients with temporal lobe epilepsy even when quantitative MRI and histopathological analysis show only mild hippocampal damage. Arch Neurol 58:933–939

Langer O, Bauer M, Hammers A, Karch R, Pataraia E, Koepp MJ, Abrahim A, Luurtsema G, Brunner M, Sunder-Plassmann R, Zimprich F, Joukhadar C, Gentzsch S, Dudczak R, Kletter

K, Muller M, Baumgartner C (2007) Pharmacoresistance in epilepsy: a pilot PET study with the P-glycoprotein substrate R-[(11)C]verapamil. Epilepsia 48:1774–1784
Lawson JA, O'Brien TJ, Bleasel AF, Haindl W, Vogrin S, Cook MJ, Bye AM (2000) Evaluation of SPECT in the assessment and treatment of intractable childhood epilepsy. Neurology 55:1391–1393
Lee JD, Kim HJ, Lee BI, Kim OJ, Jeon TJ, Kim MJ (2000) Evaluation of ictal brain SPET using statistical parametric mapping in temporal lobe epilepsy. Eur J Nucl Med 27:1658–1665
Lee JS, Juhasz C, Kaddurah AK, Chugani HT (2001a) Patterns of cerebral glucose metabolism in early and late stages of Rasmussen's syndrome. J Child Neurol 16:798–805
Lee JS, Asano E, Muzik O, Chugani DC, Juhasz C, Pfund Z, Philip S, Behen M, Chugani HT (2001b) Sturge-Weber syndrome: correlation between clinical course and FDG PET findings. Neurology 57:189–195
Lee JJ, Kang WJ, Lee DS, Lee JS, Hwang H, Kim KJ, Hwang YS, Chung JK, Lee MC (2005) Diagnostic performance of 18F-FDG PET and ictal 99mTc-HMPAO SPET in pediatric temporal lobe epilepsy: quantitative analysis by statistical parametric mapping, statistical probabilistic anatomical map, and subtraction ictal SPET. Seizure 14:213–220
Lee JD, Park HJ, Park ES, Kim DG, Rha DW, Kim EY, Kim DI, Kim JJ, Yun M, Ryu YH, Lee J, Jeong JM, Lee DS, Lee MC, Park CI (2007) Assessment of regional GABA(A) receptor binding using 18F-fluoroflumazenil positron emission tomography in spastic type cerebral palsy. NeuroImage 34:19–25
Lerner A, Bagic A, Boudreau EA, Hanakawa T, Pagan F, Mari Z, Bara-Jimenez W, Aksu M, Garraux G, Simmons JM, Sato S, Murphy DL, Hallett M (2007) Neuroimaging of neuronal circuits involved in tic generation in patients with Tourette syndrome. Neurology 68:1979–1987
Lerner JT, Salamon N, Hauptman JS, Velasco TR, Hemb M, Wu JY (2009) Assessment and surgical outcomes for mild type I and severe type II cortical dysplasia: a critical review and the UCLA experience. Epilepsia 50:1310–1335
Lin Y, Fang YD, Wu G, Jones SE, Prayson RA, Moosa ANV (2018) Quantitative positron emission tomography-guided magnetic resonance imaging postprocessing in magnetic resonance imaging-negative epilepsies. Epilepsia 59:1583–1594
Luat AF, Chugani HT, Asano E, Juhasz C, Trock G, Rothermel R (2006) Episodic receptive aphasia in a child with Landau-Kleffner Syndrome: PET correlates. Brain Dev 28:592–596
Madar I, Lesser RP, Krauss G, Zubieta JK, Lever JR, Kinter CM, Ravert HT, Musachio JL, Mathews WB, Dannals RF, Frost JJ (1997) Imaging of delta- and mu-opioid receptors in temporal lobe epilepsy by positron emission tomography. Ann Neurol 41:358–367
Majerus S, Laureys S, Collette F, Del Fiore G, Degueldre C, Luxen A, Van der Linden M, Maquet P, Metz-Lutz MN (2003) Phonological short-term memory networks following recovery from Landau and Kleffner syndrome. Hum Brain Mapp 19:133–144
Maquet P, Hirsch E, Dive D, Salmon E, Marescaux C, Franck G (1990) Cerebral glucose utilization during sleep in Landau-Kleffner syndrome: a PET study. Epilepsia 31:778–783
Maquet P, Hirsch E, Metz-Lutz MN, Motte J, Dive D, Marescaux C, Franck G (1995) Regional cerebral glucose metabolism in children with deterioration of one or more cognitive functions and continuous spike-and-wave discharges during sleep. Brain 118(Pt 6):1497–1520
Marks DA, Katz A, Hoffer P, Spencer SS (1992) Localization of extratemporal epileptic foci during ictal single photon emission computed tomography. Ann Neurol 31:250–255
Mayberg HS, Sadzot B, Meltzer CC, Fisher RS, Lesser RP, Dannals RF, Lever JR, Wilson AA, Ravert HT, Wagner HN Jr et al (1991) Quantification of mu and non-mu opiate receptors in temporal lobe epilepsy using positron emission tomography. Ann Neurol 30:3–11
McCrory E, Frith U, Brunswick N, Price C (2000) Abnormal functional activation during a simple word repetition task: a PET study of adult dyslexics. J Cogn Neurosci 12:753–762
McDougle CJ, Naylor ST, Cohen DJ, Volkmar FR, Heninger GR, Price LH (1996a) A double-blind, placebo-controlled study of fluvoxamine in adults with autistic disorder. Arch Gen Psychiatry 53:1001–1008

McDougle CJ, Naylor ST, Cohen DJ, Aghajanian GK, Heninger GR, Price LH (1996b) Effects of tryptophan depletion in drug-free adults with autistic disorder. Arch Gen Psychiatry 53:993–1000

Mimaki T, Ono J, Yabuuchi H (1983) Temporal lobe astrocytoma with infantile spasms. Ann Neurol 14:695–696

Miyauchi T, Nomura Y, Ohno S, Kishimoto H, Matsushita M (1988) Positron emission tomography in three cases of Lennox-Gastaut syndrome. Jpn J Psychiatry Neurol 42:795–804

Miyazaki M, Hashimoto T, Fujii E, Tayama M, Kuroda Y (1994) Infantile spasms: localized cerebral lesions on SPECT. Epilepsia 35:988–992

Mori K, Toda Y, Hashimoto T, Miyazaki M, Saijo T, Ito H, Fujii E, Yamaue T, Kuroda Y (2007) Patients with West syndrome whose ictal SPECT showed focal cortical hyperperfusion. Brain Dev 29:202–209

Mori K, Mori T, Toda Y, Fujii E, Miyazaki M, Harada M, Kagami S (2012) Decreased benzodiazepine receptor and increased GABA level in cortical tubers in tuberous sclerosis complex. Brain Dev 34:478–486

Moshel YA, Elliott R, Teutonico F, Sellin J, Carlson C, Devinsky O, Weiner HL (2010) Do tubers contain function? Resection of epileptogenic foci in perirolandic cortex in children with tuberous sclerosis complex. Epilepsia 51:1242–1251

Mountz JM, Tolbert LC, Lill DW, Katholi CR, Liu HG (1995) Functional deficits in autistic disorder: characterization by technetium-99m-HMPAO and SPECT. J Nucl Med 36:1156–1162

Muller RA, Chugani DC, Behen ME, Rothermel RD, Muzik O, Chakraborty PK, Chugani HT (1998) Impairment of dentato-thalamo-cortical pathway in autistic men: language activation data from positron emission tomography. Neurosci Lett 245:1–4

Muller RA, Behen ME, Rothermel RD, Chugani DC, Muzik O, Mangner TJ, Chugani HT (1999) Brain mapping of language and auditory perception in high-functioning autistic adults: a PET study. J Autism Dev Disord 29:19–31

Müller-Vahl KR, Szejko N, Wilke F, Jakubovski E, Geworski L, Bengel F, Berding G (2019) Serotonin transporter binding is increased in Tourette syndrome with obsessive compulsive disorder. Sci Rep 9(1):972

Muzik O, Chugani DC, Juhasz C, Shen C, Chugani HT (2000a) Statistical parametric mapping: assessment of application in children. NeuroImage 12:538–549

Muzik O, da Silva EA, Juhasz C, Chugani DC, Shah J, Nagy F, Canady A, von Stockhausen HM, Herholz K, Gates J, Frost M, Ritter F, Watson C, Chugani HT (2000b) Intracranial EEG versus flumazenil and glucose PET in children with extratemporal lobe epilepsy. Neurology 54:171–179

Nakamura K, Sekine Y, Ouchi Y, Tsujii M, Yoshikawa E, Futatsubashi M, Tsuchiya KJ, Sugihara G, Iwata Y, Suzuki K, Matsuzaki H, Suda S, Sugiyama T, Takei N, Mori N (2010) Brain serotonin and dopamine transporter bindings in adults with high-functioning autism. Arch Gen Psychiatry 67:59–68

Natsume J, Kumakura Y, Bernasconi N, Soucy JP, Nakai A, Rosa P, Fedi M, Dubeau F, Andermann F, Lisbona R, Bernasconi A, Diksic M (2003) Alpha-[11C] methyl-L-tryptophan and glucose metabolism in patients with temporal lobe epilepsy. Neurology 60:756–761

Nicolson RI, Fawcett AJ, Berry EL, Jenkins IH, Dean P, Brooks DJ (1999) Association of abnormal cerebellar activation with motor learning difficulties in dyslexic adults. Lancet 353:1662–1667

O'Brien TJ, So EL, Mullan BP, Hauser MF, Brinkmann BH, Bohnen NI, Hanson D, Cascino GD, Jack CR Jr, Sharbrough FW (1998) Subtraction ictal SPECT co-registered to MRI improves clinical usefulness of SPECT in localizing the surgical seizure focus. Neurology 50:445–454

O'Brien TJ, So EL, Mullan BP, Hauser MF, Brinkmann BH, Jack CR Jr, Cascino GD, Meyer FB, Sharbrough FW (1999) Subtraction SPECT co-registered to MRI improves postictal SPECT localization of seizure foci. Neurology 52:137–146

O'Brien TJ, So EL, Mullan BP, Cascino GD, Hauser MF, Brinkmann BH, Sharbrough FW, Meyer FB (2000) Subtraction peri-ictal SPECT is predictive of extratemporal epilepsy surgery outcome. Neurology 55:1668–1677

O'Tuama LA, Urion DK, Janicek MJ, Treves ST, Bjornson B, Moriarty JM (1992) Regional cerebral perfusion in Landau-Kleffner syndrome and related childhood aphasias. J Nucl Med 33:1758–1765

Ohnishi T, Matsuda H, Hashimoto T, Kunihiro T, Nishikawa M, Uema T, Sasaki M (2000) Abnormal regional cerebral blood flow in childhood autism. Brain 123(Pt 9):1838–1844

Ohta Y, Nariai T, Akimoto H, Shimohira M, Sugimoto J, Ohno K, Senda M, Hirakawa K (2001) Tuberous sclerosis: epileptogenicity and multimodal presurgical evaluations. Childs Nerv Syst 17:313–319

Ollenberger GP, Byrne AJ, Berlangieri SU, Rowe CC, Pathmaraj K, Reutens DC, Berkovic SF, Scheffer IE, Scott AM (2005) Assessment of the role of FDG PET in the diagnosis and management of children with refractory epilepsy. Eur J Nucl Med Mol Imaging 32:1311–1316

Osborne JP, Fryer A, Webb D (1991) Epidemiology of tuberous sclerosis. Ann N Y Acad Sci 615:125–127

Palm DG, Brandt M, Korinthenberg R (1988) West syndrome and Lennox-Gastaut syndrome in children with porencephalic cysts: long-term follow-up after neurosurgical treatment. In: Niedermeyer E, Degen R (eds) The Lennox-Gastaut syndrome. Alan R. Liss, New York, pp 419–426

Patil S, Biassoni L, Borgwardt L (2007) Nuclear medicine in pediatric neurology and neurosurgery: epilepsy and brain tumors. Semin Nucl Med 37:357–381

Perissinotti A, Niñerola-Baizán A, Rubí S, Carreño M, Marti-Fuster B, Aparicio J, Mayoral M, Donaire A, Sanchez-Izquierdo N, Bargalló N, Rumiá J, Boget T, Pons F, Lomeña F, Ros D, Pavía J, Setoain X (2018) PISCOM: a new procedure for epilepsy combining ictal SPECT and interictal PET. Eur J Nucl Med Mol Imaging 45(13):2358–2367

Perot P, Weir B, Rasmussen T (1966) Tuberous sclerosis. Surgical therapy for seizures. Arch Neurol 15:498–506

Philippart M, Chugani B (1995) Neuronal ceroid-lipofuscinosis: late infantile form or juvenile form? Brain Dev 17:225

Philippart M, Messa C, Chugani HT (1994) Spielmeyer-Vogt (Batten, Spielmeyer-Sjogren) disease. Distinctive patterns of cerebral glucose utilization. Brain 117(Pt 5):1085–1092

Philippart M, da Silva E, Chugani HT (1997) The value of positron emission tomography in the diagnosis and monitoring of late infantile and juvenile lipopigment storage disorders (so-called Batten or neuronal ceroid lipofuscinoses). Neuropediatrics 28:74–76

Picard F, Bruel D, Servent D, Saba W, Fruchart-Gaillard C, Schollhorn-Peyronneau MA, Roumenov D, Brodtkorb E, Zuberi S, Gambardella A, Steinborn B, Hufnagel A, Valette H, Bottlaender M (2006) Alteration of the in vivo nicotinic receptor density in ADNFLE patients: a PET study. Brain 129:2047–2060

Pinton F, Chiron C, Enjolras O, Motte J, Syrota A, Dulac O (1997) Early single photon emission computed tomography in Sturge-Weber syndrome. J Neurol Neurosurg Psychiatry 63:616–621

Richardson MP, Koepp MJ, Brooks DJ, Duncan JS (1998) 11C-flumazenil PET in neocortical epilepsy. Neurology 51:485–492

Richardson MP, Hammers A, Brooks DJ, Duncan JS (2001) Benzodiazepine-GABA(A) receptor binding is very low in dysembryoplastic neuroepithelial tumor: a PET study. Epilepsia 42:1327–1334

Rinne JO, Ruottinen HM, Nagren K, Aberg LE, Santavuori P (2002) Positron emission tomography shows reduced striatal dopamine D1 but not D2 receptors in juvenile neuronal ceroid lipofuscinosis. Neuropediatrics 33:138–141

Rintahaka PJ, Chugani HT, Messa C, Phelps ME (1993) Hemimegalencephaly: evaluation with positron emission tomography. Pediatr Neurol 9:21–28

Rintahaka PJ, Chugani HT, Sankar R (1995) Landau-Kleffner syndrome with continuous spikes and waves during slow-wave sleep. J Child Neurol 10:127–133

Romanelli P, Najjar S, Weiner HL, Devinsky O (2002) Epilepsy surgery in tuberous sclerosis: multistage procedures with bilateral or multilobar foci. J Child Neurol 17:689–692

Rowe CC, Berkovic SF, Austin M, McKay WJ, Bladin PF (1989) Postictal SPET in epilepsy. Lancet 1:389–390

Rowe CC, Berkovic SF, Austin MC, McKay WJ, Bladin PF (1991) Patterns of postictal cerebral blood flow in temporal lobe epilepsy: qualitative and quantitative analysis. Neurology 41:1096–1103

Rubí S, Costes N, Heckemann RA, Bouvard S, Hammers A, Martí Fuster B, Ostrowsky K, Montavont A, Jung J, Setoain X, Catenoix H, Hino K, Liger F, Le Bars D, Ryvlin P (2013) Positron emission tomography with α-[11C]methyl-L-tryptophan in tuberous sclerosis complex-related epilepsy. Epilepsia 54(12):2143–2150

Ruggieri V, Caraballo R, Fejerman N (1989) Intracranial tumors and West syndrome. Pediatr Neurol 5:327–329

Rumsey JM, Duara R, Grady C, Rapoport JL, Margolin RA, Rapoport SI, Cutler NR (1985) Brain metabolism in autism. Resting cerebral glucose utilization rates as measured with positron emission tomography. Arch Gen Psychiatry 42:448–455

Rumsey JM, Berman KF, Denckla MB, Hamburger SD, Kruesi MJ, Weinberger DR (1987) Regional cerebral blood flow in severe developmental dyslexia. Arch Neurol 44:1144–1150

Rumsey JM, Andreason P, Zametkin AJ, Aquino T, King AC, Hamburger SD, Pikus A, Rapoport JL, Cohen RM (1992) Failure to activate the left temporoparietal cortex in dyslexia. An oxygen 15 positron emission tomographic study. Arch Neurol 49:527–534

Rumsey JM, Nace K, Donohue B, Wise D, Maisog JM, Andreason P (1997) A positron emission tomographic study of impaired word recognition and phonological processing in dyslexic men. Arch Neurol 54:562–573

Ruottinen HM, Rinne JO, Haaparanta M, Solin O, Bergman J, Oikonen VJ, Jarvela I, Santavuori P (1997) [18F]fluorodopa PET shows striatal dopaminergic dysfunction in juvenile neuronal ceroid lipofuscinosis. J Neurol Neurosurg Psychiatry 62:622–625

Ryvlin P, Bouvard S, Le Bars D, De Lamerie G, Gregoire MC, Kahane P, Froment JC, Mauguiere F (1998) Clinical utility of flumazenil-PET versus [18F]fluorodeoxyglucose-PET and MRI in refractory partial epilepsy. A prospective study in 100 patients. Brain 121(Pt 11):2067–2081

Sakaguchi Y, Kidokoro H, Ogawa C, Okai Y, Ito Y, Yamamoto H, Ohno A, Nakata T, Tsuji T, Nakane T, Kawai H, Kato K, Naganawa S, Natsume J (2018) Longitudinal findings of MRI and PET in West Syndrome with subtle focal cortical dysplasia. Am J Neuroradiol 39(10):1932–1937

Salamon N, Kung J, Shaw SJ, Koo J, Koh S, Wu JY (2008) FDG-PET/MRI co-registration improves detection of cortical dysplasia in epilepsy patients. Neurology 71:1594–1601

Sauer L, Pereira LD, Ciasca SM, Pestun M, Guerreiro MM (2006) Dichotic listening and spect in dyslexic children. Arq Neuropsiquiatr 64:108–111

Savic I, Ingvar M, Stone-Elander S (1993) Comparison of [11C]flumazenil and [18F]FDG as PET markers of epileptic foci. J Neurol Neurosurg Psychiatry 56:615–621

Savic I, Thorell JO, Roland P (1995) [11C]flumazenil positron emission tomography visualizes frontal epileptogenic regions. Epilepsia 36:1225–1232

Sayit E, Dirik E, Durak H, Uzuner N, Anal O, Cevik NT (1999) Landau-Kleffner syndrome: relation of clinical, EEG and Tc-99m-HMPAO brain SPECT findings and improvement in EEG after treatment. Ann Nucl Med 13:415–418

Schur S, Allen V, White A, Mirsky D, Stence N, O'Neill B, Handler M, Dudley R, Laoprasert P (2018) Significance of FDG-PET hypermetabolism in children with intractable focal epilepsy. Pediatr Neurosurg 53(3):153–162

Seo JH, Holland K, Rose D, Rozhkov L, Fujiwara H, Byars A, Arthur T, DeGrauw T, Leach JL, Gelfand MJ, Miles L, Mangano FT, Horn P, Lee KH (2011) Multimodality imaging in the surgical treatment of children with nonlesional epilepsy. Neurology 76:41–48

Shiraishi H, Takano K, Shiga T, Okajima M, Sudo A, Asahina N, Kohsaka S, Fukuhara M, Saitoh S (2007) Possible involvement of the tip of temporal lobe in Landau-Kleffner syndrome. Brain Dev 29:529–533

Siegel BV Jr, Asarnow R, Tanguay P, Call JD, Abel L, Ho A, Lott I, Buchsbaum MS (1992) Regional cerebral glucose metabolism and attention in adults with a history of childhood autism. J Neuropsychiatry Clin Neurosci 4:406–414

Sinclair DB, Snyder TJ (2005) Corticosteroids for the treatment of Landau-kleffner syndrome and continuous spike-wave discharge during sleep. Pediatr Neurol 32:300–306
Singer HS, Szymanski S, Giuliano J, Yokoi F, Dogan AS, Brasic JR, Zhou Y, Grace AA, Wong DF (2002) Elevated intrasynaptic dopamine release in Tourette's syndrome measured by PET. Am J Psychiatry 159:1329–1336
Spatola M, Dalmau J (2017) Seizures and risk of epilepsy in autoimmune and other inflammatory encephalitis. Curr Opin Neurol 30(3):345–353
Stern E, Silbersweig DA, Chee KY, Holmes A, Robertson MM, Trimble M, Frith CD, Frackowiak RS, Dolan RJ (2000) A functional neuroanatomy of tics in Tourette syndrome. Arch Gen Psychiatry 57:741–748
Sturm JW, Newton MR, Chinvarun Y, Berlangieri SU, Berkovic SF (2000) Ictal SPECT and interictal PET in the localization of occipital lobe epilepsy. Epilepsia 41:463–466
Suhonen-Polvi H, Kero P, Korvenranta H, Ruotsalainen U, Haaparanta M, Bergman J, Simell O, Wegelius U (1993) Repeated fluorodeoxyglucose positron emission tomography of the brain in infants with suspected hypoxic-ischaemic brain injury. Eur J Nucl Med 20:759–765
Swartz BE, Halgren E, Delgado-Escueta AV, Mandelkern M, Gee M, Quinones N, Blahd WH, Repchan J (1989) Neuroimaging in patients with seizures of probable frontal lobe origin. Epilepsia 30:547–558
Swartz BW, Khonsari A, Vrown C, Mandelkern M, Simpkins F, Krisdakumtorn T (1995) Improved sensitivity of 18FDG-positron emission tomography scans in frontal and "frontal plus" epilepsy. Epilepsia 36:388–395
Szelies B, Weber-Luxenburger G, Pawlik G, Kessler J, Holthoff V, Mielke R, Herholz K, Bauer B, Wienhard K, Heiss WD (1996) MRI-guided flumazenil- and FDG-PET in temporal lobe epilepsy. NeuroImage 3:109–118
Szelies B, Sobesky J, Pawlik G, Mielke R, Bauer B, Herholz K, Heiss WD (2002) Impaired benzodiazepine receptor binding in peri-lesional cortex of patients with symptomatic epilepsies studied by [(11)C]-flumazenil PET. Eur J Neurol 9:137–142
Sztriha L, al Suhaili AR, Prais V (1997) Cortical hypoperfusion in symptomatic West syndrome. A SPECT study. Eur J Radiol 25:20–25
Tae WS, Joo EY, Kim JH, Han SJ, Suh YL, Kim BT, Hong SC, Hong SB (2005) Cerebral perfusion changes in mesial temporal lobe epilepsy: SPM analysis of ictal and interictal SPECT. NeuroImage 24:101–110
Theodore WH, Rose D, Patronas N, Sato S, Holmes M, Bairamian D, Porter RJ, Di Chiro G, Larson S, Fishbein D (1987) Cerebral glucose metabolism in the Lennox-Gastaut syndrome. Ann Neurol 21:14–21
Theodore WH, Carson RE, Andreasen P, Zametkin A, Blasberg R, Leiderman DB, Rice K, Newman A, Channing M, Dunn B et al (1992) PET imaging of opiate receptor binding in human epilepsy using [18F]cyclofoxy. Epilepsy Res 13:129–139
Theodore WH, Sato S, Kufta CV, Gaillard WD, Kelley K (1997) FDG-positron emission tomography and invasive EEG: seizure focus detection and surgical outcome. Epilepsia 38:81–86
Thorngren-Jerneck K, Ohlsson T, Sandell A, Erlandsson K, Strand SE, Ryding E, Svenningsen NW (2001) Cerebral glucose metabolism measured by positron emission tomography in term newborn infants with hypoxic ischemic encephalopathy. Pediatr Res 49:495–501
Tien RD, Ashdown BC, Lewis DV Jr, Atkins MR, Burger PC (1992) Rasmussen's encephalitis: neuroimaging findings in four patients. AJR Am J Roentgenol 158:1329–1332
Tomás J, Pittau F, Hammers A, Bouvard S, Picard F, Vargas MI, Sales F, Seeck M, Garibotto V (2019) The predictive value of hypometabolism in focal epilepsy: a prospective study in surgical candidates. Eur J Nucl Med Mol Imaging 46(9):1806–1816
Uijl SG, Leijten FS, Arends JB, Parra J, van Huffelen AC, Moons KG (2007) The added value of [18F]-fluoro-D-deoxyglucose positron emission tomography in screening for temporal lobe epilepsy surgery. Epilepsia 48:2121–2129
Uthman BM, Reid SA, Wilder BJ, Andriola MR, Beydoun AA (1991) Outcome for West syndrome following surgical treatment. Epilepsia 32:668–671
Valenti MP, Froelich S, Armspach JP, Chenard MP, Dietemann JL, Kerhli P, Marescaux C, Hirsch E, Namer IJ (2002) Contribution of SISCOM imaging in the presurgical evaluation of temporal lobe epilepsy related to dysembryoplastic neuroepithelial tumors. Epilepsia 43:270–276

Van Bogaert P, Massager N, Tugendhaft P, Wikler D, Damhaut P, Levivier M, Brotchi J, Goldman S (2000) Statistical parametric mapping of regional glucose metabolism in mesial temporal lobe epilepsy. NeuroImage 12:129–138

Vera P, Kaminska A, Cieuta C, Hollo A, Stievenart JL, Gardin I, Ville D, Mangin JF, Plouin P, Dulac O, Chiron C (1999) Use of subtraction ictal SPECT co-registered to MRI for optimizing the localization of seizure foci in children. J Nucl Med 40:786–792

Volpe JJ, Herscovitch P, Perlman JM, Raichle ME (1983) Positron emission tomography in the newborn: extensive impairment of regional cerebral blood flow with intraventricular hemorrhage and hemorrhagic intracerebral involvement. Pediatrics 72:589–601

Volpe JJ, Herscovitch P, Perlman JM, Kreusser KL, Raichle ME (1985) Positron emission tomography in the asphyxiated term newborn: parasagittal impairment of cerebral blood flow. Ann Neurol 17:287–296

von Oertzen TJ, Mormann F, Urbach H, Reichmann K, Koenig R, Clusmann H, Biersack HJ, Elger CE (2011) Prospective use of subtraction ictal SPECT coregistered to MRI (SISCOM) in presurgical evaluation of epilepsy. Epilepsia 52:2239–2248

Wakamoto H, Chugani DC, Juhasz C, Muzik O, Kupsky WJ, Chugani HT (2008) Alpha-methyl-L-tryptophan positron emission tomography in epilepsy with cortical developmental malformations. Pediatr Neurol 39:181–188

Wang S, Tang Y, Aung T, Chen C, Katagiri M, Jones SE, Prayson RA, Krishnan B, Gonzalez-Martinez JA, Burgess RC, Najm IM, Alexopoulos AV, Wang S, Ding M, Wang ZI (2019) Multimodal noninvasive evaluation in MRI-negative operculoinsular epilepsy. J Neurosurg 12:1–11

Weiner HL, Carlson C, Ridgway EB, Zaroff CM, Miles D, LaJoie J, Devinsky O (2006) Epilepsy surgery in young children with tuberous sclerosis: results of a novel approach. Pediatrics 117:1494–1502

Werhahn KJ, Landvogt C, Klimpe S, Buchholz HG, Yakushev I, Siessmeier T, Muller-Forell W, Piel M, Rosch F, Glaser M, Schreckenberger M, Bartenstein P (2006) Decreased dopamine D2/D3-receptor binding in temporal lobe epilepsy: an [18F]fallypride PET study. Epilepsia 47:1392–1396

Willmann O, Wennberg R, May T, Woermann FG, Pohlmann-Eden B (2007) The contribution of 18F-FDG PET in preoperative epilepsy surgery evaluation for patients with temporal lobe epilepsy: a meta-analysis. Seizure 16:509–520

Wong DF, Brasic JR, Singer HS, Schretlen DJ, Kuwabara H, Zhou Y, Nandi A, Maris MA, Alexander M, Ye W, Rousset O, Kumar A, Szabo Z, Gjedde A, Grace AA (2008) Mechanisms of dopaminergic and serotonergic neurotransmission in Tourette syndrome: clues from an in vivo neurochemistry study with PET. Neuropsychopharmacology 33:1239–1251

Wu JY, Salamon N, Kirsch HE, Mantle MM, Nagarajan SS, Kurelowech L, Aung MH, Sankar R, Shields WD, Mathern GW (2010) Noninvasive testing, early surgery, and seizure freedom in tuberous sclerosis complex. Neurology 74:392–398

Wyllie E, Comair YG, Kotagal P, Bulacio J, Bingaman W, Ruggieri P (1998) Seizure outcome after epilepsy surgery in children and adolescents. Ann Neurol 44:740–748

Yacubian EM, Marie SK, Valerio RM, Jorge CL, Yamaga L, Buchpiguel CA (1997) Neuroimaging findings in Rasmussen's syndrome. J Neuroimaging 7:16–22

Yang WH, Jing J, Xiu LJ, Cheng MH, Wang X, Bao P, Wang QX (2011) Regional cerebral blood flow in children with autism spectrum disorders: a quantitative (9)(9)mTc-ECD brain SPECT study with statistical parametric mapping evaluation. Chin Med J 124:1362–1366

You SJ, Lee JK, Ko TS (2007) Epilepsy surgery in a patient with Lennox-Gastaut syndrome and cortical dysplasia. Brain Dev 29:167–170

Yum MS, Ko TS, Lee JK, Hong S, Kim DS, Kim J (2011) Surgical treatment for localization-related infantile spasms: excellent long-term outcomes. Clin Neurol Neurosurg 113:213–217

Zhai Q, Gui J, Zhang Y, Qiao H (2010) Children treated for epileptic encephalopathies show improved glucose metabolism. Pediatr Int 52:883–887

Zilbovicius M, Garreau B, Tzourio N, Mazoyer B, Bruck B, Martinot JL, Raynaud C, Samson Y, Syrota A, Lelord G (1992) Regional cerebral blood flow in childhood autism: a SPECT study. Am J Psychiatry 149:924–930